International Mine Water Association Conference 2025

Time to Come

Braga, Portugal
Oviedo/Uviéu, Spain

6 – 11 July 2025

Teresa Valente, Ritva Mühlbauer,
Almudena Ordóñez, Christian Wolkersdorfer

Portugal IMWA Spain

2025

International Mine Water Association Conference – Time to Come

International Mine Water Association
Conference 2025 – Time to Come

Proceedings of the International Mine Water Association Conference

July 6–11, 2025

Braga, Portugal & Oviedo, Spain

Editors

Teresa Valente
Ritva Mühlbauer
Almudena Ordóñez
Christian Wolkersdorfer

International Mine Water Association Conference 2025 – Time to Come
2025, Braga, Portugal & Oviedo, Spain

ISBN 978-3-9825293-3-2

Editors
Teresa Valente, Ritva Mühlbauer, Almudena Ordóñez, Christian Wolkersdorfer

Cover design
Christian Wolkersdorfer, Anna Johanna Sotiralis

Layout and Typesetting
Jigsaw Graphic Design & Christian Wolkersdorfer

Cover Photographs
Ana Barroso, Carlos Martins, International Mine Water Association

All abstracts were reviewed by 2–6 experts of the International Scientific Committee.

All full papers were peer-reviewed by 2–3 experts from the International Scientific Committee. Authors were asked to correct their papers after the review and those that did not meet the requirements of the IMWA proceedings were rejected.

www.IMWA.info

Organizers

International Mine Water Association

University of Minho (Portugal)

Universidad de Oviedo

University of Oviedo/Uviéu (Spain)

with the support of

visit Portugal

International Scientific Committee (ISC)

Oluseyi Ayokunle Abegunde
Jamie-Leigh Robin Abrahams
Ayman Abushafa M Abufalgha
Antwi Addai
Nashon Juma Adero
Bert Allard
Ignacio Alvarez
Rodrigo Alvarez
Timothy Amangdam Anemana
John George Annandale
Margarida Horta Antunes
Norberto Jr Aquino
David Arcos
Isidora Arriagada
Tim Aubel
Okan Aygün
Abie Badhurahman
Jeff Bain
Joel Z Bandstra
Fernando Barrio-Parra
Zuzana Bártová
Maria Dolores Basallote
Sod-Erdene Bazardorj
Gabor Bekesi
Kalman Benedek
MaryBeth Berkes
Carolina Bittencourt de Abreu
Mohamed Ali Borgi
Frederik Stefanus Botha
Rob Bowell
Adrian Brown
Joanna Butlanska
Meijun Cai
Paula Carvalho
Eric Cavazza
Patricia Sekina Chagonda
Irati Chasco Díaz
Athman Gunda Chembea
Mengfang Chen
Frances Chikanda
Chan Lan Chun
Wassim Chwikhi
Maria Clara Costa
Ronan Courtney
Charles A Cravotta III
Damián Aníbal Jesús Cruz Barrientos
Roberto Pereira da Silva
Caroline Jane Dale
Priyal Dama-Fakir
Matthew John Damhuis
Camilo Raul de los Hoyos
Eduardo De Miguel
Julia Dent
Catarina Diamantino
Gareth Digges La Touche
Yanqing Ding
Qinghong Dong
Joseph J Donovan
Dayton M Dorman
Diana Mary Duthe
Sendy Dwiki
Vimbainashe Lorraine Dzimbanhete
Mariana Erasmus
Sven Eulenberger
Jodie Evans
Alissa Flatley
Hernan Flores
Rita Maria Ferreira Fonseca
Joana Fonseca Araújo
Elvis Fosso-Kankeu
Anne Gädeke
Alex Jack Gallagher
Alfredo Gallardo
Carmen C. García
Silverio García-Cortés
Mihriban Genc
Scott Gischia
Anthony Njoroge Gitii
Peter Goerke-Mallet
Saeed Golian
Cleber Jose Baldoni Gomes
Patrícia Gomes
Edward Gonzales
Andres Gonzalez Quiros
Erik Guldbech
Manuel Gutierrez
Lina Hällström
Takaya Hamai

Simon Haunch
Benjamin Hedin
Robert S Hedin
Mehrez Hermassi
Paul Hesketh
Pablo León Higueras
Xiaotong Huang
Paul Hubbard
Amy L Hudson
Ashlene Hudson
Misbah Fatima Hussain
Sheila Imrie
Yogi Irmas Pratama
Miguel Izquierdo-Díaz
Scott Jackson
Judith Liliana Jaeger Collantes
Ryan Thomas Jakubowski
Iván Jares Salguero
Fei Jin
Lucinda Johnson
David Richard Jones
Ömer Kahraman
Teemu Eemeli Karlsson
Andrea Kassahun
Hossein Kheirkhah Gildeh
Duk-Min Kim
Robert Lawrence Kleinmann
Frans Knops
Evelyn Krawczyk-Bärsch
Petr Kuznetsov
Julie Anne LaBar
Jeff Langman
Liliana Lefticariu
Jonas Enno Lehmann
Colin A Lennox
ShouQing Liu
Simon Antony Lorentz
Paul Joel Lourens
Mark Lund
Ros Lund
Rudzani Lusunzi
Joseph Ddumba Lwanyaga
Liyuan Ma
Joseph Archibald MacPhee
Godfrey Madzivire
Ann Maest
Justin Kambale Maganga
Mamile Belina Mahlohla
Tebogo Jane Makono
Abdelkabir Maqsoud
Genevieve Marchand
Johannes Philippus Maree
Paula Marinho Reis
Antonio Luis Marqués Sierra
Manny Mathuthu
Cherie McCullough
Matthew P. McGann
Federica Meloni
Javier Menendez
Thomas Metschies
Zorana Milošević
Olivia Clare Milton-Thompson
Tumelo Monty Mogashane
Lehlohonolo Mokhahlane
Patricio Ignacio Monreal
Jesus Montero
Kagiso Samuel More
Kym Lesley Morton
Alseno Kagiso Mosai
Olga Moya Aranzubia
Khuthadzo Mudzanani
Elke Mugova
Ritva Mühlbauer
Ronald H Mullennex
Festus Muturi
Shadrack Mwakio Mwagandi
Kevin Myers
Jivesh Naidu
Ivan Nancucheo
Andres Navarro
Sofia Angelina Nazaruk
Gustavo Neira-Arenas
Khashane Robert Tshishonga Netshitungulwana
Christopher Neville
Helene Flore Nguemgaing
Katarzyna Niedbalska
Erik Nixdorf
Frank Nkansah-Boadu
Candra Nugraha
Emma-Tuulia Katariina Nurmesniemi
Erastus Kiswili Nyile
Heath Marie Orcutt
Maria Almudena Ordóñez Alonso
Felip Ortuño
Oscar Osores
Michael Palmer
Michael William Palmer
Sheyla Palomino Ore
Pradeep Kumar Parhi
Kieran Parker
Agnieszka Pawlowska
Eric F Perry
Guglielmo Persiani
Benoît Plante
James Pope
Hang Qian
Hanli Qiao
Jackson Quarles
Ricardo Henryque Reginto Quevedo Melo
Mokabolane Innocent Rabohale
Madhumitha Raghav
Selaelo Jacquelene Ramugondo
Quirina Isabella Roode-Gutzmer
Sean Lloyd Rossouw
Tobias Rudolph
Eduardo Ruiz
Francisco Ruiz
Carlos Ruiz Cánovas

Humberto Antonio Saeze
Musah Salifu
David Anthony Salmon
Camille Rose Schaffer
Ivo André Homrich Schneider
Yolandi Schoeman
Ralph Schöpke
Logan Schultz
Ayanda Nomaswazi Shabalala
Melissa Shafer
Xianzhi Shi
Ivan Shubin
Eliza Liberty Siefert
Rodrigo de Almeida Silva
Alison Sinclair
Givarn Singh
Viktor Sjöberg
Jiří Slovák
Stephanie Somot
Pallavee Srivastava
Peter Clive Stanley
Gideon Steyl
Roald Alexander Strand
Wanghua Sui
Jacek Szczepiński
Małgorzata Szlachta
Salamatu Joana Tannor
Barbara M.A. Teichert
Mark John Thomasson
Craig Thompson
Lloyd Richard Townley
Tuan Quang Tran
Sereyroith Tum
Viswanath Ravi Kumar Vadapalli
Teresa Maria Valente
Estariëthe van Heerden
Rob Van Hille
Jerry Vandenberg
Orlando Vaselli
Stéphane Vaxelaire
Rens Verburg
Danie Vermeulen
Miran Veselič
Annalisa Vicente
Maria Cristina Vila
Denys Villa Gomez
Xingjie Wang
John Douglass Waterhouse
Anne Weber
Holger Weiß
Megan Dayl Welman Purchase
Thomas Wenzel
Godfred Williams-Nanyaa
Neil Allan Wolfe
Christian Wolkersdorfer
Andrew Wood
Peter Woods
Magdalena Worsa-Kozak
Qing Wu
Chao Xu
Tetsuo Yasutaka
Alan Yendell
Xiaoyun Yi
Huichao Yin
Grace Yungwirth

Local Organizing Committee (LOC)

Teresa Valente
Maria Almudena Ordóñez
Christian Wolkersdorfer
Elke Mugova
Catarina Diamantino
Carlos Martins
Ana Raquel Barosso
Amélia Paula Marinho-Reis
Margarida Antunes
Patrícia Gomes
Ritva Mühlbauer

Portugal IMWA Spain
2025

Sponsors

IMWA

Cobre
San
Rafael

dstgroup

SOMINCOR
Sociedade Mineira de Neves-Corvo, S.A.
a subsidiary of lundin mining

Malvern
Panalytical
a spectris company

srk consulting

LORAX
ENVIRONMENTAL

In-Situ

ITASCA

Technische
Hochschule
Georg Agricola

Universidad de Oviedo

ALMINA
Minas do Alentejo, SA

UIT UMWELTLEISTUNGEN

AMPHOS 21
an RSK company

Grupo I.L.C.

MUNICÍPIO DE
GUIMARÃES

edm
Empresa de Desenvolvimento Mineiro, SA

BIOSMART
soluções ambientais

Contents

Conference Papers – Peer Reviewed

Abstracts and Extended Abstracts – Reviewed

Conference Papers – Peer Reviewed

Zinc Recovery from Abandoned Mine Drainage: Insights from the Freiberg Mining Region, Germany

Janith Abeywickrama[1], Nils Hoth[1], Carsten Drebenstedt[1]

[1]*TU Bergakademie Freiberg, Gustav Zeuer Strasse 1ª, 09599, Freiberg, Germany.*

Abstract

The study was done in the Freiberg mining region of Saxony, Germany, where significant loads of zinc are released into the Elbe River. The study aimed to identify optimal conditions for zinc recovery through pretreatment of mine water, a series of 100 mL scale column experiments, and optimising the regeneration process. Initial tests showed that Aminophosphonic functionalized TP 260 resin had a high affinity for aluminium, occupying 93% of the resin's capacity, while zinc capacity was limited to 0.2 eq/L. Incomplete aluminium deloading necessitated pretreatment via selective precipitation of aluminium at pH 6.0, which resulted in increased zinc loading capacity to 1 eq/L. Under optimized conditions, a zinc concentrate of 18.5 g/L with 100% recovery was achieved, with sulfuric acid proving more effective than hydrochloric acid for elution. SEM EDX analysis indicated residual acid on the resin, suggesting the need for further study on the long-term effects of resin capacity variation. The study also revealed that three drainage galleries in the Freiberg area currently contribute nearly 85 tons of zinc load to river Elbe annually. This research elucidates the feasibility of efficient zinc recovery from these point sources of pollution via refined ion exchange processes, supporting circular economy initiatives and environmental conservation efforts.

Introduction

Old mine water discharge galleries, often referred as adits or drainage tunnels can have many importance in now a day. They basically help in managing water flow inside the mine and prevent accumulation of unnecessary levels of water in abandoned mines. However, old mines often have waste dumps and mined out areas that can generate acid mine drainage once they are exposed to water, oxygen, and necessary microbial processes (Wolkersdorfer, 2022). Therefore, sometimes the discharge galleries can transport metal loaded acidic waters to the recipient rivers causing negative impact on surrounding ecosystem and water sources. One main example of this process can be seen in Freiberg area, Germany. According to the literature, the mine water discharge galleries in the Freiberg area are particularly significant, contributing to 37% of the zinc contamination found at the end of the Elbe River (Martin *et al.*, 1994). However, due to water dilution, zinc concentrations at the mouth of the Elbe River are very low. However, if some or all of the zinc could be recovered at the discharge point, it would considerably reduce downstream contamination over the 400 km stretch and could also yield intermediate products that contribute to a circular economy.

Therefore, this study is focused on selectively recovering zinc from mining influenced water via ion exchange. As a first step, we characterized the different mine waters in the Freiberg area and compared the results with historical values from the literature (Baacke, 2000; Degner, 2003). Our results indicate that zinc loads have significantly decreased over the past two decades (Table 1). However, the Freiberg mine water galleries continue to discharge approximately 85 tons of zinc annually into the Mulde River. Moreover, sampling revealed elevated zinc concentrations of up to 20 mg/L and lower pH levels in water discharged from the VGS mine water gallery. Geochemical analyses revealed a considerable change in water composition in the VGS gallery during heavy rainfalls, while the waters in the other galleries show minimal changes (Fig. 1). Therefore, this study utilized water collected from the VGS mine water gallery (Königliche Verträgliche Gesellschaft Stollen) in Freiberg, Germany.

Based on many literatures, amino phosphonic-functionalized TP 260 resin was selected to recover zinc (Hubicki *et al.*, 2015; Jurrius *et al.*, 2014). After preliminary filtration using a 0.45-micron filter, the mining-influenced water was pumped into a 100 mL column containing TP 260 resin at a flow rate of 10 BV/h. It's important to note that in some of our earlier small-scale tests (1 BV = 10 mL), a flow rate of 10 BV/h was challenging to manage due to turbulence generated within the resin bed. However, at a 100 mL scale, the same flow rate was manageable, as the weight of the resin and the increased length of the resin bed mitigated the turbulence. Initial ion exchange experiments revealed that the TP 260 resin exhibited a strong affinity for aluminum in the water matrix (Fig. 2a), utilizing nearly 93% of its operational capacity (1.8 eq/L). The VGS water had an aluminum concentration between 4–8 mg/L. Due to the higher adsorption of aluminum, zinc was only loaded up to 0.2 eq/L. It seems that phosphonic group in the resin forms stronger coordination bond with Al^{3+} due to its higher oxidation state (+3). Therefore, most of the potentially toxic metals ions such as Cu^{2+}, Co^{2+}, and Ni^{2+}, which have lower oxidation state (+2) will be displace by the presence of Al^{3+} in a considerable concentration.

The de loading with 10% sulfuric acid was only able to elute 15% of the Al^{3+} loaded on to the resin. This result depicts that aluminum could not be entirely removed from the resin during deloading. This could mainly hinder the operational capacity and long-term sustainability of the resin. Further studies could be done with loaded resins to

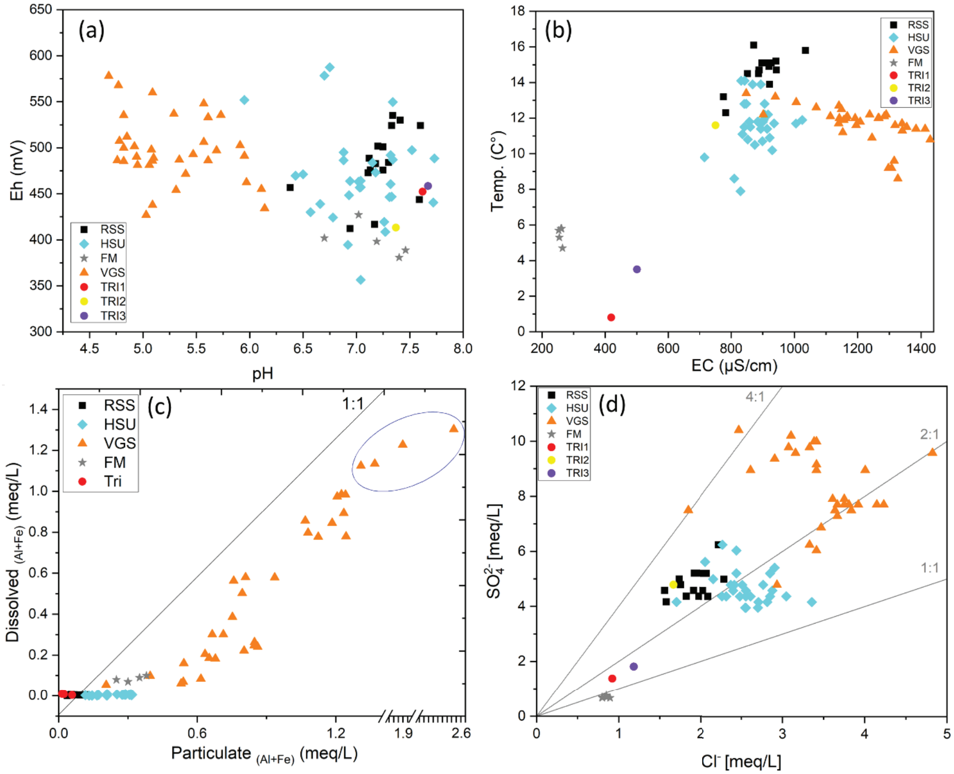

***Figure 1** a) Eh-pH diagram; b) Temperature versus electrical conductivity diagram of the Erzgebirge mine waters; c) Ratio of Particulate to dissolve Al+Fe; d) The relationship between Chloride and Sulfate (Rothschönberger Stollen – RSS; Hauptstolln Umbruch – HSU; Königliche Verträgliche Gesellschaft Stollen – VGS; Freiberger Mulde – FM; Triebisch River –Tri).*

understand the bonding between resin and Al^{3+}. However, due to the limited time, the study was primary focused on identifying a solution to remove Al^{3+} from the mining influenced water before the ion exchange process. Consequently, pretreatment step of the mining-influenced water was introduced to selectively precipitate and remove Al^{3+}. Raising the pH to 6 led to forming aluminum hydroxide precipitate, removing approximately 92% of the dissolved aluminum. Aluminum removal reached 100% at pH 7, but decreased slightly at pH 8 due to the redissolution of aluminum hydroxide. Zinc precipitation began around pH 5.5 and reached 100% at pH 8. Based on these findings, a pH of 6 was determined to be optimal for pretreatment, effectively removing most of the Al^{3+} with minimal zinc loss (approximately 15%).

When pre-treated water was introduced to 100 mL column filled with the TP 260 resin, the zinc loading capacity increased to 1 eq/L (Fig. 2b–2d). Even though some Al^{3+} were remained in the water (> 0.5 mg/L), it did generate a considerable effect on zinc loading. Under optimized conditions, the deloading process produced an 18.5 g/L zinc concentrate with 100% recovery (Fig. 2c). Sulfuric acid showed higher elution efficiency than hydrochloric acid during the deloading process. SEM EDX observation indicates that there are traces of acid composition on the resin surface even after washing the resins with distilled water, which might make the resin more acidic on the next loading cycle. Therefore, additional investigations are being conducted to evaluate the long-term sustainability of the resin and upscale the ion exchange system. The study also recommends

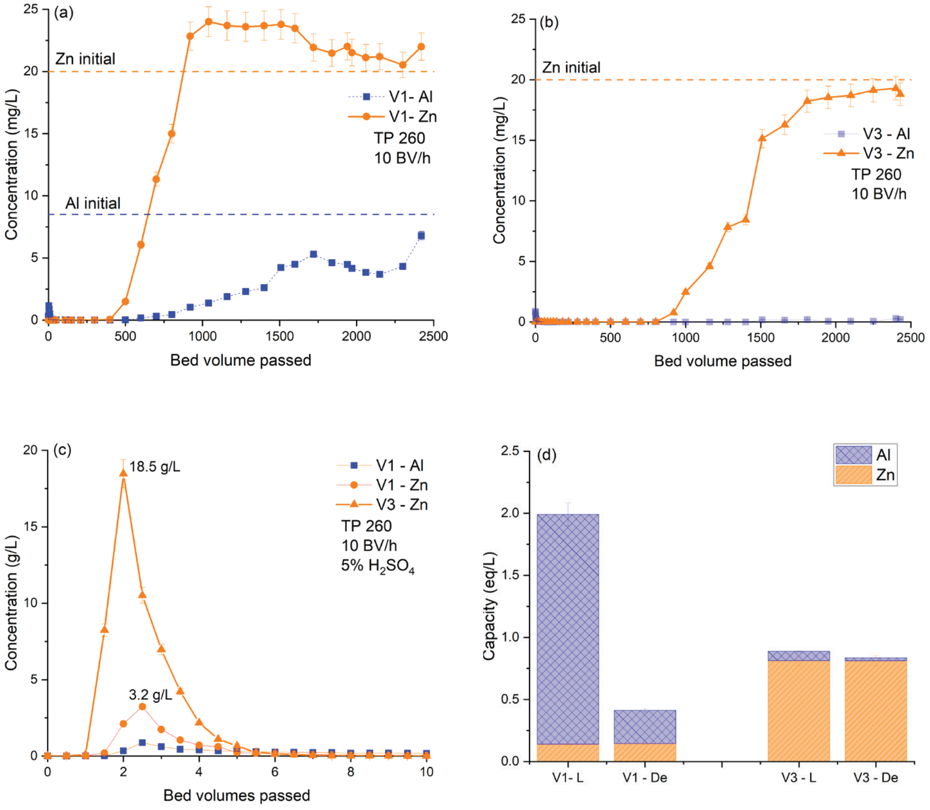

Figure 1 a) Breakthrough curves of untreated mine water (Zn and Al) loaded into IX column with TP 260 resin; b) breakthrough curves of pretreated minewater (after Al precipitation); c) De-loading curves of Zn and Al in untreated (column A) and pretreated (column B) mine waters; d) Mass balance of column A and B (L-loading, De-De-loading).

targeted sampling during extreme events and regular sampling of mine water discharges at Freiberg galleries to obtain more accurate freight determinations for recipient

Overall, through meticulous pretreatment to eliminate unwanted aluminium ions and refining deloading procedures, we have demonstrated the feasibility of efficient metal recovery from mining-influenced water via ion exchange. Scaling up the system will require evaluating water pretreatment strategies such as micro filtration or pH driven precipitation to maintain column performance while minimizing operational costs. Although aluminum was removed primarily to improve zinc recovery efficiency, future studies will examine the composition and potential value of the aluminum precipitate and its implications for material reuse or disposal. Moreover, successful implementation of this kind of technology has the potential to prevent significant amounts of metal loads from entering the recipient rivers and generate potentially exciting opportunities for metal recovery from point sources of contamination. The zinc concentrate produced in this study can be used for research purposes, such as developing new technologies or processes for zinc extraction or exploring novel applications for zinc-based materials. Moreover, it can also be used in environmental remediation such as soil stabilization where zinc can play a role in controlling pollution or promoting plant growth. Therefore, these endeavors contribute to a circular economy and serve as a pivotal measure in environmental conservation. Hence, further studies are recommended on upscaling the process.

References

Baacke, D. (2000). *Geochemisches Verhalten umweltrelevanter Elemente in stillgelegten Polysulfiderzgruben am Beispiel der Grube* [PhDThesis, TU Bergakadeime Freiberg]. https://webdoc.sub.gwdg.de/ebook/diss/2003/tu-freiberg/archiv/html/Geowissenschaften_BaackeDelf966689.html

Degner, T. (2003). *Prognose von geochemischen Auswirkungen der Nachnutzung stillgelegter Bergbau-Stollen-Systeme am Beispiel des Freiberger Grubenreviers.* https://tubaf.qucosa.de/api/qucosa%3A22433/attachment/ATT-0/

Hubicki, Z., Wawrzkiewicz, M., Wójcik, G., Kołodyńska, D., & Wołowicz, A. (2015). *Ion Exchange Method for Removal and Separation of Noble Metal Ions. In Ion Exchange – Studies and Applications*. IntechOpen. https://doi.org/10.5772/60597

Jurrius, Y., Sole, K. C., & Hardwick, E. (2014). *Removal of copper and zinc from a cobalt electrolyte by ion exchange at Kamoto Copper Company's Luilu plant*. 13.

Martin, M., Beuge, P., Kluge, A., & Hoppe, T. (1994). Grubenwässer des Erzgebirges – Quelle von Schwermetallen in der Elbe. *Spektrum Der Wissenschaften*, 5, 102–107.

Wolkersdorfer, C. (2022). *Mine Water Treatment – Active and Passive Methods*. Springer Berlin Heidelberg. https://doi.org/10.1007/978-3-662-65770-6

Table 1 *Comparison of Median Elemental Fluxes from Freiberg Mine Drainage Galleries to Receiving Rivers (This study vs Degner (2003)).*

Load (median)	HSU		VGS		RSS	
g/min	2003	2022	2003	2022	2003	2022
Na	51	96	140	67	1780	1021
K	11	16	19	10	250	141
Mg	65	80	178	76	970	697
Ca	180	261	410	240	3800	3097
Al	2.3	3	54	13	7.9	6
Fe	7.4	10	7	3	2.3	20
Mn	0.2	12	2	16	1.2	21
Si	NA	33	NA	18	NA	275
Zn	14	18	130	33	170	113
Cl	120	693	250	239	2180	2116
SO_4^{2-}	590	316	2200	851	11700	7243

Al, Fe, Mn, and Zn are given as total loads; other elements in dissolved loads; NA-: not available

Settling Characteristics and Treatment Strategies for Open-Cast Coal Mine Water in South Sumatra, Indonesia

Muhammad Sonny Abfertiawan[1], Faiz Hasan[1], Raihannisa Rizqi Meutia[2], Rizky Al Fadhli[3]

[1] *Water and Wastewater Engineering Research Group, Faculty of Civil and Environmental Engineering, Bandung Institute of Technology, Indonesia, msa@itb.ac.id*

[2] *Environmental Engineering Master Program, Faculty of Civil and Environmental Engineering, Bandung Institute of Technology, Indonesia, rrmeutia@gmail.com*

[3] *Environmental & Forestry Planning Department, PT Bukit Asam Tbk, Indonesia, rafadhli@bukitasam.co.id*

Abstract

This research investigates the efficacy of sedimentation ponds in treating mine water contaminated with suspended solids (SS). The study focuses on the design parameters of these ponds, highlighting the limitations of Stokes' law and emphasizing the importance of site-specific data. Experimental settling tests were conducted on six water samples, evaluating pH, ORP, TSS, and concentrations of iron and manganese. The results reveal that water with high acidity (pH 3.16–4.05) can naturally eliminate up to 57.4% of suspended solids within a 50-minute period. In contrast, water with neutral pH requires chemical coagulation, with dosages ranging from 20 to 200 mg/L. Following coagulation, additional settling tests were employed to establish detention time and overflow rates through the use of iso-removal curves.

Keywords: Mine water, sediment pond, settling test, suspended solid, iso-removal curve

Introduction

The management of coal mine water in Indonesia presents unique challenges due to the country's high precipitation levels. Indonesia experiences intense rainfall, with maximum daily amounts reaching 377 mm (Lubis *et al.* 2022). This substantial precipitation contributes to significant water inflow into sediment ponds, which serve as mine water treatment facilities, with peak inflows of up to 2000 L/s (Hasan *et al.* 2024). Moreover, the prevalent use of open-pit mining in Indonesia's coal industry exposes overburden and waste rock directly to rainwater, heightening the risk of adverse environmental consequences, particularly water quality deterioration (Abfertiawan *et al.* 2016).

In Indonesia, mine water typically exhibits acidic properties or high turbidity. Acid Mine Drainage (AMD) results from the interaction of sulfide minerals in overburden or waste rock with oxygen and water, producing acidic water (Abfertiawan *et al.* 2020). Additionally, the presence of colloidal clay minerals often renders mine water turbid, elevating Total Suspended Solids (TSS) concentrations (Abfertiawan *et al.* 2024). While comprehensive mine water characterization is crucial for determining optimal treatment methods, practical constraints often limit the design and monitoring of treatment systems to two primary parameters: pH and TSS. Turbid water is frequently presumed to have high TSS, prompting immediate treatment with coagulants like aluminum sulfate. However, mine water particles can be categorized as suspended or settleable solids, potentially settling naturally without chemical additives. This misconception may lead to excessive chemical use and inflated operational expenses.

The design of sediment ponds, critical for treating mine water containing suspended solids (SS), presents another challenge. These facilities are typically designed based on

Stokes' law, which assumes specific particle settling velocities or gravities. However, actual particle characteristics vary by location, and finer sediments (<2 μm) often deviate from Stokes' law due to inter-particle interactions. Consequently, site-specific designs require additional data on particle size and settling velocity. This study aims to develop a comprehensive framework for designing sediment ponds suitable for various types of coal mine water in Indonesia's South Sumatra region. By incorporating detailed particle characterization and settling behavior analysis, the research seeks to enhance coal mine water treatment efficiency and effectiveness, thereby mitigating environmental impacts and optimizing operational sustainability.

Methods

An analysis of water samples was undertaken to elucidate their physicochemical characteristics, encompassing pH, conductivity, oxidation-reduction potential (ORP), total dissolved solids (TDS), total suspended solids (TSS), and metal concentrations (Fe and Mn, in both total and dissolved forms). The Water Quality Laboratory at ITB conducted the examination, which revealed three principal water quality issues: (1) acidity (pH <6), (2) elevated turbidity (TSS >100 mg/L), and (3) a simultaneous occurrence of both conditions (pH <6 and TSS >100 mg/L). A stepwise treatment protocol was employed, contingent upon TSS concentrations. When TSS surpassed 100 mg/L, type 1 sedimentation was implemented to promote gravitational settling of discrete particles. Conversely, for TSS values ≤100 mg/L, this sedimentation step was bypassed, and the process advanced directly to jar testing using lime (CaO) for optimal dosage determination.

The sedimentation behavior of discrete particles was investigated using a Type 1 sedimentation test. This experiment employed a 7.5 L water sample in a 100 cm-high settling test column. Prior to testing, the sample underwent homogenization. Measurements were recorded at 10-minute intervals for a duration of 60 minutes, at a depth of 95 cm from the water surface. Gravimetric analysis was utilized to determine TSS concentrations, enabling the assessment of particle settling characteristics. Concurrently, a jar test was conducted using four beaker glasses, each containing varying coagulant dosages. The procedure involved a rapid mixing phase at 120 rpm for 1 minute, followed by slow mixing at 60 rpm for 10 minutes, and a 10-minute settling period. Subsequently, the supernatant was analyzed for TSS, pH, TDS, conductivity, and ORP to identify the optimal coagulant dosage. A Type 2 sedimentation test was performed to examine the settling dynamics of flocculent particles post-chemical addition. This test utilized an 8.5 L sample in a 115 cm-high column. Single sampling was conducted from five ports, positioned 20 cm apart, over a 90-minute period. The TSS removal efficiency was evaluated using overflow rate (VO) and total removal fraction (RT). Isoremoval graphs were employed to visualize TSS removal efficiency across time and depth. pH analysis was performed using a pH meter, while TSS and TDS analyses were conducted using gravimetric methods in accordance with APHA Methods 2540 Solids. Iron concentration was determined following APHA 3500 Fe B – Iron by Phenanthroline,

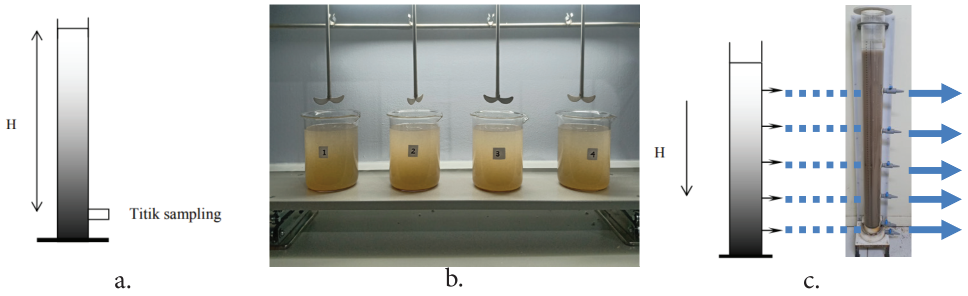

Figure 1 Illustration of (a) type 1 of sedimentation test, (b) jar test, and (c) type 2 of sedimentation test.

Table 1 Initial characterization of mine water.

No	Sample	pH	ORP (mv)	Conductivity (µS/cm)	TSS (mg/L)	Total Fe (mg/L)	Dissolved Fe (mg/L)	Total Mn (mg/L)	Dissolved Mn (mg/L)
1	A 02	5.73	274	1261	4	3.00	0.20	9.74	2.18
2	A 03	6.46	204	795.2	167.5	3.56	0.29	8.12	1.70
3	A 12	7.22	207	1576	865	37.94	4.38	9.52	1.25
4	B 02	6.45	222	761.9	252.5	4.34	0.66	6.77	2.18
5	B 04	4.05	375	1452	103.25	9.82	0.86	15.36	7.50
6	B 07	3.16	431	2130	259.5	5.72	1.63	14.74	11.70

and manganese concentration was quantified based on APHA 3500 Mn B – Manganese in Water by Persulfate and Spectrophotometry.

Results and Discussion

The mining water samples were collected using the grab sampling method, where samples were taken at a single point in time. The data presented in Table 1 represent the results of the mining water collected directly, without any prior sedimentation or treatment at the sedimentation pond inlet.

Mine water treatment encompasses three principal phases: sedimentation of discrete particles, optimization of coagulant dosage through jar testing, and sedimentation of flocculent particles. The concentration of suspended solids serves as a crucial indicator in evaluating water quality, as excessive levels of Total Suspended Solids (TSS) can obstruct the penetration of sunlight required for photosynthetic processes in aquatic flora. This obstruction may lead to a reduction in dissolved oxygen (DO) concentrations, creating an inhospitable environment for aquatic biota. Furthermore, elevated TSS levels contribute to increased surface water temperatures through the absorption of solar energy, exacerbating the depletion of DO due to the diminished solubility of oxygen in warmer water. Consequently, the elimination of suspended solids from wastewater prior to discharge is imperative to minimize detrimental environmental effects and preserve the balance of aquatic ecosystems. Initial characterization tests of the mine water samples reveal three distinct classifications: those exhibiting acidic pH, those with high turbidity, and those demonstrating a combination of both acidic pH and high turbidity (Table 2).

Type 1 sedimentation refers to the settling of discrete particles that settle independently without interacting with other particles or requiring chemical coagulants. Therefore, type 1 sedimentation tests were conducted only on samples with high turbidity (TSS > 100 mg/L), as well as those characterized by both acidic pH and high turbidity. In contrast, samples with only acidic pH issues generally had lower turbidity (TSS < 100 mg/L), making type 1 sedimentation

Table 2 Classification of mine water conditions, removal from type 1 of sedimentation, jar test results, calculation of sediment pond dimension through type 2 of sedimentation.

No	Classification	Sample Name	Removal from Discrete Settling (%)	Chemical Agent	Optimum Dosage (mg/L)
1	Acidic pH (pH <6)	A 02		Lime	14
2	High Turbidity (TSS >100 mg/L)	A 03	5.3%	Al2(SO4)3	20
3		A 12	0%		200
4		B 02	18.1%		200
5	Combination of both factors (pH <6 and TSS > 100 mg/L)	B 04	53.5%	Lime	140
6		B 07	57.4%		260

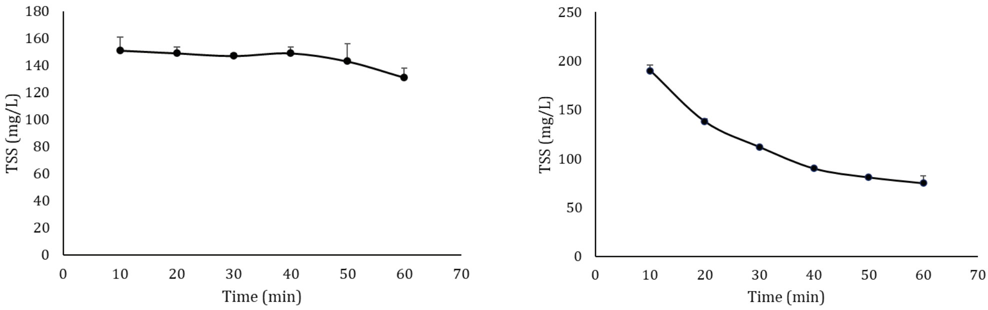

***Figure 2** Variation in TSS concentration over settling time in type 1 of sedimentation (discrete particle) for: a. sample with high turbidity (A03) and b. sample with acidic pH and high turbidity (B07) .*

unnecessary. Fig. 2 presents the variation in TSS concentration over the settling period for samples with high turbidity (A03) and those with both acidic pH and high turbidity (B07), providing critical insights into the effectiveness of the sedimentation process in improving water quality.

The results of type 1 sedimentation for the six mine water samples are presented in Table 2. Based on Fig. 2a, the type 1 sedimentation results indicate that sample A03 contains highly stable colloidal particles, making natural gravitational settling ineffective. Table 2 shows that samples with high turbidity issues had an average removal efficiency of less than 20%, suggesting the presence of stable colloidal particles that require further treatment for destabilization to enhance sedimentation and facilitate effective removal. In contrast, samples with both acidic pH and high turbidity exhibited an average removal efficiency above 50%. This is attributed to the acidic nature of mine water, which is rich in iron ions. These ions act as natural destabilizing agents for negatively charged colloidal particles, leading to the formation of larger flocs that settle more easily. This observation aligns with the study by (Dyestiana *et al.* 2023) which investigated the effects of mixing acid mine drainage with suspended solid-laden water. This study found that water with both acidic pH and high turbidity had a zeta potential exceeding -10 mV (ranging from -5 to -10 mV) at a volumetric mixing ratio of 1:1. It is well established that for optimal coagulation, the zeta potential of a solution should surpass -10 mV, approaching the isoelectric point near 0 (Kumar and Dixit 2017). The type 1 sedimentation results suggest that natural gravitational settling can be effectively utilized for samples with both high turbidity and acidic pH, minimizing the need for chemical additives. This advantage can be utilized in the design of pre-sedimentation ponds before the coagulation process to reduce chemical consumption.

The jar test was performed to determine the optimal dosage of chemical additives required for effective treatment. The primary chemicals used in this process were coagulants, which facilitate the aggregation of colloidal particles into larger flocs that can settle more efficiently. Colloidal particles are extremely small and do not settle naturally by gravity, necessitating the addition of coagulants to enhance the coagulation and sedimentation process. Additionally, pH-neutralizing agents were added to samples with acidic pH to induce chemical precipitation and increase pH levels. The key parameters analyzed in the jar test were TSS and pH levels. In this study, lime was utilized for pH neutralization, while aluminium sulfate served as the primary coagulant. The water samples with both acidic pH and high turbidity issues contains particles that naturally tend to settle through gravitational sedimentation. Therefore, the primary treatment focus is pH neutralization using lime to comply with regulatory standards. The results of the jar test, along with the chemical agent and consumption, are shown in Table 2.

Type 2 sedimentation evaluates the behavior of flocculated particles following

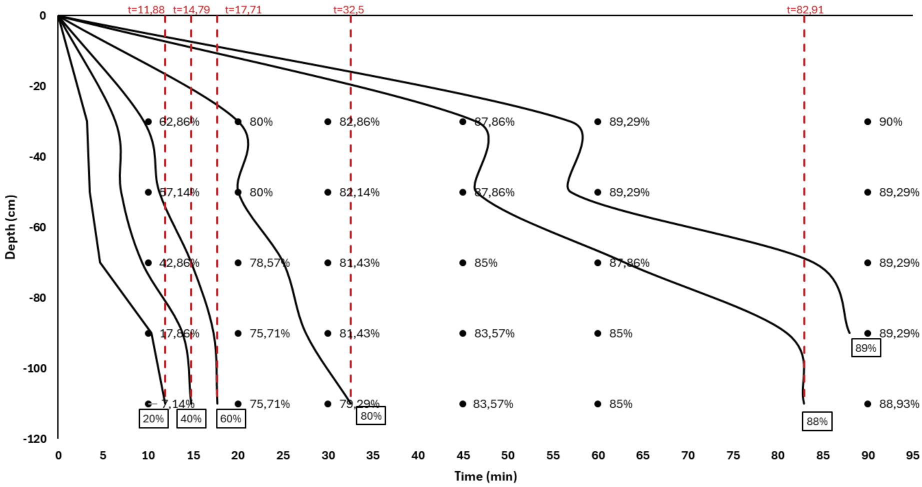

***Figure 3** Iso-removal graph for sample A03 with a target efficiency of 82.14% (achieving the water quality standard of 100 mg/L TSS concentration).*

chemical treatment. In high-turbidity water, are formed through the coagulation process, whereas in acidic water, precipitates are generated as a result of pH neutralization. This test involves sampling from five different ports at varying depths within the sedimentation tank. Samples are collected at different time intervals to observe the settling dynamics, which are then used to determine the overflow rate (vO) and total removal fraction (RT). The TSS concentration data obtained from the test is converted into percentage removal values. The determination of RT and VO is performed using an isoremoval graph, which illustrates the relationship between TSS removal efficiency, settling time, and sampling depth. Interpolation is applied to the plotted data points, allowing for the construction of a removal percentage curve. Fig. 3 illustrates an example of an iso-removal graph for sample A03. From this analysis, the relationship between overflow rate, detention time, and removal efficiency was determined, as shown in Fig. 4. In the case of sample A03, a removal efficiency of 82.14% is required to meet the water quality standard, ensuring that the TSS concentration does not exceed 100 mg/L.

The overflow rate and detention time values for a specific target removal percentage were determined. These values were then adjusted using a scale-up factor of 1.75 for detention time and 0.65 for overflow *rate* (Reynolds and Richards 1996). The adjusted detention time and overflow rate were then used to determine the pond dimensions using a formula, where A

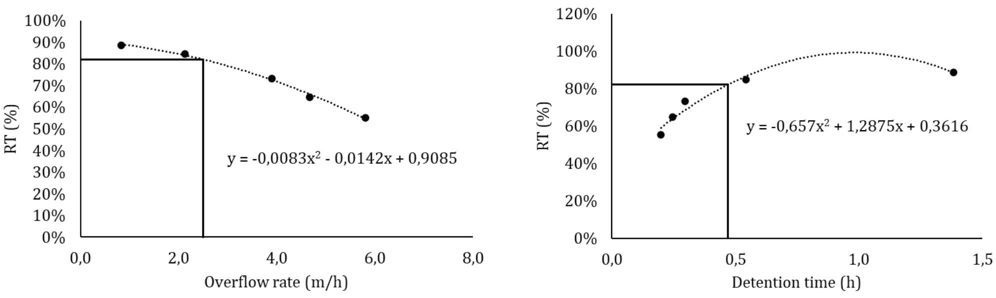

***Figure 4** The correlation between: (a) overflow rate and (b) detention time with the total solids removal fraction.*

denotes the cross-sectional area (m²), Q represents the flow rate (m³/h), v_0 is the overflow rate (m/h), H indicates the depth (m), and td is the detention time (h). The calculated sediment pond dimensions are summarized in Table 3.

$$A = \frac{Q}{v_0}\ ;\ H = \frac{Q \times td}{A}$$

From Table 3, a noticeable difference can be observed between the calculated sediment pond dimensions (column test) and the actual conditions (Stoke's law). This difference is due to variations in the calculation approach between the column test and Stokes' law, which was initially used in the sediment pond design. A widely used method for estimating theoretical settling velocity is Stokes' law, which assumes that particles are spherical in shape and smooth. However, coal mine water in Indonesia typically contains high levels of clay, which is the primary contributor of high TSS concentrations. Clay particles are often needle-shaped, plate-shaped, or flaky, which makes Stokes' law unsuitable for accurate predictions and giving incorrect results. Moreover, interactions between particles and flocculation occur due to the introduction of coagulants or precipitation resulting from pH neutralization in coal mine water treatment. When chemical agents such as coagulants or pH neutralizers are added, particles tend to bind with oppositely charged particles, forming larger aggregates that increase the settling velocity. On the other hand, Stokes' law assumes that particles settle freely without interacting with others (Ogolo *et al.* 2024). These factors highlight the need for iterative adjustments to sediment pond design based on the actual characteristics of mine water in the field rather than relying solely on Stokes' law assumptions during the initial mine plan. This approach improves the efficiency of chemical usage and enhances the operational evaluation of the sediment pond. Fig. 5 illustrates a guideline for selecting treatment methods or evaluating existing sediment pond designs using two key parameters: pH and TSS. These parameters are critical in coal mining water management, as they represent some of the most common challenges encountered by coal mining companies in Indonesia.

Conclusion

In Indonesia, pH and TSS are the most commonly observed and monitored parameters in coal mine water. However, a proper understanding of these two parameters is crucial for selecting the most effective and efficient treatment method. Not all turbid water contains suspended solids that require coagulants; some may consist of settleable solids that can naturally settle due to gravity and reducing the need for chemical usage. This can be verified through a simple field experiment using a settling test column following the Type 1

***Table 3** Calculation results of the sediment pond and the actual dimensions of the sediment pond.*

No	Sample		Removal TSS target (%)	t_d (h)	v_0 (m/h)	Existing Mine Water Discharge (m3/h)	Sediment pond dimension (Calc)		Sediment pond dimension (Act)	
							Cross sectional area (m²)	Depth (m)	Cross sectional area (m²)	Depth (m)
1	Acidic pH	A 02	55%	0.25	10.23	4680	458	2.6	3765	3
2	High Turbidity	A 03	82.14%	0.82	1.63	26640	16344	1.5	13496	2
3		A 12	99.29%	0.86	0.57	243360	426947	0.5	24268	3
4		B 02	96.57%	0.30	1.69	6480	4873	0.5	1547	5
5	Acidic pH and High Turbidity	B 04	95.33%	0.37	1.01	116640	115486	1.5	35308	6
6		B 07	87.44%	0.26	3.30	580680	175964	1	14821	3

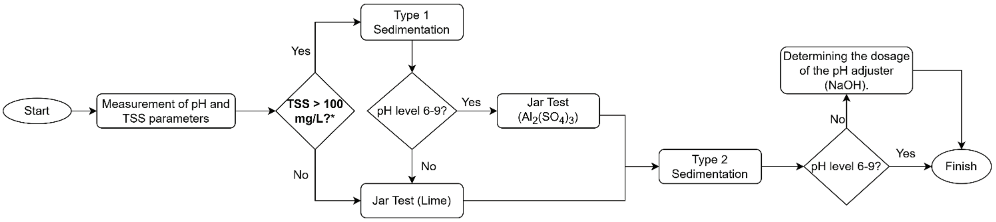

*According to water quality standards established by the Indonesian Government

Figure 5 Guideline for selecting treatment methods and evaluating sediment pond design.

sedimentation procedure, which is relatively easy to perform in the field. Additionally, choosing the right chemical treatment – whether coagulants or pH-neutralizing agents – requires compatibility testing with the mine water characteristics. This can be conducted through a jar test procedure to determine the most optimum dosage. The results of the jar test are then applied in the type 2 sedimentation procedure, which serves as a basis for evaluating the design of existing sedimentation ponds. Unlike Stokes' law, which assumes free-settling particles to determine settling velocity, the type 2 sedimentation method considers real mine water conditions in the field without relying on theoretical assumptions. These steps are expected to provide valuable insights for decision-making, optimizing chemical usage, and improving the management of coal mine water treatment in Indonesia, particularly in optimizing sediment pond operations.

Acknowledgements

This research was funded and supported by PT LAPI Institut Teknologi Bandung in collaboration with the Environmental & Forestry Planning Department, PT Bukit Asam Tbk, Indonesia, which provided resources and technical assistance throughout the study..

References

Dyestiana DC, Badhurahman A, Kusuma GJ (2023) Turbidity removal analysis and geochemical factors of mixing high turbidity mine water with acid mine drainage. Jurnal Pertambangan 7:5–12. https://doi.org/10.36706/jp.v7i1.1528 [in Indonesian]

Kumar A, Dixit CK (2017) Methods for characterization of nanoparticles. In: Advances in Nanomedicine for the Delivery of Therapeutic Nucleic Acids. Elsevier, pp 43–58

Ogolo NA, Onyekonwu MO, Michael AT (2024) Problems of Stokes' law application in determining the settling velocity of clays. Journal of Engineering Sciences and Innovation 9:277–286. https://doi.org/10.56958/jesi.2024.9.3.277

Reynolds TD, Richards PA (1996) Unit Operations and Processes in Environmental Engineering. PWS Pub. Co

Physicochemical Characterization of Nickel Mine Wastewater in South Sulawesi, Indonesia: Seasonal Variations and Treatment Potential

Muhammad Sonny Abfertiawan[1], Wahyu Sasangka Jati[1], Defita Rossa Sandriana Naseer[1], Mindriany Syafila[1], and Marisa Handajani[1]

[1] *Water and Wastewater Engineering Research Group, Faculty of Civil and Environmental Engineering, Bandung Institute of Technology*

Abstract

This study utilized ten sampling locations from nickel mine wastewater. The primary pollutants identified were Fe, Mg, Ca, and Al, with the highest concentrations observed at screening stations and processing facilities. Wastewater from Mobile Equipment Maintenance areas exhibited elevated levels of Mg, Ca, Fe, and Na, while mining sites was augmented with Al and Ni. Analyses of particle size and zeta potential revealed larger particles with higher zeta potentials during the dry season, in contrast to smaller, colloidal particles prevalent in the wet season. This investigation contributes to the development of efficacious treatment strategies for nickel mine wastewater in Indonesia.

Keywords: Nickel mine wastewater, physicochemical properties, laterite nickel

Introduction

Indonesia is the world's largest nickel producer, holding 52% of global reserves and contributing 37.04% of world production with 1 million metric tons in 2021 (USGS, 2022). Nickel is an essential resource for many industries, such as stainless steel, batteries, alloys, and metal plating. However, its high output poses a major challenge in environmental management, especially in managing mine water.

In laterite mining, environmental conditions and rainfall can increase concentrations of nickel and other metals like chromium, manganese, magnesium, and iron in mine water. Open pit mining exposes chromium, which may oxidize to toxic hexavalent chromium (Cr(VI)) and leach into water (Nasrullah *et al.*, 2017). Furthermore, the energy-intensive pyrometallurgical smelting process used for laterite ore, which cannot be processed by grinding or norgate methods, produces runoff with high metal content, thus requires treatment and management before being discharged into water bodies (Keskinkilic, 2019)

Characterizing mine water is essential to understand its environmental behavior and determine the appropriate treatment alternatives to minimize pollution. Therefore, this study examines the physical and chemical characteristics of nickel mine water from both processing and mining activities to identify suitable treatment options and guide future research.

Methods

This study analyzed nickel mine water samples from both nickel ore processing and mining activities at an open-pit nickel mine in South Sulawesi, Indonesia. Sampling was conducted using the grab sampling method at 10 ponds that collect water from mining activities, processing plants, screening stations, and mobile equipment maintenance (Tab. 1). Samples were collected within two periods: the dry season and the wet season. To preserve the samples, nitric acid was added until the pH was below 2 before they were sent to the Water Quality Laboratory at the Bandung Institute of Technology for further analysis.

Characterization of nickel mine water in this study was carried out by testing physical characteristics such as measuring pH, temperature, conductivity, using a multimeter probe. Turbidity was also measured using a turbidimeter, total suspended solids (TSS) and total dissolved solids (TDS) using the gravimetric method, particle size with dynamic light scattering method and zeta potential using electrophoresis method. Additionally, chemical characteristics were identified by assessing total and dissolved metals using Inductively Coupled Plasma Mass

Table 1 *Sampling locations.*

Type of activity	Source of Overflow	Inlet Location
Mining	Mining A (East Area) Mining B (West Area) Mining (*Crushing Quarry Washing*)	18.10
Processing Plant	Processing (*Process Plant/Smelting*)	17.30
Screening Station	Processing (*Screening Station*) A (East Area) Processing (*Screening Station*) B (West Area)	<0.04
Mobile Equipment Maintenance	Processing (*Mobile Equipment Maintenance*) A (East Area) Processing (*Mobile Equipment Maintenance*) B (West Area)	<0.04

Results and Discussion

pH and Temperature Characteristics

The pH test results for all samples in both seasons showed that the pH of mine water tended to be stable within a range of 6.8–8.7 (Fig. 1A). This falls within the acceptable limits for nickel ore mining wastewater, which is 6–9, as per the Regulation of the Minister of Environment and Forestry No. 5 of 2022. However, slight differences in pH were observed across sampling locations, likely due to variations in rock types passed through during the runoff process (Amir *et al.*, 2021). Temperature measurements (Fig. 1B) revealed seasonal differences, with dry-season temperatures ranging from 25–27 °C, slightly higher than the wet season (24.5–25.3 °C). This variation can be attributed to reduced cloud cover during the dry season, allowing the sunlight to reach the soil and water surface more directly and heat it more effectively.

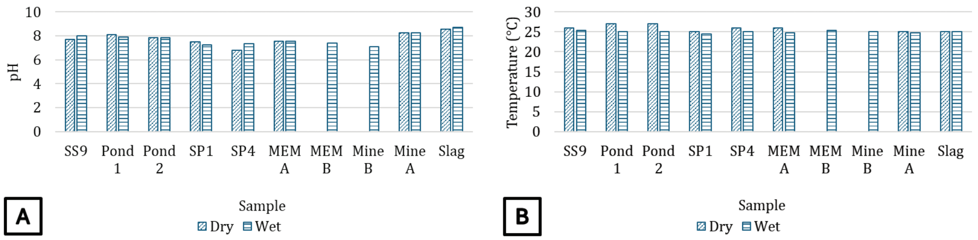

Figure 1 *Comparison of pH (A) and temperature (B) in each sample.*

Characteristics of Electrical Conductivity and Total Dissolved Solid (TDS)

Conductivity measurements revealed seasonal differences in nickel mine water quality, with wet season values (177–639 µS/cm) consistently exceeding dry season levels (150–418 µS/cm) (Fig. 2A). This increase is likely due to the higher amount of runoff in the wet season, enhancing the erosion of minerals from the surrounding soil and rocks, dissolving more minerals into the water (Loock *et al.*, 2015). The elevated mineral content directly raises the water's conductivity (Prihatno *et al.*, 2021). Among the sampled locations, the highest conductivity values were observed in water from the processing plant, screening station, then mining areas, while the lowest values were recorded in mobile equipment maintenance ponds. The higher value of conductivity at processing plants (SP1 and SP4) can be caused by the large number of dissolved substances, including metals, carried from the metal removal process at this location. Screening stations (SS9, Pond 1, and Pond 2) also exhibited high conductivity due to mineral and metal dissolution during ore crushing and grinding activity in this area, though to a lesser extent than processing plants. Mining areas (Mine A, Mine B, and Slag Dump Pond) showed moderate conductivity, likely from quarrying activities that release minerals into water. Meanwhile, mobile equipment maintenance areas (MEM A and MEM B) had the lowest conductivity, as fewer minerals and metals are introduced from heavy equipment washing compared to ore processing and mining sites.

Parallel trends were observed in TDS measurements (Fig. 2B), with wet season concentrations (89–319 mg/L) surpassing dry season levels (92–260 mg/L). This seasonal pattern results from rainfall-enhanced erosion and leaching of mining materials, which increases ionic constituents (Mg^{2+}, Ca^{2+}, Na^{+}, Cl^{-}) that contribute to both TDS and conductivity. The distribution of TDS mirrored conductivity patterns, confirming their interdependence as water quality indicators.

Characteristics of Turbidity and Total Suspended Solid

Turbidity levels in nickel mine water were generally higher in the wet season (66–115,200 NTU) than in the dry season (8.8–110,200 NTU) (Fig. 3A). This increase can be attributed to greater surface runoff, which intensifies soil and rock erosion, carrying more suspended particles into the water. The high levels of particles carried in this mine water then result in an increase in turbidity in mine water from mining activities, processing plants, and screening stations. Additionally, wet soil clinging to heavy equipment during the rainy season contributed to higher turbidity in water from equipment washing and maintenance activities.

TSS measurements using the gravimetric method (Fig. 3B) also indicated higher concentrations in the rainy season (6–136,964 mg/L) compared to the dry season (9–123,388 mg/L). This trend follows turbidity levels, as both are influenced by increased erosion and suspended particle transport. TSS quantifies the concentration

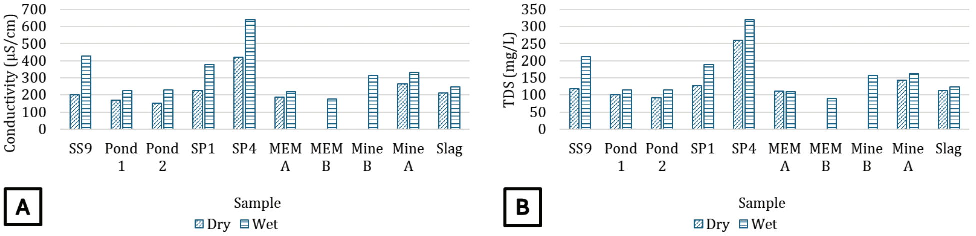

Figure 2 *Comparison of conductivity (A) and TDS (B) in each sample.*

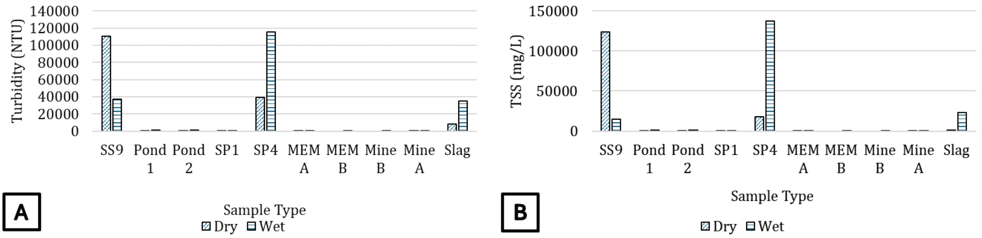

Figure 3 Comparison of turbidity (A) and TSS (B) in each sample.

of suspended solids in water, while turbidity measures light scattering by these particles. Their interdependence causes these two parameters to have the same tendency and positive correlation.

Particle Size and Zeta Potential

The results of the zeta potential and particle size measurements on nickel mining water samples show clear variations between the dry and rainy seasons, as well as between different sampling locations. During the dry season, the particle sizes are generally larger, ranging from 246.98 nm to 7,532.65 nm, with larger average sizes observed in Pond 2 and Slag Dump Pond. In contrast, during the wet season, the particle sizes tend to be smaller, with some samples, such as MEM A and Mine B Pond, showing particle sizes below 1000 nm, indicating colloidal behaviour. The zeta potential in all samples falls within a relatively high range, but not far from zero, indicating that the repulsive forces between particles are not very strong, causing the particles to aggregate and settle more easily. Larger particles (>1000 nm) tend to settle more easily, while colloidal particles require additional treatment, such as the addition of coagulants, to accelerate settling. This analysis shows that particle size and zeta potential influence mining water management processes, especially in settling strategies and further treatment. The particle size and zeta potential of each sample can be seen in the (Tab. 2).

Characteristics of Total and Dissolved Metals

Screening stations (Pond 1, Pond 2, and SS9) generally exhibited the highest levels of Mg, Fe, Ca, Ni, Al, and Cr (Fig. 4 and Fig. 5). During the dry season, Fe (9–2,468.59 mg/L) and Al (0.65–74.67 mg/L) were predominantly suspended, making them treatable via pond sedimentation. In contrast, Mg (19–169.25 mg/L) and Ca (6.36–9.62 mg/L) were mainly dissolved, requiring additional treatment such as coagulation which allow the binding of bind metal particles to form flocs that are easier to settle. During the wet season, metal concentrations were higher for Fe (413.39–5,869.59 mg/L), Mg (61.89–236.53 mg/L), and Al (26.63–168.24 mg/L). Most of these metals remained in suspended form, making sedimentation a viable treatment option.

Mine water from processing plants (SP1 and SP4) during the dry season contained high Fe, Mg, Al, and Ca levels (Fig. 4). Fe and Al metals tend to be suspended with a concentration range of 37.25–909.01 mg/L and 1.85–33.76 mg/L, respectively, allowing for sedimentation treatment. Mg (27.22–78.86 mg/L) and Ca (4.66–12.53 mg/L) were mostly dissolved, indicating the needs of coagulation process. Figure 5 shows that wet season samples exhibited increased metal concentrations for Fe (146.62–1,135.56 mg/L), Mg (69.03–110.14 mg/L), and Al (6.48–78.84 mg/L), with most metals in suspended form, making sedimentation an effective method. Additionally, Ni was detected at a fairly high levels (15.39–39.64 mg/L).

In general, nickel mine water from mobile equipment maintenance (MEM A and MEM B) had high levels of Mg, Ca, and Fe (Fig. 4 and Fig. 5). During the dry season, Fe (3.573 mg/L) was mostly suspended, allowing for sedimentation treatment, while Mg (19.29 mg/L) and Ca (10.75 mg/L) were dissolved, requiring coagulation. The concentrations of the three metals tend to be increase during the wet season, with a range of Fe metal 3.7–

Table 2 Particle Size and Zeta Potential.

Sample Type	Season	Particle Size Distribution (nm)	Average Particle Size (nm)	Zeta Potential Range (mV)	Average Zeta Potential (mV)
Pond 1	Dry	837.07 – 1,068,52	924.3	-56.5 – 3.53	-26.4
	Wet	1,068.52 – 6,667.1	2,282.3		
Pond 2	Dry	246.98 – 7,532.65	4,777.7	-43.38 – 1.54	-20.9
	Wet	2,511.05 – 5,901.02	3,576.7		
SS9	Dry	246.98 – 1,541.04	818.4	-90.32 – 53.18	-67.5 / 37.5
	Wet	4,091.63 – 7,532.65	5,433.5		
SP1	Dry	315.27 – 7,532.65	3,197.6	-28.74 – 1.23	-16.2
	Wet	2,837.04 – 6,667.1	3,896.6		
SP4	Dry	580.41 – 7,532.65	3,284.3	-44.4 – 8.42	-14.2
	Wet	402.44 – 7,532.65	3,600.8		
MEM A	Dry	39.58 – 5,901.02	3,458.9	-35.43 – 2.06	-16.1
	Wet	454.69 – 1,068.52	679.3		
MEM B	Dry	–	–	–	–
	Wet	105.1 – 6,667.1	2,870.7		
Mine A	Dry	134.16 – 7,532.65	1,982.3	-38.65 – 1.54	-11.5
	Wet	1.66 – 3,205.35	2,185.2		
Mine B	Dry	–	–	–	–
	Wet	134.16 – 193.48	155.2		
Slag	Dry	5,901.02 – 8,510.56	6,140.1	-44.89 – 3.53	-19.3
	Wet	513.71 – 8,510.56	1,847		

4.99 mg/L, Mg 22.81–23.39 mg/L, and Ca 4.71–7.53 mg/L. A fairly high concentration of Na metal was also found with a range of 5.76–6.54. Most types of Fe and Na metals are suspended metals, so the four metals have the potential to be processed using a simple pond sedimentation method. Meanwhile, Mg and Ca metals tend to be in dissolved form so that additional processing is required.

Nickel mine water from mining activities (Mine A, Mine B, Slag) contains very high concentrations of Fe, Mg, Ca, and Zn during dry season. Fe (0.14–193.18 mg/L) and Zn (0.78–0.23 mg/L) were primarily suspended, making sedimentation a viable treatment option. Meanwhile, Mg (29.42 mg/L) and Ca (3.19 mg/L) were dissolved, requiring coagulation. During the wet season, the concentration of Fe, Mg, and Al increased, with the range of Fe metal 146.62–1135.56 mg/L, Mg 69.03–110.14 mg/L, and Al 6.48–78.84 mg/L. A fairly high concentration of Ni metal was also found with a range of 15.39–39.64 mg/L. Most metals remained in suspended form, making sedimentation effective.

Conclusions

The results of the physical characterization analysis showed that the nickel mine water studied in the dry season had a pH range of 6.8–8.7, temperature 25–27 °C, conductivity 150–418 µs/cm, turbidity 8.8–110,200 NTU, TDS 92–260 mg/L, TSS 9–123,388 mg/L. Meanwhile, in the wet season it had a pH range of 6.8–8.7, temperature 24.5–25.3 °C, conductivity 177–639 µs/cm, turbidity 66–115,200 NTU, TDS 89–319 mg/L, TSS 6–136,964 mg/L mg/L. Analysis of the particle size and zeta potential in nickel mining water samples reveals variations based on season and location. During the dry season, the samples exhibit larger particles and higher zeta potentials. Conversely, in the wet season, smaller, colloidal particles with lower zeta potentials are prevalent, necessitating additional chemical treatments (e.g., using coagulants to destabilize colloids). Dry season water, with inherently more settleable particles, may only require gravity-based separation (e.g., sedimentation ponds), reducing chemical costs. Meanwhile, the results of chemical characterization analysis

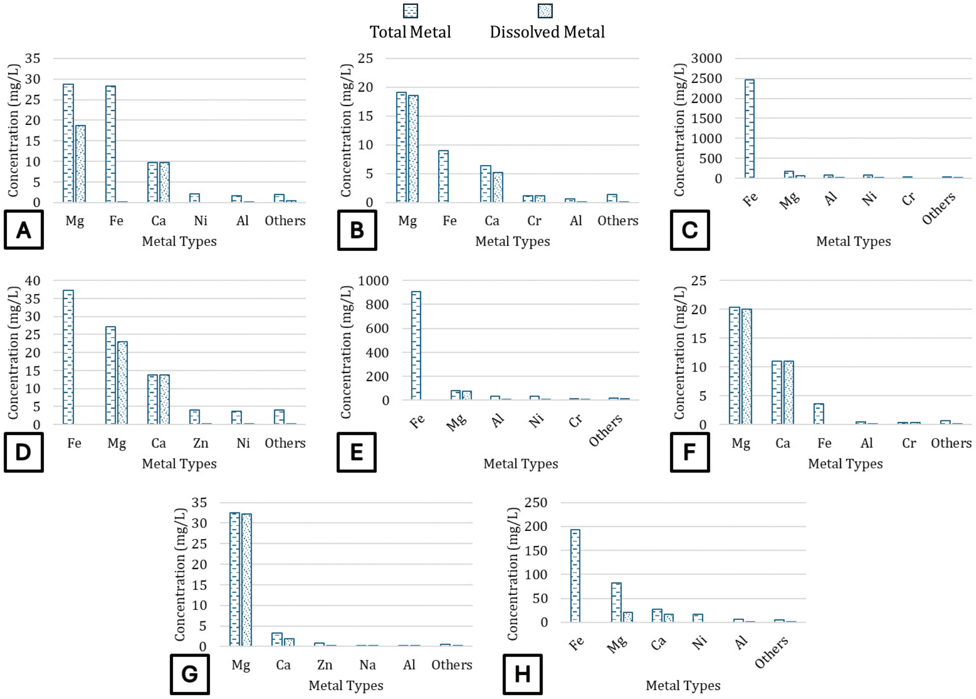

Figure 4 Characteristics of Total Metals in the Dry Season: Pond 1 (A), Pond 2 (B), SS9 (C), SP1 (D), SP4 (E), MEM A (F), Mine A (G), and Slag (H).

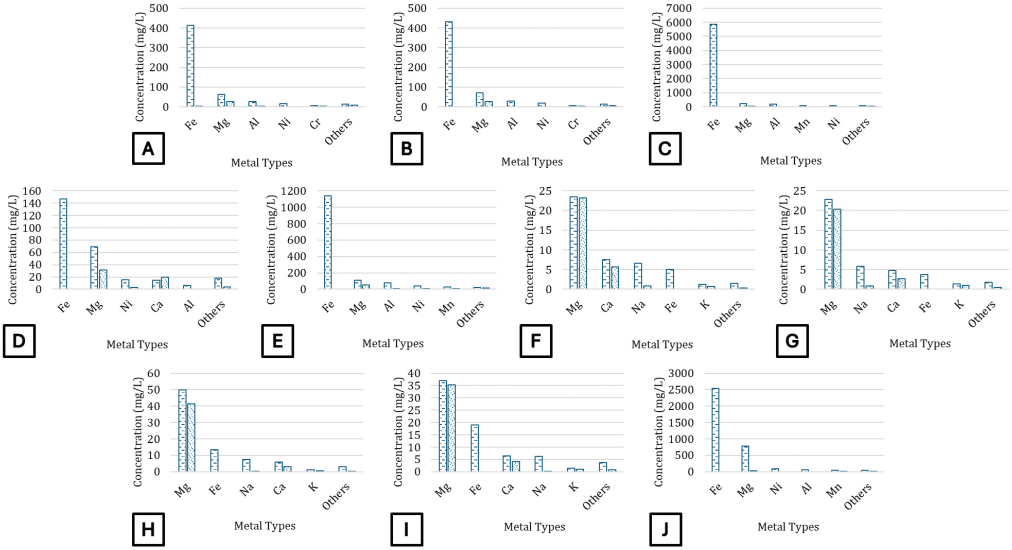

Figure 5 Characteristics of Total Metals in the Wet Season: Pond 1 (A), Pond 2 (B), SS9 (C), SP1 (D), SP4 (E), MEM A (F), MEM B (G), Mine A (H), Mine B (I), and Slag (J).

showed that the nickel mine water studied showed high concentrations of Fe, Mg, Ca, and Al metals in mine water from screening station and processing plant activities, Fe, Mg, Ca and Na metals in mine water from mobile equipment maintenance activities, and Fe, Mg, Ca, Zn, Al, and Ni metals in mine water from mining activities.

References

Amir, M. K., Prianata, Y. L. O., Dzakir, L. O., Shaddad, A. R., Aldiyansyah, A., & Kadar, M. I. (2021). Analisis Kualitas pH dan TSS Air Limbah Penambangan Bijih Nikel PT Prima Utama Lestari di Desa Ussu, Kecamatan Malili, Kabupaten Luwu Timur. *Jurnal Geomine*, 9(3), 267–274. https://doi.org/10.33536/jg.v9i3.1059

Keskinkilic, E. (2019). Nickel Laterite Smelting Processes and Some Examples of Recent Possible Modifications to the Conventional Route. *Metals*, 9(9), 974. https://doi.org/10.3390/met9090974

Loock, M. M., Beukes, J. P., & van Zyl, P. G. (2015). Conductivity as an indicator of surface water quality in the proximity of ferrochrome smelters in South Africa. *Water SA*, 41(5), 705–711. https://doi.org/10.4314/wsa.v41i5.14

Nasrullah, N., Taklim, M. K., Nurjannah, N., & Wiyani, L. (2017). Upaya Penurunan Krom Heksavalen Pada Air Tambang Nikel Dengan Menggunakan Reduktor Ferro Sulfat. *Journal Of Chemical Process Engineering*, 2(2), 45. https://doi.org/10.33536/jcpe.v2i2.166

Prihatno, H., Abida, R. F., & Sagala, S. L. (2021). Korelasi antara Konduktivitas dengan Jumlah Mineral Terlarut pada Perairan Selatan Pulau Madura. *Jurnal Kelautan Nasional*, 16(3), 211. https://doi.org/10.15578/jkn.v16i3.9975

USGS. (2022). *Mineral commodity summaries* 2022. https://doi.org/10.3133/mcs2022

Geochemical controls of potentially toxic element (PTE) release from the Gold One Tailings Dam Complex into the Randfontein area, Witwatersrand, South Africa

Jamie-Leigh R. Abrahams[1], Charles D. Okujeni[2], Oluseyi A. Abegunde[3], Changhong Wu[4], Adrian S. Williams[5]

[1]*Department of Geology, Faculty of Natural and Agricultural Sciences, University of the Free State, Bloemfontein, South Africa*

[2]*Department of Earth Sciences, Faculty of Science, University of the Western Cape, Cape Town, South Africa*

[3]*Department of Civil and Geomatics, Faculty of Engineering, Cape Peninsula University of Technology, Cape Town, South Africa*

[4]*Confucius Institute, International Relations Office, University of the Western Cape, Cape Town, South Africa*

[5]*Council for Geoscience, Minerals and Energy Unit, Cape Town, South Africa*

Abstract

This study investigated the release of potentially toxic elements (PTEs) from the Gold One Tailings Dam Complex (TDC) in Randfontein, South Africa. The Gold One TDC generally comprised a PTE-leached upper oxidized zone and PTE-enriched lower oxidized, transition and reduced zones. Acid-base accounting determined that TD materials were largely acid-generating. According to sequential extraction procedures, Co and Pb yielded the highest potentially bioavailable concentrations, compared to Cu, Ni and Zn. The results suggest that Co and Pb may pose increased threat to the health of the environment and wildlife.

Keywords: Acid-base accounting; sequential extraction procedures; Randfontein; South Africa

Introduction

Tailings are one of the largest waste products associated with mining (Dold 2014). Tailings create potential threats to the environment largely in the form of acid mine drainage (AMD). AMD, which is formed via the oxidation of sulfide minerals (such as pyrite), which readily mobilizes potentially toxic elements (PTEs) in the environment (Tutu 2003). As a result, soils, surface water bodies and groundwater in the vicinity of tailings facilities can become contaminated with PTEs over time and thereby, potentially compromise the overall environmental, ecological-and public health of the area.

The Randfontein area in West Rand, South Africa, hosts several tailings facilities linked to gold mining (Abegunde *et al.* 2016). A number of studies have reported that this area is affected by AMD (Lusilao-Makiese *et al.* 2013; Shapi *et al.* 2021). Randfontein is located close to the Krugersdorp Game Reserve. Thus, it is crucial to investigate the geochemical controls of PTE release from these tailings facilities into surrounding areas, to mitigate their potential risk to the environment and game animals.

Methods

Twenty-nine samples were collected from three drill core sections (T001, T002 and T003) in the Gold One Tailings Dam Complex (TDC) located in Randfontein, South Africa (Fig. 1). The study site lies within the Witwatersrand Basin which comprises auriferous conglomerates of the

Witwatersrand Supergroup (Tutu *et al.* 2003). TD mineralogy was determined via X-ray diffraction (XRD) analysis. Major oxide and trace element chemistry was determined via X-ray fluorescence (XRF) and inductively coupled plasma mass spectrometry (ICP-MS), respectively. Total carbon and sulfur content were determined via LECO analysis. Total carbon and sulfide-sulfur were used in acid-base accounting (ABA) to estimate the acid-generating potential of TD materials. Sulfide-sulfur was determined by digesting sulfate contents in an ammonium oxalate-oxalic acid solution at pH 3 for 2 hours at 80 °C; and the sulfate contents was then subtracted from the total LECO sulfur. Finally, sequential extraction procedures (SEPs) were used to assess the mobility and potential bioavailability of PTEs in the TDC. The five-step SEP scheme used in this study is listed below. Solutions at each step were filtered to separate the liquid from solid residue and were analyzed via graphite furnace atomic absorption spectrometry (GFAAS). Associations among extractable elements were assessed using principal component analysis (PCA).

Step 1: Water-soluble. To 5 g of solid material, 90 ml of distilled H_2O at pH 7 was added, then agitated for 90 minutes at room temperature.

Step 2: Exchangeable and carbonate (*loosely bound fraction and/or sensitive to pH changes*). To the solid residue from step 1, 90 ml of 1 M ammonium acetate- $NH_4CH_3CO_2$ (buffered to pH 5 with ≈ 37 ml acetic acid) was added, then agitated for 90 minutes at room temperature.

Step 3: Hydrous Mn-oxide (*fraction typically sensitive to redox changes*). To the solid residue from step 2, 90 ml of 0.1 M hydroxylamine hydrochloride- $NH_2OH.HCl$ (buffered with 10 ml of 10% nitric acid- HNO_3) was added, then agitated for 90 minutes at room temperature.

Step 4: Hydrous Fe-oxide (*fraction typically sensitive to redox changes*). To the solid residue from step 3, 90 ml of 0.25 M $NH_2OH.HCl$ (buffered with 25 ml of 10% HNO_3) was added, then agitated for 90 minutes at room temperature.

Step 5: Residual (*strongly bound fraction*). (i) Two rounds of 25 ml of 60% hydrofluoric acid

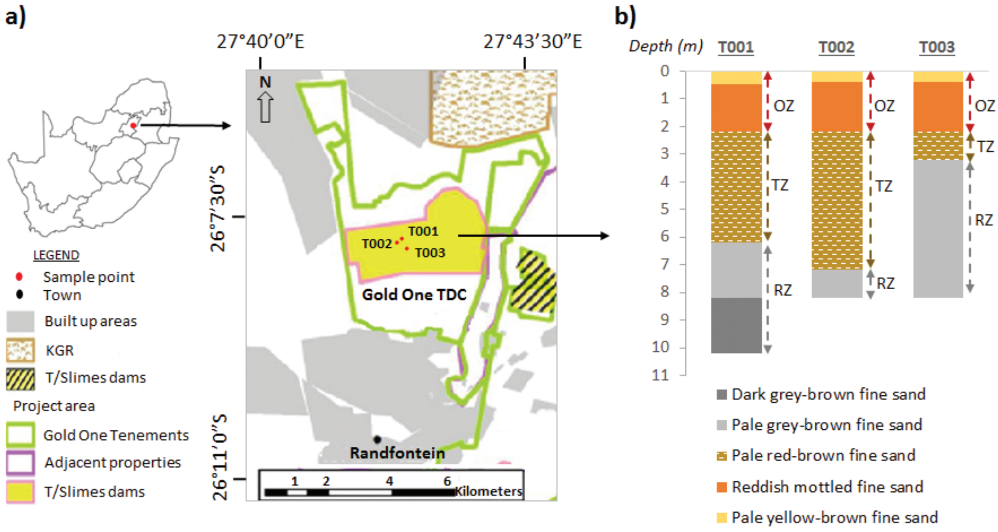

Figure 1 a) Location map of the Gold One TDC and Krugersdorp Game Reserve (KGR) near Randfontein in South Africa (modified after Gold One International Limited 2012) and b) the lithology of drill core sections T001, T002 and T003 (where 'OZ' is the oxidized zone, 'TZ' is the transition zone and 'RZ' is the reduced zone).

(HF) were added to 1 g of solid residue from step 4 and heated for 1 hr at approx. 100 °C in a sand bath; (ii) two rounds of 20 ml HF : 5 ml HNO_3 were added and heated for 1 hr at approx. 100 °C in a sand bath; (iii) 25 ml HNO_3 was added to 100 ml flasks and agitated for 5–6 hours; and (iv) flasks were topped to 100 ml with distilled water and 5 ml of 5% boric acid added to stabilize the ions.

Results and Discussion

Mineralogy and geochemistry

According to the XRD analysis, the Gold One TDC consisted of mainly quartz (41.7% – 63.7%), pyrophyllite (0.8% – 5.9%), pyrite (0.12% – 0.64%), gypsum (0.3% – 1.8%) and clinochlore (0.2% – 0.4%). These results are relatively consistent with the mineralogy of the Witwatersrand gold ore bodies (Phillips & Law 2000). However, gypsum is likely linked to the partial neutralization of AMD through liming (Tutu *et al.* 2008). Three weathering zones were distinguished in the TDC; namely, an oxidized zone 'OZ' (comprising upper pale yellow-brown fine sands and lower reddish, mottled fine sands), a transition zone 'TZ' (comprising pale red-brown fine sands) and a reduced zone 'RZ' (comprising pale to dark grey-brown fine sands) (Fig. 1). Of the drill core sections investigated, section T003 was seemingly the least weathered, showing the highest pyrite contents (approx. 0.42% – 0.64%) and the earliest onset of grey (reduced) fine sands. Paste pH ranges in the TDC were as follows: the OZ (2.9 – 5.2), the TZ (3.7 – 8.1) and the RZ (7.4 – 8.4). The acidic paste pH in the OZ is likely related to the oxidation of pyrite. Major oxide concentration ranges in the TDC were (in %): SiO_2 (81.4 – 93.3), CaO (0.02 – 1.43), Fe_2O_3 (1.37 – 4.79) and MnO (0.003 – 0.06). PTE concentration ranges in the TDC were (in mg/kg): Co (1.6 – 78.0), Ni (8.2 – 242), Zn (5.0 – 231), Cu (7.5 – 100.5) and Pb (11.4 – 67.5). Minimum PTE concentrations generally corresponded with the upper OZ; while maximum PTE concentrations generally corresponded with the lower OZ and RZ. In nearly all cases, maximum PTE concentrations coincided with maximum Fe and/or Mn oxide concentrations. Thus, Fe and/or Mn oxides, which are known scavengers of trace elements (Hall *et al.* 1996), may play important roles in the mobilization/immobilization of PTEs in the TDC.

Acid-generating potential

The acid-generating potential of the TDC was assessed using the Neutralizing Potential Ratio (NPR) which represents the ratio between acid potential (AP) and neutralizing potential (NP) (Fig. 2). Total carbon was used to represent NP (INAP 2009), with the assumption that all carbon in the sample is present as calcite ($CaCO_3$), and sulfide-sulfur selected to represent the AP. The AP ranged from 0.05 $CaCO_3$ kg/ton to 36.8 $CaCO_3$ kg/ton; while the NP ranged from 1.67 $CaCO_3$ kg/ton to 31.7 $CaCO_3$ kg/ton. The NPRs were interpreted according to Price *et al.* (1997). Thus, TD materials from sections T001, T002 and T003 were largely acid-generating. TD materials with non-acid generating potential occurred within the first 0.5 meters of sections T001 and T002. Thus, the two potentially non-acid generating samples appear consistent with the PTE-leached, pale fine sands of the upper oxidized zone, suggesting that oxidation was at its incipient stage at the time of sample collection.

PTE mobility and potential bioavailability

The bioavailable fraction of PTEs refers to the proportion of PTEs transported into, entering and accumulating in living organisms (NRC 2003). Potentially bioavailable PTE fractions are therefore considered to represent more accurately the potential toxicity of metals in the environment (Yiika *et al.* 2023). In general, water-soluble, exchangeable, carbonate and Mn/Fe oxide bound PTE fractions are considered potentially bioavailable; while residual (e.g. primary silicate)-bound PTE fractions are considered relatively stable under most environmental conditions (Siegel 2002). Fig. 3 shows that Co was largely bound to exchangeable and carbonate phases which corresponds with that of gold mine tailings in the Johannesburg area (Rösner & Van Schalkwyk 2000). Lead

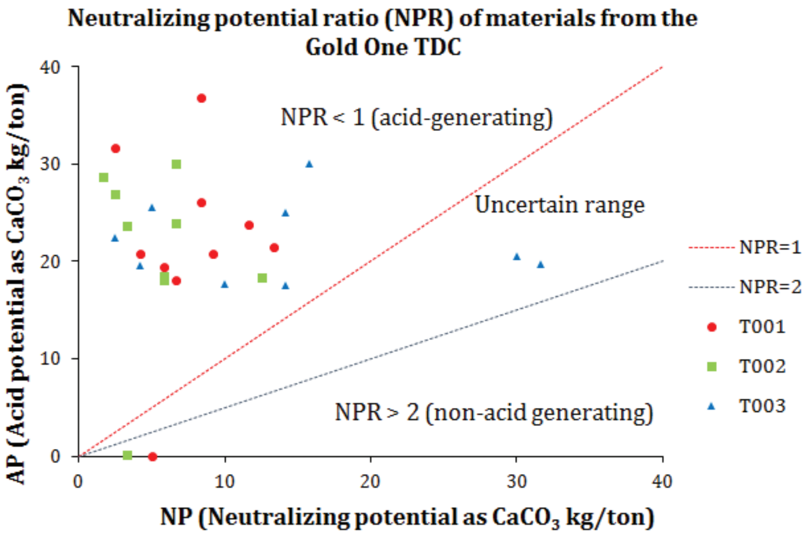

Figure 2 *Graph indicating the neutralizing potential ratio (NPR) of samples collected from the Gold One TDC.*

was largely bound to the hydrous Fe-oxide (reducible) phase which is fairly consistent with that of gold mine tailings dumps in the West Rand area (Fosso-Kankeu *et al.* 2015). Copper, Ni and Zn were largely bound to the residual phase which coincides with findings by Yiika *et al.* (2023). In general, the mobility and potential bioavailability of PTEs can be described in decreasing order as: Co > Pb >> Cu > Ni > Zn. When the weathering zones are compared with the SEP (Fig. 3), the highest water-soluble PTE fractions occurred largely within the OZ and upper TZ. This suggests that PTE fractions within the OZ and upper TZ are most susceptible to leaching by rainwater. This is important considering that the study area receives approx. 749 mm of annual rainfall (Climate-data.org 2025) and some of the highest PTE concentrations occurred within the lower OZ. PTE fractions within the lower TZ and RZ generally showed greater susceptibility to leaching under changing pH and redox conditions.

The PCA biplots of extractable elements in step 2 (the exchangeable and carbonate phase) and step 4 (the hydrous Fe-oxide phase), which were associated with the highest potentially bioavailable PTE contents, are shown in Fig. 4a and b, respectively. Fig. 4a shows that extractable Co in step 2 was associated mainly with Mn. A number of SEP-related studies have found that Co and Mn are positively correlated (Gray *et al.* 1999; Rösner & Van Schalkwyk 2000). Gray *et al.* (1999) suggested that extractable Mn in this fraction could represent Mn within carbonates, separate-phase $MnCO_3$ or highly soluble Mn oxides. Similarly, Fig. 4b shows that extractable Pb in step 4 was associated mainly with Mn which is supported by statements by Bradl (2004). The co-precipitation of Mn with Fe oxides (Sposito 1983) and incomplete dissolution of Mn oxide in step 3 (Chao 1972) provide possible explanations for the extractable Mn contents in step 4 of the SEP. The association of PTEs with Mn (Fig. 4) is consistent with the increased metal-scavenging capacity of Mn oxides, compared to Fe, which is partly attributed to their complex mineralogical structure (Hall *et al.* 1996).

Conclusions

Regarding PTE contents, the Gold One TDC was dominated by Ni and Zn, with lower concentrations of Cu, Co and Pb. The PTE contents appeared lowest in the pale yellow-brown fine sands in the upper OZ; and highest in the reddish mottled fine sands in the lower OZ and grey-brown fine sands in the RZ. According to the SEP, Co was mainly bound to the exchangeable and carbonate phase (appearing largely associated with Mn); Pb was mainly bound to the hydrous

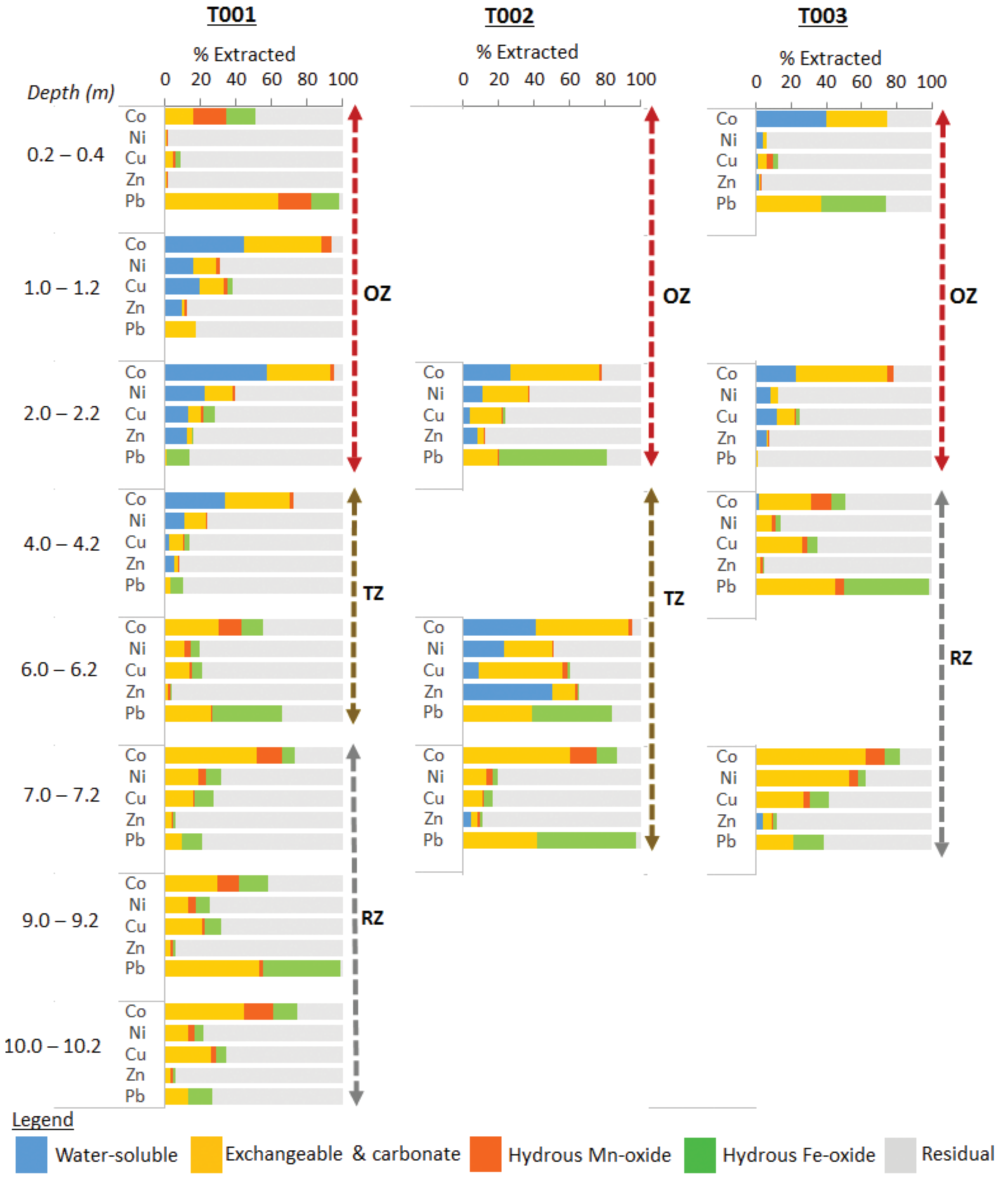

Figure 3 Results of the SEPs performed on TD materials with depth. Depths shown are consistent across T001, T002 and T003 but are not shown to scale downhole to conserve space.

Fe-oxide phase (appearing largely associated with Mn); while Cu, Ni and Zn were mainly bound to the residual phase. The results suggest that Co may have the greatest potential for release into the environment under changing pH conditions while Pb may be released into the environment under changing redox conditions. These findings are important considering that TD materials in the study site were largely acid-generating. The Gold One TDC may therefore pose potential threat to the health of animals in the nearby Krugersdorp Game Reserve. This study highlights the need to implement suitable mitigation strategies to minimize the potential environmental and ecological risks associated with the Gold One TDC. It is recommended that future

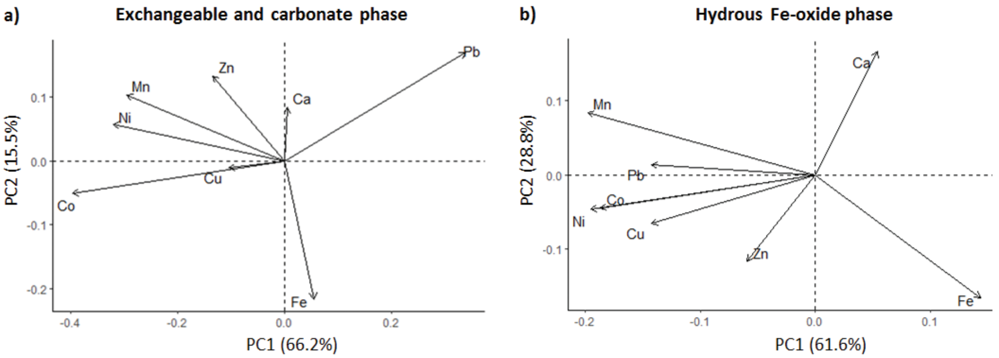

Figure 4 Principal component analysis (PCA) biplots showing element associations in a) the exchangeable and carbonate phase and b) the hydrous Fe-oxide phase.

studies incorporate leach column testing to monitor PTE release from the TDC long-term. In addition, it may be worthwhile exploring the use of hydro-geochemical modeling to predict PTE release from the TDC long-term.

Acknowledgements

The authors would like to acknowledge funding and support received from the International Science and Technology Agreement South Africa-China (2012–2014), South Africa's National Research Foundation (NRF), Inkaba-ye Africa and the Earth Sciences Department at the University of the Western Cape. We also acknowledge the Department of Water Affairs of South Africa and the Gold One mining company for granting us permission to access their tailings dam facility.

References

Abegunde OA, Okujeni CD, Wu C, Siad A (2016) Distribution patterns of contaminants in the Mogale Gold tailing dam: a case study from South Africa. Environ Earth Sci 75:1365

Bradl HB (2004) Adsorption of heavy metal ions on soils and soils constituents. J Colloid Interface Sci 277(1):1–18

Chao TT (1972) Selective dissolution of manganese oxides from soils and sediments with acidified hydroxylamine hydrochloride. Soil Sci Soc America Proc 36:764–768

Climate-data.org (2025) Randfontein Climate (South Africa). https://en.climate-data.org/africa/south-africa/gauteng/randfontein-27294/ (Accessed: 04-01-2025)

Dold B (2014) Evolution of acid mine drainage formation in sulphidic mine tailings. Minerals 4(3):621–641

Fosso-Kankeu E, Waanders FB, Munyai AH (2015) Susceptibility of Metals Release from Tailings Dumps Located In the Krugersdorp Area, 7th International Conference on Latest Trends in Engineering & Technology (ICLTET'2015) November 26–27, 2015 Irene, Pretoria (South Africa)

Gold One International Limited (2012) Randfontein Surface Operations. Analyst Site Visit 31 January 2012, 56 pp

Gray DJ, Wildman JE, Longman GD (1999) Selective and partial extraction analyses of transported overburden for gold exploration in the Yilgarn Craton, Western Australia. J Geochem Explor 67(1–3):51–66

Hall GEM, Vaive JE, Beer R, Hoashi M (1996) Selective leaches revisited, with emphasis on the amorphous Fe oxyhydroxide phase extraction. J Geochem Explor 56(1):59–78

INAP (The International Network for Acid Prevention) (2009) GARD (Global Acid Rock Drainage) Guide, http://gardguide.com/index, accessed August 2017

Lusilao-Makiese JG, Cukrowska EM, Tessier E, Amouroux D, Weiersbye I (2013) The impact of post gold mining on mercury pollution in the West Rand region, Gauteng, South Africa. J Geochem Explor 134:111–119

NRC (US National Research Council) (2003) Bioavailability of Contaminants in Soils and Sediments. In Bioavailability of Contaminants in Soils and Sediments, 420 pp

Phillips GN, Law JDM (2000) Witwatersrand Gold Fields: Geology, Genesis, and Exploration. SEG Review 13:439–500

Price WA (1997) Draft Guidelines and Recommended Methods for the Prediction of Metal Leaching and Acid Rock Drainage at Minesites in British Columbia. Reclamation Section, Energy and Minerals Division; British Columbia Ministry of Employment and Investment. Accessed October 2016, 159 pp

Rösner T, Van Schalkwyk A (2000) The environmental impact of gold mine tailings footprints in the Johannesburg region, South Africa. Bull Eng Geol Environ 59(2):137–148

Shapi M, Jordaan MA, Mbambo AT, Davies TC, Chirenje E, Dube M (2021) Determination of potentially harmful element (PHE) distribution in water bodies in krugersdorp, a mining city in the west rand, Gauteng province, South Africa. Minerals 11:1133

Siegel FR (2002) Indicator Media of Environmental Health Status In: Environmental Geochemistry of Potentially Toxic Metals, Springer, New York, p 103–129

Sposito G (1983) The Chemical Forms of Trace Metals in Soils In: I. Thornton (Ed), Applied Environmental Geochemistry, Academic Press, London, p 123–170

Tutu H, Cukrowska E, Mccarthy TS, Mphephu NF, Hart R (2003) Determination and modelling of geochemical speciation of uranium in gold mine polluted land in South Africa. 8th International Congress on Mine Water & the Environment, Johannesburg, South Africa, 137–155

Tutu H, McCarthy TS, Cukrowska E (2008) The chemical characteristics of acid mine drainage with particular reference to sources, distribution and remediation: The Witwatersrand Basin, South Africa as a case study. App Geochem 23(12):3666–3684

Yiika LP, Tita MA, Suh CE, Mimba ME, Jean-Lavenir NM (2023) Heavy Metal Speciation by Tessier Sequential Extraction Applied to Artisanal Gold Mine Tailings in Eastern Cameroon. Chem Afr 6(5):2705–2723

Prediction and Mapping of Pb Content in Overbank Sediments Affected by Coal-Mining Using Airborne Hyperspectral Imaging

Jamie-Leigh R. Abrahams[1], Emmanuel John M. Carranza[1]

[1]*Department of Geology, Faculty of Natural and Agricultural Sciences, University of the Free State, Bloemfontein, South Africa*

Abstract

Spectral absorption feature parameters (SAFPs) derived from airborne hyperspectral imaging (HSI) (396.0–2453.5 nm) were used to predict Pb contents in coalfield overbank sediments. The derived SAFPs were associated with goethite (~500 nm) and kaolinite (~1448 nm) in sediments. Sediment Pb contents correlated strongest with goethite-related absorption-depth (r = 0.6). The calibration model had a R^2 = 0.69 and standard error of estimation (SEE) = 3.97, after outlier removal. The validation model had a R^2 = 0.65 and SEE = 3.90. Overall, the results suggest that airborne HSI can complement conventional geochemical methods of detecting Pb contents in overbank sediments.

Keywords: Witbank Coalfield; reflectance spectroscopy; regression modeling

Introduction

Trace metal (TM) contamination of the environment is one of the biggest challenges related to acid mine drainage (AMD). TM analysis of sediments via conventional geochemical methods is often onerous, particularly when undertaken at large scales. Compared to conventional methods, hyperspectral imaging (HSI) sensors offer greater efficiency by rapidly measuring hundreds of contiguous spectral bands (Asadzadeh & de Souza Filho 2016), some of which can be used to predict TM contents in soils and sediments. The prediction of TM contents is based on their adsorption to minerals, such as Fe-oxides and clays in soils (Wu *et al.* 2005). The adsorption of TMs to these minerals can cause variations in the number of O^- and OH sites on the mineral's surface (Zachara & Westall 1999). These variations may cause changes in their spectral absorption feature parameters (SAFPs), namely absorption-peak depth, area, width and asymmetry, which can be linked to TM contents (Choe *et al.* 2008).

The city of Emalahleni is located in the Witbank Coalfield in South Africa, which has been mined for over a century (Hancox & Götz 2014). Thus, many rivers in the area have been affected by AMD-related TM contamination. There are limited studies on the use of airborne HSI in the vicinity of coal mines, none of which have examined overbank sediments. Among the TMs associated with coal mining, Pb is considered one of the TMs that are most hazardous to ecological and human health. Pb accumulation in the study area is linked largely to AMD related to coal mining and industrial waste (Abrahams & Carranza 2025). Thus, there is a need to efficiently monitor Pb content in the environment. This study therefore endeavoured to (i) derive SAFPs from airborne HSI for use as predictors of Pb content in overbank sediments along the Blesbokspruit River in Emalahleni, (ii) model Pb content in the study site by applying regression analysis to the airborne HSI data using GIS software and (iii) evaluate the model's predictive performance using the goodness of fit (R2) and standard error of estimation (SEE).

Methods

Overbank sediment samples

Twelve overbank sediment samples were collected at six different locations (i.e., two samples spaced approx. 5 m apart at each location), covering approx. 6 km of the Blesbokspruit River (Fig. 1). Samples were collected in this way because the spatial trends of overbank deposition can be highly variable (Simm & Walling 1998). Sample size was limited largely due to water-saturated sediments in a wetland along the stream (i.e., because high soil moisture contents typically cause interferences in spectral data) (Wu *et al.* 2005). For mineralogical analysis, air-dried samples were crushed and milled to < 75 µm and subjected to X-ray diffraction (XRD). For chemical analysis, air-dried samples were sieved (< 63 µm), treated with reverse aqua regia ($3\ HNO_3 : 1\ HCl$), which does not digest the silicate fraction (Petrović *et al.* 2022), and microwave digestion before analysis via inductively coupled plasma atomic emission spectroscopy/mass spectrometry (ICP-AES/MS).

Airborne HSI data

Airborne HSI data were collected by the Council for Geoscience of South Africa over the study site via an airplane (Fig. 1b). The flight altitude was 2.35 km with solar zenith angle of 29.4° and solar azimuth angle of 80.9°. The spatial resolution was 1 m by 1 m, with 360 bands from 396.0 nm to 2453.5 nm wavelength range. The spectra were smoothed using Savitzky-Golay filtering to reduce noise and CO_2 mitigation was applied. The HSI data were corrected for atmospheric water by applying the widely used ATCOR4 model and transformed using continuum removal analysis (Choe *et al.* 2008). Variations in absorption-band position, depth(D), width

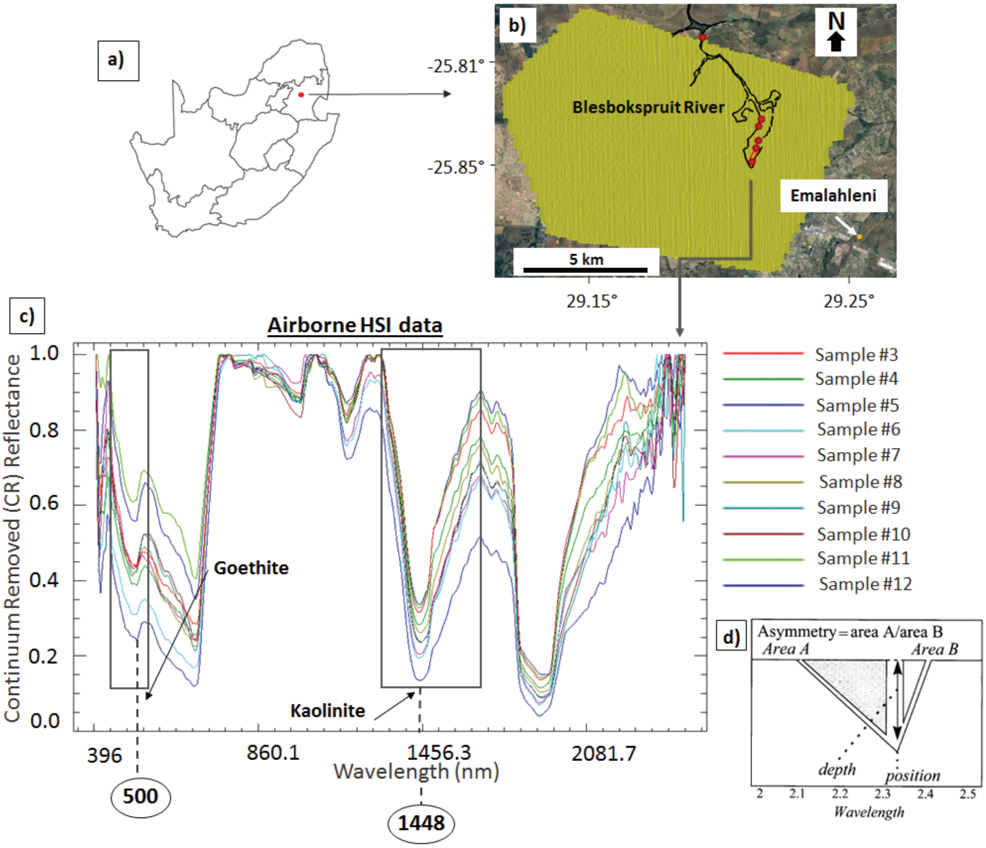

Figure 1 The study site location in the Mpumalanga Province, South Africa, b) airborne HSI coverage over the Blesbokspruit River area, c) continuum-removed reflectance data vs wavelength, and d) D and S parameters (after Van der Meer 1999). The W, which is not illustrated, is calculated as: Area A + Area B / 2D.

(W) and asymmetry (S), were derived from the most distinct SAFs at approx. 500 nm, which is associated with surface hydroxyl groups on goethite (Wu *et al.* 2005) and at approx. 1440 nm, which is associated with surface hydroxyl groups on kaolinite (Van der Meer 2004). The D, W and S were calculated according to Fig. 1d.

Statistical treatment and geochemical mapping

Pb data were *ln*-transformed to ensure that the data approximate a normal distribution, prior to correlation and regression analysis. Spearman's rank correlation analysis was performed because of the small sample size ($n = 10$) and the uncertainty quantified based on statistical significance. The minimum number of observations necessary for a single explanatory variable is $n = 10$ (Van Voorhis & Morgan 2007). Thus, relationships between Pb contents and the HSI data were modeled using univariate regression analysis. Although predictive models typically perform better using a large number of samples, models based on smaller datasets can still provide guidance for more in-depth environmental analyses (Hernandez *et al.* 2006). To calculate 'predicted' Pb contents, the regression equation generated by the best calibration model was applied and the derived *ln*-contents were back-transformed to compare with the measured Pb contents. Regression models were evaluated in terms of the R^2, SEE, root mean squared error of prediction (RMSEP) calculated using leave-one-out cross-validation (LOO-CV) and the relative model stability assessed using the Chow statistic. For the predictive map, HSI data were subjected to NDVI (normalized difference vegetation index) analysis (Cherlinka 2019) and the regression equation from the best calibration model applied to bare soils using the raster calculator in QGIS (QGIS.org 2023). Predictions were validated using pXRF (portable x-ray fluorescence) measurements collected *in-situ*.

Results and Discussion

Mineralogy and geochemistry

Overbank sediments in the study site comprised mainly quartz (up to 95%) and kaolinite (up to 5%). Thus, the overbank sediment samples had a largely sandy texture, which is supported by the findings of Bell *et al.* (2002). Overbank sediments contained considerable Al (median = 4.47%) and Fe (median = 2.57%), with minor Si (median = 0.346%). Lead contents in the study site's overbank sediments (median = 25.2 mg/kg) appeared relatively consistent with those in stream sediments in the Witbank Coalfield (mean = 24.9 mg/kg) (Bell *et al.* 2002), the Baixo Jacuí coal mining region in Brazil (median = 27 mg/kg) (Teixeira *et al.* 2001) and the Jaintia Hills coal deposit in India (mean = 27.5 mg/kg) (Sahoo *et al.* 2017).

Correlations, regression analysis and geochemical mapping

Table 1 shows the correlations between *ln*-transformed Pb contents and the airborne-derived SAFPs. Iron oxide and clay minerals typically adsorb Pb in soils and sediments (Moreno *et al.* 2006), thus, providing support for the trends observed in subsequent correlation and regression analysis. Lead contents had the strongest correlation ($r = 0.6$) with Depth500 (the goethite-related D),

Table 1 *Correlations (r) between ln-transformed Pb contents and airborne-derived SAFPs. Also shown is the goodness-of-fit (R^2) and the standard error of estimation (SEE) of the calibration models.*

Predictor	*r*	R^2	SEE
Depth500	0.6	0.39	0.26
Asym500	-0.4	0.30	0.28
Width500	-0.5	0.20	0.30
Depth1448	0.5	0.25	0.29
Asym1448	0.5	0.27	0.29
Width1448	-0.5	0.29	0.28

although it was not statistically significant. Strong correlation with goethite is consistent with findings by Covelo *et al.* (2007) that Fe-oxide adsorbed and retained greater concentrations of Pb, compared to kaolinite. Results are also consistent with the findings of Kemper and Sommer (2002) that Pb contents in soils could be estimated using correlations with iron oxide contents and the findings of Zhao *et al.* (2022) that spectral bands at approx. 500 nm had strong correlation with Pb contents in soils. Stronger correlation with the goethite- related D, compared to the W and S, is likely because the D requires a simpler calculation compared to the W and S and, thus, calculations for W and S may be prone to greater error (Van der Meer 2004).

The R^2 and SEE of the calibration regression models were consistent with the correlation analysis and showed that the best predictive model was obtained for Depth500. Based on the Chow statistic (0.095), the LOO-CV method yielded stable (i.e., $p > 0.05$) regression coefficients for airborne-predicted Pb contents. When the RMSEP (6.6 mg/kg) was evaluated in terms of the concentration range of Pb, it represented ≈20% of the concentration range. Fig. 2 shows the measured vs airborne-predicted Pb contents in overbank sediments in the study site. In general, the airborne-derived SAFPs showed a tendency to 'under'-predict higher Pb concentrations and slightly 'over'-predict lower Pb concentrations (Fig. 2a). This is consistent with the findings of Tan *et al.* (2020, 2021). The regression line and R^2 (red dotted line in Fig. 2a) were notably influenced by the high concentration outliers. Outliers (red dots) were detected using the median +- median absolute deviation (MAD) (Reimann *et al.* 2005) and were removed. Following outlier removal, the R^2 improved markedly from 0.28 to 0.69 (blue dotted line in Fig. 2a), which is consistent with Kemper & Sommer (2003), who noted a similar improvement to the R^2 when outliers were removed.

Fig. 3 shows airborne-predicted Pb contents in overbank sediments in the study site. Airborne-predicted Pb contents was calculated using the following regression equation: $y = 2.96x + 2.40$ (where x is Depth500). According to Fig. 3, the overbank sediments appeared largely dominated by Pb concentrations of 7–10 mg/kg and higher.

Predictions according to the validation model (Fig. 2b) were generally lower than measured pXRF contents. Kemper & Sommer (2003) suggested that the 'under'-prediction of higher metal concentrations is likely attributed to averaging across the area of one pixel, which can reduce higher concentrations to lower concentrations and incorporate it into the final measurement. Although the predictions were lower than the measured Pb contents and the goodness-of-fit of the validation model was only moderate ($R^2 = 0.65$), Choe *et al.* (2009) suggested that this technique is still useful because it provides a simple and rapid approximation of TM contents prior to performing more precise geochemical analysis.

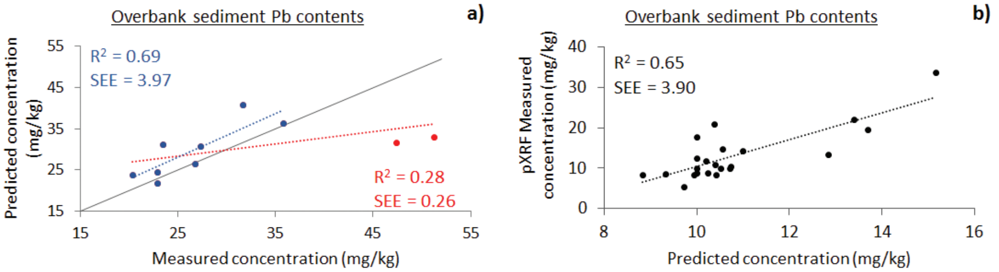

***Figure 2** a) Calibration models showing airborne HSI-predicted Pb content vs measured content in overbank sediments along the Blesbokspruit River, South Africa (the red dotted line represents the model including outliers, the blue dotted line represents the model excluding outliers and the black solid line represents the 1:1 trend line); and b) the validation model showing in-situ measured Pb contents vs. airborne HSI-predicted contents (the black dotted line represents the regression line).*

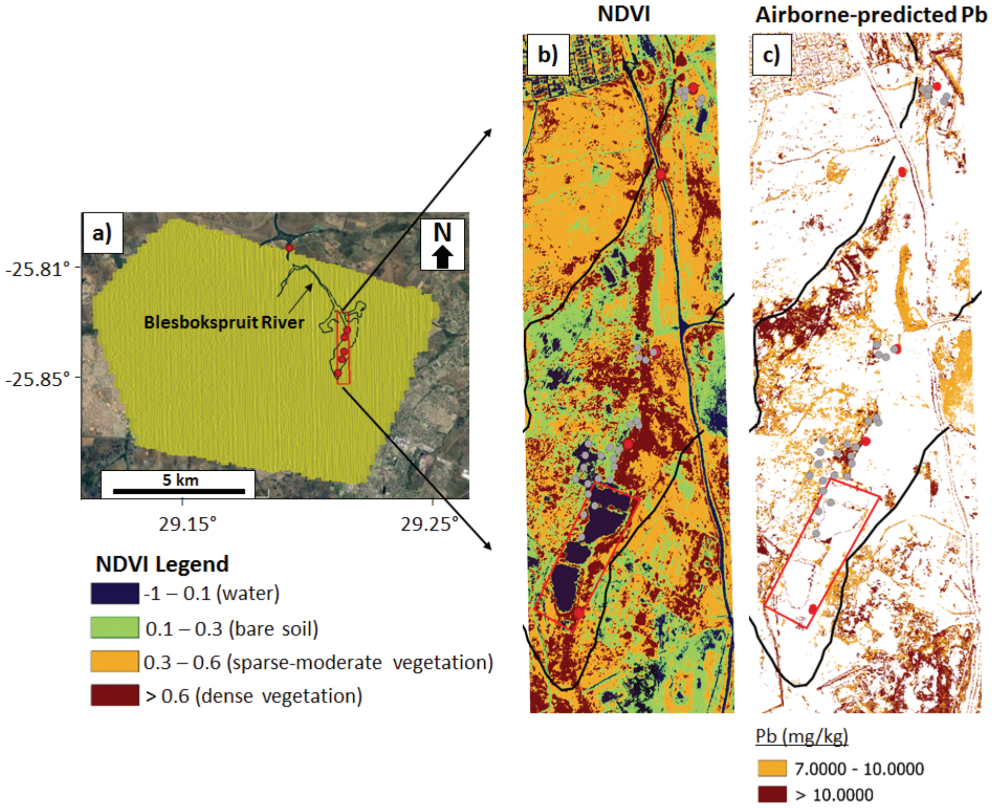

Figure 3 *a) Airborne HSI data coverage over the study area, b) NDVI and c) airborne-predicted Pb contents in exposed overbank sediments in the study site. Red dots represent ICP–MS sample sites (used in model calibration) and grey dots represent pXRF sample sites (used in model validation). The red rectangle in b) and c) highlights acid ponds in the study site.*

Conclusions

This study found that the most prominent TM-predicting SAFs were associated with goethite (at approx. 500 nm) and kaolinite (at approx. 1448 nm) in overbank sediments. Pb data correlated strongest with Depth500 (goethite-related D). The calibration model had a R^2 of 0.28 and SEE of 0.26. Outlier removal markedly improved the R^2 of the calibration model from 0.28 to 0.69. The corresponding validation model had a R^2 of 0.65 and SEE of 3.90. The results suggest that Depth500 may serve as a proxy for Pb contents in overbank sediments. Due to the small dataset (n = 10) and strong influence of outliers on the regression analysis, further research using a larger dataset is necessary to improve the calibration models. When more data are added and the models are improved, airborne HSI may be useful as a rapid screening method for detecting TM contents related to coal mining in overbank sediments prior to more intensive data collection and geochemical analysis.

Acknowledgements

The authors thank the South African National Space Agency (SANSA) for sponsoring this research project.

References

Abrahams, J-LR, Carranza EJM (2025) Assessment of trace metal contamination in overbank sediments of the Witbank Coalfield, South Africa. Environ Earth Sci 84:153

Asadzadeh S, de Souza Filho CR (2016) A review on spectral processing methods for geological remote sensing. Int J App Earth Obs and Geoinf 47:69–90

Bell FG, Hälbich TFJ, Bullock SET (2002) The effects of acid mine drainage from an old mine in the Witbank Coalfield, South Africa. Q J Eng Geol Hydrogeol 35:265–278

Cherlinka V (2019) NDVI FAQ: All You Need To Know About Index, EOS Data Analytics. Retrieved July 2023 from https://eos.com/blog/ndvi-faq-all-you-need-to-know-about-ndvi/

Choe E, van der Meer F, van Ruitenbeek F, van der Werff H, de Smeth B, Kim KW (2008) Mapping of heavy metal pollution in stream sediments using combined geochemistry, field spectroscopy, and hyperspectral remote sensing: A case study of the Rodalquilar mining area, SE Spain. Remote Sens Environ 112(7):3222–3233

Choe E, Kim KW, Bang S, Yoon IH, Lee KY (2009) Qualitative analysis and mapping of heavy metals in an abandoned Au-Ag mine area using NIR spectroscopy. Environ Geol 58(3):477–482

Covelo EF, Vega FA, Andrade ML (2007) Competitive sorption and desorption of heavy metals by individual soil components. J Hazard Mater 140:308–315

Hancox PJ, Götz AE (2014) South Africa's coalfields - A 2014 perspective. Int J Coal Geol 132:170–254

Hernandez PA, Graham CH, Master LL, Albert DL (2006) The effect of sample size and species characteristics on performance of different species distribution modeling methods. Ecography 29(5):773–785

Kemper T, Sommer S (2002) Estimate of heavy metal contamination in soils after a mining accident using reflectance spectroscopy. Environ Sci Technol 36:2742–2747

Kemper T, Sommer S (2003) Mapping and monitoring of residual heavy metal contamination and acidification risk after the Aznalcóllar mining accident (Andalusia, Spain) using field and airborne hyperspectral data. In: Habermeyer, M., Müller, A., Holzwarth, S. (Eds.) Proceedings of 3rd EARSEL Imaging Spectroscopy, Herrsching, Germany, CD-ROM ISBN 2-908885-56-5, 333–343

Moreno AM, Quintana JR, Pérez L, Parra JG (2006) Factors influencing lead sorption–desorption at variable added metal concentrations in Rhodoxeralfs. Chemosphere 64(5):758–763

Petrović S, Mrmošanin J, Pavlović A, Alagić S, Tošić S, Stojanović G (2022) The Influence of Agricultural Soil Preparation Methods on the Pseudo-Total Element Content Determined By ICP-OES. Studia Universitatis Babes-Bolyai Chemia 67(1):43–60

QGIS.org (2023) QGIS Geographic Information System. QGIS Association. Retrieved August 2023 from http://www.qgis.org

Reimann C, Filzmoser P, Garrett RG (2005) Background and threshold: Critical comparison of methods of determination. Sci Total Environ 346(1–3):1–16

Sahoo PK, Tripathy S, Panigrahi MK, Equeenuddin SM (2017) Anthropogenic contamination and risk assessment of heavy metals in stream sediments influenced by acid mine drainage from a northeast coalfield, India. Bull Eng Geol Environ, 76(2):537–552

Simm DJ, Walling DE (1998) Lateral variability of overbank sedimentation on a Devon flood plain. Hydrol Sci J 43:715–732

Tan K, Ma W, Chen L, Wang H, Du Q, Du P, Yan B, Liu R, Li H (2021) Estimating the distribution trend of soil heavy metals in mining area from HyMap airborne hyperspectral imagery based on ensemble learning. J Hazard Mater 401:123288

Tan K, Wang H, Chen L, Du Q, Du P, Pan C (2020) Estimation of the spatial distribution of heavy metal in agricultural soils using airborne hyperspectral imaging and random forest. J Hazard Mater 382: 120987

Teixeira EC, Ortiz LS, Alves MFCC, Sanchez JCD (2001) Distribution of selected heavy metals in fluvial sediments of the coal mining region of Baixo Jacuí, RS, Brazil. Environ Geol 41(1–2):145–154

Van der Meer F (1999) Can we map swelling clay with remote sensing? Int J App Earth Obs and Geoinf 1:27–35

Van der Meer F (2004) Analysis of spectral absorption features in hyperspectral imagery. Int J App Earth Obs and Geoinf 5(1):55–68

Van Voorhis CW, Morgan BL (2007) Understanding power and rules of thumb for determining sample sizes. Tutorials in Quantitative Methods for Psychology 3(2):43–50

Wu YZ, Chen J, Ji JF, Tian QJ, Wu XM (2005) Feasibility of reflectance spectroscopy for the assessment of soil mercury contamination. Environ Sci Technol 39(3):873–878

Zachara JM, Westall JC (1999) Chemical modeling of ion adsorption in soils. In Sparks DL (Ed), Soil physical chemistry, Boca Raton: CRC Press, p 47–95

Zhao D, Xie D, Yin F, Liu L, Feng J, Ashraf T (2022) Estimation of Pb Content Using Reflectance Spectroscopy in Farmland Soil near Metal Mines, Central China. Remote Sens 14(10):2420

Advancing Sustainable Tailing Management: A Comprehensive Approach to the Geochemical Characterization of Iron Ore Tailing in Dry Stacks

Rafael Cavalcanti de Albuquerque[1], Carolina Bittencourt de Abreu[1], Mariana Werle[1], Bruno César Mortatti[1], Thaís de Paula Marteleto[1], Eduardo dos Santos Costa[1], Lara Lange[1], Daniela Alcantara Machado[2], Pablo Vinícius Silva Santos[2]

[1]*Water Services and Technologies (WST), 30220-140 Belo Horizonte, Minas Gerais, Brazil, contato@waterservicestech.com*

[2]*Samarco Mineração, Germano Complex, 35420-970 Mariana, Minas Gerais, Brazil*

Abstract

Tailings dam failures in Brazil in 2015 and 2019 highlighted the critical need for safer and more sustainable tailings management practices in iron ore mining. In response, the Global Industry Standard on Tailings Management (GISTM) was established to promote best practices for ensuring the safety and integrity of tailings disposal structures. Among the innovative approaches, dry stacking has emerged as a viable alternative to conventional tailings dams, minimizing water retention within tailings and significantly reducing hydraulic risks.

This paper presents a detailed protocol for the chemical, mineralogical, and hydrogeochemical modeling—both conceptual and numerical—of iron ore beneficiation waste. Developed for one of Brazil's pioneering dry stacking facilities, implemented following the 2015 dam failure, the protocol facilitates continuous assessment of waste chemical stability. It integrates hydrochemical analyses and monitors reagents used during beneficiation processes. The systematic hydrogeochemical model consolidates data on fluid percolation and movement, encompassing geotechnical, hydrogeological, and hydrochemical factors alongside the physicochemical and mineralogical properties of the materials involved.

Three key conditions influencing the structure were identified: (1) seasonal water-level fluctuations impacting geochemical conditions, (2) the degradation of ether-amines—reagents used in the beneficiation process—altering redox environments within the structure, and (3) potential for chemical clogging in the dry stack's bottom drains. Successfully conceived and implemented, the protocol has proven effective in assessing the chemical stability of tailings, offering a comprehensive methodology for hydrochemical analysis of effluents and industrial waters while monitoring of organic reagents used in mineral processing. Results demonstrate compliance with international standards and best industry practices, reinforcing the commitment to sustainable and safe mining operations.

Keywords: Tailings, Management, Iron Ore Processing, Dam Failure, Geochemistry Characterization, Hydrogeochemical Modeling

Introduction

The Global Industry Standard on Tailings Management (GISTM, 2020) promotes best practices for tailings facility safety and environmental protection. Principle 2 emphasizes building an integrated knowledge base to support safe management throughout a facility's lifecycle, including closure. In Brazil, regulatory requirements from the National Mining Agency (ANM) have driven the adoption of innovative disposal methods, such as co-disposal in dry-stacked facilities.

While traditional research on metal leaching has focused on sulfide-rich tailings (AMIRA 2002; INAP 2009; MEND/CANMET 2009), advancements like dry stacking require new methodologies, particularly for iron ore tailings with low sulfide content. This study examines the Alegria Sul dry stack at the Germano Complex, developed after the 2015 dam failure. It establishes an approach for assessing contaminant leaching through data collection, statistical analysis, and hydrogeochemical modeling. Hydraulic and geotechnical properties, along with piezometric monitoring, were used to identify oxidizing and reducing zones affecting iron and manganese mobility. Without experimental simulations, geochemical modeling played a key role in predicting system interactions, supporting sustainable tailings management.

Geological and Climatic Setting of the Germano Complex

The Quadrilátero Ferrífero (QF) in southeastern Brazil, part of the São Francisco Craton, is a major metallogenic province composed of Archean to Paleoproterozoic rocks (Chemale and Rosière 1993; Alkmin and Marshak, 1998; Cutts *et al.* 2019). The Minas Supergroup, particularly the Itabira Group and its Cauê Formation, hosts Lake Superior-type banded iron formations (BIFs) rich in oxides (Biondi 2003). These formations originated from mid-ocean ridge exhalations and were later enriched through tectono-metamorphic events and supergene processes during the Cenozoic (Costa *et al.* 1998). The resulting itabirites underwent quartz dissolution and leaching, concentrating iron and increasing material friability. Due to natural leaching, reactive minerals like carbonates and sulfides were largely removed, leaving resistant minerals such as quartz and hematite in the Cauê Formation. For this reason, these minerals do not have relevant concentrations in the rock's composition from Caue Formation (and consequently, in the waste).

The region of the Germano Complex in Samarco experiences two well-defined seasons: a rainy season from October to March, and a dry season from April to September. The wettest period occurs from November to January, which together account for nearly 55% of the total annual precipitation. December is the month with the highest rainfall, with an average monthly precipitation of approximately 400 mm. The average annual precipitation in the Germano Mine area is approximately 1950 mm. Regarding temperature, the area experiences a tropical climate with an average annual temperature of approximately 23°C. During the rainy season (October to March), the average temperature is around 24°C, while in the dry season (April to September), the average temperature drops slightly to around 22°C.

Geochemical Assessment of Germano Complex Tailings in Accordance with GISTM

The Germano Complex, with an annual production capacity of 33 million tons of iron ore, employs a beneficiation process that includes comminution, desliming, flotation, and thickening. Desliming removes particles smaller than 10 µm, which are deposited in a mined-out pit, while larger particles undergo flotation for silica removal. Filtered tailings are thickened and deposited as a dry-stacked cake, enhancing geotechnical safety and environmental compliance in line with the GISTM. Key reagents used in beneficiation include starch, caustic soda, amines, coagulants, and flocculants, which influence flotation, dispersion, and thickening. The residual water in tailings provides critical data for assessing hydrochemical quality in bottom drains.

The protocol for characterizing shared waste rock, drained tailings, and cake samples at the Germano Complex involved extensive data collection and analysis to support conceptual and numerical modeling. Key data included beneficiation inputs, geological models, and climate records, along with solid material and hydrochemical monitoring plans. Sampling methods used representative grids, trenching for drained tailings, and drill core analysis for waste rock. Hydrochemical monitoring tracked effluents and inputs to ensure compliance with Brazilian Environmental Standards.

Chemical and mineralogical characterization was performed by an ISO/IEC 17025 certified laboratory using techniques like XRF, ICP-OES, XRD, and MLA. These methods provided detailed insights into mineral composition and geochemical processes. Statistical data treatment ensured accuracy, and MLA offered microscopic analysis of processed materials.

Geochemical characterization and numerical modeling integrated piezometric, hydraulic, and geotechnical data to predict iron and manganese mobilization. PHREEQC Interactive was used to model the chemical and mineralogical analysis of dry stack materials, filtration residues, and monitoring data, providing insights into water percolation and geochemical interactions. The potential for chemical clogging in the internal drainage system was assessed by evaluating drain geometry, porosity, and flow dynamics.

Hydrogeochemical Model

The hydrogeochemical conceptual model for the Alegria Sul dry stack integrates geotechnical, hydrogeological, hydrological, and geochemical data to understand fluid dynamics and redox processes within the structure. Drained tailings (sandy tailings) and waste rock materials (waste rock belt) deposited in the structure are moistened using sprinklers operated by water trucks to achieve optimal compaction according to geotechnical requirements.

Water outflows from the dry stack consist of drainage through drains located at the bottom of the structure (Fig. 1). The drainage system includes nine drains, classified into shallow (4) and deep (5). After percolating through the sandy tailings, water exits the structure via shallow drains. Piezometric data did not indicate a significant hydraulic connection between the deep and shallow drains. Based on this, it is inferred that the effluent percolating through the waste rock is predominantly captured by the shallow drains. A possible explanation for this behavior is the presence of a leveling platform between the drainage layers, whose low hydraulic conductivity limits the infiltration of percolated effluents towards the deep drains. Thus, the deep drains appear to primarily function in draining water from buried springs formed during the construction of the waste pile, rather than capturing significant volumes of percolated effluent.

The dry stack's predominantly unsaturated structure creates non-reducing conditions in its upper and intermediate layers, while the basal sections occasionally transition to saturation, fostering reducing conditions. Redox variations along the structure influence the transport of gases like O_2 and CO_2, driving mineral dissolution and precipitation processes. These dynamics are closely tied to factors such as groundwater level fluctuations, organic matter oxidation, and the degradation of nitrogenous compounds, which shape the system's geochemical behavior.

Specific conditions, such as organic matter burial and deep drainage points, contribute to localized reducing zones within the dry stack. The oxidation of buried organic material and amines, along with oxygen depletion, supports the mobilization of metals like iron and manganese. Hydrochemical analyses of drainage flows reveal redox-related transformations, especially between shallow and deep drainage systems. The results highlight the progressive depletion of oxygen with depth, along with changes in dissolved species concentrations. For instance, Fe^{2+}-rich solutions from deeper layers may precipitate iron oxides upon exposure to atmospheric conditions at surface drains. It is important to note that the chemistry of rainfall was not considered in the geochemical model. Instead, a more conservative scenario was adopted, using water from water trucks, which presents more saturated concentrations compared to rainfall.

The methodology adopted in this study involved geochemical modeling using the PHREEQC software (version 3; Parkhurst and Appelo, 2013) to evaluate the saturation of different mineral phases in relation to the hydrochemical conditions. The main minerals in the solid matrix and the geochemical processes influencing their dissolution and precipitation were considered.

The numerical model was structured to represent, in a one-dimensional approach, the reactive transport of water and solutes within the waste matrix. The model was based on discretizing the waste pile into cells, allowing the simulation of compositional evolution along depth. Water flow was modeled using Darcy's equation for saturated media and the van Genuchten formulation for the unsaturated zone. Solute transport was described through advection and dispersion processes, while chemical reactions were incorporated through thermodynamic equilibria and kinetic processes.

The residence time of the solution in the pile was estimated using the cross-correlation function (Padilla and Pulido-Bosch, 1995; Warner, 1998, which analyzes the relationship between the precipitation and drain flow time series from August 2023 to May 2024. The cross-correlation identifies the time lag and the intensity of the relationship between the phenomena, with statistical analysis using a p-value ≤ 0.05 to determine significance.

Hydrochemical data defined the initial conditions of aqueous solutions and parameterized the model, considering the concentrations of major and trace elements. The modeling enabled the calculation of mineral saturation indices, identifying phases that tend to remain stable, dissolve, or precipitate under the evaluated conditions. The analyzed mineral phases included carbonates, sulfates, oxides, and silicates, considering their influence on chemical equilibrium. The evaluation of saturation indices was essential for understanding the mobility of elements and the geochemical evolution of the system. Additionally, the modeling incorporated the biodegradation of organic compounds using the R-Monod kinetics, describing substrate consumption as a function of nutrient availability and microbial activity. Monitoring at Alegria Sul confirmed ammoniacal nitrogen levels remained within regulatory limits. Research by Chaves (2001) observed a decline from 31.7 mg/L to 4.7 mg/L in Samarco flotation tailings over 12 days.

The model was iteratively adjusted to represent the interaction between water and minerals, predicting the chemical composition evolution of the solution over time and under different scenarios. The results provide support for interpreting the processes controlling water quality and trends in mineral precipitation and dissolution.

Results and Discussion

The chemical and mineralogical characterization of the Alegria Sul dry stack tailings and waste rock shows a predominantly inert composition with low environmental risk. The primary components include quartz and iron oxides (hematite, goethite, and magnetite), with minimal concentrations of

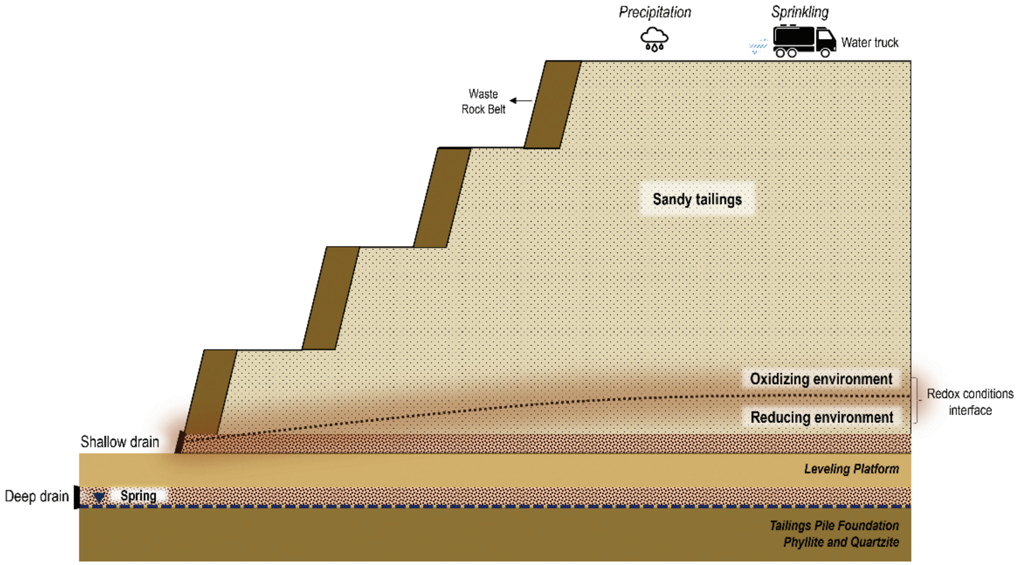

Figure 1 *Schematic representation of redox conditions at Alegria Sul dry stack.*

trace elements like arsenic, cadmium, and lead. The absence of sulfide minerals and low sulfur content indicate stability under oxidizing conditions, suggesting limited potential for acid mine drainage or pollutant release.

Hydrochemical monitoring reveals distinct chemical profiles in input (water truck) and output (drains) phases, with alkaline water truck solutions and mild acidity in deep drains. Shifts in redox conditions with depth affect dissolved iron and manganese concentrations. The degradation of organic compounds from beneficiation reagents influences these dynamics, including the destabilization of hematite under reducing conditions, releasing soluble iron.

The numerical hydrogeochemical model simulates solute transport and the degradation of ether-amines used in flotation, revealing ammonia release and stabilization. It incorporates various mineral phases, such as quartz and iron oxides, into simulations. The model also assesses transport dynamics and the residence time of solutions within the dry stack, identifying significant correlations between precipitation and drainage responses. The results indicate that at least 70% of the flow peaks in the drains are influenced by precipitation, with response times ranging from 3.5 to 5 months. Some drains show greater sensitivity, with flow increasing within 45 days after the onset of rain, peaking at 100–150 days. Other drains take 60 to 90 days to respond to precipitation. The correlation between precipitation and flow is approximately 72%, indicating a response that has not yet fully developed at these points. The analysis suggests that the correlation between the phenomena is robust, with at least 70% significant correlation.

The model further evaluates the potential for chemical clogging in the drains, predicting minimal clogging over 100 years due to $Fe(OH)_3$ precipitation. However, since most precipitation occurs outside the system, the effect on drainage efficiency is limited. Overall, the results demonstrate the environmental viability of the dry stack system and the stability of the geochemical processes within the site.

This table presents the chemical composition of different water sources in the Alegria Sul dry stack. The "Water Truck" column shows the median concentrations of water sprayed by trucks, monitored over 18 months. Q1 and Q3 represent the median concentrations within the interquartile range for shallow drains. The last two columns, "Drain Outflow" and "Equilibrium with Atmosphere", present the calibrated effluent concentrations at the drain outflow and after exposure to the atmosphere, respectively.

Conclusions

This study presents an interdisciplinary approach to address environmental

Table 1 Calibrated Water Chemistry Data for the Alegria Sul Dry Stack.

Parameters	Water Truck (median)	Q1 (Shallow Drains)	Q3 (Shallow Drains)	Drain Outflow	Equilibrium with Atmosphere
Temperature (°C)	21.90	23.20	25.20	21.90	21.90
pH	8.36	6.98	7.65	7.46	7.46
pe	6.60	2.30	6.30	-4.90	2.30
Al (mg/L)	0.10	0.01	0.04	0.10	0.10
Alkalinity (mg/L)	4.80	113.30	269.10	37.20	6.30
Ca (mg/L)	1.50	2.11	67.75	1.50	1.50
Cl (mg/L)	0.50	0.50	0.50	0.50	0.50
Fe (mg/L)	0.13	0.03	1.83	5.55	0.13
K (mg/L)	0.29	4.10	5.00	0.29	0.29
Mg (mg/L)	0.18	2.40	7.62	0.18	0.18
Mn (mg/L)	0.02	0.11	0.34	0.28	0.28
Na (mg/L)	1.40	36.00	110.50	1.40	1.40
NH_3/NH_4^+ (mg/L)	0.21	3.34	5.71	5.92	0.00

complexities in tailings management, integrating geochemistry, geotechnics, hydrogeology, geometallurgy, mine planning, and ore beneficiation. Hydrogeochemical modelling was employed to simulate interactions between sprinkler truck water and sandy tailings in the Alegria Sul dry stack, focusing on ether-amine degradation (used in Samarco's iron ore beneficiation) and mineral dissolution. Key findings included:

- Sandy tailings are predominantly quartz (≈89%), iron oxides (≈10%), silicates (≈0.7%), and trace minerals (≈0.7%), with short water residence times (100–150 days) limiting silicate dissolution.
- Ether-amine degradation is influenced by chemical structure, environmental conditions (e.g., pH, oxygen, nutrients), and microbial activity, producing organic carbon and ammoniacal nitrogen.
- Rapid degradation under reducing conditions destabilized hematite, releasing iron, while oxidizing conditions favored $Fe(OH)_3$ precipitation and nitrate formation.
- Simulations indicate ether-amines degrade within days and pose negligible environmental risks, with ammoniacal nitrogen concentrations remaining environmentally insignificant.

This methodology demonstrates a robust framework for managing uncertainties and systematically analysing data, aligned with ESG (Environmental, Social, and Governance) principles and Principle 2 of the GISTM to support safe tailings management throughout facility lifecycles.

References

Alkmin FF, Marshak S (1998) Transamazonian Orogeny in the Southern São Francisco Craton Region Minas Gerais Brazil: evidence for Paleoproterozoic collision and collapse in the Quadrilátero Ferrífero. Precambrian Research, 90:29–58.

AMIRA (2002) ARD test handbook. AMIRA P387A project: prediction and kinetic control of acid mine drainage. Melbourne, VIC: AMIRA International.

Biondi JC (2003) Processos metalogenéticos e os depósitos minerais brasileiros. São Paulo, Oficina de textos 528p.

Chaves LC (2001) Estudo de Resíduos de Sólidos Gerados na Flotação de Minério de Ferro: Quantificação e Decomposição de Aminas no Meio Ambiente. Universidade Federal de Ouro Preto. (Mestrado em Geodinâmica Superficial/Geoquímica Ambiental). Dissertação de Mestrado [Master's Thesis], 89p.

Chemale Jr. F, Rosière CA (1993) Arquitetura de domo e bacia no Quadrilátero Ferrífero no Proterozoico Inferior. Sociedade Brasileira de Geologia Boletim. Núcleo Minas Gerais 12, 172–175.

Costa AGD, Rocha JMP, Bonfioli L, Vieira CB (1998) A Importância do modelamento geológico-tipológico no controle de qualidade dos concentrados e pelotas de minério de ferro da Samarco Mineração S/A. In: XXIX Seminário de Redução de Minério de Ferro, Belo Horizonte, p. 545–555.

Cutts K, Lana C, Alkmin F, Farina F, Moreira H, Coelho V (2019) Metamorphism and exhumation of basement gneiss domes in the Quadrilátero Ferrífero: Two stage dome-and-keel evolution? Geoscience Frontiers (10), 1765–1787.

GISTM (2020) Global Industry Standard on Tailings Management. Global Tailings Review, 40p.

INAP (2009) The International Network for Acid Prevention. Global Acid Rock Drainage Guide (GARD Guide). http://www.gardguide.com

ISO/IEC 17025 (2005) General Requirements for the Competence of Testing and Calibration Laboratories. ISO, Geneva (2005).

MEND/CANMET (2009) Mining and Mineral Science Laboratory. Prediction Manual for Drainage Chemistry from Sulphidic Geologic Materials. MEND Report 1.20.1.

PADILLA, A; PULIDO-BOSCH, A. (1995). Study of hydrographs of karstic aquifers by means of correlation and cross-spectral analysis. J Hydrol, n.168, p73–89.

Parkhurst DL, Appelo CAJ (2013) Description of input and examples for PHREEQC version 3–A computer program for speciation, batch-reaction, one dimensional transport, and inverse geochemical calculations: U.S. Geological Survey Techniques and Methods, book 6, chap. A43, 497p. http://pubs.usgs.gov/tm/06/a43/

WARNER R. M. (1998). Spectral analysis of time-series data. New York, USA: Guilford Press, 225p.

Innovative Circular Economy Approach for Recovering Valuable Metals from Acid Mine Drainage and Sulfuric Acid from Mining Waste

Bárbara Ahumada-Vargas[1], Lidia Fernandez-Rojo[1], Ana Guedes[1], Eric Vilanova[1], Carlos Echevarría[1], Tamara Martínez-Santos[2], Manuel Sevilla[2]

[1]*Water Technology Center CETaqua, Cornellà de Llobregat, Spain*

[2]*Tharsis Mining, Tharsis, Spain*

Abstract

The Horizon Europe Resilex project introduces an innovative circular approach to recover Critical (and strategic) Raw Materials (CRM) from Acid Mine Drainage (AMD), reducing environmental impact while recovering valuable resources. Copper (Cu), zinc (Zn), cobalt (Co), and sulfuric acid (H_2SO_4) are recovered by combining selective precipitation, bioreactor-driven sulfide precipitation, ion exchange, nanofiltration membranes, and evapocrystallization. In the whole process, it is expected to recover up to 6.4 g of CuS and 34.7 g of ZnS per 100 L of feed water in the AnMBR, along with the production of 1.8 g of bieberite ($CoSO_4 \cdot 7H_2O$) and sulfuric acid above 50% purity.

Keywords: Metal sulfides, cobalt, sulfate-reduction, bioreactor, acid mine drainage, circular process

Introduction

Valuable metals are strategically important for the global economy, as they play a crucial role in many industries that include renewable energy, advanced manufacturing, and modern technologies. The transition to green energy systems, including wind turbines, solar panels, and electric vehicles, requires a stable supply of Critical (and strategic) Raw Materials (CRM) (Andersen et al., 2024).

Among this CRM, cobalt (Co) and nickel (Ni) plays a critical role in Li-NMC cathode materials used in electric vehicle batteries, whereas the Co increases longevity, stability, and corrosion resistance, the Ni improves energy density and storage capacity (Choi et al., 2024; Zhang et al., 2022). Meanwhile, copper (Cu) is a strategic raw material that serves an excellent thermal and electrical conductivity, and is a crucial mineral in automotive, power grid, solar photovoltaic, and bioenergy industries (Song et al., 2024). Similarly, zinc (Zn) is essential in construction, transportation, consumer electronics, and machinery industries (Nan et al., 2024).

These valuable metals are often found in the large amounts of waste generated by traditional mining and resource extraction, which frequently result in severe environmental problems such as Acid Mine Drainage (AMD) (Park et al., 2019). AMD is a highly acidic effluent characterized by low pH values (2–4) and elevated concentrations of metallic species such as iron (Fe), aluminum (Al), and Cu, and metalloids like arsenic (As) and antimony (Sb) and nonmetals like selenium (Se) (Siew et al. 2020, Hermassi et al., 2022). The conventional treatment of AMD typically involves neutralization using alkaline reagents such as lime, limestone, or sodium carbonate. (Lopez et al., 2021), generating large amounts of waste and not efficiently recovering the CRM.

Innovative technologies that enable the efficient recovery of critical metals while minimizing losses and environmental damage are crucial. To address these issues, the Horizon Europe Resilex project introduces an innovative circular treatment process aimed at recovering valuable metals such as Cu, Zn, Co and Ni from AMD, while simultaneously generating sulfuric acid from mining waste.

Materials and Methods

The Resilex technology comprises eight bench-scale units (Fig. 1), forming a circular process to treat acid wastewater and mining wastes from Tharsis mines in the Iberian Pyrite Belt.

The first unit employs a physico-chemical treatment to process acidic wastewater with a pH of 2.5, containing Fe (2 g/L), Al (30 mg/L), SO_4 (5.5 g/L), Cu (50 mg/L), Zn (260 mg/L), Co (5.6 mg/L) and Ni (1.9 mg/L). This unit is capable of treating 25 L/h and operates in two phases: the precipitation of Fe and Al using NaOH (50%), followed by a decantation process. Several experiments were conducted to determine the effect of pH on metal precipitation by raising the pH of AMD samples from 4.0 to 6.0, with a decantation time of 4 hours.

Subsequently, a 20-L anaerobic membrane bioreactor (AnMBR) is employed to produce hydrogensulfide (HS^-) from sulfates (SO_4) and organic substrate. The ultrafiltration (UF) stage is used to treat the bioreactor's product, separating it into two streams: the concentrate, which mainly consists of washed biomass, is circulated back to the bioreactor, and the permeate stream containing the HS^-. The employed tubular membrane in this step is the Berghof MO P13U, which operates with an inflow rate of 10000 L/h and a permeability of about 40 L/(m^2*h).

The produced HS^- is used to precipitate Zn and Cu as metal sulfides in the sulfide precipitation unit. Before operating the bioreactor, lab-scale experiments were conducted using 0.4 L bottles over 20 days to determine the optimal temperature, pH, inoculum-to-substrate (ISR) ratio, Chemical Oxygen Demand (COD)/SO_4 ratio, and the organic substrate for the bioreactor. Olive pomace, glycerinous water, wine residue, and cheese whey were tested as potential substrates (Fig.2). The experiment assessed their biodegradability, sulfate removal efficiency, and maximum H_2S production.

In the next stage of the treatment train, Co and Ni are captured using ion-exchange resins in a two-step process. First, the effluent from the sulfide precipitation reactor is fed into the ion-exchange unit, where metals in the solution are adsorbed to the surface of the resin. Here, the Lewatit® MDS TP 220 resin was selected for this application since it has bis-picolylamine functional groups attached to a styrene/divinylbenzene copolymer that can exchange protons from nitrogen donor atoms with cations such as Co(II) and Ni(II). In the second step, a sulfuric acid (H_2SO_4)

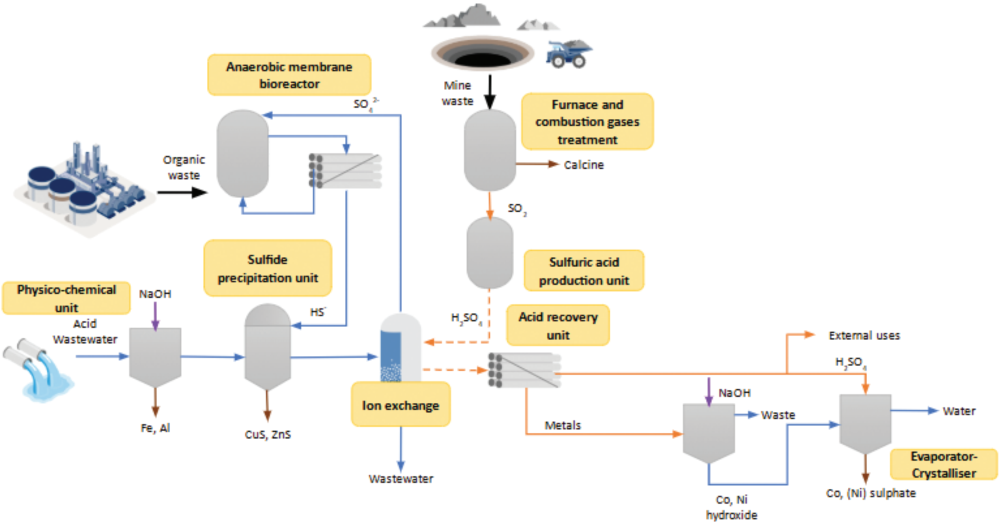

Figure 1 Resilex resource recovery treatment train.

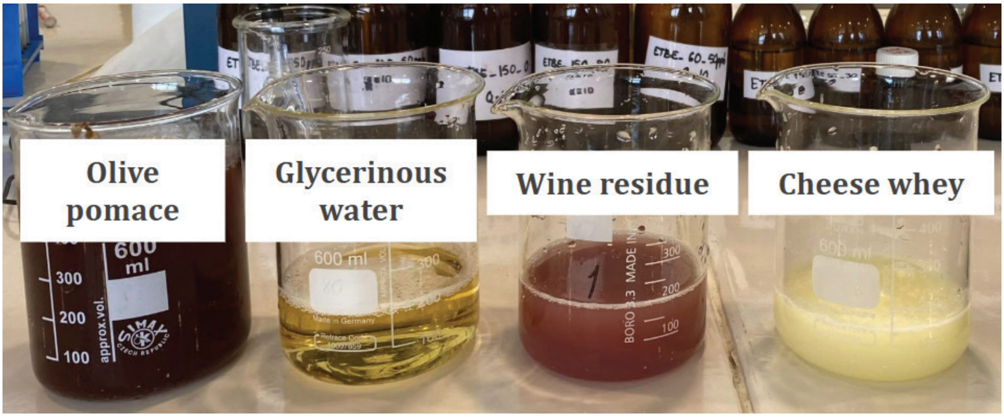

Figure 2 *Tested organic substrates for the AnMBR.*

solution is circulated through the system to desorb the adsorbed metals and regenerate the resin.

This sulfuric acid is produced from mine solid wastes with high sulfur content. The wastes are thermally oxidized in a furnace, and the resulting combustion gases are treated to produce sulfur dioxide. This sulfur dioxide is then oxidized to sulfur trioxide, using oxide beads as a catalyst, and subsequently dissolved in water through the contact process to obtain sulfuric acid.

Next, a nanofiltration (NF) membrane is employed to recover H_2SO_4 from the resin regeneration eluate using NF2540F30 Duracid membranes from Veolia WTS. These membranes are capable of operating at extremely low pH levels (as low as 0) and exhibit a positive surface charge at pH values below 4.3, making them highly suitable for the acid recovery unit. During this process, Ni and Co are concentrated in the rejected stream, while bisulfate (HSO_4^-) is recovered in the permeate and can be reused for other applications.

In the final stage, Co and Ni are precipitated as hydroxides by adding NaOH to increase the pH of the concentrate solution. The resulting hydroxide sludge is redissolved with sulfuric acid and sent to the evaporator-crystallizer, where the metals are recovered as bieberite ($CoSO_4{\cdot}7H_2O$), for market reintroduction. Preliminary simulations with PHREEQC (version 3) chemical reaction code (Parkhurst and Apello, 2013), employing the Thermoddem_V1 BRGM database (BRGM, 2012) were employed to determine the amount of NaOH to be added and the extent of the Co precipitation depending on the amount of evaporated water.

Results and discussion

The bench-scale units are currently operational and undergoing optimization of their parameters to identify the most effective settings. Below is a detailed explanation of the results obtained so far and the expected outcomes for each water treatment stage.

Physico-chemical unit

In the pH tests, iron precipitation achieved up to 99% removal across all pH levels. Aluminum also exhibited a high removal percentage reaching 70 ± 10% at pH 4.5, 97 ± 2% at pH 5, and 99% at pH 5.5 (Fig. 3). This aligns with the findings of Seo et al. (2017), who found that Fe and Al precipitated within pH ranges of 3.5–7.5 and 3.5–5.5, respectively, with concurrent precipitation around pH 4.5.

On the other hand, Co, Ni, Zn, and Cu exhibited increased precipitation with rising pH levels. Co and Ni showed minimal precipitation at pH levels of 4.5–5 but increased at higher pH levels, with Co rising from 3% at pH 4.5–5 to 11% at pH 5.5 and 21% at pH 6. Ni increased from 8% to 36% at higher pH levels. Similarly, Zn and Cu demonstrated enhanced removal; Zn's removal increased from 19% to 60%, corresponding to a decrease in concentration from 293 mg/L to 119 mg/L, respectively.

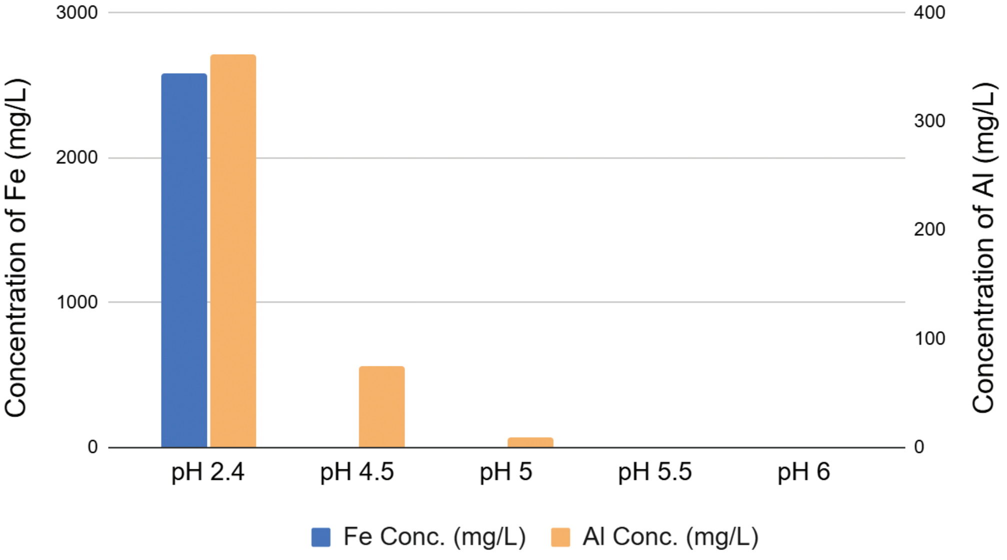

***Figure 3** Precipitation test of Fe and Al depending on pH.*

Cu exhibited the highest sensitivity to pH changes, with removal rates increasing from 45% to 99% (from 50 mg/L at pH 4.5 to 0 mg/L at pH 6).

AnMBR and sulfide precipitation unit

The lab-scale experiments determined that the optimal conditions for the anaerobic bioreactor were a temperature of 32 °C, a COD/SO4 ratio of 3.5 g/g, a pH of 7, and an inoculum-to-substrate ratio of 2 g VS (volatile solids)/g VS. Furthermore, cheese whey, with a COD of 103.4 g/L, has been identified as the most effective substrate for HS^- production in the AnMBR (Tab. 1). Blandón et al. (2014) stated that cheese whey is the most efficient substrate for achieving high biogas production levels in a shorter time. Similarly, López-Aguilar (2021), a controlled anaerobic digestion process, using animal feces sludge and cheese whey, reported that the H_2S concentration in the biogas exceeded 9,000 mg/L from day 39.

Currently, the AnMBR is in the initial phase of its operation. The initial estimated hydraulic retention time inside the bioreactor is 20 h. However, this is going to be optimised during the operation to maximise hydrosulfide production.

The HS^- produced is used to precipitate Zn and Cu as metal sulfides, enabling up to 90% removal of Cu and Zn. This process is expected to yield up to 6.4 g of CuS and 34.7 g of ZnS per 100 L of feed water.

Ion Exchange unit

Based on the literature and the resin provider's specifications, the resin is expected to remove 96–99% of Co, Ni from the eluent solution (0.004 g/L for Co and 0.001 g/L for Ni). Meanwhile, the outlet stream is expected to be mainly composed of desorbed metal

***Table 1** Organic substrate COD and biodegradability, sulfate removal and HS^- production in lab-scale experiments.*

	COD (g/L)	Biodegradability (%)	Sulfate removal (%)	Maximum H_2S production (mg/L/day)
Olive pomace	206.2	25.4	0.3	<0.1
Glycerinous water	98.4	23.9	32.2	9.2
Wine Residue	149.5	23.7	50.7	22.4
Cheese whey	103.4	55.9	78.5	52.3

ions, which are concentrated up to 3 g/L for Co, and 1 g/L for Ni, along with sulfuric acid.

Caján and Hoxana (2020) published a study evaluating the effectiveness of ion exchange in recovering Ni and Cu from acidic industrial wastewater. They concluded that at a pH between 2 and 4.5, recoveries of up to 100% for Ni and 99.81% for Cu were achievable. Botelho et al. (2019), who employed Lewatit® TP 220 resins for metal recovery, also demonstrated that the resins are effective in recovering Co and Ni, depending on the operating pH.

Furnace and sulfuric acid production unit

Solid mining waste is subjected to thermal valorization at elevated temperatures, yielding sulfuric acid with a purity exceeding 50% (w/w), which is comparable to the purity levels achieved with sulfuric acid synthesized from synthetic reagents. At industrial scales, this process is expected to release between 0.1 and 0.15 MWh/t of energy, which can be used either through a turbine connected to an electric generation or thermally to heat other fluids. The resulting acid is subsequently utilized for resin regeneration.

Acid recovery unit

The resin regeneration solution is treated using nanofiltration membranes, resulting in a final rejected solution with expected concentrations of up to 6 g/L Co(II) and 2 g/L Ni(II). Meanwhile, the permeate solution contains a bisulfate concentration of 180 g/L. This process is expected to achieve a two-fold concentration of both Co and Ni.

Evapo-Crystallizer

Given that the initial solution has a pH of 0.5 and contains up to 6 g/L Co and 2 g/L Ni, NaOH is initially added to the concentrated solution from the acid recovery unit to increase the pH to 12, resulting in the precipitation of dissolved Ni and Co as hydroxides. PHREEQC simulations indicate that 1.2 mol/L NaOH is required to achieve complete precipitation of both Co and Ni hydroxides. Subsequently, the metal hydroxide sludge, generated in the decanter tank, is redissolved using sulfuric acid, and the resulting solution is directed to the evaporator-crystallizer. Preliminary calculations suggest that, at this stage, only Co precipitates as bieberite ($CoSO_4·7H_2O$), while Ni, in the form of $NiSO_4·7H_2O$, is expected to remain undersaturated. This process is expected to yield up to 1.8 g of bieberite per 100 L of feed water.

Economic Assessment

From an economic perspective, the process requires an initial capital expenditure (CAPEX) between 950 and 1600 €/m^3/d, which includes all the bench-scale units and their integration into the complete system. The preliminary operational expenditure (OPEX) ranges between 3.6 and 6.0 €/m^3 feed, encompassing costs associated with energy consumption, chemical reagents and maintenance. While process optimization is still ongoing, the economic assessment suggests that selling recovered products can generate profit exceeding OPEX, making the recovery process economically sustainable. These economic aspects are currently under detailed evaluation.

Conclusions

The Horizon Europe Resilex project presents an innovative approach to recover CRM from AMD, integrating multiple technologies into a circular process. Currently, the pilot system is in the operational and optimization phase, with ongoing improvements aimed at maximizing metal recovery efficiency and ensuring the long-term viability of the process. First results in the physico-chemical unit showed that the pH 4.5 is optimal to efficiently remove 99% of Fe and 70% of Al, while avoiding losing valuable metals. In the whole process, it is expected to recover up to 6.4 g of CuS and 34.7 g of ZnS per 100 L of feed water in the AnMBR, along with the production of 1.8 g of bieberite ($CoSO_4·7H_2O$) and sulfuric acid above 50% purity.

Acknowledgements

This research has been conducted with the financial support of the EU through the Horizon Europe programme (HORIZON-CL4-2021-RESILIENCE-01 101058583 RESILEX).

References

Andersen EV, Shan Y, Bruckner B, et al (2024) The vulnerability of shifting towards a greener world: The impact of the EU's green transition on material demand. Sustainable Horizons 10:100087. https://doi.org/10.1016/j.horiz.2023.100087

Blandón Navarro SL, Zelaya Lanuza DS, Arranz Ramírez JC, Zamora Calero JA (2014) Evaluación de la producción de biogás a partir de suero lácteo a escala de laboratorio. Higo 4:29–35. https://doi.org/10.5377/elhigo.v4i1.8633

Botelho AB Junior, Espinosa DCR, Dreisinger D, Tenório JAS (2019) Effect of pH to recover Cu (II), Ni (II) and Co (II) from nickel laterite leach using chelating resins. Tecnol Metal Mater Min 16:135–140. https://doi.org/10.4322/2176-1523.20191575

BRGM. (2012). Phreeqc. Thermoddem. https://thermoddem.brgm.fr/databases/phreeqc

Caján S, Hoxana S (2020). Influencia del caudal de un drenaje ácido de mina sobre la remoción de metales pesados utilizando resinas de intercambio iónico (pp. 1–80).

Choi K., Jang J, Bedrossian S (2024) Impact of Impurities on Nickel Sulfate Crystallization and Strategies for Removal: Advancing Towards Battery-Grade Nickel Sulfate Production. Manuscript. Industrial & Engineering Chemistry Research

Hermassi M, Granados M, Valderrama C, et al (2022) Recovery of rare earth elements from acidic mine waters: An unknown secondary resource. Sci Total Environ 810:152258. https://doi.org/10.1016/j.scitotenv.2021.152258

López J, Gibert O, Cortina JL (2021) Evaluation of an extreme acid-resistant sulphonamide based nanofiltration membrane for the valorisation of copper acidic effluents. Chem Eng J 405:127015. https://doi.org/10.1016/j.cej.2020.127015

López-Aguilar H, Barrón A, Franco M, et al (2021) Modelación de la generación de metano a partir de suero lácteo y excreta de ganado en codigestión anaerobia. Nova Sci 13:. https://doi.org/10.21640/ns.v13i27.2791

Nan T, Yang J, Aromaa-Stubb R, et al (2024) Extracting valuable metals from zinc sulfide concentrate: A comprehensive simulation-based life cycle assessment study of oxidative pressure leaching. Miner Eng 216:108888. https://doi.org/10.1016/j.mineng.2024.108888

Park I, Tabelin CB, Jeon S, et al (2019) A review of recent strategies for acid mine drainage prevention and mine tailings recycling. Chemosphere 219:588–606. https://doi.org/10.1016/j.chemosphere.2018.11.053

Parkhurst DL, Appelo CAJ (2013) Description of input and examples for PHREEQC version 3: A computer program for speciation, batch-reaction, one-dimensional transport, and inverse geochemical calculations. Techniques and Methods. https://doi.org/10.3133/tm6a43

Seo EY, Cheong YW, Yim GJ, et al (2017) Recovery of Fe, Al and Mn in acid coal mine drainage by sequential selective precipitation with control of pH. Catena 148:11–16. https://doi.org/10.1016/j.catena.2016.07.022

Siew YW, Zedda KL, Velizarov S (2020) Nanofiltration of simulated acid mine drainage: Effect of pH and membrane charge. Appl Sci (Basel) 10:400. https://doi.org/10.3390/app10010400

Song Y, Bai W, Zhang Y (2024) Resilience assessment of trade network in copper industry chain and the risk resistance capacity of core countries: Based on complex network. Resour Policy 92:105034. https://doi.org/10.1016/j.resourpol.2024.105034

Zhang J, Said A, Han B, Louhi-Kultanen M (2022) Semi-batch evaporative crystallization and drying of cobalt sulphate hydrates. Hydrometallurgy 208:105821. https://doi.org/10.1016/j.hydromet.2022.105821

As, Sb And Aulfate Immobilization From Flotation Tailings Of An Intrusion-Related Gold Mineralization

Rodrigo Álvarez[1], José Manuel Domínguez[2], Almudena Ordóñez[1], Jorge Loredo[1], Isidro Diego[1]

[1]*University of Oviedo, Gonzalo Gutierrez Quirós, 33600 Mieres, Asturias, Spain, alvarezrodrigo@uniovi.es, ORCID 0000-0002-2651-1103; aoalonso@uniovi.es, ORCID 0000-0002-0055-1828; jloredo@uniovi.es, ORCID 0000-0001-5381-7100; diegoisidro@uniovi.es, ORCID 0000-0003-1554-4679*

[2]*Exploraciones Mineras del Cantábrico, Santa Susana St, 43, 1ºC, 33007 Oviedo, Asturias, Spain, jose.dominguez@blackdragongold.com*

Abstract

The Salave Gold Prospect is the largest unexploited and well-known gold deposit in Spain. Gold occurs almost exclusively as refractory and invisible, within the arsenopyrite crystal structure. During the closure phase, it is expected that about 2 Mt of flotation tailings (~0.1% of sulfides) will have to be allocated in an isolated dam. To assess best option to stabilize these tailings in the long-term, some leaching tests have been performed over mixtures of tailings with different binding materials. The optimum behaviour in terms of contaminant immobilization was reached by the addition of 5%(wt) Portland cement, 5% quicklime and 1% limestone filler. The release of As and Sb decreased by 98.37% and 94.68%, respectively, while sulfate release is below 5 mg/L.

Keywords: Flotation tailings management, Arsenic, Antimony, Sulfate, Leachability.

Introduction

Most of the gold-bearing ores currently being mined must undergo -before hydrometallurgy- a mineral separation process called flotation. This process usually produces a sulfide-rich concentrate containing the gold and a tailings fraction composed of milled mineral particles of the host rock, typically silicates, carbonates, or a mixture of both. While the sulfide concentrates proceed to cyanide leaching, the tailings are usually stored in engineered tailings facilities, where they accumulate until mine closure or are repurposed for backfilling mine voids using cemented paste backfilling (CPB) technology. If reuse is not feasible, flotation tailings must be properly stabilized and neutralized to prevent long-term environmental impacts

Experimental studies on the stabilization of this type of tailings, based on published data (Choi *et al.* 2009; Coussy *et al.* 2011, 2012; Kiventera *et al.* 2018, 2019; Hamberg *et al.* 2015; Tariq and Yanful 2013, among others), suggest the use of various binding materials to effectively immobilize the elements of concern present in the tailings. Ordinary Portland cement, often combined with different additives, is the most used material. The recommendations for mine sludge management outlined by the European Commission in the Best Available Techniques (BATs, Garbarino *et al.* 2018) are aligned with the findings of these studies.

The tailings used in this study come from the pilot-scale froth flotation of gold ore from the Salave gold prospect. This mineralization is considered among the most important in Europe that has yet to be exploited (measured resources are more than 1 Moz Au at 4.6 g Au/tonne). Although numerous exploration campaigns have been conducted since the 1970s, scientific literature on this mineralization is scarce, being the work of Rodríguez-Terente *et al.*. 2018 the most valuable contribution. Gold-mineralization is hosted by a variscan subalkaline and hyperpotassic granodiorite (I type granite) affected by a late hydrothermal episode. This hydrothermal activity has intensely affected the host rock, resulting in significant albitization, chloritization, and sericitization. The paragenetic sequence of the mineralization is dominated by arsenopyrite and pyrite, with appreciable amounts of molybdenite and stibnite, and occasional presence of chalcopyrite, sphalerite, berthierite and rutile. Gold is essentially refractory and is associated with sulfides, primarily arsenopyrite.

Considering the above cited background, and as a first step in developing the most effective stabilization strategy for these tailings, several preliminary tests were conducted using different concentrations of Portland cement (PC, Portland cement without additives or CEM I), quicklime and blast furnace slag (BFS) as stabilizers. These initial mixtures were analysed for mechanical properties, permeability, and leaching behaviour.

Methods

The proportional distribution of the various mineral species, along with the chemical composition and the particle size distribution of the tailings must be thoroughly analysed to design a stable tailings storage facility for long-term storage of tailings.. Grain size distribution curves were obtained by Static Light Scattering with a Laser (λ=520 nm) Particle Sizer Analyssete 22 Nano Tec Plus (FRITSCH) following the standard ISO 13320. Major elements composition was determined by Wavelength-Dispersive X-Ray Fluorescence (WDS-XRF) with a Philips PW2404 spectrometer. Minor and trace elements of the solid tailings bulk sample were assessed by Inductively Coupled Plasma Optical Emission Spectroscopy (ICP-OES, Agilent 5800 instrument). Mineralogical composition was evaluated by means of X-Ray Diffraction (XRD) using a Seifert XRD 3000 T/T Diffractometer. Energy-Dispersive X-Ray Fluorescence (ED-XRF, Inca Energy 350 module from Oxford) coupled to a Scanning Electron Microscope (SEM) was used for grain scale chemical analyses. Permeability determinations were carried out at PanTerra Geoconsultans using a digital nitrogen permeameter following the methodology described in Zhang *et al.* (2013). Leaching tests were performed according to European standards EN-12457:4 (dynamic leaching) and EN-15863 (static leaching). The filtrate resulting from these tests was analysed for the substances indicated in the Spanish Regulations for surface water quality (RD 817/2015): As, Sb, Ba, Cd, Cu, Cr, Sn, Mo, Ni, Pb, Se and Zn were analysed by Inductively Coupled Plasma Mass Spectrometry (ICP-MS) and SO_4^{2}-, F-and Cl- were analysed by Ionic Chromatography. Hg was quantified by Cold Vapour Atomic Absorption Spectrometry (CV-AAS).

Results and Discussion

Grain size distribution

As can be seen in Fig. 1, the frequency distribution of tailings particles sizes (diameters) indicates a trimodal set of measurements: there is a first mode at 10 µm, a second one at around 50 µm – which is the dominant particle size – and another one, less important, at 250 µm. D_{10} is 4.3 µm, D_{50} is 29.8 µm and D_{90} is 88.2 µm.

Chemical composition and mineralogy

XRD results show that, from a mineralogical point of view, the tailings are mainly composed by Na-rich plagioclase (albite-oligoclase) and muscovite, followed by moderate proportions of dolomite, quartz and orthoclase. Small amounts of clinochlore and sulfides can also be identified. As expected, major element composition is dominated by Si and Al. Among the alkalis, Ca and K are predominant. Calcium is primarily associated with dolomite and, to a lesser extent, with plagioclase, while K is almost entirely derived from K-feldspar. Magnesium concentrations are also high, largely due to dolomite. The predominance of muscovite among the micas contributes to relatively low Fe concentrations. Concerning trace elements, the micro-analyses carried out by ED-XRF coupled to a SEM pointed out that As and Sb appear in the form of very small particles (2-10 µm) of sulfides (stibnite and arsenopyrite) and sulfosalts.

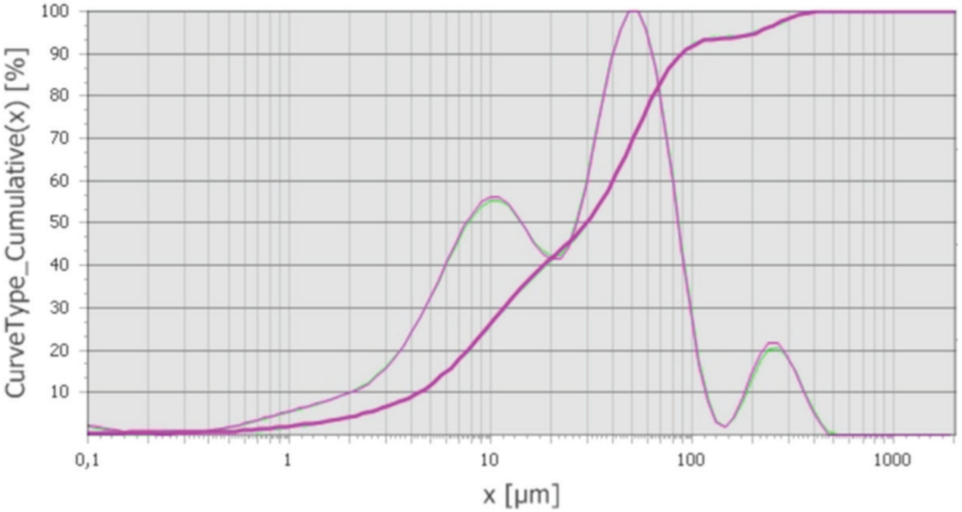

Figure 1 *Grain size distribution curve of the flotation tailings.*

Table 1 *Composition (major, minor and trace elements) of the flotation tailings.*

Oxides	Weight %	Element	mg/kg
SiO_2	54.16	As	1098
$Al2O_3$	18.38	Sb	83.6
$FeO+Fe_2O_3$	2.60	Cd	<5
MnO	0.10	Cu	32.2
MgO	3.49	Cr	11.9
CaO	4.70	Hg	<10
Na_2O	2.53	Mo	6.4
K_2O	4.41	Ni	<5
TiO_2	0.54	Pb	28.5
P_2O_5	0.20	Se	<10
Loss On Ignition	8.70	Zn	<50

Permeability and Leaching tests

Permeability and leaching tests are usually used to assess the behaviour of flotation/mine tailings that are going to be deposited in an on-land tailings impoundment after the closure of mining activities. The final disposal of this type of waste is typically achieved using a binding agent that, when properly dosed, ensures both physical and chemical stabilization of the tailings. A review of the existing scientific literature indicates that the most suitable binding agents include geopolymers, cement, quicklime and blast furnace slag. To evaluate the most suitable option among the available alternatives, a series of specimens (18 units, 160 × 40 × 40 mm) were initially prepared using Portland cement, lime and blast furnace slag as binders for the tailings, at dosages of 5% and 10% (dry weight), which are typical in such cases. The preparation of the test specimens was carried out in stainless steel molds with a longitudinal tolerance of 0.2 mm. In all cases, the specimens were demolded after 7 days of curing, with the specimens made with lime/quicklime being air-dried and those made with cement being cured in a humidity chamber at 25°C. The curing time to assess permeability in these mixtures was set at 28 days. The results are shown in Table 2 (air permeability for untreated tailings was not determined, as it depends on the degree of compaction):

As can be seen in Table 2, the reduction in water permeability – when comparing with the untreated tailings – is high in all cases, with the best values provided using PC as binding material. The reduction in permeability is not very significant (~1%, from 94.09 to 95.11) between a 5% and a 10% of PC dosage.

Leaching tests were conducted in dynamic mode (standards EN-12457:4 and

Table 2 *Results of the permeability tests conducted on the different binding materials considered.*

Sample(dosification)	**Air permeability** (mD)	**Water permeability (hydraulic conductivity, m/day)**	**Reduction (%)**
5% Quicklime	14.5	0.01064	82.26
10% Quicklime	6.95	0.00509	91.52
5% PC	4.84	0.00354	94.09
10% PC	4.00	0.00293	95.11
5% Lime+BFS	9.42	0.00689	88.51
10% Lime+BFS	10.6	0.00778	87.03
Tailings (without stabilization)		0.06	

Table 3 *Results of* ***the*** *dynamic leaching tests (DOC: Dissolved Organic Carbon; TDS: Total Dissolved Solids).*

Parameter	**Units**	**Tailings**	**7 d**	**28 d**	**Reduction (7 d)**	**Reduction (28 d)**	**Threshold**
pH (25C)		8.92	12.53	12.62			
Cl-	mg/L	<50	<50	<50.0			
F-	µg/L	<1.0	3.2	5.2			1500
Sulfate	mg/L	52.7	<5	<5	>90,51%	>90,51%	
COD	mg/L	<150	<150	<150			
TDS	mg/L	<1000	15890	15020			
Sb	µg/L	0.94	0.21	<0.05	77,66%	>94,68%	
As	µg/L	2.7	0.06	<0.05	97,77%	>98,14%	50
Ba	µg/L	<0.05	4.4	4.3			
Cd	µg/L	<0.01	<0.01	<0.01			
Cu	µg/L	<0.05	<0.05	<0.05			5
Cr	µg/L	<0.05	0.13	0.30			50
Sn	µg/L	<0.05	<0.05	<0.05			
Hg	µg/L	<0.0010	<0.0010	<0.0010			0.07
Mo	µg/L	0.16	0.28	<0.10		>37,5%	
Ni	µg/L	<0.05	<0.05	<0.05			20
Pb	µg/L	<0.05	0.09	0.06			7.2
Se	µg/L	<0.05	<0.05	<0.05			1
Zn	µg/L	<0.50	<0.50	<0.50			30

EN-15863, respectively), using the same mixtures evaluated in the permeability tests. The achieved reductions in the mobilization of As and Sb ranged between 80% and 95%, respectively, with PC being the most effective binding material for metals and metalloids. In contrast, quicklime demonstrated better performance in mitigating sulfate leaching. The reductions observed after 28 days of curing were consistently greater than those at 7 days, except in the case of Pb, where some tests showed higher reductions at 7 days.

Several studies have specifically investigated Pb immobilization in mining waste, concluding that its mobility can be minimized through calcium carbonate amendments (Martínez-Sánchez *et al.* 2014; Yun and Yu 2015) or treatment with H_3PO_4 (Navarro *et al.* 2011). Based on these findings, the proposed final mixture for large-scale implementation during mine closure consists of 5% PC, 5% quicklime and an additional 1% of limestone filler. This formulation combines the effectiveness of PC in immobilizing As and Sb with the sulfate-stabilizing properties of quicklime, while the limestone filler helps to improve the retention of Pb. The results obtained with this mixture are presented in Table 3, which includes data from untreated tailings, treated tailings at 7 and 28 days of curing, and the regulatory limit values established by Spanish legislation for these leachates. It is noteworthy that there are no threshold values for leachate pH. Nitrogen species are not considered, as the original material (flotation tailings) has not been subjected to cyanidation.

As observed in the previous Table (3), the proposed binding mixture (5% PC + 5% quicklime + 1% limestone filler) meets the environmental quality standards for surface water established in RD 817/2015 under the experimental conditions of the standard. The retention of As exceeds 98%, while that of Sb surpasses 94%. These values represent minimum estimates, considering that As and Sb were undetectable with the analytical technique used. Static leaching test (EN-15863) results, not presented here, are in no case worse than that of dynamic leaching test (EN-12457:4, Table 3). On the other hand, there are some elements whose mobility increases with the stabilization treatment. While the increases in pH and TDS can be easily explained by the binding material used and the conditions of the leaching test, there is no obvious explanation for the increase in Ba and Cr content in the leachates after applying the stabilizing agents to the tailings, as both elements are considered to be more mobile at low pH values.

PC, as a raw material, is cheaper than BSF or quicklime. From an environmental standpoint, the use of BSF would be more interesting since it is a recycled waste product. However, the better performance of PC in terms of stabilizing tailings should be a key selection criterion.

It is also important to highlight that the tailings, without any treatment (Table 3), meet the threshold values for surface water quality. In any case, the competent environmental authority points out the need to design, with proper justification, a stabilization treatment for the disposal of the tailings in a final storage facility. In the specialized literature, it is stated that, in general terms, the behavior of the tailings-PC or tailings-quicklime mixtures usually improves in the long term, concerning contaminant immobilization. In the Salave project, a long-term monitoring system will be implemented (starting from the beginning of the activity) to detect and address a potential increase in the levels of metals, metalloids, and sulfates in the leachates. The addition of the binder mix (PC + quicklime + limestone filler) to the tailings will be done at the end of the exploitation's life, and only if the tailings cannot be reused in any way

Conclusions

The tailings from the flotation process during the operational life of the Salave mine will consist of fine particles (90% smaller than 88.2 µm) and are expected to contain approximately 1000–1100 mg/kg of As and 80–90 mg/kg of Sb, in the form of arsenopyrite and stibnite, respectively.

To prevent the mobilization of these metalloids and the generation of sulfate-rich leachates at a future final disposal site, some leaching tests have been conducted using Portland cement (PC), quicklime and blast furnace slag (BFS) as binding materials. All these materials have shown good performance; however, PC exhibits the highest retention capacity for As and Sb, while quicklime is more effective in retaining sulfates. The most impermeable mixture is also achieved with PC. BFS provides the best mechanical properties, although in this case, they are of lower priority.

Using a mixture of 5% PC + 5% quicklime + 1% limestone filler, the reductions in sulfate, As, and Sb leaching exceed 90% after 28 days of curing. Additionally, the leachates obtained in the dynamic test EN-12457:4 comply with Spanish environmental quality standards for surface waters.

Acknowledgements

The authors thank all co-organisers for hosting the IMWA 2025 Conference. The authors wish also to express their gratitude to Exploraciones Mineras del Cantábrico SL for allowing the publication of the results presented in this study.

References

Choi WH, Lee SR. Park, JY (2009) Cement based solidification/stabilization of arsenic-contaminated mine tailings. Waste Manage, 29: 1766-1771. DOI: 10.1016/j.wasman.2008.11.008.

Coussy S, Benzaazoua M, Blanc D, Moszkowicz P, Bussiere, B (2011) Arsenic stability in arsenopyrite-rich cemented paste backfills: a leaching test-based assessment. J Hazard Mater, 185: 1467-1476. DOI: 10.1016/j.jhazmat.2010.10.070.

Coussy S, Benzaazoua M, Blanc D, Moszkowicz P, Bussiere, B (2012) Assessment of arsenic immobilization in synthetically prepared cemented paste backfill specimens. J Environ Manage, 93: 10-21. DOI: 10.1016/j.jenvman.2011.08.015

Garbarino E, Orveillon G, Saveyn H, Barthe P, Eder, P (2018) Best Available Techniques (BAT) reference document for the management of waste from extractive industries in accordance with Directive 2006/21/EC, EUR 28963 EN. Publications Office of the European Union, 692 p. DOI:10.2760/35297

Hamberg R, Maurice C, Alakangas C (2015) The use of low binder proportions in cemented paste backfill. Effects on As-leaching. Miner Eng, 78: 74-82. DOI: 10.1016/j.mineng.2015.04.017

Kiventera J, Sreenivasan H, Cheeseman C, Kinnunen P, Illikainen M (2018) Immobilization of sulfates and heavy metals in gold mine tailings by sodium silicate and hydrated lime. J Environ Chem Eng, 6(5): 6530-6536. DOI: 10.1016/j.jece.2018.10.012

Kiventera J, Piekkari K, Ister V, Ohenoja K, Tanskanen P, Illikainen M (2019) Solidification/stabilization of gold mine tailings using calcium sulfoaluminate-belite cement. J Clean Prod, 239: 118008. DOI: 10.1016/j.jclepro.2019.118008

Martínez-Sánchez MJ, García-Lorenzo ML, Pérez-Sirvent C, González E, Pérez V, Martínez S, Martínez L, Molina J (2014) Heavy metal immobilisation by limestone filler in soils contaminated by mining activities: Effects on metal leaching and ecotoxicity. Intl J Min Reclam Env, 28(6), 414–425. DOI: 10.1080/17480930.2014.967919

Navarro A, Cardellach E, Corbella M (2011) Immobilization of Cu, Pb and Zn in mine-contaminated soils using reactive materials. J Hazard Mater, 186(2–3): 1576-1585. DOI: 10.1016/j.jhazmat.2010.12.039.

Rodríguez-Terente LM, Martin-Izard A, Arias D, Fuertes-Fuente M, Cepedal A (2018) The Salave Mine, a Variscan intrusion-related gold deposit (IRGD) in the NW of Spain: Geological context, hydrothermal alterations and ore features. J Geochem Explor, 188: 364-389. DOI: 1016/j.gexplo.2018.02.011

Tariq A, Yanful EK (2013) A review of binders used in cemented paste tailings for underground and surface disposal practices. J Environ Manage, 131: 138-149. DOI: 10.1016/j.jenvman.2013.09.039

Yun SW, Yu C (2015) Immobilization of Cd, Zn, and Pb from soil treated by limestone with variation of pH using a column test. J Chem-NY, 641415. DOI: 10.1155/2015/641415

Zhang X, Spiers CJ, Peach CJ, Hebing A (2013) Tight rock permeability measurement by pressure pulse decay and modelling. Proceedings of the Int Symp of the Society of Core Analysts, Nappa Valley, California, USA, SCA2013-010, p. 1-12

Exploring the Potential of Hydrochar for the Removal of Toxic Metals from Mining-Influenced Waters: A Case Study on Arsenic

Álvaro Amado-Fierro[1], Antonio Luis Marqués Sierra[2], Begoña Fernandez[3], Julia Ayala[4],
Teresa A. Centeno[5]

[1]Carbon Science and Technology Institute (INCAR), CISC, Francisco Pintado Fe 26, 33011, Oviedo, Spain, alvaro.af@incar.csic.es, ORCID 0000-0002-2851-2169

[2]Institute of Space Sciences and Technologies of Asturias (ICTEA), University of Oviedo, Independencia 13, 33004 Oviedo, Asturias, Spain, marquesantonio@uniovi.es, ORCID: 0000-0003-4665-4491

[3]University of Oviedo, Gonzalo Gutierrez Quirós, 33600 Mieres, Asturias, Spain, fernandezbegona@uniovi.es, ORCID 0000-0003-1239-4839

[4]University of Oviedo, Gonzalo Gutierrez Quirós, 33600 Mieres, Asturias, Spain, jayala@uniovi.es, ORCID 0000-0002-6404-1296

[5]Carbon Science and Technology Institute (INCAR), CISC, Francisco Pintado Fe 26, 33011, Oviedo, Spain, teresa@incar.csic.es, ORCID 0000-0002-2851-2169

Abstract

The contamination of water sources by potentially hazardous elements (PHEs), especially in mining areas, poses serious environmental and health risks. This study investigates the potential of waste-derived hydrochar – a carbonaceous material produced via hydrothermal carbonisation (HTC – for the removal of arsenic (As) from mining-influenced waters.

Hydrochar's surface chemistry, rich in functional groups, enables the adsorption of various contaminants. Hydrochars derived from different biodegradable feedstocks (e.g., wood waste, green waste, municipal solid waste, grape bagasse) were produced at pilot scale and evaluated for their As adsorption capacity.

Batch experiments using synthetic As solutions assessed the performance of four hydrochars under varying pH conditions. Although none effectively removed As, the results highlighted factors such as surface charge, feedstock type, and pH as critical for adsorption performance.

Despite the limited removal in this preliminary study, hydrochar shows promise as a low-cost, sustainable adsorbent. With further optimisation—such as surface functionalisation—it could be integrated into passive treatment systems (e.g., constructed wetlands or reactive barriers) for remediation of mining-impacted waters.

Keywords: Hydrochar, Potentially Hazardous Elements (PHEs), Arsenic

Introduction

The contamination of water sources by potentially hazardous elements (PHEs) poses a substantial threat to ecosystems and public health, particularly in regions with intensive mining activity. Among these contaminants, arsenic (As) stands out due to its toxicity, mobility in aquatic systems, and longevity in the environment. Its presence in surface and groundwater originates from both natural and anthropogenic sources, including the leaching of mining waste, the oxidation of sulfides, and acid mine drainage (Ramos Ramos *et al.* 2014; Quino Lima *et al.* 2021).

Conventional techniques for PHE removal include physicochemical processes such as chemical precipitation, reverse osmosis, ion exchange, and ultrafiltration. However, these methods often present limitations in terms of operational costs, secondary waste generation, and removal efficiency in complex matrices (Ayala and Fernández 2019a; Sun *et al.* 2022). In this context, the development of sustainable and low-cost adsorbents has gained considerable interest as a viable alternative for remediating contaminated water.

Hydrochar, a carbonaceous material obtained through hydrothermal carbonisation (HTC) of residual biomass, has emerged as a promising solution due to its high porosity and abundance of oxygenated functional groups (carboxyl, hydroxyl, and carbonyl) (Akkari *et al.* 2024; Khanzada *et al.* 2024). This functional group richness is one of the key factors enhancing the adsorption capacity of PHEs. Unlike biochar, which is produced by pyrolysis, hydrochar is obtained at lower temperatures under wet conditions, allowing for better utilisation of high-moisture biomass, such as grape bagasse, municipal solid waste, and discarded wood residues (Nadarajah 2020).

Recent studies have demonstrated that the functionalisation of hydrochar through chemical or physical activation can enhance its adsorption capacity, optimising its performance in the removal of metal contaminants (Nadarajah 2020). In particular, modification with alkaline agents or impregnation with metal oxides has been shown to improve interactions with As species in aqueous solutions (Nadarajah 2020).

This study evaluates the efficiency of hydrochar derived from various biomasses for As removal under laboratory-scale and pilot-scale conditions. The adsorption capacity and As capture mechanisms are analysed, providing a detailed framework for future research on its application in mine water remediation and integration into passive treatment systems such as constructed wetlands and permeable reactive barriers. The results obtained suggest that hydrochar could play a key role in the development of innovative and sustainable strategies for water purification and the mitigation of environmental impacts in mining areas.

Materials and Methods

In this study, four types of hydrochar were produced via hydrothermal carbonisation (HTC) at 200 °C for 4 hours under autogenous conditions in the reactor shown in Fig. 1, located at the Spanish National Research Council (CSIC) facility in COGERSA (Consortium for the Management of Solid Waste in Asturias).

The first, hydrochar from wood with water (MH), was produced from shredded wood waste using water as the reaction medium. The second, hydrochar from wood with whey (LM), was obtained by using whey instead of water to assess the effect of an organic medium on the material's structure. Additionally, bio-stabilised hydrochar (BIOEST) was used, derived from the bio-stabilised organic fraction of municipal solid waste, along with a paper–cardboard hydrochar (PC), generated from paper and cardboard waste previously soaked in water.

The materials were crushed and sieved to obtain particles smaller than 250 µm, ensuring an adequate surface area for adsorption experiments (Ayala & Fernández, 2023).

To evaluate the adsorption capacity of the hydrochars, a synthetic As solution was prepared at a concentration of 900 µg/L As.

Figure 1 Reactor for hydrochar production utilising the residual steam flow from the electricity generation of the hospital waste incinerator at COGERSA (image: Álvaro Amado-Fierro).

This solution was obtained by dissolving $Na_2HAsO_4{\cdot}7H_2O$ in deionised water and adjusting the pH to 3, 4, 5, and 6 by adding H_2SO_4 or NaOH (0.01 and 0.1 M), following standardised protocols for As adsorption studies (Ayala and Fernández 2019b, c).

Each working solution was prepared and stored in sealed glass bottles to prevent pH variations before the adsorption experiments.

The adsorption experiments were conducted in a batch system using 100 mL polyethylene flasks, which were placed on a mechanical shaker to ensure homogeneous mixing of the solution. In each experiment, 10 g/L of hydrochar was added to 50 mL of contaminated solution and left in contact for 24 hours at a temperature of 25 ± 2 °C, with a constant stirring speed of 175 rpm. After the contact time, the samples were filtered, and the supernatant was analysed by ICP-MS to determine the residual metal concentration in solution. This procedure allowed the evaluation of the adsorption efficiency of each hydrochar and its potential application in the remediation of water contaminated with potentially hazardous elements (PHEs) (Nadarajah 2020).

Results and Discussion

Below (Fig. 2) are the results for the final As concentration in solution after the adsorption test with the four types of hydrochar evaluated (Bio-stabilised – BIOEST, Wood with Whey – LM, Wood with Water – MH, and Paper – Cardboard – PC).

The results (Fig. 2) indicates that none of the hydrochars effectively reduced As concentrations below 900 µg/L As. The BIOEST hydrochar exhibited the lowest concentrations; however, these remained above the initial concentration. In contrast, the paper–cardboard hydrochar (PC) displayed the highest final concentrations, reaching 990.43 µg/L at pH 6, suggesting increased desorption. Overall, no clear trend was observed as a function of pH, indicating that desorption is not strongly influenced by this parameter within the studied range.

This behaviour aligns with previous studies demonstrating that the efficiency of hydrochar in PHEs adsorption is highly dependent on its structure, surface chemistry, and working pH (Khanzada *et al.* 2023, 2024). Specifically, some hydrochars have been reported to be not only ineffective in contaminant removal but may also release metals if their surface charge is negative at certain pH values (Khanzada *et al.* 2023).

The results obtained in the As adsorption experiments with hydrochar indicate that none of the materials achieved effective removal, with most exhibiting net desorption, leading to final concentrations exceeding the initial 900 µg/L. This phenomenon may be attributed to several factors, including the surface charge of the hydrochar as a function of pH, the initial composition of the material, and the presence of impurities or functional groups unsuitable for As adsorption (Khanzada *et al.* 2023, 2024). It has been reported that the structure of hydrochar is largely influenced by the type of biomass used and the synthesis conditions, which can significantly affect its capacity to retain PHEs (Akkari *et al.* 2024).

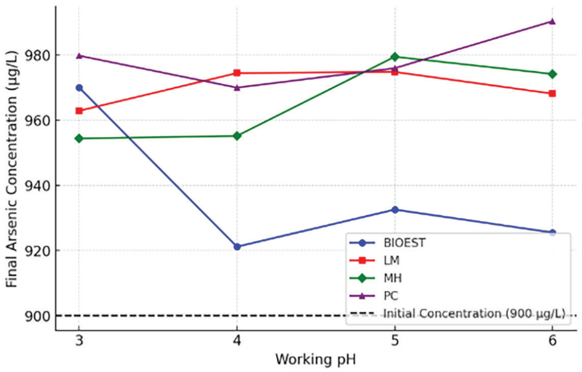

***Figure 2** Final Arsenic Concentration in Solution by Hydrochar Type.*

pH is a critical factor in PHEs adsorption, as it influences both the speciation of metals in solution and the surface charge of the adsorbent. In this study, all hydrochars were evaluated within a pH range of 3 to 6, which may have favoured the desorption of As in its arsenate form (AsO_4^{-3}), particularly if the point of zero charge (PZC) of the material was lower than the working pH (Wang *et al*., 2018). This is consistent with previous studies indicating that hydrochars with a PZC lower than the system pH tends to repel anionic species rather than adsorb them (Navas-Cárdenas *et al*. 2023; Khanzada *et al*. 2024). Additionally, it has been documented that the presence of competing anions in solution, such as phosphate or sulfate, may further reduce hydrochar efficacy in As adsorption by displacing it from active sites and promoting its release into the aqueous medium (Akkari *et al*. 2024).

Notably, the paper–cardboard hydrochar (PC) exhibited the highest desorption, with a final As concentration of 990.43 µg/L at pH 6. This may be attributed to the presence of residual compounds in its matrix, such as modified lignin, inks, or other additives, which alter its surface chemistry and reduce its affinity for As (Khanzada *et al*., 2024). Similarly, the wood hydrochar produced with whey (LM) showed high final As concentrations across all pH values tested, suggesting that the manufacturing process involving whey may have induced structural modifications that negatively affected its adsorption capacity. Previous studies have demonstrated that certain agro-industrial residues may generate hydrochars with low affinity for PHEs if the conversion process is not optimized (Adebisi 2017).

Conversely, the bio-stabilised hydrochar (BIOEST) exhibited the lowest desorption levels, though it still failed to retain As efficiently. This suggests that while bio-stabilisation may provide a more stable structure, it does not necessarily confer the appropriate functional groups required for As retention in solution (Navas-Cárdenas *et al*., 2023). The optimisation of such materials through chemical modifications, such as acid or base activation, metal doping, or nanoparticle functionalisation, has been reported as an effective strategy to enhance PHEs adsorption (Akkari *et al*., 2024).

The literature suggests that certain modifications can improve hydrochar adsorption capacity for PHEs, including chemical activation with acids or bases, the introduction of specific functional groups, and the incorporation of nanoparticles to enhance metal interactions (Khanzada *et al*., 2024; Akkari *et al*., 2024). These strategies have been successfully applied to hydrochars derived from agricultural and agro-industrial residues, yielding substantial improvements in contaminant retention in aqueous environments (Akkari *et al*., 2024).

Conclusions

The results obtained in this study indicate that none of the four hydrochars evaluated achieved effective As adsorption in solution; in fact, a desorption effect was observed in several cases. These findings clearly demonstrate that, under the tested conditions, the selected hydrochars are not suitable for As removal. However, this does not rule out the broader potential of hydrochar as an adsorbent material. Instead, it underscores the need for systematic optimisation of its physicochemical properties to improve its performance in the remediation of waters contaminated with potentially hazardous elements (PHEs) (Navas-Cárdenas *et al*., 2023; Khanzada *et al*., 2024).

The efficacy of hydrochar in PHE adsorption is known to be influenced by its chemical structure, the presence and nature of surface functional groups, its point of zero charge (PZC), and the competition with other anions in solution, such as phosphate and sulfate (Saber *et al*., 2018; Saba *et al*., 2024; Zhang *et al*., 2024). In this study, the bio-stabilised hydrochar (BIOEST) exhibited the lowest As desorption, suggesting that the stabilisation process may provide certain structural advantages, though clearly insufficient to ensure effective As retention.

Conversely, the paper–cardboard hydrochar (PC) showed the highest desorption, likely due to residual compounds such as modified lignin, inks, or additives that adversely affect its surface chemistry and affinity for As. Similarly, hydrochars derived from wood with whey (LM) and wood with water (HW-A) also exhibited poor performance, indicating that the interaction between biomass type and the reaction medium plays a crucial role in determining the resulting material's adsorption capacity (Pasipanodya *et al.*, 2024).

Since adsorption performance can be significantly enhanced through surface modification and controlled synthesis, future research should prioritise optimisation strategies such as chemical activation, pH adjustment, or impregnation with selective agents (Navas-Cárdenas *et al.*, 2023; Akkari *et al.*, 2024).

A limitation of this preliminary study is the absence of advanced physicochemical characterisation of the hydrochars, such as FTIR for functional group identification, SEM and EDS mapping for surface morphology and elemental distribution, and BET analysis for specific surface area determination. These analyses will be essential in future work to correlate structural properties with adsorption behaviour and to guide the optimisation of hydrochar production for targeted contaminant removal.

Although the present findings reveal significant limitations, hydrochar derived from biomass waste remains a promising candidate for future development as an environmentally responsible treatment material. Its valorisation supports circular economy principles and aligns with the Sustainable Development Goals (SDGs), particularly SDG 6 (clean water and sanitation), SDG 12 (responsible consumption and production), and SDG 13 (climate action).

Accordingly, the hydrochars evaluated here open new avenues for research in material engineering. Their future optimisation and possible integration into passive treatment systems, such as permeable reactive barriers and constructed wetlands, could enable their effective deployment in the long-term management of PHE contamination and contribute to the implementation of clean technologies for protecting water resources in mining-affected environments (Khanzada *et al.*, 2024; Akkari *et al.*, 2024).

References

Adebisi GA (2017) Removal of heavy metals by activated carbons prepared from hydrothermally treated biomass with phosphoric acid treatment. University of Malaya

Akkari I, Kaci MM, Pazos M (2024) Revolutionizing waste: Harnessing agro-food hydrochar for potent adsorption of organic and inorganic contaminants in water. Environ Monit Assess 196:1–28. https://doi.org/10.1007/s10661-024-13171-3

Ayala J, Fernández B (2019a) Treatment from abandoned mine landfill leachates. Adsorption technology. J Mater Res Technol 8:2732–2740. https://doi.org/10.1016/j.jmrt.2019.04.009

Ayala J, Fernández B (2019b) Removal of zinc, cadmium and nickel from mining waste leachate using walnut shells. Environ Prot Eng 45:141–158. https://doi.org/10.37190/EPE190210

Ayala J, Fernández B (2019c) Treatment of mining waste leachate by the adsorption process using spent coffee grounds. Environ Technol (United Kingdom) 40:2037–2051. https://doi.org/10.1080/09593330.2018.1435739

Khanzada AK, Al-Hazmi HE, Kurniawan TA, *et al* (2024) Hydrochar as a bio-based adsorbent for heavy metals removal: A review of production processes, adsorption mechanisms, kinetic models, regeneration and reusability. Sci Total Environ 945:. https://doi.org/10.1016/j.scitotenv.2024.173972

Khanzada AK, Rizwan M, Al-Hazmi HE, *et al* (2023) Removal of Arsenic from Wastewater Using Hydrochar Prepared from Red Macroalgae: Investigating Its Adsorption Efficiency and Mechanism. Water (Switzerland) 15:. https://doi.org/10.3390/w15213866

Nadarajah K (2020) Customized Hydrochar from Biomass Materials for Water Treatment. 1–309

Navas-Cárdenas C, Caetano M, Endara D, *et al* (2023) The Role of Oxygenated Functional Groups on Cadmium Removal using Pyrochar and Hydrochar Derived from Guadua angustifolia Residues. Water (Switzerland) 15:. https://doi.org/10.3390/w15030525

Pasipanodya D, Seedat N, Patel B, Roopchund R (2024) Production of hydrochar from the hydrothermal carbonisation of food waste feedstock for use as an adsorbent in removal of heavy metals from water. Biomass Convers Biorefinery. https://doi.org/10.1007/s13399-024-06097-w

Quino Lima I, Ramos Ramos OE, Ormachea Muñoz M, *et al* (2021) Geochemical mechanisms of natural arsenic mobility in the hydrogeologic system of lower Katari Basin, Bolivian Altiplano. J Hydrol 594:. https://doi.org/10.1016/j.jhydrol.2020.125778

Ramos Ramos OE, Rötting TS, French M, *et al* (2014) Geochemical processes controlling mobilization of arsenic and trace elements in shallow aquifers and surface waters in the Antequera and Poopó mining regions, Bolivian Altiplano. J Hydrol 518:421–433. https://doi.org/10.1016/j.jhydrol.2014.08.019

Saba B, Christy AD, Shah A (2024) Hydrochar for pollution remediation – Effect of process parameterS, adsoption modeling, life cycle assessment and terchno-economic evaluation. resouces, Conserv an Recycl 202:

Saber M, Takahashi F, Yoshikawa K (2018) Characterization and application of microalgae hydrochar as a low-cost adsorbent for Cu(II) ion removal from aqueous solutions. Environ Sci Pollut Res 25:32721–32734. https://doi.org/10.1007/s11356-018-3106-8

Sun Y, Yu F, Han C, *et al* (2022) Research Progress on Adsorption of Arsenic from Water by Modified Biochar and Its Mechanism: A Review

Zhang Y, Chen D, Xing Y, *et al* (2024) Role of Nitrate in the Production of Iron-Modified Hydrochar for Arsenic Removal. Water Air Soil Pollut 235:1–25. https://doi.org/10.1007/s11270-024-07023-6

Guidelines for Rehabilitating Mined Land to Irrigable Standard

Panayotis Patoussias[1], John George Annandale[1], Philip Dale Tanner[1]

[1]*Department of Plant and Soil Sciences, University of Pretoria, Private Bag X20, Hatfield 0028, South Africa, panayotis.patoussias@tuks.co.za, john.annandale@up.ac.za, philtanner63@gmail.com*

Abstract

Irrigation with suitable quality untreated or partially treated mine waters may be a beneficial, cost effective option for mine water management. Suitable rehabilitated mined land near such waters could be ideal for irrigation, as off-site environmental impacts are expected to be reduced relative to irrigation of unmined land falling outside of the mining footprint. Sustainable, productive irrigation requires soils to be irrigable, not just arable. Guidelines for mine land rehabilitation to irrigable standard are provided, as well as pointers for assessing the irrigability of rehabilitated land. In addition, remediation approaches for sub-optimal field areas are proposed.

Keywords: Irrigability assessment, mine influenced water, rehabilitated mined land, remediation

Introduction

Managing or treating large volumes of mine water is expensive, and irrigation may be a beneficial, cost effective option to consider (Annandale *et al.* 2002). This enhances food security, and can improve livelihoods of nearby communities, especially post-closure, thereby supporting the Just Energy Transition. Suitable rehabilitated mined land near such waters could be ideal for irrigation, as off-site environmental impacts are expected to be minimal and manageable if return flows accumulate in old pit voids and are contained. However, due to physical limitations, rehabilitated land is generally less favourable than unmined land for crop production.

The technical guidelines for irrigation with mine water (Heuer *et al.* 2021) include the Irrigation Water Quality Decision Support System (IrrigWQ-DSS) (du Plessis *et al.* 2023), which assists with assessing mine water suitability for irrigation, appropriate crop selection, and estimating the irrigable land area required to utilise the available mine water. Guidelines for obtaining regulatory approval for this practice in South Africa (Pocock and Coetzee 2021) have also been developed. The current Land Rehabilitation Guidelines for Surface Coal Mines (LaRSSA 2019) provide guidance on rehabilitation to arable standards and thus need to be supplemented with guidance on rehabilitating mined land to irrigable standard. Such guidelines should also contain procedures for assessing irrigability of rehabilitated land, and offer recommendations for remediation of sub-optimal rehabilitated areas.

The ***Guidelines for Rehabilitating Mined Land to Irrigable Standard*** presented here, exclusively consider physical land and soil characteristics, as it is assumed that chemical limitations to crop production, such as soil fertility, are easier to address than physical limitations.

Mine water is often of poor quality, requiring uniform irrigation application to minimize salinisation risk in irrigated fields. Due to the high risk of emitter blockage, mine water is unsuitable for micro-irrigation systems. Therefore, these guidelines assume that overhead centre-pivot irrigation, will be the preferred method for using mine water.

These proposed guidelines expand on the (LaRSSA 2019) guidelines, and are presented in three sections; SECTION A (summarises best soil handling practices, from stripping to replacement, as outlined in the LaRSSA

2019 guidelines), SECTION B (presents the assessment of irrigation potential of rehabilitated mined land), and SECTION C (recommends remediation approaches for areas of sub-optimal irrigability in rehabilitated mined land).

Although the development of all three sections have been guided by established and recognized practices or standards, the Rehab Irrigation Suitability (RIS) assessment model presented in section B is novel and is the main focus of this paper.

Approach

These guidelines stress the need to carefully follow the LaRSSA (2019) mine land rehabilitation guidelines to improve the chances of rehabilitating land to irrigable standard. This requires correct placement of suitable soil materials to sufficient depth, and the minimisation of compaction. Factors rendering rehabilitated mined land unsuitable for irrigation are poor surface drainage due to subsidence and low infiltrability, causing ponding, and poor internal profile drainage, causing water logging and salinisation.

Developing the Rehab Irrigation Suitability (RIS) model

The ***Rehab Irrigation Suitability (RIS)*** assessment procedure was developed by integrating the evaluation criteria of physical land and soil factors from commonly used quantitative land suitability models which evaluate the suitability of natural land for irrigation, including the Storie Index (SI) (Storie 1978) and the Parametric Model (Sys *et al*. 1991).

The ***RIS*** model evaluates six physical land and soil factors that often render rehabilitated mined land unfit for irrigation. These include: position in the landscape (PL); slope (S); depressions (Dep); infiltrability (IB); permeability or drainage rate (Perm) and water holding capacity (WHC).

Due to the expected high spatial variability of rehabilitated mined land, a 50 x 50 m sampling grid is advised at which to evaluate each of the six parameters in the desired sampling area. In-field measurements are compared to parameter-specific criteria and rated from "Ideal" to "Unacceptable". The overall irrigability class (Table 1) of an area is determined by the factor expected to most limit sustainable production. This classification system was adapted from the *Irrigation Water Quality Decision Support System* (IrrigWQ-DSS) (du Plessis *et al*. 2023), as it was considered simple, intuitive, and suitable for these guidelines.

The importance of each of the six assessment factors as well as their respective assessment criteria are presented.

Position in the landscape (PL)

Areas intended for irrigation should not be situated in low-lying areas such as floodplains, which may become water-logged and unproductive due to surface flooding after heavy rainfall. Furthermore, infiltration, erosion and sedimentation vary based on slope position (Ontl and Schulte 2012). Consequently, irrigated areas on slopes, especially those situated on backslope and toeslope regions (Fig. 1) may require up-slope drainage channels to prevent surface flow, erosion and sediment deposition, which may compromise the irrigated area (Ali 2011).

Ideally, the summit is the preferred area for irrigation, as it is expected to have more suitable infiltration, minimal sedimentation and erosion risks, subsequently requiring minimal, if any controls to reduce off-site environmental impacts.

Table 1 *Irrigability classes of the Rehab Irrigation Suitability (RIS) model.*

Irrigability class	Description
Ideal	High irrigation potential
Acceptable	Irrigable, with occasional yield penalty expected
Tolerable	Irrigable, but continuous yield penalty expected
Unacceptable	Serious yield limitations, irrigation not recommended

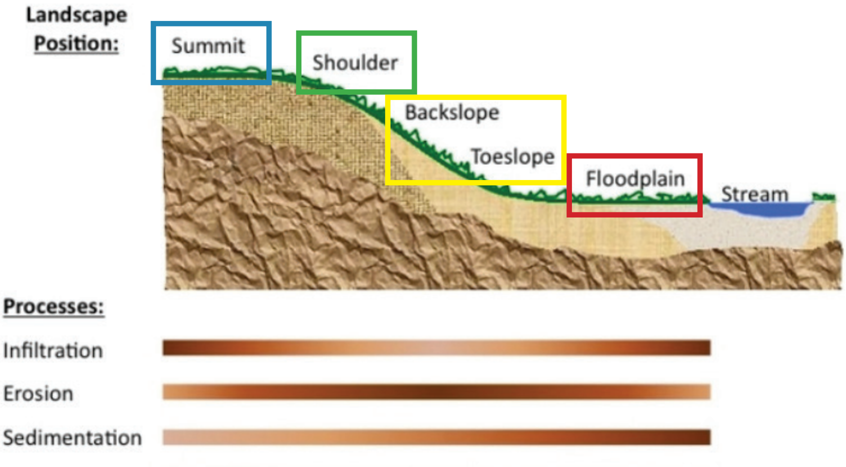

Figure 1 *Illustration of different slope positions (Ontl and Schulte 2012).*

Slope gradient (S)

When irrigating field crops with mine waters which are often saline, fields should be relatively flat (< 2%) to promote uniform distribution of irrigation water (Van Rensburg *et al.* 2012). However, the LaRSSA (2019) guidelines recommend a minimum slope of 1% to ensure effective surface drainage, preventing waterlogging and maintaining productivity in areas where subsidence or depressions may form.

Table 2, presents the RIS assessment criteria of slope gradient (%), which was adapted from the Storie Index (SI) (Storie 1978) and the Parametric Model (Sys *et al.* 1991). Moderate slopes (8–12%) were considered "Tolerable", and steep slopes (> 12%) "Unacceptable". These steeper slopes pose a higher risk of erosion and surface runoff.

Micro-relief or depressions (Dep)

Micro-relief is typically not of concern after land levelling, however, incorrectly constructed rehabilitated land is susceptible to secondary subsidence. The resettling of replaced material results in the formation of depressions which are often poorly drained, prone to waterlogging and salt build-up, making them unproductive under irrigation (LaRSSA 2019; Van Rensburg *et al.* 2012)

The risk of a depression becoming unproductive will depend on the likelihood of ponding, which is influenced by run-on, surface drainage or runoff, infiltrability and permeability. Determining both the presence of depressions, as well as the severity of ponding (Table 3), aids in better evaluating the potential risk of a depressed area becoming unproductive.

Infiltrability (IB) and permeability (Perm)

Surface soil texture, surface compaction and soil crusting will influence infiltrability, the potential rate at which water can enter the soil profile (Indoria *et al.* 2020). It is important that only the top 5 cm of the profile is assessed for infiltrability.

Permeability or internal drainage, on the other hand, is the rate water can pass through the profile and beyond the rooting zone. Poor permeability may be due to restrictive layers within the rehabilitated profile such as compacted material and stratified layers with textural contrasts (Rethman 2006). For profile

Table 2 *Assessment criteria of slope gradient (%).*

Slope gradient (%)			
Ideal	Acceptable	Tolerable	Unacceptable
<2%	2–8%	8–12%	>12%

Table 3 Assessment criteria of the occurrence and severity of depressions within a rehabilitated landscape.

Occurrence and severity of depression			
Ideal	Acceptable	Tolerable	Unacceptable
No depression	Slight depression	Medium depression	Large depression

Slight depression – Low risk of ponding and limited expected loss of productivity.
Medium depression – Moderate risk of ponding which may result in loss of productivity.
Large depression – High risk of ponding, where irrigation will most likely be unsuccessful.

permeability, textural changes down the profile are assessed, with the lowest permeability class considered the limiting layer.

The measured hydraulic conductivity ranges for Infiltrability assessment criteria (Table 4), were based on the South African Irrigation Institute's (SABI 2021) ideal surface infiltration rates of greater than 150 mm/h, specifically for centre pivot irrigation.

For Permeability (Table 5), the minimum natural soil drainage rates of greater than 2.5 mm/h recommended by soil irrigability guidelines of the USBR (2005), were adjusted to rates exceeding 5 mm/h, to ensure that rehabilitated land irrigated with poor quality mine waters will be free draining, and not prone to waterlogging and salinisation.

Using permeameters to measure hydraulic conductivity is time-consuming. A more convenient, albeit less accurate approach, involves estimating hydraulic conductivity from soil texture (Table 5). The LaRSSA (2019) guidelines assess bulk densities of various soil textures to identify levels that restrict root penetration, using this as a proxy for compaction induced impermeability.

Water Holding Capacity (WHC)

Water Holding Capacity depends on effective soil depth and the soil's ability to retain water. An approximation of WHC is often only related to effective soil depth. However, the WHC of a specific soil will be largely influenced by its soil texture. Sandy soils can

Table 4 Assessment criteria for infiltrability of the surface.

	Infiltrability (mm/h)			
	Ideal	**Acceptable**	**Tolerable**	**Unacceptable**
Hydraulic conductivity (mm/h)	> 150 mm/h	60–150 mm/h	5–60 mm/h	< 5 mm/h
Soil texture (% clay)	Coarse sand (< 5%)	Loamy sand, sandy loam (5–20%)	Loam*, silt loam*, silt*, sandy clay loam, clay loam, silty clay loam, sandy clay* (20–40%)	Silty clay, clay (> 40%)

Note: * indicates soil textures which do not strictly correlate with the clay % range specified per class.
Description: "Ideal" – Very rapid, "Acceptable" – rapid, "Tolerable" – moderate, "Unacceptable" – slow

Table 5 Assessment criteria of permeability of the most limiting layer.

	Permeability in mm/h of limiting layer			
	Ideal	**Acceptable**	**Tolerable**	**Unacceptable**
Hydraulic conductivity (mm/h)	> 50 mm/h	20–50 mm/h	5–20 mm/h	< 5 mm/h
Soil texture (% clay)	Sand, loamy sand, sandy loam* (< 10%)	Loam*, silt loam*, Sandy clay* (10–20%)	Silt*, clay loam, silty clay loam, sandy clay loam, (20–40%)	Silty clay, clay (> 40%)

Note: * indicates soil textures which do not strictly correlate with the clay % range specified.

Table 6 Soil depths (m) of different texture materials (% clay) to meet specific irrigability class requirements for provision of Readily Available Water.

	Soil depth (m) relative to % clay					
	< 5%	5–10%	10–20%	20–40%	Available Water (mm)	
Ideal	> 2.5 m	> 1.25 m	> 0.80 m	> 0.66 m	> 100	> 50
Acceptable	1.5–2.5 m	0.75–1.25 m	0.5–0.80 m	0.4–0.66 m	60–100	30–50
Tolerable	0.75–1.5 m	0.37–0.75 m	0.25–0.5 m	0.2–0.4 m	30–60	15–30
Unacceptable	< 0.75 m	< 0.37 m	< 0.25 m	< 0.2 m	< 30	< 15

Assuming the profile is irrigated to field capacity, under hot dry conditions with a full canopy cover:
Ideal: Profile can provide readily available water to the crop for a week without irrigation
Acceptable: Crop should remain productive for at least 5 – 7 days before irrigation is needed
Tolerable: Full cover crop will need irrigation every 3 to 5 days in hot dry weather
Unacceptable: Profile will need to be irrigated at intervals of less than 3 days in hot dry weather

often hold only 40 mm available water per m soil, while clayey soils easily hold 150 mm/m. Therefore, sandy soils need to be deeper than clayey soils to hold the equivalent amount of water (Sys *et al.* 1991).

Despite irrigated agriculture relying less on rainfall than dryland production, the profile still requires sufficient soil or similar root-accessible material that will store sufficient water to reduce crop water stress between irrigation cycles or even during breakdowns.

Plant Available Water (PAW) is the water held between field capacity (FC) and wilting point (WP). FC is the upper limit where drainage is negligible, while WP is the lower limit, below which plants cannot extract water. As a rule of thumb, for optimal production under irrigation, no more than half of PAW should be depleted. This is known as Readily Available Water (RAW) (FAO 1985).

Approximate PAW and RAW requirements for various irrigability classes assume that a full cover crop under hot, dry conditions, should be able to sustain optimal growth with a weekly irrigation interval. From these PAW and RAW thresholds, together with available water contents of specific soil textures (% clay) published by (Sys *et al.* 1991), one can predict the irrigation potential class from effective soil depth and texture, as seen in Table 6.

Although not included here, rehabilitated areas, may have underlying spoil material that is permeable, uncompacted and chemically suitable for root growth. This can contribute significantly to PAW, and is especially important for profiles with limited soil cover.

Remediation strategies to improve the irrigability of sub-optimal rehabilitated mined land

The guideline's final section recommends remediation actions to improve rehabilitated land with low or unsuitable irrigation potential, as identified by the RIS model. Common remediation strategies are highlighted in Table 7.

Discussion

Rehabilitating mined land to an irrigable standard from the outset is ideal, allowing for strategic site selection and suitable soil placement. However, many mines that need to manage water surplus have already rehabilitated land to different standards and must assess its suitability for irrigation using mine water. These guidelines present the six-factor ***Rehab Irrigation Suitability (RIS)*** model.

This, together with digital maps for each of the six factors assessed can create an overall Irrigation Potential/RIS map for a rehabilitated area. This map will identify suboptimal areas requiring remediation or, if the extent of area not suitable for irrigation or cost of remediation is too great, for locating areas more suitable for irrigation.

Conclusions

These draft guidelines aim to support the rehabilitation of open-cast mined land to irrigable standards, assess irrigation potential, assist with site selection, and offer guidance on improving sub-optimal sites for sustainable irrigation. Future fieldwork will assess the guidelines' validity and practicality, allowing for necessary refinements.

Table 7 Remedial recommendations to improve sub-optimal rehabilitated mined land.

Type of physical limitation	Remedial action recommendations
Position in landscape and slope	Levelling slopes greater than 12% is impractical, while slopes of 8–12% need proper irrigation systems, management, and dense perennial ground cover. Gentler slopes (2–8%), especially those with poor infiltration and erosion risks (areas on backslope to toeslope regions), may require contour ridging and upslope drainage to manage run-on and runoff and prevent sediment accumulation.
Depressions	Determine whether ponding is due to surface run-on, poor infiltration or poor drainage. If ponded due to poor infiltration and drainage, refer to respective sections. If filling and reshaping are not feasible, consider creating an outflow for excess water to drain, ensuring erosion is avoided.
Infiltrability	Soil infiltration issues caused by crusting, compaction, or clayey surfaces can be improved by adding organic matter to low-carbon soils, gypsum to sodic soils, and shallow cultivation or ripping to enhance structure and water retention (FAO 1985). Ensure irrigation rates meet the soil's infiltration capacity, while impermeable clay material should be removed and replaced with permeable material.
Drainage -Permeability (impermeable layer)	Poor drainage from impermeable layers can be addressed by deep ripping into the soil-spoil interface or installing artificial drainage systems (FAO 1985; LaRSSA 2019). If these are infeasible, alternative options include planting on ridges or using waterlogging-tolerant species like tall fescue (Mollard *et al*. 2008).
Water holding capacity	For areas with restrictive subsurface layers or shallow soil, deep ripping beyond the restrictive layer or 300 mm past the soil-spoil interface enhances root and water movement. If ineffective, suitable soil material will need to be trucked in and levelled to achieve the appropriate soil depth.

References

Volume 2. Springer New York, New York, NY, p 327–378. doi: 10.1007/978-1-4419-7637-6_9.

Annandale JG, Jovanovic NZ, Tanner PD, Benadé N, Du Plessis HM (2002) The Sustainability of Irrigation with Gypsiferous Mine Water and Implications for the Mining Industry in South Africa. Mine Water and the Environment 21(2):81–90. doi: 10.1007/s102300200023.

du Plessis HM, Annandale JG, Benadé N (2023) A Decision Support System That Considers Risk and Site Specificity in the Assessment of Irrigation Water Quality (IrrigWQ). Applied Sciences 13:12625. doi: 10.3390/app132312625.

FAO (1985) Irrigation Water Management: Training Manual No. 1 – Introduction to Irrigation. Food and Agriculture Organisation of the United States Introduction to Irrigation, Rome.

Heuer S, Annandale J, Tanner Pa, du Plessis M (2021) Technical Guidelines for Irrigation with Mine-Affected Waters, Report No. TT 855/2/21. Water Research Commission, Gezina, South Africa,

Indoria AK, Sharma KL, Reddy KS (2020) Chapter 18 – Hydraulic properties of soil under warming climate. Climate Change and Soil Interactions. Elsevier, p 473–508. doi: 10.1016/B978-0-12-818032-7.00018-7.

LaRSSA (2019) Land Rehabilitation Guidelines for Surface Coal Mines. Land Rehabilitation Society of South Africa, Coaltech, Minerals Council of South Africa.

Mollard FPO, Striker GG, Ploschuk EL, Vega AS, Insausti P (2008) Flooding tolerance of Paspalum dilatatum (Poaceae: Paniceae) from upland and lowland positions in a natural grassland. Flora 203(7):548–556. doi: 10.1016/j.flora.2007.10.003.

Ontl T, Schulte LA (2012) Soil carbon storage. Nat Educ Knowl 3(10):35.

Pocock G, Coetzee L (2021) Guidance for Attaining Regulator Approval of Irrigation as a Large Scale, Sustainable Use of Mine Water., Report No. TT 837/20. Water Research Commission, Gezina, South Africa,

Rethman NFG (2006) A Review of Causes, Symptoms, Prevention and Alleviation of Soil Compaction on Mined Land., Report No. Project-8.2.4. Coaltech, Coaltech, Johannesburg, South Africa.,

Storie RE (1978) Storie index soil rating. vol 3203. Division of Agricultural Sciences University of California, Berkeley, California

Sys C, Van Ranst E, Debaveye IJ (1991) Land evaluation, part 1: Principles in land evaluation and crop production calculation. General Administration For Development Cooperation, Brussels, Belgium

USBR (2005) Technical Guidelines for Irrigation Suitability Land Classification. United States Bureau of Reclamation: Technical service centre, Land Suitability and Water Quality Group, Denver, Colorado

Van Rensburg LD, Barnard JH, Bennie ATP, Sparrow JB, du Preez CC (2012) Managing salinity associated with irrigation at Orange-Riet and Vaalharts irrigation schemes: report to the Water Research Commission, Report No. 1647/1/12. Water Research Commission, Gezina, South Africa,

Preliminary Leaching Performance of Slag-Blended Cement for the Stabilization of Pyrite-Bearing Waste Rock

Norberto Jr Aquino[1], Dantie Claudia Butar Butar[1], Kyriaki Papadopoulou[2], Andrzej Cwirzen[2], Lena Alakangas[1]

[1]*Applied Geochemistry, Swedish School of Mines, Department of Civil, Environmental and Natural Resources Engineering, Luleå University of Technology, SE-971 87 Luleå, Sweden*

[2]*Building Materials, Department of Civil, Environmental and Natural Resources Engineering, Luleå University of Technology, SE-971 87 Luleå, Sweden*

Abstract

This study explores slag-blended cement as an alternative to Ordinary Portland Cement (OPC) for stabilizing pyrite-bearing waste rock. Over a 64-day leaching experiment, OPC-treated waste rocks produced higher pH leachates and greater major ion release due to their faster reactivity and early cement hydrate phase dissolution. Slag-blend-treated waste rocks exhibited slower ion leaching, indicating the need for extended curing. Trace element concentrations (Cu, Mn, Ni, Pb) were slightly higher in leachates from untreated waste rock, reflecting cement´s early-stage performance in metal(loids) immobilization. Further research is needed to assess slag's long-term effectiveness.

Keywords: Cement-based stabilization, Slag Cement, Portland Cement, Acid Rock Drainage, pyrite-bearing Waste Rock, Leaching Test

Introduction

Acid Rock Drainage (ARD) is a widely recognized environmental issue at mine sites, where sulfide-bearing waste rock oxidizes, releasing acidic, metal-rich waters. If left untreated, this can cause severe ecological and health effects. Stabilization/Solidification (S/S) techniques, such as the use of Ordinary Portland Cement (OPC), are commonly employed to treat hazardous wastes (Wang *et al.* 2018). In the case of waste rock stabilization, OPC can form a cementitious barrier that may reduce ARD (Sephton and Webb 2017), but its long-term effectiveness remains uncertain. Gypsum ($CaSO_4 \cdot 2H_2O$) in OPC can lead to the formation of expansive minerals like ettringite ($Ca_6Al_2(SO_4)_3(OH)_{12} \cdot 26H_2O$) and thaumasite ($Ca_3Si(OH)_6(CO_3)(SO_4) \cdot 12H_2O$), which weaken the barrier and expose sulfides to oxidation. Additionally, the high carbon emissions from cement production make OPC less ideal, highlighting the need for better alternatives.

This paper explores the use of an alternative cementitious material for stabilizing pyrite-bearing waste rock. Specifically, it investigates the potential of a supplementary cementitious material derived from granulated blast-furnace slag, which is currently used by Boliden AB in Sweden as a substitute for OPC in underground backfilling (Eriksson *et al.* 2018). Here, we compare slag-blended cement and OPC for their applicability in stabilizing waste rock in atmospheric conditions. Previous leaching tests for hazardous waste and standard leaching procedures for construction materials were conducted under saturated conditions (CEN 2015; ASTM 2018). However, in this study, we aimed to assess the leaching behavior of cement-encapsulated waste rock under atmospheric conditions rather than saturated. Thus, this study presents results from a new laboratory leaching set-up designed for monolithic cement-encapsulated waste rock. In the long term, this research seeks to provide a comprehensive understanding of the geochemical interactions within the cemented matrix, contributing to the identification of the most effective and sustainable alternative material for stabilizing sulfidic waste rock.

Methods

Encapsulation of Waste Rock by Cementitious Materials

Waste rock samples were collected from a polymetallic Cu-Zn-Au-Ag mine in Northern Sweden. For this experiment, one rock type (andesite) was selected from the collected waste rock samples, which does not necessarily represent the entire waste rock volume but was selected to represent the average S value (11 wt. %). The waste rock sample (characterization from Butar Butar *et al.* 2025) is mainly composed of quartz (36.3 wt. %), smectite (25.7 wt. %), muscovite (12.3 wt. %), chlorite (10.9 wt. %), albite (7.0 wt. %), microline (6.7 wt. %), and biotite (0.48 wt. %). Sulfur is principally associated with pyrite (0.61 wt. %), which is the most dominant sulfide in the rock sample. Most major elements (Al, Fe, K, Mg, Si) occur in rock-forming silicates, while trace elements like Co, Cu, Mn, and Ni are mostly associated with pyrite. Trace amounts of other metals (V and Zn) are also present in the sample.

The samples were cut into 3 cm × 3 cm × 3cm specimens. Waste rock samples were encapsulated with 2 cm thick of both Ordinary Portland Cement (OPC) and slag-blended cement (50% OPC, 50% Slag) in duplicate. OPC was identified as type CEM I 52.5R from Cementa (Malmoe, Sweden) while the slag was from Merox AB-Sweden (Oxelönd, Sweden). Additionally, each cement mixture was separately molded into 5 cm × 5 cm × 5 cm cubes as reference specimens. All specimens were cured for at least 28 days at 25 °C and 60% relative humidity. Determination of trace elements in solid materials was done using Inductively Coupled Plasma – Sector Field Mass Spectrometry (ICP-SFMS) by ALS Scandinavia in Luleå, Sweden.

Leaching Experiment

For the leaching experiment, encapsulated waste rock samples (including a reference untreated sample) were placed in transparent polycarbonate cells after curing. Seven cells were stored in a climate-controlled chamber at 25 °C and 60–80% relative humidity. Since no standardized leaching procedure exists for monolithic samples under atmospheric conditions, two standards were adapted: CEN/TS 15863:2015 (CEN 2015) for cell construction and experiment duration (64 days), and ASTM D5744-18 (ASTM 2018) for the weekly leaching procedure.

Milli-Q water served as the leachant, with volumes based on the sample surface area (500 mL for the reference and 600 mL for others). Cells were flooded weekly for 64 days, with water remaining in the cell for six hours before being emptied and sampled. The leachate was filtered (0.45 µm) and analyzed for main and trace elements (ICP-SFMS by ALS Scandinavia). Electrical conductivity (EC) and pH were measured immediately after sampling.

For one duplicate and the reference sample, leaching will continue beyond 64 days to assess long-term behavior and chemical interactions between the cemented matrix and waste rock. Microstructural analyses will follow after 64 days. This paper discusses results from the initial 64-day experiment.

Results and Discussion

Chemistry of OPC and Slag-Mix Cement

The initial composition of the cementitious materials and waste rock used in this study provides essential context for understanding the leaching behavior and stabilization performance using OPC and slag-blended cement. The background concentrations of major elements in OPC, slag, and waste rock are summarized in Table 1.

OPC is characterized by a high Ca content, primarily due to the presence of calcium silicates and calcium hydroxide, with smaller amounts of Si, Al, and Fe. Trace amounts of Mg, Na, K, and S are also present, reflecting the typical composition of clinker-based materials (Kothari *et al.* 2023). In contrast, slag exhibits a higher proportion of Si, Mg, and Al compared to OPC, while its Ca content is lower. This difference arises because slag relies on latent hydraulic phases rather than free lime for its cementitious properties (Chen 2007).

Table 1 Background chemical composition (wt. %) for major elements in solid samples before leaching.

Sample	Al	Ca	Fe	Mg	K	Si	Na	S
Waste Rock	4.1	0.2	6.2	1.0	1.8	28	0.1	5.1
OPC	2.8	47	2.7	2.0	0.8	9.6	0.1	1.3
Slag	7.2	28	0.2	8.4	0.6	17	0.4	1.2
Aggregates	7.5	1.2	2.8	0.5	3.4	36	2.2	0.1

Leaching Behavior and pH Trends

Overall, there is minimal variation in major element concentrations between the leachate from the reference materials (OPC and Slag-blend) and the cement-treated waste rocks (see Fig. 2). A similar trend is observed regardless of whether the cemented matrix consists solely of reference materials (OPC and Slag-blend) or contains waste rock (WROPC and WRSlag). This suggests that geochemical interactions between the cemented matrix and the waste rock that can cause the mobility of elements have been limited so far. Additionally, the release of major elements from the reference untreated waste rock remains consistently lower than that from the cement-encapsulated waste rocks, indicating that, during the first 64 days of leaching, the primary source of element release is the cementitious materials (OPC and Slag) rather than the waste rock. This can also be linked to the lag time before the oxidation occurs in the waste rock, which is after 10 weeks of wet-dry cycle leaching of crushed (1–4 mm) waste rocks (Butar Butar *et al.* 2025).

The leachate from the OPC-treated waste rock consistently exhibited a higher pH compared to slag-blend-treated waste rocks throughout the 64-day observation period, ranging between 11.5 and 10. It can be observed that the leachate from the cement-encapsulated waste rocks had a higher pH compared to the reference untreated waste rock sample (4–5). It is important to note that this low pH may not be solely attributed to the waste rock itself, as the blank sample exhibited a similar pH trend (4–5). This may be due to the residual nitric acid in the tubes and cells from the acid-cleaning process. It is therefore recommended to rinse the tubes with MQ water several times before use.

The initially elevated pH of leachate from the OPC-treated waste rocks can be attributed to the dissolution of calcium hydroxide (Ca(OH)2) from the cement (Sephton and Webb 2017), which provides an effective buffer against acidic conditions but may also lead to alkaline sulfide weathering (Butar Butar *et al.* 2025). In contrast, slag mix-treated waste rocks displayed a slightly lower pH range, decreasing from 10.5 to

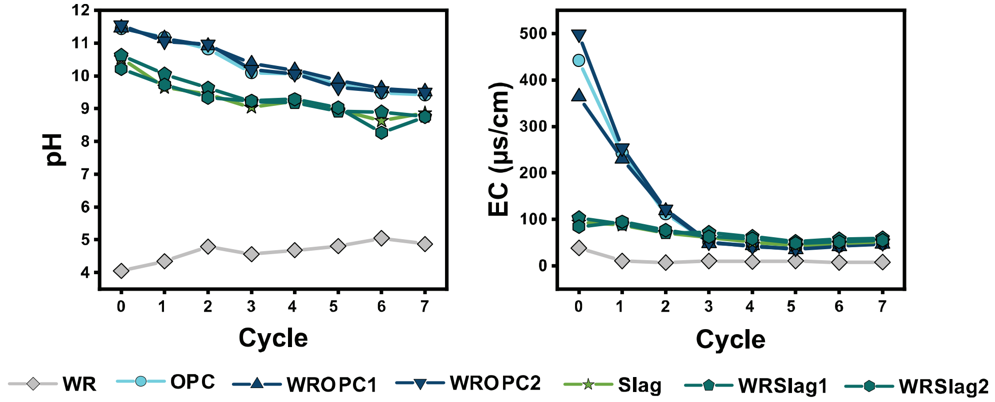

Figure 1 pH and electrical conductivity (EC) throughout the 64-day leaching experiment. One cycle represents one week except for cycle 2 to cycle 3 where there is a 2-week gap.

9.3 over the same period, probably due to the lower amount of OPC in slag-blended cement. This slightly lower pH trend may be associated with the slower activation of pozzolanic reactions, during which latent hydraulic phases react with water and Ca to form secondary binding phases (e.g., calcium silicate hydrates) (Chen 2007).

The leachate from OPC and OPC-treated waste rocks contained higher initial concentrations of Ca (Fig. 2), particularly during the first two leaching cycles, before declining to below 10 mg/L during cycles 3 and 4. The decline may be attributed to the dissolution of calcium-rich phases (during the early cycles) and the subsequent potential incorporation of Ca into stable phases, such as calcium silicate hydrates (C-S-H) (Scrivener *et al.* 2019). In contrast, leachates from slag-blend-treated waste rocks exhibited consistently lower Ca concentrations throughout the 64-day leaching period, although the concentrations became comparable to those of OPC-treated waste rocks during the final two cycles. This trend reflects the inherently lower total Ca content in slag compared to OPC. The higher initial Ca release from OPC may be due to its higher free lime content, which rapidly dissolves and releases Ca ions into the leachate. Curing time may also be a factor since slag-blended cement needs sufficient time to cure due to its slower reactivity (Wu *et al.* 1990)

The concentrations of Al and Si in the leachate were consistently higher from the OPC-treated waste rocks compared to slag-blend-treated waste rocks. The elevated levels of Al and Si in the leachate from OPC-treated waste rocks, particularly during the early stages, may be attributed to the dissolution of silicate phases in the cement. Interestingly, this higher release of Al and Si from OPC-treated waste rocks occurred despite the higher Al content in slag compared to OPC. This can be explained by the rapid dissolution of aluminate phases, such as tricalcium aluminate (C3A), in the OPC matrix (Hirsch *et al.* 2023), as well as higher pH in OPC-treated systems, which may enhance Al solubility. This trend is further supported by the higher EC values observed in the leachate from the OPC-treated waste rocks, indicating the rapid release of ions such as Al, Ca, and Si. Over time, EC in the leachate from OPC-treated waste rocks gradually decreased, consistent with the declining release of these ions. In contrast, leachate from slag-blend-treated waste rocks exhibited a more stable EC trend, likely reflecting the gradual release of major ions. This may be due to the slower reactivity of slag-blended cement which may lead to the late formation of soluble cement hydrate phases.

Both OPC- and slag-blend-treated waste rocks exhibited minimal leaching of Mg and Na, with concentrations remaining below 6 mg/L across all samples. However, leachate from slag mix-treated waste rocks demonstrated a gradual increase in Mg concentrations over time, likely due to the dissolution of Mg ions within the slag matrix which probably still has not reacted into a

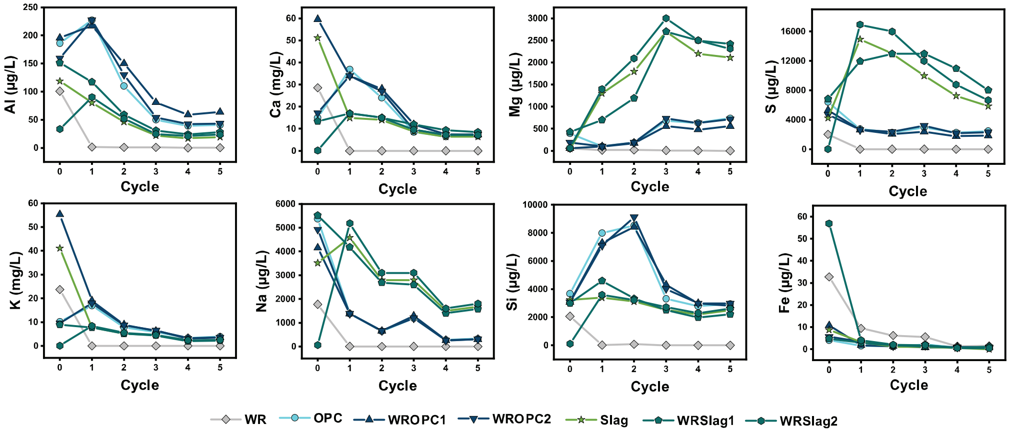

***Figure 2** Leaching trends and concentrations of major elements throughout the 64-day leaching period. One cycle represents one week except for cycle 2 to cycle 3 where there is a 2-week gap.*

stable phase (Zhai and Kurumisawa 2022). Additionally, slag-blend-treated waste rocks released higher concentrations of both Mg and Na compared to OPC-treated waste rocks, consistent with the higher initial Mg and Na content in slag. For S, slag-blend-treated waste rocks exhibited a higher release compared to OPC-treated waste rocks, despite the lower initial S content in the slag. This behavior may be attributed to the faster reactivity of OPC compared to slag facilitating the transformation of gypsum into ettringite (Sun *et al.* 2020), thereby stabilising S in the system. Due to the slower reactivity of slag, it is likely that during the early stages, gypsum in slag-blended cement still has not fully transformed to ettringite and may release S to the leachate (Ogirigbo and Black 2016). Furthermore, the release of S from the cemented waste rocks cannot be attributed to waste rock oxidation, as no evidence of oxidation has been observed in the reference waste rock yet. This interpretation is supported by the consistently low Fe release across all samples, which aligns with the absence of oxidation processes in the waste rock throughout the 64-day leaching duration.

Overall, the release of trace elements to the leachates across all samples is minimal, particularly for Cu, Mn, Ni, and Pb, with concentrations ranging from 0 to 5 µg/L per cycle. However, Mo and V exhibit slightly higher release rates in cement-treated waste rocks, likely due to the increased mobility of these elements in alkaline environments. For some trace metals (Cu, Mn, Ni, Pb), the reference untreated waste rock releases slightly higher concentrations than the cement-treated waste rocks. Although the difference is small, this still demonstrates the early-stage performance of both OPC and slag-blended cement in immobilizing trace metals. However, it is important to note that this trend represents pre-oxidation conditions, and the behavior may change once oxidation progresses.

Evaluation of New Leaching Set-Up

In this study, we tested a new leaching setup by adapting two existing standard procedures (CEN/TS 15863 and ASTM D5744). This modified setup allowed full exposure of all surface areas of the monolithic samples. The release of major elements was already evident as early as Week 0 to Week 1, providing insights into the initial performance of the cementitious materials. However, the 64-day duration is insufficient to observe sulfide oxidation in the reference waste rock sample, making it impossible to further interpret the data in terms of ARD. Therefore, the leaching duration will be extended. Additionally, a key limitation of this setup is its inability

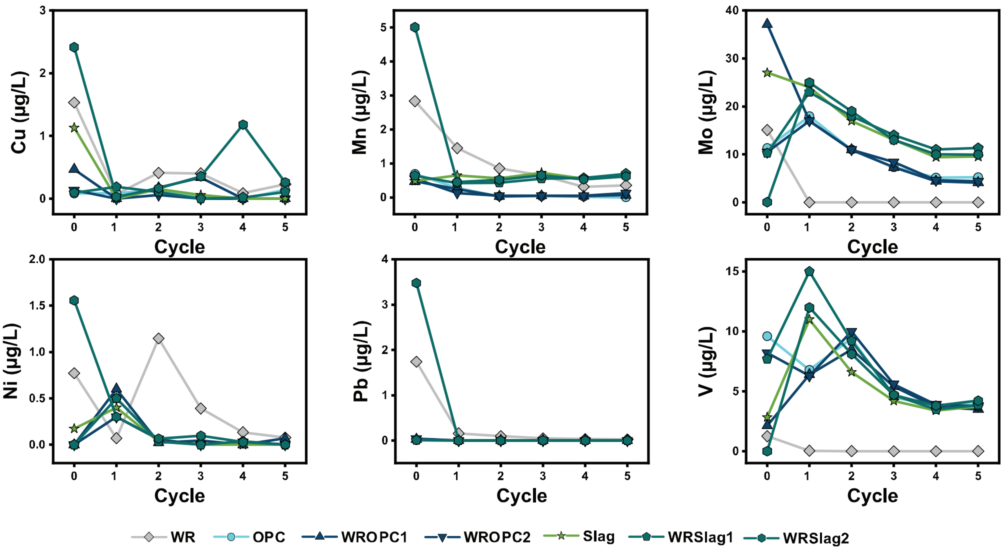

***Figure 3** Leaching trends and concentrations of major elements throughout the 64-day leaching period. One cycle represents one week except for cycle 2 to cycle 3 where there is a 2-week gap.*

to evaluate and calculate the diffusion coefficient, as diffusion calculations require a saturated leaching setup.

Conclusions

This study evaluated slag-blended cement as a potential alternative to OPC for stabilizing pyrite-bearing waste rock and mitigating ARD. While the preliminary data were inconclusive regarding ARD prevention, the leachate chemistry provided valuable early-stage insights into the performance of slag-blended cement as a potential replacement for OPC. The results highlight the importance of cement chemistry, particularly during the early stages, in identifying suitable replacements for OPC.

Leachates from both OPC- and slag-blend-treated waste rocks maintained consistently high pH levels, with OPC-treated waste rocks exhibiting slightly higher pH values. OPC-treated waste rocks also released higher concentrations of ions, likely due to the dissolution of soluble cement hydrate phases. In contrast, slag-blend-treated waste rocks exhibited a slower release of some major ions (e.g., Al, Ca, Si), which is likely a result of its slower reactivity and delayed formation of soluble hydrate phases. This suggests that slag-blended cement may require a longer curing period compared to OPC.

After 64 days of leaching, it's still unclear if slag-blended cement is a viable alternative to OPC for mitigating ARD, as the waste rock has not yet oxidized. However, the experiment provided valuable early data. Future research will focus on longer leaching tests and microstructural analyses to assess cement-waste rock interactions, long-term performance, and the effects of sulfide oxidation.

Acknowledgements

This project is co-funded by the European Union, the Swedish Agency for Economic and Regional Growth, and the Center of Advance Mining and Metallurgy (CAMM) at Luleå University of Technology.

References

ASTM (2018) Test Method for Laboratory Weathering of Solid Materials Using a Humidity Cell

Butar Butar DC, Alakangas L, Kaasalainen H, Ronne E (2025) Prevention of acid rock drainage formation through pyrite inhibition by silica coating. Environ Sci Pollut Res 32:6711–6731. https://doi.org/10.1007/s11356-025-36131-x

CEN (2015) Standard – Characterization of waste – Leaching behaviour test for basic characterization – Dynamic monolithic leaching test with periodic leachant renewal, under fixed conditions SS-EN 15863:2015 – Swedish Institute for Standards, SIS. In: Sven. Institutet För Stand. SIS. https://www.sis.se/en/produkter/environment-health-protection-safety/wastes/solid-wastes/ssen158632015/. Accessed 15 Aug 2024

Chen W (2007) Hydration of slag cement-Theory, Modelling and Application

Eriksson C, Nyström A, Jewell RJ, Fourie AB (2018) Garpenberg mine – 10 years of mining with paste backfill. Australian Centre for Geomechanics

Hirsch T, Matschei T, Stephan D (2023) The hydration of tricalcium aluminate (Ca3Al2O6) in Portland cement-related systems: A review. Cem Concr Res 168:107150. https://doi.org/10.1016/j.cemconres.2023.107150

Kothari A, Buasiri T, Cwirzen A (2023) Early Age Performance of OPC-GGBFS-Concretes Containing Belite-CSA Cement Cured at Sub-Zero Temperatures. Buildings 13:2374. https://doi.org/10.3390/buildings13092374

Ogirigbo OR, Black L (2016) Influence of slag composition and temperature on the hydration and microstructure of slag blended cements. Constr Build Mater 126:496–507. https://doi.org/10.1016/j.conbuildmat.2016.09.057

Scrivener K, Ouzia A, Juilland P, Kunhi Mohamed A (2019) Advances in understanding cement hydration mechanisms. Cem Concr Res 124:105823. https://doi.org/10.1016/j.cemconres.2019.105823

Sephton MG, Webb JA (2017) Application of Portland cement to control acid mine drainage generation from waste rocks. Appl Geochem 81:143–154. https://doi.org/10.1016/j.apgeochem.2017.03.017

Sun H, Qian J, Yang Y, *et al* (2020) Optimization of gypsum and slag contents in blended cement containing slag. Cem Concr Compos 112:103674. https://doi.org/10.1016/j.cemconcomp.2020.103674

Wang L, Yu K, Li J-S, *et al* (2018) Low-carbon and low-alkalinity stabilization/solidification of high-Pb contaminated soil. Chem Eng J 351:418–427. https://doi.org/10.1016/j.cej.2018.06.118

Wu X, Jiang W, Roy DM (1990) Early activation and properties of slag cement. Cem Concr Res 20:961–974. https://doi.org/10.1016/0008-8846(90)90060-B

Zhai Q, Kurumisawa K (2022) Effects of cation in sulfate chloride and nitrite on Ca(OH)2 activated ground granulated blast-furnace slag. Cem Concr Compos 133:104648. https://doi.org/10.1016/j.cemconcomp.2022.104648

Acid Mine Drainage Remediation with Waste Products: Laboratory Findings and Field Model Applications

Joana F. Araújo[1], Charles A. Cravotta III[2], Rita Fonseca[3], Roberto da Silva[4],
Sergio Prats A.[5], Teresa Valente[6]

[1]*AmbiTerra Laboratory, University of Évora, Institute of Earth Science, Largo dos Colegiais 2, 7004-516 Évora, Portugal, jfaraujo@uevora.pt, ORCID 0000-0003-4956-4061*

[2]*Cravotta Geochemical Consulting, 19507 Bethel, PA, USA, cravottageochemical@gmail.com, ORCID 0000-0003-3116-4684*

[3]*AmbiTerra Laboratory, University of Évora, School of Sciences and Technology University of Évora Institute of Earth Science, Largo dos Colegiais 2, 7004-516 Évora, Portugal, rfonseca@uevora.pt, ORCID 0000-0002-6389-2822*

[4]*AmbiTerra Laboratory, University of Évora, Institute of Earth Science, Largo dos Colegiais 2, 7004-516 Évora, Portugal, roberto.silva@uevora.pt, ORCID 0000-0003-3865-8724*

[5]*Biological Mission of Galicia – Spanish National Research Council (MBG-CSIC), Salcedo, Pontevedra, Spain, MED&CHANGE | MED – Mediterranean Institute for Agriculture, Environment and Development & CHANGE – Global Change and Sustainability Institute, University of Évora, Largo dos Colegiais 2, 7004-516 Évora, Portugal, sergio.prats@uevora.pt, ORCID 0000-0002-7341-877X*

[6]*Universidade do Minho, Campus de Gualtar, Institute of Earth Sciences, 710-057 Braga, Portugal, teresav@dct.uminho.pt, ORCID 0000-0002-7293-3825*

Abstract

Industrial byproducts were tested for acid mine drainage (AMD) treatment in the Iberian Pyrite Belt. Bench-scale experiments evaluated paper sludge and biochar at different AMD: material ratios (1:50, 1:100, 1:200) under oxic/anoxic conditions. Paper sludge raised pH from 1.64 to 6.23 (1:50), promoting Fe removal (100%). Biochar effectively adsorbed Cu (98%) at pH 5. A geochemical model simulated a field-scale treatment using a downflow pond with paper sludge and a biochar barrier. Results suggest these materials effectively neutralize AMD and retain potentially toxic elements, supporting their use in passive remediation.

Keywords: Passive Treatment, Industrial Byproducts Solutions, Geochemical Modeling, Iberian Pyrite Belt

Introduction

The Caveira polymetallic sulfide mine, in the northwest Iberian Pyrite Belt (IPB), faces significant environmental challenges due to historical mining. Its geology consists of an N-S-oriented antiform with a core of phyllites and quartzites (Middle-Superior Famenian) and flanks of sedimentary and volcanic sequences from the volcano-sedimentary complex (VSC). Sulfide mineralization, mainly pyrite with minor chalcopyrite, galena, and sphalerite, occurs in the VSC (Matos & Martins, 2006; Reis *et al.*, 2012). Despite its small size, the site contains extensive heap leach areas and ~2 Mt of waste (Reis *et al.*, 2012). Mining began in Roman times, initially for Au and Ag, later shifting to Cu, S, and pyrite until its abandonment in the 1960s, leaving uncontrolled acid mine drainage (AMD) that flows into the Grândola stream, dispersing potentially toxic elements (PTE) such as Cu, Pb, Zn, As, Mo, Se, Cd, Fe, and Hg (Matos & Martins, 2006; Reis *et al.*, 2012).

AMD treatment in abandoned IPB mines could involve industrial byproducts, reducing environmental impact and supporting a circular economy. The paper industry produces alkaline residues rich in lime and organic compounds, often landfilled, but capable of neutralizing AMD and facilitating metal attenuation. The most common paper sludge, from the kraft pulping process, consists primarily of organic residue with mineral impurities plus residual Ca and Na carbonates or oxides (Simão, 2018; Haile *et al.*, 2021). Likewise, biochar, which is charcoal produced from oxygen-limited biomass combustion (e.g., vineyard prunings, forestry waste, sewage sludge), has shown adsorptive potential for AMD remediation (Hu *et al.*, 2020; Qiu *et al.*, 2022). Bench-scale tests are crucial to assess these materials' feasibility. Simulating pond conditions with varying material-to-AMD ratios provides insights into their effectiveness, optimizing pH neutralization and metal attenuation. Integrating industrial byproducts into AMD treatment aligns with sustainable waste management, offering a viable alternative to conventional methods. This study investigates the effectiveness for paper sludge and biochar to be used for neutralizing AMD, with potential application in the IPB and beyond.

Methods

Bench-scale experiments evaluated the potential of industrial byproducts – paper sludge and biochar – for AMD. The study assessed their capacity to neutralize AMD and attenuate metal contaminants under controlled conditions. Batch tests were conducted in parallel under oxic or anoxic conditions to simulate a downflow pond. The pond experiments used 200ml AMD sample with material-to-AMD ratios of 1:50, 1:100, and 1:200 over 10 days, without agitation. The initial AMD had pH 1.68, SO_4 15000 mg/L, Fe 2830 mg/L, Al 583 mg/L, and Mn 63.7 mg/L, plus elevated concentrations of As (17.6 mg/L), Cd (0.528 mg/L), Co (1.01 mg/L), Cr (0.31 mg/L), Cu (33.1 mg/L), Ni (1.22 mg/L), Pb (2.29 mg/L), and Zn (146 mg/L). Effluent pH and electrical conductivity (EC) were monitored daily, while final effluent samples were analyzed by ICP-OES for metal concentrations. Solid-phase materials that accumulated in the ponds were dried at 40°C, ground, digested with *Aqua Regia*, and then analyzed by ICP-OES. Kinetic adsorption tests at pH 5 assessed metal retention by biochar and paper sludge. Using 0.4g of each material in 40ml of single-element solution, samples were shaken at 225 rpm at room temperature, with collection at intervals (5 min–24 h), followed by filtration and ICP-OES analysis.

A preliminary geochemical model was developed using PHREEQC (Parkhurst and Appelo, 2013) and the PHREEQ-N-AMDTreat+REYs water-quality tools with the wateq4fREYsKinetics.data database (Cravotta, 2022) to simulate the observed chemical changes during bench experiments. Subsequently, the model was applied to simulate a field-scale downflow pond system. Paper sludge served as a base layer to increase pH and precipitate Fe, followed by a biochar-based barrier for Cu and other metals.

Results

Kinetic Adsorption Tests

The kinetic adsorption tests assessed the adsorption rate and capacity of excess metals in Caveira mine water using the studied materials. Results revealed distinct behaviors due to their differing physicochemical properties: carbonate-rich paper sludge exhibited a different adsorption profile than highly porous, carbon-rich biochar. Copper (Cu) (Fig. 1) demonstrated similarly high retention rates for both materials, with paper sludge achieving 99.9% retention and biochar 98.3%. However, paper sludge removed nearly all Cu within 15 minutes, whereas biochar adsorbed it more slowly. Mercury (Hg) (Fig. 1) was rapidly retained by biochar (99.6% in 5 min), while paper sludge showed slower retention, reaching only 50.6% after 24 hours. Manganese (Mn) (Fig. 1) behaved differently: biochar retained just 18.4%, while paper sludge achieved complete removal (100%) within 15 minutes. Zinc (Zn) (Fig. 1) followed a similar trend, with paper sludge reaching 100% retention in 5 minutes, whereas biochar initially retained some Zn, then released it entirely after 10 hours, ending with only 21% retention after 24 hours.

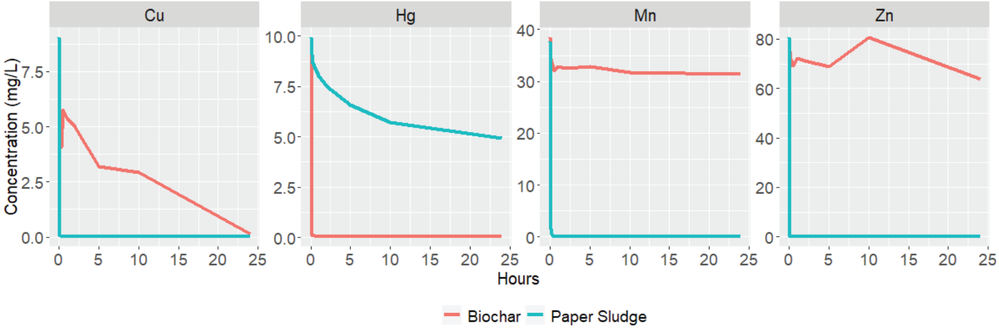

Figure 1 Adsorption kinetics of biochar and paper sludge for the studied metals over time.

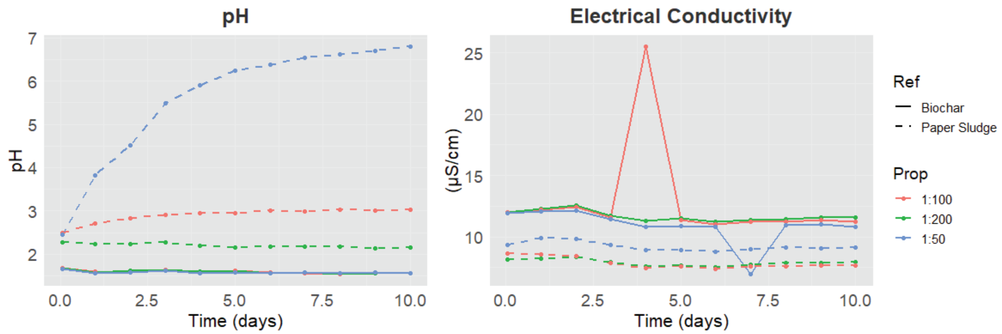

Figure 2 pH and electrical conductivity recorded in ponds under anoxic conditions over time.

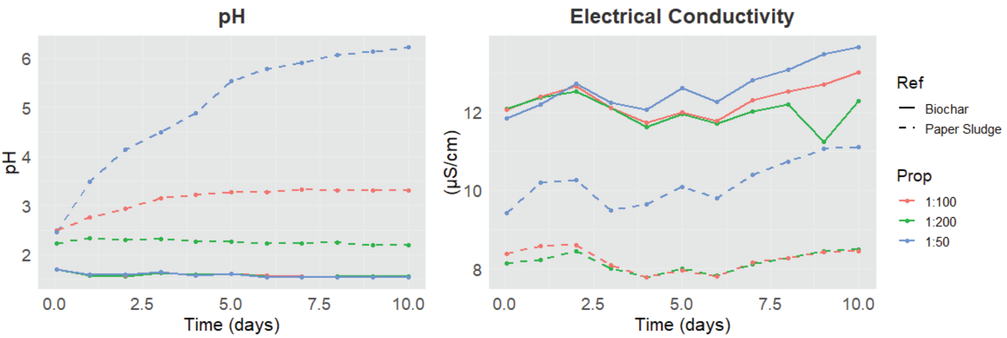

Figure 3 pH and electrical conductivity recorded in ponds under oxic conditions over time.

Pond Simulation Experiments

The primary objective of the bench-scale pond simulation experiment was to identify the optimal conditions for increasing the initial water pH (1.64) to enhance the retention capacity of metallic elements, which typically occurs at pH levels above 5–5.5. Additionally, the study aimed to assess the retention capacity of the materials for each element. The initial water EC was 11.67 mS/cm.

In biochar ponds, the initial pH (1.64) remained stable under both anoxic (Fig. 2) and oxic conditions (Fig. 3). In contrast, paper sludge ponds showed an important pH rise, especially at a 1:50 ratio, reaching 6.80 (anoxic) and 6.23 (oxic) after 10 days. Lower ratios were pH, around 3 (1:100) and 2 (1:200).

***Table 1** PTE and Alcaline Metals Removal after 10 days, ((C0-Ct)/C0 in %) in Anoxic Ponds water columns.*

	P. Sludge 1:200	P. Sludge 1:100	P. Sludge 1:50	Biochar 1:200	Biochar 1:100	Biochar 1:50
Al	-20,9	10,6	**100**	-12,4	-14,4	-12,9
As	**76,1**	**100**	**100**	**21,1**	**23,6**	**26,0**
Ca	-425,4	-277,1	-286,6	13,8	7,5	1,4
Cd	**49,5**	**66,4**	**97,1**	15,9	18,0	20,8
Co	5,0	-7,9	**86,3**	2,2	3,9	7,4
Cr	-1,5	58,2	**64,7**	-0,6	-0,5	4,4
Cu	28,2	31,8	**99,7**	**42,5**	**41,3**	**43,2**
Fe	23,2	**100**	**100**	-14,2	-16,5	-14,2
K	-2693	-11503	-23208	-2127	-2349	-6223
Mg	-196,1	-289,9	-512,7	0,5	0,5	-0,3
Mn	-23,9	-57,5	25,2	**20,6**	**19,7**	**22,8**
Na	-724,5	-1219	-2397	-24,2	-24,7	-25,8
Ni	3,9	7,6	**90,9**	10,3	10,5	15,1
Pb	**67,6**	**86,8**	**96,3**	-1,0	-12,7	-2,0
Zn	-26,2	-3,4	**98,7**	-5,2	-7,5	-6,0

In anoxic conditions (Fig. 2), paper sludge maintained stable EC (7–8 mS/cm), lower than the original water. In oxic ponds (Fig. 3), only the 1:50 ratio showed similar value (11.11 mS/cm after 10 days). Biochar conductivity in anoxic ponds (Fig. 2) was generally stable, except for peaks at 1:100 (day 4) and 1:50 (day 7). In oxic conditions (Fig. 3), this parameter increased gradually, peaking at 13.66 mS/cm for the 1:50 ratio.

PTE removal efficiencies were similar in both conditions (Tabs. 1 and 2). Biochar, particularly at the 1:50 ratio, had the lowest retention rates, while the most effective system was the 1:50 paper sludge pond with oxygenation.

The As exhibited the highest retention rates among all elements, with values ranging from 21.1% to 100% in anoxic ponds (Tab. 1) and from 0.6% to 100% in oxic ponds (Tab. 2), with

***Table 2** PTE and Alcaline Metals Removal after 10 days, ((C0-Ct)/C0 in %) in Oxic Ponds water columns.*

	P. Sludge 1:200	P. Sludge 1:100	P. Sludge 1:50	Biochar 1:200	Biochar 1:100	Biochar 1:50
Al	-81,7	-3,1	**99,9**	-19,9	-29,9	-46,8
As	**78,9**	**100**	**100**	**7,8**	**10,6**	**0,6**
Ca	-619,0	-301,2	-268,7	2,8	0,8	-26,6
Cd	**44,7**	**64,0**	**95,3**	13,6	9,2	3,2
Co	-2,3	-17,3	**93,6**	4,6	-2,8	-9,4
Cr	-3,6	60,8	**63,7**	0,5	-3,8	-8,7
Cu	24,1	30,2	**99,6**	**29,8**	**24,5**	**17,5**
Fe	20,8	**99,8**	**100**	-20,6	-30,9	-46,2
K	-2859	-10891	-27615	-2453	-5404	-8363
Mg	-346,8	-397,0	-665,2	-5,2	-14,6	-33,0
Mn	-32,6	-72,3	45,1	**9,1**	**2,5**	**-5,7**
Na	-1144	-1551	-3227	-30,6	-41,0	-67,9
Ni	-2,7	-18,0	**95,3**	11,7	3,3	2,8
Pb	**72,2**	**88,9**	**97,2**	-17,3	-14,3	-10,0
Zn	-88,8	-26,4	**99,5**	-11,5	-21,1	-38,9

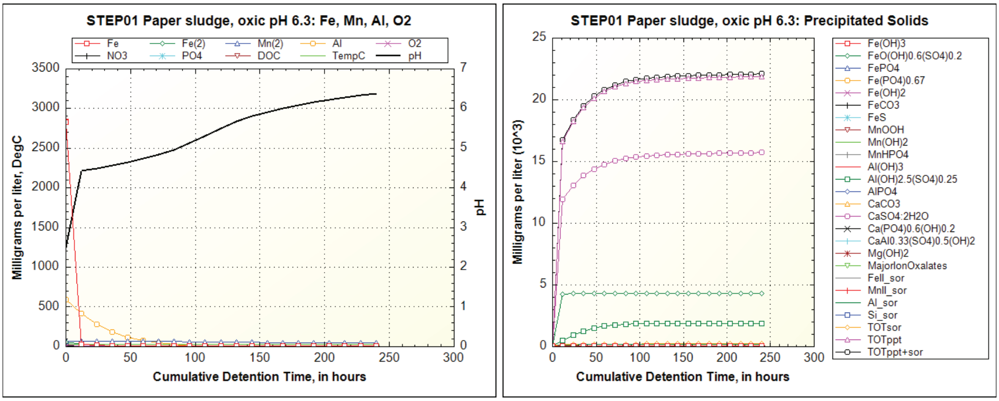

***Figure 4** Major Elements in solution (left) and precipitated solids (right) vs time, modeled in PHREEQ-N-AMDTreat + REYs for paper sludge pond.*

the highest retention observed in paper sludge systems. K and Na were the only elements not retained; instead, they were released into the environment, as indicated by their negative retention values. In the case of paper sludge, As retention was the most successful, with removal rates between 76.1% and 100% in anoxic ponds (Tab. 1) and between 78.9% and 100% in oxic ponds (Tab. 2). For biochar, the highest retention was observed for Cu, with retention rates ranging from 41.3% to 43.2% in anoxic ponds (Tab. 1) and from 17.5% to 29.8% in oxic ponds (Tab. 2).

Geochemical Modeling

To simulate remediation with paper sludge, the PHREEQ-N-AMDTreat+REYs kinetics models, TreatTrainMix2_wateq.exe and TreatTrainMix2REYs.exe were used to simulate the progressive dissolution of limestone over 240 hours combined with an excess of solid organic carbon (SOC 20 mol) under oxidizing conditions. To account for the removal of the trace elements by adsorption, a specified mass of sorbent (1000 mg) having Fe, Mn, and Al concentrations of 81.4wt%, 1.8wt%, 16.8wt%, consistent with the mass fractions in the starting solution, was assumed to be present for the duration. Fig. 4 shows an equilibrium trend for basaluminite ($Al(OH)_{2.5}(SO_4)_{0.25}$) and schwertmannite ($FeO(OH)_{0.6}(SO_4)_{0.2}$). However, it also indicated that various metal-bearing species remain in solution, leading to increased precipitation of these and other alkaline solids, with gypsum ($CaSO_4{\cdot}2H_2O$) being the most predominant.

Discussion

In the kinetic assays, biochar exhibited approximately 100% retention for Cu and Hg (Fig. 1). According to Kılıç *et al.* (2008), adsorption occurs on the biomass surface, where the release of protons and basic metal ions (Ca^{2+}, Na^+, and K^+) happens during Cu^{2+} or Hg^{2+} adsorption. This mechanism may explain the low retention rates in both oxic and anoxic biochar ponds (Tabs. 1 and 2). Biochar has a high affinity for Cu, evidenced by the kinetic assays (Fig. 1) and by Cu being the most adsorbed metal in the pond experiment (Tabs. 1 and 2). This reaction is pH-dependent (Padilla *et al.*, 2024). Mn and Zn showed approximately 20% retention in biochar assays (Fig. 1). Zn likely relies on ion exchange or electrostatic attraction, while Mn retention is hindered by high H^+ ion concentrations. Paper sludge demonstrated about 50% retention for Hg in kinetic tests (Fig. 1). Hg adsorption on cellulosic surfaces is pH-dependent, with higher pH favoring $HgOH^+$ formation and increased metal retention (Min & Ray, 2024). In contrast, Cu, Mn, and Zn retention by paper sludge reached nearly 100%. This efficiency is attributed to Ca^{2+} and Mg^{2+} release, facilitating ion exchange and promoting metal precipitation (Méndez *et al.*, 2009). Negative retention values (Tabs. 1 and 2) further suggest this. pH, a key parameter influencing adsorption interactions, was not measured during this experiment. Future studies will address this limitation.

Biochar, in the pond experiment, exhibited higher EC in both oxic and anoxic conditions (Figs. 2 and 3), indicating a higher concentration of dissolved metals, supported by Tables 2 and 3. This outcome is likely due to biochar's limited ability to increase pH, as its adsorption capacity is pH-dependent and more effective at higher values (Padilla *et al.*, 2024). However, EC was higher in oxic ponds, suggesting greater metal retention in anoxic conditions, likely due to enhanced ion reduction and metal immobilization on biochar (Zhao *et al.*, 2024). Paper sludge in the 1:50 ratio showed higher EC in an oxidizing environment (Figs. 2 and 3), indicating a greater concentration of metal ions. Higher levels of K, Na, and Mg were observed in oxic conditions (Tab. 2), likely due to oxidation reactions that accelerate organic matter breakdown and cation release (Bastviken *et al.*, 2001). This may explain why paper sludge ponds in oxygenated conditions performed slightly better than in anoxic environments (Tabs. 2 and 3).

The geochemical model generated by PHREEQ-N-AMDTreat+REYs (Fig. 4), showed that although most of the Fe precipitated at pH <3, the specified sorbent indicates this hydrous ferric oxide, as well as hydrous aluminum oxide and hydrous manganese oxide that form at higher pH, continues to be available when the pH increases to values sufficiently high for the elements to sorb. The model results are consistent with observed changes in the pH, Fe, Al, Mn, and trace elements, including nearly complete removal of Fe, Al, and most trace elements, but incomplete removal of Mn and Zn. Extrapolating the experimental results to a field model, Padilla *et al.* (2024) suggest that biochar exhibits higher retention ability at pH levels above 6.5. This supports the use of a paper sludge pond for initial mine drainage treatment, where it could effectively increase pH and retain elements. Following this, a biochar-based reactive barrier could further enhance metal adsorption by targeting the remaining dissolved elements, capitalizing on biochar’s increased retention efficiency at higher pH levels.

Conclusions

Biochar and paper sludge demonstrated promising potential for AMD treatment, each exhibiting distinct adsorption behaviors for different elements. Biochar proved particularly effective in adsorbing Cu and Hg, with its performance being pH-dependent, while paper sludge showed high retention rates for Cu, Mn, and Zn, likely due to ion exchange mechanisms and its ability to raise pH. The pond experiments highlighted the importance of environmental conditions, such as oxygen availability, in influencing metal retention and conductivity. Extrapolating to a field model, biochar’s increased efficiency at pH levels above 6.5 supports its potential role in a two-stage treatment system, where paper sludge could initially raise pH and retain PTE, followed by a reactive biochar barrier for further metal adsorption.

Acknowledgements

The authors thank to: (1) National funds through FCT – Science and Technology Foundation, I.P., in the framework of the UIDB/04683 and UIDP/04683 – Institute of Earth Sciences (IES) Programs; (2) Project GeoMinA – Implementation of a basis for defining geoenvironmental models in abandoned mining areas in the Iberian Pyrite Belt – PL23-00035 – Promove Actions Project 2023 Fundação La Caixa (2024–2027); (3) SOLVO and SOLVIT projects, based at the University of Évora, Portugal, for providing the biochar; (4) Biotek, S.A. for providing the paper sludge.

References

Bastviken D, Ejlertsson J, Tranvik L (2001) Similar bacterial growth on dissolved organic matter in anoxic and oxic lake water. Aquat Microb Ecol 24:41–49

Cravotta CA III (2022) Interactive PHREEQ-N-AMDTreat+REYs water-quality modeling tools to evaluate potential attenuation of rare-earth elements and associated dissolved constituents by aqueous-solid equilibrium processes (software download). US Geol Surv Software Release. https://doi.org/10.5066/P9M5QVK0

Haile A, Gelebo GG, Tesfaye T, Mengie W, Mebrate MA, Abuhay A, Limeneh DY (2021) Pulp and paper mill wastes: utilizations and prospects for high value-added biomaterials. Bioresour. Bioprocess. 8, 35 (2021). https://doi.org/10.1186/s40643-021-00385-3

Hu B, Ai Y, Jin J, Hayat T, Alsaedi A, Zhuang L, Wang X (2020) Efficient elimination of organic and inorganic pollutants by biochar and biochar-based materials. Biochar 2(1):47–6

Kılıç M, Keskin ME, Mazlum S, Mazlum N (2008) Hg(II) and Pb(II) adsorption on activated sludge biomass: effective biosorption mechanism. Int J Miner Process 87:1–8

Matos JX, Martins LP (2006) Reabilitação ambiental de áreas mineiras do setor português da Faixa Piritosa Ibérica: estado da arte e perspetivas futuras. Bol Geol Min 117(2):289–304

Méndez A, Barriga S, Fidalgo JM, Gascó G (2009) Adsorbent materials from paper industry waste materials and their use in Cu(II) removal from water. J Hazard Mater 165(1–3):736–743. doi:10.1016/j.jhazmat.2008.10.061

Min HS, Ray S (2024) Removal of mercury ions from wastewater using different techniques. Int J Eng Trends Technol 72(10):21–34

Padilla JT, Watts DW, Szogi AA, Johnson MG (2024) Evaluation of a pH- and time-dependent model for the sorption of heavy metal cations by poultry litter-derived biochar. Chemosphere 347:140688. doi:10.1016/j.chemosphere.2024.140688

Parkhurst DL, Appelo CAJ (2013) Description of input and examples for PHREEQC version 3—A computer program for speciation, batch-reaction, one-dimensional transport, and inverse geochemical calculations. US Geol Surv Tech Methods 6-A43. https://doi.org/10.3133/tm6A43

Qiu M, Liu L, Ling Q, Cai Y, Yu S, Wang S, Baowei D, Wang X (2022) Biochar for the removal of contaminants from soil and water: a review. Biochar 4:19. doi:10.1007/s42773-022-00139-1

Reis AP, Ferreira da Silva E, Cardoso Fonseca E, Patinha C, Barrosinho C, Matos J (2012) Environmental assessment of the Caveira abandoned mine (Southern Portugal): Part 1: Characterization of metal contaminated soil. Soil Sediment Contam 21(2):227–254

Simão L, Hotza D, Raupp-Pereira F, Labrincha JA, Montedo ORK (2018) Wastes from pulp and paper mills - a review of generation and recycling alternatives. Cerâmica 64:443–453. http://dx.doi.org/10.1590/0366-69132018643712414

Zhao Z, Lou W, Zhong D, Shi S, Zhang F, Wang L, Wu X, Sheng A, Chen J (2024) Time-varying contributions of FeII and FeIII to AsV immobilization under anoxic/oxic conditions: The impacts of biochar and dissolved organic carbon. Sci Total Environ 949:168102. doi:10.1016/j.scitotenv.2023.168102

Geochemical Monitoring to Use Waste Rock in Mine Component Construction

David Arcos[1], Pablo Quesada[2], Alonso Huamán[3], Emilie Coene[4], Ersan Demirer[5]

[1]*Amphos 21 Consulting S.L. c/ Veneçuela 103, 2ª plta., 08019 Barcelona, Spain, david.arcos@amphos21.com*

[2]*Amphos 21 Consulting Perú S.A.C. Jirón Paseo del Bosque 500 of. 201, Urb. Chacarilla del Estanque – San Borja, 15037 Lima, Peru, pablo.quesada@amphos21.com*

[3]*Amphos 21 Consulting Perú S.A.C. Jirón Paseo del Bosque 500 of. 201, Urb. Chacarilla del Estanque – San Borja, 15037 Lima, Peru, alonso.huaman@amphos21.com*

[4]*Amphos 21 Consulting S.L. c/ Veneçuela 103, 2ª plta., 08019 Barcelona, Spain, emilie.coene@amphos21.com*

[5]*Amphos 21 Consulting S.L. c/ Veneçuela 103, 2ª plta., 08019 Barcelona, Spain, ersan.demirer@amphos21.com*

Abstract

Current mining operations require the use of waste rock for the construction of components, such as the tailings dam. In the case of the mine considered in this study, the possibility of using material defined as PAG (potential acid generation) was also required. To this end, an ambitious testing program was developed for more than 8 years specially focused on the geochemical behaviour of the use of this material. As a result, innovative methodologies were developed in the industry that concluded with the definition of the characteristics of the PAG material that could be used in the construction of the tailings dam.

Keywords: Geochemistry, tailings facilities, mining operations, geochemical monitoring, large-scale tests

Introduction

Mining operations need to construct several components to operate the mine. These components include waste rock dumps, tailings deposition facilities, process plants, water reservoirs, live camps, roads, and many other infrastructures. Many of these infrastructures require large earthworks and the availability of rock material for their construction. Although, in some cases, these rocks can be extracted from quarries inside the mining area, in other cases, the only suitable material is the waste rock excavated from the mine pit. This is the case of the Mine Z in Peru, an open-pit mining operation in a porphyry copper deposit with an associated copper skarn. Mines in this type of deposits usually needs very large tailings facilities. In this case, the dam of the tailings deposit was initially designed using geotechnically acceptable waste rocks of the Non-PAG (Non-Potential Acid Generation) type. However, after several operational modifications, due to increase of mineral reserves, the change in mine planning resulted in a mismatch between tailings dam construction schedule and Non-PAG rocks availability. This led to pushing the limits of non-PAG material and evaluating the use of a material that, while being PAG, could be used during periods of time when non-PAG material was not available for the construction of the tailings dam. For this reason, a geochemical program to test the use of part of the PAG material for the dam construction was initiated. The objective of the program was to evaluate the type of PAG and its encapsulation conditions to prevent or minimize acid mine drainage and metal leaching from the tailings dam. This paper presents the results of this program and demonstrates the usefulness of environmental geochemistry in mining operations.

Methods

The geochemical program was divided in four different stages. Stage 1 consisted in the revision of all the geochemical information from waste rocks recorded by the mine, including lithological and mineralogical descriptions, and geochemical analysis and tests in 250 samples. The main source of analytical data came from ABA, NAG and SPLP tests, as well as humidity cell tests in 35 of the samples. This review allowed to define geoenvironmental units (GEUs), as rock types with equivalent lithologies and mineralogy, and similar geochemical behaviour (Arcos *et al.* 2011).

Stage 2 consisted of field tests in humidity cells. These tests used 1 m3 cells filled with the previously defined GEUs and combinations between them to evaluate the geochemical effect of the encapsulation of the PAG material (Fig. 1). A quartz gravel-filled cell was also constructed to be used as a reference cell. The cells were exposed to the site climatic conditions for over 6 years, during which they were monitored during rainfall events in the wet season. After each rainfall event, drainage water of the cells was collected in buckets, where the volume was measured, and field parameters (pH, electrical conductivity, temperature, total dissolved solids, dissolved oxygen and redox potential) were measured. In addition, a sample was taken for a complete chemical analysis of the drainage water.

In Stage 3, a layer of PAG material was installed in the dam of the tailings facility. This layer was monitored using oxygen and volumetric water content sensors. In addition to these parameters, the sensors also measured electrical conductivity and temperature. The sensors were arranged along four cross sections of the dam in three lines in each section (lower, middle and upper lines). Each line contained three pairs of sensors each one at 15, 25 and 35 m from the outer slope of the dam as shown for one of the sections in Fig. 2. It is important to note that the lower line was located in Non-PAG material and was considered as a reference line. The construction of the system, from the installation of the first line to the upper

***Figure 1** Field humidity cell tests at the mine site.*

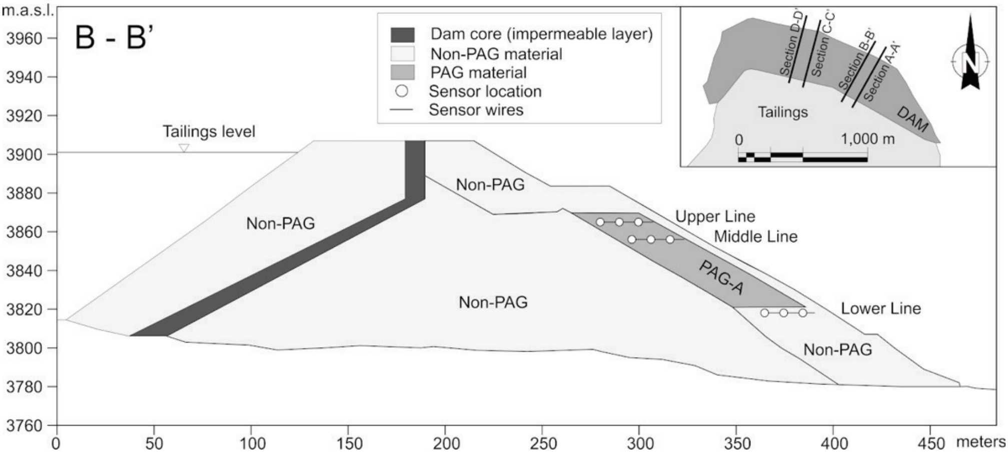

Figure 2 *Profile across the dam of the tailings facility showing the PAG layer and the location of the sensors.*

one, took approximately one year. Sensors have been recording a hourly measurements for a period of more than four years since the installation of the lower line.

Finally, the data collected throughout the previous stages have been used to calibrate a reactive transport model. This model has been implemented in the iCP interface (Nardi *et al.* 2014), which is a coupling between Comsol Multiphysics®, a general-purpose finite element simulation software for modelling coupled physics systems, and the geochemical code PHREEQC (Parkhurst and Appelo 2013). The result of this interface is a tool for solving a wide range of multiphysics and chemical problems, in this case a model of unsteady, variable-temperature reactive transport under unsaturated conditions.

Results and Discussion

Historical geochemical data from the mine reveal that results are highly dependent on lithology and its relationship to the mineralizing event. In terms of acid-generating potential, high carbonate (i.e. calcite) lithologies such as limestones, marbles and skarn alteration have been defined as Non-PAG. Post-mineralization intrusive rocks have also been defined as Non-PAG. In contrast, intrusive rocks associated with or prior to the mineralizing event, as well as some endoskarn samples, are defined as PAG or Non-PAG depending on carbonate and/or sulfide content.

In terms of metal leaching potential, based on leachates from NAG and SPLP tests, the neutralization potential ratio (NPR) has been identified as the main variable. This parameter indirectly includes lithological characteristics, since it usually presents high values for those lithologies with high calcite contents (i.e. limestones) or when the sulfide content is very low (post-mineralization intrusive rocks). The relationship between metal leaching potential and NPR shows that for a NPR > 3 this potential will be very low; while for a NPR < 0.3 the potential almost always exceeds the maximum permissible limit (MPL) defined in the legislation for mining effluents. Between both NPR values, metal concentrations gradually increase, but always below the MPL. This behaviour has been observed for all metals, although not all of them exceed the corresponding MPL value when NPR < 0.3. This allowed the differentiation of GEUs based on the NPR and sulfide content:

- **Non-PAG:** Rocks with an NPR ⩾3.0 and/or $S_{sulfide}$ ⩽0.1
- **PAG-A:** Rocks with an NPR between 0.3 and 3.0 and $S_{sulfide}$ >0.1
- **PAG-B:** Rocks with an NPR <0.3 and $S_{sulfide}$ >0.1

Field humidity cells show a similar behaviour after more than 6 years in operation (Fig. 3). Thus, the most acidic conditions and with higher concentrations of sulfate and metals in the leachates correspond to the

PAG-B material. In contrast, the Non-PAG material presents neutral to slightly alkaline conditions and very low concentrations of metals. While the PAG-A material shows an intermediate behaviour. It is important to highlight the variable behaviour of PAG-A. One of the samples shows a pH ≈ 7 over the 6 years of testing; while the other sample shows a constant decrease from pH = 7 at the beginning of the test, to pH ≈ 3 after 6 years of testing. Similarly, metals evolve to much higher concentrations in the sample with higher acidity, reaching values very similar to those of the PAG-B sample (Fig. 4). The largest difference between the two samples corresponds to the sulfide content (i.e. pyrite), being 0.4 and 0.8 wt.% for the sample kept under neutral conditions and for the sample evolving under acidic conditions, respectively. This could indicate the existence of a threshold value for the sulfide concentration, from which acid generation occurs in PAG-A and, therefore, metal concentrations increase. This is something to consider when using this material in the construction of the tailings dam.

Some of the cells were designed to evaluate the effect of encapsulating PAG material with different configurations and thicknesses of Non-PAG material. Fig. 3 shows the result of two cells in which a 0.5 m thick layer of PAG-A was placed between two 0.25 m thick layers of Non-PAG. The effect of encapsulation, in all encapsulation configurations, was to neutralize the acidity generated in the PAG layer and to reduce the concentration of metals in the drainage water by more than one order of magnitude, to values below the MPL. This behaviour was a clear argument in favour of using PAG-A type material in the construction of the tailings dam.

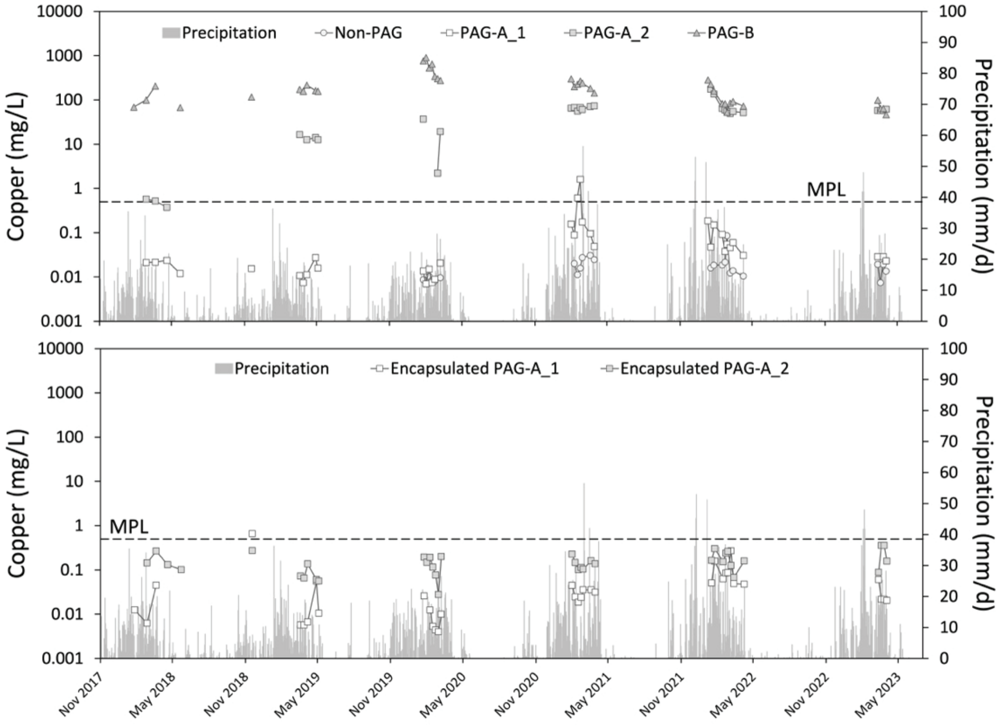

Figure 3 *Graphics showing the geochemical evolution of some of the field humidity cells. Upper graphic shows the evolution of cells representative of the three GEUs, whereas bottom graphic shows the evolution of two of the cells where a 0.5 m thick layer of PAG-A material was sandwiched between two 0.25 m thick layers of Non-PAG material. Histogram at the bottom of both graphs represents the daily precipitation MPL: maximum permissible limit.*

Installation of the PAG-A layer in the tailings dam began in December 2020. Although the variable behaviour of this material described above had already been identified, there was no possibility to limit this material to lower sulfide contents due to mine planning constraints. It should be noted that the materials used for the construction of the dam are based on the definition of GEUs, which was implemented in the mine block model. Therefore, although each 20 × 20 × 15 m block can be assigned a GEU, there may be some heterogeneity inside.

Since the installation of the lower line, most of the sensors worked perfectly for the first two years, but after two and a half years, failures began to occur in the oxygen sensors installed in the middle lines of all the profiles. As will be seen later, this was attributed to these sensors being more sensitive to the acidic conditions that were being generated in these locations, although this could not be verified for obvious reasons. The water content sensors functioned perfectly throughout the monitoring period.

The results show that the dam materials are unsaturated with respect to water content, but that during the rainy season the saturation increases, without reaching complete saturation. The response time with respect to rain events depends on the depth of the sensor at any given time (it is noting that the dam is under permanent construction according to operational needs) and the distance from the external slope of the dam, but in general it is between two weeks and a month and a half.

Oxygen measurements in the gas phase decreased towards the interior of the dam (Fig. 4). But more importantly, there was a decrease in concentration between the lower and upper lines. Thus, while oxygen contents close to atmospheric levels (21% O2) were recorded in the lower lines (in Non-PAG layers), the values in the middle and upper lines were lower (already in the PAG-A layer). Although this decrease may be due to the oxidation process of pyrite (the predominant sulfide mineral in the waste rock), it is difficult to confirm this relationship.

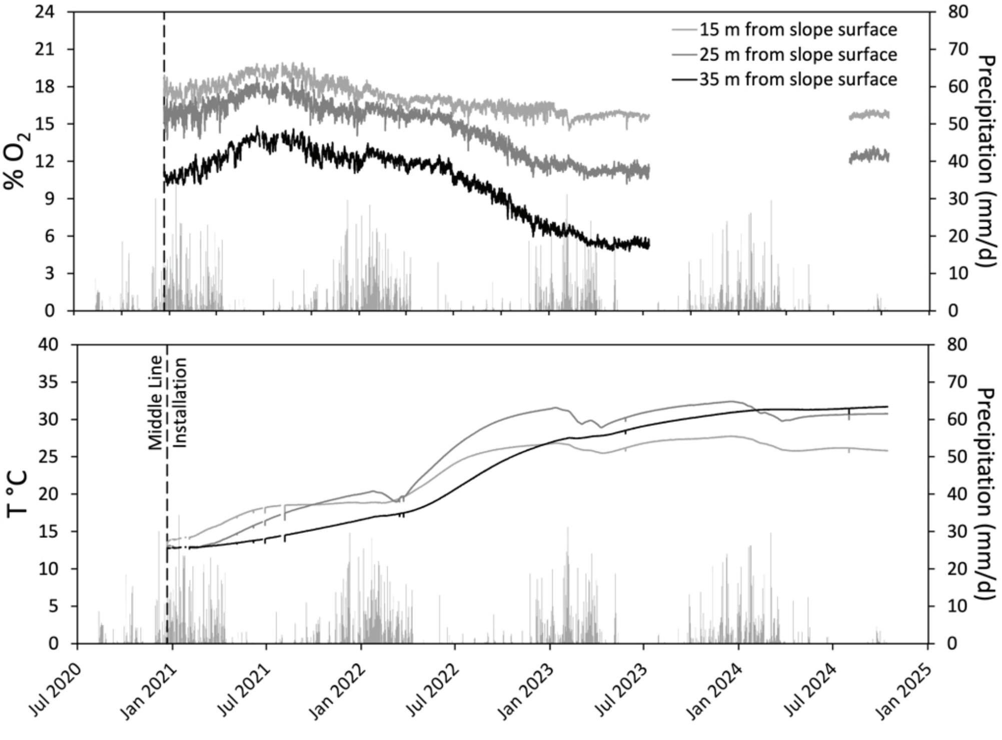

Figure 4 *Graphics showing the evolution of oxygen in the gas phase and temperature measured by sensors in one of the middle lines installed in the tailings dam.*

On the other hand, the evolution of the recorded temperature shows that in the sensors of the lower lines (in non-PAG material) the temperature increases from around 12 °C, just after the installation of the sensors, to 15–19 °C after 4 years. However, this evolution only occurs in the innermost sensors (at 35 m) with respect to the external slope of the dam, while the intermediate sensors show a smaller increase and the outermost ones (at 15 m from the external slope) do not show variation with respect to the beginning. However, the greatest changes are recorded in the sensors installed in PAG-A material. In the middle lines (Fig. 4), an increase was recorded in all the sensors from the initial 12 °C to 26–33 °C in the sensors located 25 and 35 m from the external surface. The sensor located in the outermost part (15 m) also recorded an increase, although smaller (15–26 °C). In the upper lines of sensors, an increase is also recorded up to 16–21 °C, much lower than in the case of the middle lines and more homogeneous for all the sensors in the line. It is worth noting that during the rainy season, the sensors that record higher temperatures show a slight decrease (Fig. 4), which then continues to increase during the dry season.

This temperature evolution inside the dam indicates the existence of an exothermic process and, considering the characteristics of the materials, this process consists of the oxidation of pyrite, so the temperature record is a more effective indicator to identify the existence of acid drainage generation processes. In fact, it not only allows the identification of the pyrite oxidation process but can also be used to quantify and calibrate the process in a reactive transport model.

The information generated from the geochemical tests was included in a reactive transport model for the dam. Only the downstream part of the dam was considered in the model, since the rest is separated by an impermeable layer (Fig. 2). The saturation, water and air flow parameters were calibrated using the information generated from the sensors installed in the tailings facility. The model considered the kinetic dissolution of primary minerals, mainly silicates, sulfides and carbonates, as well as the precipitation-dissolution under equilibrium conditions of secondary minerals. The model also considered the air flow in the system and the consumption of oxygen from the air by dissolution in the aqueous phase and pyrite oxidation. The pyrite oxidation process was calibrated from temperature data from the sensors, since the heat generation of the process from the enthalpy of the reaction was included in the model, so the model was run under non-isothermal conditions. Based on temperature records and to consider the high variability of the sulfide content of the PAG-A material, two subtypes of this material were included in the model, one with 1 wt.% pyrite (PAG-A1) and another with 10 wt.% pyrite (PAG-A2).

The model simulated a three-year period, and the results were compared to data on the quality of the dam drainage water, since the installation of the PAG-A layer, which is analysed monthly. The comparison showed that the model results fit the drainage data reasonably well. As shown in Fig. 5, the temperature results are equivalent to those recorded, and the metal concentrations in the waters inside the dam show that it is the PAG-A2 material that actually generates metal leaching.

It can therefore be concluded that, in this case, the use of PAG-A material with pyrite contents below 1 wt.% is geochemically acceptable for the construction of the dam since it will not generate acidic conditions in the system nor lead to the leaching of metals that may exceed the maximum permissible limits. A long-term model under closure conditions has also been developed, the results of which point in the same direction.

Conclusions

The results of this project show that geochemistry can play a very important role in the mining industry, not only in terms of environmental impact, but also in the mining operation itself, both in the engineering design of the operation and in the management and monitoring of components. In the case of this mine, this translates into a very well-calibrated definition of GEUs that allows defining their uses in the mining operation. It can also

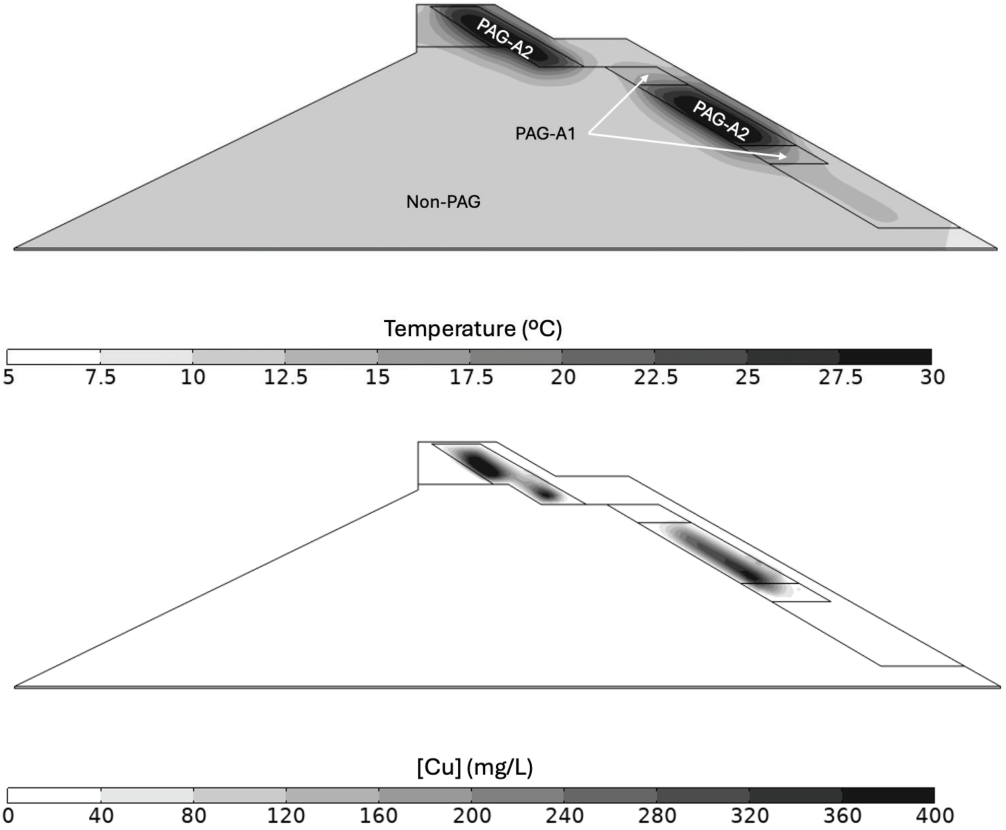

Figure 5 *Calibrated modelling results after 3 years of simulation for temperature (above) and copper concentration in water (below).*

be concluded that one of the key factors in identifying the generation of acid drainage in a mining component is temperature monitoring, which may represent a key factor in the future.

Acknowledgements

The authors thank all the staff of the mine for their support along the project, helping in the design, construction and data acquisition phases, as well as for their useful discussions on the results.

References

Arcos D, von Igel W, Flores LG, Acuña A (2011) Geoenvironmental units (GEUs) in waste dumps from Collahuasi. Proceedings of the 2nd International Seminar on Environmental Issues in the Mining Industry. Santiago, Chile, November 2011.

Nardi A, Idiart A, Trinchero P, de Vries LM, Molinero J (2014) Interface COMSOL-PHREEQC (iCP), an efficient numerical framework for the solution of coupled multiphysics and geochemistry. Computers & Geosciences 69: 10-21

Parkhurst DL, Appelo CAJ (2013) Description of input and examples for PHREEQC version 3—A computer program for speciation, batch-reaction, one-dimensional transport, and inverse geochemical calculations: U.S. Geological Survey Techniques and Methods, book 6, chap. A43, 497 p., available only at http://pubs.usgs.gov/tm/06/a43/.

Integrated Hydrogeological Fieldwork Campaign Design To Identify Infiltration From Tailings

Isidora Arriagada[1], José Luis Delgado[2]

[1]*ITASCA Chile, Providencia, Santiago, Chile, isidora.arriagada@oneitasca.com*

[2]*ITASCA Chile, Providencia, Santiago, Chile, joseluis.delgado@oneitasca.com*

Abstract

For fieldwork design, an advantage is to have a previous hydrogeological conceptualization of the study area, and enough data gathered throughout time to identify potential trends. An action plan that prioritizes tasks, leading to a staged field campaign design increases effectiveness. It has been concluded that to identify potential infiltration and seepage paths from tailings deposits the integration of continuous groundwater monitoring through hydrochemical sampling, geophysics, water level recording in monitoring wells, sonic drilling and test pits, along with tailings and natural soil analysis, improve the understanding required to assess and mitigate the infiltration potential of tailings.

Keywords: Infiltration Monitoring, Field Data, Geophysics, Tailings.

Introduction

Water management at a tailing's storage facility involves the superficial water flows and the interception, collection and treatment of seepage. Control measures may be required to prevent levels exceeding regulatory licenses and tailings guideline documents (Ritcey 1989). The liquefaction phenomenon, internal and external erosion, seepage and overtopping are some of the main waters induced failure modes of tailings facilities (ICOLD and UNEP 2001). Increasing the pulp density of the tailings typically presents a viable option for reducing water handling and subsequent storage requirements.

According to COCHILCO 2019, conventional tailings, which until a few years ago were the most frequently used, are deposited with a significant water content with solids concentrations (Cp) between 30% and 50%, while technological developments have facilitated water extraction processes, allowing thickened tailings to reach a Cp between 55% and 75%. The Cp of paste tailings can exceed 75-80%.

The application of tailings dewatering technologies to increase water recovery from tailings is an appropriate step to reduce water losses in tailings storage facilities caused by evaporation, infiltration, and retention in pore voids (Cacciuttolo and Atencio 2022), leaving a greater amount of water available for metallurgical processing. At the same time, the volume of water to be managed is limited, which not only reduces seepage but also reduces water pumping costs to and from the processing plant. A Thickened Tailings Storage Facility (TTSF) presents little water to be stored compared to conventional tailings, hence offering significant advantages by reducing stability and environmental challenges. Nevertheless, liberated water after deposition might still be available for a potential seepage and cannot be ruled out entirely.

This study aims to design an integrated field campaign to identify, monitor, characterize and prevent potential seepage challenges, estimating whether seepage is occurring or not, to be quantified and managed if necessary. The works described here could be adapted to any type of tailings deposit.

Thickened Tailings Storage Facilities

Through thickened tailings disposal (TTD) technology a sloped surface is obtained without particle segregation. For a concentration of 53% by weight, the slope at rest of the deposited tailings is 2% and can increase to 6% if the concentration rises to 65% (SERNAGEOMIN 2007). This allows self-supporting tailings storage facilities with sloping beach surfaces, requiring relatively small dams (Cacciuttolo and Atencio 2022).

In the water balance of a TTSF, the seepage and evaporation losses from the tailing's storage facility (as shown in Fig. 1) are minimised, helping to ensure the sustainable use of water. The mining industry needs to carefully manage water, because water use in the mining industry is becoming increasingly more important (Welch 2003). Copper mine tailings consist of a slurry of ground rock, water, and chemical reagents that remain after mineral processing. The composition of mine tailings varies according to the mineralogy of the ore deposit and how the ore is processed (Cacciuttolo and Atencio 2022).

This study focuses on the design of the field studies carried out at a TTSF resulting from a copper mineral process at a mining complex in an area with an arid climate. The ore is processed to produce mainly copper concentrate through a milling and flotation process completely operated with seawater. The copper mine is active, and the tailings disposal is based on thickening tailings to 65% solids using a combination of paste and high-density thickeners. Conceptually, the higher the Cp, the lower the percentage losses due to infiltration. The tailings are deposited downstream from the embankment via a spigot system in thin layers (between 10 to 20 cm thick) on beaches with 2% to 3% slopedslopes. The TTSF facility includes a drainage system, canalization structure, tailing ponds, online monitoring and environmental monitoring wells subject to local regulations.

Materials and Methods

This work was developed based on a conceptual hydrogeological model developed for the facility and its surroundings. Model development utilised fieldwork and monitoring records, operational tailings deposition data for a period of over 10 years, coupled with data collected from various hydrogeological monitoring campaigns, including geophysical campaigns and level measurements, downstream of the TTSF. In addition, geophysical surveys, sonic drilling and test pitting were conducted inside the TTSF. The latter work also provided the base details for a numerical infiltration model which is being regularly updated to assess the infiltration potential of the tailings.

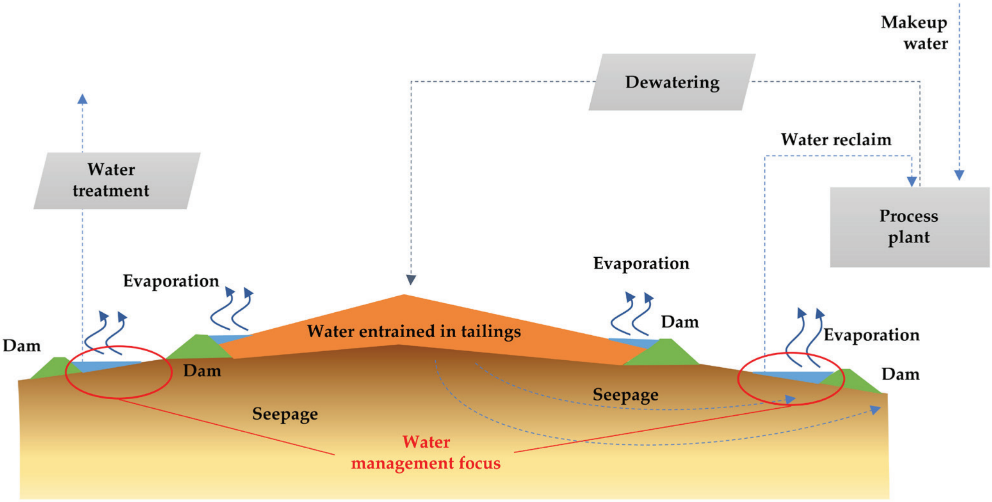

Figure 1 *Schematic of a thickened tailings storage facility (Cacciuttolo and Atencio 2022).*

Fieldwork Campaign Design

The cross-correlations between the tailings discharge zones and the environmental monitoring suggested a seepage infiltration pattern that was being developed downstream of one of the embankments. Local regulations require the monitoring of groundwater levels and groundwater quality in five monitoring wells downstream of the TTSF. The water quality from these wells is compared to process water and tailings water to identify possible infiltration from the tailings facility. The monitoring well, built 400 m downstream of the wall is called MW-1 (Fig. 2) and it began to be sampled and measured in 2020.

To design a field campaign, it is an advantage to have a previous hydrogeological conceptualization of the study area, coupled with enough data gathered throughout time to identify potential trends along with good geotechnical investigation data from the construction phases of the TSF. Assuming that the data series are long enough, the analysis can focus on their evolution over time in order to determine whether any correlations are possible. Thorough and careful analysis allows distinguishing hydrogeological or environmental issues from technical problems that may arise with field or laboratory equipment. In case of uncertainty or unclear patterns, a subsequent gap analysis helps to increase confidence in the data and strengthen the action plan.

An action plan is developed based on prioritizing the tasks according to objectives and relevance, leading to a staged field campaign design (Fig. 3). It is important to plan the sequence in which the works are carried out so that further decisions required along the workflow are well supported,

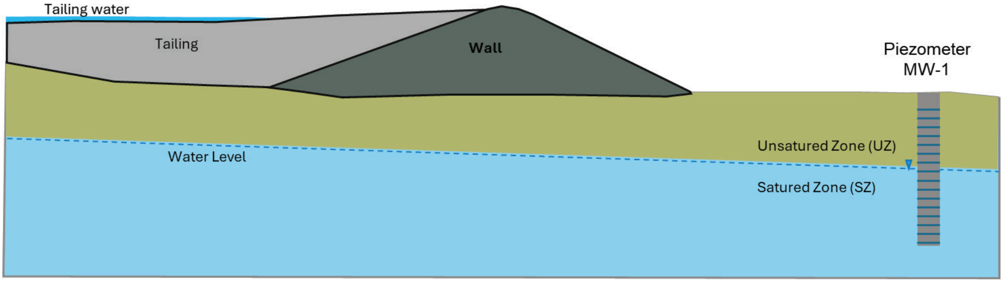

Figure 2 *Schematic diagram showing MW-1 location in initial conditions.*

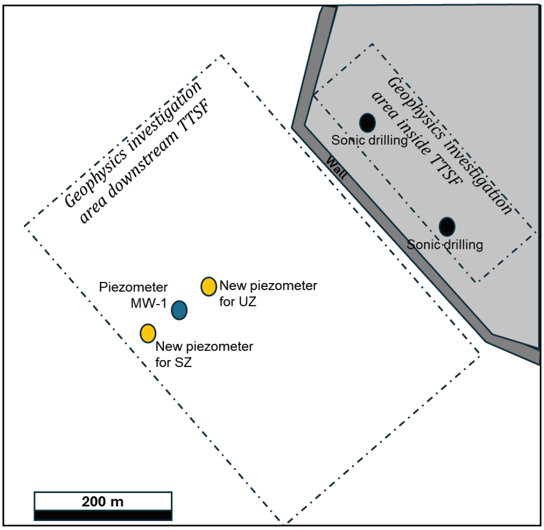

Figure 3 *Schematic diagram showing the spatial location of hydrogeological investigation activities.*

increasing the efficiency of the plan and keeping costs within budget. Wall raises are considered in the future design of the TSF.

After reviewing the available information, data and previous studies, the required field investigation tasks were developed in the following order:

1. Geophysical exploration at the beginning of the action plan allowed for the preliminary confirmation and or discarding of trends and outliers from the groundwater level and hydrochemical monitoring dataset. The TEM and SEV methods allowed for the investigation of large surface extensions and reached reasonable depths at a lower cost than drilling. Both methods proved to be suitable for tailings facilities and their surroundings, . However, better results were achieved combining TEM and NanoTEM outside of the tailings deposition area and using SEV methods inside of the deposition area and in the embankments, where the soil material is no longer in the natural condition.
2. Since geophysics requires ground truthing for technically supported interpretation, in the surroundings of the tailings deposit the drilling campaign was adjusted to cover the areas where high conductivity horizons where identified. Over the course of the drilling campaign, it could be recognized that some local high conductivity layers were related to fine grained material (clay materials) rather than humid or saturated horizons.
3. The previously installed environmental monitoring wells (e.g., MW-1) were screened along most of the well depth. This construction design does not distinguish water inflow areas between groundwater inflows and poses a vertical flow risk in the case of seepage in the UZ to SZ. New wells were constructed with specific goals, besides the groundwater level, hydrochemical and isotopic sampling capacity that the previous well already had implemented. The new monitoring wells were divided into "shallow wells" for UZ monitoring and "deep wells" screened for the SZ monitoring. All wells were implemented with pumping capacity (PVC diameter of 10"), to serve as potential mitigation control infrastructure if necessary. The design of the new monitoring wells is presented in Fig. 4.
4. A geophysical survey was also carried out into the deposition area of the TTSF; were sonic drillings and test pits were also constructed for soil sampling, instrumentalized as VWP and sealed afterwards.

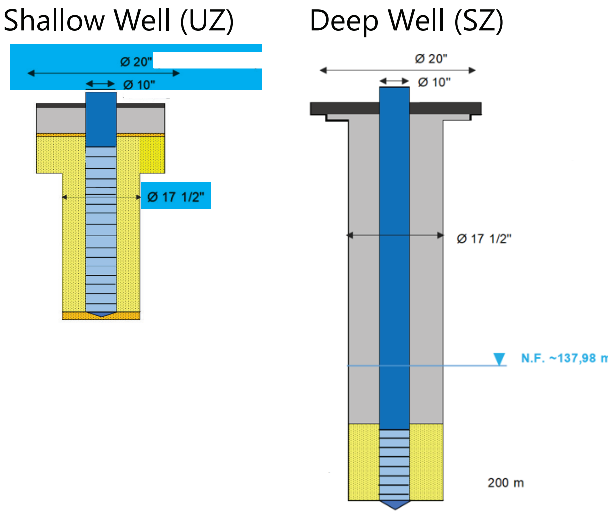

Figure 4 Shallow and deep monitoring wells design for UZ and SZ monitoring.

Results and Discussion

During the first analysis of the environmental follow-up monitoring, unexpected concentrations of certain elements such as bromide (from 5 mg/L to 60 mg/L) were detected in the water of well MW-1 (e.g. electrical conductivity EC increase from 8.000 µS/cm up to 80.000 µS/cm) as well as an increase in the water level, so additional studies were developed to determine if they corresponded to a singular phenomenon or to a more generalized trend in the aquifer (Fig. 5). Evaporation rate in this area is near to 5 mm/day.

Geophysical results downstream of the TTSF showed that the moisture was in a part of the wall that corresponded to a canalization structure and was confirmed by the investigation. Nevertheless, the field campaign continued in 2023 along with new geophysical profiles and monitoring piezometers. According to the fieldwork observations, there was a high degree of certainty that the remediation measures implemented through the drain installation eliminated the infiltration identified in the west abutment, but it was unsure if it was the only cause related to the MW-1 results, or they might be additional causes.

The soil sampling included in situ density analysis, visual humidity estimation (Fig. 6) and several geotechnical laboratory analyses (e.g. water retention curve SWCC, humidity content, granulometry, density, permeability

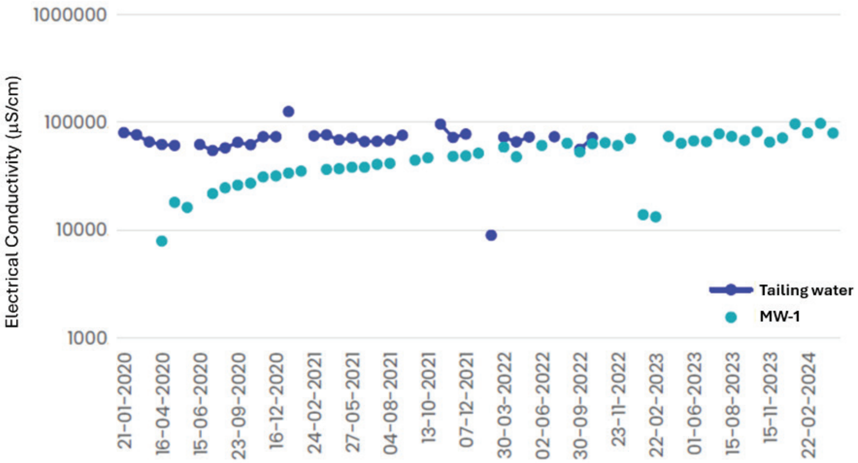

Figure 5 *Increase in EC in MW-1 compared to EC in tailing water.*

Figure 6 *In situ inspection of moisture content in sonic drilling samples (image: Claudia Mellado).*

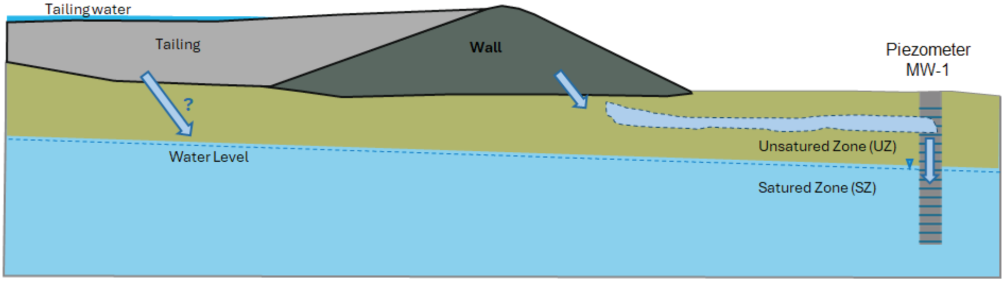

Figure 7 Schematic diagram showing the seepage mobilized by the UZ and entering the well through the screens.

and soil classification). They showed no further signs of humidity at more than 50 m depth from the surface.

Hydrochemical and isotopic monitoring provides valuable insight for the hydrogeological interpretation of potential seepage, because tailings operate with 100% seawater, to avoid extracting water from the aquifer. The water is transported from the sea into the mining facilities through a long pipeline and because of this, potential seepage from the tailings deposit has a seawater imprint, which makes it possible to differentiate between the infiltration water and the water from the aquifer due to sharp differences in their hydrochemical signature.

According to the interpretation of the results (Fig. 7), high conductivity horizons are likely associated to fine grain material and/or to infiltration recognized in the UZ. The infiltration in the drainage system in the embankment area that reached the monitoring well MW-1 and which entered through the upper screens in the UZ, was controlled in this area given that the UZ was found to be dry. However, there might be other infiltration paths that explain the on-going unexpected rising values of certain parameters on monitoring well MW-1. The UZ in this area reaches up to 150 m depth and is characterized by geological heterogeneity due to the mixture of alluvial and fluvial deposits. Some of these layers of fine grain materials with low permeability enable local flowing paths in the UZ in case seepage occurs.

Conclusions

The application of an integrated hydrogeological fieldwork campaign design has proven to be helpful to identify sources of infiltration associated with a TTSF deposit. In this case the campaign consisted in the construction of wells screened at different depths, combined with additional hydrochemistry and isotopic information obtained from the new wells which has been helpful to analyse, complement and validate previous assumptions about the site. Additional drillings are suggested to be built at the toe of the wall.

References

Cacciuttolo C, Atencio E (2022) Past, Present, and Future of Copper Mine Tailings Governance in Chile (1905–2022): A Review in One of the Leading Mining Countries in the World. Int J Environ Res Public Health 19: 13060. doi:10.3390/ijerph192013060

COCHILCO (2019) Mejores Prácticas de Gobernanza en Material de Relaves. Dirección de Estudios y Políticas Públicas de la Comisión Chilena del Cobre. Gobierno de Chile. DEPP 01/2019

ICOLD and UNEP (2001) Tailings Dams - Risk of Dangerous Occurrences, Lessons Learnt from Practical Experiences. Bulletin International Commission on Large Dams 121, Paris

Ritcey G.M. (1989) Tailings Management, Elsevier Edition

SERNAGEOMIN (2007) Guía Técnica de Operación y Control de Depósitos de Relaves. Servicio Nacional de Geología y Minería de Chile. DSM/07/31 December 2007

Welch D (2003) Advantages of Tailings Thickening and Paste Technology, Responding to Change - Issues and Trends in Tailings Management. Golder Associates Report: 5

Evaluating Climate Change Effects on Water Availability for a Proposed Mine in Eastern Canada

Okan Aygün[1], Scott Jackson[2], Colin Fraser[3], Justin Stockwell[4]

[1,2,3,4]Lorax Environmental Services Ltd. 305-1770 West 7th Avenue, Vancouver, British Columbia, V6J 4Y6. okan.aygun@lorax.ca. ORCID 0000-0003-3111-8514

Abstract

A semi-distributed hydrological model was developed to assess climate change effects on water availability for a planned mine in Newfoundland and Labrador, Canada. The model was set up using publicly available topographical and meteorological data. The potential effects of climate change on water availability were evaluated using an ensemble of CMIP6 simulations for the SSP2-4.5 and SSP3-7.0 climate change scenarios. Results show reduced annual peak discharge with earlier timing, increased winter flows from rainfall and mid-winter melts, and decreased summer water availability. These findings emphasize the need for proactive water resource management to support the mine project.

Keywords: Mine water management, hydrological modelling, climate change effects assessment

Introduction

Understanding long-term hydrometeorological conditions is crucial for assessing water resource availability and variability, particularly in the context of mining projects that rely on sustainable water management. Hydrological assessments are essential for mitigating risks associated with water scarcity, flooding, and water quality, all of which can affect operational efficiency and environmental compliance. As the changing climate continues to alter hydrological regimes, robust modelling approaches are essential for predicting future water availability and supporting proactive water resources management.

Hydrological assessment methods for mining projects often rely on lumped conceptual models, which represent an entire catchment as a single unit by averaging spatial characteristics into aggregated parameters. These models, though computationally efficient and requiring relatively low data inputs, are largely dependent on empirical relationships and generalized assumptions (Beven, 2012). While they can provide reasonable estimates under conditions similar to those used for calibration, a reliance on simplified parameterizations limits the model and its applicability to regions with differing climatic, geological, or land-use characteristics (Gupta *et al*., 2014). Moreover, their limited physical basis hinders their ability to accurately simulate hydrological responses under non-stationary conditions, such as those driven by climate change.

In contrast, fully distributed physically based models provide a more detailed representation of hydrological processes by incorporating spatial heterogeneity at finer resolution. These models offer improved predictive capabilities, particularly under changing climatic conditions, as they rely on parameters with direct physical connections to a location of interest, while explicitly accounting for spatial heterogeneity in hydrological processes (Clark *et al*., 2017). However, their application is often constrained by extensive data requirements and high computational demands, limiting practical applications in data-scarce environments.

Advancing hydrological modelling for mining projects requires an approach that integrates conceptual and physically based methods in a semi-distributed framework.

Semi-distributed models offer a compromise by representing catchment heterogeneity at a sub-basin or hydrological response unit level while maintaining a balance between computational efficiency and physical realism (Arnold *et al*., 2012). Additionally, the increasing availability of high-resolution gridded meteorological and topographical datasets provides an opportunity to enhance the accuracy of semi-distributed hydrological models, particularly in remote or ungauged regions (Mizukami *et al*., 2017).

This study evaluates the potential effects of climate change on water availability for a planned mining project in Newfoundland and Labrador, Canada. To achieve this, a semi-distributed hydrological model was developed to simulate both present and future hydrological conditions in Flora Creek, a natural (unregulated) catchment with a drainage area of 140 km^2 and located near the proposed mine site. Outputs from the semi-distributed hydrological model were then incorporated into a comprehensive mine site water balance and water quality model. Through this modelling framework, the study aims to provide insights into the potential hydrological changes and support sustainable water management strategies for mining operations.

Methods

Flora Creek basin was modelled using a customized version of the HBV-EC model emulated with the Raven Hydrological Modelling Framework version 3.7 (Craig *et al*., 2020). The Raven HBV-EC model is a semi-distributed hydrological model that is based on hydrological response units (HRUs), each defined by a distinct combination of physical attributes such as land use, vegetation cover, terrain type, soil profile and bedrock geology. The model follows a water balance approach to each HRU in the model domain, ensuring the conservation of mass. The model requires daily precipitation, as well as minimum and maximum air temperature to simulate basin hydrology. Its algorithms integrate both conceptual and physically based parameterizations. The model consists of three components: (i) a snow routine for snow accumulation and snowmelt based on the degree-day method; (ii) a soil routine that controls the proportion of rainwater and snowmelt, which generates excess water after considering soil moisture and evaporation requirements; and (iii) a runoff generation routine consisting of an upper, nonlinear reservoir that represents fast discharge and a lower linear reservoir that represents slow discharge or baseflow (fig. 1).

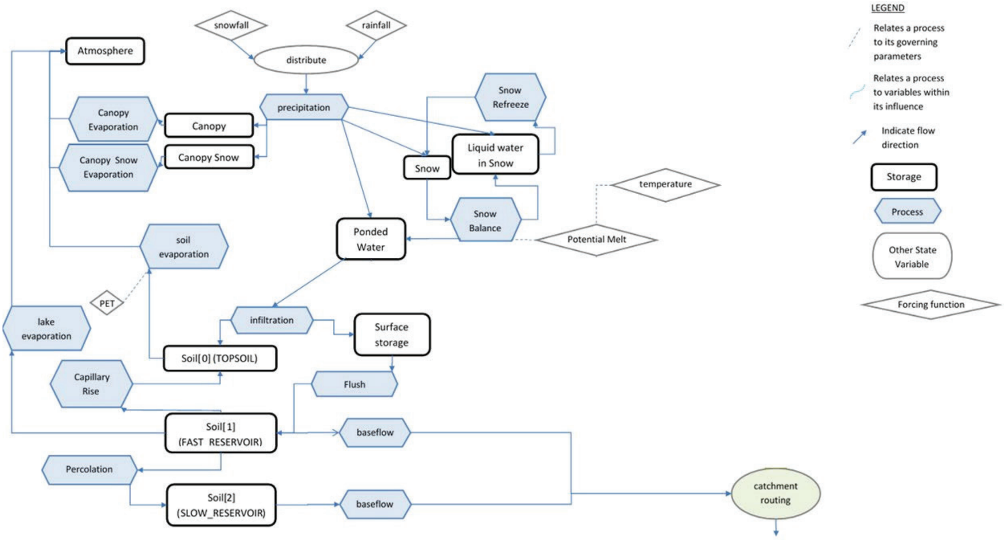

***Figure 1** The schematic of Raven HBV-EC (Craig et al., 2020).*

HRUs were defined in the Flora Creek basin by finding the unique spatial overlay of land cover type, elevation bands, aspect and slope. Land cover data were obtained from the 30m spatial resolution 2020 Land Cover Map of Canada, which is generated by the Canada Centre for Remote Sensing (CCRS). Elevation bands, slope and aspect values were derived from the Canadian Digital Elevation Model (CDEM) at 20m spatial resolution provided by Natural Resources Canada.

Daily minimum and maximum air temperatures to force the Raven HBV-EC model for the Flora Creek basin were obtained from the nearest Environment and Climate Change Canada (ECCC) climate station. Precipitation inputs to the model were derived from a combination of data from the same climate station and the Canadian Precipitation Analysis (CaPA) dataset, which integrates observations from manual and automatic ECCC stations along with the data from the radar network (Fortin *et al.*, 2018). Forward looking projections of daily precipitation and air temperature for the basin were obtained from an ensemble of downscaled and bias adjusted CMIP6 simulations, driven by SSP2-4.5 and SSP3-7.0 emission scenarios (Lavoie *et al.*, 2024). While SSP2-4.5 scenario represents an intermediate greenhouse gas emission pathway, SSP3-7.0 reflects a higher emission scenario, therefore a greater degree of future warming.

A Water Survey of Canada station is located at the outlet of the Flora Creek basin, providing mean daily streamflow observations over the past 10 years, which were utilized in this study for model calibration and validation. Additionally, a nearby snow water equivalent (SWE) record (1983–2016) was used for model verification. Data from this station were obtained from the Canadian historical SWE dataset, which compiles manual and automated SWE observations collected by national, provincial, and territorial agencies, as well as hydropower companies (Vionnet *et al.*, 2021).

Model calibration was conducted by adjusting key parameters related to evapotranspiration, soil properties, snow dynamics, and routing, based on a range of values derived from the literature. The performance of the calibrated model in simulating streamflow was assessed using the Kling-Gupta Efficiency (KGE) metric, optimized through the Dynamically Dimensioned Search (DDS) algorithm (Tolson and Shoemaker, 2007), a global optimization method with a budget of 1,000 iterations. The KGE was selected as the primary evaluation metric due to its ability to overcome the limitations of traditional measures such as the Nash-Sutcliffe Efficiency and R-squared metrics, which primarily focus on reproducing the mean and variance of observed data. The KGE ranges from negative infinity to 1, with a value of 1 indicating perfect agreement between model simulations and observed data.

Results

Simulated streamflow was compared at the outlet of the basin for the calibration (2012–2018) and validation (2019–2022) periods (fig. 2). The KGE statistic was above 0.8 over both calibration and validation periods, which suggests that the model is sufficiently reliable in generating representative hydrographs for the Flora Creek basin.

Good agreement between simulated and observed snow water equivalent (SWE) (fig. 3) demonstrates that the model performs sufficiently well in capturing snow accumulation and ablation magnitude and timing. This is particularly promising given that snowmelt runoff largely dominates the streamflow regime at the study basin. Taken together, the model developed for the Flora Creek basin adequately simulates the natural streamflow conditions in the region, along with key hydrological processes such as snowmelt, sublimation and runoff generation. Accordingly, the results also suggest the model is well suited for analysing the future hydrological conditions and can be reliably integrated into the broader mine site water balance and water quality model.

Compared to present climate conditions (defined here as 2003–2023), mean annual temperature is projected to rise across all future periods, with more pronounced warming under SSP3-7.0 (tab. 1). By the 2060–2080 period, both SSP2-4.5 and SSP3-7.0 scenarios suggest that mean annual temperature are

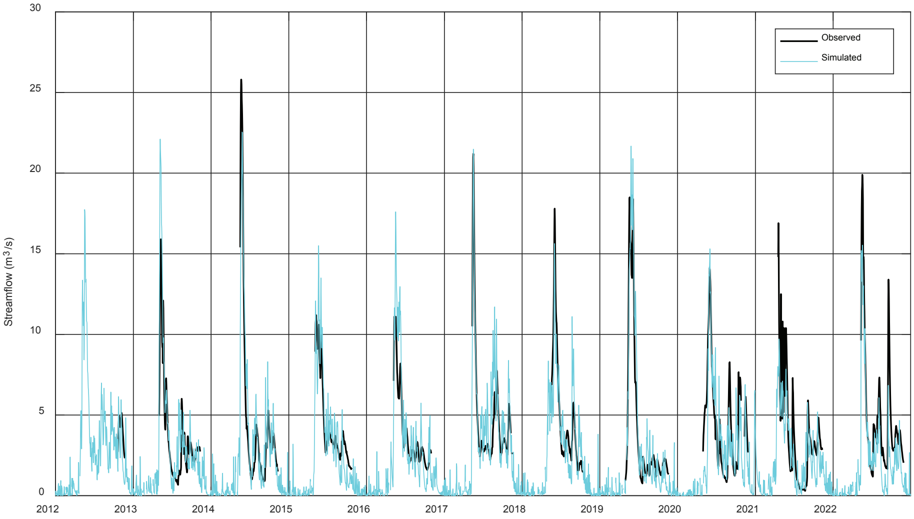

__Figure 2__ Raven HBV-EC model performance in simulating Flora Creek streamflow.

expected to surpass the freezing point, marking a shift in climatic conditions. By the end of this century, mean annual temperature is projected to increase by 3.4 °C under SSP2-4.5, whereas SSP3-7.0 predicts a much more substantial rise of 7.3 °C.

In addition to rising temperatures, mean annual precipitation is projected to increase under both scenarios (tab. 1). Relative to the present climate, precipitation is projected to increase by 5–8% by 2040–2060 and by 12–16% by the end of the century. However, snowfall as a proportion of total precipitation decreases in the future, reflecting the effect of rising temperatures. Under SSP2-4.5, snowfall declines from 394 mm (42% of total precipitation) under present climate conditions to 328 mm (32%) by the late century. This decrease is even more pronounced under SSP3-7.0, where

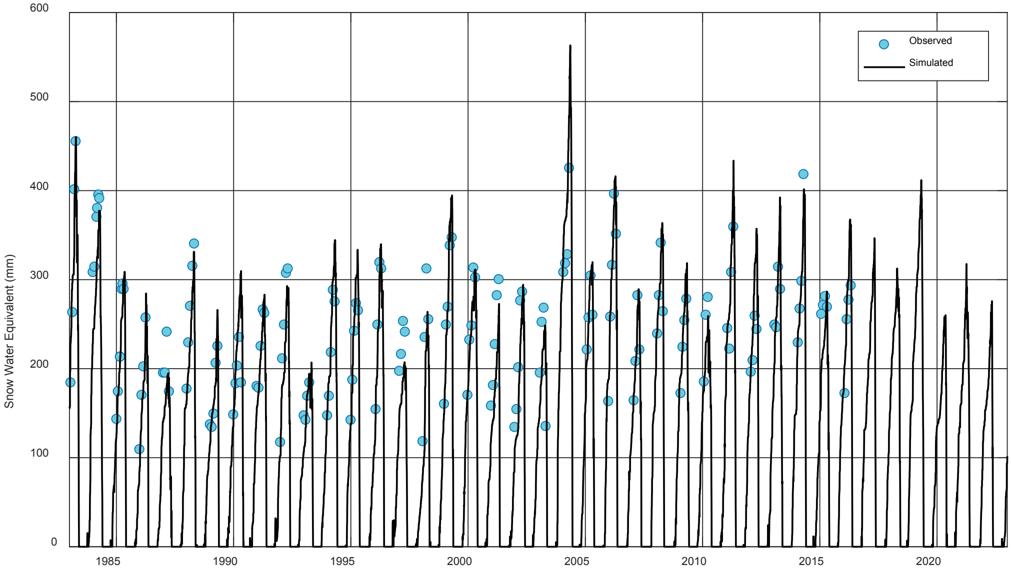

__Figure 3__ Comparison of simulated and observed snow water equivalent (SWE).

Table 3 *Mean annual temperature, precipitation and snowfall-rainfall partitioning in precipitation for the present and future simulation periods under SSP2-4.5 and SSP3-7.0 scenarios.*

Climate Variable (Annual Mean)	Present (2003–2023)	2040–2060		2060–2080		2080–2100	
		SSP2–4.5	SSP3–7.0	SSP2–4.5	SSP3–7.0	SSP2–4.5	SSP3–7.0
Temperature (°C)	-2.2	-0.3	2.2	0.4	3.6	1.2	5.1
Precipitation (mm)	931	979	1007	1010	1046	1039	1084
Rainfall (mm)	537	633	717	672	786	711	851
Snowfall (mm)	394	346	290	338	260	328	233

snowfall is projected to drop to 21% of total precipitation by 2080–2100, highlighting a stronger shift toward a rainfall dominated precipitation pattern.

Under present climate conditions, the annual peak snow water equivalent (SWE) occurs in April, reaching approximately 260 mm (fig 4). Both SSP2-4.5 and SSP3-7.0 scenarios project a decline in peak snow accumulation over time, with a more pronounced reduction under the higher-emission SSP3-7.0 scenario. By 2040–2060, peak SWE under SSP3-7.0 is projected to decline by nearly 50%, reaching approximately 130 mm, whereas under SSP2-4.5, it is expected to remain above 150 mm throughout the simulation period.

In addition to declining SWE, the timing of peak snow accumulation is expected to shift earlier in the year (fig. 4). Under SSP3-7.0, this shift becomes evident as early as 2040–2060, with peak SWE occurring one month earlier than in the present climate. The shift towards earlier peak SWE is more gradual under the SSP2-4.5 scenario, reflecting a less pronounced but still notable effect of warming temperatures (tab. 1). Furthermore, the duration of the snow-covered period is projected to shorten due to delayed accumulation in the fall and earlier melt in the spring. This reduction in seasonal snow cover is particularly pronounced under SSP3-7.0, emphasizing the greater effect of higher emissions on seasonal snow dynamics.

Projected changes in SWE have direct implications for runoff generation and overall basin yield (fig. 5). Both climate change scenarios considered here project a decline in peak yield, with SSP3-7.0 exhibiting a sharper decrease. By 2040–2060, peak yield is expected to decrease by nearly 40% under SSP3-7.0 and shift about a month earlier in the year, which is consistent with the changes in projected snow accumulation (fig. 4). Winter and early-spring flows are projected to increase under both scenarios due to enhanced rainfall and mid-winter melt events, which contribute to greater

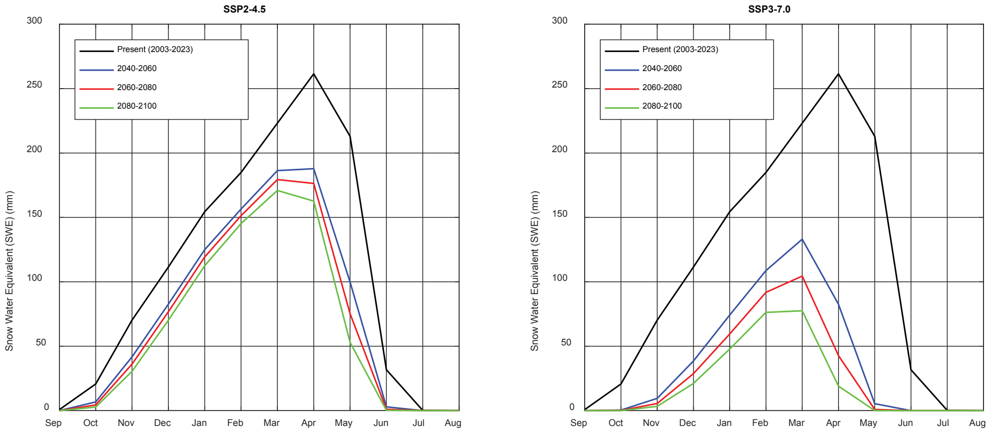

Figure 4 *Simulated snow water equivalent (SWE) under present and future climate conditions for SSP2-4.5 and SSP3-7.0 scenarios.*

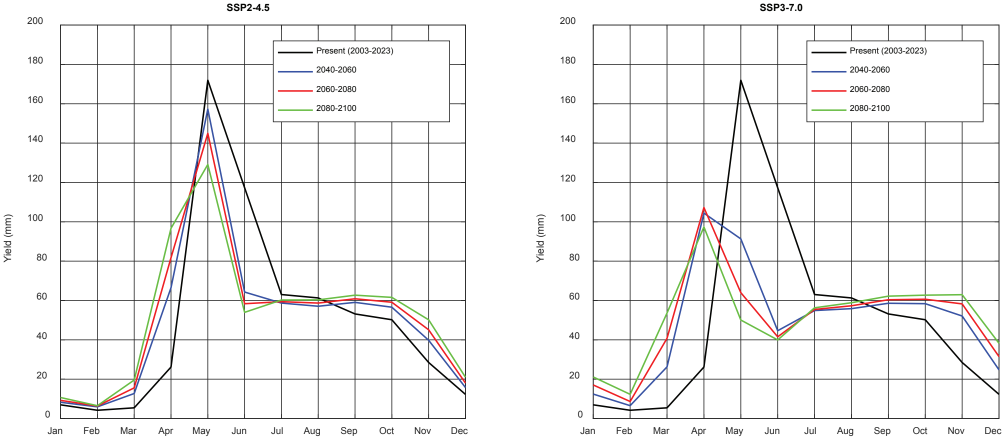

***Figure 5** Simulated basin yield under present and future climate conditions for SSP2-4.5 and SSP3-7.0 scenarios.*

runoff outside the typical snowmelt season. Conversely, summer water availability is projected to decrease by 20–40% depending on the emission scenario and projection period (fig. 5). This reduction is governed by a combination of lower snowpack levels, earlier melting, and higher evapotranspiration rates resulting from warmer temperatures.

Conclusions

The findings of this study underscore the critical need for proactive and strategic water resource management for the planned mine project considering projected climate change effects. More frequent mid-winter melt events and reduced peak snowmelt-driven flows may necessitate modifications to mine water storage infrastructure and their operational procedures, while declining summer water availability could threaten the consistency of water availability for mining operations. These hydrological changes can have direct effects on water quality, as lower flows are expected to reduce the amount dilution, resulting in higher concentrations of contaminants. The severity of these effects will depend on future warming trends, with SSP3-7.0 representing a worst-case scenario and SSP2-4.5 depicting a moderate yet still consequential shift. These scenarios provide a plausible range of potential hydrological changes that mine operators need to consider in long-term water management planning. Ensuring operational efficiency and environmental compliance while minimizing risks associated with fluctuating water resources will require adaptive strategies, including optimizing water storage systems to ensure adequate supply during drier months and improving runoff management practices during wetter months to prevent flooding or excessive runoff. Such proactive actions will be essential not only for ensuring the long-term sustainability of mining operations but also for minimizing the potential environmental and operational disruptions caused by climate variability.

The semi-distributed modelling approach adopted in this study effectively combines both conceptual and physically based methods, resulting in a robust and computationally efficient tool for assessing water availability and managing water-related risks in the mining industry. The inclusion of physical realism within the modelling framework, along with the use of publicly available topographical and meteorological data, enhances its applicability to other mine sites in the region while supporting regulatory compliance.

Acknowledgements

The authors thank all co-organisers for hosting the IMWA 2025 Conference.

References

Arnold, J.G., Moriasi, D.N., Gassman, P.W., Abbaspour, K.C., White, M.J., Srinivasan, R., Santhi, C., Harmel, R.D., Van Griensven, A., Van Liew, M.W. and Kannan, N. (2012). SWAT: Model use, calibration, and validation. Transactions of the ASABE, 55(4), pp.1491–1508.

Beven, K.J. (2012). Rainfall-runoff modelling: the primer. John Wiley & Sons.

Clark, M.P., Bierkens, M.F., Samaniego, L., Woods, R.A., Uijlenhoet, R., Bennett, K.E., Pauwels, V., Cai, X., Wood, A.W. and Peters-Lidard, C.D. (2017). The evolution of process-based hydrologic models: historical challenges and the collective quest for physical realism. Hydrology and Earth System Sciences, 21(7), pp.3427–3440.

Craig, J.R., Brown, G., Chlumsky, R., Jenkinson, R.W., Jost, G., Lee, K., Mai, J., Serrer, M., Sgro, N., Shafii, M. and Snowdon, A.P. (2020). Flexible watershed simulation with the Raven hydrological modelling framework. Environmental Modelling & Software, 129, 104728.

Gupta, H. V., Perrin, C., Blöschl, G., Montanari, A., Kumar, R., Clark, M. and Andréassian, V. (2014). Large-sample hydrology: a need to balance depth with breadth. Hydrology and Earth System Sciences, 18(2), 463–477.

Fortin, V., Roy, G., Stadnyk, T., Koenig, K., Gasset, N. and Mahidjiba, A. (2018). Ten years of science based on the Canadian precipitation analysis: A CaPA system overview and literature review. Atmosphere-Ocean, 56(3), 178–196.

Lavoie, J., Bourgault, P., Smith, T.J., Logan, T., Leduc, M., Caron, L.P., Gammon, S. and Braun, M. (2024). An ensemble of bias-adjusted CMIP6 climate simulations based on a high-resolution North American reanalysis. Scientific Data, 11(1), p.64.

Mizukami, N., Clark, M.P., Newman, A.J., Wood, A.W., Gutmann, E.D., Nijssen, B., Rakovec, O. and Samaniego, L. (2017). Towards seamless large-domain parameter estimation for hydrologic models. Water Resources Research, 53(9), pp.8020–8040.

Tolson, B. A. and Shoemaker, C. A. (2007). Dynamically dimensioned search algorithm for computationally efficient watershed model calibration. Water Resources Research, 43(1).

Vionnet, V., Mortimer, C., Brady, M., Arnal, L. and Brown, R. (2021). Canadian historical snow water equivalent dataset (CanSWE, 1928–2020). Earth System Science Data, 13(9), 4603–4619.

Improved Acidity Estimation by Integrating Comprehensive Dissolved Metal(oid) s Data: A Geochemical Modeling Case Study of Highly Mineralized Mine Waters

Ana Barroso[1], Charles A. Cravotta III[2], Patrícia Gomes[1], Isabel Margarida Horta Ribeiro[1],
Amélia Paula Marinho Reis[1,3], Teresa Maria Valente[1]

[1]*Universidade do Minho, Campus de Gualtar, Institute of Earth Sciences, 710–057 Braga, Portugal*

[2]*Cravotta Geochemical Consulting LLC, Bethel, USA, cravottageochemical@gmail.com,*
ORCID 0000-0003-3116-4684

[3]*GEOBIOTEC, Geosciences Department, University of Aveiro, Campus Universitário de Santiago,*
3810–193 Aveiro, Portugal

Abstract

This study introduces a geochemical modeling approach using PHREEQC to improve the accuracy of acidity estimates in waters influenced by acid mine drainage (AMD). AMD, common in regions like the Iberian Pyrite Belt, is characterized by low pH and high concentrations of metals, sulfate and acidity. Conventional methods, such as net acidity, often underestimate actual acidity by excluding additional metal(oid) s and bisulfate, particularly in highly mineralized waters. By incorporating factors like Fe, Al, Mn, other metal(oid)s, and bisulfate, these methods improve acidity estimation accuracy. Results demonstrate that these methods provide more precise acidity measurements, enhancing AMD monitoring and treatment strategies.

Keywords: Mine waters, acidity, PHREEQC, metal(oid)s concentration, modeling

Introduction

Acid mine drainage (AMD), which may be characterized by low pH and elevated concentrations of acidity, sulfate, and metaloids, can be a long-term environmental problem in coal or metal-mining regions (Nordstrom, 2011). The consequences of AMD include degradation of water quality, soil, and aquatic life. Portugal and Spain exemplify the environmental impact of AMD, particularly due to their long tradition of mining in the Iberian Pyrite Belt (IPB), which dates to pre-Roman times. The IPB is one of the world's largest metallogenic provinces, with approximately 90 identified massive sulfide deposits (Inverno *et al.*, 2015). A detailed geological overview of this region can be found in the works of Leistel *et al.* (1997), Barriga (1990), and Tornos (2006). Most of the mines are currently abandoned, with only a few undergoing rehabilitations. This region has been the focus of numerous studies of AMD and its possible remediation, particularly the mining-influenced waters exhibiting extremely low pH and high mineralization levels.

Acidity is one of the key parameters in the characterization, monitoring, and neutralization of mining-influenced water; it indicates the intensity and extent of mineralization and the corresponding alkalinity needed for AMD neutralization. The acidity concentration and loading are useful to determine a watercourse's capacity to neutralize AMD inflows or to estimate the necessary amount of caustic agent to achieve neutralization through treatment. Laboratory analysis involves the hot peroxide acidity method, which consists of titration of an oxidized sample with a strong base (NaOH) to a pH endpoint of 8.3 (APHA, 2012). Alternatively, estimation of this parameter can be achieved through the utilization of the computed net acidity or net alkalinity (Hedin, 2004, 2006; Kirby and Cravotta, 2005a, 2005b), which considers only pH and the concentrations of Fe, Al, Mn, and alkalinity. However, in cases of extreme mineralization, net acidity can underestimate the measured acidity due to the contributions of additional constituents that can interact with the base added. Thus, the objective of this study is to develop and demonstrate an improved method to estimate the acidity that has broad applicability to AMD with low pH and high concentrations of various solutes.

In this context, the present study proposes a geochemical modeling approach using the PHREEQC geochemical speciation program (Parkhurst and Appelo, 2013), which considers the pH, Fe, Al, Mn, additional metal(oid)s, and bisulfate (HSO_4^-). PHREEQC was used to estimate acidity according to four methods: net acidity, total acidity, acidity by speciation, and caustic titration. The net acidity uses the pH and the analytical concentrations of Fe, Al, Mn, and alkalinity, as explained by Hedin (2004, 2006). The total acidity also uses these analytical concentrations, but for an expanded list of elements, with contribution factors from -1 to +3. A factor from 0 to 1 is multiplied by the analytical sulfate concentration, depending on how much is present as HSO_4^- (factor of 1) versus SO_4^{-2} (factor of 0). Similar to total acidity, the speciated acidity assigns a contribution factor to each of the species, following the method of Kirby and Cravotta (2005a, 2005b), but considering an expanded list of constituents. Last, the caustic acidity is computed by PHREEQC as the amount of base added to reach pH 8.3, after a sample has been equilibrated with the atmosphere.

Methods

About 200 water samples were collected from two abandoned and highly contaminated mining areas of the IPB: the Trimpancho mining complex and the São Domingos mine (Barroso *et al.*, 2024; Gomes and Valente, 2022). The water samples were collected from rivers affected by AMD, pit lakes, acid lagoons, and tributary mixing sites (Fig. 1). During sampling, pH, electrical conductivity, and temperature were measured using a multiparameter instrument (Thermo Scientific Model Orion Star A Series), while oxidation-reduction potential was measured with an ORPTestr 10. Dissolved oxygen was also measured using the HACH HQ30D portable multiparameter. All instruments were calibrated with the respective standard solutions prior to each analysis. Other parameters, such as the hot peroxide acidity, alkalinity, sulfate, and metal(loid) concentrations, were analyzed

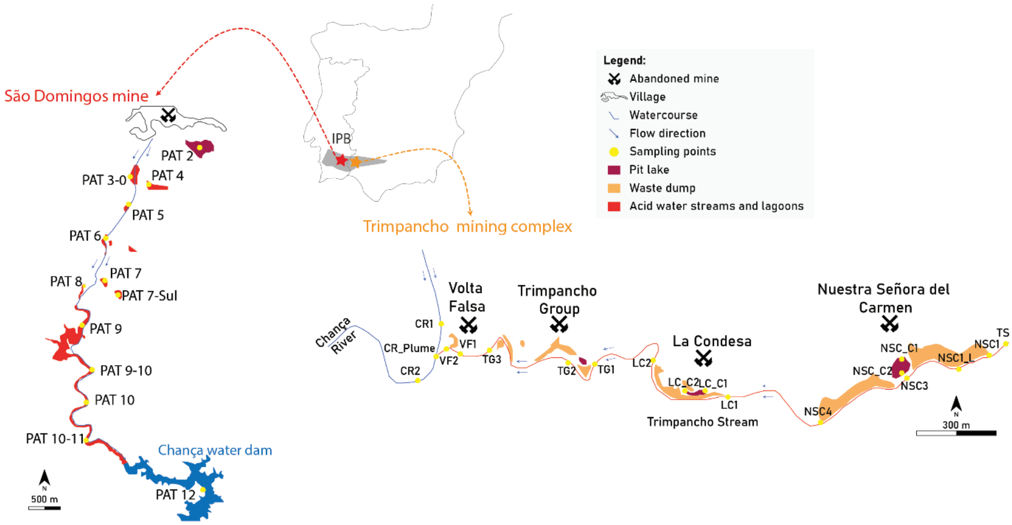

Figure 1 Location of water sampling points at the São Domingos mine (Portugal sector of IPB) and the Trimpancho Mining Complex (Spain sector of IPB).

in the laboratory. Acidity and alkalinity were determined by volumetric titration (standard method 2310 B) and sulfate concentration was obtained using turbidimetry (standard method 4500-SO4^{2-} E) (APHA, 2012). Metal(oid)s concentrations were analyzed by inductively coupled plasma optical emission spectrometry in filtered and acidified aliquots.

Results and discussion

In general, the water samples collected showed a wide range of acidity (22 to 429 250

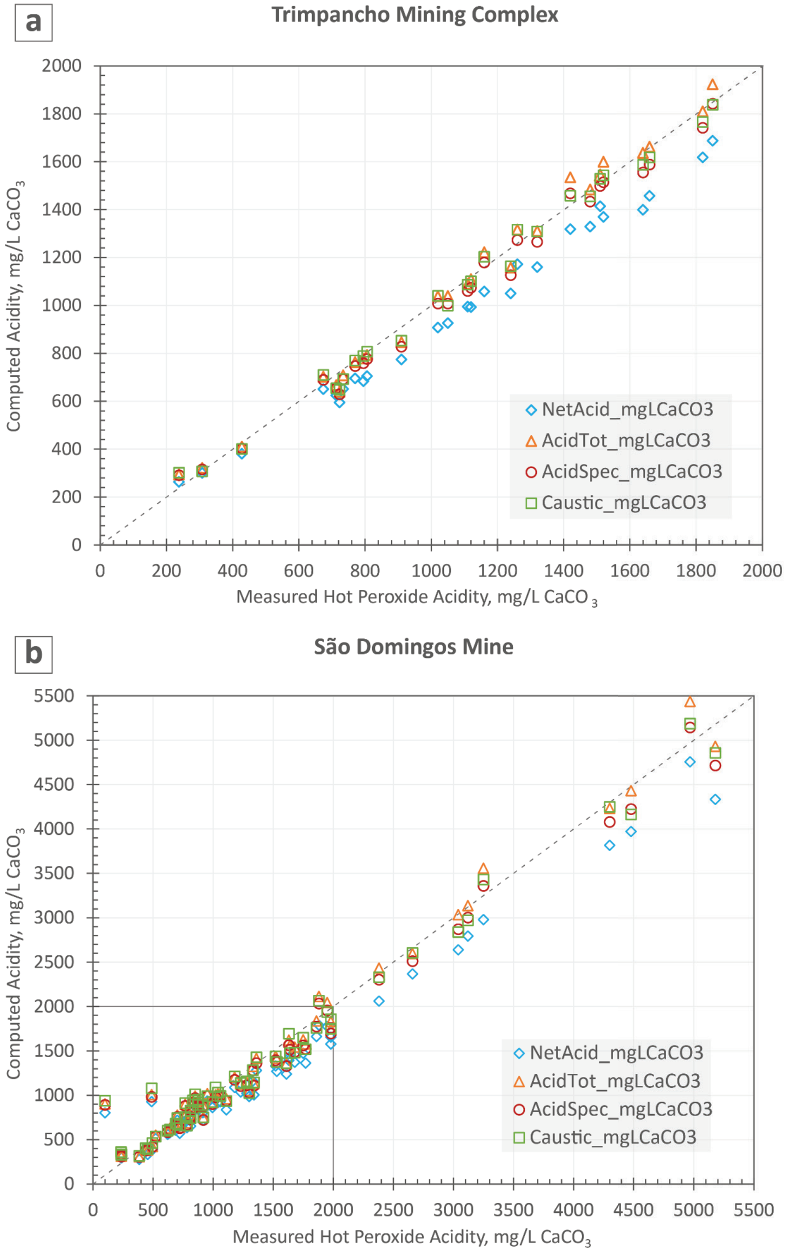

***Figure 2** Comparison between measured hot peroxide acidity and computed acidity (Net Acidity, Total Acidity, Acidity by speciation, and Caustic) using PHREEQC: (a) Trimpancho mining complex and (b) São Domingos mine.*

mg/L as $CaCO_3$), pH from 0.44 to 8.57, and sulfate concentrations up to 410 600 mg/L. The dominant dissolved cations were Fe and Al; however, many of the samples with lower pH showed high concentrations of Zn, Cu, As, Mn, Cd, Pb, and Sb. For geochemical modeling, computations with PHREEQC used the wateq4fREYsKinetics.dat database (Cravotta, 2022), which was expanded from the wateq4f.dat (Ball and Nordstrom, 1991) to include speciation data on rare earth elements and other trace elements. To ensure the accuracy of the results, the charge balance calculated by PHREEQC was verified, and only samples with a charge balance of less than ±15% were accepted for interpretations of speciation results (McCleskey *et al.*, 2023).

Fig. 2 shows the comparison of the measured hot peroxide acidity and the computed acidity results for each of the mining areas. In general, for both mining areas, the total acidity, acidity by speciation, and caustic methods show a strong agreement with the acidity measured in the laboratory. On the other hand, net acidity tends to underestimate acidity values compared to laboratory measurements. These results demonstrate the importance of potential contributions from HSO_4^- and various metal(oid)s when calculating acidity, especially highly mineralized mine waters with low pH.

The three new methods of calculation provide improved estimates of acidity and are similar in value to one another. The main difference is that speciation computations are needed for the speciated acidity and the caustic titration acidity. On the other hand, the total acidity uses only analytical concentrations, without speciation, so it may be computed using a spreadsheet or other calculator.

Conclusions

In conclusion, the developed approach provides a reliable means of estimating acidity for environments of extreme contamination. The findings show close alignment with laboratory-measured acidity values, reinforcing the validity for practical applications. Thus, by refining acidity estimation, this study contributes to effective environmental monitoring and offers insights for determination of remediation measures.

Acknowledgements

Ana Barroso acknowledges FCT – Foundation for Science and Technology, I.P., by the support of ICT through the research fellowship with reference UI/BD/151330/2021. FCT also co-funded this work in the framework of the UIDB/04683 and UIDP/04683 – Instituto de Ciências da Terra programs.

References

APHA (2012) Standard Methods for the Examination of Water and Wastewater, 20th ed.; American Public Health Association, American Water Works Association, Water Environment Federation: Washington, DC, USA.

Barriga, F. J. A. S. (1990). Metallogenesis in the Iberian pyrite belt. In Pre-mesozoic geology of Iberia (pp. 369–379). Berlin, Heidelberg: Springer Berlin Heidelberg.

Barroso, A. R., Valente, T. M. F., Reis, A. P., Antunes, I. M. H. R., & Neves, M. I. (2024). Characterization and modeling of acid mine drainage in a highly acidic stream (Trimpancho Mining Complex, SW of Spain). – *In: Kleinmann, B., Skousen, J., Wolkersdorfer, Ch.: West Virginia Mine Drainage Task Force Symposium & 15th International Mine Water Association Congress.* – p. 27–33; Morgantown, WV, USA

Cravotta CA III (2022) Interactive PHREEQ-N-AMDTreat+REYs water-quality modeling tools to evaluate potential attenuation of rare-earth elements and associated dissolved constituents by aqueous-solid equilibrium processes (software download). US Geol Surv Software Release. https://doi.org/10.5066/P9M5QVK0

Gomes, P., Valente, T., Marques, R., Prudêncio, M. I., & Pamplona, J. (2022). Rare earth elements-Source and evolution in an aquatic system dominated by mine-Influenced waters. *Journal of Environmental Management*, 322, 116125.

Hedin, R. S. (2004). The use of measured and calculated acidity values to improve the quality of AMD data sets. In *Proceedings of American Society for Mining & Reclamation conference, Morgantown*, WV, April (pp. 18–24).

Hedin, R. S. (2006). The use of measured and calculated acidity values to improve the quality of mine drainage datasets. Mine Water and the Environment, 25, 146–152.

Inverno, C., Díez-Montes, A., Rosa, C., García-Crespo, J., Matos, J., García-Lobón, J. L., Carvalho, J., Bellido, F., Castello-Branco, J. M., Ayala, C., Batista, M. J., Rubio, F., Granado, I., Tornos, F., Oliveira, J. T., Rey, C., Vítor Araújo, Sánchez-García, T., Pereira, Z., Represas, P., Solá, A. R. & Sousa, P. (2015). Introduction and geological setting of the Iberian Pyrite Belt. 3D, 4D and predictive modelling of major mineral belts in Europe, 191–208.

Kirby, C.S., and Cravotta, C.A. III (2005a) Net alkalinity and net acidity 1: Theoretical considerations: Applied Geochemistry, v. 20, p. 1920–1940. https://doi.org/10.1016/j.apgeochem.2005.07.002

Kirby, C.S., and Cravotta, C.A. III (2005b) Net alkalinity and net acidity 2: Practical considerations: Applied Geochemistry, v. 20, p. 1941–1964. https://doi.org/10.1016/j.apgeochem.2005.07.003

Leistel, J. M., Marcoux, E., Thiéblemont, D., Quesada, C., Sánchez, A., Almodóvar, G. R., ... & Saez, R. J. M. D. (1997). The volcanic-hosted massive sulphide deposits of the Iberian Pyrite Belt Review and preface to the Thematic Issue: Review and preface to the Thematic Issue. Mineralium deposita, 33, 2–30.

McCleskey, R. B., Cravotta III, C. A., Miller, M. P., Tillman, F., Stackelberg, P., Knierim, K. J., & Wise, D. R. (2023). Salinity and total dissolved solids measurements for natural waters: An overview and a new salinity method based on specific conductance and water type. Applied Geochemistry, 154, 105684. https://doi.org/10.1016/j.apgeochem.2023.105684

Nordstrom, D. K. (2011). Mine waters: acidic to circumneutral. Elements, 7(6), 393–398. DOI: 10.2113/gselements.7.6.393

Parkhurst DL, Appelo CAJ (2013) Description of input and examples for PHREEQC version 3–A computer program for speciation, batch-reaction, one-dimensional transport, and inverse geochemical calculations. US Geol Surv Tech Methods 6–A43. https://doi.org/10.3133/tm6A43

Tornos, F. (2006). Environment of formation and styles of volcanogenic massive sulfides: The Iberian Pyrite Belt. Ore Geology Reviews, 28(3), 259–307.

The Smolnik Mining Site in Slovakia: its Potential Use for the Production of Mineral Pigments

Zuzana Bártová[1]

[1]*Institute of Geotechnics of the Slovak Academy of Sciences, Kosice, Slovakia,*
bartova@saske.sk, ORCID: 0000-0001-9918-1224

Abstract

A batch cultivation of mine impacted water from the Smolnik mining site was carried out comparing the autochthonous microbial consortia to three pure acidophilic chemolithoautotrophic bacterial species. They were inoculated into the mine water together, as a bacterial consortium, in order to remove dissolved iron from the liquid phase while monitoring changes in various geochemical parameter (pH, ORP).

Overall, the final total iron concentration decreased from the initial 228.5 mg/L to 67 mg/L when bacteria were added. After a final pH increase (20% KOH) and filtration of the Fe-precipitates, the final concentration of total dissolved Fe was 2.11 mg/L.

Keywords: Mine Impacted Waters, Acidophilic bacteria, Mineral Pigments, Circular economy, Historical Mining Sites

Introduction

The riverbed of adjacent water bodies in the Smolnik region is discernibly coloured from the presence of ochreous precipitates, typical for mine impacted waters, especially in abandoned historical mining areas. This is caused by an elevated iron concentration in the mine water (237 mg/L^{-1}) and its precipitation when mixed with river freshwater.

On the walls of a sedimentation basin built for iron precipitation close to the main mine outflow, the secondary mineral Schwertmannite (Fig. 1) is naturally formed in big pieces, showing its earthy colours and hues potentially usable as a naturally reclaimed pigment.

Iron ochre precipitates are mainly formed on surfaces that are in contact with mine water, particularly in regions where flow is reduced. The dominant mineral in the outflow is the aforementioned Schwertmannite ($Fe_8O_8(OH)_8{-}2x(SO_4)x \bullet nH_2O$) (Fig. 1) (Lintnerová *et al.* 2009). Together with elements such as iron and sulfur, metalloids such as arsenic or antimony also co-precipitate with iron. After drying, its structure becomes brittle and can be easily crushed into a fine powder. It can be easily mixed with a base medium, such as oil, and the resulting colour is intense and rich. Smolnik mine waters can therefore be considered a rare raw material, which shows potential as a source of natural pigments and metals through the innovative use of bio-hydrometallurgical approaches.

Smolnik mine water contains metals, some of which are on the list of Critical Raw Materials (CRMs) issued by the European Union (European Commission 2023). CRMs are a cornerstone of circular economy and independent, self-sufficient EU. The primary pollutants in this AMD (Acid Mine Drainage) are iron, sulfates, manganese, aluminum, copper, zinc and arsenic.

The Smolnik deposit is one of only a few where mine waters were intensively used for the extraction of copper since the Middle Ages. During favourable periods, it was possible to obtain more metal from the mine water than from the ore (Jaško *et al.* 1998). Cementation technology was unique in the world at that time. According to historical records, China (1086 A.D.) was the first to use this technology (Lung 1986), but it is the Smolnik location that holds this primacy within Europe. The oldest written mention of copper production by cementation in Smolnik is from 1346 (Juck 1984). This record was therefore the second in the

Figure 1 *Secondary mineral Schwertmannite; Left – formed in the mine water on the wall of the sedimentation basin; Right – detail with its porous structure.*

world to mention the practice of copper cementation.

Mining activities at Smolnik ceased in 1994, and the area was subsequently flooded. The mining complex itself began to behave like a bioreactor, producing large amounts of acid mine drainage, where the predominant microorganism belongs to the genus *Gallionella* (Bártová 2020).

Under normal conditions, the flow of mine water reaches 10 L/s, with an average temperature of 14 °C. Sulfates and ferrous iron, which are products of pyrite leaching, are the dominant ions in this water (Kupka *et al.* 2012).

At the outflow from the main discharge shaft (Pech shaft), the total Fe concertation is currently 228.5 mg/L (225 mg/L Fe^{2+} and 3.5 mg/L Fe^{3+}) with a decreasing tendency over the years (Tab. 1). The mine water flows from underground in an anoxic form, and thus the biggest moiety of the iron is present in its Fe^{2+} form, serving as an energy substrate for iron oxidising microorganisms.

Iron is the fourth most abundant element in the Earth's crust by percent mass (Rösler and Lange 1972) and thus a common contaminant in natural waters occurring in various types of environments. Nowadays, the necessity of iron removal and recovery from such water and wastewater is currently emphasised in order to protect human health and critical infrastructure (Kaksonen and Janneck 2024). Huge opportunities connected to this endeavour lie in the use of microbial consortia facilitating iron cycling. Oxidised iron forms such as Schwertmannite can be used as valuable products (pigments, sorbents) (Reichel *et al.* 2017) and increase the value of such a material.

An example of good practice in this sector is the social enterprise True Pigments LLC in Appalachian Ohio, US (Pigments 2024).

The Truetown Discharge, located in the Sunday Creek watershed, is the largest single acid mine drainage discharge in the state of Ohio, with a flow rate of 62 L/s. The AMD treatment facility is able to treat approximately

Table 1 *Change in the composition of mine water over the years.*

Shaft Pech	SO_4^{2-} mg/L	Fe mg/L	Al mg/L	Mn mg/L	Zn mg/L
2011	2082	272	57.9	22.6	8.4
2020	1722	232	40.3	16.5	4.4
2025	1766	229	44.1	17.1	5.4

Shaft Pech	Cu µg/L	Li µg/L	Co µg/L	Pb µg/L	As µg/L	Cd µg/L	Sb µg/L	Cr µg/L
2011	1710	312	861	20.8	22	16,4	-	2.9
2020	498	253	308	36.4	73	3.8	11.2	0.4
2025	1070	290	410	12.1	28.4	0.85	<0.1	<0.1

5.3 million litres of acid mine drainage daily, cleaning up Sunday Creek while processing iron oxide for professional-grade paint pigment production and employing at least five full-time workers (Enforcement 2023).

Methods

Bacterial strains and incubation conditions

Three strains of chemolithotrophic, acidophilic, iron-oxidizing bacteria were used in the experiments: *Acidithiobacillus ferrivorans* SS3 (DSM 17398), *Acidithiobacillus ferrooxidans* (DSM 14882) and Leptospirillum feriphilum (DSM 14647). Detailed description of their growth and iron oxidation kinetics is described in detail elsewhere (Kupka *et al*. 2023). Bacteria were incubated in natural mine water from the outflow of the main discharge shaft (Pech). The cultivation took place in magnetically stirred and properly aerated baffled reaction vessels with the working volume 0,5 L with the set temperature of 25 °C and 240 RPM.

Mine water parameters

pH/ ORP analysis

A combined glass electrode (InLab Micro Mettler Toledo) was used for pH measurement. The oxidation-reduction potential (ORP) of the liquid phase during bacterial iron oxidation was measured with a combined Pt-Ag/AgCl redox electrode (InLab Redox Micro Mettler Toledo). In both cases, the Seven2Go S2 (Mettler Toledo) was used.

Iron speciation

Ferric iron was determined with a UV-spectrophotometric method at 300 nm (Basaran and Tuovinen 1986). Ferrous iron concentrations were determined by a modified o-phenantroline spectrophotometric method, insensitive to Fe^{3+} interference (Herrera *et al*. 1989).

Cell monitoring

Presence of microbial cells was confirmed by direct microscopic count using a Neubauer counting chamber with a depth of 0.01 mm. Higher densities of pure cultures facilitated faster Fe^{2+} oxidation and therefore also higher oxidation-reduction potential.

Chemical analyses

Elemental analysis of the water was done using AAS (Varian AA240Z, AA240FS) and ICP-MS 7700 (Agilent). Sulfate concentration was analyzed by ion chromatography (Dionex ICS 5000).

Results

In order to oxidise Fe^{2+} from acid mine drainage, three strains of chemolithotrophic, acidophilic, iron-oxidizing bacteria were used in a batch cultivation process. This was compared to batch cultivation without any microbial inoculation, so only natural microbial consortia were present. All batch cultivations were carried out in triplicate, with the mean value for each point plotted (Fig. 2).

Inoculation of bacterial consortium consisting of A. ferrivorans SS3, A. ferrooxidans and L. feriphilum on the third day of cultivation, accelerated Fe^{2+} complete oxidation in a span of 24 hours. Compared to the water with only native microorganisms available, even after 120 hours approximately 76 mg/L of Fe^{2+} was still present.

Once all Fe^{2+} is successfully oxidised to Fe^{3+}, the water can be used for the secondary minerals precipitation.

In order to precipitate out dissolved Fe^{3+}, pH of the oxidised solution in both cases (S; S+bb) was adjust by 20% KOH to 3.7. The pH of the Smolnik AMD from the Pech Shaft spans from 3,7 to 4,1 (Bálintová *et al*. 2019). In the experiment, the lowest value from this range was used as it is already sufficiently high for Fe precipitation.

***Table 2** Parameters of the Smolnik mine water (2025).*

pH	ORP mV	Conductivity mS/cm	Temperature °C	Flow rate L/s
4,12	289	2,09	12,1	10

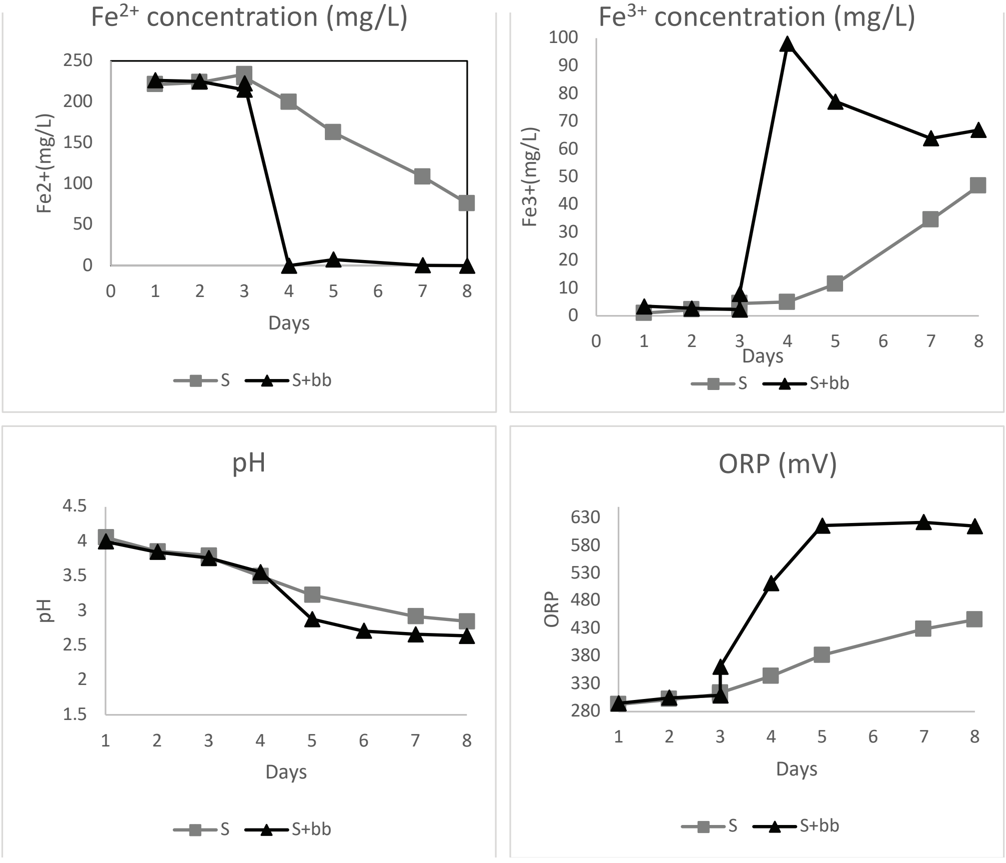

Figure 4 *Process of a batch cultivation; S- Smolnik mine water; S + bb – Smolnik mine water with 3 inoculated bacterial cultures.*

After pH adjustment to 3.7, Fe^{3+} concentration dropped to 2,11 mg/L (S+bb) and 1,74 mg/L (S), respectively.

The Fe^{2+} concentration in “S+bb” was below the detection limit already after 24 hours of bacterial inoculation but for the “S” cultivation there was still 76 mg/L present even on the 8th day. After raising the pH and subsequent filtration of precipitates (vacuum filtration through 0,23 µm membrane filter), there was still 46,75 mg/L Fe^{2+} present in the filtrate. This far exceeds the norm of 2mg/L for surface water quality according to Regulation of the Government of the Slovak Republic (269/2010 2010). The oxidized water, where inoculated bacterial consortium was used, exceeded this threshold value by only 0,11 mg/L.

Conclusion

The main purpose of this study was to remove dissolved iron by the process of bio-oxidation from the original mine water and thus minimise the risk of further iron precipitation, when mine water mixes with freshwater. To minimize the addition of chemical agents, only bacterial iron oxidation was performed.

The use of properly grown iron oxidisers in their exponential phase can effectively substitute the use of a chemical agent such as hydrogen peroxide.

Subsequently, after effective Fe2+ oxidation, selective precipitation and recovery of metals of interest can be achieved with high yields through the process of

Optimized Selective Sequential Precipitation (Macingova E. 2012) without the need for hydrogen peroxide.

Compared to the aforementioned True Pigments social enterprise, where pigments are produced from the sediments in the creek, in this research the crude mine water is being used before it reaches the water body. Intensive research is currently underway. Preliminary results show great potential for novel use of the Smolnik mine waters.

Acknowledgments

This study was funded by the EU NextGenerationEU through the Recovery and Resilience Plan for Slovakia under the projects No. 09I03-03-V04-00697

References

269/2010 (2010) Regulation of the Government of the Slovak Republic No 269/2010.

Bálintová M, Singovszká E, Holub M, Demčák Š (2019) Influence of Acid Mine Drainage on Surface Water Quality. In: Negm AM, Zeleňáková M (eds) Water Resources in Slovakia: Part I: Assessment and Development. Springer International Publishing, Cham, p 239–258. https://doi.org/10.1007/698_2017_220

Bártová Z (2020) Identifikácia Mikrobiálnych Spoločenstiev v Environmentálnych Matriciach Nekultivačnými Metódami. TECHNICKÁ UNIVERZITA V KOŠICIACH

Basaran AH, Tuovinen OH (1986) An ultraviolet spectrophotometric method for the determination of pyrite and ferrous ion oxidation by Thiobacillus ferrooxidans. Applied Microbiology and Biotechnology 24(4):338–341. https://doi.org/10.1007/BF00257060

Enforcement USDotIOoSMRa (2023) Ohio's Largest Acid Mine Drainage Site is Getting Cleaned Up. https://www.osmre.gov/news/stories/Ohio-AMD-Cleanup-Thanks-To-AMLER-BIL Accessed

European Commission D-GfIM, Industry, Entrepreneurship and SMEs (2023) Proposal for a REGULATION OF THE EUROPEAN PARLIAMENT AND OF THE COUNCIL establishing a framework for ensuring a secure and sustainable supply of critical raw materials and amending Regulations (EU) 168/2013, (EU) 2018/858, 2018/1724 and (EU) 2019/1020, Report №

Herrera L, Ruiz P, Aguillon JC, Fehrmann A (1989) A new spectrophotometric method for the determination of ferrous iron in the presence of ferric iron. Journal of Chemical Technology & Biotechnology 44(3):171–181. https://doi.org/https://doi.org/10.1002/jctb.280440302

Jaško V, Cicmanová S, Gajdoš V (1998) Smolník hydrogeologické a hydrogeochemické problémy územia po likvidácii a zatopení vydobytého ložiska pyritových rúd. Podzemná voda:118–129

Juck L (1984) Výsady miest a mestečiek na Slovensku, 1238–1350. Veda, Vydavateľstvo Slovenskej akadémie vied

Kaksonen AH, Janneck E (2024) Biological Iron Removal and Recovery from Water and Wastewater. In: Hedrich S, Wiche O (eds) Biological Metal Recovery from Wastewaters. Springer Nature Switzerland, Cham, p 31–88. https://doi.org/10.1007/10_2024_255

Kupka D, Bártová Z, Hagarová L (2023) Kinetics study comparing bacterial growth and iron oxidation kinetics over a range of temperatures 5–45 °C. Hydrometallurgy 222:106181. https://doi.org/https://doi.org/10.1016/j.hydromet.2023.106181

Kupka D, Pállová Z, Horňáková A, Achimovičová M, Kavečanský V (2012) Effluent water quality and the ochre deposit characteristics of the abandoned Smolník mine, East Slovakia. Acta Montanistica Slovaca 17

Lintnerová O, Šoltés S, Šottník P (2009) Environmentálne Riziká Tvorby Kyslých Banskyých Vôd na Opustenom Ložisku Smolník. In: Bratislave PfUv (ed). p 226

Lung TN (1986) The history of copper cementation on iron – The world's first hydrometallurgical process from medieval China. Hydrometallurgy 17(1):113–129. https://doi.org/https://doi.org/10.1016/0304-386X(86)90025-3

Macingova E. LA (2012) Recovery of Metals from Acid Mine Drainage. Chemical Engineering Transactions 28:109–114

Pigments T (2024) True Pigments LLC. https://www.truepigments.com/ Accessed

Reichel S, Janneck E, Burghardt D, Peiffer S, Kießig G, Koch T, Arnold I, Laubrich J (2017) Microbial Production of Schwertmannite: Development from Microbial Fundamentals to Marketable Products. Solid State Phenomena 262:568–572. https://doi.org/10.4028/www.scientific.net/SSP.262.568

Rösler HJ, Lange H (1972) Geochemical Tables. Edition

Opportunities to Improve Groundwater Models for Mining Assessments in South Australia: Learnings from Common Shortcomings

Gabor Bekesi[1], Juliette Woods[2], Michael Teubner[2], Mark Keppel[2],
Kent Inverarity[2], Paul Thompson[1]

[1]Department for Energy and Mining, GPO Box 618, Adelaide, South Australia 5001, Australia, gabor.bekesi@sa.gov.au

paul.thompson2@sa.gov.au

[2]Department for Environment and Water, GPO Box 1047, Adelaide SA 5001, Australia, juliette.woods@sa.gov.au, ORCID 0000-0002-3669-5049

michael.teubner@sa.gov.au

mark.keppel@sa.gov.au

kent.inverarity@sa.gov.au

Abstract

The environmental assessment and management of mines in South Australia frequently relies on groundwater modelling. Government hydrogeologists often see repeated and avoidable shortcomings in proponent modelling. These shortcomings must be identified and addressed to provide confidence that a project can be responsibly developed, particularly in South Australia, where groundwater resources are limited, and mining is economically important. Five hydrogeologists compiled a list of common errors from more than forty models. These relate to: representation of the conceptual hydrogeology, potentiometric head maps, groundwater-dependent ecosystems, potential for watertable rise, uncertainty analysis, and environmental compliance criteria.

Keywords: Hydrogeology, numerical groundwater modelling, environmental impact assessment

Introduction

The mining and energy sector is an important part of the South Australian economy: it contributed $7 billion to the state's total $18 billion of exports in 2023. Important minerals mined include copper, uranium, iron and gold. Groundwater is a critical concern of South Australia's mining sector due to the state's climate and scarce water resources. Most major mines are located in remote semi-arid and arid regions, where there is low rainfall and little data (Fig.1).

Groundwater is by far the most disputed environmental element in South Australian mining, ahead of air quality, noise, conflict with land use and traffic. This is because in the South and Coastal areas (Fig.1) the generally good quality groundwater resources are highly utilised and concerns about ongoing access to and protection of groundwater are widely held in the community. In the lower rainfall Mid-North and western Far North areas groundwater is generally brackish to saline. In recent years, competition has been developing even for saline groundwater in these parts of the state.

The environmental assessment and management of mines in South Australia frequently relies on groundwater modelling. Numerical groundwater flow models support the environmental impact assessment for both new mining applications and mining program changes for almost all major mines. These models are reviewed by government hydrogeologists to ensure that the environmental impacts of mining are assessed as reliably as possible. The reviews follow the requirements of the Mining Act 1971 and water allocation plans (if applicable), using a source, pathway and receptor approach.

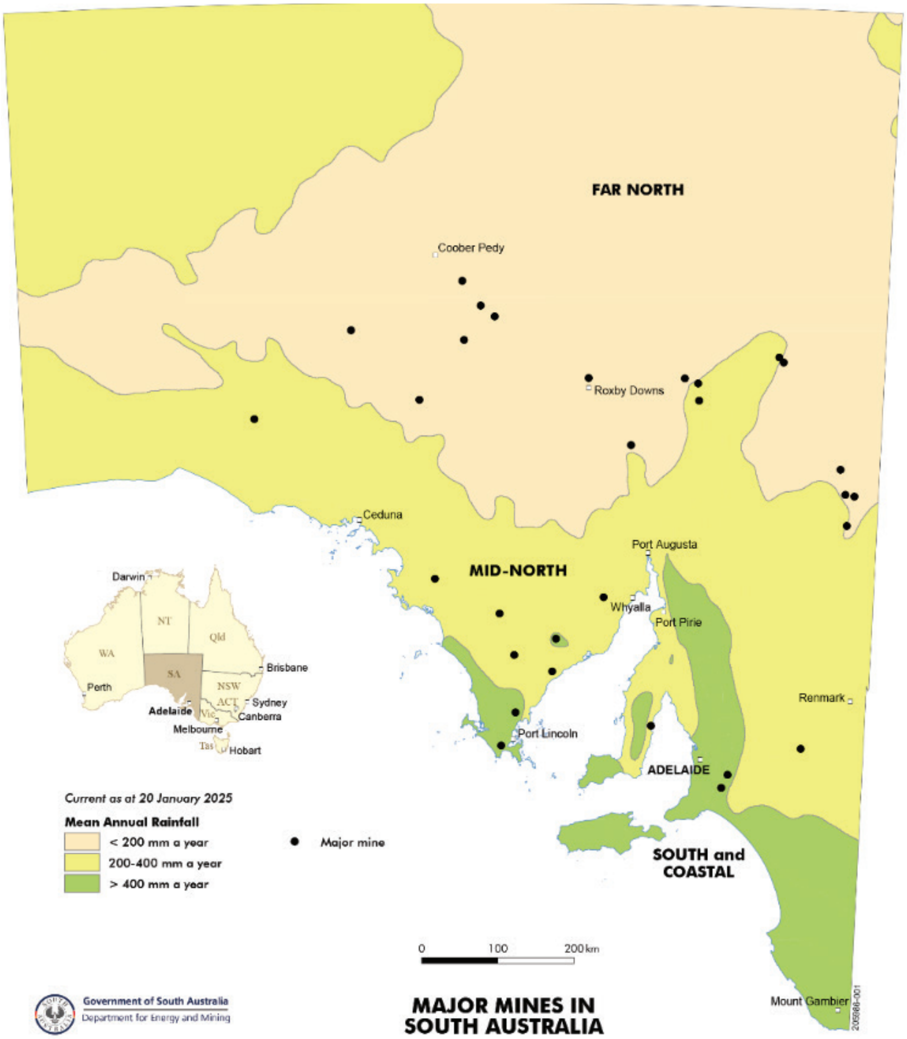

Figure 1 *Major mines in South Australia and climate zones.*

Often government reviewers repeatedly see the same avoidable shortcomings in these models. The identification and resolution of common shortcomings is important to improve modelling and provide confidence to decision makers that a project can be responsibly developed.

Methods

To improve model assessments, five hydrogeologists from two government departments, with a combined experience of approximately 150 years, compiled a list of common errors and omissions in numerical models developed for new mining applications and operational programs for existing mines. The list of errors and omissions is based on the review of more than 40 numerical groundwater flow models associated with mining applications and programs. These errors were classified into the following categories:

1. Regulatory (information required by mining regulations was not provided).
2. Data deficiency (inadequate data coverage, or the use of incorrect data).
3. Conceptual (errors and omissions in conceptual hydrogeology).
4. Errors and omissions in the conceptual hydrogeology to numerical model translation.

5. Model (errors and omissions related to the building of the model or its documentation).

Next, each of the five hydrogeologists identified the most common and important issues in their experience. Those that were identified by at least two of the hydrogeologists are presented here.

Results

The following common errors and omissions were identified in many of the reviews:

1. inconsistent representation of the conceptual hydrogeology in the numerical model;
2. insufficient model-independent groundwater potentiometric head maps for each aquifer to describe existing groundwater conditions and inform model boundary conditions;
3. lack of consideration of groundwater dependent ecosystems;
4. little focus on the damage that rising groundwater can cause to ecosystems in arid areas;
5. calibration or uncertainty analysis used in place of field data or good conceptual hydrogeology; and,
6. unnecessarily complex and difficult to enforce environmental compliance criteria that are linked to model predictions.

Each of the items above is briefly discussed in the following section.

Inconsistent representation of the conceptual hydrogeology in the numerical model

A groundwater model must start with a well-defined aim for the required model outputs. The conceptual hydrogeology is then developed, summarising and simplifying data and expert knowledge, to describe the critical hydrogeological features which will influence the required outputs. The numerical model should then embody the conceptual hydrogeology. Often the conceptual hydrogeology is informed and amended during the modelling process, as its assumptions are tested against observations. Occasionally the development of alternative concepts may be required, which in turn may help to understand conceptual uncertainties. The conceptual hydrogeology and numerical model should not be expected to match every detail of a groundwater system but should capture the salient behaviour.

The conceptual hydrogeology and the groundwater model should be consistent in the nature of hydrostratigraphic units, their hydraulic parameters, and how the groundwater system exchanges water with the surrounding environment. A simple and real mining example is a conceptual hydrogeology suggesting an aquifer – aquitard - aquifer sequence. The calibrated model, however, indicated very little contrast in hydraulic conductivity between the three hydrostratigraphic units and the numerical values suggested that all the three units were aquitards. In addition, the range for model calibrated hydraulic conductivity appears to be up to two orders of magnitude less than those interpreted from actual hydraulic aquifer tests. Such inconsistencies between the conceptual hydrogeology and the numerical model must be discussed and justified. Either the conceptual hydrogeology should be revised, with explanation, or the model calibration should be reconsidered. Where possible, conceptual and parameter uncertainties should be resolved by additional data collection.

Other examples encountered include different groundwater flow directions (horizontal or vertical) in the conceptual hydrogeology and in the model; and the model having to include processes that are not explained in the conceptualisation, such as artificially draining groundwater out of the model without explaining the physical/hydrological process that is simulated.

Probabilistic (stochastic) numerical models should also be consistent with the conceptual hydrogeology. If hundreds or thousands of realisations, each with a different parameter set, are presented as acceptable, then each realisation should be consistent with the conceptual hydrogeology. This can be difficult and time-consuming to assess.

Often inconsistency between the conceptual hydrogeology and its numerical model representation emerges at the regulatory review of the completed model.

Modellers are often reluctant to go back and change the conceptual hydrogeology as this would also trigger a model review, increase the costs and prolong the approval process. On the other hand, regulators are reluctant to approve models with unresolved inconsistencies.

Modellers often use "good" calibration of the model as a proof that there is nothing wrong with the conceptual hydrogeology. Bredehoeft (2003) concluded that good calibration of a model does not ensure a correct conceptual hydrogeology and we concur unreservedly. Both modellers and regulators should also be conscious that conceptual hydrogeology is not always immutable (Bredehoeft 2003) and sometimes even the most comprehensive uncertainty analysis cannot compensate for conceptual uncertainties.

This type of error occurs mainly because of an insufficient review process. Ideally, frequent reviews and consultation between mining proponents and regulators are required. Barnett *et al.* (2012) suggest model reviews at the completion of the conceptualisation and design stage, the calibration and sensitivity analysis, and at the completion of the project. In our experience, such frequent consultations are rare for mining proposals.

Regrettably, even when the conceptual hydrogeology and numerical model are initially consistent, later observations may invalidate both. Bredehoeft (2005) defined the *conceptualization model problem – surprise* as new data that render the prevailing conceptual hydrogeology invalid and considered that *surprise* occurs in 20 to 30% of model analyses. Hence numerical models should be revisited and revised periodically. Post-audits are recommended.

Insufficient model-independent groundwater potentiometric head maps for each aquifer to describe existing groundwater conditions and inform model boundary conditions

Boundary conditions are important and integral aspects of both the conceptual hydrogeology and the building of the numerical model. The levels, direction and gradients of flows within and between the aquifers will influence the environmental impacts of a mine.

If a model-independent and reliable groundwater head contour map cannot be constructed, the model will inadvertently be based on questionable boundary conditions, leading to unsupportable model predictions. This type of error occurs in areas with an absence of sufficient groundwater head data. South Australia, with an area of 983,000 km^2 and a population of 1.8 million (of which the capital Adelaide has 1.4 million inhabitants) has many remote areas where groundwater data are sparse.

Notwithstanding the above, if realistic boundary conditions cannot be determined in the absence of data, perhaps an interim and simple analytical solution should be developed, and efforts should be focussed on obtaining new data to aid the development of a future numerical model. New data do not necessarily require drilling if re-measuring existing wells would suffice. Hydraulic head measurements can often be obtained in the field relatively easily (Cohen and Cherry 2020) and such data can also improve the conceptual understanding.

Lack of consideration of groundwater dependent ecosystems

Addressing groundwater dependent ecosystems (GDEs) as environmental receptors is a requirement of the Mining Act (1971) of South Australia, yet GDEs are often inadequately addressed in modelling assessments.

Frequently, there is an absence of potentiometric head observations near potential terrestrial GDEs to determine depth to groundwater over time, or no consideration of streamflow data if there are potential aquatic GDEs.

Further, groundwater models for mining typically use time steps in the order of years and therefore cannot consider the seasonality and variability of the watertable, potentiometric surface, or surface water-groundwater interactions that are all important for the proper consideration of GDEs.

These inadequacies may be due to limited consideration of the model's aims at the beginning of the project. For example, mining groundwater models often focus on dewatering rates and regional drawdown, and their conceptualisation and construction reflect that. For those purposes, they concentrate appropriately on the mine site, mining actions and regional flows, with large spatial scales outside the mine, and annual or greater stress periods/timesteps. However, these may not be the most important hydrogeological features for assessing GDEs. GDE health is influenced by depth to water, spring flow and surface water/groundwater interaction near or upstream of the GDEs. Seasonal or episodic variations may be critical. Hence a model designed to estimate dewatering and regional drawdown may be a poor tool for estimating impacts to GDEs. It may be better to have a second groundwater model that captures processes important to the GDEs, which is informed by drawdown estimates from the larger-scale model.

This type of error originates from either inadequate understanding of GDEs or not including GDEs explicitly in models. The Bureau of Meteorology developed a national online dataset of Australian GDEs (http://www.bom.gov.au/water/groundwater/gde/map.shtml), providing mining proponents with an initial indication of GDEs to address in their assessment. Further, most widely available modelling software allow for the simulation of groundwater-surface water interaction and therefore aquatic GDEs (surface water, wetlands, springs) can be included in models using one of the modelling packages specifically designed for that purpose. Terrestrial GDEs can be accommodated by an evaporation package that allows evaporating the shallow water table within an extinction zone.

Little focus on the damage that rising groundwater can cause to ecosystems in arid areas

Mining related infrastructure, such as tailing storage facilities and waste rock dumps, can increase groundwater recharge and can mound the water table locally. The water table may rise as a result, up to and within the root zone of vegetation, and can cause damage or dieback to vegetation unable to cope with such changed groundwater conditions.

It is important that numerical groundwater flow models address such potential environmental impacts on vegetation and assess the resultant cumulative mounding (from tailing storage facilities and waste rock dumps) and drawdown (from dewatering or depressurisation) together. The models should consider the decades after mining ceases, as the increased recharge may persist long after the dewatering ends.

Calibration or uncertainty analysis used in place of field data or good conceptual hydrogeology

It is very challenging to robustly simulate a region where there are minimal field data to inform the conceptual hydrogeology and numerical modelling.

A simple numerical model with few parameters may calibrate well to the limited data and yet its assumptions may be incorrect. Only field work and monitoring can determine this.

More complex numerical models with many parameters may make the best use of available data during calibration, but they too may calibrate well while having incorrect assumptions. Parameters distant from observations are unlikely to be influenced by data and will revert to the modeller's initial estimates, so there is little to be gained there.

Sometimes uncertainty analysis is used to explore many possibilities in the absence of data. Unfortunately, in practice it is very difficult to demonstrate that a complex model has adequately searched all the possibilities, given that it depends on all prior assumptions and parameter distributions. Also, it is not always understood that most of these approaches are unlikely to simulate a worst or best case: if hundreds or thousands of possibilities (realisations) are simulated probabilistically to explore hundreds or thousands of parameters, it is very unlikely that the realisations will pick "worst-case" values for all parameters at the same time. If there is a clear-cut undesirable impact to be avoided, the modeller should instead consider simulating both past and future, calibrating the model to historical observations and a hypothetical future dataset in which the undesirable impact occurs. If realisations/

parameter sets are found which are consistent with conceptual hydrogeology, meet calibration criteria, and allow the undesirable impact to happen, then subsequent fieldwork should determine if those conditions are present in actuality or if they can be ruled out.

Unnecessarily complex and difficult to enforce environmental compliance criteria that are linked to model predictions

In South Australia, an environmental impact assessment is required to use the source-pathway-receptor approach. An environmental outcome and associated outcome measurement criteria are also required with details of the proposed groundwater monitoring (what, where, at what frequency and what background or control data will be used).

Sometimes unnecessarily complex and difficult to enforce outcome measurement criteria are proposed and linked to model predictions. An example is *no significant adverse drawdown above model predictions* without specifying the parameters of the relevant statistical test. Using inappropriate tests, for example using statistical methods designed for normal distribution for non-parametric data, or using linear trend estimators for non-linear temporal trends, also occurs. Difficulties also arise if subsequent model versions (for example after updates or re-calibration) vary considerably. If the outcome criteria are not changed the linkage between those and the model predictions disappears. If the model-linked criteria are varied the new criteria may allow, for example, a larger drawdown than originally; and it may have a detrimental effect on existing third party well operations or GDEs.

Most of these errors can be avoided by having an understanding of the hydrogeology, good quality baseline data and by appreciating the uncertainty in both measurements and in the model predictions.

Conclusions

Based on the compilation of errors and omissions and the contribution of five hydrogeologists, common patterns in errors from the review of more than 40 numerical groundwater flow models have emerged. Feasible solutions were provided at the end of each of the six relevant sections.

The findings from this review were already used in workshops with hydrogeologists working on behalf of mining companies and will be considered in mining guidelines and may contribute towards new Australian groundwater modelling guidelines.

To avoid common errors and omissions, more early investment in data collection, conceptual hydrogeology and modelling may be required. However, these would be recouped due to easier and faster approvals, plus it would reduce potentially expensive risks in mining construction and management. Ultimately, this will help to ensure that potential environmental impacts are reliably identified, and appropriate regulatory controls applied.

References

Barnett B, Townley L, Post V, Evans R., Hunt R, Peeters L, Richardson S., Werner A, Knapton A, Boronkay A, (2012) Australian groundwater modelling guidelines. Waterlines report 203 National Water Commission, Canberra, p.191. https://groundwater.com.au/wp-content/uploads/2023/02/australian-groundwater-modelling-guidelines.pdf

Bredehoeft JD (2003) From models to performance assessment-the conceptualization problem. Ground Water 41:571–577

Bredehoeft JD (2005) The conceptualization model problem - surprise. Hydrogeology Journal 13:37–46

Cohen AJB, Cherry JA (2020) Conceptual and Visual Understanding of Hydraulic Head and Groundwater Flow. Simple Book Publishing (https://gw-project.org/)

Management of Total System Uncertainty in Mine Water Projects

Kalman Benedek

[1]*ITASCA Australia Pty Ltd*
Level 5, Toowong Towers, 9 Sherwood Rd. Toowong QLD 4066 Australia

Abstract

Uncertainty means a lack of knowledge. Regardless of the abundance of available information, data remains restricted in both space and time. In the real world, the total uncertainty of a system is controlled by several sources, like data and parameters, conceptual models, design uncertainty, uncertainty related to the selection of modelling tools, and human behaviour.

This paper intends to address all possible sources of uncertainty by using the theory of system analysis. The system analysis can be implemented by using the so-called Features-Events-Processes (FEP) method, which is a standard approach in the nuclear industry but less known in mining applications. The approach requires the listing of all potential known and unknown features, events, and processes. Based on this comprehensive, transparent, and clear list, the relevance of each element can be evaluated, gaps can be easily identified, and by connecting elements, base case and alternative evolution pathways of a system can be developed.

In this paper a case study is presented for the development of mine-closure scenarios. It is also shown that this approach may provide several costs, business, risk reduction, and QAQC benefits for mine operators.

Keywords: System analysis, uncertainty, scenario development

Introduction

Groundwater assessment and groundwater resources are critical elements in mining operations. Groundwater is a key feature of any mining operation throughout the entire life of the mine, from exploration to the post-closure period. However, assessment of the groundwater regime is always subject to uncertainties of various sources in space and in time, and groundwater systems cannot be described in a deterministic way (Oreskes, Shrader-Frechette, & Belitz 1994). The sources of uncertainty might be, but are not limited to, limited data in space and time, conceptual uncertainty, parameter uncertainty, design uncertainty, and anthropogenic uncertainty.

Recently, there are substatntial developments to manage uncertainty associated with parameter distributions. These approaches assume parameter uncertainties and their management can compensate other sources of uncertainty. However, it is well documented in the literature that the management of one source of uncertainty can not compensate for other sources of uncertainty (Bredehoeft 2005). For example, even in case the most sophisticated statistical approaches are used to manage parameter uncertainty, if the underlying concept is wrong, the results will be invalidated by the inappropriate conceptual model selected. These problems become even more profound as the scale of interest in a particular project gets further away from observation scale in space and in time. Making a useful and applicable prediction for tomorrow is more likely than making a prediction in the scale of tens or even more (hundreds or thousands) years. The same applies to spatial scales: making good prediction at 10m away from a bore (observation) is more likely than at 100m.

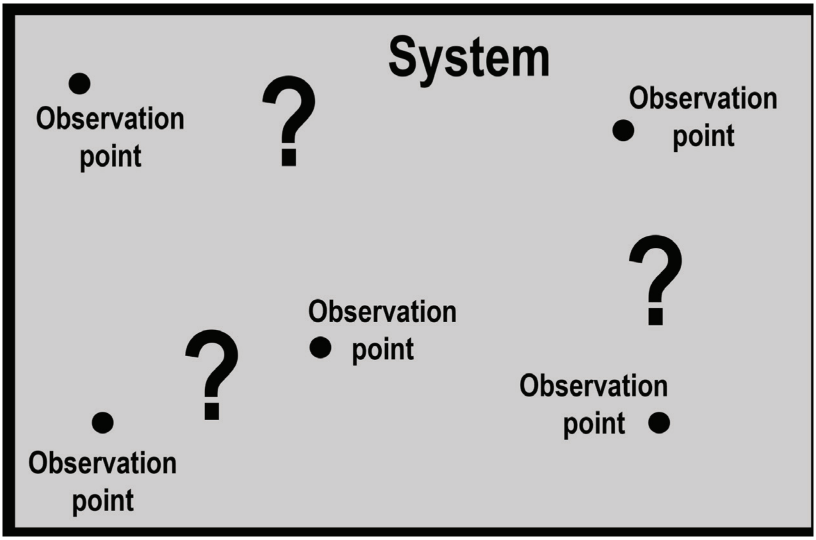

Figure 1 The difference between knowledge and theory. We know the groundwater system at discrete locations (for instance at borehole locations), but we theorise what may go on between observation points (question marks).

In general, it can be stated knowledge in hydrogeology is constrained by the spatial and temporal extent of observations and perceptions (Fig. 1). Any interpretation, interpolation, or extrapolation between the observation points in space and time cannot be fully justified and may form the basis of doubts. Assessment of the unknown is always uncertain and non-unique. As John Allen Paulos quoted, "Uncertainty is the only certainty there is" (Paulos 2003).

Beyond the parametrization of a groundwater system, which is inherently non-unique, it is even more critical to fully understand the system's key characteristics. However, conceptualisation is sometimes subjective, heavily reliant on previous experience and usually non-unique, just like system parameterization. Therefore, a method is required to manage uncertainty associated with the "lack of knowledge" in conceptualisation and with any other potential sources of uncertainty.

System analysis

The nuclear industry has developed the method of features-events-processes method (FEP catalogues) to manage this kind of uncertainty (NIREX 1998). The aim of the FEP analysis process is to provide a systematic framework for identifying all issues relevant to the evolution of a system.

A feature can be defined as an object (e.g., aquifer), structure (e.g., open pit), or condition (e.g., groundwater extraction) that has a potential effect on the system studied. An event can be defined as a natural or human-caused phenomenon that has the potential to affect the system and that occurs during an interval that is short compared to the period of the investigation (e.g., flooding, slope failure, blasting). A process can be defined as a natural or human-caused phenomenon that has the potential to affect the system and that operates during all or a part of the period of the investigation (e.g., groundwater flow, transport, seepage). The processes and events act upon features.

In general, events may define alternative scenarios, while features and processes are usually applicable across several scenarios. To identify scenarios and to develop conceptual models, a database containing the description, properties, and potential impacts of all identified FEPs and the interaction between FEPs is required. The so-called FEP catalogue lists all known, and even unknown or potential FEPs in a comprehensive database with identifiers, definitions, and short descriptions or justifications. An FEP function describes how that component contributes to the system evolution (e.g., rock may transfer fluid) (Andersson *et al.* 2009). A function indicator is a measurable or calculable property of a system component that indicates the extent to which a function is fulfilled (e.g., hydraulic conductivity of rock). A function indicator criterion is a quantitative limit such that if the function indicator to which it relates fulfils the criterion, the corresponding function is maintained (e.g., hydraulic conductivity < 1×10^{-9} m/s – sealing rock). An FEP catalogue is open; the list can be extended as more information and interpretation become available.

It is important to note that even unknown FEP elements must be included, since though these elements may not be observable recently, they may emerge as a critical element in the future. A good example of this problem is the management of climate change.

Key objectives of the FEP catalogue are comprehensiveness, traceability, and clarity (NIREX 1998). Comprehensiveness aims to consider all potential elements of a system studied. Traceability aims to provide a clear and auditable rationale supporting scenario and conceptual model development. Clarity aims to present information in a clear and accessible way such that the basis for decisions and assumptions can be readily understood.

Based on the FEP catalogue, several different system evolution pathways can be developed by using either a top-down approach or a bottom-up approach. A scenario is a description of a possible future evolution of the system; a scenario describes the system components along a potential evolution pathway. A base case scenario is a broad and reasonable representation of the natural evolution of the system and its surrounding environment; it includes all FEPs

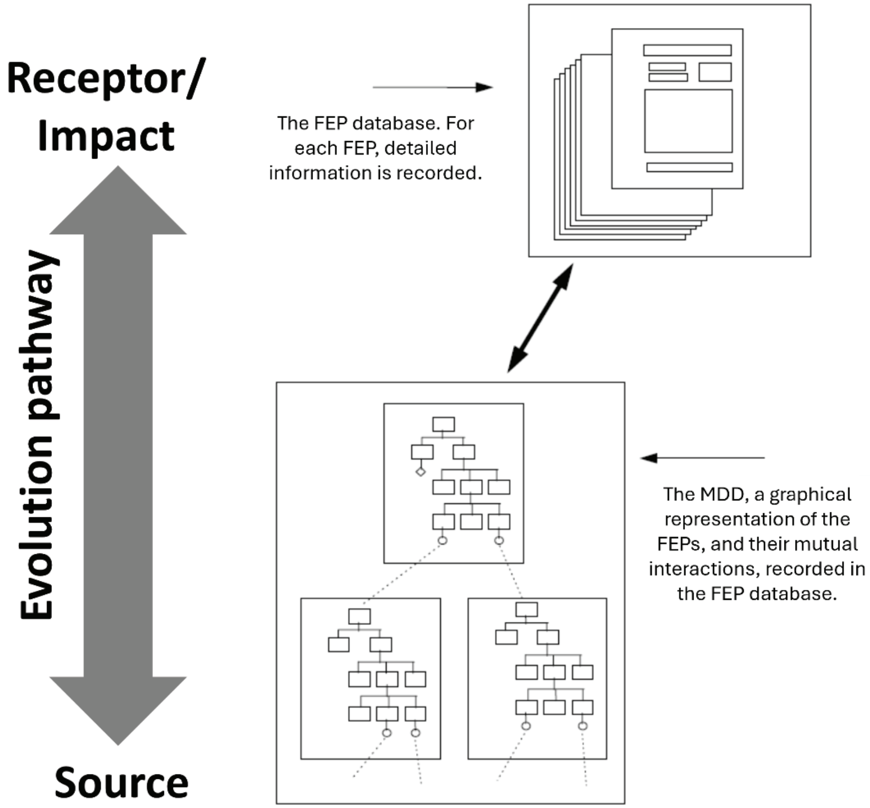

Figure 2 *Development of alternative system evolution pathways by connecting different elements of the FEP catalogue (figure modified after (NIREX 1998)). MDD stands for master directed diagram.*

that are more likely than not to be relevant to the system. Alternative scenarios are any probabilistic system evolution pathways, but the base case scenario. The individual scenarios are developed by connecting elements of the FEP catalogue in a logical way (Fig. 2).

If required, scenarios can be screened out from further analysis (modelling) by considering regulatory, low probability, low consequence or project specific criteria.

Case study

The system analysis approach presented above has been applied to a confidential site in Queensland, Australia. The client requested "the development of a qualitative hydrogeological site conceptual model detailing the potentially complete exposure pathways at the point of mine closure." This request was based on the requirements of the Progressive Rehabilitation and Closure Plan (Department of Environment and Science 2019). Regulatory guidelines usually require that all potential system evolution pathways and associated risks should be evaluated. The use of alternative scenarios (in contrast to relying on one single potential future state) has the advantage that a range of possible evolutions of the system (even including low-probability but high-consequence cases) can be explored. In addition, a good understanding of the relative importance of alternative scenarios will help clients to identify which scenarios may require further consideration (e.g., additional site investigation, modelling, etc.).

Alternative scenarios were developed for the post-closure phase, which assumed that a new hydrogeological "equilibrium" develops ("post-closure steady state") at the site. Note that this phase is different from the post-mining transient phase, which is a transient process between the operational phase and the post-closure steady-state phase. The FEP catalogue developed for the site contains six FEP categories and several elements:

- System categories:
    - General – elements that affect the entire system (e.g., time scale, spatial domain, regulatory framework).
    - Mine infrastructure elements – elements and activities in the mine (e.g., exploration holes, box cut, stockpile).
    - Geological elements (Table 1) – solid underground system (e.g., formations, faults, rock heterogeneity).
    - Hydrogeological (flow and transport) elements – groundwater system (e.g., aquifers, recharge, evapotranspiration).
    - Hydrology elements – surface water system (e.g., surface water bodies, flooding, surface water-dependent ecosystems).
    - Human activity, water use (e.g., new mining activity, site contamination, underground fire).
- Feature, event, process ID.
- Element name.
- Defining if the element is a feature, event, or process.
- Short commentary to provide added context where necessary.
- A short description to note whether the element is part of the base case scenario or not.

The geological elements of the example FEP catalogue are listed in Table 1; the schematic hydrogeological conceptualisations are shown in Fig. 3.

Based on the system element catalogue, three potential alternative scenario models (Fig. 3) have been selected for qualitative description through a series of workshops where all stakeholders were involved:

- Aquifer compartmentalisation.
- Site flooding.
- New mining activity.

A qualitative comparison of the base case and alternative scenarios is summarised in Table 2.

Table 2 clearly shows that assuming different evolution pathways for the site may result in various groundwater flow directions and groundwater quality changes. Therefore, it is critical to fully understand these alternative options to increase confidence in our predictions. Also, it is important to note that these alternative scenarios can be converted into some numerical or analytical calculations to make quantitative predictions about the potential future states of the site.

Table 1 Part of the FEP catalogue listing the geology category.

	FEP IDs	FEP Name	Feature, Event, Process	Comments/Description	Part of the Base Case Scenario?
2.0 Geology	2.1	Quaternary Sediments	F	Alluvial sediments	Yes
	2.2	Tertiary Basalts	F	4 basalt flow	Yes
	2.3	Tertiary Sediments	F	Interlayering with basalt	Yes
	2.4	Fort Cooper Coal Measures	F	Underlying the basalt with unconformity	Yes
	2.5	Moranbah Coal Measures	F	Underlying the Fort Cooper Coal Measures	Yes
	2.6	Coal Seams	F	Part of the Moranbah Coal Measures, three of the nine coal seams are economically viable	Yes
	2.7	Faults	F	Existing thrust faults up to the surface near and away the box cut. Normal faults striking east-west with vertical displacement of 5-10m, thrust faults striking north-south with 3m upthrust to east.	Yes
	2.8	Background Fracturing (Secondary Porosity)	F	Fractures are present in all geological layers.	No
	2.9	Basalt Flow Channels	F	Basalt flow over the Permian sediments.	No
	2.10	Intrusions	F	Some interpretations refer to the presence of intrusions along faults.	No
	2.11	Rock Heterogeneity	F	Basalt-sediment interlayering, sand-silt mud, clay successions.	No
	2.12	Unconformity of Geological Layers	F	Present in all geological formations.	Yes
	2.13	Primary Porosity	F	Property of each rock.	Yes
	2.14	Earthquakes	E	The possibility is considered, not the probability.	No
	2.15	Erosion, Deposition	F	Ongoing process, but no information is available.	No
	2.16	Volcanic Activity	E	The possibility is considered, not the probability.	No
	2.17	Subsidence	P	The subsurface voids may collapse, and backfilled material may get compacted.	No
	2.18	Chemical Alteration of Rocks	P	It can be assumed that waters of different origin may get in contact with various rock types. Also, backfill material may alter locally the groundwater quality. These processes may result in chemical alteration of the rocks.	No

Conclusions

Uncertainty is an inherent part of any hydrogeological project that needs to be considered at all stages of a mining operation. The proposed FEP-based system analysis is widely used in nuclear, water resource, carbon capture and storage, and geothermal projects but less known in mine water studies. In this paper it is demonstrated that developing alternative evolution pathways for a mine site may result in fundamentally different flow patterns and hydrogeological conditions. It is believed that the presented workflow can manage this kind of uncertainty, and the results may help clients in project development in the following ways:

- Consider a wide range of system components and relationships.
- Scenarios can be ranked based on their likelihood in the future in a quantitative way.
- The results may form the basis of future quantitative risk assessments.
- The underlying data set (components (features, events, processes) and relationships) may assist in preparing for alternative groundwater management scenarios.

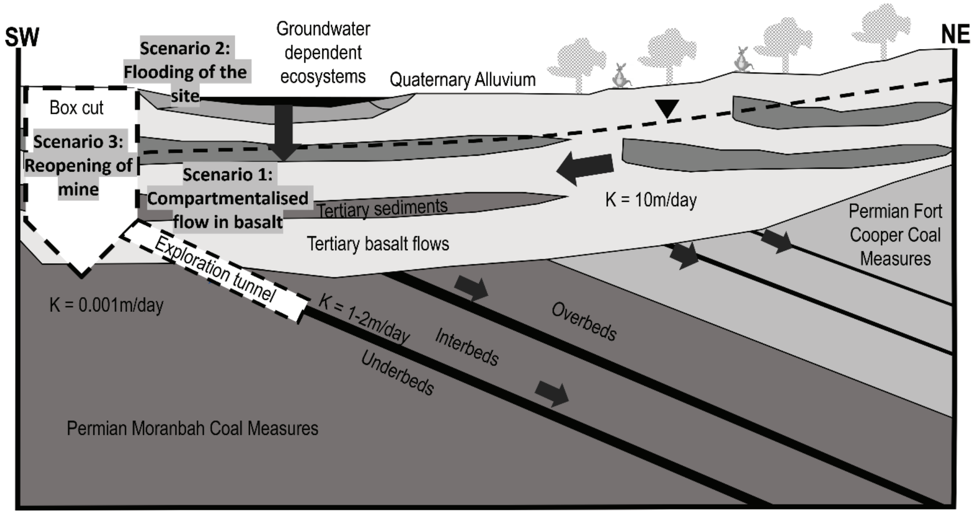

***Figure 3** Visual representation of the base case scenario and alternative scenarios.*

***Table 2** Qualitative comparison of the base case and alternative scenarios.*

Scenario	Summary of the scenario
Base Case	The box cut material is recharged from the unsaturated zone and the basalt aquifer. The two sources of recharge to the box cut may mix establishing a new blended water quality. At the horizon of the basalt – Permian aquifer interface it is assumed that low salinity basalt water mixes with more saline Permian water. Also, it is likely that water of Permian origin may not up well into the basalt layers due to its higher salt concentration and density. It is likely that this basalt water intrusion may locally dilute the more saline Permian groundwater.
Aquifer compartmentalisation	The limited extent of the aquifer may result in complete localised dewatering of the basalt aquifer during the operational phase. The vertical hydraulic gradients may be reversed leading to upwelling of more saline Permian waters into the lower section of the backfill material and basalt, resulting in water quality deterioration in the basalt aquifer
Site flooding	The local flood water infiltrates down the box cut backfill material, resulting in localised groundwater mounding around the backfilled box cut and intensified water flow back into the basalt and Permian aquifers. Any potential surface contamination may migrate into the underlying aquifers which may result in water quality decline.
New mining activity	The groundwater level declines rapidly as the new mine progresses and a cone of depression around the new mine develops. The mixed basalt-Permian water at the transitional zone of these two aquifers may intrude deeply in the basaltic aquifer resulting in poorer groundwater qualities.

- This may reduce risk and cost caused by using inappropriate water management scenarios.
- The presented system is open; as new considerations emerge, they can be added to the catalogue, and new scenarios can be investigated.

References

Andersson, J., Gunnarson, D., Hedin, A., Munier, R., Selroos, J., Ikonen, A., & Wikstrom, I. (2009) Application of host rock classification and acceptance criteria for repository layout and the safety case. Conference: 3. Amigo workshop, Nancy (France), 15–17 Apr 2008; Related Information: In:

Approaches and challenges for the use of geological information in the safety case for deep disposal of radioactive waste, 73 pages. (pp. 109–121). Nancy: Organisation for Economic Co-Operation and Development, Nuclear Energy Agency, 75 – Paris (France)

Bredehoeft J (2005) The conceptualization model problem – surprise. Hydrogeology Journal, Vol 13: 37–46, doi:10.1007/s10040-004-0430-5

Department of Environment and Science. (2019) Statutory guideline – Progressive rehabilitation and closure plans. Version 3.01, ESR2019/4964. Queensland Government, Brisbane, pp76

NIREX (1998) Overview of the FEP analysis approach to model development. Report no: S/98/009: United Kingdom Nirex Limited.

Oreskes N, Shrader-Frechette K, Belitz K (1994) Verification, validation, and confirmation of numericalmodels in the Earth sciences. Science, Vol. 263: 642–646, doi: 10.1126/science.263.5147.641

Paulos JA (2003) A Mathematician Plays the Stock Market. New York: Basic Books

Acid Mine Drainage-Background and Solutions – Global Edition

Stephen L. Benyo[1], Eric Gentis[2], Jimmy Cordova[3], Nils Schwarz[4], Robert Klug[5]

[1]Flottweg – Global Mining, Independence, Kentucky, United States of America, sbenyo@flottweg.net
[2]Flottweg – Global Mining, Independence, Kentucky, United States of America, egentis@flottweg.net
[3]Flottweg Peru – Mining & Industry Peru & Bolivia, Arequipa, Peru, cordov@flottweg.com
[4]Schwarz Global Consulting, Fairland, Gauteng 2170, South Africa, nils@sgconsulting.co.za
[5]Flottweg – Global Mining, Vilsbiburg, Germany 84137, klu@flottweg.com

Abstract

Acid Mine Drainage is a world-wide, growing, environmental problem. Passive treatment systems have been the preferred method to solving this, but the rapid decline in effectiveness of these treatments has given rise to the search for new solutions.

Active treatment solutions have been restricted to chamber filter presses which are labor-intensive to operate and have a high consumable material cost.

Utilizing centrifugation, acid mine drainage treatment systems can take advantage of technology which over the last three decades, has gained familiarity in the mining industry, after decades of established treatment in sewage, gravel washing, drilling mud and solvent extraction applications.

We share some information on this technology, in both how it operates, and its placement in AMD treatment.

Keywords: Centrifugation, Water Recovery, Active Treatment, Mobile Treatment, Solid/Liquid Separation

Introduction

Acid Mine Drainage (AMD) is a global crisis of many names – Mining Influenced Waters, Agua de Laboreo Minera and Acid Rock Drainage to name a few. The formation & movement of highly acid water rich in metals has affected waterways for thousands of years (EPA 2024). With global estimates for resolving this crisis reaching $40 billion USD the attention continues to shift towards technologies which can mitigate and prevent this compounding problem. This paper discusses basic history and technologies surrounding AMD, while providing a forward-looking view towards developing methods for treatment systems.

What is it?

The formula for the creation of Acid Mine Drainage can be classified as the introduction of a sulfide minerals to air and water, which, due to oxidation, results in the orangish/red precipitate containing sulfuric acid and metals such as Al, Mn, Zn, Cu, Pb, and Cd. To put into simple terms, when a portion of earth is exposed to oxygen for the first time, and it encounters water, a chemical reaction takes place, and results in an acidic water, which contains dissolved metals, e.g., pyrite, FeS_2, and an acidic pH level. The exposure of pyrite to oxygen and water can be a natural process, occurring due to weathering in regions such as the Yellowstone Mountains in the United States of America, or in other regions, volcanic activity, although this is not a primary source of the generation of these acid waters. Most frequently, the creation of the acid drainage is a direct result of mining activities, when earth is displaced and exposed to gather ore bodies containing valuable minerals for processing into a concentrate. When this processing area of mining, also known as a disturbed zone, is then exposed to water ingress, in the form of precipitation, stream runoff, and fracture ingress in deep wells, an environment is created which promotes the generation of acid mine waters. This can and does occur at mines which are actively producing, along with mines which have been termed "legacy" due to its inactive status.

Where is it?

While there are multiple regions affected by AMD which are facing an immediate and serious crisis, there are lingering and developing cases of affected waters globally. With tens of thousands of closed mines, thousands of active mines and many hundred in some stage of feasibility, assessment or permitting, the problem is expected to expand.

Particularly critical regions are found in the Appalachian region of the USA, along with the Gauteng Province of South Africa. In the USA, the major source of AMD comes from coal, polymetallic and copper mines. Most of the drainage in this region comes from legacy sites.

In South Africa, a region already facing a water supply shortage, the Gauteng Province has an abundance of legacy mines that once had produced precious metals and coal, now exacerbates the country's critical water shortage. The region estimates 350 million Liters of water affected per day. (Pratt 2012)

Two Major Solutions

Historically, the treatment of acid mine waters when a mine was actively producing ore was not deemed a priority, or in some cases, entirely disregarded. This occurred because the treatment of the waters was not a value-generating stream and generally viewed as a waste product. In legacy mine sites, there was a uniquely different hurdle to face, as the ownership of a closed mine is a liability, which made assigning responsibility for clean-up a challenge often left to the local communities and municipalities.

In recent years, a growing pressure has been applied to the Corporate Social Responsibility targets of active mine producers to provide solutions that mitigate and even reverse the damage created to the environment, while this increased monitoring also encouraged providing local government and communities with funding grants to begin repairing decades of damages when handling their communities' legacy sites.

These methods for addressing AMD can be broken down into two primary categories: Passive Treatment, and Active Treatment. These two methods are uniquely positioned and effective in certain circumstances, which is dependent upon flow rates, time frame, production status, number of affected sites, water quality output requirements and capital/operational funding availability. In both these systems, the primary objective is the neutralization of pH, which then allows for targeted metals to fall out of solution, creating a clear neutralized liquid discharge, and a dewatered solid.

The Passive Treatment system has been the traditional system for treatment, due to its comparatively low capital and operational expenditure for the lifetime of the system. This system operates in a series of ponds, where each pond provides an alteration to the AMD, which brings the affected waters closer to the neutralized metal-free water discharge (Fig. 1). The first set of ponds accomplish the removal of oxygen and the neutralizing of pH via the introduction of a biotic compost and variant of limestone or caustic. The solution is then oxidized in a second set of ponds, which then allow for the metals to precipitate into the final series of ponds, which are often referred to as "sacrificial zones" or polishing wetlands. Ultimately, an outlet of neutral water is produced for further transport or allocation.

The Passive Treatment is responsible for the improvements of water conditions in many regions, although it can face challenges due to its simplistic nature, which may limit the applications for which the system can be deployed. The sacrificial zone can be in defiance of environmental regulation in the region, as it creates a "dead land" which can foster limited flora and fauna, and over time, requires increasingly additional organic matter, limestone and maintenance to slow the increasing decline in water output quality. Because passive systems rely on processes that are slower than conventional treatment, they require longer retention times and larger areas to achieve similar results (Hedin *et al.* 1994). This maintenance is an intense procedure of cleaning out ponds at certain variables to ensure a consistent result, and to allow plenty of depth for static settling.

Transportation of this waste sludge is an expected challenge, especially in regions where the material must be transported via road to final location, as the waste sludge has very slow-solid settling and compaction due to the hygroscopic nature, creating instability due to the water that is retained. With these considerations, the passive system is often best positioned as a solution in closure and post-closure phases for short-term projects.

An Active Treatment System follows the same principles of neutralization, oxidizing and polishing the contaminated liquids, but carries important distinctions in both process and results.

The main distinguishing characteristic of the Active Treatment system is the utilization of a treatment plant, which has operational inputs of chemicals and electrical power. An Active Treatment system is often purpose-built for mines which are in the exploration to operational phases, and for sites in closure and post-closure phases. With centrifugation, this system eliminates the need for settling ponds, allowing for sludge to be stored in stable form, along with opportunities to compact sludge after open-air exposure, making an improved handling/disposal process.

An Active Treatment system generally introduces the acid drainage into a conditioning tank, where it is dosed with a lime slurry, neutralizing the pH. It is then transferred to neutralization reactors, where the material is oxidized, followed by a polymer-supported thickening step, in which the neutralized overflow is free of metal sludge, and the underflow is a thickened neutralized sludge. This method produces a treated water which can meet mandated water-discharge criteria and is often engineered for this specific end-goal. It is a capital-intensive system, but it has potential for cost recovery in its water production, rare earth element collection and solids transport.

***Figure 1** Construction of a passive system for AMD runoff in Pennsylvania, USA (Image: Stephen L. Benyo).*

Next examples will elaborate on a process developed for Active Treatment Systems, which deploys horizontal decanter centrifugation, to provide additional dewatering of the produced thickened neutralized sludge. With this technology employed, the solids produced from the active system is positioned for effective transportation at 50% dryness, which is effective for loader, conveyor, and truck transport to its next or final destination, while reclaiming additional neutralized water, referred to as centrate when arriving from a centrifuge.

Practical Example of Active System

An excellent example of such an active system (Fig. 2), is available for reference at an active operating mine in the mountainous region of Peru (Fig. 3).

The Active Treatment plant is part of a large polymetallic mine located between 2,200m–3,300m in a semi-dry environment, with an ambient temperature ranging from -5–25°C. The mine has been in operation for ten years, with an additional Life of Mine of 10 years. This location incurs Acid Mine Drainage because of rainwater, which washes out overburden dump creating safety and logistical concerns. 2km away from the mine site, is the processing plant. It is comprised of clarifiers, neutralization tanks, polymer dosing and a 2-phase decanter centrifuge (Fig. 4). Early in 2025, this site is moving from batch to continuous operations, as the anticipated sludge increase requires a 24/7 active treatment to alleviate the environmental effects.

A Flottweg Z4E decanter centrifuge, which

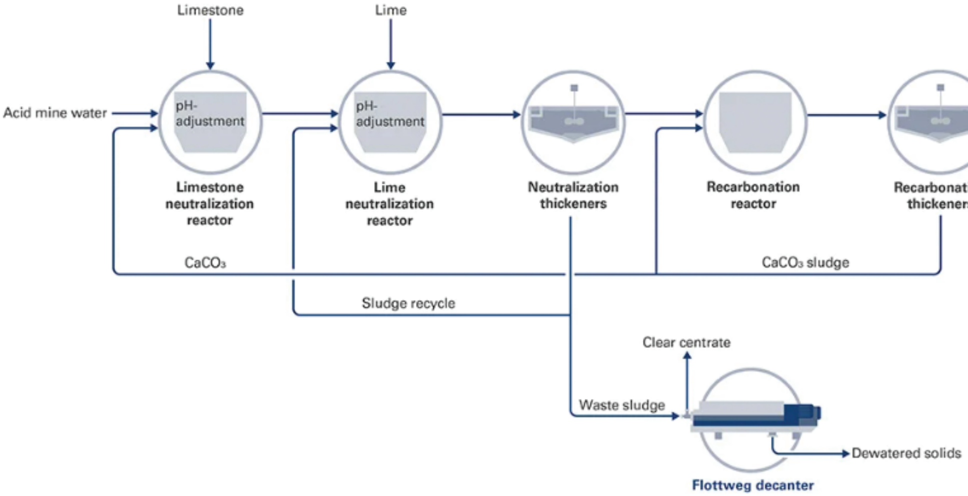

***Figure 2** Active AMD Treatment Plant Flow Diagram (Image: Flottweg SE).*

is designed to handle up to 12m3/h, receives feed from the upstream homogenizing tank, which generally produces a feed containing 3.5% solids by weight.

In start-up testing with the centrifuge, the pulp feed density was calculated at 1.1% g/cc, and the pulp feed solids content, at 1.1% solids by weight. After the feed was processed through the centrifuge, even considering the hygroscopic nature of the material, the solids content improved to 50% solids by weight, allowing for multiple modes of transport and the produced clear centrate retained a 6.9 pH, with minimal residual flocculant and essentially free of suspended solids, suitable for re-use. (Fig. 5).

Mobile Treatment Units or Systems

For AMD-affected regions with multiple legacy sites, or for active mine sites with geographic constraints, an AMD Mobile Treatment Systems serves as a compact solution which is transportable for treatment at multiple locations (Fig. 6). This system maintains key critical advantages of ease of installation, user-friendly and minimal downtime, ensuring continuous and uninterrupted production while maintaining the same levels of efficiency as a stationary system. This can be especially effective in regions which have limited funds, but require treatment at multiple sites, which demonstrate the flexible advantage of mobile treatment. This system is designed as a drop-off flat bed truck platform, which contains a clarifier, polymer dosing unit, mining-configured

***Figure 3** Active AMD Treatment Plant in Mountainous Region of Peru (Image: Emerson Huayanca).*

***Figure 4** 2-phase centrifuge processing neutralized waste sludge (Image: Jimmy Cordova).*

Figure 5 Solids discharge and centrate quality from decanter centrifuge.

centrifuge, and other ancillary equipment such as pumps, sensors and control panels.

Conclusions

The use of centrifuges for neutral sludge dewatering is a viable, effective, and economical alternative to existing technologies. When considering the environmental impact, space requirements, costs and increasing future demands, mechanical separation of solids and liquids by centrifugal force will increasingly find its way into modern mining and sludge treatment operations.

Acknowledgments

The authors wish to thank the owners, managers and especially the operations & maintenance teams at the mine in Peru for their unfailing courtesy, patience, encouragement and support during the commissioning and start-up operations.

Additional contributions & support from Messrs. Dustin Miller, Daniel Gorig, Georg Durselen, Tim Geary, Will Godby, Raul Vargas, Dan O'Brien, Andy Gralton, and Tony Kramer are all gratefully acknowledged.

References

Hedin, R.S.; Narin, R.W.; Kleinmann, R.L.P. (1994) Passive treatment of coal mine drainage. Inf. Circ. 9389. U.S. Department of the Interior, Bureau of Mines.

Pratt, Sara E (2012) All that glitters… Acid mine drainage: The toxic legacy of gold mining in South Africa. Earth Magazine, https://www.earthmagazine.org/article/all-glitters-acid-mine-drainage-toxic-legacy-gold-mining-south-africa/

U.S. Environmental Protection Agency (2024) Abandoned Mine Drainage, https://www.epa.gov/nps/abandoned-mine-drainage#:~:text=Acid%20mine%20drainage%20is%20the,minerals%2C%20resulting%20in%20sulfuric%20acid.

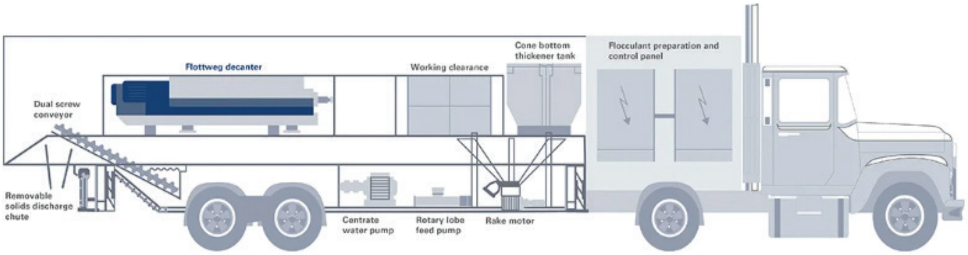

***Figure 6** AMD Mobile Treatment System.*

Floating Islands as a Tool to Promote Biodiversity in Pit Lakes

Rachele Bernasconi, Melanie L. Blanchette, Mark A. Lund

Mine Water and Environment Research Centre (MiWER), School of Science, Edith Cowan University, Perth, Western Australia, r.bernasconi@ecu.edu, ORCID 0000-0002-7973-8803

Abstract

Closure of pit lakes as aquatic ecosystems is viable, sustainable and economically responsible. Riparian vegetation and littoral areas are critical ecosystem components that cannot be established before the lake is full. Pilot-scale vegetated artificial floating islands were deployed in two moderately saline Australian pit lakes (≈5-12 mS cm^{-1}) to determine their impacts on biodiversity. Two of four plant species on the AFIs grew successfully and AFIs supported terrestrial (birds) and aquatic biodiversity (macroinvertebrates and fish). AFIs had higher sedimentation rates than lake controls. A larger-scale trial with >100 m^2 AFIs has begun incorporating lessons from this proof-of-concept pilot.

Keywords: Riparian vegetation, mine closure, birds, fish, macroinvertebrates, sedimentation

Introduction

Natural floating islands of fringing vegetation occur in many lakes globally (e.g., Inle Lake, Myanmar, Oo *et al.* 2022); they increase coverage and biodiversity of emergent plants, are resilient to water level changes, act as seed banks, and create habitat for terrestrial and aquatic animals (John *et al.* 2009). Artificial floating islands (AFIs) replicate aspects of natural floating islands, usually with artificial buoyancy and no (or limited) soil to support plants (Yeh *et al.* 2015).

Closure of pit lakes as aquatic ecosystems (see Lund and Blanchette 2023) is underpinned by the biodiversity stimulated by riparian vegetation and nutrients (Blanchette and Lund 2021). Surface contouring and revegetation is typically completed prior to filling which often takes many years (or decades) to complete. Riparian zones require proximity to the water to survive and therefore cannot be established until the lake has filled, creating a long period where the aquatic ecosystem is unlikely to meet regulator and public expectations.

As commercial AFIs have primarily been used to remove nutrients in wetlands (Stewart *et al.* 2008), AFIs in pit lakes appears initially counterintuitive to solving the problems of low nutrient levels in pit lakes. However, AFIs may provide an ongoing source of plant propagules to seed the lakes' edges during- and post-filling. Pit lake sediments typically contain very low levels of carbon (Lund *et al.* 2020) and adding C via biofilm sloughs, dead leaves, and roots from the AFIs can improve biodiversity and sediment biogenic processes (Lund and McCullough 2015).

The aim of this study was to investigate the use of pilot-scale AFIs as a proof-of-concept in saline pit lakes using both quantitative and qualitative (observational) data. Our research question was: can AFIs be successfully deployed in pit lakes, and could they enhance biodiversity? Using treatment and control AFIs, we measured: plant growth characteristics, sedimentation and C content (quantitative), and observed biodiversity (bird use, macroinvertebrates, and fish).

Methods

Study lakes and experimental design

Study coal mine pit lakes (n= 2, Lakes 'BL2' and 'BL4') were situated in the Bowen Basin (Queensland, Australia), which is Köppen-Geiger climate classification BSh (arid steppe climate with hot summers and predominantly summer rainfall (Peel *et al.* 2007)). Lake BL4

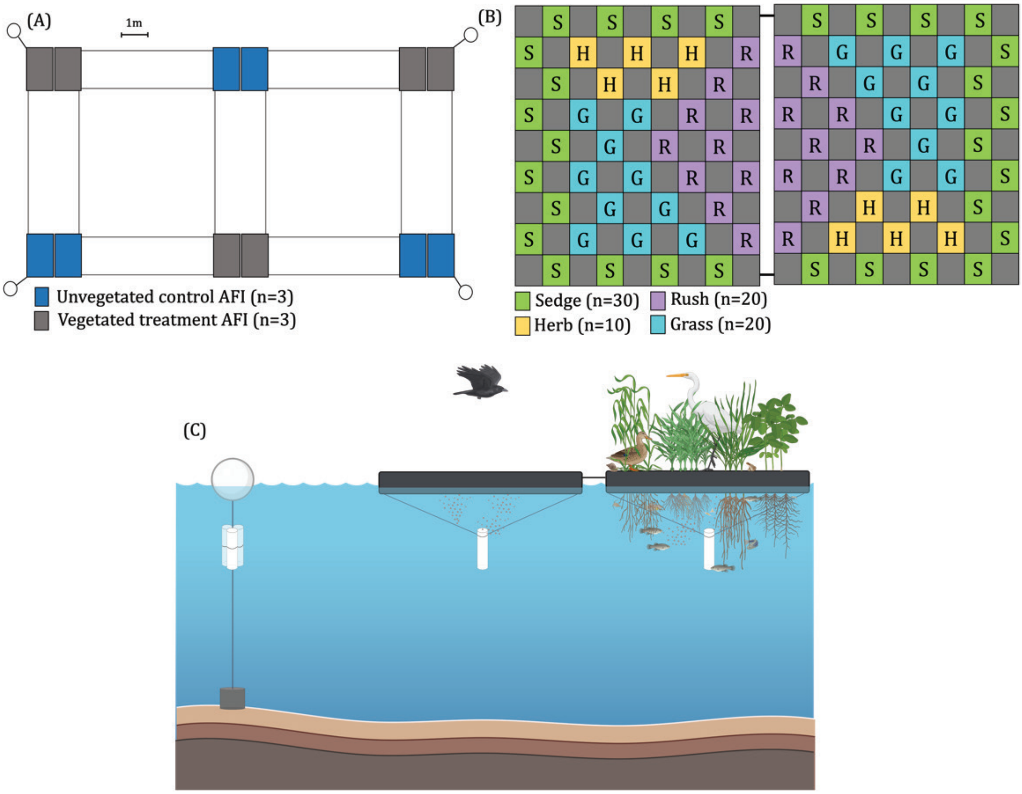

Figure 1 *Schematic representation of the* ***(A)*** *AFIs set up and* ***(B)*** *plant distribution map on the vegetated treatment AFI. Each vegetated AFI was made of 2 modules separated by 5 m (each module: 1 m x 1.5 m) with 80 plants from 4 species: P. decipiens ('herb'), L. hexandra ('grass'), J. usitatus ('rush'), and F. ferruginea ('sedge').* ***(C)*** *Sediment traps were installed ≈1 m under each AFI and as a control in the lakes' open waters (image created with BioRender.com).*

was moderately saline (≈12 mS cm^{-1}), ≈15 m deep and 10.5 ha. Lake BL2 was smaller (2.6 ha) brackish (≈5 mS cm^{-1}), and ≈12 m deep (see Blanchette and Lund 2021 for more on lakes). As of the time of this study (December 2022– April 2024), the lakes had not undergone any rehabilitation.

AFIs were installed in both lakes in December 2022. The overall construction was 6 small (3 m^2) AFIs (3 'vegetated' treatments, 3 'unvegetated' controls, arranged in a randomised block design; Fig. 1a). Each AFI consisted of 2 closely connected modules separated by 5 m (each module: 1 m x 1.5 m, polyethylene closed cell foam ≈10 mm sheets with 40 plant pots (1 plant per pot, bedded in with coir) suspended through holes in each sheet, Water Quality Solutions, Melbourne, Australia). Each vegetated AFI had 80 young plants of Australian taxa frequently used in wetland restoration projects (Barrett 2013): *Persicaria decipiens* ('slender knotweed - grass'; n= 10), *Leersia hexandra* ('swamp rice grass'; n= 20), *Juncus usitatus* ('common rush'; n= 20), and *Fimbristylis ferruginea* ('rusty sedge'; n= 30) (Fig. 1b).

In June 2023, dead plants or empty pots were replaced with the same species and sediment traps were installed. One sediment trap (0.5 m x 0.086 m int. dia. PVC tube, capped at the bottom, 2.90 L) was suspended ≈1 m beneath each AFI (n= 6) to capture fallout from islands and avoid other lake sedimentation processes. Control traps (n= 3) were deployed ≈10 m from the AFIs (≈1 m deep) held taught between a 20 kg concrete weight and a buoy (Fig. 1c).

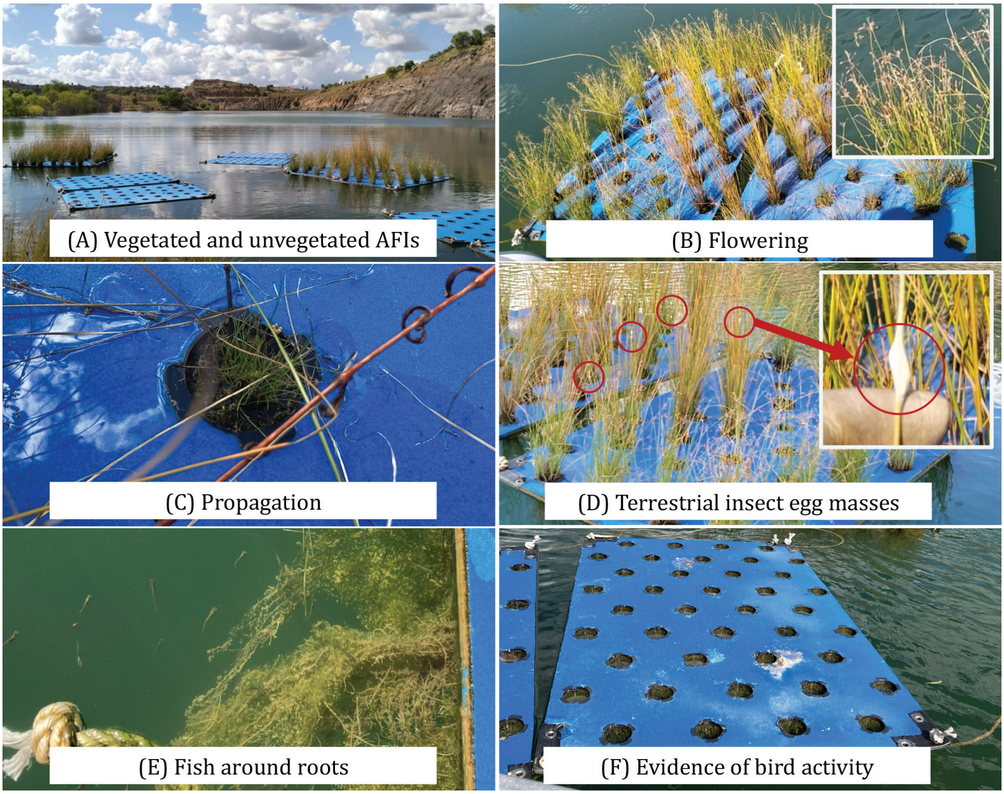

***Figure 2** Photographs of **(A)** 'vegetated' treatment and 'unvegetated' control AFIs installed at BL2; **(B)** Evidence of flowering; **(C)** propagation; **(D)** terrestrial insect egg masses (highlighted in circles); **(E)** fish around roots; and **(F)** evidence of bird activity.*

Data collection – plants, sediment, macroinvertebrates

The overall plant collection methodology was two sampling events per lake (June 2023 (both lakes), November 2023 (BL2) and April 2024 (BL4)). During each sampling event, 3 random pots containing surviving plants, per species (n= 2) were harvested from each vegetated AFI. Plants were frozen and later in the laboratory were rinsed with water to remove the soil and invertebrates. Invertebrates were preserved in 70% ethanol and identified to family or higher level. For each plant sample, the number of inflorescences, maximum length of roots, length of stems, and the number of stems were quantified. Plants were then separated into above- (stems) and below- (roots and rhizomes) ground biomass. All stems (living or dead) were counted together, as all stems were considered alive in June 2023. Biomass was measured after the plant tissue was dried in an oven at 80 °C for a minimum of 48 h until a constant weight was reached.

Sediment traps were retrieved April 2024 at BL4, and November 2023 at BL2. Upon collection, clear water was decanted from the tubes, the remaining water was shaken to homogenise and then filtered (pre-weighed 1.2 µm Glass Fibre filters (GFF), Whatman) until clogged, and the volume filtered was recorded. Filters were frozen (-20 °C) before being dried at 104 °C ± 1° C for at least 1.5 h until constant weight was achieved and sedimentation rate determined. Filters were then burnt at 500 °C for 4 h to allow determination of loss on ignition (LOI) as measure of organic matter content. Carbon content was calculated by dividing the LOI by 2 as per Pribyl (2010).

Data analyses – plant material and sediment

Plant growth data (root maximum length, mean stem length, mean number of stems, Above- and below- ground biomass, and number of inflorescences) for *J. usitatus* and *F. ferruginea* were normalised and Euclidean distance used to generate a resemblance matrix. A three-way PERMANOVA (9999 permutations; significance $p<0.05$), comparing fixed factors, 'species', 'lake' and 'date' (November 2023 and April 2024 were treated as the same time period) (Primer v7, Primer-e, New Zealand) was used to test the null hypothesis that the growth of plants was similar between species, lakes and over time. Pearson correlation coefficients were calculated between all parameters and significance tested.

The null hypotheses that sedimentation rates were not influenced by planting or lake was tested with a two-way ANOVA, with fixed factors of 'treatment' (AFI control, AFI vegetated) and 'lake' (BL2, BL4) were used to test for differences in sedimentation rates (1/x transformation) and LOI, using SPSS v29 (IBM, New York). Tukey's post hoc test was used to explore significant results.

Results and Discussion

Plant survival rates, growth and flowering

During the 12–16-month experiment at both lakes, most planted specimens of *J. usitatus* and *F. ferruginea* survived and flourished, whereas *P. decipiens* died, even after replanting with stronger specimens (Fig. 2a-c). *L. hexandra* initially died at all sites, however after replanting with better stock, 58% of specimens survived in BL2 until the end of the experiment, with none surviving at BL4. Plant survival was affected by initially small, poorly developed specimens for *P. decipiens* and *L. hexandra*, rapid change in salinity from the nursery (<1 mS cm^{-1}) to the lakes without acclimation, and excessive wave action at the anchor points, which was corrected using buoys in June 2023. Many of the empty pots were successfully colonised by propagules from mainly *F. ferruginea* (Fig. 2c).

Plant parameters were significantly different ($p<0.05$) between lakes, species, and dates, however as all interactions were also significant ($p<0.05$) the test was invalid and the relationships between the factors were investigated using PCA (Fig. 3). In *F. ferruginea* above- and below- ground biomass was positively correlated to stem count ($r= 0.98$ and $r= 0.74$ respectively; $p<0.05$), to each other ($r= 0.78$; $p<0.05$) and to inflorescences ($r= 0.91$ and $r= 0.83$ respectively; $p<0.05$). Stem length was correlated to below ground biomass ($r= -0.5$; $p<0.05$) and inflorescences ($r= 0.56$; $p<0.05$). Stem count was correlated to inflorescences ($r= 0.87$; $p<0.05$). In contrast, with *J. usitatus,* only above-ground biomass was positively correlated to stem count ($r= 0.86$; $p<0.05$) and below ground biomass was weakly correlated to maximum root length ($r= 0.55$; $p<0.05$).

In the first 6 months after planting (June 2023), *J. usitatus* parameters were tightly clustered within and between lakes in the PCA, while *F. ferruginea* grew better (in particularly above- and below- ground biomass) in BL2 compared to BL4 (raw data not shown). After another 6-10 months, *J. usitatus* in BL2 had changed little from June 2023, while those in BL4 had increased root biomass, but fewer and shorter stems and shorter roots than in June 2023, and inflorescences had increased. In contrast, *F. ferruginea* in BL4 had increased in all parameters compared to June 2023, while in BL2 increases were seen in all parameters except for stem length and inflorescences. In summary, *J. usitatus* survived over a year in BL4, but had grown little, and in BL2 the species had grown slightly. *F. ferruginea* grew well in both lakes, but slightly better in BL4; it is likely that over time, this species would have displaced *J. usitatus* and possibly *L. hexandra* in BL2.

In sum, choosing the appropriate species for the lake salinity will be important for their overall success and it may be challenging to maintain a diverse range of plants on the islands in the long term. Excessive wave action was also an issue and should be considered in terms of plant survival.

Sedimentation

Sedimentation rate was not significantly different ($F_{1,12}= 1.3$; $p= 0.27$) between lakes but was different between treatments ($F_{2,12}= 14.7$; $p<0.01$), although the interaction was

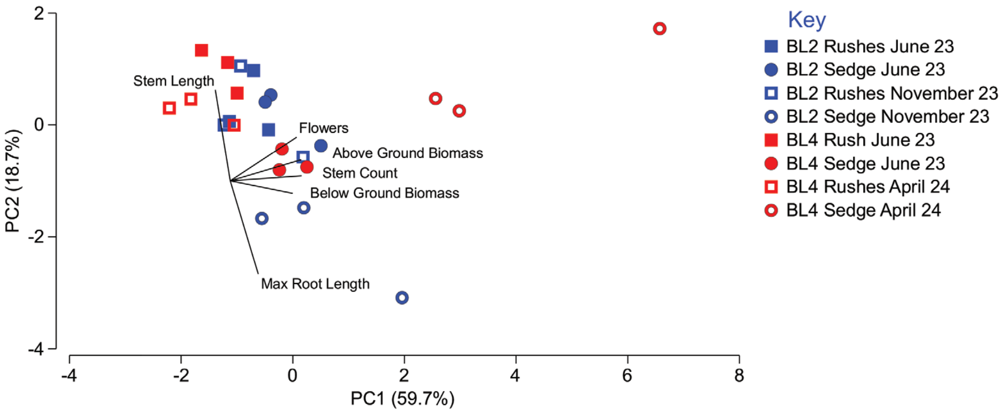

***Figure 3** PCA of average plant parameters from vegetated AFIs in BL2 and BL4 measured in June 2023 and in November 2023 or April 2024. Lines indicate positive correlations with the ordination space, with the length of the line reflecting projection into other dimensions.*

also significant ($F_{2,12}$= 7.3; p<0.01). Post hoc tests indicate that the lake sedimentation rates were lower than those from the islands, with the island treatments (AFI control, AFI treatment) were not significantly different. In BL4 the source of the high variability (coefficient of variability >82.4% compared to <33.7% in BL2) in the non-C component of the island sedimentation is not known, however the islands were located close to the old access ramp near the shore and in relatively shallow water (<3 m) which may have exposed the collection tubes to sediment resuspension caused by winds and waves or surface runoff. The sedimentation rate in lake BL2 was 3.6 ± 0.2SE g m^{-2} d^{-1} and in BL4 was 1.8 ± 0.2SE g m^{-2} d^{-1} with carbon contents of 1.9% and 3.9% respectively (Fig. 4), which was similar to those in Lake Kepwari and WO5H coal pit lakes in Collie, Western Australia (Lund *et al.* 2020; Lund *et al.* 2019).

LOI was significantly different between lakes ($F_{1,12}$= 90.7; p<0.01) and treatments ($F_{2,12}$= 11.1; P<0.01) with no significant interaction ($F_{2,12}$= 3.5; p= 0.63). Post hoc tests show the main differences were between islands and the lake and that carbon content was higher in the BL4 islands (veg.: 5.1% ± 0.1SE; control: 4.8% ± 0.1SE) compared to those in BL2 (veg.: 2.6% ± 0.2SE; control: 3.6% ± 0.4SE).

Islands appeared to promote sedimentation rates underneath them which would be a positive for the sediment development, however the sediment collected could partially have come from the soil in which the plants were planted - although as the two treatments were not statistically different this may not be an important factor.

Sediments collected from the control AFIs were characterised by a black colour and strong sulfur smell, whereas those from the vegetated AFIs were green and odourless (Fig. 4a-b). As the tubes were deployed for relatively long periods, organic breakdown may have occurred leading to an underestimation of C. The difference observed in colour and smell suggests anoxic and aerobic decomposition of organic matter occurred in the controls and vegetated islands respectively, likely due to oxygen leakage from the plant roots. The higher efficiency aerobic decomposition in the vegetated islands is likely to have resulted in greater underestimation in C content compared to the controls.

Invertebrates and birds – qualitative observations

Bird activity (no nesting) was observed via droppings (Fig. 2) on all islands (control and vegetated). Fish were observed congregating under the vegetated AFI at plant roots (Fig. 2e). Invertebrates were mainly aquatic (Dipteran larvae, Hemiptera, Odonata, Coleoptera, Gastropods), with some terrestrial Hemiptera, Coleoptera and

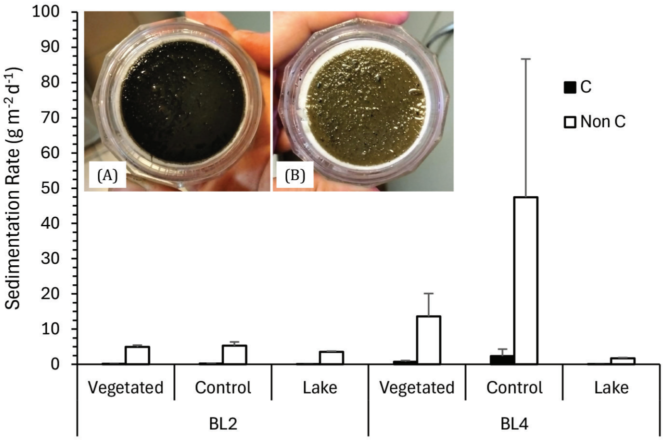

Figure 4 *Mean (± SE) sedimentation rate (g m^{-2} d^{-1}) showing proportion that was C – black bar, from sediment traps installed under the vegetated (n= 3), unvegetated control (n= 3) AFIs, and at a lake control site ≈10 m from the AFIs (n= 3) at BL2 and BL4. Photographs of filters from control **(A)**, and vegetated **(B)** AFIs at BL4.*

Arachnida. Invertebrate richness was similar between *F. ferruginea* and *J. usitatus*, in June 2023, although it was over twice as high in BL4 (e.g. 0.3 mean taxa richness per plant in BL2 vs 1.1 in BL4). Abundance (2 - 4.6 individuals per plant) and richness (0.7 - 1.4 taxa per plant) increased in both lakes in November 2023 and April 2024 and was slightly higher in *J. usitatus* in BL2 but lower at BL4.

Conclusions

Our research question was: can AFIs be successfully deployed in pit lakes, and do they enhance terrestrial and/or aquatic biodiversity? In this pilot study we used relatively inexpensive floating islands and four plant species to answer this question as a proof-of-concept with a mix of quantitative and qualitative (observational) data.

We successfully constructed and deployed AFIs. *F. ferruginea* thrived while *J. usitatus* survived and *L. hexandra* started to thrive in BL2 only - lake salinity and wave action were important factors in plant survival. Sedimentation rates were higher under the AFIs with higher C content in both lakes than 'lake controls.' Islands provided habitat for birds, fish, macroinvertebrates and could act as sources of plant propagules for rehabilitation of filling pit lakes. Bird usage could not only contribute to biodiversity, but also to nutrients that AFI plants may remove from the lake. In sum, AFIs offer potential for increasing biodiversity in pit lakes, with the greatest benefits in the littoral zone due to lake depth. The success of this pilot study has allowed us to commence a full-scale trial using more substantial (>100 m^2) islands. The upscale will consider the importance of lake water chemistry to plant survival, use camera traps to quantify bird activity, and employ tools like environmental DNA and macroinvertebrate sampling to evaluate the islands' contribution to increasing biodiversity.

Acknowledgements

This research was funded by the Australian Coal Association Research Program and supported by several mining companies and Edith Cowan University (ECU). Thanks to Andrew Lau (Yancoal Australia Ltd) and Cian Morgan (BHP Mitsubishi Alliance), Jan O'Loughlin and Vina Anfang (ECU).

References

Barrett RL (2013) Ecological importance of sedges: a survey of the Australasian Cyperaceae genus *Lepidosperma*. Annals of Botany, 111: 499-529

Blanchette ML and Lund MA (2021) Aquatic ecosystems of the Anthropocene: Limnology and microbial ecology of mine pit lakes. Microorganisms, 9(6):1207

John CM *et al.* (2009) Floating islands in a tropical wetland of peninsular India. Wetlands Ecology and Management, 17(6): 641-653

Lund MA *et al.* (2020) The importance of catchments to mine-pit lakes: Implications for closure. Mine Water and the Environment, 39(3): 572-588. DOI:10.1007/s10230-020-00704-8

Lund MA and Blanchette ML (2023) Closing pit lakes as aquatic ecosystems: Risk, reality, and future uses. WIREs Water, 10(4): e1648. DOI:10.1002/wat2.1648

Lund MA and McCullough CD (2015) Addition of bulk organic matter to acidic pit lakes may facilitate closure. 10th ICARD | IMWA – "Agreeing on solutions for more sustainable mine water management", Sanitago, Chile:1-11

Lund MA *et al.* (2019) Sedimentation rates in two pit lakes: Implications for riverine flow-through as a closure strategy. IMWA - "Mine Water: Technological and Eco. Challenges", Perm, Russia: 477-483

Oo MT *et al.* (2022) The floating garden agricultural system of the Inle lake (Myanmar) as an example of equilibrium between food production and biodiversity maintenance. Biodiversity and Conservation, 31: 2435–2452. DOI:10.1007/s10531-021-02347-9

Peel MC *et al.* (2007) Updated world map of the Köppen-Geiger climate classification. Hydrology and Earth System Sciences, 11(5):1633-1644. DOI:10.5194/hess-11-1633-2007

Pribyl DW (2010) A critical review of the conventional SOC to SOM conversion factor. Geoderma, 156(3–4):75-83. DOI:10.1016/j.geoderma.2010.02.003

Stewart FM *et al.* (2008) Floating islands as an alternative to constructed wetlands for treatment of excess nutrients from agricultural and municipal wastes – results of laboratory-scale tests. Land Contamination and Reclamation, 16(1): 25-33

Yeh N *et al.* (2015) Artificial floating islands for environmental improvement. Renewable and Sustainable Energy Reviews, 47: 616-622

Heterogeneous Oxidation and Hydrogeochemical Numerical Simulation in a Uranium Waste Rock Pile

Carolina Bittencourt de Abreu, Mariana Werle, Karen Ninanya, Rafael Albuquerque

Water Services and Technologies (WST), 30220-140 Belo Horizonte, Minas Gerais, Brazil, contato@waterservicestech.com

Abstract

This study investigates the hydrogeological and hydrogeochemical processes in Waste Rock Pile 4 (WRP4), located in the Poços de Caldas Alkaline Complex, Brazil, aiming to understand acid rock drainage (ARD) generation and contaminant transport. Formed during the operation of Brazil's first uranium mine, WRP4 exhibits complexity due to its chemical composition, particle size distribution, and interactions between gaseous, aqueous, and solid phases. Using integrated numerical models of groundwater flow and geochemical reactions, the study demonstrates that sulfide oxidation, primarily in the pile's oxidized zone, is the main mechanism driving ARD generation, resulting in acidic pH and high concentrations of metals and sulfate.

The hydrogeological model confirmed the principal groundwater flow direction from the Osamu Utsumi (OU) pit toward WRP4, with the pit significantly contributing to the system, especially during low-recharge periods. The hydrogeochemical model, developed using PHREEQC software, indicated that the internal drainage of WRP4 is predominantly influenced by the oxidized zone, with additional contributions from the pit lake. Mineral dissolution within the pile and precipitation of others, such as iron and manganese, were observed due to variations in redox conditions.

The results underscore the importance of monitoring and environmental rehabilitation strategies to mitigate ARD impacts. Incorporating mineralogical data and gas partial pressures in future models is recommended to enhance simulation accuracy. This study provides a valuable foundation for managing uranium waste rock piles, contributing to the protection of water resources and the environment.

Keywords: Acid rock drainage, numerical modeling, aqueous geochemistry, hydrogeology, uranium

Introduction

The geochemical and hydrological processes that occur in low-grade ore piles and waste rock piles share similarities, but the complexity of studying waste rock piles is amplified by factors such as size, geometry, chemical composition, particle size distribution, and the difficulty of controlling system conditions. This study focuses on the Waste Rock Pile 4 (WRP4), a uranium waste rock pile established in the 1980s during the operation of Brazil's first uranium mine, located in the Poços de Caldas Alkaline Complex, Minas Gerais. The WRP4 represents a waste disposal structure that requires an integrated approach to understand the associated groundwater flows and geochemical processes. Defining groundwater flows, combined with geochemical concepts, is important to understanding the dynamics of contaminant transport and the generation of acid rock drainage (ARD), which can negatively impact water resources and the environment.

Previous studies, such as those by Franklin (2007), Abreu (2013), and Alberti (2017), advanced the understanding of oxidation criteria and patterns in the WRP4, as well as the dynamics of flow and chemical reactions. However, none of these studies presented a numerical approach that integrated hydrogeological and hydrogeochemical models. This study aims to fill this gap by implementing and calibrating numerical models of groundwater flow and geochemical reactions, with the goal of providing a more accurate representation of the processes occurring in the WRP4. The integration of these models allows for a more robust analysis of the interaction between water flows and geochemical processes, contributing to the development of effective monitoring and environmental rehabilitation strategies.

Background

The Osamu Utsumi Mine, formerly Campo do Cercado Mine, is located near Caldas in the Poços de Caldas Alkaline Complex, Minas Gerais, Brazil. Discovered in the 1970s, uranium mining began in 1982 at the Caldas Ore Processing Unit but ceased in 1995 due to limited mineralogical understanding, achieving only 22% of its projected capacity (Cipriani 2002). Currently, INB and CNEN are engaged in environmental rehabilitation efforts.

The Poços de Caldas Alkaline Complex, the largest in South America (800 km^2, 33 km in diameter), formed during the Mesozoic and hosts uranium-, thorium-, and REE-rich lithologies, including tinguaite and phonolites (Fraenkel 1985). Uranium mineralization occurs as hydrothermal deposits in fractures and cavities or as secondary formations in redox zones, associated with pyrite, galena, sphalerite, fluorite, and barite (Franklin 2007).

The region has a tropical highland climate (16–25 °C), with 1,700 mm annual precipitation, mainly from October to March. Mining activities altered hydrology, including constructing WRP4 over Consulta Creek Valley, burying natural drainage. Bottom drains with boulders (200–1,000 mm) were installed and covered with fine-grained waste rock and clay. Additionally, a 500-meter diversion channel, lined with compacted clay, redirects Consulta Creek to the Taquari River, incorporating a retention dam for flow regulation (Franklin 2007).

Hydrogeochemical conceptual modeling

The conceptual hydrogeochemical model for the waste rock pile (WRP4) examines interactions between gaseous, aqueous, and solid phases, focusing on sulfide oxidation and metal leaching due to acid rock drainage (ARD). The pile has complex hydraulic and geochemical properties, with oxidizing conditions in the north and reducing conditions in the south, influenced by the Consulta Creek drainage system (Abreu 2013; Alberti 2017). Atmospheric oxygen enters through the slopes and is consumed by oxidation (Abreu 2013).

WRP4 spans 570,000 m^2 and holds 12 million m^3 of material, consisting of stripping material and Body B, a tubular breccia ore body. The matrix contains pyrite, fluorite, uranium minerals, molybdenum, and zirconium, with minor galena, sphalerite, and barite. Infiltration tests on the 150–200 mm clay cover confirmed low permeability. Samples were collected during the dry and rainy seasons in 2013 to 2015, and the following parameters were analyzed: Dissolved Oxygen, Turbidity, Eh, pH, Electrical Conductivity, Ca, K, Na, Mg, F, Cl, SO4, NO3, HCO3, CO3, Fe, Mn, Cd, Zn, Ba, Ti, Pb, V, Sr, Mo, Cu, Ni, Cr, Co, Hg, Si, Al, As, Y, Zr, U, Th, Ra226, Ra228, Pb210, and Rn in seven monitoring wells installed in bedrock (Alberti 2017), as shown in Fig. 1. The samples from the Osamu Utsumi pit and BNF showed mixtures of old and new water, indicating contributions from both subsurface flows and direct precipitation infiltration, suggesting a connection between WRP4 and the pit, supported by hydrochemical and isotopic similarities (Alberti 2017).

Pit waters show acidic pH at the surface, transitioning to alkaline and reducing conditions at depth. Acidic discharge fluctuates with precipitation, with peak contaminant concentrations after dry periods, consistent with the unreacted core model (Braun *et al.* 1974). pH remains acidic year-round, indicating continuous ARD generation (Abreu 2013). Geochemical assessments (paste pH, MABA, NAG) confirm advanced oxidation. The results suggest a moderate to low capacity for neutralizing acids, as indicated by the NP/AP ratio, and potential for acid generation under specific conditions, as shown by NAGpH values and sulfur content (Table 1). While sulfur content is not high, it suggests that acid drainage could occur, especially in areas with low NP/AP ratios and lower pH values.

Mineralogical analyses (ED-XRF, XRD, SEM-EDS) identified feldspars, muscovite, kaolinite, gibbsite, hematite, and goethite in the waste rock (Abreu 2013). Sulfur-rich samples showed Fe-S associations, indicating pyrite/pyrrhotite oxidation, while surface samples contained Fe oxides and aluminosilicates, reflecting advanced weathering. Pyrite oxidation drives ARD formation, while monazite and other rare earth-bearing minerals weather preferentially.

Hydrogeological conceptual modeling

The geotechnical structure under study was constructed over a lateritic soil layer ranging from 5 to 10 m in thickness, which tends to have a lower hydraulic conductivity than the saprolite layer beneath it due to the presence of clay minerals. This saprolite layer ranges from 10 – 20 m in thickness before transitioning into the underlying rock mass.

Regarding hydrogeological behavior, groundwater flow occurs primarily through two distinct pathways: (i) a shallow, unconfined flow within the granular lateritic and saprolitic materials, which can exhibit significant seasonal variability due to precipitation and evapotranspiration, and (ii) a deeper, structurally controlled flow regime governed by the fracture network within the rock mass. Table 2 resumes the aforementioned descriptions in addition to a range of expected hydraulic conductivity for this kind of material according to geological description of the area.

In a specific manner, the groundwater behavior in the study area is characterized by a principal flow through the fractures of the aquifer system, from the OU Pit toward the WRP4 as can be observed

Table 1 Acid generation potential and sulfur content of waste rock materials (Abreu, 2013).

	NP/AP	NAGpH (kg H_2SO_4 eq/t)	Sulfur content (%)
Max.	4.48	6.09	0.16
Min.	0.04	3.02	0.03
Med.	1.03	4.45	0.09

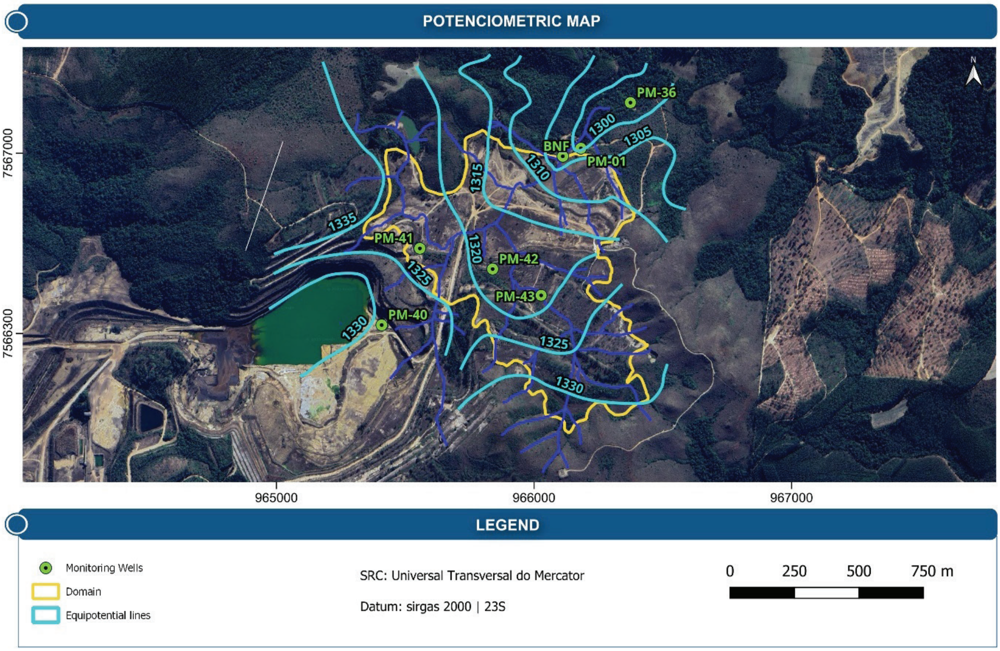

Figure 1 Potentiometric map of study area.

Table 2 Description of principal hydrogeological units.

Hydrogeological unit	Hydraulic conductivity (m/s)	Average thickness (m)	Type of flow
Lateritic soil	4.7E-9	5 – 10	Intergranular
Saprolite	5E-6	10 – 20	Intergranular
Rock mass	1E-7	-	Dual porosity
Waste rock pile	5E-7	50	Intergranular

Table 3 Hydrogeological monitoring data.

Monitoring well	Hydraulic head (m)	Date
PM-01	1292.9	December/2013
PM-10	1329.8	December/2013
PM-38	1327.1	December/2013
PM-39	1333.1	December/2013
PM-40	1334.0	December/2013

in the potentiometric map (Fig. 1). This interpretation was based on hydraulic head monitoring and the identification of discharge areas. Regarding the flow behavior within the dry stack, instrument PM41 (monitoring 1351 m) suggests the possible existence of a hydrologic divide between the pile and the pit. However, it is well known that dry stack tailings can create perched aquifers due to their compacted nature and low hydraulic conductivity. These perched aquifers may temporarily store infiltrated water, allowing for localized flow and gradual percolation into the underlying fractured aquifer system. Therefore, it is likely that PM41 is primarily monitoring superficial water rather than deeper groundwater flow. Furthermore, the potentiometric map confirms this interpretation, as it indicates that PM41 is influenced by shallow water rather than the regional groundwater system. Given this, PM41 may not provide relevant data for assessing regional groundwater flow patterns and can be considered less critical for evaluating the hydraulic connection between the OU Pit and the WRP4.

Understanding how much water infiltrates from the OU Pit toward the WRP4 is crucial for assessing the potential impact on groundwater flow and water quality. Quantifying the infiltration rate will help determine whether significant hydraulic interaction occurs between these structures, providing essential information for managing groundwater resources and evaluating potential environmental risks.

Hydrogeological numerical modeling

To further investigate the hydrogeological behavior of the study area, a two-dimensional numerical model was developed and calibrated under steady-state conditions. The calibration process relied on hydraulic head data from monitoring wells PM01, PM10, PM38, PM39, and PM40 (Table 3). As mentioned previously, PM41 was excluded from the calibration due to its shallow depth and focus on superficial water, which does not represent the deeper groundwater flow system.

The main objectives of the numerical model were to validate the conceptual understanding of the principal flow direction and quantify the contribution of water from two sources: flow from the OU Pit and effective recharge into the aquifer system. As can be observed in Fig. 2, the model helped confirm the general flow pattern described in the conceptual model. Specifically, it demonstrates that both the open pit and the dry stack pile contribute to the drainage system at the base.The quantification of water contributions revealed the following results under different recharge scenarios (Table 4). It is worth mentioning that the recharge rates were adopted through calibration in terms of water level and flow rate.

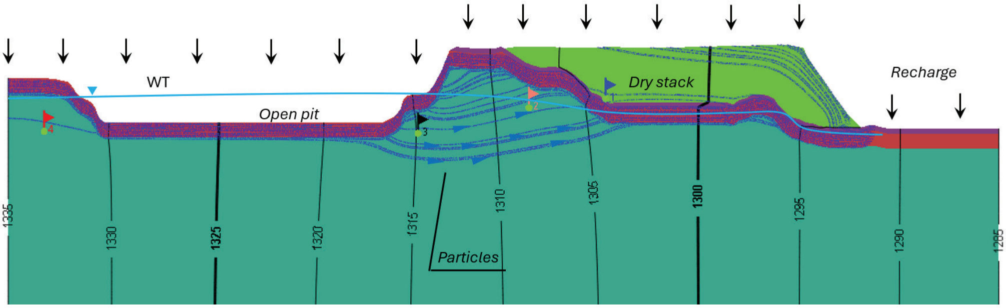

Figure 2 *2D Hydrogeological numerical model, pathlines (blue lines) and water table (sky blue line).*

Table 4 *Osamu Utsumi pit contribution.*

Recharge Rate (mm/year)	Contribution from the OU pit
100	18%
50	27%
25	35%

Table 5 *Observation points in the surrounding areas.*

Observation point	Hydraulic head (m) – 25 mm/year	Hydraulic head (m) – 50 mm/year	Hydraulic head (m) – 100 mm/year
1	1303	1305	1308
2	1308	1309	1311
3	1315	1316	1318
4	1333	1334	1334

These results show that as the recharge rate decreases, the relative contribution of water from the OU Pit increases, highlighting its importance as a significant source of groundwater under low-recharge conditions. This relationship reflects the strong hydraulic connection between the pit and the surrounding aquifer system, particularly in drier periods when natural recharge is limited. Results regarding the piezometric level in the surroundings of the study area were also studied, based on variations of the previously adopted recharge rate and the observation points shown in Fig. 2. Thus, Table 5 compiles the results in terms of hydraulic head.

The model provides a robust tool for understanding groundwater dynamics in the study area and serves as a foundation for future simulations to evaluate different management scenarios and assess the long-term impacts of hydraulic connectivity between the OU Pit and the WRP4. It is worth mentioning that the hydrogeological system was not assessed in transient regime.

Hydrogeochemical numerical modeling

The hydrogeochemical numerical modeling were performed using the software PHREEQC. The simulations involved mixing groundwater from three distinct site areas: the oxidized zone, the non-oxidized zone, and the mine's open-pit lake. According to the conceptual model, these zones influence the hydrogeochemical composition of the internal drainage of the BNF pile, which exhibits high metal concentrations, elevated sulfate levels, and acidic pH. The results of the hydrogeochemical numerical modeling indicate that the high concentrations observed in the BNF internal drainage originate predominantly from the oxidized zone, with contribution of the OU pit. The proportion of these contributions may vary depending on seasonality and precipitation.

Mixtures were simulated considering two scenarios, according with the OU pit contribution (Table 6): one with 65% of the contribution from the oxidized zone and 35% of the OU pit another with 82% of the oxidized zone and 18% of the OU pit. Based on these different proportions, the numerical modeling suggests that some dissolution is occurring within the pile, as indicated by the higher concentrations of aluminum, arsenic, and sulfate in the BNF drainage compared to the monitoring wells. Additionally, a decrease in potassium, manganese, and iron concentrations is observed in the BNF internal drainage relative to the monitoring wells, suggesting mineral precipitation. The numerical modeling results indicate a positive saturation index for $Fe(OH)_3$ (1.65), pyrolusite (3.35), barite (0.61), jarosite (10.59), and alunite (8.27), suggesting that these minerals may precipitate at the pile's outlet. This process may be driven by differences in redox conditions between the pile's interior and the bottom drain outlet.

As a next step to improve the modeling, it is recommended to incorporate mineralogical data and the partial pressure of gases. These parameters will provide more precise information, allowing for a more accurate representation of reality.

Conclusions

This study investigates the hydrogeological and hydrogeochemical processes in Waste Rock Pile 4 (WRP4) at the Poços de Caldas Alkaline Complex, Brazil. By combining groundwater flow and geochemical reaction models, it reveals that sulfide oxidation and acid rock drainage (ARD) in oxidized zones play a key role in contaminant transport. The OU pit contributes significantly to groundwater flow toward WRP4, especially in dry periods. High metal and sulfate concentrations, along with low pH in the pile's drainage, are mainly driven by the oxidized zone and further influenced by the OU pit. The findings support better environmental management and suggest incorporating mineralogical and gas data in future models.

Table 6 *Results from numerical modelling. [1]Median concentration of the parameters for the oxidized zone, [2]Median concentration of the parameters for the non-oxidized zone, [3]Median concentration of the parameters for the OU Pit, [4]Relative proportion of the effluent originating from the oxidized zone, [5]relative proportion of the effluent originating from the OU Pit.*

Parameter	Oxidized zone[1]	Non-oxidized zone[2]	OU Pit[3]	Results from numerical modelling		BNF
				65%[4] 35%[5]	82%[4] 18%[5]	
pH	4.76	6.63	5.33	4.63	4.61	4.00
Al (mg/L)	93.17	1.066	8.01	70.57	86.70	121.77
As (mg/L)	1.25	1.66	1.25	1.25	1.25	2.52
Ba (mg/L)	0.03	0.31	0.06	0.04	0.04	0.04
Ca (mg/L)	166.37	16.58	49.4	125.69	145.64	78.02
Fe (mg/L)	93.16	7.24	8.8	63.77	78.15	43.63
Mn (mg/L)	94.34	5.77	9.75	64.88	79.30	71.42
SO_4 (mg/L)	939.46	59.62	186.7	677.57	805.93	944.32
Zn (mg/L)	10.43	0.08	1.05	7.16	8.76	0.03
K (mg/L)	839.55	6.98	21.05	554.24	693.69	5.73
Mg (mg/L)	11.91	2.43	3.14	8.86	10.35	8.19
Na (mg/L)	2.57	16.9	0.815	1.96	2.26	1.31
Si (mg/L)	15.21	7.03	11.22	13.84	14.52	13.35

References

Abreu CB (2013) Influência da fase gasosa como ferramenta auxiliar no diagnóstico do potencial de geração de drenagem ácida de rocha. (Doctoral Thesis) – Engenharia Metalúrgica e de Minas, Universidade Federal de Minas Gerais – UFMG: Belo Horizonte (MG). 191p.

Alberti HLC (2017) Estudo hidroquímico e isotópico das águas subterrâneas impactadas pela drenagem ácida da mina de urânio - Osamu Utsumi, planalto de Poços de Caldas (MG). Campinas, SP, Universidade Estadual de Campinas. Instituto de Geociências. 198p.

Appelo CAJ, Postma D (2005) Geochemistry, Groundwater and Pollution. 2ed. Amsterdam: A.A. Balkema Publisher. 647 P.

Braun RL, Lewis AE, Wadsworth ME (1974) In-place leaching of primary sulfide ores: laboratory leaching data and kinetics model. Met. Trans., v. 5, p1717–1726

Cipriani M (2002) Mitigação dos impactos sociais e ambientais decorrentes do fechamento definitivo de minas de urânio. Campinas: Instituto de Geociências, Universidade Estadual de Campinas, 332p.

Fraenkel MO, Santos RC, Lourenço FEVL, Muniz WS (1985) Jazida de urânio no planalto de Poços de Caldas, Minas Gerais. In: Principais Depósitos Minerais do Brasil. DNPM, v.1, Cap.5, p.89-103.

Franklin MR (2007) Modelagem numérica do escoamento hidrológico e dos processos geoquímicos aplicados à previsão da drenagem ácida em uma pilha de estéril da mina de urânio de Poços de Caldas – MG. Rio de Janeiro: COPPE, Universidade Federal do Rio de Janeiro, 337p.

Reflooding of an Underground Mine During Closure – Analytical vs Numerical Model Estimation

Jessica Cammack, Thomas Booth

[1]WSP UK Ltd, The Mailbox, Level 2, 100 Wharfside Street, Birmingham, B1 1RT, UK, , jessica.cammack@wsp.com, thomas.booth@wsp.com

Abstract

Estimating mine inflows and reflooding rates is crucial for closure planning of underground mines, as it helps predict the mine's impact on the groundwater system and inform long-term management strategies. Both analytical and numerical methods can provide adequate estimations, with the choice depending on the complexity of the system, available information, and level of the study. This paper presents examples of high-level Excel-based analytical calculations compared to a numerical solution using FEFLOW to estimate the reflooding time of an underground mine.

Keywords: Mine, underground, reflooding, closure, modelling, analytical, numerical, FEFLOW

Introduction

To support mine closure strategies and planning, modelling is often conducted to estimate future environmental effects associated with closure. An important consideration in underground mining is the rate of reflooding of the mine and total reflooding time. Both analytical and numerical modelling methods can provide appropriate results, with the most suitable approach depending on factors such as the complexity of the system, available information, and level of the study. Understanding the rate of mine reflooding is key for defining optimal water management strategies, appropriate monitoring programmes, and potential effects on the groundwater system and nearby receptors.

As part of a closure study developed by WSP, numerical modelling was used to provide an alternative solution to an Excel-based analytical model developed by the client for estimating the reflooding time of an underground mine. The mine, primarily used to extract energy metals, reaches a maximum dewatering depth of approximately 400 meters. Longhole Open Stoping is the main mining method used, with the client estimating a total void volume of 2,150,000 m^3.

The analytical model estimated the reflooding time by dividing the total underground void volume by the estimated groundwater inflow. While a valid approximation, the analytical model assumed a constant inflow rate throughout the reflooding process equal to the current dewatering rate (5,900 m^3/d), which is expected to decline during reflooding due to a general reduction of hydraulic gradient from the rock towards the mine as mine water level rise. A total reflooding time of 1 year was estimated using the analytical model.

Numerical modelling using FEFLOW was conducted to provide a more detailed solution factoring in the complexities of the local geology, the intricate mine developments and workings, and the dynamic nearby hydraulic levels and gradients, including the time required to re-saturate the surrounding rock. An average groundwater inflow of 1,300 m3/d was obtained during the reflooding process, leading to a reflooding time of 4.5 years, considerably higher than the 1 year estimated by the analytical model. The updated results were subsequently taken into consideration for the mine closure planning.

Modelling Approach

The study was conducted through a multi-step process involving the use of Leapfrog, Excel, Python, FEFLOW and the FEFLOW Python Application Programming Interface (API). Presented below is the used modelling workflow:

1. **Representation of the underground mine in existing FEFLOW model** using the 3D mine wireframes provided by the client. The model was originally calibrated to piezometric data and dewatering rates.
2. **Creation of Volume-Elevation curves** using Leapfrog and Excel, based on the 3D mine wireframes provided by the client.
3. **Development of Python script for reflooding process and application using existing FEFLOW model**, considering the Volume-Elevation curves from Leapfrog.

Step 1: Representation of Underground Mine in Existing FEFLOW Model

A groundwater numerical model of the mine site was developed and calibrated by WSP as part of a previous stage of the study. For this purpose, WSP chose the use of the groundwater modelling software FEFLOW (Diersch, 2013), an industry standard finite element modelling code widely used in mining projects (Barnett *et al.*, 2012). Mine wireframes provided by the client were incorporated into the existing FEFLOW model, with three identified mine zones (Fig. 1). The underground mine was represented using seepage nodes for dry areas and constant head nodes for flooded areas, assuming hydrostatic conditions. As noted in Fig. 1, the three zones are connected at known depths, which is expected to affect the reflooding process. Recharge values, hydraulic conductivities and storage parameters were applied according to the conceptual model, and refined by calibrating the model to piezometric data and groundwater inflows. Recharge rates were reduced following one year of mine closure in mine facilities where covers are expected.

Step 2: Creation of Volume-Elevation Curves

Volume-Elevation curves of the underground mine were required as a key input for the modelling workflow, to determine how water ingress reflects on water level increase within the mine. For this purpose, mine wireframes in 3D CAD format were imported into Leapfrog to estimate volume versus elevation curves for the three zones independently from each other and as a whole. The obtained curves are presented in Fig. 2. It is acknowledged that the calculated void volume is an approximation derived from mine wireframes, and does not account for voids from other sources, such as fractures surrounding the mined area or the porosity of the rock mass within the depression cone. It should also be noted that a correction factor was also applied to the volumes extracted from Leapfrog to align with the total mine volume provided by the client.

Step 3: Development of Python Script for Reflooding Process and Application Using Existing FEFLOW Model

A Python script was developed to simulate the reflooding process within the numerical groundwater model using the powerful

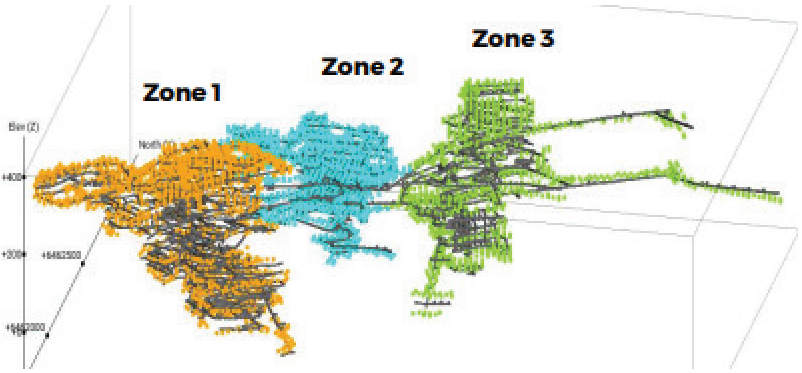

Figure 1 *Underground Mine Wireframes Provided by Client.*

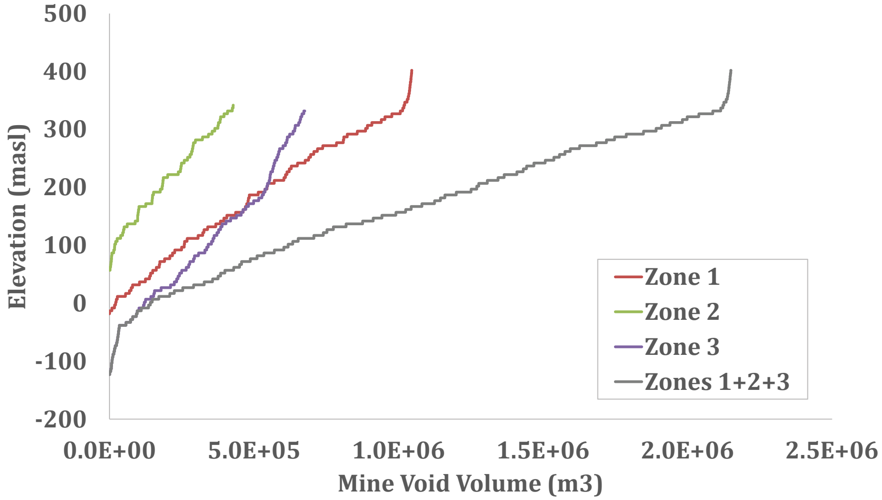

Figure 2 *Volume-Elevation Curves of Underground Mine Zones.*

FEFLOW Python API. Increases in flooded volume were calculated by FEFLOW and the Python script transiently by multiplying the mine inflows (L3/T) simulated by the model at a given timestep by the timestep length (T). The obtained volume increase was converted into an increase of flooded level using the previously determined Volume-Elevation curves. The new flooded level was used by Python to determine the new flooded areas and the necessary boundary condition conversion from seepage nodes into constant head nodes equal to the flooded level (i.e. hydrostatic assumption within the underground mine). Seepage nodes above the new flooded elevation remain unchanged to continue simulating seepage into dry (atmospheric) conditions. Flooding in each mine zone was considered to evolve independently by the script until interconnection at the identified elevations was reached, at which point water from different compartments start filling adjacent compartments with lower flooded level. When all zones reach an equilibrium, the system behaves as one unit. The model was run long enough to allow the mine time to flood completely.

3D Numerical Model Results

The simulated inflows and flooded elevations versus time were exported from the FEFLOW Python script and plotted over time (Fig. 3 and Fig. 4). Mine Zones 1 to 3 flood independently until an elevation of approximately 150 masl is reached at which point each zone becomes interconnected, flooding until an elevation of approximately 400 masl. At the beginning of the simulation inflow is equal to 5,900 m^3/d, decaying exponentially until the inflow rate reaches 0 m3/d. The numerical-based workflow estimates a total flooding time of around 4.5-years for the hydraulic parameters considered.

Alternative Analytical Approaches

It is acknowledged that the analytical approach selected by the client can be refined. Assuming a linear interpolation, an alternative method would involve using the constant average inflow rate of 2,950 m^3/day, rather than the maximum dewatering rate of 5,900 m^3/day throughout the reflooding period. This adjustment would result in an estimated reflooding time of approximately 2 years, thereby slightly improving the accuracy of the estimate.

Additionally, analytical solutions available in literature based on Darcy's Law (Darcy, 1856) can account for the reduction of hydraulic gradient from the rock into the mine over time. The Dupuit equation is a simplification of Darcy's Law (Equation 1), where Q is the discharge rate, K is hydraulic conductivity of the aquifer, dh is the head gradient, dx is the horizontal distance and A is the cross-sectional area through which groundwater

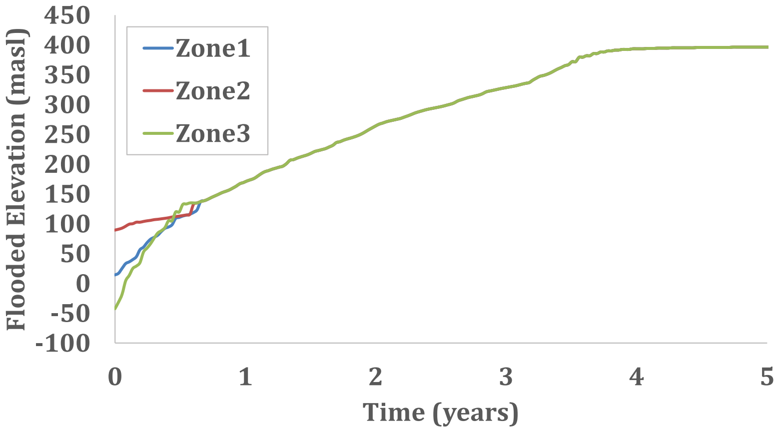

Figure 3 *Numerical Estimate of Flooded Level Throughout Time.*

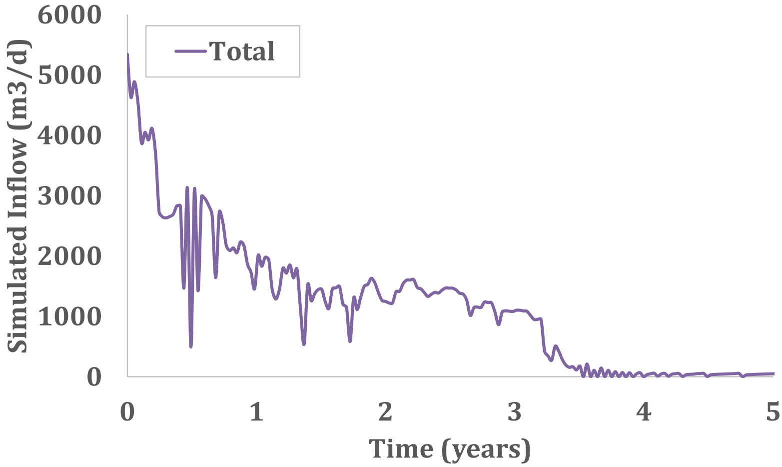

Figure 4 *Numerical Estimate of Groundwater Inflow Throughout Time.*

flows (Woessner *et al.*, 2020). Using the Dupuit (Dupuit, 1863) equation an average inflow rate of 2,020 m³/day was calculated, estimating a reflooding time of approximately 3 years.

$$Q = -K\frac{dh}{dx}A$$

Equation 1 *The Dupuit Equation (Woessner* et al., *2020).*

Comparison of 3D and 2D Results

The comparison of results from different methods for estimating reflooding time highlights variations (Table 1). The analytical method, using a constant inflow rate of 5,900 m³/day, estimates a reflooding time of 1 year. Refining this approach with an average inflow rate of 2,950 m³/day extends the estimate to 2 years. Literature-based solutions using the Dupuit equation (Dupuit, 1863), which account for the reduction of hydraulic gradient over time, predict a reflooding time of 3 years with an average inflow rate of 2,020 m³/day. In contrast, the numerical-based workflow, provides a more accurate estimate of 4.5 years, considering variable inflow rates and hydraulic parameters, with a mean inflow rate of approximately 1,300 m³/day.

Conclusion

The analytical model implemented by the client offered a simple and easy to use equation for estimating the total reflooding time, which under the right assumptions can guarantee the estimation of a minimum

Table 1 Comparison of the Analytical and Numerical Modelling Results for the Reflooding of the Underground Mine.

Model	Estimated Flooding Time year	Average Inflow Rate m³/d
Analytical (Maximum Inflow)	1.0	5,900
Analytical (Average Inflow)	2.0	2,950
Analytical (Dupuit)	3.0	2,020
Numerical	4.5	1,300

possible time for total reflooding. However, at the level of the developed study the results provided by the analytical model were considered too approximate due to the assumption of a constant inflow rate equal to the current dewatering rate. This resulted in an overestimation of the predicted average inflow rate during the duration of reflooding, and an underestimation of the total flooding time. It is recognised that the analytical approach can be improved by altering certain assumptions or by using analytical solutions available in literature based on different forms of Darcy's Law, to account for the reduction of hydraulic gradient from the rock into the mine over time.

In contrast, the developed FEFLOW-Python coupled numerical approach can easily represent the complexity of the surrounding geology, the detail of the mine workings and developments, and the dynamics of the nearby groundwater system and flooded level over time. Transient modelling captured the progression of mine flooding according within each underground zone, the connection between zones at identified levels, and the behaviour after all levels were connected. The developed workflow can easily be extended to incorporate other terms of the water balance if they exist, such as external addition of water into the mine, or pumping from the mine. Furthermore, the developed script was already extended to be applied in open pit studies, to account for atmospheric interactions (rainfall, evaporation, and snowmelt), and other terms of the water balance. It should be noted that the most appropriate modelling approach is project and site dependent. The comparison of alternate methods indicates the importance of selecting the appropriate method based on the specific requirements of the project and available data, with the 3D numerical approach offering the most realistic estimates for this study.

Acknowledgements

We would like to thank all the co-organisers for hosting the IMWA 2025 Conference. Jo Burgess, Amy Kokoska, Hetta Pieterse as well as Glenn MacLeod provided critical comments on earlier versions of this text.

References

Barnett, B., Townley, L. R., Post, V., Hunt, R. J., Peeters, L., Richardson, S., Werner, A. D., Knapton, A., and Boronkay, A. (2012). Australian Groundwater Modelling Guidelines. Waterlines Report Series No. 82. June 2012.

Darcy, H. (1856). Les fontaines publiques de la ville de Dijon. Paris: Dalmont.

Diersch, H.J.G. (2013). FEFLOW: Finite element modelling of flow, mass, and heat transport in porous and fractured media. Springer Science & Business Media.

Dupuit, J. (1863). Etudes Théoriques et Pratiques sur le mouvement des Eaux dans les canaux découverts et à travers les terrains perméables (Second ed.). Paris: Dunod.Seequent (2024). Leapfrog Geo (Version 2024.1). [Software]. https://www.seequent.com

Woessner, William W. and Eileen P. Poeter (2020). Hydrogeologic Properties of Earth Materials and Principles of Groundwater Flow. The Groundwater Project, Guelph, Ontario, Canada.

Mining: The Value of Creating a Legacy of Water Resources within Unsurmountable Challenges

Dr. FS Botha[1], Mr S Meyer[2] en Mr M Burger[3]

[1] *Water Hunters, 91 Haythorne Street, Waverley Square, Pretoria, South Africa, 0001, fanie@waterhunters.co.za*
[2] *Water Hunters, 91 Haythorne Street, Waverley Square, Pretoria, South Africa, 0001, Stephan@waterhunters.co.za*
[3] *Water Hunters, 91 Haythorne Street, Waverley Square, Pretoria, South Africa, 0001, morne@waterhunters.co.za*

Abstract

This article deals with water legacies in the mining sector within semi-arid regions and how food security may benefit from it. Water resource often results in fatal flaws for mining developments and new resources are developed, once mineral resources are depleted water resources remains available and may become part of food security plan. Water resources developed includes dams and wellfields and groundwater inflows because of mining. The case studies deal with anthropogenic aquifers, coastal sand aquifers, potassium mine in Ethiopia and gold tailings storage facilities (TSF). Finally, saltwater reclamation is discussed using greenhouse technology combined with injection wells to harvest seepage water at gold TSFs.

Keywords: Water, fatal flaws, manmade aquifers, coastal aquifers, saltwater reclamation, greenhouses

Introduction

In semi-arid regions water resources are often a fatal flaw to start new mining operations and therefore new water resources needs to be developed, however once the mineral resources are depleted then the water resources will still be available and these remaining water resources will become an integrate part of a water and food for many millennia to come.

This article deals with several case studies as examples, all situated in semi-arid to arid regions. The most common water resources developed for new mining projects are dams and wellfields therefore during feasibility studies the default water resources developed as a result mining are not always considered as part of the solution, however post-mining it often results in a water positive legacy behind. However, the water associated with mining is often considered contact water and not fit for human consumption and this is as a result of the contact water associated with gold and coal mining and created a stigma that the water resources legacies from mining is not fit for human or environmental use. There are mineral resources which that will result in post-mining water legacies that is fit for human and environmental use and they needcs to be identified in advanced and planned for as future water resources. Chrome and platinum mines within South Africa are good examples of derelict mines that result in good water quality resources and needs to be used as sustainable water resources.

The water resources typically left behind range from underground mines filled with water and new modified aquifers or AA. The case studies discussed specifically deals with the platinum mines in the Bushveld Igneous Complex (BIC), a phosphate aquifer created in the West-Coast of Southern Africa, potassium mine in Ethiopia transforming hypersaline alluvial fan to freshwater aquifers and even how a large gold TSF is harvested to aggressively reuse and reduce freshwater use. Finally, a brave step is taken into the future and consider how saltwater reclamation used in greenhouses in the Netherlands can be combined with injection wells to harvest and clean water from a large gold TSF in South Africa.

New large underground storage facilities or Anthropogenic Aquifers

South African platinum mines are mostly situated in the northern part of South Africa, with a semi-arid climate with low rainfall with significant variation in monthly and long-term annual rainfall. It therefore requires large raw/dirty water storage dams to augment process water during low rainfall and high evaporation periods. The mines were initially developed as open pits (60m deep) and currently many of these open pits are used as raw water storage facilities, however during closure, as part of the rehabilitation plan these pits are filled with waste rock and recharge again and forms man-made aquifer or AAs. AAs therefore refer to underground water storage (aquifers) that was created because of minging activity. Once these underground dams have filled, they will leak into the upper, more weathered, aquifer. Depending on the dip of the open pit floor and its extent a pit may even discharge as surface water. If not managed, it can also leak through the boundary and/or crone pillars and leak into underground workings or neighbouring mines.

The difference between *in-situ* aquifers in the BIC and the AAs is the increased porosity and subsequent increased acceptance and release of water. In-situ aquifers in the BIC have low K-values, in the order of 2.7*10−4, whereas high porosities of the backfill material estimated at 25%, lead to much higher storage and high yielding boreholes (Botha *et al*, 2011).

Nitrate levels are elevated at all platinum mines, primarily because of the explosives used, which largely consist of an ammonium nitrate emulsion. An effective natural way to deal with high nitrates is to create flooded soils or enhanced artificial wetlands or slowly run the waters through an oxygen poor anthropogenic aquifer. The AA can be used as passive denitrification cells.

The cases studies talk about similar results now found at four major platinum and chrome mining companies and the AAs all proof to be a sustainable water resources that can assist mines and communities with a sustainable water resource during prolonged drought periods and act as a natural denitrification

Figure 1 *A photo of a rehabilitated open pit mine near Rustenburg, South Africa. It is filled with backfill material covered with topsoil. It also shows three boreholes drilled into the backfill material pumping freshwater from the pit to be re-used rather than taking water from nearby agricultural irrigation channel (image: Botha et 2011).*

system. The main application of the work conducted is to transform all backfilled and rehabilitated open pits into operational AAs and take them off the mine's liability as part of their closure and rehabilitation plan. The message to take home are to reduce the cost of annual mining rehabilitation expenditure cost and leave a legacy of rehabilitated open pits behind underlain by a renewable freshwater resource, rather than a pre-mining perception of ravished contaminated mining area (Fig. 1).

Westcoast aquifer

The Westcoast aquifer is situated near the town of Hopefield, within the Westcoast of South Africa some 100 km north of Cape Town. It is a Phosphate Mine. It is a marine deposit and it is mined trough free digging and the range from 40 to 80 mbgl and 1000 m in length and 400 m in width. Initially the overburden was stockpiled on a soft stockpile and now the operation has moved to a progressive dig and fill progressive pit. Some 40 boreholes on the highwall are used to partially dewater the pit and some in pit dewatering takes place. The operation is now active for almost 8 years and the mine proved to maintain the pit water management in a sustainable manner. The water harvested is pumped into boreholes downstream and it is discharge back into freshwater aquifer that flows into sensitive freshwater/marine water interface environment.

Monitoring boreholes range from in pit monitoring and surface water monitoring to as far as 12 km at the discharge position. The current monitoring results shows zero impact on the freshwater aquifer. Challenges experienced during the project initiation was selecting the correct drilling method to enable boreholes to reach depths below the loose sandy aquifer and the right sizing of casing. During pumping of boreholes significant bioorganic growth around the casings and together with fine sand particles blinded the casing and it made dewatering ineffective. As a result, the operation had to adopt a cleaning programme with all the boreholes to be cleaned through reversed air and waterflow and mild environmentally acceptable additives.

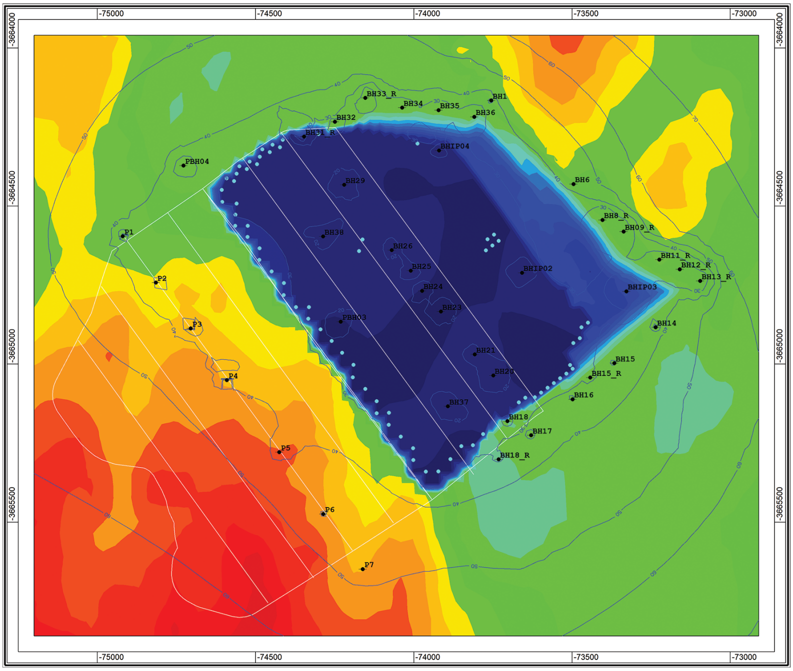

Figure 2 The calibrated model showing simulated results for December 2026 heads (blue isolines), ground elevation (contours) and residual inflow locations (blue markers). The pit is effectively dewatered, with some inflows into the pit.

Boreholes in the first phase were drilled at the edge of the open pit and not to below the targeted pit floor and resulted in less efficient dewatering. During secondary drilling phases the boreholes were drilled away from the planned pit walls and in doing so giving effect to the radius of influence not to be wide and deep enough, allowing large volumes of water to flow toward the open pit. By drilling the boreholes deeper, more water could be harvested, and the cone of depressions were deeper and wider and thereby decreasing the openings between the dewatering cones and allow less water to flow past the dewatering boreholes towards the pit.

The biggest lesson learnt were that Managed Aquifer Recharge (MAR) can be implemented within a sensitive ecosystem to conserve it, the operation requires constant monitoring and adaption based on monitoring results and initial designs needs to be adapted to meeting the conservation goals. The latest modelling (Fig. 3) demonstrate that the pit can be managed with limited water inflow and that aquifer recharge can take place to release on-contact water back into the freshwater aquifer. The aquifer is well understood, and the future use in this area may be a completely rehabilitated area and an additional water supply to an expanding Westcoast community.

Solution mine in Ethiopia

The next case study is a Potassium Mining Operation in the Danakil Dessert in the northern border between Ethiopia and Eritrea, in is well-known for its sulfuric acid volcano, the Dallol. It employs a solution mining method, and during the water resource development study conducted was part of the feasibility study a holistic water resource plan was considered. The northern border is formed by a freshwater river named the Ragali River. The project aimed to harvest saline water in alluvial fans with boreholes in the fan material and through boreholes in the orebody pumped water into the mineral deposition to dissolve the minerals and pump it back to surface and through controlled

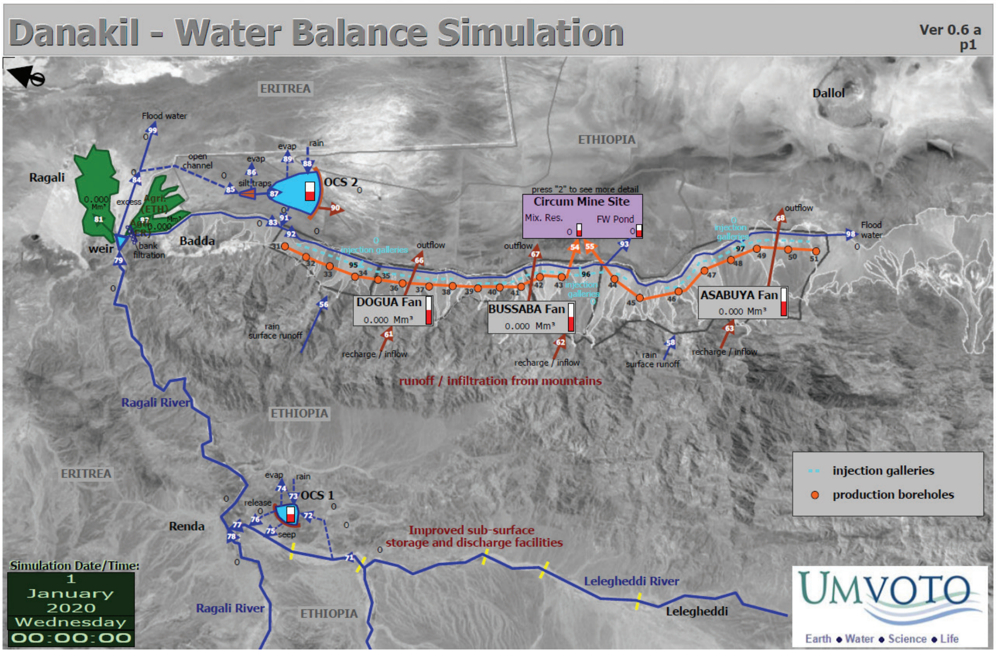

Figure 3 The flow diagram on a Google Earth Image showing the Ragali River and how the water can be harvested from the Ragali River into the different alluvial fans. It also shows the two off-channel storage facilities, one operational freshwater facility (OCS2) and one at Renda (OCS1), which will release water throughout the year to ensure constant flow in the dry season. Both OCS 1 and OCS 2 will ensure slow release of fresh water into the fans during the drier periods of the year (Botha et al*, 2017).*

crystallisation harvest potassium (Botha *et al*, 2017). During the development of the project a management approach was developed to harvest fresh water from the Ragali River (Fig. 3), flowing from the escarpment and rapidly harvest fresh water and though recharge trenches place it back into the alluvial fans to counter further salination of the alluvial fans.

The most significant lesson learnt was that although fresh water is limited, it is possible to rapidly harvest high volumes of freshwater from the Ragali River when it is available. Therefore, mining can be planned in such a way that an environment is left behind which will support the local communities with fresh water for thousands of years and if this is done then mining may become even more feasible in the most hostile environment and leaves behind a water resources legacy which may last thousands of years.

Harvesting recharged aquifer next to gold tailings Dam

The next case study is within the north-central parts of South Africa some 50 km south of Johannesburg, within the well-known gold deposits of South Africa and deals with the legacies of the old gold TSFs. The case study deals with the recharging aquifer conditions around the largest gold TSF in South Africa, with a surface area of more than 500 Ha and some 120 m high. During this case study three phases of scavenger boreholes where placed next to TSF. The aims were to ensure that the scavenger wells can be employed to harvest contaminant water in the vadose zone, reuse the water as process water and finally reduce the dependency on potable water to augment process water. The project was implemented in three phases and modelled over a period of six years to ensure scavenger boreholes were placed in optimal positions to harvest contact water. The project proofed that incremental implementation, though remodelling of monitoring data guided the team to optimise borehole positions during the project. Water harvested reduced the dependency on freshwater augmentation and make more fresh water available for municipal use, rather than industrial use.

Reclamation of freshwater using greenhouse and solar power

The last case study is still at concept stage and the plan is to take high saline contact water harvested from scavenger wells around gold TSFs and through the application of sun energy through aquaponics, greenhouse evaporation and condensation harvest fresh water and produce salts to be reused. The idea of harvesting clean water from reclaimed salt water though the use of greenhouse condensation was an idea which was first thought to be a new idea; however initial research proofed that Seawater Greenhouses harvesting through condensation was done in the Netherlands (Woodworthray (2016–2023). In the Netherlands sea water is evaporated using a radiator-like structure, blow it into a greenhouse and then harvest it using a condenser at the outlet of the greenhouse (Fig. 4). Condensed fresh water is them stored in a freshwater storage tank and pumped as drip irrigation to the greenhouse plants. Therefore, seawater is harvested to create fresh water. The saline water is discharged back into the sea and the salts that remains behind can be used as commercial evaporated sea salt.

The technology has not yet been used at a gold TSF however it has been used quite aggressively at other parts of the world. It is commonly referred to as Greenhouse Humidification – dehumidification (GHHD) (Kabeel *et al*, 2015). Solar energy is used as the electrical supply and it is proposed that solar panels must not be placed on the greenhouse and must rather be a standalone system, when it is placed on top of the greenhouse structure it may reduce the photosynthetic energy to about 52% (Kabeel *et al*, 2015). Therefore, if possible, the solar energy source needs to be a stand-alone supply to harvest sun energy. To boost the plant growth the greenhouse maybe designed as a closed system and therefore increase the CO2 in the greenhouse (Nour *et al*, 2015).

Further to this, the harvesting clean water using return water as a source at gold TSFs will become more relevant in South Africa now that new TSFs required to be lined. Prior to line TSFs, the aquifers below unlined facilities, through natural degradation played a major role in salt capturing and reduction,

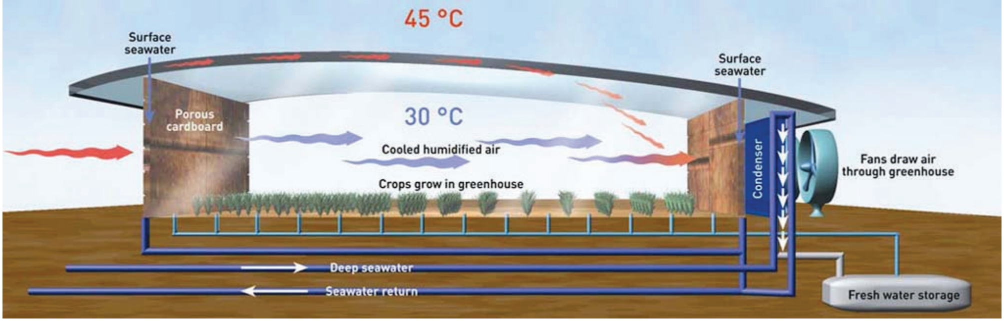

Figure 4 *Schematic view of how seawater harvesting takes place in the Netherlands produce freashwater Seawater is evaporated through a porous cardboard radiator-like structure creating water vapor and before leaving the greenhouse the humid air condensates on a cold seawater radiator as fresh water, condensate is then harvested in a freshwater storage tank and use as fresh water for the plants in the greenhouse (image: Woodworthray, 2016 – 2023).*

and water banking below the TSF. This salt sinks are eliminated when facilities are lined, and higher volumes of saline water will be recycled and reused and due to evaporation and a closed loop the salinity will increase over time. The salinity of the return water through the constant addition of salts will become too high to be used as process water and therefore desalination of return water derived from lined TSFs will become a challenge to be addressed in a cost-effective manner and the GHHD may offer a sustainable solution.

Nevertheless, the most burning question in the mining sector by all the owners and investors remains: "How to dispose the salts left behind?". The conventional and immediate answer are to harvest and dispose the salts at a certified waste disposal facility or it can be placed back on the TSF and captured within the TSF. There is also the possibility that harvested salts in the green houses may be harvested through selective crystallisation and reused.

Conclusions and recommendations

The mining sector alters the water resources environment, and the positive impact of mining is often not considered simply because society focus on the negative effect of mining. However, over the past decade operational mine water supply challenges were addressed though the development and use of AA and process water harvested next to TSFs. These options were all incorporated into site wide water management approach to harvest less water and create localised water resources. Post-mining, these local new water resources developed because of mining can then be used for various other applications to address food and water security concerns.

References

Botha FS, Gouws WJ, (2017). Danakil potash project, Danakil depression, northern Ethiopia. Integrated water balance simulation model report, SimX, February 2017

Botha FS, Maleka, L (2011). Results Results show that man-made aquifers within the platinum mining industry in South Africa can provide a solution for future water demands. Article publish IMWA 2011.

Kabeel AE, El-Said, EMS (2015). Water Production for irrigation and drinking needs in remote arid communities using closed-system greenhouse: A review. Engineering Science and Technology , an International Journal, Volume 18, Issue 2, June 2015, Pages 294–301

Nour MN, Ghanem NA, Buchholz M, Nassar M. Greenhouse based desalination for brackish water management using bittern evaporative cooling technique (2015). Water and Science Technology: Water Supply, 15.4, IMW Publishing 2015, pages 709–716.

Witthüser KT (2023). Water Hunters. Elandsfontein – Groundwater Model Update. Unpublished report Delta H. Project Number: Delh.2022.007-14, page 16.

Woodworthray (2016–2023). "Seawater Greenhouses". Appropedia. Retrieved February 1, 2025. https://www.appropedia.org/Seawater_Greenhouses

Pit Lake Prediction Case Study: Managing Insecurity in the Dataset using Bracketed Inputs

J. Larry Breckenridge[1], Meghan Blair[2] and Yuliya Subotskaya[1]

[1]*Global Resource Engineering, Colorado, United States of America*

[2]*Barr Engineering, Duluth Minnesota, USA*

Abstract

Two pit lakes formed in mine pits in an arid region. To estimate potential future pit lake water quality composition, and given uncertainties and data gaps in the dataset, eight scenarios were modelled for each pit lake using end-member input for the most-sensitive and least-understood input parameters. Key inputs were the hydraulic conductivity of the aquifer, and the acidity of pit wall runoff. In all but one scenario, both pit lakes remained circumneutral, but water quality is unlikely to meet water quality standards in any scenario because arsenic exceeds the agricultural use standard. The estimates were used to prioritize field programs to reduce uncertainty.

Keywords: Pit lake model, uncertainty, water quality

Introduction

Decisions about the management of pit lakes often must be made prior to the acquisition of robust datasets such as aquifer test results. In this case, closure and management decisions had to be made on two pit lakes due to a property transaction. This study describes methods for decision-making and analysis when data gaps exist.

Mining in Pit A began in 2013. Dewatering the pit began in late 2015 by discharging pumped water to a nearby stream. Mining ceased in March, 2016. Mining in Pit B began in 2018 and dewatering water was pumped and discharged into Pit A. Mining in Pit B ceased in 2020 and the pit lake elevations continue to equilibrate (Fig. 1). The future water surface elevations and groundwater flow rates under equilibrium conditions are unknown.

The adjacent mine pit lakes have relatively small watershed areas (0.42 km2 and 0.66 km2, respectively), which consist of natural areas, disturbed mine areas, pit walls and open water areas. Runoff from the watershed areas contacts the pit walls prior to running into the pit lakes. The mine site is located in an area with a semi-arid climate, with annual average rainfall, potential evaporation, and temperature of 490 mm, 1,990 mm, and 17.5 °C, respectively. Groundwater monitoring wells provide little information about the groundwater levels because they were specifically designed for monitoring heap leach pads and are too shallow to provide reliable information regarding the water quality or hydraulic conductivity of the deeper aquifer that the pit lakes intersect.

Seasonally-collected, depth-correlated field observations of temperature, conductivity, oxidation-reduction potential and pH suggest well-mixed conditions in both pits. With no obvious chemocline or thermocline, they classify as warm polymictic lakes.

Methods

The overall objective of pit lake water quality modeling was to forecast water chemistry in the two pit lakes and to compare these predictions to water quality standards. Specific uncertainties included:

- long-term water elevations in the pits;
- the amount of groundwater flow into and out of the pits that will occur once the pits have reached hydrologic equilibrium;
- inadequate data from kinetic cell tests to determine the amount of acidity and dissolved solutes that will be contributed to the mine pit lakes from pit wall runoff.

Figure 1 *Photograph of flooded Pit B.*

Therefore, the modeling simulates hydrologic steady-state conditions using upper and lower bounds on the anticipated future pit inflow and outflow conditions, the future equilibrium water surface elevations, and the contribution of acidity from pit wall runoff. Despite limitations, existing datasets were successfully used to provide a conceptual model and a transient water balance that accounts for inflow and outflow to the pits, and water quality simulations.

Conceptual Model

The quality of pit lake water is determined by mixed sources of inflow, evaporative concentration, and thermodynamic equilibrium reactions based on interaction with with solid- and gas-phases (Fig. 2). Because the pits are well-mixed, hydrodynamic modeling was not performed.

Preliminary speciation modeling of the existing water quality in the pit lakes at both Pit A and Pit B was conducted in the aqueous equilibrium geochemical modeling program PHREEQC with the MINTEQ.v4 database (Parkhurst and Appelo 2013). The modeling indicates that calcite is at saturation. Therefore, the mixing model of the pit lake includes calcite in the wall rock that is available to neutralize acidity from runoff.

Transient Water Balance

The present hydrologic water balance for the pit lakes was simulated for the weekly surface water elevations using climate data from on-site monitoring, evaporation calculated using the Meyer equation (Meyer 1942) and surface runoff modelling in PCSWMM (James *et al.* 2010; Fig. 3).

For the water balance, groundwater flux was the unknown term. Without information about the quantity of groundwater inflow to or out of the pits, the groundwater flow values in the water balance for each pit remain "net" groundwater flow estimates. To estimate the future equilibrium hydrologic conditions, a reasonable envelope for the future equilibrium water surface elevations was used and the groundwater inflow rates were bracketed (high and low). The transient water balances for the pit lakes were used to estimate two steady-state scenarios once final equilibrium water surface elevations are reached: 1) a "flow-through" lake condition,

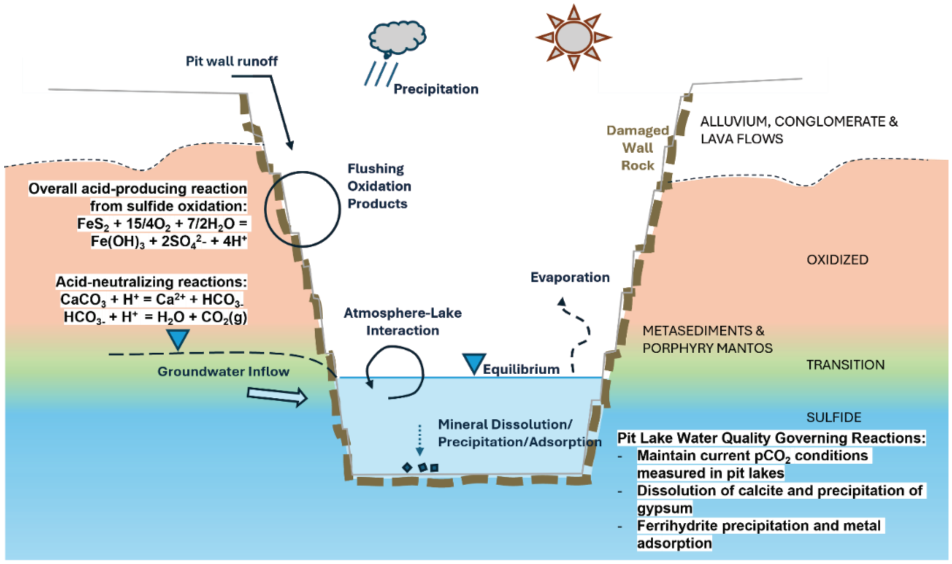

Figure 2 *Conceptual model of geochemical reactions included in pit lake simulations.*

estimated as the maximum groundwater flux needed to solve the balance during pit-filling; and 2) a terminal lake condition, where inflowing groundwater and runoff are balanced by evaporation, which is also a minimum groundwater flux condition.

For the maximum groundwater flux scenario, the inflows are balanced by outflow from evaporation and groundwater outflow. For the terminal lake scenario, inflows are balanced only by evaporation. The high and low surface water elevations bracket reasonable elevations for the anticipated final equilibrium water surfaces in each pit based on the recent monitoring. Fig. 4 shows lake elevations, groundwater flux, exchange between lakes, and evaporation totals at high and low bracketed scenarios. These flow values are used in the pit lake water quality model to specify the volumes contributed by each source.

Geochemical Model

The aqueous equilibrium geochemical modeling program PHREEQC with the MINTEQ.v4 database (Parkhurst and Appelo 2013) was used to simulate the processes of mixing the inflows and outflows for each time step and equilibrate the resulting chemistry with mineral and gas phases. The concentration of carbon dioxide gas (CO2) was constrained by the partial pressure of

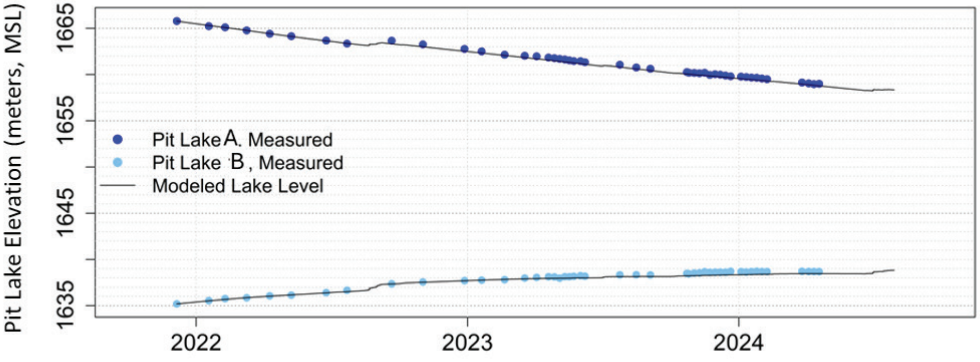

Figure 3 *Transient water balance model results.*

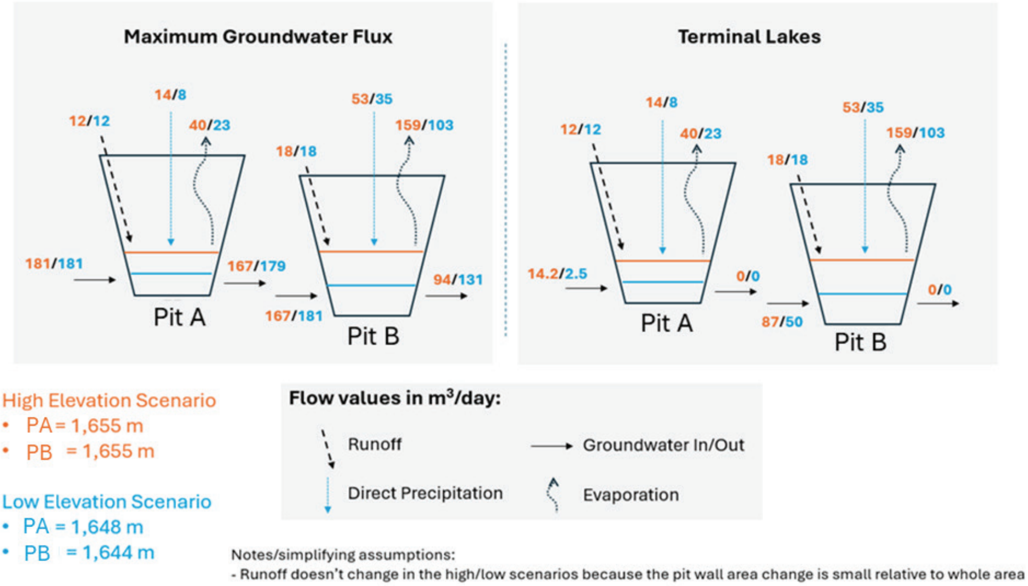

***Figure 4** End-member hydrologic scenarios for the two mine pits.*

CO2 (pCO2) calculated in the 2023 surface samples (pCO2 10–2.5) by setting the SI of CO2 to –2.5. An annual time step was used. Simulations were carried out to estimate the mixed bulk lake water quality, year-on-year, for 100 years

The future water quality was modeled by mixing inflow and outflow terms that undergo chemical reaction due to gas exchange, evaporation, mineral dissolution and precipitation, and adsorption of trace metals. The concentrations of mass assigned to each inflow and outflow term in the model are derived from site-specific water quality measurements, analyses of effluent samples from the kinetic cells, or from regional measurements. Evaporation was applied by removing the annual average volume fraction of pure deionized water.

PHREEQC was used to evaluate the speciation and saturation indexes (SIs) of relevant mineral and gas phases. The calculated SIs of carbon dioxide, calcite, gypsum, ferrihydrite, manganese carbonate, and aluminum hydroxide are used to inform the equilibration conditions specified in the future pit model. These mineral phases are those commonly known to control reactions in pit lakes associated with neutralization of acid rock drainage (ARD; Davis *et al.* 2024; Castendyk *et al.* 2015).

Insufficient laboratory analyses from the kinetic cells precluded calculation of solute release rates from wall rock or an estimate of sulfide oxidation rate. Therefore, an important assumption in the model is the proportions of runoff that are acidic and non-acidic. One of 23 kinetic cell tests of pit wall rock is characteristically acidic with a pH between 1 and 3 and high concentrations of solutes, with the rest pH neutral with moderate alkalinity. The acidic sample came from a fault zone between dacitic intrusive rock and hornfels metasediments. Available data and lithological mapping are indeterminate about the frequency of similar sulfide-rich fault zones. Therefore, a range of 5 to 20 percent ARD was selected for the model. This range was considered reasonable, with the high end of 20 percent setting a conservative upper end.

In the simulations, calcite dissolves as needed to neutralize the acidity from ARD while maintaining calcite equilibrium and the fixed pCO2. Iron, manganese, and aluminum, introduced primarily from the pit wall runoff, precipitate to maintain the designated SIs for ferrihydrite, rhodochrosite, and aluminum hydroxide, respectively.

The model includes adsorption of arsenic and cadmium onto the precipitated ferrihydrite according to the diffuse double layer model provided by Dzombak and Morel (1990) with the inclusion of a correction factor for inefficiency. The amount of ferrihydrite available for adsorption is conservatively assumed to be approximately 50 percent of the mass calculated as the acidity of the ARD is neutralized and iron precipitates.

Abundant calcite in the pit wall rocks controls the pH in each time step. Calcite dissolves over the 100-year simulation represents a 100-year calcite "demand" required to maintain a buffered pH. This demand ranges from ≈ 0.01 g/L for Pit A under "lowest risk conditions" and ≈ 26 g/L for the Pit A under "highest risk conditions". This calcite present to meet the demand was calculated from calcite availability derived from the net acid neutralizing potential from acid-base accounting tests of pit wall rock and calcium in the assay database to determine if pits remained pH neutral.

Results

In all but one scenario, the available calcite for reaction is greater than the 100-year calcite demand. Results for each pit are summarized below and in Table 1.

Pit A:

- For maximum groundwater flow conditions, due to the large annual influxes of groundwater, total dissolved solids (TDS) and sulfate concentrations decrease in all scenarios and stabilize within the first few years; the water quality in this pit quickly evolves to reflect the chemical composition of groundwater.
- For the terminal lake condition, calcite is not sufficient to maintain circumneutral pH in the scenario in which the equilibrium water surface elevation is low and the ARD proportion is high. The model indicates a decrease in pH after calcite is depleted (after approximately 30 simulated years), to a pH of 5.3 after 100 years. TDS increases in all scenarios, quickly approaching 3,000 mg/L in the first 10–30 years of the simulation, and more gradually after the water chemistry reaches equilibrium with gypsum ($CaSO_4$).
- Arsenic concentrations in Pit A for all scenarios was above agricultural use

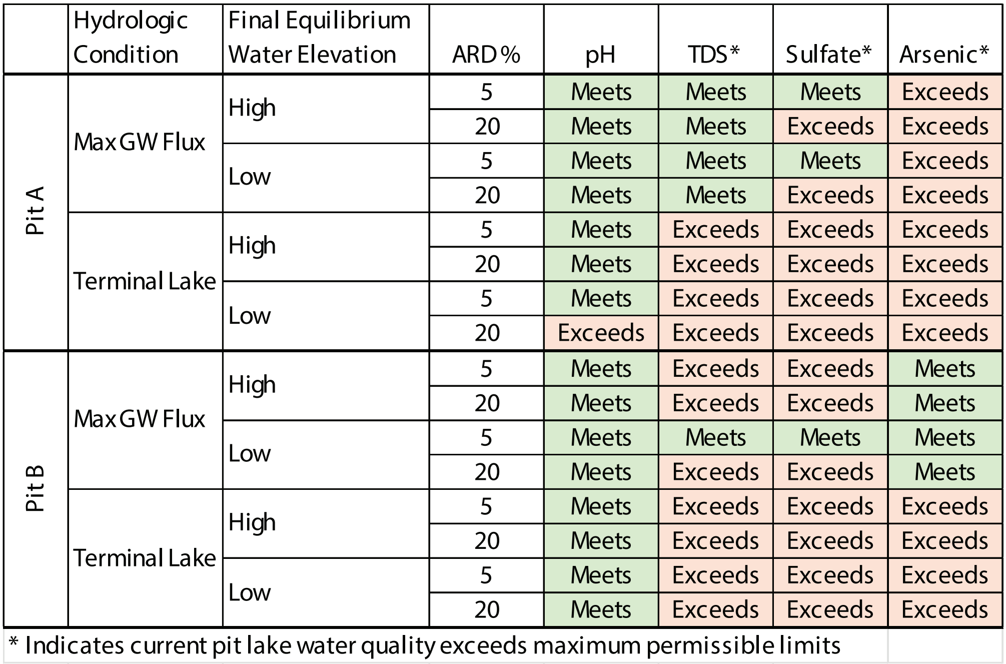

	Hydrologic Condition	Final Equilibrium Water Elevation	ARD %	pH	TDS*	Sulfate*	Arsenic*
Pit A	Max GW Flux	High	5	Meets	Meets	Meets	Exceeds
			20	Meets	Meets	Exceeds	Exceeds
		Low	5	Meets	Meets	Meets	Exceeds
			20	Meets	Meets	Exceeds	Exceeds
	Terminal Lake	High	5	Meets	Exceeds	Exceeds	Exceeds
			20	Meets	Exceeds	Exceeds	Exceeds
		Low	5	Meets	Exceeds	Exceeds	Exceeds
			20	Exceeds	Exceeds	Exceeds	Exceeds
Pit B	Max GW Flux	High	5	Meets	Exceeds	Exceeds	Meets
			20	Meets	Exceeds	Exceeds	Meets
		Low	5	Meets	Meets	Meets	Meets
			20	Meets	Exceeds	Exceeds	Meets
	Terminal Lake	High	5	Meets	Exceeds	Exceeds	Exceeds
			20	Meets	Exceeds	Exceeds	Exceeds
		Low	5	Meets	Exceeds	Exceeds	Exceeds
			20	Meets	Exceeds	Exceeds	Exceeds

* Indicates current pit lake water quality exceeds maximum permissible limits

Figure 5 *Results of pit lake model scenarios.*

standards.

Pit B:

- For maximum groundwater flow conditions, TDS and sulfate increased but reached equilibrium concentrations below water quality standards.
- For the terminal lake condition, evaporation causes TDS and sulfate to increase in all scenarios, with final TDS concentrations ranging from approximately 2,900 to 3,600 mg/L and final sulfate concentrations ranging from approximately 1,800 to 2,400 mg/L. TDS and sulfate concentrations were highest in scenarios with high ARD contribution. In all scenarios, TDS and sulfate exceed human use and agricultural contact standards.

Conclusions

Many projects lack sufficient data to perform a detailed pit lake water quality study, but many times, professionals are called upon to assess risk on a dataset with critical gaps. To assess the water quality risk of two adjacent pit lakes in an arid environment, a series of scenarios bracketing reasonable end members were constructed. The series of forward-simulations for the pit lakes and comparison with wall rock mineralogy generally suggest that pH will be buffered at circumneutral conditions in the short and long term (100 years) by the available calcite in the pit wall rocks. However, the pit lakes are unlikely to meet water quality standards for TDS and sulfate. Arsenic is unlikely to meet water quality standards in Pit A but may meet the standards in Pit B depending upon the equilibrium scenario.

The model is flexible, and run-times are short, meaning that they can be used to simulate various potential future conditions (i.e. pumping water for community use) or used to answer questions related to sensitivity of parameters. In addition, the water quality model can be easily re-run as improved hydrologic data become available to inform the water balance.

This model provided critical guidance to mine owners within a transaction to help determine the risk associated with the long-term management of Pit A and Pit B.

References

Davis A, Lengke M, Sims N, Roth M (2024) A Review of Viable Mineral Precipitates in Pit Lake Modeling. Mine Water Environ 43, 340–367. https://doi.org/10.1007/s10230-024-00989-z

Dzombak DA, Morel FMM (1990) Surface Complexation Modeling: Hydrous Ferric Oxide. New York, John Wiley, ISBN: 978-0-471-63731-8

Castendyk DN, Eary LE, Balistrieri (2015) Modeling and Management of Pit Lake Water Chemistry 1: Theory. Applied Geochemistry 57, 267–288

James W, Rossman LE, James WRC (2010) User's Guide to SWMM5. 13th Edition. Guelph, Ontario: Computational Hydraulics International.

Meyer AF (1942) Evaporation from lakes and reservoirs. St. Paul, MN: Minnesota Resources Commission.

Parkhurst DL, Appelo CAJ (2013) Description of input and examples for PHREEQC version 3 — A computer program for speciation, batch-reaction, one-dimensional transport, and inverse geochemical calculations. US Geol Surv Tech Methods, B 6, chapter A43, 497 pp

Water Driven Failure of Large Mine Slopes

Adrian Brown[1]

[1]Adrian Brown Consultants Inc., 132 West Fourth Avenue, Denver, Colorado 80223 USA
abrown@abch2o.com

Abstract

Water is an important factor in the stability of large mine slopes. Groundwater pressure on a potential failure surface in a slope reduces the effective stress on that surface, which reduces frictional strength of that surface and the Factor of Safety of the slope by as much as 40%. This effect is normally considered in standard slope stability analyses. However, water pressure acting on the surface of a potential failure mass also exerts a lateral driving force, which in saturated slopes generally exceeds the gravitational driving force, and results in a further reduction of the Factor of Safety of more than 50%. This water-drive is rarely correctly considered in standard slope stability analyses. For slopes that can have positive groundwater pressure within them, ignoring water-drive leads to dangerously under-estimating the likelihood of failure. This paper presents the theoretical basis for including water-drive in slope stability analyses, quantifies the magnitude of the failure risk that is introduced by water drive, and provides stabilization strategies that manage those risks.

Keywords: Water drive, large slope failure, slope stabilization

Introduction

Water is an important factor in the stability of large mine slopes (Hoek and Bray 1977). Groundwater pressure on a potential failure surface in a slope reduces the effective stress on that surface, which reduces frictional strength of that surface by as much as 40% (Terzaghi and Peck, 1948). This effect is normally considered in standard slope stability analyses. However, water pressure acting on the surface of a potential failure mass also exerts a lateral driving force, which in saturated slopes generally exceeds the gravitational driving force, and results in a further reduction of the Factor of Safety of more than 50%. This water-drive is often ignored in standard slope stability analyses. For slopes that can have positive groundwater pressure within them, ignoring water-drive leads to dangerously under-estimating the likelihood of failure.

Water Drive in Mine Slopes

Mine slopes in general receive water from precipitation, infiltration, snowmelt, seepage, reservoirs, rivers, and occasionally flooding. When mines are excavated the slope materials are de-stressed, in general allowing fractures to open in the materials near the mined surface. These fractures allow surface water to enter the rockmass. Mine slopes are often made up of low permeability materials, and the water entering the rockmass does not easily drain out of the fractures in the slope, or indeed the slope itself. As a result, mine slope materials at least periodically become saturated and pressurized by groundwater during their operating life.

This slope water has two effects on slope stability. First, the water “floats” the saturated portion of the rockmass, reducing its effective weight to its buoyant weight. This results in a reduction of the normal pressure on sliding surfaces, and a corresponding reduction in the frictional resistance to sliding along potential failure planes. The reduction in strength in saturated slopes is approximately equal to the ratio of the buoyant unit weight to the total unit weight of the slope materials, which for silica rocks is about 0.6, resulting in a reduction of 40% in the frictional resistance of the failure surface. This 40% reduction in the Factor of Safety may result in instability of the slope.

Second, the water "drives" the failure mass by exerting a lateral force on any potential failure surface in the interior of the slope rockmass. Water drive can be understood by considering that the potential failure mass is acting as a "dam", holding back the groundwater behind it from draining from the slope. If the slope is to remain stable, the lateral force exerted by the groundwater on the upstream side of the potential failure "dam" must be resisted, in general by shear force along the potential failure plane. The water-drive force can be large: in a saturated rock slope it is usually substantially greater than the gravitational driving force due to the weight of the rock in the potential failing portion of the slope (Brown 1969). This more than 100% increase in the driving force reduces the Factor of Safety by more than 50%, and may also result in instability of the slope.

I am going to illustrate the water drive problem by looking at the saturated slope in a different light. The slope materials are holding back the force that is exerted on the upstream section of the slope by the groundwater pressure in the un-mined portion of the slope. This is a similar function that a circular or trunnion spillway gate performs for a dam. A picture of the movable portion of such a spillway is presented in Fig. 1(a) (Vortex Hydra 2025). A notable feature of the movable gate is the large size of the bracing that resists the water pressure and holds it in place with a large pivot pin.

The size of the bracing and the pivot to which it is attached is testament to the large lateral load exerted by the water on the gate. And if they are not adequate to the task, then the outcome is starkly illustrated in Fig. 1(b) (Folsom Times 2023). In this case, the water drive is large relative to the weight of the gate, and large relative to the weight of the dam itself. Clearly designers of such gates (and the dams that contain them) need to take that water drive into account. Looking at the trunnion spillway gate as analogous to "slip circle" failure of a slope, it is equally clear that slope design engineers need to take into account the large lateral forces exerted by groundwater pressure acting on the upstream surface of any potential failure mass.

Slope stability under water drive

A powerful example of the effects of water drive on slope stability was the subject of the author's applied graduate research (Brown 1969). This study evaluated the stability of large slopes in the lignite coal measures of the Latrobe Valley in southeast Australia. The lignite in the coalfields reaches depths of 300 m, with a 15 m veneer of overburden. Beneath the lignite is a horizontal 10 m layer of clay, which in turn overlies a fine-grained sand aquifer, originally pressurized to the ground surface. Mining of the coal resulted in large-scale lateral and vertical movement of the mine slopes ("batters"), which disrupted the bucket-wheel and conveyor-belt coal-winning operation and the dewatering operations on which they depended. This in turn threatened the stability and safety of

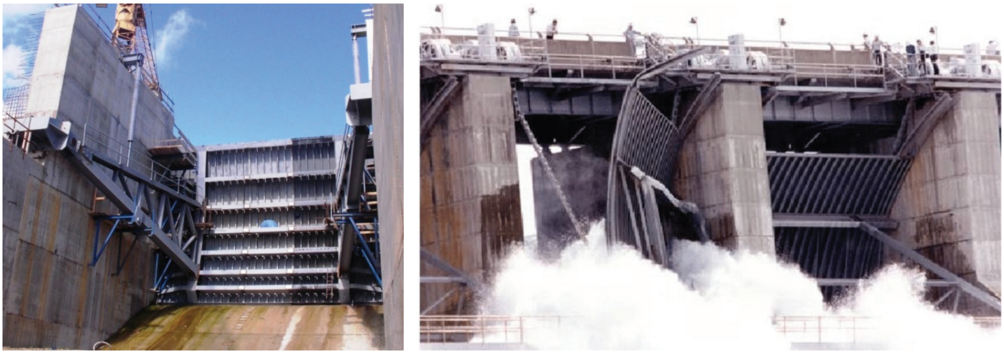

__Figure 1__ (a) Radial spillway gate (Vortex Hydra) (b) Failure of Folsom Dam Gate 3 (Folsom History).

WATER DRIVEN BLOCK SLIDING FORCE DIAGRAM

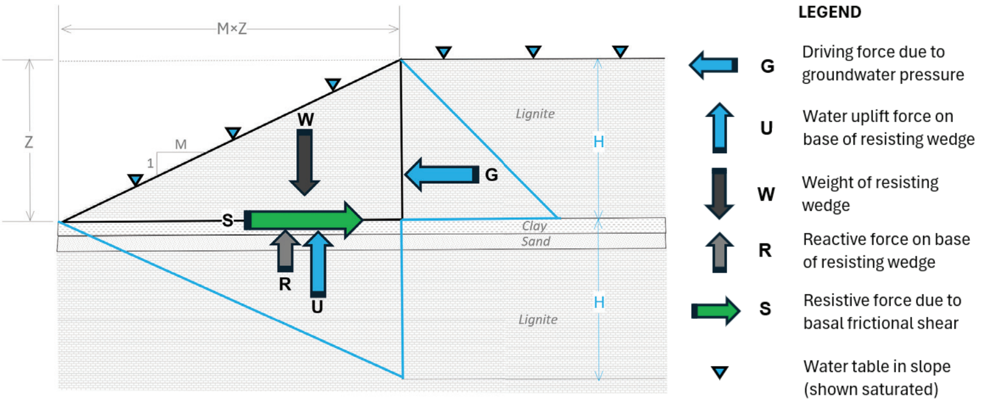

DEFINITIONS

WATER FORCES

G	Water drive due to groundwater
U	Uplift force due to groundwater

DIMENSIONS

Z	Height of slope failure wedge
T	Thickness of slice
H	Groundwater head
M	Slope (M horizontal : 1 vertical)

ROCK FORCES

W	Weight of resistive wedge
R	Reaction on base of resisting wedge
S	Shear resisting force due to friction

PARAMETERS

γw	Unit weight of water
γr	Unit weight of solid granular particles
ϕ	Effective stress friction angle
s	Degree of saturation of slope

ANALYSIS OF FACTOR OF SAFETY OF SLOPE AGAINST WATER DRIVEN G

DRIVING FORCE

The groundwater backed up behind the slope exerts a force (G) on the resisting wedge:

1) $\mathbf{G} = \frac{1}{2}\,\gamma_w\, H^2\, T$

For partial saturation (s), we have: H = s Z, so equation 1 becomes:

2) $\mathbf{G} = \frac{1}{2}\,\gamma_w\, s^2\, Z^2\, T$ where s = degree of saturation of the slope

RESISTING FORCE

The force resisting displacement of the Resisting Wedge is friction on the base of the wedge. Available base friction shear force is given by the Mohr-Coulomb relation (Hoek & Bray, 1977):

3) $\mathbf{S} = (\mathbf{W} - \mathbf{U}) \tan\phi$

The weight of the resistive wedge is given by:

4) $\mathbf{W} = \frac{1}{2}\,\gamma_r\, M\, Z^2\, T$

The groundwater upthrust on the base of the Resisting Wedge is given by:

5) $\mathbf{U} = \frac{1}{2}\,\gamma_w\, s\, M\, Z^2\, T$

Accordingly, the expression for the Resisting Force **S** is:

6) $\mathbf{S} = \frac{1}{2}\,(\gamma_r - \gamma_w\, s)\, M\, Z^2\, T \tan\phi$

FACTOR OF SAFETY

The Factor of Safety is the factor which available shear force (**S**) exceeds driving force (**G**):

7) $\mathbf{FoS} = \mathbf{S} / \mathbf{G} = [\frac{1}{2}\,(\gamma_r - \gamma_w\, s)\, M\, Z^2\, T \tan\phi] / [\frac{1}{2}\,\gamma_w\, s^2\, Z^2\, T]$

Simplifying, the FoS is found to be:

8) $\mathbf{FoS} = \mathbf{S} / \mathbf{G} = (\gamma_r/\gamma_w - s)\,(M/s^2) \tan\phi$

***Figure 2** Slope stability model for the Latrobe Valley coalfields (after Brown 1969).*

the towns, highways, rivers, and reservoirs adjacent to the mines, as well as the reliability of coal supply to mine-mouth power plants (Sullivan 2008).

All analysis methods applied to the slope at the time (including method of slices slip circle and finite element numerical analysis) incorrectly showed a high degree of stability for the slope and predicted little movement after the initial elastic strain accompanying the unloading of the slope due to mining (Brown 1969). In order to determine what mitigation is required to stabilize the mine slopes a simple force balance slope model was developed and proved able to explain the observed movement. The development of the model is presented in full in Fig. 2.

The factor of safety (FoS) against water-driven failure of the slope is given by (Fig. 2):

FoS = Resisting force / Driving force = $(\gamma_r/\gamma_w - s)\,(M/s^2)\tan\phi$

The typical clay in the Latrobe Valley has an effective stress friction angle (ϕ) of 13.5°, the lignite has a relative unit weight ($\gamma r/\gamma w$) of 1.12, and typical slopes are cut at 3H:1V ($M = 3$) (Brown, 1969). When the slope is saturated ($s = 1$), which is the worst-case situation that occurs, we have:

FoS = Resisting force / Driving force = $(1.12 - 1) \times (3/1^2) \times \tan(13.5°) = 0.09$

When the slope is thus saturated, the water drive easily exceeds the resistance offered by the clay beneath the lignite, and the lignite moves laterally towards the mine for as long as water is supplied to and retained behind the moving coal mass. This movement disturbs the coal mass and can lead to catastrophic collapse of the mine slope.

To prevent these progressive movements becoming disruptive of operations and causing the coal slopes to collapse, it was necessary to determine how much the water drive needed to be reduced to create stability ($\text{FoS} \geq 1$). Using the same parameters as above, the slope saturation that just keeps the slope stable is 60%:

FoS = Resisting force / Driving force = $(1.122 - 0.60) \times (3/0.60^2) \times \tan(13.5°) = 1.04$

Based on this finding, horizontal drains were installed along all final mine batters at multiple levels, the underlying aquifers were dewatered, and all surface water reservoirs and streams were required to be located no closer than the mine depth from the mine crest. Movements largely ceased, and production continued without serious stability incidents for 40 years.

Then a new mine operator decided to cease draining the lignite and to extend mining close to a local river. This precipitated the 6 million cubic meter failure shown in Fig. 3 (Melbourne Age 2009). Fortunately, the failure occurred at about 2 am and no mine personnel were injured. However, the State of Victoria was deprived of a substantial portion of its electrical power generation capacity for months and the estimated cost of the outage and repair of the mine was in the billions of Australian dollars (Sullivan 2008).

Could a water drive failure happen in a hard rock mine? A typical hard rock mine has an effective stress friction angle (ϕ) of 35°, a relative unit weight (γ_r/γ_w) of 2.5, and typical slopes are cut at 1H:1V ($M = 1$). When the slope is saturated ($s = 1$) we have:

Figure 3 Failure of one Latrobe Valley Open Pit slope due to water drive (Photos: Melbourne Age).

FOS = Resisting force / Driving force = $(2.5 - 1) \times (1/1^2) \times \tan(35°) = 1.05$

Still barely stable, and this is for a saturated slope with water drive alone, and horizontal sliding with a vertical crack behind the mine slope. Add in an angled fracture behind the slope, slope on the sliding plane, a coating of alteration residue on the rock joints, and some active pressure from the slope above, and that portion of the slope fails.

It appears that the collapse of the Bingham Canyon Mine in Utah in 2013 is an example of this kind of progressive failure, at least in part water driven. This mine is one of the largest in the world. To maintain stability on the slopes it incorporates an extensive mine water control system including dewatering wells, horizontal drains, and drainage tunnels (Dunn 2013). However, despite these precautions the slope was continuously moving, and failed catastrophically twice in rapid succession during the 2013 spring thaw and snowmelt (AGU 2013a). The failures occurred in almost the only portion of the slope that had no water pressure mitigation (Dunn 2013). The run out of the resulting rockslide or "sturzstrom" (literally "rock storm", per Scheidegger 1973) demolished equipment, haul roads, and operations in the mine (Fig. 4). Comprehensive real-time monitoring warned of the failure so that no life was lost (AGU 2013a). The cost of replacing equipment, rehabilitating the mine, and lost production has been estimated to be in the billions of dollars (AGU 2013b).

So, what is the lesson to be learned here? It is that water drive can provide a large force behind a saturated mine slope, which can overwhelm frictional resistance and create an unstable slope, with potentially catastrophic consequences. Any slope designer must take water drive forces into explicit consideration. Don't rely on standard slope stability packages to do it for you, because many of them do not, or do not do it correctly. Indeed, one of the most commonly used slope stability packages says of water drive: "Seepage forces in a stability analysis can create considerable confusion. The concept of seepage forces is easy to comprehend, but including seepage forces in a limit equilibrium stability analysis is fraught with misunderstanding. … [N] o attempt should be made to manually add seepage forces via concentrated point loads." (GeoSlope 2010, p. 32, 34).

Before you put your Engineer's Stamp on your computer-generated mine design, I strongly recommend that you perform a robust check on the admittedly convincing pictures that your computer analysis produces, to ensure that water drive is correctly considered. If you need assistance in this computation, I also recommend using the methodology pioneered for use in the mining industry by Evert Hoek (Hoek and Bray, 1977). The analysis presented in Fig. 2 of

***Figure 4** Landslide at Bingham Canyon Mine which occurred on April 10, 2013 (Photo: Ravell Call, Deseret News).*

this paper is a simple – but robust – example of the use of this methodology applied to slope safety under water drive.

Conclusions

1. Water drive caused by groundwater pressure behind mine slopes is a powerful factor in mine slope instability.
2. Water drive must be explicitly included in mine slope design.
3. Water drive must be explicitly included in mine slope stability mitigation.

Acknowledgements

This paper has been prepared with thanks as a tribute to Evert Hoek, who died last year after a lifetime lovingly creating and leading the science of mining rock mechanics. Evert taught me that geomechanics is both an engineering science and an art. He brilliantly and elegantly simplified it so that it is accessible to everybody in mining, allowing the larger, safer, deeper, steeper and more productive mines that provide the metals and the power for the ongoing industrial revolution that we all rely upon.

References

Brown A (1969) Earth Movement and Batter Stability in the Latrobe Valley Coalfields. M.Eng.Sci. Thesis, Monash University, August 1969

Deseret News (2013) Massive landslide stops production at Bingham Canyon Mine. Deseret News, Salt Lake City, Utah, USA, April 11, 2013. https://www.deseret.com/2013/4/11/20518052/massive-landslide-stops-production-at-bingham-canyon-mine/

Dunn J (2013) Innovative Mine Dewatering Strategies. Proceedings of Conference on Global Mining Water Management Initiatives, Las Vegas, Nevada, January 31, 2013

Folsom Times (2023) Folsom Dam spillway flaw needs $16M in repairs. https://folsomtimes.com/folsom-dam-spillway-flaw-needs-16m-in-repairs/

GeoSlope (2010) Stability Modeling with SLOPE/W – An Engineering Methodology. GEO-SLOPE International Ltd., Calgary, Alberta, Canada, Fourth Edition, February 2010

Hoek E, Bray J (1977) Rock Slope Engineering. Institution of Mining and Metallurgy, London.

Melbourne Age (2009) Experts missed obvious signs before mine collapse. The Age, Melbourne, Victoria, Australia, January 4, 2009 https://www.theage.com.au/national/experts-missed-obvious-signs-before-mine-collapse-20090103-79he.html

Petley D (2013a) The unusually large Bingham Canyon Mine landslide. AGU Blogosphere, 12 April 2013 http://blogs.agu.org/landslideblog/2013/04/12/the-unusually-large-bingham-canyon-mine-landslide-an-impressive-example-of-prediction-using-monitoring/

Petley D (2013b) Is the Bingham Canyon Mine landslide the most expensive single mass movement in history? AGU Blogosphere, 16 April 2013 http://blogs.agu.org/landslideblog/2013/04/16/is-the-bingham-canyon-copper-mine-landslide-the-most-expensive-single-mass-movement-in-history/

Rankine W (1857) On the stability of loose earth. Philosophical Transactions of the Royal Society of London, Vol. 147.

Romero M, Adams A (2013) Massive landslide stops production at Bingham Canyon Mine. Deseret News, Salt Lake City, April 11, 2013. https://www.deseret.com/2013/4/11/20518052/massive-landslide-stops-production-at-bingham-canyon-mine/

Scheidegger AE (1973) On the Prediction of the Reach and Velocity of Catastrophic Landslides. Rock Mechanics 5, 231–236 (1973)

Sullivan T (2008) Yallourn Mine Batter Failure Inquiry. State of Victoria, Australia, Victorian Government Printer No. 156, Session 2006-08. June 30, 2008

Vortex Hydra (2025) Radial Gates. https://www.vortexhydradams.com/hydraulic-works/radial-gates/

Batch Leaching to Enhance Dissolution of Siliceous Secondary Materials for Controlling AMD Formation

Dantie Claudia Butar Butar[1], Hanna Kaasalainen[2], Lena Alakangas[1], Erik Ronne[3]

[1]Applied Geochemistry, Swedish School of Mines, Dept. of Civil, Environmental and Natural Resources Engineering, Luleå University of Technology, SE-971 87 Luleå, Sweden, dantie.butar.butar@ltu.se,

ORCID 0009-0005-8576-1419; lena.alakangas@ltu.se, ORCID 0000-0001-7291-8505

[2]Department of Geology and Mineralogy, Åbo Akademi University, Åbo, Finland, hanna.kaasalainen@abo.fi, ORCID 0000-0003-3382-1764

[3]Boliden AB, SE-101 20 Stockholm Sweden, erik.ronne@boliden.com, ORCID 0000-0002-6564-5542

Abstract

Silica may be important for AMD control as it provides long-term neutralization and chemically passivating pyrite through secondary mineralization. This study tested several side streams of siliceous materials, i.e., Si-Mn slags and waste rock, in a batch leaching at various pH conditions and leaching reagents to evaluate the most optimum conditions to obtain silica through enhanced silicate dissolution. Leaching samples in MQ water resulted in a low Si release, whereas leaching of materials in carbonated MQ resulted in a high Si release. Dissolution of water-granulated slag in carbonated MQ released a high concentration of sulfur and manganese.

Keywords: Acid mine drainage, pyrite, silica, waste rock, slag

Introduction

Acid mine drainage (AMD) is a substantial environmental concern at mining sites, primarily resulting from sulfide oxidation. When exposed to oxygen, reactive sulfidic minerals, mainly pyrite, oxidize and release sulfate, acidity, and metal(oid) ions associated with the sulfide. In cases where AMD has already formed, the acidic discharge is typically treated by actively adding alkaline substances, such as lime, limestone, NaOH, or other materials capable of neutralizing the pH. However, long-term reliance on such treatments is not ideal due to the high costs associated with the continuous consumption of additives. Prevention measures to control AMD are the best available technique and are usually less costly than remediation. Passivation, also known as inhibition, is a preventive approach for controlling AMD. The principle of inhibition is based on forming a coating layer on the pyrite surface, which prevents surface oxidation, dissolution or adsorption (Li *et al.* 2024), thereby controlling long-term pyrite oxidation and AMD formation. Silica, due to its abundance in nature and environmentally benign characteristics, is considered superior to phosphate and other organic coatings.

Previous studies have demonstrated the effectiveness of silicates in inhibiting pyrite oxidation by forming a stable silicate-based coating on the pyrite surface (Butar Butar *et al.* 2025, Fan *et al.* 2017, Kollias *et al.* 2018,). Silicate coatings have been shown to remain stable within the pH range of 2.5–4.0 (Evangelou 1996), precipitate at circumneutral pH (Bessho *et al.* 2011) and form protective layers through adsorbed silicates or SiO2 precipitates (Kollias *et al.* 2018). In a study by Butar Butar *et al.* (2025), a single addition of an alkaline silicate solution without a pH buffer or adjuster, along with prolonged contact time with pyritic waste rock, managed to suppress pyrite oxidation and metal leaching by forming a silica (SiO2) layer on the waste rock surface. To ensure field applicability, which often involves complex chemical reactions that alter pH, using readily available siliceous materials rather than chemical reagents to minimize continuous amendment consumption and associated costs is preferred.

Therefore, batch leaching of siliceous materials can be employed to provide preliminary insights into enhancing the silica dissolution from several materials by evaluating the effectiveness of various leaching reagents, such as Milli-Q (MQ) water, carbonated MQ and alkaline solutions. The materials to be tested as a potential source of silica are andesitic waste rock and slags. This study aims to assess the release of silica by leaching siliceous materials under different chemical conditions to determine whether the silica released during leaching can serve a function in inhibiting pyrite surfaces. The focus of this study is to provide a preliminary understanding of siliceous materials originating from secondary sources to screen their potential suitability to be used to control AMD formation. The use of secondary resources and waste streams as sources of silica, aligns with the European Union's waste management and sustainability directive (the EU's Waste Framework Directive/Directive 2008/98/EC), promoting a circular economy and reducing overall environmental impact by waste stream valorization.

Materials and methods

Materials

The materials utilized in the batch leaching experiment consist of waste rock (herein referred to as WR) from an active polymetallic Cu-Zn-Au-Ag open-pit and underground mining operations in the Kristineberg area in Northern Sweden. The selected waste rock samples contain an average sulfur content of 11%, which corresponds to the sulfur concentration in the waste rock heap. Following collection, the waste rock underwent crushing, splitting, and homogenization.

Water-quenched, or more commonly known as water-granulated Si-Mn slag (SW) is an oxide slag produced during the manufacture of Si-Mn alloys. This slag results from the rapid cooling of molten slag through water quenching, leading to its rapid solidification and forming fine, granulated particles with a glassy, amorphous structure (*the anonymous company supplying the slag, personal communication, 14 November 2023*). Air-cooled Si-Mn slag (SA) is another by-product formed during the production of Si-Mn alloys, which results from the slow cooling of molten slag containing a mixture of Si, Mn, and other trace elements, using air. Air-cooling with water spraying gives an 90% amorphous, glassy surface whereas water-granulation gives a fine-grained, 100% amorphous and porous slag. SA and SW (herein referred to as the slags) used in this experiment were supplied by an anonymous metal company. The waste rock is andesite and contain silicate rock-forming minerals, whereas the slags comprise mainly amorphous silicate glasses (i.e., 100% amorphous glass in SW and up to 90% amorphous glass phase in SA and very few crystalline phases). For simplicity, the term silicate minerals are used throughout this article.

Methods

Before the batch leaching experiments, all solid samples were prepared and pre-treated as necessary, including size reduction to increase the reactive surface area and enhance the leachability of the materials. The waste rock was crushed to a particle size of less than 100 µm, similar to the particle size of the DST sample. The SA and SW samples, with particle sizes ranging from <100 µm to 1 mm, were used as received from the metal company and were not further reduced, except for sieving prior to use, where the <100 µm was used for the leaching experiment. To analyze the chemical composition before the batch leaching test, the solid samples were digested with two methods, i.e., acidic digestion with $HCl/HNO_3/HF$ in hotplate according to SE-SOP-0039 (SS-EN 13656:2003) and fusion with $LiBO_2$ according to SE-SOP-0060 (ASTM D3682:2013, ASTM D4503:2008) A sample weight of 100 g (± 0.001 g) was used for each leaching trial.

The leaching tests were conducted using various leaching solutions, including MQ water (herein referred to as MQ), carbonated MQ, and alkaline residual materials, to achieve initial circumneutral, acidic, and alkaline pH conditions, respectively. The leaching tests were carried out in three stages, with different liquid-to-solid (L/S) ratios and leaching durations. In the first stage, the L/S ratio was set to 0.75 (i.e., 75 mL of liquid), and the solid samples were leached for 6 hours. In every leaching stage, fresh solution and materials were added into high-density polyethene (HDPE) bottles. In the second and third stages, the L/S ratios were adjusted to 1 and 1.5, with leaching durations of 18 hours and 72 hours per stage, respectively. During the leaching process, the solid samples were mixed with the leaching solutions in HDPE bottles and agitated at 10 rpm using an end-over-end agitator. In set-ups involving carbonated MQ, MQ water was carbonated by pumping CO_2 directly into the water using a SodaStream, utilizing the principle of CO_2 dissolution in water to produce aqueous CO_2 ($CO_{2(aq)}$) and form H_2CO_3 (carbonic acid). In set-ups involving carbonated MQ, the solution added at each step was newly carbonated. The bottles were closed immediately, and lids were sealed thoroughly to limit CO_2 exchange with the atmosphere. In samples with mixtures (WR+SW), 4 wt% of SW was added to WR and was mixed homogeneously and leached in MQ.

At the end of each leaching step, leachate samples were collected and analyzed for pH and electroconductivity (EC) immediately. The leachate was filtered using a 0.2 µm filter (Merck Millipore) and subsequently analyzed for metal concentrations using Inductively Coupled Plasma – Sector Field Mass Spectrometry (ICP-SFMS) at ALS Scandinavia in Luleå, Sweden. Reagent blanks were also sampled and analyzed. The metal concentrations from all experimental setups were corrected by subtraction with the blank values to remove contributions from the reagents.

Results and discussion

Material characterization

The waste rock sample is andesite and contains several rock-forming silicate minerals, e.g., albite ($NaAlSi_3O_8$), biotite ($K(Mg,Fe)_3(AlSi_3O_{10})(OH)_2$), diopside ($CaMgSi_2O_6$), plagioclase ($(Na,Ca)(Al,Si)Si_2O_8$), microcline ($KAlSi_3O_8$), and muscovite ($KAl_2(AlSi_3O_{10})(OH)_2$), among others (Butar Butar *et al.* 2025). The primary aim is to enhance the weathering of these minerals to facilitate the release of Si for pyrite passivation. Both slag types (SA and SW) contain an amorphous glassy silicate phase, which serves as a potential Si source, as well as soluble $Ca(OH)_2$, which provides alkalinity. The slags contain minimal crystalline phases.

The concentrations of selected major elements in the starting materials are presented in Table 1. The chemical compositions of SA and SW are identical, as both samples originate from silico-manganese slag and are characterized by high Mn and Si content, although the morphology and physical properties differ. In andesite waste rock, Si is primarily hosted in silicate rock-forming minerals, whereas sulfur is only associated with pyrite (FeS_2).

Leaching characteristics of materials

Overall, leaching materials in MQ water generated leachate with varying pH levels. The dissolution of andesitic waste rock in MQ water yielded a circumneutral pH (~6) (Fig. 1). Since pH is a critical geochemical factor influencing silicate weathering rate (Dupla *et al.* 2025), this study also examined dissolution of materials under acidic and alkaline conditions to compare with leaching at circumneutral pH. The pH of solutions resulting from dissolution in carbonated MQ (Fig. 1) was influenced not only by the dissociation of carbonic acid in water but also by the dissolution of the reactive buffering minerals, such as Ca(OH)2 in slags and silicate-bearing rock forming minerals in WR, in the presence of carbonic acid.

A similar trend of high pH was observed in the leachate of the slag samples, likely due

Table 1 *Elemental analysis of WR and slag samples.*

Material	Al	Ca	Fe	K	Mg	Mn	Na	S	Si
SA	90400	169000	6440	7980	57100	63000	3880	4980	198000
SW	82600	178000	5570	6250	47500	50600	2970	4400	211000
WR	79200	4830	69200	20500	42300	1370	2340	50900	263000

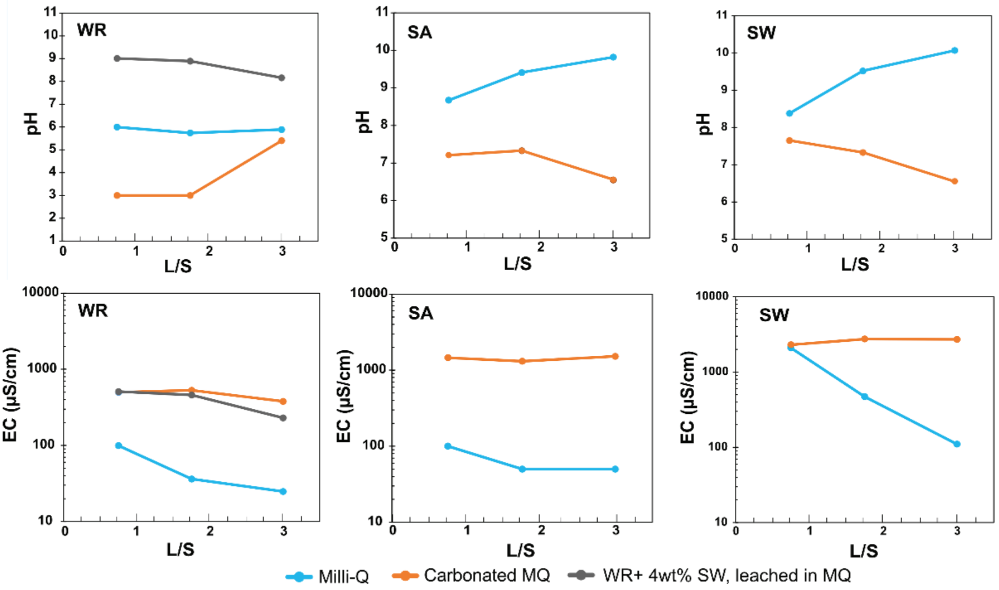

Figure 1 *pH and EC in the leachate samples, collected in the 3-step leaching test*

to dissolution of $Ca(OH)_2$. The elevated EC in the slag leachates corresponded to the increased concentration of the dissolved metals in solution (Fig. 2). The dissolution of SW in MQ resulted in leachate with a higher EC than that of SA (Fig. 1). The analysis of anions confirmed the higher EC and indicated that SW released more Cl ions compared to SA, attributed to the dissolution of salts in SW upon contact with water.

Overall, leaching the materials in MQ at circumneutral pH resulted in lower Si concentrations in solution compared to other pH conditions (Fig. 2). Fig. 2 demonstrates that silica dissolved from siliceous materials more effectively in carbonated water than in MQ water, as shown by the higher Si release observed under carbonated conditions. The batch leaching test further confirmed that carbonation of water promoted the dissolution of silicate minerals. Among the experimental setups, SA dissolution in carbonated solution yielded the highest accumulated silica concentration (~100 mg/L Si) (Fig. 2). The accumulated Si concentration in the solution followed the order: SA+ H_2CO_3 > SW+ H_2CO_3 > WR+ H_2CO_3 > WR+4wt%SW > SA in MQ > WR in MQ > SW in MQ.

In addition to Si, leaching the materials with carbonated water also resulted in a high Ca concentration in the solution (Fig. 2). Upon carbonation, Ca(OH)2 in the slags dissolved more rapidly than in MQ. Furthermore, the trilinear diagram (Fig. 3) indicates that Ca is the dominant cation in solution under acidic conditions following carbonation. The silica released during carbonation likely originated from Ca-bearing silicate minerals (Fig. 3). It is well-established that the dissolution rate of silicate minerals is pH-dependent and carbonic acid can promote silica dissolution by enhancing the dissolution of rock-forming silicate minerals through acid hydrolysis (Dupla *et al.* 2025). When silicate minerals react with carbonic acid, the accelerated weathering of silicate minerals sequesters CO2 directly in the form of alkalinity, primarily as bicarbonate ions, but also dissolves silica. The observed shift in the trend of major cations in WR (Fig. 3) likely suggests that the increased weathering rate of Mg-silicate minerals, such as biotite and diopside, occurred at low pH (Palandri and Karaka 2004) following carbonation, compared to MQ water.

Conversely, mixing waste rock (WR) samples with SW resulted in leachate with an initially alkaline pH due to the dissolution of Ca(OH)2 from the slag. However, as the available lime was depleted over time, the leachate pH gradually decreased (Fig. 1). The addition of the alkaline amendment

(SW) to WR also enhanced the dissolution of silicate minerals (Fig. 2). It is well-established that at pH>8, the Si-O bonds in silicates are weakened due to polarization from charged surface species, leading to the detachment of silicon atoms, and contributed by hydrolytic weakening by water dipoles (Brady and Walther 1989). Long-term albite dissolution, for instance, is proportional to silica surface charge above pH 8 (Brady and Walther 1989). Beyond the high Si concentrations observed in the solution, the selection of suitable materials should also consider the potential co-release of other elements upon carbonation or mixing with alkaline amendments. Although mixing materials with alkaline amendment (slags) improved silicate dissolution, it also facilitated the mobilization of deleterious elements. For instance, Mn was released in high concentrations when the materials were dissolved in carbonated water (~230 mg/L Mn in SA, ~553 mg/L Mn in SW), or when andesitic WR was mixed with SW, sulfur was released in high concentration in the leachate (~227 mg/L S) (Fig. 2). Finally, this study demonstrated that the dissolution of WR, SA, and SW in carbonated water effectively enhanced silica release.

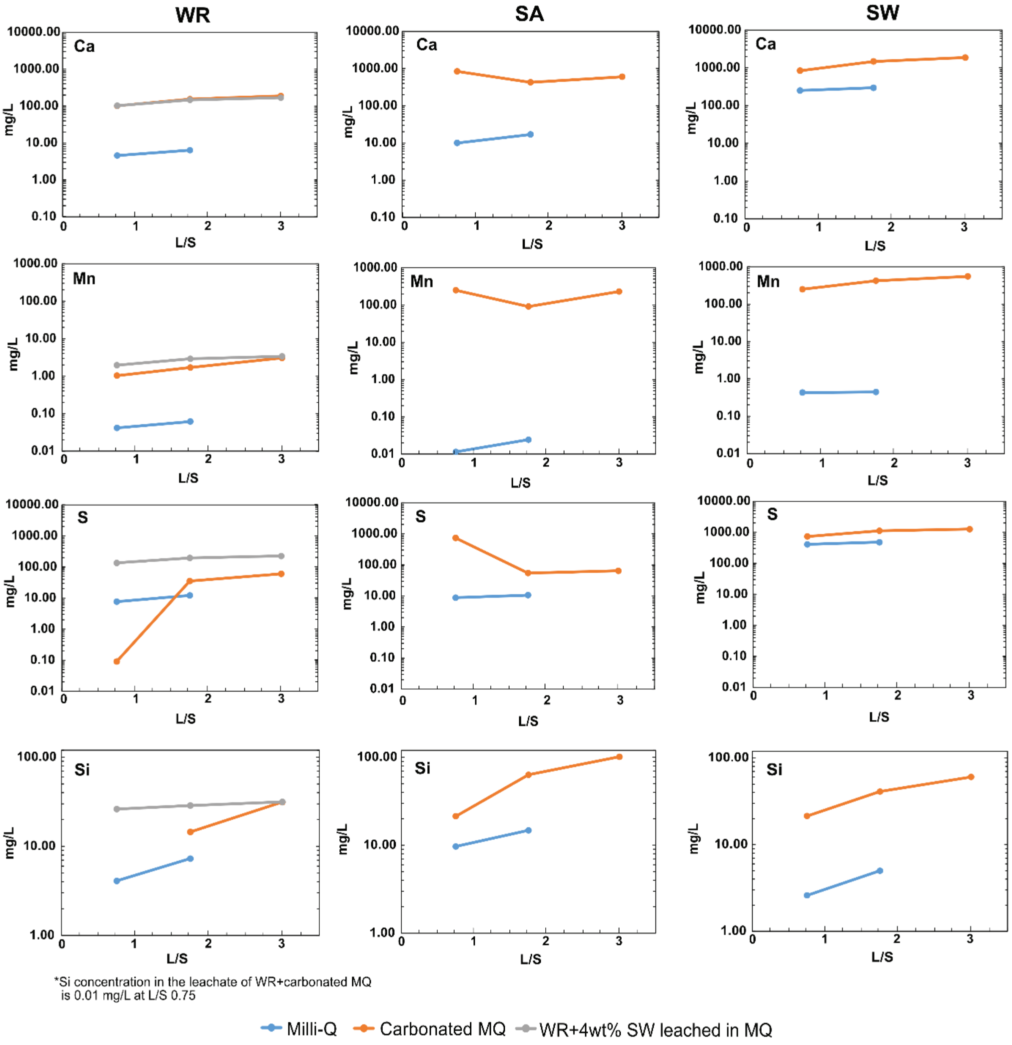

Figure 2 *Cumulative elemental concentration released to the leachate, collected in the 3-step leaching test.*

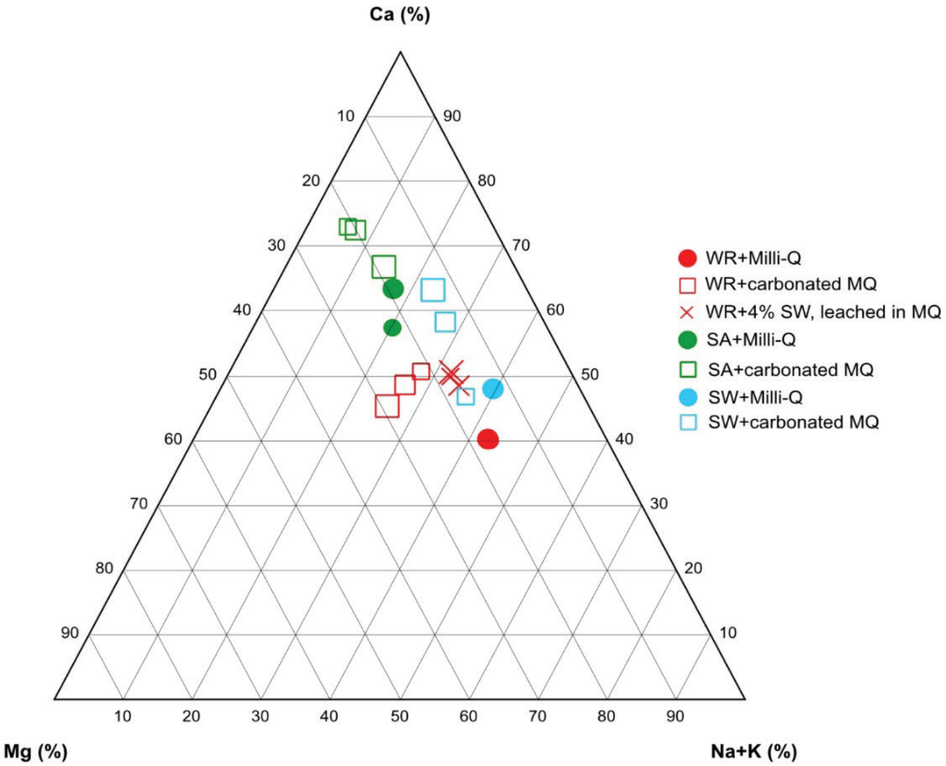

Figure 3 *Trilinear diagram of the major cations in the leachate from all collected samples.*

Conclusions

- The dissolution of siliceous materials in MQ resulted in circumneutral-alkaline leachate pH.
- The slags are inert to leaching in MQ and similarly, the dissolution of silicate minerals in andesite waste rock is slow in MQ.
- Carbonation of MQ used in the batch leaching test enhanced the dissolution of silicate minerals. Higher Si concentration was observed in samples dissolved in carbonated water than in MQ.
- Mixing WR with alkaline amendment (the slags) or using leachate from SW in the batch leaching test slightly improved silicate dissolution but is associated with a high release of Mn and S in the leachate.

Acknowledgements

Boliden Mineral AB is gratefully acknowledged for financial support and for providing research samples and access to the materials during site visits.

References

Bessho M, Wajima T, Ida T, Nishiyama T (2011). Experimental study on prevention of acid mine drainage by silica coating of pyrite waste rocks with amorphous silica solution. Environmental Earth Science 64:311–318. doi:10.1007/s12665-010-0848-0

Brady PV, Walther JV (1989). Controls on silicate dissolution rates in neutral and basic pH solutions at 25oC. Geochimica et Cosmochimica Acta: 2823–2830. doi:10.1016/0016-7037(89)90160-9

Butar Butar DC, Alakangas L, Kaasalainen H, Ronne E (2025). Prevention of acid rock drainage formation through pyrite inhibition by silica coating. Environ Sci Pollut Res. doi:10.1007/s11356-025-36131-x

Dupla X, Brantley SL, Paulo C, Möller BP, Grand S (2025). Geochemical Drivers of Enhanced Rock Weathering in Soils. Teoksessa M. Beech. Geoengineering and Climate Change, Hoboken, New Jersey: John Wiley Sons, Inc, p 207–230

Evangelou V (1996). Oxidation proof silicate surface coating on iron sulfides. US Patent No. 5, 494, 703.

Fan R, Short MD, Zeng S-J, Qian Gu, Li J, Schumann RC, Kawashima N, Smart RSC (2017). The Formation of Silicate-Stabilized Passivating Layers on Pyrite for Reduced Acid Rock Drainage. Environmental Science & Technology 51(19):11317–11325. doi:10.1021/acs.est.7b03232

Kollias K, Mylona E, Papassiopi N, Xenidis A (2018). Development of silica protective layer on pyrite surface: a column study. Environmental Science Pollution & Research 25: 26780–26792. doi:10.1007/s11356-017-0083-2

Li Y, Cao Y, Ruan M, Li R, Bian Q, Hu Z (2024). Mechanism and In Situ Prevention of Oxidation in Coal Gangue Piles: A Review Aiming to Reduce Acid Pollution. . Sustainability 16: 7208. doi:10.3390/su16167208

Palandri JL, Kharaka YK (2004). A compilation of rate parameters of water-mineral interaction kinetics for application to geochemical modeling. U.S. Geological Survey. doi:10.3133/ofr20041068

Flow Failure of TSF Brunita in 1972, SE Spain

Joanna Butlanska[1], Aldo Onel Oliva-González[2], Jose Antonio Fernández-Merodo[3],
Roberto Rodríguez-Pacheco[4]

[1,2,3,4]*Consejo Superior de Investigaciones Científicas, Centro Nacional Instituto Geológico y Minero de España, 28003 Madrid, Spain*

[1]*j.butlanska@igme.es, ORCID 0000-0003-3447-4346*

[2]*ao.oliva@igme.es, ORCID 0000-0001-6119-8602*

[3]*jose.fernandez@igme.es, ORCID 0000-0003-0642-5803*

[4]*roberto.rodriguez@igme.es, ORCID 0000-0003-3801-3213*

Abstract

The aim of this study is to analyse the influence of the drainage system on the mechanism that might have caused the flow failure of the Brunita tailings storage facility (TSF Brunita) in southeast (SE) of Spain. The TSF Brunita failed on October 20, 1972. The forensic analysis used geological, geotechnical and hydrogeological criteria to determine the causes of the flow failure. With this information the conceptual hydromechanical model was developed. The 2D stability analyses were carried out with GeoStudio software (version 2012) in two phases: (1) steady state seepage analysis to establish the reference conditions before the heavy rainfall and (2) transient seepage analysis considering the additional water from the rainfall. For both cases, factors of safety and failure surfaces were calculated using limit equilibrium methods and stress-strain analysis was performed to estimate displacements and deformations in unstable areas under changing saturation conditions. The working hypothesis was to consider that the TSF failed due to a deficient drainage system. In order to verify this, two scenarios were considered: I) insufficient drainage system and II) sufficient and efficient drainage system modelled as a drain with saturated permeability of 0.001 m/s. The results confirmed the failure hypothesis. Heavy rainfall (119 L/m^2 in one week) led to a drastic reduction of the shear strength and stability of the TSF Brunita.

Keywords: Tailings storage facility (TSF), flow failure, numerical simulations, seepage, piping

Introduction

Rain can cause slopes to collapse, which is hard to predict and can be very damaging. Heavy rain can suddenly make slopes collapse, putting lives at risk. Rainfall is a key factor in how often slopes fail. Continuous rain weakens the soil because it increases water pressure or reduces suction. Once a slide begins, it's almost impossible to stop. Moreover, if the drainage system can't remove the water, a disaster is likely to happen. On October 20, 1972, the TSF Brunita, located in the Cartagena-La Unión mining district in SE Spain, failed (Fig. 1) taking life of the cementary/church janitor José Antonio Saura Gómez. This failure has been documented in various research studies, newspaper articles, and personal testimonies. A detailed account of the events between October 17 and 20, 1972, is available in MIN (1972). Martínez-Pagán *et al.* (2011) conducted a geophysical study and geochemical characterization of four metals (Pb, Zn, Cu, Cd), along with hydrogeological characterization in two boreholes. Rodriguez *et al.* (2011) provided a description of the failure of TSFs in the mining area, including the TSF Brunita case study, and analysed the physical-mechanical properties of the tailings. Moreno-Perales

(2016) performed stability calculations using the limit equilibrium method but did not account for precipitation. An environmental characterization and description of the spatio-temporal evolution of TSF Brunita can be found in Martín-Crespo *et al.* (2018). Despite extensive research on TSF Brunita, none of the available studies have confirmed the flow failure process through numerical simulation under different boundary conditions. Hence, the objective of this work is to analyse the failure mechanisms of the tailings facility using available geological, geotechnical, and hydrogeological information, to define the conceptual model of hydromechanical operation (Rodriguez (2006)), and to perform numerical simulations of seepage, stresses, deformations, and equilibrium conditions including (i) working and (ii) failed drainage system.

Hypotheses of Flow failure of TSF Brunita

Based on the information consulted and field mapping (Fig. 1), it is hypothesized that the flow failure of the TSF Brunita was due to a poor drainage system. The Brunita's drainage system consisted of rigid, ceramic, and perforated pipes (2 m length and 20 cm inner diameter) installed at the bottom of the valley. Pipes were joined together with the cement as the deposit grew. Moreover, pipes were not protected against the entry of fines. The failure of the drainage system facilitated the development of piping around the pipes (Fig. 1d). To validate this hypothesis, two cases of TSF stability analyses were considered: I) a deficient drainage system, and II) an efficient and sufficient drainage system.

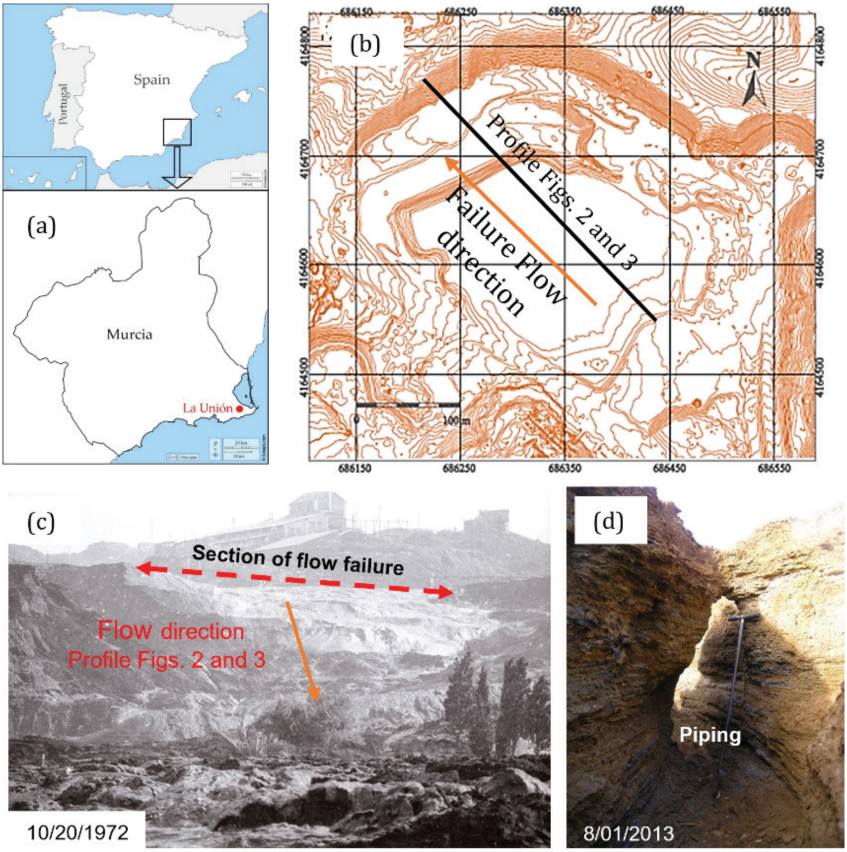

Figure 1 TSF Brunita, a) localization, b) topography of the TSF before the breach including the profile used in calculations, c) area affected by a flow failure and d) piping in TSF Brunita 50 years post-failure.

Materials

The properties of the materials that make up the tailings, the dam and the foundation were defined based on the analysis and interpretation of the information obtained from field and laboratory research and the results of various studies (Martínez-Pagán *et al.* 2011, Rodríguez *et al.* 2011, Moreno-Perales, 2016, Martín-Crespo *et al.* 2018, HORYSU, 2023 and GEOZONE, 2023). The geological, geotechnical, and hydrogeological characteristics of the tailings and the foundation materials of the TSF Brunita, used for the development of this work, are listed in Tab. 1.

Numerical model

Two-dimensional (2D) simulations were conducted using the finite element programs 'SEEP/W' and 'SIGMA/W' to model groundwater flow and stress-strain behavior, respectively. The mesh consists of 7063 elements (combination of quadrilaterals and triangles) and 7422 nodes as shown in Appendix 1 Fig. 1. Material was modelled as a linear elastic perfectly plastic Mohr-Coulomb. The program 'SLOPE/W' was used to calculate the factors of safety (FoS) using the limit equilibrium methods of Bishop (Bishop and Morgenstern 1960) and Morgenstern-Price (Morgenstern and Price 1967). The conceptual model was developed from available data, including the interpretation of aerial photographs and digital terrain models before and after the failure, as well as geotechnical and hydraulic parameters of the materials. This provided relevant information on the geometry and spatial distribution of tailings in the TSF Brunita, as shown in Figs. 2a and 3a. The main elements of the TSF were defined as a tailings basin, lagoon, a bedrock foundation, and dams/embankments. The basin was modeled with two types of tailings: a shallow layer of low plasticity silts and a deep layer of silty sands. The dams/embankments were composed of silty sand material. The maximum water level in the lagoon was fixed at 28.41 m. The drainage system was modelled as a layer of material with high permeability, having saturated permeability of 0.001 m/s. The vertical part extended to the maximum level of the lagoon's water table (28.41 m), and the horizontal part was extended through all deposit length, both with a width of 0.65 m. The deformability, shear strength, and hydraulic properties of each material are provided in Tab. 1.

Results

In the geotechnical-structural stability analysis, pore pressures, phreatic surfaces, hydraulic gradients, seepage rates, factors of safety (FoS), potential failure surfaces, and horizontal displacements, were determined under different saturation conditions (Figs. 2 and 3). The analysis considered two hypotheses: I) an insufficient drainage system, and II) a sufficient and efficient drainage system. The analysis considering the maximum level of the lagoon (and working drains) before heavy rains was used as the base simulation. This base simulation allowed to obtain the initial pore pressures (Appendix 1 Fig. 2). The calculated safety factor was around 3. Subsequently, seepage analysis was performed considering the water input from rainfall to calculate changes in water tables and safety factors over time. The effect of

Table 1 *Geotechnical and hydraulic parameters: solid specific gravity (G_s), porosity (n), saturated unit weight (γ_{sat}), dry unit weight (γ_{dry}), cohesion (c), friction angle (ϕ), Young's modulus (E), Poisson's ratio (v), saturated hydraulic conductivity – horizontal (k_h^{sat}) and vertical (k_v^{sat}).*

Material	G_s kN/ m³	n %	γ_{sat} kN/m³	γ_{dry} kN/m³	c kPa	φ °	E kPa	ν –	k_v^{sat} m/s	k_h^{sat} m/s
Low plasticity silts (tailings)	28.9	42	18.5	16.84	15.14	28.25	1000	0.31	6.59×10^{-9}	6.59×10^{-10}
Silty sands (tailings)	28.9	40	19.1	17.38	38	29.25	3500	0.31	6.99×10^{-7}	6.99×10^{-8}
Silty sands (dam)	28.7	33	21.0	19.11	49	31	4000	0.31	8.31×10^{-5}	8.31×10^{-6}
Graphite schist and Quartzites (Foundation)		12	22.0	20.02	150	40	100000	0.28	1.15×10^{-11}	1.15×10^{-12}

rainfall was modeled by performing transient seepage analysis, accounting for the increase in water table height produced by 119 L/m^2 (119 mm) of rainfall in one week. This rainfall was recorded at the Algar (Murcia) weather station, located 4 km from the TSF Brunita and was equivalent to an infiltration rate of 1.97×10^{-7} m/s.

Hypothesis I: an insufficient drainage system

The results of the numerical simulation (Fig. 2) confirmed that the hypothesis regarding the insufficiency of the drainage system as the main cause of the failure was correct. The simulation indicated that the drainage system in place at the time of the rainfall was inadequate to evacuate the water stored within the facility. Fig. 2b shows a distribution of pore water pressure resulting from the saturation of the tailings from heavy rain, with the flooded surfaces of dams 1 and 2. The loss of stability is confirmed by the drop in the safety factor of the TSF (Figs. 2c and d). As shown in Fig. 2d, the factor of safety (FoS) reached 1 (limit equilibrium) 48 hours after the onset of rainfall, which aligns with the first landslide experienced by the TSF Brunita as described by MIN (1972). The slipped zone shows displacements of the mass of embankment 1 of 0.18 m (Fig. 2e),

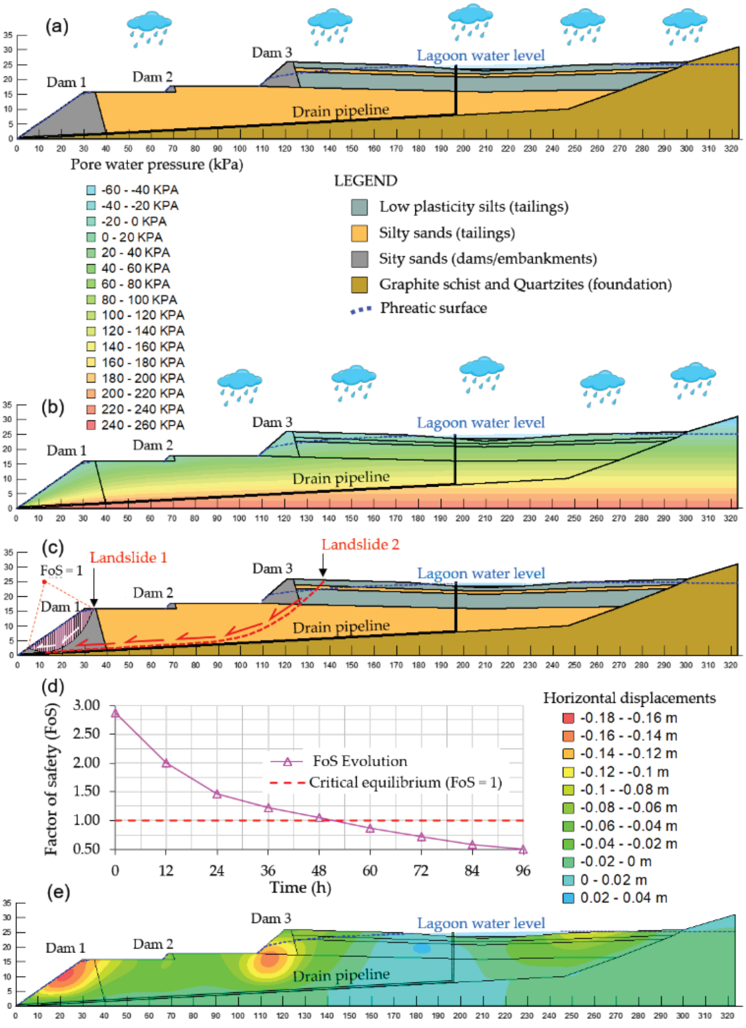

Figure 2 *Behaviour of the TSF Brunita with an insufficiently drainage system: (a) conceptual model, (b) pore water pressure resulting from tailings saturation (time = 48 h), (c) slip surface of TSF Brunita, (d) reduction of FoS of the dam 1 of TSF, (e) displacements computed in TSF (time = 48 h).*

while the displacements at the base of dike 3 are 0.12 m. The water flow through the dam 1 slope at the time of failure was 11.27 m³/s (Appendix 1 Fig. 3).

Hypothesis II: a sufficient and efficient drainage system

In this case, a drain with a saturated hydraulic conductivity of 0.001 m/s was installed. When the drain is functioning, there is no increase in pore pressures (Fig. 3b). As shown, all three embankments remain in an unsaturated condition. If the drainage system can evacuate the volume of infiltrated water throughout the period of heavy rainfall, the factor of safety (FoS) remains higher than 2 (Fig. 3c). As seen in Fig. 3d, no large deformations occur in embankment 1. The largest deformations occur in embankment 3, which is consistent with the increased saturation of the tailings.

Conclusion

The numerical analysis of the TSF Brunita highlights the critical importance of a good drainage system for the stability of TSFs, especially during intense rainfall. The numerical simulation confirmed that the 1972 failure was due to fault drainage (did not

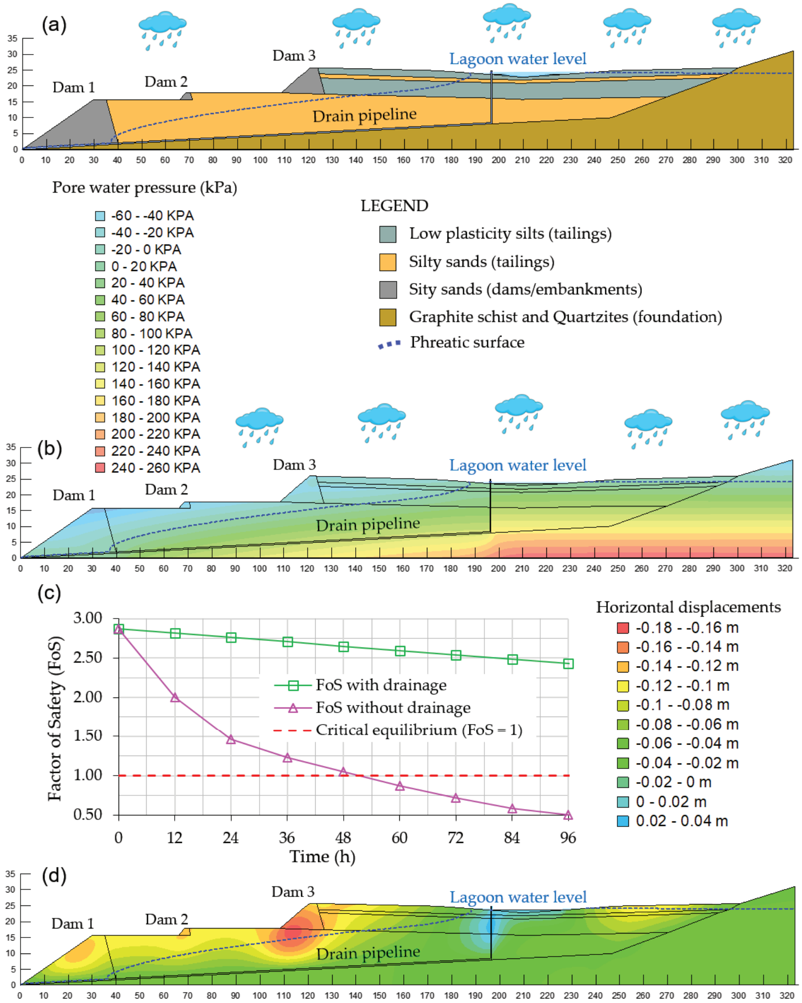

***Figure 3** Behaviour of the TSF Brunita with a sufficiently drainage system (a) conceptual model, (b) pore water pressure resulting from tailings saturation (time = 48 h), (c) comparison of the safety factor of tailings dam 1 for the case with and without drainage, (d) displacements computed in TSF (time = 48 h).*

comply with the regulations) that could not handle the water from the rains. Key points:

- Poor drainage: The rains increased the water pressure in the tailings, reducing their strength, causing slope instability and ultimately flow failure. Moreover, the drainage system consisting only of subsurface drains (that not comply with the drainage design regulations) was not sufficient to evacuate water from the deposit. The drains might have clogged/break at some point, causing seepage through the face of the tailings facility. Hence, the usage of only subsurface rigid drains should be discouraged from being used.
- Sufficient and efficient drainage: A good drainage system may keep the slopes unsaturated and provides a high safety factor, even during extreme rainfall. Although, the finite element method cannot predict piping around the drain, it is expected that piping that developed around the pipe was the cause of failure.
- Design and maintenance: It is essential to design and maintain adequate drainage system that should include more elements to evacuate water (impermeable membranes, drainage canals, tailings dewatering, etc.) to mitigate the risks of severe weather events, which are increasingly common due to climate change.

Acknowledgements

The authors thank to Ministry for Ecological Transition and Demographic Challenges (MITECO), Dirección General de Biodiversidad for funding this research: TD by PRTR Medida C04.I03 belonging to “Asesoramiento en actuaciones de restauración de zonas mineras en el entorno del Mar Menor” Project (Joanna Butlanska) and “Estudio de las materias primas críticas y estratégicas para la transición ecológica y el suministro de las principales cadenas de valor industrial en España” Project – MPMIN ref. 3263 (Aldo Onel Oliva-González). This work was also supported by grant PID2022-138197OB-100 funded by MICIU/AEI/10.13039/50100011033 and by ERDF/E (Jose Antonio Fernández-Merodo and Roberto Rodríguez-Pacheco).

References

Bishop AW, Morgenstern NR (1960) Stability coefficients for earth slopes. Géotechnique 10(4):129–150. doi:10.1680/geot.1960.10.4.129

GEOZONE, 2023. Estudio geofísico mediante tomografía eléctrica, polarización inducida y MASW para proyecto de remediación ambiental de residuos mineros y emplazamientos afectados por la minería en los TT. MM. de Cartagena – La Unión. Informe Técnico, GEOZONE ASESORES S.L. 2023, 115p.

HORYSU, 2023 Sondeos exploratorios con pruebas de penetración estándar y ensayos de laboratorio para estudio geológico y geotécnico en la cuenca del Mar Menor, La Unión, Murcia. LABORATORIOS HORYSU Inversiones de Murcia, S.L.

Martín-Crespo T, Gómez-Ortiz D, Martín-Velázquez S, Martínez-Pagán P, De Ignacio C, Lillo J, Faz A (2018) Geoenvironmental characterization of unstable abandoned mine tailings combining geophysical and geochemical methods (Cartagena-La Union district, Spain). Engineering Geology 232:135—146. doi:10.1016/j.enggeo.2017.11.018

Martínez-Pagán P, Faz A, Acosta JA, Carmona DM, Martínez-Martínez S (2011) A multidisciplinary study for mining landscape reclamation: A study case on two tailing ponds in the Region of Murcia (SE Spain). Physics and Chemistry of the Earth, Parts A/B/C 36(16):1331—1344. doi:10.1016/j.pce.2011.02.007

MIN (1972). Informe sobre accidente ocurrido en el dique de estériles del lavadero “Brunita”, propiedad de la Empresa Eloy Celdrán Conesa, en término municipal de la Unión (Murcia). Ministerio de Industria.

Moreno-Perales A (2016) Stability calculation of the “Brunita” tailings dam, La Unión, Murcia, Spain. Master's Thesis Polytechnic University of Cartagena.

Morgenstern NR, Price VE (1967) A numerical method for solving the equations of stability of general slip surfaces. Computer Journal 9(4): 388–393. doi:10.1093/comjnl/9.4.388

Rodríguez R (2006) Hydrogeotechnical characterization of a metallurgical waste. Canadian Geotechnical Journal 43(10): 1042–1060. doi:10.1139/t06-061

Rodríguez R, García-García C, Zarroca M, Roqué C, Linares R, Oldecop L (2011) Características geológicas y geotécnicas de los lodos de flotación de la Sierra Minera de Cartagena-La Unión (SE España). Boletín Geológico y Minero 122 (2).

SEEP/W (2012). Seepage Modeling with SEEP/W. An Engineering Methodology. March 2012 Edition. GEO-SLOPE International Ltd. Alberta, Canada.

SLOPE/W (2012). Stability Modeling with SLOPE/W. An Engineering Methodology (July 2012 edition), GEO_SLOPE Internacional Ltd, Alberta, Canada, p. 246.

SIGMA/W (2013). Stress-Deformation Modeling with SIGMA/W. An Engineering Methodology (July 2013 edition), GEO_SLOPE Internacional Ltd, Alberta, Canada, p. 223.

Screening-Level Economic Evaluation of Critical and Strategic Raw Materials stored in Iberian Pyrite Belt Pit Lakes, Spain

Devin Castendyk[1], Skyler Sorsby[2], Javier Sánchez-España[3]

[1]WSP USA Inc., 7245 West Alaska Drive, Suite 200, Lakewood, Colorado, 80226, USA,
devin.castendyk@wsp.com, ORCID 0000-0002-8150-5566

[2]WSP USA Inc., 10 Lake Center Drive, Suite 205, Marlton, New Jersey, 08053, USA,
skyler.sorsby@wsp.com, ORCID 0000-0003-4612-3199

[3]Centro de Astrobiología, Spanish National Research Council (CSIC), Carretera de Ajalvir, Km 4,
Torrejón de Ardoz, 28850 Madrid, Spain, jsanchez@cab.inta-csic.es, ORCID 0000-0001-6295-1459

Abstract

The recovery of metals from pit lakes can potentially generate circular economies, improve water quality, provide critical materials, and demonstrate corporate investments in Environmental-Social-Governance objectives. A screening-level assessment of copper recovery from thirteen pit lakes in the Iberian Pyrite Belt, Spain, using copper cementation, solvent extraction-electrowinning and sulfide precipitation extraction methods, found copper cementation from Corta Atalaya could generate approximately €14.9 million over 5.8 years after a combined expenditure of €12.5 million. The approach used a novel, artificial intelligence, Pit Lake Decision Tool to calculate returns. The Tool can be used to prospect for metal recover from pit lakes.

Keywords: Pit lakes, copper recovery, return on investment, AI, Iberian Pyrite Belt stratification, lessons learned

Introduction

Pit lakes that store large volumes of acid rock drainage and metal leachate may provide unique opportunities for the recovery of critical raw materials (CRMs) and strategic raw materials (SRMs). Researchers in Spain have been exploring opportunities to recover CRMs and SRMs from historic mine tailings, waste rock, and mine water to prompt domestic production, clean up abandoned mine sites, build circular economies and reduce national supply chain risks (Rosario-Beltré *et al* 2023). This work includes acidic pit lakes of the Iberian Pyrite Belt (IPB), Spain (Fig. 1) which have been studied for potential metal recovery for nearly two decades (Sánchez España *et al* 2008), notably, Corta Atalaya Pit Lake (Santofimia *et al* 2023), which has high concentrations of dissolved cobalt, copper, nickel and zinc (Table 1). The European Union identifies cobalt as a CRM and copper and nickel as SRMs.

Conceptually, the extraction of CRMs and SRMs from pit lake water may be less energy intensive and have a lower carbon footprint than extraction from tailings or waste rock which require mechanical excavation, haulage, and potentially, regrinding. Instead, lake water with high dissolved concentrations of metals can be pumped to a dedicated metal recovery facility. Recovery options for copper include: cementation, ion exchange, electrowinning, solvent extraction-electrowinning and sulfide precipitation. The operational life of the metal recovery facility is proportional to the volume stored in the lake plus the volume stored in flooded historic workings that are hydrogeologically connected to the pit lake.

Montana Resources (MR) used copper cementation to recover copper from the Berkeley Pit Lake in Montana, USA, from 1998 to 2013 (Gammons and Icopini 2020). This process lowered the average concentration of dissolved copper from approximately 180 mg/L to 50 mg/L and may be the first reported example of metal recovery from pit lake water. Over the ten-year period from 2003 to 2013, MR recovered 15 million kg of copper using this process, worth an estimated €126 million today. Sánchez-España *et al* (2022) demonstrated copper cementation to be the most efficient Cu-recovery method for acid mine waters in the IPB. Other recovery operations for zinc, copper and rare earth elements are currently being investigated at two pit lakes in former open pit copper mines in the western United States (Castendyk *et al* 2025).

For stakeholders to consider metal recovery options, at a minimum, the expected return on investment (ROI) must be positive, meaning the revenue generated must exceed the combined capital expenses (CAPEX) and operational expenses (OPEX) over the duration of the project. Whereas several studies identify CRMs and SRMs in mine wastes, few studies report the expected ROI from these operations, which can generate unrealistic expectations.

This study presents a screening-level approach to estimate the stored value of CRMs and SRMs in pit lakes and to estimate the ROI for copper recovery. The approach uses a novel, artificial intelligence (AI) application, called the Pit Lake Decision Tool (PLDT), to estimate ROI. We demonstrate the approach for thirteen acidic (pH<5) IPB pit lakes, provide an analysis for Corta Atalaya Pit Lake, and recommend "next steps" for pit lakes passing the screen tool.

Method

The screening approach has three steps: (1) Estimate the mass and current value stored in the pit lake. If the metal value is ≥ €10 million, proceed to Step 2; (2) Compare the stored metal mass in the pit lake to the mass stored in an equivalent volume of Earth's crust. If the mass stored is ≥ 2× crustal mass, proceed to Step 3; and (3) Estimate the ROI over time. Lakes that generate a positive ROI and cross the break-event point within a reasonable period (e.g., 2 years) pass the screening process and should be further investigated (see Discussion). Thirteen pit lakes in the IPB listed in Table 1 were screened for potential copper recovery using these steps.

The first step uses available pit lake volumes (m^3) and published dissolved metal concentrations (mg/L) (Table 1) to calculate the mass (kg) stored in pit lake water. Lake volume is best derived from a high-resolution stage-storage relationship produced from a recent bathymetric survey of the pit lake or from the mine plan at the time of closure

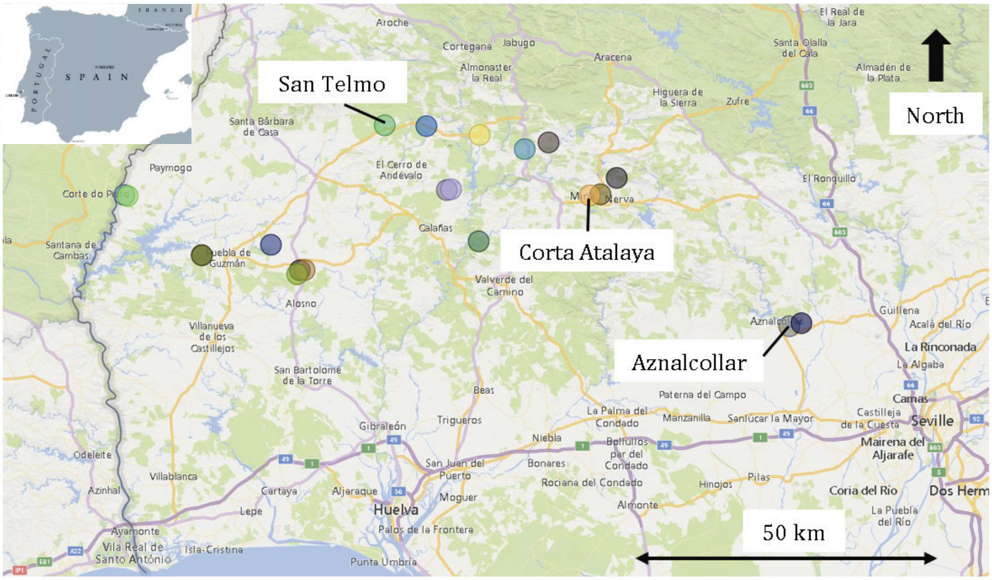

Figure 1 Map of Southwest Spain showing 20 pit lakes (colored circles) in the Iberian Pyrite Belt.

(provided no pit wall failures or mine waste deposition has occurred over time). In the absence of these data, an approximate volume can be generated using the surface area and maximum depth assuming the pit lake has the geometry of a right-circular cone.

If published metal concentrations are not available, concentrations (specifically, copper) can be estimated via the PLDT using a tree-based ensemble machine-learning method (XGboost) applied to the International Network for Acid Prevention (INAP), Pit Lakes Database (Richards and Castendyk 2024) and other data sources. The Database contains chemical analyses from >2,600 water samples collected from over 270 pit lakes located in 25 different ore deposit types. These data are used to predict dissolved copper concentrations in surface waters around the world. The fitted machine-learning model predicts low, best-fit, and optimistic copper concentrations for a user-selected pit lake which informs the initial stored metal mass estimate for the ROI calculations. The current commodity price (€/kg) is multiplied by the stored mass and a recovery efficiency factor (assumed to be 95%) to estimate the present-day stored value.

In Step 2, the mass of each metal stored in pit lake water is compared against the mass stored in an equivalent volume of rock at a concentration equal to the average crustal abundance on Earth. We assumed a bulk rock density of 2,600 kg/m^3 and a copper concentration of 68 ppm (https://periodictable.com/Properties/A/CrustAbundance.al.html; March 31, 2025).

In Step 3, the PLDT is used to estimate the ROI for various copper recovery methods using the machine-learning derived estimates of low, best-fit, and optimistic concentrations as initial estimates. To calculate the ROI over time, the user selects the predicted copper concentrations or provides an observed concentration. The user also provides the lake volume, a realistic influent flow rate to the recovery system (e.g., 750 gal/min or 0.047 m^3/sec), and a realistic recovery period (e.g., ≈10 years) for operations. Finally, the user selects the copper recovery method from a drop-down list which currently includes: cementation (C), solvent extraction-electrowinning (SX-EW), chemical sulfide precipitation (CSP), and biological sulfide

***Table 1** Properties of thirteen acidic pit lakes in the Iberian Pyrite Belt.*

Name	Area	Depth	Volume	pH	Co	Cu	Ni	Zn
	Ha	m	m^3		mg/L	mg/L	mg/L	mg/L
Corta Atalaya[1]	16	106	5.8E + 06	2.2-2.8	27	405	6	5,500
Filon Centro[2]	3.8	40	6E + 05	2.4	1.4	17	0.8	33
Confesionarios[2]	2.48	80	1E + 06	2.5	2.7	2	0.1	7
Pena del Hierro[2]	1.87	>50	*3.1E + 05*	2.5	0.7	5	0.0	22
Ntra. Sra. Del Carmen[2]	0.7	32	1E + 05	2.5	1.0	19	0.4	5
La Zarza-W[2]	1.77	>40	*2.4E + 05*	2.6	6.0	151	5.0	207
Cueva de la Mora[2]	1.78	40	3E + 05	2.6	1.1	8	0.5	17
La Zarza-E[2]	0.7	>40	*9.3E + 04*	2.6	2.5	80	2.5	102
Herrerias I[2]	0.81	50	2E + 05	2.8	2.2	25	1.8	101
San Telmo[2]	14.36	107	7E + 06	2.9	0.9	21	0.5	89
Concepcion[2]	1.2	15	4E + 5	3.0	0.9	10	0.1	28
Aznalcollar[2]	28.4	38	6E + 06	3.6	6.7	35	2.6	834
Hererias II[2]	1.42	15	1E + 5	4.7	1.1	8	0.9	27

[1] Volume and monimolimnion chemistry from Santofimia *et al* (2023)

[2] Volumes from Sánchez España *et al* (2009); surface water chemistry from Sánchez España *et al* (2008)

Italicized volumes were estimated assuming a circular surface area and geometry of a right-circular cone precipitation (BSP). The PLDT stores default scalable CAPEX (linked to pump rate) and fixed and variable OPEX for each method based on costs for similar projects in the western United States (Table 2).

The PLDT calculates the daily ROI in US dollars (USD) over time using the market value of the commodity in today's prices minus the CAPEX and cumulative OPEX. Of importance, the Tool identifies the break-even point (ROI = $0; ignoring inflation) and the net gain/loss over the duration of recovery. Pit lakes worth further investigation will exceed the break-even point within the first few years and show an initial increase in ROI with time.

Results

Table 3 lists IPB pit lakes (from Table 1) that store over €1 million in cobalt, copper, nickel and zinc. Consistent with work by Santofimia *et al* (2023), this study finds that Corta Atalaya Pit Lake has the most potential for metal recovery among IPB pit lakes, storing approximately €20 million in copper and over €118 million in combined metals. Although not listed as a CRM or SRM, zinc makes up 80% of the stored value in Corta Atalaya Pit Lake. The second and third most valuable IPB pit lakes are Aznalcollar Pit Lake, which stores €18 million in combined metals, and San Telmo Pit Lake, which stores €3 million in combined metals. Corta Atalaya Pit Lake was the only pit lake in Table 1 to store over €10 million in copper and was advanced to Step 2.

With a volume of 5.8 million m^3, Corta Atalaya Pit Lake stores approximately 2.3 million kg of copper. An equivalent volume of average Earth's crust with a copper concentration of 68 mg/kg would store approximately 1 million kg of copper. With 2.3 times more copper mass stored compared to an equal volume of average crustal rock, Corta Atalaya was advanced to Step 3.

Fig. 2 compares the estimated ROI (in $US millions) over a fifteen-year period for Corta Atalaya Pit Lake using four methods generated by the PLDT: C, SX-EW, CSP and BSP. Design criteria assumed an initial copper concentration of 405 mg/L (Table 1) and a pump rate of 0.047 m^3/sec. Copper-depleted effluent from the recovery process is assumed to return to the pit lake, resulting in an overall decrease in stored copper concentration (and value) with time.

This analysis shows that copper cementation is likely to generate a profit for 5.8 years. The CAPEX for plant startup would be $4.1 million USD (Table 2). The value of copper produced would exceed the CAPEX plus cumulative annual OPEX over the first 5.8 years, increasing the net ROI over time. After approximately two years of operation, the value of copper recovered would equal the combined value of CAPEX plus cumulative OPEX, called the "break-even point." At 5.8 years of operations, the value generated from

Table 2 *Costs in $USD millions for copper recovery at 750 gallons/minute (Castendyk et al 2025).*

Cost	C	SX-EW	CSP	BSP
CAPEX	$4.1	$28.5	$4.3	$7.8
OPEX (annual)	$1.6	$3.1	$8.5	$3.7

Table 3 *IPB pit lakes storing over €1 million in CRMs, SRMs and zinc, assuming 95% recovery.*

Name	Co	Cu	Ni	Zn
	(€21.87/kg)[1] € million	(€8.87/kg)[1] € million	(€14.99/kg)[1] € million	(€3.14/kg)[1] € million
Corta Atalaya	3.3	20	0.5	95
San Telmo	0.1	1	-	2
Aznalcollar	0.8	2	0.2	15

[1] Commodity prices from London Stock Exchange Global (LSEG), September 9, 2024

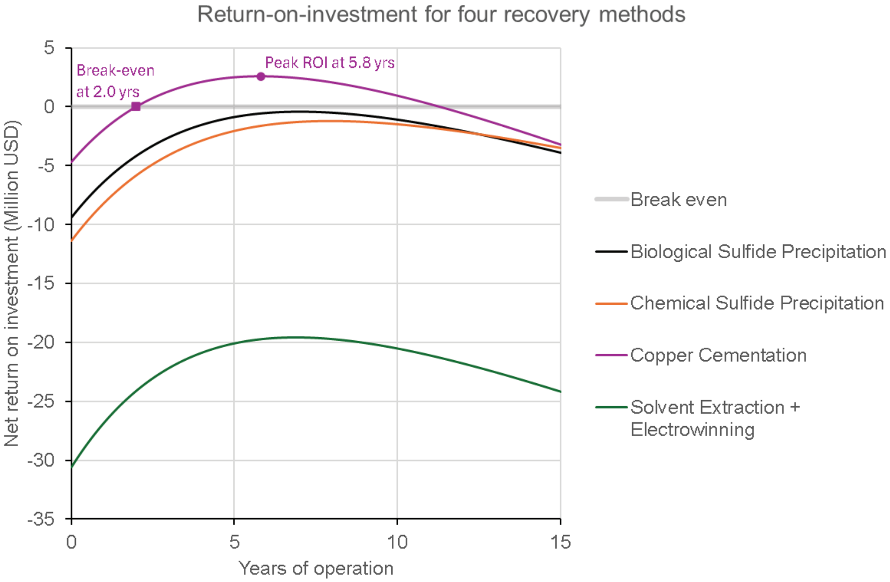

Figure 2 *Estimated net ROI using four different copper recovery methods at Corta Atalaya Pit Lake.*

copper recover would peak at approximately \$16.0 million USD (€14.9 million) after an expense (CAPEX and cumulative OPEX) of \$13.4 million USD (€12.5 million) for a peak ROI of \$2.6 million USD (€2.4 million). Beyond 5.8 years, the ongoing OPEX costs would exceed the value generated by continued copper recovery, eroding the net ROI over time. After 12 years of operations, the net ROI would reduce to zero.

The value of copper recovered using other methods also exceeds the annual OPEX over the first five to seven years. However, the initial CAPEX is significantly higher for these methods (Table 2) resulting in a large, negative ROI at time zero. As a result, the net ROI from these methods did not pass the break-even point, suggesting these methods may not be profitable at present time.

Discussion

When applied to thirteen pit lakes in the IPB, the screening tool found that one pit lake, Corta Atalaya (the biggest and most metal-rich pit lake in this mining district) has the potential to generate a positive ROI using copper cementation methods. For ESG benefits, circular economy development, and resource resiliency, some stakeholders may be willing to invest in copper recovery even if the net ROI is low. For other methods (SX-EW, CSP, BSP), the ROI produced from metal recover did not pass the break-even point, which makes metal recovery less interesting for stakeholders.

In addition to costs, there are two important differences between the copper recovery methods considered: the form of the final product and effluent pH. Although initially more expensive, SX-EW produces a salable product of nearly 99.5% pure copper, whereas copper cementation and sulfide precipitation produce concentrates that must be sent to a smelter for refinement. Smelter costs decrease the ROI of both cementation and sulfide precipitation methods. The sulfide precipitation process decreases the pH of the process effluent, whereas SX-EW and copper cementation have little impact on pH. Treatment of acidic effluent can increase the cost of sulfide precipitation unless effluent is directly discharged back to the pit lake.

For stratified, meromictic pit lakes like Corta Atalaya, copper-rich water stored in the deep layer (monimolimnion) could be pumped to the copper recovery plant and copper-depleted water could be returned to the shallow layer (mixolimnion). This could ensure a (more or less) constant copper concentration in influent to the recovery plant over the first few years of operation.

It may be possible to combine copper recovery with the recovery of additional metals to increase the value obtained from a pit lake. Castendyk *et al* (2025) discuss a plan for a pit lake in the United States where copper will be recovered by cementation, followed by the precipitation of aluminum hydroxide by titration, followed by the recovery of zinc by ion exchange and sulfide precipitation. A similar process at Corta Atalaya could increase value by recovering zinc.

The volume of a pit lake is a critical factor influencing ROI. For Corta Atalaya Pit Lake, the analysis used copper concentrations for water in the monimolimnion, the deepest part of the pit lake (Santofima *et al* 2023). Because pit lakes have a cone-shaped bathymetry, where stored volume decreases with depth, the use of the monimolimnion concentration overestimates the stored mass and economic value of copper in Corta Atalaya Pit Lake. That said, most pit lakes in the IPB intersect historic workings which may store additional mass, such that lake volume alone may underestimate the value of the resource. Inclusion of the mass stored in connected mine workings, if applicable, would increase the estimated ROI.

The PLDT is shown to be a useful tool for rapid estimation of ROI from pit lakes, allowing the prospecting of metal recovery from pit lakes on a global scale. However, the CAPEX and OPEX used in the Tool are based on a similar pit lake in the western United States (Castendyk *et al* 2025) and require additional refinement to ensure applicability to Spain. Key factors include: electricity costs, distance from mine site to a smelter for the processing of concentrate, reagent costs, and environmental permitting. A detailed review of potential environmental effects, carbon footprint (from transportation), etc, would be needed as part of an advanced analysis. Future updates to the PLDT will include (1) provide CAPEX and OPEX for additional CRMs, SRMs and economic metals such as zinc, (2) factor inflation on initial CAPEX into ROI, and (3) add more copper recovery methods such as electrowinning and ion exchange.

For pit lakes that pass the three-step screening process presented here, the following "next steps" should be completed: (4) Collect a new water quality profile to verify concentrations and update the screening level estimate. Water samples should be collected at a high resolution (e.g., one sample per five meters depth) and/or a high-resolution profile of specific conductance should be collected and correlated to available metal concentrations to plot the metal concentration as a function of depth for the entire water column; (5) Define a high resolution stage-storage relationship for the pit lake using a recent bathymetric survey or mine plans; (6) Plot the incremental mass stored as a function of depth and sum to obtain the true stored value; (7) Conduct a desk-top study on available recovery methods to estimate site-specific costs; and (8) collect new samples and submit to a laboratory for a bench-scale study of copper recover using the most economical recovery method. This work would then lead to an advanced analysis and conceptual design for a copper recovery system. The authors hope this approach will facilitate more utilization of existing pit lake resources leading to improved ESG practices.

Conclusions:

A three-step screening method using a novel, AI-based, PLDT found that copper recovery from Corta Atalaya Pit Lake using copper cementation could potentially generate a positive ROI, leading to a circular economy and beneficial use for mine impacted water. The PLDT can be rapidly applied to other pit lakes to prospect for other metal recovery opportunities.

Acknowledgements

The authors thank INAP for permission to use the Pit Lakes Database to develop the PLDT. We also thank WSP for support to develop the PLDT, and Robert Kimball (WSP), Jack Lindauer (WSP), Bridgette Hendricks (WSP) and Alan Drake (Wood PLC) for technical discussions.

References

Castendyk D, Kimball R, Lindauer J (2025) Metal recovery from pit lakes; prospecting, ROI and ESG. Proc 2025 Soc Mining, Metallurgy and Exploration, Annu Conf & Expo, Denver, Colorado

Gammons CH, Icopini GA (2020) Improvements to the water quality of the acidic Berkeley pit lake due to copper recovery and sludge disposal. Mine Water and the Environment 39:427-439

Richards A, Castendyk D (2024) Update to the INAP Pit Lakes Database. Proc International Conference on Acid Rock Drainage, ID 153, Halifax, Nova Scotia

Rosario-Beltré AJ *et al* (2023) Critical Raw Materials recovery potential from Spanish mine wastes: A national-scale preliminary assessment. Journal of Cleaner Production 407: 137163

Sánchez España J, López Pamo E, Diez M, Santofimia E (2009) Physico-chemical gradients and meromictic stratification in Cueva de la Mora and other acidic pit lakes of the Iberian Pyrite Belt. Mine Water Environ 28(1):15-29

Sánchez España J, López Pamo E, Santofimia Pastor E, Diez Ercilla M (2008) The acidic mine pit lakes of the Iberian Pyrite Belt: an approach to their physical limnology and hydrogeochemistry. App Geochem 23: 1260-1287

Sánchez-España, J.; Ilin, A.; Yusta, I. (2022) Metallic Copper (Cu[0]) Obtained from Cu^{2+}-Rich Acidic Mine Waters by Two Different Reduction Methods: Crystallographic and Geochemical Aspects. Minerals 2022, 12, 322

Santofima E, Rincón-Tomás B, López-Pamo E, González F, Amils R (2023) Geochemical and limnological characterization of the Corta Atalaya Pit Lake (Riotinto Mines, Spain). Mater Proc 15(1), 66

The Treatment Strategies of Acid Mine Drainage Based on Resource Utilization

Mengfang Chen, Hongping Chen, Yulu Ai, Yudong Feng, Jing Li

State Key Laboratory of Soil and Sustainable Agriculture, Institute of Soil Science,
Chinese Academy of Sciences, Nanjing 210008, China

Abstract

Acid mine drainage (AMD) poses major environmental challenges due to its acidity, high sulfate, and metal concentration. This study developed multifunctional remediation materials using natural attapulgite and alkaline residues, enhancing the performance of constructed wetlands (CWs). The materials improved sulfate and metal ion removal, stabilized pollutants, and supported microbial communities, enabling long-term treatment efficiency. In-situ mineralization further converted AMD into valuable layered double hydroxides (LDHs), aiding arsenic (As) and antimony (Sb) fixation. This low-cost, sustainable approach offers promising applications for AMD remediation and industrial wastewater management, advancing green solutions for environmental protection.

Keywords: Acid mine drainage, constructed wetlands, layered double hydroxides, arsenic, antimony

Introduction

Acid mine drainage (AMD) is a persistent environmental issue caused by the oxidative leaching of sulfide minerals in mining residues such as tailings, waste rocks, and underground excavations (Kefeni *et al.* 2017). It is characterized by strong acidity, high sulfate concentrations, and elevated levels of toxic metal(loid)s (Nordstrom *et al.* 2015). Globally, AMD has severely affected water resources and ecosystems, with regions like the United States, Australia, and China facing widespread contamination due to abandoned mines (Kefeni *et al.* 2017). This widespread pollution emphasizes the urgent need for effective and sustainable AMD remediation technologies.

Traditional AMD treatment methods are classified into active and passive systems (Johnson and Hallberg 2005). Active treatments, such as chemical neutralization using lime or sodium hydroxide, are effective but often incur high operational and maintenance costs (Naidu *et al.* 2019). In contrast, passive systems like constructed wetlands (CWs) offer low-cost, energy-efficient alternatives (Skousen *et al.* 2017). However, the extreme acidity and high concentrations of metals and sulfates in AMD can harm plants and microorganisms in CWs, reducing their treatment efficiency if not properly pre-treated. Therefore, optimizing CW configurations to improve their tolerance and purification capacity for AMD is of great scientific and practical importance.

Substrate optimization is a critical factor in improving CW performance. Organic carbon sources and inorganic media not only provide microbial attachment sites but also facilitate pollutant removal through adsorption, filtration, and complexation (Sheoran and Sheoran 2006). However, few studies have focused specifically on optimizing inorganic media in CWs. Conventional materials such as gravel and sand mainly serve to trap larger particles but are largely ineffective in removing metals and sulfate from AMD. Therefore, incorporating multifunctional materials with superior properties presents a promising strategy to improve CW efficiency in AMD treatment. In our previous studies (Chen *et al.* 2022), attapulgite-soda residue (ASR) composites showed strong metal removal and acid neutralization capacities. Combining ASR with organic carbon sources as CW substrates is expected to enhance the simultaneous removal of sulfate, metals, and acidity. However, it remains unclear whether ASR can alleviate AMD-induced stress on plants and microorganisms within CWs. Moreover, further research is needed to clarify whether pollutant removal in ASR-based CWs is driven primarily by substrate adsorption or microbial metabolism.

Although AMD is widely recognized as a major pollution source, it is also a potential resource for valuable metal ions and sulfates (Hedrich and Johnson 2014). Harnessing AMD for resource recovery aligns with the principles of green and sustainable remediation. Studies have shown that under actual mining conditions, layered double hydroxides (LDHs)-a type of secondary mineral-can form naturally in AMD-impacted rivers (Chikanda *et al.* 2021). LDHs are considered promising adsorbents for oxygen-containing anions such as arsenate, antimonate, and chromate, owing to their high surface area, abundant hydroxyl groups, and excellent anion exchange capacity (Fang *et al.* 2021). However, most LDH synthesis methods rely on pure chemical reagents, leading to high material costs and limiting their large-scale application in water remediation (Maziarz *et al.* 2019). Given its composition, AMD can serve as a low-cost source of sulfate, Fe, Mg, and Mn for synthesizing sulfate-intercalated iron-based LDHs, potentially reducing production costs significantly. Nevertheless, the synthesis of such LDHs directly from field AMD, as well as their mechanisms for As and Sb removal, remain largely unexplored.

This study aims to develop multi-functional remediation materials by combining natural attapulgite with industrial by-product alkaline residues, evaluate their effectiveness in enhancing sulfate and metal removal, stabilizing pollutants in AMD, and supporting microbial communities in CWs. Additionally, the study explores the in-situ formation of LDHs from AMD for direct immobilization of As and Sb, providing insights into pollutant removal mechanisms and contributing to sustainable strategies for AMD remediation and resource recovery.

Methods

Materials: Attapulgite was sourced from Xuyi County, Jiangsu Province, China, and soda residue SR, a by-product of the ammonia-soda process, was obtained from Lianyungang, Jiangsu Province. The ASR composites were prepared by mixing attapulgite and SR at a 5:5 ratio with 7.5% sodium carbonate as a binder, followed by granulation, drying at 105 °C for 12 h, and calcination at 450 °C for 2 h. AMD samples were collected from a pyrite mine in Sichuan Province, China. The AMD exhibited high sulfate (2198 mg L^{-1}) and metal concentrations (Fe 268 mg L^{-1}, Mn 66.4 mg L^{-1}, Cu 91.7 mg L^{-1}, Zn 79.8 mg L^{-1}, Cd 4.28 mg L^{-1} and Pb 0.33 mg L^{-1}) with pH 2.08.

Construction and operation of laboratory-scaled CWs: Laboratory-scale horizontal subsurface flow constructed wetlands (HSSF-CWs) were set up in a net house in Nanjing, China, under uncontrolled environmental conditions to simulate real scenarios. Each CW consisted of a polypropylene box (57 × 26 × 42 cm) with a water inlet and outlet, filled in layers: coarse gravel, fine gravel or ASR composites mixed with organic fertilizer (2:1, v/v), soil, and overlying water. Nine *Typha* seedlings were planted in each CW after a 4-week acclimatization period. CW systems operated for 9 months in continuous flow mode with a hydraulic retention time (HRT) of 7 days. Influent and effluent water samples were collected weekly to measure pH using pH probes, and sulfate and metal concentrations using ion chromatography and inductively coupled plasma optical emission spectrometry (ICP-OES) after filtration and acidification. Soil and substrate samples were analysed post-experiment for total and chemical fractions of metals using a modified BCR sequential extraction method (Wang *et al.* 2019), X-ray diffraction (XRD), and ICP-OES. Plant photosynthetic pigments, catalase (CAT), peroxidase (POD), superoxide dismutase (SOD), and malondialdehyde (MDA) were measured spectrophotometrically. Metal concentrations in plant tissues were measured by ICP-MS. Substrate DNA was extracted for microbial community analysis via 16S rRNA sequencing. OTUs were clustered (97% similarity), and species were annotated using the RDP classifier.

Resource utilization of field AMD: Sulfate and metal ions from field-collected

AMD were used to synthesize LDHs for the direct immobilization of As and Sb within the AMD matrix. In-situ immobilization was carried out via coprecipitation in a four-necked flask. AMD samples (200 mL) containing 10.6 mg L^{-1} Sb and 7.8 mg L^{-1} As were mixed with 0.8 M NaOH under vigorous stirring at 40 °C, maintaining a pH of 8.8-9.3. The resulting As- and Sb-loaded LDHs were separated, thoroughly cleaned, freeze-dried, and analyzed. Elemental composition was analyzed by ICP-MS, crystal structures by XRD, and morphology by scanning/transmission electron microscopy (SEM/TEM). Functional groups were identified using Fourier transform infrared spectroscopy (FTIR), surface area was measured via nitrogen adsorption–desorption, and surface binding energies were examined by X-ray photoelectron spectroscopy (XPS). Additionally, density functional theory (DFT) calculations were performed to explore the interactions of As and Sb with LDHs, with particular focus on anion exchange mechanisms and the potential formation of brandholzite.

Results and Discussion

Performance of CWs for AMD treatment: The effluent pH of constructed wetlands filled with gravel (CWs-G, as the control) ranged from 5.5 to 6.1 (average 5.9) during the first 200 days but gradually declined to 4.5 afterward (Fig. 1a). The sulfate concentration showed an inverse trend, decreasing from 2096 to 1161 mg L^{-1} initially but rising to 1569 mg L^{-1} after 200 days, with an average removal efficiency of 42% (Fig. 1b). High sulfate concentrations (> 2000 mg L^{-1}) have been a major challenge in AMD treatment (Fernando *et al.* 2018). Removal efficiencies for Fe, Mn, Cu, Zn, Cd, and Pb were 88%, 26%, 71%, 77%, 64%, and 60%, respectively (Fig. 1c-h). These results indicate that traditional constructed wetlands (filled with gravel and organic substrates) have limited long-term purification efficiency for AMD. In comparison, constructed wetlands filled with ASR composites (CWs-ASR) exhibited a higher effluent pH, consistently ranging from 7.7 to 8.4 throughout the operation period (Fig. 1a), meeting the pH requirement of China's Integrated Wastewater Discharge Standard (6 < pH < 9). Furthermore, sulfate removal efficiency substantially improved to 72%, and the removal efficiencies of all six metals exceeded 96% (Fig. 1), with concentrations meeting the Class I limits of the same standard.

Removal pathway of metals in CWs: Except for Fe and Mn, metal concentrations in wetland substrates were obviously higher than those in surface soil. In CWs-G substrates, the concentrations of Fe, Mn, Cu, Zn, Cd, and Pb were 5147, 599, 2864, 1540, 213, and 103 mg kg^{-1}, respectively (Fig. 2). The addition of composites to the substrate in CWs-ASR substantially enhanced the

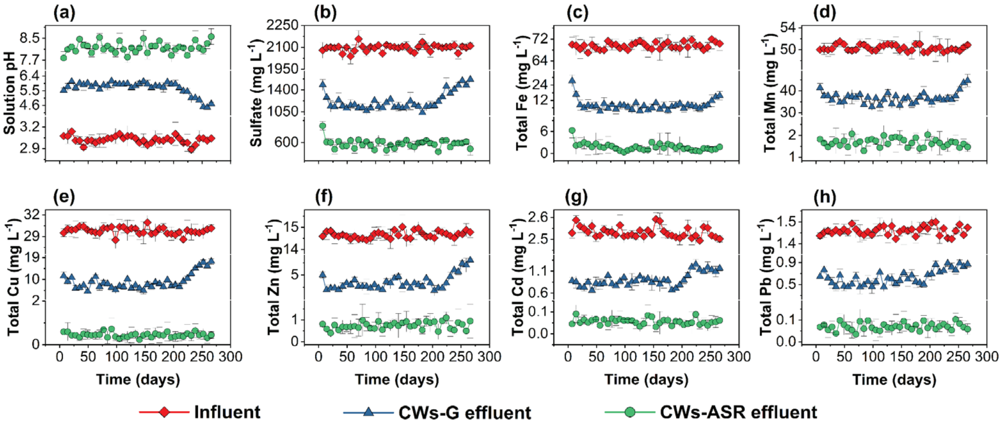

Figure 1 *Temporal variations of pH (a) and concentrations of sulfate (b), total Fe (c), Mn (d), Cu (e), Zn (f), Cd (g) and Pb (h) in different CWs during the whole experiments.*

removal of all metals, increasing Fe, Mn, Cu, Zn, Cd, and Pb concentrations to 6055, 2304, 4092, 2053, 329, and 172 mg kg^{-1}, respectively, representing increases of 18-285% compared to CWs-G (Fig. 2). Sequential extraction analysis revealed changes in the chemical forms of metals in soil and substrate. In CWs-G, metals primarily existed as exchangeable (14-36%), carbonate-bound (11-17%), Fe-Mn oxide-bound (31-56%), and organic/sulfide-bound forms (9-28%) (Fig. 2). However, in CWs-ASR, exchangeable metals were reduced to 1–5%, while metals associated with carbonates (19-32%) and organic/sulfides (29-34%) substantially increased (Fig. 2). Compared to CWs-G, plants in CWs-ASR exhibited substantially lower metal contents in both roots and shoots. These results indicate that the addition of composites substantially reduces the bioavailability of metals, consistent with findings from sequential extraction.

Responses of plants and microorganisms in CWs: The response of plants to AMD stress was evaluated by analyzing changes in photosynthetic pigments and biochemical indicators in CWs-G and CWs-ASR. As shown in Fig. 3a, the concentrations of photosynthetic pigments in CWs-G plants, including chlorophyll a (1.73 mg g^{-1}), chlorophyll b (0.62 mg g^{-1}), and carotenoids (0.52 mg g^{-1}), were substantially lower than those in CWs-ASR plants (2.45, 0.93, and 0.78 mg g^{-1}, respectively). Similar trends were observed in the activities of SOD, CAT, and POD (Fig. 3b-d). Specifically, SOD (78.24 U g^{-1}), CAT (43.21 U g^{-1}), and POD (32.46 U g^{-1}) activities in CWs-G plants were markedly lower than those in CWs-ASR plants, which reached 114.56, 65.34, and 36.17 U g^{-1}, respectively. These differences indicate that plants in CWs-G experienced abiotic damage when exposed to AMD (Jia *et al.* 2020), whereas the application of composites in CWs-ASR alleviated this abiotic stress.

The microbial community diversity was higher in CWs-ASR, indicating that the application of composites promoted microbial growth, which contributed to the improved AMD treatment performance in CWs-ASR. The abundance of Proteobacteria, closely associated with sulfur cycling due to

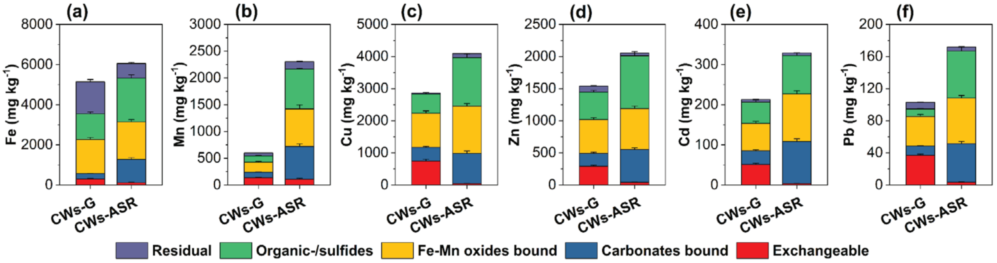

Figure 2 *Metal speciation in the CWs substrates determined by sequential extraction.*

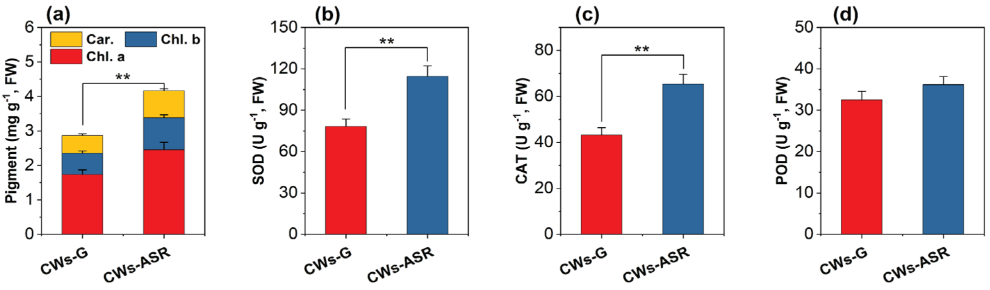

Figure 3 *Variations of physiological indexes of wetland plants in different CWs, including photosynthetic pigments (a), SOD (b), CAT (c) and POD (d).*

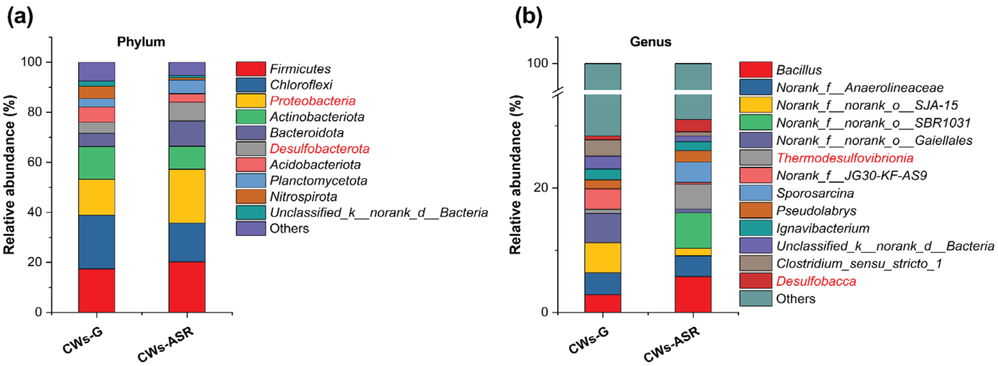

Figure 4 *Percentages of community abundance in different CWs at phylum (a) and genus (b) levels.*

its sulfate-reducing species (Jia *et al.* 2022), was higher in CWs-ASR (21.5%) compared to CWs-G (14.3%) (Fig. 4a). Additionally, the relative abundance of *Desulfobacterota*, critical for sulfate and metal removal (Jia *et al.* 2022), was greater in CWs-ASR (7.5%) than in CWs-G (4.4%) (Fig. 4a). At the genus level, CWs-ASR also exhibited a higher relative abundance of sulfate-reducing bacteria (SRB) (Fig. 4b). The Circos plot further highlighted the distribution of SRB genera across different wetlands. Besides *Thermodesulfovibrionia* and *Desulfobacca*, CWs-ASR had a greater relative abundance of *Desulfosarcinaceae, Desulfurivibrionaceae, Desulfatitalea,* and *Desulfosporosinus*, all of which are associated with sulfate reduction (Jia *et al.* 2022). In summary, the application of composites enhanced microbial diversity in CWs-ASR, and the increased abundance of these microorganisms likely played a key role in AMD treatment.

In situ immobilization of As and Sb containing AMD by forming LDHs: After inducing the formation of LDHs in AMD, the concentrations of Fe, Mg, sulfate, As, and Sb decreased from initial values of 1690, 1524, 2055, 7.8, and 10.6 mg L^{-1} to 1.3, 12.4, 623, 0.006, and 0.004 mg L^{-1}, achieving reduction rates of 69.7–99.9%. Both As and Sb concentrations in the treated AMD were below the limits set by China's drinking water standards (GB 5749-2022). The desorption and TCLP tests showed dissolution rates of Fe, Mg, As, and Sb below 1%, indicating excellent chemical stability of the As/Sb-LDHs under both acidic and alkaline conditions, with controlled risks of secondary pollution. XRD analysis of As/Sb-LDHs revealed a hydrotalcite crystalline phase (Fig. 5a). Differences in interlayer spacing were attributed to variations in the ionic radii of sulfate, As, and Sb, suggesting partial replacement of interlayer sulfate by As and Sb (Fig. 5b). New peaks in the XRD spectrum of Sb-LDH corresponded to $MgSb_2(OH)_{12}\cdot 6H_2O$, indicating that surface Mg ions formed complexes with Sb (Fig. 5a). FTIR spectra of As-LDHs showed weakened intensities of S-O groups at 1116 cm^{-1} and -OH groups at 3456 cm^{-1}, alongside the appearance of an As-O band at 820 cm^{-1}, suggesting that As was captured by LDHs through complexation with -OH functional groups (Fig. 5c). In the O 1s spectra of As/Sb-LDHs, an additional As-O peak was observed, and the relative peak area of Fe/Mg-OH decreased from 49.4% to 32.3%, indicating Mg-OH bond breakage and the formation of $MgSb_2(OH)_{12}\cdot 6H_2O$ (Fig. 5d). A reduction in Fe $2p_3/_2$ and Fe $2p_1/_2$ binding energies post-reaction suggested Fe-OH bond cleavage and Fe-O-As bond formation (Fig. 5d). In coexisting conditions, Sb obviously interfered with the fixation of As by LDHs, while As had no notable effect on Sb fixation. DFT calculations showed that the formation energies (E_{form}) for Sb via anion exchange and complexation were substantially lower than those for As, indicating that Sb fixation on LDHs is more favorable and explaining Sb's interference with As fixation.

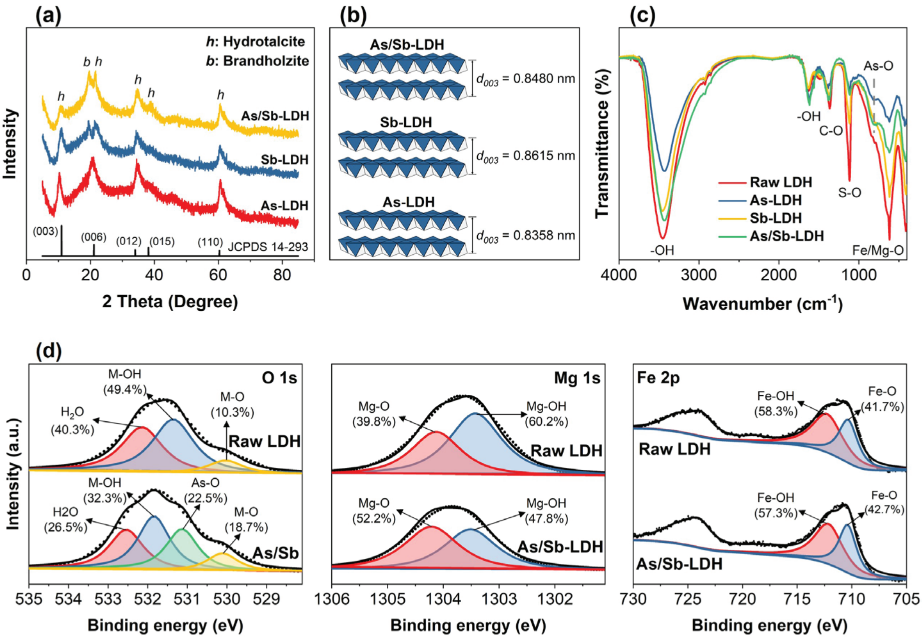

Figure 5 The X-ray diffraction patterns (a), interplanar spacing (b), FTIR spectra (c) and XPS spectra (d) of the LDHs loaded with As and/or Sb.

Conclusions

The application of ASR composites as substrates in CWs is a cost-effective and efficient method to improve AMD treatment. ASR composites neutralize AMD, reduce metal bioavailability, alleviate oxidative stress on wetland plants, and enhance microbial diversity. Sulfate-reducing bacteria (SRB) regenerates active sites on saturated ASR, further enhancing CW efficiency through synergistic adsorption and microbial sulfate reduction. The in-situ formation of LDHs in AMD is a simple and effective method for immobilizing As and Sb. The As- and Sb-loaded LDHs exhibit high chemical stability under acidic and alkaline conditions, minimizing secondary pollution risks. While Sb may interfere with As immobilization, LDH performance is largely unaffected by pH or coexisting ions. As is immobilized by anion exchange and complexation with -OH groups, whereas Sb interacts with Mg through ionic bonding. This innovative approach provides a practical solution for in-situ remediation of AMD from sulfate-rich, As- and Sb-contaminated abandoned mines.

Acknowledgements

The study was financially supported by the Natural Science Foundation of China (Grant No. 42207093) and the Natural Science Foundation of Jiangsu Province (Grant No. BK20210995). The authors thank all co-organisers for hosting the IMWA 2025 Conference.

References

Chen HP, Ai YL, Jia YF, Li J, Gu MY, Chen M (2022) Effective and simultaneous removal of heavy metals and neutralization of acid mine drainage using an attapulgite-soda residue based adsorbent. Sci Total Environ 843:157120. doi:10.1016/j.scitotenv.2022.157120

Chikanda F, Otake T, Koide A, Ito A, Sato T (2021) The formation of Fe colloids and layered double hydroxides as sequestration agents in the natural remediation of mine drainage. Sci Total Environ 774:145183. doi:10.1016/j.scitotenv.2021.145183

Fang QZ, Ye SJ, Yang HL, Yang KH, Zhou JW, Gao Y, Lin QY, Tan XF, Yang ZZ (2021) Application of layered double hydroxide-biochar composites in wastewater treatment: Recent trends, modification strategies, and outlook. J Hazard Mater 420:126569. doi:10.1016/j.jhazmat.2021.126569

Fernando WAM, Ilankoon IMSK, Syed TH, Yellishetty M (2018) Challenges and opportunities in the removal of sulphate ions in contaminated mine water: A review. Miner Eng 117:74-90. doi: 10.1016/j.mineng.2017.12.004

Hedrich S, Johnson DB (2014) Remediation and selective recovery of metals from acidic mine waters using novel modular bioreactors. Environ Sci Technol 48:12206-12212. doi:10.1021/es5030367

Jia LX, Liu H, Kong Q, Li M, Wu SB, Wu HM (2020) Interactions of high-rate nitrate reduction and heavy metal mitigation in iron-carbon-based constructed wetlands for purifying contaminated groundwater. Water Res 169:115285. doi:10.1016/j.watres.2019.115285

Jia YY, Wang PD, Ou YY, Yan YJ, Zhou SN, Sun LP, Lu H (2022) Insights into the microbial response mechanisms to ciprofloxacin during sulfur-mediated biological wastewater treatment using a metagenomics approach. Water Res 223:118995. doi:10.1016/j.watres.2022.118995

Johnson DB, Hallberg KB (2005) Acid mine drainage remediation options: A review. Sci Total Environ 338:3-14. doi:10.1016/j.scitotenv.2004.09.002

Kefeni KK, Msagati TAM, Mamba BB (2017) Acid mine drainage: Prevention, treatment options, and resource recovery: A review. J Clean Prod 151:475-493. doi:10.1016/j.jclepro.2017.03.082

Maziarz P, Matusik J, Straczek T, Kapusta C, Woch WM, Tokarz W, Radziszewska A, Leiviska T (2019) Highly effective magnet-responsive LDH-Fe oxide composite adsorbents for As(V) removal. Chem Eng J 362:207-216. doi:10.1016/j.cej.2019.01.017

Naidu G, Ryu S, Thiruvenkatachari R, Choi Y, Jeong S, Vigneswaran S (2019) A critical review on remediation, reuse, and resource recovery from acid mine drainage. Environ Pollut 247:1110-1124. doi:10.1016/j.envpol.2019.01.085

Nordstrom DK, Blowes DW, Ptacek CJ (2015) Hydrogeochemistry and microbiology of mine drainage: An update. Appl Geochem 57:3-16. doi: 10.1016/j.apgeochem.2015.02.008

Sheoran AS, Sheoran V (2006) Heavy metal removal mechanism of acid mine drainage in wetlands: A critical review. Miner Eng 19:105-116. doi:10.1016/j.mineng.2005.08.006

Skousen JG, Zipper CE, Rose A, Ziemkiewicz PF, Nairn R, McDonald LM, Kleinmann RL (2017) Review of passive systems for acid mine drainage treatment. Mine Water Environ 36:133-153. doi:10.1007/s10230-016-0417-1

Wang J, Wang PM, Gu Y, Kopittke PM, Zhao FJ, Wang P (2019) Iron-manganese (oxyhydro)oxides, rather than oxidation of sulfides, determine mobilization of Cd during soil drainage in paddy soil systems. Environ Sci Technol 53:2500-2508. doi: 10.1021/acs.est.8b06863

Geochemical Processes in Iron-Rich Mine Drainages: Enhancing Passive Treatment Systems through Colloid Stability and CO Reduction

Frances Chikanda[1,2], Hajime Iwaki[1], Hkaung Htut San[1], Ryosuke Kikuchi[1],
Yoko Ohtomo[1], Tsubasa Otake[1], Tsutomu Sato[1]

[1]Division of Sustainable Resources Engineering, Hokkaido University, 006-0080, Sapporo, Japan, franceschikanda2@eng.hokudai.ac.jp, ORCID 0000-0003-2596-274 iwaki.hajime.k7@elms.hokudai.ac.jp; hkaunghtut.earthlover@gmail.com, ORCID 0009-0001-2984-646X; rkikuchi@eng.hokudai.ac.jp, OCRID 0000-0001-7151-0735; ohtomoy@eng.hokudai.ac.jp, ORCID 0000-0002-1237-2042; totake@eng.hokudai.ac.jp, ORCID 0000-0001-9596-4141; tomsato@eng.hokudai.ac.jp, ORCID 0000-0002-3279-3696

[2]Creative Research Institution, Hokkaido University, 060-0812, Sapporo, Japan

Abstract

Mine drainage, especially from abandoned sites, poses a substantial environmental challenge. Passive treatment systems are effective but require understanding geochemical processes. This study focuses on two Japanese abandoned mine sites: the Ainai mine (neutral pH, rich in iron) and the acidic Shojin River. Iron (Fe) colloids play a key role in sequestering toxic elements like arsenic (As) and zinc (Zn). In Ainai, Fe colloids were stable, promoting effective treatment, but in the Shojin River, the colloids were unstable. To address this, basalt was added to raise pH and stabilize Fe colloids, enhancing water quality while also contributing to carbon dioxide removal (CDR).

Keywords: Mine drainages, Passive treatment, Fe Colloids, Enhanced Rock Weathering (ERW), Carbon dioxide removal (CDR)

Introduction

Mine drainage, particularly from abandoned sites, poses an environmental threat due to its potential to contaminate water sources with toxic metals (Nordstrom 2011). Understanding the geochemical processes governing mine drainage is critical for developing effective and sustainable remediation strategies. While active treatment methods, such as chemical dosing and mechanical aeration, provide immediate mitigation, they are often expensive and require continuous maintenance (Johnson and Hallberg 2005). In contrast, passive treatment systems harness natural geochemical and biological processes to improve water quality in a more cost-effective and environmentally sustainable manner (Gandy *et al.* 2016).

Although Iron (Fe) colloids can act as transportation vectors for toxic elements, they also play a crucial role in passive treatment, by sequestering toxic elements such as arsenic (As) and zinc (Zn), thereby reducing their mobility in aquatic systems (Hsu *et al.* 2010). Additionally, the dissolution of silicate rocks, such as basalt, contributes to carbon dioxide (CO_2) removal through enhanced rock weathering (ERW), a process that facilitates long-term carbon sequestration (Beerling *et al.* 2020). However, the stability and efficiency of Fe colloids are highly dependent on pH conditions, which vary across different mine drainage environments (Younger *et al.* 2002).

A novel aspect of this study is the integration of ERW with acid mine drainage (AMD) remediation, leveraging the concept that the carbon dioxide removal (CDR) efficiency of ERW is directly linked to the mineral dissolution rate in ultramafic rocks(in this case, basalt). Studies on water-rock interactions suggest that mineral dissolution occurs more rapidly in acidic, dynamic systems such as AMD compared to stagnant, neutral environments like agricultural soils (Renforth *et al.* 2015). Consequently, ERW may achieve higher carbon sequestration efficiency in AMD settings, providing an additional environmental benefit beyond conventional mine drainage treatment.

This study investigates mine drainage at two abandoned sites in Japan (Fig. 1): the Ainai Mine, characterized by neutral pH and Fe-rich conditions, and the acidic Shojin River (Fig. 1). The Ainai mine drainage system utilizes aeration to promote Fe oxidation and precipitation, while the Shojin River employs a limestone bed to neutralize acidity and remove Fe, As, and Zn. Given the acidic nature of the Shojin River, basalt was put into the river to increase pH and consequently, stabilize Fe colloids.

Based on this background, this study aims to (i) characterize the nature of Fe colloids in neutral and acidic mine drainage systems, (ii) assess the sequestration efficiency of Fe colloids for toxic metal removal and (iii) investigate the efficiency of basalt in stabilizing Fe colloids in acidic environments. By integrating ERW with AMD remediation, this approach not only enhances the sequestration of toxic elements but also contributes to CO_2 reduction, demonstrating the additional environmental benefits of passive treatment strategies.

Methods

Onsite measurements were conducted at the sampling sites, including pH, electrical conductivity (EC), dissolved oxygen (DO), redox potential (ORP), turbidity, alkalinity, and temperature. Alkalinity, expressed as HCO_3^-, was determined by titrating a 50 mL water sample (filtered through a 0.45 µm filter) with 0.16 N HNO_3, following the USGS guidelines (Rounds 2012). Dissolved ferrous iron (Fe^{2+}) was measured using an ion-selective pack from Kyoritsu Chemical Check Lab., Corp.

Water samples were collected for the analysis of various parameters, including cations, anions, and dissolved colloidal fractions. The collected water was filtered using 0.20-micrometer membrane filters and stored in 50 mL acid-washed polyethylene bottles. Samples for dissolved colloidal fraction analysis underwent additional filtration using nano-membrane filters with a molecular weight cutoff of 200 kDa. To preserve cation samples, 1% (v/v) ultrapure nitric acid was added.

Precipitated sediments from the drainage were collected for mineralogical and chemical characterization. Additionally, ultrafiltration at each sampling point enabled the collection and physical observation of colloids retained on the ultrafilters.

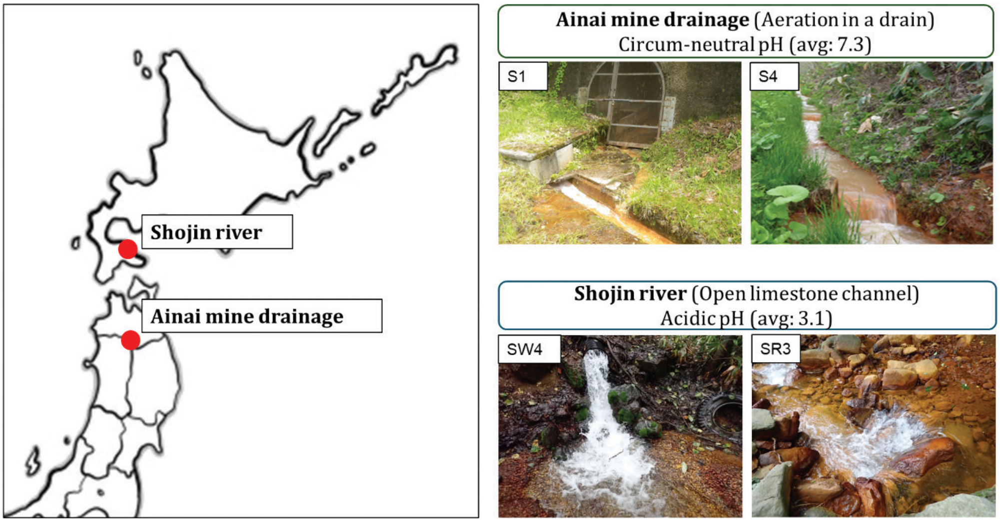

***Figure 1** Location of Shojin river and Ainai mine drainage, along with their field pictures.*

For the field trial, approximately 1 ton of crushed basalt particles (5 cm in diameter) was introduced into the Shojin River. Water samples were analyzed before and after interaction with the basalt to assess changes in water chemistry. Sampling was conducted over a period of two months to evaluate the long-term effects of basalt addition on pH stabilization, Fe colloid stability, and toxic metal sequestration.

Results and Discussion

Trends of Fe and As in dissolved and colloidal fractions

Ainai Mine Drainage

The onsite measurements at the Ainai Mine indicate a neutral to alkaline system, with pH values ranging from 6.20 to 7.91 (Fig. 2a). Downstream, the pH increases while alkalinity decreases, suggesting carbonate buffering effects. The geochemical analysis indicates that Fe^{2+} concentrations decrease downstream, accompanied by increasing turbidity, implying Fe (oxy)hydroxide nanoparticle formation and aggregation. The inverse relationship between turbidity and Fe^{2+} concentrations suggests that oxidation of Fe^{2+} to Fe^{3+} leads to precipitation and increased turbidity (Hsu *et al.* 2010).

Arsenic (As), primarily present as arsenite [As(III)], follows Fe in its distribution (Fig. 2b). The formation of Fe colloids at sites S2 and S3 suggests that Fe colloids act as primary carriers, while As behaves as a pseudo-colloid, its mobility largely governed by Fe colloids. The inverse correlation between Fe and As concentrations suggests that As removal occurs through adsorption, co-precipitation, and aggregation with Fe colloids (Gandy *et al.* 2016). However, further downstream, As persists in the dissolved phase, likely due to Fe-Si associations that reduce Fe oxide affinity for As (Younger *et al.* 2002).

Shojin River

In contrast, the Shojin River represents an acidic mine drainage system (Fig. 3a). The background site (SR1) has a near-neutral pH (6.9), but wastewater from the abandoned mine is highly acidic (pH: 2.8). The wastewater samples (SW1, SW2, SW4) contain elevated Fe and As concentrations, exceeding WHO limits (Fe: 10 mg/L, As: 10 µg/L). Upon mixing with uncontaminated river water at SR2, elemental concentrations decrease progressively downstream, reaching levels below WHO limits by SR9.

Colloidal and dissolved fractions, absent in initial wastewater and river water, emerge from SR2 onward. Fe and As exist in both dissolved and colloidal forms but transition predominantly to the dissolved phase from SR6. Element concentrations inversely correlate with pH, decreasing as pH increases. The formation of Fe colloids initially facilitates As sequestration (Fig. 3b); however, in the Shojin River, Fe colloids appear unstable (Fig. 3b, SR3 to SR5) and prone to dissolution, potentially re-releasing As into the water column (Nordstrom 2011).

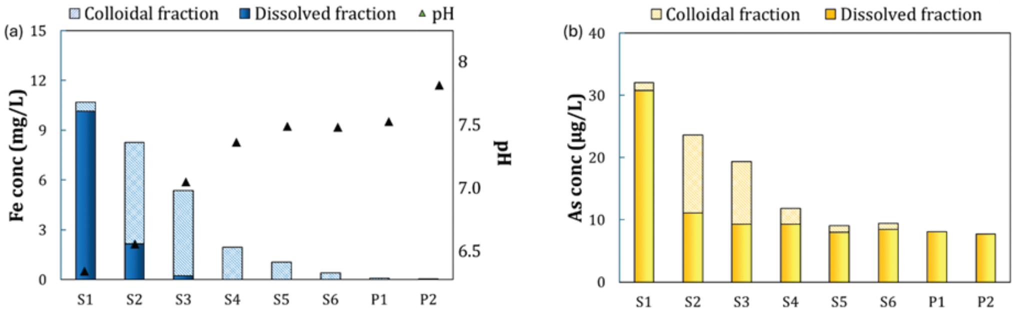

Figure 2 *Trends of dissolved and colloidal fractions of (a) Fe and (b) As concentrations at Ainai mine drainage. S1 to S6 represent the sampling points at Ainai mine drainage. P1 and P2 are ponds set up at the downstream of the aeration channel before the water flows to a nearby river.*

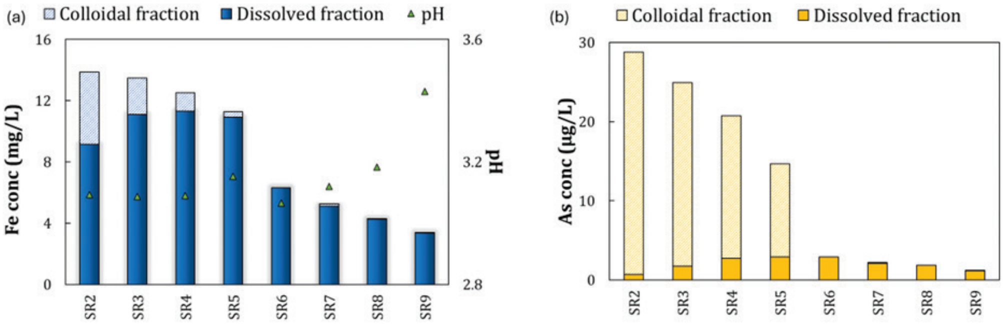

Figure 3 *Trends of dissolved and colloidal fractions of (a) Fe and (b) As concentrations at Shojin river. SR represents sampling location from SR2 (mixing point with background river water) and flows towards the downstream at SR9, before emptying into the Japan sea.*

Mineralogy of colloids, sediments, and suspended particles

Microscopic analysis of the collloids collected on the ultrafilters confirmed that mineralogy in the mine drainage is pH-dependent, with schwertmannite forming in acidic conditions and ferrihydrite dominating at neutral to slightly alkaline pH (Fig. 4a and b). At the Shojin River, schwertmannite was identified in both sediments and colloids, exhibiting its characteristic fibrous structure. TEM analysis further revealed schwertmannite as fibrous aggregates with spheroidal hedgehog morphologies, composed of Fe, S, C, O, and minor As, as detected by EDS. These particles measured 50–80 nm on average. The formation of schwertmannite is primarily controlled by Fe^{3+} hydrolysis under acidic conditions (Bigham *et al*. 1996). Solid-phase analyses suggest that schwertmannite plays a crucial role in As scavenging, making it a key component in AMD environments (Regenspurg *et al*. 2004).

In contrast, at the Ainai mine drainage, XRD analysis of sediments and suspended particles identified 2-line ferrihydrite as the dominant Fe hydroxide mineral. Ferrihydrite formation is favored under circumneutral conditions, resulting from Fe^{2+} oxidation and subsequent hydrolysis (Cornell and Schwertmann, 2003). EDS analysis confirmed that the colloids in Ainai drainage primarily consist of 2-line ferrihydrite, which exhibits high affinity for toxic element sequestration (Webster *et al*., 1998). The stability and reactivity of ferrihydrite make it a key

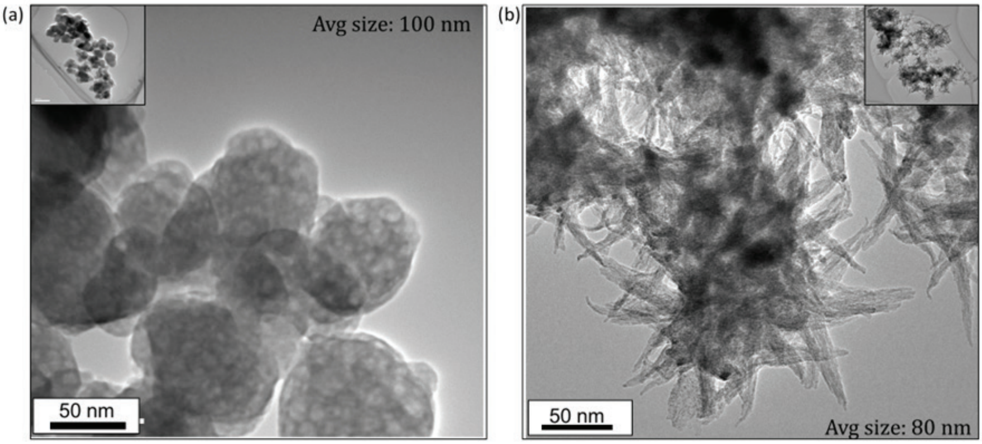

Figure 4 *Morphology (a) Core-shell ferrihydrite aggregates at Ainai mine drainage and (b) fibrous schwertmannite colloids at Shojin.*

component in passive treatment systems (Legg *et al.*, 2014).

Integration of mine drainage treatment with CO_2 reduction

Schwertmannite colloids formed in the acidic Shojin River system exhibited dissolution behavior, primarily influenced by the low pH of the system. The state of schwertmannite in strongly acidic environments is well-documented, as it tends to dissolve and release previously adsorbed elements, including arsenic (As) (Regenspurg *et al.*, 2004). To improve water quality and enhance colloid stability, basalt was introduced to the system to promote pH buffering (Fig. 5).

On-site measurements revealed a gradual increase in pH following basalt addition, a key factor in stabilizing schwertmannite colloids and enhancing As sequestration. After one month of this flow through-basalt interaction, the pH increased to an average of 3.7from 3.2, a trend attributed to the dissolution of basaltic minerals, which release alkaline species into the water (Renforth *et al.*, 2015). This increase in pH facilitates the transformation of schwertmannite into more stable Fe hydroxides, thereby reducing the risk of As remobilization (Bigham *et al.*, 1996).

Continued interaction between acidic mine drainage and basalt results in the dissolution of silicate minerals, contributing bicarbonate ions (HCO_3^-) to the system. These ions eventually reach downstream environments, where they enhance ocean alkalinity, potentially increasing CO_2 sequestration through enhanced weathering processes (Beerling *et al.*, 2020). This mechanism highlights the dual benefit of basalt addition—not only improving the stability of Fe colloids in AMD systems but also contributing to global carbon cycle regulation.

Conclusions

This study highlights the crucial role of Fe colloids, particularly schwertmannite and ferrihydrite, in the sequestration of toxic elements such as arsenic (As) in mine drainage systems. The findings demonstrate that pH plays a fundamental role in controlling the mineralogy and stability of Fe colloids, with schwertmannite dominating in low-pH environments and ferrihydrite forming under neutral conditions.

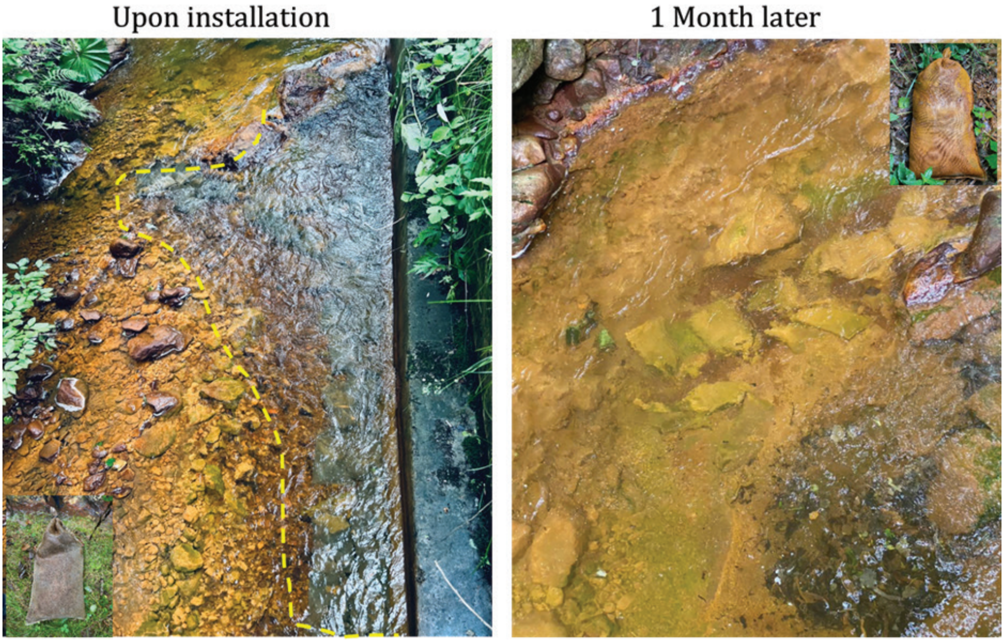

Figure 5 *Pictures of increased precipitation at the Shojin river on the surface of basalt bags. (Left) Gray-ish basalt bags along the river and (right) 1 month after basalt application.*

In the acidic Shojin River, schwertmannite was found to be unstable, leading to potential As re-release. However, the introduction of basalt improved water quality by increasing pH, thereby enhancing the stability of Fe colloids and promoting As sequestration. The interaction between basalt and acidic drainage facilitated the dissolution of silicate minerals, releasing bicarbonate ions that contribute to ocean alkalinity and CO_2 reduction.

Overall, this study underscores the potential of enhanced rock weathering as a dual-benefit strategy for mine drainage remediation and climate change mitigation. By integrating geochemical processes with passive treatment approaches, this method offers a sustainable solution for managing mine-impacted waters while contributing to long-term carbon sequestration.

Acknowledgements

The authors thank all Hokkaido Research Organization for their cooperation during the research. We extend our gratitude to all those who contributed to our research, particularly Mr. F Nakamura, Ms. N. Kimotsuki and Mr. Naito for their assistance with our field work and some analysis. This research was supported by a Joint research grant from Research Grant of the "Nanotechnology Platform" Program of the Ministry of Education, Culture, Sports, Science and Technology (MEXT) of Japan; New Energy and Industrial Technology Development Organization (NEDO); the Japan Society for the Promotion of Science (JSPS) KAKENHI.; and the Japan International Cooperation Agency (JICA). The authors also thank all co-organisers for hosting the IMWA 2025 Conference.

References

Beerling DJ, Kantzas EP, Lomas MR, Wade P, Eufrasio RM, Renforth P, Banwart SA (2020) Potential for large-scale CO_2 removal via enhanced rock weathering with croplands. Nature 583:242–248

Bigham JM, Schwertmann U, Carlson L, Murad E (1996) A poorly crystallized oxyhydroxysulfate of iron formed by bacterial oxidation of Fe(II) in acid mine waters. *Geochim Cosmochim* Acta 60:2111–2121

Cornell RM, Schwertmann U (2003) The Iron Oxides: Structure, Properties, Reactions, Occurrences, and Uses. *Wiley-VCH*

Gandy CJ, Smith JWN, Jarvis AP (2016) Attenuation of mining-derived pollutants in the hyporheic zone: a review. *Sci Total Environ* 547:414–425

Hsu LC, Jang CS, Lin HR, Wang MK (2010) The formation of iron colloids in acid mine drainage. *Environ Earth Sci* 59:883–895

Johnson DB, Hallberg KB (2005) Acid mine drainage remediation options: a review. *Sci Total Environ* 338:3–14

Nordstrom DK (2011) Mine waters: acidic to circumneutral. *Elements* 7:393–398

Regenspurg S, Brand A, Peiffer S (2004) Formation and stability of schwertmannite in acidic mining lakes. *Geochim Cosmochim Acta* 68:1185–1197

Renforth P, Pogge von Strandmann PAE, Henderson GM (2015) The dissolution of olivine added to soil: implications for enhanced weathering. *Appl Geochem* 61:109–118

Rounds SA (2012) Alkalinity and acid neutralizing capacity. *US Geological Survey Techniques of Water-Resources Investigations* Book 9, Chapter A6, Section 6.6

Younger PL, Banwart SA, Hedin RS (2002) Mine Water: Hydrology, Pollution, Remediation. *Springer Science & Business Media*

From Novel Laboratory Methodologies to Field Implementation: Assessing CO_2 and O_2 Flux in Northern Europe Mine Waste

Logan Clancy[1,2], Steven Pearce[2], Daniel Schoen[3], Ben Gersten[3], Evangelos Mouchos[2], Andrew Barnes[3] and Rosalia Shiimi[2]

[1]*Cardiff University, Cardiff, UK*

[2]*Mine Environment Management (MEM) Ltd., Denbigh, UK, rshiimi@memconsultants.co.uk, emouchos@memconsultants.co.uk, spearce@memconsultants.co.uk*

[3]*Geochemic Ltd., Pontypool, UK, abarnes@geochemic.co.uk*

Abstract

The demand for metals in net-zero technologies has increased mining waste. This study examines carbon sequestration in ultramafic mine waste in Northern Europe. In collaboration with research partners, innovative methods assess CO_2 sequestration and emissions. Closed-system experiments showed O_2 depletion from 21% to negligible values (mg/L) due to sulfide oxidation. CO_2 removal is evaluated by monitoring atmospheric CO_2 and carbonate formation, considering CO_2 from acid mine drainage neutralisation. Results suggest carbonation can reduce CO_2 emissions, informing scalable carbon management. Open-barrel tests simulate field conditions, supporting sequestration strategies and contributing to the EU-funded C-SINK project.

Keywords: Gas flux monitoring, Carbon sequestration, Mine waste, Carbonation, Field trials

Introduction

This study expands on prior carbon capture and sequestration (CCS) research by Mine Environmental Management (MEM) Ltd. and Geochemic Ltd., focusing on CO_2 removal through mine waste materials. The increasing demand for metals essential to net-zero technologies has intensified mining activities, leading to significant waste production. Mine waste, particularly from ultramafic deposits, has the potential to sequester atmospheric CO_2 through mineral carbonation. However, challenges remain in quantifying CO_2 removal, understanding O_2 flux changes due to sulfide oxidation, and developing scalable carbon management strategies. Building on previous studies (e.g., Savage, 2019, 2023; Shiimi, 2022; Schoen, 2022), this study further investigates CO_2 sequestration potential using laboratory-scale and mesocosm experiments. The research integrates enhanced weathering (EW) techniques with improved monitoring, reporting, and verification (MRV) frameworks. Additionally, preparations for field-scale testing aim to refine carbon dioxide removal (CDR) strategies in mining contexts, bridging the gap between controlled experiments and real-world applications.

Methods

Sample Preparation, Collection and Characterisation

Mine waste samples, obtained from waste rock storage facilities (WRSF) and tailings storage facilities (TSF) at Northern European mine sites, were characterised according to British (BS) and European (EU) standards. Characterisation focused on mineralogical (SEM-EDX, optical microscopy), elemental (ED-XRF for elemental distribution and carbon capture potential), geochemical (NAG, ANC, total carbon and sulfur, pH, EC), and geotechnical (specific gravity, particle size distribution, water content) properties. These analyses identified oxidation and carbonation potential, assessed carbon sequestration capacity, and informed experimental design. Tailings were tested in Xylem WTW OxiTop®-C/B (Oxitops and Carbitops) and open-barrel setups, while waste rock underwent similar experiments. Historical MSc and PhD data (e.g., Savage *et al.* 2019, Chmielarski 2020, Schoen 2022, Shiimi 2022, Savage 2023, Cole 2023) supported sample selection and methodology

Closed-System Experiments

Laboratory-scale closed experiments utilised established methodologies to evaluate carbon capture. Oxitops experiments, conducted over 30 days at 8–10 °C, followed the WTW Soil BOD manual (2010a, 2010b) to measure O_2 consumption and CO2 produced using a NaOH solution. Carbitops experiments, also lasting 30 days, were performed at 5% CO_2 and 8–10 °C to assess CO_2 consumption under elevated conditions. Sealed barrel experiments, spanning over 365 days, employed bespoke vessels developed by Schoen *et al.* (2023), using controlled starting gas compositions (O_2, CO_2) at 8–10 °C. Throughout these experiments, pressure and gas concentration changes were monitored to evaluate CO_2 production and consumption rates, enabling detailed carbon balance calculations.

Open-System Experiments

An open barrel mesocosm test (Fig. 1) was designed to simulate field conditions, in Northern Europe, providing a platform to evaluate sensor performance before upscaling to field trials. The experiment operated under atmospheric O_2 and CO_2 conditions at 8–10 °C, with the objective of developing and setting up an open-barrel equipment test to monitor gas flux and geochemical behavior in mine tailings under semi-controlled open system conditions. This development represents a new approach to understanding carbonation processes in mining contexts. As part of a broader EU-funded carbon sequestration project, open system experimentation is considered part of the plans for an upscaled field trial at a Northern European mine site.

Results

Characterisation of ultramafic mine waste

Waste rock samples had a moisture content of 7.5% added before experiments, as water is necessary for the carbonation process. Carbon dioxide dissolves in water to form carbonic acid, which reacts with Mg- and Ca-bearing silicates to produce secondary carbonate minerals. Particle size distribution (PSD) curves for waste rock revealed well-graded material ranging from gravel to fines, with smaller particle sizes contributing increased surface area for oxidation and

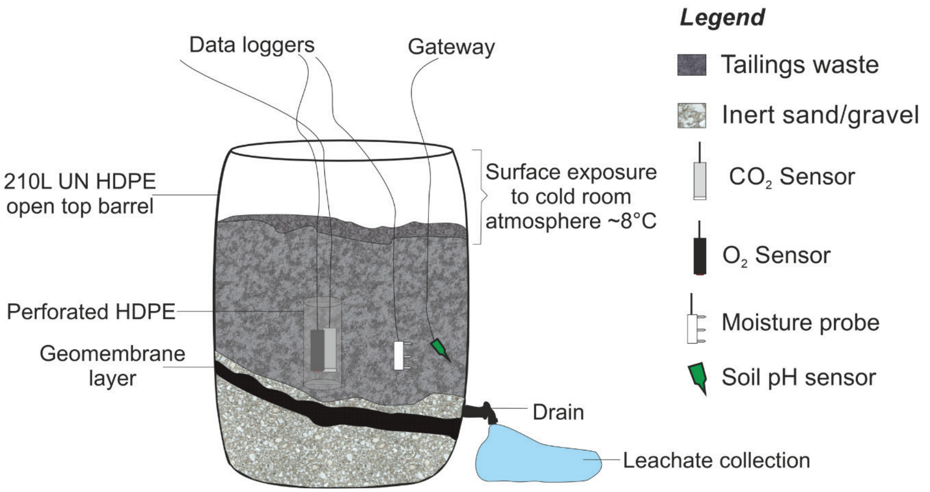

Figure 1 *Open barrel schematic (designed and submitted as part of first author's MSc dissertation for Cardiff University).*

carbonation reactions. Elemental analysis from prior studies was used to evaluate the carbon capture potential (CCP) for waste rock and tailings. Waste rock demonstrated a higher CCP (~370 kg CO_2/tonne) compared to tailings (~330 kg CO_2/tonne). Calcium concentrations remained consistent (~10%) across both materials. Magnesium content was higher in waste rock, potentially explaining its elevated CCP due to magnesium's role in carbon capture. The mineralogical compositions of waste rock and tailings were broadly similar featuring sulfides, silicates and carbonates. Target minerals such as pyrrhotite, pyrite, calcite, and dolomite were identified, alongside gangue minerals including diopside, enstatite, tremolite, serpentine, and chlorite. These minerals are critical for carbonation reactions, as sulfides generate acidity, carbonates neutralise it to produce CO_2, and magnesium silicates react with CO_2 to form carbonates.

Carbon Balance by Oxitops and Carbitops

Under low-temperature conditions (10 °C), the carbon balance of the analysed Oxitops and Carbitops mine waste samples demonstrated net CO_2 sequestration potential (Fig. 2). CO_2 production rates estimated from both the back titration and TIC methods were estimated between 0.40 and 1.24 kg CO_2/tonne/year for tailings and less than 0.10 kg CO_2/tonne/year for waste rock. In a 5% CO_2 atmosphere, CO_2 consumption rates ranged from 1.90 to 2.11 kg CO_2/tonne/year for tailings and 1.16 to 1.25 kg CO_2/tonne/year for waste rock. Net CO_2 sequestration rates were higher in waste rock, ranging from 1.09 to 1.20 kg CO_2/tonne/year, driven by limited CO_2 production from sulfide oxidation and carbonate dissolution, coupled with notable CO_2 uptake by silicate minerals. For tailings, net sequestration rates were estimated between 0.67 and 1.71 kg CO_2/tonne/year, with higher CO_2 production from sulfide oxidation offset by greater CO_2 uptake via carbonation reactions.

Passive Carbonation in Closed Barrels

Two sealed barrels (Fig. 3) stand out as they directly compare to the hypotheses for atmospheric conditions developed by Schoen *et al.* (2023). A waste rock barrel, exposed to atmospheric conditions, showed O_2 concentrations starting at ~20% (≈278 mg/L), in November 2022, which gradually decreased over time due to sulfide oxidation, reaching complete depletion by April 2024. This aligns with the hypothesis for atmospheric CO_2 conditions, which predicted that O_2 concentrations would fall as sulfides were oxidised, leading to a reduction in available O_2. CO_2 concentrations in this barrel began at ~400 ppm (≈0.56 mg/L) and steadily increased, peaking at ~1.6% (≈16,000 mg/L) in April 2024, coinciding with the complete O_2 depletion. This supports the hypothesis that CO_2 levels would initially increase due to the rapid occurrence of sulfide oxidation and primary carbonate dissolution, releasing CO_2 before passive carbonation (CO_2 uptake) becomes dominant. From mid-April 2024 onward, CO_2 concentrations began to decline, reaching ~1.3% (≈13,000 mg/L) by November 2024. A control barrel, which contained quartz chips, showed little change

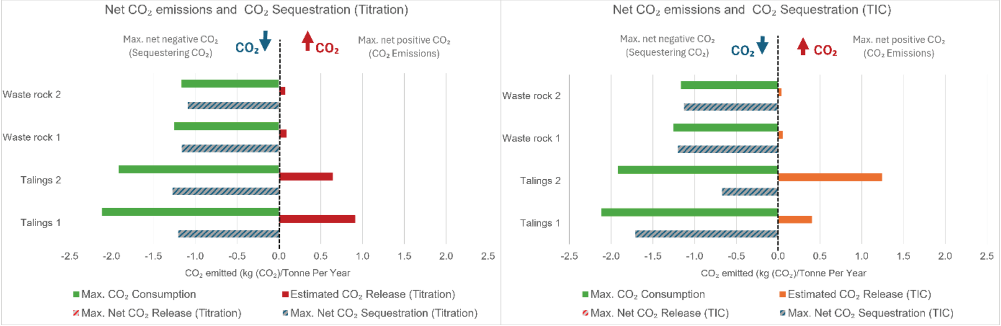

***Figure 2** Net CO_2 emissions and sequestration results via titration and total inorganic carbon (TIC) methods.*

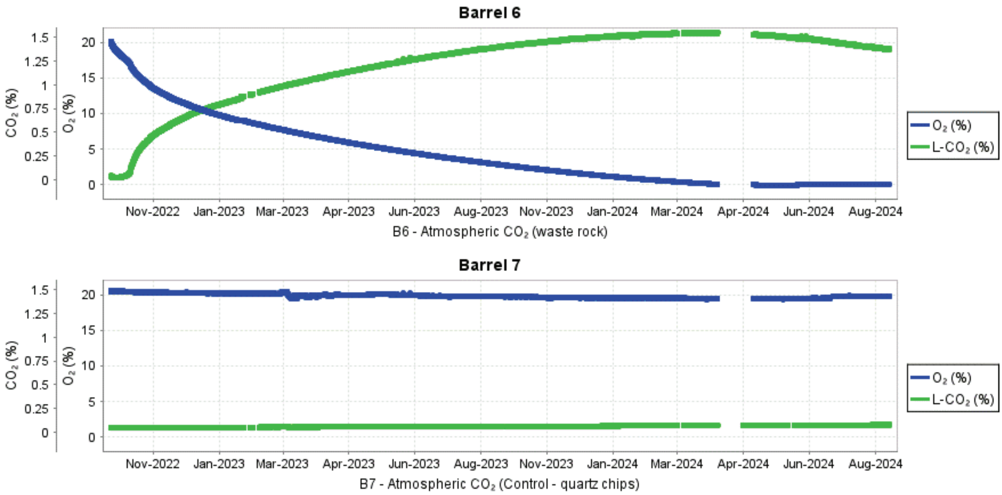

Figure 3 *Sealed barrel results after prolonged monitoring of the gas flux.*

in O_2 and CO_2 concentrations over the two-year period. A minor deflection in O_2 levels between November 2023 and May 2024 was attributed to sensor corrosion, confirming that no reaction-driven gas exchange occurred in this control barrel.

Commissioning the Open Barrel Equipment Test

The open barrel was commissioned and filled with mine tailings sourced from a Northern European mine site. The barrel is instrumented with O_2, CO_2, pH, temperature, and soil moisture sensors (Fig. 4). The barrel will be irrigated, and leachate collected for geochemical analysis. The open barrel contains 120 kg of homogenised mine tailings at 20% moisture content, with a base layer of 25 kg of DI-rinsed river aggregate gravel and 20 kg of inert sand mix. The system also includes a geomembrane to contain and prevent contamination of the materials. The open barrel mesocosm test will enable more precise measurements of the factors influencing carbonation processes, which is vital for optimising carbon sequestration strategies. Real-time monitoring results from this new approach will provide valuable insights into CO_2 removal efficiency in mining contexts, paving the way for more sustainable practices and effective carbon management across the industry.

Key Observations/Discussion

Critical characterisation of ultramafic mine waste

The characterisation of waste rock and tailings include the importance of moisture content, as water is essential for carbonation by enabling CO_2 dissolution and subsequent reactions with magnesium- and calcium-bearing silicates to form carbonates. The particle size distribution showed a range of material sizes, with smaller particles offering a larger surface area for oxidation and carbonation. Elemental and mineralogical analyses revealed similarities between the materials, with both containing mafic minerals like pyroxene and amphibole, though tailings had a higher presence of olivine. Various key minerals, including pyrrhotite, pyrite, calcite, and dolomite, were identified as important for carbonation processes. These characteristics suggest that both waste rock and tailings possess the necessary conditions for carbonation, with mineral composition playing a considerable role in their carbon sequestration potential.

Nature of the closed system experiments

The Oxitop and Carbitop tests demonstrated that both tailings and waste rock have the potential for CO_2 sequestration. Waste rock exhibited higher net CO_2 uptake due to lower CO_2 production from sulfide oxidation and

Figure 4 *Open barrel equipment setup.*

greater carbonation of silicate minerals. In contrast, tailings generated more CO_2 from sulfide oxidation but also underwent substantial carbonation, resulting in net sequestration. The saturated nature of the tailings likely restricted CO_2 diffusion, enhancing its uptake by silicate minerals. The largely saturated conditions in the tailing's facility likely limited CO_2 diffusion relative to O_2, allowing CO_2 produced during sulfide oxidation to be consumed by silicate minerals. These findings indicate that both waste rock and tailings can achieve net CO_2 sequestration under the studied conditions, with tailings exhibiting higher carbonation rates than waste rock.

The sealed barrel tests further supported these findings. The waste rock barrel followed expected trends, with O_2 depletion due to sulfide oxidation and an initial CO_2 increase from sulfide oxidation and carbonate dissolution. Over time, CO_2 concentrations declined as carbonation reactions became dominant. The control barrel, containing quartz chips, exhibited negligible gas fluctuations, confirming the absence of reaction-driven gas exchange.

The future of the open system experiments

While initial sensor readings for the open barrel equipment test are being recorded, the timeline for carbonation development remains uncertain, and the full trends will emerge as data collection continues. The future field trials will provide more information to refine carbonation process insights and carbon sequestration strategies.

Conclusion

The project has made substantial contributions to the advancement of carbon sequestration strategies by utilizing mine waste materials. By building on prior research, this study has refined methodologies for monitoring CO_2 and O_2 fluxes, a critical aspect of assessing the carbon capture potential of mine waste. These efforts not only address Measurement, Reporting, and Verification (MRV) challenges but also enhance Enhanced Weathering (EW) frameworks for Carbon Dioxide Removal (CDR). The novel open-barrel experiment, along with upcoming field trials at the mine site, marks a crucial step in validating these strategies in real-world settings. The data gathered from these trials will offer valuable insights that will shape future carbon sequestration technologies, including those supported by the EU-funded C-SINK project. This work establishes a solid foundation for improving carbon sequestration methods and advancing efforts to mitigate atmospheric CO_2 levels. Future research should focus on modelling existing CCS data (e.g. using PHREEQC) to identify emerging trends and further refine conclusions. Additionally, enhancing O_2 and CO_2 consumption rate models using techniques such as differential or integrated rate laws will considerably improve carbon sequestration models. Investigating parameters like temperature,

O_2/CO_2 content, particle size, and mineralogy will be essential in developing more accurate and robust consumption estimation models for future carbon capture strategies.

Acknowledgement

The authors would like to acknowledge Cardiff University for providing support for this study as part of an MSc course placement. We also extend our gratitude to the external anonymous mining operator who funded this experimental work as part of the first author's MSc placement. Additionally, the authors thank all the organisers for hosting and accepting this paper into the IMWA 2025 Conference.

References

Chmielarski M (2019) An assessment of the carbon sequestration potential of ultramafic nickel mine waste rock: Investigation of impacting environmental factors (Unpublished MSc dissertation). Cardiff University.

Cole J (2023) Investigating the rate of passive carbonation and assessment of the carbon balance of metalliferous mine waste (Unpublished MSc dissertation). Cardiff University.

Savage RJ, Pearce S, Mueller S, Barnes A, Renforth P, and Sapsford D (2019) Methods for assessing acid and metalliferous drainage mitigation and carbon sequestration in mine waste: A case study from Kevitsa mine, Finland. In: Proceedings of the International Conference on Mine Closure. Australian Centre for Geomechanics:1073–1086. doi: 10.36487/ACG_rep/1915_86_Savage.

Savage R (2023) Humidity cell testing of mine wastes under a CO2 supplemented atmosphere (PhD dissertation). Cardiff University.

Schoen D (2022) Investigating the rate of passive carbonation of mine wastes with focus on a metal mine in Finland (Unpublished MSc dissertation). Cardiff University.

Schoen D, Savage R, Pearce S, Shiimi R, Gersten B, Roberts M, Barnes AK (2023) A novel empirical approach to measuring pore gas compositional change in mine waste storage facilities: A case study from northern Europe. Proceedings of the International Conference on Mine Closure. https://doi.org/10.36487/acg_repo/2315_070

Shiimi R (2022) Development of a method to assess the carbon balance of typical waste storage facilities at the Boliden Kevitsa mining operation (Unpublished MSc dissertation). Cardiff University.

Shiimi R, Savage R, Pearce S, Barnes A, Roberts M, Schoen D, Sapsford D (2023) The development of a multi-parameter respirometric laboratory testing method to estimate site-specific net carbon dioxide flux from metalliferous mine waste. International Mine Water Association (IMWA) 2023 Proceedings. Retrieved from https://www.imwa.info/docs/imwa_2023/IMWA2023_Shiimi_471.pdf

WTW, a Xylem brand (2010a) BOD application report: Respiration activity of soils (basic principles, process characteristics). Germany: 1–16.

WTW, a Xylem brand (2010b) BOD application report: Respiration activity of soils (standard test preparation). Germany: 1–8.

Biologic Treatment Of Acid Mine Drainage: A Perspective Of Two Decades Of Research, Challenges And Opportunities

Maria Clara Costa[1,2], Tânia Palma[2], Jorge Carlier[2]

[1]Faculdade de Ciências e Tecnologia, ed. 8, Universidade do Algarve, Campus de Gambelas, 8005-139 Faro, Portugal, mcorada@ualg.pt, ORCID 0000-0003-1340-5237

[2]Centro de Ciências do Mar, Universidade do Algarve, Campus de Gambelas, 8005-139 Faro, Portugal, tcpalma@ualg.pt, ORCID 0000-0001-8614-570X

jcarlier@ualg.pt, ORCID 0000-0003-0675-2716

Abstract

This article briefly reviews the work carried out over the last 20 years by the Environmental Technologies group at the Centre for Marine Sciences at the University of the Algarve on the biological treatment of acidic water from the São Domingos mine using sulfate-reducing bacteria. In a chronological sequence, its main challenges are presented, which included the search for and enrichment of metal-resistant sulfate-reducing bacteria and the search for efficient and available wastes as low-cost carbon sources. The opportunities that have resulted from these studies, namely the synthesis of functional nanoparticles of metal sulfides and the recovery of metals, among others, are also presented.

Keywords: São Domingos mine, acid mine drainage treatment, sulfate-reducing bacteria, carbon sources, metals and metal sulfide nanoparticles

Introduction

Mining activities are ancient in Portugal, dating back to the Pre-Roman and Roman periods. They played an important role in the Portuguese economy of the 19th and 20th centuries associated mainly with polymetallic sulfides in the south, and uranium minerals in the north. In the second half of the twentieth century, almost all the mining activities were suspended and consequently many mine sites were left untreated. The fact that much of Portugal mineralization is associated with sulfide minerals provided great potential for acid mine drainage (AMD) production and an estimate of about 14 % of the Portuguese mines were found to generate acidic waters (Pinto 2005). São Domingos mine, a deposit of polymetallic sulfides explored for Cu, Pb, Zn, S, Fe, Ag, and Au, located in Southeast Portugal in the Iberian Pyrite Belt, is an example of this situation. The inactive open-pit from the mining operations resulted in the creation of a large pit-lake with acid water with pH close to 2 containing high concentrations of sulfate and metals (mainly aluminium, iron, zinc and copper). The contamination is not only confined to the pit-lake since other water bodies located in the downstream area nearby (Fig. 1) are also affected (Tab. 1).

The problems associated to AMD in Portugal and in specially in São Domingos were the driving force that stimulated the studies of our research group for the development of alternative treatment processes based on the use of Sulfate-Reducing Bacteria (SRB), since traditional neutralization with alkaline agents do not address the reduction of sulfate, are expensive and result in the formation of high volumes of relatively soluble sludge. Moreover, the use of biologic techniques offers several opportunities, such as the possibility to recover the metals, namely as metal sulfides with functional applications.

Since our first studies several carbon sources have been tested, mainly wastes locally

Figure 1 Aerial view of São Domingos mining area, AMD sampling and water bodies.

available. In addition to the characterization of the consortia and their dynamics, other improvements were introduced to the bioremediation systems aiming to improve the efficiency of the process and the quality of the effluents, resulting in the installation *on-situ* of a pilot plant at São Domingos mine.

The present review gives a summarized perspective of the work evolution started twenty years ago by the Environmental Technologies research group of Centre of Marine Sciences at the University of Algarve, with the aim of developing simple and low-cost processes, based on the use of SRB, for the treatment of AMD from São Domingos mine site.

The biologic treatment of AMD using SRB: The main challenges

Selection of low-cost matrices

The research work of the Environmental Technologies group, started in 2004, has always been focused on the treatment of AMD from São Domingos mine and used bench scale fixed-bed column bioreactors, initially in a semi-continuous mode. Sewage, anaerobic sludge and soil from the mining area were tested as solid matrices, inoculum for SRB and as sources of substrates. Lactose was also added as a supplementary carbon and energy source because it could be easily available at zero or even at negative cost in

***Table 1** AMD typical composition collected in Site 1-6 (see Fig. 1) in different seasons.*

Chemical species	Concentration (mg/L)	
	Summer	Winter
Al	211	138
Fe	178	45
Zn	38	28
Cu	21	30
SO_4^{2-}	2323	1848
pH	2.58	2.48

effluents of local cheese industries. The results showed that in those conditions AMD was neutralized, and that the sulfide produced was enough for the precipitation of the main dissolved metals (Costa 2005). The use of soil as solid support suggested the possibility of using that system for the decontamination of both waters and soils, although the effluents have high organic load.

Later, the behavior of that bioreactor was compared with other three filled with "more inert" packaging materials: coarse sand, glass spheres and cereal straw in the absence or presence of three added carbon sources: lactate, ethanol and lactose (Costa 2008). The data confirmed that it was possible to grow SRB in the bioreactor containing sewage, anaerobic sludge, and soil in the absence and in the presence of the carbon sources, to remove the main metals present in AMD, although an incomplete sulfate removal was observed. When coarse sand or glass spheres were utilized, efficient copper and zinc removal was observed. Nevertheless, the incapacity of both systems to generate enough alkalinity did not allow to maintain their good performances in terms of iron removal and sulfate reduction. Thus, the incorporation of neutralizing and buffer capacity materials to the column matrices was recommended. Due to its low density, cereal straw was not suitable to obtain the necessary anaerobic environment inside the column for SRB activity and thus, coarse sand was selected as the preferable column matrix.

Selection of highly-metal resistant sulfate-reducing bacteria

Due to the high concentration of metals in AMD, the search for metals-resistant SRB was, at that time, considered important for the development of efficient bioremediation technologies. Therefore, samples from distinct anaerobic environments (sediments from the mining area, sludge from wastewater treatment plants and soil from a thermal place) were tested in batch aiming to obtain an SRB consortium resistant to Fe, Cu and Zn. The consortium enriched from an anaerobic lagoon of a local wastewater treatment plant was selected as the best metals-resistant SRB inoculum and its phylogenetic analysis of the dsr gene sequence revealed the presence of SRB species affiliated to *Desulfovibrio desulfuricans* and *Desulfobulbus rhabdoformis* (Martins 2009a). The results demonstrated that usually lethal concentrations of Fe (400 mg/L), Zn (150 mg/L) and Cu (80 mg/L) were not toxic and a very good efficiency in terms of sulfate reduction and metals removal was observed, while for other consortia enriched from different samples sulfate reduction was inhibited by the presence of copper and zinc. Both ethanol and lactate were efficiently used by the selected consortium. This highly metal-resistant SRB community was then used in the subsequent studies to inoculate the bioreactors to carry out AMD decontamination.

Neutralizing adjuvant for the biologic treatment of AMD

Marble stone powder (calcite tailing), a residual material resulting from the cutting and polishing of marble stone, an important Portuguese industry located not far from several national mining areas, was tested as a possible low-cost adjuvant for the biologic treatment of AMD. The performance of a combined chemical/biologic packed bed reactor containing the selected SRB inoculum and calcite tailing as neutralising agent mixed with coarse sand was assessed (Barros 2009). This work emphasized the key role played by the calcite waste in the inlet of the reactor by adjusting the pH to values adequate for SRB activity with low energy demand which would be impossible without its neutralisation action. Later the neutralizing and the biologic steps were separated to better control each stage of the treatment process, using two individual and sequential columns in an upflow continuous mode. Even later, during process optimization, the calcite column was replaced by a neutralization tank to avoid clogging (Fig. 2).

Selection of efficient low-cost carbon source

AMD is deficient in carbon sources/electron donors and thus requires the external addition for biologic sulfate reduction. However, the need of a carbon source is likely the most critical issue in AMD biologic treatment, determining the economic viability of the process which efficiency is highly dependent of the type of carbon and energy source utilized. To guarantee a viable economic process, wastes locally available at zero or even negative costs from the local food industry (wine wastes and cheese whey) were tested in batch as carbon sources (Martins 2009b). The results showed that these wastes could be efficiently used by these bacteria if calcite tailings were present as a neutralizing and buffer material: 95% and 50 % sulfate reduction were achieved within 20 days of experiment on media containing wine waste and cheese whey, respectively. Identification of the dissimilatory SRB community using the dsr gene revealed the presence of the species *Desulfovibrio fructosovorans*, *Desulfovibrio aminophilus* and *Desulfovibrio desulfuricans*. These findings demonstrated the potential of using wastes from the winery industry combined with calcite tailing for the development of cost-effective and environmentally friendly bioremediation processes.

The BIOMETAL DEMO project

Later, in the framework of BIOMETAL DEMO international project (Ballester 2017) five alternative industrial by-products and wastes from Portugal and Spain were tested: molasses from orange, molasses from sugar-beet, carbocal, domestic wastewater and olive mill wastewater (Carlier 2019). This work demonstrated the potential of new substrates largely available in the Iberian Peninsula and the respective required doses to feed SRB bioreactors in special for long-term passive bioremediation processes. Although relatively efficient, no one was able to compete with wine waste (Costa 2009), which remained the selected carbon source for the subsequent active systems tested in the laboratory (Fig. 2a) and for the pilot plant resulting from the process scale up further installed on situ in São Domingos. The pilot plant, set-up in collaboration of AGRI.PRO Ambiente, consisted of two serial neutralization tanks of 0.75 m^3 each filled with 450 kg of limestone followed by the biological treatment with SRB in one up-flow anaerobic packed bed reactor (UAPB) made of PEAD, with 4.5 m^3 capacity, filled with 8 metric tons of river stone, coarse sand, and limestone (Fig. 2b). In steady state conditions, water well below by the maximum values allowed by Portuguese legislation for irrigation (Decreto-Lei n.º 236/98, from 1 August, [SO_4^{2-}] = 575 mg/L; [Al] = 20 mg/L; [Fe] = 5 mg/L; [Zn] = 10 mg/L; [Cu] = 5 mg/L) was produced with one-week hydraulic retention time. When wine wastes were replaced by the domestic wastewater of the treatment plant where the pilot was installed, in a ratio of wastewater to AMD close to 1:1, about two weeks of hydraulic retention time was required to obtain water with similar quality. However, during operation, the system

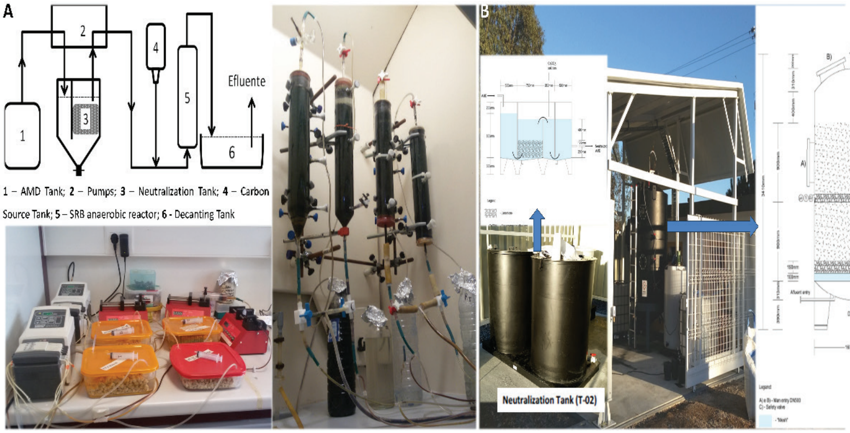

Figure 2 Lab scale continuous systems (A) to treat AMD using SRB and Pilot installation (B) at São Domingos.

faced problems mainly related to the low temperatures in winter and others associated to inefficient pH neutralization.

Dynamics of the bacterial populations

The dynamics of the bacterial populations in the UAPB during AMD treatment using wine wastes and ethanol as carbon source was investigated to better understand the bioremediation process (Martins 2011). The results demonstrated that the type of carbon source modulated the bacterial community. The bacterial diversity was higher in the bioreactor fed with wine waste where the dominant community was composed by bacteria affiliated with *Desulfovibrio* sp.. The presence of SRB and fermentative bacteria (*Clostridium* sp., Bacteroidales order, *Citrobacter* sp. and *Cronobacter* sp.) suggests a synergistic interaction between these bacterial groups and may be associated to the efficiency of such complex organic substrate.

The opportunities

Synthesis of metal sulfides NPs

During AMD treatment an excess of toxic hydrogen sulfide is produced which was the main reason to investigate its use to produce functional metal sulfides. Hence, batch tests where sulfide biologically generated by SRB was added to several unimetallic solutions demonstrated that ZnS (mainly sphalerite, 20–30 nm) (Costa 2012) and CuS (covellite, with a mean size of ~3.5 nm) (Costa 2013) nanocrystals could be synthesised in a simple way. Afterwards, the UAPB system used in AMD treatment was adapted (an "add-on" to the regular bioremediation system) to take advantage of the surplus H_2S contained in the treated effluent to produce zinc sulfide NPs (Vitor 2015) and other metal sulfides, or even NPs of reduced metals (Assunção 2016), under atmospheric temperature and pressure. With this, the environmental issue caused by the most problematic residue produced in AMD bioremediation, is not only minimized, but is also turned into an economic advantage, with the added benefit of dismissing the use of expensive and toxic chemicals and/or any sophisticated apparatus.

Recover of metals from extreme AMD

AMD waters have been regarded as a potential resource of metals due to the urgent need to recover or recycle metals from secondary resources benefiting the environment and stimulating circular economy and sustainability. Due to the presence of extreme AMD at São Domingos mine (impoundment next to the sulfur factory ruins at Achada do Gamo), with concentrations of copper higher than 5 g/L and zinc close to 2 g/L (Nobahar 2022a), a combination of chemical and biologic strategies based on the use of liquid-liquid extraction followed by SRB action was designed. In that process copper was first selectively extracted by ACORGA M5640 and then stripped using sulfuric acid to a purified aqueous phase, from where it was further precipitated and recovered as nanosized covellite with high purity, which may be used in a plethora of applications from medicine, catalysis and renewable energy devices.

Zinc recovery from the extreme copper free AMD was then attempted, but the high concentration of iron and their coextraction with several commercial extractants were the main drawbacks. The solution relied on the potential of AliCy, an ionic liquid, used to separate Fe(III) from the acidic multimetallic solution, followed by pH increase of the aqueous raffinate to values in the range of 3.25 to 3.50 (Nobahar 2022b). With this approach more than 90% of Fe(III) was separated and the remaining was removed by precipitation, with Zn losses lower than 18%. Thereafter, the highest Zn recovery from the medium resulting from such combination of processes was attained by precipitation using biogenic sulfide at pH = 3.5. The precipitates were identified as NPs of wurzite and sphalerite (ZnS) with sizes between 2 and 22 nm agglomerated into larger structures. These NPs may have applications as photocatalysts in H_2 production and in the degradation of toxic organic compounds, electrochemical sensors, among others.

Our group is currently investigating novel recovery options, focused on critical metals, and prioritizing green technologies, or others more environmentally friendly than those used until now, involving the use of new biomass and/or innovative materials not yet explored.

Cotreatments and acidophilic SRB

Since the BIOMETAL DEMO project where several wastes and domestic wastewater were used as carbon sources, the possibility of AMD cotreatment is being considered. We assessed the cotreatment of AMD and Olive Mill Wastewaters (OMWW), both coexisting in the same region, in SRB-enriched bioreactors (Carlier 2020). The process required a neutralizing agent to create optimal pH conditions for successful removal of the AMD's main contaminants. Sulfate, Al, Fe, Cu and Zn decreased below Portugal's maximum admissible values for irrigation waters, while phenol concentrations, the main pollutants in OMW, dropped to half their initial concentrations. Recently, an acid-tolerant SRB consortium, able to growth at pH 4.5 in the presence of methanol and mainly composed by *Desulfosporosinus* spp. was enriched from sediments from the confluence zone between its flow and treated sewage in São Domingos (Nobahar 2024). The use of acidophilic SRB may be promising for cotreatments by decreasing the required amounts of neutralizing agents and the ratios of wastewater:AMD. Presently, the potential use of acidophilic SRB consortia is under investigation and new projects aiming at their utilization in the cotreatment of AMD and other wastes are envisaged, expecting to bring new challenges and opportunities.

References

Assunção A, Vieira B, Lourenço JP, Costa MC (2016) Recovery of gold(0) nanoparticles from aqueous solutions using effluents from a bioremediation process. RSC Advances, 6(114):112784–112794, doi:10.1039/C6RA24503J

Ballester A, Castro L, Costa MC, Carlier JD, Roig MG, Péres-Galende PP, Alvarez A, Bertagnolli C, Guibal E (2017) Design of remediation pilot plants for the treatment of industrial metal-bearing effluents (BIOMETAL DEMO project): Lab tests. Hydrometallurgy 168:103–115, doi:10.1016/j.hydromet.2016.10.010

Barros RJ, Jesus C, Martins M, Costa MC (2009) Marble stone processing powder residue as chemical adjuvant for the biologic treatment of acid mine drainage. Process Biochemistry 44:477–480, doi:10.1016/j.procbio.2008.12.013

Carlier JD, Alexandre LM, Luís AT, Costa MC (2019) Potential of industrial by-products and wastes from the Iberian Peninsula as carbon sources for sulphate reducing bacteria. International Journal of Environmental Science and Technology 16(8):4719–4738, doi:10.1007/s13762-018-02197-z

Carlier JD, Luís AT, Alexandre LM, Costa MC (2020) Feasibility of co-treating olive mill wastewater and acid mine drainage. Mine Water and the Environment 39:859–880, doi:10.1007/s10230-020-00719-1

Costa MC, Duarte JC (2005) Bioremediation of acid mine drainage using acidic soil and organic wastes for promoting sulphate-reducing bacteria activity on a column reactor. Water, Air, and Soil Pollution 165(1–4):325–345, doi:10.1007/s11270-005-6914-7

Costa MC, Martins M, Jesus C, Duarte JC (2008) Treatment of acid mine drainage by sulphate-reducing bacteria using low-cost matrices, Water, Air, and Soil Pollution 189:149–162, doi:10.1007/s11270-007-9563-1

Costa MC, Santos ES, Barros, Pires C, Martins M. (2009) Wine wastes as carbon source for biological treatment of acid mine drainage. Chemosphere 75:831–836, doi:10.1016/j.chemosphere.2008.12.062

Costa JP, Girão AV, Lourenço JP, Monteiro OC, Trindade T, Costa MC (2012) Synthesis of nanocrystalline ZnS using biologically generated sulfide. Hydrometallurgy 117–118:57–63, doi:10.1016/j.hydromet.2012.02.005

Costa JP, Girão AV, Lourenço JP, Monteiro OC, Trindade T, Costa MC (2013) Green synthesis of covellite nanocrystals using biologically generated sulfide: Potential for bioremediation systems. Journal of Environmental Management 128:226–232, doi:10.1016/j.jenvman.2013.05.034

Martins M, Faleiro ML, Barros RJ, Veríssimo AR, Barreiros MA, Costa MC (2009a) Characterization and activity studies of highly heavy metal resistant sulphate-reducing bacteria to be used in acid mine drainage decontamination. Journal of Hazardous Materials 166:706–713, doi:10.1016/j.jhazmat.2008.11.088

Martins M, Faleiro ML, Barros RJ, Veríssimo AR, Costa MC (2009b) Biological sulphate reduction using food industry wastes as carbon sources. Biodegradation 20(4):559–567, doi:10.1007/s10532-008-9245-8

Martins M, Faleiro ML, Silva G, Chaves S, Tenreiro R, Costa MC (2011) Dynamics of bacterial community in up-flow anaerobic packed bed system for acid mine drainage treatment using wine wastes as carbon source. International Biodeterioration & Biodegradation 65:78–84, doi:10.1016/j.ibiod.2010.09.005

Nobahar A, Melka AB, Pusta A, Lourenço JP, Carlier JD, Costa MC (2022a) A new application of solvent extraction to separate copper from extreme acid mine drainage producing solutions for electrochemical and biological recovery processes. Mine Water and Environment 41(2):387–401, doi:10.1007/s10230-022-00858-7

Nobahar A, Melka B, Marín-Beltrán I, Neves V, Costa MC, Carlier J (2022b) Zinc recovery from an extreme copper free acid mine drainage: Studying the prior separation of ferric iron by solvent extraction using AliCy and/or alkalinization. Journal of Sustainable Metallurgy 8(4):1509–1531, doi:10.1007/s40831-022-00588-8

Nobahar A, Fitas ET, Costa MC, Carlier JD (2024) Acid mine drainage bioremediation using bacteria enriched from the confluence zone between its flow and treated sewage. International Journal of Environmental Science and Technology 6 Nov, doi:10.1007/s13762-024-06160-z

Pinto MC, Silva MV (2005) Contemporary reviews of mine water studies in Europe, Part 3, Overview of mining in Portugal. In: Wolkersdorfer C, Bowell C (Eds), IMWA Springer-Verlag, Mine Water and the Environment 24: 58–76, doi: 10.1007/s10230-005-0074-2

Vitor G, Palma TC, Vieira B, Lourenço JP, Barros RJ, Costa MC (2015) Start-up, adjustment and long-term performance of a two-stage bioremediation process, treating real acid mine drainage, coupled with biosynthesis of ZnS nanoparticles and ZnS/TiO2 nanocomposites. Minerals Engineering 75:85–93, doi:10.1016/j.mineng.2014.12.003

Water-Quality Modeling Tools to Evaluate Attenuation of Dissolved Constituents by Precipitation and Adsorption Reactions During Treatment of Acid Mine Drainage

Charles A. Cravotta III[1]

[1]*Cravotta Geochemical Consulting, Bethel, PA, USA, cravottageochemical@gmail.com,*
ORCID 0000-0003-3116-4684

Abstract

An understanding of geochemical reactions and environmental factors that control water quality is required for management and mitigation of environmental effects from acid mine drainage (AMD). This paper describes water-quality modeling tools that were developed to aid in the evaluation of key hydrogeochemical processes and their relative importance in controlling concentrations of dissolved metals and associated constituents in AMD and the effluents from treatment systems.

Keywords: Critical minerals, rare earth elements, equilibrium, kinetics, speciation, AMDTreat, PHREEQC

Introduction

Knowledge of the interactive processes that account for variations in pH and attenuation of dissolved metals is essential for the prediction of aquatic toxicological effects (e.g. Smith and Huyck, 1999) and the identification of strategies for treatment of acid mine drainage (AMD) to minimize impacts and control costs (e.g. Cravotta et al., 2015; Cravotta, 2021). To address aquatic toxicity concerns from excessive concentrations of metals, treatment of AMD is widely practiced to increase pH (> 6) and remove Fe (< 7 mg/L), Al (<1.5 mg/L), Mn (< 5 mg/L) and associated trace elements before discharging the effluent to receiving water bodies (e.g. Cravotta and Brady, 2015; Skousen et al., 2019; Nordstrom, 2020). Untreated, net-acidic AMD having pH < 5 frequently has elevated concentrations of rare-earth elements, yttrium, and scandium (REYs) plus various other trace elements, including cobalt (Co), copper (Cu), chromium (Cr), nickel (Ni), and zinc (Zn) that generally decrease as pH is increased through typical AMD treatment steps (Cravotta, 2008b; Cravotta and Brady, 2015; Vass et al., 2019a, 2019b; Hedin et al., 2020). The REYs and trace metals tend to be attenuated by adsorption to hydrous ferric oxides (HFO), hydrous aluminum oxides (HAO), and/or hydrous manganese (III–IV) oxides (HMO) that precipitate as the AMD is neutralized, forming AMD treatment solids (Smith et al., 1999; Cravotta, 2008b; Pourret and Davranche, 2013; Ayora et al., 2016; Cravotta et al., 2024; Hedin et al., 2024).

The REYs, Co, Cu, Cr, Ni, and Zn are among more than 50 "critical minerals" that are essential for modern industrial, transportation, energy, and electronics products and for which global supplies are vulnerable to disruption (Schulz et al., 2017; Nassar et al., 2020; White et al., 2024). Recovery of major metals plus REYs and other potentially valuable constituents from AMD could offset some treatment costs while addressing domestic supply concerns (Fritz et al., 2021). Nevertheless, the determination of optimal conditions for economic recovery of valuable trace components tends to be complicated because major components in typical AMD solutions and associated treatment solids tend to interact with and dilute the concentrations of more valuable trace components, particularly REYs. Although adsorption is the primary mechanism for REYs attenuation in passive systems and freshwater environments (Ayora et al., 2016; Hedin et al., 2024), precipitation of REYs with hydroxide, phosphate, carbonate, or oxalate compounds may also be feasible, especially through active chemical treatment (Zhang and Honaker, 2018; Josso et al., 2018; Edahbi et al., 2018; Royer-Lavallée et al., 2020; Wang et al., 2021; Leon et al., 2021; Mwewa et al., 2022; Hermassi et al., 2022).

Methods

This study employs the interactive PHREEQ-N-AMDTreat (v.1.4.5) and PHREEQ-N-AMDTreat+REYs (v.1.0.5) water-quality modeling tool sets (Cravotta, 2021, 2022) that use PHREEQC (Parkhurst and Appelo, 2013) with a customized thermodynamic database including new adsorption constants (Tasker et al., 2025). These models simulate changes in pH, dissolved metals, and associated solutes resulting from passive and active treatment of AMD. In addition to Fe, Al, Mn, and major elements, the PHREEQ-N-AMDTreat+REYs tools consider various trace elements and REYs. Each tool set consists of a caustic titration model and a sequential reaction model. Stand-alone models are available from the U.S. Geological Survey (Cravotta, 2020, 2022), and modified versions will be accessible as "new" tools through radio buttons in the final version of the AMDTreat 6.0 cost-analysis model, now available as a beta release (Office of Surface Mining Reclamation and Enforcement, 2022).

A user interface (UI), which automatically displays a default dataset, facilitates the input of user-defined water-chemistry and flow data for one or two solutions and the adjustment of important system variables, such as reaction rates, mineral solubility, and sorbent characteristics. Adsorption of cations and anions is computed for freshly precipitated HFO, HAO, and HMO having specified surface area, plus previously accumulated sorbent that has known mass of HFO, HAO, and HMO components. Fresh HFO is formed by precipitation of schwertmannite and $Fe(OH)_3$, HAO by hydrobasaluminite and $Al(OH)_3$, and HMO by manganite and $Mn(OH)_2$, at a selected saturation index.

The CausticTitration and CausticTitrationMix2REYs tools compute the equilibrium concentrations of elements among dissolved, precipitated, and sorbed fractions as a function of pH and other solution characteristics. The pH is automatically increased by 0.25-unit intervals from the initial pH to a maximum pH of 11 by the incremental addition of an acid-neutralizing agent (NaOH, $Ca(OH)_2$, CaO, Na_2CO_3, or $CaCO_3$). For both tools, the amount of caustic reacted to achieve the target pH is included in the output with other information such as the concentrations of elements in solution and solids. Graphical and tabular output for each of the water-quality tools indicates the pH, specific conductance, total dissolved solids, alkalinity, net acidity, metals, and other solute concentrations of treated effluent plus the mass and generalized composition of precipitated solids as a function of retention time and/or the amount of caustic (or oxidizing) agent added.

The TreatTrainMix2 and TreatTrainMix2REYs tools incorporate equilibrium aqueous and surface speciation *plus kinetics models* for gas exchange, iron and manganese oxidation and precipitation, limestone dissolution, and organic carbon oxidation combined with reduction of nitrate, sulfate, and ferric iron. Reactions with caustic chemicals or hydrogen peroxide (H_2O_2) coupled with aeration may be simulated separately or combined with additional kinetic steps. Sludge recirculation or reactive coatings on limestone surfaces are modeled by indicating a mass of previously accumulated sorbent.

Results

Equilibrium models using the "CausticTitrationMix2REYs.exe" tool accurately indicated the observed attenuation of REYs over pH ~4.5 to 6 for AMD containing SO_4 (820 mg/L), Fe (103 mg/L), Al (9.5 mg/L), Mn (2.9 mg/L), and individual REE of 58.9 ± 10.3 mg/L titrated with NaOH (Fig. 1). Because of presumed "instantaneous" oxidation, however, the equilibrium model did not accurately simulate observed Fe and Mn concentrations. To better account for redox disequilibrium, a kinetic model was applied to simulate gradual oxidation of FeII and MnII over the 24-hour reaction period. The kinetic model yielded reasonable agreement with observed results for Fe and Mn, but with relatively unchanged results for REYs. In this particular example, almost all the REYs adsorption could be accounted for solely by the precipitation of the initial 3 mg/L Fe^{III} that formed HFO at pH <4, with less than 2% of sorption by more abundant HAO. All the REYs had been attenuated before Mn oxidation and hydrolysis, so none were attenuated by HMO.

Highly acidic leachate (10,500 mg/L as $CaCO_3$) with elevated concentrations of Fe, Al, Mn, and REYs discharged at a coal-refuse facility was considered as a test case to evaluate treatment strategies that could produce a concentrated REYs extract. This facility currently utilizes lime neutralization, which causes precipitation of Fe, Al, and REYs into complex Fe-Al-Ca rich sludge mixture. The lime treatment and two hypothetical strategies that could feasibly concentrate REYs were simulated with the "TreatTrainMix2REYs.exe" tool (Fig. 2). The lime treatment to pH ~8.7 rapidly removes REYs with the sludge mixture. In contrast, alternative strategies using H_2O_2 to oxidize Fe^{II} demonstrate potential for removal of most Fe and Al without initial removal of REYs. In one case, NaOH is added to attain pH 3 followed by aeration to precipitate Fe and Al oxyhydroxides while maintaining pH <4.5. Subsequent aeration and further increasing pH with limestone promotes adsorption of REYs by HAO and HMO that form thereafter. In another case, NaOH and NaH_2PO_4 were added to precipitate REY-PO_4 after H_2O_2 addition (e.g. Hermassi et al., 2022). In both cases, REYs-enriched solids produced by the alternative treatments contain a small fraction of the initial Fe and Al and most of the REYs. Using these results as guidance, bench-scale testing of the modeled treatment steps to concentrate REYs into solids may be considered to test the results and optimize extraction of the REYs from the various solid components (e.g. Rushworth et al., 2023; Boothe et al., 2024).

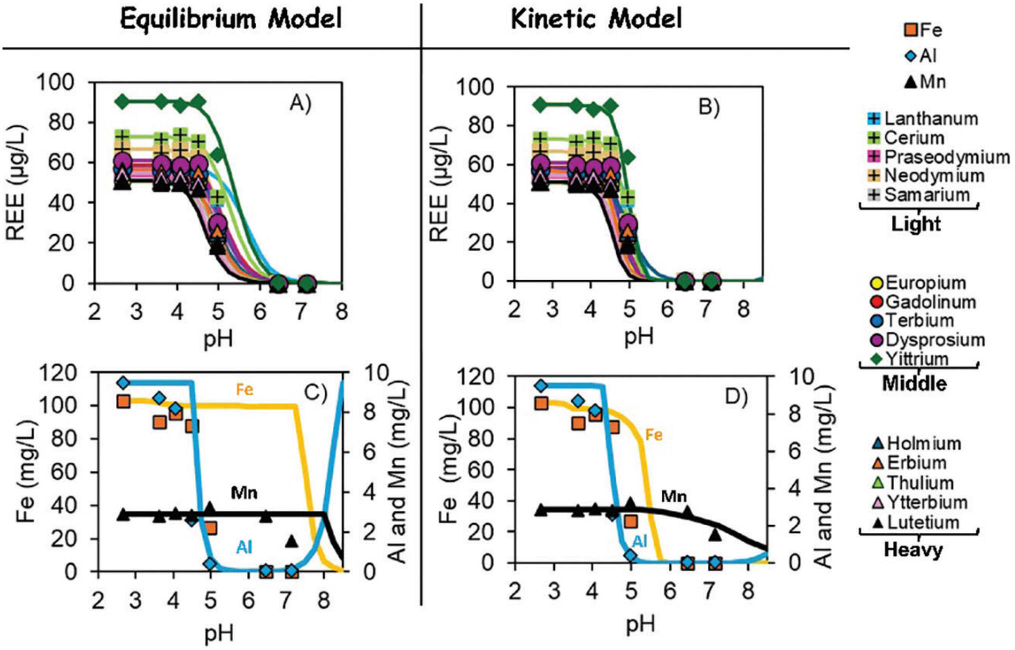

Figure 1 Comparison of measured (symbols) and PHREEQ-N-AMDTreat+REYs simulation results (curves) for pH and concentrations of dissolved Fe, Al, Mn, and REYs in AMD from the Hughes Borehole (after Tasker et al., 2025). Oxidation of FeII and MnII is instantaneous for the equilibrium model but varies with pH for kinetic model.

Considering the design flow with the modeled reaction time estimates for each of the treatment system components in the TreatTrainMix2 or TreatTrainMix2REYs model, the size (land area, pond volume, limestone bed volume, etc.) of a treatment component can be estimated (Cravotta, 2021). Now, a user may use these reaction times in the AMDTreat 6.0 cost-analysis model (Office of Surface Mining Reclamation and Enforcement, 2022) to readily (1) estimate the sizing and quantities of reactive materials for specific treatment steps; (2) compute the land-area and costs for installation and operation of relevant components; and (3) evaluate the cost-effectiveness of alternatives for AMD treatment that could meet effluent discharge limits and also result in effective recovery of Fe, Al, Mn, and various critical minerals.

Conclusions

Water-quality modeling tools are now freely available to aid in the evaluation of key hydrogeochemical processes and their relative importance for controlling concentrations of dissolved metals and associated constituents in AMD through sequential steps in treatment systems. By adjusting the modeled chemical dosing or kinetic variables, such as aeration rate and duration, the effects of independent and sequential treatment steps that have different retention times or quantities of reactive solids, such as limestone or sorbing substrates, can be simulated. The reaction

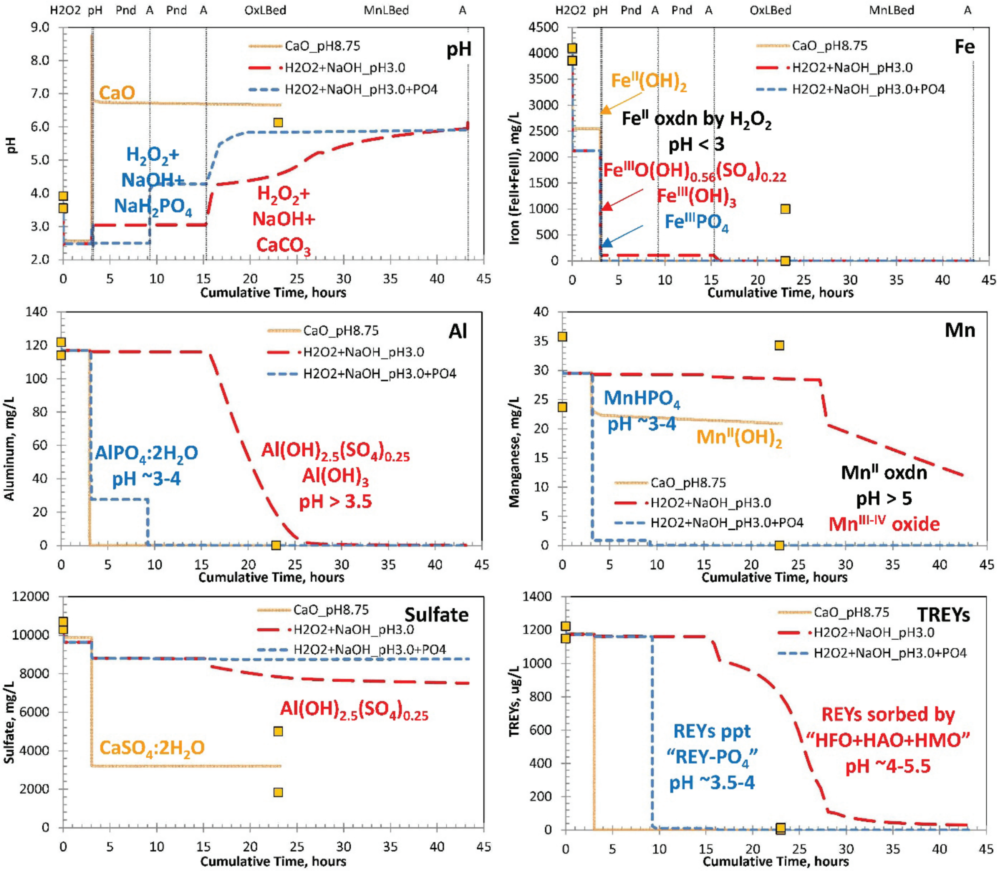

Figure 2 Comparison of measured (symbols) and PHREEQ-N-AMDTreat+REYs simulation results (curves) for pH and dissolved Fe, Al, Mn, SO4, and total REYs concentrations at a coal-refuse disposal facility. Measured values are for lime treatment without H2O2, sampled on two different dates (adapted from Cravotta et al., 2024).

times considered for the kinetics models correspond to retention times for the modeled treatment steps. The retention times can be used with known or anticipated AMD flow rates to estimate the dimensions of the system components, such as a limestone bed or pond, the quantities of reactive materials consumed or sludge generated, and corresponding installation and operation costs for individual components and the overall treatment system.

References

Ayora C, Macías F, Torres E, Lozano A, Carrero S, Nieto JM, Pérez-López R, Fernández-Martínez A, Castillo-Michel H (2016) Recovery of rare earth elements and yttrium from passive-remediation systems of acid mine drainage. Environ Sci Tech 50:8255–8262. https://doi.org/10.1021/acs.est.6b02084

Cravotta CA III (2008a) Dissolved metals and associated constituents in abandoned coal-mine discharges, Pennsylvania, USA – 1. Constituent concentrations and correlations. Appl Geochem 23:166–202. https://dx.doi.org/10.1016/j.apgeochem.2007.10.011

Cravotta CA III (2008b) Dissolved metals and associated constituents in abandoned coal-mine discharges, Pennsylvania, USA – 2. Geochemical controls on constituent concentrations. Appl Geochem 23:203–226. https://dx.doi.org/10.1016/j.apgeochem.2007.10.003

Cravotta CA III (2020) Interactive PHREEQ-N-AMDTreat water-quality modeling tools to evaluate performance and design of treatment systems for acid mine drainage (software download). US Geol Surv Software Release https://doi.org/10.5066/P9QEE3D5

Cravotta CA III (2021) Interactive PHREEQ-N-AMDTreat water-quality modeling tools to evaluate performance and design of treatment systems for acid mine drainage. Appl Geochem 126:104845. https://doi.org/10.1016/j.apgeochem.2020.104845

Cravotta CA III (2022) Interactive PHREEQ-N-AMDTreat+REYs water-quality modeling tools to evaluate potential attenuation of rare-earth elements and associated dissolved constituents by aqueous-solid equilibrium processes (software download). US Geol Surv Software Release. https://doi.org/10.5066/P9M5QVK0

Cravotta CA III, Brady KBC (2015) Priority pollutants and associated constituents in untreated and treated discharges from coal mines in Pennsylvania, U.S.A. Appl Geochem 62:108–130. https://doi.org/10.1016/j.apgeochem.2015.03.001

Cravotta CA III, Means B, Arthur W, McKenzie R, Parkhurst DL (2015) AMDTreat 5.0+ with PHREEQC titration module to compute caustic chemical quantity, effluent quality, and sludge volume. Mine Water Environ 34:136–152. https://doi.org/10.1007/s10230-014-0292-6

Cravotta CA III, Tasker TL, Hedin BC (2024) Laboratory and field observations inform geochemical models of treatment strategies to recover rare-earth elements from acid mine drainage. – In: Kleinmann, B., Skousen, J., Wolkersdorfer, Ch.: West Virginia Mine Drainage Task Force Symposium & 15th International Mine Water Association Congress, Morgantown, WV, USA, p. 98–104. https://www.imwa.info/docs/imwa_2024/IMWA2024_CravottaIII_98.pdf.

Edahbi E, Plante B, Benzaazoua M, Ward M, Pelletier M (2018) Mobility of rare earth elements in mine drainage: Influence of iron oxides, carbonates, and phosphates. Chemosphere 199:647-654. https://doi.org/10.1016/j.chemosphere.2018.02.054

Fritz AG, Tarka TJ, Mauter MS (2021) Technoeconomic assessment of a sequential step-leaching process for rare earth element extraction from acid mine drainage precipitates. ACS Sustainable Chem Engineer 9:9308-9316. https://doi.org/10.1021/acssuschemeng.1c02069

Hedin BC, Hedin RS, Capo RC, Stewart BW (2020) Critical metal recovery potential of Appalachian acid mine drainage treatment solids. Int J Coal Geol 231:103610. https://doi.org/10.1016/j.coal.2020.103610

Hedin BC, Stuckman MY, Cravotta CA III, Lopano CL, Capo RC (2024) Determination and prediction of micro scale rare earth element geochemical associations in mine drainage treatment wastes: Chemosphere 346:140475. https://doi.org/10.1016/j.chemosphere.2023.140475

Hermassi M, Granados M, Valderrama C, Ayora C, Cortina JL (2022) Recovery of rare earth elements from acidic mine waters: An unknown secondary resource. Sci Tot Environ 810:152258. https://doi.org/10.1016/j.scitotenv.2021.152258

Josso P, Roberts S, Teagle DAH, Pourret O, Herrington R, Ponce de Leon Albarran C (2018). Extraction and separation of rare earth elements from hydrothermal metalliferous sediments. Min Eng 118:106–121. https://doi.org/10.1016/j.mineng.2017.12.014

Leon R, Macias F, Canovas CR, Perez-Lopez R, Ayora C, Nieto JM, Olias M (2021) Mine waters as a secondary source of rare earth elements worldwide: The case of the Iberian Pyrite Belt. J Geoch Explor 224:106742. https://doi.org/10.1016/j.gexplo.2021.106742

Mwewa B, Tadie M, Ndlovu S, Simate GS, Mitinde E (2022) Recovery of rare earth elements from acid mine drainage: A review of the extraction methods. J Environ Chem Eng 10:107704. https://doi.org/10.1016/j.jece.2022.107704

Nassar NT, Brainard J, Gulley A, Manley R, Matos G, Lederer G, Bird LR, Pineault D, Alonso E, Gambogi J, Fortier SM (2020) Evaluating the mineral commodity supply risk of the U.S. manufacturing sector. Sci Adv

6:eaay8647. https://doi.org/10.1126/sciadv.aay8647

Nordstrom, DK (2011) Hydrogeochemical processes governing the origin, transport and fate of major and trace elements from mine wastes and mineralized rock to surface waters. Appl Geochem 26, 1777–1791. https://doi.org/10.1016/j.apgeochem.2011.06.002

Nordstrom DK (2020) Geochemical modeling of iron and aluminum precipitation during mixing and neutralization of acid mine drainage. Minerals 10:547. https://doi.org/10.3390/min10060547

Office of Surface Mining Reclamation and Enforcement (2022) AMDTreat 6.0 Beta. https://www.osmre.gov/programs/reclaiming-abandoned-mine-lands/amdtreat

Parkhurst DL, Appelo CAJ (2013) Description of input and examples for PHREEQC version 3–A computer program for speciation, batch-reaction, one-dimensional transport, and inverse geochemical calculations. US Geol Surv Tech Methods 6-A43. https://doi.org/10.3133/tm6A43

Pourret O, Davranche M (2013) Rare earth element sorption onto hydrous manganese oxide: a modeling study. J Colloid Interface Sci 395:18–23. https://doi.org/10.1016/j.jcis.2012.11.054

Royer-Lavallée A, Neculita CM, Coudert L (2020) Removal and potential recovery of rare earth elements from mine water. J Indust Chem Eng 89:47–57. https://doi.org/10.1016/j.jiec.2020.06.010

Schulz KJ, DeYoung JH Jr., Seal RR II, Bradley DC, eds. (2017) Critical mineral resources of the United States – Economic and environmental geology and prospects for future supply: US Geol Surv Prof Paper 1802. https://doi.org/10.3133/pp1802I

Skousen JG, Ziemkiewicz PF, McDonald LM (2019) Acid mine drainage formation, control and treatment: Approaches and strategies. Extr Ind Soc 6:241–249. https://doi.org/10.1016/J.EXIS.2018.09.008

Smith KS, Huyck HLO. (1999) An overview of the abundance, relative mobility, bioavailability, and human toxicity of metals. In: Plumlee, G..S., Logsdon, M.J. (Eds.), The Environmental Geochemistry of Mineral Deposits – Part A.Processes, methods, and health issues. Reviews in Economic Geology 6A, 29–70.

Smith KS, Ranville JR, Plumlee GS, Macalady DL (1998) Predictive double-layer modeling of metal sorption in mine-drainage systems. In. Metal Adsorption by Geomedia, Jenne, E.A. (Ed.). San Diego, Academic Press, 521–547.

Tasker TL, Cravotta CA III, Roman B (2025) Sorption of rare-earth elements and yttrium (REE) with hydrous ferric oxide and hydrous aluminum oxide – Roles of sulfate and pH. Appl Geochem, submitted.

Vass CR, Noble A, Ziemkiewicz PF (2019a) The occurrence and concentration of rare earth elements in acid mine drainage and treatment byproducts: Part 1 – Initial survey of the northern Appalachian coal basin. Mining Metal Explor 36:903–916. https://doi.org/10.1007/s42461-019-0097-z

Vass CR, Noble A, Ziekiewicz P (2019b) The occurrence and concentration of rare earth elements in acid mine drainage and treatment byproducts. Part 2 – regional survey of northern and central Appalachian coal basins. Mining Metal Explor 36:917–929. https://doi.org/10.1007/s42461-019-00112-9

White SJ, Kane T, Campbell K, Croteau MN, Iacchetta M, Blake J, Cravotta CA, Kunz B, Alpers CN, Jenkins J, Walton-Day K (2024) A multidisciplinary approach that considers occurrence, geochemistry, bioavailability, and toxicity to prioritize critical minerals for environmental research. Environmental Science & Technology 58, 22519–22527. https://doi.org/10.1021/acs.est.4c11211

Zhang W, Honaker RQ (2018) Rare earth elements recovery using staged precipitation from a leachate generated from coarse coal refuse. International Journal of Coal Geology 195:189–199. https://doi.org/10.1016/j.coal.2018.06.008

Physicochemical Characterisation of Pit Lakes Using Google Earth Engine: Chilean Case Study

Damián Cruz Barrientos[1], Oscar Benavente Zolezzi[2,3], Álvaro Navarrete Calvo[1], Camilo Sánchez Yáñez[1]

[1]*Universidad Mayor, Escuela de Geología, Cam. La Pirámide 5750, Huechuraba, Santiago, Chile, damian.cruz@mayor.cl.*

2SRK Consulting – Denver, GeoEnvironmental Group, 1125 17th St Ste 600, Denver, USA, obenavente@srk.com.

3SRK Consulting Spa – Chile, Cierre de Minas y Geoquímica, Av. Vitacura 2939, Piso 5, Las Condes, Santiago, Chile, obenavente@srk.com.

Abstract

This study uses satellite imagery and the HSV color model to assess pit lake water quality. Water color results from sunlight interactions influenced by dissolved ions and suspended particles. Transition metals form distinct complexes (Fe^{2+}: olive green, Cu^{2+}: blue-green, Fe^{3+}: brown-yellow), while oxyhydroxide colloids scatter specific wavelengths (Fe: red-orange, Al: white). Because pH and redox conditions affect ion complexation and mineral phase formation, HSV variations can reflect physicochemical changes. Validation at Berkeley Pit Lake showed correlations between satellite-derived HSV and known events. The method is being applied to Chilean pit lakes for environmental monitoring, aiding early detection of environmental changes.

Keywords: Mine Closure Plan, Pit Lakes Monitoring, Satellite Imagery, Acid Mine Drainage, Water Quality

Introduction

A large portion of the environmental issues linked to mining stem from the waste generated during extraction, with pit lakes being among the most challenging mining legacies to manage. These water bodies are prone to physicochemical changes due to prolonged exposure to minerals like pyrite, which can lead to acidic conditions and elevated sulfate and trace element concentrations in the pit lake and nearby water bodies. This study aims to develop a robust methodology and numerical dataset to analyze, monitor, and determine the physicochemical characteristics of pit lakes using satellite imagery.

The innovation of this research lies in its development of a cost-effective methodology for monitoring pit lakes through the color of the water in the HSV (Hue, Saturation, Value) model. Several studies have shown that the true color of the water can indicate the hydrochemical conditions of water bodies. For instance, Murphy *et al.*, (2018), and Ohsawa *et al.*, (2009) found that dissolved Fe^{2+} gives water a green olive hue due to light absorption, while native sulfur particles scatter a blue hue in volcanic crater lakes. Castellón *et al.*, (2013) observed that aluminium colloids influence water color by reflecting light in all visible wavelengths (i.e., whitish color to the water), producing the unusual sky-blue color of Celeste River in Costa Rica. Additionally, the reddish color of iron oxides, oxyhydroxides, and hydroxides is a well-known characteristic of these mineral phases, used as pigments since prehistoric times (Torrent & Barrón, 2002). These findings suggest that the physicochemical characteristics of pit lakes can be inferred from satellite imagery, as mineral speciation and ion complexation are pH and redox-dependent.

Time series of HSV values for each pit lake under study were calculated using surface reflectance data from Landsat and Sentinel-2 missions, processed via the Google Earth Engine with Python. By correlating the H, S and V of the water with physicochemical properties such as pH, redox, metal concentrations and stratification states. This methodology was validated using the publicly available dataset from Berkeley Pit Lake, Montana, USA, compiled by INAP in the Pit Lakes Database. This acidic pit lake has historical water quality records dating back to the 1980s, overlapping with publicly available satellite data from Landsat 4, 5, 7, 8, and 9, and Sentinel-2 satellites. Following this validation, the methodology was applied to Chilean pit lakes with data in situ identified through web scraping, allowing for a broader assessment of its applicability in diverse mining environments.

Method

Satellite imagery from Landsat 4, 5, 7, 8, 9, and Sentinel-2, stored in Google Earth Engine (GEE), was analysed to determine the true colour of pit lakes.

The process starts with the identification and delineation of the pit lake under study over multi scenes. To do so, a two-steps method involving the uses of Normalised Difference Water Index (NDWI) and a supervised machine learning technique, Random Forest, were employed.

The first step corresponds to the identification and segmentation of the pit lakes using the NDWI histogram, calculated as (GREEN – NIR) / (GREEN + NIR), and the OTSU algorithm (Otsu, 1979). Metadata, including acquisition date, scene name, solar azimuth, cloud cover percentage, and water surface area, was extracted and stored in an Excel database for each scene. Scenes without detected water were assigned an NDWI value of 10, and each scene was validated manually by assigning 1 for correct mapping and 0 for incorrect mapping. This process is applied to each of the six satellite collections, independently.

Validated scenes (i.e., scenes where the NDWI threshold value found by the OTSU algorithm properly identifies water and non-water pixels) were then used as training cases of a Random Forest algorithm. This supervised machine learning technique uses all the available bands in each satellite collection to derive a suitable algorithm capable to distinguish water and non-water pixels. An optimum number of seven validated scenes are recommended to be used in the training process with sufficient temporal spacing among them to capture possible changes in colour and surface variations of the water body. This process is also applied to each of the six satellite collections independently.

After identifying and segmenting the pit lakes, water pixels were processed to extract HSV color values by converting RGB to HSV (Fig. 1), enabling a more detailed interpretation of lake color variations, following the method used in Murphy *et al.*, (2018).

A grid of points was generated on the lake to extract HSV values and then were stored in an Excel template for inter-satellite comparisons, compiling the following dataset:

- Mean HSV values across all points
- HSV at the lake's central point (determined by Euclidean distance)
- 5th, 50th, and 95th percentile values of HSV

For a better representation of hue (0–1), a polar histogram was used, where hue values

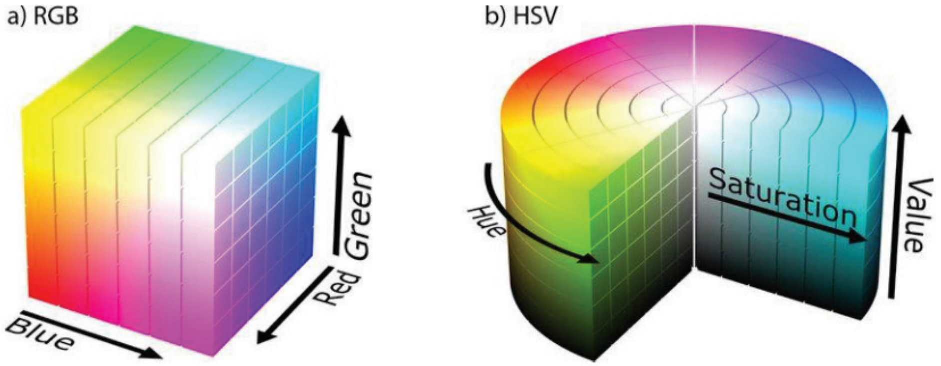

***Figure 1** RGB and HSV model color (Extracted from Saraullo* et al., *2019).*

Table 1 *Summary of satellite images analysed and classification accuracy of NDWI and Random Forest.*

Remote Sensor	Landsat 5	Landsat 7	Landsat 8	Landsat 9	Sentinel 2	Total images
Images Evaluated	159	610	52	107	235	1163
NDWI Correct (%)	26 (16.35%)	41 (6.72%)	10 (19.23%)	12 (11.21%)	103 (43.82%)	192 (16.5%)
RF Correct (%)	125 (78.61%)	599 (98.19%)	36 (69.23%)	48 (44.85%)	162 (68.93%)	970 (83.4%)

were transformed by multiplying by 360. The transformed dataset was subjected to QA/QC filters to improve data reliability and select the most representative images of each pit lake.

The validation process was conducted using the INAP Pit Lakes Database, which provided access to comprehensive historical data. Berkeley Pit was selected as the validation site due to its large surface area, extensive temporal data in situ, and documented studies of its evolution. Hydrochemical modelling of Berkeley Pit Lake data using PHREEQC allowed for an improved understanding of the redox conditions, mineral saturation indices and co-precipitation processes affecting water colour dynamics.

Once validated, the methodology was applied to Chilean pit lakes with available public data. To identify these lakes, a Python-based web scraping script was developed to extract relevant information from the SEA (Servicio de Evaluación Ambiental) website. The validated methodology was then applied to these sites, ensuring a systematic remote sensing approach for assessing physicochemical characteristics in pit lakes across Chile.

Results

Validation – Berkeley Pit Lake Case

The methodology was validated using satellite imagery of Berkeley Pit Lake. A total of 1163 images were found for Berkeley Pit Lake between May 1984 to September 2024, with NDWI correctly identifying water bodies in only 16.5% of the total cases. In contrast, the Random Forest algorithm achieved a significantly higher accuracy of 83.4% (Tab. 1).

To ensure an accurate representation of pit lake color, a QA/QC filtering process was applied to the 1163 images. The first filter, based on mean color variation below 35°, removed 433 images, leaving 730 valid scenes. The second filter, applying a dispersion coefficient threshold ($R > 0.95$), further reduced the dataset to 439 images. The third filter, incorporating manual area mapping with a 20% error margin, gives in a final dataset of 311 images for analysis (Tab. 2).

The evolution of HSV reveals the occurrence of four stages (Fig. 2), which are closely associated with changes in hydrochemistry over time:

- **Stage 1 (1984–1988):** Green olive hues ($H = 0.25$, $S = 0.35$, $V = 0.05$) indicate a dominant presence of Fe^{2+}, with more dissolved iron suggesting the onset of acid conditions due to groundwater contact with sulfide rocks. This phase exhibits a meromictic state, defined by the establishment of a deep chemocline.
- **Stage 2 (1988–1997):** Increase of the Fe^{3+}/Fe^{2+} ratio due to oxidation, changing the color of the water to yellow-brown ($H = 0.15$, $S = 0.35$, $V = 0.04$). This transformation is supported by an increase in the pe values of the water while maintaining an almost constant pH.
- **Stage 3 (1997–2013):** The introduction of alkaline tailings sludge into the pit lake during this stage resulted in the co-precipitation of Fe-oxyhydroxides and Fe-oxyhydroxide-sulfate. This process is

Table 2 *QA/QC filtering process for satellite images used in the evaluation.*

Remote Sensor	Landsat 5	Landsat 7	Landsat 8	Landsat 9	Sentinel 2	Total images
Images Evaluated	159	610	52	107	235	1163
1st QA/QC Filter	131	451	30	49	69	730
2nd QA/QC Filter	72	241	29	39	58	439
3rd QA/QC Filter	54	169	23	19	46	311

evident from the saturation indexes of Schwertmannite, Goethite, Jarosite and Ferrihydrite, and the colloidal particles of these minerals produced scattering effects that shifted the lake's hues towards red-orange and lower V values observed in this period (H = 0.07, S = 0.45, V = 0.03). Due to the alkaline tailings disposal the lake returned to a holomictic state in 2010, with a rise in pH from 2.5 to 4 and a decline in Fe concentrations from 1000 mg/L to 0.5 mg/L, accompanied by the disappearance of the chemocline. These changes were further corroborated by the vertical homogeneity of the water column, indicating the absence of chemical stratification.

- **Stage 4 (2013–Present):** The most recent stage is characterised by a marked increase in H, S, and V values (H = 0.45, S = 0.8, V = 0.1), reflecting near-complete co-precipitation of Fe-oxyhydroxides and Fe-oxyhydroxide-sulfates, and the initiation of the co-precipitation of Al-oxyhydroxides and Al-oxyhydroxide-sulfates (Jurbanite – Alunite). This transition alters the light reflectance properties of the pit lake, as Al-oxyhydroxides-sulfates scatters the lights in all the visible wavelengths (increase in S and V), enhancing the color given by both dissolved Fe^{2+} and Cu^{2+}.

Application on Chilean Pit Lakes

Currently, Chile does not have an official registry of pit lakes. In this study, a numerical

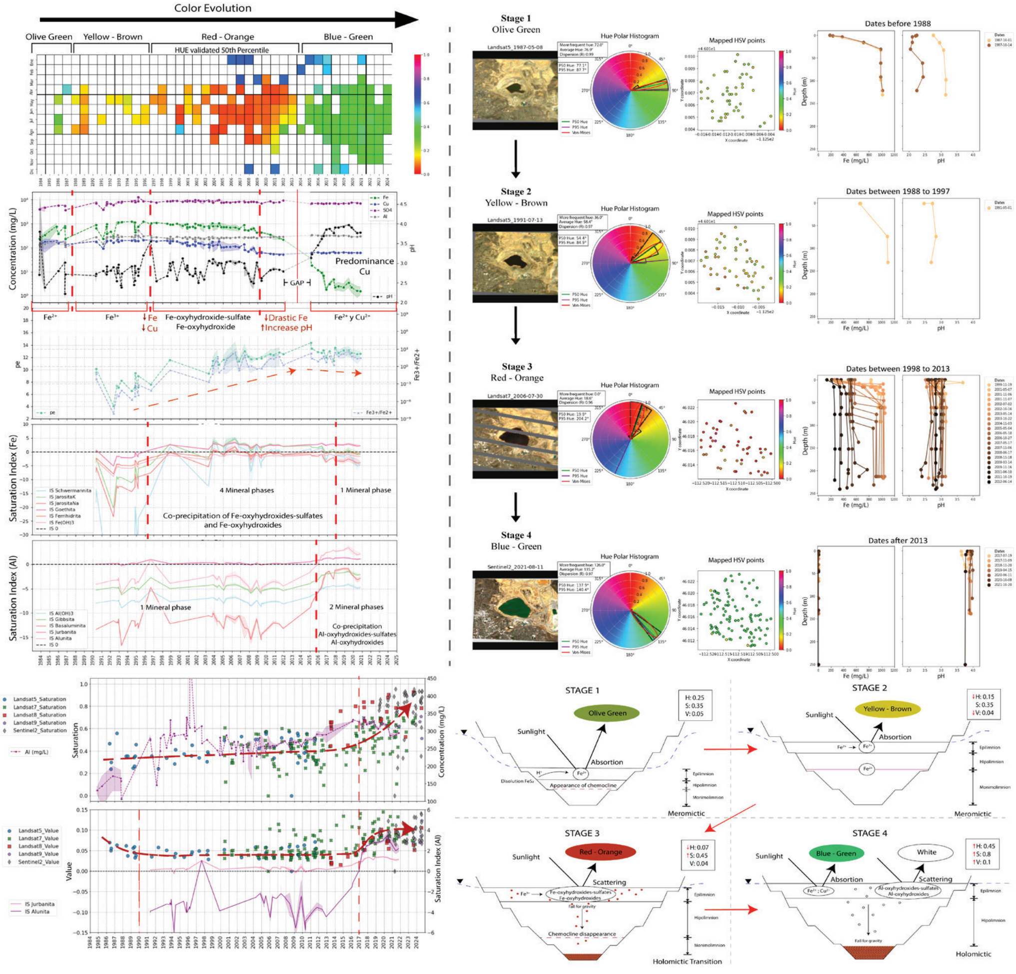

Figure 2 Correlation between true-color pit lake and in situ physico-chemical parameters.

database was established, identifying a total of 111 pit lakes across 46 mining sites. At these 46 mining sites, a web scraping approach was applied to search for available environmental data. This process identified 23 pit lakes (20.4%) with reported physicochemical parameters, allowing the methodology to be applied to those with in situ data (Tab. 3).

The analyzed pit lakes predominantly exhibit sulfate-calcium water types, with pH values ranging from acidic to neutral-alkaline (1–9), electrical conductivity (500 –140000 µS/cm), and concentrations of SO_4 (40–185000 mg/L), Cu (0.001–4000 mg/L), Fe (0.001–4300 mg/L), and Al (0.005–7800 mg/L).

Most pit lakes in Chile have an olive green hue (H = 0.3), indicating the presence of dissolved Fe^{2+}. In some cases, on limited dates, the color changes to blue-green, suggesting the presence of dissolved Cu^{2+}, typically associated with neutral to alkaline pH conditions (Fig. 3).

In two specific cases (Mina Sur and Quebrada Blanca) the color of the pit lake was initially olive green, then changed to a yellow-brown and finally to a red-orange. Given the red-orange color, this indicates the presence of colloids Fe hydroxides, suggesting that the pH conditions are acidic (Fig. 3).

The application of this method made it possible to determine the time of occurrence of the pit lake (i.e., "Cerro Blanco"), its seasonal occurrence being only between September and February. It also made it possible to determine backfill times in different pit lakes (i.e., "Andacollo").

One of the limitations of the application of this methodology in Chilean pit lakes is the presence of shadows projected on the lake. This effect is particularly pronounced in winter due to the steep slopes of the Andean range and the low solar azimuth, which complicates the accurate segmentation of water bodies, as observed in the case of "El Soldado" (Fig. 4).

Another limitation is the low surface area of the pit lakes, which results in poor segmentation using random forest, due to the low number of pixels representing the water body. Therefore, for a reliable representation of the data, a minimum threshold of 10 pixels is recommended, resulting in an area of approximately 9000 m^2 in Landsat images and

Table 2 Summary of data collected through web scraping of pit lakes in Chile.

Mining Site	Type of deposit	Number of samples	Data type	No. of pit lakes with data
Andacollo	Copper Porphyry	4	Tables	4
Candelaria	IOCG	108	Database	1
Cerro Blanco	Calcium Carbonate (Others)	1	Database	1
Cerro Colorado	Copper Porphyry	12	Modeling	2
Chuquicamata	Copper Porphyry	4	Database	1
Collahuasi	Copper Porphyry	39	Database	1
El Salvador	Copper Porphyry	16	Writings and Laboratory Certificates	3
El Soldado	Stratabound	3	Laboratory Certificates	1
La Coipa	Porphyry / Epithermal Au	4	Modeling	1
Los Bronces	Copper Porphyry	4	Database	1
Mina Sur	Copper Porphyry	9	Database	1
Quebrada Blanca	Copper Porphyry	54	Database	3
Santo Domingo	Stratabound	2	Tables	2
Zaldívar	Copper Porphyry	3	Database	1
Total	**5**	**260**	**5**	**23**

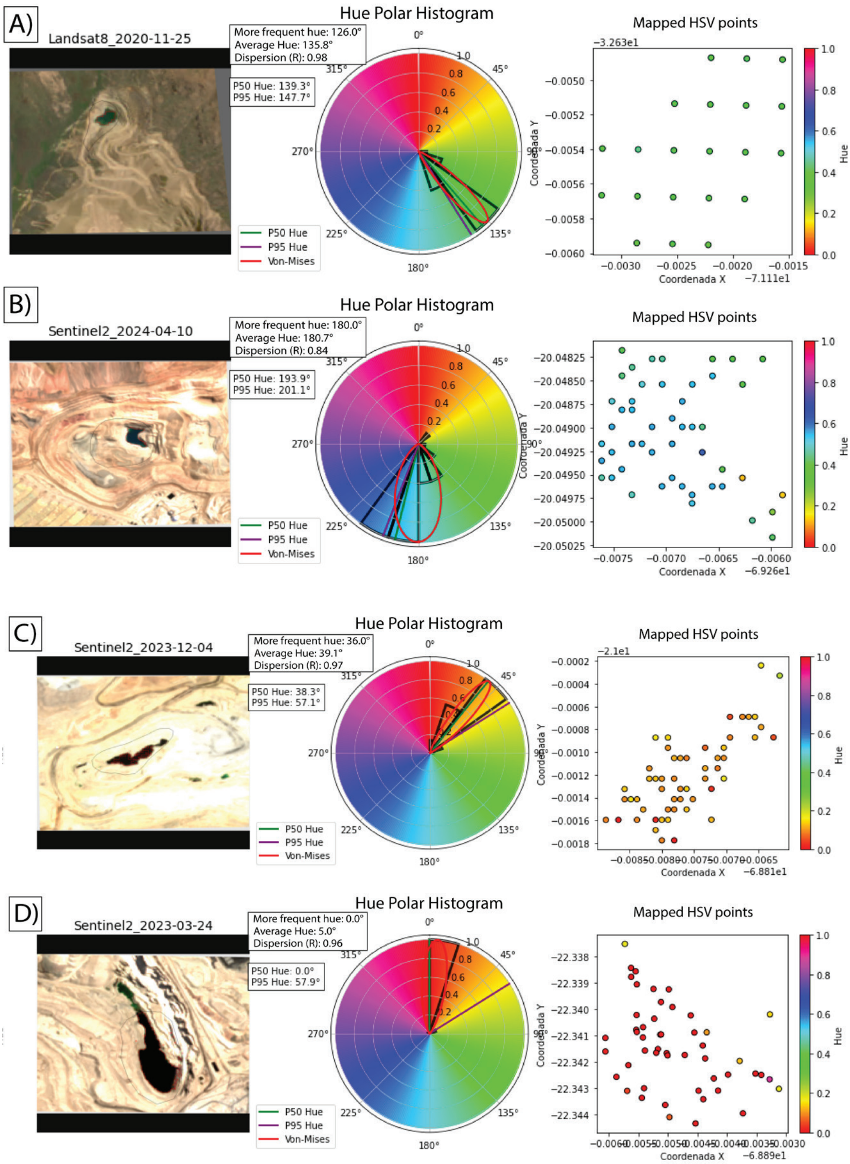

Figure 3 Examples of olive green, blue-green, yellow-brown and red-orange colors. A) El Soldado, B) Cerro Colorado, C) Quebrada Blanca, D) Mina Sur.

1000 m^2 in Sentinel-2 images. This limitation arises from the low spatial resolution of the different satellites.

Conclusions

This study emphasizes the use of remote sensing for the physicochemical characterisation of pit lakes, utilizing true color analysis using the HSV model and the Random Forest machine learning algorithm. The use of QA/QC filters improves the segmentation of pit lakes in satellite images, certifying a correct color representation. The validation was performed at Berkeley Pit Lake, as it contains extensive historical data, has many studies, and has a large area. It also demonstrated that physicochemical characteristics can be inferred from the absorption of sunlight by dissolved chemical elements such as Fe^{2+} (Olive Green), Cu^{2+} (Blue-Green), and Fe^{3+} (Yellow-Brown). Mineral colloids such as

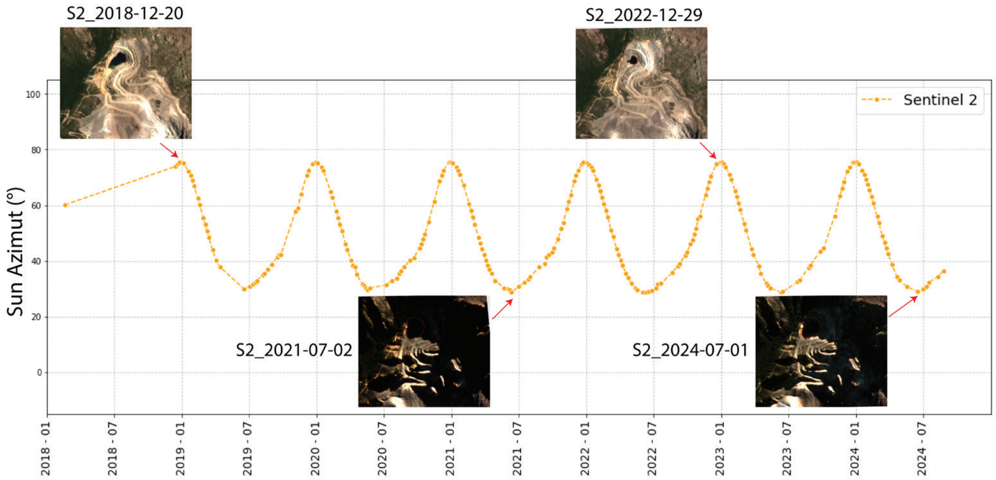

***Figure 4** Presence of shadows that affected the segmentation of the pit lake by the azimuth of the Sun in "El Soldado".*

Fe and Al oxyhydroxide-sulfates also affect the color spectrum, as Fe-oxyhydroxide-sulfates disperse the orange-red color, while Al-oxyhydroxide-sulfate colloids influence the color of water by reflecting light at all visible wavelengths, increasing S and V in the HSV model.

This methodology has been successfully applied in Chilean pit lakes, although its main limitation lies in the spatial resolution of Landsat and Sentinel images, particularly for smaller pit lakes. To improve monitoring, the use of hyperspectral drones is recommended to obtain higher resolution images, allowing for more accurate analysis of surface waters. Continuous monitoring with the HSV model offers a cost-effective alternative to in situ methods, facilitating long-term environmental assessment and improving pit lake management.

Acknowledgements

Thanks to INAP for granting access to the Pit Lake Database, which was essential for the validation of this methodology.

References

Castellón, E., Martínez, M., Madrigal-Carballo, S., Arias, M. L., Vargas, W. E., & Chavarría, M. (2013). Scattering of Light by Colloidal Aluminosilicate Particles Produces the Unusual Sky-Blue Color of Río Celeste (Tenorio Volcano Complex, Costa Rica). PLoS ONE, 8(9). https://doi.org/10.1371/journal.pone.0075165

Murphy, S., Wright, R., & Rouwet, D. (2018). Color and temperature of the crater lakes at Kelimutu volcano through time. *Bulletin of Volcanology*, 80(1). https://doi.org/10.1007/s00445-017-1172-2

Ohsawa, S., Saito, T., Yoshikawa, S., Mawatari, H., Yamada, M., Amita, K., Takamatsu, N., Sudo, Y., & Kagiyama, T. (2009). Color change of lake water at the active crater lake of Aso volcano, Yudamari, Japan: Is it in response to change in water quality induced by volcanic activity? *Limnology*, 11(3), 207–215. https://doi.org/10.1007/s10201-009-0304-6

Otsu, N. (1979). *A threshold selection method from gray-level histograms. Automatica*, 11(285-296), 23–27.

Saraullo, F. A. V., Larosa, F. S., Ghignone, R. A., & Lanzillotta, L. (2019). *Diseño, implementación y ensayo de un lector de colores de bajo costo para personas ciegas y disminuidas visuales.*

Torrent, J., & Barrón, V. (2002). *Diffuse reflectance spectroscopy of Iron Oxides.*

Reactive Barriers for Mine Waters Treatment: an Approach using Alternative and Nature-Based Materials

Roberto da Silva[1], Rita Fonseca[2], Joana Araújo[3], Joanna Gmitrowicz-Iwan[4]

[1]*AmbiTerra Laboratory, University of Évora, Institute of Earth Sciences, Évora, Portugal, roberto.silva@uevora.pt, ORCID 0000-0003-3865-8724*

[2]*AmbiTerra Laboratory, Dep. Geosciences, School of Sciences and Technology, University of Évora, Institute of Earth Sciences, Évora, Portugal, rfonseca@uevora.pt, ORCID 0000-0002-6389-2822*

[3]*AmbiTerra Laboratory, University of Évora, Institute of Earth Sciences, Évora, Portugal, jfaraujo@uevora.pt, ORCID 0000-0003-4956-4061*

[4]*Institute of Soil Science, Environmental Engineering and Management, University of Life Sciences, Lublin, Poland, joanna.gmitrowicz-iwan@up.lublin.pl, ORCID 0000-0001-7202-3250*

Abstract

This work aims to reduce the influence of Acid Mine Drainage in two mining areas in the Iberian Pyritic Belt, specifically the Caveira Mine System in Portugal, and the Trimpancho Mining Complex in Spain, which both stopped operations in the 1960s. Since then, acid drainage from exposed waste piles has released toxic elements into nearby waterways, causing widespread contamination. Laboratory tests were conducted to find the best materials for neutralization of the acid drainage and subsequently retain Potentially Toxic Elements (PTE). Water samples from both mines showed high levels of toxic metals like As, Fe, Cu, Pb, and Zn, with very low pH levels, so laboratory scale ponds were created where various byproducts and nature-based materials were used to test the ability to neutralize acid drainage from the mines. With these tests it was verified that paper sludge was a great pH neutralizer, increasing mine water pH from 1.64 to 6.23 in 11 days and that industrial activated carbon, biochar, three different sludges and two different clays had great PTE removal ratios for As, Cu, Pb, Mn and Zn. Therefore, column tests with different materials simulated reactive barriers to determine the best combinations for this PTE removal. The tests indicated that sludges and industrial activated carbon are effective for retaining PTE and that multilayered reactive barriers are recommended for large-scale field applications to remediate contaminated water after increasing pH with paper sludge-based ponds.

Keywords: Acid mine drainage, potential toxic elements, byproducts, reactive barriers, remediation

Introduction

Environmental wealth is increasingly a factor of concern for us, combined with the needs to explore the geological heritage, essential for modern industry. This work is mainly focused on testing byproducts and nature-based materials, which otherwise had no practical use, to remediate watercourses, and water sources, from the Caveira Mine System (CMS) in Grândola, Portugal, and Trimpancho Mining Complex (TMC) in Spain. These mining sites (Fig. 1), located in the Iberian Pyrite Belt (IPB) – a volcanogenic massive sulfide province, in the southwestern part of the Iberian Peninsula – were explored since the period of Roman occupation, with particular incidence in the last two centuries (Oliveira & Matos 2002; Matos & Sousa 2008; Salmerón *et al.* 2014). CMS is embedded in Palaeozoic formations, in the NW region of the IPB, about 10 km SE of Grândola, Portugal (Mateus *et al.* 2008; Reis *et al.* 2012). This local has sediments predominantly of sandy nature, with few presences of clays in samples collected around the exploring area (da Silva *et al.* 2025). TMC is located in the SE region of the IPB, more precisely in the Huelva Province, in the SW of Spain, where a stream, that crosses the complex, flows to the Chança river in Portugal (Pérez Ostalé 2014). In this region the sediments are mostly of coarse sandy nature with a very few silts and clays mixed in their composition (da Silva *et al.* 2025).

Both mining sites have not undergone any mining exploration work since the 1960s, when different companies ceased mining operations in several mines in the IPB, due to the collapse of the copper market worldwide (Oliveira & Matos 2002), leaving them without proper supervision, poor management and absence of policies to contain contaminants. After comprehending the level of contamination in both regions, the aim of this work is to contribute with essential understanding on selecting the best tools to be applied, such as the use of byproducts and nature-based materials, to retain Potentially Toxic Elements (PTE) present in the effluents, which are responsible for the contamination not only of the surrounding watercourses, but also of the sediments that comprise them (da Silva *et al. in press*).

Preliminary Study

Initially, element concentrations were quantified to understand the level of contamination in the watercourses. To do so, Partial Digestion with Aqua Regia was carried out on water samples collected from the effluents for total quantification (dissolved and particulate forms). The same samples were also filtered through 0.45 µm filters, to quantify the dissolved forms (Tab. 1). In addition to element concentrations pH and SO4 was also measured in the effluents. Both effluents were acidic with CMS (pH 1.64) being slightly less acidic compared to TMC (pH 1.1). CMS has an average of 1251.22 mg/L in SO4 concentration, ranging from 0 to 14967,46 mg/L, and TMC has an average of 3665,08 mg/L, ranging from 47,38 to 9598.03 mg/L.

The ability of different byproducts, to neutralize the acidic effluents, was then tested through kinetic tests, simulating small ponds in 250 ml Erlenmeyer flasks with different ratios between water and byproducts used,

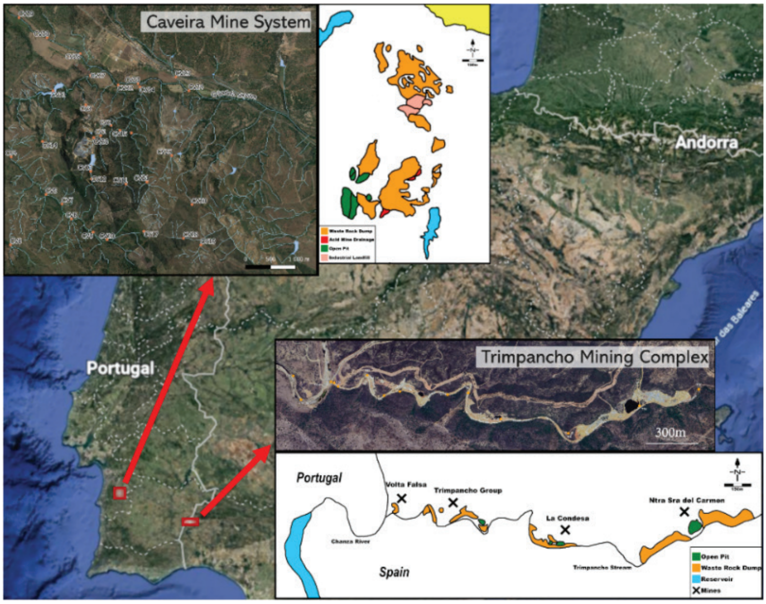

Figure 1 Geographical representation of the CMS (adapted from: Ferreira da Silva et al. *2015) and TMC (adapted from Grande* et al. *2017).*

Table 1 *PTE in original waters from CMS and TMC – filtered and digested.*

	Al	As	Ca	Cd	Co	Cr	Cu	Fe	K	Mg	Mn	Na	Ni	Pb	Zn
								mg/L							
CMS Filtered	583.3	17.66	123.3	0.5	1.0	0.3	33.1	2831.7	0.5	194.1	63.7	84.1	1.2	2.3	146.0
CMS Digested	604.6	15.6	101.1	0.8	1.0	0.4	29.2	2652.3	3.7	183.4	47.5	73.7	1.4	5.2	145.3
TMC Filtered	2507.9	<0.1	474.5	2.7	2.1	0.8	206.0	2958.0	0.6	1934.8	252.1	68.4	3.0	0.2	2402.1
TMC Digested	2300.0	<0.3	464.8	3.0	3.0	1.3	210.0	2691.0	4.9	1789.0	255.4	68.1	3.5	0.9	2207.3

such as paper, marble and limestone sludges, industrial activated carbon, biochar and two different clays. Tests lasted for 11 days until the pH of the waters stabilized to verify the best materials to increase pH (Fig. 2A-C) and to take the opportunity of carrying out preliminary analysis of the materials' PTE retention potential (Fig. 2D).

These preliminary tests showed us that paper sludge has great potential to increase pH in mine waters and that the byproducts can decrease the concentration of PTEs in the waters.

Lab-scale Testing Ponds and Reactive Barriers

Verifying that paper sludge had the best performance in increasing pH of mine waters, lab-scale ponds were constructed using inert plastic trays, holding 10 L of mine water (water from CMS was used to make this experiment, due to its higher concentration in PTE) with 200 g of paper sludge (Fig. 3). In the first pond experiment, paper sludge was used raw, conglomerated, in its original state. For the second pond, paper sludge was crushed before being combined with the mine water. The water in the first pond remained in contact with the byproduct for over two weeks, when it attained a pH value of 6,55. The water in the second pond attained a pH value of 7.52 just after 3 days. After neutralizing the pH, the water's clarity became practically translucent, losing its characteristic dark brownish colour and turbidity (Fig. 4). Then, after the water was separated from the residue at the bottom of the pond, samples were collected from both water and residue to be analysed by ICP-OES. The water was then used to perform the reactive barriers test, to

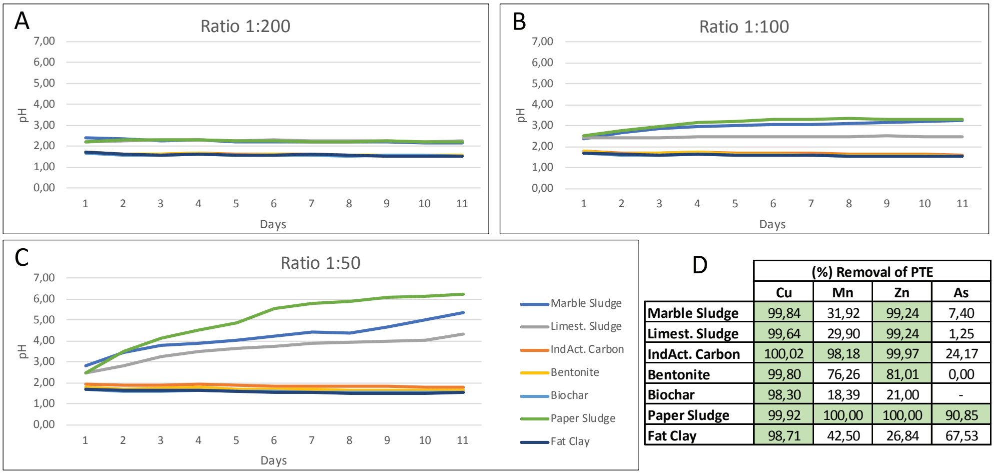

	(%) Removal of PTE			
	Cu	Mn	Zn	As
Marble Sludge	99,84	31,92	99,24	7,40
Limest. Sludge	99,64	29,90	99,24	1,25
IndAct. Carbon	100,02	98,18	99,97	24,17
Bentonite	99,80	76,26	81,01	0,00
Biochar	98,30	18,39	21,00	-
Paper Sludge	99,92	100,00	100,00	90,85
Fat Clay	98,71	42,50	26,84	67,53

Figure 2 *A–C; Results of the first pH increment tests, with different ratios of water (200; 100; 50 ml) to 1 g of byproduct. D; results from the preliminary analysis on main PTE removal after pH increment tests for each byproduct.*

Figure 3 *Lab-scale Pond with mine water from CMS and paper sludge. First precipitation of iron oxides.*

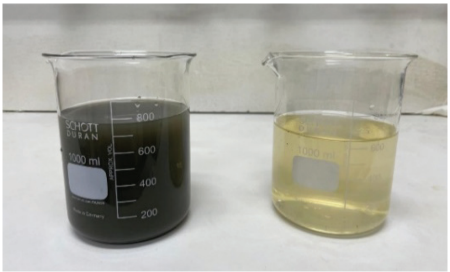

Figure 4 *Mine water before (left) and after (right) Pond experiment.*

check for the maximum PTE removal from these contaminated waters.

Therefore, for the last experiment, different columns were created (Fig. 5) simulating reactive barriers, with the following combinations:

- Column 1 – Marble Sludge + Biochar
- Column 2 – Marble Sludge + Fat Clay
- Column 3 – Limestone Sludge + Industrial Active Carbon
- Column 4 – Limestone Sludge + Bentonite

All byproducts were separated with fine gravel, to prevent direct contact between them, and water was pumped against gravity in each column through a peristaltic pump, at 1.20 rpm in a 4mm tubes, resulting in a flowrate of 2.77 ml/min. These combinations were created with insight from the preliminary study, to understand which byproduct would make the best combination to attain a total, or close to a total, PTE removal from the contaminated waters. In the end, and for each column, samples were taken from the four final waters and for each byproduct, to be chemically analysed.

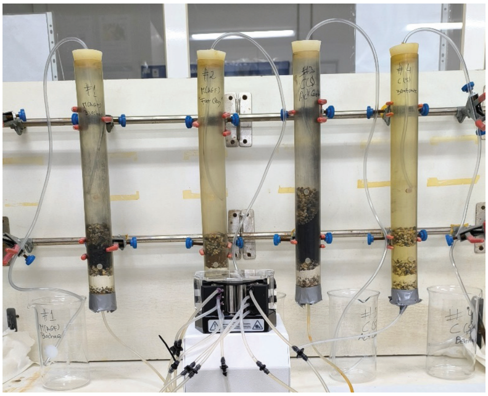

Figure 5 *Reactive Barriers experiment with 4 different byproducts combinations.*

All collected samples, waters and byproducts, were digested through Partial Digestion with Aqua Regia, and then analysed by ICP-OES, allowing us to verify that PTE were mostly retained in the pond residue (iron hydroxide film over the paper sludge) after the 11 days of contact, between the water and paper sludge, and yet, that some of the other byproducts still managed to retain PTE during the reactive barrier experiment, after the pond (Fig. 6).

In the end of the whole experiment, most PTE were removed from the mine water. As, Cu and Pb reached minimum values in all experiments and Fe reached very low amounts after passing through the columns with marble sludge. Zn and Mn were considerably retained at the end of all experiments, although with a lower performance compared to the other elements (Fig. 7).

In a first instance, it was noticed that the paper sludge has a great potential to increase pH in mine waters, influencing a greater retention of PTE by other materials. With just the contact of mine water with paper sludge, in the pond experiment, it made Fe precipitate by 95%, and then it was still retained after passing through the reactive barriers. Best results were attained in the first two columns, with marble sludge, and also with biochar and fat clay, attaining a removal over 99% of this element, going from an initial amount of around 2800 mg/L to just around 20 mg/L by the end of the whole experiment. Same happened for Cu and Pb, in which most part of each element was retained in the pond experiment, by the paper sludge. In the end, values decreased from around 30 mg/L (Cu) and 5 mg/L (Pb) to

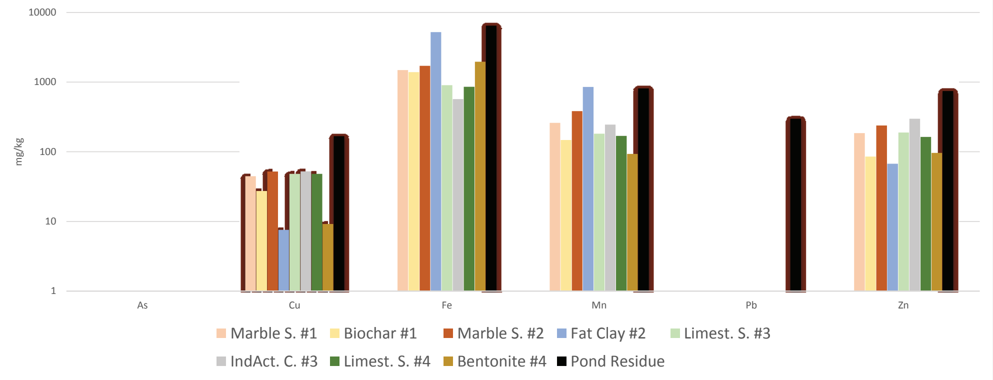

Figure 6 Results, in logarithmic scale, from Partial Digestion with Aqua Regia analysed through ICP-OES in byproduct samples from the after-pond and after-reactive barriers experiments.

8 mg/L and 0,40 mg/L, respectively. Meaning that Cu was removed by about 73% and Pb by about 92%. Arsenic was 100% removed from the water, going from about 15 mg/L to near 0 (all analysis were under the detection limit of the ICP-OES) and, Zn and Mn had a removal of 37,93% and 60,53%, dropping from 145 mg/L to 90 mg/L (Zn) and 190 mg/L to 75 mg/L (Mn).

Discussion

After performing the digestion of all samples collected from the pond/reactive barriers experiment, it's noticeable that PTE were mainly retained during this process, in which it was possible to reduce the amounts of As, Fe, Cu, Mn, Pb and Zn, in water contaminated by the influence of the mine and its wasting piles, to values below those recommended by the Decree-Law 236/98 (Portugal) on surface water quality.

The absence of arsenic values in all analyses during, and after the whole experiment, may indicate that this element may have undergone complexation, binding to iron oxides and precipitating with them during contact with paper sludge. The values of Mn and Zn may show a lower retention rate, compared to the other elements, this may be because paper sludge has high levels of these elements in its composition (4631,94 mg/Kg and 97,76 mg/Kg, respectively), which may have influenced its retention capacity.

Also, it was noticed that crushing the paper sludge before mixing with mine waters show better results, that may be because of the increment of specific area of the byproduct, leading to a pH increment within fewer days

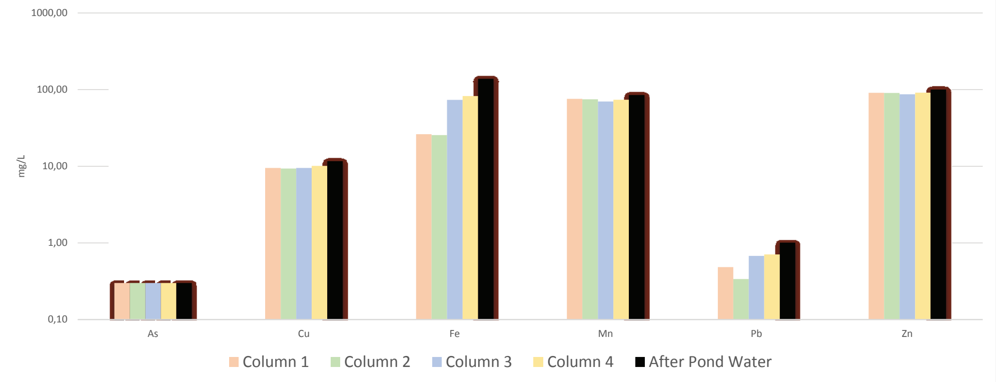

Figure 7 Results, in logarithmic scale, from Partial Digestion with Aqua Regia analysed through ICP-OES in CMS water samples from the after-pond and after-reactive barriers experiments.

of contact. And a slower speed when pumping water to the columns should also be tested to see if it can enhance PTE retention, allowing the water to remain in contact with the materials for longer periods of time, giving more time for retention to occur.

Conclusions

This shows that some byproducts and nature-based materials can be repurposed as a cost-effective material for environmental remediation in cases of Acid Mine Drainage, to increase water pH and remove PTE from it. According to this study, paper sludge was the best material for pH increment and a prior PTE removal, such as Fe, Cu and Pb. After pH increment using paper sludge, other materials such as industrial activated carbon, fat clay and marble sludge, showed high potential for retaining PTE. Furthermore, their homologous (Biochar, Bentonite and Limestone Sludge), despite having also performed well, they did not prove to be as good as the first ones in relation to PTE removal. However, it may be scientifically interesting to combine each homologous material and check if the potential for PTE removal improves. In conclusion, the experiment proved to be valid in the treatment of contaminated water affected by acid mine drainage in mining environments in a controlled laboratory-scale environment. Further experiments are underway to verify the removal potential, real-scale applicability and retention capacity of the materials that will determine the lifespan of the barriers.

Acknowledgements

The authors acknowledge: National funds through FCT – Science and Technology Foundation, I.P., in the framework of the UIDB/04683 and UIDP/04683 – Institute of Earth Sciences (IES) Programs; Project GeoMinA – Implementation of a basis for defining geoenvironmental models in abandoned mining areas in the Iberian Pyrite Belt – PL23-00035 – Promove Actions Project 2023 Fundação La Caixa (2024–2027).

References

Grande J A, Santisteban M, Valente T, De la Torre M L, Gomes P (2017) Hydrochemical characterization of a river affected by acid mine drainage in the Iberian Pyrite Belt. Water Sci Technol 75 (11): 2499–2507, doi:10.2166/wst.2017.097

Mateus A, Figueiras J, Matos J X, Gonçalves M A, Lopes R, Labaredas J, Beleque A (2008) Condicionantes impostas à dispersão de metais acumulados em escombreiras mineiras: o exemplo de Caveira, Faixa Piritosa Ibérica. A Terra: conflitos e ordem

Matos J X, Sousa P (2008) Prospecção de sulfuretos maciços no sector português da Faixa Piritosa Ibérica. In CLME'2008-5º Congresso Luso-Moçambicano de Engenharia e IICEM-2º Congresso de Engenharia de Moçambique, livro de resumos, Maputo, p 2–4

Oliveira M L F, Matos J X (2002) The exploitation of copper ores and the settlements of Estremadura and south of Portugal during the calcolithic. Ciências Históricas, Univ Portucalense, Porto, p 123–138

Pérez Ostalé E (2014) Caracterización ambiental de estructuras mineras en la Faja Pirítica Ibérica como soporte metodológico de gestión territorial. (Doctoral dissertation, Universidad de Huelva)

Reis A P, Ferreira da Silva E, Cardoso Fonseca E, Patinha C, Barrosinho C, Matos J (2012) Environmental Assessment of the Caveira Abandoned Mine (Southern Portugal). Part 1: Characterization of Metal Contaminated Soil, Soil and Sediment Contamination. An International Journal, 21: 2, p 227–254

da Silva R, Fonseca R, Araújo J, Silva N, Albuquerque T (in press) Avaliação do nível de contaminação nos sedimentos de cursos de água do Sistema Mineiro de Caveira (Grândola). Comunicações Geológicas, ISSN: 0873-948X

da Silva R, Fonseca R, Araújo J, Valente T (2025) The Enrichment of Potentially Toxic Elements in the Iberian Pyrite Belt's Abandoned Mines: Geomaterials as Purpose for Their Remediation. Battelle Proceedings of the 2025 Sediments Conference in Tampa, Florida

Salmerón I, Valente T, Grande J A, De la Torre M L, Santistebán M, Lobo A, Sánchez-Requena J (2014) Four abandoned mines, one acid mine drainage affected river and an unsolved issue for a water supply reservoir. Energy and Environment Knowledge Week

Breaking the Toxicity Barrier: A Gold Mine’s Journey to Sustainable Wastewater Treatment

Myriam De Ladurantaye-Noël[1], Marc Laliberté[2], Alain Gadbois[2], David Oliphant[2]

[1]*Veolia Water Technologies Canada, Canada, myriam.deladurantaye@veolia.com*
[2]*Veolia Water Technologies Canada, Canada*

Abstract

In gold mining operations, contaminants such as cyanide species, ammonia, and metals can generate a toxic effluent. A Canadian gold mine operating in a very cold climate faced recurring toxicity issues and was pressed by regulations to address the issue. This case study highlights the journey to understand the sources of toxicity and identify a suitable solution, taking into account constraints such as climate and footprint. It presents the approach that leads to a compliant full-scale application, and demonstrates the effectiveness of the combined moving bed biofilm reactors (MBBR) and metals removal for toxicity remediation.

Keywords: Toxicity, mine water discharge, ammonia, thiocyanate, cyanate, biological treatment, MBBR

Introduction

In Canada, the federal regulation requires that treated mine effluent water meet specific criteria such as pH, TSS and concentrations of a few metals, and must not be acutely lethal prior to discharge to the environment. Two aquatic species, which are deemed representative of most of the native aquatic life in Canada, are used to evaluate the acute lethality potential of an effluent in freshwater discharge; *Oncorhynchus mykiss* (fish) and *Daphnia magna* (crustacean) (Metal and Diamond Mining Effluent Regulations, 2024).

With consideration of the Canadian regulation, a new mine must identify and eliminate any source of acute toxicity in its effluent prior to discharge. This is the story of a mine journey to understand and solve toxicity issues not addressed by traditional contaminants removal.

Context

A mine, located in the Canadian Shield, was being designed and was expected to produce a toxic effluent. It was located in an area with no other mine nearby, in a subarctic climate. Such climate results in long, cold winters with large quantities of snow, strong freshets, and warm summers.

During the feasibility study of the mine, detailed geochemical and hydrological studies tried to predict the composition and flow rate of mine effluent. Preliminary results from the studies led to the conclusion that copper and arsenic were concerns for toxicity, and that cyanide and explosive residuals would likely be at concentrations of no concern. The mine effluent treatment plant was therefore centred on metal removal (copper and arsenic). However, due to the uncertainties around the preliminary studies, the mine water treatment plant was designed to allow implementation of additional equipment at a later stage, once a better understanding of the water quality was achieved. At start-up of the mine effluent treatment plant, the treated water met all the metals criteria and was not acutely lethal (hereafter referred to as “non-toxic”).

However, when the mine ramped up its production and started its concentrator, the mine effluent started to be toxic first to *Daphnia magna*, and then to *Oncorhynchus mykiss*. Within a year of starting production, the treated mine effluent was failing every toxicity test, no matter the modifications done to the concentrator operation or the mine effluent treatment plant.

Starting Point Hypotheses

The Canadian gold mine presented in this case study employs the MacArthur-Forrest process, which utilizes cyanide as a leaching agent for gold extraction in ore slurry. The resulting gold-barren solution is largely recirculated to the concentrator, but a portion must be purged to optimize the mill operation. This purged water contains high levels of cyanide, a highly toxic contaminant to wildlife (Pandey, 2013), necessitating detoxification at the source. The INCO Sulphur Dioxide/Air process provides such detoxification. It employs sulfur dioxide and a copper catalyst in the presence of air to oxidize cyanides to cyanates. In addition to copper, this process adds cyanates into the water. Furthermore, the interaction between the cyanide solution and sulfides in the ore generates another cyanide by-product, thiocyanates (Habashi, 1967).

Although cyanates and thiocyanates are less toxic compared to free cyanide, especially to mammals and birds, they remain toxic to crustaceans such as *Daphnia magna* (Dauchy, 1980, Hemming, 1989). In addition, cyanates and thiocyanates naturally hydrolyse/oxidize to ammonia, which is toxic to fish, particularly in its un-ionized form (Constable, 2023).

The treated effluent started failing toxicity tests first to *Daphnia magna* and then to *Oncorhynchus mykiss*. Ammonia being more toxic to fishes than to crustaceans, this indicates that while ammonia was likely a cause of toxicity, it was also likely not the only one. Analysis of the toxic treated water quality confirms that not only ammonia was present in concentrations to be a source of toxicity, but cyanate (OCN^-) and thiocyanate (SCN^-) were as well.

Identification of the toxicity sources is a key for treatment, as many options exist for each of the contaminants of concern. Simultaneous removal of the three contaminants could be achieved either by biological hydrolysis of cyanates followed by oxidation of ammonia and thiocyanates or reverse osmosis separation. While reverse osmosis is a universal solution for many contaminants, the cost of evaporating and disposing of the final concentrated solution is often prohibitive and only used as a last resort solution. Therefore, an active biological treatment, requiring limited chemical addition and limiting the quantity of generated wastes, was selected to enhance the natural degradation of nitrogen contributors. The use of a biological system also gives better sustainability to the treatment plant, mainly due to its limited impact on the environment and its performance improvement in time with few maintenance over the years.

Moving bed biofilm reactors (MBBR) have been used for nitrogen removal in municipal and industrial applications for decades. Operation of MBBR has been done in challenging environments, such as conditions close to freezing and while experiencing recurring toxic shocks (Kwofie, 2021). MBBRs are fixed film biological reactors where suspended media (typically made of HDPE) serves as biomass support. Since the biomass is attached instead of free floating, its concentration within the reactor is stabilized even under fluctuating loads and flows. A structured biofilm also provides a protected environment for bacteria, providing higher resistance to toxic shocks, and ensuring optimal conditions for slow-growing nitrifying bacteria to develop and thrive in shorter retention times. Additionally, the MBBR technology facilitates the implementation of multiple reactors in series, each optimized for specific microbial communities required for the removal of pollutants at higher removal rates (Rusten, 2000). For all these reasons, it was selected as a prime solution for the mine water treatment plant.

Validation and Investigation

The first step of the validation was the confirmation of the nitrogen contributor induced toxicity at laboratory scale. During these tests, reactors with a volume of three to five litres were fed with the mine effluent. The objective was to validate the viability of the MBBR technology in such an application. The main conclusions from the laboratory test were the following:

- Biological nitrification is inhibited by copper. Copper concentration over 0.25 mg/L resulted in a slow start-up and ammonia and nitrites accumulation. Oxidation of cyanide and thiocyanates, as well as cyanate hydrolysis were not impacted by copper.

- When the MBBR reactors were the same size, ammonia and cyanides species were removed with over 99% efficiency once metal precipitation was implemented. However, nitrification was incomplete, resulting in nitrous acid inhibition for nitrite oxidation. The nitrite build-up resulted in a toxic effluent. The oxidation of nitrites to nitrates is the slowest of all the biological reactions. More time must be allowed for completion of both nitrification reactions in a single biological reactor.
- Once the MBBR reactors were sized to consider the nitrite oxidation kinetic, full removal of ammonia and cyanide species was achieved. The treated effluent was non-toxic.
- Biological activity decreased at lower water temperatures, as expected, but with the same removal performances. The effluent was still non-toxic.

Laboratory testing had proven the possibility of biological removal of the toxicity sources using the MBBR technology, resulting in a non-toxic effluent. There were still uncertainties related to process performance in fluctuating conditions. A six month pilot was therefore conducted to evaluate the response of the biological treatment in varying water composition and load, and operating during the cold season. The MBBR pilot was fed from the clarified water of the existing metal removal plant. The pilot was started up in early fall (water temperature of close to 20 °C) through late winter (down to 5 °C). The main observations and conclusions were the following:

- While the clarified metal removal effluent failed all toxicity tests (100% mortality), the MBBR effluent had no mortality for both *Daphnia magna* and *Oncorhynchus mykiss*.
- Complete oxidation of thiocyanates and cyanates, as well as the complete degradation of ammonia nitrogen to nitrates, was consistently achieved during six months of operation.
- The MBBR process can fail if not protected from biological offset, such as toxic shocks (chemical spills) and pH excursions. Both were experienced during piloting and resulted in biological oxidation failure, highlighting the importance of their early detection.
- Biological recovery to short-term toxic shocks is fast, recovering full capacity within a week.

The pilot test highlighted the importance of control over operating conditions and pretreatment efficiency to prevent harm to the biomass. The test also demonstrated the ability of the MBBR system to recover from process offsets and toxic shocks. Interested readers are referred to a narrative of the case study by the authors of this paper (De Ladurantaye-Noel, 2025).

Full-scale application

Commissioning of the full-scale MBBR was completed in November 2017. The biological reactors are installed between the two existing metal precipitation stages; the first providing copper removal for biomass protection and the second removing sloughed biomass and excess of phosphorus in addition to metal polishing of the final effluent. A visual representation of the flow diagram is represented in Fig. 1.

MBBR thrive by optimizing natural biological reactions to enhance the biomass

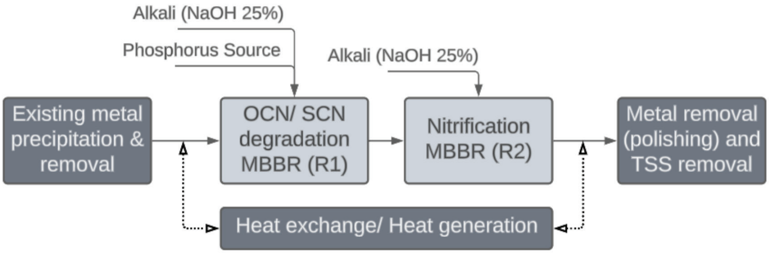

***Figure 1** Full-scale plant process schematic*

growth and efficiency. In order to help this optimization, some design considerations are implemented:

- Due to their size, the MBBR reactors are insulated field erected tanks to be installed outdoors. In winter, the water is close to 0 °C, being held in a large pond outside prior to treatment. For these reasons, water heating with heat recovery are used when required: it prevents freezing (tanks and pipes are not heat-traced) as well as having the capacity to quickly increase the biomass activity. An increase of the water temperature results in a 5% to 8% treated load increase per °C of water temperature increase.
- An alkali must be dosed in both MBBR reactors to control pH, as nitrification causes acidification of the mine effluent. While a calcium-based alkali could be used, sodium hydroxide was selected to avoid potential scaling issues (gypsum and calcite).
- A phosphorus source is supplemented in the first reactor as a nutrient to the biomass, since the mine effluent is devoid of an easily available phosphate source.

The base of design for the full scale application are the following:

- A hydraulic flow rate of 1 083 m³/h.
- A nitrogen load of 147 kg N/d at 8 °C (17% as CN^-, 56% as SCN^-, 27% as OCN^-) in R1.

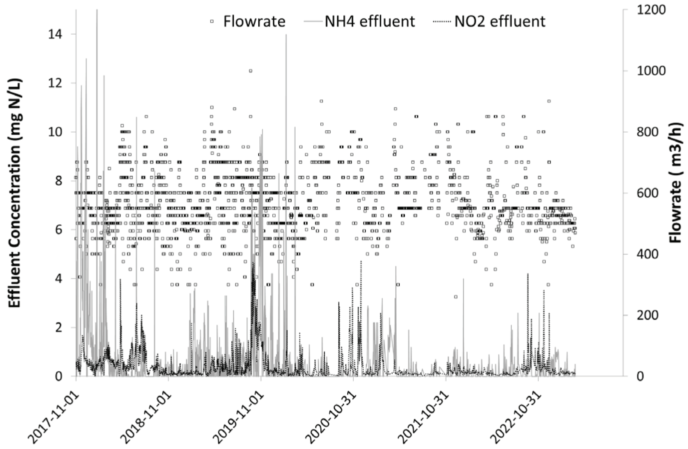

Figure 2 *Flowrate fluctuation and effluent ammonia and nitrite concentration.*

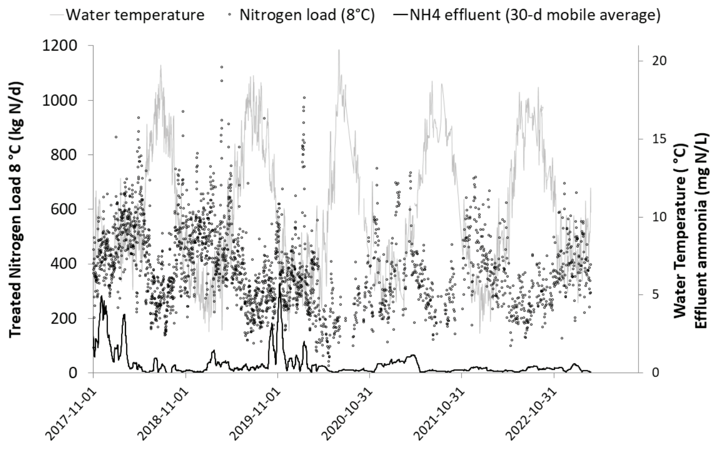

Figure 3 *Nitrogen treated load (corrected at 8 °C), water temperature variation seen and ammonia concentration at the effluent (represented as a 30-d moving average to lighten the graph).*

- An ammonia load of 462 kg N/d at 8 °C (combining mine effluent ammonia and by-product ammonia from the cyanide species degradation) in R2.

The conditions of operation were expected to vary based on the operation of the mine and on precipitations. The flowrate variation, as well as its impact on the biological treatment (effluent ammonia and nitrite concentrations) are illustrated in Fig. 2. Fig. 3 presents the variation of treated nitrogen load from the MBBR with the effluent ammonia concentration.

Main observations from five years of operation, as illustrated in Fig. 2 & 3, are the following:

- Substantial flow variations were observed over time. As expected, the fixed film biological treatment was not impacted through these hydraulic variations and provided robust nitrogen removal without harmful biomass entrainment.
- As the biomass matures, ammonia and nitrite peaks in the final effluent reduce in frequency and intensity. This is likely due to the increase in biodiversity in the biomass, which provides a variety of species that can respond to changes in condition.
- Load variations could be managed as long as the biomass is allowed to adapt through the increase. Sudden load variations (> 15% increase in 24 hours) have resulted in episodes of decreased performance until the biomass can stabilize its activity; this is illustrated in Fig. 3 with a small increase in ammonia concentration through fast load variations.
- Applied load was over the design load on several occasions. Nitrogen load up to 1 000 kg N/d (> 200% increase) was treated without impacting the effluent quality. This is due to biomass specialization and maturation, resulting in increased treatment capacity.
- The water heating system is used to boost bacterial activity, either to resolve a biological offset or to speed the load increase that could be managed by the biological system.
- Operation of the MBBR at 3 °C is possible with no impact on the system's performance. Limitations on lowering the temperature further are due to risks of freezing.

Previous analysis was mainly focused on the final effluent composition. It is however also interesting to look at the evolution of cyanate (OCN$^-$) and thiocyanate (SCN$^-$) through both MBBR reactors, as illustrated in Fig. 4, for a better understanding of the biological reactions.

Overall performance for cyanide species is high. Thiocyanate oxidation was complete in R1 shortly after commissioning. On the other hand, cyanate hydrolysis is not completed in R1 but in R2. Hydrolysis in R1

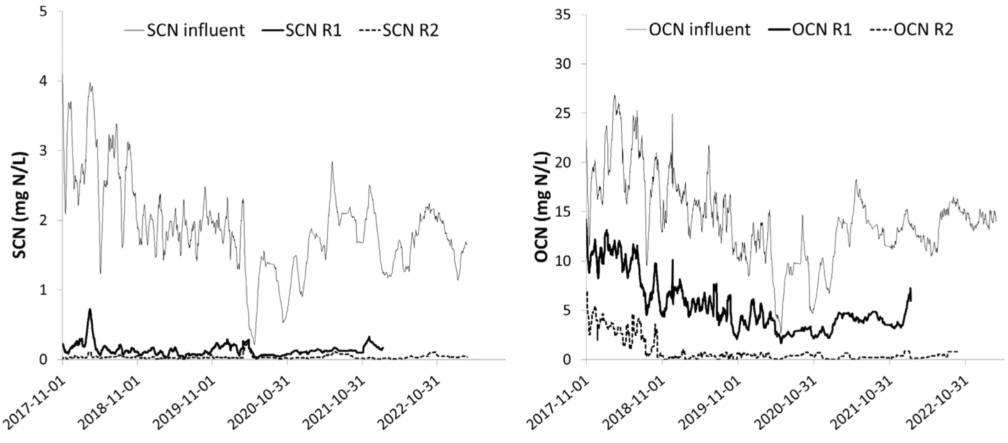

Figure 4 *Cyanide species degradation evolution through the full-scale MBBR treatment; thiocyanate on the left and cyanate on the right (data shown as moving average, 30-d)*

keeps improving over time after four years of operation. This cyanate hydrolysis evolution is a good example of biomass specialization and maturation over time.

The last element of concern is toxicity. Toxicity results from the full-scale operation are summarized in Table 1.

The following conclusions can be highlighted from the toxicity results:

- Prior to the MBBR installation, toxicity was a major issue with > 60% of mortality for both *Daphnia magna* and *Oncorhynchus mykiss*. An effluent is legally toxic when more than 50% of the test organisms die.
- During the commissioning of the MBBR, while the biomass is not yet acclimated, mortality dropped for both organisms to compliance and results show less variation.
- After completion of the commissioning period, mortality for both *Daphnia magna* and *Oncorhynchus mykiss* dropped significantly and results are stable over time. During this period, an improvement of arsenic removal was also seen, as shown by the reduction of the standard deviation, as arsenic is oxidized and easier to remove in the second metal precipitation following biological oxidation.

Conclusions

Mine development is complex and predicting its effluent water quality is challenging. When developing a water treatment plant, the mine's process chemistry needs to be considered from an early stage and should not be limited to metals. This case study highlights that no matter the water chemistry uncertainties, the possible sources of toxicity should be part of a contingency plan for the treatment plant and its integration should be thought of from the initial design.

This case study illustrates its benefices, as it started developing toxicity after the start-up of its concentrator. Investigations revealed a combination of ammonia, thiocyanate and cyanate in the mine effluent, none of which were removed by the existing physico-chemical treatment plant, to be causes for toxicity. A MBBR technology, which integration had already been planned in the initial design, was selected for the removal of these nitrogen species. Positive results from both laboratory and pilot tests led to its full-scale application, the performance of which confirmed its robustness, with no toxicity breach for years since its commissioning.

Mining effluent water treatment can be wrongly simplified to metal precipitation only, assuming that the toxicity of the process water is due to metals alone. This project demonstrated the removal efficiency of biological reactors for contaminants that can't be precipitated but are known to be biodegradable, such as cyanide species and ammonia.

This project focused on toxicity removal. However, to further increase the sustainability of the water treatment chain, nitrate removal should also be considered. While not toxic, it is a known source of eutrophication in receiving environments. Along the toxicity testing assessment, the pilot scale test did prove that biological denitrification was efficient to reach low total nitrogen concentration at the final effluent (< 5 mg N/L). Future implementation of a denitrification biological reactor was planned for in the design of the biological toxicity removal.

Table 1 Toxicity evolution in time, from the mine start-up to stabilization of the MBBR process

Effluent Water Parameters	Mortality *Daphnia magna (%)*			Mortality *Oncorhynchus mykiss (%)*			Total Arsenic (mg/L)		
	Average	*SD*	*Nb. data*	*Average*	*SD*	*Nb. data*	*Average*	*SD*	*Nb. data*
Metal removal only	61	45	137	69	423	137	0.025	0.062	202
Commissioning of MBBR	36	38	23	10	23	23	0.009	0.008	26
Stable MBBR Operation	0.7	3.2	57	0	1.9	57	0.006	0.005	390

References

Constable, M, Charlton, M, Jensen, F (2003) An Ecological Risk Assessment of Ammonia in the Aquatic Environment. Human and Ecological Risk Assessment 9 (2):527-548

Dauchy, JW. Waller, WT, Piwoni, MD (1980) Acute Toxicity of Cyanate to Daphnia magna. Bull Environm Contam Toxicol 25:194-196

De Ladurantaye-Noël, M, Laliberté, M (2025) From Toxicity to Compliance: a Case Study in Gold Mining Wastewater Management. World Gold Conference Proceedings (in press)

Habashi, F (1967) Kinetics and Mechanism of Gold and Silver Dissolution in Cyanide Solution; Montana College of Mineral Science and Technology. Butte, MT, 1–42

Hemming, TA, Blumhagen, KA (1989) Factors Influencing Thiocyanate Toxicity in Rainbow Trout. Bull Environ Contam Toxicol 43(3):363-369

Kwofie, IA, Jogand, H, De Ladurantaye-Noël, M, *et al.* (2021) Removal of Cyanide and Other Nitrogen-Based Compounds from Gold Mine Effluents Using Moving Bed Biofilm Reactor (MBBR). Water 13(23):3370

Metal and Diamond Mining Effluent Regulations SOR/2002-222 https://laws-lois.justice.gc.ca/eng/regulations/sor-2002-222/FullText.html

Pandey, G, Govind, P (2013) Toxicity of cyanide in fishes: An overview. Univers J Pharm 2(2):23–26

Rusten, B, Hellström, BG, Hellström, F, *et al.* (2000) Pilot testing and preliminary design of moving bed biofilm reactors for nitrogen removal at the FREVAR wastewater treatment plant. Water Sci Technol 41(4-5):13–20

Hydrogeological Research and Mine Design to Prevent the Impact of the Future Integrated Lithium Project “San Jose de Valdeflórez Project” to “El Calerizo” Aquifer (Cáceres, Spain)

Carlos Del Olmo[1], Jesús Montero[2], David Valls[3].

[1]*Ingemisa, cdelolmo@ingemisa.es 2Mining Sense, j.montero@mining-sense.com*
[3]*Infinity Lithium. dvalls@extremaduranewenergies.es*

Abstract

This article describes the methodologies and results of the site characterization work carried out to define the substrate of both the underground exploitation and surface facilities areas of the San José de Valdeflórez Project (the Project) and the main mine design measures developed to prevent affections to "El Calerizo" karstic aquifer. The hydrogeological and hydrogeochemical research programme has allowed the formulation of a Conceptual Hydrogeological Model and the definition of its main parameters.

Keywords: Site characterization, unsaturated zone, low permeability, karstic aquifers.

Background and objectives

The San José de Valdeflórez Project (Cáceres, Spain) seeks to conduct a rational and sustainable exploitation of the Valdeflórez lithium deposit, integrating technical innovations and social sensitivities to guarantee its acceptance and mitigate risks.

Geologically and hydrogeologically, is in the Cáceres Syncline. The Armorican and Silurian quartzite outcrops draw the North and South flanks. Both have been the object of mining exploration and exploitation, mainly for tin and phosphates, in the last century.

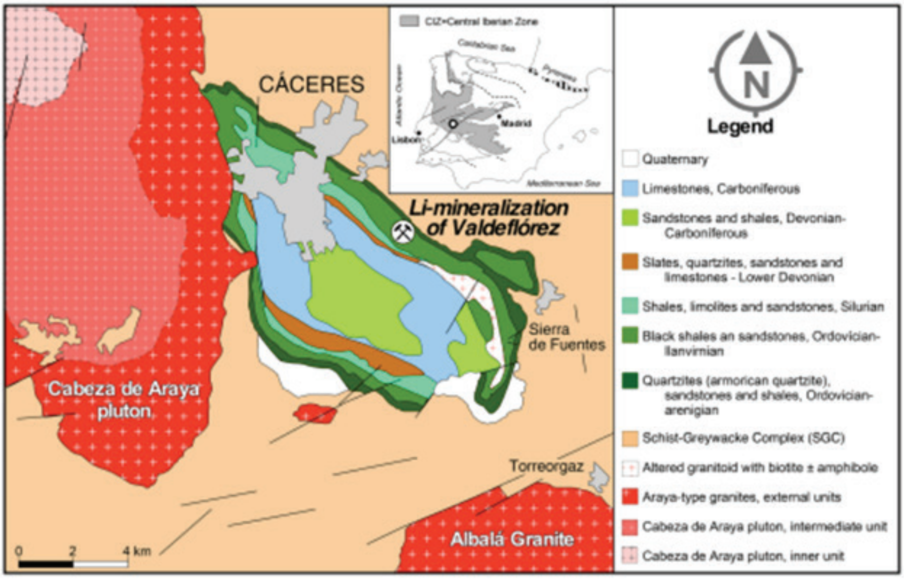

***Figure 1** Simplified Geological setting (Pesquera* et al.*, 2020).*

The northern flank forms a narrow valley between two quartzite ridges, in the middle of which an Ordovician psammopelitic sequence (Valhondo unit) hoists the Li deposit. In between the psamopelites it appears, interlayered, quartzite levels in which Li-rich quartz-micas and Quartz and greisen type veins are the main Li sources (Pesquera *et al.*, 1999, 2020).

Hydrogeologically, it is an impermeable to very low permeability environment. The Li deposit, which outcrops on the surface, extends to at least 450 m deep, has been exhaustively investigated through a detailed structural geological characterization, including more than 10,500 m of drillholes and the analysis of more than 4,200 samples, which has allowed the set-up of a geological model that has revealed a 111.3 Mt resource (indicated and inferred included) and an average grade of 0.61 wt% Li2O (JORC Resource), one of the largest in Europe. (*Pesquera et al.*, 2020).

Methods

Valdeflórez mining complex is in two hydrogeological units (U.H.-1 El Calerizo and U.H.-2 Valhondo) in the Salor and Guadiloba basins rivers, respectively. The mining exploitation works are in the U.H.-2 (Valhondo), on the northern flank of the syncline, while the tailings (TMF), treatment plant and other facilities will be located on the U.H.-1 (El Calerizo), also on the northern flank of the syncline. (Fig. 2).

For the study of the karstic aquifer, a specific hydrogeological and hydrogeochemical characterization program has been developed, starting by the establishment of the geological-structural model based on various field campaigns of controlled source geophysical techniques: Electrical boreholes, Microgravimetry, Electrical Tomography… A total of 4,000 m of Electrical Tomography profiles were done, in order to determine the thickness of the decalcification clays surficial layer and to make an assessment of the possible existence of karst cavities at depths of up to 15–20 m. These investigations have been complemented by an Audio-Magneto-Telluric Tomography (AMDT) campaign with a total of about 5,000 m, with the aim of studying the characteristics of the substrate up to 300 m deep and establishing the most favourable locations for the implementation of trenches and hydrogeological boreholes.

This has allowed the definition of the substrate geometry of both the unsaturated and the saturated zones of the karst aquifer in the Project area and its surroundings. The hydrogeological research program began with the water points inventory and sampling to determine their piezometric characteristics and chemical quality, and then the determination of hydrogeological parameters through specific "in situ" tests.

Results and discussion

Fig. 3 to 5 (*INGEMISA, 2024*) summarize the results of the piezometric measurements

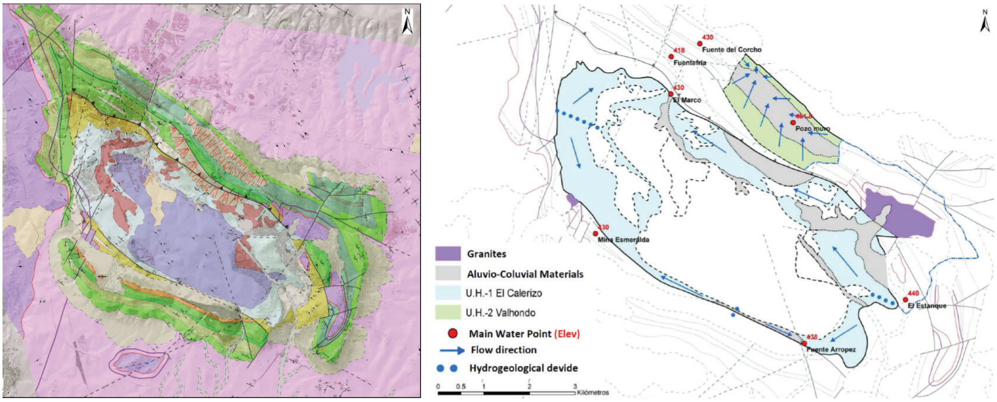

Figure 2 Cáceres anticline Geological Map and Hydrogeological Units (INGEMISA, 2024).

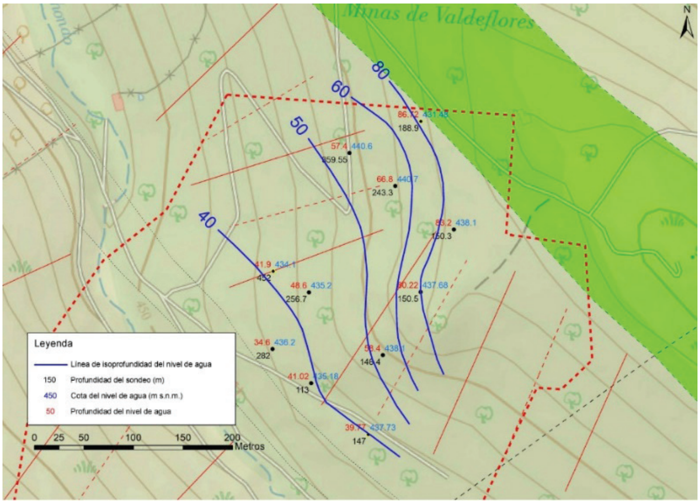

Figure 3 *Mining Area (UH-2. Valhondo Unit). Depths to the water table.*

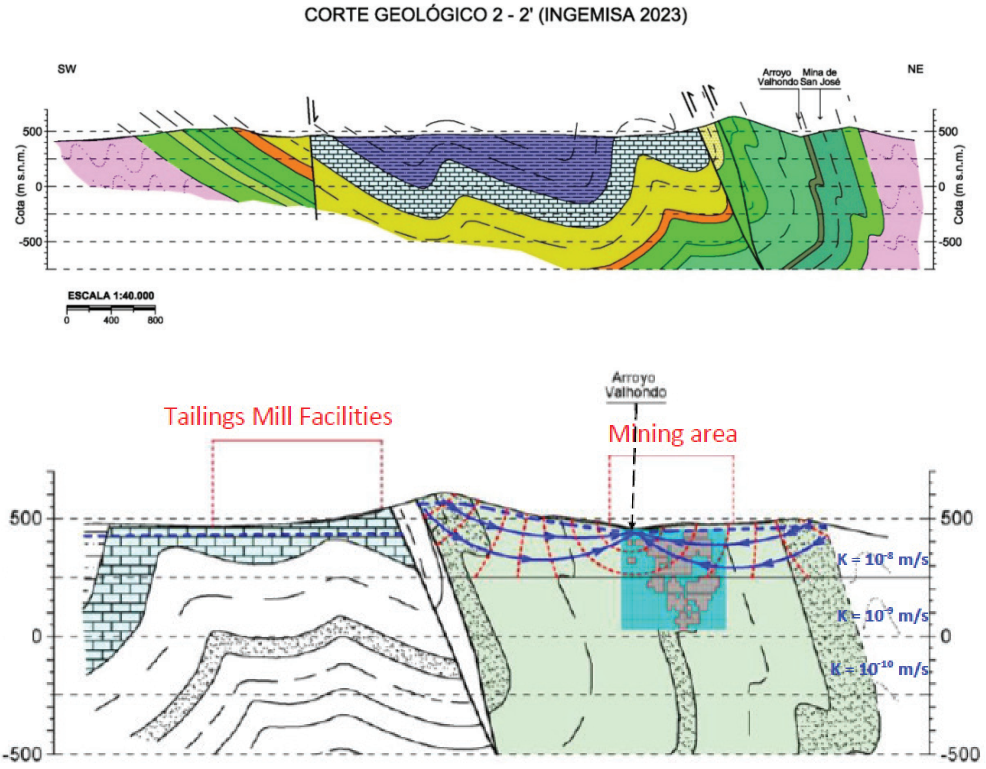

Figure 4 *Cross section (Fig. 2) and Hydrogeological Profile based in the Conceptual Model.*

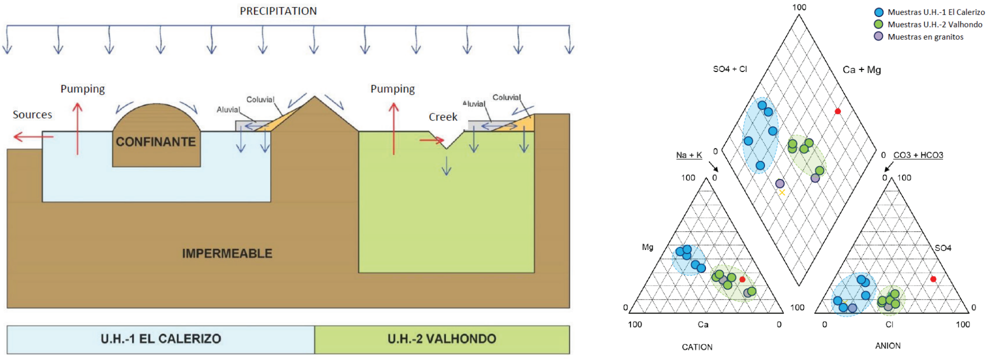

Figure 5 *Relationship between Hydrogeological Units and their hydrochemical character.*

in the mining area, a cross-section NE-SW and hydrogeological profile trough the mining and mill tailings areas, the conceptual model from them deduced, and a chemical quality diagram that shows the differences between the two hydrogeological units. As may be observed, both units (El Calerizo and Valhondo) are not hydraulically connected, as are separated by levels of slates and vulcanite of exceptionally low permeability that guarantee the individualization of their hydrogeological functioning.

The planned mining area is in the UH-2 (Valhondo), formed by a main aquifer of a multilayer type, permeable by mechanical fracturing and free regime, with local effects of confinement and marked anisotropy, both vertically and horizontally. Horizontal anisotropy is due to the different permeability of the different lithological layers of the aquifer. Permeability values between 10^{-9} m/s and 10^{-7} m/s are attributed, with the highest values corresponding to the fractured quartzite layers and the lowest to the shales. Intermediate values ($K = 10^{-8}$ m/s) correspond to slates and quartzites intercalations. The average permeability of the unit in the exploitation area is in the order of $K = 4{\cdot}10^{-8}$ m/s, compatible with a medium of low permeability. The depths of the wells inventoried in this area reach a maximum of 150 m, with variable flows between 0.1 and 0.2 L/s. The specific flow rate is estimated to be between 0.01 L/s/m and 0.02 L/s/m, so, the most frequent value for the transmissivity will be T = 0.1 to 0.2 m^2/d.

In the area planned for the Tailings Management Facility (TMF), treatment plant and other facilities, 4 pumping tests has been carried out, in which transmissivity values of less than 1 m^2/d have been obtained. In addition, two Air Lift tests have been conducted in two nearby boreholes, which yielded higher transmissivities: 16 to 100 m^2/d, values later confirmed by pumping tests. It is observed that, in the central and northern sectors of this area, the values of transmissivity and permeability are low, while in the southern sector they acquire higher values, compatible with the hydraulic characteristics attributed to the aquifer. This confirms the marked anisotropy of the environment and its compartmentalization into blocks of different hydrogeological characteristics. (Fig. 6).

For the investigation of the unsaturated zone of the substrate of the TMF zone, eleven “in situ” infiltration tests have been carried out on the decalcification clays that cover the carbonate outcrops, in trenches (Porchet and by the double ring methods). All of them were instrumented with pressure sensors in continuous sampling and with recording periods of up to 3 days. They show permeability values in a range of $K = 10^{-7}$ m/s and $K = 10^{-6}$ m/s. TDR and FDR (Time and Frequency Domain Reflectometry) have determined the moisture content.

Given that the average piezometric level of El Calerizo aquifer in this area is located at 35 m, the water flows that eventually reach the substrate under the decalcification clays

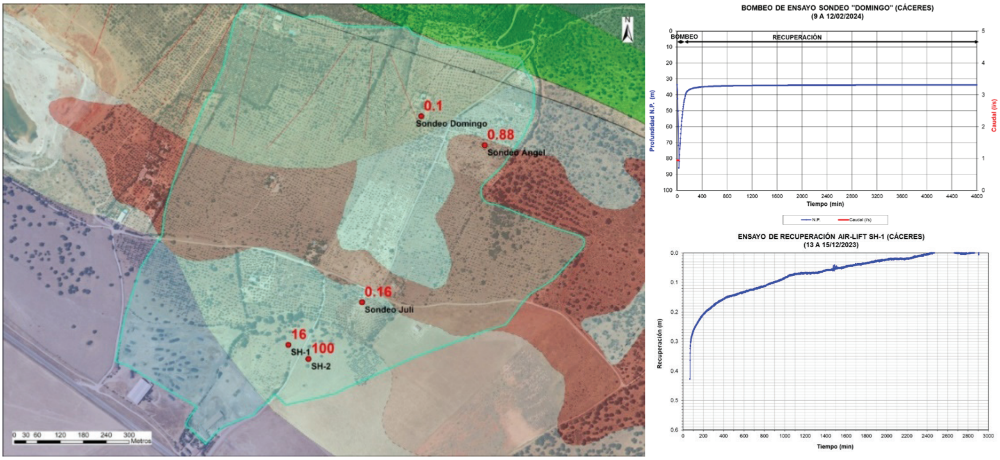

Figure 6 *Karst aquifer transmissivities (m2/d): pumping and air lift test diagramms (INGEMISA, 2024).*

would circulate through the unsaturated zone, until they reach the piezometric level, with a speed dependent on the permeability of the medium. For the values indicated above, transit times would be in the order of one year.

Mine design

The exploitation of the deposit will be carried out by the well-known underground mining method sub-level stoping, with paste backfilling. This mining method increases the ore recovery. The materials used for backfilling are the tailings produced in the processing plant, so the Project uses its own natural resources, minimizing the dependence on external materials. The stopes will be divided into primary and secondary, so that the secondary stopes will serve as a pillar while the stopes already exploited are filled with paste with a variable cement content, pumped with an optimum humidity that allows the flow through a pipe system but reduces the water consumption, afterwards, the secondary stopes are mined. The mine is divided into 60m height levels, subdivided in sub-levels. Each level is mined from the lower to the upper sub-level. Once a level is fully mined, and backfilled, the accesses not needed for mine services are closed for this level. The mine access will be through two ramps (services and transport), *Mining Sense Global (2024)*, (Fig. 7).

The geographical constrains for the mine facilities dictate that the project infrastructure is located to the South of the orebody. To

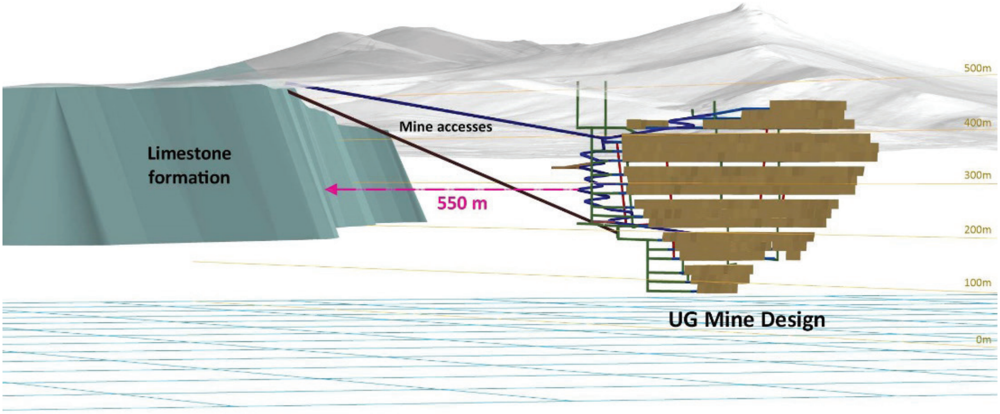

Figure 7 *Mine design (Mining Sense 2024)*

avoid that the mining works are developed through the Calerizo aquifer, the mine portal is to the North of the contact between the Calerizo limestone levels and the slate and vulcanic levels. Both, the galleries, ventilation shafts, and the exploitation area itself, are located in the low permeability materials that compose the U.H.-2 (Valhondo Unit), which has a hydrogeological behaviour independent of the El Calerizo aquifer. Mining works that need to be drained are, hence, developed on materials with low transmissivities and low affection to the surrounding users.

But the Valdeflórez Project has not only avoided to cross the lithologies in which El Calerizo aquifer is; in addition, a series of action protocols will be implemented, focused on:

1. Minimizing the impact of rock blasting in the vicinity of the excavation, and the development of secondary permeability due to fracturing.
2. "In advance" investigation, using geophysical techniques, oriented boreholes, and eventual sealing of fractures that may act as preferential pathways. In that sense the use of pre-grouting, where the investigation shows it appropriate, will have an important impact, with three main advantages: to control water inflow, to limit groundwater drawdown above the galleries, and to make tunnelling progress more predictable since rock mass quality is improved (*Barton et alia*, 2019).
3. Internal drainage system that guarantees that underground works are carried out in a drained environment, so that the water generated in the mine itself can never infiltrate outside the mine, as it acts as a sump during the exploitation phase.
4. Mine filling with low permeability paste material, to minimise the possibility of water contamination during the closure and post-closure stages.

Groundwater management will consist of the collection of water inflows and water produced by the mining works in pumping stations, provided by settling ponding compartments, to reduce solids. This water is pumped to the mine water deposit on the mine gate, from which the water is used back for mining works, the excess of water is used of other mining activities mainly for paste backfill, ore treatment of dust suppression. This makes the underground mining works self-sufficient in terms of water needs.

Conclusions and future research lines

In the San José de Valdeflórez Project a significant effort has been dedicated to the development and optimization of a mining and surface facilities design that allow the exploitation of the Li resources in a responsible and sustainable way. The characterization of the project substrate has been conducted, defining its geological-structural context based on surface geology, remote sensing techniques, application of various geophysical methods and borehole drilling.

The hydrogeological and hydrogeochemical research programme carried out has allowed the formulation of a Conceptual Hydrogeological Model and the definition of its main parameters. One of the most important efforts has been the definition of the unsaturated zone, where the surface facilities will be located and its role in the protection of El Calerizo aquifer, using Electrical Tomography, Infiltration tests, TDR & FDR, AMDT…

The integration of the available geological-structural and hydrogeological information in a calibrated hydrogeological model, with predictive capabilities, together with the Groundwater Control Network drilling program, will allow, through their instrumentation and monitoring, to continue the performance assessment of the facilities to demonstrate that they do not affect the evolution of El Calerizo aquifer through appropriate measurements and sampling.

This investigation will be continued during the construction phase, by the implementation and integration of protocols focused on the reduction of impacts, both, on the water drawdown impact, ground stability, water inflow and work progress prediction, taking the control measures in the case of deviations.

References

Pesquera, A., Roda-Robles, E., Gil-Crespo, P.P. *et al*. The metasomatic enrichment of Li in psammopelitic units at San José-Valdeflórez, Central Iberian Zone, Spain: a new type of lithium deposit. Sci Rep 10, 10828 (2020). https://doi.org/10.1038/s41598-020-67520-6

Pesquera, A., Torres-Ruiz, J., Gil-Crespo, P. P. & Velilla, N. Chemistry and genetic implications of tourmaline and Li–F–Cs micas from the Valdeflores area (Cáceres, Spain). American Mineralogist, vol 84, no1–2, 1999, pp 55–69. https://doi.org/10.2138/am-1999-1-206

INGEMISA (2024). Actualización del Modelo Conceptual del acuifero del Calerizo y su relación con las actividades mineras en Valdeflorez (Cáceres). (Unpublished)

Mining Sense Global, SL for Castilla Mining (2024). Proyecto General de Explotación de San José de Valdeflórez (Unpublished)

Barton, N. Quadros, E. Understanding the need for pre-injection from permeability measurements: What is the connection? Journal of Rock Mechanics and Geotechnical Engineering 11 (2019) https://www.sciencedirect.com/science/article/pii/S1674775518304219?via%3Dihub

An Overview of Active and Passive Mine Water Treatment at Urgeiriça Uranium Legacy Mine (Portugal)

Catarina Diamantino[1], Carlos Martins[1], Edgar Carvalho[1]

[1]*EDM – Empresa de Desenvolvimento Mineiro, S.A., Rua Sampaio Pina, nº 1, 7º andar, 1070-248 Lisboa, Portugal, catarina.diamantino@edm.pt, carlos.martins@edm.pt, edgar.carvalho@edm.pt*

Abstract

Environmental remediation of legacy mining sites in Portugal has been done since 2001 by EDM – Empresa de Desenvolvimento Mineiro, a state-owned company, including radioactive and sulfide polymetallic mines. One of the main focuses of the remediation design projects is the control and treatment of mine water using combined active and passive treatment systems. This paper presents the mine water treatment processes and monitoring that are implemented at Urgeiriça uranium legacy site.

Keywords: Urgeiriça mine, Mine water treatment, Environmental remediation

Introduction

Exploitation of radioactive ores in Portugal initiated with the discovery of the first radium deposit in 1907 and was concluded in the early nineties. Since 2001, EDM – Empresa de Desenvolvimento Mineiro, S.A. (EDM), a Portuguese State-Owned Company, has been granted the responsibility for the environmental remediation of all mining legacy sites in Portugal, under a concession contract established by the Decree-Law 198-A/2001. The implementation of remediation aims for the reduction of risks to people and to the environment and to contribute to the reuse of these areas for different beneficial end-uses, such as restoration of landscapes and habitats, or other public subsequent uses (Carvalho *et al.* 2023).

In the scope of the concession contract are included 199 legacy mining sites, including 62 radium and uranium legacy sites, which have been exploited between 1912 and 1991. Since the beginning of concession, EDM remediated 55 radioactive mining sites and 10 radioactive and polymetallic mining sites are planned to be remediated until 2030.

One of the main focuses of the remediation design projects is the control and treatment of mine water using combined active and passive treatment systems (Diamantino, 2016). This paper presents the mine water treatment processes and monitoring that are implemented at Urgeiriça uranium legacy site.

The treatment system is divided into two lines, active treatment and passive treatment. The active treatment includes pH neutralization with calcium hydroxide and addition of barium chloride followed by sedimentation for solid-liquid separation. The secondary passive treatment system, includes several steps such as aeration, sedimentation, filtration in adsorbent media and phytoremediation in aerobic wetlands.

Both systems are monitored before, in the intermediate steps and at the end of the treatment, and the water quality control programme includes in situ analysis of parameters such as pH, electrical conductivity, temperature, redox potential, total dissolved solids and flow rate and laboratory analysis of chemical and radiological parameters as total uranium, U238, U234 and Ra226 radionuclides, sulfate, chloride, manganese, calcium and sodium. These elements were identified in previous studies as the best indicators of hydrogeochemical contamination related to the legacy uranium mining sites in Centro Region, Portugal (Diamantino *et al.* 2016).

This paper will present an overview on the evolution of the mine water quality and treated volume, including assessment on the effects of the implementation of the remediation of two tailings dams, waste rock piles, uranium mill and other affected areas in the Urgeiriça legacy mining site and the resulting water quality improvement, specific removal efficiency rates and compliance with regulatory limits for water discharge. Also, it will present the quantities of used chemical reagents and operation and maintenance costs of mine water treatment.

Brief description of the Urgeiriça legacy mine site

Urgeiriça mine site is located in the village of Canas de Senhorim, in the municipality of Nelas and district of Viseu, in the central Portugal. Considered at one point to be one of the most important uranium mines in Europe, the Urgeiriça mine was registered in 1912 by a French group for radium exploration. In 1929, ownership of the mine passed into the hands of the Companhia Portuguesa de Radium (CPR) which was formed by English capital. By 1944 exploration restarted, interrupted by the outbreak of World War II, with the production of uranium concentrate. In 1962, the mine passed into the hands of the Portuguese State, through the Junta de Energia Nuclear (JEN), created to promote and develop nuclear energy studies. Around 1977, the National Uranium Company (ENU) took over the management of the mine until its closure in 1991.

Geologically, the Urgeiriça mine is characterized by the presence of porphyroid granites that host the quartz vein being explored, which is 7 kilometers long, 3 to 7 meters thick and oriented N 60º E. It is composed of of quartz, jasper, microbotrioidal pitchblende, uranitite, autunite, torbenite, and sulfides such as pyrite, marcasite, galena and chalcopyrite.

Exploration took place over a length of more than 1.6 kilometers, to a depth of 570 meters in 19 levels of galleries, with an average spacing of 30 meters. The mine had 6 shafts, the main one being the Sta. Bárbara shaft. Conventional underground mining was used until 1973, when in situ leaching with sulfuric acid was introduced.

A total of 4.370 tonnes of uranium oxide was produced in Portugal, of which 25% was mined at Urgeiriça and 75% from the surrounding mines located in the central region of Portugal, which were also processed at the Urgeiriça mill.

Environmental remediation of Urgeiriça legacy mine site

Mining operations from these past activities left environmental impacts caused by two tailings dams, waste rock piles, sludge deposits and various mining facilities, a uranium mill and related buildings and equipment in the industrial area, as well as risks due to the physical and safety stability of some buildings. Radiological and chemical contamination in the surrounding area, including contamination of surface water and groundwater, air, soil and sediments, had resulted in an existing exposure situation, mainly due to external gamma radiation, indoor and soil exhalation of radon gas and inhalation of dust.

Environmental remediation of the Urgeiriça mining area began in 2001 and comprises a phased, stepwise approach, as defined in the Master Plan of the Mining area of Urgeiriça, that aimed to remediate the risks to health and the environment from past mining activities. The implementation was concluded in 2022, with a total investment of more than 33 million euros. Funding was provided by EDM, mining royalties from current mining operators in Portugal, and the European Commission Cohesion Funds.

Urgeiriça Mine Water Treatment Plant details

Mine Water Treatment Plant (MWTP) new facilities were constructed in 2016, as part of the final phase of the environmental remediation works at the Urgeiriça mine (Fig. 1). The treatment system is divided into two lines, active treatment and passive treatment carried out through sedimentation and aeration tanks and phytoremediation ponds. Division criteria results from a balance between the installed treatment capacity and operation costs. In average 80% of flow rate is directed to the passive treatment and 20% to the active treatment. Mine effluents consists in subsurface outflows from two sealed tailings dams, which are collected via underground drains and directed to a leached well, from where they are pumped for treatment (Diamantino *et al*. 2023). Mine water treatment was complemented with a passive system in order to evaluate a gradual transition to a more sustainable solution in the long term, if adequate contaminant removal could be achieved without the need for continuous operation, reagent addition and energy consumption, and benefiting from a natural attenuation process in terms of effluent quality.

Active treatment line includes processes for treatment and separation between the liquid and the solid phases. Treatment of the liquid phase (Fig. 2) includes pH neutralization by adding calcium hydroxide ($CaOH_2$) to increase the pH and barium chloride ($BaCl_2$) to promote precipitation of Ra-226 and uranium, followed by decantation for solid-liquid separation, with monitoring of the effluent quality at the end of the treatment line. Two reactors for pH correction and two reactors for the addition and mixing of barium chloride are installed inside the MWTP building.

MWTP generates sludges that require additional thickening and dewatering operations prior to disposal. After chemical treatment, effluents are directed to a decantation system consisting of two circular decanters. The sludge accumulated at the bottom of the clarifier is directed to the sludge pumping well and pumped to a circular gravity thickener silo. Solid phase treatment process involves gravitational thickening of the sludges in a silo, followed by dewatering with a filter press and the use of filter bags for storage. Effluent from the thickening and dewatering of the sludge is recirculated. In order to improve the efficiency and speed

Figure 1 *Mine water treatment station at Urgeiriça mine site (Diamantino* et al. *2023).*

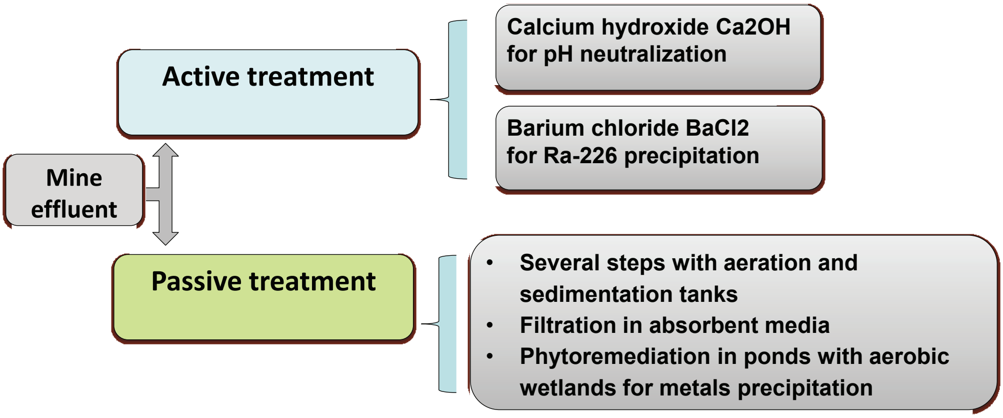

***Figure 2** Mine water treatment scheme at Urgeiriça mine site (Diamantino* et al. *2023).*

of the sludge dewatering process, polymer dosing is used on the sludge to be dewatered.

Passive treatment system

The passive treatment system essentially corresponds to a water treatment structure using principles of aeration, sedimentation, neutralization, and filtration in adsorbent media and phytoremediation. It consists of several interconnected tanks with gravitational effluent circulation.

The effluent is pumped from the leachate well through aeration cascades to primary and secondary sedimentation tanks. Aeration promotes the precipitation of iron oxides as well as other contaminants and metals. The effluent is them discharged into to the neutralization and filtration line, which consists of different filling materials, such as limestone, barite, and activated carbon, placed in big bags inside the tanks, protected at the top and bottom by limestone gravel. The total hydraulic retention time in the neutralization and filtration process, taking into account the average annual flow rate of 30 m^3/h, is approximately 126 hours.

Then the effluent from passive treatment is mixed with the effluent from active treatment before being pumped to the two phytoremediation ponds to improve the quality of the treated water. Biological treatment ponds consist of floating strips of macrophytes planted with *Juncus effusus*, *Iris pseudacorus*, and *Typha latifolia*. This solution has the advantage of providing phytoremediation of the water through a passive, natural, low-maintenance, and very simple to operate process, i.e. a phytoextraction process that consists of extracting the contaminant elements from the effluent and accumulating them in the biomass produced by the installed vegetation.

At the end of the last pond, the effluent passes through a monitoring station for continuous water quality and flow control before being released into the watercourse. If the water quality does not allow for discharge into the watercourse, the effluent can be recirculated through an existing pumping station to the beginning of the active treatment. The system was designed for an average influent flow rate of 30 m^3/hour and a maximum flow rate of 60 m^3/hour.

Chemical and radiological composition of mine effluent

Water quality control programme started in 2001. The effluent to be treated is generally acidic (with an average pH of 3.00 and electrical conductivity of 1313 μS/cm for 2018–2024), with high concentrations of metals such as manganese and iron and radionuclides. Table 1 shows the annual average concentration of chemical and radiological elements and in situ parameters, in 2023, for the effluent before and after treatment, with sampling frequencies of monthly and every two weeks, respectively.

Fig. 3 shows the annual variation of average concentrations in mine effluent, before and after treatment over the last 7 years, for sulfate, manganese, pH and total

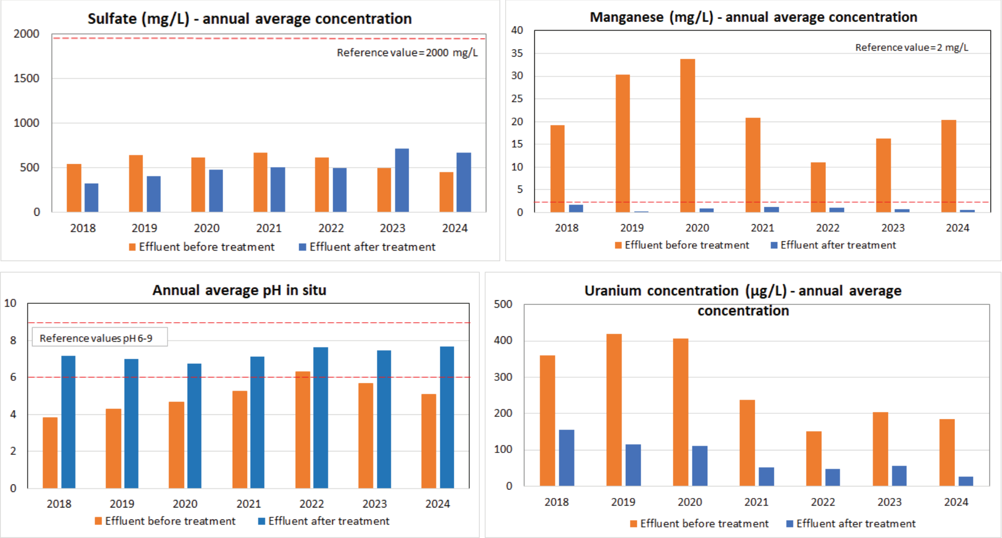

Figure 3 Annual variation of average concentrations in mine effluent before and after treatment. Dashed lines in red colour are the respective parameter reference values from permit licence for treated mine effluent discharge.

uranium concentration, with a decreasing tendency for uranium concentration and a smaller increasing tendency for pH values. Long historical data series can document this natural attenuation process after environmental remediation (Diamantino et at. 2023).

Removal efficiency rates and compliance with regulatory limits for mine effluent water discharge

The removal efficiency rates of mine water treatment, calculated on the basis of available laboratory results of chemical and radiological analysis, for the main contaminants and considering average annual concentrations in 2023, are the following: 100% for iron, 95% for manganese, 73% for total Uranium and 75% for Ra-226 (Table 1). With regard to the reference limit values for the discharge of treated mine effluent, a license permit has been issued by the national Regulatory Body for the management and protection of water resources and radiological protection (Environmental Protection Agency, Agência Portuguesa do Ambiente – APA). Table 1 shows these reference limit values defined for pH, sulfate, iron, manganese, TSS, radionuclides and Indicative Dose calculation. For radiological parameters, compliance is established for water for human consumption, taking into account the contamination history of the site. The results of this control and monitoring programme are reported annually to the Regulatory Body for compliance evaluation.

Quantities of chemical reagents and operation and maintenance costs for mine water treatment

Chemical reagents used in the active treatment are calcium hydroxide ($CaOH_2$) and barium chloride ($BaCl_2$). Fig. 4a shows the monthly evolution of the quantities of reagents used in 2023. In total, 58 m^3 of $CaOH_2$ and 2400 kg of $BaCl_2$ are used annually. As expected, higher amounts are used during the winter season when precipitation and discharge rates increase. Fig. 4b shows the monthly evolution of discharge rate and total precipitation in 2023. October was the wettest month, but this was not reflected in the increase of treated flow until the following month. The average flow rate was 21,5 m^3/h in 2023.

The operation costs in Urgeiriça MWTP, considering only the consumption of chemical reagents are shown in Table 2 and are around 16.800€/year (1400€/month). Other costs include technical staff, maintenance and cleaning operations and management of sludge produced, estimated at 14.000€/month, but shared and optimized

Table 1 Mine effluent composition before and after treatment, annual average values in 2023. Calculated efficient rate for contaminants removal. Reference values from permit licence for treated mine effluent discharge.

Parameter	Mine effluent before treatment	Mine effluent after treatment	Efficient rate	Effluent reference limits
N.º samples	12	24	–	–
pH	5.68	7.48	24%	5–9
EC (µS/cm)	1361	1086	20%	
Redox potential (mV)	179	137	–	
Temperature (ºC)	16.88	18.31	–	
Sulfate (mg/L)	715	498	30%	<2000
Chloride (mg/L)	33.20	34.99	–	
Sodium (mg/L)	42.40	35.68	–	
Calcium (mg/L)	201	181	10%	
Iron (mg/L)	11.83	0.05	100%	<2
Manganese (mg/L)	16.23	0.78	95%	<2
Total Suspended Solids TSS (mg/L)	31.6	3.95	87%	<60
Uranium total (µg/L)	203.8±30	55.8±8.0	73%	–
U-238 (Bq/L)	2.518±0.39	0.689±0.01	73%	3.0
U-234 (Bq/L)	2.213±0.35	0.593±0.01	73%	2.8
Ra-226 (Bq/L)	0.062±0.02	0.015±0.01	75%	0.5
Pb-210 (Bq/L)	–	0.05±0.02(b)	–	0,1
Indicative Dose (mSv) (a)	<0.10 conformity for water consumption – 15 in 20 analyses >0.10 conformity for water consumption – 5 in 20 analysis			<0.10

(a) Indicative Dose is calculated accordingly with Decree Law nº 69/2023, 21 August, from the measured radionuclide concentrations and dose coefficients set out in Table A of Annex iii to Council Directive 96/29/EURATOM of 13 May 1996. If [Σ Ci(obs)/Ci(der) ≤1] them Indicative Dose <0.10 mSv. Considering the sum of main radionuclides: U-238, U-234, Ra-226, Po-210. (b) average concentration considering 20 samples.

between other smaller mine sites, mainly with passive treatment systems. Permanent technical staff represent approximately 60% of the total operation and maintenance costs.

Conclusion

This paper presents an interesting mine effluent control and treatment plant that was implemented during the environmental remediation of the Urgeiriça legacy mine site, which combines a common and effective solution of an active system with the addition of chemical reagents and a more sustainable passive treatment system with aeration, sedimentation and phytoremediation processes. Operation and maintenance costs are high in the post-remediation phase, but the long-term reduction in concentrations of contaminants such as uranium is expected to allow a gradual transition to passive treatments. Mine water discharge limits are generally accomplished, for chemical and radiological parameters, but for radiological parameters compliance reference limits are very restrictive.

Table 2 Costs of chemical reagents consumption in 2023.

Reagents	Unitary Costs	Consumption	Total costs
$CaOH_2$	286€/m³	58 m³	16.588€
$BaCl_2$	2,77€/25kg	2400 kg	286€

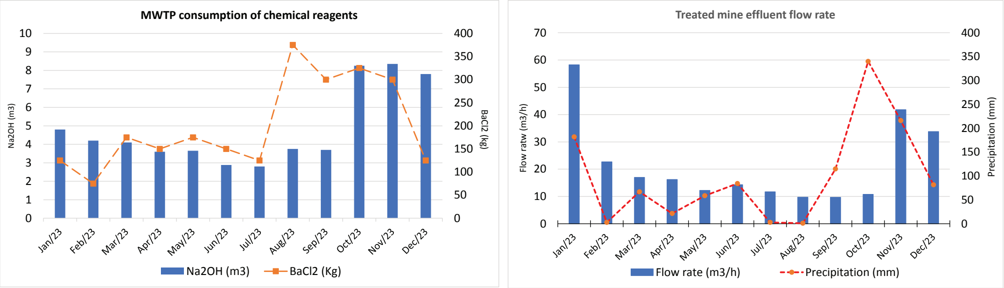

Figure 4 a) Consumption of chemical reagents in 2023. b) Treated mine effluent flow rate in 2023.

References

Carvalho E, Diamantino C (2023) Perspectives and challenges for sustainable post-remediation management of uranium legacy sites in Portugal. International Conference on the Safety of Radioactive Waste Management, Decommissioning, Environmental Protection and Remediation: Ensuring Safety and Enabling Sustainability. IAEA CN-318/244. Nov 6–10, IAEA International Atomic Energy Agency. Vienna, Austria.

Diamantino C, Carvalho E, Pinto R, (2016) Water resources monitoring and mine water control in Portuguese old uranium mines. Annual Conference of the International Mine Water Association IMWA2016, Leipzig, Germany.

Diamantino C, Carvalho E, Martins C (2023) An overview of active and passive treatment mine water treatment at Urgeiriça uranium legacy mine (Portugal). WISSYM 2023 Re-thinking mining remediation. Innovative approaches towards sustainability. WISMUT, 25–28, September. Dresden, Germany. Poster.

The Application of Quantitative Risk Assessment to Assessing the Impact of Tailings Management Facilities on Groundwater Resources

Gareth Digges La Touche[1], Sofia Nazaruk[2], Thomas Booth[2], Tom Demmer[2], Alireza Nickman[2], Jessica Cammack[2]

[1]*WSP UK Ltd, 7 Lochside View, Edinburgh, EH12 9DH, United Kingdom, garethdiggeslatouche@wsp.com, ORCID 0000-0002-4889-1581*

[2]*WSP UK Ltd, The Mailbox, Wharfside Street, Birmingham, B1 1RQ, United Kingdom*

Abstract

Tailings Management Facilities may pose a risk to water resources. This paper discusses the use of probabilistic simulation within quantitative analytical risk assessment models, especially in scenarios where limited data may undermine confidence in the predictive outcomes.

The application of probabilistic modelling is demonstrated through case studies that evaluate closure and remediation strategies for a tailings management facility, as well as quantifying uncertainty. The impact of different liner and cover systems and the importance of considering facility design holistically is considered, recognising that factors such as landform and cover design are as integral to mitigating risk as liner design.

Keywords: Tailings, risk, closure, water resources, water quality

Introduction

Tailings Management Facilities (TMF), also known as Tailings Storage Facilities (TSF), are engineered structures used for the containment of residues (tailings) from mineral processing. Tailings are often deposited as a slurry, though in recent years as the result of some well publicised facility failures (e.g. Samarco in 2015 and Brumadinho in 2019, both in Brazil (Sliva Rotta *et al.*, 2020)) there has been a shift towards the use of filtered tailings (also known as "dry" stack facilities).

Whilst termed a "dry" stack facility, it should be noted that filtered tailings are not dry but are tailings that have been dewatered, often by filter press. Filtered tailings should be compacted after placement to reduce the liquefaction risks and have a water content close to (or drier than) the Standard Proctor Optimum water content (Ulrich (2019)). As such a filtered tailings stack can readily have a water content of 15% (defined as geotechnical moisture content, i.e. mass of water / mass of solids) or more (Crystal *et al.*, 2018). The moisture content of filtered tailings can both increase or decrease depending on the environmental setting and facility design.

Historically tailings have been deposited directly on natural ground, contained behind a dam or embankment structure though in recent years, facilities are increasingly engineered with low permeability liners based on an assessment of risk to water resources. For example, the European Directive 2006/22/EC (European Union, 2006) on mine water requires the demonstration of no significant risk of polluting soil, groundwater or surface water as the result of operation of a mine waste facility. This risk assessment may comprise a qualitative assessment of risk based on analogue facilities or more typically an assessment based on the results of a numerical or analytical model of groundwater flow and contaminant transport.

The nature of the hazard, i.e. the concentrations of contaminants in the tailings and resultant leachate arising from percolation of infiltration through the waste mass or in arid settings the drain down of entrained pore water may be determined from geochemical characterisation and modelling to predict leachate quality. Such processes are industry standard (e.g. European Commission 2018) and the Global Acid Rock Drainage (GARD) Guide (International Network for Acid Prevention 2014) outlines a process for predictive modelling as summarised in Fig. 1.

The common approach to environmental risk assessment is to consider the source, pathway and receptor linkages, with the source being, in this instance, a tailings facility and the pathway and receptor both being groundwater, as in the case described in this paper. The assessment methodology should include a robust model that adequately represents the physical system based on the available data, that enables a prediction of water quality and thus risk at the identified receptors. Ideally such a risk assessment should consider both operational and closure phases of the mine operation, taking into consideration for example the evolution of engineering controls over time and in particular the degradation of engineered components such as liners or cover systems.

The use of probabilistic (stochastic) calculation approaches using the Monte Carlo simulation method in analytical contaminant transport models to understand the interaction of a TMF with the groundwater environment provides a powerful tool for the assessment of risk and the likelihood of that risk being realised. This can be implemented

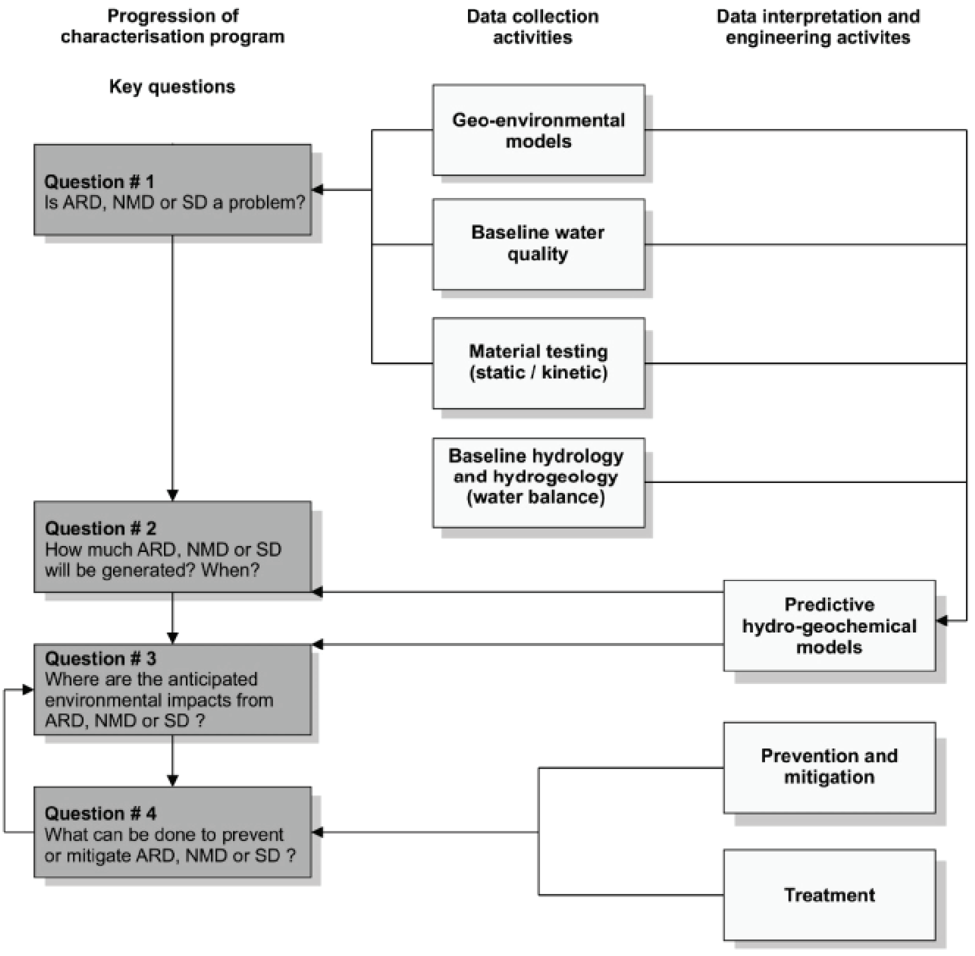

Figure 1 *Characterisation process road map (after INAP (2014). ARD – acid rock drainage; NMD – neutral mine drainage; SD – saline drainage.*

in both dynamic, i.e. time variant, and steady state models. Both approaches are illustrated in this paper.

Risk assessment and probabilistic models

Probabilistic modelling is employed to manage the inherent uncertainty in most of the input parameters needed for groundwater and impact or risk assessments. This approach allows for the prediction of potential outcomes and their likelihood, providing insight into the risk posed to the water environment by a TMF. Parameters that are not precisely known due to limited sampling or variability (e.g., in geological or hydraulic properties) can be represented through stochastic inputs that capture the estimated value at the relevant scale.

Probabilistic simulation tools use stochastic methods to randomly sample statistical distributions of input parameters and perform model calculations with the selected values. This Monte Carlo analysis process is repeated numerous times, generating a set of output values that can be statistically analyzed to describe the probability of certain outcomes (see Fig. 2).

The range of likely results can be presented based on their probabilities and an understanding of the sensitivity of the model parameters, providing quantitative information to inform decision making. The approach of using probabilistic simulation for groundwater risk assessment has been central to the regulatory approach to groundwater protection in the UK for over 25 years (e.g. Environment Agency, 1999).

As outlined above a groundwater risk assessment comprises three components: the source (in this case, tailings), the pathway or pathways connecting the source to any receptors, and the receptors themselves (such as groundwater and surface water bodies like rivers and streams). If any component of the source-pathway-receptor system is absent from a site, the risk to the groundwater and surface water environment will be negligible.

The starting point for any TMF risk assessment is the development of a conceptual model that describes the hydrological and hydrogeological setting and identifies the source-pathway-receptor linkages. A probabilistic analytical model may then be created for the risk assessment process, using site characterisation data to parameterise the model. For groundwater assessments, the model typically includes a one-dimensional contaminant transport model representing advection and attenuation processes such as dilution, dispersion, sorption, precipitation, and biodegradation along a specific migration pathway. It is possible to build complex models that combine multiple models each representing different components of the system such as changes in infiltration through cover systems and evolution in source term chemistry, this can include coupling

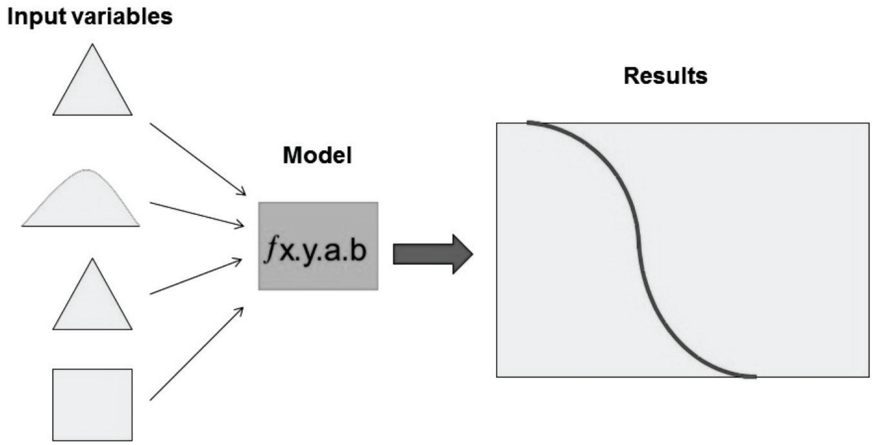

Figure 2 *Components of a probabilistic simulation.*

to geochemical modelling codes such as PHREEQC.

Probabilistic risk assessment using a steady state contaminant transport model

To understand the potential risks to the wider groundwater and surface water environment from an existing TMF, located in northern Europe, and to provide a rational basis for risk management (including further characterisation studies) a simple spreadsheet based contaminant transport model was developed. Contaminant transport for a number of potential contaminants of concern (PCOC) was simulated using the Domenico (1987) equation simulating advection, dispersion, diffusion and retardation. As many variables were not well constrained, such as hydraulic conductivity, hydraulic gradient, aquifer thickness and chemical properties (such as the soil water partition coefficient) the model was set up to consider these based on the most likely value and an estimate of the standard deviation from that value, assuming a normal distribution. The resulting model was run for 1000 iterations to allow adequate sampling of the probability functions.

Based on the calculations it was identified that at the 95% confidence level the chloride concentration 100 m downgradient of the TMF would be less than 115 mg/L (Fig. 3a) and the nickel concentration 0.023 mg/L (Fig. 3b), compared to initial concentrations at source of 300 mg/L and 0.06 mg/L respectively. The calculated 50%ile or most-likely concentrations were 106 mg/L and 0.021 mg/L for chloride (Fig. 3a) and nickel (Fig. 3b) respectively. Calculated travel times for breakthrough of the plume were approximately 50 years and approximately 27,400 years for chloride (Fig. 3c) and nickel (Fig. 3d) respectively at the 95% confidence level and 38 years and 19,600 years at the 50%ile (Fig. 3c and d).

The results of the calculations, illustrated in Fig. 3, indicate that it is unlikely that the chloride concentrations will exceed the regulatory criteria of 120 mg/L downgradient of the facility, whereas the nickel concentrations will exceed the regulatory limit of 0.01 mg/L, although not for many (thousands) years. The relative travel times are significant in that while based on the chloride travel time, as a conservative tracer, breakthrough is most likely to occur in approximately 38 years, it is unlikely that there will be an impact from nickel for a much longer period. This allowed risk

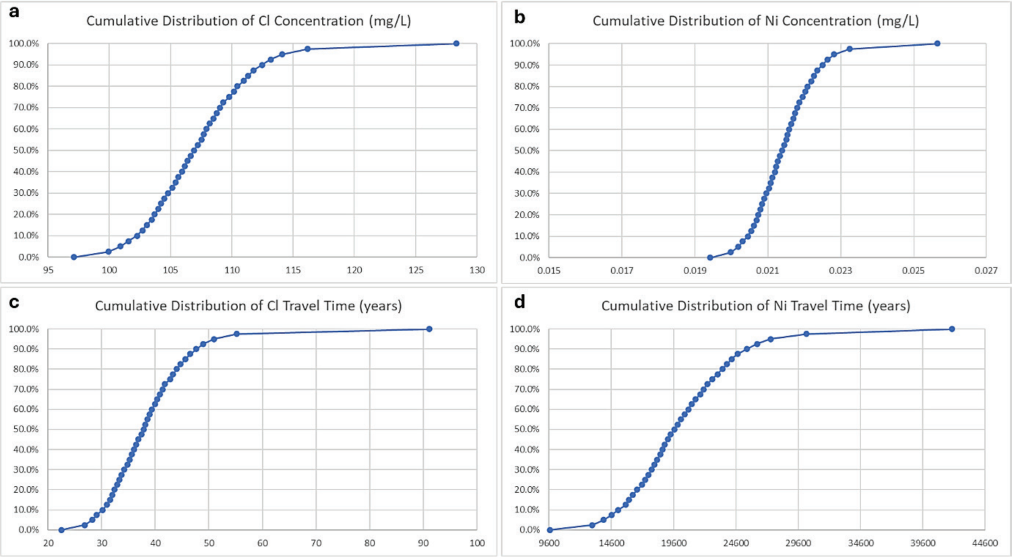

Figure 3 Selected output from a probabilistic simulation of steady state contaminant transport, showing the cumulative distribution of Chloride and Nickel Concentrations (a and b respectively) and Travel Times (c and d respectively).

management actions, such as source control, to be prioritised on the basis there was not an immediate risk from nickel contamination in groundwater arising from the TMF.

The use of dynamic probabilistic risk assessment

As discussed in Digges La Touche and Garrick (2011) a dynamic probabilistic model of contaminant transport was used to model the risks arising from an unlined TMF in South America and the residual risks following remediation of the facility by removal of the tailings to a new contained facility. The conceptual model is illustrated in Fig. 4. It was considered that following the removal of the tailings that a residual long-term risk would remain due to contamination of the underlying weathered bedrock. The evolution of concentrations at the monitoring point downgradient of the facility was simulated, using a dynamic probabilistic simulation model, and used as the basis for calibration against 7 years of existing monitoring data. It was found necessary to reduce the assumed partition coefficients for a number of PCOC to achieve a reasonable calibration.

The benefit of using a dynamic probabilistic model is that it allows the simulation of time variant problems. As can be seen from Fig. 5, without removal of the tailings it is predicted that concentrations of lead would continue to increase over time. Simulations of concentrations at the surface water receptor approximately 1 km from the TMF showed consistent results although it was noted that the travel times varied by an order of magnitude between the 95%ile and the 50%ile, most-likely, simulations. On this basis it was possible to demonstrate to the regulator that the remedial action was proportionate.

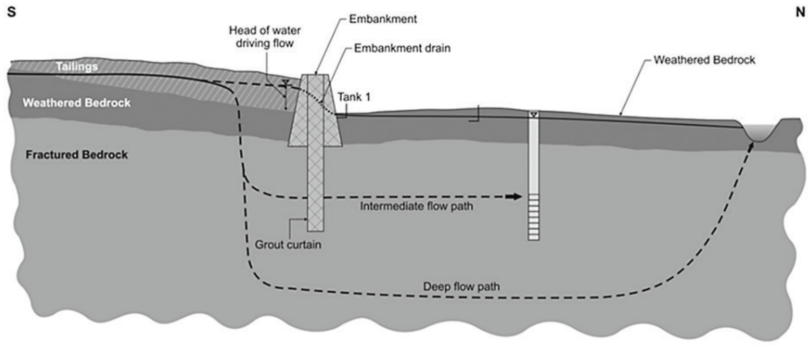
Ⓐ Conceptual hydrogeological model when tailings are present

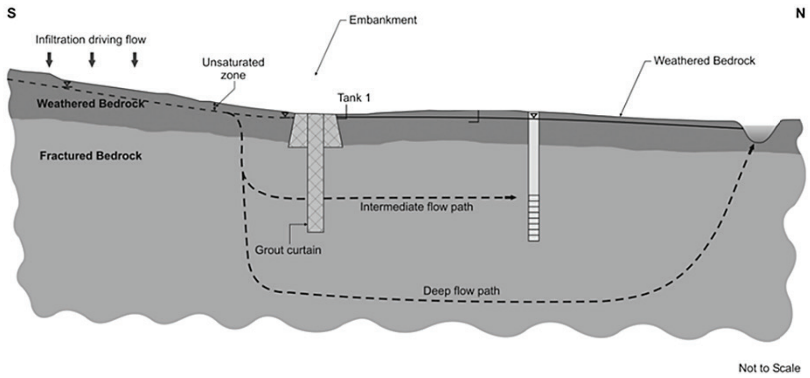
Ⓑ Conceptual hydrogeological model when tailings are removed

Figure 4 *Tailings Management Facility Conceptual Model during operation and following remediation (after Digges La Touche and Garrick (2011).*

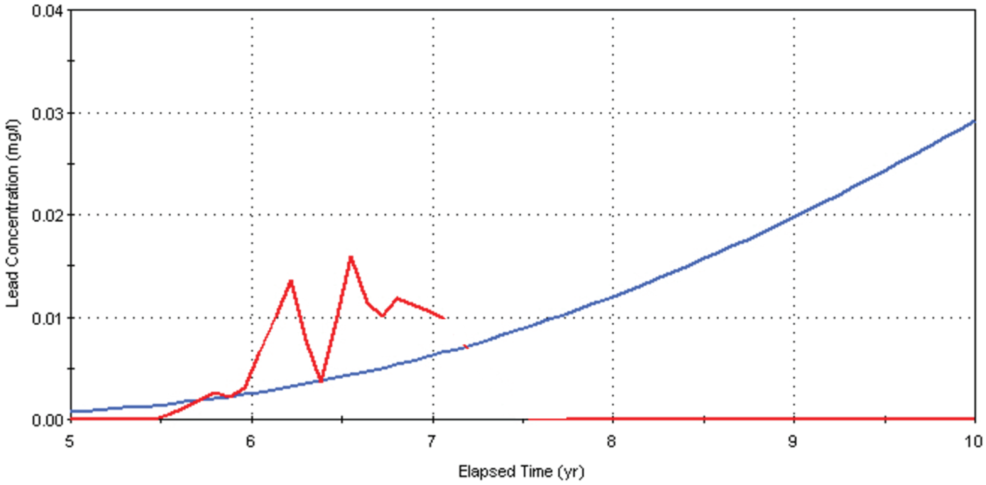

***Figure 5** Modelled 95%ile lead concentrations in groundwater (blue line) compared to measured concentrations (red line).*

Conclusions

The use of probabilistic models for the assessment of the impact of TMFs on, and thus risk to, water resources can be applied using relatively simple and cost-effective tools. The use of probabilistic simulations allow the natural variation in physical and chemical properties of the system to be taken into account and also allows for the quantification of uncertainty in those properties and thus also in the predicted impacts. While in both of the examples presented the models do not consider geochemical reaction pathways, it is considered that as screening models that can be calibrated to a sufficient degree based on simple retardation factors that the models are fit for their intended purpose. That is to inform short term decision making rather than trying to represent the details of the system and its evolution.

References

Crystal, C, Hore, C, Ezama, I (2018) Filter-pressed dry stacking: design considerations based on practical experience. Proceedings of the 22nd international conference on tailings and mine waste, Keystone, Colorado, USA, September 30–October 2, 2018.

Digges La Touche, G, Culshaw, H, Lansley, R (2011) Probabilistic modelling for tailings remediation and restoration. Proceedings of the International Mine Water Association Conference, Aachen, Germany.

Domenico, PA (1987) An analytical model for multidimensional transport of a decaying contaminant species. Journal of Hydrology, 91:49–58

Environment Agency (1999) Guidance on assigning values to uncertain parameters in subsurface face and transport modelling. National Groundwater and Contaminated Land Centre Report NC/99/38/3.

European Commission (2018) Best Available Techniques (BAT) Reference Document for the Management of Waste from Extractive Industries in accordance with Directive 2006/21/EC.

European Union (2006) Directive 2006/21/EC of the European Parliament and of the Council of 15 March 2006 on the management of waste from extractive industries and amending Directive 2004/35/EC.

International Network for Acid Prevention (2014) Global Acid Rock Drainage Guide (GARD Guide), http://www.gardguide.com/images/5/5f/TheGlobalAcidRockDrainageGuide.pdf

Silva Rotta, LH. Alcântara, E, Park, E, Negri, RG, Lin, YN, Bernardo, N, Susse, Mendes, TSG, Filho, CRS (2020) Álvarez H, Domínguez G, Ordóñez A, Menéndez J, Álvarez R, Loredo J (2020) The 2019 Brumadinho tailings dam collapse: Possible cause and impacts of the worst human and environmental disaster in Brazil. Int J Appl Earth Obs Geoinformation 90: 1–12, doi.org:10.1016/j.jag.2020.102119.

Ulrich, B (2019) Practical thoughts regarding filtered tailings. Proceedings of Paste 2019, the 22nd International Conference on Paste, Thickened and Filtered Tailings, Cape Town, 8–10 May 2019.

Comprehensive Study on the Electrical Characteristics and Full-Spectrum Tracing of Water Sources in Flooded Coal Mines

Donglin Dong [1,2] , Qiang Wu[1,2]

[1]*College of Geoscience and Surveying Engineering, China University of Mining & Technology-Beijing, Beijing 100083, China*

[2]*Inner Mongolia Research Institute, China University of Mining and Technology (Beijing), Ordos 017004, China*

Abstract

This study proposes a novel spectral tracing technique to identify inrush water sources in Donghuantuo coal mine. Electrical characteristics of the mine floor were analyzed, and spectral data from main aquifers were used to build a source database. A CSSOA-optimized random forest model (CSSOA-RF) was developed, achieving 100% accuracy in tests. The method enables rapid and reliable identification of single and mixed water sources, offering technical support for mine safety and water hazard prevention. While effective in this relatively simple geological setting, further validation is needed for broader application.

Keywords: Identification of Inrush water Sources; Spectral Tracing Technology; Chaotic Sparrow Search Optimization Algorithm (CSSOA)

Introduction

Traditional methods for studying inrush water, which rely on inrush water data and physical parameters, have proven effective in distinguishing relatively simple water sources. However, in cases where the water quality is complex and physical parameters are similar, or where the water quality of different inrush sources is alike, traditional methods often fail. This necessitates the use of alternative approaches for identifying inrush water sources (Sun 1965; Sun and Zheng 1996). By analysing the basic components of aquifers and the chemical composition of water samples from inrush points, suitable discriminant functions are selected, and discriminant formulas are established based on specific criteria. These formulas are then used to classify unknown samples, employing methods such as fuzzy mathematics, grey relational analysis, extension identification, Geographic Information Systems (GIS), support vector machines, and artificial neural networks (Panagopoulos *et al.* 2016; Zhang *et al.* 2019; Ju and Hu 2021).

In recent years, with the rapid advancement of computer technology, neural networks have gradually been used to identify inrush water sources in mines. Common artificial neural network models include BP neural networks, RBF neural networks, ELM, and Elman neural networks, which are valuable for accurately identifying multiple water sources in mines. Deep learning algorithms represent an evolution of artificial neural networks, with common approaches including deep neural network (DNN) analysis, convolutional neural network (CNN) analysis, and probabilistic neural network (PNN) analysis. Scholars often use these methods to determine the origin of water samples. Optimization algorithms such as genetic algorithms, ant colony algorithms, and particle swarm algorithms are frequently used for function optimization and combinatorial optimization of discriminant models. For example, Zhang Di applied a genetic algorithm-optimized support vector machine to identify inrush water sources, which improved the accuracy of parameter selection for support vector machines in inrush water source identification. However, this method still has drawbacks, such as tracing detection times exceeding one hour, inability to trace mixed water and its proportions, and loss of the optimal rescue window post-inrush.

This study aims to explore a new method that abandons the traditional approach of concentration testing. Instead, it focuses on the rapid and accurate identification of inrush water sources, proposing a novel method for identifying mixed inrush water sources.

Methods

Study Area and Water Sampling

Donghuantuo mine is located in the city of Tangshan in North China's Hebei Province. The southeast wing of the mine extends 13.5 km in strike length and 3 km in dip width, while the northwest wing stretches 8 km in strike length and 0.5 km in dip width. The mining area covers 40.5 km². The terrain within the mining boundary is quite flat, with no rivers traversing the area. Additionally, there are no surface water systems within the Donghuantuo mining boundary, as illustrated in Fig. 1. The Donghuantuo mining field hosts multiple aquifers, including the Quaternary alluvial pore-confined aquifer, the Carboniferous–Permian sandstone fissure-confined aquifer, and the Middle Ordovician limestone karst fissure-confined aquifer. These aquifers are divided into seven aquifer groups, as shown in Fig. 1.

In the preliminary phase of this study on spectral tracing of inrush water sources, four water samples were collected from the primary aquifers of the Donghuantuo mine. These samples were taken from the 12–2–14–1 aquifer, the 5 coal roof aquifer, the Quaternary aquifer, and the Ordovician limestone aquifer, with each sample measuring 1000 mL. Each of the four samples was labeled and numbered accordingly.

Transient Electromagnetic Method for Inrush Water Sources

In this study, the enhanced TEM67 transient electromagnetic method was employed. The transmitter used was the TEM57-Mk2, augmented with two TEM67 power modules, capable of reaching an emission voltage of up to 240 V and a maximum emission current of 28 A. This configuration allowed the use of large-sized or large effective area transmitter coils, achieving greater exploration depths. The table below compares the transmission power of the TEM67 and the enhanced TEM67. It shows that with a transmission frame size of 2000 m × 2000 m (equivalent to an exploration depth of 2000 m), the magnetic moment M (I × S) of the enhanced TEM67 can reach up to 36,363,636 A·m².

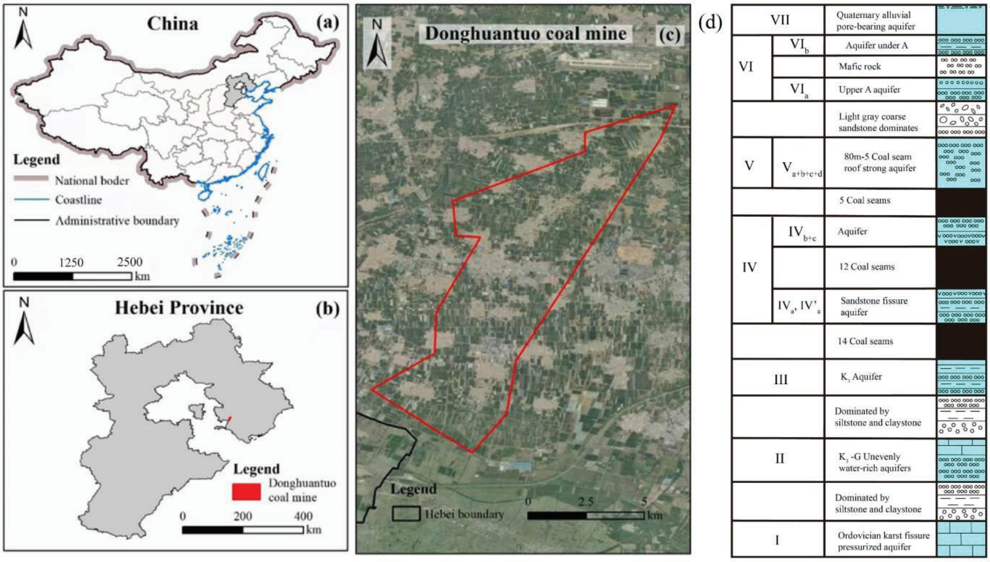

Figure 1 Geographical location of the study area.

Chaos Sparrow Search Optimization Algorithm

The sparrow search algorithm (SSA) faces challenges such as a tendency to get trapped in local optima, a lack of randomness in the search process, and slow convergence. To address these issues, researchers including Xin introduced the tent chaotic sequence and Gaussian distribution into the SSA, forming the chaos sparrow search optimization algorithm (CSSOA). This method uses tent chaotic mapping during the population initialization stage to maintain a uniform distribution of initial individuals. When the population exhibits convergence or divergence, chaotic perturbations and Gaussian mutations are applied to alleviate local optima problems.

Random Forest (RF) Algorithm

Random forest (RF) is an ensemble learning algorithm commonly applied to classification tasks. It constructs a large number of decision trees from training samples to form a collective discriminative model, which is then used for classifying unknown samples. In UV–Visible spectrum classification, RF can effectively handle non-linear relationships and, through its built-in feature importance metrics, select the most informative features from large datasets, thus enabling efficient processing of high-dimensional spectral data while ensuring classification accuracy.

Electrical Characteristics of Water-Rich Inrush Water Source

Electrical Characteristics of Water-Rich Inrush Water Sources at the 20223 and 3015 Working Face

The current retreating working faces are 20223 and 3015. To ensure safe and efficient mining, it is necessary to conduct electrical resistivity surveys on the roof and floor of these working faces to accurately delineate their water-bearing properties. The enhanced TEM67 transient electromagnetic method was used to detect water-rich areas at the 20223 and 3015 working faces. These surveys were complemented by data from four drill holes and tunnel exposure data. The water-bearing characteristics of the roof and floor of these working faces are illustrated in the following Fig. 2.

According to Fig. 2, a relatively low-resistivity zone, designated as DF-1, was identified within the 0 to 80 m vertical detection range of the floor at the 20223 working face. Analysis of related hydrogeological data suggests that this zone corresponds to a sandstone fissure-confined aquifer. Comparisons with the fault lines in the profile and cross-section diagrams indicate that this zone is likely connected by faults, warranting focused investigation. Verification through four drill holes confirmed that this is indeed a fault zone.

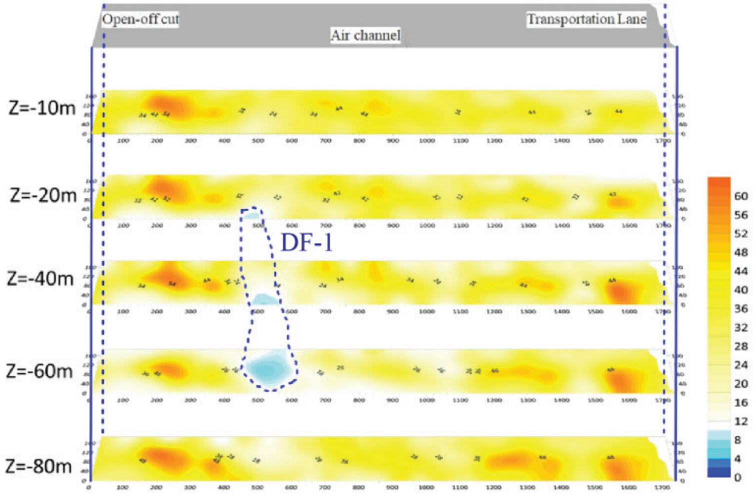

Figure 2 *3D Electrical resistivity tomography (ERT) image of the 20223 working face floor.*

Spectral Characteristics of Various Inrush Water Sources

A vacuum filtration apparatus was used to filter each water sample solution through a 0.45 μm PTFE hydrophilic filter membrane to remove particulate impurities. The filtered water samples were then dispensed into sample bottles that had been washed with ultrapure water and air-dried. To increase the sample size for subsequent machine learning, each type of water sample was divided into eight sample bottles, resulting in eight sets of spectral data for each type of water sample. To ensure accuracy, each sample was measured three times, and the arithmetic mean of these measurements was used as the spectral curve data for that sample. For ease of data processing and result interpretation, samples were assigned hierarchical numbers, e.g., the first sample of water sample type 1 was labeled 1–1, and its two repeated measurements were labeled 1–1–1 and 1–1–2, respectively. In total, 32 sets of water samples were prepared for subsequent classification model training in this tracing study.

The prepared samples were subjected to spectrophotometric measurement. After the instrument completed its self-check and warm-up, the measurement parameters of the spectrophotometer were set: the starting wavelength was set to 320 nm, the ending wavelength to 650 nm, and the scanning interval to 1.0 nm. Zero-line calibration was then performed. Each sample was measured sequentially, with three repeated measurements. The data were then imported into a computer using a USB drive and labeled accordingly. After measuring each type of sample, the cuvette and other instruments were cleaned with ultrapure water. Upon completing the measurements of all water samples, the repeated measurement data for each sample were organized and averaged arithmetically, resulting in 32 sets of single-source spectral data, as shown in Fig. 3.

Analysis of Fig. 4 reveals significant differences in the spectral data of the four aquifer types within the measured wavelength range of 320–650 nm. The absorbance

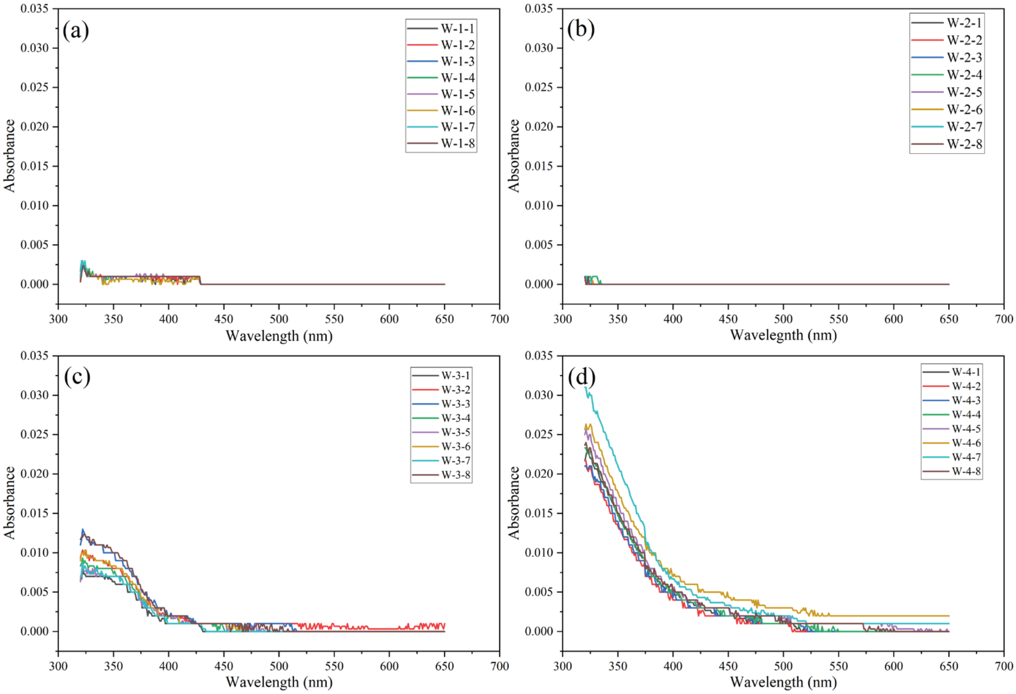

Figure 3 Original spectral data of each aquifer. (a) 12-2~14-1 aquifer water samples, (b) 5 coal roof aquifer water samples, (c) quaternary aquifer water samples, (d) Ordovician limestone aquifer water samples.

fluctuations for water samples W-1 and W-2 are minimal, distributed within the range of 0 to 0.005, with most absorbance values being 0. Specifically, the absorbance for W-1 drops to 0 after 429 nm and remains unchanged, while for W-2, it remains at 0 beyond 335 nm. In contrast, water samples W-3 and W-4 exhibit significant absorbance variations, with both reaching maximum absorbance values around 320 nm and then gradually decreasing to their minimum values. The absorbance range for W-3 is between 0 and 0.015, while for W-4, it is between 0 and 0.0325. The absorbance variations for all four water samples are concentrated in the ultraviolet region (<400 nm), aligning with the visual characteristics of colorless and transparent water samples.

Water samples W-3 and W-4, which are from shallower locations, experience more frequent water–rock interactions compared to the deeper W-1 and W-2 samples. As a result, W-3 and W-4 have higher ion concentrations and more complex ionic compositions, leading to more pronounced spectral variations. The distinct spectral differences among the four water samples ensure the accuracy of the subsequent machine learning tracing model's classification and identification.

Based on the hydrogeological conditions, hydraulic connections, and actual geological situations of the four main aquifers sampled from the Donghuantuo mine, the study investigated the mixing of the Quaternary water sample W-3 and the 12–2~14–1 aquifer water sample W-1. The preparation method for these mixed samples was consistent with that of the single-source samples. W-1 and W-3 samples were mixed in ratios of 1:9, 2:8, ..., 8:2, and 9:1. To ensure sufficient training samples for the subsequent tracing model, 10 samples were prepared for each mixing ratio, resulting in a total of 90 mixed spectral data entries, as shown in Fig. 4.

Construction and Evaluation of the Tracing Identification Model

Using the preprocessed sample data, we constructed the CSSOA-RF spectral tracing identification model based on the Python language. The CSSOA algorithm was employed to optimize the key parameters of the RF model, achieving adaptive parameter optimization for the tracing identification model. This phase involved steps such as da-taset partitioning, CSSOA algorithm optimization, and the construction of the CSSOA-RF tracing identification model.

The parameters of the RF model, including *n_estimators, max_depth, min_samples_leaf*, and *min_samples_split*, were optimized based on the training set. The CSSOA algorithm's objective function was set to the average error obtained from five-fold cross-validation on the training set. The population size was set to 60, with a discoverer ratio of 0.7 and a warning reconnaissance ratio of 0.2. The optimization process is illustrated in Fig. 5. After 67 iterations, the model achieved the minimum average error value of 0.1596, which remained stable. Therefore, the parameter combination at this point was chosen as the optimal parameter values for the RF model.

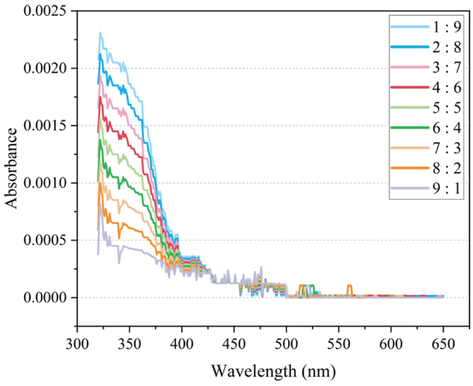

Figure 4 *Original spectral data of different aquifers.*

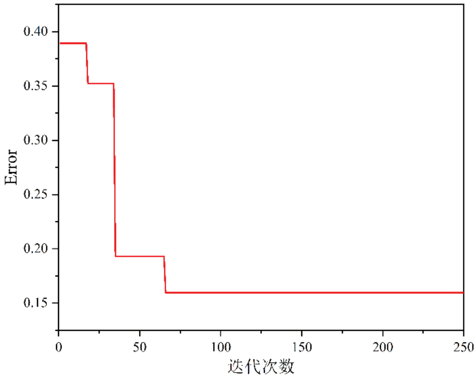

Figure 5 *CSSOA parameter optimization curve.*

Conclusion

CSSOA-RF Spectral Tracing Identification Model: By using the chaos sparrow search optimization algorithm (CSSOA) to optimize the key parameters of the random forest (RF) model, the CSSOA-RF spectral tracing identification model was constructed. The CSSOA algorithm, through the introduction of chaotic perturbations and Gaussian mutations, overcame the limitations of traditional sparrow search algorithms that tend to get trapped in local optima. This improved optimization efficiency and the model's global search capability. The optimized RF model achieved optimal parameter selection, providing reliable technical support for tracing identification. In the test set, the CSSOA-RF model demonstrated excellent classification performance, achieving 100% accuracy, with only one sample misclassified, indicating the model's outstanding classification ability and generalization performance. The confusion matrix visualization further confirmed the model's accuracy and stability in practical applications. This result validates the effectiveness and practicality of spectral tracing technology in identifying mine inrush water sources.

Innovative and Reliable Method for Inrush Water Source Identification: This research provides a new, more accurate, and reliable method for identifying inrush water sources, addressing the shortcomings of traditional methods in handling complex water quality conditions. The model helps in quickly identifying inrush water sources in coal-bearing regions of North China, reducing disaster losses and enhancing mine safety. Additionally, the spectral database and CSSOA-RF model developed in this study offer valuable references for future related research.

Thanks to the National Key Research and Development Program 2023YFC30121 for funding this study.

References

Sun HL (1965) Characteristics of karst water inrush channels in coal seam fractures. China Coal Soc 2: 51–57.

Sun FY, Zheng SY (1996) Research on the characteristics of mine water quality and its application in identifying water sources. Coal Sci. Technol 10: 27–30.

Panagopoulos G, Angelopoulou D, Tzirtzilakis E, Giannoulopoulos P (2016) The Contribution of Cluster and Discriminant Analysis to the Classification of Complex Aquifer Systems. Environ Monit Assess 188: 591. doi:10.1007/s10661-016-5590-y

Zhang H, Xing H, Yao D, Liu L, Xue D, Guo F (2019) The Multiple Logistic Regression Recognition Model for Mine Water Inrush Source Based on Cluster Analysis. Environ. Earth Sci 78–612. doi:10.1007/s12665-019-8624-2

Ju Q, Hu Y (2021) Source Identification of Mine Water Inrush Based on Principal Component Analysis and Grey Situation Decision. Environ Earth Sci 80: 157. doi:10.1007/s12665-021-09459-z

Comparison of Optimised Models for the Investigation of Heating Potential in Abandoned Mines Using Mine Water

Tom Ebel, Willi Krause, Aline Jünger, Lukas Oppelt, Timm Wunderlich, Fritz Raithel,
Thomas Grab, Tobias Fieback

Chair for technical thermodynamics, Institute of thermal engineering,
TU Bergakademie Freiberg, Chair for technical thermodynamics, Gustav-Zeuner-Straße 7, 09599 Freiberg, Germany

Abstract

After decommissioning and natural flooding, mines become large water reservoirs thermally coupled to the underground. Although the energy storage capacity enables significant heating or cooling potential, high drilling and construction costs require precise plant design. Many stakeholders lack the resources for detailed thermohydraulic modeling approaches. This paper presents a reduced, numerical model using an implicit finite volume method, balancing speed and accuracy. Verified against CFD simulations, it achieves less than 2.5% deviation in laminar flow cases. It can lay the basis of an accessible tool for preliminary geothermal assessments, aiding stakeholders in taking the first step in realising efficient mine water energy systems.

Keywords: Geothermal, Energy, Modelling, Thermodynamics

Introduction

In mining regions, many abandoned mines undergo flooding due to infiltrating surface water [Macklin *et al.* 2023]. The water collects in the mine workings, where it takes on the temperature of the rock and is therefore geothermally coupled to the underground. To gain access and utilize the stored heat in this mine water, drilling into the mine and abstracting the water with pumps is a common method [Ghoreishi-Madiseh *et al.* 2012, Rodríguez & Díaz 2009]. Mine water is then reinjected into the mine at another seam or a distant gallery to create a backflow to the abstraction point, which restores the mine water´s temperature.

Drilling into a mine for mine water access brings its own set of challenges, including regulatory, drilling precision, and safety aspects [Grab *et al.* 2018]. This directly affects how the project is evaluated financially, as dealing with the challenges creates costs, which need to be matched or outperformed by the expected returns. Therein lies a continuous challenge of using geothermal resources, as methods of determining the expected energy gain over the mine water system's lifetime are not easily accessible by many stakeholders. This is especially important since the mine can be thermally exhausted, putting the energy supply at a crucial risk. Cities, energy suppliers, or private firms in small mining regions often lack the necessary personal and financial capacity to carry out pilot studies to investigate the potential yield from the heating and cooling energy [Moulli-Castillo *et al.* 2024]. This is especially driven by a lack of accessible stakeholder tools for conducting initial thermodynamic evaluations for mining.

In order to develop an accessible tool, an underlying thermodynamical model is required that combines accuracy, flexibility and computation speed. Suitable models are found both in the analytical [Pruess & Bodvarsson 1984, Rodríguez & Díaz 2009] and the numerical model domain [Renz *et al.* 2009, Małolepszy 2003, Ghoreishi-Madiseh *et al.* 2012]. Since the researched numerical approaches model the physical system in fine detail, they are not suited for integration into a fast and user-oriented model. Analytical models, however, possess unique advantages. State-of-the-art models like the model from Rodríguez and Díaz (ROD-model) show high computation speed and sufficient accuracy for evaluating heat extraction from mine galleries [Pruess & Bodvarsson, Rodríguez & Díaz 2009]. On the other hand, because of their analytical nature, they lack variability, unable to include varying time-dependent parameters like heat load. The goal of this paper is to introduce a reduced numerical simulation model, tailored for use in preliminary mine water system investigations. This model and the aforementioned analytical model are compared, and their results benchmarked against a 3D computational fluid dynamics (CFD) simulation.

Model Development Approach

The newly developed model (TUBAF-model) needs to approximate the conditions present in a mine water geothermal system. To be comparable to the ROD-model, a cylindrical gallery shape with a finite rock layer surrounding it is used, the gallery being flooded with water. The system therefore integrates conductive heat transfer in the rock mass and diffusive heat transfer to water. This mechanism of coupling solid and fluids enables the simplification that they can be solved independently and subsequently be coupled with the convective heat transfer boundary condition at the gallery wall. The fluid is approximated with an analytical solution for the distribution of the temperature along the gallery. For the solid domain, an implicit Finite Volume Method (FVM) scheme is used. An implicit approach ensures numerical stability when varying the time step and spatial resolution, while the FVM scheme provides flexibility in terms of geometric spacing of the grid. Lastly, the spatial dimensions were investigated for possible reduction in simulation load. The subsequent characteristics of the system were utilized:

- Rotational symmetry
- Quasi-adiabatic conditions in the axial direction within the solid (only heat flow to and from the gallery is considered) [Krause 2024]

The numerical simulation within the solid is therefore simplified to a 1-dimensional (1D) grid. The spatial grid in the whole of the solid domain consists of several 1D layers lined up and coupled through the fluid domain, resulting in a quasi 2D grid. An overview of the modelling approach is given in Fig. 1.

To ensure the accuracy of the results, both spatial and temporal grid independence tests were conducted. The requirement for an applicable grid size was a deviation of 0.15% or less in heat output from a very fine grid after 20 years of continuous heat extraction. Resulting maximal grid sizes were 10 m and 0.2 m in the axial and radial gallery directions, respectively. In the temporal dimension, results yielded the defined accuracy with a timestep of 63,072 s. For simulation efficiency, the model was implemented in the coding language C.

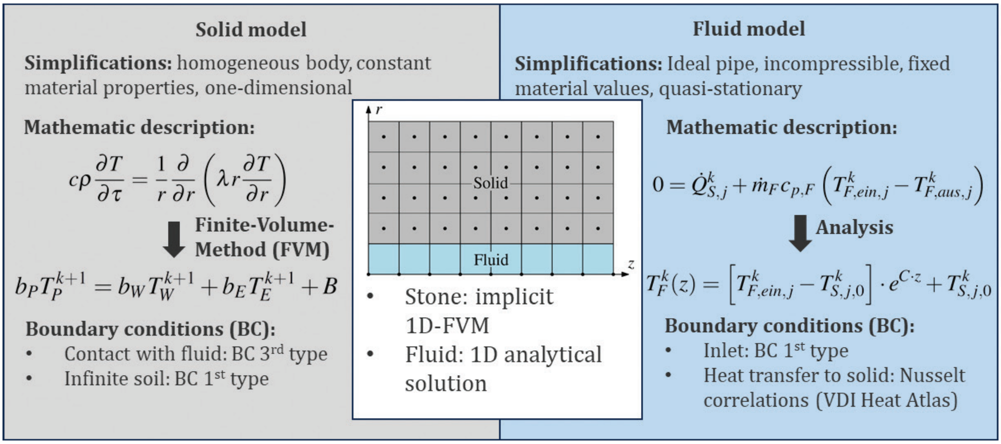

Figure 1 *Overview of the approach for the simplified mine water thermodynamic TUBAF model.*

CFD-Benchmark Model

In order to evaluate the numerical TUBAF and the analytical ROD-model mine water models, a 3D-CFD model is used. The model was set up using the commercial software STAR-CCM+ [Siemens 2025]. In the fluid, the continuity, momentum and energy equations are solved. For the solid domain, the heat conduction equation for three-dimensional bodies is solved. The model equations are discretized over polyhedral control volumes using the Finite Volume Method (FVM). Prismatic extruder cells, which expand in the axial direction, were used to enlarge the possible simulation geometry. The model consists of a total of 4.2 million cells. The large-scale model mesh with the extruder cells is shown in Fig. 2 a). The fluid-side boundary between the solid and fluid includes additional flat, prismatic cells to better resolve the developing boundary layer and steep parameter gradients, which are shown in Fig. 2 b).

Model evaluation

Using the benchmark model, the TUBAF developed model can be compared to the analytical mine water model. Therefore, the analytical ROD-model is also implemented in C to ensure comparability. Furthermore, the model was modified by flow dependent heat transfer correlations as suggested by [Loredo *et al.* 2017].

To evaluate the models on performance, a reference case was defined, which included model geometry and material properties, as well as flow characteristics. The parameters chosen are based on values as proposed in the initial ROD-model and conform to realistic rock values for the context of mine water geothermal utilization [Rodríguez & Díaz 2009, Krause 2024]. Case parameters for the following comparisons are described in Table 1.

If not specified, the listed parameters apply in the following investigations. The TUBAF and the literature model are then compared to the 3D-CFD benchmark simulation results.

Laminar Flow

Initially, long-term operation of a mine water geothermal plant with only heat extraction is simulated. In this case, mine water is abstracted and reinjected with a lower temperature at the constant value of 7 °C. In order to simulate heat extraction at a laminar flow regime, the flow rate of Table 1 applies, yielding a Reynolds number of 1438. Model results are shown in Fig. 3 and Table 2.

The analytical approach has the shortest calculation time, being several orders of magnitude lower than the TUBAF model. Simplifications in the calculation of the wall temperatures and the assumptions of a finite radius of thermal influence in the rock lead to a better computational performance. One drawback is the mentioned simplifications do not represent the physical processes as accurately as the TUBAF model. The TUBAF model yields a deviation of −2.5% in comparison to −6.7% of the ROD-model.

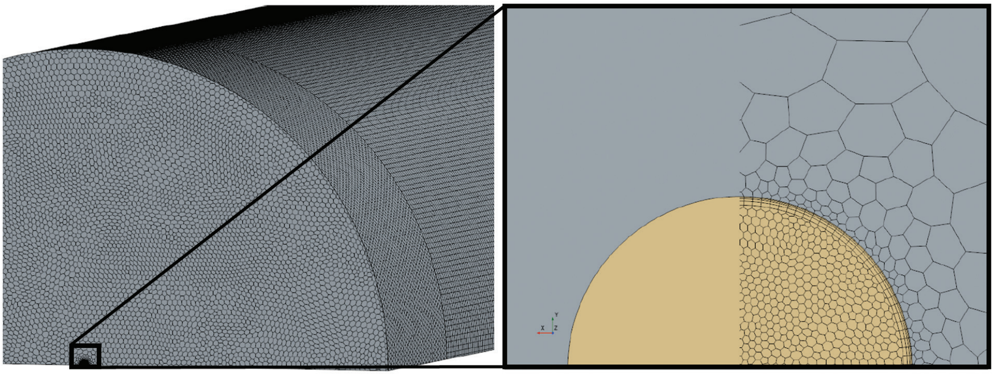

a) b)

Figure 2 a) Angled large-scale view of the model with the gallery inlet and solid domain; b) Detailed frontal view of the model with the gallery inlet and solid domain.

Table 1 *Reference case parameters for the model comparison.*

Parameter	Unit	Fluid domain	Solid domain
Radius gallery	m	1	100
Length of gallery	m	1,000	1,000
Start temperature	K	300.15	300.15
Heat conductivity	W/(m·K)	0.58	2.78
Specific heat capacity	J/(kg·K)	4,186	800
Density	kg/m^3	1,000	2,500
Kinematic viscosity	mm^2/second	1.24	–
Volume flow	L/second	2.80	–

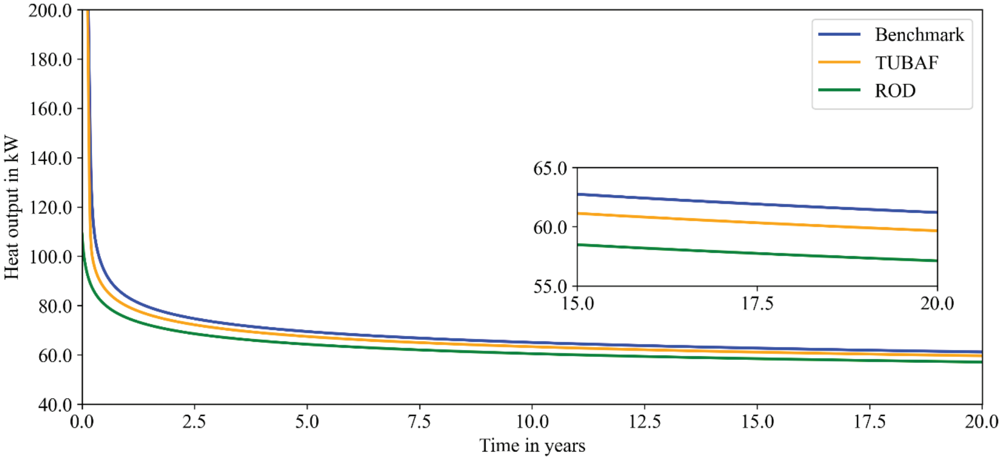

Figure 3 *Development of the heat extraction rate with laminar flow over a period of 20 years according to the models, inlet temperature constant at 7 °C.*

Table 2 *Evaluation parameters of the laminar reference case simulation.*

Evaluation Parameter	Benchmark model	Comparison models	
		TUBAF	ROD
Calculation time in seconds	24,743.3	66.0	< 0.1
Heat output in kW at 20 years	61.2	59.7	57.1
Deviation from benchmark model in %	–	-2.5	-6.7

The TUBAF model is therefore applicable for laminar modelling.

Turbulent Flow

In the practical operation of a mine water system, the geometry and the roughness of the wall surfaces change continuously. Depending on those circumstances and the induced flow rate, the heat transfer changes accordingly. To test the models considering turbulent conditions, the mass flow of the mine water was set to 28 L/s, raising the Reynolds number accordingly to 14380. Results of the simulations are shown in Fig. 4 and Table 3.

Due to the improved heat transfer in turbulent flow, the heat output is continuously higher than for laminar flow. Compared to the laminar case, the computation time remained at the same level, while the deviation from

Table 3 *Evaluation parameters of the turbulent reference case simulation.*

Evaluation Parameter	Benchmark model	Comparison models	
		TUBAF	ROD
Calculation time in seconds	24,911.7	66.2	< 0.1
Heat output in kW at 20 years	85.4	100.4	76.9
Deviation from benchmark model in %	–	+ 17.7	- 9.9

comparison to benchmark models underwent a change. While the analytical model calculates less heat output, the TUBAF model overestimates the heat output by almost 18%. This deviation shows the limits of the TUBAF mine water calculation code. The higher heat output in the turbulent case is likely a result of the fixed Nusselt correlations that calculates the heat transfer coefficient. Until more specific Nusselt correlations for turbulent flow regimes are tested, only simulations in the laminar flow range can be considered valid. For laminar flow, the code can be used for seasonal heat load investigations, including heat extraction and heat injection.

Conclusions and Outlook

Since there is currently no basis for an inexpensive load-flexible and reduced thermodynamical calculation code for mine water, the goal of this investigation was to establish a reduced numerical calculation code and evaluate its applicable simulation range. It was compared with a state-of-the-art analytical model to a detailed 3D-CFD benchmark model in terms of heat output when applying laminar and turbulent flow regimes. According to the results, the developed model can be used for laminar flow conditions. When this applies, the model can be used for quick investigations of seasonal heat load variations, which can then be compared to a benchmark simulation using detailed physics models. In turbulent flow, the deviation from the benchmark suggests improvement potential in the heat transfer between fluid and solid. After improving the reduced model to fit the results of the benchmarkings, efficiency measures such as the implementation of non-equidistant grids can be considered. The improved model can therefore become the foundation for an easy-to-access tool, which can help to analyze mines in quick pilot studies, thereby creating a better decision basis for use by municipalities and energy suppliers.

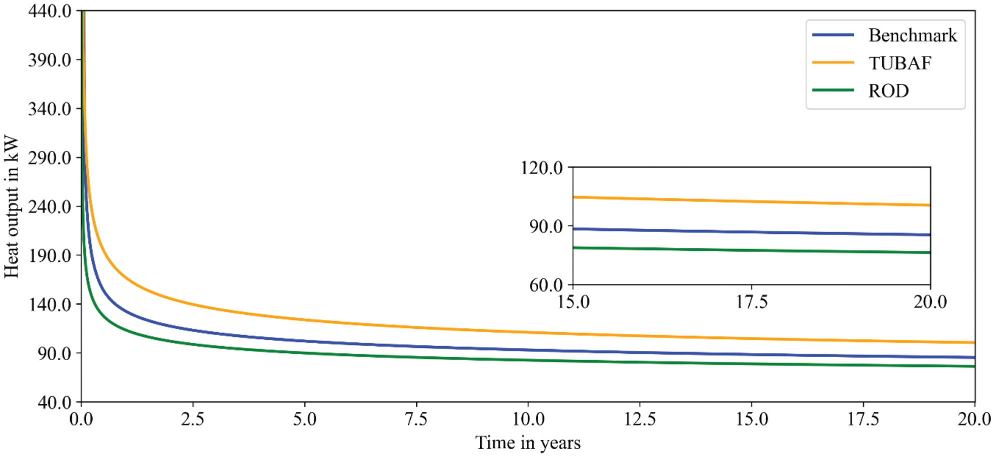

Figure 4 *Development of the heat extraction rate with turbulent flow over a period of 20 years according to the models (volume flow at 28 L/s), inlet temperature constant at 7 °C.*

References

Ghoreishi-Madiseh S A, Ghomshei M, Hassani F P, Abbasy F (2012) Sustainable heat extraction from abandoned mine tunnels: A numerical model. J. Renewable Sustainable Energy 1 May 2012; 4 (3): 033102. https://doi.org/10.1063/1.4712055

Grab T, Storch T, Groß U (2018) Energetische Nutzung von Grubenwasser aus gefluteten Bergwerken. In Handbuch Oberflächennahe Geothermie, von Bauer, Freeden, Jacobi & Neu, 523–586. Berlin: Springer Spektrum

Krause W (2024) Entwicklung und Vergleich von Modellen zur Berechnung des Wärmeentzugs in Strecken mit Grubenwasser – Development and Comparison of Models for Calculating Heat Extraction in Mine-Water Galleries, Diploma Thesis, TU Bergakademie Freiberg

Loredo C, Banks D, Roqueñí N (2017) Evaluation of analytical models for heat transfer in mine tunnels, Geothermics, Volume 69, 2017, Pages 153–164, ISSN 0375-6505, https://doi.org/10.1016/j.geothermics.2017.06.001

Macklin M G, Thomas C J, Mudbhatkal A, Brewer P A, Hudson-Edwards K A, Lewin J, Scussolini P, Eilander D, Lechner A, Owen J, Bird G, Kemp D, & Mangalaa K R (2023) Impacts of metal mining on river systems: a global assessment. Science, 381(6664), 1345-1350. https://doi.org/10.1126/science.adg6704

Małolepszy Z (2003) Low Temperature, Man-Made Geothermal Reservoirs in Abandoned Workings of Underground Mines. Conference Paper

Moulli-Castillo J, van Hunen J, MacKenzie M, Sear T, Adams C (2024) GEMSToolbox: A novel modelling tool for rapid screening of mines for geothermal heat extraction, Applied Energy, Volume 360, 2024, 122786, ISSN 0306-2619, https://doi.org/10.1016/j.apenergy.2024.122786.

Pruess K, Bodvarsson G S (1984) Thermal Effects of Reinjection in Geothermal Reservoirs with Major Vertical Fractures. J Pet Technol 36 (1984): 1567–1578. doi: https://doi.org/10.2118/12099-PA

Renz A, Rühaak W, Schätzl P (2009) Numerical Modeling of Geothermal Use of Mine Water: Challenges and Examples. Mine Water Environ 28, 2–14 (2009). https://doi.org/10.1007/s10230-008-0063-3

Rodríguez R, Díaz M B (2009) Analysis of the utilization of mine galleries as geothermal heat exchangers by means a semi-empirical prediction method, Renewable Energy, Volume 34, Issue 7, 2009, Pages 1716-1725, ISSN 0960-1481, https://doi.org/10.1016/j.renene.2008.12.036

Siemens Industries Digital Software (2025) Simcenter STAR-CCM+, version 18.04

Geo-Environmental Characterization of Coal Mine Waste Rock: Assessing its Potential to Generate Acid Mine Drainage

Ayoub El Aallaoui[1],*, Mustapha El Ghorfi[1,2], Abdellatif Elghali[2], Yassine Taha[2], Mostafa Benzaazoua[2] and Rachid Hakkou[2,3]

[1]Laboratory of Geo resources, Geo environment and civil engineering, Faculty of Science and Technology Gueliz, Cadi Ayyad University, Avenue A. Elkhattabi, BP549, 40000 Marrakech, Morocco

[2]Geology sustainable mining laboratory institute (GSMI), Mohamed 6 polytechnic university (UM6P), Benguerir, Morocco

[3]Materials and Environmental Chemistry Laboratory (IMED-Lab), Faculty of Science and Technology Gueliz, Cadi Ayyad University, Avenue A. Elkhattabi, BP549, 40000 Marrakech, Morocco

**ayoub.elaallaoui@ced.uca.ma*

Abstract

Coal mining generates coal mine waste rock (CMWR), which can pose environmental risks like acid mine drainage (AMD), contaminated neutral drainage (CND), or saline drainage, depending on pH and metal(loids) concentration. The Jerada T08 CMWR pile, deposited over 50 years ago, exemplifies this issue. To assess its environmental impact, a geo-environmental characterization was conducted, leading to a 3D model that highlights zones prone to acidity. Results identified 3.8 Mt of potentially acid-forming (PAF) materials, distributed heterogeneously mainly in highly oxidized upper zones. This approach enhances management strategies and reduces costs by enabling targeted mitigation and minimizing remediation efforts.

Keywords: Coal Mine Waste Rock, Acid Mine Drainage, Geochemistry, Environment, 3D modeling

Introduction

Mining provides significant economic benefits through the extraction of valuable elements, but it also generates substantial amounts of waste, leading to critical environmental challenges (Worlanyo and Jiangfeng 2021). Mining waste is broadly categorized into two types: waste rock (WR) and tailings. WR, produced during mineral extraction, is typically deposited in large piles with a wide particle size distribution. Although it is generally physically stable, it often lacks chemical stability (Amos *et al.* 2015; Elghali *et al.* 2019). Tailings, on the other hand, are fine-grained residues from flotation processes, usually deposited in slurries in impoundments. Wet tailings stored behind dams can exhibit low mechanical stability, and many tailings dam failures around the world have resulted in extensive environmental damage; tailings can also have low chemical stability (Aubertin *et al.* 2002; Lindsay *et al.* 2015). Coal mine waste rock (CMWR) from coal mining frequently contains iron sulfide minerals, which present significant environmental hazards due to their potential to generate acid mine drainage (AMD) (Nordstrom *et al.* 2015). AMD, a major mining environmental issue, occurs when sulfide minerals (primarily pyrite) are exposed to air and water in the absence of sufficient neutralizing minerals (Evangelou and Zhang 1995; Dold 2017). This process produces sulfuric acid and releases various contaminants, such as iron, copper, zinc, arsenic, and cadmium, into the environment. AMD is characterized by an acidic pH (below 4), which enhances the solubility of metals and facilitates their mobility (Nordstrom *et al.* 2015). Once initiated, it can persist for decades or even centuries after mine closure, posing a long-term threat to water resources (Bouzahzah *et al.* 2014).

Mitigating environmental concerns related to AMD in CMWR requires a thorough characterization of their physical, chemical, and mineralogical properties. Key physical parameters, such as particle size distribution (PSD), density, porosity, and specific surface area (SSA), are critical for understanding reactivity and AMD generation potential (Elghali *et al.* 2019, 2023). Chemical analyses, focusing on sulfur content and trace element concentrations, are essential for assessing leaching risks and acid production potential, which are crucial for predicting AMD formation and designing targeted remediation strategies (Escobar *et al.* 2021; El Aallaoui *et al.* 2024b). Mineralogical evaluations play a pivotal role in identifying sulfide minerals, the identification of oxidized zones, the presence of neutralizing minerals that buffer acidity, and the degree of sulfide liberation (Parbhakar-Fox *et al.* 2013; El Aallaoui *et al.* 2024a). Additionally, geochemical assessments using static and kinetic tests provide insights into the acid generation potential of CMWR and help pinpoint potentially acid-forming (PAF) zones (Benzaazoua *et al.* 2017; Tabelin *et al.* 2020). Mapping the distribution of PAF zones through 3D modeling enables the identification of highly reactive areas and enhances understanding of the factors influencing AMD rates and extent, offering a more effective approach to managing environmental risks (Blannin *et al.* 2023; El Aallaoui *et al.* 2024b). However, heterogeneity, limited understanding of oxidation pathways, and insufficient field data further hinder predictive accuracy of the models (Dold 2014; Simate and Ndlovu 2014). Addressing these gaps requires advanced modeling techniques, long-term field and laboratory studies to enhance AMD prediction.

This study introduces a novel approach for the Jerada province, focusing on the abandoned Jerada coal mine (closed since 2000) and its oldest waste pile (T08), deposited over 50 years ago (Fig. 1A). It offers a cost-effective strategy for managing CMWR by integrating environmental protection with sustainability. A baseline for PAF distribution and AMD risk was established through detailed chemical, mineralogical, and environmental analyses. Drone imagery provided topographic data and enabled PAF volume estimation (Fig. 1B), while 3D modeling uncovered spatial variations in acid generation potential (AGP), identifying previously unrecognized PAF zones within

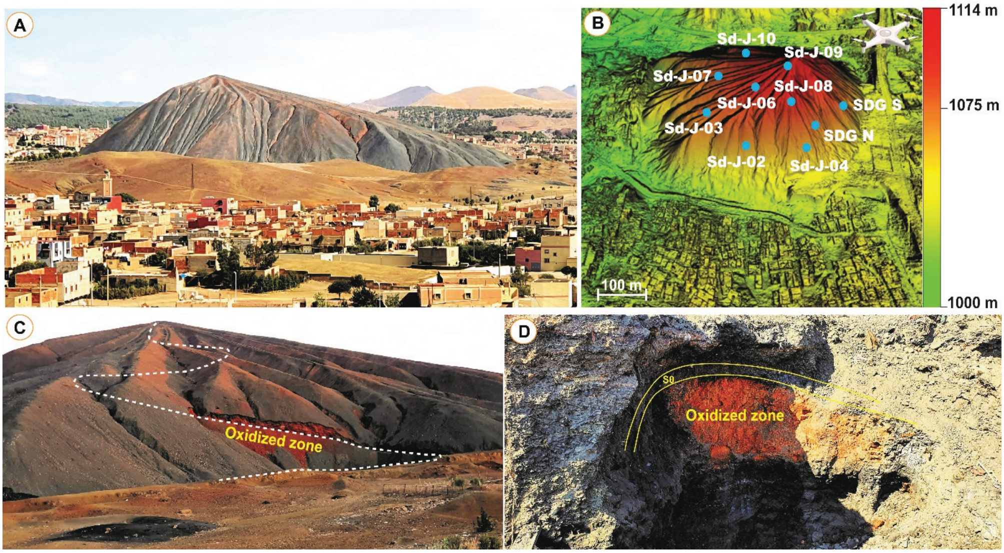

Figure 1 *Real image of the T08 CMWR pile; B: Topo-photogrammetric survey of T08 conducted via drone, highlighting the height of the pile and location of selected drillholes; C and D: On-site images of T08 showcasing the effects of oxidation.*

the CMWR pile. Samples from distinct oxidized zones (low and high oxidation) were analyzed for physical, chemical, and mineralogical characteristics using acid-base accounting (ABA) and net acid generation (NAG) tests to assess their environmental behavior (Fig. 1C, D).

Materials and Methods

The Jerada basin in eastern Morocco faces environmental and socio-economic challenges due to ten unrehabilitated CMWR piles, T01 to T10 (Jerada Archives 1990). T08, the largest, contains around 7.3 Mt of CMWR (Aallaoui *et al*. 2024; El Aallaoui *et al*. 2025) and reaches 100 m in height. Despite arid conditions, AMD remains a concern. A drone survey of 120 ha enabled precise topographic mapping and volume estimation of T08. Reverse circulation drilling retrieved 432 samples (~20 kg/m) (Tab. 1) that were dried, crushed to 100 µm, and analyzed to assess the potential environmental behavior of the pile. Two composite samples represented distinct oxidation zones. The low-oxidized sample (Sd-J-02, Sd-J-03, Sd-J-10, SDG N) exhibited black coal characteristics with relatively low pyrite and iron oxide content. Conversely, highly oxidized sample (SDG R, SDG A, Sd-J-06, Sd-J-08) showed more iron oxides content and reddish color, suggesting advanced oxidation. Analyses covered physicochemical, mineralogical, and environmental aspects. Particle size distribution was determined via wet sieving (for particles between 50 µm and 2 mm) and laser diffraction (for <500 µm). SSA was measured using the BET method. Major elements (SiO_2, Al_2O_3, TiO_2, Fe_2O_3, CaO, MgO, MnO, Na_2O, K_2O) were analyzed via XRF-EDS. Total carbon and sulfur were quantified using an induction furnace. Sulfates were measured via acid digestion (HCl) and spectrophotometry (at 650 nm). Trace elements were analyzed using ICP-MS following HNO_3-$HClO_4$ digestion, followed by controlled evaporation and dilution (1:8000) to prevent ICP-MS oversaturation. The AGP was assessed using static test (ABA) and NAG test. The NAG test, performed with H_2O_2 digestion, measured pH and electrical conductivity (EC) to further predict acid generation. Using 3D modeling, AGP zones were identified, correlating with oxidation areas to improve waste management through early PAF detection, targeted mitigation, and cost reduction. Geochemical and environmental data from over 200 points were processed in Datamine Studio RM to interpolate parameters like S-sulfate, S-sulfide, acidification potential (AP), and net neutralizing potential (NNP). Variogram analysis determined data distribution, and ordinary kriging was used for interpolation between and among measurements. Results were presented as wireframes with 6 × 6 × 2 m blocks and sub-blocks for precision.

***Table 1** Drill hole locations, depths, and inclinations for the T08 waste pile.*

Pile	Holes ID	X (m)	Y (m)	Z (m)	Depth (m)	Inclination (°)
T08	SDG A	796814.47	416002.24	1036.10	18	0
	SDG B	796856.30	416025.38	1032.42	52	0
	SDG N	797067.95	415939.83	1036.92	26	0
	SDG R	796930.50	416020.16	1039.59	58	0
	SDG S	797049.19	415994.44	1030.00	46	0
	Sd-J-02	797000.00	415700.00	1043.90	10	90
	Sd-J-03	796900.00	415700.00	1049.45	20	90
	Sd-J-04	797100.00	415800.00	1031.01	2	90
	Sd-J-06	796900.00	415800.00	1084.50	50	90
	Sd-J-07	796800.00	415800.00	1034.26	8	90
	Sd-J-08	797000.00	415900.00	1089.50	60	90
	Sd-J-09	796900.00	415900.00	1103.31	74	90
	Sd-J-10	796800.00	415900.00	1037.47	8	90

Results and discussion

The physical assessment of the CMWR pile revealed slight differences in particle size distributions between low-oxidized and high-oxidized zones. In low-oxidized areas, the D90 (particle diameter at 90% passing) was 353.3 µm, compared to 409 µm in high-oxidized zones (Fig. 2A). Mineral grain sizes ranged from 6 to 32 µm, with pyrite grains slightly larger in low-oxidized zones (8–18 µm). Iron oxide grains, particularly hematite, ranged from 10 µm in high-oxidized zones to 33 µm in low-oxidized areas (Fig. 2B). Finer pyrite particles in highly oxidized zones increased surface area, accelerating pyrite oxidation, though secondary iron oxide coatings often slowed further reactions, creating redox disequilibrium (Cravotta 1994; Evangelou and Zhang 1995). Chemical analysis revealed up to 13 wt.% carbon, with total sulfur ranging from 0.5–2 wt%, highest in SDG A, SDG B, and SDG R. Sulfate content varied from 0.12–16 wt%, peaking in SDG A, SDG B, and Sd-J-06, with concentrations decreasing with depth. ICP-MS analysis detected Cu (41 mg/L), Zn (122 mg/L), Pb (93 mg/L), Fe (66,556 mg/L), Ni (54 mg/L), Co (25 mg/L), and As (49 mg/L), while Cd and Ti were below detection limits. These trace element levels raise concerns about metal leaching during and after rainfall events. While previous toxicity leaching characteristic procedure (TCLP) studies (Taha *et al.* 2018) indicated that concentrations generally fall below hazardous leaching thresholds, long-term monitoring remains essential.

Mineralogical analysis highlighted the dominance of silicates minerals, with quartz constituting 37.1–38.3 wt% and clay minerals accounting for 31.7–33.1 wt%. Mica content ranged from 14.2 to 16.2 wt%, while plagioclase and chlorite were present in smaller percentages (4.92–5.34 wt% and 1.25–2.32 wt%, respectively). Calcite content varied from 2.32 wt% in low-oxidized zones to 3.55 wt% in high-oxidized zones. Iron oxides, such as hematite (1.53–1.8 wt.%) and goethite (2.17–3.2 wt.%), were more abundant in high-oxidized zones (Fig. 3A, B). QEMSCAN imagery provided further insights, highlighting a significant presence of iron oxides (Hematite and goethite). Traces of pyrite grains were observed in both low and high-oxidized zones, closely associated with surrounding gangue minerals (Fig. 3C, D). Furthermore, the limited presence of neutralizing minerals, such as carbonates, in these CMWR reduces the capacity to buffer acidity, increasing the vulnerability to acid generation.

The ABA results showed AP values of 14–41 kg $CaCO_3$/t, with lower levels (14–17 kg $CaCO_3$/t) in low-oxidized zones. NP was limited, and NNP ranged from −35 to −12 kg $CaCO_3$/t, classifying most samples as uncertain (−20 < NNP < 20), except SDG A, SDG B, SDG R, and Sd-J-09 (PAF, NNP < −20) (Fig. 4B). The neutralization potential ratio (NPR) varied from 0.16 to 0.36, confirming all samples as PAF (NPR < 1). NAG pH values ranged between 2.4 and 6.1, with solution acidity values of 4.32–42.5 kg H_2SO_4/t, exceeding standard limits. NPR plotted against

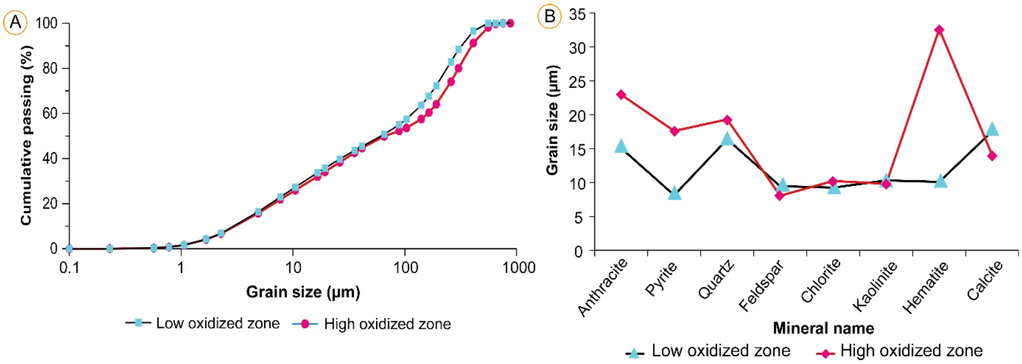

Figure 2 *A: Particle size distribution for low and high oxidized zones, B: Minerals grain size distribution for low and high oxidized zones.*

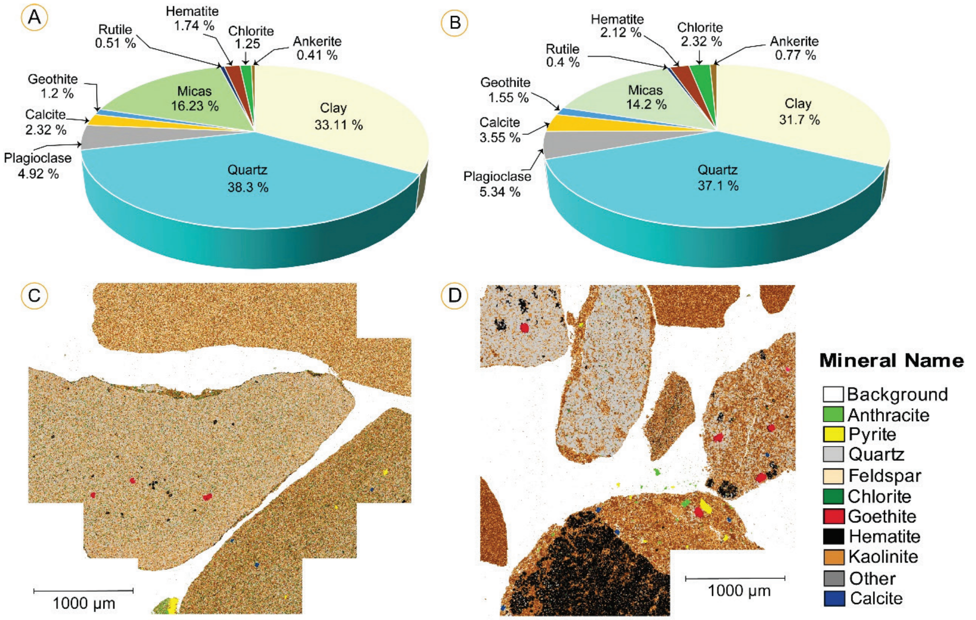

***Figure 3** Mineralogical phases identified using QEMSCAN for A: low-oxidized and B: high-oxidized zones; QEMSCAN imagery for C: low oxidized and D: high oxidized zones.*

NAG pH in Fig. 4A, showed most samples between uncertain classification (UC) and PAF, with NPR ranging from 1.61 to 79.33 and SDG R, Sd-J-06 exhibiting the highest AGP. EC varied from 0.12 to 1.28 µS/cm, peaking in SDG R, SDG A, and Sd-J-06. Jerada's CMWR exhibits predominantly AGP properties, with some areas falling within UC range. Therefore, long-term kinetic tests are crucial for further understanding of environmental behavior over time. A 3D geochemical block model was developed using 3D photogrammetric imagery and chemical analysis of drilled samples to map the spatial distribution of S-sulfate, S-sulfide, AP, and NNP. The model identified high S-sulfide content areas, indicating significant AMD potential. Ordinary kriging was used to interpolate these parameters, assuming a density of 1.60 kg/m^3. Results showed low S-sulfate contents in the core (<0.034 wt%) and higher near the surface due to oxidation. Total S-sulfide was estimated at 6.01 Mt (0.48 wt% average), with approximately 3.8 Mt of PAF material concentrated in the upper sections, while the remaining (approximately 3.5 Mt) were classified as uncertain (Fig. 4C, D).

Conclusion

This study pioneered the use of 3D mapping and modeling to identify PAF zones in the Jerada CMWR pile (T08). By integrating physical, chemical, and mineralogical data with high-resolution drone imagery, it mapped approximately 3.8 Mt of PAF material, mainly in the upper zones where high oxidation has increased sulfate content and AP. These findings enable targeted mitigation strategies to minimize long-term environmental and financial impacts.

Acknowledgements

This research was financially supported by the International Research Chairs Initiative, sponsored by Canada's International Development Research Centre (IDRC) and coordinated through the Canadian Research Chairs Program under Grant Numbers 108469-001 and 109418-006.

References

Aallaoui AE, El Ghorfi M, Elghali A, *et al* (2024) 3D Modeling and Resources Estimation of Coal Old Piles in Jerada Mine, Oriental Morocco. In: Çiner, A., *et al.* Recent Research on Sedimentology, Stratigraphy, Paleontology, Geochemistry, Volcanology, Tectonics,

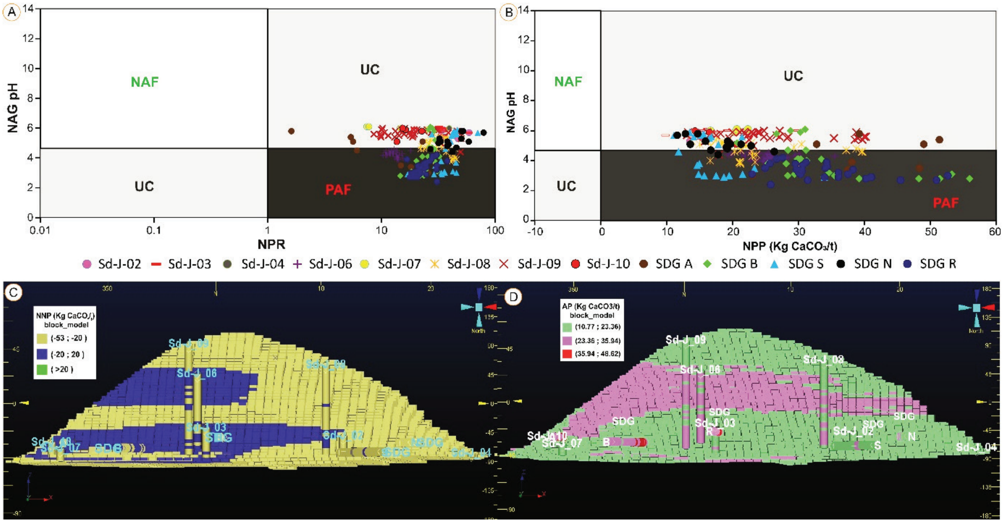

Figure 4 AMD prediction results for the T08 CMWR pile: (A) NPR vs. NAG pH, (B) NPP vs. NAG pH, (C) estimated block model of NNP (kg CaCO3/t), and (D) estimated block model of AP (kg CaCO3/t). NAF = non-acid forming, UC = uncertain classification, PAF = potentially acid forming.

and Petroleum Geology. MedGU 2022. Advances in Science, Technology & Innovation. Springer, Cham.

Amos RT, Blowes DW, Bailey BL, *et al* (2015) Waste-rock hydrogeology and geochemistry. Appl Geochemistry 57:140–156. https://doi.org/10.1016/j.apgeochem.2014.06.020

Aubertin M, Bussière B, Bernier L, *et al* (2002) La gestion des rejets miniers dans un contexte de développement durable et de protection de l'environnement. Congrès Annu la Société Can génie Civ GE-045:1–10

Benzaazoua M, Bouzahzah H, Taha Y, *et al* (2017) Integrated environmental management of pyrrhotite tailings at Raglan Mine: Part 1 challenges of desulphurization process and reactivity prediction. J Clean Prod 162:86–95. https://doi.org/10.1016/j.jclepro.2017.05.161

Blannin R, Frenzel M, Tolosana-Delgado R, *et al* (2023) 3D geostatistical modelling of a tailings storage facility: Resource potential and environmental implications. Ore Geol Rev 154:105337. https://doi.org/10.1016/j.oregeorev.2023.105337

Bouzahzah H, Benzaazoua M, Bussiere B, Plante B (2014) Prediction of Acid Mine Drainage: Importance of Mineralogy and the Test Protocols for Static and Kinetic Tests. Mine Water Environ 33:54–65. https://doi.org/10.1007/s10230-013-0249-1

Cravotta CA (1994) Secondary iron-sulphate minerais as sources of sulphate and acidity. In: Environmental Geochemistry of Sulfide oxidation

Dold B (2017) Acid rock drainage prediction: A critical review. J Geochemical Explor 172:120–132. https://doi.org/10.1016/j.gexplo.2016.09.014

Dold B (2014) Evolution of acid mine drainage formation in sulphidic mine tailings. Minerals 4:621–641. https://doi.org/10.3390/min4030621

El Aallaoui A, El Ghorfi M, Elghali A, *et al* (2024a) Investigating the reprocessing potential of abandoned zinc-lead tailings ponds : A comprehensive study using physicochemical , mineralogical , and 3D geometallurgical assessments. Miner Eng 209:108634. https://doi.org/10.1016/j.mineng.2024.108634

El Aallaoui A, El Ghorfi M, Hakkou R, *et al* (2024b) Integrated 3D geo-environmental assessment of acid-forming materials in historic coal waste piles for sustainable management. Chemosphere 370:143947. https://doi.org/10.1016/j.chemosphere.2024.143947

El Aallaoui A, Elghali A, Hakkou R, *et al* (2025) 3D geometallurgical characterization of coal mine waste rock piles for their reprocessing purpose. Int J Coal Sci Technol 12:. https://doi.org/10.1007/s40789-025-00756-7

Elghali A, Benzaazoua M, Bussière B, Bouzahzah H (2019) Determination of the available acid-generating potential of waste rock, part II: Waste management involvement. Appl. Geochemistry 100:316–325

Elghali A, Benzaazoua M, Taha Y, *et al* (2023) Prediction of acid mine drainage: Where we are. Earth-Science Rev 241:104421. https://doi.org/10.1016/j.earscirev.2023.104421

Escobar GA, Jorge E, Álvaro MRSR, Mafalda MMP (2021) Physical – Chemical Characterization of the Neves Corvo Extractive Mine Residues : A Perspective Towards Future Mining and Reprocessing of Sulfidic Tailings. J Sustain Metall 7:1483–1505. https://doi.org/10.1007/s40831-021-00428-1

Evangelou VP, Zhang YL (1995) A review: Pyrite oxidation mechanisms and acid mine drainage prevention A Review: Pyrite Oxidation Mechanisms and Acid Mine Drainage Prevention. Crit Rev Environ Sci Technol 25:37–41. https://doi.org/http://dx.doi.org/10.1080/10643389509388477

Jerada Archives (1990) Historique de la mine de Jerada. In: Charbonnages du Maroc (CDM) report – Exploitation et Enrichissement. pp 9–15

Lindsay MBJ, Moncur MC, Bain JG, *et al* (2015) Geochemical and mineralogical aspects of sulfide mine tailings. Appl Geochemistry 57:157–177. https://doi.org/10.1016/j.apgeochem.2015.01.009

Nordstrom DK, Blowes DW, Ptacek CJ (2015) Hydrogeochemistry and microbiology of mine drainage: An update. Appl Geochemistry 57:3–16. https://doi.org/10.1016/j.apgeochem.2015.02.008

Parbhakar-Fox A, Lottermoser B, Bradshaw D (2013) Evaluating waste rock mineralogy and microtexture during kinetic testing for improved acid rock drainage prediction. Miner Eng 52:111–124. https://doi.org/10.1016/j.mineng.2013.04.022

Simate GS, Ndlovu S (2014) Acid mine drainage: Challenges and opportunities. J Environ Chem Eng 2:1785–1803. https://doi.org/10.1016/j.jece.2014.07.021

Tabelin CB, Corpuz RD, Igarashi T, *et al* (2020) Acid mine drainage formation and arsenic mobility under strongly acidic conditions: Importance of soluble phases, iron oxyhydroxides/oxides and nature of oxidation layer on pyrite. J Hazard Mater 399:122844. https://doi.org/10.1016/j.jhazmat.2020.122844

Taha Y, Benzaazoua M, Edahbi M, *et al* (2018) Leaching and geochemical behavior of fired bricks containing coal wastes. J Environ Manage 209:227–235. https://doi.org/10.1016/j.jenvman.2017.12.060

Worlanyo AS, Jiangfeng L (2021) Evaluating the environmental and economic impact of mining for post-mined land restoration and land-use: A review. J Environ Manage 279:111623. https://doi.org/10.1016/j.jenvman.2020.111623

Geochemical Characterization of Tailings, Pit Lake Sediments and Waters using PHREEQC in Nador Abandoned Mine (Morocco)

Fatima zohra El houfy, Abdelilah Dekayir, Mohamed Rouai, Abdelmouiz Ech-charef

Geo-explorations & Geotechnics Lab, Faculty of Sciences, University Moulay Ismail, Zitoune, BP. 11201, Meknes, Morocco

Abstract

In north of Morocco, Nador abandoned Fe-mines are well known for their acid mine drainage (AMD). Geochemical and mineralogical investigations show that tailings are dominated by jarosite, gypsum and quartz. Low quantities of hematite, magnetite, and titanomagnetite are also identified. Axara pit lake sediments comprise gypsum, quartz, langbeinite, morenosite, bianchite, and dolomite. Copiapite and jarosite are indicators of extreme acidic conditions. Fe and S constitute the main chemical composition of the studied samples. Mn is the predominant metal in tailings with values ranging from 198.49 to 638.65 µg/g, followed by As (606.93 to 16.12 µg/g); Cu (576.24 to 40.70 µg/g); Co (411.22 to 31.54 µg/g); Ni (144.70 to 16.94 µg/g); Zn (120.31 to 30.92 µg/g); and Pb (70.83 to 6.05 µg/g). Waters from Axara pit lake are characterized by acidic pH (3.12) with high conductivity (29160 µS/cm), and very high sulfate contents (31506.23 mg/l). As, Ni and Fe have exceeded the water-quality standard (WHO, 2011). PHREEQC modeling of waters shows that Fe, As, and Ni exist in solution as $FeSO_4$, As^{3+} and $NiSO_4$ species respectively.

Keywords: Acidic pit lake, PHREEQC, Jarosite, Contamination, Tailings

Introduction

Since the 1900s, the iron district of Beni Bou Ifrour-Ouixane located southwest of Nador city has played an important role in the mining history and economy of Morocco (Bouabdellah *et al.* 2016). This district consists of three highly productive iron mines, with Ouixane and Axara being open-pit mines, and Setolazar being underground (Benidire *et al.* 2022). Between 1914 and 1967, this district produced 1.5 Mm^3 of mining waste annually and over 65 Mt of ore with a Fe content of over 50% (Lakrim *et al.* 2011). The mining wastes are scattered in the landscape, resulting from abandonment without rehabilitation for more than 32 years (Tarik *et al.* 2023). The intensive mining has left pit lakes filled with water like Axara which is strongly acidic (pH = 3) (Lakrim *et al.* 2011). Tailings heaps are composed of high percentages of iron oxides, hydroxides, and sulfides (pyrite, pyrrhotite, and chalcopyrite) (Khafouri *et al*, 2011) and are directly exposed to weathering. The oxidation of sulfide-rich minerals leads to the production of sulfuric acid (H_2SO_4) and decreases in the pH of water with high contents of dissolved metals which impact soil, water, and plants (Lakrim *et al.* 2011; Air *et al.* 2021; Tarik *et al.* 2023). Thus, the main objectives of this study are to 1) investigate in detail the mineralogy and chemical composition of mine tailings and lake sediments (2) chemical speciation of PTEs in pit lake waters.

Materials and Methods

Study Area

The Beni Bou Ifrour-Ouixane mining district is close to Nador city in north of Morocco (Fig. 1). The most productive mines were Ouixane, Axara, and Setolazar (Bouabdellah *et al.* 2013). The area is characterized by a mediterranean humid climate (annual rainfall of around 346 mm/year) (El Yaouti *et al.* 2009). The geology of the study area consists of a regular alternation of schist layers interspersed with limestone lenses, along with occasional levels of acidic tuff from volcanic eruptions. All these units are covered by Barremian limestone. During the Miocene, porphyritic intrusive microdiorite was introduced into the previous sequence. Significant hydrothermal alteration halos developed accompanying the emplacement of this intrusive suite, impacting both the intrusive bodies (endoskarns) and their carbonate and sandstone-carbonate protolith host rocks (Jabrane 1993; Bouabdellah *et al.* 2013). The ore deposit is stratiform and presents banded textures where mineralized iron bands are alternated with sterile shale bands. Primary ore paragenesis is characterized by a predominance of iron oxides (hematite, magnetite) and hydroxides (goethite), locally accompanied by significant quantities of sulfides (sphalerite, chalcopyrite, bornite, marcasite, pyrite, pyrrhotite, and galena).

Sample collection and analysis

Tailings and pit lake sediments

Seven samples of mine tailings were collected in the vicinity of the Bokoya-Setolazar mine in May 2023. Samples T1, T2, T3, T4, and T5 were located on the same tailings dam. Samples T6 and T7 were collected inside the treatment unit area of Setolazar. All the mine tailings have a rust-orange color indicating their advanced oxidation state, except sample T7 which was characterized by a dark gray color. Three sediment samples were collected from the Axara pit lake (Sed 1, Sed 2, Sed 3) and one was taken from the Ouiksane pit lake (Sed 4). An additional soil sample (REF) was taken approximately 4 km far away from the mining area to serve as a non-contaminated reference sample (Fig. 1).

Mineralogical characterization was performed using X-ray diffraction (XRD) with a BRUKER Advance Diffractometer equipped with a copper anticathode. The ICP-OES Agilent 5800 VDV spectrometer was used for chemical analysis of Ca, Fe, K, Mg, Na, Al, and S. The concentrations of Mn, Co, Ni, Cu, Zn, As, and Pb were determined using ICP-MS (Perkin Elmer NexIon 300 X).

Pit lake waters

Five water samples were collected from the Axara pit lake. Samples have been collected using polyethylene bottles. Temperature (T), pH, electrical conductivity (EC), dissolved oxygen (DO), and redox potential (Eh) values were measured on-site using an HQ40d portable multi-meter. The samples were analyzed for some ions (Ca^{2+}, F^{-}, Cl^{-}, SO_4^{2}, NO^{2-}) by ion exchange chromatography using ICS 3000 Thermo Fisher detector. The total element content of As, Sn, Cr, Zn, Cd, Pb, Ni, Ca, Fe, Mg, Cu, Ti, Al, Na, and K were measured by ICP-AES (ICP ULTIMA EXPERT).

Geochemical modeling

The PHREEQC 3.7.3 software (PHREEQC.DAT) was used to examine the current speciation of PTEs in the solution. The saturation Index (SI) was calculated using temperature, pH, electron activity (pe), and metal concentration to predict precipitating minerals (Luo *et al.* 2020). SI > 0 indicates that water is supersaturated, SI = 0 indicates that the mineral and the water are in equilibrium; SI < 0 indicates that the water is undersaturated, allowing the mineral to dissolve into the solution.

Results and discussion

Mineralogy of tailings and floor lake sediment

The mineralogical compositions of mine tailings and lake sediments are represented in Fig. 2. The mineralogy of the tailings is dominated by jarosite (14-88 %), gypsum (2-80 %), and quartz (10-13%). Low quantities of hematite, magnetite, and titanomagnetite are also identified. The high content of sulfate minerals (jarosite) is produced by the oxidation of sulfide minerals (Hakkou *et al.* 2008). In tailings, high dissolved SO_4^{2-} and calcium released during silicate dissolution at low pH may lead to the precipitation of gypsum (Moncur *et al.* 2005). XRD data indicate the presence of copiapite in tailing T2. The formation of this mineral instead of jarosite is due to high concentrations of sulfate,

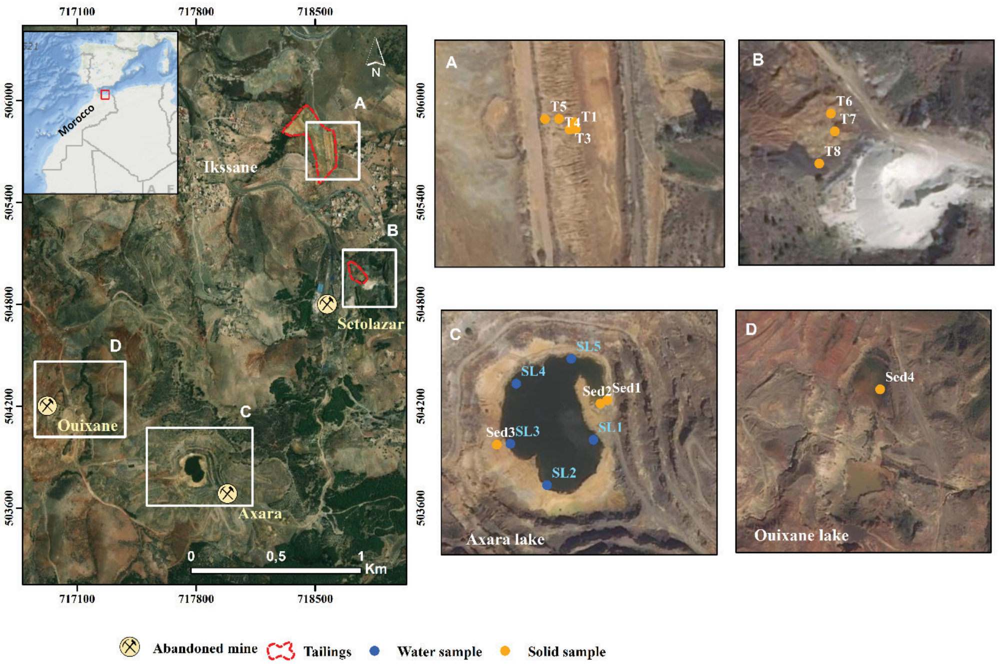

Figure 1 *Samples location in the study area.*

with both Fe^{3+} and Fe^{2+} in aqueous solution. Copiapite and jarosite are relatively soluble and indicate extremely acidic conditions (Nordstrom *et al.* 2015; Lim *et al.* 2024). Sample T7 presents significant quantities of hematite (69%) and magnesioferrite (22%), which explain the dark gray color of the tailing. Axara floor sediments are dominated by gypsum, quartz (32%), langbeinite (15%), jarosite (16%), and quartz (10%). The sample taken from the dried part of the lake contains morenosite (32%) bianchite (26%) and dolomite (9%). Ouiksane pit lake sediment contains aluminosilicate (albite (34%), paragonite (16%), and smaller amounts of kaolinite (5%), and clinochlore (8%)).

Chemical composition of sediments and tailings

The chemical analyses of the studied samples are illustrated in Table 1. Fe and S constitute the main chemical composition of the studied samples. The highest Mn, Zn, and Pb amounts were recorded in lake sediments. Ni, Co, and Zn concentrations in Sed 3 are related to the occurrence of the moorhouseite, Bianchite and morenosite. The Sample Sed 4 records the high value of Pb concentration (85.75 µg/g) followed by As, Cu, Co; Ni; Zn; and Pb. Sample T7 shows a high Fe content, confirmed by the presence of hematite. Significant amounts of Co, Cu, Ni, and Zn are found in sample T2. These trace elements could be associated with copiapite through coprecipitation and adsorption (Jamieson *et al.* 2005). This significant amount of As may be associated with jarosite,(Savage *et al.* 2005). All the PTEs largely exceed the reference sample.

Geochemistry of pit lake waters

The pit lake waters Axara are highly acidic (pH = 3) with high conductivity (29160 µS/cm) and less oxidizing conditions. The Eh values likely indicate variations in the dominant Fe^{2+}/Fe^{3+} redox couple, as iron concentrations are generally elevated (Yucel and Baba 2013). Sulfate is the predominant anion of Axara pit lake (31506.23 mg/l). As, Ni and Fe are found to exceed the water-quality standard (WHO, 2011), whereas the other elements amounts does not exceed their respective limits (Table 2). The high iron content can be attributed to the oxidation of pyrite (FeS$_2$) or other sulfide minerals, which releases Fe^{2+} and Fe^{3+} in solution. Ni could

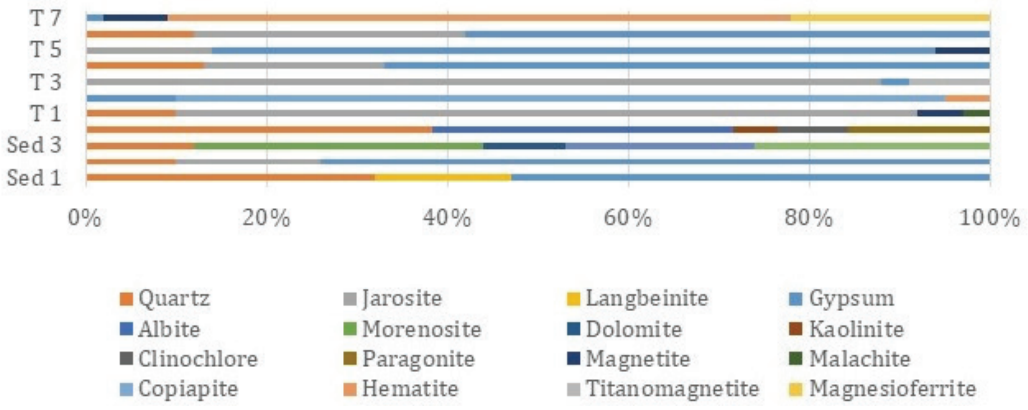

Figure 2 *Mineralogical characterizations of tailings and pit lake sediments.*

be originated from the oxidation of sulfide minerals (waste rocks, ore minerals) or from leaching from morenosite found in sediment Sed 3 in Axara pit lake.

PTEs chemical speciation in Axara pit lake

Chemical speciation was done using PHREEQC. The molalities of metal species and As that exceed the WHO standards are shown in Table 2. In this study, the main As species in solution were As^{3+}, $HAsO_2$, and $As(OH)_3$, implying a strongly reducing environment. The As^{5+} is less toxic in comparison with As^{3+} because trivalent As compounds are more soluble in water (Chaudhary *et al.* 2024).

Chemical speciation shows that Fe exists as sulfate ($FeSO_4$) and chloride ($FeCl^+$). The re-dissolution of previously formed unstable precipitates or the leaching of iron from the tailings and ore minerals are the two main causes of the higher iron contents in water (Obiefuna and Orazulike 2010). The Ni^{2+}, $NiSO_4$, and $NiCl^+$ are the predominant species. These potentially toxic metals (PTMs) can be found as sulfate species. the distribution of PTMs in water is influenced substantially by the dissolving of sulfate minerals (Hu *et al.* 2021).The calculated SI shows that Axara pit lake remains oversaturated with anatase, cassiterite, and rutile (SI>0) and they are likely to precipitate from the solution (Fig.5). These minerals require extremely little dissolved ions to reach oversaturation because of their low solubility products (K_{sp}). Gypsum (SI = -0.71) and Anhydrite (SI =

Table 1 *Chemical element concentrations in tailings and lake sediments.*

Sample		T 1	T 2	T 3	T 4	T 5	T 6	T 7	Sed 1	Sed 2	Sed 3	Sed 4	REF
Al		9.79	11.58	10.06	10.07	5.90	12.39	6.77	15.96	7.90	3.73	19.84	23.32
Ca		31.81	6.31	36.23	36.44	33.06	42.62	11.44	56.40	89.78	0.54	7.32	42.31
Fe		232.40	166.80	214.18	191.39	210.59	208.19	546.45	118.99	108.51	23.38	59.19	56.76
K	mg/g	4.81	0.90	4.34	5.14	4.83	5.87	1.33	16.94	10.81	0.01	10.81	15.67
Mg		5.54	6.73	4.29	3.72	7.78	3.73	6.21	5.92	10.09	20.99	2.25	2.77
Na		4.87	0.78	4.61	5.56	4.42	6.08	1.28	14.50	7.77	8.97	11.78	15.52
S		106.36	143.49	104.34	156.08	87.95	98.80	10.06	62.99	111.51	130.15	2.67	0.33
Mn		441.57	597.96	284.73	198.49	695.34	539.83	638.65	197.73	189.92	2130.60	507.79	881.81
Co		126.02	411.22	126.29	207.19	129.73	108.44	31.54	15.80	10.61	245.02	26.10	19.96
Ni		44.20	144.70	45.25	87.03	47.66	37.58	16.94	16.87	5.02	98.42	35.99	22.44
Cu	μg/g	361.96	576.24	329.52	152.50	307.93	234.60	40.70	206.15	305.63	413.27	146.36	25.45
Zn		66.66	120.31	51.75	30.92	84.82	70.69	51.82	31.31	40.61	330.22	245.03	82.09
As		197.72	98.59	311.61	119.88	606.93	157.11	16.12	31.11	32.36	0.92	30.67	7.24
Pb		45.53	6.05	25.82	45.39	26.79	70.83	11.26	10.22	25.21	0.00	85.75	30.74

Table 2 *Hydrochemical data and chemical species molalities of the Axara pit lake water.*

	Mean	WHO, 2011)	Species	Molality
pH	3.126	7.5	As^{3+}	1.47E-06
Eh(mv)	228.08		$HAsO_2$	7.87E-07
T(°C)	24.44		$As(OH)_3$	6.83E-07
Cond.(µS/cm)	29160	1500	As^{5+}	2.11E-11
Cl^- (mg/l)	3841.97		$H_2AsO_4^-$	1.94E-11
SO_4^{2-} (mg/l)	31506.22		H_3AsO_4	1.73E-12
As(mg/l)	0.10	0.01	Fe^{2+}	5.63E-04
Sn(mg/l)	0.006		$FeSO_4$	3.75E-04
Cr(mg/l)	0.03	0.05	Fe^{+2}	1.85E-04
Zn(mg/l)	3.09	3	$FeCl^+$	3.38E-06
Cd(mg/l)	0.016	0.003	Fe^{3+}	2.15E-12
Pb(mg/l)	0	0.01	$FeOH_2^+$	1.25E-12
Ni(mg/l)	1.15	0.07	Ni	2.05E-05
Ca(mg/l)	51.02	75	$NiSO_4$	1.30E-05
Fe(mg/l)	30.33	0.3	Ni^{+2}	7.44E-06
Mg(mg/l)	44.53	50	$NiCl^+$	1.99E-08
Cu(mg/l)	1.59	2		
Ti(mg/l)	0.008			
Al(mg/l)	25.33	0.2		
Na(mg/l)	32.77	200		
K(mg/l)	45.36	12		

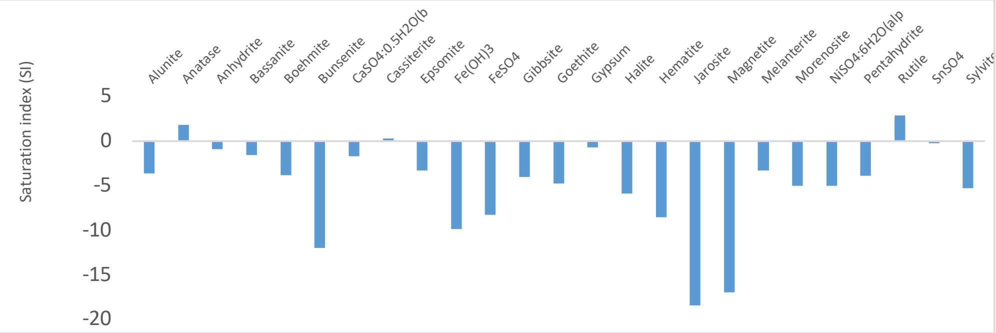

Figure 3 *Saturation index of Axara pit lake waters predicted by PHREEQC*

-0.88) are close to equilibrium. The pit lake is significantly undersaturated with other minerals (SI<0) indicating that they do not form or tend to dissolve (Jarosite, magnetite, and hematite).

Conclusions

In Beni Bou Ifrour abandoned mines, the tailings are dominated by jarosite, gypsum generated by AMD, and quartz, with low quantities of hematite, magnetite, and titanomagnetite. The Axara floor sediment show varying mineral compositions. They are composed mainly by gypsum, jarosite, and quartz, with Ni-Zn sulfates. Chemical analysis revealed low contents of Al, Na, K, and Mg. Fe and S occur as the main elements in both tailings and pit lake sediments. Mg occurs in mine tailings, followed by As, Cu, Co, Ni, Zn, and Pb.

In Axara pit lake the most common anion in waters is sulfate, while As, Ni, and Fe exceed water-quality Standards. A^{3+}, $HAsO_2$, and $As(OH)_3$ are the most common forms of As in water. Fe^{2+} occurs as sulfate (FeSO4) and chlorides ($FeCl^+$) where Ni+, NiSO4, and $NiCl^+$ are the most common species of Ni. The distribution of PTMs is greatly impacted by SO_4^{2-}. The SI analysis indicates that the studied waters are oversaturated with anatase, cassiterite, and rutile. Gypsum and Anhydrite are close to equilibrium, while other minerals are significantly undersaturated.

References

Air W, Khafouri A, Talbi EH, Abdelouas A (2021) Assessment of Heavy Metal Contamination of the Environment in the Mining Site of Ouixane (North East Morocco). https://doi.org/10.1007/s11270-021-05318-6

Benidire L, Benidire L, Boularbah A (2022) Impacts of mining activities on soil properties : case studies from Morocco mine sites Impacts of mining activities on soil properties : case studies from Morocco mine sites

Bouabdellah M, Jabrane R, Margoum D, Sadequi M (2016) Skarn to Porphyry-Epithermal Transition in the Ouixane Fe District , Northeast Morocco : Interplay of Meteoric Water and Magmatic-Hydrothermal Fluids.

Bouabdellah M, Lebret N, Marcoux E, *et al* (2013) Les mines des Beni Bou Ifrour-Ouixane (Rif Oriental) : un district ferrugineux néogène de type skarns The Beni Bou Ifrour-Ouixane mines (Eastern Rif), Neogene Skarn Type Iron Deposits To cite this version : HAL Id : insu-00812110

Chaudhary MM, Hussain S, Du C, *et al* (2024) Arsenic in Water: Understanding the Chemistry, Health Implications, Quantification and Removal Strategies. ChemEngineering 8:78

Edition F (2011) Guidelines for drinking-water quality. WHO Chron 38:104–108

El Yaouti F, El Mandour A, Khattach D, *et al* (2009) Salinization processes in the unconfined aquifer of Bou-Areg (NE Morocco): A geostatistical, geochemical, and tomographic study. Appl Geochemistry 24:16–31.

Hakkou R, Benzaazoua M, Bussière B (2008) Acid mine drainage at the abandoned kettara mine (Morocco): 1. environmental characterization. Mine Water Environ 27:145–159.

Hu J, Zhu C, Long Y, *et al* (2021) Interaction analysis of hydrochemical factors and dissolved heavy metals in the karst Caohai Wetland based on PHREEQC, cooccurrence network and redundancy analyses. Sci Total Environ 770:145361.

Jabrane R (1993) Etudes génétiques de la mineralisation en fer de Nador (Maroc nord oriental)

Jamieson HE, Robinson C, Alpers CN, *et al* (2005) Major and trace element composition of copiapite-group minerals and coexisting water from the Richmond mine, Iron Mountain, California. Chem Geol 215:387–405.

Lakrim M, Laila M, Omar EA, Garouani a el (2011) etude d ' impact des dechets miniers de la mine de nador sur l ' environnement (Nord-Est du Maroc).

Lim J, Sylvain K, Pabst T, Chung E (2024) Effect of waste rock particle size on acid mine drainage generation: Practical implications for reactive transport modeling. J Contam Hydrol 267:104427

Luo C, Routh J, Dario M, *et al* (2020) Distribution and mobilization of heavy metals at an acid mine drainage affected region in South China, a post-remediation study. Sci Total Environ 724:138122.

Moncur MC, Ptacek CJ, Blowes DW, Jambor JL (2005) Release, transport and attenuation of metals from an old tailings impoundment. Appl geochemistry 20:639–659

Nordstrom DK, Blowes DW, Ptacek CJ (2015) Hydrogeochemistry and microbiology of mine drainage: An update. Appl Geochemistry 57:3–16

Obiefuna G, Orazulike D (2010) Chemical Speciation of Some metal ions in Groundwaters of Yola Area Using Geochemical Model. J Appl Sci Environ Manag 14:. https://doi.org/10.4314/jasem.v14i2.57846

Savage KS, Bird DK, O'Day PA (2005) Arsenic speciation in synthetic jarosite. Chem Geol 215:473–498.

Tarik M, Noureddine E, Ahmed B, *et al* (2023) Heavy Metals Analysis and Quality Evaluation in Drinking Groundwater around an Abandoned Mine Area of Ouichane (Nador ' s Province , Morocco). 24:118–127

Yucel DS, Baba A (2013) Geochemical characterization of acid mine lakes in northwest turkey and their effect on the environment. Arch Environ Contam Toxicol 64:357–376. https://doi.org/10.1007/s00244-012-9843-7

Groundwater Water Quality Around an Existing Mine: From Current Conditions to Mine Closure

Rodrigo F. Embile Jr.[1], Ingar Walder[2]

[1]*DHI Group – Sweden, Skeppsbron 28, 111 30 Stockholm, roem@dhigroup.com, ORCID 0000-0003-2121-5468*

[2]*Kjeoy Research and Education Center, Kjeoy 8412 Vestbygd, Norway, ingar.walder@nmt.edu*

Abstract

Groundwater quality around a mine constitutes a major part of a mine environmental permit. Understanding mine-water quality and its environmental impacts must be investigated not just during the mine operation but until stable state is reached that can be 100 years or more after closure. In this study, diffuse leakage water quality from a tailings management facility of an iron ore mine was modelled from the current condition, increased production and closure. Results show that while major elements will eventually decrease, trace elements will be attenuated via sorption to oxyhydroxides in the sediments which will improve the groundwater quality in time.

Keywords: Groundwater, PhreeqC, mine closure, reactive transport

Introduction

Modelling of groundwater quality is generally a complex task that involves several phases and expertise both from external consultants and the mine staff itself. A good hydrological model including a water balance model is generally a prerequisite to any water quality modelling work. This is to ensure that the flow rates and volumes are properly accounted for in calculating water mineral interactions, dilution effect, mass loading, and final concentrations to receiving environments such as a rivers and groundwater resources. Understanding and knowing factors contributing to water quality during operation and its closure is a pre-requisite to any mine-permit application.

An active tailings management facility (TMF) of an iron ore mine was used as the study area. The mine has been in production for over a century, producing iron concentrate from magnetite-hematite ore. Diffuse leakage coming from the TMF is observed based on the high concentration of Cl (82 mg/L) in some monitoring wells at the base relative to process water average concentration of 137 mg/L that enters the TMF during tailings deposition. The diffuse leakage quality is a result of the geochemical reactions within the tailings dam, in the support dike, the mineral processing, and mine water used in the ore processing.

Regional groundwater flows perpendicular to the tailing management facility and into the recipient river (Figure 1). According to current data, the groundwater is affected by the diffuse leakage coming from the TMF. The diffuse leakage contains elevated concentrations of major constituents such as Cl, SO4, and Ca as well as notable trace metals such as U and Ni. The mine plans to increase production which could directly affect the diffuse leakage and thereby the groundwater water quality through the increase in concentration of these constituents. This will also result in increased flow rates and water volume coming from the TMF into the river. In order to address these issues, the mine plans to implement protection measures to the groundwater and river by pumping contaminated water and cleaning that in the clarification pond prior to release in the receiving environment.

Groundwater quality was modelled downstream of the TMF towards the river with the goal of understanding the effect on water quality around the mine during its current operation, mine production expansion, and closure. The groundwater hydrology of the mine was first modelled using MIKE-SHE where particle tracking simulation of the diffuse leakage was also performed. A multi-component reactive transport modelling was performed using PHREEQC (Parkhurst, D. and Appelo, C., 2013) incorporating the transport parameters obtained from the results of the groundwater hydrogeology.

Methods

Prior to the modelling work, a conceptual model was first developed. The conceptual model was designed and agreed to by all stakeholders involved from the mining company side and the consultants working on the project. This ensures that the conceptual model is in line with the understanding of the current conditions as well as the past and future scenarios based on the identified mine plan and closure scenario. Input data and parameters were obtained from the site, either from field investigation or from literature and public sources.

Conceptual Model

The onset of water-mineral interactions begins within the tailings and support dike when mine process water enters these areas during tailings deposition via spigots. The resulting water quality from the water-mineral interactions between the tailings and support dike materials is what flows further down into the dam and then reacts with the underlying sediments. Based on geologic information as well sonic drilling data, moraine underlies the dam facility. It is within this moraine that major changes to the diffuse leakage water quality occur. Sorption and attenuation of most metals including Ni and U occur as the diffuse leakage intercepts the moraine. This is mainly due to the presence of iron oxyhydroxides and clay minerals within the moraine. Conservative elements such as SO4 and Ca generally retain their level of concentration within the moraine. As the diffuse leakage flows through the glaciofluvial sediments, sorption still occurs but at a lesser degree. The water quality that exits the glaciofluvial sediments is what reports to the recipient river.

Hydrological model

The MIKE-SHE integrated groundwater program simulated the diffuse leakage from the tailings dam to the recipient river using a particle tracking tool. This tool produced the total travel time and distance of the diffuse leakage from the source to the recipient, which was then subdivided into each zone of interest (tailings, support dike, moraine, glaciofluvial sediment). The average of these parameters provide basis for the residence time of the reacting water in each zone.

There is an increase in the travel time and distance during the applied scenario which is directly related to the increased height of the tailings dam from the current setting. This will also result in an increased height of the water table in the dam. During closure, the water table in the dam will eventually go down, increasing the thickness of the unsaturated zone. These changes in the TMF

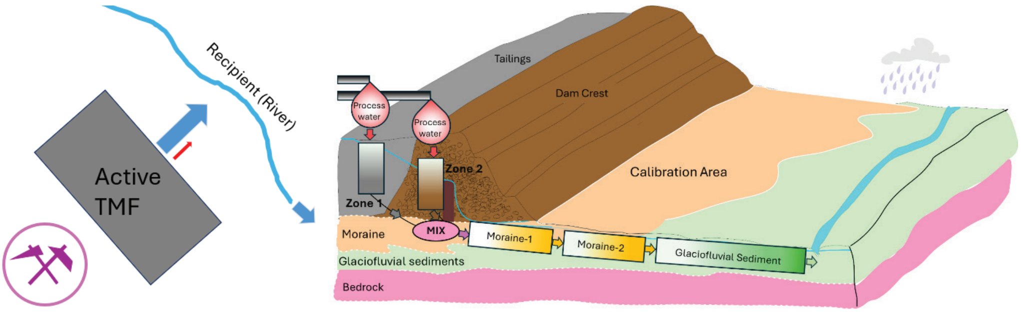

Figure 1 *Left: Schematic diagram showing the mine, tailings management facility (TMF) and the general direction of groundwater flow to the recipient river. The small red arrow denotes the contaminated diffuse leakage. Right: Flow path and modelling zones from the input of mine process water into the tailings pond until it reaches the recipient river.*

hydrogeology are included in the predictive modelling of the water quality.

PhreeqC reactive transport model

The design of the reactive transport model with PhreeqC tracks the source of the diffuse leakage as it flows through the different geologic materials until it reaches the river. These different geologic materials (tailings, support dike, moraine, and glaciofluvial sediments) correspond to zones or columns in the PhreeqC modelling.

Each zone was assigned as a column containing these materials of interest. For the current scenario, the mine process water input water quality is based on measured data. Similarly, calibration data was based on an average of wells downstream from the dam facility. During the applied setting, modelled mine process water was used as input water quality. The process water quality for the current and applied scenarios are used as the existing water quality within the tailings and support dike. During the closure scenario, only precipitation infiltrates the tailings dam, resulting to an improved water quality in time.

Geochemical characterization of the tailings, support dike (wall rocks from the mineral exploitation), moraine, and glaciofluvial sediments were obtained from sonic drilling data and literature. Mineralogical tests, XRD and full chemical analysis were performed for these materials. This information was used as input parameters for the mineralogy of the materials and their weight percentage in the columns.

Hydrological data such as travel time and distance of the diffuse leakage as it flows through the different zones were obtained from MIKE-SHE hydrogeological modelling. This information was used as input for the reactive transport modelling in PhreeqC.

Calibration and Validation

Calibration of the diffuse leakage water quality was carried out using the average concentration of selected wells downstream of the dam facility. These wells were selected based on the direct influence of the diffuse leakage which was based on the concentration of conservative elements such as Cl.

Groundwater quality during different time scenarios

The concentration of most constituents of the diffuse leakage during the current setting is seen to increase by as much as 50–100% for most constituents for the applied setting (maximum expansion of the mine). This is primarily attributed to the increased concentration of most constituents in the process water resulting from the change in the ore mix and increased volume of the ore that will be processed during the applied setting. The concentrations of these constituents are, however, seen to significantly decrease by as much 90% during closure, for example, 80 years after the mining operation has ceased (Figure 2). This decrease is primarily linked to the cessation of process water input into the tailings, with rainwater being the only incoming solution after that. An observed increase in some constituents, especially the trace elements during closure, is attributed to the continuous oxidation of sulfide minerals that will be exposed during the lowering of the phreatic water table in the TMF during the closure scenarios.

Generally, the variation in the relative percentage of increase or decrease of these constituents during the different time scenarios modelled is dependent on the heterogeneous nature of the materials modelled, including, but not limited to, mineral reaction rates, changes in physicochemical conditions and changes in hydrological conditions. A proposed cover system on top of the tailings facility is seen as an important measure to limit further oxidation and reactions brought about by increased oxygen and water infiltration.

Conclusion

Groundwater modelling from a tailings dam facility to a recipient river was performed for the current, applied and closure scenarios for an iron ore mine. A potential increase in mine production will also increase constituent elements in the modelled groundwater. Attenuation of metal transport was notable in the moraine and glaciofluvial sediments likely due to the strong presence of iron oxyhydroxides mineral. The closure and post-closure scenarios of the mine shows lowering

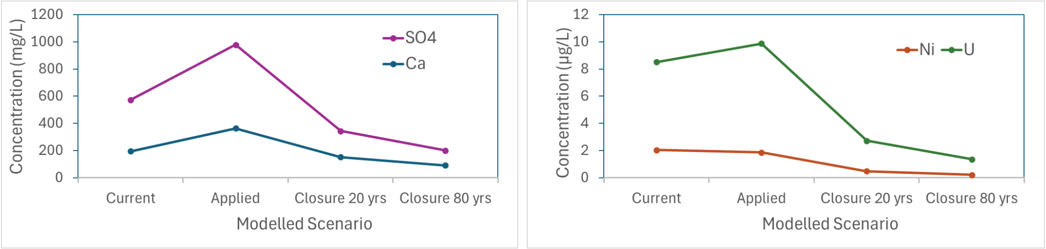

***Figure 2** Concentration of major constituents SO4 and Ca as well as trace elements U and Ni for the current condition, applied scenario and closure setting (20 and 80 years after closure).*

concentration of all constituents largely due to reduced diffuse leakage influence and continuous precipitation infiltration.

The results from these models provide a basis for a mine environmental permit application. These models also provide guidance on potential water quality risks that must be addressed and water management measures that must be implemented to make sure water quality around the mine remains within the set limits of regulatory agencies. In addition, these models provide a good picture of the hydrodynamics and water quality, their effect to mine operation, natural ecosystems surrounding the mine, communities and other stakeholders.

Acknowledgements

The authors would like to thank the mining company that owns all pertinent data in this study for allowing us to use them for this article.

References

Parkhurst, D. and Appelo, C., (2013) Description of Input and Examples for PHREEQC Version 3 – A computer program for speciation, batch reaction, one dimensional transport, and inverse geochemical calculations. USGS Techniques and Methods. Book 6 Chapter A43, 497 p

Investigation of a Heap Leach Facility leak using Finite Element Seepage Analysis

Jacob Erickson[1], J Larry Breckenridge[1]

[1]*Global Resource Engineering, 17301 W Colfax Ave, Suite 400, Golden, Colorado, 80401, jerickson@global-resource-eng.com, lbreckenridge@global-resource-eng.com*

Abstract

Gold heap leach facilities (HLFs) are susceptible to environmental releases of gold-cyanide pregnant leach solution (PLS) if deformities and perforations in the engineered liner systems occur. This case study presents how the two-dimensional, finite-element, variably saturated seepage modeling program, SEEP/W, predicted PLS fate and transport. Results demonstrated PLS does not reach a groundwater well downgradient of an HLF even after increasing leakage rates and 30 years of post-heap closure. These results helped regulators develop a response and management plan and demonstrated the importance of fate and transport modeling when HLF leaks occur.

Keywords: Cyanide, fate and transport, unsaturated hydrogeology.

Introduction

Cyanide leaching through HLFs is a widely applied method for recovering gold from oxide ore (Hiskey 1985). HLFs are engineered to collect and transport any and all PLS from the heap to the processing facility. A standard leachate collection system (LCS) consists of four layers (Lupo 2010):

1. The over liner, boulder to cobble-sized material which collects PLS and protects underlying leachate collection pipes from stacked ore;
2. The composite liner, high-density polyethylene (HDPE) or similar material which is an impermeable layer for PLS to accumulate atop while it is collected by the leachate collection pipe system;
3. The under liner, engineered low-conductivity clay layer (LCCL), compacted to a hydraulic conductivity of approximately 1×10^{-6} cm/s, provides a final barrier to protect any PLS from percolating into the substrate; and,
4. The leak detection system (LDS), consisting of perforated drainpipes, monitors for any PLS that may flow through the LCCL and into the environment.

During LCS installation and subsequent additions of ore, it is common for deformities and perforations to exist throughout the LCS or, more specifically, the composite liner (Rowe *et al.* 2013). If these failures expand to great enough size or occurrence, the LDS will start to detect PLS leakage.

Different jurisdictions have varying leakage rates of PLS that are not considered a hazardous release into the environment. For example, one jurisdiction in the United States reports 25 gallons/day (94.64 L/d) as the actionable limit.

For this case study, an HLF in a confidential location detected a leakage rate in two HLF leaching cells that were above the actionable limit. However, due to the placement of the LDS at this HLF, which was installed *above* the LCCL (it is typically installed below the LCCL), this leakage rate did not necessarily equate to a release to the environment. Ultimately, the HLF owners needed to know the risk of environmental contamination from the liner breach. Therefore, a predictive seepage analysis of the fluid dynamics of the PLS through the HLF, the LCS, and the underlying substrate was executed.

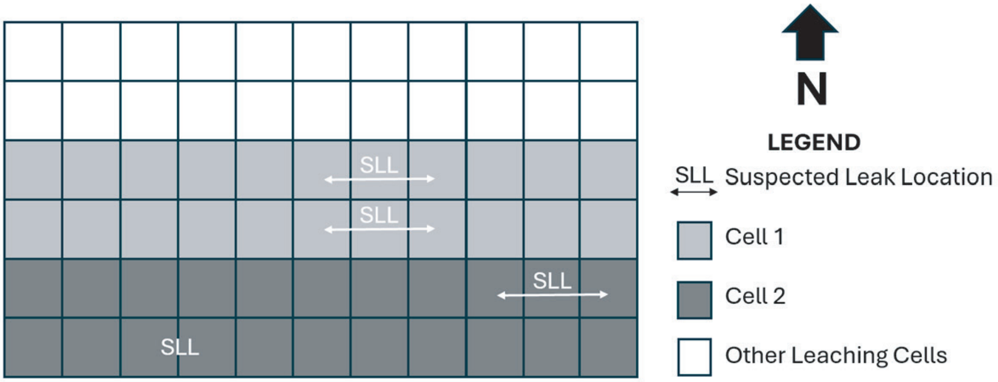

Figure 1 *Overhead HLF Grid with Cell 1 and Cell 2 Suspected Leak Locations.*

Methods

Leak Detection

Before the seepage analysis could be performed, the location of the leak had to be determined. Using historical leach application records, and historic PLS collection results for different HLF cells, many arrays were created in Microsoft Excel to model when different sections of each cell were actively leached. The approximate location of the leak for each leaching cell (Fig. 1) was ascertained using the Excel arrays with leachate application time-series records and LDS leachate collection rate observations. Most notably, the Cell 1 leakage rates and application schedules suggested only one central location for the leak while Cell 2 suggested one to two major leak locations.

The locations of the leaks, and their magnitude, was considered in all future modelling and mitigation evaluations.

Conceptual Model

Since the detected leaks were found to occur in horizontally adjacent cells, and because the gradient is consistently vertical within the vadose zone, and to one compass direction in the saturated zone, 2D cross-sections can be used to conceptualize the leak mobility during and between phases of the HLF. The HLF evaluation considered three phases of operation: the current configuration (under leach), ultimate configuration (with more ore, and also leached), and closure (capped without leaching.) (Fig. 2). The mine does not anticipate placing much more ore on this area of the HLF. As a result, the ultimate configuration of the HLF will occur several months after the current configuration. If operations were to continue as planned, the closure (capped) configuration would occur two years after the end of ore placement and residual leaching.

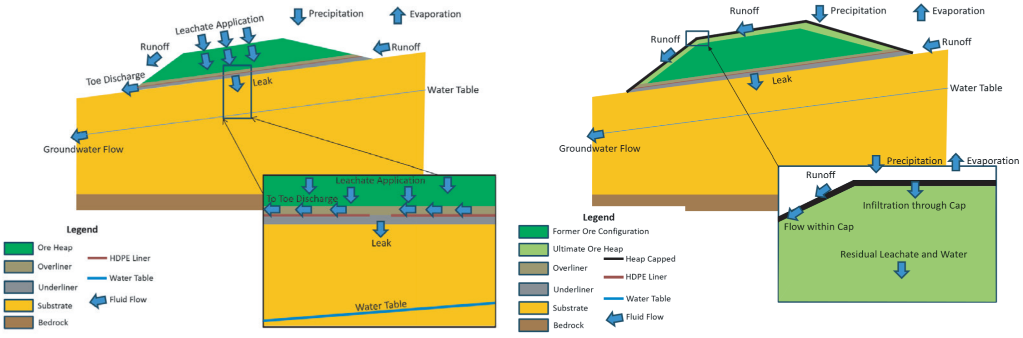

Figure 2 *Conceptual Models of the Current Configuration (left) and Closure (Capped) Configuration of the HLF (right).*

During operations, the greatest amount of fluid flow travels through the ore into the LCS to the toe discharge, which delivers PLS directly to the processing facility. Only a small fraction of the fluid flows through the breach in the liner. This is because there is a several order-of-magnitude difference between the over liner next to the leachate collection pipes (1×10^{-2} cm/s) and the LCCL below the liner (1×10^{-6} cm/s).

After a short period where new ore is stacked and leached, the HLF has a two-year period of residual PLS leaching to extract more gold. Finally, the HLF leaching ceases, and the amount of fluid flowing through the HLF decreases exponentially as the ore drains out. Post-leaching and after drain-down, there is no longer PLS sitting atop the leak. This results in an exponential decrease in the PLS moving through the breach in the liner.

Potential mitigation measures were also considered. It is possible to install an inter-lift liner prior to the ultimate configuration of the HLF (Fig. 2) to divert the flow of PLS applied to the heap away from the breach and towards the LCS. In this conceptual layout (Fig. 3), only residual leachate stored in Cell 2 encounters the liner breach because PLS above Cell 2 is diverted horizontally by the inter-lift liner. The inter-lift liner concept does not consider stability and structural integrity of the HLF, which must be evaluated separately before it can be applied to the HLF. This mitigation measure was presented to the client as a solution (if required) to lower the potential release of PLS to substrate.

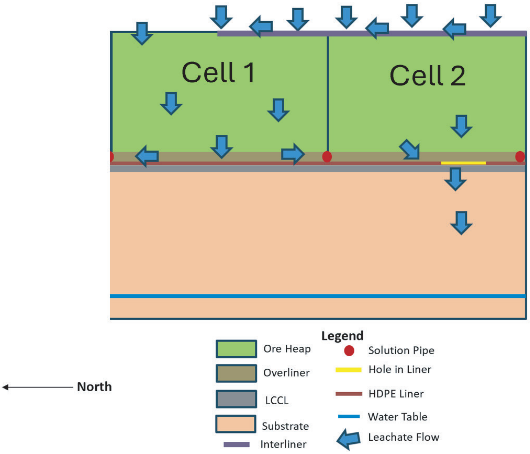

Figure 3 Conceptual Model of an Inter-lift Liner for Cell 2.

Predictive Groundwater Model

To conduct the seepage analyses, the two-dimensional, finite-element, variably saturated seepage modeling program SEEP/W was chosen because it is capable of assessing the non-linear dynamics of unsaturated groundwater flow through steady-state and transient state analyses (GEO-SLOPE International Ltd. 2015). The program uses a mesh of nodes to quantify the flow dynamics of water within the model domain. Additionally, a two-dimensional model is sufficient for this case study due to the direction of flow being either vertical (to the water table) or downgradient towards the toe of the heap.

To construct the model, several features needed to be implemented into the program. These included HLF and geologic cross-sections, material properties, finite-element mesh for each material, and boundary conditions (BCs). Geologic cross-sections of the HLF foundation were acquired from previous geotechnical studies and monitoring wells drilled around the HLF. The HLF cross-section was acquired from HLF as-built drawings.

Properties for the unsaturated and saturated materials were based on soil water characteristic curves (SWCCs) and hydraulic conductivity values (K-values) derived from lab-analyzed samples of the materials used in the heap (ore) and the LCS (unconsolidated cobble over liner and clay under liner). Substrate properties were assumed based on core samples analyzed during drilling of monitoring wells (silty sand with gravel) with a porosity value of 0.25 (Heath 1983) and a K-value 6.8×10^{-4} cm/s (Domenico and Schwartz 1990). These materials were then assigned to different regions in the model according to layers presented in the conceptual models.

Once each material was incorporated into the model, an appropriate finite-element mesh was applied to each region. A finite-element mesh is used in SEEP/W to calculate fluid and mass transfer within each region.

Finer meshes result in longer run times, but more refined results especially for modeled locations of concern. Focusing on the breaches in the liner, a coarse mesh was assigned to parts of each region that were outside the breach, while a fine mesh was assigned to the over liner, LCCL, and substrate regions near the liner breach.

Several BCs were implemented to simulate PLS application and PLS collection. The leachate application rate of 2.7 × 10^{-6} $m^3/s/m^2$ was directly reported by the HLF owners, while precipitation (applied to the heap when leachate application was "turned off") was calculated based on the average yearly precipitation. Because the HLF is in an arid region, precipitation is not a significant factor. A 10% infiltration rate was chosen during current and ultimate heap configurations, while a 1% infiltration rate was chosen for the closure (capped) configuration. PLS collection pipes were zero pressure boundaries, which would cause any PLS to preferentially flow towards these collection points. Hydraulic head boundaries were defined from monitoring wells located upgradient and downgradient of the HLF. The difference between these boundaries generated a water table oriented properly with the HLF and other material geometries.

Steady-state calibration was performed to a "snapshot" of HLF operations, but the steady state model was not relevant to the results. The transient model contains the following time steps:

- Ore loading and active leaching (day 1 to day 1048);
- Active leaching in the ultimate configuration (day 1049 to day 1778);
- Residual drain down, calibrated to state-approved HLF drain down model (day 1779 to day 3603);
- Uncovered (day 1 through day 1778) with 10% precipitation infiltration;
- Covered (day 1779 through day 12728) with effectively zero infiltration.

Using this time series, historic and future PLS fate and transport was simulated.

Results

Flow Modeling of the Leak

Initial results of the transient models for the Cell 1 leak show moisture migration is clearly visible under the HDPE liner in the area of the breach. A modeled pressure head of 0.38 m above the liner and breach is also observed (Fig. 4).

However, the moisture does not significantly penetrate the Cell 1 LCCL, even after two years of PLS application. This is because (as mentioned above) the LCCL is specifically compacted and conditioned to be a secondary backup liner to the HDPE. The results show that even the substrate, despite the fact that it contains coarse-grained material, acts as an impediment to PLS flow. Under vadose zone flow physics, dry materials have a lower conductivity than wet materials often by several orders of magnitude (Brady 1990). The leak from the Cell 1 HDPE breach going through the LCCL does not have enough moisture to "wet" the substrate to a point where it augments the hydraulic conductivity. This causes the moisture front to stay stored in the LCCL and upper substrate.

For Cell 2, which had a larger breach in the liner, there is a much greater PLS plume in the substrate (Fig. 5).

Upon reception of these results, the HLF owners requested several sensitivity analyses be simulated to minimize any Cell 2 PLS release into the environment. These included cessation of leaching activities two years after

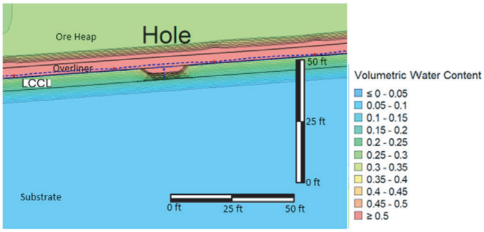

***Figure 4** Moisture and Particle Tracking from Cell 1 after 2 years of Leak Detection. The blue dashed line above the LCCL is the hydraulic head above the liner.*

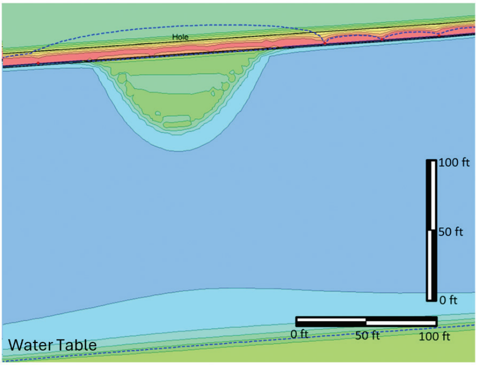

Figure 5 *Moisture Tracking from Cell 2 after 2 years of Leak Detection.*

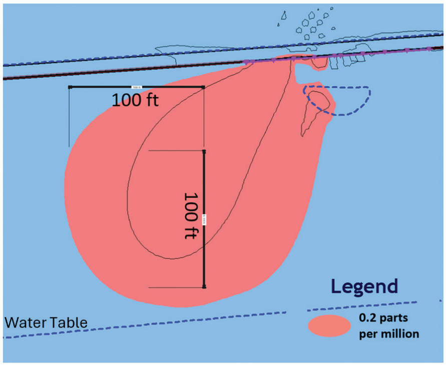

Figure 6 *PLS plume extent, 30 years after Closure Configuration.*

the leak was detected and the application of an inter-liner. The most-reasonable mitigation was a shorter PLS application time even though this resulted in some loss of gold recovery. According to the model, approximately 2260 L of residual leachate remains in the HLF after 10 years of drain down.

Chemical Fate and Transport Modeling

Considering the results presented in Fig. 5, additional contaminant fate and transport modeling was simulated to ensure PLS did not reach the water table below the LCS. The chosen program was CTRAN/W, a finite-element program for simulating the transport of a dissolved constituent or gas through porous media by advection and diffusion. The model also includes a half-life for cyanide degradation of one year. This half-life is representative of cyanide degradation in the atmosphere (Razanamahandry *et al.* 2017). Since the vadose zone is mostly composed of air and not water, the environment for the fate and transport of the PLS plume reflects atmospheric conditions.

A 0.2 parts per million minimum concentration plume was then simulated in CTRAN/W. This minimum value was selected as the United States national drinking water standard is 0.2 parts per million (Agency for Toxic Substances and Disease Registry 2006). A minimum concentration plume refers to a plume with the extent set to a minimum concentration value. Thus, anything inside the plume is greater than the extent (red, Fig. 6) while everything outside the plume is set to 0 parts per million (blue, Fig. 6). Results from the model indicate that 30 years after the closure configuration, the plume would not reach the water table and is about 229 meters away from the toe of the HLF (Fig. 6).

Conclusions and Discussion

Upon presentation of the flow plus fate and transport modeling results to the regulators, the mine formulated an action plan, consisting of monitored natural attenuation which involved the observation of changes to water quality from monitoring wells downgradient of the HLF.

The results show that, even though liner breaches may occur, heap leach facilities are designed and constructed to mitigate PLS release with a multiple-tier protection system. In this case, the HDPE liner and the LCCL work together to mitigate environmental release, even when an HDPE breach occurs.

This case study showed that it is possible to detect the location of the leak from the leaching history, and to simulate the effects of a liner breach on the transport and fate of PLS. The driving factor in the result was the engineered low conductivity of the LCCL (compacted and tested to < 1×10^{-6} cm/s) and the power the unsaturated zone and relative permeability function combined with a low flux rate into the substrate to mitigate long-term PLS transport.

Acknowledgements

We would like to acknowledge our anonymous client for their support on this project.

References

Brady NC (1990) Nature and Properties of Soils. 10. New York: MacMillan Publishing Company.

Domenico PA, Schwartz FW (1990) Physical and Chemical Hydrogeology. John Wiley & Sons, New York:824.

GEO-SLOPE International Ltd. (2015) Leakage from a Pond with a Clay Liner (PDF).

Heath RC (1983) Basic ground-water hydrology. U.S. Geological Survey Water-Supply. Paper 2220:86.

Hiskey JB (1985) Gold and Silver Extraction: the Application of Heap-Leaching Cyanidation. Arizona Bureau of Geology and Mineral Technology Fieldnotes 15(4):1–5.

Lupo JF (2010) Liner system design for heap leach pads. Geotextiles and Geomembranes 28(2):163–173. doi: 10.1016/j.geotexmem.2009.10.006

Razanamahandry LC, Karoui H, Andrianisa HA, Yacouba H (2017) Bioremediation of soil and water polluted by cyanide: A review. African Journal of Environmental Science and Technology 11(6):272–291. doi: 10.57897/AJEST2016.2264.

Rowe KR, Brachman RWI, Irfan H, Smith ME, Thiel R (2013) Effect of underliner on geomembrane strains in heap leach applications. Geotextiles and Geomembranes 40:37–47. doi: 10.1016/j.geotextmem.2013.07.009.

Agency for Toxic Substances and Disease Registry, US (2006) Toxicological Profile for Cyanide. Table 8–1.

Surface Runoff Observations at Rock Covered Overburden Stockpiles and Implications to Hydrologic Modeling

Jared Erickson[1], Made Mahayasa[2], Nathan Haws[3]

[1]*Stantec Consulting International LLC, 2890 East Cottonwood Parkway, Suite 300, Salt Lake City, Utah, USA, jared.erickson@stantec.com*

[2]*Freeport McMoRan, Inc. 333 North Central Avenue, Phoenix Arizona, USA, mmahayas@fmi.com*

[3]*Geosystems Analysis, Inc. 3393 North Dodge Boulevard, Tucson Arizona, USA, nwhaws@gsanalysis.com*

Abstract

This study evaluated the changes in catchment response to progressive reclamation of the Upper Wanagon overburden stockpiles at the Grasberg Mine in Indonesia. Reclamation activities alter surface water runoff and accounting for these alterations in predictive runoff models is a challenge for the Upper Wanagon reclamation design. A runoff test plot was constructed to measure rainfall runoff response within the reclaimed area. A rainfall gauge and a surface water runoff flume have also been installed to provide measurements of stormwater response. This paper demonstrates how these data sources have been leveraged to inform hydrologic models and improve reclamation designs.

Keywords: Mine Reclamation, Stormwater, Hydrology, Drainage Design

Introduction

The Upper Wanagon overburden stockpiles (UWOBS) are located at the Grasberg Mine in Indonesia at approximately 4000 meters above mean sea level within the Maoke Mountain range in Central Papua. The climate of this area is wet, with rain falling almost daily and a total annual precipitation average of approximately 4 meters. Average daily rainfall depths range between 9- and 16 millimetres per day and the largest daily rainfall depths generally occur between January and March. The topography is steep, and the geology is dominated by formations of karstic limestone.

The UWOBS occupy approximately 350 hectares and store overburden stockpile (OBS) material produced in the Grasberg open pit. Progressive reclamation of the stockpiles commenced when OBS placement ended in 2018. As of 2024, reclamation work has been completed for approximately 250 hectares. Fig. 1 illustrates the stockpiles prior to the beginning of reclamation in 2018 and as reclamation work has progressed through areas of the stockpiles in 2021 and 2024.

Reclamation includes regrading to direct surface runoff into engineered channels that are armored with riprap. The regraded OBS surfaces are capped with a rock cover consisting of blasted limestone rock and then vegetated. The rock cover is coarse gravel to boulder material with interstitial sands mined from a nearby limestone quarry. The rock cover thickness is 5 meters.

Hydrologic models were developed to characterize runoff during storm events to aid design of stormwater conveyance infrastructure and to evaluate erosional stability of the rock cover. The hydrology models were calibrated to simulate runoff events during large storms recorded prior to 2018 at a rainfall gauge and flow monitoring flume (locations shown in Fig. 1). Typically, calibration of a hydrologic model using locally recorded data increases confidence in the model's ability to predict runoff rates during the design storm events. This may not be the case for a reclamation site such as the UWOBS because the closure activity alters surface water runoff characteristics. For example, UWOBS regrading alters drainage pathways and removes surface depressions that store water which is likely to increase runoff. Further, the rock cover is more coarse and more permeable than the overburden material and the cover could increase rainfall losses, causing total runoff rates to decrease. Accounting for the influence of the closure activities in predictive runoff models is essential for a robust and cost-effective closure design.

Test Plots

A reclamation test plot was constructed to aid understanding of the influence of the rock cover on surface water hydrology. The test plot was instrumented to measure the hydrologic response during design rainfall events. The test plot was constructed on a 2:1 slope where rock cover was installed over OBS fill. A base channel with a low permeability geosynthetic liner was installed to capture surface runoff. In addition, a perforated pipe underlain by a geosynthetic liner was installed below the rock cover (at the rock cover – OBS interface) near the base of the slope such

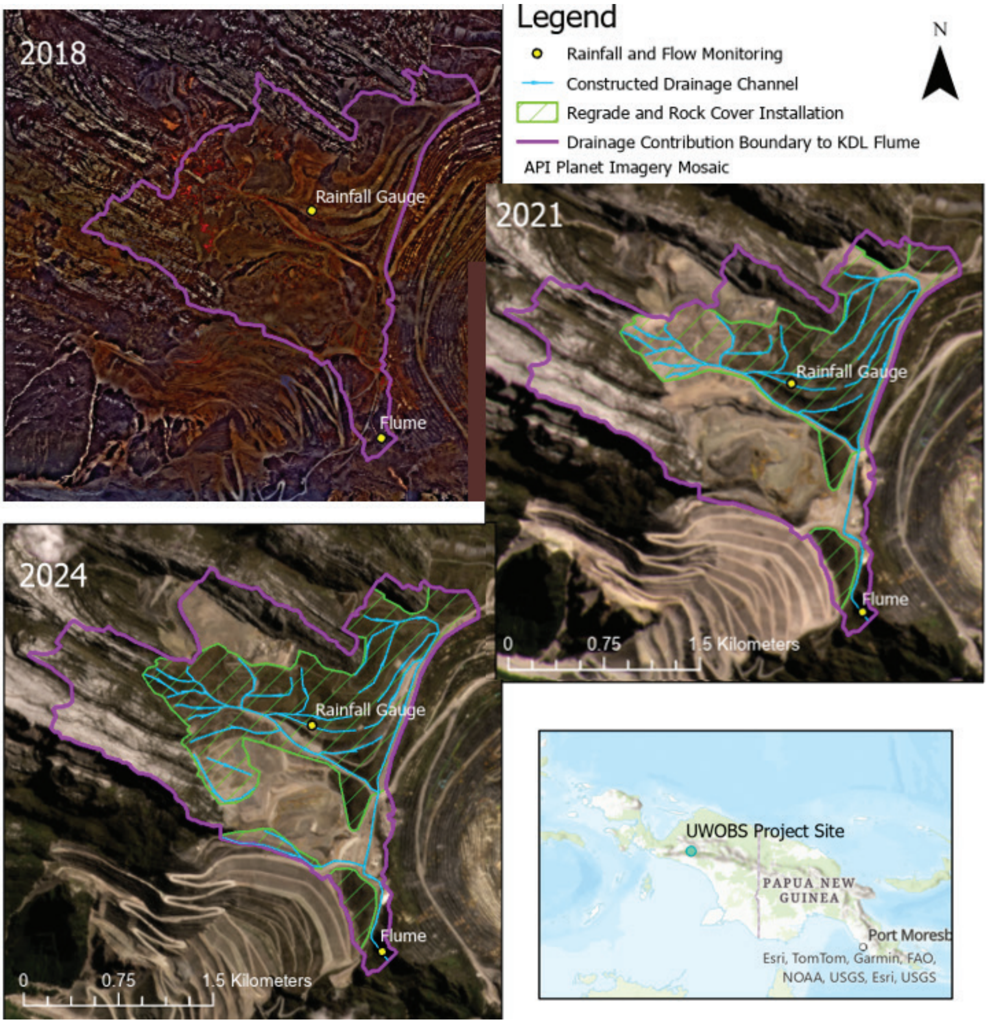

Figure 1 Images of UWOBS Conditions in 2018, 2021 and 2024.

that flow running along the rock cover – OBS interface also would be captured and measured. Flows from the base channel and the interface perforated pipe were directed to separate H-style flumes. Arrays of wobbler-type sprinklers were installed on the surface to simulate design rainfall intensities. Several pressure regulators were installed along the sprinkler delivery pipes so that the sprinkler spray would be uniformly distributed across the plot. Fig. 2 provides images of the test plot.

During testing, nearly zero runoff was observed on the rock cover surface even during the highest simulated intensity events (simulated rainfall intensity with an estimated annual exceedance probability 0.01). Runoff along the rock cover – OBS interface was observed and accounted for a substantial portion of the to total applied water during the highest simulated intensities (between 30% and 60%).

Based on these observations, a hydrologic conceptual model for the LWOBS area was hypothesized in which all precipitation infiltrates into the rock cover and, depending on the rainfall intensity, a portion of the infiltrated water is captured at the OBS surface beneath the rock cover and is re-expressed as surface water at the toe of the slope as illustrated in Fig. 3. Surface water is produced as accumulated flow along the rock cover - OBS interface saturates the rock cover layer.

Figure 2 *Test Plot Constructed to Simulate Runoff Response on Rock Covered Surface.*

Rainfall and Runoff Observations

The UWOBS designers have continued to review rainfall and surface runoff measurements from the UWOBS area as reclamation work has been completed. The record extends from late 2013 (several years prior to the start of reclamation activities) and continues as reclamation work is completed. Fig. 4 provides a summary of average monthly flow rates measured at the KDL Flume and total monthly rainfall depths measured at the Rainfall Gauge.

Fig. 5 provides observations of daily average flow rates. Flow measurements shown using BLUE dots represent average daily flow measured below 650 L/s and RED dots represent daily average flow rates measured above. The data shown in Fig. 5 is summarized in Tab. 1.

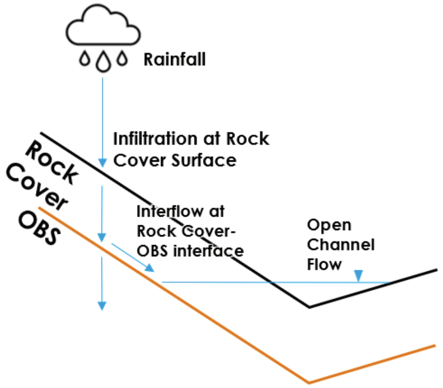

Figure 3 Illustration of Conceptual Model for UWOBS Rainfall Runoff.

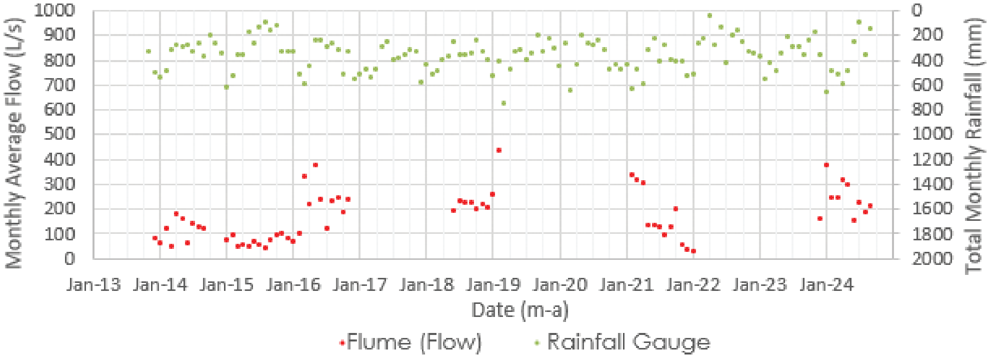

***Figure 4** Record of Average Monthly Flow Rate (Flume) and Monthly Total Rainfall Depths (Rainfall Gauge).*

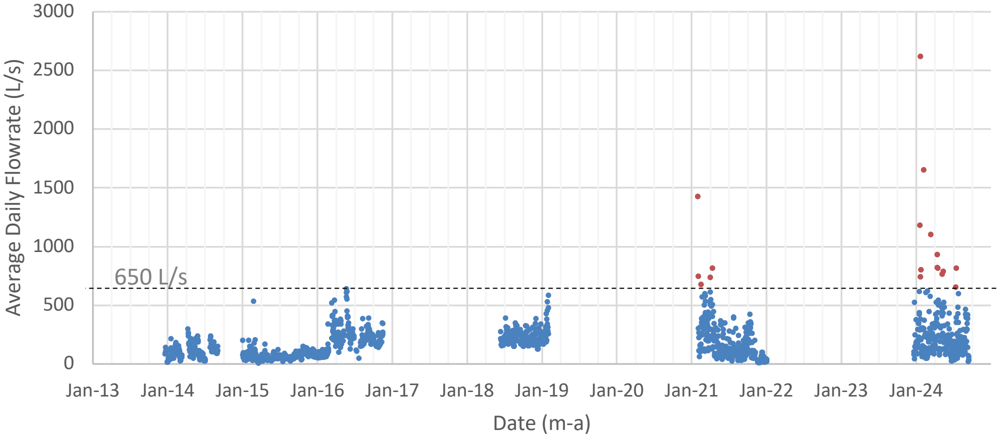

***Figure 5** Daily Average Daily Flow Rate at the Flume.*

Table 1 Summary of Average Daily Flow Rate at the Flume.

Date Range	Days with Flow Measurements	Days with Average Measured Flow Greater than 650 L/s	Percent of Days with Average Measured Flow Greater than 650 L/s
2013 through 2016	766	0	0.0%
2018 through 2019	225	0	0.0%
2021 through 2022	323	5	1.5%
2023 through 2024	270	13	4.8%

The monthly average flows show little change with time however, observations of the daily average flow rates show that the frequency of high daily flows (i.e. flow rates greater than 650 L/s) has increased as reclamation work has been completed. In fact, about 5% of the daily average flows recorded after significant reclamation had been completed between 2023 and 2024 are higher than the largest average daily flow recorded in the period prior to the start of reclamation and during the early reclamation period (i.e. prior to 2019).

The flume record and the observations from the test plot support a conceptual model where typical precipitation intensities are absorbed and attenuated within the rock cover material, resulting in a fairly constant long-term average flow rate through the flume. During rainfall events of relatively high intensity, a portion of the rainfall is captured on the OBS surface and accumulates as it runs downslope, eventually saturating the rock cover and surface water runoff is produced.

Implications for Hydrologic Modeling

Stormwater hydrology models were updated to reflect the conceptual model. The most influential update was in characterizing the time for drainage runoff to accumulate at design points of interest (i.e. time of concentration). This was achieved in the model by estimating flow velocities within the interstitial voids of the rock cover material (Leps, 1973). The model estimates a contributing area at which the voids in the rock cover would saturate causing surface flow. Travel times below the estimated rock cover saturation point are estimated assuming surface flow velocity methods (e.g. Manning's equation).

Fig. 6 on the next page provides comparative results of observed runoff at the flume versus predicted runoff using the calibrated stormwater model during recorded rainfall events after reclamation work in areas of the LWOBS had been completed.

The calibrations results demonstrate the hydrology model's ability to reproduce observed runoff conditions during isolated rainfall events with elevated rainfall intensity. The modeled runoff peak times are within 30-minutes and the peak values are within 20% of the observed flow rate.

Conclusions

Reclamation activities to regrade stockpiles and install a rock cover has affected the hydrologic response characteristics within the UWOBS area. Review of flow records presented herein suggest the affects can most clearly be observed by review of daily averaged runoff rates from the LWOBS area which have increased in correlation with progressing LWOBS reclamation. Insights to better understand these changes in site runoff patterns are provided by observations from a test plot constructed to study runoff characteristics on a rock covered slope. The test plot shows that high infiltration rates at the rock surface combined with interflow along the rock cover – OBS interface is the dominate flow path for the hydrologic response at the base of a reclaimed slope.

The information presented herein illustrates the importance of obtaining precipitation and runoff data for site-specific conditions. This study demonstrated how site-specific data can be leveraged to improve

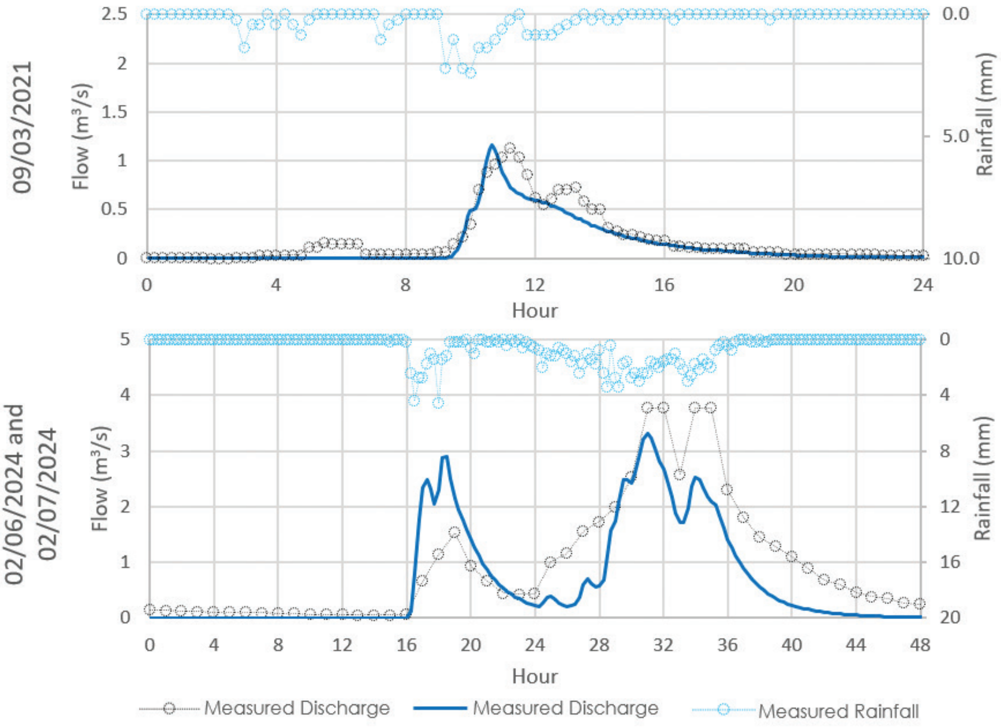

Figure 6 *Stormwater Runoff Model Calibration Results during Rainfall Events in 2021 and 2024.*

hydrologic models and ultimately drainage design. The findings of this study are specific to the UWOBS reclamation but may be broadly relevant to reclamation design of mine facilities using a thick rock fill cover.

References

Leps, T.M., “Flow through Rockfill.” Embankment Dam Engineering, John Wiley and Sons, P. 87–107, 1973.

Phytoremediation Potential of Aquatic Plants in a Tropical River Basin: Metals Bioaccumulation and Translocation from Mine Water

Ibtisani Farahnaz, Muhammad Sonny Abfertiawan,
Mindriany Syafila, Marisa Handajani

*Water and Wastewater Engineering Research Group, Faculty of Civil and Environmental Engineering,
Bandung Institute of Technology, Jl. Ganesha No. 10, Bandung, West Java 40132*

Abstract

This study aimed to evaluate aquatic plants that receive nickel mine runoff in Akelamo River, Obi Island, North Maluku, Indonesia, using Bioaccumulation Factor (BAF) and Translocation Factor (TF) to determine their phytoremediation potential. The predominant aquatic plant species identified in the Akelamo River belong to the grass family (Poaceae), specifically *Echinochloa* sp. This species accumulated primarily for Ni, Zn, Fe, Mn, Cu, with a high translocation potential for from roots to stems for Ni and Zn metals. These findings indicate that *Echinochloa* sp. plants, which grows naturally in rivers within nickel mining regions, can accumulate, and have the potential to phytoremediate, various metal.

Keywords: Aquatic plant, metal, bioaccumulation, phytoremediation

Introduction

Mining that employs open-pit methods has greater challenges when operating in countries within tropical rainforest regions, wherein rainfall is relatively high. Indonesia, as one of the tropical countries with the world's largest nickel reserves, has an average rainfall of up to 3000 mm per year, which is very high compared to sub-tropical countries with an average of 800 - 1000 mm per year (Eccles *et al.*, 2019; ESDM, 2020; USGS, 2021). The complexity of tropical ecosystems and high rainfall can accelerate the process of moving various materials from mine water into water bodies, which has an impact on the balance of aquatic ecosystems that act as transport routes and transport various materials and pollutants (Abfertiawan *et al.*, 2023; Karim *et al.*, 2020).

Aquatic plants in river ecosystems act as bioindicators for the level of pollution due to their adaptation and tolerance mechanisms to metals. Being sedentary, relatively long-lived, and able to accumulate metals, aquatic plants are ideal for pollution monitoring. This also opens up opportunities to explore the potential of phytoremediation to absorb, accumulate and neutralise metal pollutants from the environment (Prasad, 2005; Singh *et al.*, 2017; Qian, 2015).

This study evaluates the extent of metal accumulation in plant biomass to understand its phytoremediation capacity that grow naturally in a river that drains a nickel mining area. By understanding bioaccumulation mechanisms through Bioaccumulation Factor (BAF) and Translocation Factor (TF), we hope that effective mitigation approaches can be developed to reduce the impact of nickel mining activities on river ecosystems.

Methods

Study Area

The aquatic plants that were the subject of this metal bioaccumulation study were collected from a river that is the receiving water body of nickel mining activities on Obi Island, North Maluku, Indonesia (1°33’08.84‘‘S and 127°25’52.50‘‘E). While there are several mining catchment areas in the location (A-G) (Fig. 1), catchment area G is a mining area that specifically drains its outlet directly into

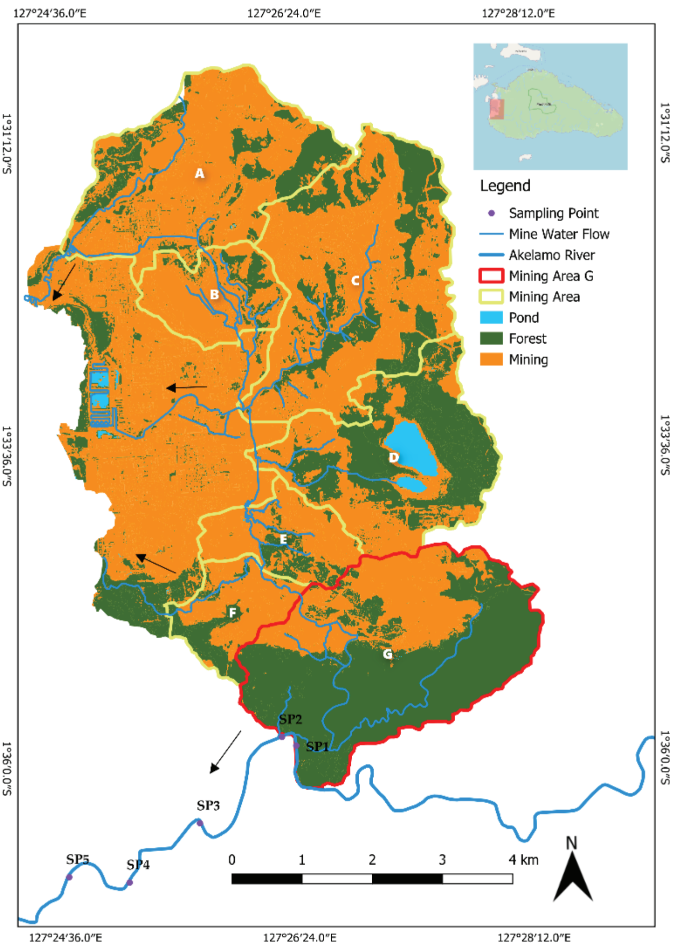

Figure 1 Distribution of sampling site and location in study area.

the main river, the Akelamo River. Samples of aquatic plants, sediments, and water were taken from five sampling points from the river upstream to downstream.

Sample Collection

The sampled aquatic plant parts include roots, stems, and leaves, using a shovel from the surface of river sediments. Samples of aquatic plants growing in the research area were collected, washed under running water, and placed in plastic bags for identification. The samples were dried at 95 °C to a constant weight, and crushed into fine powder for metal content analysis. Metals in aquatic plants were measured after acid digestion of the dried samples with an acid mixture (HNO3:H_2SO_4:$HClO_4$ dalam 5:1:1) at 85 °C until a clear solution was obtained. The solution was then filtered using 0.45 micron for analysis.

A total of 1 litre of river water were sampled and stored in polyethylene bottles. Sediment samples were taken using a shovel at a depth of 0-10 cm from the river surface. Wet samples were prepared by drying at 105 °C to constant weight, crushing to <63µm size, and digesting with aqua regia (HCl:HNO_3 dalam 3:1) (USEPA 3050B). Metal content for all samples was analysed using Inductively Coupled Plasma-Mass Spectrometry (ICP-MS) (APHA 3125).

Data Analysis

Metal bioaccumulation was evaluated using the Bioacumulatiion Factor (BAF) approach which refers to the efficiency of aquatic plants to accumulate metals from the environment into their tissues. The BAF of different metals from sediment to aquatic plant and water to aquatic plant was calculated based on the dry weight of aquatic plant samples with the equation given by Wilson and Pyatt (2007) as follows:

$$\mathrm{BAF} = \frac{\text{C plant tissue}}{\text{C sediment / water / soil}}$$

where $C_{\text{plant tissue}}$ is the concentration of metals in plant tissue (roots/stems/leaves) and $C_{(\text{sediment/water/soil})}$ is the concentration of metals in sediment, water, or soil.

Translocation Factor (TF) was used to describe the accumulation of metal concentrations from roots to other plant parts, such as stems and leaves/shoot. Its value was calculated based on the following equation (Zacchini *et al.*, 2009):

$$\mathrm{TF} = \frac{\text{C aerial parts}}{\text{C root}}$$

where $C_{\text{aerial parts}}$ is the metal concentration in the leaves/shoot or stems and C_{root} is the metal concentration in the roots.

Result and Discussion

Aquatic Plant Identification and Metal Content

The identification of aquatic plants at the sampling point of Akelamo River showed that the grass species (Poaceae) *Echinochloa* sp. was the most abundant among aquatic plants. The genus *Echinochloa* consists of more than 250 species of plants that are widely distributed throughout the world, especially in tropical areas with dry or waterlogged soil conditions. These aquatic plants have fibrous roots, flat stem, and hairy, glabrous, nodes, which are characteristics that enable the plants to survive and adapt to various environments (Damalas *et al.*, 2008; Marambe and Amarsinghe, 2002). A population of *Echinochloa colona* is known to grow naturally in the former chromite mine area (Rout *et al.*, 2000), in which this species has developed tolerance to metals. According to Rout *et al* (2000), this tolerance is maintained by a genetic system that is balanced by natural selection, making it suitable in restorations designed to produce effective vegetation cover to improve mined land and reduce erosion. Other studies have also shown that this plant can be useful in phytoextraction and revegetation programs on mining waste containing metals, due to its ability to accumulate metals (Peng *et al.*, 2017; Subhashini *et al.*, 2016; Sultana *et al.*, 2015). Metal concentrations in aquatic plants, sediment, and surface water collected from Akelamo River are shown in Table 1.

Among the various sampling points, the highest concentration of metal Fe (14018.5 mg/kg), Mn (475.40 mg/kg), Cr (79 mg/kg), Cu (29 mg/kg) was recorded in the root of *Echinochloa* sp., and Ni (17.63 mg/kg), Zn (62.22 mg/kg) was found in *Echinohloa* sp. stem. Minimum metal contents were found in *Echinochloa* sp. leaves. In this aquatic plant, metals were primarily accumulated in the roots, followed by stems and leaves. Metal concentration of sediment follows this order: Fe (6582.98 mg/kg) > Mn (238.37 mg/ kg) > Cr (72.89 mg/kg) > Zn (22.87 mg/kg) >

Table 1 *Metal concentration in aquatic plant, sediment, and surface water.*

Metal Element	***Echinochloa* sp. (mg/kg) (Mean ± SE)**			**Sediment (mg/kg) (Mean ± SE)**	**Water (mg/L) (Mean ± SE)**
	Root	**Stem**	**Leaf**		
Ni	14 ± 11	17.6 ± 13.4	9.7 ± 8.1	6.1 ± 3.6	0.01 ± 0.00
Fe	14018.5 ± 16570	5229 ± 73.8	4035.5 ± 6243.2	6582 ± 826	0.43 ± 0.24
Mn	475.4 ± 471.8	245.8 ± 293.5	10.4 ± 97.2	238.3 ± 88.5	0.06 ± 0.03’
Cr	79 ± 60.4	37.6 ± 43.7	33.2 ± 44.7	72.9 ± 30.1	0.05 ±0.03
Cu	29 ± 30.8	16.3 ± 21.8	10.4 ± 12.9	19.3 ± 3.1	0.01 ±0.00
Zn	52.7 ± 56.9	62.2± 57.4	32.9 ± 28.4	22.8 ± 6.5	1.14 ± 0.39

Cu (19.29 mg/kg) > Ni (6.12 mg/kg), while decreasing trend of various metals in surface water was observed in this order: Zn > Fe > Mn > Cr > Ni > Cu.

Metals can be absorbed by aquatic plants or macrophytes through roots from sediments or leaves/shoots directly from the water column. Metal uptake by roots and leaves increases as the metal concentration in the medium (water or sediment) increases. However, uptake is not always linear with increasing concentration because metals are bound to tissues with saturation or tolerance limits (Greger, 2004).

Bioaccumulation and Translocation Factor

Bioaccumulation Factor (BAF) is commonly used to describe how much a plant is able to store pollutant materials such as metals, whereas its phytoremediation ability is generally characterised by Translocation Factor (TF). The BAF and TF for metals found in the aquatic plants of *Echinochloa* sp. in Akelamo River are shown in Table 2.

As shown in Table 2, the BAF values for *Echinochloa* sp. plants of metals found are ranging from 1.08 to 7.19 according to the following order, from the largest: Ni (2.35) > Zn (2.31) > Fe (2.13) > Mn (1.99) > Cu (1.50) > Cr (1.08). BAF < 1 or BAF = 1 indicates that plants are able to absorb metals, but do not always accumulate them, while BAF > 1 indicates the plant ability to accumulate metals in its tissues, categorising the plant as a hyperaccumulator (Satpathy *et al.*, 2014). With BAF > 1, *Echinochloa* sp. that grows naturally in Akelamo River is able to accumulate metals, the three with the highest values being Ni, Zn, and Fe. A previous study by Subhashini *et al* (2016) also confirmed that *Echinochloa colona* is effective in absorbing Zn and Ni.

TF with a value > 1 is categorised as an indicator of high efficiency in translocating metals from roots to other parts such as stems and leaves/shoots (Majid *et al.*, 2016). This study showed that the order of TF values from roots to stems was Ni > Zn > Cu > Mn > Cr > Fe, while from roots to shoots Ni > Zn > Cr > Cu > Fe > Mn. The findings showed that the TF value from root to stem was more than one for Ni (1.23) and Zn (1.18), indicating high translocation ability. Plants with Bioaccumulation Factor and Translocation Factor of more than 1 (BAF and TF > 1) have a phytoextraction potential, while plants with Bioaccumulation Factor value above one but a Translocation Factor less than one (BAF > 1 and TF < 1) have a phyto-stabilisation potential (Subhashini *et al.*, 2016; Yoon *et al.*, 2006). The success of the phytoextraction process depends on the plant's ability to move metals to tissues other than roots (Ma *et al.*, 2001; Majid *et al.*, 2014). *Echinochloa* sp. growing naturally around the Akelamo River can therefore be considered as a hyperaccumulator for phytoremediation and has the potential for phytoextraction, especially for Ni and Zn metals, since they tend to accumulate higher in the stem than in the roots.

In contrast, the metals Fe, Mn, Cr, and Cu have TF values less than 1, indicating that the amount of metals accumulated in root tissues

***Table 2** Bioaccumulation and Translocation Factor of metals in aquatic plants from Akelamo River.*

Metal Element	*Echinochloa* sp.		
	BAF (Root/Sediment)	TF (Leaf/Root)	TF (Stem/Root)
Ni	2.35	0.68	1.23
Fe	2.13	0.29	0.37
Mn	1.99	0.02	0.52
Cr	1.08	0.42	0.48
Cu	1.50	0.36	0.56
Zn	2.31	0.62	1.18

is greater than the amount found in stem or shoot tissues. Thus, although plants are able to accumulate metals in root tissues (BAF > 1), the ability of plants to translocate metals to other plant tissues is still limited (TF < 1), as such that they accumulate more of Fe, Mn, Cr, and Cu metals in root tissues and have more potential for phytostabilisation.

We think that the high concentration of Fe metal measured in the roots is due to the high concentration of Fe in the sediment (Table 1). The nickel mine that discharges water into the Akelamo River is a nickel laterite known to produce large amounts of Fe from the laterisation process (Elias, 2002). Despite high Fe concentrations in the roots, TF to the stem or leaves was low, characterised by TF < 1 (Table 2). Fe translocation from roots to stems or shoots depends on the level of Fe treatment and is specific to aquatic plants (Mnafgui *et al.*, 2022; Siquera-Silva *et al.*, 2012). We suspect that the roots in these aquatic plants may act as a barrier that prevents Fe translocation to other tissues. Oxygen released by the roots can increase oxidising conditions resulting in the deposition of metallic elements on the root surface (Chauduri *et al.*, 2014; Machado *et al.*, 2005).The high productivity of BAF and TF in the tropical region may be due to the thermocline that tends to be stable throughout the year. In addition, the combination of intensive sunlight exposure and high rainfall effectively recycles nutrients through plant biomass (Pau *et al.*, 2018).

Conclusions

As a tropical nation with high rainfall and the largest nickel reserves in the world, nickel mining in Indonesia has the potential to manage mine water entering rivers with a natural biota-based approach. This study demonstrates that *Echinochloa* sp, which grows naturally in the Akelamo River-a receiving water body of nickel mining effluent-is able to accumulate the metals Ni, Zn, Fe, Mn, Cu, and Cr, as indicated by Bioaccumulation Factor (BAF) values > 1. In addition, this plant has a high potential to translocate metals from roots to stems, especially for Ni and Zn metals, as indicated by Translocation Factor (TF) values > 1. Therefore, *Echinochloa* sp. can be considered as a hyperaccumulator for phytoremediation and has the potential for phytoextraction especially of Ni and Zn metals, as those metals tend to accumulate higher in the stem than in the root.

References

Abfertiawan MS, Palinggi Y, Syafila M, Handajani M, & Pranoto K (2023). A Comparison dataset on static test using two concentrations of hydrogen peroxide for prediction of acid mine drainage. Data in Brief, 51, 109706.

Eccles R, Zhang H, & Hamilton D (2019). A review of the effects of climate change on riverine flooding in subtropical and tropical regions. Journal of Water and Climate Change, 10(4), 687-707.

Elias M (2002). Nickel laterite deposits-geological overview, resources and exploitation. Giant ore deposits: Characteristics, genesis and exploration. CODES Special Publication, 4, 205-220.

Chaudhuri P, Nath B, & Birch G (2014). Accumulation of trace metals in grey mangrove Avicennia marina fine nutritive roots: The role of rhizosphere processes. Marine pollution bulletin, 79(1-2), 284-292.

Damalas, CA, Dhima KV, & Eleftherohorinos IG (2008). Morphological and physiological variation among species of the genus Echinochloa in Northern Greece. Weed Science, 56(3), 416-423

ESDM (2020). Booklet Tambang Nikel 2020. https://www.esdm.go.id/id/booklet/booklet-tambang-nikel-2020

Fayiga AO, & Ma LQ (2006). Using phosphate rock to immobilize metals in soil and increase arsenic uptake by hyperaccumulator Pteris vittata. Science of the Total Environment, 359(1-3), 17-25.

Ma LQ, Komar KM, Tu C, Zhang W, Cai Y, & Kennelley ED (2001). A fern that hyperaccumulates arsenic. Nature, 409(6820), 579-579.

Machado W, Gueiros BB, Lisboa-Filho SD., & Lacerda LD (2005). Trace metals in mangrove seedlings: role of iron plaque formation. Wetlands Ecology and Management, 13, 199-206.

Majid, SN, Khwakaram AI, Rasul GAM, & Ahmed ZH (2014). Bioaccumulation, enrichment and translocation factors of some heavy metals in Typha angustifolia and Phragmites australis Species growing ALONG Qalyasan stream in Sulaimani City/IKR. Journal of Zankoy Sulaimani-Part A, 16(4), 93-109.

Marambe B, & Amarasinghe L (2002). Propanil-resistant barnyardgrass [Echinochloa crus-galli (L.) Beauv.] in Sri Lanka: Seedling growth under different temperatures and control. Weed Biology and Management, 2(4), 194-199

Mnafgui W, Rizzo V, Muratore G, Hajlaoui H, de Oliveira Schinoff, B., Mnafgui K., ... & Hussain S. (2022). Trigonella foenum-graecum morphophysiological and phytochemical processes controlling iron uptake and translocation. Crop and Pasture Science.

Pau S, Detto M, Kim, Y, & Still CJ (2018). Tropical forest temperature thresholds for gross primary productivity. Ecosphere, 9(7), e02311.

Peng Q, Chen W, Wu L, & Bai L (2017). The Uptake, Accumulation, and Toxic Effects of Cadmium in Barnyardgrass (Echinochloa crus-galli). Polish Journal of Environmental Studies, 26(3).

Rout GR, Samantaray S, & Das P (2000). Effects of chromium and nickel on germination and growth in tolerant and non-tolerant populations of Echinochloa colona (L.) Link. Chemosphere, 40(8), 855-859

Satpathy D, Reddy MV, & Dhal SP (2014). Risk assessment of heavy metals contamination in paddy soil, plants, and grains (Oryza sativa L.) at the East Coast of India. BioMed research international, 2014(1), 545473.

Siqueira-Silva AI, da Silva LC, Azevedo AA, & Oliva M A (2012). Iron plaque formation and morphoanatomy of roots from species of restinga subjected to excess iron. Ecotoxicology and Environmental Safety, 78, 265-275.

Subhashini V, & Swamy AV V S (2016). Efficiency of Echinochloa Colona in the removal of heavy metals from contaminated soils. International Journal of Scientific Research, 5(3), 689.

Sultana R, Kobayashi K, & Kim KH (2015). Comparison of arsenic uptake ability of barnyard grass and rice species for arsenic phytoremediation. Environmental monitoring and assessment, 187, 1-9.

USGS (2021). Mineral commodity summaries 2021: U.S. Geological Survey, 200 p., https://doi.org/10.3133/mcs2021.

Wilson B, & Pyatt FB (2007). Heavy metal bioaccumulation by the important food plant, Olea europaea L., in an ancient metalliferous polluted area of Cyprus. Bulletin of environmental contamination and toxicology, 78, 390-394.

Yoon J, Cao X, Zhou Q, & Ma LQ (2006). Accumulation of Pb, Cu, and Zn in native plants growing on a contaminated Florida site. Science of the total environment, 368(2-3), 456-464.

Zacchini, M., Pietrini, F., Scarascia Mugnozza, G., Iori, V., Pietrosanti, L., & Massacci, A. (2009). Metal tolerance, accumulation and translocation in poplar and willow clones treated with cadmium in hydroponics. Water, Air, and Soil Pollution, 197, 23-34.

Zhang W, Cai Y, Tu C, & Ma LQ (2002). Arsenic speciation and distribution in an arsenic hyperaccumulating plant. Science of the total Environment, 300(1-3), 167-177.

Ion Exchange to Recover Rare Earth Elements from Acid Mine Drainage

Elaine Cristina Batista Felipe[1], Luciano Bernado José[2], Clauson Souza[1], João Gabriel Niquini Cordeiro[1], Ana Claudia Queiroz Ladeira[1]

[1]Center for Development of Nuclear Technology, CDTN – Av. Antônio Carlos 6627, CEP 31270-901, Campus UFMG, Belo Horizonte, Brazil, ecbf@cdtn.br, clauson.souza@cdtn.br, jgncordeiroufmg@gmail.com, acql@cdtn.br

[2]Universidade Pungue, Departamento de Química, Chimoio, Manica, Moçambique, lucianobernardojose@yahoo.com.br

Abstract

Current research addresses the study of the recovery of rare earth elements from AMD using a cationic exchange resin. The AMD has a total REE concentration of 0.35 and total impurities of 7.4 mmol L^{-1} at pH 3.5. The elution was performed using 0.02 mol L^{-1} NH_4EDTA at pH 8.5 in systems with a loaded column and a fraction column connected in series. Elution was demonstrated to be selective for REE over impurities and to separate heavy REE from light REE. Oxalic acid precipitation proved to be highly efficient for the selective recovery of REE over Al.

Keywords: Cation resin, loading, elution, NH_4EDTA, oxalic acid.

Introduction

Since 2011, rare earth elements (REE) have been included in the European Commission's list of critical raw materials. These materials are essential for advancing strategic sectors such as renewable energy, electric mobility, defense, and digital technologies (Bobba *et al.* 2020). In long-term decarbonization scenarios, REE are indispensable for enabling a clean energy economy. However, the global supply chain for these elements is highly vulnerable to disruptions caused by economic fluctuations and geopolitical challenges. The concentration of REE in AMD makes it a promising alternative source for REE recovery (Moraes *et al.* 2020; Middleton *et al.* 2024).

Numerous studies have investigated the separation of REE using ion exchange, demonstrating that this method is highly effective for achieving such separations. The process can be broadly described as follows: initially, the REE is adsorbed onto the resin-packed column bed. Subsequently, an eluting solution is introduced into the column, promoting individual or grouped REE desorption. Finally, the eluted REE are collected, in fractions, from the column. Various types of resins are employed during the loading and fractionation stages. Recent research on REE recovery from AMD has highlighted the effectiveness of strong acidic resins, particularly the Lewatit MDS 200H resin, owing to its remarkable loading capacity and excellent selectivity for REE compared to other metallic impurities such as aluminum, calcium, and magnesium frequently found in AMD (Felipe *et al.* 2020; José *et al.* 2024; Silva *et al.* 2024).

The eluting solution is critical in promoting the desorption of ions bound to the resin and their fractionation. Therefore, the choice of a suitable eluent is of paramount importance. Stability constants of REE complexes with specific eluents provide valuable insights into the separation efficiency and aid in identifying the most effective eluent. For instance, EDTA and DCTA, due to their high stability constants, notably enhance the separation of REE (Dezhi 2018). This study explores the recovery of REE from an AMD through the ion-exchange process, emphasizing the elution and fractionation steps using a suitable eluent to achieve selective separation of the elements, followed by precipitation of REE oxides.

Methods

Materials: The AMD sample was provided by Indústrias Nucleares Brasileiras (INB) and was collected from a decommissioned uranium mine located in Caldas Municipality, Minas Gerais State, Brazil. Table 1 provides an overview of the REE concentrations (mmol L^{-1}) and the main metallic impurities present in the AMD. The sulfate concentration is approximately 14 mmol L^{-1} (1.3 g L^{-1}) and pH 3.5. A detailed chemical characterization of the AMD can be found in the work by José *et al.* (2024). The resin used was Lewatit MDS 200 H, a strongly acidic cation exchange resin with sulfonic acid functional groups ($-SO_3H$), supplied by Lanxess Company.

Loading experiments: The loading experiments were conducted in glass columns with an inner diameter of 11 mm, wet-packed with resin Lewatit MDS 200H to a bed volume (BV) of 8 mL (6.25 g dry basis). AMD solution containing 0.35 mmol L^{-1} of total REE and 7.4 mmol L^{-1} of total impurities was pumped through the resin at a flow rate of 0.78 ± 0.01 mL min^{-1} (residence time of 10.2 min). Samples were collected periodically by an automatic fraction collector and analyzed for chemical composition using inductively coupled plasma optical emission spectrometry ICP-OES (SPECTRO model ARCOS®).

Elution experiments: Elution was conducted with the loading and fractionation columns connected in series, wet-packed with the resin at BV of 8 mL and 15.5 mL, respectively. The fractionation column was pre-activated with 10% NH_4OH. The elution was carried out with 0.02 mol L^{-1} NH_4EDTA at pH 8.5, 25 ± 5 °C, a flow rate of 0.38 ± 0.02 mL min^{-1}, and a residence time of 21 min. Samples were collected from the effluent of the fractionation column every 45 min.

Precipitation of oxalates: The experiments were based on Nawab *et al.* (2022), which utilized 1.91 mol of oxalic acid per mole of total metals (REE + impurities) at a fixed pH of 2.5, adjusted with 10% NH_4OH. The composition of the precipitates was determined based on ICP-OES analysis (SPECTRO model ARCOS®).

Table 1 *Composition, Loading (Q) and percentage of removal of REE and Impurities from the AMD, and economic data.*

Loading Data											
	Rare Earth Elements								Impurities		
Elements	La	Ce	Pr	Nd	Sm	Gd	Dy	Y	REE_{Total}	Ca	Al	Mg
AMD Molality (mmol L^{-1})	0.22	0.01	0.02	0.05	0.007	0.003	0.003	0.04	0.35	2.8	4.3	0.31
Molar (g mol^{-1})	139	140	141	144	150	157	163	89	140	24	27	24
AMD Composition (mg L^{-1})	30.8	1.4	2.8	7.2	1.1	0.5	0.5	3.6	47.8	67.2	116.1	7.44
AMD Composition (%)	2.8	0.1	0.3	0.6	0.1	0.04	0.04	0.5	4.5	36.1	55.4	4.0
Q (mmol g^{-1})	0.174	0.005	0.012	0.032	0.004	0.001	0.001	0.022	0.25	0.79	1.71	0.15
Q (mg g^{-1})	24.17	0.70	1.69	4.62	0.60	0.16	0.16	1.96	35.10	31.66	46.14	3.65
Recovery (%)	81	71	71	81	70	58	58	65	71.2	33.0	58.0	48.0
Economic Data												
Price for metal (1) (USD/Kg)	$5.30	$5.50	$105.00	$64.50	$13.75	$25.50	$380.00	$15.00	$4.50	NC	$1.91	$2.26
Gross Values of REE in ADM (USD/1000 L)	$0.16	$0.01	$0.30	$0.47	$0.01	$0.01	$0.19	$0.05	$1.20	NC	$0.22	$0.02
Net Values of REE in ADM (USD/1000 L)	$0.13	$0.01	$0.21	$0.38	$0.01	$0.01	$0.11	$0.03	$0.88	NC	$0.13	$0.01
Net Values of REE in ADM (USD/1000 gal²)	$0.60	$0.02	$0.96	$1.71	$0.05	$0.03	$0.49	$0.16	$4.01	NC	$0.58	$0.04

(1) Prices: https://en.institut-seltene-erden.de/aktuelle-preise-von-seltenen-erden/; (2) gal (4.546L); NC - not calculated; LREE (La, Ce, Pr, Nd, Sm); HREE (Gd, Dy, Y).

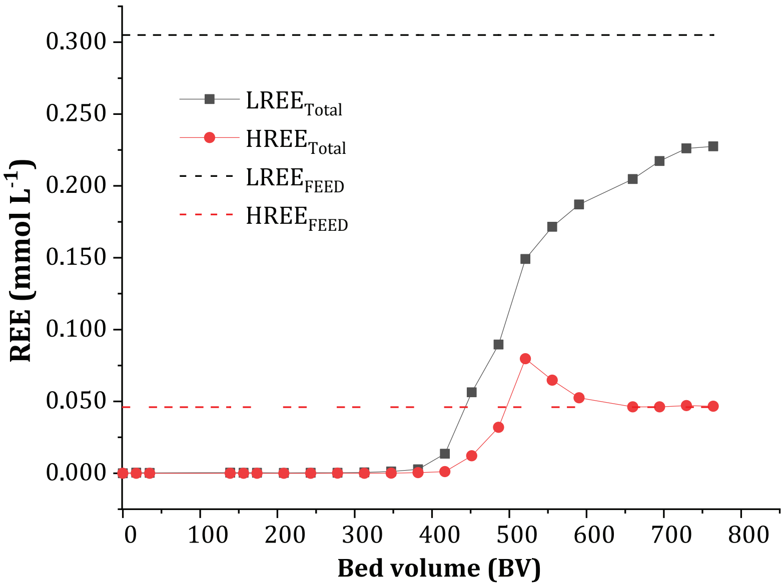

Figure 1

Results and discussion

Loading of REE and impurities

The loading (Q) for total REE after the percolation of approximately 800 BV of AMD was 0.25 mmol·g^{-1}, corresponding to 0.23 mmol·g^{-1} of light REE (LREE) and 0.02 mmol g^{-1} of heavy REE (HREE) (Tab. 1). These results indicate a high affinity of the resin for light REE over heavy REE, consistent with previous studies utilizing this resin for REE recovery from the same effluent (Felipe *et al.* 2020; José and Ladeira 2021; José *et al.* 2024). Regarding impurities, the loading amount was 2.7 mmol g^{-1}.

The loading profiles for REE were plotted based on the sum of the outlet concentrations of La, Ce, Pr, Nd, and Sm for LREE, and Gd, Dy, and Y for HREE. As previously reported, the loadings profile for LREE and HREE confirm the resin's selectivity for LREE (Fig. 1).

Valuation of AMD REE components

AMD has an estimated gross REE metal value per 1000 L of approximately US$1.20, with a recoverable metal value of around US$0.88. The extractable REE value as metals per 1000 gallons of AMD is $4.01. This value falls within the mid-range of AMD treatment costs in the U.S., which vary from US$1 to US$10 per 1000 gallons (Kefeni *et al.* 2017). These values suggest that REE present in AMD could represent a potentially viable economic resource.

Elution and fractionation of REE and impurities

The fractionation profiles of REE and impurities using 0.02 mol L^{-1} NH_4EDTA at pH 8.5 were determined (Fig. 2). It is evident that selective elution favors HREE over LREE, followed by a minor elution of aluminum. This suggests that NH_4EDTA exhibits an elution selectivity order of HREE > LREE. Several studies in the literature attribute this behaviour to the preferential formation of HREE-EDTA complexes compared to those formed with LREE (La, Ce, Pr, Nd, Sm) and impurities (Al, Ca, Mg) (José *et al.* 2024; Moore 1995).

Nd, Pr, Sm, and Ce elution occurs mainly between 10 and 20 BV, while La elutes up to 30 BV, with its maximum concentration peak at 20 BV. Calcium is eluted after all REE, in the 29 to 41 BV range. The fractions of eluate were analysed for REEs and impurities, and their composition was established (Fig 3).

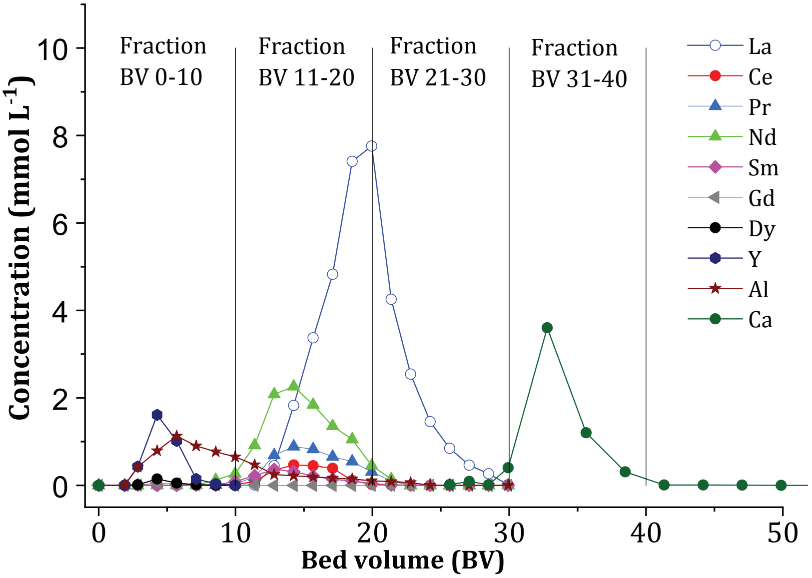

Figure 2

The composition of fraction 0–10 BV consists of 43% HREE, 4.6% LREE, and 52.4% Al (Fig. 3A). Similar to the loading column, the fractionation column activated with NH_4^+ also exhibits a preference for LREE retention over HREE retention. The fraction 11–21 BV comprises 95.5% LREE and 4.5% Al (Fig. 3B). Regarding the LRRE, La is the major component with approximately 53.5%, followed by Nd, Pr, and Sm. The fraction 21–30 BV (Fig. 3C), which concludes the elution of REE, is composed of 91.9% of La, 4.6% of (La, Ce, Nd, Pr), and 3.5% of impurities (Ca, Al). The direct comparison between the composition of the AMD and the composition of each fraction revealed that, in addition to the recovery of REE, there was separation and enrichment of heavy and light REE in distinct fractions. The composition of the last fraction, i.e., 31–40 BV, indicates an almost complete separation of Ca (Fig. 3D) from the other REE.

Each fraction of the eluate was used to produce REE oxalates through the addition of oxalic acid to one specific fraction, resulting in the formation of REE precipitates (eq. 1).

$2REE^{3+} + 3H_2C_2O_4 + 10H_2O \rightarrow REE_2(C_2O_4)_3 \cdot 10H_2O\downarrow + 6H^+$ (1)

The precipitation was carried out at pH 2.5 adjusted with NH_4OH. According to Nawab *et al.* (2022), at a pH of 2.5, REE precipitation reached 98.4%. Table 2 presents the composition of the solids obtained after precipitation. The precipitation process was more efficient for REE compared to impurities, particularly aluminum, which forms a stable soluble complex with oxalic acid ($Al(C_2O_4)_3^{3-}$ $Al(C_2O_4)_2^-$; $Al(C_2O_4)^+$).

The oxalate obtained from the fraction BV 11–20 was selected and then calcined at 900 °C. Fig. 4 presents the REE oxide obtained after calcination and its composition.

Conclusions

The findings of this work established a chemical route to selective recovery of REE from AMD. This route involves adsorption using ion exchange resin, oxalate precipitation, and calcination to produce REE oxides. The results of REE and impurity loading demonstrated higher recovery efficiency for REEs. Elution experiments using 0.02 mol L^{-1} NH_4EDTA in a column system connected in series showed selective elution of REEs over impurities. Regarding fractionation, it was

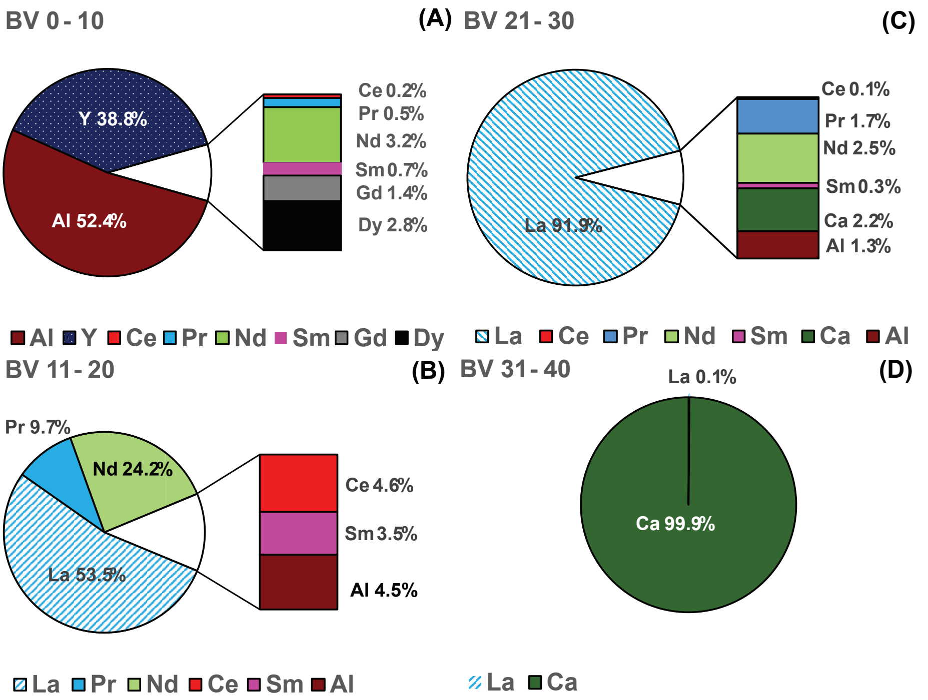

Figure 3

possible to obtain different eluate fractions, yielding distinct REE compositions in each collected fraction. Precipitation in oxalates was more effective and selective for REE, with aluminum accounting for only 5% of impurities in the REE oxalate. The precipitation of the eluate with oxalate acid increased the REE content from 47.6%, i.e., fraction 0 to 10 BV, to 99%. Results of the solids after calcination confirmed the efficiency of REE fractionation from AMD.

Acknowledgements

The authors would like to thank CNPq, FAPEMIG, FINEP, INCTAcqua, INCT-Patria, RenovaMin Project, REGINA Project, INCT-Matéria, World Bank, Unipung and MCTESTP-Mozambique, for financial support and the reviewers for the valuable suggestions.

Table 2 Composition of the precipitates obtained with oxalic acid for each fraction of the eluate.

Oxide	Composition of precipitate (%)		
	Fraction 0–10 BV	Fraction 11–20 BV	Fraction 21–30 BV
La_2O_3	0.0	53.1	94.3
CeO_2	0.7	4.9	0.1
Pr_6O_{11}	2.1	10.8	1.8
Nd_2O_3	13.4	27.4	2.6
Sm_2O_3	2.9	3.8	0.3
Gd_2O_3	6.0	0.0	0.0
Dy_2O_3	9.2	0.0	0.0
Y_2O_3	65.3	0.0	0.0
total oxide REE	99.6	99.9	99.1
Impurities	0.4	0.1	0.9

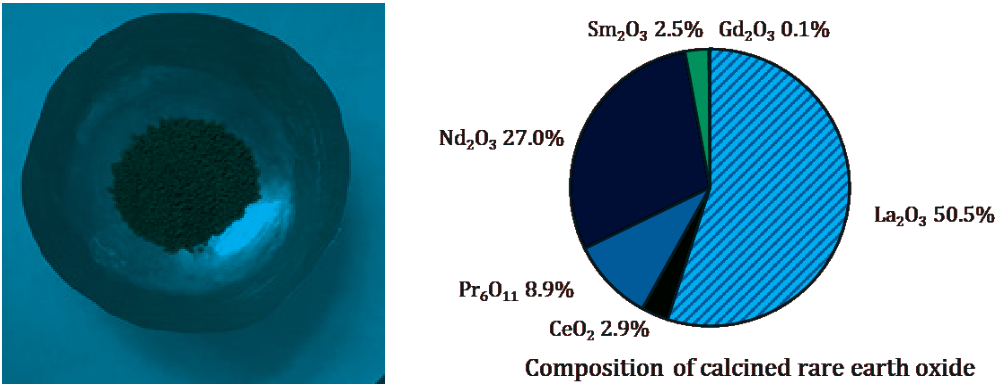

Figure 4

References

Bobba S, Carrara S, Huisman J, Mathieux F, Pavel C (2020) Critical Raw Materials for Strategic Technologies and Sectors in the EU – A Foresight Study. Publications Office of the European Union. https://www.europeansources.info/record/critical-raw-materials-for-strategic-technologies-and-sectors-in-the-eu-a-foresight-study/ Accessed 2025-01-10

Current prices of rare earths. ISE Institut Fur Seltene Erden Und Metalle AG. https://en.institut-seltene-erden.de/aktuelle-preise-von-seltenen-erden/ Accessed 2025-03-20

Dezhi Qi (2018) Ion-Exchange and Extraction Chromatography Separation of Rare Earth Elements. In: Dezhi Qi (ed) Hydrometallurgy of Rare Earths, Elsevier, 631–669

Felipe E, Batista K, Ladeira A (2020) Recovery of rare earth elements from acid mine drainage by ion exchange. Environ Technol. 42(17), 2721–2732. https://doi.org/10.1080/09593330.2020.1713219

José L, Ladeira A (2021) Recovery and separation of rare earth elements from an acid mine drainage-like solution using a strong acid resin. J. Water Process Eng. 41, 102052.https://doi.org/10.1016/j.jwpe.2021.102052.

José L, Silva G, Ladeira A (2024) Pre-concentration and partial fractionation of rare earth elements by ion exchange. Miner. Eng. 205:1–13. https://doi.org/10.1016/j.mineng.2023.108477

Kefeni K, Msagati T, Mamba M (2017) Acid mine drainage: Prevention, treatment options, and resource recovery: A review. J. Clean. Prod. 151. https://doi.org/10.1016/j.jclepro.2017.03.082.

Middleton A, Hedin B, Hsu-Kim H (2024) Recovery of Rare Earth Elements from Acid Mine Drainage with Supported Liquid Membranes: Impacts of Feedstock Composition for Extraction Performance. Environ. Sci. Technol. 2024, 58, 6, 2998–3006 https://doi.org/10.1021/acs.est.3c06445

Moraes M, Murciego A, Álvarez-Ayuso E, *et al.* (2020) The role of Al13-polymers in the recovery of rare earth elements from acid mine drainage through pH neutralization. Applied Geochemistry. 113. 104466. 10.1016/j.apgeochem.2019.104466.

Moore BW (2000) Selective Separation of Rare Earth Elements by Ion Exchange in an Iminodiacetic Resin. US Patent 6,093,376, 25 July 2000.

Nawab A, Yang X, Honaker R (2022) Parametric study and speciation analysis of rare earth precipitation using oxalic acid in a chloride solution system. Miner. Eng. 176, 107352. https://doi.org/10.1016/j.mineng.2021.107352.

Silva G, Souza C. Ferreira P, Ladeira A (2024) Effect of fractionation columns on the elution of rare earth elements recovered from acid mine drainage. Minerals. 14(4), 451. https://doi.org/10.3390/min14050451

The Indicative Significance of Sulfate and its Stable Isotope to Antimony in the Water and Soil System of Xikuangshan Mining Area in Hunan Province

Chenxin Feng[1], Jianwei Zhou[1], Xingjie Wang[2], Peng Liu1, Wanyu Li[1], Xueyan Pang[1]

[1]*School of Environmental Studies, China University of Geosciences, Wuhan, China, fcxaptx4869@163.com, jw.zhou@cug.edu.cn, pengliu@cug.edu.cn, wy_li@cug.edu.cn, x8pang@uwaterloo.ca*

[2]*Institute of Geological Survey, China University of Geosciences, Wuhan, China, Wangxingjie@cug.edu.cn*

Abstract

Sulfate has important indicative significance for the environmental behavior of antimony (Sb). Using sulfur and oxygen isotopes, combined with the valence state test of antimony, the groundwater of Xikuangshan in Hunan Province was analyzed. The results show that 50–75% of the $\delta^{18}O$ in groundwater and surface water comes from water, and the $\delta^{18}O$ in mine water mainly comes from sulfate. As sulfate concentration increased, the Sb(III)/Sb(total) ratio rose from 2.39% to 88.63%, and antimony is more sensitive to the response mechanism of endogenous sulfate. This research offers new insights for preventing groundwater antimony pollution.

Keywords: Migration and transformation, water environment, sulfate, stable isotope, valence state analysis

Introduction

Hunan Xikuangshan in China is the world's largest antimony deposit, known as the 'antimony capital of the world'. Nearly a hundred years of mining activities have caused a series of mine geological environment problems, among which the problem of antimony pollution in groundwater and other water environment is particularly prominent (Jia *et al.*, 2022; Jia *et al.*, 2024; Zhou *et al.*, 2022;Zhou *et al.*, 2024a).

However, the source of Sb in the water environment and its migration and transformation are very complex processes, and traditional hydrogeochemical methods such as hydrochemistry are difficult to study in depth and systematically (Wen, 2017; Li *et al.*, 2022; Zhou *et al.*, 2023). Therefore, the selection of typical isotope tracers based on the geological characteristics of the Xikuangshan deposit and the biogeochemical behavior of antimony is a necessary means to study the source, migration and transformation process of antimony in the water environment of the Xikuangshan deposit. Antimony minerals in Xikuangshan are mainly stibnite (Sb2S3) (Zhou *et al.*, 2024b; Jia *et al.*, 2023). Sulfur is the main associated element of antimony minerals in Xikuangshan. The oxidation of sulfide minerals (stibnite) will release a large amount of SO_4^{2-} into the water body. Therefore, the sulfur and oxygen isotopes of sulfate are the direct media to study the source and migration and transformation process of Sb in the water environment of Xikuangshan.

Methods

The hydrochemical data obtained in the process of this study are derived from the field collection work in 2024, including groundwater (spring) samples and surface water (ore-bearing drainage) samples, which are strictly preserved in accordance with the sampling requirements and tested and analyzed in the first time. Among them, the analysis and test of anion and cation and antimony valence state were tested by the laboratory, and the stable isotopes $\delta^{2}H_{H2O}$, $\delta^{18}O_{H2O}$, $\delta^{34}S_{SO4}$ and $\delta^{18}O_{SO4}$ were tested by the State Key Laboratory of Biogeology and Environmental Geology of China University of Geosciences (Wuhan).

Results and Discussion

The $\delta^{34}S_{SO4}$ values of mine drainage ranged from −7.29‰ to +7.86‰, with an average of +6.2‰, and the $\delta^{18}O_{SO4}$ values ranged from +1.1‰ to +11.1‰, with an average of +6.2‰. The $\delta^{34}S_{SO4}$ values of groundwater ranged from-3.10‰ to +7.82‰, with an average of +3.79‰, and the $\delta^{18}O_{SO4}$ values ranged from +2.1‰ to +5.8‰, with an average of +3.5‰. The $\delta^{34}S_{SO4}$ values of surface water ranged from -8.04‰ to +3.56‰, with an average of 0.0‰, and the $\delta^{18}O_{SO4}$ values ranged from +1.4‰ to +5.1‰, with an average of +3.8‰ (Fig. 1a). Both surface water and groundwater are controlled by sulfate oxidation, and part of the mine drainage is distributed around atmospheric precipitation, which is presumed to be directly recharged by atmospheric precipitation. It can be seen from Fig. 1b that 50–75% of $\delta^{18}O$ in groundwater and surface water comes from water. However, two sets of data in mine drainage show that only 0–25% of $\delta^{18}O$ comes from water, mainly from sulfate, which indicates that the formation process of mine drainage is mainly controlled by the oxidation process of stibnite, and the $\delta^{18}O$ of other mine drainage is in the range of 50–75% H_2O, indicating that the formation process of mine drainage is affected by atmospheric precipitation leaching.

Through sulfur and oxygen isotopes, it is found that the hydrochemical samples in the study area are mixed by background surface water, atmospheric precipitation and ore-bearing groundwater (Fig. 2). Further analysis of the three-end element mixing ratio of different types of water shows that the contribution of atmospheric precipitation is higher in TG and XG than in BG. It's due to the aquifer in the Batangshan River Basin belongs to the limestone layer, the core is relatively complete, and the cracks are not developed. The aquifer in the Tanjiaxi River Basin belongs to the siliceous limestone layer, and the karst is more developed. The aquifer in the Xuanshan River Basin is argillaceous limestone layer, which is easier to be eroded, so that the atmospheric precipitation in the Tanjiaxi and Xuanshan River basins can enter the aquifer faster to form a recharge. XR receives 61% of the upstream background value, mainly receiving upstream water supply, and is weakly recharged by atmospheric precipitation and groundwater lateral runoff. On the contrary, the contribution of atmospheric precipitation to the TR is as high as 80%, and the contribution of the upstream background value is only 6%. It shows that the slope confluence process of atmospheric precipitation has a great influence on the water body during the runoff process of Tanjiaxi, and the water body has changed

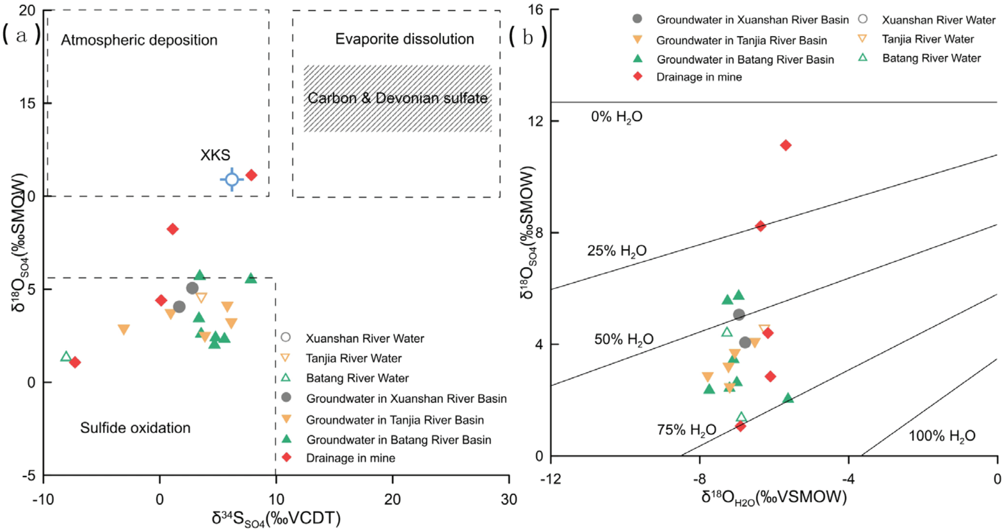

Figure 1 $\delta^{34}S_{SO4}$–$\delta^{18}O_{SO4}$*(a) and* $\delta^{18}O_{H2O}$–$\delta^{18}O_{SO4}$ *(b) correlation diagram(Li* et al.*, 2022).*

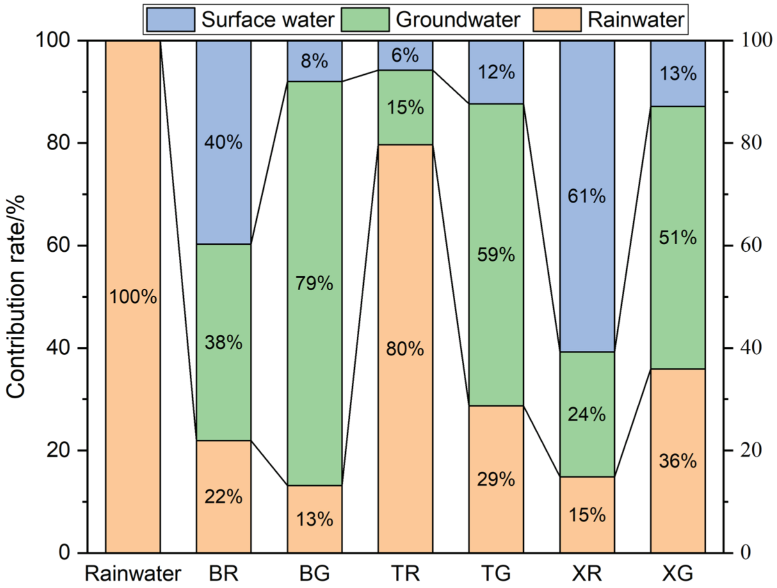

Figure 2 The contribution of three endmembers (background surface water, atmospheric precipitation and ore-bearing groundwater) in different types of water (BR - Batangshanxi River, BG – Batangshanxi Groundwater, TR- Tanjiaxi River, TG – Tanjiaxi Groundwater, XR – Xuanshan River, XG – Xuanshan Groundwater).

greatly during the runoff process.

By analyzing the correlation between the ratios of the main ions, the source of the leaching effect experienced during the formation of the water body can be identified, as shown in Fig. 3. The surface water and groundwater in the study area are closer to the mixing of carbonate rocks and evaporite rocks. It is worth noting that 80% of the contribution of TR comes from atmospheric precipitation. In addition to direct recharge, the more important process of atmospheric precipitation recharge to surface water is slope confluence. This process occurs on the surface so that the slope confluence can take away part of the evaporated salt formed on the surface of the slope, making TR closer to the dissolution of evaporated salt rock. The drainage formation process is not entirely a natural process, and is greatly affected by human activities. Therefore, it is not completely controlled by three types of rock salt.

When we shifted the research question from how groundwater is formed to how antimony is released and migrated during the formation of groundwater, we began to explore the migration process of antimony by exploring the changes of antimony and related parameters along the runoff path. In Fig. 4a of the TR, the source is characterized by high antimony (Sb) concentrations and a certain degree of reducing properties due to the influence of waste dumps and extensive livestock breeding by surrounding residents. During the runoff process, the antimony is gradually diluted and oxidized. However, after passing through TJ3, a direct discharge of high Sb-containing water occurs, which leads to an increase in antimony concentration in the river. The characteristics of XR are quite different from those of TR (Fig. 4b). Since the aquifer in the Xuanshan River Basin does not contain ore-bearing layers and there is no slag heap in the upstream, the concentration of antimony in the upstream section is extremely low. After flowing through XS5 (a large tailings reservoir nearby), the concentration of antimony increased significantly. In order to further confirm the impact of the tailings pond on the river, we tested the water directly discharged from the tailings pond into the river. A large amount of polyferric sulfate (PFS) was added to make the antimony concentration

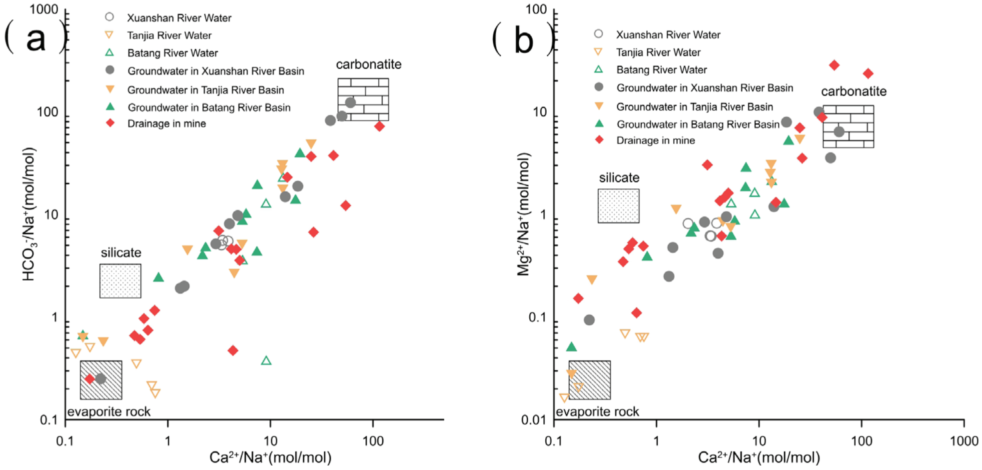

Figure 3 The relationship between different types of rocks and the main ion types of groundwater(a–γ(HCO_3^-/Na^+)-γ(Ca^{2+}/Na^+), b-γ(Mg^{2+}/Na^+)-γ(Ca^{2+}/Na^+)).

lower than 0.5 mg/L, and the whole was in an acidic anaerobic environment, indicating that the tailings pond can cause a large amount of antimony to enter the water environment through other ways besides direct discharge, such as atmospheric precipitation leaching, bottom leakage and other uncontrollable ways.

Atmospheric precipitation recharge, slag heap leaching and antimony-containing wastewater recharge need to be considered in the process of surface water runoff, while the reason for the increase of antimony in the process of groundwater runoff is relatively simple. It is usually due to the oxidation of stibnite in the aquifer during the groundwater runoff process through the silicified limestone section of the ore-bearing layer-Shetianqiao Formation, which causes a large amount of antimony to be transformed into free state and enter the groundwater. This is the case for TG and BG (Fig. 4d, e). In this process, in addition to the increase of antimony concentration, sulfate concentration and $\delta^{34}S_{SO4}$ will also increase, which is due to the large amount of SO_4^{2-} produced during the oxidation of stibnite. However, the increase of antimony concentration in XG does not belong to this situation. Considering that

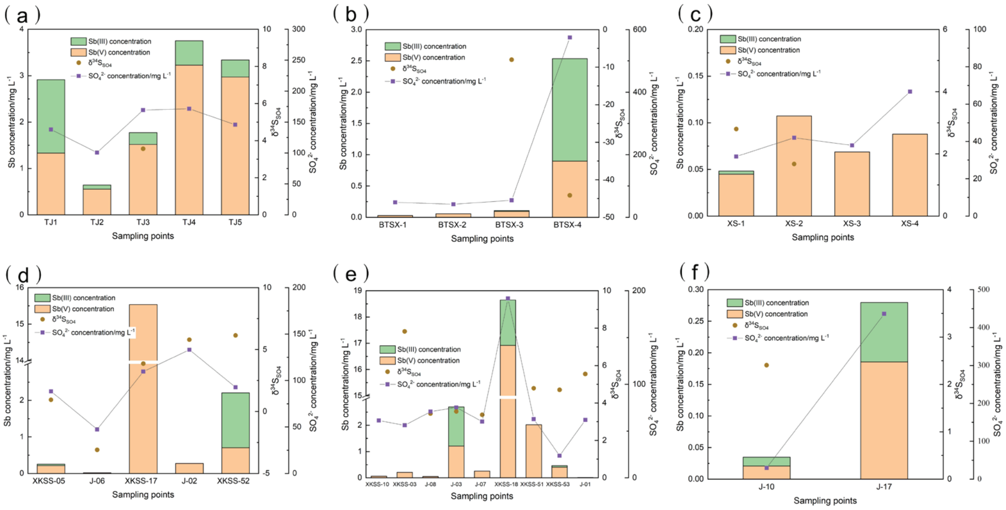

Figure 4 The change process of antimony, sulfate and $\delta^{34}S_{SO4}$ along the runoff path (a-TR, b-BR, c-XR, d-TG, e-BG, f-XG).

J17 is located not far downstream of XS5, it is speculated that the increase of J17 concentration is affected by the tailings pond, or there is an interaction process between surface water and groundwater, which is affected by the high antimony surface water downstream of XR.

We define the sulfate produced during the oxidation of stibnite as the endogenous sulfate produced by the hydrochemical process in the aquifer, and the sulfate injected into the PFS agent to regulate the Sb concentration in the water body is defined as the exogenous sulfate caused by human activities. Due to the strong correlation between endogenous sulfate and exogenous sulfate and the migration and transformation process of Sb, there is a certain relationship between the occurrence form of Sb in water and the concentration of sulfate. The specific performance is that with the increase of SO_4^{2-}concentration, the ratio of Sb (III)/Sb(V) in the water body increases, the proportion of Sb (III) in the water is higher, and the water body is more inclined to the reducing environment. The variation of Sb(III)/Sb(V) in groundwater (under the control of endogenous sulfate) is more sensitive to the nonlinear response trend of SO_4^{2-}concentration change than that in mine drainage and surface water (under the control of exogenous sulfate). However, this can only show that there is a strong correlation between sulfate and the occurrence of antimony, and it is not enough to show that sulfate can affect the occurrence of antimony in water, which needs further research to confirm.

Based on the content described above and previous research, the conceptual model of antimony migration and transformation on the two-dimensional profile of the study area was optimized(Wen, 2017). After atmospheric precipitation, slag heap leaching occurs on the surface, which causes antimony to dissolve from the solid phase medium and enter the surface water for migration. The underground aquifer can accept part of the antimony released by the slag heap leaching carried by the infiltration of atmospheric precipitation, and more of it comes from the oxidation of stibnite to directly produce free antimony. In the process of migration, the occurrence form of antimony changes with the change of redox conditions.

Conclusions

The formation process of groundwater in the study area is controlled by the lithology of the aquifer. The lithology of the Batangshan River Basin is relatively complete, and it is basically not recharged by surface water and atmospheric precipitation. The Tanjiaxi and Xuanshan River Basins are able to receive atmospheric precipitation recharge. The formation process of surface water is mainly affected by the upstream background surface water and atmospheric precipitation. The water of the Xuanshan River is mainly recharged by the upstream

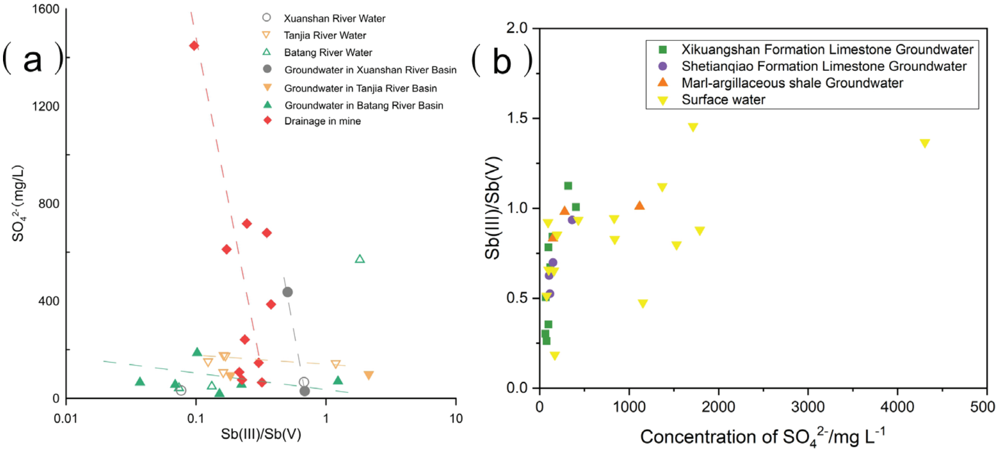

Figure 5 *Synergistic relationship between sulfate and Sb(III)/Sb(V) in water(a-groundwater in different basins,b-groundwater from different aquifers).*

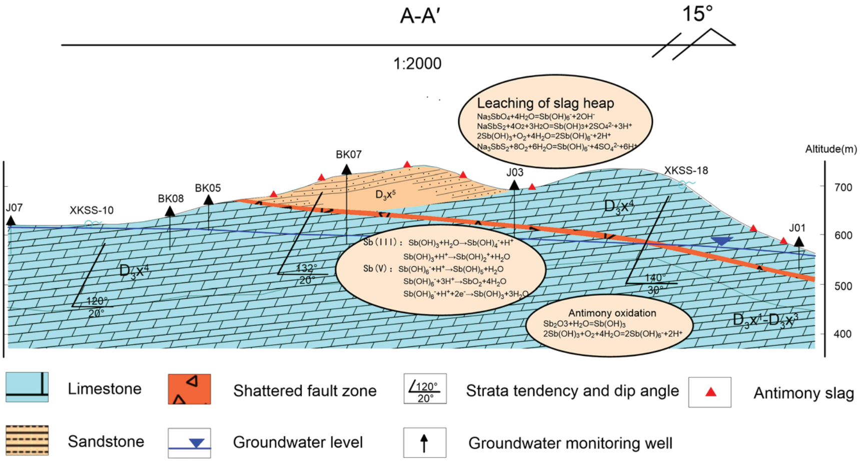

Figure 6 *Conceptual model of antimony migration and transformation in tin mine.*

water, while the Tanjiaxi River is recharged by the slope confluence of atmospheric precipitation. During the recharge process, the slope confluence can leach part of the surface evaporation salt, which makes the ion composition of the Tanjiaxi River closer to the end member of the evaporation salt rock.

In the process of surface water runoff, the concentration of antimony can be increased by the direct supply of external high antimony water or the interaction process of surface water and groundwater. In the process of groundwater runoff, the channel for the release of antimony is usually the oxidation of stibnite. The solid phase Sb_2O_3 is oxidized to free antimony and enters the aquifer. In this process, a large amount of SO_4^{2-} is produced, which increases the sulfate concentration and a. The source analysis of sulfur and oxygen isotopes on the drainage of high antimony ore also confirms this conclusion.

In the process of groundwater migration, the valence state of sulfate and antimony showed a high degree of regularity, and the fluctuation of antimony valence state in summer was more intense in response to sulfate concentration. Further study of the effect of sulfate sources on antimony found that Sb(III)/Sb(V) was 91.91% and 59.28%, respectively, at high endogenous sulfate concentration and high exogenous sulfate concentration, indicating that the valence state of antimony was more sensitive to the response of endogenous sulfate.

Acknowledgements

This research was supported by the National Key R&D Program of China (2022YFC3702203), The stable isotope correlation test was completed by the State Key Laboratory of Biogeology and Environmental Geology, China University of Geosciences (Wuhan).

References

Jia X, Kaufmann A, Lazarov M, Wen B, Weyer S, Zhou J, Ma L and Majzlan J (2024) Antimony Isotope Fractionation during Kinetic Sb (III) Oxidation by Antimony-Oxidizing Bacteria Pseudomonas sp. J1. Environ Sci Technol doi:10.1021/acs.est.3c10271

Jia X, Ma L, Liu J, Liu P, Yu L, Zhou J, Li W, Zhou W and Dong Z (2022) Reduction of antimony mobility from Sb-rich smelting slag by Shewanella oneidensis: Integrated biosorption and precipitation. J Hazard Mater 426, 127385, doi: 10.1016/j.jhazmat.2021.127385

Jia X, Majzlan J, Ma L, Liu P, Fan P, Li W, Zhou J and Wen B (2023) Novel insights into the mechanisms for Sb mobilization in groundwater in a mining area: A colloid field study. J Hazard Mater 459, 132212, doi:10.1016/j.jhazmat.2023.132212

Li X, Pan G, Zhou A, Fang L and He N (2022) Stable sulfur and oxygen isotopes of sulfate as tracers of antimony and arsenic pollution sources related to antimony mine activities in an impacted river. Appl Geochem 142, 105351 doi:10.1016/j.apgeochem.2022.105351

Zhou W, Liu P, Ye Z, Wen B, Beckie RD, Zhou A, Zhou Z and Zhou J (2024a) Antimony mobility in soil near historical waste rock at the world's largest Sb mine, Central China. Sci Total Environ 921, 171194, doi: 10.1016/j.scitotenv.2024.171194

Zhou W, Liu P, Zhou J, Liu J, Wang C, Mu H, Jia H and Zuo J (2024b) Characteristics and environmental significance of sulfur isotope signatures in the water environment of typical pyrite mines. J Environ Sci doi: 10.1016/j.jes.2023.12.012

Zhou W, Zhou A, Wen B, Liu P, Zhu Z, Finfrock Z and Zhou J (2022) Antimony isotope fractionation during adsorption on aluminum oxides. J Hazard Mater 429, 128317 doi:10.1016/j.jhazmat.2022.128317

Zhou W, Zhou J, Feng X, Wen B, Zhou A, Liu P, Sun G, Zhou Z and Liu X (2023) Antimony isotope fractionation revealed from EXAFS during adsorption on Fe (oxyhydr) oxides. Environ Sci Technol 57(25), 9353–9361, doi:10.1021/acs.est.3c01906

Wen B (2017) Implications of isotope for sources, migration and transformation of antimony in the water environment of the Xikuangshan, Hunan. China University of Geosciences, Wuhan. PhD dissertation (in Chinese).

.

Cyanide and Metal Removal from Gold Cyanidation Effluents

Linda A. Figueroa[1], Inge Delius[2], Christopher Bellona[3]

[1]Department of Civil and Environmental Engineering, Center for Mining Sustainability, Colorado School of Mines, Golden, Colorado, 80401 lfiguero@mines.edu, ORCID 0000-0003-3588-6705

[2]Department of Civil and Environmental Engineering, Center for Mining Sustainability, Colorado School of Mines, Golden, Colorado, 80401 ideliuscordova@mines.edu, ORCID 0000-0002-8185-3712

[3]Department of Civil and Environmental Engineering, Center for Mining Sustainability, Colorado School of Mines, Golden, Colorado, 80401 cbellona@mines.edu, ORCID 0000-0003-3366-3559

Abstract

Gold cyanidation effluent often contains high levels of cyanide and metals. While removal in synthetic water is well demonstrated, real process water introduces complexities that need further study. Batch tests with process waters from three Peruvian sites evaluated an electrochemical approach for contaminant removal. Cyanide destruction was two orders of magnitude slower in real water, and copper removal varied with water composition. The results underscore the need to understand process water chemistry to create a reliable treatment design framework. Additional research is essential for optimizing cyanide and metal removal in practical applications.

Keywords: Copper, metal cyanide complex, electrochemical treatment, process water chemistry

Introduction

Cyanide is commonly used in the mining industry to extract gold from gold-bearing ores, particularly low-grade ores where gold cannot be extracted through processes such as crushing and gravity separation. Cyanidation is the most common lixiviant for gold extraction and is added in excess. At alkaline pH, the cyanide ion (CN^-) dissolved the gold contained in the ground ore under mildly oxidizing conditions by forming water soluble gold-cyanide complexes such as $NaAu(CN)_2$. After recovery of the gold cyanide complex, the remaining process water (barren solution) contains the excess cyanide and metals extracted from the gold ore.

Cyanide discharge standards vary with the receiving environment. The International Cyanide Management Code has designated a limit of 50 mg/L in process water storage facilities. In the US, pretreatment standards for discharge into a publicly owned treatment works is 1.2 mg/L. Additional, drinking water and aquatic limits are 200 ppb and 50ppb, respectively. Copper and Zinc are the major metals observed in cyanidation process waters. Drinking water limits for copper and zinc are relatively high, 1 mg/L and 5 mg/L, respectively. Aquatic limits on copper and zinc are the primary drivers of treatment. Specific values depend on the discharge and receiving water chemistry. Copper limits are on the order of 10 of mg/L with zinc limits on the order of 100 mg/L. The release or reuse of barren solutions from gold cyanidation processing requires reduction of the cyanide and metals to discharge standards.

Electrochemical oxidation of cyanide along with the formation of copper and zinc solid phases has the potential to meet the treatment goals without chemical addition. Investigations with synthetic waters have demonstrate the ability to concurrently removal both contaminants. However, real process waters introduce complexities that require further investigation (Sierra-

Alvarado *et al.* 2022). Batch tests with process waters from three Peruvian sites evaluated an electrochemical approach for contaminant removal.

Methods

Real process wastewater samples came as barren solutions from three different small gold processing facilities in the Arequipa region of Peru. These waters were transported to the lab facility in Arequipa for electrochemical experiments. The initial pH of real wastewater solutions was adjusted and throughout the experiments maintained at approximately 11.5 by addition of 1M NaOH to avoid release of HCN gas. Each experimental condition was implements over a 2-day period. Ten experimental conditions in all were evaluated, only experiments where pH 11.3–11.5 was maintained were assessed, Tab. 1.

Experiments were carried out in a 1L beaker which worked as the electrolytic cell. The pH and temperature of the water were measured using a pH meter equipped with a temperature probe (Thermo Scientific Orion model 520A and 420A+) which was suspended by a swing arm electrode holder. Electrical power was supplied using a DC Power Supply made by EXTECH (model 382202, 0 to 18V, 0 to 3A). The beaker was placed on a magnetic stirring plate to keep the solution well mixed throughout the experiment. The anode was composed of pure graphite plate sheets while the cathode was composed of pure copper sheets. All experiments were carried out at ambient temperature, 20 ± 2°C. The electrode cross sectional area was approximately 15×3 cm with a 3mm width for graphite sheets and 1mm width for copper sheets. The electrodes were held at about 3cm from each other. The submerged area of the electrodes in the solution was 19.5 cm^2.

The current efficiency describes the efficiency in which electrons are transferred in an electrochemical system to facilitate a reaction. To calculate current efficiency (E_C), the number of Coulombs used by the reaction of interest is divided by the total number of Coulombs available in the electrochemical system.

$$E_C = \frac{Coulombs\ used\ by\ reaction\ of\ interest}{Available\ Coulombs} \times 100$$

The current efficiency for cyanide, copper and zinc reactors were based on the stoichiometries shown below (Marsden 2006).

$CN^- + 2OH^- \rightarrow CNO^- + H_2O + 2e^-$

$Cu^+ + e^- \rightarrow Cu$

$Zn^{2+} + 2e^- \rightarrow Zn$

Results and Discussion

Samples were collected at the beginning and end of each experiment. The initial measured concentrations varied some with each experiment conducted. The average values for each site are presented in Tab. 2. Cyanide, copper and zinc removal are shown along with the current efficiency in Tab. 3. Initial and final molar concentrations of the different forms of cyanide along with copper and zinc are shown in Fig. 3.

Reduction of all cyanide forms and metals was higher at 5V applied compared to the application of 2V. In experiments with synthetic water, copper removal is higher at lower voltages (Felix-Navarro 2003). Lower removal of cyanide and metals were observed at 2V for Site 1 relative to Site 2. The metal-cyanide complex concentrations were double the values at Site 1. Concurrent destruction of free and WAD cyanides was observed at 5V for all sites and at 2V for Site 1. However, only free cyanide destruction was observed

***Table 1** Experiments conditions for real process water samples.*

Experimental Condition	Site	Voltage	pH	Conductivity (mS/cm)
1	1	2	11.5	13.3
2	1	5	11.5	
3	1	5	11.5	
4	2	2	11.3	5.0
5	2	5	11.4	
6	3	5	11.5	24.5

Table 2 *Average values for real process water samples.*

Component	Site 1	Site 2	Site 3
Initial pH	10.8	11.3	9.7
WAD+Free Cyanide	1180	2390	2290
Total Cyanide	1440	2670	2780
Free Cyanide	790	1530	1510
Cl^-	820	680	20500
NO^{3-}	130	60	540
NO^{2-}	220	100	120
SO_4^{2-}	6000	4500	13800
PO_4^{3-}	90	190	0
Ca	1030	1610	1920
Na	4950	3190	15200
Sr	10	10	120
K	170	290	360
Si	210	230	220
Zn	130	620	150
Mg	240	240	470
Fe	10	20	2
Cu	230	180	580
As	12	1	4

Table 3 *EPercent of cyanide and metal removal and current efficiency.*

	% removal				% current efficiency		
ID	Free CN	WAD CN	Copper	Zinc	Free CN	Cu	Zn
Site 1@5V	90	92	96	73	14	1	1
Site 1@ 2V	45	60	69	69	71	4	4
Site 2@5V	59	58	67	45	32	1	4
Site 2@2V	11	0	0	0	82	0	0
Site 3@5V	86	79	94	0	98	9	0

for Site 2 at 2V. Additional investigation is needed on the impact of metal cyanide complexes concentrations at low and high applied voltages.

Current efficiency results are consistent with the hierarchy of electro potential of the reactions: Cyanide > Copper > Zinc. Site 3 process water current efficiency was 100% for the observed removals. A longer reaction time may have resulted in subsequent zinc removal when additional electrons (current) are provided. Copper and zinc removals greater than 65% and 40%, respectively were observed when current efficiency was 20–80%. Higher removal of the cyanide and metals at current efficiencies < 100% may still require longer reaction times if the limitation is kinetic.

Conclusions

The effects of applied voltage, initial cyanide and copper concentrations and composition of the electrolyte on the degradation rates of cyanide and removal of metals from real gold cyanidation wastewater were studied. In general, cyanide degradation rates

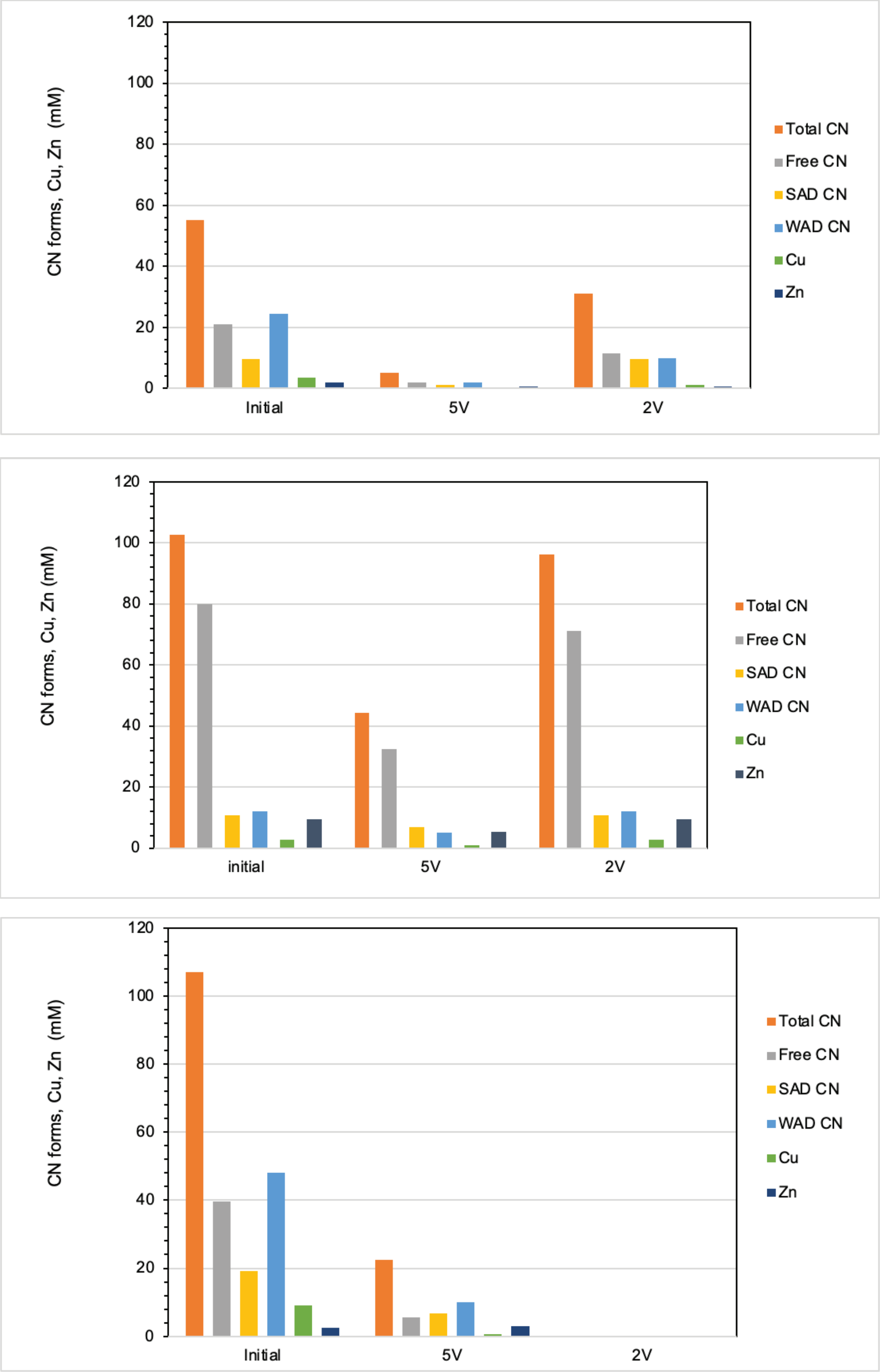

Figure 1 *Initial and final concentrations of cyanide and metals from the field sites: (a) Site 1, (b) Site 2 and (c) Site 3 (no data at 2V).*

increased with conductivity and higher applied voltages. Real wastewater contained additional constituents and higher the rate of cyanide degradation had more complex relationships with voltage and conductivity than observed in studies with synthetic waters. In process wastewater, more metal removal occurred at higher applied voltage which is opposite compared to synthetic waters. Zinc and copper were the only metals removed from process wastewater during the electrochemical experiments. Real wastewater with the highest measured conductivity removed over 90% copper and 80% cyanide at 5 V. Additional work is needed with real gold cyanidation process wastewater to determine optimal conditions based on water composition.

Acknowledgements

The authors thank our collaborators from the Center for Mining Sustainability affiliated with the Colorado School of Mines and the Universidad Nacional de San Agustín de Arequipa.

References

Felix-Navarro RM, Lin SW, Castro-Ceceña AB, Casco-Carrete JA (2003) Cyanide destruction and simultaneous recovery of copper with an electrochemical reactor. J Electrochem Soc 150(8): D149. https://doi.org/10.1149/1.1590994

Marsden, MO (2006) The chemistry of gold extraction, SME, CO.

Sierra-Alvarado EG, Valle-Cervantes S, Lucho-Chigo R, Rodríguez-Rosales MDJ, Rojas-Montes JC, Fuentes-Aceituno JC, Martínez-Gómez VJ (2022) A kinetic-mechanistic study of cyanide degradation which can be contained in mining tailings dams using a divided electrolytic cell. Minerals Engineering 188:107833. https://doi.org/10.1016/j.mineng.2022.107833

Multi-Scale Characterization of Mine Waste in a Circular Economy: Challenges and Opportunities

Hernan Flores[1,2], Tobias Rudolph[1], Jörg Benndorf[2]

[1]*Research Center of Post-Mining (FZN), Technische Hochschule Georg Agricola (THGA), Herner Straße 45, 44787 Bochum, Germany*

[2]*Department of Mine Surveying and Geodesy, TU Bergakademie Freiberg, Fucksmühleweg 9B, 09599 Freiberg, Germany; Correspondence author: hernan.flores@thga.de*

Abstract

The growing demand for critical raw materials (CRMs) for a climate-neutral economy has intensified challenges in waste generation and management. Traditional mine waste characterization, focused on environmental risk assessment within a linear economy framework ("take-make-dispose"), contrasts with the circular economy approach ("make-use-return"), which aims to minimize waste and recover valuable materials. However, unlocking the potential of mine waste requires robust, multi-scale characterization techniques. In this study, we review multi-scale characterization protocols to assess mine waste streams in support of a circular economy. In particular, we highlight the use of hyperspectral imaging as a key monitoring technique, enabling the semi-quantitative assessment of hydrogeochemical parameters and metals in mine water, identification of mineral associations in waste rock, and mapping of metal concentrations in tailings. Although challenges remain regarding sensor sensitivity, cost, and large-scale integration, addressing limitations and improving on standardization of such advanced monitoring tools can enhance mine waste management by improving environmental risk monitoring and enabling resource recovery.

Keywords: Mine waste, hyperspectral imaging, remote sensing, unmanned aerial system, tailing ponds, post-mining

Introduction

The European Union's ambition to achieve a climate-neutral economy by 2050, sustain green and digital transitions, and ensure strategic autonomy hinges on reliable, secure, and resilient access to critical raw materials (CRMs) (Ragonnaud 2023). CRMs, while not inherently scarce, are of immense economic importance for key industries. However, they face significant supply risks due to dependence on imports and a lack of viable substitutes. The growing demand for digital and green technologies has further intensified the focus on CRMs, leading to an expansion of the official list of these materials (European Commission, 2018). To meet global climate goals, mineral production may need to increase by nearly 500% by 2050 (Hund *et al.* 2020). Yet, Europe's limited mining activity for CRMs contrasts with its abundance of active and abandoned mines for other minerals. These large volumes of waste – such as waste rock, tailings, slurry ponds, and metallurgical residues – are often heterogeneous in composition and properties (Hudson-Edwards *et al.*, 2011) and are typically discarded as non-valuable, yet they may contain significant amounts of valuable CRMs (such as rare earth elements, lithium, and cobalt ore (Tayebi-Khorami *et al.* 2019)). This presents a unique opportunity to address supply challenges by revalorizing mining waste within a circular economy framework.

The transition from a linear economy model ("take, make, dispose") to a circular economy ("make, use, return") offers a transformative approach to mine waste management. In this framework, waste is minimized, and materials are continuously reintegrated into production cycles. Mining, traditionally seen as a resource-intensive industry, has the potential to play a pivotal role in advancing circular economy principles by recovering valuable materials from waste streams and reducing environmental liabilities(Schreck and Wagner 2017). Despite this possibility, the management of mine waste remains a significant challenge. Incomplete or inadequate mine closure practices can lead to severe environmental impacts, underscoring the need for improved understanding of the chemical and physical properties of mine waste. Without this knowledge, engineering solutions for waste containment and rehabilitation are likely to fail (Jamieson *et al.* 2015). Multi-scale characterization techniques, such as remote sensing, hyperspectral imaging, and geophysical methods offer promising solutions for mine waste management. However, their implementation is often limited by high costs associated with advanced sensor technologies and data processing. Early integration of these techniques throughout the mining cycle is essential for mitigating environmental risks, optimizing waste management, and advancing circular economy principles in CRMs recovery.

Methodology

In this work we explore a set of monitoring tools to characterize mine waste across different dimensions. We review innovative and sensor technology at different scales, highlighting their limitations, uncertainties, and the need for improved standardization and integration of such advanced monitoring techniques in mining operations to enhance environmental risk monitoring and enable resource recovery. Specifically, we summarize how hyperspectral imaging serves as a key technique due to its versatility and multi-scale adaptability, and show case studies that demonstrate their advantages when monitoring different mine waste constellations: semi-quantitative assessment of hydrogeochemical parameters and metals in mine water, identification of mineral associations in waste rock, and mapping of metal concentrations in tailings. A comprehensive characterization approach that requires the integration of macro, meso, and micro-scale methodologies, each providing different levels of detail (Fig. 1).

At the macro scale, large-scale monitoring techniques such as satellite imagery and airborne remote sensing enable the assessment of waste deposits and their environmental impacts. The meso scale involves site-specific assessments using drone-based hyperspectral imaging and geophysical methods to achieve detailed surface and subsurface characterization. Finally, at the micro scale, high-resolution laboratory techniques allow for the precise analysis of mineralogical, geochemical, and metallurgical properties, providing critical insights into material composition and resource recovery.

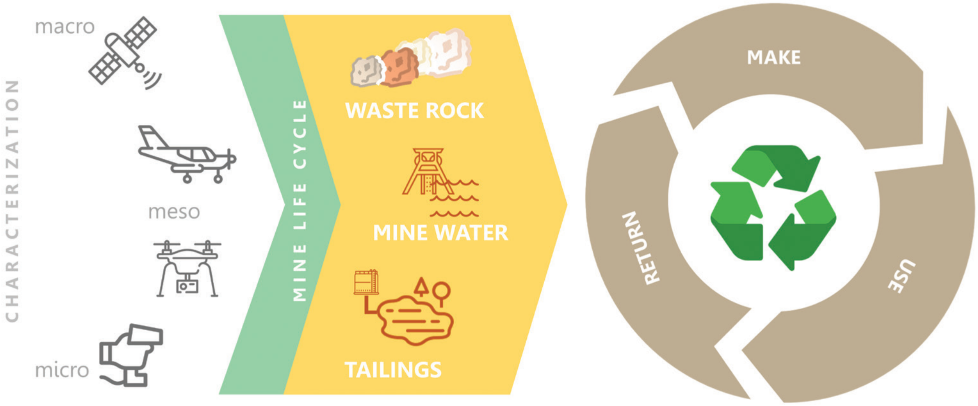

Figure 1 *Schematic concept of multi-scale characterization of mine waste constellations to support a circular economy.*

Macro Scale Approaches: Remote Sensing and Regional Assessments

Due to the extensive nature of mine waste, remote sensing technologies provide essential large-scale monitoring capabilities. Satellite sensors has proven effective for environmental monitoring, with hyperspectral sensors enabling the detection of metal-bearing minerals indicative of contamination. Studies have demonstrated the feasibility of using spectroscopy for detecting iron-bearing minerals in mining areas (Swayze *et al.* 2000) and for identifying acid-generating waste rock to protect water resources (Montero *et al.* 2005). More recently, hyperspectral airborne sensors have been applied to map tailings and waste materials, focusing on minerals responsible for acid formation and secondary mineral distribution (Khosravi *et al.* 2021). Reflectance spectroscopy techniques have been used to assess environmental pollution based on the presence of minerals such as jarosite, ferrihydrite, and goethite/hematite (Choe *et al.* 2008). Additionally, large-scale remote sensing studies have categorized over 1,000 waste rock dumps and tailings storage facilities worldwide (Morrill *et al.* 2022)

Meso Scale Approaches: In-Field Characterization and Geophysical Techniques

Meso-scale techniques bridge the gap between macro-scale remote sensing and micro-scale laboratory analyses, providing critical insights into the physical and chemical properties of mine waste. Hyperspectral imaging (via drones and field scanners) enables high-resolution mineralogical mapping, offering a non-invasive method for characterizing waste materials across mining sites. Geophysical methods, including Electrical Resistivity Tomography (ERT), Ground Penetrating Radar (GPR), and LiDAR, provide valuable subsurface information, detecting fractures, fluid movement, and material distribution (Martin *et al.* 2017). Drilling techniques (core, sonic, vibratory) allow for physical sampling, providing direct insights into stratigraphy and material properties(Benndorf *et al.* 2022; Khomiak *et al.* 2024). In-field spectroscopic analyses, such as Infrared Spectroscopy (IR) (Kamps *et al.* 2024) and portable Laser-Induced Breakdown Spectroscopy (pLIBS), enable rapid, on-site chemical characterization, reducing reliance on laboratory testing (Kuhn *et al.* 2015). Geometallurgical assessments integrate mineralogical, chemical, and metallurgical data to evaluate mine waste for CRM recovery while predicting environmental risks (Parbhakar-Fox *et al.* 2019).

Micro Scale Approaches: High-Resolution Laboratory Analyses

Micro-scale laboratory techniques are essential for detailed mine waste characterization, enabling precise assessments. Computed Tomography (CT) provides non-destructive 3D imaging of mine waste, revealing internal structures such as porosity and fractures, which are crucial for understanding leaching behavior (Jamieson *et al.* 2015). X-Ray Diffraction (XRD) and X-Ray Fluorescence (XRF) identify mineral phases and elemental composition, aiding in contamination assessment and mineral stability predictions. Mineral Liberation Analysis (MLA) evaluates mineral associations for reprocessing. ICP-MS and ICP-OES provide sensitive trace element detection for monitoring hazardous metals in mine waste. Hyperspectral imaging at the laboratory scale provides detailed mineralogical mapping, supporting large-scale assessments of waste-rock dumps (Flores and Möllerherm 2023).

Results

This section presents findings from three case studies, each applying multi-scale spectral sensing technologies on different mine waste constellations. By integrating spectral characterization routines, these studies demonstrate how advanced spectral monitoring techniques can improve the characterization of different mine waste constellations. Flores *et al.* 2021 employed drone-based hyperspectral imaging to monitor acid mine drainage (AMD)-impacted river systems in the Rio Tinto region (Fig. 2). Regression analysis on hyperspectral data enabled the estimation of hydrogeochemical parameters, providing valuable insights into water quality in the Iberian Pyrite Belt, southern Spain.

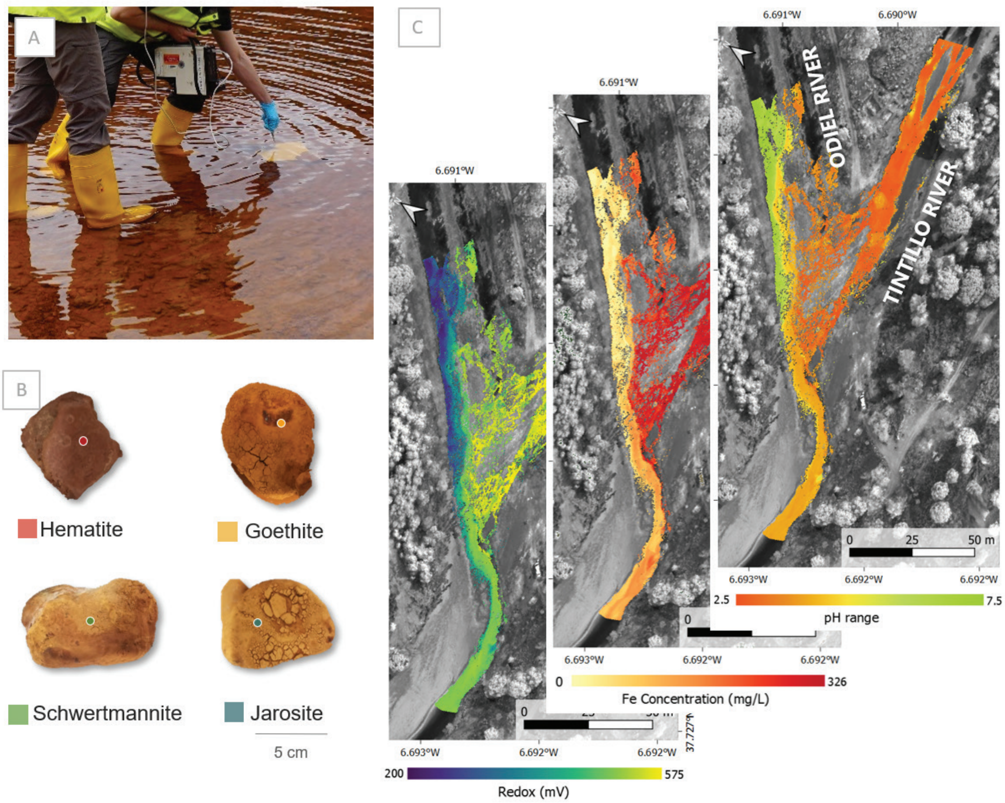

Figure 2 (A) In-field spectroscopy of Acid Mine Drainage affected waters. (B) main secondary iron-minerals detected in the river borders at the Odiel-Tintillo Confluence (southern Spain). (C) Catalogue of hydrogeochemical parameters of water derived from drone-borne hyperspectral imaging (Modified from Flores et al., 2021*).*

Laboratory-scale analyses of mine dumps have been conducted to assess both environmental risks and economic beneficiation (Benndorf *et al.* 2022; Flores and Möllerherm 2023). Using multiple sensors, these studies quantified metal content and identified key mineral associations (Fig. 3). A multi-method characterization approach was applied to study tailings in Ibbenbüren, Germany (Fig. 4). The workflow combined hyperspectral imaging (visible-to-near infrared and thermal), ground validation, and compositional analysis. This approach generated high-resolution mineral maps and semi-quantified iron content, identifying critical minerals associated with secondary iron by-products, which may be viable for secondary prospecting (Flores *et al.* 2024).

Conclusions

This contribution reviews various multi-scale characterization techniques applied to mine waste repositories to support both environmental monitoring and resource recovery. By integrating remote sensing, in-field spectral analysis, and laboratory-based mineralogical assessments, we demonstrate how mine water, waste rock dumps, and tailings can be effectively characterized and monitored. The results highlight the value of hyperspectral imaging for detecting hydrogeochemical parameters and metals in mine water, multi-sensor laboratory analyses for determining the composition of waste dumps, and combined imaging and geochemical methods for the semi-quantification of metal composition in tailings. Future work should focus on

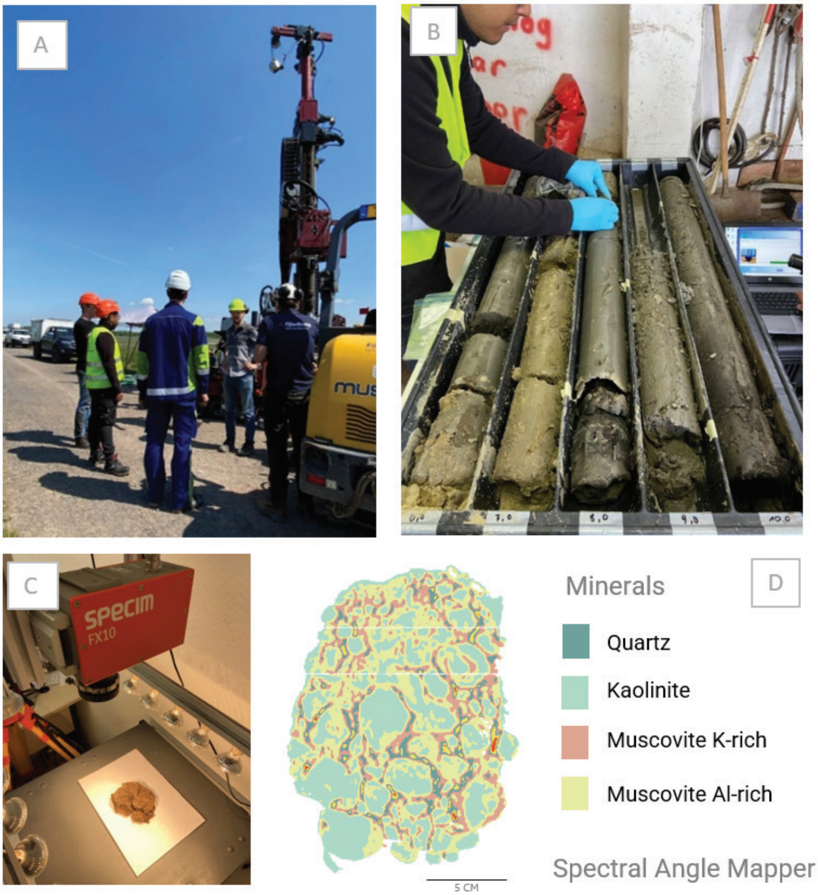

Figure 3 (a) Drilling campaign at waste dump location. (b) Drill-core inspection and sample selection. (c) Sensor assembly at TU Bergakademie Freiberg, Department of Mine Surveying and Geodesy, Germany. (d) SAM classification over waste dump sample.

standardizing spectral-based monitoring routines, refining pre-processing methods, and integrating machine learning for automated mineral classification. Expanding case studies to further validate the applicability and reproducibility of these techniques across different mining regions will be key to strengthening the link between characterization and reprocessing strategies, ultimately enhancing the role of mine waste management within a circular economy.

References

Benndorf J, Restrepo DA, Merkel N, *et al* (2022) TRIM4Post-Mining: Transition Information Modelling for Attractive Post-Mining Landscapes – A Conceptual Framework. Mining 2:248–277. https://doi.org/10.3390/mining2020014

Choe E, van der Meer F, van Ruitenbeek F, *et al* (2008) Mapping of heavy metal pollution in stream sediments using combined geochemistry, field spectroscopy, and hyperspectral remote sensing: A case study of the Rodalquilar mining area, SE Spain. Remote Sens Environ 112:3222–3233. https://doi.org/10.1016/j.rse.2008.03.017

European Commission (2018) European Innovation Partnership on Raw Materials Raw Materials Scoreboard. https://doi.org/10.2873/13314

Flores H, Lorenz S, Jackisch R, *et al* (2021) Uas-based hyperspectral environmental monitoring of acid mine drainage affected waters. Minerals 11:1–25. https://doi.org/10.3390/min11020182

Flores H, Möllerherm S (2023) TRIM4Post-Mining: Mine Waste Management and Risk Monitoring – A lignite mine case. 1–5. https://doi.org/10.3997/2214-4609.2023101158

Flores H, Reker B, Pawlik M, *et al* (2024) Hyperspectral UAV-sensing for monitoring tailing ponds: Towards

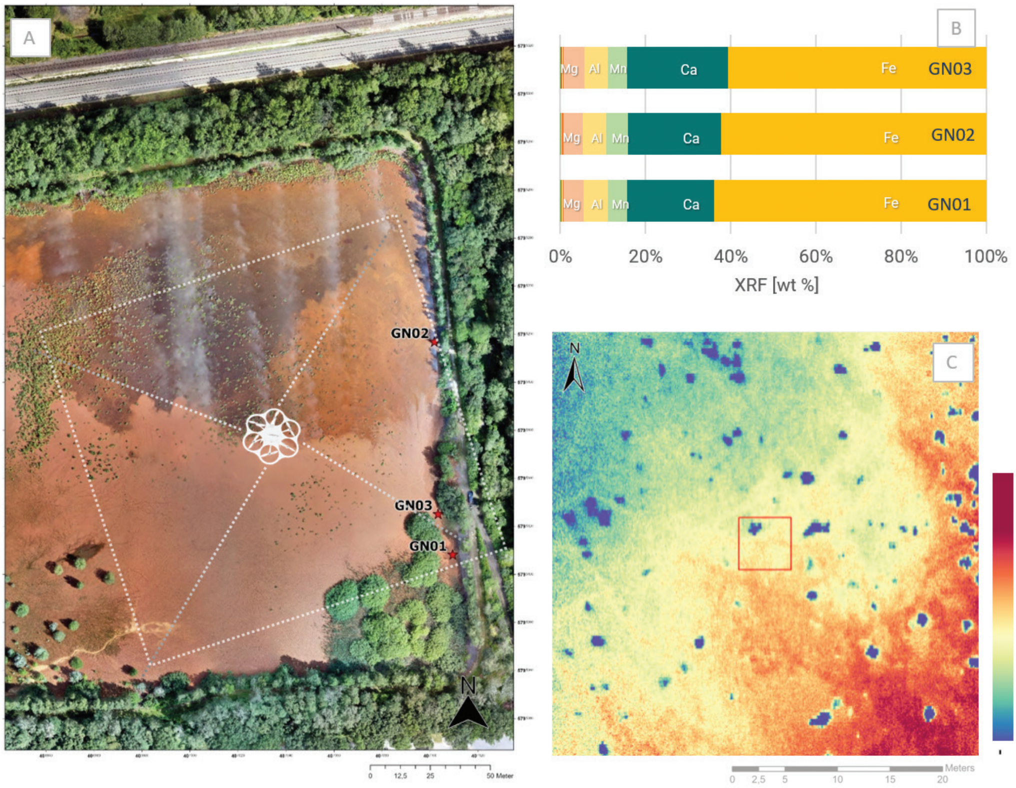

Figure 4 *(A) Orthophoto of the Tailing facility at Ibbenbüren showing the UAS-borne hyperspectral scanned scene and sampling locations (red-starts). (B) Chart of the main element fractions of three sludge samples determined by the XRF analysis. (C) Fe band ratio (650/735 nm) derived from hyperspectral scene (Modified from Flores et al., 2024).*

responsible resource repurposing. In: Kleinmann, B, Skousen, J, Wolkersdorfer, Ch: West Virginia Mine Drainage Task Force Symposium & 15th International Mine Water Association Congress – p 196 – 202; Morgantown, WV, USA (International Mine Water Association)

Hudson-edwards KA, Jamieson HE, Lottermoser BG (2011) Mine Wastes : Past , Present , Future ENVIRONMENTAL IMPACT OF. 375–380. https://doi.org/10.2113/gselements.7.6.375

Hund K, La Porta D, Fabregas T, *et al* (2020) Minerals for Climate Action: The Mineral Intensity of the Clean Energy Transition. World Bank Publications 110

Jamieson HE, Walker SR, Parsons MB (2015) Mineralogical characterization of mine waste. Applied Geochemistry 57:85–105

Kamps O, Desta F, Maghsoudi Moud F, Buxton M (2024) Multi-Level Characterization of Lignite Mine Waste by the Integration of Wide Wavelength Range Infrared Spectroscopy. Mining 4:588–612. https://doi.org/10.3390/mining4030033

Khomiak O, Benndorf J, Verbeek G (2024) Sub-Surface Soil Characterization Using Image Analysis: Material Recognition Using the Grey Level Co-Occurrence Matrix Applied to a Video-CPT-Cone. Mining 4:91–105. https://doi.org/10.3390/mining4010007

Khosravi V, Doulati Ardejani F, Gholizadeh A, Saberioon M (2021) Satellite imagery for monitoring and mapping soil chromium pollution in a mine waste dump. Remote Sens (Basel) 13:. https://doi.org/10.3390/rs13071277

Kuhn K, Meima JA, Rammlmair D, Ohlendorf C (2015) Chemical mapping of mine waste drill cores with laser-induced breakdown spectroscopy (LIBS) and energy dispersive X-ray fluorescence (EDXRF) for mineral resource exploration. J Geochem Explor 161:72–84. https://doi.org/10.1016/j.gexplo.2015.11.005

Martin V, Bussière B, Plante B, *et al* (2017) Controlling water infiltration in waste rock piles: Design, construction, and monitoring of a large-scale in-situ pilot test pile

Montero IC, Brimhall GH, Alpers CN, Swayze GA (2005) Characterization of waste rock associated with acid drainage at the Penn Mine, California, by ground-based visible to short-wave infrared reflectance spectroscopy assisted by digital mapping. Chem Geol 215:453–472. https://doi.org/10.1016/j.chemgeo.2004.06.045

Morrill J, Personius P, Sampat P, *et al* (2022) Safety First Guidelines for Responsible Mine Tailings Management Safety First Guidelines for Responsible Mine Tailings Management ACKNOWLEDGMENTS Thank you to

Parbhakar-Fox A, Gilmour S, Fox N, Olin P (2019) Geometallurgical characterization of non-ferrous historical slag in Western Tasmania: Identifying reprocessing options. Minerals 9:. https://doi.org/10.3390/min9070415

Ragonnaud G (2023) Securing Europe's supply of critical raw materials

Schreck M, Wagner J (2017) Incentivizing secondary raw material markets for sustainable waste management. Waste Management 67:354–359. https://doi.org/10.1016/j.wasman.2017.05.036

Swayze GA, Smith KS, Clark RN, *et al* (2000) Using imaging spectroscopy to map acidic mine waste. Environ Sci Technol 34:47–54. https://doi.org/10.1021/es990046w

Tayebi-Khorami M, Edraki M, Corder G, Golev A (2019) Re-thinking mining waste through an integrative approach led by circular economy aspirations. Minerals 9

Monitoring, Control, and Prevention of Excess Hg in Acid Mine Drainage (AMD) in an Abandoned Metal Sulfide Mine (SW Portugal), using Nature-Based Solutions

R. Fonseca[1], J. Araújo[2], R. da Silva[2]

[1]*AmbiTerra Laboratory, Institute of Earth Science, Dep. Geosciences, School of Sciences and Technology University of Évora, Évora, Portugal. rfonseca@uevora.pt. ORCID 0000-0002-6389-2822*

[2]*AmbiTerra Laboratory, Institute of Earth Science, University of Évora, Évora, Portugal. jfaraujo@uevora.pt, ORCID: 0000-0003-4956-4061; roberto.silva@uevora.pt ORCID: 0000-0003-3865-8724*

Abstract

This study aims to monitor the behavior of Hg in watercourses drained by a huge pile of tailings in an abandoned mine located in the Iberian Pyritic Belt (IPB), and to test the most effective low-cost technology in retaining Hg. The water collected in two consecutive years from the watercourses showed meaningful values in areas near the tailings (16-28µgL-1), above the reference value, 0.3µgL-1 (EU Regulation, 2009). Bench scale tests were conducted to evaluate the effectiveness of nature-based materials in retaining Hg by analyzing ion exchange capacity, kinetic tests, and simulating "ponds" containing different proportions of materials vs mine water.

Introduction

Metal Pollution affects all mining sectors, has a combined worldwide economic impact and its impacts can continue for more than 2,000 years (Taylor, 2012). This kind of pollution, in metallic ores, is in general associated with acid mine drainage (AMD), a multi-factor pollution formed from complex chemical, physical, and biological interactions that takes place under ambient conditions in abandoned and active mines (Ighalo *et al.*, 2022). The producing of acid metal-rich waters, their spread in the environment, and the interconnectivity of water systems, has environmentally significant consequences on the delicate and highly vulnerable aquatic systems (Ferreira da Silva *et al.*, 2015), contaminating local surface waters, groundwaters and stream sediments.

In areas impacted by mining of metal sulfides, mercury (Hg) is one of the most critical contaminants in the environment, due to its potential toxicity and the easiness with which it leads to a widespread contamination over a wide area (Sørmo *et al.*, 2022). In water systems, the conversion to more toxic Hg-forms, as methylmercury (MeHg), is dominated by biotic methylation under anoxic conditions. In this process, sulfur reducing bacteria have been identified as the main methylators (Sørmo *et al.*, 2022), which increases the overall risk of Hg in aquatic environments affected by metallic sulfides mining sites. To avoid this major threat to water systems, the Hg present in acid drainage resulting from the leaching of mining waste must be retained before it reaches groundwater and surface water bodies. This study aims to (1) monitor the spatial and temporal behavior of Hg in the watercourses affected by a huge pile of mining wastes at Caveira Mine (SW Portugal), located in the Iberian Pyritic Belt, and (2) test the most effective technology in retaining Hg, using nature-based materials.

Case Study

The Caveira mine is in South Portugal, in the SW extreme limit of the Iberian Pyritic Belt (IPB), one of the most important metal bearing areas in the world, due to the unusual polymetallic (Cu, Pb, Zn, Fe, As, Sb, Co, Mn) sulfides concentration (Fig.1) in large and medium sized mineral deposits (Ferreira da Silva *et al.*, 2015). The mine is embedded in Paleozoic formations and the geological sequence is represented from bottom to top by phyllites and quartzites, followed by a volcanic sedimentary complex sequence, hosted of the polymetallic massive sulfide mineralization. It has a long exploitation history that started in the Roman period and past mining activities included pyrite (FeS_2) and Cu extraction. The mine ceased operations in the 1960s and the lack of maintenance of the large volumes of tailings and waste dumps produced by the mining activities (estimated to be higher than 2 Mt), has contributed to its identification as one of the most problematic abandoned mining areas in the IPB, with evidence of intense long-term acid mine drainage (AMD) and other impacts on the surface environment. Rainwater circulates and percolates easily over and through these tailing materials causing significant erosion and transport of debris, harmful compounds and potentially toxic elements (PTE), posing severe environmental problems to nearby soils and waterways of the Sado watershed. Previous studies conducted by Ferreira da Silva *et al.* (2005), reported the occurrence of stable forms of mercury (such as cinnabar and other mercury sulfides) at the surface around the mine. Different materials deposited along the main streams and in the dump areas trace the historical evolution of ore processing in those sites.

Methods

A total of 49 water samples (18 in 2022 and 31 in 2023) were collected from a grid of 1 km × 1 km, in small and narrow creeks, that receive the drainage waters from the mine tailing piles, also including points outside the mining activity that represent the background of the area tributaries (Fig. 1). These streams flow to the Grândola Stream, in Sado basin, the second-largest hydrographical basin in Southern Portugal. The samples were taken in two consecutive years (2022–2023) representing different climate scenarios: 2022 reflects a very dry winter with anomalous values in terms of precipitation and temperature, and 2023 a regular rainy winter. Sampling was followed by immediate readings of pH, redox potential, dissolved oxygen (mg/L), conductivity (µS/cm), resistivity (KΩcm), total dissolved solids (mg/L), temperature (ºC) and turbidity (NTU), using a portable multi-parameter (Hanna Instruments, HI98494/10) and a turbidimeter (Hanna Instruments HI98713-02). Mercury (Hg) was analyzed in refrigerated samples stored in dark glass

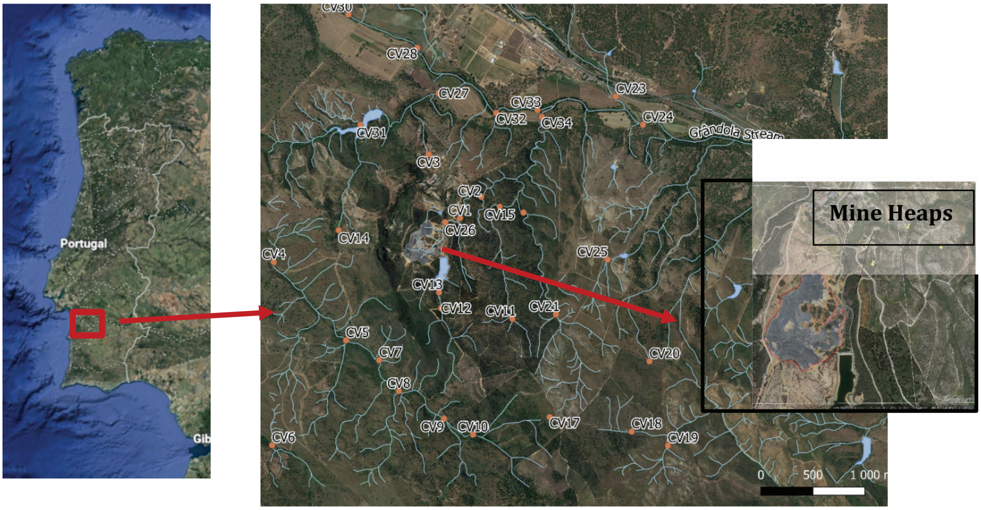

Figure 1 Location of the mine heaps of Caveira and sampling design in the watercourses affected by the AMD.

containers, using a mercury analyzer (NIC MA-3000) based on thermal decomposition, gold amalgamation, and cold vapor atomic absorption spectroscopy detection. The accuracy and analytical precision of all the analyses were checked through the analysis of reference materials and duplicate samples in each analytical set.

To better control and prevent the excess of Hg found in watercourses, a bench-scale evaluation of the effectiveness of twelve nature-based and waste materials was carried out, considering their retention capacity for Hg. The goal of these tests is to identify the most appropriate materials to be used in the upstream sections of waterways to restore water quality. The selected materials have different mineralogical composition, always following the principle of easy availability and low cost: powders of carbonate rocks (limestone and marble), terra rossa, iron oxides, clays (bentonite and illitic clay with quartz, K-feldspar, kaolinite, goethite), cellulose wastes, acacia biochar, activated carbon from coconut shell in powder and pellets. Before contact with the mining water, all the materials were analysed for: 1) contents of the chemical elements in extractable forms through partial digestion with bi-acid hydrochloric and nitric solution in a high-pressure microwave digester, followed by ICP-OES analyses; 2) determination of their retention capacity by analysing the cation exchange capacity; 3) Hg content. The evaluation of the effectiveness of these materials, included:

1. **kinetic tests:** The main objective was to determine the rate and capacity of adsorption of excess Hg in mine waters, for each material, and the most suitable chemical and physical conditions for its adsorption. These tests were carried out by shaking each material with a mono elemental solution of the same concentration as the sample with the highest level (CV1: 10mg/L) with a pH adjusted to pH5.5. Each material, in contact with the Hg solution at a ratio of 10g material/1L Hg solution, was placed in an orbital shaker at room temperature in distinct containers corresponding to different time intervals: t_1–5 min, t_2–15 min, t_3–30 min, t_4–1h; t_5–2h; t_6–5h; t_7–10h and t_8–24h. At the end of each time interval, the samples were analyzed in the mercury analyzer. Based on the concentrations found, the adsorption capacity of each material was calculated for each element.
2. **Simulation of retention ponds:** Ponds were simulated in which the 12 natural/waste materials set in laboratory beakers, were covered with water collected in the point closer to the mine heaps (CV1), characterized by critical PTE levels including Hg, and very low pH (pH1.64), in order to evaluate their ability to increase pH, just by being in contact with it for 10 days. The materials were tested individually under the same conditions, varying only two parameters: i) different proportions of materials: mine water (1:50, 1:100, 1:200), *ii*) different conditions of contact with atmospheric oxygen (direct contact vs. isolation). Throughout the contact period, pH and conductivity were measured daily and the water was analyzed for Hg content after the 10 days of contact with the materials. These values were compared with the actual Hg concentration in the mining water before contact, and the percentage of element removal was calculated.

Results and Discussion

The physicochemical parameters of the water column show slight differences in the two periods (Table 1): a decrease in the lowest pH values is observed at points located nearest the heaps, ranging from 1.10–3.30 during the drier period (2022) and 1.42–4.53 during the wetter period (2023), while an inverse variation pattern is observed in relation to the higher pH values, observed at points further away from the heaps, with the highest values occurring during the wetter period (6.26–8.33). The extreme acidification (pH1–3) rich in metals is typical for the mining areas of the IPB, resulting from the oxidation of metal sulfides, producing metal(loid)s, sulfate ions, sulfuric acids, precipitates of Fe-Al-Ca-Mg (Mn, Co), sulfates and Fe-Al oxyhydroxides (Valente *et al.*, 2013). In the Caveira area, this acidification comes from the leaching of the tailing piles, which is higher during the rainy season, but with a greater impact in the streams during the driest periods due to the lower dilution effect. This effect is also noticeable in the 2022 campaign, where the waters, especially those closer to the tailings, have higher conductivity values (median: 889 µS/cm) when compared with the values in 2023 (median: 583 µS/cm). The variation of these two parameters reflects the complex interaction between mining wastes and hydrogeochemical conditions, showing a deterioration of the water quality in the drier year 2022, and a leaching and dilution effect in 2023, which slightly improves its quality.

The analysis of metals (Fe, As, Cd, Co, Cr, Cu, Mn, Ni, Pb, Zn) in water samples from both periods, carried out in previous studies (Araújo *et al.* in *litt.*), showed that these metals are mainly present in dissolved form. This increases metals mobility in watercourses and, consequently, their bioavailability and environmental hazard. At sampling points near the heaps, elements such as As, Al, Cd, Ni, Mn, Cu, Pb and Zn exceed the regulatory limits established by Portuguese legislation (Decree-Law No. 236/98), classifying the water as extremely polluted. Concentrations of the more mobile elements, such as As, Cd, Mn, Cu and Zn, are higher during the period of increased precipitation, in the points close to the heaps, due to an extensive leaching and runoff of metals from the waste material.

The Hg levels in the waterways are very similar in both sampling campaigns (2022: 16–18 µgL-1, 2023: 26–28 µgL^{-1}), following the same distribution pattern, with higher values in areas located near the Caveira waste pile, gradually decreasing with distance. For all the other metals, there is also evidence of a plume migration between the two sampling periods. These results suggest that the large waste dump in the area, rich in metal sulfides, is the main source of pollution affecting these waterways and the entire surrounding area.

The increase of several metals in the water column during the wetter period is also observed in relation to the sediments of the watercourses, especially those closest to the Caveira mine tailings. In these areas, the sediments are classified as contaminated to very contaminated for As, Cu, Pb and Hg,

Table 1 *Variation of pH, conductivity and mercury levels in the waters of the waterways affected by the Caveira Mine, in the 2 study periods, 2022 and 2023.*

2022				2023							
Samples	pH	Conduct. µS/cm	Hg µg/L	Samples	pH	Conduct. µS/cm	Hg µg/L	Samples	pH	Conduct. µS/cm	Hg µg/L
CV1	1.23	8250	10,000	CV1	1.58	23.22	27.320	CV21	6.07	1206	<0.01
CV2	1.10	8315	15.175	CV2	1.68	19.26	2.19	CV22	6.33	610	26.110
CV3	3.31	4761	18.185	CV3	4.53	2539	28.310	CV23	6.54	752	1.350
CV5	6.64	789	11.975	CV4	6.68	816	<0.01	CV24	5.93	618	3.460
CV10	7.29	490	0.79	CV5	6.73	822	<0.01	CV26	1.42	31.47	<0.01
CV13	8.33	673	0.17	CV6	6.57	1075	<0.01	CV27	6.96	896	<0.01
CV15	5.76	156	3.665	CV7	6.55	720	<0.01	CV28	7.07	517	<0.01
CV22	8.25	1315	0.45	CV8	6.45	764	<0.01	CV29	6.45	524	<0.01
CV23	6.96	896	0.215	CV9	6.59	748	<0.01	CV30	7.08	512	<0.01
CV24	6.26	1008	0.835	CV10	6.61	573	<0.01	CV31	6.94	583	<0.01
CV26	1.33	85.46	7.985	CV11	5.48	220	3.230	CV32	6.65	577	<0.01
CV27	7.24	1752	0.365	CV12	5.6	91	<0.01	CV33	5.85	585	<0.01
CV28	7.19	870	0.065	CV13	7.04	691	<0.01	CV34	1.78	11.78	<0.01
CV29	7.45	863	0.78	CV15	5.77	403	<0.01				
CV30	7.92	882	0.045	CV16	4.94	935	<0.01				
CV31	8.28	749	0.095	CV18	6.21	391	<0.01				
CV32	7.23	929	0.055	CV19	6.5	271	<0.01				
CV33	7.28	930	<0.01	CV20	6.17	84	<0.01				

according to the Portuguese legislation for dredged sediments (Regulation 1450/2007). For Hg, the concentrations range from 2 to 12 times higher than the critical limit established by the Portuguese legislation (10 $mgkg^{-1}$) and high concentrations were also found in the pore water of these sediments (1600–4000 μgL^{-1}), with much higher levels than those analyzed in the water column. Given the dynamic behavior of Hg in these watercourses, as evidenced by the fractionation analysis of this element in the sediments (Fonseca *et al.*, 2025), the very high concentrations in the soluble fraction, and its high mobility and toxicity, it became clear that this element should be considered as one of the highest priorities to be included in the remediation strategies to be proposed for this mining area

A large number of bench scale tests have been conducted using twelve low-cost and readily available nature/waste materials, to identify the most suitable for the remediation of this contaminated water system for a range of PTE, including Hg. The chemical characteristics of these materials were evaluated by analyzing the contents of Hg and of other metallic elements in extractable forms (Table 2). The retention capacity of the materials in terms of PTE was determined by analyzing their cation exchange capacity (Table 2). Except for mineralized iron oxides (ORA2) with low exchange capacity and three other materials – biochar, marble sludge (M(AGF)) and limestone sludge (C(S)), with adsorption capacity within normal values, the remaining materials have high to very high adsorption and cation exchange capacity. This group includes activated carbon in powder and in pellets, bentonite clay and ferrihydrite.

Regarding the adsorption capacity for the 5 elements found above the critical limits in the Caveira mine water (Cu, As, Mn, Zn, Hg), the 12 materials behave differently for each element, due to their mineralogical and chemical characteristics and the chemical behavior of the elements, namely their greater or lesser solubilization capacity and the conditions necessary for their retention and the chemical form in which they occur in solution. This paper presents only the Hg retention tests.

The kinetic tests carried out with a mono elemental solution of Hg at a concentration of 10 mg/L show that, except for limestone sludge (retention of 13.7%) and marble sludge (retention of 2.79%), all the other materials were able to retain Hg, although activated carbon in powder and in pellets, were the only ones able to retain almost 100% (respectively 99.99% and 94.38%) after 15 minutes of contact with the synthetic Hg-solution,

***Table 2** Characterization of the "pure" geo and waste materials before contact with mine water: contents of Hg and other metals found above the critical limits in Caveira mine water (Portuguese legislation, Decree-Law No. 236/98), and Cation exchange capacity.*

Pure natural/waste materials							
Samples	**Description**	**Hg µg/Kg**	**As mg/Kg**	**Cu mg/Kg**	**Pb mg/Kg**	**Mn mg/Kg**	**CEC cmolc/kg**
C(S)	Limestone sludge	5.41	<2.50	8.16	1.70	14.72	23.19
M(AGF)	Marble sludge	14.23	<2.50	6.94	2.07	158.63	21.22
BVV	*Terra Rossa*	66.51	2.50	3.77	5.858	177.15	47.87
B#2	Bentonite	5.91	<2.50	0.20	<0.50	113.37	166.08
ORA2	Fe-oxides	22.12	<2.50	<0.50	14.39	311.44	5.81
Lagoa	*Terra Rossa*	47.03	<2.50	23.96	3.01	203.02	63.97
Fat clay	Illitic clay	29.11	<2.50	6.49	3.32	1650.04	74.75
Celulose	Waste of Celulose	38.88	<2.50	128.32	16.11	5300.21	42.60
CF03	Ferrydrite	50.11	11,907.9	4.93	43.11	353.95	87.59
Biochar	Acacia Biochar	13.20	4.90	3.95	3.67	129.63	14.90
Pellets carbon	Activated Carbon in Pellets	21.50	<2.50	31.62	2.96	107.64	72.66
Powder carbon	Activated Carbon in powder	7.29	<2.50	17.00	2.35	29.67	87.31

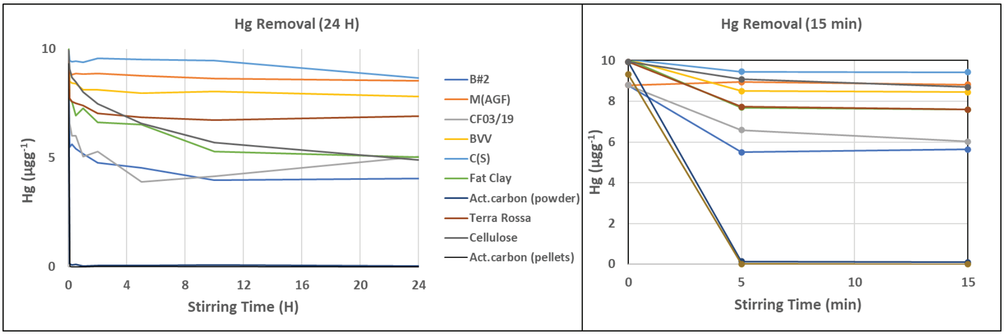

***Figure 2** Hg removal from the mine water, by nature and waste products*

followed by bentonite (53.83%) and cellulose (50.64%). The amount of Hg removed by each material is shown in Fig. 2.

Mercury in solution forms mainly anionic complexes but can also occur as the free cation Hg^{2+}. It is therefore preferentially retained by positively charged materials but can also be adsorbed by electronegative materials. This behavior is confirmed by the adsorption capacities of the 12 materials tested. A pond simulation evaluated the ability of the materials to (1) increase the initial pH (1.56) to reduce element solubility and (2) retain excess Hg after 10 days of contact with mine water at three material-to-water ratios (1:50, 1:100, 1:200). The results showed that:

- Cellulose, limestone, and marble sludges were most effective in raising water pH, increasing it from 1.56 to 6.6 after 7 days. The highest increase occurred at the lowest water/material ratio (50 mL:1g) in both oxic and anoxic conditions, with similar values. For example, cellulose, the most efficient, raised pH to 6.80 in an anoxic pond and 6.23 in an oxic pond.
- In Caveira mine water, with low initial conductivity, this parameter decreases at first and remains lower only in three geomaterials (limestone and marble sludge, ferrihydrite). In others, it stays unchanged or slightly increases, likely due to the high ion exchange capacity and exchange bases that most materials have (e.g., cellulose: Na, Mg, K) transferring to the water.
- Analysis of Hg in the water after the contact with these materials, showed a greater efficiency in reducing the original levels ($461 µgL^{-1}$) for limestone, marble, activated carbon and cellulose ($2 µgL^{-1}$-$3 µgL^{-1}$). The slight difference in the Hg retention compared to the kinetic tests is due to: (1) some materials significantly increased the water pH when in contact, while others did not (e.g. activated carbon) and (2) chemical competition at the adsorption sites of materials between Hg and other elements also present in excess (As-Fe-Cu-Zn-Pb).

Conclusions

Contamination control of waterways affected by the Caveira Mine should occur only after intervention upstream of the tailings and dumps. Based on our studies, it is proposed to intervene in drainage water to reduce particle transport with high metal content and discharge of highly acidic water (pH 1–2) with dissolved metals. This intervention should occur where runoff water converges before entering watercourses, in two ways:

1. *Pond to increase pH:* In extreme acidity, metals cannot be adsorbed by any material. Depending on their availability at the remediation sites, any of the 3 materials that have shown good efficacy in raising the pH, cellulose and limestone and marble sludges (1:50 ratio) can be placed at the pond bottom in contact with air. These industrial waste materials have no economic value, and costs relate only to transport and placement. Though pH increase is somewhat slower in contact with oxygen, an open pond is more economical and aids iron oxidation, which is highly concentrated in these waters.
2. *Further treatment before discharge:* With improved pH and lower iron concentration, water should be pumped to

selected structures based on topography, before being discharged to watercourses: 1) a pond in flat terrain, or 2) a reactive barrier, preferably permeable, in rugged areas. The bottom should be capped with a layer of effective Hg-removing geomaterials, like activated carbon. Since these waters contain other harmful metals (Fe, Cu, Zn, Pb, As), a multi-layer coating can be applied, including cellulose and/or limestone and marble sludges, which have shown good efficacy in retaining these elements (Araújo *et al*., 2025), in addition to activated carbon. In ponds, layers can be arranged sequentially controlled by zig-zag baffles, to direct the water flow and increase retention time of water for decontamination.

Acknowledgements

The authors thank: (1) National funds through FCT-Science and Technology Foundation, I.P., in the framework of the UIDB/04683 and UIDP/04683 – Institute of Earth Sciences (IES) Programs; (2) Project GeoMinA – Implementation of a basis for defining geoenvironmental models in abandoned mining areas in the Iberian Pyrite Belt – PL23-00035 – Promove Actions Project 2023 Fundação La Caixa (2024–2027).

References

Araújo J, Fonseca R, Albuquerque, Silva N, Silva R (in litt) T *et al.* in litt Influence of sulphide mine tailings on drainage water quality, 60 years after its abandonment. A Case study in SW Portugal. Comunicações Geológicas, ISSN: 0873-948X; e-ISSN: 1647-581X

Sørmo E, Silvani L, Fredrik H, Braaten V, Bryntesen T, Eek E, Cornelissen G (2022) Formation and availability of methylmercury in mercury contaminated sediment: effects of activated carbon and biochar amendments. Journal of Soils and Sediments ,22, 1041–1053.

Ferreira da Silva E, Durães N, Reis P, Patinha C, Matos J, Costa MR (2015) An integrative assessment of environmental degradation of Caveira abandoned mine area (Southern Portugal). J. Geochem. Explor. 159, 33–47. https://doi.org/10.1016/ j.gexplo.2015.08.

Fonseca R, Araújo J, Silva R, Albuquerque T (2025) Innovative Approaches to Remediate Waterways contaminated with Mercury in a Mining Area in the Iberian Pyritic Belt, SW Portugal. Abstract I96, Twelfth International Conference on the Remediation and Management of Contaminated Sediments, Tampa, FL (USA) 27–30 January 2025, Battelle.

Ighalo JO, Adeniyi AG (2020) A comprehensive review of water quality monitoring and assessment in Nigeria. Chemosphere 260, 127569.

Taylor JR (2012) Global Heavy Metal Pollution (AMD / ARD) Impacts. 1st International Acid and Metalliferous Drainage Workshop in China – Beijing 2012.

Valente T, Grande JA, de la Torre ML, Santisteban M, Cerón JC (2013) Mineralogy and environmental relevance of AMD-precipitates from the Tharsis mines, Iberian Pyrite Belt (SW, Spain). Applied Geochemistry, 39, 11–25.

Seepage and water quality observations from three lysimeters constructed at a coal mine in northeastern, British Columbia, Canada

Colin Fraser[1] and Justin Stockwell[2]

[1]Lorax Environmental Services Limited, 305-1770 West 7th Avenue, Vancouver, BC, Canada V6J 4Y6
colin.fraser@lorax.ca ORCID 0009-0000- 9292-1656

[21]Lorax Environmental Services Limited, 305-1770 West 7th Avenue, Vancouver, BC, Canada V6J 4Y6
justin.stockwell@lorax.ca

Abstract

At a coal mine in northeastern British Columbia, Canada, three mine rock lysimeters were constructed to evaluate the relative performance of soil covers in reducing net infiltration, seepage volumes, and chemical loads potentially requiring treatment. Data collection is ongoing at the study site with interim results indicative that mine rock with an engineered cover produces less seepage than mine rock with a standard reclamation cover and a control pile without cover. Relevant hydro-climatic and loading data are presented for the mine rock lysimeters, and a water quality dataset spanning more than ten years is discussed.

Keywords: Waste rock, runoff, lysimeters, reclamation, cover systems, water quality

Introduction

Infiltration through waste rock piles mobilizes sulfide oxidation products as well as blasting residues (Wellen *et al.* 2015; Mahmood *et al.* 2017). Accordingly, parameters of concern at coal mines often include sulfate, nitrate and selenium, with mitigative measures such as passive and active treatment, waste submergence, seepage interception, and the application of cover systems, employed to achieve compliance with effluent standards and broader ecosystem health goals.

Work by others illustrates the utility of lysimeters in ground-truthing laboratory studies, while bridging understanding regarding flow and chemical processes occurring in mine waste at a large scale (e.g., Hansen *et al.* 2000; Smith *et al.* 2013, Muniruzzaman et al. 2021). Studies in the open scientific literature also report on the research objectives, experimental design, and/or general progress of lysimeter experiments involving cover system trials (e.g., Okan and Barbour 2003; Urrutia *et al.* 2011; Kahale *et al.* 2022).

At a coal mine in northeastern British Columbia (BC), three mine rock lysimeters were constructed to explore whether earlier application of soil covers reduces contaminant loading without substantive additional cost. The research objectives of this study include: i) measuring flow and water quality from covered and uncovered mine rock piles; and ii) comparing the relative performance of differing cover systems, in terms of volume and water quality of drainage output. Cover placement at the study site is hypothesized to reduce net infiltration into mine rock, thus reducing seepage volumes and chemical loads potentially requiring treatment.

Methods and Data Sources

A flat area of 100 m by 100 m on the 1,490 m elevation bench of the coal mine was selected for the mine rock lysimeters. Each lysimeter consists of an ~4 m tall mine rock pile built on a 17 m by 17 m base, complete with liner systems, a network of collection pipes, and containment berms. The lysimeters were constructed with non-PAG mine rock (i.e., siltstone, shale, sandstone and conglomerate) from the Middle and Lower Gates Formation (Stott, 1968), subunits which constitute ~85% of all mine rock at the study site. Median sulfur content (% S) and neutralization potential ratios (NPR, kg CaCO3/t) for mine rock is as follows: Middle Gates (0.09% S, NPR = 32); and Lower Gates (0.1% S, NPR = 62). Parameters of interest established through compliance monitoring include Se associated with pyrite oxidation and NO_3 associated with explosive use.

Seepage volume emanating from each lysimeter is first piped to a holding tank, then directed through a tipping bucket measuring device (1 tip = 1 L) where volumetric data is recorded by dataloggers. Lysimeter seepage water quality when sampled is analyzed for general parameters (e.g., pH and specific conductance), nutrients, major ions, and total and dissolved metals. To allow direct comparison between experimental piles, lysimeters were constructed from the same material (i.e., representative and <1 year old mine rock (0.5 m D90); bulk density ~1.7 t/m^3), using the same excavating equipment. Additional details for the lysimeters are provided in Tab. 1, noting pile masses and volumes are the same at L2 and L3 lysimeters, whereas owing to steeper side slopes and different morphometry, L2 and L3 tonnages are ~30% less than L1.

Precipitation data used in the study (e.g., to compute ratios of rainfall to seepage) are sourced from the mine site climate station (2016 through 2024). The mine site also maintains local hydrometric gauges and water quality sampling stations, with high quality and multi-decadal climate and streamflow data (e.g., daily yield data for Flatbed Creek; WSC 07FB009 (1982-2024)) also recorded by government monitoring agencies at several nearby stations.

Results

Climate conditions at the study site are characterized as continental, with cold snowy winters, warm summers, and a frost-free period of 120 days (GoBC 2021). Mean annual temperature at the study site is 1.0 °C, mean annual precipitation is 1,050 mm (60% of total is snowfall), and annual evaporation is on the order of 400 mm. Local watercourses exhibit a freshet dominated runoff regime, punctuated by periodic- high flow events, coinciding with large convective summer rainfall events. Mean annual runoff estimated for a local- high elevation monitoring station (i.e., 40 km^2, mean catchment elevation = 1,532 m asl) is 478 mm.

Representative seepage and water quality data for the lysimeters are shown in Fig. 1 and Fig. 2, respectively. Water quality data span the period 2013 to 2024, with sampling effort limited to the late-May through early-October period, when the underdrains of lysimeters are ice-free. Seepage records for lysimeters were also seasonal, with record periods as follows per lysimeter: L1 (Control; 2017 and 2019-2024); L2 (Standard reclamation cover; 2016, 2017 and 2019-2024); and, at L3 (Engineered cover; 2019, 2020 and 2024).

Fig. 1 shows seepage data in time series (upper panel; m^3/day) and cumulative volume (middle panel; m^3) formats, six-years after construction of the lysimeters. The lysimeters have been exposed to a wide range of hydro-climatic conditions. Standardized annual streamflow anomalies for a nearby hydrometric gauge (Flatbed Creek, 07FB009) confirm recent drier than average years to include 2014, 2021, 2022, 2023 and 2024, with wetter conditions evident in 2015, 2016, 2017, 2018 and 2020.

Table 1. Design basis for lysimeters constructed at study site.

Station ID	Mine Rock Size	Cover Description	Slope Angles
L1 (Control)	0.5 m D90	Uncovered	Angle of repose (37° slopes)
L2 (Standard reclamation cover)		0.3 m topsoil, reclamation vegetation	2:1 grade (27° slope angles)
L3 (Engineered cover)		0.3 m compacted till below 0.3 m topsoil, reclamation vegetation	2:1 grade (27° slope angles)

The three lysimeters exhibit unique flow signatures. For example, L3 (Engineered cover) exhibits a dampened seepage response to large rainfall event (i.e., less preferential flow) and less baseflow (or matrix flow). In comparison, the L1 and L2 lysimeters clearly report more seepage overall and are more responsive to rainfall events than L3. For a congruent ~3-month period depicted in Fig.1, cumulative precipitation reporting to each lysimeter, expressed as a volume over their footprints was 120 m^3, whereas cumulative seepage volumes at L1 (44 m^3) and L2 (51 m^3) were generally similar, and three-times greater than cumulative seepage measured at L3 (14 m^3).

Averaged over the ice-free period shown in Fig. 1, seepage at L3 was approximately 12% of measured precipitation, whereas L1 seepage (37%) and L2 seepage (43%) were roughly a factor of three higher. With the available data it was possible to develop a more fulsome comparison of cumulative seepage for the L1 (111 m^3) and L2 (109 m^3) lysimeters based on more than 600 days of overlapping data. This extended analysis provides added confidence that seepage production at L1 and L2 to date has been generally similar – rather than materially different.

Fig. 2 shows time series plots for pH, total alkalinity, chloride, calcium, nitrate, sulfate, and selenium from the three lysimeters. Time series for several parameters (e.g., TSS (not shown), total alkalinity (Fig. 2, panel 2), chloride (Fig. 2, panel 3) and calcium (Fig. 2, panel 4)) show considerable variability for five years, prior to showing more stable conditions post-2019. Post-2019 seepage from the lysimeters is slightly basic (pH 8.0 to 8.5; Fig. 2, panel 1)) and similar between sites, while total alkalinities vary seasonally and show similarity. Similarly, post-2019 calcium and sodium (not shown) signatures are also very similar and relatively stable interannually, suggesting that quasi-equilibrium conditions have been attained at the piles.

Flushing of blasting residues occurred much sooner at L1 (Control) versus the two covered lysimeters (Fig. 2, panel 5; nitrate). Nitrate concentrations at L1 remained elevated to a threshold of ~5 mg/L through autumn 2015, while concentrations remained elevated to the same threshold at L2 and L3 through autumn 2017.

Time series plots for magnesium (not shown), sulfate (Fig. 2, panel 6) and selenium (Fig. 2, panel 7) show several commonalities. Of note, Mg, SO_4 and Se concentrations at L2 and L3 are very similar for the post-2019 period. These two lysimeters are covered, have similar morphometry and same tonnages of mine rock on their pads. Given the similar sulfate and selenium concentrations at L2 and L3 while acknowledging seepage production at L3 (Engineered cover) is lower than at L2 (Standard reclamation cover), field data support a conclusion that sulfate and selenium loading at L3 lysimeter is less than loading at L2 (Fig. 1, lower panel).

Mg, SO_4 and Se plots show consistently higher concentrations at L1 (Control) compared to L2 and L3, for the post-2019 period. Greater mass and different morphometry at L1 versus L2 and L3 lysimeters may explain the higher seepage concentrations at L1. By applying a scaling factor to L1 concentration data that accounts for the mass differences at the lysimeters, Mg, SO_4 and Se data show far better alignment across the three sites. Additionally, it is also plausible that ingress of the oxidation front in L1 is promoting sulfide weathering, which is more pronounced in the uncovered pile (L1), due to unimpeded convective oxygen flow.

Regarding recent upward trending in Mg, SO_4 and Se, at all three lysimeters, the collection of additional data may confirm continued upward trending, or alternatively, it is plausible that quasi-steady state conditions have been reached and a return to more typical hydro-climatic conditions will be commensurate with better (lower concentration) seepage water quality. Generally dry conditions have prevailed locally since 2021, with extreme drought conditions occurring in 2024.

Discussion

This paper presents interim water balance and chemical findings from this multi-year research initiative. Data collected thus far indicates the engineered cover pile (L3) produces less seepage than the standard reclamation covered lysimeter (L2) and control pile (L1). While hypothesized that seepage production at L2 would be lower than L1 on account of cover placement, several years of field data confirm seepage production at L1 and L2 to be more similar than different.

Chemistry data from the lysimeters for several parameters (e.g., TSS, total alkalinity, chloride and calcium) showed considerable variability over the first five years of measurement, then reached quasi-equilibrium conditions from 2019 onward. Flushing of blasting residues occurred much sooner at uncovered L1 (Control) compared to the two covered lysimeters. Mg, SO_4 and Se concentrations at L2 and L3 are very similar for the post-2019 period, while concentrations for these same parameters were higher at L1. Owing to lower seepage production at L3 versus L1 and L2 and given that seepage chemistry is either the same (L2) or elevated (L1) compared to L3, load reductions appear achievable by placing engineered cover systems over mine rock (e.g., 30 cm compacted till, 30 topsoil, vegetated).

Future study phases should continue the monitoring of lysimeter seepage and water quality, while considering integration of additional sensors in piles (e.g., soil moisture and oxygen probes), as well as autosamplers and continuously recording sensors (e.g., specific conductance and water temperature), to advance overall study objectives. A portion of seepage reporting from the lysimeters is associated with infrequent, but episodic, seepage events attributable to large storms (e.g., convective rainfall event >30 mm/day). However, the water quality database for the lysimeters is currently biased toward low-moderate seepage conditions, and future sampling efforts should aim to fill this knowledge gap.

At the conclusion of mining and should cover systems be broadly applied to waste rock facilities, design specifications for cover systems merit careful contemplation of datasets developed at the experimental scale while reconciling learnings with conceptual understanding garnered for entire facilities and at larger spatial scales. In addition, future reclamation activities need to be cognizant of the climate conditions forecasted for mine closure and beyond. Forward looking climate change projections (e.g., downscaled 8-GCM ensemble, SSP3-7.0) indexed to a baseline of 1991-2020 predict warmer conditions at the study site (+3°C), coincident with increases in precipitation (+35%) and evaporation (+25%) by 2100.

Acknowledgements

The authors thank the support of staff at the Trend mine site in preparing and presenting findings from the lysimeter trials. Mr. Scott Jackson, Mr. Timo Kirchner and two anonymous referees provided critical comments on earlier versions of this manuscript.

References

Government of British Columbia (GoBC) (2021) Biogeoclimatic Ecosystem Classification (BEC) Zone Map (version 12, September 2, 2021). Forest Analysis and Information Branch. Victoria, BC.

Hansen JB, Holm PE, Hansen EA, Hjelmar, O (2000) Use of lysimeters for characterization of leaching from soil and mainly inorganic waste materials. Nordtest Techn. Rep. 473, 49.

Kahale T, Ouedraogo O, Neto MD, Simard V, Cabral AR (2022) Field-based assessment of the design of lysimeters for landfill final cover seepage cover control. Journal of the Air & Waste Management Association, Vol 72, No. 12, 1477-1488.

Mahmood FN, Barbour SL, Kennedy C, Hendry MJ (2017). Nitrate release from waste rock dumps in the Elk Valley, British Columbia, Canada. Sci Total Environ. Dec 15:605-606:915-928. doi: 10.1016/j.scitotenv.2017.05.253. Epub 2017 Jul 6.S

Muniruzzaman M, Karlsson T, Ahmadi N, Kauppila PM, Kauppila T, Rolle M (2021) Weathering of unsaturated waste rocks from Kevitsa and Hitura mines: Pilot-scale lysimeter experiments and reactive transport modeling. Applied Geochemistry. Vol 130:104984.

O'Kane M and Barbour SL (2003) Predicting field performance of lysimeters used to evaluate cover systems for mine waste. 6th Proceedings ICARD, Cairns, QLD, Pages 327–39.

Smith LJD, Bailey BL, Blowes DW, Jambor JL, Smith L, Sego DC (2013) The Diavik waste rock project: Initial geochemical response from a low sulfide waste rock pile. Applied Geochemistry, Vol 36, Pages 210-221, ISSN 0883-2927

Stott, DF (1968) Lower Cretaceous Bullhead and Fort St. John Groups between Smoky and Peace Rivers, Rocky Mountain Foothills, Northeastern BC. Geological Survey of Canada, Bulletin 152, 279 pp.

Urrutia P, Wilson W, Aranda C, Peterson H, Blackmore

S, Sifuentes F, Sanchez M (2011) Design and Construction of Field-Scale Lysimeters for the Evaluation of Cover Systems at the Antamina Mine, Peru. Proceedings of Tailings and Mine Waste 2011, Vancouver, BC, November 6 to 9, 2011.

Wellen CC, Shatilla NJ, Carey SK (2015) Regional scale selenium loading associated with surface coal mining, Elk Valley, British Columbia, Canada. Science Total Environ. Volume 532, pp. 791-802.

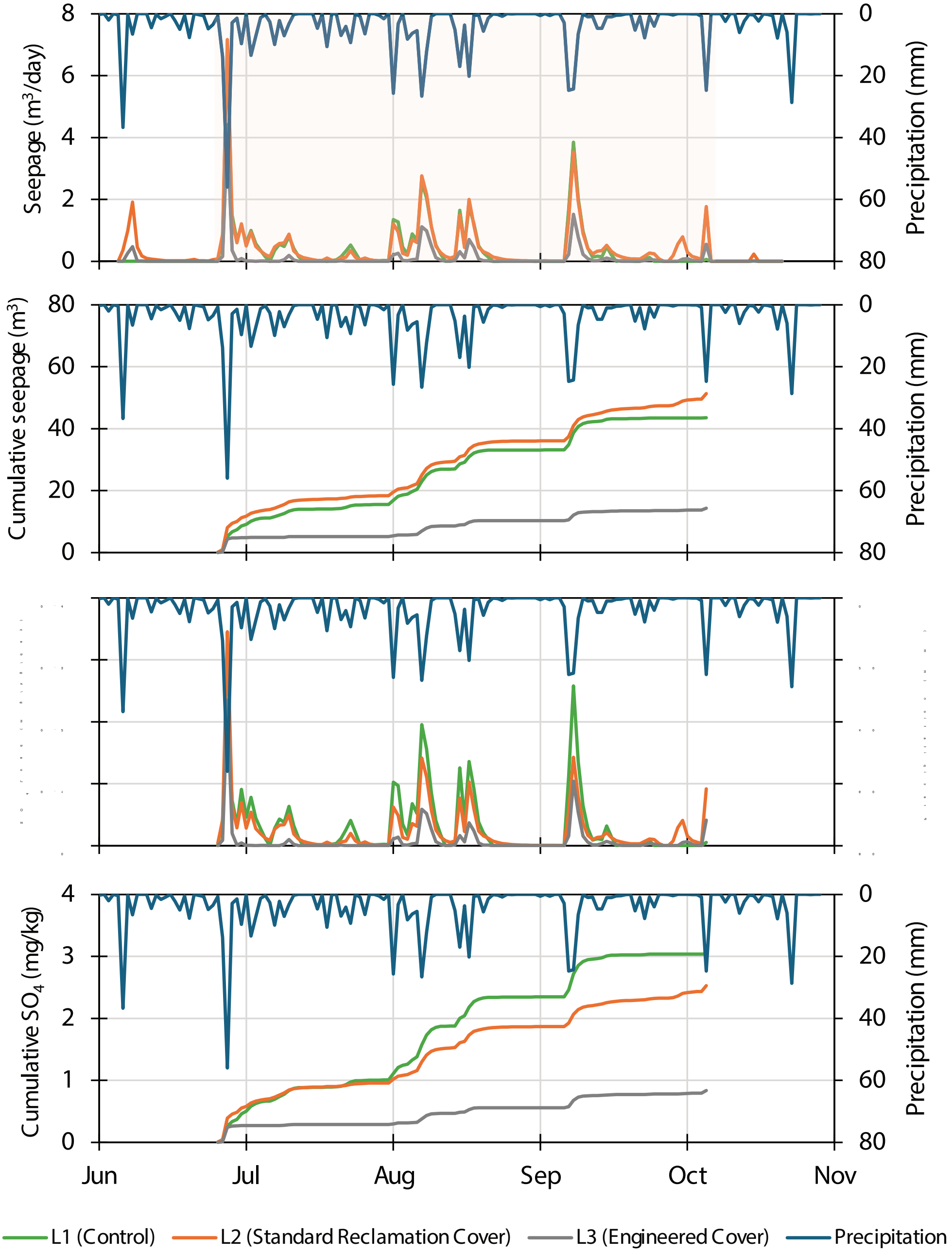

Figure 1: Time series illustrating patterns of seepage and precipitation (upper panel), cumulative seepage and precipitation (second panel), daily sulfate loading (third panel) and cumulative sulfate loading (lower panel), 6-years following commissioning of the three lysimeters. SO$_4$ data shown in the third and lower panels are standardized by mass per mine rock lysimeter.

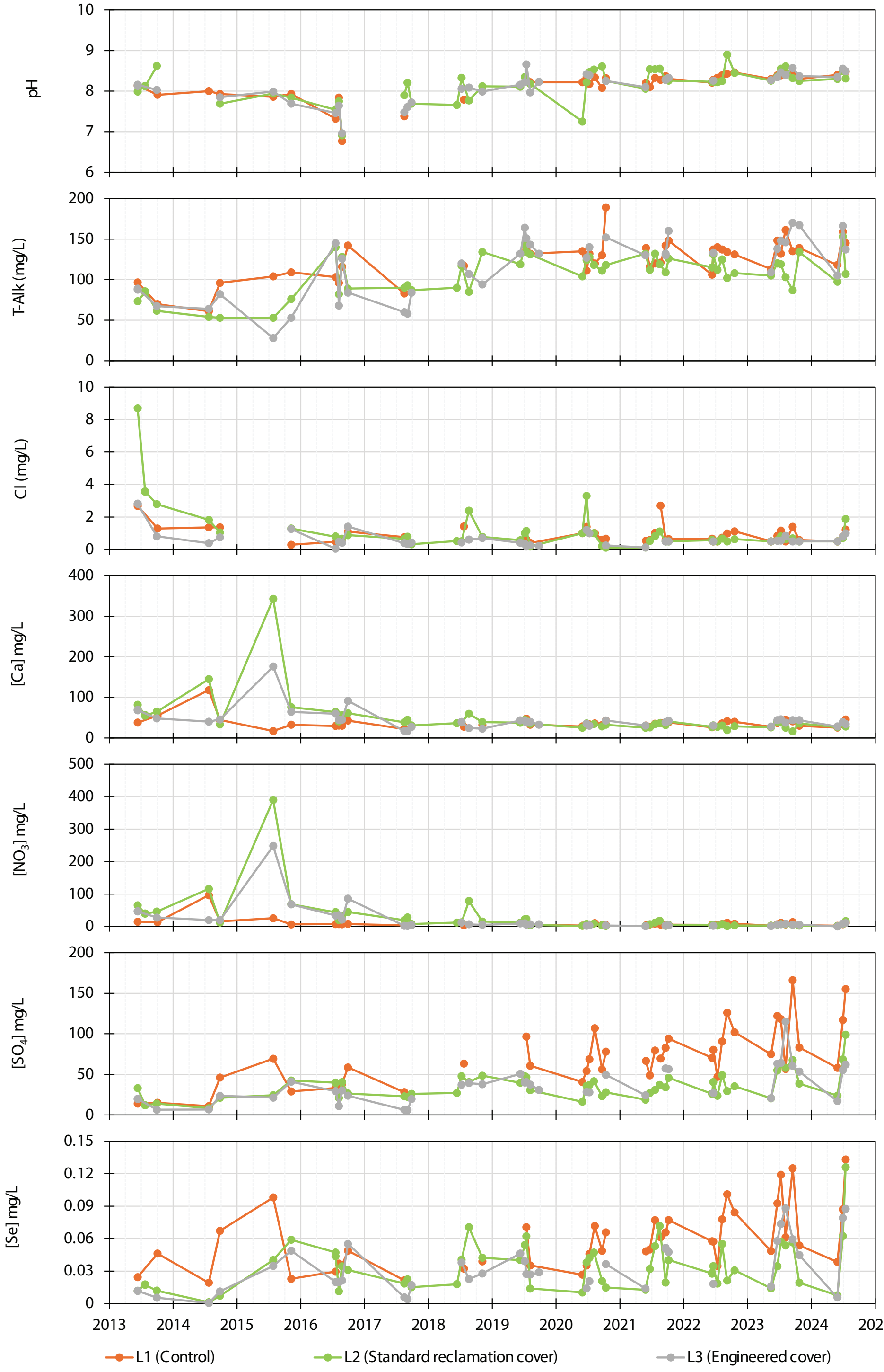

Figure 2: *Time series plots showing pH, total alkalinity, chloride, calcium, nitrate, sulfate and selenium measured for the period 2013-2024 at three mine rock lysimeters.*

Preliminary Analysis of Stable Water Isotope Patterns in the Lusatian Lignite Mining District (Germany)

Anne Gädeke[1], Maike Groeschke[2], Paul Koeniger[3]

[1]*Federal Inisitute for Geosciences and Natural Resources, Research and Development Centre for Post-Mining Areas, Gaglower Str. 17/18, 03048 Cottbus, Germany, anne.gaedeke@bgr.de, ORCID 0000-0003-0514-2908*

[2]*Federal Inisitute for Geosciences and Natural Resources, Research and Development Centre for Post-Mining Areas, Gaglower Str. 17/18, 03048 Cottbus, maike.groeschke@bgr.de, ORCID 0000-0003-3488-4310*

[3]*Federal Inisitute for Geosciences and Natural Resources, Groundwater Resources – Quality and Dynamics, Wilhelmstraße 25–30, 13539 Berlin, Germany, paul.koeniger@bgr.de, ORCID 0000-0002-1197-6274*

Abstract

This study presents preliminary findings from a large-scale survey comprising over 1,000 samples of precipitation, surface water, groundwater, and post-mining lakes in the Lusatian lignite mining district (Germany). All samples were analyzed for stable water isotopes (δ^2H, $\delta^{18}O$) to refine our understanding of hydrological connectivity among surface and groundwater as well as evaporation loss from post-mining lakes. Our results show distinct isotopic differences among water sources, identifying post-mining lakes primarily recharged by groundwater and areas where groundwater is influenced by surface water. These insights highlight the potential of isotope analysis as a valuable tool for adaptive water resource management.

Keywords: Stable water isotopes, Lusatian lignite mining district, post-mining lakes, surface-groundwater interactions, lake evaporation

Introduction

The EU aims to have a net-zero greenhouse gas (GHG) economy by 2050, with 55% reduction on 1990 levels by 2030. At present, heating and cooling represent over 50% of the nd cooling supply, two conceivable well locations were derived based on the mine layouts.

Conclusions

The lignite-mining region of Lusatia is characterized by i) low precipitation (less than 600 mm a-1, compared to the German average (820 mm a-1), 1981–2010, National Meteorological Service), ii) a negative climatic water balance in most years (MLUL 2018), iii) predominantly sandy soils with a low water storage capacity covered by highly managed ecosystems (forest and agricultural monocultures), and iv) long-term, large-scale open cast lignite mining activities. The lignite mining activities have significantly affected the water resources, both in terms of water quantity and quality, in the Lusatian river basins of the rivers Spree, Schwarze Elster and Lusatian Neiße (Grünewald 2001). Recent extreme heatwaves, coupled with low precipitation, have exacerbated water management challenges in this already water-scarce region (Creutzfeldt *et al.* 2021; MLUK 2021).

Stable water isotopes (δ^2H, $\delta^{18}O$), can serve as environmental tracers for investigating groundwater-surface water interactions and evaporation loss in (post-mining) lakes (Baskaran *et al.* 2009). The isotopic composition of precipitation, groundwater, and surface water can be used to trace the movement and mixing as well as the residence times of these water sources. This analysis potentially enables the identification of groundwater discharge pathways into surface water bodies and vice versa (Gat 1996). In addition, stable isotopes can support the quantification of evaporation loss from surface water and lakes (Koeniger *et al.* 2021), as the isotopic signature of the water sources (surface and groundwater, precipitation) differ. Evaporation is causing enrichment of heavier isotopes in source water, thus creating distinct gradients. These gradients provide insights into the rate of evaporation, the influence of climate variability, and the dynamics of the water balance within lake ecosystems. Stable isotopes thus offer a non-invasive method to better understanding hydrological processes.

The aim is this study is to refine our understanding of hydrological processes in mining-affected watersheds by using stable water (δ18O, δ2H) isotopic signatures of precipitation, surface water, groundwater, and post-mining lakes. The (long-term) aim is to assess the groundwater-surface water interaction and evaporation loss of the post-mining lakes. Our analysis focuses on the Lusatian mining district, located in northeastern Germany.

Study Area

The Lusatian mining district is located approximately 100 km southeast of the German capital Berlin, extending across the federal states of Brandenburg and Saxony and three watersheds: Spree, Schwarze Elster and Lusatian Neiße (Fig. 1 a) covering together an area of approximately 20,000 km². Lusatia experiences a temperate climate with both maritime and continental influences. Since the 1960s, significant air temperature increases were observed, while total annual precipitation remained unchanged (Gädeke *et al.* 2017). Industrial-scale open-cast lignite mining has been ongoing since the early 20th century in the Lusatian mining district. The open-cast lignite mining has had a profound impact on watersheds, resulting in extensive groundwater depletion, modified river courses, and changes in discharge patterns (Grünewald 2001; Schoenheinz *et al.* 2011; Pohle *et al.* 2019). To safely extract the lignite in the open-cast mines, groundwater is lowered below the coal seams, often reaching depths of up to 100 m below the ground surface. Part of the groundwater pumped has been used to augment surface water discharge over decades, especially of the Spree River. At the peak of mining, the groundwater drawdown cone extended across 2,100 km² and the total water deficit was about 9 × 109 m³. After the German reunification (1990), 12 out of 17 mines were closed resulting, among others, in a considerable reduction in the mine drainage water. Currently, the average proportion of mine drainage water in the Spree River at Cottbus is ~ 50%, increasing to ~75% during dry summer months (Uhlmann *et al.* 2023). The mass deficit following lignite extraction results in open pits, which are generally transformed into post-mining lakes in Lusatia. Once flooded, these lakes will collectively cover an area of approximately 350 km². The three still active open-cast mines will have to be shut down by 2038. Several water management challenges are overlapping in the Lusatian mining district, including, among others: further reduction of mine drainage waters to augment surface water flow, mitigation of the remaining mining-related water deficit, mining-related water quality problems, climate change, socioeconomic impacts.

Data and Methods

In 2024, more than 1,000 water samples, consisting of ~400 groundwater, ~260 surface water and ~450 post-mining lake samples, were collected in the Lusatian mining district (Fig. 1) as part of the standard montane hydrological monitoring of the LMBV (Lausitzer und Mitteldeutsche Bergbau-Verwaltungsgesellschaft mbH). The survey covers an area of approximately 4,000 km². In addition, the Federal Institute for Geosciences and Natural Resources operates a weekly precipitation sampling since 2023 in the city of Cottbus (Fig. 1 a).

A total of approximately 75 post-mining lakes were sampled using boats, helicopters, or onshore techniques (Fig. 1 b). Within each lake, samples were systematically collected from multiple locations and depths. Sampling followed the lakes' seasonal circulation patterns, including spring turnover, the start and end of summer stagnation, and autumn circulation, to capture temporal variations in water composition. Surface water sampling includes 68 streams, with sampling intervals ranging from biweekly to quarterly (Fig. 1 c). Groundwater samples were obtained from depths between 2.5 and 114 meters below the surface, representing different aquifer systems: aquifers formed in mining dumps and natural systems surrounding the post-mining lakes (Fig. 1 d).

All samples were analysed in the isotope laboratory of the German Federal Institute for Geosciences and Natural Resources (BGR), utilizing a Picarro L2130-i laser spectrometer. Results are expressed as parts per thousand deviations from the VSMOW (Vienna Standard Mean Ocean Water) with analytical precisions of 0.2‰ and 0.8‰ for $\delta^{18}O$ and $\delta^{2}H$ values, respectively.

Here, we present a subset of the samples (886 samples) as sample processing and data analysis are still ongoing (groundwater: 253 (~63% of collected samples), surface water: 217 (~84%), post-mining lakes: 363 (~81%), precipitation (53 weekly samples (January 2023 – April 2024), sampling ongoing)).

Mean precipitation of Cottbus presents the precipitation amount-weighted average of weekly isotope values ($\bar{\delta}$) from the total

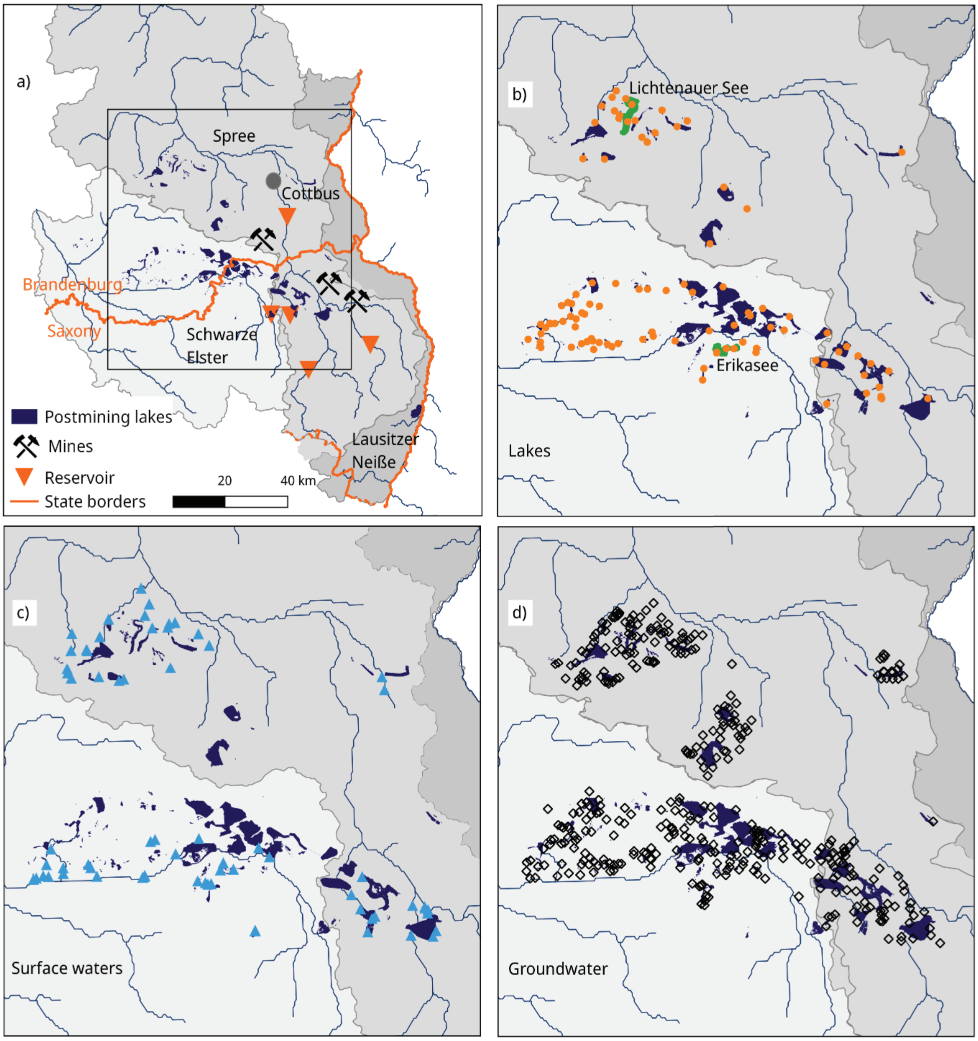

Figure 1 *Overview of the study area a) and the sampling locations for post-mining lakes b), surface c) and groundwater d). The black box in a) presents the section that is zoomed into in b), c) and d). In b) the lakes shown in green colour present the Erikasee and the Lichtenauer See.*

Table 1 Statistical properties of the samples (886 in total).

	Precipitation		Lakes		Surface waters		Groundwater	
	$\bar{\delta}$18O	$\bar{\delta}$2H	δ^{18}O	δ^{2}H	δ^{18}O	δ^{2}H	δ^{18}O	δ^{2}H
Minimum	-19.5	-147	-8.6	-62	-9.4	-66	-9.9	-69
25. Percentile	-9.8	-71	-5.1	-43	-7.7	-57	-9.1	-65
Median	-8.0	-57	-4.0	-37	-6.5	-51	-8.8	-63
Mean	-8.0	-57	-4.0	-38	-6.3	-50	-8.2	-60
75. Percentile	-5.8	-36	-3.0	-31	-4.8	-41	-8.1	-59
Maximum	1.3	-9	0.8	-17	-2.1	-28	-3.0	-30

weekly precipitation (P) and isotope values (δ) as follows:

$$\bar{\delta}[‰] = \frac{\sum_{i=1}^{N} \delta_i \times P_i}{\sum_{i=1}^{N} P_i} \qquad (1)$$

Results and Discussion

Table 1 provides an overview of the statistical properties of the isotopic signatures of precipitation, post-mining lakes, surface and groundwater. Overall, post-mining lakes have the most enriched (less negative) isotopic signature, followed by surface waters. Groundwater and precipitation isotopic signatures are most depleted (more negative). In addition, precipitation isotopes show a distinct variability characteristic for stations in a continental-influenced climate in the Northern Hemisphere: More positive δ-values occur during summer compared to the winter.

The dual-isotope plot, which includes all samples, reveals that there are distinct isotopic signatures depending on the water source (Fig. 2).

- The majority of surface, and especially the post-mining lakes water samples deviate from the meteoric water lines (MWL) due to evaporative enrichment (lower slope compared to the Global MWL and Local MWL)
- Groundwater samples, and also surface water samples, that plot near the GMWL and LMWL present locations where no

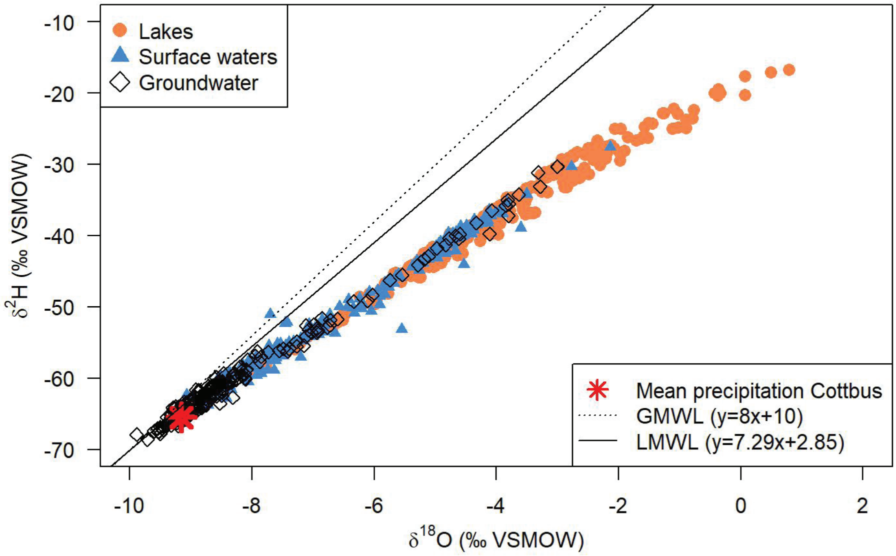

***Figure 2** Dual isotope plot (δ^{18}O vs. δ^{2}H) showing the post-mining lake, surface and groundwater samples, the Global (GMWL) and Local (LMWL) Meteorological Water Line, and the mean weighted precipitation of Cottbus (01/2023-04/2024). Precipitation is <600 mm a^{-1}.*

mixing with surface/post-mining lake water has occurred (minimal evaporative losses)

- Groundwater samples that plot away from the GMWL and LMWL indicate that mixing processes with surface/post-mining lake water have occurred (intermediate isotopic signatures)

To evaluate a subset of the post-mining lakes in more detail, we preselected 24 lakes. Out of these 24 lakes, the "Erikasee" samples plot nearest to the LMWL. This observation supports the fact that the Erikasee was primarily flooded by groundwater instead of surface water. A total of 11 samples were collected from the "Erikasee" at three different locations (shore, southwestern part, lake center (close to an inlet of a trench)) and different periods (March, May, June, August, September). The analysis reveals the following: samples collected close to the lake surface become more enriched during summer compared to winter. At the sampling point in the center of the post-mining lake for example, an increase in δ18O (δ2H) of 40% (28%) was identified between March and September. Furthermore, sampling points near the lake's surface are more enriched compared to those at greater depths. Opposite to the enrichment process taking place close to the lake surface, the samples collected at depths greater 10 m become more depleted during summer (Fig. 3). For the most enriched lakes, e.g. "Lichtenauer See", two possibilities and their combined effect exist: large evaporation demand and surface water input/flooding of lake with surface water to keep water levels as well as to ensure a satisfactory water quality. Based on 16 samples collected between March and September, the spatio-temporally analysis reveals the same patterns as for lake "Erikasee": more enriched (depleted) values closer to the lake surface (bottom) and as the year advances. In terms of morphology, the "Erikasee" and "Lichtenauer See" are similar, though they differ in size ("Erikasee" ~40% of the size of "Lichtenauer See") and the "Erikasee" is characterised by a large internal in-pit dump. Both lakes are fully flooded. The other most enriched lakes, present the larger post-mining lakes of Lusatia, some of which, are still actively flooded by surface water and/or are characterised by channels connecting different lakes. In addition, due to their size, large evaporation loss is expected.

Conclusions

Our study shows the potential of using stable water isotope tracers to investigate the spatial and temporal variability of the dominant

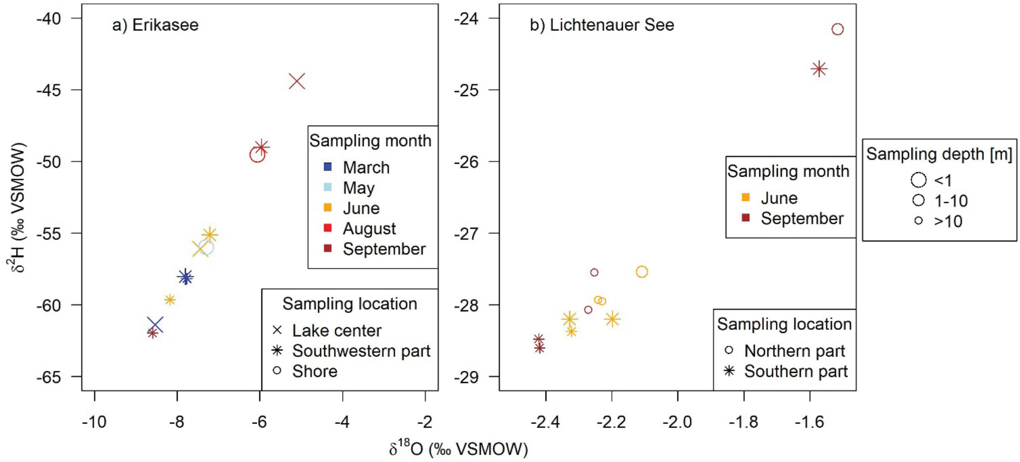

Figure 3 *Dual isotope scatter plot for the Erikasee (a) and Lichtenauer See (b) showing differences based on sampling month, location and depth.*

hydrological processes in watersheds affected by large-scale lignite mining. The simultaneous sampling of precipitation, lake, surface and groundwater allows the identification of isotopically distinct regions: effluent (groundwater infiltration into surface water) and influent (surface water infiltration into groundwater) systems, reflecting the state of flooding the post-mining lakes and rising groundwater levels in the groundwater depression cone (ongoing, completed). Our preliminary results also reveal that isotopic signatures of post-mining lakes, surface and groundwater samples differ considerably: clear enrichment of heavier isotopes and more thus more positive δ-values indicate progressive enrichment due to evaporation of water, especially close to the postmining lake surfaces. This approach enables a more detailed characterisation and interpretation of the current status of post-mining lakes in the Lusatian lignite mining district.

Acknowledgements

We would like to thank the LMBV (Lausitzer und Mitteldeutsche Bergbau-Verwaltungsgesellschaft mbH) for providing the opportunity to collect the water samples.

References

Baskaran S, Ransley T, Brodie RS, Baker P (2009) Investigating groundwater–river interactions using environmental tracers. Aust J Earth Sci 56:13–19. https://doi.org/10.1080/08120090802541887

Creutzfeldt B, Pohle I, Zeilfelder S, *et al* (2021) Die Niedrigwasser 2018, 2019 und 2020 – Analysen und Auswirkungen für das Land Berlin. Senatsverwaltung für Umwelt, Verkehr und Klimaschutz, Abteilung Integrativer Umweltschutz, Referat Wasserwirtschaft, Wasserrecht und Geologie, Berlin

Gädeke A, Pohle I, Koch H, Grünewald U (2017) Trend analysis for integrated regional climate change impact assessments in the Lusatian river catchments (north-eastern Germany). Reg Environ Change 17:1751–1762. https://doi.org/10.1007/s10113-017-1138-0

Gat JR (1996) Oxygen and Hydrogen Isotopes in the Hydrological Cycle. Annu. Rev. Earth Planet. Sci. 24:225–262

Grünewald U (2001) Water resources management in river catchments influenced by lignite mining. Ecol Eng 17:143–152. https://doi.org/10.1016/S0925-8574(00)00154-3

Koeniger P, Hamutoko J, Post VEA, *et al* (2021) Evaporation loss along the Calueque-Oshakati Canal in the Cuvelai-Etosha Basin (Northern Namibia): evidence from stable isotopes and hydrochemistry. Isotopes Environ Health Stud 57:53–66. https://doi.org/10.1080/10256016.2020.1830082

MLUK (2021) Niedrigwasser 2018 und 2019 in den Flussgebieten Schwarze Elster, Spree und Lausitzer Neiße – Eine länderübergreifende Auswertung. Ministerium für Landwirtschaft, Umwelt und Klimaschutz des Landes Brandenburg, Potsdam

MLUL (2018) Klimawandelmonitoring im Land Brandenburg – Basisbericht. Potsdam

Pohle I, Gädeke A, Schümberg S, *et al* (2019) Management Influences on Stream-Flow Variability in the Past and Under Potential Climate Change in a Central European Mining Region. Water Resour Manag 33:5191–5206. https://doi.org/10.1007/s11269-019-02432-3

Schoenheinz D, Grünewald U, Koch H (2011) Aspects of Integrated Water Resources Management in River Basins Influenced by Mining Activities in Lower Lusatia. ERDE – J Geogr Soc Berl 142:163–186

Uhlmann W, Zimmermann K, Kaltofen M, *et al* (2023) Wasserwirtschaftliche Folgen des Braunkohleausstiegs in der Lausitz. Umweltbundesamt Texte | 90/2023:266

Hydrodynamic Modelling of Rising Lower Triassic Sandstone Groundwater in the Lorraine Coal Basin (France)

Pauline Galas[1], Bastien Morin[2], Laurent Vaute[2], Olivier Lefebvre[1], Marsia Joder[3], Maxime Hirsch[4]

[1]*GEODERIS, 1 rue Claude Chappe, 57000 Metz, France, pauline.galas@geoderis.fr, olivier.lefebvre@geoderis.fr*

[2]*BRGM, 1 rue Jean Zay, 54500 Vandœuvre-lès-Nancy, France, b.morin@brgm.fr, l.vaute@brgm.fr*

[3]*BRGM, DPSM/UTAM Est, 2 avenue de la Moselle, 57800 Freyming-Merlebach, m.joder@brgm.fr*

[4]*DREAL Grand-Est, 5 rue Hinzelin, 57009 Metz, maxime.hirsch@developpement-durable.gouv.fr*

Abstract

The cessation of mining operations and associated dewatering, combined with a reduced demand for groundwater from the Lower Triassic sandstone aquifer by local authorities and industries in the Lorraine coalfield (France), has led to a rising water table and a long-term risk of flooding in several urban areas. GEODERIS and BRGM developed a three-dimensional numerical hydrodynamic model to identify flood-prone areas and estimate the time frame within which the water table could eventually reach the surface, both with and without the progressive implementation of a pumping infrastructure. A major update of the model was conducted between 2023 and 2024.

Introduction

The Lorraine coalfield, located in northeastern France along the border with Germany, was the site of intensive coal mining from the late 19th century to the early 21st century. Prior to mining activities, the area was largely covered by wetlands and swamps. Groundwater abstraction for mining operations, industrial use, and municipal supply significantly lowered the water table of the Lower Triassic Sandstone aquifer, leading to the drying up of wetlands. Urban development subsequently took place in these areas without fully considering the long-term unsustainability of this situation with a possible water table replenishment.

The gradual shutdown of water-intensive industries in the 1980s and 1990s, the cessation of coal mining in the 2000s, and increasing water conservation efforts have contributed to the ongoing recovery of the sandstone aquifer. The reestablishment of a new piezometric equilibrium, potentially at or above the topographic surface, must be taken into account.

In this context, GEODERIS was commissioned by the French government, which is fully responsible for post-mining risk management, to conduct various groundwater rise forecasts. In collaboration with BRGM, a three-dimensional (3D) numerical hydrodynamic model has been under development since 2015−2018 to simulate groundwater dynamics across the entire Lorraine coalfield (BRGM 2018, GEODERIS 2018, GEODERIS 2022). Based on the results of this model, areas where groundwater recovery is expected to reach depths of less than 3 meters were delineated. Subsequently, in 2021, pumping strategies were assessed and designed to lower the water table to depths greater than 3 meters within these so-called 'commitment zones.' A major update of the model was conducted between 2023 and 2024 to improve forecasts of both the rising groundwater level in the sandstone aquifer and the required withdrawal volumes (BRGM 2025, GEODERIS 2025). The progressive deployment of the drawdown wellfield will be accompanied by a phased expansion of the piezometric monitoring network to refine predictions through future iterations of the 3D model.

Methods

Structure of the model

The Lower Triassic sandstone groundwater model, which forms the basis of our work, has been developed by BRGM since 1993 using the MARTHE software. MARTHE, developed by BRGM, is a numerical modeling tool for simulating groundwater flow and mass transport (Thiéry 2015). The model covers a large portion of the Lorraine region, primarily corresponding to the confined section of the aquifer. The main model uses a grid of 500-meter square cells for regional-scale representation, while the Lorraine coalfield is represented with a refined grid of 50-meter square cells over an area of approximately 750 km². The model operates in a transient (non-steady-state) regime.

Four geological layers are considered (Fig. 1), listed from the most recent to the oldest (i.e., from top to bottom):

- Alluvial deposits: sandstone facies with occasional impermeable peat horizons.
- Lower Triassic sandstone: predominantly fine to coarse sandstones with clay layers in the upper section, conglomeratic levels in the central part, and clay lenses at the base.
- Permian: clayey sandstones with very low permeability.
- Carboniferous mining works (where present): this formation is considered to have low permeability, with flow occurring only within mining galleries or fractured zones created by mining operations.

Several aquifers are present in these formations: the alluvial domain, the Lower Triassic sandstones and the mining reservoir. The latter was implemented because of the mine induced fracturing of the overlying sandstones, creating infiltration of the water into the mine through so-called "aquifer-mine exchange points". When the mines closed, pumping stopped, leading to the flooding of mines, which was completed at the end of 2009 in the western sector and in 2012 in the central-eastern sector. Three pumping stations are still in place in the mining reservoir to control its level and maintain it below the Lower Triassic sandstone water level. It allows to avoid the formation of mineralized plumes at the aquifer-mine exchange points.

The Lower Triassic sandstone aquifer is recharged both by outcrops within the basin and by more distant outcrops in surrounding mountain ranges. It is confined where it is overlain by the low-permeability marl formations of the Muschelkalk (considered as impermeable in the modelling). On a regional scale, groundwater flows from the south-southwest to the north-northeast.

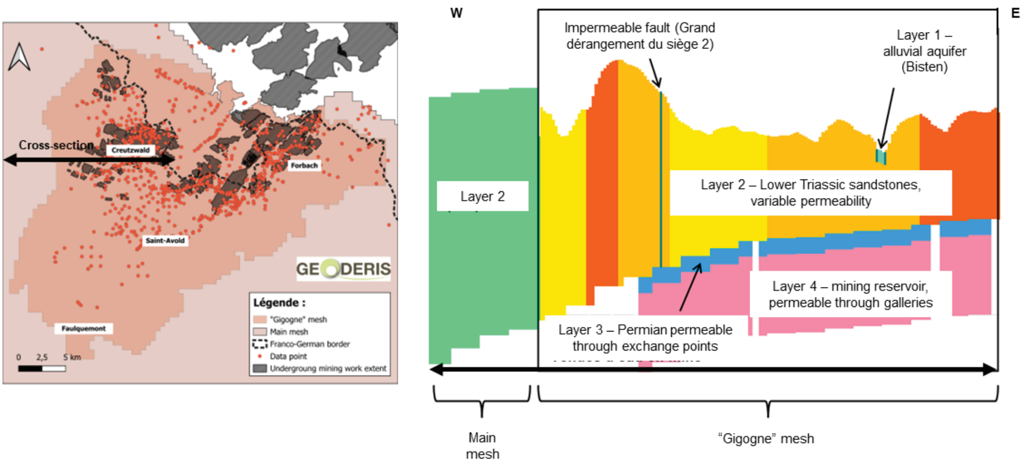

Figure 1 West-East cross-section of the Lower Triassic sandstone groundwater model through the city of Creutzwald (BRGM, 2015).

The model explicitly accounts for the hydrogeological role of major faults, including the Hombourg-Longeville, Saint-Nicolas, and Grand Dérangement du Siège 2 faults. Notably, the Longeville-Hombourg fault hydraulically divides the basin into two distinct sectors: the western sector, where the water table is close to the surface, and the eastern sector, where it remains deep (over 40 m).

Interactions between alluvial aquifers (and surface water bodies), the sandstone aquifer, and mining reservoirs via the fractured Permian formations are also modeled. The surface layer is represented using a LIDAR-derived Digital Terrain Model (DTM), the minimum elevation was applied to the center of each 50-meter square cell (safe for the rising groundwater calculations).

Automated history calibration (1976–2022)

In 2023–2024, an update of the 2018 version of the model was carried out (alluvial domain redefinition, change in faults modelling, consideration of climate change). A re-calibration step of the 2018 version of the model was also performed (Fig. 2) based on those major changes and new data acquisition. This process involves adjusting parameters related to the geological formations or the model structure to reproduce observed water level data.

The main parameters used for model calibration include the permeability of the various geological layers and faults, as well as the vertical anisotropy of the alluvial deposits, which represents its capacity to exchange water with the underlying sandstone formation. These parameters were initially assigned uniform values throughout the model. The mean value of vertical anisotropy obtained during the calibration of the latest model version (2018) was retained, while permeability was defined based on the average Lower Triassic sandstone permeability value from the literature in the Lorraine coal basin (1.10^{-5} m·s^{-1}, Noël 1997).

Calibration was conducted using the PEST tool (PEST: Model-Independent Parameter Estimation and Uncertainty Analysis, https://pesthomepage.org/), an algorithm designed to automate incremental adjustments of calibration parameters. The

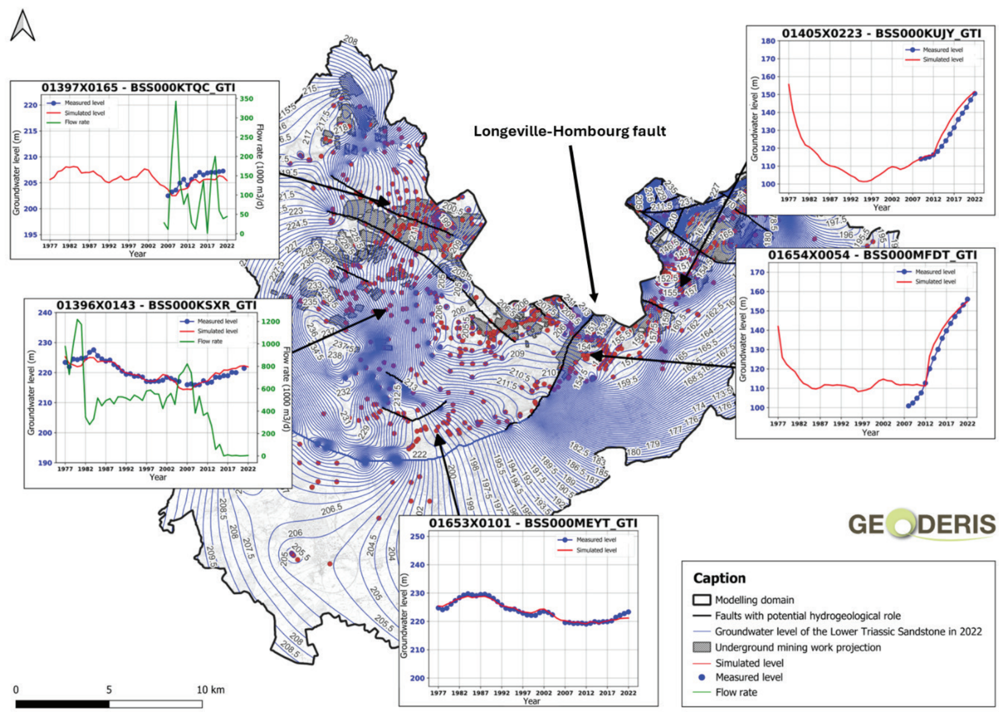

Figure 2 *Examples of history matching results (comparison of measured and simulated levels).*

algorithm iterates multiple times, varying permeability and anisotropy to minimize the difference between model results and observed data. Other parameters, such as stream infiltration and fault permeability, were adjusted manually. The calibration process was considered complete when the parameters stabilized and showed no significant further variation. At the end of this step of calibration, errors vary between 1,68 m and 5,93 m according to the sectors (mean of medians of absolute deviations weighted by number of annual observations, without considering a part of German territory which presents only few piezometric chronicles).

Simulations

The simulation scenarios combine various climate and withdrawal scenarios. The climatic scenario used for forecasting simulations of the effects of changes in withdrawals from the sandstone aquifer and the mining reservoir integrates two distinct climatic periods, each modeled with specific infiltration chronologies based on French IPCC climate projections (DRIAS):

- A so-called "stabilized period", designed to forecast the long-term influence of reduced withdrawals under a fixed average infiltration rate, once the water table has reached equilibrium.
- An "exceptional period", intended to assess the additional influence of recurrent extreme rainfall events by applying a maximum infiltration rate.

The RCP 4.5 (Representative Concentration Pathway) emission scenario from DRIAS was selected. This corresponds to a moderate stabilization scenario in which global efforts are made to limit greenhouse gas emissions.

Regarding the withdrawal scenarios, an initial simulation was conducted using a water demand projection collected by national authorities. This simulation aimed to estimate the evolution of the rising water table in the absence of any active control measures. Based on the results obtained, a second modeling phase was carried out to design a pumping network capable of maintaining the water table at a depth of more than 3 meters in the commitment zones.

Results

The results are presented as calculated isodepth maps for different dates and simulation scenarios, namely: 2023, 2030, 2065, the stabilized period, and the exceptional period.

Fig. 3 and 4 illustrate some key results. Fig. 3 depicts the water table depth in the sandstone aquifer at the end of the stabilized period. The stabilized water level—defined as the point where the rate of water level rise is less than 3 cm per year across the entire basin – is expected to be reached by 2147. Fig. 4 shows the water table depth in the sandstone aquifer under high rainfall conditions, taking into account the progressive deployment of the pumping network. In the model, the pumped water leaves the system whereas in reality it will be discharged into the watercourses.

By 2023, the sandstone water table has stabilized in the Grossbach valley. It is potentially outcropping in the Bisten valley, although impermeable layers within the sandstone or alluvial formations may prevent direct observation of groundwater at the surface. The remainder of the basin was not expected to experience a shallow water table this year.

According to the first simulation scenario – without drawdown measures to control the water table – the eastern sector will be affected by groundwater levels shallower than 3 meters by 2044.

The second type of simulation was used to determine the number of boreholes required to lower the water table to a depth of more than 3 meters below the commitment zones. In the western sector, by 2030, 9 pumping boreholes would be necessary to meet the commitments. Most of these are located in the Bisten valley, with an additional borehole required near the eastern boundary of the Longeville-Hombourg fault. Subsequent modeling indicates that by 2065, 7 more boreholes would be installed in the Bisten valley. By the time the water table stabilizes, a total of 16 pumping wells will be operational in the model. The results also suggest that under a future exceptional rainfall scenario, it may be necessary to install 3 additional pumping wells in the Bisten valley.

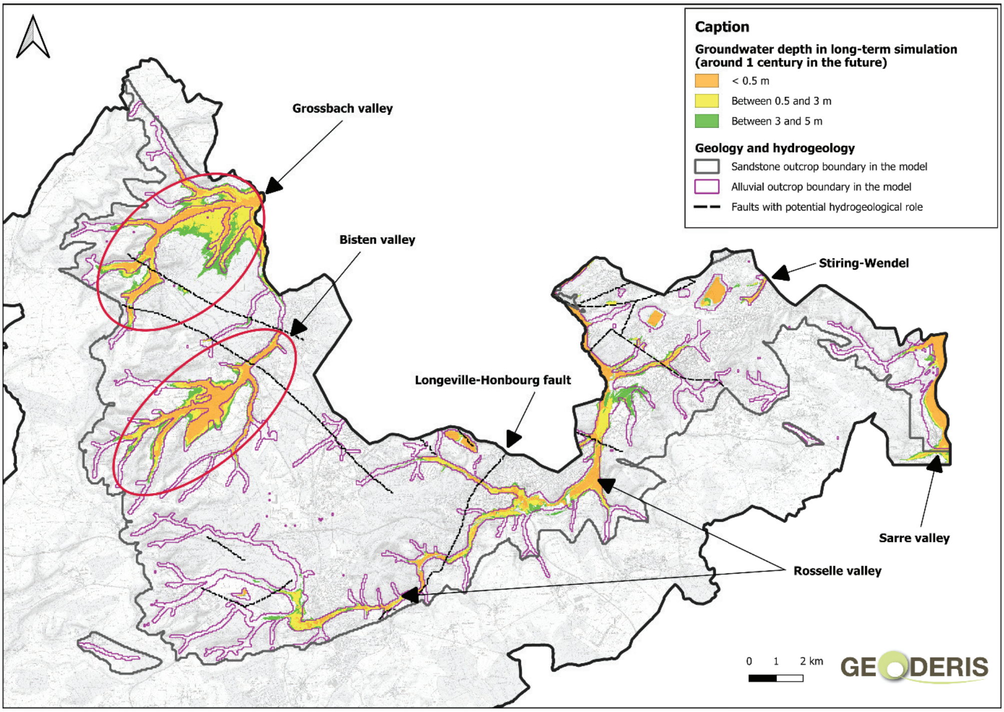

Figure 3 *Sandstone groundwater level simulated at the end of the stabilized period (around one century from today).*

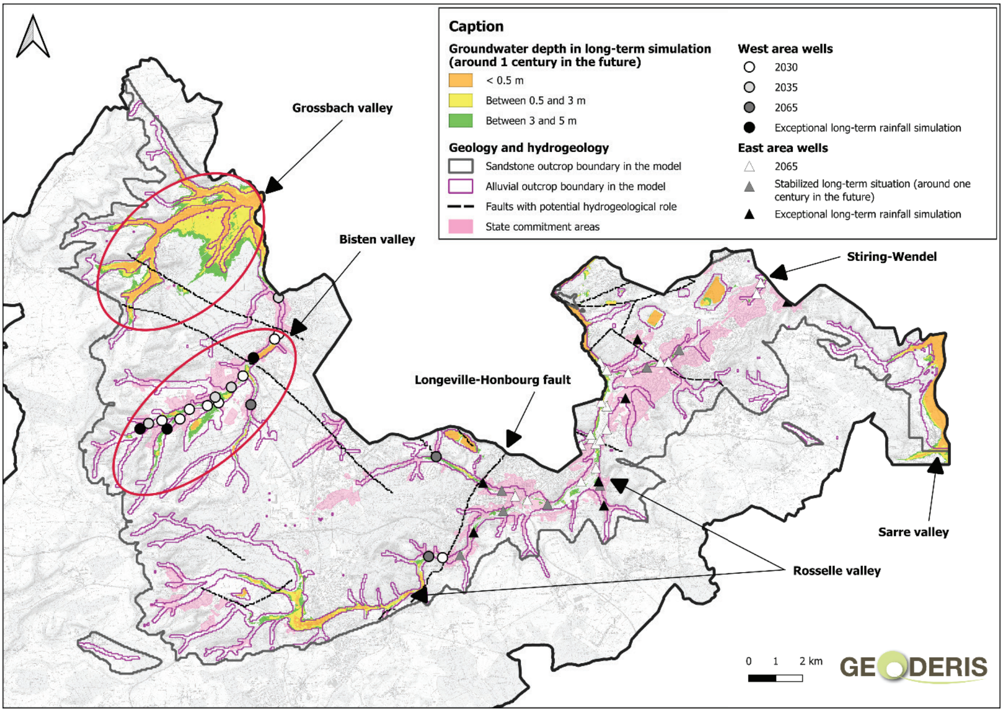

Figure 4 *Sandstone groundwater level simulated at exceptional period, considering gradual installation of pumping areas.*

In the eastern sector, pumping to maintain the sandstone water table at a depth of more than 3 meters should begin by 2044. By 2065, approximately 20 pumping structures would need to be progressively activated, extending from the Rosselle valley to the Stiring-Wendel township. Under stabilized water conditions, expected to be reached within a century, 5 additional boreholes would need to be activated. In the event of high rainfall conditions, a further 5 boreholes would be required.

Perspectives

In total, approximately 50 drawdown boreholes would be required to maintain the water table at a depth of more than 3 meters below the commitment zones across the Lorraine coalfield. This would correspond to an annual extraction volume of approximately 21 million m^3 under stabilized conditions and up to 40 million m^3 in an exceptional rainfall scenario. These estimates take into account 2 existing boreholes in the Bisten valley, which also tap into the Lower Triassic sandstone aquifer.

To support the progressive deployment of an optimal wellfield, a dense piezometric network will be gradually established, comprising around 200 piezometers throughout the Lorraine coalfield. This expanded monitoring network will allow for precise measurement of rates of water table rise and assessment of the actual effect of drawdown boreholes. Additionally, it will provide valuable data on the geological formations encountered, including peat horizons, improving our understanding of localized confinement of the water table, whether within alluvial deposits or sandstone formations.

Pumping tests and chemical analyses will also be conducted to enhance knowledge of the hydrogeological functioning of different sectors and to determine the origin of the extracted water. Furthermore, chemical analyses will provide critical information on water quality, as compliance with regulatory standards is required before any discharge into surface water bodies.

References

Noël Y. (1997) Modèle de gestion de la nappe des grès du Trias inférieur en Lorraine, Phase 1 – Acquisition des données. Rapport BRGM R 39228.

BRGM (2015) Evaluation des zones à risque lié à la remontée de nappe consécutive à la baisse des prélèvements d'eau dans le bassin houiller lorrain, secteur de La Houve, RP-64573-FR

Thiéry D. (2015) – Code de calcul MARTHE – Modélisation 3D des écoulements dans les hydrosystèmes - Notice d'utilisation de la version 7.5. BRGM/RP-64554-FR, 306 p., 150 fig.

BRGM (2018) Evaluation des zones soumises au phénomène de remontée des nappes du grès du Trias inférieur et des alluvions sus-jacentes dans le bassin houiller lorrain, RP-67630-FR.

GEODERIS (2018) Cartographie des zones soumises au phénomène de remontée des nappes dans le bassin houiller lorrain (57), E2018/034DE.

GEODERIS (2022) Remontée de nappe dans le bassin houiller lorrain. Réponse à la saisine de la DREAL Grand Est du 11/08/2021 concernant les engagements de l'Etat Vision « projet » à un horizon de 10 ans, 2021/165DE.

BRGM (2025) Evaluation des zones soumises au phénomène de remontée des nappes du grès du Trias inférieur et des alluvions sus-jacentes dans le bassin houiller lorrain – Version 2024, RP-73887-FR.

GEODERIS (2025) Mise à jour 2024 de la cartographie des zones soumises à la présence de la nappe des Grès du Trias Inférieur à faible profondeur dans le bassin houiller lorrain (57), 2024/168DE.

The use of geomorphology as the basis of mining closure: a case study of Waste Rock Facility rehabilitation at the Santa Bárbara mine (Perú)

Alfredo Gallardo[1], Juan del Río[2], John Melgarejo[3]

[1]*Amphos 21 Consulting Peru SAC, Jr. Paseo del Bosque 500, of. 201, Lima, Perú,* alfredo.gallardo@amphos21.com, *ORCID 0000-0002-7293-3825*

[2]*Amphos 21 Consulting Peru SAC, Jr. Paseo del Bosque 500, of. 201, Lima, Perú,* juan.delrio@amphos21.com, *ORCID 0000-0002-7293-3825*

[3]*Compañía de Minas Buenaventura SAA, Ca. Las Begonias 415, Lima, Perú,* john.melgarejo@buenaventura.pe, *ORCID 0000-0002-0055-1828*

Abstract

Compañía de Minas Buenaventura is custodian of the Santa Bárbara mine located in the Departament of Huancavelica in Peruvian central highlands. Santa Bárbara is – one of the first gold and silver mines exploited by the Spanish conquistadors upon their arrival in the Americas – In 2021 Compañía de Minas Bubenaventura commissioned Amphos 21 to conduct basic and engineering studies for the design of a closure project. This project is focused on three waste rock dumps and an open pit. A novel geomorphological restoration approach was proposed, unifying these deposits and shifting from a standard regulatory closure framework to one that is more harmonious with the natural environment. The open pit was not part of the geomorphological rehabilitation.

The most outstanding feature of this pioneering and innovative project is the elimination of the need for concrete channels for surface water management. Instead, an organic soil cover layer was designed, with varying thicknesses tailored to the various slopes of the terrain. This solution is complemented by the use of native high Andean species (stipa ichu), which enhance the ecological integration of the site. This approach not only reduces post-closure maintenance costs but also minimizes socio-environmental risks typically associated with traditional infrastructure components. By prioritizing natural solutions, the project demonstrates a commitment to both sustainability and environmental harmony, setting a new benchmark for mining closure practices.

Keywords: Environmental liabilities, innovation, geomorphology, rehabilitation, runoff

Photography 1: *View of typical closure of mining environmental liabilities*

Introduction

The regulations governing mine closure in Peru were established in 2003, followed by the guidelines for the closure of environmental liabilities in 2005. These regulations were accompanied by respective closure guides, which serve as reference documents providing guidelines, suggestions, and minimum directives proposed by the state. These documents are widely used by mining companies and, particularly, by the consulting firms responsible for designing mine closure plans.

However, Peruvian closure legislation tends to be static, emphasizing the development of component engineering over specific, site-specific studies. Specialized consultancies often treat the guidelines and standards as strict compliance requirements, adhering to them to the letter. This approach overlooks numerous variables and natural aspects that are not adequately evaluated or incorporated into rehabilitation and closure designs.

Over the past two decades of activities related to the closure of mining environmental liabilities, the industry has largely operated within the framework of these guidelines and the predefined parameters for the shape and structure of components, such as waste rock facilities (WRFs). Most of these facilities have been remediated according to the following criteria:

- Total or partial removal of rock material.
- Profiling and physical stability of slopes
  - Covering with natural waterproofing material (clays, gravels and topsoil).
  - Waterproofing with geosynthetics and topsoil.

Many of these projects remain under restricted access and continuous surveillance, as none have successfully achieved stable closure conditions that harmonize with the natural environment. Common issues include soil erosion, limited vegetative growth, failures in concrete channels, and the presence of acid rock drainage, among others. These challenges force mining companies to incur permanent maintenance costs for infrastructure and water treatment, undermining the long-term sustainability of the closures process.

In contrast, this project aims to rehabilitate the site by integrating the waste rock facilities (WRFs) with the natural slopes (geo-shapes) of the surrounding environment. This innovative approach involves the implementation of a natural cover composed solely of topsoil and native species, such as Stipa ichu, eliminating the need for concrete channels and other artificial water collection, management, and discharge systems. By prioritizing natural solutions, the project not only reduces maintenance costs but also fosters a more sustainable and ecologically integrated closure, setting a new standard for mining rehabilitation practices.

Background

Santa Bárbara holds a significant place in mining history as one of the first Spanish mines in the Americas, with operations beginning shortly after the arrival of Conquistadors in the 16th century (1532). Over the centuries, Santa Barbara has played a pivotal role in the history of Huancavelica and Peruvian mining, standing out as the only quicksilver (mercury) mine in Peru during the viceroyalty period.

In the 20th century, the mine transitioned into private ownership and was converted into an open-pit copper operation. It operated from 1960 until 1982, when activities ceased. By 1998, the site was officially declared an environmental liability. Due to its historical and cultural significance, the mine was designated as Cultural Heritage of the Nation by the Peruvian Institute of Culture in 2005.

Since 2009, closure works have been underway at the site. In 2021, Amphos 21 was commissioned to design and engineer the geomorphological rehabilitation of two waste rock facilities (WRFs), DSB-02 and DSB-14, covering an area of approximately 20 hectares. This project represents a groundbreaking effort to restore the site in a way that harmonizes it with its natural and historical context, setting a new benchmark for the closure of mining sites.

Design and Engineering

WRF DSB-14, was first “closed” in 2015, under the closure criteria mentioned in the introduction. However, the field works undertaken in 2015 presented the following problems:

- Soil erosion within the reservoir
- Low vegetative growth
- Clogging of concrete channels
- Discharge of water over the existing road
- Sediment entrainment on natural soils
- Permanent maintenance and control costs
- Constant supervision and nonconformities issued by the Peruvian Environmental Evaluation and Control Agency (OEFA).

Buenaventura, the custodian of Santa Bárbara, decided to incorporate this component as part of geomorphological rehabilitation, aiming to propose a comprehensive closure solution. This decision was driven by the recognition that previous design criteria had proven ineffective in achieving long-term stability and environmental integration.

The WRF DSB-02 was divided into two distinct sectors: DSB-02A and DSB-02B (Fig. 1). Sector A corresponded to a waste rock dump located on natural terrain without regular slope control or proper conformation, resulting in an irregular and unstable structure. In contrast, Sector B maintained a well-organized and managed waste rock dump, with a more controlled and stable configuration. This division allowed for a tailored rehabilitation approach, addressing the unique challenges of each sector while ensuring a cohesive and sustainable closure design.

The new design criteria for the geomorphological rehabilitation of these WRFs were as follows:

- Restore the functionality of the hydrological network and the promotion of biodiversity through the recovery of the natural hydrological regime.
- Avoid the use of terraces or banks
- Design a drainage network with hydrological criteria (incorporating maximum storn events and climate change).
- Use the surrounding natural area as a reference
- Generate concave or convex-concave slopes (Fig. 2).
- Avoid the use of anthropic or artificial elements such as pipes, ditches or concrete channels, etc.

In 2021, Amphos 21 conducted a comprehensive geochemical study of the entire Santa Bárbara mine site, including the two waste rock facilities (DSB-02 and DSB-14). The results revealed that the rock material contained in these facilities is not expected to generate acid rock drainage (ARD), results that are consistent with the site, since during more than 40 years of mine abandonment, there was never acid drainage. This condition significantly simplifies the rehabilitation

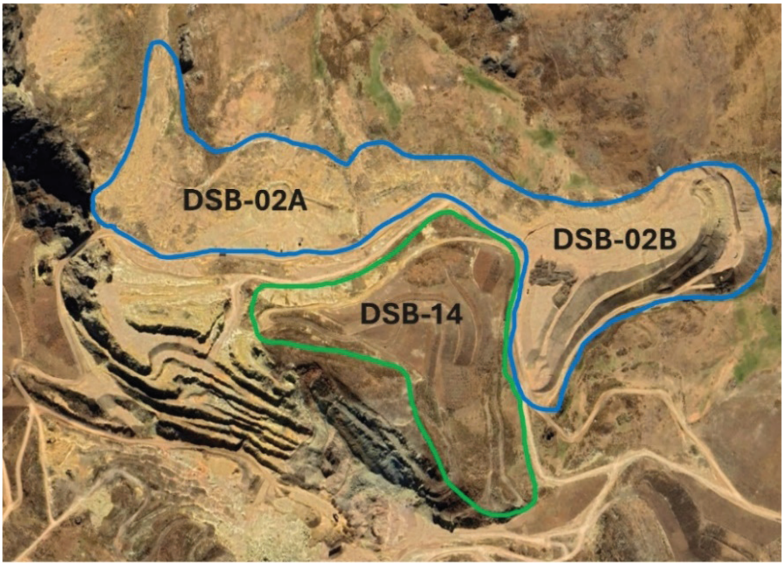

Figure 1: Design sectors Santa Barbara waste rock facilities DSB-02A and DSB-02B

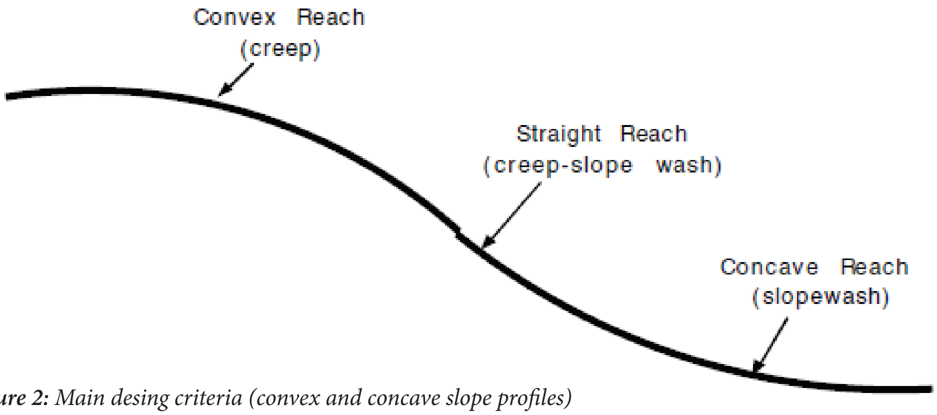

Figure 2: *Main desing criteria (convex and concave slope profiles)*

challenge, as the focus shifts from designing a complex cover system to restoring the water and landscape functionality of the environment.

However, the tools available in the market for modeling and designing such an alternative are limited, often tied to patents and licenses from specific suppliers. Faced with this constraint, Amphos 21's project management decided to take an innovative approach by conducting the design modeling exclusively using Civil 3D (Autodesk), leveraging the expertise of Peruvian civil engineers. This decision not only demonstrates adaptability but also highlights the commitment to developing locally-driven solutions for sustainable mine closure.

The integration of these waste rock facilities (WRFs) required the removal of the access road that previously divided the two components. This road was identified as a key factor contributing to erosion and sediment drag, exacerbating the environmental challenges at the site. Its removal was a critical step in ensuring the long-term stability and ecological integration of the area.

Between 2023 and 2024, extensive engineering and earthmoving works were carried out under the supervision of Amphos 21. A total of approximately 314,000 m^3 of waste material was moved, balancing cut and fill operations during this period (Table 1). The process resulted in a surplus of 18,700 m^3, which was repurposed as fill material in the open pit of the unit being closed. This approach not only optimized the use of available materials but also contributed to the overall geomorphological restoration of the site.

Photography 2: *Front view of the WRFs*

***Table 1** Earthwork for geomorphologic conformation (Buenaventura. Dec. 2024).*

Earthwork Activity	**Year 2023** m^3	**Year 2024** m^3	**Total** m^3
Cut	43 982.28	122 518.14	166 500.42
Backfill	25 271.61	122 530.95	147 802.56
Total	69 253.89	245 049.09	**314 302.98**

By the end of December 2024, all earthmoving activities, including cutting, filling, and surface shaping, were successfully completed. These tasks were carried out with contracted heavy machinery, such as motor graders, tractors, rollers, excavators, and dump trucks. The remaining task for 2025 involves the final shaping of the topsoil layer and the establishment of native herbaceous vegetation, as illustrated in Photograph 3. This step will mark the culmination of the geomorphological rehabilitation efforts, ensuring the site's seamless integration with the natural environment.

Next steps

By the end of 2025, the project is expected to be fully completed with the final formation of the topsoil layer and the subsequent revegetation using native species. To ensure the success of this phase, Amphos 21 conducted a comprehensive soil characterization study of the surrounding soils. This study aimed to identify and understand the limiting factors of the soils, particularly considering the challenging environmental conditions of the area, which is located at an altitude of over 4,200 meters above sea level.

The study also had two additional objectives: first, to determine the characteristics and properties of the soils intended for use as cover material, and second, to evaluate the limitations of these soils from both a geochemical and productivity perspective. From a geochemical standpoint, the study assessed the soils ability to control underlying materials, while from a productivity perspective, it focused on their suitability to support vegetation growth. These insights are critical for ensuring that the topsoil layer not only stabilizes the site but also fosters the successful establishment of native vegetation, contributing to the long-term ecological restoration of the area.

To achieve this, 17 nearby points in the Santa Bárbara near area were evaluated. The results of these evaluations provided critical data to establish the final design of the soil cover composition, tailored to the specific requirements of different areas based on both the slopes and elevation of the sites.

According to the final design (Fig. 2), a total of 16,320 m^3 of topsoil will be required to complete the project. The project is

***Photography 3:** View of the WRF (DSB-02B and DSB-14)*

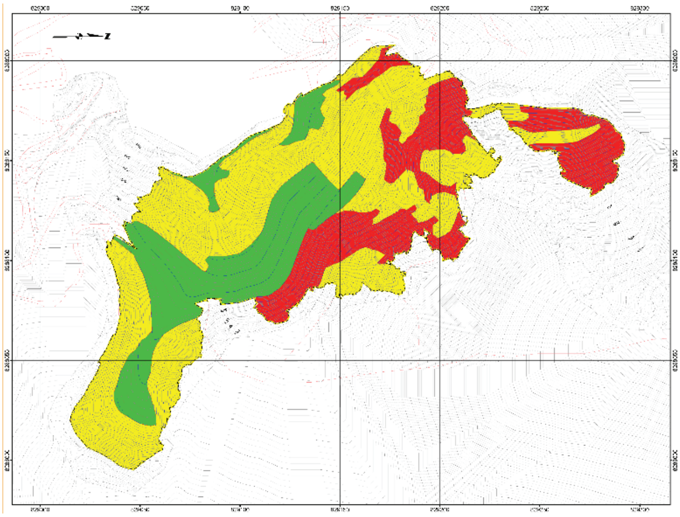

Coverage				
Class	Height (m)	Area (m²)	Volume (m³)	Color
Class 1 - 4 S < 25%	0.15	42,450	6,368	🟩
Class 5 S < 25% - 55%	0.70	105,570	7,390	🟨
Class 6 S > 55%	0.20 a 0.50	50,870	2,544	🟥

Figure 2: *Design of the surface to be covered with topsoil*

scheduled to resume in July 2025, with the goal of completing the revegetation process using Stipa ichu by November and December of 2025. This timeline ensures that the vegetation will be well-established before the onset of the rainy season in the area.

Conclusions

Geomorphological rehabilitation represents a groundbreaking and sustainability-focused approach that eliminates the need for traditional concrete structures and water management ponds, which are commonly used in the post-closure control. This innovative method not only reduces long-term maintenance costs but also promotes a more harmonious integration with the natural environment.

The implementation of this project in Peruvian mining marks a significant milestone in the design and closure planning of waste rock facilities (WRFs). After many years of remediation and closure activities in Perú, there has yet to be a fully successful case of WRF closure. This project aims to establish a new standard for sustainable and effective mine closure practices.

Acknowledgements

The authors thank all the staff of the Buenaventura mines company, for their support along the project, helping in the design, construction and data generation, as well as for their useful discussions on the results.

References

El Peruano Official Newspaper (2017) Approval of Environmental Quality Standards (EQS) for Soil

FAO (2009) Guide for the description of soils. Fourth edition. Rome

Ministry of Energy and Mines of Peru (2009) Approved the Closure Plan of Mining Environmental Liabilities of the "Santa Barbara" mining unit.

National Institute of Culture of Peru (2005) Declares the Santa Barbara mine installations a National Cultural Heritage.

Buenaventura Mining Company SAA (2008), Closure Plan for Environmental Mining Liabilities of the former Santa Barbara mining unit.

Pilot study of improved soils as a cover alternative for mine closure of waste rock dump, Peru

Alfredo Gallardo[1], Eduardo Ruiz[2], David Arcos[3]

[1]Amphos 21 Consulting Peru S.A.C. Jirón Paseo del Bosque 500 of. 201, Urb. Chacarilla del Estanque – San Borja, 15037 Lima, Peru, alfredo.gallardo@amphos21.com

[2]Amphos 21 Consulting Peru S.A.C. Jirón Paseo del Bosque 500 of. 201, Urb. Chacarilla del Estanque – San Borja, 15037 Lima, Peru, eduard.ruiz@amphos21.com

[3]Amphos 21 Consulting S.L. c/ Veneçuela 103, 2ª plta., 08019 Barcelona, Spain, david.arcos@amphos21.com

Abstract

This study proposes the use of improved soils as an alternative to the more traditionally used cover layers for sulfide waste rocks. The theoretical advantage of these improved soils lies in their capacity for self-regeneration, so that they do not require maintenance. In addition, the design of the improved soil layers is based on the site conditions and focuses on reducing infiltration into the underlying system and also generating anoxic conditions that help to reduce the rate of sulfide oxidation.

To this end, a testing program was developed and started in 2015, in which, a cover was designed and installed on the backfilled surface of an exhausted open-pit section at a mining operation. In addition, a monitoring system was designed and installed to evaluate the effectiveness of the cover. This paper describes and discusses the monitoring results and the implications for the strategy to ensure an environmentally and economically sustainable closure of the mining operation, highlighting some of the key findings.

Keywords: Improved soils, mining closure, hydrogeochemical monitoring, full-scale test.

Introduction

In Peru, the guidelines for closure of mining operations suggest the use of a defined cover developed in layers, where the priority is to reduce infiltration with low permeability materials (GDMEA 2006). However, there are alternative concepts that are possible which are based on imitating nature. With these concepts the very structure of some soils promotes water retention and evapotranspiration, thereby limiting infiltration and reactivity with the organic fraction that promotes oxygen consumption.

In this context, a pilot project has been developed for the closure of a section of the pit in a gold mine in a high sulfidation epithermal deposit. This type of deposit is known to present lithologies with a large variety of hydrothermal alterations all of them with elevated potential acid generation (PAG) as indicated by Plumlee et al. (1999). Closing the pit area consists of backfilling a pit area of approximately 80,000 m^2 with sulfide waste rocks and which are covered with improved soils, known as technosols (Santos et al. 2019, Macías et al. 2023). The project consists of evaluating the effectiveness of this technosol with respect to its capacity to minimize infiltration (target hydraulic conductivity is in the range of 10^{-2} to 10^{-3} m/d) and also reduce the oxidizing capacity of waters that may infiltrate using different types of instrumented boreholes.

Figure 1 Site view before (above), during (lower left) and after (lower right) cover implementation.

Methods

The target pit area was backfilled with waste rock and then covered with a combination of three 15 cm-thick manufactured soil layers (Fig. 1) being, from bottom to top: 1) a lower layer of andic technosol, whose purpose is both to neutralize the generation of acids and also reduce the mobility of anions; 2) a reducing technosol, to reduce the rate of sulfide oxidation (i.e., pyrite) and, 3) an eutrophic-calcareous technosol, whose objective is to promote local plant growth (a feasibility study with local vegetation was conducted) and increase microbial activity and biodiversity, as well as to buffer the system to alkaline conditions.

To test the effectiveness of the improved soil cover, a monitoring system was designed and installed (Fig. 2). This monitoring system consisted of:

1. **Near-surface boreholes:** just below the soil cover and isolated from the waste rock by a layer of quartz gravel. The purpose of these instrumented boreholes is to evaluate the effect of the cover on oxygen consumption and the quality of the infiltration water, before encountering the waste rock.
2. **Deep boreholes in the backfill:** Their purpose is to allow for the sampling of water that might infiltrate to the base of the backfill inside the pit basin.
3. **Instrumented wells**: These wells included a series of continuous measurement sensors (temperature, conductivity, suction pressure, water, oxygen and CO_2 content), as well as suction lysimeters at different depths in the backfilling; and
4. **External piezometers:** Drilled upstream and downstream of the pilot test area and at different depths to monitor the potential impact on the groundwater quality.

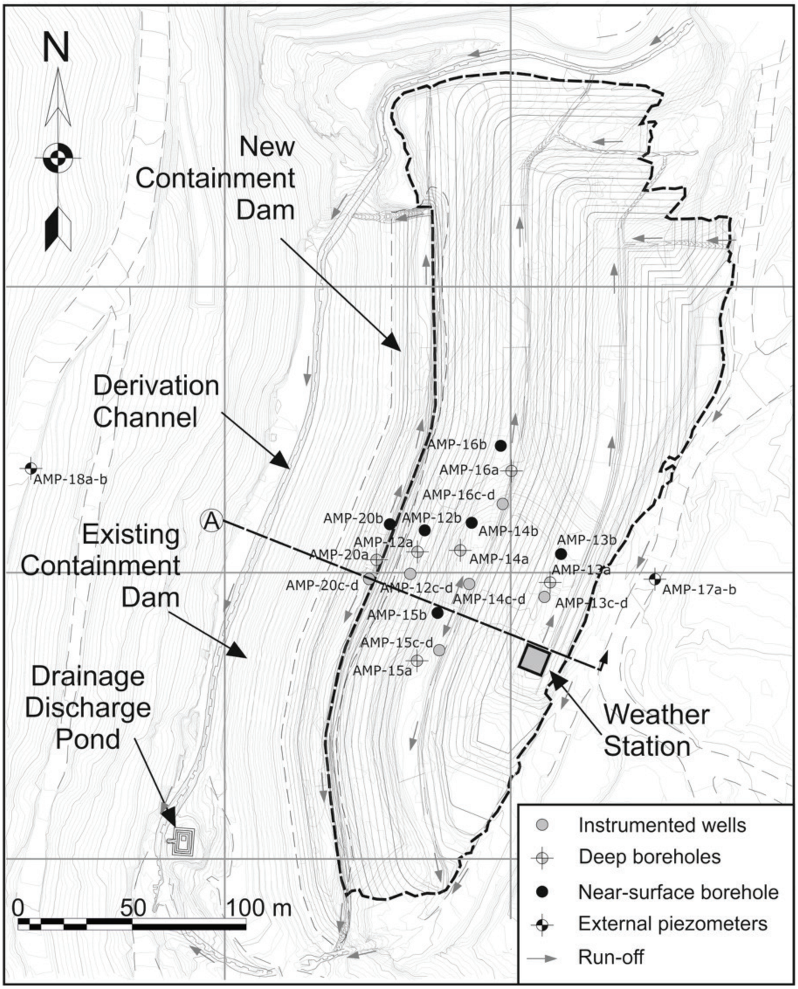

Figure 2 Map of the full-scale cover test with location of the different types of boreholes.

5. **Drainage and groundwater collection pond:** This is the outlet of the drainage system where water samples and field measurements are periodically taken.
6. **A weather station:** Installed on the pilot area.

This project started reporting water quality indicators in 2018. The sensors in the project were programmed to generate daily information. Additionally, during the wet season, more exhaustive monitoring was carried out with specific measurements of some of the parameters and water sampling from the suction lysimeters, deep boreholes and external piezometers.

Results and Discussion

Geology in the open pit and its surroundings correspond to volcanic tuffs, ignimbrites, andesites with small patches of Quaternary alluvial cover. The first 5 to 20 meters of rock depth present a high degree of weathering and fracturing, giving it a high contrast of permeability with respect to the deeper fresh bedrock, favouring the circulation of water through this surficial layer.

The climate of the area is characterized by two distinct seasons, a dry season from June to October and a wet season from November to May, with an average annual rainfall of approximately 1,200 mm. Fig. 3 shows the difference in precipitation between dry and

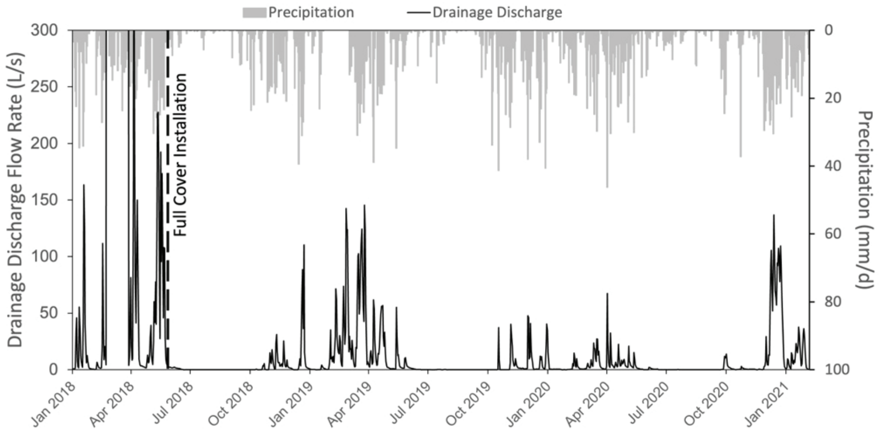

***Figure 3** Monitoring of the discharge flowrate of the pilot.*

wet season, leading to a rapid response to rainfall events in the drainage system of the pilot area. Monitoring results show that the overburden is not saturated with respect to water content, but increases briefly after each rainfall event, without reaching saturation. The time and magnitude of response to rainfall events depends on the depth of the sensor in each borehole. It is also worth noting in Fig. 3 the difference in flow rate before (beyond the scale limits) and after the cover is installed.

Also, the geochemical information of waste rocks used in the backfilling, including lithological and mineralogical descriptions, and geochemical analysis and tests was reviewed. The main source of analytical data came from ABA, NAG and SFE tests and hydrochemical analysis (Table 1) confirming their PAG (Potential Acid Generation) behaviour.

The results from the surface boreholes indicate that, as expected, a decrease in redox conditions (ORP) is recorded since the first half of February 2018. The decrease recorded is 200-300 mV. Furthermore, in most of these boreholes, the water is kept at a near-neutral to slightly alkaline pH (pH = 7 – 8), while the conductivity values remain relatively low (0.5 – 3.5 mS/cm).

Most of the instrumented boreholes show similar results, with lower oxygen contents at the bottom of the backfill. This means that oxygen consumption is also occurring in the waste rock and not only in the cover (Fig. 4). However, at the sampling points of the borehole drilled in the containment dam location, the behaviour is different, with higher oxygen contents at the lowest point of the backfill, at 20 m depth (nearly atmospheric values). This behaviour indicates that the toe of the dam constitutes an air entry zone, likely due to the larger granulometry, especially at the base, and therefore greater air permeability. Furthermore, the high temperatures recorded in this borehole (40 – 50 °C) indicate that pyrite oxidation is taking place. The temperature gradient generated may result in enhanced air circulation.

The quality of the drainage water from the system has been monitored by systematic sampling at the drainage discharge pond. The results indicate that, in addition to the decrease in drainage flow indicated above (Fig. 3), sulfate and metal concentrations show a significant decrease since the installation of the cover (Fig. 5). Specifically, sulfate presents a decrease from concentrations >10,000 mg/L to concentrations <5,000 mg/L, just four years after the installation of the cover. Similarly, copper concentrations decrease from >200 mg/L to <80 mg/L, similar decreases occur with the other metals. It is noteworthy that the first samples of each wet season show higher concentrations, which decrease throughout the season (Fig. 5). This effect is characteristic of this type of system (Nordstrom 2007), where, during the dry season, the wastewater continues to react with

Table 1 *Baseline drainage water compositions prior to installing the improved soil cover (concentration values in mg/L).*

	pH	Eh(mv)	SO_4	TSS	Pb	Cu	Zn	Fe	Mn
Baseline (Jan 2016)	1.8	603.4	11,542	150	2.2	187.7	3	910.5	27.1
Average values	1.7	591.4	5,307	91	0.7	197.4	7.3	2,234.9	18.6

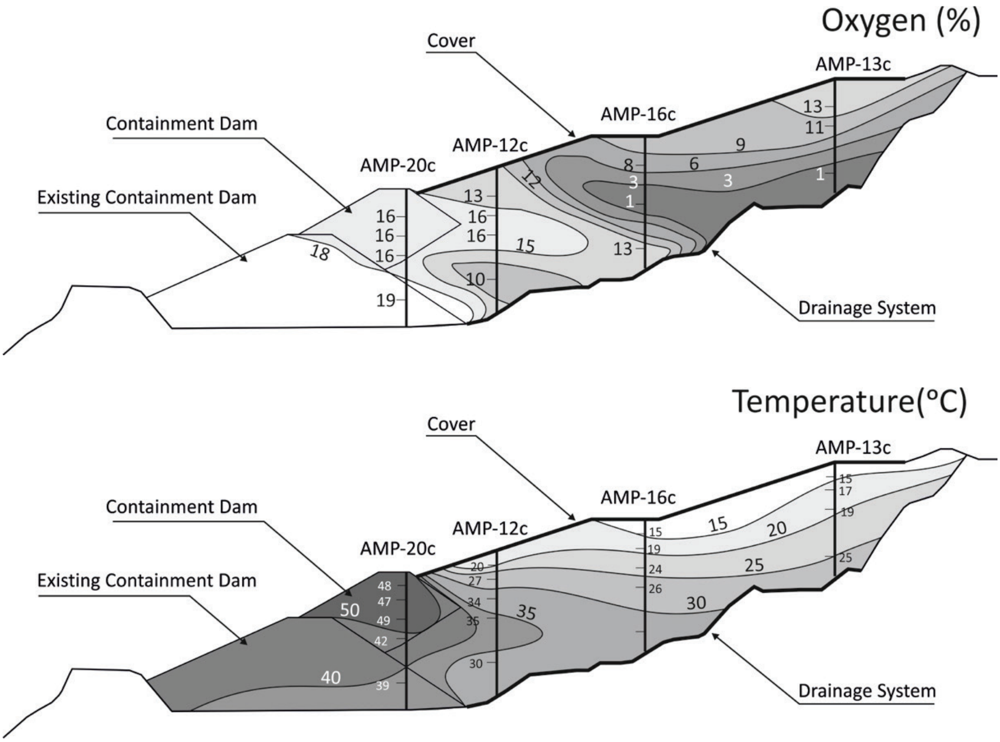

Figure 4 *Cross section A of the backfill – cover system as shown in Fig. 2, with mean data of the last half year recorded for oxygen content (above) and temperature (below).*

the waste rock and the solutes accumulate in the form of precipitated secondary phases and, at the beginning of the wet season, the first filtrations redissolve these phases producing this effect of increased concentrations.

From the implementation point of view, the cover can be considered successful. One of the aspects to highlight is the healthy development of a vegetation cover, its integration into the landscape and without requiring additional maintenance. This vegetative cover increased evapotranspiration, while reducing water infiltration. The drainage flow at the base of the backfill decreased by more than an order of magnitude. In addition, the decrease in oxygen entry through the cover decreased the rate of sulfide oxidation, reducing the concentration of metals in the drainage water. Although trends are positive, values remain above the maximum permissible Peruvian values, indicating that restoration remains a long-term path.

Conclusions

The use of improved soils as cover material can be considered a viable option since, in addition to promoting the phytostabilization of metals and good revegetation in general, it facilitates oxygen consumption, generating anoxic environments to minimize

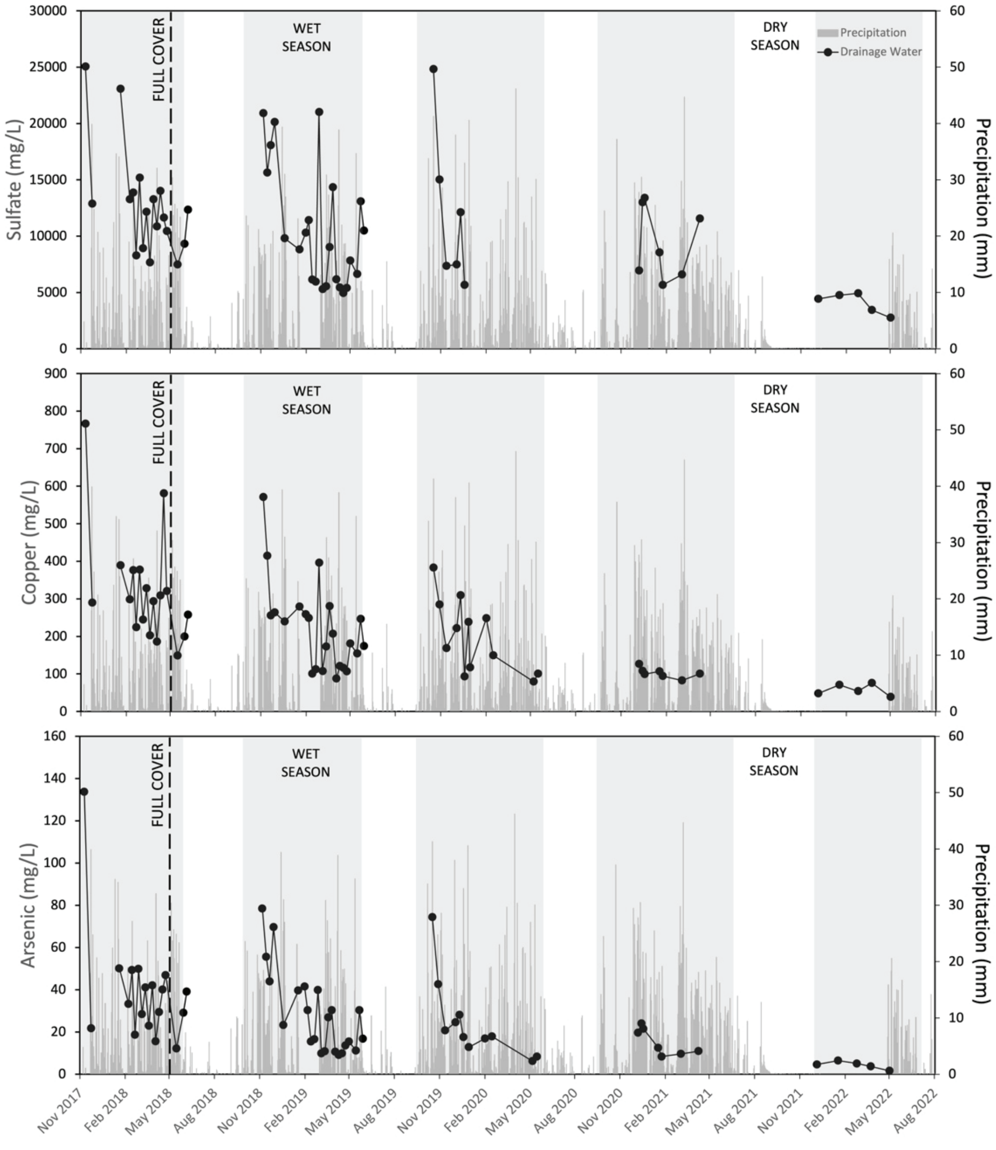

Figure 5 Graphics presenting chemical evolution for selected components in the water collected at the drainage discharge pond.

acid rock drainage. The increase in the evapotranspiration rate due to vegetation growth and, therefore, the reduction of percolation has been shown to be efficient, showing another benefit of using this cover concept.

The evolution of water quality indicators, infiltration, runoff and evapotranspiration, have been similar or better than those obtained by traditional systems of layers with low permeability materials such as clays, which are used in many cases of mine closure in Peru. In this case without the added cost of material acquisition (often outside the mining units), transport and disposal, becoming a living pilot study that continues to yield results that can be used to focus other cases of closure based on sustainable solutions.

On the other hand, although the results are satisfactory, areas for improvement have been identified. For example, alkaline irrigation could be considered prior to the installation of the cover, this approach would help to eliminate very acidic water and therefore deactivate the oxidising capacity of the ferric ion, which is much more powerful than oxygen. For the case study, in a context of advanced ARD (pH<2) and after several years of monitoring, the investigation confirms that facility closure is a long-term process and the guarantees of restoration of the conditions prior to mining operations are difficult to achieve solely with the installation of the cover.

Acknowledgements

The authors thank all the staff of the mine for their support along the project, helping in the design, construction and data acquisition phases, as well as for their useful discussions on the results.

References

García FM, García IM, Vázquez FM (2023) Environmental and Productive Applications of Tailor-Made Technosols: Biosphere Learnings. In: Chaminé HI, Fernandes JA (eds) Advances in Geoengineering, Geotechnologies, and Geoenvironment for Earth Systems and Sustainable Georesources Management. Advances in Science, Technology & Innovation, pp. 219-225.

MINEM (2016) Guide to developing mine closure plans (in Spanish). https://cdn.www.gob.pe/uploads/document/file/5217286/Guía Cierre de Minas.pdf

Nordstrom DK (2007) Effects of seasonal and climatic change on water quality from acid rock drainage in the western United States. In: Cidu R, Frau F (eds.) Water in Mining Environments. pp. 11-16, Cagliari (Mako Edizioni).

Plumlee GS, Smith KS, Montour MR, Ficklin WH, Mosier EL (1999) Geologic controls on the composition of natural waters and mine waters draining diverse mineral-deposit types. En The environmental geochemistry of mineral deposits. Part B: case studies and research topics. Littleton, Colorado: Society of Economic Geologists, Reviews in Economic Geology, v.6-B, pp. 373-432.

Santos ES, Abreu MM, Macías F (2019) Rehabilitation of mining areas through integrated biotechnological approach: Technosols derived from organic/inorganic wastes and autochthonous plant development. Chemosphere 224: 765-775.

Mine Water Injection and Storage in Ordos Basin, China

Chen Ge[1], Sun Yajun[2], Sui Wanghua[3], Xu Zhimin[4], Gao Liang[5]

[1]*School of Resources and Geosciences, China University of Mining and Technology, 221116, Xuzhou, Jiangus, China, cg5@cumt.edu.cn, ORCID 0000-0003-0260-8987*

[2]*School of Resources and Geosciences, China University of Mining and Technology, 221116, Xuzhou, Jiangus, China, syj@cumt.edu.cn*

[3]*School of Resources and Geosciences, China University of Mining and Technology, 221116, Xuzhou, Jiangus, China, suiwanghua@cumt.edu.cn, ORCID 0000-0001-7004-1877*

[4]*School of Resources and Geosciences, China University of Mining and Technology, 221116, Xuzhou, Jiangus, China, xuzhimin@cumt.edu.cn*

[5]*State Key Laboratory of Internet of Things for Smart City and Department of Ocean Science and Technology, University of Macau; Macao, 999078, China, gaoliang@um.edu.mo*

Abstract

This paper explores the application of mine water injection and storage technology in the Ordos Basin, focusing on its hydro-geological framework and practical implementation strategies. 15 hydro-geological frameworks of mine water injection and storage are systematically delineated. The sandstone and limestone types are categorized and described. Based on projects, the study also evaluates six different well construction methods and operational modes. And the case study of the MC-1 well in the Muduchaideng coal mine provides insights into the challenges and successes of long-term mine water injection. The detailed implementation plans, hydro-geological testing, operation timelines and consideration for re-operation were presented to provide the option methodology for sustainable mine water resource management in the arid and semi-arid areas.

Keywords: Mine water injection, storage, hydro-geological framework, mode

Introduction

Ordos Basin is currently the most important coal resource base for China. The Jurassic coal measures are widely mined for energy supply. Huge roof sandstone water drainage induced by mining activities is drained due to the typical hydro-geological framework. The total amount of mine water drainage nearly is 50% of the regional water consumption (Chen *et al.* 2020). Managed Aquifer Recharge (MAR) is generally adopted in the over-abstraction of groundwater, CO_2 storage, oil and gas recovery, salt mining, surface subsidence, saltwater intrusion and so on. Mine water injection and storage is a method that similar to the MAR, but the main and key technique is different from this conventional approach. According to an inventory of 27 mines using or considering MAR for current or future operations in the review paper (Sloan *et al.* 2023), only Garzweiler open coal mine at Rhine land area of German is one project in the coal field, the others are all referring to metallic mines (Yungwirth *et al.* 2017). While some public papers have explored the geological storage of mine water (Chen *et al.* 2022; Chen *et al.* 2022; Chen *et al.* 2022; Li *et al.* 2024; Li *et al.* 2024), a systematic exploration of the hydro-geological framework and geological storage mode remains a critical research priority, necessitating further interdisciplinary studies to address unsolved complexities. This paper systematically delineates the aforementioned research components through theoretical analysis, laboratory experiment and empirical projects validation.

Materials and methods

The concept of coal mine water injection and storage

Mine water injection and storage is a treatment method for mine water that is coming to the mining space by the disturbances of coal resource extraction. Water will be injected and stored in the deep underground space of these strata through artificial interventions or the nature-based function of the hydro-geological framework in the coal mine. Generally, when the target aquifer is deeper than the coal measures, the model will be qualified as deep injection and storage.

Key elements, guiding principles and technical characteristics are summarized based on the existing engineering cases. Key elements include mine water sources, deep-storage pathways, deep-storage spaces and impermeable caprocks. Guiding principles include Coal mine safety prioritization, environmental protection through quality-stratified storage and resource exploitation compatibility. Technical characteristics include water quality stability, adequate reservoir capacity, controllable permeability and cost-effectiveness.

The hydro-geological framework of mine water injection and storage in China

The hydro-geological framework (Kihm *et al.* 2024) of mine water injection and storage specifically refers to the spatial positions and combinational relationships among the target aquifers (categorized as shallow, deep, and those at the same layer), the coal seams being mined or already mined , the deep storage sites (surface or underground), as well as the aquifers and aquitards at different depths, various water filling sources (such as water inrush bodies) in the mine, the pathways (channels and wells), the hydro-geological boundaries, the mining spaces, etc. The spatial arrangements and combinational relationships of those elements collectively determine the effectiveness and safety of mine water injection and storage.

Drawing on the extant mine water injection and storage projects, the author has meticulously collated and comprehensively summarized the types of hydro-geological framework associated with mine water injection and storage in China. The detailed information is explicitly presented in Table 1.

Typical hydro-geological framework of mine water injection and storage in the deep sandstone aquifer

The hydro-geological framework for mine water injection and storage in the deep sandstone aquifer in the Ordos Basin is as follows: Groundwater from Yan'an Formation (with a TDS content of 7000 mg/L to 9000 mg/L) and Zhiluo Formation (with a TDS content of 1000 mg/L to 3000 mg/L) within the vertical scope of caving zone and water-conducting fracture zone induced by mining activities for No.3 coal seam of Yan'an Formation, will flow through the mining-induced fractures or drainage boreholes to the surface/ underground ponds by the drainage system. The mine water will be injected and stored in the Triassic Liujiagou Formation sandstone aquifers by deep wells (such as vertical, inclined and branch wells).

Different well structures and modes for mine water injection and storage in Ordos Basin

The implementation of mine water injection and storage projects in Muduchaideng mine, Nalinhe No.2 mine and Dahaize mine shows that 6 applicable well constructions for sandstone mode are summarized as shown in Figure 2.

The mine water injection and storage has been applied in some coal mines with different modes, which is determined by the TDS content of mine water, well structure, injection flow, wellhead pressure, injection time and frequency as well as the permeability & capacity increasing condition of the target aquifers. The projects of mine water injection and storage in the Muduchaideng mine and Nalinhe No. 2 are classified as the type of high TDS content, moderate flow rate and high pressure. Based on field trials and risk assessments, the solution is validated as technically feasible with safety parameters within acceptable thresholds.

Table 1 The hydro-geological framework of mine water injection and storage in China..

Water-inrush body in coal mines	The target layers of mine water injection and storage	Type description	Remarks
Surface water	Unconsolidated aquifer Sandstone aquifer Karst aquifer Burnt rocks Unconsolidated aquifer	Surface water into the deep unconsolidated aquifer Surface water into the deep sandstone aquifer Surface water into karst aquifer Surface water into the deep burnt-rocks Quaternary water into the unconsolidated aquifer	Zhanihe coal mine
Groundwater from roof aquifer of coal seams	Sandstone aquifer Delamination space induced by mining activities Unconsolidated aquifer	Roof sandstone water into another sandstone aquifer Roof sandstone water into the delamination space	A specific coal mine in Maowusu deset of Ordos basin
	Sandstone aquifer	Sandstone water into the unconsolidated aquifer Limestone water into the unconsolidated aquifer Sandstone water into the deep sandstone aquifer	Muduchaideng mine, Nalinhe No. 2 mine, Mataihao mine, Dahaize mine and Xiaobaodang mine
Groundwater from floor aquifer of coal seams	Karst aquifer Mixed aquifer Roof goaf	Limestone water into the deep sandstone aquifer Sandstone water into the deep aquifers of Taiyuan Formation, Ordovician, and Cambrian limestone Limestone water into the deep aquifers of Taiyuan Formation, Ordovician, and Cambrian limestone Sandstone water into the deep mixed aquifers of sandstone and limestone Goaf water into the roof goad	Lilou mine-Wutongzhuang mine and Xiaoyun coal mine Laoyingyan coal mine
Goaf water in the same coal seams	Goal in the same level Floor goaf	Goal water into another goaf of the same level Goaf water into the floor goaf	Underground reservoirs in mines, Lingxin coal mine
Other types	Burnt-rock aquifer	Water-inrush body into the burnt-rock aquifers	Shendong mining area

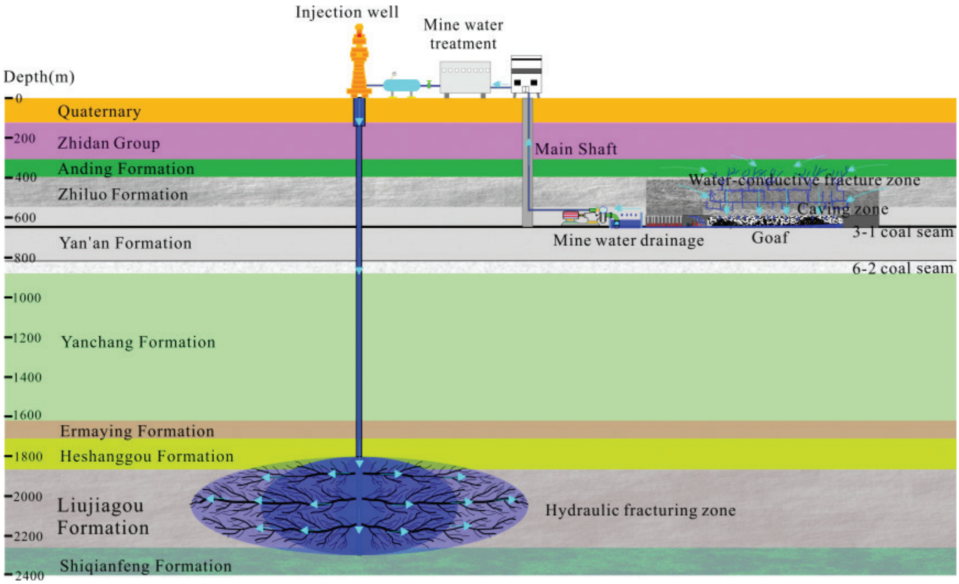

Figure 1 Schematic diagram of the typical hydro-geological framework of mine water injection and storage in the deep sandstone aquifer.

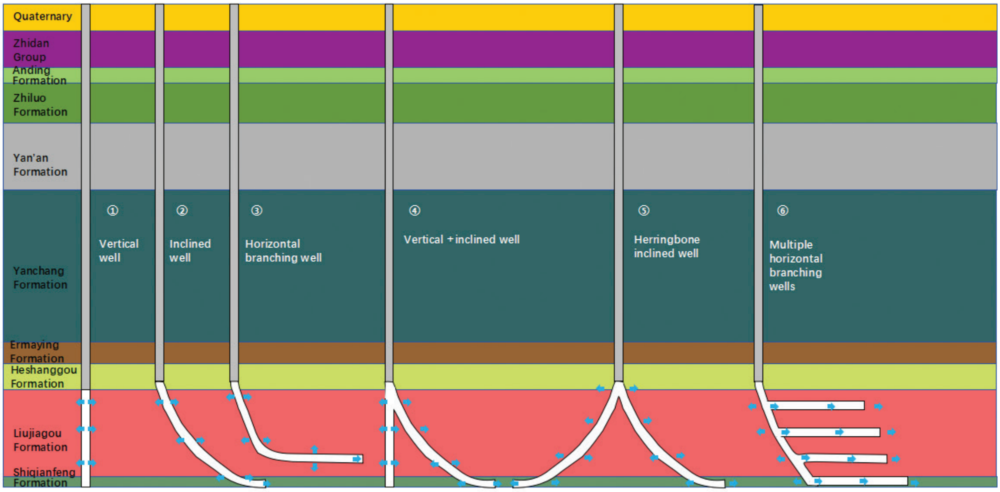

Figure 2 *Different well constructions for mine water injection and storage.*

Results and discussion

Construction of MC-1 well and in-situ hydro-geological testing in Muduchaideng coal mine

The MC-1 well was constructed from 1st October 2019 to 8th March 2020, with a total length of 2299.5 m. The target Liujiagou Formation was buried from 1800 m to 2290 m, with 113 sub-layers. The typical lithology was characterized by the brown, pinkish-red, red and gray sandstone and mudstone. Due to the low-porosity and low-permeability for this tight target layer, the conventional pumping tests were infeasible (flow rates too low) , prompting a shift to the natural water-level recovery test, which further confirmed the low-permeability characteristics. The original Liujiagou Formation was low porosity at 7.5% and lower permeability at 5.31×10^{-6} m/d to 6.19×10^{-6} m/d. Subsequent variable-pressure injection tests were conducted to derive hydro-geological parameters. After hydraulic fracturing, the permeability significantly greater 1788 to 2858 times greater than natural. We found that the critical pressure of hydraulic fracturing should be greater than 31.5 MPa.

Operation of mine water injection and storage from March 2020 to July 2021

Observations of injection flow rates and pressures during March 2020 to July 2021, revealed persistent dynamic variations, indicating that under high-pressure and large-volume re-injection conditions, the fracture network within the deep target layer remained in a state of continuous evolution. The fracture network was comprised with natural fractures and hydraulic fractures. The limited storage capacity of the reservoir necessitated repeated hydraulic fracturing to induce rock damage, thereby utilizing hydraulic pressure to gradually displace water radially, expanding the influence radius and creating additional storage space for mine water.

As demonstrated by the trend analysis of wellhead pressure versus injection flow rate (Figure 3), the wellhead pressure dynamics exhibited a gradual stabilization from an initial 6.2 MPa to a final equilibrium of 8.0 MPa, indicating progressive pressure buildup under controlled injection conditions. The flow rate demonstrated a sustained increase from 54 m^3/h to a steady-state plateau at 98 m^3/h, reflecting optimized hydraulic conductivity by hydraulic fracturing or operational adjustments. During this period, the cumulative mine water injection volume exceeded 1 million cubic meters, demonstrating significant sequestration potential. Storage and containment of mine water resources were partially achieved, enabling large-scale hydraulic management. Mine water treatment costs per ton were reduced by 80% through optimized injection protocols.

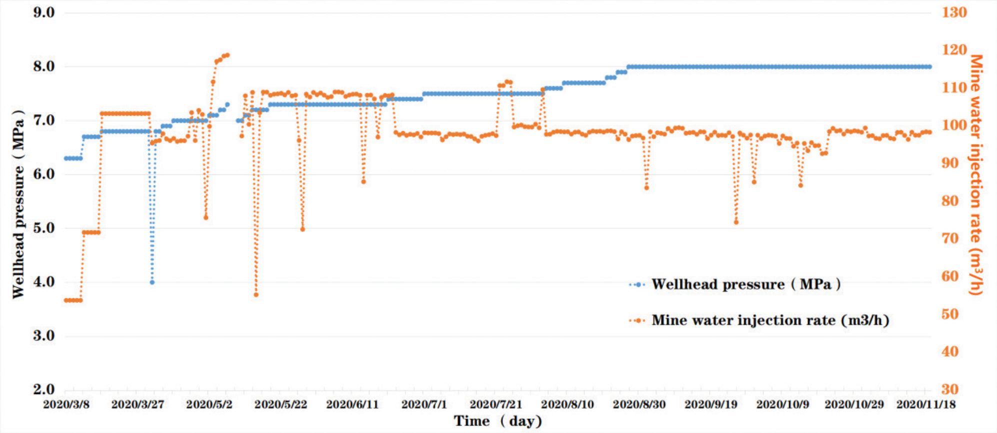

Figure 3 *Wellhead pressure and injection flow rate for MC-1 well.*

Operation from October 2024 to now

Prior to re-operation of MC-1 well, controlled water release was conducted by adjusting the valves at a flow rate of 100 to 200 m^3/h. Water quality analysis indicated that the TDS concentration exceeding 10,000 mg/L, but different from the original baseline of 65,111 mg/L for Liujiagou Formation water. The water temperature was recorded at 64 °C, which corresponded to a burial depth of approximately 2,100 – 2,200 meters from the previous logging data from MC-1 well. It was observed that there was no reduction in water discharge, so the professional oilfield service crew was engaged to perform the modification work on the MC-1 well. The cumulative volume of water release reached approximately 1,340,000 m^3.

The MC-1 well commenced re-injection on 4th October 2024, until now, a cumulative volume of 88,000 m^3 mine water had been injected. The typical operating wellhead pressure (at the roadway of -600 m level) ranged from 16 MPa to 18 MPa, accompanied by a flow rate from 60 m^3/h to 70 m^3/h. When the wellhead pressure was up to 22 MPa, the injection flow rate would decline to 50–60 m^3/h. We considered that the intermittent re-injection might induce sandstone fracture closure and re-opening. The existing fracture network and pores were saturated with high-pressure water, limiting the storage capacity. Elevated wellhead pressure could force new fractures to initiate based on the natural fracture network. High-pressure mine water may preferentially migrate along dominant fracture pathways (such as natural fractures), forming a hydraulic barrier when encountering low-permeability interlayers (such as mudstone).

Conclusions

The definition of mine water injection and storage was presented and 15 hydro-geological frameworks of in China were illustrated, especially the deep sandstone and limestone types were indicated with the operated project. As for the project of MC-1 well, the detailed implementation plans, hydro-geological testing, operation timelines and consideration for re-operation were presented to assess the feasibility and expectation of this proposed methodology.

Acknowledgements

This work was funded by the National Key Research and Development Project of China [grant number 2023YFC3012103 and 2019YFC1805400]; the National Natural Science Foundation [grant number 42202268]; general project of China Post-doctoral Science Foundation [grant number 2023M742937] and the National Science Foundation of Jiangsu Province [grant number BK20210524].

References

Chen G, Sun Y, Xu Z, Li X. 2022. Hydrogeological feasibility of mine water deep geological storage in Baotashan coarse sandstone: A case study in Ordos Basin. *Deep Underground Science and Engineering*, 1(2): 148–164.

Chen G, Xu Z, Rudakov D, Sun Y, Li X. 2022. Deep Groundwater Flow Patterns Induced by Mine Water Injection Activity. *International Journal of Environmental Research and Public Health*, 19(23): 15438.

Chen G, Xu Z, Sun Y, Sui W, Li X, Zhao X, Liu Q. 2022. Minewater deep transfer and storage. *Journal of Cleaner Production*, 332: 129848.

Chen X, Jiang J, Lei T, Yue C. 2020. GRACE satellite monitoring and driving factors analysis of groundwater storage under high-intensity coal mining conditions: a case study of Ordos, northern Shaanxi and Shanxi, China. *Hydrogeology Journal*, 28(2): 673–686.

Kihm J, Kim J, Kim Y, Kim S, Yeh G. 2024. Hydrogeologic Framework Model-Based Numerical Simulation of Groundwater Flow and Salt Transport and Analytic Hierarchy Process-Based Multi-Criteria Evaluation of Optimal Pumping Location and Rate for Mitigation of Seawater Intrusion in a Complex Coastal Aquifer System. *Water Resources Research*, 60(6): e2023WR035486.

Li X, Chen G, Wei W, Tan X, Xu Z, Zhang L, Zhang F, Liu Q, Sun Y. 2024. Feasibility of Injecting Pretreated Mine Water into a Deep Ordovician Aquifer in the Lilou Coal Mine, China. *Mine Water and the Environment*, 43(1): 168–182.

Li X, Chen G, Xu Z, Liu Q, Chen T, Sun Y. 2024. Paradigm for Determining the Optimal Ultradeep and Super-thick Saline Aquifer for High-TDS Mine Water Geological Storage. *Acta Geologica Sinica – English Edition*, 98(3): 771–785.

Sloan S, Cook P G, Wallis I. 2023. Managed Aquifer Recharge in Mining: A Review. *Groundwater*, 61(3): 305–317.

Yungwirth G, Austin E, Preene M, Corcoran F, Birch J. *Aquifer reinjection scheme for excess mine water: design methodology and outcomes*. Finland: 2017.

Improving Early Mine Design using Reference Class Forecasting of Mine Water

Gischia, Scott. Tamara Diedrich. Xiang Li.

MineraLogic, LLC. 306 West Superior Street, Suite 900. Duluth, Minnesota.
sgischia@mnlogic.com, tdiedrich@mnlogic.com, xli@mnlogic.com

Abstract

Integrating projections of mine water chemistry early into the mine design process—prior to relevant site-specific data being available—provides the greatest opportunity for improving environmental outcomes with the lowest increases to overall schedule and cost. An approach derived from behavioral economics, "Reference Class Forecasting" (RCF), is applied here in a mine water quality context to identify a preliminary design basis for rock stockpiles. The RCF evaluation, as demonstrated in this paper, required a relatively low level of project definition, yet identified order of magnitude reductions necessary for constituents of interest and screened out other constituents from further review.

Keywords: Mine water scoping design reference class forecast

Introduction

Hydrogeochemical forecasts of future mine water chemistry can provide valuable technical bases for the design of future mining projects. However, construction of a hydrogeochemical model requires a high degree of project-specific and site-specific knowledge to establish the conceptual framework for modeling and to inform model parameter values. Developing the mine plan, site water balance, baseline water quality evaluation, and results from a geochemical characterization program requires considerable time and resources before model results are available.

Further, mine development timelines continue to lengthen (Heijlen *et al.* 2021). The current average lead time to operations for a new nickel mine is over 17 years, with increasingly complex environmental review and permitting (ER&P) occupying a substantial part of that timeline. The combined effect of extended development timelines and commitment to a specific project definition during ER&P creates an inherent conflict: either the ER&P-committed mine design is out of date by the time permit decisions are imminent; or that ER&P must begin so far in advance of mine design that probabilistic modeling is hindered by numerous unconstrained assumptions that unduly restrict the subsequent mine design. Both are undesirable situations from the perspectives of the project, the regulator and the public process.

This conflict between state of project knowledge and project timelines exists in other contexts. Budget forecasting for major multi-year capital projects requires cost estimates long in advance of detailed project design. The general rule of thumb is that the earlier in the project lifecycle that problem areas are identified, the more effectively management of those issues can be integrated into the project – resulting in better decision making, better design, and lower overall project cost. However, the conflicts between mine design and extended ER&P effectively constrain projects from applying best informed design principles for water management at the most advantageous stage of the process (Fig. 1).

An alternative approach for early mine water quality design is presented in Reference Class Forecasting (RCF). RCF is borne out of economic theories originally by Kahneman & Tversky (Tversky and Kahneman 1974) (Kahneman 1979) and further developed by Flyvbjerg (2007) in transportation project

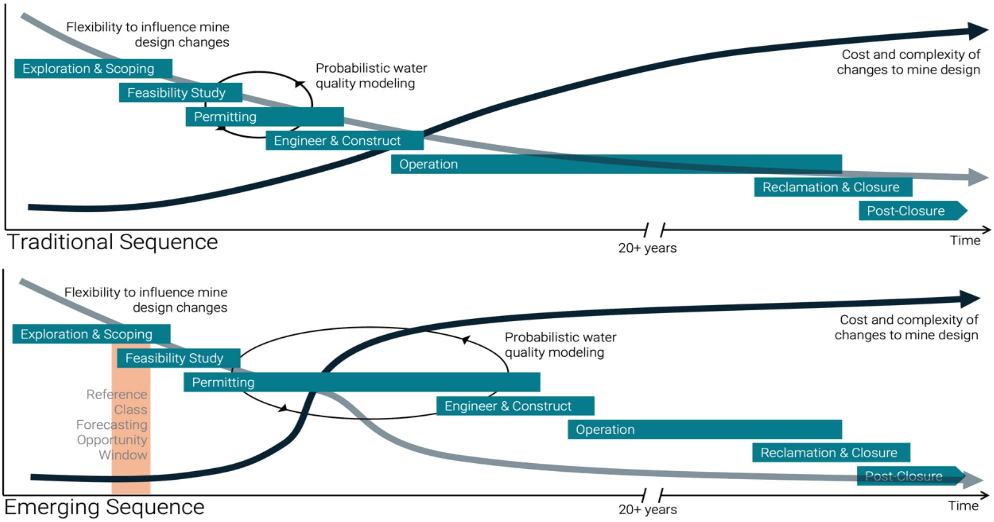

***Figure 1** Mine development sequence with respect to design flexibility and cost to integrate changes. The inflection point between flexibility to integrate design changes and cost/complexity of executing changes is shifting earlier in project timelines as the permitting processes become longer and contingent on modelling.*

cost forecasting. It provides an alternative to 'inside' (or bottom up) cost buildups, which rely on a detailed breakdown of steps and assignment of cost to each, by instead looking for 'outside' similar projects that create a reference class from which costs for the project of interest may be more accurately estimated.

Once a target project is identified, RCF is approached as a 3-step process per Flyvbjerg:

(1) Identifying a relevant reference class of past, similar projects. The class must be broad enough to be statistically meaningful but narrow enough to be truly comparable with the specific project.

(2) Establishing a probability distribution for the selected reference class. This requires access to credible, empirical data for a sufficient number of projects within the reference class to make statistically meaningful conclusions.

(3) Comparing the specific project with the reference class distribution, in order to establish the most likely outcome for the specific project.

The principle of RCF was adopted here for scoping-level assessments of mine project water quality to more effectively integrate water quality design into mine planning. Early RCF-based planning (See Fig. 1, lower panel) brings the benefit of limiting the scope of water modeling requirements to streamline ER&P scopes without increasing water quality risk. The outcomes of a scoping-level mining project water quality RCF are threefold: (1) screen out constituents that are unlikely to influence project design, (2) identify constituents that are likely to drive project design, including an order of magnitude of the reductions required, and (3) identify constituents for which a forecast is unclear and further review is necessary.

Methods

Development of Mine Water Quality Database

Globally, mining companies regularly sample and measure water as part of permitting requirements and in many jurisdictions those data become publicly available through local regulatory agencies. However, those water quality data tend to lack the contextual framing necessary to enable comparative use of the information.

A database of mine water quality was constructed targeting ore from magmatic nickel-copper-platinum group elements (Ni-Cu-PGE) deposits. Available water quality measurements were associated with site metadata that include the local climate, primary ore mineralogy, dominant sulfide mineralization, host lithology, characteristic waste lithologies, mining and processing types and rates, and USGS mineral deposit type. In addition, water samples were associated with proximal mine features (mine pits, rock stockpiles, tailings basins, catchment ponds) that may influence water chemistry. This information was sourced from mine permit applications, financial reporting, environmental review documents and published research findings and efficiently extracted from those sources via automated machine algorithms. The digital data were scrutinized through a quality assurance / quality control process that involved multiple review criteria, including order of magnitude error, analyte mismatch, and digit rounding issues. The database presently contains information from 39 unique mines, 1,556 unique sample locations, covers 108 unique analytes and includes a total of 1,374,045 unique water quality measurements – all with the associated contextual metadata.

Application of RCF Approach

The mine feature targeted for this demonstrative RCF evaluation is a waste rock stockpile generated from an open pit Ni-Cu-PGE magmatic sulfide ore mine. This theoretical mine ("Project mine") will obtain ore from a deposit located in the upper latitudes of the United States.

Identify a reference class

The RCF approach echoes prior work on geoenvironmental models (for example, Plumlee and Nash (1995)), which posit that geological characteristics and their associated geochemical processes exert a fundamental control on the "environmental behavior" of mineral deposits, with factors such as climate, and mining and milling methods representing potentially subordinate controls on the same. This evaluation leverages operational data from a reference class of four Ni-Cu-PGE deposits. Due to the orogenesis of this deposit type, these mines are expected to broadly share lithological characteristics of both the host intrusive body and, less so, the surrounding country rock (Naldrett 2004). Table 1 summarizes a comparison between the mines selected to comprise the reference class for this evaluation and the Project mine. Criteria in Table 1 are:

- **Description:** Indicates mining method.
- **Climate:** Indication of net precipitation and temperature at site.
- **Deposit Type:** All mines in this evaluation are mining Ni-Cu-PGE deposits. Criterion indicates the "Secondary Deposit Type", per Appendix 3 of Mudd and Jowitt (2022).
- **Waste Rock Lithologies:** General lithologic context for rocks that report to the waste rock stockpile and/or waste rock management area. All mines are expected to manage mafic to ultramafic (M-UM) igneous compositions, with or without additional rock types.
- **Stockpile Contact Water Characteristics:** Select general water chemistry parameters associated with waste rock storage. While all mines have waste rock contact water with neutral pH, there is notable variability in specific conductance and, consistent with this, sulfate concentration.

Establish a distribution of expectations

The mine water quality database was queried to obtain a dataset consisting of water quality observations from the reference class at sampling locations associated with waste rock stockpile seepage or runoff. Sampling locations selected were upstream of water treatment or other mitigative approaches. Analytes reported as below method detection limits were assessed as half of the respective limit. Observations were averaged on a monthly time basis, although this resulted in aggregation of a negligible portion of the dataset as most data were recorded on a monthly or longer frequency. For each analyte, concentrations were ordered numerically and plotted as a probability distribution. Due to the overall similarity between the Project mine and those in the reference class, no site-specific adjustments to probability distributions were applied.

Compare project to reference class

This evaluation was intended to identify the chemical constituents which will comprise the design basis for water treatment or other mitigative measures to be applied to a future waste rock stockpile ("constituents of interest") by comparing likely untreated future water quality relative to one or more benchmarks. Therefore, in addition to the probability distribution of water quality expectations, evaluation thresholds are needed to serve as evaluation benchmarks, and decision criteria are selected to formally define the acceptable level of uncertainty under which the comparison is made.

Set evaluation thresholds. Evaluation thresholds were derived in this evaluation from twenty-two potentially relevant water quality standards and incorporated project risk tolerance (see example under "Set decision criteria"). Two sets of evaluation thresholds were used. One set of evaluation thresholds ("Primary" threshold) was set to be equal to the most restrictive of the potentially applicable water quality standards. A second set of evaluation thresholds ("Secondary" threshold) was defined at 25% of these same standards. These thresholds were selected as aligned with acceptable project risk at a scoping level of evaluation.

Set decision criteria. Decision criteria are an expression of risk tolerance that balance the value of the consequence of a wrong decision against the cost/time to obtain additional certainty.

For this evaluation, the goal was to inform mine design based on water quality expectations. Under-projections (i.e., falsely rejecting an expectation that stockpile contact water will be above a water quality standard) were deemed to be of greater potential consequence than over-projections (falsely accepting the same), as they carry risks of a mine design that will result in exceedances to water quality criteria. However, both under and over projections have negative consequences, and thus, both risks of false acceptance and rejection are managed through establishment of decision criteria.

Table 1 Project site and associated reference class mine stockpile features.

	Project Mine	Mine A	Mine B	Mine C	Mine D
Description	Open pit	Open pit to underground	Underground	Open pit	Open pit to underground
Climate (Country, Köppen-Geiger code)	United States, Dfb	Spain, Csa	United States, Dfb	Finland, Dfc	Canada, ET
Deposit Type	Small M-UM Intrusion-related	Small M-UM Intrusion-related	Small M-UM Intrusion-related	Layered Intrusive	Small M-UM Intrusion-related
Waste Rock Lithologies	M-UM intrusives, metasediments	Breccia with M-UM fragments, calc-alkaline volcanics, and carbonates	Peridotite, metasediments	M-UM intrusives, mica schists, shales	M-UM intrusives, gneiss
Stockpile Contact Water Characteristics					
pH	---	7.9	7.5	6.6	7.3 – 7.7
Specific Conductance	---	3,300	2,500	5,000	200
Sulfate	---	1,700	1,100	1,600	Not available

Constituents are excluded from the design basis if the 99th percentile (P99) is *less than* the Primary threshold (i.e., the water quality standard). This is intended to limit the probability of falsely rejecting an expectation of water quality exceedances to less than 1%.

Constituents are included in the design basis if the P99 observation of the Reference Class probability distribution is *greater than* the Primary threshold, *and* the 50th percentile (P50) observation *is greater* than the Secondary threshold (i.e., 25% of the water quality standard). This set of decision criteria isolates constituents for which there is greater than a 1% chance of being observed above the water quality standard, and no more than 50% chance of being present at or above 25% of the water quality standard. The use of the Secondary threshold in this case manages the risk of overengineering the system by limiting "acceptance" to constituents that are likely to be present at concentrations near the standard.

Constituents are classified "undetermined" (i.e., more study is needed) if the P99 observation of the Reference Class probability distribution is *greater than* the Primary threshold, *and* the 50th percentile (P50) observation *is less* than the Secondary threshold. In this case, observations are too variable; while at least 1% are above the water quality standard, half or more are well below it. Either additional information is required, or a decision may be made to adopt an adaptive management approach for the risk of overengineering for this constituent.

Results and Discussion

Example cumulative distribution function (CDF) plots of water quality constituents from the identified reference class of mine stockpiles are shown in Fig. 2 (Step 2 of the RCF process). The primary and secondary water quality thresholds defined for each constituent are displayed within the CDF plots as a solid and dashed vertical line, respectively. The full results of the RCF constituent screening according to the defined acceptance criteria for the project are summarized in Table 2 (Step 3 of the RCF process).

In this evaluation, the RCF narrowed the scope of constituents from a starting list of twenty-two by ruling out eight constituents that were unlikely to have any bearing on mine design, six with likely design influence and eight for which further site-specific evaluation would be recommended including an indication of degree of necessary reduction for each of the latter two groups. The

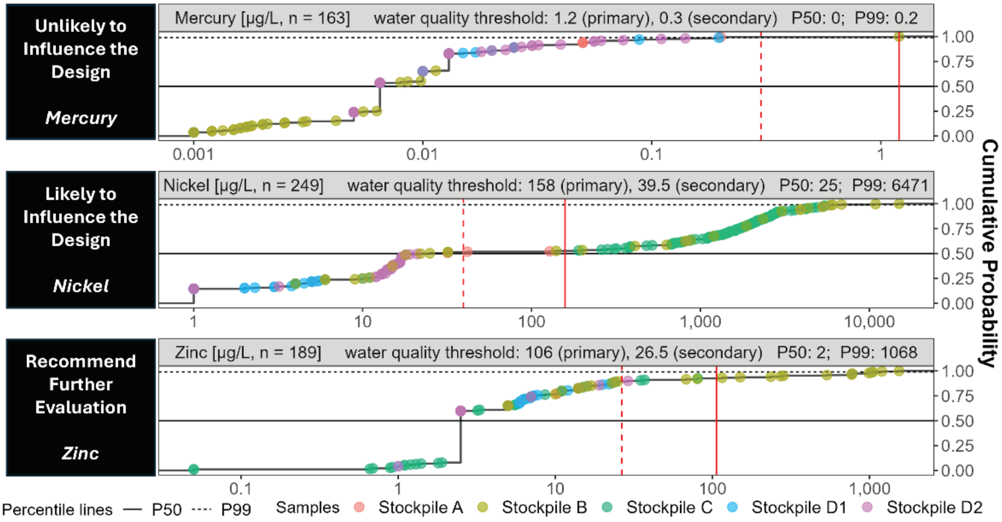

Figure 2 Example CDF plots for water quality constituents from mine stockpile reference class. Primary and secondary evaluation thresholds are identified by solid and dashed vertical lines, respectively.

resultant list of focus areas can be integrated into early mine planning to evaluate a range of management techniques and associated cost/benefits to best inform the mine plan and upcoming ER&P processes which may include: formal regulatory applicability assessments of target water quality standards, reassessing mine design to limit exposure of constituents of concern, evaluation of source control techniques that limit mobilization to water, passive/semi-passive/active control technology evaluations, regulatory relief options and adaptive risk management approaches that evolve over time.

Limitations. Data availability to construct mine feature reference classes is the current limiting factor on broader application of RCF. In this example, four sites were identified for which stockpile data across the range of constituents of interest were available where a pool size approaching 20-30 sites would be ideal. Data availability is increasing as social and governance interests in data transparency drive industry and regulatory bodies to make large datasets publicly available. For example, an industry-led group has recently been assembling a database of pit lake water quality. Reference classes that are comprised of larger pools of mine feature sources will improve confidence in the outcomes of the methodology.

Conclusion

Reference class forecasting provides a rapid, empirical-based method for early-in-design projections of mine water quality. Such forecasts inform mine design for water quality at the most advantageous stage of the planning process and focus ER&P exercises on the constituents of highest interest.

In the example application in this paper, the RCF established a focus on specific constituents and a scale to which those constituents are likely to affect stockpile performance. This provides numeric goals for the design team to integrate water quality solutions at a time when full project lifecycle cost-benefits are most actively assessed. RCF can also focus the permitting team on constituents that merit a deeper evaluation during ER&P. On a more nuanced basis, RCF also prompts a project team to make conscious decisions about acceptable risk tolerance in mine water quality design.

The RCF process is most limited at this point by the availability of mine data from which to build statistically robust reference classes, but its potential for application is expected to grow as data transparency and industry interests drive more mine water quality data into the public realm.

Table 2 Water quality acceptance criteria and RCF-identified constituents in each outcome category.

Constituent Outcome	Acceptance Criteria			Constituents (scale of reduction expressed as P99/primary threshold)
	P99		P50	
Constituent is unlikely to influence design	< primary water quality threshold	---	---	antimony, barium, beryllium, chromium, fluoride, lead, mercury, pH
Constituent is likely to influence design	> primary water quality threshold	AND	> secondary water quality threshold	arsenic (2x), copper (8x) manganese (130x), nickel (38x) silver (4x), sulfate (14x)
Further evaluation is recommended	> primary water quality threshold	AND	< secondary water quality threshold	aluminum (8x), cadmium (5x) chloride (3x), cobalt (90x) selenium (10x), thallium (4x) TDS (7x), zinc (10x)

References

Flyvbjerg B (2007) Curbing Optimism Bias and Strategic Misrepresentation in Planning: Reference Class Forecasting in Practice. European Planning Studies 16(1):3-21. https://doi.org/10.1080/09654310701747936

Heijlen W, Franceschi G, Duhayon C, Van Nijen K (2021) Assessing the Adequacy of the Global Land-Based Mine Development Pipeline in the Light of Future High-Demand Scenarios: The Case of the Battery-Metals Nickel (Ni) and Cobalt (Co). Resources Policy 73. https://doi.org/10.1016/j.resourpol.2021.102202

Kahneman D, A Tversky (1979) Prospect Theory: An Analysis of Decision under Risk.". Econometrica 47:263-291

Mudd GM, Jowitt SM (2022) The New Century for Nickel Resources, Reserves, and Mining: Reassessing the Sustainability of the Devil's Metal. Economic Geology 117(8):1961-1983. https://doi.org/10.5382/econgeo.4950

Naldrett A (2004) Magmatic Sulfide Deposits: Geology, Geochemistry and Exploration. Springer-Verlag Berlin Heidelberg. https://doi.org/10.1007/978-3-662-08444-1

Plumlee GS, Nash JT (1995) Geoenvironmental Models of Mineral Deposits: Fundamentals and Applications. In: U.S. Geological Survey (ed).

Tversky A, Kahneman D (1974) Judgment Under Uncertainty: Heuristics and Biases. Science 185(4157):1124-1131

Influence of Mine Geometry and Working Type on Groundwater Flow and Heat Transport for Geothermal Exploitation

Andres Gonzalez Quiros[1], Mylene Receveur[1], Alison Monaghan[1], Vanessa Starcher[1], Kyle Walker-Verkuil[1], Jeroen van Hunen[2]

[1]*British Geological Survey, Edinburgh, Scotland, UK 2Durham University, Durham, England, UK*

Abstract

The UK Geoenergy Observatory in Glasgow is a unique at-scale research facility to study mine water geothermal and thermal energy storage. In this work we present results from two heat injection experiments performed at two mine levels characterised by different mine workings. The experiments resulted in different thermal breakthrough times, even under similar test conditions. We compare the results and discuss the influence of the mine geometry and working types on the groundwater flow and heat transport processes with support from numerical modelling. This quantification is important to assess the long-term sustainability and potential of flooded mines for geothermal exploitation.

Keywords: Geothermal, UKGEOS Glasgow, Heat transport, Thermal Breakthrough, Mine workings

Introduction

Flooded disused mines have potential to be used for mine water geothermal and thermal energy storage, contributing to the decarbonisation of heating and cooling. Various installations around the world (Walls *et al.* 2021) have confirmed the potential of these underground resources in the energy transition. These have not, however, been fully deployed, partly because of the uncertainties relevant to post-closure conditions in the subsurface, drilling success and flow output, flow and heat transport processes and potential risk of thermal breakthrough or long-term sustainability of the resource (NE LEP 2022, Monaghan *et al.* 2025). In addition, for mine thermal energy storage, there is uncertainty about the extent of the thermally affected volume in both the mine workings and the rock mass as well as its storage and recovery efficiency.

The UK Geoenergy Observatory, in Glasgow (UK) (www.ukgeos.ac.uk) is an at-scale facility to study mine water geothermal energy and thermal energy storage in mines. The facility consists of 12 boreholes (5 of them screened in two levels of mine workings) and a geothermal centre for flexible experimentation (Fig. 1) (Monaghan *et al.* 2022). The boreholes are equipped with downhole hydrogeological loggers, and those drilled to the depths of the mine workings have installed fibre optic distributed temperature sensing and electrical resistivity cables. The geothermal infrastructure consists of a heat pump / chiller, three different heat exchangers, submersible pumps in two of the mine boreholes screened at two different mine levels (GGA07, screened in the Glasgow Upper, and GGA05 in the Glasgow Main), and reinjection mains in four of the mine working boreholes (GGA01, GGA05, GGA07 and GGA08).

The Observatory can be used to perform heat abstraction or injection experiments with multiple configurations: abstraction-reinjection in the same mine workings (i.e., GGA01 and GGA07 in the Glasgow Upper, and GGA05 and GGA08 in the Glasgow Main) (Fig. 2), or abstracting from one of the mine workings and reinjecting into the other, both in heating and cooling modes. This allows the possibility of performing experiments based on actual supply conditions (for example with seasonal thermal storage). All in all, the

Observatory provides data to measure heat transport mechanisms, estimate the hydraulic and thermal properties at real world scale and de-risk mine related energy installations.

In this work we present the results of two in-seam (i.e. abstraction and reinjection in two boreholes screened at the same mine level) heat injection experiments performed at the Glasgow Observatory, one performed in the Glasgow Upper mine workings in 2023 and the other in the Glasgow Main in 2024.

Methods

Mine water reservoir characterisation

Up to seven coal seams were worked in the area between 1805 and 1928. The mine boreholes of the Observatory targeted two of the shallower mine workings: the Glasgow Upper (approx. 50 m bgl, i.e below ground level) and the Glasgow Main (approx. 85 m bgl). Another level of mine workings, the Glasgow Ell (approx. 74 m bgl) was also intersected by the deeper boreholes but these are not screened at this level (Monaghan *et al.* 2020a).

The extent and distribution of mine workings was interpreted from the available working and mine abandonment plans from 1880s and 1930s obtained from the Mining Remediation Authority (formerly the Coal Authority). Plans were digitised and georeferenced (with some challenges to accurately georeferencing the plans; see Monaghan *et al.* 2022 for more details). The analysis included the identification of the coal seams, working methods (pillar and stall, shortwall, followed by total extraction), roadways and shafts.

After analysis, the mine was divided in zones (Fig. 1) that were used as reference for the parameterisation of the numerical models. The working method and post-abandonment conditions (backfilled compaction, collapse, pillar spalling, floor lift) define the current distribution and properties that influence the groundwater flow and heat transport. These conditions were defined with support from other methods, including analysis of legacy records, historical mining narratives, analysis of exposed coal sites, and, more directly with the information from the construction of the Observatory that included the drilling of the boreholes, well logging, borehole camera data and initial hydrogeological testing.

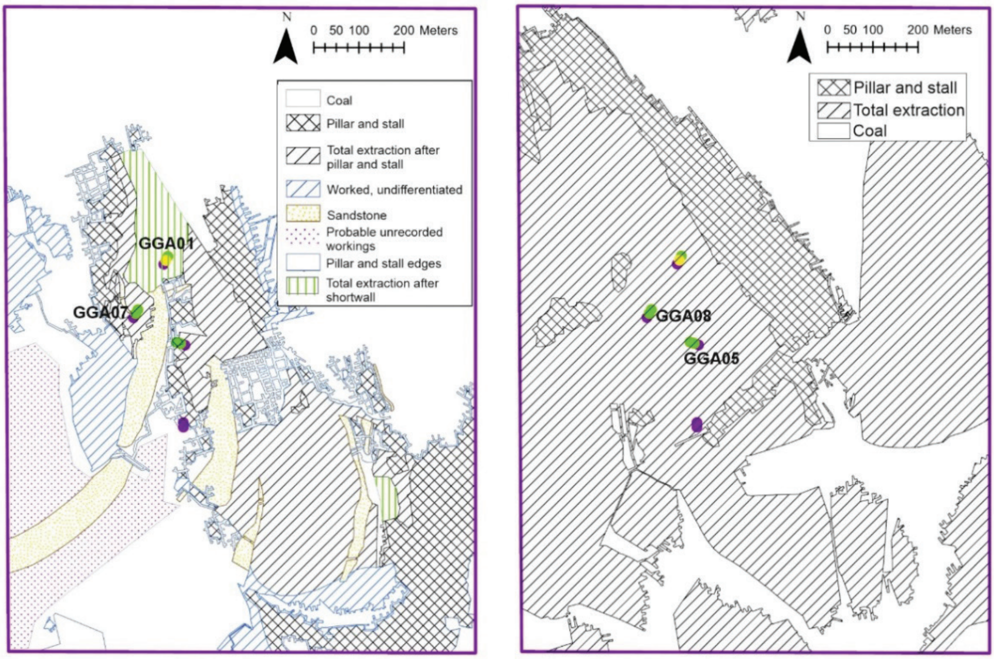

Figure 1 *Zonation of mine workings developed from the mine working plans and the drilling data for the Glasgow Upper (left) and Glasgow Main (right) mine workings. The four sites of Observatory boreholes are shown, with the boreholes used at each heat injection experiment labelled. BGS©UKRI 2025.*

At-scale heat injection experiments

Two heat injection experiments in a doublet mode were performed at the Observatory. Two, boreholes GGA07 and GGA05, screened at the Glasgow Upper and Glasgow Main intervals, respectively, and equipped with a submersible pump were used for abstraction, while a different borehole screened across the same mine workings, GGA01 and GGA08, were used for re-injection. The abstracted water was circulated via buried surface pipes and passed through a heat exchanger linked to the heat pump / chiller to increase the water temperature before reinjection (Fig. 2).

The heat injection experiment using the Glasgow Upper mine workings was conducted in September 2023 and had a duration of 17 days (Table 1 for details). The abstraction borehole was GGA07, and the reinjection borehole was GGA01 (Fig. 2), located at about 135 m distance. The average injection temperature was 17.4 °C, although it varied between a maximum of 17.9 °C and a minimum of 16.7 °C, and at two times problems in the heat pump resulted in very short (<5 minutes) cooler injection temperatures that reached 9.6 and 10.1 °C (Fig. 3 – left). Temperatures were measured at the wellhead and the downhole logger located below the reinjection main, both providing near identical readings. The shell and tube heat exchanger was used in this experiment.

The experiment at the Glasgow Main mine workings started at the end of August 2024 and ran for 5 days. Abstraction was from borehole GGA05, and reinjection at borehole GGA08 (Fig. 2B), located at about 119 m distance. The initial reinjection temperature was 17.2 °C. The average injection temperature was 16.8 °C, but more unstable for the duration of the experiment than in the Glasgow Upper test, with maximum measured T of 17.5 °C and minimum of 15.6 °C. The plate heat exchanger was used in this experiment.

Numerical Modelling

Numerical models of the UKGEOS site were developed using the FEFLOW software. Two different models were used to evaluate each experiment, under the assumption that no connectivity between the Glasgow Upper and Glasgow Main exist (Gonzalez Quiros *et al.* 2024). The mine working plans and the conceptual hydrogeological model were used

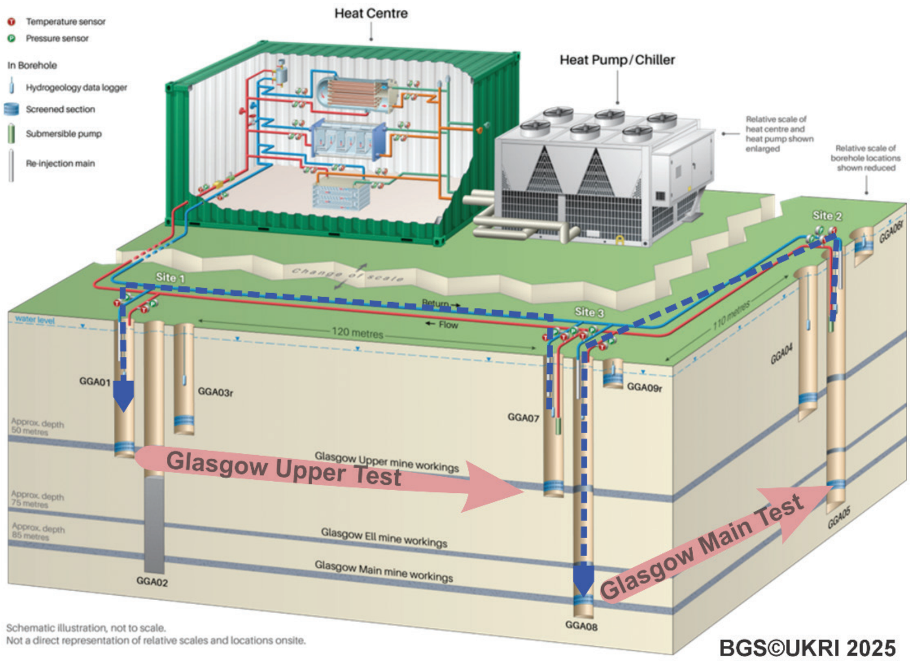

***Figure 2** Schematic diagrams of the heat injection tests at the Glasgow Upper and Main mine workings.*

Table 1 *Experimental conditions in the two tests.*

	Glasgow Upper Test	Glasgow Main Test
Start date	12/09/2023 11:00	30/08/2024 12:30
Run time	411 h	121 h 48 mins
Abstraction borehole	GGA07	GGA05
Reinjection borehole	GGA01	GGA08
Distance abstraction – reinjection	135 m	119 m
Flow-rate	12 L/s	12 L/s
Initial abstraction T	11.92 °C	12.49 °C
Final abstraction T	12.51 °C	12.93 °C
Average injection T	17.37 °C	16.78 °C
ΔT (initial abstraction T – average reinjection T)	5.45 °C	4.29 °C
Heat exchanger	Shell and Tube	Plate
Thermal breakthrough time (0.1 °C change at abstraction)	116 h (4.8 d)	56 h (2.3 d)

to delineate the geometry and implement the boundary conditions. The proposed zonation of mine workings (Fig. 1) was used to delineate zones of parameters for automatic calibration, that was performed using PEST (Doherty 2018) with the hydraulic heads measured in the Observatory boreholes.

Using this setup, forward heat transport numerical models were simulated with the conditions of the experiment. Thermal properties were assigned to the model using the mine working descriptions. A percentage of materials and voids were assigned based on the zonation, expert knowledge and drilling data. Literature and laboratory values for the lithologies and their percentages were later used to obtain a representative thermal conductivity and volumetric heat capacity at for each zone. The temperature observations at the abstraction boreholes for the duration of the experiment were used as reference.

Results

Experiment Results

Fig. 3 shows the temperature measured at the wellhead sensors of the abstraction and reinjection boreholes during the two experiments. The temperature in the abstraction borehole records the change in temperature related with the arrival of the thermal plume and the timing and character of thermal breakthrough. The temperature change relative to the initial abstraction temperature (ΔT) is shown to facilitate the identification of thermal breakthrough.

In the Glasgow Upper experiment, the initial abstraction temperature at GGA07 was 11.92 °C. The temperature fluctuated in the first 6 h of the experiment (less than 0.1 °C increase), probably because of borehole circulation effects, but stabilised again at 11.92 °C until it started to increase constantly after approximately 3 d (Fig. 3 left). After 4.8 d, the measured temperature increase at the abstraction borehole was more than 0.1 °C and reached a 0.5 °C increase after 14 d, with a maximum of 0.59 °C at the end of the experiment, after 17 days.

In the Glasgow Main experiment, the initial abstraction temperature measured at the wellhead was 12.49 °C, suggesting a temperature approximately 0.5 °C higher in the deeper of the Glasgow Main mine workings compared to the shallower Glasgow Upper mine workings, and reflecting the geothermal gradient in the area. After approximately 2 d the abstraction temperature started to increase, reaching 0.1 °C change after 2.3 d, and a maximum of 0.44 °C at the end of the experiment, after approximately 5 d (Fig. 3 right).

Numerical Modelling

The numerical model was calibrated for the hydraulic properties using the hydraulic heads measured at the boreholes screened in

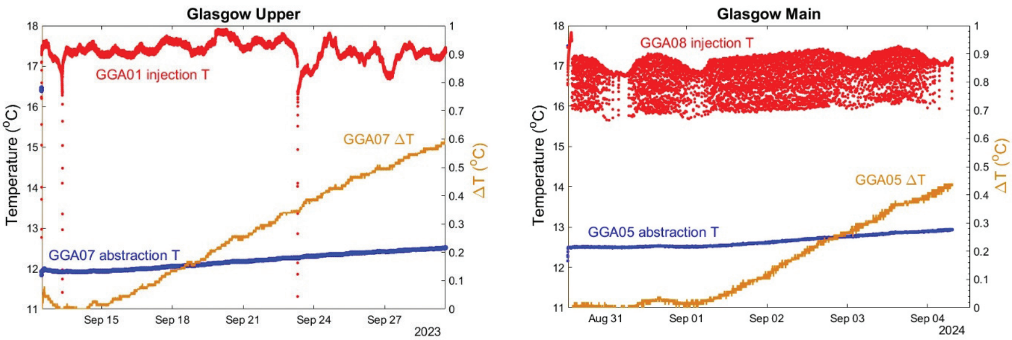

Figure 3 *Abstraction and reinjection temperatures during the Glasgow Upper (left) and Glasgow Main (right) heat injection tests. Experiment duration (x axis) was different. BGS©UKRI 2025.*

the mine working intervals. The calibration with hydraulic heads from GGA01, GGA04 and GGA07 produced a very good fit and resulted in hydraulic conductivity estimates for the areas around the GGA01 and GGA07of 3.2×10^3 m/d and 3.3×10^3 m/d, respectively, of similar magnitude to those obtained from the pumping test characterisation (Shorter *et al.* 2021, Gonzalez Quiros *et al.* 2024). An example of the distribution of hydraulic conductivities at the Glasgow Upper level is shown in Fig. 4 left.

Results of the heat transport models resulted in good estimate of the thermal plume arrival times and temperature changes of similar magnitude to those observed in the experiment (an example of results is shown in Fig. 4 right). However, there is still some uncertainty about the combination of parameters to produce the best possible fit. Assigning very high dispersity values resulted in smoother thermal plumes and more attenuated changes, similar to the observations.

Discussion

The time arrival of the thermal breakthrough (considering a temperature change of 0.1 °C) was interpreted in the Glasgow Upper after 4.8 days and in the Glasgow Main after 2.3 days. The longer thermal breakthrough time in the Glasgow Upper mine workings aligns with the interpretation of a greater percentage of backfilled mine workings (Monaghan *et al.* 2020) and abstraction-injection boreholes located transverse to the direction of former coal pillars, compared to Glasgow Main mine working interpreted to have a greater percentage of open voids. The character of the thermal breakthrough in both cases is small and gradual, as opposed to a single pulse of water that is 5 °C hotter.

The results of the numerical modelling produced good estimates of arrival time of

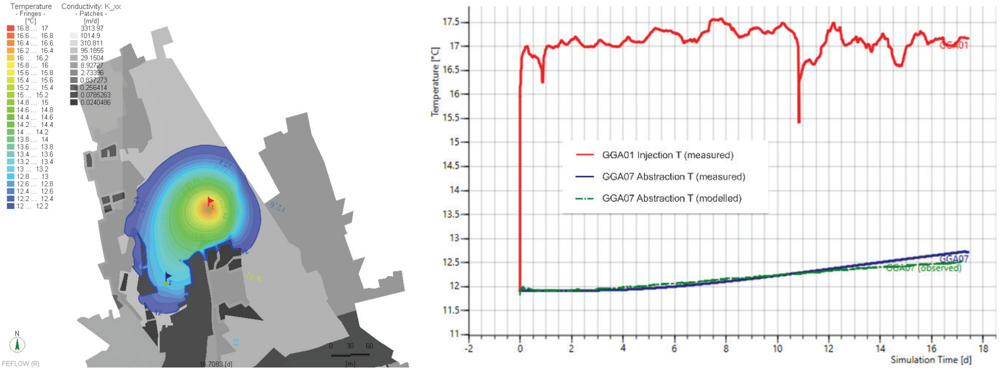

Figure 4 *Numerical model results: (left) distribution of temperatures in the Glasgow Upper mine workings at the end of the experiment; and (right) modelled (blue) and observed (green) temperatures in the abstraction borehole. In red injection temperature. BGS©UKRI 2025.*

the thermal plume at the abstraction borehole and acceptable temperature variation compared with the observations. This shows that the parameterisation of the mine working heterogeneity is a reasonable approximation and important control on heat processes. However, the differences in modelled temperatures might be a consequence of some processes not being fully represented or not fully representative parameterisation.

Internal heterogeneities (e.g. fractures, open voids, conduits) and the limits of how these can be represented using a zoning and equivalent porous media approach needs to be further investigated. The effect on heat transport (heat loss in the heat injection experiment) of the surrounding rock mass, including the fractured roof, is also uncertain. These and other effects, such as local thermal non equilibrium (LTNE) (Gossler *et al.* 2020, Heinze 2024) reported in aquifers at high flow velocities and large grain materials (such conditions are typical of a flooded mine) might result on increasing the effective heat dispersion, while not influencing the advective velocity.

Conclusions

Two heat injection experiments performed at the UK Geoenergy Observatory in Glasgow have revealed the influence of mine working geometry and type in the heat transport processes. Both experiments were conducted under very similar conditions, but thermal breakthrough times were more than twice as long in the mine workings interpreted to have a greater percentage of backfilled mine workings and where boreholes were across the direction of former coal pillars. The results are important to understand the processes of heat transport and assess the long-term sustainability and potential of flooded mines for mine water geothermal and mine thermal energy storage. However, there still remains uncertainty about parameter distribution and magnitude and scale of the thermal processes that requires further research and experimentation.

Acknowledgments

This work has been funded by the EPSRC, United Kingdom grant number EP/V042564/1 Geothermal Energy from Mines and Solar-Geothermal heat (GEMS). An extended version with more detailed results is to be submitted to "Mine Water and the Environment" (IMWA journal).

References

Doherty J (2018) PEST: Model Independent Parameter Estimation User Manual, 7th edition. Australia. Watermark Numerical Computing.

Gonzalez Quiros A, MacAllister DJ, MacDonald A, Palumbo-Roe B, Bearcock J, Ó Dochartaigh B, Callaghan E, Kearsey T, Walker-Verkuil K and Monaghan A (2024) De-risking green energy from mine waters by developing a robust hydrogeological conceptual model of the UK Geoenergy Observatory in Glasgow. Hydrogeology Journal, 32. 1307–1329. doi: 10.1007/s10040-024-02778-y

Gossler MA, Bayer P, Rau GC, Einsiedl F and Zosseder K (2020) On the limitations and implications of modeling heat transport in porous aquifers by assuming local thermal equilibrium. Water Resources Research, 56(10), e2020WR027772. doi: 10.1029/2020WR027772

Heinze T (2024) Multi-phase heat transfer in porous and fractured rock. Earth-Science Reviews, 104730. doi: 10.1016/j.earscirev.2024.104730

Monaghan AA, Barron HF and Starcher V (2020) UK Geoenergy Observatories Glasgow: express data release, mine water and environmental baseline monitoring boreholes at Cuningar Loop (updated June 2020). British Geological Survey Open Report, OR/20/02. 17pp.

Monaghan AA, Starcher V, Barron HF, Shorter K, Walker-Verkuil K, Elsome J, Kearsey T, Arkley S, Hannis S and Callaghan E (2022) Drilling into mines for heat: geological synthesis of the UK Geoenergy Observatory in Glasgow and implications for mine water heat resources. Quarterly Journal of Engineering Geology and Hydrogeology, 55(1), pp.qjegh2021-033. doi: 10.1144/qjegh2021-033

Monaghan AA, Adams CA, Bell RA, Lewis MA, Boon D, González Quirós A, Starcher V, Farr G, Wyatt LM, Todd F and Walker-Verkuil K (2025) Geological factors in the sustainable management of mine water heating, cooling and thermal storage resources in the UK. In Geological Society, London, Energy Geoscience Conference Series (Vol. 1). The Geological Society of London. doi: 10.1144/egc1-2023-39

NE LEP (2022) The Case for Mine Energy – unlocking deployment at scale in the UK. A mine energy white paper. North East LEP.

Shorter KM, MacDonald AM, O Dochartaigh BE, Elsome J and Burke S (2021) Data release and initial interpretation of test pumping of boreholes at the Glasgow UK Geoenergy Observatory. British Geological Survey Open Report, OR/21/016. 104pp. doi: 10.5285/315c716a-8bc5-4071-ad67-62da22e4b6ab

Walls DB, Banks D, Boyce AJ and Burnside NM (2021) A review of the performance of minewater heating and cooling systems. Energies, 14(19), 6215. doi: 10.3390/en14196

Challenges and Opportunities for High-Temperature Mine Thermal Energy Storage with Focus on Regulatory Barriers for Implementation

Andres Gonzalez Quiros[1], Margaret Stewart[1], Thomas Olver[2], Stefan Klein[3], Elke Mugova[3], Corinna Abesser[4]

[1]British Geological Survey, Edinburgh, Scotland, United Kingdom
[2]Geothermal Engineering Ltd., Cornwall, United Kingdom
[3]Fraunhofer IEG, Bochum, Germany
[4]British Geological Survey, Keyworth, England, United Kingdom

Abstract

Mine thermal energy storage (MTES) is an innovative solution to use flooded mines to temporarily store heat during periods of low heating demand for later use during periods of high demand. Its implementation has associated technical and regulatory challenges that must be tested and understood. The PUSH-IT project is piloting the implementation of high-temperature thermal energy storage in aquifers, boreholes and mines. Two MTES sites are being assessed, a demonstration site in Bochum (Germany) and a follower site in Cornwall (UK). This paper presents a summarised review of the regulatory frameworks and barriers for MTES development in these two countries.

Keywords: Thermal Energy Storage, MTES, Regulation, PUSH-IT project

Introduction

A challenge for the decarbonisation of heating is balancing heat production with seasonal variations in heat demand, characterised by periods of very high heat demand in winter and very low heat demand in summer. Underground Thermal Energy Storage (UTES) is an innovative solution to use the subsurface space for thermal storage in periods of excess heat production and low heat demand (e.g. Kallesøe and Vangkilde-Pedersen, 2019).

Various technologies are grouped within UTES, including the storage of heat in aquifers (ATES), boreholes (BTES), and mines (MTES). Mine thermal energy storage (MTES) (e.g. Hahn *et al.* 2024) takes advantage of the mine water filling the void space in flooded mine workings and/or shafts, as well as the surrounding host rock to store heat.

MTES systems can be implemented using various technological solutions (e.g. Walls *et al.* 2021). Typically, mine water, used as heat carrier, is abstracted using boreholes or mine shafts. Heat is transferred to the water (e.g. when the mine water is used for cooling or as carrier for waste heat from industrial processes) via a heat exchanger, and the heated water is then reinjected back into the mine for storage. The process is reversed to recover the heat during periods of higher heating demand.

As mine water geothermal, the MTES concept has been tested at a few sites, but it is still not widely implemented. Commercial uptake is relatively slow due to multiple technical, economic and regulatory barriers. In this work we review existing regulatory frameworks for mine thermal energy storage, as part of the PUSH-IT project, with focus on Germany and the United Kingdom, where the two MTES sites are located.

The PUSH-IT Project

Project Overview

PUSH-IT (**P**iloting **U**nderground **S**easonal **H**eat storage **I**n geo**T**hermal reservoirs)

(Bloemendal *et al.*, 2024) is an EU-funded project that aims to demonstrate the full-scale application of high temperature underground thermal energy storage (HT-UTES) in geothermal reservoirs.

The project includes three types of HT-UTES technologies: Aquifer Thermal Energy Storage (ATES), Borehole Thermal Energy Storage (BTES) and Mine Thermal Energy Storage (MTES), with three demonstrator sites and three follower sites (one per technology). HT-ATES in Delft (Netherlands) and Berlin (Germany), HT-BTES in Darmstadt (Germany) and Litoměřice (Czechia) and HT-MTES in Bochum (Germany) and Cornwall (United Kingdom).

In parallel with the scientific and technical activities at each site, the project aims to investigate the regulatory landscape as well as social aspects of HT-UTES projects, such as public awareness and perception of the technology. As with other new technologies, the lack of specific regulation and limited technological awareness among stakeholders and users are factors that can prevent faster market upscaling.

This work summarises the regulatory frameworks for mine water geothermal and mine thermal energy storage in Germany and the United Kingdom. More specifically in the two MTES sites in the PUSH-IT project, the demo-site in Bochum (Germany) and the follower site in Cornwall (UK). As the moment only in Bochum it is planned to develop a MTES system.

Bochum

In Bochum (North Rhine Westphalia, NRW, Germany), the MTES will be installed at the technical centre of the Ruhr University Bochum (RUB). Boreholes are being drilled to a depth of 120 m into the Mansfeld Colliery, located directly under the RUB.

The system will be integrated in the university's heating and cooling network, currently fed by gas fired boilers and a CHP (combined heat and power) unit with a capacity of 9 MW. The local heating network also supplies heat to approximately 4,800 apartments, 760 houses and 115 other buildings, with supply temperatures in the range 80–120°C. The aim is to use the mine water from the colliery to store waste heat, at approximately 30°C, from the technical/data centre (700 kW peak load) (Fig. 1). The target storage capacity is between 2 and 8 TJ (considering an available storage volume of 5,000–7,000 m^3).

United Downs

In Cornwall (UK), the project is evaluating solutions to store the residual heat from deep geothermal power production at the United Downs Deep Geothermal Project (Olver and Law 2025) in nearby flooded metal (tin and copper) mines. To evaluate the feasibility of the installation of MTES technologies in this location, investigations are being carried in the Consolidated Mines, closed in the 19th century. The activities being carried out include water sampling, temperature logging

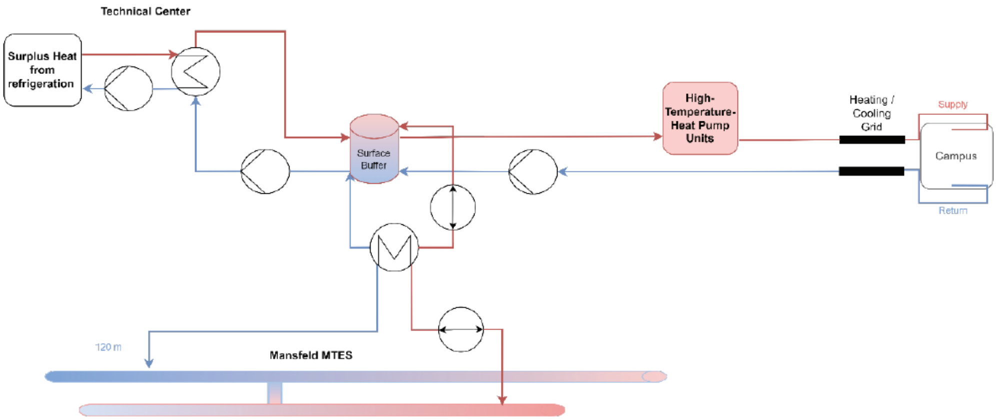

Figure 1 *Schematic diagram of the MTES integration in the heating and cooling network at RUB (F-IEG).*

and tracer testing using accessible shafts, supported by conceptual and numerical modelling undertaken to develop an understanding of the system and assess its potentiality for HT-MTES.

Regulatory Framework of Mine Thermal Energy Storage

Germany

Germany's regulation is decentralised, with national laws setting broad standards and implementation carried out by state (Länder) authorities.

Shallow geothermal projects which use groundwater require notification and permission from the Lower Water Authority (LWH), as stated by the Act on the Regulation of Water Resources (WGH – *Gesetz zur Ordnung des Wasserhaushalts*). The LWH must be notified of any activities that might be affecting groundwater quality and flow. In Bochum, both the WGH and the LWG (*Landeswassergesetz* – North Rhine Westphalia Water Resources Act) regulate the notification and approval obligations for the construction and operation of a shallow geothermal system. Deeper projects require authorisation from the mining authority.

According to the Mining Act (BBergG – *Bundesberggesetz*), drilling to depths of more than 100 m and developments across more than one property require the supervision of the Mining Authority. In NRW an online platform (https://www.bohranzeige.nrw.de/online/) is available to notify drilling activities. Potential issues related to methane must be considered. The drilling is supervised by the Mining Authority, Department 6 Mining and Energy of the Arnsberg District Government in NRW.

The geological information obtained during the investigation and construction of the project must be deposited (Geological Data Act – *GeolDG*) with the local geological survey (*Geological Survey of NRW* – Geologischer Dienst NRW) no more than 3 months after the end of the investigation.

The HT-MTES project in Bochum also obtained permissions from the land and mine owners and agreements with the main beneficiary of the project, the Ruhr University Bochum, prior to obtaining the necessary permits from the authorities.

New legislation in form of the Geothermal Heat Acceleration Act (GeoWG) ("Gesetz zur Beschleunigung der Genehmigung von Geothermie-Anlagen, Wärmepumpen sowie Wärmespeichern, GeoWG") (Deutscher Bundestag 2025) is being drawn up in Germany aiming to facilitate project development and simplify the permitting process. The proposed new law includes various amendments to the BBergG and the WGH aiming to facilitate and accelerate the approval and deployment of geothermal and heat storage systems.

United Kingdom

Geothermal energy is not recognised as a natural resource in UK legislation, and there is no regulator with allocated remit for geothermal and thermal energy storage. Regulatory oversight in the United Kingdom is devolved to the nations, with the nation's environmental regulators playing a key role in regulating potential environmental impact alongside local planning authorities.

In Great Britain (i.e. England, Scotland, Wales), any activity which intersects, disturbs or enters coal seams also requires prior notification and written authorisation from the Mining Remediation Authority (MRA), formerly the Coal Authority (IEA 2023). The MRA is a non-departmental public body that manages the UK's coal assets and legacy, including liabilities associated with past coal mining and unworked coal. In addition to the drilling permit, the abstraction of heat from closed coal mines requires a heat access agreement from MRA (MRA 2024). To support future licensing and regulation, the MRA has built a Living Lab in Gateshead (NE England), located between two mine water heat schemes in the area, the Gateshead Energy Company Network and Lanchester Wines. The site will provide data to help in understanding thermal and hydraulic interactions and support the MRA permitting, environmental regulators and new developers. Access to mine workings in Northern Ireland required authorisation from the Department of the Economy. When the mine water is abstracted from a borehole, a supplementary agreement for the actual borehole location is required.

Metalliferous mines, such as the Consolidated Mines in Cornwall, do not require permission from the MRA. As currently, there is no legislation relating to the ownership of geothermal energy in the UK (Abesser *et al.* 2023a, b), accessing these mines for geothermal / thermal energy storage only requires permission from the land and mine owner as well as planning permission from the responsible mineral planning authority (this is the scenario for a hypothetical MTES project in Cornwall). Planning permission is necessary for most construction works, such as a mine water geothermal or MTES system involving drilling. The competent authority, most likely the local planning authority is the responsible for planning, development management and enforcement. The authority can also ask for additional requirements such as an Environmental Impact Assessment (EIA) or a Habitat Regulation Assessment. Health and Safety regulations (regulated by the Health and Safety Executive) apply to all construction workplaces.

The Environment Agency (in England), or the equivalent environment agencies in the other nations (Scottish Environment Protection Agency, SEPA in Scotland; Natural Resources Wales, NRW in Wales; Northern Ireland Environment Agency, NIEA in Northern Ireland) are the responsible for protection and regulation of groundwater related activities. For geothermal use, borehole construction, abstraction and discharge require authorisation from the relevant environment agency. In England, open loop systems require a groundwater investigation consent, an abstraction license (for abstractions of more than 20 m3 per day) and an environmental permit for the discharge of water from the EA (some exceptions apply) (McClean and Pedersen 2023, EA 2023).

In addition to the previous requirements, the British Geological Survey (BGS) must be notified of the intend to drill boreholes of more than 15 m depth, and the records must subsequently be deposited with the BGS.

Discussion and Conclusion

The increased use of the subsurface for energy applications, as in the case of geothermal energy and thermal energy storage, require an appropriate regulatory framework that both achieves its purpose (e.g. protect people or the environment, prevents interference with other users) while at the same time does not introduce additional excessive administrative burden for projects to be developed.

The project PUSH-IT aims to demonstrate the full-scale application of high-temperature underground thermal energy storage, including the potential of mines to store excess heat. In parallel with site construction and development and related technical activities, the project intends to reduce the potential regulatory barriers for HT-UTES development.

This work has presented a summary of the regulatory and permitting regimes of HT-MTES systems at the project sites: the demonstrator site in Bochum (Germany) and the follower site in Cornwall (UK).

In Germany and the UK there is not bespoke regulation for mine thermal energy storage. Geothermal legislation is under review in Germany (GeoWG expected to enter into force in 2025). In the UK regulation is still evolving drawing on existing frameworks developed for related activities and involves a mix of national, regional, and local authorities. Some authorities, such as the Mining Remediation Authority, consider heat resources as part of managing and granting access to their assets (i.e. flooded coal mines) but there is no national regulation for the abstraction and storage of heat. Although guidance exists for project developers (e.g. IEA 2023; ScotGov 2024), new technologies such as MTES must follow permit workflows with specific requirements set for each project by the competent authorities, leading to project delays and excess costs.

The regulatory review presented in this work will be used in combination with site specific learnings obtained during construction and interviews with authorities and project developers, to identify gaps and inefficiencies in the regulation and develop a set of recommendations for UTES project success.

References

Abesser C, Gonzalez Quiros A and Boddy J (2023a) The case for deep geothermal energy-unlocking investment at scale in the UK: a deep geothermal energy white paper. https://evidencehub.northeast-ca.gov.uk/downloads/668/nel1435a-geothermal-white-paper-report-v12.pdf

Abesser C, Gonzalez Quiros A and Boddy J (2023b) Evidence report supporting the deep geothermal energy white paper: the case for deep geothermal energy – unlocking investment at scale in the UK. Nottingham, UK, British Geological Survey, 134pp. (OR/23/032) https://nora.nerc.ac.uk/id/eprint/535567

Bloemendal M, Bruhn D, Bossennec C, Huhn F, Klein S, Kranz S, Meier N, Peach-Gibson A, Olver T, Peresty V and Pham H (2024) The PUSH-IT project: Geothermal energy storage demonstration and advances for different storage technologies and geological settings (No. EGU24–18418). Copernicus Meetings. doi: 10.5194/egusphere-egu24-18418

Deutscher Bundestag (2025) Gesetz zur Beschleunigung der Genehmigungsverfahren von Geothermieanlagen, Wärmepumpen und Wärmespeichern sowie zur Änderung weiterer rechtlicher Rahmenbedingungen für den klimaneutralen Ausbau der Wärmeversorgung. https://dip.bundestag.de/vorgang/gesetz-zur-beschleunigung-der-genehmigungsverfahren-von-geothermieanlagen-w%C3%A4rmepumpen-und-w%C3%A4rmespeichern/315288 (last accessed 5 February 2025)

EA (2023) Environment Agency Guidance. Open loop heat pump systems: apply to install one. https://www.gov.uk/guidance/open-loop-heat-pump-systems-permits-consents-and-licences (last accessed 4 February 2025)

International Energy Agency (2023) Summary of the regulatory framework for coal mine water geothermal developments in the UK. IEA Geothermal Mine Water Energy Expert Group, June 2023. https://drive.google.com/file/d/1G1j3psBJYQawQVmExWbEkCnwAjV4LKim/view (last accessed 4 February 2025)

Hahn F, Klein S, Mannke, K, Verhoeven R, Güldenhaupt J, Seidel T, & König T (2024) Mine thermal energy storage (MTES) systems in abandoned collieries within the Ruhr area. In West Virginia Mine Drainage Task Force Symposium & 15th International Mine Water Association Congress (pp. 249–250).

Kallesøe A.J. & Vangkilde-Pedersen, T. (eds.) (2019) Underground Thermal Energy Storage (UTES) – state-of-the-art, example cases and lessons learned. HEATSTORE project report, GEOTHERMICA – ERA NET Cofund Geothermal. 130 pp + appendices.

McClean, A., & Pedersen, O. W. (2023) The role of regulation in geothermal energy in the UK. Energy Policy, 173, 113378. doi: 10.1016/j.enpol.2022.113378

MRA (2024) Mine water heat access agreement. https://www.gov.uk/government/publications/mine-water-heat-access-agreement (last accessed 4 February 2025)

Olver, T., & Law, R. (2025, February) The United Downs Geothermal Power Plant, Cornwall, UK: Combining the Generation of Geothermal Electricity and Heat, with the Extraction of Critical Raw Materials. In Proceedings of the 50th Workshop on Geothermal Reservoir Engineering, Stanford, CA, USA.

ScotGov (2024) Scottish Government. Accessing Scotland's geothermal resource: regulatory guidance. https://www.gov.scot/publications/accessing-scotlands-geothermal-resource-regulatory-guidance/ (last accessed 4 February 2025)

Walls, D. B., Banks, D., Boyce, A. J., & Burnside, N. M. (2021). A review of the performance of minewater heating and cooling systems. Energies, 14(19), 6215. doi: 10.3390/en14196215

Using Geophysics Methods to Analyze Evolution of Infiltration from a Tailing Storage Facility

Manuel Gutierrez[1], Laura Tapias[2]

[1]Itasca Chile, Providencia, Santiago, Chile. manuel.gutierrez@oneitasca.com

[2]Itasca Chile, Providencia, Santiago, Chile. laura.tapias@oneitasca.com

Abstract

Tailing storage facility (TSF) infiltration poses a significant environmental risk. This study investigates infiltration plume evolution from a TSF under investigation since 2016. Geophysical methods, specifically NanoTEM and electrical resistivity tomography, were used to characterize subsurface anomalies indicative of infiltration. These techniques offer high-resolution data and allow for temporal monitoring of the plume's migration. Results demonstrate the effectiveness of geophysics in delineating the infiltration's spatial extent, identifying areas of high concentration, and assessing groundwater potential contamination. Temporal analysis reveals contaminant migration rates, informing mitigation strategies and suggesting new control measures. This approach provides valuable insights for improved TSF management and environmental monitoring.

Keywords: Tailings, Infiltration, Geophysics, Groundwater Contamination.

Introduction

Tailings storage facilities (TSF) are indispensable components of modern mining operations. However, they also represent a significant environmental liability due to the potential for seepage and infiltration. One of the primary concerns associated with TSFs is the risk of tailings-derived water infiltrating underlying groundwater systems. This infiltration can introduce a range of contaminants, including pollutants and other potentially harmful substances, into aquifers, posing substantial risks to both water resources and sensitive ecosystems.

While modern TSF design incorporates various measures to minimize seepage, achieving complete elimination of infiltration is often a significant challenge. The complex and frequently heterogeneous nature of the foundation soils beneath TSFs, coupled with the evolving chemical and physical properties of the tailing's material itself, contributes to the complexity of predicting and effectively monitoring infiltration processes. These factors make it difficult to accurately assess the potential for contaminant migration and the long-term effects on groundwater quality.

Traditional monitoring methods, such as installation of monitoring wells, while providing valuable data, can be hard to implement, spatially limited in their coverage, and potentially disruptive to the TSF structure itself. These limitations highlight the need for alternative approaches that can provide more comprehensive and non-invasive monitoring of infiltration.

This study explores the application of geophysical methods, specifically geoelectrical techniques, as a non-invasive and effective approach to characterize and monitor the evolution of infiltration plumes emanating from a TSF that has been under study since 2016, providing a valuable temporal dataset for analyzing the long-term behavior of infiltration. The study aims to demonstrate the utility of geophysics in enhancing our understanding of infiltration processes and improving the management of potential risks associated with TSFs

Infiltration Monitoring Complexity

Monitoring infiltration from TSFs represents a complex challenge due to the interplay of numerous influencing factors. These factors include hydraulic properties of tailing's material, hydrogeological characteristics of the underlying soils (such as permeability, porosity, and degree of saturation), specific design and operational practices of the TSF, and climatic conditions. A thorough understanding of these factors and their complex interactions is crucial for effectively understanding and managing the infiltration process.

However, the unsaturated zone, where much of the initial infiltration occurs, poses a particular challenge for characterization. This zone, located between the ground surface and the water table, is notoriously difficult to investigate due to its dynamic nature and the complex interactions between water, air, and soil particles. Traditional methods, while providing valuable information, have inherent limitations. Soil sampling and laboratory testing, for example, offer insights into soil properties but are limited in spatial extent and can be disruptive to the TSF structure. Furthermore, these methods may not adequately capture the dynamic nature of the infiltration process, which can vary significantly over time in response to changing conditions.

These limitations have driven the exploration and development of more comprehensive and, importantly, non-invasive monitoring techniques. The need for methods that can provide continuous, spatially distributed information about infiltration processes without disturbing the TSF has led researchers and practitioners to investigate the potential of geophysical methods. These methods offer the promise of characterizing the subsurface in a non-destructive manner, providing valuable insights into the evolution of infiltration plumes and informing more effective management strategies.

Geophysical Methods: A Powerful Tool for Infiltration Analysis:

A Geophysical methods offer a non-invasive and cost-effective way to investigate the subsurface and identify anomalies associated with infiltration. This study focuses on the use of geoelectrical methods, specifically NanoTEM and ERT, to map the spatial distribution of electrical resistivity.

These methods are widely used in hydrogeological exploration contexts. Both ERT and NanoTEM are indirect and non-invasive methods that measure the variation of electrical resistivity in the subsurface. This property, electrical resistivity, will depend mainly on the porosity of the rocks, the degree of lithification and, in the case of sediments, granulometry (Telford *et al.* 1990). Furthermore, the relative water content in the rocks (i.e. saturated, partially saturated or unsaturated layers) and the chemistry of the groundwater (electrical conductivity) allow for significant variations in resistivity with depth (Telford *et al.* 1990). In this way, the layers with the highest water content will provide low resistivity values (< ~30 Ω-m), compared to those less saturated (between 30 and 250 Ω-m approx.) and unsaturated (> ~250 Ω-m). Some examples can be seen in works carried out in Northern Chile (Taucare, 2015; Ruthsatz *et al.* 2018; Viguier *et al.* 2018).

- NanoTEM (Transient Electromagnetic Method): NanoTEM measures the decay of an electromagnetic field induced in the ground. It is particularly sensitive to conductive materials at depth and can be used to map the overall extent of a conductive plume associated with infiltration.
- Electrical Resistivity Tomography (ERT): ERT involves injecting electrical current into the ground and measuring the resulting voltage differences. By analyzing these measurements, a 2D or 3D image of the subsurface resistivity distribution can be generated. ERT provides higher spatial resolution than NanoTEM and can be used to delineate the detailed structure of the infiltration plume.

Study Site and Methodology:

This study focuses on a specific TSF that has been monitored since 2016. Geological setting, TSF design, and operational history are important factors considered in the interpretation of geophysical data.

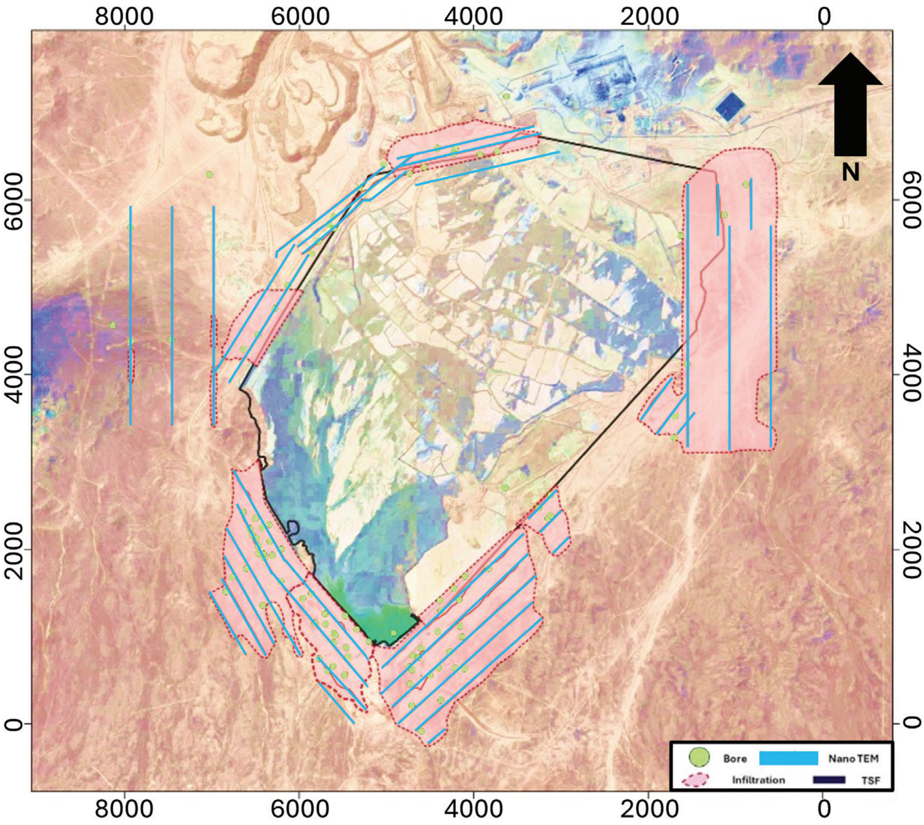

Figure 1 *Geophysical survey's locations around TSF area.*

The methodology involves repeated geophysical surveys using NanoTEM and ERT at key locations around the TSF (Fig. 1). Baseline surveys were conducted to establish background resistivity distribution before significant infiltration was observed. Subsequent surveys were conducted at regular intervals to monitor the temporal evolution of the infiltration plume. The data were processed and interpreted using specialized software to generate maps and cross-sections of resistivity. These results were then integrated with existing hydrogeological data, including information from monitoring wells, to develop a comprehensive understanding of the infiltration dynamics.

Results and Discussion:

Multiple geophysical surveys successfully delineated the spatial extent of the infiltration plume emanating from the TSF, with multiple interpretations of the resistivity (Fig. 2). NanoTEM data provided a regional overview of the conductive anomaly, while ERT data revealed the detailed structure of the plume, including areas of higher contaminant concentration.

Fig. 2 shows the delimitation of the plume based on the resistivity interpretation of one of the multiple surveys. Results of this interpretation were also compared with data from bores P4 and P4A, drilled and screened in the unsaturated zone, but their current situation shows presence of water that is associated with infiltration from the TSF. It must be noted that close to bore P4A there is a lack of data due to field complications. This same procedure was repeated with the different surveys shown in Fig. 1. With all this information it was possible to delimitate the areas of the infiltration as presented in the same figure.

Temporal analysis of the data showed the plume's migration pathways and its rate of advance. Results were compared with data from monitoring wells, confirming the effectiveness of the geophysical methods in detecting and characterizing infiltration. The study also revealed the influence of geological structures, such as faults or preferential flow paths, on the plume's migration. This was not the focus of the study and will be analyzed in future studies.

As shown (Fig. 2) this infiltration flows at the first 25 m to 50 m below ground surface, while regional water level in this area is currently at 200 m of depth or lower. The climate of the area is desertic, with less than 5 mm of precipitation per year in average, leading to the main conclusion that the only source of water that can produce this infiltration is the water contained in the tailings.

Implications for TSF Management:

The findings of this study have important implications for the management of the TSF. The comprehensive understanding of infiltration dynamics provided by the geophysical methods allows for the development of more effective strategies for preventing and mitigating groundwater contamination risks. For example, the identification of high-risk areas can inform the placement of additional monitoring wells or the implementation of targeted remediation measures. Temporal monitoring data can also be used to assess the effectiveness of existing mitigation measures and to optimize water management strategies.

Conclusions

This study demonstrates the effectiveness of geophysical methods, particularly NanoTEM and ERT, as valuable tools for monitoring the evolution of infiltration plumes from TSFs. These methods provide high-resolution data without the need for intrusive sampling, enabling the capture of both spatial and temporal dynamics of infiltration. The results of this research contribute to a better understanding of the complex processes governing infiltration and provide valuable information for developing improved TSF management strategies. Further research could explore the integration of geophysical data with hydrogeological models to enhance predictive capabilities and optimize water management practices.

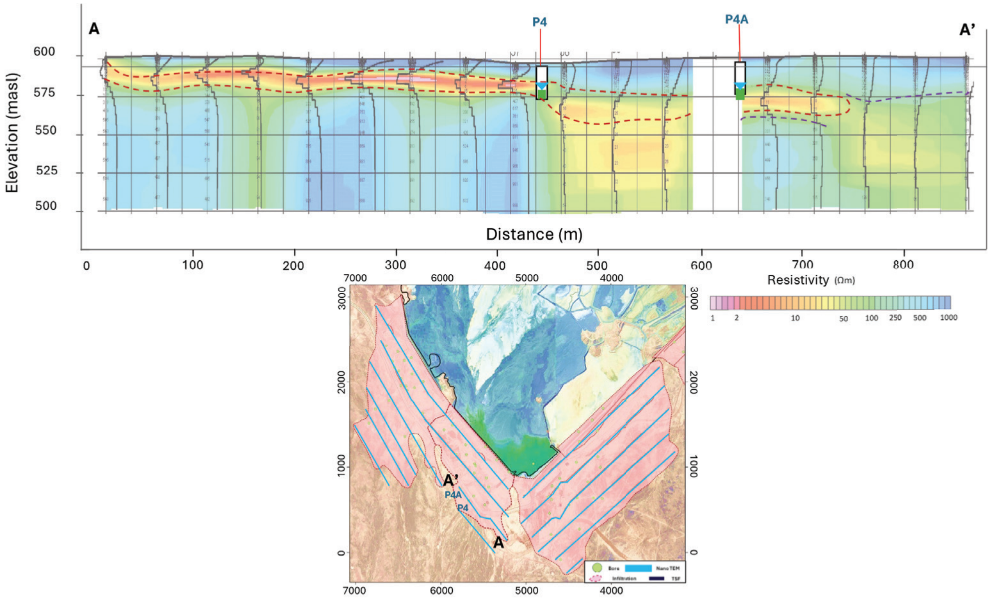

Figure 2 *Interpretation of resistivity for one of the geophysical surveys.*

References

Ruthsatz A.D., Samiernto-Flores A., Diaz D., Salazar-Reinoso P., Herrera C. & Brasse H. 2018. Joint TEM and MT aquifer study in the Atacama Desert, North Chile. Journal of Applied Geophysics 153, 7-16. https://doi.org/10.1016/j.jappgeo.2018.04.002

Taucare M. 2015. Hidrogeología y aplicación del método TEM para el reconocimiento de acuíferos en la Quebrada de Camiña, Región de Tarapacá, Chile. Tesis para optar al título de geólogo, Universidad Católica del Norte, Antofagasta, Chile.

Telford W.M., Geldart L.P. & Sheriff R.E. 1990. Applied Geophysics (2nd edition). Cambridge University Press, 770 pp. https://doi.org/10.1017/CBO9781139167932

Viguier B., Jourde H., Yáñez G., Lira E.S., Leonardi V., Moya C.E., García-Pérez T., Mari0ngue J. & Lictevout E. 2018. Multidisciplinary study for the assessment of the geometry, boundaries and preferential recharge zones of an overexploited aquifer in the Atacama Desert (Pampa del Tamarugal, Northern Chile). Journal of South American Earth Sciences 86, 366-383. https://doi.org/10.1016/J.JSAMES.2018.05.018

Portugal IMWA Spain
2 0 2 5

Multi-Variable Analysis For Fault Identification And Hydraulic Characterization

Manuel Gutierrez[1], Laura Tapias[2]

[1]Itasca Chile, Providencia, Santiago, Chile. manuel.gutierrez@oneitasca.com
[2]Itasca Chile, Providencia, Santiago, Chile. laura.tapias@oneitasca.com

Abstract

Fractured aquifers, especially those containing faults, pose significant challenges in hydrogeological studies. This study investigates a tailing storage facility overlying a fault system potentially acting as a preferential flow path. A comprehensive review of existing geological, hydrochemical, geophysical, and piezometric data, collected over several years, was conducted to identify the presence of a potential fault. Results indicate distinct geological units on either side of the fault, confirmed by both geological models and geophysics. Hydrochemical and piezometric data suggest the fault acts as a barrier to regional groundwater flow. This multi-variable approach demonstrates the value of integrating diverse datasets for fault identification and characterization, informing risk assessments and mitigation strategies.

Keywords: Fractured Aquifers, Field Data, Geophysics, Tailings.

Introduction

Fractured rock aquifers represent complex hydrogeological systems where groundwater flow is predominantly governed by the intricate network of fractures and faults (Beale & Read 2013). A thorough understanding of the geometry and hydraulic properties of these features is essential for effective groundwater management, particularly when considering potential contamination from sources such as tailings storage facilities (TSFs).

Faults, depending on factors like their internal structure, the degree of fracturing, and the surrounding stress field, can function as either conduit for preferential groundwater flow or barriers to groundwater movement. In the present study, a TSF located above a suspected fault system raises concerns regarding potential preferential flow paths for infiltration.

While regional geological maps may indicate the presence of faults, detailed characterization of these features is often lacking. This paper addresses this gap by presenting a multi-variable approach. This approach integrates diverse datasets collected over several years to identify, characterize, and ultimately understand the hydraulic role of the fault system situated beneath the TSF.

The Challenge of Fault Characterization in Hydrogeology

Characterizing faults within hydrogeological investigations presents a multitude of challenges. Traditional methods, while valuable, often fall short in providing the comprehensive understanding needed for effective groundwater management. Geological mapping and core drilling, for example, offer valuable insights into fault locations and lithological characteristics, but these methods are often limited in their spatial extent and can be prohibitively expensive, especially when investigating deep or complex fault zones. As described by Fetter (2001), spatial variability of hydraulic conductivity in fractured rock is difficult to characterize This limitation becomes particularly acute when dealing with faults, which can exhibit significant variations in hydraulic properties along their strike and dip.

Furthermore, these traditional methods may not adequately capture the complex three-dimensional geometry of fault systems. Faults rarely exist as simple, planar features; they are often comprised of multiple interconnected fractures, brecciated zones, and gouge material, creating intricate pathways for groundwater flow. The geometry of fractures is highly variable and complex, making it difficult to describe mathematically (Freeze and Cherry 1979). This complexity makes it challenging to accurately represent faults in groundwater flow models (Fig 1), leading to uncertainty in predictions of groundwater flow paths and contaminant transport.

Moreover, these methods may struggle to fully characterize the hydraulic properties of faults, such as their transmissivity and storativity. These properties, which govern the rate and volume of groundwater flow through the fault zone, are crucial for assessing the potential for contaminant migration.

The lack of detailed information regarding fault geometry and hydraulic properties creates significant uncertainty in groundwater flow models (Fig. 2). This uncertainty makes it difficult to accurately assess the potential for contaminant migration along faults, particularly in situations like the present study where a TSF is situated above a suspected fault system. To address these challenges, this study adopts a multi-faceted approach, integrating multiple data sources. These include geological data from existing maps and reports, water level and piezometric data from monitoring wells, hydrochemical data to identify potential flow paths and mixing zones, and geophysical data, such as seismic surveys and electrical resistivity tomography, to provide insights into the subsurface structure and geometry of the fault system. By integrating these diverse datasets, the study aims to provide a more comprehensive and robust understanding of the fault system beneath the TSF, ultimately improving the assessment of potential risks and informing effective groundwater management strategies.

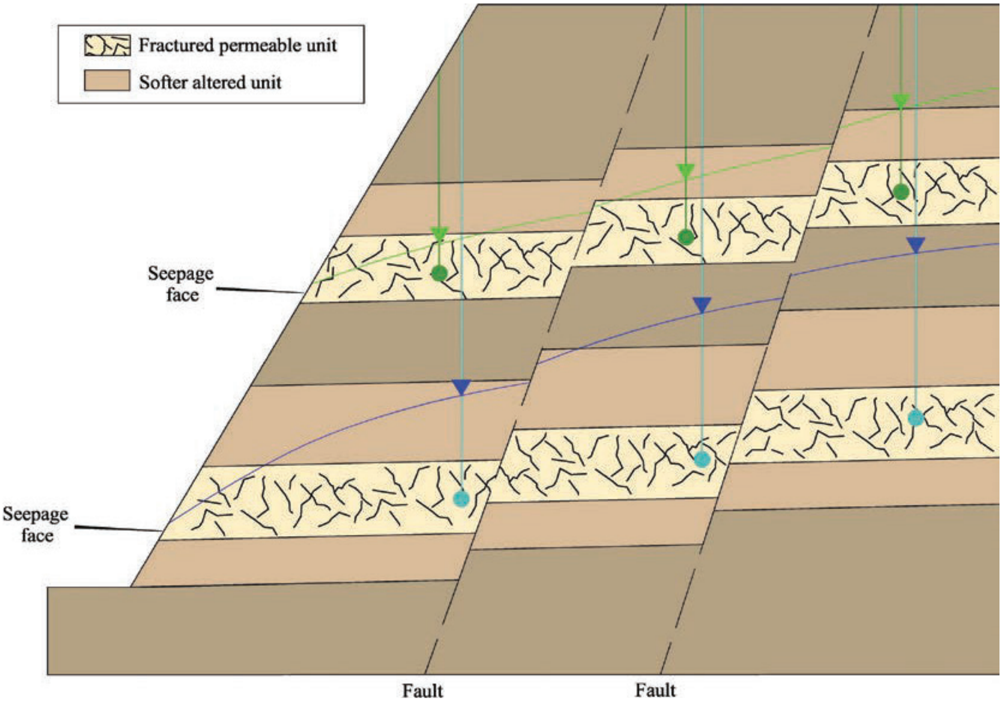

Figure 1 *llustration of vertical and lateral compartmentalization due to faults and bedding planes (Beale & Read 2013).*

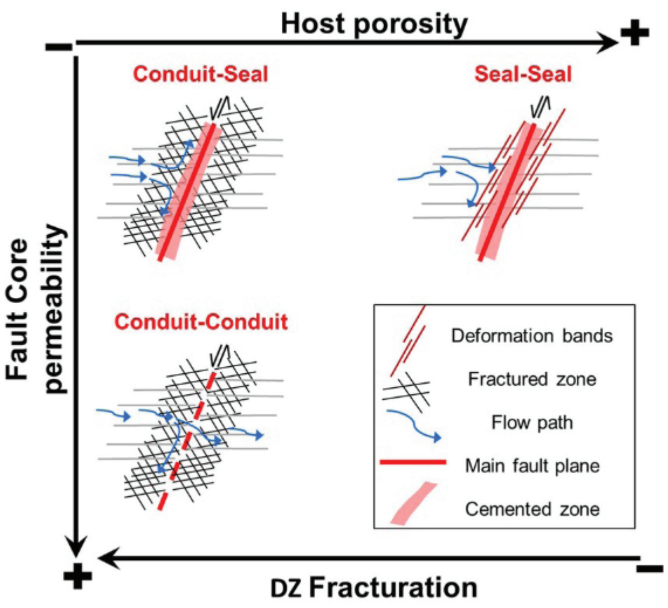

Figure 2 Classification of main conceptual models for fault zone's representation (Rohmer et al. 2015).

Multi-Variable Approach and Data Integration

This study involved a comprehensive review of existing data collected over several years with varying objectives. The review process focused on identifying relevant and high-quality data for fault characterization. The following datasets were integrated:

- Geological Characterization: Data from geological mapping, drill core logs, and surface exposures were used to identify different geological units and their spatial relationships. This information was crucial for determining the fault's geometry and identifying the materials juxtaposed across the fault plane.
- Water Levels and Piezometry: Water level data from monitoring wells and piezometers provided insights into the groundwater flow patterns and hydraulic head distribution in the area. This information was used to assess the potential for the fault to act as a barrier to groundwater flow.
- Hydrochemistry: Hydrochemical data, including major ion concentrations and isotopic signatures, were used to identify distinct groundwater sources and flow paths. Differences in water chemistry across the fault could indicate hydraulic isolation.
- Geophysics: Geophysical data, such as seismic surveys or electrical resistivity tomography, can provide information about subsurface structures, including faults. These data were used to map the location and extent of the fault system.

Results and Discussion

The integration of these diverse datasets yielded valuable insights into the fault system.

- Fault Geometry: The combined geological (Fig. 3) and geophysical (Fig. 4) data allowed for the delineation of the fault's geometry The presence of distinct geological units on either side of the fault, identified in both geological models and geophysical surveys, provided clear evidence of fault displacement.
- Hydraulic Barrier: Analysis of water level and piezometric data revealed a significant difference in hydraulic head across the fault (Fig. 3), suggesting that the fault acts as a barrier to regional groundwater flow. This interpretation was supported by hydrochemical data (Fig. 4), which showed distinct water chemistry signatures on either side of

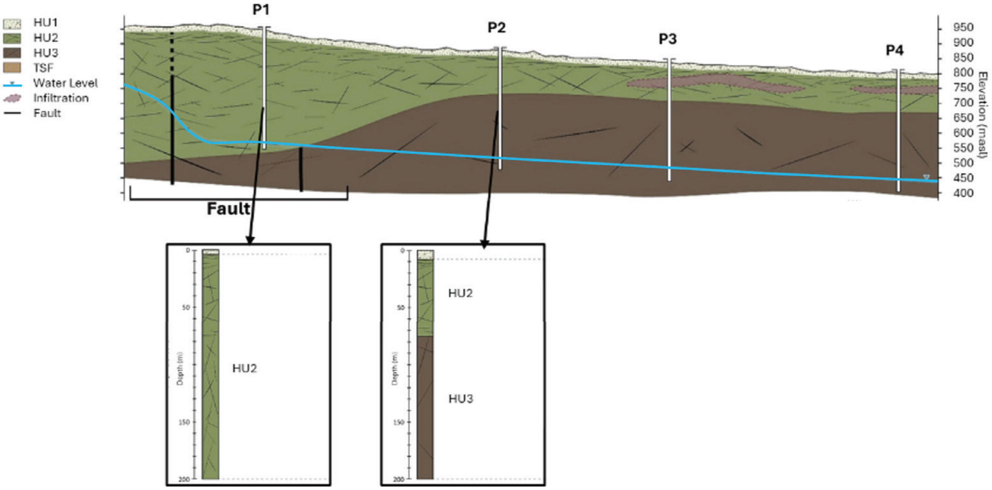

Figure 3 Geological interpretation.

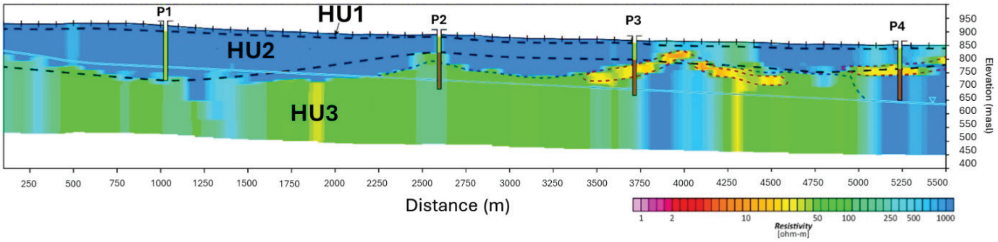

Figure 4 Geophysical survey.

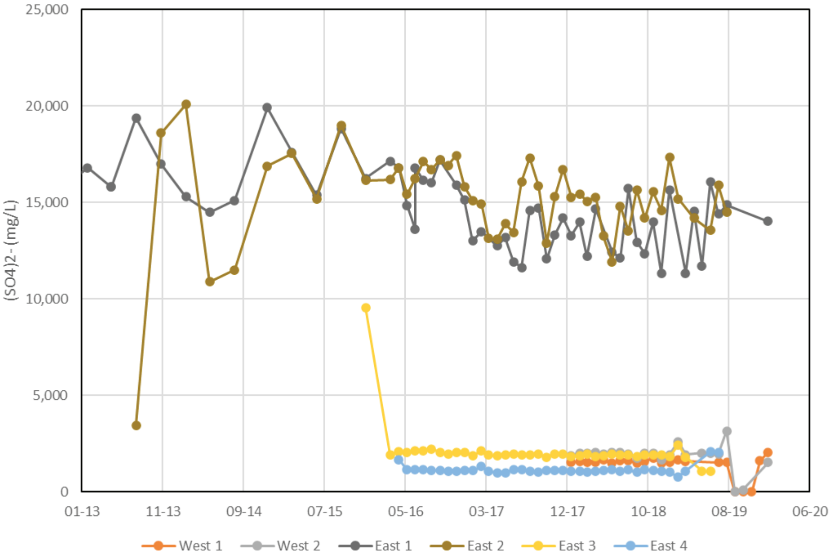

Figure 5 Sulfate concentrations in east and west bores.

the fault, indicating limited groundwater mixing. These findings suggest that the fault may be impeding groundwater flow and potentially influencing the migration of infiltration from the TSF.

Implications for Risk Assessment and Mitigation:

The detailed characterization of the fault system has important implications for risk assessment and mitigation related to the TSF. Understanding the fault's geometry and hydraulic properties allows for a more accurate assessment of the potential for contaminant migration along the fault. The finding that the fault acts as a hydraulic barrier suggests that infiltration from the TSF may be preferentially channelled along the fault zone, potentially affecting specific areas. This information can be used to inform the design and placement of monitoring wells and to develop targeted mitigation strategies to prevent groundwater contamination.

Conclusions

This study demonstrates the value of a multi-variable approach for characterizing complex hydrogeological systems, particularly in the presence of faults. By integrating diverse data sources, this work has provided valuable insights into the geometry and hydraulic properties of a fault system beneath a TSF. The findings highlight the importance of considering fault structures in groundwater flow models and risk assessments related to potential contamination. The results of this study can inform current and future management strategies for the TSF and contribute to the protection of groundwater resources. Further research could explore the use of numerical modelling to simulate groundwater flow and contaminant transport along the characterized fault system.

References

Barnett *et al.* (2012). Australian groundwater modelling guidelines, Waterlines report, National Water Commission, Canberra.

Beale, G., Read, J. (2013) Guidelines for evaluating water in pit slope stability. CSIRO Publishing, Collingwood.

Fetter, C.W. (2001). Applied Hydrogeology. 4th Edition. Prentice-Hall Inc.

Freeze, R.A. and Cherry, J.A. (1979) Groundwater. Prentice-Hall Inc., Englewood Cliffs, Vol. 7632, 604.

Rohmer, Jérémy & Nguyen, Trung-Kien & Torabi, Anita. (2015). Off-fault shear failure potential enhanced by high-stiff/low-permeable damage zone during fluid injection in porous reservoirs. Geophysical Journal International. 202. 10.1093/gji/ggv225.

Feasibility Study: Geothermal Local Heating with Mine Water for the Development Area Richtericher-Dell in Aachen, Germany

* Florian Hahn[1], Stefan Klein[1], Kevin Mannke[1], René Verhoeven[1], Marco Braun[2]

[1]Fraunhofer IEG, Bochum, Germany, florian.hahn@ieg.fraunhofer.de

[2]STAWAG, Aachen, Germany, marco.braun@stawag.de

Abstract

This feasibility study explores the potential of utilizing geothermal energy from mine water for heating the Richtericher-Dell development area in Aachen, Germany. In light of the EU's goal for a net-zero greenhouse gas economy by 2050, and the significant contribution of heating and cooling to Germany's energy demand, this study proposes the implementation of a fifth generation district heating and cooling (5GDHC) network. The project aims to leverage mine water from a depth of 270 meters, employing an electrical submersible pump to circulate water through an energy center, while integrating a pit thermal energy storage system to enhance capacity during peak loads. The planned heating grid is designed to support approximately 850–900 residential units, with an anticipated annual consumption of 9.5 GWh. The study concludes that the proposed system can operate independently of fossil fuels, relying solely on sustainable energy sources and a power-to-heat backup system. This model serves as a blueprint for future heating grid expansions in the Aachen region, promoting the reutilization of mine water and the integration of decentralized energy systems.

Keywords: Coal mines, mine water, geothermal energy, fifth generation district heating and cooling (5GDHC) networks

Introduction

The EU aims to have a net-zero greenhouse gas (GHG) economy by 2050, with 55% reduction on 1990 levels by 2030. At present, heating and cooling represent over 50% of the final energy demand in Germany and are mainly supplied by fossil fuel derived energy (BMWK, 2022). The implementation of mine water in fifth generation district heating and cooling (5GDHC) networks is a possibility to counterbalance this effect.

The feasibility study for the planned development area Richtericher-Dell in Aachen, Germany aims at the supply of heating and cooling via mine water with the focus on the underground development of geothermal energy in conjunction with a 5GDHC network.

5GDHC refers to a modern approach to district energy systems that focuses on improving energy efficiency, integrating renewable energy sources, and reducing greenhouse gas emissions.

Relevance to Sustainable Energy:

- **Energy Efficiency:** 5GDHC systems utilize advanced technologies such as heat pumps and thermal energy storage to optimize energy use.
- **Renewable Integration:** They can incorporate a higher share of renewable energy sources, such as solar thermal and geothermal energy.
- **Decentralization:** Promotes local energy production and consumption, reducing transmission losses.
- **Flexibility:** Adaptable to varying energy demands and the integration of smart grid technologies.
- **Lower Emissions:** Contributes to climate goals by reducing reliance on fossil fuels.

In summary, 5GDHC networks play a

crucial role in transitioning to sustainable energy systems by enhancing efficiency and promoting the use of renewables, e.g. mine water.

Mine water utilization concepts

Utilizing the thermal potential of mine water from abandoned mines is generally possible with different technical systems. If the mine water is to be used as a heat source, either a closed or an open system can be employed. In closed systems the mine water is indirectly utilized by borehole heat exchangers (BHE), which are installed in shafts (Fig. 1). These are usually tubular heat exchangers made of metal or plastic, in which a heat transfer medium is circulated (secondary circuit), which absorbs the heat, e.g. from the backfill column of a former shaft. It is also conceivable to tap into the existing water column via a tubular heat exchanger, which is fed through a degassing pipe that is e.g. still accessible.

The volume flow of the circulating heat transfer medium is generally the limiting factor for the indirect use of the geothermal energy present in the subsurface, due to an optimum extraction rate depending on the flow rate (VDI, 2019).

The direct thermal utilization of mine water in an open doublet system should be favored at an early stage, due to significantly higher thermal extraction rates. For this purpose, the available mine water potential in the subsurface must be estimated.

In an open system with direct utilization of the existing ambient heat in the subsurface, it must be ensured that the extraction and injection wells are not hydraulically connected to each other, as this can result in a “thermal short circuit”, which can significantly reduce the performance of the mine water scheme. It is therefore highly recommended to position the wells in different levels of the mine layout.

Study area

Urban development plans for the Richtericher Dell area in Aachen, Germany (Fig. 2) led to the adoption of a master plan in 2005. A final partial or overall plan with a binding development scheme still has to be finalised by the City of Aachen.

However, residential development is still planned, supplemented by sites for daycare centers, a retirement home and retail. In consultation with the City of Aachen, it was highlighted that the energy requirements of the development scheme will be in line with the already provided data from 2005. For the feasibility study, it was therefore assumed that the future development is in accordance with the elements of the previous planning, which was utilized for the expected heat demand and the planning of the heating network.

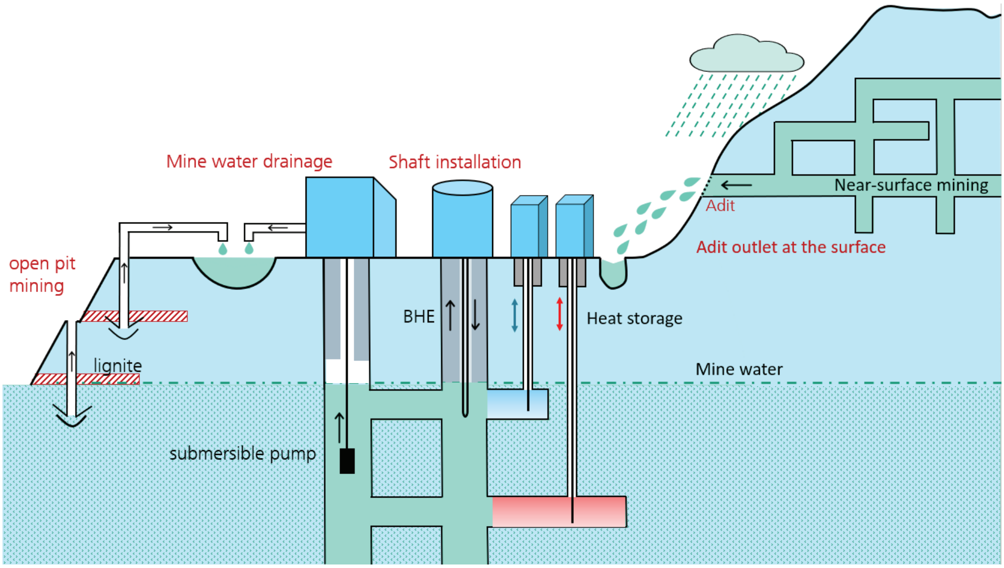

Figure 1 *Mine water utilization concepts (modified after LANUV, 2018).*

The following cartographic representation (Fig. 3) shows the Richtericher Dell master plan with the foreseen housing scheme. For the feasibility study, the master plan was the basis for the planned heating network and the spatial integration of the mine water utilization concept. The layout of the planned heating and possible cooling network was set in the streets of the master plan (dashed in different shades of blue).

The heating scheme of the newly built houses can be freely selected and adapted to the conditions of supply from a low temperature heating source. Surface heating systems are assumed for the heating distribution within the housing units, so that only a low flow temperature (max. 35 °C) will be required.

The planned heating grid within the Richtericher-Dell development allocates an area of 37 ha with approx. 850–900 new residential units. A maximum grid capacity of approx. 4.2 MW with a simultaneity of 83% was based on the net energy balance of the foreseen buildings (with an anticipated annual consumption of approx. 9.5 GWh). As an innovation, it should be emphasized that the influence of an additional pit thermal energy storage (with a constructible surface that can be reused as a parking lot in the vicinity of the energy center) was specifically investigated and evaluated within the feasibility study. This could significantly support the anticipated 40 °C grid temperature during peak loads by providing an additional hydraulically separated temperature circuit for more than 24 hours at a time. In combination with the pit thermal energy storage system, the output of the anticipated mine water system and heat pumps could be reduced by approximately 50%.

The integration of mine water into the Richtericher Dell development scheme is an integral part of the 5GDHC network and could be achieved by pumping mine water from the deeper 270 m level using an electrical submersible pump, feeding it to an energy center and then discharging the cooled mine water into the 200 m level (Fig. 1).

The actual heat or cooling medium for supplying the new development area circulates in a secondary circuit from the energy center to the consumer points and

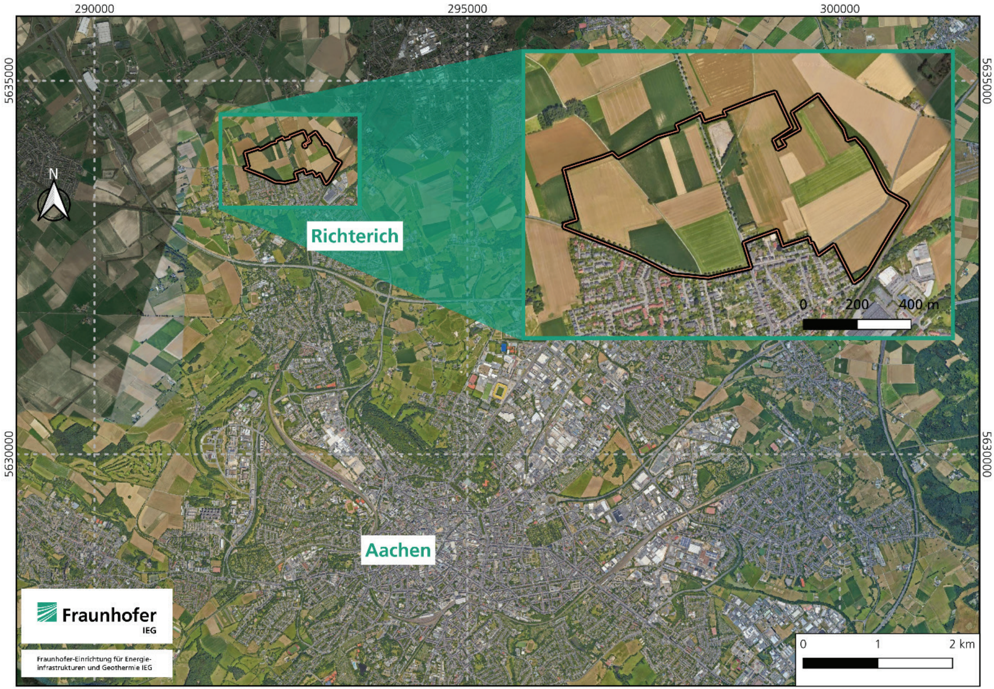

Figure 2 Geographical location of the planned Richtericher Dell development area in Aachen, Germany.

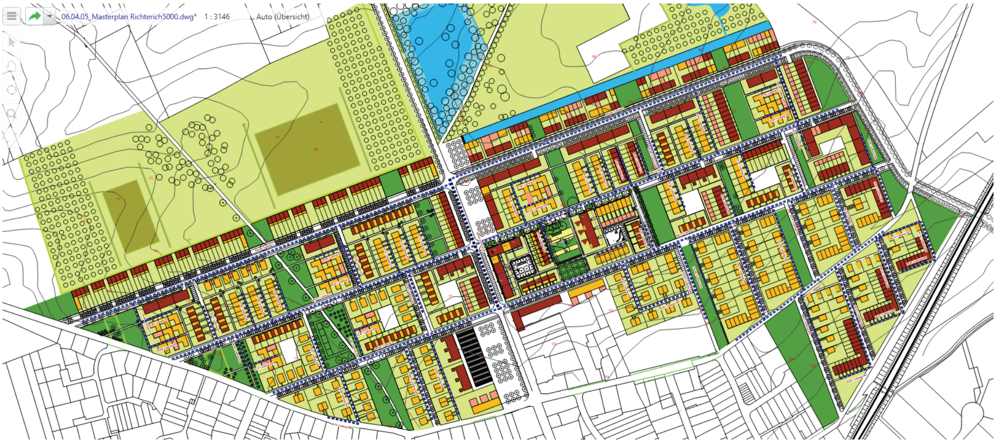

Figure 3 *Urban development draft of the Richtericher Dell development scheme (from 2005).*

after thermal use in the return flowline back to the energy center.

In an open doublet system, both wells would be equipped with an electrical submersible pump including a line for pumping or re-injection, so that the investment costs are minimized.

The same principle could be considered reversibly in the summer months for a possible cooling supply, so that cooler mine water is pumped from the 200 m level, fed to the energy center and then reintroduced into the 270 m level by absorbing the surplus heat from the cooling network.

In order to characterize the geohydraulic productivity of the mine workings, the old mining situation at the site was examined. Based on the mine layouts provided, including information on the coal production rates of the mines, the existing potential was assessed to be favorable.

After analyzing the geological and hydrogeological framework conditions, together with the planned above-ground development, including the grid design for the heating and cooling supply, two conceivable well locations were derived based on the mine layouts.

Conclusions

The feasibility study for geothermal local heating using mine water in the Richtericher-Dell development area demonstrates a viable pathway toward sustainable energy solutions. By implementing a 5GDHC network, this project effectively utilizes geothermal resources to meet the heating demands of approximately 850–900 residential units, with an anticipated annual consumption of 9.5 GWh. The innovative integration of a pit thermal energy storage system significantly enhances the network's capacity to manage peak loads, reducing reliance on fossil fuels.

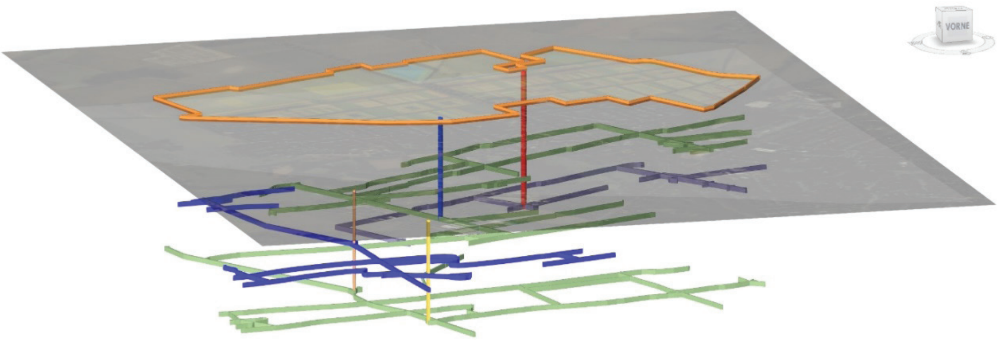

Figure 4 *3D representation of the 100 m, 200 m and 270 m level.*

Moreover, the dual functionality of the proposed system allows for cooling in warmer months by reversing the flow of mine water, thus optimizing the use of available geothermal energy year-round. The findings indicate that the existing geohydraulic conditions are favorable for the successful implementation of this concept, reinforcing the potential for similar projects in the Aachen region.

Overall, this study serves as a blueprint for future heating grid expansions, advocating for the reutilization of mine water and the establishment of decentralized energy systems. The integration of sustainable practices within urban development aligns with the EU's climate goals, contributing to a more resilient and low-carbon energy future.

Acknowledgements

This feasibility study was supported by the BAFA funding scheme Wärmenetze 4.0.

References

BMWK (2022) Endenergieverbrauch nach Anwendungsbereichen: https://view.officeapps.live.com/op/view.aspx?src=https%3A%2F%2Fwww.bmwk.de%2FRedaktion%2FDE%2FBinaer%2FEnergiedaten%2Fenergiedaten-gesamt-xls-2022.xlsx%3F__blob%3DpublicationFile%26v%3D8&wdOrigin=BROWSELINK. Accessed 20 July 2022.

LANUV (2018) Landesamt für Natur, Umwelt und Verbraucherschutz Nordrhein-Westfalen Potentzialstudie Warmes Grubenwasser: LANUV Fachbericht 90.

VDI (2019) Verein Deutscher Ingenieure e.V. standard 4640 sheet 2

Unlocking the Geothermal Potential of Abandoned Flooded Mines: A Path to Renewable Energy and Regional Revitalization in Wallonia, Belgium – Methodology and Modeling Approaches

Virginie Harcouët-Menou[1], Nicolas Dupont[2], Olivier Kaufmann[2], Edgar Hernandez[1], Philippe Orban[3], Caroline De Paoli[3], Yanick N'Depo[2], Thierry Martin[2], Gert Moermans[1], Thomas Neven[1], Clémentine Schelings[4], Jacques Teller[4], Alain Dassargues[3], Thomas Waroux[5]

[1]VITO, Boeretang 200, 2400 Mol, Belgium, virginie.harcouet-menou@vito.be, ORCID 0000-0001-7250-8581

[2]Geology & Applied Geology, Faculty of Engineering, University of Mons, Rue de Houdain 9, 7000 Mons, Belgium, nicolas.dupont@umons.ac.be, ORCID 0000-0003-4938-8686

[3]Hydrogeology & Environmental Geology, Urban & Environmental Engineering Unit, University of Liège, Quartier Polytech 1, Allée de la Découverte, 9, Bât. B52 – Sart Tilman 4000 Liège, Belgium, p.orban@uliege.be, ORCID 0000-0002-4338-0870

[4]LEMA, Urban & Environmental Engineering Unit, University of Liège, Quartier Polytech 1, Allée de la Découverte, 9, Bât. B52 – Sart Tilman 4000 Liège, Belgium, clementine.schelings@uliege.be, ORCID 0000-0001-7718-4539

[5]Town and Regional Planning, Faculty of Architecture and Urban Planning, University of Mons, Rue d'Havré 88, 7000 Mons, Belgium, thomas.waroux@umons.ac.be, ORCID 0009-0004-7043-6827

Abstract

Geothermal energy from mine water can transform former mining regions into renewable energy hubs, supporting 5th generation heat networks. Wallonia, with its rich coal mining history, is well-suited for this approach. A 2019 study identified strong geothermal potential in the Couchant de Mons, Charleroi, and Liège basins, leading to three feasibility studies. These highlighted both opportunities and limitations of geothermal mine water projects, depending on demand and subsurface conditions. The most promising site in the Liège basin was selected for a pilot project to showcase how abandoned flooded mines can drive the energy transition, offering sustainable energy and storage while revitalizing post-mining areas in Wallonia.

Keywords: Mine water, geothermal, modelling, potential assessment

Introduction

The transition to sustainable energy as alternative to fossil fuel sources requires innovative solutions to meet growing energy demand while reducing environmental impacts. Geothermal energy from mine water represents a promising opportunity, repurposing abandoned flooded mines as geothermal energy sources and reservoir for seasonal thermal storage. Ideally this geothermal source is integrated into 5th generation energy networks to ensure high efficiency of this solution. These flexible networks allow buildings to exchange heat and cold with each other through a low-temperature grid, using smart controls to balance energy needs efficiently.

Belgium's Walloon region, with its coal mining history, has shown strong interest in this energy system. A key milestone was the 2019 regional study assessing the geothermal potential of mine water for energy production and storage (Dupont *et al.* 2021). This study laid the foundation for detailed feasibility studies of pilot projects in the coal districts of Liège, Couchant de Mons and Charleroi.

This paper presents a methodology for regional geothermal mine water potential assessment and site-specific feasibility studies. It explores models integrating subsurface characteristics and energy demand to optimize production and storage and discusses the modelling methods.

Estimation of the geothermal potential of mine water at the regional scale in Wallonia

The methodology used to estimate the potential of the Walloon coal mines developed by Dupont *et al.* (2021) is summarized in this section. In general, to estimate the geothermal potential of mine water a series of parameters must be defined, the methodology varies depending on the investigated scale and the energy use considered (heating, cooling or both).

At the project scale, geothermal potential can be estimated using key parameters like accessible water volume, temperature range, reservoir connectivity, and flow rates (Verhoeven *et al.* 2014). This requires detailed mining and hydrogeological data.

For mapping geothermal potential on the Walloon region scale, the large number of mine plans (tens of thousands) and limited hydrogeological data make this approach impractical. Thus, only mining void volumes and temperature ranges are considered key parameters as the accessible water volumes and their temperature are assumed to be derivable from these parameters.

The applied approach uses the number of exploited coal seams (n) per unit area as a proxy for mining void volumes, assuming homogeneous average thickness of a coal seam at basin's scale.

For minimum and maximum temperatures, the proxies used are the minimum and maximum mining depths for each unit area, respectively (*depth_min and depth_max*). This approach assumes a uniform geothermal gradient of 30°C/km across the Walloon coal basins, which is generally valid for this region.

The source data used to determine the geothermal potential of mine waters are the cross-sections of the "Mining Administration", drawn every 100 meters from east to west at a scale of 1:5000. In practice, all cross-sections were examined and sampling was carried out using a 100 m grid. This resolution allows for a local to highly localized assessment of geothermal potential.

After data acquisition and validation, the information was imported into a Geographic Information System (GIS) for spatial analysis. Fig. 1 illustrates the maximum extraction depths obtained for eastern Wallonia and the number of exploited coal seams in the same area.

With the aim of utilizing mine water for both heating and cooling potential, the following proxy was selected to estimate the

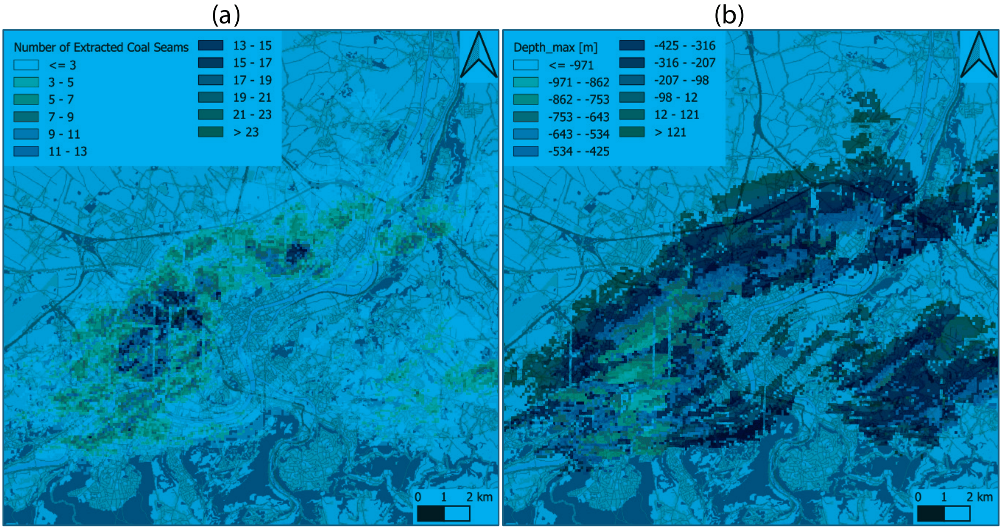

Figure 1 (a): Distribution of maximum extraction depths in the Liège district. (b): Distribution of the number of extracted coal seams in the Liège district. Source: Dupont et al. *2021.*

geothermal potential: (*depth_max –depth_min*) * n. Simplified, this proxy represents the total recoverable energy within a 100 m grid cell. The distribution of the geothermal potential proxy for mine water in eastern Wallonia is illustrated in Fig. 2a (left part).

By definition, the proposed proxy for representing the geothermal potential of mine water is a local measure, reflecting conditions at each sampled point. To scale up potential estimates for hypothetical geothermal mine water projects, a decision-support tool was developed for site selection. The approach assumes a simplified 5th-generation network, including a deep well (hot) and a shallow well (cold) connected to a backbone (primary network) within a defined radius.

Given the adopted simplifications, for a hypothetical site connected to such a system, the maximum geothermal potential of mine water is estimated by determining the minimum and maximum extraction depths within the radius and integrating the number of exploited coal seams:

$$\textit{proxy of "Site" geothermal potential of mine water} = \frac{(depth\_max - depth\_min).\sum n}{\int search\ area}$$

In Fig. 2a (right part), the “site” potential estimated for a radius of 800 m is illustrated. This methodology enables us to highlight the most favorable areas for implementing geothermal projects using mine water connected to 5th-generation networks. The exercise was conducted for the main coal districts in the region. The study's key finding is that, under conservative assumptions, Wallonia has the technical subsurface potential to develop several geothermal projects like the pioneering geothermal project using mine water in Heerlen.

Feasibility studies in the Walloon coal basins: Liège case study

Based on this positive geothermal potential regional evaluation, in 2021, the Walloon Administration launched three feasibility studies for pilot geothermal projects using mine water in the three most significant mining districts, namely Couchant de Mons, Charleroi, and Liège basins.

The main difference between the regional-scale potential study and local feasibility studies lies in considering surface demand, local reservoir detailed mapping and modelling. A similar methodology has been followed for the three studies (Fig. 3).

First, basin-scale assessments were conducted, progressively narrowing down to identify the most promising locations for potential pilot projects in each basin. This process involved aligning the mine’s geothermal potential with surface demand.

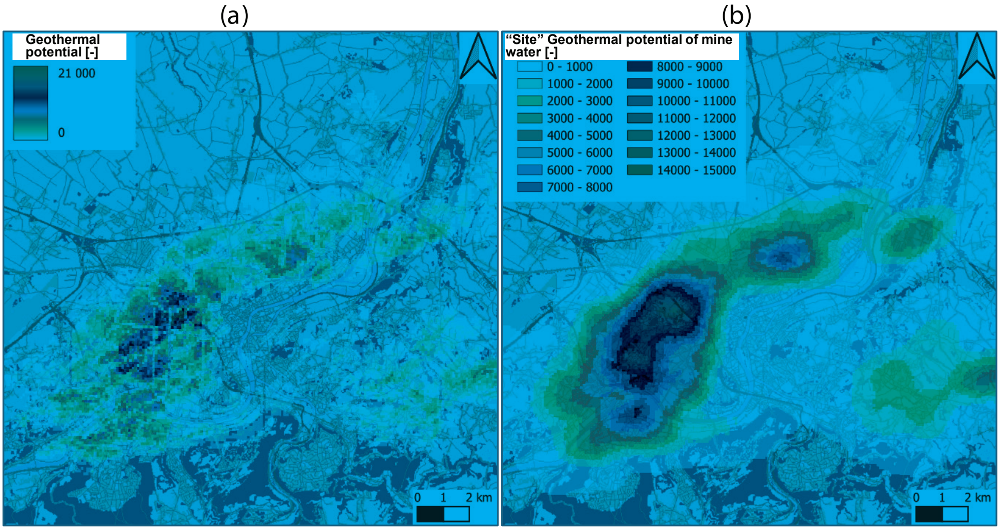

Figure 2 *(a): Distribution of the geothermal potential of abandoned flooded mines in the Liège District. (b): Distribution of the "Site" geothermal potential of mine water in the Liège district for a radius of 800 m. Source: Dupont* et al. *2021.*

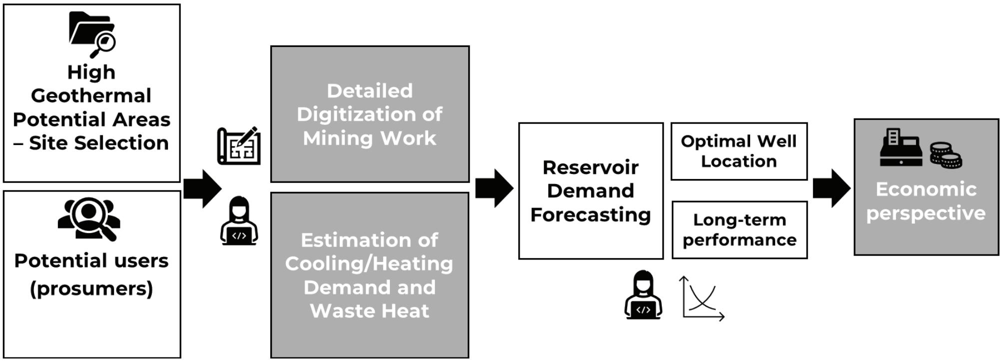

Figure 3 Methodology for conducting the feasibility studies.

For each basin, three potential pilot locations were evaluated with the most viable one chosen for a detailed feasibility study. Fig. 4 presents the conceptual design developed for the mine water project as part of the feasibility studies.

Second, surface and subsurface data related to the site's perimeter was collected and synthetized. The heat and cold prosumers to be connected were identified as well as their demand profiles. The model of the mine reservoir was elaborated by digitizing and conceptualizing the geometry of the interconnected galleries, shafts, and extracted coal panels of the flooded mine in the fractured Westphalian formations. This step is time-consuming but essential to describe the mine reservoir as realistically as possible to ensure the reliability and robustness of the results and its behavior under defined exploitation scenarios.

Two modeling approaches were then used to predict the reservoir's behavior (Fig. 5). One assumes that flow occurs mainly through mine galleries, considering only the interconnected gallery network. In this case, wells must target these galleries and are linked exclusively through this network. A second approach is a numerical model that includes both galleries and mined panels as well as the host rock, treating the system as a multi-domain discretized porous media similar to the discrete fractured network approach (Karimi-Fard *et al.* 2004). Here, wells can target either galleries, mined panels, or both. These two approaches are complementary. The first enables rapid screening and well placement optimization, allowing numerous simulations in a short time but simplifying fluid-rock interactions. In contrast, the second approach better represents complex thermal and hydrological exchanges within the reservoir, considering

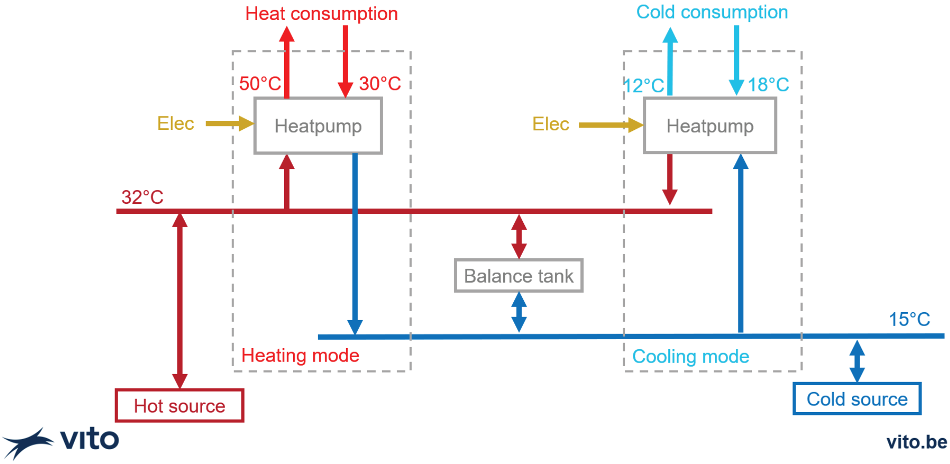

Figure 4 Conceptual design of the investigated mine water geothermal system, called GEOMINE system.

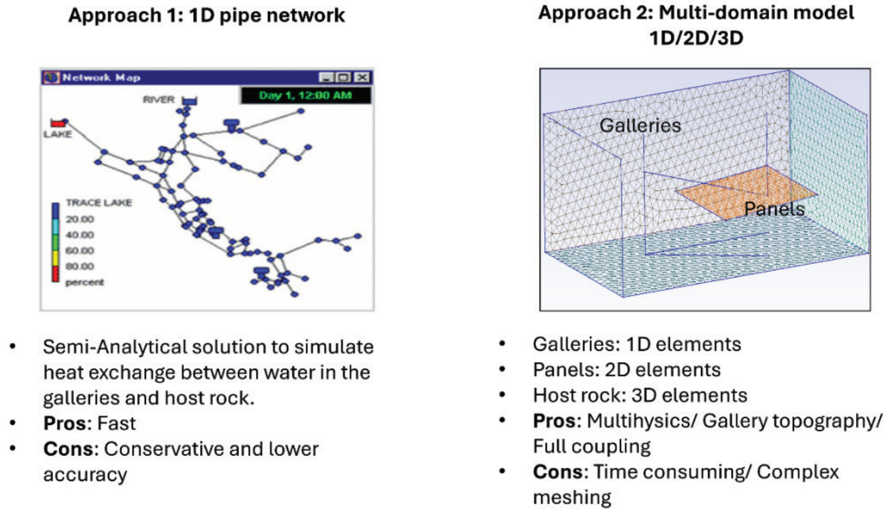

Approach 1: 1D pipe network

- Semi-Analytical solution to simulate heat exchange between water in the galleries and host rock.
- **Pros:** Fast
- **Cons:** Conservative and lower accuracy

Approach 2: Multi-domain model 1D/2D/3D

- Galleries: 1D elements
- Panels: 2D elements
- Host rock: 3D elements
- **Pros:** Multihysics/ Gallery topography/ Full coupling
- **Cons:** Time consuming/ Complex meshing

Figure 5 Modelling approaches followed in the feasibility studies.

the geological properties governing heat transfer and fluid flow.

The first simulations, coupled to Python optimization scripts, enabled us to identify and optimize the positioning of the wells of the geothermal system. A modified in-house version of the open-source code EPANET is used to run the simulations. It requires the network of galleries, shafts, blind shafts, and other connecting mine structures as input to accurately define the reservoir geometry. This model can be used as well to evaluate, in a conservative way, the project's sustainability by assessing the thermal breakthrough risks for defined production scenarios. Results provide essential insights for planning, risk management and system design.

The second approach simulates coupled groundwater flow and heat transfer. In this case, the 3D highly heterogeneous rock domain is complemented with discrete 1D and 2D elements representing mine galleries

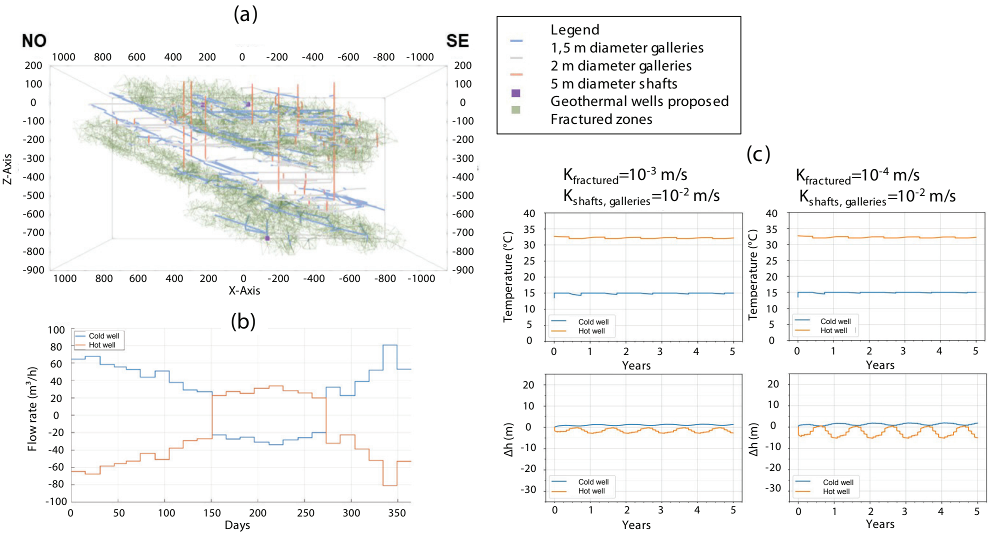

Figure 6 (a): Representation of the mine reservoir. (b): Example of demand flow profiles. (c): Resulting simulated production temperature and head variations at the two wells of the system over a 5-year period for defined hydraulic properties of existing shafts and galleries of the mine reservoir and of fractured zones resulting from coal exploitation.

and panels respectively. Feflow© is used to allow temperature-dependent density and viscosity, in a complex 3D heterogeneous domain. This second approach allows to test additional options for the wells, such as wells targeting panels, galleries or both. Its main drawback lies in the time-consuming nature of the simulations and the complexity of the required meshing procedure.

For wells targeting galleries, the results in terms of production temperature and head variations of the two approaches are relatively similar in case the host rock is considered as very low permeability. The main difference is the head response at the wells of the system, which is generally lower when considering the host rock, due to diffuse flow in the rock that is not considered in the first model.

The response in temperature and in head for a realistic demand scenario in the Liège's case is illustrated in Fig. 6. The system concept foresees using a reversible heat pump and a geothermal doublet. Hot water is pumped from the deepest parts of the open network, and cold water is re-injected at 15 °C in the shallower parts comprising galleries or fractured rocks. A seasonal inversion is planned to cool the buildings during summer, considering reinjection of hot water at 32 °C. Overall, production temperatures remain relatively stable, and the expected pressure variations are acceptable for the modeled scenarios. The surface demand can be fulfilled by the GEOMINE system.

One of the lessons learned is that the main challenge to design the whole geothermal project and to assess its future efficiency is the uncertainties inherent to such a highly heterogeneous underground reservoir, such as: the permeability in backfilled mine wells, extension and location of fractured zones and permeability of panels. They can impact the simulation results of short-, mid-, and long-term temperature evolution in pumping and injection zones. This case study highlights the importance of relying on modeling approaches using detailed mine data to provide reliable predictions. Uncertainties in temperature, pressure, and flow rates affecting GEOMINE design and operation should be addressed in the follow-up exploratory phase.

Conclusion

This paper outlines the Walloon region's approach to demonstrating how abandoned mines can drive the energy transition, provide sustainable energy and storage solutions, and revitalize post-mining areas. The region adopted a step-by-step strategy, beginning with a regional potential assessment, followed by multiple feasibility studies. The presented work has major implications for renewable energy in former mining regions. In Liège, the implementation of the proposed project is expected to cut CO2 emissions by 55–72% and reduce primary energy consumption by 31–44%. The findings have led to a call to implement a pilot geothermal project at the location of the Liège selected site, which intends to serve as a model for similar initiatives across Wallonia or Europe. This research highlights the potential for abandoned mines to play a central role in the energy transition, providing both a sustainable energy source and storage solution while addressing environmental and economic challenges in post-mining areas.

Acknowledgement

The authors thank Service Public de Wallonie for funding the study on the regional geothermal potential of mine water and the three feasibility studies and for providing the data for publication.

References

Dupont, N., Kaufmann, O., Harcouët-Menou, V., Matthijs, J. (2021) La géothermie des eaux des mines et son potentiel en Wallonie (sud de la Belgique). Géologues, 211 : 82–89.

Harcouët-Menou, V., Hernandez, E., Moermans, G., Neven, T., Schelings, C., Teller, J., De Paoli, C., Dassargues, A., Orban, P., Kaufmann, O., N'depo, Y., Martin, T., & Dupont, N. (2024) Étude de faisabilité dans le bassin de Liège en vue de lancer un projet pilote en géothermie minière. Belgium: EDIWALL.

Verhoeven, R., Willems, E., Harcouët-Menou, V., De Boever, E., Hiddes, L., Op't Veld, P., Demollin, E. (2014) Minewater 2.0 project in Heerlen in Netherlands: transformation of a geothermal mine water pilot project into a full-scale hybrid sustainable energy infrastructure for heating and cooling. Energy Procedia, 46: 58–67. doi.org/10.1016/j.egypro.2014.01.158

Karimi-Fard, M., Durlofsky, L.J., Aziz (2004) An Efficient Discrete-Fracture Model Applicable for General-Purpose Reservoir Simulators. SPE Journal. SPE-88812-PA. doi.org/10.2118/88812-PA

Integrating Hydrogeological and Geophysical Modeling for Sustainable Water Management in Phosphate Mining: A Case Study of the Beni Amir Deposit, Morocco

Ouissal Heddoun[1*], Majid El Baroudi[1], Anasse Ait Lemkademe[1] & Mostafa Benzaazoua[1]

[1]*Geology & Sustainable Mining Institute, Mohammed VI Polytechnic University, Benguerir, Morocco*
** Email: Ouissal.heddoun@um6p.ma*

Abstract

Mining operations below the water table poses critical groundwater management challenges, particularly in semi-arid regions like Morocco's Beni Amir phosphate deposit, where water volumes partially or completely submerge phosphate layers. A multidisciplinary study integrating Electrical Resistivity Tomography (ERT), Magnetic Resonance Sounding (MRS), and hydrogeological data from 580 wells and 692 boreholes characterized groundwater conditions. Findings indicate 73% of the deposit is at least partially submerged. Combined geophysical and hydrogeological analyses delineated aquifer geometry and hydrodynamic properties, identifying submerged phosphate layers and multi-aquifer systems. This approach provides detailed insights for optimizing dewatering strategies, aiding sustainable groundwater management in mining operations.

Keywords: Groundwater management, submerged phosphate layers, Electrical Resistivity Tomography (ERT), Magnetic Resonance Sounding (MRS), aquifer characterization, dewatering strategies.

Introduction

Water management is a critical challenge for the global mining industry, particularly in water-stressed semi-arid regions like Morocco 's Oulad Abdoun Basin (Bahir *et al.* 2020). As a leading phosphate producer (Lee *et al.* 2023), Morocco, faces complex hydrogeological challenges in the Beni Amir deposit (Fig. 1), where mining operations often encounter water-saturated layers.

In open-pit mines below the static groundwater level, groundwater inflows from surrounding strata (Bahrami *et al.* 2014) can impede production, increase equipment failures, compromise slope stability, increased explosive usage and create hazardous working conditions. These challenges demand efficient dewatering strategies to maintain safe and stable operations (Unsal and Yazicigil, 2016), particularly as mining advances from the northern zones to deeper submerged southern sections in the Ben Amir deposits. To provide safe and stable conditions for mining during the operational period (Unsal and Yazicigil, 2016), developing an efficient dewatering system is necessary, with groundwater level prediction playing a crucial role in its design (Najafabadipour *et al.* 2022). Effective dewatering operations is directly linked to an understanding of the geological structure and hydrogeological systems that govern water movement within the deposit (Morton and van Mekerk 1993). Traditional hydrogeological characterization methods often prove insufficient in sedimentary environments like phosphate deposits. ERT provides high-resolution lithological contrasts (e.g., distinguishing dry from saturated zones), while MRS directly quantifies hydraulic parameters, critical data unobtainable from sparse boreholes alone. To address this gap, geophysical methods such as Electrical Resistivity Tomography (ERT) and Magnetic Resonance Sounding

(MRS) are increasingly used to investigate near-surface conditions (Gomo *et al.* 2024) and groundwater pathways (Villain *et al.* 2011). The integration of these methods, combined with conventional geological and hydrogeological data help delineate aquifer geometry, identify submerged phosphate layers, and assess hydrodynamic parameters. This integrated approach is particularly relevant in North Africa, where research on hydrogeological processes in phosphate mining regions has been limited. This study integrates geophysical, geological, and hydrogeological data to improve groundwater characterization in the Beni Amir phosphate deposit. By combining conventional and advanced techniques, it aims to enhance water management strategies, providing mining operators with better tools for sustainable resource extraction.

Geological & Hydrogeological setting of the Study area

The Beni Amir deposit is situated within the Oulad Abdoun phosphate basin, located in Morocco's western Meseta structural region. The deposit measures approximately 22.5 km east to west and 8 km north to south, representing one of 13 phosphate deposits (Fig. 1) in the basin ranging from Late Cretaceous to Eocene age. The stratigraphic sequence of the basin comprises five main lithological units: (i) Cenomanian series of alternating marl and limestone, (ii) Turonian series of dolomites and massive limestones with occasional marly intercalations and karst features, (iii) Senonian series primarily of marl from the Coniacian to Campanian age, (iv) Maastrichtian to Ypresian series containing phosphate beds and barren interbeds, and (v) Lutetian series of marine biocalcarenites within the "Thersite slab"(Moutaouakil and Giresse 1993). The exploitable phosphate series in Beni Amir consists of multiple layers (Tab.1): Layer 3 (marl matrix-rich), Layer 2 (Danian-Thanetian loose phosphates), Layer 1 (two-part structure of loose and marly phosphates), Layer 0' (loose to indurated phosphates), Layer 0 (loose to calcified phosphates), and Furrows A and B (characterized by loose, coarse to fine-grained phosphates). Hydrogeologically, four main aquifers characterize the region: the Mio-Plio-Quaternary, Eocene, Senonian,

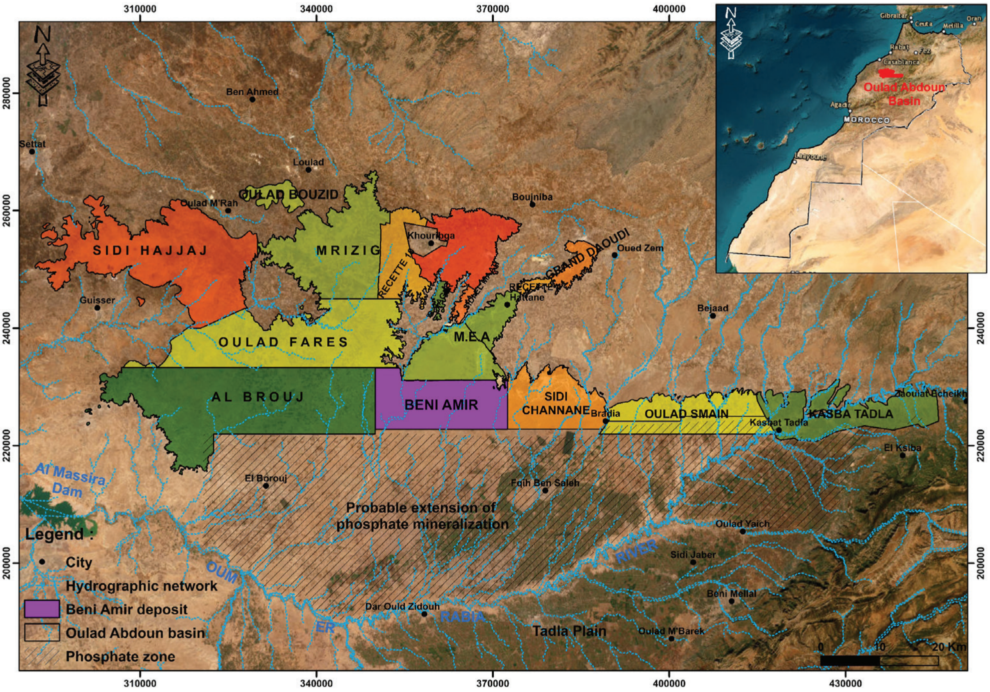

Figure 1 Map showing the location of the Oulad Abdoun phosphate basin and the Beni Amir deposit.

and Turonian aquifers. Unlike the northern and central parts of the Oulad Abdoun basin, the Beni Amir deposit, along with other southern deposits (EL Brouj, Sidi Chennane, Oulad Smain, and Kasba Tadla), regularly encounters water table interactions with phosphate layers.

Methods

The study employed an integrated methodology to assess submerged areas and hydrodynamic parameters in the Beni Amir phosphate deposit, combining multiple data sources and advanced geophysical techniques. The research utilized 580 piezometric measurements collected during September–October 2023 and elevation data from 694 drilling operations, with ERT profile and MRS surveys conducted in data-scarce locations identified during field reconnaissance.

Conceptual model of the study area

A comprehensive conceptual hydrogeological model was developed using Visual Modflow Flex 9.0, serving as a foundation for future numerical groundwater flow model. This approach involved defining the study area through polygon data, interpolating phosphate layer boundaries using drilling data, and creating three-dimensional geological zones. The resulting model (Fig. 3) illustrates the intersections between phosphatic layers and the piezometric level, delineating the deposit's drowned and dry zones.

Electrical Resistivity Tomography (ERT)

ERT was utilized to map subsurface structures by measuring electrical resistivity distribution (Loke *et al*., 2021). The ERT survey employed Syscal Pro Switch equipment with six multi-core cables, featuring 16 electrodes spaced 5 meters apart and using an inverse Wenner-Schlumberger array to achieve investigation depths of 70–80 meters. Data processing involved filtering through ProsysIII software and inversion using RES2DINV, with root mean square errors maintained below 15%. Final visualization and validation were accomplished using Surfer 13, integrating borehole and piezometric data to ensure comprehensive hydrogeological characterization.

Magnetic Resonance Sounding (MRS)

Complementing the ERT, MRS detects groundwater by measuring nuclear magnetic resonance signals from hydrogen atoms (Legchenko *et al*., 2002). Using a NUMIS Plus system with a 100-meter square loop antenna, we transmitted currents at the local Larmor frequency (1758.41 Hz at 41,276.15 nT) to excite subsurface water molecules. The resulting relaxation signals (16–20 pulse moments, 80–120 stackings) were processed through Samovar software using notch and bandpass filters to determine the volume of free water content and estimate permeability to 100 m depth.

Results & Discussion

The conceptual model (Fig. 2) developed by integrating piezometric map with phosphatic layers, provides detailed insights into subsurface structure and water distribution. Submersion patterns (defined as layers below the water table) vary across phosphatic layers. Some layers are fully submerged, while others remain partially or completely dry. For instance, Layer 3 (Maastrichtian), shown in Fig. 2(a), is 46.88% submerged, while Layer 2, depicted in Fig. 2(b), has 29.4% submerged. In contrast, Layer 1, shown in Fig. 2(c), is predominantly dry with only 13.3% submerged. Layer 0'and Layer 0, illustrated in Fig. 2(d) and Fig. 2(e), shows a gradual reduction in submerged areas, with 10.9% and 5.2% submerged, respectively, leaving the majority of their extents in dry zones. Finally, the Furrow A/B layers (Fig. 2(f)) exhibit minimal submersion, with dry zones dominating. The conceptual model highlights a southward slope of the phosphate layers, where the deposits increasingly submerge into the Beni Amir aquifer. A cross-section from east to west (Fig. 2), located in the southern part of the deposit and based on the generated 3D model, shows that the piezometric level is above most phosphate layers, indicating extensive submersion in this region. The aquifer primarily lies in the central study area, fully covering most deposits, while the water table only partially intersects Layer 3 in the western and northwestern regions. These variations in water distribution and submersion present significant implications for mining operations, particularly as they necessitate tailored water management strategies.

To assess the geometry and hydrodynamic properties of the aquifer, an Electrical Resistivity Tomography (ERT) profile and a Magnetic Resonance Sounding (MRS) surveys were conducted in the southern region where the data is scares (Fig. 3 and Fig. 4). The ERT profile, spanning 795 meters from East to West, reveals subsurface structure variations: a high-resistivity zone (>460 ohm·m) in the upper 10 meters corresponds to Lutetian limestone formations, followed by a medium-resistivity band (50–150 ohm·m) linked to dry Ypresian formations. A near-surface conductive zone suggests the presence of a recharge area or a shallow aquifer, possibly influenced by a nearby stream. Deeper low-resistivity zones indicate wet marl, clay, and phosphate facies from Maastrichtian formations, with localized high-resistivity zones interrupt these conductive layers, suggesting the presence of limestone blocks or geological disruptions.

Building on the insights from the ERT profile, the MRS surveys provided complementary hydrogeological data by quantifying the volumetric water content and permeability at different depths. Since MRS directly measures free water content, the results primarily represent the saturated zones within the formations. The estimation of hydraulic conductivity (K) was derived from the relaxation time, which serves as a proxy for pore size distribution. At MRS Site 1, located in the eastern part of the deposit, the inversion results reveal three

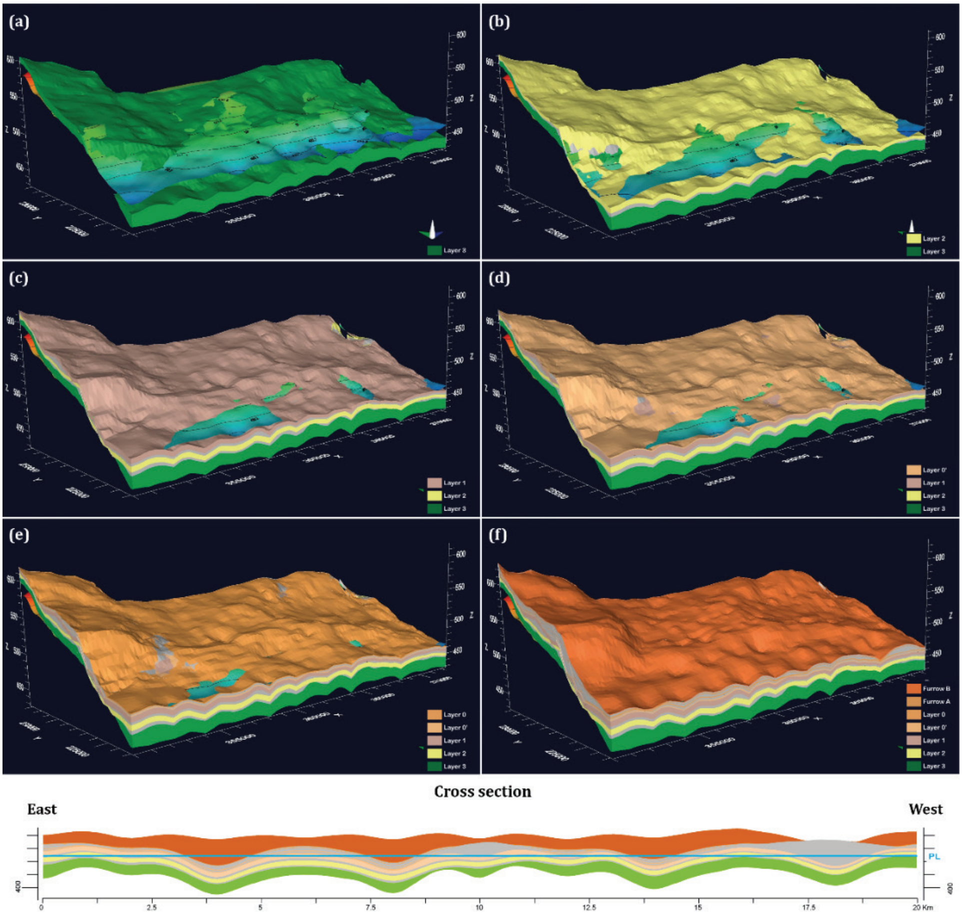

Figure 2 Conceptual model showing the dry zone and drowned zone of each phosphatic layer starting from the bottom ((a): Layer 3 to the top (F): Furrow A/B) within the Beni Amir deposit.

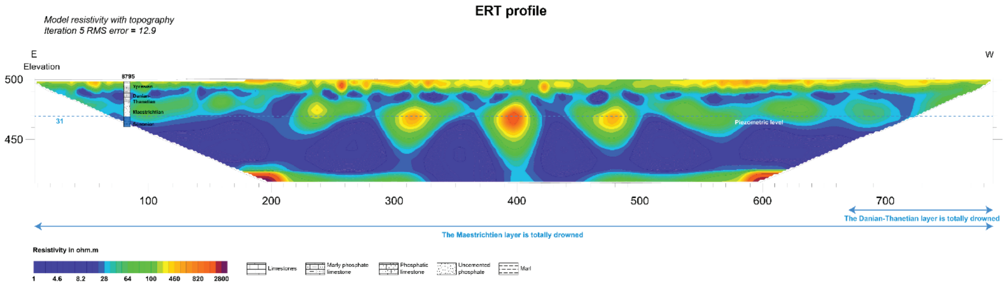

Figure 3 *Model resulting from ERT data inversion calibrated to lithological boreholes columns. The dashed blue line indicates the on-site measured piezometric level.*

distinct saturated zones. The first aquifer, associated with the Ypresian formation, lies between 4 and 18 meters depth and exhibits a water content of 0.3% with a permeability of 1.5 × 10^{-5} m/s. Below this, the primary Maastrichtian aquifer is found between 32 and 50 meters depth, with a water content of 0.9% and a permeability of 3.9 × 10^{-5} m/s. These results align well with a nearby borehole located 400 meters from the MRS site, which confirms the water level at approximately 35 meters. Deeper still, a third aquifer associated with the Senonian formations spans from 50 to 102 meters depth, with a water content of 0.6% and a permeability of 2.9 × 10^{-5} m/s. At MRS Site 2, three aquifers were identified. The first two occur within the Danian-Thanetian and Maastrichtian formations and are located between 16–20 meters and 20–35 meters depth, respectively. These aquifers exhibit water contents ranging from 1.2% to 1.9% and a permeability of 7.3 × 10^{-4} m/s. The third and deepest aquifer, associated with the Senonian formation, extends from 35 to 100 meters depth. It shows a higher water content of 2.9% and a significantly elevated permeability of 1.9 × 10^{-3} m/s, likely influenced by its proximity to a stream. The observed water levels at this site correspond well with the piezometric map, although borehole logs indicate a slightly deeper water level. In the southeastern part of the

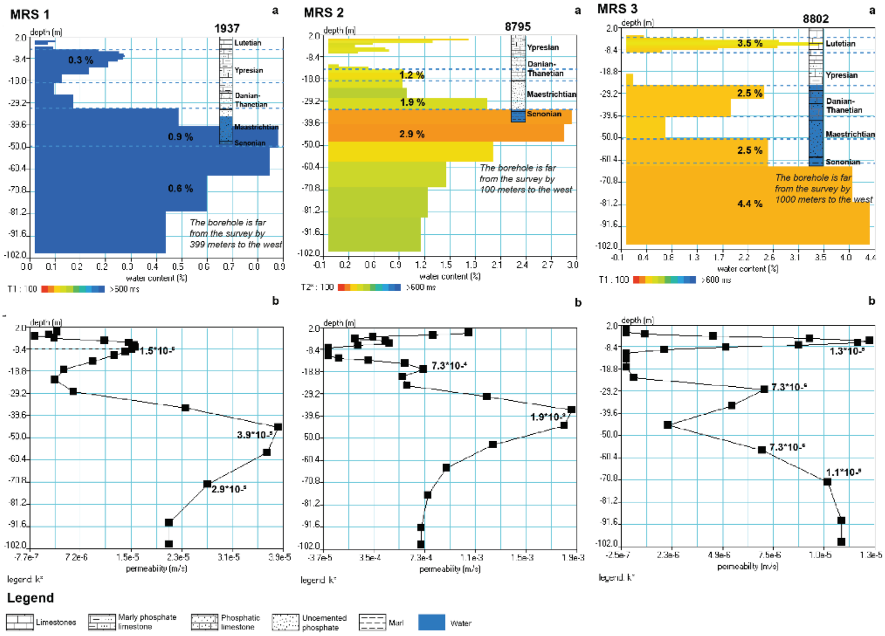

Figure 4 *MRS data measured in the deposit (a) Model resulting from MRS data inversion and its correlation with the hydrogeological column;(b) Permeability curves versus depth.*

Table 1 Synthetic table of the various divisions of the phosphate series of Beni Amir.

Chronostratigraphic division			**Mining division**
Era	**Period**	**System**	
		Lutetian	**Cover layer**
Tertiary (Cenozoic)	Eocene		Furrow B
			Furrow A
			Layer 0
			Layer 0′
		Ypresian	Layer 1
	Paleocene	Thanetian - Danian	Layer 2
Secondary (Mesozoic)	Upper Cretaceous	Maastrichtian	Layer 3

deposit, MRS Site 3 reveals the presence of multilayered aquifers. A shallow aquifer lies between 4 and 10 meters depth, with a water content of 3.5% and a permeability of 1.3 × 10^{-5} m/s. Beneath this, an aquifer located between 25 and 62 meters depth features an impermeable layer between 40 and 50 meters, associated with the upper part of the Maastrichtian formation. This intermediate aquifer, linked to the Danian-Thanetian and Maastrichtian phosphate layers, has a water content of 2.5% and a permeability of 7.3 × 10^{-6} m/s. The deepest aquifer, situated between 62 and 100 meters, lies within the Senonian formation and exhibits a higher water content of 4.4% with a permeability of 1 × 10^{-5} m/s. This aquifer demonstrates relatively higher permeability compared to the overlying phosphate layers. Notably, the water levels in this area align well with both borehole logs and the piezometric map, further validating the findings.

Conclusions

The study highlights the critical groundwater challenges faced in Morocco's Beni Amir phosphate deposit, where 73% of the area is partially submerged. By integrating geophysical techniques, such as ERT and MRS, with geological and hydrogeological data, the research provided a detailed understanding of aquifer geometry and hydrodynamic properties. Geophysical methods significantly enhanced the conceptual model by revealing multi-aquifer systems, impermeable layers, and direct measurements of volumetric water content and permeability, which traditional hydrogeological techniques could not provide. Developing conceptual models, especially for complex multi-layered sedimentary systems, is crucial for understanding the subsurface, and the 3D stratigraphic model created here offers valuable insights for future investigations. The study also highlights that the phosphate layers in the Beni Amir area slope southward under the Tadla plain, becoming gradually covered by the Beni Amir aquifer, with thickness variations from north to south. These findings will help optimize dewatering strategies, mitigate groundwater impacts, and inform sustainable resource management. This work supports global efforts in phosphate mining by enhancing our understanding of the hydrogeological and geological interactions, contributing to more effective groundwater management strategies in semi-arid regions.

Acknowledgements

The authors thank all co-organisers for hosting the IMWA 2025 Conference.

References

Bahir M, Ouhamdouch S, Ouazar D, El Moçayd N (2020) Climate change effect on groundwater characteristics within semi-arid zones from western Morocco. Groundwater for Sustainable Development 11, 100380. https://doi.org/10.1016/j.gsd.2020.100380

Bahrami S, Doulati Ardejani F, Aslani S, Baafi E (2014) Numerical modelling of the groundwater inflow to an advancing open pit mine: Kolahdarvazeh pit, Central Iran. Environ Monit Assess 186, 8573–8585. https://doi.org/10.1007/s10661-014-4025-x

Gomo S, Mutshafa N, Dildar J, Manzi MSD, Bourdeau JE, Brodic B, James I, Cooper GRJ, Durrheim RJ (2024) Integration of ground geophysical methods to characterize near-surface aquifer zones within an active mine. Near Surface Geophysics 22, 521–538. https://doi.org/10.1002/nsg.12314

Lee S H, Assi AT, Mohtar RH, Hamane M, Yoon PR, Yoo SH (2023) Development of WEF-P Nexus based on product-supply chain: A case study of phosphorous fertilizer industry in Morocco. Science of The Total Environment 857, 159520. https://doi.org/10.1016/j.scitotenv.2022.159520

Legchenko A, Baltassat JM, Beauce A, Bernard J (2002) Nuclear magnetic resonance as a geophysical tool for hydrogeologists. Journal of Applied Geophysics, Surface Nuclear Magnetic Resonance: What is Possible? 50, 21–46. https://doi.org/10.1016/S0926-9851(02)00128-3

Loke M H, Rucker D F, Chambers J E, Wilkinson P B, Kuras O (2021) Electrical Resistivity Surveys and Data Interpretation, in: Gupta, H.K. (Ed.), Encyclopedia of Solid Earth Geophysics. Springer International Publishing, Cham, pp. 344–350. https://doi.org/10.1007/978-3-030-58631-7_46

Morton KL, van Mekerk FA (1993) A phased approach to mine dewatering. Mine Water and the Environment 12, 27–33. https://doi.org/10.1007/BF02914796

Moutaouakil D, Giresse P, (1993) Petrology and sedimentary environments of Mesocenozoic phosphorites from Ouled Abdoun Basin, Morocco. Bulletin – Societe Geologique de France 164, 473–491.

Najafabadipour A, Kamali G, Nezamabadi-pour H (2022) Application of Artificial Intelligence Techniques for the Determination of Groundwater Level Using Spatio–Temporal Parameters. ACS Omega 7, 10751–10764. https://doi.org/10.1021/acsomega.2c00536

Unsal B, Yazicigil H, (2016) Assessment of Open Pit Dewatering Requirements and Pit Lake Formation for the Kışladağ Gold Mine, Uşak, Turkey. Mine Water Environ 35, 180–198. https://doi.org/10.1007/s10230-015-0345-5

Villain L, Sundström N, Perttu N, Alakangas L, Öhlander B (2011) geophysical investigations to identify groundwater pathways at a small open-pit copper mine reclaimed by backfilling and sealing. Mine Water.

Constructed Wetlands for Treatment of Alkaline Bauxite Residue Leachate: Ten Years of Monitoring a Single Cell System and Optimising Designs for a Multi-Cell Approach

A. Hudson[1], J.G. Murnane[2], R. Courtney[1]

[1]*Department of Biological Sciences and Bernal Institute, University of Limerick*
[2]*School of Engineering, University of Limerick*

Abstract

Limited data are available for long term constructed wetland (CW) use for alkaline leachates. This paper summarises monitoring from a single cell CW operating for 10 years to treat bauxite residue leachate, successfully dropping pH from 11.5 to 7.14 (±0.14). Lessons from the single cell informed the construction of two new multi-celled systems with differing substrate mixes: one with 8% organic matter content, the other 12%. The new systems came online in 2024 with the first 6 months monitoring showing pH reductions from ≈11.2 to 7.41 (8% OM) and 7.14 (12% OM) alongside trace element (Al, As and V) reduction.

Keywords: Bauxite residue leachate, alkaline leachate, constructed wetlands

Introduction

Mining and processing of minerals for metal production has generated in excess of 100 billion tonnes of waste and tailings globally: with annual quantities projected to increase as demand for metals rises (Hund *et al.* 2020; Valenta *et al.* 2023). The alumina industry accounts for >4.6 billion tonnes of bauxite residue (BR), with >170 million tonnes generated annually (International Aluminium Institute 2022; Qin *et al.* 2023). Due to the use of sodium hydroxide (NaOH) to extract Aluminium (Al), leachates formed from BR are inherently alkaline (pH 9-13.2) and contain elevated concentrations of Al, arsenic (As), vanadium (V) and sodium (Na) (Burke *et al.* 2013; Higgins *et al.* 2017).

Long term management of leachates from BR and other mine waste storage facilities poses a challenge to operators and regulators, as leachates may form for decades post closure (Di Carlo *et al.* 2019; Mayes *et al.* 2008). Each facility must be assessed to ensure the post-closure plan is appropriate for site specific parameters (leachate chemistry, space constraints, climatic conditions, other treatments/remediation works to waste piles) and may include active or passive treatment technologies. Increasingly, passive approaches, such as constructed wetlands (CWs), are preferred due to lower long term operational costs, but equivalent treatment performance efficiencies (Hedin 2020).

Relative to acidic and neutral drainages, CW treatment of alkaline leachates has received less attention, and consequently there are a lack of long term datasets available (Vymazal *et al.* 2021). Treatment of BR leachate (average influent pH 11.5) to achieve a discharge of pH<9 using a passive CW has been demonstrated over a 7.5 year timespan, with a single cell CW achieving an effluent of pH of 7.1 (Hudson *et al.* 2023b). However, monitoring the efficacy of CW operation and associated substrate saturation for longer periods is necessary to determine their ongoing operation and potential lifespans. Additionally, further design optimisations, such as increased organic matter in the substrate to aid both pH reduction (Buckley *et al.* 2016) and retention of trace elements of increasing interest such as V, have been demonstrated at lab scale (Hudson *et al.* 2024). However, further investigations are necessary to determine whether these findings are scalable.

This paper presents the findings of two ongoing CW pilot studies treating BR leachate at an operating alumina refinery: a single cell CW which has been operational for 10 years, and the initial 6 months monitoring of 2 new multicell systems (3 cells each) built using different substrate OM contents.

Methods

Site Description-Single Cell:

The single cell pilot, which has been operating for 10 years, is 4 m × 11 m constructed at a bauxite residue disposal area (BRDA) at Aughinish Alumina, Ireland. The substrate was a transplanted local soil (pH = 6.7, EC = 188μS cm^{-1}, CEC 38 cmol kg^{-1}, and 2.8% organic C content), planted with *Phragmites australis*, *Typha latifolia* and *Sparangium erectum* supplied locally (FH Wetland Systems Ltd). Vegetation was acclimatised over 6 months with fresh water.

The CW inflow is controlled by a PLC mixing system and three 1000L tanks: a leachate tank, a mixing tank and a dosing tank. Alkaline leachate and deionised water were mixed until the target pH of ~11.5 was reached. Leachate is then pumped to the dosing tank, where it was discharged to the CW at a summer (May-September) rate of 45-55L h^{-1} or winter rate (October-April) of 10-30L h^{-1}. Varied rates are due to increased winter precipitation.

Site Description- Multi-cell systems:

Two parallel multi-cell systems were constructed at a separate location on the same BRDA facility. Each system contains three cells of approximately 8m × 4m each, with a spillway between each cell. The feed system loading the cells is the same as the single cell, feeding both systems at the same rate and target pH, currently averaging 11.2.

The substrate in one system consists of 8% OM and the other system contains 12% OM. Both systems were planted with *P. australis*, *T. laitifolia* and *S. erectum*. A PLC system of the same configuration also feeds the two multicell systems.

Monitoring and Sampling-Single Cell:

Inflow and outflow pH was measured from May 2015 using a field probe, with monthly averages reported over the 10-year operating period. Additional samples of water and sediments were taken throughout the operational period for elemental analysis, with samples filtered through 0.45μm filters and determined by ICP-MS. Detailed analyses (pH EC, trace elements, microbial community) of the sediments after 4 and 5 years of operation are available separately (Hudson *et al.* 2023a; O'Connor and Courtney 2020). Monitoring of inflow and outflow for pH, conductivity and trace elements on a bi-weekly basis has been conducted since June 2024.

Monitoring and Sampling-Multi-Celled Systems:

Loading of the new multi-cell systems began in April 2024, where monitoring of the pH and EC of the inflow and outflows were taken daily. Additional water samples were collected from the inflow and outflow of each cell and system on a bi-monthly basis since June 2024 (6-month period) for elemental analysis to assess pH, conductivity and trace element removal rates.

Results

Single Cell

Average monthly outflow pH (7.14±0.18, Fig. 1) was consistently far lower than the upper pH9 discharge limit. Removal of Al (96%), As (85%) and V (71%) has been sustained over the 10-year operating period while Na concentrations also decreased by an average 22% and was mostly found in soluble forms in the substrate (up to 60% of total). Na removal efficiency has decreased as time has passed, with removal decreasing from significant reductions of 31% after year 1 and 13% in year 5, to negligible removal of Na and release (-8% ±22) in the past 6 months monitoring. Monitoring from June 2024-Dec 2024 showed Al, As and V concentrations in the effluent were significantly reduced compared to the influent, decreasing by 99, 90 and 73% respectively (Fig. 2), with no significant difference between the influent and effluent Na concentrations.

Multi-celled Systems:

Over the 6-month sampling period, the 12% OM system has shown greater pH reduction in the final outflow (pH=7.1±0.14) when compared with the 8% OM system (pH=7.41±0.17). Both systems effectively reduced pH below the pH 9 threshold within the first cell (Fig. 3).

Removal rates of Al and V at the outflows were 99.9% and 99.2% in both substrate systems. Arsenic concentrations were below the limit of detection in all samples of the inflows and outflows across the sampling period. Initial measurements show the V and Al are removed to below the limit of detection

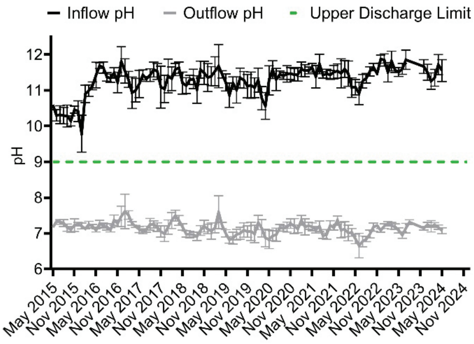

Figure 1 *Monthly average of inflow and outflow pH values from May 2015, with the upper discharge limit of pH 9 marked. Error bars denote standard deviation.*

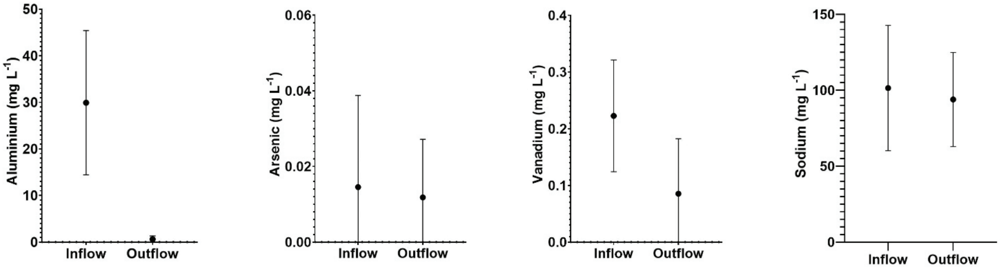

Figure 2 *Average inflow and outflow concentrations of Al, As, V and Na of the single cell system over a 6-month operating period from June to December 2024. Error bars denote standard deviation.*

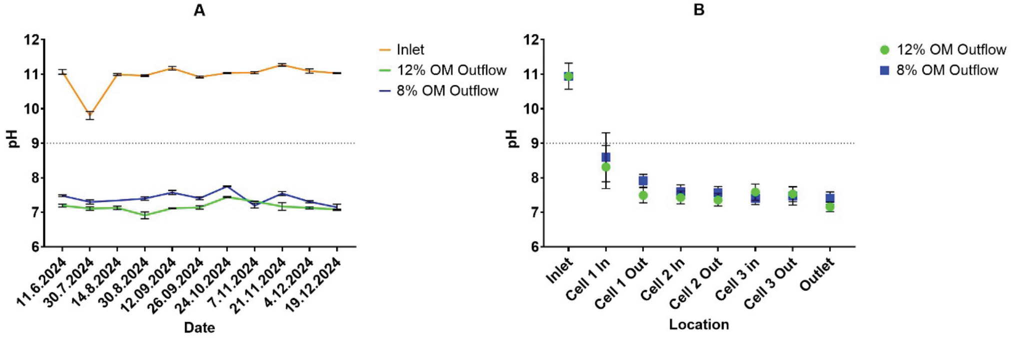

Figure 3 *A) Average pH over 6-month period at inflow and outflow points of the multi-celled systems whose substrate contains 12% and 8% organic matter respectively and B) average pH across the CW cells, with pH threshold of 9 denoted on both graphs. Error bars denote standard deviation.*

at the outflow of the second cells in both treatments, with the 12% OM system showing a greater reduction of V within the first cell (Fig. 4). There was an efflux of Na from both systems (inflow= 42.2±11.7 mg L^{-1}, 12% OM= 56.01±19.4 mg L^{-1}, 8% OM=50.54±17.9 mg L^{-1}) but it is likely that this was due to release of Na from the substrate material as the system adjusted to increased pH.

Discussion

Passive nature-based solutions are increasingly becoming the preferred design of choice for remediation and treatment of industrial leachates, particularly where long term post closure management is required. However ongoing monitoring of CW systems for pH reduction and trace element removal is often reported through sporadic sampling campaigns across a systems operation, with limited published data on systems over 10 years old (Pat-Espadas *et al.* 2018). The single cell pilot demonstrates the capacity of CWs to consistently reduce the pH of alkaline BR leachate from ~11.5 to pH<9 over a 10-year period. With over 2000 pH sampling dates from commissioning to present this dataset provides one of the most continuous monitoring datasets for any CW, and the longest, to the authors knowledge, for an alkaline system. Possible mechanisms of pH reduction are microbial respiration, production of organic acids and carbonation, which have all been supported by elevated microbial activity and biomass and carbonates formed within the system (Higgins *et al.* 2018; Hudson *et al.* 2023a).

Reductions of influent Al, As and V in the 10-year-old single celled pilot CW indicates that the system is still providing the additional benefit of reducing trace element load. The removal rates of Al concur with other findings in alkaline steel slag systems (Gomes *et al.* 2019), as well as acidic coal mine drainage (Hedin 2020) and with domestic wastewaters (Kröpfelová *et al.* 2009). V removal efficiency exceeds that reported in field scale CWs treating steel slag leachate (Gomes *et al.* 2019) and municipal water (Kröpfelová *et al.* 2009), and is comparable to rates reported in lab investigations (Chi *et al.* 2024; Zhang *et al.* 2024). Albeit removal efficiency of Na has decreased in the single cell system, the quantity of Na (110 mg L^{-1}) is still far below the threshold of 200 mg L^{-1} for Drinking Water (Environmental Protection Agency 2014). Trace removal processes within these wetlands include precipitation as oxides, sedimentation and microbial processes, with limited plant uptake displayed (Higgins *et al.* 2017; Hudson *et al.* 2023b; O'Connor and Courtney 2020).

Multicell monitoring reveals that the substrate with the 12% OM had a higher pH reduction, with average outflow pH 0.3 units less than that of the 8% mix. This field scale approach corroborates with lab scale studies (Buckley *et al.* 2016), demonstrating the concept is scalable. Removal of trace elements, of Al and V remained high over the 6 months, but further monitoring is needed to determine whether rates are maintained over a longer period. V retention was shown to be greater in the first cell of the 12% OM substrate when compared with the 8% OM mix (Fig. 4). This result is corroborated with a batch study which shows that V retention increases for substrates that contain higher proportions of compost (Hudson *et al.* 2024). This effect is also seen in modified biochars where enhanced surface area and pore volume, and surface modification of the biochar

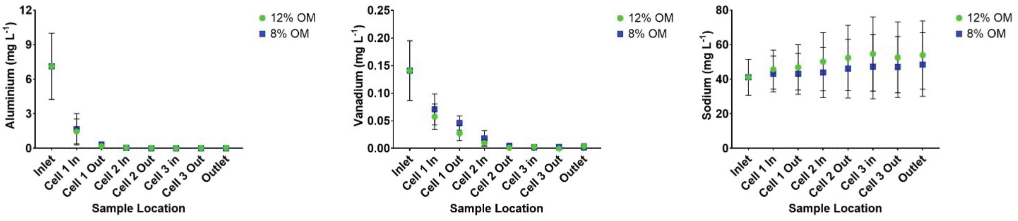

Figure 4 Average water concentrations of Al, V and Na within the two multi-celled systems. Error bars denote standard deviation.

increase the amount of adsorption sites and the opportunity to optimise the removal of V from waters (Ghanim *et al.* 2020). V removal is also noted to be correlated with the organic carbon in natural wetlands (Shaheen *et al.* 2016; Telfeyan *et al.* 2017), supporting the findings and rationale behind employment of increased organic matter to increase removal by adsorption.

Monitoring of these pilots over time is essential to determine the point at which the primary objective of pH reduction is no longer achieved, if indeed such a point is reached. As it stands, the use of a predominantly topsoil only system has achieved successful pH reduction over the past 10 years in the single cell. The new multi-cell systems require long term monitoring to determine whether pH reduction is achieved to a greater degree in one of the treatment types, and with greater co-benefits (i.e. trace element removal). At present, the multi-cell design appears to give the added benefit of the second cell acting as a polishing bed to remove any trace elements (Al and V) still present, with pH already being below the necessary pH 9 limit in the first cell outlet. It is hypothesised that the second and third cells may help increase the lifespan of a treatment system compared with a single cell CW, as trace elements can be accumulated in the second and third beds upon saturation of the first. However, only continued future monitoring will determine whether this occurs.

Passive treatment systems such as CWs can provide cost savings to operators and regulators over time due to reduced operational costs. Similarly, CWs are more environmentally friendly compared to active treatment systems which have emissions due to reagent and electricity generation and transport and require routine sludge disposal. Additionally, such systems provide a potential means of capture of rare earth elements that may otherwise be released to the environment, and further investigation into such retrieval of these elements from wetland substrates is needed.

Conclusions

Monitoring of a single cell CW treating alkaline bauxite residue leachate has demonstrated effective pH reduction from > 11 to pH 7.14 over a 10-year sampling period. Additionally, reductions in trace elements Al, As and V have been sustained. New multicell CWs comparing substrate mixes have so far demonstrated effective pH reduction, with a 12% organic matter content substrate producing an additional 0.3 unit reduction when compared with an 8% organic matter content. So far, the multicell configuration demonstrates enhanced capture of trace elements Al and V, with the first cell removing most and the second cell removing any remaining traces from the outflow of the first. Further monitoring is needed to determine whether effluent quality will be maintained over time and whether differences in treatment efficiencies arise due to differing substrate organic matter contents.

Acknowledgements

This work was supported by funding from Aughinish Alumina.

References

Buckley R, Curtin T, Courtney R (2016) The potential for constructed wetlands to treat alkaline bauxite residue leachate: laboratory investigations. Environ Sci Pollut Res Int 23(14):14115–22. https://doi.org/10.1007/s11356-016-6582-8

Burke IT, Peacock CL, Lockwood CL, Stewart DI, Mortimer RJ, Ward MB, Renforth P, Gruiz K, Mayes WM (2013) Behavior of aluminum, arsenic, and vanadium during the neutralization of red mud leachate by HCl, gypsum, or seawater. Environ Sci Technol 47(12):6527-35. https://doi.org/10.1021/es4010834

Chi Z, Li W, Zhang P, Li H (2024) Simultaneous removal of vanadium and nitrogen in two-stage vertical flow constructed wetlands: Performance and mechanisms. Chemosphere 367:143663. https://doi.org/https://doi.org/10.1016/j.chemosphere.2024.143663

Di Carlo E, Boullemant A, Courtney R (2019) A field assessment of bauxite residue rehabilitation strategies. Science of The Total Environment 663:915-926. https://doi.org/https://doi.org/10.1016/j.scitotenv.2019.01.376

Environmental Protection Agency (2014) Drinking Water Parameters. Microbiological, Chemical and Indicator Parameters in the 2014 Drinking Water Regulations 2014. An overview of parameters and their importance. Environmental Protection Agency., Wexford

Ghanim B, Murnane JG, O'Donoghue L, Courtney R, Pembroke JT, O'Dwyer TF (2020) Removal of vanadium from aqueous solution using a red mud modified saw dust biochar. Journal of Water Process Engineering 33:101076. https://doi.org/10.1016/j.jwpe.2019.101076

Gomes HI, Mayes WM, Whitby P, Rogerson M (2019) Constructed wetlands for steel slag leachate management: Partitioning of arsenic, chromium, and vanadium in waters, sediments, and plants. Journal of Environmental Management 243:30-38. https://doi.org/https://doi.org/10.1016/j.jenvman.2019.04.127

Hedin RS (2020) Long-term Performance and Costs for the Anna S Mine Passive Treatment Systems. Mine Water and the Environment 39(2):345-355. https://doi.org/10.1007/s10230-020-00676-9

Higgins D, Curtin T, Burke I, Courtney R (2018) The potential for constructed wetland mechanisms to treat alkaline bauxite residue leachate: carbonation and precipitate characterisation. Environmental Science and Pollution Research 25(29):29451-29458

Higgins D, Curtin T, Courtney R (2017) Effectiveness of a constructed wetland for treating alkaline bauxite residue leachate: a 1-year field study. Environmental Science and Pollution Research 24(9):8516-8524. https://doi.org/10.1007/s11356-017-8544-1

Hudson A, Murnane JG, Courtney R (2023b) Constructed Wetlands For Treatment Of Bauxite Residue Leachate: 7.5 Years Of Monitoring. Paper presented at the IMWA 2023 – Y Dyfodol | The Future, Casnewyydd/Newport, Wales,UK:215-219.

Hudson A, Murnane JG, O'Dwyer T, Courtney R (2024) Influence of organic matter in wetland substrate on vanadium removal: A batch and column study. Journal of Water Process Engineering 68:106359. https://doi.org/https://doi.org/10.1016/j.jwpe.2024.106359

Hudson A, Murnane JG, O'Dwyer T, Pawlett M, Courtney R (2023a) Influence of sediment quality and microbial community on the functioning capacity of a constructed wetland treating alkaline leachate after 5.5 years in operation. Science of The Total Environment 867:161259. https://doi.org/https://doi.org/10.1016/j.scitotenv.2022.161259

Hund K, La Porta D, Fabregas TP, Laing T, Drexhage J (2020) Minerals for Climate Action: The Mineral Intensity of the Clean Energy Transition, Report № 112 p

International Aluminium Institute (2022) Sustainable Bauxite Residue Management Guidance. 2 edn

Kröpfelová L, Vymazal J, Švehla J, Štíchová J (2009) Removal of trace elements in three horizontal sub-surface flow constructed wetlands in the Czech Republic. Environmental Pollution 157(4):1186-1194

Mayes WM, Younger PL, Aumônier J (2008) Hydrogeochemistry of alkaline steel slag leachates in the UK. Water Air and Soil Pollution 195(1-4):35–50. https://doi.org/10.1007/s11270-008-9725-9

O'Connor G, Courtney R (2020) Constructed wetlands for the treatment of bauxite residue leachate: Long term field evidence and implications for management. Ecological Engineering 158:106076. https://doi.org/10.1016/j.ecoleng.2020.106076

Pat-Espadas AM, Loredo Portales R, Amabilis-Sosa LE, Gómez G, Vidal G (2018) Review of constructed wetlands for acid mine drainage treatment. Water 10(11):1685

Qin D, Tan X, Zhao X, Qian L, Nie Y, Pan X, Gao Q, Peng M, Liu Y, Han X (2023) Biological neutralization of bauxite residue with fermented waste sludge and bio-acid, and the microbial ecological restoration. Chemical Engineering Journal 474:145758. https://doi.org/https://doi.org/10.1016/j.cej.2023.145758

Shaheen SM, Rinklebe J, Frohne T, White JR, DeLaune RD (2016) Redox effects on release kinetics of arsenic, cadmium, cobalt, and vanadium in Wax Lake Deltaic freshwater marsh soils. Chemosphere 150:740-748. https://doi.org/https://doi.org/10.1016/j.chemosphere.2015.12.043

Telfeyan K, Breaux A, Kim J, Cable JE, Kolker AS, Grimm DA, Johannesson KH (2017) Arsenic, vanadium, iron, and manganese biogeochemistry in a deltaic wetland, southern Louisiana, USA. Marine Chemistry 192:32-48. https://doi.org/10.1016/j.marchem.2017.03.010

Valenta RK, Lèbre É, Antonio C, Franks DM, Jokovic V, Micklethwaite S, Parbhakar-Fox A, Runge K, Savinova E, Segura-Salazar J, Stringer M, Verster I, Yahyaei M (2023) Decarbonisation to drive dramatic increase in mining waste–Options for reduction. Resources, Conservation and Recycling 190:106859. https://doi.org/https://doi.org/10.1016/j.resconrec.2022.106859

Vymazal J, Zhao Y, Mander Ü (2021) Recent research challenges in constructed wetlands for wastewater treatment: A review. Ecological Engineering 169:106318. https://doi.org/https://doi.org/10.1016/j.ecoleng.2021.106318

Zhang S, Qi J, Jiang H, Chen X, You Z (2024) Improving vanadium removal from contaminated river water in constructed wetlands: The role of arbuscular mycorrhizal fungi. Environmental Pollution 347:123804. https://doi.org/https://doi.org/10.1016/j.envpol.2024.123804

Optimisation of Prediction-Driven Monitoring Programs

Rui Hugman[1], Cecile Coulon[2], Johanna Zwinger[3], Eduardo de Sousa[4]

[1]INTERA Inc, 8000-254 Faro, Portugal, rhugman@intera.com, ORCID 0000-0003-0891-3886

[2]INTERA SAS, 69760 Limonest, France, ccoulon@intera.com, ORCID 0000-0001-9722-9976

[3]INTERA Inc, 6000 Perth, WA, Australia, jzwinger@intera.com, ORCID 0000-0003-0891-3886

[4]INTERA Inc, 6000 Perth, WA, Australia, edesousa@intera.com

Abstract

Data acquisition optimisation in a decision-support modelling context is demonstrated. Groundwater model forecasts can accrue substantial uncertainty. Whilst assimilating field data can reduce this uncertainty, data collection can be expensive. In this paper an approach for optimal data collection that minimizes costs, maximizes informational value, and supports long-term resource sustainability is demonstrated. Using Ensemble Variance Analysis within a multi-objective optimisation framework, cost-effective monitoring locations for a real-world site are identified. Outcomes are a set of monitoring configurations which provide the optimal trade-off between cost and uncertainty reduction. From these, a monitoring program is selected that achieves 90% of possible uncertainty reduction at 30% of total cost.

Keywords: Monitoring, optimisation, uncertainty, decision-support, modelling, groundwater

Introduction

Effective groundwater management at mine sites often relies on numerical modelling to support decision-making, including designing dewatering systems, securing water supplies for mining operations, and evaluating potential environmental impacts of mining activities. Groundwater models, being simplifications of reality, are inherently uncertain, particularly given the scarcity of information about real-world system properties and stresses. This uncertainty can typically be reduced by assimilating data from system state measurements. However, data collection and monitoring programs can be costly, and from a decision-support perspective, not all data holds equal value.

Value of data in model-based decision-making is proportional to its capacity to reduce the uncertainty of model predictions. Data Worth Analysis (DWA) provides a systematic approach to evaluating the potential of new data to achieve this objective. Data worth based on linear analysis are well established in the groundwater modelling literature (e.g., Dausman *et al.* 2010; Fienen *et al.* 2010). However, they are limited by the assumption of linearity between changes in model parameters and predictions and come with the computational cost of filling out a Jacobian (e.g., sensitivity) matrix. The latter become particularly prohibitive when using high-dimensional parameterisation schemes, required to express hydrogeological heterogeneity and uncertainty.

More recently, He *et al.* (2018) introduced the Ensemble Variance Analysis (EVA) approach to assess data worth. EVA operates under the assumption that forecasted and measured values jointly follow a multi-Gaussian distribution. And that to estimate the change in forecast uncertainty, it is not necessary to know the value of future measured data, only the covariance between the forecast and the measured data. Using this assumption, the variance (i.e., the uncertainty) and covariance (i.e., how knowing about one value changes uncertainty in another value) of model outputs can be estimated from an ensemble of simulations without requiring prior knowledge of the measured values. This ensemble of model outputs is generated by running a model many times with different samples of plausible parameter values. Each sample is referred to as a realisation.

From a practical perspective, EVA offers a significant advantage over linear methods: it relies on ensembles of model outputs rather than finite difference derivatives, making its computational cost independent of the number of model parameters and removing the assumption of linearity. This can reduce the number of model runs required for DWA from the order of a few thousands to a few hundred.

The current paper discusses the application of EVA to optimise a monitoring network at an undisclosed mine site. Measured data is used for history matching a decision-support groundwater model. The model is used to support management of extraction wells, with potential effects on several environmental receptors. As data collection is expensive, the objective is to rationalize the monitoring network to ensure high-quality forecasts whilst minimizing cost. Although we focus here on groundwater level data, this same approach is readily extendible to any datatype that can be employed to inform a model.

Methods

In summary, a numerical groundwater model is constructed to simulate predictions of management interest, as well as potential as-of-yet uncollected data from the monitoring network. This model is simulated many times with different parameter realisations. The combination of parameter realisations is referred to as an "ensemble". The simulated outputs from the ensemble of models are used to calculate the co-variance between predictions of interest and potential new data. This enables calculation of the expected predictive uncertainty, if the as-of-yet uncollected data is collected.

Subsequently, multi-objective optimisation is undertaken by calculating the expected predictive uncertainty many times, assuming different combinations of collected data, searching for the combination of monitoring locations that maximize uncertainty reduction at the minimum cost. Note this does not require re-running the numerical model, only the EVA calculations which have a low computational cost.

Site and Numerical Modelling

Due to confidentiality reasons, details of the site cannot be disclosed. However, this should not detract from the approach and outcomes. The mine site is located in an arid area and relies on a well-field to maintain water supply throughout the project's lifespan. The well-field extracts groundwater from a paleochannel aquifer, overlain by low-permeability calcretes and a phreatic aquifer. Annual recharge is low and sustainability of the well-field yield relies on storage and lateral inflow to the paleochannel. Management of the well-field is additionally constrained by needing to ensure that nearby environmental receptors are not affected by drawdown, and that the confined paleochannel is not desaturated.

A numerical model for the site is used to support management of the well-field and forecast sustainable yields. The model simulates historical and future project lifespan. History matching is undertaken for the historical period using an iterative ensemble smoother (IES), as implemented in the open-source software PESTPP-IES (White *et al.* 2018). IES provide computationally efficient approaches to condition model parameters to measured data. Information from available field data is assimilated (including hydraulic heads, site characterisation tests and other soft data). Hydraulic properties and unknown stresses (e.g., recharge, poorly documented extraction rates, external boundary conditions) are represented with a high-dimension parameterisation scheme to express spatial heterogeneity. Following history matching, model forecasts are made with the ensemble of models, providing quantified uncertainty of the predictions of interest.

Ensemble Variance Analysis

EVA operates on the assumption of a multivariate Gaussian relationship between the observation data and the prediction. It quantifies the expected reduction in uncertainty using covariance information derived from a set of simulations (i.e., an ensemble of model outputs). Thus, to conduct EVA, an ensemble of model-simulated outputs is required. This ensemble must include simulated outputs for both potential future data and the forecasts of interest. Conveniently, when using PESTPP-IES, an ensemble of model outputs is a byproduct of predictive uncertainty analysis.

Let the vector composed of the sub-vectors $\boldsymbol{s}$ and $\boldsymbol{d}$ denote outputs generated by a model $\boldsymbol{Z}$ simulated with uncertain parameters represented by the vector $\boldsymbol{k}$.

$$\begin{bmatrix}\boldsymbol{s}\\\boldsymbol{d}\end{bmatrix} = \mathbf{Z}(\boldsymbol{k}) \qquad (1)$$

Vector $\boldsymbol{s}$ contains model outputs that correspond to predictions of interest. The vector $\boldsymbol{d}$ contains simulated outputs that correspond to as-of-yet uncollected data.

If the model $\boldsymbol{Z}$ is simulated many times, each time with a different sample of $\boldsymbol{k}$, the ensemble of model outputs can be collected into a matrix from which the covariance between predictions and as-of-yet uncollected data can be calculated as:

$$\boldsymbol{C}\left(\begin{bmatrix}\boldsymbol{d}\\\boldsymbol{s}\end{bmatrix}\right) = \begin{bmatrix}C_{ss} & C_{sd}\\C_{ds} & C_{dd}\end{bmatrix} \qquad (2)$$

From the above, and assuming a multi-Gaussian distribution between a prediction s and measured data *d*, the expected posterior variance of the prediction can be calculated as:

$$\sigma_{s|d}^2 = \sigma_s^2 - C_{sd}C_{dd}^{-1}C_{ds} \qquad (3)$$

Under the assumption of multi-Gaussian distribution, posterior variance of the prediction s is independent of the value of measured data *d*. Expected variance is the average variance of s given a value of ***d***, across the ensemble. Thus, it provides a conservative lower bound of expected uncertainty reduction. Different values of s can be computed assuming different combinations of d to assess their relative value in reducing predictive uncertainty. As these calculations are computationally cheap, it becomes feasible to wrap them within global optimizer algorithms, as described below.

Monitoring Network Optimisation

Multi-objective optimisation was undertaken employing particle swarm optimisation (PSO; Kennedy and Eberhart 1995)—a population-based, stochastic search algorithm inspired by natural swarm behaviour—and the NSGA-II algorithm (Deb *et al.* 2002), which uses fast non-dominated sorting to efficiently handle trade-offs among multiple objectives. The workflow is implemented using the open-source software PESTPP-MOU (White *et al.* 2022).

Optimisation objectives are quantities that the optimisation algorithm aims to minimise or maximise. The monitoring optimisation was formulated as a two-objective optimisation:

1. maximise total uncertainty reduction, and
2. minimise cost.

For the case described herein, we consider the total uncertainty reduction as an aggregate of the "percentage uncertainty reduction" across all forecasts. It is calculated by summing percentage uncertainty reductions across all forecasts. For this case, we simply aim to minimize aggregate uncertainty. However, more complex formulations of the objective function are possible, such as aiming to achieve a minimum variance for a given prediction.

Cost is calculated as the total number of samples from all sites, multiplied by the average cost per sample. This value does not account for variable costs, such as distance travelled between sites, as they were not available – however, it could. For this site an assumption of one sample per year was made. However, more complex parameterisations are possible, such as optimising for sampling frequency and duration.

The optimisation algorithm explores the solution space by testing different combinations of monitoring locations, calculating their cost and assessing their worth at reducing uncertainty. Outcomes are combinations that provide the maximum uncertainty reduction for a given cost (or a minimal cost for a given uncertainty reduction).

Results

The optimal trade-off between cost and uncertainty reduction is shown in Fig. 1. Referred to as the "pareto front", this curve represents the set of optimal solutions in a multi-objective optimisation problem, where no objective can be improved without worsening at least one other. In other words, at any point along the curve, it is impossible to reduce uncertainty without incurring greater cost (and vice versa).

The y-axis on Fig. 1 is scaled to percentage of the maximum possible uncertainty reduction achievable by collecting data from all available sites. Outcomes show that approximately 85% of possible uncertainty reduction can be achieved with around 20% of the monitoring locations. This represents a substantial saving in terms of cost. As the number of sites in the monitoring network increases, there are diminishing returns. Most of the information gains are achieved from a small portion of the monitored sites.

For comparison, the outcomes for an expert-knowledge (i.e., "manual") designed monitoring plan are displayed in Fig. 1. The proposed plan provides sub-optimal uncertainty reduction. In other words, uncertainty could be reduced substantially further for cheaper.

It remains incumbent on the decision-maker to determine the acceptable trade-off. This will always be case specific. For the site, a desired uncertainty reduction of at least 90% of achievable was specified by the decision-maker. The proposed monitoring configuration was reduced to 65 sites, approximately 30% of the total projected cost, assuming an average cost per sample over the project lifespan.

Conclusions

Data worth optimisation using EVA was employed to optimize data collection to inform prediction-driven modelling. This approach provided a sub-set of monitoring locations that would provide 90% of the information content of the entire network at 30% of the cost. Furthermore, the optimised monitoring locations achieved better results than previously proposed "expert knowledge" derived locations, both in terms of cost and uncertainty reduction.

The approach described herein provides an effective and computationally cheap approach to inform the design of data acquisition programs within a prediction-driven modelling context. Although here it is employed for an existing network and targeting groundwater level measurements, the approach is readily extendible to other contexts and datatypes.

Acknowledgements

The authors thank all co-organisers for hosting the IMWA 2025 Conference and the reviewers and editors for providing constructive comments on this text.

References

Dausman AM, Doherty J, Langevin CD,Sukop MC (2010) Quantifying data worth toward reducing predictive uncertainty. Groundwater, 48: 729–740. https://doi.org/10.1111/j.1745-6584.2010.00679.x

Deb K, Pratap A, Agarwal S, Meyarivan, TAMT (2002) A fast and elitist multiobjective genetic algorithm: NSGA-II. *IEEE transactions on evolutionary computation*, 6(2), 182-197. https://doi.org/10.1109/4235.996017

Fienen MN, Doherty J, Hunt RJ, Reeves HW (2010) Using pre-diction uncertainty analysis to design hydrologic monitoring networks: Example applications from the Great Lakes water availability pilot project. Technical Report. US Geological Survey.

He J, Sarma P, Bhark E, Tanaka S, Chen B, Wen X, Jaira K (2018) Quantifying expected uncertainty reduction and value of information using ensemble-variance analysis. SPE J. 23 428–448. doi: https://doi.org/10.2118/182609-PA

Kennedy J, Eberhart R (1995) Particle swarm optimization. *In Proceedings of ICNN95-international conference on neural networks* (Vol. 4, pp. 1942–1948). IEEE. http://dx.doi.org/10.1109/ICNN.1995.488968.

White JT, Fienen MN, Doherty J (2016) pyEMU: a python framework for environmental model uncertainty analysis, version .01: U.S. Geological Survey software release, https://dx.doi.org/10.5066/F75D8Q01.

White JT (2018) A model-independent iterative ensemble smoother for efficient history-matching and uncertainty quantification in very high dimensions. *Environmental Modelling & Software,* 109, 191–201.

White JT, Hunt RJ, Fienen MN, Doherty J (2020) Approaches to Highly Parameterized Inversion: PEST++ Version 5, a Software Suite for Parameter Estimation, Uncertainty Analysis, Management Optimization and Sensitivity Analysis: *U.S. Geological Survey Techniques and Methods* 7C26., https://doi.org/10.3133/tm7C26.

White JT, Knowling MJ, Fienen MN, Siade A, Rea O, Martinez G (2022). A model-independent tool for evolutionary constrained multi-objective optimization under uncertainty. *Environmental Modelling & Software*, 149, 105316.

Proposing a Design and Planning Method for Mine and Tunnel Drainages

Juan Pablo Hurtado-Cruz[1], Sebastián Pérez-Cortés[2], Gonzalo Yañez Aravena[3], Gonzalo Alfaro Troncoso[4]

[1]Department of Mining Engineering, University of Santiago de Chile. Av. Lib. Bdo. O'Higgins 3363, Estación Central, Santiago, Chile. juan.hurtado@usach.cl. 0000-0001-7602-8278

[2]Department of Mining Engineering, University of Santiago de Chile. Av. Lib. Bdo. O'Higgins 3363, Estación Central, Santiago, Chile. sebastian.perez@usach.cl. 0000-0001-6542-3481

[3]Department of Mining Engineering, University of Santiago de Chile. Av. Lib. Bdo. O'Higgins 3363, Estación Central, Santiago, Chile. gonzalo.yanez@usach.cl. 0000-0001-2045-2234

[4]Department of Mining Engineering, University of Santiago de Chile. Av. Lib. Bdo. O'Higgins 3363, Estación Central, Santiago, Chile. luis.alfaro@usach.cl. 0000-0001-2045-2234

Abstract

Around the world, both mining and underground civil works require excavating tunnels or ramps, whether for access, ore mining, rail or road connectivity, ventilation, water supply, among other applications. During this process, it is common to intercept groundwater, which must be removed to achieve the final excavation objectives. If the tunnel slope or ramp is positive or zero, drainage can be done through a lateral channel or pipe without major impacts. However, when the slope of the ramp or tunnel is negative, the water must be removed as soon as possible to avoid accumulation due to gravity. It is common that when the underground works depth exceeds the hydraulic capacities of a simple pumping system, pumping stations are used to remove the water in stages to the surface or to the final accumulation or drainage site. This paper describes a methodology for the design, sizing and planning of pumping stations for underground drainage in mines with depths that require the use of pumping stations, due to the high hydraulic pressures above 10 bar. This methodology consists of determining the hydraulic design variables of the system from the initial project proposed setting up as the maximum depth reached, ramp slope and maximum expected infiltration flow. With the maximum depth and the total head losses estimated by the proposed design variables, the total head loss to overcome is determined. In this way, total losses can be subdivided according to the number of pumping stations proposed, based on the same height and flow to be overcome by each pumping station. This last allows the engineers to takes advantage of available resources, maintenance, geological conditions of the site and drainage needs in terms of flow and depth, considering potential anomalous situations and response capacities in the event of emergencies or faults. It also is aligned with the treatment and reuse of water to be used as "industrial water". Based on extensive field observations across various projects, this methodology provides a comprehensive solution for sustainable water management in mining, civil, and military operations, enabling water treatment and reuse while addressing both routine drainage and emergency scenarios.

Keywords: Pumping stations, groundwater, mine drainage, underground projects, ramp excavation, underground mining, piping

Introduction

Hard rock tunnel or ramp excavation often encounters groundwater that must be removed to meet project objectives and the maintain safe working conditions for the underground miners. Positive or zero slopes allow for straightforward drainage using a lateral channel or pipe. However, negative slopes necessitate pumping systems. Encountering one or more aquifers further increases the water volume requiring extraction. Therefore, a thorough hydrogeological study is essential to determine the anticipated inflow at depth. This involves established methods for testing and estimating parameters like permeability, transmissivity, and storage capacity (Dupuit, 1863; Thiem, 1906; Theis, 1935; Todd, 1959). Once these parameters are determined, steady-state groundwater inflows can be estimated using the Goodman *et al.* (1965) formulation.

When tunnel depth exceeds the capacity of simple pumping systems, pumping stations are required for staged drainage to the surface or a designated discharge point. Some authors discuss tunnel dewatering through articles and reports on underground pumping stations design (Cashman and Preene, 2013; Powers *et al.*, 2007), they offer useful but limited detail on pumping stations for ramps or mine tunnels.

The proposed methodology for drainage and water resource utilization involves a structured approach and an initial suggested pumping station design. This design aims to standardize hydraulic elements across all stations, including pump type and operating point, pipe dimensions, and fitting quantity. This work draws upon years of field observations at multiple mines and incorporates good practices from mining companies and their engineers, often based on practical experience (Palta Araya, 2015; Tapia Cid, 2018).

Proposed Drainage System Philosophy

Operational philosophy for excavating negatively sloped ramps considers a maximum vertical depth achievable with a generally consistent slope, often determined by the uphill grade capacity of the development equipment (excluding rest areas and curves). This defines the ramp length. As excavation progresses through aquifers or water-bearing geological structures, infiltration begins. This water, along with water from drilling equipment, must be removed from the excavation face. Submersible pumps designed for sludge or debris transport the water to a nearby mobile or temporary accumulation and pumping station for discharge to the surface or the nearest pumping station. As excavation deepens, permanent pumping and accumulation stations become necessary due to the hydraulic limitations of pumping systems. Furthermore, if properly designed, these stations could partially clean and treat the water for reuse as industrial water for drilling equipment. To achieve this, the stations require a minimum water accumulation volume to supply drilling operations and to accommodate downtime for pump system maintenance, mechanical or electrical failures, and unforeseen events. Additionally, from an operational point of view, the design is determined by the storage capacity required to manage the maximum number of stop-starts the pump system is designed to maintain. Too small volume results in excessive stop-starts and more likely system failure. At some Chilean underground mines, is observed at least one full day of accumulation capacity and the pumping system capacity should be sufficient to pump the entire accumulated volume within a fraction of a day. It can be operating less than 50% of the day, sometimes with multiple pumps in parallel. This redundancy allows for partial capacity pumping during maintenance, failures, or underestimating the total infiltration flow rate. Additionally, is frequently to find the maximum working hydraulic pressure not exceed 10 bar for operational feasibility and avoid leakages, because PVC Class 10 (10 bar) and HDEP (6–20 bar) are commonly used.

Proposed Methodology

The following outlines the proposed methodology, based on the philosophy described above:

Determine the tunnel or ramp design parameters, such as vertical depth and ramp slope, to calculate the total ramp length. These are typically defined by the project design.

Quantify maximum expected infiltration flow rate based on hydrogeological studies for flow and recharge estimations, that can be additionally influenced by different mining units like old mines and abandoned areas. The idea is to estimates a maximum capacity design for the pumping stations.

Estimate maximum accumulation period for the pumping stations, considering the maximum expected infiltration flow rate, and then calculate the maximum expected accumulation volume. Providing one full day of accumulation capacity is recommended to address potential failures, planned maintenance, or to avoid underestimating the total infiltration water flow rate.

Select a daily pump operating percentage, representing the pumps' daily operational time. A value below 50% is recommended, ensuring the pumps can drain the entire volume within a fraction of a day to cover underestimating the total infiltration water flow rate.

Select a pipe diameter based on the maximum pumping flow rate, daily pump operating percentage, and maximum expected infiltration flow rate, or the desired emptying time for the pumping station. An economical flow velocity range within the pipes is suggested to be between 0.5 and 2.5 m/s (Cengel & Cimbala, 2018) (Crane Co., 2018).

Estimate friction and minor losses as if the entire ramp were a single pipe, using the chosen diameter. This provides an initial approximation of total system losses.

Estimate the total head loss as the sum of the friction and minor losses for the entire ramp plus the total vertical lift.

Select the pump curve and operating point, based on the maximum working pressure per station established by engineering and operations (agreed-upon manageable pressure limit defined by the company experience and cost evaluation).

Determine the number of pumping stations vertically by dividing the total head loss by the head at the selected pump's operating point. This will likely result in a non-integer value. If the number is close to the lower integer, rounding down is recommended. For example, 4.05 or 4.1 could be approximated to 4. However, for larger non-integer values, assess the margin between the installation's required point and the chosen pump's operating point. Thea goal is to stay within the agreed-upon manageable pressure limit. Several design iterations may be necessary to optimize this value, as excavating and constructing a pumping station represents a significant investment. Once an acceptable value is reached, adjust the pump operating point according to the final number of stations.

Determine the recirculation volume for equipment water consumption, such as horizontal drilling jumbos, ground support equipment, hydraulic splitters, and radial and/or vertical drilling rigs. In the latter case, some equipment may require substantial water volumes for operation and may be supplied using the infiltration water, which can be partially recirculated to the nearest pumping station as an option. Optionally, the mine water may be cleaned of mud on surface to be introduced by gravity.

Design the pumping station, considering the accumulation volume, solids settling system, and water treatment for supplying industrial water to equipment.

Determine the operational parameters of the mobile pumping station based on the development characteristics to size its capacities, such as average and maximum flow rate, maximum lift, sludge removal, transportability, and rapid installation capability. This will determine the pump sizing, dimensions and design of the housing, and electrical power requirements. Commercial products are available, or they can be developed in-house.

Pumping System Design

The pumping system consists of three main parts: pumping at the working face to the mobile station, pumping from the mobile station to the nearest operational pumping station, and staged pumping to the tunnel exterior or final discharge point. The design of each stage is addressed below (see Fig. 1).

Pumping Station Design

The pumping station design comprises several components, detailed in Fig. 2. The

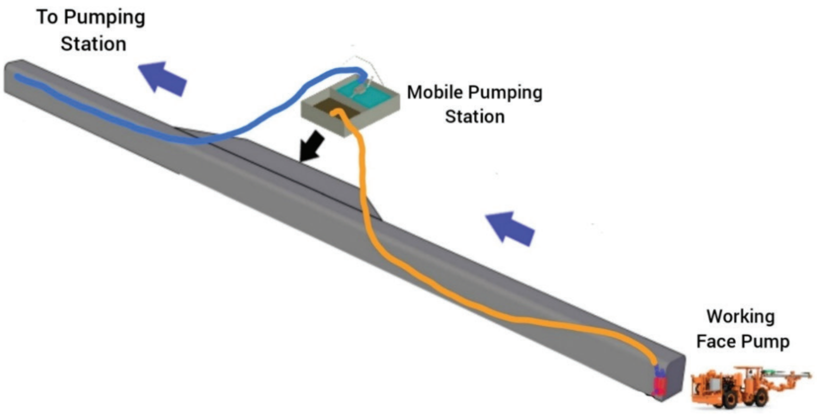

Figure 1 *Pumping System Schematic.*

station is located laterally to the main tunnel or ramp, with a slope to accommodate water accumulation. It includes a settling pond where dirty water from the face drains and solids settle. Cleaner water overflows the settling pond into the pumping area. A centrifugal pump located in the pumping area propels the water to the upper level or the next higher pumping station.

Solids or Sludge Wall

The sludge wall, as mentioned, retains the coarse fraction of the drainage water, allowing cleaner water to overflow. This wall should be constructed of high-quality concrete to provide the necessary stability for sediment removal and withstand impacts from cleaning equipment buckets (see Fig. 3). A minimum concrete compressive strength of 17 MPa, or category G17, is recommended (Instituto Nacional de Normalización – Chile, 2016).

Pumping Station Sizing

Pumping station dimensions depend on the established accumulation volume, geomechanical stability requirements (height "y," width "b"), which typically do not exceed those of the main tunnel or ramp, and the station slope. This slope must allow development equipment access during construction. Fig. 4 illustrates the usable storage area within a pumping station, which can be divided into two volumes.

These volumes relate to the station's design geometry and quantify its capacity, with Vt, the total volume, being the sum of Volume 1 (V1) and Volume 2 (V2). In this schematic, Volume 1's length is directly related to the station slope, tunnel width, and height, but only half contributes to usable volume. This

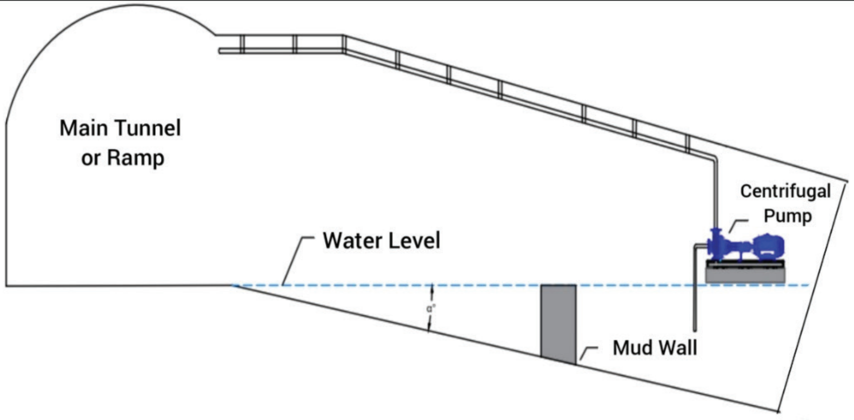

Figure 2 *General Pumping Station Schematic.*

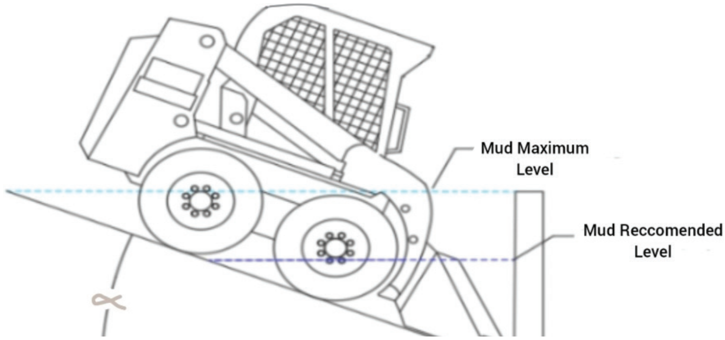

Figure 3 *Sediment cleaning equipment at the sludge wall.*

can be calculated directly using the slope and tunnel dimensions to estimate length L1:

$\text{Slope} = y / L1$ Then $L1 = y / \text{Slope}$

$V1 = (y*L1*b) / 2$

If Volume 1 is insufficient to accommodate the total accumulation volume, Volume 2 must be estimated. This can be considered a parallelepiped, with a volume given by:

$V2 = (y*L2*b)$

Length L2 is derived from $V2 = Vt - V1$.

Furthermore, before operations commence, waterproofing the tunnel walls exposed to water is recommended, especially near geological structures that could cause significant water infiltration. This is also crucial in areas with nearby mining activity or conditions that alter rock mass stresses, potentially activating geological structures and causing seepage to under levels.

Water Treatment and Utilization

The water recovered and stored in the pumping area can be treated for use as industrial water, supplying drilling equipment and other operations. Treatment occurs in the accumulation area. The first step is pH neutralization. Low pH acidity can corrode equipment materials, pipes, valves, and fittings. Acidic water is common in sulfide mines due to the presence and degradation of pyrite. Conversely, high pH or alkaline conditions are also corrosive and tend to precipitate Mg and Ca salts in pipes, valves, and fittings, potentially causing complete blockage through internal accretion by scaling. After pH neutralization, suspended solids must be settled to prevent their circulation through the system, which can cause blockages or accretion. While the sludge wall retains a significant portion of solids, some (primarily fines) enter the accumulation area due to flow turbulence in the sludge zone.

Pump and Staged Pumping

The pump lifts water from the accumulation area to the next station. It should be easily accessible for maintenance; a platform

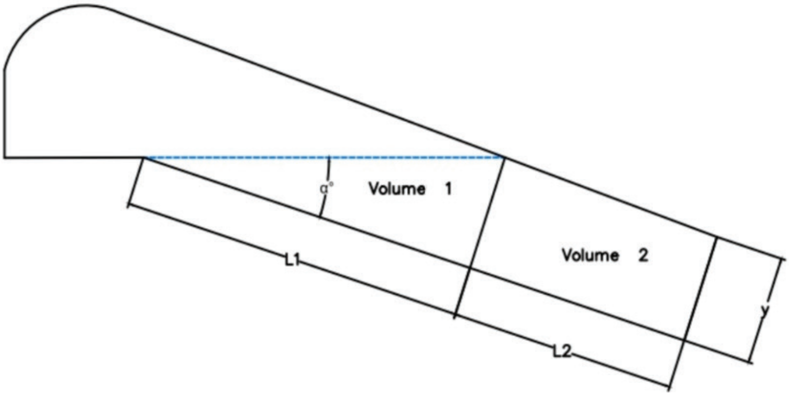

Figure 4 *Storage Area Schematic.*

above the flooded area can facilitate this. A centrifugal pump is suggested, standby operating in parallel with another for redundancy during repairs or maintenance. The station length may be determined by the pump's NPSH (Net Positive Suction Head) requirements. In this case, a floating pump on a raft or a submersible backup pump can be installed. Using a primary submersible pump is not recommended due to their lower hydraulic pressure output, which would limit the distance between pumping stations.

Staged pumping conveys drainage water to the exterior. This can be manual, semi-automated, or fully automated, depending on the implemented sensors, PLC (Programmable Logic Controller), and communication system available in the tunnel. It's crucial to consider that the stations operate in series; failure at one station halts drainage until the issue is resolved. Therefore, the accumulation volume should account for potential failure scenarios, providing time for intervention and solve them.

Sump pumping at the working face

When ramp is developing at the lower level, working face requires one or more submersible sludge pumps operating continuously to manage infiltration. These pumps must be designed for abrasive solids; otherwise, their lifespan will be significantly shortened by drilling debris. Submersible sludge pumps typically have a limited hydraulic lift capacity, so their role is to transfer water from the face to a nearby pumping station. Hydraulic lift calculations must account for head losses and vertical elevation.

Mobile Pumping Station

The mobile pumping station is crucial in this drainage system. It should be located as close as possible to the working face to receive water and convey it to the nearest pumping station. Positioning it in an auxiliary drift prevents obstructing tunnel traffic. Careful consideration should be given to matching the hydraulic pressure of the face pumps with the maximum distance to the mobile pumping station to facilitate planning during tunnel development. The station design should include a receiving tank and a booster pump. For solids separation, the tank should be divided by a settling wall, allowing cleaner water to overflow for pumping. The pump must handle abrasive solids, have a flow rate exceeding the infiltration rate to accommodate various scenarios, and a hydraulic lift capacity greater than the separation between pumping stations. This is because when the design distance between stations is reached, the next station may not yet be constructed or operational, requiring additional time beyond the main tunnel or ramp development (at least one week).

Final Discussion and Conclusions

This document has outlined the key design elements for drainage in descending tunnels or ramps. The methodology and design enable drainage water utilization through accumulation and treatment. Variations and alternative designs may be necessary depending on site-specific characteristics, such as complex spatial layouts often found in mines. This method can be combined with other techniques like vertical drainage wells from the surface or the horizontal directional drilling (HDD) method to support drainage in more complex areas. Similarly, aquifer waterproofing where the tunnel intersects is an option for reducing infiltration rates.

If high accumulation volumes lead to excessively long pumping stations, shorter parallel stations in a "Y" or cross configuration, or even bilaterally on both sides of the ramp, can be considered. Adequate geomechanical and hydrogeological studies are also essential, as high-quality information enables proper system sizing to meet requirements and ensure tunnel stability. The entire project requires economic evaluation, considering excavation, equipment, instrumentation, operation, and maintenance costs, which could be the subject of a separate, in-depth article.

Acknowledgements

The authors wish to express their gratitude to the Mining Engineering Department of the University of Santiago, Chile for support funding for conference attendance.

References

Cashman, P. M., & Preene, M. (2012). Groundwater lowering in construction: A Practical Guide to Dewatering, Second Edition. CRC Press.

Cengel, Y. A., & Cimbala, J. M. (2018). Fluid Mechanics: Fundamentals and Applications (4th ed. ed.). (U. o. Nevada, Ed.) Reno, USA: McGraw-Hill Education.

Crane Co. (2018). Flow of Fluids Through Valves, Fittings, and Pipe (Technical Paper No. 410). Crane Co.

Darcy, H. (1856). Lee fontaines publiques de la ville de Dijon. V. Dalmont, Paris.

Dupuit, J. (1863). Etudes théoriques et pratiques sur le mouvement des eaux dans les canaux découverts et á travers les terrains perméables. 2éme édition. Dunod, Paris.

Goodman, R. E., Moye, D. G., Van Schalkwyk, A. and Javendel, I. (1965). Ground water inflows during tunnel driving. Bull. Assoc. Engineering Geologists, vol. 2, No 1.

Instituto Nacional de Normalización de Chile (2016). Hormigón – Requisitos Generales. Norma Chilena (NCh 170) Cuarta edición.

Powers, J. P., Corwin, A. B., Schmall, P. C., & Kaeck, W. E. (2007). Construction dewatering and groundwater control: New Methods and Applications. John Wiley & Sons.

Palta Araya, V. M. (2015). Estudio y operativización sistema de ventilación y drenaje para construcción túnel conveyor (Vol. 1). (J. P. Hurtado Cruz, Ed.) Santiago, Región Metropolitana, Chile: Universidad de Santiago de Chile.

Tapia Cid, S. I. (2018). Estimación del período de autoabastecimiento hídrico total para (Vol. 1). (J. P. Hurtado Cruz, Ed.) Santiago, Región Metropolitana, Chile: Unviersidad de Santiago de Chile.

Theis, C. V. (1935). The relation between the lowering of the piezometric surface and the rate and duration of discharge of a well using groundwater storage. Amer. Geophys. Union., vol. 16, pp. 519–524.

Thiem, G. (1906). Hydrologische methoden. Gebhardt, Leipzig.

Todd, K. (1959). Groundwater hydrology. John Wiley & Sons, New York.

Diffusive Gradients in Thin Films (DGT) as an Aid to Risk Assessment in Watercourses Affected by Mine Drainage

Miguel Izquierdo-Díaz[1], Almudena Ordóñez[2], Humberto Serrano-García[1], Rodrigo Álvarez[2], Carmen García-Fernández[2], Efrén García-Ordiales[2], Eduardo De Miguel[1], Fernando Barrio-Parra[1]

[1]*Universidad Politécnica de Madrid, ETS de Ingenieros de Minas y Energía, 28003 Madrid, Spain, miguel.izquierdo@upm.es, ORCID 0000-0003-2695-0779*

[2]*University of Oviedo, Escuela Politécnica de Mieres, 33600 Mieres, Asturias, Spain, aoalonso@uniovi.es, ORCID 0000-0002-0055-1828*

Abstract

This study evaluates the environmental quality of river water and sediments in the Caudal River basin (NW Spain), historically affected by Hg and Cu mining. Initial sampling revealed high metal(oid) concentrations, especially downstream of former Hg mines. A second campaign used DGT (Diffusive Gradients in Thin Films) passive samplers to assess bioavailable fractions at selected points. Results showed a strong correlation between As and Cu in DGT and pore water, with As showing up to 75% transfer at low concentrations, indicating its nearly fully bioavailable chemical form. This highlights the usefulness of DGT samplers for determining bioavailability.

Keywords: Bioavailability, DGT, Ecological Risk, River Sediments, Trace Elements

Introduction

River sediments are essential components of aquatic ecosystems, serving as both habitats and food sources for a variety of organisms. However, their ability to act as sinks for pollutants, including trace metals and metalloids, can lead to considerable ecological risks. These risks are particularly pronounced in regions affected by historical mining activities, where sediments continue to harbour contaminants long after the cessation of mining operations. Such contamination can severely affect benthic organisms and the broader ecosystem by influencing the bioavailability of harmful elements (Banaee *et al.* 2024; Eyong 2008).

Traditionally, environmental assessments have concentrated on water column quality, but this approach often overlooks the potential for sediments to act as reservoirs and sources of pollutants. Changes in physicochemical conditions, whether natural or anthropogenic, can trigger the remobilization of contaminants from sediments into the overlying water, amplifying ecological hazards (García-Ordiales *et al.* 2020; Kim *et al.* 2006). Given these dynamics, sediment assessments that account for bioavailability, i.e. the fraction of contaminants available for biological uptake, are critical for accurately evaluating environmental risks (Ali *et al.* 2024).

Bioavailability is influenced by the chemical forms of contaminants and their interactions with sediment matrices and pore water. Therefore, various analytical methods have been developed to estimate bioavailable fractions, ranging from leaching and extraction methods to advanced in situ technologies. Sequential extraction techniques using weak acids, such as acetic acid, have been widely adopted to target exchangeable, water-soluble, and acid-soluble fractions of metals, which are presumed to represent bioavailable forms (Rauret *et al.* 1999). However, these traditional methods may fall short in capturing the dynamic interactions between contaminants and their surrounding environment.

Diffusive Gradients in Thin Films (DGT) technology has emerged as a powerful alternative, offering dynamic and time-integrated measurements of bioavailable contaminants. This technique not only provides insights into the mobility and speciation of metals in sediments but also minimizes sample handling and potential contamination (Davison & Zhang 2012). DGT's ability to quantify labile metal fractions with high spatial resolution has made it a preferred tool in environmental monitoring (Huang *et al.* 2019; Taylor *et al.* 2020).

The primary objective of this research is to compare methodologies for evaluating the bioavailability of key contaminants in river sediments. By integrating traditional extraction techniques and advanced DGT-based assessments, this work aims to identify the most effective approaches for estimating ecological risks. The study's findings will contribute to the ongoing discourse on sediment contamination, with implications for risk management in mining-affected aquatic systems. Specifically, this work explores the dynamic interplay between sediment-bound and dissolved contaminants, highlighting the advantages and limitations of different analytical approaches in characterizing bioavailable fractions.

Methods

Study Area

The research was conducted in the Caudal River basin, located in Asturias, northwest Spain. This area has a long history of mining activities, particularly mercury (Hg) and copper (Cu) extraction, which have left a lasting environmental legacy (mining waste still remains in uncovered spoil heaps, exposed to mechanical and chemical weathering). The basin's geological substrate primarily comprises Carboniferous sedimentary rocks, including sandstones, shales, and graywackes, interspersed with calcareous outcrops. These rocks exhibit low permeability, which, combined with the region's humid climate and high annual rainfall exceeding 1,000 mm, results in predominantly surface runoff-dominated hydrology.

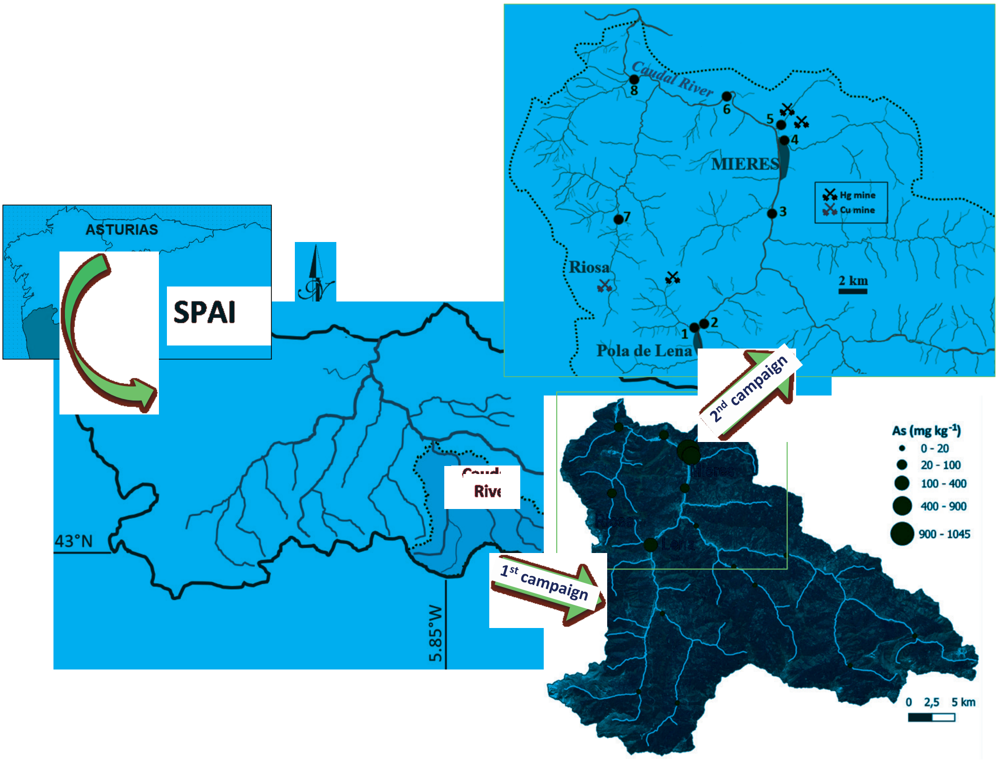

Figure 1 Caudal River basin; As concentrations found in the first sediment sampling campaign; Location of sampling points of the second campaign (mod. Escudero et al., 2024; Alvarez et al. 2024).

Mining operations in the basin ceased decades ago; however, residual contamination persists. Spoil heaps and unremediated mine facilities continue to release pollutants, including arsenic (As), mercury (Hg), and copper (Cu), into the river system. These elements are originally present in various mineral forms, such as cinnabar (HgS) for Hg, arsenopyrite (FeAsS) for As and Chalcopyrite ($CuFeS_2$) for Cu, which contribute to the complex contamination profile. The Hydrological Planning Office reports that the Caudal River is in poor ecological condition, especially in its lower section. Macroinvertebrate studies show low biodiversity, suggesting that old mine sites are negatively affecting aquatic life (Escudero *et al*. 2024). Sampling points were strategically located downstream of the Hg mining sites in Mieres and Pola de Lena and the Cu mine at Riosa (Fig. 1) to identify the extent of contamination and its ecological implications.

Sampling and Analysis

In a first campaign, water and bulk sediment samples were collected on the banks of the main watercourses of the basin (Fig. 1), using plastic tools. The area where the highest concentrations of elements of concern (Hg, As and, to a lesser extent, Cu) were found (see next section), was selected for the second sampling campaign (Fig. 1). This second phase includes the bioavailability study, so eight sediment sampling points were critically selected in the most affected areas (Fig. 1), including 2 field duplicates (samples 4 & 5). Each sampling event involved the collection of bulk sediments, pore water, and in situ deployment of DGT devices.

1. Bulk Sediments: Approximately 1 kg of sediment was manually collected from the uppermost layer (≤3 cm depth) using plastic tools to minimize contamination. Samples were air-dried, sieved to isolate the fine fraction (<63 µm), and subjected to pseudo-total digestion using aqua regia. Metal(loid) concentrations were analysed using inductively coupled plasma optical emission spectroscopy (ICP-OES).
2. Pore Water: Sediment pore water was extracted through centrifugation under anoxic conditions to prevent oxidation. The extracted water was filtered, acidified to pH 2 with nitric acid, and stored at 4 °C until analysis. Trace metals were quantified using inductively coupled plasma mass spectrometry (ICP-MS).
3. DGT Deployment: DGT devices were deployed at the sediment-water interface for a period of four days. The DGT units contained binding gels tailored to capture specific contaminants, including Chelex-100 for trace metals and ferrihydrite for arsenic. After retrieval, the binding gels were eluted, and the accumulated contaminants were quantified to determine time-averaged bioavailable concentrations.
4. Acetic Acid Extraction: A subset of samples from the bulk sediments underwent a selective extraction using 0.11 M acetic acid to isolate exchangeable and acid-soluble fractions. This method simulates conditions conducive to bioavailability and provides a comparative benchmark against DGT measurements.

Results and discussion

The results of the first campaign revealed that stream waters downstream the mine sites (with up to 0.76 mg L^{-1} As) exceed concentrations established by the US Environmental Protection Agency (EPA) and Spanish regulations for the protection of human health and the environment. Hg and As concentrations in sediments (up to 195 and 1045 mg kg^{-1}, respectively) exceeded the thresholds set by the Canadian Sediment Quality Guidelines (CCME 2023) and the US Environmental Protection Agency (US EPA 2022) guidelines, indicating possible adverse and chronic effects on aquatic life (Escudero *et al*. 2024). In addition, the concentrations found downstream the mines are high above the background values found for the whole basin: 14.7 mg kg^{-1} As, 0.23 mg kg^{-1} Hg and 16.65 mg kg^{-1} Cu (Barrio-Parra *et al*. 2025). The Hydrological Planning Office reports that the Caudal River is in poor ecological condition, especially in its lower section. Macroinvertebrate studies show low biodiversity, suggesting that old mine sites are negatively affecting aquatic life, despite being inactive for decades (Escudero *et al*. 2024).

Table 1 Analytical results (after Álvarez et al. 2024)

	Sediment (mg kg^{-1})			Acetic acid extract (mg kg^{-1})			Pore water (µg L^{-1})			DGT (µg L^{-1})		
Sample	**As**	**Hg**	**Cu**	**As**	**Hg**	**Cu**	**As**	**Hg**	**Cu**	**As**	**Hg**	**Cu**
1	313	8.76	28.5	15.8	0.0011	0.52	221	0.043	2	75	0.013	1.6
2	218	7.72	25.7	6.72	0.0009	0.61	144	0.074	4	34	0.018	0.9
3	34.5	1.57	26.4	<0.20	<0.0004	1.20	<5	0.063	2	5.6	0.004	1.0
4	39.7	1.88	24.6	0.22	0.0007	0.35	14	0.080	2	4.7	0.002	0.9
4dup	16.1	<0.20	12.8	<0.20	<0.0004	0.33	10	0.105	3	<2.9	0.005	1.8
5	1080	80.7	22.5	33.9	0.0205	1.17	746	0.263	2	580	0.059	1.7
5dup	921	78.0	21.2	24.7	0.0029	1.07	649	0.255	4	220	0.034	1.0
6	38.4	1.31	27.3	0.40	<0.0004	0.52	13	0.069	2	11	0.006	1.1
7	17.9	<0.20	54.3	<0.20	<0.0004	4.64	6.0	0.032	14	7.6	0.007	2.7
8	34.9	3.76	25.4	0.28	<0.0004	1.59	10	0.071	2	7.5	0.006	1.2

In sediments sampled in the second campaign, As and Hg levels surpassed Probable Effect Levels (PELs), with concentrations up to 1080 mg/kg for As and 80 mg/kg for Hg. These findings underscore the critical need to evaluate not only the total contaminant load but also the bioavailable fractions that directly influence ecological risks.

Comparison of Methods

Pore water concentrations revealed remarkable spatial variability, particularly for As and Cu. The highest concentrations of As and Hg were detected downstream of Hg mining sites, while elevated Cu levels were identified downstream of the Cu mine. The dynamic interaction between pore water and sediment phases was evident, emphasizing the role of pore water as a critical reservoir for bioavailable contaminants (Bufflap & Allen 1995). Pore water analysis effectively captured the soluble metal fraction but was influenced by sampling conditions and temporal variability.

Acetic acid method, widely accepted as a proxy for bioavailable metal fractions, revealed that bioavailability varied notably among elements. For As, the acetic acid-extractable fraction represented up to 5% of the total sediment content in areas near mining activities, compared to less than 1% in less contaminated locations. Cu exhibited slightly higher mobility, with extractable fractions reaching up to 8.5% in the most affected areas. In contrast, Hg showed negligible extractable fractions (≤0.2%), reflecting its low mobility and bioavailability under the studied conditions. Acetic acid extraction provided a straightforward, cost-effective means to estimate the labile metal fraction. However, it underestimated bioavailability for elements like As and Cu when compared to DGT (i.e. the fractions of As and Cu extracted by acetic acid from the sediment are lower than the fractions of these elements retained from the pore water in the DGT).

DGT technique provided in situ, time-averaged measurements of bioavailable metal fractions, offering a dynamic perspective on contaminant exchange at the sediment-water interface. Strong correlations were observed between As and Cu concentrations in DGTs and pore water (≥75% transfer efficiency for As at low concentrations), indicating a substantial bioavailable fraction. Conversely, Hg transfer to DGTs was negligible, regardless of sediment concentrations, likely due to its limited mobility and strong association with sediment particles (Davison & Zhang 2012). DGTs emerged as the most robust tool for assessing bioavailability, particularly for As and Cu. By integrating diffusion and kinetic replenishment processes, DGTs offered a more comprehensive understanding of dynamic contaminant exchange between sediment and water phases (Gu *et al.* 2023). Fig. 2 shows a comparison of results for the 3 samples closest to the Hg mines in Lena and Mieres and to the Cu mine.

Element-Specific Observations

Arsenic exhibited a complex behaviour across methods. While total sediment concentrations were consistently high, the bioavailable fraction measured by DGT and pore water analysis was more pronounced at sites with low total As levels, suggesting a dynamic equilibrium between solid and liquid phases. This equilibrium appeared disrupted at highly contaminated sites, where particulate-bound As dominated.

Copper showed moderate mobility and bioavailability, with DGT and pore water measurements aligning closely. The acetic acid-extractable fraction was relatively consistent, highlighting Cu's moderate affinity for sediment binding sites. Elevated Cu concentrations near the Cu mine in Riosa were particularly concerning, given their potential ecological implications.

Mercury demonstrated minimal mobility and bioavailability across all methods. The negligible transfer to DGTs, despite high total concentrations in sediments, underscores Hg's tendency to form stable, non-labile complexes within the sediment matrix (Chaudhary *et al.* 2020). This limited bioavailability suggests that Hg poses less immediate risk to aquatic biota, although long-term risks associated with remobilization cannot be discounted.

For the field replicates, the calculated coefficients of variation for As and Cu are high, reaching up to 60% for As in the sediment and the DGT, while remaining low in other cases.

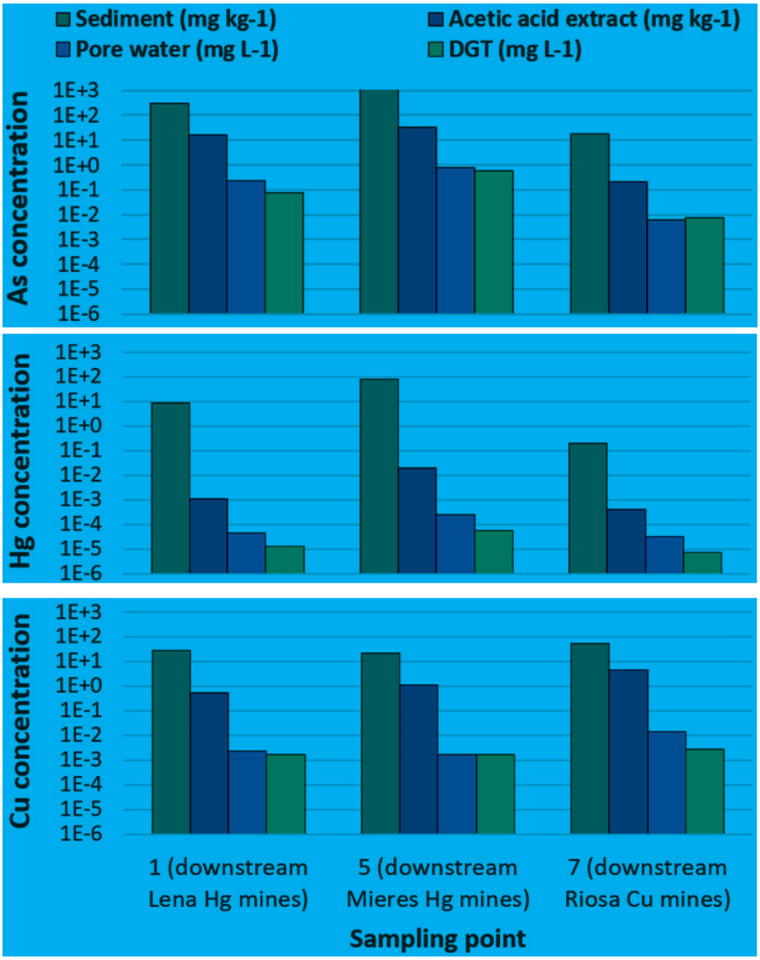

Figure 2 *As, Hg and Cu concentrations (same logarithmic scale) in sediment, pore water, DGT and acetic acid extract in three sampling points.*

Conclusion

The study highlights remarkable contamination levels of As, Hg and Cu in the Caudal River basin, a region heavily affected by historical mining activities. Total metal(loid) concentrations in sediments downstream of former Hg and Cu mining sites often exceed thresholds established by globally accepted guidelines, suggesting a high likelihood of adverse ecological effects.

These findings underscore the importance of integrating multiple methodologies to accurately assess ecological risks in mining environments. While total metal concentrations provide a baseline for contamination levels, bioavailability data are critical for understanding actual ecological effects. The superior performance of DGTs in capturing dynamic bioavailability highlights their potential as a standard tool in environmental monitoring and risk assessment frameworks.

The study demonstrates that dynamic techniques like DGTs offer substantial advantages over traditional methods, by allowing in situ and continuous measurements of available metal(loid) concentrations with high spatial resolution, enabling more accurate assessments of ecological risks posed by potentially toxic elements in river sediments, particularly in basins affected by mine drainage. The integration of these findings into environmental management strategies can aid in prioritizing remediation efforts and mitigating long-term influences on aquatic ecosystems.

Notwithstanding, the variability in field replicates, particularly for As, highlighted the influence of site-specific factors and methodological limitations. High coefficients of variation were found for some measurements, emphasizing the need for standardized deployment protocols and additional replicates to enhance reliability. Future research should focus on refining DGT calibration for elements like Hg and exploring correlations between DGT measurements and biological uptake in aquatic organisms.

Acknowledgements

The present study has been funded through the PID2020-115313RB-I00/AEI/10.13039/501100011033 research grant of the Spanish Ministry of Science and Innovation, and the CARESOIL-CM [TEC-2024/ECO-69] programme, funded by the regional government of the Community of Madrid (Spain).

References

Ali J, Tuzen M, Shaikh Q, Jatoi WB, Feng X, Sun G, Saleh TA (2024) A review of sequential extraction methods for fractionation analysis of toxic metals in solid environmental matrices. TrAC Trends Anal. Chem. 173, 117639, doi: 10.1016/j.trac.2024.117639

Álvarez R, Izquierdo M, Serrano H, García-Ordiales E, García C, Alberquilla F, Barrio F, De Miguel E, Charlesworth S, Ordóñez A (2024) Comparison of sediment bioavailable methods to assess the potential risk of metal(loid)s for river ecosystems. Ecotoxicol Environ Saf 281: 116614, doi: 10.1016/j.ecoenv.2024.116614

Banaee M, Zeidi A, Mikusková N, Faggio C (2024) Assessing metal toxicity on crustaceans in aquatic ecosystems: a comprehensive review. Biolog. Trace Elem. Res, doi: 10.1007/s12011-024-04122-7

Barrio-Parra F, Álvarez R, Serrano-García H, Izquierdo-Díaz M, Ordóñez A, García-Fernández CC, De Miguel E (2025) A proposed methodology for the definition of background and reference values for trace elements in fluvial sediments. Ecotoxicol Environ Saf 290: 117517, doi: 10.1016/j.ecoenv.2024.117517

Bufflap SE, Allen HE (1995) Sediment pore water collection methods for trace metal analysis: a review. Water Res 29(1):165–177, doi:10.1016/0043–1354(94)E0105-F

CCME (Canadian Council of Ministers of the Environment), 2023. Canadian Environmental Quality Guidelines – Sediment. https://ccme.ca/en/resources/water-aquatic-life#

Chaudhary M, Quanz M, Williams J, Maltby E, Oakes K, Spooner I, Walker TR (2020) Assessment of metal(loid) concentrations using diffusive gradient thin (DGT) films in marine, freshwater and wetland aquatic ecosystems impacted by industrial effluents. Case Stud. Chem. Environ. Eng. 2, 100041, doi: 10.1016/j. cscee.2020.100041

Davison W, Zhang H (2012) Progress in understanding the use of diffusive gradients in thin films (DGT)—back to basics. Environ Chem 9:1–13, doi:10.1071/EN11084

Escudero L, Ojanguren AF, Álvarez R, García C, Pañeda J, Alberquilla F, Ordóñez A (2024) Assessment of hydrological, geological, and biological parameters of a river basin impacted by old Hg mining in NW Spain. Environ Sci Poll Res 31: 11081–11095, doi: 10.1007/s11356-024-31888-z

Eyong BE (2008) Distribution of arsenic and other heavy metals in sediments and their effects on benthic macroinvertebrates in the Gallinas River, San Miguel County, New Mexico. New Mexico Highlands University, 162 p.

García-Ordiales E, Covelli S, Braidotti G, Petranich E, Pavoni E, Acquavita A, Loredo J (2020) Mercury and arsenic mobility in resuspended contaminated estuarine sediments (Asturias, Spain): a laboratory-based study. Sci Tot Environ 744: 140870, doi: 10.1016/j.scitotenv.2020.140870

Gu YG, Jiang SJ, Jordan RW, Huang HH, Wu FX (2023) Nonmetric multidimensional scaling and probabilistic ecological risk assessment of trace metals in surface sediments of Daya Bay (China) using diffusive gradients in thin films. Sci. Total Environ. 867, 161433, doi: 10.1016/j.scitotenv.2023.161433

Huang JY, Franklin H, Teasdale PR, Burford MA, Kankanamge NR, Bennett WW, Welsh DT (2019) Comparison of DET, DGT and conventional porewater extractions for determining nutrient profiles and cycling in stream sediments. Environ. Sci. Process. Impacts 21 (12), 2128–2140, doi: 10.1039/c9em00312f

Kim EH, Mason RP, Porter ET, Soulen HL (2006) The impact of resuspension on sediment mercury dynamics, and methylmercury production and fate: A mesocosm study. Mar Chem 102(3–4): 300–315, doi: 10.1016/j.marchem.2006.05.006

Rauret G, López-Sánchez JF, Sahuquillo A, Rubio R, Davidson C, Ureb A, Quevauvillerc P (1999) Improvement of the BCR three step sequential extraction procedure prior to the certification of new sediment and soil reference materials. J Environ Monitor 1:57–61, doi: 10.1039/A807854H

Taylor AC, Fones GR, Mills GA (2020) Trends in the use of passive sampling for monitoring polar pesticides in water. Trends Environ. Anal. Chem. 27, e00096, doi: 10.1016/j.teac.2020.e00096

US EPA, 2022. Freshwater Sediment Screening Benchmarks. https://www.epa.gov/risk/freshwater-sediment-screening-benchmarks.

Practical Guidance for Adjusting Rainfall Annual Exceedance Probability Estimates for Climate Change

Scott Jackson[1], Colin Fraser[2], Okan Aygün[3]

[1,2,3]*Lorax Environmental Services Ltd., 305 – 1770 W 7th Avenue Vancouver, British Columbia, Canada, V6J 4Y6. Scott.Jackson@lorax.ca. ORCID 0009-0002-8387-8478*

Abstract

Mine water management infrastructure is commonly designed to pass or retain runoff resulting from a design rainfall event. The annual exceedance probabilities for these events are developed using a historical record of extreme rainfall. Extreme rainfall events are increasing in magnitude globally at a non-linear rate of approximately 7%/degree Celsius, consistent with the Clausius-Clapeyron relationship. This trend is expected to continue with projected climate change and may lead to water management upset conditions if not properly accounted for in design criteria calculations. This paper provides guidance to aid practitioners in addressing this developing issue.

Keywords: Climate change, rainfall, annual exceedance probabilities, risk management, mine water management

Introduction

The likely range of human caused warming from 1850–1900 to 2010–2019 is between 0.8 °C and 1.3 °C, with a globally averaged increase in precipitation since 1950, and a faster rate of increase since 1980 (IPCC, 2023). The globally averaged 20th and early 21st century rate of increase in annual maximum daily rainfall intensity is estimated to be 5.9 to 7.7% per °C of average near-surface atmospheric temperature warming (Westra *et al.*, 2013a), with higher rates of increase noted in the high latitudes of the Northern Hemisphere and the tropics, and lower rates in the arid mid-latitudes.

The intensity of high-magnitude rainfall events is a function of the moisture content of an air mass (*i.e.*, precipitable water), which in turn is a function of the air mass temperature. This relationship can be described by the Clausius-Clapeyron (CC) equation, which shows the moisture capacity of air will increase by approximately 5–8% for each 1 °C increase in temperature, depending on the baseline air temperature value. Specifically, the CC equation [Equation 1] expresses the saturation pressure of water vapour as a function of atmospheric pressure, where:

$$\ln\left(\frac{P_1}{P_2}\right) = \frac{\Delta H_{vap}}{R}\left(\frac{1}{T_2} - \frac{1}{T_1}\right) \qquad \text{[Equation 1]}$$

- P_1 and P_2 are vapour pressures (in standard atmospheres) at temperatures T_1 and T_2;
- ΔH_{vap} is the enthalpy of vapourization (40.7 kJ mol^{-1});
- R is the gas constant (8.3145 J mol^{-1} K^{-1});
- T_2 is equal to the vapour pressure of water (1.0 atmosphere or 1013.25 mb) at the boiling point (373 K (100°C); and,
- T_1 is set to the temperature for which the vapour pressure is to be calculated.

In general terms, the CC equation returns an exponential rise in vapour pressure with increasing air temperatures (Fig. 1), which means that with future warming, extreme precipitation events may be expected to increase in a non-linear fashion and could be higher for rarer events. Such projected increases will vary at regional scales depending on the amount of regional warming, changes in atmospheric circulation, and storm dynamics (Seneviratne *et al.*, 2021). This has relevance to the design and operation of both existing and proposed mine water management infrastructure, which are commonly designed to handle runoff events that fall within the historical rainfall distribution based on annual exceedance probabilities (AEPs; e.g., 1:100-year 24-hour rainfall event).

Derivation of rainfall AEPs for current conditions are subject to several sources of uncertainty, including:

- Underrepresented spatial variability and magnitude of rainfall due to sparse monitoring networks in most regions, particularly for highly localized convective storms;
- Under catch due to wind effects and undersized gauge orifices, and relatively short-duration climate record lengths;
- Application of statistical distributions to represent high-magnitude events, particularly those located on the tails of the distributions, where representative samples from the monitoring records are limited or unavailable; and,
- A chaotic climate system exhibiting natural (internal) variability, which is intrinsic to the climate system and therefore irreducible.

Consideration of projected climate change adds further uncertainty regarding rainfall AEPs, as a changing climate may lead to changes in storm dynamics and shifts in synoptic storm tracks (e.g., atmospheric rivers, hurricanes), and therefore local rainfall distributions that deviate from historical conditions.

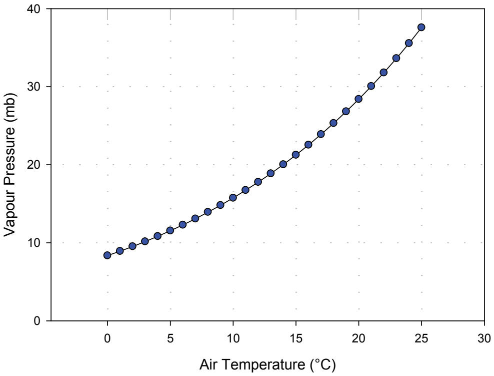

Figure 1 *Clausius-Clapeyron relationship.*

Global standards or accepted research methodology to determine how future extreme rainfall events of less than 1-day in duration may change in frequency and intensity over local areas are lacking (CSA, 2019). Furthermore, General Circulation Models (GCMs) are currently unable to fully resolve local scale convective processes and synoptic scale systems that lead to extreme precipitation and therefore, estimates of short duration rainfall derived from recent GCM outputs (at time of writing) are not reliable (Li *et al*., 2019). Recent attempts to estimate Probable Maximum Precipitation amounts for < 1-day duration using modelling approaches have shown promise (e.g., Hiraga *et al*., 2025), however the intensive data and modelling requirements are often not practical for use in developing inputs to mine water management infrastructure design.

The guidance outlined herein aims to address the gap between current state of knowledge with respect to the relationship between air temperature increases and precipitation event magnitude, and current approaches to developing rainfall AEP estimates, while providing practitioners a means to scale these estimates for a range of potential climate change outcomes.

Methods

There are three primary components to this guidance (Fig. 2):

1. Evaluate the original AEPs that an existing piece of infrastructure was designed to and determine whether the AEPs are appropriate for continued use.
2. Confirm the design life of the infrastructure in question.
    - If the design life < 10 years, apply an AEP scalar based on a +1 °C air temperature increase above the reference period; and,
    - If design life > 10 years, conduct a standard risk assessment for the infrastructure in question, using a probability: consequence matrix, and developing AEP scalars as outlined below.
3. Estimate future AEPs for relevant time scales and emissions scenarios.
    - Conduct a risk assessment for current conditions;

- Characterize site-specific changes to climate regime (historical and projected);
- Select a climate change emission scenario for scalar development;
- Apply climate change scalars to precipitation AEPs; and,
- Review of triggers for additional or future assessment.

The first step is the evaluation of both the original AEP estimates that the infrastructure of interest was designed to handle, and if available, current AEP estimates for the site. This should be completed by a qualified practitioner and ideally, should take into consideration all available site and regional climate data, industry best practices, technical guidance and relevant regulatory standards. If relevant to the site of interest, high-magnitude snowmelt events and the potential for overlap with extreme rainfall events should also be quantified. Next, a review of site-specific trends in air temperature, precipitation, and relevant changes in local synoptic patterns, including storm track changes, duration, and rainfall magnitude should be undertaken to provide a baseline understanding of changes already occurring.

Once the above evaluation steps are completed, a determination of the infrastructure design life should be made. Given that projected increases in air temperature and air moisture capacity are expected to progress throughout the next century (Seneviratne *et al.*, 2021), the magnitude of derived rainfall scalars are expected to increase under all emissions scenarios over the next several decades. As a result, determination of the expected design life is foundational to the recommended approach to developing rainfall AEP scalars. In summary, the longer the design life, the greater the uncertainty in climate change projections, and therefore higher emissions scenario projections are recommended for use in these circumstances.

Given the relatively low variation in projected temperature changes between emissions scenarios over the next 10-years (out to approx. 2040), a simplified approach is recommended whereby a +1 °C air temperature increase from the reference period is assumed, with scalars developed using this temperature change as input to the CC equation (Fig. 2).

If the design life is greater than 10 years, then a risk assessment is recommended to be conducted, taking into consideration the cumulative probability of exceedance (PoE) of a given rainfall AEP over the full design life (n in Equation 2).

$\mathrm{PoE} = 1 - (1 - AEP)n$ [Equation 2]

Accordingly, the cumulative probability of exceedance increases with each successive year of operation, such that the likelihood of failure may become relatively high, should the works be in use for a long period of time. The PoE can be applied within a risk matrix to determine the Likelihood of an event occurring (Tab. 1), which can then be cross-referenced against the consequence of infrastructure failure resulting from a rainfall event exceeding design criteria.

For example, a structure with a design life of 25 years designed to a 1:100-year event would have an expected 22% PoE over a 25-year operational period, returning a Likelihood of Unlikely (Tab. 1). The association between Likelihood and PoE is based upon standard risk assessment practices and probabilities of occurrence.

Once the risk categorization has been completed, the next step is to select the emissions scenario to be used for developing the AEP scalars. Emissions scenario selection is based upon both the design life and risk categorization for the infrastructure in question (Fig. 2).

Forward looking projections of future climate outcomes are generated using GCMs, which are driven by greenhouse gas forcings. These forcings are based upon scenarios that envision various Shared Socioeconomic Pathways (SSPs). These emissions pathways begin in 2015 and are summarized below for the scenarios recommended for use in this guidance:

- SSP2-4.5: Intermediate greenhouse gas emissions, with CO_2 emissions remaining around current levels until mid-century, then decreasing;
- SSP4-6.0: Higher emissions than SSP-4.5, with CO_2 emissions peaking in 2050 and declining thereafter;

Table 1 Likelihood and Cumulative Probability of Exceedance.

Likelihood	Cumulative Probability of Exceedance
Almost Certain	≥ 95%
Likely	≥ 75% to < 95%
Possible	≥ 25% to < 75%
Unlikely	≥ 5% to < 25%
Highly Unlikely	≥ 0.1% to < 5%
Extremely Remote	< 0.1%

- SSP3-7.0: High greenhouse gas emissions, with CO_2 emissions doubling from current levels by 2100; and,
- SSP5-8.5: Very high greenhouse gas emissions, with CO_2 emissions doubling from current levels by 2050.

These SSPs translate to projected global average temperature increases of 1.5 °C over the near term (all SSPs; 2021–2040), a range of 1.6 to 2.4 °C over the mid-term (2041–2060), and a range of 1.4 °C to 4.4 °C over

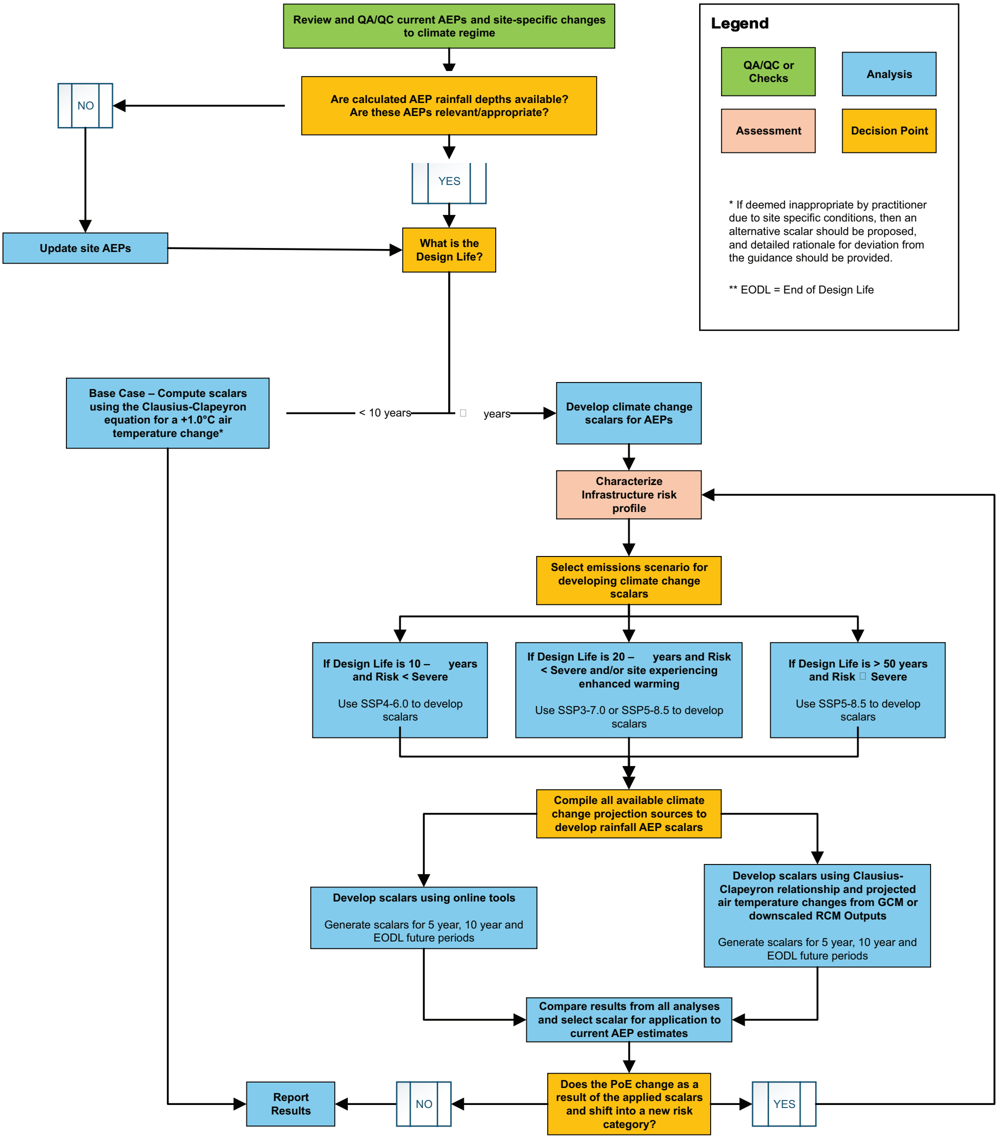

Figure 2 *Decision tree showing assessment process for scaling rainfall annual exceedance probability estimates for projected climate change based on the infrastructure design life.*

the long-term (2081–2100). These projected temperature increases are directly linked to the atmospheric moisture capacity, as defined by the CC equation.

Minimal difference in the projected global temperature change by 2050 is expected between emissions scenarios, but beyond this point, divergence between scenarios becomes pronounced. By the end of this century, the projected global temperature increase is approximately 2.8 °C for the SSP2-4.5 scenario, and 4.7 °C for the SSP5-8.5 scenario. Therefore, the recommended conservative approach to selecting emissions scenarios is based primarily on the design life of the structure. A shorter design life is linked to lower emissions scenarios, and a longer design life (i.e., > 20 years) linked to higher emissions scenarios (Fig. 2). In cases where the design life is > 50 years, the SSP5-8.5 scenario is recommended outright, in alignment with the guidance in ECCC (2020).

Once the emissions scenario has been selected, rainfall AEP scalars are derived using the following methods:

1. Using downscaled projection data for the study region supplied in online tools (if available); and,
2. Applying the Clausius-Clapeyron equation to local estimates of air temperature change.

It is assumed that the practitioner will apply professional judgement when assessing the utility of available online tools. If no downscaled products providing climate change scaled estimates of precipitation are available for the study area, then the current AEPs can be adjusted using the air temperature change projections and the CC relation as a conservative, physically based approach. The CC equation is applied to calculate the potential vapour pressure of an air mass at a given temperature, which is directly proportional to the precipitation depths that air mass can generate. This is recommended to be done for the current reference period, and for the future periods that scalars are required for (generally for the 5-year, 10-year and end of design life periods). Once these vapour pressure potential values have been generated, a scalar can be developed by:

$$Climate\ Scalar = \frac{Future\ Vapour\ Pressure\ Potential}{Current\ Vapour\ Pressure\ Potential} \qquad \text{[Equation 3]}$$

This approach should also be taken as a check on scalars derived from online products. Once this has been done, the practitioner should compare the results from all analyses (e.g., online tools, CC equation) and select the most appropriate scalar values to be applied to the current AEP estimates.

After the current AEPs have been scaled for projected climate change under the selected emissions scenario, a final check should be conducted to determine whether the updated AEPs shift the Likelihood into a higher category (Tab. 1) and therefore have the potential to increase the assessed risk profile for the infrastructure (Fig. 2).

The state of knowledge surrounding climate change induced increases in extreme rainfall is continually evolving. Similarly, mine sites and associated water management infrastructure are in a constant state of flux. Accordingly, the following events should be considered as triggers for revisiting the rainfall scalar assessment:

- An increase in structure design life of > 10 years;
- Future IPCC assessment reports provide significantly different (i.e., higher) temperature delta predictions;
- An update to the risk assessment matrix used in the analysis or underlying components; and,
- The occurrence of one or more significant rainfall event(s) that alters the underlying frequency distribution, and therefore the current AEP estimates.

Conclusions

It is likely that rainfall AEPs developed using historical data will not be representative of future conditions as the global climate continues to warm. Given the importance of these values for the safe design and operation of mine water management infrastructure, it is critical that a science-based methodology be employed to develop robust estimates of future rainfall magnitude.

A methodology is presented herein to guide practitioners through the process of developing future scalars for rainfall AEPs based on infrastructure design life considerations, standard risk assessment practices, climate change projections from the International Panel on Climate Change's Sixth Assessment Report, and the well-established relationship between air temperature, moisture capacity and extreme rainfall depths.

Acknowledgments

The authors thank all co-organisers for hosting the IMWA 2025 Conference and the opportunity to present this paper.

References

Canadian Standards Association (CSA) (2019). CSA PLUS 4013:19 Technical Guide: Development, interpretation, and use of rainfall intensity-duration-frequency (IDF) information: Guideline for Canadian water resources practitioners. September 2019. 126 pp.

Hiraga, Y., Tahara, R., and Meza. J. (2025). A methodology to estimate Probable Maximum Precipitation (PMP) under climate change using a numerical weather model. Journal of Hydrology. 652. doi.org/10.1016/j.jhydrol.2024.132659

IPCC. (2023). Summary for Policymakers. In: Climate Change 2023: Synthesis Report. Contribution of Working Groups I, II and III to the Sixth Assessment Report of the Intergovernmental Panel on Climate Change [Core Writing Team, H. Lee and J. Romero (eds.)]. IPCC, Geneva, Switzerland, pp. 1–34, doi: 10.59327/IPCC/AR6-9789291691647.001

Li, C., Zwiers, F., Zhang, X., & Li, G. (2019). How much information is required to well constrain local estimates of future precipitation extremes? Earth's Future, 7. https://doi.org/10.1029/2018EF001001

Seneviratne, S.I., X. Zhang, M. Adnan, W. Badi, C. Dereczynski, A. Di Luca, S. Ghosh, I. Iskandar, J. Kossin, S. Lewis, F. Otto, I. Pinto, M. Satoh, S.M. Vicente-Serrano, M. Wehner, and B. Zhou. (2021). Weather and Climate Extreme Events in a Changing Climate. In Climate Change 2021: The Physical Science Basis. Contribution of Working Group I to the Sixth Assessment Report of the Intergovernmental Panel on Climate Change [Masson-Delmotte, V., P. Zhai, A. Pirani, S.L. Connors, C. Péan, S. Berger, N. Caud, Y. Chen, L. Goldfarb, M.I. Gomis, M. Huang, K. Leitzell, E. Lonnoy, J.B.R. Matthews, T.K. Maycock, T. Waterfield, O. Yelekçi, R. Yu, and B. Zhou (eds.)]. Cambridge University Press, Cambridge, United Kingdom and New York, NY, USA, pp. 1513–1766, doi:10.1017/9781009157896.013

Westra, S., L. V. Alexander, and F. W. Zwiers (2013). Global increasing trends in annual maximum daily precipitation, J. Clim., 26, 3904–3918.

Treatment of AMD Liming Sludge for Metals Recovery and Mining Site Rehabilitation

J. Jacob[1], D. Pino-Herrera[1], E. Plat[1]

[1]BRGM, F-45060 Orléans, France, j.jacob@brgm.fr

Abstract

Acid mine drainage treatment by liming generates sludge that accumulates over time and may contain valuable metal concentrations high enough to justify recovery. This study explores a remediation and valorization process for AMD sludge from a former mining site in France. Selective leaching with H2SO4 recovered over 80% of Cu and Zn, followed by selective precipitation with Na2S to produce metal concentrates. While the process is technically viable and can be economically feasible, residual Zn levels in the sludge hinder off-site valorization and waste management remains an issue. Further research should focus on improving the management of the remaining matrix, either by stabilizing it, identifying off-site applications compatible with its composition, or developing processes to separate clean gypsum from the residual material.

Keywords: AMD, liming, rehabilitation, recovery

Introduction

Acid mine drainage (AMD) is a major environmental challenge that can persist for centuries (Tabelin *et al*. 2019). However, AMD can also contain valuable metals, making metal recovery an attractive but often difficult objective due to the typically low flow rates and/or low metal concentrations in these effluents. As highlighted by Plumlee *et al*. (1999), higher acidity in the treated effluent is positively correlated with increased metal concentrations in the water, particularly for Cu, Zn, Ni, and Mn. Lime treatment is one of the most widely used methods for AMD treatment worldwide (Skousen *et al*. 2014). This process effectively neutralizes acidity and precipitates metals, but it also generates sludge composed primarily of gypsum, which can accumulate over time and reach large volumes.

In this study, we focus on a remediation and valorization process targeting AMD lime treatment sludge that has accumulated over decades. Instead of addressing metal recovery directly from AMD or from freshly produced sludge, our approach aims to process an existing sludge deposit in a single, bigger short-term treatment campaign. This allows for the efficient extraction of valuable metals while also addressing the long-term environmental challenges posed by the sludge storage.

Mine site description

The old Chessy mine is located near Lyon in France. It was active from 1414 to 1877, first for copper exploitation, then for sulfuric acid production (Bayle *et al*. 2003). The ore deposit is characterized by a stockwork of barite, galena, sphalerite, and chalcopyrite hosted within altered soda-dacitic lavas. An acid mine drainage has been discharging from a water adit for an unknown but distant period. Its average characteristics (n = 134) are as follows: flow rate of 7.2 m^3/h, pH 2.7, and concentrations of Al at 50 mg/L, Cu at 32 mg/L, Fe at 255 mg/L, SO_4 at 2339 mg/L, and Zn at 210 mg/L. Lime treatment of the AMD began in the mid-19th century and continues to this day. The sludge generated over more than 150 years of treatment has been stockpiled on-site. Fig. 1 shows the sludge dump along with the locations of six core samples drilled up to 8 m deep.

Twenty-two samples coming from the core samples were analysed by alkaline fusion and ICP-AES. The sludge mainly contain; Al at 1.8%, Si at 1.6%, Ca at 17.0% Fe at 12.2%, SO_4 at 31.9% Zn at 5.1%, Cu at 1.3%, Cd at 107 mg/kg. Moisture content at 105 °C was 59.8%. The size of the sludge deposits was estimated using GIS software, incorporating data from various sources, including bibliographic references (maps from different periods, settling pond cleaning reports, etc.), an elevation model, and the depths of six sludge core samples. The total sludge volume was estimated at 77,000 m^3, equivalent to approximately 154,000 tonnes. The mine site is managed by the department for mine safety and risk prevention of BRGM (DPSM) on behalf of the State.

Methods

Selective leaching

Leaching experiences of Chessy liming sludge were done first in 250-mL shake flasks at low-solid content, then in 2L stirred reactor. Sulfuric acid was used as a sole leaching agent. A broad range of key leaching parameters were studied: solid/liquid ratio from 0.7 to $20\%_{m/m}$, acid/solid ratio from 40 to 650 g_{acid}/kg_{solid}, temperature 22 °C to 60 °C and leaching time from 6h to 48h. The main goal was to maximize Cu, Zn and Cd dissolution yield and consequently to minimize the concentration of these metals in the residue. For metal concentration measurements, about 2 mL of pulp were filtrated at 0.45 µm and diluted ten times using 1% HNO_3 and placed at 4 °C. Metal concentrations (Al, Cu, Fe and Zn) were then measured on the filtrate with a 4210 MP-AES (microwave plasma atomic emission spectroscopy) from Agilent Technologies and used to calculate dissolution yields. Cadmium was analysed by AAS (SpectrAA–220FS, Varian). The detailed methodology and results of the leaching optimization are detailed in Jacob *et al.* (2025).

Finally, a 20L stirred reactor was used to produce enough pregnant leach solution (PLS) for selective precipitation tests. Operating parameters of this operation were solid load $20\%_{m/m}$, temperature 22°C, leaching time 24h, acid concentration 143 g_{acid}/kg_{solid} and an agitation speed of 300 rpm.

Selective precipitation

The methodology for selective precipitation was developed through small-scale tests and subsequently validated using 16.7 L of PLS to produce sufficient amount of the different precipitates for characterization. All precipitation steps were performed in a 20-L stirred tank reactor operating at 300 rpm, with a reaction time of approximately 10 minutes per step. The selective precipitation protocol began with the addition of a fixed quantity of Na2S, in a 1:1 stoichiometric ratio to the Cu concentration in the PLS, to precipitate copper sulfide, which was separated by filtration. For Cd and Al precipitation, another dose of Na_2S, in a 1:1 stoichiometric ratio to the Cd concentration, was added, followed by NaOH addition to adjust the pH to 4.5, and the resulting precipitate was filtered. Finally, the pH was raised to 9.0 with NaOH to precipitate zinc hydroxide. The precipitates were filtered using Whatman® GF/A glass microfiber filters. All precipitates were dried

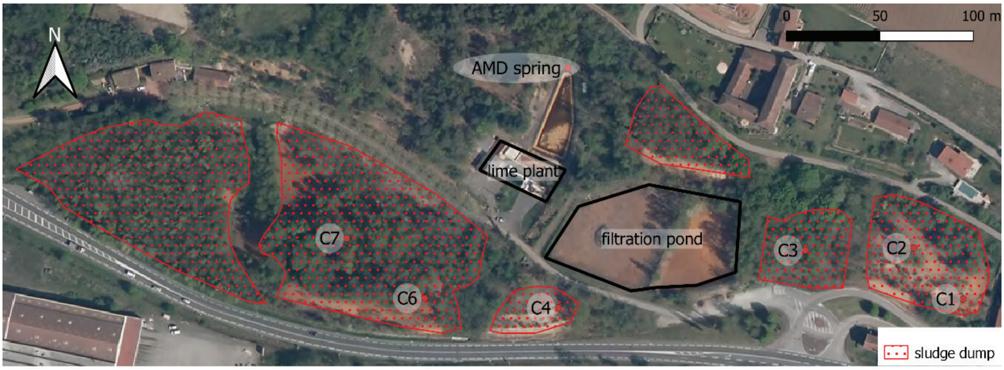

***Figure 1** Sludge dump and core sampling locations on the mining site.*

at 40 °C without prior washing of the filter cakes. Due to the difficulty of filtering the zinc hydroxide precipitate, it was recovered using semi-continuous centrifugation at 8000 rpm (Avanti JXN-26, Beckman Coulter).

Results

Selective leaching

Leaching tests conducted in the 20-L reactor under relatively optimized conditions yielded promising results. The resulting PLS was at pH 3.0 and contained 1.4 g/L of Cu, 8.7 g/L of Zn, 17 mg/L of Cd, and 937 mg/L of Al, while Fe remained below detection limits. The leaching efficiencies achieved were 65.2% for Cu, 80.3% for Zn, 85% for Cd, and 11.3% for Al. The residual solids contained 0.4% Cu, 1.0% Zn, and 20 mg/kg of Cd.

Overall results of the whole test plan indicate that this process enables the leaching of over 80% of Cu and Zn from the sludge under optimal conditions, with a solid content of 5–15% and an acid dosage of 150–200 g H_2SO_4 per kg at room temperature. Increasing the acid concentration beyond this range provides only marginal improvements in dissolution rates but greatly increases acid consumption due to the dissolution of iron, leading to a loss of selectivity. Acid/solid ratio is the most important parameter of the process. Under these economically optimal conditions, the Cu, Zn and Cd contents in the residue after leaching are around 0.2%, 0.8% and < 15 mg/kg respectively.

Selective precipitation

In terms of recovery efficiency relative to the PLS composition, 97% of the Cu was recovered in the Cu concentrate, with the remaining 3% retained in the Al/Cd waste. For Zn, 84% was recovered in the Zn concentrate, while 13% co-precipitated in the Cu concentrate, and 3% ended up in the Al/Cd waste. These results demonstrate the overall efficiency of the selective precipitation process but also underline the need for optimization, particularly in zinc recovery. The purity of Cu and Zn products were assessed against target specifications provided by two potential buyers to determine their marketability as concentrates (Fig. 2).

The Cu concentrate contained 38% Cu, 4% Zn, and 122 mg/kg Cd, meeting the objective of at least 30% Cu and less than 200 mg/kg Cd. The other major components were sulfates (23%) and sulfides (18%). The loss on ignition at 1025 °C was 39%, primarily due to the thermal decomposition of copper sulfates and sulfides. XRD analysis (supplementary

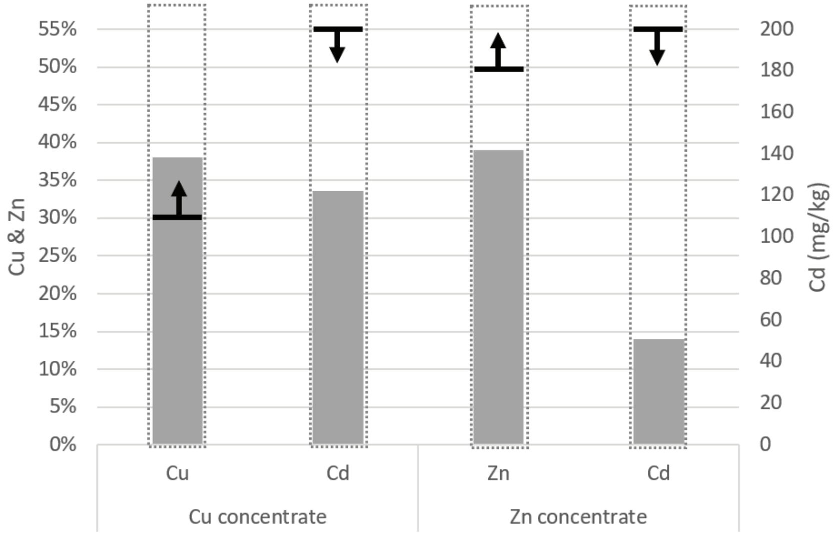

__Figure 2__ Cu, Zn, and Cd concentrations in concentrate compared to target values. The arrows indicate threshold requirements: Cu and Zn concentrations must meet or exceed the target, while Cd concentrations must remain below the target.

material S1) showed that the sulfate fraction mainly consisted of hydrated and anhydrous copper sulfates, including chalcanthite ($Cu(SO_4)(H_2O)_5$), poitevinite ($Cu(SO_4)(H_2O)$), and brochantite ($Cu_4(SO_4)(OH)_6$).

The Zn concentrate contained 39% Zn and 51 mg/kg Cd, compared to the target of 50% Zn and less than 200 mg/kg Cd. It is therefore necessary to increase the purity of the concentrate. The other major components were sulfates (29%) and Na (10%). Loss on ignition at 1025 °C of 27%, was likely due to sulfate thermal decomposition. A notable observation during the large-scale (20 L) selective precipitation experiment was the behavior of the recovered zinc hydroxide during drying. When dried at 40°C, it lost 90% of its mass, highlighting its high initial water content and the associated challenges in filtration and handling. XRD analysis (supplementary material S2) revealed a complex mineralogy with poorly crystallized phases, making it difficult to precisely identify all present compounds. However, the analysis confirmed the presence of thenardite (Na_2SO_4) and suggested the likely presence of phases similar to sodium sulfite (Na_2SO_3) and hydrated zinc hydroxy-sulfate ($ZnSO_4 \cdot 3Zn(OH)_2 \cdot 4H_2O$).

The Al/Cd waste contained 0.3% Cu, 4.6% Zn, 0.26% Cd, 24% S, 14% Al, and 5% Si, with a loss on ignition at 1025 °C of 49%.

The main challenges of the precipitation steps are related to the Zn concentrate, which does not fully meet our purity objective and is also difficult to filter, necessitating energy-intensive centrifugation and extensive drying. Potential improvements to the selective precipitation step include precipitating zinc as sulfide using Na2S, which is likely easier to filter, washable, and less hydrated, and separating Al and Cd to optimize waste management costs. Recycling the rinse water in the selective leaching and selective precipitation process could also help recover dissolved Cu and Zn and improve the overall recovery rates.

Preliminary Economic Evaluation

A preliminary economic assessment of the process was conducted, assuming the complete treatment of the accumulated sludge (154,000 t at 40% moisture) according to the flowsheet presented in Fig. 3. The evaluation considered the leaching, and precipitation yields of Cu and Zn, as well as their concentrations in the recovered concentrates, under the assumption that Zn is precipitated as sulfide.

The calculation of metal sales prices was based on smelter terms, including payable percentages, deductions, and treatment charges set by Nyrstar for Zn and Boliden for Cu, using publicly available data from their websites. Metal prices were averaged over the period 2018–2023 based on historical Cu and Zn prices from the London Metal Exchange (LME).

Operating expenses (OPEX) included the costs of reagents and the operation of reactors, filters, and excavators, estimated using the CostMine© (2019) estimation guide. Capital

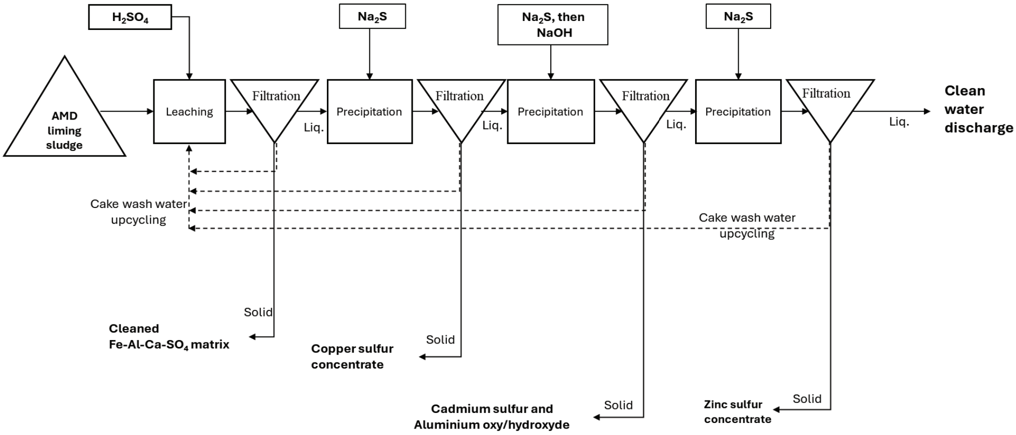

Figure 3 *Process flowsheet for selective leaching and precipitation of Cu, Zn, and Cd from AMD liming sludge.*

expenses (CAPEX) were calculated based on the cost of major equipment (reactor tanks, agitation systems, filters) evaluated using CostMine© (2019). Additional CAPEX components, such as installation and erection, steelworks and structures, civil works, piping, electrics, instrumentation, insurance, and freight, were accounted for using Lang's factor method.

The evaluation was conducted under the assumption of on-site treatment with leaching performed at 10% solid content. Four scenarios were considered, combining two different operational durations (1 and 2 years) and two leaching techniques: conventional stirred-tank reactor (CSTR) leaching and pond leaching inspired by Guezennec *et al.* (2023).

The results of the preliminary economic assessment are presented in Table 1. Changing the operational duration has little effect on OPEX, as reagent costs constitute the majority of operational expenses. The project remains relatively small, both in terms of duration and financial scale, especially when compared to typical mining industry standards. Depending on the scenario, uncertainties, and fluctuations in metal prices, the profitability of the operation is not guaranteed. However, beyond its economic viability, this project should also be considered as a mine site remediation operation.

Waste management

Waste management remains the most substantial challenge of this project. Despite a substantial reduction in Cu, Zn, and Cd concentrations, the post-leaching matrix still qualifies as hazardous waste under current French regulations. Attempts to find off-site valorization options – particularly in cement production or plaster manufacturing due to the high gypsum content – have so far been unsuccessful, mainly due to residual Zn concentrations remaining too high (0.8%).

The site continues to accumulate sludge, and although it will not reach full capacity for several years, a long-term solution must be identified. The disposal of newly generated sludge in hazardous waste storage facilities would represent a heavy financial burden for public authorities. Moreover, the mass of metals removed from the site through the valorization process (Cu, Zn, Al, Cd) is minimal compared to the overall mass of the remaining Fe-Al-Ca-SO_4 matrix.

At this point and based on our experience, the most viable remediation strategy probably involves covering the sludge to isolate it from the environment. Additionally, exploring alternative water treatment technologies that generate less waste and/or produce residues that are more easily valorized should be a priority for future research. A key aspect of these treatments would be the selective precipitation of valuable and/or hazardous elements, and inert matrix components.

Conclusions

This study demonstrates the feasibility of selectively leaching and precipitating Cu and Zn from AMD lime treatment sludge accumulated over decades. The results show that over 80% of Cu and Zn can be efficiently recovered through an optimized leaching process while maintaining selectivity by minimizing Fe and Al dissolution. The subsequent selective precipitation process achieved high recovery rates for Cu and Zn, although precipitating zinc as sulfide using Na_2S would be necessary to enhance the purity of the Zn concentrate and improve its filtration properties.

***Table 1** Preliminary Economic Evaluation.*

Treatment	Total CAPEX (k€)	Total OPEX (k€)	Metal sales (k€)	ROI
1 year & CSTR	≈ 4 300	≈ 7 800	≈ 13 200	≈ 14%
1 year & pond leaching	≈ 2 900	≈ 7 800	≈ 13 200	≈ 37%
2 years & CSTR	≈ 2 100	≈ 7 800	≈ 13 200	≈ 80%
2 years & pond leaching	≈ 1 500	≈ 7 800	≈ 13 200	≈ 117%

Despite the successful metal recovery, the management of the residual sludge remains a challenge. While the process substantially reduces Cu, Zn, and Cd concentrations in the solid residues, the final material still qualifies as hazardous waste under current French regulations. Attempts to valorize the matrix off-site were unsuccessful mainly due to residual Zn concentrations exceeding acceptable thresholds. Given the ongoing accumulation of sludge at the site, a long-term remediation strategy must be identified. This could include covering the existing waste with a geomembrane and/or a thick layer of clean topsoil as well as replacing the existing lime plant with a more efficient technology, such as sulfate-reducing bioreactor that generates denser waste and enable selective metal precipitation.

Beyond the specific case of this site, this study highlights a broader opportunity: AMD treatment sludges accumulate over long time represent an anthropogenic ore, where valuable metals concentrate. Similar deposits exist worldwide (Aubé & Zinck, 1999), suggesting that this approach could be applied to other AMD lime treatment residues and potentially to other water treatment technologies, such as sulfate-reducing bioreactors or Dispersed Alkaline Substrate for rare earth (Ayora *et al.*, 2016).

In an era where environmental priorities are being challenged worldwide, developing AMD treatment strategies that facilitate waste valorization—by leveraging the long-term accumulation of valuable metals in sludge—could make these essential environmental obligations more sustainable.

Acknowledgements

Financial support for this study was provided by BRGM's Department for Mine Safety and Risk Prevention (DPSM) within the framework of its mission as delegated post-mining operator on behalf of the French state.

References

Aubé BC, Zinck JM (1999) Comparison of AMD treatment processes and their impact on sludge characteristics. In proceedings for Sudbury (Vol. 99, pp. 261–270)

Ayora C, Macías F, Torres E, Lozano A, Carrero S, Nieto JM, Castillo-Michel H (2016) Recovery of rare earth elements and yttrium from passive-remediation systems of acid mine drainage. Environmental science & technology, 50(15), 8255–8262

Bayle LD, (2003). Mines et minéraux de Chessy (Rhône). Le Règne minéral. Hors Série IX. Éditions du Piat

CostMine. (2019). Mine and Mill Equipment Cost Calculator. Spokane Valley, WA, InfoMine USA, Inc.

Guezennec AG, Hubau A, Pino-Herrera D, Heikkinen V, Dew D, Falagan C, Mines P (2023) Pilot-scale demonstrations of innovative biohydrometallurgy for sustainable valorisation of mining waste: main outcomes from H2020-NEMO project Biomining 2023

Jacob J, Pino-Herrera D, Greffié C, Wille G, Plat E (2025) Reprocessing of the waste produced during acid mine drainage lime Comptes Rendus, Chimie 27(S4), 1-18

Lardeau M, (1987). Mineralogie et petrogenese du minerai sulfure du gisement volcano-sedimentaire a zn-cu-ba-(pb-ag) de chessy-les-mines (rhone): application a l'etude des amas sulfures metamorphises (Doctoral dissertation, Orléans)

Plumlee GS, Smith KS, Montour MR, Ficklin WH, Mosier EL (1997) Geologic controls on the composition of natural waters and mine waters draining diverse mineral-deposit types. The Environmental Geochemistry of Mineral Deposits: Part A: Processes, Techniques, and Health Issues Part B: Case Studies and Research Topics

Skousen J, (2014) Overview of acid mine drainage treatment with chemicals. Acid mine drainage, rock drainage, and acid sulfate soils: Causes, assessment, prediction, prevention, and remediation, 325–337

Tabelin C, Sasaki A, Igarashi T, Tomiyama S, Villacorte-Tabelin M, Ito M, Hiroyoshi N (2019) Prediction of acid mine drainage formation and zinc migration in the tailings dam of a closed mine, and possible countermeasures. In MATEC Web of Conferences (Vol. 268, p. 06003). EDP Sciences

Probabilistic Analysis of Human Health Risks Linked to Procambarus Clarkii Consumption in Almaden Hg Mining District

Judith L. Jaeger[1], José I. Barquero[1], Samantha T. Jiménez-Oyola[2], Feliciano M. Bacale[1],
Efrén García-Ordiales[3], Pablo L. Higueras[1]

[1]*Instituto de Geología Aplicada, Universidad de Castilla-La Mancha. Pl. Manuel Meca,*
1. 13400 Almadén (Ciudad Real), Spain

[2]*Escuela Superior Politécnica del Litoral, ESPOL, Facultad de Ingeniería en Ciencias de La Tierra,*
Campus Gustavo Galindo km 30.5 vía Perimetral, P.O. Box 09-01-5863, Guayaquil, Ecuador

[3]*Centro universitario de Investigación del agua (CUIDA), Escuela Politécnica de Mieres.*
C/ Gonzalo Gutiérrez Quiros s/n. 33600 Mieres

Abstract

The American crayfish (*Procambarus clarkii*) is considered a bioindicator of Potentially Toxic Elements (As, Hg, Cd, Pb, Cu, Zn, and Sb); on this basis, this study aims to assess the human health risk associated with its consumption by the local population in the Almadén mercury mining district, in terms of Hazard Quotient and Cancer Risk. A probabilistic Bayesian approach was applied based on the concentrations of each PTE in the sampled crayfish and survey data collected from the local population. The results show that consumption of crayfish represents a health risk, mainly due to its As, Hg and Sb content.

Keywords: Bayesian probabilistic approach, mercury pollution, bioaccumulation, food safety, human health risk, potentially toxic elements

Introduction

The Almadén Mercury Mining District (AMMD), located in Spain, has been historically impacted by intense mercury mining activities. These impacts have been exacerbated by inadequate mine closure practices, leading to widespread contamination of soil, water, sediments, and biota with potentially toxic elements (PTEs) such as mercury (Hg), arsenic (As), and cadmium (Cd) (Higueras *et al*., 2016; Jiménez-Oyola *et al*., 2020; Barquero *et al*., 2023). This contamination poses significant ecological and human health risks, particularly for populations living in proximity to the mining district.

Among the various exposure pathways, dietary intake of contaminated aquatic species has emerged as a critical concern. In the AMMD, the freshwater crayfish Procambarus clarkii is frequently consumed by the local population. This species is known for its high capacity to bioaccumulate PTEs, especially mercury, in its tissues (Anandkumar *et al*., 2020). While several studies have assessed environmental contamination in the region, there is a notable lack of research evaluating the health risks associated with the consumption of bioindicator species such as *Procambarus clarkii*, particularly in historically contaminated mining environments.

This study aims to assess both carcinogenic and non-carcinogenic human health risks in adults associated with the consumption of abdominal muscle (AbM) from Procambarus clarkii in the AMMD. To address this objective, a Bayesian probabilistic framework is employed. Bayesian statistics provide a robust method for incorporating uncertainty and prior knowledge into the analysis of environmental health risks. Based on Bayes' theorem, this approach allows the estimation of the probability of health outcomes while correcting for potential errors or limitations in empirical data (Wu *et al*., 2014). Importantly, it is especially suitable for cases where sample sizes are limited, as it enables the integration of prior information to enhance the reliability of results (Aven and Eidesen, 2007).

In this study, probabilistic distributions were assigned to both the concentrations of PTEs measured in crayfish tissues and the exposure parameters obtained from surveys conducted among the local population. These distributions were constructed by combining in situ data with well-established probability density functions (PDFs) from the scientific literature (Iribarren *et al.*, 2009). This framework was used to estimate key health risk metrics, including the Hazard Quotient (HQ), Cancer Risk (CR), Hazard Index (HI), and Total Cancer Risk (TCR) for each sampling point.

The results contribute to a deeper understanding of the long-term environmental and public health implications of historical mining activities in the AMMD. Furthermore, the findings highlight the value of *Procambarus clarkii* as a reliable bioindicator species, providing a basis for future monitoring programs and environmental health assessments in similarly impacted regions.

Methods

The study area was located along a stretch of the Valdeazogues River and its tributaries within the AMMD area in Ciudad Real, Spain. A total of 10 sites (S1, S2, S3, S4, S5, S6, S7, S8, S9, and S10) were sampled.

A total of 300 *Procambarus clarkii* specimens were collected. The crayfish were rinsed with Milli-Q water and stored in airtight polyethylene bags. Upon arrival at the laboratory, they were euthanized by hypothermia.

After a minimum of one week, the crayfish were dissected using a stainless-steel dissection kit to extract the AbM. The extracted tissues were weighed to calculate parameters for the Hazard Quotient (HQ). They were then freeze-dried using a Telstar Cryodos apparatus (at 0.1 mbar and approximately -50 °C). The dried samples were powdered and homogenized with a KINEMATICA Microtron MB 800 B blade mill for further analysis.

The AbM samples were analyzed using Energy Dispersive X-ray Fluorescence (ED-XRF) to determine the concentrations of Potentially Toxic Elements (PTEs), including

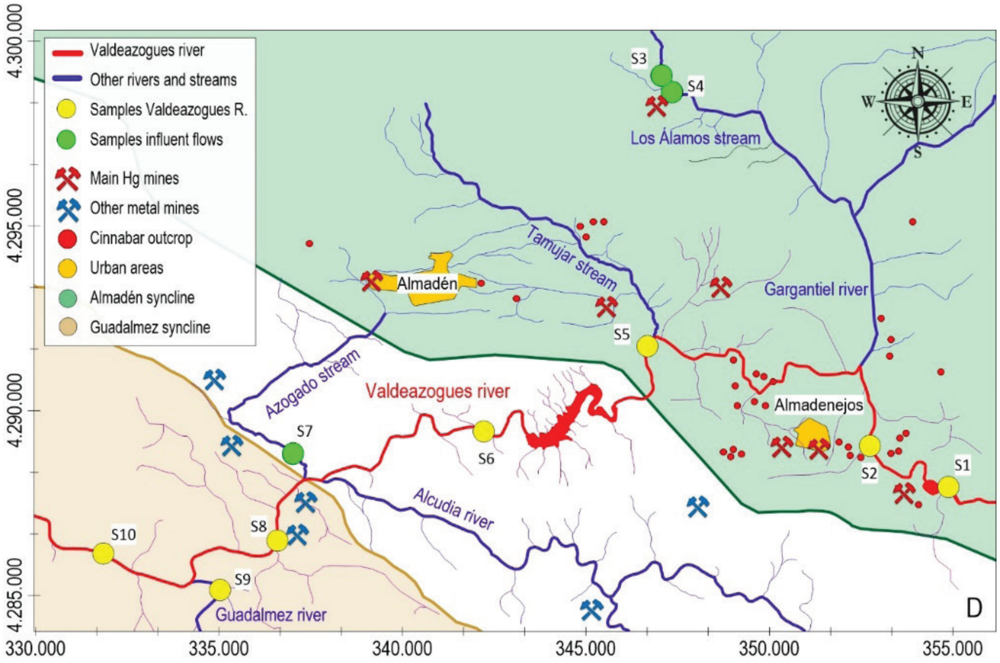

Figure 1 *Location of the sampling sites, main mines and Hg outcrops.*

As, Cd, Pb, Cu, Zn, and Sb. Additionally, total mercury (HgT) concentration was quantified using Zeeman-corrected atomic absorption spectrometry (Sholupov and Ganeyev, 1995).

A structured survey was administered to the adult local population, following the privacy policy of Spain, to gather key exposure parameters, including body weight (BW), exposure frequency (EF), ingestion rate (IR), and exposure duration (ED). These variables are essential for characterizing the population in the context of human health risk assessment.

In order to perform the risk assessment, it has been done the estimation of the absorbed dose (ADD: mg kg^{-1} day^{-1}) which was estimated using the equation:

$$\mathrm{ADD} = \frac{\mathrm{C} \times \mathrm{EF} \times \mathrm{IR} \times \mathrm{ED}}{\mathrm{AT} \times \mathrm{BW}} \tag{1}$$

Where C is the concentration (mg kg^{-1}), EF is the exposure frequency (days year^{-1}), IR is the ingestion rate (kg day^{-1}), ED is the exposure duration (years), AT is the average exposure time (365 days × 30 years for non-carcinogenic or 365 days × 70 years for carcinogenic risk assessment) and BW is the body weight (kg).

The non-carcinogenic (HQ) and carcinogenic risk (CR) were calculated according to equation 2 and 3, respectively.

$$\mathrm{HQ} = \frac{\mathrm{ADD}}{\mathrm{RfD}} \tag{2}$$

$$\mathrm{CR} = \mathrm{ADD} \times \mathrm{SF} \tag{3}$$

The oral reference dose (RfD) and the slope factor (SF) were obtained from the Risk Assessment Information System Website (RAIS, 2020). RfD: 0.0003 mg kg^{-1} for As, 0.001 mg kg^{-1} for Cd, 0.04 mg kg^{-1} for Cu, 0.0001 mg kg^{-1} for Hg, 0.004 mg kg^{-1} for Pb, 0.0004 mg kg^{-1} for Sb and 0.3 mg kg^{-1} for Zn. And the SF: 1.5 mg kg^{-1} day^{-1} for As and 0.0085 mg kg^{-1} day^{-1} for Pb.

Finally, the cumulative non carcinogenic risk, expressed as the Hazard Index (HI), has been calculated ($\mathrm{HI}=\Sigma \mathrm{HQ}_i$). Similarly, the Total Carcinogenic Risk (TCR) has been estimated ($\mathrm{TCR}=\Sigma \mathrm{CR}_i$). The acceptable threshold values are 1 for HI and 1E-05 for the TCR. (USEPA 2004a, 2001)

The probabilistic distributions used in the risk assessment were selected based on previous documentation and expert opinion. Additionally, EasyFit 5.5 software was used

Table 1 *Probabilistic distributions and their priors used for each parameter.*

Parameters	Distributions
C_{As}, C_{Cd}, C_{Hg}, C_{Pb}, C_{Sb}	LogNormal (muC, tauC)
	C = LogNormal (0, 0.1)
	tauC = Gamma (1.0E-04, 1.0E-04)
C_{Cu}, C_{Zn}	Gamma (alpha, beta)
	alpha = Gamma (1, 1)
	beta = Gamma (1, 1)
IR	Normal (muIr, tauIr)
	Ir = Normal (0, 0.1)
	tauIr = Gamma (0.07, 1.0E-04)
BW	Normal (muBw, tauBw)
	Bw = Normal (1, 1)
	tauIR = Gamma (2, 1)
EF	Beta (a, b)
	a = Normal (5, 1.0E-04)
	b = Normal (5, 1.0E-04)

to determine the best-fit distributions for collected data. The distributions and priors used for each parameter are found in Table 1. The probabilistic modelling was conducted in RStudio using the RJags package, obtaining 1000 values for each parameter (Jiménez-Oyola *et al*., 2021).

Results and discussion

The metal concentrations detected at the sampling points are summarized in Table 2. Since measurements were taken on a dry weight basis, and assuming a water content of 70% for all analyzed samples, appropriate adjustments were made. Zn and Cu exhibited the highest concentrations, as they are essential elements required in trace amounts by organisms (Anadkumar *et al*., 2020). In contrast, more than 50% of the samples exceeded the legal limit for Hg, Pb, and Cd (0.5 mg kg^{-1}, fresh weight), as established by the European Union (UE 2023/915, 2023).

As shown in the Fig. 2a, the HQ_{As} and HQ_{Sb} exceeds the acceptable limit of 1 at 97.5 percentile and HQ_{Hg} at 75 percentile. HQ_{Cu} also exceeds the limit in the 99.8 percentile. As regards the carcinogenic risk, the CR_{As} exceeds the permissible value of 1.E-05 (USEPA 2004a) in the 75 percentile, while Pb doesn't represents a carcingenic risk as it doesn't exceed this value (Fig. b). These results indicates that the consumption of crayfish in the Almadén mercury mining district may represent a risk for consumers.

As shown in Table 3, the HI exceeds the permissible value of 1 at each sampling site. In the case of the carcinogenic risk, all the sampling points also surpasses the limit for TCR of 1E-05.

Although all values exceed the maximum permissible limit, each site can be categorized into three levels based on HI values: low (1 to 2), medium (2 to 3), and high (≥3). Specimens from sampling site S3 exhibits the lowest HI value, placing it within the low-level category, probably because it's a point of non-influence, upstream Las Cuevas mine. Sampling sites S1, S2, S5, S6, S8, and S9 fall within the medium level, while sites S4, S7, and S10 are classified as high-level sites, all of them downstream a mining affected zone.

Among the high-HI sites, S7 (Arroyo Azogado) receives wastewater from nearby towns and runoff from the Almadén Hg mine, which likely contributes to its elevated HI value. Similarly, site S10 (Presa Mendoza) is located downstream the main mining zones; acting like a barrier as it receives water from the DMMA and the Alcudia Valley.

Among the medium-HI sites, S2 collects water draining from El Entredicho mine, potentially leading to a significant influx of As and Hg into the Valdeazogues River at this location. Unlike S7, which is affected by the Almadén Mercury mine—a site with historical metallurgical activity—S2 is influenced solely by El Entredicho mine, where no metallurgy was present. The S5 site, on the other hand, is influenced by two distinct sources: treated wastewater from the town of Almadén and runoff from the industrial area of the same town; this combination of inputs may explain its classification within the medium-HI range.

A significant difference in HI and TCR values can also be observed between sites S3 and S4, with S3 located upstream of Las Cuevas mine and S4 downstream of it. This contrast highlights the strong influence of

Table 2 *Metal concentrations of the sampled points (mg kg^{-1}, f.w.)*

	Minimum	p50	Mean	p97.5	Maximum
As	0.46	2.11	2.45	6.44	7.46
Cd	0.21	0.70		1.84	1.89
Cu	50.85	112.37	125.50	219.59	227.71
Hg	0.48	1.02	1.22	2.47	2.50
Pb	0.28	0.70		2.95	3.15
Sb	1.61	5.53	5.76	9.34	10.33
Zn	91.91	253.75	261.37	332.57	355.63

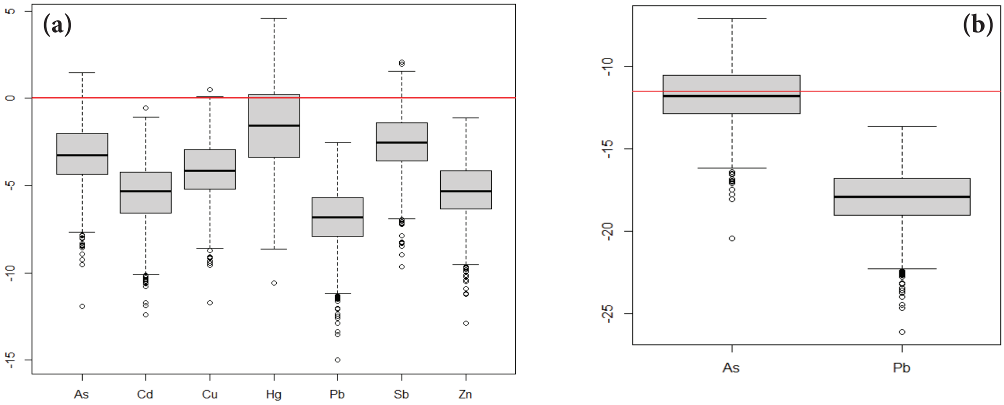

Figure 2 Boxplot of the (a) Hazard Quotient and (b) Cancer Risk (values in logarithm scale). The red line represents the safe exposure threshold.

Table 3 Values of the HQ, CR, HI, and TCR for each PTE and sampling site.

Sampling Site	HQ							HI	CR		TCR
	As	Cd	Cu	Hg	Pb	Sb	Zn		As	Pb	
S1	0.47	0.06	0.13	0.46	0.03	1.06	0.06	2.27	9.10E-05	3.66E-07	9.13E-05
S2	0.22	0.09	0.14	1.23	0.01	1.06	0.06	2.81	4.18E-05	1.69E-07	4.19E-05
S3	0.22	0.02	0.14	0.53	0.02	0.48	0.03	1.45	4.18E-05	3.16E-07	4.21E-05
S4	0.61	0.06	0.34	1.59	0.01	0.91	0.05	3.56	1.17E-04	1.69E-07	1.17E-04
S5	0.38	0.09	0.17	0.80	0.01	1.23	0.07	2.75	7.31E-05	1.41E-07	7.32E-05
S6	0.43	0.06	0.21	0.58	0.02	0.73	0.05	2.07	8.20E-05	2.20E-07	8.22E-05
S7	0.46	0.03	0.31	0.97	0.01	1.23	0.07	3.08	8.95E-05	1.30E-07	8.96E-05
S8	0.68	0.05	0.18	0.43	0.02	1.30	0.06	2.73	1.32E-04	3.55E-07	1.32E-04
S9	0.61	0.06	0.14	0.35	0.02	0.89	0.06	2.13	1.18E-04	2.65E-07	1.19E-04
S10	1.34	0.06	0.31	1.15	0.02	0.65	0.07	3.59	2.59E-04	2.76E-07	2.59E-04

abandoned mines on the aquatic ecosystem in the region and, consequently, their potential implications on human health through the trophic chain.

Conclusions

The findings suggest that consumption of crayfish sampled in the context of the AMMD pose a health risk, primarily due to their As, Hg and Sb content. Arsenic contributes to a cancer and non-cancer risk at all sampling sites. On the other hand, Hg and Sb are the main contributors to non-cancer risk. This finding suggests that sediments in the crayfish habitat may contain elevated levels of these PTEs.

The primary driver of human health risks associated with crayfish consumption through the food chain appears to be the large number of abandoned mines in the region. Due to inadequate closure, these sites continue to influence the aquatic ecosystem, particularly downstream of the mines, where the highest HI and TCR levels are recorded.

Upstream sampling points exceed the maximum permissible limit for HI, indicating that although pollution levels are lower in these areas, they remain significant. This contamination is likely influenced by both anthropogenic and geogenic sources within the exploitation zone.

References

Anandkumar A, Li J, Prabakaran K, Jia ZX, Leng Z, Nagarajan R, Du D (2020) Accumulation of toxic elements in an invasive crayfish species (Procambarus clarkii) and its health risk assessment to humans. J Food Compos Anal 88:103449. doi:10.1016/j.jfca.2020.103449

Aven, T., Eidesen, K., 2007. A predictive Bayesian approach to risk analysis in health care. BMC Med. Res. Methodol. 7, 1–8. https://doi.org/10.1186/1471-2288-7-38.

Barquero JI, Hidalgo JJ, Esbrí JM, Higueras PL, García-Ordiales E (2023) A Preliminary Assessment of Mercury, Methylmercury, and Other Potentially Toxic Elements in Largemouth Bass (Micropterus salmoides) from the Almadén Mining District. Environ Geochem Health. doi:10.1007/s10653-024-02326-3

European Parliament and Council of the European Union (2023). Regulation (EU) 2023/915 of 25 April 2023 on maximum levels of certain contaminants in foodstuffs and repealing Regulation (EC) No 1881/2006. Official Journal of the European Union, L 119, 103–111. https://doi.org/10.2875/469065

Higueras PL, Amorós JA, Esbrí JM, Pérez-de-los-Reyes C, López-Berdonces MA, García-Navarro FJ (2016) Mercury transfer from soil to olive trees: A comparison of three different contaminated sites. Environ Sci Pollut Res 23(7):6055–6061. doi:10.1007/s11356-015-4357-2

Iribarren I, Chacón E, De Miguel E (2009) A Bayesian approach to probabilistic risk assessment in municipal playgrounds in Madrid, Spain. Arch Environ Contam Toxicol 56(1):165–172. doi:10.1007/s00244-008-9161-2

Jiménez-Oyola S, García-Martínez MJ, Ortega MF, Bolonio D, Rodríguez C, Esbrí JM, Llamas JF, Higueras P (2020) Multi-pathway human exposure risk assessment using Bayesian modeling at the historically largest mercury mining district. Ecotoxicol Environ Saf 201. doi:10.1016/j.ecoenv.2020.110833

Jiménez-Oyola S, García-Martínez MJ, Ortega MF, Chávez E, Romero P, García-Garizábal I, Bolonio D, García-Martínez F (2021) Probabilistic multi-pathway human health risk assessment due to heavy metal(loid)s in a traditional gold mining area in Ecuador. Ecotoxicol Environ Saf 224 doi:10.1016/j.ecoenv.2021.112629

RAIS, 2020. Toxicity profiles. Risk Assessment Information System. URL: http://rais.ornl.gov

Sholupov SE, Ganeyev AA (1995) Zeeman atomic absorption spectrometry using high frequency modulated light polarization. Spectrochim Acta B 50(10):1227–1236. doi:10.1016/0584-8547(95)01316-7

USEPA, 2001. Risk Assessment Guidance for Superfund (RAGS) Volume III (Part A). Process for Conducting Probabilistic Risk Assessment. Washington, DC.

USEPA, 2004a. What you need to know about mercury in fish and shellfish.

Wu, J., Long, S. C., Das, D., & Dorner, S. M. (2014). Integrating quantitative PCR and Bayesian statistics in quantifying microbial risk. Science of the Total Environment, 468–469, 479–488. https://doi.org/10.1016/j.scitotenv.2013.08.071

Recovery of Sands from Gold Mining Tailings for Clinker Manufacture

Natalia Jaramillo[1]; Óscar Jaime Restrepo[1]; Antonio Luis Marqués [2]; Begoña Fernández[3]; Julia Ayala[3]

[1]Universidade Nacional de Colombia, Facultad de Minas, njaramilloz@unal.edu.co

[1]Universidad Nacional de Colombia, ojrestre@unal.edu.co ORCID 0000-0003-3944-93

[2]Institute of Space Sciences and Technologies of Asturias (ICTEA), University of Oviedo, Independencia 13, 33004 Oviedo, Asturias, Spain, marquesantonio@uniovi.es, ORCID 0000-0003-4665-4491

[3]University of Oviedo, Gonzalo Gutierrez Quirós, 33600 Mieres, Asturias, Spain, fernandezbegona@uniovi.es, ORCID 0000-0003-1239-4839

[3]University of Oviedo, Gonzalo Gutierrez Quirós, 33600 Mieres, Asturias, Spain, jayala@uniovi.es, ORCID 0000-0002-6404-1296

Abstract

Gold mining in Antioquia, Colombia, is prominent, especially in Bajo Cauca and Nordeste. This study, a collaboration between the National University of Colombia and the University of Oviedo, used materials from the "El Molino" plant. It aimed to optimize gold mining sands for clinker manufacture by identifying waste parameters affecting production, determining optimal raw material proportions using Bogue's moduli, and comparing the mechanical performance of cement from mining waste with conventional Portland cement. Results indicated the necessity of thermal pre-treatment to reduce contaminants and highlighted the high energy input required for effective silica reaction.

Keywords: Mining waste, clinker, circular economy, environment

Introduction

Mining operations have been identified as a significant source of environmental liabilities, defined as abandoned mining activities (Yurupari, 2003; Cruzado-Tafur *et al.*, 2021). The inadequate management of these liabilities is associated with the generation of acid drainage, which can be detected between 2 and 5 years after the commencement of mining operations (Abiahu, 2019).

In the context of gold mining, these liabilities, otherwise known as tailings, are constituted of a mixture of crushed rock and processing fluids from mills and concentrators (Kossoff, 2014). It is noteworthy that these tailings frequently contain elevated concentrations of toxic elements and compounds, including cadmium, copper, zinc, lead and chromium (Abiahu, 2019; Okereafor, 2020).

The properties of these waste materials vary according to the protolith from which they originate, but they generally exhibit high angularity and abundance of grains with sizes between 0.625 mm and 2.0 mm, and variable densities between 2.5 g/cm³ and 2.6 g/cm³ (Kossoff, 2014). Mineralogically, they are classified into three groups: gangue (mainly quartz and plagioclase), sulfides (such as pyrite, pyrrhotite and arsenopyrite) and secondary minerals formed by interaction in the depositional medium. The waste-to-concentrate production ratio is high, sometimes around 200:1, and can increase as the market price of metal rises (Lottermorser, 2010; Kossoff, 2014).

A number of studies have explored potential new applications for these by-products. However, the process of obtaining gold follows a linear design where the ore is beneficiated and the residue is discarded or stored in dams, sometimes used as backfill material without adequate knowledge of its physical, chemical and mineralogical characteristics (Kossoff, 2014). This has resulted in these tailings being considered as inefficient materials, with a low impact on waste reduction

In Colombia, gold mining is active in approximately 17 departments and 80 municipalities across diverse scales (Casallas & Martinez, 2014). In 2023, the department of Antioquia ranked as the leading gold producer, with the municipalities of Caucasia and Buriticá reporting gold yields of 9,365.7 kg and 6,501.9 kg, respectively (UPME, 2024). This suggests that Antioquia, as the largest gold producer in the country, has a significant amount of mining waste in its territory.

Cement production requires a carefully balanced chemical composition in the raw mix to ensure optimal clinker mineralogy and performance. The main components – lime, silica, alumina, and iron oxide – must be present in specific ratios to form desirable phases such as alite and belite. However, naturally occurring raw materials often lack this ideal composition, particularly in terms of reactive silica and alumina contents. Considering that the raw materials for cement production are not chemically ideal, it is necessary to add corrective materials. These include silica-rich materials such as quartzites and quartz sandstones, although softer minerals or amorphous silica like opal are preferred due to their higher reactivity during sintering (Tobón & López, 2007). Mining waste has potential for clinker production due to its high silica content and significant amounts of iron and alumina, which are essential components for clinker manufacturing.

This study, a collaborative endeavor between the National University of Colombia and the University of Oviedo, explores the utilization of mining waste from the 'El Molino' facility for the fabrication of clinker. The objective is to propose a sustainable alternative for the management of gold mining waste in the region, in alignment with the 2030 Sustainable Development Goals and the principles of the circular economy

Materials and Methods

Materials

The material used in this research corresponded to samples taken from the gold mining waste storage ponds at the ‘El Molino’ processing plant. The plant is located in the rural area of the village of Santa Rita, located 10 km northwest of the municipality of Andes in the department of Antioquia – Colombia (Fig. 1).

Artisanal miners in the area travel to the plant to process the material extracted from the mines. The concentrate is marketed and the tailings from the process are stored in storage yards within the plant. Finally, the tailings from the artisanal miners' beneficiation process that was stockpiled become the raw material for processing at the “El Molino” beneficiation plant.

Sampling points were randomly selected and with the help of a sampling shovel, approximately15 kilograms of material was extracted and packed in bags. XRD, XRF and SEM were used for characterization.

X-Ray Diffraction (XRD)

The XRD test confirmed the presence of quartz, plagioclase and magnetite. A content of micas such as Illite and Muscovite was also detected (Fig. 2).

***Figure 1** El Molino Mine.*

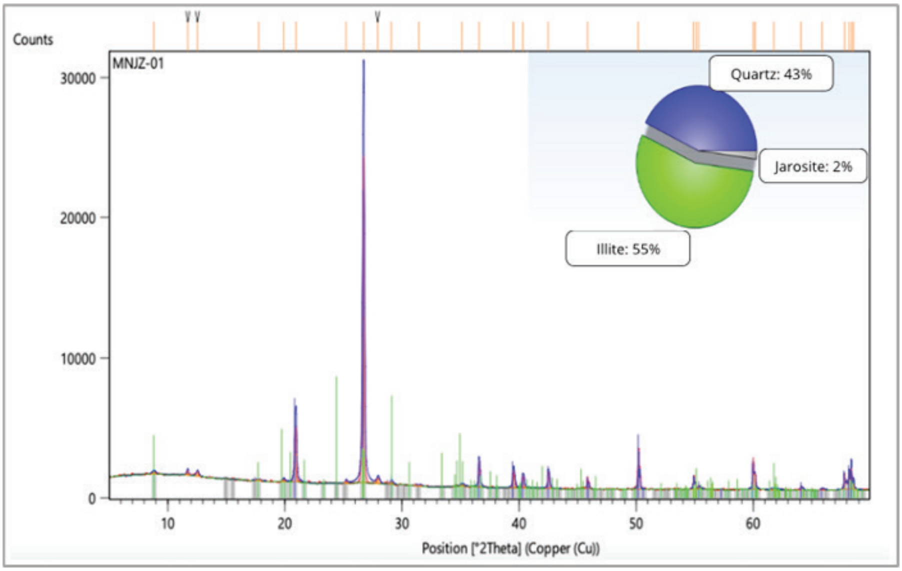

Figure 2 *Diffractogram of the mining residue.*

Table 1 *XRF results of the mining waste.*

	Mg	Al	Si	P	S	Cl	K	Ca	Ti	Mn	Fe	Cu	Zn	As	V
%	6,49	11,71	57,97	0,86	4,31	0,25	1,94	0,55	0,518	0,03	11,25	0,04	0,17	2,45	0,03

Scanning Electron Microscopy (SEM)

Scanning electron microscopy (SEM) confirmed the presence of quartz, arsenic and sulfur in the form of pyrite and arsenopyrite. The quartz grains (QZ) were identified surrounded by arsenopyrite (As).

The complementary raw material for clinker production came from different sources located in Asturias. The calcite was supplied by the La Belonga mine located in the city of Oviedo, the silica sand was obtained from the company 'Sílices La Cuesta' where it is used for glass production and the alumina from the company 'Arciresa', Arcillas Refractarias S.A. located in Lugo de Llanera. These raw materials were all characterised by their high purity.

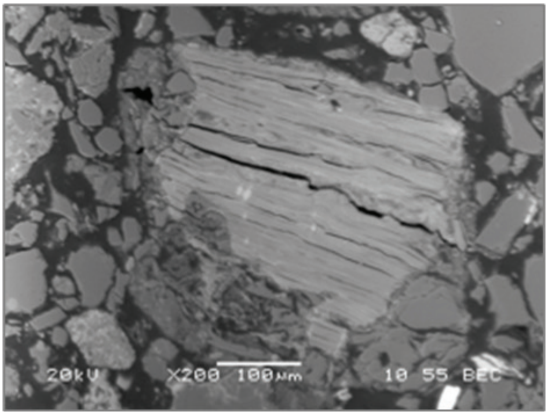

Figure 3 *Micrograph of the waste particles.*

Element	Weight%	Atomic%
O K	36.21	56.82
Mg K	3.10	3.20
Al K	9.09	8.46
Si K	17.83	15.94
Cl K	0.25	0.18
K K	0.88	0.57
Ti K	2.26	1.18
Fe K	30.38	13.66
Totals	100.00	

Table 2 Contribution to clinker meal from gold mining waste sands.

CaO (%)	Al_2O_3	Fe_2O_3	SiO_2
0,1	0.0	94.7	5.2

Table 3 Dosage of complementary materials to clinker meal.

Calcite (g)	Alumina (g)	Silica (g)	Sand (g)
0,1	0.0	94.7	5.2
MH (%)	**MS (%)**	**MA (%)**	**LFS (%)**
1.9	1.6	1.2	90.85

Method:

Using Boggue's method for the calculation of the dosage of the raw materials in the manufacture of Clinker, the calculations of the necessary dosages of both the mining waste Table 2 and the rest of the material necessary to reach the values required to obtain the Clinker with the modules presented in Table 3.

After the compression of the tablets with the prepared mixture, the specimens were subjected to different heating ramps from room temperature with a ramp of 10 °C per minute until they reached maximum temperature and were kept at this constant temperature for 45 minutes. After this time, the clinked specimen was removed from the furnace. The maximum temperatures used were 1250 °C and 1300 °C.

Results

After the clinkering tests, the sample did not reach a complete reaction at 1250°C, as granules and pores of different sizes and colors were found inside the sample without showing homogeneity of the firing and therefore in the final coloring. Fig. 4a

Similarly, the product shown in Fig. 4b showed a darker color due to the interaction of the raw materials in the sintering process in the kiln, however, some unreacted particles were still observed, which led to an additional test with a ramp to ensure the decarbonation process of the flour.

As a result of testing the sample with the stepped ramp at a maximum temperature of 1300°C, the product shown in Fig. 4c was obtained, which exhibits a more intense brown color, less unreacted granules and a higher reaction of the components. For the step ramp, the equipment was programmed with a ramp of 10 °C per minute until 800 °C was reached. At this temperature remained constant for 30 minutes and at the end of this time it was increased again at 10 °C per minute until it reached a maximum temperature of 1300 °C, remaining constant for 45 minutes.

Each of the products obtained from the sintering process in the linear heating ramps at 1250 °C and 1300 °C, as well as the product from the stepped ramp at 1300 °C, were characterized by XRD and SEM in the equipment of the University of Oviedo in order to verify in greater detail the formation of the mineral phases of the clinker.

Figure 4 Specimens obtained at 1250 °C (a), 1300 °C linear (b) and 1300 °C staggered (c).

Table 4 XRD identification.

Phase name	Identification COD	Identified 2θ peaks	2θ correlated reference peaks
Heating ramp to 1250 °C			
Larnite	96-901-2790	32,6017° y 32,0288°	32,598° y 32,075°
Gehlenite	96-101-1003	31,3307° y 29,0424	31,347° y 29,061°
Calcite	96-900-9668	29,390° y 47,1236°	29,390° y 47,092°
Merwinite	96-900-0286	33,4894°	33,409° y 33,568°
Heating ramp to 1300 °C			
Larnite	96-901-2790	32,1361° y 32,6338°	32,598° y 32,075°
Gehlenite	96-900-6114	31,3702° y 29,1217°	31,347° y 29,061°
Merwinite	96-900-0286	33,4978°	33,409° y 33,568°
Heating ramp to 1300 °C Stepped			
Larnite	96-901-2790	32,6345° y 32,1475°	32,598 y 32,170
Gehlenite	96-900-6114	31,384° y 29,083°	31,347 y 29,061
Merwinite	96-900-0286	33,4953°	33,409° y 33,568°

Scanning Electron Microscopy (SEM)

On the matrix, there is a growth of grains with an approximate size of 1µm and a lighter color than the matrix, forming in some sectors agglomerations in the form of rosettes. The presence of gehlenite is observed in the form of well-defined needles with sizes between 1µm and 5µm, as well as cracks due to the cooling process.

Conclusions

This study addresses the possibility of reusing gold mining waste, a major environmental liability, for application as a raw material for clinker production. The study identified the critical parameters affecting clinker production, concluding that waste cannot fully replace raw materials and requires high purity supplements. Therefore, not all deposits are suitable; a complete mineral characterization of the waste to be used in each case is needed.

On the other hand, once the final clinker obtained has been studied, it is concluded that controlling the temperature, the amorphous phases and promoting the formation of belite during sintering could improve the properties of the final product.

This study highlights the potential of gold mining waste for clinker production, contributing to sustainable waste management and circular economy

References

Abiahu, C. F. (2019). Mine waste: sources, problems and mitigations. EPH – International Journal of Applied Science, 5, 3, 01–12. https://doi.org/10.53555/eijas.v5i3.112

Casallas, M., & Martinez, J. (2014). Panorama de la minería del oro en Colombia. Ploutos 5 (1): 20–26

Cruzado-Tafur, E., Torró, L., Bierla, K., Szpunar, J., & Tauler, E. (2021). Heavy metal contents in soils and native flora inventory at mining environmental liabilities in the Peruvian Andes. Journal of South American Earth Sciences. 106, 103107. https://doi.org/10.1016/j.jsames.2020.103107.

Kossoff, W. D.-E. (2014). Mine Tailings Dams: Characteristics, Failure, Enviromental Impacts, and Remediation. Applied Geochemistry, 51, 229–245. https://doi.org/10.1016/j.apgeochem.2014.09.010

Okereafor, U., Makhatha, M., Mekuto, L., & Mavumengwana, V. (2020). Gold mine tailings: A potential source of silica sand for glass making. Minerals, 10(5). 448. https://doi.org/10.3390/min10050448

Lottermoser, B. G. (2010). Mine Wastes: Characterization, Treatment and Environmental Impacts. Springer. 400p.

Tobón, J. I., & López, F. (2007). Replanteamiento de las ecuaciones de bogue en el cálculo mineralógico del clinker para una cemetera colombiana. Dyna, 74, 153:53–60.

Unidad de Planeación Minero-Energética UPME. (2024). Plan Estratégico de Tecnologías de la Información (PETI) 2024–2026. UPME. https://www.upme.gov.co/PETI_2024–2026.pdf

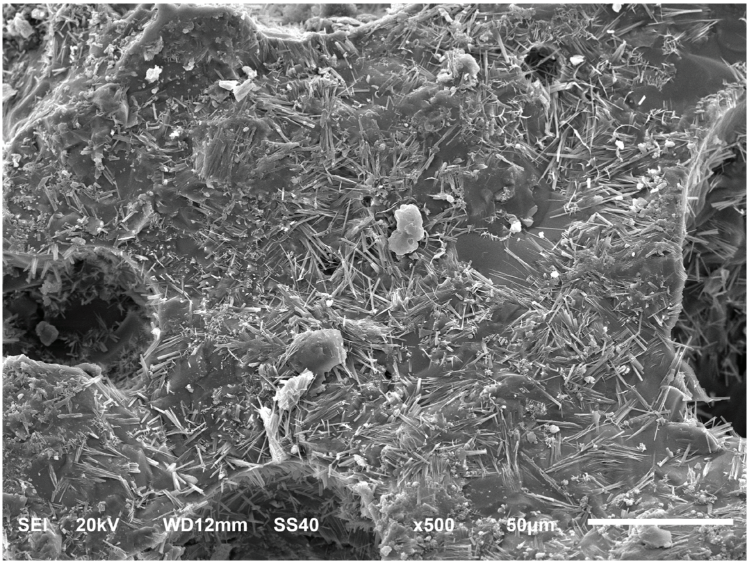

Figure 5 *Micro grains of gehlenite with belite in sintering product at 1300°C.*

Yupari, A. (2021). Pasivos ambientales mineros en Sudamérica. CEPAL, Servicio Nacional de Geología y Minería (SERNAGEOMIN), Instituto Federal de Geociencias y Recursos Naturales (BGR). https://1library.co/document/z1remoeq-informe-pasivos-ambientales-mineros-en-sudamerica.html

An Approach to Green Corrosion Inhibitors in Acid Mine Drainage (AMD)

Iván Jares[1], Efrén García[2], Luis González[1], Guillermo Laine[3], Juan José del Campo[1]

[1]*Instituto STEM MinesTech. Casa de las Artes y las Ciencias de Bueño s/n, 33171 Ribera de Arriba. Principado de Asturias, ivan.jares@gmail.com, luisgong@outlook.es, delcampo@cordes.es., ORCID 0009-0000-5849-3352*

[2]*University of Oviedo, Gonzalo Gutierrez Quirós, 33600 Mieres, Asturias, Spain, garciaefren@uniovi.es, ORCID 0000-0001-9138-7076*

[3]*University of Oviedo, Gonzalo Gutierrez Quirós, 33600 Mieres, Asturias, Spain, laineguillermo@uniovi.es, ORCID 0009-0002-8794-1630*

Abstract

Corrosion of metals and alloys represents a significant economic burden, accounting for approximately 3–4% of the annual GDP in developed countries, according to the European Commission. Among the various forms of corrosion, one of particular concern is that caused by acid mine drainage (AMD). Due to the thermodynamic instability of metals submerged in water, corrosion is inevitable. This phenomenon becomes even more critical in AMD-affected environments, where low pH and dissolved ions accelerate material degradation. Therefore, developing sustainable and cost-effective methods to mitigate AMD-induced corrosion is essential.

This study investigates the effectiveness of a green corrosion inhibitor derived from spent coffee grounds, in reducing the corrosion rate of mild steel exposed to AMD. The primary goal is to explore a low-cost, eco-friendly alternative to conventional inhibitors, aiming to enhance the durability of metallic infrastructure in mining and industrial settings. The research methodology involves weight-loss analysis of mild steel samples immersed in AMD, with and without the green inhibitor, to quantify its protective effect.

The results demonstrate a significant reduction in material degradation when the inhibitor is present, as it forms a protective film that shields the metal from direct interaction with the acidic environment. Compared to untreated samples, the inhibited specimens show a substantial decrease in weight loss, indicating improved corrosion resistance. This protective layer, attributed to organic compounds in the coffee waste, acts as a barrier against aggressive ions in AMD.

The findings of this study highlight the potential of waste-derived inhibitors as a viable solution for mitigating AMD-related corrosion. The practical implications extend to mining operations and industrial facilities where metallic structures and machinery are at risk of premature failure due to corrosive conditions. By enhancing the service life of steel components, this research contributes to reducing maintenance costs and promoting sustainable waste management practices.

This work underscores the feasibility of using green inhibitors for corrosion protection, paving the way for further exploration of organic waste-based solutions in industrial applications.

Keywords: Corrosion, steel, AMD, green inhibitors.

Introduction

Corrosion is a widespread problem that affects the durability of metal structures, leading to economic losses of 3–4% of the annual GDP in developed countries (Kumari *et al.*, 2025). Among the various forms of corrosion, one of the most severe is acid mine drainage (AMD)-induced corrosion, which occurs in mining environments where sulfide mineral oxidation generates acidic waters rich in sulfate and metal ions [09]. This low-pH environment significantly accelerates the degradation of metallic infrastructure, particularly mild steel, commonly used in industrial and mining applications (Miguel Sarmiento *et al.*, 2024).

To promote a corrosive process, it is mandatory the formation of an electrochemical cell which is composed of an anodic zone, a cathodic zone, an electrolyte and a metal (Jares Salguero *et al.*, 2024b). In a corrosion process, usually, the anodic reaction is the one show in Equation 1 (M is the corroded metal specie). However, the most common cathodic reactions (Eq. 2 aerated neutral or alkaline aqueous medium, Eq. 3 acid aerated aqueous medium, Eq. 4 acid medium) depends on the environmental conditions which are dependent on the pH (Pancorbo, 2010).

(Eq. 1) $M \leftrightarrow M^{n+} + ne^-$
(Eq. 2) $O_2 + H_2O + 4e^- \rightarrow 4OH^-$
(Eq. 3) $O_2 + 4H^+ + 4e^- \rightarrow 2H_2O$
(Eq. 4) $2H^+ + 2e^- \rightarrow H^2$

AMD is primarily caused by the oxidation of pyrite (FeS_2) in the presence of water and oxygen, leading to the formation of sulfuric acid and dissolved metal ions (Younger *et al.*, 2002):

(Eq. 5) $2FeS_2 + 7O_2 + 2H_2O \rightarrow 2Fe^{2+} + 4SO_4^{2-} + 4H^+$

These aggressive conditions promote pitting corrosion, stress corrosion cracking, and material failure in industrial equipment (Miguel Sarmiento *et al.*, 2024). Studies show that mild steel exposed to AMD experiences significant weight loss and tensile strength reduction, which can lead to catastrophic failures in mining infrastructure (Miguel Sarmiento *et al.*, 2024). Given the high economic and environmental costs, developing effective corrosion mitigation strategies is crucial (Ling *et al.*, 2024).

Given the highly corrosive nature of AMD environments, effective mitigation strategies are crucial. Traditionally, inorganic inhibitors such as chromates and phosphates have been widely used. However, due to their toxicity and environmental impact, regulatory restrictions have increase and research has shifted toward green alternatives, particularly plant-derived inhibitors (Kharbouch *et al.*, 2024). Organic inhibitors, including quinolinium derivatives and imidazole-based compounds, function by adsorbing onto metal surfaces and forming a protective barrier [11]. However, their high cost and potential bioaccumulation have driven interest toward green corrosion inhibitors derived from sustainable sources (Parangusan *et al.*, 2024).

Plant-based inhibitors have emerged as a promising alternative due to their biodegradability, low toxicity, and cost-effectiveness (Mungwari *et al.*, 2024). Many natural inhibitors contain polyphenols, flavonoids, and alkaloids, which adsorb onto metal surfaces and reduce corrosion rates (Mungwari *et al.*, 2024). Among biomass-based inhibitors, spent coffee grounds (SCG) have shown significant potential due to their high polyphenol and melanoidin content, which facilitates the formation of a protective film on mild steel (Elhady *et al.*, 2024).

Electrochemical studies demonstrate that coffee waste extracts can achieve up to 96% inhibition efficiency in acidic environments. Tafel polarization and electrochemical impedance spectroscopy (EIS) tests confirm that coffee waste reduces the double-layer capacitance (Cdl) and increases charge transfer resistance (Rct), indicating strong adsorption on the metal surface. Furthermore, using coffee waste as an inhibitor aligns with circular economy principles, reducing industrial waste while providing a low-cost corrosion control method (Elhady *et al.*, 2024).

This study evaluates the corrosion inhibition efficiency of coffee waste extract in AMD environments, identifying and evaluating its protective efficiency. By assessing weight-loss measurements, electrochemical behaviour, and inhibitor-film formation, this research aims to provide a sustainable alternative to conventional inhibitors, extending the lifespan of metallic structures in mining and industrial applications.

Materials and methods

In this study carbon steel coupons with the same composition and from the same piece were prepared. Those coupons were mechanically cut into 25 mm × 25 mm × 0.75 mm (±1). Then, they were polished with silicon carbide emery papers and commercial sandpapers of different granulometry, after cleaned with distilled water and finally dried in an airflow.

Based on earlier used procedures (Cordeiro *et al.*, 2018; Elhady *et al.*, 2024; Jares Salguero *et al.*, 2024a; Ramos *et al.*, 2019; Torres *et al.*, 2011), the extraction of spent coffee was used to perform the experiments. Aqueous extract of spent coffee was obtained by infusion method.

The present investigation was carried out using commercial coffee which was used for conventional extraction in an electric coffee maker. After the extraction, it is performed a re-extraction process harnessing 200mL of distilled water for each 100g of spent coffee. The infusion method involves boiling the coffee for 10 minutes, followed by filtration through a commercial coffee filter. Finally, the second and definitive aqueous extract is filtered with a Whatman filter of 20-25 µm.

***Table 1** Characterization of the Sao Domingos AMD.*

Parameter	Value
H	2,3
Al	241.000 µg/L
As	1.090 µg/L
Cu	25.700 µg/L
Fe	214 mg/L
Hg	<0,05 µg/L
Mg	86,8 mg/L
Mn	12.850 µg/L
Ni	512 µg/L
Pb	39,9 µg/L
U	6,22 µg/L

The extracts of spent coffee grounds were used as corrosion inhibitors for carbon steel in a Sao Domingos AMD. The sample was taken at the following coordinates: 631823 X, 4169012 Y.

Triplicate carbon steel coupons were fully immersed in the São Domingos AMD in the absence and presence of the green corrosion inhibitor based in aqueous spent coffee extracts at room temperature (20±2°C). The samples were placed in a static environment without agitation. For the experiment, they are prepared three borosilicate vessels with only 50 ml of the Sao Domingos AMD and other three additional borosilicate vessels with a solution prepared with 50 ml of AMD and 5 ml of green inhibitor. It should be noted thar the pH after the inhibitor addition does not vary, thus, the pH of both solution remains in 2,3.

Weight loss was determined using a scale with an accuracy of 0,02 mg. The efficiency of the inhibitor is determined by the following expression (Torres *et al.*, 2011):

$$\text{(Eq. 6)}\quad E\,[\%] = \frac{W_0 - W_i}{W_0}$$

Where W_0 and W_i are the weight loss in the absence and inhibitor presence respectively.

In order to evaluate significant figures, the mean of the three results obtained is the value used for the representation of each result.

Results

Fig. 2 presents the variation in corrosion rate for steel coupons exposed to AMD, with and without the inhibitor, over different immersion times. Under identical electrolyte conditions and exposure times, the spent coffee extracts form a protective layer, reducing the corrosion rate. (R_{corr}).

However, experimental data indicate that as exposure time increases, the corrosion inhibitor's efficiency decreases substantially. This fact indicates that the passivation layer form over the metallic surface is degraded over time. This result suggests that, for a real AMD a dispenser could be recommended.

Furthermore, the SEM images support the thesis of the efficiency reduction by time. As it is shown in Fig. 3, the presence of oxides over the metallic surface is similar for both samples.

Figure 1 Experimental extraction and set-up.

Conclusion

The efficiency of aqueous spent coffee extracts is proven by different researchers for acidic solutions (Cordeiro *et al.*, 2018; Elhady *et al.*, 2024; Jares Salguero *et al.*, 2024a; Ramos *et al.*, 2019; Torres *et al.*, 2011), however, this investigation evidenced it's performance in an AMD environment. This inhibition action is attributed to the blocking action of the protective layer form by the spent coffee extract. Moreover, the inhibition efficiency decreases with increasing the exposure time.

For further research, it is advisable to repeat the current experiment simulating an AMD flow and dosing the coffee extract periodically in order to avoid the efficiency decrease due to the passage of time.

References

media. International Journal of Electrochemical Science 13, 12188–12207.

Elhady, S., Zaki, E., El-Azabawy, O.E., Fahim, I.S., 2024. Electrochemical evaluation of green corrosion inhibitor based on ground coffee waste in Petroleum fields. Results in Engineering 21, 101880.

Jares Salguero, I., González Genicio, L., García Ordiales, E., Laine Cuervo, G., del Campo Gorostidi, J.J., 2024a. Utilización de residuos como inhibidores verdes de la corrosión en medios ácidos. Posibilidades para

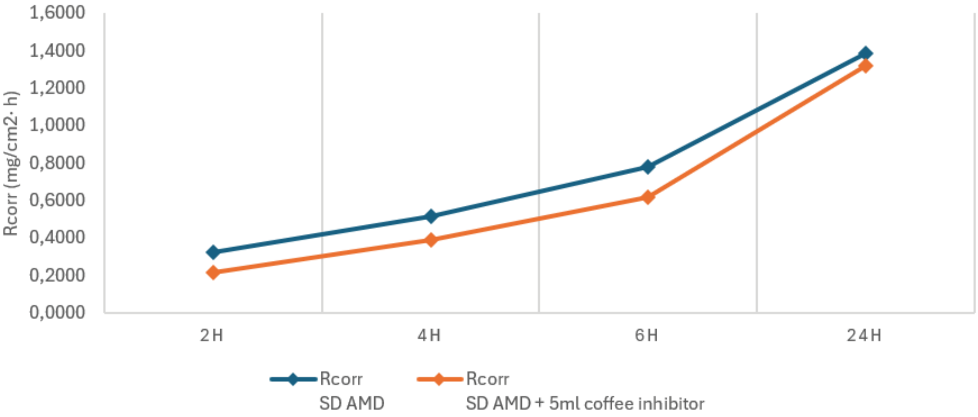

Figure 2 Variation of the corrosion rate of test coupons.

Table 2 *Variation of the corrosion rate of test coupons.*

Elapsed time and electrolyte **h**	**R$_{corr}$** ***mg·cm^{-2}·h^{-1}***	**R_corr SD AMD + inhibitor** ***mg·cm^{-2}·h^{-1}***
2	0,3227	0,2187
4	0,5147	0,3920
6	0,7787	0,6160
24	1,3840	1,3200

Table 3 *Inhibitor efficiency at 2, 4, 6 and 24 hours.*

Elapsed time and electrolyte	**R$_{corr}$** ***mg·cm^{-2}·h^{-1}***	**Efficiency (E)** **%**
SD AMD, 2h	0,3227	–
SD AMD + 5 ml inhibitor, 2h	0,2187	32,2
SD AMD, 4h	0,5147	–
SD AMD + 5 ml inhibitor, 4h	0,3920	23,8
SD AMD, 6h	0,7787	–
SD AMD + 5 ml inhibitor, 6h	0,6160	20,9
SD AMD, 24h	1,3840	–
SD AMD + 5 ml inhibitor, 24h	1,3200	4,6

Asturias. Presented at the Congreso de Sostenibilidad y Economía Circular Aplicada 2024, Madrid.

Jares Salguero, I., Laine Cuervo, G., del Campo Gorostidi, J.J., 2024b. Revisión de los tipos de corrosión en proyectos fotovoltaicos. Presented at the Congreso Nacional de Medioambiente 2024.

Kharbouch, O., Aribou, Z., Ferraa, S., Alotaibi, N.H., El-alouani, M., Hsissou, R., Al-Maswari, B.M., Galai, M., Touhami, M.E., Aziz, Z., 2024. Enhancing copper corrosion resistance in highly caustic environments: Evaluation of environmentally friendly inorganic inhibitors and mechanistic insights. International Journal of Electrochemical Science 19, 100815.

Kumari, A., Kaur, N., Kaur, M., Husain, F.M., Bhowmik, P.K., Sohal, H.S., 2025. Sustainable corrosion prevention of mild steel in acidic media with Rumex Nepalensis herb extract. RSC advances 15, 924–937.

Ling, H., Li, X., Xue, H., Sun, Q., Liu, L., Du, C., Li, K., 2024. The effect of acid mine drainage on the properties of an all-solid waste paste backfill body based on oil shale residue. Construction and Building Materials 425, 136017.

Miguel Sarmiento, A., Rodriguez-Perez, A.M., Davila, J.M., Luisa de la Torre, M., 2024. Effect of acid mine drainage on the mechanical properties of AISI 1020 carbon steel and AW6060 aluminium. Journal of Materials Research and Technology 32, 541–549. https://doi.org/10.1016/j.jmrt.2024.07.099

Mungwari, C.P., Obadele, B.A., King'ondu, C.K., 2024. Phytochemicals as green and sustainable corrosion inhibitors for mild steel and aluminium. Results in Surfaces and Interfaces 100374.

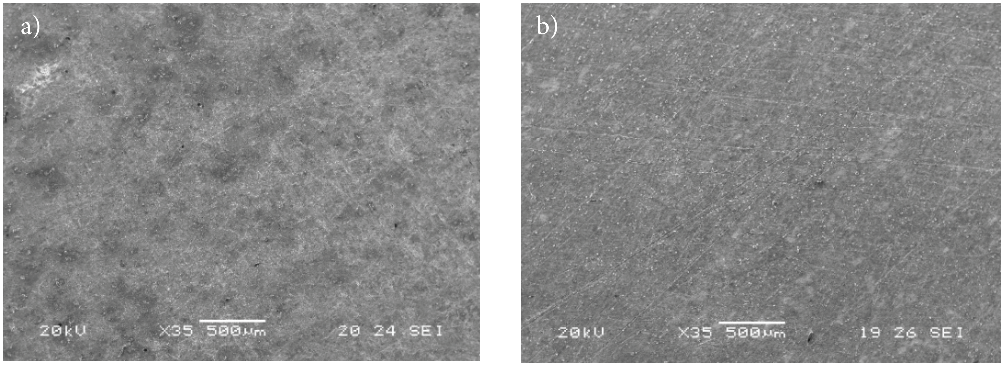

Figure 3 *SEM micrographs of mild steel after 24 hours of immersion in AMD: (a) untreated sample showing extensive corrosion; (b) sample treated with spent coffee extract.*

Pancorbo, F.J., 2010. Corrosión, degradación y envejecimiento de los materiales empleados en la edificación. Marcombo.

Parangusan, H., Sliem, M.H., Abdullah, A.M., Elhaddad, M., Al-Thani, N., Bhadra, J., 2024. Plant Extract as Green Corrosion inhibitors for Carbon steel substrate in different environments: A systematic review. International Journal of Electrochemical Science 100919.

Ramos, S.A.F., Senna, L.F. de, Lago, D.C.B. do, 2019. Evaluation of aqueous coffee husks extracts as a corrosion inhibitor of 1020 carbon steel in 1 mol L-1 HCl solution. Materials Research 22, e20180839.

Torres, V.V., Amado, R.S., De Sá, C.F., Fernandez, T.L., da Silva Riehl, C.A., Torres, A.G., D'Elia, E., 2011. Inhibitory action of aqueous coffee ground extracts on the corrosion of carbon steel in HCl solution. Corrosion Science 53, 2385–2392.

Younger, P., Banwart, S., Hedin, R., 2002. Mine water, Hidrology, Pollution, Remediation. Environmental Pollution 5.

The Environmental and Financial Aspects for the Use Of Pit Lakes for Sustainable Mine Closure

Andrew Johnstone[1]

[1]GCS (Pty) Ltd, 63 Wessel Road, Rivonia, Johannesburg, 2128, South Africa
andrewj@gcs-sa.biz

Abstract

Mine closure has become an integral part of mine planning to ensure sustainable closure of mines and to avoid post closure social and environmental risks and to minimize closure financial liabilities. Opencast mining operations result in a final mine void which on closure fill with water, forming a pit lake. Pit lakes are becoming an increasingly acceptable form of mine closure provided that long-term environmental risks are acceptable especially water quality degradation. In addition, pit lakes may negate cost associated with backfilling of the final mine void and potential water treatment costs. Case studies have shown that terminal pit lakes can reduce closure costs by 50 to 85%. Sustainable mine closure is assessed in terms of the appropriate mitigation measures to ensure no long-term environmental liabilities.

Keywords: Mine closure, pit lakes, water management, financial provision

Introduction

To ensure sustainable mining, all mines require a closure plan that must be environmentally, legally and socially sustainable and is suitably funded. In assessing the environmental aspect of closure, one of the most important factors is the management of post closure water impacts and liabilities. The potential post closure water impacts are dependent on the mining method and the mineral being mined. In general, sulfide ores have the greatest impact on water quality and open cast mining the largest impact on water quantity. Sulfide ores often lead to acid mine drainage as seen in copper mines in Canada and Spain. Pit lakes are an internationally acceptable from of mine closure for example lignite mines in Germany, gold pits in Australia and sulfide mines in Canada.

The main concern regarding potential water impacts on the closure of a mine is determining the impact of rebounding water. The forecasting is required to determine if the rebounding water will discharge on surface. If the rebounding water will discharge on surface predictions are required to determine the time, location, volume and the quality. The water management strategy is then included in the mine closure plan and budgeting the financial provision for the rehabilitation quantum.

Pit lakes form when dewatering ceases and mine voids fill with water. Correctly designed pit lakes provide a sustainable water management option for mine closure and may avoid long-term treatment costs. Correctly designed pit lakes minimise environmental impact and long-term post closure financial liabilities. Pit lakes also offer potential uses of the water for domestic, off channel storage, agriculture, fish farming, recreation and biodiversity. (Blanchette and Lund 2016).

The aim of the paper is to evaluate pit lakes as a cost effective, environmentally sustainable closure option through South African case studies. The paper discusses 4 case studies for the closure of a coal, diamond, chrome and a manganese mine in South Africa using pit lakes

Types of Pit Lakes

There are three main types of pit lakes, and these are largely dependent on the hydrological regime and the pit lakes water balance. (See Fig. 1).

Type 1: Terminal sinks have no surface outflow due to a net negative water balance

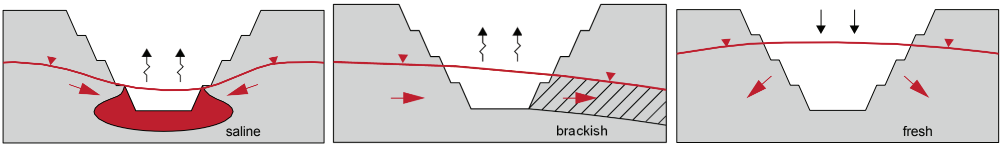

Type i: Groundwater sink **Type ii: Groundwater throughflow** **Type iii: Groundwater recharge**

Figure 1 Sink, Throughflow and Recharge Pit lakes (Johnson and Wright 2003).

Type 2: Throughflow pit lakes result in flow of groundwater from the pit lake Type 3: Recharge pit lakes result in groundwater recharge and potential discharge on surface

South African Climate

South Africa's climate varies from a humid climate in the southeast to very arid in the west. In general, the decrease in rainfall is associated with an increase in the potential evaporation resulting in a net water deficit over the majority of South Africa. On average South Africa receives 500mm/a with a mean potential evaporation of 1800mm/a. The magnitude of the water deficit depends on the location in South Africa and offers the opportunity for the design of terminal sink pit lakes as a closure option. This relationship applies to many global locations including Australia, Chile and West Africa. Terminal sink pit lakes offer an alternative to long term water treatment with the associated carbon footprint and disposal of waste.

Pit lake Water Balance

Pit lake water balances in South Africa are largely controlled by evaporation as evaporation exceeds precipitation by a factor of 2 to 3 (depending on the location). As a result, if the inflow into a pit lake is managed and the net evaporation from the pit lake surface area is greater than the sum of the inflows, it is highly unlikely that the pit lake will discharge onto the surface and into the catchment. This deficit in arid climates support terminal sinks reducing discharge risks as seen in wetter climate like Scandinavia and Germany. The water balances of the pit lakes are calculated based on a generalized mathematical expression after Gamons *et al.* (2009) where:

$\Delta S = (P + SWin + GWin) - (E + (T) + SWout + GWout)$

ΔS is change in storage, which is the volume of water in the lake.

Water In is a sum of:
P is the precipitation falling onto the pit lake.
SWin is the sum of any surface water inputs which include runoff and diverted streams.
GWin is groundwater entering the lake (which includes groundwater flow from historical workings).
Water Out:
E is the evaporation from the lake.
T is plant transpiration (negligible in arid pit lakes and significant in wetter climates)
SWout is surface water discharged from the pit lake and includes pumpage.
GWout is the groundwater leaving the pit lake.

In the above equation if **SWin** is managed by minimizing runoff into the pit lake and **GWin** is reduced by allowing groundwater levels to rebound decreasing the groundwater gradient (inflow) and evaporation exceeds the sum of all inflows into the pit lake, the pit lake will be a terminal sink. SWin can be minimised inflow management techniques such as diversion channels to discharge clean water into the catchment. The arid climatic conditions in southern Africa favour the use of terminal pit lakes for mine closure.

Pit lake Water Quality

A major consideration is the pit lake water quality after the closure of the mine. The pit lake water quality affects the environmental classification and as a result the environmental sustainability of the lake. Models of pit lake geochemistry are described by external and internal processes of which many of the internal processes are mediated by algae and microbes (Gammons *et al.*, 2009). External processes are described as wall rock runoff and wall rock leaching in the Kriel case study detailed below. The quality of the inflows (surface and groundwater) into the pit lake also affects the evolution of the pit lake water quality (See Fig. 2)

Pit lakes generally exhibit stratification in the water column which is also dependent on the depth of the pit lake. Shallow pit lakes exhibit less stratification than deep pit lakes. The stratification results in a variation in the water quality and temperature with depth (Gammons 2009). The aspect ratio of pit lakes determines the relationship between the surface area and depth of the pit lake (Castendyk *et al.* 2015). Shallow lignite pit lakes in Germany exhibit very little stratification and due to wind related mixing (Muller 2017) while deep pit lakes in Navada form meromictic layers. Fig. 2 shows the varying water quality and geochemical process that occur in pit lakes in the epilimnion, hypolimnion and monimolimnion.

Considerations for Using Pit lakes as a Sustainable Closure Option

Assessing a mine closure plan that includes pit lakes requires evaluating, quantifying, and prioritising various factors to determine their suitability for sustainable closure (ICMM, 2019). Water quality is typically the most critical consideration.

South African Regulatory Requirements

South Africa has a complex regulatory framework for the use of pit lakes in mine closure. The regulatory requirements include the Mineral and Petroleum Resources Act 28 of 2002 (mandates mine closure), National Water Act 36 of 1998 (mandates water licences) and the National Environmental Act 107 of 1998 (mandates ESIA). To obtain the regulatory approval for the use of pit lakes in the mine closure multiple authorisations are required for all the acts. A working group involving Coaltech, Minerals Council and some mining companies are engaging with the relevant South African Authorities to streamline the process for the approval of pit lakes for mine closure. Unlike Australia's streamlined EIS process, South Africa requires multi-act approvals and draft regulations are expected in late 2025

Case Studies

To illustrate the implementation of pit lakes into mine closure programs several South African case studies are discussed. As each pit lake is unique but is governed by the same broad classifications and the author has selected several case studies to illustrate various options. The case studies are included in the mine closure plan and the associated financial provision. Only in the diamond and one of the coal mines cases have the mine closed, while in all the other case studies involve operational mines. The case studies vary in locations, nature of the ore body,

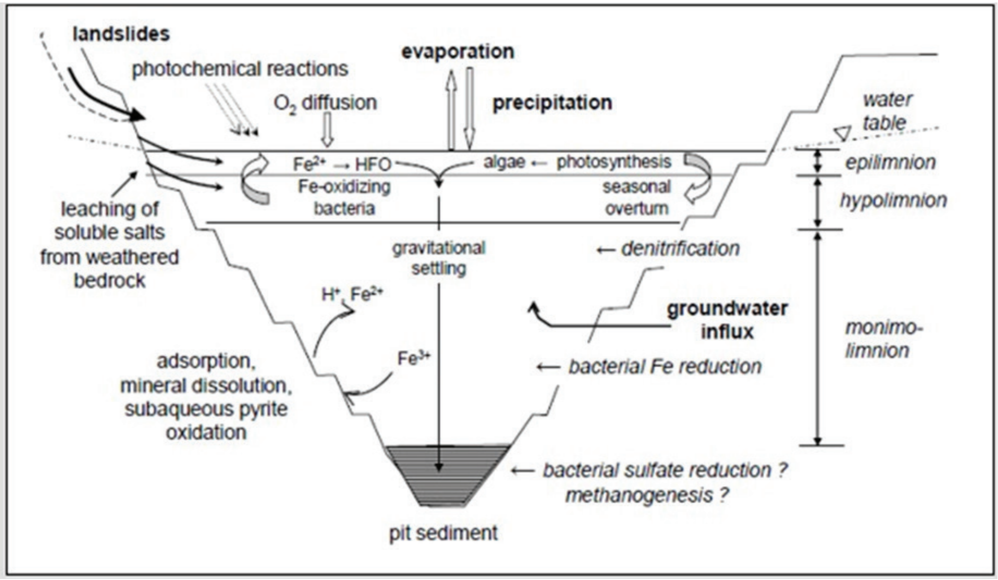

Figure 2 Chemical Process in a pit lake. (Gammons (2009).

Table 1 Factors to be considered regarding the use of pit lakes as a mine closure option.

Water quality, stratification, mixing	Long-term treatment liabilities	Post-mining employment	Site water balance
Mine water management	Catchment resources	Hydrology and hydrogeology	Geochemistry
Integrated closure planning	Microbiology	Pit lake bathymetry	Licensing and legislation
Biodiversity	Closure cost reduction	Social impact	
Health and safety	Alternative land use	Site water balance	

environment, social and financial aspects. The following case studies from different mining environments are discussed for a Coal, Diamond, Chrome & Manganese Mine in South Africa

Case Study 1: Coal Mine Pit lakes

The case study involves a study of three pit lakes in various coal basins in South Africa with different mining methods and climatic regimes. The studies were funded by the South African Water Research Commission and details are detailed in WRC publications K5/2577//3 (2019) and TT 797/2/19 (2019) and Coaltech (2021).

In general coal mines and spoils have the potential to generate poor quality leachate and acid rock drainage. Closure plans are required to management of the post closure liabilities, especially the water impacts and associated liabilities. The three mines investigated were:

- Mafuta Mine is situated in the Waterberg coalfield and is a single pit. The pit lake is a terminal sink
- Kriel Colliery is situated in the Mpumalanga coalfield and the comprised roll over open cast mining with a final void. The pit lake is a terminal sink
- Rooikop Mine in the KwaZulu-Natal coalfields and was open cast mine with underground operations developed from the high wall. The pit lake discharges onto surface during the summer rainfall months

In all cases the pit lake water was neutral to alkaline, and the total dissolved solid (TDS) content varied depending on the mining method. The highest TDS (3443mg/L) was recorded in pit lakes resulting in the role over method where the pit lake was in direct hydraulic contact with the backfilled material. The lowest TDS (1000mg/L) was recorded in the single open pit and intermediate TDS (1208mg/L) where the pit lake was in direct hydraulic contact with underground operations (Table 2). These are pit lake water quality where water levels have stabilized. Variable pit lake water quality can be expected during the rebound of water levels and before a steady state as in the case of Kriel. In all cases regulatory exemption is required as the pit lake does not comply with catchment water quality standards and all cases supports aquatic life.

Case Study 2: Diamond Mine Pit Lake

The diamond mine case study where a pit lake in included the mine closure plan is a single pit open cast mine. When mining ceased in the late 2010's groundwater levels were allowed to rebound in the open pit. Pit lake water levels and quality are monitored

Table 2 Coal mine Pit Lake Water Quality .

Pit lake	Mafuta	Kriel	Rooikop
pH	8.4	8.4	7.9
TDS (mg/L)	1000	3443	1208
Sodium (mg/L)	301	434	18
Total Alkalinity (mg/L)	326	197	118
Sulfate (mg/L)	94	1930	608
Chloride (mg/L)	314	35	2.5
Nitrate- NO$_3$ (mg/L)	9.7	0.24	<0.1

regularly and do not comply with catchment water quality standards (Table 3). The pit lake water balance was calculated and is a terminal sink. A cost comparison was completed where the cost of backfilling the open pit was compared to the use of a pit lake in the closure planning. The orders of magnitude for backfilling of the open pit are R3.4 billion compared to an estimated R500 million if the pit lake is accepted as a closure option. The closure costs of the pit lake option include revegetation of waste/spoils, storm water diversions, slope benching and fencing to address safety concerns.

The major considerations against the pit lake closure option were pit side wall stabilities, sterilisation of resource with backfilling and loss of some 20 ha of arable land. Studies proved that the pit lake closure option was environmentally sustainable, financially preferable and potential safety concerns could be mitigated. At present, the mine is undergoing extensive applications for regulatory approval.

Case Study 3: Chrome Mine Pit Lake

The case study involves a large open cast chrome mine in the Western Bushveld Igneous Complex of South Africa. The mine plans to develop an underground extension from the open pit high walls. During the underground development, the mine will leave the associated waste in the open pit. Geochemical assessment of the chrome seams, roof, floor and overburden proved that lithologies are largely inert and do not pose any risk of water contamination (ABA results less than 0.5% S). During the closure planning, numerous post mining land uses were identified, feasibility studies undertaken and costed. One of the post closure land uses is to use the pit as a water resource where storm water and other sources of water could be stored and used during winter to meet regional domestic demand. Other potential post closure land uses involved agricultural irrigation, out of pit fish farming and recreation. The financial provision for backfilling of the open cast was calculated to be R5.5 billion compared to an estimated R1 billion for the use of a pit lake for closure.

Case Study 4: Open Cast Manganese Mine

The manganese mine is in the arid Northern Cape Province of South Africa. The current mine closure plan states that the open pit should be rehabilitated with backfill. Detailed geochemical assessments to determine the risk of acid rock drainage and generation of poor-quality leachates identified no risks from the pit, waste and overburden rock dumps other than nitrate from the explosives. Due to the climate of the area and the hydrogeological regime, the pit lake would be a terminal sink. The water quality in the pit lake would decline over time due to evapo-concentration of salts in the pit lake (Table 5). Case studies modelled in the arid USA the indicate that pit lake salt concentrations are likely to double every 50 years. In the case of terminal sink pit lakes, the groundwater gradients are into the pit lake posing no thread to the surrounding land use largely game and stock farming with a low population density and land value. The zone of impact of the terminal pit lake on the surrounding groundwater users is limited

Table 3 *Diamond Mine Pit Lake water quality.*

	Pit lake (2017)	Ambient Groundwater (April 2017)
pH	7.1	7.9
TDS (mg/L)	1934	615
Electrical Conductivity (mS/cm)	294	102
Sodium (mg/L)	432	53
Total Alkalinity as $CaCO_3$ (mg/L)	1403	480
Sulfate (mg/L)	44	27
Chloride (mg/L)	242	33
Nitrate as N (mg/L)	0.1	0.25

Table 4 Summary of Groundwater Quality for Open Pit Chrome Mine.

Constituents of Concern	Prediction of pit lake water quality (2050)
pH	7 to 8
Total dissolve Solids mg/L	500 to 640
Sulfate (mg/L)	80 to 100
Nitrate as N (mg/L)	20 to 30

(Water quality will vary depending on supplementary sources of water to be stored in the pit lake)

due the low aquifer potential The side wall of the open pit would be sloped for safety to the groundwater rebound level.

Conclusions

The use of correctly designed pit lakes will result in sustainable mine closure. Pit lakes offer various benefits including but not limited to water management, biodiversity, alternative land uses, post mining employment and an overall reduction in closure cost. Post closure water management benefits of pit lake are the control of surface discharge, avoidance of long-term water treatment costs and the associated carbon footprint, plus alternative uses for the water resource. Pit lakes also offer potential to increase both the aquatic and terrestrial biodiversity of a historical mined area. Pit lakes result in a reduction in closure liabilities when compared to backfilling of the open pit and long-term water treatment of up to 85% in the diamond mine case study and 80 % in the chrome mine case study. The author would like to stress that the potential use of pit lakes as a closure option must be included in the mining feasibility study to allow for the correct pit lake designs. The inclusion of pit lakes in the closure plan will decrease regulatory delays and compliance with ICMM Closure goals

References

Coaltech (2021) GCS Water and Environmental (Pty) Ltd and Gunn Attorneys. A Manual for the Authorisation of Pit Lakes as a Closure Option for South African Coal Mines.

Gammons CH, Harris LN, Castro JM, Cott PA, Hanna BW (2009) Creating Lakes from Open Pit Mines: Processes and Considerations, Emphasis on Northern Environments.

International Council on Mining & Metals (2019) Integrated Mine Closure Good Practice Guide.

Johnstone AC, Kennedy L, Mpetle M (2019) An Investigation to Determine if South African Coal Mine Pit Lakes are a Viable Closure Option. Water Research Commission Report No. 77 797/1/19 Vol 1.

Johnson K, Wright P (2003) Hydrological Classification of Pit Lakes.

Blanchette ML, Lund MA (2016) Pit Lakes are a Global Legacy of Mining: An Integrated Approach to Achieving Sustainable Ecosystems and Value for Communities. Sci Total Environ.

Lund MA, Blanchette ML (2023) Closing Pit Lakes as Aquatic Ecosystems: Risk, Reality, and Future Uses.

Müller M (2013) Modeling Pit Lake Water Quality – How Do We Solve Multi-Disciplinary Problems? IMWA.

WRC (2019) GCS Water and Environmental (Pty) Ltd. A Preliminary Manual for the Design of Coal Mine Pit Lakes as an Environmentally Stable Closure Option in South African Mines.

Table 5 Results of Predicted Water Chemistry for 100 years (Concurrent Backfill and Pit Lake Formation).

Constituents of Concern	Initial	100 years
pH	8.9	7.0
Total Dissolved Solids (mg/L)	1365	5 460
Sulfate (mg/L)	127	508
Nitrate as N (mg/L)	15	60

Potential Generation and Consumption of Carbon Dioxide during Treatment of Mine Drainages in South Korea

Duk-Min Kim[1], Ki-Rim Lee[1], Ju-In Ko[2]

[1]*Department of New Energy and Mining Engineering, Sangji University, Wonju, Gangwon state, Republic of Korea, kdukmin8@sangji.ac.kr, ORCID 0000-0002-1537-6866*

[2]*Korea Mine Rehabilitation and Mineral Resources Corporation, Wonju, Gangwon state, Republic of Korea*

Abstract

In this study, direct CO_2 emissions from mine drainages and indirect CO_2 emissions from the potential consumption of hydrated lime were modeled using PHREEQ-N-AMDTreat based on chemical compositions and flow rates at most mine drainage sites (n = 395) across South Korea. When considering CO_2 emissions, passive treatment methods were found to be substantially more advantageous than (semi-)active treatment methods using hydrated lime. Additionally, implementing pre-aeration is a preferable approach for most mine drainages from the perspective of CO_2 emission reduction.

Keywords: Carbon footprint, CO_2 emission, PHREEQ-N-AMDTreat, hydrated lime, pre-aeration

Introduction

Mine drainages often act as CO_2-emission sources because of pyrite oxidation and H^+ production, which enhances the dissolution of carbonate minerals. Although the treatment of mine drainage with hydrated lime is a common practice to increase pH, the production of lime can generate considerable amount of CO_2, during calcination of limestone.

Lime dosages have been studied and modeled in various mine drainage treatment facilities (Cravotta, 2021; Kim *et al.*, 2023), and life-cycle assessment studies have indicated substantially lower CO_2 emissions associated with passive treatment compared to active treatment using lime (Tuazon and Corder, 2008; Hengen *et al.*, 2014). Unlike active and semi-active methods (e.g., automated lime dosing systems that operates without labor, often accompanied by a large settling pond), which require continuous input of chemicals or energy, passive treatment systems function without such inputs (Younger *et al.*, 2002). Specifically, to increase pH, passive systems typically utilize limestone or steel slag within SAPS (Successive Alkalinity Producing Systems), slag reactors, or SLBs (Slag Leach Beds), whereas active treatment systems rely heavily on hydrated lime. Despite the growing awareness of CO_2 emissions from industrial lime use, the potential effects of different mine drainage treatment strategies on CO_2 emissions—including the conversion of CO_2 to other species due to pH increase and the indirect CO_2 emissions from lime production—remain largely unassessed. To the best of the authors' knowledge, this gap highlights a critical need for further research.

Thus, the objectives of this study are (1) to calculate CO_2 emissions from most mine drainages in South Korea and evaluate the effect of CO_2 removal through pH elevation, (2) to estimate indirect CO_2 emissions associated with the use of hydrated lime for treating these drainages, and (3) to assess the suitability of pre-aeration as a mine drainage treatment strategy, focusing on its potential to reduce lime dosage and associated CO_2 emissions.

Methods

Survey on mine drainages

In 2016, the Korea Mine Rehabilitation and Mineral Resources Corporation (KOMIR) investigated 395 mine drainages across South Korea. Mine drainages with relatively high contamination and/or flow rates were surveyed four times a year, while those with lower contamination and/or flow rates were surveyed twice a year. The majority of the mine drainages were adit discharges, while some were leachates from dumps of waste rock or tailings.

Data analysis

Seasonal water quality and quantity data of the 395 mine drainages were assessed. Dissolved CO_2 concentrations and the dosages of hydrated lime required to reach specified target pH values were assessed using the Caustic Titration module of PHREEQ-N-AMDTreat version 1.4.5 (Cravotta, 2020, 2021). For this study, the aeration to equilibrium condition with a steady-state partial pressure of CO_2 (pCO_2) of $10^{-3.4}$ atm was applied. When assessing dissolved CO_2 concentrations in mine drainage, samples with a pH lower than 4.5 or without alkalinity were excluded.

To predict maximum CO_2 concentrations that could potentially be degassed from mine drainages by natural aeration ($C_{CO2(degas)}$), dissolved CO_2 concentration at the equilibrium pCO_2 of $10^{-3.4}$ atm ($C_{CO2(eq)}$) was subtracted from the modeled initial concentration of dissolved CO_2 ($C_{CO2(dissolved)}$) (Equation 1). The CO_2 flux ($F_{CO2(degas)}$) was then computed by multiplying this difference in concentration by the cumulative annual flow rate expressed in L yr^{-1} (Q_{annual}).

The mine drainages were classified into two categories: (1) potential (semi-)active treatment with hydrated lime, which includes 11 (semi-)active treatment facilities under operation, and (2) others (indicated as “Others” in the relevant plots), which include (a) mine drainages expected to meet discharge criteria in South Korea (excluding arsenic and fluoride) after aeration, (b) mine drainages being successfully treated by passive treatment facilities, and (c) stagnant mine drainages without surface flow.

After the geochemical modeling of each seasonal data subset which is described above, annual averages were used for each mine drainage site (n=395).

Calculation of CO_2 emission from hydrated lime consumption

Emissions of CO_2 from hydrated lime production facilities, categorized as Scope 1 emissions (direct greenhouse gas emissions from sources controlled or owned by the organization), were examined. To focus on the primary and direct sources of CO_2 emissions, calcination and fuel combustion were included, while electricity consumption and limestone quarrying were excluded from the carbon budget.

To convert the amount of quicklime (CaO) to CO_2 generation, an emission factor of 0.75 for lime during thermal decomposition ($EF_{Lime(decom)}$) was applied. This factor was derived from the stoichiometric ratio (SR) of CO_2 to CaO (0.785), and adjusted for the purity (P) of quicklime at 0.95 (IPCC, 2006, 2021; GGIRC, 2022). Subsequently, $EF_{Lime(decom)}$ was multiplied by a conversion factor (CF) for hydrated lime from quicklime (0.757) to obtain the final emission factor for hydrated lime ($EF_{HL(decom)}$) of 0.57 during thermal decomposition (Equation 2; IPCC, 2006, 2021).

Moreover, CO_2 generation from fossil fuel combustion during the calcination of limestone was added to the total CO_2 emission (Shan *et al.*, 2016; Laveglia *et al.*, 2022; Wu *et al.*, 2023). Shan *et al.* (2016) reported mass

$$F_{CO2(degas)} = C_{CO2(degas)} \times Q_{annual} = (C_{CO2(dissolved)} - C_{CO2(eq)}) \times Q_{annual} \quad (1)$$

$$EF_{HL(decom)} = EF_{Lime(decom)} \times CF = SR \times P \times CF \quad (2)$$

$$EF_{HL(coal)} = EF_{Lime(coal)} \times CF = R_{C-L} \times EF_{Coal} \times CF = \frac{M_{Coal}}{M_{Lime}} \times EF_{Coal} \times CF \quad (3)$$

ratios ($R_{C\text{-}L}$) of coal consumption (M_{Coal}) to lime production (M_{Lime}) ranging from 0.12 to 0.16 in China, with a weighted average of 0.15. The emission factor for coal combustion (EF_{Coal}) was 1.85 t CO_2 per t coal (Shan *et al.*, 2016), resulting in an emission factor for lime during fuel combustion ($EF_{Lime(coal)}$) of 0.27 t CO_2 per t lime (Equation 3). By applying the conversion factor (CF) from quicklime to hydrated lime, we calculated the emission factor for hydrated lime during fuel combustion ($EF_{HL(coal)}$) to be 0.21 t CO_2 per t hydrated lime.

Thus, summing the emission factors for hydrated lime during thermal decomposition ($EF_{HL(decom)}$, 0.57) and coal combustion ($EF_{HL(coal)}$, 0.21) yields 0.78 t of CO_2 directly generated per tonne of hydrated lime produced. When considering the total CO_{2eq} emissions over the entire production process, Laveglia *et al.* (2022) calculated 0.94 t of CO_{2eq} during hydrated lime production in four EU countries. Additionally, Wu *et al.* (2023) estimated 0.89 t of CO_{2eq} during hydrated lime production in the Yangtze River basin in China. Therefore, the CO_2 directly generated during hydrated lime production ($C_{CO2(HL)}$) was calculated by multiplying the hydrated lime dosage (D_{HL}) by the emission factor for hydrated lime (EF_{HL} = 0.78) (Equation 4).

$$C_{CO2(HL)} = D_{HL} \times EF_{HL} = D_{HL} \times 0.78 \qquad (4)$$

Results and discussion

The total potential amount of CO_2 generated from the mine drainages was 481 t yr^{-1}, of which 95% was from coal mines. Modeled concentrations of potential CO_2 degassing from mine drainages are plotted against the pH and alkalinity of untreated mine drainages in Fig. 2. The logarithm of the potential CO_2 concentrations degassing from

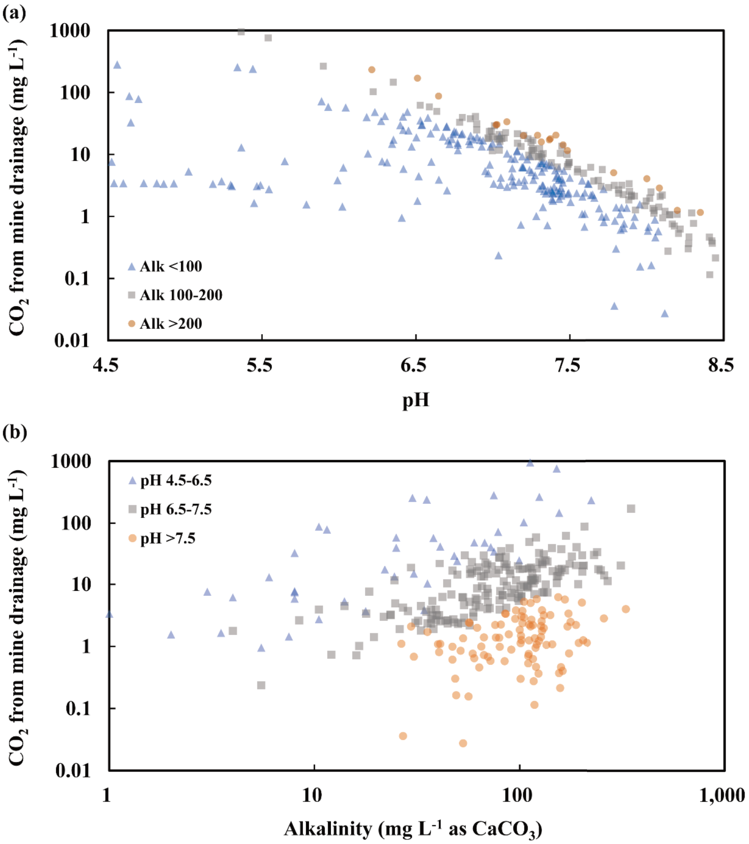

*Figure 2 Relationship between modeled concentrations of potentially degassed CO_2 and (**a**) pH and (**b**) alkalinity in untreated mine drainages in South Korea. The samples are classified by alkalinity and pH ranges.*

mine drainages exhibited a predominantly linear negative relationship with pH within each alkalinity range (Fig. 2a). Similarly, within each pH range, the logarithm of CO_2 concentrations demonstrated a linear positive relationship with the logarithm of alkalinity (Fig. 2b).

Fig. 2a also demonstrate that degassing CO_2 concentrations, which are closely related to dissolved CO_2 concentrations in mine drainage, decrease significantly with increasing pH. This suggests that mine drainage treatment by increasing pH mitigates CO_2 degassing through conversion to HCO_3^- and/or calcite precipitation.

Indirectly generated CO_2 concentrations were calculated based on the modeled consumption of hydrated lime during treatment. The accuracy of predicting hydrated lime consumption using the same model (Caustic Titration module in PHREEQ-N-AMDTreat) was verified against actual measurements from a full-scale treatment facility in South Korea (Kim *et al.*, 2023). The concentrations of generated CO_2 were compared with pH and alkalinity (Figs. 3 and 4). A notable trend was observed at pH values below 5.5, where decreasing pH corresponded to increased acidity and associated lime dosages, resulting in increasing concentrations of generated CO_2 by lime usage. Similarly, at a given alkalinity, sample groups with lower pH values exhibited higher potential CO_2 generation from lime usage (Fig. 4b). Additionally, a positive relationship was observed between CO_2 generation by lime usage and alkalinity of mine drainages (Figs. 3b and 4b).

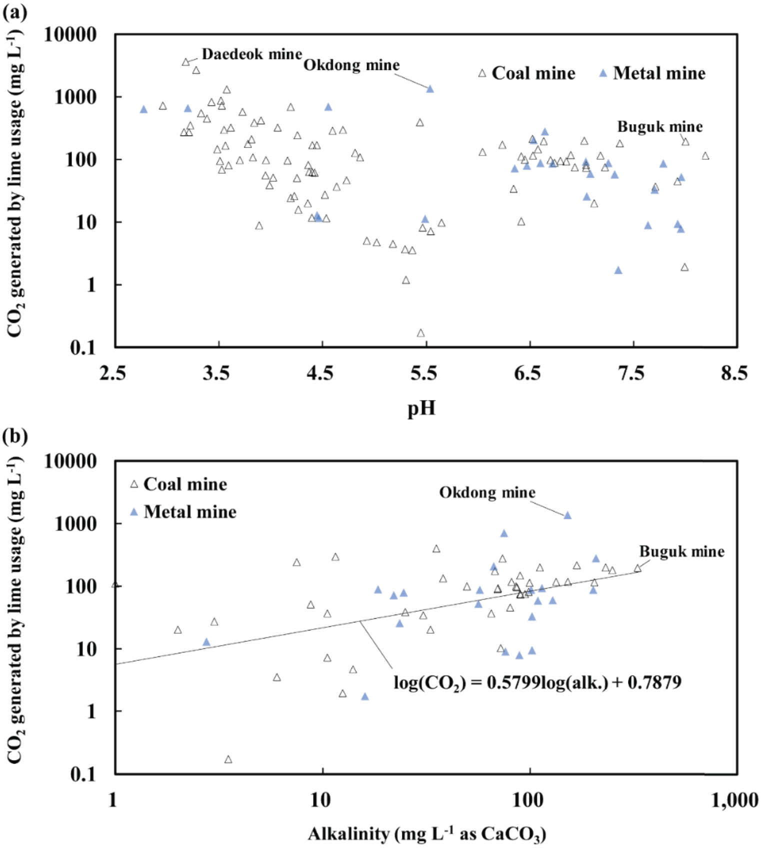

Figure 3 *Relationship between calculated indirect emission (in mg L^{-1}) of CO_2 from modeled usage of hydrated lime and (**a**) pH and (**b**) alkalinity in mine drainages. The samples are classified based on mine types.*

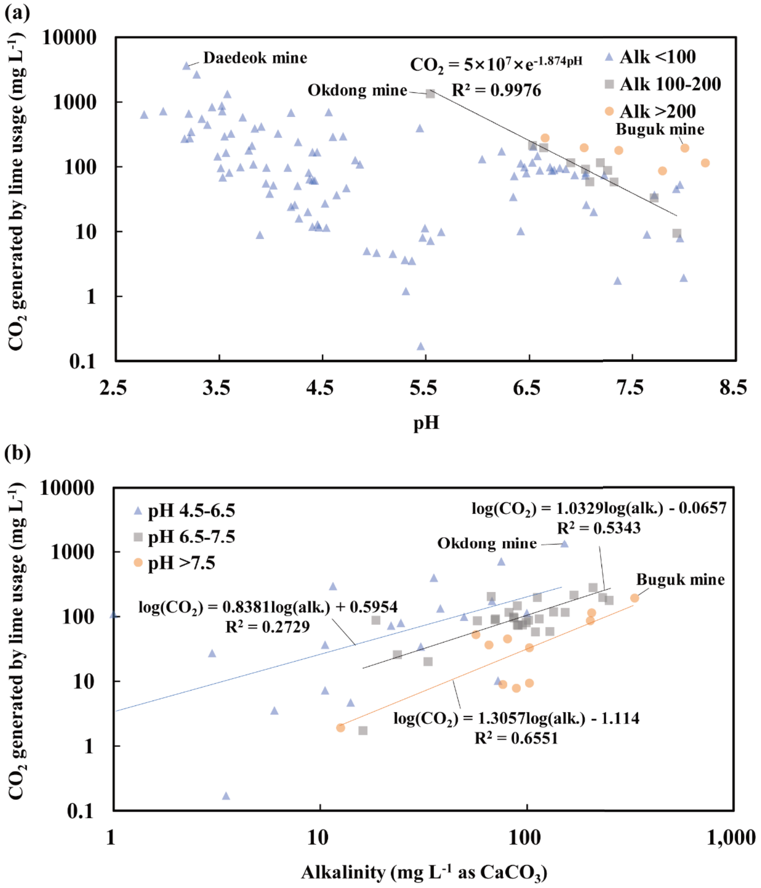

Figure 4 *Relationship between calculated indirect emission (in mg* L^{-1}*) of* CO_2 *from modeled usage of hydrated lime and (**a**) pH and (**b**) alkalinity in mine drainages. The samples are classified based on alkalinity and pH ranges, and samples with pH <4.5 are excluded in (**b**). Regression lines correspond to the samples with alkalinities of 100–200 mg* L^{-1}*1 as* $CaCO_3$ *in (**a**) and to samples with three different pH ranges in (**b**).*

Potential consumption of hydrated lime to treat all the sampled mine drainages could generate 2,230 t CO_2 yr^{-1}, which was more than 12 times the CO_2 degassed from drainages, assuming atmospheric equilibrium under surface conditions. Moreover, constructing (semi-)active treatment facilities using hydrated lime consumes substantial amount of cement and electricity.

Pre-aeration to degas CO_2 prior to the treatment of mine drainages has been reported to substantially reduce lime consumption, owing to the decrease of H_2CO_3. We compared direct CO_2 emissions during pre-aeration with indirect CO_2 emissions resulting from hydrated lime usage. The estimated CO_2 emissions from most drainages were less than 13% of the indirect CO_2 emissions from hydrated lime. As the ratio (13%) was lower than the reported reduction of hydrated lime consumption (22%–50%) by the pre-aeration step of the treatment, the step was preferable for most mine drainages concerning CO_2 emission. Samples with higher alkalinity and pH seem to benefit from pre-aeration in terms of reducing CO_2 emission.

Conclusions

Regarding CO_2 emission, passive treatment is substantially more beneficial than (semi-) active treatment using hydrated lime. Although mine drainages with pH below 4.5

or without alkalinity could not be assessed, pre-aeration was preferred with respect to CO_2 emission for mine drainages with high pH and high alkalinity among the mine drainages with pH above 4.5.

Acknowledgements

This work was supported by an R&D project of the Korea Mine Rehabilitation and Mineral Resources Corporation from 2022 to 2025 and by the Graduate School of Sangji University. The authors gratefully acknowledge the contributions of the people at Korea Mine Rehabilitation and Mineral Resources Corporation for conducting sampling, pretreatment, and analyses. We thank Charles Cravotta for creating the PHREEQ-N-AMDTreat model and for his comments on an early draft of the manuscript.

References

Cravotta, C.A., 2020. Interactive PHREEQ-N-AMDTreat water-quality modeling tools to evaluate performance and design of treatment systems for acid mine drainage (software download): U.S. Geological Survey Software Release. https://doi.org/10.5066/P9QEE3D5

Cravotta, C.A., 2021. Interactive PHREEQ-N-AMDTreat water-quality modeling tools to evaluate performance and design of treatment systems for acid mine drainage. Appl. Geochem. 126, 104845. https://doi.org/10.1016/j.apgeochem.2020.104845

GGIRC, 2022. 2022 National Greenhouse Gas Inventory Report of Korea, Cheongju.

Hengen, T.J., Squillace, M.K., O'Sullivan, A.D., Stone, J.J., 2014. Life cycle assessment analysis of active and passive acid mine drainage treatment technologies. Resour. Conserv. Recycl. 86, 160–167. https://doi.org/10.1016/j.resconrec.2014.01.003

IPCC, 2006. IPCC Guidelines for National Greenhouse Gas Inventories, Geneva, Switzerland.

IPCC, 2021. Climate Change 2021: The Physical Science Basis. Contribution of Working Group I to the Sixth Assessment Report of the Intergovernmental Panel on Climate Change, Cambridge. https://doi.org/10.1017/9781009157896

Kim, D.-M., Kwon, H.-L., Park, M.-S., 2023. Underestimation of alkaline dosage and precipitate amount during water treatment: Role of inorganic carbon and use of PHREEQ-N-AMDTreat. J. Clean. Prod. 433, 139683. https://doi.org/10.1016/j.jclepro.2023.139683

Kim, D.-M., Lee, K.-R., Park, M.-S., 2005. Potential generation and consumption of carbon dioxide during treatment of mine drainages in South Korea. Sci. Total Environ. under rev.

Laveglia, A., Sambataro, L., Ukrainczyk, N., De Belie, N., Koenders, E., 2022. Hydrated lime life-cycle assessment: Current and future scenarios in four EU countries. J. Clean. Prod. 369, 133224. https://doi.org/10.1016/j.jclepro.2022.133224

Shan, Y., Liu, Z., Guan, D., 2016. CO2 emissions from China's lime industry. Appl. Energy 166, 245–252. https://doi.org/10.1016/j.apenergy.2015.04.091

Tuazon, D., Corder, G.D., 2008. Life cycle assessment of seawater neutralised red mud for treatment of acid mine drainage. Resour. Conserv. Recycl. 52, 1307–1314. https://doi.org/10.1016/j.resconrec.2008.07.010

Wu, E., Wang, Q., Ke, L., Zhang, G., 2023. Study on carbon emission characteristics and emission reduction measures of lime production—A case of enterprise in the Yangtze River basin. Sustainability 15, 10185. https://doi.org/10.3390/su151310185

Younger, P.L., Banwart, S.A., Hedin, R.S., 2002. Mine Water: Hydrology, Pollution, Remediation, Kluwer Academic Publishers, Dordrecht, Netherlands. https://doi.org/10.1007/978-94-010-0610-1

Modelling of Mine Water Discharges with Integrated Pump Management

Christoph Klinger[1], Julia Nicolina Sunten[1], Nele Pollmann[1], Christine von Kleinsorgen[2]

[1]DMT GmbH & Co. KG, Natural Resources: Hydrogeology and Water Resource Management, Am TÜV 1, 45307 Essen, Germany, Christoph.Klinger@dmt-group.com, JuliaNicolina.Sunten@dmt-group.com, Nele.Pollmann@dmt-group.com

[2]V-WH-SK Grubenwasserkonzepte, RAG Aktiengesellschaft, Im Welterbe 10, 45141 Essen, christine.vonkleinsorgen@rag.de

Abstract

Mine water levels are currently rising to an optimized level in large parts of the Ruhr region in Germany, with the aim of reducing the number of pump stations and shift to submersible pump management from surface. These developments also pose new demands on mine water discharge management into receiving waters and the numerical quality and quantity modelling of the pumped mine water. Therefore, a method has been developed to be able to calculate the pump management typical for submersible pumps using numerical modeling with the established Boxmodell. This method is illustrated using a site example, which demonstrates the effects that the interaction of pump management, the location of the pump site and the hydraulic conditions can have on mine water discharge.

Keywords: Mine flooding, pump management, mine water management, model calculation, mass transport modelling

Introduction

During the active period of hard coal mining in the Ruhr region, the mine workings were kept dry by dewatering the deepest mine areas (Coldewey 1994, Drobniewski 2017). Nevertheless, dams to former mining areas induced higher water levels locally. The water levels in the mines were thus constant over a long period of time. Following the closure of the last mines in the region in 2018, water levels rise almost everywhere or discharge into zones with lower water levels (Vogt 2020).

The DMT mine water modelling software "Boxmodell" calculates the mine water rises based on the known initial conditions (water levels, inflows) and using numerous model input data on the condition of the host rock and the residual mine voids (Eckart 2007). Extensive reference and monitoring data are available for this purpose and are used to calibrate the model.

In some mine water provinces, the target level has now been reached and the water is discharged into the receiving waters. Some older dewatering systems use underground pump stations for this purpose, in which the water levels in the catchment area are kept constant, as was previously the case in active mining. Depending on the exposure of the mines to the surface, only the water inflows or extraction rates vary, which is also considered by the models in the affected regions on the basis of groundwater recharge rates (Bedford 2022). Despite the variable flow rates, the hydraulic and chemical conditions in the catchment area of the pumps are comparatively stable under these conditions.

In new facilities, submersible pumps have been and also continue to be installed, which are lowered from the surface into the rising mine water. As most systems have several pumps installed with a fixed pumping capacity the pumps are switched on and off as required to pump the inflowing water. In most cases this does not correspond to the rate of mine water inflow to the mine (in part influenced by groundwater recharge). As a result, the water levels rise when the pumping capacity is smaller than the inflow and fall when the pumping capacity is higher than the inflow (Fig. 1). While this has no relevant consequences for the chemical composition of the discharged water at some locations, current modelling studies show that this can certainly be the case under sensitive site conditions.

Location

The last mine water pump station in the eastern Ruhr area was discontinued in 2019. Since then, the water levels have been rising depending on the regional distribution of inflows and the volume of residual voids that can be filled as well as the hydraulic connections within the mine water province. The site of the future pump station is centrally located between the two most recently active mines. Fig. 2 shows a clear focus of the inflows in the western area, which resulted in mine water flowing from the west over many years and contributing to the filling of the eastern cavities.

In addition to the quantities, the compositions of the mine waters to the west and east of the future pump station also differ substantially. While the mine water in the western part is characterized by low-salinity and seasonally fluctuating inflows from the overburden, the hydrochemical situation in the east is dominated by highly saline waters from the carbonate layers. Another special feature of the western inflow water is the occurrence of sulfide, which has been detected in the discharge water over a period of more than 10 years. The occurrence of hydrogen sulfide (H2S) is explained by bacterial sulfate reduction and is calculated in this way by the model. The mobilization of pyrite oxidation products (sulfate, iron, manganese, other metals) during the mine water rise is also considered for the entire area.

Modelling of a future pump station

Once a target level for the rising water has been reached, the mine water must be pumped again and discharged into the receiving water (Balzer 2019). Earlier modelling calculations for this scenario used the steady state approach with a constant water level and variable but only slowly changing flow rates due to the inflows (Fig. 1). For a possible use of submersible motor pumps, the resulting hydraulic conditions and the effect on the quality of the discharged mine water should be examined by using numerical modelling. The initial step requires reprogramming of the pump module in the model code, with which the pumps are activated or switched off depending on the inflow and the upper and lower water level limits.

To model this correctly, it is necessary to specify the hydraulic properties of the flow paths. Overall, the naturally flowing water volumes are already very large, averaging more than 20 m³/min. However, the flow rates induced by the pumps will be much higher at up to 50 m³/min. The current situation already allows the permeability coefficients between the model boxes to be calibrated in this respect due to gradients within the province (Fig. 3). Even if, according to the current state of knowledge, it is not necessary

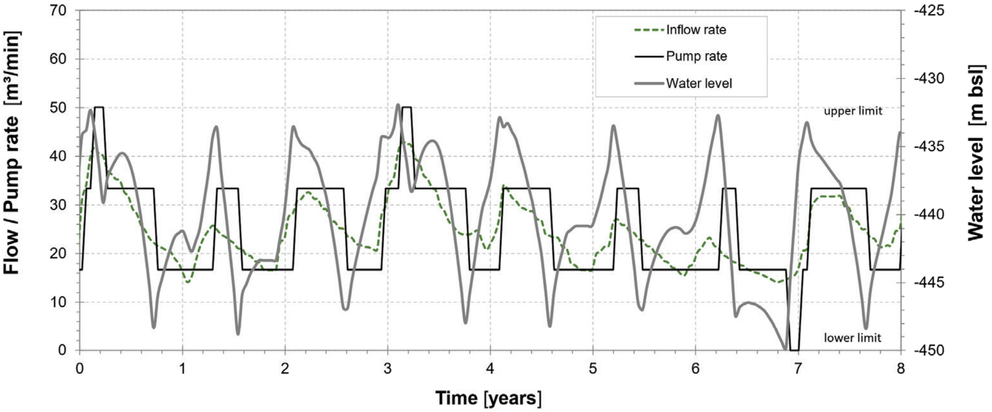

Figure 1 *Test calculation on the interaction of mine water inflow and pumping rate with the water level.*

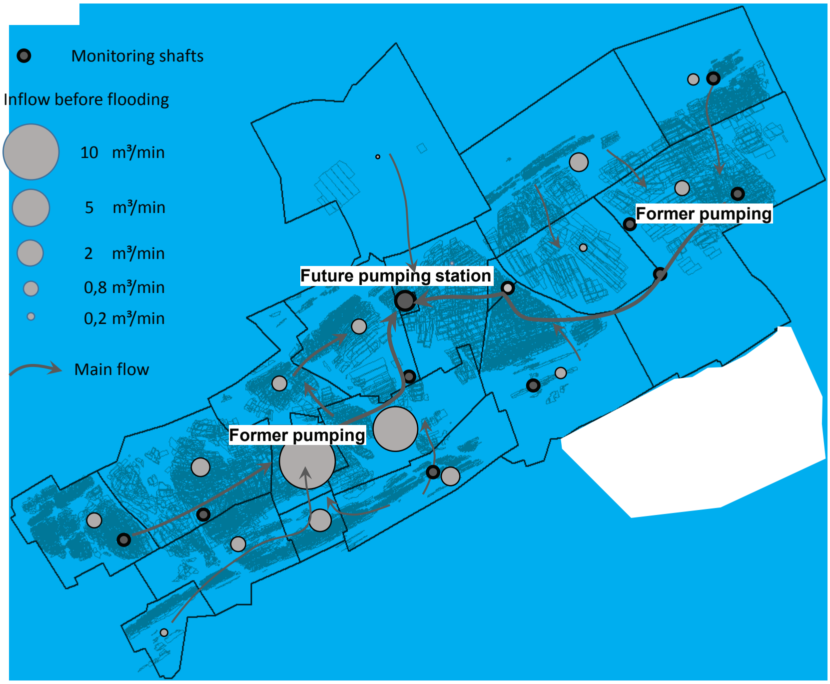

Figure 2 *Water province with distribution of inflows and flow directions to the future pump station.*

to assume that there are any breaks or other plugs in the gallery system, there are still water level differences of approx. 10 m along the flow gradient from west to east. Such effects have not yet been observed and calibrated at other locations due to the usually much lower flow rates.

In a future operation, this will lead to water level differences of up to several tens of meters between the extraction site and the periphery of the water province (Fig. 4). The inertia of the flow system within the water province, which extends over a total of about 33 km, leads to various effects. Particularly in phases of high-water withdrawal and lowering of the mine water level in the pump shaft, the directly neighboring areas will follow the water movements in the shaft. At the peripheral areas with high inflow in the west, however, the changes will only be damped, and the water levels will remain generally higher. This dynamic not only influences the storage volume during pumping operations, but also the quality of the water flowing to the extraction point.

A preliminary evaluation of the substance emissions made it clear that high mine water discharges in summer during low flow rates in the receiving water could lead to exceedance of environmental limits. It would therefore not be possible to lower the mine water level once the upper limit is reached. For this reason, a concept has been developed that utilized higher pumping rates during phases with higher flow rates in receiving waters (mainly in winter and spring). Due to the storage volume of the residual mine voids, it is then possible to slowly raise the water level in summer with low pumping rates and thus minimize the load on the receiving water.

The modelling approach for this concept is based on fixed dilution factors between the water flow in the receiving water and the amount of mine water discharged (Fig. 5). The dilution factor was selected such that the water level can be maintained in a defined level range in the long term with a feasible pumping cycle. In the past, this range was often selected too small during planning, which reduced the degrees of freedom in pump operation. For the site conditions, the pump clearance should therefore be at least 50 m to be able to bridge longer dry phases with low discharges in the receiving water (Fig. 6). This concept of variable, stepless mine water extraction can be realized by

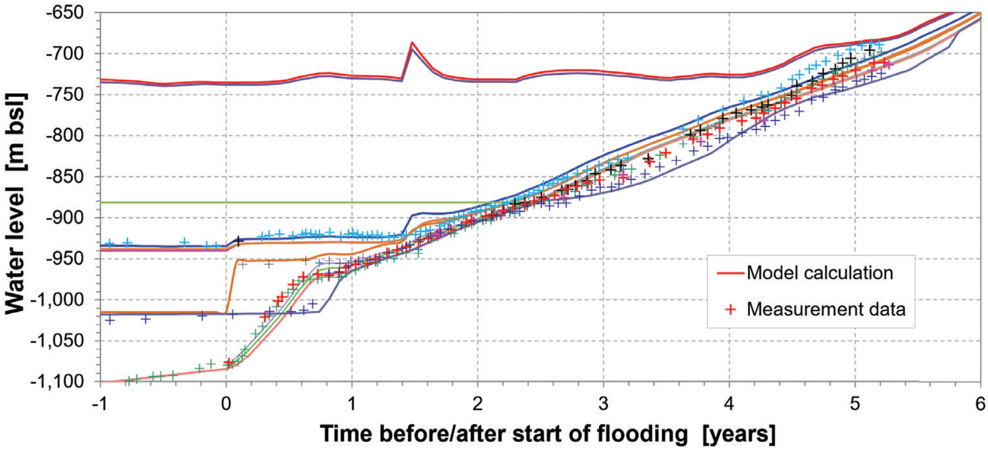

Figure 3 Water level development in the water province.

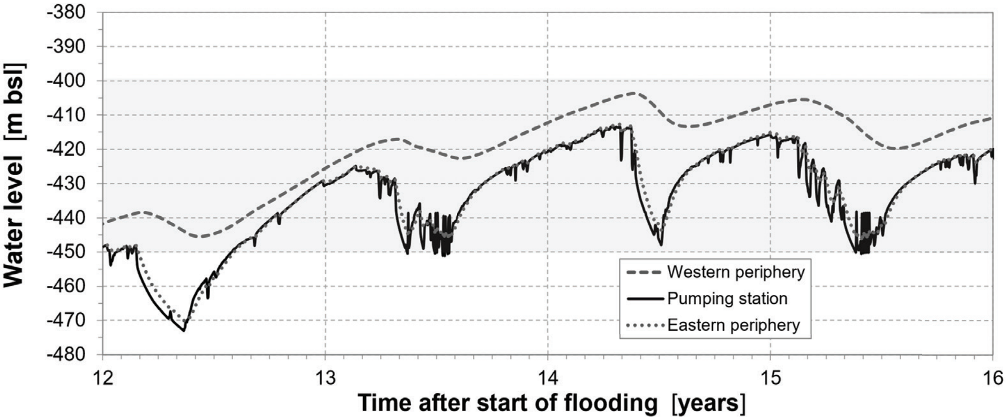

Figure 4 Spread of water levels in the water province during pumping operation.

using frequency-controlled pumps with a defined performance interval with variable pumping rates.

However, it is difficult to forecast the climatic conditions in the coming years or decades with sufficient accuracy to provide a suitable basis for such forecasts. Such modelling can therefore only be used to cover the possible range of scenarios and to test sensitivity to extreme situations. In the context of two climatically controlled hydraulic systems, as in this particular case, the temporal parallelism of the underlying reference data for mine water and receiving water is particularly important. The model therefore cyclically repeats an 11-year period 2008–2018, which is fully covered by data on mine water discharge, receiving water flow and regional climate data and for which a sufficiently good calibration could be achieved. This period contains both pronounced dry periods and years with high precipitation and is therefore a suitable basis for estimating future mine water discharges.

The inflow situation into the mine shows an attenuation and temporal shift of the maxima/minima compared to the groundwater recharge and even more so to the surface runoff. However, the described method (Bedford *et al.* 2022) ensures that both data series are based on the same climatic conditions. The main variable is then the rate of mine water pumped, while the chemical composition is calculated by the model.

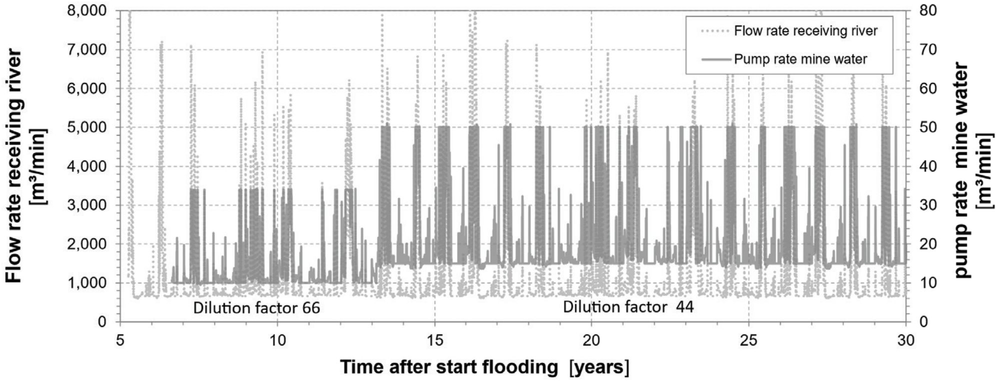

Figure 5 *Flow rates in the receiving river and adjusted pumping rate of the mine water.*

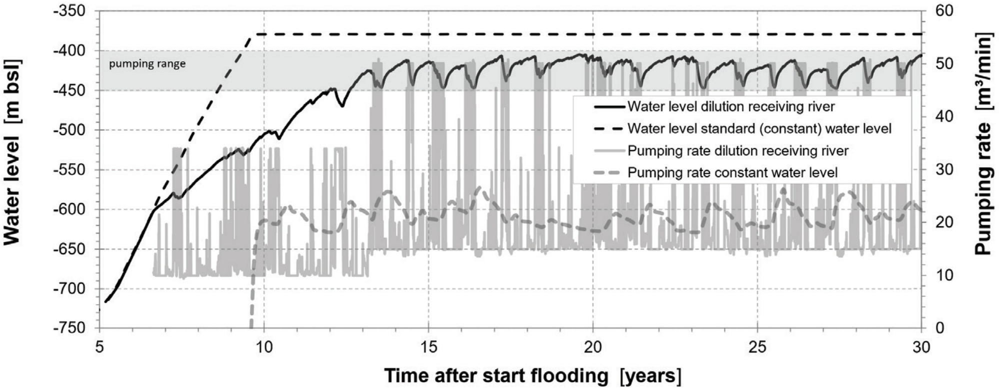

Figure 6 *Pumping rate of the mine water and resulting water levels.*

Quality Calculation

Calculations on reactive mass transport were carried out using this hydraulic concept. These show that, in contrast to constant pumping rates, the model calculates pronounced jumps in concentration in the discharged mine water. This is not limited to individual parameters, but also affects pyrite oxidation products and sulfide in addition to primary dissolved components of the inflows (example chloride in Fig. 7). The relevant higher salt concentrations in the eastern inflow are clearly visible. The substance content of the western catchment area forms the base concentration of the mixed water in the pump.

A higher temporal resolution analysis of the interaction between the extraction rate, which is forced by water levels and the receiving water discharge (Fig. 8), and the resulting concentrations in the mine water (Fig. 9) provides a simple and plausible explanation of this phenomenon. In phases of low extraction rate (with low flow rate in the receiving water), less water is extracted than flows in with the western partial flow. The remaining quantity pushes into the eastern mine areas and thus contributes to the filling of the cavities as the mine water rises. As a result, almost exclusively the low-salinity water is then pumped from the western sub-province.

If the pump rate exceeds the total inflow, the water level is lowered and, in addition to the current inflow, water is also withdrawn from the storage volume. This increases the proportion of water from the eastern sub-province to up to 30% of the total extraction rate. However, the average inflows are distributed west:east at a ratio of 95%:5%. Even if the model considers the fact that

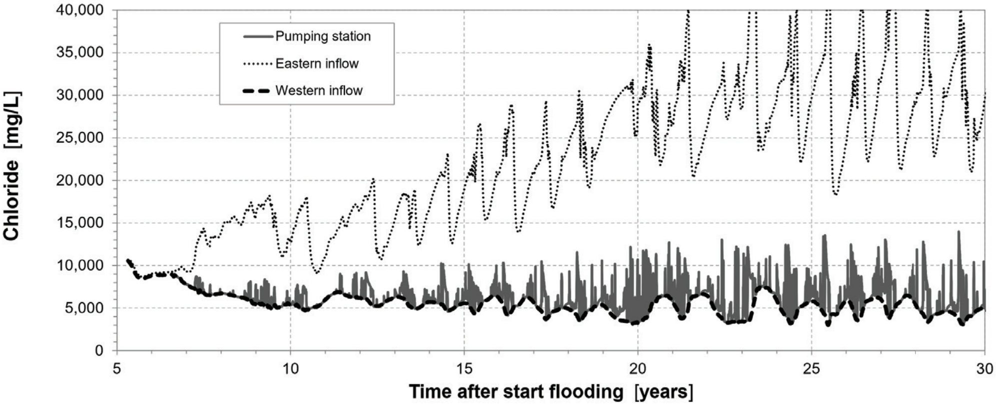

Figure 7 *Calculated development of chloride in the pumped mine water and the partial streams.*

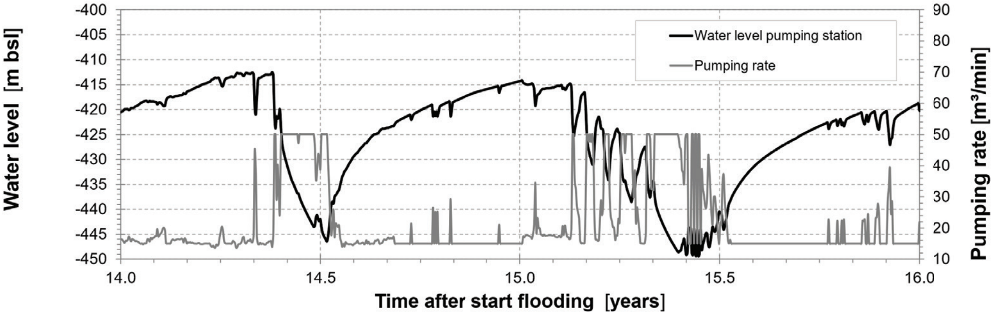

Figure 8 *Detailed analysis of pump rate and water level.*

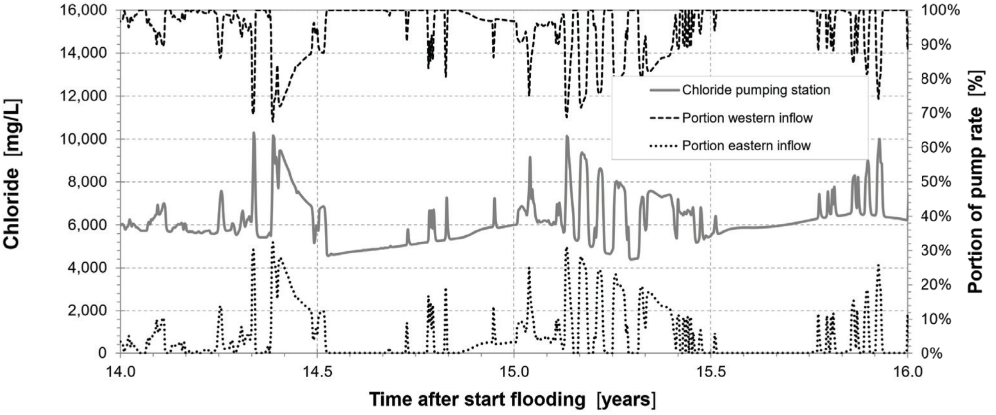

Figure 9 *Detailed analysis of inflow proportions and resulting mine water concentration of chloride.*

western water also flows back again from voids in the east, this leads to peaks in the concentrations but even more such in the discharged loads. As a result, the loads and thus also the mixed water concentrations in the receiving water exceed the equalization actually aimed for via the flow rate ratio.

These fluctuations influence not only dissolved salts, but also secondary releases or formations of iron and sulfide. After washing out the iron mobilized in the rising water, the model again calculates the continuously formed sulfide appearing again in the western inflow. The eastern inflow is likely to have persistently high iron concentrations due to low flow and flush rates. The model does not expect only a mixture associated with FeS precipitation, but a constant change between sulfide and iron surplus in the discharged mine water. If the discharge into the receiving water requires treatment of the mine water regarding these components, this would also mean a constant change between two operation modes in a processing plant.

Conclusions

This site example clearly demonstrates the effects that the interaction of pump management, the location of the pump site and the hydraulic conditions can have on mine water discharge. It is therefore advisable to carefully assess the site conditions and review the plans for the final design of a water province. Various scenarios can be easily checked in advance using numerical models. This requires reactive mass transport models, whose water extraction strategy is developed in coordination with the environmental impact assessments of the water discharge and the technical planning.

References

Bedford M, Markowska M, *et al.* (2022) TEXMIN HANDBOOK. A Guide to Managing the Risks Posed to Working and Abandoned Mining Facilities, and to the Surrounding Environment, Caused by Climate Change. Central Mining Institute (GIG), University of Exeter: Exeter, UK

Balzer IMR (2019) Mine Water in the Ruhr Area-Opportunities for the Future. Min. Rep., 155, 254–261

Coldewey WG, Semrau L (1994) Mine Water in the Ruhr Area (Federal Republic of Germany); University of Nottingham, Department of Mineral Resources Engineering, Nottingham, UK, pp. 613–629

Drobniewski M, Balzer I, Frankenhoff H, Witthaus H (2017) Mine Water Management in the Ruhr Coalfield. In Proceedings of the Mine Water and Circular Economy; IMWA: Lappeenranta, Finland

Eckart M, Gzyl G, Kories H, Metz M, Rengers R, Paul M (2007) Das Boxmodell-Konzept – Von der Modellbasierten Flutungskonzeption des Wismut-Standorts Ronneburg zur Anwendung in der Deutschen Steinkohle. In: Proceedings of the Internationales Bergbausymposium WISMUT, Gera, Germany, pp. 439–446

Vogt M, Lange GbR (2020) Machbarkeitsstudie Zentrale Wasserhaltung Lohberg. RAG Aktiengesellschaft: Essen, Germany

Annual Treatment Performances of Sulfate-Reducing Process Under Ethanol Addition Conditions with Rice Bran for Zinc-Containing AMD in Japan

Masataka Kondo[1], Yusei Masaki[2], Kana Hagihara[1], Koki Iguchi[1], Takaya hamai[2], Yuki Semoto[2], Taro Kamiya[1], Nobuaki Ishikawa[1], Masao Okumura[2], Naoki Sato[2]

[1]Metals Technology Center, Japan Organization for Metals and Energy Security, Furudate 9-3 Kosaka-kozan, Kosaka, Akita, Japan, kondo-masataka@jogmec.go.jp

[2]Metals Environment Management Department, Japan Organization for Metals and Energy Security, Toranomon 2-10-1, Minato-ku, Tokyo, Japan

Abstract

This study compares three nutritional conditions – ethanol alone and ethanol supplemented with two different proportions of rice bran – in a large-scale anaerobic sulfate-reducing process. pH neutralization and soluble Zn removal were consistently effective throughout the study period. Sulfate reduction and total Zn removal performance during winter varied depending on the nutrient conditions. The ethanol-only nutrient conditions resulted in insufficient sulfate reduction for total Zn removal during winter, whereas ethanol supplemented with rice bran was effective for sufficient sulfate reduction and subsequent total Zn removal. Supplementing ethanol with rice bran improved ethanol consumption efficiency and sustained treatment performance during winter.

Keywords: Passive Treatment, Ethanol, Rice Bran, Sulfate-Reducing Process, Total Zinc

Introduction

In Japan, active treatment is used to continuously treat mine water at approximately 100 abandoned mine sites. The Japan Organization for Metals and Energy Security (JOGMEC) has been researching and developing passive treatment systems to reduce treatment costs, focusing on processes that offer a short hydraulic retention time (HRT) and a small footprint for application in Japan. A large-scale, multi-step passive treatment test, consisting of a 2-hour aerobic iron (Fe) oxidizing/removal process followed by a 22.5-hour anaerobic sulfate-reducing process, was initiated in 2020 (Hayashi *et al.* 2021). The water flow rate during this test was set to 100 L/min. After the Fe oxidizing/removal process, acid mine drainage (AMD) was directed into the anaerobic process within vertical-flow biochemical reactors (BCRs) filled with a mixture of rice husk and limestone. Three different nutritional conditions with a continuous ethanol feed have been tested since 2020. Ethanol and rice bran have been used as direct, indirect, and supplemental nutrients for sulfate-reducing bacteria (SRB) (Masaki *et al.* 2023, Sato *et al.* 2024). The objective of this study is to investigate the annual treatment performance among three nutritional conditions based on ethanol feed, with or without the addition of rice bran.

Methods

Test site and chemistry of acid mine drainage

A large-scale passive treatment test was conducted at an abandoned metal mine in northern Japan (Fig. 1). The annual temperature at the test site varies from −10 to +40 °C. During winter, the site experiences heavy snowfall. AMD containing Fe, zinc (Zn), copper (Cu), and cadmium (Cd) was partially discharged from an adit into the passive treatment system via a pipe (Table 1). The AMD was first introduced into an aerobic vertical flow BCR filled with a mixture of rice husks and limestone for Fe removal. In this

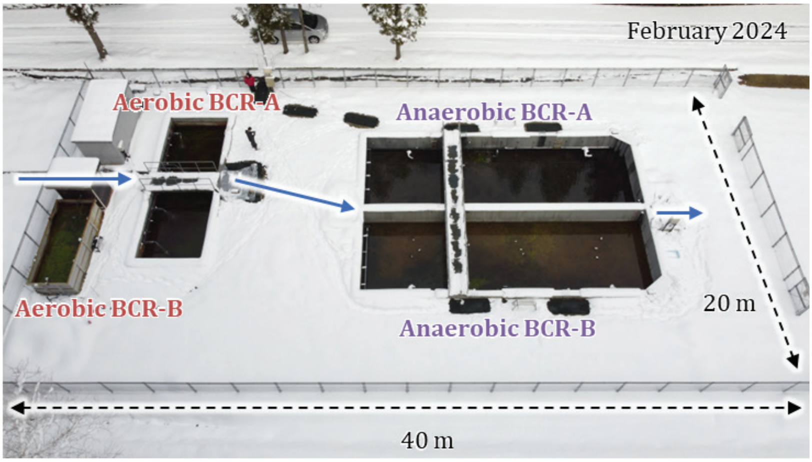

Figure 1 Large-scale, multi-step passive treatment test (image courtesy of Masataka Kondo). The blue arrows indicate the direction of flow. BCR, biochemical reactor.

process, ferrous iron (Fe^{2+}) was oxidized to ferric iron (Fe^{3+}) by Fe-oxidizing bacteria and precipitated primarily as schwertmannite (Masaki *et al.* 2021). The effluent from this process was then introduced into anaerobic BCRs for sulfate reduction. Fifty L/min of water, following Fe removal, was introduced into each anaerobic reactor, and the HRT in the reactor media was calculated to be 22.5 h. This study focused on the treatment results of the anaerobic BCR-A.

Anaerobic biochemical reactor structures

Two anaerobic BCRs were constructed with concrete walls and floors below the ground surface to maintain a minimum water temperature of 4 °C (Fig. 2). Each reactor was 5 m wide, 16 m long, and 3.5 m deep (total volume of 280 m3). At the bottom of the reactors, perforated pipes and limestone (20–40 mm) with a thickness of 0.15 m were installed to correct effluent water. A mixture of rice husk and limestone (20–40 mm) was then added to the reactors, divided into a lower layer (thickness of 1 m) and an upper layer (thickness of 0.5 m), with varying mixture weight ratios. Starting in 2020, the rice husk/limestone weight ratios in the lower and upper layers were set to 1/4 and 1/8, respectively. In 2022, limestone was added to the upper layers, and the rice husk/limestone weight ratio was changed to 1/16. The total media volume in each reactor was 120 m^3.

Carbon source nutrition conditions

Three different nutrient conditions with continuous ethanol feed were tested in the anaerobic BCR-A from 2021 to 2024. The first condition (Condition I) involved continuous ethanol feed using a metering pump, which introduced ethanol into the reactor from the surface, setting final feed concentrations of 36 mg/L (November 2021 to July 2022) and 24 mg/L (July 2022 to September 2022). The second condition (Condition II) involved continuous ethanol feed (final concentration of 24 mg/L) with an initial addition of 300 kg (0.3 wt% of the mixture media) of rice bran as supplemental nutrition (for approximately 26000 m^3 of annual water flow). The rice bran

Table 1 Average water quality of acid mine drainage (AMD) and the influent to the anaerobic BCRs from November 2021 to September 2024. Fe, iron; Zn, zinc; Cu, copper; Cd, cadmium; DO, dissolved oxygen.

	Temp. C°	pH	Fe mg/L	Zn mg/L	Cu mg/L	Cd mg/L	Sulfate mg/L	DO mg/L
AMD	13.2	3.6	38	17	4.9	0.1	296	–
Influent to the anaerobic BCRs	12.2	3.2	5.2	17	4.6	0.1	284	2.2

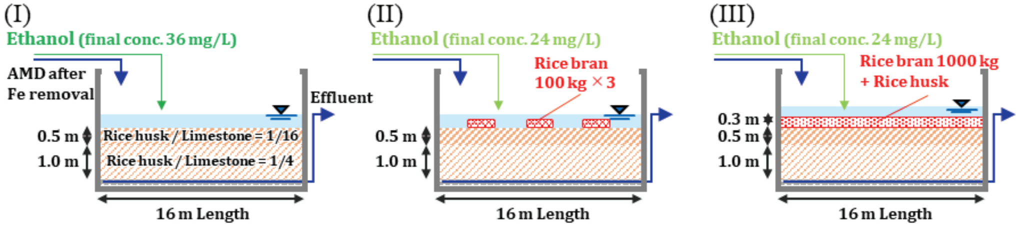

Figure 2 Cross-sectional structure of anaerobic BCR-A under three conditions: (I) 36 mg/L of ethanol, (II) 24 mg/L of ethanol supplemented with 300 kg of rice bran, and (III) 24 mg/L of ethanol supplemented with 1000 kg of rice bran.

was divided into three lines across the surface of the media (September 2022 to September 2023). In September 2023, the old rice bran was collected on one side, and 800 kg of new rice bran was added to the other side. Each batch of rice bran was then mixed with rice husk to form a 0.3-meter nutrition layer. Considering the remaining nutrients in the old rice bran, the third condition (Condition III) involved continuous ethanol feed (final concentration of 24 mg/L) with the addition of approximately 1000 kg (0.8 wt% of media) of rice bran addition (September 2023 to September 2024).

Monitoring parameters and analytical conditions

Temperature, pH, and oxidation–reduction potential (ORP; vs. Ag/AgCl) were measured on-site using a portable multi-water quality meter (MM-42DP, DKK-TOA Corp., Japan), and dissolved oxygen (DO) was measured using a portable DO meter (HQ1130, Hach Company, CO., USA). Filtered (0.45 µm) and unfiltered water samples were collected in high-density polyethylene bottles. The concentrations of Zn, Cu, and Cd were determined through inductively coupled plasma optical emission spectroscopy (Agilent 5110 ICP-OES, Agilent Technologies Inc., CA, USA). The sulfate concentrations in the filtrates were determined via ion chromatography (Dionex ICS-6000, Thermo Fisher Scientific, Waltham, MA, USA). The concentrations of organic acids and ethanol in the filtrates were determined by ultra-performance liquid chromatography using an ion exclusion column (ICPak Ion Exclusion Column: 7 µm, 7.8 mm × 300 mm; Waters Corp., USA), equipped with photodiode array detection (λ=210 nm) and refractive index detection, respectively.

Results and discussion

Treatment performance of the anaerobic process under three nutrition conditions

The water temperature of the effluent from the anaerobic BCRs ranged between 4.6 and 21.0 °C from 2021 to 2024, varying with changes in ambient temperature (Fig. 3). The pH in the effluents increased steadily due to the dissolution of limestone, and ranged between 6.2 and 7.4, with no remarkable differences observed across the nutrient conditions. Anaerobic conditions were maintained, with the ORP remaining at approximately −250 to −300 mV throughout the entire period under all nutrition conditions. During winter, the maximum ORP values were −193 mV under Condition (I), −208 mV under Condition (II), and −255 mV under Condition (III), respectively. The minimum sulfate reduction concentrations for each nutrient condition during winter were 24, 26, and 61 mg/L, respectively.

The stoichiometric requirement for sulfate reduction to remove metals as sulfides from the influent water was approximately 30 mg/L. Under conditions (I) and (II), the sulfate reduction concentration occasionally fell below 30 mg/L. For Zn removal performance, soluble Zn concentrations in the filtered effluent water remained below 0.2 mg/L across all seasons, regardless of nutrient conditions. The total Zn concentration sharply increased to 7.4 mg/L under Condition (I) and gradually increased to 1.9 mg/L under Condition (II). Under Condition (III), the maximum total Zn concentration remained below 0.1 mg/L, even during winter.

The concentration of ethanol in the effluent showed a trend similar to that of the total Zn concentration in the winter season, reaching 31 mg/L (86% of feed) under Condition (I) and 11 mg/L (46% of feed) under Condition (II). The results indicated that the activity of SRB decreased owing to the effect of lower water temperatures, and ethanol, as a carbon source, was no longer consumed. However, the presence of rice bran as a supplemental nutrient source increased the efficiency of ethanol consumption and slowed the increase in total zinc concentration in the effluent. Under Condition (III), the ethanol concentration in the effluent was below the detection limit in nearly all seasons, except during the start-up period.

Table 2 lists the differences in treatment performance for Zn and other parameters during winter across the three nutrient conditions. The total Zn concentration had not exceeded 2 mg/L (the domestic discharge standard) under conditions (II) and (III) throughout the study period, whereas exceeded under Condition (I). Under Condition (II), total Zn concentration

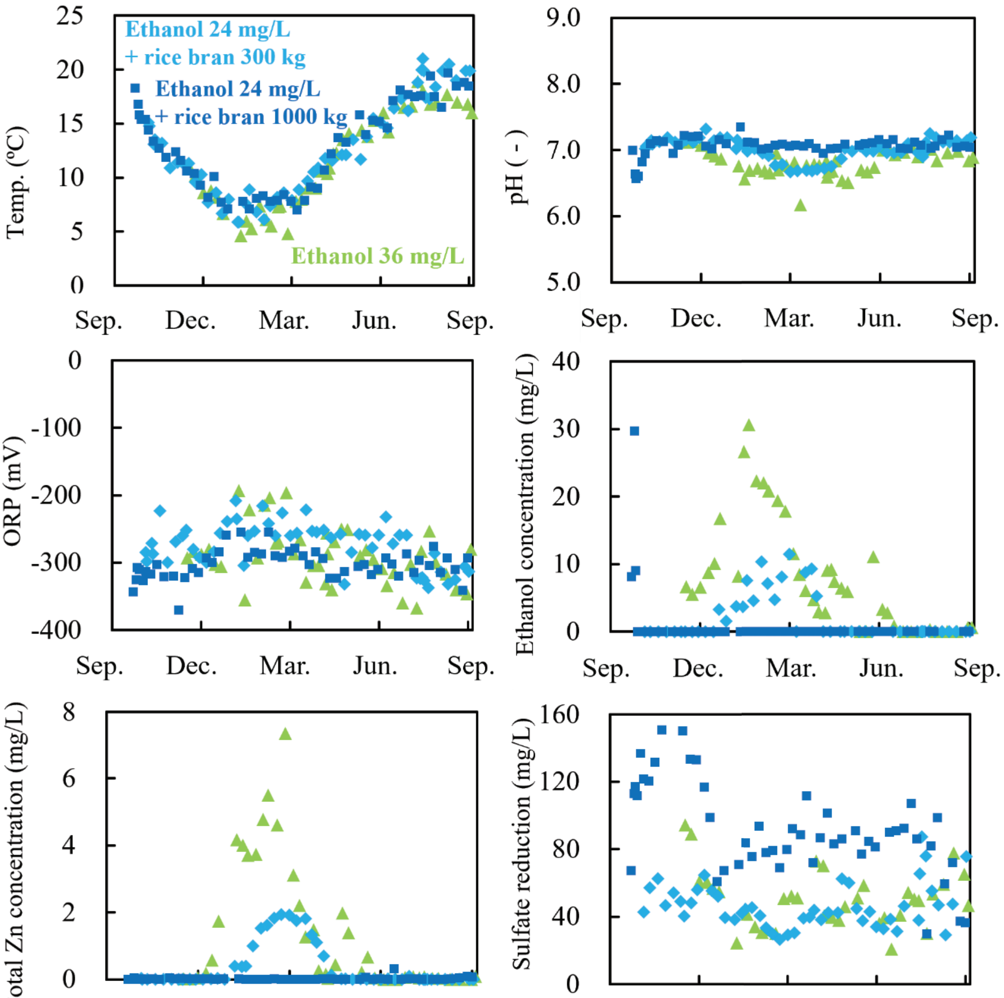

Figure 3 *Changes in temperature, pH, oxygen–reduction potential (ORP), concentrations of ethanol and total Zn, sulfate reduction, and effluent characteristics of anaerobic BCR-A. Light green triangle: 36 mg/L of ethanol; light blue square: 24 mg/L of ethanol with 300 kg of rice bran; blue square: 24 mg/L of ethanol with 1000 kg of rice bran.*

increased and approached 2 mg/L, suggesting that at least 300 kg of rice bran was required for this test scale, and that a larger amount of rice bran was needed for stable Zn treatment. The total amounts of organic carbon added to the BCRs each year were calculated, assuming an organic carbon content ratio of 45wt% in rice bran based on feed analysis. This amounted to 489 kg-C/y under Condition (I), 460 kg-C/y (325 kg from ethanol and 135 kg from rice bran) under Condition (II), and 775 kg-C/y (325 kg from ethanol and 450 kg from rice bran) under Condition (III).

The total supplied organic carbon was lower under Condition (II) than Condition (I); however, sulfate reduction was higher, and the maximum Zn concentration was lower under Condition (II) compared to Condition (I). This suggested that rice bran supplied not only ethanol but also several types of carbon sources, along with trace elements such as nitrogen (N) and phosphorus (P), which resulted in a diverse community of SRB. As a result, sulfate-reducing activity was maintained even at low water temperatures (Sato *et al*. 2024). It was also assumed that this helped maintain the activity of ethanol-utilizing SRB, resulting in the low concentration of unutilized ethanol at the outlet, as shown in Fig. 3. Therefore, the efficiency of metal removal under Condition (II) surpassed that under Condition (I), which involved ethanol alone, despite the lower amount of organic carbon. Under Condition (III), the high total organic carbon content and the presence of rice bran across the entire surface layer led to a more uniform nutrient supply from the rice bran, resulting in the most stable treatment performance during winter.

Sulfate reduction concentration with depth

A comparison of sulfate reduction across different depths showed that sulfate reduction was higher at depths shallower than 1 m (half the depth of the lower layer) during non-winter seasons under all nutrient conditions (Fig. 4). In contrast, during winter, sulfate reduction decreased at depths shallower than 1 m and increased at depths greater than 1 m under conditions (I) and (II). This indicated that the region of sulfate reduction activity shifted to deeper layers owing to the decrease in water temperature. Under Condition (III), sulfate reduction in areas deeper than 1 m did not decrease substantially during winter, and the total amount of sulfate reduction was the highest among the three nutrient conditions. It was assumed that organic nutrient sources, including ethanol, were consumed at shallower depths due to the addition of rice bran, resulting in more active sulfate reduction. This may have resulted in the precipitation of metal sulfides at shallower depths, trapping them on the rice husk surface over a wider area. Consequently, the total Zn concentrations were lower with rice bran than with ethanol alone (Fig. 3), suggesting that the sulfides were less likely to be released as suspended solids. Considering the capture area of the suspended solids, the reaction by SRBs should occur primarily on the upper side of the contents. To facilitate this, nutrient sources must be present in sufficient quantities during winter.

Conclusions

In this study, the annual treatment performance of the anaerobic BCR under three nutrient conditions with continuous ethanol feeding was investigated. We

***Table 2** Summary of treatment performance under three nutrient conditions during winter (December to February).*

		Condition (I) 36 mg/L of ethanol	Condition (II) 24 mg/L of ethanol + 300 kg of rice bran	Condition (III) 24 mg/L of ethanol + 1000 kg of rice bran
Domestic discharge standard of Zn	–	Over	Under	Under
Average ORP in winter	mV	259	253	281
Average sulfate reduction in winter	mg/L	42	42	81
Total amount of organic carbon	kg/y	489	460	775

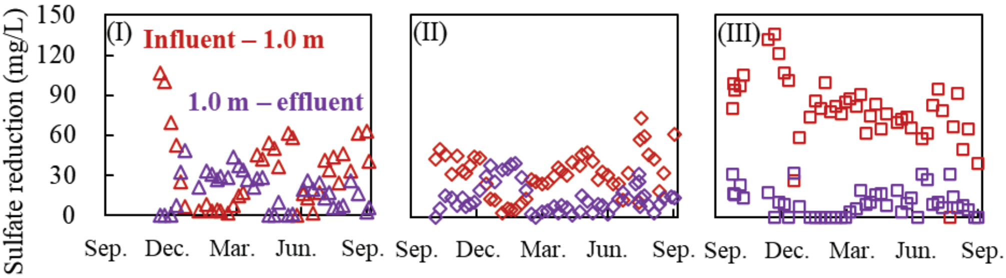

Figure 4 Changes in sulfate reduction with depth: Condition (I) 36 mg/L of ethanol, Condition (II) 24 mg/L of ethanol supplemented with 300 kg of rice bran, and Condition (III) 24 mg/L of ethanol supplemented with 1000 kg of rice bran.

observed no appreciable difference in the treatment performance for metal removal under any of the nutrient conditions during the non-winter period. Sulfate reduction activity, the concentration of unused ethanol, and total Zn concentration exhibited different behaviours during winter. Under 36 mg/L of ethanol (Condition I), sulfate reduction activity decreased to a minimum of 24 mg/L, and the total Zn concentration increased sharply to a maximum of 7.4 mg/L. Under 24 mg/L of ethanol supplemented with 300 kg of rice bran (Condition II), sulfate reduction activity decreased to a minimum of 26 mg/L; however, the total Zn concentration increased gradually to a maximum of 1.9 mg/L meeting Japan domestic discharge standard. Under 24 mg/L of ethanol supplemented with 1000 kg of rice bran (Condition III), sulfate reduction activity was sufficiently high during the winter season, with a minimum of 61 mg/L, and the total Zn concentration increased to only a maximum of 0.1 mg/L. It was found that the addition of rice bran as a supplemental nutrient source, alongside ethanol, improved winter treatment performance without substantial differences in the annual organic carbon supply. Comparing sulfate reduction activity with depth, sulfate reduction in the upper media layer decreased during winter under conditions (I) and (II), with the active sulfate reduction area shifting downward. In contrast, sulfate reduction activity in the upper layer remained relatively high under Condition (III) during winter. It was also found that sulfate reduction activity in the upper layer was maintained during winter, ensuring the preservation of the thickness of the layer where suspended metal sulfide solids were trapped, thereby sustaining effective treatment performance. Other nutrient source conditions, including modifications to the timing of ethanol and rice bran addition, will be tested in future research.

References

Hayashi K, Washio T, Masaki Y, Hamai T, Sakata T and Sato N (2021) Full-scale compact passive treatment system for a Japanese AMD by aerobic bioreactor for Fe removal and sulfate reducing bacteria bioreactor for Zn removal. Proceedings of the 14th International Mine Water Association. Cardiff, Wales, United Kingdom. July 12–15, 2021. (Online)

Masaki Y, Hayashi K, Hamai T, Washio T, Sakata T, Kanayama A, Horiuchi K, Sakoda M, Masuda N and Sato N (2021) A full-scale test of iron removal from acid mine drainage using iron-oxidizing bacteria. Proceedings of The Mining and Materials Processing Institute of Japan. Minato-ku, Tokyo, Japan. March 8–10, 2021. (Online)

Masaki Y, Washio T, Hagihara K, Hamai T, Horiuchi K, Semoto Y, Kamiya T, Takamoto K and Sato N (2023) A Biological Sulfate-Reducing Process for Zinc-Containing AMD in Japan: Comparison of Annual Treatment Performances Among Nutrient Conditions of Ethanol, Rice Bran and Their Hybrid for Sulfate-Reducing Bacteria. Proceedings of the International Mine Water Association. Newport, Wales, United Kingdom. July 17–21, 2023.

Sato Y, Hamai T, Masaki Y, Aoyagi T, Inaba T, Hori T and Habe H (2024) Replacing rice bran with low-molecular-weight substrates affected the performance and metabolic feature of sulfate-reducing bioreactors treating acid mine drainage. J Environ Chem Eng 12 (2): 112118, doi: 10.1016/j.jece.2024.112118.

Multisensor-based Surface Water Quality Monitoring: A Case Study for the Chalkidiki, Greece

Veronika Kopačková-Strnadová[1], Martin Kýhos[1,2], Jan Jelének[1], Giannis Zabokas[3], Athina Agali[3], Kostas Gounaris[3]

[1]*Czech Geological Survey, Klárov 131/3, Malá Strana, 118 00 Praha 1, Czech Republic*

[2]*CZU, Faculty of Environmental Sciences, Kamýcká 129, 165 00 Prague 6, Czech Republic*

[3]*Hellas Gold, Stratoni, Chalkidiki, 63074, Greece*

Abstract

This study investigates the application of multisource and multiscale Earth Observation (EO) technologies for monitoring water quality in the Kassandra Mining District, Chalkidiki, Greece. We integrate spectral data from various platforms: high-resolution water spectral libraries from an OceanOptics STS-VIS-VIS spectrometer (337–823 nm) on a DJI Phantom 3 UAV, multispectral imagery from a Parrot Sequoia camera (4 bands) on a DJI Phantom 4 Pro UAV, and 8-band multispectral Planet Labs satellite data at 3-meter resolution. These datasets are combined with in situ surface water samples from field campaigns and long-term monitoring by Hellas Gold (HG). Initial results indicate that Total Suspended Solids (TSS), serving as a proxy for estimating arsenic high/medium/low (As) levels, can be predicted at high accuracy using Partial Least Square Regression (PLSR) on the water spectral libraries ($R^2 = 0.85$). Modified spectral indices based on the most important wavelengths identified by PLSR achieved an R^2 of 0.82, while original multispectral indices from PlanetScope imagery yielded an R^2 of 0.78. These findings suggest strong potential for utilizing these data and methods in water quality monitoring at local and regional scales.

Keywords: Mine water tracer test, Tyrol/Austria, underground mine, density stratification, lessons learned

Introduction

Water monitoring is a crucial task for mining companies. Mining operations can affect local water resources, so regular monitoring is vital for ensuring compliance with environmental regulations. Additionally, water quality assessments are essential for pollution prevention, allowing companies to identify contamination from potentially toxic metals or toxic chemicals early on. Immediate corrective actions can then be taken to prevent broader environmental damage affecting ecosystems and public health (Mogimi *et al.* 2024).

Remote sensing techniques offer numerous advantages in water monitoring, including comprehensive coverage, cost efficiency, and real-time monitoring capabilities. Imaging spectroscopy presents an effective alternative to traditional laboratory analyses, enabling the detection of various environmental parameters, such as total suspended solids (TSS), using spectral sensors (Adjovu *et al.* 2023). Many case studies focused on surface water quality have primarily utilized satellite data (Wirabumi at. al. 2021). Additionally, the use of UAV-sensed data has rapidly emerged, highlighting its significant potential for the water pollution monitoring (Guimarães *et al.* 2019, Zeng *et al.* 2017).

In this study, we explored the integration of various UAV-based spectral data and developed spectral models suitable for real-time monitoring of surface water quality. We also evaluated the feasibility of up-scaling these spectral models to match the spectral and spatial resolution of high-resolution multispectral satellite data from Planet Labs, thereby facilitating water monitoring over larger areas.

Test Site

The study was conducted in the Kassandra Mining District on the Chalkidiki Peninsula in northern Greece, known for its rich mineral resources. It hosts one active underground mine, one underground mine in care and maintenance and one open pit / unground mine under construction, all operated by Hellas Gold (HG): Olympias, Stratoni, and Skouries. Olympias primarily extracts gold (Au), lead (Pb), and zinc (Zn), focusing on gold and base metal production. Stratoni specialized in lead (Pb), zinc (Zn), and silver (Ag), establishing itself as a key silver producer; however, it is currently under maintenance. Skouries, which focuses on copper (Cu) and gold (Au), serves as an important source of these minerals but is currently under construction.

Data

This section outlines the field data acquisition methods, including UAV-based and water sampling, conducted from April 11th to 17th, 2024, in the Kassandra Mining District of Chalkidiki (Fig. 1).

UAV-Based Water Spectral Data Acquisition

The lightweight OceanOptics STS-VIS spectroradiometer (40 mm × 42 mm × 24 mm, 60 g) was mounted on a DJI Phantom 3 UAV to acquire water spectral libraries, capturing data across 1,024 spectral bands in the 337–823 nm range with an optical resolution of 1.5 nm and a 25° field of view (FOV). Powered by an external battery and operated with a Raspberry Pi 3, it features a Wi-Fi-enabled web interface for ground control. A custom 3D-printed mount was designed for optimal weight distribution and stability. Data were collected at 15 sites (Fig. 1) across three rivers and streams, flying at 3 meters above the water for minimal disturbance and achieving a spatial resolution of 1.2 meters. Data were systematically collected at two-second intervals along three transects: 50 meters upstream, 50 meters downstream, and diagonally across each water body. A customized Python script in Jupyter Notebook processed the radiance data from *.txt files, calculating final reflectance using input files for dark body, white reference, and sample measurements per the OceanView manual. The Savitzky-Golay filter (SGF) was applied to smooth the collected spectra using the ‘scipy.signal.savgol_filter’ function in Python.

Concurrently, multispectral imagery was captured at 13 sites near the mining pits using a lightweight (72 g) Parrot Sequoia camera mounted on a DJI Phantom 3 UAV. This 4-band sensor operates in the Green, Red, Red Edge, and Near-Infrared (NIR) ranges and was paired with a 35-gram sunshine sensor to measure incident solar radiation. Data were collected at 35 meters altitude, with 11-meter line spacing and 2-second

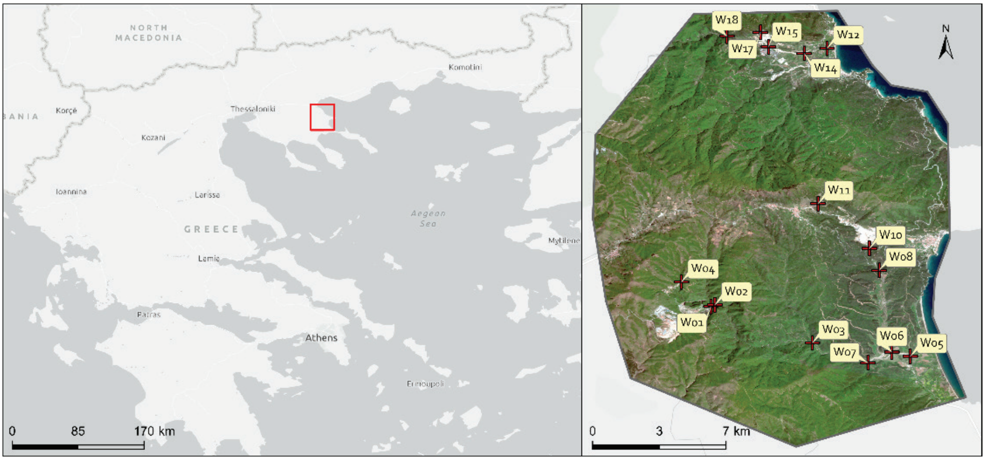

***Figure 1** Areas of the interest: Water Quality sampling and UAV data acquisition sites.*

capture intervals to ensure adequate overlap. Calibration images were recorded before each flight with an Airnov VIS-NIR greyscale calibration panel. All multispectral data were processed and calibrated using Agisoft Metashape Professional, resulting in high-resolution mosaicked reflectance images (2.5 cm) for detailed spatial insights into the study sites.

Satellite Data

An 8-band multispectral surface reflectance mosaic from PlanetScope, harmonized to the Sentinel-2 sensor, was obtained in GeoTIFF format (Planet Labs PBC, 2024). This mosaic, acquired on April 11th, was specifically chosen to align with the UAV data collection timeframe. The data were accessed through the PlanetScope Explorer platform under a student scientific license.

Water in-situ samples

Water samples were collected during field-work from April 11th to 17th, 2024, in conjunction with UAV data acquisition at all 15 locations that matched the UAV sites (Fig. 1), including sections of the Olympias, Stratoni, and Skouries streams in active mining areas. These samples were analyzed at HG laboratories for the same parameters as in long-term monitoring, including potentially toxic metals and Total Suspended Solids (TSS) concentrations. However, organic carbon, another important water quality parameter, was not possible to analyse at HG laboratories. The results were statistically evaluated to identify key relationships relevant to water quality assessment. Additionally, we examined long-term environmental data from the HG monitoring system, covering January 2015 to April 2024, which includes a wide variety of parameters also analyzed in the April 2024 water samples.

Methods

Statistical analysis of laboratory water analysis

A common statistical assessment was applied to the in-situ water sample data, which included correlation analysis, linear regression, and calculation of the coefficient of determination.

Partial Least Squares Regression (PLSR)

To assess the high-spectral resolution data from the OceanOptics STS-VIS (water spectral libraries), Partial Least Squares Regression (PLSR) was employed. PLSR is a quantitative chemometric method designed to analyze data with strong correlations and noise. Its main advantage over other multivariate methods is its ability to manage datasets with more variables than samples, making it ideal for spectroscopic data containing hundreds to thousands of reflectance values. PLSR utilizes two matrices: X (independent variables, such as spectral libraries) and Y (dependent variables, such as chemical laboratory analyses). It applies a technique similar to Principal Component Analysis (PCA) to reduce the dimensionality of the X matrix while maximizing its covariance with Y.

Band indices

PLSR was conducted on the OceanOptics STS-VIS high-spectral resolution data (water spectral libraries) to identify spectral wavelengths most strongly correlated with selected water parameters. The most sensitive wavelengths were then used to modify existing multispectral indices, including the Normalized Difference Vegetation Index (NDVI; Rouse *et al.*, 1973), Normalized Difference Water Index (NDWI; McFeeters, 1996), Normalized Difference Suspended Solids Index (NDSSI; Hossain *et al.*, 2010), and Water Ratio Index/ red-band modification (WRI; Shen and Li, 2010). These indices were applied to imaging data from the multispectral Parrot Sequoia and PlanetScope sensors; however, NDSSI was not calculated for the Parrot Sequoia due to its lower spectral resolution. Finally, water indices from all three datasets were statistically analyzed using linear regression to assess their relationships with the tested water parameters.

Results

Selection of the water environmental indicators

After analyzing laboratory results, TSS was the only optically active constituent (OAC) that consistently exceeded detection limits across most samples, showing significant variation among sampling sites. A linear regression analysis revealed a correlation between TSS and As values ($R^2 = 0.33$), which improved after excluding samples with low TSS (<5 mg/L) and As (<15 µg/L) concentrations, leading to high RMSE values. With these thresholds, the correlation strengthened, achieving an R^2 of 0.43 and 0.44 for both water sample analysis and long-term monitoring, respectively (Fig. 2). These findings suggest that TSS can serve as a proxy for estimating arsenic concentrations (Nasrabati *et al.* 2018), enabling predictions of low, medium, and high As levels based on TSS measurements.

Spectral data analysis

PLSR was applied using high-resolution spectral data from water spectral libraries. In this analysis, reflectance served as the independent variable (X), while TSS and As were the dependent variables (Y). The derived regression coefficients (Fig. 3a-b) indicated that wavelengths from the red to near-infrared regions were the most significant for predicting TSS as well as for As. Consequently, a PLSR model was established for TSS prediction, achieving an R^2 of 0.99 for the training dataset and R^2 of 0.85 for the validation dataset (Fig. 3c) using the Leave-One-Out method (Kopačková-Strnadová *et al.* 2021). In the case of As, we could only establish a training model, achieving an R^2 of 0.97 (Fig. 3d). Unfortunately, validation was not feasible due to the dataset lacking representative values that fall in the middle range between low and high values.

To assess the estimation of TSS, potentially also As, using spectral indices, four commonly used multispectral indices were adapted to suit the high spectral resolution of the water spectral libraries. Rather than broader spectral regions for the blue, green, red, and near-infrared bands, we used wavelengths most sensitive to TSS, identified by PLSR: 460.5 nm, 530.7 nm, 674.2 nm, and 805.9 nm (Tab. 1). These spectral indices were then also applied to images from the Multispectral Planet using the original spectral bands (Tab. 1). For Parrot Sequoia images, the NDSSI index wasn't used due to the limited number of spectral bands available.

When comparing the regression results between the in-situ data and the analyzed spectral datasets (Tab. 2), the water spectral libraries—characterized by high spectral resolution and high spatial detail—to those obtained from multispectral imaging data, it is evident that models with higher R^2 values were achieved using the water spectral libraries. However, this trend does not hold for the NDSSI index, which seems that may perform better with broader wavelength ranges (e.g., spectral bands) as it was specifically designed for multispectral data. This will be the focus of further analysis. Overall,

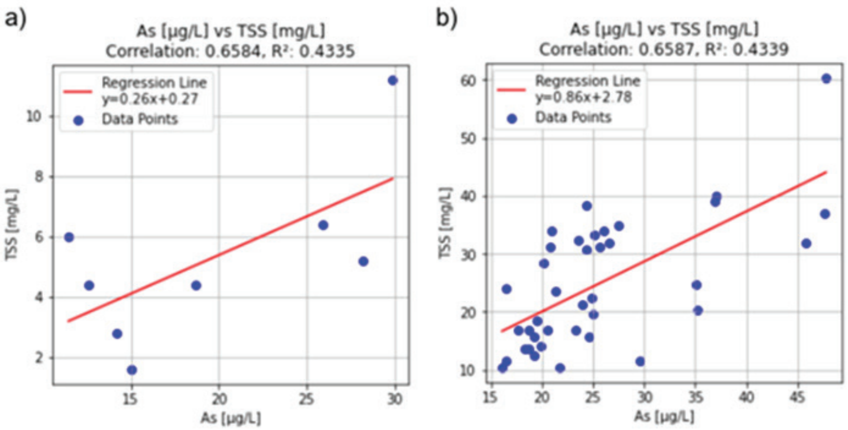

Figure 2 *Correlation between TSS and As: 2024 In-situ samples, r=0.66, R2=0.43 (a), Long-term monitoring 2015-2024, r=0.66, R2=0.44 (p<0.001) (b).*

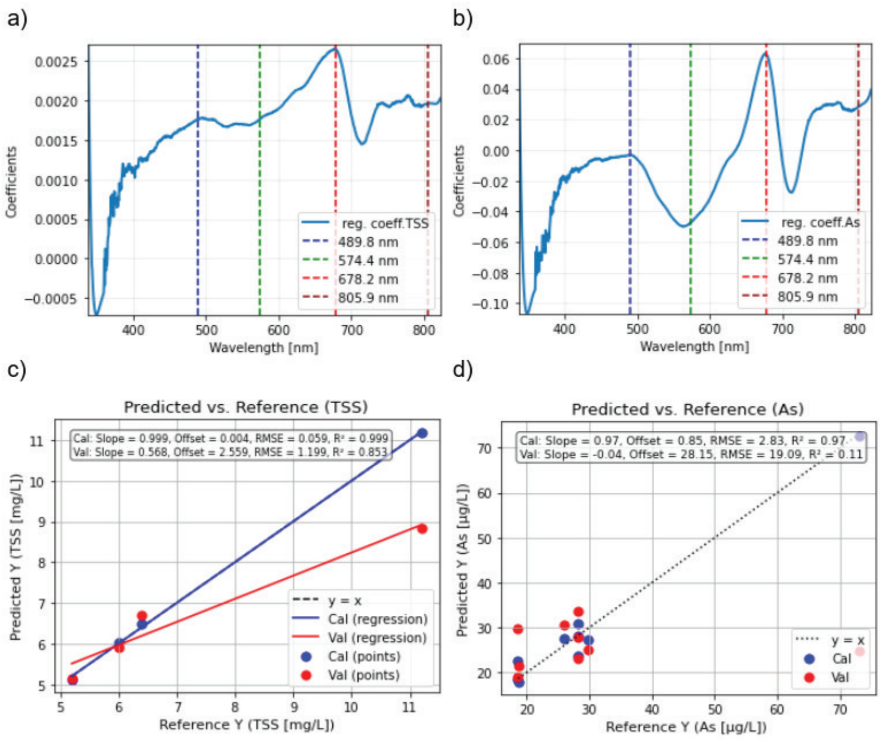

Figure 3 PLSR analysis and predictions applied to high-resolution spectral data - water spectral libraries: (a) Regression coefficients for TSS prediction, (b) Regression coefficients for As prediction, (c) PLSR predictions for TSS (blue – calibration, red – validation), and (d) PLSR predictions for As (blue – calibration, red – validation).

Table 1 Indices definition and adjusted formula used for the water spectral libraries/STS-VIS data.

Indices	Standard formula	Reference	Adjusted formula to STS-VIS data
NDVI	$\frac{\rho_{NIR} - \rho_{RED}}{\rho_{NIR} + \rho_{RED}}$	Rouse *et al.*, 1973	$\frac{\rho_{805.9} - \rho_{674.2}}{\rho_{805.9} + \rho_{674.2}}$
WRI (Red)	$\frac{\rho_{GREEN} - \rho_{RED}}{\rho_{NIR} + \rho_{RED}}$	Shen and Li, 2010	$\frac{\rho_{530.7} + \rho_{674.2}}{\rho_{805.9} + \rho_{674.2}}$
NDWI	$\frac{\rho_{GREEN} - \rho_{NIR}}{\rho_{GREEN} + \rho_{NIR}}$	McFeeters, 1996	$\frac{\rho_{530.7} - \rho_{805.9}}{\rho_{530.7} + \rho_{805.9}}$
NDSSI	$\frac{\rho_{BLUE} - \rho_{NIR}}{\rho_{BLUE} + \rho_{NIR}}$	Hossain *et al.*, 2010	$\frac{\rho_{460.5} - \rho_{805.9}}{\rho_{460.5} + \rho_{805.9}}$

Table 2 Statistical evaluation of the linear regressions performed between water in-situ analysis and the spectral indices from the water spectral libraries (STS-VIS), Parrot Sequoia, and Planet Lab data.

Indices	R^2/Regression		
	STS-VIS data	Parrot Sequoia	Planet Lab data
NDVI	0.815 / y = 0.05x – 0.09	0.721 / y = 0.11x – 0.51	0.493 / y = 6.11x + 1.76
WRI	0.731 / y = -0.02x + 1.02	0.309 / y = -0.08x – 1.76	0.647 / y = -18.49x + 17.60
NDWI	0.781 / y = -0.02x + 0.01	0.623 / y = -0.07x + 0.58	0.775 / y = -23.49x – 2.83
NDSSI	0.288 / y = -0.10x – 0.09	X	0.715 / y = -24.00x – 3.93

reliable TSS predictions were obtained when scaling the tested indices to Planet Lab and Parrot Sequoia data, with the NDWI index achieving the highest R^2 of 0.78 and 0.62 respectively.

Conclusion

This study examined the feasibility of estimating Total Suspended Solids (TSS) correlated with arsenic (As) using high spectral and spatial resolution data, specifically water spectral libraries (STS-VIS) and multispectral imaging data from PlanetScope. The results confirm the significant potential of these contactless technologies for water quality monitoring, leading to the following conclusions: a) TSS is an important parameter correlating with As ($r = 0.66$, $R^2 = 0.44$, $p < 0.001$), indicating TSS can serve as a proxy for semiquantitative As estimations (high-medium and low values); b) TSS predictions can achieve an R^2 of 0.85 using PLSR on the water spectral libraries; c) Generally good predictions were observed with multispectral indices and PlanetScope data (Fig. 4), with the NDWI yielding the best results ($R^2 = 0.78$).

Acknowledgment

The presented analysis was conducted under the support of the EC grant MultiMiner. The MultiMiner project is funded by the European Union's Horizon Europe research and innovation actions programme under Grant Agreement No. 10109137474.

References

Adjovu, G.E., Stephen, H., James, D., Ahmad, S., 2023. Measurement of Total Dissolved Solids and Total Suspended Solids in Water Systems: A Review of the Issues, Conventional, and Remote Sensing Techniques. Remote Sensing 15, 3534.

Hellas Gold S.A., 2016. Environmental Monitoring Program. Available at: https://environmental.hellas-gold.com/ [Accessed 20 Jul. 2024].

Hossain, A. K. M. A., Jia, Y., & Chao, X. (2010, September). Development of remote sensing based index for estimating/mapping suspended sediment concentration in river and lake environments. In Proceedings of 8th international symposium on ECOHYDRAULICS (ISE 2010) (Vol. 435, pp. 578-585).

Jackisch, R., Heincke, B. H., Zimmermann, R., Sørensen, E. V., Pirttijärvi, M., Kirsch, M., ... & Gloaguen, R. (2021). Drone-based magnetic and multispectral surveys to develop a 3D model for mineral exploration at Qullissat, Disko Island, Greenland. Solid Earth Discussions, 2021, 1-51.

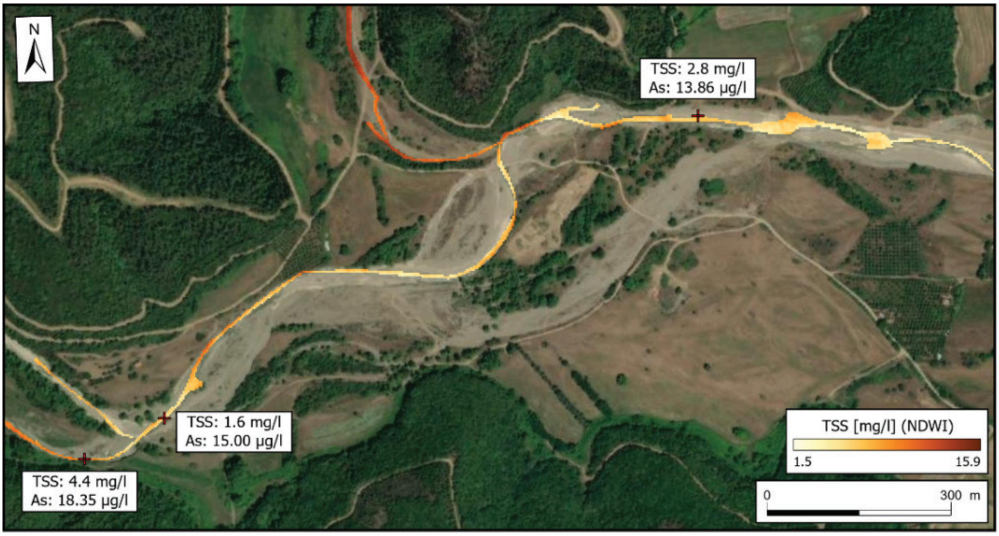

Figure 4 TSS estimated employing NDWI to PlanetScope data (11th of April 2024, Skouries).

Kopačková-Strnadová, V., Rapprich, V., McLemore, V., Pour, O., & Magna, T. (2021). Quantitative estimation of rare earth element abundances in compositionally distinct carbonatites: Implications for proximal remote-sensing prospection of critical elements. International Journal of Applied Earth Observations and Geoinformation, 103, 102423

McFeeters, S. K. (1996). The use of the Normalized Difference Water Index (NDWI) in the delineation of open water features. International journal of remote sensing, 17(7), 1425-1432.

Planet Labs PBC, 2024. Scene Level Normalization and Harmonization of Planet Dove Imagery. Retrieved from https://assets.planet.com/docs/scene_level_normalization_of_planet_dove_imagery.pdf

Rouse, J. W., Haas, R. H., Schell, J. A., & Deering, D. W. (1974). Monitoring vegetation systems in the Great Plains with ERTS. NASA Spec. Publ, 351(1), 309.

Shen, L., & Li, C. (2010, June). Water body extraction from Landsat ETM+ imagery using adaboost algorithm. In 2010 18th International Conference on Geoinformatics (pp. 1-4). IEEE.

Wirabumi, P., Kamal, M., Wicaksono, P., 2021. Determining effective water depth for total suspended solids (TSS) mapping using PlanetScope imagery. International Journal of Remote Sensing 42, 5784–5810.

Zeng, C., Richardson, M., King, D.J., 2017. The impacts of environmental variables on water reflectance measured using a lightweight unmanned aerial vehicle (UAV)-based spectrometer system. ISPRS Journal of Photogrammetry and Remote Sensing 130, 217–230.

Efficient Earth Observation System for Acid Mine Drainage

Veronika Kopačková-Strnadová[1], Martin Kýhos[1], Jan Jelének[1]

[1]Czech Geological Survey, Prague 11821, Czech Republic, veronika.strnadova@geology.cz, https://orcid.org/0000-0001-9317-5990

Abstract

Acid Mine Drainage (AMD), a significant water pollutant from sulfide mineral oxidation in mining areas, generates sulfuric acid and harmful substances. Effective AMD management involves careful material handling, treatment, and water management. Imaging spectroscopy provides a practical alternative to traditional chemical analysis, identifying pyrite oxidation "hot spots" and sulfate mineral formation. This research develops robust AMD monitoring systems using machine learning techniques on optical multi- and hyperspectral data. We use hyperspectral (PIKA L camera, UAV) and multispectral (Sentinel-2, orbital) datasets at the Lítov post-mine dump (Sokolov lignite basin, Czech Republic). Validated against XRD mineralogy and Google Earth-identified hotspots, Radial Basis Function Support Vector Machine (RBF SVM) outperforms other ML methods in identifying AMD hot spots and class separation. RBF SVM effectively detects AMD discharge and distinguishes mineral mixtures (oxy-hydroxides and oxides) using both Pika L and Sentinel-2 data.

Keywords: Acid Mine Drainage, multispectral data, hyperspectral data, Machine Learning, classification

Introduction

Acid Mine Drainage (AMD) is a significant environmental issue that arises when water flows over or through sulfur-bearing rocks, such as coal or metal ores, which have been exposed to air and water during mining operations. This exposure leads to the oxidation of sulfide minerals, producing sulfuric acid. The generated acid reacts with surrounding rocks, releasing various toxic metals and metalloids, including arsenic, lead, and cadmium, into the water. Consequently, the discharged water becomes highly acidic and contaminated, posing severe ecological risks. Acidic water can devastate aquatic habitats, harm fish and other aquatic organisms, and significantly degrade overall water quality. It can also contaminate drinking water sources, leading to adverse effects on human health, including neurological and developmental issues. Addressing AMD requires implementing appropriate measures during mining operations, such as effective handling and treatment of mined materials and the establishment of robust water management systems. Additionally, post-mining remediation techniques, such as neutralizing the acid and removing harmful substances, are employed to minimize environmental impact and restore affected ecosystems.

Recent advancements in remote sensing technologies have revolutionized the monitoring of AMD. Imaging spectroscopy serves as an efficient alternative to traditional chemical analyses for mine characterization and assessing potential AMD discharge, as well as for acid sulfate soil mapping. Spectroscopic approach focuses on identifying minerals that indicate subaerial oxidation of pyrite (e.g., jarosite), often referred to as "hot spots," and the subsequent formation of the other oxidation products (such as oxy-hydroxides and oxides) (Swayze *et al.* 2000).

To date, effective methods have been demonstrated to detect potential AMD hotspots using hyperspectral systems deployed on Unmanned Aerial Vehicles (UAVs, Flores *et al.* 2021) and aerial platforms (Kopačková

2014). Moreover, the availability of current satellite systems that provide free multispectral data, such as Sentinel-2, and hyperspectral imaging data from platforms like EnMap and PRISMA, offers novel opportunities for monitoring AMD from space. Furthermore, a feasibility study by Chalkey *et al.* (2023) highlighted the potential of multi-scale AMD monitoring using various remote sensing platforms, including UAV-based systems, PlanetScope, and Sentinel-2. Their research emphasized the importance of integrating multiple datasets for comprehensive monitoring, which can enhance the accuracy and efficiency of AMD detection.

In this study, we aim to advance the development of innovative and highly efficient AMD monitoring systems by exploring the application of Machine Learning (ML) techniques to imaging spectral data acquired by different platforms, including UAV-based hyperspectral data (PIKA L) and multi-spectral imagery from Sentinel-2 satellite. By leveraging these technologies, we aim at improving the detection and management of AMD, ultimately contributing to more sustainable mining practices and better protection of the environment.

Test site

The study was conducted at the Lítov post-mine dump, located in the western part of the Sokolov lignite basin in the Czech Republic. This site is notable for its inclusion in the Czech-Bavarian "Geopark" program, which highlights the unique characteristics of man-made landscapes. The Lítov dump is particularly remarkable due to its highly acidic substrates (Kopačková 2014, Kopačková and Hladíková 2014), sparse vegetation, and the presence of a unique semi-desert environment that supports exceptional flora and fauna.

Remote sensing data

In September 2023, **UAV-based hyperspectral data** were collected using a DJI Matrice 600 Pro hexacopter with a Ronin MX gimbal. The imaging was performed with a Resonon Pika L camera (Fig. 1), covering a spectral range of 380–1000 nm across 150 spectral bands. The camera had a 17 mm focal length lens, a 17.6-degree field of view (FOV), and an instantaneous field of view (IFOV) of 0.71 mrad. Data were collected at a constant altitude of 120 m and a flight speed of 1.3 m/s, with flight paths designed using Litchi for DJI Mission Hub to run south to north, minimizing the Bidirectional Reflectance Distribution Function (BRDF) effect. Due to the survey area size, data acquisition occurred over two days: September 6 and 25, 2023, between 12:00 and 14:00 to maximize sunlight and reduce shadows. Flight lines were spaced 15 m apart to ensure a 70% overlap between adjacent hyperspectral cubes. After acquisition, we used Spectronon Pro (v. 3.4.11) for pre-processing, converting radiance to reflectance with calibration target spectra and georectifying hyperspectral cubes using GPS data from the SBG Ellipse IMU and the UAV's onboard GPS. The final hyperspectral mosaic achieved a spatial resolution of 0.2 m.

Multispectral **Sentinel-2 (S-2) data** (Fig. 1), specifically the 2A surface reflectance product, were extracted from the Copernicus Data Space Ecosystem. The selected datasets were captured under cloud-free conditions in

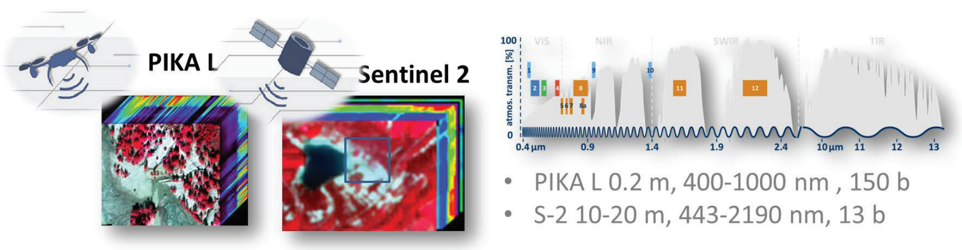

***Figure 1** Schematic illustrating: high spatial resolution hyperspectral data (400-1000 nm) were acquired via UAV using a PIKA L scamera and multispectral Sentinel-2 satellite data, highlighting the spectral range and band positions.*

September 2023, ensuring a rain-free period of at least two days prior to data acquisition.

In-situ and calibration/validation data

Soil and substrate samples were collected as part of long-term research initiatives (2010–2018). Additional samples were gathered during the UAV data acquisition in September 2023. To resolve the sample mineralogy, a Philips X'Pert X-ray Diffractometer (XRD) at the Czech Geological Survey was utilized. The XRD patterns were generated using monochromatic radiation and a graphite secondary monochromator. Random patterns were collected over an angular range of 2° to 70° (2θ), with increments of 0.05° (2θ).

Based on detailed sample mineralogy, we categorized the samples into three distinct classes (Tab. 1, Fig. 2). This classification facilitated precise determination of AMD/pH by monitoring pH stability in Fe sulfates, oxy-hydroxides, and oxides (Swayze *et al.* 2000). We selected different scenarios to train/validate ML models using high spectral and spatial resolution PIKA L data and multispectral 10-m resolution S-2 data. For both datasets, we used sample locations to create regions of interest (ROIs) for training (1 sample per class with established mineralogy) and validation (5 samples per class with established mineralogy) of the Machine Learning (ML) classifications. For high-resolution PIKA L data, mineral classes represented areas of a few meters. In contrast, for S-2 data, we selected more homogenous areas of tens of meters to train the models (Fig. 3).

In addition to mineral samples, we visually identified AMD hotspots using high-resolution orthophotos from Google Earth. While XRD analysis wasn't performed on these hotspots, we confirmed their AMD-generating activity in the field, and this dataset was also used for ML classification validation.

Machine Learning (ML) classifications

Four ML classifications (Shirmard *et al.* 2022) were tested using the ENVI Machine Learning toolbox (v. 5.7) and the Regions of Interest (ROIs) outlined in the previous section were used as labeled data.

Random Forest (RF) is a machine learning technique that uses multiple decision trees trained on different subsets of data. It helps avoid overfitting and works well with large datasets, providing better accuracy and robustness to outliers. However, it can be slow with large forests, may handle categorical variables poorly, and produces larger models. **Extra Trees (ET)**, or Extremely Randomized Trees, is similar to Random Forest but splits nodes randomly without seeking optimal splits. This method samples the entire dataset and is faster than Random Forest, though it shares some disadvantages, such as slow performance with large forests and larger model sizes. **Support Vector Machine (SVM)** is a linear classifier that finds the optimal hyperplane to separate data into classes. It works well when data is linearly separable or nearly so. On the other hand, **Radial Basis Function Support Vector Machine RBF SVM** is a classification algorithm that uses a nonlinear boundary to separate classes, making it effective in high-dimensional spaces. While powerful, it has long training times, limiting its use for large datasets.

Results

The machine learning (ML) classifications were validated using XRD analysis and field-

Figure 2 Lítov dump site - AMD" hot spot" illustrating the field situation and how the mineral classes 1-3 (Tab. 1) look like (A), detailed photo of the class 1 (jarosite-rich) (B).

Table 1 *Mineral classes defined for the Machine Learning classifications and their mineral composition.*

Mineral class	AMD minerals XRD	Other minerals XRD
Class 1	jarosite, jarosite>>goethite	gypsum, kaolite, quartz, mica
Class 2	jarosite, goethite/ goethite, jarosite	kaolite, quartz, mica
Class 3	hematite, goethite	kaolite, quartz, mica, lignite

verified AMD hotspots identified visually in Google Earth. Using either PIKA L (Tab. 2, Fig. 4) or S-2 (Tab. 3, Fig. 5) as input, RBF SVM consistently outperformed the other tested ML approaches. With high-resolution PIKA-L data, RBF SVM correctly identified almost all AMD hotspots (6 out of 7 from Google Earth) and accurately matched all mineral classes with XRD-determined mineralogy. The performance of other models, in descending order of accuracy, was: ET, RF, SVM.

Similar results were observed with S-2 data (Tab. 3, Fig. 5), where RBF SVM correctly mapped most AMD hotspots (13 out of 18 from Google Earth) and matched 10 out of 20 mineral compositions determined by XRD. As expected, the precision of AMD mapping decreased with the lower spatial and spectral resolution of the S-2 data. The performance order for other models with S-2 data was: RF, ET, and SVM.

These initial results indicate that RBF SVM excels at detecting AMD discharge and distinguishing mineral mixtures in both multi- and hyperspectral datasets. Its strength likely stems from its ability to effectively define class margins using a nonlinear boundary, making it a robust kernel within the SVM family for high-dimensional data. This allows for accurate differentiation of overlapping classes. While RF and ET classifiers also performed well, they were less accurate in differentiating between jarosite (stable under acidic pH) and goethite/hematite (indicating increasing pH).

Conclusion

The study validated machine learning (ML) classifications for identifying Acid Mine Drainage (AMD) hotspots using XRD analysis and field-verified hotspots from Google Earth. The Radial Basis Function Support Vector Machine (RBF SVM) consistently outperformed other ML approaches, accurately identifying nearly all AMD hotspots with high-resolution PIKA L data (6 out of 7) and matching all mineral classes determined by XRD. For Sentinel-2 (S-2) data, RBF SVM mapped most AMD hotspots (13 out of 18) and matched 10 of 20 mineral compositions from XRD, though its precision decreased due to the lower resolution of S-2 data. The order of performance for other models was Elastic Trees (ET), Random Forest (RF), and Support Vector Machine (SVM) for PIKA L data, and RF, ET, and SVM for S-2 data. uture research will aim to establish connections between AMD mineralogy and specific pH ranges

Figure 3 *Training dataset (ROIs) selected for the PIKA L (A) and Sentinel-2 (B) data classifications.*

Table 2 Validation statistics for the ML classifications (PIKA L data used as the input).

ML classification	Number of correctly/ incorrectly classified AMD hotspots (jarosite-rich class 1) XRD	Number of correctly/ incorrectly classified AMD hotspots Google Earth high-res. imagery	Number of correctly/ incorrectly classified mineral classes 2 and 3 XRD
RBF SVM	6/1	5/0	4/0
SVM	1/6	1/4	1/3
RF	2/5	1/4	4/0
ET	3/4	3/2	4/0

and explore machine learning techniques on extended multi-temporal datasets, broaden training and validation datasets for scalability, and assess model transferability to other locations, such as the Kirki post-mining site in Greece.

Acknowledgement

The presented analysis was conducted under the support of the EC grant MultiMiner. The MultiMiner project is funded by the European Union's Horizon Europe research and innovation actions programme under Grant Agreement No. 10109137474.

References

Flores, H., Lorenz, S., Jackisch, R., Tusa, L., Contreras, I. C., Zimmermann, R., & Gloaguen, R. (2021). UAS-based hyperspectral environmental monitoring of acid mine drainage affected waters. Minerals, 11(2), 182.

Chalkley, R., Crane, R. A., Eyre, M., Hicks, K., Jackson, K. M., & Hudson-Edwards, K. A. (2022). A multi-

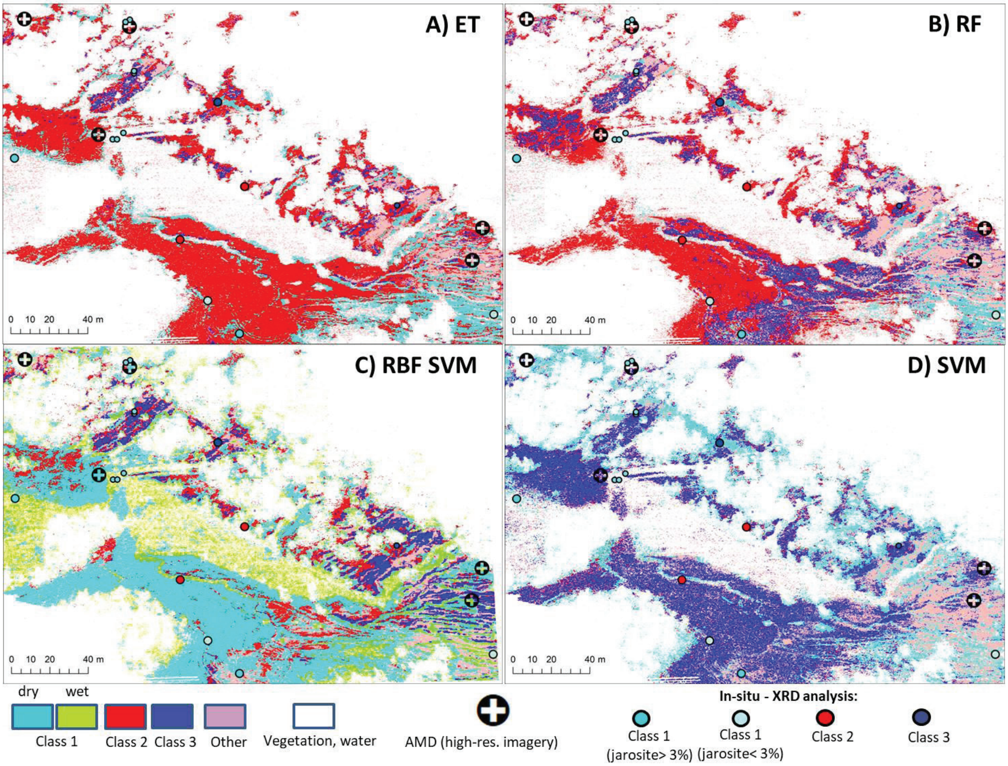

Figure 4 Machine learning classification results for PIKA L data, overlaid with sample locations where XRD analysis was performed for mineralogical determination. The locations of visually identified AMD hotspots from Google Earth imagery are also shown.

Table 3 Validation statistics for the ML classifications (Sentinel-2 data used as the input).

ML classification	**Number of correctly/ incorrectly classified AMD hotspots (jarosite-rich class 1)** XRD	**Number of correctly/ incorrectly classified AMD hotspots** Google Earth high-res. imagery	**Number of correctly/ incorrectly classified mineral classes 2 and 3** XRD
RBF SVM	13/5	5/6	5/4
SVM	11/7	4/7	3/6
RF	12/6	5/6	4/5
ET	10/8	3/8	5/4

scale feasibility study into acid mine drainage (AMD) monitoring using same-day observations. Remote Sensing, 15(1), 76.

Kopačková, V. (2014). Using multiple spectral feature analysis for quantitative pH mapping in a mining environment. *International Journal of Applied Earth Observation and Geoinformation*, 28, 28–42.

Kopačková, V., & Hladíková, L. (2014). Applying spectral unmixing to determine surface water parameters in a mining environment. *Remote Sensing*, 6(11), 11204–11224.

Shirmard, H., Farahbakhsh, E., Müller, R. D., & Chandra, R. (2022). A review of machine learning in processing remote sensing data for mineral exploration. Remote *Sensing of Environment*, 268, 112750.

Swayze, G. A., Smith, K. S., Clark, R. N., Sutley, S. J., Pearson, R. M., Vance, J. S., ... & Roth, S. (2000). Using imaging spectroscopy to map acidic mine waste. *Environmental Science & Technology*, 34(1), 47–54.

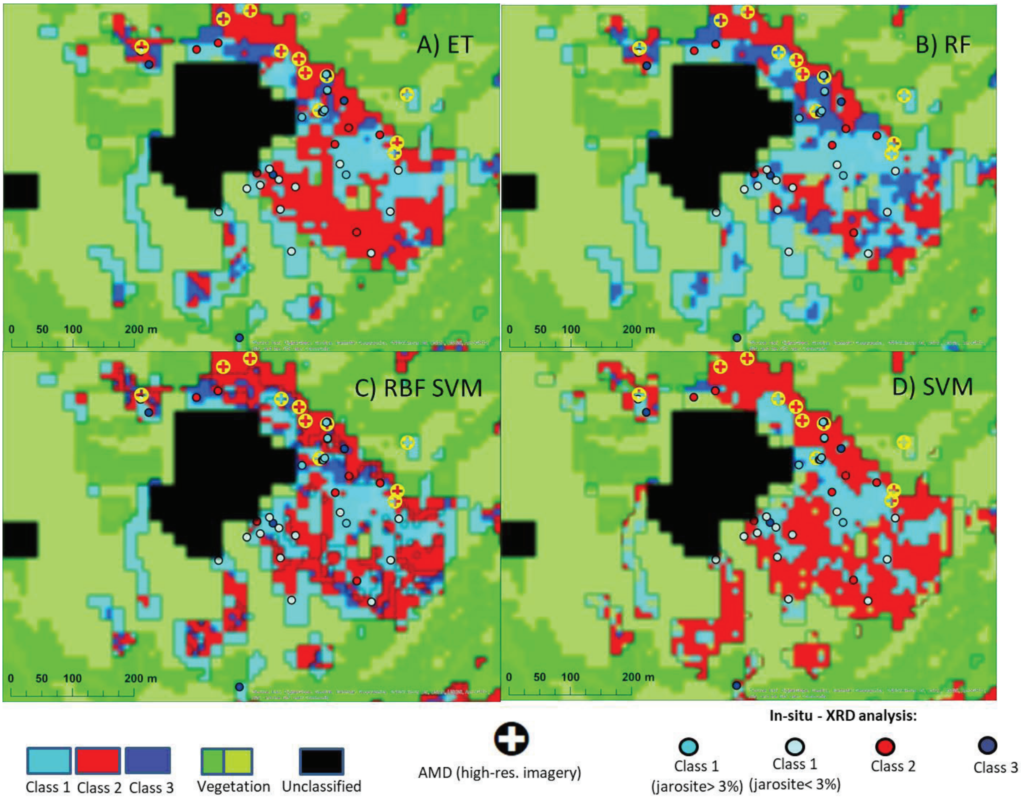

Figure 5 Machine learning classification results for Sentinel-2 data, overlaid with sample locations where XRD analysis was performed for mineralogical determination. The locations of visually identified AMD hotspots from Google Earth imagery are also shown.

Bioremediation of Uranium-Contaminated Water: Magnetic Bacteria as Potential Supporters

Evelyn Krawczyk-Bärsch, Björn Drobot, Johannes Raff

Helmholtz-Zentrum Dresden-Rossendorf, Institute of Resource Ecology, Bautzner Landstraße 400, 01328 Dresden, Germany, e.krawczyk-baersch@hzdr.de, ORCID: 0000-0001-8249-0506; b.drobot@hzdr.de, ORCID: 0000-0003-1245-0466; j.raff@hzdr.de, ORCID: 0000-0002-0520-3611

Abstract

The ability of magnetotactic bacteria to remove dissolved uranium(VI) from U-contaminated water appears to be very effective, even in a broad pH range. High amounts (78–96%) of uranium were removed from a bacterial suspension in laboratory experiments after one day of exposure and bound in the cell wall of the bacteria showing a stable immobilization of uranium(VI). Our findings may initiate new remediation strategies on effective immobilization of uranium(VI). In combination with the magnetic properties of these bacteria, a simple technical water purification process can be realized not only for uranium(VI), but probably also for other metals.

Keywords: Mine water, uranium, magnetotactic bacteria, bioremediation

Introduction

Uranium mining activities and the processing of ores have left a legacy of environmental contamination. Radionuclides can migrate into surrounding aquifers and soils, thus representing a human health risk. Conventional technologies based on physicochemical treatments are traditionally used to remediate contaminated mine water. However, these approaches are cost-intensive and ineffective particularly for low uranium concentrations. Bioremediation, on the other hand, is a promising alternative to remove uranium from contaminated waters that is less expensive, easy to implement and effective at low uranium concentrations (Sánchez-Castro *et al*. 2021; Newman-Portela *et al*. 2024). Several mechanisms of interactions of microorganisms with radionuclides are known, like biosorption on functional groups of the cell surface (Lloyd and Macaskie, 2002), bioaccumulation, where the metal is taken up into the cell (Suzuki and Banfield, 2004), the enzymatic reduction of metals, which is called bioreduction (Beyenal *et al*., 2004), and biomineralization, where radionuclides can precipitate with microbial generated ligands, e.g., phosphate, sulfide or carbonate (Merroun *et al*., 2011). The investigated microorganisms included bacteria as well as fungi. The organisms can interact with uranium, transforming it into less soluble and toxic forms. Thus, bioremediation is considered a more sustainable and less invasive environmental remediation strategy than other traditional technologies. In a unique combination of analytical methods and transmission electron and fluorescence microscopy as well as various spectroscopic techniques, the ability of magnetotactic bacteria to remove uranium from contaminated waters was tested. Important indications were gained on possible binding sites in the bacterial cell walls. Findings from the present study suggest a promising method to support or outperform the physicochemical treatments. By utilizing the magnetic properties of magnetotactic bacteria (e.g. *Magnetospirillum magneticum* AMB-1), it appears to be possible to biologically remediate uranium-contaminated mine water.

Methods

For analytical, microscopic and spectroscopic studies, a cell suspension of *Magnetospirillum magneticum* AMB-1 was prepared in laboratory experiments, using sterile tap water at different pH values (3.5, 4.5, 5.5, 6.5 and 7.5), and combined with a 0.1 M stock solution of $UO_2(NO_3)_2$ to adjust an initial uranium(VI) concentration of 0.1 mM. During the incubation on a rotary shaker at 30 °C, cell suspension was collected at distinct time points (5, 15, 30 and 45 min, as well as after 1, 2, 3, 4, 5, 6, 24 and 25 hours) and centrifuged at 13.000 x g for 1 min. The supernatants were sampled for inductively coupled plasma mass spectrometry (ICP-MS) measurements to determine the residual uranium(VI) concentration. For cryo-time resolved laser-induced fluorescence spectroscopy (cryo-TRLFS) the pellets were transferred into a copper holder. The cryo-TRLFS method was chosen due to the high sensitivity toward uranium(VI) complex formation in aqueous solutions (Moulin *et al.* 1995). In addition, important ligands of the cell wall, e.g., peptidoglycan, lipopolysaccharide, L-rhamnose, D-(+) galactose, D-(+) mannose were used as reference ligands and measured for comparison and interpretation of possible binding sites of uranium(VI) to *Magnetospirillum magneticum* AMB-1 cell walls (Krawczyk-Bärsch *et al.* 2022). The mixed cryo-TRLFS spectra were analysed by parallel factor (PARAFAC) analysis to extract single component spectra from the total emission spectra data sets (Drobot *et al.* 2015). In addition, during the uranium(VI) interaction experiments, samples were taken at the beginning of the experiments and after 1, 3, 6 and 24 hours to check the viability of *Magnetospirillum magneticum* AMB-1 cells depending on the uranium(VI) incubation time and on the pH. For this purpose, the cells were tested by live-dead staining (SYTO®9/propidium iodide). The cell viability was observed using a confocal laser scanning microscope (CLSM). Transmission electron microscopy (TEM) and energydispersive X-ray spectroscopy (EDXS) studies were performed to locate uranium in *Magnetospirillum magneticum* AMB-1 cells. For this study, ultrathin sections of *Magnetospirillum magneticum* AMB-1 cells were prepared and loaded with 0.1 mM uranium at pH 6.5 for 5 hours. Detailed sample preparation protocols are available in Krawczyk-Bärsch *et al.* (2022).

Results and discussion

The removal efficiency of dissolved uranium(VI) by *Magnetospirillum magneticum* AMB-1 cells is very effective and independent of the pH. High amounts of uranium(VI) were removed from the suspension at all pH values tested. As shown in Fig. 1, the removal of uranium(VI) takes place within the first hour, where at pH 6.5 almost 78% of the uranium(VI)

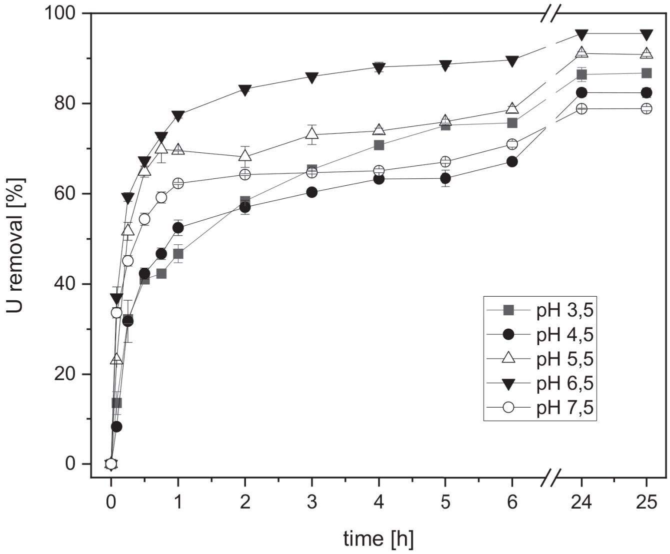

Figure 1 Uranium(VI) removal from contaminated water by Magnetospirillum magneticum AMB-1 cells versus time in sterilized tap water at different pH and 30 °C; initial uranium(VI)conc. = 0.1 mM.

is eliminated from the contaminated water. After 24 h, almost all of the initial uranium(VI) concentration (96%) is removed by *Magnetospirillum magneticum* AMB-1 cells. In contrast, at a pH of 3.5, only 46% U(VI) is bound in the first hour. Nevertheless, 86 % of the U(VI) was removed from the suspension at the end of the experiment, which even indicates efficient removal of U(VI) by *Magnetospirillum magneticum* AMB-1 cells at low pH.

As the cell viability test showed, the majority of the cells, with the exception of those treated at pH 3.5 as well as pH 7.5, were still alive after 24 hours, despite being exposed to high concentrations of uranium(VI). The bright-field TEM image in Fig. 2a shows a typical elongated *Magnetospirillum magneticum* AMB-1 cell with up to five crystals, which are visible as black dots. EDXS analysis clearly confirms that these dots exclusively consist of Fe. They are so-called magnetosomes consisting of magnetic mineral crystals, which were synthesized intracellularly as a special feature by magnetotactic bacteria and are responsible for the magnetic property of the bacteria (Balkwill *et al.* 1980). Studies have shown that they are not involved in the removal of uranium. Rather, analysis of the elemental distribution of uranium at pH 6.5 clearly indicated the predominant binding of uranium to the cell wall (Fig. 2b).

After the incubation of *Magnetospirillum magneticum* AMB-1 cells with 0.1 mM uranium(VI) at different pH values (3.5–7.5) and different contact times (0.5, 2, 5 and 24 h), the cells were used for cryo-TRLFS measurements. A subsequent analysis of all emission spectra from the TRLFS data set by PARAFAC extracted the single component spectra of five uranium(VI) species, which were probably formed during the uranium(VI) biosorption of *Magnetospirillum magneticum* AMB-1 cells. Since EDXS elemental distribution analysis clearly indicate that uranium(VI) is predominantly bound in the cell wall, important ligands were considered as possible complexants for uranium(VI) and used as reference spectra of potential ligands (peptidoglycan, lipopolysaccharide, L-rhamnose, D-(+) galactose, D-(+) mannose). The luminescence properties have shown that there is no correspondence with most ligands, with the exception of peptidoglycan. The results reveal that peptidoglycan, a key ligand in the cell wall, plays a crucial role in uranium biosoption. The formation of three characteristic species were determined over a wide pH range. The

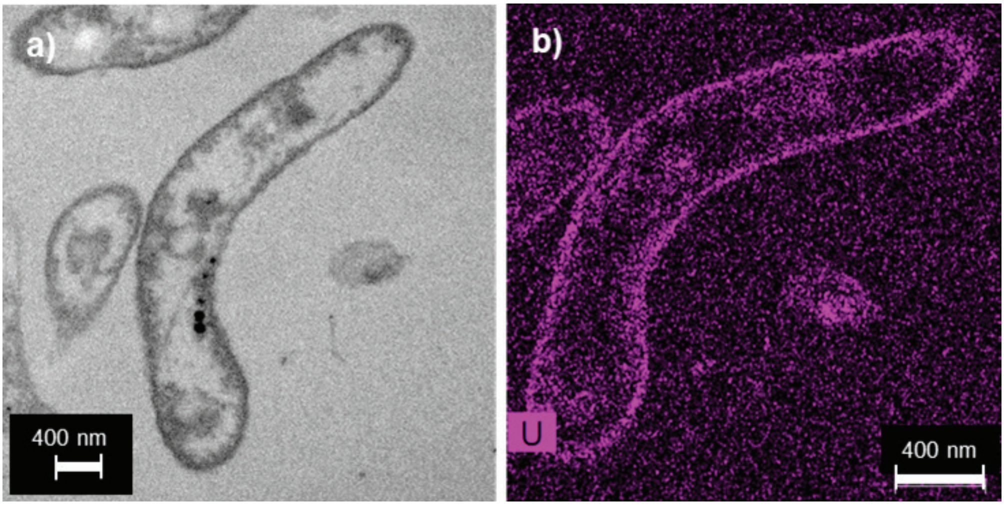

Figure 2 *Bright-field TEM image of a thin sectioned Magnetospirillum magneticum AMB-1 cell (a) with magnetosomes (black dots) together with EDXS-based element distribution analysis of U (b). Sterilized tap water, pH 6.5; initial uranium(VI) conc. = 0.1 mM; duration: 5 h at 30 °C.*

relative luminescence intensity distribution of the three uranium-peptidoglycan reference species versus pH show that uranium-peptidoglycan species (1) is mainly important in the acidic pH range and is rather negligible in the neutral and basic pH range. Species (2) dominates the bioassociation of uranium(VI) in the mentioned broad pH range, with a dominance at pH 5.5 being emphasized. Species (3), on the other hand, only gains significance in the basic pH range (s. Fig. 3).

Conclusions

With regard to the development of innovative bioremediation strategies of contaminated water, the presented studies show clearly that magnetotactic bacteria, such as *Magnetospirillum magneticum* AMB-1, are suitable candidates. They can survive as planktonic cells both in a wide pH range and with relatively high uranium(VI) concentrations of up to 0.1 mM, while effectively and almost completely immobilizing uranium(VI). Uranium is bound on the bacterial cell wall almost entirely, showing a stable immobilization of uranium. An outstanding feature however, is the formation of nanoscopic magnetic crystals within the cell of magnetotactic bacteria, which were proved by TEM/EDXS. Thus, in combination with its magnetic properties, magnetotactic bacteria offer many advantages for the development of various bioassociation technologies. The magnetic properties could be harnessed for straightforward magnetic separation of uranium-loaded bacteria from contaminated water. Consequently, a simple technical water purification process could be realized, not only for uranium(VI), but probably also for other metals with the objective of potential industrial applications in the field of microbiological purification of water.

Acknowledgements

The authors are grateful to Damien Faivre and Sandra Prévéral (CEA Cardarache, France) for providing the strain of *Magnetospirillum magneticum* AMB-1.

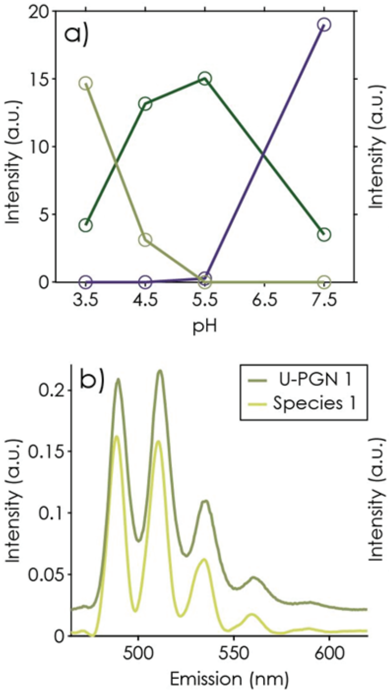

***Figure 3** a): Relative luminescence intensity distribution of three uranium-peptidoglycan (U-PGN) reference species versus pH. b, c, d): Main PARAFAC extracted species in comparison to the appropriate U-PGN reference spectra. Sterilized tap water, initial uranium(VI) conc. = 0.1 mM at 30 °C.*

We thank Sabrina Beutner and Sylvia Schöne (both Helmholtz-Zentrum Dresden-Rossendorf, Germany) for ICP-MS analysis. Robin Steudtner´s skilful work on cryo-TRLFS measurements is gratefully acknowledged. The Biotechnology Center of the Technical University Dresden (Germany) is thanked for the preparation of the TEM samples. We thank also René Hübner from the HZDR Ion Beam Center TEM facilities for the measurements of the TEM samples. Special thanks to Justus Ramtke from the University of Applied Sciences Zittau/Görlitz, Faculty of Natural and Environmental Sciences (Germany) for his support with the experimental work.

References

Balkwill DL, Maratea D, Blakemore RP (1980). Ultrastructure of a magnetic spirillum. J. Bacteriol. 141, 1399–1408.

Beyenal H, Sani RK, Peyton B., Dohnalkova A., Amonette J., Lewandowski Z (2004). Uranium immobilization by sulfate-reducing biofilms. Environ. Sci. Technol. 38, 2067–2074.

Drobot B, Steudtner R, Raff J, Geipel G, Brendler V, Tsushima S (2015). Combining luminescence spectroscopy, parallel factor analysis and quantum chemistry to reveal metal speciation – a case study of uranyl(vi) hydrolysis. Chem. Sci. (6), 964. doi:10.1039/C4SC02022G.

Krawczyk-Bärsch E, Ramtke J, Drobot B, Müller K, Steudtner R, Kluge S, Hübner R, Raff J (2022). Peptidoglycan as major binding motif for Uranium bioassociation on *Magnetospirillum magneticum* AMB-1 in contaminated waters. J. Hazard. Mater. 437, 129376. doi:10.1016/j.jhazmat.2022.129376.

Lloyd JR, Macaskie LE (2002). Biochemical basis of microbe-radionuclide interactions. In: Miranda, J. (Ed.), Interactions of Microorganisms with Radionuclides. Keith-Roach, M.J. and Livens, F.R., Elsevier Sciences, Oxford, UK, pp. 313–342.

Merroun ML, Nedelkova M, Ojeda JJ, Reitz T, Fernandez M-L, Arias JM, Romero-Gonzalez M, Selenska-Pobell S (2011). Bio-precipitation of uranium by two bacterial isolates recovered from extreme environments as estimated by potentiometric titration, TEM and X–ray absorption spectroscopic analyses. J. Hazard. Mater. 197, 1–10.

Moulin C, Decambox P, Moulin V, Decaillon JG, (1995). Uranium speciation in solution by time-resolved laser-induced fluorescence. Anal. Chem. 67 (2), 348–353.

Newman-Portela AM, Krawczyk-Bärsch E, Lopez-Fernandez M, Bok F, Kassahun A, Drobot B, Steudtner R, Stumpf T, Raff J, Merroun ML (2024). Biostimulation of indigenous microbes for uranium bioremediation in former U mine water: multidisciplinary approach assessment. Environ. Sci. Pollut. Res. 31(5):7227-7245. doi:10.1007/s11356-023-31530-4.

Sánchez-Castro I, Martínez-Rodríguez P, Abad MM, Descostes M, Merroun ML (2021). Uranium removal from complex mining waters by alginate beads doped with cells of Stenotrophomonas sp. Br8: Novel perspectives for metal bioremediation. J. Environ. Manag. 296:113411. doi:10.1016/j.jenvman.2021.113411.

Suzuki Y, Banfield JF (2004). Resistance to and accumulation of, uranium by bacteria from a uranium-contaminated site. Geomicrobiol. J. 21, 113–121.

Settling Characteristics and Physic-Geochemical Stability of Fly Ash for Acid Mine Drainage Neutralization in Pit Lakes: A Laboratory-Scale Study

Ginting Jalu Kusuma[1], Dian Febriana[1], Sendy Dwiki[1], Abie Badhurahman[1], Rudy Sayoga Gautama[1], IK Dwika Parananda[1]

[1]*Institute Technology of Bandung, Faculty of Mining and Petroleum, Mining Engineering Department, Bandung, Indonesia*

Abstract

This study examines the use of Fly Ash (FA), a byproduct of coal combustion, as an in-situ neutralizing agent for AMD in pit lake. Due to its alkaline composition, FA is well-suited for AMD treatment. Although FA is no longer classified as hazardous waste under Indonesian regulations, proper management is crucial to avoid potential environmental impacts. This research focuses on the sedimentation characteristics and physic-geochemical stability of FA in AMD under controlled laboratory conditions.

The experimental setup consisted of acrylic tubes with a diameter of 11.2 cm, each containing varying volumes of AMD (5, 10, and 15 L) resulting in different water heights, while maintaining a consistent solid-to-water ratio of 1:5. FA was allowed to settle for 24 hours, during which its settlement velocity and stratification of FA in AMD were monitored. The pH of AMD was recorded hourly for 12 hours, with a final measurement at 24 hours. After stabilization, the grain size distribution, mineralogical composition, and chemical properties of the FA were analysed. Post-treatment water samples were analysed using Ion Chromatography (IC) and Inductively Coupled Plasma Mass Spectrometry (ICP-MS).

The results demonstrated significant improvements in water quality, with pH levels rising from 2.77 to 6.24, 6.81, and 7.65 in the three different acrylic tubes, and the concentrations of Fe and Al decreasing by over 100%. Manganese concentrations were reduced by 19.88% to 40.06%, highlighting the effectiveness of FA as a neutralizing agent for AMD. Remarkably, the pH improvement to near-neutral levels occurred within the first hour, with a stable pH recorded over the next 24 hours. The contact time between FA and AMD is directly proportional to the improvement in water quality. Smaller FA particles have a larger surface area in contact with AMD, resulting in longer settling times. The settling velocity of FA particles ranged from 15.38 to 21.88 cm/s. After neutralization, iron precipitated as goethite ($FeOOH$), hematite (Fe_2O_3), and hydrohematite, while aluminum precipitated as gibbsite ($Al(OH)_3$), and manganese as pyrolusite ($Mn(OH)_2$) and manganite ($MnOOH$). These results confirmed the formation of secondary minerals through the precipitation of Fe, Al, and Mn.

Keywords: Pit Lake, Fly Ash, Neutralization, Acid Mine Drainage, In-situ Treatment

Introduction

Open-pit mining often results in the formation of pit lakes, which, if not properly managed, can accumulate acid mine drainage (AMD). Once AMD develops, treatment is required to neutralize acidity and remove dissolved metals to comply with environmental standards. Various AMD treatment methods are available and are generally classified as active, passive, or in situ. The selection of an appropriate method depends on site-specific conditions and treatment objectives.

One in situ approach for AMD neutralization in pit lakes involves the dispersion of an alkaline neutralizing agent across the water surface. This method has been implemented in a former coal pit lake in South Kalimantan (Gautama, 2014). Among potential neutralizing agents, fly ash (FA), a by-product of coal combustion, has demonstrated effectiveness due to its alkaline mineral content. Calcium oxide (CaO), a primary component of FA, reacts with sulfuric acid (H_2SO_4) to reduce acidity, making FA a promising material for AMD treatment.

Despite significant production, the utilization of fly ash and bottom ash (FABA) in Indonesia remains low, accounting for only 0.47% in 2012. Although FABA applications have expanded in construction materials, such as lightweight concrete, paving blocks, and bricks, as well as in soil improvement, its use remains below production levels (Aisyana, 2022). Given the prevalence of open-pit mines and the widespread formation of pit lakes, enhancing FABA utilization for AMD neutralization presents a strategic opportunity for sustainable environmental management.

This study aims to investigate the in-situ treatment mechanism of FA surface-spreading in pit lakes. Furthermore, the research will examine the physical and chemical properties of FA before and after exposure to AMD, determine the settling velocity of FA particles, and analyse the chemical reactions involved. The findings are expected to contribute to the development of more effective AMD treatment strategies, promoting the utilization of FA in pit lake management.

Methods

Samples Characterization

Fly ash (FA) samples were sourced from a coal-fired power plant in Tanjung Enim, South Sumatra, Indonesia, and oven-dried prior to characterization. XRD analysis identified quartz as the dominant mineral phase (90%), with minor amounts of nepheline (4.8%), goethite (4.4%), and hematite (0.8%). XRF results showed Si (46.6 wt%) as the major element, followed by Al (23.1 wt%) and Fe (12.1 wt%), with trace levels of Na, Mg, K, Ca (4.06%), and Sr. The main oxides were SiO_2 (52.9 wt%), Al_2O_3 (27.9 wt%), and Fe_2O_3 (6.23 wt%).

Static testing revealed a paste pH of 8.07. Net Acid Generation (NAG) testing indicated low acid-forming potential, with NAG pH values of 4.5 and 7 producing 0 and 3.67 kg H_2SO_4/ton, respectively. The Net Acid Producing Potential (NAPP) was −92.4 kg H_2SO_4/ton. The Acid Buffering Characteristic Curve (ABCC) showed rapid initial pH decline with acid addition, suggesting high initial reactivity.

The FA had a specific gravity of 2.48 and was predominantly silt-sized (57%), with sand (33.17%) and clay (8.08%) fractions, classifying it as poorly graded. AMD was generated via column leaching of potentially acid-forming (PAF) overburden using distilled water. The resulting leachate was analyzed using multiparameter probes, ion chromatography (IC), ICP-MS, and strong acid-base titration. Summary of AMD characteristics is presented in Table 1.

***Table 1** AMD sample for neutralization test.*

Parameter	Value	Parameter	Value
pH	2,77	K^+	3,39 mg/L
TDS	1,46 ppt	SO_4^{2-}	1.258,41 mg/L
ORP	254,4 mV	Cl^-	6,32 mg/L
EC	2,93 mS/cm	HCO_3^-	-
Temperatur	27,9 oC	F^-	4,8 mg/L
Acidity	1.939,33 mg CaCO3/L	Al	90,47 mg/L
Na^+	27,57 mg/L	Fe	80,94 mg/L
Ca^{2+}	75,63 mg/L	Mn	15,5 mg/L
Mg^{2+}	224,65 mg/L		

Settling of FA and AMD Neutralization Test Set-up

For the settling test, a custom-designed acrylic tube was used with three variations of AMD and FA volumes, each maintaining a constant solid-to-water ratio of 1:5 (Fig. 1). The tubes had a uniform diameter of 11.2 cm, while the height varied based on the volume requirements for each variation. The first acrylic tube (Tab1) was filled with 5 L of AMD, and 1 kg of FA was introduced at the start of the test (0 hours). The second tube (Tab2) contained 10 L of AMD, with 2 kg of FA added in two stages: 1 kg at 0 hours and another 1 kg at 4 hours. The third tube (Tab3) held 15 L of AMD, with 3 kg of FA added incrementally in three stages: 1 kg at 0, 4, and 8 hours.

After the FA was introduced into the AMD-filled test tubes, it was left to settle for 24 hours. During this period, observations were made on the settling rate and precipitate stratigraphy. To ensure accuracy and minimize errors, the testing process was documented. Additionally, the physical parameters of the AMD were measured hourly from the 1st to the 12th hour using a multiparameter device.

Post-Neutralization Testing

Following the 24-hour settling period, the sediment precipitates and treated water were analysed. The sediment was divided into two portions for physical and chemical assessments. The post-neutralization FA samples were examined for physical characterization, static test, and mineralogical composition. The treated AMD samples were analysed for pH and oxidation-reduction potential (ORP) using a multiparameter device, while IC and ICP-MS were employed for further chemical characterization.

Results and Discussions

The results of pH and ORP measurements for Tab1, Tab2, and Tab3 are presented in Fig. 3. In general, all test variations showed an increase in pH and a decrease in ORP, indicating a progressing neutralization process. In Tab1, the pH increased sharply from 2.77 at hour 0 to 6.03 at hour 1 and then stabilized around this value until hour 24, demonstrating rapid and effective neutralization. Meanwhile, ORP decreased significantly from 254.4 mV at hour 0 to 58.2 mV at hour 1 and stabilized between 42.3 and 61.6 mV, reflecting a shift in oxidation-reduction conditions.

In Tab2, the pH increased more gradually from 2.77 at hour 0 to 4.36 at hour 1, then increased sharply to 6.15 at hour 5 and remained stable until hour 24. The ORP decreased from 254.4 mV at hour 0 to approximately 159 mV at hour 1, followed by a steady decline to near zero at hour 24. Meanwhile, in Tab3, the pH increase was slower than in the other tubes but ultimately achieved more optimal results. The trends in pH and ORP across all tubes followed a similar pattern, with pH increasing and ORP decreasing as neutralization progressed.

The differences in pH progression were influenced by the solid-to-water (S/W) ratio applied over time. In Tab1, a constant S/W ratio of 1:5 was maintained throughout the experiment. In Tab2, the ratio shifted from 1:10 at hour 0–4 to 1:5 from hour 4–24. In Tab3, the S/W ratio varied from 1:15 at hour 0–4, 1:7.5 at hour 4–8, and 1:5 from hour 8–24. These variations in FA addition influenced

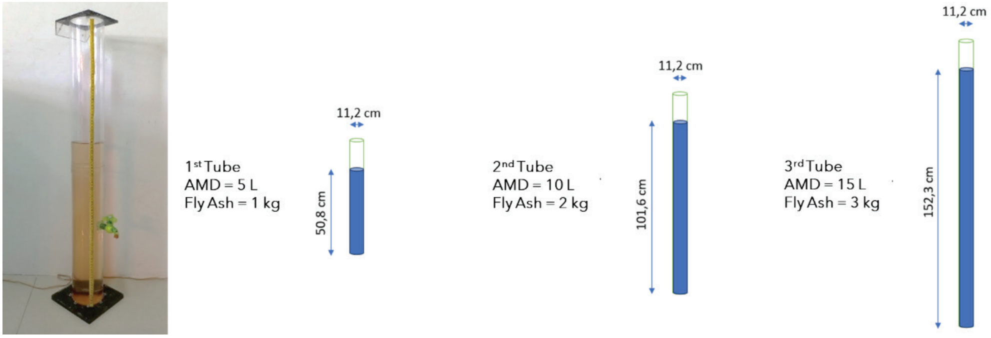

***Figure 1** AMD sample in an acrylic test tube with configuration.*

the rate and efficiency of pH increase. The percentage error for all three neutralized water samples was minimal, ranging between 0.5% and 0.7%. The ion balance error of the final samples is presented in Fig. 4.

The height of FA sediment was monitored over time, as shown in Fig. 5. Sedimentation began approximately one hour after FA addition, aligning with the peak period of AMD neutralization. Sediment height initially increased as particles settled, followed by a gradual decrease due to compaction.

In each of the precipitates, quartz was identified as the dominant mineral. The respective percentages were 97.9% in the upper sediment and 90.1% in the lower sediment of Tab1, 88.6% in the upper sediment and 87.4% in the lower sediment of Tab2, and 81% in the upper sediment and 77.8% in the lower sediment of Tab3. In addition to quartz, other minerals not previously detected in the FA were formed, including gypsum, goethite, hematite, and gibbsite.

XRF analysis showed that the fly ash sample contained 4.06% CaO. When CaO react with water, they form hydroxides such as $Ca(OH)_2$, which generate hydroxyl ions (OH^-) that contribute to pollutant degradation and acid neutralization (Shirin, 2021). XRD analysis also detected 4.8% aluminosilicate, primarily nepheline ($KNa_3Al_4Si_4O_{16}$). Nepheline dissolution can raise pH without CO_2 release (Noort *et al.*, 2018), though its reactivity is relatively low. Compared to lime, aluminosilicates dissolve more slowly, are kinetically controlled, and provide long-term buffering capacity (Petronijevic *et al.*, 2022).

According to Stokes' Law, the settling velocity of a particle in a fluid is directly proportional to its diameter. However, in addition to particle size, the density of the material also plays a significant role in determining settling velocity. The average settling velocities of FA particles observed in this study are presented in Fig. 6. The results indicate that the frequency of FA addition influences the uniformity of particle size distribution within the sediment, subsequently affecting the overall settling behaviour. This finding aligns with previous research by Koch *et al.* (2008), which highlights the importance of reaction time in the effective neutralization of acid mine drainage using fly ash.

The concentrations of alkali and alkaline earth metals in AMD increased after neutralization with fly ash, with the highest levels observed at elevated pH. The most notable increase occurred in Tab3, where the final pH reached 7.65, indicating the active role of these metals in the neutralization process. Their oxide forms promoted

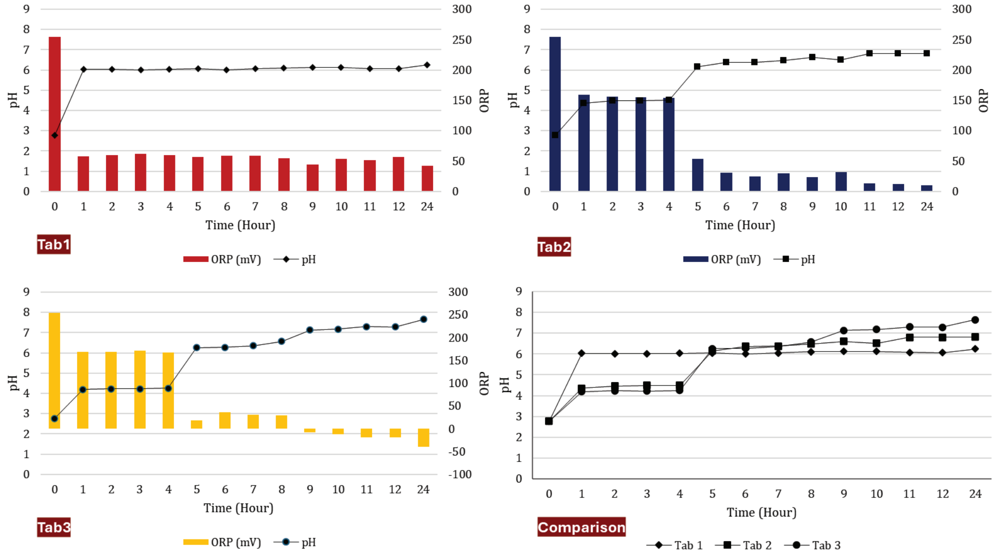

Figure 2 *pH and ORP measurement results of three tubes and the comparison.*

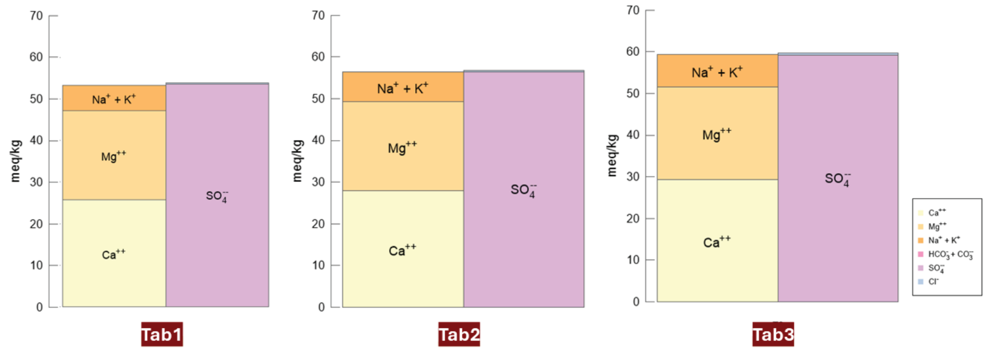

Figure 3 *The ion balance after neutralization.*

hydroxyl generation, contributing to pH elevation. Variations in metal concentrations are shown in Fig. 7.

Additionally, the NAPP values of sediment from Tab1, Tab 2 and Tab3 increased compared to the original FA, suggesting the dissolution of sulfur species during AMD interaction. This is supported by elevated sulfate concentrations in the treated water.

Based on acidity measurements, the AMD sample showed an acidity value of 1,030.33 mg $CaCO_3$/L. In contrast, the acid neutralization capacity (ANC) of the FA sample was determined to be 104.7 kg H_2SO_4/ton, equivalent to 106.84 kg $CaCO_3$/ton. This indicates that a minimum of 10 g of FA is required to neutralize 1 L of AMD. However, only 10 kg H_2SO_4/ton of the total neutralization capacity of FA demonstrated high reactivity. This limited reactivity can be attributed to the composition of reactive neutralizing components, such as Ca and Mg, which constitute only 9.14% of the total FA mass.

Conclusions

This study demonstrated the potential of fly ash (FA) to neutralize acid mine drainage (AMD) in a pit lake. Post-treatment pH increased to 6.24 in Tab1, 6.81 in Tab2, and 7.65 in Tab3. Static test showed a decrease in acid-neutralizing capacity in the sediment, though it remained classified as Non-Acid Forming (NAF) with retained neutralization potential. A reduction in alkali and alkaline earth metal content was also observed in the sediments.

The proposed protocol for studying the leachates provides useful information for designing mitigation strategies and environmental monitoring in mining areas.

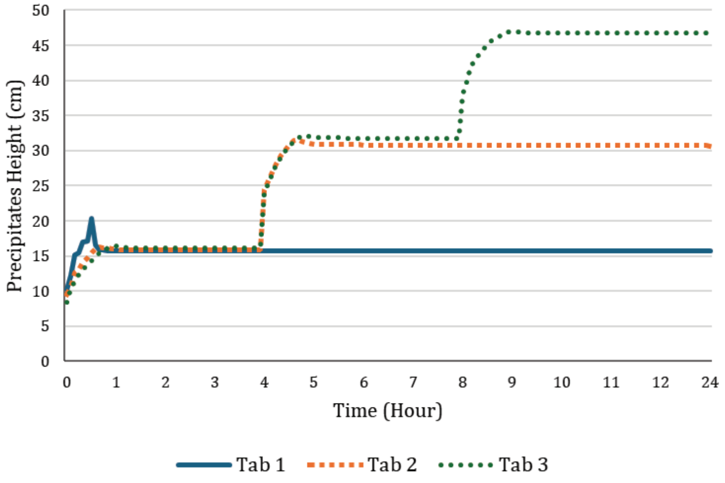

Figure 4 *FA sediment height in the three test tubes.*

Table 2 XRD result of sediments

Mineral	Weight Percentage (%)					
	Upper Tab1	Lower Tab1	Upper Tab2	Lower Tab2	Upper Tab3	Lower Tab3
Quartz (SiO_2)	97,9	90,1	88,6	87,4	81,0	77,8
Gypsum ($CaSO_4$)	0,4	1,4	3,7	3,7	1,5	3,7
Goethite (FeOOH)	0,4	2,0	3,6	3,6	1,9	2,5
Hematite (Fe_2O_3)	0,5	1,4	0,7	0,7	11,6	1,9
Gibbsite ($AlOH_3$)	0,8	5,1	4,5	4,5	4,0	14,1

Table 3 Effectiveness of Fly Ash in AMD Neutralization.

Criteria	Tab1	Tab2	Tab3
Acidity (mg $CaCO_3$/L)	40,8	37,51	33,45
Neutralization Efficiency (%)	96,04	96,36	96,75
FA needed in 1 L of AMD (kg)	0,5	1	1,5
FA Utilization Efficiency (%)	50,48	50,48	50,48

The highest settling velocity (21.88 cm/s) occurred in the lower sediment layer of Tab3, associated with coarser particles. In contrast, the upper layers of Tab1 and Tab2 showed slower settling (15.52 cm/s and 15.38 cm/s) due to finer particle sizes. Longer contact time between FA and AMD improved water quality, with finer particles enhancing neutralization efficiency through increased surface area and extended settling time.

References

Aisyana, M. (2022). Politik Kebijakan Limbah Energi: Analisis Kebijakan Penghapusan Limbah FABA dari Daftar Limbah Berbahaya di Indonesia. Jurnal Ilmu Sosial Indonesia (JISI), Vol. 3, No 90–98.

Gautama, R. S. (2014). Pembentukan, Pengendalian, dan Pengeloaan Air Asam Tambang. Penerbit ITB.

Koch, C., Graupner, B., Werner, F. (2008). Pit Lake Treatment Using Fly Ash Deposits and Carbon Dioxide. 10th International Mine Water Association Congress.

Shirin, S., Jamal, A., Emmanouil, C., & Yadav, A. K. (2021). Assessment of Characteristics of Acid Mine Drainage Treated. Applied Sciences.

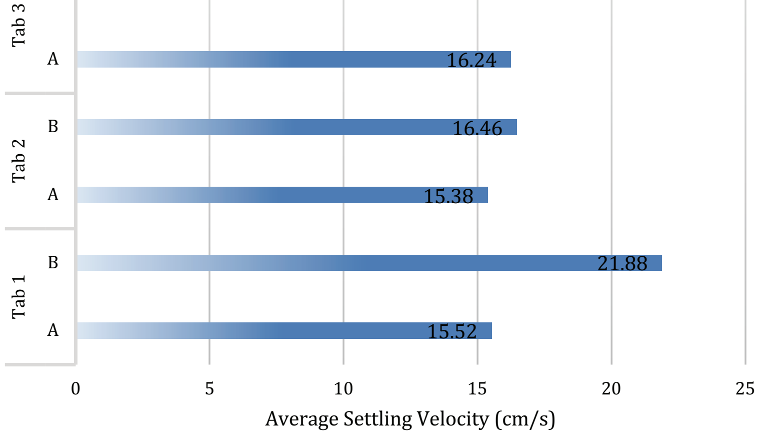

Figure 5 Average settling velocity of FA.

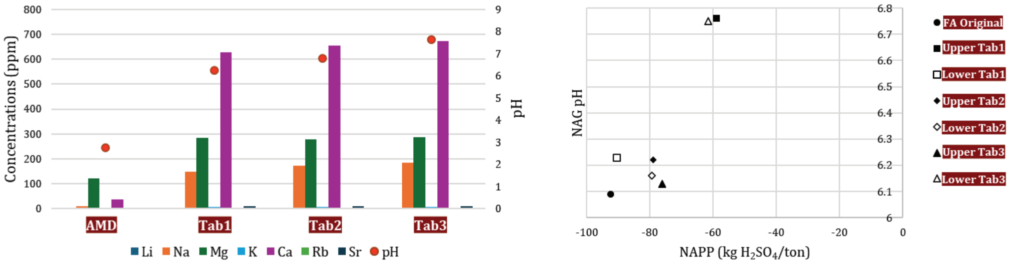

***Figure 6** (a) Left – Post-Neutralization Concentrations of Alkali and Alkaline Earth Metals in AMD (b) Right – Initial Fly Ash and Post-Neutralization Sediment Samples.*

Noort, R. V., Morkved, P. T., and Dundas, S. H. (2018). Acid Neutralization by Mining Waste Dissolution under Conditions Relevant for Agricultural Applications. Geosciences 8, 308.

Petronijevic, N., Radovanovic, D., Stulovic, M., Sokic, M., Jovanovic, G., Kamberovic, Z., Stankovic, S., Stopic, S., & Onjia, A. (2022). Analysis of the Mechanism of Acid Mine Drainage Neutralization Using Fly Ash as an Alternative Material: A Case Study of the Extremely Acidic Lake Robule in Eastern Serbia. Water 14, 3244.

Experimental Approach to Designing a Flushing System for SAPS Pond

Dong-Kil Lee, Youngwook Cheong, Sangwoo Ji, Giljae Yim, Yong-chan Cho

Korea Institute Geoscience and Mineral Resources (KIGAM), 124 Gwahang-no, Yuseong-gu, Daejeon 34132, South Korea, ldk@kigam.re.kr

Abstract

Successive alkalinity-producing systems (SAPS) effectively treat acid mine drainage but suffer reduced efficiency and lifespan due to sludge accumulation in the limestone layer. Flushing systems, comprising perforated pipes, periodically discharge water to restore limestone porosity. However, existing designs lack scientific rigor. This study introduces a hydrodynamic approach to optimize flushing system design by evaluating orifice size and spacing. A novel performance index, orifice influence radius, was developed to calculate optimal configurations. The results provide a practical framework for improving flushing efficiency, extending SAPS lifespan, and enabling predictable facility management, offering critical insights into the engineering of mine drainage treatment systems.

Keywords: Successive alkalinity-producing system, acid mine drainage, flushing system, sludge removal, orifice influence radius

Introduction

The successive alkalinity-producing system (SAPS) is a widely implemented passive treatment method for mitigating acid mine drainage (AMD), utilizing stratified layers of water, organic matter, and limestone. While SAPS initially exhibits high treatment efficiency, the gradual accumulation of sediment in the organic and limestone layers significantly diminishes its performance and reduces its operational lifespan, which is typically designed for 20–25 years (Kepler and McCleary 1994; Zipper 2001). To mitigate these challenges, flushing systems have been introduced, comprising perforated pipes embedded within the limestone layer that periodically discharge accumulated sediment and AMD through controlled flushing (Weaver *et al*. 2004).

The efficacy of a flushing system depends on several interrelated factors: the physical properties of the limestone layer, sediment characteristics, system flow dynamics, and the design parameters of the flushing device, including orifice size and spacing. However, existing research often evaluates system performance as a whole without isolating the contribution of individual design elements, limiting the ability to optimize system configurations. A deeper understanding of these mechanisms is critical to advancing SAPS design and improving long-term performance.

This study modified from Lee and Cheong (2021) focuses on the specific role of flushing device characteristics in sediment removal. By standardizing the basic experimental conditions for the limestone layer, sediment properties, and flow dynamics, the investigation isolates the impact of orifice design and proposes a radius of influence for orifices as a guiding parameter for the optimal design of flushing systems. These findings offer practical insights for enhancing the efficiency and predictability of SAPS operation, addressing a critical gap in current treatment methodologies.

Experimental methods

To isolate the influence of flushing device characteristics, the experiment was conducted under controlled conditions, ensuring consistent properties for the limestone layer, sediment, and flow dynamics. Glass beads of uniform size and shape were utilized to simulate the limestone layer, while sediment with consistent density and origin was employed to represent the sludge. A constant hydraulic head was maintained to replicate natural drainage conditions in SAPS.

The experimental apparatus consisted of a rectangular tank (1 m × 0.5 m × 1.2 m) equipped with adjustable pipe connections and valves shown in Fig. 1. A 19 cm-thick layer of glass beads, with a spherical diameter of 20 mm and porosity of 39.0%, was placed above the pipe network to simulate the limestone layer. Three pipe diameters (16 mm, 25 mm, 50 mm) and orifice sizes (3 mm, 6 mm, 9 mm) were tested at varying orifice spacings (100 mm, 200 mm, 300 mm) to evaluate their effects on flushing efficiency. The lateral spacing of the pipe is 250 mm.

The sediment used in this study, primarily composed of iron oxide, was sourced from the Hwangji-Yoochang passive treatment facility in South Korea. Its dry density was 3.85 g/cm^3. For each test, a fixed dry weight of sediment (740 g) was mixed with water and uniformly distributed over the water surface in the tank. The sediment was allowed to settle completely into the glass bead layer before flushing commenced.

Flushing was initiated by rapidly opening the valve connected to the pipe network, allowing water to flow and mobilize the sediment. The expelled sediment-water mixture was collected, and the sediment was separated, dried at 80 °C, and weighed to quantify removal efficiency. This procedure was repeated for each combination of orifice spacing and pipe diameter. Prior to sediment flushing, flow consistency was verified against theoretical models such as the Bernoulli and Blake–Kozeny equations using water-only tests.

Experimental results

Volumetric Flow Rate Without Sediment

The discharge flow rate exhibited a direct relationship with orifice diameter, as illustrated in Fig. 2. A proportional increase in flow rate was observed with both larger orifice diameters and an increased number of orifices, consistent with theoretical predictions. The measured and calculated values showed strong agreement, demonstrating the robustness of the employed experimental framework.

Flow Rate Reduction Through the Glass Bead Layer

The introduction of the glass bead layer resulted in a measurable reduction in discharge flow rate due to the additional flow resistance, as depicted in Fig. 3. The calculated flow

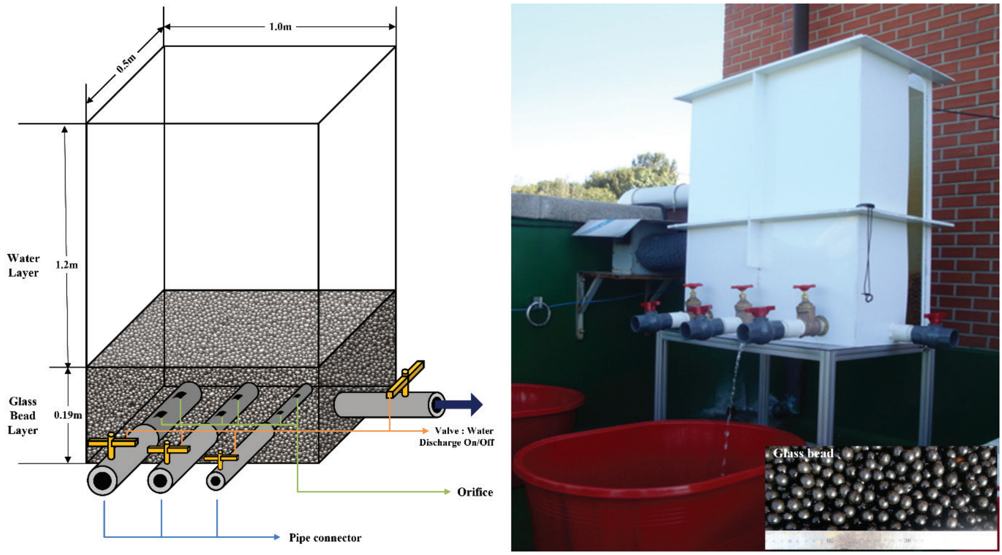

Figure 1 *Schematic diagram and photograph of the flushing experiment apparatus.*

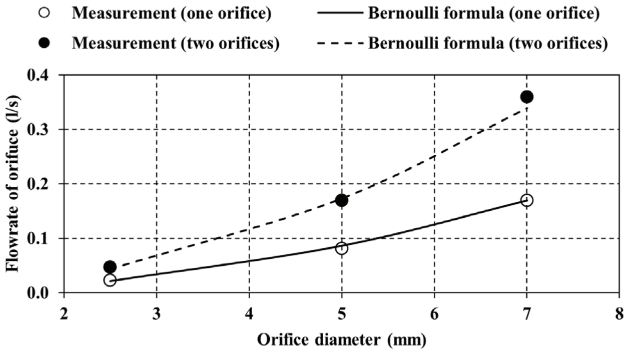

Figure 2 *Discharge flow rate according to orifice diameter and number of orifices in the case without deposits.*

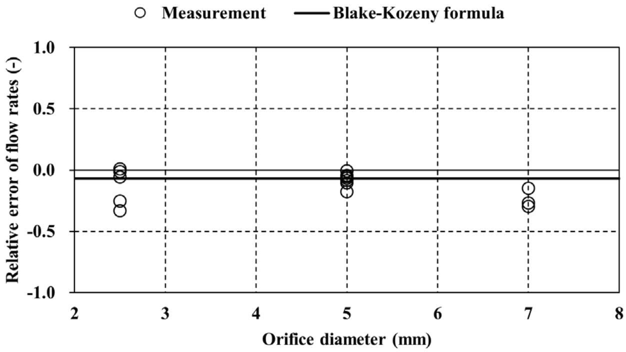

Figure 3 *Relative error of flowrate according to orifice diameter when water flows through the glass bead layer.*

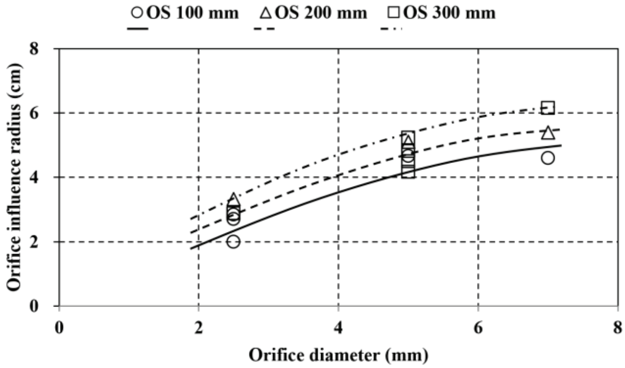

Figure 4 *Orifice influence radius according to orifice diameter.*

rate showed an approximate 6.9% decrease under identical conditions, corroborating experimental measurements. Deviations in the measured results were attributed to occasional blockage of orifices by glass beads. Nevertheless, a consistent alignment between theoretical and experimental values validated the methodology.

Orifice Influence Radius for Sediment Removal

The orifice influence radius, representing the effective sediment removal zone, was quantitatively assessed using Equation (1). Fig. 4 demonstrates that larger orifice diameters yielded greater influence radii, although the rate of increase diminished beyond a diameter of 5 mm due to limitations imposed by the dynamic flow behavior. This trend underscores the need to optimize orifice size to balance sediment removal efficiency and hydraulic constraints.

$$R_I = \sqrt[3]{\frac{3}{4\pi}\,\frac{W_S}{n_o \rho_D}} \qquad (1)$$

where, $\mathbf{W_S}$: dry weight of the iron sediment recovered at the orifice (g)

$\boldsymbol{\rho_D}$: distribution density of the iron sediment in the glass bead layer (g/m^3)

$\mathbf{n_o}$: number of orifices

Impact of Orifice Spacing

As shown in Fig. 5, the influence radius expanded with increasing orifice spacing before reaching a plateau. This behavior reflects the reduction of overlapping influence zones as spacing increases. Smaller orifices exhibited limited overlap separation at shorter distances, whereas larger orifices required greater spacing to achieve similar separation. Under the conditions of this study, the maximum influence radii were determined to be 3.2 cm, 5.3 cm, and 6.1 cm for orifice diameters of 2.5 mm, 5 mm, and 7 mm, respectively. These findings provide critical insights for designing flushing systems with optimized orifice configurations.

Discussion

This study established an orifice influence radius of up to 7 cm under an average hydraulic head of 0.99 m within a glass bead layer. Consequently, the optimal orifice spacing was determined to be 14 cm, which is slightly smaller than the 15 cm recommended by Weaver *et al.* (2004). It should be noted that these experimental results were obtained using glass beads with a diameter of 20 mm, which may differ from actual conditions where limestone aggregates are used. Nevertheless, the findings underscore the feasibility of employing the experimentally derived influence radius as a fundamental parameter in the design of lateral pipe configurations for flushing systems.

Furthermore, the results indicate that the influence radius is significantly affected by key factors such as hydraulic head, orifice diameter, and the effective porosity of the limestone layer. For instance, an increase in hydraulic head was observed to enhance the discharge flow rate, thereby expanding the influence radius and potentially permitting larger orifice spacing. Traditionally, flushing system designs have largely overlooked these complex interdependencies. By adopting the methodological framework developed in this study, engineers can systematically integrate these critical parameters into design considerations, thereby improving the efficiency and adaptability of flushing systems.

Conclusions

This study confirmed that the flow rates through orifices embedded in a porous glass bead layer under constant head conditions closely align with theoretical predictions based on the Blake–Kozeny equa-

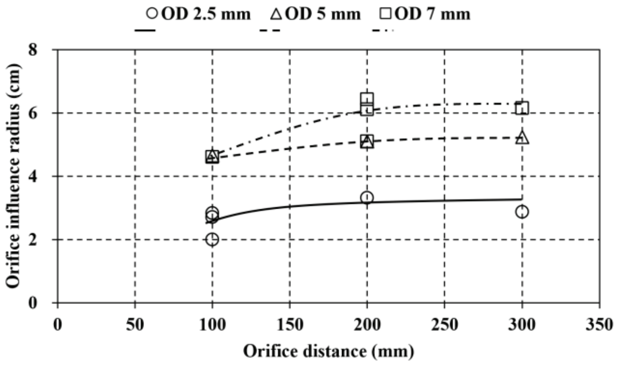

***Figure 5** Orifice influence radius according to orifice spacing.*

tion. Additionally, the study introduced the concept of the orifice influence radius as a quantitative performance index and provided a comprehensive methodology for its evaluation. Experimental findings demonstrated that, at an average hydraulic head of 0.99 m, the maximum influence radius was 7 cm, corresponding to an optimal orifice spacing of 14 cm or less in the glass bead layer. This result is consistent with, albeit slightly more conservative than, previously proposed guidelines. It is important to acknowledge that these experimental results may not fully replicate real-world scenarios where limestone aggregates are utilized.

The proposed design methodology offers a practical framework for optimizing orifice configurations, including spacing and distribution, tailored to specific operational conditions. Moreover, this study highlights the crucial influence of key parameters such as differential head, orifice diameter, and limestone layer porosity on the performance of flushing systems. The application of this experimental approach paves the way for more scientifically robust and operationally efficient designs, ultimately enhancing the longevity and effectiveness of successive alkalinity-producing systems.

Acknowledgements

This research was supported by the Basic Research Project (25-3414) of the Korea Institute of Geoscience and Mineral Resources (KIGAM) funded by the Ministry of Science, ICT of Korea and Korea Mine Rehabilitation and Mineral Resources Corporation (KOMIR).

References

Kepler DA, McCleary EC (1994) Successive alkalinity-producing systems (SAPS) for the treatment of acid mine drainage. Proc Int Land Reclamation and Mine Drainage Conf, Apr 24–29, Pittsburgh, PA, USA, pp. 195–204

Lee DK, Cheong YW (2021) Experimental study of the adoption of flushing technique in successive alkalinity-producing systems with a focus in influence radius of orifice. Environ Earth Sci 80:805

Weaver KR, Lagnese KM, Hedin RS (2004) Technology and design advances in passive treatment system flushing. 2004 National Meeting of the American Society of Mining and Reclamation and the 25th West Virginia Surface Mine Drainage Task Force, Apr 18–24, Morgantown, WV, USA.

Zipper C, Skousen J, Jage C (2011) Passive Treatment of Acid-Mine Drainage with Vertical Flow Systems. Virginia Cooperative Extension Publication No. 460-133, June 2001.

A Comprehensive Approach to Fluoride Treatment in Mine Drainage: Chemical Precipitation and Adsorption

Ki-Rim Lee[1], Duk-Min Kim[1], Hye-Lim Kwon[1], Nam-Kyu Kim[1], Young-Min Kim[1], Dae-Gyu Im[2], Sin-Dong Kim[3], Seul-Ki Koo[4]

[1]*Department of New Energy and Mining Engineering, Sangji University, Wonju, 26393, Gangwon state, Republic of Korea, kdukmin8@sangji.ac.kr, ORCID 0000-0002-1537-6866*

[2]*Department of Earth and Environmental Sciences, Korea University, Seoul, 02841, South Korea, daegull1995@korea.ac.kr*

[3]*Environment Energy & Chemical Solution, Pocheon, 11154, South Korea, catalite@hanmail.net*

[4]*Korea Mine Rehabilitation and Mineral Resources Corporation (KOMIR), Wonju, 26464, South Korea, skkoo@komir.or.kr*

Abstract

Fluoride in mine drainage poses substantial environmental risks, often exceeding South Korea's regulatory discharge limit of 3.0 mg/L. This study assessed treatment processes combining precipitation and adsorption for fluoride and toxic metals from the Samwon mine drainage. To treat aluminum, manganese, and fluoride, experiments involving injection of calcium hydroxide and reaction with slag-limestone mixture were conducted. Subsequently, to treat remnant fluoride, experiments involving precipitation/adsorption using aluminum sulfate and lanthanum chloride as well as adsorption using Al-rich coal mine drainage sludge and domestic water purification sludge were conducted. The results demonstrated substantial fluoride reduction, with adsorption kinetics following a pseudo-second-order model.

Keywords: Fluoride removal, adsorption, precipitation, coprecipitation, aluminum sludge

Introduction

Fluoride and toxic metals in mine drainage present persistent environmental challenges due to their toxicity and potential long-term effects on ecosystems and human health (Hamamoto *et al.*, 2015; Tang *et al.*, 2009). The World Health Organization (WHO, 2017) recommends a fluoride concentration of less than 1.5 mg/L in drinking water, but some mine drainages can exceed this threshold. In addition to fluoride, metals such as manganese, iron, and aluminum are commonly found in elevated concentrations in mine drainage, contributing to water quality deterioration. At the Samwon mine, located in South Korea, mine drainage contains high levels of fluoride (up to 20.5 mg/L), as well as manganese and iron concentrations that exceed national discharge limits. Although aluminum does not have a defined discharge standard, it was included as a treatment target due to its potential to cause environmental issues such as whitening. The geology of the Samwon area consists of Cretaceous granitic rocks and metamorphosed sedimentary rocks, both of which are known sources of fluoride. Fluoride occurs in granitic rocks primarily in Si–F bonds, and its mobility depends on surrounding geochemical conditions, including pH, redox potential, and the presence of competing ions. Once released into groundwater, fluoride may exist as soluble species or precipitate as fluorite (CaF_2).

To address these challenges, this study assessed and compared the performance of different treatment approaches for fluoride and metal removal. In the primary treatment, two separate processes were tested and compared: (1) active precipitation using calcium hydroxide ($Ca(OH)_2$), and (2) passive precipitation using a slag-limestone mixture. These processes were assessed based on their ability to remove aluminum, manganese, iron, and fluoride. In the secondary treatment, two different fluoride removal methods were applied to the water that remained after each primary treatment: (1) chemical precipitation and/or adsorption induced by the addition of aluminum sulfate ($Al_2(SO_4)_3$) or lanthanum chloride ($LaCl_3$), and (2) adsorption using aluminum sludge-based adsorbents from an Al-rich coal mine drainage treatment facility and from a domestic water purification facility (Fig. 1). This study aims to assess and compare each treatment step – both primary and secondary – by examining removal efficiency, economic feasibility, and potential for practical application in mine drainage treatment.

Methods

Adit drainage used in this study was collected from the Samwon mine, South Korea. The water exhibited a near-neutral to slightly acidic pH (average: 6.2) and high electrical conductivity (EC), with elevated concentrations of fluoride (up to 20.5 mg/L), manganese, iron, and aluminum (Tab. 1).

Temperature, oxidation-reduction potential (ORP), pH, EC, and dissolved oxygen (DO) concentrations were measured using an HQ40D multi-portable meter (Hach). Alkalinity was measured using a digital titrator (Hach), and fluoride was analyzed with a DR-900 colorimeter (Hach). Major cations and anions were analyzed by ICP-OES (Varian 720-ES) and ion chromatography (Metrohm 850), respectively.

In the primary treatment stage, two separate processes were assessed and compared. The first method involved active treatment by adding calcium hydroxide ($Ca(OH)_2$) in batch experiments to increase the pH and induce the precipitation of metals and fluoride. The second method applied passive treatment using a slag-limestone mixture at a volumetric ratio of 4:6 in a lab-scale column setup, where hydraulic retention times (HRTs) ranged from 2 to 12 hours. The slag was basic oxygen furnace (BOF) steelmaking slag generated in South Korea. Geochemical modeling using PHREEQC was performed to predict the saturation indices of potential precipitates including gibbsite (Al(OH)3), goethite (FeOOH), magnetite (Fe_3O_4), and fluorite (CaF_2), to understand the dominant removal mechanisms.

Following the primary treatments, two different approaches were tested for secondary fluoride removal. The first method involved chemical dosing using aluminum sulfate ($Al_2(SO_4)_3$) or lanthanum chloride ($LaCl_3$) in batch experiments, which induce

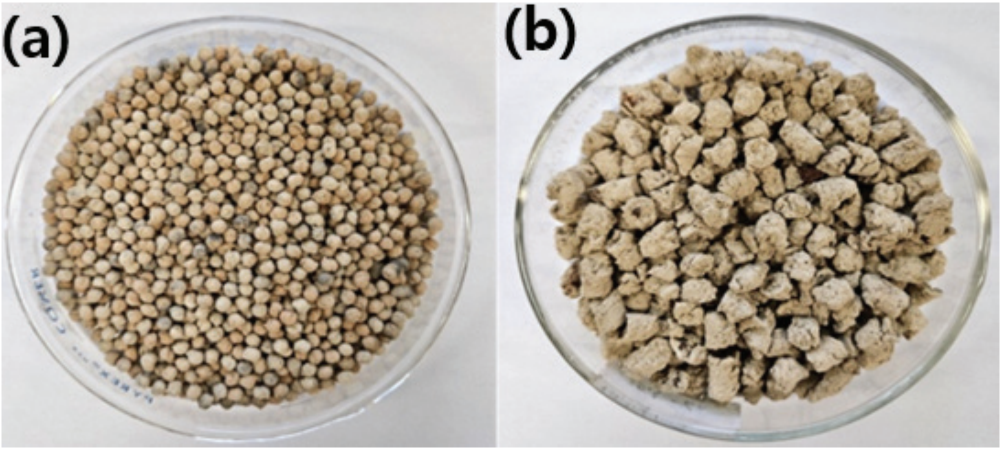

Figure 1 Photographs of the adsorbents used in the secondary treatment process: (a) adsorbent made from sludge of a domestic water purification facility and (b) from sludge of a coal mine drainage treatment facility.

Table 1 Physicochemical characteristics and ion composition of mine drainage collected from the Samwon mine.

Average physicochemical characteristics of mine drainage						Flow rate (m^3/day)	
T (°C)	pH	EC (µS/cm)	DO (mg/L)	Alkalinity (mN)	SS (mg/L)	Avg.	Max.
18.4	6.2	1028.2	6.7	0.87	4.0	129.6	1065.7
Ion concentration (mg/L)							
Fe	Mn	Al	Ni	Cu	Zn	F^-	SO_4^{2-}
4.07	10.75	12.52	0.07	0.01	0.38	35.93	523.80

precipitation and/or adsorption. Dosages were varied to evaluate fluoride removal efficiency and sludge generation. The second method employed two aluminum-based adsorbents: ST, derived from sludge of Samtan (ST) mine drainage treatment facility, and DENS-10, obtained from alum sludge in a domestic water purification facility. Adsorbents were characterized via Brunauer-Emmett-Teller (BET) surface area analysis, Barrett-Joyner-Halenda (BJH) pore distribution, and scanning electron microscopy/energy dispersive X-ray spectroscopy (SEM-EDS). Batch adsorption experiments were conducted under varying pH and solid-to-liquid (S/L) ratios, and adsorption behaviors were assessed using pseudo-first-order and pseudo-second-order kinetic models as well as Langmuir and Freundlich isotherm models.

Results and discussion

Primary treatment using calcium hydroxide effectively increased the pH of mine drainage and facilitated the removal of aluminum, manganese, iron, and fluoride through precipitation. As the pH rose to approximately 10.5, aluminum precipitated as hydroxides, which was supported by PHREEQC modeling. Iron, initially present at 5.8 mg/L, was completely removed at pH above 8.0, likely due to the formation of iron (oxy)hydroxides. While manganese concentrations exceeded 2 mg/L at pH 9.5, they decreased below 0.15 mg/L at pH 10.5, meeting regulatory discharge limits. Fluoride concentration decreased from 20.5 mg/L to 13.7 mg/L after calcium hydroxide addition, and PHREEQC results indicated possible fluorite (CaF2) formation as a key removal mechanism. Although the fluoride concentration decreased after primary treatment, it still exceeded both the WHO guideline of 1.5 mg/L and South Korea's regulatory discharge limit of 3.0 mg/L for high-quality water bodies, indicating the necessity of a secondary treatment process. This study was conducted in accordance with South Korea's regulatory standards for wastewater discharge, and the treatment performance was evaluated based on the national discharge limit of 3.0 mg/L for fluoride.

In the passive treatment using a slag-limestone mixture, the removal of aluminum and manganese was effective at hydraulic retention time (HRT) of ≥4 hours in the column, but fluoride concentrations remained between 13.0 and 17.1 mg/L, again indicating the need for additional treatment.

For chemical-based secondary treatment, the addition of 1,200 mg/L of aluminum sulfate ($Al_2(SO_4)_3$) reduced the fluoride concentration from 13.7 mg/L to 2.8 mg/L within 30 minutes, but produced a large volume of aluminum hydroxide sludge. In contrast, lanthanum chloride ($LaCl_3$) at 400 µL/L achieved similar fluoride removal below 3.0 mg/L with substantially less sludge production. While both reagents were effective, lanthanum chloride showed an advantage in sludge management.

In the adsorption-based secondary treatment, ST and DENS-10 adsorbents were applied to batch experiments. ST showed a higher surface area (168.94 m^2/g) and pore volume (0.53 cm^3/g) than DENS-10 (39.96 m^2/g, 0.14 cm^3/g) (Table 2). Kinetic analysis revealed that both materials followed pseudo-second-order (PSO) kinetics, suggesting chemisorption as the dominant mechanism. ST showed rapid initial uptake but reached saturation earlier, while DENS-10 exhibited more stable adsorption over time. Adsorption

Table 2 BET and BJH analytical results for the DENS-10 and ST adsorbents.

Adsorbent	BET (m^2/g)	Total pore volume (cm^3/g)	dp, peak (nm)	Avg. pore size (nm)	Reference
DENS-10	40	0.14	18.5	14.8	This study
ST	169	0.53	43.6	13.7	This study
GASA$_{(100\ mesh)}$ [1)]	177	0.73	<180.0	–	(Cho et al., 2020)
ASBA[2)]	87	0.11	–	3.6	(Lee et al., 2020)
Activated alumina	357	0.44	–	46.4	(Kim et al., 2005)

1) A granular composite adsorbent prepared from PAC and starch gel

2) Alum-sludge based adsorbent

isotherm results indicated DENS-10 followed Langmuir isotherm implying uniform monolayer adsorption, with a maximum adsorption capacity (qmax) of 12.3 mg/g. In contrast, ST exhibited combined mechanisms involving both surface adsorption and mineral precipitation, supported by SEM observations of fluorite formation on its surface. This may be attributed to residual calcium from the hydrated lime treatment in the Samtan treatment facilities, which reacted with fluoride during adsorption.

Conclusions

This study assessed and compared multiple treatment strategies for fluoride and metal removal from the Samwon mine drainage. The primary treatment using calcium hydroxide and a slag-limestone mixture demonstrated effective removal of aluminum, manganese, iron, and partial fluoride reduction through pH adjustment and precipitation. In the secondary stage, both chemical reagent addition ($Al_2(SO_4)_3$ and $LaCl_3$) and adsorption using aluminum-based materials (ST and DENS-10) were tested. Lanthanum chloride achieved similar fluoride removal to aluminum sulfate while generating less sludge, making it advantageous for sludge management. Between the adsorbents, DENS-10 showed q_{max} of 12.3 mg/g, while ST offered a combined mechanism of surface adsorption and mineral precipitation. Overall, this study demonstrated that the proposed treatment approaches are effective and adaptable depending on site-specific conditions. Future work will focus on field-scale validation and long-term stability.

Acknowledgements

This research was supported by the Development of Source Identification and Apportionment Methods for Toxic Substances in Marine Environments Program of the Korea Institute of Marine Science & Technology Promotion (KIMST), funded by the Ministry of Oceans and Fisheries (RS-2022-KS221655), and by the Korea Mine Rehabilitation and Mineral Resources Corp. (KOMIR) in 2024.

References

Bhatnagar A, Kumar E, Sillanpää M (2011) Fluoride removal from water by adsorption—A review. Chem Eng J 171:811–840. https://doi.org/10.1016/j.cej.2011.05.028

Cho, D.-W., Han, Y.-S., Lee, J., Jang, J.-Y., Yim, G.-J., Cho, S., Lee, J.-S., & Cheong, Y.-W. (2020). Water defluorination using granular composite synthesized via hydrothermal treatment of polyaluminum chloride (PAC) sludge. Chemosphere, 247, 125899. https://doi.org/10.1016/j.chemosphere.2020.125899

Hamamoto S, Kishimoto N, Ueki M (2015) Mechanistic consideration of fluoride removal using aluminum sulfate. J Water Environ Technol 13:15–24. https://doi.org/10.2965/jwet.2015.15

Kim, S.-Y., Kim, J. H., Kim, H.-J., & Cho, Y.-S. (2005). A study on the removal of low-concentration fluoride-ion by modified alumina. Journal of Korean Society of Environmental Engineers, 247–252.

Kumar R, Kang CU, Mohan D, Khan MA, Lee JH, Lee SS, Jeon BH (2020) Waste sludge derived adsorbents for arsenate removal from water. Chemosphere 239:124832. https://doi.org/10.1016/j.chemosphere.2019.124832

Lee G, Cui M, Yoon Y, Khim J, Jang M (2018) Passive treatment of arsenic and heavy metals contaminated circumneutral mine drainage using granular polyurethane impregnated by coal mine drainage sludge. J Clean Prod 186:282–292. https://doi.org/10.1016/j.jclepro.2018.03.156

Lee, J. H., Ji, W. H., Lee, J. S., Park, S. S., Choi, K. W., Kang, C. U., & Kim, S. J. (2020). A study of fluoride and arsenic adsorption from aqueous solution using alum sludge-based adsorbent. Economic and Environmental Geology, 53(6), 667–675. https://doi.org/10.9719/EEG.2020.53.6.667

Tang Y, Guan X, Su T, Gao N, Wang J (2009) Fluoride adsorption onto activated alumina: Modeling the effects of pH and some competing ions. Colloids Surf A Physicochem Eng Asp 337:33–38. https://doi.org/10.1016/j.colsurfa.2008.11.027

Turner BD, Binning P, Stipp SLS (2005) Fluoride removal by calcite: Evidence for fluorite precipitation and surface adsorption. Environ Sci Technol 39:9561–9568.

World Health Organization (WHO) (2017) Guidelines for drinking-water quality: Incorporating the 1st addendum, 4th ed. WHO Press, Geneva.

The Role of Colloidal and Particulate Fractions in REE Enrichments in Coal-Based Acid Mine Drainage Systems

Liliana Lefticariu[1*], Ryan L. Bowman[1], Madeline Lewinski[1],
Jerome Specht[1], and Paul T. Behum[2]

[1]School of Earth Systems and Sustainability, Southern Illinois University, Carbondale, 62901 USA

[2]Office of Surface Mining Reclamation and Enforcement, Alton, Alton, IL 62002 USA (retired)

*Corresponding author lefticar@siu.edu, ORCID 0000-0003-3413-654X

Abstract

This work investigated the distribution, modes of occurrence, and relative extractability of rare earth elements (REE) from aqueous and solid waste at Tab Simco, an abandoned coal mining operation in Illinois, U.S.A. We found a preferential enrichment of REE-bearing phases in the aluminum-rich solid waste, which can contain up to 300 mg/kg of REE (corresponding to 0.04% REO), thus making it an attractive target for REE extraction. Additionally, existing technologies can sequester >90% of REE from AMD and concentrate them by a factor of 1000 in the solid precipitates. Coal-based waste could become a REE unconventional source.

Keywords: Rare earth elements, acid mine drainage, colloids, REE recovery stratification

Introduction

The rare earth elements (REE) are a group of 17 elements that include the lanthanides (Ln, atomic numbers 57 through 71), scandium (21), and yttrium (39) (IUPAC, 2005). The REE have similar atomic structure and geochemical behavior in natural systems and most are relatively abundant in the Earth's crust (McLennan, 2001). REE are essential in many industrial applications, including clean energy technologies, communications, and medical science (Kolker *et al*., 2024). The REE global demand is predicted to increase up to seven times above the current levels by 2040 (U.S. DOE, 2023). Lately, the REE international market is challenged by continuously growing demand and limited supply, which could lead to shortages and engagements (Kolker *et al*., 2024). Based on their economic prospect, Nd, Pr, Dy, and Tb are considered critical rare earths (i.e., *critical*-REE, U.S. DOE, 2023).

Coal mining waste (CMW), traditionally considered a byproduct of electric power generation, often contains REE and other critical materials (Kolker *et al*., 2024). In CMW, REE are associated with REE-bearing minerals (i.e., bastnäsite, monazite, xenotime, apatite, and zircon) or adsorbed onto clay minerals (Kolker *et al*., 2024). In the Illinois coal basin, CMW at abandoned mining lands (AML) exhibited elevated REE contents ranging from 100 to over 300 mg/ kg (Bowman, 2025). The REE concentration value of 300 mg/kg is considered the lower limit for economic profitability (U.S. DOE, 2023). Weathering of CMW materials, primarily those containing high amounts of pyrite (Lefticariu *et al*., 2006), produces coal-based acid mine drainage (AMD), which is of environmental concern in coal basins worldwide. Although AMD is characterized by high acidity and elevated sulfate and iron contents, it may also contain economically relevant elements, including REE (Lefticariu *et al*., 2020). It is uncertain what physical and biogeochemical processes exert primary control on the distribution of REE at AML sites.

In this contribution, we investigated the distribution, modes of occurrence, and relative extractability of REE from coal-based waste products, including AMD and CMW, at Tab Simco, an abandoned coal mining operation in the Illinois Basin, U.S.A. (Behum *et al.*, 2011; Lefticatiu *et al.*, 2020). We show that the preferential enrichments of REE-bearing phases occurs in the clay-rich particulate fraction, which can contain up to 300 mg/kg of total REE (corresponding to 0.04% REO), making it an attractive target for REE extraction. Existing technologies can sequester >90% of REE from AMD and concentrate them by a factor of 1000 in solid precipitates from which REE can be extracted using current technologies (Fujita *et al.*, 2024 and references therein). Together these data support the idea that coal-based waste materials at AML sites could become a promising secondary source of REE.

Methods

Multiple coal-based solid and aqueous samples were collected at different locations at Tab-Simco, an abandoned coal mining operation in the Illinois Basin, U.S.A. Details about sample locations are presented elsewhere (Lefticariu *et al.*, 2017; Bowman, 2025). The Tab Simco AML site is well suited for this study because it contains multiple AMD seeps and an AMD treatment system that includes a sulfate-reducing bioreactor and a wetland system designed to remediate AMD pollution (Behum *et al.*, 2011). Our team has studied the site and collected data for over fifteen years and the comprehensive breakdown of the methodology used for sample collection and analysis is available in our earlier work (Burns *et al.*, 2012; Lefticariu *et al.*, 2015; 2017; 2019; 2020;).

Briefly, the aqueous AMD samples were collected in 250-mL Nalgene™ HDPE bottles at various locations at the Tab Simco site following previously described procedures (Lefticariu *et al.*, 2017; Bowman, 2025). After collection, the samples were immediately transported on ice back to the SIUC Geochemistry Laboratory and filtered through 0.22 µm cellulose acetate membrane (Millipore® HAW). The filtered samples were analyzed for pH and conductivity by Mettler Toledo S400 Benchtop pH meter and dissolved sulfate by ion chromatography (IC). Cations analyses, including REE, were performed on filtered, acidified to pH < 2 using ultra-pure HNO_3 (Fisher Scientific™) solution by Inductively Coupled Plasma Mass Spectroscopy (ICP-MS) at the ACME Laboratories, Inc. (Bureau Veritas Commodities), Vancouver, British Columbia, Canada. The solid samples derived from the weathering and passive treatment of CMW were collected across the Tab Simco AML site (Bowman, 2025). Additionally, multiple sediment cores were retrieved from the bioreactor representing mixtures of in situ precipitates and sediments generated by the weathering CMW and transported to the bioreactor (i.e., Lefticariu *et al.*, 2017; 2018). The retrieved samples were transported to SIUC, sectioned, dried at 50 °C, ground via mortar and pestle, and saved for further analyses. The metal, including REE, contents of solid matrix materials were determined by ICP-MS using a sodium peroxide fusion digestion method at Activation Laboratories, Inc. (Actlabs), Ancaster, Ontario, Canada. The mineralogical characterization was performed by powder X-ray diffraction (XRD) using a Rigaku Ultima IV X-ray diffractometer with CuKα radiation (Lefticariu *et al.*, 2017) and scanning electron microscopy with energy-dispersive X-ray spectroscopy (SEM-EDS) analyses using a Hitachi FlexSEM1000 SU1000 unit, with a Bruker EDS Unit attached for EDS analysis with a detection limit of 100 ppm (Bowman, 2025).

Results and Discussion

At the Tab Simco AML site, the weathering of CMW transferred its organic and inorganic constituents to the solution, which are transported as dissolved, colloidal, and/or particulate components by AMD and deposited across the site. Previous work showed that the primary dissolved (<0.22 µm) components in AMD were sulfate, SO_4, and ferrous iron, Fe(II), (Behum *et al.*, 2011) both sourced by pyrite oxidation (Lefticariu *et al.*, 2006). XRD analysis showed that the phyllosilicate minerals and quartz (Al-rich detrital phases, dNP) dominated the AMD colloidal and particulate fractions (Bowman, 2025). Additionally, the CMW-sourced aqueous Fe(II) was oxidized to ferric iron Fe(III), which through a series of microbially mediated processes that promoted the formation of Fe-rich phases (i.e., schwertmannite, goethite), precipitated as neoformed nano- and micro-scale particles (nNP) (Lefticariu *et al.*, 2017). The field-scale bioreactor plays a key role in accumulating these dNP and nNP colloidal and particular fractions transported by AMD (Fig. 1a, b), such that over time, a thick sediment layer storing the accumulating dNP and nNP formed at the bottom of the pond above the bioreactor. Probing these AMD sediments allowed us to decipher the nature of the colloidal and particulate fractions as well as the biogeochemical processes that contributed to their formation and transformation (Lefticariu *et al.*, 2017)

The total concentration of REE (ΣREE) of various waste materials varies across the Tab Simco AML site (Bowman, 2025). The ΣREE of AMD samples from Tab Simco main seep ranged from 744.2 to 1000.2 µg/L with an average of 898.3 µg/L (n = 8) while *critical*-ΣREE (Nd, Pr, Dy, and Tb) varied between 192.5 and 258.1 µg/L with an average of 224.9 µg/L. Overall, similar average ΣREE in AMD were noted from Tab Simco (ΣREE_{avg} = 898 µg/L) and Illinois basin AMD samples (ΣREE_{avg} = 1059 µg/L) (Lefticariu *et al.*, 2018).

The ΣREE contents of the AMD sediments at Tab Simco varied from 7 to 245 mg/kg (Bowman, 2025). Significantly, the concentrations of REE inversely correlate with Fe (R^2 = 0.82, n = 18) (Fig. 1c) and directly correlate with Al (R^2 = 0.91, n = 18) (Fig. 1d), a trend consistently observed in AMD and CMW materials at AML sites throughout the Illinois Basin both (Lefticariu *et al.*, 2020; Bowman, 2025).

The normalized REE values to those of the Upper Continental Crust Reference (UCC; McLennan, 2001) further showed the large gap of the individual REE contents between the Al-rich and Fe-rich sediments (Fig. 1e). The Fe-rich sediments show an overall flat REE pattern, with value generally lower than 0.5, while Al-rich sediments exhibit more varied patterns displaying a Ce negative anomaly and enrichments in middle REE, namely Nd, Sm, Eu, and Gd (Fig. 1e). However, in terms of relative abundance of individual REE, similar patterns emerged for Fe-rich and Al-rich sediments, with the most abundant REE being Ce (33-36%), Ln (18-22%), Nd (14-16%), Y (11-13%), Pr (3- 4%), Gd (2%), and Dy (2%). This surprising result suggests that contrary to the overall distinct mineralogy of the Al- and Fe-rich sediments, the REE may be hosted by similar phases. *The critical*-ΣREE (Nd, Pr, Dy, and Tb) contents varied between 1.7 and 7.7 mg/kg with an average of 4.8 mg/kg for Fe-rich sediments and between 27.2 and 48.7 mg/kg with an average of 40.2 mg/kg for Al-rich sediments. Overall, the Al-rich sediments contain one order of magnitude more REE than the

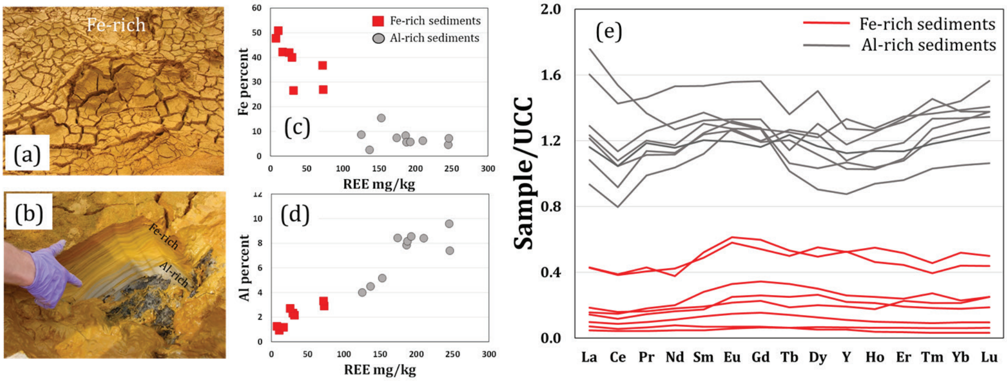

Figure 1 *Composite picture depicting (a) and (b) close-up view of the Fe-rich and Al-rich sediments accumulated in the upper part of Tab Simco bioreactor (Lefticariu et al., 2018); the dark material below the Al-rich sediment is the top of the organic compost layer (c) and (d) comparison REE values and Fe and Al, respectively of the AMD sediments; (e) REE patterns of Fe-rich and Al-rich sediments normalized to Upper Continental Crust Reference (UCC; McLennan, 2001).*

Fe-rich sediments. In terms of the relative abundance of individual *critical*-REE, all AMD sediments exhibit similar patterns for Nd (69-74%), Pr (17-19%), Dy (8-10%), and Tb (1-2%).

The AMD sediments were further examined in detail by SEM and additional data were collected at the X-ray microprobe at Beamline 13-ID-E (GSECARS) at the Advanced Photon Source (APS), Argonne, IL (for details see Lefticariu *et al.*, 2017; 2018). The REE-bearing particulates were observable as trace phases by scanning electron microscopy and we measured the contents of REE in the particulates (Table 1; Bowman, 2025).

Our SEM analysis showed that the Fe-rich sediments contained no any discernible REE particles. Conversely, in the AL-rich AMD sediments, we were able to identify several REE-bearing particles, which were embedded within the clay-rich regions (Fig. 2a). These nano-and micro-scale REE-bearing particles were often embedded within the clay mineral assemblages (Fig. 2). The EDX-SEM measurements showed that REE-bearing particles exhibited elevated REE contents (Bowman, 2025), with values up to 5,535 ppm for La, 1845 ppm for Ce, and 73,994 for Nd (Table 1). Moreover, the high Al, Si, O, and low Fe contents suggest that the REE-bearing particles were embedded within the clays. Further mineralogical investigations revealed that phosphates, such as monazite ((Ce, Nd)PO_4), were the main (Ce,Nd)-bearing minerals in these sediments (Bowman, 2025).

Results of synchrotron X-ray analysis of the AMD sediments were previously reported (Lefticariu *et al.*, 2017; 2018). In terms of REE contents, we present here the Y spatial distribution in an Al-rich sediment sample as a Y-Ka µXRF map (Fig. 2b). We used Y as a proxy for the REE since it has similar behaviour with the lanthanides (Kolker *et al.*, 2024). The map shows randomly distributed high-Y hot spots with sizes ranging from microns to nanometres (Fig. 2b). In the AMD sediments, Y was most probably incorporated into xenotime (YPO_4) and Y-bearing zircon ($ZrSiO_4$), which probably originated in the weathering CMW. Previously, we showed zircon, a ubiquitous accessory mineral in CMW, was present all AMD sediments as nano- and micro-scale particles. However, the particles' size and abundance were much higher in the Al-rich sediments (Lefticariu *et al.*, 2017).

The source of REE at the Tab Simco AMD system was the weathering CMW. Our recent investigation revealed that *ΣREE* of the CMW from the Illinois coal basin ranges from 100 to 310 mg/kg (Bowman, 2025). The common REE-bearing minerals in CMW include phosphates (i.e., monazite, rhabdophane, xenotime, apatite, and crandallite), silicates

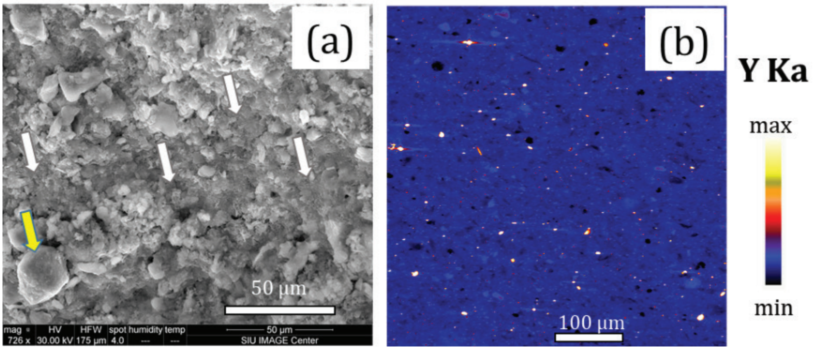

***Figure 2** (a) SEM image of the sample from the Al-rich layer of the AMD sediments. The yellow arrow point to a quartz grain while the white arrows point to clay regions that host REE-bearing particulates. (b) Synchrotron X-ray fluoresce (XRF) elemental map of Yttrium (Y) in an Al-rich sediment sample (Lefticariu et al. in preparation).*

Table 1 Chemical composition of REE-bearing particulate fraction in Al-rich samples from Tab Simco AML sites. Values in parts per million (ppm) (data from Bowman 2025).

Sample ID	C	O	Al	Si	Fe	La	Ce	Nd
Point #35	65675	537435	147574	229548	0	5535	1376	0
Point #38	105060	361644	153055	331257	0	303	675	0
Point #39	41071	270282	175780	348317	86085	2622	1845	73994
Point #40	84260	444743	107811	388262	23381	1529	12	0
Point #41	55340	416188	139550	331955	29963	787	82	26132
Point #42	55498	347804	155977	307194	62281	1221	1571	62140
Point #43	45515	529049	142525	223825	0	851	367	44953

(i.e., allanite, titanite, and zircon) and adsorption on clays (Kolker *et al.*, 2024). Physical and biogeochemical processes and mineral solubility controlled the weathering and partition of REE-beating phases among various fractions. At Tab Simco, after the REE were released from their host minerals, they were transported as dissolved aqueous sulfate complexes and colloidal and particulate fractions. Highly acidic (pH <4) solutions, such as Tab Simco AMD (pH<3) are required to mobilize substantial amounts of REE due to the low solubility of REE-bearing minerals in neutral pH solutions. Phosphates usually weather rapidly in natural environments, releasing REE as either aqueous complexes or microscopic mineral particulates, which can adsorb onto clays and then be transported by AMD (Bowman, 2025).

In terms of CMW volume, the Fe-rich sediments are prevalent at Tab Simco (Lefticariu *et al.*, 2017) and may represent an important sink for REE. However, recent work has demonstrated that REE adsorption onto Fe(III) precipitates is trivial at pH values lower than 5 (Lozano *et al.*, 2020). At Tab Simco, acidic waters characterized both the AMD, with pH <3, and the porewater of Fe-rich sediments, with pH <3.5, and therefore, the adsorbed REE fraction on Fe(III)-nNP is probably insignificant. Thus, ΣREE for Fe-rich sediments probably was the contribution of the detrital colloidal and particulate fraction. Clay minerals, particularly kaolinite and illite, can also sequester REE through weakly adsorption on their surfaces (Borst *et al.*, 2020). Clay-hosted REE deposits, a product of igneous rocks weathering in subtropical areas, are a major source of REE ores worldwide. As with Fe(III) sediments, the adsorption processes are controlled by pH, with clay's sequestration capacity for REE increasing at higher pHs (Bishop *et al.*, 2024). At Tab Simco, two factors could have controlled in the enhanced REE adsorption onto clays: the Al-rich sediments which contain high amounts of clays (i.e., kaolinite) and the pH values of their porewater were >5.5 (Lefticariu *et al.*, 2017). In addition to REE adsorption on clays, the colloidal and particulate REE fraction markedly contributed to elevated ΣREE of the Al-rich sediments (Table 1). These processes resulted in the enhanced capacity of Al-rich sediments to sequester REE with ΣREE values ten times higher than those of Fe-rich sediments. Moreover, across the Illinois basin at the AML site, an accumulation of Al-rich sediments was observed, and in all cases, they contained higher REE contents (Bowman, 2025). Together, these results indicate that clay minerals could play an important role in the transport and sequestration of REE in AMD systems.

Conclusions

In this study, we show that in addition to the dissolved REE, there is a substantial fraction of REE carried as colloids and fine suspended particles that partition the REE between a truly dissolved fraction (<0.01 µm) and the solid phases (>0.45 µm). The preferential enrichments of REE-bearing phases in the Al-rich sediments, which can contain up to 300 mg/kg of REE (corresponding to 0.04% REO) make it an attractive target for REE extraction. Additionally, existing technologies can sequester >90% of REE from AMD and concentrate them by a factor of 1000 in the solid precipitates (i.e., Fujita *et al.*, 2024 and references therein). Together these data strongly support the idea that Al-rich AMD sediments can become a promising secondary source of REE.

Acknowledgments

Synchrotron X-ray fluoresce (XRF) elemental maps were collected using the X-ray microprobe at Beamline 13-ID-E (GSECARS) at the Advanced Photon Source (APS), Argonne, IL. This research was supported by grants from the Department of Energy (DE-FE0032049) and NASA (80NSSC21K180).

References

Behum PT, Lefticariu L, Bender KS, Segid YT, Burns AS, Pugh CW (2011) Remediation of coal-mine drainage by a sulfate-reducing bioreactor: A case study from the Illinois coal basin, USA. Appl. Geochem. 26: S162-S166.

Bishop BA, Alam MS, Flynn SL, Chen N, Hao W, Ramachandran SK, Swaren, L., Gutierrez RD., Konhauser KO, Alessi DS, Robbins LJ (2024). Rare Earth Element adsorption to clay minerals: mechanistic insights and implications for recovery from secondary sources. Environ. Sci. Technol. 58(16):7217-7227.

Borst AM, Smith MP, Finch AA, Estrade G, Villanova-de-Benavent C, Nason P, Marquis E, Horsburgh NJ, Goodenough KM, Xu C, Kynický J (2020) Adsorption of rare earth elements in regolith-hosted clay deposits. Nat. Commun. 11(1):4386.

Bowman RL (2025) Illinois abandoned mine lands: possibilities for sourcing critical minerals in coal mining waste. Ph.D. thesis, Southern Illinois University, Carbondale, Illinois.

Burns AS, Pugh CW, Segid YT, Behum PT, Lefticariu L, Bender KS (2012) Performance and microbial community dynamics of a sulfate-reducing bioreactor treating coal generated acid mine drainage. Biodegradation 23:415-429.

Fujita Y, Park D, Lencka M, Anderko A, Reed D, Thompson V, Das G, Eslamimanesh A, Jiao Y (2024) Beneficiation of Rare Earth Elements: Prospects for Biotechnology Deployment. In Rare Earth Elements: Sustainable Recovery, Processing, and Purification (pp.251-297). American Geophysical Union: Willey Publishing.

IUPAC (2005) In: Connelly, N.G. Hartshorn, R.M. Damhus, T. Hutton A.T. (Eds.) Nomenclature of Inorganic Chemistry-IUPAC Recommendations.

Kolker A, Lefticariu L, Anderson ST (2024) Energy-Related Rare Earth Element Sources. In Rare Earth Metals and Minerals Industries: Status and Prospects (pp. 57-102). Cham: Springer International Publishing.

Lefticariu L, Klitzing KL, Kolker A (2020) Rare Earth Elements and Yttrium (REY) in coal mine drainage from the Illinois Basin, USA. Int. J. Coal Geol. 217:103327.

Lefticariu L, Pratt LM, Ripley EM (2006) Mineralogical and sulfur isotopic effects accompanying oxidation of pyrite in millimolar solutions of hydrogen peroxide at temperatures from 4 to 150 C. Geochim. Cosmochim. Acta 70(19):4889-4905.

Lefticariu L, Sutton SR, Bender KS, Lefticariu M, Pentrak M, Stucki JW (2017) Impacts of detrital nano-and micro-scale particles (dNP) on contaminant dynamics in a coal mine AMD treatment system. Sci Total Environ. 575:941-955.

Lefticariu L, Sutton SR, Lanzirotti A, Flynn TM (2019) Enhanced immobilization of arsenic from acid mine drainage by detrital clay minerals. ACS Earth Space Chem. 3(11):2525-2538.

Lefticariu L, Walters ER, Pugh CW, Bender KS (2015) Sulfate reducing bioreactor dependence on organic substrates for remediation of coal-generated acid mine drainage: Field experiments. Appl. Geochem. 63:70-82.

Lozano A, Ayora C, Fernández-Martínez A (2020) Sorption of rare earth elements on schwertmannite and their mobility in acid mine drainage treatments. Appl. Geochem. 113:104499.

McLennan SM (2001) Relationships between the trace element composition of sedimentary rocks and upper continental crust. Geochem. Geophys. Geosyst. 2(4), doi:10.1029/2000GC000109

U.S. Department of Energy, DOE (2023) Critical Materials Assessment, https://www.energy.gov/sites/default/files/2023-07/doe-critical-material-assessment_07312023.pdf

New Insights at the Molecular Level: The Impact of Dom On Antimony Migration and Enrichment in Water Environments of Antimony

Wanyu Li[1], Jianwei Zhou[1,*], Xingjie Wang[2], Chenxin Feng[1], Haibo Feng[3], Weiqing Zhou[1]

[1]*China University of Geosciences (Wuhan), School of Environmental Studies, 68 Jincheng Road, Wuhan, PR China, wy_li@cug.edu.cn, jw.zhou@cug.edu.cn, fcxaptx4869@163.com, wq.zhou@cug.edu.cn*

[2]*China University of Geosciences (Wuhan), Institute of Geological Survey, 388 Lumou Road, Wuhan, PR China, wangxingjie@cug.edu.cn*

[3]*China University of Geosciences (Wuhan), School of Geography and Information Engineering, 68 Jincheng Road, Wuhan, PR China, haibo_feng@cug.edu.cn*

Abstract

Dissolved organic matter (DOM) significantly influences the migration and transformation of antimony (Sb) in aquatic environments. This study integrated hydrogeochemical analysis with DOM characterization to explore its role in Sb enrichment in mining areas. Results indicated that (1) water contained tryptophan-like proteins and humic substances; (2) CHON and CHO type compounds enhanced Sb enrichment in groundwater, while photodegradable compounds affected Sb in surface water; and (3) non-bioactive compounds and photodegradation products were key to Sb complexation. These findings enhance understanding of Sb biogeochemistry and support pollution control efforts in mining areas.

Keywords: Antimony mining; dissolved organic matter; EEMs; FT-ICR MS

Introduction

Antimony (Sb) is a metalloid element with potential toxicity and carcinogenicity (Lai *et al.* 2022). It and its compounds have a wide range of applications and are important strategic materials. Antimony pollution in the water environment mainly originates from human activities such as mining, smelting, and the combustion of fossil fuels (Quiroz *et al.* 2016). Long-term exposure to high levels of Sb could cause severe damage to the human immune system and development (Wang *et al.* 2020). The U.S. Environmental Protection Agency, the European Union, the World Health Organization, and China have set limits for antimony concentrations in drinking water at no more than 6, 5, 20, and 5 µg/L, respectively (Filella *et al.* 2002).

Dissolved organic matter (DOM) is an important and ubiquitous active component in aquatic ecosystems, containing functional groups such as hydroxyl and carboxyl groups. DOM can serve as a microbial substrate or as an electron donor or acceptor, thereby indirectly affecting the biogeochemical processes of antimony by controlling microbial activities in the water environment (Wang *et al.* 2023). Moreover, DOM can bind with Sb both directly and indirectly. Sb forms bidentate chelating rings with oxygen-containing organic ligands in DOM, such as O = C-OH and C-OH, resulting in the formation of OM-Sb complexes (Tella and Pokrovski 2008). Alternatively, negatively charged organic matter and $Sb(OH)_6^-$ species can interact with metal oxides, forming OM-metal-Sb complexes (Karimian *et al.* 2019). Through these interactions, DOM influences the geochemical processes of Sb. Additionally, under light-induced conditions, the generation of triplet states, phenoxyl radicals from organic matter, and quinone species under dark conditions can all oxidize Sb(III) (Wu *et al.* 2019). However, these studies are all based on laboratory experiments, and the impact of DOM in natural water environments on the biogeochemical cycling of Sb remains unclear.

This study, leveraging water chemistry, DOM spectroscopy, and molecular analysis techniques, aims to elucidate the sources, spectral characteristics, and molecular features of DOM in the water environment of a typical antimony mining area. It analyses the impact of DOM on the migration and enrichment of Sb.

Methods

The samples were collected from Xikuangshan, the largest antimony mine in China, including 10 groups of groundwater and 6 groups of surface water, and the sampling work was completed in June 2022. The aquifer in Xikuangshan is composed of siliceous limestone, with antimony sulfide being the main ore type. The surface was covered with waste rocks and slag piles, which have been disposed of in recent years after being piled up for many years.

The pH, DO, EC, ORP, anions and cations, trace elements, and DOC concentrations in the water environment were tested. For some samples, DOM was analysed using Three-dimensional fluorescence and Fourier-transform ion cyclotron resonance mass spectrometry (FT-ICR MS). The pretreatment for three-dimensional fluorescence testing involved filtering the samples through a 0.45 μm filter membrane into 40 mL brown glass bottles, followed by the addition of concentrated phosphoric acid of superior purity for preservation. For FT-ICR MS samples, the field samples were filtered through a 0.45 μm filter membrane and then acidified with high-purity hydrochloric acid, followed by storage in the dark at 4°C. The pretreatment was completed within 12 hours, and the steps were as follows: (1) Activation of the SPE column by sequentially washing it with three column volumes of methanol and three column volumes of acidified ultrapure water (pH = 2) at a flow rate of 2 mL/min. (2) Extraction of the water sample with a flow rate controlled at 2 mL/min. (3) Drying of the SPE column by washing it with three column volumes of acidified ultrapure water and removing the moisture from the column using nitrogen gas. (4) Elution of the sample with one column volume of methanol, followed by storage in a brown glass bottle in the dark at -18 °C for submission (Dittmar *et al*. 2008).

The three-dimensional fluorescence results were analyzed using the parallel factor analysis (PARAFAC) method in the DOMFluor toolbox. The FT-ICR MS results were processed using Data Analysis 4.0 (Bruker Corporation).

Results and discussion

Chemical characteristics of the water environment and distribution of antimony

The water environment of the antimony mining area was neutral to slightly alkaline (average pH 7.61), mainly influenced by the limestone aquifer, which neutralized the acidic mine water generated by mining activities. The important ions in the water

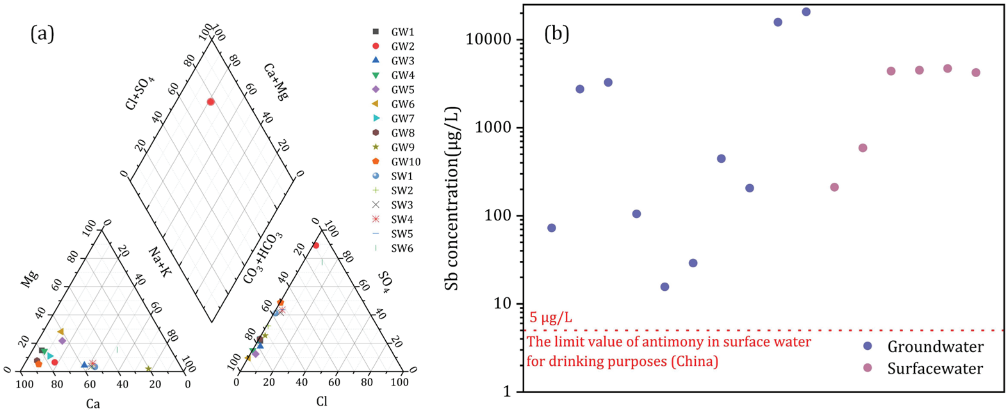

Figure 1 *(a) Piper diagram in the water environment of Xikuangshan; (b) Distribution of antimony in the water environment of Xikuangshan.*

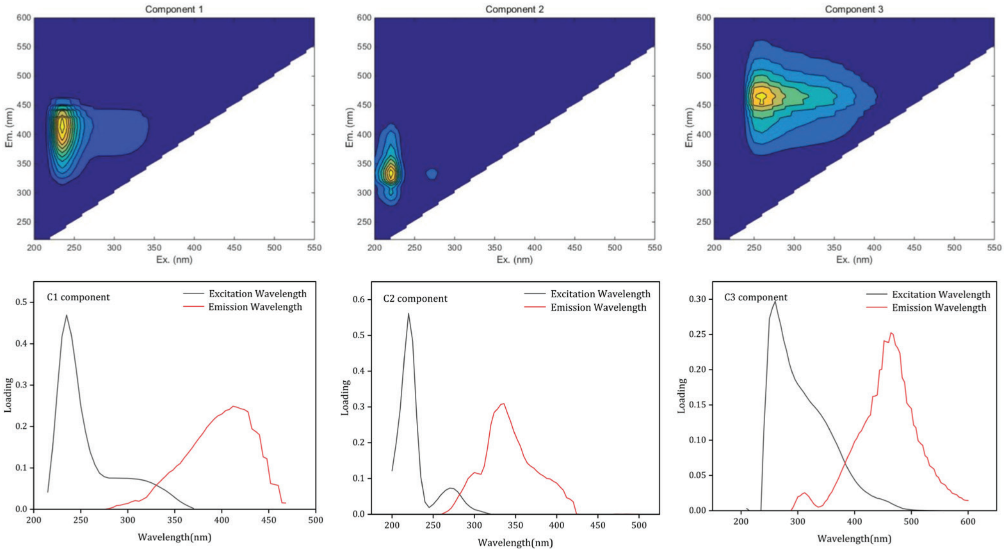

Figure 2 Common components of DOM in the water environment resolved by Parallel Factor Analysis.

environment were Ca^{2+}, Na^+, SO_4^{2-}, and HCO_3^-. The main hydrochemical type of groundwater was primarily Ca-HCO_3, while Na^+ and SO_4^{2-} ions were more prominent in surface water. This was mainly influenced by the leaching of surface waste residues and waste rock piles or the recharge of mine wastewater (Fig. 1a) (Wen *et al.* 2023).

The concentrations of Sb in the water environment of Xikuangshan (15.62–20752.18 μg/L) was far above the limit value for drinking water in China (5 μg/L). The Sb concentration in groundwater had a large degree of dispersion. The surface water samples were taken from a stream, and the Sb concentration increased gradually along the flow direction (Fig. 1b).

Spectral characteristics of DOM and its indicative role in antimony migration and enrichment

Using Parallel Factor Analysis, we could resolve three common components in the water environment of Xikuangshan (Fig. 2). Component C1 was a terrestrial humic-like substance (Ex./Em. 235 nm/412 nm), which was a photochemical product of terrestrial organic matter and represented the smallest molecules generated during the biodegradation process (Coble 1996). Component C2 was a protein-like tryptophan substance (Ex./Em. 220 nm/336 nm), which was an autochthonous product of microbial activity and was associated with the structure of aromatic amino acids (Murphy *et al.* 2008). Component C3 was a terrestrial aromatic humic-like substance (Ex./Em. 260 nm/464 nm), with a larger molecular weight, and it readily formed metal ion-organic complexes with metal ions (Ishii *et al.* 2012).

The average maximum fluorescence intensity relative to the content of the three common DOM components in the water environment followed the order: C1 > C2 > C3, with values of 43.70%, 37.77%, and 18.53%, respectively. The relative distribution of DOM fluorescence components in surface water was more concentrated than in groundwater (Fig. 3a). In groundwater environments with high Sb concentrations (>3 mg/L), the proportions of C1 and C3 components were significantly higher, indicating that humic-like components in groundwater might have influenced the enrichment of Sb through complexation. In contrast, the relative content of the C2 component was significantly lower, suggesting that the binding of tryptophan-like proteins with Sb led to fluorescence quenching, resulting in a notable decrease in fluorescence intensity (Fig. 3b).

In surface water, the relative contents of C1 and C3 components exhibited a trend consistent with Sb concentration along the flow path, whereas the C2 component showed an opposite pattern (Fig. 3c). Similar

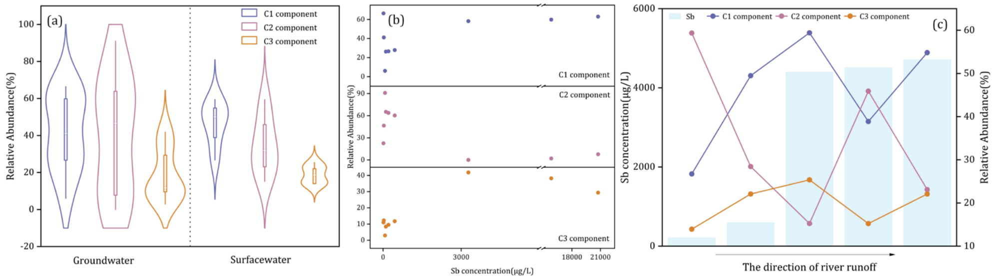

Figure 3 *(a) Boxplot of the relative content distribution of common DOM components in groundwater and surface water environments; (b) Relationship between the relative content of common DOM components in groundwater and Sb concentration; (c) Characteristics of changes in Sb concentration and the relative content of common DOM components along the flow path in surface water runoff.*

to groundwater, the humic-like components represented by C1 and C3 were important complexing species of Sb, and a co-migration process of Sb with these components occurred in surface rivers. Additionally, the fluorescence quenching effect of Sb on tryptophan-like proteins was also significant. At the fourth sampling point, the relative contents of all components changed abruptly due to a shift in the river's surrounding environment from a human activity area to a waste residue and waste rock dumping area, altering the DOM sources and enhancing microbial activity in this region.

Molecular characteristics of DOM and its indicative role in antimony migration and enrichment.

The correlation between individual DOM molecules and Sb concentration in the aquatic environment indicated that Sb enrichment was associated with various types of organic matter (OM). In groundwater, Sb enrichment was primarily related to highly unsaturated compounds, polyphenols, and polycyclic aromatic hydrocarbons (Fig. 4a), with nitrogen-containing compounds being dominant. These compounds were recalcitrant, non-biologically active organic substances that could facilitate Sb migration and enrichment in groundwater through electron shuttling, complexation, and competitive adsorption (Mao *et al.* 2024), while the influence of biological activity on Sb was not significant. The number of OM molecules associated with Sb enrichment in surface water was far lower than in groundwater (Fig. 4b) and was mainly composed of low unsaturated, saturated, and aliphatic compounds, with biological activity playing a more prominent role.

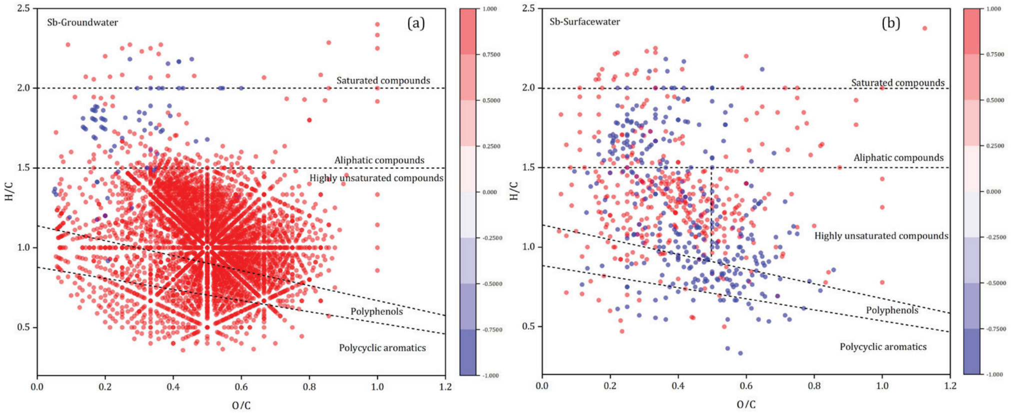

Figure 4 *Correlation between individual molecules and Sb concentration in groundwater (a) and surface water (b).*

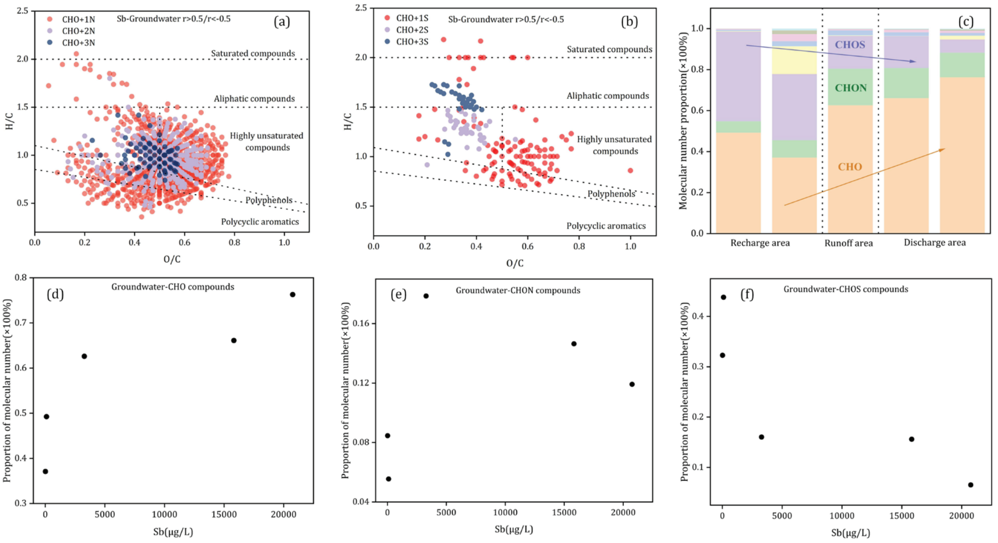

__Figure 5__ Correlation between individual molecules of CHO+1N, CHO+2N, CHO+3N compounds and Sb concentration in groundwater (r > 0.5 or r < -0.5) (a), and CHO+1S, CHO+2S, CHO+3S compounds and Sb concentration in groundwater (r > 0.5 or r < -0.5) (b); Stacked bar chart of the proportion of molecular numbers of different elements in different regions of groundwater (c); Correlation between the proportion of molecular numbers of CHO (d), CHON (e), and CHOS (f) compounds and Sb concentration in groundwater.

In the groundwater environment, the correlation between CHON and CHOS type organic compounds and Sb concentration (Fig. 5a, b) indicated that the recalcitrant, non-biologically active organic compounds that were strongly associated with Sb in the groundwater of the tin mining area were primarily composed of nitrogen- and sulfur-containing organic compounds. Along the groundwater recharge, runoff, and discharge zones, the proportion of CHOS compounds gradually decreased, while the proportion of CHON and CHO compounds gradually increased (Fig. 5c). This suggested that sulfur-containing organic compounds were unfavorable for Sb migration in the saturated zone. When Sb concentrations were relatively low (< 5 mg/L), nitrogen-containing organic compounds facilitated Sb migration, whereas at higher Sb concentrations, CHO type organic compounds played a more significant role in influencing Sb migration or enrichment.

In the surface water environment, the correlation between CHON, CHOS, and CHO type organic compounds and Sb concentration was shown in Fig. 6a, b, and c. The high unsaturation, polyphenol, and polycyclic aromatic components associated with Sb were primarily nitrogen-containing and unsaturated CHO compounds, while the sulfur-containing compounds related to Sb were key components of low-unsaturation, aliphatic, and saturated compounds. During the surface water runoff process, the proportion of CHON and CHO compounds initially decreased and then increased, whereas CHOS compounds exhibited the opposite trend, first increasing and then decreasing. This pattern was mainly influenced by changes in the river's flow path and the inflow of mining wastewater. These findings suggested that, compared to human activity areas, organic matter in solid waste dumping areas, particularly those containing nitrogen and unsaturated functional groups, more effectively complexed with high-concentration Sb, facilitating co-migration.

Conclusions

This study investigated the impact of dissolved organic matter (DOM) on the migration and enrichment of antimony (Sb) in the water environment of an antimony mining area from

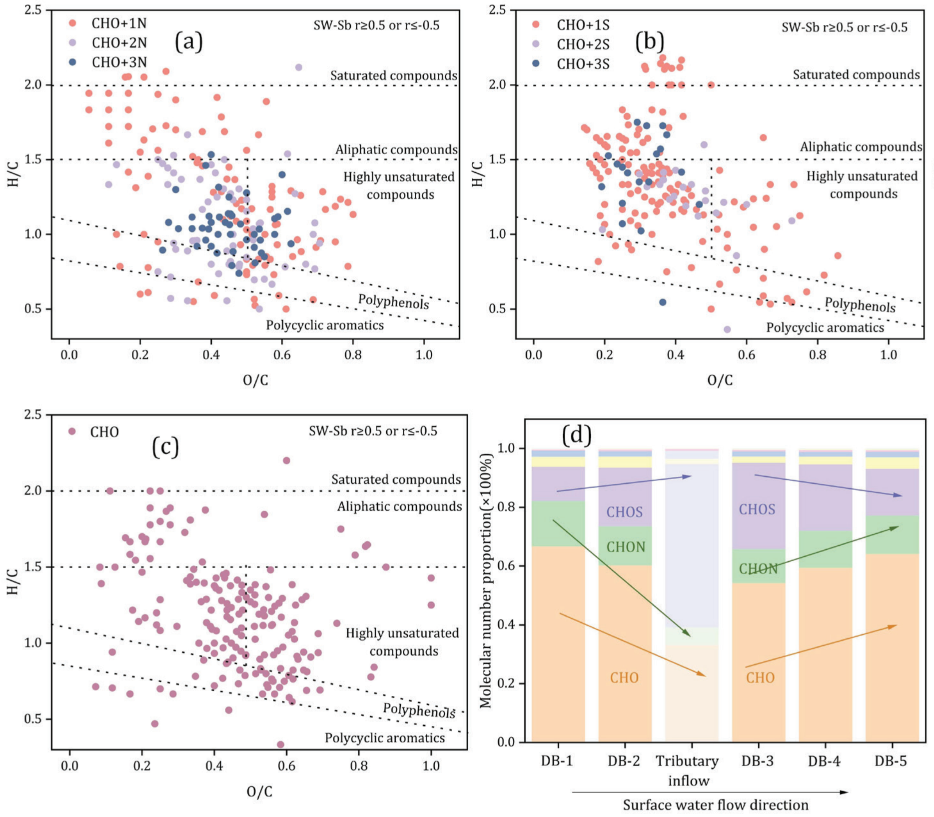

Figure 6 *Correlation between individual molecules of CHO+1N, CHO+2N, and CHO+3N compounds and Sb concentration in surface water (r > 0.5 or r < -0.5) (a); CHO+1S, CHO+2S, and CHO+3S compounds and Sb concentration in surface water (r > 0.5 or r < -0.5) (b); CHO compounds and Sb concentration in surface water (r > 0.5 or r < -0.5) (c); and stacked bar chart of the proportion of molecular numbers of different elements along the surface water flow path (d).*

the perspectives of water chemistry, DOM spectroscopy, and molecular characteristics. The results showed that the migration and enrichment of Sb in groundwater were associated with recalcitrant, non-biologically active compounds, such as unsaturated compounds, polyphenols, and polycyclic aromatic hydrocarbons, which were primarily composed of nitrogen (N)- and sulfur (S)-containing organic compounds. Compared to CHOS compounds, CHON and CHO compounds were more conducive to the enrichment of Sb in groundwater. In surface water, humic-like components played a crucial role in the complexation and co-migration of Sb, with N-containing functional groups and unsaturated bonds being the primary contributors. Additionally, fluorescence quenching of protein-like components was observed. Overall, complexation was an important mechanism for the enrichment of Sb by DOM in the water environment, with recalcitrant compounds, photodegradation products of organic matter, and protein-like components serving as key complexing species.

Acknowledgments

This research was supported by the National Natural Science Foundation of China (NO. 42030706 and 42077182).

References

Coble P (1996) Characterization of marine and terrestrial DOM in seawater using excitation-emission matrix spectroscopy. Marine Chemistry 51(4):325–346. https://doi.org/10.1016/0304-4203(95)00062-3

Dittmar T, Koch B, Hertkorn N, Kattner G (2008) A simple and efficient method for the solid-phase extraction of dissolved organic matter (SPE-DOM) from seawater. Limnology and Oceanography: Methods 6(6):230–235. https://doi.org/10.4319/lom.2008.6.230

Filella M, Belzile N, Chen Y-W (2002) Antimony in the environment: a review focused on natural waters: I. Occurrence. Earth-Science Reviews 57(1):125–176. https://doi.org/https://doi.org/10.1016/S0012-8252(01)00070-8

Ishii SK, Boyer TH (2012) Behavior of reoccurring PARAFAC components in fluorescent dissolved organic matter in natural and engineered systems: a critical review. Environmental Science & Technology 46(4):2006-2017. https://doi.org/10.1021/es2043504

Karimian N, Burton ED, Johnston SG (2019) Antimony speciation and mobility during Fe (II)-induced transformation of humic acid-antimony (V)-iron (III) coprecipitates. Environmental Pollution 254:113112. https://doi.org/10.1016/j.envpol.2019.113112

Lai Z, He M, Lin C, Ouyang W, Liu X (2022) Interactions of antimony with biomolecules and its effects on human health. Ecotoxicology and Environmental Safety 233:113317. https://doi.org/10.1016/j.ecoenv.2022.113317

Mao W, Wang D, Wu P, Zhu J, Liao P, Lai K, Ding Z, Zhang Y, He Z, Zheng R, Chen Y (2024) Co-transport of ferrihydrite-organic matter colloids with Sb (V) in saturated porous media: implications for antimony mobility. Environmental Science: Nano 11(4):1462–1476. https://doi.org/10.1039/D3EN00701D

Murphy KR, Stedmon CA, Waite TD, Ruiz GM (2008) Distinguishing between terrestrial and autochthonous organic matter sources in marine environments using fluorescence spectroscopy. Marine Chemistry 108(1–2):40–58. https://doi.org/10.1016/j.marchem.2007.10.003

Quiroz W, Astudillo F, Bravo M, Cereceda-Balic F, Vidal V, Palomo-Marín MR, Rueda-Holgado F, Pinilla-Gil E (2016) Antimony speciation in soils, sediments and volcanic ashes by microwave extraction and HPLC-HG-AFS detection. Microchemical Journal 129:111–116. https://doi.org/10.1016/j.microc.2016.06.016

Tella M, Pokrovski GS (2008) Antimony(V) complexing with O-bearing organic ligands in aqueous solution: an X-ray absorption fine structure spectroscopy and potentiometric study. Mineralogical Magazine 72(1):205–209. https://doi.org/10.1180/minmag.2008.072.1.205

Wang K, Min D, Chen G, Liu D, Yu H (2023) Oxidation of Sb(III) by Shewanella species with the assistance of extracellular organic matter. Environmental Research 236:116834. https://doi.org/10.1016/j.envres.2023.116834

Wang R, Zhang L, Chen Y, Zhang S, Zhuang T, Wang L, Xu M, Zhang N, Liu S (2020) Elevated non-essential metals and the disordered metabolism of essential metals are associated to abnormal pregnancy with spontaneous abortion. Environment International 144:106061. https://doi.org/10.1016/j.envint.2020.106061

Wen B, Zhou A, Zhou J, Huang J, Long T, Jia X, Zhou W, Li W (2023) Sources of antimony contamination and its migration into water systems of Xikuangshan, China: Evidence from hydrogeochemical and stable isotope (H, O, S, and Sr) signatures. Environmental Pollution 337:122381. https://doi.org/10.1016/j.envpol.2023.122381

Wu T, Qin W, Alves ME, Fang G, Sun Q, Cui P, Liu C, Zhou D, Wang Y (2019) Mechanisms of Sb(III) oxidation mediated by low molecular weight phenolic acids. Chemical Engineering Journal 356:190–198. https://doi.org/10.1016/j.cej.2018.09.008

Improved Mine Water Quality Predictions Using Available International Hydrochemical Datasets

Chazanne Long[1], Phil Burris[1]

[1]*Wardell-Armstrong a part of SLR, London, clong@wardell-armstrong.com*

[2]*Wardell-Armstrong a part of SLR, Truro, pburris@wardell-armstrong.com*

Abstract

Mine waters exhibit variable compositions with a range of pH and dissolved solutes. Waters with pH less than six are referred to as acid mine drainage (AMD), and waters with pH greater than six are classified as saline drainage (SD) or neutral mine drainage (NMD) depending on the concentration of dissolved solutes. Plumlee *et al.*, (1999) developed a set of trace elements that when compared with pH, enabled definition of mine waters into twelve categories and later developed this into a geo-environmental model using mine sites from a limited geography within North America. This study uses a wider international sample-set of surface water drainage from mines to assess whether this model has global applicability.

Hydrochemical data from thirty-eight mines located on four continents were plotted onto the Plumlee model to assess the boundaries of each field. Early geology-based classification schemes (e.g. Cox and Singer, 1986) have evolved into mineral deposit models that classify deposits using geologic, geophysical and geochemical characteristics that consider the overall 'geodynamic' context of ore deposits (Gessner *et al.*, 2018).

The results of this study correlate well with the fields set out in the original Ficklin diagrams from the 1990s. This approach helps move towards more refined mine water quality predictions early on in a project development and allows easy revision of the model throughout the project life cycle. These models can be used as an improved predictive tool by researchers including consultants, mining professionals, regulators and other stakeholders.

Keywords: Ficklin Diagrams, Mine water, water quality prediction, international dataset

Introduction

Mine waters exhibit variable compositions with a range of pH and dissolved solutes, where waters with pH less than six are referred to as acid mine drainage (AMD), and waters with pH greater than six are classified as saline drainage (SD) or neutral mine drainage (NMD) depending on the concentration of dissolved solutes (Plumlee et al., 1994; Verburg et al., 2009, INAP, 2009). Increasing demand for metals and minerals to assist with the energy transition, and new methods and economic drivers for commodity recovery from former wastes and tailings make it more important than ever that mineral development is progressed responsibly. (e.g. World Economic Forum 2015, Arvanitidis et al., 2017). Planning and regulatory requirements across jurisdictions require a good understanding of the potential geochemical outcomes from the mining lifecycle, meaning predictive tools for geochemical evolution need to be accessible and robust for different situations.

Background

Ficklin diagrams showing sum of metal versus pH were originally developed to characterise surface water drainage from mineral deposits and classify waters into 1 of 12 fields (Fig. 1). Over the past three decades, these classifications have become widely used by an increasing range of consultants and academics working on geo-environmental studies, many of which are mining projects, but now also include other applications, including industrial processing and anthropogenic influences on environmental backgrounds.

Within the mining industry, Ficklin diagrams are used to characterise ground water and surface water types and are applied to baseline (pre-project) natural waters as well as modified water quality, throughout the entire mine life cycle, including closure and post-closure of a project. Static and kinetic laboratory test results are also plotted onto Ficklin diagrams to predict future mine waters and leachates from various facilities such as waste rock dumps (WRDs), pit lakes, and process plants. Collectively, these results are used to develop mine water and mine waste management plans, along with associated strategic risk assessments, mitigations where necessary, and stewardship of resources.

Geoenvironmental models and integration of mineralisation styles

Plumlee *et al.*, (1994) correlated water chemistry ranges into defined fields and related these to specific mineralization styles based on a limited geographic dataset, and these are displayed in grey fields presented in Fig. 1. Considering the wide application of Ficklin diagrams, which could be more widely used for resource and reserve definition of varying mineralisation styles, coupled with the need for robust prediction tools to derisk mining projects in the 21st century, this study

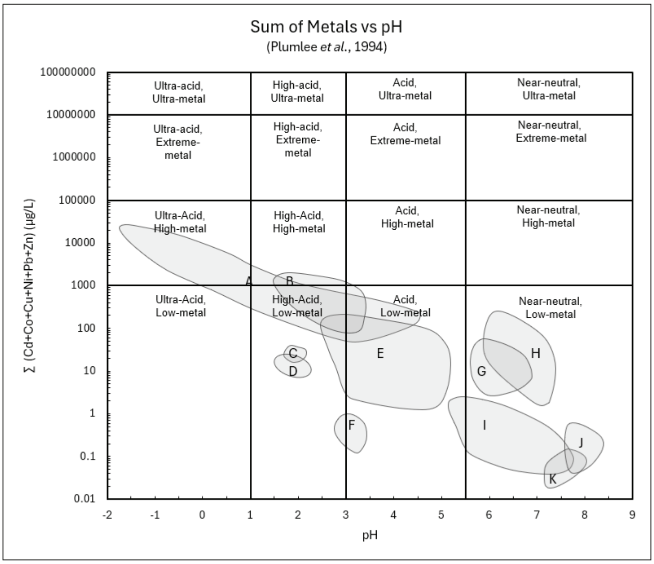

Figure 1 Plumlee et al (1994) mineralisation fields for: A Pyrite rich massive sulfides; B sulfide rich ores (with pyrite, enargite, bromite etc) in wallrock highly altered to silica, alunite, kaolinite and clays; C high-sulfide, low-base metal hot spring ores in acid-altered wallrock; D high-sulfide low-base metal, porphyry Mo ores in igneous wallrock; E pyrite- and base metal- rich polymetallic veins and disseminations in wallrock with low acid-buffering capacity; F pyrite-rich, base metal-poor veins and disseminations in wallrock with low acid-buffering capacity; G Pyrite- and base metal-rich, polymetallic veins that are carbonate-rich or occur in wallrock altered to contain carbonate; H Pyrite- and base metal-rich, polymetallic replacements and veins in carbonate-rich sediments; I polymetallic veins with moderate to low pyrite and base metal content that's all carbonate rich or occur in carbonate rich wallrock; J pyrite-poor, polymetallic replacements in carbonate-rich sediments; K pyrite-poor, Au-Te veins and breccias with carbonate gangue

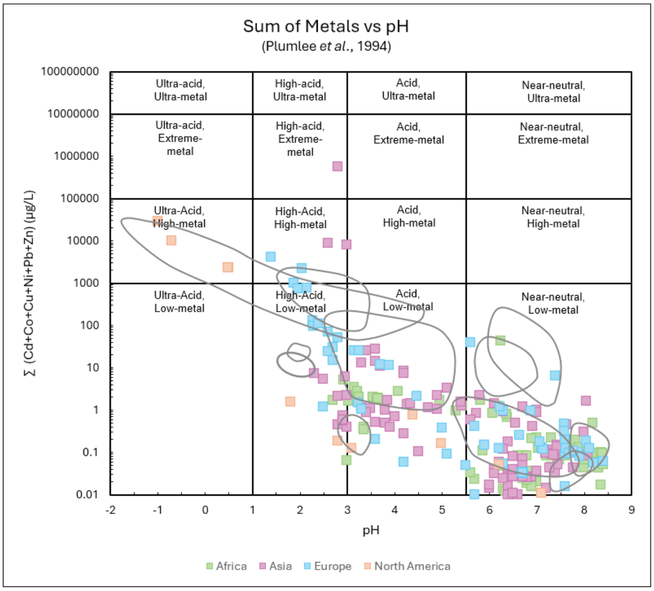

Figure 2 Global dataset displaying continent from which it originates compared to the fields in Plumlee et al (1999)

aims to further define these fields using a wider and more varied dataset collected from a range of published international projects.

A desktop investigation was performed using Google scholar and various other resources to access publicly available river water, groundwater and mine water data associated with mining activities, distributed across different continents. Additionally, unpublished data and internal Wardell-Armstrong International mine water data was used with permission from our client-base. This international dataset comprises 287 samples across four continents, including 89 from Africa, 97 from Asia, 62 from Europe and 39 from North America (Fig. 2), and reflecting 12 commodities (Au, Co, Cu, Fe, Mn, Pb, S, U, Zn, coal, dolomite and fluorite) (Fig. 3).

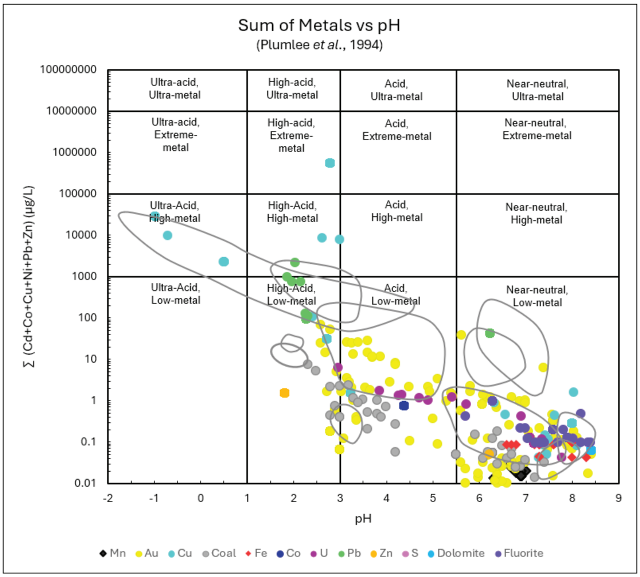

Figure 3 Plumlee mineralisation fields compared with an international dataset displaying main commodity extracted at each project

Results

The international dataset is graphically displayed in Fig. 2, showing the geographical distribution and comparing this with Plumlee's (1994) original mineralisation fields. There is generally a good correlation between the international dataset and Plumlee's fields. There are also some key differences, across the continents, notably North American mines report the lowest recorded pH values while Asian mines record the highest concentrations of dissolved metals.

There are several mine waters which plot outside, but near, to Plumlee's fields. More work needs to be done to collect robust internationally relevant data that can be scrutinised against mineralisation types. This information is often not available in public domain published hydrochemistry studies.
Like the geographically based dataset, the general fit of the international commodity dataset shows good correlation with Plumlee's mineralisation fields. In the section below we present a series of graphs showing different "major commodities" and compare these against Plumlee's mineralisation fields.

Zinc deposits typically exhibit a lower sum of metal concentrations in comparison to the lead and copper deposits. There is some overlap between copper and zinc deposits where copper deposits show more variability with pH, ranging from ultra-acid to near-neutral pH and the sum of metals extending from low-metal to extreme-metal concentrations (Fig. 4).

Fig. 5 shows gold mineralisation extends from high-acid, low-metal to near-neutral, low-metal pH and the sum of metal concentration is positioned within the low metal range. Gold and copper exhibit similar trends (Fig. 4). Uranium deposits (Fig. 6) are defined as near-neutral, low-metal to high-acid, low-metal compositions. These data form a narrow band that superimposes the Au and Cu deposits. A single Co deposit is characterised by an acid, low-metal composition, and partially overlaps with the U deposit field (Fig. 9).

Iron and manganese ore deposits (Fig. 7) all plot within the near-neutral, low metal range, with the pH for iron ore deposits extending to more alkaline pH (up to 8.5), whereas manganese ores exhibit constrained pH between 6 and 7.5. These fields are like those observed for fluorite and dolomite, which also plot within the near-neutral, low-metal field (Fig. 9).

Coal fields range from near-neutral, low-metal to high-acid low-metal, and typically exhibit lower sum of metals compared to Au, U and Cu deposits (Fig. 8), but have a similar trend to zinc deposits (Fig. 4).The similar Plumlee fields observed for Cu (C,D,F,G,H), Au (A,E,F,H,I,J,K) and Pb (A,B,H) are all high-sulfide / pyrite-rich base-metal poor to rich fields.

Uranium deposits (E,I) partially superimposes the pyrite (low-medium) with low to high acid buffering capacity which occur associated with carbonates. Mn (I,K,H), Fe (I,J,K), dolomite (I,J,K) and fluorite (I,J,K)

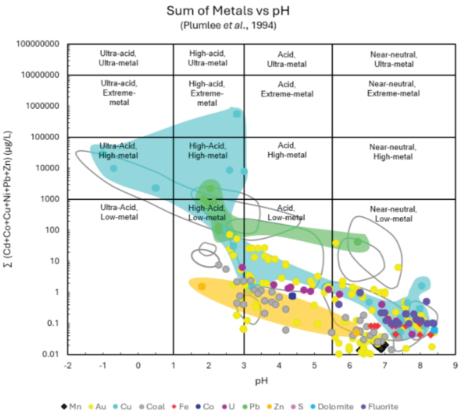

Figure 4 *Zn, Pb and Cu deposits*

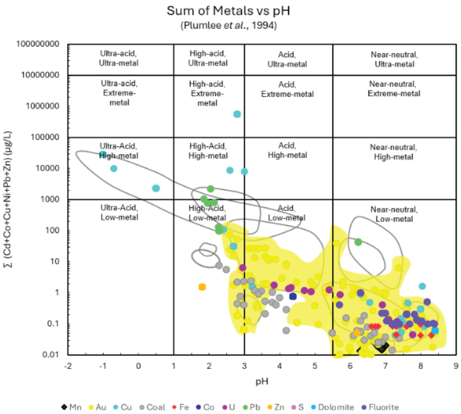

Figure 5 *Au deposits*

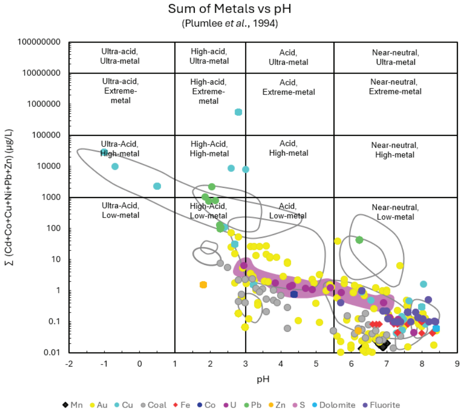

Figure 6 *U deposits*

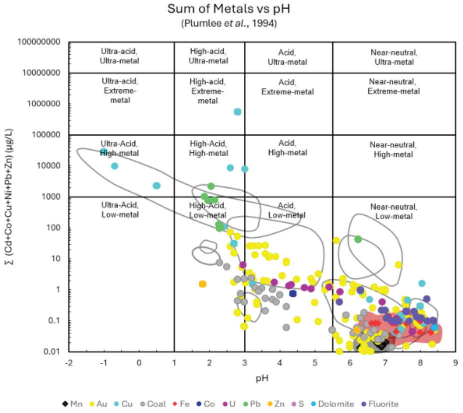

Figure 7 *Iron ore and manganese deposits*

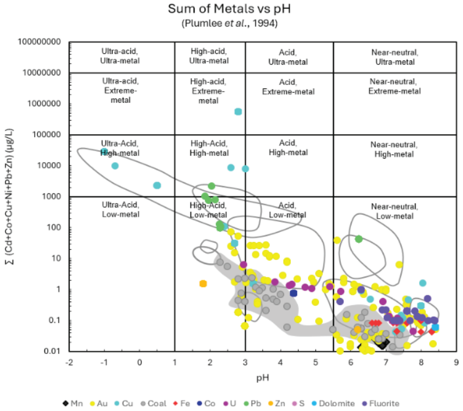

Figure 8 *Coal fields*

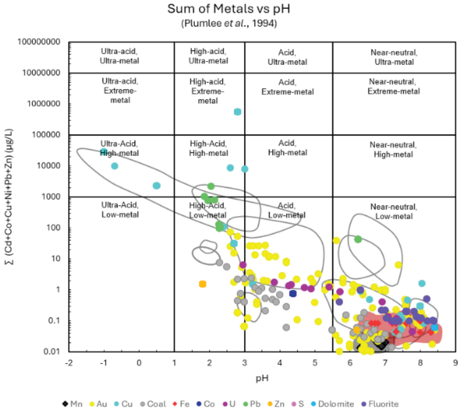

Figure 9 *Co, fluorite and dolomite deposits*

all partially superimpose the pyrite poor with high buffering capacity, possibly associated with carbonates. Coal (D,E,F,I,K) exhibits trends that range from pyrite poor to pyrite rich, with poor to high buffering capacity. The trends observed generally fit well with the mineralisation styles as noted by Plumlee *et al.* (1994). The analysis shows a clear basis for distinction between ore types and their hydrogeochemical signature. Further work would be needed to confirm the statistical strength of the classifications, for instance using analysis of variance (ANOVA).

Conclusions

By including hydrochemical characterisation of surface waters and groundwaters, which are routinely monitored at advanced exploration and PFS stages of projects today, this approach moves toward more refined predictions of water quality early in project development. This allows mitigatory steps to be implemented sooner for higher-risk projects and later for lower-risk projects as well as allocation of appropriate risk and budget to be spent in accordance with mine project development. Surface and groundwater hydrochemistry data collected at the PFS stage can be used to generate environmental baselines that are deposit-specific and help develop environmental quality standards that are robust for closure, and free-from legislative criteria which sometimes are not available, except as international best practices. Since these data are usually collected, it represents an opportunity to gain additional insights into geochemical characterisation.

While this model is only as good as the diversity of mineral deposits and commodities used to define each trajectory, these models can be used as an improved predictive tool by researchers including consultants, mining professionals, regulators and other stakeholders. This dataset is comparatively small and does not cover all the mineralisation styles listed in Cox and Singer (1986), as it represents clients that Wardell Armstrong International have represented, together with published data in the public domain, mostly from academic papers. To improve the predictive ability of this approach, it is recommended that an improved global mine water database is generated and made available for public use.

References

Arvanitidis N, Boon J, Nurmi P, Di Capua G (2017) White Paper on Responsible Mining. IAPG - International Association for Promoting Geoethics, http://www.geoethics.org/wp-responsible-mining.

Cox DP, Singer DA (Eds) 1986. Mineral deposit models, US Geological Survey Bulletin 1693. https://doi.org/10.3133/b1693

Gessner K, Blenkinsop T, Sorjonen-Ward P (2018). Characterization of ore-forming systems – advances and challenges. Geological Society, London, Special Publications. Volume 453, p 1-6, https://doi.org/10.1144/SP453.16

International hydrochemical database available upon request.

Plumlee WH, Smith GS and Ficklin KS (1994). Geoenvironmental models of mineral deposits and geology - based mineral - environmental assessments of public lands, US Geological Survey. Denver: USGS.

Plumlee GS *et al.* (1999) 'Geologic controls on the composition of natural waters and mine waters draining diverse mineral – deposit types', in The environmental geology of mineral deposits. 1st edn. Denver: Society of Economic geologists, 373 – 432.

The International Network for Acid Prevention (INAP) (2009). Global Acid Rock Drainage Guide (GARD Guide).http://www.gardguide.com/

Verburg R *et al.* (2009) 'The global acid rock drainage guide (GARD Guide)', Mine Water and the Environment, 28(4), p 305–310. doi:10.1007/s10230-009-0078-4

World Economic Forum (2015). Mining and Metals in a Sustainable world, http://www3.weforum.org/docs/WEF_MM_Sustainable_World_2050_report_2015.pdf [last accessed 10 October 2024].

Operation of a Continuous Sulfidogenic System for Treating Mine Water with a High Concentration of Chloride

Marjory López[1], Iván Nancucheo[1]

[1]*Facultad de Ingeniería, Universidad San Sebastián, Lientur 1457, Concepción 4080871, Chile*

Abstract

In Chile, coal was extracted from underground mines beneath the Pacific Ocean, in the Arauco Basin in the Southern Biobío Region, with the operation ceasing in 1997. The mine "Chiflón del Diablo" is an abandoned coal mine and part of the Lota mining complex, registered on the tentative list to be awarded UNESCO World Heritage status. The mine has been a tourist attraction due to the exploitation beneath the coastal area. Unfortunately, since the last massive earthquake that hit the Biobio Region (February 2010), flooding of the mine was observed, requiring saline groundwater to be dewatered directly into the nearshore zone to maintain tourist activities. This water pumped from the mine out onto the beach, possessed a high concentration of chloride (~600 mM; 21.272 ppm) as a consequence of the seawater intrusion process into the shafts, a phenomenon reported at many mines near the coast. The mine water discharged to the sea from the Chilean mine additionally contained elevated ferrous iron (between 2–5 mM; 112–279 ppm) and sulfate (~33 mM;) due to the oxidation of pyrite, the main sulfide mineral associated with the Arauco Basin. This study describes the removal of iron and sulfate in mine water with high chloride concentration by using a continuous sulfidogenic biofilm reactor inoculated with sediment samples from the "Salar of Huasco," Chile. In the samples analyzed in the biofilm, *Desulfomicrobium*, a genus belonging to the order Desulfovibrionales, was the most abundant SRB, with a relative abundance of about ~30%. Feeding the mine water, with a hydraulic retention time of 25 h, it was possible to remove more than 90% of sulfate and iron by using lactate as electron and carbon source. This study highlights the use of a halophilic sulfate-reducing consortium to promote sulfidogenesis in mine water with a high chloride concentration.

Keywords: Sulfate reduction, Chloride, Continuous system

Introduction

Chile's mining industry faces important challenges in terms of environmental sustainability and water resource management that must be addressed. In the current scenario, one of the biggest environmental problems is the generation of mine drainage. In addition, climate change has led to increased water scarcity, affecting the use of water in industrial processes with the mining industry being forced to use different water sources for mineral extraction, including seawater. A major problem associated with this strategy is that few reports have evaluated the impact of seawater on mine drainage mitigation strategies (Texeira *et al.*, 2023). In the southern part of Chile, mine water impacted by seawater ("Chiflón del diablo" mine) is currently being discharged into the coastal sea. This is an example of untreated saline mine water that generates a plume containing highly visible ochre particles, where mine water treatment has yet to be implemented. Conventional AMD treatment is not cost-effective, pointing to the urgent need for a sustainable solution, particularly for mine waters impacted with seawater. A sustainable alternative approach for the removal of sulfate in mine drainage compared with other physicochemical treatment technologies is bioreactors promoting sulfate reduction. By doing this, sulfate is reduced to sulfide that can be used as metal precipitant or oxidized to elemental sulfur as demonstrated in different studies and full-scale applications using sulfate-reducing microorganisms (SRMs) at moderately low pH. While sulfidogenic bioreactors are becoming increasingly targeted for the remediation of (i.e., Johnson and Santos, 2020), few reports targeting sulfate-reducing consortia with the ability to grow under saline conditions to remediate the mine drainage originating from mine operations impacted with seawater have been described. In a recent study by Barton and Fauque (2022), on polyextremophilic microorganisms, it was found that *Desulfovibrio tunisiensis* and *Desulfohalobium retbaense* are sulfate reducers that can survive in moderately acidic pH ranging from 4.5 to 5.5 with optimal salinities of 4% and 10% NaCl, respectively. Chile harbors a huge diversity of salars in the Altiplano and Atacama Desert. The Salar de Huasco is an athalassohaline system, high-altitude (3.800 m above sea level) salt flat with neutral pH, water salinities ranging from freshwater to saturated salt waters. The concentration of sulfate up to ~70 mM was determined within the Salar the Huasco, and neutrophilic SRMs have been detected (belonging to the order of Desulfovibrionales and Desulfobacterales) in ponds with mats (Molina *et al.*, 2018). In this study, microbial enrichments were obtained from sediment samples from the Salar de Huasco, possessing dissimilarity sulfate reducing bacteria to set up and operate a sulfidogenic metal remediation process for the treatment of the water discharged from the mine "Chiflón del Diablo" characterized with elevated concentrations of iron, sulfate and chloride.

Materials and Methods

Sulfidogenic bioreactor

An upflow sulfidogenic biofilm bioreactor (Electrolab, UK) with a working volume of 2.3 L was set up and operated under continuous flow mode, based on a system previously described by Gonzalez and colleagues (2019). A pre-trial bioreactor was set up housing sulfidogenic bacteria obtained from different ponds in Salar de Huasco (Nancucheo *et al.*, 2023) with occurrence of blackened sediments that served as source material to enrich for sulfate reducing microbial communities. Enrichments were grown on 1–2 mm diameter porous beads made from recycled glass (Poraver Dennert GmbH, Germany), which occupied ~50% of the total volume of the vessel. The bioreactor was filled with SRMs medium with 10 mM of sulfate at pH 7 and 5 mM of lactate as electron donor and carbon source. The medium was maintained in batch mode for 20 days, recirculating the liquid through the bioreactor to encourage attachment to the beads. The bioreactor was maintained at 30 °C and stirred at 50 rpm with a continuous stream of nitrogen to remove H_2S produced. A pre-trial continuous bioreactor was operated and fed with synthetic water, with chloride increased from 150 to 500 mM, and pH modified from 6 to 8. During this period, the HTR was decreased by up to 25 hours prior to feeding with the real mine water. For 50 days, the sulfidogenic bioreactor system was fed with real mine water discharged from the "Chiflón del Diablo mine" which contained sulfate (~33 mM) and chloride (~600 mM) with an HRT of 25 h. Due to the variable amount of iron for each discharge process (ranging from 2.3 to 5 mM), mine waters were collected three times over a period of 40 days to fed the reactor with "fresh" iron water. During this phase, the feed liquor was sparged with N2 to minimize ferrous iron oxidation. An additional bottle was used to supply essential nutrients for the SRMs, including salts/trace elements (Nancucheo *et al.*, 2016), lactate (45 to 90 mM) and yeast extract (0.1 to 0.3 %).

Miscellaneous analysis

The pH of the filtered liquid samples was measured using a pH meter (model HI 2221; Hanna Instrument, Inc.). The concentration of sulfate was determined with Sulfaver Kits (HACH, based on SM4500-SO42- E, APHA, 2005). Lactate and acetate in the effluent liquor were measured by HPLC coupled with a UV detector (Agilent Technologies, Santa Clara, CA, USA), although acetate was not detected during the course of the experiment. Total iron was quantified by the method of o-phenanthroline. A sample from the bioreactor was collected at the end of the experiments to analyze the microbial community using high-throughput 16S rRNA gene sequencing targeting the V4 region, as described elsewhere (Schwarz *et al.*, 2020).

Results and discussion

Fig. 1 shows the measured values of total iron in the influent and effluent liquor, as well as sulfate removal. During the operation to remove high concentrations of sulfate in the influent liquor (33 mM), two steady states were observed. Between days 10 and 35, approximately 60% of the sulfate was removed, and lactate was entirely consumed as a carbon and electron donor (data not shown). Between days 35 and 50, the major objective was to increase the removal of sulfate. by increasing the amount of lactate (45 to 90 mM) and yeast extract (0.1 to 0.3 %) on day 35, it was possible to remove up to approximately 95%. Under these conditions, the rate of sulfate reduction was 3 g sulfate L-1 day-1, which is higher than those reported for other sulfidogenic bioreactors. Importantly, no acetate was found in the effluent, which typically appears as a waste product in sulfate-reducing bioreactors. This presence leads to chemical oxygen demand, which is undesirable. During the operation, most of the iron was removed, presumably as FeS, due to the black coloration observed in the sulfidogenic bioreactor. Although FeS can be unstable, its recovery has attracted widespread interest due to its excellent biocompatibility and multifunctionality in biomedical applications.

Fig. 2 shows the relative abundance of the bacterial community at the end of the operation. The analysis confirmed the presence of two genera of SRMs capable of thriving in high chloride concentrations. *Desulfomicrobium*, a non-spore-forming, gram-negative sulfate-reducing genus, was identified as the dominant microorganism in the bioreactor. One challenge is to increase the abundance of *Desulfomicrobium*, promoting the removal of sulfate and the consumption of carbon sources rather than allowing the growth of other heterotrophs that do not contribute to the sulfidogenesis process.

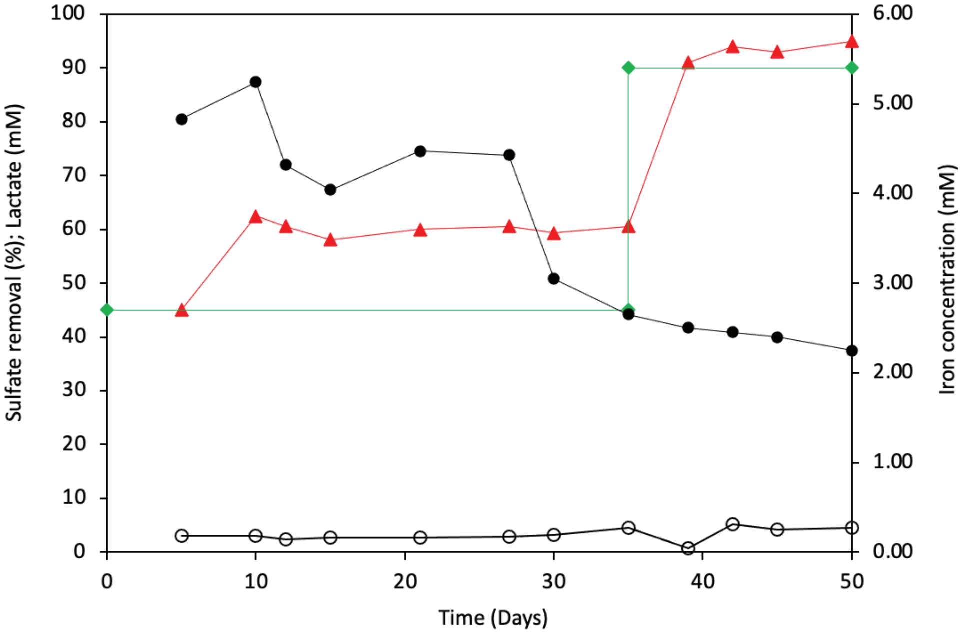

Figure 1 *Removal of sulfate (▲) and concentrations of iron in the feed liquor (●) and in the outflow (❍) of the bioreactor, along with lactate (●) supplied with the mine water with high concentration of chloride.*

Conclusions

The experimental work demonstrated a simple and efficient process for removing sulfate and iron from actual mine water with a high chloride concentration. For this particular and extreme mine, water is crucial for the microbial community that thrives in high concentrations of chloride obtained from a salar in the Atacama Desert in Chile.

References

Texeira, L., Calisaya-Azpilcueta, D., Cruz, C., Botero, Y.L., Cisternas, L.A. 2023. Impact of the use of seawater on acid mine drainage from mining wastes. Journal of Cleaner Production. 383, 135516

Johnson, D.B., A.L. Santos, A.L. 2020. Biological removal of sulfurous compounds and metals from inorganic wastewaters. P.N.L. Lens (Ed.), Environmental Technologies to Treat Sulfur Pollution: Principles and Engineering, IWA Publishing, London. 215–246

Barton, L.L., Fauque, G.D. 2022. Sulfate-reducing bacteria and archaea. Cham: Springer International Publishing

Gonzalez, D., Liu, Y., Villa, D., Southam, G., Hedrich, S., Galleguillos, P., Colipai, C., Nancucheo, I., 2019. Performance of a sulfidogenic bioreactor inoculated with Indigenous acidic communities for treating extremely acidic mine water. Minerals Engineering. 131, 370–375.

Molina, V., Eissler, Y., Cornejo, M., Galand, P.E., Dorador, C., Hengst, M., Fernandez, C., Francois, J.P. 2018. Distribution of greenhouse gases in hyper-arid and arid areas of northern Chile and the contribution of the high altitude wetland microbiome (Salar de Huasco, Chile). Antonie Van Leeuwenhoek. 111, 1421–1432.

Nancucheo, I., Segura, A., Hernández, P., Canales, C., Benito, N., Arranz, A., Romero-Sáez, M., Recio-Sánchez, G. 2023. Bio-recovery of CuS nanoparticles from the treatment of acid mine drainage with potential photocatalytic and antibacterial applications. Science of The Total Environment. 902, 166194.

Schwarz A., Suárez J I., Aybar M., Nancucheo I., Martínez P., Rittmann B E. 2020. A membrane-biofilm system for sulfate conversion to elemental sulfur in mining-influenced waters. Science of The Total Environment. 740, 140088

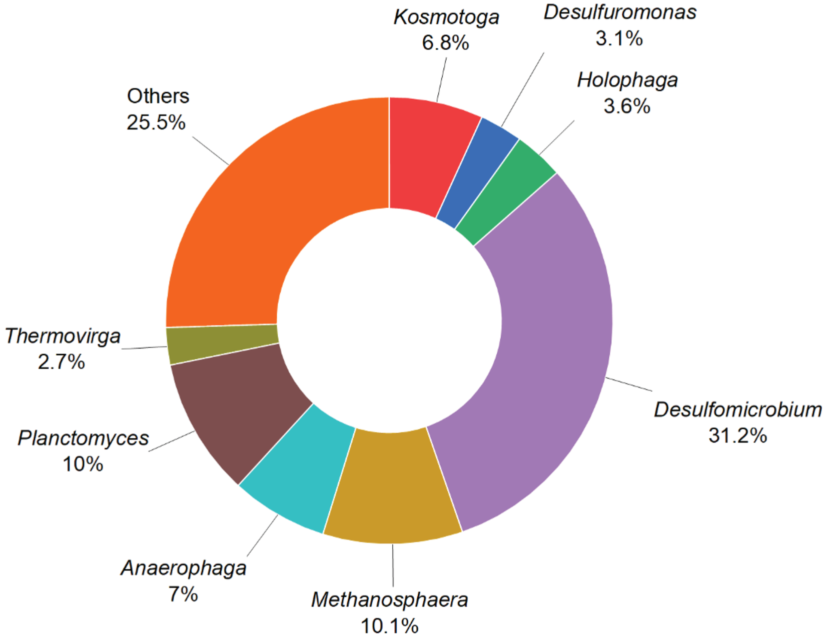

Figure 2 Microbial population determined in the sulfidogenic system.

MCA – Water Quality Risk Assessment Tool

Paul Joël Havemann Lourens, Petrus Daniel Vermeulen

Institute for Groundwater Studies, University of the Free State, PO Box 339, Bloemfontein, 9300, South Africa, lourenspjh@ufs.ac.za, vermeulend@ufs.ac.za

Abstract

Industrial, mining and agricultural industries in South Africa are legally obligated by the Constitution of South Africa and Environmental Legislation to identity, quantify, monitor, and manage their pollution sources and the potential environmental impact of these sources. A risk assessment, based on the Monte Carlo analysis (MCA) of random sampling, was developed to characterize, quantitatively, the uncertainty and variability in assessing possible environmental impacts and risk. The program is a screening tool applied to historical time-series monitoring data for a monitoring site to determine the risk of probability of environment impact on water quality parameters for the groundwater regime.

Keywords: Risk assessment, Monte Carlo analysis, monitoring programmes

Introduction

Handling, processing, and storage of different type of wastes and end-products of all industrial, agricultural, and mining facilities can release contaminants into the natural water environment. It is for this reason that these industries are legally obligated by the Constitution of South Africa and Environmental Legislation to identify, quantify, monitor, and manage these pollution sources and potential environmental impact of these sources on the natural environment.

Apart from the initial capital cost for the installation of a monitoring network, the cost for analyzing the water quality for different industries can outweigh the cost for sampling, data processing, storage, and reporting. The cost for analyzing the water quality can be reduced if it is possible to identify water quality parameters that have a high risk of impacting the groundwater regime and modify the water quality parameters to be monitored, and the frequency of monitoring according to the risk of probable impact. The aim of this research was to develop a quantitative risk assessment tool to assist geohydrologists in the optimization of groundwater monitoring programmes.

Approach to the Quantitative Risk Assessment

The Monte Carlo analysis of random data sampling was used in this research to characterize, quantitatively, the uncertainty and variability in assessing possible impacts and risk. The U.S. Environmental Protection Agency (1997) defines the Monte Carlo analysis as a random data sampling techniques in obtaining a probabilistic approximation to the solution of a mathematical equation/model. The random sampling Monte Carlo Algorithm applied in the Microsoft Excel Program for this research study is given below (equation 1, see more Microsoft (2022) and EXCELTV (2022) for a detailed explanation).

{NORM.INV[RAND(), A, Sdev.]} -
{NORM.INV[RAND(), A, Sdev.]}

Equation 1

Where NORM.INV = the Normal Inversion Function, RAND () = function that elicit a random number (probability) based on the other criteria within the distribution, A = arithmetic mean of the selected/input water quality parameter, Sdev. = the standard deviation of the selected/input water quality parameter.

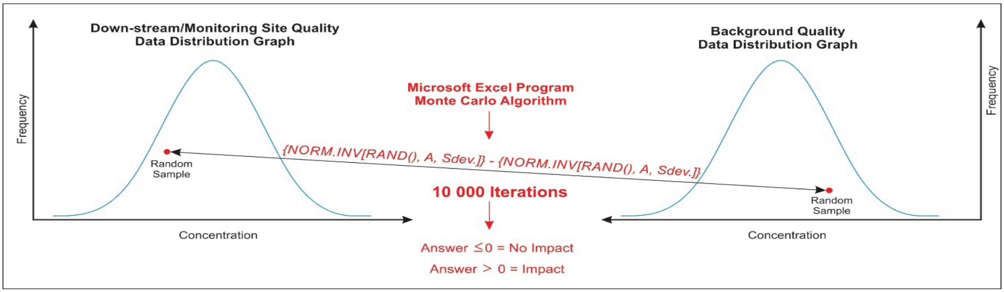

Figure 1 *Illustration explaining the concept of the Monte Carlo random sampling analysis.*

Table 1 *Results of the Monte Carlo algorithm versus a selected standard.*

Value/Answer	Frequency	Probability of Impact
>0	8524	85.24%
Value/Answer	**Frequency**	**Probability of Impact exceeding first limit of standard**
>250	6631	66.31%
Value/Answer	**Frequency**	**Probability of Impact exceeding second limit of standard**
>500	4082	40.82%

The concept of the algorithm in Equation 1 is illustrated in Fig. 1. The algorithm takes a random sample from the distribution of the downstream/monitoring site quality data and a random sample from the distribution of the upstream/background quality data. The random sampling points is then subtracted from each other. This process is repeated 10 000 times for each water quality parameter. A value equal or less than zero is regarded as no impact, and a value greater than zero is regarded as an impact (Fig. 1)

The algorithm is applicable to data that is normally distributed (Gaussian or Bell-Shaped Curved distribution). According to Reimann, Filzmoser and Garrett (2005), geochemical data distributions are generally symmetrical (normally distributed) or can be logarithmic transformed to be symmetrical. The distribution of each water quality parameter in terms of non-normality (skewness) was evaluated by calculating the coefficient of variation (COV). If the COV is smaller than 100% a normal distribution is assumed and when greater than 100%, a logarithmic scale was prepared (Reimann, Filzmoser and Garrett, 2005) and the Normal Inversion Function in Equation 1 was replaced by the Log-Normal Inverse Function (LOGNORM.INV)(EXCELTV, 2022).

The frequency percentage of the values above zero equals the percentage of probability of impact (see Tab. 1). The values are then evaluated in terms of the limits of a selected standard. The frequency percentage of the values above the limit of the standard equals the percentage of probability of impact exceeding the limit of the selected standard (Tab. 1).

The probability percentages are then converted to a value between one and five based on the percentage intervals shown in Tab. 2. Based on these ratings, the basic concept of a risk equals the probability multiplied by the severity of consequence (Duijm, 2015) are then used to compute a risk rating for each water quality parameter. The probability of impact is regarded as the probability, where the probability of the exceedance of the limits of the selected standard is regarded as the severity of consequence. In the case where a water quality parameter has two limits, the sum of the ratings assigned to each of these two categories are then multiplied by the probability. The computed risk ratings are then classified according to the intervals shown in Fig. 2.

Monitoring data from two different Industrial Facilities within South Africa, with varies types of waste management facili-

Table 2 *Rating of probability percentage.*

Probability Percentage	0-20	20-40	40-60	60-80	80-100
Rating	1	2	3	4	5

Risk Rating (Probability × Severity)				
Very Low 1-2	Low 3-9	Medium 10-15	High 16-20	Very High >20

Figure 2 *Risk rating categories.*

ties was used to test the approach of the quantitative risk assessment. The number of monitoring points of the two different sites ranges between 200 and 350, with a data coverage period ranging between 15 and 20 years. This research is part of an unpublished PhD thesis completed at the University of the Free State, South Africa.

MCA – Water Quality Risk Assessment Tool Interface

The MCA-Water Quality Risk Assessment Tool is a Microsoft Excel-based program. The tool consists of the nine sheets that will be discussed in the paragraphs below.

Title Sheet (MCA_WQRAT) – When the MCA-Water Quality Risk Assessment Tool is opened, it will show a Title sheet (Fig. 3). The sheet also indicates the information and data input sequence to be followed. The user should read through the sequence, and once familiar they can continue by clinking on the "START" button. The user will then be navigated to the General Info sheet.

Menu Sheet – the MENU sheet (Fig. 4) enables the user to navigate between the different worksheets. These worksheets include the General Inf, BH-ID, CHEM, and RESULTS sheets.

General Info Sheet – The user is navigated to the General Info sheet (Fig. 5) by clicking on the "START" button in the Title sheet. This is where the user defines the general information for the monitoring

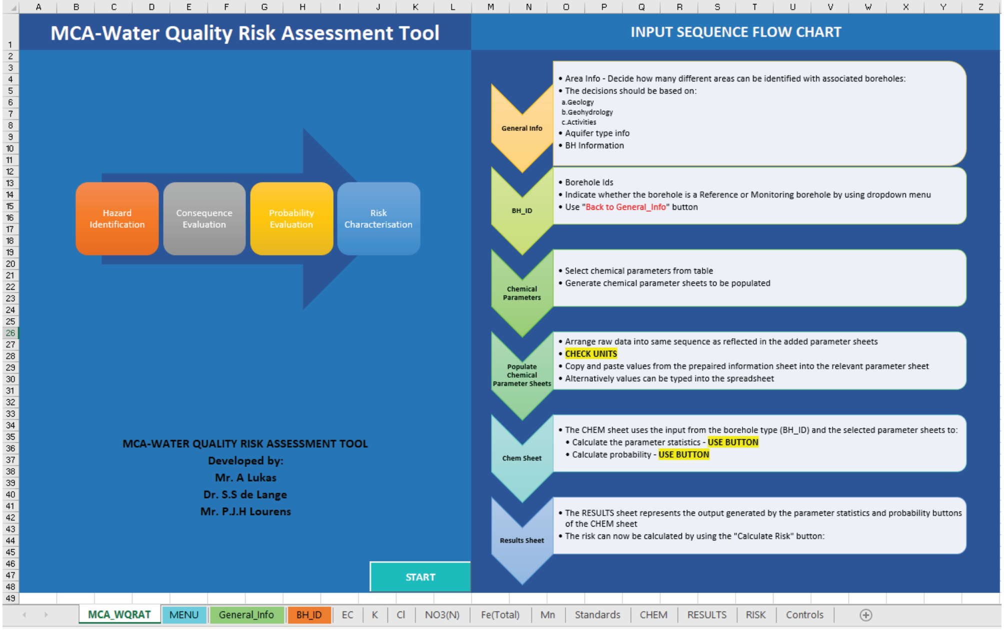

MCA-WATER QUALITY RISK ASSESSMENT TOOL
Developed by:
Mr. A Lukas
Dr. S.S de Lange
Mr. P.J.H Lourens

INPUT SEQUENCE FLOW CHART

General Info
- Area Info - Decide how many different areas can be identified with associated boreholes:
- The decisions should be based on:
  a.Geology
  b.Geohydrology
  c.Activities
- Aquifer type info
- BH Information

BH_ID
- Borehole Ids
- Indicate whether the borehole is a Reference or Monitoring borehole by using dropdown menu
- Use "Back to General_Info" button

Chemical Parameters
- Select chemical parameters from table
- Generate chemical parameter sheets to be populated

Populate Chemical Parameter Sheets
- Arrange raw data into same sequence as reflected in the added parameter sheets
- CHECK UNITS
- Copy and paste values from the prepaired information sheet into the relevant parameter sheet
- Alternatively values can be typed into the spreadsheet

Chem Sheet
- The CHEM sheet uses the input from the borehole type (BH_ID) and the selected parameter sheets to:
  - Calculate the parameter statistics - USE BUTTON
  - Calculate probability - USE BUTTON

Results Sheet
- The RESULTS sheet represents the output generated by the parameter statistics and probability buttons of the CHEM sheet
- The risk can now be calculated by using the "Calculate Risk" button:

Figure 3 *Title sheet of the MCA-Water Quality Risk Assessment Tool.*

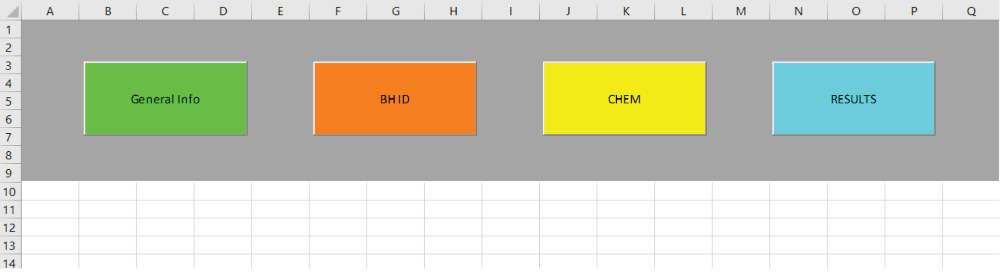

Figure 4 MENU sheet of the MCA-Water Quality Risk Assessment Tool.

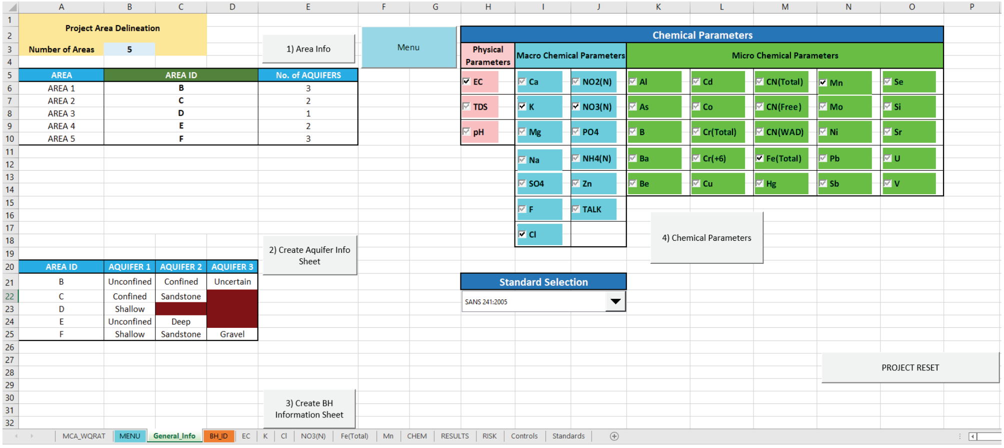

Project Area Delineation

Number of Areas 5

AREA	AREA ID	No. of AQUIFERS
AREA 1	B	3
AREA 2	C	2
AREA 3	D	1
AREA 4	E	2
AREA 5	F	3

AREA ID	AQUIFER 1	AQUIFER 2	AQUIFER 3
B	Unconfined	Confined	Uncertain
C	Confined	Sandstone	
D	Shallow		
E	Unconfined	Deep	
F	Shallow	Sandstone	Gravel

Chemical Parameters

Physical Parameters	Macro Chemical Parameters		Micro Chemical Parameters				
☑ EC	☐ Ca	☐ NO2(N)	☐ Al	☐ Cd	☐ CN(Total)	☑ Mn	☐ Se
☐ TDS	☑ K	☑ NO3(N)	☐ As	☐ Co	☐ CN(Free)	☐ Mo	☐ Si
☐ pH	☐ Mg	☐ PO4	☐ B	☐ Cr(Total)	☐ CN(WAD)	☐ Ni	☐ Sr
	☐ Na	☐ NH4(N)	☐ Ba	☐ Cr(+6)	☑ Fe(Total)	☐ Pb	☐ U
	☐ SO4	☐ Zn	☐ Be	☐ Cu	☐ Hg	☐ Sb	☐ V
	☐ F	☐ TALK					
	☑ Cl						

Standard Selection

SANS 241:2005

Figure 5 General Info sheet of the MCA-Water Quality Risk Assessment Tool.

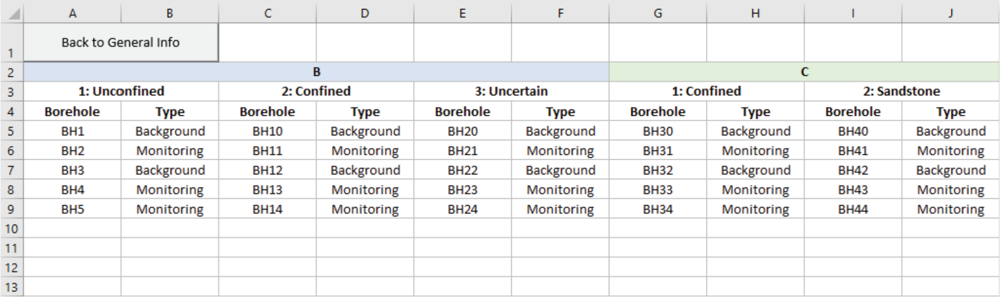

B						C			
1: Unconfined		2: Confined		3: Uncertain		1: Confined		2: Sandstone	
Borehole	Type	Borehole	Type	Borehole	Type	Borehole	Type	Borehole	Type
BH1	Background	BH10	Background	BH20	Background	BH30	Background	BH40	Background
BH2	Monitoring	BH11	Monitoring	BH21	Monitoring	BH31	Monitoring	BH41	Monitoring
BH3	Background	BH12	Background	BH22	Background	BH32	Background	BH42	Background
BH4	Monitoring	BH13	Monitoring	BH23	Monitoring	BH33	Monitoring	BH43	Monitoring
BH5	Monitoring	BH14	Monitoring	BH24	Monitoring	BH34	Monitoring	BH44	Monitoring

Figure 6 BH_ID sheet of the MCA-Water Quality Risk Assessment Tool.

site. Information includes area information, aquifer classification, and chemical parameter and standard selection.

Borehole-ID Sheet (BH_ID) – This is where the user lists the borehole names per area and per aquifer as defined in the General Info sheet. The user should also select or indicate if the borehole is a reference (background) or monitoring borehole by using the dropdown menu (Fig. 6).

CHEM Sheet – The CHEM sheet (Fig. 7) is where the user calculates the parameters statistics and probability of impact per chemical parameter. This can only be completed if the chemical parameter sheets (generated when the chemical parameters were selected in the General Info sheet) have been populated. First the user should click on the "Calculate Parameter Statistics" button. The average, standard deviation and

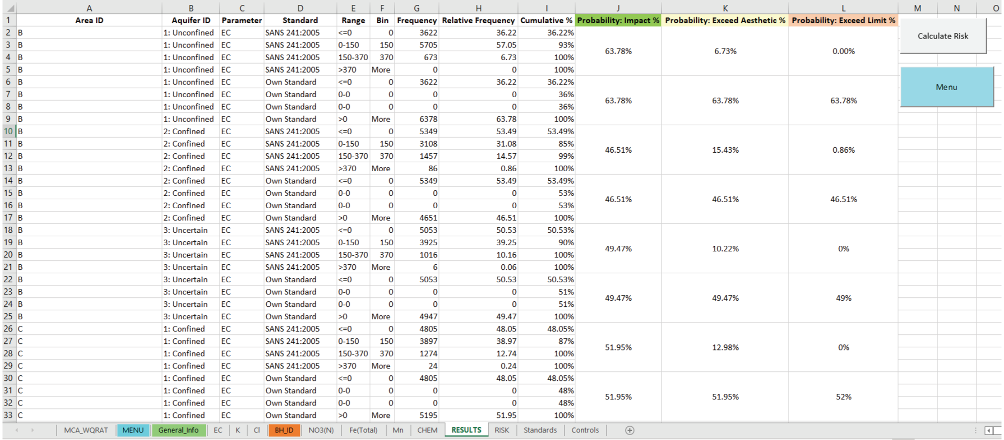

	Area ID	Aquifer ID	Parameter	Standard	Range	Bin	Frequency	Relative Frequency	Cumulative %	Probability: Impact %	Probability: Exceed Aesthetic %	Probability: Exceed Limit %
2	B	1: Unconfined	EC	SANS 241:2005	<=0	0	3622	36.22	36.22%	63.78%	6.73%	0.00%
3	B	1: Unconfined	EC	SANS 241:2005	0-150	150	5705	57.05	93%			
4	B	1: Unconfined	EC	SANS 241:2005	150-370	370	673	6.73	100%			
5	B	1: Unconfined	EC	SANS 241:2005	>370	More	0	0	100%			
6	B	1: Unconfined	EC	Own Standard	<=0	0	3622	36.22	36.22%	63.78%	63.78%	63.78%
7	B	1: Unconfined	EC	Own Standard	0-0	0	0	0	36%			
8	B	1: Unconfined	EC	Own Standard	0-0	0	0	0	36%			
9	B	1: Unconfined	EC	Own Standard	>0	More	6378	63.78	100%			
10	B	2: Confined	EC	SANS 241:2005	<=0	0	5349	53.49	53.49%	46.51%	15.43%	0.86%
11	B	2: Confined	EC	SANS 241:2005	0-150	150	3108	31.08	85%			
12	B	2: Confined	EC	SANS 241:2005	150-370	370	1457	14.57	99%			
13	B	2: Confined	EC	SANS 241:2005	>370	More	86	0.86	100%			
14	B	2: Confined	EC	Own Standard	<=0	0	5349	53.49	53.49%	46.51%	46.51%	46.51%
15	B	2: Confined	EC	Own Standard	0-0	0	0	0	53%			
16	B	2: Confined	EC	Own Standard	0-0	0	0	0	53%			
17	B	2: Confined	EC	Own Standard	>0	More	4651	46.51	100%			
18	B	3: Uncertain	EC	SANS 241:2005	<=0	0	5053	50.53	50.53%	49.47%	10.22%	0%
19	B	3: Uncertain	EC	SANS 241:2005	0-150	150	3925	39.25	90%			
20	B	3: Uncertain	EC	SANS 241:2005	150-370	370	1016	10.16	100%			
21	B	3: Uncertain	EC	SANS 241:2005	>370	More	6	0.06	100%			
22	B	3: Uncertain	EC	Own Standard	<=0	0	5053	50.53	50.53%	49.47%	49.47%	49%
23	B	3: Uncertain	EC	Own Standard	0-0	0	0	0	51%			
24	B	3: Uncertain	EC	Own Standard	0-0	0	0	0	51%			
25	B	3: Uncertain	EC	Own Standard	>0	More	4947	49.47	100%			
26	C	1: Confined	EC	SANS 241:2005	<=0	0	4805	48.05	48.05%	51.95%	12.98%	0%
27	C	1: Confined	EC	SANS 241:2005	0-150	150	3897	38.97	87%			
28	C	1: Confined	EC	SANS 241:2005	150-370	370	1274	12.74	100%			
29	C	1: Confined	EC	SANS 241:2005	>370	More	24	0.24	100%			
30	C	1: Confined	EC	Own Standard	<=0	0	4805	48.05	48.05%	51.95%	51.95%	52%
31	C	1: Confined	EC	Own Standard	0-0	0	0	0	48%			
32	C	1: Confined	EC	Own Standard	0-0	0	0	0	48%			
33	C	1: Confined	EC	Own Standard	>0	More	5195	51.95	100%			

Figure 7 *CHEM sheet of the MCA-Water Quality Risk Assessment Tool.*

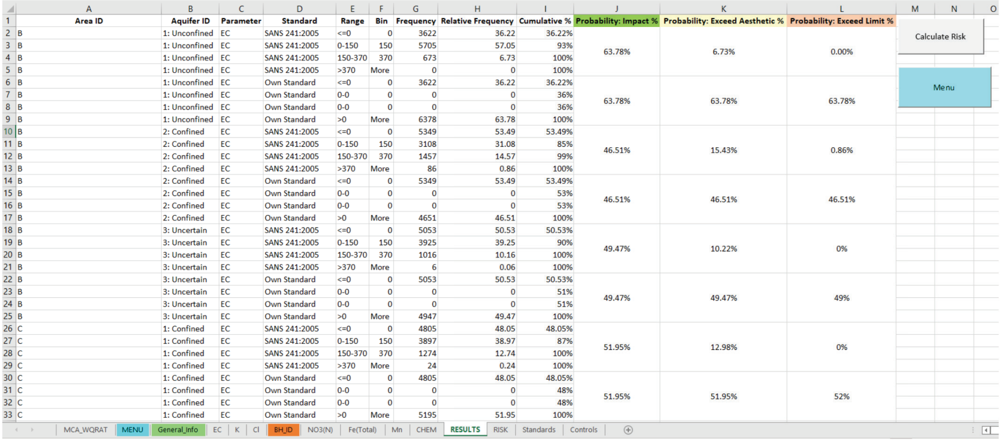

	Area ID	Aquifer ID	Parameter	Standard	Range	Bin	Frequency	Relative Frequency	Cumulative %	Probability: Impact %	Probability: Exceed Aesthetic %	Probability: Exceed Limit %
2	B	1: Unconfined	EC	SANS 241:2005	<=0	0	3622	36.22	36.22%	63.78%	6.73%	0.00%
3	B	1: Unconfined	EC	SANS 241:2005	0-150	150	5705	57.05	93%			
4	B	1: Unconfined	EC	SANS 241:2005	150-370	370	673	6.73	100%			
5	B	1: Unconfined	EC	SANS 241:2005	>370	More	0	0	100%			
6	B	1: Unconfined	EC	Own Standard	<=0	0	3622	36.22	36.22%	63.78%	63.78%	63.78%
7	B	1: Unconfined	EC	Own Standard	0-0	0	0	0	36%			
8	B	1: Unconfined	EC	Own Standard	0-0	0	0	0	36%			
9	B	1: Unconfined	EC	Own Standard	>0	More	6378	63.78	100%			
10	B	2: Confined	EC	SANS 241:2005	<=0	0	5349	53.49	53.49%	46.51%	15.43%	0.86%
11	B	2: Confined	EC	SANS 241:2005	0-150	150	3108	31.08	85%			
12	B	2: Confined	EC	SANS 241:2005	150-370	370	1457	14.57	99%			
13	B	2: Confined	EC	SANS 241:2005	>370	More	86	0.86	100%			
14	B	2: Confined	EC	Own Standard	<=0	0	5349	53.49	53.49%	46.51%	46.51%	46.51%
15	B	2: Confined	EC	Own Standard	0-0	0	0	0	53%			
16	B	2: Confined	EC	Own Standard	0-0	0	0	0	53%			
17	B	2: Confined	EC	Own Standard	>0	More	4651	46.51	100%			
18	B	3: Uncertain	EC	SANS 241:2005	<=0	0	5053	50.53	50.53%	49.47%	10.22%	0%
19	B	3: Uncertain	EC	SANS 241:2005	0-150	150	3925	39.25	90%			
20	B	3: Uncertain	EC	SANS 241:2005	150-370	370	1016	10.16	100%			
21	B	3: Uncertain	EC	SANS 241:2005	>370	More	6	0.06	100%			
22	B	3: Uncertain	EC	Own Standard	<=0	0	5053	50.53	50.53%	49.47%	49.47%	49%
23	B	3: Uncertain	EC	Own Standard	0-0	0	0	0	51%			
24	B	3: Uncertain	EC	Own Standard	0-0	0	0	0	51%			
25	B	3: Uncertain	EC	Own Standard	>0	More	4947	49.47	100%			
26	C	1: Confined	EC	SANS 241:2005	<=0	0	4805	48.05	48.05%	51.95%	12.98%	0%
27	C	1: Confined	EC	SANS 241:2005	0-150	150	3897	38.97	87%			
28	C	1: Confined	EC	SANS 241:2005	150-370	370	1274	12.74	100%			
29	C	1: Confined	EC	SANS 241:2005	>370	More	24	0.24	100%			
30	C	1: Confined	EC	Own Standard	<=0	0	4805	48.05	48.05%	51.95%	51.95%	52%
31	C	1: Confined	EC	Own Standard	0-0	0	0	0	48%			
32	C	1: Confined	EC	Own Standard	0-0	0	0	0	48%			
33	C	1: Confined	EC	Own Standard	>0	More	5195	51.95	100%			

Figure 8 *RESULTS Sheet of the MCA-Water Quality Risk Assessment Tool.*

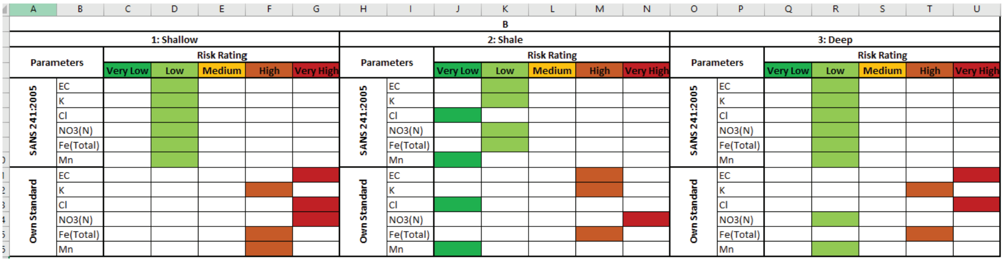

B

1: Shallow							2: Shale							3: Deep						
Parameters		Risk Rating					Parameters		Risk Rating					Parameters		Risk Rating				
		Very Low	Low	Medium	High	Very High			Very Low	Low	Medium	High	Very High			Very Low	Low	Medium	High	Very High
SANS 241:2005	EC		🟩				SANS 241:2005	EC		🟩				SANS 241:2005	EC		🟩			
	K		🟩					K		🟩					K		🟩			
	Cl		🟩					Cl	🟩						Cl		🟩			
	NO3(N)		🟩					NO3(N)		🟩					NO3(N)		🟩			
	Fe(Total)		🟩					Fe(Total)		🟩					Fe(Total)		🟩			
	Mn		🟩					Mn	🟩						Mn		🟩			
Own Standard	EC					🟥	Own Standard	EC				🟧		Own Standard	EC					🟥
	K				🟧			K				🟧			K				🟧	
	Cl					🟥		Cl	🟩						Cl					🟥
	NO3(N)					🟥		NO3(N)					🟥		NO3(N)		🟩			
	Fe(Total)				🟧			Fe(Total)				🟧			Fe(Total)				🟧	
	Mn				🟧			Mn	🟩						Mn		🟩			

Figure 9 *RISK Sheet of the MCA-Water Quality Risk Assessment Tool.*

coefficient of variance is calculated for each chemical parameter for the monitoring boreholes and reference boreholes and the sheet is automatically populated. If the coefficient of variance is greater than 100% the log-transformed statistics is selected by default for the probability calculation (Monte Carlo analysis). Then the user should click on the "Calculate Probability" button. The user is then navigated to the RESULTS sheet (Fig. 8).

RESULTS Sheet – this is where the probability percentages calculated is presented and where the user can calculate the risk. The user should click on the "Calculate Risk" button. The risk is then calculated based on the probability percentages and the user is navigated to the RISK sheet (Fig. 9).

RISK Sheet – This sheet represents the final product of the risk assessment process, which is the calculated risk matrix per monitoring area, indicating the probable risk of impact per chemical parameter.

Application for Groundwater Monitoring Programme Optimization

Based on the risk rating calculated by the MCA-Water Quality Assessment Tool, a monitoring programme can be optimized by applying the following rules:

- Water quality parameters with a risk rating of high to very high should be monitored at minimum on a quarterly basis.
- Water quality parameters with a risk rating of medium should be monitored at a minimum on a biannual basis (wet and dry season).
- The water quality parameters with a risk rating of very low to low should be monitored on an annual basis – if the concentration of these parameters exceed the limits of the selected standard at one of the monitoring localities, then the frequency of monitoring for that parameter at that specific locality should be increased to determine if it was a once off occurrence or if the concentration is increasing over time.

Conclusions

The MCA-Water Quality Risk Assessment Tool should be regarded as a screening tool applied to historical time-series monitoring data for a specific monitoring site to determine the risk of probability of impact for the inorganic water quality parameters. The Tool can be applied to varies industries that have the potential to impact or have impacted the groundwater regime if historical time-series monitoring data is available. Other applications include:

- Determination of which potential pollution source at an industrial and/or mining facility is impacting the water resources (surface-and groundwater) the most or which one have the highest risk of possible impact.
- Industrial and/or mining post-closure screening tool to estimate which water quality parameters have the highest risk of impacting the water resources of the area.
- Incorporation into monitoring reports to assist management in identifying problem areas and the management thereof.

Acknowledgements

A special thanks to our colleagues, Dr. Fanie de Lange and Dr. Anton Lukas, at the Institute for Groundwater Studies, for their assistance with the coding of Microsoft Excel to develop the MCA-Water Quality Risk Assessment Tool.

References

Duijm, N.J. (2015) 'Recommendations on the use and design of risk matrices', Safety Science, 76 (July 2015), pp. 21–31. https://doi.org/10.1016/j.ssci.2015.02.014.

EXCELTV (2022) Monte Carlo Simulation Formula in Excel - Tutorial and Download. Available at: https://excel.tv/monte-carlo-simulation-excel-tutorial-download/ (Accessed: 13 October 2022).

Microsoft (2022) Introduction to Monte Carlo simulation in Excel, Office Support. Available at: https://support.microsoft.com/en-us/office/introduction-to-monte-carlo-simulation-in-excel-64c0ba99-752a-4fa8-bbd3-4450d8db16f1 (Accessed: 13 October 2022).

Reimann, C., Filzmoser, P. and Garrett, R.G. (2005) 'Background and threshold: Critical comparison of methods of determination', Science of the Total Environment, 346(1–3), pp. 1–16. https://doi.org/10.1016/j.scitotenv.2004.11.023.

U.S. Environmental Protection Agency (1997) 'Guiding Principles for Monte Carlo Analysis', Risk Assessment Forum [Preprint] (EPA/630/R-97/001).

Irrigation With Witwatersrand Goldmine Waters

Lesego Madiseng[1], John Annandale [1], Phil Tanner[1], Corleen van Aswegen[1] and Sakhiwo Sukati[1]

[1]*Department of Plant and Soil Sciences, University of Pretoria, Private Bag, X20, Hatfield, 0028, South Africa, u28424868@tuks.co.za Bd de l'université, J9X 5E4 Rouyn-Noranda, QC, Canada, abdelkabir.maqsoud@uqat.ca*

Abstract

Irrigation has been proposed as a cost-effective, long-term option for managing mining-influenced waters in the Witwatersrand Goldfields. However, there are concerns about the suitability of these waters for crop production as well as the safety of the produce for consumption. To address these concerns, A glasshouse pot trial was established where crops were irrigated with untreated and HDS-treated mine water from the Eastern, Central and Western Basins of the Witwatersrand Goldfields. The findings of this study indicate that crops that are safe to consume can successfully be produced with treated mine waters from the Witwatersrand Goldfields. Furthermore, the findings suggest that untreated mine waters from these goldfields can be utilized for irrigation if soils are strategically limed.

Keywords: Irrigation, Crops, Mine water.

Introduction

Cessation of mining activities in the Witwatersrand Goldfields led to the flooding of underground mine workings, posing a risk of acid mine drainage (AMD) discharge. Since many of the mines are ownerless and derelict, the management of AMD is a taxpayer liability. In 2010, three of the basins in the Witwatersrand goldfields – the Eastern, Central, and Western Basins were identified as posing the greatest AMD discharge risk. This was after AMD from the Western Basin discharged into a nearby nature reserve, making national news and prompting emergency interventions (Coetzee *et al.* 2010). These interventions included setting environmental critical levels (ECL), which are threshold water levels that need to be maintained in the underground mine workings to prevent AMD discharge. In addition, three high-density sludge (HDS) treatment plants, one in each basin, were constructed to pump and treat approximately 185 ML/day of AMD from the Witwatersrand basins. A major concern with the AMD from the Witwatersrand basins was the acidity and the high concentration of sulfate, total dissolved solids and trace elements.

HDS treatment addresses the acidity and reduces the concentration of most trace elements. However, the sulfate and total dissolved solids in the waters remain high, resulting in an increase in the dissolved salt load to receiving water bodies. This is a major concern in the Eastern and Central basins, where an average of 140 ML/day of treated mining-influenced water is discharged into tributaries of the Vaal Barrage, which supplies water to many parts of the country (Rand Water 2024; TCTA 2024). The treated mining-influenced water from these basins reportedly contributes 2500 mg/L of total dissolved solids (TDS) to the Vaal Barrage. This increased dissolved salt load often necessitates dilution with expensive Lesotho Highlands water to maintain a TDS of 600 mg/L in the catchment (DWS 2024; Rand Water 2024). The discharge of HDS-treated mining-influenced water is, therefore, not sustainable and long-term solutions are sought. Desalination using Reverse Osmosis is the preferred long-term management option. However, this technology is expensive and energy-intensive, making it unaffordable and possibly unfeasible, considering the ongoing energy crisis. Irrigation has been proposed as a cost-effective option with opportunities for great socioeconomic benefits (Annandale et al, 2023). However, there are concerns about the productivity of crops irrigated with mine water and their safety for consumption.

Irrigation with circumneutral, Ca^{2+} and SO_4^{2}-enriched mining–influenced water has successfully been demonstrated in the Mpumalanga Coalfields. Additionally, long-term modelling by Annadale *et al.* (2023) showed that HDS-treated mining-influenced water from the Witwatersrand Goldfields is suitable for irrigation. According to Annadale *et al.* (2023), even untreated mining-influenced water can be utilized if liming materials are applied to the soil to manage acidity. The productivity of crops irrigated with mining-influenced water has not been demonstrated in the Witwatersrand Goldfields. Furthermore, the food and feed safety of crops irrigated with treated and untreated mining-influenced water from the Witwatersrand basins requires investigation. Therefore, this study aimed to investigate crop responses to irrigation with untreated and HDS-treated mining influenced water from the Witwatersrand basins and to assess the food and feed safety of the produce.

Methods

Glasshouse pot trials were established in July 2024 at the University of Pretoria Innovation Africa Experimental Farm. Oat was selected as a salt-tolerant winter crop suitable for food and feed. The oat was planted in 6 L pots filled with 8 kg of red sandy loam soil from the experimental farm. Soils irrigated with untreated mine water were limed with reagent grade $CaCO_3$ to counteract the acidity from the water. Lime application rates were determined based on the acidity of the water and seasonal crop water requirements. The trial consisted of six treatments of treated and untreated mine water collected from the three Witwatersrand treatment plants for irrigation. The mine waters were analysed three times during the trial at an accredited laboratory, and the average quality is presented in Table 1. Analysis methods are listed in the laboratory accreditation certificate (Waterlab 2024). Deionised water was used as a control treatment. Each treatment was replicated four times.

The pots were irrigated when soil water was depleted by at least 40%. A crop and water-specific leaching fraction, determined using the leaching requirement equation proposed by Ayers and Westcot (1985), was applied with each irrigation. Once a week, the crops were irrigated to field capacity with a nutrient solution instead of the treatment irrigation waters. Therefore, crops with higher water requirements received more of the nutrient solution.

The crop was harvested at maturity, and above-ground biomass and grain yield were determined. Composite samples of the stems plus leaves and the grain were analysed for elements of concern. Trace element concentrations were determined in the shoots and seeds to assess the food and feed safety of the crops. Composite samples of each water treatment were analysed to determine the effect of the mine water treatments on pH (KCl), saturated paste electrical conductivity (ECe), phosphorus (P bray 1) as well as Melich III extractable macro and micronutrients.

Statistical analyses were performed in SAS® Studio. Analysis of variance (ANOVA) was used to assess the effects of the mine water on above-ground biomass production and seed yield. Mean comparisons were performed using Tukey's Studentized Range (HSD) Test.

Results and Discussion

Effect of mine water irrigation on selected soil chemical properties

Selected soil chemical properties of soils irrigated with mine water are presented in Table 2. The pH of the soils irrigated with untreated AMD was greater than 7, indicating

***Table 1** Average qualities of mine water collected from the EB (Eastern Basin), CB (Central Basin), and WB (Western Basin). Concentrations are in mg/L, acidity as mg/L CaCO3 eq., EC in mS/m and pH without units.*

Parameter	EB untreated	EB HDS treated	CB untreated	CB HDS treated	WB untreated	WB HDS treated
pH	6.36	7.81	5.79	8.14	6.29	9.33
EC	283	257	384	375	342	331
Ca	328	321	538	785	616	697
Mg	112	97	162	138	94	71
Na	185	188	157	155	165	159
SO4	1328	1254	2317	2280	1882	1864
Cl	109	110	57	56	47	47
Acidity	130	9	427	5	100	5
Al	0.06	0.057	0.140	0.100	0.100	0.129
As	0.17	0.003	0.239	0.056	0.300	0.011
B	0.26	0.249	0.451	0.169	0.075	0.074
Cd	<0.001	<0.001	<0.001	<0.001	<0.001	<0.001
Cr	<0.025	<0.025	<0.025	<0.025	<0.025	<0.025
Cu	0.010	0.021	0.010	0.010	0.010	0.010
Fe	78	0.18	276	0.69	46	0.55
Pb	<0.001	<0.001	<0.001	<0.001	<0.001	<0.001
Mn	4.2	1.7	19	1.47	17	0.48
Hg	<0.001	<0.001	<0.001	<0.001	<0.001	<0.001
Mo	<0.009	<0.009	<0.009	<0.009	<0.009	<0.009
Ni	0.053	0.031	0.308	0.025	0.032	0.025
U	0.059	0.047	0.004	0.001	0.105	0.015
Zn	0.028	0.026	0.063	0.025	0.032	0.029

that the application of limestone was efficient in neutralizing the waters. Irrigation with the mine water did increase the ECe of the soils. However, the ECe of the soils was within the ideal and acceptable range as predicted by (Annandale *et al.* 2023). Melich III extractable concentrations of selected trace elements in soils irrigated with mine water were generally similar to those of the control. This is likely due to the addition of limestone in soils irrigated with untreated AMD and the generally circumneutral pH of the soils irrigated with HDS treated AMD reducing the availability of the elements.

Above-ground biomass production and grain yield of crops irrigated with mine waters

Irrigation with mine water had no substantial effect on crop biomass production except in oats irrigated with the Eastern Basin mine waters. Oats irrigated with these waters yielded substantially greater biomass than the control. There were no substantial differences in biomass between the mine water treatments except for oats irrigated with Central Basin AMD, which yielded substantially less biomass than oats irrigated with treaded Eastern Basin AMD.

Irrigation with the mine water had no substantial effect on crop yield except in oats irrigated with treated water from the Eastern and Central basins, which produced higher yields than the control. Oats irrigated with CB AMD had substantially lower yields than those irrigated with treated CB AMD.

The biomass production and yield of crops irrigated with Eastern Basin mine water are consistent with predictions made by Annandale *et al.* (2023), which indicated

Table 2 Soil pH, ECe and selected Melich III extractable elements. Concentrations are in mg/kg, ECe in mS/m and pH without unit.

Parameter	Control	EB HDS treated	CB HDS treated	WB HDS treated	EB untreated	CB AMD untreated	WB AMD untreated
pH	6.83	7.24	5.93	6.58	7.66	7.27	7.52
ECe	25.9	181	220.8	189.5	188.2	254	173.2
P	148	86	86	113	60	52	98
K	44	60	63	53	71	71	52
Ca	1309	1762	1288	2013	1742	2513	2069
Mg	127	502	626	316	700	992	508
S	26	907	1534	1369	1295	2260	1401
Na	21	264	279	229	336	384	220
Fe	64.07	61.21	48.32	60.94	60.24	108.31	65.4
Mn	145.9	54.2	40.91	74.69	69.86	89.62	102.03
Cu	4.11	4.22	3.4	3.62	3.79	3.71	3.56
Zn	8.57	5.22	4.52	5.53	5.52	5.52	5.26
B	0.33	0.9	0.33	0.34	0.87	0.56	0.41
Mo	0.5	0.66	0.55	0.37	0.21	0.42	0.35

that these waters were the most suitable for crop production. Annandale *et al.* (2023) predicted that irrigation with CB AMD could negatively affect yield. However, in this study, these waters had no significant effect on the yield. Overall, these results indicate that mine water from the Witwatersrand Goldfields can successfully be used for crop irrigation with no effect on productivity.

Food and feed safety of crops irrigated with mine waters

Local and International food and safety feed safety regulations cite As, Cd, Hg, and Pb as contaminants in food and animal feed (DAFF 2010; FAO-WHO 2023). Therefore, food and feed safety assessments focused on these elements. Uranium was also included in the analyses, as the concentration in some of the waters exceeded irrigation and drinking water quality thresholds (DWAF 1996a, 1996b).

Table 3 shows the concentration of As, Cd, Cr, Hg, Pb, Ni and Zn concentrations in the plant material compared to food and feed safety thresholds. As, Hg and Pb were below food and safety thresholds in all plant materials analysed, indicating that irrigation with the mine waters did not result in the bioaccumulation of these elements in the edible parts of oats. Cd concentrations exceeded food safety thresholds in oats irrigated with untreated WB mining-

Table 2 Mean above-ground biomass production and yield of oats. Means with the same letter are not significantly different (p-value=0.02). Units are g/pot.

Treatment	Aboveground biomass	Yield
Control	149(bc)	35 (b)
EB HDS treated	201 (a)	61(a)
EB untreated	198(a)	60 (ab)
CB HDS treated	193(ab)	73 (a)
CB untreated	138(c)	34(b)
WB HDS treated	185 (ab)	54(ab)
WB untreated	194 (ab)	51 (ab)

Table 3 As, Cd, Cr, Hg, Pb, Ni and Zn concentrations in oats compared to food and feed safety thresholds. Units are mg/kg on a dry mass basis. Shaded cells indicate an exceedance of the relevant threshold(s).

	As	Cd	Hg	Pb	U
Food safety threshold	—	0.1	0.1	0.2	—
Feed safety threshold	2	0.5	0.1	5	—
Leaves and stems					
Control	<0.01	<0.01	<0.01	<0.01	<0.01
EB HDS treated	<0.01	<0.01	<0.01	<0.01	<0.01
CB HDS treated	<0.01	0.24	<0.01	<0.01	<0.01
WB HDS treated	<0.01	<0.01	<0.01	<0.01	<0.01
EB untreated	<0.01	0.14	<0.01	<0.01	<0.01
CB untreated	<0.01	<0.01	<0.01	<0.01	<0.01
WB untreated	<0.01	0.18	<0.01	<0.01	<0.01
Grain					
Control	<0.01	<0.01	<0.01	<0.01	<0.01
EB HDS treated	<0.01	<0.01	<0.01	<0.01	<0.01
CB HDS treated	<0.01	<0.01	<0.01	<0.01	<0.01
WB HDS treated	<0.01	<0.01	<0.01	<0.01	<0.01
EB untreated	<0.01	0.09	<0.01	<0.01	<0.01
CB untreated	<0.01	<0.01	<0.01	<0.01	<0.01
WB untreated	<0.01	0.29	<0.01	<0.01	<0.01

influenced water. This suggests that irrigation with untreated mining-influenced water from the Western Basin can result in the bioaccumulation of cadmium, posing a food safety risk. Nonetheless, cadmium concentrations were below feed safety thresholds. Uranium concentrations were below the detection limit (0.01 mg/kg). However, this detection limit is greater than typical concentrations found in staple foods (0.002 mg/kg), as reported by the WHO (2001).

Although substantial amounts of As and U were added to the soil through irrigation, this did not result in the bioaccumulation of these elements in the plant material, suggesting limited mobility of these elements in soils and or limited translocation to the edible portions of the crop. In contrast, there was substantial bioaccumulation of Cd in the plant material despite the waters containing low concentrations of the element.

Cd availability is pH dependent, and the concentration of plant-available cadmium is typically higher in acidic soils (pH < 5.5)(Gu *et al.* 2022; Kicińska *et al.* 2022; Zhang *et al.* 2023). Cadmium concentrations in the mine waters were below the detection limit, and soil pH was greater than 5.5. The relatively high concentrations of Cd in the plant material may be a result of the soils containing substantial amounts of the element and/or the mine waters increasing the availability. Additionally, studies have shown that plants can accumulate substantial amounts of Cd even though the soil concentrations of the elements are low (Liu *et al.* 2016; Niu *et al.* 2023; Rolka 2015).

The food safety assessments suggest that crops irrigated with HDS-treated mining-influenced water from the Witwatersrand Basins should be safe for consumption, as predicted by Annadale et.al (2023). The food safety risk of crops irrigated with untreated WB untreated water as well as the food safety risk posed by U in the EB waters and the untreated WB untreated water require further investigation. More sensitive water and crop analyses are required to explore the magnitude of the risk.

Conclusions

Irrigation offers a mine water management option that will support water and food security, with the potential to create livelihoods. This study demonstrated that crops can successfully be produced with treated mine water from the Witwatersrand Goldfields. Furthermore, the untreated mine water from these goldfields can be utilized for irrigation if soils are strategically limed. Concentrations of major elements of concern were generally below the food and feed safety thresholds. However, food safety risks posed by Cd and U, particularly in crops irrigated with untreated mining-influenced water, require further investigation.

Acknowledgements

The authors thank the Water Research Commission (WRC) for their continued support of the mine water irrigation group at the University of Pretoria. We also thank Mr Ayanda Mtetwa from the Department of Water and Sanitation (DWS) for facilitating access to mine water for use in our study.

References

Annandale J, Du Plessis M, Tanner P, Heuer S, Madiseng L (2023) Irrigation Should be Explored as a Sustainable Management Solution to the Acid Mine Drainage Legacy of the Witwatersrand Goldfields. Mine Water and the Environment. https://doi.org/10.1007/s10230-023-00961-3.

Ayers RS, Westcot DW (1985) Water quality for agriculture. vol 29. Food and Agriculture Organization of the United Nations Rome

Coetzee H, Hobbs P, Burgess J, Thomas A, Keet MM (2010) Mine water management in the Witwatersrand Gold Fields with special emphasis on acid mine drainage.

DAFF (2010) Fertilizers, Farm Feeds, Agricultural Remedies And Stock Remedies Act, 1947 (Act No. 36 Of 1947). In: Department of Agriculture Forestry and Fisheries SA (ed).

DWAF (1996a) South African Water Quality Guidelines – Volume 1: Domestic Use. In: Department of Water Affairs and Forestry SA (ed). vol Volume 1: Domestic Use. Department of Water Affairs and Forestry, Pretoria

DWAF (1996b) Volume 4: Agricultural Use: Irrigation. In: Department of Water Affairs and Forestry (South Africa) (ed). Department of Water Affairs and Forestry, Pretoria

DWS (2024) National State of Water Report. In: Department of Water and Sanitation SA (ed).

FAO-WHO (2023) Joint FAO/WHO Food Standards Programme Codex Committee on Contaminants in Food (2023). In: FAO-WHO (ed). The Hague, The Netherlands

Gu J, Zou G, Su S, Li S, Liu W, Zhao H, Liu L, Jin L, Tian Y, Zhang X, Wang Y, Zhao T, Du L, Wei D (2022) Effects of pH on Available Cadmium in Calcareous Soils and Culture Substrates. Eurasian Soil Science 55(12):1714-1719. https://doi.org/10.1134/s1064229322601391

Kicińska A, Pomykała R, Izquierdo-Diaz M (2022) Changes in soil pH and mobility of heavy metals in contaminated soils. European Journal of Soil Science 73(1). https://doi.org/10.1111/ejss.13203

Liu H, Wang H, Ma Y, Wang H, Shi Y (2016) Role of transpiration and metabolism in translocation and accumulation of cadmium in tobacco plants (Nicotiana tabacum L.). Chemosphere 144:1960-1965. https://doi.org/https://doi.org/10.1016/j.chemosphere.2015.10.093

Niu L, Li C, Wang W, Zhang J, Scali M, Li W, Liu H, Tai F, Hu X, Wu X (2023) Cadmium tolerance and hyperaccumulation in plants – A proteomic perspective of phytoremediation. Ecotoxicology and Environmental Safety 256:114882. https://doi.org/https://doi.org/10.1016/j.ecoenv.2023.114882

Rand Water (2024) Integrated Annual Report 2024. Retrieved from https://www.randwater.co.za/annualreports.php

Trans Caledon Tunnel Authority (TCTA) (2024) Integrated Annual Report 2024. Retrieved from https://www.tcta.co.za/annual-reports/

Waterlab (2024) Certificate of Accreditation. South African National Accreditation System Retrieved from https://www.waterlab.co.za/index.html

WHO (2001) Depleted uranium: Sources, Exposure and Health Effects. In: World Health Organisation (ed).

Zhang Z, Chen X, Qin X, Xu C, Yan X (2023) Effects of Soil pH on the Growth and Cadmium Accumulation in Polygonum hydropiper (L.) in Low and Moderately Cadmium-Contaminated Paddy Soil. Land 12(3):652. https://doi.org/10.3390/land12030652.

Benthic Diatoms as Indicators of Groundwater-Surface Water Connectivity in Coal Mining Wetlands: Case of depression wetlands in Belfast, Mpumalanga Province, South Africa

Tebogo Madlala[1,2] Thokozani Kanyerere[2], Paul Oberholster[3], Harrison Pienaar[1,3]

[1]CSIR, Water Centre, Smart Water Use Research Group, 11 Jan Cilliers Rd, Stellenbosch, 7599, Western Cape Province, South Africa.

[2]Institute for Water Studies, Department of Earth Science, University of the Western Cape, Bellville, Cape Town, 7535, South Africa.

[3]Centre for Environmental Management, Faculty of Natural and Agricultural Science, University of the Free State, Bloemfontein, 9300, South Africa. Corresponding author email: tmadlala@csir.co.za

Abstract

The applicability of diatoms as bioindicators to assess hydrological connectivity between groundwater and surface water in wetlands affected by coal mining was examined. Benthic diatoms were identified as effective indicators due to their sensitivity to water chemistry, flow, and nutrient dynamics. Field and lab analyses of hydrochemistry, isotopes, and diatom assemblages revealed that wetlands near mining activities had acidic water, higher EC, and diatoms indicative of mining, suggesting mine-affected groundwater influence (i.e. *Craticula Budari*). In contrast, distant wetlands showed nutrient-associated diatoms and atmospheric recharge signatures. This multidisciplinary approach demonstrates the value of diatoms in monitoring ecosystem health and managing wetlands in mining regions.

Keywords: Diatoms, groundwater-surface water interaction, coal mining, wetlands, hydrological connectivity, bio-indicators, hydrochemistry, isotopes, mine pollution.

Introduction

Coal mining can disrupt wetland ecosystems, affecting groundwater-surface water interactions and water quality. While chemical and isotopic analyses are commonly used to study these connections (Madlala et al. 2021), the potential of benthic diatoms as biological indicators remains largely underexplored. Limited research exists on their effectiveness in detecting groundwater influence in mining-impacted wetlands (Pfister et al. 2017; Oberholster 2019; Oberholster et al. 2020). The purpose of this study was to determine whether benthic diatoms, in conjunction with chemical and isotopic techniques, could accurately detect groundwater-surface water connection in wetlands that were used for coal mining. Understanding these dynamics is crucial for wetland conservation and sustainable water management in mining areas.

Methods

Study site description

The Exxaro Belfast Implementation Mining Rights Area is in the headwaters of the Komati River catchment in Mpumalanga Province, South Africa. The coal mine is situated 55 km east of Middelburg and 20 km southwest of Belfast, south of the N4 highway (Fig. 1). The area includes two catchments with southward-flowing streams, namely the Witkloofspruit and the Klein Komati, along with various wetland types such as depressional, valley bottom, and hillslope wetlands (Golder Associates Africa 2011).

Wetland occurrence in mining areas like the Exxaro Belfast Implementation

Mining Rights Area is shaped by geology and hydrogeology, which control water availability, flow, and storage. The area's Karoo Supergroup sedimentary rocks (sandstone, shale, and coal) along with dolerite dykes and sills (Steenekamp 2009), influence water movement and accumulation in the subsurface. Sandstone and shale act as water-bearing layers or confining units, while coal seams, with high porosity, can store and release groundwater, supporting wetlands. Dolerite dykes create barriers that force groundwater to the surface, aiding wetland formation. However, mining operations that remove these geological layers can disrupt natural hydrological balance, draining wetlands or altering their water supply.

The hydrogeology of the area includes two key aquifer systems. The shallow, semi-confined weathered zone aquifer, with static water levels of 0.2–35 mbgl and low groundwater yields (<0.3 l/s), sustains surface-dependent wetlands, like depressional and valley-bottom wetlands. The deeper fractured aquifer, yielding up to 2 l/s, supports wetlands relating to groundwater discharge (Golder Associates Africa 2018). Groundwater follows the Klein Komati River's flow, linking riparian and floodplain wetlands. Fractures and faults in the Karoo bedrock can create groundwater pathways, supplying wetlands even where surface water is limited.

Land use in the mining rights area is primarily cattle grazing, crop cultivation, and coal mining. Natural grasslands provide habitats for wildlife, including the endangered African Grass Owl. Vegetation consists of Mesic and Dry Highveld Grasslands, with indigenous grasses, biesies (*Juncus effuses*), and cattails (*Typha capensis*). Alien invasive species, including blue gum (*Eucalyptus globulus*) and poplar (*Populus sp.*), are also present.

The climate of the region is characterized by summer rainfall (October–April), with the highest temperatures occurring in wet summer months and lower temperatures in dry winter periods. Rainfall is influenced by convective storm systems.

Data Collection Methods

A comprehensive approach to assess the physicochemical and biological characteristics of water systems, focusing on wetlands, piezometers was followed. In situ physicochemical parameters, including pH, electrical conductivity, and total dissolved solids (TDS), were measured using a handheld Hanna HI991300™ multi-meter, depending on water availability at

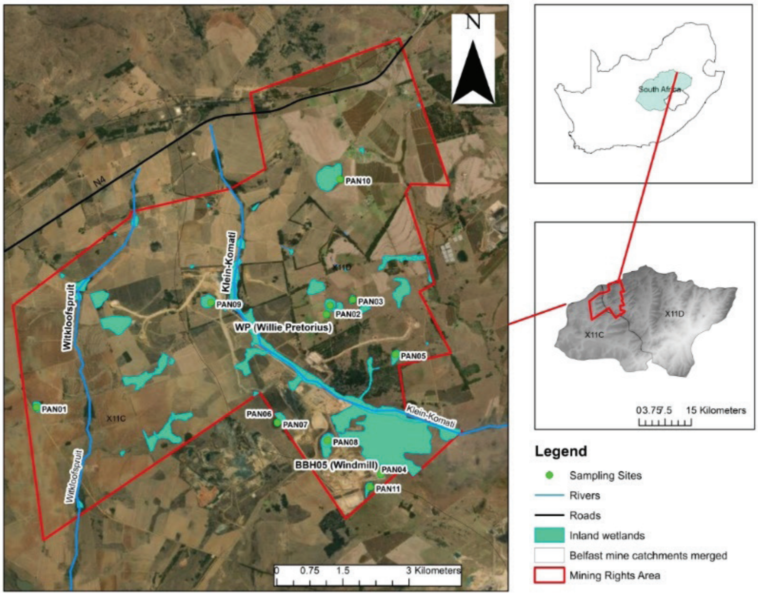

Figure 1 Study area map of the Upper Komati River catchment (X11C and X11D) with the study mine (red box) Belfast Implementation Mining Rights Area.

the sampling location. Water samples for hydrochemical analysis were collected using a grab sampling technique, with 1L acid-washed polyethylene bottles used to obtain representative samples from flowing water within wetlands. Sampling points were carefully selected to avoid stagnant water, and bottles were rinsed three times with site water prior to collection. For piezometers and boreholes, a bailer was used to collect samples after purging at least three well volumes to ensure representative groundwater and subsurface water samples (Brassington 2007). A total of 27 water samples were collected from various sources, including pan wetland surface water, rainwater, and piezometers, to identify the sources sustaining the pan wetlands (Table 3 in Appendix). The collected samples were immediately labelled, stored in a cooler box with ice to minimize chemical alterations, and transported to the CSIR chemistry laboratory in Stellenbosch, South Africa for analysis of major ions, metals, and nutrients to characterize water types and assess spatial variations in water chemistry.

Environmental isotope analysis was conducted to complement hydrochemical data. Water samples for isotopic analysis were collected in 50-100 mL double-sealed polyethylene bottles and transported to iThemba Labs at the University of Witwatersrand for analysis using mass spectrometry. To maintain consistency, both hydrochemical and isotopic samples were collected from the same water sources, ensuring comparability and minimizing variability in results.

Benthic microalgal communities, categorized as epipelic (motile) or epipsammic (attached to sand or rock surfaces), were sampled to evaluate their ecological role. Epilithic and epipsammic algae were collected from submerged substrates at depths of 5-20 cm using a hand auger, following established protocols (Oberholster 2019). Five random samples per site were pooled into composite samples, which were then divided into subsamples for specific analyses: (a) unpreserved samples for culturing and identification of filamentous algae, (b) preserved samples for microscopic identification of soft algae, and (c) unpreserved samples for diatom identification. Soft algae subsamples were fixed in 2.5% glutaraldehyde in the field and stored under cold, dark conditions to preserve integrity until laboratory analysis. This multi-faceted sampling and analytical approach ensured a robust characterization of the aquatic environment, integrating physicochemical, isotopic, and biological data to provide a comprehensive understanding of the studied ecosystems.

Data Analysis Methods

Water samples were analysed for major ions, nutrients, and dissolved metals at the CSIR SANAS-accredited laboratory following standard procedures (Younger 2007). Chemical analysis included cations (Ca^{2+}, Mg^{2+}, K^+, and N^+) and anions (HCO_3^-, Cl^-, SO_4^{2-}), nutrients (nitrates and phosphates), and dissolved metals (Al, Ba, Fe, Mn, Si, Sr). Analytical techniques included Inductive Coupled Plasma Optic Emission Spectroscopy (ICP-OES), Inductive Coupled Plasma Mass Spectroscopy (ICP-MS), and Flow Injection Colorimetric detection using a HACH D3900 Spectrophotometer.

Stable hydrogen ($^2H/^1H$) and oxygen ($^{18}O/^{16}O$) isotope ratios were analysed at iThemba Laboratories, Gauteng, using a Los Gatos Research (LGR) Liquid Water Isotope Analyzer. Laboratory standards were calibrated against international reference materials, with analytical precision of ±0.5‰ for $\Delta^{18}O$ and ±1.5‰ for Δ^2H. Results were expressed in delta-notation (‰ deviation from Standard Mean Ocean Water, SMOW)

Diatom samples were processed by removing organic matter with potassium dichromate and sulfuric acid, followed by rinsing and mounting in Pleurax medium for microscopic analysis. Identification was performed at 1250 × magnification (Carl Zeiss, Germany) following taxonomic references (Van Vuuren 2006; Taylor et al. 2007; Oberholster et al. 2022). Species abundance was categorized from rare (≤50 cells/5 cm^2) to predominant (5,001–25,000 cells/5 cm^2). Only diatom species classified as scarce to predominant were selected for statistical analysis. To explore groundwater-surface water interactions, Canonical

Correspondence Analysis (CCA) was used to assess relationships between diatom community composition and water chemistry in coal mining environments.

Results and Discussion

The hydrochemical analysis of sampled water revealed a freshwater system dominated by naturally occurring constituents, suggesting minimal anthropogenic influence. Major ions such as Na, SO_4^{2-}, Cl^-, and HCO_3^- dominated the total dissolved components in boreholes, wetland surface waters, and piezometers, resulting from natural processes like dissolution, ion exchange, and subsurface biological activity. Metal concentrations varied significantly (Table 2 in Appendix: Al ranged from 0.04 to 62 mg/L (mean = 5.89 mg/L), B from 0.02 to 0.08 mg/L (mean = 0.03 mg/L), Ba from 0.03 to 0.7 mg/L (mean = 0.24 mg/L), Fe from 0.34 to 71 mg/L (mean = 10.43 mg/L), Mn from 0.01 to 2.4 mg/L (mean = 0.45 mg/L), and Si from 1.1 to 81 mg/L (mean = 12.01 mg/L).

Comparison with South African Water Quality Guidelines revealed that while most parameters were within permissible limits for aquatic ecosystems, industrial, irrigation, domestic, and livestock uses, certain elements exceeded thresholds (Table 2 in Appendix). TDS, Cl^-, Fe, and Si surpassed industrial use limits; Al, Fe, and Mn exceeded irrigation and livestock watering standards; and Al, Fe, and Mn were above domestic use limits. Al and Mn also exceeded aquatic ecosystem guidelines. Notably, groundwater exhibited higher metal concentrations than wetland piezometers and surface water, with elevated levels of Fe, Al, and Mn likely linked to mining activities, particularly overburden stripping during mine development, which impacts wetland water quality. These findings highlight the need for monitoring and mitigation to address metal contamination and ensure water suitability for various uses.

Water samples from wetlands, piezometers, and groundwater exhibited similar mineralization, dominated by Na, Ca, K, and HCO_3^-, indicating prolonged subsurface residence times and extensive water-rock interactions. Ion exchange processes facilitated the leaching of these geologically derived elements. While HCO_3^- presence could suggest geological or anthropogenic buffering of natural acidity,

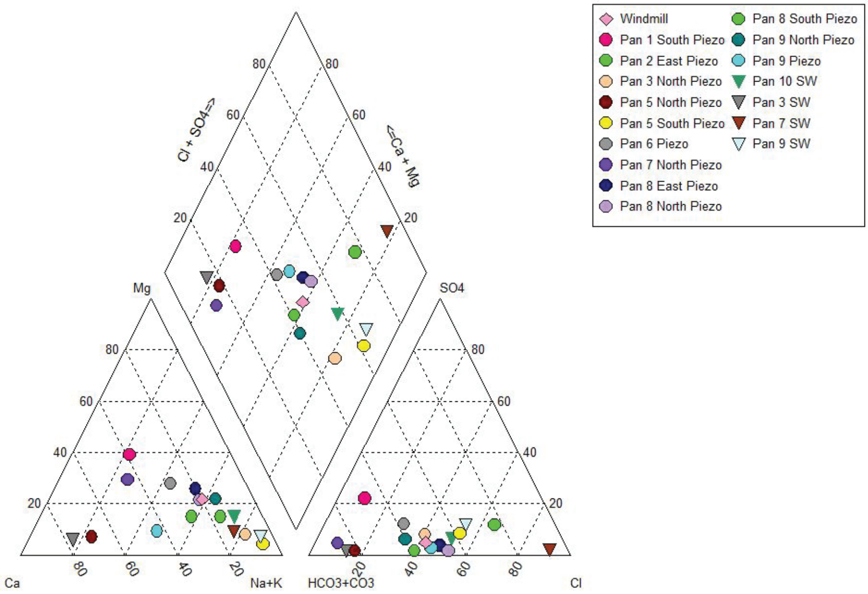

Figure 2 *Piper diagram showing hydrochemical facies of sampled water.*

pH levels in groundwater and surface water ranged from 5.58 to 6.69, reflecting naturally acidic conditions. However, biological activity, geological heterogeneity (e.g., coal seams), and varying soil buffering capacities resulted in circumneutral pH ranges (6–8). This suggests the upwelling and discharge of more basic deeper groundwater into the wetlands, consistent with findings by (Marques et al. 2004)

The isotopic variations in Δ¹⁸O and Δ²H across different sampling sites indicate that some wetlands were sustained by depleted subsurface water, while others received enriched atmospheric water. During the dry season, isotopic signatures showed that certain piezometers had been submerged and exhibited enrichment due to evaporative effects, suggesting a mix of surface and subsurface water. Few samples aligned with the evaporation line, indicating reduced evaporative influence on water sources. The clustering of surface water with pan piezometers and groundwater sources suggests groundwater exfiltration into the wetlands, with delayed discharge attributed to subsurface flow paths.

Diatoms are a highly diverse group of algae, often the most species-rich component of aquatic ecosystems, making them valuable biological indicators due to their distinct habitat preferences. Their diversity enhances ecological assessments by providing redundancy in data, increasing confidence in environmental inferences. Three dominant diatom functional groups in the depression wetlands were identified: mobile, motile, and high-profile taxa, with *Nitzschia tripunctata*, *Navicula rhynchocephala*, and *Fragilaria tenera* being the most abundant species. High-profile diatoms, particularly *Gomphonema* species, were highly sensitive to environmental disturbances, including fluctuating water levels, elevated ionic concentration, and nutrient scarcity, aligning with findings from previous studies (Stenger-

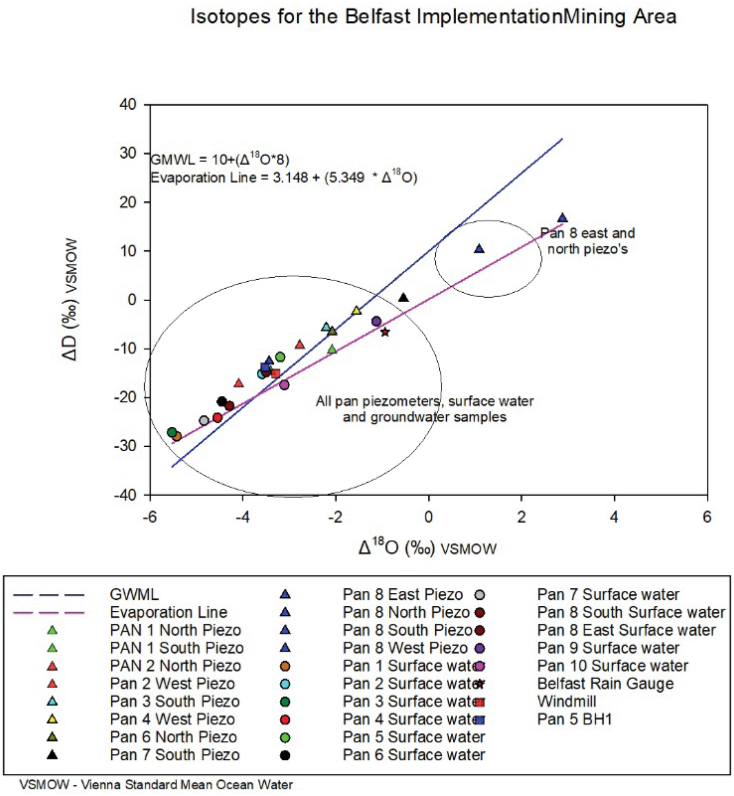

VSMOW - Vienna Standard Mean Ocean Water

Figure 3 *Biplot showing the Isotope ratios for Pans and local groundwater against the Global Meteoric Water Line and Evaporation Line (Craig 1961).*

Kovács et al. 2018; Oberholster et al. 2022). The phytoplankton community (Table 4 in Appendix) was dominated by *Bacillariophyta* (diatoms), *Euglenophyta* (small flagellates), and *Chlorophyta* (green algae), with *Euglenophyta* flourishing in wetlands enriched with organic matter from decaying macrophytes, which contributed to water coloration and lower pH levels. The seasonal presence of *Trachelomonas* suggested elevated organic matter and nutrient concentrations in the dry season, mirroring trends observed in other eutrophic wetland ecosystems.

Unlike many depression wetlands in Mpumalanga, which experience seasonal hydroperiods, the studied wetlands remained inundated throughout the year, indicating passive groundwater contributions during the dry season. The detection of *Craticula buderi* at Pan 7 (near the abandoned mine) suggested potential contamination, as this taxon is commonly linked to mine water seepage (Oberholster et al. 2022). CCA ordination (See Fig. 1 in Appendix) revealed that and associated with agricultural activity were closely associated with diatom species indicative of nutrient enrichment, while species resistant to elevated electrolyte concentrations were associated with mining activity diatom indicators.

Conclusion

Hydrochemical, isotopic and benthic phytoplankton analyses confirmed the influence of mining on the wetland's hydrology. A total of 65 phytoplankton taxa were identified, with 25 species indicating eutrophic conditions likely driven by agricultural activities, including organic matter accumulation, fertilizer runoff, and cattle grazing. The presence of Craticula buderi and isotopic indications of groundwater influx at a wetland near an abandoned mining site suggests its impact on wetland hydrology. These findings highlight the necessity of an integrated monitoring framework to evaluate wetland ecological integrity, considering both groundwater-surface water interactions and anthropogenic influences on phytoplankton dynamics.

References

Brassington R (2007) Field Hydrogeology: Third Edition. John Wiley and Sons, West Sussex, England.

Craig H (1961) Isotopic variations in meteoric waters. Science (1979) 133:1702–1703.

Golder Associates Africa (2011) NBC Belfast Ecological Baseline and Impact Assessment. Pretoria.

Golder Associates Africa (2018) Exxaro Coal Mpumalanga (PTY) LTD Belfast Implementation Project: Groundwater and Surface Water Quarterly.

Madlala T, Kanyerere T, Oberholster P, Butler M (2021) Assessing the groundwater dependence of valley bottom wetlands in coal-mining environment using multiple environmental tracers, Mpumalanga, South Africa. Sustain Water Resource Management 7.

Marques J, Matias M, Basto M, RC (2004) Water-rock interaction responsible for the origin of high pH mineral waters (S. Portugal).

Oberholster P, Melusi T, Tebogo M, Ndlela L (2020) Using pollution tracers to determine the origin of wastewater seepage in the vicinity of the SASOL, Sigma mine: ad hoc dry season monitoring.

Oberholster PJ, Schoeman Y, Truter JC, Botha AM (2022) Using Periphyton Assemblage and Water Quality Variables to Assess the Ecological Recovery of an Ecologically Engineered Wetland Affected by Acid Mine Drainage after a Dry Spell. Processes 10.

Oberholster PPJ (2019) Using hydrological and phytobenthic indicators to determine the natural and anthropogenic stressors to depressional wetlands in the vicinity of the EXXARO, North Block Complex mine, Belfast.

Pfister L, Wetzel CE, Klaus J, et al (2017) Terrestrial diatoms as tracers in catchment hydrology: a review. Wiley Interdisciplinary Reviews: Water 4:e1241.

Steenekamp G (2009) Belfast Project: Baseline Report on Geohydrological Investigation as part of the EIA and IWULA for the proposed mining operation. Riversdale.

Stenger-Kovács C, Körmendi K, Lengyel E, et al (2018) Expanding the trait-based concept of benthic diatoms: Development of trait- and species-based indices for conductivity as the master variable of ecological status in continental saline lakes. Ecol Indic 95:63–74.

Taylor JC., Harding WR., Archibald CGM. (2007) An illustrated guide to some common diatom species from South Africa. Water Research Commission, Pretoria.

Van Vuuren SJanse (2006) Easy identification of the most common freshwater algae: a guide for the identification of microscopic algae in South African freshwaters. Resource Quality Services (RQS) 2.

Younger PL (2007) Groundwater in the Environment: An Introduction. Wiley-Blackwell, Newcastle.

Appendix

Table 1 *Results from hydrochemical analysis of surface water sampled from wetlands at the Belfast Implementation mine site used for Canonical Correspondence Analysis (CCA). Table shows the concentrations for Potassium (K), Sodium (Na), Calcium (Ca), Magnesium (Mg), Sulfate (SO4-), Chloride (Cl), Bicarbonate (HCO3-),*

Parameter	K	Na	Ca	Mg	SO_4^-	Cl	HCO_3^-	TN	EC mS/m	pH	P	Al	Fe	Si
Pan 1	1.5	11	18	11	26	9.2	102.48	1.1	24	8	0.025	7.8	14	15
Pan 2	37	72	12	10	16	97	136.64	0.8	60	7.3	0.025	1.4	1.8	11
Pan 3	16	7.2	3.4	1.9	5.8	24	14.64	3.3	4	6.1	0.22	0.08	0.58	3.1
Pan 4	0.4	14	56	2.6	2.7	18	192.76	1.1	36	7.3	0.22	5.6	1.8	6.5
Pan 5	0.6	15	39	2.4	2.1	17	140.3	0.8	27	7.4	0.17	2.8	1.9	4.3
Pan 6	5.3	4.9	0.4	0.2	2.3	11	13.42	16	5	6	1.2	5	7.4	6.2
Pan 7	5.4	8.6	6.8	4	6.5	12	39.04	1.8	12	7.1	0.23	0.12	0.57	4.8
Pan 8	0.05	19	6.2	4.8	2.6	25	42.7	1.2	16	6.9	0.22	0.04	0.34	2.1
Pan 9	24	13	5.4	4.9	4.8	20	61	6.4	19	6.7	0.94	0.66	24	2.5
Pan 10	31	213	11	10	67	227	250.1	5.5	114	8	1.2	33	32	69

Table 2 Descriptive statistics of hydrochemical analysis for water samples collected from boreholes, wetland piezometers and wetland surface water.

Statistic	Units	Minimum	Maximum	Mean	Standard deviation (n-1)	Industrial	Irrigation	Livestock	Domestic	Aquatic Ecosystems
K	mg/l	132	0.1	11.99	22.01	*	*	*	>50	*
Na	mg/l	334	2	33.13	59.15	*	>70	>2000	>100	*
Ca	mg/l	56	0.4	12.45	13.08	*	*	>1000	>32	*
Mg	mg/l	25	0.2	5.34	4.71	*	*	>500	>30	*
SO4	mg/l	245	0.1	19.65	39.50	>30	*	>1000	>200	*
Cl	mg/l	426	2	40.45	72.87	>20	>100	>3000	>100	*
HCO3	mg/l	309.88	6.831	75.18	75.01	*	*	*	*	*
EC	µS/cm	250	2	30.61	40.84	>150	>400	*	>70	*
pH	mg/l	8.2	6	7.00	0.55	7.0-9.0	6.5-8.4	*	6.0-9.0	*
TDS	mg/l	1418	5	185.44	240.12	>100	*	>2000	>450	*
Al	mg/l	62	0.04	5.89	11.39	*	>5	>5	>0.15	>0.1
B	mg/l	0.08	0.02	0.03	0.01	*	>0.5	>5	*	*
Ba	mg/l	1.2	0.03	0.24	0.24	*	*	*	*	*
Fe	mg/l	71	0.34	10.43	13.76	>0.1	>5	>10	>0.1	*
Mn	mg/l	2.4	0.01	0.45	0.61	>0.5	>0.02	>10	>0.05	>0.18
Si	mg/l	81	1.1	12.01	17.25	>0.5	*	*	*	*

Table 3 *ΔD (‰) and δ18O (‰) SMOW isotope ratios for water samples collected from boreholes, wetland piezometers and wetland surface water.*

Sample	ΔD (‰) SMOW	Δ^{18}O (‰) SMOW	GWML	EL
PAN 1 NP	-10.30	-2.08	-6.699	-10.989
PAN 1 SP	-14.59	-3.40	-17.304	-18.063
PAN 1 SW	-28.0	-5.4	-33.514	-28.874
PAN 10 SW	-17.45	-3.11	-14.929	-16.479
PAN 2 NP	-17.18	-4.09	-22.821	-21.742
PAN 2 SW	-15.18	-3.59	-18.778	-19.046
PAN 2 WP	-9.27	-2.78	-12.288	-14.717
PAN 3 EP	-11.91	-3.13	-15.140	-16.619
PAN 3 SP	-5.69	-2.21	-7.709	-11.663
PAN 3 SW	-27.18	-5.53	-34.341	-29.425
PAN 4 WP	-2.36	-1.56	-2.491	-8.183
PAN 4 SW	-24.16	-4.55	-26.493	-24.191
PAN 5 SW	-11.74	-3.20	-15.633	-16.948
PAN 6 NP	-6.56	-2.08	-6.691	-10.984
PAN 6 SW	-20.86	-4.45	-25.709	-23.668
PAN 7 South/Open	0.29	-0.55	5.613	-2.778
PAN 7 SW	-24.77	-4.84	-28.811	-25.737
PAN 8 EP	16.62	2.88	33.109	15.561
PAN 8 NP	10.27	1.09	18.712	5.959
PAN 8 RG	-6.57	-0.94	2.433	-4.899
PAN 8 South 8	-14.79	-3.50	-18.076	-18.578
PAN 8 SP	-12.62	-3.44	-17.566	-18.237
PAN 8 SW	-21.75	-4.29	-24.418	-22.807
PAN 8 WP	-13.78	-3.50	-18.099	-18.593
PAN 9 SW	-4.41	-1.13	0.957	-5.883
Windmill	-15.03	-3.29	-16.399	-17.459
BH 1 Belfast	-13.76	-3.52	-18.254	-18.696

Table 4 Composition of epilithic algal communities of the pan sites at the Belfast Implementation mine site. The relative abundance of each epilithic algal taxa was grouped as follows: + = ≤ 50 (rare); ++ = 51- 250 (scarce); +++ = 251-1000 (common); ++++ = 1001-5000 (abundant); and +++++ = 5001-25 000 (predominant) cells/5 cm^2..

Species	Autecology of common benthic algae	Pan 1	Pan 2	Pan 3	Pan 4	Pan 5	Pan 6	Pan 7	Pan 8	Pan 9	Pan 10
Bacillariophyta											
Cocconeis pediculus	Water with a moderated to high electrolyte content. Taylor et al. (2007)		++								
Craticula buderi	Occurs in mine effluent with moderated to elevated electrolyte content. Taylor et al. (2007)						+	++++			
Craticula cuspidate	Eutrophic water with moderate to high electrolyte content Taylor et al. (2007)		++								++
Cyclotella meneghiniana	Eutrophic water. Taylor et al. (2007)		++							++	++
Cocconeis placentula	Meso –to eutrophic standing water. Taylor et al. (2007)		+++							+++	++
Diploneis elliptica	Oligotrophic standing water with moderated electrolyte content. Taylor et al. (2007)						+++	++			
Eunotia pectinalis var. undulata	Found in circumneutral to weakly acidic, electrolyte-poor waters. Taylor et al. (2007)							++	+++		
Eunotia bilunaris	Oligotrophic standing waters. Taylor et al. (2007)						++		+++		
Encyonopsis leei var. sinensis	Oligo- to mesotrophic water with low to moderate electrolyte content. Taylor et al. (2007)							++	+++		
Flagilaria ulna	Mesotrophic to eutrophic alkaline water. Taylor et al. (2007)	++	+++								++
Fragilaria tenera	Meso- to eutrophic water. Taylor et al. (2007).		+++							++++	++
Frustulia vulgaris	Oligotrophic to highly polluted water. Taylor et al. (2007)						++	+++			
Gomphonema laticollum	Slightly eutrophic water. Taylor et al. (2007).	++				+++					
Gomphonema venusta	Oligo- to mesotrophic water with low to moderated electrolyte content. Taylor et al. (2007).					++	++++	++			

Gomphonema italicum	Found in slightly eutrophic habitats. Taylor et al. (2007).		+++							+++	++
Gomphonema parvulum	Found in acidic, oligotrophic, electrolyte poor water. Taylor et al. (2007).							+++	++		
Hantzschia amphioxys	Favour periodically dry habitats. Taylor et al. (2007).										+++
Melosira variance	Eutrophic water. Taylor et al. (2007).		+++								
Navicula capitatoradiata	Tolerant of critical levels of pollution. Taylor et al. (2007).						++				
Navicula notha	Circumneutral, oligotrophic electrolyte poor water Taylor et al. (2007).				++++						
Navicula rhynchocephala	Oligo-to eutrophic water with low to moderated electrolyte content. Taylor et al. (2007).	++++			+++						
Navicula angusta	Weakly acidic, oligotrophic, clean, un-impacted water. Taylor et al. (2007).								+++		
Navicula riediana	Alkaline, eutrophic electrolyte-rich water. Taylor et al. (2007).		++				+				++
Navicula tripunctata	Good indicator of eutrophic water with a moderate to high electrolyte content. Taylor et al. (2007).		+++							++++	+
Nitzschia littorea	Mining effluent. Oberholster et al. (2017).							+++			
Nitschia pura	Weakly to moderately polluted waters with moderate electrolyte content. Taylor et al. (2007).	+++		++							
Nitzchia closterium	Brackish water. Taylor et al. (2007).	++									
Nitzschia intermedia	Eutrophic water with moderated to high electrolyte content. Taylor et al. (2007).		++							+++	
Nitzchia gracilis	Eutrophic, electrolyte rich water Taylor et al. (2007)									++	
Pinnularia viridiformis	Oligo-to mesotrophic water with low to moderate electrolyte content Taylor et al. (2007); Oberholster et al. (2010)		+++		++++	+++		+++	++++	++++	

Pinnularia divergens	Oligotrophic electrolyte poor water. Taylor et al. (2007).					+	++	++		
Pinnularia viridis	Found in circumneutral water with a low to moderated electrolyte content. Taylor et al. (2007)								+++	
Pinnularia subcapitata	Oligotrophic electrolyte poor water Taylor et al. (2007)		+++		+++					
Tabellaria flocculosa	This taxon flourish in oligotrophic, circumneutral or slightly acidic water. Taylor et al. (2007)								++	
Melosira variance	Eutrophic water. Taylor et al. (2007).		++							
Chlorophyta										
Closterium margaritiferum	Oligo-to mesotrophic water (Oberholster et al., 2010)								++	
Closterium peracerosum	Eutrophic water (Brook, 1965)				++				+++	
Cosmarium hammeri	Eutrophic water (Brook, 1965)						+++		++++	
Cosmarium pseudopraemorsium	Oligo-to mesotrophic water (Oberholster et al., 2010)			+++			++		+++	
Euastrum evolutum	Mesotropic water (Brook, 1965)				+++					
Actinastrum lagerheim	Not none				+++					
Cosmarium quadrum	Eutrophic water (Brook, 1965)								++	
Dictyosphaeium sp.	Not none			++++						
Eudorina elegans	Found in meso to eutrophic water. Van Vuuren et al .(2006)			+				+++	++	++
Eudorina unicocca	Found in meso to eutrophic water. Van Vuuren et al .(2006)									++++
Scenedesmus armatus	Found in meso to eutrophic water. Van Vuuren et al .(2006), Palmer, (1969)								++	
Oedegonium crassum	Eutrophic water (Simons, 1994)	++								+++
Spirogyra adnata	Oligo-to mesotrophic water (Oberholster., 2011)							+++	++	

Spirogyra reticulata	Oligo-to mesotrophic water (Oberholster, 2011)								+++		
Spirogyra rugulosa	Oligo-to mesotrophic water (Oberholster, 2011)						+++				
Staurastrum anatinum	Oligotrophic water (Brook, 1965)								+++		
Spondylosium sp.	Oligotrophic water (Brook, 1965)								+++		
Euglenophyta							++				
Euglena sociabilis	Organic pollution or brackish water rich in organic matter (Palmer, 1969; Effiong and Inyang, 2015)					++					
Euglena mutabilis	Organic pollution or brackish water rich in organic matter (Palmer, 1969; Effiong and Inyang, 2015)							+++			
Phacus acuminata	Organic pollution or indicator of moderate to strong pollution water (Effiong and Inyang, 2015); (Valadez et al., 2010)		+++								
Phacus pleuronectes	Organic pollution or indicator of moderate to strong pollution water (Effiong and Inyang, 2015); (Valadez et al., 2010)					+++		+++	+		
Trachelomonas intermedia	Eutrophic water (Wolowski and Grabowska, 2007)	++	++++	+++					+++++	+++	++++
Trachelomonas hispida	Eutrophic water (Effiong and Inyang, 2015)					+++					
Trachelomonas volvocina	Eutrophic water (Wolowski and Grabowska, 2007)			++++	+++						
Trachelomonas sp. 1				++					++		++
Cyanophyta											
Merismopedia punctate	Indicator of poor water quality (Begum and Hossain, 1993)									++	
Oscillatoria tenuis	Organic pollution, Eutrophic water (Palmer, 1969, Douterelo, I, Perona, E., Mateo, P. 2004)		++								
Microcystis aeruginosa	Eutrophic water (Oberholster et al., 2012)				+++						
Nostoc sp.	Oligotrophic water (Douterelo, I, Perona, E., Mateo, P. 2004)	++									

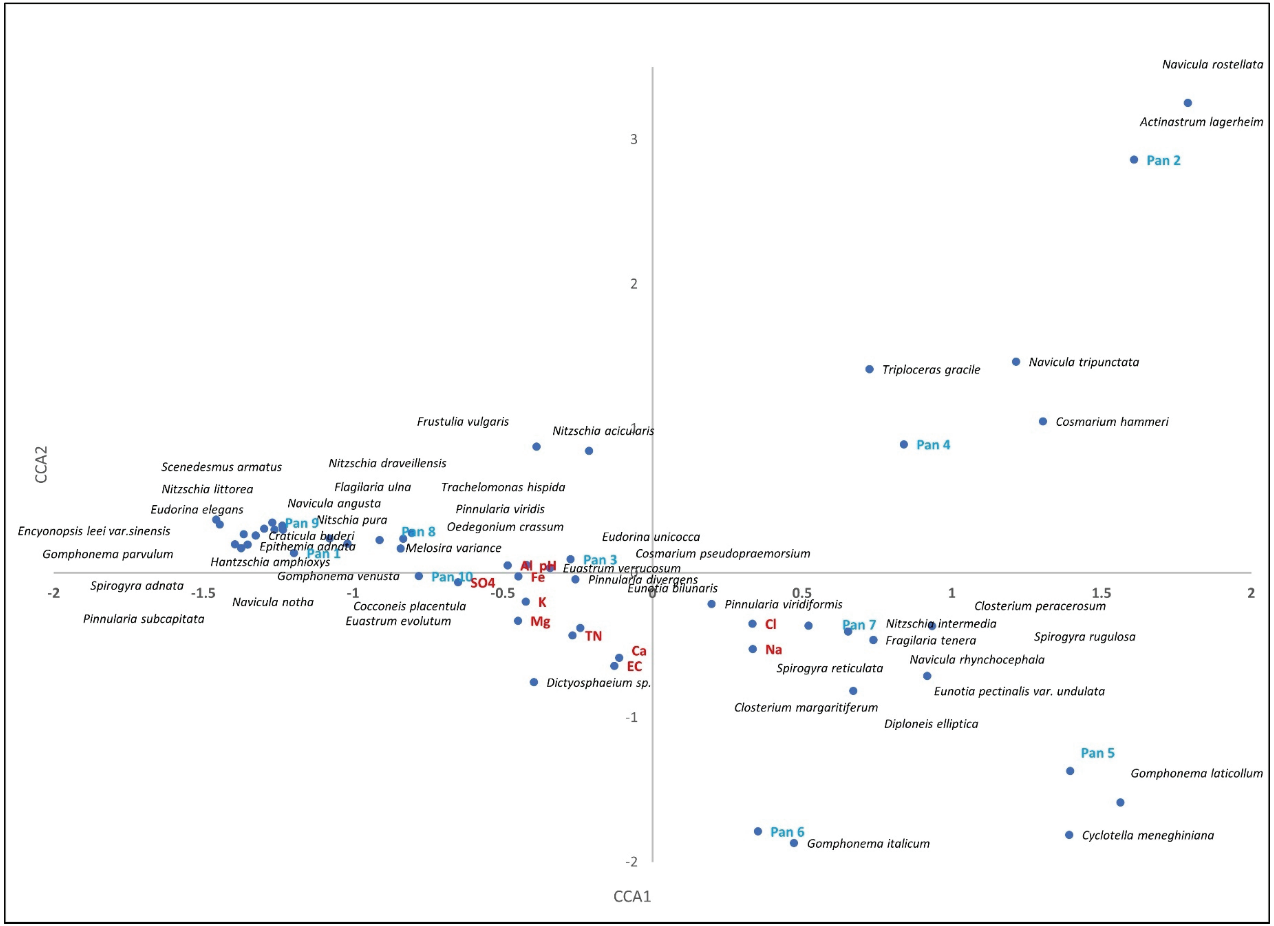

Figure 1 Canonical Correspondence Analysis of benthic diatoms and water quality parameters sampled from wetlands at the Belfast Implementation mine site.

Remining for Renewable Energy Metals: An Update

Ann Maest

Buka Environmental, Telluride, Colorado, USA, amaest@buka-environmental.com, ORCID 0000-0002-9707-2435

Abstract

More metals are needed to accelerate the pace of using renewable energy sources to combat the climate crisis. The recovery of renewable energy metals and materials from mining wastes can become an important part of the supply chain. This updated review reports on remining efforts in four areas, with a focus on the United States and Europe: geochemical and physical characterization, estimates of the recovery potential for valuable minerals, remining examples and processing approaches, and environmental and health effects. If properly conducted, remining can improve circularity and environmental conditions in areas affected by existing and legacy mining activity.

Keywords: Remining, renewable energy, circular economy, reprocessing, characterization

Introduction

Remining can be defined as the use of mine waste, including solid waste and mine-influenced waters, as the source material from which to extract metals or create other materials with economic value. Remining sources for renewable energy metals (e.g., Co, Cu, Ni, Ga, In, Li, Mn, REEs) that are needed to expand solar and wind power and electric vehicles usage include legacy and existing mine wastes and associated mine waters, coal mine residues, and byproduct and primary production materials. Tailings are of greatest interest due to their abundance globally and the fact that they are already crushed and ground, which lowers energy and water use. Currently, remining operations are largely focused on gold; the potential for extracting renewable energy metals and minerals from mine wastes is enormous but needs more emphasis and commitment from government agencies, mining companies, and business interests.

The advantages of remining are environmental, political, and economic and include reducing dependency on foreign imports, accomplishing cleanup of the long-term environmental effects of mining while funding the cleanup through economic gain, reducing energy and water use relative to the amount of metal produced, and improving circularity – which aims to eliminate or greatly reduce wastes by creating useful products from wastes remaining from original mining and remining operations.

A paper published in 2023 (Maest 2023) examined the state of remining potential, approaches, and efforts globally in four areas: geochemical characterization, the potential for recovery of valuable minerals, remining examples and processing approaches, and environmental and health effects. This paper provides a current update on the four topics, with an emphasis on the United States and Europe.

Geochemical and physical characterization

The first step in any remining project is characterizing the volume of waste and its chemical and physical characteristics such as total metal content, mineralogy, physical stability, and worker safety issues. Phosphate, uranium, and other wastes can be radioactive, and radiologic characterization is important. Geochemical characterization methods typically applied at proposed and active mines for predicting pollution potential (e.g., acid-base accounting, short- and long-term leach tests) should be expanded to include mineral liberation analysis and bench-scale process testing for remined materials.

The U.S. Geological Survey (USGS), through its Earth Mapping Resources Initiative (Earth MRI), which began in 2019, is aiming to create a National Mine Waste Inventory (USGS 2024a). Their characterization includes bulk geochemistry for 61 elements, mineralogy by x-ray diffraction, and acid-base accounting. Water samples will be analyzed for major cations and anions, trace elements including precious metals, and alkalinity/acidity. The U.S. Environmental Protection Agency's (US EPA) Toxics Release Inventory (TRI) now has information on releases to air, land, and water from currently active mines through 2023 (US EPA 2025), but legacy mines are not included, and the data are not amenable to estimating resource potential of the mine wastes.

The European Union (EU) passed the Critical Raw Materials Act (EU 2024), which includes Article 27: Recovery of critical raw materials from extractive waste. The Article calls for establishing a database of closed extractive waste facilities in each Member State by 24 November 2026. In terms of physical and chemical characterization of the wastes, the database is to include the location, areal extent and waste volume; approximate quantities and concentrations of all raw materials; and information to enable the recovery of critical raw materials (CRMs) from the extractive waste facility.

Estimates of the potential for recovery of valuable minerals

The amount of tailings in storage worldwide was estimated at 282.5 billion tonnes in 2020, based on 8500 total tailings storage facilities (active, inactive, closed) worldwide (Franks *et al* 2020). The annual growth in tailings around the world has been estimated at between 7 and 14 billion tonnes (Maest 2023), demonstrating a wide variability due to lack of careful accounting and other factors. More recent updates on these global figures are not available.

Pollutant registries in the United States, Europe, and elsewhere can be used to get a very rough estimate of the amount of specific renewable energy metals and materials in mine wastes, but reporting improvements are needed to better estimate the metal "reserve" and to determine economic viability. The most comprehensive estimate of the amount of CRMs in tailings dates from 2019 (Blengini *et al.* 2019), and the data used in the analysis are from 2015. An update is clearly needed. Using those outdated estimates, approximately 1000 tonnes of cobalt, 2000 tonnes of gallium, 200 tonnes of indium, and 100 tonnes of natural graphite are contained in EU tailings. The preliminary economic assessment of the recovery of CRMs from extractive waste and the creation of the associated database required as part of the recently passed EU Critical Raw Materials Act will promote the recovery of CRMs from extractive waste and greatly improve estimates (European Parliament 2024).

In the United States, the US EPA updates its TRI annually. The most recently available data are from 2023. Using the TRI Explorer for all releases from the Metal Mining sector (NAICS 327), Table 1 shows the tonnes of renewable energy metals released or disposed at currently active metal mines in the United States.

Table 1 shows that total TRI releases of the selected renewable energy metals/metalloid increased from 2022 to 2023 for Sb, Cu/Cu compounds, Mn, Ni, Ag, and Zn, while all others decreased. The identity of the compounds for each chemical is not specified, and neither is the concentration of the chemical in the wastes. To better understand the potential economic value of these wastes and releases from active mines in the United States, these issues would need to be included, and other characterization methods, such as mineralogy and liberation would need to be added. Again, TRI only reports releases from active metal mines, but it does provide a picture of the amount of potentially valuable products that are thrown away and that could be added to the supply chain for renewable energy minerals.

Remining examples and processing methodology

Recent but non-exhaustive examples of remining projects in the United States and Europe are included in Tables 2 and 3. The USGS continues to expand its work under

Table 1 Total TRI releases from metal mines for select renewable energy metals: 2022, 2023, and 1998–2023

Chemical	Total TRI Disposal or Other Releases, 2022 tonnes	Total TRI Disposal or Other Releases, 2023 tonnes	Total TRI Disposal or Other Releases, 1998–2023 tonnes
Sb compounds	2289	2373	116,809
Cr	809	767	36,999
Cr compounds	4526	4372	168,593
Co	127	95.5	477
Co compounds	937	765	31,415
Cu	72	82.0	132,886
Cu compounds	38,486	39,685	2,916,356
Mn	337	392	35,560
Mn compounds	58,800	31,935	1,074,253
Ni	374	448	11,170
Ni compounds	5327	4210	141,906
Ag compounds	93	102	5968
Zn compounds	182,794	210,656	6,024,630

US EPA (2025), Maest (2023)

Earth MRI in terms of the number of sites examined for remining potential (see Tab. 2). All projects started between 2022 and 2024 are currently in progress and are still in the characterization phase. The focus on deriving value from mine wastes extends across the country from states not currently active in mining such as Iowa, to the top mining state, Nevada.

Efforts in the EU have included characterization and processing (see Tab. 3). The focus of NEMO (2025) is sulfidic wastes, and three case studies are currently underway: two in Finland and one in Ireland. Four pilot studies are demonstrating processing of the sulfidic wastes to recover metals and minerals and to emphasize circularity by creating cement and building products. Bioleaching is being demonstrated in ponds and heaps from heap leach operations and in tanks using tailings. Additional metals are being recovered from pregnant leach solution from heap leach operations. The RAWMINA Project shut down in 2024 with their final conference presentation in Barcelona in October 2024. The broad-reaching project included 19 partners in nine countries and included waste characterization, bioleaching, and selective recovery of critical minerals using four methods (see Tab. 3).

Bioleaching appears to still be the leading choice for processing of mine wastes to recover critical minerals because of its lower costs, energy use, and environmental effects, although regrinding and flotation are being used at some current remining operations (Maest 2024, Table 4 and Supplemental Materials).

In addition to governmental efforts, mining and remining companies have engaged in remining operations. Mining companies are especially well situated to evaluate the economic potential of mineral extraction wastes – whether theirs or others. A recent example is the news announcement from Cerro de Pasco Resources that their Phase 1 drilling program at the Quiulacocha Tailings Project in Peru is nearly completed (Globe Newswire 2024). Silver grades in the tailings are promising; in addition to Zn, Pb, Ag, Cu, and Au, they are focusing on Ga and In, which are important renewable energy metals. Their drilling will extend to depth in the large deposit. Mean grades to the 19-m depth drilled thus far indicate the following: Ag 1.91 oz/t, Zn 1.80%, Pb 0.77%, Cu 0.07%, Au 0.07 g/t, Ga 30.6 ppm, and In 18.4 ppm. Metallurgical testing and additional drilling (recently up to 42 m depth) are planned for 2025. The facility is estimated to contain

Table 2 Examples of mine waste and mine water remining projects in the United States. All projects are in progress.

US State	Target Mineral/ Metals	Target Waste	Mines/ Districts	Project Description/ Status
Illinois	Ba, Cd, Ga, Ge, In, Pb, Ag, U, Zn	tailings	Upper Mississippi Valley lead-zinc District	Characterization of geochemistry/ mineralogy. Started 2023
Nevada	Critical minerals	5 types of mine waste	11 sites with 4 different mineral systems	Volume, geochemical, mineralogic, deportment, resource estimate studies; Started 2024
New York	REEs	tailings	Fe, Fe-Ti, and Pb-Zn mines	Waste characterization. Started 2023
Florida	REEs, P	gypsum stacks, tailings, waste rock piles, clay settling ponds	Central and north Florida phosphate mines	Geochemical, mineralogic characterization; water samples from mine/ processing ponds. Started 2022
Montana	REEs, Ge, Zn, others	tailings	Nine mines in southwestern/ western Montana	Sampling for grade and tonnages of critical minerals, mineralogy. Started 2023
Colorado	Cd, Cu, Pb, Mg, Mn, REEs, Zn	tailings, waste rock, metallurgical waste, "perpetual mine-related water"	Ten inactive mines discharge sites, six waste pile areas (sites include three Superfund sites)	Concentrations of critical minerals in waste piles, mine effluent, and water treatment plant sludges. Started 2022.

USGS (2024b)

approximately 75 million tonnes of tailings from the 1920s to the 1990s.

Environmental and health effects

The positive environmental and health consequences of remining are mentioned much more often than the negative effects, but because the field is relatively new, few detailed examples or evaluations are available. Understanding the potential positive and negative effects of remining on the environment, ecological systems, communities, and workers is a data gap that needs to be filled as remining operations become more common.

Despite the data gap in this area, some of the same adverse effects known to occur from virgin extraction can result from remining operations, including tailings dam failures and water quality degradation. However, other adverse effects are less likely to occur from remining operations, such as creation of open pits and modification of stream flows and groundwater levels.

Because tailings are currently the primary target of remining operations, environmental and health risks associated with these mine facilities must be carefully evaluated before, during, and after remining projects. Worker safety is an especially high concern for sampling efforts. Two known tailings impoundment failures have occurred from remining operations thus far: the 2022 Jagersfontein Mine in South Africa (recovery of diamonds from old diamond mine spoil heaps) and the 2000 tailings dam failure in Baia Mare, Romania, which contaminated the drinking water of more than 2 million

Table 3 *Examples of remining projects in Europe.*

Countries	Target Mineral/Metal	Mine/Target Wastes	Processing Approach	Outputs / Circularity
Finland1	Cu, Co, Zn, Ni, REEs, Mn, Mg, Al, Fe, Sc	Sotkamo Ni-Co-Zn-Cu Mine / heap leach residues, pregnant leach solution	Bioleaching, secondary heap bioleaching	Critical metals and sulfates; products including backfill, cement, construction materials
Finland1	Co, Ni, Cu, Zn	Luikonlahti Mine: Cu-Zn-Ni-Co-Au ore processing facility/ high-sulfur tailings	Tank bioleaching	Critical metals and sulfates; products including backfill, cement, construction materials
Ireland1	Secondary products	Tara Mines/ tailing slimes	Flash-calcination of tailings, granulation of tailings	Cement, concrete, composite cement, artificial aggregates, ready-mix concrete
EU with partners in the UK and South America2	Co, Sb, Ge, W; additional recovery of Au, Ag	Wastes from active and abandoned mines	Mine waste characterization; bioleaching; Fe removal (magnetic); selective recovery using, e.g., nanofibrous composite materials, electrowinning, electrocoagulation	Critical metals; Fe-based byproducts

1 NEMO (2025); 2 RAWMINA (2024)

people in Hungary (WISE Uranium Project 2025). No newer tailings dam or mine facility failures related to remining operations have been reported.

Additional environmental and health risks associated with remining include leaching of metals and other contaminants to groundwater and surface water and potentially affecting aquatic life, wildlife, and drinking water sources; adverse effects on Indigenous communities, which disproportionately live close to virgin extraction projects for renewable energy minerals (Owen *et al*. 2023) and could therefore live near similar remining operations; and increased transportation, noise, and exposure effects on communities, including to radioactivity for certain kinds of deposits (phosphate, uranium).

Where remining projects also remediate existing pollution from abandoned or inactive operations, benefits can multiply. Best practices for all phases of remining operations, including for facility design, water management, worker safety, and environmental and human health protections are needed for remining projects. Many of these practices can be borrowed from those required at leading mining projects, but site-specific evaluations and approaches are always needed.

Conclusions

In addition to expanded virgin extraction for renewable energy metals and minerals around the world, recovery for mining wastes can become an important part of the value chain. Projects underway and recently completed in the United States and Europe are characterizing the “reserve” in extractive wastes, and some projects in the EU have completed or are investigating effective processing approaches. Policies are needed at the national level to encourage remining and to require environmental and worker safety protections and information transparency.

References

Blengini GA, Mathieux F, Mancini L, Nyberg M, Viegas HM, (Editors), Salminen J, Garbarino E, Orveillon G, Saveyn H, Mateos Aquilino V, Llorens González T, García Polonio F, Horckmans L, D'Hugues P, Balomenos E, Dino G, de la Feld M, Mádai F, Földessy J, Mucsi G, Gombkötő I, Calleja I (2019) Recovery of critical and other raw materials from mining waste and landfills: State of play on existing practices. JRC116131 (Joint Research Centre), EUR 29744 EN, Publications Office of the European Union, Luxembourg, ISBN 978-92-76-08568-3. doi:10.2760/600775

European Parliament (2024) Briefing: Implementing the EU's Critical Raw Materials Act. European Parliamentary Research Service (13 pgs). Author: Guillaume Ragonnaud. November.

European Union (2024) Regulation (EU) 2024/1252 of the European Parliament and of the Council of 11 April 2024 establishing a framework for ensuring a secure and sustainable supply of critical raw materials and amending Regulations (EU) No 168/2013, (EU) 2018/858, (EU) 2018/1724 and (EU) 2019/1020. https://eur-lex.europa.eu/legal-content/EN/TXT/PDF/?uri=OJ:L_202401252; accessed 9 February 2025

Franks, D.M.; Stringer, M.; Baker, E.; Valenta, R.; Torres-Cruz, L.A.; Thygesen, K.; Matthews, A.; Howchin, J.; Barrie, S. (2020) Lessons from tailings facility data disclosures. In Toward Zero Harm. A Compendium of Papers Prepared for the Global Tailings Review; Global Tailings Review: St Gallen, Switzerland, 2020; Chapter VII; 135p. https://globaltailingsreview.org/wp-content/uploads/2020/09/GTR-TZH-compendium.pdf

Globe Newswire (2024) Cerro de Pasco Resources Reports Initial Assay Results from its Quiulacocha Tailings Drill Campaign. October 15. https://www.globenewswire.com/news-release/2024/10/15/2963082/0/en/Cerro-de-Pasco-Resources-Reports-Initial-Assay-Results-from-its-Quiulacocha-Tailings-Drill-Campaign.html (accessed 10 February 2025)

Maest AS (2023) Remining for renewable energy metals: A review of characterization needs, resource estimates, and potential environmental effects. Minerals (13): 1454. doi:10.3390/min13111454

NEMO (2025) Near-zero-waste recycling of low-grade sulfidic mining waste for critical metal, mineral and construction raw material production in a circular economy. https://h2020-nemo.eu/project-2/; accessed 9 February 2025

Owen JR, Kemp D, Lechner AM, Harris J, Zhang R, Lèbre E (2023) Energy transition minerals and their intersection with land-connected peoples. Nat. Sustain. (6): 203–211. doi:10.1038/s41893-022-00994-6

RAWMINA (2024) An integrated, innovative pilot system for recovery of critical raw materials from mine waste. https://rawmina.eu/; accessed 9 February 2025

U.S. Environmental Protection Agency (2025) TRI Explorer. Release Reports. https://enviro.epa.gov/triexplorer/tri_release.chemical; accessed 9 February 2025.

U.S. Geological Survey (2024a) Earth MRI Progress. https://www.usgs.gov/special-topics/earth-mri/science/earth-mri-progress; accessed 9 February 2025

U.S. Geological Survey (2024b) Earth MRI Acquisitions Viewer. (Select Mine Waste). https://ngmdb.usgs.gov/emri/#3.2/38.09/-99.46; accessed 9 February 2025

Wise Uranium Project (2025) Chronology of major tailings dam failures: 1960–2025. https://www.wise-uranium.org/mdaf.html (accessed 10 February 2025)

Direct Cooling of Brine with Primary Refrigerant During Freeze Crystallization

Mlungisi Mahlangu[1], Johannes P. Maree[1,2], Martin Botha[3],
Kagiso S. More[1] and Bheki B. Mamba[1]

[1]*Institute for Nanotechnology and Water Sustainability, College of Science, Engineering and Technology, University of South Africa, Private Bag X6, Science Campus, Florida, Johannesburg, 1709, South Africa.*

[2]*ROC Water Technologies, 28 Keramiek Street, Clayville, Olifantsfontein, 1666, South Africa.*

[3]*A-Thermal Retort Technologies, 28 Keramiek Street, Clayville, Olifantsfontein, 1666, South Africa.*

11968680@mylife.unisa.ac.za(ORCID: 0000- 0002-0270-8227), mareejp@unisa.ac.za(ORCID: 0000-0002-8901-2512), moreks@unisa.ac.za(ORCID 0000-0003-2803-7983), mambabb@unisa.ac.za(ORCID: 0000-0003-2534-2579)

Abstract

To achieve zero waste disposal, this study explores pipe freeze crystallization as a cost effective and energy efficient solution for brine treatment. The key objectives were to assess chiller capacity, evaluate the impact of brine composition on salt and ice recovery, and measure energy consumption. Results showed that the chiller operated at 43.7 kW, enabling the recovery of 519.9 kg/day of $Na_2SO_4 \cdot 10H_2O$ (60%) from high TDS (131.9 g/L) brine at a flow rate of 200 L/h. For lower TDS (117.5 g/L) brine, 119.4 kg/day of $Na_2SO_4 \cdot 10H_2O$ and 313.2 kg/day of ice were recovered. The total energy required for cooling, salt crystallization, and ice formation was only 5.7 kW, demonstrating the efficiency of this method compared to conventional brine management techniques.

Keywords: Industrial wastewater treatment, brine treatment, zero waste, salt recovery, ice recovery, energy efficiency

Introduction and Background

In coal washing plants, water is used to separate coal fines from coal and transport them to waste disposal sites, where fines settle in dumps, and water returns through penstocks or seepage to the washing plant. Since the dump walls are built from coal discard with high pyrite (FeS_2) content, the leachate generated contains Fe^{2+}, Fe^{3+}, Al^{3+}, Mn^{2+}, Ca^{2+}, Mg^{2+}, Na^+, SO_4^{2-}, and Cl^- (Qureshi *et al.* 2016; Seo *et al.* 2017). This acid wastewater must be neutralised to prevent acid corrosion and undergo desalination to remove gypsum forming compounds before being safely discharged into public water systems. To achieve zero waste disposal, brine from desalination cannot be stored in evaporation ponds. Instead, it requires advanced treatment technologies such as crystallization. A study supported by the Wader Programme of the WRC demonstrated that coal leachate with a total dissolved solids (TDS) concentration of 12,540 mg/L can be effectively neutralised with Na_2CO_3 to produce stable water (Maree *et al.* 2021). Additionally, $Fe(OH)_3$ sludge was processed for pigment recovery. The neutralised water, free of scale forming compounds like gypsum, $CaCO_3$, and metal hydroxides, was then treated with reverse osmosis, yielding purified water and a concentrated brine stream with a TDS of 90 g/L. This brine was further treated using a low temperature crystallization approach to recover $Na_2SO_4 \cdot 10H_2O$ and clean water through ice formation.

Crystallization based separation presents a more energy efficient and sustainable alternative to evaporation or distillation for saline wastewater treatment. It provides several advantages, including: i) it enables zero waste operations by concentrating brines to the point of selective salt crystallization, ii) it allows different salts to be recovered based on their solubility differences (Lewis *et al.* 2010; Randall *et al.* 2009, 2011), and iii) it consumes substantially less energy, only 123 kWh per ton of ice, compared to the 715 kWh per ton of water vaporised through evaporation (Table 1). Researchers have demonstrated that $Na_2SO_4·10H_2O$ can be efficiently recovered through cooling with a secondary refrigerant (Maree 2018). A 300 L/h Pipe Freeze Crystallization (PFC) plant was designed, constructed, and has been operational since 2018 (Fig. 1). The plant consists of key components such as an 18 kW chiller, a cooler reactor with a high density polyethylene (HDPE) pipe heat exchanger (120 m long, 32 mm diameter), a clarifier, and an ice filter. The efficiency of the PFC system depends on several factors, including i) the recycle flow rate of the secondary refrigerant, ii) pipe dimensions, iii) feedwater temperature, iv) freeze temperature, v) TDS concentration, vi) SO_4^{2-}/Cl^- and SO_4^{2-}/SO_3^{2-} mole ratios, vii) refrigerant type, and viii) ambient temperature. Fig. 1 illustrates the variations in salt recovery over a 66-month period, which correlate with changes in these key process parameters.

Objectives

The primary objectives of this study were to evaluate the chiller capacity required for effective cooling, assess the impact of brine composition on the recovery of salt ($Na_2SO_4·10H_2O$) and ice, analyse energy consumption across different operating conditions, and determine the purity of recovered ice. These factors are critical for optimising the efficiency and scalability of the crystallization process while ensuring minimal energy use and maximum resource recovery.

Methods and Materials

Saline water with a composition of approximately 75 g/L Na_2SO_4 and 75 g/L NaCl was used as the feedstock for this study. The experimental setup consisted of an 18 kW chiller containing a refrigerant mixture of 30% MeOH/70% H_2O, a cooler reactor equipped with an HDPE coil pipe, and a supporting metal skeleton to ensure structural stability, and a clarifier. The chiller was responsible for lowering the temperature of the secondary refrigerant to -10 °C, which was then circulated between the chiller and the cooler reactor. A long HDPE pipe, submerged in the secondary refrigerant, facilitated the controlled cooling of the saline water, circulating between the cooler reactor and clarifier, enabling the crystallization of $Na_2SO_4·10H_2O$ and the formation of ice (Fig. 2).

The plant was operated continuously to evaluate the impact of brine composition on salt and ice recovery, energy consumption, and ice purity. TDS and chloride concentrations were analysed following Standard Methods (American Public Health Association 2012) to monitor water quality changes. Additionally, OLI ESP software simulations were conducted to predict the equilibrium concentration of Na_2SO_4 in the brine under varying cooling

Table 1 Comparison of energy consumption between freeze crystallization and evaporation/distillation.

Parameter	Unit	Freezing	Evaporation/Distillation
Flow (m/t)	m^3/h	1	1
Flow (m/t)	kg/s	0.28	0.28
T_1	°C	25	100
T_2	°C	-2	25
C_p	kJ/kg.K	4.18	4.18
H_v	kJ/kg	330	2 260.00
Energy for cooling/heating ($E = m/t.C_p.dT$)	kWh/t	31.35	87.08
Energy for freezing/evaporation ($E = m/t.H_v$)	kWh/t	91.67	627.78
Total Energy	kWh/t	123.02	714.86

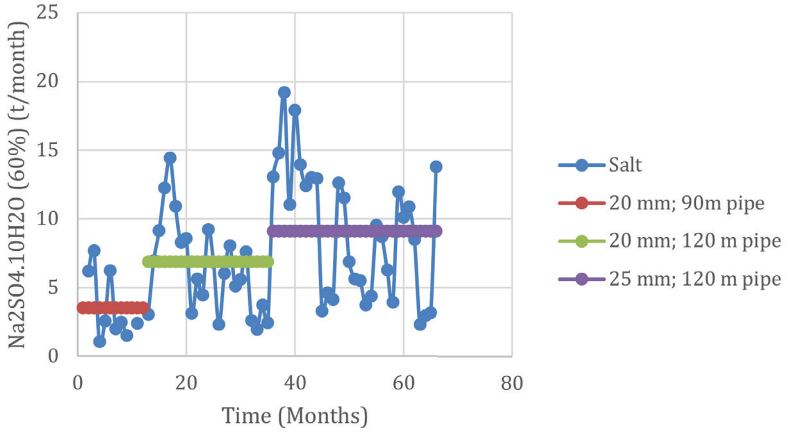

Figure 1 *Salt recovery with cooling over time (from More et al. 2025).*

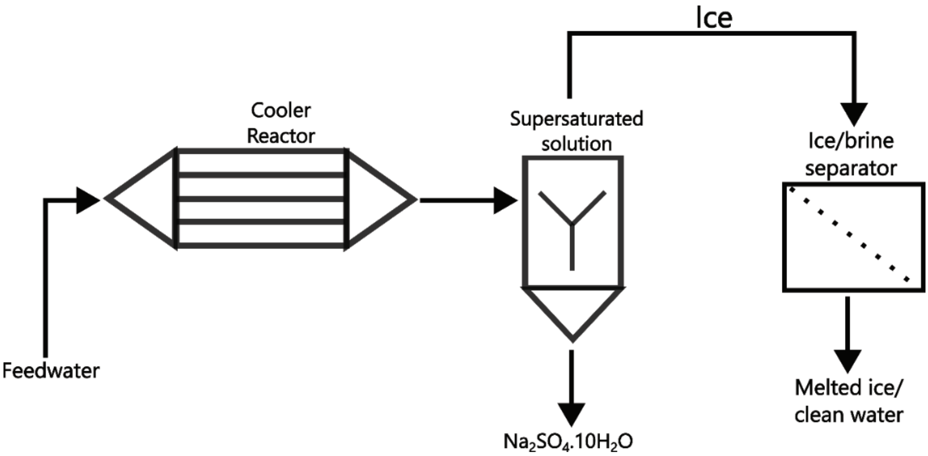

Figure 2 *Schematic diagram of the experimental setup.*

conditions. These simulations were validated by comparing predicted crystallization outcomes with actual experimental results, ensuring the accuracy of the process modelling and optimisation.

Results and Discussion

Chiller Capacity

The chiller's primary refrigerant transferred cooling energy to the secondary refrigerant through copper spirals in the chiller bath, which in turn cooled the brine through an HDPE coil heat exchanger in both the cooler reactor and clarifier. Temperature sensors placed at key points in the system monitored temperature variations, confirming the effectiveness of heat exchange between the chiller bath, secondary refrigerant, and brine. The chiller capacity was determined under zero load conditions by temporarily removing the HDPE heat exchanger from the cooler reactor. This assessment provided insight into how efficiently the system could maintain low temperatures necessary for crystallization.

As shown in Table 2, the chiller's energy transfer capacity decreased from 43.73 kW to 8.19 kW as the temperature dropped from 7.4 °C to -12 °C. This decline was reflected in the coefficient of performance (COP), which fell from 3.6 to 0.7 due to increased heat losses at lower temperatures. The system's efficiency was constrained by the flow rate of the secondary refrigerant and the length of the HDPE coil. Although the recycle pump had a capacity of 20,000 L/h, only 6,200 L/h could be processed through the chiller bath without overloading the cooler reactor. Increasing the length of the HDPE pipe and improving insulation could enhance heat transfer efficiency, allowing for better cooling performance and improved crystallization rates.

Salt Recovery

The brine treatment plant was specifically designed to remove Na_2SO_4 through cooling, facilitating the crystallization of $Na_2SO_4 \cdot 10H_2O$. A secondary refrigerant mixture (50% methanol and 50% water) was continuously recycled between the chiller bath and the cooler reactor at a rate of 6,200 L/h. The brine was cooled by passing through a 120 m long HDPE pipe (32 mm OD), which was submerged in the cooler reactor. This setup enabled efficient heat exchange and facilitated salt precipitation. The brine was then recycled between the HDPE coil in the cooler reactor and a 1,000 L clarifier, where the crystallized salt settled and was subsequently removed.

During a typical operational week (2024-12-23 to 2024-12-29), the system processed brine with a high TDS concentration at a rate of 200 L/h (Table 3). The feedwater contained 131.9 g/L TDS, with 63.2 g/L NaCl and 68.6 g/L Na_2SO_4. As the brine was cooled from 25 °C to -2.0 °C, $Na_2SO_4 \cdot 10H_2O$ crystallized, reducing Na_2SO_4 concentrations from 68.6 g/L to 40 g/L, yielding 519.9 kg/ day of $Na_2SO_4 \cdot 10H_2O$ (60%). The total energy consumption for cooling and salt production amounted to 7.9 kW, closely matching the measured electrical energy consumption of 7.33 kW. The cold energy generated by the chiller was calculated at 12.5 kW. Additionally, chloride concentrations were reduced from 61 g/L in the feed to 12 g/L in the melted ice, indicating substantial impurity separation. These findings confirm that the system operates efficiently, with salt recovery rates aligning closely with OLI simulation predictions.

Ice Recovery

The primary goal of brine treatment plant was to remove Na_2SO_4 through cooling. With a chiller capable of reaching -30 °C, tests were conducted to assess ice recovery alongside salt crystallization. These findings were critical for upgrading the plant to recover not only $Na_2SO_4 \cdot 10H_2O$ but also NaCl and ice. During a typical operational week (2024-08-19 to 2024-08-25), the system processed brine at 171 L/h with a high TDS concentration (Table 3). The feedwater contained 117.5 g/L TDS, composed of 98.9 g/L NaCl and 18.6 g/L Na_2SO_4. As the brine was cooled from 20 °C to

***Table 2** Determination of the chiller capacity.*

Time	Temperature		Volume	Energy			COP
	Chiller Bath	Cooler Reactor			Electrical	Thermal	
h	°C	°C	L	kWh	kW	kW	
0.00		7.40	1 696	0.00	0.0	0.00	
0.33	-3.00	-1.70	1 696	4.11	12.3	43.73	3.55
0.83	-4.30	-3.60	1 696	8.59	10.3	21.14	2.05
1.33	-5.70	-5.10	1 696	14.74	11.1	15.02	1.36
1.83	-7.40	-7.10	1 696	24.04	13.1	12.67	0.97
2.33	-8.60	-8.30	1 696	27.49	11.8	10.78	0.91
2.83	-10.90	-9.70	1 696	34.24	12.1	9.67	0.80
3.33	-11.60	-11.10	1 696	41.16	12.3	8.89	0.72
3.83	-12.50	-12.20	1 696	45.99	12.0	8.19	0.68

Table 3 *Energy balance between heat transfer from the secondary refrigerant to the brine.*

Parameter	Unit	Salt recovery							
No		1	2	3	4	5	6	7	Average
Date		23-Dec-24	24-Dec-24	25-Dec-24	26-Dec-24	27-Dec-24	28-Dec-24	29-Dec-24	
TDS Feed	g/L	150.5	150.0	100.0	117.5	127.0	149.0	129.0	131.9
Cl^-	g/L	45.4	44.5	20.4	34.4	41.1	46.3	37.4	38.5
NaCl	g/L	74.6	73.1	33.5	56.5	67.5	76.0	61.4	63.2
Na_2SO_4 Feed	g/L	75.9	76.9	66.5	61.0	59.5	73.0	67.6	68.6
Na_2SO_4 Treated	g/L	47.7	45.9	35.4	26.3	20.8	53.0	50.9	40.0
Na_2SO_4 OLI	g/L	10.9	11.0	15.4	12.8	11.7	10.9	12.2	12.1
q1	L/h	6 200	6 200	6 200	6 200	6 200	6 200	6 200	6 200
Chiller bath	°C	-8.2	-8.1	-8.1	-7.6	-7.7	-8.1	-7.2	-7.8
Cooler Reactor	°C	-6.0	-6.2	-5.9	-5.9	-5.7	-5.5	-5.3	-5.8
E1 = q1.Cp.dT	kW	13.32	11.33	12.84	10.25	12.00	15.79	11.81	12.5
q2	L/h	200	200	200	200	200	200	200	200
Feed	°C	25.0	25.0	25.0	25.0	25.0	25.0	25.0	25.0
Treated	°C	-3.2	-2.1	-2.5	-2.2	-0.2	-2.7	-1.3	-2.0
Salt (60% $Na_2SO_4 \cdot 10H_2O$)	kg/d	513.0	562.0	565.0	630.0	703.0	363.0	303.0	519.9
Ice	kg/d	0	0	0	0	0	0	0	0.0
E2a q1.Cp.dT	kW	6.44	6.19	6.30	6.22	5.76	6.34	6.02	6.2
E2b m.Hv (Salt)	kW	1.65	1.80	1.81	2.02	2.26	1.17	0.97	1.7
2Ec m.Hv (Ice)	kW	0.00	0.00	0.00	0.00	0.00	0.00	0.00	0.0
E2 Total	kW	8.09	8.00	8.12	8.24	8.01	7.51	6.99	7.9
E3	kWh	176.0	176.0	176.0	176.0	176.0	176.0	176.0	176.0
E4	kW	7.33	7.33	7.33	7.33	7.33	7.33	7.33	7.3
		Ice recovery							
No		8	9	10	11	12	13	14	Average
Date		19-Aug-24	20-Aug-24	21-Aug-24	22-Aug-24	23-Aug-24	24-Aug-24	25-Aug-24	
TDS Feed	g/L	114.0	108.0	110.8	126.0	84.4	136.6	142.8	117.5
Cl-	g/L	59.6	65.2	43.1	48.2	53.6	73.7	78.3	60.2
NaCl	g/L	97.9	107.1	70.8	79.2	88.0	121.0	128.6	98.9
Na_2SO_4 Feed	g/L	16.1	0.9	40.0	46.8	-3.6	15.6	14.2	18.6
Na_2SO_4 Treated	g/L	7.1	-9.1	36.9	46.8	-3.6	15.6	-17.5	10.9
Na_2SO_4 OLI	g/L	6.1	0.9	6.1	6.1	0.0	5.9	5.9	4.4
q1	L/h	6 200	6 200	6 200	6 200	6 200	6 200	6 200	6 200
Chiller bath	°C	-14.7	-14.6	-13.2	-14.3	-14.9	-12.9	-13.5	-14.0
Cooler Reactor	°C	-12.6	-12.3	-10.2	-11.6	-12.3	-11.3	-10.8	-11.6
E1 = q1.Cp.dT	kW	13.02	13.80	17.96	16.03	15.31	10.01	16.09	14.6
q2	L/h	171	171	171	171	171	171	171	171
Feed	°C	20.0	20.0	20.0	20.0	20.0	20.0	20.0	20.0
Treated	°C	-6.1	-7.6	-7.3	-8.1	-7.4	-8.7	-6.5	-7.4
Salt (60% $Na_2SO_4 \cdot 10H_2O$)	kg/d	140.0	156.0	47.9	0.0	0.0	0.0	492.0	119.4
Ice	kg/d	201	257	115	438	449	550	183	313.2
E2a q1.Cp.dT	kW	5.10	5.40	5.35	5.50	5.35	5.61	5.19	5.4
E2b m.Hv (Salt)	kW	0.45	0.50	0.15	0.00	0.00	0.00	1.58	0.4
2Ec m.Hv (Ice)	kW	0.77	0.98	0.44	1.67	1.71	2.10	0.70	1.2
E2 Total	kW	5.55	5.90	5.50	5.50	5.35	5.61	6.77	5.7
E3	kWh	176.0	176.0	176.0	176.0	176.0	176.0	176.0	176.0
E4	kW	7.33	7.33	7.33	7.33	7.33	7.33	7.33	7.3

-7.4 °C, the secondary refrigerant temperature increased from -14.0 °C to -11.6 °C, demonstrating efficient heat exchange. This cooling process facilitated the formation of 313.2 kg/day of ice and 119.4 kg/day of $Na_2SO_4·10H_2O$ (60%), effectively reducing the Na_2SO_4 concentration from 18.6 g/L to 10.9 g/L (Fig. 3). The experimental results closely matched OLI simulation predictions, confirming the system's efficiency.

The total energy consumption for cooling, salt, and ice recovery amounted to 7.3 kW, aligning well with the measured electrical energy consumption of 7.33 kW. The cold energy generated in the chiller was calculated at 14.6 kW. While the chiller's full 18 kW capacity was not utilised, primarily due to limitations in the flow rate of the secondary refrigerant through the cooler reactor, the system still achieved substantial ice and salt recovery. These results demonstrate that freeze crystallization is a viable and energy-efficient method for recovering ice and salts from high TDS brines, providing both economic and operational benefits.

Conclusions

The study demonstrated that freeze crystallization is an effective and energy efficient method for brine treatment, achieving substantial salt and ice recovery. The chiller capacity was determined to be 43.7 kW at 7.4 °C, supporting stable cooling operations. For high TDS brine (131.9 g/L) at a flow rate of 200 L/h, 519.9 kg/day of $Na_2SO_4·10H_2O$ (60%) was recovered, reducing Na_2SO_4 concentration from 68.6 g/L to 40 g/L, with total energy consumption of 7.9 kW. Similarly, for lower TDS brine (117.5 g/L) at 171 L/h, 119.4 kg/day of $Na_2SO_4·10H_2O$ (60%) and 313.2 kg/day of ice were recovered, lowering Na_2SO_4 concentration from 18.6 g/L to 10.9 g/L, with a total energy use of 5.7 kW. These findings confirm that pipe freeze crystallization is a viable solution for sustainable brine treatment, optimising resource recovery while minimising energy consumption.

Recommendations

To enhance system efficiency and maximise salt and ice recovery, it is recommended to improve insulation on open pipes to reduce heat losses. Additionally, increasing the length of the HDPE pipe in the cooler reactor from 120 m to 270 m would allow for greater cold energy transfer from the secondary refrigerant to the brine, improving crystallization efficiency. Finally, after implementing these improvements, the plant should be evaluated for NaCl recovery to further optimise the freeze crystallization process and enhance overall resource recovery.

Acknowledgements

The authors acknowledge the valuable input of the following parties: THRIP for providing funds for the upgrade of the freeze crystallization plant, Innovation Hub for funding the procurement of the 18 kW Chiller, UNISA (iNanoWS), A-Thermal Retort Technologies for providing a site, saline water and technical support, ROC Water Technologies for providing job opportunities, ROC Water Technologies plant operators (Sabelo

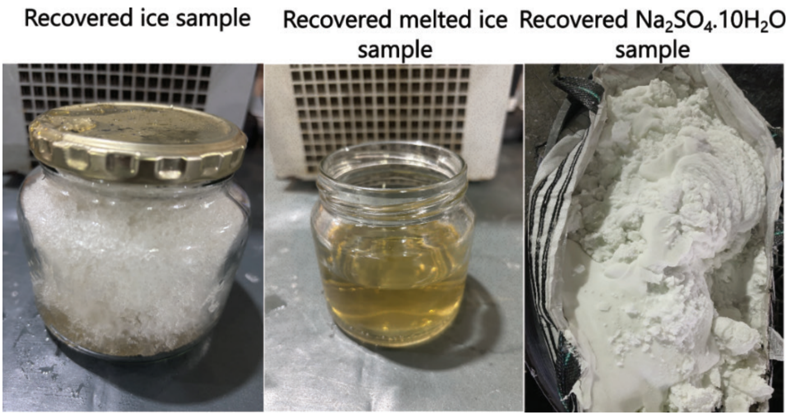

Figure 3 *Samples of the recovered ice, melted ice and $Na_2SO_4·10H_2O$ (60%).*

Mdumbe, Zola Shikweni, Akani Chauke, Banele Ntshangase, Josaphat Mulumba, Mxolisi Malale, Thatego Mohlamonyane) for the operation of the plant and monitoring of its performance.

References

American Public Health Association (2012) Standard methods for the examination of water and wastewater. vol 10. American Public Health Association, Washington, DC

Lewis AE, Nathoo J, Thomsen K, Kramer HJ, Witkamp GJ, Reddy ST, Randall DG (2010) Design of a Eutectic Freeze Crystallization process for multicomponent waste water stream. Chem Eng Res Des 88(9):1290-1296. https://doi.org/10.1016/j.cherd.2010.01.023

Maree JP (2018) Pipe Freeze Crystallization. South Africa, Australia, Canada, USA. Patent Provisional Appl. No: 2018/04084. RSA No: 2019/03795, Australia No: 201204324 (pending), Canada No: 3,092,764 (pending), USA No: 17,027,873

Maree JP, Letjiane SL, Ramothole R, Oyewo AO, Mogashane TM, Sebothoma PS, Vellem S, Ntumba N, Germanis J (2021) Treatment for the recovery of drinking water and valuable products from mine water, Report № C2019/2020-00033, Wader. Water Research Commission, Pretoria

More KS, Maree JP, Mahlangu M (2025) Optimising Salt Recovery—Four-Year Operational Insights into Na_2SO_4 Recovery from Saline Waters Using Pipe Freeze-Crystallization. Water 17(1):101. https://doi.org/10.3390/w17010101

Qureshi A, Maurice C, Öhlander B (2016) Potential of coal mine waste rock for generating acid mine drainage. J Geochem Explor 160:44-54. https://doi.org/10.1016/j.gexplo.2015.10.014

Randall DG, Nathoo J, Lewis AE (2009) Seeding for selective salt recovery during eutectic freeze crystallization. Paper presented at the International Mine Water Conference, Pretoria, South Africa, 19:639-646.

Randall DG, Nathoo J, Lewis AE (2011) A case study for treating a reverse osmosis brine using Eutectic Freeze Crystallization—Approaching a zero waste process. Desalination 266(1):256-262. https://doi.org/10.1016/j.desal.2010.08.034

Seo EY, Cheong YW, Yim GJ, Min KW, Geroni JN (2017) Recovery of Fe, Al and Mn in acid coal mine drainage by sequential selective precipitation with control of pH. CATENA 148:11-16. https://doi.org/10.1016/j.catena.2016.07.022

Recovery of Poly-Cationic Metal Sulfate from Acid Mine Drainage and its Beneficiation as a Coagulant for Water Treatment

Mamile Belina Mahlohla[1,2], Vhahangwele Masindi[1,2]; Memory Tekere[1], Spyros Foteinis[3]

[1]Department of Environmental Sciences, College of Agriculture and Environmental Sciences, University of South Africa (UNISA), P. O. Box 392, Florida, 1710, South Africa

[2]Magalies Water, Scientific Services, Research & Development Division, Erf 3475, Stoffberg street, Brits, 0250,

[3]Research Centre for Carbon Solutions, School of Engineering and Physical Sciences, Heriot-Watt University, Edinburgh EH14 4AS, United Kingdom.

Abstract

Acid mine drainage (AMD) is an acidic effluent enriched with high metal content, posing noteworthy environmental risks. However, AMD treatment can be coupled with resource recovery, promoting circular economy strategies. This study demonstrates the recovery of Fe(III) from AMD using MgO nanoparticles, followed by FeCl_3 synthesis for river water treatment. The optimized conditions (0.2 mL/L FeCl_3, 100 rpm, 5 min contact time) achieved the removal efficacies in the following order: turbidity (99.6%) > Al (99.5%) > Fe (99.4%) > Cr (99.2%) > Ni (98.2%) > Mn (91.5%) > Cu (90.7%) > As (80.5%) > color (46.4%). This study highlights the feasibility of producing $FeCl_3$ from AMD and its effectiveness for drinking water treatment, offering an innovative approach to AMD valorization.

Keywords: Acid mine drainage, resource recovery, ferric chloride, water treatment, circular economy

Introduction

Acid mine drainage (AMD) is a problem in both abandoned and active mines that can greatly affect the ecosystem quality (Simate and Ndlovu, 2014) and particularly surface water and groundwater (Yadollahi *et al.*, 2021). Different technologies have been employed for the treatment of AMD and they include active, passive, and integrated systems (Masindi, 2022). Each approach has different ecological, economic, and social impacts hence there is a need to come up with closed loop systems that seek to omit or minimize the release of waste into the environment. Furthermore, during AMD treatment sludge that is rich in metals and minerals is also produced and this sludge could be beneficiated to produce valuable products that have variety of industrial applications. previous research has demonstrate the feasibility of recovering valuable minerals such as hematite, goethite, magnetite (Akinwekomi *et al.*, 2020) which, among others, can be used to produce Fe-based catalysts (Aslam *et al.*, 2023), as well as gypsum (Masindi *et al.*, 2018a), and clean water (Pino *et al.*, 2020). Recovery is also governed by the dominance of chemical species. Fe and S are the commonly recovered elements, although others valuable elements such as rare earth elements(REE) could also be recovered but in trace concentrations (Mwewa *et al.*, 2022). This study seeks to recover ferric iron (Fe (III)) from AMD using magnesium oxide (MgO) nanoparticles and explore its application to produce ferric chloride ($FeCl_3$) for water treatment.

Methods

Masindi *et al.*, (2018b) confirmed the feasibility of recovering Fe (III) and other elements from AMD using a sequential and fractional approach and this was employed herein for Fe(III) recovery. To this end, AMD was collected from an active coal mine in Mpumalanga, South Africa, using 25 L containers. The samples were pre-filtered using Macherey Nagel (MN 615-Ø125 mm diameter) filter papers and the filtrate was then used for Fe (III) recovery. Surface water samples were collected from the Wilge River Dam, Gauteng Province, South Africa and used to test the efficacy of the AMD-derived FeCl3. Similarly, surface water was collected using 25 L containers. For quality control, sampling containers were rinsed using the same water during the sampling procedure to avoid contamination.

Analysis of AMD and river water

For the characterization of the collected AMD, the river water, and the FeCl3 treated water a multi-parameter probe (Hach Company HD40D) was used to measure the pH and electrical conductivity (EC). Turbidity was recorded using a tungsten lamp turbidimeter (Hach Company TL2350). Metal and non-metal fractions were determined using inductively coupled plasma mass spectrometry (ICP-MS) (Thermo Scientific XSERIES 2 ICP-MS, coupled to ASX-520 auto sampler) and inductively coupled plasma – optical emission spectrometry (ICP-OES) (Agilent Technologies 5110 ICP-OES coupled with SPS 4 auto sampler), as required based in their concentrations.

Recovery of Fe(III) ions and production of ferric chloride

The Fe(III) rich sludge was recovered from AMD by selective precipitation using MgO nanoparticles. Specifically 100 mL of AMD were transferred into a reactor, and a defined dosage of MgO-nanoparticles was added to enact the optimum Fe(III) recovery (Masindi *et al.*, 2018b). After that, the mixture was stirred for 30 minutes at 500 rpm by means of an overhead agitator (stirrer). To separate the sludge from the supernatant, the mixture was allowed to settle for another 30 min. In order to recover valuable minerals, the supernatant was filtered through a Whatman filter. The Fe(III) rich was then dried and stored until utilization for $FeCl_3$ production. The production of $FeCl_3$ solution for this study was achieved by calcining the recovered Fe(III)-rich sludge at 1200 °C in a furnace. The calcination step ensures phase transformation, improved Fe(III) purity, and removal of residual volatiles, enhancing $FeCl_3$ yield. Then, the calcined Fe(III)-rich sludge was reacted with industrial grade hydrochloric acid (HCl) towards $FeCl_3$ synthesis, as described elsewhere (Almeida and Schneider, 2020).

Stock solution preparation, optimization studies, and removal efficiency

The stock solution was prepared by adding 0.7 mL of $FeCl_3$ solution into a 1000 mL volumetric flask, filled with deionised water. The solution was kept in the fridge until utilization for optimization studies.

The removal efficiency (%) was calculated using the subsequent equation (Eq.1):

$$\%\text{Removal} = \frac{C_{\text{initial}} - C_{\text{final}}}{C_{\text{initial}}} \times 100 \qquad (1)$$

***Table 1** The chemical composition of raw mine water.*

Parameter	Units	Real AMD
pH	–	2.1
Sulfate	mg/L	8000
Fe	mg/L	2800
Mn	mg/L	190
Al	mg/L	280
Cr	mg/L	11
Cu	mg/L	0.9
Ni	mg/L	2.1
Zn	mg/L	4.7
Pb	mg/L	1.1
Acidity	mmol $CaCO_3$	26.2

Where, $C_{initial}$ and C_{final} represent initial concentration (level) and final concentration (level), respectively.

For the determination of optimum conditions for contaminants removal from the river water, several operational parameters were optimized, i.e., $FeCl_3$ dosage, mixing speed, and contact time. Batch experiments were conducted in the laboratory using one-factor-at-a-time (OFAT)method to identify those conditions. The experiments were conducted in triplicate, and the obtained results are reported as mean values.

Effect of dosage

Six 1000 mL aliquots of the collected AMD were spiked with different $FeCl_3$ dosages, i.e., 0.1, 0.2. 0.4, 0.6, 0.8 and 1.0 mL. Then, using a jar test stirrer, the mixtures were stirred for 1 min at 200 rpm. Thereafter, the samples were afforded 60 min for the suspended solids to settle. The turbidity was first determined and the supernatant was then filtered using a Whatman gravity filter. After filtration, the pH and EC were measured.

Effect of mixing speed

Similarly, six 1000 mL aliquots of the collected AMD were used, but these were now spiked with different 0.2 mL $FeCl_3$. The mixtures were mixed for 1 min each at different mixing speeds, i.e.,25, 50, 100, 150, 200 and 250 using the jar test stirrer. Thereafter, the samples were afforded 60 min for the suspended solids to settle and the supernatant was filtered using a Whatman gravity filter. The turbidity, pH, and EC were again measured.

Effect of contact time

Congruent to the effect of dosage and mixing speed, six 1000 mL aliquots of the collected AMD were spiked with 02 mL $FeCl_3$ and stirred at 100 rpm for the following durations, i.e., 1, 2.5, 5, 10, 15, 30 min at the jar test stirrer. Similarly, the samples were afforded 60 min to equilibrate and then filtered, while the turbidity, pH, and EC were also measured

Results and discussion

Effect of FeCl3 dosage

The results on the effect of FeCl3 dosages on river water treatment are shown in Fig. 1. As mentioned above, various FeCl3 dosages were examined, i.e., 0.1, 0.2, 0.4, 0.6, 0.8, and 1.0 mL.

As shown in Fig. 1, there was a variation in the percentage removal of contaminants as a function of dosage. The different chemical species reach equilibrium, in terms of percentage removal, at different FeCl3 dosages. Specifically, turbidity, Al, Fe and Zn, were practically removed at 0.2 mL dosage, at the next dosage (0.4 mL) Fe removal reach equilibrium, while Ni reached equilibrium at 0.6 mL dosage. The overall removal efficacy followed this sequence, Al (100%), Fe (100%), turbidity (99.9%), As (99.8%), Mn (99.4%), Cr (98.6%), Ni (98.5%), Cu (88.2%), Zn (50%) and colour (25%), respectively. There was a decrease in pH with an increase in $FeCl_3$ dosage. Overall, results in Fig. 1 suggest that the optimum dosage is 0.2 mL and this was considered in the subsequent experiments.

Effect of mixing speed

Fig. 2: The effect of mixing speed on the removal of chemical species contained in real river water (conditions: 1 min of mixing, 0.2 mL, and 60 min settling).

The results on the effect of the mixing speed are shown in Fig. 2. As mentioned above, six different mixing speed were considered, i.e., 25, 50, 100, 150, 200, and 250 rpm. Essentially, it was identified that the reduction in contaminants concentration is a function of mixing speed. Specifically, from 0–25 rpm there was a reduction in turbidity, Fe and Al in river water, while Mn, As, and Cu removal increases with increasing mixing speed and at 100 rpm Ni reaches equilibrium. The removal efficacy for the parameters registered the following sequence: As (99.9%), Fe (99.8%), turbidity (99.7%), Al (98.6%), Ni (94.4%), Mn (86.3%), Cr (84.2%), Cu (81.7%), colour (14.3%) removal efficacies. As such, 100 rpm was taken as the optimum mixing speed and will be used in subsequent experiments.

Effect of contact time

The results for the effect of contact time, when using the following durations: 1, 2.5, 5, 10, 15 and 30 min, are shown in Fig. 3.

As illustrated in Fig. 3, increasing the mixing durations are beneficial for the

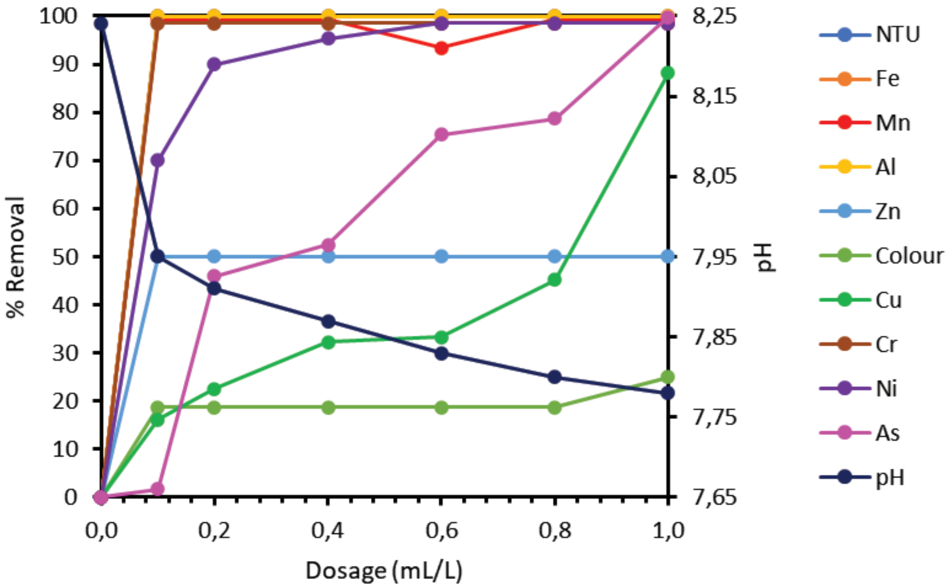

Figure 1 The effect of $FeCl_3$ dosages on the removal of contaminants contained in real river water (conditions: 1 min of mixing, 200 rpm mixing speed, and 60 min settling).

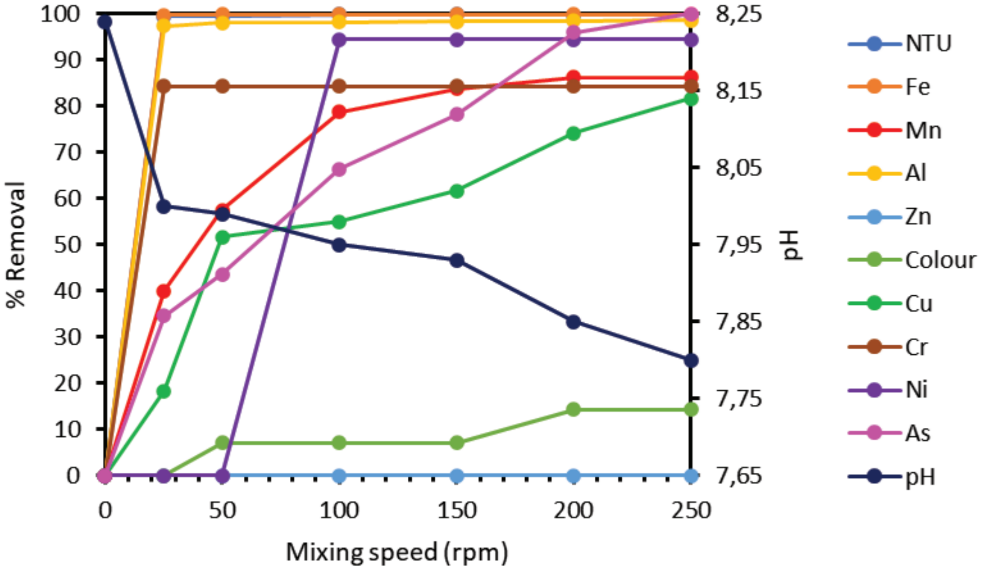

Figure 2 The effect of mixing speed on the removal of chemical species contained in real river water (conditions: 1 min of mixing, 0.2 mL, and 60 min settling).

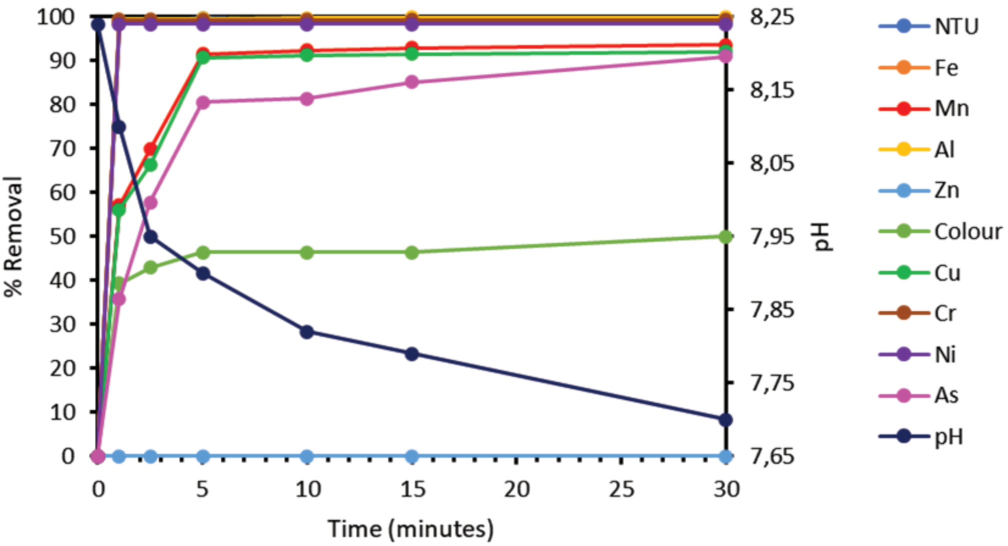

Figure 3 Percentage removal and pH variations in river water when treated for different contact times using FeCl3 synthesized from mine water (Conditions: 0.2 mL: L dosage at 100 rpm mixing speed, followed by 60 min settling time at ambient temperature and pH.)

removal of contaminants, since the percentage removals for all examined contaminants/indicators increase with increasing mixing durations. In more detail, it was observed that turbidity, Fe, Al, Cr and Ni removal plateaus at the first examined mixing duration (1 min), whereas colour removal was observed to reach equilibrium at 5 min mixing duration. The removal percentage efficacies are as follows: turbidity (99.6%), Al (99.5%), Fe (99.4%), Cr (99.2%), Ni (98.2%), Mn (91.5%), Cu (90.7%), As (80.5%) and Colour (46.4%), respectively. The pH also appears to decrease with increasing contact times, and this can be traced back to FeCl3 increasing dissolution with increasing contact times. On the other hand, As removal steeply increase at up to 5 min contact time and then gradually increases until the last examined mixing duration. Based on the aforementioned results 0.2 mL of FeCl3, 100 rpm, and 5 min of mixing are the optimum conditions for river water treatment. Under those conditions the system registered the following sequence in terms of the percentage removal of contaminants; turbidity (99.6%), Al (99.5%), Fe (99.4%), Cr (99.2), Ni (98.2%), Mn (91.5%), Cu (90.7%), As (80.5%) and Colour (46.4%), respectively. These removals render the treated river water within the South African specifications for drinking water quality (SANS 241:2015).

Conclusions

The results from this study illustrate the feasibility of recovering ferric iron (Fe(III)) from acid mine drainage (AMD) and use it for ferric chloride ($FeCl_3$) production. The synthesized $FeCl_3$ was used to treat river water. Its application as a coagulant for treating drinking water was effective at 5 min of contact time, 100 rpm mixing speed, and 0.2 mL/L FeCl3 dosage. The results also highlighted that the AMD-derived $FeCl_3$ can be used for water treatment, as the treated river water was within the South African specifications for drinking water quality (SANS 241:2015).

Acknowledgements

The authors of this study would like to convey their sincere gratitude to the University of South Africa and Magalies Water for extending their facilities towards the accomplishment of the objectives of this project.

References

Akinwekomi V, Maree JP, Masindi V, Zvinowanda C, Osman MS, Foteinis S, Mpenyana-Monyatsi L, Chatzisymeon E (2020) Beneficiation of acid mine drainage (AMD): A viable option for the synthesis of goethite, hematite, magnetite, and gypsum – Gearing towards a circular economy concept. *Minerals Engineering*, 148.

Almeida VO, Schneider IAH (2020) Production of a ferric chloride coagulant by leaching an iron ore tailing. *Minerals Engineering*, 156, 106511.

Aslam T, MasindI V, Ahmad AA, Chatzisymeon E (2023) Valorization of Acid Mine Drainage into an Iron Catalyst to Initiate the Solar Photo-Fenton Treatment of Municipal Wastewater. *Environments* – MDPI, 10.

Masindi V (2022) Challenges and avenues for acid mine drainage treatment, beneficiation, and valorisation in circular economy: A review. *Ecological Engineering,* pp. 106740–2022.

MasindI V, Madzivire G, Tekere M (2018a) Reclamation of water and the synthesis of gypsum and limestone from acid mine drainage treatment process using a combination of pre-treated magnesite nanosheets, lime, and CO_2 bubbling. *Water Resources and Industry*, 20, 1–14.

Masindi V, Ndiritu JG, Maree JP (2018b) Fractional and step-wise recovery of chemical species from acid mine drainage using calcined cryptocrystalline magnesite nano-sheets: An experimental and geochemical modelling approach. *Journal of Environmental Chemical Engineering*, 6, 1634–1650.

Mwewa B, Tadie M, Ndlovu S, Simate GS, Matinde E (2022) Recovery of rare earth elements from acid mine drainage: A review of the extraction methods. *Journal of Environmental Chemical Engineering*, 10, 107704.

Pino L, Beltran E, Schwarz A, Rui MC, Borquez R (2020) Optimization of nanofiltration for treatment of acid mine drainage and copper recovery by solvent extraction. *Hydrometallurgy*, 195, 105361.

Simate GS, Ndlovu S (2014) Acid mine drainage: Challenges and opportunities. *Journal of Environmental Chemical Engineering*, 2, 1785–1803.

Yadollahi A, Abdollahi H, Ardejani FD, Mirmohammadi M, Magdouli S (2021) Bio-oxidation behavior of pyrite, marcasite, pyrrhotite, and arsenopyrite by sulfur- and iron-oxidizing acidophiles. *Bioresource Technology Reports*, 15, 100699.

Depression and Dewatering Characteristics of Kaolinite in View of the Reprocessing of Ultrafine Colliery Waste

Malibongwe S. Manono

Centre for Minerals Research, Department of Chemical Engineering, University of Cape Town, Private Bag X3, Rondebosch 7701, South Africa, malibongwe.manono@uct.ac.za, ORCID 0000-0002-2928-9368

Abstract

Coal holds an important position within South Africa's commodities due to its current role as the primary energy source. Nevertheless, the beneficiation and processing of South African coals result in substantial wastes in the form of discards and ultrafine coal slurries. Previous research has shown the potential of coal ultrafines to serve as an energy resource if suitably beneficiated, given their comparable quality to run-of-mine coal. The issue of long-term environmental impact from these ultrafine coals also comes to the forefront, particularly concerning the substantial sulfidic content in coal ultrafines, which can contribute to the generation of acid rock drainage (ARD). In addressing these complexities, froth flotation is seen as a promising technique for the beneficiation of ultrafine coal waste. However, this technique is not without its challenges. Coal ultrafines often encompass a significant proportion of clay minerals, with kaolinite being a prominent phyllosilicate clay mineral. The prevalence of kaolinite as a gangue mineral in South African coal ultrafines adds an intricate layer to the beneficiation process, as effectively depressing kaolinite during flotation can prove intricate. Efficient depression of kaolinite is thus necessary to separate it from ultrafine coal particles during flotation. Furthermore, considerations of pulp chemistries, such as process water quality in ultrafine coal flotation would be of paramount importance, especially given that there is water scarcity in regions within which coal mining occurs in South Africa. Because of this, the implementation of closed water circuits in flotation and effective dewatering of tailings for water recovery and dry stacking of tailings have gained much prominence owing to the need to minimise water consumption and enhance waste management practice in line with SDG 6, 9, 12, 13, 14 and 15. Therefore, it stands to reason that effective depression of kaolinite during ultrafine coal flotation is crucial in achieving high-quality coal products with reduced impurities with an understanding of the influence of different flotation chemistries. This research considers kaolinite depression and dewatering characteristics in inorganic electrolyte concentrated process water in view of process water recirculation in coal flotation and the need for the dewatering of tailings. Laboratory scale tests such as zeta potential measurements and depressant adsorption studies were considered. Understanding the behaviour of kaolinite in these contexts is vital for sustainable coal processing and environmental stewardship.

Keywords: Coal flotation, coal processing discards, kaolinite flotation, tailings dewatering, water recirculation

Introduction

South African coals contain high amounts of kaolinite, present as gangue mineral, its composition can be as high as 90 wt.%(Mpofu *et al*. 2004). Kaolinite is a clay mineral made up of ultrasmall particles which are too fine to separate using conventional hydrocyclones or screens, due to kaolinite particles passing through all the beneficiation processes during coal beneficiation. It is thus important to selectively depress this kaolinite in fine coal processing through separation processes such as froth flotation where fine clay minerals are rejected to the tails. The nature of the froth flotation process ensures a separation fine particles by manipulating the chemistry of the system through the addition of reagents such as collectors, depressants, flocculants and frothers (Bulatovic, 2007). The manipulation of the pulp chemistries ensures that particles are either hydrophobic or hydrophilic such that the hydrophilic particles attach to air bubbles rising through the pulp and float while the hydrophilic particles remain in the pulp and are rejected out of the system through the tailings stream (Wills and Napier-Munn 2006).

Since flotation is water intensive, previous studies have investigated how process water recirculation and the consequential increase in ionic strength of the plant water affect the overall coal flotation performance and found that the accumulation of inorganic electrolytes affects the mineral surface, reagent action, and pulp chemistry (Arnold and Aplan 1986; Celik and Somasundaran 1986; Yoon and Sabey 1989; Ozdemir 2013; Çelik and Ozdemir 2018; GUNGOREN *et al*. 2020). To induce the depression of clay minerals like kaolinite in coal flotation, depressants such as polysaccharides are added to induce the hydrophilicity of kaolinite. Several studies have revealed factors that may improve the adsorption of polysaccharide type depressants onto clay minerals include an alkaline pH, higher ionic strength of process water and the presence of polyvalent cations in solution (Arnold and Aplan 1986; Yoon and Sabey 1989; Kawatra and Eisele 1992). Ultrafine colliery waste has potential to be a useful energy source due to comparable coal to that of run-of-mine (ROM) coal. Due to the predominant kaolinite minerals and ultrafine size of the coal waste, current conventional South African methods in the coal industry are not able to separate these ultrafine particles, coal waste also contains sulfidic compounds such as pyrite which pose an environmental hazard due to the acid rock drainage (ARD) formation. It is thus suggested to use froth flotation which is being used globally for coal waste. Considering the intensive water use of the flotation process and scarce water availability, water recirculation has become a trend to mitigate fresh water use. This however leads to ion and reagent accumulation in the water, thus changing the water quality which plays an important role in the pulp chemistry and thus flotation performance. This study aims to consider the impact of selected ions at different pH values to the **surface chemistry of kaolinite** in view of the **depression of kaolinite during fine particle coal processing** and **dewatering characteristics of kaolinite laden tailings** emanating out of repurposed coal fine particles.

Methods

Mineral Sample Preparation

A kaolinite powder-like sample of analytical grade was provided from a supplier in Cape Town. The sample was then screened according to the appropriate sizes required for zeta potential measurements, sodium carboxy methyl cellulose (CMC) adsorption tests and particle flocculation tests. Particle sizes between -75 to 38 µm were used for CMC adsorption tests and flocculation tests while -38 µm were used for the zeta potential studies as these have been chosen to be suitable for these tests (October *et al*. 2019).

Reagents

De-ionised water was used to prepare single salt solutions of sodium chloride (NaCl), magnesium chloride ($MgCl_2$) and calcium chloride ($CaCl_2$), sodium hydroxide (NaOH) and hydrochloric acid (HCl) for pH control, and sodium carboxymethyl cellulose as depressant.

Single Salt Solution Preparation

In order to study the effect of selected ions or water quality on the depression and dewatering characteristics of kaolinite, single salt solutions of NaCl, $MgCl_2$ and $CaCl_2$ in concentrations of 0.01 mol/L were used. These single salt solutions were prepared using de-ionised water as the baseline. These salts were supplied by Merck and were of analytical grade.

pH Modifiers

Buffer solutions of sodium hydroxide (NaOH) and hydrochloric acid (HCl) were used for pH adjustment.

Depressant Preparation

CMC, SENDEP-30E, supplied by Senmin, was used as a depressant. A stock solution of 1% (w/v) was prepared by adding 1 g of CMC in 100 mL of deionised water in a beaker and stirred for 3 h on a magnetic stirrer until completely dissolved. The stock solution was refrigerated at the end of every test day and a new batch was prepared every 5 days to ensure it does not expire (Dzingai *et al.* 2020).

Acid and Phenol Solution Preparation for CMC Adsorption

The DuBois calorimetric method used for the determination of the adsorption of CMC requires the use of sulfuric acid and phenol. To prepare the solutions used in the DuBois calorimetric method, concentrated sulfuric acid (H_2SO_4) was poured into a test beaker under a fume hood. The volume was measured according to the number of tests performed daily since the acid could not be reused the following day. For the phenol preparation, 5 g of phenol salt were weighed and added to a 100 mL glass beaker with de-ionized water under a fume hood (du Bois *et al.*, 1956). The contents were transferred to a volumetric flask and closed with a cap to ensure that the fumes are not released. The solution was then magnetically stirred until full dissolution of phenol salt was achieved. The phenol solution was placed in the fume hood and used daily as needed.

CMC Adsorption on Kaolinite

Adsorption of CMC onto kaolinite was measured by determining the concentration of the CMC that remained in suspension. A tool used to measure this is the UV spectrophotometer which is based on the theory of ultraviolet rays being absorbed by a substance and this results in an apparent spectrum. This theory is based on Beer's law explained by Mayerhöfer and Popp (2019), relating absorbance and concentration as shown in Eq (1), A is the absorbance and c, is the concentration(c). Another essential element is the wavelength determined at the highest absorbance which is used in absorption studies to be able to determine the concentration (L).

$$A = \varepsilon L c \quad (1)$$

For the adsorption tests performed, four calibration curves were first generated for all water types, i.e., deionised water, NaCl, $MgCl_2$ and $CaCl_2$. The samples were poured into beakers at a volume of 30 mL, CMC was then added from 1 mL to 5 mL in increments of 1 mL in five separate beakers for each water type. The contents were then mixed. Using a syringe, 1 mL per sample was measured out into test tubes and then transferred to the fume hood.

Following the DuBois calorimetry method, 2 mL of a phenol solution and 10 mL of sulfuric acid were added to the test tubes with CMC samples. The reaction is almost immediate and is exothermic giving off a warm touch to the test tubes. The samples were left in the fume hood for 40 min to allow the reaction to come to completion. When the reaction time was over, small amounts of the samples were poured into quartz cuvettes for absorbance measurements in a UV-Vis spectrophotometer. Maximum absorbances were recorded and observed in the 483–489 nm frequency range. This was slightly different to the 490 nm frequency for CMC reported by du Bois *et al.* (1956) but close and this might be due to residual components in the industrial make-up of CMC, SENDEP-30E.

The measured absorbances were recorded alongside the corresponding CMC concentrations. Calibration curves were then used in the adsorption studies to obtain residual CMC in solution following kaolinite adsorption to CMC. A total of 16 samples were prepared for the four water types: de-ionised (DI), NaCl, $CaCl_2$ and $MgCl_2$ and at four different pH values, namely, pH 4, 6, 8, and 10. To start, the waters were poured into 16 flasks as marked appropriately according to water type and pH to be tested, 3 mL of CMC and 3 g of kaolinite of 38–75 µm particle size were added to 30 mL of water then mixed, the mixture was then adjusted to required pH values. The top of the flasks was covered with tin foil and placed in an Ecobath shaker at a controlled temperature of 20°C and speed of 141 rpm for 15 min. After 15 min in the water bath, a plastic syringe was used to draw out enough slurry such that 1 mL filtered solution can be collected to be analysed for residual CMC. A 0.45 µm filter was attached at the end of the syringe and the filtrate was collected in a sample container. The sample was then poured into a test tube at an amount of 1 mL and the DuBois colorimetric procedure was followed as already described by adding 2 mL of phenol and 10 mL of sulfuric acid and allowing the reaction to come to completion, after which the samples were poured into cuvettes for absorbance measurements. The concentration of CMC in solution for unknown samples was then calculated using measured absorbances and generated calibration curves. Adsorption tests were done in triplicate to minimise experimental error.

Zeta Potential Determination

To analyse the electrokinetic behaviour of the particle suspension, zeta potential measurements were conducted. An amount of 30 mL of four water types were poured into four beakers, DI, NaCl, $MgCl_2$ and $CaCl_2$, an amount of 3 g kaolinite was added to the solutions and mixed. The four samples were then taken for zeta potential tests. This process was repeated four times for the following pH values, 4, 6, 8, and 10. Using a pipette, a small amount of the suspension was poured into a folded capillary cell and closed tightly. The cell was wiped on the outside to ensure that no solution was leaking or flowing out of the cell, then inserted into a Malvern Zeta-sizer which was then closed. On the desktop, the Malvern Zeta-sizer application was opened and set up by selecting the mineral of interest (kaolinite), the parameter to be measured (zeta potential), dispersant (water), cell (folded capillary cell), measurement (automatic, 3 times), data processing (general/default), the ok and start prompts were then selected to start the analysis. The machine read a single sample three times as selected and reported the potential in mV together with a graph showing the total potential versus the total counts. The cell was removed from the machine and flushed using de-ionised

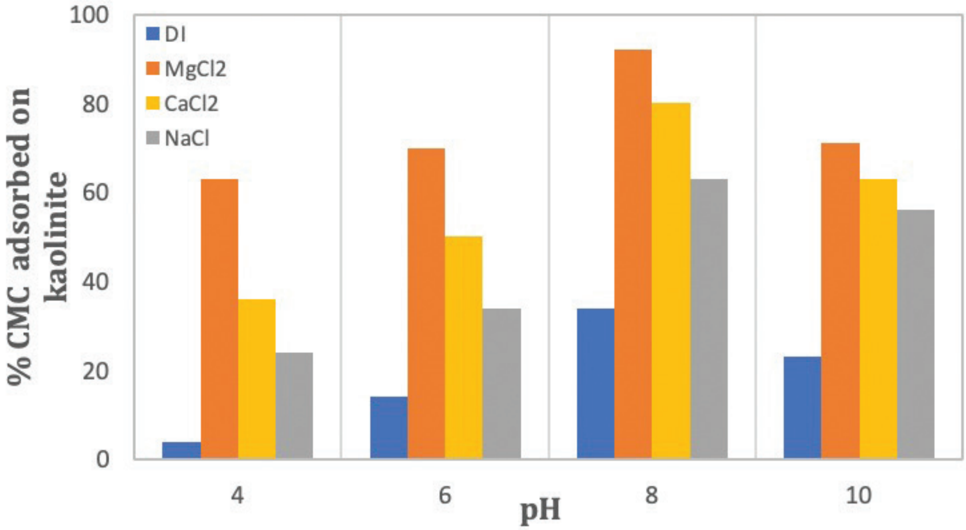

Figure 1 CMC Adsorption onto Kaolinite at varying pH.

water to ensure that the next sample was not contaminated. The zeta potential studies were repeated two times for each test condition to increase the accuracy of results.

Results and Discussion

Effect of Solution Chemistry and pH on CMC Adsorption

Fig. 1 shows a comparison of CMC adsorption to kaolinite at pH 4, 6, 8, and 10 for different water types.

$MgCl_2$ shows the best adsorption performance across all pH values. This trend is followed by $CaCl_2$. NaCl and de-ionised (DI) water both showed lower adsorption performance with NaCl showing better performance than DI. It can also be seen that for all water or solution types, the adsorption of CMC on kaolinite increased as pH increased from 4 to 8 and then took a deep at pH 10. The results shown in Fig. 1 also show that the divalent ions from $MgCl_2$ and $CaCl_2$ showed better adsorption performance of CMC to kaolinite compared to the monovalent NaCl and the DI, these observations agree with the literature that polyvalent ions are effective at improving depressant adsorption to minerals (Laskowski *et al.* 2007; Burdukova *et al.* 2008; Manono *et al.* 2019).

Effect of Solution Chemistry and pH on the Zeta Potential of Kaolinite

Fig. 2 shows a comparison of the zeta potential of kaolinite at pH 4, 6, 8, and 10 for different water types.

It can be seen from Fig. 2 that both $MgCl^2$ and $CaCl^2$ had less negative zeta potential values and closest to the isoelectric point (0 mV) when compared to NaCl and DI water. These results agree with the observed higher percentage adsorption for CMC to kaolinite; these trends are similar to earlier work on talc by (Manono *et al.* 2020). $CaCl_2$ resulted in a more negative zeta potential than $MgCl_2$ after pH 8, this can be attributed to the different speciation occurring as the pH changes. The DI water showed the most negative magnitude in zeta potential at pH 6 and 7 and less negative lower than NaCl above pH 7. The zeta potential trend suggests that kaolinite particles are more flocculated in $CaCl_2$ and $MgCl_2$ and thus kaolinite dewatering would be more effective in divalent cations and possibly even better in the presence of CMC as CMC has been shown to possess flocculant-polymer-like properties (Sharma *et al.* 2006; Salehizadeh *et al.* 2018; Guo *et al.* 2021).

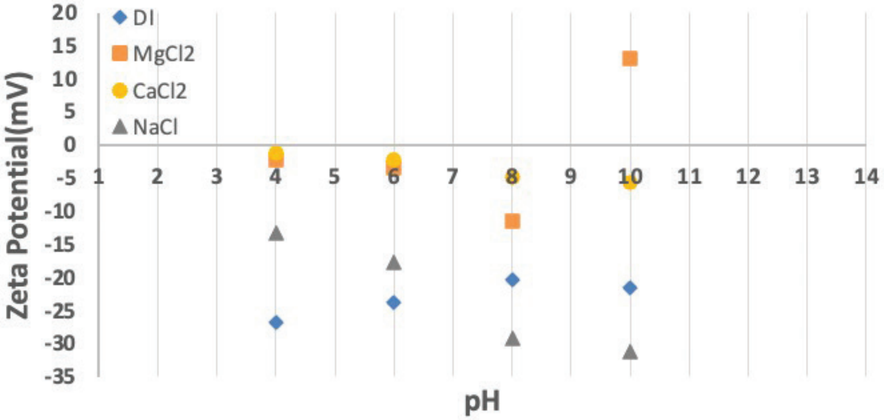

Figure 2 *Zeta potential of Kaolinite at varying pH.*

Conclusions

The effect of different ionised water and varying pH on **CMC adsorption to kaolinite** was studied. De-ionised water was doped with three salts $MgCl_2$, $CaCl_2$, and NaCl at 0,01 M separately, and depressant CMC was added and measured for adsorption to kaolinite, pH was also varied at 4, 6, 8, and 10 to observe it effect. **Zeta potential** was measured to assess the inherent repulsive forces of the kaolinite particles in the different waters at varying pH values: 4, 6, 8, and 10 in the absence of the depressant. **Adsorption studies** and **zeta potential measurements** were necessary in terms of predicting the effects that **varying pH and inorganic electrolytes** would have on the **hydrophilicity, depression and flocculation of kaolinite** particles.

Adsorption studies showed that water containing Mg^{2+} resulted in the best adsorption performance across all pH values followed by Ca^{2+}, Na^{+}, and DI performed poorly. **Zeta potential results** showed that both Ca^{2+} and Mg^{2+} water types had zeta potential values lower and closest to the isoelectric point (0 mV) when compared to Na^{+} and DI water types in agreement with the observed higher percentage adsorption of CMC to kaolinite.

This study showed that CMC adsorption increased with **alkaline pH** although a threshold was seen. Both divalent ions Mg^{2+} and Ca^{2+} showed the best adsorption performance and less negative zeta potential compared to Na^{+} and DI water. Thus, process water with Ca^{2+} and Mg^{2+} ions may be recommended for CMC adsorption to kaolinite at ~pH 8; this could result in the necessary depression of kaolinite particles in ultrafine colliery waste beneficiation through froth flotation and may also impart better flocculation or dewatering behaviour on kaolinite bearing tailings after flotation.

Acknowledgements

The author would like to acknowledge the University of Cape Town for supporting this work. Queen Sekudu is acknowledged for conducting the test work as part of her final year project towards the degree of BSc(Eng) in Chemical Engineering at the University of Cape Town.

References

Arnold, B.J. & Aplan, F.F. 1986. The effect of clay slimes on coal flotation, Part II: the role of water quality. *International Journal of Mineral Processing*. 17(3–4):243–260.

du Bois M, Giles, K A, Hamilton, J K, Rebers, P A, Smith, F. 1956. Colorimetric method for determination of sugars and related substances. *Analytical Chemistry*. 28(3):350–356.

Celik, M.S. & Somasundaran, P. 1986. The Effect of Multivalent Ions on the Flotation of Coal. *Separation Science and Technology*. 21(4):393–402. DOI: 10.1080/01496398608057170.

Dzingai, M., Manono, M. & Corin, K. 2020. Simulating the Effect of Water Recirculation on Flotation through Ion-Spiking: Effect of Ca^{2+} and Mg^{2+}. *Minerals*. 10(11):1033. DOI: 10.3390/min10111033.

Harvey, P.A., Nguyen, A. V. & Evans, G.M. 2002. Influence of electrical double-layer interaction on coal flotation. *Journal of Colloid and Interface Science*. 250(2):337–343. DOI: 10.1006/jcis.2002.8367.

Kadagala, M.R., Nikkam, S. & Tripathy, S.K. 2021. A review on flotation of coal using mixed reagent systems. *Minerals Engineering*. 173. DOI: 10.1016/j.mineng.2021.107217.

Kawatra, S.K. & Eisele, T.C. 1992. Recovery of pyrite in coal flotation: Entrainment or hydrophobicity? *Mining, Metallurgy & Exploration*. 9(2):57–61. DOI: 10.1007/BF03402970.

Mpofu, P., Addai-Mensah, J. & Ralston, J. 2004. Temperature influence of nonionic polyethylene oxide and anionic polyacrylamide on flocculation and dewatering behavior of kaolinite dispersions. *Journal of Colloid and Interface Science*. 271(1):145–156. DOI: 10.1016/j.jcis.2003.09.042.

October, L., Corin, K., Schreithofer, N., Manono, M. & Wiese, J. 2019. Water quality effects on bubble-particle attachment of pyrrhotite. *Minerals Engineering*. 131. DOI: 10.1016/j.mineng.2018.11.017.

Ozdemir, O. 2013. Specific ion effect of chloride salts on collectorless flotation of coal. Physicochemical *Problems of Mineral Processing*. 49(2):511–524. DOI: 10.5277/ppmp130212.

Ozdemir, O., Taran, E., Hampton, M.A., Karakashev, S.I. & Nguyen, A. V. 2009. Surface chemistry aspects of coal flotation in bore water. *International Journal of Mineral Processing*. 92(3):177–183. DOI: https://doi.org/10.1016/j.minpro.2009.04.001.

Wills, B.A. & Napier-Munn, T. 2006. *Mineral Processing Technology. An Introduction to the Practical Aspect of Ore Treatment and Mineral Recovery*. V. 7th. Elsevier Science & Technology Books.

Yoon, R.H. & Sabey, J.B. 1989. Coal flotation in inorganic salt solutions. In *Interfacial Phenomena in Coal Technology*. V. 32. G.D. Botsaris & Y.M. Glazman, Eds. Surfactant Science Series. 87–114.

Assessment Of The Efficacy Of Superabsorbent Polymers In The Treatment Of Metal Mining Effluents

Abdelkabir Maqsoud[1], Nor el hoda Addi[1], Tikou Belem[1], Mamert Mbonimpa[1]

[1]Université du Québec en Abitibi-Témiscamingue, Research Institute in mines and Environment, 445 Bd de l'université, J9X 5E4 Rouyn-Noranda, QC, Canada, abdelkabir.maqsoud@uqat.ca

Abstract

Several techniques are commonly employed to treat AMD, including raising the pH by adding alkaline materials, precipitating dissolved metals by introducing sulfide reagents, and using biological processes. Superabsorbent polymers (SAPs), known for their high water absorption and retention capacity, offer a promising alternative for treating mining effluents due to their unique properties. In this study, synthetic metal solutions were used to assess the effectiveness of SAPs in effluent treatment using artificial solution. Investigation results demonstrate the effectiveness of SAPs in sequestering metal ions. The sequestration capacity of metals is influenced by pH, the ionic radius of the element, and the availability of binding sites in the SAPs.

To better understand the relationship between absorption rates, metal and metalloid sequestration and these chemical factors, equations have been proposed that consider both ionic radii and the concentrations of the elements analyzed. These equations provide highly accurate predictions of the metallic ion absorption rate.

Keywords: Superabsorbent polymers, water absorption, metal sequestration .

Introduction

Acid Mine Drainage (AMD), which results from mine wastes, is one of the most challenging environmental problems currently faced by the mining industry. Mining operations generate large amounts of waste, such as waste rock and tailings, which must be properly managed to protect the environment. Special attention is required when these wastes contain sulfidic minerals, such as pyrite and pyrrhotite. The oxidation of sulfides exposed to atmospheric conditions tends to acidify water, making it more prone to the mobilization of metals contained in the rock. These processes generate an acidic leachate known as acid mine drainage (AMD) or Acid Rock Drainage (ARD) (e.g., Aubertin *et al.*, 2002). AMD is characterized by high levels of sulfate and metals at low pH, and if not properly managed, it can negatively affect surrounding soils, surface water, and groundwater (Maqsoud *et al.*, 2016).

Acid mine drainage generally requires treatment before being discharged into the natural environment (Ben Ali *et al.*, 2019; USEPA, 2014). This treatment primarily involves increasing the pH (when applicable) and alkalinity, along with removing metals and sulfates. Several active and passive treatment technologies are well known and have been successfully applied to achieve these objectives (Wolkersdorfer, 2022; Skousen *et al.*, 2017; USEPA, 2014; Genty, 2012; Ben Ali *et al.*, 2019). The selection of a treatment technology is site-specific and must account for various parameters, including flow rate and water quality, while also considering economic, environmental, regulatory, and social factors.

Another technique that can be used in effluent treatment is the application of superabsorbent polymers (SAP). These polymers have high water retention as well as metal and metalloid sequestration capacities

(Ismi *et al.*, 2015; Addi *et al.*, 2019; Rifi *et al.*, 2005; Kanny-Diallo *et al.*, 2024). The sequestration of chemical elements is also linked to the water retention capacity of the polymers. This property could be utilized in the management of mine tailings (tailings densification) to enhance the geotechnical stabilization of mine tailings (Sahi *et al.* 2019).

This paper aims to assess the absorption rate and sequestration capacity of SAP for metals and metalloids and to establish a relationship between metal ion absorption rates and various chemical factors. To achieve this, an experimental study was conducted using an artificial solution and recycled superabsorbent polymers (SAP).

Materials and Methods

Materials

The superabsorbent polymers (SAPs) used in this study are based on sodium polyacrylates (PaNa). They are sourced from the recovery of defective diapers by Recyc PHP Inc. in Drummondville, Quebec, Canada. For these SAPs, the point of zero charge (PZC) was evaluated to determine the optimal pH for SAP sorption. This parameter was assessed using the salt addition method (Belviso *et al.*, 2014). The pH_{pzc} is the point where there are equal amounts of positive and negative charges. As shown in Fig. 1, the point of zero-charge corresponds to 5.83 for PANa coming from diapers. At this pH, SAPs would be more appropriate to capture cations, and this optimal pH was used for all tests performed.

Adsorption and sequestration tests

Salt solutions of different concentrations were prepared separately in deionized water. A volume of 200 ml of each saline solution was used, into which 0.50 g of hydrogel (dry PA-Na) was placed for 1 hour.

After this contact time, hydrogels containing trapped metal ions and water were separated from the saline solution by vacuum filtration. The resulting hydrogel was then weighed to determine the mass of the SAP at equilibrium swelling ($M_{SAP\text{-}eq}$).

From this, the absorption rate (Q^{eq}) can be calculated using equation (1) (see Sahi *et al.* 2019):

$$Q_{eq} = \frac{M_{SAPeq-}\,M_{SAPDry}}{M_{SAP-Dry}} = \frac{M_{water-absorbed}}{M_{SAP-Dry}} \quad (1)$$

Where MSAPeq corresponds to the mass of the SAP at equilibrium swelling.

Also, the concentrations of salt ions in the solution (after absorption) were evaluated using ICP-AES. By the initial concentrations measured in the solution, including the

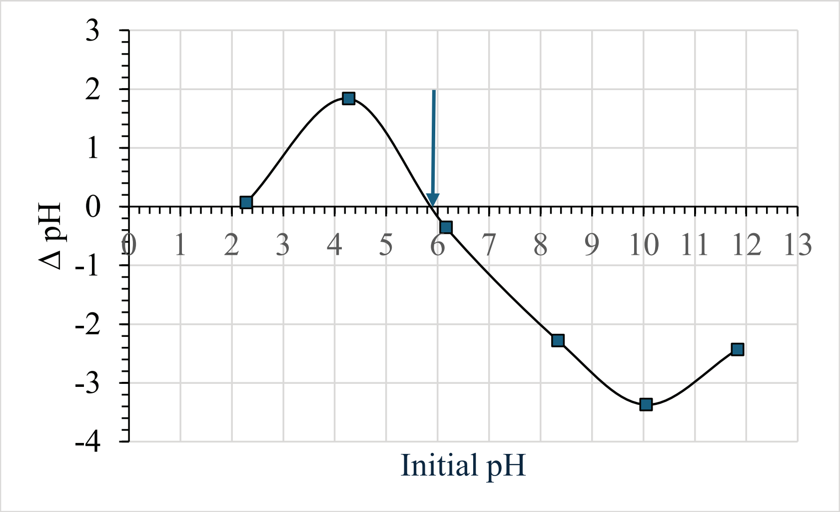

Figure 1 Evaluation of pH pzc of SAP.

volume used in each test, the initial mass ($M_{0\text{-ion}}$) for each element was defined. After the absorption test, final mass ($M_{f\text{-ion}}$) was determined using the same technique.

$$SP\ (\%) = \frac{M_{0-ion} - M_{f-ion}}{M_0 - ion} \times 100 \qquad (2)$$

These masses were used to evaluate the ion sequestration potential using the following equation:

Implications for Risk Assessment and Mitigation:

The detailed characterization of the fault system has important implications for risk assessment and mitigation related to the TSF. Understanding the fault's geometry and hydraulic properties allows for a more accurate assessment of the potential for contaminant migration along the fault. The finding that the fault acts as a hydraulic barrier suggests that infiltration from the TSF may be preferentially channelled along the fault zone, potentially affecting specific areas. This information can be used to inform the design and placement of monitoring wells and to develop targeted mitigation strategies to prevent groundwater contamination.

Results

In this section, we present the results related to the absorption and sequestration capacity of metals and metalloids by SPA.

Absorption rate (Q_{eq})

Absorption rates of Zinc, Arsenic, Lead, Nickel, Copper, Cadmium, Iron, and Cobalt are presented in Fig.2. This figure shows that for the tested element one can observe a decrease of Qeq by comparison to absorption in the deionised water. Also, one can observe that the absorption rate is also affected by the increase in the concentration

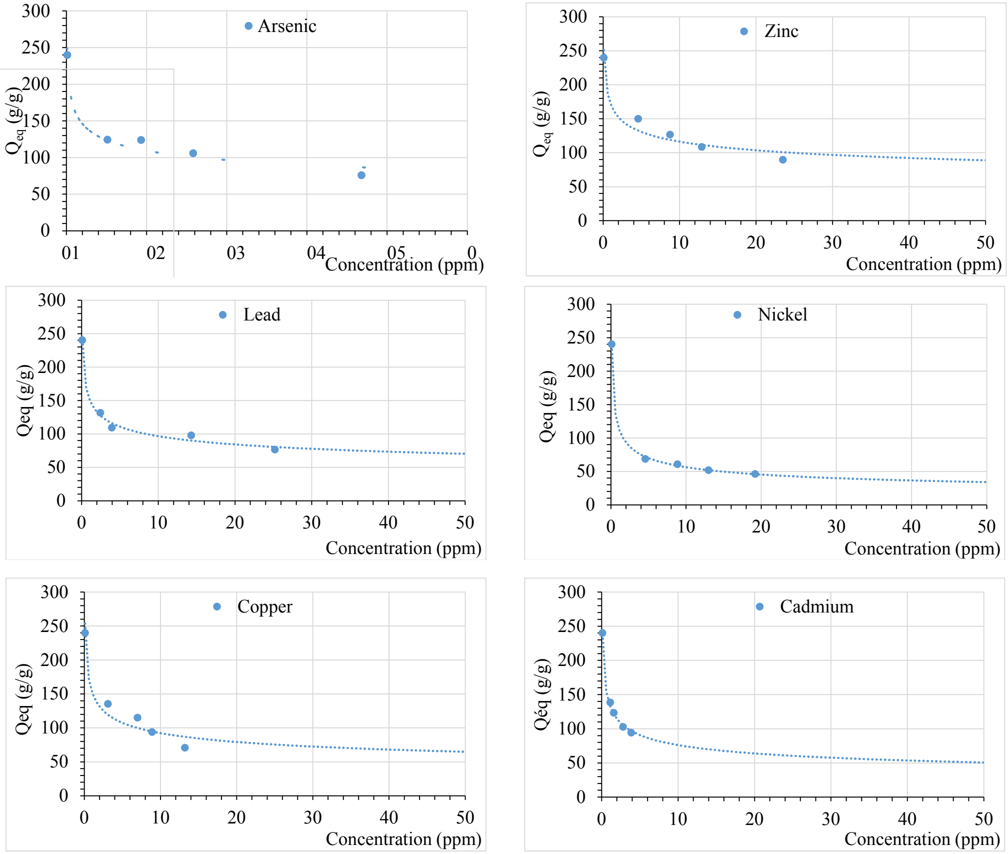

Figure 2 Absorption rate of different elements using SAP

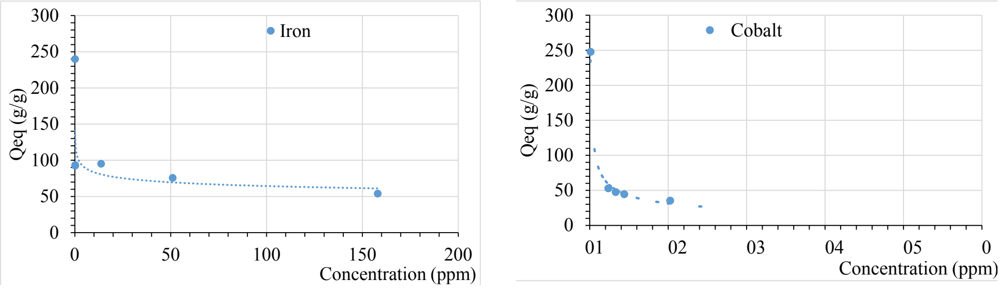

Figure 2 Absorption rate of different elements using SAP (continued)

of the analysed elements. This reduction is included between 146 and 205 g/g for cadmium and Cobalt respectively. This reduction in Qeq can probably be explained by the occupation of sites by metal ions or even by the closure of polymeric meshes, thus preventing absorption.

For the different elements, adjustments were made to the measured values, and all the elements analysed fit adequately using a power model.

Sequestration potential (SP)

The sequestering potential by PSAs of chemical elements depends on the ionization degree of SAPs, pH, chemical concentration, ionic and charge state of the element, and the molar amount (Taouil, 2014). The metal and metalloid sequestration potential was calculated using Formula 2, and the results are shown in Fig. 3. This last figure shows that the sequestration potential ranges from 33 to 40% for Co, 11 to 16% for Cu, 0 to 83% for Pb, 52 to 69% for Zn, 17 to 30% for As, 48 to 69 % for Cd, and 47 to 62 % for Ni.

The sequestration potential exhibits two types of behavior:

- An increase in concentrations is accompanied by a decrease in SP. This behavior is observed for arsenic, zinc, nickel, and cadmium.
- An increase in solution concentrations is accompanied by an increase in SP. This behavior is observed for copper, lead, and cobalt.

The sequestration capacity of PA-Na is due to the forces of diffusion and electrostatic attraction between the carboxyl groups

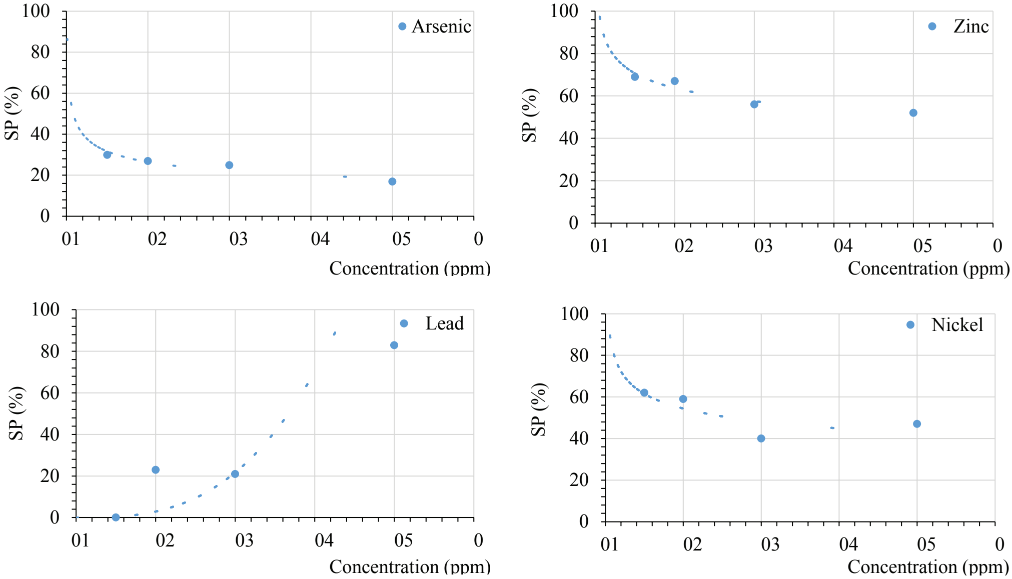

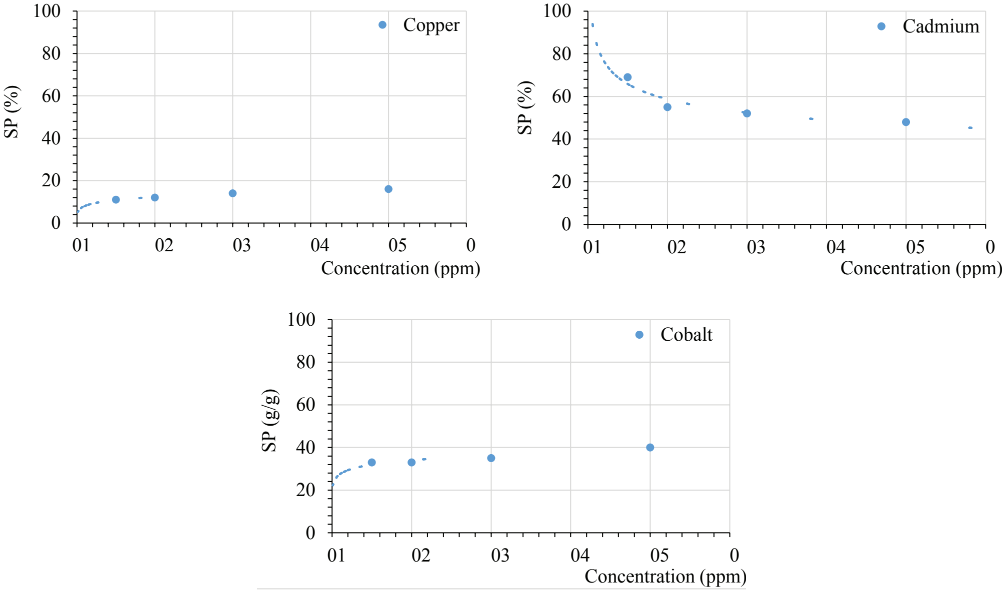

Figure 3 *Sequestration potential of metal and metalloids by SAP*

(COO-) and the metal ions, which favors the penetration of metal ions into the hydrogel network.

Discussion

The presence of metal ions reduces the absorption rate (see Fig. 2), as inter-chain reactions with carboxylate groups restrict the expansion of the polymer network.

Also, the evolution of sequestration potential as a function of metal ion concentration primarily depends on the pH of the medium, the ionic radius of the element, and the available sites in the polymer.

To illustrate the relationship between the absorption rate (Q^{eq}) and the corresponding chemical elements, an equation has been proposed that incorporates both the ionic radii (r) and the initial concentrations (C_i) used in the analysis:

$$Q_{eq} = K_1 \times r + (K_2 / r^3) + K3 \times C_i + (K4 \times \ln(C_i^3)) \tag{3}$$

With K_1 =96.84, K_2 = 14.22 and K_3 =0.3116 et K4 =-1.023.

The proposed equation was used to calculate Q^{eq} for all the analyzed elements, and the results are presented in Fig. 4a. This figure compares the measured and predicted Q^{eq} values. As indicated by the coefficient of determination R^2 (R^2 = 0.98), the predictions are highly accurate, leading to the conclusion that the proposed equation allows for a highly precise calculation of the absorption rate. However, to generalize this equation, it is necessary to validate it using additional data that were not included in the development of Equation 3.

Also, to illustrate the relationship between the absorption rate (Qeq), the initial mass ($M_{0\text{-ion}}$) and final mass ($M_{f\text{-ion}}$) (both used for the calculation of SP), an equation has been proposed:

$$M_{f-ion} = AM_{0-ion} + BQ_{eq}^2 \tag{4}$$

Where A = 0.84 and B = -0.2E^{-4}

The proposed equation was used to calculate the final mass for all the analyzed elements, and the results are presented in Fig. 4b. This figure compares the measured and predicted values of final mass of metal and metalloid. As indicated by the coefficient of determination R2 (R2 = 0.9978), the predictions are highly accurate, leading to the conclusion that the proposed equation allows for a highly precise calculation of the final mass used for the calculation of the SP.

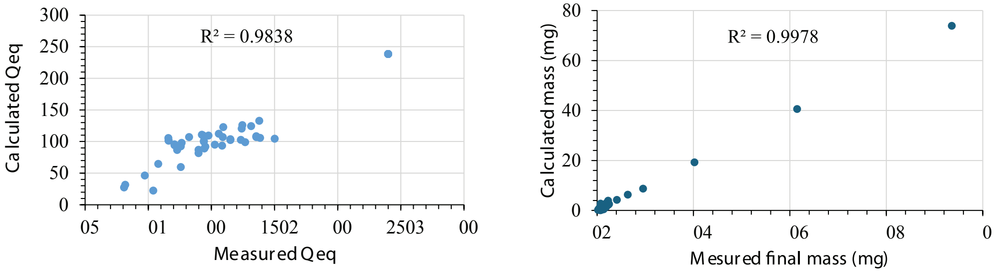

Figure 4 Measured and calculated values: a) Absorption rate (Qeq) b) final metal and metalloid mass

Conclusions

Investigation results demonstrate the effectiveness of SAPs in the absorption water and the sequestering of metal and metalloid. The sequestration capacity of metals is influenced by the ionic radius of the element, and the availability of binding sites in the SAPs and the initial concentration of element.

To better understand the relationship between absorption rates, (Qeq), the potential sequestration (SP) and these chemical factors, equations have been proposed that considers both ionic radii and the concentrations of the elements analyzed. These equations provide highly accurate predictions of absorption rate and sequestration potential of metal and metalloid. However, further validation using data not included in the equation's development is required to generalize their applicability

References

Addi N E, Maqsoud A, Belem T, Mbonimpa M, El Mahboub K, Kabamba CN, Poudama L É, Lemay J F (2019) Évaluation du potentiel de séquestration des métaux lourds contenus dans des pulpes de résidus miniers par les polymères superabsorbants (PSA). Proc. of GeoSt.John's 2019, the 72nd Canadian Geotechnical Conference, St. John's, Newfoundland and Labrador, Canada, September 29 - October 2,

Aubertin M, Bussière B, & Bernier L (2002) Environnement et gestion des rejets miniers. Presses Internationales Polytechnique Montréal, Canada, CD-ROM.

Belviso C, Cavalcante F, Di Gennaro S, Lettino A, Palma A, Ragone P, Fiore S (2014) Élimination du manganèse d'une solution aqueuse à l'aide de cendres volantes et de sa zéolite synthétique hydrothermale. Journal of Environmental Management, 137, 16-22.

Ben Ali H E, Neculita C M, Molson JW, Maqsoud A, Zagury G J (2019) Performance of passive systems for mine drainage treatment at low temperature and high salinity: a review. Miner. Eng. 134, 325–344.

Genty T (2012) Comportement hydro-bio-géo-chimique de systèmes passifs de traitement du drainage minier acide fortement contaminé en fer. Doctorat, Université du Québec en Abitibi-Témiscamingue.

Ismi I, Rifi E, Lebkiri A, & Oudda H (2015) Spectral characterization of PA–Cu under two polymeric forms and their complex PA–Cu. J. Mater. Environ. Sci, 6(2), 343-348.

Kanny Diallo F-B, BelemT, Maqsoud A, Mbonimpa M (2024). Investigation of the potential for removal of heavy metals and metalloids from mine waters using sodium polyacrylate superabsorbent polymers. MEDGU 2024.

Maqsoud A, Neculita C, Bussière B, Benzaazoua M (2016) Hydrochemical evolution of the Abandoned Manitou Mine site during and after tailings deposition. Environmental Science and Pollution Research, 23 (9), 9054-9072.

Rifi E-H, Lakkis D, & Leroy J M (2005) Extraction de l'argent par des gels d'acide polyacrylique–polyacrylate de sodium. Application à l'élimination des ions chlorures. Comptes Rendus Chimie, 8(5), 917-921.

Sahi A, El Mahboub K, Belem T, Maqsoud A, & Mbonimpa M (2019) Dewatering of Mine Tailings Slurries Using Superabsorbent Polymers (SAPs) Reclaimed from Industrial Reject of Baby Diapers: A Preliminary Study. Minerals, 9(12), 785.

Skousen J, Zipper C E, Rose A, Ziemkiewicz P F, Nairn R, McDonald L M, Kleinmann R L (2017) Review of passive systems for acid mine drainage treatment. Mine Water Environ. 36, 133–153.

USEPA (United States Environmental Protection Agency), 2014. Reference Guide to Treatment Technologies for Mining-Influenced Water. pp. 94 EPA 542-R-14-001.

Wolkersdorfer C (2022) Mine water treatment – Active and passive methods. Springer Book, ISBN 978-3-662-65772-0.

Geochemical Modelling Applied to the Study of Arsenic Mobilization in Abandoned Mines

Antonio Luis Marqués[1], Begoña Fernández[2], Ángeles Fernández-González[3], Julia Ayala[4]

[1]Institute of Space Sciences and Technologies of Asturias (ICTEA), University of Oviedo, Independencia 13, 33004 Oviedo, Asturias, Spain, marquesantonio@uniovi.es, ORCID: 0000-0003-4665-4491

[2]Department of Materials Science and Metallurgical Engineering, University of Oviedo, Independencia 13, 33004 Oviedo, Asturias, Spain, fernandezbegona@uniovi.es ORCID 0000-0003-1239-4839

[3]Department of Geology, University of Oviedo, C/ Jesús Arias de Velasco s/n 33005 Oviedo, Asturias, Spain, mafernandez@uniovi.es, ORCID 0000-0002-2009-0870

[4]Department of Materials Science and Metallurgical Engineering, University of Oviedo, Independencia 13, 33004 Oviedo, Asturias, Spain, jayala@uniovi.es ORCID 0000-0002-6404-1296

Abstract

The end of mercury mining activities in the Spanish region of Asturias from the 1970s has left significant sources of arsenic contamination in tailings piles, some of which are abandoned. The mobility of arsenic in water and its incorporation into the hydrological cycle add to the hazards of the leachates that continue to be produced constantly in many of these tailings piles. This work proposes a protocol for characterizing the leachates, which are regularly sampled in the field, analysed in the laboratory and geochemically modelled. The proposed methodology has been applied to the dumps of La Soterraña mine, which contributes concerning amounts of arsenic to the natural waters in its surroundings. Although the results presented here are still considered to be preliminary, the protocol seems to be ideal for evaluating the leachates and their hazards, offering explanations regarding the mobility of the contaminants and the formation of efflorescences that appear in the tailings piles during certain periods of the year.

Keywords: Geochemical modelling, abandoned mines, arsenic, mine tailing pile.

Introduction

The region of the Principality of Asturias (NW Spain) has been an important mercury producer since ancient times. By the late 1960s, it produced 5% of the world's mercury. However, from that point on, the economic conditions that led to the drop in the price of this metal caused the gradual closure of all the mining operations, and the last mercury mine in the region, La Soterraña, ceased its activity in 1974. A characteristic feature of many mercury mines in Asturias is a strong geochemical anomaly in arsenic, which was also exploited as a byproduct and has left significant contamination in the spoil heaps, recognized as an important source of local pollution (Marques, 2020).

The La Soterraña mine, currently inactive, is located in the municipality of Lena, on the southwest slope of a mountain called Las Campusas, next to the AS-231 road. In the field and on satellite photographs, it is identified by the abundance of mining facilities in ruins and by an impressive waste dump (43°11'31.6"N 5°50'37.7"W), which reveals the significant volume of material extracted during an extended mining period. The small stream Muñón runs along the western edge of the spoil heap, collecting leachate water that is permanently channeled in the roadside ditch. The spoil heap is heterogeneous, with almost no vegetation, and recurrent efflorescences, more or less ephemeral, develop on it, although their nature has not been completely determined. Currently, actions are being taken regarding the spoil heap in connection with a remediation and decontamination project (SUBproducts4LIFE) funded by the European Union.

From a geological point of view, the La Soterraña deposit is classified by Luque (1985) and Luque-Cabal and Gutiérrez – Claverol (2010) as part of the Central Coal Basin. The materials in which the mineralization is hosted are sandstones and shales from the Lena Group, of Carboniferous age, which also contains some carbonated banks and coal seams (Luque 1985). The main tectonic structure in the area is the Muñón anticline, with an approximate N-S direction, affected on its western flank by two fault systems: one with an approximate NNE-SSW trace (like the Pajares fault, according to Alonso *et al.* 2009) and another with a predominant E-W direction (like the Aramo fault). The deposit, which is considered of tardi-Hercynian epithermal character (Luque *et al.* 1989), has cinnabar, realgar, and orpiment mineralization, generally associated with limestone beds.

This work proposes a protocol for the geochemical modelling of natural waters that have leached the spoil heaps of these abandoned mines, aimed at understanding their current state after several decades of mining abandonment. The focus is on arsenic, which is highly dangerous and mobile in water, in a hydrogeologically complex context, of rural nature and strong human alteration. It has been applied to the La Soterraña mine, and here we present the main results, which, although preliminary in some aspects, are of interest for potential remediation efforts or actions on the spoil heaps and in the hydrogeological system.

Methods

The methodology applied in this study primarily involves sampling leachate waters at different times of the year, their chemical analysis, and geochemical modelling using the PHREEQC code. The results are interpreted and discussed in correlation with meteorological conditions. The following details the procedure followed for each of these tasks; however, it is important to note that the selection of sampling points, which is not discussed here as it is outside the scope of this study, requires a deep understanding of the regional and local geological and hydrogeological context. Additionally, it is stated that the sampling period extended from late December 2022 to late April 2023, a time of year when precipitation is more likely, according to data from the Spanish State Meteorological Agency. Within this period, efforts were made to maintain regularity, with sampling approximately every 10 days.

Two sampling points, very close to each other, were selected. At the first point (P1), leachate water is directly collected from the lowest point of the waste dump, and at the second (P2), at the same level, from the stream described above, which borders the dump at its most western part. The mixing of waters occurs practically at the sampling site; that is, the leachates are discharged directly into the stream, with no specific treatment currently in place (Marques *et al.* 2018). Fig. 1 shows the location of the collection sites on a satellite image, along with its coordinates.

Water samples were collected and preserved according to a standardized procedure that ensures the absence of contamination and the stability of the sample. Essentially, the procedure requires constant water flow, in-situ measurement of pH and water temperature, the use of gloves,

Figure 1 *Detailed location of the sampling points at La Soterraña on the Google Earth satellite image.*

the addition of three drops of nitric acid (1N) per 200 mL to prevent precipitation, and preservation in decontaminated polypropylene containers, stored in a refrigerator at 8 °C until the chemical analysis is performed. For each collection, 500 mL of sample was obtained per sampling point.

All water samples collected were analysed at the Technical Services of the University of Oviedo. The samples were filtered using a 0.45-micron PTFE syringe filter, and the arsenic concentration was determined in all of them by ICP-MS, using an Agilent Technologies HP 7700 instrument. Additionally, based on the results, a complete analysis of the concentrations of B, Na, Mg, Al, K, Ca, Ti, V, Cr, Mn, Fe, Co, Ni, Cu, Zn, As, Se, Sr, Mo, Ag, Cd, Sn, Sb, Ba, Hg, Tl, Pb, and U was conducted in one of the samples using the same instrumental technique, along with the determination of the anions F^-, Cl^-, and SO_4^{2-} by ion chromatography with a METROHM 883 Basic IC plus system. For this complete analysis, the sample with the arsenic concentration closest to the mean of all the samples was selected.

From the results of analyses, geochemical modelling was carried out using the PHREEQC Interactive code version 3.7.3 (Parkhurst and Appelo 2013), from the USGS (United States Geological Survey). The modelling utilized the llnl.dat database, which includes a comprehensive set of thermodynamic data compiled by the Lawrence Livermore National Laboratory and is considered an ideal database for mine water modelling.

Calculations of the effective rainwater, that is, water that percolates into the waste dump, were obtained using the TRASERO 2.0 code, developed by the Alicante County Council. The input data were obtained from the Spanish meteorological service (AEMET) website, *meteosolana.net*, for the station nearest to La Soterraña mine, called Lena-Ronzón. The code uses an empirical correlation method known as the *Thornthwaite approximation*, whose fundamentals and detailed development can be found in the manual (Diputación de Alicante 2005) and the references therein.

Results

The arsenic content in the samples from the water of the tailings piles at the two locations is shown in Tab. 1. A variation in the data is observed, but within the same order of magnitude, without any major gradients or values that could be considered anomalous within the data series. The arsenic content in all samples is several orders of magnitude above the tolerable levels for water intended for human consumption (not exceeding 10 µg/L according to Spanish regulations in Real Decreto 3/2023 and WHO recommendations), or even for uses such as irrigation (not exceeding 25 µg/L according to Spanish regulations Real Decreto 60/2011).

The full analysis of the sample selected as the most representative in terms of arsenic concentration yields the results shown in Tab. 2. Both the arsenic content data and the data for other elements are consistent with those found in historical records from monitoring conducted at La Soterraña (Marqués, 2020).

The complexity of the waters whose analyses are shown in Tab. 2 and the high number of species and phases that can

***Table 1** As concentration in the water collected from the tailings of the abandoned La Soterraña mines.*

As content µg/L (LQ=2 µg/L)		
Date	**P1 (dump)**	**P2 (stream)**
29/11/2022	35322.35	41532.55
10/12/2022	36634.21	34116.58
20/12/2022	34625.11	33250.48
02/01/2023	35250.36	32928.79
11/01/2023	31667.58	29985.45
20/01/2023	29514.29	29754.02
31/01/2023	31725.43	32260.17
09/02/2023	39533.81	34599.84
18/02/2023	43552.76	40837.89
02/03/2023	36237.60	32906.1
11/03/2023	39472.46	36680.75
20/03/2023	40260.21	42168.88
31/03/2023	41685.37	49421.26
20/04/2023	40266.83	43360.43
27/04/2023	40534.92	43518.9

form presents a complicated geochemical modelling. The modelling with PHREEQC predicts that native mercury (Hg), barite ($BaSO_4$), tiemannite (HgSe), $Sb(OH)_3$, and Sb_2O_4 could precipitate. The saturation indices for each of these are shown in Tab. 3, that also includes the saturation indices for the phases containing arsenic.

Thus, according to modelling, all arsenic species are dissolved, and therefore, their mobility in the natural environment is very high. Based on the PHREEQC modelling, an attempt has been made to determine the hypothetical precipitation sequence of arsenic phases in a system where water is removed through evaporation. However, the concentration required for the precipitation of these phases is so high that the ionic strength increases significantly. When this ionic strength reaches such high levels, the database used in the modelling becomes insufficient, and thus the simulation cannot be performed. Consequently, it can be concluded that arsenic phases will only appear when the presence of water is minimal. In the event that they precipitate, and due to their high solubility, these phases can be considered ephemeral in the tailings, and with any rainfall episode, they would re-enter the aqueous system. Probably, some of these phases appear as efflorescences in the tailings during dry periods.

Discussion

In light of the data presented in the Results section, the situation regarding arsenic at the mining waste dump of the abandoned La Soterraña mine is concerning. The data from this study are consistent with historical records and with those from several research projects that have been developed and are still ongoing to try to mitigate the situation. Focusing solely on arsenic content, the waters circulating around the tailings pile and collecting its leachates are heavily contaminated with arsenic, and the Muñón stream exceeds legal limits for human consumption or even irrigation by more than three orders of magnitude. The efflorescences that recurrently appear are soluble, and instead of permanently fixing arsenic, they re-enter the water system when the short dry periods in the valley end.

The graph in Fig. 2 shows the concentration of arsenic in the analysed samples from La Soterraña along with effective rainfall data as calculated by TRASERO 2.0. Although the discussion is qualitative, it is clear that arsenic concentrations increase during dry periods. The amount of water flowing through the Muñón stream, and the percolation in

__Table 2__ Composition of a representative sample of the leachates from La Soterraña dump.

Element or ion	Concentration µg/L	LQ µg/L
B	56.81	20
Na	21904.54	200
Mg	27234.02	200
K	14896.46	200
Ca	235837.12	200
V	11.91	2
As	36634.21	2
Se	3.67	2
Sr	3247.53	2
Mo	8.97	2
Sb	59.88	2
Ba	28.51	2
Hg	0.56	0.2
U	0.82	0.2
	mg/L	**mg/L**
F^-	0.680	0.02
Cl^-	12.33	0.2
SO_4^{2-}	616.47	0.2
NO^{3-}	2.804	0.2

__Table 3__ Saturation indices for As species and the possible phases that could precipitate in lixiviates.

Phases	Saturation Index
Barite	0.52
Hg (native)	4.9
$Sb(OH)_3$	0.79
Sb_2O_4	6.4
Tiemannite (HgSe)	4.4
Arsenolite (As_2O_3)	-22.66
As	-33.04
As_2O_5	-24.77
As_4O_6 (cubic.)	-45.17
As_4O_6 (monocl.)	-44.95

the tailings pile increases during the rainy season, and the concentration of dissolved phases decreases. Establishing a quantitative correlation of data requires a longer sampling period, and most likely, the actions being carried out at the tailings pile and its surroundings in connection with ongoing projects complicate the achievement of a good quantitative correlation between rainfall and arsenic concentration, beyond the merely qualitative correspondence.

Conclusions

In light of the data presented in the Results section, the situation regarding arsenic at the tailings pile of According to the geochemical modelling, all the arsenic is in dissolved chemical species, making it highly mobile. Arsenic phases will only precipitate during very dry periods. Due to their high solubility, rainfall carries them back into the aqueous system.

Although the available data are preliminary, a correlation has been found between the arsenic leached from the La Soterraña tailings pile and the effective rainfall during the sampling period.

The proposed protocol for studying the leachates provides useful information for designing mitigation strategies and environmental monitoring in mining areas.

Acknowledgements

This study was supported by the Ministry of Science and Innovation (Spain) under CI-MCI-21-PID2020-113558RB-C41.

References

Alonso JL, Marcos A, Suarez, A (2009) Paleogeographic inversion resulting from large out of sequence breaching thrusts: The León Fault (Cantabrian Zone, NW Iberia). A new picture of the external Variscan Thrust Belt in the Ibero-Armorican Arc. Geologica Acta, 7(4):451–473, doi: 10.1344/105.000001449.

Diputación de Alicante (2005) Tratamiento y gestión de series temporales hidrológicas. Simulación de Modelos de flujo en Acuíferos. Manual del usuario de la aplicación TRASERO. Available at https://ciclohidrico.com/descargas/aplicaciones/

Luque C (1985) Las Mineralizaciones de Mercurio en la Cordillera Cantábrica. PhD. Thesis, University of Oviedo 1531 p.

Luque C, García-Iglesias J, Garcia-Coque P (1989). Características geoquímicas de los cinabrios de la cordillera cantábrica (NW de España): Utilidad en prospección. Trabajos de Geología 18:3–11.

Luque Cabal C, Gutiérrez-Claverol M (2010) Riquezas geológicas de Asturias. 416 p. ISBN 978-693-8520-3

Marques AL (2020) Modelización de la incidencia de la minería abandonada de mercurio en la cuenca del río Nalón: correlación de eventos y análisis de riesgos. PhD. Thesis, University of Oviedo 311 p. https://digibuo.uniovi.es/dspace/handle/10651/60418.

Marqués AL, Ribeiro L, Roqueñí N, Fernández JJ, Loredo J, (2018) A new graphic methodology to interpret the multivariate data analysis of hydrochemical data in orphan mine areas, Journal of Geochemical Exploration, 191:43–53, https://doi.org/10.1016/j.gexplo.2018.06.001.

Parkhurst DL, Appelo, CAJ (2013) Description of input and examples for PHREEQC version 3–A computer program for speciation, batch reaction, one-dimensional transport, and inverse geochemical calculations: U.S. Geological Survey Techniques and Methods, Book 6, Chap. A43, 497 p. https://doi.org/10.3133/tm6A43

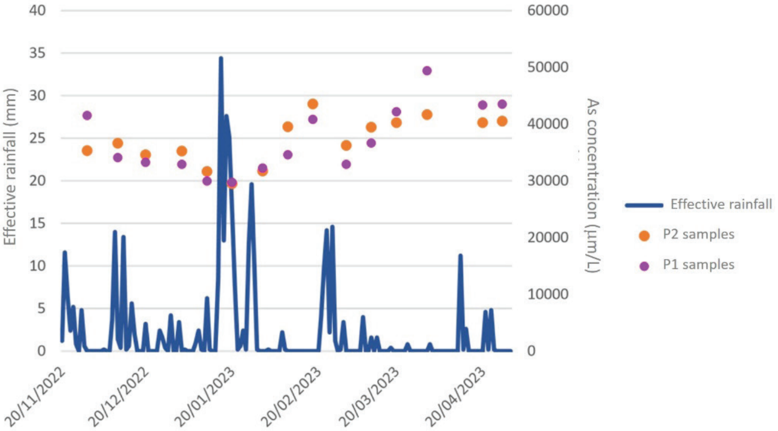

***Figure 2** Correlation between effective rainfall and arsenic concentration at the two sampling points.*

Environmental Challenges and Remediation Operations at the Former Antimony-mine of Le Cetine di Cotorniano (Tuscany, Italy): Monitoring and Water Treatment Solution at Laboratory and Field Scale

Federica Meloni[1,2], Giordano Montegrossi[2], Barbara Nisi[2], Jacopo Cabassi[2]., Francesco Bianchi[3], Stefano Mirri[4], Andrea Profeti[5], Orlando Vaselli[1,2]

[1]*University of Florence, Via G. La Pira 4, Florence, Italy*

[2]*CNR-IGG Institute of Geosciences and Earth Resources, Via G. La Pira 4, Florence, Italy*

[3]*S.B.C. Geologi Associati, Via XX Settembre 78, Florence, Italy*

[4]*Regione Toscana, Via di Novoli 26, Florence, Italy*

[5]*Ingegno P&C S.r.l. , Via A. Gramsci 49, Ponte a Egola (Pisa), Italy*

Abstract

The main criticality at the former Sb-mine of Le Cetine (Tuscany, Italy) is the high content of Sb in surface and shallow ground waters (up to 24 mg/L). To minimize the Sb concentration, a laboratory-scale Permeable Reactive Barrier (PRBL) was built to mimic the effect of a full-scale PRB, which is expected to be operative in the forthcoming months to abate the initial Sb content up to 75%. A kinetic model to verify the fate of Sb into the PRB is presented and highlighted that the minimum residence time of waters to reduce Sb in PRB is 168 hours.

Keywords: Antimony, kinetic reactions, geochemical monitoring, permeable reactive barrier

Introduction and study area

The exploitation of Sb at Le Cetine di Cotorniano mine (Southern Tuscany, Italy, Fig. 1A) began in 1878 and ceased in 1948 (Menchetti *et al*. 2015). Over time, even though the Sb demand was mostly related to weapons manufacturing, the mining activity was discontinued due to poor technology and complexity of the geological environment. The Le Cetine mine is part of a series of epigenetic Sb-rich ore deposits characterizing the southern part of Tuscany and generated by hydrothermal fluids related to the "Tuscan Magmatic District". These deposits are located on a structural high mainly due to direct and oblique faults, developed after post-collisional extensional tectonic activity (Middle Miocene) (Menchetti *et al*. 2015). In particular, the mine expanded at the contact with the Calcare Cavernoso Fm (CC, a Rhaetian vacuolar dolomitic limestone) where an intense silicification produced jasperoids. Permian siliceous schists and Oligocene-Cretaceous Ligurian and Sub-Ligurian Units are unconformably under- and overlying CC, respectively (Menchetti *et al*. 2015). The latter two formations are made up by ophiolitic fragments, clays, gabbro, and marls (Fig. 1B). The mineralization, with a content of Sb between 5 and 50%, mainly consisting of stibnite (Sb_2S_3), was found within the jasperoids. Sometimes, stibnite and calcite veins were recognized in fractured areas or within non-silicified dolomitic zones. Where altered, stibnite turns into Sb-oxides and sulfates (Menchetti *et al*. 2015). Many Sb bearing minerals, including cetineite (a Sb-oxysulfide hydrate: $NaK_5Sb_{14}S_6O_{18}(H_2O)_6$, Sabelli and Vezzalini, 1987), cervantite (Sb^{3+} Sb^{5+} O_4, first reported by D'Achiardi, 1901), onoratoite ($SbO_{11}Cl_2$, Belluomini *et al*. 1968), and other minerals e.g. rosenbergite ($AlF[F_{0.5}(H_2O)_{0.5}]*H_2O$, Omi *et al.* 1993) and dacostaite ($K(Mg_2Al)[Mg(H_2O)_6]_2(AsO_4)_2F_6*2H_2O$, Biagioni *et al.* 2025), have been found over the years in this mine. The Corsaioli Creek (Fig. 1B) is the main receptor of the surface run-off of Le Cetine, limiting the mining area to the south, and it flows into the main watercourse in the study area: the Rosia River (Fig. 1C).

The high secondary permeability of CC favors the infiltration of meteoric waters circulating on the surface. This indeed provokes an irregular inflow. In particular, during the summer months (July to September), little or no water is feeding the Corsaioli Creek and the few occurring springs. The absence of water in the mining system was both an advantage (the tunnels were not flooded during mining operations) and a disadvantage (rainwater collecting areas were placed and used for various mining operations, Menchetti *et al.* 2015). Given the high solubility of Sb minerals, from a geochemical point of view, the lack of water is beneficial. Issues arise when mineralization in streams or mining tailings interact with meteoric and run-off waters in autumn-winter months. During these periods, Sb concentrations in surface water greatly exceeded the threshold concentration (CSC) of 5 µg/L for surface water imposed by Italian law (Lgs D. 152/06). In 2011, a preliminary characterization plan was carried out for both soils and waters from the mining area, which led to define an exhaustive reclamation project that is currently going on. Among other reclamation operations, the project includes the reshaping of the mine tailings, to be covered by an impermeable capping, followed by the construction of a reactive permeable barrier (PRB) to drain surface and ground

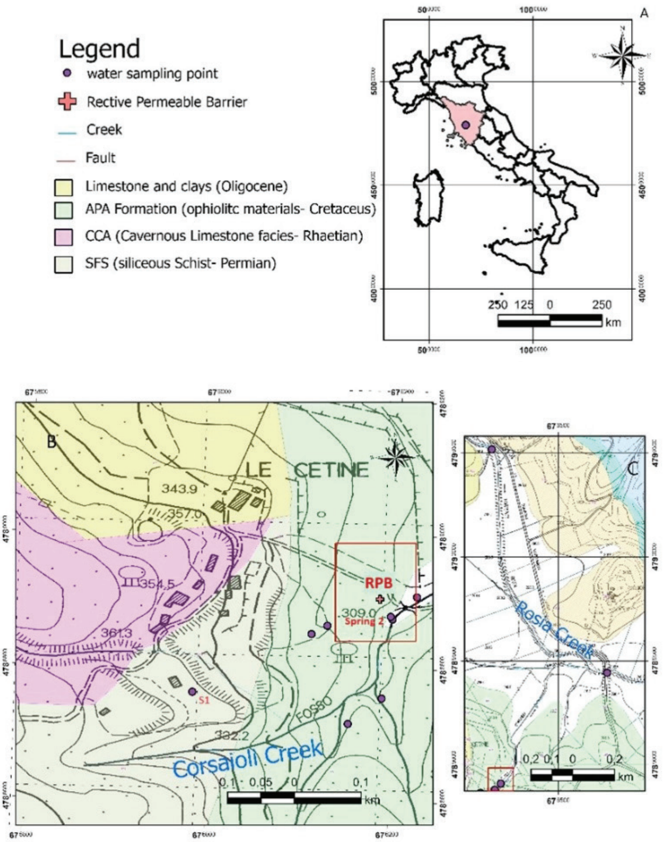

Figure 1 Simplified geological maps of Le Cetine di Cotorniano mine. The violet circles represent the water sampling points and the red cross the location of the Permeable Reactive Barrier.

waters. The PRB to abate Sb is expected to be done early this year. Since June 2024, a monthly geochemical survey of the waters within the mining area and nearby (violet circles in Fig. 1B and 1C) has been carried out and a PRB, at laboratory scale, was built to test the efficiency of the PRB on-site.

The aims of this work were to: i) geochemically characterize the surface and ground waters in the Le Cetine mine, ii) investigate the reaction kinetics of the various minerals characterizing the study area to optimize the PRB functionality with the aim to reduce the Sb concentrations by least 75% before discharging the treated waters into the local watercourse.

Methods

For the geochemical monitoring of the waters from the former mining area, ten sampling points were selected, as follows: two piezometers (i.e., S1 in the tailing body, and S6 at the foot of the tailing body); one spring; seven surface waters, i.e., five from the Corsaioli Creek (respectively named F1, F2, F3, FCP, F4) and two from the Rosia Creek (one upstream and one downstream after the confluence of the Corsaioli Creek). During the various surveys, F1, S6, and the spring could not be sampled because they were dry. In October 2024, however, a new spring, named “spring 2”, was found with a flow rate of 0.1 L/min. For each sampling, measurements of pH, electrical conductivity (EC), redox potential (Eh), temperature (T), and in the case of sample S6 hydraulic head, were carried out in situ. The main cations and anions, as well as Fe, Al, Mn, Hg, As, Sb, Se and some other trace metals, were analyzed. The software PHREEQC version 3.5.0 (Parkust and Appelo, 1999) with Minteq.v database, modified by Meloni *et al.* (2024), was used to calculate the Saturation Index (SI) and determine Sb speciation. Furthermore, four mine tailings samples (named from Cet1 to Cet4), with different grain sizes, were collected and leached (ratio soil-MilliQ-water 1:10) to study the reaction kinetics of the minerals contained in the tailings. The leaching tests were performed on the four samples after 1 hour, 1 day, and 7 days. The leaching tests were carried out progressively (from 1 hour to 7 days) on the same sample aliquot after filtration at 0.45 µm. In total, the material was leached for 8 days and 1 hour. For each leaching test, the main cations and anions, as well as the same trace elements as those measured in the water samples, were analyzed. Subsequently, the kinetic model that best represented the mineral dissolution was calculated. Additionally, by using the PHREEQC software, the reaction conditions leading to the mineral dissolution were reconstructed. This process allowed us to define the origin of the Sb-pollution in

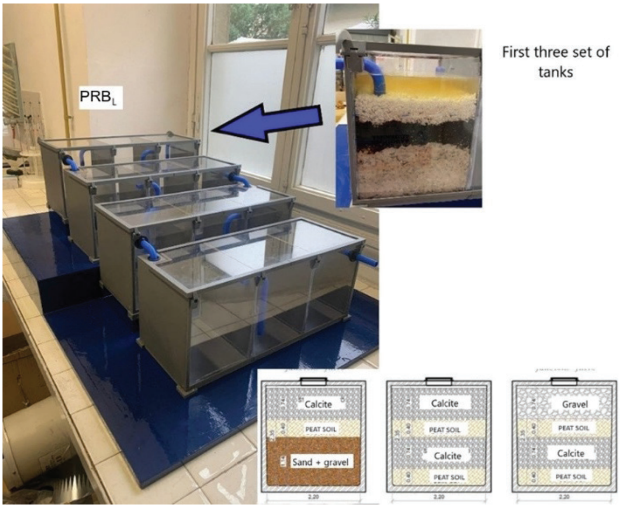

Figure 2 Laboratory-scale Permeable Reactive Barrier (PRBL) and a schematic representation of the tanks and relative proportions of the materials to be filled with.

spring 2, and the runoff waters that are going to be conveyed to the PRB. As part of the reclamation project, the PRB is constructed with four cascading tanks, each one divided into three smaller compartments. The first set of tanks consists of alternating layers of gravel + sand, peat soil, and calcite with mixed grain sizes (Fig. 2). The second and third sets are composed by alternating layers of peat soil and calcite with mixed grain sizes (each of this layer is repeated twice). The final set of tanks is composed by peat soil, calcite with mixed grain sizes, and a final layer of gravel. All tanks are sealed airtight to create reducing redox conditions. This model was recreated at a laboratory scale using a 3D printer (Fig. 2) and filled with the previously described materials. A peristaltic pump was used to circulate the water through the barrier by setting the flow rate to the downscaled version of the PRBL, preserving the interaction time as the water passes through the PRB (ca. 8 days).

Results and discussion

The surface waters exhibited a Ca(Mg)-HCO_3 geochemical facies. Sample S6, on the other hand, had a Ca(Sb)-SO_4 composition, while spring 2 showed an intermediate (Ca(Sb)-$HCO_3(SO_4)$) composition between S6 and the surface waters. All waters, except for the samples from the Rosia stream in July, consistently exceeded the Sb concentrations for CSC limits. Specifically, the concentration of Sb in S1 was 24,407 µg/L, whilst that of spring 2 was 10,993 µg/L. The Corsaioli creek showed a Sb content of 865 µg/L after the inflow of spring 2 into the creek. All analyzed waters were relatively low in Fe and Al (up to 220 and 68 µg/L, respectively). Notably, spring 2 and sample S1 were characterized by Fe and Al concentrations below the detection limit (5 µg/L).

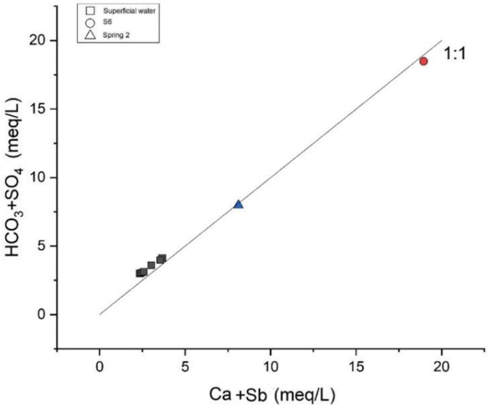

Figure 3 Binary diagram Ca+Sb (meq/L) vs. HCO_3+SO_4 (meq/L) for the October 2024 water samples. Th stoichiometric line is also drawn.

By calculating the SI of the waters and the speciation of Sb and given the generally basic pH of the waters and an oxidizing Eh (always above 200 mV), Sb was found as Sb^{5+}, in the form of romeite ($Ca_2Sb_2O_7$) or SbO_2. Occasionally, tripuhyite ($FeSbO_4$) appeared to be slightly oversaturated. If we consider Sb^{5+} dominating over Sb^{3+} and construct a binary graph of Ca+Sb vs. HCO_3 + SO_4 (in meq/L, Fig. 3, with concentrations relative to the October 2024 sampling), the sampled waters distribute uniformly along the stoichiometric 1:1 line, demonstrating that the waters derive from water-rock interaction processes involving meteoric water, carbonate, sulfide, and sulfate.

Scanning electron microscopy (SEM) of the four sampled tailings showed that antimony was found as metallic Sb, Sb bound to Ca and S (likely as romeite) and occasionally as stibnite, and Sb-oxides. However, the presence of Sb sulfosalts cannot be ruled out, as they were found in both the mine and the landfill materials. Gypsum, calcite, pyrrhotite, and pyrite (sometimes containing As) were also present.

Currently, X-ray powder diffraction (XRD) and quantitative XRF analysis are in progress. The leaching tests on the tailing samples showed a change in the geochemical facies over time, i.e., transitioning from Ca(Sb)-SO_4 to Ca(Sb)-HCO_3 (Fig. 4A,B C). Unlike Fig. 3, Fig. 4C shows a deviation of the leachate samples from the 1:1 stoichiometric line to a Ca+Sb enrichment. When Ca is removed from the graph (Fig. 4D), the samples realign along the stoichiometric line, indicating a greater contribution of Ca due to an increased presence of calcite, gypsum and romeite. From the kinetic model, it is observed that Sb follows a second-order kinetics equation (Eq. 1), while the main anion and cation components follow a first-order kinetics equation (Eq. 2):

$y = B(1-e^{(-x/c)})$ Eq.1

$y = B \times log(C \times x) + A$ Eq.2

By entering the obtained parameters into PHREEQC, it is evident that the dissolution kinetics of the minerals are governed by the dissolution of pyrite (FeS_2) and the precipitation of magnetite. Calcite buffers the acidity of sulfides (primarily Sb_2S_3 and FeS_2), raising the pH up to > 9.3.

Calcium ions are related to the dissolution of gypsum. Sulfate is also likely related to the chemical oxidation of FeS_2. In some cases, an excess of sulfate is found due to the presence of soluble salts (e.g. mirabilite, peretaite, batoniite), which immediately increase their concentration in the aqueous phase. The kinetic model indicates that after 168 hours the concentration of Ca^{2+}, Sb^{5+}, $Fe^{3+ \text{ or } 2+}$, SO_4^{-2}, HCO_3^{-} in the leachates tends to be stabilized. Therefore, this coincides with the minimum residence time of the water with a flow rate of 0.00167 L/s (i.e., the flow from "spring 2") in the PRB to achieve a reduction of Sb concentrations. To test the PRB_L, synthetic waters with increasing concentrations of Sb (i.e., 20, 50, 100 µg/L) were produced. After the required contact time with the barrier filling material had passed, an aliquot of water was collected for pH, EC, Eh, and T measurements, and main cations and anions and trace metals analysis. The water flowing through the barrier showed a reduction in Sb of approximately 75%. Tests with concentrations of around 1000 µg/L are also planned.

Conclusion

This study presented the results of geochemical surveys of surface and piezometer waters at the former Sb mine of Le Cetine di Cotorniano. The waters had high concentrations of Sb largely exceeding the Italian CSCs. The remediation project, which is still ongoing, includes the creation of a PRB to channel run-off and spring waters and to reduce Sb concentrations in the nearby river. To optimize the PRB, reaction kinetics of minerals, characterizing the mine tailings, were investigated. In addition, a laboratory-scale PRB was tested with a

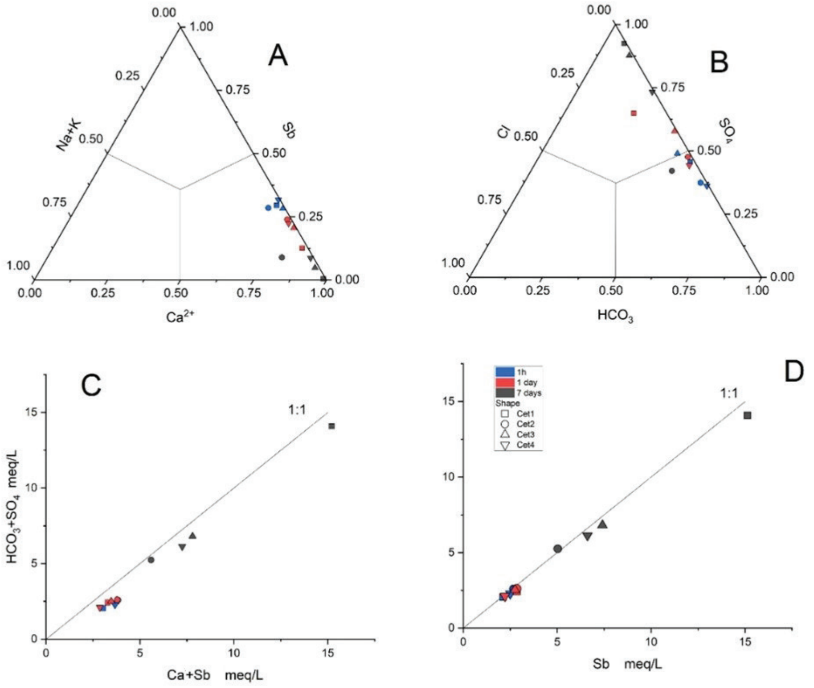

Figure 4 A) Main cation ternary diagram, B) main anion ternary diagram, C) binary diagram Ca + Sb (meq/L) vs. HCO_3 + SO_4 (meq/L), D) binary diagram Sb (meq/L) vs. HCO_3 + SO_4 (meq/L) of the four tailing leachates.

synthetic water at increasing concentrations of Sb to assess whether the designed PRB would be able to reduce the initial concentration of Sb. The barrier is currently able to retain approximately 75% of the Sb input. Forthcoming studies involving waters with higher Sb concentrations are already planned by also adding As and Se, the latter two exceeding the Italian CSCs. Whether the physicochemical processes that retain Sb in the barrier are related to adsorption or precipitation of mineralogical phases are also to be investigated.

References

Belluomini G, Fornaseri M, Nicoletti M (1968) Onoratoite, a new antimony oxychloride, from Cetine di Cotorniano, Rosia (Siena, Italy). Minaral Mag 36:1037–1044, doi:10.1180/minmag.1968.036.284.01

Biagioni C, Mauro, D, Sejkora J, Dolníček, Z, Dini A, Škoda R (2025) Dacostaite, K (Mg2Al)[Mg (H2O)6]2 (AsO4) 2F_6 2H2O, a new fluoride–arsenate mineral from the Cetine di Cotorniano Mine (Tuscany, Italy). Eur J Min 37(1):39–52, doi:10.5194/ejm-37-39-2025

D'Achiardi G. (1901): Cenni sui minerali della miniera di antimonio delle Cetine di Cotorniano. Atti della Società Toscana di Scienze Naturali, Processi Verbali, 12:232–236 (In Italian)

Meloni F, Montegrossi G, Cabassi J, Bianchi F, Nisi B, Rappuoli D, Vaselli O (2024) Geochemical Surveys of Ground and Surface Waters in the Abandoned Hg-Mine of Abbadia San Salvatore (Central Italy): A Preparatory Investigation before Remediation. Water 16(9):1210, doi:10.3390/w16091210

Menchetti S, Batoni M, Batacchi C, Borselli A, Ceccantini L, Fassina B, Marchesini M, Rossellini A, Ruggeri G (2015) Le Cetine di Contorniano. Miniera e Minerali; Associazione Micro-Mineralogica: Cremona, Italy, p 354 (In Italian). ISBN: 978-88-905541-3-1

Olmi F, Sabelli C, Trosti-Ferroni R. (1993) Rosenbergite, AlF [F0. 5 (H2O) 0.5] 4· H2O, a new mineral from the Cetine mine (Tuscany, Italy): description and crystal structure; Rosenbergite, AlF[F0.5(H2O)0.5]4·H2O, a new mineral from the Cetine mine (Tuscany, Italy): description and crystal structure. Eur J Min 5(6):1167–1174

Parkhurst DL, Appelo CAJ (1999) User's guide to PHREEQC (Version 2)-A computer program for speciation, batch-reaction, one-dimensional transport, and inverse geochemical calculations: U.S. Geological Survey. Water Res Inv 312:99–4259, doi: 10.3133/wri994259

Sabelli C, Vezzalini MG (1987) Cetineite, a new antimony oxide-sulfide mineral from Cetine mine, Tuscany, Italy. Neu Jahr Min Monat 9:419–425.

Application of Unsupervised Machine Learning Methods to Mine Water Quality Data

Tom Meuzelaar[1], Allie Wyman[1], and Shannon Zahuranec[1]

[1]Life Cycle Geo, LLC., 729 Main Street, Longmont CO 80501, tom@lifecyclegeo.com (ORCID 0000-0003-3119-8390), allie@lifecyclegeo.com, shannon@lifecyclegeo.com

Abstract

Mine water quality data is both ubiquitous and highly under-used. Water quality data is typically collected on a regular basis starting early in the mine project life cycle all the way into post-closure. The data is spatially extensive, multivariate and highly dimensional in nature, making it ideal for analysis by modern unsupervised methods. Application of unsupervised machine learning methods to water quality data in four different parts of the mine project life cycle (baseline and compliance, feasibility and permitting, operations and closure) at various project sites indicates that the multivariate approach succeeds where traditional methods fail and provides considerable additional insight and value to mine operators. The methods are highly effective in identifying unique water quality fingerprints, the existence of mine influence, and mixing and various reactive processes that occur in water. Example use cases are provided herein and demonstrate that the methods have been successfully used to reduce water treatment capital and operating expense, prevent and mitigate expensive environmental liability and provide significant forecasting insight.

Keywords: Mine water quality, unsupervised machine learning, life cycle water management

Introduction

Surface water, groundwater, process water and other water quality data types are collected throughout the mine project life cycle at regular, recurring intervals (e.g., MEND 2009). During early exploration stages, water quality is collected for baselining purposes. In the mine planning and stage, water quality data collected from material characterization testing is combined with the baseline data to develop models that predict water quality associated with future mining activities. Prediction outcomes support material and water management strategies, as well as permitting needs. During operations, water quality data is collected to monitor mine facility seepage, water treatment performance, and compliance at site boundaries. In closure, water quality is collected to assess closure strategy effectiveness and employ adaptive water management strategies. Water quality data is ubiquitous through the project life cycle and yet remains highly underutilized. Employment of multivariate approaches to analyzing water quality data remains the exception and not the rule.

The abundance of this data is ideally suited to using machine learning approaches to maximize its value. Water quality data is typically collected at regular intervals throughout the project life cycle. Furthermore, compliance and operational requirements dictate that water quality be collected at sufficient spatial density (MEND 2009). Finally, water quality data is multi-dimensional, commonly including measurements for 20 to 40 (or more) different parameters. The large number of parameters makes for a “wide” dataset with considerable statistical and geochemical variance, which facilitates application of innovative unsupervised machine learning methods.

In this study, unsupervised machine learning methods are applied to evaluate mine water quality during four separate stages of the mine life cycle. The names of mine sites, operators, and other location-specific details are often not divulged as many of these analyses have yet to be reviewed by respective regulatory stakeholders. As such, the unsupervised analyses must, for now, remain in the confidential domain (except where explicitly stated).

Methods

All water quality data was analysed using Principal Component Analysis (PCA) using various Python (Van Rossum *et al.* 2009) libraries including pandas, numpy, pyrolite (Williams *et al.* 2020), sklearn, matplotlib and seaborn. Unsupervised multivariate data analysis is a typical first step in a machine learning project, primarily aimed at exploring data structure and identifying classes of related samples (often referred to as "domains"). Numerous methods exist that can be applied to water quality data (Huang *et al.* 2022) which offer various strengths and weaknesses, primarily the extent to which they preserve local and global data structures. PCA is highlighted in this study because statistical relationships between water quality parameters are easily observed on a biplot and add considerable interpretability to the results. However, it should be noted that other multidimensional methods can add considerable insight during a multivariate analysis. PACMaP (Pairwise Controlled Manifold Approximation and Projection; Wang *et al.* 2021), for instance, is recognized to be one of the most optimal methods for preserving both local and global data structure.

However, PCA is perhaps most widely used as its output can add considerable elements of explainability to the results, which is critical for machine learning work. PCA is a dimensionality reduction technique that simplifies a dataset to its irreducible, basic structure (i.e., principal components) in terms of statistical variance. Typically, the bulk of the dataset geochemical variance is accounted for by principal components 1 and 2, although for datasets with deeper statistical variance, additional components can add relevance in an analysis. The biplot is a graphic tool that displays how individual chemical elements relate to one another in principal component space. The position of chemical vectors on a biplot indicate whether elements are closely related or inversely related. Elements with longer vectors exert greater control over the overall dataset statistical variance. Individual sample factor scores can be plotted on the biplot as well which helps indicate which samples exert the greatest influence on a dataset for a particular set of parameters. For groundwater and surface water data, when sample points for a given location cluster in one area of the biplot, it indicates that water quality is not changing much over the sampling period. Locations with highly variable sample scores over time are likely undergoing some chemical changes, such as being influenced by mine impacted water, mixing with another water, or other geochemical reactions.

All water quality datasets required data cleaning and transformation prior to statistical analysis to address issues such as data censoring (detection limits), missing values, outliers and implicit numeric correlation (e.g., Aitchison, 1982).

Results

Fig. 1 provides a biplot for water quality collected for a large underground mine permitting project, where several groundwater types are expected to be encountered that might require eventual treatment during operations.

The mine will be developed in fractured bedrock (Deeper Aquifer) below a thick layer of alluvium (Shallow Aquifer). The future operator was unable to distinguish groundwater quality between the two layers using simple time series evaluation and requested a more sophisticated analysis. Fig. 1 presents results of this analysis and shows that unsupervised methods are clearly able to distinguish between deeper aquifer water, with arsenic and fluoride particularly diagnostic, and shallow waters that are more defined by their carbonate mineral composition, as indicated by the alkalinity, calcium and magnesium vectors; these trends can be directly related to logged lithology and bulk geochemical data for the boreholes. PCA results underscore the importance of dissolved trace element concentrations in identifying each forensic signature. Furthermore, one well (Aquifer Mixing) has a very long well screen that is open to both the Shallow and Deeper aquifer – PCA clearly shows that water quality in this well exhibits both aquifer forensic signatures and makes it possible to tell during which sampling intervals the water carries one signature or the other.

Fig. 2 shows the multivariate signature of humidity cell test (HCT) data collected during the feasibility/permitting stage for the proposed Pebble mine in the USA (this mine was never permitted). This data is publicly available through a published EIS.

The PCA results displayed on the biplot are augmented by multivariate clustering (colored panels in background of Fig. 2). Multivariate analysis of HCT data has, to our knowledge, not been published and yet is highly useful. This Pebble HCT dataset was published and first presented in 2024 (Meuzelaar and Wyman, 2024) and clearly shows geochemical transitions that mine waste materials undergo in humidity cells over time in the process of becoming acid generating. The four broad clusters speak to this, with cells typically starting out at stable pH (Cluster 1), being buffered by alkalinity available in the materials. If the waste materials have negligible or low sulfide content, cell leachate quality remains in this cluster for the duration of testing. Cells with higher sulfide, however, begin to oxidize over time and enter the yellow transition zone characterized by the sulfate vector, which represents sulfide oxidation, and the magnesium, calcium and barium vectors, which represent buffering of acidity by neutralizing carbonate minerals. Once material neutralization potential is depleted, the cells start to become acid generating and enter the cluster 3 domain on the biplot – this transition is typically very fast. This cluster is defined by acidity and all

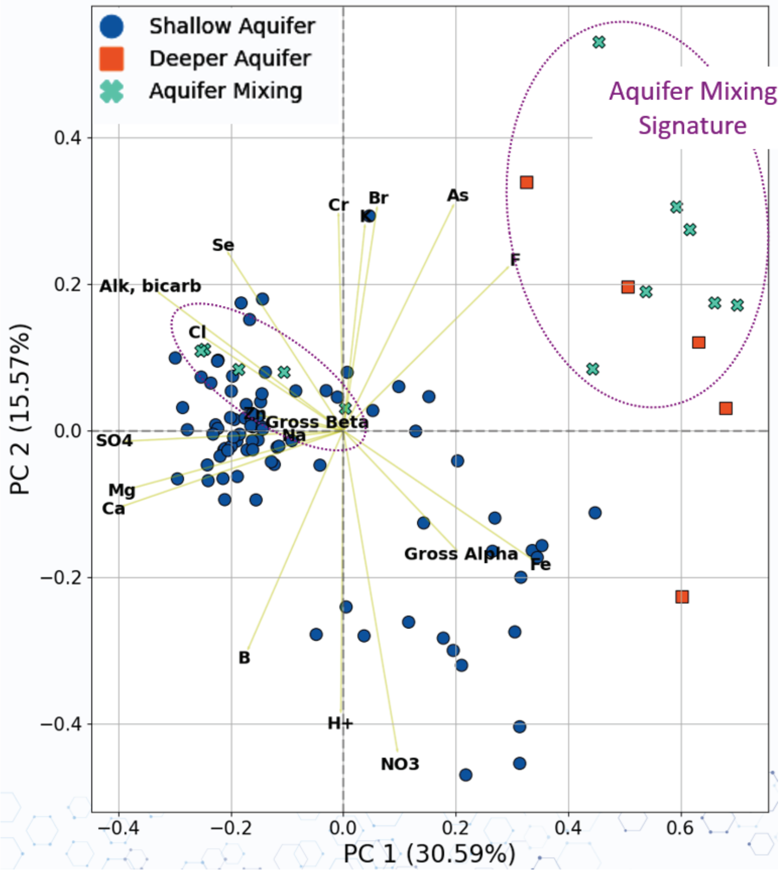

Figure 1 *Water Quality Signatures of Shallow Alluvial, Deep Bedrock and a Mixed Zone.*

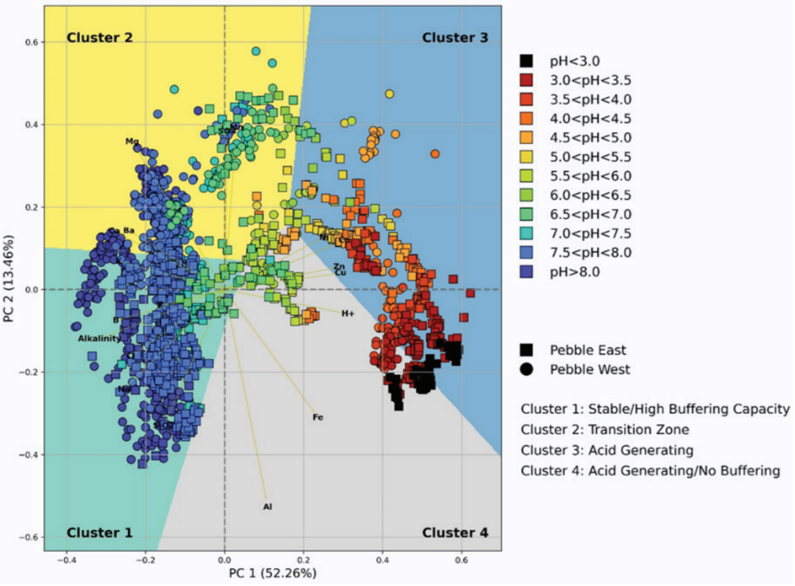

Figure 2 *Water quality signatures of the Pebble HCT dataset over time (Meuzelaar and Wyman 2024).*

the chalcophile trace metals that are typically released from sulfide minerals and remain in solution as the pH lowers. It is important to note that changes in HCT chemistry can be observed on the biplot that are often not evident based on leachate pH alone – results from unsupervised multivariate analysis can serve as an early warning indicator of ARD onset, where HCT pH often cannot. Finally, the iron and aluminum vectors (which plot towards the southeast) define cluster 4 and are consistent with a humidity cell running out of 'fuel' (sulfide content) which eventually leads to pH recovery – as pH recovers, iron precipitates out first (above pH 3–3.5), followed by aluminum (pH 4–4.5).

Fig. 3 illustrates HCT permitting data (grey symbols) collected for a confidential mine site with operational seepage data (purple symbols). The operational seepage data is overlain as the larger purple symbols in Fig. 3 and represents drainage from a lined waste rock facility consisting of materials that have long-term ARD potential. Laboratory HCT tests indicate that materials have a propensity to become acid-generating within a decade, however this has not been observed at the operational scale.

The operator is concerned that their waste rock pile will become acidic in the next few years and requested development of a seepage water quality analysis tool that will predict onset of ARD before it happens based on monthly monitoring of seepage from the waste rock pile. Early warning will give them time to respond adaptively and proactively – once ARD starts, it is extremely difficult to reverse. Because the HCTs represent accelerated weathering that generates ARD in the lab, it provides an excellent laboratory proxy for the geochemical "direction" (on the biplot) that seepage water quality is likely to move in if the waste rock pile begins to generate acid. The biplot looks somewhat similar to the previous Pebble HCT dataset, except these rocks are much more mafic in nature, so trace metals such as copper and nickel tend to predominate in leachate chemistry.

Unsupervised analysis of actual seepage data, overlain on the permitting-stage laboratory data, allows the operator to see, on a monthly basis, whether waste rock pile seepage is moving closer to acidic conditions or further away. This allows the operator to respond proactively (i.e., add lime to the pile) to prevent ARD formation which could result in costly compliance penalties.

Fig. 4 shows the final unsupervised analysis, representing four decades of groundwater and surface water quality data being collected at a mine that is going into closure.

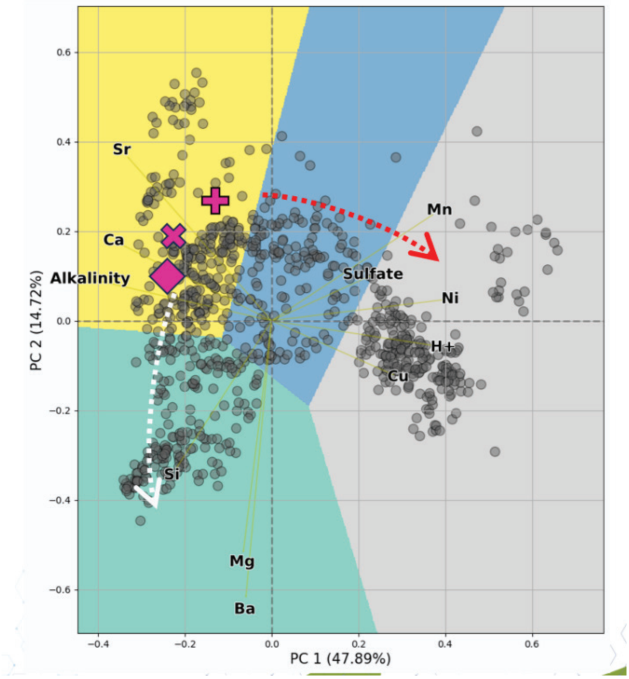

Figure 3 *Waste Pile Seepage plotted over HCT data to predict onset of ARD.*

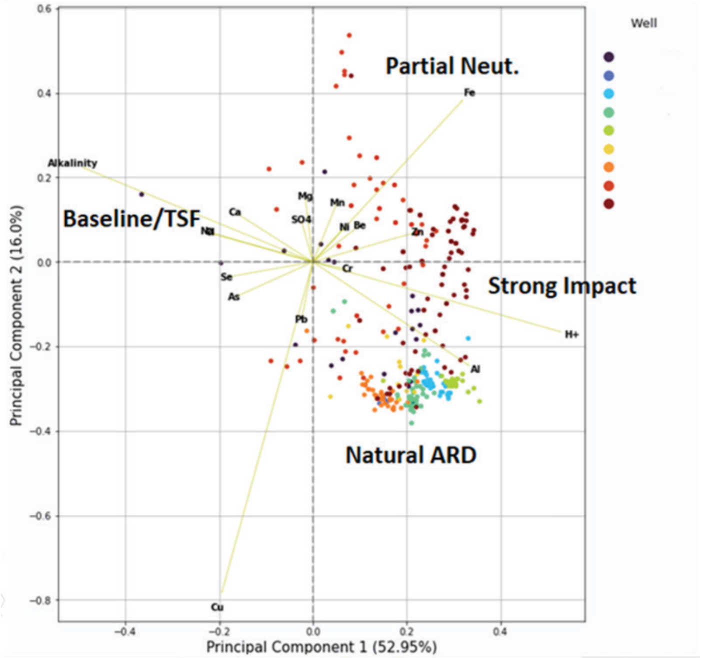

Figure 4 *PCA biplot clearly delineating natural ARD from MIW.*

The mine has known pre-mining natural ARD, as established by field observation. Large ferricrete deposits of geologic age, speak to a "fossil" acid drainage that has been partially neutralized resulting in precipitation of iron from solution, and co-precipitation of a number of metals. Once the mine went into operation, the highly reactive waste rock also began to generate acidity and MIW. Over time, the operator has been unable to separate the older, geologic waters from MIW.

Unsupervised machine learning readily differentiates natural ARD from MIW, based on the aluminum and copper signature of the former, and the fact that natural, geologic waters tended to retain highly stable water quality over the course of mining. MIW, on the other hand, displays a highly variable chemical signature over time. Pit waters (which plot towards the right and northeast corners of the biplot) especially, are highly variable over the sampling period. This is consistent gradual formation of ARD and declining pH over time, as indicated by the proton and base metal vectors on the biplot. Unsupervised analysis is also able to differentiate MIW of different types, as tailings seepage and background groundwater are defined more by alkaline, acid-buffering (calcium) and cation exchange (sodium) processes. Further unsupervised analysis of just the tailings and baseline groundwater dataset (not shown here) yields further success in delineating tailings MIW from natural baseline groundwater; the latter often has high sulfate and chlorite due to strong evaporative ambient conditions and is again not easy to discriminate from tailings MIW using traditional, lower-dimensional analysis methods.

Separation of natural ARD from pit-generated MIW indicates that all MIW is generated within the pit hydraulic capture zone. Additional analysis of area water quality signatures further indicate that waste rock dumps are not generating seepage or impacts. The fact that all impacts are hydrologically contained changed the project closure strategy significantly as the initially perceived need for future active water treatment is now likely eliminated. This is a very significant savings for the client, that was made possible by using more sophisticated data analysis methods.

Conclusions

Application of unsupervised methods to various water quality data types collected in four different parts of the mine project life cycle indicates that the multivariate approach is highly effective in identifying different water quality domains, breakthrough of MIW, mixing effects and various reactive processes that occur in water.

The four use cases have application and implications as follows:

- **Baseline and compliance:** machine learning methods are applied to separate pre-mining water quality in different hydrostratigraphic units and to detect vertical transmissivity between units, providing the future operator considerable flexibility and power in future water treatment planning, and also providing significant insight to the site hydrogeologic conceptual model.
- **Feasibility and permitting:** unsupervised analysis of a large laboratory HCT dataset provides considerable insight to the nature and timing of acid conditions; this information is highly valuable in making HCT termination decisions as lag time to acidity can be challenging to predict using standard methods (depletion calcs, monitoring changes in leachate pH).
- **Operations:** comparison of waste rock seepage leachate to HCT data generated during permitting allows for regular monitoring of seepage quality and provides early warning to potential acidic conditions, allowing the operator to react and respond proactively.
- **Closure planning:** multivariate analysis of decades of groundwater and surface water quality resulted in successful delineation of natural ARD signatures from various types of MIW. The ability to identify these water types influences the long-term closure strategy and is likely to result in considerable water treatment cost savings.

Acknowledgements

The authors wish to thank its confidential clients for allowing use of their datasets for this type of complex analysis and for being forward thinking and open to these more sophisticated approaches. We also thank our LCG colleagues Alice Alex, Morgan Warren and Sam Wright for assisting with various aspects of data analysis and review.

References

Aitchison, J. 1982. The statistical analysis of compositional data (with discussion). Journal of the Royal Statistical Society, Series B (Statistical Methodology), v. 44, 139–177

Huang, H., Yingfan, W., Rudin, C., Browne, E. 2022. Towards a comprehensive evaluation of dimension reduction methods for transcriptomic data visualization. Communications Biology, v. 5, no 719

MEND. 2009. Prediction Manual for Drainage Chemistry from Sulphidic Geologic Materials. MEND Report 1.20.1. December 2009.

Van Rossum, G., Drake, F. L. 2009. Python 3 Reference Manual. Scotts Valley, CA: CreateSpace. https://docs.python.org/3/reference/.

Wang, Y., Huang, H., Rudin, C., Shaposhnik, Y. 2021. Understanding how Dimension Reduction Tools Work: An Empirical Approach to Deciphering t-SNE, UMAP, TriMap, and PaCMAP for Data Visualation

Williams *et al.* 2020. pyrolite: Python for geochemistry. Journal of Open Source Software, 5(50), 2314. https://doi.org/10.21105/joss.02314

Wyman-Feravich, A., Meuzelaar, T. 2024. The Spiral toward Acidity: A Machine Learning Approach to Analyzing Humidity Cell Test Results, International Conference for Acid Rock Drainage (ICARD 2024), Halifax Canada.

Innovation in Characterization-Proyecto Touro – Galicia, Spain

Tom Meuzelaar[1], Pablo Núñez Fernández[2], Morgan Warren[1]

[1]Life Cycle Geo, LLC., 729 Main Street, Longmont CO 80501, tom@lifecyclegeo.com, ORCID 0000-0003-3119-8390

[2]Cobre San Rafael SL, B70491121, La Mina, S/N 15822, Touro (San Xoan), La Coruña, Spain, pablo.nunez@atalayamining.com, ORCID 0000-0002-6218-0479

Abstract

Mine waste characterization tests conducted on metamorphosed mine materials can substantially underpredict acid generation potential and overpredict acid neutralization potential if improper laboratory methods are used. Supervised machine learning methods were used to correct 60,000 such erroneous sulfur assay data points for the Proyecto Touro exploration assay dataset. A trained machine learning model showed excellent results, being able to predict sulfur concentrations with up to 93% accuracy. The innovative methods used in this study indicate that erroneous data generated from use of improper laboratory characterization tests does not necessarily need to be discarded, as machine learning algorithms can sometimes be used to correct them.

Keywords: Waste characterization, environmental geochemistry, unsupervised machine learning, supervised machine learning, digital transformation, artificial intelligence, data science

Introduction

Environmental characterization testing must be conducted on future mine waste material to determine its potential acid rock drainage (ARD) and metals leaching characteristics. When carrying out such tests on metamorphosed mine materials it is important to select the correct laboratory methods as tests that do not fully digest metamorphosed sulfides (e.g., pyrrhotite) can lead to substantially underpredicted acid generation potential (AGP) while tests that don't account for metalliferous carbonates (e.g., rhodochrosite, siderite) or graphite can lead to overpredicted acid neutralization potential (ANP); this can lead to considerable underprediction of overall material ARD potential (Meuzelaar *et al.*, 2021a).

When Cobre San Rafael obtained the Touro copper property[1], it also acquired multiple legacy assay datasets. The legacy waste and ore sulfur assay data from Proyecto Touro in Galicia, Northwestern Spain were frequently obtained using weak acid methods that did not fully digest metamorphosed sulfide minerals (principally pyrrhotite). Additionally, the presence of both graphite and manganese–iron carbonates in Touro added considerable risk of ANP overestimation. While environmental characterization tests conducted on newer ore and waste samples collected by Cobre San Rafael for Proyecto Touro aimed to properly address these risks, the older legacy dataset contained considerable inaccuracy, especially in sulfur measurement. Accordingly, there was a need to correct the underestimated and erroneous legacy sulfur data. The cost to re-assay 60,000 erroneous sulfur data points was deemed prohibitive, therefore innovative machine learning algorithms were employed to attempt to correct this data. The innovative approach relied on re-analysis of a small subset of samples, and training a machine learning model to 1) predict sulfur concentrations based on concentrations of other chemical components in the data subset, and 2) predict corrected sulfur values for the entire exploration assay database.

---

[1] Atalaya Mining currently owns 10% but has a phased earn-in agreement for up to 80% ownership

Background

Proyecto Touro is located in the Galicia province in northwest Spain. It is a brownfield copper project, having been historically mined from 1973 to 1986. The mine footprint comprises six separate deposits (Arinteiro, Vieiro, Bama, Brandelos, Monte de las Minas and Arca). Among them, Monte de las Minas and Arca have not been mined yet. Regionally, the deposits are located in the Órdones Complex, an extensively metamorphosed allochthnous unit within the larger northwest Iberian Massif. Member units are predominantly meta-sedimentary (paragneiss) and meta-volcanic (amphibolite) lithologies. Copper mineralization occurs as chalcopyrite mostly within the meta-volcanics in a Besshi-type volcanogenic massive sulfide configuration. Both paragneiss and amphibolite contain considerable metamorphosed pyrite, as pyrrhotite, and this represents the primary mineral that gives future Touro waste rock ARD potential. Cobre San Rafael aims to properly characterize and understand waste rock ARD potential as part of its long-term water and materials management plan, and to assist with permitting.

Methods

For this study, Cobre San Rafael provided assay data for 5,880 samples comprising eight different ore and waste lithologies (Table 1, below) with measurements of 49 different chemical elements. Some samples contained very little sulfur (<0.01 wt. %), while others such as the Massive Sulfide lithology samples contained sulfur concentrations as high as 11.8 wt. %. The original legacy data sulfur analyses were obtained using a three-acid aqua regia digestion that was insufficient to fully digest the metamorphosed pyrite and pyrrhotite in the samples.

As is typical for a geochemical dataset being prepared for machine learning analysis, considerable data wrangling was required to address the issue of numeric closure (Aitchison 1982) and the presence of censored data (i.e. detection limits). Major element compositional data sums to a constant of 100% which introduces artificial collinearity that need to be removed prior to statistical modeling. This collinearity, termed numeric closure, may be addressed by transforming the data using log-transforms such as the centered-log ratio (Pawlowsky-Glahn and Egozcue 2006). Censored data include those that are either above or below a laboratory detection limit. While techniques such as use of whole or half the detection limit are commonly used to address censored data, a preferred method is to impute (predict) numeric values in place of the censored constants, based on the bulk chemistry of the sample (Sanford *et al.* 1993). This imputation employs the expectation-maximization (EM) algorithm (Palarea-Albaladejo and Martin-Fernandez 2015). All data cleaning, transformation and machine learning-based analysis was performed using the R statistical computing environment (R Core Team 2017); scripts were executed with the Microsoft Azure Machine Learning Studio platform.

Machine learning algorithms are particularly useful for identifying patterns in high dimensional datasets, such as

***Table 1** Sulfur Assay Data, by Lithology.*

Logged Lithology	Number of Samples	Median Sulfur Concentration (wt. %)
Amphibolite	1742	1.9
Garnet Amphibolite	716	3.0
Ca-poor Amphibolite	1361	3.5
Breccia-Massive Sulfide	32	11.7
Biotitic Schist	297	4.3
Massive Sulfide	155	5.9
Pelitic Paragneiss	1305	0.8
Pelitic paragneiss with sulfide	272	10.4

multivariate chemical composition. The conceptual model for supervised machine learning predictions were based on the hypothesis that material sulfur concentrations are dependent on mineral type and abundance and can be predicted based on other chemical elements that are also associated with minerals that control sulfur abundance. Given that elements such as sulfur are typically found in the structure of multiple different minerals, the relationship between sulfur and other assay elements is not readily predicted by simpler methods. To achieve optimal predictive accuracy, multiple machine learning algorithms were tested including artificial neural networks (ANNs) boosted decision trees (BDTs), multiple linear regression and random forest (RF). The primary statistical criteria used to assess the accuracy of sulfur predictions were the coefficient of determination (r2) and mean squared error (MSE). To aid in interpretation, variable influence was calculated for each of the algorithms employed using a feature importance algorithm provided within the Azure environment.

Results

MSE and r^2 values for each of the algorithms are provided in Table 2. The results clearly indicate that BDTs and ANNs (both with r^2 values of 0.93 and order of magnitude lower MSE) considerably outperform multiple linear regression and the RF algorithm.

Given their high predictive accuracy, BDTs and ANNs were selected for further analysis. A comparison between machine learning-predicted sulfur and the raw training data is given in Fig. 1, which indicated that both models are least accurate in predicting low sulfur concentration data (<0.1 wt. %). Given that mine materials with sulfur concentrations below this threshold have very low ARD potential, model underperformance at these lower concentrations is considered less critical. However, it is noted that the BDT is a bit better at predicting low sulfur concentrations than the ANN algorithm.

Results of the variable influence analysis are given in Table 3 for both algorithms. For both analyses iron is, by some measure, the most critical element necessary to predict sulfur concentrations. Given that iron is one of the two primary elements comprising pyrrhotite (the other being sulfur), this result is intuitive. Beyond this, variable influence for the BDT algorithms are more intuitive as most variables are chalcophile or siderophile elements that are commonly found substituting for iron and sulfur in the crystal lattice of sulfide minerals (and also represent the primary risk for metals leaching when sulfides oxidize). The compositional variables that contribute to ANN predictive accuracy are less intuitive – they may possible have something to do with rock forming or secondary (hydrothermal) processes, but this is not immediately known.

However, the results generally validate the hypothesis that the chemical elements used to predict sulfur concentrations are, as expected, broadly controlled by mineral concentrations and crystal structure. As such, using a multivariate machine learning-based approach is a powerful tool for predicting elemental concentrations. This approach could also be used for many similar applications with environmental implications, including:

- Training a combined bulk chemistry/mineralogical composition database to predict graphite or various metal-bearing carbonates
- Predicting trace element concentrations within specific minerals (e.g., leachable

Table 2 Machine Learning Prediction Results.

Supervised Machine Learning Algorithm	Mean Squared Error MSE	Regression Coefficient r^2
Multiple Linear Regression	2.47	0.66
Random Forest	9.56	0.22
Boosted Decision Trees (BDT)	0.46	0.93
Artificial Neural Network (ANN)	0.43	0.93

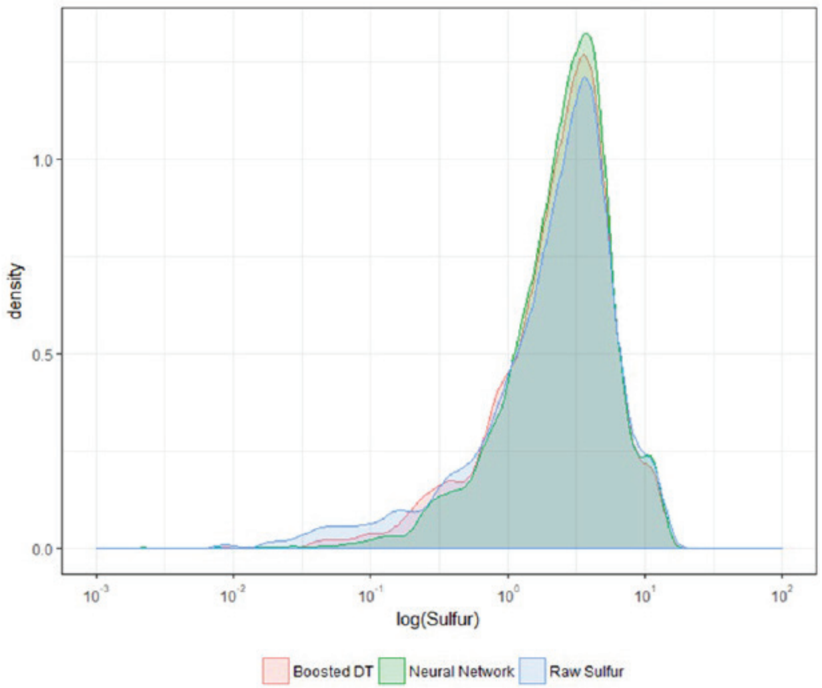

***Figure 1** Distribution of Predicted and Raw Sulfur Concentrations.*

selenium in sulfide minerals vs. “locked” selenium in silicates)

- Predicting acid-generating soluble alunite vs. non-soluble “hydrothermal” alunite vs. other acid sulfate minerals

Finally, with modern field spectroscopy-based instrumentation, an IoT (Internet of Things) configuration that includes field data acquisition, upload to a cloud-hosted database, machine learning analysis on the cloud and rapid results to support quicker decision-making, should be viable.

Conclusions

The trained machine learning model showed excellent results being able to predict sulfur concentrations with 93% accuracy. The high accuracy is the result of having sufficient assay data points and chemical parameters, as well as the fact that sulfide mineral concentrations

***Table 3** Variable Importance Analysis Results for ANN and BDT sulfur predictions*

Ranking	Boosted Decision Tree BDT		Artificial Neural Network (ANN)	
	Element	Ranking	Element	Ranking
1	Fe	0.23	Fe	0.28
2	Cd	0.13	Sr	0.09
3	Zn	0.11	Th	0.07
4	Co	0.07	Ti	0.07
5	Ag	0.06	Tl	0.05
6	Cr	0.05	Cr	0.05
7	Al	0.05	Ca	0.03
8	Ni	0.03	Ba	0.03
9	Na	0.03	U	0.03
10	Se	0.03	Rb	0.03

(largely pyrrhotite) correlate strongly with the concentrations of trace metals which substitute into the sulfide lattice.

The innovative supervised sulfur prediction, LECO digestion and Modified Sobek titration methods employed in this study indicate that erroneous data generated from use of improper laboratory tests does not necessarily need to be discarded. Rather, such methods offer a pathway to correction of erroneous data.

Acknowledgements

The authors acknowledge provision of legacy sulfur data by Cobre San Rafael. Specifically, Fernando Diaz-Riopa and Julian Sanchez of Cobre San Rafael are acknowledged, as well as Alan Nobel and Monica Barrero. Much of this work was completed as an internal Golder Associates research and development project. Microsoft graciously provided access to their Azure cloud-based analytics environment for this work.

References

Aitchison, J. (1982) The statistical analysis of compositional data (with discussion). Journal of the Royal Statistical Society, Series B (Statistical Methodology), v. 44, 139–177

Meuzelaar, T., Núñez-Fernández, P., Martín-Izard, A., Arias-Prieto, D., Díaz-Riopa, F. (2021) The Waste rock of the Touro copper deposit in Galicia, Spain: challenges for its environmental characterization. Geochemistry: Exploration, Environment, Analysis v. 21, p. 1–14 doi:10.1144

Palarea-Albaladejo J., Martin-Fernandez, J.A. (2015) zCompositions – R package for multivariate imputation of left censored data under a compositional approach. Chemometrics and Intelligent Laboratory Systems, v. 143, 85–96.

Pawlowsky-Glahn V., Egozcue J.J. (2016) Compositional data and their analysis: an introduction, in Buccianti, A., Mateu-Figueras, G. and Pawlowsky-Glahn, V. (eds) Compositional Data Analysis in the Geosciences: From Theory to Practice. Geological Society, London, Special Publications, v 264, 1–10.

R Core Team (2017) R: A language and environment for statistical computing. R Foundation for Statistical Computing, Vienna, Austria. https://www.R-project.org/.

Sanford, R.F., Pierson, C.T., Crovelli, R.A. (1993) An objective replacement method for censored geochemical data. Mathematical Geology, v 25, 59–80.

Integrated 3D Laser Scanning Implementation for Monitoring Tailing Dams

María José Cabrera[1], Patricio Monreal[2], Rainier Ramírez[3]

[1]Maptek Sudamérica, Viña del Mar, Valparaíso, Chile. 2520274. Mine Measurement mariajose.cabrera@maptek.cl

[2]Maptek Sudamérica, Viña del Mar, Valparaíso, Chile. 2520274. Mine Measurement patricio.monreal@maptek.cl

[3]Maptek Sudamérica, Viña del Mar, Valparaíso, Chile. 2520274. Mine Measurement rainier.ramirez@maptek.cl

Abstract

Tailings or mine waste storage dams are structures designed to store discarded material from various stages of ore concentration, which accumulates into large volumes. This is primarily due to the fact that, over time, the metal grades decrease significantly (< 1%). In this context, where storage demands continue to grow, effective risk management for these large and dynamic structures becomes crucial. These dams evolve in shape and size over time, and their stability is influenced by hydrometeorological and seismic events, which directly affect safety, and, consequently, the population near the tailings ponds. Over the past two decades, incidents involving tailings dams have prompted the industry to address the risks associated with efficient operational management, environmental impact, and safety concerns stemming from potential collapses.This article discusses the integration of a system through the application of 3D laser scanning and monitoring software, which delivers accurate results for both monitoring the stability of tailings dams and managing their operations. The process involves measuring millimetric deformations by calculating base data at critical points on the dam's wall. The objective of the 3D laser scanning system is to provide a decision-support tool that helps professionals manage geotechnical risks, monitor in real-time, and report movements caused by slope instability that could disrupt mining operations and result in material and human losses.The system provides safe, real-time alerts through a network predefined by the geotechnical professional. Additionally, the system's point cloud database allows for subsequent analysis, meaning that each scan performed by the equipment can be reviewed and reconstructed if there is a need to investigate a displacement event. This enables the monitoring of surface changes as remedial work is carried out, offering a risk management tool that ensures the safety of the team and personnel.

Keywords: Laser scanning 3D, monitoring, tailing dams, hazard

Introduction

The system presented in this paper integrates both software and hardware technologies, specifically designed to monitor, analyze, and report displacements in critical areas or zones of interest, as identified by the geotechnical professional. In this case, it is applied to the containment walls of tailings dams, which are defined as storage structures where the wall is constructed from the coarser fraction of the tailings, compacted through a process that separates coarse solids from finer ones via water-driven flow.

Containment walls are structures designed to contain the solid waste discharged during the final stages of mining. These walls are also referred to as "Resistant Prisms," as they form the peripheral area of the tailings storage facility. They are artificially constructed to complement the natural perimeter, thus forming the basin area. These walls contain waste deposits that evolve over time due to factors such as an increase in volume, embankment heightening, or exposure to various hydrometeorological and seismic events that can affect the dam's structural stability. As a result, strict monitoring and control of embankment walls and potential rupture or failure zones are necessary.

Currently, large dams require continuous and meticulous surveillance and control through an instrumentation and/or geotechnical monitoring system (Oliva, 2015). The need for instrumental monitoring, as well as the number and placement of monitoring devices, depends on the uncertainties related to site conditions and the behavior of the structures under normal operating conditions or in the presence of external events. This paper focuses on an integrated monitoring system that enables the study and oversight of tailings dams, aimed at enhancing both operational safety and the safety of surrounding populations. The 3D laser technology offers a decision-support system that assists professionals in managing geotechnical risks, provides real-time monitoring, and facilitates the reporting of movements caused by instability that could disrupt mining operations and result in material and human losses.

Methodology

Laser Technology

The methodology employed for displacement monitoring and control involves the use of 3D laser scanners and specialized software to capture and process point cloud data with Gaussian weighting. The Deployable Monitoring System integrates a 3D laser scanner that generates high-resolution point clouds, which are visualized in real-time through the associated software. This software allows the configuration of monitoring windows, within which alarms can be set to notify users via email if displacement occurs beyond a predefined range, enabling quick responses to high-risk operational events.

The system collects detailed data on the tailings dam embankment walls, utilizing cells that are ideally composed of 36 points. The distance and diameter of these points depend on the resolution, the monitoring distance, and the data acquisition speed, all of which are influenced by the reflectivity of the material being scanned.

Data acquisition is governed by both the reflectivity of the materials and the scan acquisition speed. For this process, a standard scan mode of 50 kHz was used, allowing the

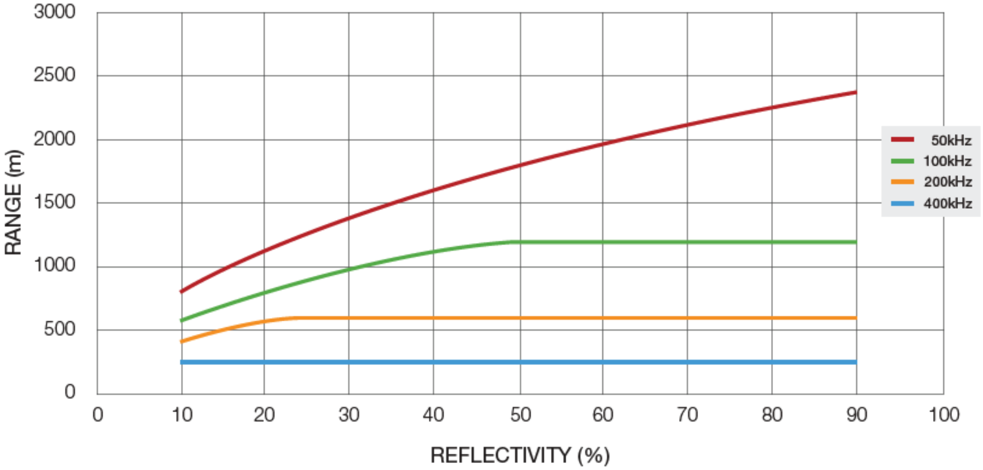

Figure 1 *Graph of reflectivity versus distance range in meters (Sentry Field Operator Manual).*

scanner to achieve a range of approximately 1600 to 1800 meters with a reflectivity of 40 to 50%, as shown in Fig. 1.

Implementation Process

The implementation process for the Geotechnical Monitoring System follows a series of key steps, as outlined in Fig. 2. First, it is crucial to assess the geological, geotechnical, and structural conditions of the area to be monitored, including the properties of the soil and the environment that will require monitoring. The next step is to determine whether visual monitoring or instrumental monitoring is needed. If instrumental monitoring is chosen, the following step involves identifying the specific parameters to be measured. Given that the focus is on monitoring tailings dam walls, a monitoring plan must be established using a laser scanner. This plan should include, at a minimum, the following key points:

- **Control Areas:** The monitoring system should be installed in critical areas where key parameters need to be measured.
- **Threshold Values:** The measurements obtained through monitoring will serve as an early warning mechanism within the risk management program. Maximum reference values will be set, which must not be exceeded.
- **Scan Frequency:** Regular monitoring and analysis of data enable the detection of abnormal trends in mass behavior, allowing for timely corrective actions when necessary.
- **Contingency Plan:** A response protocol will be developed for situations where deformation thresholds are exceeded. This protocol will include clear communication among all parties involved in controlling the mass movements

Selection of Monitoring Areas on the Tailings Dam Wall

For monitoring the tailings dam wall, the following surface measurements are recommended:

1. **Measurement of Freeboard:** This refers to the vertical distance from the crest of the dam to the surface of the tailings or water, specifically the distance from the dam's crest, which is situated above the water level in the pond.
2. **Measurement of Horizontal and Vertical Movement:** This includes monitoring the initial crest of the dam and the downstream slope for any horizontal or vertical movement.
3. **Measurement of Vertical Movements in Tailings Deposits:** These movements are significant due to the compaction from self-weight and consolidation of the tailings deposits.

Once the monitoring process is initiated, data is collected daily for post-processing. This allows for back analysis, which involves reviewing the data day by day to identify trends in the displacement curves. These trends can indicate various conditions, such as inactive, regressive, transgressive, linear, progressive, or critical behavior. Each curve is based on the accumulated displacement observed in each zone created at the start of the monitoring, or whenever the geotechnical professional decides to establish a new zone. Zones can be created at any point during monitoring, and they will reflect all data from the beginning of the monitoring until the zone creation date. Since the system continuously stores and preserves the data, the point cloud is always accessible for evaluating and interpreting the accumulated displacement in the monitored area.

In addition to graphically representing displacement, the software also provides information on inverse velocity and displacement velocity of the data. To ensure accurate data interpretation, it is recommended to capture as many point clouds as possible. In other words, the more data available, the more precise the interpretation of the displacement curves will be.

Results

The results obtained from the monitoring solution provide a real-time representation of the monitored area through the point cloud captured every 12 minutes, with photographic coloring, as shown in Fig. 3. Thanks to the system's high accuracy and reliability, it enables real-time tracking of millimeter-scale

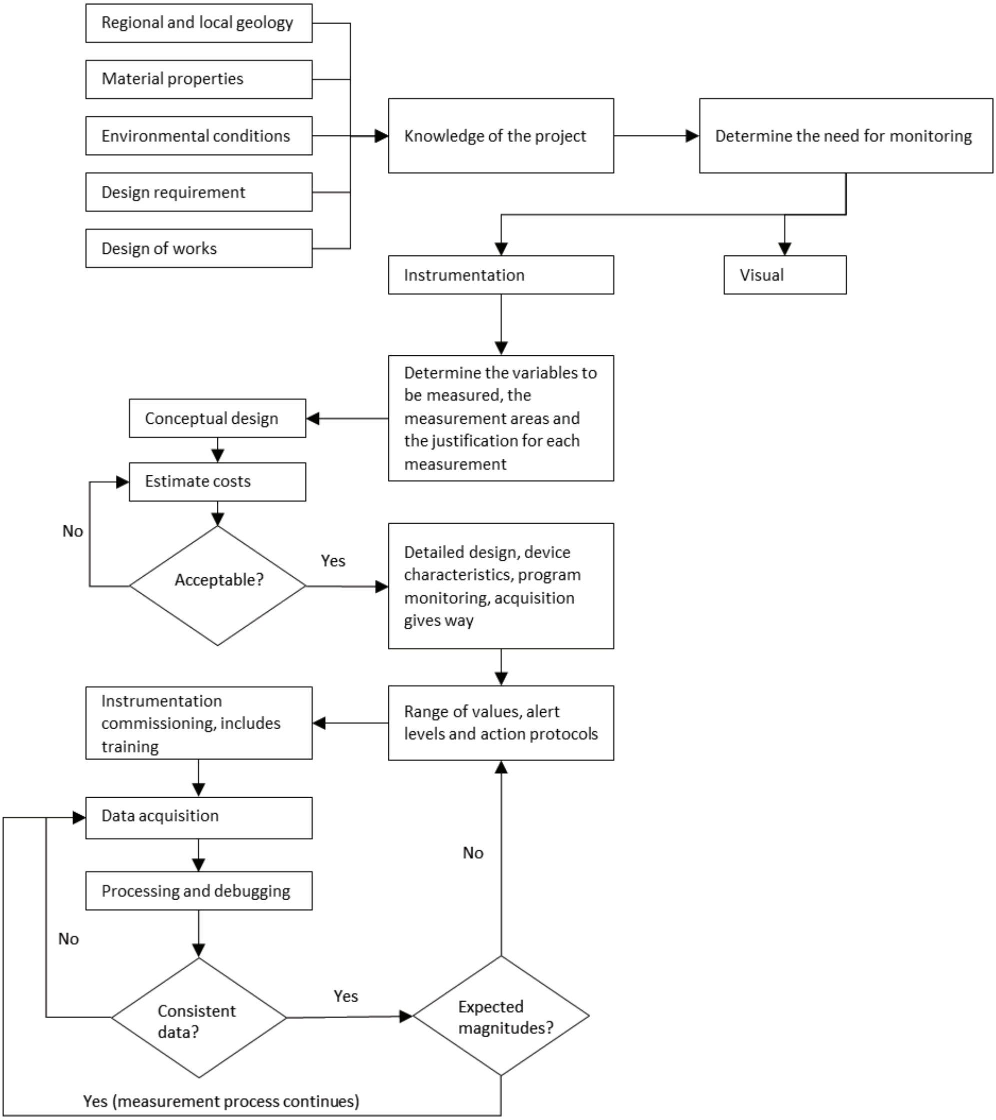

Figure 2 *Sequential diagram for implementing instrumental monitoring.*

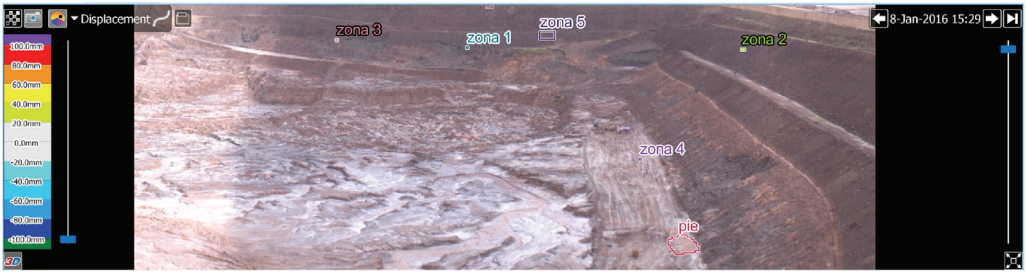

Figure 3 *Monitoring zone, Tailings dam wall with photographic color.*

deformations in the dam, with timely updates according to the predefined threshold values.

In Fig. 4 and 5, the monitored area is divided into subzones labeled Zone 1, Zone 2, Zone 3, Zone 4, Zone 5, and Pie. These subzones are depicted in colors indicating either positive or negative displacement. Positive displacement represents forward movement of the material, while negative displacement indicates a setback in the monitored sector. The warm colors in the legend correspond to positive displacement, meaning that the cells within the Foot zone have moved approximately 40 mm closer to the monitoring equipment over a span of 4 days

In Fig. 6, the displacement graph shows the monitored zones as a function of time. Zones 1, 2, 3, and 4 exhibit a regressive to inactive trend over time. However, starting from January 12th, the Pie zone transitions from an inactive state to a critical condition, with the curve indicating instability at the base of the wall. On that date, the Pie zone shows a positive displacement of 30 mm, signaling a potential issue.

By January 15th, the area labeled "Pie" reaches an average accumulated displacement of 61 mm across an area of 61.60 m^2, making it the region with the highest displacement on the dam wall. The average point count per cell in this area is 35 points. Fig. 7 illustrates the color variation in a northward view of the wall. In the first image, the Pie zone appears gray, indicating no movement or a displacement of less than 20 mm. The second image, taken on the last day of monitoring, shows that the displacement in the central zone has exceeded an accumulated 100 mm.

Conclusion

The primary objective of this monitoring solution is to assist geotechnical professionals in making informed decisions based on displacement data derived from highly accurate point clouds captured using long-range laser technology. This provides reliable information that optimizes time, financial resources, and personnel. Additionally, the system streamlines processes, reduces operational costs, and enhances productivity within mining operations, all while maintaining a strong focus on safety in areas that require the most attention from a geotechnical perspective. The safety of personnel in fields such as surveying, geology, geotechnics, and other mine-related roles is consistently prioritized.

The laser scanner operates 24/7, continuously collecting valuable data and

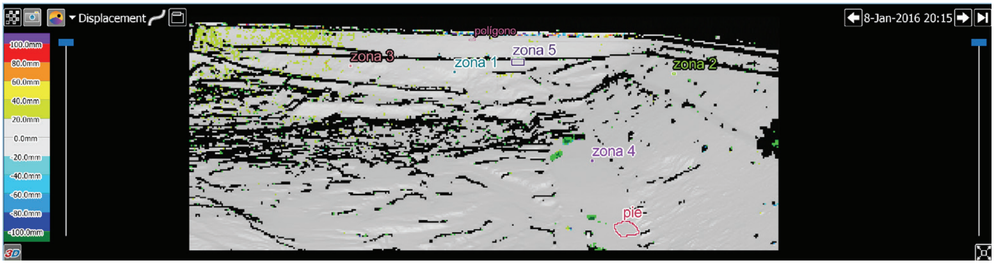

Figure 4 *Monitoring zone, Tailings dam wall with color legend by displacement. Date: January 8, 8:15 p.m.*

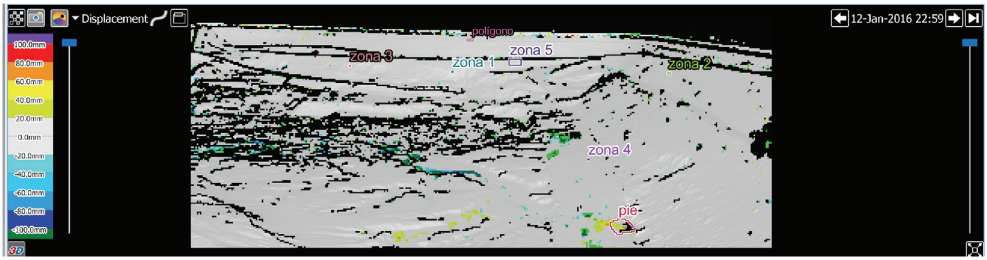

Figure 5 *Monitoring zone, Tailings dam wall with color legend by displacement. Date: January 12, 10:59 p.m.*

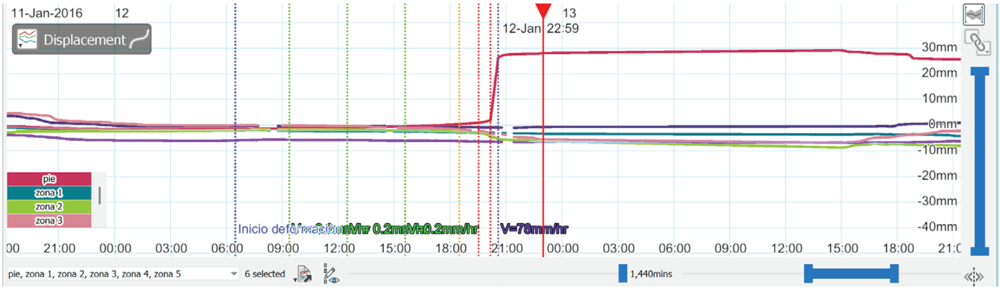

Figure 6 Monitoring zone, Tailings dam wall with color legend by displacement. Date: January 12, 10:59 p.m.

offering exceptional versatility for the mine's operational teams. It provides comprehensive monitoring of the tailings dam wall, capturing all essential geotechnical parameters required for stability analysis. The hardware's practicality and portability enable it to be swiftly relocated to monitor events in real time, offering a robust decision-support system for safe and efficient mining operations. This system can be rapidly deployed to any area that requires continuous, 24-hour monitoring.

Acknowledgements

We would like to thank all the co-organizers for the organization of IMWA 2025, and O. Burgess, Amy Kokoska, Hetta Pieterse, and Glenn MacLeod for their critical contributions to the preparation and drafting of the template for this document.

References

Carvajal Arroyo, M. I. (2018). Desarrollo de una metodología para análisis de estabilidad física de depósitos de relaves.

SERNAGEOMIN. (2015). Preguntas Frecuentes sobre Relaves.

Zandarin Iragorre, M.T., 2021. Normativa, gestión de riesgos y experiencia sobre depósitos de relaves en Chile, 132 (4): 573-581 ISSN: 0366-0176 DOI: 10.21701/bolgeomin.132.4.012

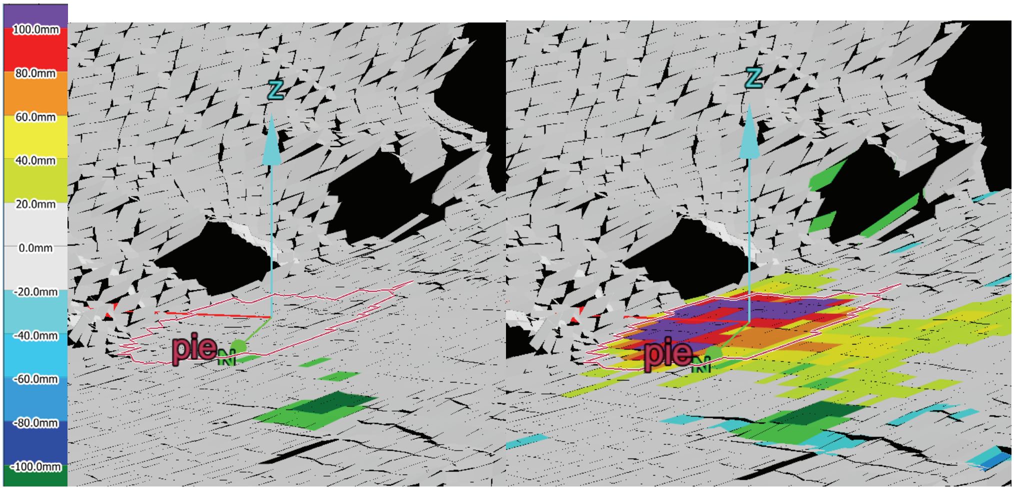

Figure 7 A comparative image, from the first day of monitoring versus the last day in the same "Pie" area.

The Importance of Understanding the Implications of the Carbonate Balance on Active Mine Water Treatment

Richard Morgan[1], Richard H Coulton[2]

[1]*Sand Separation Systems Ltd, Caldicot, Wales, UK, Richard.morgan@m-rs.co.uk*

[2]*Sand Separation Systems Ltd, Caldicot, Wales, UK, Richard.H.Coulton@sandseparationsystems.co.uk*

Abstract

The importance of carbonate chemistry and its role in passive mine water treatment is well understood and is supported by numerous publications (Hedin, Narin, Kleinmann 1994). However, there is less published information on its importance in active mine water treatment. In particular, the role carbonate chemistry plays in dictating alkali consumption and sludge generation

Keywords: IMWA 2025, HDS, Active Treatment, Decarbonisation, Degassing

Introduction

Studies on UK mines have shown that dissolved inorganic carbon and the corresponding carbonate chemistry has an important and often overlooked role in the active treatment of both net alkaline and acidic waters. Historically the differences between theoretical and measured alkali demand and sludge generation rates put down to process inefficiencies and/or parasitic “secondary reactions”. In cases which Carbon dioxide (CO_2) stripping has been incorporated in active plants, the benefits have typically been established experimentally, often without a full appreciation of the underlying chemistry. The purpose of this paper is to explore the importance carbonate chemistry in active mine water treatment and discuss how these “secondary reactions” can either be minimised or used advantageously.

Most active treatment plants operate with either one or two reactors with retention times of circa 20–40 mins to precipitate dissolved metals as metal hydroxides following the addition of an alkali with changes in the dissolved metal concentration and carbonate chemistry occurring simultaneously. This paper aims to demonstrate that by analysis the various carbonate reactions on an individual stepwise manner it is possible to:

- Assess the effect dissolved CO2 has on alkali demand and sludge generation
- Assess the effect metal precipitation on pH without alkali addition
- Predict calcium carbonate precipitation
- Demonstrate how the carbonate buffer can be used to reduce alkali demand and sludge generation.

Method

By considering the carbonate $CO_2/HCO_3^-/CO_3^{2-}$ buffer reactions (Younger, 2002) along with pH, total inorganic carbon (TIC) and alkalinity it is possible to predict changes in the carbonate species and the effect these have on the plant performance. Knowing two of these parameters (pH and TIC for example) it is possible to calculate the remainder. For example, by assuming air stripping reduces the CO2 concentration to an assumed value, this together with the alkalinity value can be used to predict the pH and carbonate species concentrations. Fig. 1 illustrates how these vary for a process comprising the following treatment stages:

- Carbon dioxide air stripping (degassing)
- Iron precipitation using hydrogen peroxide (thereby avoiding the need to raise the pH to accelerate the iron oxidation reaction with oxygen)
- Raising pH to promote precipitation of other dissolved metals (such as manganese)
- Precipitation of these other metals and calcium carbonate

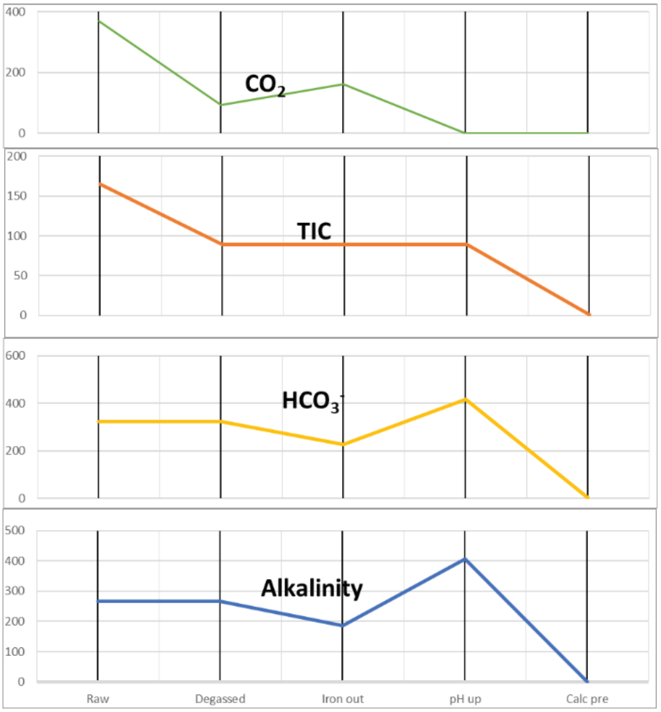

Figure 1 Concentration changes for an iron and manganese removal process using CO2 stripping a hydrogen peroxide to promote iron oxidation and precipitation.

The application of this technique and its relevance to active treatment plant design is illustrated in the following 4 case studies.

Case Study A – Highly Acidic Mine Water flowing from a Pyritic Orebody

This case study explores the treatment of a highly acidic mine water (pH circa 3). At the time of closure, the metal concentrations peaked at circa 5,000 mg/L iron, 200 mg/L zinc plus aluminium, cadmium and other metals. Immediately following closure an ad-hoc temporary treatment system was implemented, with the addition of lime slurry into the pipe carrying the water to the nearby tailings dam. Process control was implemented by manually checking the discharge pH and adjusting the lime addition accordingly. This simple process achieved 99.9% metal removal and has a lime efficiency of 85% (defined as the theoretical dose/actual dose).

Some 8 years later this process was replaced by a high density sludge (HDS) plant. To achieve the new manganese consent (< 1 mg/L) an operational pH > 9 was required. At that point the iron concentration had reduced to around 200 mg/L. However, despite implementing the HDS process the lime efficiency had deteriorated to 72%. By 2024, the iron concentration had stabilised at around 80 mg/L and the lime efficiency had further deteriorated to less than 50%.

Whilst not in area dominated by carbonate geology, laboratory analysis revealed an average total inorganic carbon (TIC) concentration of 30 mg/L (which at the incoming pH 3 is present as dissolved CO2). On raising the pH to 9.3 to ensure manganese removal, the plant effectively acted as a lime softener precipitating the CO2 as calcium carbonate (Evans, Morgan, Coulton, 2019)

To confirm the implication of the dissolved CO2 on lime/alkali demand, an assessment of the changes in the carbonate chemistry with and without CO2 stripping was undertaken (as summarised in table 1)

The low mine water pH allows for a reduction of CO2 within the mine water without increasing the pH and concentration of bicarbonate ions resulting a best-case scenario for CO2 stripping. This data was

Table 1 Case Study A – Predicted Carbonate Chemistry.

	Fe^{2+} mg/L	pH	TIC mg/L	CO_2 mg/L	HCO_3^- mg/L -	CO_3^{2-} mg/L	Alkalinity mg/L as $CaCO_3$
Raw Mine Water	80	3	30	110	0	0	0
Without CO_2 Stripping							
pH increase	80	9.3	30	0	138	12	135
Fe precipitation	0	9.3	30l	0	138l	12	135
Calcium precipitation	0	9.3	0	0l	0	01	0
With 90% CO2 stripping							
Degassed	80	3	3	11	0	0	0
pH increase	80	9.3	3	0	12	1	13
Fe precipitation	0	9.3	3	0	12	1	13
Calcium precipitation	0	9.3	0	0	0	01	0

Table 2 Case Study A – Theoretical reduction in lime demand and sludge generation.

	Without CO_2 stripping	With CO_2 stripping	Predicted reduction
Lime demand	384 mg/L	219 mg/L	42%
Sludge generation	344 mg/L	222 mg/L	35%

then used to estimate the resultant changes in lime consumption and sludge generation that could be achieve by stripping 90% of the CO_2 (as summarised in Table 2 below). Due to the elevated levels of calcium the addition of lime still has a softening effect but with a reduced precipitant volume.

Case Study B – Treatment of a Net Alkaline Mine Water with and without CO2 stripping

In contrast to Case Study A this study considers the effect of CO_2 stripping on a circum neutral net alkaline mine water. The plant was constructed over a decade ago to treat water containing 50 mg/L dissolved iron. And included a pre-treatment stage to air strip CO_2. After period of successfully operation, problems were encountered with the CO_2 stripping stage, which was switched off and the HDS plant operated without the benefit of degassing.

This provided an opportunity to confirm the applicability of the stepwise methodology and compare the results with the actual plant performance. Table 3 summarises the predicted carbonate chemistry with and without CO_2 stripping.

Table 4 provides a comparison of the predicted alkali/lime consumption for these two scenarios. In comparison the actual lime dose when the plant was operated without degassing was 290 mg/L (9% greater than the predicted value of 266mg/l).

Given the high influent alkalinity, it would be possible to operate the HDS plant using hydrogen peroxide as an oxidant rather than air (provided the treated water pH remained above lower consent limit of 6). Thereby avoiding the need for pH adjustment to accelerate the iron/oxygen kinetics. Table 5 summarises the predicted changes in the carbonate chemistry and the estimated final pH – which at 6.2 is still within consent. Importantly, whilst the unit price of hydrogen peroxide is more expensive that lime, it offers additional advantages in avoiding use of the CO_2 stripping mixers and blowers and potentially reducing the amount of sludge generated.

Case Study C – Comparison of Predicted and Measured Values for a highly Alkaline Water

Case Study C relates to a former coal mine which following abandonment was allowed to flood and overflow at a rate of up to 200 L/s into the receiving watercourse. After

Table 3 Case Study B Predicted Carbonate Species.

	Fe^{2+} mg/L	pH	TIC mg/L	CO_2 mg/L	HCO_3^- mg/L -	CO_3^{2-} mg/L	Alkalinity mg/L as $CaCO_3$
Without CO_2 Stripping							
Raw Mine Water	50	6.4	174	300	467	0	382
pH Adjust + Fe precipitation	0	7.3	174	64	795	0.7	652
With 80% CO2 stripping							
Raw Mine Water	50	6.4	174	300	467	0	382
Degassed	50	7.1	108	60	465	0.3	382
pH Adjust + Fe precipitation.	0	7.3	108	40	493	0.5	405

Table 4 Table 4 Case Study B – Lime Consumption

	Predicted lime dose	Lime efficiency
With CO_2 stripping	83 mg/L	79.5%
Without CO_2 stripping	266 mg/L	25%

optioneering potential treatment solutions, it was decided that due to its location the only viable treatment option was active treatment using the HDS process.

Laboratory screening tests confirmed that to achieve the required dissolved iron and manganese concentrations of <1 mg/L it would be necessary to operate the plant at up to pH 9.3. At this pH, calcium carbonate precipitation will occur (increasing the alkali demand and sludge generation rate) making it critical to understand and control the carbonate chemistry. To provide meaningful process design data a 1m3/hr pilot plant (designed to replicate the HDS process) was mobilised to site to test a series of different treatment scenarios thereby optimising of the treatment process.

Table 6 contains a summary of the predicted carbonate species for each step of the proposed treatment process considering both the iron and calcium carbonate precipitation.

This data was used to predict both the lime consumption and sludge generation rates and comparison with pilot plant results as shown in Table 7. Lime/alkali demand from the pilot plant data was within 10% of the predicted values validating the calculation methodology. The predicted sludge generation at pH 7.5 is in reasonable agreement with the measured value, simply because at this pH very little carbonate precipitation takes place. However, at pH 9.3 the calculation over predicted the sludge generation as the methodology assumed all the calcium was fully precipitated. When back calculated using the measured residual calcium concentration the theoretical and actual values almost converge with the remaining difference possibly due to the short reactor residence time and the reaction kinetics.

Case Study D Treatment of Mine Water from Net Alkaline Metalliferous Mine

This case study provides a comparison of the treatment options for a circum neutral mine water with elevated dissolved Iron, Arsenic and Manganese concentrations. This plant was required to treat water at a rate of 1050 m3/hr whilst achieving total arsenic and dissolved manganese concentrations of 50 µg/L and 20 µg/l respectively.

Pilot testing of a traditional HDS process demonstrated that consent compliance could only be achieved by coprecipitating all metal using calcium carbonate at pH10. This resulted in a lime demand of 296 mg/L and a sludge generation rate of around 400 mg/L (i.e. a daily lime consumption of 7.2tpd and a dry sludge maas of 10tpd some 100 m3/day of sludge at the achieved settled solids concentration of 10%w/v).

Table 5 *Case Study B Predicted in Carbonate Species for Hydrogen Peroxide based Iron precipitation.*

	Fe^{2+} mg/L	pH	TIC mg/L	CO$_2$ mg/L	HCO$_3^-$ mg/L -	CO$_3^{2-}$ mg/L	Alkalinity mg/L as CaCO$_3$
Raw Mine Water	50	6.4	174	300	467	0	382
Fe precipitation	0	6.2	174	375	360	0	295

Table 6 *Case Study C – Predicted Carbonate Species Distribution.*

	Fe^{2+} mg/L	pH	TIC mg/L	CO$_2$ mg/L	HCO$_3^-$ mg/L -	CO$_3^{2-}$ mg/L	Alkalinity mg/L as CaCO$_3$
Raw Mine Water	45	6.15	165	370	324	0	266
Degassed	45	6.75	89	93	324	0	266
Iron out	0	6.35	89	163	226	0	186
pH increase	0	9.3	89	0.3	415	38	405
Calc precipitation	0	9.3	12	0	59	12	58.5

Further pilot testing to demonstrate the effect of CO$_2$ stripping revealed it was no longer possible to rely on this approach to achieve consent compliance. Instead, a two stage HDS process was developed with separate arsenic and manganese removal HDS circuits. Making use of the available carbonate buffer, this approach achieved iron coprecipitation of arsenic without the need for alkali addition. Table 8 shows the calculated stepwise approached used to calculate the chemistry changes. In comparison the actual reactor pH was 6.8. Importantly because the arsenic/iron removal stage did not require an increase in pH it was possible to concurrently precipitate the iron/arsenic whilst simultaneously stripping the CO$_2$ in a single reactor simplifying the process. (Morgan, 2024)

On leaving iron/arsenic HDS stage, the pH was raised to 10 in the secondary HDS circuit to precipitate the manganese. Table 9 summarises the measured alkali/lime demand and sludge generation rates for both the original traditional HDS circuit and subsequently adopted two stage HDS process. This clearly demonstrates benefit achieved by utilising the carbonate buffer in the first HDS circuit, with the lime demand and sludge generation rates reduced by 80% and 60% respectively.

Conclusion

The case studies presented above illustrate the benefits of process engineers using a simple stepwise methodology to understand and manage the carbonate chemistry when designing and optimising active treatment

Table 7 *Case Study C Comparison of Theoretical and Actual Pilot plant Results.*

	Degassing	pH	Lime Demand		Sludge Generation	
			Actual	Theoretical	Actual	Theoretical
Iron precipitation	Yes	7.5	130 mg/L	122 mg/L	100 mg/L	85 mg/L
Iron + Manganese precipitation	Yes	9.3	≈ 400 mg/L	377 mg/L[1] 413 mg/L[2]	651 mg/L	657 mg/L[1] 814 mg/L[2]
	No	9.3		841 mg/L[2]		1.324 mg/L[2]

Notes

[1]Calculated using the measured residual Calcium concentration of 58.5 mg/L

[2]Calculated on the assumption that all the calcium is precipitated as calcium carbonate

Table 8 Case Study D – Theoretical Carbonate balance for simultaneous carbon dioxide stripping and iron precipitation with hydrogen peroxide oxidation

	Fe^{2+} mg/L	pH	TIC mg/L	CO_2 mg/L	HCO_3^- mg/L -	CO_3^{2-} mg/L	Alkalinity mg/L as $CaCO_3$
Raw Mine Water	33	6.3	35.6	69.1	85.4	0	70.0
Degassed	33	7.0	20.5	13.8	85.3	0	35.6
Iron out	0	5.5	20.5	65.0	13.7	0	11.1

Table 9 Case Study D – Reduction in lime demand and sludge generation achieved by beneficially using the carbonate buffer

	Original HDS concept without CO_2 stripping and use of carbonate buffer	Two stage process with CO_2 stripping and beneficial use of carbonate buffer
Lime Demand	296 mg/L	59 mg/L
Sludge generation	400 mg/L	162 mg/L

systems. As degassing with the short retention times available can only remove dissolved CO_2, in low pH net acidic mine water degassing alone can provide a vast reduction of inorganic carbon. In circum neutral and net alkali water degassing can only remove a proportion of the inorganic carbon with reactions of bicarbonate ions raising the pH and limiting further CO_2 removal. Importantly the methodology shows in these cases where sufficient alkalinity is available the use hydrogen peroxide (instead of air/oxygen) for iron oxidation and precipitation can remove the need for alkali addition offering potential significant cost saving in terms of reduced process complexity and operating cost.

References

Hedin, R, Narin, R, Kleinman, R, (1994). Passive Treatment of Coal Mine Drainage, US Department of The Interior – Bureau of Mines Circular

Younger, P, Banwart, S, Hedin, R, (2002). Mine Water – Hydrology, Pollution, Remediation. ISBN – 978-1-4020-0137-6

Evans, J, Morgan, R, Coulton, R, (2019). The Effects of Using Hydrogen Peroxide to Provide an Improved HDS Process, 14th IMWA Congress (postponed) – Mine Water Solutions, p152–15

Morgan, R, Coulton, R, Kingstone K, Watson N, (2024). Development of a single stage High Density Sludge (HDS) process for the reopening of South Crofty Tin Mine, Cornwall, UK, 15th IMWA Congress Proceedings of the International Mine Water Association Conference & West Virginia Mine Drainage Task Force Symposium, p452

Deep Physico-Chemical Profiling in a Flooded Mine Shaft: Understanding Water Dynamics in Gardanne Lignite Mine (France)

Bastien Morin[1,2], Laurent Vaute[2], Pauline Collon[1]

[1]BRGM, French Geological Survey, 1 rue Jean Zay, 54500 Vandœuvre-lès-Nancy, France, b.morin@brgm.fr, l.vaute@brgm.fr

[2]RING, GeoRessources, Université de Lorraine, CNRS, ENSG, rue du doyen Marcel Roubault, 54500 Vandœuvre-lès-Nancy, France, pauline.collon@univ-lorraine.fr

Abstract

Neutral Mine Drainage (NMD) in the flooded Gardanne lignite mine (Southern France) remains poorly understood, with persistently high Fe (30 mg/L) and SO_4 (2000 mg/L) concentrations. In 2024, a field campaign conducted in the Gérard shaft, using in-situ profiling and water sampling, reveals a deep stratification. Comparisons with 2011 data indicate a shift from a predominantly static regime with diffusive processes in the deeper part to a more dynamic system, characterized by convective loops and forced convection driven by pumping. Persistent inflows seem to influence the water column structure, shaping its stratification and internal dynamics.

Keywords: Gardanne, lignite, post-mining water management, physico-chemical log, stratification, shaft

Introduction

Acid mine drainage (AMD) is widely recognized for its environmental impact. However, in carbonate-rich systems, neutral mine drainage (NMD) can also occur, posing distinct risks to water quality despite its neutral pH. Long-term management of post-mining sites requires a deep understanding of the hydrogeochemical processes controlling water chemistry. Therefore, extensive localized studies are essential to identify key water-rock interactions, sources of dissolved elements, and the role of bacterial populations in the geochemical cycles of each abandoned mine.

Gardanne underground lignite mine, located near Marseille (Southern France), operates in an NMD context. The flooding of the mine in 2003 led to a deterioration of water quality, characterized by persistent high iron and sulfate concentrations. Hydrogeochemical studies conducted at the time of the mine closure predicted a fast decline in these concentrations over time. More than two decades later, iron and sulfate levels measured at the pumping outlet remain unexpectedly high (Fe: 30 mg/L; SO_4: 2000 mg/L), suggesting the persistence of unaccounted geochemical processes, additional mineralized water inputs within the mine reservoir, and/or insufficient knowledge of the hydrogeological system.

This work investigates the evolution of water quality in the Gardanne mine water reservoir through the analysis of vertical variations in physico-chemical parameters. These variations help understand water-rock interactions, groundwater flow dynamics, and mixing processes within the reservoir. To achieve this, in-situ profiling was conducted along the water column, complemented by chemical analyses of water samples collected at different depths in the Gérard shaft, the only remaining access to the mine water reservoir.

Site description

The Arc Basin is a large east-west syncline, located about ten kilometers north of Marseille (Fig. 1(a)). It extends 75 km east-west and 20 km north-south. It consists of fluvio-lacustrine deposits, including the Upper Cretaceous sub-stages: Valdonnien, Fuvélien, Bégudien, Rognacien (oldest to youngest), and Eocene formations. This structure lies on a substratum of Jurassic and Cretaceous formations. The eastern part of the Arc Basin, known as the Gardanne Basin (Ancel *et al.* 2004), was a coal mining area from the early 19th century until 2003. Although this basin is only slightly affected by major tectonic faults, it is structurally bounded to the north by the Sainte-Victoire mountain, resulting from a thrust system, and to the south by the Étoile massif, also formed by thrust tectonics (Fig. 1).

The Fuvélien formation, which was exploited during mining operations, is a local term referring to the Upper Campanian (about 74 Ma). This formation is present in the autochthonous part of the Gardanne Basin, where it dips north-northwest. It is also found in the southern part of the basin, within a tectonic slice known as the "Lambeau charrié" (thrust sheet), which is bounded by the Diote fault to the north and the Safre fault to the south. This thrusted structure, formed simultaneously with that of the Étoile massif, induced a southward dip of the Fuvélien layers in this area (Fig. 1(b)). The Fuvélien is an approximately 300 m thick formation composed of 96% limestone, divided into five distinct types, and 4% lignite (Gaviglio 1985). The lignite layers are mainly concentrated in its basal part, where they form seven distinct horizons with specific petrographic and sedimentological characteristics (Gonzalez

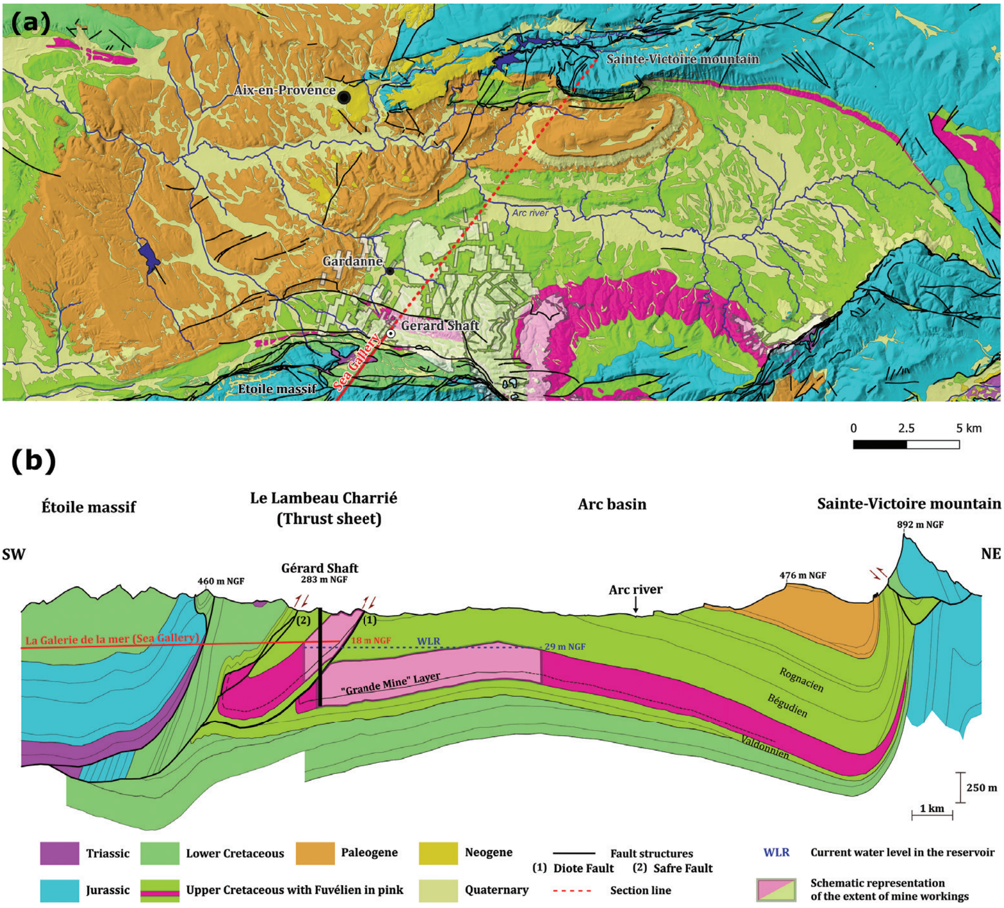

Figure 1 Simplified geological map (a) and cross-section (b) of the Gardanne basin, illustrating the main lithological units and structural features; (b) adapted from J-P Durand (1980, Houillères du Bassin de Centre-Midi) (NGF: French altimetric reference based on the mean Mediterranean Sea level).

1981). These layers were exploited to varying degrees depending on their thickness. The most intensively mined was the 'Grande Mine' lignite layer, which is 2.5 m thick in the autochthonous deposit and 4 m in the thrust sheet.

The Gardanne basin has a complex hydrogeological setting, with multiple superimposed aquifers compartmentalized by low-permeability formations. The most important and deepest aquifer is the Upper Jurassic unit, composed of karstified limestones, with a recharge occurring in the Sainte-Victoire Mountain (Fig. 1). In some areas (mainly in the north), the localized absence of Lower Cretaceous formations results in a direct contact between Jurassic and Upper Cretaceous units (Ancel *et al.* 2004). The Fuvélien, the main karstic aquifer of the Upper Cretaceous, is separated from the Jurassic by the Valdonnien, a marl formation acting as an aquitard. No natural outlet of the Fuvélien has been identified. Above it, the Bégudien forms the second Upper Cretaceous aquifer unit.

Mining operations revealed heterogeneous permeability in the Fuvélien: behaving as an active aquifer in the east near outcrops, but drier in the deeper western part (Chalumeau 2000). During the 1970s and 1980s, major groundwater inflows (sources "90" and "Sainte-Victoire") were encountered in the eastern part of the mine, temporarily disrupting operations. These inflows likely originate from the Jurassic karst aquifer, and reach the mine through localized connections (fractures or karst conduits) between the Fuvélien and Jurassic formations (Chalumeau 2000; Dewandel *et al.* 2017). These exchanges, still active today, influence the flow dynamics within the mine water reservoir. When mining operations ceased in 2003, pumping was stopped, initiating a gradual rise of the water table within the underground workings. This process resulted in the progressive flooding of the mine, substantially altering the hydrogeochemical conditions within the system. As expected, iron and sulfate concentrations increased due to water-rock interactions, with peak values reaching 55 mg/L for iron and 3000 mg/L for sulfate. During active mining, various water inflows were mainly drained by gravity through the Galerie de la Mer, a historical drainage gallery that discharged directly into the port of Marseille. Once the mine was flooded, the risk of mine water overflowing into this pathway became problematic, as the iron-rich water could oxidize and precipitate, potentially causing visible staining in the port. To prevent this uncontrolled discharge, a pumping system was established in 2010 at the Gérard shaft, located upstream of the gallery, to transport the pumped water to the sea via a pressurized pipeline under anoxic conditions, preventing any risk of iron oxidation. The Gérard shaft is the only access point to the entire mine water reservoir and intersects both the autochthonous and thrust sheet sections of the Fuvélien formation. It features multiple gallery levels along its 700 m depth, providing a unique opportunity to investigate the hydrogeochemical processes within the flooded mine. A field campaign was conducted at this site to identify the sources of mineralized water, characterize mixing processes, and assess ongoing water-rock interactions within the mine system.

Methods

To investigate the hydrogeochemical conditions in the flooded Gardanne lignite mine, a field campaign was conducted in October 2024 at the Gérard shaft, the only access point to the mine water reservoir. Based on the framework proposed by Mugova and Wolkersdorfer (2022) for studying flooded shafts and stratification, a specialized mobile setup was deployed. This system consisted of a 1.5 km winch mounted on a field truck and equipped with an electrified cable for data transmission and real-time monitoring. This setup allowed for precise depth control, ensuring accurate in-situ measurements and water sample collection.

To avoid some undesirable interactions between the equipment and the pumps, the water extraction system was shut down 92 hours before the field measurements. A multiparameter probe (Idronaut 303, GeoVista) was then deployed to perform a detailed continuous physico-chemical log along the water column. The recorded parameters included pH, temperature and conductivity. The probe was calibrated beforehand and deployed at a speed of approximately 5 m/min. The probe provides high-resolution (±0.005 °C, ±1 µS/cm, ±0.05 for pH). A similar logging approach was conducted in several shafts of the Lorraine coal basin (Reichart 2013).

Based on physico-chemical profiling, water samples were collected at specific depths corresponding to major transitions (Fig. 2). Sampling was performed using remotely operated, pre-vacuumed stainless-steel bottles, which were opened at depth via a solenoid valve. This ensured passive filling with minimal air contact, preserving redox-sensitive species such as dissolved ferrous iron. The collected samples were analyzed for dissolved gases (free gases, CFCs, SF_6), carbon species (TOC, TIC, DOC, DIC), alkalinity (CO_3^{2-}, HCO_3^-), major anions (Cl^-, F^-, NO_3^-, NO_2^-, SO_4^{2-}, PO_4^{3-}), major cations (Ca^{2+}, Fe^{2+}/Fe^{3+}, K^+, Mg^{2+}, Na^+, NH_4^+, Si), trace elements (Ag, Al, As, B, Ba, Be, Br, Cd, Co, Cr, Cu, Li, Mn, Ni, Pb, Sr, Zn), isotopic ratios (δ^2H/δ^1H, $\delta^{18}O/\delta^{16}O$ in water; $\delta^{13}C/\delta^{12}C$ in DIC; $\delta^{34}S$, $\delta^{18}O$ in SO_4^{2-}; $\delta^{34}S$ in dissolved sulfides; $^{87}Sr/^{86}Sr$, $^7Li/^6Li$, $\delta^{11}B/\delta^{10}B$), and microbiological parameters (bacterial biodiversity via DNA sequencing, microflora abundance). Only dissolved iron concentrations will be discussed in this paper.

Results and Discussions

Physico-chemical profiles from 2024 can be compared with a 2011 log, recorded about a year after mine flooding ended and pumping started (Fig. 2). Temperature, conductivity and pH of both datasets are presented in Fig. 2. The Fe^{2+} concentrations in different zones of the Gérard shaft (precise depths shown in Fig. 2) are presented in Table 1. Dissolved iron, analysed by ICP-AES within one month after sampling, was measured on samples filtered on-site at 0.45 µm and acidified to pH <2 with ultrapure nitric acid immediately after collection.

The 2024 log reveals five distinct zones (Fig. 2), which will structure our following discussion. These zones appear to be strongly related to different mining levels, corresponding to former access galleries in the shaft. In 2011, Zone 1 (above pumps) has a uniform temperature of 21.73°C with a low temperature gradient (0.2 °C/100 m). Zone 2 (between the pumps and level 250) is stable at 22.45°C down to -183 m NGF, then decreases irregularly to 21.8°C at -250 m NGF. Zone 3 (level 250 to -315 m NGF) displays a nearly linear but unstable gradient (2.57°C/100 m) extending to -276 m NGF, followed by a temperature jump and another gradient (1.87°C/100 m) to -309 m NGF, before rising abruptly to 24.1°C at -314 m NGF. Zone 4 (-315 to -335 m NGF) shows a uniform temperature (24.15°C) with a low gradient (0.04°C/100 m). Finally, in Zone 5 (-335 to -421 m NGF), temperature increases irregularly with depth (0.74°C/100 m), reaching 24.79°C at -421 m NGF. The 2024 log shows notable changes. Zone 1 remains uniform, with a temperature of 20.77°C and a low gradient (0.2°C/100 m). Zone 2 is stable at 21.3°C (0.028°C/100 m). In Zone 3, temperature is stable but slightly noisy (~21.76°C) with a gradient of 0.06°C/100 m. Zone 4 reveals a staircase-like structure: the upper part has two large steps (~3.5 m), followed by four smaller ones (~1.5 m) with a gradient of 11.8°C/100 m. At -329.5 m NGF, the gradient steepens (24.2°C/100 m) with smaller steps (~50 cm). In Zone 5, temperature remains stable at 25.02°C (0.09°C/100 m). Conductivity and pH follow a similar trend to

Table 1 Fe^{2+} Concentration evolution in different Gérard shaft zones (2011 & 2024).

			Fe^{2+} (mg/L)	
Zone n°	Sampling Depth 2011	Sampling Depth 2024	2011	2024
1	-17 m NGF	-35 m NGF	< 0.05	< 0.02
2	-247 m NGF	-247 m NGF	43	32.9
3	–	-310 m NGF	–	29.7
4	-317 m NGF	–	27.8	–
5	-417 m NGF	-419 m NGF	2.2	13.0

temperature, except in Zone 1, where the pH is higher (6.76 in 2011 and 7.35 in 2024) than in the rest of the shaft and slightly decreases from top to bottom in 2024. Additionally, a 2 m-thick intermediate layer (Wolkersdorfer 2008, Mugova and Wolkersdorfer 2022) appears between Zones 1 and 2, and a 1.5 m-thick one between Zones 2 and 3. Between the two periods, a general cooling and decrease in conductivity are observed throughout the water column, except in Zone 5, along with an overall increase in pH. The dissolved iron concentration in the shaft (Table 1) is very low in Zone 1, reaches a maximum in Zone 2, then tends to decrease with depth. It is contrary to what is generally observed (Nuttall *et al.* 2004), stating that dissolved iron concentrations typically increase with depth.

In 2011, an inflow of cold, fresh water clearly appeared at -250 m NGF, cooling both the upper and lower parts of the shaft. Since the Gérard shaft is cased and supposed

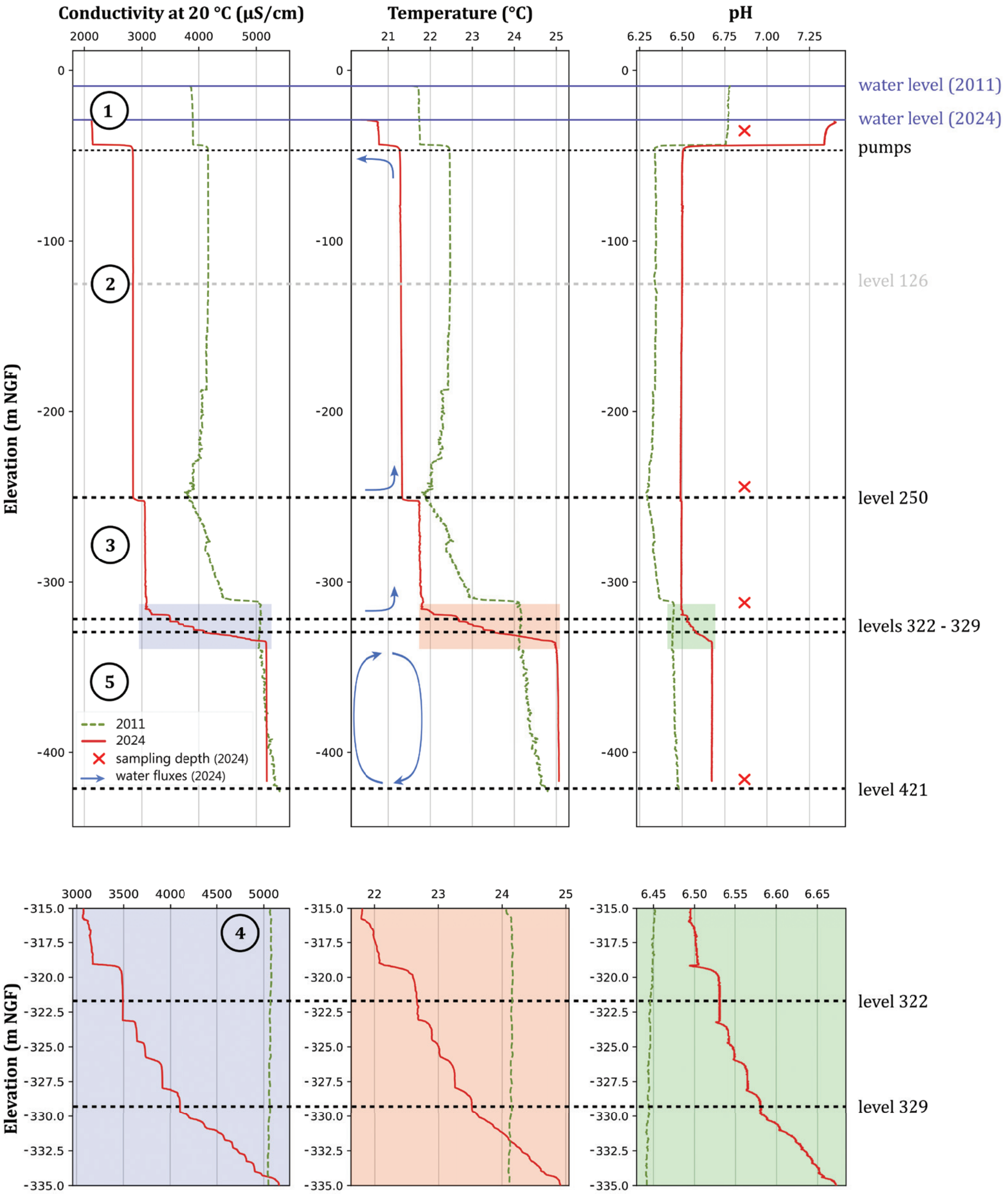

Figure 2 *Comparison of pH, Conductivity and Temperature logs in the Gérard Shaft (2011 & 2024).*

hydraulically sealed, water exchanges are only possible through intersecting galleries. This inflow corresponds to one such gallery, likely fed by groundwater from the Jurassic karst aquifer (sources 90 and Sainte-Victoire), through the former main drainage gallery (Travers Banc 250). Between 2011 and 2024, temperature, conductivity, and pH have homogenized up to the pumps level (Zone 2), indicating an upward forced convection regime in this water column (Reichart 2015, Bao *et al.* 2019a). The progressive deepening of this forced convection suggests that pumping has extended its influence over time, creating a homogeneous layer as a balance between the inflow at level 250 and the outflow at the pump. Stratification occurs when water layers form due to density contrasts from temperature, salinity, or turbidity variations (Wolkersdorfer 2008). The 2011 data indicate a predominantly diffusive regime in Zone 3, characterized by the absence of vertical water fluxes, as evidenced by the observed temperature gradient. The sharp transition between Zones 3 and 4 at -315 m NGF, followed by a uniform temperature in Zone 4, suggests the influence of a warmer inflow through the gallery at level 322 interacting with the gallery at level 329 to form a localized convection loop (similar to the Ronneburg Uranium mine; Wolkersdorfer 2008). Zone 5 was primarily governed by a diffusive regime. Between 2011 and 2024, important changes occurred in these deeper zones. Zone 3 has now stabilized into a homogeneous layer, possibly due to the influence of pumping extending to level 322, which would now direct its inflow upward. This shift has disrupted the dynamic exchanges between levels 322 and 329, giving rise to a thermohaline staircase structure in Zone 4. This type of stratification typically results from local opposing temperature and salinity gradients, triggering double-diffusive convection, which generates a sequence of oscillatory convection cells (Reichart 2015, Bao *et al.* 2019a, Bao *et al.* 2019b). The stable conditions observed in Zone 5 in 2024 now suggest the presence of a large convection loop between levels 421 and 329, or inter-level connections at the mine scale. The staircase structure in Zone 4 effectively isolates Zone 5 from the upper part of the shaft (Wolkersdorfer 2008, Reichart 2015, Bao *et al.* 2019b). The two identified inflows at levels 250 and 322 potentially share a similar origin due to their comparable iron concentrations. In its upper part (above level 322), the mine appears to be supplied by recharge zones and major inflows encountered during mining operations, likely originating from the Jurassic karst aquifer. Water circulates through the gallery network before reaching the shaft openings at levels 250 and 322, where it is pumped out. Lower concentrations in the deepest part may indicate other water sources and/or specific biogeochemical processes.

Conclusions

The comparative analysis of physico-chemical profiles between 2011 and 2024 highlights changes in the organization of water masses within the Gérard shaft. For thirteen years of pumping, the water column has evolved towards a stable stratification. This structuring appears to reflect a differentiated convection regime depending on the shaft zones, with the upper part being primarily influenced by anthropogenic pumping, while the deeper section results from natural stratification processes. Two inflows at levels 250 and 322, seemingly originating from similar sources, have been identified. Additionally, the deepest zone appears to be isolated from the rest of the shaft, potentially influenced by distinct biogeochemical processes or different water inputs. These preliminary interpretations, although supported by the literature, concern complex systems that remain challenging to understand. The forthcoming interpretation of chemical, isotopic, and bacteriological analysis results, coupled with their modeling, should help refine the understanding of flow dynamics within the shaft and its exchanges with the rest of the mining network.

Acknowledgments

The authors thank all contributors to this research. Special thanks go to BRGM, and more specifically to DPSM, for funding this work. We are also grateful to Benjamin Edwards and Hervé Boullée from DPSM for their expertise and invaluable support during the field campaign.

References

Ancel A, Moulin M, Rampnoux N (2004) Bassin d'Aix-Gardanne: état des connaissances géologiques, structurales et hydrogéologiques. Rapport de phase 1: Synthèse des données hydrogéologiques. Rapport BRGM/RP-53238-FR, 114 p.

Bao T, Liu Z (2019a) Geothermal energy from flooded mines: Modeling of transient energy recovery with thermohaline stratification. Energy Conversion Management 199:111956. https://doi.org/10.1016/j.enconman.2019.111956

Bao T, Liu Z (2019b) Thermohaline stratification modeling in mine water via double-diffusive convection for geothermal energy recovery from flooded mines. Appl Energy 237:566–580. https://doi.org/10.1016/j.apenergy.2019.01.049

Chalumeau A (2000) Fonctionnement hydrogéologique des exploitations de lignite du bassin de Fuveau (Bouches-du-Rhône). PhD thesis, Université de Franche-Comté.

Dewandel B, Ladouche B, Lanini S (2017) Projet de recherche ARK – Amélioration de la connaissance de l'aquifère du bassin d'Aix-Gardanne. Rapport final BRGM/RP-65884-FR.

Gaviglio P (1985) La déformation cassante dans les calcaires Fuvéliens du bassin de l'Arc (Provence). PhD thesis, Université de Provence.

Gonzalez G (1981) Étude sédimentologique du lignite Fuvélien du bassin de l'Arc et de l'encaissant calcaire (Bouches-du-Rhône, France). PhD thesis, Université de Provence.

Mugova E, Wolkersdorfer C (2022) Density stratification and double-diffusive convection in mine pools of flooded underground mines – A review. Water Research 214:118033. https://doi.org/10.1016/j.watres.2021.118033

Nuttall CA, Younger PL (2004) Hydrochemical stratification in flooded underground mines: an overlooked pitfall. J Contam Hydrol 69:101–114. https://doi.org/10.1016/S0169-7722(03)00152-9

Reichart G (2015) Modélisation thermo-hydrodynamique d'un réservoir minier profond ennoyé – Le cas du Bassin Houiller Lorrain. PhD thesis, Université de Lorraine.

Wolkersdorfer C (2008) Water management at abandoned flooded underground mines. Springer-Verlag, Heidelberg.

Characterization of Old Tailings Materials for Li-Sn Extraction and Sustainable Environmental Management: A Case Study of the Bielatal Tailings Dam, Altenberg, Eastern Ore Mountains, Saxony, Germany

Kofi Moro[1], Nils Hoth[2], Marco Roscher[3], Carsten Drebenstedt[4]

[1]TU Bergakademie Freiberg, Institute for Mining and Special Construction Engineering, Gustav-Zeuner-Straße 1a, Freiberg 09596, Germany, Kofi.Moro@mabb.tu-freiberg.de, ORCID 0000-0003-2851-9405

[2]TU Bergakademie Freiberg, Institute for Mining and Special Construction Engineering, Gustav-Zeuner-Straße 1a, Freiberg 09596, Germany, Nils.Hoth@tu-freiberg.de

[3]TU Bergakademie Freiberg, Institute for Mining and Special Construction Engineering, Gustav-Zeuner-Straße 1a, Freiberg 09596, Germany, Marco.Roscher@mabb.tu-freiberg.de

[4]TU Bergakademie Freiberg, Institute for Mining and Special Construction Engineering, Gustav-Zeuner-Straße 1a, Freiberg 09596, Germany, Carsten.Drebenstedt@mabb.tu-freiberg.de

Abstract

Reprocessing potential and environmental risk of Bielatal tailings material, Altenberg, Germany, were assessed using percussion core samples (7 m depth), analyzed for geochemical, mineralogical composition, particle size, and milieu parameters (pH, Eh, EC). Tin (0.12 wt%) and lithium (0.10 wt%) were valuable elements, while arsenic (0.04 wt%) posed environmental concerns. Tin and lithium were associated with cassiterite and mica phases respectively. Samples were composed of 56% silt, 35% fine sand, and 9% clay, with enrichment of tin, lithium, and arsenic in fine fractions. Weak acidity (pH 6) and low oxidation (Eh 160 mV) suggest minimal acid mine drainage risk.

Keywords: Bielatal tailings dam, geochemical characterization, mineralogical characterization, lithium, tin

Introduction

Comprehensive characterization of historical tailings is essential for effective environmental management and resource recovery. Understanding their chemical, mineralogical, and physical properties helps mitigate environmental risks and identify opportunities for extracting valuable elements (e.g. Li, Sn) while assessing potential toxic metal (e.g. As, Pb) content (Jackson and Parbhakar-Fox 2016). Physical property analysis also ensures storage facility stability, preventing dam failures and promoting sustainable mining practices to protect ecosystems and communities (Anawar 2015). Each tailings storage facility (TSF) has a unique depositional history, structure, and composition influenced by processed ore characteristics, processing technology, and deposition methods (Büttner *et al.* 2018; Redwan *et al.* 2012). Exploration and feasibility studies, similar to those for primary ore deposits, rely on understanding material characteristics such as grade, particle size, mineral liberation, and metal deportment to minimize investment risks in tailings reclamation (Büttner *et al.* 2018).

To date, there has been no characterization studies of the Bielatal TSF, and that there is little or no literature been published about the reprocessing potential of this tailings body, hence its selection as a case study in this work. The interest in reprocessing the tailings coexists with the necessity to reduce harmful

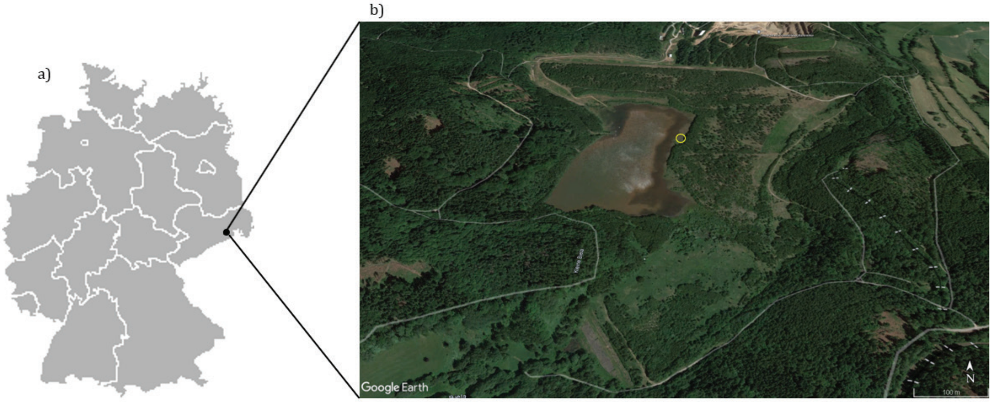

Figure 1 (a) Location of the Bielatal tailings dam in Germany, (b) oblique Google satellite image of the surface of the dam with marked (yellow) sampling area (modified after Google Inc. (2024)).

environmental impacts caused by the high arsenic contents which were completely discharged into the Bielatal tailings dam during the mining operation. Furthermore, it is important to investigate the current condition of the tailings material to ascertain its potential risk with respect to acid mine drainage. The findings from this preliminary study is compared to literature to check the correlations between survey data and site-specific materials examined. This would highlight the importance of combining historical data with detailed geochemical and mineralogical analyses to assess the potential for resource recovery and environmental risks in mine tailings.

Study area

The Bielatal TSF in Altenberg, Saxony (Fig. 1), was built by Volkseigener Betrieb (VEB) Zinnerz Altenberg and operated from 1967 until 1991. The dam stored processing wastes from the Altenberg Sn deposit, a world-class greisen deposit in the Eastern Erzgebirge, Saxony, Germany (Weinhold 2002). It measures around 73,000 m^2 by surface area, a height of 80 m, and an average width of 680 m. It holds about 10.5 Mio m3 of flushed-in tailings material. Located 1.5 km north of Altenberg, one-third of the TSF surface is covered by a residual lake (Fig. 1b) with a flushing beach as part of its reclamation strategy.

Materials and Methods

Sampling was conducted in Oct.–Nov. 2023 on the eastern side of the residual lake (Fig. 1b) at five points (RKS1–RKS5) using percussion coring to a depth of 7 m and about 5 m apart, yielding about 100 kg of material. Samples were dried at 105 °C, deagglomerated, and homogenized for analysis. Particle size distribution was determined using a laser particle size analyzer and pH, redox potential (Eh), and electrical conductivity (EC) were measured in a 1:2 solid-liquid ratio. Eh values were corrected to the standard hydrogen electrode (Blowes *et al.* 1998).

Bulk chemical composition was analyzed using a hXRF analyzer, while Li was measured by Na-peroxide fusion. Strong agreement was observed between Na-peroxide fusion and hXRF for Sn and major elements. Mineral phases were identified via Scanning Electron Microscopy (SEM) with Energy Dispersive X-ray spectroscopy (EDX) analysis.

Results and discussion

Geochemical characterisation

A summary of the chemical composition of the tailing samples is presented in Tab. 1. The results indicate that, the main components of the tailing samples (RKS1-RKS5) are Si with average concentration of 33 wt%, Al 8 wt%, Fe 5 wt%, and K 2 wt%. The valuable elements in the tailing samples like Sn and Li have average concentrations of 0.12 wt% and 0.10 wt% respectively. All other elements have an average concentration < 0.1 wt%. The results show that, the major environmentally concerning element is the Arsenic (As) content present in the tailings with the average

Table 1 Average metal concentration of tailing samples, (combined hXRF and Na-peroxide fusion (*) data from individual drill holes).

Sample	Al %	As %	Bi %	Ca %	Fe %	K %	Li* %	Mn %	Mo %	Rb %	S %	Si %	Sn %	Ti %	W %
RKS1	7.57	0.04	0.02	0.78	4.45	1.90	0.10	0.09	0.02	0.06	0.06	32.32	0.09	0.04	0.02
RKS2	7.72	0.04	0.01	0.79	4.70	1.96	0.10	0.08	0.01	0.11	0.05	32.60	0.10	0.04	0.02
RKS3	7.49	0.04	0.01	0.77	4.63	1.94	0.10	0.08	0.01	0.11	0.05	33.25	0.10	0.04	0.02
RKS4	8.04	0.04	0.01	0.76	4.75	2.03	0.09	0.08	0.01	0.11	0.06	32.85	0.11	0.04	0.02
RKS5	7.83	0.04	0.02	0.77	4.90	2.02	0.10	0.08	0.01	0.11	0.06	31.91	0.19	0.04	0.02

concentration of 0.04 wt%. From the results it can be seen that, the element distribution values in all 5 drill core bulk samples are quite similar, indicating a relatively even element distribution in these sampling locations. A more deep and extensive drilling campaign is needed to further confirm this for the entire tailings body.

Correlation of Rb-Li in tailings material

Conventional lithogeochemical techniques often result in delays between sample collection and laboratory analysis, creating a gap between data acquisition and application (Kalnicky and Singhvi 2001). Since Li, a lighter element, is not directly measurable by XRF, its correlation with Rb (by hXRF) plays a crucial role. Weinhold (2002) reported strong Li-Rb correlations (R^2 = 0.95–0.99) in the Altenberg ore deposit, where Li is primarily associated with mica phases like zinnwaldite. Correlation between Rb and Li can be seen in Fig. 2. Similarly, a high correlation (R^2 = 0.95) in the investigated samples is confirmed, indicating that high Rb samples are also richer in Li. This validates the use of hXRF-measured Rb to predict Li content using the correlation equation, particularly for rapid decision-making in process steps. Furthermore, the establishment of such a kind of correlation equation has not only the potential to reduce the time between sampling and result gathering but can also substantially reduce analytical costs in extensive sampling campaigns. It is worth noting that, the prediction is reliable within the range of 0.07–0.14 wt%, but new dataset is needed to validate the equation for values outside this range.

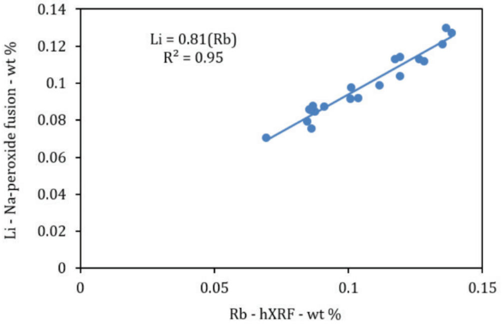

Figure 2 Rb-Li correlation in tailing samples.

Particle size distribution related to geochemical composition

The geochemical composition of tailings samples is bound to minerals that passed the ore processing procedures. These multi-stage treatments result in different grain sizes.

Fig. 3a shows the relevant particle size data (d50) and element (Li, Sn, As) concentration against depth from drill core samples RKS5. For simplicity, only the data for d50 is shown. Basically, the results for the 5 different drill core samples show the same trend, therefore, only one drill hole (RKS5) is shown. The general tailings samples are very heterogeneous with regard to grain size ranging from 0.35 to 300 µm. The silt fraction (2 to 63 µm) represents the highest content (56–60%). The fine sand (63 to 300 µm) and clay (< 2 µm) content ranges from 30–35% and 6–9% respectively. Fig. 3b is a correlation between element concentration (Li, Sn, As) and particle size distribution (d50). Note that, Li data are predicted values from the Rb-Li correlation equation for reasons mentioned above. A vertical fractionation layered structure is clearly evident in the drill profile (Fig. 3a) with an alternating layer structure of coarse and fine-grained materials. This could be attributed to the tailings spilling (deposition) process.

From 3a, it is clear that, Li, Sn and As concentrations are higher in the finer particle size fractions. However, there exit a poor correlation between Sn-As and the entire size distribution (Fig. 3b). Li on the other hand shows a consistent correlation across all size fractions. This means that the processing technology (flotation) used for the extraction of Sn was very efficient for the coarser particles, resulting in a higher enrichment only in a specific fraction (fine particles). Li, which was not a target element at the time was not attacked by flotation, resulting in a uniform distribution of Li-bearing minerals within the sample and broke down proportionally during size reduction, hence, the consistent correlations across all size fractions. This implies that, the extraction of Sn from the tailing samples should be targeted in the fine fraction while Li should be targeted across all particle size streams. For environmental reasons, the fine particles should be of major concern as As is highly enriched in the fine fraction.

Determination of mineral content by SEM-EDX

According to Weinhold (2002), the Bielatal tailing materials consist mainly of quartz, mica, topaz and alkali feldspars with minor hematite, and clay minerals resulting from feldspar alterations (Redwan 2022). Of particular importance to this study are the minerals cassiterite, mica and some relevant arsenic bearing mineral phases. Therefore, SEM-EDX analysis was conducted to further confirm the presence of these mineral phases in the tailing samples. From Fig. 4, it can be seen that, silicates are homogeneously distributed in the sample and associated to most elements such as K, Al, Fe, F, Na, Ca, Mg and Ti. In this regard, the following mineral phases could be present; quartz, topaz, feldspar, mica, and kaolinite. Tin is bound to the cassiterite phase (SnO_2) represented as strongly bright, discrete particles in the Backscattered Electron (BSE) mode. Fe to some extent shows an association with sulfur and arsenic which could indicate the probable presence of pyrite and/or arsenopyrite. A homogeneous S and As distribution observed is likely due to the low content and peak overlap making it difficult to identify specific As-S rich phases in the sample. A more detailed analysis of these materials would be performed using XRD to further confirm the presence of these probable mineral phases.

Environmental (milieu) parameters

Fig. 5 shows the pH, Eh and EC measured values in the eluates against profile depth for one drill core sample. These parameters are key indicators of the geochemical

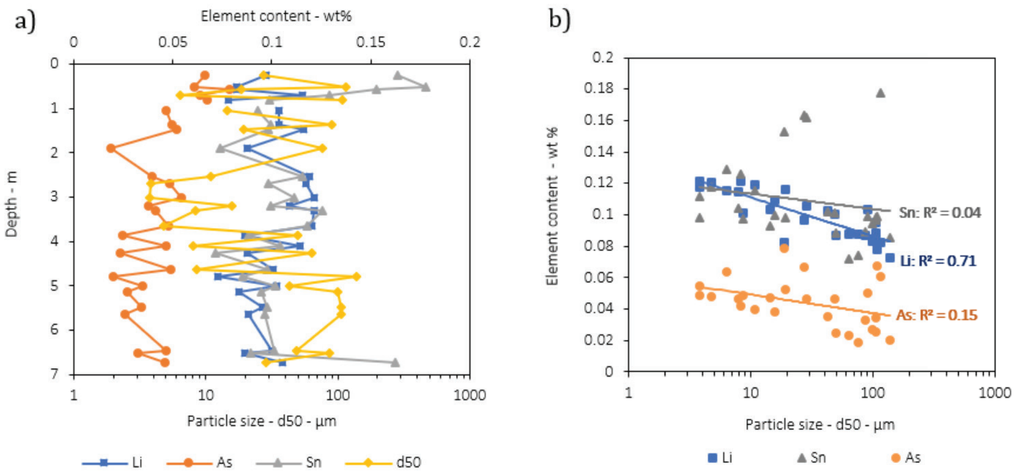

Figure 3 *(a) Particle size distribution and concentration of Li, Sn and As of drill core RKS5 by depth (b) correlation between particle size distribution and concentration of Li, Sn and As on a logarithmic scale.*

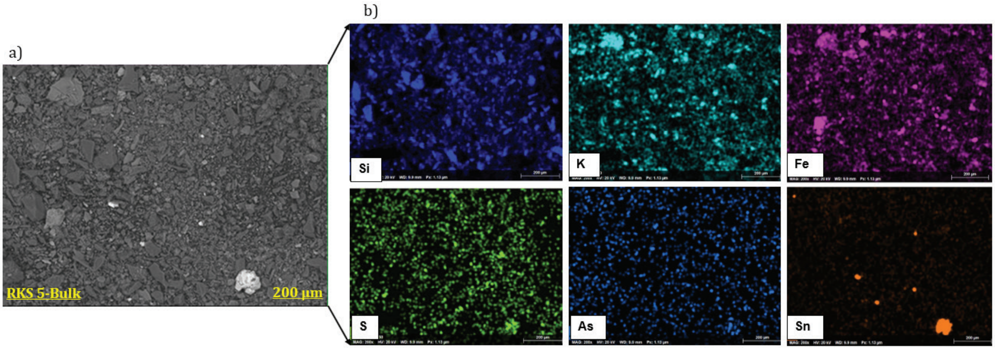

Figure 4 *Mapping of tailing sample (RKS5 bulk sample) at x100 magnification (a) SEM image (BSE) (b) EDX.*

environment in the tailings. The pH increases gradually from 5.5 at the top to 6.8 at depth, indicating a weak acidic to neutral conditions in the tailings body. This can be attributed to the buffering effect of the primary ore processed at the time (Modabberi 2018), the processing technology used and or only to the infiltration of meteoric waters (pH 5.6). The Eh to some extent decreases with increasing depth from 486 mV to less than 200 mV, indicating a highly oxidized condition at the upper part of the tailings body. This could lead to certain weathering effects at the upper part of the tailings body. The lower part of the tailings body is less oxidized. The electrical conductivity fluctuates in a range of 38–68 µS/cm suggesting relatively low levels of dissolved ions in the tailings body. An average moisture content of 35% was recorded for the drill core samples which indicates that the tailings are relatively moist, but not in a fully saturated state. Under these above described conditions, the tendency for acid mine drainage and metal mobility is minimal. However continuous monitoring and management is paramount to minimize environmental risks.

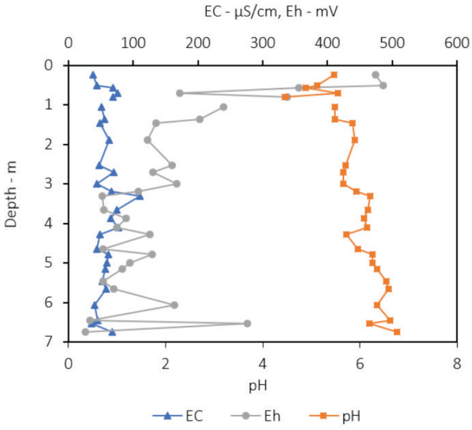

Figure 5 *Milieu parameters (EC, pH and Eh) measured with depth – RKS5.*

Conclusion

This study evaluated the Bielatal tailings dam material to assess its potential for valuable metal recovery and environmental management. The material consists mainly of quartz, mica, topaz, feldspars, hematite, and clay minerals, reflecting its greisen origin, with economically relevant concentrations of Li and Sn enriched in finer grain fractions. A Rb-Li correlation equation was developed to address challenges in direct Li measurement, aiding rapid decision making in process control and analytical cost reductions. The material is predominantly fine-grained, with silt and fine sand dominating. Based on the findings, it is recommended that Sn extraction from the tailing samples should be focused on the fine fraction, while Li extraction should be considered across all particle sizes.

Environmental assessment revealed weak acidity, moderate oxidation, and minimal acid mine drainage risk, with arsenic being the primary element of environmental concern. The fine particles of the tailings require special attention, as As is notably enriched in this fraction. Low metal mobility is expected under the current tailing's conditions. These findings align with historical data, confirming the resource potential of the tailings and emphasizing the need for further studies and ongoing monitoring to guide sustainable reclamation strategies and minimize environmental risks.

Acknowledgments

The authors acknowledge that, this work as part of the TEVLiS project was funded by the German Federal Ministry for Education and Research (BMBF) as part of the rECOmine research project initiative (funding number 03WIR1912C). The authors are also sincerely grateful for discussion and contribution by project partners BEAK GmbH, UVR-FIA GmbH, ERZLABOR GmbH and Zinnwald Lithium GmbH and the site (Bielatal tailings dam) owner, LMBV, for their permission and cooperation in material sampling.

References

Anawar HM (2015) Sustainable rehabilitation of mining waste and acid mine drainage using geochemistry, mine type, mineralogy, texture, ore extraction and climate knowledge. J Environ Manag 158:111–121, doi:10.1016/j.jenvman.2015.04.045

Blowes DW, Jambor JL, Hanton-Fong CJ, Lortie L, Gould W (1998) Geochemical, mineralogical and microbiological characterization of a sulphide-bearing carbonate-rich gold-mine tailings impoundment, Joutel, Québec. Appl Geochem 13:687–705, doi:10.1016/S0883-2927(98)00009-2

Büttner P, Osbahr I, Zimmermann R, Leißner T, Satge L, Gutzmer J (2018) Recovery potential of flotation tailings assessed by spatial modelling of automated mineralogy data. Miner Eng 116:143–151, doi:10.1016/j.mineng.2017.09.008

Google Incorportaion (2024). Google Earth (online). earth.google.com accessed on August 27, 2024

Jackson LM, Parbhakar-Fox A (2016) Mineralogical and geochemical characterization of the Old Tailings Dam, Australia: Evaluating the effectiveness of a water cover for long-term AMD control. Appl Geochem 68:64–78, doi:10.1016/j.apgeochem.2016.03.009

Kalnicky DJ, Singhvi R (2001) Field portable XRF analysis of environmental samples. J Hazard Mater 83:93–122, doi:10.1016/S0304-3894(00)00330-7

Modabberi S (2018) Mineralogical and geochemical characterization of mining wastes: remining potential and environmental implications, Muteh Gold Deposit, Iran. Environ Monit Assess 190:734. doi:10.1007/s10661-018-7103-7

Redwan M (2022) Geochemical and mineralogical characteristics of some gold mine tailings in the Eastern Desert of Egypt. Front Earth Sci 16:906–915, doi:10.1007/s11707-021-0968-3

Redwan M, Rammlmair D, Meima JA (2012) Application of mineral liberation analysis in studying micro-sedimentological structures within sulfide mine tailings and their effect on hardpan formation. Sci Total Environ 414:480–493, doi:10.1016/j.scitotenv.2011.10.038

Weinhold G (2002) Die Zinnerz-Lagerstätte Altenberg/Osterzgebirge. In: Bergbau in Sachsen, Band 9, Sächsisches Landesamt für Umwelt und Geologie, Dresden

Advances in integrated performance monitoring of Tailings Storage Facilities

Alastair Bovim[1], Kym L Morton[2], Philip Marais[3]

[1]Insight Terra, 42 Oxford Street, Durbanville, 7550, South Africa, alastair.bovim@insightterra.com

[2]KLM Consulting Services Pty Ltd, 22 Central Road, Sunrella AH, 1748, South Africa, kmorton@klmcs.co.za, ORCID 0000-0002-5865-1979

[3]Independent Researcher, South Africa, marais.philip@outlook.com

Abstract

Since the initiation of the Global Industry Standard on Tailings Management (GISTM), the adoption by mining companies of advanced monitoring technologies has expanded. These systems utilize continuous, near-real-time data from diverse sensors, integrating geotechnical, hydrological, and environmental measurements. Enhanced by real-time data fusion and advanced statistical analysis, the technology enables the detection of subtle structural deviations, improving the accuracy of quantitative risk assessments, and reducing false positives. Dynamic, tailored response plans are activated based on detected anomalies and forward-looking statistical trend analysis, enabling swift, informed decision-making. This approach enhances safety and proactive risk management for tailings storage facilities and promotes regulatory compliance, operational efficiency, and sustainability.

Keywords: GISTM, Tailings Management, Advanced Analytics, Sustainability

Introduction

Tailings storage facilities (TSFs) have attracted increasing attention from international investors, insurers and the United Nations due to catastrophic failures, prompting industry changes. One key outcome was the publication of the Global Industry Standard on Tailings Management (GISTM), which emphasizes integrated performance monitoring as a safety measure (GISTM, 2020). Guidelines for TSF monitoring have been established, promoting best practices and effective oversight (Zare *et al.*, 2024). As a result, new monitoring technologies have emerged, including:

- Real-time sensor data collection
- Data integration and management in the cloud
- Real-time statistical analysis
- Anomaly detection
- Machine Learning and AI

These innovations offer benefits like reducing false positives, improving risk assessments, speeding decision-making, automating response plans, enhancing disaster preparedness, reducing compliance efforts, and cutting operational costs. This paper focuses on the value of these technologies for safety, monitoring, proactive risk management, and automated responses.

Monitoring Techniques for Tailings Storage Facilities

Before the widespread availability of sensors and Internet of Things (IoT) devices enabling automated monitoring, visual assessments and manual measurements were the primary tools used in surveillance monitoring. These processes were manual and time consuming, resource-intensive, and introduced the possibility of human error. The clear need for implementation of more effective monitoring systems, coupled with the affordability and scalability of IoT-enabled sensor networks, has propelled the industry toward digitized and automated data collection.

A systematic review by Cacciuttolo *et al.* (2024) analyzed 52 studies from Web of

Science (WoS) and Scopus databases, highlighting the widespread use of modern technologies. 90% of the papers analysed specified the use of real-time automatic measurements.

These new advanced monitoring technologies create the potential for a greater understanding of critical failure mechanisms, or modes, enable early detection of potential triggers, and support tailings dam design and expansion. By integrating these systems, the industry can transition from reactive to proactive risk management, ensuring safer and more efficient operations.

Automated Data Processing

The typical monitoring data flow from TSF instrumentation is **collection**, **transformation**, **validation**, **processing**, and **visualisation** (Insight Terra, n.d.). Automated data collection from TSF instrumentation begins with data collection through local wireless gateways and networks. This data at site level is normalized, and compressed, ensuring efficient and secure transmission to the cloud via either terrestrial or satellite connectivity. Upon reaching the cloud, each raw measurement enters a real-time data pipeline and undergoes validation and transformation against predefined accuracy thresholds before processing.

Following validation, the data is enriched with installation details and other relevant metadata to produce contextualised data with the correct engineering units. Raw data persists, whilst the calculated engineering metrics progress to the next step of real-time analysis by logic algorithms, which are designed to extract contextual information, generate insights, identify anomalies, and trigger alerts when predefined thresholds are exceeded. The processing and analysis of each metric in real-time differ substantially from retrospective analysis. Analysing the data quality through each step reduces the potential for false positives. Invalid data is stored separately from valid data for further analysis. Finally, the processed data is made available to other systems and visualisation tools, allowing users to create dashboards and use the data for informed decision-making and processes like root cause analysis.

Advanced Data Processing and Analysis

Historically, each retrieved parameter would be evaluated individually to determine any structural changes in the TSF. However, more recently multi-dimensional data sources are being integrated into a single framework for improved analysis. As demonstrated by Mwanza *et al.* (2024), the combination of geotechnical, environmental, and hydrological parameters through digital twin simulation and machine learning enables a more comprehensive analysis of TSF stability. This integration allows for real-time monitoring as well as predictive insights that weren't possible with traditional single-parameter assessments.

Unified data frameworks derive new insights via advanced analytics. As the proliferation of IoT sensors and instrumentation broadens data availability, previously unrecognized correlations among parameters become apparent. This evolution is demonstrated in contemporary TSF monitoring methodologies, where enhancements in real-time data acquisition, coupled with machine learning (ML), are significantly advancing failure prediction capabilities. By integrating digital twin technology and ML algorithms, TSF management is transitioning from straightforward parameter monitoring to sophisticated predictive analytics. This allows the detection of early warning signs across various failure modes, thereby enabling more proactive risk management and strengthening safety measures. This represents a substantial progression from traditional monitoring techniques, which primarily depended on explicit mathematical correlations among single parameters.

Fig. 1 on the next page depicts the processing steps of a single payload of data containing measurement metrics from a geotechnical instrument with several data points, such as an inclinometer.

The received data payload, which includes multiple metric measurements (e.g., from a MEMS inclinometer), undergoes the following processing steps:

1. Quality assurance: Each metric within a data point is initially checked to ensure accuracy and reliability.

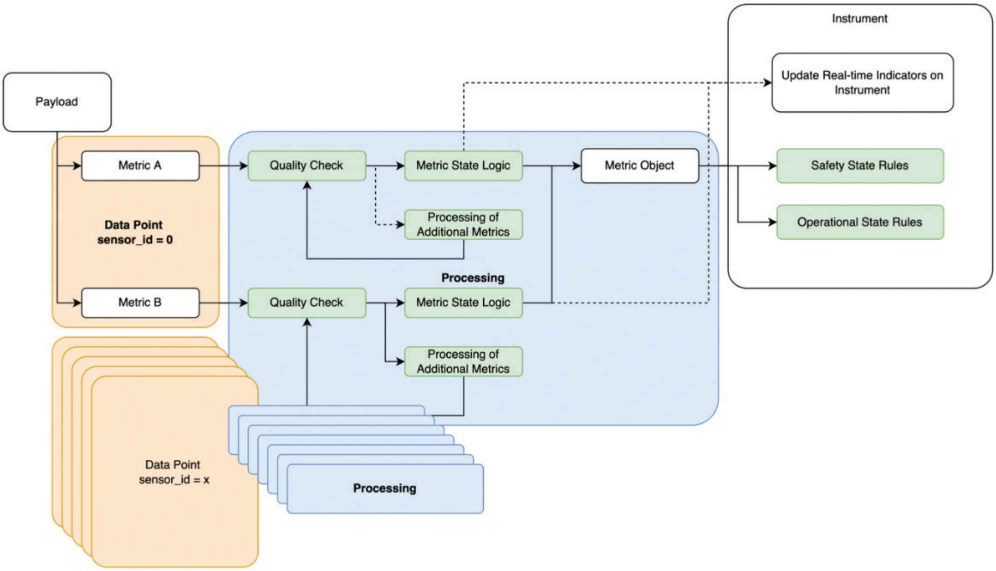

Figure 1 Data Processing Step for a Payload.

2. Metric state analysis: After quality assurance, each metric is subjected to state logic analysis for detecting abnormalities and trends. This analysis also updates the real-time indicators of the instrument.
3. Extended metric processing: Further metrics are generated for each data point using a processing script. This includes querying historical data, enhancing the depth of analysis, and conducting additional logical validations.
4. Data persistence and rule application: After processing, metrics are stored and subsequently integrated into a rules engine. This engine activates safety and operational state protocols.
5. Complex scenario execution: The safety and operational states execute comprehensive analyses across all metrics and data points, determining the appropriate indicators for monitoring system integrity and operational safety.
6. Virtual device handoff: The payload may also be transferred to virtual devices for additional processing. These virtual devices handle multiple payloads from various instruments, each running through its own designated processing script and generating a new set of metrics.
7. Nested entity triggering: Any nested monitoring entities are triggered for processing once the initial instrument entity completes its safety and operational state processing.
8. Data point group invocation: Groups of data points can be created from new payloads from one or more similar instruments, to undergo the same process, including safety and operational state processing.

Micro Trend Analysis

Geotechnical instrumentation metrics are implicitly slow to change. They require long-term analysis to identify macro trends. However, by the time these trends become clear, addressing their impact may be costly and disruptive. Real-time analysis, enabled by the availability of real-time data, can be implemented to detect micro trends in time-series data. A trend change can serve as an early warning for large incidents.

Statistical Process Control (SPC) approaches can track data fluctuations and identify anomalies that may signal abnormal conditions in the tailings structure. These methods detect potential dangers by analysing characteristics such as tailings density, settlement rates, and groundwater levels (Harvey, 2023). More particularly, the Nelson Rules, first introduced in Lloyd S. Nelson's publication The Shewhart Control

Chart: Tests for Special Causes (Nelson, 1984), provide a formal framework for finding exceptional causes of variation in a process through microtrend analysis. The Nelson Rules can be used inside SPC to discover early warning signs of impending problems. This allows stakeholders to be proactive in maintaining the safety of tailings facilities.

Limited research has been published on the application of these rules in the mining industry. Other industries have however successfully implemented these practices. The paper, "*Condition Monitoring of Internal Combustion Engines in Thermal Power Plants Based on Control Charts and Adapted Nelson Rules*" (Vilas Boas *et al.*, 2021), is an example of a successful application of Nelson Rules. Their findings highlight how SPC and Nelson Rules can be used for early failure detection, predictive maintenance, and decision-making to prevent costly breakdowns. It is reasonable to conclude that this process is similarly useful for tailings management.

How these rules can apply to tailings management is discussed next, focusing on Rules 1 to 4 due to their relevance to sensor performance and geotechnical stability.

1. Extreme Deviation (One point is more than 3 standard deviations from the mean)
   a. Geotechnical Implications: This may indicate sudden instability, such as excessive pore pressure.
   b. Sensor Implications: Possible sensor malfunction.
2. Prolonged Bias (9+ consecutive points on one side of the mean)
   a. Geotechnical Implications: Suggests a new norm has been reached, requiring a recalculation of the mean.
   b. Sensor Implications: Could indicate sensor drift
3. rending Data (6+ consecutive points increasing or decreasing)
   a. Geotechnical Implications: Reflects progressive changes such as soil consolidation, tailings compaction, or embankment settlement.
4. Oscillations (14+ points alternating in direction)
   a. Geotechnical Implications: Unlikely to be caused by natural factors
   b. Sensor Implications: This likely points to a faulty sensor.

In addition to the Nelson Rules, various statistical techniques can be used to analyse trends and determine TSF stability. Comparative stability analysis methods, such as those described in "Comparative Stability Analysis of Tailings Storage Facilities" (Vega Vergiagara *et al.*, 2021), offer alternate means of monitoring TSF behaviour. Raw data can be turned into useful information about the sensor network and TSF stability by using various statistical methodologies.

To aid in proactive decision-making, an automated notification system can be built to alert stakeholders when anomalies are identified. These notifications then connect stakeholders to a dashboard that shows key performance indicators (KPIs) relating to TSF conditions. Such dashboards enable engineers and decision-makers to monitor trends, identify abnormalities, and take proactive measures. By leveraging real-time analytics and SPC techniques, TSF management can become more proactive, reducing the risk of major incidents and ensuring long-term stability.

Creating and Enhancing Response Plans

Trigger Action Response Plans (TARPs) can be employed to systematically manage risks in TSFs by defining clear actions based on predefined safety or operational thresholds. Integrating TARPs with real-time data is essential for enhancing the safety and efficiency of TSFs. As highlighted by Nunes *et al.* (2023), TARPs are designed to address deviations from normal operating conditions through a tiered response system, ensuring timely interventions that reduce the likelihood of structural failures and restore safe conditions.

The Response Plan Data Model in Fig. 2 ensures a structured approach to risk management by linking safety states, responder types, monitoring entities, and supporting documentation. Each response plan is linked to an Operational/Safety State Indicator, defining risk levels, categorized by colour levels (e.g., Red for critical conditions). It is assigned to a Responder Type, which mimics a persona, e.g. Engineer of Record (EOR) or Responsible Tailings Facility Engineer (RTFE). This ensures that correct actions are taken by the appropriate individuals. Monitoring entities, including sensors, interface nodes, physical and virtual devices, and data point groups, visualise their safety or operational states (Red, Orange, Yellow, Blue, Green) in real-time based on the predefined trigger conditions. Monitoring entities activate response plans when they detect a specific state. Furthermore, attachments such as procedural documents and schematics are linked to response plans, guiding responders.

Fig. 3 illustrates how the above data model is used for Monitoring Entity A. If Monitoring Entity A triggers a RED safety state, all the relevant responders (in this case Responder A and B) will be allocated their respective RED response plans. If the safety state were to later change to YELLOW, different responders (e.g. Responders B and C) would be assigned their associated YELLOW response plans. The same goes for the ORANGE, BLUE, and GREEN states. Email notifications and monitoring applications ensure that the appropriate details are conveyed to the designated responders in real-time.

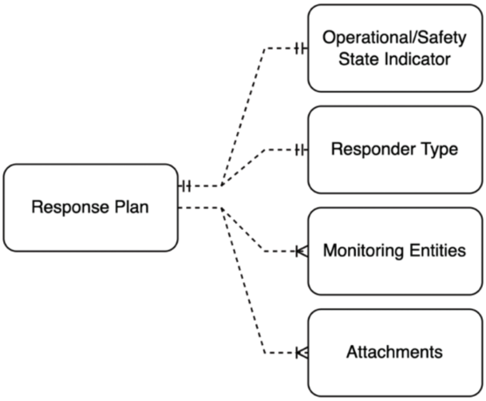

Figure 2 *Response Plan Data Model.*

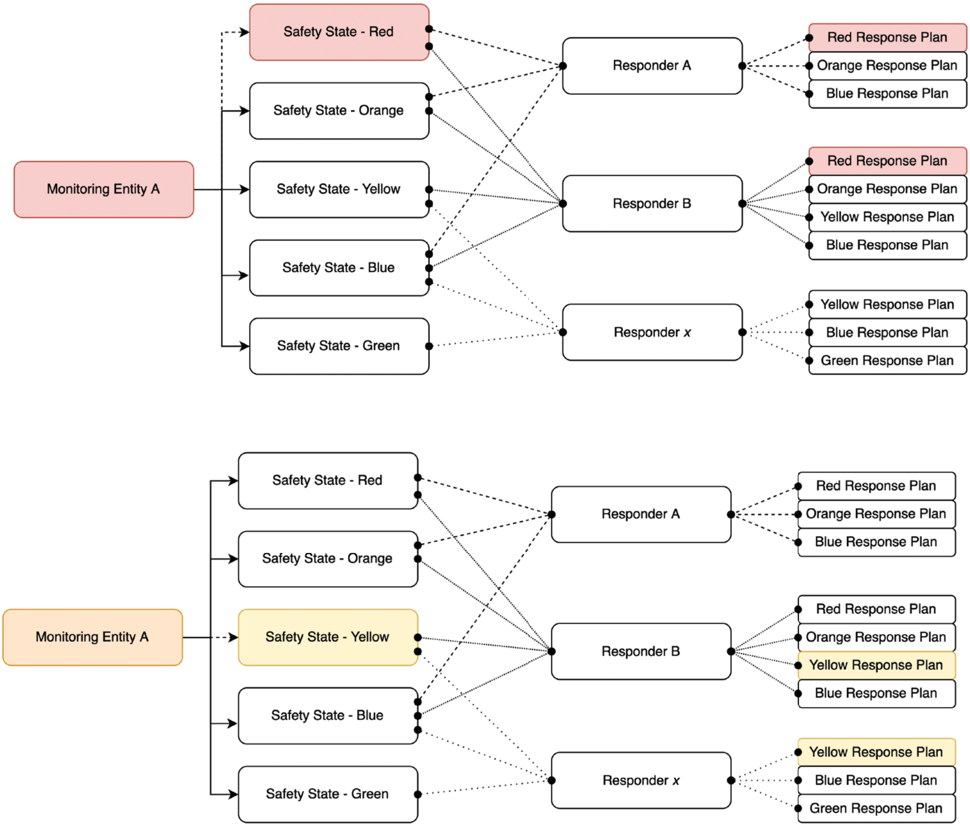

Figure 3 *Trigger Action Response Plan Example.*

Applications, Broader Implications, and Industry Transformation

The adoption of advanced monitoring technologies in TSFs is reshaping industry practices, enhancing safety, sustainability, and operational efficiency. The industry is making steady progress in integrating these technologies, particularly following the implementation of the GISTM.

Despite the clear benefits of these advancements, challenges remain regarding widespread adoption across all facilities, particularly among smaller operators facing budget constraints. Nonetheless, the industry's commitment to improving safety standards through technology is evident as it progresses towards more sustainable and efficient TSF management solutions.

The future of TSF management lies in the implementation of advanced technologies such as automated instrumentation, AI, and digital twins. Digital twins, which create virtual replicas of physical systems, offer predictive insights and enhance monitoring capabilities. The integration of ML/AI and IoT technologies into mining automation presents opportunities for improved data security, transparency, and operational efficiency (Cacciuttolo 2024).

Conclusions

Advancements in integrated monitoring of TSFs have transformed risk management into a proactive process. By leveraging near real-time data, advanced SPC, and automated response plans, the industry can detect anomalies earlier, reduce false positives, and implement dynamic mitigation strategies. The implementation of multi-dimensional data analysis and ML/AI-driven insights that are integrated into the overall surveillance and performance monitoring processes enhances TSF safety and optimizes response planning, ensuring compliance with evolving industry standards such as the GISTM. Beyond safety improvements, these innovations offer cost savings, environmental benefits, and operational efficiencies that drive broader industry transformation. As technology advances, the incorporation of predictive analytics, ML/AI, and digital twin modelling will further refine TSF management practices, paving the way for a safer, more sustainable future in the mining sector.

Acknowledgements

The authors would like to thank Etienne Bruwer, Director of Solution Engineering at Insight Terra, for his valuable contributions and insights. His expertise and support were instrumental in refining key technical aspects of this paper.

References

Cacciuttolo C, Guzmán V, Catriñir P, Atencio E (2024) Sensor Technologies for Safety Monitoring in Mine Tailings Storage Facilities: Solutions in the Industry 4.0 Era. Minerals 14(5):446. https://doi.org/10.3390/min14050446

Global Industry Standard on Tailings Management. (2020) *Global industry standard on tailings management*. Retrieved from https://globaltailingsreview.org/global-industry-standard/

Harvey D (2023) Data management and insights for effective tailings storage facility management. *SAIMM Conference Proceedings*. Retrieved from https://www.saimm.co.za/Conferences/files/tailings-2023/21%20585_Harvey.pdf

Insight Terra. (n.d.). *How it works*. Retrieved January 29, 2025, from https://www.insightterra.com/platform/how-it-works

Mwanza J, Mashumba P, Telukdarie A (2024) A framework for monitoring stability of tailings dams in real-time using digital twin simulation and machine learning. Procedia Computer Science 232:2279–2288. https://doi.org/10.1016/j.procs.2024.02.047

Nelson, L. S. (1984). The Shewhart control chart: Tests for special causes. *Journal of Quality Technology*, 16(4), 238-239.

Nunes AJC, Cavalieri F, dos Santos Lopes HL, Lima AP, Rodrigues RS (2023) Deterministic and statistical analysis in the definition of triggered action response plans in tailings dams. *In Proceedings of Tailings and Mine Waste 2023*. Vancouver, Canada: University of British Columbia. https://doi.org/10.14288/1.0438144

Vergiagara V, Yulianto MR, Anggara R, Saptono S (2021) Comparative stability analysis of tailings storage facilities. *AIP Conference Proceedings*, 2363, 030014. https://doi.org/10.1063/5.0061808

Vilas Boas FM, Borges-da-Silva LE, Villa-Nova HF, Bonaldi EL, Lacerda Oliveira LE, Lambert-Torres G, Assuncao FO, Costa CIA, Campos MM, Sant'Ana WC, Lacerda J, Marques da Silva Junior JL, Gomes da Silva E (2021) "Condition monitoring of internal combustion engines in thermal power plants based on control charts and adapted Nelson rules," Energies 14(16): 4924. https://doi.org/10.3390/en14164924

Zare M, Nasategay F, Gomez JA, Moayedi Far A, Sattarvand J (2024) A Review of Tailings Dam Safety Monitoring Guidelines and Systems. *Minerals* 14(6):551. https://doi.org/10.3390/min14060551

Possible Value Recovery from Abundant Gold Mine Dumps and Waterbodies in Krugersdorp, South Africa

Alseno K. Mosai[1], Mildred Phasha[1,2]

[1]*Department of Chemistry, Faculty of Natural and Agricultural Science, University of Pretoria, Lynwood Road, Pretoria, 0002, South Africa, Alseno.Mosai@up.ac.za, ORCID 0000-0002-2762-9437*

[2]*Department of Geology, University of Pretoria, Hatfield campus, Pretoria, 0002, South Africa*

Abstract

The current study focused on identifying valuable elements that can be recovered from Lancaster Dam and gold mine dumps in Krugersdorp, a city in Gauteng Province, South Africa. The mine dumps considered are from closed and abandoned mines and have been existing for many decades. The area is also known for high volumes of acid mine drainage. The concentrations of valuable and base elements were measured. Rare earth elements (REEs), Ni, Co, Ag, Li, Cu and Cr among others were detected and found to be in concentrations that can be recovered to help meet their demand. Salvaging REEs and other valuable elements from mine waste can help improve the economies of many countries since, the elements are in demand due to improving technologies and growing population. Other elements including those that are toxic at very low concentrations were also detected. Thus, suitable techniques for the recovery of valuable elements in the study area, are those that have high selectivity and efficiency.

Keywords: Mine dumps, mine waste, contaminated waterbodies, rare earth elements, valuable elements

Introduction

Krugersdorp, a city in South Africa, located on the western ridge margin of the Witwatersrand Basin is known as the territory of gold mining (Shapi *et al.* 2021). The closed, abandoned and operating mines in this region have led to serious air, soil and water pollution due to large amount of waste in the form of solid (mine dumps) and liquid (wastewater, acid mine drainage) released into the environment either directly or indirectly (Fig. 1). High amount of waste in this region was left untreated by the previous mine owners, who cannot be identified since mining laws and regulations have only been implemented in recent years. Thus, the responsibility now rests with the local government to protect local residents from the negative effects of mining waste (Mabaso 2023). The rehabilitation of mining areas is often expensive, however, without it, mining has long lasting negative impact on the environment and on living organisms. Without rehabilitation, toxic elements will continue to migrate to waterbodies (e.g., groundwater and surface water) which should be protected, especially in countries with waters shortages (Lusilao-Makiese *et al.* 2013). Some of the toxic elements can be transported through the air and reach residential areas, nature reserves, agricultural areas and waterbodies, leading to ease of access to living organisms including humans, livestock and wild animals. Residents in the vicinity of mining areas have been found to suffer from serious health effects due to continuous ingestion of toxic elements (Munyai *et al.* 2016). Thus, there is an urgent need to rehabilitate closed and abandoned mines.

Precious and valuable elements including rare earth elements (REEs), gold, platinum group elements, nickel and cobalt among others, have been found in some mining waste (Watson and Beharrell 2006). The profit from the recovery of these elements using cheap and efficient methods and techniques can boost the economies of many countries and assist the government with the funds required for rehabilitation. This is because, the natural resources of these precious elements have been depleting, but their demand is increasing due to population growth and improving technologies (De Boer and Lammertsma 2013).

This study is based on identifying precious and valuable elements in Krugersdorp and concluding on their potential for recovery. The concentrations of toxic elements were also measured in order to determine the urgency of rehabilitation in the area.

Methodology

Study area and sampling

The study was conducted in Krugersdorp (S 26°07.8321', E 027°46.6774'), a city in Gauteng Province, South Africa. Krugersdorp is known as a mining city due to large amount of gold reserves which were discovered in 1887. The study site is in the vicinity of an abandoned gold mine, which is characterized by a number of mine dumps and acid mine drainage (Fig. 1a). There are also illegal artisanal miners in the area, who have been operating for decades, indicating that there is still gold in the area (Fig. 1b). Lancaster Dam, which is situated in the study area, was considered for the collection of liquid samples. Samples were collected from five sites which include the Lancaster Dam (Fig. 2). GPS coordinates were recorded using GPSMAP 65 TopoActive Af (Garmin, USA). A multiparameter was used to measure temperature, pH, conductivity, redox potential and total dissolved solids (TDS) in the Dam and wetlands. Both solid and liquid samples were collected and their colours were recorded. The containers used for the samples were acid washed, following a cleaning protocol. Liquid samples were collected in triplicates using polypropylene containers with caps and immediately preserved in a cooler at 4 °C. Solid samples including tailings and plant stems were collected. Tailings were collected at a depth of between 10 and 50 cm below surface using an auger. The parameters recorded in the field were also recorded in the laboratory after transportation, to account for any changes.

Analysis of samples

The solid samples collected were dried at room temperature for a week and digested using Multiwave GO Plus microwave digester (Anton Paar, Germany). 0.25g of the ground sample was digested with 10 ml HNO_3 and 2.5 ml H_2O_2 for 45 minutes at 180 °C. The collected liquid samples were filtered using 0.22 µm microfilters and stored in the refrigerator until required. Inductively coupled plasma optical emission spectroscopy (ICP-OES) (Spectro Genesis, Germany) was used to measure the concentration of elements (REEs and other elements). The anions were measured using ion chromatography (IC) (Metrohm, South Africa). Fourier transform infrared spectroscopy (FTIR) was used to determine the functional groups on the collected samples.

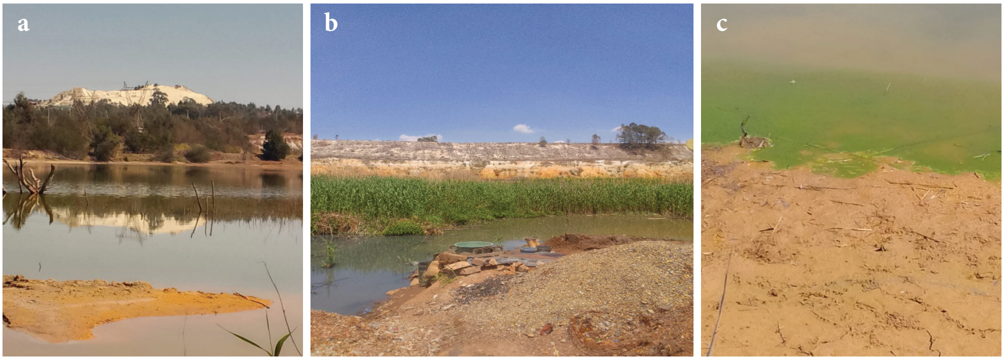

***Figure 1** Solid and liquid waste in Krugersdorp.*

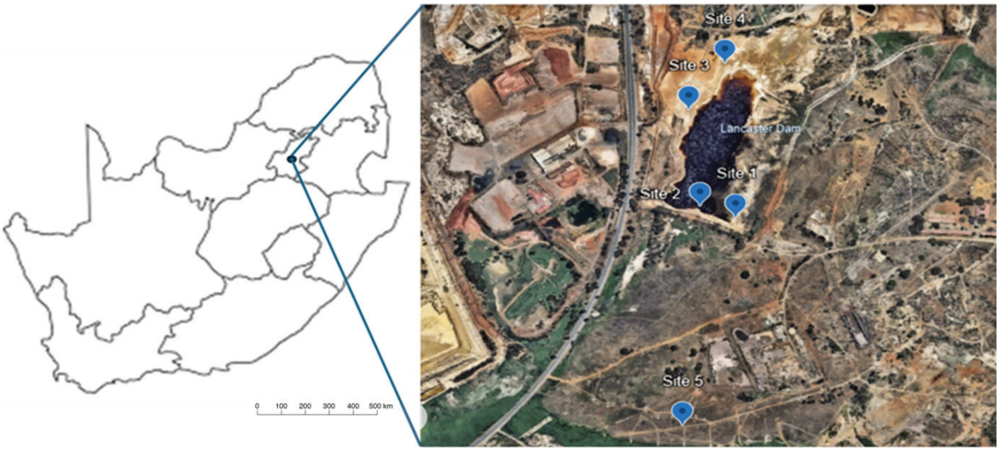

Figure 2 *The study area and sampling sites.*

Results and discussions

The results of the samples collected from different sites in the study area are presented in Table 1. Liquid samples were collected around the Dam in sites 1-3 (Fig. 2). The Dam was found to be acidic with a pH of less than 3. Moreover, the Dam was characterized by high content of dissolved inorganic and organic substances, as indicated by the high TDS (Table1). High TDS means that water cannot be used for supporting biodiversity, ecosystem services, recreation, agriculture and farming among others (Adjovu *et al.* 2023). High TDS can also result in harmful green algae and eutrophication, which was observed in the Dam (Fig. 1c). The redox potential in the Dam was greater than 200 mV, which indicates that there are more oxidizing species in the water. Some of the solid and liquid samples had greenish blue colour, which might be due to the cyanide which was used during mineral processing. Moreover, the operations of illegal miners in the study area (site 5) (Fig. 2) can negatively affect the environmental quality of the area.

The results indicating the concentrations of REEs from the study site are presented in Fig. 3. Samples indicated by site 1a-3a were collected from the dam. The concentrations ranged between 0 and 2 mg L^{-1}. Ce and Tb were the dominant REEs in the Dam (Fig. 3a). Other REEs i.e., Y, La, Nd and Dy were also detected in higher concentrations. It is highly likely that high concentrations of REEs have settled at the bottom of the dam. The concentrations of REEs were also determined in the vicinity of artisanal mining in the area, however, the concentrations were very low. REEs found in the dam were also detected in nearby mine dumps but, at significantly ($p<0.05$) higher concentrations (0- >300 mg L^{-1}) (Fig. 3b). This indicates that there is a higher chance that the REEs migrated from the mine dumps to the dam, through the air and the soil.

There is a wetland around the artisanal mining site (site 5), and some plants were tested for the concentrations of REEs. Certain REEs (Sc, Er, Pr and Tb) were detected in higher concentrations (>3 mg L^{-1}) in the stems

Table 1 *Colours observed and parameters measured in the field.*

Site Name	Temperature (°C)	pH	Conductivity (mS cm^{-1})	Redox potential (mV)	TDS (mg L^{-1})	Colour
1	25.9	2.7	4	220.15	>2000	Dark brown
2	21.4	2.9	4	219.77	>2000	Light brown
3	22.2	2.8	4	219.90	>2000	greenish blue

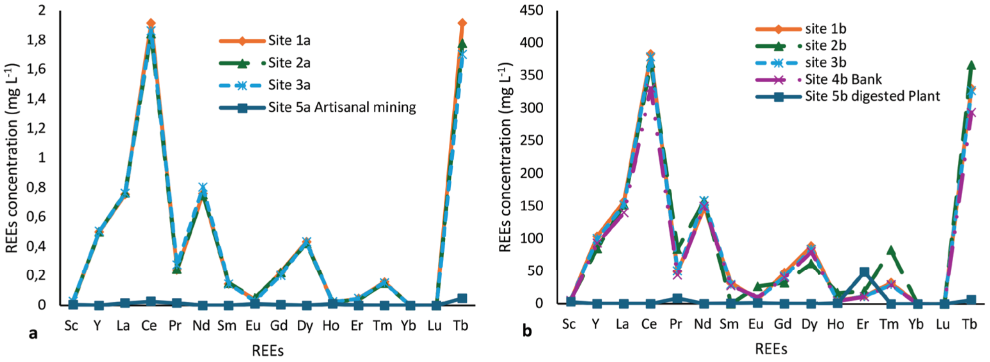

***Figure 3** Concentrations of REEs in the (a) liquid and (b) solid samples ($n = 3$, RSD < 5%).*

of the plants. Thus, REEs can be taken up by plants. The results indicated that the REEs around Krugersdorp are in concentrations which can be considered for recovery and can help meet their demand. REEs can be found in many parts of the world but large REEs reserves are found in few countries including China, USA and Brazil (De Boer and Lammertsma 2013). As a result, the price of REEs has been increasing over the years. This is also heightened by their demand. Thus, mining waste and waterbodies in the vicinity of mining sites rich in REEs can be considered as potential secondary sources of REEs to help meet demand and help improve the economies of many countries including South Africa.

The concentrations of other elements including Ag, Al, Ca, Co, Cu, Zn, Ni, Fe, Li, Na, K, Mg and Mn were also measured, and the results are shown in Table 2. It is important to know the presence and concentrations of some of these elements as they can negatively impact the recovery of precious elements. Ag, Zn, Co, Cu, Li and Ni are known as some of the most valuable elements used in different technologies including batteries, catalysts and pharmaceuticals (Li *et al.* 2019). The concentrations of these elements were high in solid samples, and good enough for recovery. Al, Na, K, Mg and Fe were observed to be the most dominant elements in the study area.

To recover REEs and other valuable elements from waterbodies, adsorbents and ion exchange techniques might be beneficial due to efficiency and less time required. However, recovery could be challenging due to the high content of other elements which can act as competing ions. To successfully recover the valuable elements, functionalized and highly selective techniques should be used. Cheap and efficient bio-surfactants, flushing, microbial leaching and phytoremediation can be used to recover valuable elements in the areas (Lima and Ottosen 2021).

Very toxic elements including Pb, Cd and Tl were also found in the solid and liquid samples. Their concentrations were low (<0.5 mg L^{-1}), however, their toxicity and effect to living organisms can be severe at low levels (≈1 µg L^{-1}) (Nava-Ruíz and Méndez-Armenta 2013). When ingested by humans, these elements can lead to cancer and liver, kidney and nervous system failure (Aloke *et al.* 2019). Their presence in both solid and liquid samples, means that they can be easily accessible to local residents as they travel through the air, especially in windy seasons. Depending on environmental conditions, Cr can be oxidized to Cr^{6+} which is very toxic in small concentrations. The oxidation process is very likely to occur in the Dam which was characterized by positive redox potential. Thus, the dam and the mine dumps are not safe for local residents. Moreover, these elements can migrate to groundwater through the soil profile, which increases their accessibility to humans and livestock dependent on groundwater. South Africa is a water scarce country; therefore, the available natural water resources should be protected from pollution. Rehabilitation may be the best process to apply immediately after the recovery techniques in order to prevent further environmental

Table 2 Concentrations of other elements found at different sites in the study area (n = 3, RSD < 5%).

Sample	Ag	Al	Ca	Co	Cu	Zn	Ni	Fe	Li	Na	K	Mg	Mn
Site 1a	0.184	170.005	0	4.127	1.696	11.236	9.406	28.601	0.92	105.617	63.365	63.245	24.637
Site 2a	0.186	118.594	0	3.196	1.034	7.985	7.089	28.775	0.894	72.95	57.907	63.913	18.479
Site 3a	0.186	101.07	0	2.602	0.881	6.684	5.869	25.265	0.821	60.056	50.577	57.619	15.558
Site 5a	0.189	0.361	15.562	0.098	0.237	0.069	0.071	0.15	0.602	46.407	12.773	15.11	2.746
Site 1b	35.4	16905.6	974.6	26	108.2	64.6	48	3057.6	142.4	235.8	684.6	301	40.2
Site 2b	35.2	22498.6	1071.6	40.4	191.2	132.4	96.4	46701	574	531	3232.6	1222.6	173.4
Site 3b	35.4	3314	109.6	17.2	69.2	19	18.4	4136.6	143.4	319.4	660.8	141	24
Site 4b	35.2	5819.8	2255.6	41	51.4	43	19.4	11384.6	184.4	600.8	507	1806	157.2
Site 5b	37	39750.6	1571.6	54.2	251	1942.4	1735.6	7102.2	196.2	19463.8	13612.2	13031.4	329.6
Site 5b Plant	36.4	1666.2	2659.4	25	47	80.8	14.8	30.4	120.6	10278	2889	3203	2306.4
Site 5b stem	37	129.8	2314	18.2	75	214.4	128.6	1760.2	121	2389.4	244498	9314	392.2

Site 1a-3a = Lancaster Dam Site 5a = artisanal mining wastewater Site1b-3b = Mine dump (>500 m from Lancaster Dam) (solid waste)
Site 5b = artisanal mining site (solid waste)

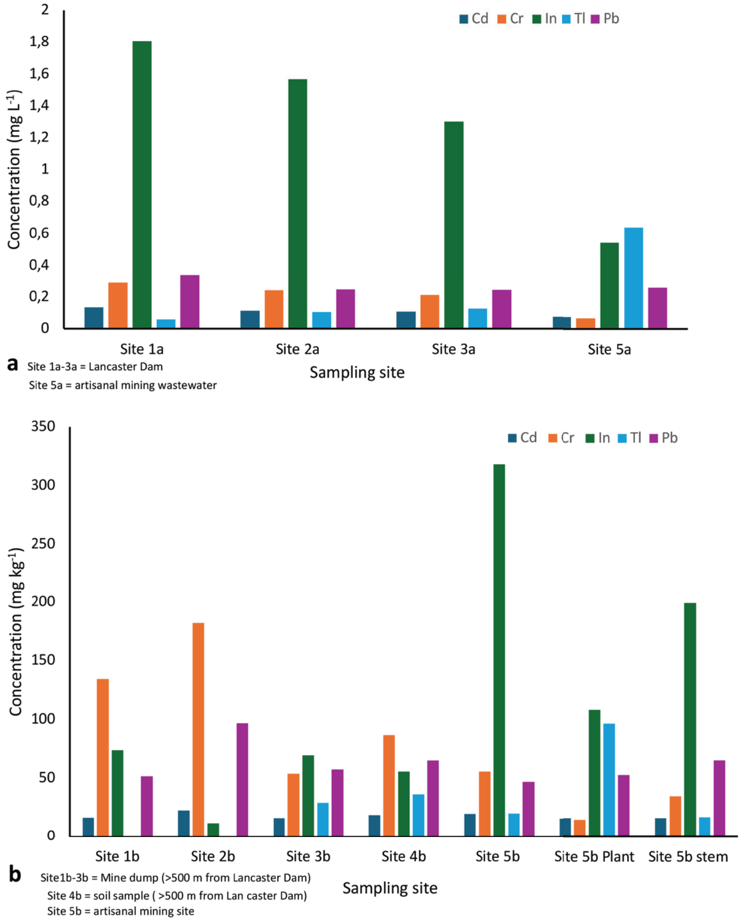

Figure 4 Concentrations of toxic elements in (a) liquid and (b) solid samples collected in the study area (n = 3, RSD < 5%).

pollution. The profit from the recovery of valuable elements including REEs can help with the implementation of rehabilitation in Krugersdorp.

Conclusions

Krugersdorp, a city in South Africa is known for gold mining. The area is characterised by numerous closed and abandoned mine sites due to depleted reserves. There are also a number of mine dumps and large volumes of acid mine drainage. This study focused on identifying and quantifying valuable elements that can be recovered from mine dumps and a dam in the area. The dam was characterised by low pH, high conductivity, high total dissolved solids and positive redox potential. Rare earth elements and other valuable elements (Ni, Co, Mn, Li and Ag) were detected in the dam and mine dumps. The study area can be considered as a potential place for the recovery of valuable elements to meet their global demand. The conditions of the mine dumps and the dam which were determined in this study, will help select the best recovery techniques for valuable elements. Selective ion exchange resins, membranes and functionalised adsorbents can be used as cost-effective and efficient recovery techniques in the study area. Other elements including Al, Na, K, Mg and Fe were detected in high concentrations and can be considered as potential competing ions when recovery techniques are applied. Moreover, toxic elements were detected, and their concentrations indicate that the residents and other living organisms in the area might not be safe. Thus, there is an urgent need for rehabilitation, which can be quickened by using the profits made from the recovery of valuable elements.

Acknowledgements

The authors would like to thank the National Research Foundation (NRF) Thuthuka (grant number: TTK23040489225) and the University of Pretoria for financial assistance.

References

Adjovu GE, Stephen H, James D, Ahmad S (2023). Measurement of total dissolved solids and total suspended solids in water systems: A review of the issues, conventional, and remote sensing techniques. Remote Sens 15(14):3534

Aloke C, Uzuegbu IE, Ogbu PN, Ugwuja EI, Orinya OF, Obasi IO (2019) Comparative assessment of heavy metals in drinking water sources from Enyigba Community in Abakaliki Local Government Area, Ebonyi State, Nigeria. Afr J Environ Sci Technol 13(4):149-154

De Boer MA, Lammertsma K (2013) Scarcity of rare earth elements. ChemSusChem 6(11):2045-2055

Li G, Yang H, Zheng Y, Chen XH, Yang JA, Zhu D, Ruan L, Takashima K (2019) Challenges in the use of zinc and its alloys as biodegradable metals: Perspective from biomechanical compatibility. Acta biomaterialia 97:23-45

Lima AT, Ottosen L (2021) Recovering rare earth elements from contaminated soils: Critical overview of current remediation technologies. Chemosphere 265:129163

Lusilao-Makiese JG, Cukrowska EM, Tessier E, Amouroux D, Weiersbye I (2013) The impact of post gold mining on mercury pollution in the West Rand region, Gauteng, South Africa. J Geochem Explor 134:111-119

Mabaso SM (2023) Legacy Gold Mine Sites & Dumps in the Witwatersrand: Challenges and Required Action. Nat Resour 14(5):65-77

Munyai AH, Fosso-Kankeu E, Waanders F (2016) Biological influence on the mobility of metals from mine tailing dump located in Krugersdorp area. Int J Sci Res ISSN:2319-7064

Nava-Ruíz C, Méndez-Armenta M (2013) Cadmium, lead, thallium: occurrence, neurotoxicity and histopathological changes of the nervous system. Pollutant diseases, remediation and recycling 321-349.

Shapi M, Jordaan MA, Mbambo AT, Davies TC, Chirenje E, Dube M. (2021) Determination of potentially harmful element (PHE) distribution in water bodies in Krugersdorp, a Mining City in the west Rand, Gauteng Province, South Africa. Minerals 11(10):1133.

Watson JHP, Beharrell PA (2006) Extracting values from mine dumps and tailings. Miner Eng 19(15): 1580-1587

Coal Acid Mine Drainage – Passive Treatment Lime Compost Drains – Three abandoned coal mined sites in Southern Illinois

Olga Moya Aranzubía[1]

[1]*Illinois Department of Natural Resources, Office of Mines and Minerals, Abandoned Mined Lands Reclamation Division, 503 East Main Street, Benton, Illinois, 62812, United States of America, olga.aranzubia@illinois.gov*

Abstract

Coal mining has been occurring in the United States, in earnest, for well over two hundred years. It has been estimated that 5.5 billion tonnes of coal have been mined in Illinois from 1883 to 2004. As a result of this historic industry, legacy coal mining environmental impacts continue to afflict Illinois' communities and landscape. This is evidenced by the three different abandoned coal mine sites significantly affected by acid mine drainage presented below. The aim of this paper is to provide an overview of the implemented passive treatments at these three project sites. These constructed passive treatments should simply be considered practical case studies, where legacy acid mine drainage needed abatement, but due several constraints, no other type of treatment was to be considered. These case studies present some long-term positive results of the implemented passive treatment systems. Recommendations for future construction, modelling of these systems to offer improvements in sizing, based on flow and acid mine discharge chemical characteristics, as well as additional research on the use of different construction materials are proposed.

Introduction

A 1668 map from Father Louis Hennepin's expedition, down the Illinois River, mentions a "cole mine" (Coal Report 1954). Coal has been instrumental in the overall growth of the state of Illinois, with initial coal mining beginning in the early 1800s. Until the mid-1950s, Illinois was ranked third in the United States, in all time bituminous coal production, behind only Pennsylvania and West Virginia (Kolata 2010). Prior to the passage of the 1977 Surface Mining Control and Reclamation Act (SMCRA), by the United States Congress, there was no federal regulatory oversight over coal mining activities and what happened to those mine sites once mining stopped. Since the passage of SMCRA, states and tribes, with current or historic coal mining, are eligible to apply for abandoned mined land reclamation grants, funded primarily by fees generated by active mining production.

Marshall Equipment, Richardson Coal Company, and Beecher Williams No. 1, are three different abandoned coal mined sites, located in Saline County, in southeastern Illinois. These three legacy coal mine sites were eligible for reclamation, under SMCRA, by the Abandoned Mined Land Reclamation Division (AMLRD), in the state of Illinois.

These three sites mined the Davis and Dekoven coal seams. The Davis and Dekoven coal seams are frequently 3 to 7,6 meters apart and are most often surface mined, in tandem, in Saline and Gallatin counties, in southeastern Illinois. These two coal seams represent an estimated 3,7 billion tonnes of coal resources remaining in these two Illinois counties (Jacobson 1993). The Davis and Dekoven coal seams vary in thickness between 1 to 1,5 meters each, with ash content ranging from 8 to 13%, sulfur content in the range of 3 to 5%, and heating values from 12.500 to 13.500 kilojoules. (Jacobson 1993)

All three of these abandoned mined sites were contour surface mined, with some auger and deep mining also occurring, to remove the Davis and Dekoven coal seams, at a depth varying from 1,5 to 35 meters. These three coal mine sites were in operation from the early 1950s to the early 1960s.

Legacy coal mining at these three locations resulted in acid mine drainage seeps, with average flows of less than 37,9 Liters per minute. While the seeps had low water flows, the water chemistry of the Davis and Dekoven coal seams has proven to be extremely destructive.

Both coal seams produce highly acidic seepage, with high iron, aluminium and sulfate concentrations associated with the inter-burden material separating the two coal seams. The acid forming material associated with these coal seams had proven to be challenging to treat with traditional passive treatment methods and required a slightly different approach.

Methods

These abandoned coal mine sites present very similar post mining conditions, because of all different types of mining, surface, auger, and underground coal extraction occurred at all three sites. These locales all include dangerous vertical highwalls, averaging in height between 6 and 25 meters, often with shallow acid water filled pits and acid seeps along the highwall toe.

The abandoned coal mine sites presented acid mine drainage seeps with similar water chemistry produced by the Davis and Dekoven coal seam and its inter and overburden. An overview of the pre-reclamation acid mine drainage characteristics at each site, are presented in Table 1 below. Due to the Illinois AMLRD program funding and personnel limitations, only some form of passive treatment system was deemed possible to abate the acid mine drainage at the above-mentioned sites. After a careful review of the coal mine acid seepage data, with very low pH, overall high concentrations of iron, and aluminum, well above the recommended limits, less than 1 mg/L, designing a traditional passive treatment drain system was dismissed. Traditional passive drains systems do not remain anoxic and allow for oxidation, as pH increases along the treatment system. The oxidation process allows most iron, in ferrous form (Fe^{+2}), to precipitate out of solution, as ferric hydroxide ($Fe(OH)_3$), forming a rust coloured gelatinous solid, that coats alkaline rock material, eventually clogging the system, and rendering the passive drain network as ineffective. Aluminum (Al^{+3}), when present at higher concentrations, and low pH, such as is present at these three sites, can undergo hydrolysis and precipitation of the aluminum, to form aluminum hydroxide (Al(OH)3), which can also contribute to clogging of traditional passive drain systems. To prevent iron oxidation and aluminum hydrolysis, and avoid any solid precipitate clogging the system, a modified passive system for treatment of the acid seepage produced at these sites was needed. A Lime Compost Drain (LCD) was proposed as the passive treatment system on these three legacy coal mines sites, which was incorporated as part of the overall reclamation design at each project location.

The main proposed concept of the LCD chemical processes is to create a very low oxygen, high alkaline and high pH environment, within the drain, through which acid seepage is directed, with any oxygen present being consumed by the slow degradation of organic matter. Keeping the drain composition as anoxic as possible, would prevent iron (Fe^{+2}) from oxidizing and precipitating out, minimizing coating of the high alkalinity treatment material. Within the LCD, aluminum (Al^{+3}) would travel through a highly alkaline, high pH environment, maintaining the metal in

***Table 1** Pre-Reclamation Coal Acid Mine Drainage Data*

Site Name (date)	Acidity mg/L	pH	Aluminum mg/L	Iron mg/L
Marshall Equipment (2005)	784,0	2,68	41,00	154,00
Richardson Coal Company (2013)	122,3	3,38	12,51	42,98
Beecher Williams No. 1 (2021)	460,0	3,04	42,33	29,32

solution. Both metals, iron and aluminum would undergo oxidation and/or hydrolysis, when the pH drops to ranges 6.5 to 7.5, as treated water exits the LCD anoxic treatment system into the newly constructed open air sediment basins. Traditionally iron hydroxide ($Fe(OH)_3$), would settle out first, as a reddish-brown solid, followed by aluminum hydroxide ($Al(OH)_3$).

A Lime Compost Drain (LCD) consists of a two-layer system, wrapped by a permeable material, such as filter fabric. The bottom most layer contains 75mm, high alkalinity coarse aggregate, with 90% or greater calcium carbonate ($CaCO_3$) content and minimum thickness of 0,3 meters. The top layer, also 0,3 meters in thickness, consists of a well-blended mixture of 50% compost material, such as mulch, and 50% of 25mm high alkalinity coarse aggregate, with 90% or greater calcium carbonate ($CaCO_3$) content.

Mixing of these materials is done on site. Backfilling over the LCD is completed in such manner as not to compromise the integrity of the newly constructed drain. During construction, if possible, it is best to keep the LCD construction area free from water during the placement of the limestone, compost, filter fabric and cover soil. Both layers are then draped by an impermeable polyethylene liner, with a minimum thickness of 0,75 mm, to reduce surface runoff infiltration into the passive treatment. This is then, followed by carefully placed backfill material.

The LCD flow is then routed to an outlet basin/s where oxidation and hydrolysis occurs, precipitated solids are settled, and water is discharged to a nearby waterway and/or existing stream. To keep the LCD, drain anoxic at the basin outlet, the discharge elevation of the basin is kept a minimum 0,3 meters above of the LCD outlet elevation. Both drain layers vary in width and length, depending on existing highwall conditions, flow, and slight variations of the acid mine water chemistry at each location.

These drains are usually placed as close as possible to the exposed highwall face and on the pit floor. The trench bottom is excavated to the rock layer of the mined pit floor. Prior to any backfill activities, the trench floor, sides slopes, and adjacent highwall are made as clear as possible of any sediment, debris, or vegetation. Detail drawings for the drain construction are shown on Fig. 1. This LCD system was constructed on all three sites with great improvement to chemistry of the coal acid mine drainage discharging from the passive LCD system.

During implementation of the first LCD design, at the Marshall Equipment project, construction challenges arose. The original design included a 50mm perforated pipe system throughout the drain. This pipe system included vertical sampling ports to the surface. Pipe sampling ports were kept anoxic by using a 180˚ pipe elbow at the surface. The large amount of compacted backfill material that needed to be placed in and around these vertical pipe sampling ports, to abate the existing vertical highwall, made it nearly impossible to ensure proper construction. This piping for sampling ports proved to be very hard to maintain completely vertical

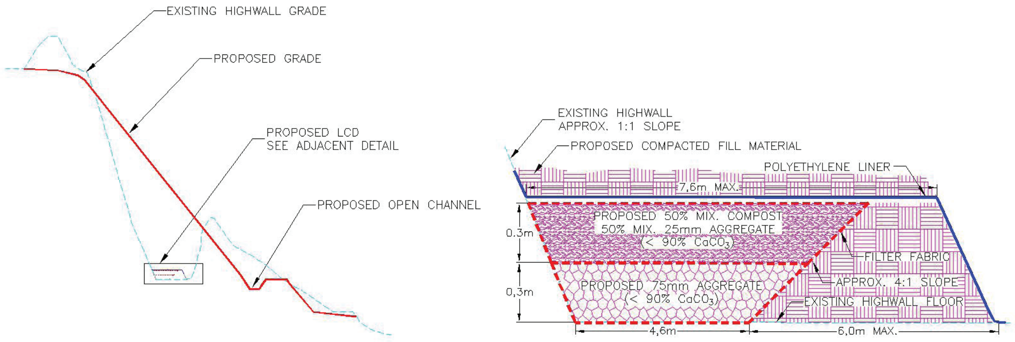

Figure 1 Lime Compost Drain (LCD), Typical Cross Section and Profile, Not to Scale (image: Olga Moya Aranzubia).

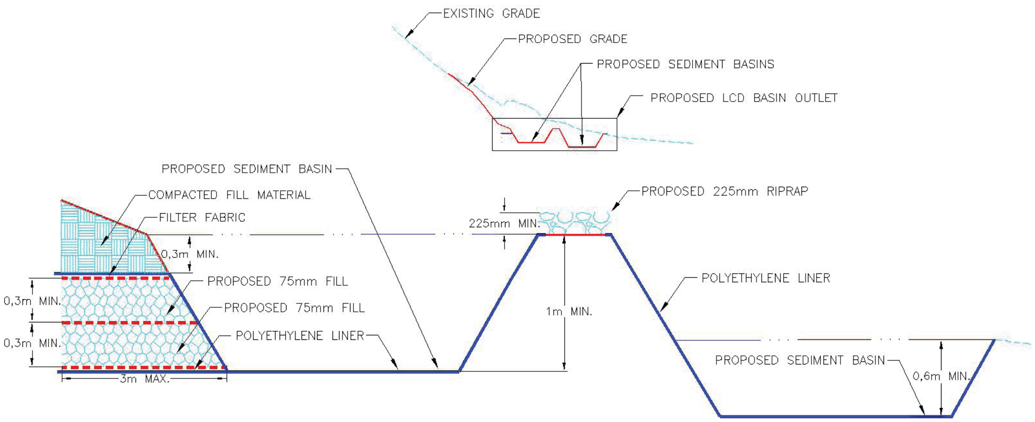

Figure 2 Lime Cost Drain Basin (LCD), Typical Cross Section and Profile, Not to Scale (image: Olga Moya Aranzubia).

to the surface. It was also very difficult to ensure the connection between the vertical pipes for these sampling ports and the main pipe network, running within the drain, remained in place and functioning, once backfill material was placed and compacted. The entire pipe system was removed from subsequent designs.

Another challenging aspect identified, post-construction of the LCD system, was the removal of settled solids. While riprap lined settling basins were very practical and easy to construct, they became difficult to maintain. These three LCD systems were built without any type of modelling for sizing, making it difficult to estimate the amount of precipitate that would be dropping out of solution at the outlet basins. While the original system at the Marshall Equipment site remains functional and precipitate sediment is being adequately handled, the Richardson Coal Company LCD system basins reached capacity after six years. A remedial project was completed to remove existing sediment from the basins at the Richardson Coal Company site. The clean out proved to be time consuming, due to the riprap lining of the basins, making it costly. The most recently designed and constructed LCD passive treatment included the lining of the outlet basins with high density polyethylene, instead of the previously used 225mm riprap. This new lining material was introduced in an effort to ease the maintenance removal of precipitated solids settled, from the basin, as it will accumulate over time.

The following figures illustrate pre-reclamation conditions, Figs. 1 and 2, construction activities, Fig. 3, and post reclamation results, Fig. 4.

Conclusions

These three constructed LCD passive treatments should simply be considered practical case studies, where legacy acid mine drainage needed abatement. Due to several constraints, such as program budget and lack of field and maintenance budget and personnel, only a passive treatment, with little or no maintenance, was to be considered. Research modelling of this passive treatment system would allow for the study of a method to properly size the

Table 2 Post-Reclamation LCD Discharge Drainage Data.

Site Name (date)	Acidity mg/L	pH	Aluminum mg/L	Iron mg/L
Marshall Equipment (2024)	0,0	6,44	0,05	25,70
Richardson Coal Company (2024)	0,0	6,05	0,40	29,90
Beecher Williams No. 1 (2024)	0,0	7,87	0,05	0,10

Figure 3 *Marshall Equipment Acid Mine Drainage Seep 2007 (image: Olga Moya Aranzubia).*

Figure 4 *Marshall Equipment Phase Acid Mine Drainage Seep 2007 (image: Olga Moya Aranzubia).*

Figure 5 *Richardson Coal Company LCD Construction (image: Olga Moya Aranzubia).*

Figure 6 *Marshall Equipment Reclaimed Highwall and LDC Sediment Basin 2010 (image: Olga Moya Aranzubia).*

width of the drain and the thickness of the treatment layers. Investigating the rate of decay of the organic matter, that keeps the system anoxic and functional would also be very beneficial. A study based on different parameters, such as flow, acid mine water chemistry and organic content, could lead to a better way to calculate the optimal mixture ratio of the organic material and alkaline rock material, while maintaining the integrity of this layer within the drain, and still be able to receive large amounts of backfill material. Additional examination of the drain system discharge would allow for more appropriate sizing of the outlet basins, to accommodate settling precipitate, based on the drain outlet water chemistry. Further investigation on the use of different lining material, for the sediment basins, to optimize the ease of precipitate removal, would also improve the overall design of the system. The introduction of a viable sampling system would provide measured parameters in the field, that could prove instrumental in estimating organic matter decay and the estimated life of a fully functional LCD.

Acknowledgements

Support for the development, design, and construction of the Lime Compost Drain passive treatment for the abatement of legacy acid mine drainage in Southern Illinois goes to supervisory staff at the Illinois Abandoned Mined Reclamation Division. Continued helpful review and support resources of Paul T. Behum, Senior Hydrologist, Office of Surface Mining Reclamation and Enforcement, U.S. Department of Interior, to the design of this passive treatment system, so it could be implemented as part of the overall reclamation at these sites.

References

Behum PT, Mick A, (2018) Oral paper, Investigations of Acidic Discharges from the Historic Mining of the Davis and Dekoven Coal Beds in Southern Illinois, presented at the 2018 National Meeting of the American Society of Mining and Reclamation, St. Louis, MO: The Gateway to Land Reclamation, June 3 – 7, 2018, Published by ASMR; 1305 Weathervane Drive, Champaign, IL

Jacobson, RJ, Treworgy CG, Chenoweth C, Bargh MH (1998) Availability of Coal Resources in Illinois: Mt.

Carmel Quadrangle, Southeastern Illinois, Illinois Minerals, Department of Natural Resources, Illinois State Geological Survey, Champaign, IL

Kolata DR, Nimz CK, (2010) Geology of Illinois, Institute of Natural Resources Sustainability, Illinois State Geological Survey, Univ of Illinois at Urbana-Champaign p 261–280

Ray BT, (1995) Environmental Engineering, Southern Illinois University, Carbondale, IL, Water Quality, p 224– 230

Exploring Geothermal Application in Flooded Underground Mines with an Analogue Model Mine

Elke Mugova[1], Christian Wolkersdorfer[2], Florian Hahn[1]

[1]Fraunhofer IEG, Competence Center for Post-Mining-Exploitation, Am Hochschulcampus 1, 44801 Bochum, Germany, elke.mugova@ieg.fraunhofer.de, ORCID: 0000-0001-6019-9945
florian.hahn@ieg.fraunhofer.de

[2]South African Research Chair for Acid Mine Drainage Treatment, Tshwane University of Technology (TUT), Private Bag X680, Pretoria 0001, South Africa, @wolkersdorfer.info,
ORCID: 0000-0003-2035-1863

Abstract

Geothermal use of flooded underground mines is gaining popularity, particularly utilising warm mine water for heating purposes. A current example is the former colliery Dannenbaum in Bochum, Germany. The “Agricola Model Mine” in Pretoria, South Africa, was set up to replicate conditions at the Dannenbaum colliery. With this model mine it was possible to monitor parameters like temperature, electrical conductivity and change of tracer concentration while warm, mineralised mine water was reinjected in the upper mine water body and caused breakdown of the existing density stratification. These findings indicate that a change in the water chemistry, due to geothermal pumping, is possible.

Keywords: Mine water, analogue model, numerical modelling, stratification, geothermal, mine water heat

Introduction

In recent years, there has been an increase in the reuse of former mine sites for various purposes, including flooded mines. This trend recognises the potential of mine water as a valuable resource. Two main applications have emerged: the extraction of raw materials from mine water and the geothermal use of mine water. Typically, warm mine water is utilised for heating, although cooling or mine thermal energy storage (MTES) is possible as well (Banks *et al.* 2017; Grab *et al.* 2018; Hahn 2024b; Walls *et al.* 2021)(Fig. 1). Understanding the hydrodynamic processes within flooded underground mines is crucial for all types of geothermal utilisation. Density stratification, defined as the presence of water bodies with different physico-chemical properties within the flooded mines, is one of these processes (Mugova and Wolkersdorfer 2022; 2025). It has been shown, that density stratification can be disturbed or caused to breakdown by the use of pumps, ultimately leading to a deterioration of water quality. The aim of this paper is to use analogue modelling to investigate whether geothermal pumping activities could influence density stratification and discharge water quality.

Methods

In order to investigate the potential stratification breakdown in a flooded mine, it is essential to establish baseline parameters that closely resemble real-world conditions, thereby enabling the results to be applicable to other mining sites. For this reason, an applied analog model was based on the former Dannenbaum colliery in Bochum, Germany.

The colliery is an old mine site, where coal extraction began in the 14th century and transitioned to underground mining in 1843, with shaft depths exceeding 600 m. In 1963, the mine was closed following the amalgamation of several neighbouring collieries. Today, the area, which later housed the Opel car factories, is being economically developed under the name Mark 51°7. With the objective of supplying a sustainable geothermal heat and cooling system to

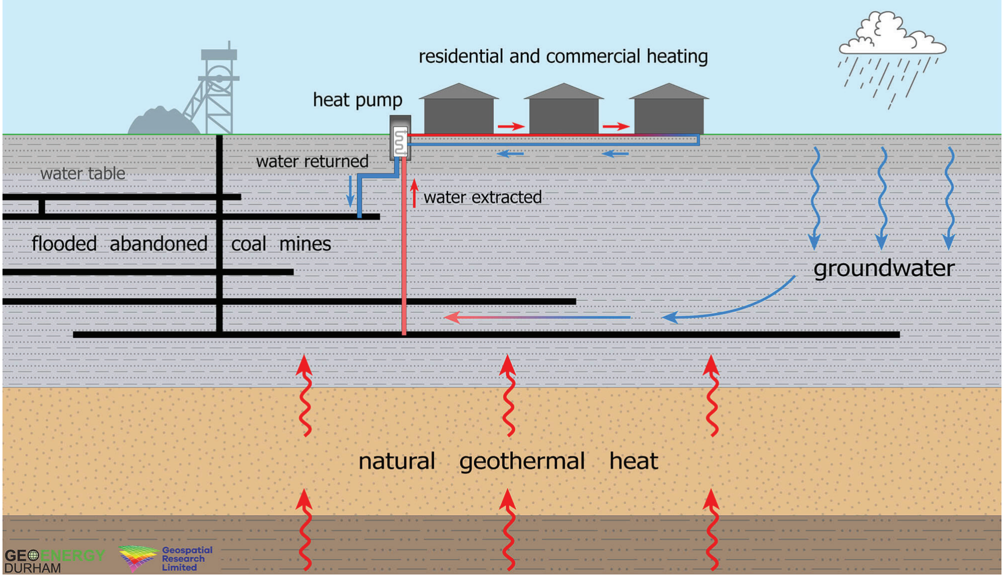

Figure 1 *Schematic overview on how to utilise mine water for geothermal heating (from Geospatial Research Ltd. 2025).*

Mark 51°7, two directional wells (GT1 and GT2, Fig. 2) have been drilled into the mine workings (Hahn 2024a). The long-term vision for the flooded mine is to utilise it for geothermal heating and cooling in a LT-MTES (low temperature mine thermal energy storage). However, it should be noted that these associated pumping activities will affect the hydraulic system. Current observations indicate the existence of density stratification within the flooded mine, characterised by the presence of at least two distinct water bodies: an upper CF (cold-fresh) water body with a temperature of 16.4 °C and an electrical conductivity of 1.7 mS/cm, and a lower WM (warm mineralised) water body with a temperature of 26.0 °C and an electrical conductivity of 10.4 mS/cm. This study will investigate whether the stratification is affected by pumping activities and what implications this may have on the discharged water quality.

The Agricola Model Mine (AMM) is a scaled-down reconstruction of a flooded underground mine, measuring 6 × 4 m. Since 2021, it has been operational at Tshwane University of Technology (TUT) in Pretoria, South Africa. Designed to replicate conditions in a flooded underground mine, the model utilises dimensions scaled-down according to the Reynolds number. With depths of 65 cm, 145 cm, 225 cm, and 305 cm, and a diameter of 90 mm, the four horizontal levels are connected to four shafts. Constructed from insulated, transparent PVC tubes, the AMM can accommodate a total water volume of 153 L. To simulate rainwater inflow, a peristaltic pump continuously supplied water to the upper part of the AMM, while natural discharge is replicated at the outflow of shaft #1. A total of 36 sampling ports are incorporated into the model for comprehensive water monitoring and sampling. Heating foils are placed in the sumps of all four shafts in order to create geothermal gradients, achieving maximum water temperatures of 42 °C (Molaba 2022; Mugova *et al.* 2024).

All four shafts and four horizontal levels were incorporated into the experimental set-up to ensure a representation of the Dannenbaum colliery. Initially, mine pool conditions with density stratification were established, using parameters that closely imitate those of the Dannenbaum site. After 10 days of undisturbed conditions, different fluorescent tracers were injected into the upper CF water body (above level 145) and WM water body

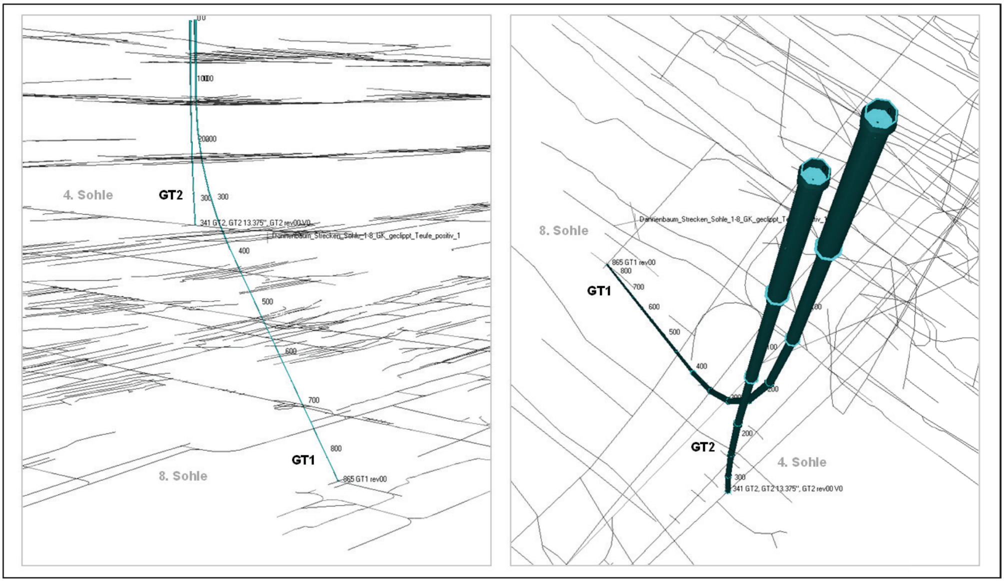

Figure 2 Directional wells GT1 & GT2 at Dannenbaum colliery (Hahn 2024a).

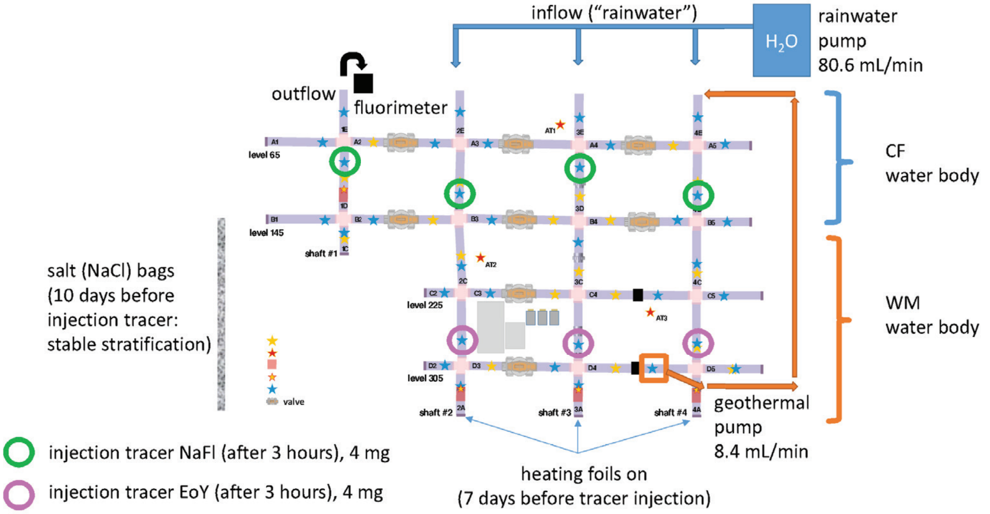

Figure 3 AMM set-up of the experiment with tracers Sodium Fluorescein (NaFl) and EosinY (EoY).

(below level 145). Subsequently, analogue to geothermal pumping activities, warm, higher mineralised mine water was extracted from the WM water body and reinjected into the CF water body (Fig. 2). Throughout a 49-day monitoring period, changes in water parameters were tracked using 10 electrical conductivity and temperature probes, as well as through continuous tracer concentration measurements.

Results and Discussion

A clear separation was observed in the temperature data when the heating foils were activated, indicating a lower water body with temperatures ranging from 22.8 to 23.3 °C and an upper water body with temperatures between 17.6 and 18.7 °C. However, this stratification was disrupted by the extraction of warm water from the WM water body and its reinjection into the CF water body.

Following the activation of the geothermal pump on day 7.0, a rise in temperature was observed in the WM water body until day 7.6, after which a rapid decline was evident in sections 2C, 3C, and 4C within approximately 14.4 hours. By 19.2 to 33.4 hours post geothermal pumping, the temperatures in these sections equalled those in the CF water body, indicating a swift mixing of the upper WM water body. Sections 2B and 4B showed a similar trend, initially rising to a maximum of 24.9 °C on day 8.4 before mixing with cooler water, which led to a temperature drop. The mixing process took longer in the lower WM compared to the upper sections. In the CF water body, the introduction of warm water resulted in a uniform temperature increase across all sections. By day 10.8, 92.9 hours after the geothermal pump was activated, complete mixing occurred, leading to a temperature range of 21.1 to 21.5 °C. There was no recovery of stratification observed for the remainder of the experiment, and post-breakdown temperatures fluctuated between 19.9 and 25.3 °C, primarily influenced by changes in room temperature and the temperature of the incoming tap water (Fig. 3). A similar mixing process could be determined from the electrical conductivity data.

Continuous monitoring of sodium fluorescein (NaFl) concentrations at outflow shaft #1 revealed three distinct peaks. The first peak resulted from flushing NaFl added before rainwater influx, while the second, higher peak came from additional NaFl introduced into the CF water body, leading to a quick tracer flush. The third peak around day 16 is unexplained, likely due to disturbances from geothermal pumping. Following the initial sodium fluoride (NaF) injection, even distribution was achieved within a few days, with minimal detection in sump section 1C. However, the presence of NaFl in the WM water body was minimal, with an average of 0.85 µg/L after three days, in comparison to 17.96 µg/L in the CF water body. Rainwater further flushed NaFl in the CF water body out, while concentrations in the WM water body remained stable. Notably, the geothermal pump had only minimal effect on NaFl concentrations in the CF water body. Following the injection of EoY dye tracer in the WM water body, the tracer was evenly distributed in the WM until the geothermal pump was switched on, with an average concentration of 46.72 µg/L recorded after 6.9 days. Subsequent to pump activation, EoY concentrations in the WM

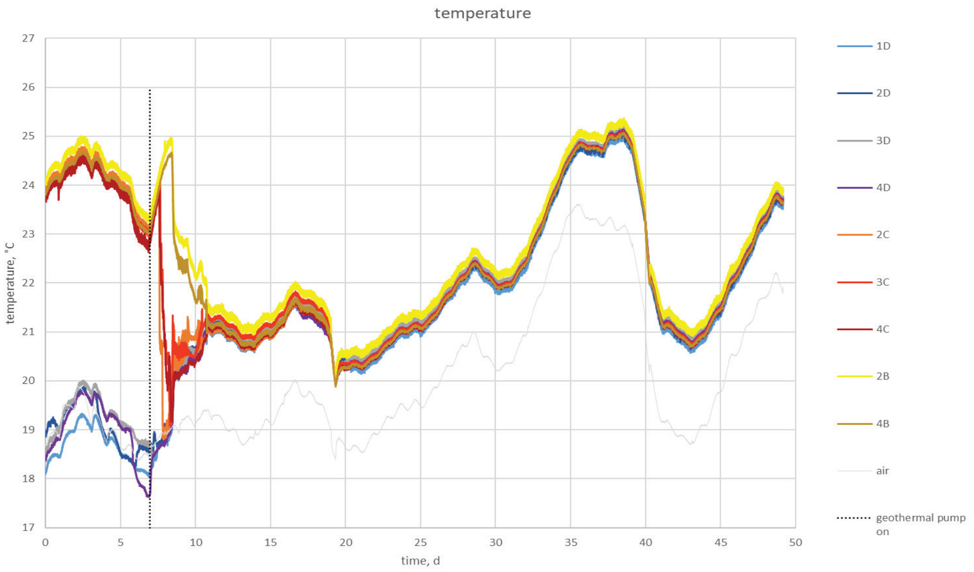

Figure 4 *Temperature curve before and after the geothermal pump was switched on (dotted line) with probes above level 145 (1D, 2D, 3D, 4D) and probes below level 145 (2C, 3C, 4C, 2B, 4B).*

underwent a substantial decrease (averaging 0.80 µg/L by day 49), predominantly in sections directly beneath the CF, due to dilution from CF water. Geothermal pumping also resulted in the transfer of water from the WM to the CF water body, thereby raising EoY concentrations in the CF water body. With exception of section 2E, EoY rapidly disseminated throughout the CF. Within 24 hours after pump activation, the average EoY concentration in the CF water body was 8.27 µg/L. However, it decreased to 1.41 µg/L by day 49 due to influx of fresh water.

Overall, the geothermal pumps, i.e. the extraction of water from the WM water body and its reinjection into the CF water body, caused rapid mixing. This resulted in a mixed water body. Larger temperature fluctuations occurred in the mixed water body due to lab conditions. In contrast, the electrical conductivity, which can be seen as an indicator of mine water mineralisation, decreased over time, caused by the permanent supply of fresh water and the forced flow from pumping. The mineralised water was flushed out over time, whilst "geothermal" heat by the heating foils was supplied continuously.

Conclusions

Through analogue modelling in the AMM, it was possible to understand the conditions in the flooded Dannenbaum colliery. These include the presence of density stratification and the future withdrawal and injection of water for geothermal use from the lower WM water body and the upper CF water body. Based on the AMM results, it can be assumed that the pumping activities in the Dannenbaum colliery will cause mixing of the currently existing water bodies. Due to the high electrical conductivity in the WM water body, an increase in mineralisation is to be expected when the WM water body is reinjected into the CF water body. This change in chemistry must be taken into account when configuring the heat exchangers. Temporal predictions regarding a potential stratification breakdown within the flooded mine remain uncertain at this time. Water is only used from a small area of the Dannenbaum mine workings (394 km in total), suggesting that it is negligible in relation to the overall hydraulic system (Prinz Regent colliery with 288 km and Friedlicher Nachbar colliery with 320 km of mine workings additionally to Dannenbaum). However, geothermal pumping must not be mistaken with mine dewatering pumping activities. Mine water drainage takes place at the former colliery Friedlicher Nachbar, about 7 km away und connected via several other abandoned coal mines. The water of all surrounding former mines is pumped centrally at this site. Despite the potential for increased mine water mineralisation directly at the Dannenbaum mine, dilution effects over the extended inflow distance suggest that no detrimental changes in mine water quality at Friedlicher Nachbar are to be expected. Once the geothermal pump at the Dannenbaum mine (Mark 51°7) commences operation, a monitoring programme for water quality should be initiated, encompassing both the immediate vicinity of the mine and the Friedlicher Nachbar site. In addition, numerical modelling with SPRING is planned to compare both the AMM results and the real data available so far. Having the possibility to model both, flooding scenarios and utilisation of mine water in an analogue way, provides a good opportunity to better understand the complex hydraulic system of a flooded mine and to support mine water management decision-making.

Acknowledgements

The authors thank their respective research institutions for providing support in conducting this research. The German foundation "Forum Bergbau und Wasser" in the Deutscher Stifterverband made travel funds available through the International Giving Foundation. Furthermore, the NRF SARChI chair for Mine Water Management, Department of Environmental, Water and Earth Sciences, Tshwane University of Technology under Grant № 86948 supported this research.

References

Banks D, Athresh A, Al-Habaibeh A, Burnside N (2017) Water from abandoned mines as a heat source: practical experiences of open- and closed-loop strategies, United Kingdom. Sustainable Water Resources Management 5(1):29-50 doi:10.1007/s40899-017-0094-7.

Geospatial Research Ltd. (2025) Mine-Water Heat. www.geospatial-research.com/mine-water-heat/ Accessed 06.02.2025

Grab T, Storch T, Groß U (2018) Energetische Nutzung von Grubenwasser aus gefluteten Bergwerken. In: Bauer M, Freeden W, Jacobi H, Neu T (eds) Handbuch Oberflächennahe Geothermie. Springer, Heidelberg, p 523–586

Hahn F (2024a) Geothermal reutilization of an abandoned colliery coupled with a district heating grid and a high-temperature underground storage.

Hahn F, Klein S, Mannke K, Verhoeven R, Güldenhaupt J, Seidel T, König T (2024b) Mine thermal energy storage (MTES) systems in abandoned collieries within the Ruhr area. In: Kleinmann B, Skousen, J., Wolkersdorfer, Ch., (ed) West Virginia Mine Drainage Task Force Symposium & 15th International Mine Water Association Congress, Morgantown, WV, USA, 2024. International Mine Water Association, 249 – 250 p

Molaba LE (2022) Determining Controlling Factors for Water Stratification in Flooded Underground Mines in an Analogue Model Mine. MSc Thesis, Tshwane University of Technology

Mugova E, Molaba LE, Wolkersdorfer C (2024) Understanding the Mechanisms and Implications of the First Flush in Mine Pools: Insights from Field Studies in Europe's Deepest Metal Mine and Analogue Modelling. Mine Water Environ 43(2):73–86 doi:10.1007/s10230-024-00969-3.

Mugova E, Wolkersdorfer C (2022) Density Stratification and Double-Diffusive Convection in Mine Pools of Flooded Underground Mines – A Review. Water Res 214 doi:10.1016/j.watres.2021.118033.

Mugova E, Wolkersdorfer C (2025) Understanding the influence of stratification for mine water management: a comparative study. Scientific Reports 15(1):2757 doi:10.1038/s41598-024-82293-y.

Walls DB, Banks D, Boyce AJ, Burnside NM (2021) A review of the performance of minewater heating and cooling systems. Energies 14(19):6215.

Enhancing Ammonia Nitrogen Removal from Saline Mining Effluents: A Hybrid Approach with Ozone Microbubbles and Precipitation

Maher Mzoughi[1], Mehrez Hermassi[1], Étienne Bélanger[1], Thomas Genty[1],
Catherine N. Mulligan[2] Carmen M. Neculita[1]

[1]*Research Institute on Mines and Environment (RIME), University of Québec in Abitibi-Témiscamingue (UQAT), Canada*

[2]*Department of Building, Civil and Environmental Engineering, Concordia University, Montreal, QC H3G 1M8, Canada*

Abstract

Mining activities generate effluents with high ammonia nitrogen (NH_3^-N) concentrations, presenting substantial environmental risks. This study investigates the use of ozone microbubbles for ammonia removal from mining effluents. The treatment achieved over 99% ammonia removal in 15 L of effluent at a pH of 9, with treatment times ranging from 60 to 150 min. Ozone microbubbles demonstrated stable ammonia removal efficiency across varying salinity conditions, which were assessed to simulate the typical salinity levels of mining effluents. Following ozonation, Friedel's salt precipitation was applied to reduce chloride concentrations by 35% to 45%, addressing post-treatment concerns regarding effluent quality. These results suggest that ozone microbubbles, complemented by Friedel's salt precipitation, offer a promising solution for ammonia removal, particularly in cold climates where conventional methods face limitations.

Keywords: Ozone microbubbles, Ammonia nitrogen, Mining effluents, Advanced oxidation processes (AOPs), Salinity, Cold climates, Removal efficiency, Precipitation

Introduction

Mining operations are crucial for global mineral production, but they pose substantial environmental challenges, particularly in terms of effluent generation. Among the most concerning contaminants in mining effluents is NH3-N, which is highly toxic to aquatic life, even at low concentrations (0.4–3 mg/L) (CWQ 2010). Ammonia is introduced to waste streams in mining using the common blasting agent (ANFO-ammonium nitrate fuel oil) and emulsion-based products, as well as through cyanide degradation (Jermakka *et al.* 2015; Kuyucak and Mubarek 2013). As environmental regulations become increasingly stringent, the mining industry faces growing pressure to implement effective water treatment methods. The Metal and Diamond Mining Effluent Regulations (MDMER) require that discharged water must not be acutely toxic and set a criterion of 0.5 mg/L of NH3-N (Minister of Justice, 2024). At the provincial level in Quebec, mining companies must comply with the guidelines outlined in Quebec's Directive 019 for the mining industry (D019 2005; Ryskie *et al.* 2021). In addition to ammonia, salinity is another primary concern in mining effluents. Elevated salinity levels, as measured by total dissolved solids (TDS) or electrical conductivity (EC), pose considerable risks to aquatic life and the environment (Van Dam *et al.* 2014). Several advanced treatment technologies, including biological, physical, and chemical methods, have been employed to address ammonia and salinity in mining effluents (Elsahwi *et al.* 2022; Kuyucak and Mubarek 2013). Biological treatment methods are commonly used due to their cost-effectiveness; however, their effectiveness is often limited in colder climates, where low temperatures can inhibit microbial activity (Zha *et al.* 2020). However, ozonation with microbubbles effectively treats ammonia and other contaminants, generates no toxic byproducts, and adds no residual salinity (Neculita *et al.* 2020). Due to the presence of competing contaminants, such as cyanide and its derivatives from gold extraction, the ozonation process can be affected, necessitating further optimization of operational parameters. Additionally, pH levels have been found to play a critical role in ammonia removal, with optimal pH ranges of 9 to 11 yielding the most effective results (Ryskie *et al.* 2020). These findings underscore the need for continuous research to refine ozonation systems and adapt them to various effluent compositions and environmental conditions, particularly in colder regions. Controlling salinity levels remains a crucial challenge in managing mining effluents. Friedel's salt precipitation has been explored as a post-treatment to limit chloride and sulfate concentrations (Alhinaai *et al.* 2025; Wang *et al.* 2018), offering a means to control residual salinity in treated effluents and improve the quality of discharge water. By precipitating specific ions, Friedel's salt precipitation helps mitigate the environmental risks of high salinity, contributing to more responsible effluent management practices. This process works by reacting chloride ions with calcium or aluminium compounds to form Friedel's salts, which are insoluble and can be easily removed from the effluent.

This study aims to evaluate the effectiveness of microbubble ozonation in removing NH3-N from mining effluents, with a focus on the impact of varying chloride and sulfate salinity levels. It also examines the application of Friedel's salt precipitation as a post-treatment method to mitigate residual salinity. By evaluating synthetic and real mining effluents, the study seeks to contribute to the development of more efficient and sustainable treatment technologies, ensuring compliance with environmental regulations and minimizing the impact on aquatic ecosystems.

Methods and materials

Microbubble ozonation unit for effluent treatment

Trials were carried out using a pilot unit for microbubble ozonation, consisting of a medical oxygen cylinder supplying the Primozone GM1 ozone generator, which has an ozone production capacity adjustable between 20% and 100% of its full output (equivalent to 35 g O_3/h at 20% wt concentration, or 300 g/Nm^3 at 20% wt) (Ryskie *et al.* 2023). The generator has a cooling system, as the ozone production reaction is exothermic. The system also features a microbubble pump and a static mixer, which work together to enhance and control the size of the bubbles, thereby optimizing ozonation efficiency. The ozonation reactor has an 18 L capacity and is made of polycarbonate. The gas flow rate for the tests was 1.3 L/min, and the ozone generator produced ozone at a rate of 22 g/h. The reactor was maintained at 10 °C using the cooling system to preserve ozone solubility, as temperature increases would otherwise reduce it. A total of 15 L of effluent was treated. The pH was maintained at 9 using a 2.5 N NaOH solution, with a hydraulic residence time (HRT) ranging from 1 to 2.5 h.

Synthetic and real effluents for ozonation tests

Two distinct types of effluents were utilized in two separate experimental series for the ozonation tests. ***Synthetic effluents:*** The first experimental series was performed using synthetic effluents (solutions) prepared from deionized water and high-purity ACS-grade chemicals (Thermo Fisher Scientific). Ammonia nitrogen was introduced in the form of NH_4Cl or $(NH_4)2SO_4$, while sodium thiocyanate (NaSCN) was added in select cases to achieve a targeted concentration of thiocyanate (SCN^-). To simulate varying salinity levels, appropriate salts such as NaCl and Na_2SO_4 were incorporated, depending on whether the salinity was attributed to chloride (Cl^-) or sulfate (SO_4^{2-}) ions. The primary objective of this series was to assess the efficiency of microbubble ozonation in treating synthetic effluents, each containing varying concentrations of NH_3^-N, SCN^-, and different salinity profiles. A summary of the elemental concentrations used in these tests is provided in Table 1. ***Real effluents:*** The second series of four tests involved three real effluents, R1, R2, and R3, along with a 40% diluted version of effluent R3 (denoted as R4), all sourced from several mines in Canada (Table 1). These effluents varied in chemical composition, ammonia concentrations, and salinity sources. For effluent R_1, with high metal concentrations, the metals were precipitated before ozonation to prevent interference with the ammonia removal process. This pre-treatment prevents metal interference in microbubble ozonation; however, its industrial-scale necessity requires further evaluation.

Salinity treatment via Friedel's Salt precipitation: Jar test procedure

A jar test was conducted to investigate chloride precipitation as Friedel's salt, specifically testing the effect of salinity treatment on effluent R_3, which has high chloride salinity, following ozonation. A 250 mL sample of effluent R3 was treated with $NaAlO_2$ and $Ca(OH)_2$ using a Ca/Al/Cl molar ratio of 2/1/1, with constant stirring at 150 rpm for 24 h. During the experiment, liquid samples (1 mL each) were collected at regular intervals: every 5 min during the initial hours and every 30 min thereafter. All samples were filtered through a 0.45 µm filter before liquid analysis. At the end of the experiment, the solution was filtered through a Buchner funnel in an Erlenmeyer flask using a cellulose filter (0.22 µm; Mixed Cellulose Ester filter, Filter-Lab), and the solid was separated. All chemicals used in the experiments were of ACS-grade quality (Thermo Fisher Scientific).

Physicochemical measurements and analytical laboratory techniques

This study used various analytical techniques to monitor the physicochemical properties of synthetic and real effluent samples throughout the experimental treatment process. Initial concentrations of the effluents were measured before the experiment began, establishing baseline values for comparison. During the experiment, liquid samples were collected from synthetic and real effluents at regular intervals for analysis every 15 min, depending on the treatment process (ozonation or Friedel's salt precipitation). NH_3-N concentrations were measured using an ammonia-selective electrode (ISE Orion ThermoFisher Scientific) to track ammonia levels. Anion concentrations, including Cl^-, NO_3^-, and SO_4^{2-}, were analyzed using ion chromatography at the experiment's start and end. SCN^- concentrations were determined by UV-VIS spectrometry at 460 nm after the addition of nitric acid (HNO_3) and ferric nitrate ($Fe(NO_3)_3$), which formed a cyano ferric complex. pH was continuously monitored using a pH electrode connected to a multimeter (Symphony B30PCI). The initial and final concentrations of the effluents, along with the observed changes during the experiment, were used to assess the effectiveness of the treatment process. These analyses provided crucial data on the chemical dynamics throughout the treatment under varying conditions.

Table 1 *Composition of synthetic and real effluents.*

Effluent	Type	pH	$[Cl^-]$ (mg/L)	$[N\text{-}NH_3]$ (mg N/L)	$[SCN^-]$ (mg/L)	Br^- (mg/L)	SO_4^{2-} (mg/L)
S1	Synthetic	6.40	–	55.0	50.0	–	2400
S2	Synthetic	6.16	–	100.0	50.0	–	2400
S3	Synthetic	8.03	–	110.0	–	–	2400
S4	Synthetic	6.86	2400	110.0	–	–	–
S5	Synthetic	5.93	18000	110.0	–	–	–
R1	Real	7.88	247	67.5	54.9	3.3	1899
R2	Real	9.88	220	76.0	52.7	2.2	2221
R3	Real	7.88	36329	392.3	<1	260.8	1208
R4	Real	7.12	14237	153.8	<1	102.2	325

Data treatment and calculation of treatment efficiency

The treatment efficiency of different elements (e.g., NH_3-N) was calculated using the equation 1:

$$Efficiency = \frac{C_i - C_f}{C_i} \times 100 \qquad (1)$$

where C_i and C_f represent the concentrations of NH_3-N before and after treatment, respectively.

The mass of elements (e.g., N-NH_3) treated was calculated using the equation 2:

$$\text{Mass treated} = (C_0 - C_x) \times V \qquad (2)$$

where C_0 is initial concentration, C_x is the remaining concentration, and V is the volume treated.

The ozone consumption (O3) was calculated using the equation 3:

$$\text{Ozone consumption} = \frac{T_1}{60} \times Q \times \frac{Mass\ Treated}{1000} \quad = (3)$$

where T_1 is the treatment time, and Q is the ozone flow rate.

Results and discussion

Ozonation tests using synthetic effluents

Fig. 1 shows the treatment efficiency and ozone consumption for five synthetic effluents (S1 to S5). The treatment duration ranged from 90 to 165 min, successfully reducing NH_3-N concentrations to below 0.5 mg/L. Effluent S1, which contained 62.09 mg N/L of NH_3-N and 50.61 mg N/L of SCN^-, required 2 h to remove 99.4% of NH_3-N, with SCN^- rapidly oxidized within the first 30 min. In effluent S2, with an initial NH_3-N concentration of 103.9 mg N/L and 44.7 mg N/L of SCN^-, the treatment achieved 99.6% removal efficiency after 150 min, decreasing NH_3 to 0.378 mg N/L. The presence of SCN^- in both S1 and S2 extended treatment times, as SCN^- consumed ozone during the oxidation process. Effluent S3, containing 117 mg N/L of NH_3-N and SO_4^{2-}, achieved 99.7% NH_3-N removal in 105 min, with ozone consumption measured at 77.2 g O_3/g N-NH_3. Effluent S4, which contained 2.4 g/L of Cl^- and 118.3 mg N/L of NH_3, reached nearly 100% NH_3-N removal in 105 min, with ozone consumption of 68.3 g O_3/g NH_3. The NO_3^- concentration increased from 32.9 mg/L to 191 mg/L in S4, indicating effective NH_3 oxidation. Effluent S5, which had 17.7 g/L of Cl^- and 116.8 mg N/L of NH_3-N, required 90 min to achieve near-complete NH_3 removal, reaching 99.9% efficiency, with ozone consumption of 57.8 g O_3/g NH_3. The addition of SO_4^{2-} and Cl^- across all effluents did not crucially affect treatment efficiency. No chlorinated by-products, such as chlorates (ClO_3^-) or perchlorates (ClO_4^-), were detected, even at high concentrations of Cl^-. These results demonstrate that microbubble ozonation is highly effective for treating saline and non-saline effluents. The presence of SCN^- was the only factor contributing to longer treatment times, but it did not deteriorate treatment efficiency. According to previous studies (LeBourre 2020; Ryskie 2017), the treatment duration required for synthetic effluents containing 246 mg N/L and 100 mg N/L of NH_3, respectively, were similar in effluents that only contained NH_3-N, without the

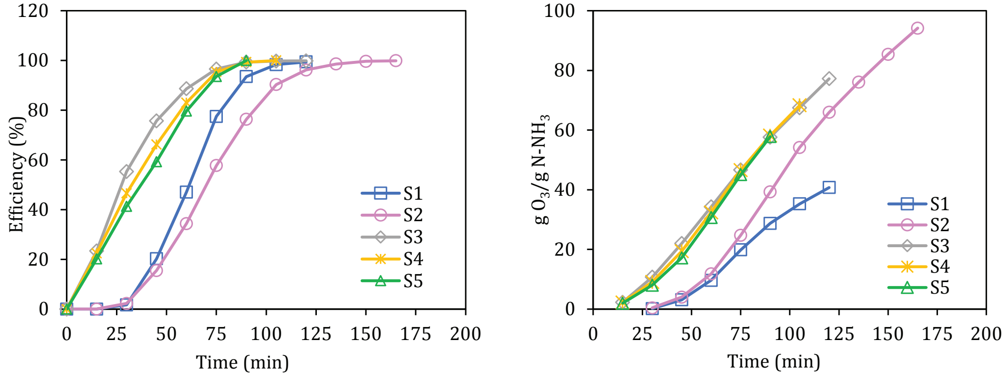

Figure 1 *a) Treatment efficiency as a function of time for five synthetic effluents containing different concentrations of NH_3, SCN^-, and various salinities (S1 to S5), b) O_3 consumption as a function of time for the same synthetic effluents (S1 to S5).*

addition of salts. This indicates that treatment times were almost identical for saline and non-saline synthetic effluents, and the treatment efficiency remained consistently high. Therefore, the introduction of SO_4^{2-} and Cl^- did not reduce the effectiveness of the microbubble ozonation process. The relatively longer treatment times observed in effluents S1 and S2 can be primarily attributed to the presence of SCN^-, which consumed ozone during the oxidation process. Moreover, trials with synthetic effluents demonstrated no important effect from sulfates or chlorides, and no chlorinated by-products were detected, even at high concentrations of Cl^-. These findings underscore the robustness of the microbubble ozonation process across various effluent compositions. To further validate the process's effectiveness, additional trials with real effluents, which were more complex, were conducted.

Ozonation tests with real effluents

Ozonation tests were conducted on three real effluents: R1, R2, R3, and R4 (R3 was tested at a 40% dilution prior to treatment). These effluents differ in their concentrations of NH_3-N and have various sources of salinity. Additionally, thiocyanates are present in two effluents (Fig. 2). In all cases, the treatment efficiency was around 99%, and an NH_3-N concentration of less than 0.5 mg N/L was achieved. In the first stage for effluent R1, high metal concentrations were precipitated to prevent interference with the ozonation process. The precipitation effectively reduced the residual metal levels (data not presented). Afterwards, ozonation was performed, during which SCN^- rapidly oxidized, dropping from 54.9 to 0 mg N/L within 30 min. This oxidation contributed to a slight increase in NH_3-N concentration, from 67.5 to 71.4 mg N/L during the same period. The treatment efficiency for NH_3-N was high, decreasing from 67.5 to 0.3 mg N/L, representing a 99.5% efficiency within 2 h. This was accompanied by an O_3 consumption of 44.3 g O_3/g N-NH_3. Concerning effluent R2, which has a similar NH_3-N composition to R1, the treatment time was longer, reaching 135 min. The initial pH was high, around 9.88, and NaOH was added only after the first 15 min. Initially, the NH_3-N concentration increased slightly from 75 to 77 mg N/L due to the transformation of SCN^-, which degraded within 30 min, dropping from 52.74 to 0.05 mg N/L. The treatment of this effluent was also effective, reducing the NH_3-N concentration from 76 to 0.2 mg N/L, with an average O_3 consumption of 56.2 g O_3/g N-NH_3, as shown in Fig. 2b. At the start of the test, the effluent was white and opaque, gradually turning pink by the end. This color change is likely due to the formation of metal oxide nanoparticles, which could pose a toxicity risk to Daphnia magna (Ryskie *et al.* 2023). For effluent R4 (R3 at 40% dilution), which had a salinity mainly due to the presence of chloride at 14 g/L and did not contain SCN^-, the treatment was nearly 100% effective in just 60 min, with an O_3 consumption of 50.7 g O_3/g N-NH_3. Between 45 and 60 min, the N-NH_3 concentration

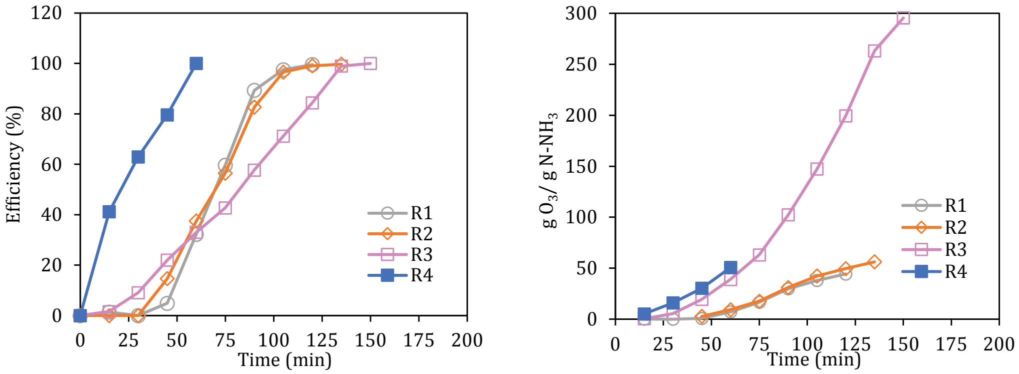

Figure 2 *a) Treatment efficiency as a function of time using real effluents (R1, R2, R3 and R4 (R3 at 40% dilution)). b) O_3 consumption as a function of time using the real effluents.*

dropped sharply from 31.2 to 0.02 mg N/L. The oxidation of N-NH_3 was accompanied by an increase in the NO_3^- concentration, which increased from 252 mg/L (relatively high relative to R1 and R2) to 338 mg N/L. For undiluted effluent R3, the treatment duration was relatively short despite the high initial NH_3-N concentration of 392.3 mg N/L. The ozonation with microbubbles lasted 150 min, decreasing the NH_3-N concentration from 392.3 to 0.008 mg N/L, indicating near 100% efficiency. The O_3 consumption was 295.6 g O_3/g N-NH_3. Between 120 and 135 min, the N-NH_3 concentration dropped from 61.2 to 4.2 mg N/L. Thus, despite high salinity, higher initial NH_3-N concentrations result in faster kinetics, while the presence of contaminants like SCN- may increase treatment time due to their faster oxidation. Future studies should examine solution aging and complexation in real effluents, as these factors may impact treatment effectiveness.

Salinity treatment with Friedel's salt

Following the ozonation of effluent R3, high chloride salinity was treated using Friedel's salt precipitation, resulting in a chloride removal efficiency of 35 ± 6%, indicating some decrease in chloride levels. The chemical reaction responsible for the formation of insoluble Friedel's salt, triggered by the addition of $Ca(OH)_2$ and $NaAlO_2$ to the chloride-rich effluent, is as follows (Wang *et al.* 2018):

$$CaCl_2 + 3Ca(OH)_2 + 2NaAlO_2 + 8H_2O \rightarrow 2Ca_2Al(OH)_6Cl \cdot 2H_2O + 2NaOH \quad (4)$$

This reaction is based on the theoretical molar ratio of Ca:Al:Cl of 2:1:1. In addition to chloride removal, the treatment led to a reduction in sulfate concentrations, underscoring the broader potential of Friedel's salts for salinity management in mining effluents. Despite the promising results, further investigations are necessary to optimize and enhance chloride removal efficiency.

Conclusion

This study focused on enhancing NH3-N removal from saline mining effluents through a hybrid approach combining microbubble ozonation and precipitation. Initial tests were conducted with synthetic effluents in batch mode to simulate real-world conditions, followed by trials with effluents from various Canadian mines. The results revealed a high treatment efficiency of 99% across all tests. The main variation in treatment times was attributed to the rapid oxidation of SCN^-, which occurred before NH_3-N oxidation. SO_4^{2-} and Cl^- ions did not considerably influence the treatment time or the overall effectiveness of ozonation. Notably, no chlorinated by-products were detected during the ozonation of chloride-containing effluents, likely due to the operating temperature of approximately 10°C, which is not conducive to ClO_3^-formation. Furthermore, post-treatment of ozonated effluent R3 using Friedel's salts demonstrated moderate chloride removal, showcasing the potential of combining ozonation with precipitation techniques. This hybrid approach presents a promising solution for addressing both ammonia nitrogen and salinity challenges in managing mining effluents. While tests demonstrate high NH3-N removal efficiency, scaling up may pose challenges that require further study.

Acknowledgement

This work was funded by the Natural Sciences and Engineering Research Council of Canada (NSERC), the Canada Research Chairs Program (Carmen M. Neculita), and the industrial partners of the Research Institute on Mines and Environment (RIME) - University of Québec in Abitibi-Témiscamingue (UQAT)-Polytechnique Montréal, including Agnico Eagle, Canadian Malartic Mine, Iamgold Corporation, Newmont, Raglan Mine-Glencore, and Rio Tinto.

References

Alhinaai MA, *et al.*, (2025) Chloride removal from stormwater and lakes impacted by road salt application: Experimental assessment of Friedel's salt reactions. Environmental Science & Technology Letters (in press).

CWQ (2010) Canadian water quality guidelines for the protection of aquatic life: Ammonia. (No. 1299).

D019 (2005) Directive 019 sur l'industrie minière. Government of Quebec.

Elsahwi ES, Hopp CE, Dawson FP, Kirk DW (2022) Electrochemical oxidation of ammonia-laden wastewater in the mining industry. In: IEEE Transactions on Industry Applications, vol 58, 4225–4232.

Jermakka J, Wendling L, Sohlberg E, Heinonen H, Vikman M (2015) Potential technologies for the removal and recovery of nitrogen compounds from mine and quarry waters in subarctic conditions. Critical Reviews in Environmental Science and Technology 45(7):703–748.

Kuyucak N, Mubarek IT (2013) Separation technologies for inorganic compounds contained in industrial wastewaters including metal ions, metalloids, thiosalts, cyanide, ammonia and nitrate. Separating Pro-Environment Technologies for Waste Treatment, Soil and Sediments Remediation, p 139–171.

LeBourre B (2020) Traitement de l'azote ammoniacal par ozonation et de la salinité résiduelle par filtration membranaire sur des effluents miniers réels. Université du Québec en Abitibi Témiscamingue (UQAT), Canada, 62p.

Minister of Justice (2024) Metal and Diamond Mining Effluent Regulations (MDMER), Canada.

Neculita CM, *et al.*, (2020) Future Prospects for Treating Contaminants of Emerging Concern in Water and Soils/Sediments. In: Advanced Nano-Bio Technologies for Water and Soil Treatment. Filip, J., Cajthaml, T., Najmanová, P., Černík, M., Zbořil, R. (Eds.) Springer, pp. 589–605.

Ryskie S (2017) Traitement de l'azote ammoniacal dans les effluents miniers contaminés au moyen de procédés d'oxydation avancée. MASc thesis, Université du Québec en Abitibi Témiscamingue (UQAT), Québec, Canada, 129p.

Ryskie S, Bélanger E, Neculita CM, Couture P, Rosa E (2023) Influence of ozone microbubble enhanced oxidation on mine effluent mixes and Daphnia magna toxicity. Chemosphere 329:138559.

Ryskie S, Gonzalez-Merchan C, Neculita CM, Genty T (2020) Efficiency of ozone microbubbles for ammonia removal from mine effluents. Minerals Engineering 145:106071.

Ryskie S, *et al.*, (2021) Active treatment of contaminants of emerging concern in cold mine water using advanced oxidation and membrane-related processes: A review. Minerals 11(259):1–23.

Van Dam RA, Harford AJ, Lunn SA, Gagnon MM (2014) Identifying the cause of toxicity of saline mine water. PLoS ONE 9(9):e106857.

Wang LP, *et al.*, (2018) Removal of chloride ions from an aqueous solution containing a high chloride concentration through the chemical precipitation of Friedel' salt. Materials Transactions 59(2):297–302.

Zha X, Ma J, Lu XW (2020) Use of a low-cost and energy-efficient device for treating low-strength wastewater at low temperatures focusing on nitrogen removal and microbial community. Science of the Total Environment 722:137916.

Selective Recovery Of Rare Earth Elements From Mining Influenced Water Using A Sulfonic Acid Resin: Evaluating Competitive Adsorption With Iron

Tamlyn S. Naidu[1,5], Ed Hardwick[2,3], Peter E. Holm[1], Craig Sheridan[4,5]

[1]*Department of Plant and Environmental Sciences, University of Copenhagen, Denmark*

[2]*School of Chemical and Metallurgical Engineering, University of the Witwatersrand, Johannesburg, South Africa*

[3]*CwengaTechnologies (Pty) Ltd, 28 Boeing Road East, Dunvegan, 1609, South Africa*

[4]*School of Geography, Archaeology and Environmental Studies, University of the Witwatersrand*

[5]*Centre in Water Research and Development, University of the Witwatersrand*

Abstract

Rare earth elements (REEs) are critical for modern technologies but sourcing them is environmentally hazardous and monopolized by certain regions. Mining influenced water (MIW) presents a potential sustainable alternative source. This study evaluates ion exchange (IX) for REE extraction in the presence of high iron (Fe) concentrations, assessing the selectivity of a sulfonic acid IX resin. Batch adsorption experiments were conducted, and equilibrium data were fitted to multicomponent isotherm models. Results indicate that while Fe exhibited high adsorption due to abundance, it had low selectivity, whereas REEs showed significantly stronger affinities. These findings highlight the potential of IX for sustainable REE recovery from MIW.

Keywords: Rare earth elements (REEs); Acid mine drainage (AMD); Ion exchange technology; Circular economy.

Introduction

Rare Earth Elements (REEs) Click or tap here to enter text.are essential for the production of high-performance magnets, electric vehicle (EV) batteries, wind turbines, and various electronic components. Their unique magnetic, optical, and catalytic properties make them indispensable in a wide array of industries, from renewable energy to defence applications (McLeod and Krekeler 2017). The global supply of REEs faces mounting challenges (including geopolitical tensions, environmental concerns, and economic dependencies) that threaten long-term sustainability (Massari and Ruberti 2013). A small number of regions dominate REE production (Fig. 1), creating a geographic monopoly that leaves global markets vulnerable to trade restrictions and political shifts (United States Geological Survey 2024).

Traditional REE extraction and processing generate hazardous waste, necessitating strict environmental regulation. Historically, REEs have been sourced from mineral ores such as bastnäsite, monazite, loparite, and lateritic ion-adsorption clays (Balaram 2019). However, with increasing pressure to reduce reliance on single-source suppliers, mitigate ecological impacts, and address the depletion of high-grade deposits, attention is shifting toward secondary sources. This strategy enables recovery from industrial waste, e-waste, and mine tailings. A particularly promising source is mining-influenced water (MIW), which often contain REEs and CRMs (Naidu *et al.* 2023). These streams offer both resource recovery and pollution mitigation by bypassing conventional processing, making them an attractive route for sustainable extraction.

Previous studies on REE recovery from MIW have focused on, and primarily

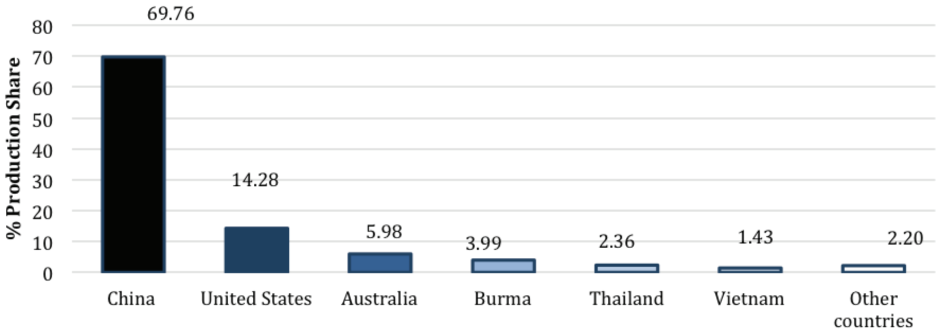

Figure 1 *Global REE Production Share 2023*

extracted, a select few elements, namely Y, La, Ce, Pr, and Nd, along with co-occurring metals such as Ca, Mg, and Fe (Smith *et al.* 2023). Techniques such as ion exchange (IX) have proven effective under specific conditions and are favoured in hydrometallurgy due to their metal affinity, stability, and reusability (El Ouardi *et al.* 2023). REEs span the lanthanide series, and each have distinct characteristics and uses – Eu in phosphors, Tb in magnets, and Gd in MRI contrast agents (Rademaker *et al.* 2013). Given their broad applications, a more inclusive recovery strategy is needed. This study aims to broaden this lens, focusing on the selectivity of a sulfonic acid cationic resin in extracting the full range of REEs from MIW in the presence of high amounts of Fe. This study evaluates resin selectivity using adsorption isotherms, specifically the Langmuir model, as well as empirical data.

Use of the Langmuir Model: The Langmuir isotherm describes monolayer adsorption on homogeneous surfaces, assuming no interaction between adsorbed species (Dada *et al.* 2012). Although these assumptions limit its use in complex, multicomponent systems, it remains a valuable predictive tool. Despite deviations from ideal behaviour, it has been shown to reasonably estimate adsorption capacities and equilibrium constants by capturing general trends. In MIW systems with competitive adsorption, it can still approximate equilibrium partitioning among available sites, offering insight into dominant interactions (Tangpromphan *et al.* 2016). Variants like the Multicomponent Competitive Langmuir Isotherm (MCL) improve applicability by incorporating ion competition (Misak 1995). Langmuir-based models have also been successfully applied to IX processes under non-ideal conditions (Jasim and Ajjam 2024).

In this study, the Langmuir model was selected due to its demonstrated success in similar systems (Calzaferri and Brühwiler 2024). While its assumptions limit predictive accuracy in complex, multicomponent systems like MIW, it is used here primarily as a tool to interpret adsorption behaviour and identify selectivity trends. Model refinements were introduced based on experimental data to better capture competitive effects; however, it is acknowledged that modifying isotherms outside their theoretical foundations (by empirically adding terms) compromises their general applicability. As such, the model's role here is illustrative rather than strictly predictive, with the core aim being the determination of REE selectivity coefficients.

Materials and Methods

A strongly acidic, gelular cation exchange resin, Lewatit® MonoPlus S 108 H (S108H), was sourced from CWENGA Technologies, South Africa, and Lanxess Deutschland. This styrene-divinylbenzene copolymer-based resin in H+ form was selected for its proven efficiency in metal removal and water demineralization, as supported by previous studies (Naidu *et al.* 2023). AMD samples were collected from a coal mine storage area in Emalahleni, Mpumalanga. Samples were stored in sealed polytetrafluoroethylene (PTFE) containers under constant temperature conditions. Seasonal and temporal variations in AMD composition were not accounted for, as these represent natural fluctuations encountered in real-world scenarios. To minimize adsorption losses in samples taken during the experiment, samples were preserved using nitric acid (0.6%), ensuring that dissolved metal adsorption onto container surfaces was negligible. Given that the MIW volume, the starting MIW conditions, resin quantity, and vessel type remained constant across all experiments, any potential variation was considered uniform and was assumed to not affect comparative adsorption results. The behavioural parameters of the IX system were evaluated through the following methods:

REE Content in AMD: The concentrations of REEs in the AMD samples were analysed using inductively coupled plasma optical emission spectroscopy (ICP-OES) and inductively coupled plasma mass spectrometry (ICP-MS), following the methodology reported by Smith (2023).

Isotherm Parameters and Competitive Adsorption: Batch adsorption experiments were conducted using 900 mL AMD samples placed in glass bottles containing 45 mL of S108H resin. Samples were agitated for 72 hours at 23 °C at 200 RPM, after which the liquid phase was filtered through 0.45 µm syringe filters and analysed. Adsorption data were fitted to multiple isotherm models, including the extended MCL model to evaluate REE and CRM selectivity. To further enhance predictive accuracy, an interaction term was introduced into the MCL model. This term was iteratively determined by minimizing the difference between predicted and experimental adsorption results using nonlinear least squares optimization via the Levenberg-Marquardt algorithm. Additionally, empirical evidence, based on ratios of initial vs. final concentrations for each element, was used to validate the model predictions. Seven different AMD solutions with varying initial conditions (labelled 1–7) were used to assess system behaviour under different competitive adsorption scenarios.

Statistical analysis of adsorption variability was not conducted, as experiments were performed as single-pass trials without replicates; however, analytical precision was maintained through consistent experimental conditions and validated instrumental methods.

Results and Discussion

Initial Concentrations and Model Performance: The initial concentrations of selected elements in each experiment are presented in Table 1.

Adsorption data, representing equilibrium concentrations in each vessel, were fit to the simple Langmuir model. The residual plot for Nd illustrates the goodness-of-fit, with predicted values closely aligning with observed data (Fig. 2). This outcome confirmed the results of prior studies, reinforcing the Langmuir model's potential robustness in describing REE adsorption behaviour in multicomponent systems. Following the application of the simple Langmuir model, a modified Langmuir model was introduced to account for competitive adsorption effects. The resultant

Table 1 Initial concentrations of Fe, Mg and select REEs in solution prior to resin contact

	Elemental Concentration (mg/L)							
Experiment	Fe	Mg	Ce	Nd	Eu	Gd	Yb	Lu
1	6462	493.9	6.61	1.25	0.07	0.53	0.139	0.02
2	4006	477.4	8.27	1.18	0.07	0.53	0.128	0.018
3	1692.2	202.2	2.66	0.63	0.03	0.17	0.061	0.00913
4	781.3	101.3	1.27	0.30	0.01	0.08	0.029	0.00426
5	451.1	59.4	0.76	0.18	0.01	0.05	0.017	0.00259
6	187.9	26.3	0.34	0.08	0.004	0.02	0.008	0.00115
7	98.1	13.7	0.17	0.04	0.002	0.01	0.004	0.00057

equation from the iterative modeling process is presented below.

$$Q_{e,i} = \frac{Q_{m,i} K_{L,i} C_{e,i}}{1 + \sum_{j=1}^{N} K_{L,j} C_{e,j}^{\eta_{L,j}}}$$

Where $Q_{e,i}$ is the equilibrium concentration of component i on the resin (mg/L), $Q_{e,i}$ is the maximum adsorption capacity for component *i* (mg/L), $K_{l,i}$ is the Langmuir affinity constant for component *i* (L/mg), $C_{e,i}$ is the equilibrium concentration of component *i* in solution (mg/L), $\eta_{l,i}$ is the interaction factor for component i, which modifies the competitive effect, and *N* is the total number of competing components in the system. The modification followed a similar approach to that used by Singh *et al.* (2024) for PFAS competitive adsorption equilibria on colloidal activated carbon. The equation quantifies how concentration-based competition (i.e., the presence of other ions) influences the Langmuir affinity constant (K_l) and maximum adsorption capacity (Q_m) for each element.

Initial guesses for Q_m and K_l were determined using the simple Langmuir model. Regression techniques were then used to obtain the optimal value for each term as well as the competition coefficient (η_l). Fig. 3 shows the normalized affinity coefficients obtained from this study which demonstrate that the resin exhibits a strong preference for REEs, with Fe and Mg showing substantially lower selectivity. Fe and Mg have selectivity coefficients which are 1 227 994 and 127 400 times less, respectively, than the REE with the highest affinity – Tm. Empirical data further support this trend; when comparing the average ratio of initial to final solution concentrations, Fe and Mg exhibited the lowest average adsorption relative to their initial concentrations (71 % and 76% respectively). Notably, in terms of measured concentrations, Ce demonstrated the highest average removal from solution (97%), deviating from model predictions. This discrepancy is likely due to Cerium's unique ability to exist in multiple oxidation states (Ce^{2+}, Ce^{3+} and Ce^{4+}), whereas other REEs predominantly exist in the trivalent state. The higher stability of Ce^{4+} in solution may result in enhanced adsorption relative to Ce^{2+} and Ce^{3+}, a factor not explicitly accounted for in the Langmuir model, which assumes a uniform adsorption mechanism. Consequently, the model provides an overall affinity for Ce without distinguishing between its oxidation states, potentially leading to an underestimation of its true selectivity. Further modelling or experimental validation is required to support this hypothesis.

Fit Assessment: Assessing the goodness of fit for non-linear models remains challenging, even when linear forms are applied. It is

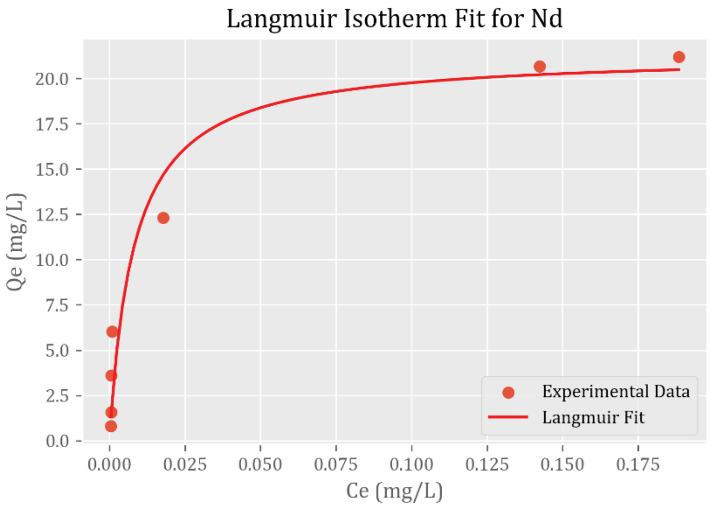

***Figure 2** Langmuir Isotherm Fit for Nd Adsorption onto Resin: Experimental Data vs. Model Prediction.*

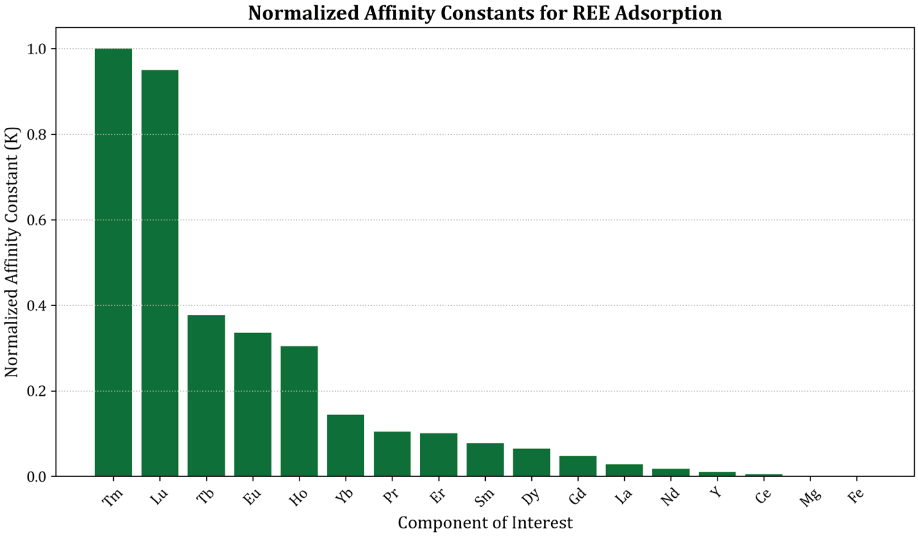

Figure 3 *Normalized selectivity of ions of interest in AMD solution using a modified extended Langmuir isotherm model.*

debatable whether using linear metrics like R^2 is mathematically valid post-linearization. Ideally, non-linear models should be evaluated in their original form for accuracy. During preliminary data analysis, multiple linearized versions of the Langmuir equation were explored (Mohammadi *et al.* 2012), to estimate initial Q_m and K_L values. Despite differences in transformation, a trend emerged: K_L values followed the same relative pattern, with Tm consistently showing the highest affinity. For mathematical reference, R^2 values for the linear fits are presented in Fig. 4.

The R^2 values indicate strong Langmuir fits for most REEs (all >0.99), except for Ce (0.96), Fe, and Mg (0.89–0.92). Ce's deviation is likely due to its variable oxidation states, which affect its adsorption behaviour compared to other predominantly trivalent REEs. Fe and Mg showed poorer fits due to several factors. Fe's high concentration, possible presence in both Fe^{3+} and Fe^{2+} forms, and low selectivity

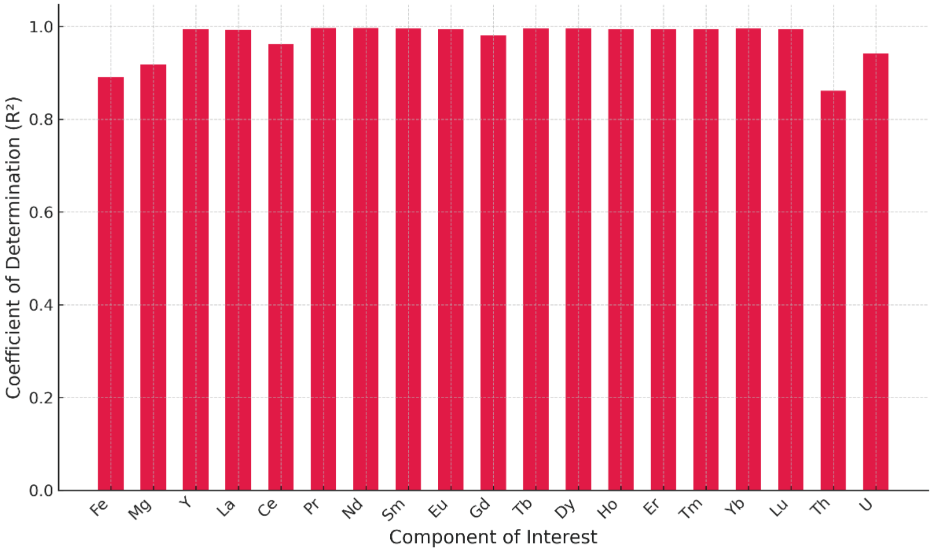

Figure 4 *Coefficient of Determination for all Elements analysed when fit to the simple Langmuir isotherm.*

for the resin likely led to non-ideal adsorption, including potential multilayer formation and competitive displacement. Mg, as a divalent ion, also deviates from the trivalent REE trend, weakening model applicability. These results underscore the limitations of the Langmuir model in complex systems with oxidation-state variation, competitive interactions, and non-monolayer adsorption.

Conclusions

Isotherm constants showed that Fe had high adsorption capacity (Q_m), consistent with its abundance in solution, but low selectivity (K_L), indicating adsorption driven by concentration rather than resin affinity. In contrast, REEs exhibited much higher selectivity, demonstrating strong binding to the resin even in the presence of excess Fe. The established selectivity sequence was: Tm > Lu > Tb > Eu > Ho > Yb > Pr > Er > Sm > Dy > Gd > La > Nd > Y > Ce >> Mg >> Fe. As shown in Fig. 4, REEs were adsorbed over Fe by several orders of magnitude, highlighting the S108H resin's potential for REE recovery. This sequence differs from earlier binary system studies (e.g., Hubicki *et al.* (1968)), likely due to the complex ion matrix of real AMD, which includes high sulfate levels and competing ions. Factors such as redox conditions, Al, Ca, and Total Organic Carbon may also influence selectivity, though not explicitly assessed here.

This study met its aim of evaluating REE selectivity in Fe-rich AMD using Langmuir-based modelling and empirical data. While Fe showed significant uptake, its poor selectivity reinforces the resin's potential for REE-focused separation. Future work should explore competing ion effects, optimize IX conditions, and assess performance in column systems. Cerium's unique behaviour, likely tied to redox variability, also merits deeper investigation.

Acknowledgements

The authors express their gratitude to the Danida Fellowship Centre for supporting the Acids to Value project through Grant 21-M10-KU, and to Nkosilomusa Moyo for his initial laboratory work on REE extraction from AMD.

References

Balaram V (2019) Rare earth elements: A review of applications, occurrence, exploration, analysis, recycling, and environmental impact. Geoscience Frontiers 10:1285–1303. 10.1016/j.gsf.2018.12.005

Calzaferri G, Brühwiler D (2024) A unified description of ion exchange and complete adsorption isotherms, including cluster growth and cavity filling. Microporous and Mesoporous Materials 377:113223. 10.1016/j.micromeso.2024.113223

Dada AO, Olalekan AP, Olatunya AM, DADA O (2012) Langmuir, Freundlich, Temkin and Dubinin–Radushkevich Isotherms Studies of Equilibrium Sorption of Zn 2+ Unto Phosphoric Acid Modified Rice Husk. IOSR Journal of Applied Chemistry 3:38–45. 10.9790/5736-0313845

El Ouardi Y, Virolainen S, Massima Mouele ES, *et al* (2023) The recent progress of ion exchange for the separation of rare earths from secondary resources – A review. Hydrometallurgy 218:106047. 10.1016/j.hydromet.2023.106047

Felipe ECB, Batista KA, Ladeira ACQ (2021) Recovery of rare earth elements from acid mine drainage by ion exchange. Environmental Technology (United Kingdom) 42:2721–2732. 10.1080/09593330.2020.1713219

Hubicki Z, Kołodyńska D, Ion Exchange Technologies (1968) Selective Removal of Heavy Metal Ions from Waters and Waste Waters using Ion Exchange Methods. In: Hellferich F (ed) Ion Exchange. McGraw-Hill

Jasim AQ, Ajjam SK (2024) Removal of heavy metal ions from wastewater using ion exchange resin in a batch process with kinetic isotherm. S Afr J Chem Eng 49:43–54. 10.1016/j.sajce.2024.04.002

Massari S, Ruberti M (2013) Rare earth elements as critical raw materials: Focus on international markets and future strategies. Resources Policy 38:36–43. 10.1016/j.resourpol.2012.07.001

McLeod C, Krekeler Mark (2017) Sources of Extraterrestrial Rare Earth Elements: To the Moon and Beyond. Resources 6:40. 10.3390/resources6030040

Misak NZ (1995) Adsorption isotherms in ion exchange reactions. Further treatments and remarks on the application of the Langmuir isotherm. Colloids Surf A Physicochem Eng Asp 97:129–140. 10.1016/0927-7757(94)03073-9

Mohammadi M, Ameri Shahrabi MJ, Sedighi M (2012) Comparative study of linearized and non-linearized modified Langmuir isotherm models on adsorption of asphaltene onto mineral surfaces. Surface Engineering and Applied Electrochemistry 48:234–243. 10.3103/S1068375512030088

Naidu TS, Moyo N, Hardwick E, *et al* (2023) Exploring the Potential for Rare Earth Element Recovery from Coal Mine Acid Mine Drainage using Ion Exchange Technology. In: Stanley P, Wolkersdorfer C, Wolkersdorfer K (eds) IMWA 2023 Conference – "Y Dyfodol | The Future". IMWA, Newport, Wales, pp 376–382

Rademaker JH, Kleijn R, Yang Y (2013) Recycling as a Strategy against Rare Earth Element Criticality: A Systemic Evaluation of the Potential Yield of NdFeB Magnet Recycling. Environ Sci Technol 47:10129–10136. 10.1021/es305007w

Singh M, Hakimabadi SG, Van Geel PJ, *et al* (2024) Modified competitive Langmuir model for prediction of multispecies PFAS competitive adsorption equilibria on colloidal activated carbon. Sep Purif Technol 345:127368. 10.1016/j.seppur.2024.127368

Smith J, Hardwick E, Falconer J, *et al* (2023) The Development of a Sample Preparation Technique for the Analysis of Trace Elements in Mine Impacted Waters containing High Levels of Iron. In: Stanley P, Wolkersdorfer C, Wolkersdorfer K (eds) Y Dyfodol | The Future. International Mine Water Association, Newport, Wales, pp 484–490

Tangpromphan P, Kaewchada A, Jaree A (2016) Competitive effect of glucose–fructose adsorption in a fixed-bed chromatographic column. J Sep Sci 39:4314–4324. 10.1002/jssc.201600572

United States Geological Survey (2024) Mineral Commodity Summaries 2024

Passive Treatment of Acid Mine Drainage Integrated with Carbon Dioxide Removal by Enhanced Rock Weathering in Acid Mine Drainage

Fugo Nakamura[1], Hkaung Htut San[1], Hajime Iwaki[1], Monthicha Rawangphai[1], Naomi Kitagawa[2], Shinichiro Morimoto[2], Takao Nakagaki[3], Tsutomu Sato[1]

[1]*Laboratory of Eco-Materials and Resources, Course of Sustainable Resources Engineering, School of Engineering, Hokkaido University*

[2]*Environmental and Social Impact Assessment Team, Global Zero Emission Research Center, The National Institute of Advanced Industrial Science and Technology, Department of Energy and Environment*

[3]*Nakagaki Laboratory, Department of Mechanical Engineering, School of Creative Science and Engineering, Waseda University*

Abstract

Interest is growing in Enhanced Rock Weathering (ERW) as a Carbon Dioxide Removal (CDR) strategy already applied to terrestrial and marine environments. Research shows that most silicate minerals dissolve several orders of magnitude faster under strongly acidic conditions like those found in acid mine drainage (AMD). An advantage of this approach is that silicate mineral dissolution from basalt increases AMD pH, potentially enabling passive treatment systems. To investigate both CDR potential and passive treatment possibilities of basalt-based ERW in AMD, we conducted one-dimensional reactive-transport modeling (1D-RTM) as a case study using the Amemasu River downstream from the abandoned Shojin mine. Using 1D-RTM, we estimated annual basalt weathering rates, CDR potential, and secondary schwertmannite formation. Life cycle assessment (LCA) and techno-economic evaluation (TEA) were then performed to determine net CDR and economic feasibility. We applied a surface complexation model (SCM) to evaluate contaminant adsorption by schwertmannite precipitates. Results show that ERW in AMD provides sufficient net CDR to be economically viable. Moreover, schwertmannite formation efficiently removes arsenic through adsorption while simultaneously releasing protons that maintain the acidic conditions necessary for enhanced mineral weathering. These dual benefits—carbon sequestration and contaminant removal—offer substantial economic incentives for treating AMD sites, particularly those contaminated with arsenic, iron, and sulfate. AMD treatment with limestone can be a major challenge to carbon neutrality in terms of economic burden and emissions. Our findings suggest the possibility of replacement of some active AMD treatment with limestone.

Keywords: ERW, CDR, 1D-RTM, SCM, LCA/TEA, schwertmannite

Introduction

The urgent need for cost-effective AMD treatment has driven interest in passive remediation approaches that utilize natural attenuation processes. In AMD treatment using limestone, the reaction of limestone with acid emits CO_2 gas. As limestone is the most common neutralizing agent, if carbon pricing is imposed on limestone-derived CO_2 emissions, its cost may rise, further increasing the economic burden of AMD treatment. Meanwhile, Enhanced Rock Weathering (ERW) is emerging as a promising Carbon Dioxide Removal (CDR) technology for carbon neutrality. Current

ERW applications focus on agricultural and marine sites with moderately acidic to alkaline environments.

Studies show that most silicate minerals dissolve much faster in strongly acidic environments such as AMD. Fig. 1 illustrates the relationship between the dissolution rate of major minerals in basalt and pH. For example, labradorite, an abundant mineral in basalt, dissolves approximately 1000 times faster at pH 2 compared to pH 7. This pH-dependent dissolution behavior suggests that applying ERW to strongly AMD could dramatically enhance mineral weathering rates. Moreover, adding basalt could enable passive treatment, continuously removing harmful elements while meeting wastewater standards. In our case study, we conducted geochemical modeling, life cycle assessment (LCA), and techno-economic assessment (TEA) of ERW in the Amemasu River, an AMD-affected river in Hokkaido where our research group is conducting field experiments, and our study clarified the effectiveness of ERW regarding both CDR and passive AMD treatment.

Methods

Modeling concept

This study evaluates CDR through the following steps. Basalt powder added to AMD releases cations (Ca, Mg, Na, K) while simultaneously removing sulfate ions through schwertmannite formation. Following the reaction, the treated river water enters the ocean, enhancing alkalinity without further basalt dissolution or schwertmannite formation. Total alkalinity is directly proportional to the concentration of dissolved inorganic carbon (DIC) because increased ocean alkalinity enhances CO_2 dissolution, raising dissolved inorganic carbon (DIC) concentrations. This relationship, defined by the proportionality constant η, is represented in Equation 1. Here ΔA_(T by ERW) is the total alkalinity change due to ERW (Beerling *et al.* 2020). Kanzaki *et al.*, (2023) suggests that up to 90% of the carbon initially sequestered via enhanced silicate weathering remains stored in the ocean for 100 to 1,000 years, indicating that the ocean is a semi-permanent carbon store for human timescales and CDRs. The release of highly charged cations from basalt, along with sulfate removal via schwertmannite formation, contributes to increased seawater alkalinity. The change in alkalinity is defined by Equation 2 when described in terms of the conservative ions involved in this study. In this study, the change in alkalinity defined by Equation 2 was substituted into Equation 1 to calculate the CDR of the ocean due to ERW in the Amemasu River. The value η was set to 0.86 (Beerling *et al.* 2020).

$$\mathrm{CDR} = \Delta \mathrm{DIC} = \eta \times \Delta A_{\mathrm{T\ by\ ERW}}$$

$$\Delta A_{\mathrm{T\ by\ ERW}} = 2 \times \Delta[\mathrm{Ca}^{2+}, \mathrm{Mg}^{2+}] + \Delta[\mathrm{Na}^{+}, \mathrm{K}^{+}] - 2 \times \Delta[\mathrm{SO_4}^{2-}]$$

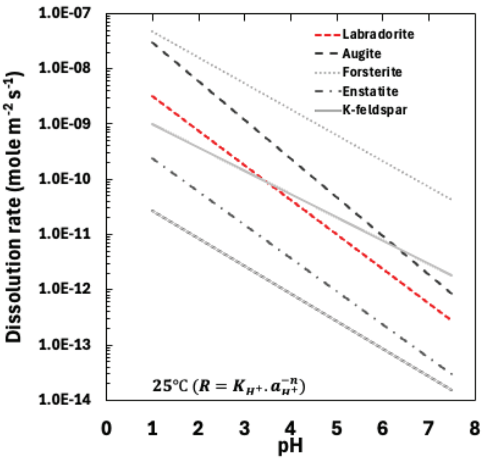

Figure 1 *Dissolution rate of major minerals in basalt as a function of pH (Palandri and Kharaka, 2004; Brantly* et al.*, 2008).*

Reactive Transport Modeling for basalt dissolution and CDR via ERW in AMD

A 1D-RTM was constructed to simulate alkali basalt dissolution in a flow-through system. The model was adapted from a published RTM for basalt dissolution in agricultural land (Beerling *et al.* 2020). X1t in the Geochemists' Workbench® 2023 Release 17.0 was used for modeling (Bethke, 1998). In the present calculations, only labradorite, augite, and forsterite, which are the minerals that contribute to the CDR reaction and account for 76% by weight of the alkali basalt, were considered and using kinetic parameters from Beerling *et al.* (2020). We selected these minerals because they dissolve within one year, releasing calcium and other cations.

In addition, schwertmanite, commonly observed in AMD with pH 3–4 and high sulfate concentrations (Bigham *et al.*, 1990), was included as a secondary mineral and set the kinetics data according to Sánchez-España *et al.*, 2011. The 15th of Dec. 2020 Thermoddem version of the thermodynamic database (Blanc, 2017; Blanc *et al.*, 2012) was used. We defined maximum annual basalt dissolution as the point where 99.9% of CDR-relevant minerals dissolve. Equation 3 (Beerling *et al.*, 2020) defines the dissolution rate, ri for any mineral i. The specific surface area, a key dissolution rate variable, follows Equation 4 by assuming that the specific surface area is equal to the specific surface area calculated with a uniform 80% passing particle size (Beerling *et al.* 2020).

$$r_i = w_i SSA_i m_i \tag{3}$$

$$SSA_i = \lambda(a\rho^{-1}r^{d-3}) \tag{4}$$

Where w_i is the mineral weathering rate, λ the roughness coefficient of the particle surface, SSAi is the specific surface area of mineral i (cm^2/g), mi is the mass of mineral i (g), ri is the radius of the particle (cm), a is a geometric variable for which the particle is assumed to be spherical, d (dimension) is 2, ρ is density, 3.0 (g/cm^3) (Beerling *et al.* 2020). This study compared basalt powder (a commercial product) with basalt dust (a mining by-product from crushing and sorting). First, the 80% passing particle size of the smallest basalt product defined by Beerling *et al.* 2020 was set to 10 µm, and the 80% passing particle size was set to 10 µm for basalt products (Beerling *et al.*, 2020) and 100 µm for basalt dust, a manufacturing by-product. The dimensions of the river were 0.5 m in height, 2.0 m in width, and variable length. Water quality parameters used in the model are presented in Table 1. These data come from laboratory analyses using inductively coupled plasma atomic emission spectroscopy (ICP-AES), inductively coupled plasma mass spectrometry (ICP-MS), and ion chromatography, as well as from field measurements of dissolved oxygen (DO), pH, and temperature.

Approach for LCA/TEA of ERW in AMD at Amemasu River

We used the LCATEA tool to calculate CO_2 emissions and costs (both operational and capital) for implementing ERW in the Amemasu River. The LCATEA tool was developed in collaboration with the National Institute of Advanced Industrial Science and Technology (AIST) using the IDEA® ver3.3 emissions and cost unit database of the AIST (Tahara *et al.* 2010). For this assessment, we established system boundaries including mining, crushing, and transport activities. Basalt was assumed to be dumped directly from the truck into the Amemasu River, generating no additional emissions or costs. For basalt dust scenarios, mining and crushing were excluded from calculations as dust is a manufacturing by-product. Emissions and costs were calculated by multiplying the unit, which is the emissions and costs generated in each activity, by the activity amount, which is the raw materials, energy, and travel distance used in the construction process associated with ERW on the AMD. Of the activity amounts, the amount of

***Table 1** Chemistry of the AMD (Amemasu River) used in the 1D-RTM.*

Species in fluid	Concentration[mg/L]	Species in fluid	Concentration[mg/L]
Ca^{2+}	15.09	$O_{2(aq)}$	5.1
Mg^{2+}	2.31	Fe^{2+}	16.22
K^{+}	2.33	SO_4^{2-}	549.69
Na^{+}	4.3	$Ti(OH)_{4(aq)}$	1×10^{-14}
Al^{3+}	10.42	Pb^{2+}	0.101
Cl^{-}	6.04	$H_4SiO_{4(aq)}$	20.75
As^{3-}	102.8×10^{-3}	HCO^{3-}	3.16×10^{-3}
pH (-)	3.04	Flow rate (m/s)	0.19
Temperature (°C)	25		

basalt mining, crushing, and transportation is the amount of basalt that can be dissolved per year, calculated by 1D-RTM, and the transportation distance is the round-trip distance calculated from the road distance from Amemasu River to the nearest basalt mining site. A 10-ton truck was used for transport. Here, the only processes for which new construction costs were considered were mining and crushing, which may need to be newly established for ERW.

Surface Complexation Modeling of schwertmannite Adsorption in Amemasu River

To evaluate passive treatment potential, we constructed a surface complexation model (SCM) simulating arsenic adsorption over a one-month period in the Amemasu River. The model primarily examined arsenic removal through schwertmannite surface complexation, which is well known to remove arsenic from wastewater (Miyata *et al.* 2018). Khamphila *et al.* (2017) found that arsenic adsorption on schwertmannite occurs through internal complex formation, similar to adsorption on ferrihydrite. They also reported that arsenate binds more selectively than sulfate. Therefore, we used the FeOH.sdat dataset for iron hydroxide surface complexes (Bethke, 1998) in our arsenic adsorption modeling without considering sulfate adsorption, which is less competitive than arsenic. We compared arsenic concentrations in AMD treated with schwertmannite to Japanese effluent standards.

Results

Basalt dissolution and schwertmannite formation at Amemasu River (AMD)

Results illustrated in Fig. 2 show that for the 10 µm particle size, up to 900 t/year of basalt was dissolved and 191 t/year of schwertmannite was precipitated. For the 100 µm particle size, up to 400 t/year of basalt was dissolved and 108 t/year of schwertmannite was precipitated. The CDR was calculated to be 334 t-CO_2/year and 155 t-CO_2/year for the 10 µm and 100 µm particle sizes, respectively.

Net CDR(LCA) and TEA of ERW in Amemasu River

Considering the industrial process that inputs these basalt volumes into Amemasu River, the net CDR is shown in Fig. 3. Fig. 3 demonstrates the net CDR for both the 10µm particle size product and the 100µm particle size dust. Results indicate that the CO_2 removal by weathering is sufficient compared to the emissions in both cases. The balance between net sales and the cost of carbon credits, assuming a carbon credit price of 250 US dollars, is shown in Fig. 4. Utilizing both product and dust is economically feasible, with sufficient benefits even after considering the main operational and capital costs.

Changes in Arsenic Concentration by Schwertmannite Adsorption in Amemasu River

Fig. 5 illustrates the amount of schwertmannite formed and the change in the concentration of dissolved arsenic in the Amemasu

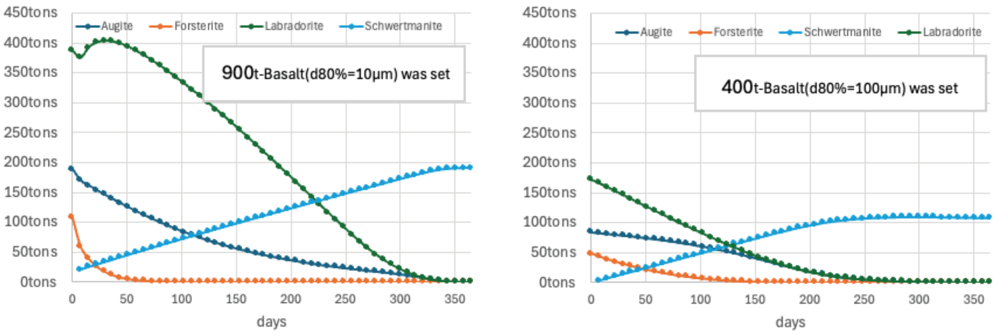

Figure 2 *Annual changes in mineral contents in the alkali basalt and schwertmannite formation (900t with 10µm particle size left; 400t with 100µm particle size: right).*

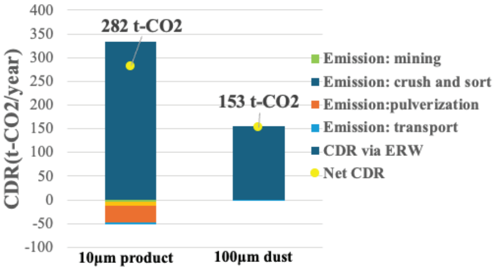

***Figure 3** The balance between CDR via ERW in Amemasu River and emissions from engineering processes involved.*

River due to arsenic adsorption at the amount of schwertmannite formed. When comparing arsenic removal via schwertmannite adsorption to Japanese effluent standards, the amount of schwertmannite needed to achieve the effluent standard for one month is about 8 tons. In other words, the amount of schwertmannite formed in both cases when the basalt particles to be spread is 100μm and 10μm is 12 times greater than the amount of schwertmannite needed to achieve the effluent standard for one month. This result suggests that passive treatment may be achievable.

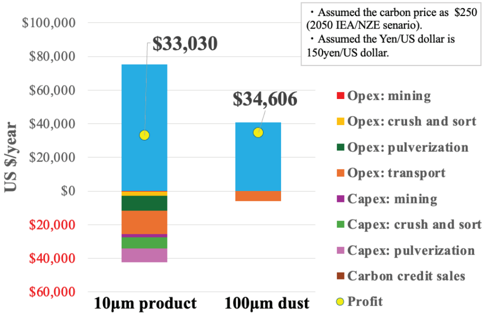

***Figure 4** The balance between Sales via carbon credits assuming the price as 250 US dollars/t-CO_2 in IEA/NZE 2050 scenario and Opex/Capex of engineering processes involved.*

Discussions

Our results demonstrate that the acidic conditions in AMD substantially accelerate basalt weathering, resulting in substantial net CDR, and ERW via AMD may be feasible. Furthermore, as shown in Eq. 5, the schwertmannite-forming reaction (Schoepfer and Burton, 2021) could simultaneously supply protons and lead to large amounts of basalt dissolution by maintaining acidic conditions favorable for ERW. Results also suggest that passive treatment could be achieved for a certain period by schwertmannite adsorption. These two results indicate that passive treatment can be technically integrated with CDR via ERW in AMD.

$$8Fe^{3+} + SO_4^{2-} + 14H_2O \rightarrow Fe_8O_8(OH)_6(SO_4) + 22H^+ \quad (5)$$

Conclusions

This study demonstrates two main implications: the possibility of large-scale CDR and simultaneous passive treatment by AMD. These dual benefits provide substantial economic incentives, especially

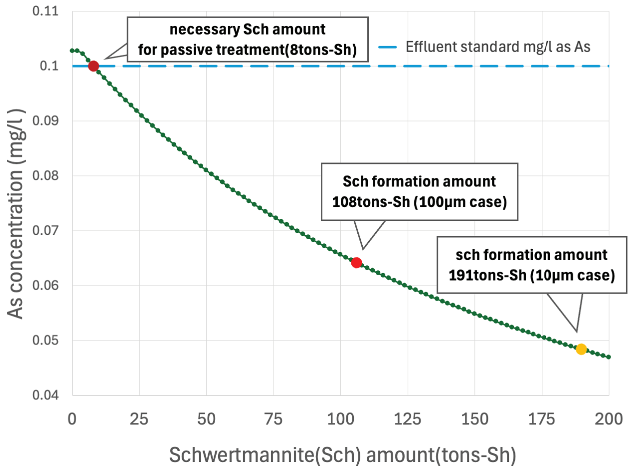

***Figure 5** Arsenic concentration changes by adsorption of schwertmannite precipitated in Amemasu River.*

for AMD sites dealing with arsenic, iron, and sulfate contamination. As the model has uncertainties, validation should be performed using data obtained after basalt dispersal in the Amemasu River. Furthermore, future studies should also be applied to activation treatment and compare the proposed activation treatment combined with ERW with the current active treatment in AMD treatment plants using limestone.

Acknowledgments

The paper is based on results obtained from a project, JPNP18016, commissioned by the New Energy and Industrial Technology Development Organisation (NEDO).

References

Beerling, D.J., Kantzas, E.P., Lomas, M.R., Wade, P., Eufrasio, R.M., Renforth, P., Sarkar, B., Andrews, M.G., James, R.H., Pearce, C.R., *et al.* (2020). Potential for large-scale CO_2 removal via enhanced rock weathering with croplands. Nature, 583, 242–248.

Bethke, C.M. (1998). The Geochemist's Workbench: A User's Guide. University of Illinois, Urbana, IL.

Bigham, J.M. (1995). Formation mechanisms and stability of iron hydroxide-sulfate precipitates in acid mine waters. Physica B: Condensed Matter, 208–209, 481–483.

Bigham, J.M., Carlson, L., Murad, E. (1990). Schwertmannite, a new iron oxyhydroxy-sulfate from Pyhäsalmi, Finland, and other localities. Mineralogical Magazine, 54(375), 355–365.

Blanc, P. (2017). Update for the 2017 version. Report BRGM/RP-66811-FR.

Brantley, S.L., Kubicki, J.D., White, A.F. (Eds.). (2008). Kinetics of Water-Rock Interaction. Springer, Dordrecht, Netherlands. https://doi.org/10.1007/978-0-387-73563-4

IEA (International Energy Agency). (2024). Global Energy and Climate Model. Paris. Available from: htßtps://www.iea.org/reports/global-energy-and-climate-model. Licence: CC BY 4.0.

Kanzaki, Y., Planavsky, N.J., Reinhard, C.T. (2023). New estimates of the storage permanence and ocean co-benefits of enhanced rock weathering. PNAS Nexus, 2(4), pgad059. https://doi.org/10.1093/pnasnexus/pgad059

Miyata, N., Akita, T., Komai, T. (2018). Arsenate adsorption and structural changes in synthetic schwertmannite: EXAFS and ATR-FTIR analysis. Environmental Science & Technology, 52(9), 5356–5363.

Palandri, J.L., Kharaka, Y.K. (2004). A compilation of rate parameters of water-mineral interaction kinetics for application to geochemical modeling. U.S. Geological Survey Open File Report, 2004-1068.

Sánchez-España, J., Yusta, I., Diez-Ercilla, M. (2011). Schwertmannite and hydrobasaluminite: a re-evaluation of their solubility and control on the iron and aluminum concentration in acidic pit lakes. Applied Geochemistry, 26, 1752–1774.

Schoepfer, V.A., Burton, E.D. (2021). Schwertmannite: A review of its occurrence, formation, structure, stability and interactions with oxyanions. Earth-Science Reviews, 221, 103811.

Tahara, K., Onoye, T., Kobayashi, K., Yamagishi, K., Tsuruta, S., Nakano, K. (2010). Development of inventory database for environmental analysis (IDEA). Proceedings of the 9th International Conference on Ecobalance, Nov 2010, Tokyo, Japan, 119.

Environmental Geochemical Impact Of Tailings Spills In Natural Streams In Chile (Mapocho River Case)

Álvaro Navarrete-Calvo[1], Natalia Bustamante-Penagos[2], Camilo Sánchez-Yáñez [1],
Ringo Maturana1, Max Hidalgo[1], Santiago Montserrat[3]

[1] *Universidad Mayor, Escuela de Geología, 367 Manuel Montt, Chile, alvaro.navarrete@umayor.cl*

[2] *Universidad de La Frontera, Departamento de Obras Civiles, 1145 Francisco Salazar, Temuco, Chile, natalia.bustamante@ufrontera.cl, ORCID 0000-0002-9977-1432*

[3] *Advanced Mining Technology Center, University of Chile, Avda. Tupper 2007, 8370451 Santiago, Chile santiago.montserrat@amtc.uchile.cl*

Abstract

This study investigates abandoned tailings deposit from 1978, located near Santiago, Chile, posing environmental and public health risks. The tailings dam, situated on the banks of the Mapocho River and near a residential area, discharges effluents directly into the river. A partial collapse of the collapse of tailings impoundment in 1987 released approximately 400,000 m^3 of material, containing potentially toxic elements and identified as a source of acid drainage.

The primary objective of this study was to assess the downstream dispersion and geochemical stability of the collapsed tailings. To achieve this, a photogeomorphological map and a digital elevation model (DEM) were developed to locate potential tailings accumulation sites. Trial pits were excavated at several points along the river (0 to 2 meters depth), where tailings and sediment samples were collected for granulometric, geochemical, and mineralogical analyses. Excavations revealed two distinct tailings layers: one 5 cm thick and the other exceeding 1 metre.

These findings suggest that the tailings have been transported and deposited in unmonitored and unremediated fluvial bars and floodplains. However, geochemical analysis indicates that this material does not exhibit the high metal or sulfur concentrations characteristic of the tailings. Additionally, neutral paste pH values suggest a low potential for acid generation. The presence of reducing redox conditions in the buried material further supports its geochemical stability.

The integration of geological, geochemical and hydraulic methods proves effective for assessing the transport and fate of collapsed tailings, offering valuable tools for similar environmental assessments in Chile.

Keywords: Abandoned tailings, Acid drainage, Potentially toxic elements, Sediment geochemistry, Mine closure planning.

Introduction

In Chile, numerous tailings storage facilities built using the upstream method throughout the 20th century are at potential risk for physical instability due to natural events such as extreme precipitation, floods, and earthquakes. Several failures have been recorded in Chile, including the collapse of 200,000 m^3 of tailings at the Las Palmas facility after the 2010 earthquake (Pizarro *et al.*, 2010), the 1985 failure of the Cerro Negro dam releasing 500,000 m^3 (WISE Uranium Project, 2025), and the 1987 collapse of the Pudahuel dam due to extreme rainfall, discharging 400,000 m^3 of tailings into the Mapocho River (Nueva Pudahuel S.A, 2009).

Despite these significant environmental events, there is a lack of geochemical records of affected soils and fluvial sediments in Chile, hindering the assessment of long-term geochemical stability and potential environmental impacts. This issue is particularly complex for tailings spills from decades ago, where materials may have been buried or transported downstream without a detailed geochemical characterization of original materials.

This study focuses on an abandoned tailings dam impoundment, active from 1978 to 1987, located near Santiago, Chile. The tailings originate primarily from an epigenetic hydrothermal vein-type copper deposit. The site, which lacks adequate mitigation measures, poses significant risks to the environment and public health. The facility extends along the Mapocho River on a gentle hillside that drains directly into the river, contributing to contamination of fluvial sediments, particularly through the release of potentially toxic elements (PTEs) and acid mine drainage (AMD), as identified in prior evaluations (CIMMT & S, 2006). A residential area housing approximately 2,000 people is situated nearby, while agricultural fields covering an estimated 68 hectares extend 1.5 km downstream along the river. Therefore identifying and characterizing the accumulation zones of these tailings is crucial for understanding the associated risks.

Methods

A sampling campaign was conducted on August 16-17, 2024, collecting 40 sediment samples from seven points—two upstream control points and five downstream. Upstream points were sampled to establish a chemical baseline for fluvial sediments unaffected by tailings. Downstream points were selected within sediment depositional areas based on photogeomorphological mapping (Fig. 1) and high-resolution Digital Elevation Models (DEMs) from ALOS PALSAR (12.5 m resolution) and drone-based photogrammetry (4.73 cm resolution, Appendix A, Supplementary Material).

Sampling was carried out through trial pits along channels in lateral bars of the Mapocho River, with depths ranging from 0 to 190 cm, using an Edelman auger for more compact substrates. Samples weighed around 2 kg for trial pits and 80-500 grams for auger samples. Depth sampling was based on textural and

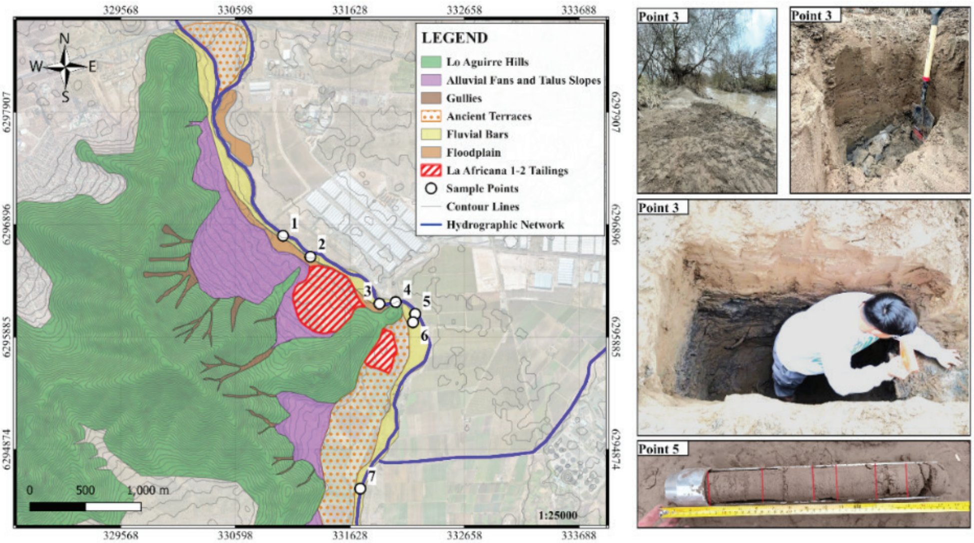

Figure 1 *The geomorphological map of the western slope of the Mapocho River highlights sampling points (1 to 7), key geomorphological units (fluvial bars, terraces, and alluvial fans), and the Pudahuel tailings deposit. Photographs show trial pit examples, with an edited image of sampling point 3 to enhance the paste-like tailings material at depths below 47 cm, and sampling point 5 demonstrating the use of an Edelman auger for sediment separation.*

color variations, compaction, and moisture. All samples, except for point 6, were collected within 2 meters of the river channel.

Sample preparation was conducted at the HEMERA Center and the CNAP Center at Universidad Mayor in Chile, following standard methods (Smodis *et al.*, 2003). The process involved quartering, drying at 40°C, and sieving with a Ro-Tap W.S. Tyler RX-29 shaker to separate gravel, sand, and silt/clay fractions. Geochemical analysis of the sand and fine silt/clay fractions was performed using X-ray fluorescence (XRF) with a SciAps X-200 portable analyzer. Instrument calibration was performed using fundamental parameters with Compton normalisation. Prior to each use, calibration was verified using a 316 stainless steel plate as a reference standard Descriptive statistics were applied to elements with over 90% data above the detection limit, calculating the minimum, maximum, median, mean, and standard deviation.

The paste pH measurement was conducted using 20 g of dried sample mixed with 20 mL of deionized water in a Falcon tube, ensuring homogenization. Once the solid material settled, the pH of the solution was measured with a Hanna HI 98194 multiparameter device, after verifying calibration with pH 4.01 and 7.00 buffer solutions.

X-ray diffraction (XRD) analysis was performed on the silt/clay fraction (#230 mesh) of dried samples using a Bruker D2 PHASER powder diffractometer at the VREMAS laboratory, Universidad de La Frontera. The analysis employed Cu Kα radiation ($\lambda = 1.5418$ Å) over a 2θ range of 5°–70° with a step size of 0.02° for high-resolution diffraction patterns. The XRD results helped identify crystalline mineral phases in four sediment samples, focusing on sulfide minerals, oxidation products, and silicate gangue minerals. One sample was collected upstream, and three separated samples from a deep trial pit near the tailings.

The environmental quality of the sediments was evaluated using two reference guidelines: the Consensus-Based Sediment Quality Guidelines (MacDonald *et al.*, 2000), which assess the potential effects of sediment chemical composition on aquatic ecosystems, and the Canadian Sediment Quality Guidelines, designed to evaluate potential risks to human health in residential and industrial areas.

This study used a two-dimensional model of an incompressible Newtonian fluid for hydraulic modeling, solving the Saint-Venant equations with Manning's resistance law using HEC-RAS software. The digital elevation model (DEM) was obtained from the ALOS PALSAR satellite product with a spatial resolution of 12.5 m × 12.5 m, and a channel incision was applied to address vegetation-related issues. Bedload sediment transport was analyzed using the Meyer-Peter and Müller equation. A structured mesh with 22 m cell size was used in areas away from the Mapocho River channel, while a non-structured mesh with refined cells down to 12 m was used within the channel. Monthly mean discharge time series from March 2004 to May 2016 were used as the upstream boundary condition, and normal depth was set as the downstream boundary condition. The hydraulic model was calibrated considering Manning's roughness and the depth correction of the digital elevation model, through the validation of flow levels during high and low flow periods. Additionally, different mesh sizes were evaluated to optimize computational time and the quality of the hydraulic modeling.

Results

The sediment distribution was 60% sand and 40% silt/clay. The paste pH of tailings samples was acidic (1.5–2.7), while sediment samples were near-neutral to slightly alkaline (6.7–8, average 7.2). Samples with paste pH below 5 can be considered evidence of immediate acidity. The major elements in river sediment samples were Si (average 15.5%), Al (average 4.6%), Fe (average 3.8%), and Ca (average 2.3%), while the most abundant potentially toxic elements (PTEs) had mean concentrations of Mn (874.6 mg/kg), S(433.8 mg/kg), Cu (199.2 mg/kg), V (140.8 mg/kg), Zn (96.0 mg/kg), and Pb (13.7 mg/kg), mainly found in the silt/clay fraction. A detailed breakdown of sediment chemistry is available in the supplementary material (Appendix B, Table 1).

XRD analysis showed river sediments predominantly composed of quartz, followed by iron oxides and minor calcite, while tailings consisted mainly of iron oxides with quartz and trace sulfides, as bornite. Tailings samples had higher sulfur content, with average concentrations of Fe (13.2%), S (8.4%), Si (6.3%), Al (1.9%), and Ca (0.9%). Among PTEs, Cu (3950.3 mg/kg), Zn (56.7 mg/kg), and As (42.6 mg/kg) were most abundant.

Bedload sediment transport estimated using the Meyer-Peter and Müller equation, shows sediment transport downstream of the tailings dam, with a sedimentation area identified upstream. The modeled area in HEC-RAS 2D is shown in brown in Fig. 2, with purple points representing sediment sampling locations. A raster in Fig. 2 illustrates sediment transport rates, with red indicating high transport and green low transport. Transparent pixels highlight sedimentation zones, particularly between sampling points 2 and 3, where tailings deposition is expected after dam failure or spills.

Sediment transport occurs in both the river channel and floodplain, with tailings particles not remaining long due to flow-driven transport. Further downstream, additional sediment accumulation zones may exist, requiring an expanded model area and higher DEM resolution for more detailed assessment.

We focus on Cu and S as proxies for identifying mining-related sources, given the very high concentrations of residual Cu and S in the local tailings impoundment. Fig. 3 shows that Cu concentrations are higher

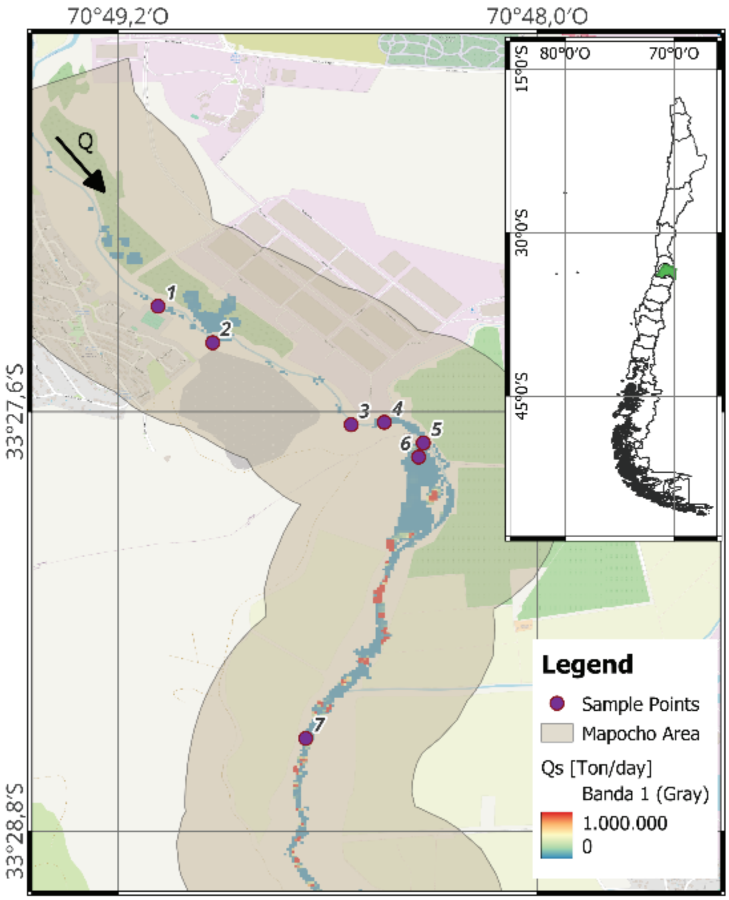

Figure 2 Bedload sediment transport in the Mapocho River was estimated using the Meyer-Peter and Müller equation, with sample point locations marked by purple points.

in the fine fraction than in the sand fraction. Three distinct patterns were observed:

- Sampling point 1 (upstream of the tailings site) shows higher Cu concentrations at 5–10 cm and below 30 cm, compared to other depths within the same sample point.
- Sampling point 5 exhibits increased Cu concentrations below 20 cm, particularly in the fine fraction.
- Sampling points 3 and 4 show elevated Cu concentrations near the surface, especially in the fine fraction (>350 mg/kg), with lower concentrations in buried tailings.

For S concentrations, Fig. 3 shows a similar pattern to Cu upstream, with higher surface values and below 20 cm, but S concentrations are similar in both fractions. Sampling point 3 shows peak S concentrations in the sand fraction at the surface and in buried paste-like tailings (~700 mg/kg), while the fine fraction has lower values (250–500 mg/kg), except at the surface.

The buried paste-like tailings, possibly from the 1987 spill, suggest minimal oxidation and preservation of sulfide minerals due to reduced redox conditions. This is supported by paste pH measurements, which showed no acidic conditions at depth. Oxidation could have occurred during droughts, mobilizing sulfates.

Sampling point 4 shows distinct Cu variations, with high concentrations (>750 mg/kg) at three depths, especially in the fine fraction. Sampling point 5 has lower Cu concentrations across all depths. Cu and S in the buried material at point 3 may originate from tailings but with differing geochemical patterns. The hydraulic model suggests tailings deposition between points 2 and 3, explaining the Cu variations at different depths.

Elevated Cu and S concentrations at point 1 suggest a potential upstream metal source, possibly linked to seasonal acid drainage in the Mapocho River (Correa-Burrows *et al.*, 2021) or nearby mining activities.

Conclusions

The chemical analysis of Mapocho River sediments reveals that Cu concentrations are significantly elevated at surface levels or below 20 cm, surpassing the PEC parameter of consensus-based sediment quality guideline (SQG) (MacDonald *et al.*, 2000) for potentially toxic elements (PTEs). Mn follows with slightly elevated concentrations in some surface samples downstream of the tailings deposit, also exceeding the SQG.

The buried tailings layers show low PTE concentrations and lack reactivity in terms of acid release upon contact with water, likely due

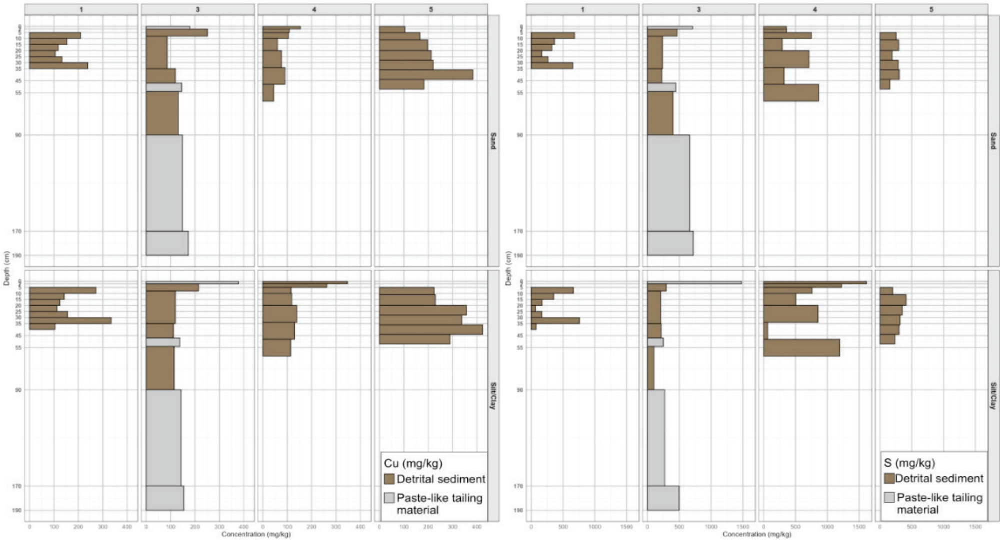

Figure 3 *Depth profiles of Cu and S concentrations (mg/kg) in trial pits along the river, with each column representing a sampling point. The upper section shows the sand fraction, and the lower section shows the silt/clay fraction. Brown indicates detrital river sediment, and grey represents buried paste-like tailings.*

to the reducing conditions from burial, which may stabilize sulfide minerals. However, further research is necessary to determine if the tailings-like material originates from the Pudahuel tailings deposit or another source. Isotopic analysis is recommended to confirm the source. If linked to the Pudahuel tailings, future studies will investigate the geochemical processes responsible for the mobilization and reduction of Cu and S concentrations in the buried material. A reanalysis of surface sediments before the next seasonal rains will help assess if concentrations stabilize or decrease naturally, aiding predictions of the buried material's seasonal behavior.

Geochemical data reveal high concentrations of Cu, Fe, Mn, and S in the upper centimeters of riverbed sediments, exceeding the PEC threshold for freshwater environments. Extreme precipitation accelerates tailings erosion and deposition in river sediments. Hydrodynamic modeling shows how these events transport sediments downstream and create hazards for the surrounding ecosystem and human health. Elevated Cu concentrations upstream of the tailings deposit suggest a potential alternative source and additional mobilization events. Future research will focus on examining Cu concentrations in the river upstream.

The hydraulic model successfully identified sediment accumulation and erosion zones. However, it did not fully align with transport patterns observed during the 1987 and 2001 flood events, and ongoing refinements are necessary. This study emphasizes the synergy between hydraulic modelling and geochemistry, highlighting its potential to investigate other historical tailings spills in Chile.

Acknowledgements

C.I(e) Leonardo Torres y al laboratorio Vremas de la Universidad de La Frontera.

We express our gratitude to the Applied nanotechnology Center (CNAP) and the HEMERA Center of Universidad Mayor for providing laboratory facilities and analytical equipment essential to this research.

References

CIMM T & S S.A. (2006, marzo). Muestreo del relave de Minera La Africana y aplicación del test ABA. (Informe final, Proyecto 51/10-128). Preparado para Compañía Minera Nueva Pudahuel.

Correa-Burrows, J. P., Navarrete-Calvo, Á., Valenzuela-Díaz, M. J., Zapata-Aguiló, V. A., Montserrat, S., Navarro-Valdivia, L., ... & Caraballo, M. A. (2021). The role of local geochemical and mineralogical backgrounds as essential information to build efficient sediment quality guidelines at high-mountainous hydrothermally-altered basins (Mapocho basin, Chile). *Science of the Total Environment*, 785, 147266.

MacDonald, D.D., Ingersoll, C.G., Berger, T.A., 2000. *Development and evaluation of consensus-based sediment quality guidelines for freshwater ecosystem*. Arch. Environ. Contam. Toxicol. 39, 20–31. https://doi.org/10.1007/s002440010075.

Maturana, R. (2024). *Quantification of eroded material in abandoned tailings deposits and its environmental implications. Case study: La Africana tailings, Metropolitan Region* [Thesis for the degree of Geologist]. Universidad Mayor.

Nueva Pudahuel S.A. (2009). Environmental Impact Declaration: Environmental remediation of La Africana tailings deposit, Project Congo. Servicio de Evaluación Ambiental, Región Metropolitana. Retrieved from https://seia.sea.gob.cl/expediente/ficha/fichaPrincipal.php?modo=normal&id_expediente=3985782

Pizarro, G., Pasten, P., & Bonilla, C. (2010). Preliminary contingency assessment in Las Palmas tailings dam, Pencahue sector, Maule Region: Phase I. Final report. Retrieved from https://bibliotecadigital.ciren.cl/handle/20.500.13082/32496

Price, W. A. (1997). *Guidelines and recommended methods for the prediction of metal leaching and acid rock drainage at minesites in British Columbia*. Ministry of Employment and Investment, Reclamation Section, Energy and Minerals Division.

Smodis, B., Annareddy, V. R. R., & Rossbach, M. (2003). *Collection and preparation of bottom sediment samples for analysis of radionuclides and trace elements*. International Atomic Energy Agency.

Valenzuela-Diaz, M. J., Navarrete-Calvo, A., Caraballo, M. A., McPhee, J., Garcia, A., Correa-Burrows, J. P., & Navarro-Valdivia, L. (2020). Hydrogeochemical and environmental water quality standards in the overlap between high mountainous natural protected areas and copper mining activities (Mapocho river upper basin, Santiago, Chile). *Journal of Hydrology, 588*, 125063.

WISE Uranium Project. (2025, February 5). Chronology of major tailings dam failures. WISE Uranium Project. https://www.wise-uranium.org/mdaf.html

Analysis of mine closure practices and the regulatory mining framework in the Córdoba province – Colombia

Gustavo Neira-Arenas[1], Sebastián Navarro-Martínez[2]

[1]*Universidad Nacional de Colombia – Facultad de Minas, Medellín, Colombia –* gneira@unal.edu.co, *ORCID 0000-0003-1178-1917*

[2]*Universidad Nacional de Colombia – Facultad de Minas, Medellín, Colombia -* sebastian.navarro@eia.edu.co

Abstract

Mining has been a traditional economic activity in the province of Córdoba, in the north of Colombia, representing in average 1.83% GDP of the region and producing over US$4.920 million in annual royalties for the country. Nickel, coal, gold, limestone, clays and building materials are resourced, and there are great expectations to produce copper. It faces, however, critical environmental challenges, particularly in water management, due to inadequate regulatory frameworks and the rise of informal mining activities. This study analyzes environmental licenses issued in Córdoba over the past two years by the regional environmental bodies, focusing on coal and building materials extraction, to assess compliance with national and international standards. The findings reveal significant gaps in Colombia's regulatory framework, especially in water management, compared to global best practices outlined by organizations such as the International Council on Mining and Metals (ICMM) and the Asia-Pacific Economic Cooperation (APEC).

Key deficiencies include the lack of detailed strategies for water resource monitoring, prevention of acid mine drainage (AMD), and long-term water quality protection. Current closure plans often fail to incorporate site-specific water monitoring, such as tracking pH levels, potentially toxic metals concentrations, and total dissolved solids, which are crucial for early contamination detection. Additionally, the absence of robust financial assurances and climate change adaptation measures further exacerbate the risks of long-term environmental liabilities.

The study highlights the need for Colombia to align its regulatory framework with international standards, emphasizing integrated water management, stakeholder engagement, and post-closure monitoring. Addressing these gaps is essential for ensuring sustainable mining practices, mitigating environmental and social risks, and safeguarding water resources in mining regions like Córdoba. The findings underscore the importance of adopting global best practices to enhance environmental stewardship and achieve long-term ecological rehabilitation in Colombia's mining sector.

Keywords: Water management, Mine closure practices, legacy issues, community engagement, socioeconomic effects, Colombia

Introduction

The province of Córdoba, located in northern Colombia between the Andes Mountains and the Caribbean Sea, is a region where mining plays a significant economic role, contributing 1.83% to the regional GDP. Key minerals extracted include coal, gold, nickel, limestone, and building materials, with emerging interest in copper production. As of 2017, there were 146 active mining contracts, predominantly for building materials (42%) and coal (15%), alongside gold (26%) and

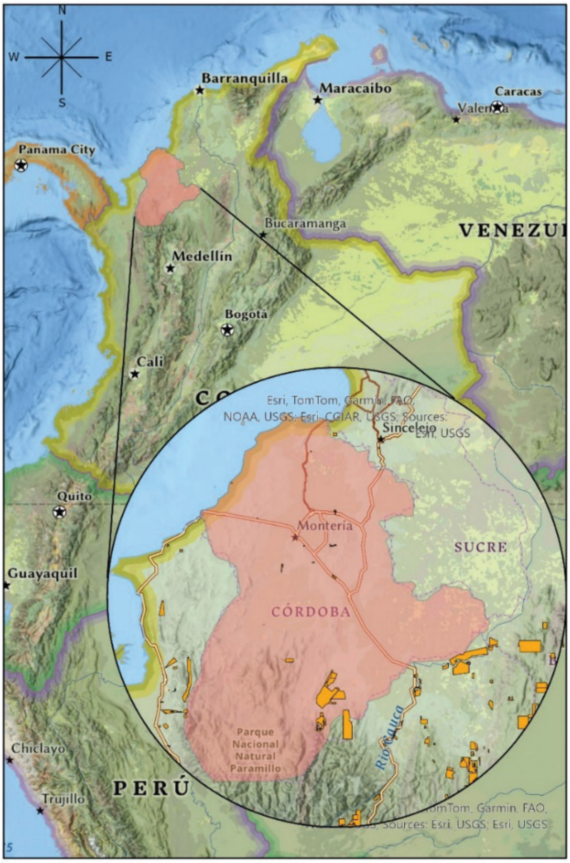

Figure 1 *Geographic location of the Córdoba province - Colombia. Source: National Mining Agency (ANM), Colombia.*

nickel (4%). However, the sector faces growing challenges, including environmental degradation, particularly in water resources, exacerbated by informal mining activities and outdated regulatory frameworks.Water management in mining has become a critical issue in Córdoba, with documented cases of uncontrolled discharge of contaminated wastewater from coal mines into local water bodies. This has led to negative effects on ecosystems and communities, as mine waters often mix with surface runoff, accumulating in ponds and posing significant environmental and health risks. The lack of robust regulatory mechanisms to address these issues, combined with the rise of illegal mining, has further complicated water resource management in the region.

Colombia's mining sector is governed by the Mining Code (2001) and the Political Constitution (1991), with environmental oversight provided by the Ministry of Environment and Sustainable Development (MADS) through instruments such as Decree 1076 (2015) and guidelines for Environmental Impact Assessments (EIA). Despite recent efforts to modernize regulations, including the 2022 ANLA guide for mine closure, significant gaps remain, particularly in water management, climate change adaptation, and stakeholder engagement. These shortcomings contrast sharply with international standards, such as those from the International Council on Mining and Metals (ICMM) and the Asia-Pacific Economic Cooperation (APEC), which emphasize integrated water management, acid drainage prevention, and post-closure monitoring.

This study examines environmental licenses issued in Córdoba over the past two years, focusing on coal and building materials extraction, to assess compliance with national and international standards. Key areas of analysis include water management, ecological rehabilitation, socioeconomic effects, and air quality, with a particular emphasis on mine closure practices. By identifying gaps and proposing alignment with global best practices, this research aims to contribute to the development of more sustainable and environmentally responsible mining practices in Colombia.

Methods

The study was conducted through an analysis of environmental licenses granted within the last two years in this province by environmental regional authorities. The licenses correspond to medium scale mining projects, as defined in the respective Colombian law: coal up to 850,000 t per year (open pit) or 650,000 t per year (underground) and building materials up to 350,000 m^3 per year (MME 2016). The licenses were analyzed in terms of the current regulation framework in Colombia, including the recently issued guide for the formulation of the closure and abandonment plan that mining users must present in the EIA (ANLA 2022). Due to the evident weakness of the current regulation, closure activities were also compared with guidelines provided by international organizations such as APEC (Asia-Pacific Economic Cooperation) (APEC 2018) and ICMM (International Council on Mining and Metals) (ICMM 2019). This analysis aimed to identify areas of convergence and divergence between local environmental licenses and international mine closure standards in key aspects, including water management, socioeconomic monitoring, ecological rehabilitation, air quality, and terrain stability. The results, also applicable to other regions, highlight a list of aspects that are persistently absent in mine closure plans and could serve as a global reference framework to evaluate the effectiveness and sustainability of mine closure plans in the Córdoba province. This methodological approach facilitated a comprehensive and rigorous assessment, highlighting areas that could benefit from increased alignment with international best practices in mine closure.

The mining regulation framework in Colombia

Colombia's mining sector is regulated primarily by the Mining Code (2001), which governs mineral exploration and exploitation. The National Mining Agency (ANM), under the Ministry of Mines and Energy, oversees mineral resources and grants permits through the approval of a Work and Infrastructure Program (PTO) and the signing of Mining Concession Contracts. Environmental regulation falls under the Ministry of Environment and Sustainable Development (MADS), guided by Decree 1076 (2015), Mining and Environmental Guides (2005), and Terms of Reference for EIA (ANLA, 2016). Both the National Authority of Environmental Licenses (ANLA) and Regional Autonomous Corporations (CARs) issue environmental licenses, but CARs deal with smaller-scale projects.

Mining projects require both a Mining Concession Contract and an Environmental License. The Closure and Abandonment Plan is integrated into the EIA but is not independently requested. While consultation with Indigenous and local communities is mandatory for projects with significant environmental or social repercussions, general community engagement is limited and cannot block project development. Financial assurances are required but are insufficient, with miners obliged to provide environmental policies equivalent to 5% of exploration and construction investments and 10% of production value. These provisions do not adequately cover closure and post-closure costs, highlighting a critical gap in ensuring long-term environmental and financial accountability.

Results

Analysis of mine closure practices

Mine closure practices in Córdoba, Colombia, are guided by comprehensive Final Closure Plans that address physical stabilization, ecological rehabilitation, waste disposal, and facility dismantling, in line with national regulations. However, environmental licenses often lack specificity in critical areas, particularly water management, air quality, socioeconomic monitoring, and stakeholder engagement. The application of the APEC (2018) mine closure checklist reveals significant gaps in current practices. These include the absence of mechanisms to prevent or mitigate acid and mine drainage, insufficient monitoring of water resources during and after closure, and inadequate financial assurances to cover long-term liabilities, such as water treatment and site maintenance. A key deficiency is the lack of detailed strategies for water management, particularly in preventing acid mine drainage (AMD), which can persist for decades if not properly addressed. International guidelines, such as those from the ICMM (2019), emphasize the need for integrated water management from the early stages of mining operations, including measures to protect water resources and monitor water quality post-closure. In contrast, current practices in Córdoba often fail to include site-specific water monitoring plans, such as tracking pH levels, potentially toxic metals concentrations, and total dissolved solids, which are critical for early detection of contamination.

Another area for improvement is the incorporation of climate change considerations into closure plans. Internationally, frameworks like those from ICMM and APEC recommend using climate change models to assess site-specific risks, such as increased rainfall or drought, which could have a great influence on water management and long-term site stability. Colombia's regulatory framework does not yet mandate such assessments, leaving closure plans vulnerable to future climate-related challenges.

Stakeholder engagement is another critical gap. While Colombian regulations require community consultation during the licensing phase, there is no formal mechanism to involve local communities in the verification of closure activities. International best practices, such as those outlined by ICMM, stress the importance of ongoing engagement with stakeholders, including minority groups, to ensure that closure plans align with community expectations and needs. This is particularly important in Córdoba, where mining activities often intersect with vulnerable ecosystems and marginalized communities.

Financial assurances for closure and post-closure activities also fall short. Current regulations require miners to provide environmental policies equivalent to a percentage of project investment, but these amounts are often insufficient to cover long-term liabilities, such as water treatment or ecosystem restoration as they are not directly related to the real nature and extension of the affected area. International standards, such as those from APEC, recommend more robust financial mechanisms, including bonds or trusts, to ensure that funds are available for unforeseen post-closure costs.

The 2022 ANLA guide introduces improvements by recommending the inclusion of climate change, circular economy, and risk analysis in closure plans. However, its non-binding nature limits its influence on licensing decisions. To address these gaps, Colombia must strengthen its regulatory framework by aligning it with international best practices, particularly in water management, climate change adaptation, stakeholder engagement, and financial assurances. These measures are essential for ensuring sustainable mine closure and minimizing long-term environmental and social risks in Córdoba and other mining regions.

Water use monitoring and management

Despite the frequent reference to water quality and quality control, the closure plans show a weakness in the implementation of an appropriate set of indicators, especially in the case of groundwater. The effective monitoring of water and terrain during closure and post-closure phases is imperative to ensure environmental integrity and site stability. However, the closure activities described in the mining license fail to include strategies for water resourcing, management, and monitoring. This represents a significant gap when compared to international standards. The "Integrated Mine Closure: Good Practice Guide" of the International Council on Mining and Metals (ICMM, 2019) emphasizes that closure planning must incorporate water management from the early stages, including measures for acid drainage prevention and water resource protection. However, current closure practices in Córdoba do not include any detailed and clear strategies to address these critical aspects.

In addition to these deficiencies, current mine closure plans do not specify any methodologies for addressing potential effects on the hydrological balance and aquifer connectivity, which are essential for long-term water resource sustainability. International standards, such as those outlined by ICMM, emphasize the need for hydrogeological modeling to predict changes in groundwater flow post-closure and to mitigate potential contamination risks. Additionally, the absence of predictive models for water contamination and advanced risk assessment methodologies, as recommended by APEC, limits the ability to anticipate and proactively manage long-term water quality challenges. Furthermore, closure plans fail to require the implementation of passive water treatment systems, such as artificial wetlands and metal retention systems, which are widely recognized by ICMM and APEC as cost-effective, sustainable solutions for managing contaminated mine water over extended periods. Strengthening these aspects within the regulatory framework would significantly enhance the effectiveness of water management strategies in post-mining landscapes.

A deficient water management strategy in mine closure can lead to contamination of surface and groundwater sources, with long-term consequences for local communities and dependent ecosystems. Acid mine drainage, for instance, can persist for decades if preventive measures are not adequately implemented. The "Mine Closure Checklist for Governments" from APEC (2018) underlines the necessity of evaluating and mitigating these risks to safeguard water quality after mine closure. Without robust control mechanisms, mining sites may become sources of perpetual environmental liabilities, requiring expensive remediation efforts and posing significant socio-environmental risks.

A robust post-closure monitoring program is essential to ensure long-term site stability and environmental sustainability. According to ICMM (2019), an effective monitoring framework should include parameters such as pH, potentially toxic metals concentrations, and total dissolved solids, with site-specific sampling frequencies tailored to local hydrological conditions. However, current closure plans in Córdoba lack explicit guidelines on these critical aspects. The absence of a comprehensive monitoring approach jeopardizes the ability to detect early warning signs of contamination and implement corrective actions in a timely manner. Addressing these deficiencies by incorporating international best practices will significantly strengthen water management in mine closure plans in Córdoba. Aligning regulatory frameworks with global guidelines will enhance environmental stewardship, mitigate long-term liabilities, and ensure the sustainable rehabilitation of former mining sites.

Conclusions

The analysis of mine closure practices in Córdoba, Colombia, reveals significant gaps in water management, particularly in monitoring, prevention of acid drainage, and long-term water resource protection. Current closure plans lack detailed strategies for groundwater and surface water monitoring, as well as measures to mitigate contamination risks, such as acid mine drainage. This contrasts sharply with international standards, such as those outlined by ICMM and APEC, which emphasize integrated water management from the early stages of mining operations. Without robust water management strategies, mining sites risk becoming sources of perpetual environmental liabilities, threatening local ecosystems and communities.

The study also highlights the broader regulatory weaknesses in Colombia's mine closure framework, including insufficient stakeholder engagement, inadequate financial assurances, and a lack of binding guidelines for post-closure land use. While the 2022 ANLA guide introduces some improvements, its non-binding nature limits its effectiveness. Furthermore, the guide lacks explicit methodologies and technical specifications necessary to ensure effective hydrological rehabilitation and long-term water quality protection. The absence of clear, enforceable measures leaves room for inconsistent implementation, undermining the sustainability of closure practices. To ensure sustainable mining practices, Colombia must align its regulatory framework with international best practices, particularly in water management, and enforce stricter compliance to mitigate long-term environmental and social risks. Addressing these gaps is crucial for achieving environmental integrity and safeguarding water resources in mining regions like Córdoba.

References

MME (2001). MINISTRY OF MINES AND ENERGY. Colombian Mining Code Law 685 of 2001. Bogotá, Colombia. 40 p.

MME (2016). MINISTRY OF MINES AND ENERGY. Decree 1666 of 2016, Bogotá, Colombia. 4 p.

ANLA (2022). Guide for the preparation of closure and abandonment plans of mining projects. Bogotá, Colombia. 2022. 55 p.

APEC (2018). Mine Closure Checklist for Governments. Asia Pacific Economic Consortium. (APEC), Canada. 70p.

ICMM (2019). Integrated Mine Closure: Good Practice Guide. 2nd edition. International Council on Mining and Metals (ICMM), London, UK. 132p.

MADS (2015). MINISTRY OF ENVIRONMENT AND SUSTAINABLE DEVELOPMENT (MADS). Decree 1076 of 2015. Bogotá, Colombia. 1055 p.

MME (2005). MINISTRY OF MINES AND ENERGY. Mining Environmental Guides – Exploration, exploitation, Beneficiation and Transformation. Bogotá, Colombia. 360 p.

ANLA (2016). Terms of Reference for the preparation of EIA. Agencia Nacional de Licencias Ambientales (ANLA). Ministry of Environment and Sustainable Development. Bogotá, Colombia. 159 p.

Multitemporal Remote Sensing Assessment of Fluvial Dynamics and the Effects of Alluvial mining in the Guaviare River Basin, Colombia

Gustavo Neira-Arenas[1], Sebastián Navarro-Martínez[2]

[1]Universidad Nacional de Colombia – Facultad de Minas, Medellín, Colombia – gneira@unal.edu.co, ORCID 0000-0003-1178-1917

[2]Universidad Nacional de Colombia – Facultad de Minas, Medellín, Colombia -sebastian.navarro@eia.edu.co

Abstract

According to official figures, aggregate extraction has intensified along the Guaviare River to meet Colombia's growing infrastructure demands (ANM 2024), raising concerns about its geomorphological stability and the socio-environmental wellbeing of riverine communities. This study combines multitemporal Landsat imagery (1984–2023) with official mining data to evaluate channel migration, erosion, and deposition across a 230 km river reach. Seven meanders were classified according to their distance from principal mining hotspots – high, medium, and low influence – revealing that meanders nearest to extraction sites exhibit up to 60–70 % higher migration rates and nearly double the erosion observed in more distant meanders. A distinct peak in deposition at a medium-influence meander (24.5 km downstream) further underscores the heterogeneity of fluvial responses, which are affected by both direct mining impacts and localized sediment accumulation. Temporal analyses demonstrate a threefold increase in erosion between 2008 and 2013, coinciding with the onset of heightened production (~2012), followed by elevated deposition from 2013 to 2018 and a renewed surge in erosion after 2018. Minimal correlation with deforestation or river discharge levels suggests that aggregate mining is the primary driver of these channel adjustments. However, potential unreported or illicit extraction beyond officially documented sites complicates the assessment, indicating that official records may underestimate the full extent of mining-related impacts. The results highlight an urgent need for integrated management and enforcement strategies that balance economic imperatives with ecological and cultural preservation along the Guaviare River.

Keywords: Alluvial mining, Guaviare river, Remote sensing, Gravel extraction, fluvial dynamics, river water

Introduction

The extraction of sand and gravel, essential materials for global infrastructure development (Padmalal and Maya 2014), has intensified in Colombia due to the growing demand from urbanization, road construction, and civil engineering projects. The Guaviare River, strategically located between the Orinoquía and Amazon regions, plays a critical role as a source of these materials (Minambiente 2023). However, this activity has led to significant socio-environmental challenges, including alterations to river morphology, biodiversity loss, and conflicts with indigenous communities who depend on these ecosystems for their livelihoods(Kondolf 1994, 1997; Kondolf et al. 2002). Despite existing regulatory frameworks, gaps in enforcement and a lack of detailed, multitemporal data hinder effective management of aggregate mining along the Guaviare River. This study leverages remote sensing methodologies, including Landsat (Nagel et al. 2023) imagery from 1984 to 2023, to analyze river dynamics – erosion, sedimentation, and channel migration –

over time. By correlating these changes with extraction intensity and socio-environmental impacts, this research aims to provide evidence to inform sustainable policies and conservation strategies that balance economic development with ecological and cultural preservation.

Methods

The primary dataset consisted of Landsat images acquired from the earliest available date through the present, covering a five-year period. The study area (see Fig. 1) begins at the headwaters of the Guaviare River and extends 230 km downstream, encompassing 170,495.67 hectares distributed across the departments of Meta and Guaviare and the municipalities of San José de Guaviare, Mapiripán, and Puerto Arturo. Within this region, mining hotspots along the river were identified, including key stakeholders, and all relevant features were georeferenced. Special attention was given to estimating extraction volumes, although these figures are incomplete due to the prevalence of informal mining activities that are not reported to government authorities.

Subsequent to data acquisition, a preprocessing stage was carried out to ensure optimal image quality. This included applying cubic resampling to smooth the imagery, adjusting contrast parameters, and using indices such as NWDI (Gao 1996) , MNDWI (Zhou et al. 2015), and various modifications thereof to enhance water feature delineation. The central channel lines and both left and right riverbanks were then manually delineated for every available image within the demarcated area. River migration, erosion and deposition were subsequently determined by overlaying channel riverbanks and centerlines from two different time periods and analyzing channel migration directions.

All riverine areas within the defined study region were then classified. Seven meanders were selected based on their more pronounced and quantifiable meandering behaviors, facilitating measurement and trend analysis; in contrast, other sections exhibited strongly braided morphologies that obscured the identification of clear patterns. Mining-related geographic information was integrated into this analysis to delineate

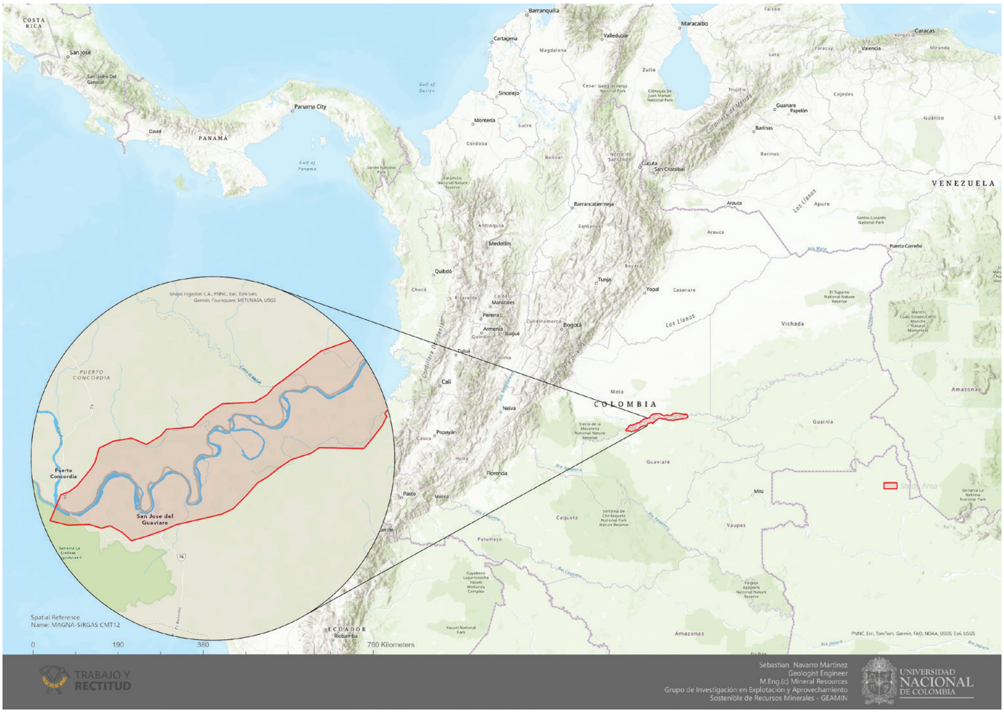

Figure 1 Study Area – a segment of the Guaviare River, Colombia.

areas according to their mining activity. A **direct influence zone** was established for regions where mining titles and active operations intersect the river channel. This zone captures the immediate sections of the channel where extraction activities occur. From this direct zone, a **high-influence zone** was defined by referencing adjacent meanders, resulting in the selection of three proportionally representative meanders near titled areas. Although these meanders are somewhat removed from direct operations, their proximity suggests potential exposure to certain mining-related impacts.

Two **medium-influence zones** were then demarcated. One encompasses the urban center of the municipality of Mariripan; its classification as a medium-influence zone stems from nearby applications for ilegal mining and the likely extraction of construction materials such as sand. The other medium-influence zone, further downstream, includes three additional meanders situated at greater distances from the principal mining activities at San José del Guaviare, where more diffuse impacts may be observed. Finally, two low-influence zones were identified, representing the areas farthest from both mining zones and the meanders in the high- and medium-influence zones. While these more distant areas are less likely to be affected, potential long-term impacts cannot be entirely ruled out, albeit at lower intensities relative to nearer regions.

All available datasets were ultimately integrated, including annual mining production data, total erosion (for each bank), total deposition, and river migration metrics. Hydrological monitoring stations were also considered to investigate possible correlations between fluvial behavior and hydrological trends(IDEAM 2024), thereby providing a more comprehensive analysis of the Guaviare River's response to mining activity and natural geomorphological processes.

Results

The results of this study reveal several notable patterns regarding the spatial distribution of meanders, fluctuations in mining extraction volumes, channel migration rates, and accompanying processes of erosion and deposition. First, the proximity of each meander to the primary mining hotspot allowed for a classification into high-, medium-, and low-influence zones. In Fig. 2, Meanders 1 (4 km downstream) and 2 (8.9 km downstream) were categorized as high-influence due to their relative closeness to intensive extraction areas, whereas Meander 3 (24.5 km downstream) exhibited medium influence, and Meanders 4 (54.8 km) and 5 (63 km), as in Fig. 3, were considered low-influence zones. Although Meanders 6 (152 km) and 7 (205 km) lie substantially farther from the documented mining focal point, reports of illicit or unregulated mining between Meanders 5 and 6 introduce uncertainty, suggesting that these more distant segments may also experience some level of mining-related impacts.

Official data from the National Mining Agency (ANM) on material extraction for the municipality of San José del Guaviare indicate that production volumes of riverine materials followed a rising trend from 2012 through 2019, peaking near the end of this interval, then declining until 2022, and rebounding in 2023. These fluctuations likely reflect shifting economic conditions, regulations, and possibly technological changes influencing both legal and unreported mining activities. Given the potential for unregistered extraction in remote areas, the official records should be interpreted as indicative rather

Table 1 Some of the Landsat images used are shown, with more than 30 in total.

landsat image	Source
LMO5_L1TP_007058_19841209 20200902 _02 T2	https://earthexplorer.usgs.gov/
LTO5_L1TP_006058_19850103_20200918_02 T1	https://earthexplorer.usgs.gov/
LTO4_L25P_006058_19880104_20200917_02 T1	https://earthexplorer.usgs.gov/
LEO7_L1TP_007058_20030104_20200916_02 T1	https://earthexplorer.usgs.gov/
LEO7_L2SP_007058_20080203_20200913_02 T1	https://earthexplorer.usgs.gov/

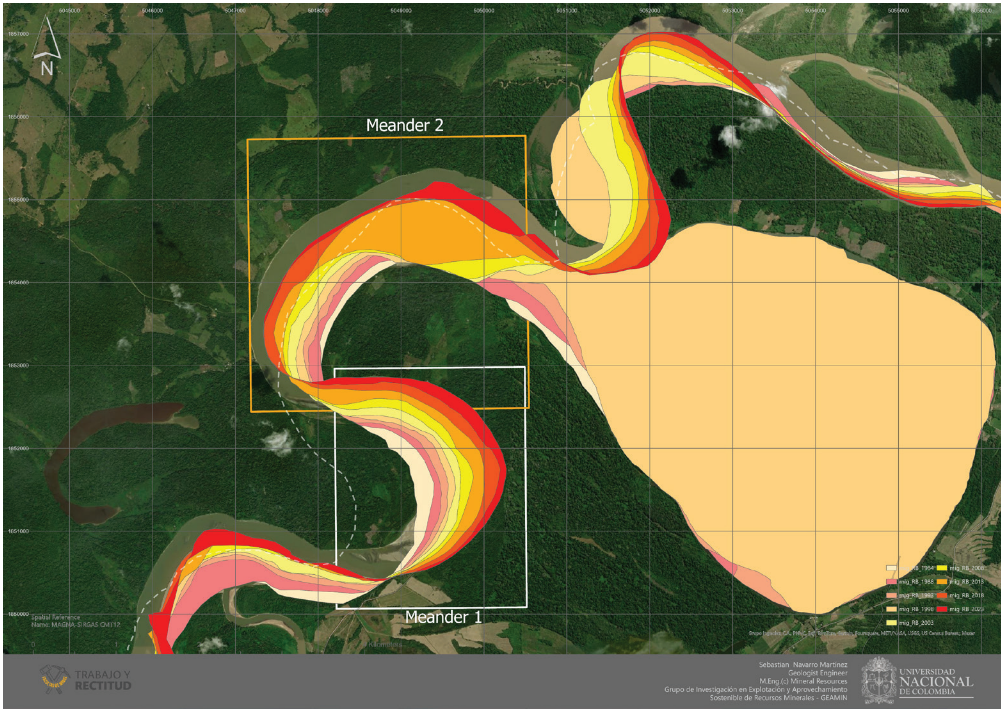

***Figure 2** High mining influence segment: the right bank migration of the river was calculated by analyzing differences between two distinct time periods. Same methodology was applied to assess the migration of the centerline and the left bank.*

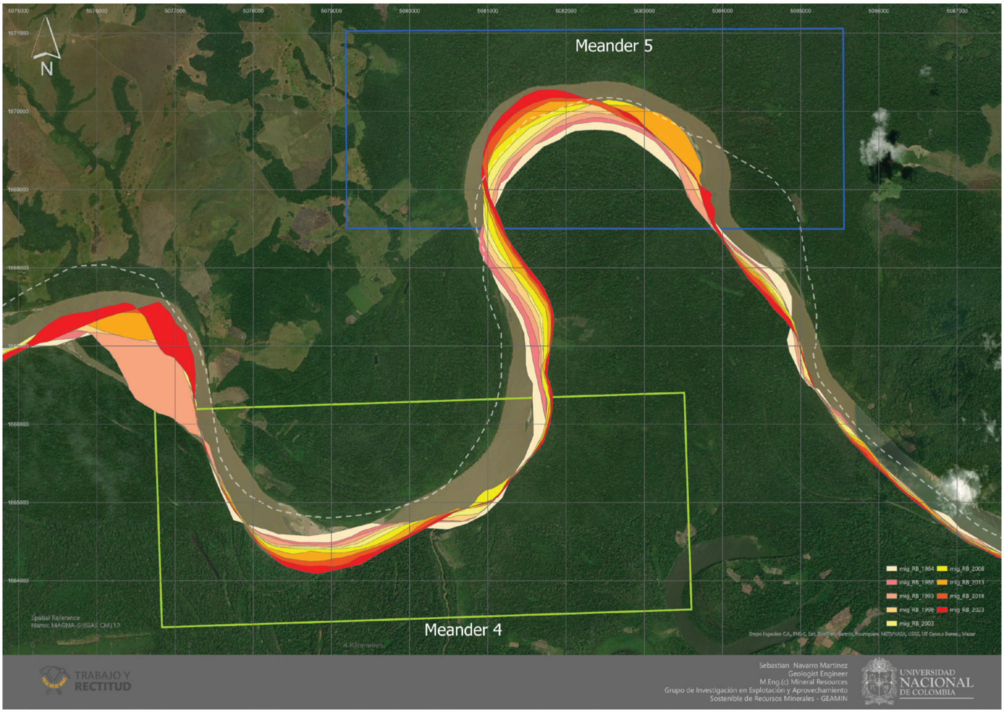

***Figure 3** Low mining influence segment – Meanders 4 and 5.*

than exhaustive. Meanders with high mining influence (1 and 2) show 7% more migration than the meander with medium influence (3) and 64% more than the average of those with low influence (4 and 5). In terms of erosion, the high-influence meanders nearly double the values observed in those with low influence and exceed meander 3 by 25%. In contrast, regarding deposition, meander 3 exhibits such a significant peak (particularly from 2013 to 2018) that it surpasses the average of meanders 1 and 2 by 2% and almost doubles the values of meanders 4 and 5. With respect to migration, between 1984 and 1988 and between 1988 and 1993 it nearly doubles (from about 0.96 to about 1.48 million m^2), while from 1988 to 1993 and from 1993 to 1998 it decreases. Until 2003, the values remain around 1.2 to 1.4 million m^2. Then, between 2003 and 2008 and between 2008 and 2013 there is a jump from about 1.40 to about 1.75 million m^2. From 2008–2013 to 2013–2018, there is a slight increase (from about 1.75 million m^2 to about 1.78 million m^2), followed by a decrease from 2013–2018 to 2018–2023 (from about 1.78 million m^2 to about 1.52 million m^2). These phases partially coincide with mining extraction between 2012 and 2019, which covers the second half of 2008–2013 and almost all of 2013–2018, during which migration went from about 1.75 to about 1.78 million m^2 and remained stable. Subsequently, in 2018–2023, migration declined, mirroring the drop in extraction between 2020 and 2022 despite the uptick in 2023. Erosion, meanwhile, gradually increases up to 2003 (1.26 million m^2, then 1.67 million m^2, 1.66 million m^2, and 1.91 million m^2) and remains high (about 1.85 million m^2) in 2003–2008. However, in 2008–2013 it shows a peak of about 5.22 million m^2—almost triple the previous period—then decreases to 2.00 million m^2 in 2013–2018, and rises again to about 4.20 million m^2 in 2018–2023. Regarding deposition, it fluctuates around 1.7 to 2.5 million m^2 up to 2008, stands at moderate levels (about 2.27 million m^2) from 2008–2013, and then surges (about 5.10 million m^2) in 2013–2018, doubling the previous record. Finally, it drops to about 1.41 million m^2 in 2018–2023, the lowest value in the entire series.

Additionally, certain observations suggest that unreported mining activity may be influencing fluvial dynamics beyond the officially recognized hotspots (Fig. 4). High values of erosion and pronounced trends of increased erosion and deposition in Meanders 6 and 7, which lie far downstream, could be indicators of undocumented or illegal mining, potentially distorting the geomorphic patterns observed in these reaches. Field observations also showed that when a meander cutoff occurs, downstream scouring can intensify; however, while there was a recent cutoff near Meanders 6 and 7, the trend toward higher erosion and deposition appears to have been established beforehand. A similar cutoff event took place near Meander 3 in the medium-influence zone, briefly altering local fluvial dynamics. In that case, channel processes stabilized after a short period, illustrating the variability and resilience of the river's response to both natural adjustments and anthropogenic impacts.

Deforestation processes were also analyzed using the same images to determine whether the observed changes in fluvial dynamics were linked to deforestation or were intrinsic river processes. No significant deforestation was identified in the selected meanders during the periods of heightened erosion. Additionally, river levels and discharge, obtained from IDEAM stations (Institute of Hydrology, Meteorology, and Environmental Studies of Colombia), were examined; however, no correlation was found between river levels and the intensification of fluvial dynamics.

Conclusions

This research highlights the multifaceted influences of aggregate mining on the Guaviare River. Proximity to the principal extraction hotspot correlates strongly with greater channel migration and erosion, with Meanders 1 and 2 showing migration rates approximately 7 % higher than those of Meander 3 and 64 % higher than low-influence meanders. Erosion near these high-influence meanders is nearly double that of low-influence meanders and roughly 25 % greater than at Meander 3. In contrast,

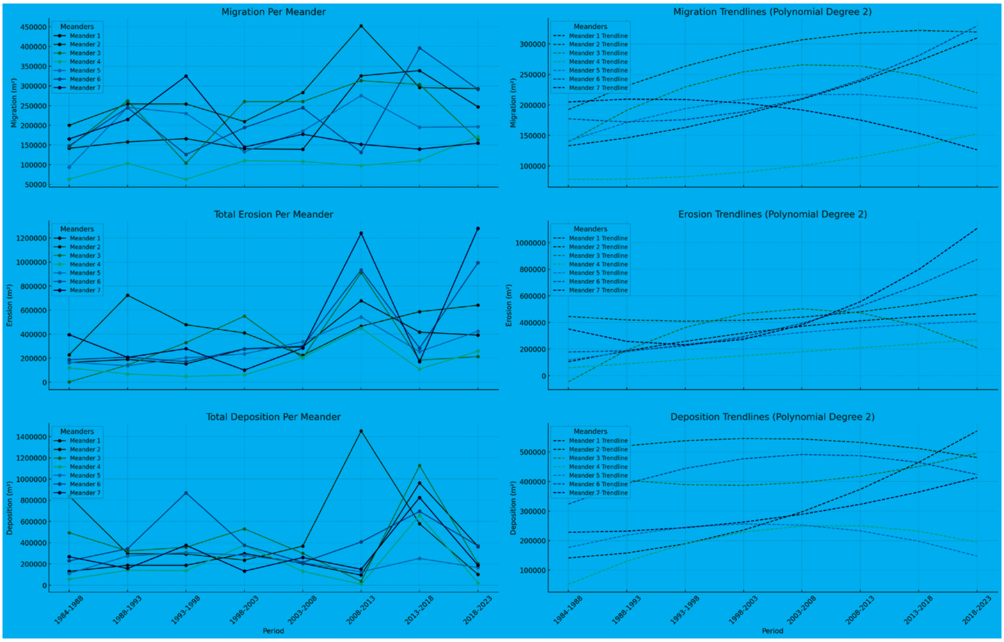

Figure 4 Graphs of Fluvial Dynamics Analysis.

Meander 3 exhibits intense deposition – particularly during 2013–2018 – that exceeds by about 2 % the average of Meanders 1 and 2 and nearly doubles the values for Meanders 4 and 5, suggesting localized sediment accumulation driven by both natural processes and mining pressures.

The temporal patterns echo the official ANM data: between 2012 and 2019, extraction volumes increased substantially, coinciding with marked shifts in channel morphology. From 2008 to 2013, erosion rates tripled relative to previous averages; from 2013 to 2018, deposition peaked, while erosion temporarily decreased; and after 2018, erosion again intensified as extraction levels rebounded. These fluctuations underscore the non-linear nature of fluvial response to mining activities. Further downstream, high erosion and deposition values in Meanders 6 and 7 hint at unregulated mining, suggesting that official records may underestimate the actual magnitude and spatial extent of extraction impacts.

Additional analyses reveal minimal deforestation within the examined meanders during the periods of heightened erosion, indicating that the observed fluvial changes are not primarily linked to land-cover alterations. Likewise, correlations with river discharge or levels from IDEAM stations were negligible, implying that mining-driven channel adjustments surpass the influence of short-term hydrological variations. Overall, these findings underscore the necessity for integrated management approaches – encompassing remote sensing, field verification, and robust regulatory oversight – to maintain the ecological integrity of the Guaviare River while acknowledging its central role in economic development.

References

ANM (2024) ANM Volumen de Explotación de Minerales Asociados a Pagos de Regalías | Datos Abiertos Colombia. https://www.datos.gov.co/Minas-y-Energ-a/ANM-Vol-men-de-Explotaci-n-de-Minerales-Asociados-/r85m-vv6c/about_data

Gao BC (1996) NDWI – A normalized difference water index for remote sensing of vegetation liquid water from space. Remote Sens Environ 58:257–266. https://doi.org/10.1016/S0034-4257(96)00067-3

IDEAM (2024) Consulta y Descarga de Datos Hidrometeorológicos. http://dhime.ideam.gov.co/atencionciudadano/

Kondolf G (1994) Geomorphic and environmental effects of instream gravel mining. Landsc Urban Plan 28:225–243. https://doi.org/10.1016/0169-2046(94)90010-8

Kondolf GM (1997) Hungry water: Effects of dams and gravel mining on river channels. Environ Manage 21:533–551. https://doi.org/10.1007/S002679900048/METRICS

Kondolf GM, Smeltzer M, Kimball L (2002) Freshwater Gravel Mining and Dredging Issues

minambiente (2023) Los ríos, claves para la salud del planeta – https://www.minambiente.gov.co/galeria-imagenes-minambiente/

Nagel GW, Darby SE, Leyland J (2023) The use of satellite remote sensing for exploring river meander migration. Earth Sci Rev 247:104607. https://doi.org/10.1016/J.EARSCIREV.2023.104607

Padmalal D, Maya K (2014) Environmental Science and Engineering Sand Mining Environmental Impacts and Selected Case Studies

Zhou W, Li Z, Ji S, et al (2015) A New Index Model NDVI-MNDWI for Water Object Extraction in Hybrid Area. Communications in Computer and Information Science 482:513–519. https://doi.org/10.1007/978-3-662-45737-5_51

Uranium Reduction in Mine Water via Glycerol Biostimulation: Spectroscopic Evidence of U(IV) Formation

Antonio M. Newman-Portela[1], Andrea Kassahun[2], Björn Drobot[1], Robin Steudtner[1], Johannes Raff[1], Mohamed L. Merroun[3], Evelyn Krawczyk-Bärsch[1]

[1]*Helmholtz-Zentrum Dresden-Rossendorf e.V., Institute of Resource Ecology, Dresden, Germany. a.newman-portela@hzdr.de, ORCID: 0000-0001-9381-1280; b.drobot@hzdr.de, ORCID: 0000-0003-1245-0466; r.steudtner@hzdr.de, ORCID: 0000-0002-3103-9587; j.raff@hzdr.de, ORCID: 0000-0002-0520-3611; e.krawczyk-baersch@hzdr.de, ORCID: 0000-0001-8249-0506*

[2]*WISMUT GmbH, Chemnitz, Germany. a.kassahun@wismut.de*

[3]*University of Granada, Faculty of Science, Department of Microbiology, Granada, Spain. merroun@ugr.es, ORCID: 0000-0003-4553-5976*

Abstract

Uranium (U) contamination in mine water remains a challenge despite conventional remediation efforts. This study explores the biostimulation of the indigenous microbial community in Schlema-Alberoda mine water using glycerol, vanillic acid, and gluconic acid as electron donors to promote microbial U(VI) reduction. Glycerol demonstrated the highest efficiency, leading to a near-complete decrease in U concentration in the supernatant. Cryo-TRLFS and UV/Vis analyses confirmed the reduction of U(VI) to U(IV) through glycerol. The results highlight the potential of biostimulation for U remediation and its viability as an efficient and sustainable strategy for low-level U contaminated mine water.

Keywords: Uranium, mine water, bioremediation, spectroscopy, tetravalent uranium

Introduction

Anthropogenic activities have left radionuclide-contaminated environments worldwide and uranium (U) contamination from mining activities poses serious environmental and human health risks. The Schlema-Alberoda mine (WISMUT GmbH, Saxony, Germany) was a major U mining site until the 1990s. After mining ceased, conventional remediation efforts were applied to mitigate U contamination in mine water (Newman-Portela *et al.* 2024). However, U remains in the mine water at 1 mg/L. In aqueous environments U exists mainly as soluble U(VI) and less soluble U(IV). Under oxidizing conditions, U(VI) forms uranyl (UO_2^{2+}) complexes, enhancing mobility, whereas under reducing conditions, U(IV) precipitates as uraninite (UO_2), limiting its transport.

Over the past three decades, bioremediation has emerged as a cost-effective and efficient strategy for addressing U contamination (Banala *et al.* 2021). Its success relies on biogeochemical processes mediated by microorganisms, which can alter U solubility through different biochemical interactions. The primary approaches for U bioremediation involve biomineralization in oxic environments and enzymatic reduction under anoxic conditions (Banala *et al.* 2021). Additionally, microbial enzymatic U reduction can be enhanced by the addition of electron donors, accelerating environmental detoxification and improving the overall bioremediation process (Newsome *et al.* 2014). Therefore, bioremediation presents itself as a viable, sustainable, and scalable approach, offering an effective microbiological technology to complement conventional remediation techniques.

Schlema-Alberoda mine water has a circumneutral pH and redox potential that favor U mobility. It contains high sulfate and iron concentrations, with a diverse microbial community linked to carbon, sulfur, iron, and nitrogen cycles, which may play a role in U cycling. In this study, we investigate the potential of the indigenous microbial community in Schlema-Alberoda to reduce U in mine water contaminated with low U concentrations (1 mg/L) by stimulating its activity with different electron donors (gluconic acid, vanillic acid, and glycerol) in various experiments. Additionally, we assess the effectiveness of glycerol as an electron donor for biostimulation using a spectroscopic approach. The results demonstrate that glycerol is highly effective in stimulating the native microbial community, leading to the near-complete removal of soluble U(VI) and the formation of U(IV).

Methods

The chemical composition of the mine water from a former U mine in Saxony (Germany) was determined by inductively coupled plasma-mass spectrometry (ICP-MS) and high-performance ionic chromatography (HPIC). Microcosms (1 L serum bottles) were prepared with fresh mine water (1 mg/L U) and amended separately with 10 mM glycerol, 10 mM gluconic acid, or 10 mM vanillic acid as electron donors. Additionally, abiotic controls were prepared using sterile mine water from Schlema-Alberoda amended with 10 mM glycerol, vanillic acid, and gluconic acid to evaluate whether these electron donors influenced mine water chemistry. The microcosms were incubated at 28 ± 2 °C for four months in darkness. Redox potential (E_h) and pH were measured, and aliquots were taken to determine U, Fe, As, and SO_4^{2-} concentrations using ICP-MS and HPIC. At the end of the experiment, a black precipitate was observed at the bottom of the glycerol-amended microcosm.

To further investigate the black precipitate using a spectroscopic approach, a new set of biostimulated anaerobic microcosms was established. These microcosms contained Schlema-Alberoda mine water (1 mg/L U) supplemented with 10 mM glycerol. They were incubated at 28 ± 2 °C for four months in darkness. U concentrations were monitored at the end of the experiment using ICP-MS. A microcosm was terminated when the soluble U concentration decreased by 20%, 60%, or 90%. U(VI) in the aqueous phase of the microcosm was investigated using cryo-time-resolved laser fluorescence spectroscopy (cryo-TRLFS). Samples for cryo-TRLFS were collected in single-use 2 mL plastic cuvettes, and measurements were performed under cryogenic conditions using a Nd:YAG pulsed laser system, and luminescence spectra in the wavelength range of 350 to 650 nm were recorded with an iHR550 spectrograph and an amplified CCD-camera system. Ultraviolet–visible (UV/Vis) spectroscopy was used to detect the formation of U(IV) in the black precipitate formed at the bottom of the microcosms during the experiment. Samples were prepared by dissolving the black precipitate in 5 M HCl, and the spectral range between 500 and 750 nm was captured by the Cary 5G UV/Vis-NIR spectrophotometer. An aquo ion U(IV) solution of 100 µM in 5 M HCl was used as the reference spectrum.

Results and discussion

The biostimulation experiments showed a notable decrease of soluble U(VI) in Schlema-Alberoda mine water. The pH values ranged from neutral to slightly basic values (7.00 to 8.01). However, adding glycerol, the E_h of the mine water showed a sharp drop; from 445 mV to −246 mV. Among the tested electron donors, glycerol showed the highest efficiency, achieving nearly complete U(VI) removal (99%), whereas vanillic acid led to a reduction of approximately 90% (Tab. 1). However, in the gluconic acid microcosm, no decrease in U(VI) concentration was observed. The electron donor may promote the growth of bacteria involved in glycerol fermentation, leading to the production of organic compounds that can be utilized by sulfate-reducing bacteria (SRB) or iron-reducing bacteria (IRB), which play a key role in U reduction. For example, IRB such as *Geobacter* can utilize acetate as an electron donor for U(VI) reduction (Anderson *et al.* 2003). Similarly, bacteria such as *Desulfovibrio*, an SRB also capable of iron reduction, can oxidize glycerol while coupling it to sulfate reduction (Santos *et al.* 2018; Lovley *et al.* 1993). Indirectly, the sulfide produced in this process could facilitate the indirect reduction of U(VI) to U(IV) (Boonchayaanant *et al.* 2010). However, further studies on the microbial community are needed to identify the bacterial genera involved in this process.

On the other hand, no notable changes were observed in the abiotic controls. This is because vanillic acid and gluconic acid do not form stable complexes with U(VI) under the given physicochemical conditions, as thermodynamic speciation calculations reported by Newman-Portela *et al.* (2024) predict no coordination between these compounds and U. In the case of glycerol, there were no thermodynamic data for complexation with U(VI). However, no formation of U(VI)-glycerol complexes was expected since glycerol exhibits only three hydroxyl groups that do not deprotonate in aqueous solutions (Newman-Portela *et al.* 2024).

Cryo-TRLFS analysis (Fig. 1) reveals distinct fluorescence bands at 480, 501, 519, 542, and 566 nm, matching the spectral features previously identified for $Ca_2UO_2(CO_3)_3(aq)$ (Newman-Portela *et al.* 2024). The UV/Vis spectra (Fig. 2) show a well-defined peak at 650 nm, which aligns with the characteristic signal of U(IV) when compared to the reference. Additionally, a peak at 560 nm is observed, consistent with prior reports of U(IV) formation (Gao and Francis 2008). A separate peak between 675 nm and 700 nm suggests potential U(IV) interaction with chloride, likely influenced by the elevated HCl concentration used during sample preparation (Tutschku *et al.* 2003).

Overall, the UV/Vis spectra provide clear evidence of U(IV) formation, with its bands becoming more pronounced as soluble U(VI) decreases in the supernatant (Fig. 2). In contrast, the cryo-TRLFS spectra exhibit a reduction in fluorescence intensity as soluble U(VI) decreases (Fig. 1). These spectral changes clearly indicate a progressive transformation of U(VI) to U(IV) under biostimulated conditions using glycerol as electron donor, supporting the effectiveness of the selected electron donors in promoting microbial U(VI) reduction to U(IV). The observed shifts in spectral features are consistent with previous studies on U speciation, reinforcing the role of microbial activity in controlling U mobility. Further investigations using advanced spectroscopic and microscopic techniques, along with microbial community analyses, could offer a more comprehensive understanding of the mechanisms governing U bioreduction in mine water environments.

Conclusions

This study demonstrates the effectiveness of biostimulation in promoting U(VI) reduction in Schlema-Alberoda mine water. Among the tested electron donors, glycerol was the most efficient, leading to a near-complete removal of soluble U(VI) and the formation of U(IV). The sharp decrease in redox potential upon glycerol addition suggests the stimulation of anaerobic microbial activity, likely involving sulfate- and iron-reducing bacteria. The UV/Vis and cryo-TRLFS analyses confirm the

Table 1 *Geochemical parameters observed in the original mine water and at the end of the experiment after the electron donor biostimulation (glycerol, vanillic acid and gluconic acid). Data presented in mg/L and* E_h *in mV.*

	Schlema-Alberoda mine water	Glycerol	Vanillic Acid	Gluconic Acid
pH	7.32	7.99	7.00	8.01
E_h	445	-246	218	-248
Fe	0.99	0.05	0.32	0.35
As	0.92	0.46	0.40	0.17
U	1.05	0.01	0.10	1.37
SO_4^{2-}	335	141	338	144

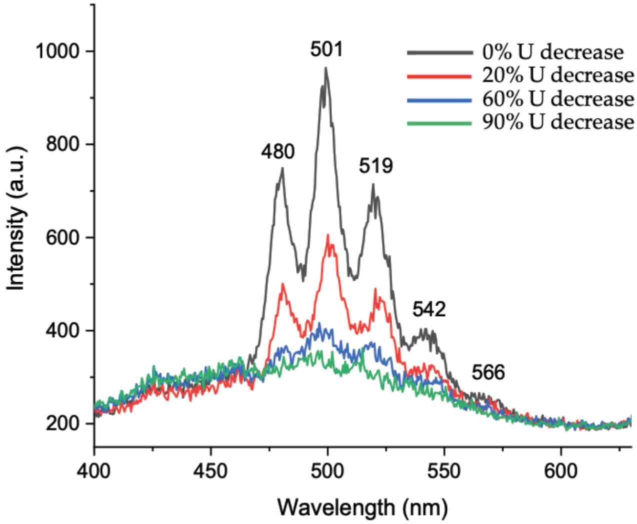

Figure 1 *Cryo-TRLFS spectra of the aqueous phase (supernatant) at different stages of uranium(VI) reduction in glycerol-amended microcosms. The sample with no U decrease in the supernatant is shown in black, while samples with 20%, 60%, and 90% uranium decrease are represented in red, blue, and green, respectively.*

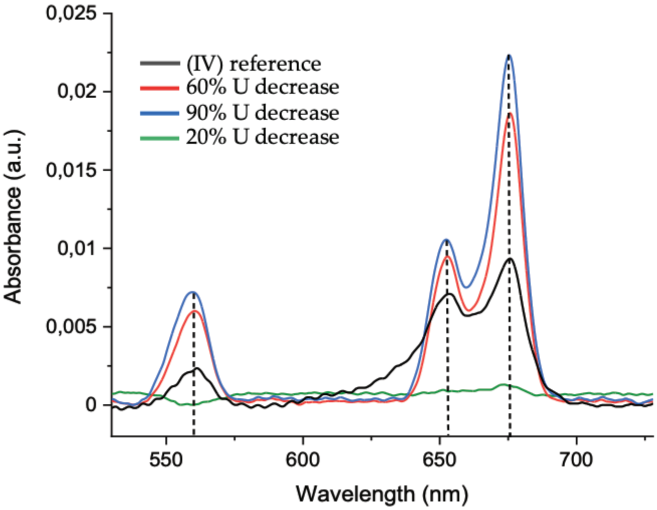

Figure 2 *UV/Vis absorption spectra of the black precipitate samples with different levels of uranium decrease at the supernatant in glycerol-amended microcosms. The U(IV) reference is shown in black, while samples with 20%, 60%, and 90% uranium decrease are represented in green, red, and blue, respectively.*

reduction of U(VI) to U(IV), highlighting the role of microbial processes in controlling U mobility. The findings emphasize the potential of bioremediation as a complementary strategy to conventional remediation techniques for low-level U-contaminated environments. However, further studies on the microbial community composition and metabolic pathways are necessary to refine biostimulation strategies and optimize U immobilization. Additionally, the long-term stability of reduced U(IV) should be evaluated to ensure its environmental persistence and effectiveness as a remediation approach.

Acknowledgements

WISMUT GmbH (Germany) is gratefully acknowledged by the authors for providing the case study, sharing relevant remediation site information, and technical support during the sampling campaigns. Furthermore, the authors express their appreciation to the staff at Helmholtz-Zentrum Dresden-Rossendorf (Germany), especially Sabrina Beutner and Sylvia Schöne for analytical measurements. This research was funded by the RadoNorm project under the Euratom research and training programme 2019–2020 (grant agreement No 900009). Additional support was provided by the mobility grants programme of the European Radioecology Alliance (ALLIANCE).

References

Anderson RT, Vrionis HA, Ortiz-Bernad I, Resch CT, Long PE, Dayvault R, Karp K, Marutzky S, Metzler DR, Peacock A, White DC, Lowe M, Lovley DR (2003) Stimulating the in situ activity of *Geobacter* species to remove uranium from the groundwater of a uranium-contaminated aquifer. *Appl Environ Microbiol* 69(10):5884–5891. doi:10.1128/AEM.69.10.5884-5891.2003

Banala UK, Das NPI, Toleti SR (2021) Microbial interactions with uranium: Towards an effective bioremediation approach. *Environ Technol Innov* 21:101254. doi:10.1016/j.eti.2020.101254

Boonchayaanant B, Gu B, Wang W, Ortiz ME, Criddle CS (2010) Can microbially-generated hydrogen sulfide account for the rates of U(VI) reduction by a sulfate-reducing bacterium? *Biodegradation* 21(1):81–95. doi:10.1007/s10532-009-9283-x

Gao W, Francis AJ (2008) Reduction of uranium (VI) to uranium (IV) by *Clostridia*. *Appl Environ Microbiol* 74:4580–4584. doi:10.1128/aem.00239-08

Lovley DR, Roden EE, Phillips EJP, Woodward JC (1993) Enzymatic iron and uranium reduction by sulfate-reducing bacteria. *Mar Geol* 113(1–2):41–53. doi:10.1016/0025-3227(93)90148-O

Newman-Portela AM, Krawczyk-Bärsch E, Lopez-Fernandez M, Bok F, Kassahun A, Drobot B, Steudtner R, Stumpf T, Raff J, Merroun ML (2023) Biostimulation of indigenous microbes for uranium bioremediation in former U mine water: multidisciplinary approach assessment. *Environ Sci Pollut Res*. doi: 10.1007/s11356-023-31530-4

Newsome L, Morris K, Lloyd JR (2014) The biogeochemistry and bioremediation of uranium and other priority radionuclides. *Chem Geol* 363:164–184. doi:10.1016/j.chemgeo.2013.10.034

Santos SC, Liebensteiner MG, van Gelder AH, Dimitrov MR, Almeida PF, Quintella CM, Stams AJM, Sánchez-Andrea I (2018) Bacterial glycerol oxidation coupled to sulfate reduction at neutral and acidic pH. *J Gen Appl Microbiol* 64(1):1–8. doi:10.2323/jgam.2017.02.009

Tutschku J, Hennig C, Geipel G, Bernhard G (2004) UV-Vis measurements of uranium (VI) and uranium (IV) in concentrated chloride solution prepared with the electrochemical cell. FZR – IRC *Annu Rep* 12. Retrieved from: https://www.hzdr.de/db/Cms?pOid=25166&pNid=142

Geochemical Modelling of Sulfur Cycling Processes During Mine Water Rebound in Former Hard Coal Mines of the Ruhr and Saar Regions, Germany

Simon E. Nikutta[1], Barbara M. A. Teichert[1], Henning Jasnowski-Peters[1], Harald Strauss[2], Sebastian Westermann[1]

[1]*Research Center of Post-Mining, Technische Hochschule Georg Agricola University, , 44787 Bochum, Germany, simon.nikutta@thga.de*

[2]*Universität Münster, Institut für Geologie und Paläontologie, 48149 Münster, Germany, hstrauss@uni-muenster.de, ORCID 0000-0003-2639-1225*

Abstract

A controlled mine water rebound is conducted in former hard coal mines of the Ruhr and Saar regions. To avoid risks for humans and the environment, the identification of old mine workings, which are prone to hydrogen sulfide (H_2S) formation is important. Thus, the sulfur content in coal is implemented in a geochemical model to assess future H_2S formation. Given the natural variability within a coal seam, mean sulfur contents for each mine water dewatering catchment area shall be used. For the southern Ruhr area, an influence of precipitation on the mine water geochemistry could be made visible.

Keywords: Geochemical modelling, sulfur cycling, pyrite oxidation, sulfate reduction, mine water rebound

Introduction

With the closure of the last active hard coal mines in 2018, the post-mining phase in the German hard coal mining areas began. Mine water management was no longer necessary to ensure mining operation, but to prevent an uncontrolled rise of mine water. Continuous maintenance of mine water management is therefore part of the perpetual tasks outlined in the legacy agreement between RAG AG (formerly Ruhrkohle AG) and the federal states of North Rhine-Westphalia and Saarland from 2007 (Balzer and Roth 2019; Jasnowski-Peters and Melchers 2022).

The RAG AG presented a concept for the long-term optimization of mine water management in order to achieve the perpetual tasks as sustainably and efficiently as possible. This concept establishes objectives aimed at protecting both human health and the environment from potential risks imposed by mine water, as well as a plan to allow for a controlled mine water rebound (RAG 2024). Rising mine water levels result in a series of beneficial effects for the whole mine water management. The depth from which mine water must be pumped is reduced, consequently decreasing the required energy and the respective costs (Balzer and Roth 2019). Furthermore, flooding of deeper mine workings can potentially limit the mobility of any remaining contaminants in those zones. Density differences between highly mineralized water from deeper parts of the mine and lower mineralized water from inflows closer to the surface cause the formation of density stratification (Kessler *et al.* 2020).

During the mine water rebound, previously dewatered areas of the mine workings come back into contact with the mine water body over time (Jasnowski-Peters and Melchers 2022). In these previously dewatered areas of the mine, weathering processes have led to the formation of easily soluble mineral phases like sulfates, hydroxides and carbonates which are consequently dissolved by the rising, often acidic, mine water (Wolkersdorfer and

Mugova 2023). The acidity results from pyrite oxidation. Hard coal usually has a total sulfur content ranging from 0.5 to 5 wt.-%, whereof pyrite sulfur is the major fraction (Chou 2012). As the dewatered mine workings are in contact with air, pyrite oxidation, which is described by equations [1] – [4], takes place (Evangelou and Zhang 1995).

[1] $2\ FeS_{2\ (s)} + 7\ O_{2\ (aq)} + 2\ H_2O \rightarrow 2\ Fe^{2+} + 4\ SO_4^{2-} + 4\ H^+$

[2] $2\ Fe^{2+} + ½\ O_2 + 2\ H^+ \rightarrow 2\ Fe^{3+}\ H_2O$

[3] $2\ Fe^{3+} + 6\ H_2O \leftrightarrow 2\ Fe(OH)_{3\ (s)} + 6\ H+$

[4] $14\ Fe^{3+} + FeS_2 + 8\ H_2O \rightarrow 15\ Fe^{2+} + 2\ SO_4^{2-} + 16\ H^+$

During abiotic pyrite oxidation, equation [2] is the rate limiting step. Fe^{3+} reacts with pyrite faster than it can be reproduced by reaction with O_2 (Evangelou and Zhang 1995). Additionally, oxidation can be catalysed by bacteria to a factor of $>10^6$ (Singer and Stumm 1970). With the rise of mine water levels and the ongoing depletion of oxygen in the (newly) flooded parts of the mine workings, pyrite oxidation will slow down (Wolkersdorfer and Mugova 2023). In anoxic regions of the mine workings, the sulfate resulting from pyrite oxidation, is released into the mine water (eq. [4]) and will be utilized as electron acceptor by sulfate-reducing bacteria (SRB). The sulfate reduction can either take place with an organic electron donor like lactate (eq. [5]) or an inorganic electron donor like elemental hydrogen (eq. [6]).

Chemo-organotrophic sulfate reduction with organic electron donor:

[5] $C_3H_5O_3^- + SO_4^{2-} + 3\ H+ \rightarrow C_2H_3O_2^- + HCO_3^- + HS^- + H_2O$

Sulfate reduction with inorganic electron donor:

[6] $SO_4^{2-} + 4\ H_2 + 2\ H^+ \rightarrow HS^- + 4 + H_2O$

In order to ensure groundwater quality, it is crucial to monitor the formation of hydrogen sulfide, which has strong adverse effects to (ground)-waterbodies. This is particularly important as the Haltern Formation aquifer in the region is used for drinking-water production (Drobniewski *et al.* 2018). In the context of the planned rise of mine water levels, it is important to predict whether and where sulfate reduction might occur as well as quantitatively estimating H_2S formation.

In order to achieve this, a hydrogeochemical model will be developed to account for the sulfur content of the coal seams, following an approach with two main objectives:

1. Determination of sulfur concentrations in the coal seams to identify areas within the mine workings that may be prone to increased pyrite oxidation and subsequent sulfate reduction during the rise of mine water.
2. Depth-dependent sampling of the mine shafts in order to enhance the understanding of the different geochemical zones in the mine workings and to investigate if density stratification has already developed.

Methods

Modelling

Sulfur concentrations were kindly provided by RAG AG and were partially derived from exploration drillings or from samples taken during mining operations. No discrimination between organic and inorganic sulfur species was possible, since the sulfur content was given in wt.-%. Hence, the values were interpreted as pyrite sulfur, as it is the major sulfur fraction in coal. Modelling the spatial distribution of sulfur contents was carried out using the Software ArcGIS Pro (version 3.3.2). Ordinary kriging was applied using a spherical function, where at least two and not more than ten neighbours were included. Initially, it was carried out for a larger area, using data available from exploration drillings and subsequently for a longwall mining operation in the same coal seam.

Seasonal influence of precipitation in the southern Ruhr area

In order to estimate the influence of precipitation on mine water geochemistry in two southern water provinces Friedlicher Nachbar (FN) and Robert Mueser (RM) in Bochum, precipitation data from the station of the German Weather Service (DWD) in Bochum was used to compare with the with the mine water geochemistry (Deutscher Wetterdienst 2025). From the daily precipitation the 6-weeks-sum was calculated, to allow for a better recognition of time periods with high precipitation.

Results and Conclusions

Modelling

For the input data, the sulfur content observed in the exploration drillings ranged from 0.61 to 1.93 wt.-% sulfur, with a mean value of 1.01±0.32 wt.-% sulfur. The sulfur content varies widely between the drillings without a discernible spatial trend. This led to a bullseye effect: In the centre of the modelled area, a pattern of concentric rings can be seen in Fig. 1. This can be attributed to one high sulfur concentration value with 1.86 wt.-%. The sample just south has almost half the sulfur content with 0.94 wt.-%. At the same time, the data density surrounding this point is low, which further enhances the bullseye effect.

To further revise the calculated sulfur content from the kriging interpolation, sulfur concentrations of samples of a longwall mining operation of the coal seam President 1 were investigated. The area of the operation is located in the west of the interpolated area, had an approximate extent of 2 km × 1 km and is depicted in Fig. 1 and 2. The measured sulfur values ranged from 0.57 to 1.73 wt.-%, with a mean value of 1.01±0.24 wt.-%. When compared to the sulfur map in Fig. 1, the modelled sulfur content in the mining field varied substantially, even when considering a smaller area. This leads to the conclusion, that the sulfur is unevenly distributed within the coal seam, resulting in highly variable sulfur contents even within relatively small areas. Highly variable sulfur contents within coal seams reflect the heterogeneity of fluvial and marine delta plains during coal formation and the varying intrusion of sea water (Casagrande 1987; Spears 2015; Dai *et al.* 2020). Consequently, ordinary Kriging interpolation is not the suitable method for this application. The same conclusion can be drawn when considering the Kriging interpolation carried out with the same parameters for the sulfur values in the longwall mining operation of coal seam President 1. Fig. 2 shows zig-zag patterns, which may be a result of high local variability in the observed data. A comparison of the mean sulfur contents in the exploration drillings and in the mining samples showed a very good agreement. In order to further substantiate this agreement, sulfur data for ten coal seams in the Ruhr area reported by Suess *et al.* (2007) were considered for comparison in Fig. 3. In general, a good agreement of the mean values was observed, certainly within the error margins.

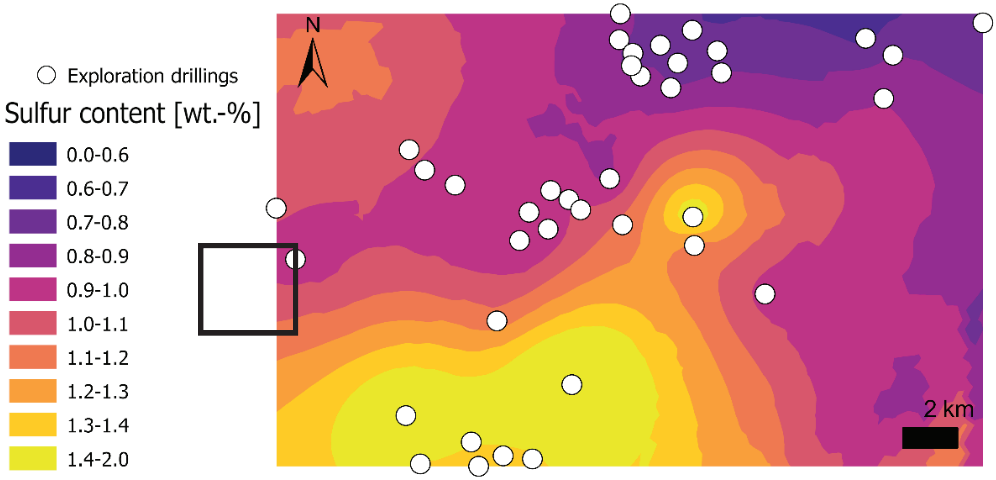

Figure 1 *Spatial distribution of the sulfur content in the coal seam President 1 resulting from Kriging interpolation of data from 45 exploration drillings in the western Ruhr area, depicted by the white circles. The black rectangle roughly represents the area of the longwall mining operation.*

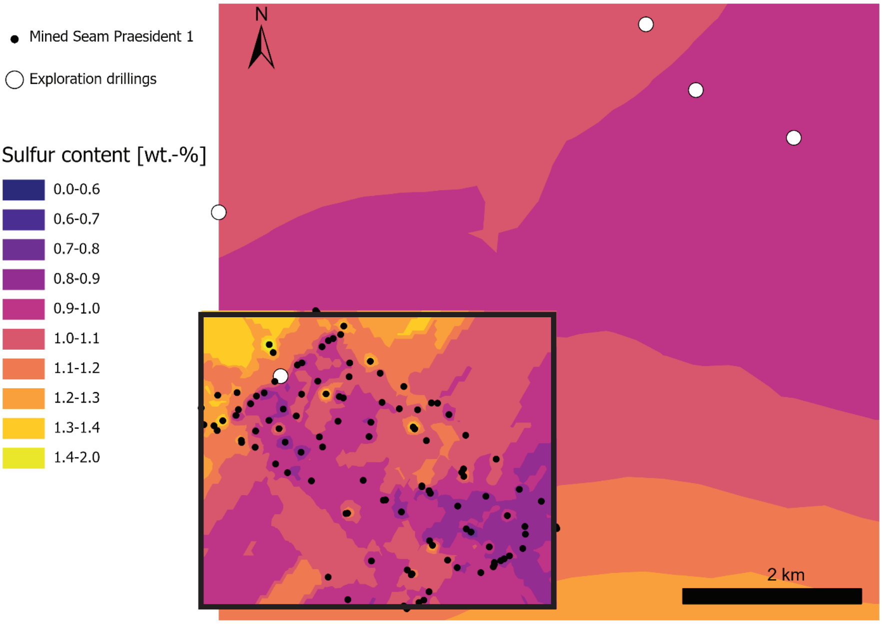

Figure 2 Kriging interpolation for the spatial distribution of sulfur contents resulting from Kriging interpolation of observations for seam Praesident 1 from a longwall mining operation in the western Ruhr Area, depicted by the black circles.

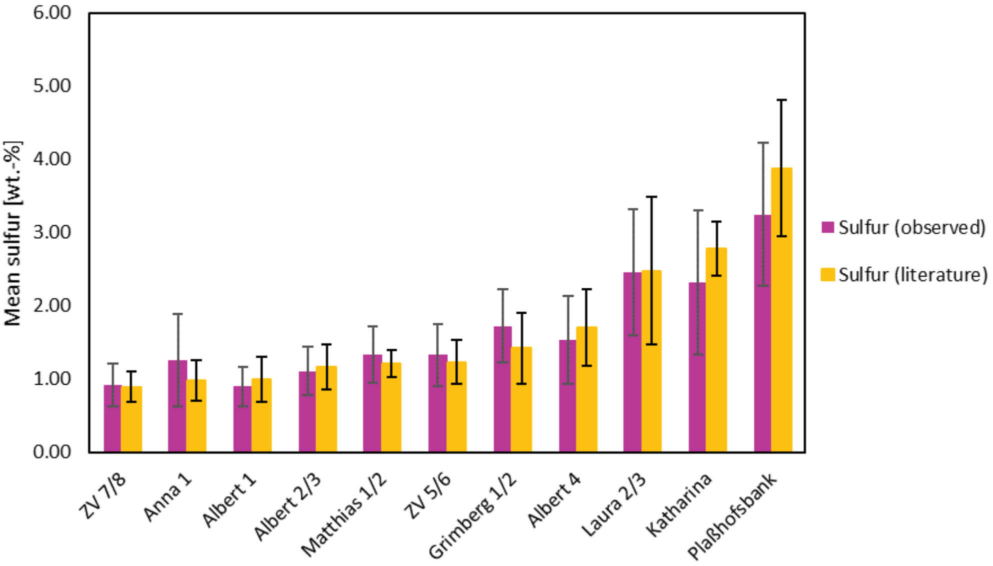

Figure 3 Comparison of average sulfur contents observed in this study (orange) compared to average values reported by Suess et. al. (2007; purple) for several coal seams of the Ruhr Area. The error bars indicate the standard deviation.

Consequently, for further modelling, mean sulfur contents will be used for each coal seam in each water management province, as the local variations of the sulfur content are too high to allow a more detailed geostatistical analysis.

Seasonal influence of precipitation in the southern Ruhr area

During the time period from November 2022 to December 2023 the sulfate concentrations ranged from 70 mg/L to 88 mg/L in RM and from 205 mg/L to 236 mg/L in FN, respectively.

The amount of precipitation was higher in the winter of 2023/2024, compared to the to the winter of 2022/2023. Additionally, the spring of 2024 had a high amount of precipitation, which was evenly distributed over a prolonged time period. This shows in the elevated baseline of the 6-weeks-sum of the precipitation, which was mostly higher than 100 mm from October 2023 to June 2024. The higher amounts of precipitation and its evenly distribution led to an increased ground water recharge and consequently to more water reaching the mine workings. This observation is consistent with the sulfate concentrations in the mine water, which showed rising values up to 210 mg/L in RM and 360 mg/L in FN, respectively. Iron-sulfide oxidation products from dewatered parts of the mine, which are in contact with air, were washed into the mine water body and led to a rise in concentrations. Sulfate concentrations seemed to start to decline again on the last available data point, however more samples will be necessary to confirm this trend.

Summary and outlook

Sulfur contents are highly variable even in close proximity within the same hard coal seam. This, in combination with a heterogenous data density, renders the interpolation of sulfur data inconclusive. However, the mean sulfur concentration for individual coal seams is somewhat consistent and within the same range as literature data (Suess *et al.* 2007). Therefore, the application of mean values will be more suitable for the development of a geochemical model.

An effect of precipitation on mine water geochemistry in the southern mine water provinces of the Ruhr region could be identified. After extended periods of precipitation the sulfate concentrations showed a rise, after a certain lag time. In order to gain further insight on the sources

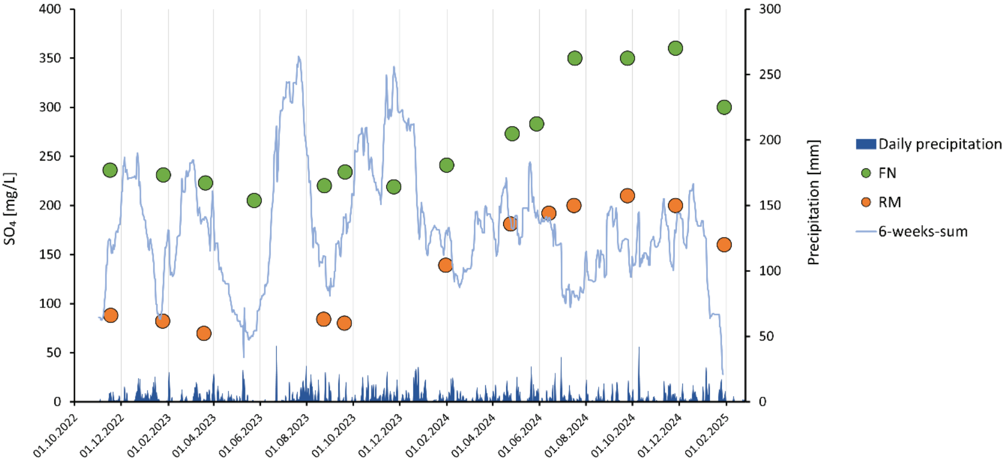

Figure 4 Sulfate concentrations in mine waters of the water provinces RM, FN and daily precipitation, 6-weeks-sum of daily precipitation in mm over time.

of the sulfate isotope measurements of the sulfate will be carried out.

Future work will comprise mine water sampling in shafts at discrete depths providing a better understanding of the sulfur turnover in different depths of the mine workings, if these measurements are possible and scientifically reasonable.

Acknowledgements

We sincerely thank RAG AG for providing the data used in this study, enabling valuable insights into mine water management processes and for providing financial support for this project.

References

Balzer I, Roth M (2019) Mine Water in the Ruhr Area-Opportunities for the Future. Mining Report 155

Casagrande DJ (1987) Sulphur in peat and coal. Geological Society, London, Special Publications 32:87–105

Chou C-L (2012) Sulfur in coals: A review of geochemistry and origins. International journal of coal geology 100:1–13

Dai S, Bechtel A, Eble CF, Flores RM, French D, Graham IT, Hood MM, Hower JC, Korasidis VA, Moore TA (2020) Recognition of peat depositional environments in coal: A review. International journal of coal geology 219:103383

Deutscher Wetterdienst (2025) Monatliche Niederschlagswerte. https://opendata.dwd.de/climate_environment/CDC/observations_germany/climate/monthly/more_precip/. Accessed 3 February 2025

Drobniewski M, Karus C, Löchte J (2018) Retreat to the future: shaping the post-mining era. Mine Water and the Environment 37:866–867

Evangelou VP, Zhang YL (1995) A review: pyrite oxidation mechanisms and acid mine drainage prevention. Critical Reviews in Environmental Science and Technology 25:141–199

Jasnowski-Peters HJ, Melchers C (2022) Mine Water Rebound in the Former Hard Coal Mining Area of the Ruhr District—Hydrogeochemical Monitoring for a Sustainable, Ecological and Economical Feasible Post-Mining Approach. Min. Rep. Glückauf 158:333–343

Kessler T, Mugova E, Jasnowski-Peters H, Rinder T, Stemke M, Wolkersdorfer C, Hilberg S, Melchers C, Struckmeier W, Wieber G (2020) Groundwater in former German coal mining areas—a scientific perspective on mine floodings. Grundwasser 25:259–272

RAG (2024) Konzept zur langfristigen Optimierung der Grubenwasserhaltung der RAG Aktiengesellschaft für Nordrhein-Westfalen. https://geodaten.rag.de/bid/tree/GenV/Grubenwasserkonzept%20NRW/Konzept%20%E2%80%93%20Grubenwasserhaltung%202024.pdf. Accessed 12 December 2024

Singer PC, Stumm W (1970) Acidic mine drainage: the rate-determining step. Science 167:1121–1123

Spears DA (2015) The geochemistry and mineralogy of high-S coals, with examples mainly from the East Pennines Coalfield in Yorkshire and Nottinghamshire, UK: an overview. Proceedings of the Yorkshire Geological Society 60:204–226

Suess MP, Drozdzewski G, Schaefer A (2007) Sedimentary environment dynamics and the formation of coal in the Pennsylvanian Variscan foreland in the Ruhr Basin (Germany, Western Europe). International journal of coal geology 69:267–287

Wolkersdorfer C, Mugova E (2023) Untersuchungen zum Verständnis von Grubenflutung und der Barrierewirkung von Dichteschichtung. 21. Albergbaukolloqium Essen:197–204

Partners in Sustainability: The Benefits of a Collaborative Relationship Between a Mine, Consultant, and Supplier in Water Management

Magnus Nilsson[1], Myriam De Ladurantaye-Noel[2]

[1]*Envidan, Sweden*

[2]*Veolia Water Technologies Canada, Canada*

Abstract

Water treatment in mining is crucial for environmental sustainability, as untreated water can harm ecosystems, which can affect permitting. A Swedish metal mine exemplifies innovation and collaboration in tackling water treatment challenges. Key elements of concern include metals, which seems common yet is complex for efficient application. Designing of an effective process involves selecting appropriate precipitation mechanisms and solids removal technologies, which has proven to be effective and robust for the presented case study, delivering high-quality effluent. By adopting proactive strategies, mining companies can ensure sustainable, efficient, and environmentally responsible operations, serving as models for others in the industry.

Keywords: Metal precipitation, synergy, water treatment

Introduction

In Sweden, many mines operate under outdated environmental permits or are in interim periods while awaiting new ones. When applying for new permits, mines commit to feasibility studies and water testing while adhering to provisional conditions. The regulatory framework involves multiple authorities and stakeholders who can provide input on water quality before the environmental court makes a decision. Environmental Quality Standards (EQS) are crucial in guiding efforts to ensure functionality and preservation of ecosystems, which often requires water quality improvements. The principle of non-deterioration mandates that the current status of water bodies must not worsen. Regulatory changes aim to align with these standards and address evolving environmental impact understandings, promoting sustainable mining practices.

In this case study, the mine was enhancing the treatment of existing tailings and clarification ponds in response to the provisional conditions entering in 2015. Thus, the mine began adding caustic soda to the tailings pond to precipitate metal hydroxides, which were then settled out in the clarification pond. However, in 2017, the mine effluent was experiencing non-compliances to the permit requirements, most specifically during higher flows and colder water periods.

This was the starting point to the formation of a partnership, bringing together the client, a consultant, and a technologies supplier to develop a sustainable solution also compliant with requirements from regulators and local community. The objective of the partnership was to fix and follow a comprehensive timeline of approximately five years, which included stages such as the preliminary feasibility study (PFS), trials, feasibility study (FS), definitive feasibility study (DFS), design and build phases, and commissioning, in implementing a robust and compliant water treatment strategy with limited waste management requirement and limited chemical dosing requirement to ensure flexibility of the treatment plant over time and it sustainability.

The overview of the project workflow presented in this case study is illustrated in Figure 1.

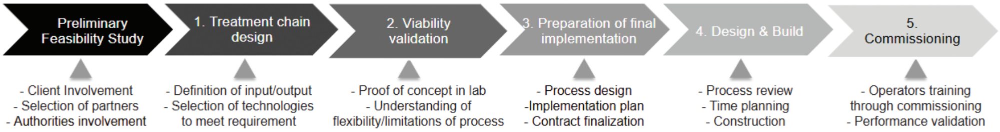

***Figure 1** Overview of the project workflow.*

Definition of the project- Preliminary Feasibility Study

In the process of selecting parties for the design of the water treatment system, a collaborative approach was adopted involving the client, the consultant, and the technologies supplier from early on. The mining company sought a partner capable of delivering a comprehensive turnkey solution, which included civil engineering, piping, machinery, electrical systems, and automation, while excluding programming and groundwork, in which the client wanted to be actively involved.

The selection of the partners was based on key criteria, including a proven track record and robust technical support capabilities. The client prioritized a consultant with extensive experience in industrial projects within Sweden and a good knowledge of local regulations. The consultant required a well-established network and partnered up with a technologies supplier familiar with the mining sector with relevant references. The work ethics of both partners was also important, to ensure alignment of the client's engagements on social and environmental performances.

The objective of collaboration early in the project timeline is to allow the client, consultant and supplier to work closely together, giving each the possibility to fully contribute to their expertise in developing the most effective solution. The stability in the design team also allows a solid understanding of the project through entire timeline, reducing risks of schedule and budget slips.

Furthermore, through the complete duration of the project, and in compliance with Swedish authorities (Geological Survey of Sweden (SGU) and Swedish Agency for Marine and Water Management (HaV)), the mining operation was required to monitor an extended list of parameters. This follow-up was integrated into the planning and execution process, ensuring that the solution met not only the current regulatory standard, but plan ahead for future needs.

Step one: Treatment chain design- Preliminary Feasibility Study

The first step of this process is the determination of what should be expected on the site and what the required output of the water treatment plant are. The information used for the design of the system, in collaboration with the consultant and the technologies supplier, are summarized in Table 1. Criteria (in brakets) are future targets and are not regulated on the actual permit.

The parameters of concern are metals. Several precipitation mechanisms are available to achieve metal removal. The main precipitation mechanisms seen in such application are the following:

- Hydroxide: metal hydroxide is the simplest precipitation mechanism. It relies on the pH of the solution to precipitate the metal to hydroxides (OH^-), mainly in alkaline conditions. Hydroxides precipitation has a fast kinetic and only requires alkali dosing and pH control. Its main limitation is its sensibility to pH as it impacts the solubility of the precipitate, thus the efficiency of the metal removal (Lewis, 2010). This could also lead to metals leaching out of sludge. The efficiency of hydroxide precipitation depends on the solubility of its precipitate, which does not allow to steadily reach µg/L levels (Kurniawan, 2006).
- Sulfide: sulfide precipitation relies on the addition of a sulfide source to bind metals and form precipitates. Sulfide chemistry does not rely as much on pH (Lewis, 2010), but pH should be monitored to prevent hydrogen sulfide gas release. The main drawbacks from sulfide precipitation is

Table 1 Influent composition of the mine effluent water and regulatory limitation.

Parameters	Units	Mine Effluent Average	Water Quality Design	Regulation – Criteria Monthly Average
pH	–	7.8	6.0 – 8.0	6.5 – 8.5
Temperature		7	2 - 22	–
Total Suspended Solids (TSS)	mg/L	12	1000	5
Chloride	mg/L	34.7	–	–
Total Calcium (Ca)	mg/L	248	450	–
Sulfate (SO_4)	mg/L	1.3	–	–
Total Arsenic (As)	mg/L	0.015	0.090	(0.010)
Total Cadmium (Cd)	mg/L	0.0014	0.0047	0.0005
Total Copper (Cu)	mg/L	0.0064	0.028	0.010
Total Lead (Pb)	mg/L	0.154	1.30	0.060
Total Nickel (Ni)	mg/L	0.028	0.090	(0.020)
Total Zinc (Zn)	mg/L	0.800	1.70	0.400

the toxicity of its residual in water, as well as its colloidal precipitates. A performant clarification step must be implemented to capture these fine precipitates. The main advantage of sulfide precipitation is its very low solubility, making it attractive in low metal concentration effluent (Lewis, 2010).

- Surface complexation: surface complexation is an adsorption mechanism. It relies on the adsorption of the metal of concern on a charged metallic surface. The metallic surface is formed using a metallic coagulant, mostly ferric iron, and is called ferric oxyhydroxide. It is a transitional crystal formed during iron precipitation of the form Fe_2O_3 x H_2O (Randall, 1999). Once oxyhydroxide is formed, according to the pH of the solution, it is either charged positive for oxyanions removal, or negative for metal removal. The main advantage of surface complexation is the absence of a solubility limitation. As long as there is binding surfaces available, metals will be adsorbed and captured. However, it is highly pH dependant; sludge management must prevent pH drifts to prevent metals leach.
- Phosphate precipitation: phosphate precipitation is effective for metal removal. However, it is useless for arsenic removal. It is also susceptible to delayed onset of precipitation, and increase the phosphorus discharge to the environment, which when not regulated is a source of eutrophication in the environment. Given that other precipitation mechanisms are unaffected by these problems, phosphate precipitation was not considered.

In the case of the Swedish mine, the metals of concern are zinc, cadmium, copper and lead. Arsenic and nickel are also expected to be added to the regulation to a further date. The main elements of concern for the metal precipitation step were the following:

- Very low criteria: most of the hydroxide solubilities are over the criteria. Therefore, this mechanism is not enough; it must be combined to other mechanisms.
- Several metals to be removed: metal hydroxides and surface complexation both relies on the pH to precipitate/adsorb the right metals. For surface complexation, fair removal can be achieved for all the main contaminants of concern at a slightly alkaline pH. However, adding arsenic removal, it cannot cover oxyanions and metals in a single stage.

The metal precipitation mechanisms selection is based on several considerations; the central point of focus is the limitation on the number of stages required to address all the metals of concern and providing flexibility for future requirements. Stability of the sludge as well as limitation of the sludge production is also considered in the selection of the precipitation mechanisms, to a lesser extent as it was not designated as a priority concern. The selected design was a combination of hydroxide precipitation and surface complexation until permit modification. Contingencies to add sulfide precipitation was included in the design to cover its addition to support metals and arsenic removal at a later date.

Once the metals out of solution, care must be taken for the solids separation step. Regulations are mainly based on total metal concentrations, thus adequate removal of the particulate metals is essential. The level of solids separation efficiency required must be evaluated to reach the balance between performance and cost. Therefore, the design must consider the following:

- Expected flow variations: fluctuating water composition as well as fluctuating flows require operation adjustment to the solid separation system. Conventional clarifiers, with long retention times, operate best in steady conditions and could be negatively impacted by sudden variations. Short retention time reacts faster and thus are favourable in applications with important turndowns.
- Efficiency to capture metal precipitate: sulfide precipitates require a cohesive chemical conditioning to efficiently capture these through the solid separation step.
- Particulate metals versus inert suspended solids: the higher the inert solids are, the lower is the metallic fraction in total solid load. The solids separation system let solids out to effluent no matter which. The higher the metallic precipitate fraction is, the higher will be the particulate metal concentration, and thus total metal concentration, at final effluent.
- Solids load: mine effluent solid load and precipitates generated in the metal precipitation step must be handled by the solids separation step. Systems such as ballasted flocculation requires customization to operate at higher extraction rate for very high solids loads, while clarifiers such as clarifier/thickener thrive in higher solids load conditions.
- Footprint availability.

For the Swedish mine, the metal criteria are stringent but not prohibitive to physico-chemical approaches. The treatment chain is been installed between a tailing pond and a clarifier pond, resulting in a low inert solids load and a limited footprint availability. The site location also lead to seasonal and fluctuating flows. The selected technologies in this application were ballasted flocculation, for its efficiency in tight space and its quick response in varying conditions, combined with a discfiltration polishing which provides over 50% removal of remaining solids out of the clarified water. In order to optimize the ballasted flocculation step and efficiently implement surface complexation, part of the sludge extracted is recirculated back to the metal precipitation step, allowing sufficient retention time for oxyhydroxide formation in a limited footprint.

To increase the robustness of the proposed treatment chain, sludge management is also key. Due to the selection of combined hydroxide precipitation and surface complexation, the sludge must be managed against leaching. Sludge out of the ballasted flocculation is sent directly to a centrifuge for dehydration. The dry cake falls into a container to be moved to the tailings for final disposal and centrate is sent back to the metal precipitation reactor, for zero liquid discharge.

The flow diagram of the water treatment plant for the Swedish mine is illustrated in Figure 2.

Step 2: Viability validation- Trials and Feasibility Study

Bench-scale tests has been carried out by the technologies supplier, using water from the site, to understand the capabilities of proposed treatment chain. The tests have been carried out at different pHs and using different coagulant dosages, as well as testing additional flexibility of the treatment by addition of a sulfide source. Results of interest from these tests are presented in Table 2. All metal concentration results are from an external accredited laboratory. The selected sulfide source is Hydrex 6909, a carbamate-based metal chelatant. Criteria (in brackets) are future targets and are not regulated on the actual permit. All criteria are as monthly averages.

Early involvement of the technologies supplier in the design team increases the understanding of the process capability at full-scale application. For this particular

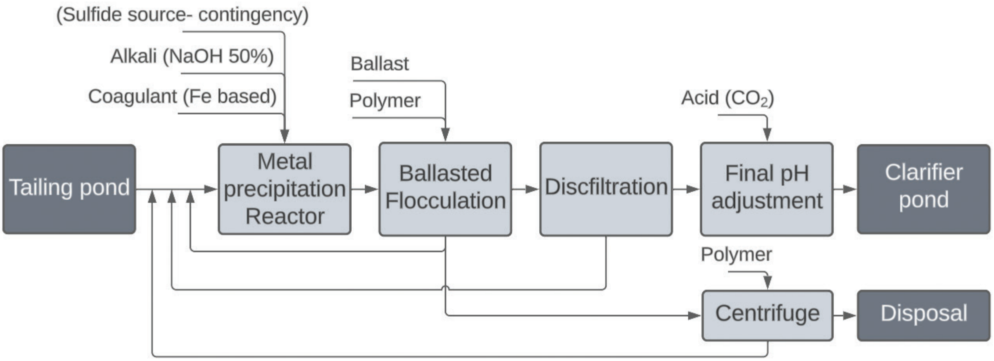

Figure 2 *Treatment chain flow diagram.*

application, results from the laboratory tests has shown compliancy to all criteria operating at pH 9.0, with a low chloride ferric concentration. The addition of carbamate has shown good performances at a lower pH (pH= 8), increasing the efficiency of the overall treatment efficiency, thus allowing for additional flexibility of treatment plant if needed. The laboratory testing can also be used for an operation cost (OPEX) estimation of ±30%, providing understanding of the chemistry of the mine effluent.

Step 3: Preparation of final implementation- Definitive Feasibility

Once the process chain has been validated and its flexibility capabilities better defined by the technologies supplier, detailed engineering could carry-on. At this stage, lists (equipment, instruments, valves), P&ID, layouts and process design are worked in collaboration of all parties.

End result of this step is a precise process treatment with an implementation plan. At this stage, estimation of the capital costs (CAPEX) and operating costs (OPEX) within ±10% is available. The client signs a contract of delivery with the consultant, acting as a contractor. Once the contract is finalised between the parties for execution of the project, the design and build step is initiated.

Step 4: Design and build

The first part of the design and build step is the process reviews and construction preparation. During this phase, effective communication between the client, consultant, and technologies supplier is essential; in-person and virtual meetings were conducted to finalize the design of the process train and the architectural aspects of the building, to align details prior to construction.

After finalizing process reviews and construction preparation, the client initiated the groundwork. To avoid concrete work during the winter months and prevent any kind of downtime on the construction site, the project schedule was carefully managed. Detailed design work was largely completed during the definitive feasibility study phase, ensuring that construction proceeded

Table 2 *Main results from the laboratory testing for risk mitigation of the water treatment plant.*

	Coagulant dose mg Fe/L	Sulfide dose mL/L	pH	Total As µg/L	Total Cd µg/L	Total Cu µg/L	Total Pb µg/L	Total Ni µg/L	Total Zn µg/L
Criteria				**(10)**	**0.5**	**10**	**60**	**(20)**	**400**
RW	–	–	7.5	4.42	0.21	0.744	13	11.1	1 160
Test 3	5	–	9.08	1.93	< 0.01	0.418	1.91	6.67	87.4
Test 4	5	–	8.02	2.2	0.0281	0.377	3.11	10.5	528
Test 7	10	–	9.03	1.45	< 0.01	0.402	1.52	5.78	60.8
Test 20	5	0.1	8.04	1.76	< 0.008	< 0.1	0.424	0.59	39.9

smoothly. The main focus at this stage is on time completion. This efficient planning allowed for the timely installation of all necessary equipment, ensuring the project schedule stayed on track.

Step 5: Commissioning

Commissioning of the plant was successfully completed by the staff from the mine, the consultant and the technologies supplier. Operators of the plant were hired by the client prior to construction and they were trained all through construction of the plant. They were also an active part of the commissioning alongside the consultant and technologies supplier. Commissioning is not yet completed, but preliminary results are showing complete compliance of the treatment chain, as shown in Table 3. Results are presented as dissolved metals, to give better appreciation of the process variation with fluctuating pH of operation. Total metal concentrations criteria (monthly average) are also presented for reference. pH compliance is not considered as the water quality is measured prior to final pH adjustment. Criteria (in brackets) are targets and are not regulated yet.

Results from commissioning shows great performances of the water treatment chain even if the process is not tuned in yet. It is interesting to note that operation at pH < 8.5, without sulfide addition, results in higher metal concentration for zinc, lead and cadmium. These metals were showing great removal with sulfide precipitation during bench test at pH 8.0 (refer to Table 2).

Key Insights

The main conclusions and implications from the collaboration are as follows:

- Effective Collaboration: Strong cooperation across all stages and disciplines, such as project managers and process specialists, among the three parties facilitated problem-solving and maintained project momentum over the five-year period. Collaboration of all parties had also strengthened validation of the process, understanding of it and identification of its limitations.
- Achievements: The project delivered a high-quality plant with an excellent working environment and robust process solutions, due to the practical experience of all parties in consulting, design, construction, supply, commissioning, and operation.
- Success Factors: The project's success was driven by a collaborative approach from the outset, supported by a fixed-price agreement. Regular meetings ensured alignment and prompt issue resolution.
- Areas for Improvement: Allocating more time for the design phase would have benefited the integration of internal components like ventilation, piping, and electrical systems. Extending the design phase by two months due to initial delays proved advantageous, underscoring the need for adequate planning time.

***Table 3** Preliminary performance of the treatment chain through commissioning.*

	TSS mg/L	pH	Diss. As µg/L	Diss. Cd µg/L	Diss. Cu µg/L	Diss. Pb µg/L	Diss. Ni µg/L	Diss. Zn µg/L
Criteria	**5**	**–**	**(10)**	**0.5**	**10**	**60**	**(20)**	**400**
2024-12-09	1.2	7.2	0.97	0.032	0.42	0.21	2	4.2
2024-12-16	1.1	8.6	0.88	0.02	0.44	0.038	1.8	3
2024-12-20	5.3	7.6	1.4	0.068	0.32	0.33	2.7	76
2024-12-27	5.2	7.6	1.3	0.11	0.47	0.83	2.3	79
2025-01-02	1.3	8.4	0.69	0.04	0.51	0.13	1.5	3.2

Conclusion

The case study highlights the advantages of a collaborative and structured approach in developing a robust and flexible water treatment plant. The project adeptly addressed regulatory and technical challenges through effective communication and cooperation among the client, consultant, and technologies supplier. The project delivered a high-quality plant, benefiting from the practical experience and expertise of all parties involved. This collaborative approach ensured alignment and facilitated problem-solving, highly contributing to the project's success.

Nonetheless, the experience revealed areas for improvement, particularly in allocating adequate time for the design phase. Lessons learned offer valuable insights for future projects, highlighting the importance of comprehensive planning and strong partnerships to achieve sustainable mining practices that protect aquatic ecosystems.

References

Lewis, A (2010) Review of metal sulphide precipitation. Hydrometallurgy. 104 (2): 222–234

Randall, S, Sherman, D, Ragnarsdottir, K, Collins, C (1999) The mechanism of cadmium surface complexation on iron oxyhydroxide minerals. Geochimica et Cosmochimica Acta 63 (19–20): 2971-2987

Kurniawan, T, Chan, G, Lo, W, Babel, S (2006) Physico–chemical treatment techniques for wastewater laden with heavy metals. Chemical Engineering Journal 118 (1–2): 83-98

A Hydrogeochemist's Mindful Toolkit: Conceptualization, Characterization, And Modeling Of Mine Sites Producing Acid Mine Drainage

D. Kirk Nordstrom[1]

[1]*formerly emeritus, U.S. Geological Survey, Boulder, Colorado, 80303 USA, dkirknordstrom@comcast.net, ORCID 0000-0003-32835136*

Abstract

After 50 years of studying acid mine drainage, three themes need improvement for more effective and cost-efficient mine-waste remediation: conceptualization, characterization, and modeling.

Conceptualization depends on one's background and experience with geology, hydrology, chemistry, hydrogeochemistry, microbiology, mining, and mineral processing.

Characterization builds on conceptualization using detailed knowledge of best practices.

Modeling always contains assumptions and misconceptions that become clearer through hypothesis testing and further data collection.

Two important skill sets stand out the most: a solid knowledge of the field of hydrogeochemistry, and humility when facing complexity. Then many of the costly mistakes of the past can likely be avoided.

Keywords: Remediation, conceptualization, characterization, modeling

Introduction

Acid metal-rich discharges from mining activities are one of the largest and most difficult problems to prevent and remediate. Nriagu and Pacyna (1988) estimated that 6,000 metric tons of Zn, 2,500 metric tons of Pb, and 900 metric tons of Cu per year were discharged to worldwide surface waters from metal mining activities. Berner and Berner (1996) estimated that 48% of the annual global sulfate flux of the world's rivers to the oceans was man-made pollution (acid rain, fertilizers, and acid mine drainage) and amounts to 77 x 1012 metric tons. Of that, a substantial portion is from mining and smelting activities. To date we still do not know approximately how much global sulfate flux is from metal mining compared to other anthropogenic activities or natural sources. Nieto *et al.* (2013) reported that 35,682 metric tons/a of sulfate out of an anthropogenic global 1.24 x 108 metric tons/a (Meybeck, 2003), or 0.03%, is discharging from the combined Tinto and Odiel Rivers when rainfall flush-out events are included. They also reported 649 metric tons/a of Zn, or nearly 3% of the global flux came from these rivers alone. Galvan *et al.* (2012) evaluated the mass flux of metals and sulfate in the Meca subbasin of the Odiel River Basin, SW Spain and for the water year 2000–2001, the sulfate flux was 18,645 metric tons/a, more than half of the two much larger basins. More recent studies indicate that sulfate flux from pyrite weathering and from pollution sources may be seriously underestimated (Burke *et al.*, 2018).

The number of disasters resulting from failed waste impoundments that have been addressed by several experts such as Davies (2002) and appear to be on the rise. The resulting spills can have both physical and chemical detrimental effects down gradient. Kossoff *et al.* (2014) list a dozen examples of well-known impoundment failures and a list of toxic chemical substance concentrations for eight of these. More spills have occurred since their paper was published. The pore water in sulfidic tailings waste can contain very high concentrations of sulfuric acid and metals. Mine portals can discharge water with pH values below 1.0 and underground massive sulfide mines have produced waters of negative pH (Nordstrom, 2011).

The purpose of this paper is to review the general approach to remediation of complex mine waste sites which generate acid mine drainage and, from my own experience, make a few suggestions. My suggestions fall into the categories of conceptualization, characterization and modeling.

Conceptualization

How one conceives of mine waste material, especially acid mine drainage, depends on several factors. There is documentation available on site-specific properties, visual observations from site inspections and maps and photographs, etc. Each person also brings their own perspective obtained through education and experience that shape how one conceives of the problem at hand and interprets the documentation. Every expert tends to understand things from a particular viewpoint that could be as much deleterious as helpful. A microbiologist tends to think of waste processes as always catalyzed by microbes. A geologist considers the rocks, rock structure, and mineralogy but not so much the microbes. A hydrogeologist looks at the rocks as a bounding structure to flowpaths but not so much as reactive material. The chemist sees chemical composition in both rocks and waters but might not see the importance of flowpaths or microbes. The mining engineer understands the operations of mining and mineral processing but not the need for additional expertise. Remediation of complex mine sites typically requires expertise from all of these areas – geology, hydrology, chemistry, hydrogeochemistry, microbiology, mining and mineral processing. The conceptual model addresses what is known, what is unknown and needs to be known, what sources and sinks of contaminants exist and what actions should be on the priority list.

A mine waste site can be a hydrogeochemical mess and although many books and papers have addressed the subject, these publications can be limited in terms of the authors' perspectives. For a single book, Lottermoser (2010) integrates quite well most all these important factors. Because these subjects are typically not courses covered by civil engineering curricula — consulting companies, mining companies, and regulatory agencies must either hire this expertise or learn these skills through training. Progress has been slow in recognizing the importance of conceptualization.

At the Iron Mountain mines superfund site, the potentially responsible parties advocated mine plugging for a legacy mine actively producing large quantities of acid mine drainage. The concept, still promoted today, was that the mine pool created by plugging would cover the remaining massive sulfide and block the access of oxygen and prevent the formation of acid mine drainage. The site was the worst possible site for mine plugging for a host of reasons (Nordstrom and Alpers, 1999). Mining had excavated a complex array of mines leaving numerous adits and drillholes that would allow strongly acidic water (pH<1) from a mine pool to leak out in all different directions into two different catchments and not easily contained. The mine pool would be well above the groundwater table. An active landslide existed above the main workings and several steam vents can be seen in winter, allowing easy entrance for water and oxygen. The country rock has no helpful buffering capacity against this acid water. After considerable deliberation, the mine was not plugged. Instead, a lime treatment facility was set up to neutralize the acid mine drainage which primarily discharged from two portals, and it was relatively easy to capture and treat. Many other mines in the western US having similar hydrogeochemical characteristics were plugged, the mine pool backed up and became enriched in acid and metal concentrations, was not contained and the consequent pollution of receiving streams and rivers became worse. Alternative treatment had to be installed for these sites, usually a lime neutralization plant, while the mine pool was dewatered. The predicted Iron Mountain mine plugging scenario was done and confirmed for other sites; it is often not a preferred option.

One disturbing aspect of neutralization plants is that they cost millions of dollars to build and maintain. At Iron Mountain, the amount of time it would take to exhaust the production of acid mine drainage at current weathering rates is approximately 3,000 years. Neutralization will not be supported in perpetuity because the cost is far greater than what can be supported by society and orders of magnitude higher than the value of the metals mined. A practical long-term remedial solution has yet to be determined for this site and many others.

Another example of mistaken conceptualization was on the Questa project (2001–2007) when the US Geological Survey was asked to determine the pre-mining groundwater quality of an active mine site. The Questa mine produced molybdenum ore concentrate. A proximal analog catchment that had not been mined was used to understand the pre-mining groundwater composition. Prior to the USGS participation a consultant was estimating the pre-mining groundwater quality by gathering surface sediments over a large area of mineralized ground and using analyses of quick water leach tests as a proxy for groundwater compositions. These test results bore little resemblance to actual groundwater compositions, and it points out the importance of informed conceptualization. Of course, one can change the water composition of leach tests by simply changing the ratio of solids to water, but it still did not mimic actual groundwater compositions.

Conceptualization should include a source-sink-receptor or flux-reservoir schematic of contaminant sources and pathways of mobility. The first schematic will be primitive, and as more and more site data are gathered it can be refined and improved. Examples of these schematics can be found in Nordstrom and Nicholson (2017).

Characterization

Characterization builds on conceptualization to formulate a plan with high and low priorities for what is needed to best quantify contaminant reactivity and mobility. In other words, to put numbers on amounts, reactivities and transport for the conceptualization. Characterization fills in the gaps and makes a strong case for the importance of remediation. Decisions must be made on what samples to collect, how to collect the samples, from what locations should the samples be collected, and for what purposes. Even though plenty of information is available on protocols for sampling, preservation, and analysis, protocols are not always followed and sometimes the protocols themselves are deficient. For example, EPA holding times for chloride and sulfate in water samples has been 28 days. If the sample has been filtered and kept in a cool or refrigerated space, those water samples can be held for many months without any change in concentration. I tried to find out why there were such restrictive holding times and discovered that there was no documentation. Even the EPA QA/QC director did not know where the holding time numbers came from. The USGS holding time on the same constituents is 6 months and the only reason they have a time limit is because there is not enough storage space to hold the bottles longer than that. I resolved my particular issue by taking a small sample set and analyzing them for sulfate within the holding time period and months after. The results were exactly the same within analytical error. I then explained why certain major ions are conservative in the sense that they will not change over time if the water is collected properly. Those results were found acceptable to both regulators and industry representatives. The last time I checked, chloride and sulfate holding times were still 28 days without explanation or reference.

When water samples are being collected from a site, certain field parameters must be obtained such as pH, temperature, specific conductance, and often dissolved oxygen. I experienced a situation where a non-USGS person was asked to collect a groundwater sample from a well and measure field parameters. The person reported a pH of 4. Several subsequent samples were collected by USGS personnel in which there was no discernible difference in water composition except that personnel following protocols always reported a pH slightly above 6. That much difference in pH is unacceptable when the procedures have been spelled out for decades (Bates, 1973). Another explanation is that in this example the well was not adequately purged before sampling.

Regulators do not usually require routine Fe(2/3) determinations on acid mine water samples. Consequently, charge balances on acid water samples might not be adequately balanced and the behavior of one of the most important cations in the water will not be characterized sufficiently. Ferrous iron, Fe(II), is highly soluble and mobile at any pH, whereas ferric iron, Fe(III), is highly insoluble at moderately acid to neutral pH values. Charge balance on a water sample is a simple QA/QC (quality assurance/quality control) procedure that helps to confirm the reliability of the analysis for major ions. Because of the control of trace metal sorption by freshly precipitating ferric oxides and hydroxides, analytically determining and understanding iron redox chemistry is a critical requirement for characterizing acid mine drainage. The analytical procedure for this requirement is both simple and robust. There is every reason to collect and preserve (with HCl) samples for Fe(2/3) redox determinations.

Other routine QA/QC procedures for water and sediment samples should be readily available in submitted reports, such as field and lab blank determinations, detection limits, methods of field and lab analyses, spiked recoveries, and, most importantly, results from standard reference samples (for both waters and solids). When the full suite of major ion determinations have been completed for a water sample, the conductance can be calculated and compared with the measured value as an accuracy check in addition to the charge balance assessment (McCleskey *et al.*, 2012) in addition to the charge balance.

I have seen examples of the dissolved concentration of potentially toxic metals and metalloids greater than the "total" concentration, i.e. the concentration on an acidified unfiltered sample. This result reflects problems with sample collection or preservation or analytical procedures and should be resolved. As a footnote, US Geological Survey field and lab teams rarely observe this difference. It seems to be more apparent when the contractor who collects the samples is different from the contractor who analyses the samples and different from the QA/QC auditor who screens the samples. When there are serious disconnects in communication between field teams and lab teams, it is easier for mistakes to occur in analytical results. One or two people who are responsible for data interpretation should accompany the field team and visit the analytical lab to follow the chain of custody for confirmation of protocols and to understand if there were any unexpected field or lab issues that could have caused unacceptable analytical determinations.

As the data is compiled it should be incorporated into a site model that addresses flux/reservoir (or stocks/flows) and identifies the dominant sources, pathways, and receptors. Seasonal trends and storm events should be sampled to determine the effects of weather and climate change.

The next level above sampling and analysis is interpretation of the data in a fashion that allows a manager, regulator, or non-technical person to understand the meaning of the results. At this point, the schematic conceptualization of the data is revisited and any serious knowledge gaps reported. Interpretation involves being intimately familiar with the analytical data, the field site, and what plots and diagrams are most useful. Hence, the characterization phase may include hydrogeochemical modelling for interpretation and it certainly does include modeling when considering scenarios for planning remediation or answering site specific questions about hydrogeochemical site behavior.

Modeling

Modeling is a complex subject that begins with the development of conceptual models, analogous to the conceptualization described above. It is essential to remember that (1) a model is not a computer code, (2) models are not unique, (3) models, if not tested, lack meaning, (4) if models are tested and predictions agree with independent observations, this result is not "validation", and if they don't agree, the models are not invalidated, (5) models and scenarios should not be confused with each other, (6) poor model predictions usually result from poor conceptual models, and (7) models are inherently "incorrect" but can be useful (Nordstrom, 2012; Nordstrom and Campbell, 2014; Nordstrom and Nicholson, 2017).

The importance of the conceptual model cannot be overemphasized. I can do no better than to quote (Bredehoeft, 2005).

"Every model has as its foundation a conceptual model."

"The conceptual model is based on the subjective judgment of the analyst."

"A numerical model provides a tool by which to test the appropriateness of the prevailing concept."

"One can expect the conceptual model to be continuously updated as new information is acquired."

To these I would simply add that all models are incomplete, and deficiencies are addressed with implicit or explicit assumptions. These assumptions can be unimportant or seriously deleterious to the calculations or unknown as to their effect on the result. What matters most is that they are transparent and better to be made explicit. Uncertainty analysis can help to identify what are the most sensitive variables which might point to more field and analytical data to better constrain the model.

A strong or reliable model is one that has been well tested for a wide range of conditions. If we are interested in an environmental model, it must field tested. For how long? Some have suggested around 25 years to make sure that extreme weather events and changing climate conditions are monitored and understood. I tend to agree. A better approach is to recycle and reuse these waste materials in ways that are safe for human health and the environment. Modeling is well-educated guesswork, and too many modelers view their models as immutable. I prefer the wisdom of Erica Thompson (2022) who stated:

"Model Land provides us with maps of the future, but they are not always the maps that we need. Some are plain and simple; some are elaborate and embellished; most are in some ways misleading; all were drawn by someone fallible; all have limits beyond which we can only write 'Here Be Dragons.' The terrain outside Model Land is bumpy and disputed. While our models can predict, warn, motivate or inspire, we must ourselves navigate the real-world territory and live up to the challenge of making the best of our imperfect knowledge to create a future worth living in."

I have reviewed reports where an elaborate scheme of transport equations, combined with rate and equilibrium equations for geochemical reactions and other equations for physical processes to predict metal and/or acid concentrations, present a remediation scenario that gives a highly optimistic viewpoint. But when the question is asked: Has there been a demonstration project to show the feasibility of such a scheme? It doesn't exist. There has been no testing of the complex model to find out if it works as planned, if the assumptions are adequate, and what are the major limitations and weaknesses. Hence, it is only a possible scenario or thought experiment and not even a scenario to which you can assign a vague uncertainty. There are models and scenarios that can be tested because they are short-term experiments and there are others that can never be tested in a human lifetime of 70 or 80 years, such as a high-level radioactive waste repository because it must last a few hundred thousand years without harming the biosphere. If they cannot be tested, they cannot be confirmed, and they certainly cannot be validated.

If we don't plan for on site reuse and recycling of mine wastes as the mine plan is developed before any extraction begins, it is a missed opportunity and will likely lead to an environment that is more expensive to manage at and following mine closure.

References

Bates RG (1973) Determination of pH: Theory and Practice. John Wiley & Sons, New York

Berner EK, Berner RA (1996) Global Environment: Water, Air, and Geochemical Cycles. Prentice-Hall, Upper Saddle River, NJ

Bredehoeft JD (2005) The conceptualization model problem – surprise. Hydrogeol J 13(1): 37–46

Burke A, Present TM, Paris G, Rae CM, Sandilands BH, Gaillardet J, Peuker-Ehrenbrink B, Fischer WW, McClelland JW, Spencer RGM, Voss BM, Adkins JF (2018) Sulfur isotopes in rivers: Inisghts into global weathering budgets, pyrite oxidation, and the modern sulfur cycle. Earth Planet Sci Let 496:168–177, 10.1016/j.epsl.2018.05.022

Davies MP (2002) Tailings impoundment failures: are geotechnical engineers listening? Waste Geotechnics: 31–36

Galvan L, Olias M, Canovas CR, Torres E, Ayora C, Nieto JM, Sarmiento AM (2012) Refining the estimation of metal loads dissolved in acid mine drainage by continuous monitoring of specific conductivity and water level. Appl Geochem 27: 1932–1943

Kossoff D, Dubbin WE, Alfredsson M, Edwards SJ, Macklin MG, Hudson-Edwards KA (2014). Mine tailings dams: Characteristics, failure, environmental impacts, and remediation. Appl Geochem 51: 229–245

Lottermoser BG (2010) Mine Wastes: Characterization, Treatment and Environmental Impacts. 3rd ed. Springer, Heidelberg, doi 10.1007/978-3-642-12419-8

McCleskey RB, Nordstrom DK, Ryan JN, Ball JW (2012) A new method of calculating eletrical conductivity with applications to natural waters. Geochim Cosmochim Acta 77: 369–382

Meybeck M (2003) Global occurrenced of major elements in rivers. In: Drever JI (Ed.), Surface and Groundwater, Weathering and Soils, Treatise on Geochemisry. Elsevier, New York, 27–68, 10.1016/B0-08-043751-6/05164-1

Nieto JM, Sarmiento AM, Canovas CR, Olias M, Ayora C (2013) Acid mine drainage in the Iberian Pyrite Belt 1. Hydrochemical characteristics and pollutant load of the Tinto and Odiel rivers. Environ Sci Poll Res 20: 7509–7519

Nordstrom DK (2011) Mine waters: Acidic to circumneutral. Elements 7(6): 393-398, doi.org/10.2113/gselements.7.6.393.

Nordstrom DK (2012) Models, validation, and applied geochemistry: Issues in science, communication, and philosophy. Appl Geochem 27(10): 1899–1919, doi.org/10.1016/j.apgeochem.2012.07.007

Nordstrom DK, Alpers, CN (1999) Negative pH, efflorescent mineralogy, and consequences for environmental restoration at the Iron Mountain Superfund site, California. Proc natl Acad Sci USA 96: 3455–3462

Nordstrom DK, Campbell KM (2014) Modeling low-temperature geochemical processes. In: Drever JI (Ed.), Surface and Groundwater, Weathering and Soils, Treatise on Geochemisry. Elsevier, New York, 27–68, dx.doi.org/10.1016/B978-0-08-095975-7.00502-7

Nordstrom DK, Nicholson A (2017) Geochemical modeling for mine site characterization and remediation. Society for Mining, Metallurgy & Exploration, Englewood, Colorado, USA

Nriagu JO, Pacyna JM (1988) Quantitative assessment of world-wide contamination of air, water and soils by trace metals. Nature 333: 134–139

Thompson E (2022) Escape from Model Land: How Mathematical Models Can Lead Us Astray and What We Can Do About It. Basic Books, NY

Study Of The Flooding Of Coal Mines In Asturias – Possibilities For The Use Of Mining Reservoirs

Almudena Ordóñez[1], Rodrigo Álvarez[1], Carmen García-Fernández[1], Silverio García-Cortés[1]

[1]University of Oviedo, Escuela Politécnica de Mieres, 33600 Mieres, Asturias, Spain aoalonso@uniovi.es, ORCID 0000-0002-0055-1828; alvarezrodrigo@uniovi.es, ORCID 0000-0002-2651-1103; garciafercarmen@uniovi.es, ORCID 0000-0002-3598-9790; sgcortes@uniovi.es, ORCID 0000-0001-5695-1268

Abstract

This study focusses on the water and energy utilisation possibilities of the coal mines in the central sector of Asturias, most of which are already flooded. In order to estimate the potential for exploitation, the capacities of the mining reservoirs and the water recharge they receive have been estimated, highlighting the importance of hydrogeological studies of mining reservoirs for their use. Several examples illustrate a way to enhance the value of mining heritage after mine closure, creating wealth in often depressed areas, in line with the European Union's roadmap for energy transition.

Keywords: Underground mining reservoir, Flooding, Hydrogeological characterization, Mine water energy use, Coal mines

Introduction

The reduction of greenhouse gas emissions and the increase in the implementation of renewable energies is aligned with the EU proposals for 2030, as well as with the Paris Agreement. The EU Energy Efficiency Directive 2023/1791 requires Member States to increase the use of renewable energy and obliges them to migrate their district heating and cooling systems to 100% renewable energy, waste heat or a combination of both by 2050. Geothermal energy, often underestimated in the renewable energy scene, stands out as an innovative and sustainable alternative to meet energy demands, e.g. that used for space and district heating/cooling by means of a heat pump (low and very low enthalpy resources). Resolution 2023/2111(INI) adopted by the European Parliament calls for a European strategy to accelerate deployment and investment in geothermal energy. In addition, more support is requested for regions whose economies are dependent on fossil fuels, in order to help them make the transition to geothermal energy. This could be the case in Asturias (NW Spain), whose core industries have traditionally been coal mining and power generation through thermal power plants. Mine water, traditionally seen as waste, is increasingly being recognized as a valuable resource. In the context of the global shift toward clean energy, the energy market is pursuing creative solutions for its generation and storage. Underground pumped hydroelectric energy storage systems (UPHS) are gaining attention as efficient, flexible options for managing the intermittency of renewable energy sources.

It is worth highlighting the Asturian geothermal mine water systems as thermal energy storage applications (Menéndez *et al.* 2019, 2020). Near the Barredo shaft (Mieres), the company HUNOSA implemented more than a decade ago the first district heating using mine water, which has served as an example for other similar systems in Europe. Subsequently, another district heating associated with the Fondón shaft (Langreo) has been implemented. Accumulated experience has shown that the distance from mining reservoirs to consumers greatly influences the viability of the project. Therefore, this study considers systems with potential customers close to the reservoirs, such as the aforementioned Barredo and Fondón and others such as Carrio (Laviana), San Antonio (Aller) or La Camocha (Gijón). In addition to the above, it is also possible to consider the use of UPHS in mining infrastructures, as well as considering the mine water as a water resource. This work highlights the need and relevance of carrying out a complete hydrogeological study of mining reservoirs prior to their water and energy use.

Methods

Study Area

For over two centuries, up to 70% of Spain's coal production came from the Asturian Central Coal Basin (CCB), but all the mines are closed now. Underground mining progressed reaching depths up to 1,000 m. This process fractured the rock, increasing rainwater infiltration, which required constant drainage through pumping while the mines were operational. In total, about 40 Mm^3 per year of water were pumped when the mines were active. When the mines were closed, pumping stopped, leading to gradual flooding or 'groundwater rebound' (Younger *et al.* 2002). The flood rate is influenced by seasonal infiltration and void volume, slowing near large underground galleries and rising faster between them (Ordóñez *et al.* 2012). If pumping were not restarted, mine water would eventually come to the surface through the lowest mine adit or any connected permeable rock, leading to uncontrolled discharge. To prevent this, controlled pumping is often reinstated in the Asturian coal mines, balancing discharge with recharge to maintain a stable water level and creating an underground 'mining reservoir'. This regulated underground reservoir can serve various purposes, such as water supply, river flow support, and energy -mainly geothermal- applications.

Hydrogeological characterisation of mining reservoirs

From a hydrogeological perspective, the CCB consists mainly of Carboniferous rocks with low permeability, preventing the formation of major aquifers. The undisturbed rock mass is nearly impermeable, with only certain sandstones acting as small, confined aquifers due to surrounding mudstones and shales. As a result, groundwater primarily flows through mining voids and open fractures. Mining operations have created artificial, pseudo-karstic aquifers where most stored water is found in mining-induced voids (Ordóñez *et al.* 2012). Additionally, the hydrogeological properties, such as porosity or permeability of the originally low-permeability materials improve considerably due to mining. Therefore, these mining reservoirs can be considered isolated systems, surrounded by nearly impermeable Carboniferous rocks, which prevent lateral groundwater inflow. Thus, the infiltration of effective rainfall is considered its source of recharge.

The basin linked to a reservoir refers to the area where rainfall can infiltrate into the mine workings. Its boundaries are defined by topographic divides and the extent of the mined area, which may enhance permeability in the overlying materials. Firstly, it is necessary to carry out a climatic study to determine the effective rainfall (total rainfall minus evapotranspiration) in the basin affected by the mining reservoir. This effective rainfall divides between infiltration into the reservoir (recharge) and runoff into the basin's watercourses. The average pumped flow from the shafts in the reservoir during the mine's active period must be determined. As mentioned, in this area the pumped water can be made equivalent to the infiltrated effective rainfall, representing the reservoir's average recharge (Ordóñez *et al.* 2012). The geology of the area and the effect of potential loosing rivers must be taken into account. Once all these parameters have been estimated, it is possible to define a conceptual hydrogeological model of the operation of the mining reservoir.

To predict flooding and determine potential uses, the reservoir's storage capacity must be estimated. This involves assessing mining voids, considering historical mining activity and connections to adjacent workings. The volume of voids of the mining reservoir determines the usable water storage capacity and influences regulation possibilities by adjusting recharge and withdrawal rates. One method to determine void volume at different depths involves estimating the infiltrated water volume during flooding -if it has already occurred-. This requires monitoring groundwater rebound (measuring water level rise in shafts) and assessing effective rainfall infiltration during the flooding period. On the other hand, this volume can be also estimated by calculating the volume of mining galleries using their total length (several hundreds of km, Table 1) and an average cross-section as well as estimating the voids from coal extraction based on historical production data and coal density, taking into account the void loss due to backfilling, compaction, or collapse, depending on the mining method used (Álvarez *et al.* 2016).

According to the conceptual model, after pumping stops, the groundwater level in the mining reservoir will gradually rise, filling the voids over time. Using the gathered information, the flooding process can be predicted, considering its typically slow nature due to the extensive mine workings and related volume of voids relative to water inflow. A rough estimate of the time required to fill the reservoir, and its average filling velocity can be calculated based on the void volume and the average recharge rate. In addition, the expected flood evolution can be modelled using specific software, such as the GRAM model (Groundwater Rebound in Abandoned Mineworkings; Adams and Younger, 2001) or the software FEFLOW (Finite Element subsurface FLOW system; Andrés et al 2015).

Potential uses of mine water

Water supply: Mining reservoirs are often located near urban settlements, allowing treated mine water to be used as a water source. By considering average recharge, the reservoir's annual supply curve can be determined and compared to demand. Regulation through reservoir capacity enhances supply by offsetting seasonal water deficits with stored water from other periods.

Energy resource: Mine water has significant geothermal potential due to its stable temperature and flow. Using it as a low-enthalpy resource for heating and cooling through heat pumps can reduce energy consumption, CO_2 emissions and costs by more than 50% compared to conventional systems (Matas-Escamilla *et al.* 2023). Additionally, if some of the water used for geothermal purposes is returned to the reservoir, hydraulic power can be efficiently generated using a turbine during peak-load hours. Energy storage using mining reservoirs in UPHS systems is especially advantageous for mines requiring continuous pumping. These systems help address the intermittency of renewable sources like solar and wind while also revitalizing abandoned mines through job creation and community development.

Apart from the temperature of the mine water, for the long-term geothermal exploitation of the reservoirs, it is very important to know the thermal conductivity of the rock mass, particularly for modelling the thermal exploitation of the reservoir (Andrés *et al.* 2015, 2016), as well as some hydrochemical parameters. In particular, the Barredo-Figaredo mine waters are near neutral, net alkaline, high metal waters of Na-HCO^3 type. Their suspended and dissolved solids and particularly their iron content have caused some scaling and clogging on heat exchangers of the geothermal installations.

Results

Fig. 1 shows simplified examples of conceptual model of two Asturian mining reservoirs, considering the water balance in the basin affected by each of them.

Fig. 1 Recharge basin and conceptual hydrogeological model of the Candín-Fondón (A) and the Lieres (B) mining reservoirs

The capacity of the studied underground mining reservoirs in Asturias varies between 5 and 9 Mm3 and the water recharge they receive varies between 0.8 and 5.6 Mm^3/year (through an area of the associated basin that ranges from 9 to 47 km^2), so by means of regulation, a large capacity of water is available as a water resource for urban or industrial uses (Table 1). The flooding periods of these systems vary from 1 to more than 15 years, depending on the hydrogeological characteristics and the exploitation schemes.

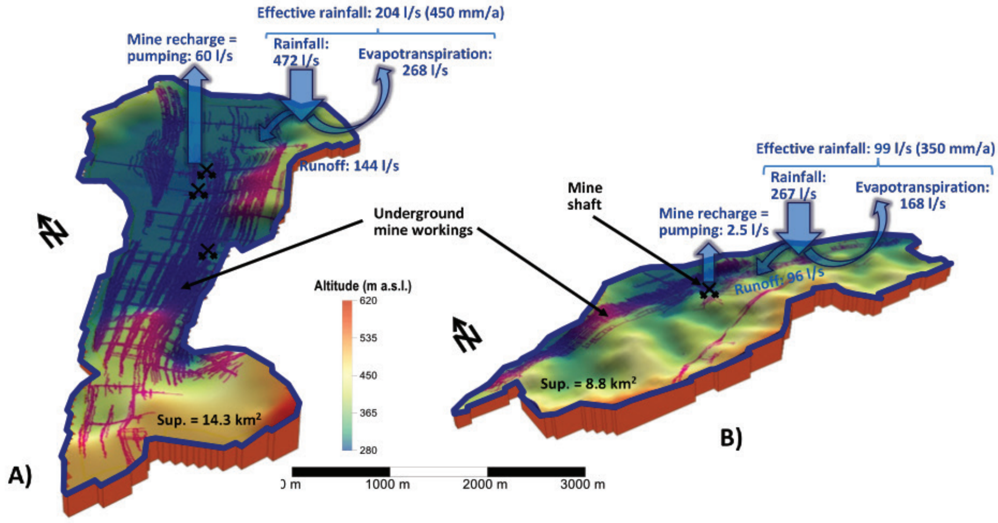

Figure 1 Recharge basin and conceptual hydrogeological model of the Candín-Fondón (A) and the Lieres (B) mining reservoirs

It is observed that the estimation of the flooding time of a mining reservoir depends on its volume of voids but is mainly negatively correlated with the water recharge it receives, which in turn depends primarily on the recharge area of the reservoir, as well as other factors such as the precipitation regime and the unexploited rock mass below the surface that will limit infiltration into the mining voids. All the considered mining reservoirs are located in the CCB, excepting La Camocha, that belongs to another sedimentary basin.

Fig. 2A shows the actual evolution of the Candín-Fondón reservoir flooding compared

Table 1 Comparison of (approximate) data from different mining reservoirs

Mining reservoir	Max. depth (m)	Length of galleries (km)	Aprox. volume of voids (Mm³)	Area of recharge (km²)	Water recharge (Mm³/year)	Aprox. flood duration (years)
Barredo-Figaredo (Mieres)	647	400	5.8	16.4	4.0	1
Candín-Fondón (Langreo)	700	598	8.0	14.3	1.8	5
Carrio-S. Mamés-Cerezal (Laviana-SMRA)	960	567	7.1	46.6	4.5	1
Santiago-S. Jorge-S. Antonio (Aller)	614	583	9.1	37.7	5.6	1.6
La Camocha (Gijón)	612	158	7.8	15.9	0.8	>15
Lieres (Siero)	780	242	7.0	8.8	0.08	>15

with that previously predicted with the GRAM and FEFLOW models. Analogies can be seen in the rise of the piezometric level and a good estimation of the total flooding period. However, accurately predicting the water level evolution is nearly impossible, and errors from using average values (recharge, hydrogeological parameters) must be considered. Model accuracy depends on the precision of input data, especially the hydraulic properties of the mined areas. Higher permeability and lower void volume (porosity, storage coefficient) lead to a faster water level rise, with the model being particularly sensitive to the storage coefficient (Álvarez *et al.* 2016).

Considering the recharge of the Mina La Camocha mining reservoir and assuming a constant daily consumption of 134 liters per person (average for Asturias), the minimum monthly recharge could supply over 4,200 people after proper water treatment. This estimate does not account for reservoir storage, but if it is considered, regulation becomes possible – allowing surplus water to be stored during high-infiltration months for use during drier periods. As shown in Fig. 2B, by storing excess water from October to February, the available supply could double to nearly 35,800 m^3 per month, meeting the needs of approximately 8,900 people. This would require only 0.05 Mm^3 of the reservoir's total 7.8 Mm^3 capacity.

The temperature of the mine water in the Asturian coal mines usually exceeds 20 °C and, considering all the mines in the CCB, geothermal energy of more than 200 thermal GWh/year could be produced by means of heat pumps, while consuming only 40 GWh of electricity (Jardón *et al.* 2013). The thermal conductivity of the rock mass varies between 1 and 5 W m^{-1} K^{-1} (Fig. 3A). Fig. 3B shows a thermal FEFLOW model of the Barredo-Figaredo reservoir obtained after a simulation of 30 years, where the sub-superficial areas keep low temperatures. Figaredo shaft is cooler due to the influence of the recharge coming from the Turón River. The coolest

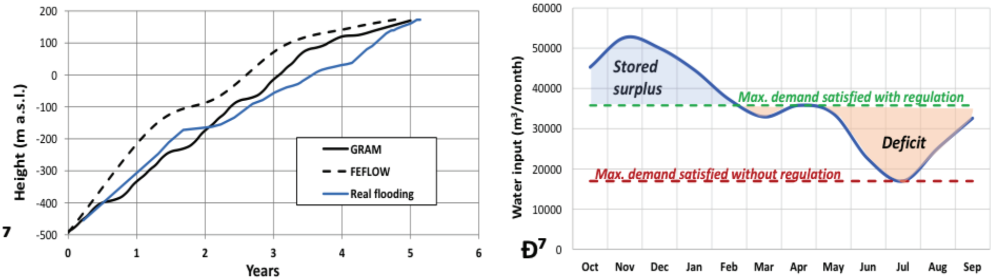

Figure 2 *Modelling of the flooding of the Candín-Fondón reservoir (A); Annual regulation of La Camocha reservoir for water use (B)*

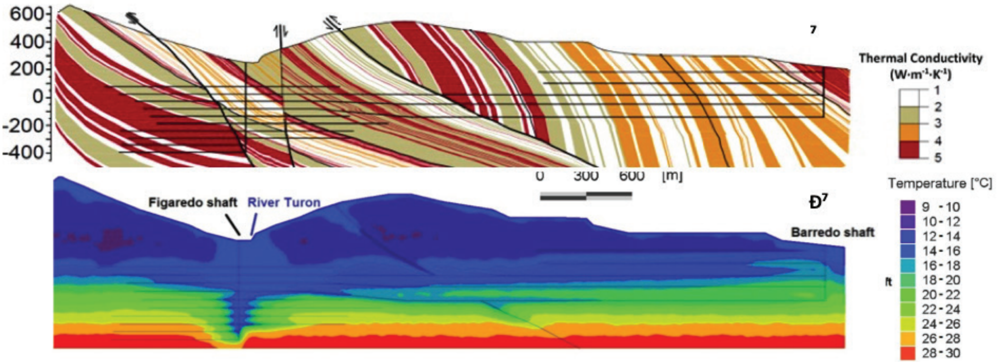

Figure 3 *Cross-sectional view of the Barredo-Figaredo reservoir depicting the thermal conductivity of the geological units (A) and thermal map of the reservoir after 30 years of simulated geothermal exploitation (B) (mod. Andrés et al. 2016)*

water is located near the shaft and advances through the horizontal galleries.

Álvarez *et al.* (2021) proposed a UPHS system for the Lieres coal mine in Asturias, featuring a 520 m net hydraulic head and a 40 MW capacity. The system's estimated cost is €75 million, but when integrated with wind turbines as a hybrid system, its economic viability improves, achieving a 19-year payback period and an NPV of €54 million. Following a hydrogeological study, this mine was chosen due to its depth, proximity to potential consumers, and low water recharge rate, which reduces pumping costs for controlled flooding. The design utilizes existing mine infrastructure to house most of the installation and the lower reservoir, cutting civil engineering costs, while the upper reservoir is located at the surface within the mining site.

Conclusions

A comprehensive hydrogeological characterization of the mining reservoirs improves the understanding of the flooding process, enabling its application to other mines for predictive purposes before flooding occurs. Additionally, a detailed reservoir assessment, is essential for managing mine water as both a water supply and energy resource.

Renewable energy storage is crucial for the future, and public-private partnerships are essential to rebuild economies towards greater sustainability. Geothermal and UPHS systems can be implemented in closed coal mines, but this requires prior hydrogeological characterisation of the reservoir. The methodology proposed here has potential applicability across various regions. These examples illustrate the value of heritage after mine closure, in line with the European Union's roadmap for energy transition.

Acknowledgements

The authors would like to thank the organisers of the IMWA 2025 congress, as well as the Principality of Asturias for their support in funding the AYUD/2021/51460 research grant.

References

Adams R, Younger P (2001) A Strategy For Modeling Ground Water Rebound In Abandoned Deep Mine Systems. Ground Water 39:249–261, doi: 10.1111/j.1745-6584.2001.tb02306.x

Álvarez H, Domínguez G, Ordóñez A, Menéndez J, Álvarez R, Loredo J (2021) Mine Water for the Generation and Storage of Renewable Energy: A Hybrid Hydro–Wind System. Int J Environ Res Public Hlth 18(13):6758. doi:10.3390/ijerph18136758

Álvarez R, Ordóñez A, De Miguel E, Loredo C (2016) Prediction of the flooding of a mining reservoir in NW Spain. J Environ Manage 184:219-228, doi: 10.1016/j.jenvman.2016.09.072

Andrés C, Álvarez R, Ordóñez A (2016) Estimation of thermal conductivity of rocks from their mineralogical composition (Asturian Coal Basin, NW Spain) for modelling purposes. Environ Earth Sci 75:266-275, doi: 10.1007/s12665-015-5037-8

Andrés C, Ordóñez A, Álvarez R (2015) Hydraulic and Thermal Modelling of an Underground Mining Reservoir. Mine Water Environ 36:24-33, doi: 10.1007/s10230-015-0365-1

Jardón S, Ordóñez A, Álvarez R, Cienfuegos P, Loredo J (2013) Mine Water for Energy and Water Supply in the Central Coal Basin of Asturias (Spain). Mine Water Environ 32:139–151, doi: 10.1007/s10230-013-0224-x

Matas-Escamilla A, Álvarez R, García-Carro F, Álvarez-Alonso L, Cienfuegos P, Menéndez J, Ordóñez A (2023) Mine water as a source of energy: an application in a coalfield in Laciana Valley (León, NW Spain). Clean Technol Environ Policy 25:2747-2760, doi: 10.1007/s10098-023-02526-y

Menéndez J, Ordóñez A, Álvarez R, Loredo J (2019) Energy from closed mines: Underground energy storage and geothermal applications. Renew Sust Energ Rev 108:498–512, doi: 10.1016/j.rser.2019.04.007

Menéndez J, Ordóñez A, Fernández-Oro JM, Loredo J, Díaz-Aguado MB (2020). Feasibility analysis of using mine water from abandoned coal mines in Spain for heating and cooling of buildings. Renew Energ, 146: 1166–76, doi:10.1016/j.renene.2019.07.054

Ordóñez A, Jardón S, Álvarez R, Andrés C, Pendás F (2012) Hydrogeological definition and applicability of abandoned coal mines as water reservoirs. J Environ Monit 14:2127–2136, doi: 10.1039/c2em11036a

Younger PL, Banwart SA, Hedin RS (2002) Mine water, Hydrology, Pollution, Remediation. Kluwer Academic Publishers, Dordrecht, The Netherlands

Integrated Water Balance, Streamflow and Quality Model for Holistic Determination of Security of Water Supply and Ecological Flow Requirements at a West African Mineral Sands Mine

Michael Palmer[1], Caroline Bladen[1]

[1]Jones & Wagener (Pty) Ltd Engineering and Environmental Consultants, 59 Bevan Road, Rivonia, 2191, Johannesburg, South Africa, palmer@jaws.co.za

Abstract

Management of water resources within the area of influence of mining is critical to ensure sufficient water at the correct quality for all stakeholders, including the mine itself and the associated ecological systems. To achieve this, a multi-disciplinary team of hydrologists, hydrogeologists, ecologists and engineers was assembled to determine the required ecological flows and water quality in the freshwater, wetland and estuarine systems surrounding the mine. An integrated GoldSim-based model was compiled to simulate streamflow and the mine water and salt balance, and utilised as the central tool to ensure that both the mining and environmental water objectives were met.

Keywords: Water balance, salt balance, streamflow model, water quality, ecological flow, ecological reserve, dam sizing, water security, mine water management

Introduction

Availability of the right volume of water, at the right quality, at the right time is essential for sustaining both aquatic and riparian ecosystems. The same can be said of mining operations. However, mining activities can negatively affect water resources by degrading land, altering watercourses, and exposing water to ore and tailings. Surface water in West Africa is an essential resource for both natural systems and local communities affected by mining. A comprehensive understanding of these competing needs was developed during the mine planning stage of Sierra Rutile Limited's (SRL) Sembehun project, with the aim to minimise environmental consequences and balance the mine's water requirements with those of the surrounding environment.

SRL intends to mine their Sembehun reserve, a mineral sands deposit, by open pit mining methods over a period of approximately 13 years (i.e. 2026 to 2039). Several watercourses flow through the mining area, transitioning from freshwater in the upper reaches to estuarine in the lower reaches and incorporating a complex combination of sensitive wetland, peat and mangrove habitats.

To ensure sufficient water supply for the mining operation, while ensuring the preservation of habitat and the associated aquatic fauna and flora, a multi-disciplinary team of specialists was assembled to work with the mine team, in a co-operative relationship, to achieve a mine design that would satisfy both mining and environmental objectives. A multi-disciplinary approach was adopted for the determination of the Ecological Flow (E-Flow) requirements of the surrounding watercourses, which consider both water quality and quantity requirements to preserve the surrounding habitat and associated aquatic fauna and flora. The process demonstrated the value of a detailed and integrated model (incorporating catchment runoff (streamflow), in-stream water quality, and the mine water and salt balance), when utilised as the key interfacing tool between mine planning and environmental teams. Such a model enables the assessment of mining scenarios and environmental mitigations, in an iterative manner, to mitigate the threat of mining-related environmental impacts in the form of, amongst others, reduction in catchment area (water quantity) and discharge of mine affected water (water quality).

Site Characterisation

Sembehun mine will occupy an area approximately 45 km2 in extent, shown on Fig. 1. Several watercourses drain through the proposed mining area, in a south-westerly direction. These watercourses are tributaries of the Bagru River, which drains into the Sherbro estuary. Tidal conditions dominate the Bagru River as it flows past the mining area and extend a substantial distance up the tributaries. Upstream of the tidal influence, freshwater conditions persist, where the in-stream water quality can be described as near pristine.

Rainfall, and the associated streamflow, in the Sembehun region is highly seasonal, with a Mean Annual Precipitation (MAP) of 2,811 mm. The high seasonality results in water security concerns for mining and industrial activities during the dry season (J&W 2024).

Several open pits are planned, where the ridges between the watercourses will be mined. Ore will be processed at a Wet Concentrator Plant (WCP). Pits will be backfilled with overburden material, as well as tailings material from the WCP for selected open pits, with in-pit Tailings Storage Facilities (TSFs), being established. In addition, an Initial TSF (ex-pit) will be required for the first three years of mining, until pit development is sufficient for in-pit tailings deposition.

Water required for minerals processing at the WCP will be sourced first from return water from the TSFs, with make-up water being sourced from an in-stream Process Water Dam (PWD), situated on the Solaieyea Creek. To minimise the influence of the PWD and water abstraction on the downstream aquatic environment, environmental releases from the PWD will be required.

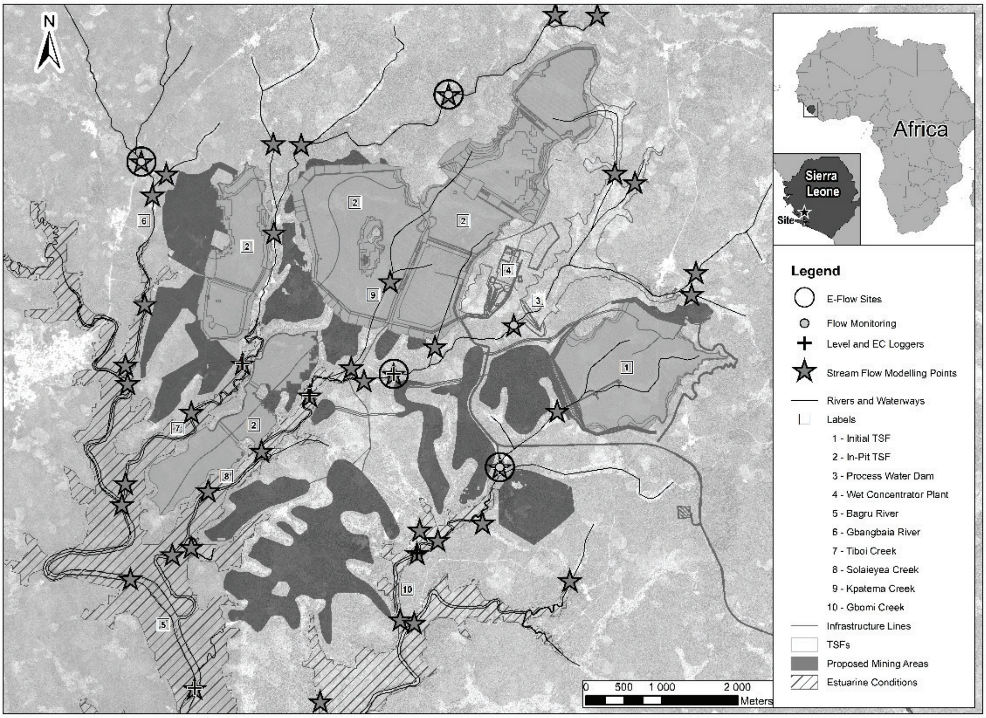

Figure 1 *Map of mining area.*

Groundwater and stormwater encountered within the open pits will be pumped into the adjacent watercourses, once suspended solids have been removed. Initial mine planning was that TSF return water and stormwater would be pumped to the PWD, for reuse in the WCP.

Potential threats due to mining were recognised by the mine planning team. These are expected to include direct loss of flow in the watercourses, due to abstraction of water for mining, loss of flow due to catchment reduction from the open pits and TSFs, change in baseflow to the watercourses due to the mine's interference with the groundwater regime, change in flow dynamics of the aquatic systems (for example seasonality and the freshwater-saltwater interface), deterioration in water quality and erosion as a result of mining, with consequent sediment deposition in watercourses and wetlands. These threats, in turn, can result in changes to the abundance and/or distribution of sensitive species, particularly in the dry season.

Overall Project Approach

With the key objective of supporting the mine design (in terms of availability of water and the associated required PWD capacity), while, at the same time, mitigating environmental impacts, a list of specialist studies required to determine the E-Flows requirements in the watercourses was compiled. Required studies comprised the following: hydrology, hydrogeology, geochemistry, wetlands, freshwater ecology and estuarine ecology. Several supporting studies were also required to provide data that would instill a greater degree of confidence in the outcomes of the studies and modelling. These studies included hydrological monitoring (rainfall, streamflow, water quality), estuary and river bathymetric survey, and sediment transport and geomorphology modelling. Mine design (i.e. Life of Mine (LoM) plan, stormwater planning, water management planning) was also required.

An integrated model was developed, incorporating catchment runoff and streamflow modelling for the mining area and the associated watercourses, as well as mine water and salt balance modelling. This model was used as the central interface between the mine design and the environmental studies determining the E-Flow requirements. It modelled the effects of the mining on the

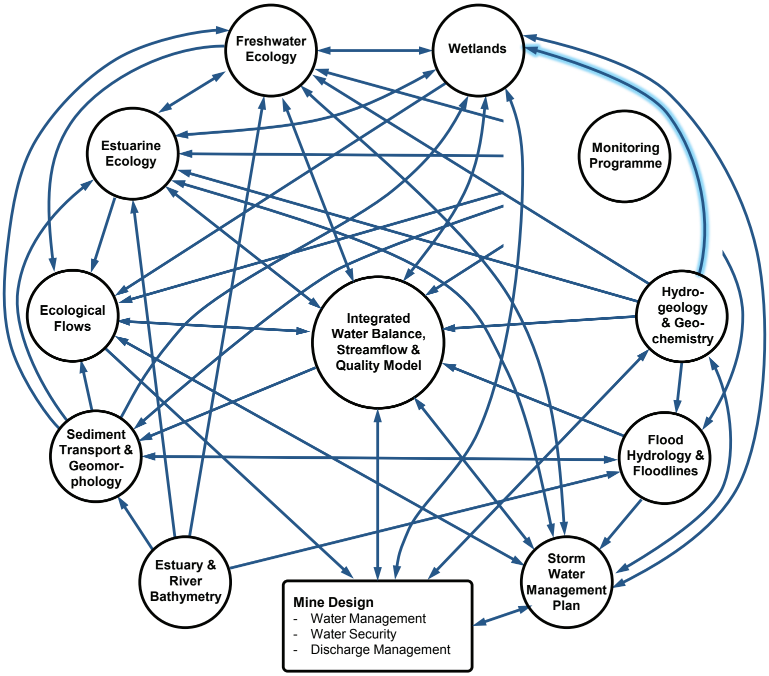

Figure 2 *Study inter-dependencies and flow of information (arrows indicate direction of flow of information, with double-headed arrows indicating flow in both directions in an iterative manner).*

water systems, providing this to the E-Flows team, and feeding the outcomes of the E-Flows assessments back to mine planning in an iterative process. Inter-dependencies and flow of information, including requirements for iteration between the various specialists, as well as the mine design team, were determined in an optimised, integrated approach. In this way the integrated model provided valuable input to the mine design team, in terms of the achievable assurance of supply and associated required capacity of the PWD, as well as input to the E-Flows team in terms of the baseline mining effects on streamflow and water quality. The E-flows teams provided feedback, in terms of acceptability of the anticipated changes in streamflow and water quality, with proposed mitigations. These were subsequently modelled in the integrated model. Associated influences on mining were then determined and fed back to the mining design team.

The specialist studies and flow of information are illustrated in Fig. 2. This complex network of information flows illustrates the inter-connectedness of the various studies and how the integrated model was a key input to the various studies and the mine design.

Integrated Model

GoldSim systems modelling software was used to develop a dynamic, daily time-step model for the mine and the associated catchments. The model comprised three main components, namely a catchment runoff and streamflow model, utilizing the Australian Water Balance Model (AWBM) (Boughton 2004) modelling algorithms, the mine water balance, and a water quality component modelling both the mine salt balance and the in-stream water quality. Utilizing the LoM plan, the effects of the mining activities on streamflow and water quality, over time, could be modelled.

Daily rainfall data, recorded at SRL's Area 1 operations, was available in a record spanning from 2000 to present. While this record was relatively short, spanning 23 years, it was determined by Golder (2018) and Jones & Wagener (2024) to be the most reliable rainfall record available in the region. A stochastic rainfall generator model, derived from Boughton (1999), was used in the model to generate statistically relevant synthetic rainfall data sets, which were used in Monte Carlo simulations to generate probabilistic water balance and streamflow output.

Inputs in the form of in-stream water quality monitoring data were obtained from the Environmental, Social and Health Impact Assessment (ESHIA) (Digby Wells 2023). This was used, along with typical mine water quality analysis results from Area 1, as input to the salt balance. In addition, mining inputs, such as, but not limited to, production, open pit, dam and TSF inputs, water management, demands and discharges, were obtained and incorporated in the modelling.

Output from the hydrogeology and geochemistry study were also utilised as inputs to the integrated model. These included anticipated groundwater ingress volumes and quality to the pits, streamflow losses due to mining and expected water quality in TSF return and seepage.

A streamflow monitoring programme was designed and implemented. Monitoring locations were identified, distributed across the mining area, including both freshwater

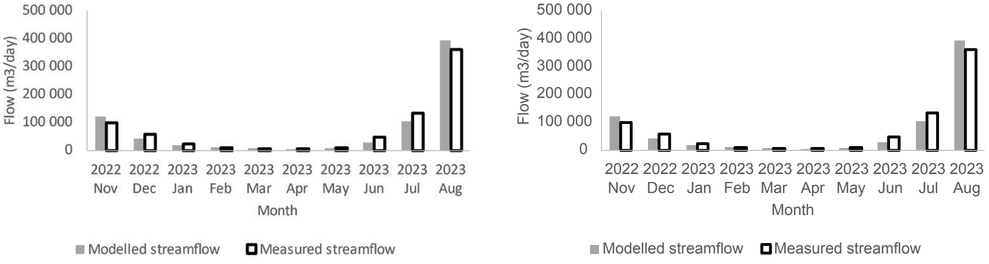

Figure 3 Streamflow calibration – modelled vs measured flows, Solaieyea Creek downstream of PWD (full period - left), (dry season – right).

and tidally influenced zones. A combination of continuous monitoring by means of water level loggers and EC probes, and weekly in-stream flow measurement using a hand-held velocity meter, was employed to monitor streamflow and EC for a period of 12 months (WCS 2023). This data was used to calibrate the streamflow model. It is acknowledged that one year is too short a period for calibration and validation of a streamflow model. However, the period was dictated by project time constraints.

The information was incorporated into the integrated model and the calibration achieved was considered reasonable, with the model considered suitable for predictive modelling. Fig. 3 illustrates the calibration achieved, by comparing the modelled versus measured streamflow, on a monthly basis, in the Solaieyea Creek, downstream of the proposed PWD.

Model Runs and Integration with Mine Planning and Specialist Teams

Baseline Model Outputs

Current status model runs were undertaken to develop reference (pre-mining) flows in the watercourses at each of the selected "Modelling Points" (MPs) (refer to Fig. 1). Monthly flows, expressed as various percentiles, based on the stochastic rainfall, were produced for each MP.

A preliminary storage-yield analysis was undertaken for the PWD, and it was determined that, at the initially planned PWD capacity of 2.9 Mm3, an assurance of supply of 93.5% would be achieved. To provide the desired assurance of supply of 95%, the PWD capacity would need to be 3.1 Mm^3.

Three water quality constituents were modelled, namely total dissolved solids (TDS), sulfate and aluminium (Al). It was determined by the hydrogeological and geochemical modelling that oxidation of sulfide in the ore and overburden material would result in mine water with low pH and elevated TDS, sulfate and metals (with Al used as a key indicator of metals toxicity to aquatic species, as directed by the freshwater ecologist (Tate 2024a)). Further, a lack of pH buffering capacity in the freshwater systems meant that should mine or tailings water be discharged directly into the freshwater reaches of the watercourses, without treatment, this would result in low pH and elevated TDS, sulfate and metals concentrations in the watercourses themselves.

Modelling results indicated TDS concentrations in the watercourses reaching up to 310 mg/L, from a pre-mining concentration of 50 mg/L and Al reaching up to 15 mg/L, from a pre-mining concentration of 0.03 mg/L. Similarly, the discharge of TSF return water into the PWD would result in TDS concentrations of up to 250 mg/L, with Al reaching 1.1 mg/L. These changes would be expected to have acute effects on the freshwater species, with an acute effect Al concentration being 0.1 mg/L (Tate 2024b). On the other hand, the discharge of mine water into the estuarine watercourse reaches was not considered by the estuarine ecology team to be problematic, given the high salinity and buffering capacity of sea water. The TDS concentration of the mine water was considered immaterial in relation to the TDS of sea water and Al (and other metals) would be expected to precipitate due to the high pH buffering capacity of the sea water (Clark 2024).

Iteration for Optimised Mine Design and E-Flows

Model results for each of the E-Flow sites were provided to, and utilised by, the E-Flows team. It was found that the freshwater system was most vulnerable to changes in streamflow, as well as quality, and the E-Flows assessment became driven by the freshwater system requirements.

Desired E-flows were determined by the freshwater specialists, accounting for seasonality, baseflow, freshets and floods, and confirmed in terms of available habitat (Tate 2024a). These were fed back into the integrated model and the required environmental releases, from the PWD, to achieve these flows, were determined. Mine assurance of supply was then re-assessed on this basis. It was found that the desired E-Flows resulted in an assurance of supply of only 85%, based on a PWD capacity of 2.9 Mm^3 – substantially lower than the mine's desired 95%. Through iteration in the integrated model, it was found that by reducing the E-Flows requirement by 10% during the dry season (November to May) an assurance of supply of 93.5% could be achieved – similar to the baseline assessment, though lower than desired. To achieve 95%, a PWD capacity of 3.1 Mm^3 would be required, at substantial additional cost.

A further workshop was held with the E-Flows team to assess the consequence of reducing the E-Flows requirement. These reduced E-flows were re-assessed by the freshwater specialists and the results indicated that this reduction could be tolerated by the system. This compromise was therefore presented to the mine design team, i.e. a reduction in assurance of supply, as well as environmental releases, without the need to increase the storage capacity of the PWD.

E-Flows could not be met in the Gbomi Creek, downstream of the Initial TSF, primarily due to the reduction in catchment due to the TSF. It was concluded that the only viable mitigation would be to reduce the duration of the flow reduction as much as possible by rehabilitating the facility as soon as possible, to return the surface runoff to the watercourse. This could reduce the impact by approximately four years (assuming a one-year rehab. period) (i.e. from eight to four years).

The above process addressed the water quantity aspects. Water quality in the watercourses was found to be affected primarily due to the intent to discharge pit water directly into the closest watercourse, as well as due to the mixing of TSF return water and freshwater in the PWD. It was recommended that pit water should not be discharged into the freshwater reaches, but rather conveyed by pipe to the tidal, estuarine zone and discharged at riverbed level to ensure that it makes contact with saline water, which lies below the freshwater due to its higher density. To address the water quality issues in the PWD it was recommended that a separate facility be provided at the WCP, to receive TSF return water and ROM stockpile runoff and feed it directly to the WCP, with only makeup water being drawn from the PWD.

The above mitigations were assessed in the integrated model and found to substantially improve the water quality predictions, achieving concentrations below the Al acute effect limit of 0.1 mg/L in all watercourses. This is shown in Fig. 4 for the MP located downstream of the PWD (LTC5) on the Solaieyea Creek. The exception to this is at the end of LoM, as mining ramps down, TSF returns will need to be managed to avoid water quality deterioration.

Conclusions

The integrated model was utilized as the pivotal tool for quantifying the effects of the mine and its planned water management practices on the flow and water quality regimes in the watercourses flowing through the mining area. Water management alternatives and mitigations were tested, allowing for rational decision-making on the part of the mine design team.

By adopting key mitigations, including balancing assurance of supply against cost and required E-Flows, adopting an accelerated TSF rehabilitation strategy, separating TSF return water and ROM stockpile runoff from the PWD by providing a separate facility for these, and only discharging pit water into the tidal reaches of the watercourses, at river bed level, it was shown that the mine's influence

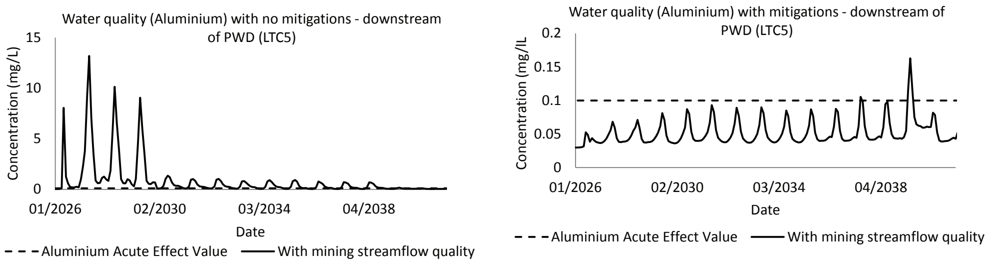

Figure 4 *Comparison between water quality (Al) with mining, no mitigation (left), with mitigation (right).*

on stream flow and water quality could be maintained at an acceptable level.

This study underscores the value of an integrated model as an essential tool to support mine planning and the management of the impacts on water resources. With a multi-disciplinary approach and a co-operative relationship between the mining and environmental teams, it is possible to achieve outcomes that satisfy both mining and environmental objectives.

References

Clark BM, Hutchings K, Dawson J and Bovim LA (2024) Sembehun II Environmental Flow Assessment (EFA): Estuarine Health & Scenario Assessment. Report no. 2076/3 prepared by Anchor Environmental Consultants (Pty) Ltd for Sierra Rutile Limited. 96 pp. Report No. 2076/3.

Boughton W (1999) A daily rainfall generating model for water yield and flood studies. Report no. 99/9.

Boughton W (2004) The Australian Water Balance Model. Environmental Modelling & Software 19 943–956.

Digby Wells (2023) Surface Impact Assessment Sembehun ESHIA Update. SRL7709.

Golder Associates, 2018. *Iluka Resources Limited, Hydrologic and Hydraulic Studies for Sembehun Project including SD1 Storage*, Sierra Leone. Golder Associates Report No. 1781577-019-R-RevA.

Jones & Wagener (2024) Sierra Rutile Limited Sembehun Definitive Feasibility Study Integrated Mine Water and Salt Balance Project Report. Report No. JW474/23/J888 – Rev1.

Tate R, Clark T, Patton P, Coertzen L, Verburgt L (2024a) Ecological Flow Requirement Study for The Proposed Sierra Rutile Limited Sembehun Project, Moyamba Region, Sierra Leone. Report no. 2053/5.

Tate R (2024b) SRL eFlow Project – Scenario Analysis Habflo Outputs.

Wetland Consulting Services (WCS) (2023) Interim Report of the Hydrological Monitoring at Area 5 of SRL.

Autonomous Robotic Exploration in Flooded Mines

Richárd Zoltán Papp[1], Máté Koba[2]

[1]*UNEXMIN Georobotics Ltd. 1045 Budapest, Hungary, ricsi@unexmin-georobotics.com,*
ORCID 0000-0002-1920-3567

[2]*UNEXMIN Georobotics Ltd. 1045 Budapest, Hungary, mate.koba@unexmin-georobotics.com,*
ORCID 0000-0002-8977-877X

Abstract

Underwater mine exploration is a complex task due to the confined space, the need for high precision and the extreme environmental conditions. Traditional human-based methods are not only risky but also inefficient in submerged environments. This abstract introduces UNEXMIN Georobotics's underwater robotic technology, which provides a safe, non-invasive, and highly efficient alternative to manual exploration, particularly in abandoned, flooded, or hard-to-access mine workings. The introduced robotic system allows us to collect valuable geological and structural data while substantially reducing human exposure to dangerous conditions. This work is important as it addresses the growing need for cost-effective, automated solutions in the mining industry.

This approach is centred around a novel underwater robotic platform designed for confined and extreme environments, specifically tight mine shafts that are often submerged and inaccessible by traditional means (Martins *et al.* 2018). The UX robotic technology incorporates advanced navigation systems, including a Doppler Velocity Log (DVL), inertial measurement units (IMU), multibeam sonar, 360° imaging sonar and high-precision laser modules. The robots are equipped with six cameras and optical cable connection to ensure precise, real-time data acquisition up to 1500 m water depth. What sets this methodology apart is the combination of these technologies in a modular, compact egg-shaped design that can access areas as small as 1 meter in diameter.

The technology's key findings include successful deployments in several test environments and active mine sites, where the introduced robotic system demonstrated its ability to navigate complex underwater environments, collect high-resolution 3D data, and perform tasks autonomously. In 2022, the robot set a world record by reaching 450 meters in depth during a dive in the Hranice Abyss, the world's deepest underwater cave, showcasing its capability to operate in extreme conditions.

The implications of the work done by UNEXMIN georobotics are broad. This technology can be applied to flooded mine exploration, water management in underground environments, geological surveys, and archaeological missions to preserve submerged historical structures. Additionally, it has the potential to substantially shorten the process of reopening flooded mines by providing detailed, real-time data without the need for dewatering or large-scale manual inspections. This technology enhances safety and efficiency. It offers new avenues for industries and governments to explore submerged environments while decreasing the risk and high cost associated with traditional and mostly non-applicable diving methods. As such, UNEXMIN Georobotics' underwater robots represent a breakthrough in the way we approach and manage flooded and confined spaces in mining and beyond.

Keywords: Robotics, underwater, autonomous, mapping, survey

Introduction

Overview of underwater mine exploration requirements

Underwater exploration poses a wide variety of technical and environmental tasks which needs to be addressed, this method is far more complicated than surface or aerial exploration. A principal factor to be resolved is the absence of natural light in deep waters, necessitating the employment of advanced sonar and laser-based mapping technologies. Furthermore, the high pressure encountered in deep environments restricts the utilisation of conventional equipment, thereby necessitating robust robotic systems with pressure resistance as a key attribute. The use of radio signals in water is severely limited, necessitating the development of alternative methods of communication such as optical cables or acoustic signals (Goh *et al*. 2009). The risks posed by flooded mines or underwater cave systems are exacerbated by the confined nature of these environments, which often have narrow passageways that restrict movement and increase the chances of entrapment. The presence of silt and debris as shown in (Fig. 1) can extremely reduce visibility, making navigation highly dependent on advanced sensors and rely more on sonar data instead of visual information to navigate properly.

Another concern is structural instability, as abandoned mines may have collapsed sections or unpredictable water currents that pose additional risks. Furthermore, the absence of standardised maps for many flooded mines means that robotic explorers must rely entirely on real-time data collection to construct navigable models. These difficulties make underwater mine and cave exploration one of the most demanding applications for autonomous robotic systems (Thomas Scott J. C. C. Day and Teague 2017).

The innovative robotic technology developed by UNEXMIN Georobotics Ltd. represents a pioneering approach to underwater mine and cave exploration, facilitating the creation of geo-referenced, highly accurate 3D maps. This capability is of considerable importance for several reasons. Firstly, flooded mines and underwater cave systems frequently lack existing maps or possess outdated and imprecise records due to structural collapses and sediment shifts over time. The employment of an autonomous underwater robot has the potential to facilitate non-invasive exploration of cave systems, a task that is of considerable scientific value. The unique adaptations exhibited by cave organisms to low food availability, hypoxic waters and darkness, make them a subject of particular interest.

The deployment of a robot equipped with cameras and sensors could assist in the documentation of biodiversity, the monitoring of population distributions and the collection of environmental data, without causing disturbance to fragile ecosystems (Pérez-Moreno *et al*. 2017). Utilising advanced navigation systems, including Doppler Velocity Logs (DVL), inertial measurement units (IMU), and multibeam sonar, UNEXMIN's robotic solution can generate detailed spatial models that provide a clear and up-to-date representation of these treacherous environments. In addition to mapping, the robotic system is capable of collecting critical environmental data, such as salinity, pH levels, and oxygen concentration. These parameters are critical for comprehending the geochemical conditions of submerged sites, which in turn influences decisions related to mine reopening, water management, and preservation efforts. For instance, measuring oxygen levels can assist in evaluating the potential for microbial activity that might lead to structural degradation, while pH and salinity data provide insight into corrosion risks for existing infrastructure. The integration of these environmental factors into a geo-referenced model, facilitated by this technology, has the potential to enhance exploration, as well as to provide informed decision-making support to industries, researchers and policymakers in the domains of resource management, safety and conservation of these hidden underwater worlds.

Importance of autonomous robotic solutions

The deployment of robots for the purpose of underwater mine and cave exploration offers outstanding advantages over traditional

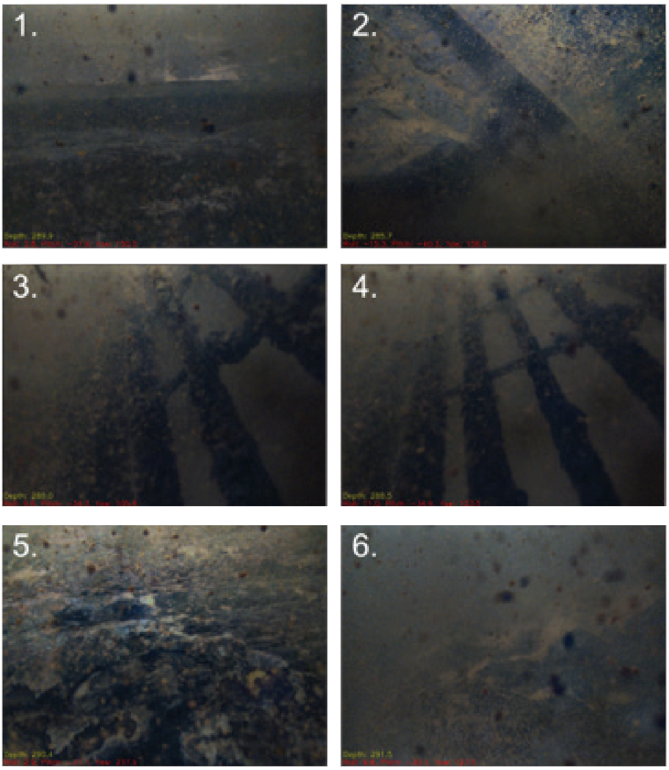

Figure 1 *Low visibility during a dive caused by murky water and sediments.*

human-based methods, primarily in terms of safety, efficiency, and data quality. A primary benefit is the elimination of human risk. Flooded mines and underwater caves present life-threatening conditions, including structural instability, low visibility, strong currents, and extreme pressure. By using autonomous or remotely operated robots, human divers are not exposed to these hazards, reducing the likelihood of accidents and fatalities (Courtenay *et al.* 2012).

Furthermore, the deployment of robots ensures unparalleled efficiency in exploring such environments. In contrast to human divers, who are limited in endurance and require extensive support systems, robotic systems possess the capacity to operate continuously for extended periods, thereby enabling the collection of high-resolution data without the necessity of decompression stops or breaks and of course to risk human life (Mcleod and Jacobson 2011). The integration of advanced sonar, laser scanning, and imaging technologies enables the generation of precise 3D maps of submerged structures, thereby facilitating insights that would be almost impossible to obtain manually. Furthermore, the ability of robots to access areas that are too tight, deep, or hazardous for divers is a notable advantage, rendering them indispensable for investigating abandoned mines, collapsed tunnels, or unknown cave systems. Their autonomy, capacity to adapt to unexpected obstacles, and the ability to relay real-time data make them a highly effective tool for exploring and managing underwater environments.

The robotic platform

Navigation and mapping

Sonar, an acronym for Sound Navigation and Ranging, is a technique that uses sound waves to detect and locate objects underwater. Initially, a sonar system emits sound waves, typically in the form of short pulses or continuous waves, through a transducer. The transducer serves to convert electrical energy into acoustic energy, thereby transmitting the sound waves into the water (Gray *et al.* 2019).

The sound waves travel through the water until they encounter an object, such as the seabed, a submerged structure, or marine life. The speed of sound in water is faster than in air, typically around 1 500 m/s. When the sound waves hit an object, they are reflected toward the source. The sonar system incorporates a receiving transducer that detects these returning sound waves, known as echoes. The echoes are then processed by the sonar system to create a visual representation of the underwater environment, including the determination of water depth, location of objects and identification of their shapes and sizes based on the strength and timing of the echoes.

The employment of advanced sonar systems, such as multibeam sonar, facilitates the emission of multiple sound beams concurrently, thereby ensuring comprehensive coverage of a vast area and enabling precise mapping of the seafloor and submerged objects. 360° imaging sonar, on the other hand, provides real-time visualisation of the surroundings by generating a comprehensive image of the underwater environment. Sonar technology finds extensive application in diverse fields, including underwater exploration, navigation, fishing, and search and rescue operations. Its value is particularly evident in environments where visibility is limited, such as turbid waters or deep-sea conditions, where it is indispensable for marine research and exploration.

In the context of underwater mine exploration, a considerable technological problem arises from the absence of GPS signals, thereby rendering these environments GPS-denied. To navigate and map such areas, the robotic system relies on a manually marked location provided by geologists, who base their information on accurate GPS data obtained from the surface. To effectively operate in these conditions, the robotic system utilises a combination of advanced technologies. To create detailed 3D models of the environment, the system employs a structured light system and sonar technology. The functioning of the structured light system is based upon the projection of a known pattern of light onto surfaces, with the subsequent capture of the resulting deformations by means of cameras. The analysis of these deformations enables the system to construct high-resolution 3D representations of submerged mine structures. Furthermore, sonar technology is used for the detection and location of objects underwater. The robot is equipped with a multibeam sonar, which emits multiple sound beams to cover a wide area, and a 360° scanning sonar, providing real-time visualisation of the surroundings for obstacle avoidance. Together, these technologies enable the robot to create accurate and detailed 3D maps of the underwater environment (Franchi *et al.* 2021).

Accurate positioning and navigation in GPS-denied environments rely on the Doppler Velocity Log (DVL) and a highly precise Inertial Measurement Unit (IMU). The DVL is a sonar-based instrument that measures the robot's velocity relative to the seabed or water column by emitting acoustic signals and analysing the Doppler shift of the returned echoes. The data gathered from this process is then integrated over time to estimate the robot's position using a method known as dead reckoning, which is critical in the absence of GPS. Simultaneously, the IMU provides highly precise measurements of the robot's orientation, acceleration, and angular velocity, information which is fundamental for maintaining a stable course and correcting any drift, thereby ensuring reliable navigation and positioning. The integration of a structured light system and sonar technology for 3D modelling with the DVL and IMU for accurate positioning and navigation enables the robotic solution to effectively explore and map environmentally testing underwater locations, such as those without GPS, ensuring safe and efficient exploration of previously inaccessible areas (Kok *et al.* 2017).

Instrumentation

The technology facilitates the deployment of multiple sensors, enabling in-situ analysis of mine water. This analysis is imperative for the monitoring and management of the environmental impact of mining activities. The sensors employed include a pH meter, an oxygen concentration meter, a temperature sensor, and a conductivity sensor and there is also a possibility for hyperspectral imaging. pH is a principal parameter in evaluating water quality, as it influences the solubility and bioavailability of nutrients and contaminants. For instance, acidic waters have been observed to leach harmful metals from mine waste, while alkaline waters have been found to indicate the presence of certain minerals. Monitoring pH levels is, therefore, a key aspect of environmental risk identification and ensuring that water quality remains within acceptable limits for aquatic life (Nordstrom 2011). The oxygen concentration meter measures the amount of dissolved oxygen in the water. In mining operations, the presence of pollutants can deplete oxygen levels, so monitoring this parameter helps assess the health of the aquatic ecosystem and the impact of mining activities. The robot is also equipped with a high precision temperature sensor that can measure water temperature with an accuracy of ±0.1 °C. The conductivity sensor quantifies the electrical conductivity of water, which is directly proportional to the concentration of dissolved ions. Elevated conductivity levels may be indicative of high salt or pollutant concentrations, which can result from mining operations. Conductivity monitoring facilitates the assessment of water quality and the identification of potential contamination. In-situ mine water analysis using these methods is imperative for several reasons. Primarily, it enables real-time monitoring of water quality, facilitating timely responses to potential environmental issues. Secondly, understanding the chemical and physical properties of mine water is essential for assessing its impact on local ecosystems and ensuring compliance with environmental regulations. By utilising these sensors, the robot contributes to a comprehensive understanding of the water quality in and around mining sites, supporting sustainable mining practices.

Hyperspectral imaging represents a sophisticated technological advancement that facilitates the acquisition and analysis of a broad spectrum of wavelengths across the electromagnetic spectrum. In contradistinction to conventional cameras, which are limited to the capture of images in three primary colours (red, green, and blue), hyperspectral imaging employs the collection of data across a multitude of contiguous spectral bands, thereby enabling comprehensive analysis of the materials present in the environment (Zawada 2003). The operational principle of this technology entails the utilisation of a specialised sensor to capture light reflected from surfaces in the form of a spectrum. The unique spectral signature of each material is characterised by its specific pattern of reflectance at different wavelengths (Tschannerl *et al.* 2019). By comparing these spectral signatures to those of known reference materials, the system can identify the composition and characteristics of the observed materials (De La Rosa *et al.* 2021). In the context of identifying mineralisation, hyperspectral imaging is particularly valuable. When the robot surveys an area, it can detect various minerals based on their spectral signatures. For instance, distinct reflectance patterns are exhibited by minerals such as silicates, carbonates, and oxides, which can be identified through hyperspectral analysis. This capability enables the robot to map and characterize mineral deposits with a high degree of precision.

Results

A 3D point cloud generated by the robotic system, illustrates the spatial configuration of a mine (Fig. 2). The dataset clearly shows a decline leading to two horizontal tunnels and a smaller chamber. The colour gradient in the point cloud clearly shows elevation variations, with the transition from red to blue indicating depth changes. This visualization supports precise geospatial mapping, aiding in the navigation of autonomous systems and facilitating further geological or mineralogical studies within the mine.

As described, with the help of the robotic platform, photogrammetric models also could be generated (Fig. 3). The model accurately depicts the geological features of the tunnel walls, revealing fine details such as miner-inscribed markings, structural

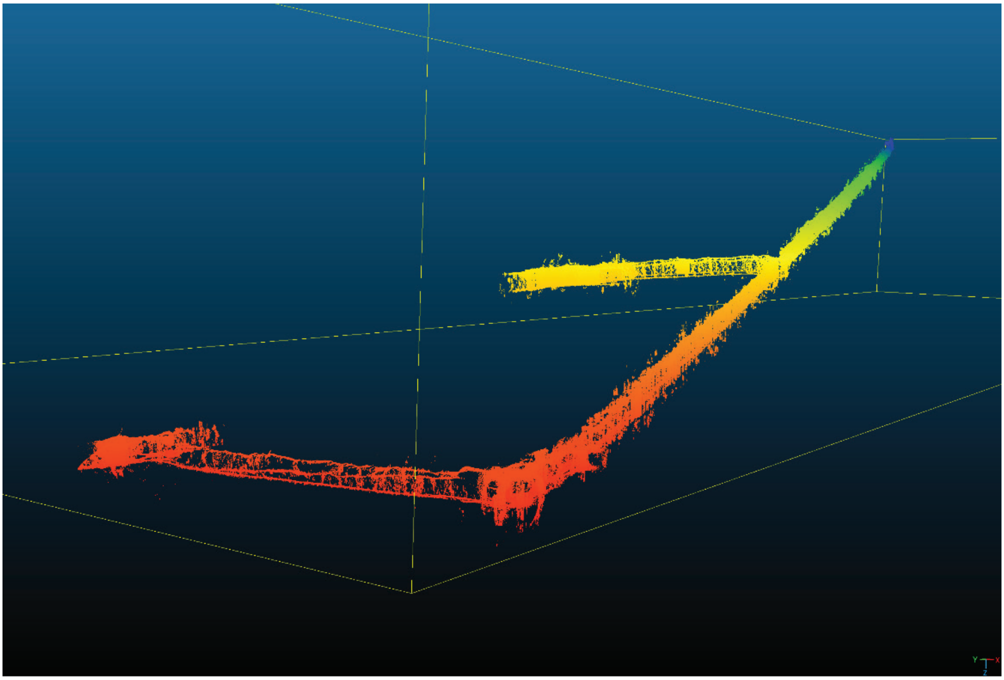

Figure 2 *3D point cloud of an underwater mine section.*

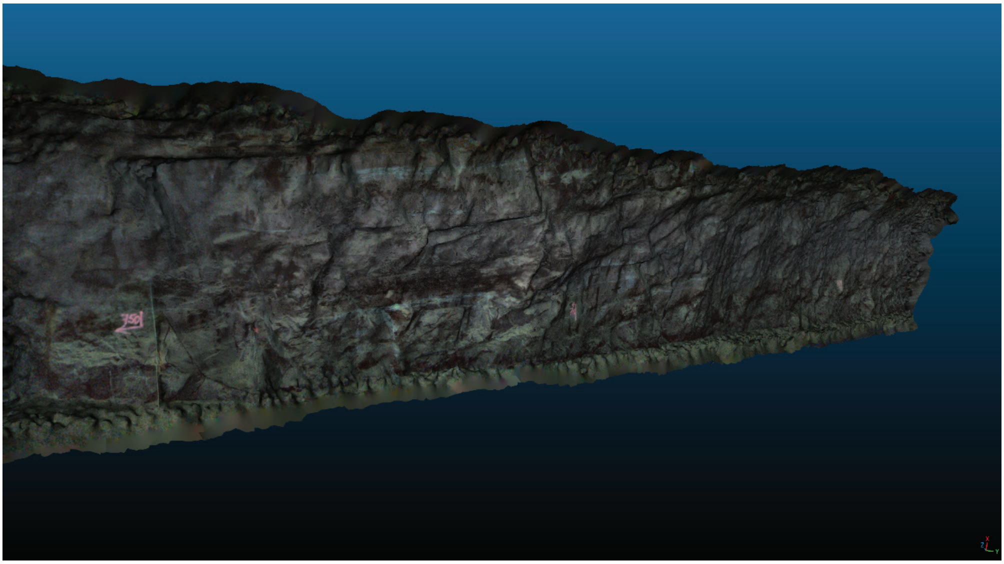

Figure 3 *3D Photogrammetric model of a mine decline.*

discontinuities, and surface textures. This high-fidelity representation facilitates a multifaceted analysis, including geological analysis, structural integrity assessments, and historical documentation of submerged mining environments.

Conclusion and prospective developments

At present, a major focus of development at UNEXMIN Georobotics Ltd. is to increase the level of autonomy for its robotic systems. Efforts are being made to enhance onboard decision-making capabilities using machine learning algorithms that enable the robot to assess its surroundings, navigate obstacles, and adjust its course dynamically without external input. The integration of advanced sensors and automated pattern recognition aims to minimise the necessity for remote human intervention, thereby enabling robots to execute missions autonomously, even in highly unpredictable environments. This enhancement is expected to markedly boost operational efficiency, rendering underwater exploration safer and more effective by empowering robots to adapt to unforeseen scenarios in real time. Also, the team is working towards to set a new world record by exploring the depths of the Hranice Abyss, the world's deepest known underwater cave, with the aim of reaching an unprecedented depth of 1,500 metres in a natural freshwater cave. This mission is not only seeking to set a new world record, but also to collect valuable geological and environmental data, thereby facilitating a more profound understanding of the cave system's structure and conditions. The insights gained from this exploration will contribute to scientific knowledge and advance the capabilities of autonomous underwater robotics in extreme environments.

UNEXMIN Georobotics Ltd has already developed advanced robotic solutions that have been adopted by gratified commercial clients in the mining sector. The company is now seeking to establish new partnerships with organisations in the mining industry with a view to exploring abandoned mines and conducting detailed underwater surveys. The aim of these collaborations is to provide cost-effective and highly precise assessments of flooded or hard-to-reach mining sites. These partnerships will enable safer, faster, and more efficient decision-making regarding mine reactivation, resource estimation, and hazard identification. The company's ongoing dedication to innovation and strategic collaborations is integral to its mission of shaping the future of autonomous exploration, while concurrently providing the mining industry with state-of-the-art technological solutions.

References

Courtenay G, Smith DR, Gladstone W (2012) Occupational health issues in marine and freshwater research. Journal of Occupational Medicine and Toxicology 7:4. https://doi.org/10.1186/1745-6673-7-4

De La Rosa R, Khodadadzadeh M, Tusa L, *et al* (2021) Mineral quantification at deposit scale using drill-core hyperspectral data: A case study in the Iberian Pyrite Belt. Ore Geol Rev 139:104514. https://doi.org/10.1016/J.OREGEOREV.2021.104514

Franchi M, Ridolfi A, Allotta B (2021) Underwater navigation with 2D forward looking SONAR: An adaptive unscented Kalman filter-based strategy for AUVs. J Field Robot 38:355–385. https://doi.org/10.1002/rob.21991

Goh JH, Shaw A, Al-Shamma'a AI (2009) Underwater wireless communication system. J Phys Conf Ser 178:012029. https://doi.org/10.1088/1742-6596/178/1/012029

Gray AC, Anderton M, Crane CD, Schwartz EM (2019) Design, construction, and implementation of an inexpensive underwater passive SONAR. Applied Acoustics 148:251–263. https://doi.org/10.1016/J.APACOUST.2018.12.022

Kok M, Hol JD, Schön TB (2017) Using Inertial Sensors for Position and Orientation Estimation. Foundations and Trends® in Signal Processing 11:1–153. https://doi.org/10.1561/2000000094

Martins A, Almeida J, Almeida C, *et al* (2018) UX 1 system design - A robotic system for underwater mining exploration. In: 2018 IEEE/RSJ International Conference on Intelligent Robots and Systems (IROS). IEEE, pp 1494–1500

Mcleod D, Jacobson JR (2011) The Role of Autonomous Underwater Vehicles in Deepwater Life of Field Integrity Management. In: All Days. OTC

Nordstrom DK (2011) Mine Waters: Acidic to Circmneutral. Elements 7:393–398. https://doi.org/10.2113/gselements.7.6.393

Pérez-Moreno JL, Balázs G, Wilkins B, *et al* (2017) The role of isolation on contrasting phylogeographic patterns in two cave crustaceans. BMC Evol Biol 17:247. https://doi.org/10.1186/s12862-017-1094-9

Thomas Scott J. C. C. Day PMDC, Teague J (2017) Autonomous vehicles for ore prospecting: robots in the air and water. Applied Earth Science 126:91–92. https://doi.org/10.1080/03717453.2017.1306291

Tschannerl J, Ren J, Zhao H, *et al* (2019) Hyperspectral image reconstruction using Multi-colour and Time-multiplexed LED illumination. Opt Lasers Eng 121:352–357. https://doi.org/10.1016/J.OPTLASENG.2019.04.014

Zawada DG (2003) Image processing of underwater multispectral imagery. IEEE Journal of Oceanic Engineering 28:583–594. https://doi.org/10.1109/JOE.2003.819157

Mine Closure Strategy for Pit Lakes Formation in Indonesia: Initial Framework for Open Pit Coal Mine

IK Dwika Paramananda, Sarah Hasanah, Lerian Nisa, Ginting Jalu Kusuma, Rudy Sayoga Gautama, Abie Badhurahman, Salmawati, Sendy Dwiki, Intan Nurul Rizki

Department of Mining Engineering, Faculty of Mining and Petroleum Engineering,
Bandung Institute of Technology, Indonesia

Abstract

The formation of pit lakes during coal mine closure poses complex environmental, hydrological, geological, and socio-economic challenges that require integrated and proactive planning. This study develops a strategic framework for pit lake formation in Indonesia by combining hydrological modelling, geochemical assessment, and regulatory analysis. A key focus is the use of nearby river water for controlled pit filling to mitigate acid mine drainage (AMD) and enhance long-term landscape sustainability. The framework is applied to Pit D2 in the Binungan River watershed, evaluating two scenarios: precipitation-only and river-supplemented filling. Hydrological modelling using HEC-RAS identifies an optimal diversion channel elevation of +4 masl to manage flood risks. Water quality modelling with PHREEQC demonstrates that river supplementation significantly improves water chemistry, reducing Fe concentrations from 211.57 to 0.94 mg/L, sulfate from 459.46 to 28.83 mg/L, and increasing pH from 5.64 to 6.07—approaching regulatory standards. Beyond improving water quality, the study highlights the potential of pit lakes as flood retention systems in high-rainfall areas such as Kalimantan. Given limited regulatory guidance on river use for pit lake filling, this research underscores the importance of considering such approaches within mine closure planning. Future efforts should further integrate pit lake development into early-stage mine design to support sustainable, multi-functional post-mining land use.

Keywords: Pit-lake, mine closure, coal mine, flood retention

Introduction

Open-pit coal mining in Indonesia commonly results in residual mine voids due to high overburden-to-coal stripping ratios. According to the Ministry of Energy and Mineral Resources (ESDM, 2020), there were 1,164 coal mining permit areas (WIUP) nationwide, many of which are expected to convert mine voids into pit lakes as part of mine closure. However, Indonesia's coal is geochemically prone to generating acid mine drainage (AMD), primarily due to the exposure of potentially acid-forming (PAF) material and its imbalance with non-acid-forming (NAF) material during mining operations.

To guide pit lake development, the government has established regulatory frameworks such as ESDM Regulation No. 7 of 2014, mandating reclamation, water quality monitoring, and mine void water management, and Government Regulation No. 22 of 2021, which sets water quality standards based on intended water use. The formation of pit lakes requires integrated planning of both water quantity and quality. While precipitation, runoff, and groundwater recharge are typical filling sources, these are often insufficient and slow, especially for large voids. Additionally, PAF exposure on pit walls can worsen water quality over time. Thus, engineered solutions such as controlled catchments and surface water supplementation must be considered.

This study evaluates the feasibility of using nearby rivers to fill a coal mine void in Berau Regency, primarily to prevent the formation of acidic pit lakes caused by the exposure of PAF materials. River water supplementation is explored as a geochemical mitigation strategy to reduce AMD risk while also supporting more sustainable post-mining land use.

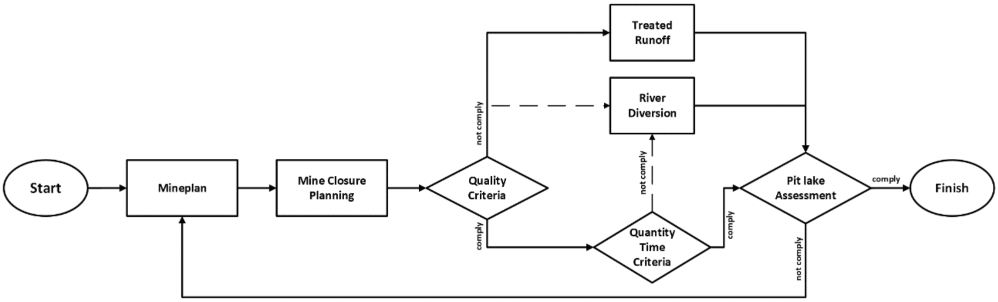

Figure 1 *Flowchart Pit Lake Formation Decision Making Tree.*

Methods

The methodology used in this study is based on the implementation of a decision-making tree strategy for pit lake formation, as illustrated in Fig. 1.

1. The primary output of mine planning and operations is an open residual void, which is typically documented in the mine closure plan. This plan includes dimensions and the proposed utilization of the remaining pit.
2. The conversion of the residual void into a pit lake requires consideration of several critical factors, particularly the water quality that will develop. The selection of an appropriate filling method is based on water quality modelling, assuming precipitation and surface runoff as the default inflow conditions.
3. If the modelled water quality of the pit lake does not comply with environmental standards as regulated by Government Regulation No. 22 of 2021, alternative runoff management strategies must be considered. These may include enhancing alkalinity to neutralize pit wall leachate or utilizing nearby water bodies with suitable quality.
4. Additionally, the timeframe for pit lake filling, which is generally proportional to the pit dimensions, must be considered. The use of nearby water bodies can be considered as an option to accelerate the filling process.
5. Once the pit lake filling model has been developed, a final evaluation against pit lake criteria must be conducted. If the established criteria are not met, the mine planning process must be reassessed iteratively to ensure the feasibility of pit lake formation.

Study Area

The Binungan Coal Mine site, which has been in production since 1996, is located in Pegat Bukur Village, Sambaliung District. This study focuses on Binungan Mine Operation - 01, specifically Pit D2, which is projected for conversion into a pit lake. Pit D2 commenced operations in 2012 and was ceased production by September 2022. It serves as the study location for implementing the pit lake formation strategy framework outlined previously. Pit D2 covers a surface area of 122.1 hectares, with a depth of 90 meters and an approximate volume of 41 million cubic meters. The pit is situated between two rivers—Kelai River and the downstream section of Binungan River—both of which are part of the Kalimantan V River Basin (Berau-Kelai). The location and longitudinal profile of Pit D2 are illustrated in Fig. 2.

According to data from the Berau-Kelai River Basin Authority, the Kelai River does not meet the Class 2 raw water quality standard based on East Kalimantan Regional Regulation No. 02 of 2011 (PUPR, 2019), primarily due to land-use pressures from settlements, agriculture, plantations, and mining in the upstream catchment. Interestingly, the elevated sulfate levels in the Kelai River could potentially stimulate sulfate-reducing bacteria (SRB) activity, which may help mitigate acidification within pit lakes. However, due to concerns over other contaminants, variable flow conditions,

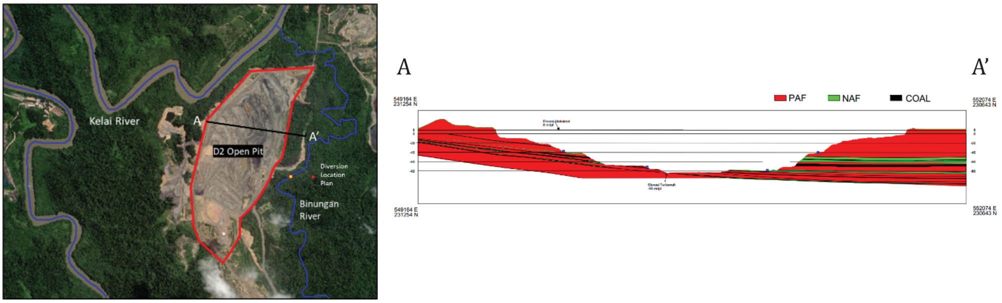

Figure 2 *Location of Pit D2 Relative to Surrounding Water Bodies and PAF-NAF Distribution.*

and long-term ecological risks, the Binungan River was selected as a more stable and environmentally suitable water source for controlled pit lake filling.

Data

The data used in this study include the geochemical model of Pit D2, the leachate conditions of PAF and NAF rocks in Pit D2, the catchment area conditions of the Binungan Watershed (DAS Binungan), and the current state of the Binungan River.

Geochemical Model and Leachate Water Quality of Pit D2

The PAF and NAF rock mapping for Pit D2, previously conducted by the company, has been validated using rock samples to develop a geochemical model. The geochemical modelling and leachate water quality assessment were conducted using kinetic testing on four rock samples through the Free Draining Column Leach Test (FDCLT) using AMIRA standards. These results serve as the basis for predicting the water quality of the future pit lake.

The leachate water quality data were obtained from four rock samples, which were analyzed using the FDCLT kinetic test method. These results form the basis for modelling the water quality of the post-mining lake and are presented in Table 1.

Binungan Watershed Conditions

The Binungan Watershed covers an area of 136 km^2, predominantly consisting of secondary dryland forest with a slope range of 0-5%. Within this watershed, the Binungan River extends approximately 35 km in length. The river has a slope gradient of approximately 0.04%, with a riverbed elevation of +2.5

Table 1 *Leachate Water Quality Results of Pit D2 Rock Samples Using FDCLT.*

No	Parameter	Unit	PAF-A	NAF-B	NAF-C	PAF-D
1	Aluminium	mg/L	27.87	2.84	1.27	15.79
2	Iron	mg/L	771.15	<0.1	1.57	308.31
3	Manganese	mg/L	7.85	<0.1	<0.1	1.03
4	Calcium	mg/L	13.64	182.93	57.35	7.87
5	Magnesium	mg/L	13.12	362.67	96.36	6.27
6	Natrium	mg/L	5.94	<0.01	3.22	1.13
7	Potassium	mg/L	1.70	<0.01	5.22	10.13
8	Sulfate	mg/L	684.32	7,428.22	1,409.64	1,730.59
9	Alkalinity as $CaCO_3$	mg/L	-	516.00	117.00	-
10	Chlorine	mg/L	2.35	<0.01	2.44	2.29
11	pH		5.65	8.20	8.06	2.87

Table 2 Binungan Rainfall and River Water Quality.

No	Parameter	Unit	Rainfall	Binungan River	No	Parameter	Unit	Rainfall	Binungan River
1	Aluminium	mg/L	0.001	3	7	Potassium	mg/L	0.2	0.98
2	Iron	mg/L	0.01	0.001	8	Sulfate	mg/L	2.1	2.32
3	Manganese	mg/L	0.01	0.04	9	Alkalinity as $CaCO_3$	mg/L	6.7	26.7
4	Calcium	mg/L	1.2	12.5					
5	Magnesium	mg/L	1.3	11	10	Chlorine	mg/L	0.1	41.8
6	Natrium	mg/L	0.6	3.67	11	pH		5.8	7.01

masl at the planned diversion point. The river's maximum width reaches 48 meters, while its baseflow discharge is approximately 10 m^3/ second, resulting in a water column height of about 1.5 meters. Binungan river and rainfall water quality that will be used for pit lake filling model are presented in Table 2.

Pit Lake Filling Model

The filling model was developed based on the geochemical classification, as outlined in Table 1, and follows the decision-making framework presented in Fig. 1. Based on these considerations, the pit lake filling scenarios are divided into two approaches: filling through precipitation and filling through a combination of precipitation and river diversion. The Binungan River's baseflow discharge of 10 m^3/second provides sufficient flow capacity to support controlled filling without significantly altering regional hydrology. However, recognizing that watersheds support diverse life forms and that population growth and land-use changes may increase future reliance on this ecosystem, post-mining lake development must prioritize long-term ecological sustainability, ensuring minimal impacts on aquatic habitats and surrounding biodiversity.

The water quality modelling expected to develop in Pit D2 as a post-mining lake based on geochemical characteristics follows the process illustrated in Fig. 3 and Fig. 4.

A hydrograph analysis of the Binungan River was conducted using HEC-RAS software, utilizing the SCS hydrograph method to determine the optimal elevation for the diversion channel. This was done to effectively capture flood discharge and volume flow passing through the Binungan River segment near Pit D2 (A-A'), as shown in Fig. 5. Using a 10-year return period rainfall, the maximum water level in the Binungan River was determined to be +6 masl. Additionally, baseflow data at the diversion cross-section indicated a water surface elevation of +3.5 masl. Based on this information, the optimal diversion channel level for the Binungan River was determined to be +4 masl.

Result and Discussion

Following the two previously designed scenarios as mentioned in methodology section, the water quality modelling for Pit D2 was carried out using PHREEQC software through Inverse Modelling, Forward Modelling, and Mixing Simulations. The results of the modelling are presented in Table 3.

Discussion

Several key water quality parameters of the proposed pit lake, as presented in the Table 3, meet the applicable environmental standards. However, dissolved iron (Fe) concentrations exceed the regulatory limits. Previous studies have demonstrated that this issue can be mitigated through various treatment approaches (Berg et al., 2019; Fan et al., 2018). Additionally, Government Regulation No. 22 of 2021 outlines specific chemical and biological parameters that must be met, some of which are beyond the scope of this study.

Based on the decision-making framework for pit lake filling (Fig. 1), the utilization of river water as a supplementary filling method can be considered, particularly in cases where geochemical constraints in the

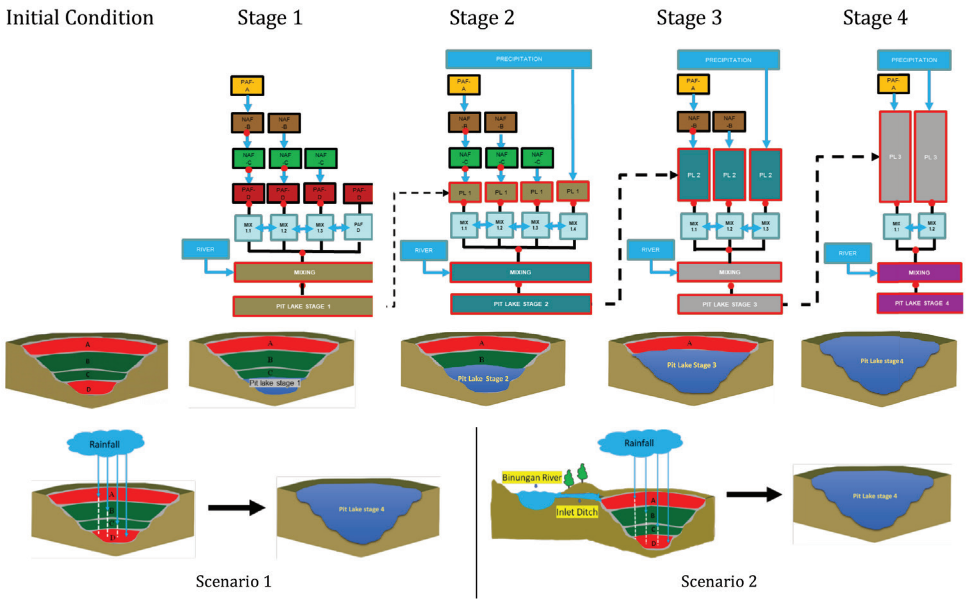

Figure 3 Pit Lake Filling Scenario.

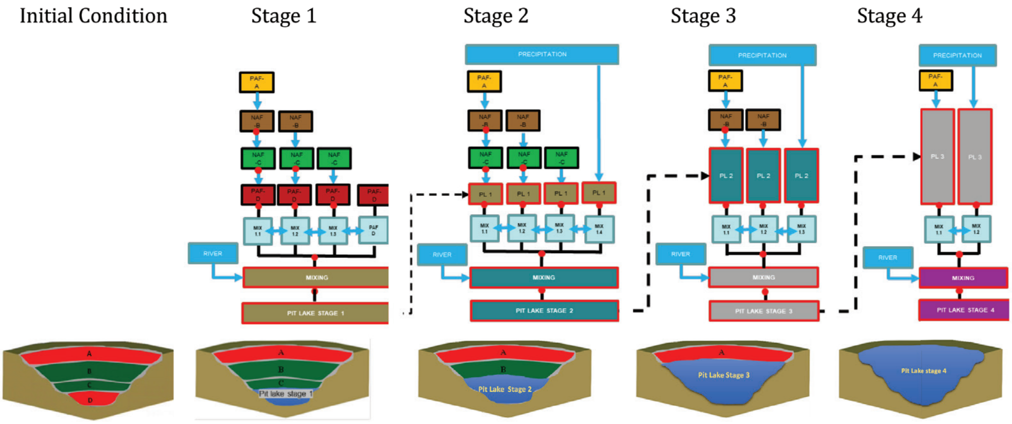

Figure 4 Pit Lake Water Quality Formation Model.

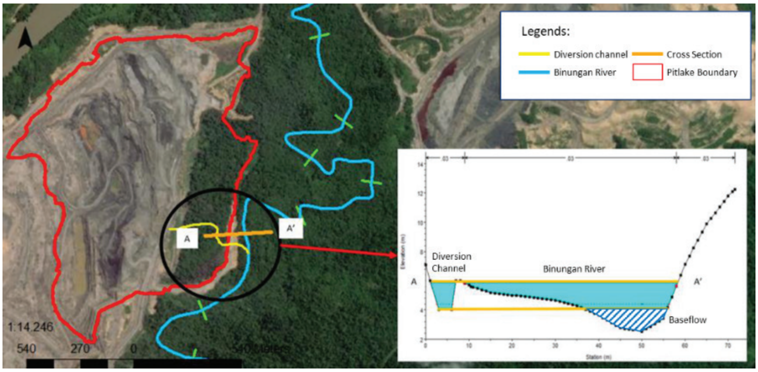

Figure 5 Diversion Channel Location from Binungan River to D2 Pit Lake.

Table 3 *D2 Pit Lake Water Quality Model.*

		Pit Lake Water Quality		Water Quality Standards*			
Parameter Scenario 1 Precipitation Only		Scenario 2 (Precipitation + River Diversion)	Class 1	Class 2	Class 3	Class 4	
pH		5.64	6.07	6-9	6-9	6-9	6-9
Sulfate	mg/L	459.46	28.83	300	300	300	400
Iron	mg/L	211.57	0.94	0.3	-	-	-
Manganese	mg/L	3.51	0.14	0.4	0.4	0.5	1

*The water quality classification according to Government Regulation No. 22 of 2021 is as follows:

- Class 1: Water suitable for drinking water sources and other uses requiring similar water quality.
- Class 2: Water suitable for water-based recreation facilities, freshwater aquaculture, livestock, irrigation, and other uses requiring similar quality.
- Class 3: Water suitable for freshwater aquaculture, livestock, irrigation, and other uses requiring similar quality.
- Class 4: Water suitable for irrigation and other uses requiring similar quality.

pit limit natural water quality improvement. This approach not only ensures that the resulting pit lake meets environmental carrying capacity standards as required by Government Regulation No. 22 of 2021 but also enhances the potential function of the lake as a flood retention system.

Currently, Indonesian regulations permit river diversions under specific conditions. Regulation of the Minister of Public Works and Public Housing Number 4 of 2024 on River Diversion stipulates that any modification to river flow must include a hydrological and hydraulic assessment, considering factors such as design flood discharge, flow profiles (including depth, velocity, and pattern), erosion, and sedimentation dynamics. Given these regulatory frameworks, the use of river water for pit lake filling, as outlined in the proposed strategy, presents a viable and potentially sustainable solution for post-mining land use.

Conclusions

Based on the analysis conducted, the utilization of rivers as an alternative for pit lake filling is feasible. This decision should be grounded on the pit lake model, particularly if precipitation-based filling alone results in water quality below environmental standards for pit lakes. Additionally, the use of pit lakes for flood retention should be considered. Currently, Indonesian regulations do not explicitly govern this aspect, leading to limited recognition by coal mining companies and the government. Given Indonesia's high rainfall, the prevalence of PAF rock formations, and the massive dimensions of former mining pits, the potential for pit lakes as flood retention systems remains largely untapped.

However, several key considerations must be addressed, including regional watershed water balance, accurate geochemical modelling, social and environmental impacts assessment of river diversion, both in terms of flood discharge and full river redirection, and criteria for pit lake feasibility, including dimensions, water quality, and filling duration.

Future research should focus on integrating pit lake formation models into mine planning as an iterative approach to minimize long-term management requirements. Additionally, studies should examine the long-term hydrological, hydrogeological, and ecological impacts of river utilization for pit lake filling and pit lake function as flood retention systems.

Acknowledgements

The authors would like to thank PT Berau Coal for providing data and assistantships through the ITB-PT Berau Coal Mine Closure Planning Project Scheme.

References

Berg, J. S., 1¤, I. D., Zé Quel, J., Duverger, A., Lamy, D., Laberty-Robert, C., & Miot, J. (2019). Microbial diversity involved in iron and cryptic sulfur cycling in the ferruginous, low-sulfate waters of Lake Pavin. https://doi.org/10.1371/journal.pone.0212787

Fan, Y. Y., Li, B. B., Yang, Z. C., Cheng, Y. Y., Liu, D. F., & Yu, H. Q. (2018). Abundance and diversity of iron reducing bacteria communities in the sediments of a heavily polluted freshwater lake. Applied Microbiology and Biotechnology, 102(24), 10791–10801. https://doi.org/10.1007/s00253-018-9443-1

Indonesia Government (2024). Pengalihan Sungai. Regulation of the Minister of Public Works and Public Housing Number 4 of 2024.

Indonesia Government (2021). Penyelenggaraan Perlindungan dan Pengelolaan Lingkungan Hidup. Government Regulation Number 22 of 2021.

McCullough, C. D., & Schultze, M. (2018). Engineered river flow-through to improve mine pit lake and river values. Science of The Total Environment, 640–641, 217–231. https://doi.org/10.1016/J.SCITOTENV.2018.05.279

Paramananda, I. K. D., Badhurahman, A., Kusuma, G. J., Dwiki, S., Salmawati, & Gautama, R. S. (2023). Modelling of Coal Pit Lake Quantity and Quality for Mine Closure (Case Study ON2 Area, Lati Mine Operation, Berau Coal). https://www.imwa.info/imwaconferencesandcongresses/proceedings/332-proceedings-2023.html

Tuheteru, E. J., Gautama, R. S., Kusuma, G. J., Kuntoro, A. A., Pranoto, K., & Palinggi, Y. (2021). Water balance of pit lake development in the equatorial region. Water (Switzerland), 13(21). https://doi.org/10.3390/w13213106

Wulandari, D., Gautama, R. S., Kusuma, G. J., & Badhurahman, A. (2024). Simulasi Pengisian Lubang Bekas Tambang Pit D2 Site Binungan 01 Kalimantan Timur. Jurnal Pertambangan, 7(4), 191–197. https://doi.org/10.36706/JP.V7I4.1536

Brine Migration from Deep Flooded Abandoned Salt Mines and its Influence on Surface Stability

Kieran Parker[1], Rebecca Ní Chonchubhair[2] , Alessandro Novellino[3]

[1]*Geological Survey of Northern Ireland/British Geological Survey, Adelaide House, 39-49 Adelaide Street, Belfast BT2 8FD, UK, kiepar@bgs.ac.uk ORCID 0000-0001-8314-816*

[2]*Geological Survey of Northern Ireland/British Geological Survey, Adelaide House, 39-49 Adelaide Street, Belfast BT2 8FD, UK, rebch@bgs.ac.uk ORCID 0009-0008-3177-0178*

[3]*British Geological Survey, Environmental Science Centre, Keyworth, Nottingham, NG12 5GG, UK alessn@bgs.ac.uk ORCID 0000-0001-9682-9056*

Abstract

Historic salt mining at Carrickfergus, Northern Ireland has left a legacy of hazards including surface subsidence and land contamination through brine water discharges. Three abandoned salt mines, hydrologically connected, pose a risk to overlying infrastructure and properties and the environment. Post closure, the mines are undergoing active subsidence resulting in crown-hole development and a series of extensive brine discharges at surface contaminating the surrounding lands and watercourses. Numerous assessments and monitoring methods, conducted over decades, have been implemented to understand the processes of instability with the results indicating a cyclic direct connection between surface instability and brine discharges.

Keywords: salt mines, ground stability, brine discharge, multiphysics integration, geodetic monitoring

Introduction

The abandoned Duncrue, French Park and Maiden Mount salt mines are located directly adjacent to each other within the town of Carrickfergus, Northern Ireland. Situated on an elevated slope Maiden Mount is the upper and mostly northly mine working and Duncrue the lower mine with French Park located between the two (Fig. 1). There is an elevation difference of 50m between the three mines. Operating from 1853 to 1958, all three mines initially worked independently using conventional methods, later changing to solution mining methods. Brining operations have left a legacy of instability as a result of dissolution of the mine support pillars due to water injection. Surface monitoring data collected since 1991 shows the area overlying the mines are undergoing active subsidence and heave. A public road, public water supply intake, residential properties and the Belfast Gas Transmission Pipeline are located on the lands overlying and adjacent to the mine site

Geological setting

Carrickfergus is situated on the south-eastern edge of the Antrim Plateau on a low lying coastal plain rising in elevation to the west. The superficial geology is dominated by boulder clay till and tidal flat deposits of clay and sand (Table 1). The bedrock geology is dominated by lava flows of the Lower Basalt Formation at elevations towards the north-west and the Triassic Mercia Mudstone Group on the coastal plains. Between these two dominant features, at elevations above 100 meters, is the Cretaceous Ulster White Limestone Formation (UWLF), Waterloo Mudstone Formation (WMF) and Triassic mudstones of the Penarth Group (PNG) and Mercia Mudstone Group (MMG). A number of north-south trending faults cut across the greater Carrickfergus area (Mitchell *et al.* 2004).

Carrickfergus is predominately MMG bedrock, a fine-grained mudstone with silty horizons which, from an engineering

Table 1 Summary geology of the greater Carrickfergus area. (Mitchell, 2004)

Age	Group/Formation	Lithology
Quaternary	Till	Boulder clay, sand & gravels
Paleogene	Lower Basalt Formation	Basalt
Cretaceous	Ulster White Limestone Formation	Limestone, hard white chalk, with flints and basal glauconite-rich beds
Jurassic	Waterloo Mudstone Formation	Grey mudstone with thin limestone beds
Triassic	Penarth Group	Dark grey mudstone
Triassic	Mercia Mudstone Group	Red and green mudstone and marl with thick salt bands

perspective, has a high bearing strength (Cigna et al, 2017). Gypsum occurs in veins and anhydrite as irregular nodules. Halite beds occur in the lower sequences of the MMG ranging in thickness up to 40 m.

The Maiden Mount, French Park and Duncrue mine workings are situated on the MMG with the northern boundary containing PNG and WMF. Maximum superficial till coverage is 20 m at Maiden Mount and 15 m at French Park (Griffith *et al.* 1983).

History of mining

Mine development started in 1853 and by 1870 three salt mines operated directly adjacent to each other. Both Maiden Mount and French Park mines extracted two halite beds while Duncrue extracted one. The mines initially operated using conventional mining methods using room and pillar design. As the mines developed, French Park and Duncrue mines became hydrologically connected to facilitate a change to uncontrolled brining operations. Maiden Mount continued to operate independently, adopted solution mining however, it did not develop any engineered connection to the adjacent French Park mine.

- ***Maiden Mount mine*** operated from 1869 to 1937 using conventional room and pillar methods. In 1953 brine production started at the mine and continued until 1958. The depth to the workings is 278 m below ground level (bgl) with an extraction height of 13 m, in areas worked out, and 33 m within the brined void (Atkins, 2004). The last recorded mine plan, based on underground surveying is dated 1937. Production records show 47,270 t of salt was produced during the brine operations between 1953 and 1958, equating to a further volume of 21,000 m3 halite removed (Atkins, 2009).
- ***French Park mine*** opened in 1870. A tunnel to extract brine was constructed within the mine in 1896 to connect the adjacent, closed Duncrue mine. The tunnel stopped short of the Duncrue mine and was connected via a series of inclined boreholes. Brining operations continued until 1952. Average depth of workings is 203 m bgl with an extraction height of 10 m, in areas worked out, and 28 m within the brined void (Atkins, 2004).
- ***Duncrue mine*** opened in 1853. Instability is first recorded in 1865 with the failure of a pillar close to the shafts which then propagated to adjacent pillars. Due to concerns on the stability of the workings, underground operations ceased in 1871. From 1896, brine was pumped from the mine through connections to French Park mine. Brine operations ceased in 1938 following a collapse which destroyed the connection to French Park mine. The average depth of workings is 180 m bgl with an extraction height of 11 m (Atkins, 2004).

Monitoring and assessment methods

The assessment and monitoring of the three mines include:

- Precise levelling and sub-surface extensometer
- Ultrasonic, sonar cavity and Close Circuit Television surveys
- Groundwater level monitoring and mine water salinity
- Multi geophysics: seismic, electrical resistivity and electrical self-potential
- Interferometry Synthetic Aperture Radar (InSAR)

Data from these surveys is used to determine ground motion at various locations, ascertain the structure and migration of the mine voids and assess the interior condition of the mines and evolution of mine water processes and pathways.

Six probe boreholes were developed into Maiden Mount (3) and French Park (3) mines. Each probe hole contained extensometers and facilitated access to collect groundwater levels, measure saline concentrations at various levels and enable ultrasonic and CCTV surveys of the mine to be carried out. Ultrasonic and CCTV show the mines to be flooded, and all support pillars completely dissolved or are in a very poor state due to dissolution as a direct result of brining. At each probe hole it is noted that limited salt is retained on the mine roof, resulting in the exposure of the MMG at various points and this is more pronounced at freshwater injections points such as old shafts and injection hole (Atkins 2009). Sonar cavity surveys carried out in the 1990's identified the Maiden Mount mine cavity had migrated towards surface (Arup and Partners 1992). This void migration led to the development of crown holes in 2001 and 2006 resulting in surface depressions exceeding 100 m in diameter and 18 m in depth.

Results

The results of precise levelling show a steady downward trend of the surface overlying Maiden Mount, while at French Park the same trend occurs at a number of monitoring points however, a number of others points record variable periods of recurrent heave and subsidence. Data from Duncrue shows relative stability across the site with one monitoring station, located at its boundary with French Park, recording significant cumulative subsidence.

Brine Seepages

Four notable large scale brine seepages occurred at French Park, two in 2001, one in 2004 and 2005 continuing for periods exceeding 18 months. Smaller scale discharges and salt patches at surface are routinely observed on a regular basis (Parker 2023). In the months prior to crown holes developing at Maiden Mount, salt patches were reported on lands adjacent to the shafts at French Park and following collapse saline springs developed at the same areas (Atkins 2003). At the same time, there was an increased rate of heave at monitoring stations across French Park (Atkins 2004). There is no direct evidence of any interconnections between the two mines, however, the data indicates an apparent relationship between the crown hole appearing and the emergence of brine springs downslope. At the time of the 2006 crown hole, water levels at Maiden Mount decreased by more than 9 m while at the same time, at French Park it rose by almost 8 m.

The crown hole at Maiden Mount is primarily fed by surface water. Salinity levels within the crown hole are stratified with saline concentrations greater with depth, however, concentrations are vastly lower than those measured at the saline springs down slope. This rules out the possibility of water within the crown hole infiltrating pathways within

***Table 2** Laboratory results of water analysis of samples taken at various points within the three probe holes (FP1, FP2 & FP3) at French Park.*

Sample	Depth (m bgl)	Temp (°C)	pH	Na (g l^{-1})	Cl (g l^{-1})
FP1-A	192.65	15.7	7.14	54.4	82.2
FP1-B	189.50	14.8	7.06	58.2	27.5
FP1-C	186.50	14.8	7.02	74.8	35.3
FP1-D	183.50	15.7	7.08	82.7	38.9
FP1-E	180.50	14.2	7.05	61.0	28.5
FP2-A	197.90	14.9	7.04	80.1	43.4
FP2-B	192.00	14.6	7.02	76.7	35.4
FP2-C	188.00	14.8	7.00	89.9	39.3
FP3-A	227.00	15.3	7.29	85.3	37.6
FP3-B	122.96	13.1	7.36	12.4	52.9

the shallow quaternary till and springing out downslope to create the saline springs. Salinity measurements taken from within the French Park mine indicate a near saturation brine within the flooded sections (Table 2).

Structure and groundwater pathways

The borehole records for the monitoring wells note heavy fluid loss during drilling suggesting some form of mining induced fracturing of the mudstones has occurred. It is proposed migrating voids that have reached surface has resulted in the overlying MMG to be severely brecciated above the mine. This is supported by the borehole logs which details heavily fractured rock. The MMG, recorded within the area, is of low permeability and does not act as a good pathway for fluid movement (Mitchell *et al.* 2004) however brecciation and fracturing as a result of void migration will have developed additional groundwater pathways to surface. Regular monitoring also shows old mine shafts and probe holes act as good pathways to surface for groundwater.

Multi-geophysical techniques using seismic and electrical resistivity surveys combined with electrical self-potential (SP) surveys were conducted to characterize the geological and hydrological processes driving the mining hazards. Resistivity and seismic refraction were acquired to characterise the subsurface structures while patterns within SP profiles and resistivity-velocity images of the subsurface were used to identify brine plumes, groundwater flow and underground cavities. Results from the geophysical surveys identified compositional changes and deformation altering the geochemistry of the groundwater. Water ingress to the underlying strata from crown holes has led to gravitational slumps as a result of dissolution of the halite bearing strata. This has resulted in deformation and stepped thrusts coincident with brine migration to surface. The occurrence of brine migration to surface at French Park is more prevalent following Maiden Mount surface subsidence as a hydraulic head in the deep mine induced by freshwater injection to the crown hole at surface promotes the movement of saline waters through pathways created by weaknesses within the strata, boreholes and shafts leading to extensive land contamination events (Meju *et al.* 2023).

Interferometry Synthetic Aperture Radar (InSAR)

Surface levelling data combined with subsurface extensometer and mine water levels have shown to provide an indicator of brine transport to surface. Decreasing surface and water levels at Maiden Mount in combination with uplift in surface and water levels act as a precursor to large brine seepages at surface. To better understand how monitoring surface motion can be utilised to maximum effect and provide a near-real time early warning of both subsidence and brine discharge events, satellite InSAR data was evaluated using historic data from three European Space Agency satellites spanning the four decades: ERS (1992-2000), ENVISAT (2002-2010) and Sentinel 1 (2014-2022). InSAR provides regular ground deformation measurements with millimetric accuracy that allow users to reconstruct the kinematics of the motion and correlate it to environmental factors such as mining. One of the main drawbacks of InSAR is its reliance on stable targets to provide reliable measurement points (Parker *et al.* 2024), and it generally does not provide reliable deformation data over areas of vegetation (Garthwaite 2017).

InSAR provides regular ground motion data and wide coverage to millimeter scale without the requirement to visit the site, providing a cost-efficient technique. The results returned from the three satellites showed relative stability however target coverage is poor (figure 2) so we cannot exclude the possibility of the area moving. The results however did identify those areas of land where no acquisitions are being recorded due to the absence of stable ground reflector targets and were InSAR artificial targets might be placed in the future to improve coverage.

Conclusions and future work

The mine site at Carrickfergus poses a risk to infrastructure through instability while also posing an environmental risk to the overlying lands due to contamination. Research and

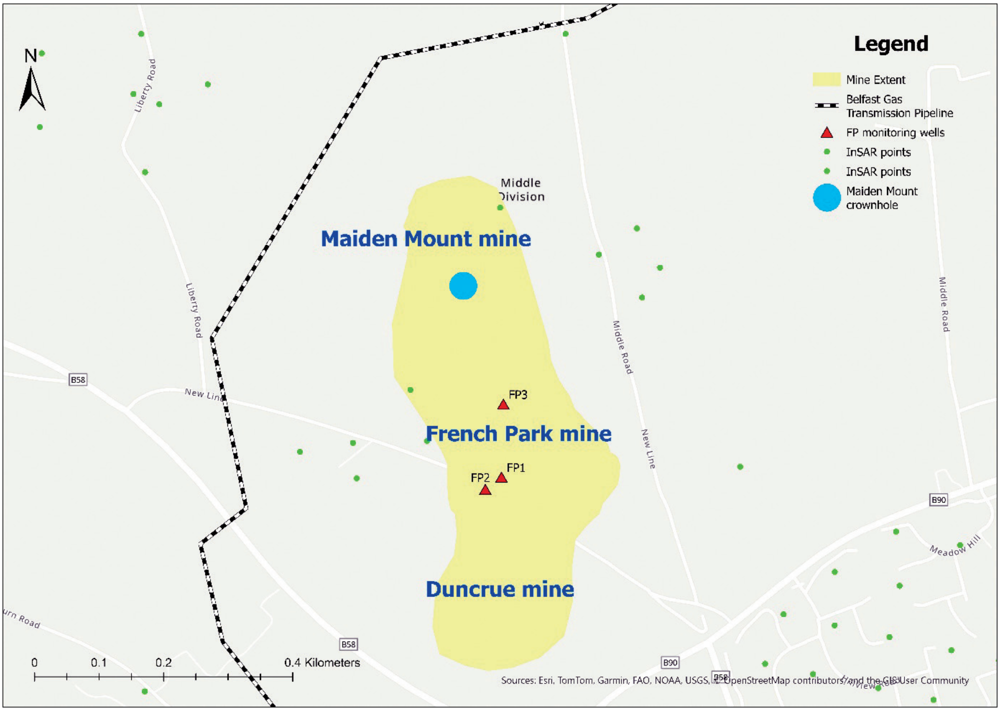

Sources: Esri, TomTom, Garmin, FAO, NOAA, USGS, © OpenStreetMap contributors, and the GIS User Community

Figure 1 Layout of the mine complex at Carrickfergus showing the location of the mines extent and proximity to the BGTP. Monitoring wells at French Park are lie downslope from the crownhole at Maiden Mount mine. InSAR results for the Carrickfergus area show the low reflector response for the area of interest with very limited return acquisitions over the mine extent and area extending across the BGTP.

investigations have shown processes at the mine site to be complex and inter-connected. The major factor leading to instability is considered to be infiltration of freshwater via mine shafts, fractures and areas of crown holes at Maiden Mount. These hydraulic processes occurring at Maiden Mount may then be influencing those at French Park which is impacted by active ground motion, fluctuating water levels and contamination of the overlying lands through large scale brine seepages. The hydraulic head driven by freshwater injection is entering the Maiden Mount mine at depth, transporting through pathways, the nature of which is not clear, to the French Park mine, and is then driven up through the fractured mudstones to the surface. These discharges create space within the mine voids leading to surface subsidence, infiltration of freshwater, creating further dissolution within the mine, and the process continues in a cycle of subsidence, water injection, discharges, subsidence. Trends are identified within the results from surface stability monitoring and water levels which indicates a source of information that can be used to predict seepages at surface, future evolution of ground deformation and impact to the overlying infrastructure.

To investigate further and gain a better understanding of the interconnecting relationship between surface stability and groundwater processes, a newly developed monitoring network, designed on this and other previous work, is at present being implemented. This will include a high-density network of twenty-five monitoring stations across the site. Each station will be equipped with permanent GNSS stations, InSAR reflector target and precise levelling point. These stations will investigate the reliability and comparability of each geodetic method which will be important, given the varying costs and constraints with each method. Flow meters are installed up slope and down slope of the site to monitor changes in surface water flow which could indicate freshwater injection from surface to the mine site. Further flow meters will be installed at various points across the two streams directly over the site. Water levels will continue to be monitored at a number of points using the monitoring wells. Further analysis of mine water geochemistry will be undertaken at regular intervals to assess stratification, brine levels and the evolution of mine water, particularly following brine seepages and following freshwater injection. Sub-surface monitoring using the extensometer monitoring boreholes are to be continued to assess stability and void migration. Combined with regular topographic, aerial LiDAR, aerial photogrammetry surveys, the network will provide an important research observatory to understand processes within flooded abandoned salt mines.

The greater Carrickfergus area contains a further five abandoned salt mines as well as an extensive active salt mine which has been in operation since 1965. The knowledge gained from the work at Maiden Mount-French Park will have implications for the management of these assets while also providing critical knowledge for the management of salt mines globally.

Acknowledgements

This work, including mine surveys, is funded by the Northern Ireland Governments, Department for the Economy. Some of the results presented are part of a project funded by the Natural Environment Research Council (NERC) under the Environmental Risks to Infrastructure Innovation Programme (ERIIP). NERC grants: NE/N013018/1 and NE/N013042/1: *InSAR for geotechnical infrastructure: enabling stakeholders to remotely assess environmental risk and resilience* (February 2016–July 2017). ERS and ENVISAT satellite data were provided by the European Space Agency (ESA). Sentinel-1 InSAR results are available through the European Ground Motion Service.

References

Arup and Partners (1992) Report on the site investigation (Phase 2) of the Duncrue, Maiden Mount, Burleigh Hill and Black Pit salt mines, Carrickfergus, County Antrim, Northern Ireland. Department for Commerce.

Atkins, 2003. Maiden Mount mine, Infilling crown hole with PFA: Hydrogeological risk assessment. Department for Enterprise, Trade and Investment.

Atkins, 2004. Potential subsidence for BMAP plan, 2004/17. Department for Enterprise, Trade and Investment.

Atkins, 2009. Maiden Mount mine settlement prediction. Department for Enterprise, Trade and Investment.

Cigna F, Banks VJ, Donald AW, Donohue S, Graham C, Hughes D, McKinley JM, Parker K, 2017. Mapping Ground Instability in Areas of Geotechnical Infrastructure Using Satellite InSAR and Small UAV Surveying: A Case Study in Northern Ireland. Geosciences. 2017; 7(3):51.

Garthwaite, M.C., 2017. On the design of radar corner reflectors for deformation monitoring in multi-frequency InSAR. Remote Sensing, 9(7), p.648.

Griffith, A.E., Wilson, H.E., Bennett, J.R.P., 1983. Geology of the country around Carrickfegus and Bangor: Sheet 29. Memoirs of the Geological Survey of Northern Ireland.

Meju, M. A., Kulessa, B., Gallardo, L., Thompson, S., Ruffell, A., Parker, K. 2023. Improved imaging of ground deformation and brine seepage around abandoned flooded salt mines by joint inversion of multiphysics data, Journal of Applied Geophysics, Volume 219, 2023, 105217.

Mitchell, W. I. (ed), 2004. The geology of Northern Ireland – Our natural foundation, Geological Survey of Northern Ireland, Belfast.

Parker, K. 2023. Ground stability analysis review of Carrickfergus abandoned mines potential impact on the Belfast Gas Transmission Pipeline: Monitoring network proposal. Geological Survey of Northern Ireland.

Parker, K., Novellino, A., McAllister, E., Bateson, L., Lemon, K. 2024. Carrickfergus abandoned salt mines: Assessment of ground stability and implications to the Belfast Gas Transmission Pipeline, British Geological Survey

Interaction Between Bacteria And Minerals In Post-Mining Heaps In View Of Metal(Loid) Release

Agnieszka Pawlowska[1], Jakub Kaźmierczak[2]

[1] *Wrocław University of Science and Technology, Wybrzeże Wyspiańskiego 27, 50-370 Wrocław, Poland, agnieszka.pawlowska@pwr.edu.pl, ORCID 0000-0003-1025-5851*

[2] *Wrocław University of Science and Technology, Wybrzeże Wyspiańskiego 27, 50-370 Wrocław, Poland, jkazmierczak2002@gmail.com*

Abstract

Bioleaching of mining waste using acidophiles was studied, yielding 586.8 mg/L of arsenic. Bacterial mobility was analyzed in unmodified and surfactant-treated beds using hexadecyltrimethylammonium bromide (CTAB), sodium dodecyl sulfate (SDS), polyoxyethylenesorbitan monooleate (Tween 80), and rhamnolipids. Electrostatic interactions influenced adhesion, with mineral waste maintaining a negative zeta potential at pH 2–12. Bacterial cells exhibited a positive charge at highly acidic pH and a negative above pH 2.6, where the isoelectric point was determined. CTAB enhanced bacterial retention, SDS reduced it due to electrostatic repulsion, and rhamnolipids did not affect migration, suggesting additional adhesion mechanisms.

Keywords: Arsenic leaching, Bacterial migration, Surfactant adsorption, Zeta potential

Introduction

Releasing toxic elements from mining waste heaps presents environmental challenges, particularly in regions with a long history of ore processing. Waste heaps are generally located outside and exposed to weather conditions. For this reason, these areas risk becoming sites of enhanced microbial activity since the presence of acidophilic microorganisms accelerates the formation of acid mine drainage and acid rock drainage due to the sulfide and ferrous oxidation, which facilitates mineral dissolution.

Immobilization of bacterial cells on the mineral surface improves the bioleaching efficiency by creating a specific micro-environment for biooxidation (Watling 2006). Chemicals that prevent bacterial attachment and promote bacterial transport are important, e.g. for successful bioaugmentation (Zhong *et al.* 2017). Cell adhesion to the surface facilitates the colonization of bacteria, improving their ability to leach metals. On the other hand, increased mobility of microorganisms in mineral medium hinders their bio-oxidation capabilities and participates in subsurface migration of contaminants. Therefore, understanding interactions between bacteria and minerals is needed to explain the microbial cell deposition onto solid supports (Katsikogianni *et al.* 2004).

Surfactants were previously used for bacterial transport enhancement in geological media using Tween 20 and sodium dodecyl sulfate, SDS (Gross and Logan 1995) and rhamnolipids (Bai *et al.* 1997; Chen *et al.* 2004). The effect of Tween 20, Tween 80, Plurafac® LF 120, Plurafac® LF 600 and Lutensol® XL 90 on the growth of mixed thermophilic culture consisting mainly of *Metallosphaera hakonensis* was studied by Ghadiri *et al.* (2019). The influence of SDS on bacterial adsorption characteristics was also studied during the bioleaching process of vanadium-bearing shale by *Bacillus mucilaginosus* (Cai *et al.* 2022). Nevertheless, surface electrostatics is investigated to a much lesser extent. The presence of specific chemical groups on the particle surface determines its polar or hydrophobic character and possible electrostatic potential.

Our previous studies showed that the adsorption of lipopolysaccharides and rhamnolipids onto mineral surface changed in the electrical double layer structure and zeta potential, affecting bioleaching (Pawlowska and Sadowski 2020; Pawlowska *et al.* 2021). Therefore, insight into microbial-mineral interactions highlights the importance of controlling bacterial activity in mining waste management. An improved understanding of these processes could lead to more effective strategies for minimizing environmental contamination from mining heaps and optimizing metal recovery through biotechnological applications.

This study investigated the potential for arsenic leaching from mining waste using a microbial consortium isolated from a post-mining environment. There is still limited research on bacterial behaviour in porous media in the presence of surface active compounds, especially in multimineral beds. To address this gap, surfactants of different types were used to determine the conditions that promote bacterial adhesion to mineral surfaces and those that enhance microbial cell migration through the bed.

Methods

The mineral waste material used in the research originated from a heap in southwest Poland, where gold-bearing arsenic ore was previously mined. A particle size of 0.2-0.5 mm was used in the study. The selected fraction contained mg/kg: 19581 As, 56465 Fe, 211.8 Pb, and 74.71 Zn.

A consortium of acidophilic microorganisms dominated by the genera *Acidithiobacillus* and *Acidiphilium* was used. Bacteria prior to leaching were grown on a modified Silverman-Lundgren mineral medium composed of 44.8 g/L $FeSO_4{\cdot}7H_2O$, 3.0 g $(NH_4)_2SO_4$, 0.5 g $MgSO_4{\cdot}7H_2O$ g/L, 0.5 g/L K_2HPO_4, 0.1 g KCl. Inoculum content was 10% (v/v), pH 2.0. Microorganisms were cultivated in shaken flasks at 35 °C for 24 h. Leaching was conducted in glass columns, with a solid content of 50 g and 500 mL of medium. The control sample was deionized water of pH 2.0. Ferrous and ferric iron concentration was determined, as reported previously (Pawlowska *et al.* 2023).

In order to obtain a pure cell suspension for adsorption studies (without culture medium), the cultures were separated on a Whatmann no. 1 paper filter. Then, the solution was centrifuged for 10 minutes at 10°C, 9000 rpm. The supernatant was poured off, and bacterial cells were re-suspended in a water solution of pH 2.5 and centrifuged again. This procedure was repeated until high-purity microorganisms were obtained, which were finally suspended in 2 mL of water with a pH of 3 (Jin *et al.* 2019). The cell concentration was determined by measuring the absorbance at 500 nm.

For surface modification, four surface-active agents were used: i) cetyltrimethylammonium bromide (CTAB), ii) sodium dodecyl sulfate, iii) polyoxyethylenesorbitan monooleate (Tween 80) and iv) rhamnolipids. CTAB was purchased from Thermo Fisher Scientific (USA), SDS and Tween 80 from Sigma-Aldrich (USA), and biosurfactant 90% pure from AGAE Technologies, LLC (USA). Mineral surface modification was done by suspending 25 g of mineral sample in 100 mL of 0.001 M surfactant solution and placed in a rotary shaker for 3 h at 155 rpm. The surfactant solution was decanted, solid dried at 35 °C for 24 hours, and placed in glass columns. Migration through the bed was carried out with 70 mL of bacterial suspension (IS 10^{-3} KCl) and an initial 2 mL/min flow. After the experiment was completed, the solid was left to dry at 30 °C for about 48 hours.

The pH and redox potential were measured using a pH/Eh metre Elmetron CX-401. Element content in liquid samples was determined using the Agilent 5110 ICP-OES (United States) instrument. The solid was analyzed after mineralization with nitric acid. Zeta potential was determined using Zetasizer 2000 (Malvern, United Kingdom) at a constant ionic strength of 10^{-3} M KCl and 20 °C. The final result was the average of five measurements.

Results

Bioleaching experiments

Results of arsenic extraction are presented in Fig. 1a. The final solutions were also tested for zinc and lead content. Waste bioleaching yielded 586.8 mg/L As, 6.380 mg/L Pb and 3.479 mg/L Zn in 21 days. In the control, 50.44 mg/L As, 1.345 mg/L Zn, and 0.379 mg/L Pb were leached. There was a rapid drop of ferrous iron with a simultaneous increase in ferric iron due to bacterial activity (Fig. 1b). After the fifth day of the process, a slight decrease in Fe(III) concentration was observed, most likely due to iron precipitation. In bioleaching, the pH remained constant at an average of 2.16 (±0.12). A continued rise in pH was observed for control sample with a final pH of 4.4, which might be due to the neutralizing capacity of mineral waste or acid leaching (Fig. 1c). The Eh values for abiotic control was within range of 238 – 365 mV (Fig. 1d). Redox potential during bioleaching rapidly increased within the first two days and remained constant until the end of the process, within a range of 552-584 mV.

Zeta potential and migration experiments

Measurements of the zeta potential allowed us to indirectly determine the surface charges of microorganisms and mineral material at the conditions of the experiments (Fig. 2). The mineral suspension had a negative electrical potential within the tested pH range. At pH 6.5, the zeta potential of mineral waste was -29.1. The suspension of microorganisms exhibited slightly positive values at highly acidic pH. The isoelectric point was identified at pH 2.6, and above this point, bacterial cells had negative zeta potential, reaching a maximum of -23.1 mV at pH 11.4.

Migration experiments were conducted on an unmodified bed with adsorbed surfactants

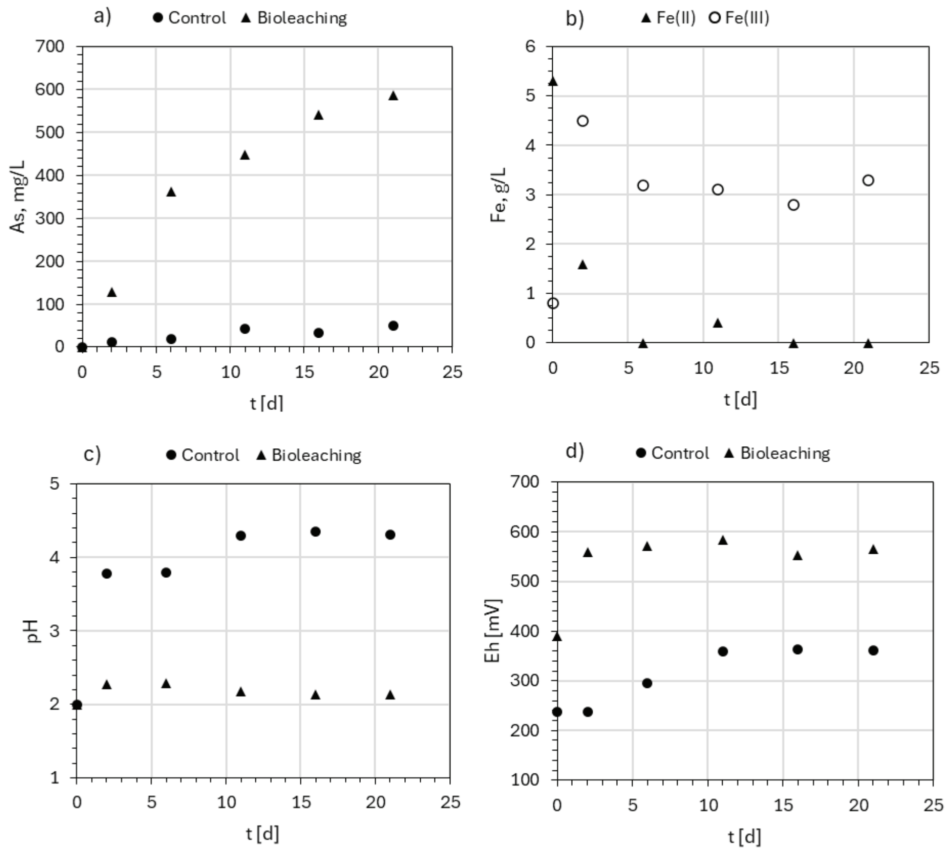

Figure 1 Results of mineral waste leaching: a) arsenic concentration, b) ferrous and ferric changes during bioleaching, c) pH, and d) Eh versus time

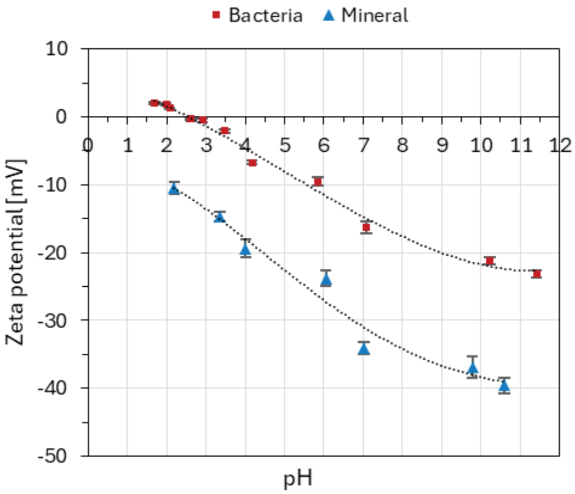

Figure 2 *Zeta potential of bacteria and mineral waste depending on pH. Ionic strength 10^{-3} M KCl*

and a constant ionic strength of 10^{-3} KCl. The results are presented as plots of the relative concentration of cells passing through the bed (*C*) against their initial concentration (C_0). Changes are shown as a function of time and depicted in Fig. 3. As can be seen, bacterial cells migrate best through the bed modified with SDS. In the initial phase, the cell concentration in the filtrate increases; after 10 minutes, it reaches a fixed level. Only 7.06% of cells were attached, the lowest value obtained (Tab. 1). This effect was attributed to increased electrostatic repulsion between the negatively charged mineral surface and bacterial cells. The use of SDS decreased particle zeta potential to -39.3 mV (Tab. 2) due to negatively charged sulfate polar heads of the anionic surfactant. The facilitated migration led to a decrease in total flow time compared to other experiments.

The highest percentage, 17.4%, of cells was adsorbed when the mineral was previously conditioned with CTAB (Tab. 1). It was due to the negatively charged surface of bacterial

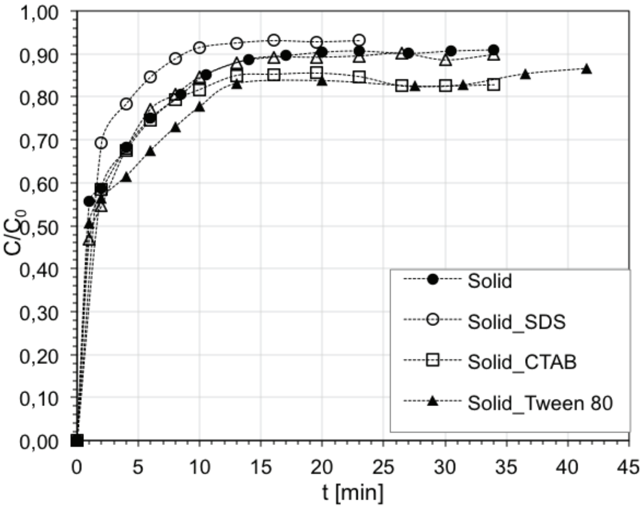

Figure 3 *A normalized concentration C/C_0 versus reaction time for bacterial adsorption in various mineral beds, pH 6.5; ionic strength 10^{-3} KCl*

Table 1 Summary of transport experiments

Surfactant	Total time min	Cells adsorbed %	Molar mass g/mol
-	34	9.42	-
CTAB	34	17.4	364.4
SDS	23	7.06	288.4
Tween 80	42	16.0	1310
Rhamnolipids	34	10.6	650.8

Table 2 Zeta potential of selected samples at pH 6.5 and ionic strength 10^{-3} KCl

Sample	Zeta potential mV
Bacterial cells	-17.7
Pure mineral waste	-29.1
Mineral waste with CTAB	27.2
Mineral waste with SDS	-39.3
Mineral waste with Tween 80	-20.5
Mineral waste with rhamnolipids	-45.9

molecules at pH 6.5, which has a zeta potential of -17.7 mV and remains retained on the bed due to electrostatic interactions with the positively charged mineral surface (27.2 mV). The negative zeta potential of bacterial cells was due to anionic surface groups, such as carboxyl and phosphate (Zhong *et al.* 2017). In the case of cationic surfactant, the CTAB-charged cation head group ($N^+(CH_3)_3$) was responsible for a positive electrical potential of modified particles.

Tween 80, a non-ionic surfactant, increased bacterial retention. The percentage of adsorbed cells was 16.0%. The mineral surface showed a negative charge, as did the bacteria, so the retention effect in the bed may have been caused by pore-clogging by surfactant molecules, as Tween 80 is characterized by a much larger molar mass than other tested surface active agents. Confirmation of this phenomenon requires further research.

Biosurfactants are gaining popularity as eco-friendly alternatives for their chemical counterparts. Therefore, except for chemical surfactants, rhamnolipids were also tested. Surprisingly, using rhamnolipids showed no major changes in cell migration through the bed. The retention time was comparable to an unmodified bed. The zeta potential of the mineral with biosurfactant adsorbed decreased to -45.9 mV due to negatively charged carboxyl groups in the biomolecule. Nevertheless, the effect of its presence differed from that of SDS or Tween 80. It suggests that other interactions occur when biosurfactants are present, which will be the subject of further research.

Conclusions

The preliminary tests showed that mineral waste might be a secondary source of arsenic, one of the critical raw materials identified by the European Union. The material to be bioleached is currently stored in heaps under atmospheric conditions, so it should be considered that toxic elements such as arsenic might, under favourable conditions, be released into the environment. Therefore, the ability to control these phenomena is very important. The use of surface-active compounds can help to control the above-mentioned processes. The retention of acidophilic microorganism cells favours bioleaching processes, and their leaching from the deposit will have the opposite effect.

Preliminary experiments on cell migration through a bed modified with surfactant compounds of different types have shown that electrostatic factors partially control the adhesion process. The zeta potential showed that the tested mineral waste maintains a constant negative charge across the pH range with no isoelectric point. The microbial suspension exhibited a slightly positive charge at highly acidic pH, with an isoelectric point at pH 2.6, after which the bacterial cells became negatively charged.

The study demonstrated that surfactants influence bacterial retention on mineral surfaces due to electrostatic interactions and physical effects. Modification with CTAB, a cationic surfactant, resulted in the highest bacterial adsorption due to electrostatic attraction between the positively charged surface and negatively charged bacterial cells at pH 6.5. In contrast, SDS, an anionic surfactant, reduced bacterial retention to the lowest level, probably due to increased electrostatic repulsion. The biosurfactant on the mineral surface did not affect cell retention, suggesting that electrostatic factors alone do not control adhesion. These findings highlight the potential of surfactant modification in controlling microbial behaviour in historical waste heaps and suggest the need for further research on bacterial interactions in heterogeneous mineral systems.

Acknowledgements

The research was realized within grant no. 2021/43/D/ST10/02784, financed by the National Science Centre, Poland.

References

Bai G, Brusseau ML, Miller RM (1997) Influence of a rhamnolipid biosurfactant on the transport of bacteria through a sandy soil. Appl Environ Microbiol 63:. https://doi.org/10.1128/aem.63.5.1866-1873.1997

Cai Z, Wang Y, Zhang Y, Tian H (2022) Effects of surfactant on Bacillus mucilaginosus adsorption characteristics during vanadium bioleaching process. J Environ Chem Eng 10:. https://doi.org/10.1016/j.jece.2022.108961

Chen G, Qiao M, Zhang H, Zhu H (2004) Bacterial desorption in water-saturated porous media in the presence of rhamnolipid biosurfactant. Res Microbiol 155:. https://doi.org/10.1016/j.resmic.2004.05.001

Ghadiri M, Harrison STL, Fagan-Endres MA (2019) Effect of surfactant on the growth and activity of microorganisms in a heap bioleaching system. Miner Eng 138:. https://doi.org/10.1016/j.mineng.2019.03.028

Gross MJ, Logan BE (1995) Influence of different chemical treatments on transport of Alcaligenes paradoxus in porous media. Appl Environ Microbiol 61:. https://doi.org/10.1128/aem.61.5.1750-1756.1995

Jin D, Liu L, Zheng G, *et al.* (2019) A rapid method to quantify the biomass of viable Acidithiobacillus ferrooxidans in iron-based bioleaching matrix of sewage sludge. Biochem Eng J 152:. https://doi.org/10.1016/j.bej.2019.107360

Katsikogianni M, Missirlis YF, Harris L, Douglas J (2004) Concise review of mechanisms of bacterial adhesion to biomaterials and of techniques used in estimating bacteria-material interactions. Eur Cell Mater 8

Pawlowska A, Sadowski Z (2020) Effect of schwertmannite surface modification by surfactants on adhesion of acidophilic bacteria. Microorganisms 8:. https://doi.org/10.3390/microorganisms8111725

Pawlowska A, Sadowski Z, Winiarska K (2023) Microbial communities of acidic post-mining environments and their use in laterite bioreduction. Acta Montanistica Slovaca 28:918–928

Pawlowska A, Sadowski Z, Winiarska K (2021) Effect of rhamnolipids and lipopolysaccharides on the bioleaching of arsenic-bearing waste. Minerals 11:1303. https://doi.org/10.3390/min11121303

Watling HR (2006) The bioleaching of sulphide minerals with emphasis on copper sulphides – A review. Hydrometallurgy 84:. https://doi.org/10.1016/j.hydromet.2006.05.001

Zhong H, Liu G, Jiang Y, *et al.* (2017) Transport of bacteria in porous media and its enhancement by surfactants for bioaugmentation: A review. Biotechnol Adv 35

Coupled Groundwater-Surface Water Modelling Workflow to Support Risk Assessment of an Abandoned Underground Coal Mine Due to Natural Water Rebound

Nachayada Phonseela[1], Thomas Booth[1]

[1] *WSP, United Kingdom*

Abstract

This study aims to develop a coupled groundwater-surface water flow and solute transport modelling tool to evaluate the influence of mine water rebound from an abandoned underground coal mine sitting under limestone and sandstone aquifers and nearby streams. The developed workflow relies on MODFLOW6 and the FloPy Python library and aims to identify contaminant migration pathways towards potential receptors of mine water discharge by estimating increases in chloride concentration. The results indicate that if poor-quality mine water rises to levels where it can discharge into the local and regional aquifers, it will primarily travel through the limestone aquifer and streams and pose a risk of pollution to extensive regions of the aquifers and surface water bodies. Furthermore, significant groundwater-surface water interaction is expected to occur downstream of the mine, with contaminants migrating from the aquifer into streams close to the mine location and from the streams into the aquifer downstream of the mine.

Keywords: Risk assessment, groundwater, modelling, transport, coal, abandoned, underground mine

Introduction

Mine water rebound refers to the process where water floods abandoned deep mines after the cessation of dewatering operations (Merritt & Power 2022; Younger & Adams 1999). This often leads to polluted water either discharging to the surface or contaminating nearby aquifers (Younger & Adams 1999). Therefore, development of predictive groundwater flow and solute transport modelling tools that identify contaminant migration pathways and potential receptors of mine water discharge is essential for the effective planning of mitigation strategies.

The primary objective of this study is to develop and implement a coupled groundwater-surface water flow and solute transport modelling tool to evaluate the influence of mine water rebound from an abandoned underground coal mine on the overlying limestone and sandstone aquifers and nearby streams. The modelling workflow aims to identify contaminant migration pathways towards potential receptors of mine water discharge, by estimating increases in chloride (Cl) concentrations.

The solute transport model is based on an existing regional groundwater flow model, developed using MODFLOW6 (MF6) and the FloPy Python library. This approach allows a dynamic representation of groundwater-surface water interactions in both space and time, for both flow and solute transport. As part of this study, the regional groundwater flow model was adapted and imported into Groundwater Vistas 9 (GWV9) to provide a user-friendly modelling interface for the client. Solute transport capabilities were added to GWV9, to represent the evolution of chloride. This integration allows the model to be used as an effective predictive tool and ensures seamless compatibility with MF6, facilitating the efficient and straightforward implementation of management scenarios.

Modelling Framework

The study area is an abandoned underground coal mine, located below regionally important limestone and sandstone aquifers. Since the cessation of dewatering operations during post-closure, the mine has been facing natural mine water rebound, with highly saline waters with high concentrations of chloride.

The modelling work focuses on chloride, with a source concentration of 16,500 mg/L, assuming non-reactive behaviour. The study considers the following pollution source cases, as shown in Fig. 1 and Table 1:

- The risk of mine water rebounding into the limestone aquifer (overlying the coal unit) where the distance between mine workings and the base of the limestone aquifer is less than 50 meters, in locations A and B (see Fig. 1).
- Unused shafts as a source of contaminants into groundwater.
- Potential diffusion of contaminants throughout the entire mining block.
- The risk of artesian mine water discharge near the unused shaft, leading to overflow into the nearby river.

Four predictive scenarios were conducted, considering the discharge locations described above for different combinations of discharge rates per location, adding to a total of 28 L/s estimated for the considered worst-case scenario (see Table 1). The simulation of mine water rebounding into the limestone aquifer used injection well boundary conditions. For Scenario 4, the potential artesian mine water was modelled by introducing a direct inflow into the nearby river.

Flow and Solute Transport Modelling Workflow

Import of Regional MODFLOW6 Groundwater Flow Model into Groundwater Vistas

The regional groundwater flow model covers an area of approximately 7,000 square kilometres (km^2) and consists of four layers representing three geological units that sit above an underground coal mine. These geological units comprise mudstone (layer 1), sandstone (layer 2), and limestone (layers 3 and 4).

The regional groundwater flow model was imported into GWV9 using Python scripting based on the FloPy library. The hydraulic parameters from the original groundwater flow model were directly incorporated into the developed GWV9 model without any alterations.

In the GWV9 model, the surface water component is integrated within the model to simulate the dynamic interactions between surface water and groundwater. This integration allows for a coupled process where changes in surface water bodies, such as rivers and lakes, directly influence groundwater levels and vice versa. The model uses the Streamflow Routing (SFR) Package to represent these interactions, ensuring that

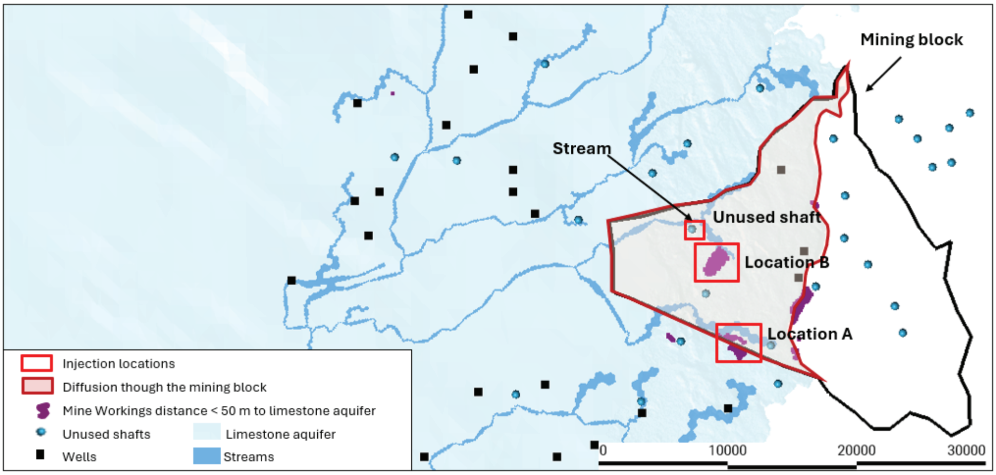

Figure 1 Sources of pollution considered as part of this study.

Table 1 *Mine water discharge per scenario.*

	Discharge location				
Scenario	**Aquifer at Location A***	**Aquifer at Location B***	**Aquifer at unused shaft***	**Artesian water into nearby river****	**Re-infiltration artesian water****
Scenario 1 (28 L/s)	9.3 L/s	9.3 L/s	9.3 L/s	–	–
Scenario 2 (28 L/s)	–	28 L/s	0.0 L/s	–	–
Scenario 3 (28 L/s)	28 L/s diffuse throughout eastern mining area			–	–
Scenario 4 (28 L/s)	–	–	5 L/s	16.3 L/s	6.7 L/s

* See Figure 1.

** Scenario assumes artesian water moving as runoff into river, with a fraction re-infiltrating before reaching the river.

both surface water and groundwater systems are accurately simulated.

Implementation of Steady State Version of the Model

The developed transport modelling tool was configured to simulate 100 years under the mean annual conditions observed during 2009–2019. To achieve this, the developed GWV9 model was converted into a steady-state model by implementing the mean boundary conditions of the original groundwater flow model from 2009–2019. This steady-state model represents conditions at the beginning of the solute transport model. The piezometric heads generated by the developed GWV9 model were compared to the average annual heads from the original groundwater flow model for the same timeframe. This comparison revealed an almost identical match for the calibration targets, as illustrated in Fig. 2.

Implementation of Solute Transport Modelling

Solute transport capabilities were integrated into the developed GWV9 model, with transport porosities considered equal to specific yield values. Dispersivity values were derived from the study of Arriaza and Ghezzehei (2013), based on a potential plume dimension of up to 10 kilometres. The model employed a longitudinal dispersivity of 100 m, a transverse dispersivity of 10 m, and a vertical dispersivity of 1 m. Chloride was treated as non-reactive, with no consideration for sorption or degradation processes, and modelled as increase in concentration from a zero-background concentration.

To accommodate the solute transport modelling process within the current capabilities of GWV9, external modifications were required for specific MF6 packages. These include the Streamflow Routing (SFR), Streamflow Transport (SFT), Dispersion (DSP), and Iterative Model Solution (IMS) packages.

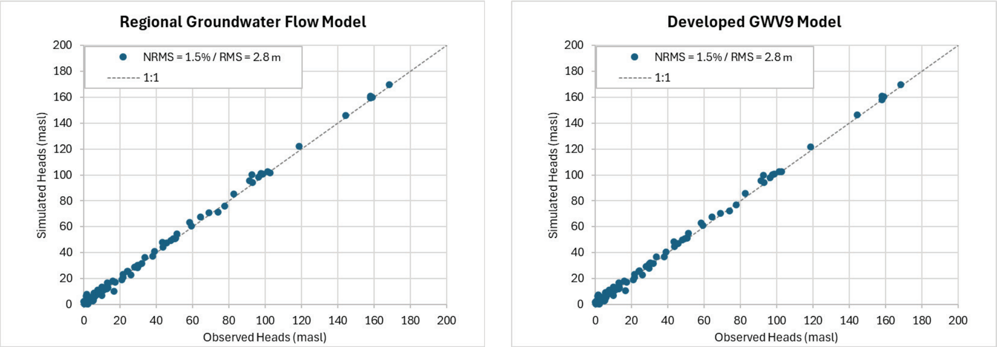

Figure 2 *Calibration results for the regional groundwater flow model period 2009–2019 (average) (left) and developed GWV9 model (right).*

Modelling Results

The chloride concentration results presented in Fig. 3, Fig. 4, Fig. 5 and Fig. 6 show increase of chloride concentrations in aquifers and streams relative to background levels, exceeding the standard drinking water limit of 250 mg/L set by the US Environmental Protection Agency (EPA) (1988). The simulation results indicate that for the considered worst-case scenario potential pollution from the mining block could affect the water quality of the overlying aquifers and nearby streams. Elevated concentrations are particularly noted in nearby streams for the artesian mine water discharge scenarios (Scenario 4) (Fig. 6).

According to the simulation results, mine water leakage from potential sources mainly moves through the limestone aquifer and streams, ultimately reaching potential receptors such as principal aquifers (limestone and sandstone), streams and rivers, and groundwater abstractions. In the mining area, the stream functions as a gaining stream, allowing contaminated groundwater to enter and cause surface water contamination. As contaminants travel along the streams, they can discharge

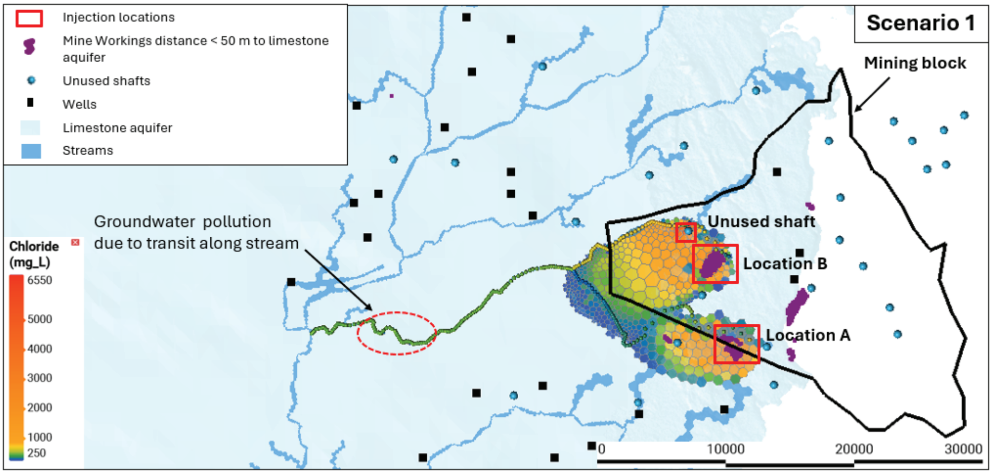

Figure 3 *Simulated concentration results of chloride for Scenario 1, considering an inflow of 28 L/s into the aquifer equally distributed between Location A, B, and the unused shaft. Chloride source is 16,500 mg/L.*

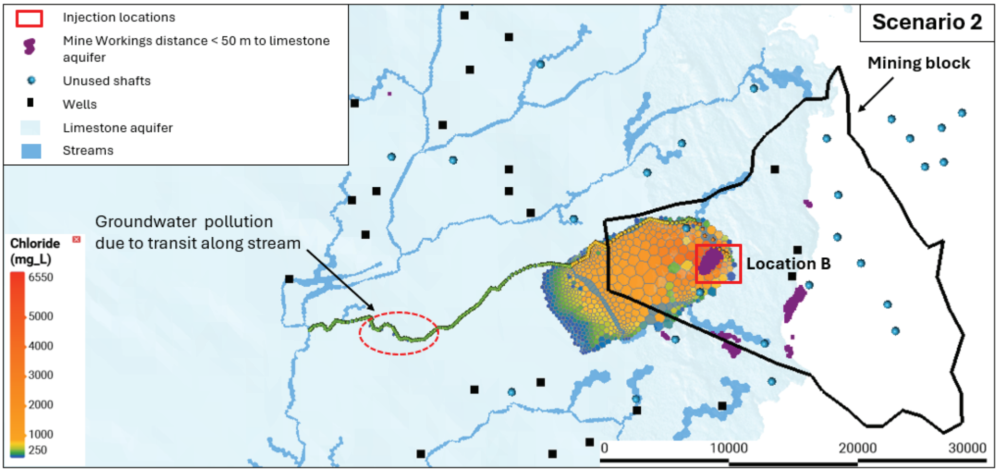

Figure 4 *Simulated concentration results of chloride for Scenario 2, considering 28 L/s into aquifer at Location B. Chloride source is 16,500 mg/L.*

into the aquifer downstream of the mining block, where the stream transitions to a losing stream. This results in the aquifer becoming contaminated as it receives polluted surface water. This interaction between groundwater and surface water is visible in Scenarios 2 (Fig. 4) and 4 (Fig. 6). It is crucial to highlight that modelling was based on mean annual conditions, and consequently concentrations could be higher during dry periods when flow conditions are low.

Conclusions and Recommendations

A summary of the solute transport modelling outcomes is presented below, including the main conclusions and recommendations.

- The model suggests that extensive regions of the aquifer and streams could be at risk of pollution if poor-quality mine water, which travels primarily through the limestone aquifer and streams, rises to levels where saline mine water discharges into the local and regional aquifers, either diffusely or from specific areas within the mining block above the coal unit.

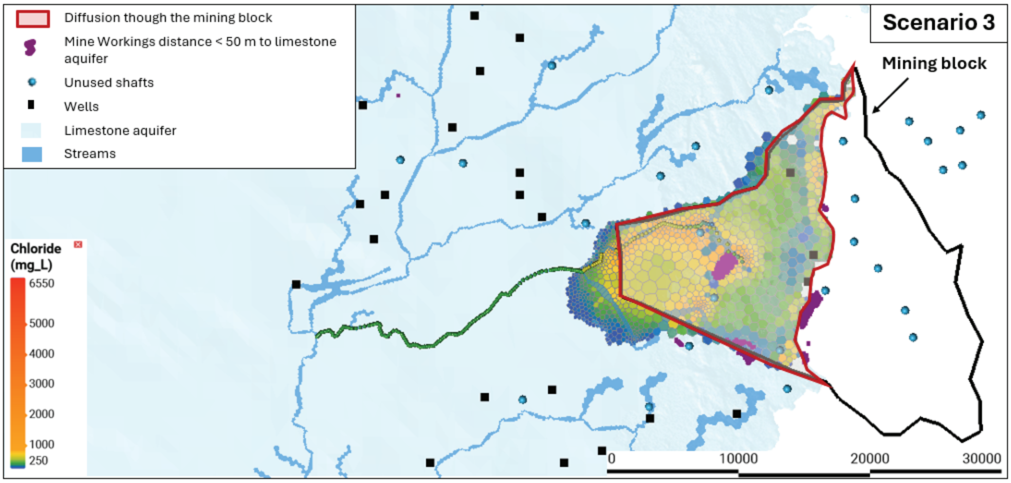

Figure 5 *Simulated concentration results of chloride for Scenario 3, considering 28 L/s into aquifer diffused across the eastern mining block. Chloride source is 16,500 mg/L.*

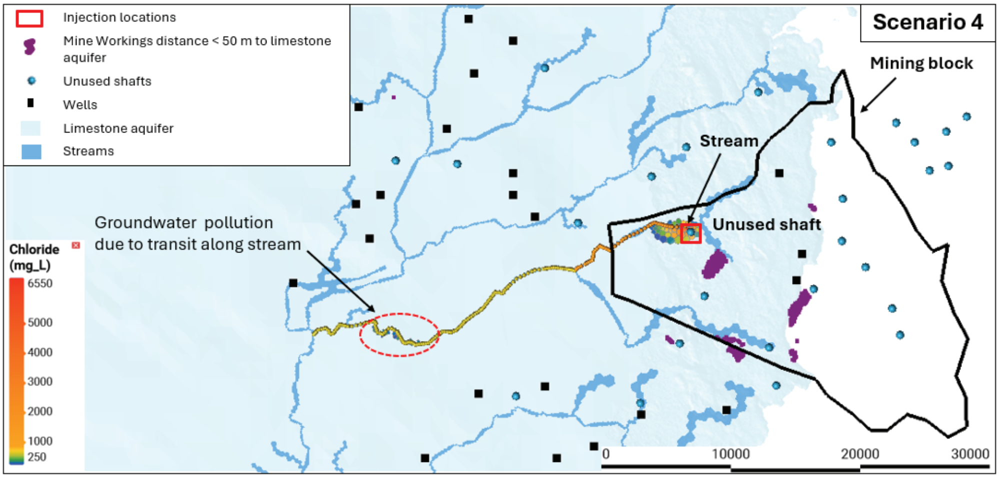

Figure 6 *Simulated concentration results of chloride for Scenario 4, considering 5 L/s into aquifer at unused shaft and 23 L/s of mine water as runoff into nearby river. Chloride source is 16,500 mg/L.*

- Substantial groundwater-surface water interaction is expected, where contaminants migrate from the aquifer into the stream and vice versa depending on the location and time of the year, with relatively fast travel times in the streams.
- The modelling results are based on mean annual conditions. Therefore, both groundwater and stream concentrations could be higher than predicted during low flow conditions. Thus, implementation of a transient version of the developed GWV9 model is recommended to be able to simulate seasonal variations of concentrations.
- The study is based on a theoretical scenario; thus, the modelling results do not reflect actual conditions. However, the simulations suggest severe potential consequences, necessitating the consideration of risk management measures, including monitoring and mitigation strategies.
- The developed GWV9 model was run as a deterministic model for each scenario, producing a single outcome based on the input parameters. Deterministic models do not account for variability or uncertainty. Conducting sensitivity analyses is recommended to understand the impact of key parameters and capture the range of possible outcomes and inherent uncertainties.

References

Arriaza, J.L. & Ghezzehei, T.A. (2013). Explaining longitudinal hydrodynamic dispersion using variance of pore size distribution. *Journal of Porous Media*, 16(1).

Merritt, P., & Power, C. (2022). *Assessing the long-term evolution of mine water quality in abandoned underground mine workings using first-flush based models.* (Vol. 864). Science of The Total Environment.

United states environmental protection agency. (1988). Manual, *Waste Minimization Opportunity Assessment*. Government Institutes Inc.

Younger, P L., & Adams, R. (1999). *Predicting mine water rebound*. Environment Agency, Bristol (United Kingdom); Northumbrian Water Ltd. (UK).

A Physics- and Chemistry-Informed Neural Network for Simulating Mine Waste Weathering: Application to Pyrite Oxidation Modeling

Hanli Qiao[1], Mohammad Jooshaki[1], Massimo Rolle[2], Timo Lähivaara[3], Marko Vauhkonen[3], Tommi Kauppila[1], Muhammad Muniruzzaman[1,4]

[1]*Geological Survey of Finland, Vuorimiehentie 5, 02151, Espoo, Finland*

[2]*Institute of Applied Geosciences, Technical University of Darmstadt, Schnittspahnstraße 9, 64287, Darmstadt, Germany*

[3]*Department of Technical Physics, University of Eastern Finland, Yliopistonranta 1, 70211, Kuopio, Finland*

[4]*Institute of Geosciences, University of Bonn, Kirschallee 1–3, 53115 Bonn, Germany*

Abstract

Mining environments involve complex hydro-bio-geochemical systems. Reactive transport modeling (RTM) is essential to rigorously describe these processes. Yet, process-based RTM is computationally intensive and limited in practical applications. To mitigate such challenges, this paper provides a novel deep learning-based surrogate accelerator, hidden-reactive-transport-neural-network (HRTNet), to simulate pyrite oxidation, a process of key importance for acid mine drainage. HRTNet relies on a flexible two-network architecture integrating chemical and physical equations. The model can effectively capture the desired spatio-temporal dynamics in a considerably reduced computation time (almost eight-fold). Additionally, HRTNet shows a good generalization capability covering a wide range of conditions beyond the training datasets.

Keywords: Mine waste weathering, machine learning, physics-chemistry-informed neural network, pyrite oxidation, reactive transport modeling

Introduction

In mining settings, intricate geochemical and hydrogeological conditions interact at multiple scales. These systems usually involve mineral dissolution and precipitation, contaminant release and transport, gaseous species migration, and the eventual formation of acid mine drainage (AMD), which poses a severe pollution issue due to high concentrations of sulfate, elements of potential concern such as metals and metalloids, and low pH. The oxidation of sulfide minerals is one of the primary sources of AMD, where pyrite and pyrrhotite are principal minerals that generate acidic drainage in mine waste (Moncur *et al.* 2009; Kefeni *et al.* 2017; Simate and Ndlovu 2014). Pyrite oxidation is thus a main driver of the environmental and economical challenges associated with AMD (Chandra and Gerson 2010). Effectively capturing the dynamics of these processes enables accurate prediction and monitoring of their environmental influences, thereby facilitating mitigation of pollution risks. Reactive transport modeling (RTM) is a sophisticated approach that can resolve these coupled processes, by integrating a wide range of physical, chemical, and biological processes in mining waste and mining-affected subsurface systems (Steefel *et al.* 2005; Xu *et al.* 2000; Battistel *et al.* 2019; 2021).

While these process-based models are accurate and represent a rigorous formulation, they are often computationally intensive, resulting in limitations in many practical applications that require multiple model-based evaluations and risk assessments (Steefel 2019; Muniruzzaman and Pedretti, 2021). These challenges mainly stem from the demand for solving a suite of highly coupled partial differential equations (PDEs). In recent years, numerous efforts have been devoted to mitigating the computational burden associated with the process-based RTM simulations, with surrogate models presenting promising potentials. Among these techniques, machine learning (ML) and deep learning (DL) based accelerators have received increasing attention, including successful applications in geochemical calculations (Jatnieks *et al*. 2016; Laloy and Jacques 2022; Demirer *et al*. 2023; Guérillot and Bruyelle 2020; Leal *et al*. 2020), parameter upscaling (Prasianakis *et al*. 2020), and uncertainty and sensitivity analysis (Degen *et al*. 2022). So far, purely data-driven surrogate models have been the primary approach in diverse geochemical and transport problems like in hyporheic zone (Moeini *et al*. 2024), electrokinetic transport (Sprocati and Rolle 2021; Sprocati *et al*. 2025), dolomitization process (Li *et al*. 2022), porous media transport (Marcato *et al*. 2023), and riparian zone (Yu *et al*. 2024). Unlike fully data-driven models, strategies combining geochemical or physical knowledge were developed to improve prediction accuracy while promising large speedups. These formulations consider governing knowledge either as a priori (De Lucia 2024) or a trigger of fully physical simulation when the surrogate predictions are implausible (De Lucia and Kühn 2021). Additionally, physics-based ML is another model that has been developed for geoscientific systems by integrating the solutions of the governing PDEs and data-driven methods using the non-intrusive reduced-basis model (Degen *et al*. 2023). Finally, physics-informed ML (PIML) has been a promising technique, which explicitly integrates governing physical laws into the learning process. This can be achieved by embedding PDE residuals in the loss function, as demonstrated by Raissi *et al*. (2019) in their work on physics-informed neural networks (PINNs), or by encoding these laws directly into the neural network architecture (Rao *et al*. 2023; Liu *et al*. 2024).

Recently, PIML techniques have been successfully applied in various systems, yet contributions to accelerating process-based RTM are still scarce and require systematic studies. The work in this paper aims to contribute to this research gap. The study was inspired by the Hidden Fluid Mechanics (HFM) model provided by Raissi *et al.* (2020) to propose an intelligent surrogate model, the Hidden Reactive Transport Neural Network (HRTNet), which integrates the governing physical and chemical reaction laws. To this end, HRTNet is applied and tested for pyrite oxidation examples to evaluate its performance. HRTNet results were compared against the process-based RTM simulations to assess the accuracy and generalization capability of the proposed surrogate modelling approach.

Methods

We consider the study by Battistel *et al.* (2019) as a model problem, relevant for mine waste weathering processes, for investigating pyrite oxidation reactive fronts in 1-D and 2-D porous media. The left panel in Fig. 1 shows the 1-D and 2-D flow-through experiments described by Battistel *et al.* (2019). In 1-D case, a cylindrical glass column was used, where a pyrite inclusion (4 cm long, placed in the middle, with 67.63 mol/Lwater pyrite) was embedded within a sandy matrix. In contrast, a quasi two-dimensional flow-through chamber, packed with a sandy matrix containing a rectangular pyrite inclusion (located at 5 cm from the inlet and 10 cm from bottom, with 33.82 mol/Lwater pyrite), was used for the 2-D experiment. These experiments were performed by continuously injecting an oxic solution, and a non-invasive optode technique was used to monitor oxygen front propagation at high-spatial and temporal resolution. O_2 sensor strips adhered to the inner walls of the flow-through setups are shown in pink color in Fig. 1. A physically homogeneous but chemically and mineralogically heterogeneous system is generated by keeping the same grain sizes of the sand and pyrite.

We leverage the same process-based RTM as used by Battistel *et al.* (2019) to simulate the 1-D and 2-D flow-through experiments. The model is a basis for generating the

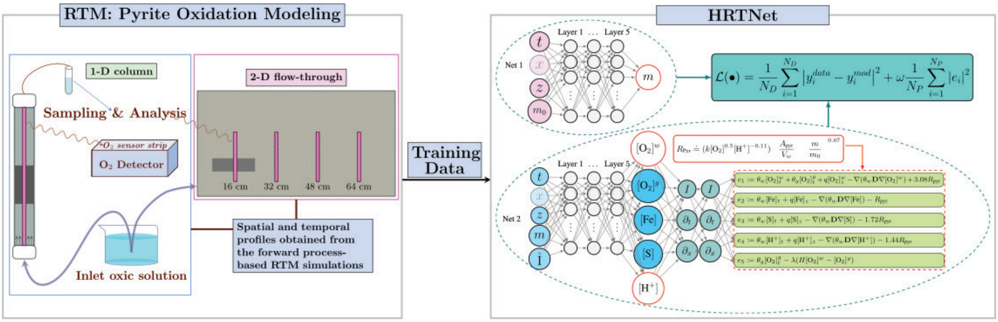

***Figure 1** Schematic diagram of the problem setup and overall workflow of the proposed surrogate modeling approach. The left panel displays exemplary reactive transport systems involving 1-D and 2-D flow-through setups by Battistel* et al. *(2019). The right panel is the surrogate model architecture showing its learning mechanism.*

training data fed into the HRTNet (Fig. 1, right panel). The RTM process relies on the chemical reaction:

$$FeS_{1.72} + 3.08O_2 + 0.72H_2 \; Fe^{2+} + 1.72SO_4^{2-} + 1.44H^+ \qquad (1)$$

where Fe^{2+}, SO_4^{2-}, and H^+ are the main released oxidation products, implying O_2 consumption and acidity generation. Pyrite oxidation was simulated as kinetically controlled reactions with the rate law proposed by Williamson and Rimstidt (1994):

$$R_{\text{pyr}} = (k[O_2]^{0.50}[H^+]^{-0.11})\left(\frac{A_{\text{pyr}}}{V_w}\right)\left(\frac{m}{m_0}\right)^{0.67}(1-\Omega_{\text{pyr}}) \qquad (2)$$

According to the chemical reactions and the rate law, the governing mass conservation equations for reactive transport in 1-D and 2-D flow-through systems are expressed as:

$$\theta_w\frac{\partial c_{w,i}}{\partial t} + \theta_g\frac{\partial c_{g,i}}{\partial t} + \mathbf{q}\cdot(\nabla c_{w,i}) - \nabla\cdot(\theta_w \mathbf{D}_i \nabla c_{w,i}) = -\sum_{j=1}^{N_j} v_{ij}R_j \qquad (3)$$

$$\theta_g\frac{\partial c_{g,i}}{\partial t} = \lambda(Hc_{w,i} - c_{g,i}) \qquad (4)$$

where H (= 31.25) is Henry's coefficient for oxygen. Note that a mass transfer term taking into account the exchange of oxygen between the aqueous and gaseous phases was considered in the transport equations to account for the effect of entrapped gas bubble in the porous media. We integrate the pyrite reaction law and the governing PDEs into the neural networks by designing a tailored two-network architecture (Net 1 and Net 2) shown in Fig. 1 (right panel). HRTNet aims to learn a mapping $f(t, \boldsymbol{x}, m_0) \rightarrow c$, where $\boldsymbol{x}$ is a spatial vector with component z for the 1-D column and x, z for the 2-D flow-through system. m_0 is the initial pyrite concentration, which is zero in the purely sandy media where pyrite is absent, and c represents the target concentrations. This architecture ensures that HRTNet approximates f and adheres to the underlying chemical and physical laws.

Net 1 is a pure data-driven network that outputs the pyrite concentration, m, which acts as one of the inputs of Net 2, and is used in the pyrite reaction rate calculations. The input layer of Net 2 contains an extra variable $\overset{0}{\mathrm{I}}$, an identifier to disambiguate where pyrite is absent when multiple training datasets are used. Net 2 first predicts the target concentrations. R_{pyr} is subsequently calculated by m, $O_2]^w$ and $[H^+]$, which is further used in calculating the PDE residuals obtained with the help of automatic differentiation to construct the loss function. The two networks interplay with each other by minimizing the loss. Thus, HRTNet incorporates the chemistry- and physics-informed learning in a flexible way to capture the spatial and temporal dynamics with various initial pyrite concentrations. The half-transparent neuron x in both networks (Fig. 1) allows identifying between 1-D and 2-D cases. Table 1 lists the parameters with their values used to calculate the PDE residuals for 1-D and 2-D flow-through setup.

Results

We trained HRTNet based on the results of the forward process-based reactive transport simulations in 1-D and 2-D systems. In 1-D column, the training data consists of four datasets with various initial

Table 1 Parameters and their values used in the PDE residuals of HRTNet in 1-D and 2-D flow-through setup.

Parameter	Description	1-D column	2-D flow-through
θ_w [-]	Volumetric water content	0.347	0.358
θ_g [-]	Volumetric gas content	0.033	0.022
q [m/s]	Specific discharge	6.03×10^{-6}	6.60×10^{-6}
D [m²/s]	Dispersion coefficient	2.50×10^{-9}	4.41×10^{-9}; $1.02 \times 10^{-9\#}$
λ [1/s]	Mass transfer coefficient	1.95×10^{-6}	4.26×10^{-6}

#The first and second value refers to the longitudinal and transverse dispersion coefficients respectively

pyrite concentrations, [30; 45; 60; 75] mol/L$_{water}$. Fig. 2 compares HRTNet prediction results and the process-based simulation at different reaction hours with an initial pyrite concentration of 52 mol/L$_{water}$, which was not part of the training data.

HRTNet performs consistently with RTM in all cases considering the prediction of dissolved oxygen O_2^w, oxygen concentration in the gaseous phase O_2^g and remaining pyrite concentration. Slight discrepancies between HRTNet and RTM in iron, sulfur, and proton profiles after the reaction zone can be observed, especially at early time (t = 3.2 *h* in Fig. 2). Overall, HRTNet can accurately capture the spatiotemporal dynamics with varying initial pyrite concentrations, a remarkable achievement among the existing DL-based surrogate models. This strong performance stems from HRTNet's flexible and generalized learning mechanism. Its two-network structure effectively integrates governing physics and chemistry principles, enabling HRTNet to achieve outstanding predictions beyond the training conditions.

Similarly, in the 2-D flow-through case, HRTNet was trained on training data consisting of multiple datasets from RTM, with initial pyrite concentrations, [10; 20; 30; 40] mol/Lwater. Fig. 3 compares the HRTNet's predictions on the second row with ground truth from RTM on the first row.

The initial pyrite concentration is 33.82 mol/L$_{water}$, the same as in the experimental setup. The outstanding agreement demonstrates that HRTN*et als*o performs very well in 2-D flow-through.

Conclusion

The proposed HRTNet approach systematically integrates the governing chemical and physical equations with neural network architecture to allow transport and geochemistry-aware learning. The model relies on a flexible architecture based on two networks sharing a common loss function, allowing the incorporation of data-driven and physics-chemistry-informed contributions.

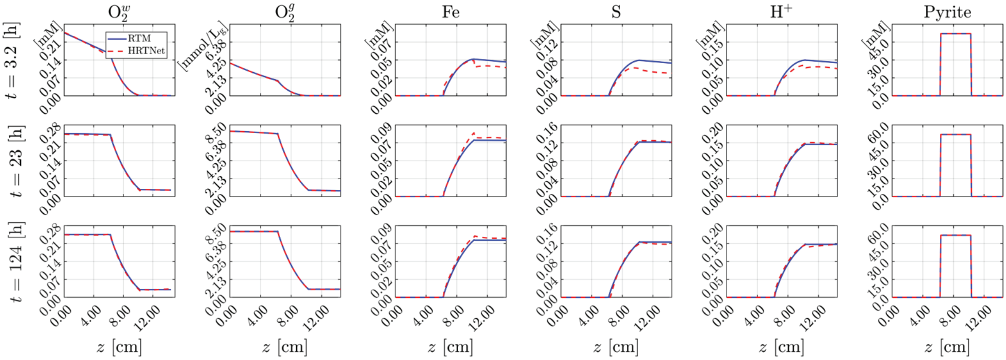

***Figure 2** Comparison between HRTNet predictions and RTM simulations with initial pyrite concentration of 52 mol/L$_{water}$ in 1-D column setup. Blue lines show ground truth from RTM simulations and the red dashed lines present the predictions obtained from the intelligent surrogate model.*

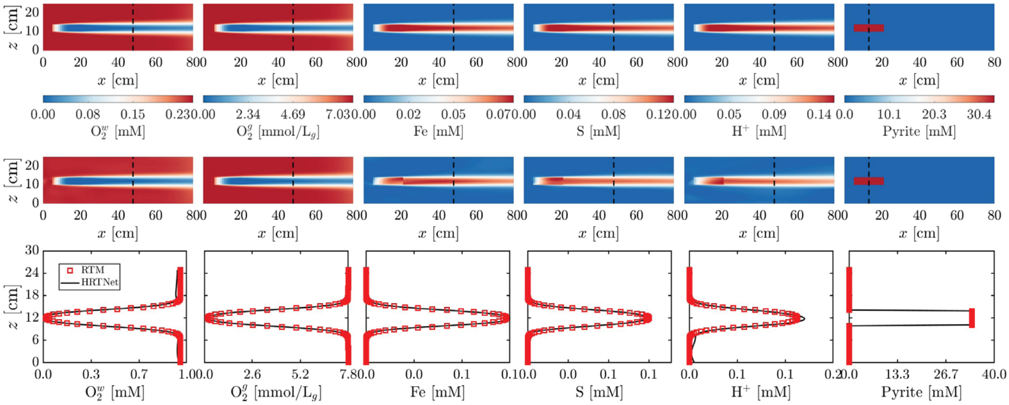

Figure 3 *HRT Predictions in 2-D flow-through chamber at t=50 h: top row – RTM, middle row – HRTNet, bottom row – vertical profiles at x = 13 cm for pyrite and x = 48 cm for others. The black dashed lines represent the cross section where oxygen sensor is placed at x = 48 cm, except for pyrite for which profile at x=13 cm is shown: the corresponding results are on the third row. The red squares represent ground truth from RTM and the black lines are the predictions of HRTNet.*

The two components can effectively capture the data patterns and the reactive transport dynamic features.

We considered examples including pyrite oxidation in 1-D and 2-D geochemically heterogeneous domains to evaluate HRTNet's performance. The results reveal that the predictions obtained by the trained surrogate model agree well with those from mechanistic RTMs. Furthermore, the physics- and chemistry-informed learning was promising to achieve a good generalization capability, because HRTNet could predict the desired spatio-temporal dynamics for a wide range of initial concentrations beyond the training datasets. Based on these encouraging results, the proposed approach could be extended to more complex systems in which not only pyrite oxidation but also other reactive processes control the formation of acid mine drainage.

Acknowledgements

This study is funded by Jane and Aatos Erkko Foundation (grant no. 220021). This work has also been supported by the Research Council of Finland (Finnish Centre of Excellence of Inverse Modeling and Imaging), Flagship of Advanced Mathematics for Sensing Imaging and Modelling (grant no. 358944), and the Research Council of Finland project 321761. M.M. acknowledges the support from the Research Council of Finland through HiFi-MuTaNTS (grant no. 364773) project. Finally, the authors thank the IT Center for Science, Finland (CSC), for generously sharing their computational resources.

References

Battistel M, Muniruzzaman M, Onses F, Lee J, Rolle M (2019) Reactive fronts in chemically heterogeneous porous media: Experimental and modeling investigation of pyrite oxidation. Applied Geochemistry 100: 77–89

Battistel M, Stolze L, Muniruzzaman M, Rolle M (2021) Arsenic release and transport during oxidative dissolution of spatially-distributed sulfide minerals. J Hazardous Materials 409: 124651

Chandra AP, Gerson AR (2010) The mechanisms of pyrite oxidation and leaching: A fundamental perspective. Surface Science Reports 65(9): 293–315

De Lucia M (2024) DecTree: a physics-based geochemical surrogate for surface complexation of uranium on clay. Advances in Geosciences 65: 45–54

De Lucia M, Kühn M (2021) DecTree v1.0 – chemistry speedup in reactive transport simulations: purely data-driven and physics-based surrogates. Geoscientific Model Development 14: 4713–4730

Degen D, Cacace M, Wellmann F (2022) 3D multi-physics uncertainty quantification using physics-based machine learning. Scientific Reports 12: 17491.

Degen D, Caviedes Voullième D, Buiter S, Hendricks Franssen HJ, Vereecken H, González-Nicolás A, Wellmann F (2023) Perspectives of physics-based machine learning strategies for geoscientific applications governed by partial differential equations. Geoscientific Model Development 16(24): 7375–7409

Demirer E, Coene E, Iraola A, Nardi A, Abarca E, Idiart A, de Paola G, Rodríguez-Morillas N (2023) Improving the performance of reactive transport simulations using artificial neural networks. Transport in Porous

Media 149: 271–297

Guérillot D, Bruyelle J (2020) Geochemical equilibrium determination using an artificial neural network in compositional reservoir flow simulation. Computational Geosciences 24: 697–707

Jatnieks J, De Lucia M, Dransch D, Sips M (2016). Data-driven surrogate model approach for 733 improving the performance of reactive transport simulations. Energy Procedia 97: 447–453

Kefeni KK, Msagati TAM, Mamba BB (2017) Acid mine drainage: Prevention, treatment options, and resource recovery: A review. J Cleaner Production 151: 475–493

Leal AMM, Kyas S, Kulik DA, Saar MO (2020) Accelerating reactive transport modeling: on-demand machine learning algorithm for chemical equilibrium calculations. Transport in Porous Media 133: 161–204

Laloy E, Jacques D (2022) Speeding up reactive transport simulations in ce- ment systems by surrogate geochemical modeling: Deep neural networks and k-nearest neighbors. Transport in Porous Media 143: 433–462

Li Y, Lu P, Zhang G (2022) An artificial-neural-network-based surrogate modeling workflow for reactive transport modeling. Petroleum Research 7(1): 13–20

Liu XY, Zhu M, Lu L, Sun H, Wang JX (2024) Multi-resolution partial differential equations preserved learning framework for spatiotemporal dynamics. Communications Physics 7:31

Marcato A, Santos JE, Boccardo G, Viswanathan H, Marchisio D, Prodanović M (2023) Prediction of local concentration fields in porous media with chemical reaction using a multi scale convolutional neural network. Chemical Engineering Journal 455: 140367

Moeini F, Ershadnia R, Rubinstein RL, Versteeg R, Li P, McGarr JT, Meyal A, Wallace CD, Dai Z, Carroll KC, Soltanian MR (2024) Employing generative adversarial neural networks as surrogate model for reactive transport modeling in the hyporheic zone. J Hydrology 639: 131485

Moncur MC, Jambor JL, Ptacek CJ, Blowes DW (2009) Mine drainage from the weathering of sulfide minerals and magnetite. Applied Geochemistry 24(12): 2362–2373

Muniruzzaman M, Pedretti P (2021). Mechanistic models supporting uncertainty quantification of water quality predictions in heterogeneous mining waste rocks: a review. Stochastic Environmental Research and Risk Assessment 35 (5): 985-1001.

Prasianakis NI, Haller R, Mahrous M, Poonoosamy J, Pfingsten W, Churakov SV (2020) Neural network based process coupling and parameter upscaling in reactive transport simulations. Geochimica et Cosmochimica Acta 291: 126–143

Raissi M, Perdikaris P, Karniadakis GE (2019) Physics-informed neural networks: A deep learning framework for solving forward and inverse problems involving nonlinear partial differential equations. J Computational Physics 378: 686–707

Raissi M, Yazdani A, Karniadakis GE (2020). Hidden fluid mechanics: Learning velocity and pressure fields from flow visualizations. Science 367: 1026–1030

Rao C, Ren P, Wang Q, Buyukozturk O, Sun H, Liu Y (2023). Encoding physics to learn reaction–diffusion processes. Nature Machine Intelligence 5: 765–779

Simate GS, Ndlovu S (2014) Acid mine drainage: Challenges and opportunities. J Environmental Chemical Engineering 2(3): 1785–1803

Sprocati R, Rolle M (2021) Integrating process-based reactive transport modeling and machine learning for electrokinetic remediation of contaminated groundwater. Water Resources Research 57: e2021WR029959

Sprocati R, Guadagnini A, Ceresa L, Gallo A, Rolle M (2025) Global sensitivity analysis of mass transfer and reaction dynamics for electrokinetic transport in porous media. Advances in Water Resources doi.org/10.1016/j.advwatres.2025.104887

Steefel CI (2019) Reactive transport at the crossroads. Reviews in Mineralogy and Geochemistry 85: 1–26

Steefel CI, DePaolo DJ, Lichtner PC (2005) Reactive transport modeling: An essential tool and a new research approach for the earth sciences. Earth and Planetary Science Letters 240: 539–558

Williamson MA, Rimstidt J (1994) The kinetics and electrochemical rate-determining step of aqueous pyrite oxidation. Geochimica et Cosmochimica Acta 58, 5443–5454

Xu TF, White SP, Pruess K, Brimhall GH (2000) Modeling of Pyrite Oxidation in Saturated and Unsaturated Subsurface Flow Systems. Transport in Porous Media 39: 25–56

Yu Z, Dai H, Yang J, Zhu Y, Yuan S (2024) Global sensitivity analysis with deep learning-based surrogate models for unraveling key parameters and processes governing redox zonation in riparian zone. J Hydrology 638: 131442

Radiological Assessment of Copper Mining Wastes from the Iberian Pyrite Belt

Juan Antonio Ramírez Pérez[1], Alejandro Barba Lobo[2],
Manuel Jesús Gázquez González[3], Juan Pedro Bolívar Raya[4]

[1]*Universidad de Huelva, Campus El Carmen, Facultad de Ciencias Experimentales, 21007 Huelva, Spain, juan.ramirez@dci.uhu.es, ORCID 0009-0003-6757-7066*

[2]*Universidad de Huelva, Campus El Carmen, Facultad de Ciencias Experimentales, 21007 Huelva, Spain, alejandro.barba@dci.uhu.es, ORCID 0000-0001-8335-1532*

[3]*Universidad de Cádiz, Campus de Puerto Real, Instituto de Investigación Marina (INMAR), 11510 Puerto Real, Cádiz, Spain, manueljesus.gazquez@uca.es, ORCID 0000-0002-0198-5732*

[4]*Universidad de Huelva, Campus El Carmen, Facultad de Ciencias Experimentales, 21007 Huelva, Spain, bolivar@uhu.es, ORCID 0000-0001-9258-6341*

Abstract

The Iberian Pyrite Belt (IPB) is in the southwest Iberian Peninsula. Due to heavy mining and processing of sulfide ores, large amounts of historic mining wastes are dispersed along this area, which are called as "legacy sites". Many of these wastes contain large quantities of metals and metalloids (e.g. As, Cd, Cu) including some potentially Naturally Occurring Radioactive Materials (NORM), which can constitute an important environmental threat and a substantial potential public health. Therefore, a novel radioactive and physicochemical characterization of the most relevant mining wastes was performed, including potential lines of valorization.

Keywords: Mining wastes, radioactive characterization, Iberian pyrite belt, radionuclides, radiological hazard index

Introduction

The Iberian Pyritic Belt (IPB), located in the southwest of the Iberian Peninsula, hosts the largest concentration of polymetallic massive sulfides deposits in the world. This area has been heavily mined for some 5000 years, but was particularly intense during the English period, especially between 1870 and 1930 (Yesares *et al*. 2015), generating a large amount of mining waste, belonging to the more than 100 mines located in this area, most of them abandoned. These wastes have a high content of metals/metalloids such as As, Cu, Zn, and Pb. Moreover, they are Naturally Occurring Radioactive Materials (NORM) wastes since metals extraction from mined minerals can generate materials with naturally occurring radioactive activity according to the EU regulation. Therefore, its radiological implications have to be evaluated. In addition, the toxic metals, metalloids, and associated contaminants as sulfursuppose a potential environmental risk and problems for public health, as they are close to towns and sensitive aquatic ecosystems(Álvarez-Valero *et al*. 2009).

Considering the potential environmental and human health problems related to these wastes, the main objective of this work has been to perform a comprehensive radioactive characterization of the different mining wastes located at these mines, as well as the evaluation of their radiological risks.

Methods

Three mining complexes representative of the mines developed in the IPB were selected for study: 1) Sotiel Coronada (SC), 2) Cueva de la Mora (CM), and 3) Tharsis (TH) (Almodóvar *et al*. 2019). The main processes developed by these mine complexes were extraction of polymetallic ores producing shales rejects (SH), pyrite flotation sludges (FP), roasted pyrite for sulfuric acid production (RP), pyrites leached with sulfuric acid (PY) and slags from minerals smelting (SL) (Tornos *et*

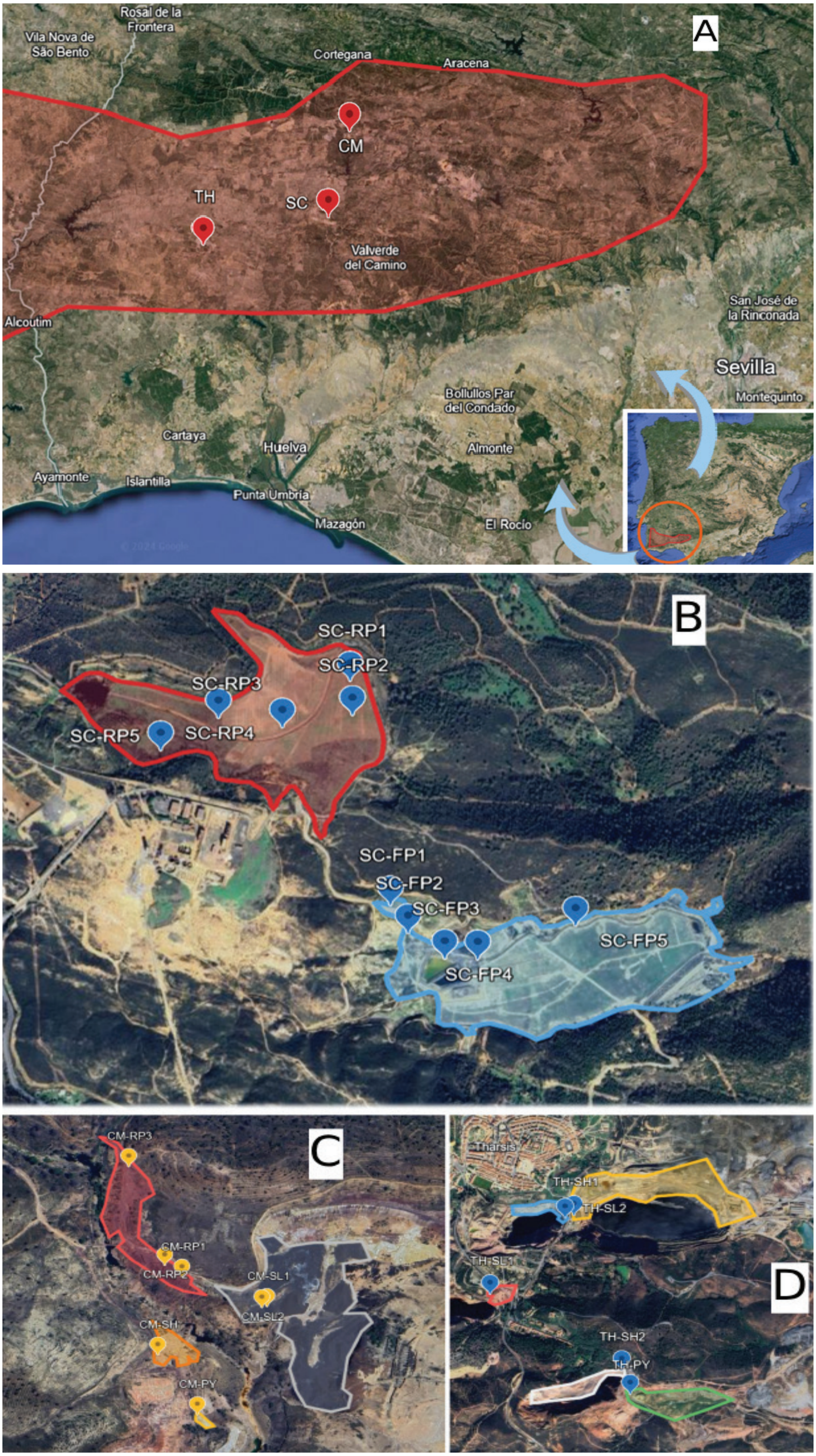

Figure 1 *Locations of studied mines in the Iberian Pyrite Belt (A), and associated mine waste sample sites at Sotiel Coronada (B), Cueva de la Mora (C) and Tharsis (D). Each colour represents an area with the same type of waste.*

al. 2000). In Fig. 1 can be seen the locations of mines in relation to the IPB and associated samples.

Regarding the methodology, first the most characteristic waste piles in the area were sampled. One sample (1 kg) was taken per mound, but in case the extent was too large, several samples were taken from that area for better comparison. The mining wastes were collected subsurface with a shovel, eliminating the upper 5 cm most affected by weathering. The samples were stored in hermetically sealed bags. Subsequently, pre-treatment (drying, milling…) and the measurement of physicochemical parameters were carried out. Afterwards, multi-elemental analysis was carried out by ICP-MS/ICP-OES & XRF and radionuclide concentrations measurement by alpha and gamma spectrometry. Radiological risk indices (Ra_{eq}, Hex, Hin and Ic; Eke *et al.* 2024 ; Paschoa & Steinhäusler 2010) were also calculated. Quality control was applied through blanks, replicates, certified reference samples (IAEA-375 & IAEA-327) and inter-comparisons.

Results

The average concentrations of the major elements in percentage are shown in Fig 2. Each residue has characteristic concentrations for each element. The main elements are Fe, Si and Al. The leached pyrites and flotation residues have a high sulfur content, 3-4 orders of magnitude higher than undisturbed soil. The pyritic waste could generate a possible environmental impact from acid mine drainage (AMD) (Moreno-González *et al.* 2022). Also, all wastes have concentrations 3-4 orders of magnitude above typical soil in metals/metalloids such as As, Cu, Zn and Pb, which could lead to high toxicity (Álvarez-Valero *et al.* 2009).

The mean values of natural radionuclide activity concentrations for different wastes are shown in Fig 3 and Fig 4. For the ^{238}U series, it can be seen that there is secular equilibrium between the radionuclides, and that each waste has distinctive activity concentrations, with slag and leached pyrites having the highest activity concentrations. The observed values for the waste are consistent with those of typical soil (^{238}U: 26-82 Bq/kg ; Monty 2001). For the ^{232}Th decay series and for ^{40}K the same conclusions can be applied, distinctive values for each residue are those expected for undisturbed soil (^{232}Th: 11-84 Bq/kg; ^{40}K: 25-1650 Bq/kg; Charles 2001).

The radiological risk indices calculated were radium equivalent activity (Ra_{eq}), the external (H_{ex}) and internal (H_{in}) radiation indices and the activity concentration index for building materials (Ic) (Fig 4). These are defined by the expressions (Eke *et al.* 2024; Paschoa & Steinhäusler 2010):

trations measurement by
ectrometry. Radiological
ex, Hin and Ic; Eke *et al.*
Steinhäusler 2010) were
lity control was applied
icates, certified reference
& IAEA-327) and inter-

ntrations of the major
age are shown in Fig 2.
haracteristic concentra-
nt. The main elements are
eached pyrites and flota-

highest activity concentratio
values for the waste are consi
of typical soil (^{238}U: 26-82
2001). For the ^{232}Th decay
^{40}K the same conclusions
distinctive values for each r
expected for undisturbed s
Bq/kg; ^{40}K: 25-1650 Bq/kg; C
The radiological risk in
were radium equivalent act
external (H_{ex}) and internal
indices and the activity conc
for building materials (Ic) (I
defined by the expressions (
Paschoa & Steinhäusler 2010

Major elements

***Figure 2** Average concentrations in percentage of the major elements of pyrite flotation (FP), pyrite roasting (RP), smelting slags (SL), leached pyrite (PY) and shale rejects (SH).*

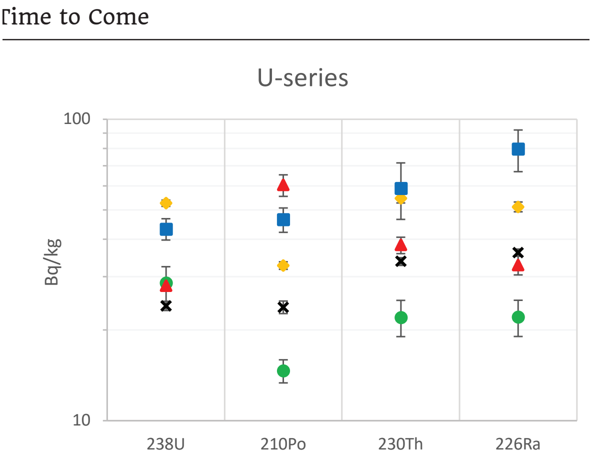

Figure 3 *^{238}U series activity concentrations of pyrite flotation (FP), pyrite roasting (RP), smelting slags (SL), leached pyrite (PY) and shale rejects (SH).*

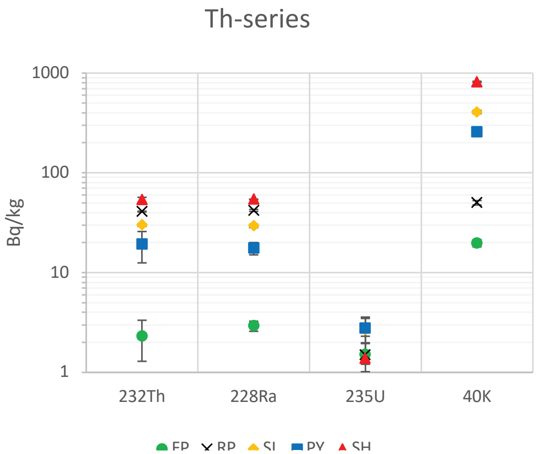

Figure 4 *^{232}Th series and ^{40}K activity concentrations of pyrite flotation (FP), pyrite roasting (RP), smelting slags (SL), leached pyrite (PY) and shale rejects (SH).*

$$Ra_{eq}\ (\mathrm{Bqkg^{-1}}) = C_U + 1.43C_{Th} + 0.077C_K \qquad (1)$$

$$H_{ex} = \frac{C_U}{370} + \frac{C_{Th}}{259} + \frac{C_K}{4810} \qquad (2)$$

$$H_{in} = \frac{C_U}{185} + \frac{C_{Th}}{259} + \frac{C_K}{4810} \qquad (3)$$

$$I_C = \frac{C_{Ra}}{300} + \frac{C_{Th}}{200} + \frac{C_K}{3000} \qquad (4)$$

where C_U, C_{Th}, C_K and C_{Ra} are the activity concentrations of ^{238}U, ^{232}Th, ^{40}K and ^{226}Ra respectively in Bq/kg. The Ra_{eq} values obtained are less than 370 Bq/kg, so they can be marketed in the USA. The H_{ex} and H_{in} values are below the limit value 1, so they do not pose a radiological risk (Eke *et al.* 2024). Likewise, the Ic being less than 1 in all samples, they can be used as building materials without radiological restrictions (Santos *et al.* 2022).

Conclusions

A multi-elemental analysis of different mining wastes from 3 mines located in the FPI: Sotiel Coronada, Cueva de la Mora and Tharsis has been carried out, with the following conclusions:

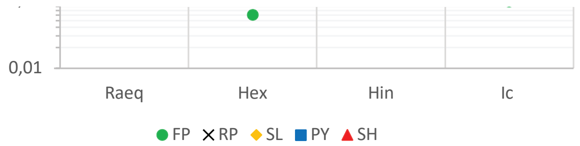

ıes of radiological risk indices Ra_{eq} (Bq/kg), H_{ex}, H_{in} and I_c for pyr
melting slag (SL), leached pyrite (PY) and slate rejects (SH).

concentrations 3-4 orders
above typical soils for
ds with high toxicological
tes have been radioactively
with results for activity

Eke, B. C., Akomolafe, I. R., Uk
Onyenegecha, C. P. (2024). Asses
Hazard Indices Due to Natural
Soil Samples from Imo State U
Nigeria. Environmental Healt
11786302231224581.

Figure 5 *Average values of radiological risk indices* Ra_{eq} *(Bq/kg),* H_{ex}*,* H_{in} *and* I_c *for pyrite flotation (PF), pyrite roasting (RP), smelting slag (SL), leached pyrite (PY) and slate rejects (SH).*

1. All wastes have concentrations 3-4 orders of magnitude above typical soils for metals/metalloids with high toxicological implications.
2. The mining wastes have been radioactively characterised, with results for activity concentrations of natural radionuclides in the range for typical Spanish soils.
3. The calculated radiological risk indices demonstrate that the wastes do not pose a radiological risk.
4. Finally, these wastes comply with the Spanish regulations required for gamma radiation emitted as construction materials.

Acknowledgements

This work has been supported by the project "Diagnosis and proposals for the environmental recovery of areas affected by industrial and mining activities; Implications for the Huelva estuary" (RESTOREHU), Ref.: TED2021-130361B-I00.

References

Almodóvar, G. R., Yesares, L., Sáez, R., Toscano, M., González, F., & Pons, J. M. (2019). Massive sulfide ores in the Iberian Pyrite Belt: Mineralogical and textural evolution. Minerals, 9(11), 653.

Álvarez-Valero, A. M., Sáez, R., Pérez-López, R., Delgado, J., & Nieto, J. M. (2009). Evaluation of heavy metal bioavailability from Almagrera pyrite-rich tailings dam (Iberian Pyrite Belt, SW Spain) based on a sequential extraction procedure. Journal of Geochemical Exploration, 102(2), 87-94.

Eke, B. C., Akomolafe, I. R., Ukewuihe, U. M., & Onyenegecha, C. P. (2024). Assessment of Radiation Hazard Indices Due to Natural Radionuclides in Soil Samples from Imo State University, Owerri, Nigeria. Environmental Health Insights, 18, 11786302231224581.

Charles, M. (2001). UNSCEAR Report 2000: sources and effects of ionizing radiation.

Moreno-González, R., Macías, F., Olías, M., & Cánovas, C. R. (2022). Temporal evolution of acid mine drainage (AMD) leachates from the abandoned tharsis mine (Iberian Pyrite Belt, Spain). Environmental Pollution, 295, 118697.

Paschoa, A. S., & Steinhäusler, F. (2010). legal Aspects of natural Radiation. In Radioactivity in the Environment (Vol. 17, pp. 141-151). Elsevier

Santos, Á. M., Teresa, L. C. A., Llácer, J. M. M., Romero, M. I., Manjón, M. D. M. P. P., & del Llano, S. L. L. Real Decree 1029/2022 of 20 December, approving the Regulation on health protection against the risks arising from exposure to ionising radiation: Questions and answers?

Tornos, F., Barriga, F. J. A. S., Marcoux, E., Pascual, E., Pons, J. M., Relvas, J. M. R. S., ... & Blundell, D. (2000). The Iberian pyrite belt. Database on Global VMS Districts, Codes-Geode, 19-52.

Yesares, L., Sáez, R., Nieto, J. M., De Almodovar, G. R., Gómez, C., & Escobar, J. M. (2015). The Las Cruces deposit, Iberian Pyrite Belt, Spain. Ore Geology Reviews, 66, 25-46.

Solar Evaporation of Brine

M.G. Rapeta[1], J. P. Maree[1,2], T.A.M Msagati[1], T.T.I Nkambule[1]

[1]*Institute for Nanotechnology and Water Sustainability (iNanoWS), College of Science, Engineering and Technology, University of South Africa, Private Bag X6, South Africa*

[2]*ROC Water Technologies, 28 Keramiek Street, Clayville, Olifantsfontein, 1666, South Africa.*

61958239@mylife.unisa.ac.za (ORCID: 0000-0002-6757-0783); mareejp@unisa.ac.za (ORCID: 0000-0002-8901-2512); msagatam@unisa.ac.za (ORCID: 0000-0002-9621-5051); nkambtt@unisa.ac.za (0000-0001-9633-1733)

Abstract

The leachate from coal and waste dumps is highly polluted with mine water, creating significant environmental challenges. Current methods involve storage in evaporation ponds, aiming to reduce immediate impacts. This research proposes an innovative approach using the combination of evaporation, to decrease leachate volume, oxidation of Fe^{2+} to Fe^{3+} with iron-oxidizing bacteria and pH adjustment by using $CaCO_3/Ca(OH)_2$. Key findings include solar evaporation, oxidation achieving a 1:2 molar ratio of Fe^{2+}/Fe^{3+} to recover magnetite using sodium or calcium alkalis, and improved sludge separation characteristics. This method enhances acid mine water treatment efficiency, reduces energy costs, and simplifies management, making it a promising strategy for sustainable practices in mining and environmental management.

Keywords: Leachate, evaporation, solar heating, Fe(ll) oxidation, magnetite

Introduction

The mine water produced in South Africa by gold mines and coal mines, discloses that the existing and previous gold mines in Gauteng produce 350 ML/d. This is produced by the Western (40 ML/d), Central (82 ML/d), Eastern (102 ML/d) and Far Western (126 ML/d) Basins (Mogashane *et al.*, 2020). The coal mines in Mpumalanga produced 200 ML/d of mine water of which 100 ML/d is further treated with reverse osmosis to produce water of drinking quality and brine that are stored in evaporation ponds (Maree *et al.*, 2013). Storage of brine in evaporation ponds is not encouraged by Department of Water and Sanitation as ground water can be contaminated when the plastic liners get damaged (Ahmed *et al.*, 2000).

Leachate from mine tailings, which typically contains high concentrations metal ions, is often subjected to evaporation processes to effectively reduce its overall volume. To facilitate this, water spray cannons are employed, creating micro-sized droplets that are dispersed into the atmosphere, thereby promoting evaporation. While this method can help in concentrating the leachate and minimizing the volume of waste, it has significant drawbacks (Jiang *et al.*, 2023). One major concern is that the saline-rich spray produced during this process can be carried by wind, potentially impacting neighboring areas. This unintended dispersal can lead to soil and water salinization, adversely affecting local ecosystems and agricultural lands. Consequently, while evaporation strategies may seem beneficial for waste management, careful consideration of their environmental impacts is essential (Nalukui and Besa, 2024).

In South Africa and elsewhere, brine from desalination plants is typically stored in evaporation ponds; however, this practice is not favored by authorities due to the potential leakage of plastic liners, which raises significant concerns about environmental contamination and long-term sustainability. Similarly, in mining operations, the management of leachate containing high levels of iron ions is critical, especially after the oxidation process. Efficient recovery of magnetite from this oxidized leachate can significantly mitigate its environmental impact while transforming it into a valuable resource. By implementing effective recovery techniques, both practices address the need for sustainable waste management. This approach not only enhances resource utilization but also reduces the overall volume of waste generated, promoting a more responsible and environmentally friendly mining and desalination industry (Mos, 2018).

Maree has proposed a system for the evaporation of iron rich acid mine water and brine and for the recovery of good quality water and salt (Fig. 1), existing out of the following stages: (i) Solar heating of the brine in a coil shaped pipe, (ii) Evaporation of the brine in a pipe system, (iii) Condensation of humid air through cooling with ambient air or melted ice from freeze crystallization units. The purpose of this investigation was to evaluate and to improve the proposed design.

Objectives

The following objectives were set for the project: (i) Evaluate process configuration for solar evaporation (ii) Determine rate of heating in a pipe (iii) Determine effect of temperature and air volume on vapor fraction.

Materials and Methods

Feedstock. Leachate from a waste coal dump and tap water was used for paper and laboratory studies.

Equipment. HDPE pipes of different diameter, steel plate and thermometer were used.

Experimental. The effect of the following parameters was investigated: (i) Solar heating of the brine, (ii) Evaporation of the brine in a pipe system.

Analytical. Standard procedures were used to collect samples at various phases, filter them (Whatman No. 1), and measure their concentrations of Fe(II), Fe(III), pH, Ca, and alkalinity (APHA, 2012). Metals were analyzed using inductively coupled plasma atomic emission spectroscopy (ICP-OES) (iCAP-7000 Series, ANATECH, South Africa). The pH/EC meters were calibrated before the start of each set of experiments and during the experiment using calibration buffers.

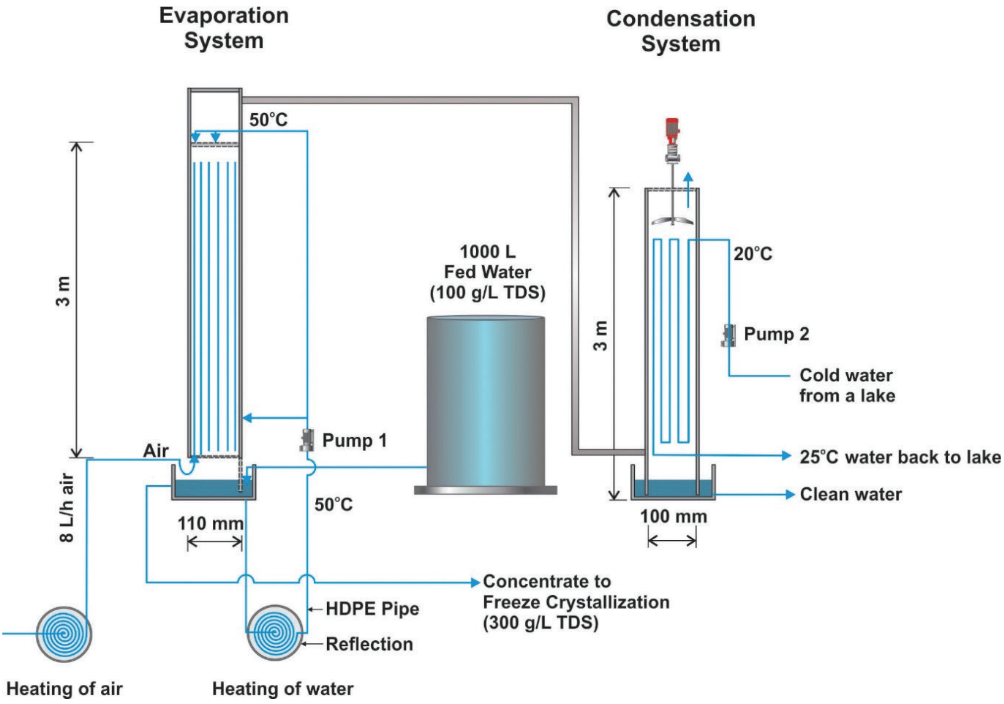

Figure 1 Process configuration for solar evaporation.

OLI Software simulations. The OLI ESP software program was used to predict the conditions needed for evaporation of the leachate (OLI, 2021). OLI is an aqueous equilibrium chemistry estimator with an interactive and self-instructive interface for clarifying reactions, the ability to work with all kinds of common equilibrium reactions, a strong solution algorithm, expressive and easily understandable displays for results, and the ability to produce results in multiple formats according to different uses.

Results and Discussion

Up-concentration of saline waters

The up concentration of saline waters needs a combination of treatment steps, depending on its chemical composition. For mine water rich in metals with a low pH, metals need to be removed through pH adjustment. For brine from desalination plants, up concentration through evaporation can be applied directly.

Magnetite from coal mine leachate

Leachate from a waste coal dump that contained 9 270 mg/L Fe^{2+}, 100 mg/L Fe^{3+}, 328 mg/L Al^{3+} and 600 mg/l Ca^{2+}, 486 mg/L Mg^{2+}, 43 788 mg/L SO_4^{2-} and 200 mg/L Cl^- was treated with the aim to recover magnetite (Fe_3O_4) from Fe^{3+}-rich water (Table 1).

In Step 1, 70% of the water was evaporated at 60 °C through contact with air in a column reactor. Fe^{2+} was oxidised to Fe^{3+} (Eq. 1) due to the presence of 20% O_2 in the air. In Step 2 the Fe^{3+}-rich oxidised water was treated with Na_2CO_3 to precipitate Fe^{3+} as $Fe(OH)_3$ (Eq. 2). In Step 3, a specific volume of the Fe^{2+}-rich feed water was treated with NaOH to precipitate Fe^{2+} as $Fe(OH)_2$ (Eq. 3). The volume of Fe^{2+}-rich feed water needed to result in a $Fe(OH)_3$/$Fe(OH)_2$ mole ratio of 2, was calculated to be 0.8 L out of a total volume of 1 L. In Step 4 the product water from Steps 2 and 3 was mixed to form the $Fe(OH)_2$/$Fe(OH)_3$ sludge, which was allowed to settle and separated from the liquid. In Step 5 the $Fe(OH)_2$/$Fe(OH)_3$ mixed sludge was heated to form magnetite (Fe_3O_4) at 100 °C (Eq 4). An OLI simulation was used to determine chemical dosages and to predict water qualities. At a dosage of 45 423 mg Na_2CO_3, Fe^{2+} was reduced from 9 270 to 60 mg, Al^{3+} from 328 to 1 mg. A dosage of 26 129 mg NaOH was needed to reduce Fe^{2+} from 60 to 1 mg, Fe^{3+} from 1 to 0 mg and Al^{3+} from 1 to 0 mg. The TDS concentration increased from 55 010 mg/L to 212 488 mg/L when 1 L of feed water was evaporated to a final volume of 0.3 L.

$$2Fe^{2+} + \tfrac{1}{2}O_2 + 2H^+ \rightarrow 2Fe^{3+}\ H_2O \qquad (1)$$

$$2Fe^{3+} + 3H_2O + 3Na_2CO_3 \rightarrow$$
$$2Fe(OH)_3 + 3CO_2 + 6Na^+ \qquad (2)$$

$$Fe^{2+} + 2NaOH \rightarrow Fe(OH)_2 + 2Na^+ \qquad (3)$$

$$Fe(OH)_2 + 2Fe(OH)_3 \rightarrow Fe_3O_4 + H_2O \qquad (4)$$

$$Fe(OH)_3 \rightarrow FeOOH + H_2O \qquad (5)$$

$$Fe(OH)_3 \rightarrow Fe_2O_3 \qquad (6)$$

Pigment from Coal Mine Leachate

Pigment can be recovered from iron in mine water as an alternative to magnetite. Only Steps 1 and 2 will be needed. Steps 3 and 4 will be obsolete. Step 5 will need higher temperatures for processing $Fe(OH)^3$ to goethite (yellow pigment) at 200 °C (Eq. 5) or to hematite (red pigment) at 800 °C (Eq. 6) (Rapeta *et al.*, 2024).

Brine

Brine from reverse osmosis plants has a TDS of 30 000 to 90 000 mg/L and contains mainly Na_2SO_4 and NaCl. Such brine is stored in evaporation ponds, which are not environmentally accepted. Such brine can be treated with Freeze Crystallization (FC) for the recovery of water and salt. Since FC required 120 kWh/ton ice, it is advantageous if the RO brine can be concentrated further prior to treatment with FC.

Solar Heating

Evaporation is energy intensive as 2 256 kJ is needed for evaporation of 1 kg H_2O, which amounts to 713.8 kWh/ton H_2O. At an electricity price of R2.00/kWh, evaporation cost (heating from 25 °C to 100 °C + evaporation) amounts to R1 427.50/ t H_2O. This high cost of evaporation with electricity serves as motivation for solar evaporation.

Table 2 shows the effect of pipe diameter on the rate of heating with solar energy in HDPE pipes. It also shows pipe cost. It was noted that water can be heated in a 16 mm ID HDPE pipe within 25 min from ambient temperature (21 to 28 °C) to 49 °C compared to 26 min in a 46 mm Dia. HDPE pipe (Fig.

Table 1 Treatment of Fe^{2+}-rich leachate through evaporation to form magnetite.

Parameter	Unit	Feed 1a	Step 1 Evaporation + Fe^{2+}-oxidation	Step 2 $Fe(OH)_3$ formation	Feed 1b	Step 3 $Fe(OH)_2$ formation	Step 4 2+3	Step 5 Magnetite
Temp	°C	25.0	60.0	60.0	25.0	25.0	60.0	120.0
H_2O	L	1.0	0.3	0.3	0.8	0.8	1.1	
H_2O	g	0.0	1.5					
Feed 1								
Na_2CO_3	mg			45 423.0				
NaOH	mg					26 129.0	0.0	
O_2	mg		1 319.2					
Solution								
pH		5.0			5.0			
Acidity	mg $CaCO_3$	43 035.6	43 044.5	166.0	32 675.0	0.0	166.0	
H^+	mg	486.6	321.8	1.0	369.0	0.0	0.0	
Na^+	mg	0.0	0.0	19 712.0	0.0	15 024.0	34 736.0	
Mg^{2+}	mg	486.0	486.0	486.0	369.0	369.0	855.0	
Ca^{2+}	mg	351.0	100.0	100.0	266.0	266.0	366.0	
Fe^{2+}	mg	9 270.0	60.0	60.0	7 038.0	0.0	0.0	
Fe^{3+}	mg	100.0	9 310.0	1.0	76.0	0.0	0.0	
Al^{3+}	mg	328.0	328.0	1.0	249.0	0.0	0.0	
SO_4^{2-}	mg	43 788.0	43 186.0	43 186.0	33 246.0	33 246.0	76 432.0	
Cl^-	mg	200.0	200.0	200.0	152.0	152.0	352.0	
TDS	mg	55 010.0	53 991.0	63 746.0	41 766.0	49 058.0	112 741.0	
TDS	mg/L	55 010.0	179 971.0	212 488.0	55 010.0	64 613.0	106 434.0	
Fe^{3+}/Fe^{2+}								
Cations	me	917.9	905.4	905.0	697.0	697.0	1 599.0	
Anions	me	917.9	905.3	905.0	697.0	697.0	1 602.0	
Vapor								
H2O	g		0.7					
CO2				18 855.0				
Solids								
CaSO4			853.4					
$Fe(OH)_2$				0.0		11 323.0	11 323.0	
$Fe(OH)_3$				17 810.0		145.0	17 955.0	
Fe^{3+}/Fe^{2+}							2.0	
$Al(OH)_3$							2.9	2.9
Fe_3O_4								22 696.0

2.a). The pipe cost for heating 1 m^3/h from 20 °C to 44 °C at ambient t temperature of 29 °C was calculated to be R5 215 in the case of a 50 mm Dia HDPE pipe. Fig. 2.b showed the effect of heat reflection with a steel plate. With a steel plate a higher temperature of 53 °C was reached, compared to 48 °C without the reflecting plate. Similar runs were carried out to determine the rate of heating air in a pipe. A temperature of 42 °C was reached within 30 min. The lower temperature in the case of air, compared to water, can be ascribed to the smaller heat transfer coefficient of air (10 – 100 $W/(m^2K)$ compared to that of water (500 – 10 000 $W/(m^2K)$.

Table 2 *Heating of water and with solar energy in a pipe.*

Parameter	I.D. (mm)		
	16.0	46.0	106.0
O.D. (mm)	20.0	50.0	110.0
Volume/m (L)	0.2	1.7	8.8
Heating time1 (min)	25.0	26.0	100.0
Volume heated per h in 1 m pipe (L)	0.5	3.8	5.3
Pipe needed for 1 m3/h (m)	2 072.0	261.0	189.0
Pipe price (R/m)	5.0	20.0	60.0
Pipe cost for heating (R/m^3)	10 362.0	5 215.0	11 332.0

Further studies will focus on how the rate of heating can be increased by passing the water through coil pipe, placed in a concave shaped ball, with a reflecting surface, covered with glass, to minimise heat losses to the atmosphere.

Evaporation

Table 3 shows the effect of temperature and gas volume on the H_2O_{vap} fraction in gas phase (OLI simulation). The cells in bold shows the gas volume and temperature where near 50% of the water was in the gas phase and 50% in the liquid phase. If the target is to do evaporation at 55°C, a mass of 4 000 g N_2 (3 200 L) will need to be contacted with 1 000 g H_2O to produce 433 g of H_2O_{vap} and 567 g H_2Ol. To evaporate 100 L/h water at 55°C, 320 m^3/h dry air will be required.

Conclusion

The following conclusion were made: (i) Saline water can be heated in an HDPE pipe. The rate and temperature to achieve is influenced by the pipe dia, pipe length, water feed rate and sun reflection. (ii) Evaporation of saline water is influenced by temperature of the water and air, surface area of the medium and air flow rate. (iii) The estimated cost of solar evaporation amounted to R103/m^3. If this can be used to up-concentrate the feed to freeze crystallization, its cost of R614/m^3 can be reduced. It is estimated that the cost of freeze crystallization can be reduced by 40% if combined with solar evaporation.

Recommendation

It is recommended to design and construct a 100 L/h unit for solar heating, evaporation and condensation

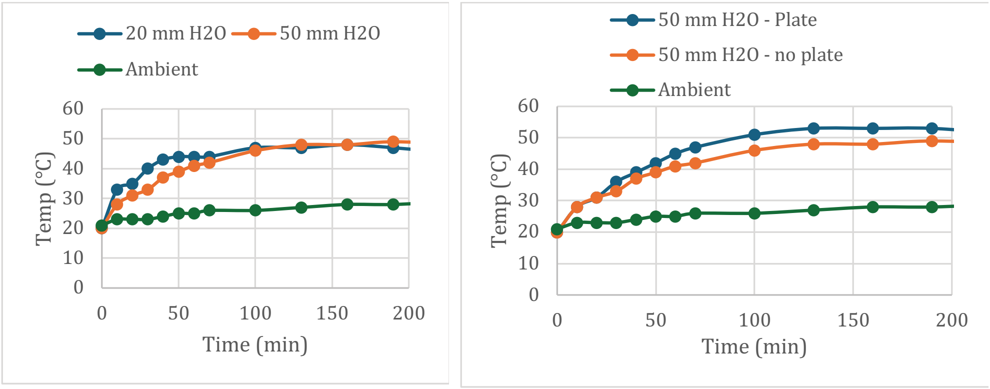

a. Dia varied with no steel reflection

b. Reflection varied (Dia. = 50 mm)

Figure 2 *Heating of water and with solar energy in a pipe (a. Dia varied with no steel reflection, b. Reflection varied (Dia. = 50 mm).*

Table 3 Effect of temperature and gas flow on evaporation from 1 kg water, 50 g Na_2SO_4 and 50 g.

Temperature [°C]	48	55	62	69
H_2O – Vap [g] – N2 = 0.0 g	0.0	0.0	0.0	0.0
H_2O – Vap [g] – N2 = 800.0 g	61.0	90.0	134.0	200.0
H_2O – Vap [g] – N2 = 1600.0 g	121.0	179.0	264.0	390.0
H_2O – Vap [g] – N2 = 2400.0 g	181.0	266.0	389.0	**560.0**
H_2O – Vap [g] – N2 = 3200.0 g	240.0	351.0	**506.0**	693.0
H_2O – Vap [g] – N2 = 4000.0 g	298.0	**433.0**	610.0	798.0
H_2O [g] – N2 = 0.0 g	1 000.0	1 000.0	1 000.0	1 000.0
H_2O [g] – N2 = 800.0 g	939.0	910.0	866.0	800.0
H_2O [g] – N2 = 1600.0 g	879.0	821.0	736.0	610.0
H_2O [g] – N2 = 2400.0 g	819.0	734.0	611.0	**440.0**
H_2O [g] – N2 = 3200.0 g	760.0	649.0	**494.0**	307.0
H_2O [g] – N2 = 4000.0 g	702.0	**567.0**	390.0	202.0

Acknowledgements

The authors acknowledge the valuable input of the following parties: THRIP, UNISA (iNanoWS) for providing with research facilities, NRF for financial support for IMWA Conferences at Morgantown, USA in 2024 and Bragg, Portugal in 2025 and Prof Steffan Panglisch, MAMDIWAS, Germany.

References

Ponds For Brine Disposal In Desalination Plants. *Desalination*, 130, 155-168.

Apha, N. E. W. E. F. 2012. *Standard Methods For The Examination Of Water And Wastewater* (), Washington: American Water Works Association, American Public Health Association.

Jiang, S., Chen, Y., Chen, S. & Hu, Z. 2023. Removal And Reclamation Of Trace Metals From Copper And Gold Mine Tailing Leachates Using An Alkali Suspension Method. *Water*, 15, 1902.

Maree, J. P., Mujuru, M., Bologo, V., Daniels, N. & Mpholoane, D. 2013. Neutralisation Treatment Of Amd At Affordable Cost. *Water Sa*, 39, 245-250.

Mogashane, T. M., Maree, J. P., Mujuru, M. & Mphahlele-Makgwane, M. M. 2020. Technologies That Can Be Used For The Treatment Of Wastewater And Brine For The Recovery Of Drinking Water And Saleable Products. *Recovery Of Byproducts From Acid Mine Drainage Treatment*, 97–156.

Mos, Y. M. 2018. *Magnetite Crystallization Through Oxidation And Bioreduction: Processes For Iron Recovery From Groundwater*. Wageningen University And Research.

Nalukui, S. & Besa, B. 2024. Effects Of Tailings Disposal On The Environment: A Case Study Of Nampundwe Mine. *Journal Of The Southern African Institute Of Mining And Metallurgy*, 124, 527-534.

Oli. 2021. Https://Downloadly.Net/2020/04/11634/04/Oli-Systems/16/?#/11634-Oli-Syst-122115014831.Html. *Https://Downloadly.Net/2020/04/11634/04/Oli-Systems/16/?#/11634-Oli-Syst-122115014831.Html [Online]. [Accessed 01 31].*

Rapeta, M. G., Maree, J. P. & Msagati, T. M. 2024. Removal Of Iron (II) As Magnetite From Acid Mine Water. *Minerals* (2075–163x), 14.

Re-Mining of Mine Water Sludges in Germany: An Opportunity?

Bastian Reker[1], Sebastian Westermann[1]

[1]Technische Hochschule Georg Agricola, Research Center of Post-Mining, Herner Straße 45, 44787 Bochum, Germany, Bastian.Reker@thga.de

Abstract

Many natural resources are critical for the economy and the technologies of our daily lives. The utilization of deposits or resources that were until recently considered waste materials may contribute to a secure and sustainable supply of these resources. Against this background, the RAG-Stiftung has funded the IAW3^3 project at THGA Bochum to conduct an initial screening and evaluation of whether mine water and its sludges from the former hard coal mining areas in the Ruhr region, the Saarland, and Ibbenbüren (NRW) offer an opportunity to extract metals classified as critical.

Keywords: Critical elements, natural resources, hard coal mining, Ruhr area, Saar area, Ibbenbueren

Introduction

Rising prices due to the depletion of natural resources, continuously increasing demand, and strong dependence on third-party countries led the European Commission in 2011 to publish a list of critical elements, most of which are metals. This list is updated every two years and, as of 2023, comprises 34 elements (EC 2023), predominantly (transition) metals, including Rare Earth Elements (REE). Other parts of the world are also aware of the strong dependence on critical metals from third-party countries, which has led to several investigations – e.g., in the USA (Cravotta III 2007, Ziemkiewicz *et al.* 2016, Stewart *et al.* 2017), Portugal (Prudêncio *et al.* 2015), and South Africa (Dube *et al.* 2020) – to determine whether mine water sludges in old tailing ponds provide sufficient enrichment factors for some of these metals, particularly REEs. This concept was adopted for the former hard coal mining regions in Germany (Ruhr and Saar areas, Ibbenbüren), where the last two active collieries were closed at the end of 2018. In 2022, the project "IAW33" was launched at the Research Center of Post-Mining at THGA Bochum, funded by the RAG-Stiftung for three years. This project systematically screens and evaluates, for the first time, whether critical metals show similar enrichment tendencies in mine water sludges and deposits in old tailing ponds in the former hard coal mining regions of Ruhr, Saarland (ongoing investigation), and Ibbenbüren (NRW).

Methods

For the collection and sampling of mine water sludges, two types of precipitation reactors were constructed to facilitate the oxygenation of mine waters and the precipitation of dissolved iron species within a defined volume. The first reactor was designed for low-mineralized mine waters (i.e., iron concentrations < 5 mg/L, no dissolved NaCl). It consists of two commercial 600 L IBC containers connected to each other and equipped with a solar-powered pump for aeration. This design enables operation in remote areas without access to a stationary power supply. A key advantage of this setup is its relatively large volume of 1,000 L, which allows for larger-scale experiments. This reactor was used for the mine waters from the former mining sites "Friedlicher Nachbar" and "Robert Müser" in Bochum, as well as "Heinrich" in Essen (all located in the Ruhr area). The second type of reactor was designed to prevent iron ochre deposition in the pumps of the first reactor when handling highly mineralized mine waters (i.e., Fe concentrations > 5 mg/L, presence of dissolved NaCl). These reactors consist of a single 600 L IBC container, where aeration is facilitated by an external oxygen compressor (HighBlow® HP-80) with six outlets installed inside the container (Fig. 1). This reactor type has been used for the mine waters from the former mining sites "Walsum" in Duisburg (Ruhr area), "Duhamel" in Saarland (still in operation), and Ibbenbüren (NRW). Additionally, several sludge samples were collected and analyzed from two tailing ponds at the "Friedlicher Nachbar" site and in Ibbenbüren.

The collected sludge samples were dried overnight at 100 °C and analyzed by ICP-MS (Inductively Coupled Plasma Mass Spectrometry) at the German Mining Museum in Bochum (Deutsches Bergbau-Museum, DBM). For analysis, the dried and pulverized sludge was dissolved in aqua regia and examined for 55 elements, including alkaline and alkaline earth metals, transition metals (including REEs), metals, and semimetals. To enhance readability and interpretation, the results (originally in weight percent) were converted to grams of the respective metal per ton of dried sludge. It is important to note that the total metal concentration only accounts for the analyzed elements and does not include certain semimetals (e.g., B, Si, As) or some alkaline and alkaline earth metals (e.g., Na, K, Ca). Moreover, selected samples were analyzed using X-ray Diffraction (XRD) to identify impurities and by-products. Experiments for the actual extraction of metals from the sludge were conducted in cooperation with the Max Planck Institute for Sustainable Materials in Düsseldorf, using an innovative technology approach (Jovičević-Klug *et al*. 2024). In this process, the dried and pulverized sludge is pressed into a 10 g pellet and heated in an arc furnace (Edmund Bühler GmbH, type Arc-Melting AM200) under a reducing atmosphere (90% Ar, 10% H_2) at approximately 3.6 kW (18 V, 200 A).

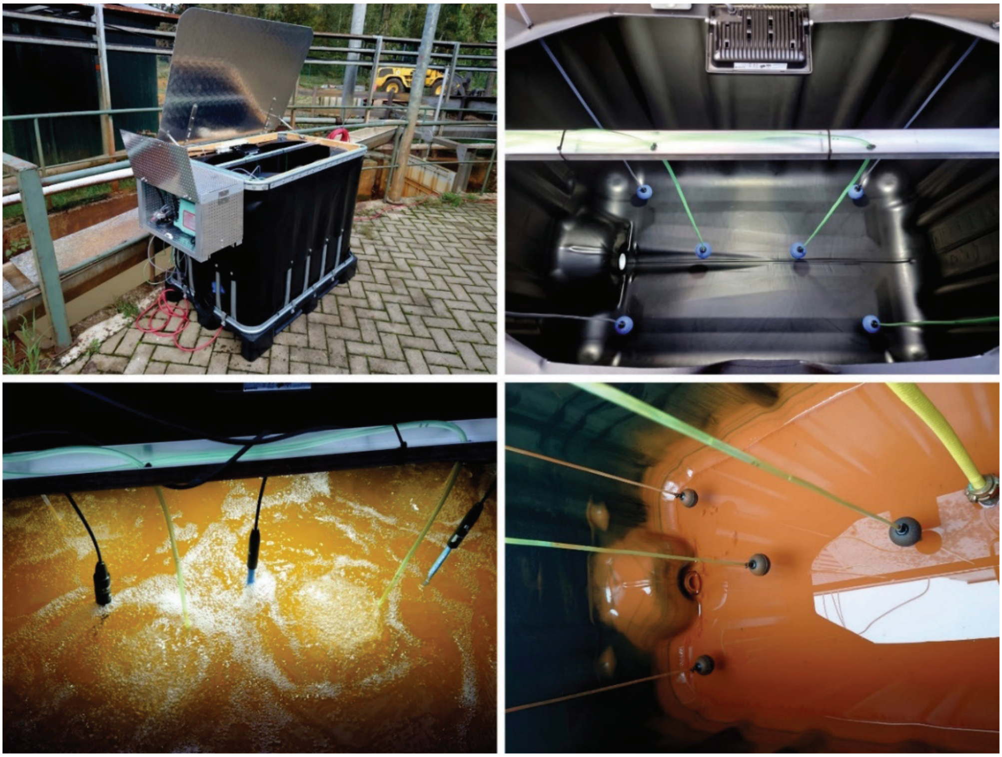

Figure 1 *Type 2 precipitation reactor at the Ibbenbüren site. The lower images show the active process (left) and the sampling procedure (right).*

The resulting products will be analyzed by ICP-MS at the DBM, following the same procedure as for the original sludge samples

Results Ruhr area

In the Ruhr region, four mine water pumping stations were evaluated: "Friedlicher Nachbar" (FN) (including its tailing pond, FN-TP) and "Robert Müser" (RM) within the city of Bochum, "Heinrich" (HR) in Essen, and "Walsum" (WS) in Duisburg (located in the western part of the Ruhr area). As expected, each site exhibits distinct characteristics, leading to varying results. While the sludges from FN, RM, and HR show relatively low total metal concentrations ranging between 2% and 5%, FN-TP and WS demonstrate significantly higher concentrations of 68% and nearly 74%, respectively (Table 1).

The high total metal concentrations observed in FN-TP and WS are primarily due to the iron and manganese fractions, which account for 99.0% and 98.6%, respectively. In contrast, the other samples (FN, RM, and HR) exhibit high levels of impurities, including lime, gypsum, and anhydrite, which significantly reduce their total metal concentrations. This is further supported by the relatively high proportions of alkaline and alkaline earth metals in these samples compared to FN-TP and WS. Additionally, all samples from the Ruhr area lack valuable and critical transition metals, rare earth elements (REEs), and semi-metals (e.g., cobalt, nickel, titanium).

Results Ibbenbueren

The analysis results of sludge samples from the former Ibbenbüren mining area, collected from both the precipitation reactor and the tailing ponds, indicate potential for secondary raw material production. The total metal concentration in the tailing pond (Table 1) reaches nearly 50%, with significant portions of transition metals (including approximately 15,273 g/t Mn, 383 g/t Ti, 323 g/t Co, and 472 g/t Ni), (semi-)metals (12,044 g/t Al), and rare earth elements (about 100 g/t). Conversely, the sample from the precipitation reactor also exhibits a high total metal concentration of about 63% (Table 1); however, it lacks critical and valuable metals. This can be attributed to a pH drop during the experiment from 6.7 to 3.1, caused by the hydrolysis of dissolved iron (initial concentration: 150–200 mg/L in the mine water), which led to the release of protons. As a result, most other metals remained in solution. To address this, a second experiment was conducted using a staggered precipitation approach to account for the varying solubilities of different metal species at different pH levels (Wolkersdorfer 2021). After each pH adjustment (using lime milk at pH 3, pH 5, pH 7, pH 9, and pH 11), the water was transferred to a second reactor, and the corresponding sludge was sampled and analyzed (Table 2):

- The pH 3 sequence produced results similar to those observed for IB in Table 1, as expected.

***Table 1** The table below presents the summarized analysis results for the mining sites: "Friedlicher Nachbar Tailing Pond" (FN-TP), "Friedlicher Nachbar" (FN), "Robert Müser" (RM), "Heinrich" (HR), and "Walsum" (WS) (all located in the Ruhr area), as well as "Ibbenbüren Tailing Pond" (IB-TP) and "Ibbenbüren" (IB). All data are given in grams of metal per ton of dried sludge (g/t). The total metal concentration (expressed as a percentage) is calculated as the sum of the individual metal concentrations divided by 10,000.*

g/t	FN-TP	FN	RM	HR	WS	IB-TP	IB
Alkaline (earth) metals	5,276	10,363	18,766	14,000	5,159	11,821	493
Transition metals (excl. Fe)	30,962	1,803	1,979	2,648	4,710	17,726	210
(Semi-)metals	387	121	101	195	4,349	12,075	1,485
Rare Earth Elements	8	1	1	1	1	100	5
Iron	644,600	21,300	2,106	31,182	722,000	441,574	627,926
Sum	681,234	33,588	22,953	48,025	736,218	483,296	630,120

Table 2 Summarized analysis results for the staggered precipitation experiment at Ibbenbueren. All data in grams of metal per ton of dried sludge (g/t). The total metal concentration in percent equals the sum divided by the factor 10,000.

g/t	IB pH3	IB pH5	IB pH7	IB pH9	IB pH11
Alkaline (earth) metals	1,084	1,495	9,047	16,626	20,068
Transition metals (excl. Fe)	316	719	23,882	31,964	2,665
(Semi-)metals	2,203	5,980	43,822	9,740	8,102
Rare Earth Elements	9	28	840	53	34
Iron	609,153	799,028	277,284	7,935	5,313
Sum	612,764	807,250	354,875	66,265	36,148

- At pH 5, the highest total metal concentration of nearly 81% was recorded, mainly due to the high iron content. Additionally, metals, semi-metals, and REEs showed slight enrichment (Table 2, Fig. 2).
- At pH 7, the total metal concentration dropped significantly, as most of the iron had already precipitated at lower pH levels. However, the concentration of transition metals increased by a factor of 33 (including titanium and cobalt, Fig. 2). Moreover, the levels of (semi-)metals (mostly aluminum) and rare earth elements peaked (Table 2, Fig. 2), making this near-neutral pH – or slightly above – the optimal condition for potential metal recovery from mine water.
- As the pH increased further, the concentration of transition metals rose again, primarily due to the highest manganese precipitation at this stage. Additionally, the increasing levels of alkaline and alkaline earth metals were largely a result of reactions between dissolved magnesium and the added lime milk used for pH adjustment.

Taking these results into account, the large tailing ponds in close proximity to the mine water treatment plant in Ibbenbüren present an opportunity for the future extraction of critical and valuable raw materials. With a total area of 236,000 m^2 (Fig. 3), these ponds contain a big volume of sludge, which has been deposited since the early 1980s. The sludge depth is between 2 m and 4 m, resulting in an overall deposit volume ranging

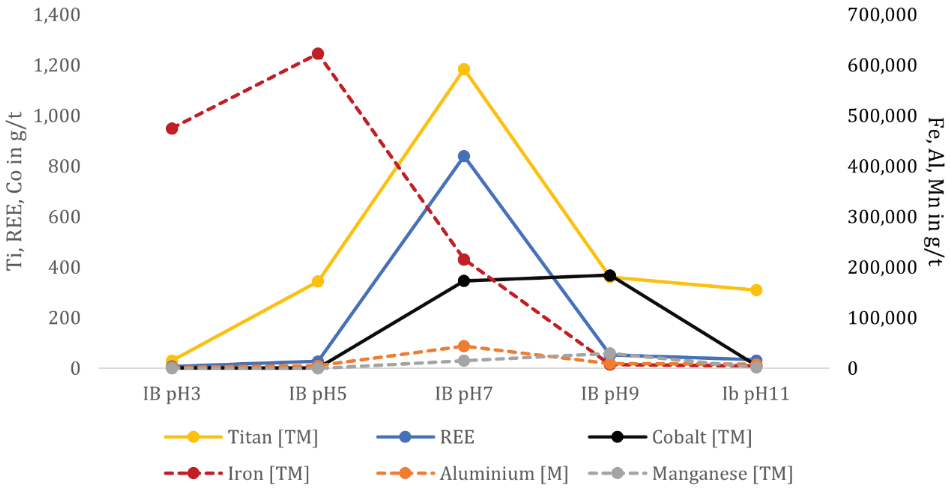

Figure 2 Concentration trends for selected (transition-)metals in the staggered precipitation process in Ibbenbueren. All data in grams of metal per ton of dried sludge (g/t). The dotted lines refer to the right y-axis (Fe, Al, Mn), the solid lines to the left y-axis (Ti, REE, Co). [TM] = Transition metal; [M] = Metal.

from 472,000 m^3 to 944,000 m^3. Based on this volume range, the analysis results, and taking into account the density and solid-to-water ratio of the sampled sludge (67.5% water, 32.5% solids), the expected recoverable amounts of pure metals can be estimated as follows: 88,000–176,000 t of Fe, 2,400–4,800 t of Al, 3,000–6,000 t of Mn, 90–180 t of Ni, 75–150 t of Ti, 65–130 t of Co and 20–40 t of Rare Earth Elements.

Considering that the tailing pond samples were collected only from the surface (for safety reasons) and that the western hard coal field of Ibbenbüren was flooded in the early 1980s, a clear first flush effect (Younger 1997) has been detectable for the past 40 years (Reker *et al.* 2022). As a result, the calculated tonnages likely represent a lower-end estimation

Metal extraction

In cooperation with the Max Planck Institute for Sustainable Materials in Düsseldorf, experiments were conducted using a novel CO_2-neutral approach for metal extraction from these sludges (Jovičević-Klug *et al.* 2024). As a result, two 10 g sludge pellets yielded a 4.7 g "nugget" of pure iron with a purity of over 98% (with minor impurities of Co and Ni), along with 4.3 g of slag (Fig. 4). Further experiments and analysis of the slag are currently ongoing.

Conclusion

This research project represents the first systematic screening and evaluation of mine water sludges in the former hard coal mining areas of the Ruhr, Saarland, and Ibbenbüren. The results indicate potential for the extraction of critical and valuable raw materials such as manganese, cobalt, nickel, titanium, and rare earth elements – particularly from old tailing ponds like those in Ibbenbüren. A new, sustainable, and climate-neutral extraction method utilizing electrical energy without emitting greenhouse gases was successfully tested. However, further work is required, particularly in upscaling the extraction process to optimize energy consumption (e.g., reducing thermal losses) and facilitate the treatment of larger material volumes. Overall, the re-mining of tailing ponds

Figure 3 *Tailing Ponds at the mine water treatment plant in Hoerstel (Ibbenbueren). The mine water treatment plant in Hörstel processes mine water from the "Dickenberger Stollen," which has been dewatering the western field of the hard coal deposit since the early 1980s. The samples presented in this study were collected from the western side of the pond, near the center, which covers an area of 53,288 m².*

not only provides a valuable opportunity to enhance the independence of critical raw materials from third-party countries in a climate-neutral way, but it also helps reduce land consumption for the deposition of new mine water sludges – which will continue to accumulate in the future – while simultaneously lowering the costs of mine water treatment.

Acknowledgement

The authors express their gratitude to the RAG-Stiftung for funding this research project over a period of three years and to RAG AG for their valuable collaboration and support. Furthermore, we sincerely thank Dr. Michael Bode from the Deutsches Bergbau-Museum (DBM) for conducting the ICP-MS analyses and the Max Planck Institute for Sustainable Materials for carrying out the metal extraction experiments.

References

Cravotta III CA (2007): Dissolved metals and associated constituents in abandoned coal-mine discharges, Pennsylvania, USA. Part 1: Constituent quantities and correlations. Appl Geochem 23 (2008), p 166–202, doi:10.1016/j.apgeochem.2007.10.011

EC (European Commission) (2023): Critical raw materials. Online: https://single-market-economy.ec.europa.eu/sectors/raw-materials/areas-specific-interest/critical-raw-materials_en (11.03.2025)

Dube G, Vadapalli VRK, Malatji M, Mothupi T (2020): Recovery of Rare Earth Elements (REE) from Acid Mine Drainage (AMD) passive treatment systems – A review. Presentation on the SAIMM Conference (online) on 12.11.2020

Jovičević-Klug M, Souza Filho IR, Springer H, Adam C, Raabe D (2024): Green steel from red mud through climate-neutral hydrogen plasma reduction. Nature 625, p 703–717

Prudêncio MI, Valente T, Marques R, Sequeira Braga MA, Pamplona J (2015): Geochemistry of rare earth elements in a passive treatment system built for acid mine drainage remediation. Chemosphere 138 (2015), p 691–700

Reker B, Westermann S, Melchers C (2022): Grubenwässer als Ressource kritischer Rohstoffe in Deutschland. GeoResources 4/2022, p. 43–47

Stewart BW, Capo RC, Hedin BC, Hedin RS (2017): Rare earth element resources in coal mine drainage and treatment precipitates in the Appalachian Basin, USA. Int J Coal Geol 169 (2017), p 28–39, http://dx.doi.org/10.1016/j.coal.2016.11.002

Wolkersdorfer C (2021): Grubenwasserreinigung – Beschreibung und Bewertung von Verfahren. Heidelberg (Springer), https://doi.org/10.1007/978-3-662-61721-2

Younger PL (1997) The longevity of minewater pollution – a basis for decision-making. Sci Total Environ 194–195:457–466. https://doi.org/10.1016/S0048-9697(96)05383-1

Ziemkiewicz P, He T, Noble A, Liu X (2016): Recovery of Rare Earth Elements (REEs) from Coal Mine Drainage. Online: https://wvmdtaskforce.com/wp-content/uploads/2016/04/2016-etd30-pfz-a.pdf (11.03.2025)

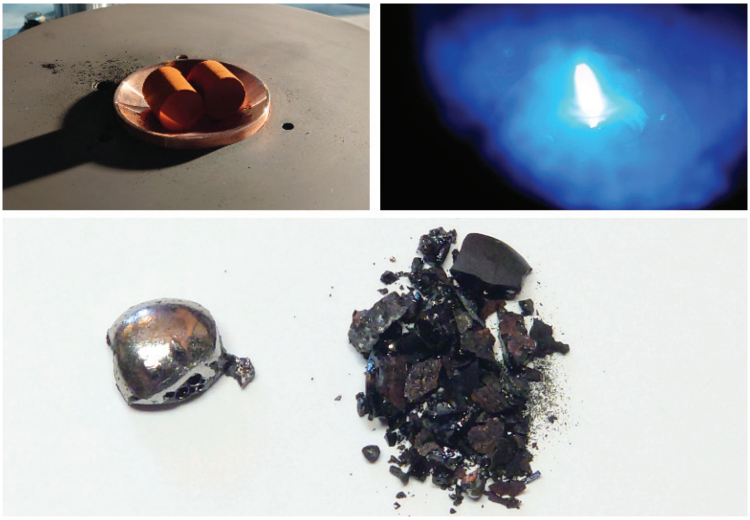

Figure 4 *Two pellets of sludge in the copper crucible of the arc furnace before the experiment conducted at the Max Planck Institute for Sustainable Materials (upper left); plasma-arc during the experiment (upper right) and the final products: pure iron nugget and slag (lower picture).*

Application of X-Ray-Tomography and Geochemical Modeling to Optimize AMD Treatment Design Using DAS at a former Tin Mine Site in France

K. Rhino, J. Jacob, A. Lassin, F. Duré, J. Engevin, J. Huron, V. Guérin

BRGM, 3 av. Claude-Guillemin – BP 36009 – 45060 ORLÉANS Cedex

Abstract

First pilot-scale trials of Dispersed Alkaline Substrate (DAS) reactors for treating acid mine drainage (AMD) at a closed Sn mine in Abbaretz, France revealed notable iron precipitation and clogging over time (Jacob et al., 2023). To address this, a fixed-bed limestone reactor was used to estimate precipitate volume via X-ray tomography, linking iron precipitation to porosity reduction. A second DAS reactor (with new condition) was conducted and a geochemical model, developed with PHREEQC, was used to simulate calcite dissolution, AMD neutralization, and iron hydroxide precipitation under varying residence times. DAS results aligned with experimental data, offered insights into DAS efficiency and lifespan, and helped identifying the main mechanisms that control the fate of iron and metals at the different stages of the process. These findings inform the design of robust passive treatment systems for long-term AMD management.

Keywords: Acid mine drainage, DAS, geochemical modelling, iron precipitation, Clogging

Introduction

AMD poses a substantial environmental challenge due to its high acidity and metal and metalloid content, which can contaminate water resources. DAS reactors offer a promising passive treatment solution by neutralizing acidity and facilitating metal precipitation through calcite dissolution (Ayora *et al.*, 2013). Compared to classical anoxic limestone bed, DAS can handle to an extent passivation/clogging due to ferric iron and aluminum thanks to inert wood chips. However, over time iron precipitation can still lead to clogging, limiting system efficiency and lifespan. Understanding the interplay between residence time, precipitate formation, and porosity evolution is critical for optimizing DAS reactor performance. This study combines laboratory experiments and X-ray tomography to estimate molar volume of precipitate, providing insights to enhance the design and long-term viability of AMD treatment systems.

Methods

Iron precipitate investigations

A 0.25 L fixed-bed limestone reactor was used to simulate AMD treatment (neutralization and iron precipitation). The downflow glass column (diameter 4.5 cm, total height 46 cm) contained 390 g of limestone (500 µm–4 mm particles) with a 262 mL bed volume and 40.8% porosity. A synthetic AMD (pH 2.45, 75 mg/L of Fe(III)) was pumped at 55 mL/h for 72 h, then at 28 mL/h for 53 h. Outlet pH was monitored every 5 minutes. Inlet and outlet samples were collected at 9, 24, 30 and 95 h, filtered (0.45µm) and acidified. Dissolved Fe and Ca were quantified by Agilent 4210 MP-AES. Setup photo is in supplementary material S1. A 6 mm-thick water layer coated the limestone bed. Residence time was about 2h in the column.

Following this experiment, the first 55 mm of the limestone column were scanned in an

X-ray microtomograph (ULTRATOM from RX-solutions (Chavanod, France)) with a 28.4 µm voxel size. Scanning parameters were 120 kV (voltage) and 200 µA (tube current) with a 1 mm Al filter. ImageJ software (Schneider *et al.*, 2012) and voxel counter plugin were used to calculate porosity and precipitate volume based on X-ray absorption differences among air, limestone and precipitate.

The apparent molar volume of the precipitates was estimated using the measured volume from computer tomography (CT) scans and the amount of iron precipitated, acknowledging that the precipitates consist of iron oxyhydroxides with an uncertain exact composition, hydration state, nature of the mineral and according to the following equation:

$$apparent\ molar\ volume\ = \frac{Volume\ of\ AMD\ treated\ \times ([Fe_{in}] - [Fe_{out}])}{Volume\ of\ precipitates}$$

Where Fe_{in} and Fe_{out} are inlet and outlet Fe dissolved molar concentration.

DAS reactor

A 60 cm high square column (30 cm × 30 cm) was filled with calcite (17% vol. grain size 0–4 mm) and wood (83% vol. grain size 0–30 mm). The average composition of the water in the inlet was pH = 2.75, 206 mg/L of Fe, 19 mg/L of Ca and 18 mg/L of Al. The output effluent was on average pH = 6.4, 86 mg/L of Fe, 290 mg/L of Ca and 0.1 mg/L of Al. The residence time in the DAS is 30 h. A 5 cm-thick water film coated the limestone bed.

Modelling of DAS reactor

Geochemical modelling was performed using the PHREEQC code (Parkhurst and Appelo, 2013) in conjunction with a modified version of the Thermoddem database (Blanc *et al.*, 2012). This database decouples Fe(II) and Fe(III) redox valencies, allowing for detailed simulation of non-equilibrium redox-sensitive processes. The model was designed to simulate the injection of AMD into a DAS reactor. The primary objectives were to predict iron depletion at the column outlet, evaluate changes in porosity over time, and simulate the neutralization of acidity within the column.

The column was divided into five cells. The first cell contained a 5 cm water layer in equilibrium with the atmosphere, with a porosity of 100%. The remaining cells represented layers filled with calcite (wood was not specifically modelled, because considered inert), with a total porosity of 54%. An average AMD composition was used for modelling despite natural variations. Hydrological parameters were calibrated using a conductivity residence time test with low conductivity water, later replaced by AMD. The model simulated acid neutralisation, iron redox reactions, and mineral process. The first cell modelled Fe(II) oxidation to Fe(III) by oxygen using Singer and Stumm (1970) rate law. Calcite dissolution and acid neutralization reactions followed rate laws derived from Marty *et al.* (2015). Precipitation processes included only ferrihydrite ($Fe(OH)_3$) and gibbsite ($Al(OH)_3$), as the main precipitation process occurring in the column

The model calibration used experimental data collected during the first 50 days of the experiment, during which the DAS was operational without notable issue including clogging.

Results

Iron precipitate investigations

The fixed-bed limestone reactor presented good performances throughout the duration of the experiment with effluent pH increasing from 2.5 to 6.7, Ca concentration increasing from 61 to 341 mg/L and Fe concentration decreasing from 75 to less than 5 mg/L (detection limit). After 72 hours, a rise in the water level in the column caused by an increase in pressure drop was observed, it was probably due to a decrease in porosity of the fixed-bed. The AMD flow rate was then halved to avoid an overflow during the next 53 hours. By the end of the experiment, the water level rose from 6 mm to 28 mm above the limestone.

Fig. 1 (obtained with X-ray Computational microtomography, CT) overlays the evolution of porosity and precipitates (expressed as a percentage of the total area of each horizontal slice) with depth on a vertical CT slice of the column. Precipitates are highlighted in red. Image processing did not allow for a clear distinction between the precipitates and the interface of the limestone grains. This was accounted for in the calculation of the percentage and volume of precipitates by subtracting a baseline measurement taken at the bottom of the column (between 45 and 55 mm from the top). Minimum porosity was found at between 10 and 15 mm depth (approximately 26%), then gradually increased downwards to about 37.9% near the base of the column, a value close to the pre-neutralization porosity (40.8%). No effect of carbonate dissolution was observed (due to limited operation time and the uncertainty of the measurements). The precipitates were most concentrated at the top of the column, where the iron-laden AMD entered, occupying a maximum of approximately 20% of the column volume. The slice with the most precipitates is shown in supplementary material S2. This proportion steadily decreased toward the bottom, becoming nearly negligible after 35 mm. Interestingly, the minimum porosity occurred approximately 10 mm below the maximum precipitate concentration, likely due to the irregular surface of the limestone packing.

The apparent molar volume of the precipitates was calculated as 825 cm^3/molFe. Assuming the precipitate is primarily ferrihydrite (given the near-neutral pH conditions), this value was compared to the molar volume of ferrihydrite (reported in the Thermoddem database, Fe(OH)3: 34.36 cm^3/mol). The calculated in-situ value was 24 times higher, reflecting the loose nature of the undried precipitate in place within the reactor. This 1:24 ratio (or ≈4%) is consistent with the typical solid content of iron sludge found in passive mine water settling ponds (Zinck *et al.* 1997). This highlights the consequence of the low density of the precipitate and absence of structure on the operational performance and lifespan of the treatment system as pressure drop became measurable after only 3 days of experimentation. This confirms the importance of wood chips in the DAS mixture for maintaining open porosity.

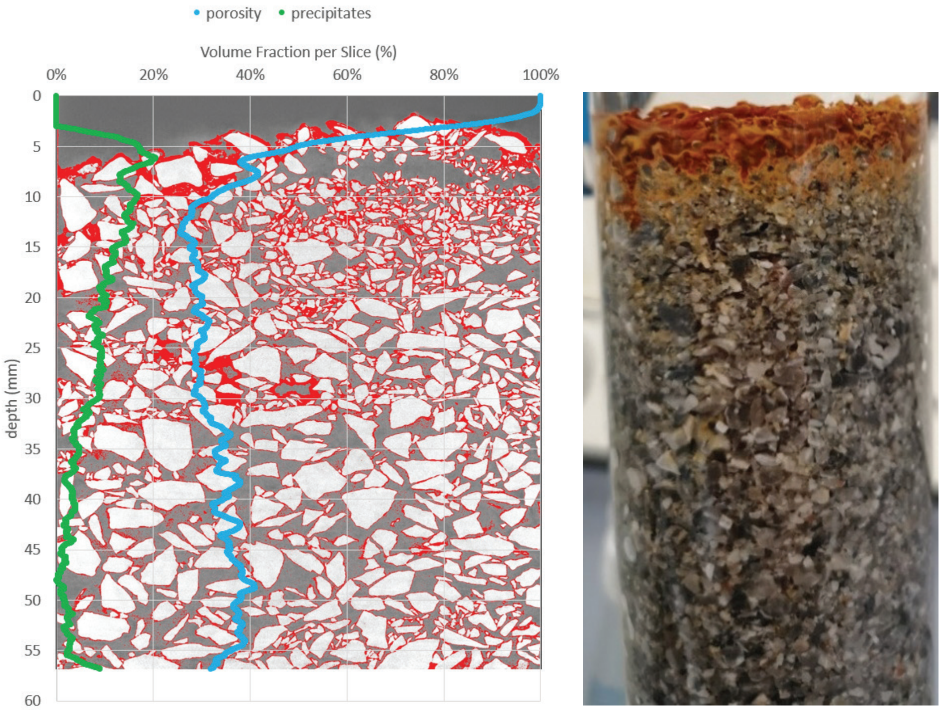

Figure 1 *On the left, evolution of porosity and precipitates (expressed as a percentage of the total area of each horizontal slice) with depth on a vertical CT slice of the middle of the column. In red the iron precipitate, and in white and grey limestone grains and porosity respectively; on the right, photo of the top of the column by the end of the experience.*

Modelling of DAS reactor

The hydrodynamic parameters required for modelling were established using an electrical conductivity test. The initial total porosity is 54%, hydraulic conductivity is estimated to 2×10^{-6} cm/s, and the dispersivity was 0.01 m.

Simulations for residence times of 24, 30 (experimental residence time), 36, and 48 hours revealed key insights into iron depletion, pH evolution, and mineral precipitation (Fig. 2). Overall, the simulations showed that the overall column reached a steady reactivity after 5 days of experimentation, suggesting that the interaction between the AMD effluent and the DAS is the result of a chemical equilibrium. Iron retention increased with longer residence times: for example, 24-hour simulations showed 55% retention, while 48-hour simulations showed 65%. The simulation for the experimental residence time (30 hours) matched the observed data well (58% of iron retention). The pH evolution was consistent across residence times, driven by the kinetic dissolution of calcite with a simulated final pH of 6.8 compared to the experimental pH of 6.4 (30 h residence time). This difference may result from local variations in chemical composition or edge effects, the square

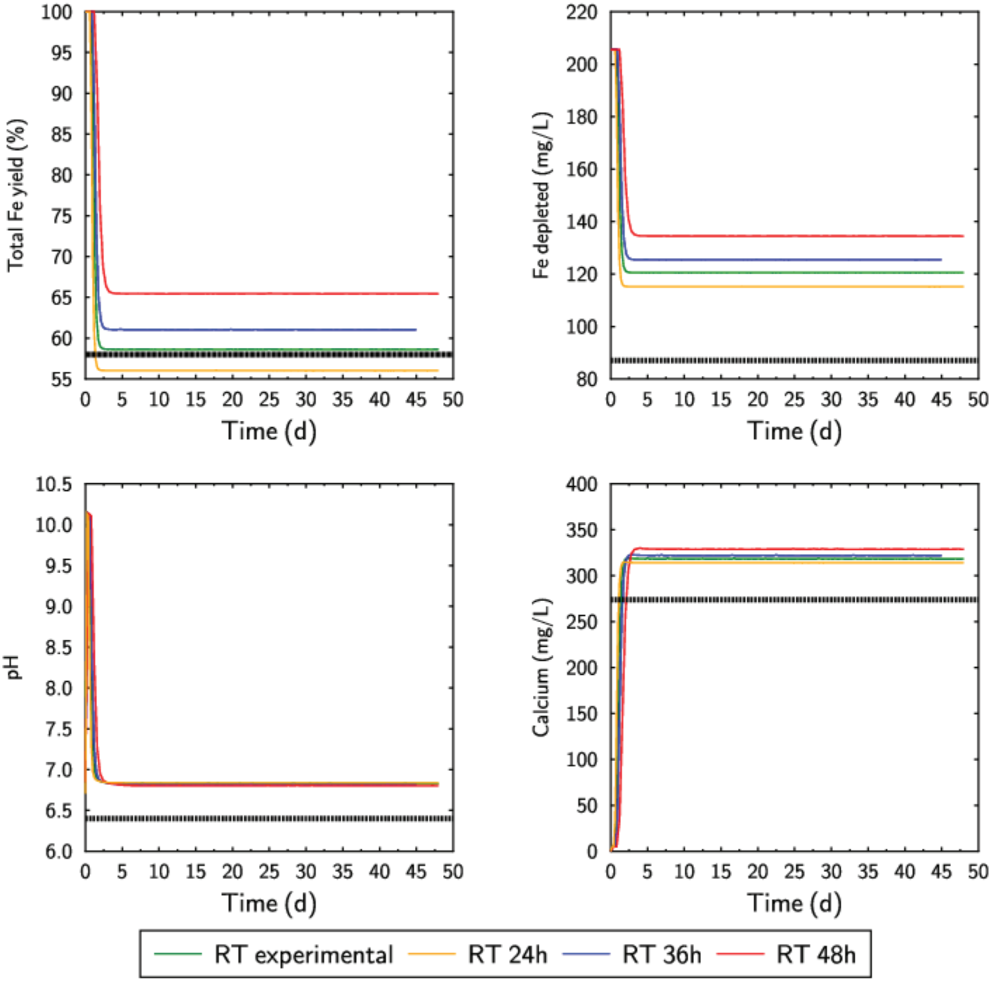

Figure 2 *Simulation of the evolution of the Total Fe yield, Fe depletion, pH and calcium concentration as a function of residence time. Black dashed lines represent the experimental value after 50 days of experimentation. Green, yellow, blue and red lines represent the results for respectively the experimental residence time (30 hours), and residence time of 24, 36 and 48 hours.*

reactor shape may allow a portion of the injecting solution to bypass reactions with calcite. Mixing the final output solution with 5–10% of unreacted AMD gave a pH of 6.5 approaching the experimental pH of 6.4. Iron precipitation trends aligned with iron retention: the 24-hour simulation exhibited 120 mg/L of iron removal from the injected AMD, while the 48-hour simulation showed 140 mg/L of iron removal. These simulated values were higher than the experimental result of 85 mg/L Fe removed from the injected water. Accounting for 5–10% AMD bypass at the reactor edges brought simulated values closer to experimental data.

Calcium concentration is similar across all simulations with a final value fluctuating around 325 mg/L whereas experimental data shows a final value of 275 mg/L in the effluent. This gap in Ca concentration can be attributed to the edge effect which limits the dissolution of calcite in the edges. This result aligns with the pH findings which reveal that less dissolved calcium leads to a more acidic final pH or calcite specific surface area was different in the experiment.

The volume mass of the in situ undried precipitates estimated by X-ray microtomography (825 cm^3/mol Fe) was incorporated into the simulation to assess porosity changes over time. This was performed instead of considering the mass density of each mineral precipitating and dissolving into the system. While this kind of calculation in PHREEQC is typically used for diffusion-dominated processes, here the simulation was adapted to estimate porosity changes across the DAS under flow conditions. However, it is important to note that the simulations did not account for the feedback effect of porosity reduction on flow rates, meaning that decreased porosity did not lead to a simulated decreased residence time in the layer.

The simulation results showed that shorter residence times considerably accelerated porosity reduction (Fig. 3), attributable to a greater flow of fresh AMD, leading to increased dissolution of calcite. This apparent contradiction with calcium and iron concentration in the effluent can be explained by the higher influx of dissolved iron with a shorter residence time. For instance, with a residence time of 24 hours, the iron influx was 147 mg/h, with 55% (80.8 mg/h) depleted at the outlet. Conversely, at a 48-hour residence time, the influx was 84 mg/h, with 65% (54.6 mg/h) depleted. Despite the higher depletion efficiency at longer residence times, the greater absolute iron precipitation in the shorter residence time scenario led to faster porosity decline due to increased

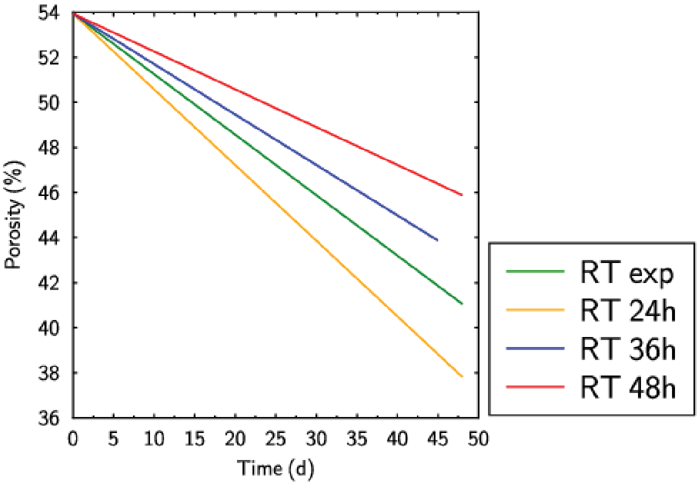

Figure 3 Evolution of porosity as a function of residence time. Experimental results show a final porosity of 48%. Green, yellow, blue and red lines represent the results for respectively the experimental residence time (30 hours), and residence time of 24, 36 and 48 hours.

precipitate formation within the DAS reactor. Considering the experimental final measured porosity was about 48% after functioning for 100 days, Fig. 3 shows that the simulations (50 days) overestimates the porosity change. The model does not consider the edge effect or the passivation of the grain which could slow down the overall decrease of porosity. Although the code has its limitations, it provides a useful approximation of porosity changes and highlights the critical role of residence time in DAS performance.

Conclusions

This study underscores the importance of residence time and iron precipitation on DAS reactor performance for AMD treatment. Laboratory experiment and X-ray microtomography revealed porosity reduction due to precipitate build up, while reactive transport modeling captured key geochemical processes. Shorter residence times could accelerate clogging and increase porosity decline, emphasizing the need for careful optimization of operational parameters. Furthermore, these insights enable a better-informed choice between smaller, less costly reactors with shorter lifespans, which require more frequent replacement of the packing material, and larger, more expensive reactors designed to last longer due to slower clogging rates. By quantifying precipitate volume and porosity effects, this study offers practical guidance for enhancing DAS reactor efficiency and ensuring sustainable AMD treatment.

Acknowledgements

The authors would like to thank the DPSM for funding and supporting this research. We also extend our gratitude to the MIMAROC platform of BRGM for providing access to the X-ray microtomography facilities used in this study. We thank Stephane Gaboreau for the µ-tomography acquisition.

References

Jacob J, Moreau U, Duré F, Engevin J, Huron J, Lassin A, Guérin V (2023, July). AMD passive treatment using DAS at an old tin mine in France. In IMWA 2023.

Ayora C, Caraballo MA, Macias F, *et al* (2013) Acid mine drainage in the Iberian Pyrite Belt: 2. Lessons learned from recent passive remediation experiences. Environ Sci Pollut Res 20:7837–7853. https://doi.org/10.1007/s11356-013-1479-2

Schneider CA, Rasband WS, Eliceiri KW (2012) NIH Image to ImageJ: 25 years of image analysis. Nat Methods 9:671–675. https://doi.org/10.1038/nmeth.2089

Parkhurst D.L., Appelo C.A.J. (2013) Description of input and examples for PHREEQC version 3: a computer program for speciation, batch-reaction, one-dimensional transport, and inverse geochemical calculations (No. 6-A43), U.S. Geological Survey, Techniques and Methods. Reston, VA.

Blanc Ph, Lassin A, Piantone P, *et al* (2012) Thermoddem: A geochemical database focused on low temperature water/rock interactions and waste materials. Applied Geochemistry 27:2107–2116. https://doi.org/10.1016/j.apgeochem.2012.06.002

Marty NCM, Claret F, Lassin A, *et al* (2015) A database of dissolution and precipitation rates for clay-rocks minerals. Applied Geochemistry 55:108–118. https://doi.org/10.1016/j.apgeochem.2014.10.012

Singer PC, Stumm W (1970) Acidic Mine Drainage: The Rate-Determining Step. Science 167:1121–1123. https://doi.org/10.1126/science.167.3921.1121

Zinck JM, Wilson JL, Chen TT, Griffith W, Mikhail S, Turcotte AM (1997, May) *Characterization and stability of acid mine drainage treatment sludges*; MEND Report 3.42.2a; Natural Resources Canada (CANMET): Ottawa, Ontario, Canada, 73 pp.

Towards Sustainable Recovery of Rare Earth Elements from Acidic Mine Waters: A Circular Treatment Approach Integrating Selective Precipitation and Ion Exchange

Alexandra Roa[1], Julio López[2], José Luis Cortina[3]

[1]Universitat Politècnica de Catalunya (UPC), Campus Diagonal-Besòs, Chemical Engineering Deparment, C/Eduard Maristany 10-14, 08930 Barcelona, Spain, alexandra.roa@upc.edu, ORCID 0000-0003-3325-2709

[2]Universitat Politècnica de Catalunya (UPC), Campus Diagonal-Besòs, Chemical Engineering Deparment, C/Eduard Maristany 10-14, 08930 Barcelona, Spain, julio.lopez.rodriguez@upc.edu, ORCID 0000-0001-6739-7960

[3]Universitat Politècnica de Catalunya (UPC), Campus Diagonal-Besòs, Chemical Engineering Deparment, C/Eduard Maristany 10-14, 08930 Barcelona, Spain, CETaqua, Carretera d'Esplugues 75, 08940 Cornellà de Llobregat, Spain, jose.luis.cortina@upc.edu, ORCID 0000-0002-3719-5118

Abstract

Acidic Mine Waters (AMWs) pose a great environmental risk due to their acidity and metal content. Traditional treatments neutralize acidity but produce hazardous sludge. This study introduces a sustainable, circular approach for treating AMWs, focusing on recovering valuable Rare Earth Elements (REEs) and other Critical Raw Materials (CRMs). Using AMWs from the Aznalcóllar Open Pit (SW, Spain), metals like Fe, Al, and Zn were removed through precipitation and sulfide formation, achieving >99% efficiency. Ion exchange resins separated heavy and light REEs, which were recovered as >90% pure oxalates. This eco-friendly process minimizes sludge, mitigates pollution, and supports CRM demand, demonstrating global applicability.

Keywords: Acid mine waters, rare earth elements recovery, heavy rare earth elements, light rare earth elements, selective precipitation, ion exchange, TP272, S930, rare earth elements oxalates

Introduction

Rare Earth Elements (REEs), despite their importance for modern technologies, are scarce, and only a few countries (China, USA and Myanmar) hold reserves (Ayora *et al.* 2016; Voncken 2016). Due to their increasing demand and cost, the European Union (EU) has classified them as Critical Raw Materials (CRMs). Therefore, to reduce the dependency on other countries, the EU is promoting treatment schemes to recover CRMs from secondary sources through circular economy processes (León *et al.* 2021).

Acidic Mine Waters (AMW) are a by-product of the mining industry, which result from the oxidation of sulfide minerals such as pyrite (Sánchez-Andrea *et al.* 2014). Not only they are characterised by their acidic pH, but also by their high concentration of REEs (several orders of magnitude higher than in other water sources) (Ayora *et al.* 2016). Due to that, they represent a great environmental hazard. Conventional AMW treatment focus on prevention or remediation. However, green technologies such as selective precipitation or ion exchange (IX) are being explored for metal recovery (Simate and Ndlovu 2014).

By using selective precipitation, metals can be recovered as hydroxides (Hermassi *et al.* 2022), sulfides (Luptáková *et al.* 2010) or oxalates (Chung, Dong-Yong; Kim, Eung-Ho; Lee, Eil-Hee; Yoo 1998). For instance, researchers (MacIngova and Luptakova 2012) have achieved removals >99% of Cu, Zn, Fe, Al and Mn through staged precipitation, which involved pH adjustment and chemical reagents. Regarding the recovery of REEs, due to the relatively low contents (mg/L to µg/L), the use of IX as selective extraction and post-concentration stage is a promising option.

This study focuses on the fractionation of REEs into Heavy REEs (HREEs) and Light REEs (LREEs) by using two commercial IX resins, one impregnated resin with bis-(2,4,4-trimethylpentyl-) phosphinic acid (TP272) and a chelating one containing iminodiacetic functional groups (S930). For that, a pre-treatment for the removal of the major elements (Fe, Al) and recovery of the valuable elements (Zn, Cu, Co, Ni) present in the AMW was performed. Followed by an optimization of the elution process of the resins. To conclude the work, a crystallization process was performed to recover REEs as oxalates.

Methods

The AMW used came from the Aznalcóllar open-pit in Seville, Spain and was provided by the company *Minera Los Frailes*. The AMW was characterized by an acidic pH (2.7-2.8) and a high content of Mg (1628.5 mg/L), S (3653.8 mg/L), Al (215.7 mg/L), Fe (47.1 mg/L), Zn (547.5 mg/L), and REEs (18.5 mg/L). The content of REEs, separated in LREEs and HREEs can be seen in Table 1.

To avoid interferences during the IX process, and to maximize the resin capacity towards REEs, Fe, Al and Zn were removed (see Fig. 1). For the removal of Fe and Al the process consisted of the addition of H_2O_2 (4 ml/L AMW) to oxidise Fe(II) to Fe(III), followed by an increase of pH (up to 4.5) using NaOH 5 mol/L. Selection of NaOH instead of CaO(s), a cheapest and widely alkali was done to reduce the content of Ca(II) in the treated AMW as it could cause the reduction of the IX resins' capacity. For the removal of Zn, a dosage of 66.6 mmol/L of NaHS was added to the solution at constant pH of 2. The reaction was carried out for at least 10 min or until no variations of the oxidation-reduction potential were noticed. In both processes, after the precipitation, solutions were filtered through a Mixed Cellulose Esters (MCE) filter with 0.45 µm of porous size to remove suspended solids.

For the selective recovery of REEs, two commercially available resins were selected to fractionate REEs into HREEs and LREEs. These were the Lewatit TP272 from *Lanxess*, presenting high selectivity towards HREEs, and the S930 from *Purolite*, used to focus on the retention of LREEs. The experimental set-up consisted of two columns with the same dimensions (2.16 cm of diameter and 11.3 cm of height) allocated in an in-series configuration. The first column contained 15 g of the Lewatit TP272 and the second column contained 16 g of the Purolite S930. Moreover, the inlet of the columns was connected to a peristaltic pump (Miniplus 3 from *Gilson*) and the outlet to a fraction collector (Fraction Collector 204 from *Gilson*). Continuous tests were performed using the AMW depleted of Fe, Al and Zn at a flow-rate of 3 PV/h. Afterwards, the resins were regenerated with a H_2SO_4 solution at 1 PV/h. The chosen concentration for the regeneration of each resin (0.4 mol/L for the TP272 and 0.15 mol/L for the S930) was due to an optimization process. In there,

Table 1 *REEs content in the Aznalcóllar open-pit (Seville, Spain)water (mg/L), average of 5 samples collected along one year.*

LREEs				HREEs			
La	2.3	±	0.1	**Y**	2.5	±	0.2
Ce	6.3	±	0.3	**Tb**	0.12	±	0.01
Pr	0.89	±	0.04	**Dy**	0.54	±	0.04
Nd	3.5	±	0.3	**Ho**	0.09	±	0.01
Sm	0.76	±	0.04	**Er**	0.20	±	0.02
Eu	0.12	±	0.01	**Tm**	0.020	±	0.002
Gd	0.93	±	0.07	**Yb**	0.12	±	0.01
				Lu	0.020	±	0.001

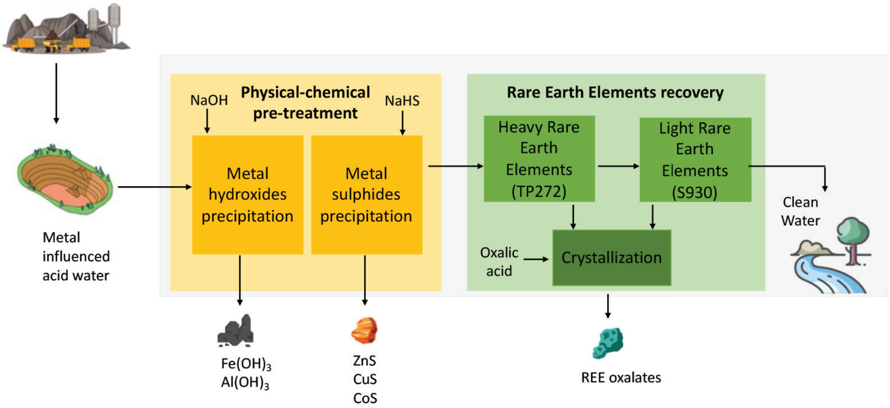

Figure 1 *Followed experimental procedure for the selective recovery of REEs from AMWs.*

the focus was to balance the concentration factors achieved during the elution step and the minimization of the excess of acid to reduce the cost of the alkali solution in the crystallization process. More information could be found in Roa *et al.* (Roa *et al.* 2024a)

The crystallization process focused on the selective recovery of REEs from the eluate as oxalates. For that, after the regeneration of the resins, the samples with higher content of REEs were mixed and an excess of 100% of oxalic acid was added to ensure the complete precipitation. After the addition of oxalic acid, the pH was corrected to 1 using NH_3 instead of NaOH to avoid the precipitation of sodium oxalates (e.g. $NaHC_2O_4.H_2O(s)$) and to not compromise the purity of the resulting solid. When the precipitation was completed, the solution was filtered through a 0.22 µm MCE filter and the solids were dried at 70 °C for 24 h. More details are provided in Roa *et al.* (Roa *et al.* 2024b)

Results

The removal percentages attained during the selective precipitation of Fe, Al and Zn can be seen in Fig. 2, where the blue sections are the metal removals as hydroxides and hydroxysulfates at pH 4.5 and the green ones are as sulfides at pH 2. From there, it can be observed that Al, Fe, and Si were mainly removed as hydroxides. The selected pH of operation was a compromise between removing the maximum amount of Fe(III) and Al(III) and minimizing the losses of valuable elements such as Ce. On the other hand, Cu, Zn, Cd, Ni, Co, and Ce were removed as sulfides. Overall, after those two steps of pre-treatment

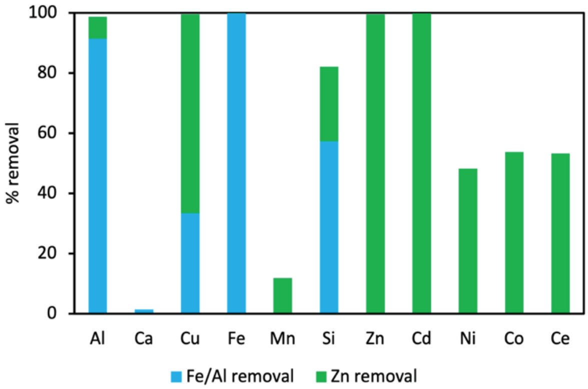

Figure 2 *Removal % for the selective precipitation of Fe and Al at pH 4.5 using NaOH 5 mol/L and removal of Zn at pH 2 using 66.6 mmol/L of NaHS.*

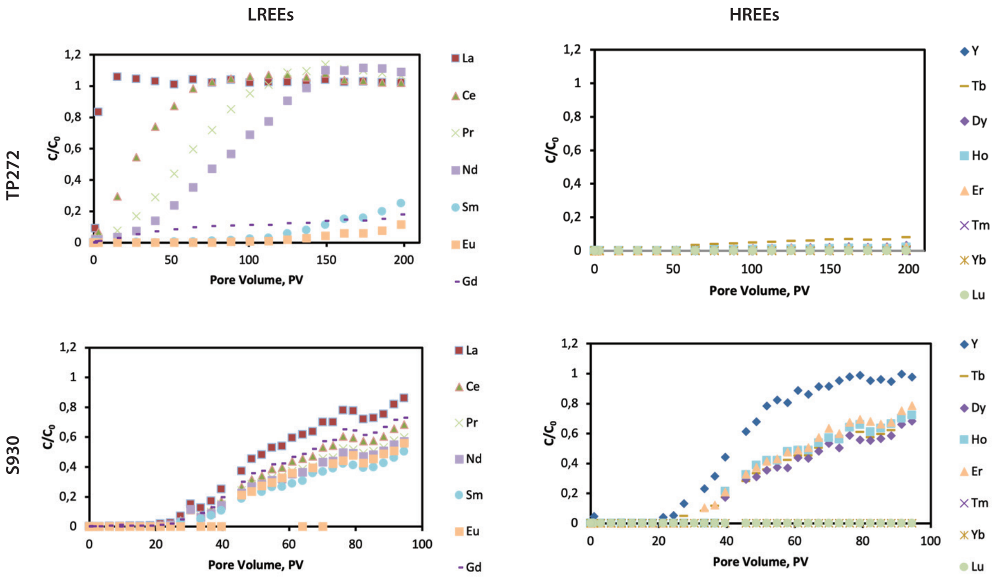

***Figure 3** Breakthrough curves of HREEs and LREEs for TP272 and S930 resins when treating pre-treated AMW depleted of Fe, Al, and Zn.*

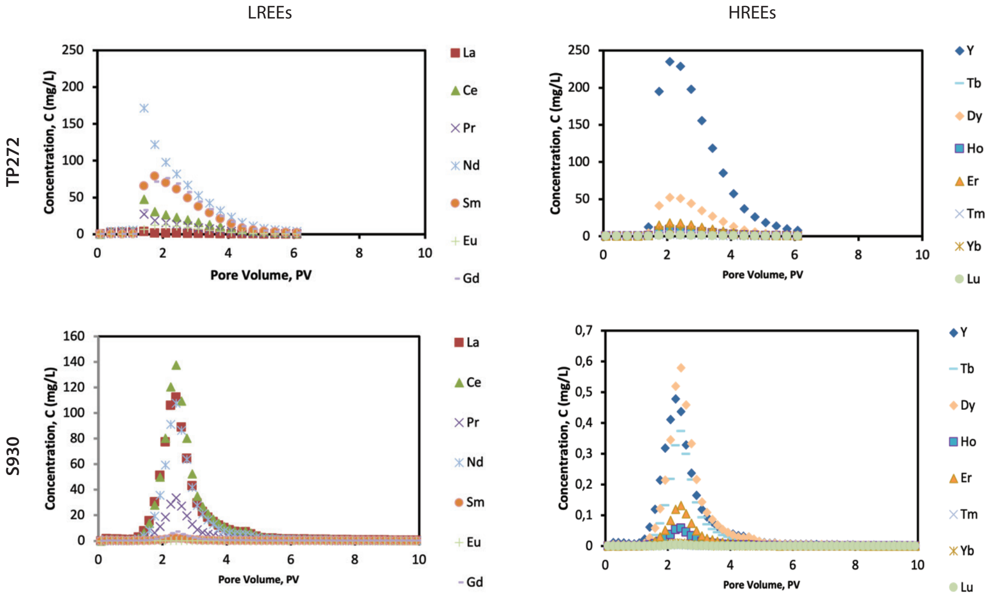

***Figure 4** Elution curves of TP272 with 0.4 mol/L and S930 with 0.15 mol/L of H_2SO_4.*

the removals attained were >99% for Fe, Cu, Zn and Cd, >95% for Al and >40% for Ni, Si, Co, and Ce. However, as reported before the losses of certain REEs were expected during this step by sorption and co-precipitation phenomena (Ayora *et al.* 2016; Lozano *et al.* 2020). No significant losses were observed for the remaining REEs (<2%).

For the fractionation of the REEs into HREEs and LREEs, after bibliography research (Page *et al.* 2017; Hermassi *et al.* 2021), it was decided to test the columns in

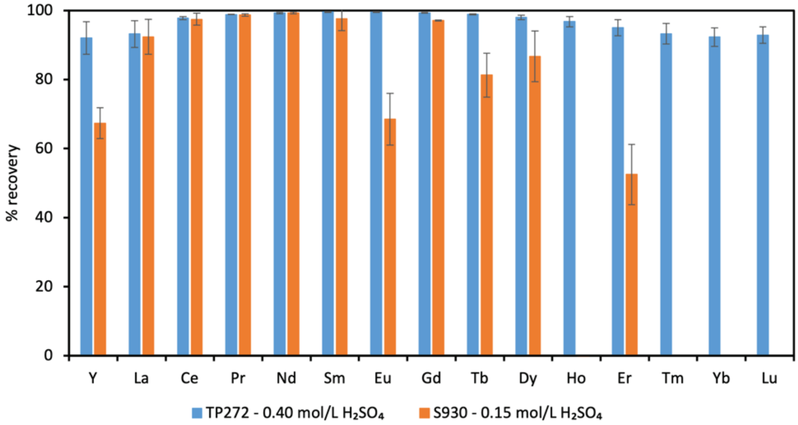

Figure 5 *Recovery percentage of REEs as oxalates from TP272 and S930 when using 0.4 mol/L and 0.15 mol/L of H_2SO_4, respectively in the eluation process.*

series, where the first resin was the TP272 to extract the HREEs, while the S930 was able to extract the remaining LREEs. It was decided to operate the first resin until reaching 200 PV ($C/C_0 = 0.1$), as seen in Fig. 3, to maximize its uptake of HREEs. If the resin was left until saturation, some of the HREEs would have passed to the second column containing the S930, reducing the uptake of LREEs of this one.

After the breakthrough, the regeneration of the TP272 and S930 was done with 0.4 mol/L and 0.15 mol/L of H_2SO_4, respectively (see Fig. 4). In the case of the TP272 the regeneration was completed after 6 PV. In the case of the S930 it was regenerated after 4 PV, which is in accordance with the bibliography (Page *et al.* 2017). In both cases, the curves were quite narrow and uniform, and from them, the selectivity of the TP272 towards the HREEs can be clearly seen. After the regeneration the maximum concentration of Y recovered was near 250 mg/L whereas for the S930 did not reach 1 mg/L.

The recovery percentage REEs as oxalates at the optimum elution conditions for both resins can be seen in Fig. 5. From the samples originated from the TP272 impregnated resin, recoveries higher than 90% were achieved for all the REEs. However, an almost complete recovery for Ce, Pr, Nd, Sm, Eu, Gd, and Tb was obtained. Regarding the S930 chelating resin, recoveries higher than 80% were attained for La, Ce, Pr, Nd, Sm, Gd, Tb, and Dy. Moreover, recoveries between 50% and 60% were achieved for Y, Eu, and Er. Nonetheless, it is worth mentioning the fact that, even though REEs such as Ho, Tm, Yb, and Lu were in low concentration in the initial AMW (<0.15 mg/L), they were completely retained by the TP272 resin. Hence, at that concentration the S930 is not able to extract them from the treated AMW.

After the solution was filtered and dried, the solid was analysed and it was observed that for both resins, the solid was a mixture of REEs oxalates. However, the proportion of LREEs or HREEs was different depending if the solid came from the TP272 resin or the S930, showcasing the affinities of each one. With the AMW depleted of Fe, Al, Zn and REEs, a post-treatment, focusing on the reclamation of water would be the following step. In addition, a techno-econimical analysis must be performed in order to ensure the feasability of the proposed treatment train.

Conclusions

This study shows the possibility of implementing a method to valorise AMW based on the integration of selective precipitation and IX processes to selectively recover REEs.

During the pre-treatment, removals of 90% and 99% of Fe and Al, respectively, as hydroxides were attained. In addition, the removal of Zn and other transition metals as sulfides was carried out, obtaining removals higher than 99% for Zn and Cd and higher than 40% for Ni, Co, and Ce.

Regarding the IX process, it was observed that the resin TP272 presented a high selectivity towards the HREEs, whereas the S930 could concentrate both HREEs and LREEs. Therefore, by integrating both resins in series, REEs could be fractionated into HREEs and LREEs. Afterwards, they were recovered as oxalates by the addition of oxalic acid, achieving recoveries higher than 90% and solids that were a mixture of them.

This work demonstrated the technical viability of recovering REEs (considered critical elements in USA, Canada, Australia and the EU, among others) from secondary sources associated to mining wastes.

Acknowledgements

This project has been financed by the Spanish Agency of Research (AEI) through the REEsources (PDC2021-120869-I00), UPCYCLING (PID2023-147160OB-C21) and MET4LIBS (TED2021-131583B-I00) projects., as well as by the REEcovery project (PN-21033) financed by the EIT-Raw Materials. The work of A. Roa was supported by the Ministerio de Ciencia e Innovación (MCIN) and the AEI within the scope of the grant PRE-2021-097794. Support for the research of J.L. Cortina was also received through the "ICREA Academia" recognition for excellence in research funded by the Generalitat de Catalunya. Additionally, the authors acknowledge the project CEX2023-001300-M funded by MCIN/AEI/10.13039/501100011033. Finally, the Catalan Government (ref. 2021-SGR-596) is also acknowledged. The authors also acknowledge Minera Los Frailes for providing the AMWs.

References

Ayora C, Macías F, Torres E, *et al* (2016) Recovery of Rare Earth Elements and Yttrium from Passive-Remediation Systems of Acid Mine Drainage. Environ Sci Technol 50:. https://doi.org/10.1021/acs.est.6b02084

Chung, Dong-Yong; Kim, Eung-Ho; Lee, Eil-Hee; Yoo J-H (1998) Solubility of RE oxalate in oxalic and nitric acid media. 277–284

Hermassi M, Granados M, Valderrama C, *et al* (2022) Impact of functional group types in ion exchange resins on rare earth element recovery from treated acid mine waters. J Clean Prod 379:134742. https://doi.org/10.1016/j.jclepro.2022.134742

Hermassi M, Granados M, Valderrama C, *et al* (2021) Recovery of Rare Earth Elements from acidic mine waters by integration of a selective chelating ion-exchanger and a solvent impregnated resin. J Environ Chem Eng 9:105906. https://doi.org/10.1016/j.jece.2021.105906

León R, Macías F, R. Cánovas C, *et al* (2021) Mine waters as a secondary source of rare earth elements worldwide: The case of the Iberian Pyrite Belt. J Geochemical Explor 224:. https://doi.org/10.1016/j.gexplo.2021.106742

Lozano A, Ayora C, Fernández-Martínez A (2020) Sorption of rare earth elements on schwertmannite and their mobility in acid mine drainage treatments. Appl Geochemistry 113:. https://doi.org/10.1016/j.apgeochem.2019.104499

Luptáková A, Bálintová M, Jenčárová J, *et al* (2010) Metals recovery from acid mine drainage. Nov Biotechnol Chim 10:23–32. https://doi.org/10.36547/nbc.1060

MacIngova E, Luptakova A (2012) Recovery of metals from acid mine drainage. In: Chemical Engineering Transactions

Page MJ, Soldenhoff K, Ogden MD (2017) Comparative study of the application of chelating resins for rare earth recovery. Hydrometallurgy 169:275–281. https://doi.org/10.1016/j.hydromet.2017.02.006

Roa A, López J, Cortina JL (2024a) Selective separation of light and heavy rare earth elements from acidic mine waters by integration of chelating ion exchange and ligand impregnated resin. Sci Total Environ 954:. https://doi.org/10.1016/j.scitotenv.2024.176700

Roa A, López J, Luis Cortina J (2024b) Recovery of Rare Earth Elements from Acidic Mine Waters: A Circular Treatment Scheme Utilizing Selective Precipitation and Ion Exchange. Sep Purif Technol 126525. https://doi.org/10.1016/j.seppur.2024.126525

Sánchez-Andrea I, Sanz JL, Bijmans MFM, Stams AJM (2014) Sulfate reduction at low pH to remediate acid mine drainage. J Hazard Mater 269:98–109. https://doi.org/10.1016/j.jhazmat.2013.12.032

Simate GS, Ndlovu S (2014) Acid mine drainage: Challenges and opportunities. J Environ Chem Eng 2:1785–1803. https://doi.org/10.1016/j.jece.2014.07.021

Voncken JHL (2016) Physical and Chemical Properties of the Rare Earths. In: The Rare Earth Elements: An Introduction. Springer International Publishing, Cham, pp 53–72

Use of Industrial By-Products to Prevent/ Reduce Water Contamination with As and Hg

Rafael Rodríguez[1], Efrén García[1], Begoña Fernández[2], Julia Ayala[2]

[1]Department of Mining Exploitation and Prospecting, Polytechnical School of Mieres, University of Oviedo, Gonzalo Gutiérrez Quirós s/n, 33600 Mieres, Asturias, Spain; rrodrifer@uniovi.es, ORCID 0000-0002-5518-1481; garciaefren@uniovi.es, ORCID 0000-0001-9138-7076

[2]Department of Materials Science and Metallurgical Engineering, Polytechnical School of Mieres, University of Oviedo, Gonzalo Gutiérrez Quirós s/n, 33600 Mieres, Asturias, Spain; fernandezbegona@uniovi.es, ORCID 0000-0003-1239-4839, jayala@uniovi.es, ORCID 0000-0002-6404-1296

Abstract

Based on two real scale trials carried out in an abandoned mercury mine waste dump, a solution to prevent and reduce the contamination of water with arsenic (As) and mercury (Hg) is proposed. First, the waste surface is covered with a layer of fly ash preventing 90% of the water to be contaminated. Second, the leachate is treated in filtering channels with fly ash and steel slags to reduce the As concentration in four stages with reduction of 60% in each stage. The results demonstrate the feasibility and usefulness of the proposed solution.

Keywords: Fly ash, steel slag, physical remediation, abandoned mines, passive mine water treatment

Introduction

The European Union produces about 64 million tons per year of fly ash (ECOBA, 2016) and 15 million tons per year of slags (EUROSLAG, 2022). About 57% and 12% respectively are not reused with the problem of its storage and very expensive management. It has been demonstrated that some byproducts can fix potentially toxic elements. On the other hand, there are in Europe many mining dumps containing high concentrations of toxic elements being a problem both for the environment and human health. In this context, the SUBproducts4LIFE project was developed within the LIFE program of the European Union. First, the use of fly ash from coal burning power plants and slags from blast furnace and steel making were tested at a laboratory scale with positive results, Ayala and Fernández (2020). Then, several real scale tests were carried out in an abandoned mercury mine (Fig. 1) to demonstrate the reuse of byproducts to reduce the contamination of leachates produced in waste dumps.

The main problem is that rainwater is contaminated by the waste producing leachate with very high concentration of As and Hg, which becomes a very serious environmental problem. The average annual rainfall P in the area is of about 900 mm/a (Chazarra *et al.*, 2018), and the average evapotranspiration ET_0 is of about 800 mm/a (Sancho *et al.*, 2012). Under these conditions, the main goal is to prevent and reduce this contamination of the water.

Materials and Methods

The mine, located in Asturias (Spain), is a paradigmatic case of arsenic (As) and mercury (Hg) contamination that has been studied many times during the last years, i.e. Loredo *et al.* (1999, 2006), Fernández *et al.* (2020), García *et al* (2021), Rodríguez *et al.* (2021). In the present work the test was carried out in the upper waste dump with about 13,000 t of solid waste from metallurgical process highly contaminated with As and Hg. Seven soil samples were collected as described in Fernández *et al.* (2020) with the results shown in Table 1.

Two different tests were carried out. The first consisted in covering the waste with fly

Table 1 Arsenic and mercury concentration in the waste.

Potentially Toxic Element	N	Average mg/kg	Min mg/kg	Max mg/kg	SD
Arsenic (As)	7	16,107	2594	38,841	13,312
Mercury (Hg)	7	3646	240	7266	2645

ash to prevent water contamination. This measure is quite interesting because it has also the advantage of preventing gaseous Hg emissions to the atmosphere after Rodríguez *et al.* (2023).

For this purpose, two areas of about 1000 m^2 each one, were selected in the waste dump. One was covered with a layer of 30 cm of ash (Fig. 2) to prevent the rainwater infiltration. Under this layer another layer 30cm thick of blast furnace slag was put as a drainage. In this case, ash, with porosity of 58.8% and permeability of 2.83×10^{-6} m/s, act as physical barrier preventing the entry of water. No loss of efficiency of the materials has been observed; in no case are the slags or ashes loaded with As or Hg. Although slags were also used, the more important role is due to ashes. Slags contribute to the stability and drainage.

Water samples were collected from the ditch at the toe of the dump in each area. The ditches receive surface run off as well as leachates that have passed through the waste materials. Due to ditches are independent, the comparison between As and Hg concentration in leachate in both ditches allowed determine the efficiency of the ashes to prevent contamination.

In the second test the contaminated water passed through filtering channels to reduce the Hg and mainly As concentration as much as possible. The channels consisted in a half of a 40 cm diameter pipe, 6 m long, arranged with a slope of approximately 10%.

These channels were filled with two layers of steel making slags 3–4 cm thick alternating with two layers of fly ash 1–2 cm thick. The steel slag base layer is shown in the Fig. 3. In total, 189 kg of material were used (45 kg of ash and 144 kg of slag). The composition of the material is as follows:
80 kg of slag + 27 kg of ash + 64 kg of slag + 18 kg of ash.

In this case, the removal of As and Hg from the water is due to physicochemical reactions, and the byproducts retain these elements (Ayala and Fernández, 2020). Therefore, as they work, they become loaded with As and Hg, reaching a point where they are exhausted, and their efficiency is null. The efficiency and the life span of the byproducts are determined by comparing the As and Hg concentration at the inlet and outlet of the channel.

Figure 1 La Soterraña mercury mine facilities (image: courtesy of Quercus Media).

Figure 2 The two areas (covered and uncovered) of the waste dump (image: courtesy of Ax1 Ahora).

Results

Four campaigns of water sampling in ditches of waste dump were carried out. Campaigns 1, 3 and 4 are related to days with intense raining while campaign 2 is related to rain of moderate intensity for several days (Fig. 4). The cumulative rain for each period was 42.8, 6.6, 45.6 and 53.4 mm respectively.

Nine samples of water were taken in each ditch. The results show that there is a huge variability in the concentration of As and Hg for different samples. High concentrations of As and Hg are usual when it rains after a dry period. The relationship between Hg concentration in waste and Hg concentration in leachate is according to Vaselli *et al.* (2017).

The results (Tables 3 and 4) show the effect of the ash capping: the contamination of the water was reduced more than 90%, from 10,203 to 1040 µg/L for As, and from 5.46 to 0.1 µg/L for Hg. This is in accordance with a study in another area described in Rodríguez *et al* (2025). When $P/ET_0 \approx 1$, with a 30 cm of ash layer, only 10% of the rainwater crosses

Figure 3 One of the channels used for trials (image: R. Rodríguez).

Table 2 *Chemical composition of fly ash (FA), and blast furnace and steel making slags (BFS, SMS) after Ayala and Fernández (2020).*

	Weight percentage (%)									Concentration (mg/kg)								
	SiO2	Fe2O3	MgO	K2O	Al2O3	CaO	SO3	TiO2	MnO	Hg	As	Zn	Cu	Cr	Pb	Ni	Cd	pH
FA	56.5	9.5	0.9	2.61	23.9	3.4	2.04	0.85	-	2	59	90	57	83.6	16	65.4	1.84	10.9
BFS	34.2	0.34	5.7	0.44	12.8	42	3.29	0.64	0.31	5.5	10.3	4	2.18	27	1	0.4	-	11.3
SMS	13.8	37.9	1.1	0.3	2.1	38.3	1.14	0.53	3.49	16.3	37.8	57.5	26	49	9	24	0.16	11

the ash, contact to the waste and become contaminated.

This result is very important because this solution reduces the Hg concentration from 5.46 to 0.10 µg/L, which is lower than 1 µg/L which is the maximum allowable concentration of Hg in water before being discharged in a river.

It must be taken in mind that companies which supply byproducts have a huge experience in managing these materials. More concretely in Asturias there are several large landfills in which these byproducts are deposited and consequently their potential effects on the environment, of very low intensity, and the measures to avoid them are well known. The main goal, more difficult to achieve, is to reduce the high concentration of Hg and As in water, mainly in the later which can reaches 400 times the maximum allowable value.

The effectiveness of the filtering channel was also analysed. Due to Hg concentration (0.38 µg/L) was lower than the maximum allowable value, only the As removal is analysed. The test was conducted over a period of two weeks (334 hours), with a total volume of 11,234 L of water flowing through the channel (average flow rate of 0.56 L/min). Samples were also collected on the initial days to ensure the representation of high adsorbent dosages.

A total of six water samples were collected at the inlet and outlet of the channel to analyse

Table 3 *Arsenic concentration in the ditch water.*

Sampling point (ditch)	N	Average (mg/L)	Min (mg/L)	Max (mg/L)	SD
Uncovered waste dump area	9	10,203	1525	26,304	6965
Ash-covered waste dump area	9	1040	23	220	980

Table 4 *Mercury concentration in the ditch water.*

Sampling point (ditch)	N	Average (mg/L)	Min (mg/L)	Max (mg/L)	SD
Uncovered waste dump area	9	5.46	0.67	23.25	9.00
Ash-covered waste dump area	9	0.10	0.00	0.29	0.12

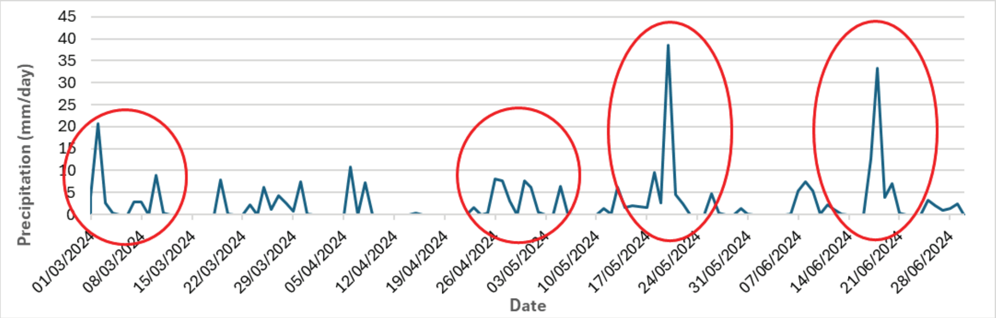

Figure 4 *Daily precipitation in the area (according to Spanish Meteorological Agency AEMET).*

the As concentration by Inductively Coupled Plasma Mass Spectrometry (ICP-MS). The average concentration of As was reduced from 21,510 to 11,192 µg/L with an average global efficiency of 47.9%. According to Ayala and Fernández (2020) ashes and steel slags exhibit comparable retention curves, suggesting that about half of the arsenic was retained in the slags and half in the ashes.

If it is assumed that the entire mass of material (189 kg) is involved in removing As, the relationship between the volume of water treated at a given time and the mass of material represents the adsorbent concentration which diminishes with time. According to these results, if the volume of water is limited to an adsorbent concentration of 25 g/L, the As reduction reaches the 60% (Fig. 5).

Case study

Based on the previous results, we can carry out a case study assuming the use of filtering channels in conjunction with the use of fly ash capping to prevent and diminish the contamination of the rainwater over 1000 m^2 of a dump with waste from mercury metallurgical process. We can consider that the yearly precipitation is 900 mm/a, and the total rainwater volume over the 1000 m^2 of waste surface is 900 m^3/a.

Let us assume that the concentration of As and Hg in leachate from the waste dump is 10,000 and 5.0 µg/L respectively. The maximum allowable concentration for As and Hg to discharge water into a river are 25 and 1 µg/L respectively according to Spanish regulations.

The waste surface is covered a layer of ash 30 cm thick which means that only 10% of water is contaminated. The water collected in the ditch is driven to a filtering channel with steel making slag and fly ash. The efficiency of the channel is 60% for a dosage of 25 g/L.

Under these hypotheses, the concentration of Hg in leachate after covering the waste with ash would be 0.5 µg/L, lower than the maximum allowable value 1 µg/L. Nevertheless, the concentration of As would be 1000 µg/L, so it is necessary the treatment in a filtering channel to reduce the As concentration to 25 µg/L. We can achieve this by using 4 stages in series:
1000 µg/L × $(1 – 0.60)^n$ = 25 µg/L *µ* then n ≈ 4
The total mass of adsorbent material is:
4 × 900 m^3/a × 25 g/L = 4 × 900 m^3/a × 25 kg/m^3 = 90,000 kg/a = 90 t/a

Each stage must have 22.5 t of ashes and slags with a total volume of about 11.2 m^3. An example of a possible distribution could be four channels of 25 m ×2.5 m × 0.2 m.

The result could be improved if the layer of ashes covering the waste is of 40 cm thick. In this case, the water infiltrating through the ash would be 5%, the As concentration in the ditch would be 500 µg/L and only 3 stages should be necessary. After using, the exhausted byproducts should be stored in the site and covered with clean ash.

Conclusions

The solution described for the elimination of As and Hg from the leachate produced in a waste dump has been demonstrated to be feasible and useful to reduce mainly the As contamination by reducing the concentration of As from 10,000 to 25 µg/L.

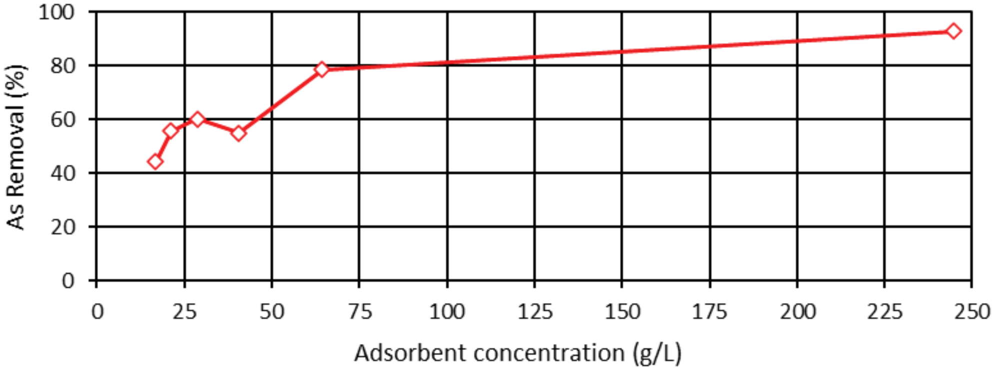

***Figure 5** Relationship between As removal and adsorbent dossage.*

On the other hand, it must be considered that the results achieved are perfectly replicable since they were carried out under real conditions without taking special precautionary measures like in a laboratory.

Acknowledgements

Authors would like to thank the collaboration of the institutions and private companies that participated in the project SUBproducts4LIFE funded by the European Union (Ref. LIFE16 ENV/ES/000481).

References

Ayala, J, Fernández B (2020) Industrial waste materials as adsorbents for the removal of As and other toxic elements from an abandoned mine spoil heap leachate: a case study in Asturias. Journal of Hazardous Materials, 384, 121446. doi:10.1016/j.jhazmat.2019.121446

Chazarra A, Flórez E, Peraza B, Tohá T., Lorenzo B, Criado E, Moreno JV, Romero R, Bote R (2018) Mapas climáticos de España (1981–2010) y ETo (1996–2016). Ed.: Ministerio para la Transición Ecológica, Agencia Estatal de Meteorología. Madrid, 2018. 75 pp.

ECOBA 2016. https://www.ecoba.com/ecobaccpprod.html. Accessed: 19/03/2025.

EUROSLAG, 2022. https://www.euroslag.com/products/statistics/ . Accessed: 19/03/2025.

Fernández B, Lara L, Menéndez-Aguado J, Ayala J, García-González N, Salgado L, Colina A, Gallego JL (2020) A Multi-Faceted, Environmental Forensic Characterization of a Paradigmatic Brownfield Polluted by Hazardous Waste Containing Hg, As, PAHs and Dioxins. Sci. Total Environ. 726, 138546. doi:10.1016/j.scitotenv.2020.138546

Loredo J, Ordóñez A, Gallego JL, Baldo C, García-Iglesias J (1999) Geochemical Characterisation of Mercury Mining Spoil Heaps in the Area of Mieres (Asturias, Northern Spain). J. Geochem. Explor., 67, 377. doi:10.1016/S0375-6742(99)00066-7

Loredo J, Ordóñez A, Álvarez R (2006) Environmental impact of toxic metals and metalloids from the Muñón-Cimero mercury-mining area (Asturias, Spain). J. Hazard. Mater., 136, 455–467. doi:10.1016/j.jhazmat.2006.01.048

Garcia-Gonzalez H, García-Ordiales E, Rodríguez R (2022) Analysis of the Airborne Mercury and Particulate Arsenic Levels Close to an Abandoned Waste Dump and Buildings of a Mercury Mine and the Potential Risk of Atmospheric Pollution. SN Appl. Sci. 4, 76. doi:10.1007/s42452-022-04964-7

Rodríguez R, Garcia-Gonzalez H, García-Ordiales E (2022) Empirical Model of Gaseous Mercury Emissions for the Analysis of Working Conditions in Outdoor Highly Contaminated Sites. Sustainability 14, 13951. doi:10.3390/su142113951

Rodríguez R, Hernández Z, Fernández B, Bascompta M (2023) A Novel Solution to Avoid Mercury Emissions Produced by Highly Contaminated Demolition Debris in Mining Site. Environments 10, 187. doi:10.3390/environments10110187.

Rodríguez R, Bascompta M, García-Ordiales E, Ayala J (2025). Use of fly ash layer as a barrier to prevent contamination of rainwater by contact with Hg-contaminated debris. Environments 12, 107. doi:10.3390/environments12040107.

Sancho JM, Riesgo J, Jiménez C, Sánchez MC, Montero J, López M, (2012) Atlas de Radiación Solar en España utilizando datos del SAF de Clima de EUMETSAT. Ed.: Agencia Estatal de Meteorología (AEMET). Madrid, 162 pp.

Vaselli O, Nisi B, Rappuoli D, Cabassi J, Tassi F (2017) Gaseous Elemental Mercury and Total and Leached Mercury in Building Materials from the Former Hg-Mining Area of Abbadia San Salvatore (Central Italy). Int. J. Environ. Res. Public Health 2017, 14, 913 425. doi:10.3390/ijerph14040425.

Advances in Mine Dewatering Design and Monitoring at Tharisa Chrome Mine Rustenburg South Africa

Mark Roebert[1], Nathi Mntungwa[1], Moses Msitsini[2], Pieter Holtzhausen[2]
Kym L Morton[2], Wayne van Heerden[2]

[1]*Tharisa Minerals, Rustenburg South Africa, mroebert@tharisa.com*

[2]*KLM Consulting Services Pty Ltd, 22 Central Road, Sunrella AH, 1748, South Africa, kmorton@klmcs.co.za, ORCID 0000-0002-5865-1979*

Abstract

Tharisa Minerals is a chrome and platinum group metals (PGM) open-pit mine near Rustenburg, South Africa. The mine dewaters three pits and a planned underground mine. Historic workings under the mine's active East pit also require proactive water management to ensure safe mining operations.

Tharisa's dewatering strategy integrates stormwater control, in-pit pumping (boreholes and sumps), and pit perimeter dewatering boreholes. Automated monitoring of water levels record success in meeting drawdown targets. Water re-use enables a phased approach to zero discharge.

Tharisa is a good example of pro-active dewatering design. There are valuable insights on dewatering for surface and underground transition mines.

Keywords: Chrome, Dewatering, Pit-Perimeter, Monitoring, In-Pit Pumping, PGMs

Introduction

South Africa's Tharisa Minerals operates a large chrome and platinum group metals (PGM) open pit mine near Rustenburg, situated in the western limb of the Bushveld Complex (BC). The BC holds over 70% of the world's platinum and chrome resources. Tharisa mine is situated on the south-western limb of the BC and is underlain by the Middle Group (MG) and Upper Group (UG) chromitite layers straddling the boundary between the Marikana and Rustenburg facies (Dildar *et al.* 2023). Tharisa mines and processes about 5.6 million tonnes/yr (Mt/a) from five MG chromitite seams within the layered mafic and ultramafic intrusions, producing about 1.7 Mt of chrome and about 120 000oz of PGMs (4E) per annum.

The MG chromitite layers outcrop on the property striking roughly east to west with a gentle change in strike to northwest-southeast in the far west. These layers dip at between 9° and 15° to the north. The stratigraphy typically narrows to the west and the dip steepens to the western edge of the outcrop. The dip shallows out at depth across the whole mine area.

Despite the region's low rainfall of about 600 mm/yr, the mine must continually dewater its three pits and planned underground mine, ahead of mining operations. The proximity to old underground mining voids under the eastern area of the East pit requires dewatering in advance of mining, to ensure risk-free ore extraction. Fig. 1 shows the mine location and main rivers.

Fig. 2 shows the three pits, local geology, geological structures and the underlying old Samancor chrome workings. There are three pits: East pit, West pit, and Far West pit. The East pit will be mined to an elevation of 980 meters above mean sea level (mamsl), while the West pit will be mined to an elevation of 1 025 mamsl. Tharisa's planned underground mine will be mined to an elevation of 790 mamsl in the first 10 years.

The main aquifers at Tharisa are the weathered zones of the upper BC, faults and dyke contacts, and the ore body contacts. The eastern side of the East pit is underlain by

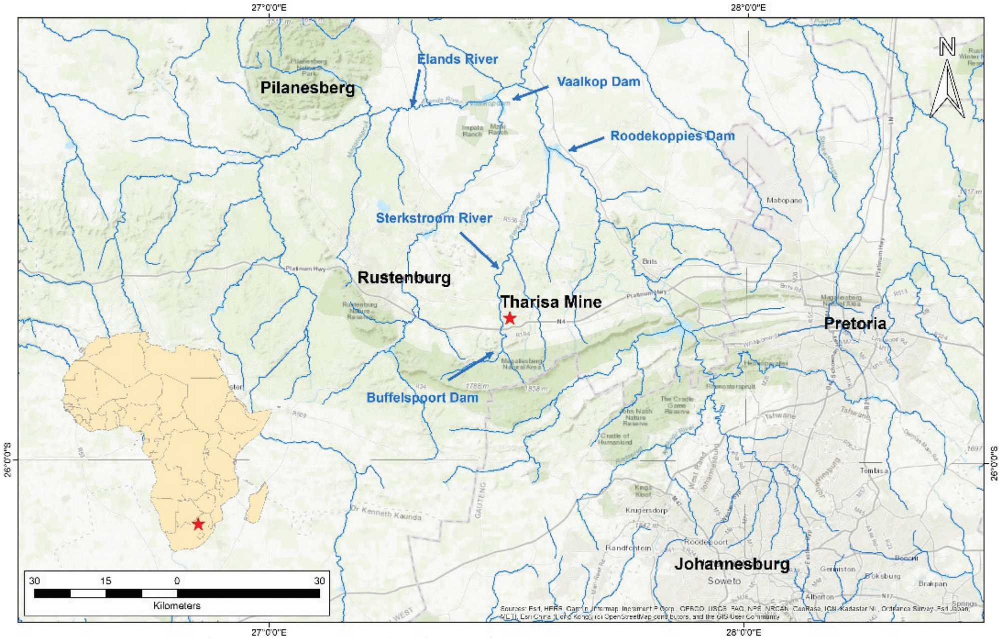

Figure 1 Location of Tharisa Mine in South Africa (Tharisa Minerals 2018).

flooded, mined-out workings (known as the Samancor workings). Groundwater flow is from south to north. Recharge is from rainfall, stored water in waste rock dumps, and from the Sterkstroom River which separates the East and West pits. The Sterkstroom is fed by the Buffelspoort dam, so it has a constant head. Rainfall is between 240 to 850 mm/a with most of the rain falling in November to April. During Summer rainfall months, the pits can become flooded. Water pumped out of the pit is classified as calcium sulfate

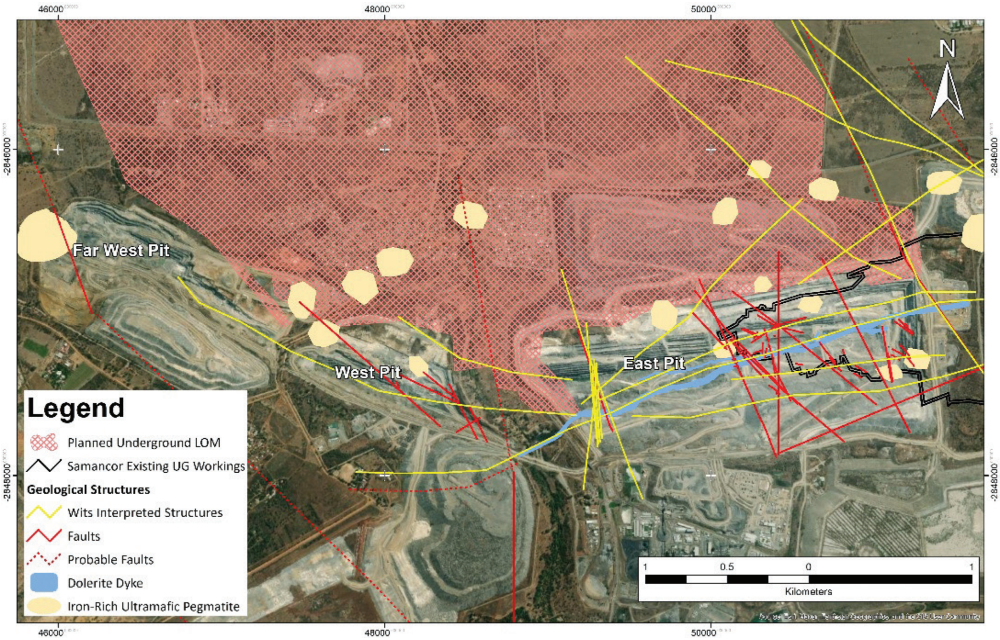

Figure 2 Tharisa Mine geology and pits.

dominant; as the major cation and anions are calcium (Ca^{2-}) and sulfate (SO_4^{2-}). Traces of nitrate are common. The water is used in the process plant and dust suppression.

The design of the dewatering strategy addresses four objectives:

1. Cutting off recharge through detailed stormwater diversion and shallow borehole pumping.
2. Exploitation of permeability by pumping from deeper water-bearing zones.
3. Monitoring groundwater levels within and along the pit perimeter to evaluate dewatering success, and maintain targets for monthly drawdowns.
4. Starting early – dewatering in advance of mining, with accurate management of the flooded Samancor workings, seasonal rainfall and elevated groundwater levels.

A phased approach to achieve a cost-effective dewatering design, has been used (Morton 2024) to develop the detailed strategy for the Tharisa surface mine which comprises:

- Diversion of surface runoff using accurate stormwater drainage and grading of roads.
- Pumping from sumps and in-pit dewatering boreholes to collect pit water and intercept the Samancor workings' water.
- Pumping from pit-perimeter dewatering boreholes (shallow and deep).
- Monitoring of groundwater levels using dedicated monitoring boreholes.
- Target setting for maintaining groundwater levels below planned mining blocks, in monitoring boreholes within the pits and around the perimeter.
- Regular review and upgrade of the pumping network to intercept water in advance of mining.

Fig. 3 shows the layout of the 2024 dewatering boreholes.

Detailed structural geological mapping was done to identify the main conduits carrying the groundwater into the mine. The structural mapping followed the guidelines outlined in Morton *et al.* (2023). The main conduits are NE-SW fault zones, dyke contacts, bedding planes and ore body contact zones.

Conceptual model

Geological, structural and hydrogeological information was used to create a conceptual hydrogeological model. This model provides a comprehensive understanding of the groundwater system in and around the mining area, and provides a framework for

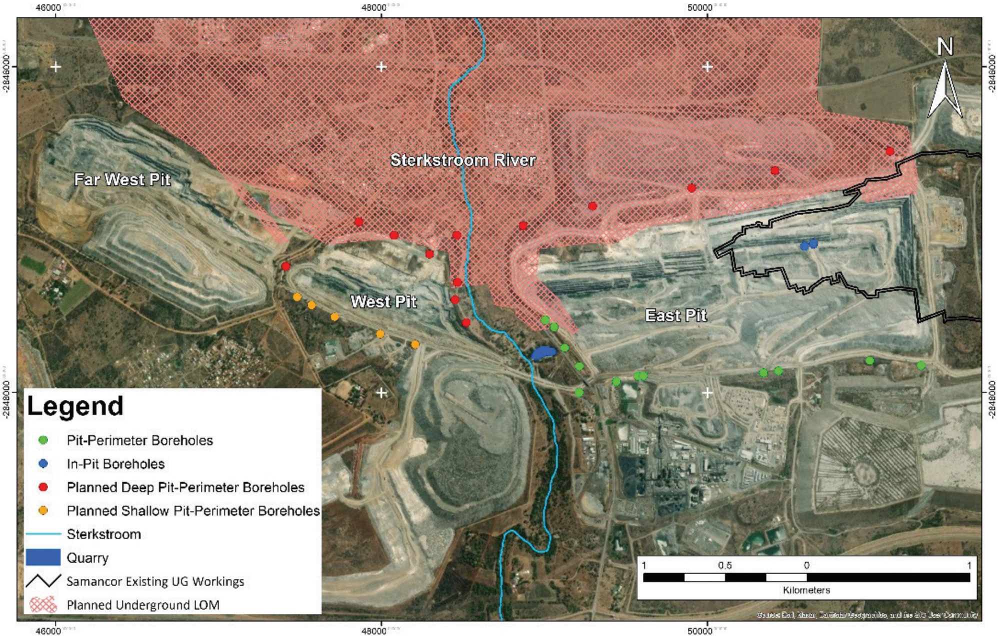

Figure 3 *Tharisa Mine Dewatering boreholes 2024.*

interpreting hydrogeological data detailing: where the water comes from, what it moves along and where it is stored. Sources of water include near-surface groundwater seepage; the Sterkstroom River; waste rock dumps; recycling from an old quarry; deeper fractured rock aquifer contribution and direct precipitation. Conduits for water flow include open faults and chromitite and dyke contacts, and water storage areas include high porosity rocks, old mining voids such as the old Samancor workings, tailings storage facilities and waste rock dumps. Tailings and waste rock dumps release water into the workings over time through structural connection, even during the drier periods.

Site specific transmissivity was estimated between 15 to 30 m^2/d in the shallow weathered zone (about 0 to 33 m thick), and between 2 to 4 m^2/d in the deeper fractured zone matrix. This value can be as high as 250 m^2/d along open faults and fracture zones. The hydraulic head ranges between 1 171 to 1 208 mamsl. A conceptual illustration of the hydrogeology of a North-South (N-S) cross section through the East pit is shown in figure 4.

Numerical model

A numerical model, based on the conceptual model was built using FEFLOW® to simulate the probable inflow to the pits up to the year 2041, and inform the design of the required pumping capacity. Three different dewatering scenarios (base case and 1 and 2) were modelled to simulate reducing the predicted passive inflow into the pits, as shown in figure 5 for the East pit.

These scenarios simulated the effect of twelve shallow dewatering boreholes south of the East pit, five additional deep dewatering boreholes north of the East pit, and two in-pit dewatering boreholes targeting the old underground Samancor workings.

The deep boreholes are designed to cut off recharge from geological structures. In-pit boreholes were drilled to lower water levels in the flooded Samancor workings and intercept the dyke contacts. Shallow boreholes were drilled into geological structures, identified through geophysical surveys and mapping, to cut off recharge from the river and capture groundwater seepage.

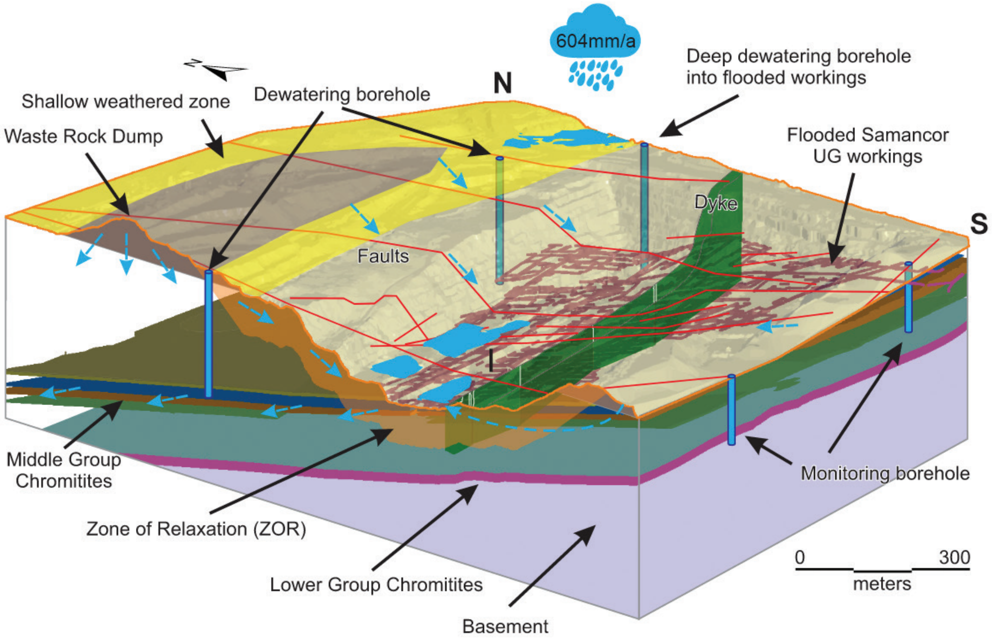

Figure 4 Conceptual illustration of groundwater flow regime (N-S).

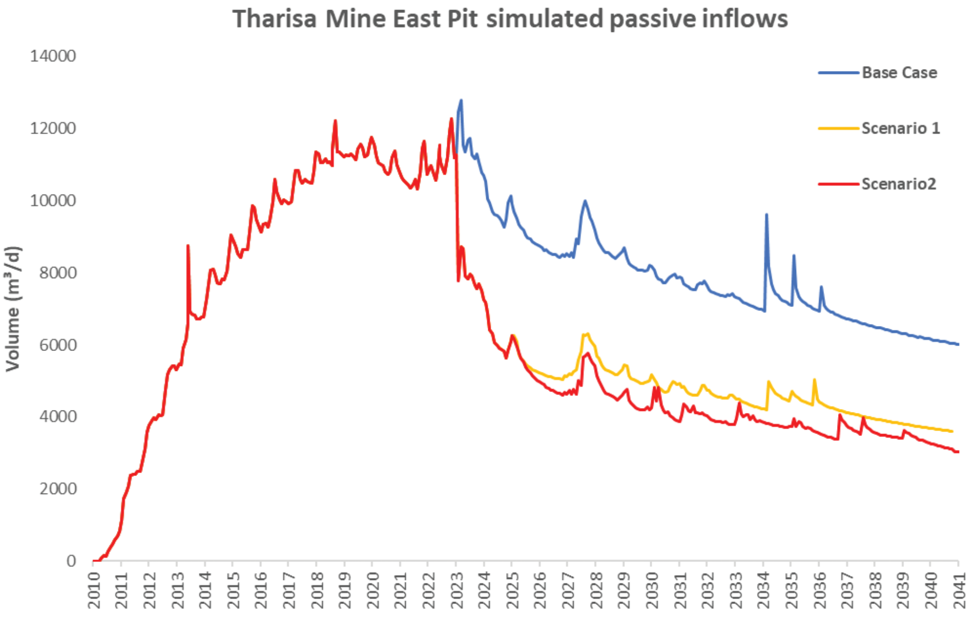

Figure 5 *Output from 2024 numerical model showing the East pit simulated passive inflows.*

Output from the 2024 numerical model for the East pit includes:

- Base case: Pit sump pumping and dewatering from two boreholes drilled into the Samancor workings.
- Scenario 1: When the 12 shallow dewatering boreholes are operational, passive inflow decreases by 3 500 m^3/day.
- Scenario 2: An additional decrease of approximately 1 000 m^3/day in simulated passive inflows, is observed when the five additional deep dewatering boreholes are implemented.

Dewatering implementation

Following the site investigation and the development of the conceptual model, numerical modelling was used to calculate the number of boreholes required to keep the groundwater level below the pit bottom in advance of mining. Because the ore body dips to the north, the northern dewatering boreholes are drilled deep enough to intercept water on structures and bedding planes targeted below the planned mine level.

In 2025 two dewatering boreholes were drilled into the Samancor workings from the East pit and equipped to extract 6 720 m^3/d. Twelve shallow boreholes were sited, using Electrical Resistivity Tomography (ERT) to intercept the shallow weathered aquifer on the southern and western sides of the East pit. Five deep boreholes are in progress to intercept the deep groundwater on the northern side of the East pit. On the West pit perimeter, thirteen boreholes are planned. These boreholes were also sited using ERT.

The twelve boreholes on the East pit perimeter and the two in-pit boreholes were drilled using rotary percussion, cased, developed and aquifer tested. Water is pumped to the plant and an old nearby quarry. The 2025 pumping strategy is a combination of:

1. East pit: a central sump, two in-pit boreholes, and seventeen pit-perimeter boreholes.
2. West pit: a central sump and thirteen planned pit perimeter boreholes.
3. Far West pit: a central sump.

Conclusions

Tharisa mine needs to pump between 7 000 – 10 000 m^3/d to keep the groundwater level below pit bottom in advance of mining. The dewatering strategy incorporates a phased installation of pit perimeter boreholes, in-pit boreholes, and sumps to intercept water effectively. By cutting off recharge through detailed stormwater diversion, utilizing accurate water level monitoring networks, and starting dewatering operations well in advance of mining, the strategy ensures efficient dewatering of the pit in advance of mining. A conceptual and numerical model (developed using FEFLOW®) which included groundwater flow mapping, recharge sources, and identification of storage areas, enables the optimization of borehole placement and design of pumping capacities. This phased approach has proven to be a cost-effective method for managing groundwater inflows, reducing environmental discharge, and supporting Tharisa's mining operations across multiple pits and the planned underground mine. Successful implementation of this dewatering design highlights its applicability to other surface and surface-to-underground transition mines.

Acknowledgements

The authors thank Tharisa management for the permission to publish the information from Tharisa.

References

Dildar J, Manzi MSD, Abiye T, Gomo S, Rapetsoa MK, Drennan G (2023) Groundwater circulation in the shallow crystalline aquifer of Tharisa Mine, South Africa: evidence from environmental isotopes and near-surface geophysics. Water 15, 2876, https://doi.org/10.3390/w15162876

Morton KL, Millsteed BD, van Heerden WL, Msitsini M (2023) Structural logging and modelling for use in simulation of inflows in underground hard rock mines. In: Stanley P; Wolkersdorfer C; Wolkersdorfer, K, Mugova E: IMWA 2023 – The Future p. 365-370. Newport, Wales, UK (International Mine Water Association).

Morton KL (2024) A phased approach to mine dewatering – updated from IMWA 1993. West Virginia Mine Drainage Task Force Symposium & 15th International Mine Water Association Congress 2024 p. 458–463

Tharisa Minerals (2018) Mineral resources and mineral reserve statement. Online available at: https://www.tharisa.com/reporting/annual-report-2018/mineral-resources-and-mineral-reserve-statement.php

Carbonate Reactions that Dictate Drainage Chemistry and Carbonate Consumption Under Variable System Conditions

Cheryl Ross[1], Jennifer Thompson[2], and Ryan Jakubowski[3]

[1]*WSP USA Inc., Redmond, Washington, USA, cheryl.ross@wsp.com*
[2]*WSP USA Inc., Denver, Colorado, USA, Jennifer.thompson@wsp.com, ORCID 0000-0002-0953-0468*
[3]*Freeport-McMoRan Inc., Phoenix, Arizona, USA, rjakubow@fmi.com*

Abstract

A material's potential to generate acidity is predicted based on the balance of acid-generating and acid-neutralizing minerals. The standard acid-base accounting and depletion calculations assume that pyrite and calcite are the primary reactive phases and that the relative rates of pyrite oxidation and calcite dissolution follow a specific reaction pathway associated with a defined pH and carbon dioxide partial pressure. This paper evaluates the effects of changes in system conditions on acid-base accounting using results from both laboratory-kinetic testing and reactive-transport modeling.

Keywords: Pyrite, calcite, oxidation, MIN3P

Introduction

In acid rock drainage (ARD) assessments, a principal objective is to determine whether the system of interest has sufficient neutralization potential (NP) to counteract the acidity generated by sulfide oxidation to maintain circumneutral pH. Assessments of ARD potential use available laboratory- and field-scale information, which are often supported by geochemical and hydrologic modeling (Pieretti *et al*. 2022). Inherent with these assessments is a tacit consideration regarding how variable boundary conditions may affect the hydrogeochemical behavior of the system.

Typically, kinetic testing is conducted to study the weathering of sulfidic mine materials in contact with oxygen and water. These tests provide an indication of a material's ability to effectively counteract the acidity generated by sulfide oxidation. Many minerals are capable of acid neutralization; however, mineral reaction mechanisms and rates vary widely (Jambor *et al*. 2006). Carbonate minerals (e.g., calcite and dolomite) provide effective NP (when present) due to their generally fast reaction kinetics and are often found at equilibrium in surface water and groundwater systems.

Standard kinetic testing methods use prescribed solid to water ratios that may not be representative of field conditions. Two widely adopted kinetic testing methods are the ASTM (2018) humidity cell test (HCT) and the AMIRA (2002) column test. Results from these tests are commonly used to confirm material classification with respect to ARD potential, estimate the lag time to the development of acidic conditions, if applicable, and to assess potential drainage chemistry during operations and post-closure.

Standard acid-base accounting (ABA) and depletion calculations are based on the reaction stoichiometry for pyrite (FeS_2) and calcite ($CaCO_3$) as shown in Equation 1.

$$FeS_2 + \frac{15}{4}O_2 + \frac{7}{2}H_2O + 2CaCO_3 = Fe(OH)_3 + 2SO_4^{2-} + 2Ca^{2+} + 2H_2CO_3 \quad \text{(Equation 1)}$$

This reaction applies at pH values <6.3 when dissolved carbonate is present as carbonic acid (H_2CO_3). Standard ABA calculations assume that acidity (hydrogen ions) produced by pyrite oxidation are partially neutralized by calcite to a pH not greater than approximately 6 (i.e., two moles of calcite consumed per mole of pyrite oxidation, as shown in Equation 1). At pH values >6.3, dissolved carbonate is present as bicarbonate (HCO_3^-) wherein four moles of calcite are consumed to neutralize the acidity produced from the oxidation of one mole of pyrite.

Standard ABA calculations assume that calcite depletion is attributed to a single mechanism, specifically pyrite oxidation. This paper evaluates the potential for calcite depletion due to two mechanisms, referred to as "sulfide oxidation" (i.e., calcite dissolution to counteract the acidity generated by pyrite oxidation) and "carbonate flushing" (i.e., dissolution of calcite to maintain solution equilibrium conditions). For the conditions evaluated in this study, it is demonstrated how laboratory kinetic testing design can affect the contribution of carbonate flushing to total calcite depletion. Laboratory kinetic testing and reactive-transport modeling of a mine waste sample containing high concentrations of pyrite and calcite are presented.

Methods

The ASTM (2018) HCT methodology, which specifies a 2:1 or 1:1 solid to water ratio (1,000 g material flushed weekly with 500 mL or 1,000 mL of deionized water), is designed to thoroughly flush sulfide-oxidation products. The desired pore volume and generation of sufficient leachate for analytical purposes are among the factors for consideration in the selection of the weekly lixiviant volume. The AMIRA (2002) free-draining column method uses a monthly leach cycle and incorporates heat lamps to increase the system temperature. Laboratory testing for this study was based on the AMIRA column methodology (Fig. 1). Study conditions, as compared to ASTM (2018) and AMIRA (2002), are shown in Table 1. Lixiviant addition was increased during the latter weeks of laboratory column operation to evaluate the effects of a change in water to solids ratio on leachate composition.

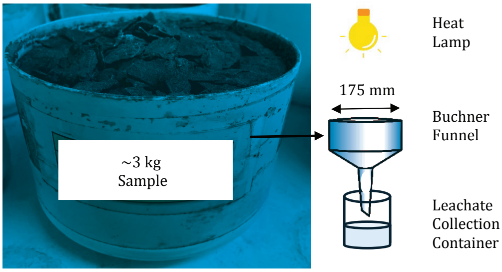

Figure 1 Column testing photograph and schematic.

For this study, the sample composition and laboratory-column procedure were designed to test extreme conditions and promote fast reaction kinetics (e.g., elevated sulfide concentration and higher temperature than field conditions). Column testing of a sample containing pyrite (~25%), calcite (~5%) and dolomite (~2%) was conducted over a period of nine years (118 leach cycles). Column leachates collected monthly were analyzed for a comprehensive suite of parameters including pH, major ions and metals. Geochemical modeling, using a reactive-transport code, was conducted to evaluate potential reactions occurring within the columns. The modeling, conducted when 7.7 years (100 leach cycles) of column-test data were available, focused on the investigation of the relative rates of sulfide- and carbonate-mineral depletion under variable system conditions. At the completion of the modeling study, the rate of lixiviant addition to the column was increased to evaluate changes in system behavior following a change in flow conditions and to examine the findings of the geochemical modeling. Week 4 lixiviant addition was increased from 800 mL to 1,600 mL for leach cycles 114 to 118.

MIN3P was used to evaluate the processes occurring in the laboratory column. MIN3P is a general-purpose reactive-transport model for simulating variably saturated water flow and transport, diffusive and advective gas flow, and thermodynamic and kinetic reactions between aqueous, mineral, and gas phases (Mayer *et al.* 2002). The MIN3P code also includes dissolution-precipitation, oxidation-reduction, and surface-complexation reactions. The ability of MIN3P to account for variably saturated flow conditions, gas transport, and the simultaneous simulation of flow, mineral weathering and transport reactions makes it a valuable tool (e.g., Steefel *et al.* 2015) to generate robust simulations of mine wastes and predict changes in mine water through time.

Table 1 *Study column test procedure design as compared to standard kinetic testing methods.*

Test Method (standard or study)	Solids Mass kg	Cycle Leach Water Volume L	Leach Cycle Time weeks	Temp. °C	Annual Water Volume L	Equivalent Annual Water Depth $^{(d)}$ mm
Humidity Cell – Option A (ASTM 2018)	1	0.5 – 1.0	1	25 (±2)	26 – 52	803 – 3,182; 1,607 – 6,364
Free Draining Column (AMIRA 2002)	2 $^{(a)}$	1.4 $^{(b)}$	4	30 – 35	18.2	757
Free Draining Column (current study)	3	1.4 – 2.2 $^{(c)}$	4	~49	18.2 – 28.6	757 – 1,189

(a) 2 to 2.5 kg (typically)

(b) 0.7 L per kg of sample; for a 2-kg sample, 0.2 L in weeks 1 to 3 and 0.8 L in week 4

(c) 0.2 L in weeks 1 to 3 and 0.8 or 1.6 L in week 4

(d) Annual water volume converted to a depth in mm based on humidity cell (10.2 or 20.3 cm inner diameter for coarser [material screened or crushed to 100% passing 6.3 mm] and finer [<150 µm] materials, respectively) or column (17.5 cm inner diameter) surface area.

The model simulated a one-dimensional profile with a height equivalent to the height of the column (10 cm). Model parameterization of selected physical and chemical components of the system is shown in Table 2. Initial mineral concentrations were as follows: pyrite (24.6 wt.%), calcite (5.2 wt.%), and dolomite (2.2 wt.%). Gypsum and ferrihydrite (amorphous) were included in the model simulations with initial concentrations of 0 wt.%.

MIN3P simulates the weathering reactions of sulfide minerals using a shrinking core model (SCM) (Wunderly *et al.* 1996). As sulfide minerals react, a rind of secondary oxidation minerals forms on the exterior faces of the reacted sulfide-mineral grains. The oxidation rind forms a barrier that slows the transport of sulfide oxidation reactants (e.g., O_2, Fe^{+3}, H_2O) to the unreacted mineral surface as well as the transport of sulfide oxidation products (e.g., acidity, sulfate, and trace elements) away from the reacting mineral surface. The unreacted portion of the mineral grain shrinks as the sulfide mineral oxidizes and the oxidation rind thickens, consequentially decreasing the reaction rate through time.

MIN3P modeling included both calibration and predictive simulations. During model calibration (~8-year simulation period), input parameters were adjusted to achieve a match between simulated and measured leachate concentrations. Factors affecting the rate of pyrite oxidation (e.g., the effective diffusion coefficient that defines the rate of oxygen diffusion into the pyrite grain and pyrite grain size) and carbonate mineral reaction rates were adjusted until an acceptable match between simulated and measured leachate concentrations was achieved.

Table 2 *MIN3P model parameterization (selected parameters).*

Model Input	Value	Description
Dimensions – Height	10 cm	Column height
Boundary Conditions –		
Top – Infiltration Rate	3.1×10^{-9} m/s	Average column inflow
Bottom		Free draining column
Hydraulics –		
Porosity	0.46	Based on field-measured values
Hydraulic Conductivity	5.5×10^{-4} m/s	Richards' Equation parameterization
Lixiviant Composition	pH 5.6 PCO_2 (atm) $10^{-3.5}$ PO_2 (atm) 0.21	Deionized water at equilibrium with atmospheric carbon dioxide and oxygen

Selenium is present in column leachates, which is attributed to its occurrence as an impurity within the pyrite-crystal lattice. As a result, selenium was incorporated into pyrite as defined within the model. Selenium concentrations in column leachate, in addition to sulfate leachate concentrations, were matched during model calibration. Conservative transport of selenium was assumed. Following model calibration, the simulation period was extended from 10 years to 150 years (i.e., an extended period of time to allow for carbonate depletion). Sensitivity analyses were conducted to evaluate the effects of a change in flow rate through the columns.

Laboratory Testing Results

Column kinetic testing results (dissolved concentration and load for the full period of record) are shown in Fig. 2. Only a small fraction of the 1,800 mL of water added monthly (cycles 1 to 113) was recovered. Monthly water storage within the column was calculated to be small, thereby indicating a high amount of water loss due to evaporation. The increase in recovered leachate volume from cycle 114 onward corresponded to the period of higher lixiviant addition. An increase in constituent loading (results shown for sulfate, calcium and alkalinity) was observed in association with an increase in lixiviant volume.

Based on the column leachate results, speciation modeling of column leachates, and visual observations, the conceptual model for reactions occurring in the column is as follows:

- **Sulfide Oxidation** – Pyrite oxidation is occurring and releases sulfate, iron, and metals (e.g., Se). The gradual decrease in sulfate concentrations over time is attributed to oxidation rind development (e.g., shrinking core) and consequent decrease in the rate of pyrite oxidation.
- **Carbonate Dissolution** – Calcite and dolomite dissolution are occurring, resulting in the neutralization of acidity generated by sulfide oxidation. Circumneutral pH conditions are sustained within the column. Geochemical speciation modeling indicates that the leachates are often in equilibrium with calcite.
- **Secondary Mineral Reactions** – Some sulfide oxidation products are likely retained within the column. The low concentrations of iron in column leachates indicate iron attenuation within the col-

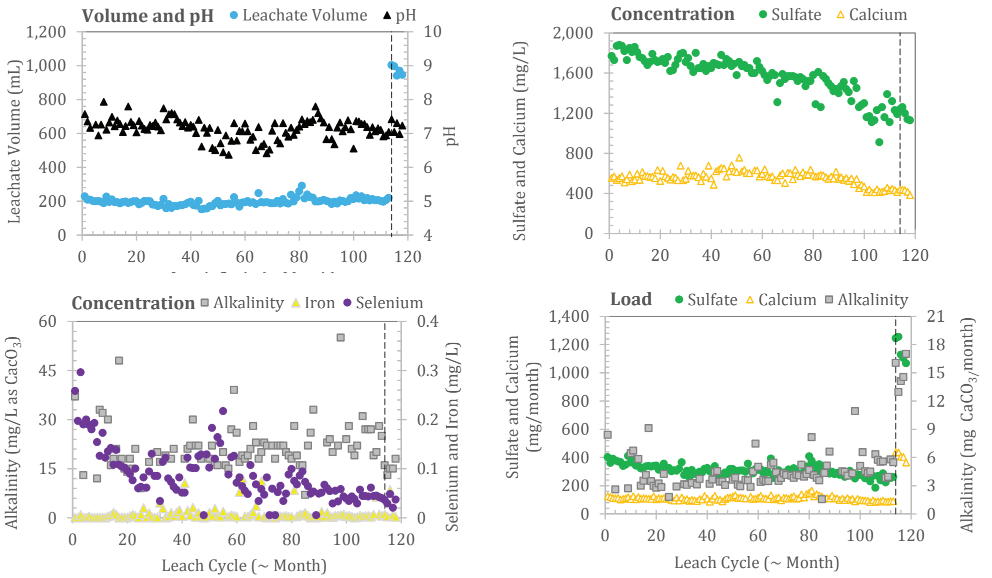

***Figure 2** Column leachate chemistry. Dashed line at 114 months indicates when week 4 lixiviant addition increased from 800 to 1,600 mL.*

umn, which is supported by geochemical modeling indicating the leachates are supersaturated with respect to ferrihydrite (amorphous). The early-time column leachates are in equilibrium with gypsum, suggesting gypsum precipitation. Mineralogical analysis of the sample did not identify the presence of gypsum; however, sulfate was detected as part of standard ABA sulfur speciation analysis. Early-time gypsum equilibrium may, therefore, be due to gypsum dissolution.

Reactive Transport Modeling Results

Calibrated model results compared to measured column leachate concentrations are shown in Fig. 3 (10-year simulation period). Because the model simulated a consistent flow rate through the column, the variability observed in column leachate concentrations due to changes in flow dynamics is not represented by the model. Mineral concentrations are shown in Fig. 4 (150-year simulation period). The model predicts pyrite oxidation through the full depth of the column at the same (or very similar) rate, indicating that oxygen diffusion into the column is not a limiting factor for sulfide oxidation. This is expected due to the very low modeled column saturation (i.e., average saturation of 6% does not limit oxygen ingress) and shallow column depth (10 cm). Calcite depletion also occurs through the full column depth, but calcite depletion is faster at the top of the column, attributed to equilibration of the lixiviant (deionized water) with calcite (i.e., flushing mechanism). Gypsum precipitation occurs within the first few years; however, as the rate of pyrite oxidation decreases over time, undersaturated conditions with respect to gypsum are predicted. Ferrihydrite precipitation is predicted over the ~8-year calibration period.

The effect of an increase in flow through the column was investigated through a series of sensitivity analyses. The infiltration rate into the column was increased by 2 times, 10 times, and 50 times compared to the base case simulation (Figs. 3 and 5) over a 150-year simulation.

An increase in flow increases the rate

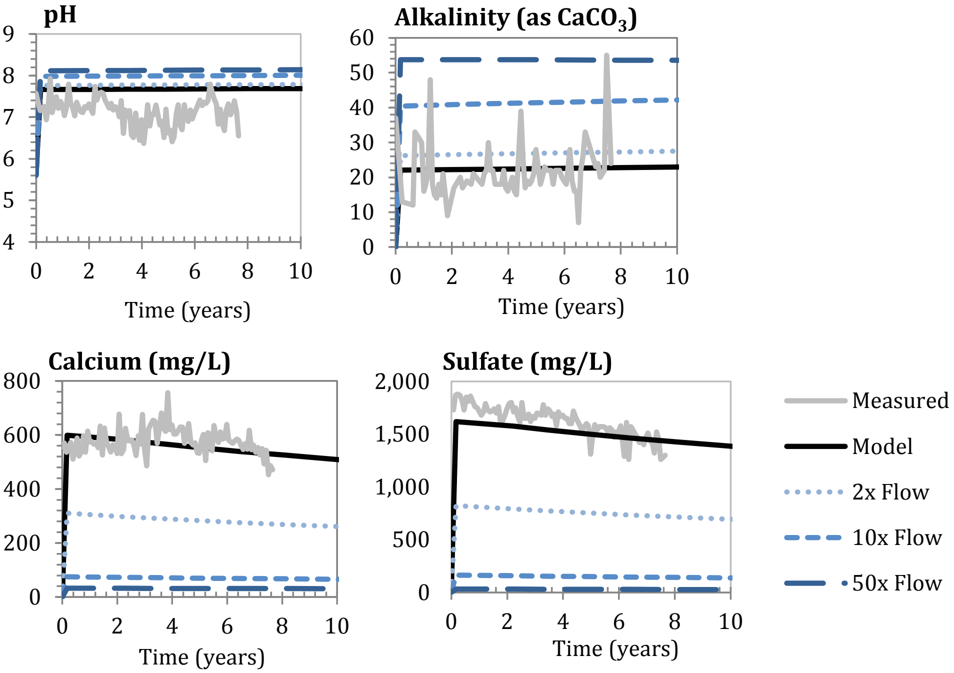

Figure 3 *Calibrated MIN3P model results (black line) compared to measured column leachate concentrations (grey line). Sensitivity model results for an increase in lixiviant volume (2x, 10x or 50x increase) represented by blue dashed lines.*

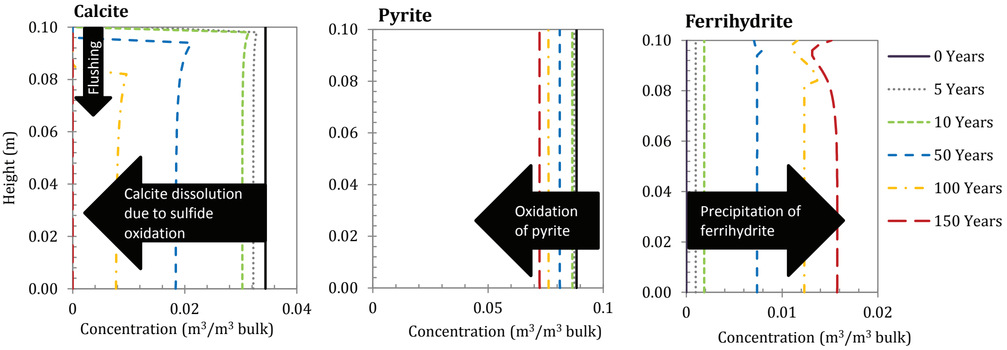

Figure 4 *Base case model mineral reactions (150-year simulation period).*

of calcite depletion and decreases the lag time to acidic conditions. However, based on the hydraulic properties of the material, the degree of saturation of the material is not affected by the higher flow rates and no significant change in the rate of pyrite oxidation is predicted. Fig. 5 shows the molar ratio of carbonate to pyrite depletion for each model simulation. At the lowest flow rate (base case model), the ratio of carbonate depletion to pyrite depletion initially is 2, consistent with Equation 1. As the rate of flow increases, equilibration of a higher volume of water with calcite increases the ratio of carbonate depletion to pyrite oxidation. The simulated flow volumes are representative of infiltration rates ranging from 0.2 (2x) to 4.9 m/a (50x). The simulated high range of flow (representative of a very wet climate) is within the standard HCT design (Table 1) but exceeds typical infiltration rates observed in most engineered mine waste facilities.

To test the behavior predicted by the model, the week 4 lixiviant volume was increased by a factor of two from cycle 114 onward. Results are available for five leach cycles (cycles 114 to 118). Similar to the MIN3P model results, an increase in alkalinity loading is observed with an increase in flow (Fig. 2). These empirical observations confirm that the rate of carbonate depletion is affected by the column test design.

Conclusions

Laboratory investigations and hydrogeochemical modeling of the weathering behavior of a mine waste sample containing pyrite and calcite have demonstrated that under the conditions evaluated, the rate of calcite depletion is sensitive to the water to rock ratio used in testing. Calcite depletion is interpreted to occur due to two mechanisms: (1) to counteract the acidity generated by pyrite oxidation and (2) dissolution to maintain calcite equilibration, termed flushing. Equilibration of calcite with larger flushing volumes of deionized water increases the rate of calcite depletion compared to that associated with neutralization of the acidity generated by pyrite oxidation alone. Consequently, the potential for calcite consumption due to flushing may warrant

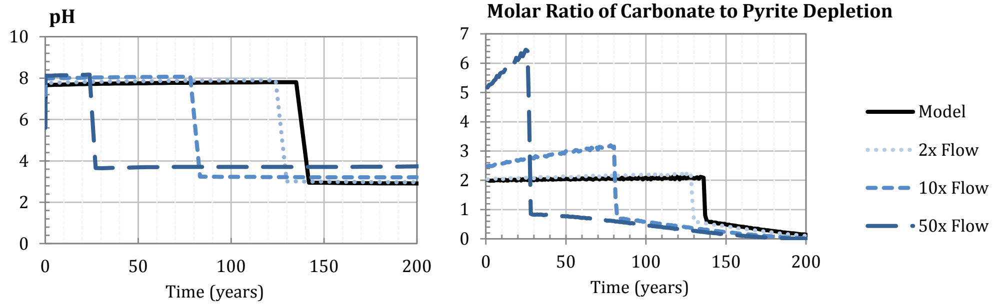

Figure 5 *Sensitivity model results following an increase in lixiviant volume (2x, 10x or 50x).*

consideration under some laboratory and field conditions. It is recommended that in addition to sulfide oxidation, consideration of the other factors that may affect NP consumption be incorporated into the interpretation of kinetic testing results and development of the conceptual model of system behavior.

Acknowledgements

The authors would like to thank Freeport-McMoRan Inc. for permission to publish this work, which would not have been possible without the dedicated assistance of the laboratory team managing the columns.

References

American Society of Testing Materials (ASTM) (2018) Standard Test Method for Laboratory Weathering of Solid Materials Using a Humidity Cell, D5744–18

AMIRA International Ltd. (AMIRA) (2002) ARD Test Handbook – Project P387A Prediction and Kinetic Control of Acid Rock Drainage (Appendix F). May

Jambor JL, Dutrizac JE, Raudsepp M (2006) Comparison of measured and mineralogically predicted values of the Sobek neutralization potential for intrusive rocks. In: Barnhisel RI (Ed), Proceedings of the 7th ICARD, St. Louis, MO, USA, p 820–832

Mayer KU, Frind EO, Blowes DW (2002) Multicomponent reactive transport modeling in variably saturated porous media using a generalized formulation for kinetically controlled reactions. Water Resour Res 38(9):1174

Pieretti M, Karlsson T, Arvilommi S, Muniruzzaman M (2022) Challenges in predicting the reactivity of mine waste rocks based on kinetic testing: Humidity cell tests and reactive transport modeling. J Geochem Explor, 237, 106996

Steefel CI, Appelo CAJ, Arora B, Jacques D, Kalbacher T, Kolditz O, Lagneau V, Lichtner PC, Mayer KU, Meeussen JCL, Molins S, Moulton D, Shao H, Simunek J, Spycher N, Yabusaki SB, Yeh GT (2015) Reactive transport codes for subsurface environmental simulation. Comput Geosci 19:445–478

Wunderly MD, Blowes DW, Frind EO, Ptacek CJ (1996) Sulfide mineral oxidation and subsequent reactive transport of oxidation products in mine tailings impoundments: A numerical model. Water Resour Res 32(10):3173–3187

An Novel Approach to Hydrogeochemical Risk Assessment Based on short-term tests

Francisco Ruiz Allén[1]

[1]*Consultoría Geológica, S.L. (CONGEO), Real Oviedo 10, 33013 Oviedo, Spain, fruizallen@congeo.es*

Abstract

An approach has been followed that attempts to obtain as much information as possible from the static tests. During the process some questions arise: the role of project site water analysis in a geochemical study, the inadequacy of standard ABA tests for estimating the effective neutralization potential of rock samples with silicates and little or no carbonates, the possibility of using the NAG test to help the geochemist to predict which lithologies release what, and to establish risk levels that help to define waste management and water treatment measures, before the results of long-term kinetic tests are available.

Keywords: Static testing, silicates, mineralogy, neutralization potential, NAG leaching.

Introduction

In Spain, it is not uncommon for environmental impact studies of metallic mines to be based on a set of geochemical tests consisting of ABA according to the European standard EN15875, rock analysis by aqua-regia and leaching test according to the European standard EN12457 (leaching test in deionised water for 24 hours). Mineralogical analysis of environmental samples is not included, and no account is taken of the additional information for the hydrogeochemical characterization that may be provided by actual site waters. Budgetary constraints, but above all the lack of involvement of a geochemist and the fear of misuse of the data by environmental groups may be part of the reasons.

A comprehensive set of geochemical static tests, together with site water data, has been used for the geochemical risk assessment of a lithium mine project located in northern Spain. In the project area there are old mining works of very small size. Lithium is found in pegmatites hosted in schists.

Of all the work done, the approach based on mineralogical estimation of the neutralization potential of silicates, which is considered challenging by several authors (Jambor 2006, Karlsson 2019, Morin 2007 and 2024), and the use of a risk index based on NAG eluates are discussed here. It also highlights the importance of verifying the NAG procedure followed by the laboratory and ensuring the complete oxidation of the samples.

Materials and Methods

The rock materials analyzed consisted of 24 drill core samples, 3 waste rock samples and 2 sediment samples. Drill core samples were dried at 60°C, crushed to below 2 mm and quartered to approximately 200 grams which were subjected to grinding to below 75 microns to obtain the subsamples required for the various analyses. In the case of the dump samples, the dry sample was previously sieved at 10 mm and at 2 mm for the sediment samples. The rest of the preparation was carried out on the finer fractions as indicated above.

Drill core samples were selected by the projects geologists based on dominant rock units and 3D spatial distribution. The position of the projected underground workings was considered, looking for the closest corresponding sample intervals in the drill-cores.

There is no seepage from the old waste dumps. Instead, there was information available of the quality of surface (streams) and ground waters (piezometers).

The selected geochemical tests were X-ray diffraction (XRD, Rietveld refinement method) mineralogy; ABA (acid-base accounting), using the European EN 15875 procedure; NAG (Net Acid Generation test) and leachability tests such as EN 12457, widely used for landfills, which would give immediate solubility or leachability, and the analysis of the eluate obtained in the NAG test, following the instructions of the AMIRA P387A Handbook (Smart *et al.*, 2002). Chemical analysis of the samples was carried out by extraction with aqua regia, a 3:1 mixture of hydrochloric acid and nitric acid, which is the most commonly used method in Spain for mine waste and soils pollution characterization. We think, however, that it would have been better to perform whole rock analysis to verify the mineralogical information and also to allow the application of the silicate neutralization model (Morin 2024).

The European standard for acid-base accounting – EN 15875 – requires reducing the size of the samples to less than 0.125 mm in 95% of particles. The final titration pH for the assessment of the Neutralization Potential (NP) is 8.3. Also, it differs from the Sobek and other modified methods in that it uses the carbonate content, calculated from the inorganic carbon, to assess the amount of hydrochloric acid to be used in the titration for measuring the NP, instead of using a Fizz test.

The single addition NAG test was used. The NAG method requires adjusting the pH at the beginning of the test between 4.5 and 6.0 by NaOH solution (AMIRA 2002, MEND 2009). This may give rise to a relevant inaccuracy in the test, as the pH obtained in the NAG test is compared with 4.5. For this reason, the laboratory was asked to regulate the pH as close to 4.5 as possible and to record that initial pH in addition to the NAG pH. Additionally, the eluates obtained in duplicates of the NAG test were analyzed to evaluate the release of sulfur and metals and to evaluate the complete oxidation of sulfides.

Results and Discussion

Acid-Base Accounting

Acid-base accounting (ABA) tests, either according to the American EPA 600 (Sobek) standard and its modifications, or the European standard EN15875, do not adequately reflect the solid-phase neutralization potential (NP) that silicates may have. This is because, in the short duration of the static laboratory tests, the silicates do not react – or react only to a limited extent – with the hydrochloric acid used (Morin 2024). This is a key issue, as lag times to the onset of acidity are usually calculated from the total NP and AP derived from the ABA standard and their depletion in humidity cell tests (HCT).

Inspired by the work of Karlsson *et al.* (2019), an approach following Kwong (1993), rather than Lawrence and Scheske (1997), was attempted here. Interestingly, both approaches use data from Sverdrup (1990), but Lawrence and Scheske assign an order of magnitude less reactivity to intermediate weathering silicates than Kwong. XRD mineral concentrations were converted to moles/kg according to their ideal formula molecular weight, and then to moles of H+ using the Kwong formula according to Sverdrup. The results were converted to moles of $CaCO_3$ equivalent (1 mol $CaCO_3$ equivalent = 2 mol aqueous H+, pH < 6.3) and then to kg $CaCO_3$/t.

Similarly, Jambor *et al.* (2006) have proposed their own mineral-specific NP values, based on performing the Sobek procedure on freshly prepared monomineralic samples of some minerals, but using a protocol to standardize the time and temperature of the acidification step in the Sobek method. The NPs according to Jambor *et al.* were assigned to the minerals, the NP of the whole sample was obtained by addition of the NPs according to the weight content of the different silicate minerals in the sample.

Lawrence and Scheske state that the Sobek test may overestimate NP availability under real field conditions for many samples. Also, Jambor *et al.* show that NP results for most plagioclase series increase linearly with increasing Ca in the formula. Both statements are contrary to the NP model presented by Morin (2024), according to which Sobek usually underestimates the NP of plagioclase silicates, and plagioclase reactivities increase exponentially with Ca content (which is also shown in the data used by Kwong and Lawrence and Scheske).

The NPs calculated after Kwong show consistently higher values than those obtained by EN 15875 (Fig. 1), even when quartz has been assigned 0 and not 0.004 as reactivity. The NPs calculated according to Jambor are very low, presumably because quartz varies between 35 and 58% in the schist samples, and between 21 and 32% in the pegmatites. Other minerals present are muscovite, biotite, K-feldspar and albite, all of which are assigned 1 after Jambor, except for quartz (0) and biotite (which is assigned 8 as phlogopite). Jambor NPs are based on the Sobek procedure (granulometry 0.250 mm, acid digestion at 85ºC, titration pH at 7.0), whilst EN 15875 is done on <0.125 mm sample, 24 h at room temperature, titration pH at 8.3).

All these approaches used in this work have shown some drawbacks. First, the actual effective NP in samples with silicates cannot be known from static tests. The rate of oxidation of sulfides and the amount of sulfides present are critical. This is largely a site-specific and kinetically determined parameter. So, there is no reference to compare with. Second, there are some minerals not considered in the mentioned publications so, when there were no data, the assignment of reactivities was based on similarities in the mineral formula, considering the presence of Ca and Mg mainly. Third, the results differed between mineralogical approaches (Fig. 1). Four, XRD proved to be blind to the different plagioclases present, which were reported generically as albite. Analysis of rocks with aqua-regia, showed that Ca was present up to 0.56% in the schists samples. Unfortunately, digestion with aqua-regia provides limited dissolution of the silicates, depending also on the mineralogy. Whole-rock analysis should have been used instead to verify the calcium concentration. The ongoing HCTs on two samples are showing that Ca is the main cation released on a molar basis. Therefore, it is very likely that Ca plagioclase is present in the samples. Calcium molar ratios using SEM/EDX should have been carried out (Morin 2024).

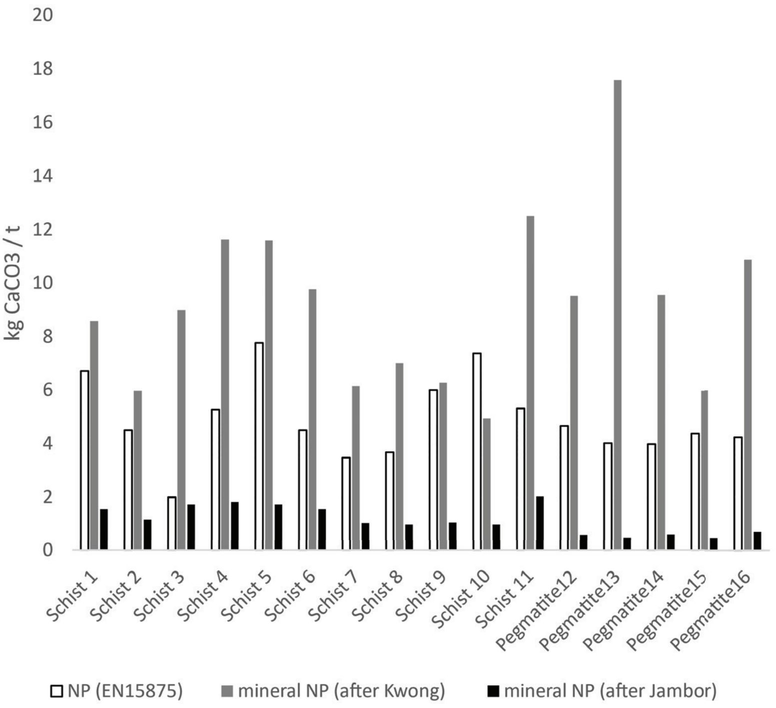

Figure 1 Neutralization potentials of samples from the mine project.

Leaching tests

The "Manual for risk assessment of closed or abandoned extractive industries" (IGME, 2014), among other tests to assess the risk in former mine dumps, calculates a mean hazard quotient (CPPlab) from the leachability test following the EN 12457 standard on waste dump samples. This test consists of putting 90 g of the material, crushed to less than 10 mm, in contact with 900 ml of deionized water. The mixture is stirred for 24 hours and filtered at 0.45 mm for analysis.

The average hazard quotient is calculated from the relationships between the concentrations in the leachate and the Spanish environmental quality standards (EQS) for the protection of the aquatic environment, which are derived from the European Water Framework Directive and are the same in several European countries.

$$\mathrm{CPP}_{\mathrm{LAB}} = \frac{1}{\mathrm{n}} \sum^{n} \frac{[X]_{LIX-LAB}}{NCA_X} \quad \text{(IGME 2014)}$$

Where $[\mathrm{X}]_{\mathrm{LIX-LAB}}$ is the concentration measured in the leachate resulting from applying the EN 12457–2 laboratory procedure to the waste for element X; NCAX is the target concentration in the receiving watercourse corresponding to element X; and n is the number of elements for which the concentration measured in the eluate is higher than the value adopted as a standard. On the other hand, the Gard Guide (INAP, 2009) presents the Geochemical Abundance Index (GAI) as an indication of elemental enrichment. The GAI for an element is calculated as follows:

$$\mathrm{GAI} = \log_2\left[\frac{\mathrm{C}}{1.5\times\mathrm{S}}\right] \quad \text{(INAP 2009)}$$

where C is the concentration of the element in the sample and S is the median content for that element (mean world soil, crustal abundance, etc). A GAI of 0 indicates that the element is present at a concentration similar to, or less than, median abundance and a GAI of 6 indicates approximately a 100-fold, or greater, enrichment above median abundance (INAP, 2009).

The drawback of the GAI is that it is not related to the mobility of metals and hence, it does not really give any indication of the elements that may actually affect the water quality in a future mining project.

Recognizing the shortcomings of the GAI identified above, an index has been developed using a formulation analogous to that of the GAI but applied to NAG test eluates.

$$NagI = \log_2\left[\frac{C}{1.5 \times EQSx}\right]$$

Where, C is the concentration of the parameter in the NAG eluate and EQSx, as in the IGME procedure applicable to EN 12457, the Environmental Quality Standard, i.e. the maximum allowable or target concentration in the receiving watercourse corresponding to parameter X. In this case, a NagI of 3 represents 12 to 24 times the water quality target.

Another logarithmic formula was previously tried, but the sensitivity was not enough for the work. Using the following formula, a NagI of 3 represents 250 to 1250 times the water quality target concentration and table 1 showed no numbers except for Cu in some samples.

$$I = \log_5\left[\frac{C}{2 \times EQSx}\right]$$

The sulfate concentrations in the NAG eluates were compared with those of the mining-influenced waters at the site as a reference for possible upscaling between the laboratory and the field. This also helped to choose the first logarithmic formula as the appropriate one. Also, the site water analyses and the mineralogy were used to verify that no parameters are missing in the levels of risk identified in the NAG eluates. The influence of elements that may be volatilised under the NAG test conditions (which requires heating on a hot plate), such as mercury and its compounds, has not been evaluated.

At the mine project, after comparison with EQS, the elements that had been found to be relevant in the groundwater analyses were Cu and Zn in some borehole water samples. Using the approach proposed here, in addition to Al and Fe, Cu and Zn appear as elements of concern in the NAG eluates of the analyzed rock samples (Table 1). The pHs obtained in the NAG eluates do not suggest that significant metal precipitation may have occurred, except for aluminum

Table 2 Risk indexes calculated from NAG eluates for the mine project.

			pH –	pH –	F mg/L	Sulfate mg/L	Al µg/L	Sb µg/L	As µg/L	B µg/L	Cd µg/L	Co µg/L	Cu µg/L	Cr µg/L	Fe µg/L	Mn µg/L	Hg µg/L	Mo µg/L	Ni µg/L	Pb µg/L	Se µg/L	U µg/L	Zn µg/L
Sample	**Lithology**	**Depth (m)**	**NAG**	**NAG eluat**	**1,7**	**250**	**200**	**10**	**50**	**1500**	**0,45**	**20**	**5**	**50**	**200**	**50**	**0,07**	**70**	**35**	**14**	**1**	**30**	**30**
1	Schist	29	5,35	4,62	–	–	1	–	–	–	–	–	–	–	–	–	–	–	–	–	–	–	–
2	Schist	41	6,47	4,97	–	–	1	–	–	–	–	–	1	–	–	–	–	–	–	–	–	–	–
3	Schist	16	5,27	4,76	–	–	1	–	–	–	–	–	–	–	–	–	–	–	–	–	–	–	–
4	Schist	25	5,60	4,37	–	–	1	–	–	–	–	–	3	–	–	–	–	–	–	1	–	–	–
5	Schist	178	4,62	3,98	–	–	1	–	–	–	–	–	3	–	1	–	–	–	–	–	–	–	–
6	Schist	8	4,95	4,38	–	–	1	–	–	–	–	–	1	–	–	–	–	–	–	–	–	–	–
7	Schist	15	5,33	4,25	–	–	2	–	–	–	–	–	3	–	1	–	–	–	–	–	–	–	2
8	Schist	255	5,93	4,53	–	–	1	–	–	–	–	–	2	–	1	1	–	–	–	–	–	–	1
9	Schist	275	5,78	4,25	–	–	1	–	–	–	–	–	3	–	1	–	–	–	–	–	–	–	–
10	Schist	12	5,04	4,49	–	–	1	–	–	–	–	–	1	–	1	–	–	–	–	–	–	–	–
11	Schist	43	5,59	4,45	–	–	1	–	–	–	–	–	2	–	1	–	–	–	–	–	–	–	1
12	Schist	55	5,56	4,62	–	–	1	–	–	–	–	–	2	–	1	–	–	–	–	–	–	–	–
13	Schist	108	5,82	4,41	–	–	1	–	–	–	–	–	2	–	1	–	–	–	–	–	–	–	–
14	Schist	249	6,22	4,52	–	–	1	–	–	–	–	–	3	–	1	–	–	–	–	–	–	–	–
15	Pegmatite	78	5,10	4,50	–	–	2	–	–	–	–	–	1	–	–	–	–	–	–	–	–	–	2
16	Pegmatite	57	5,08	4,62	–	–	2	–	–	–	–	–	2	–	–	–	–	–	–	–	–	–	2
17	Pegmatite	299	5,91	4,71	–	–	2	–	–	–	–	–	1	–	–	1	–	–	–	–	–	–	–
18	Pegmatite	196	5,78	4,76	–	–	2	–	–	–	–	–	1	–	1	2	–	–	–	–	–	–	1
19	Pegmatite	156	4,98	4,84	–	–	2	–	–	–	–	–	2	–	–	–	–	–	–	–	–	–	–

and iron, which would explain the observed drift in pH between the NAG assay for the ABA classification, and the duplicate for the analysis of the NAG eluates, which is assayed one day later. This precipitation of Al and Fe could potentially result in losses from solution by adsorption or co-precipitation of some metals, e.g. arsenic, but no arsenic was found in the site waters above D.L. nor arsenopyrite in the deposit.

Conclusions

This study investigated the possibility of using an XRD mineralogy neutralization potential (NP) based on Kwong (1993), comparing also with Jambor (2006) as a preliminary approach to verify the NP obtained by standard ABA methods. However, the results were very different and actual effective NP remains unknown. Also, XRD proved to be blind to the different plagioclases that may be present, which were reported as albite. However, ongoing HCT has shown that the main cation released is Ca. Nevertheless, the NP values were higher than those obtained by EN15875, and this may be useful to check whether silicate neutralization is being underestimated in the ABA assay. An approach such as the model suggested by Morin (2024) is likely to be much more accurate. It requires the use of SEM-EDX to identify Ca content on selected silicate mineral particles, which was not carried out in this study.

Along with mineralogy, site water analyses are considered essential for a comprehensive approach and very useful as a reference or to calibrate risk assessment models. Test procedures should be carefully checked in continuous communication with the analytical laboratory. This is especially relevant with the NAG procedure. The recommendation to use a multiple addition test has been confirmed, even for samples with low sulfide content (Parbhakar-Fox 2018). In addition, for the initial hydrogen peroxide solution, the NAG procedure states: “Aim for a pH of 4.5 and no higher than 6.0” AMIRA Manual P387A (Smart *et al.*, 2002). We recommend asking the laboratory to bring it as close to 4.5 as possible.

The application of an index based on the comparison of element concentrations in NAG eluates with the Environmental Quality Standards for water, is considered very promising as a tool to identify which lithologies release what, at what level of risk, and to design waste management measures, on a risk-based approach rather than on water quality prediction.

Acknowledgements

The author thanks the mining company for participating in these investigations and for facilitating the necessary field work. Special thanks to Dr. Kevin A. Morin, Mine Drainage Assessment Group, for his expertise, open publications and technical discussions over the recent years.

References

Alberruche ME (2014). Manual for risk assessment of closed or abandoned extractive industries [Manual para la evaluación de riesgos de instalaciones de residuos mineros cerradas o abandonadas]. Instituto Geológico y Minero de España (IGME)

Jambor JL, Dutrizac JE, Raudsepp M (2006) Comparison of measured and mineralogically predicted values of the Sobek neutralization potential for intrusive rocks. 7th International Conference on Acid Rock Drainage (ICARD), March 26–30, 2006. American Society of Mining and Reclamation (ASMR).

Karlsson T, Räisänen M L, Lehtonen M, Alakangas L (2019) Comparison of static and mineralogical ARD prediction methods in the Nordic environment. Environmental Monitoring and Assessment 190:719.

Kwong J (1993) Prediction and Prevention of Acid Rock Drainage from a Geological and Mineralogical Perspective. MEND Project 1.32.1. Canmet, Ottawa, Canada.

Lawrence R, Scheske M (1997) A method to calculate the neutralization potential of Mining wastes. Environmental Geology 32 (2) September 1997 7 Q Springer-Verlag.

Morin KA (2024). Silicate Neutralization Potential Focussing on Plagioclase, and the MDAG Silicate NP Model. MDAG Internet Case Study #80.

Morin KA, Leroux J, Lamontagne A, Michaud ML, Dy E, Huang C (2024). Predictions of ARD Potential Dominated by Silicate Neutralization Potential at the Troilus Gold Minesite, Québec, Canada. ICARD 2024.

Parbhakar-Fox A, Fox N, Ferguson T, Hill R, Maynard B (2018) Dissection of the NAG pH Test: Tracking Efficacy Through Examining Reaction Products. IMWA proceedings 2018.

Smart *et al.* (2002) ARD Test Handbook Project P387A, Prediction and Kinetic Control of Acid Mine Drainage. AMIRA International, Melbourne.

The International Network for Acid Prevention (INAP), 2009. Global Acid Rock Drainage Guide (GARD Guide).

Environmental implications of acid mine drainage in the Middle Urals, Russia

Liudmila S. Rybnikova[1], Petr A. Rybnikov[2], Vera Yu. Navolokina[3]

[1]*Institute of Mining of the Ural Branch of the RAS, Yekaterinburg, Russia,620075, luserib@mail.ru, ORCID 0000-0002-4221-7879*

[1]*Institute of Mining of the Ural Branch of the RAS, Yekaterinburg, Russia,620075, ribnikoff@yandex.ru, ORCID 0000-0002-7829-5035*

[1]*Institute of Mining of the Ural Branch of the RAS, Yekaterinburg, Russia, 620075, vunavolokina@gmail.com, ORCID 0000-0002-1547-9451*

Abstract

The abandoned copper-pyrite mines of Levikha and Degtyarsk are located in the Ural fold mountains within the catchment areas of large water reservoirs. Acid mine waters have been discharged here for over 20 years. The AMD treatment systems of these mines are identical, involving neutralization and settling. However, the quality of the mine waters after treatment differs: in the area of the Degtyarsk mine almost all indicators at the point of discharge into the river network comply with regulatory requirements, whereas the discharge from the Levikha mine contains metal concentrations that exceed the standards by 2–3 orders of magnitude. The main factors that influence the water treatment efficiency at these mines are anthropogenic (mine water flow rate and acidity), natural (catchment area), and technological (amounts of reagent, volume of clarification ponds).

Keywords: Acid mine drainages, hydrosphere, copper-pyrite mines, clarifier pond, treatment, catchment area

Introduction

Acid mine drainage (AMD) occurs not only during the operation of mines but also after their closure. This is one of the leading environmental problems globally. The main cause of AMD is the presence of sulfide minerals in rocks. During the mining process, the structure of the rock mass is disrupted, which leads to sulfuric acid weathering of sulfide minerals in the course of interaction with water and air. Mine waters tend to have low pH values, thus further contributing to the dissolution of rocks and enrichment of the water with metals. Reaching landscapes and water bodies, these effluents cause significant harm to both the hydrosphere and the entire surrounding ecosystem.

In the Middle Urals (Russia), a large number of copper pyrite mines have been closed and flooded over the past decades. This has caused serious hydrogeoecological problems. The lack of groundwater resources in the Ural fold mountains accounts for the fact that the main, and sometimes the only source of water supply (especially for large cities) are water reservoirs. In terms of environmental impact on such reservoirs in the region, the Levikha and Degtyarsk copper pyrite deposits are considered to be the most dangerous ones.

The Degtyarsk deposit is located within the catchment area of the Volchikhinskoye reservoir, which supplies water to Yekaterinburg (population 1.5 million people). Following treatment, the AMD flows from the area of the Levikha deposit into the Lenevsky pond, which is used to supply water to the city of Nizhny Tagil (population 350 thousand people). To prevent emergencies from happening and ensure the proper quality of discharged mine water, work is being conducted at these mines at the expense of the regional budget to localize surface runoff, pump out mine water and neutralize it. These deposits are located in identical geological conditions and have a similar history of development using the same methods (open-pit mining and underground block caving methods, with the mining depth of about 600 m and the mining period of 80 years). After the cessation of drainage and filling of the cone of depression, localized AMD discharges formed at each of them in the lowest part of the mining landscape (in sinkholes). Although the overall AMD flow rate is now lower (by approximately 2 times) than during mine development and drainage, it can reach several thousand cubic meters per day. Without treatment, this AMD may cause degradation of the landscape and unacceptable pollution of the hydrosphere over large areas. The AMD is neutralized with lime milk, followed by settling in clarification ponds that were built in the middle of the last century (Fig. 1). However, the quality of the purified mine water at these two mines is fundamentally different: in the area of the Degtyarsk mine, almost all indicators at the point of discharge into the river network meet the regulatory requirements. At the Levikhinsky mine the treatment efficiency was lower both in period of deposit development and in period of flooding. Mg, Cu, Zn and Al content in water exceeded content standards 2-3 times. The first flush effect only made this situation worse (Rybnikova 2021).

The aim of this work is to assess the factors that determine the processes of AMD formation at the Degtyarsk and Levikha mines and identify the main natural and technological parameters that would allow better water quality indicators to be attained at the discharge into the water bodies.

Methods

At the Degtyarsk and Levikha deposits, water chemistry observations have been conducted both during the period of mining and after flooding. The observation points are confined to the areas where the water chemistry undergoes an essential change: AMD outlets (surface discharge), AMD neutralization, settling in the clarification ponds, and discharge into the river network (the mouths of the Yelchevka River at the Degtyarsk deposit and the Levikha River at the Levikha deposit).

The main pollution indicators are

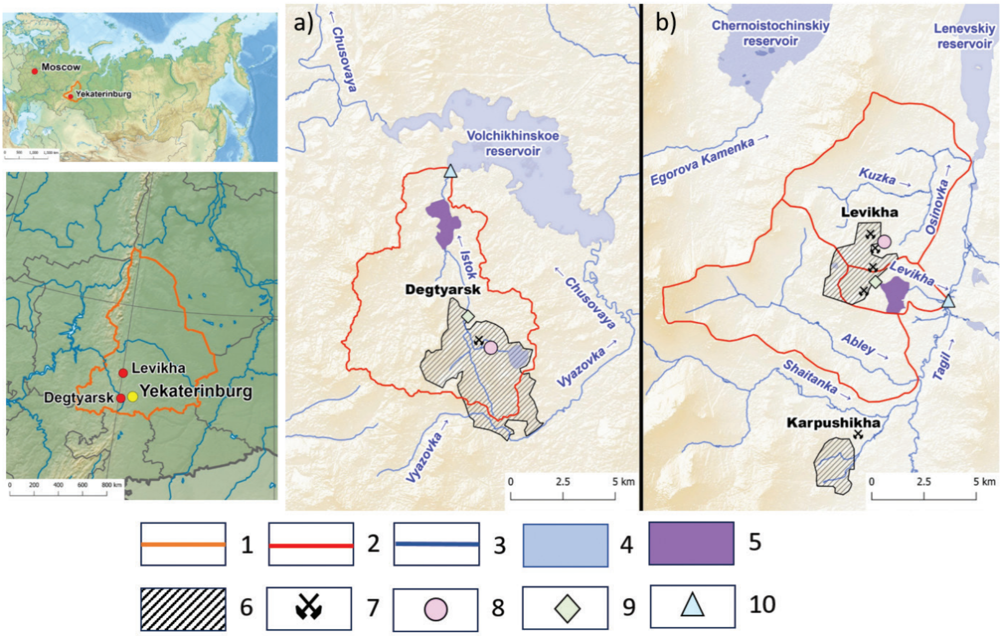

Figure 1 Layout of the objects under study: a) Degtyarsk mine, b) Levikha mine. 1 – border of the Sverdlovsk region, 2 – local catchments, 3 – rivers, 4 – reservoirs a) Volchikhinskoye reservoir, b) Lenevskiy reservoir, 5 – clarification pond, 6 – towns, 7 – abandoned mines, 8 – AMD discharge zone, 9 – Ca(OH)2 neutralization, 10 – the mouths of the Leivikha and Yelchevka rivers.

determined on a monthly basis starting from the beginning of AMD discharge as follows: pH, Cu, Zn, Fe, Cl, SO4, Mn, As, suspended solids, total dissolved salts and oil products. In addition, we regularly carry out a detailed analysis of mine, underground and surface waters for an extended list of components.

Analysis for Na and K is carried out using flame emission spectrometry; Ca, Mg are determined by flame atomic absorption spectrometry; and Fe by atomic adsorption spectrometry. Inductively coupled plasma mass spectrometry is used for analysis for a wide range of elements, including: Al, Be, Cd, Co, Mn, Cu, As, Ni, Pb, Se and Zn. Nitrogen-containing substances (such as NO_2 and NO_3) are determined by ion-selective potentiometry. Gravimetric analysis is used to determine SO4, and argentometric titration to determine Cl. Measurements of t (°C), Eh (μV), pH, TDS are performed on site.

AMD acidity (AC) and the amount of alkaline reagent needed for AMD neutralization (RE) were determined by the formula (Hedin 1994):

$$AC = 50 \times \left(\frac{2Fe^{2+}}{56} + \frac{3Fe^{3+}}{56} + \frac{2Mn^{2+}}{55} + \frac{3Al^{3+}}{27} + \frac{2Cu^{2+}}{64} + \frac{2Zn^{2+}}{65} + 1000 \times (10^{-pH})\right),$$

where the estimated acidity AC is expressed in mg/L of $CaCO_3$; Fe^{2+}, Fe^{3+}, Al^{3+}, Mn^{2+}, Cu^{2+}, Zn^{2+} are metal concentrations in the solution, mg/L; 50 is a coefficient for conversion of acidity in mg-eq into mg/L $CaCO_3$.

Required amount of reagent (RE) was estimated by the formula (Taylor 2005):

$$RE = Q \times AC \times 0.0864,$$

where the estimated RE is expressed in kg $CaCO_3$/day; Q is the flow rate, L/s; AC is the acidity, mg/L of $CaCO_3$; 0.0864 is the conversion factor.

Treatment efficiency (TE) was estimated by the formula:

$$TE = \frac{C_{in} - C_{out}}{C_{in}} \times 100\%,$$

where C_{in}, C_{out} are the concentrations of pollutants in the AMD discharge zone and in the effluent at the mouths of the rivers Yelchevka and Levikha, respectively, mg/L.

For the cumulative assessment of water pollution, we used the total pollution index (Zc):

$$Z_c = \sum_{i=1}^{n} \frac{C_i}{C_{MAC}} - (n-1)$$

where C_i is the actual concentration of a substance in water, mg/L; C_{MAC} is the maximum allowable concentration (MAC) for a pollutant in fishery water bodies, mg/L; n is the number of substances determined.

Results and Discussion

When the acidic waters reached the surface, they were found to have high concentrations of all components. In recent years, these concentrations have shown a slow gradual decrease. This process is called 'first flush' and is observed in many abandoned mines (Younger 1997, Gzyl 2007, Wolkersdorfer 2022, Rybnikova 2019).

The AMD from the Degtyarsk mine (the caved area of the «Kolchedannaya» shaft) are sulfate, the predominant cations being calcium, or magnesium, or iron, pH=2.3-3.3, mineralization ranges from 3.7 to 16 g/L. At the mouth of the river Yelchevka, the mine waters are characterized as sulfated magnesium-calcium, pH = 7.2-7.5 (neutral medium). Mineralization is from 0.9 to 1.2 g/L (Fig. 2).

At the Levikha mine, in the discharge zone (the collapse area of the Levikha II shaft), the mine waters are sulfate magnesium-iron-aluminum (the ratio of cations can vary). The water is less acidic (pH = 3.6-3.9), with a higher mineralization from 14.2 to 20.0 g/L. At the mouth of the Levikha River, water after treatment is characterized as sulfated magnesium-calcium, pH = 6.6-7.6. Mineralization is from 0.5 to 9.2 g/L (Fig. 2).

Treatment efficiency at the Degtyarsk mine reaches 99%, and the maximum allowable concentration (MAC) excess factor ranges from 10 (for Cu, Zn) to 20 (for Mn). At the Levikha mine, a similar scheme leads to worse results: treatment efficiency varies from 59% (for Mn) to 93% (for Fe, Cu). As a result, pollutant concentrations at the mouth of the Levikha River at the point of discharge into the Tagil River exceed the MAC 11 thousand times for Zn; 1.4 thousand times for Mn; and hundreds of times for Cu.

As a result, the total pollution index demonstrates that the degree of purification at the Degtyarsk mine is 300 times higher than at the Levikha mine, whereas it is only two times higher in the AMD discharge zone.

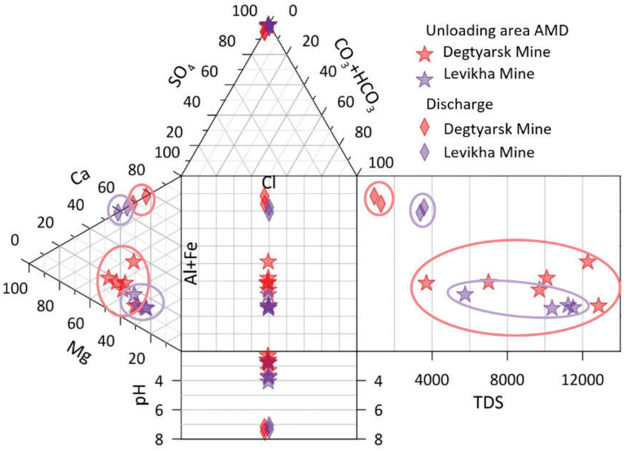

Parameter	Unloading area		Discharge	
	Degtyarsk Mine	Levikha Mine	Degtyarsk Mine	Levikha Mine
pH	2.6	3.8	7.4	7.2
Fe, mg/L	899	1 455	0.1	95
Mn, mg/L	39	82	0.2	34
Cu, mg/L	11	19	0.01	1.0
Zn, mg/L	121	280	0.1	107
SO_4, mg/L	7 110	7 493	704	2 133
∑M, mg/L	11 188	16 534	628	4 557

***Figure 2** Chart showing the chemical composition of water in the AMD discharge zone and after treatment, %-eq/L.*

We have identified the following reasons for this discrepancy.

Water acidity and amount of reagent used

At the Degtyarsk mine, the pH values are lower, but the water acidity is 5 times lower (the all metals content is lower). Therefore, it takes 1.58*10^6 kg/year of $Ca(OH)_2$ to neutralize 50 L/s of mine water from the Degtyarsk mine, whereas the Levikha mine needs 3,5 times more of $Ca(OH)_2$ to neutralize 32 L/s, or 5.46*10^6 kg/year (Fig. 3).

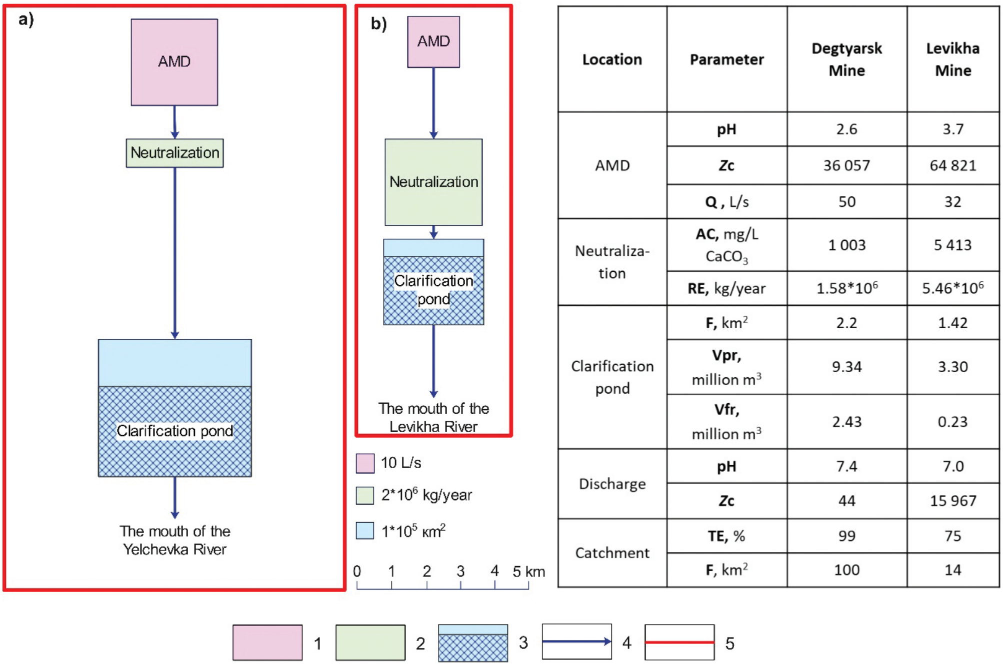

Location	Parameter	Degtyarsk Mine	Levikha Mine
AMD	**pH**	2.6	3.7
	Zc	36 057	64 821
	Q, L/s	50	32
Neutralization	**AC,** mg/L $CaCO_3$	1 003	5 413
	RE, kg/year	1.58*10^6	5.46*10^6
Clarification pond	**F,** km^2	2.2	1.42
	Vpr, million m^3	9.34	3.30
	Vfr, million m^3	2.43	0.23
Discharge	**pH**	7.4	7.0
	Zc	44	15 967
Catchment	**TE,** %	99	75
	F, km^2	100	14

***Figure 3** AMD purification chart and parameters: a) Degtyarsk mine, b) Levikha mine. 1 – AMD discharge zone, 2 – $Ca(OH)_2$ neutralization, 3 – clarification pond (shading – volume of bottom sediments, blue – free volume), 4 – surface streams, 5 – catchment area of the Yelchevka and Levikha rivers. Q – flow rate, F – area, Vpr – project volume, Vfr – free volume, AC – estimated acidity, RE – required amount of reagent, Zc –total pollution index, TE – treatment efficiency.*

Area and volumes of clarification ponds

To settle the water after neutralization, clarification ponds were built in the 1950s. They have been in operation without cleaning for several decades. After neutralization of highly mineralized acidic mine waters, hydrates and oxides are precipitated in the form of a finely dispersed silt-like suspension of a brick-orange color. These sediments have filled the southern part of the Yelchevka clarification pond (design area 2.2 km^2, total volume 9.34 million m^3) and formed a beach with dried sludge in the western part of the Levikha pond (design area 1.42 km^2, total volume 3.2 million m^3) (Fyodorova 2014, Rybnikova 2023). The clarification ponds are filled to 74 and 93%, respectively. The free volume is 2.43 million m^3 at the Degtyarsk mine and only 0.23 million m3 at Levikha (Fig. 3). As a result, the available free volume of the Levikha clarification pond is 10 times less than that of Yelchevka.

It is obvious that this volume of the Levikha clarification pond is not enough for settling the water after neutralization and ensuring interaction of pollutants with reagents. At the discharge from the pond, we observe increased concentrations of Zn (107 mg/L), Fe (95 mg/L), Mn (34 mg/L), and Cu (1 mg/L) (Fig. 2).

Passive purification and dilution

The passive purification stage involves settling the water after neutralization in streams and dilution with surface and groundwater in the catchment area. The catchment area of the river basin where the Yelchevka clarification pond is situated is about 100 km^2, with the AMD discharge zone located in the upper part of the catchment. The river network is long and has relatively high flow rates, which ensures a good degree of effluent dilution. The catchment area of the Levikha River where the Levikha clarification pond is built, is as small as 14 km^2. The AMD discharge zone here is located in the neighboring private catchment area of the Kuzka River (also a tributary of the Tagil River), from where the acidic waters are pumped across the local watershed into the Levikha River valley. In fact, the flow rate of the Levikha River is increased 3 times due to the inflow of acidic waters, whereas the possibility of diluting the purified effluent in the catchment area is very low. At the mouth of the river Yelchevka, the total pollution index is over 350 times lower than that at the mouth of Levikha (44 and 1.6*10^4, respectively).

For the Degtyarsk mine, the current two-stage system is quite effective. To improve the treatment efficiency at the Levikha mine, it is necessary to switch to a more advanced scheme of three-stage purification, for example: 1 – treatment facilities with aerators, 2 – radial settling tanks, 3 - a cascade of ponds (Rybnikova 2024).

Conclusion

At the Degryatsk and Levikha mines, now depleted and abandoned, AMD is being discharged to surface streams. The waters are sulfate, and calcium, magnesium, iron or aluminium may dominate among the cations.

AMD treatment at both sites is carried out in two stages: neutralization with lime milk and settling in clarification ponds. However, the treatment efficiencies are different. At the Degtyarsk mine, it reaches 99%, while at the Levikha mine it varies from 59% to 93%. Accordingly, the quality of the water discharged into the Tagil river system does not meet the standards: the concentrations of manganese, copper, zinc, and aluminum exceed the standards hundreds and thousands of times.

The main factors influencing the efficiency of the treatment system are as follows: anthropogenic (mine water flow rate and acidity), natural (dilution with clean water in the catchment areas), and technological (amount of reagent used for neutralization, volume of the clarification ponds).

Acknowledgements

This work was supported by State Assignment of The Institute of Mining, Ural Branch of the Russian Academy of Sciences 075-00410-25-00 PR. Theme 2 (2025-2027) “Geoinformation support for systemic assessment of environmental conservation strategies in the development of subsoil resources” (FUWE-2025-0002) s. r. 1022040300092-1-1.5.1.

References

Fyodorova OI, Davydov VA (2014) Diagnostics of Ground Water-Work Facilities with Electric and Seismic Methods with the Elchevsk Dam as a Study Case. Water Sector of Russia 6:44–55

Gzyl G, Banks D (2007) Verification of the "first flush" phenomenon in mine water from coal mines in the Upper Silesian Coal Basin, Poland. Journal of Contaminant Hydrology 92(1-2):66-86, doi: 10.1016/j.jconhyd.2006.12.001

Hedin RS, Nairn RW, Kleinmann RLP (1994) Passive Treatment of Coal Mine Drainage. Washington: United States Department of the Interior, 52 p.

Rybnikova LS, Rybnikov PA (2019) Regularities in the Evolution of Groundwater Quality at Abandoned Copper Sulfide Mines at the Levikha Ore Field, Central Urals, Russia. Geochemistry International 57 (3):298–313, doi: 10.31857/S0016-7525643282-299

Rybnikova LS, Rybnikov PA (2021) Assessment of hydrosphere formation factors in nature-and-technology systems: A case-study of the upstream basin of the Tagil River in the Sverdlovsk Region. Mining Informational and Analytical Bulletin 5-2: 257–272, doi: 10.25018/0236_1493_2021_52_0_257

Rybnikova LS, Rybnikov PA, Navolokina VY (2023) Rehabilitation of man-made formation of abandoned copper pyrite deposits on the example of Levikhinsky mine (Middle Urals). Bulletin of the Tomsk Polytechnic University. Geo Assets Engineering 334(8):137–150, doi: 10.18799/24131830/2023/8/4089

Rybnikova LS, Rybnikov PA, Navolokina VYu (2024) Assessment of the efficiency of acid mine

drainage purification (using the example of copper-pyrite mines in the Middle Urals). Journal of Mining Institute267: 388-401.EDN SBKRCK

SanPiN 1.2.3685-21 "Hygienic standards and requirements for ensuring the safety and (or) harmlessness of environmental factors to humans", as amended on December 30, 2022

Taylor J., Pape S., Murphy N (2005) A summary of passive and active treatment technologies for acid and metalliferous drainage (AMD). Fremantle, Werstern Australia, 49 p.

Wolkersdorfer C (2022) Mine Water Treatment – Active and Passive Methods. Springer Berlin, Heidelberg: 328, doi: 10.1007/978-3-662-65770-6

Younger PL (1997) The longevity of minewater pollution – a basis for decision-making. Sci Total Environ 194–195:457–466, doi: 10.1016/S0048-9697(96)05383-1

Post-closure water management in Chelyabinsk Coal Basin (Russia)

Petr A. Rybnikov[1], Liudmila S. Rybnikova[1], Alexander Yu. Smirnov[1]

[1]The Institute of Mining, Ural Branch of the Russian Academy of Sciences, 58 Mamin-Sibiryak Street, Yekaterinburg, 620075, Russia, ribnikoff@yandex.ru, ORCID 0000-0002-7829-5035

[1]The Institute of Mining, Ural Branch of the Russian Academy of Sciences, 58 Mamin-Sibiryak Street, Yekaterinburg, 620075, Russia, luserib@mail.ru, ORCID 0000-0002-4221-787

[1]The Institute of Mining, Ural Branch of the Russian Academy of Sciences, 58 Mamin-Sibiryak Street, Yekaterinburg, 620075, Russia, alexsm94@gmail.com, ORCID 0000-0002-9015-0816

Abstract

In the early 21st century, coal mining in the Chelyabinsk coal basin (Southern Urals, Russia) was terminated. Mining and associated dewatering occurred for over a century across the 1,300 km2 area of the basin.

This paper describes the development of the first regional groundwater flow model for the Chelyabinsk coal basin. Its objective was to assess the consequences of water table rebound and underground mine and open-pit flooding post mine closure. Climate change is accounted for in the model by considering changes in precipitation patterns.

Keywords: Coal deposits, Drainage, Hydrogeological conditions, Mines, Geo-ecological problems, Open-pits, Waterlogging, Landslide, Leakage, Water-carrying utilities.

Introduction

During 1993–1994 in Russia was started restructuring coal industry. This led to closure of 203 coal mining enterprises (188 underground and 15 open-pit mines). The negative consequences of mine liquidation and flooding in Russian coal basins vary depending on a combination of geological, geomorphological, hydrogeological and mining factors (Rybnikova 2020, Rybnikov 2020, Melchers 2015). Similar processes have been observed in other countries (Wolkersdorfer 2008).

The Chelyabinsk coal basin covers an area of 1,300 km^2 and located on the eastern slope of the Ural Mountains (Fig. 1). The landscape of the region presents a gently rolling forest-steppe plain, broken by hillocks and saucer-shaped hollows. In hydrographic terms, the region is characterized by an extremely sparse river network and an abundance of endorheic lake basins with areas ranging from fractions of a hectare to dozens of square kilometers. Rivers are represented by the Miass River in the northern part of the basin (average annual flow rate of 18 m3/s), and the Uvelka River in the southern part (11 m3/s). The other rivers are intermittent, disappearing into swampy lake basins. Over the past 20 years, precipitation has been between 281 mm/year (2021) and 588 mm/year (2014). Average precipitation has been 460 mm/year.

The Chelyabinsk coal basin deposits were discovered in 1832 and their commercial development was started in 1907. The cities of Kopeysk (150,000 people) and Korkino (35,000 people) grew on the basis of the mining settlements near the mines. Coal peak production was reached in the 1960s. Nowadays all opencasts and mines have ceased operation.

The geological structure of the Chelyabinsk coal basin represents as graben within Paleozoic rocks of the eastern slope of the Urals and is filled coal sediments lower Mesozoic ages.

During mining operations, the average annual water outflow rate from all mines and workings reached 2,363 m^3/hour. This water was discharged into three lakes, lake Kurlady, lake Tretye, and lake Kurochkino, and into the river Chumlyak, and the Ulamovo swamp.

The cessation of mine dewatering with the closure of the Kopeysk and Korkino opencast coal mines has resulted in groundwater table rebound with ecological and hydrogeological impacts such as the flooding of the opencast pits, infrastructure, and sinkholes.

Methods

There are three depression cones within the Chelyabinsk coal basin. They are located in the North (Kopeyskiy open pit, “Zentralnaya” shaft), at the center of coal basin (Korkinsky open pit), in the South (Emanzhelinsk). Total water inflow to the north depression cone was 6 times more compare to the central cone (1200 and 200 m3/hour, accordingly). Despite the fact that depth of the Korkinsky open pit is 500 meters an area of the central depression cone was smaller compare to the northern depression cone. During mine development river flow consumption of the Chymlyak river wasn’t found and the center depression cone was outside of the river. At the same time in the northern depression cone the Miass river is draining groundwater flow. The flooding forecast for the Korkinsky mine was carried out in the reclamation project (Sokolovsky 2018).

For estimation of flooding rate of the Kopeysk open-pit mine groundwater flow model had been developed. The purposes of modeling were as follows: to predict maximum flood level in the Kopeyskiy open pit, to define the speed and duration of depression cone filling. Groundwater flow modeling was performed using the Processing ModFlow 8 software. The model boundaries were defined by watersheds according to the position of the natural streams and reservoirs for Lake Kurlady in the East, Lake Smolino in the West, and the Miass River in the North (Fig. 2). The total number of blocks was equaled 700 blocks along the X axis and 500 blocks along the Y axis. The block size was determined as 50 × 50 m. The model area was 440 km^2.

The groundwater flow model has two-layer stricture. The upper layer is associated

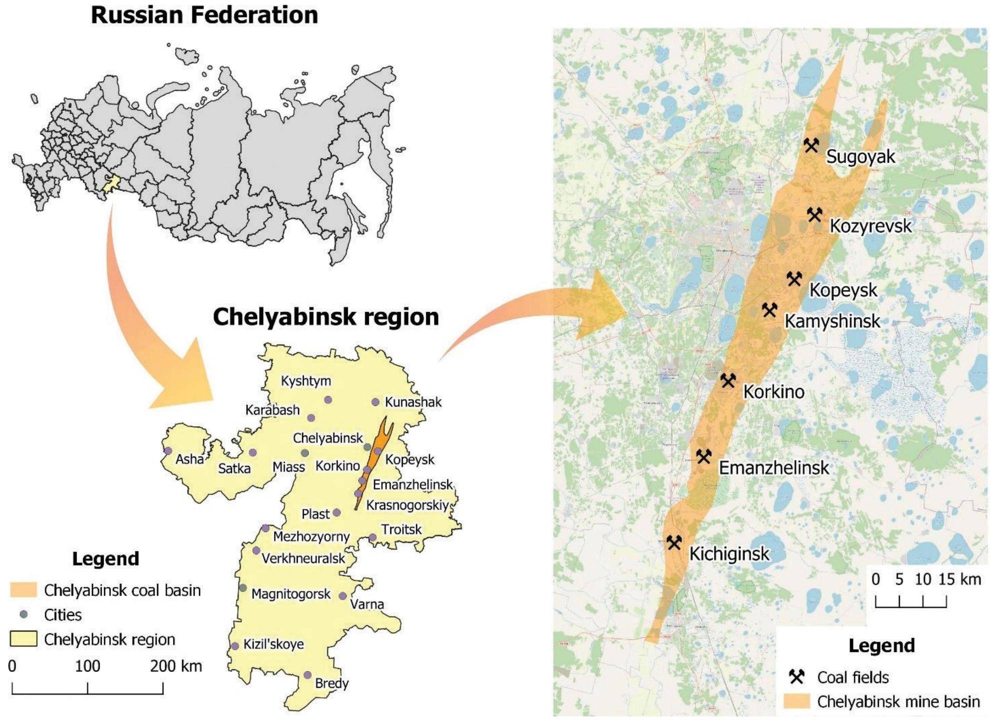

Figure 1 The Chelyabinsk Coal Basin location map.

with Eocene-Upper Cretaceous sediments (argillites), and the bottom one is confined to Triassic-Jurassic deposits (sandstones with interlayers of clays and gaizes). The first layer thickness was defined as 50 m and the second as 100 m. Hydraulic conductivities of the top layer vary from 0.2 to 1 m/day and from for the bottom layer 0.05 to 0.15 m/day, accordingly. The groundwater recharge modulus is taken to be 1.25 L/s per square kilometer. The model was calibrated based on the mining period with stable mine water inflows (steady-state solution). The model storage parameters for transient flow of open-pit flooding process were calibrated in the model by simulating the flooding period from 2010 to 2021. Forecasting for flooding rate of the Kopeysk open pit was aimed

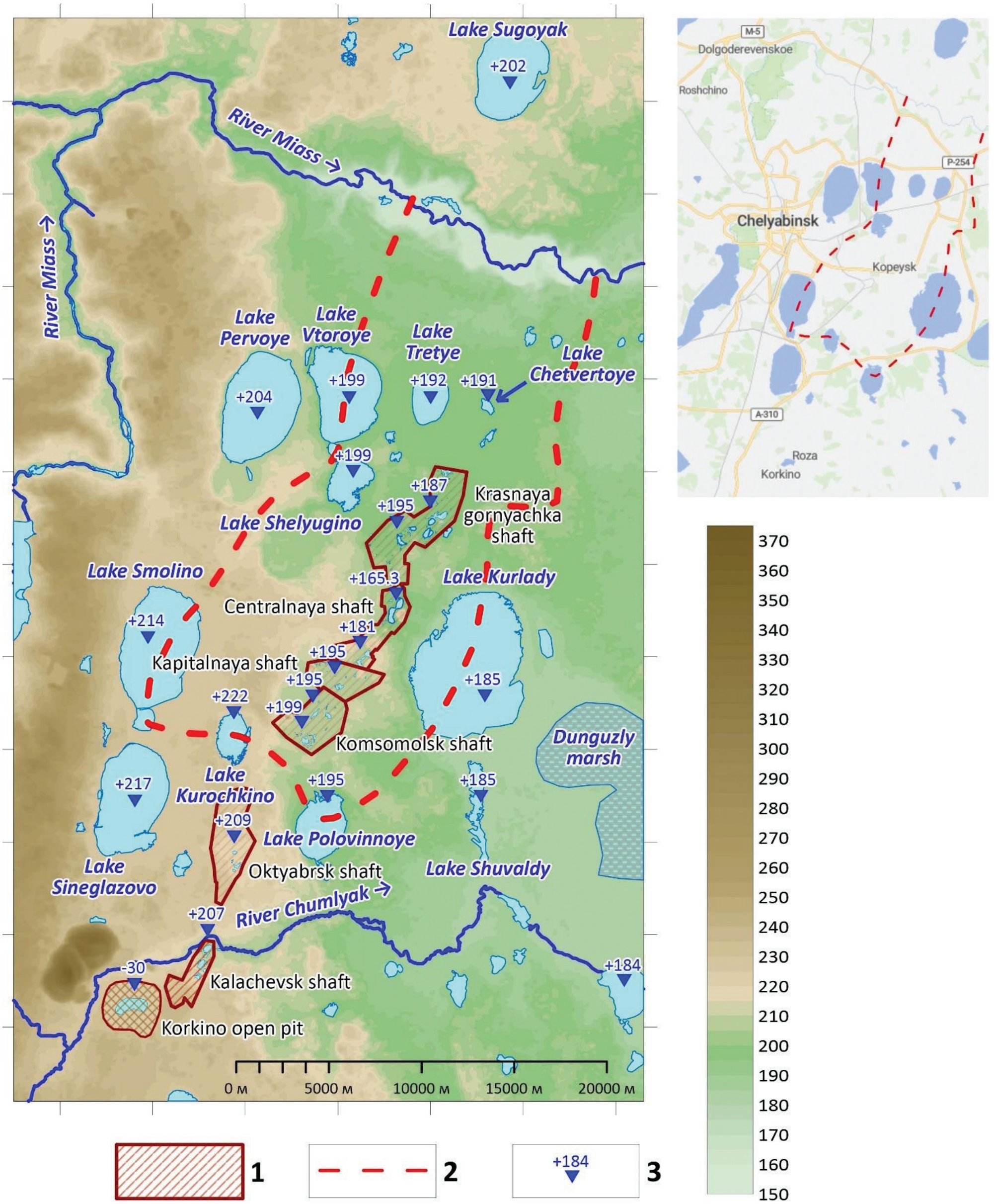

Figure 2 *Hydrographic network of the region and minefield location map. 1 – mining allotment; 2 – mine catchment area boundary in the northern part of the Chelyabinsk Coal Basin (groundwater flow model boundary); 3 – reservoir water level mark.*

under three scenarios: without taking any actions; for the open pit filled to half storage capacity (with stabilization of the open-pit's western side prone to sliding); and complete backfilling of the open pit. To determine the influence of the period's precipitation, we considered three scenarios (for half-filled open pit): 10 years of high precipitation; normal precipitation over the entire flooding period; 10 years of low precipitation. The maximum flooding value is the same for all scenarios at 194.5 m.

Results

Kopeysk open-pit mine, shaft "Tsentralnaya". The facilities of this opencast are located within the city's developments and industrial infrastructure. The flooding of the Kopeysk open-pit mine has been going on since 2004; drainage from the shaft "Tsentralnaya" was stopped in 2006. The western side of the open pit is occupied with an industrial plant. Several landslides have occurred here during the flooding. After the largest landslide in 2015, the daylight surface near the plant's territory subsided by 15 m. It was established that there had been leaks of hot water from the plant's cooling tower, discharged onto the terrain. This led to the flooding of the territory and waterlogging of the previously backfilled mass on the side slope, which provoked further landsliding. The slope of the landslide area was stabilized by backfilling in the spring of 2019. After the shutdown of the cooling tower, leakage ceased, and no movements of the ground reference marks have been recorded since then.

Based on the modeling results was shown that the open-pit flooding (starting from 2021) will make 70 years without organization any actions and will make 5 years with complete backfilling of the open pit (Fig. 1). Provided that any measures will be taken to stabilize the western slope of the open-pit the water mark will be reached at 194.5 m (in scenarios of 50% filling of the mined-out space) in 25 years with a probability of 70% (Rybnikova 2023). In case of combination of unfavorable factors (e.g., a series of years with high precipitation) the water mark will be reached in 6 years. If very low precipitation years will be repeated (such as 2021) the flooding will continue for 31 years.

External boundaries of the model are impermeable except the Miass river and the Kurlady lake where the groundwater flow is discharged. Incoming model balance terms are infiltration and leaks from water-carrying communications in city areas. Outcoming model balance terms are evapotranspiration, discharge into the Kurlady lake and the Miass river, filling the volume of the Kopeyskiy open pit. The groundwater flow is directed to the open pit during the flooding process. When the volume of the Kopeyskiy open pit will be filled, the groundwater flow will direct

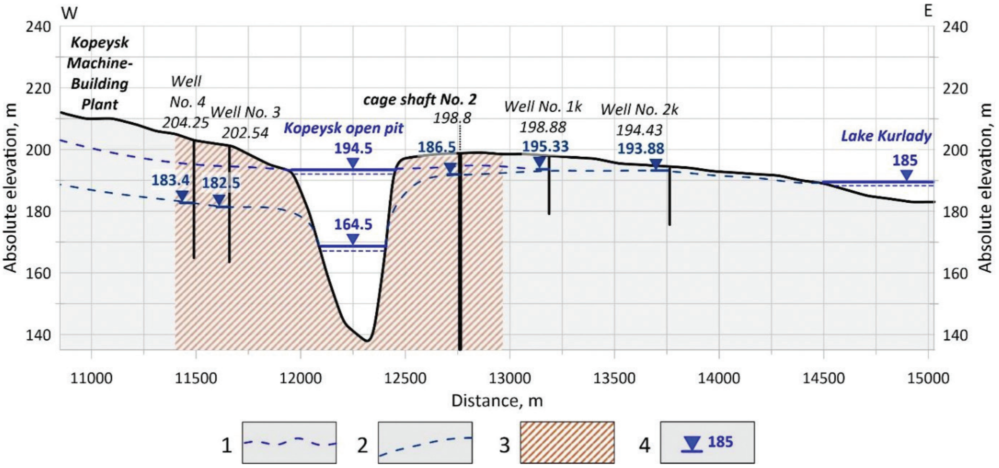

***Figure 3** Schematic cross section along the line Kopeysk Machine-Building Plant – Kopeysk open pit – Lake Kuraldy. 1 – current groundwater level; 2 – predicted groundwater level; 3 – mining allotment for the shaft Tsentralnaya; 4 – absolute water-level elevation.*

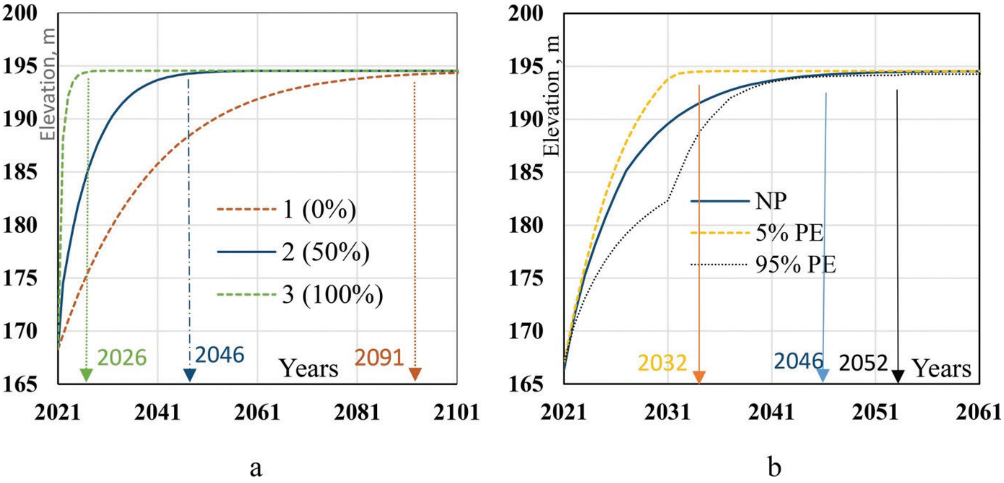

Figure 4 Prediction of Kopeysk open pit flooding for different scenarios allowing for: a degree of pit backfilling (1—without backfilling, 2—with 50% backfilling, 3—with 100% backfilling); b variation in natural water recharge (1—normal period (NP), 2—water-rich period with 5% probability of excess for 10 years (5% PE), 3—water-short period with 95% probability of excess for 10 years (95% PE). The number at the arrow means the year of peak water mark.

to the open pit, Kurlady lake and the Miass river. The local watershed between the lake and the open pit will be kept, groundwater flow from the open pit into the Kurlady lake won't be proceed.

The Korkino open-pit mine. The Korkino mine is the deepest opencast coal mine in Eurasia: its depth is 493 m, more than 3 km long on the surface, and 2.5 km wide. Over the period of operation for 70 years (since 1934), it produced 250 million tons of coal and excavated 1.5 billion tons of ground material. The excavation volume amounted to about 3 billion m^3. The mine ceased operation in 2017. In addition to open-pit production, the Korkino deposit was also worked by the underground method at the shaft Korkino. The first major landslide occurred in 1945 on the northwestern side; the shaft Korkino was condemned as unfit for use, and the buildings collapse has begun. A decision of resettle Roza village and Korkino city settlements and phase out the open-pit facilities was made.

Endogenous fires occurred regularly in the open-pit's sides, the consequences of which were felt at a distance of dozens of kilometers. For the purposes of reclamation, a project was developed that provided for the filling of the mine workings and preventing spontaneous combustion by backfilling such zones with material based on tailings from the Tominsky Mining and Processing Plant (Sokolovsky 2018). At present, a 14-km long slurry pipeline is used for filling open-pit. This technique resolves several environmental problems at once: copper porphyry ore extraction and processing wastes are utilized; fires are extinguished; reclamation of the man-made workings is carried out.

The backfilling of the open-pit is planned to be completed by 2045. By then, open-pit will contain 479 million m3 of backfill

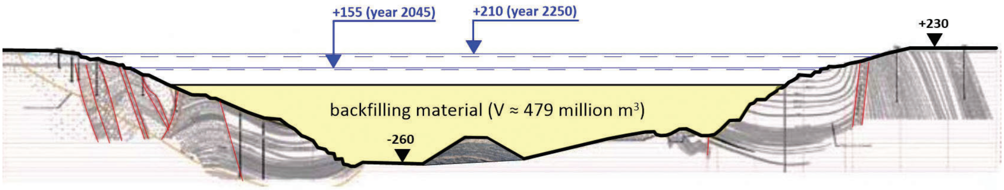

Figure 5 Korkino open pit space in the course of reclamation.

and 212 million m3 of water and the water mark will reach +155 m (Rybnikova 2023). The estimated flooding level of the Korkino open-pit will be no higher than +210 m. The groundwater inflows will occured 200 m^3/hour and the flooding time from +155 m (water surface area of 4.7 km^2) to +220 m (water surface area 7.4 km2) water mark will take at least 200 years.

Conclusion

The flooding of the Kopeysk open-pit to the maximum level of +194.5 m will continue until 2091. It is necessary to prevent the water level in the open pit from rising above the level of +190.0 m to prevent the flooding of the residential developments on its eastern side of the Kopeysk open-pit. Mining activity was not the main cause of landslide slope waterlogging and adjacent area flooding.

Reclamation of Eurasia's largest Korkino opencast mine is being conducted by backfilling of the mine workings with material based on tailings from the Tominsky Mining and Processing Plant, which are delivered to the open pit via a slurry pipeline. The backfilling of the mined-out workings is planned to be completed by 2045 at a mark level of +155 m. Estimated flooding level of +210 m will occurred no earlier than 2250 year.

It has been shown for the first time that the cause of an urban area flooding is the geological and geomorphological structure of the territory characterized by the presence of natural lakes and poor drainage of the area.

The combination of geological structural features with geomorphological conditions, hydrometeorological factors and mining methods leads to the formation of new hydrogeoecological conditions at the post-operational stage, which may last for dozens and hundreds of years. Due to the filling of the cone of depression, man-made reservoirs are formed, areas are flooded, and landslide processes develop. At the same time, lakes that form due to mine drainage tend to dry up, and the quality of the water in them deteriorates radically.

Acknowledgements

This work was supported by State Assignment of The Institute of Mining, Ural Branch of the Russian Academy of Sciences 075-00410-25-00 PR. Theme 2 (2025-2027) "Geoinformation support for systemic assessment of environmental conservation strategies in the development of subsoil resources" (FUWE-2025-0002) s. r. 1022040300092-1-1.5.1.

References

Melchers C, Kretschmann J, Goerke-Mallet P, Kleinberg K, Tyulenev MA (2015) Elements and aspects of the post-operational period of mining enterprises. Bulletin of the Kuzbass State Technical University 6(112):3–13. (In Russ., abstract in Eng.)

Rybnikov PA, Rybnikova LS, Maksimovich NG, Demenev AD (2020) Study of the hydrogeological conditions of coal deposits at thepost-operational stage using hydrodynamic modeling (on theexample of the Kizel coal basin, western Urals, Russia). GIABMin Info Anal Bull. 3.1:488–500 doi.org/10.25018/0236-1493-2020-31-0-488-500 (In Russ., abstract in Eng.)

Rybnikova LS, Rybnikov PA (2020) Pit Lake and Drinking Water Intake: Example of Coexistence (Middle Urals, Russia). Mine Water and the Environment. 39:464–472, doi:10.1007/s10230-020-00691-w

Rybnikov PA, Rybnikova LS, Smirnov AYu (2023) Post-mining of Chelyabinsk Coal Basin (Russia): The Effects of Mine Flooding Mine Water and the Environment. 42:472–488, doi.org/10.1007/s10230-023-00947-1

Rybnikova LS, Rybnikov PA, Smirnov AYu (2023) Flooding of Open Pit and Underground Mines in the Chelyabinsk Coal Field. Consequences, Problems and Solution. Journal of Mining Science. 3:497–504.

Sokolovsky AV, Lapaev VN, Temnikova MS, Gordeev AI (2018) Technological features of liquidation of the Korkino open-cast. Coal 3(1104):91–95. doi.org/10.18796/0041-5790-2018-3-91-95 (in Russ.)

Wolkersdorfer C (2008) Water management at abandoned flooded underground mines. Fundamentals. Tracer tests. Modelling. Water treatment. Springer. 465 p.

Iber as a Flood Nowcasting and Forecasting Software Suite for Mine Managers

Marcos Sanz-Ramos[1], Ernest Bladé[2]

[1]Flumen Research Institute, Universitat Politècnica de Catalunya (UPC-BarcelonaTECH) – Centre Internacional de Mètodes Numèrics en Enginyeria (CIMNE) 08034 Barcelona, Spain, marcos.sanz-ramos@upc.edu, ORCID 0000-0003-2534-0039

[2]Flumen Research Institute, Universitat Politècnica de Catalunya (UPC-BarcelonaTECH) – Centre Internacional de Mètodes Numèrics en Enginyeria (CIMNE) 08034 Barcelona, Spain, ernest.blade, ORCID 0000-0003-1770-3960

Abstract

Iber is a two-dimensional numerical tool for the simulation of free surface water flows. Widely used for numerical modelling of environmental flows, Iber has been recently enhanced to simulate non-water flows such as mudflows and debris flows by implementing rheological models oriented to compute the resistance forces. This new extension is freely distributed, fully integrated into a user-friendly guided interface, and enables practitioners to analyze mine-tailings spill propagation, providing valuable information for assessing flood hazard and risk in the event of tailing storage facilities failure. This work shows the new features and capabilities of Iber.

Keywords: Risk management, hazardous situations, mine-tailings, numerical modelling, Iber

Introduction

Mine tailings, a by-product of mine activities, are commonly stored, temporally or permanently, in Tailing Storage Facilities (TSF). The failure or malfunctioning of TSF can release large amounts of water containing high concentrations of pollutants into the environment, which often behave as non–Newtonian fluid flows. Preventing and mitigating these hazardous situations is challenging for the mining industry for both active and closured TSF (Klose 2007).

The complexity and scale of tailings disasters present enormous challenges for emergency services, environmental regulators, mine managers, and affected communities (Penman *et al.* 2001). Efforts to provide effective response and recovery require a thorough understanding of the behaviour of tailings materials, including their transport mechanisms, dispersion patterns and the potential for further environmental degradation over time. Advances in numerical modelling tools, together with improvements in computational capacity, allow for the development of strategies to reduce the risk to the environment and population based on more accurate predictions of mine tailings behaviour and propagation (Hungr 1995; Adewale *et al.* 2017).

Numerical modelling tools allow simulating the dynamics of non–Newtonian fluids by solving mass and momentum conservation equations. This is an essential step in flood risk management, providing reliable flood information for mine planning in existing or new facilities (e.g. maximum flood extent, depth, and flow velocity). Iber is a software suite widely extended –but not limited– for simulating hydrodynamic processes of water flows (Bladé *et al.* 2014), and particularly to simulate dam-break scenarios (Sanz-Ramos *et al.* 2023b). This two-dimensional hydrodynamic numerical tool has been recently enhanced to simulate non–Newtonian shallow flows (Sanz-Ramos *et al.* 2023a, 2024a), especially those related to mine tailings by incorporating rheological models that reflect the fluid's properties (e.g. Bingham).

The purpose of this work is to demonstrate the new features of Iber for simulating shallow non–Newtonian flows, such as mine tailings spill propagation. The code integrates several rheological models to consider different flow behaviours and a specific numerical scheme that achieves the fluid detention according to the rheological properties of the fluid. It is fully integrated in a user-friendly guide user interface and freely distributed for practitioner in general, and specifically for mine managers. (www.iberaula.com). The performance of the numerical tool is shown throughout a benchmark, showing good results and the valuable information to assess flood hazard and risk in mine-tailings spill propagation scenarios.

A software suite for mine managers

Numerical tool: IberNNF

Iber is a two-dimensional software for the simulation of hydrodynamics originally developed for shallow water flows (www.iberaula.com). The application fields of Iber also extend to transport processes, morphodynamics, hydrological processes, soil erosion in watersheds, urban drainage and eco-hydraulics. Fig. 1 depicts a schematic interrelationship of the different calculus modules, being the hydrodynamics the main module. IberNNF is a new calculation module that works as hydrodynamic module separated from the rest of modules of Iber. It integrates a specific numerical scheme and rheological models for the numerical modelling of non–Newtonian shallow flows, or non-water shallow flows. A detailed description can be found in Sanz-Ramos *et al.* (2023a).

Rheological models

Rheology is the science in charge of studying the deformation and flow of matter under variations in temperature, pressure and shear stress (Adewale *et al.* 2017). Omitting the temperature and pressure terms, fluid behaviour is only a function of shear stress, which is proportional to the shear rate through the viscosity. Non–Newtonian fluids can be classified into 4 large groups: Newtonian (constant viscosity), Dilatant (viscosity increases when shear stress increases), pseudoplastic (viscosity reduces when shear stress increases), and Bingham-type (the fluid movements starts when the shear stress is greater than the yield stress).

From the simplest Potential law to the full –and complex– Bingham model, several rheological models exist in the literature, the development of each one being oriented to achieve the particular reproduction of a fluid behaviour. The aim of IberNNF is not to include as rheological models as possible—or exist—; however, it implements the flowing 8 rheological models to attempt representing the resistance forces that act against flow motion of non–Newtonian flows.

The *Manning* equation can be applied for both water and non-water flows, since it was utilised by several authors for simulating hyperconcentrated flows (e.g. Takahashi 1985; Syarifuddin *et al.* 2018). Macedonio and Pareschi (1992) considering constant sediment concentration and uniform flow, derived the following expression: $\tau = \tau_y + \mu_1 (dv/dz)^{\alpha}$, where τ_y is the yield stress,

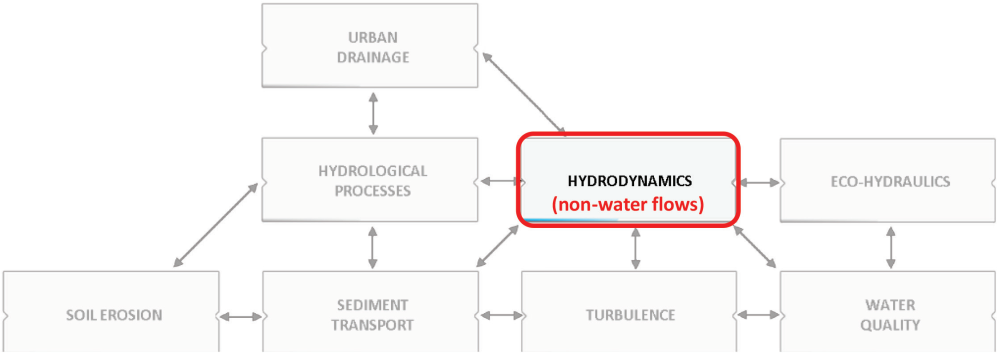

Figure 1 *Calculation modules of Iber for (a) water flows, and (b) non-water flows (IberNNF).*

μ_1 is a proportionality coefficient and α is the flow behaviour index. When α = 1 a model for *Viscous* flows is developed; while α = 2 a *Dilatant* flow behaviour is expected.

O'Brien and Julien (1988) derived an expression for the representation of the shear stress of mudflows, being a quadratic equation that integrates the Mohr–Coulomb term, the viscous term and the turbulent term through the Manning equation. In this sense, the formulation of Herschel and Bulkley (1926) is a generalization of various expressions in which e.g. dilatant, viscous or plastic behaviours can be derived depending on the value of the coefficient α.

Since the proposal of the Bingham (1916) rheological model, several approaches have been introduced to deal with the difficulties on directly obtaining the shear stress proportional to the flow velocity (Pastor *et al*. 2009). IberNFF implements a Bingham simplified model (O'Brien and Julien 1988; Pitman *et al*. 2003), which is a explicit equation that considers the viscous and the Mohr–Coulomb contributions.

The rheological model of Voellmy (1955) considers the Mohr–Coulomb and the turbulent contributions, being this last one equivalent to the Manning model. Finally, the Bartelt model (Bartelt *et al*. 2015) accounts for resistance generated by the cohesion, a physical property of the fluid. This rheological model is commonly used together with the Voellmy model.

Workflow

The utility and practical application of any numerical code necessarily requires its integration in a graphical user interface (GUI). This facilitates the model build-up, setup and results visualization. Iber is fully integrated in the multi-dimensional pre- and post-process GUI software called GiD. The interface is adapted for Iber to make a simple, easy and user-friendly experience for a 2D-hydrodynamic modelling process. Three main steps define the workflow of Iber, and thus IberNNF: the first step (pre-process) is where the user creates the model and implements all conditions; the second step (calculation) is the place for time parameters definition, calculation module selection and simulation run; and finally (post-process) is when all results can be analysed in the GUI or/and export to third party software.

The activation IberNNF (Fig. 2a) adapts the GUI to show the particular tools and options to carry out a simulation considering the fluid as non–Newtonian. A new tab on the Problem data appears allowing the selection of the different rheological models, the fluid properties, and additional options (Fig. 2b). Depending on the rheological model selected, different parameters must be imposed, particularly those related to the friction slope which follow the same definition of Land uses concept (Fig. 2c). This provide identical benefits as for Newtonian fluids, allowing to assign it manually in the model geometry/

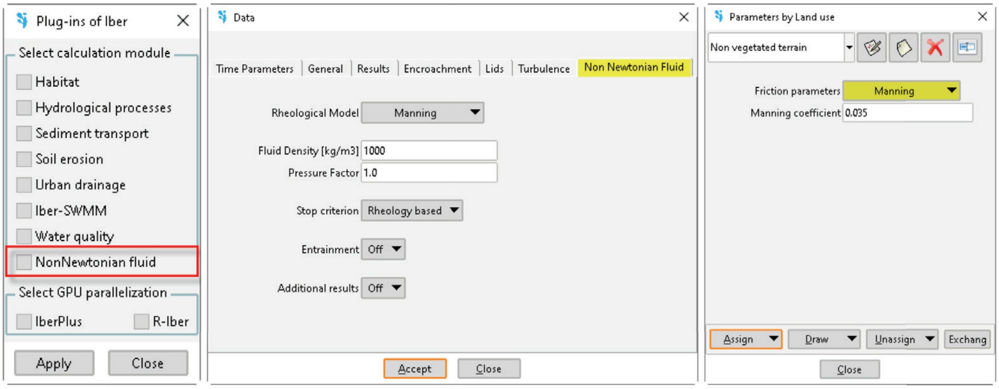

Rheological Model: Manning
Fluid Density [kg/m3]: 1000
Pressure Factor: 1.0
Stop criterion: Rheology based
Entrainment: Off
Additional results: Off

Non vegetated terrain
Friction parameters: Manning
Manning coefficient: 0.035

(a) (b) (c)

Figure 2 GUI of IberNNF: (a) activation of the module; (b) definition of main parameters; and (c) definition of non-dependent parameters of the rheological model.

mesh or automatically to the mesh by importing raster files. Nevertheless, the Land uses database has been particularised to this module removing land uses typically used for flood analysis or hydrological processes, e.g. “river”, “concrete” or “urban fabric”.

Evaluating past, present and future hazardous situations

Since 1961, more than 150 major TSF failures have been reported (WISE 2024), with an average of 2.5 failures per year and 82 of them occurring between 2000 and 2024. This highlights the strong need for enhance and comprehensive management, monitoring, prevention, and planning strategies to mitigate the flood risks associated with mining activities.

IberNNF can be applied to simulate mine-tailings spill propagation after a TSF failure (Sanz-Ramos *et al.* 2024b, a) and, thus, it can be a useful tool for mine managers to analyse past events, plan and design actions to mitigate hazardous situations of existing or future TSF. To that end, IberNNF couples the hydrodynamics with a specific option that implements the breach formation in the simulation process (Sanz-Ramos *et al.* 2023b), the dam-break process and the subsequent fluid propagation being simulated jointly. This allows mine managers to identify and assess the potential flood extent and environmental damages

The numerical tool provides the evolution of hydrodynamic variables (e.g. depth, velocity, and fluid elevation) at each element of the calculation mesh, the base to assess the flood hazard and risk at each element at risk (EaR) of computational domain. The results can be analysed directly in the GUI or can be exported to other software to provide additional features and greater versatility for the users. This can help to apply the specifications and verify criteria of guidelines of each country or region worldwide to prevent dangerous situations for people and the environment (Penman *et al.* 2001; Klose 2007; Kheirkhah Gildeh *et al.* 2021).

Application & results

The performance of the numerical tool was exemplified through, first, the idealised dam-break of a visco-plastic fluid ($\rho = 1835$ kg/m^3) presented by Bryant (1983), which consists in a stored fluid (30.5 m in height and 305 in length) immediately released over a fully flat terrain with a runout distance of 1896 m. The parameters of the different rheological models implemented into IberNNF were defined according to Naef *et al.* (2006) with the aim of reproducing the results of the analytical solution of Hungr (1995). According to Hungr (1995), a simulation considering a total steady-state shear strength of 2390 Pa was carried out.

Table 1 summarises the values of the rheological models, and the maximum runout and fluid elevation at the end of the simulation, together with the detention time. In all simulations the fluid was released instantaneously and stopped a few seconds later. The fluid motion, runout and detention

Table 1 *Maximum runout and height at the end of the simulation and detention time according to the values of the rheological models of Bingham (simplified), O’Brien & Julien, and Voellmy. *Bingham simplified with a factor of 1.5 in the yield stress contribution (Naef et al. 2006).** Bingham simplified with a factor of 1 in the yield stress contribution (O’Brien and Julien 1988). ***Bingham simplified model was forced to a total steady-state shear strength of 2390 Pa.*

Model	**Bingham* (simplified)**		**Bingham** (simplified)**		**Bingham*** (simplified)**	**O’Brien & Julien**				**Voellmy**	
Parameter	$1.5 \cdot \tau_y$	μ_B	τ_y	μ_B	$\rho g h S_{rh}$	n	τ_y	η	K	μ	ξ
Value	1500	100	1500	100	2390	0.02	1500	100	24	0.02	2500
Runout [m]	1748		2066		1875	1893				1738	
Time [s]	126		148		130	146				168	
Height [m]	9.59		8.14		9.69	8.25				12.75	

τ_y: yield stress; μ_B: viscosity; ρ: density; h: depth; n: Manning coefficient; η: O’Brien’s viscosity; K: resistance parameter.

time were according to the rheological properties of the fluid.

The shape of the fluid at the end of the simulation was non-horizontal (Fig. 3a), the elevation in Bingham and O'Brien & Julien approaches being higher at intermediate distances (1250-1750 m) than upstream (500-1250 m) and decreasing almost vertically at the leading edge. The results of Voellmy were smoother than the others, being necessary to use a very low value of the Coulomb friction coefficient. Tn terms of runout, two approaches provided the best fit in comparison with the analytical solution: considering a total steady-state shear strength of 2390 Pa (Bingham***) and O'Brien & Julien. Only differences in the maximum height at the upstream part of the channel are remarkable due to velocity-dependent terms of the O'Brien & Julien rheological model. The results were also compared with DAN model (Hungr 1995), showing a good performance of IberNNF in representing an idealised dam-break scenario with non-Newtonian flow.

The second example is the gypsum TSF failure presented by Jeyapalan *et al.* (1983), which geometry was idealized according to Wu *et al.* (2020). A constant height of 11 m, released instantaneously, was imposed as initial condition considering a Bingham type fluid (τ_y = 1000 Pa and μ = 50 Pa·s). A mesh density of 5500 els./ha was used to discretize the computational domain. Fig. 3b shows a 3D view of the free surface at the end of the simulation, revealing a non-horizontal shape with the fluid at rest. The simulated runout was 300 m and the fluid front detention was produced at 50 s, in agreement with Jeyapalan *et al.* (1983). The fluid was fully stopped at 102 s.

Although the freezing time aligns with the observations, uncertainties in the breach formation –such as the breaking time and the evolution of the breach shape– along with the potential fluidization of the stored fluid (Ayala-Carcedo 2004), could result in an incomplete representation of the fluid behavior during both the dynamic and static phases (Sanz-Ramos *et al.* 2022).

Conclusions

New capabilities of Iber, particularly through the hydrodynamic module IberNNF for non-water flows, provide practitioners and mine managers a free distributed software to assess flood hazard and risk scenarios. This module is fully integrated in a user-friendly guide user interface (GUI) allowing the analysis of mine-tailings spill propagation over the environment, whether in its own GUI or exporting the results to other software.

Both dynamic and static phases of the fluid are result only of the rheological model, obtaining a free surface with the fluid at rest. The current version of IberNNF implements the equations of Bingham (simplified), O'Brien and Julien, Manning and Manning-like formulas (Viscous and Dilatant fluid behaviours), Voellmy, Bartelt and Herschel-Bulkley, providing practitioners a wide range of formulations to properly represent particular fluid behaviors.

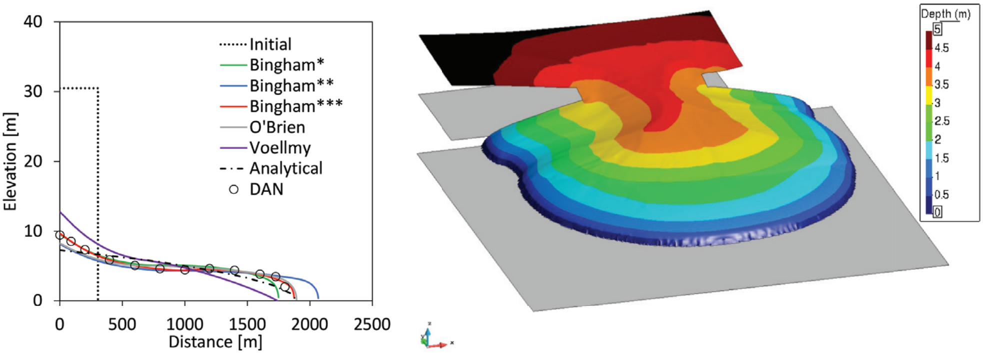

(a) (b)

Figure 3 *Results of the numerical simulations: (a) idealized dam-break presented by Bryant (1983), and (b) gypsum TSF failure presented by Jeyapalan et al. (1983).*

References

Adewale FJ, Lucky AP, Oluwabunmi AP, Boluwaji EF (2017) Selecting the most appropriate model for rheological characterization of synthetic based drilling mud. Int J Appl Eng Res 12:7614–7629

Ayala-Carcedo J (2004) La rotura de la balsa de residuos mineros de Aznalcóllar (España) de 1998 y el desastre ecológico consecuente del río Guadiamar: causas, efectos y lecciones. Bol Geol y Min 115:711–738

Bartelt P, Valero CV, Feistl T, *et al* (2015) Modelling cohesion in snow avalanche flow. J Glaciol 61:837–850. https://doi.org/10.3189/2015JoG14J126

Bingham EC (1916) An investigation of the laws of plastic flow. Bull Bur Stand 13:309–353. https://doi.org/10.6028/bulletin.304

Bladé E, Cea L, Corestein G, *et al* (2014) Iber: herramienta de simulación numérica del flujo en ríos. Rev Int Métodos Numéricos para Cálculo y Diseño en Ing 30:1–10. https://doi.org/10.1016/j.rimni.2012.07.004

Bryant SM (1983) Application of tailings flow analyses to field conditions. University of California, Berkeley. United States of America

Herschel WH, Bulkley R (1926) Konsistenzmessungen von Gummi-Benzollösungen. Kolloid-Zeitschrift 39:291–300. https://doi.org/10.1007/bf01432034

Hungr O (1995) A model for the runout analysis of rapid flow slides, debris flows, and avalanches. Can Geotech J 32:610–623. https://doi.org/10.1139/t95-063

Jeyapalan JK, Duncan JM, Seed HB (1983) Investigation of Flow Failures of Tailings Dams. J Geotech Eng 109:172–189. https://doi.org/10.1061/(ASCE)0733-9410(1983)109:2(172)

Kheirkhah Gildeh H, Halliday A, Arenas A, Zhang H (2021) Tailings Dam Breach Analysis: A Review of Methods, Practices, and Uncertainties. Mine Water Environ 40:128–150. https://doi.org/10.1007/s10230-020-00718-2

Klose CD (2007) Mine Water Discharge and Flooding: A Cause of Severe Earthquakes. Mine Water Environ 26:172–180. https://doi.org/10.1007/s10230-007-0006-4

Macedonio G, Pareschi MTT (1992) Numerical simulation of some lahars from Mount St. Helens. J Volcanol Geotherm Res 54:65–80. https://doi.org/10.1016/0377-0273(92)90115-T

Naef D, Rickenmann D, Rutschmann P, McArdell BW (2006) Comparison of flow resistance relations for debris flows using a one-dimensional finite element simulation model. Nat Hazards Earth Syst Sci 6:155–165. https://doi.org/10.5194/nhess-6-155-2006

O'Brien JS, Julien PY (1988) Laboratory Analysis of Mudflow Properties. J Hydraul Eng 114:877–887. https://doi.org/10.1061/(ASCE)0733-9429(1988)114:8(877)

Pastor M, Haddad B, Sorbino G, *et al* (2009) A depth-integrated, coupled SPH model for flow-like landslides and related phenomena. Int J Numer Anal Methods Geomech 33:143–172. https://doi.org/10.1002/nag.705

Penman ADM, Brook D, Martin PL, Routh D (2001) Tailings dams. Risk of dangerous occurrences. Lessons learnt from practical experiences. Commission Internationale des UNEP/ICOLD. Grands Barrages – 151, bd Haussmann, 75008 Paris

Pitman EB, Nichita CC, Patra A, *et al* (2003) Computing granular avalanches and landslides. Phys Fluids 15:3638–3646. https://doi.org/https://doi.org/10.1063/1.1614253

Sanz-Ramos M, Blade E, Dolz J, Sánchez-Juny M (2022) Revisiting the Hydraulics of the Aznalcóllar Mine Disaster. Mine Water Environ 41:335–356. https://doi.org/10.1007/s10230-022-00863-w

Sanz-Ramos M, Bladé E, Oller P, Furdada G (2023a) Numerical modelling of dense snow avalanches with a well-balanced scheme based on the 2D shallow water equations. J Glaciol 1–17. https://doi.org/10.1017/jog.2023.48

Sanz-Ramos M, Bladé E, Sánchez-Juny M, Dysarz T (2024a) Extension of Iber for Simulating Non–Newtonian Shallow Flows: Mine-Tailings Spill Propagation Modelling. Water 16:2039. https://doi.org/10.3390/w16142039

Sanz-Ramos M, Bladé E, Silva-Cancino N, *et al* (2023b) A Probabilistic Approach for Off-Stream Reservoir Failure Flood Hazard Assessment. Water 15:2202. https://doi.org/10.3390/w15122202

Sanz-Ramos M, Vales-Bravo JJ, Bladé E, Sánchez-Juny M (2024b) Reconstructing the spill propagation of the Aznalcóllar mine disaster. Mine Water Environ 43:. https://doi.org/10.1007/s10230-024-01000-5

Syarifuddin M, Oishi S, Hapsari RI, Legono D (2018) Empirical model for remote monitoring of rain-triggered lahar at Mount Merapi. J Japan Soc Civ Eng Ser B1 (Hydraulic Eng 74:I_1483-I_1488. https://doi.org/10.2208/jscejhe.74.I_1483

Takahashi T (1985) Debris flow: mechanics and hazard mitigation. In: ROC-JAPAN Joint Seminar on Multiple Hazards Mitigation. National Taiwan Univerisity, Taipei, Taiwan, ROC, pp 1075–1092

Voellmy A (1955) Über die Zerstörungskraft von Lawinen. Schweizerische Bauzeitung 73:15. https://doi.org/10.5169/seals-61891

WISE (2024) Chronology of major tailings dam failures. WISE Uranium Proj. World Inf. Serv. Energy

Wu T, Vuong T, Wang C, *et al* (2020) Model development for simulating mudslide and the case study of the failure of the gypsum tailings dam in East Texas in 1966. 1–24. https://doi.org/10.5194/nhess-2020-126

Can Ecological Engineering Redefine Wetland Recovery in Mining?

Yolandi Schoeman[1,2], Paul Johan Oberholster[1,2]

[1]*Centre for Mineral Biogeochemistry, University of the Free State, P.O. Box 339, Bloemfontein, 9300, South Africa, SchoemanY1@ufs.ac.za (ORCID 0000-0002-5844-059X), OberholsterPJ@ufs.ac.za (0000-0001-5369-4497)*

[2]*Ecological Engineering Institute of Africa, University of the Free State, P.O. Box 339, Bloemfontein, 9300, South Africa*

Abstract

Wetlands altered by mining provide critical services such as water purification, biodiversity support, and flood regulation, yet traditional monitoring tools inadequately capture interactions in these altered ecosystems. This study presents an innovative framework integrating the Ecological Integrity Index and Ecological Engineering Index to assess and guide ecological recovery. Applied at the Leeuspruit wetland near Gold Fields South Deep Gold Mine, the indices identified key areas for intervention. Findings revealed severe degradation, with elevated uranium and Total Dissolved Solid levels. Proposed interventions, including hybrid constructed wetlands and bioremediation, aim to enhance biodiversity and water quality. This framework offers a replicable model for sustainable mining wetland restoration globally.

Keywords: Ecological engineering, wetland restoration, ecosystem health, mining wetlands, sustainability monitoring

Introduction

Mining activities can substantially alter wetland ecosystems, reducing their ability to provide critical services such as water purification, flood regulation, and biodiversity support (Belle *et al.* 2023; Schoeman *et al.* 2025). Traditional monitoring approaches often fail to account for the interactions between natural and engineered systems, hindering effective restoration efforts. Ecological engineering provides a structured framework for addressing these challenges through targeted interventions (Jansen van Vuuren *et al.* 2024).

This study integrates the Ecological Integrity Index (EII), Ecological Engineering Index (EEI), and Ecological Engineering Nexus Accounting Framework (EENAF) to guide wetland recovery strategies. By incorporating financial valuation, the framework demonstrates how ecological improvements can support both environmental sustainability and economic decision-making.

Methods

To develop a comprehensive framework for wetland recovery, a combination of ecological and engineering assessment tools was applied. The approach involves evaluating baseline ecological conditions using the EII and identifying potential improvements through the Ecological Engineering Index EEI. This dual-index system provides a structured pathway for planning and prioritizing interventions based on both ecological and operational needs. The framework is further strengthened by the integration of financial and ecosystem service valuation under the EENAF, allowing stakeholders to link ecological outcomes with long-term sustainability and economic feasibility.

The Ecosystem Condition Index (ECI) is the computational core of the Ecological Integrity Index (EII). While the EII represents the broader conceptual framework that includes metric selection, weighting, and interpretation, the ECI provides the quantitative calculation that produces the final ecological condition score used within the EII.

Ecological Integrity Index (EII)

The Ecological Integrity Index (EII) is a composite assessment tool that evaluates the current ecological state of wetland ecosystems using a weighted metric system. It provides an overall ecological health score by combining scores from key biophysical indicators such as biodiversity, water quality, soil health, and hydrological connectivity.

A key component of the EII is the Ecosystem Condition Index (ECI), which aggregates individual metric scores into a single value using a weighted average approach, as shown in the equation below:

$$ECI = \frac{\sum_{i=1}^{n} Wi \, . Ni}{\sum_{i=1}^{n} Wi}$$

Where:

- N_i is the score for metric i ,
- W_i is the assigned weight for metric i,
- n is the total number of metrics.

To explain further, in this equation, (Ni) refers to the measured score of the ecological metric (i), not to be confused with the number of metrics, which is denoted by (n). This distinction is important to avoid misinterpretation: (Ni) represents the actual ecological condition of a specific parameter (e.g., water quality, biodiversity), while (n) indicates the total number of such parameters included in the calculation.

The EII evaluates the current ecological state of wetland ecosystems by analyzing critical biophysical metrics. Biodiversity is a key indicator, reflecting the ecosystem's resilience and ability to provide services through species richness, keystone species presence, and the effect of invasive species. A diverse biological community supports stability and enhances natural recovery processes. Water quality measures, including uranium concentration, total dissolved solids (TDS), and nutrient loads, indicate pollution levels and inform priorities for remediation efforts. Soil health is assessed via organic matter content and erosion rates, both of which influence nutrient cycling and support for vegetation. Finally, hydrological connectivity measures flow continuity and retention capacity, critical factors for maintaining wetland functionality and mitigating the risks of habitat fragmentation. Together, these metrics guide targeted interventions by identifying areas of vulnerability and potential ecological enhancement.

To clarify for general readers, the Ecological Engineering Index (EEI) uses Normalized Improvement (NI) as its core computational tool. While EEI is a broader decision-making framework evaluating the potential effectiveness of various ecological interventions, NI quantifies how much improvement a specific intervention could produce relative to baseline and target values.

Ecological Engineering Index (EEI)

The Ecological Engineering Index (EEI) is a decision-support tool designed to evaluate the effectiveness of proposed ecological interventions. It builds upon the EII by projecting how each intervention is expected to improve the current ecological metrics. The EEI is guided by ecological engineering principles (Schoeman *et al.* 2025) such as ecosystem connectivity, self-sustainability, energy efficiency, and resilience.

A central part of the EEI is the Normalized Improvement (NI) calculation, which quantifies how much a specific ecological metric is expected to improve due to a given intervention. This allows direct comparison of potential interventions. NI is calculated as follows:

$$NI = \frac{M(post) - M(baseline)}{M(target) - M(baseline)}$$

Where:

- $M_{baseline}$ is the initial condition of the metric,
- M_{post} is the expected value after intervention,
- M_{target} is the defined goal or optimal ecological condition.

NI results are then used within the EEI framework to prioritize interventions based on the degree of projected ecological improvement, adherence to design principles, and practical feasibility.

The EEI (Schoeman & Oberholster, 2024a) assesses the effectiveness of ecological interventions by projecting improvements in key metrics and aligning solutions with core ecological engineering principles. These include ecosystem connectivity, energy efficiency, resilience, and self-sustaining design (Schoeman *et al.* 2025). Constructed wetlands are selected to reduce pollutants and enhance biodiversity through natural processes like sedimentation and microbial uptake. Riparian buffers stabilize soils and support habitat continuity, while bioremediation targets pollutant breakdown using microbial activity. By grounding interventions in these principles, the EEI supports both immediate recovery and long-term ecosystem resilience.

Intervention Design

The intervention design at Leeuspruit was developed based on the EEI, which identified critical ecological deficits in water quality, biodiversity, and hydrological connectivity. Constructed wetlands were recommended to be implemented to reduce elevated uranium and TDS by enhancing natural filtration processes and nutrient cycling. Riparian buffer zones were recommended to be established to stabilize soils, mitigate erosion, and provide habitat corridors to promote biodiversity recovery. Bioremediation techniques were recommended to be applied where microbial processes could degrade pollutants effectively, improving both soil and water quality. These proposed interventions, aligned with ecological engineering principles, can address immediate restoration needs while enhancing long-term ecosystem resilience.

Integration with EENAF

The EENAF (Schoeman & Oberholster, 2024b) provides a structured approach to link ecological recovery efforts with financial and socio-economic outcomes. It achieves this through three key components:

- The Extent and Condition Accounts document changes in wetland area and ecological state, helping stakeholders assess the physical improvements resulting from restoration interventions. This data enables long-term tracking of ecosystem health and capacity for service provision.
- The Service Flow Accounts measure the ongoing performance of ecosystem services such as water purification, carbon sequestration, and flood mitigation. These services are vital for both environmental sustainability and human well-being, providing measurable indicators of ecological functionality.
- Finally, the Monetary Valuation component translates improvements in ecosystem services into economic terms.

This component supports investment decisions, regulatory compliance, and sustainability reporting by assigning financial value to these benefits. This valuation helps stakeholders justify ecological interventions by demonstrating clear returns on investment (ROI), enhancing business cases for continued environmental stewardship and project funding.

Results and Discussion

Interpretation of ECI Scores

To aid interpretation of calculated ECI values, a standardized classification system is used to link ECI with ecological condition categories (Tab.1). These categories reflect levels of ecosystem modification and functionality, ranging from natural (Category A–B) to critically degraded (Category F). This classification is adapted from ecological benchmarking systems such as WET-Health guidelines, and provides a transparent basis

***Table 1** Ecosystem Condition Index (ECI) and EII Score Interpretation.*

ECI Score	EII Category	Interpretation
0.80–1.00	A–B	Natural or near-natural ecosystem
0.60–0.79	C	Slightly modified; functioning mostly intact
0.40–0.59	D	Moderately degraded; impaired but restorable
0.20–0.39	E	Seriously modified; high loss of ecological value
0.00–0.19	F	Critically degraded; ecosystem collapse

Table 2 Baseline conditions and projected improvements.

Key metric	Baseline value	Target value	Projected value	Normalized improvement (%)
Uranium concentration	0.09 mg/L	0.03 mg/L	0.045 mg/L	66.67
Total dissolved solids	950 mg/L	500 mg/L	600 mg/L	70.00
Biodiversity score	0.2	0.8	0.6	75.00
Vegetation coverage	0.4	0.8	0.7	60.00
Hydrological and terrestrial connectivity	0.3	1.0	0.8	83.33

for evaluating the severity of degradation and prioritizing restoration actions.

Baseline Assessment

The EII assessment classified the Leeuspruit wetland as seriously modified (Category E). Key findings include:

- Uranium concentration: 0.09 mg/L, exceeding safe thresholds.
- TDS: 950 mg/L, indicating severe mineral pollution.
- Biodiversity: Dominance of invasive species with reduced native species richness.
- Hydrological connectivity: Disrupted flow patterns due to mining infrastructure.

Projected Outcomes

Tab. 2 summarizes baseline conditions, target goals, and projected improvements based on EEI assessments.

Range and Outcomes for the EEI

The EEI serves as a predictive decision-support tool, guiding the prioritization of ecological engineered interventions based on projected ecological gains. It operates through the NI metric, which evaluates how much improvement an intervention is expected to deliver relative to a desired target. The EEI framework enables stakeholders to assess the effectiveness of proposed ecological engineering solutions, helping to strategically allocate resources. The classification table below outlines the range of EEI/NI scores and their associated outcomes, from highly effective interventions to those with minimal return.

The ecological engineering approach (Fig. 1) applied at Leeuspruit is designed to transform the degraded wetland into a resilient post-mining futures zone. Phased interventions focus on adaptive hydrological modeling and integrated ecological monitoring to ensure long-term functionality. A dual remediation strategy – combining phycoremediation and phytoremediation – is proposed alongside compact hybrid constructed wetlands in key buffer zones. These solutions align with broader sustainability goals by promoting carbon sequestration, biodiversity conservation, and landscape connectivity. With EEI/NI scores ranging from 0.60 to 0.80, the proposed interventions indicate substantial potential for ecological recovery. Additionally, the ability to generate over USD 1.08 million annually from ecosystem services highlights the financial viability of these actions, linking ecological restoration with carbon and biodiversity market opportunities.

Table 3 Ecological Engineering Index (EEI) Score Interpretation.

EEI / NI Score	Projected outcome	Intervention priority
0.80–1.00	High potential for full functional recovery	Highest priority intervention
0.60–0.79	Good improvement expected	Recommended for scaling
0.40–0.59	Moderate improvement	Consider with other options
0.20–0.39	Limited gains	Low return, limited impact
0.00–0.19	Very low effectiveness	Not suitable / low priority

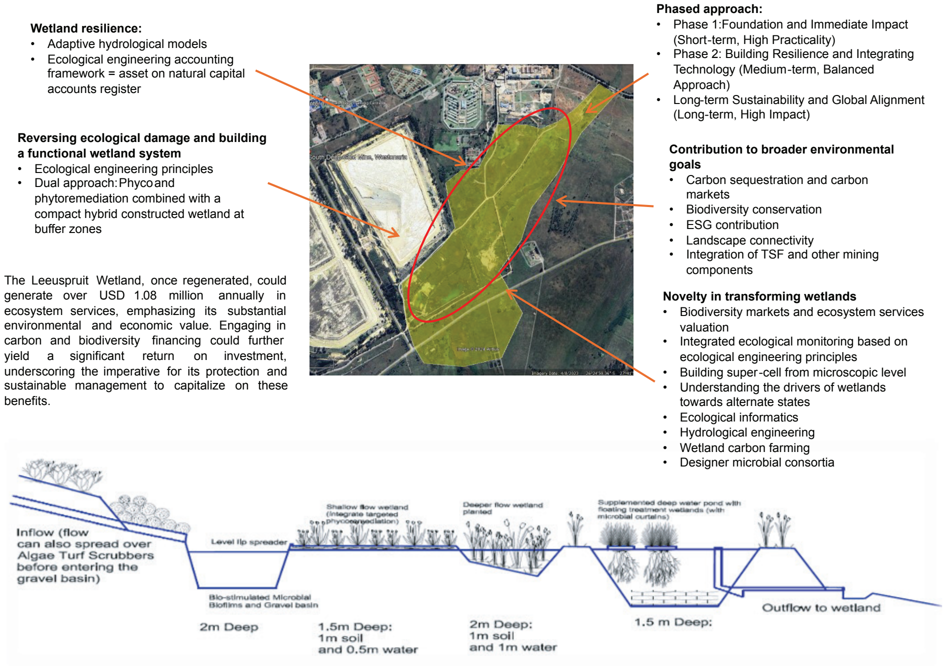

Wetland resilience:
- Adaptive hydrological models
- Ecological engineering accounting framework = asset on natural capital accounts register

Reversing ecological damage and building a functional wetland system
- Ecological engineering principles
- Dual approach: Phyco and phytoremediation combined with a compact hybrid constructed wetland at buffer zones

The Leeuspruit Wetland, once regenerated, could generate over USD 1.08 million annually in ecosystem services, emphasizing its substantial environmental and economic value. Engaging in carbon and biodiversity financing could further yield a significant return on investment, underscoring the imperative for its protection and sustainable management to capitalize on these benefits.

Phased approach:
- Phase 1:Foundation and Immediate Impact (Short-term, High Practicality)
- Phase 2: Building Resilience and Integrating Technology (Medium-term, Balanced Approach)
- Long-term Sustainability and Global Alignment (Long-term, High Impact)

Contribution to broader environmental goals
- Carbon sequestration and carbon markets
- Biodiversity conservation
- ESG contribution
- Landscape connectivity
- Integration of TSF and other mining components

Novelty in transforming wetlands
- Biodiversity markets and ecosystem services valuation
- Integrated ecological monitoring based on ecological engineering principles
- Building super-cell from microscopic level
- Understanding the drivers of wetlands towards alternate states
- Ecological informatics
- Hydrological engineering
- Wetland carbon farming
- Designer microbial consortia

***Figure 1** Ecological engineering approach to redefine wetland recovery (Schoeman & Oberholster, 2024c).*

Financial Valuation and Project Support

The financial evaluation using the EENAF highlights the economic viability of restoring the Leeuspruit wetland. Estimated annual savings include USD 500,000 from reduced water treatment costs, USD 200,000 from erosion control and vegetation recovery, and revenue potential from carbon credits, with approximately 1,200 tonnes of CO_2 equivalent offset annually. Additionally, improved hydrological connectivity is expected to lower flood-related infrastructure maintenance costs. The site also holds the potential for participation in emerging biodiversity credit and market schemes, further enhancing its long-term ecological and financial value. These outcomes present a compelling return on investment (ROI), strengthening the case for funding ecological interventions and positioning mining operations as leaders in sustainability and compliance.

Conclusion

This study demonstrates the potential for integrating the Ecological Integrity Index, Ecological Engineering Index, and Ecological Engineering Nexus Accounting Framework to redefine wetland recovery strategies in mining contexts. By linking ecological and financial metrics, the framework supports both environmental sustainability and economic decision-making.

The Leeuspruit case study highlights that targeted interventions can improve ecosystem functionality while reducing long-term operational risks. This integrated approach provides a replicable model for global wetland recovery in mining-altered landscapes, aligning with sustainability and biodiversity conservation goals.

Future research should explore refining these indices and extending financial valuation models to other ecosystems and industrial contexts.

Acknowledgments

The authors would like to thank Gold Fields South Deep Gold Mine for their support and collaboration in this project.

References

Belle G, Schoeman Y, Oberholster PJ (2023) Potential toxic element pollution in surface water and its implications for aquatic and human health: Source-Pathway-Receptor Model. Water 15:3100. doi:10.3390/w15173100

Jansen van Vuuren M, Schoeman Y, Botha AM, Oberholster PJ (2024) Revealing the protective dynamics of an ecologically engineered wetland against acid mine drainage: A case study in South Africa. Appl Sci 14:7441. doi:10.3390/app14177441

Oberholster PJ, Schoeman Y, Truter JC, Botha AM (2022) Using periphyton assemblage and water quality variables to assess the ecological recovery of an ecologically engineered wetland receiving acid mine drainage before and after a dry spell. Processes 10:1–22. doi:10.3390/pr10010001

Schoeman Y, Erasmus M, Naidoo N, Oberholster PJ (2025) Novel hybrid nature-based solutions for the sustainable treatment of industrial wastewater: alkaline and acid mine drainage. In: Fosso-Kankeu E, Masindi V, Maree J, Mamba B (Eds), Customized technologies for sustainable management of industrial wastewater: Circular economy approach. Scrivener Publishing, p 39–110 (In Press)

Schoeman Y, Oberholster PJ (2024a) Special session presentation: Bridging the gap: Ecological Engineering Index for enhanced monitoring of nature-based and ecologically engineered systems. 25th Waternet/WARFSA/GWP-SA Symposium, 30 Oct–1 Nov 2024, Maseru, Lesotho

Schoeman Y, Oberholster PJ (2024b) Advancing mining sustainability metrics: The Ecological Engineering Nexus Accounting Framework (EENAF). In: Das AP, Van Hullebusch ED, Akcil A (Eds), Sustainable management of mining waste and tailings: A circular economy approach. CRC Press

Schoeman Y, Oberholster PJ (2024c) Pre-feasibility study for optimizing the Leeuspruit wetland area at South Deep Gold Mine. Unpublished Report. UFS:Bloemfontein.

Performance of Pilot-Scale Passive Treatment Tests of a Contact Oxidation Manganese-Oxidizing Bacteria for Manganese-Containing Mine Water

Yuki Semoto[1], Takaya Hamai[1], Yusei Masaki[1], Manami Ikeda[1], Masao Okumura[2], Naoyuki Miyata[2], Tetsuo Yasutaka[3], Taiki Katayama[3]

[1]*Metals Environment Management Department, Japan Organization for Metals and Energy Security, Toranomon 2-10-1, Minato-ku, Tokyo, Japan, semoto-yuki@jogmec.go.jp*

[2]*Department of Biological Environment, Akita Prefectural University, 241–438, Shimoshinjo-Nakano, Akita, Japan*

[3]*Institute for Geo-Resources and Environment, National Institute of Advanced Industrial Science and Technology (AIST), Tsukuba, Ibaraki, Japan*

Abstract

The performance of a pilot-scale passive treatment system consisting of a limestone bioreactor and fiber filter material bioreactor in series and employing a contact oxidation method utilizing Mn-oxidation bacteria was evaluated for neutral mine water containing Mn and Zn over approximately one year of operation. In the limestone bioreactor, the maximum Mn removal rate reached 49.7 g/m^3/day under aeration at water temperatures of approximately 20 °C. Even under low water temperatures of around 5 °C, the average Mn removal rate of the system reached 5.65 g/m^3/day at a hydraulic retention time of 3 days in a limestone bioreactor.

Keywords: Passive treatment, Mn-oxidizing bacteria, Contact oxidating process, Mn removal, Zn removal

Introduction

Passive treatment (PT) has been developed as an alternative to active treatment (AT) for mine water due to the lower treatment costs. For example, for the treatment of mine water containing manganese (Mn), AT typically involves adding alkaline reagents to raise the pH above 9, precipitating Mn as an oxide or hydroxide, and then neutralizing by adding acidic reagents (Deepti *et al*., 2016). In contrast, PT using Mn-oxidizing bacteria (MnOB), which oxidize soluble Mn at circumneutral pH (Bradley *et al*., 2005), offers a more cost-effective approach.

In Japan, mine water treatment is conducted at approximately 100 abandoned mines to meet the domestic discharge standard. However, the reliance on AT results in high operational costs (Ministry of Economy, Trade and Industry, Japan, 2023). At an abandoned mine in Japan, pilot-scale PT tests using a contact oxidation method utilizing MnOB were performed for neutral mine water containing Mn and zinc (Zn), and the effectiveness of Mn and Zn removal was confirmed (Watanabe *et al*., 2024, Tum *et al*., 2024). However, further studies are required to investigate the removal of different concentrations of Mn and Zn.

This study builds upon these findings by evaluating the performance of pilot-scale PT tests at different locations of the same abandoned mine as the above studies for neutral mine water containing higher concentrations of Mn (average 64.1 mg/L) and Zn (average 10.1 mg/L) over an operation period of approximately one year.

Methods

Test site and water profile of the target mine

A pilot-scale PT test was conducted in a test garage in an abandoned mine in a cold Japan region. The annual room temperature

Table 1 Water profile of the target mine.

	pH (-)	Temp. (°C)	Soluble Mn (mg/L)	Soluble Zn (mg/L)	Total Fe (mg/L)	Sulfate (mg/L)
Average	7.18	12.3	64.1	10.1	0.633	370
Maximum	7.79	19.1	78.0	13.0	2.91	441
Minimum	5.83	6.1	53.0	8.0	0.102	300

[1]Temp: temperature; Fe: iron.

ranged from -2 to 30 °C. A portion of the targeted mine water (Table 1) was distributed to a water tank using a pipe in the garage. The system was the same as that in previous reports (Watanabe *et al.*, 2024, Tum *et al.*, 2024) and consisted of two sequential biological processes: a limestone bioreactor (LBR) and a fiber filter material bioreactor (FBR). The system was divided into two parallel test series (X and Y). Mine water first introduced into each LBR (X-1 and Y-1) using an electric pump from the top and the LBR effluents then introduced naturally into each FBR (X-2 and Y-2) from the top.

Pilot-scale test

The LBRs (X-1 and Y-1) and FBRs (X-2 and Y-2) in each series (series X and Y) used the same reactor vessel made of fiber-reinforced plastics measuring 1.6 m wide, 0.97 m long, and 0.75 m deep, with a working volume of 630 L. The surface of each reactor was opened to take atmospheric oxygen. A partition wall was installed at the center of each reactor. Water that was introduced from one side of reactor passed under the partition wall and drained from the opposite side of reactor. The LBRs were filled with 800 kg of limestone (20–40 mm) supplied by Okubo Rozai Co., Ltd., Japan, for pH stabilization. The FBRs were suspended in 400 m polypropylene and vinylon fibers (Biocord PP+K-45, TBR Co., Japan) as inorganic carriers to enhance microbial activity. Pilot-scale PT tests were conducted from September 2023 at mine water flow rates of 30 to 650 mL/min, corresponding to hydraulic retention times (HRT) in the LBR of 0.3 to 7 days. Prior to the test, the LBRs and FBRs were filled with mine water, and a suspension of Mn deposits collected from the mine drainage ditch was inoculated as a source of MnOB. The details of the test conditions are presented in Table 2.

Operating conditions for pilot-scale test

The pilot-scale PT tests were performed in two ways during the Mn removal start-up period: continuous-flow operation (series X) and batch operation (series Y). Under continuous-flow operation, an electric pump was used to continuously pump a specified amount of mine water into the LBR and the HRT was set to the HRT in the LBR. Under batch operation, a large electric pump was used to quickly introduce mine water into the LBR, which remained in the LBR and FBR for a certain period, before repeating the cycle. During batch operation, mine water was introduced at twice the effective volume of the LBR to replace the water inside the LBR and FBR. The residence time of the mine water in the LBR after water replacement was considered as the HRT in the batch operation. After the Mn removal start-up, a continuous-flow operation was performed in series X and Y. The water flow was stopped

Table 2 Test contents of series X and Y.

	Series X		Series Y	
	X-1	X-2	Y-1	Y-2
Media	Limestone	Polypropylene and vinylon fibers	Limestone	Polypropylene and vinylon fibers
Working volume (L)	630	630	630	630
Porosity (%)	45	92	45	92
Effective volume (L)	283.5	579.6	283.5	579.6

from June to early July 2024. An air pump was used to provide aeration from the bottom of the LBRs and FBRs to increase the dissolved oxygen for microbial activity, depending on the conditions.

Monitoring parameters and analytical methods

Temperature, pH, oxidation-reduction potential (ORP, vs. Ag/AgCl), and dissolved oxygen (DO) were monitored using a portable multi-water quality meter (MM-42DP, DKK-TOA Corp., Japan). Un-filtered and filtered (pore size of 0.45 µm) water samples were regularly collected to measure the total and soluble concentrations of Mn and Zn using inductively coupled plasma optical emission spectrometry (ICP-OES; Agilent 5110 ICP-OES, Agilent Technologies Inc., USA). The sulfate concentrations and total organic carbon (TOC) in the filtrates were determined using an ion chromatograph (IC; Dionex ICS-6000, Thermo Fisher Scientific Inc.) and TOC analyzer (TOC-L, Shimadzu Corp.), respectively.

Results and Discussion

Mn removal start-up with continuous-flow operation and batch operation

Pilot-scale PT tests were initiated under continuous-flow operation (series X) and batch operation (series Y) at an HRT of 7 days in the LBR to investigate the differences in Mn removal. The soluble Mn concentration in the effluent of X-1 LBR gradually decreased from the beginning of the operation and fell below Japan's domestic discharge standard of 10 mg/L after four weeks. The soluble Mn removal performance in the effluent of Y-1 LBR was higher than that of X-1 LBR from the beginning of the test and the soluble Mn concentration remained below Japan's domestic discharge standard after 3 weeks. Soluble Zn removal followed the same trend in X-1 and Y-1 LBR. It is assumed that the batch operation maintained a stable bacterial community in the LBR compared to the continuous-flow operation, leading to the faster establishment of sufficient microorganisms. Similar results were reported in laboratory tests by

Figure 1 *Pilot-scale PT test system. Test series: X and Y; X-1 and Y-1: limestone bioreactor (LBR); X-2 and Y-2: fiber filter materials bioreactor (FBR).*

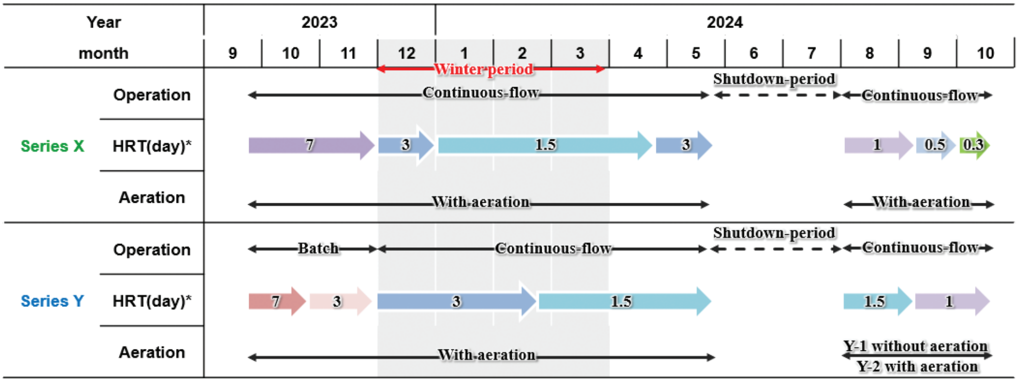

*HRT in the Limestone BioReactor

Figure 2 *Changes under the operating conditions in series X and Y.*

Obey *et al.* (2024), suggesting that batch operation was effective for fast Mn removal start-up, even on a pilot scale. As the test progressed, the limestone surfaces of X-1 and Y-1 LBR gradually became covered with blackish deposits. It is estimated that MnOB acclimated in each LBR over time; soluble Mn was oxidized and deposited as Mn oxides, such as birnessite (δ-MnO¬$_2$); and Zn was adsorbed on the surface of the Mn oxides or coprecipitated Mn oxides containing Zn, such as woodruffite ($ZnMn_3O_7·H_2O$), as reported by Watanabe *et al.* (2024) and Tum *et al.* (2024).

Treatment performance of series X and Y in winter periods

From December 2023 to March 2024, after the Mn removal start-up, water was introduced under continuous-flow operation in series X and Y. From December 2023 to March 2024, series X operated at an HRT of 1.5 days in the X-1 LBR from January 2024 to March 2024, whereas series Y operated at an HRT of 3 days in the Y-1 LBR from December 2023 to February 2024. The water temperature in each period ranged from 2.3 to 6.3 °C (average 4.8 °C) and 1.9 to 6.5 °C (average 4.0 °C) in the effluent of X-1 LBR and X-2 FBR and 1.9 to 6.4 °C (average 4.7 °C) and 6.3 to 0.4 °C (average 3.6 °C) in the effluent of Y-1 LBR and Y-2 FBR, corresponding to changes in room temperature. During the operation of series X during the winter period at an HRT of 1.5 days in the X-1 LBR, the soluble Mn in the effluent of the X-2 FBR remained below 10 mg/L in the early period but dramatically increased after 3 months. This was presumably due to a decrease in microbial activity at lower water temperatures compared to the PT tests in the non-winter periods described below. The maximum Mn removal rate in series X during this period was 9.3 g/m3/day. For series Y during the winter period at an HRT of 3 days in the LBR, the soluble Mn in the effluent of the Y-2 FBR remained below 10 mg/L, with an average Mn removal rate of 5.65 g/m3/day. This suggests that the PT system can function well for the Mn removal below Japan's domestic discharge standard by setting an appropriate Mn loading rate, even under conditions with average water temperatures below 5 °C. The treatment performance of soluble Zn in series X and Y showed the same trend as that of soluble Mn.

Treatment performance of LBR in non-winter periods

Following the water shutdown period from June to early July 2024, the pilot-scale PT tests were resumed in series X and Y from August to October 2024 to investigate the maximum Mn removal rate of the LBR with aeration at an HRT of the X-1 LBR from 0.3 to 1 day and without aeration at an HRT of the Y-1 LBR from 1 to 1.5 days. The water temperatures in the effluent of X-1 and Y-1 LBRs in this period ranged from 18.4 to 21.9 °C and 19.2 to 22.9 °C, respectively, corresponding to changes in room temperature. For X-1 LBR with aeration, the Mn removal rate remained stable up to an Mn loading rate of approximately 30.0 g/m^3/day. However, at higher Mn loading rates, the Mn removal rate gradually decreased. Within the tested HRT of X-1 LBR, a maximum Mn removal rate of 49.7 g/m^3/day was obtained when the Mn loading rate was 94.4 g/m^3/day. Based on the correlation between the Mn removal rate and Mn loading rate, the maximum Mn removal rate for the LBR with aeration is expected to be approximately 50.0 g/m3/day. However, for the Y-1 LBR without aeration, the Mn removal rate increased with the Mn loading rate within the tested HRT, with a maximum Mn removal rate of 27.7 g/m^3/day. Since no noticeable decline in Mn removal was observed relative to the Mn loading rate at HRT in the Y-1 LBR from 1 to 1.5 days, an improved Mn removal rate can be expected in the LBR without aeration. The trends showed that the LBR with or without aeration in this system achieved high Mn removal rates up to Mn loading rates of about 30.0 g/m^3/day under water temperatures of approximately 20 °C.

Conclusions

Pilot-scale PT tests were conducted to treat mine water containing Mn and Zn in an abandoned mine in a cold district in Japan using a contact oxidation method utilizing MnOB. The Mn removal start-up phase in the LBR of the system required approximately four weeks under continuous-flow operation and three weeks under batch operation. Soluble Zn removal followed the same trend as Mn removal. It is estimated that the batch operation maintained a stable bacterial community in the LBR compared to the continuous-flow operation, leading to the faster establishment of sufficient microorganisms. Even at an average water temperature below 5 °C in the winter period, a maximum Mn removal rate of 9.3 g/m^3/day was obtained, with an Mn removal rate of 5.65 g/m^3/day. The results suggest that the system can remove Mn to levels under

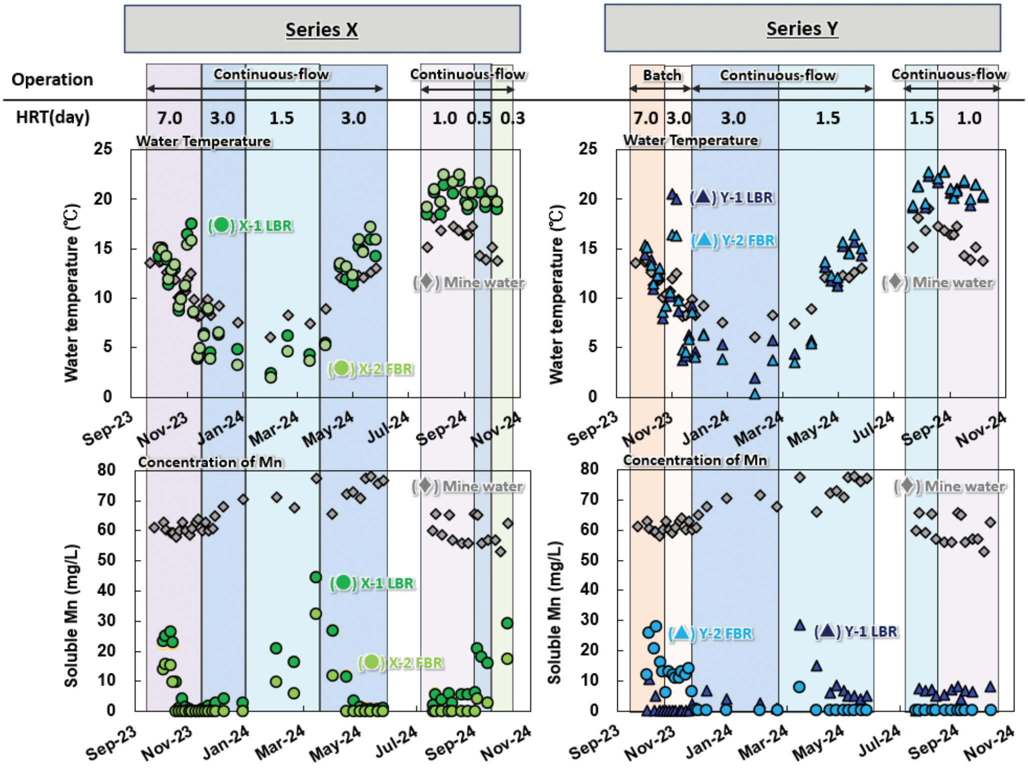

Figure 3 *Changes in water temperature, concentrations of soluble Mn in series X and Y. Grey color: mine water; green color: X-1 LBR; light green color: X-2 FBR; blue color: Y-1 LBR; Light blue color: Y-2 FBR.*

Japan's domestic discharge standards by setting an appropriate Mn loading rate. During the non-winter periods, at an average water temperature of approximately 20 °C, the Mn removal rate in the LBR increased with the Mn loading rate until approximately 30.0 $g/m^3/day$ regardless of aeration. With aeration, the Mn removal rate gradually decreased in the LBR at higher Mn loading rates. The results showed that, regardless of aeration, the LBR in the system achieves high Mn removal rates up to Mn loading rates of about 30.0 $g/m^3/day$ under water temperatures of 20 °C. Future PT tests will investigate the maximum Mn loading rate in FBR and evaluate the long-term treatability and maintainability of the system.

Acknowledgements

This study was funded by Ministry of Economy, Trade, and Industry, Japan (METI) under the research project on Advanced Technology for Mine Drainage Treatment in Closed Mines for the year 2023 and 2024. The funders had no role in the study design, data collection, data analysis, or decision to publish.

References

Ministry of Economy, Trade and Industry, Central Mine Safety Committee in Japan. “Mine pollution control.” https://www.meti.go.jp/policy/safety_security/industrial_safety/sangyo/mine/2017_newpage/kogaiboshi.html, 22 July 2023

Deepti S. Patil, Sanjay M. Chavan, John U. Kennedy Oubagaranadin. (2016). A review of technologies for manganese removal from wastewaters, Journal of Environmental Chemical Engineering. 4(1), 468-487

Bradley M. Tebo, Hope A. Johnson, James K. McCarthy, Alexis S. (2005). Templeton, Geomicrobiology of manganese(II) oxidation, Trends in Microbiology. 13(9), 421–428,

Watanabe Miho, Tum Sereyroith, Katayama Taiki, Gotore Obey, Okano Kunihiro, Matsumoto Shinji, Yasutaka Tetsuo, Miyata Naoyuki. (2024). Accelerated manganese(II) removal by in situ mine drainage treatment system without organic substrate amendment: Metagenomic insights into chemolithoautotrophic manganese oxidation via extracellular electron transfer. Journal of Environmental Chemical Engineering. 12, 113314. 10.1016/j.jece.2024.113314.

Gotore Obey, Watanabe Miho, Okano Kunihiro, Miyata Naoyuki, Katayama Taiki, Yasutaka Tetsuo, Semoto Yuki, Hamai Takaya. (2024). Effects of batch and continuous-flow operation on biotreatment of Mn(II)-containing mine drainage. Journal of Environmental Sciences. 152. 10.1016/j.jes.2024.05.038.

Tum Sereyroith, Katayama Taiki, Miyata Naoyuki, Watanabe Miho, Hashimoto Yohey, Nishikata Miu, Yasutaka Tetsuo. (2024). Geochemical insights and model optimisation for pilot-scale passive treatment of manganese and zinc in a legacy mine in Japan. Heliyon. 10. e40363. 10.1016/j.heliyon.2024.e40363.

The Evaluation of a Pilot Pervious Concrete Treatment System for Acid Mine Drainage Treatment

Ayanda Shabalala[1], Monica Ngomane[2], Nokuthula Khanyile[3]

[1] *University of Mpumalanga, School of Biology and Environmental Sciences, Mbombela, South Africa, 1200*
Ayanda.shabalala@ump.ac.za, ORCID 0000-0002-3539-2943

[2] *University of Mpumalanga, School of Biology and Environmental Sciences, Mbombela, South Africa, 1200*
201757281@ump.ac.za, ORCID 0000-0003-3205-273X

[3] *University of Mpumalanga, Faculty of Agriculture and Natural Sciences, Mbombela, South Africa, 1200*
nokuthula.khanyile@ump.ac.za, ORCID 0000-0002-9647-9006

Abstract

The high costs involved in Acid Mine Drainage (AMD) remediation have led to a search for low-cost liming alternatives. A pervious concrete (PERVC) reactive barrier system was designed and evaluated for the remediation of AMD at an abandoned coal mine site. The results showed that following treatment with PERVC, the pH increased from 2.6 to 12. Al, Fe, Zn, Ni, Co, Cu, and Mn were effectively removed from the mine water with efficiency levels of 97% to 100%. PERVC offers alternative technology for polluted mine waters that can be marketed to the mining industry for full-scale implementation.

Keywords: Acid mine drainage, contaminant removal, low-cost technology, pervious concrete, pilot study

Introduction

The United Nations recently recognized AMD as the second most critical global issue after climate change, emphasizing the severity of this environmental challenge (Daraz *et al.*, 2023). The primary indicator of AMD contamination in surface water bodies is low pH and high sulfate and metal loading (Kefeni *et al.*, 2015). Most existing AMD treatment regimens make use of active treatment methods. However, these are expensive, generate large amounts of toxic sludge, require a continuous supply of chemicals and substantial energy for production (Seervi *et al.*, 2017; Turingan *et al.*, 2022). Consequently, while addressing AMD, active treatment methods introduce new pollution, rendering them highly unsustainable for environmental management (Yang *et al.*, 2023). Therefore, greater emphasis should be placed on finding the most effective, cost-efficient, and simple methods for successfully treating AMD.

Recent approaches emphasize the use of raw or natural materials to treat AMD, a strategy that is expected to promote greener and more sustainable treatment solutions, such as the use of porous pavements. Porous pavements or pervious concrete (PERVC) have demonstrated high efficiency in the containment of runoff and the reduction of stormwater accumulation in urban areas. They have also been shown to be good pollution sinks owing to their high particle retention capacity. Since porous pavement has minimal environmental impact, the US Environmental Protection Agency (EPA) has endorsed its use for water purification (Lee *et al.*, 2022). PERVC, which is a mixture of granite stone or gravel, cement, little to no sand, and water, has been shown to be highly effective in filtering out metallic micro-pollutants from runoff water. Correctly built PERVC may effectively treat polluted or acidic water by eliminating most of the undesired impurities such as sulfate, Fe, Zn, salt, Mg, Mn, and most other metals, in addition to raising the pH value (Shabalala *et al.*, 2017; Dash and Kar, 2018; Shabalala and Ekolu, 2019). While PERVC has proven to be an effective solution for AMD in controlled laboratory settings, its efficacy in field-scale or pilot studies remains unexplored. The aim of the study was to design and evaluate the application of a PERVC permeable barrier system for the remediation of AMD at an abandoned coal mine site. Furthermore, the study aimed to show that PERVC can effectively treat polluted mine water to meet the national limits applicable to wastewater discharge into a water resource.

Methods

Materials and sample preparation

The concrete mixture was prepared using Ordinary Portland Cement (CEM I 52.5R), 9.5 mm granite aggregates, and Ground granulated blast furnace slag (GGBS). The commercially available South African Portland cement (52.5 R) and GGBS (50 kg) products were purchased from Pretoria Portland Cement Company and AfriSam Ltd, respectively. Before use, the Portland cement and GGBS were milled and sieved until the maximum particle diameter was <90 µm. To achieve optimum porosity, a water-to-cement ratio of 0.27 was used for all mixes. The dry ingredients were mixed for one minute in a 400 L concrete mixer, then water was gradually added and mixed for another minute. Chryso Fluid Premia 310 superplasticizer was added for workability.

Pervious concrete reactive barrier design and installation

A pilot study to evaluate the potential application of PERVC-PRB for the remediation of acid mine drainage was installed at an abandoned coal mine site at Emalahleni, a town located in Mpumalanga, South Africa. The pilot plant consisted of a pre-treatment zone (PTZ) overlying a PERVC reactive barrier zone, as shown in Fig. 1. The dimensions of the PTZ were 7m long, 0.6 m wide, and 0.5m deep. From the PTZ compartment, the AMD seeped into the pervious concrete reactive barrier, which was 7 m long, 1.8 m wide, and 1 m deep. The AMD delivery system consisted of one elevated 2000L tank connected to a pipe system through which the acidic mine water was continuously injected into the gravel layer at a flow rate of 50 ml/min, ultimately through the pervious concrete reactive zone. The performance of the PERVC system was monitored for 180 days. The system was completely passive as all flows relied on gravity, with no need for pumps or electrical components. This also added to the ease of maintenance of the plant.

Analytical methods

The raw and treated AMD samples were analysed for Al, Fe, Zn, Mn, Na, Mg, K, Ca, Mn, Fe, Co, Ni, and Cu using the Perkin Elmer SCIEX (Concord, Ontario, Canada) ELAN 6000 inductively coupled plasma mass spectrometer to accuracy of 0.01 mg/L. The concentration of sulfate was determined using ion chromatography, Dionex QIC-IC (Thermo Fisher Scientific, Massachusetts, USA). Measurement of pH, electrical conductivity and total dissolved solids was conducted using the MP-103 microprocessor-based pH/mV/Temp tester. The mineralogical, and microstructural properties of pervious concrete before and after coming into contact with the AMD were determined using the Pan Analytical X-ray X'pert PRO PW3830 diffractometer (Malvern Panalytical Ltd., Malvern, UK) and the Scanning Electron Microscopy (SEM) coupled with Electron Dispersion Spectroscopy (EDS), TESCAN VEGA3SEM with AZtec EDS (Tescan Orsay Holding, Brno, Czech Republic). Mine tailings and product solids were oven-dried at 50 °C for 24 hours before characterization. Portland cement and pervious concrete samples (0.08 g each) were vacuum-dried, carbon-coated for 30 minutes, and mounted on carbon tape affixed to an aluminum stub for SEM-EDS analysis.

Results and Discussion

The pH of the raw AMD was 2.6, while its composition showed high concentrations of Fe (199 mg/L), Al (73 mg/L), Mn (17 mg/L), and SO_4 (1124 mg/L). Fig. 2a presents the pH results of treated AMD water samples versus time. Upon contact with pervious concrete, the pH value of the untreated AMD increased rapidly from 2.6 and reached a pH value of 11.72 within 24 hours. The pH of the treated mine water remained high throughout the 180 days of treatment being reported. The neutralising capacity of PERVC is attributed to the large quantity of portlandite phase which adds alkalinity to the solution. (Song

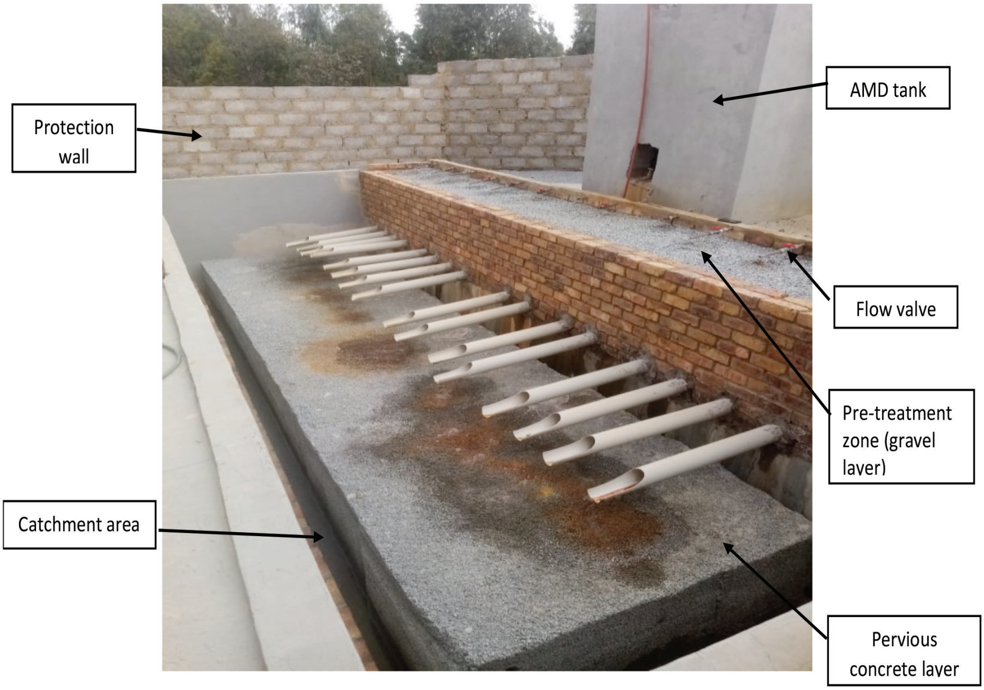

Figure 1 Pervious concrete reactive barrier system.

et al., 2021). Fig. 2b gives the change in concentration of Al, Fe and Mn in the mine water after treatment with pervious concrete. Most of the Al, Fe and Mn contained in the AMD precipitated rapidly out of solution due to the formation of Al $(OH)_3$, $Fe(OH)_3$ and $Mn(OH)_2$, respectively. Aluminium in mine water was reduced from 73 mg/l to 0.112 mg/L. The iron concentration in acidic water decreased from 199 mg/l to 0.051 mg/L, which is below the national limits applicable to the discharge of wastewater into a water resource (NWA, 1999). The Fe (III) in AMD may form iron (III) hydroxide ($Fe(OH)_3$) and Hematite (Fe_2O_3) during the treatment, which results in iron removal. Mn was reduced from 17 mg/L to below the detection limit (<0.025 mg/L). Cu, Co, and Ni concentrations in raw AMD were generally low and decreased to undetectable levels after pervious concrete treatment (Fig. 2c). The concentrations of Al, Fe, Mn, Zn, Cu, Co, and Ni decreased as the pH of the solution increased. Precipitation of metal hydroxides and oxides may explain the observed reductions in concentrations of these contaminants. Ni, Cu, and Zn may have precipitated as $Ni(OH)_2$, $Cu(OH)_2$, and $Zn(OH)_2$, respectively. The removal of cobalt is probably due to its adsorption / co-precipitation upon or with iron and aluminium hydroxides and hydrosulfate. At pH values between 8 and 9, Ni is adsorbed onto calcite in solution (Kefeni *et al.*, 2015). An increase in Cu, Co, Ni, and Zn concentrations is observed after day 60 of the experiment. This may be attributed to the seasonal transition from a wet summer to dry winter months, which are characterised by reduced water flow and decreased metal dilution, potentially leading to higher pollutant concentrations. However, the concentration of these metals remained below detection for the 180 days of treatment being reported. After 180 days of running the treatment plant, the concentration of SO_4 had been reduced from 1124 mg/L to 339 mg/L (Fig. 2d). This was possibly caused by the release of calcium ions due to the dissolution of portlandite in concrete, which was then followed by the formation of gypsum ($CaSO_4.2H_2O$). At pH above 3.75, gypsum precipitates out of solution, which results in the removal of sulfate from the acidic water (Chatla *et al.*, 2023). The high neutralising ability of pervious concrete resulted in 69.8% removal of the sulfate content in the raw AMD. Laboratory column studies have indicated that the PERVC barrier has about twice the lifespan of the commonly used ZVI barrier. The minimum expected lifespan of the PERVC treatment system is 10 years (Ekolu & Katadi, 2018).

Removal efficiency

At day 180, pervious concrete effectively removed Al, Fe, Zn, Ni, Co, Cu and Mn with efficiency levels of 97% to 100%. It is clear from Table 1 that the major metals present in AMD were completely removed or reduced to negligible concentrations following treatment with pervious concrete. The concentrations of these metals remained low or below detection during the 180 days of the treatment with PERVC.

Characterization of the pervious concrete before and after exposure to the AMD

The XRD analysis of reacted pervious concrete shows a massive formation of gypsum and close mixtures of gypsum, sodium sulfate and iron oxide (Fig. 3a). These inter-mixtures seem to be metal precipitate complexes from AMD, possibly adsorbed by gypsum. The microstructural feature of concrete after exposure to AMD is seen in Fig. 3b and 3c, and it indicates the presence of an intermixture of alkali metals such as Na, Al, K, Mg, Ca and Si. These observations show that the precipitation of metals with an increase in pH, along with their possible adsorption onto calcium silicate hydrate, are the main mechanisms for metal removal by pervious concrete.

Conclusions

After 180 days of treatment of the AMD with pervious concrete, the levels of Al, Fe, Mn, Co, Cu, Ni, Co, Cu and SO_4 were reduced to limits below the NWA criteria for discharge of wastewater into the environment. The metal removal efficiency levels for Al, Fe, Mn, Zn, Cu, Co and Ni were 99.9%, 99.9%, 99.0%, 97.5%, 97.1%, and 98.2%, respectively, while 69.8% of SO_4 was removed. These findings indicate that pervious concrete technology is effective in treating mine water. However, the pH levels of the treated mine water exceeded the maximum permissible range of 5.5 to 9.0 for

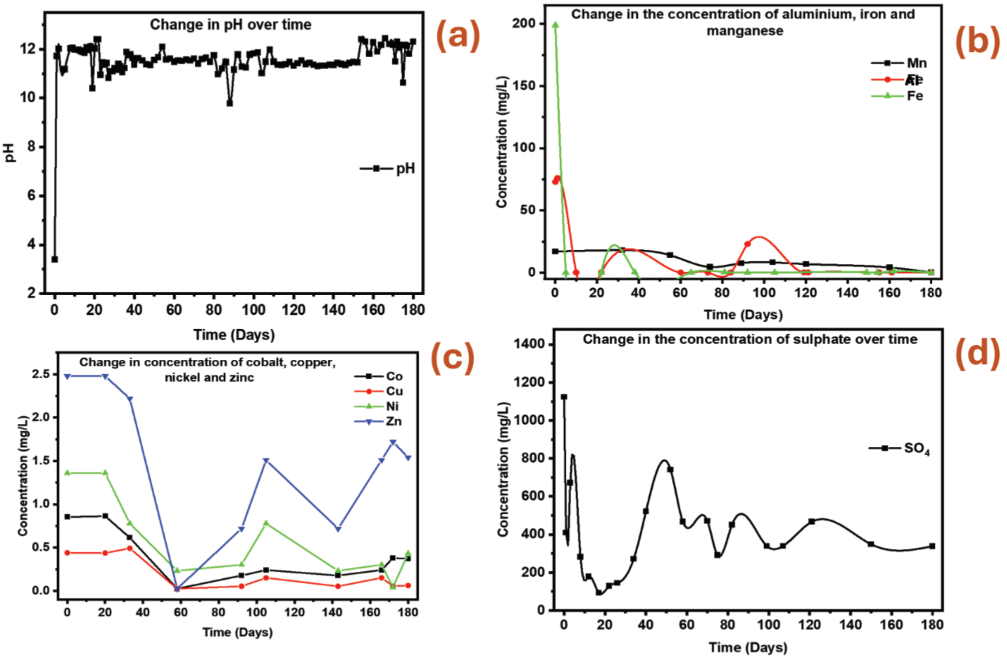

***Figure 2** Change in the pH and the concentrations of Mn, Al, Fe, Co, Cu, Ni, Zn and SO_4 with time.*

Table 1 Contaminant removal efficiency levels of pervious concrete.

	Contaminant Removal Efficiency							
Day	Al (%)	Fe (%)	Mn (%)	SO_4 (%)	Ni (%)	Co (%)	Cu (%)	Zn (%)
33	50.7	99.5	17.7	-10.9	42.8	28.0	-11.8	10.5
105	68.5	99.9	68.2	63.5	42.8	72.0	65.9	39.1
143	69.9	99.9	89.4	54.1	82.9	79.3	88.0	71.1
180	99.9	99.9	99.9	69.8	98.2	97.1	97.5	99.0

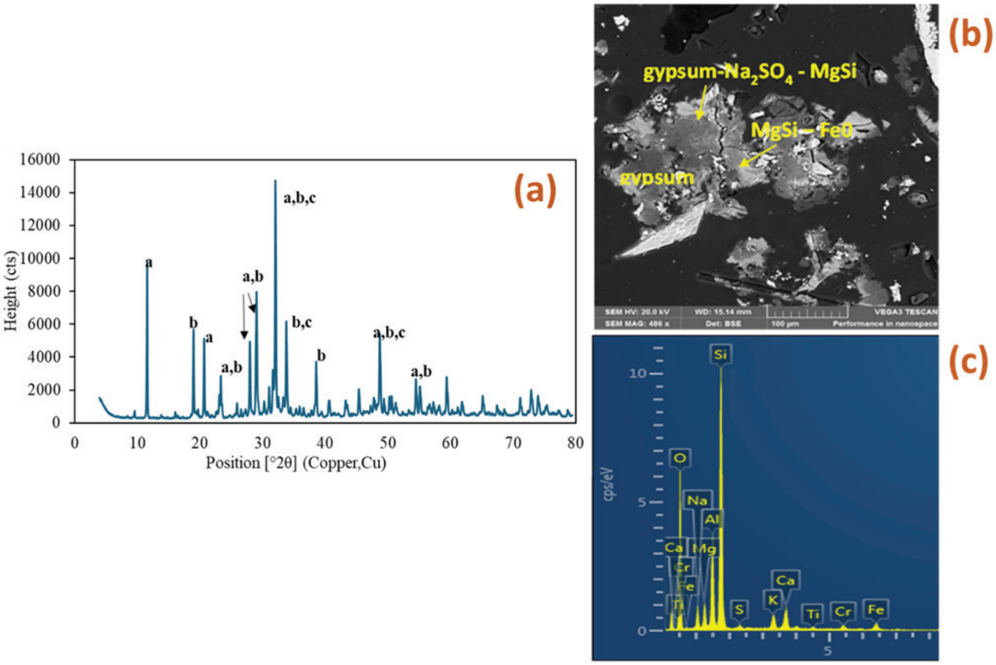

Figure 3 *XRD patterns of pervious concrete after exposure to AMD: (a) XRD analysis of residues from: a - gypsum ($CaSO_4{\cdot}2H_2O$); b - Thernadite (Na_2SO_4); c- calcite; (b) and (c) SEM examination of pervious concretes after 180 days of use in acid mine drainage treatment.*

the discharge of pollutants to a water resource. Further improvement of the treatment system is required to enable attenuation of the high alkalinity in the treated water.

Acknowledgements

The research work presented in this paper was financially supported by the National Research Foundation (NRF) of South Africa, Grant No. 138409, Water Research Commission (WRC), project No. WRC 2020/2021-0021 and the University of Mpumalanga (UMP). The authors are grateful for the support given by NRF, WRC and UMP.

References

Chatla A, Almanassra IW, Abushawish A, Laoui T, Alawadhi H, Atieh MA, Ghaffour N (2023) Sulphate removal from aqueous solutions: State-of-the-art technologies and future research trends. Desalination 558:116615.

Dash S, Kar B (2018) Environmental Friendly Pervious Concrete for Sustainable Construction. IOP Conference Series. Mater Sci Eng 410: 012005

Daraz U., Yang L, Iftikhar A., Iqbal R., Ditta A (2023) Remediation technologies for acid mine drainage: Recent trends and future perspective. Chemosphere 311: 137089.

Ekolu SO, Katadi BL (2018) Prediction of longevities of ZVI and pervious concrete reactive barriers using the transport simulation model. J Environ Eng 144(9).

Kefeni KK, Msagati TM, Maree JP, Mamba BB (2015) Metals and sulphate removal from acid mine drainage in two steps via ferrite sludge and barium sulphate formation. Miner. Eng. 81:79-87.

Lee MG, Wang WC, Wang YC, Hsieh YC, Lin YC (2022) Mechanical properties of high-strength pervious concrete with steel fiber or glass fiber. Buildings 12(5):620. doi.org/10.3390/buildings12050620

National Water Act (1999) Discharge limits and conditions set out in the National Water Act, Government Gazette No. 20526, 8 October. Department of Water Affairs (DWA), Pretoria, South Africa.

Shabalala AN, Ekolu SO, Diop S, Solomon F (2017) Pervious concrete reactive barrier for removal of heavy metals from acid mine drainage – column study. J Hazard Mater 323: 641 - 653.

Shabalala AN, Ekolu SO (2019). Assessment of the Suitability of Mine Water Treated with Pervious Concrete for Irrigation Use. Mine Water Environ 38:798-807.

Seervi V, Yadav HL, Srivastav SK, Jamal A (2017) Overview of active and passive systems for treating acid mine drainage. Int Adv Res J Sci Eng Technol 4 (5):131 – 137.

Song J, Huang G, Han D, Hou Q, Gan L, Zhang M (2021) A review of reactive media within permeable reactive barriers for the removal of heavy metal(loid)s in groundwater: Current status and future prospects. J Clean Prod. Volume 319: 128644.

Turingan COA, Cordero KS, Santos AL, Tan GSL, Tabelin CB, Alloro RD, Orbecido AH (2022) Acid Mine Drainage Treatment Using a Process Train with Laterite Mine Waste, and Limestone as Treatment Media. Water 14(7):1070.

Yang Y, Li B, Li T, Liu P, Zhang B, Che L (2023) A review of treatment technologies for acid mine drainage and sustainability assessment. J Water Process Eng 55(4):104213.

Release of Uranium from a Former Iron Mine, 30 Years after Flooding

Viktor Sjöberg[1,2], Bert Allard[1,2]

[1]Remedy by Sweden AB, Libergsgatan 6, SE-632 21 Eskilstuna, Sweden
[2]Örebro University, Man-Technology-Environment, SE-701 82 Örebro, Sweden,
viktor.sjoberg@oru.se, bert.allard@oru.se

Abstract

The Stripa mine, located in Bergslagen, Sweden operated from the Middle Ages until 1977 and later served as a research facility for SKB until 1991, after which it was flooded. Recent studies show a notable increase in uranium concentrations in the mine water, reaching nearly 1 mg/L at 200 m depth, compared to historical levels of 10 µg/L. This increase is linked to uranium(IV) oxidation by elevated dissolved oxygen. Further research should investigate key biogeochemical processes controlling uranium transport and long-term environmental persistence. The findings highlight regional environmental risks, including potential contamination of wells, emphasizing the mine's long-term environmental impact.

Keywords: Uranium, mine water, environmental impact, biogeochemical processes, environmental risks

Introduction

The Stripa mine, situated in Bergslagen in the Guldsmedshyttan region, Sweden (59.70617, 15.09578) has a long history of iron ore extraction dating back to the 1400s (Willim 2008). Mining operations ceased in 1977, leaving behind a 490-meter-deep mine. The mine was subsequently repurposed by the Swedish Nuclear Fuel and Waste Management Company (SKB) as a research facility until 1991. During this period, extensive hydrogeological studies were conducted with a focus on groundwater flow, radionuclide transport, and engineered barriers for nuclear waste isolation in granitic rock (Nordstrom *et al*. 1989, Waber & Nordstrom 1992). This has provided some fundamental knowledge on solute transport in fractured crystalline rock, highly relevant to the present study. After the research concluded, the mine was flooded, leading to clear hydrogeochemical changes, and the surface facilities were used for industrial purposes (Eriksson & Larsson 2007). In 2006, the remaining structures were declared buildings of historical value, preserving their industrial heritage (Willim 2008).

The mine's geological setting features uranium-rich granitic bedrock, interspersed with hematite, magnetite, and quartz. Historical investigations in the 1950s identified uranium mineralization, particularly pitchblende at the 350-meter level. Compared to other regional rock is the content of uranium in the Stripa mine clearly elevated (Tab. 1) (as cited in: Allard, Sjöberg, Karlsson 2017). Recent water quality assessments and geochemical modeling have indicated changes in uranium concentrations and speciation, warranting further evaluation of the mine's environmental impact.

***Table 1** Abundance of uranium in regional bedrock and in the Stripa mine.*

Bedrock	Regional, granite	Regional, metamorphic	Stripa, shallow	Stripa, deep	Stripa, 107 m	Stripa, 408-456 m	Stripa, 760 m
Uranium (g/ton)	18+15	6+1	27+6	37+6	32	31	35

The key objective of this study is to synthesize historical data and data from recent sampling in an attempt to further characterize the mine-water and understand its potential environmental impact on the surroundings upon release from the mine.

Methods

Sampling and Analysis

Water samples were collected during multiple campaigns, including those conducted in 2017 and earlier SKB-led studies from 1979 to 1986. Samples were obtained from streams near the site, the mine shaft overflow, and within the mine shaft itself down to a depth of 200 meters (Fig. 1). Analyses included measurements of pH, dissolved oxygen, metal concentrations, and anions. Advanced methods, such as inductively coupled plasma mass spectrometry (ICP-MS), were used for uranium quantification.

Geochemical Modeling

Geochemical modeling using Visual Minteq was conducted to determine uranium speciation in the mine water. The model incorporated measured concentrations of dissolved oxygen, carbonate, and other geochemical parameters. It predicted the dominant uranium species in both the shaft water and discharge water, providing insights into uranium mobility under current conditions.

Results and Discussion

Hydrogeological Characteristics

The mine's groundwater can be categorized into three distinct types based on historical data (1979–1986) (cf. Fritz, Barker & Gale 1979, Nordström 1983, Gale *et al.* 1987):

1. Shallow Oxic Water: Shows influence from surface water, with low salinity and pH 5–7.

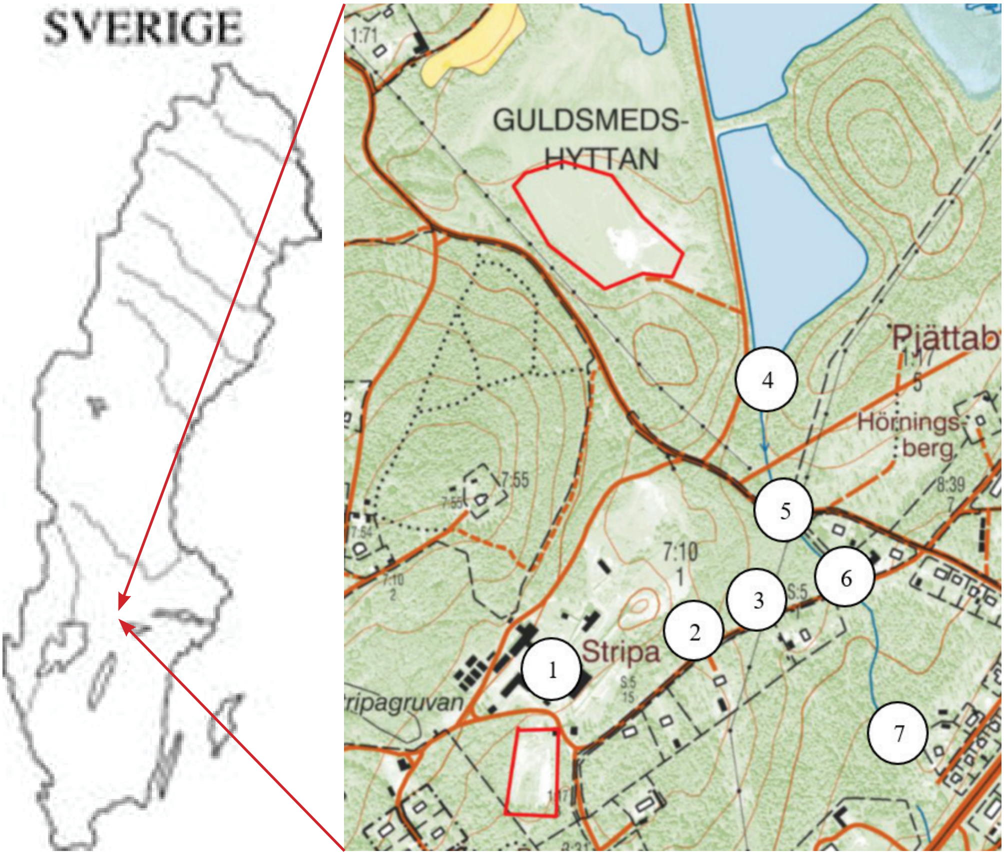

Figure 1 *Map over sampling locations. The old mine site is located in mid/southern Sweden, some 170 km west of Stockholm.*

Table 2 Groundwater composition, historical (pre-1991) and recent (2017) data.

	Year	pH (range)	Na^+	K^+	Mg^{2+}	Ca^{2+}	Cl^-	SO_4^{2-}	HCO_3^-	SiO_2
Shallow	Pre-1991	5.2-8.1	5.7	1.7	3.8	16.3	4.6	10.9	68.1	10.9
Intermediate	Pre-1991	8.6-9.2	46.2	0.2	0.2	19.1	56.3	2.7	72.7	11.2
Deep	Pre-1991	9.3-10.1	224	0.7	0.1	125	513	71.5	12.2	13.7
0–200m	2017	7.4-7.5	18.2	2.2	9.2	55.2	24.7	27.3	189	4.4

2. Intermediate Anoxic Water: Exhibits Ca-HCO3 composition, low salinity, and pH 7–8.
3. Deep Anoxic Water: Characterized by Na-Ca-Cl composition, high salinity, and pH >9. The water is 8,000–30,000 years old and unaffected by modern surface water infiltration.

In 2017, shifts were observed in groundwater composition (mg/L, Tab. 2). Elevated concentrations of K, Mg, Ca, HCO_3, Cl, and SO_4 were detected, with a reduction in depth-dependent gradients. This suggests mixing of shallow and deeper waters in the mine shaft.

Uranium Dynamics

Recent measurements reveal a dramatic increase in uranium concentrations, reaching nearly 1 mg/L at 200 m depth. This marks a tenfold increase from historical averages. Dissolved oxygen levels were measured at 37.2% saturation at 15 m depth, 23.1% at 200 m, and 87.7% in the discharge water, indicating mixing with surface water. The oxidation of uranium(IV) to uranium(VI) appears to be the primary driver of elevated uranium levels. This process is facilitated by the mine's transition from anoxic to oxic conditions. Geochemical modeling confirms that uranium exists predominantly as carbonate complexes in the mine water, with carbonate complexes being the dominant species (Tab. 3).

The dominance of carbonate complexes highlights the role of elevated carbonate levels in enhancing uranium mobility and solubility. Historical uranium concentrations ranged from 1 to 10 µg/L, peaking at 90 µg/L in oxic waters collected in drillholes in the mine as well as private wells (PW1–5) within 2 km radii from the mine shaft. , while current concentrations exceed 900 µg/L due to these geochemical shifts (Tab. 4).

Environmental Risks

Elevated uranium concentrations pose potential risks to the surrounding environment. While uranium levels in streams and surface waters remain within acceptable limits (Tab. 5), the potential contamination of private wells in the vicinity is concerning. With the estimated flow out of the mine the input of uranium to the downstream recipient is in the range of 10 to 100 kg of uranium annually. Further studies are required to evaluate the extent of uranium mobility and its environmental impact on regional water quality.

Table 3 Uranium speciation in shaft and discharge water.

Species	% in shaft surface water	% in discharge water
$Ca_2UO_2(CO_3)_3$ (aq)	68.0	60.4
$CaUO_2(CO_3)_3^{-2}$	28.7	28.7
$UO_2(CO3)_2$-2	1.59	4.16
$(UO_2)_2CO_3(OH)_3^-$	0.85	3.03
UO_2CO_3 (aq)	0.50	3.06
$UO_2(CO_3)_3^{-4}$	0.33	0.34
$UO_2(OH)_2$ (aq)	0.04	0.18
UO_2OH^+	0.02	0.12
$UO_2(OH)_3^-$	0	0.02

Table 4 Historical (pre-1991) (as compiled in Allard, Sjöberg, Karlsson 2017) and recent (2017) concentrations of uranium in groundwater, in and around the mine according to depth.

			Uranium (µg/L)	
	Year	Depth (m)	Average range	Maximum
PW1–5	pre-1986	40–60	0.8–8	90
Mine	1986–91	0–80	n.d.	90
Mine	1986–91	89–104	0.8–11	n.d.
Mine shaft	2017	0–200	929–987	n.d.
M3	pre-1986	336–350	8–11	12
E1	pre-1986	357–385	2–10	13
N1	pre-1986	357–401	1–2	9
V1	pre-1986	449–863	0.1–2	35
mine	1986–91	765–861	0.1–2	n.d.
mine	1986–91	908–969	0.1–0.8	n.d.
V2	pre-1986	792–1232	<0.1–0.8	8

Recommendations

To address the environmental risks associated with the Stripa mine, several immediate actions and future research initiatives are recommended. First, it is essential to establish a long-term groundwater monitoring program that focuses on tracking uranium concentrations, dissolved oxygen levels, and other key parameters. This will provide critical data to assess ongoing changes in water quality and potential contamination risks. Additionally, raising public awareness is crucial; local communities should be informed about the potential risks associated with using private wells near the mine site to ensure they can take necessary precautions.

Looking ahead, further research is needed to better understand and mitigate the environmental impact of uranium contamination. One key area of study is the biogeochemical processes driving uranium mobility in the mine's groundwater, which will help clarify the mechanisms controlling its transport and persistence. Moreover, it is important to assess the feasibility of in situ remediation techniques, such as reactive barriers, to limit uranium release and prevent further environmental impact. Lastly, comprehensive sediment and biota studies should be conducted to evaluate the ecological consequences of uranium contamination in downstream environments, ensuring that the long-term effects on aquatic ecosystems are well understood and properly managed.

Conclusion

The Stripa mine presents a unique case study in the long-term environmental impacts of flooded mines in granitic rock. While historical operations and recent research activities have provided valuable insights, the recent rise in uranium concentrations underscores the need for ongoing monitoring and targeted remediation. Geochemical modeling indicates that carbonate complexes dominate uranium speciation, contributing

Table 5 Average concentration of uranium, pH and electrical conductivity (EC) in sampling points, in (1) and around the mine (2–7) according to Fig. 1.

	1	2	3	4	5	6	7
	mine		downstream	creek			
	shaft	discharge	discharge	upstream		mixing point	downstream
Uranium (µg/L)	966	227	266	5.7	4.9	9.4	6
pH	7.44	7.15	7.39	6.48	6.91	6.92	7.24
EC (µS/cm)	370	235	253	88.2	88.2	88.8	94.2

to its mobility. Collaborative efforts between researchers, local authorities, and the community will be essential in ensuring the site's safe integration into the surrounding region while preserving its historical and industrial significance.

Acknowledgements

The authors want to thank personal from Lindesbergs Kommun and Structor Miljöteknik AB for granting access to the mine site and for help during sampling campaigns.

References

Nordstrom DK, Ball JW, Donahoe RJ, Whittemore D (1989) Groundwater chemistry and water-rock interactions at Stripa. Geochim Cosmochim Acta 53:1727–1740

Allard B, Sjöberg V, Karlsson S (2017) Groundwater and surface water from Stripa. Water quality in the mine and outflow of metals from the premises. RBS 17-06 R, Remedy by Sweden AB

Eriksson I & Larsson P (2007) Stripa gruva, Översiktlig miljöteknisk markundersökning, 29pp, Internal Report 6242-001, Structor Miljöteknik AB

Willim A (2008). Stripa – från järnmalmsgruva till industriminne. Geoarchaeological Research Report. UV Uppsala rapport 2008:12

Fritz P, Barker JF, Gale JE (1979) Geochemistry and isotope hydrology of groundwaters in the Stripa granite. Results and preliminary interpretations. Swedish-American Coopertive Program on Radioactive Waste Storage in Mined Caverns in Crystalline Rock. Earth & Environmental Sci. Stripa Reports 1977–86, KBS/LBL

Gale J, MacLeod R, Welhan J, Cole C, Vail L (1987) Hydrogeological characterization of the Stripa site. Stripa Project TR 87-15, SKB, Stockholm

Nordström DK (1983) Geochemical characteristics of groundwater at Stripa. Proc. Symp. Geological Disposal of Radioactive Waste. In Situ Experiments in Granite. OECD/NEA, Paris, p 143–153

Waber N, Nordstrom DK, 1992. Geochemical modeling of granitic ground waters at the Stripa site (Sweden) using mass balance approach. In Kharaka YK, Maest AS (Eds). Proc. 7th Internat. Symp. on Water-Rock Interactions (WRI-7), Internat. Assoc. Geochem. Cosmochem. p 243–246

Novel Developments in High-Shear Degassing Using Carbon Dioxide-Depleted Air to Precipitate Metal Contaminants: Sustainable Active Treatment Strategies for Circum-neutral Mine Water

Victoria Smyth[1], Max Gerke[1], Ryan Schultz[1], Julia Dent[1], Steven Pearce[1], Ben Gersten[2], Tom Williams[3] , Andrew Barnes[2]

[1]*Cambrian Environmental Technologies, UK, jdent@cambrianenvirotech.co.uk*

[2]*Geochemic Ltd., UK, abarnes@geochemic.co.uk*

[3]*Natural Resources Wales, UK, tom.williams@naturalresourceswales.gov.uk*

Abstract

The Sustainable Active Treatment (SAT) system has been developed as a novel process for treating circum-neutral mine water (CNMW) and recovering metals. The system's degassing process raises the pH of CNMW to alkaline levels, enabling the precipitation of metals such as zinc and lead. Recent developments introduce the use of carbon dioxide (CO_2)-depleted air, by a device stripping CO_2 from compressed air, that more effectively increases pH. Laboratory trials using CNMW from the disused Nant y Mwyn mine site in Mid Wales confirm the effectiveness of this technique, achieving enhanced metal precipitation compared with conventional air degassing. These advancements demonstrate SAT's potential as a sustainable and effective alternative treatment method for improving water quality and resource recovery from CNMW..

Keywords: Water treatment, zinc, degassing, abandoned mines

Introduction

Circum-neutral mine water (CNMW) is typical of historical metal mines in Mid Wales due to the presence of carbonate gangue and absence of sulfides such as pyrite (Warrender *et al.* 2011). CNMW often has high concentrations of metals such as zinc, lead, cadmium and copper due to their solubility over a wide pH range. Cambrian Environmental Technologies (CET) are developing a modular system for treatment of CNMW and recovery of metals, by combining treatment steps into a "treatment train" approach which include degassing and sorption (Dent *et al.* 2023, Marsden *et al.* 2021).

Industrial applications in mineral processing have readily demonstrated that the high shear reactor is an efficient aeration step. The creation of bubbles in water or droplets in air means the surface area for gas exchange is significantly increased, improving the gas transfer rate. The dispersion of bubbles in a liquid also minimises the distance that molecules need to move in order to come into contact with the gas-liquid interface, increasing reaction rates. CNMW from underground mine workings often contains higher levels of dissolved carbon dioxide (CO2) than typical surface conditions, resulting in depressed pH even in the presence of excess alkalinity. The excess CO2 can be removed by degassing, resulting in a rise in pH because of the presence of latent alkalinity. Reducing CO2 concentrations in mine water could therefore reduce the chemical demands of typical treatment systems (Geroni *et al.* 2011).

Henry's gas law states that the amount of dissolved gas in a liquid is directly proportional to its partial pressure above the liquid. Minimisation of the partial pressure of a gas above a liquid shifts the equilibrium of the dissolved gas, encouraging it to be released from the liquid. The implications of this gas law were incorporated into modification of the SAT system to determine if the aeration step could be made more effective at degassing CO2. A series of laboratory experiments were set-up to test different media to 'scrub' compressed air of CO2 at different laboratory scales. The degassing step using 'scrubbed' compressed air was tested on CNMW from the Nant y Mwyn site in Mid Wales.

The Nant y Mwyn Mine is near Rhandirmwyn, 10 km north of Llandovery, Carmarthenshire. The mine consists of both underground workings and extensive spoil heaps, which are a source of zinc loading to the nearby river system. The portal of the Lower Boat Level drainage adit is blocked and water discharges from the crown hole of an air shaft in-bye of the blockage. Water from the Lower Boat Level was used in this trial. The minewater is circum-neutral and contains an average of 13 mg/L zinc.

Methods

A series of laboratory-scale trials using the SAT system were completed using mine water collected from the site in sealed intermediate bulk containers (IBCs). The chemistry of the mine water at Nant y Mwyn has been described previously (Dent *et al.* 2023, Marsden *et al.* 2021), abridged details are presented in Results Tab. 2. The SAT system uses the Aeroblast reactor which utilises high shear technology to aerate the mine water. The high shear conditions increase the generation of nanobubbles and the efficacy of degassing of CO_2 due to the increased surface area at the water/gas interface. Compressed air has previously been used as the main gas feed for the degassing step.

A flow gauge attached to the Aeroblast was continuously monitored to determine when 100 L has gone through the shearing column; this loop is referred to as one 'Pass'. The length of each batch run (BR) was determined by the number of 'Passes' the same 100 L of minewater went through. At the end of each BR the mine water was drawn from the top of the tank into waste storage, the tank was cleaned and then re-filled with mine water from the IBCs.

The primary form of analysis was real-time pH from the top of the Aeroblast tank, which was monitored using a Metler-Toledo meter (pH Sensor InLab® 413 IP67). Gas and water pressures within the Aeroblast circuit (system gauges) were continuously monitored for consistency. Dissolved oxygen (YSI multiparameter probe), temperature (Metler + YSI), and atmospheric pressure (YSI) were also noted.

To test the theory that the concentration of CO_2 in the input gas was limiting the pH raise in the degassed water, three different trials were completed. An initial trial to test the concept utilised a pressurised nitrogen (N_2) gas canister connected to the Aeroblast circuit as this would supply 0% CO_2. Secondly, two different vessels were filled with milled waste concrete to act as a chemical "scrubber" to remove CO_2 from compressed air. Resultant gas from one large column of milled concrete (50 cm media length, saturated with water) was fed to a 1 L mine water sample. A system consisting of smaller columns, in-series, which were filled with damp, milled concrete (3x 18 cm media length) between an air compressor and the Aeroblast circuit were used to affect a pH change in 100 L mine water samples. Up to two in-line vessels, utilising commercially available (dry) scrubbing media were also installed between an air compressor and the Aeroblast circuit, ultimately, to a higher flow rate and air pressure. Each means of supplying CO_2-depleted gas to the mine water sample was tested independently from the other, with various gas pressures and flow rates. The scenarios included in the trials are shown in Tab. 1.

The ability of the scrubbers to remove CO2 was monitored using a Vaisala GMP252 CO2 monitoring probe and Insight™ software. The commercial scrubbing media was a mixture of calcium hydroxide and sodium hydroxide. The waste concrete was freshly milled by jaw crusher to reduce the impact of weathering and generate media 'pellets' of less than 3 cm.

Water samples were collected at regular intervals from the top of the Aeroblast tank for analysis by ICP-MS to assess how the gas mix trials affected contaminant precipitation. The difference between the dissolved metals concentrations and the total metal

Table 1 Overview of degassing scenarios assessing reduction in the concentration of CO2 within input gasses via various 'scrubbing media'.

Scrubbing Media	CO_2 min. (µg/L)	CO_2 mean (µg/L)	Media length (cm)	Column diameter (cm)	Mean gas flow rate (L/hr)	Max. air pressure (Bar)	Mine water vessel size (Litres)
Nitrogen (N_2)	n/a	n/a	n/a	n/a	15	4.5	100
Commercial (dry)	0	14	36	7	20	4.5	100
Concrete (damp)	0	60	54	7	6	6	100
Concrete (saturated)	0	14	50	15	Unavailable	2	1

concentration indicates the amount that has precipitated i.e. is no longer dissolved. The amount of precipitation was calculated from the dissolved and total metals in the initial mine water source and then again at 10 Passes, 20 Passes and 30 Passes.

Results

Changes in pH and dissolved metals concentrations of the trials using CO_2-depleted air or N2 gas are shown in Fig. 1 and Tab. 2. Overall, all three trials successfully raised the pH to over 8, which is required for the precipitation of ionic zinc in the mine water. The trials were compared where those where only compressed air was used as the gas source (no depletion of CO_2).

Trials with compressed air in the 100 L Aeroblast circuit ran at higher flow rates and pressures than N2 and scrubbed air (i.e. CO_2-depleted) in the same apparatus, yet the pH of the mine water failed to surpass pH 8 at 20 Passes. When trialled with N2 pH 8 was surpassed within approximately 8 Passes. When using air scrubbed with commercial scrubbing media, the pH of the mine water

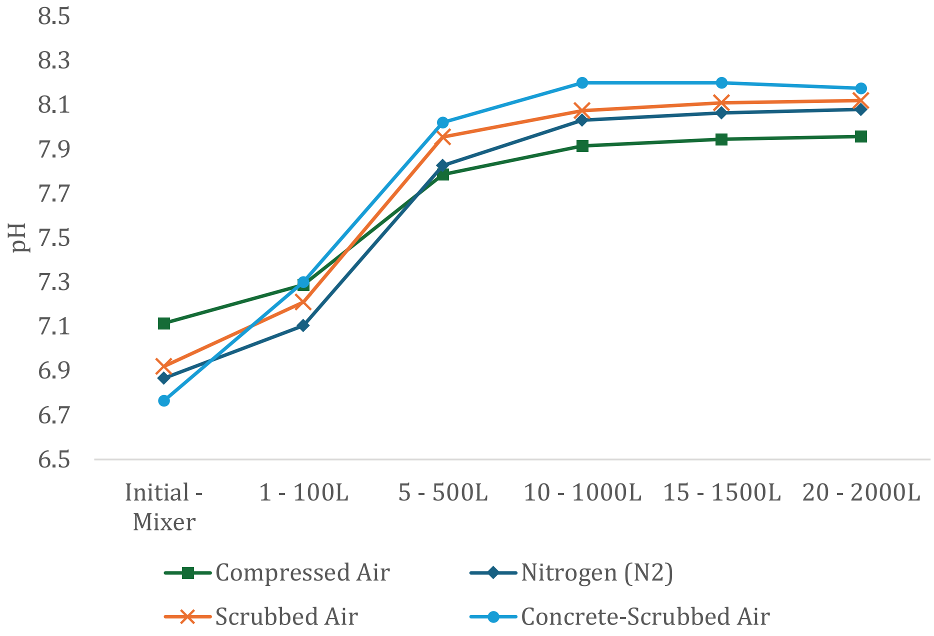

Figure 1 *Spatial distribution of the sulfur content in the coal seam President 1 resulting from Kriging interpolation of data from 45 exploration drillings in the western Ruhr area, depicted by the white circles. The black rectangle roughly represents the area of the longwall mining operation.*

surpassed pH 8, in a similar number of passes as when N2 (0% CO_2) was used as the input gas (Fig. 1).

At the lowest flow rates, the input exhaust gas mix generated by the larger column of crushed concrete (50 cm length, saturated) reduced the CO_2 concentration to 0 mg/L, which was maintained at < 20 mg/L (0.002%) for almost 80 hours. For the smaller columns of crushed concrete media (3x 18 cm, damp), installed in series for the 100 L Aeroblast circuit, flow rates were low but pH 8 was surpassed after 6 Passes. The maximum pH achieved (pH 8.16) was very similar to when N_2 and compressed air scrubbed with commercial (dry) media had been installed in the Aeroblast circuit. Homogeneity of the grain size of the milled waste concrete was improved upon for the smaller vessels, from the larger one, by selective sieving but flow rates could not exceed 10 L/min, which is too low to reach the target pH of 8.3.

It was noted during the experiments that the use of a stirrer within the Aeroblast tank appeared to draw CO_2 from the atmosphere and kept the pH lower.

Alongside the complete removal of CO_2 from the gas input, the air flow rate was proven to play an important role in the pH increase (Tab. 2). Further investigations using compressed air scrubbed by the dry, commercial media were able to reach higher gas flow rates, yielding pH results above the target 8.3.

The increase in pH for each 100 L mine water sample had a marked effect on the quantity of metal precipitate. When the pH was raised over 8, a fine, pale, precipitate formed in the 100 L mine water sample, obscuring the view of the agitator and the base of the Aeroblast tank. This precipitate did not form in the 100 L trials using only compressed air as the mine water remained close to pH 8, even after 45 Passes. It is theorised that this precipitate is a zinc hydroxide based on the chemistry of the inflow and outflow water (confirmation due with ongoing testing).

Implications of the pH increase for metals precipitation are considered in more detail in Fig. 2 and Fig. 3. The starting concentration of zinc per sample ranged from approximately 10 mg/L to 14 mg/ L. Almost all zinc (Fig. 2) was precipitated in the higher flow rate trials, where the tank pH went above 8.3 in BRs of 30 Passes. Lead, copper and cadmium also readily precipitated at this pH. Fig. 3 illustrates the precipitation of these three metals (Pb, Cu, Cd) by the reduction in dissolved concentrations.

Discussion

These trials confirm that a crucial driver for the removal of CO_2 from CNMW, and therefore increase in mine water pH, is the proportion (or partial pressure) of CO_2 in the gas used in degassing. Nitrogen has the largest partial pressure differential (100% gas is not CO_2) however, the use of compressed N_2 canisters in remote environments, where this system is proposed to be used, are impractical for use and maintenance.

The CO_2 proportion in air is anticipated to be variable but approximately 0.03–0.04%. Following the scrubbing processes utilised in these degassing trails, the difference in CO_2 concentration from the original gas composition (i.e. air) appears negligible compared with the marked effect the change has on the reaction to increase the mine water pH. The correlation between the reduction in CO_2 concentrations in the gas feed and the largest increase in pH change in the mine water, indicate the importance of CO_2 in regulating mine water pH.

The concrete media seemed to outperform other options but higher flow rates are required to reach the target pH than those

Table 2 *Results for pH (averaged maxima) and selected dissolved metal concentration changes in mine water by gas flow rate.*

	Aeroblast 'Passes'	pH	Zinc µg/l	Lead µg/l	Cadmium µg/l	Copper µg/l
Initial mine water	n/a	6.86	10750	113	37.2	24.5
Lower gas flow	20	8.13	5656	31.3	31.3	4.6
Higher gas flow	30	8.54	2070	8.4	28.0	1.5

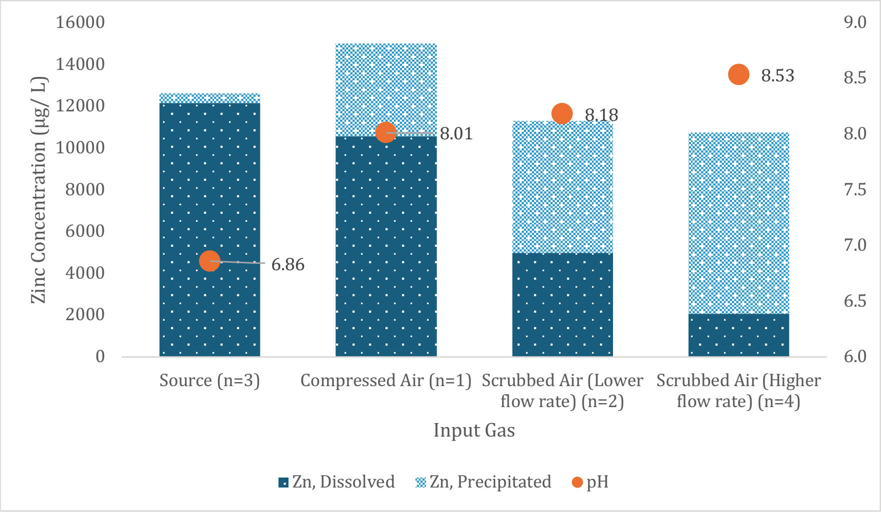

Figure 2 *Zinc precipitate in mine water at batch run end by gas mix, against pH in 100 L tank.*

employed in the BRs. The higher pH reached at low flow rates was also when no agitation occurred within the 100 L in the Aeroblast tank. Results therefore look similar to the initial tests with commercial media, which were agitated, but did not work effectively at the higher flow rates necessary to consistently surpass 8.3.

At the higher air flow rates, the residence time through the concrete scrubbing media was greatly reduced and as such, the CO_2 removal was not as effective. The reactivity of the recycled concrete is linked to the homogeneity of the material both in terms of reactive surface area and reactivity of available minerals, which will need to be

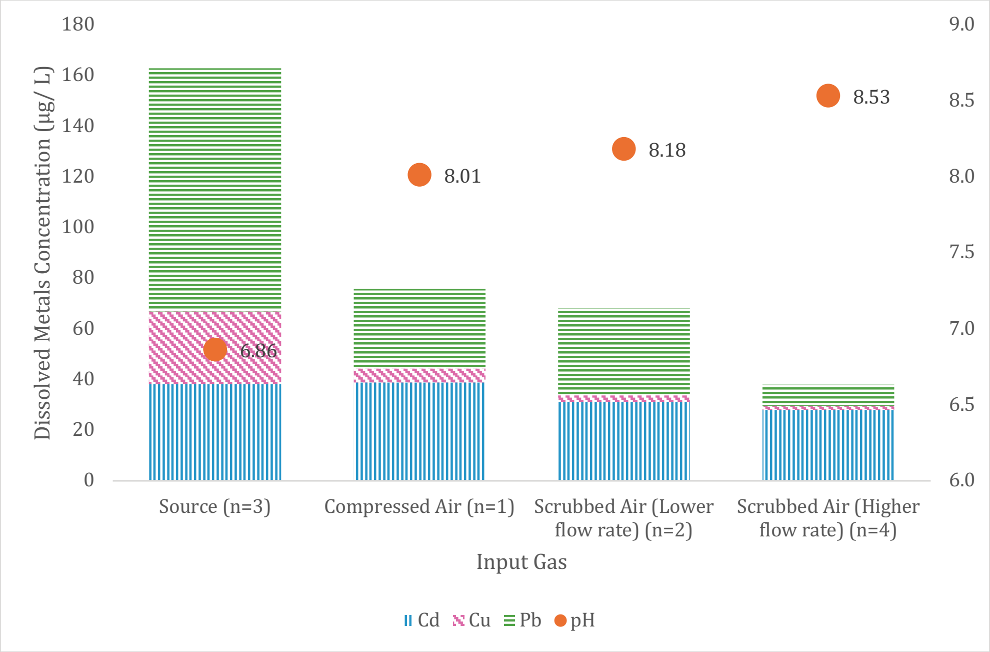

Figure 3 *Select metals concentrations at batch run end by gas mix, against pH in 100 L tank.*

compensated by material preparation and gas residence time.

Further investigations will use a larger volume for the scrubber system to improve residence times (both soda lime and concrete) and ensure this element is working as effectively as possible.

Conclusions

The findings from this study demonstrate that the gas mix used in degassing plays an important role in altering the condition of mine water pH because adjustments to pH are highly sensitive to CO_2 concentrations in the gas input. The incorporation of a "scrubber" to reduce CO_2 concentrations was therefore an effective means to increase pH during degassing. Re-purposing of used concrete, to act as a CO_2 scrubbing media, in the degassing step of the SAT system exhibits feasibility although requires further investigation to improve current constraints.

This paper only describes the recent trials on the degassing stage of the SAT system. Ultimately, the SAT system will incorporate two more stages to maximise the removal and recovery of contaminant metals (primarily zinc) via filtration and sorption elements. Investigations are still ongoing to finalise the design of the "treatment train" that will reduce the dissolved zinc from 10 mg/L to a target of 10–100 µg/L. Parameters for continuous running of the system have been chosen based on the results from the BRs that achieved a pH raise beyond 8.3 and are ongoing.

Overall, the trials demonstrated that a semi-active treatment system using scrubbed air or N_2 to degas CO_2 from mine water was effective at raising pH within the range required for precipitating metals of interest. This system could reduce reagent consumption associated with traditional treatment systems.

Acknowledgements

The authors thank the Wales Metal Mines Programme, funded by Welsh Government, for allowing these results to be published.

References

Coal Authority (2020) Metal Mine Failing Waterbodies Assessment. – Overview Report OP16-154/F13/0.

Geroni JN, Sapsford DJ, Florence K (2011) Degassing CO_2 from mine water: implications for treatment of circumneutral drainage. Mine Water

Dent, Julia; Pearce, Steven; Savage, Rhys; Marsden, James; Schultz, Ryan; Williams, Tom; Stanley, Peter; Roberts, Mark; Barnes, Andrew; Gersten, Ben (2023): Optimising Circum-Neutral Mine Drainage Treatment By Implementing High Shear Degassing Into A Sustainable Active Treatment System. – In: Stanley, P.; Wolkersdorfer, C.; Wolkersdorfer, K., Mugova, E.: IMWA 2023 – Y Dyfodol | The Future. – p. 129–134; Newport, Wales, UK (International Mine Water Association)

Marsden J, Pearce S, Sambrook T, Dent J, Barnes A (2021) Site specific optimisation assessment of cirucm-neutral water treatment using a cost-treatability curve assessment. IMWA 2021 Proceedings: Mine Water Management for Future Generations (2021) 334–339.

Warrender R, Pearce N, Perkins W, *et al* (2011) Field Trials of Low-cost Reactive Media for the Passive Treatment of Circum-neutral Metal Mine Drainage in Mid-Wales, UK. Mine Water and the Environment 30:82–89. https://doi.org/10.1007/s10230-011-0150-8

Evapotranspiration Cover Design Optimization – A Case Study

Yuliya Subotskaya[1], Larry Breckenridge[2]

[1]*Staff Mine Water Scientist, Global Resource Engineering, Golden, Colorado, ysubotskaya@global-resource-eng.com*

[2]*Principal Environmental Engineer, Global Resource Engineering, Golden, Colorado, lbreckenridge@global-resource-eng.com*

Abstract

Evapotranspiration (ET) covers are an industry-standard tool for mine waste leachate mitigation in arid and semi-arid climates. A new ET cover was designed, field-tested, and optimized with computer modeling for the tailings storage facility (TSF) at the Zangazeur Copper-Molybdenum Complex (ZCMC) in Kapan, Armenia. Collected field data from ET cover test cells, soil characteristics, and climate data were combined to create a variably saturated groundwater flow model which simulated the effectiveness of the new cover for over 10 years. The model was validated to the field-observed measurements of moisture. A minimum thickness of cover that would prevent breakthrough was recommended.

Keywords: Evapotranspiration cover, vadose zone groundwater modelling, closure cover

Introduction

The TSF at ZCMC is an upstream-raise TSF with a 5.7 km^2 exposed surface area in need of reclamation. Tailings impounded in the TSF are not acid-generating, but they do produce a leachate that is high in some regulated metals which has the potential to affect downstream water quality, and, therefore, must be managed to eliminate the mobilization of dissolved metals. The site receives an average of 550 mm of rain a year, making it a semi-arid environment that is suited for ET cover installation.

It is industry standard practice to mitigate metal leaching (ML) of mine tailings through the installation of an ET cover which is designed to absorb and store wet-season moisture. The cover is vegetated so that direct evaporation and plant transpiration can remove stored moisture during the dry season to prevent breakthrough (defined as infiltration through the cover into the tailings). Mining projects and the US Environmental Protection Agency (EPA) have shown that, if properly designed, ET covers can virtually eliminate infiltration of precipitation into lower layers of material in arid and semi-arid environments (Benson *et al.* 2002).

Much of the existing tailings dam face is covered with a reclamation soil cover. The original cover was designed in 1975 and relied on the use of a compact clay layer with low saturated hydraulic conductivity to prevent leachate into the tailings. From top to bottom, it consisted of 20 cm of topsoil and 50–70 cm of compacted clay.

Since the time of the cover's design, it has been shown that a compacted clay barrier placed directly atop of fine-grain waste often does not maintain its protective functionality, especially in arid or semi-arid environments (Bolen *et al.* 2001) (Albright *et al.* 2004) (Bonaparte *et al.* 2004). Repeated wetting and drying cycles in combination with root intrusion by vegetation can result in an increase in hydraulic conductivity up to two orders of magnitude (Maine Bureau of Remediation and Waste Management 1997) (Albrecht Benson 2001). As a result, ZCMC hired Global Resource Engineering (GRE) to update their original cover design to one with a coarse-grained capillary break layer that takes advantage of the difference in pore sizes at the boundary between the finer storage material and the coarser capillary break material to minimize the infiltration of stored moisture into the tails. While the cover with the capillary break may be negatively affected by root intrusion and subterranean fauna, this paper assumes that these elements will not affect the performance of the cover over time.

Field Programming

GRE designed a field program to confirm the necessity for a new ET cover, and to properly characterize available onsite material. Two instrumented ET cover test cells, 3 m by 3 m, were installed on the surface of the TSF to compare the efficacy of the existing and new cover design, and to gather in-field data on moisture changes throughout the cover soil profile. 3 m by 3 m was chosen due to its ease of construction and amount of instrumentation available. The test cells were installed as detailed in Fig. 1, with moisture sensors and lysimeters installed to monitor water infiltration and seepage through the two covers. GRE realized that pan lysimeters, even when fitted with diversion control collars and installed with a natural capillary break at the point where the pan collection occurs, could be inaccurate due to the formation of a zero-tension boundary layer within the soil that disrupts natural flow paths in unsaturated soils (Kahale *et al.* 2022). However, logistical constraints including long-lead times for fabrication and shipping limitations made a wicking lysimeter impossible to acquire prior to ground freezing in the winter.

The existing cover test pit was dug into the prior concurrent cover, with instruments placed horizontally within the cover to measure conditions with minimal disturbance. Installation of the soil lysimeter in the existing cover test pit was done by digging a pit adjacent to the test column area, then placing the lysimeter into a dug-out cavern at 120 cm below the layer of compacted clay and topsoil (Fig. 1). Before installation, an access port and hose were installed and checked, and the divergence control collar was backfilled with mine tailings. The remaining space around the lysimeter was backfilled with mine tailings. Moisture sensors were placed 80 cm and 120 cm below the ground surface in a similar fashion before backfilling the adjacent access pit with the same layers. Due to the way the instrumentation was installed, the vegetative cover remained undisturbed atop the test pit.

In the second test pit, a new cover was installed in accordance with the guidance for Engineered Covers within the Global Acid Rock Drainage Guide, with instruments placed within the cover during the installation process (INAP 2014). The pan lysimeter was placed in the center of the pit, 120 cm below ground surface, then backfilled with mine tailings (Fig. 1). Soil probes were installed at 150 cm, 110 cm, 70 cm, and 20 cm below ground surface by digging into the backfilled soil and placing the sensor at the proper location as planned in Fig. 1. Due to the design of the new cover, it was impossible to have undisturbed vegetation atop the new cover cell as was possible with the existing cover test cell. This difference was taken into consideration upon data analysis.

Measurements of the soil moisture content and soil temperature were taken twice daily from November 2022 to October 2023. Fig. 2 and 3 show the change in moisture

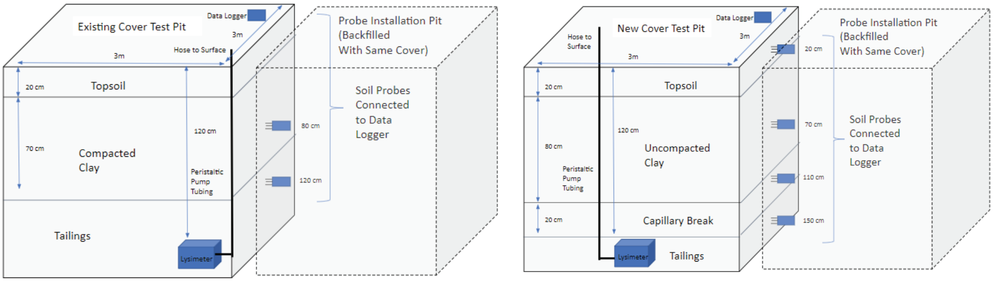

Figure 1 *Design and Instrumentation of Existing and New Cover Test Cells.*

content at the moisture probe locations in the existing cover test pit and the new cover test pit respectively. Both pits show an increase in soil moisture content in the upper layers of soil starting in early May, which is then followed by the wetting of deeper soil layers as water moves downward. There is an increase in moisture in the mine tailings in the new cover test pit, up to 0.25 m3/m3 (volumetric moisture content), but smaller in magnitude than the breakthrough event in the existing cover pit, which wetted up to 0.37 m3/m3. The soil moisture changes in the new cover test pit also represent an underperformance of the new cover, as it does not have established vegetation to further mitigate water infiltration.

The pan lysimeters installed in the test pits proved to be ineffective at collecting meaningful and accurate leached water volume for the two test pits, as the collected water volume did not correspond to the volumetric water content measured by the soil moisture probes. These pan lysimeters collected water from under the existing cover, but none under the new cover. As seen in Fig. 3, the surge in moisture seen in the capillary break and the mine tailings in mid-summer 2023 should have resulted in moisture collection in the new cover pan lysimeter, but none was measured. This disconnect between the moisture probe data and the pan lysimeter data remains a weak point in the study and will be discussed later in this paper.

Soil Characterization

For the construction of an ET cover, ZCMC must excavate and utilize soil and subsoil from the perimeter of the existing TSF. Because the area is large, and because different alluvial/colluvial materials are available around the TSF perimeter, a borrow material suitability study was conducted. 25 soil samples were taken from locations all over the site and included samples of topsoil, tailings, and other available material for use in the new cover. The samples were compacted to 80% standard proctor before testing, which is consistent with truck dumped and bladed material. All samples were sent to Lernametalurgiai Institute (LMI) geotechnical lab for analysis. LMI performed the gradation, compaction, hydraulic conductivity, plasticity, and moisture content tests of every sample. Additionally, the Soil Water Characteristic Curve (SWCC) (ATSM D6836-16 2016) was measured of 5 of the samples of the most-favorable borrow material.

The geotechnical and SWCC data was used to determine the range of soil types available onsite. The results show there are a variety of soils present on site, from very fine-grained clay to coarser grained sand and sandy gravel that would be suitable as borrow sources for topsoil, capillary break material,

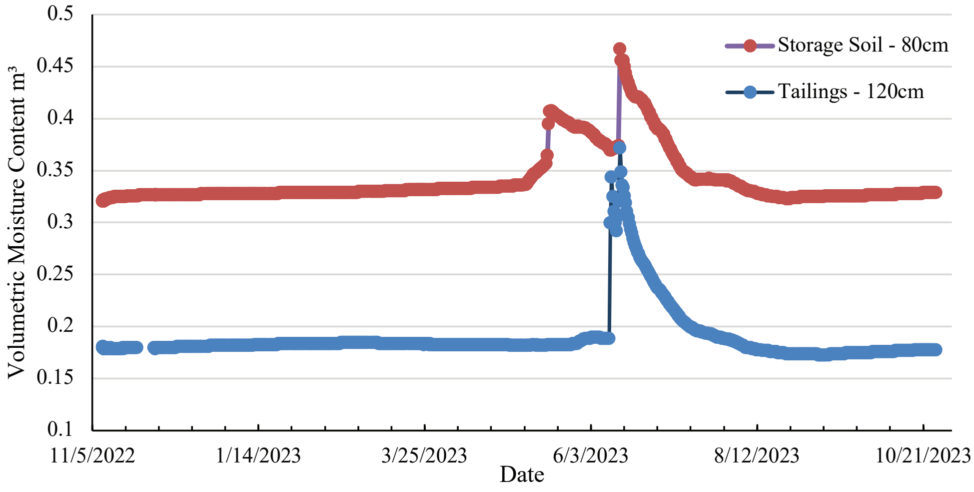

Figure 2 Soil moisture changes in existing cover.

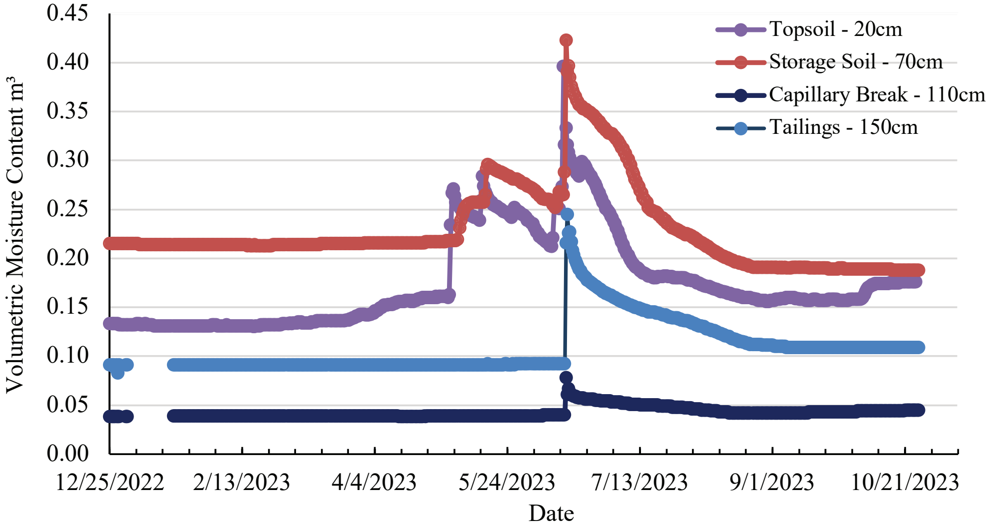

Figure 3 Soil moisture changes in new cover.

or storage soil. GRE determined that soil with between 45% and 80% of fine-grained material that passed through the 0.075 sieve, but still with a wide range of particle size that allowed for their hydraulic conductivity to be in the range of 10–5 –10–6 cm/s would be most suitable for use as storage soil.

Model Design

GRE created a computer simulation using GeoStudio's SEEP/W software which allows for the modeling of variably saturated groundwater flow and has a long history of application in the mining industry. The model can effectively simulate many years of climate effects on the cover, can elucidate the movement of water within the cover, and can be used to evaluate the viability of different thicknesses of ET covers. The computer model calculations are done using known scientific relationships of evaporation, transpiration, and soil-specific interactions with water.

2D column models of the existing and new cover were designed to be 1 m thick and 3 m wide to correspond to the dimensions of the two test cells and to minimize computing time. Soil layers within the model were created to replicate the corresponding new and existing ET cover designs.

Results of the onsite soil testing program were used to define materials within the model. The Van Genuchten equation was fitted to the SWCC lab results to produce a function that was representative over a wide range of soil matric pressures that would be present during the simulation. The SWCC for the remaining samples was estimated in GeoStudio using LMI-tested grain size data and liquid limits. The saturated water content of each soil was estimated based on each soil type (Heath 1983). Hydraulic conductivity functions were developed in GeoStudio using the preexisting SWCC functions and measured saturated hydraulic conductivity of each soil. The Fredlund-Xing-Huang estimation was used for clayey soils, and the Van Genuchten estimation was used for all other soils as is considered best in engineering practice (Zhang 2015). Thermal conductivities and volumetric heat capacity of soils are dependent on volumetric water content and were estimated based on soil type and measured water content.

The model is capable of simulating climate effects on water balance including solar radiation, precipitation, soil temperature, snowmelt, and transpiration. 10 years of daily precipitation, solar radiation, wind speed, and temperature data was provided by the meteorological station in Kapan, Armenia. This data was used to create a typical year, as well as a representative 90th percentile wet year for the site. 90th percentile wet year was selected to evaluate the impact of higher precipitation on the cover, but to not overestimate future rainfall events. Additional climate and biological parameters necessary for the land-climate interaction function were filled in using available online data and site observations. It is important to note that the resulting average climate was representative of a typical year, and not specific to the 2022–2023 climate in the area.

Model Calibration

Collected in-field data from the installed soil moisture probes was used to calibrate the model. Discrepancies between the model-predicted data and the field data were noted and the model parameters were adjusted until the model represented empirical conditions as closely as possible while retaining fidelity to the lab testing and the climate data.

The model was able to predict the magnitude of soil moisture changes over time, but not the transient dynamics. Fig. 2 and 3 show a very rapid response to spring moisture that could not be easily duplicated in the model without substantial alteration of the material properties outside of the range of the tested values. GRE hypothesizes that the very rapid increase in moisture content measured by the probes may have been the result of preferential flow pathways, or a limitation of the modeling software to simulate a rapidly migrating moisture font traveling through the soil. The model is limited by the data that was available to GRE for input and calibration, as climate data was only available from one weather station and in-field soil moisture content measurements were only collected for one year.

Model Results

Despite the challenges in calibrating the model to the field data, GRE proceeded to simulate the new ET cover with a capillary break. The input geometry, material, and climate information were used by the GeoStudio software to calculate the climate effects on the existing and new ET covers over ten years. Single-particle tracking was also used to monitor the movement of a representative particle of water through the column and to track breakthrough through the ET cover into the tailings. The moisture content of locations within the model columns that coincided with locations of the in-field soil probes in the test pits were monitored. Additionally, the percentage of mass balance error in the simulation was monitored to have errors of less than 1% of the total water within the system.

The sample water balance, including the water balance error for the new cover, is shown in Fig. 4. Although the model could not be calibrated to match the in-field moisture probe data exactly, this was reconciled by the water balance data and the general moisture content patterns exhibited by the model system. Both the new and existing cover were designed to prevent breakthrough with repeated wet years (with 90th percentile rainfall). The total moisture infiltration and storage in the modeled cover was more than observed in the field.

Fig. 4 shows that the new ET cover can evaporate and transpire out all the moisture in the soil. The cover water volume increases with snowmelt in spring, but this moisture is then mitigated by evaporation and transpiration that both work to dry the soil and return it to the same water volume as at the beginning of the year. The simulation of the new cover shows near-zero vertical infiltration into the mine tailings and is predicted to function in a manner similar to the effectiveness of other capillary break covers (Benson *et al.* 2002).

Conclusion

Field instrumentation revealed that the existing cover on the site could be improved to meet the project goal of minimizing leachate and protecting groundwater quality. However, the study faced challenges in obtaining quality field data. The installed pan lysimeters did not comport with moisture content readings, and extremely rapid changes in moisture content observed in the installed moisture content probes could not be duplicated in groundwater models. For future studies, in place of of the pan lysimeters, wicking lysimeter should be installed, and a wider array of moisture content probes should be installed within both cover pits to be monitored for over a calendar year. However, a conservative model was built that demonstrated the effectiveness

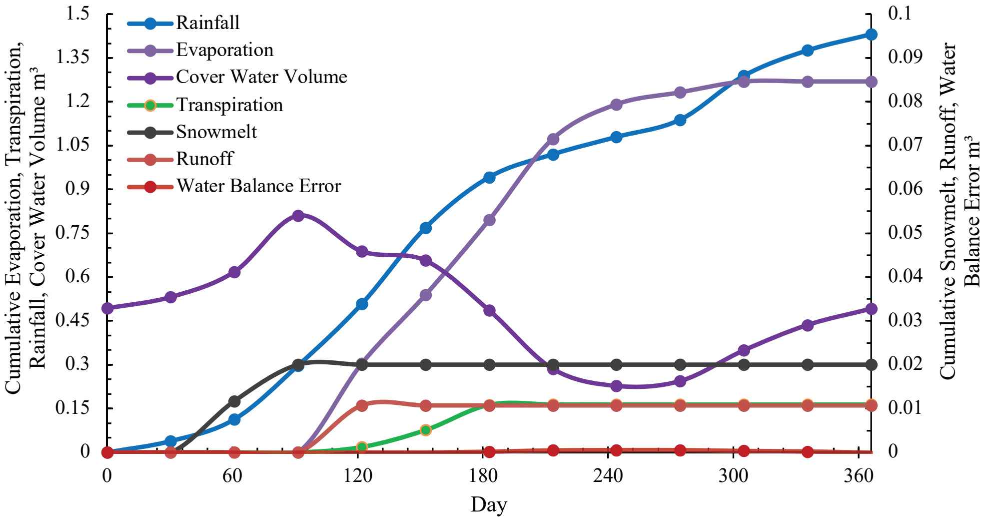

Figure 4 *Water balance in 0.5 m storage soil ET cover, year 10.*

of the new cover design at preventing leachate over 10 years. More work should be done to improve confidence in modeling results, as well as confirm this study's findings.

Despite these limitations, the study furthered the understanding of a best practice cover for the tailings facility. The ET cover model with the on-site borrow materials and the capillary break was robust, and it performed well with various material types and over a wide range of potential climate conditions. Switching to an industry-standard ET cover is part of ZCMC's continuing effort to achieve the ICMM international guidelines for concurrent and final mine closure (ICMM 2019).

Acknowledgements

GRE would like to thank ZCMC and LMI for their support of this project, with special thanks to Asya Ghazaryan, Armen Stepanyan, and Suren Yeritsyan.

References

Albrecht BA, Benson CH (2001) Effect of Desiccation on Compacted Natural Clays. Journal of Geotechnical and Geoenvironmental Engineering. 127(1):67–75

Albright WH, Benson CH, Gee GW, Roesler AC, Abichou T (2004) Field Water Balance of Landfill Final Covers. Journal of Environmental Quality. 33(6):2317–2332

ATSM D6836-16 (2016) Standard Test Methods for Determination of the Soil Water Characteristic Curve for Desorption Using Hanging Column, Pressure Extractor, Chilled Mirror Hygrometer, or Centrifuge. West Conshohocken, PA USA: ASTM International.

Benson CH, Albright WH, Roesler AC, Abichou T (2002) Evaluation of Final Cover Performance: Field Data from the Alternative Cover Assessment Program (ACAP). Waste Management Conference, Tuscon, Arizona.

Bolen ME (2001) Alternative Cover Assessment Program Phase II Report, Madison Wisconsin USA: Department of Civil and Environmental Engineering, University of Wisconsin, Madison.

Bonaparte R, Gross BA, Daniel DE, Koerner RM, Dwyer SF (2004) Draft Technical Guidance for RCRA/CERCLA Final Covers. US Environmental Protection Agency. National Risk Management Research laboratory, Cincinnati OH.

Heath RC, (1983) Basic Ground-Water Hydrology. U.S. Geological Survey Water-Supply Paper 2220, p86.

International Council of Mining and Metals (ICMM) (2019) Integrated Mine Closure Good Practice Guide, 2nd Edition.

International Network for Acid Prevention (INAP) (2014) The Global Acid Rock Drainage Guide, 2nd Edition.

Kahale T, Ouédraogo O, Duarte Neto M, Simard V, Cabral AR (2022) Field-based assessment of the design of lysimeters for landfill final cover seepage control. Journal of the Air & Waste Management Association, 72(12):1477–1488. doi:10.1080/10962247.2022.2126557

Maine Bureau of Remediation and Waste Management (1997) An Assessment of Landfill Cover System Barrier Layer Hydraulic Performance. Augusta, Maine

Zhang, F (2015) Examination of the estimation of relative permeability for unsaturated soils. Canadian Geotechnical Journal. doi:10.1139/cgj-2015-0043

Water Disaster Control with Grouting in Bed Separation due to Deep Mining

Wanghua Sui, Yonghui Wu, Baofu Wu

China University of Mining and Technology, Xuzhou, China, suiwanghua@cumt.edu.cn, ORCID 0000-0001-7004-1877

Abstract

This paper investigates the overburden bed separation evolution and grouting propagation in the Menkeqing coal mine, China, using laboratory test, numerical, and field monitoring methods. Bed separation develops vertically from low-order to high-order and aligns with the mined-out area horizontally, forming stable separations in the Zhidan Formation. A comprehensive evaluation of water inrush disaster risk was conducted for the panel 11-3101. Grouting with coal gangue slurry effectively mitigated groundwater inrush and surface subsidence. Results confirm grouting as a viable measure for controlling bed-separation water inrush hazards.

Keywords: Overburden bed separation; Water inrush disaster evaluation; Grouting

Introduction

With the increasing depth of coal resource mining in China, mine water hazards have become more prominent, posing important constraints on the safe extraction of coal. Bed separation water hazards, as a new type of water hazard, severely threaten coal mine safety due to their characteristics of high concealment, suddenness, and large instantaneous water inflow. It is generally believed that the occurrence of static water pressure-induced bed separation water inrush hazards requires three basic conditions: sufficient water sources, stable separation spaces, and unstable aquicludes (Bai *et al*, 2021; Gao *et al*, 2023).

Grouting is one of the effective measures for preventing and controlling bed separation water inrush hazards. By filling and reinforcing the separation space through grouting, the prevention and control of bed separation water hazards can be achieved, ensuring mining safety. To improve the precision of bed separation treatment, various comprehensive methods can be used to determine and monitor the separation location on-site. Using coal gangue as a component of the grout not only handles large amounts of coal gangue but also prevents bed separation water hazards in advance. This is a highly green and environmentally friendly filling mining method, achieving efficient utilization and harmless treatment of solid waste (Cao *et al*,2024; Qiao *et al*, 2021).

This paper takes the panel 11-3101 of the Menkeqing coal mine as the research background. Through multiple methods, including numerical simulations, and on-site monitoring, the development, localization, and characteristics of bed separation spaces in deep coal mines are analysed in depth. A risk assessment of bed separation water hazards and coal gangue grouting treatment is conducted, and the effectiveness of the treatment is evaluated. Ultimately, effective prevention and control of bed separation water hazards in complex strata and green treatment of coal gangue are achieved.

The strata of the Menkeqing coal mine mainly consist of conglomerate sandstone, sandstone, sandy mudstone, mudstone, and coal seams. The geological structure is a monocline inclined to the west. The faults are mainly NW-trending normal faults, which are neither water-bearing nor water-conductive. The panel 11-3101 of the Menkeqing coal mine is bounded by solid coal on both sides, with a tendency width of 260.4 m, a burial depth of 693–721 m, a coal seam dip angle of 1°–4°, and an average thickness of 4.92 m.

The water-filled aquifers affected by mining activities in the Menkeqing coal mine are the clastic rock confined aquifers of the Yan'an Formation and the Zhiluo Formation. These aquifers have limited hydraulic connection with the overlying phreatic aquifer and atmospheric precipitation, weak water abundance, and poor groundwater recharge conditions, posing minimal threat to mine exploitation. The maximum unit water inflow is 0.2068 L/s·m (The facility' s drainage capacity, expressed in liters per second per meter). The aquicludes include the Middle Jurassic Anding Formation, the aquiclude from the floor of the Anding Formation to the roof of the No. 2 coal seam, and the aquiclude from the base of the No. 2 coal seam to the roof of the No. 3 coal seam in the Yan'an Formation.

Materials and Methods

Laboratory Test

Coal gangue was used as the primary grouting material. It was initially crushed with a ball mill to achieve a particle size under 10 mm before being combined with cement to form the slurry.The slurry' s waterproofing capability was governed by its post-solidification physical properties, including water-solid ratio, density, viscosity, and mass concentration. The experimental results were summarized in Table 1. Based on field grouting tests, a slurry formulation with a water-solid ratio of 2:1 and an average density of 1.3 g/cm^3 was selected for production.

Numerical simulation

The development of roof bed separation in the panel 11-3101 was simulated using three-dimensional discrete element technology. The model dimensions were 800 m × 460 m × 685 m (Fig. 1). Given the stratum dip angle of only 1°–2° in this area, the dip angle was simplified to 0° for modelling purposes. To improve the computational efficiency of the model, the Quaternary system was equivalently treated as a uniformly distributed load of 0.44 MPa applied to the top of the model. Except for the top boundary, which was free, all other boundaries were fixed. The model included the following layers: a 10 m thick floor of the No. 3–1 coal seam in the Yan'an Formation, a 5 m thick No. 3–1 coal seam, a 40 m thick layer from the roof of the No. 3–1 coal seam to the top boundary of the Yan'an Formation, a 160 m thick Zhiluo Formation, a 60 m thick Anding Formation, and a 410 m thick Cretaceous system.

Field Monitoring

The development of bed separations was investigated using drilling mud loss, ultrasonic imaging, and borehole television. The phenomenon of complete mud loss indicated that rock layer movement led to the formation of overburden bed separation. After flushing with clean water and allowing it to settle, downhole colour television imaging logging and ultrasonic imaging were conducted to observe fractures. Prior to mining, drainage boreholes were drilled in the roof to dewater the aquifer, and continuous drainage was carried out for nearly three months. During this period, changes in water discharge were recorded, and water samples were collected for quality analysis.

Table 1 *Experimental results of coal gangue slurry ratio.*

Particle size 0.125 mm				Particle size 0.106 mm			
Water-solid ratio	Density /g/cm^3	Viscosity/s	Mass concentration	Water-solid ratio	Density /g/cm^3	Viscosity /s	Mass concentration
1.6:1	1.32	19.5	43.4%	1.6:1	1.33	20.0	43.4%
1.8:1	1.30	17.4	40.0%	1.8:1	1.31	18.0	40.0%
2.0:1	1.29	16.9	37.0%	2.0:1	1.30	18.0	37.0%
2.2:1	1.28	17.0	34.4%	2.2:1	1.28	17.5	34.4%
2.4:1	1.26	16.5	32.0%	2.4:1	1.26	16.9	32.0%

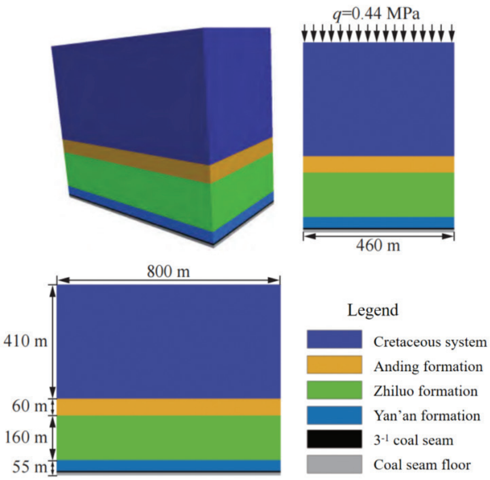

Figure 1 Numerical simulation model of the panel 11-3101.

Zoning Evaluation

The evaluation of bed separation water hazards is typically divided into five steps: ① Analysis of geological and hydrogeological conditions: understand the structural development of the panel and analyse the water inrush processes in adjacent mines within the mining area. ② Extraction of influencing factors: based on previous water inrush cases, analyse the necessary conditions for the formation of bed separation water. Combine this with the actual geological conditions of the mine to screen suitable influencing factors and normalize them. ③ Weight determination: use a combination of the Analytic Hierarchy Process (AHP) and the Entropy Weight Method to determine the weights. ④ Weight assignment: comprehensively calculate the weights obtained from each algorithm to determine the final weight values. ⑤ Risk zoning: utilize a Geographic Information System (GIS) to overlay different influencing factors according to their weights and create a risk zoning map for bed separation water hazards.

Results

Positioning of Bed Separation

Fig. 2 shows the numerical simulation results. When the panel advanced to 100 m, the immediate roof of the No. 3–1 coal seam caved, along with the No. 25 fine sandstone and No. 24 sandy mudstone of the Yan'an Formation. Transverse and vertical fractures developed, extending to the top of the Yan'an Formation. At 200 m of advancement, the fractures propagated upward to the No. 21 fine sandstone. By 300 m, the interconnected fractures reached the No. 20 sandy mudstone, and the water-conducting fractured zone reached its maximum extent. At this stage, uneven settlement occurred between the No. 16 sandy mudstone and No. 17 fine sandstone at the base of the Anding Formation, forming temporary transverse fractures. At 400 m of advancement, the overburden subsidence range expanded, the caved zone compacted, and the temporary transverse fractures closed. At 500 m, two bed separation spaces formed: the first separation between the No. 16 sandy mudstone and No. 17 fine sandstone at the base of the Anding Formation, and the second separation between the No. 13 medium sandstone and No. 14 sandy mudstone at the base of the Zhidan Formation. Numerous small fracture sets developed within the Anding Formation, likely due to the interbedded sandstone and mudstone structure. At 600 m of advancement, the bed separation further propagated upward, forming the third separation between the No. 8 fine sandstone and No. 9 medium sandstone in the middle of the Zhidan Formation.

Before conducting bed separation grouting, observation boreholes were drilled in Panel 11-3101 to validate the results of numerical simulations, thereby obtaining the actual development of bed separation on-site (sequence of treatment: mining and simulations, on-site verification, and grouting). It was found that the theoretical calculations were in good agreement with the measured results, except for the Class II (Jia *et al*, 2023) bed separation at the base of the Anding Formation (burial depth of 450–500 m), where the drilling fluid consumption was not large. This is because the Anding Formation consists of interbedded sandstone and mudstone, lacking thick sandstone layers, resulting in minimal grout leakage. Most small bed separations were also observed in the borehole color television imaging (Fig. 3).

Water Inrush Zoning

Three main factors influencing bed separation water hazards were identified: aquifer water

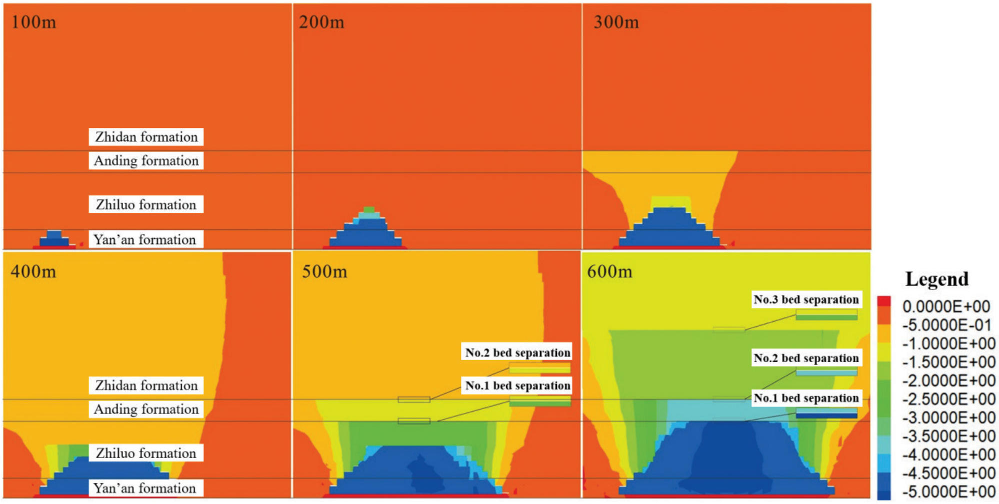

Figure 2 Vertical displacement of overburden rock of the panel.

pressure (weighting of 0.4), aquiclude thickness (weighting of 0.2), and height of the water-conducting fractured zone (weighting of 0.4). Based on borehole data around panel 11-3101, the computational datasets for each influencing factor were statistically analysed. The greater the aquifer water pressure, the stronger the recharge capacity to the bed separation space, and the higher the risk of water inrush. The water pressure distribution ranges from 3.33 to 3.97 MPa, with an average of 3.73 MPa (danger threshold of 3.95 MPa).

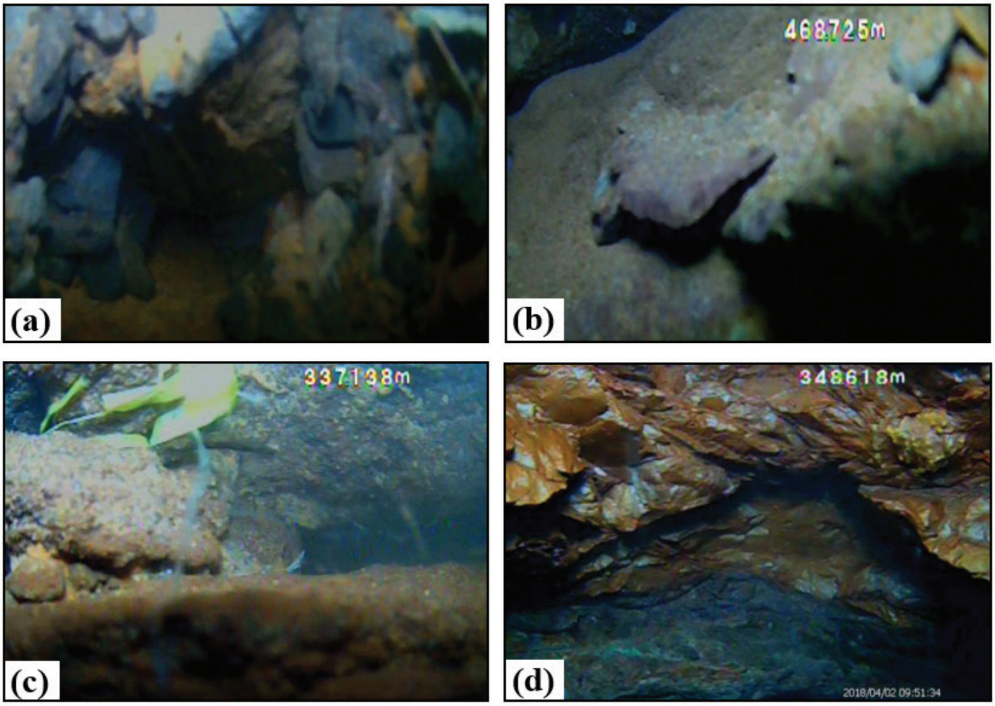

Figure 3 Borehole TV and ultrasonic imaging reveal bed separation and fracture development.

(a) (b) Multiple small bed separations at the bottom of the Anding Formation, (c) (d) bed separations at the junction of the Zhidan and Anding Formation.

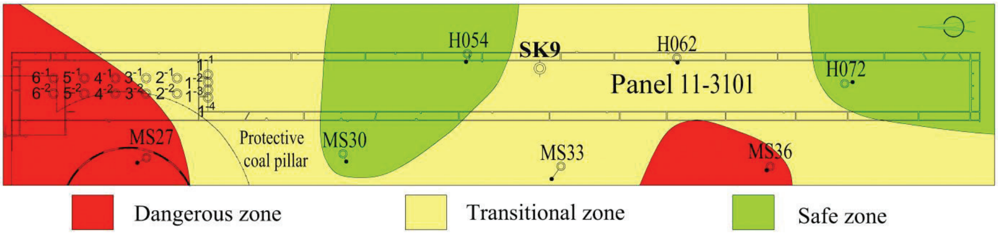

Figure 4 *Water inrush risk zoning.*

Aquiclude thickness refers to the distance between the bottom of the bed separation and the top boundary of the water-conducting fractured zone. The thinner the aquiclude, the weaker its resistance to deformation and failure, increasing the likelihood of bed separation water hazards. The thickness distribution ranges from 179.14 to 238.06 m, with an average of 204.6 m (danger threshold of 234 m). When the bed separation layer is fixed, the higher the water-conducting fractured zone, the thinner the aquiclude, and the greater the risk of water hazards. The height distribution ranges from 112.1 to 129.16 m, with an average of 124.5 m (danger threshold of 127 m). The panel was divided into five zones (two dangerous, two safe and one transitional zone) based on the risk intensity of water inrush from bed separation (Fig. 4). At the MS27 borehole located near the stopping line of the panel, there is a high risk of bed separation water hazards due to the high aquifer water pressure (3.96 MPa), thin aquiclude thickness (210 m), and development height of the water-conducting fractured zone (128 m). To ensure the safe mining of the panel, it is necessary to implement bed separation grouting in this area in advance.

Water Inflow and Quality

Fig. 5 shows that water from the Yan'an Formation-Zhiluo Formation aquifer flowed into the panel space as the water-conducting fractured zone gradually developed upward after grouting and during mining. When the panel advanced to 263 m, the water inflow was 187 m^3/h. At an advancement distance of 430 m, the water inflow reached 296 m^3/h, followed by a slight continuous increase. When the panel advanced to 3,300 m, the water inflow increased to 686 m^3/h. As the panel continued to advance, the water inflow gradually decreased. By the end of grouting and during mining, the water inflow in the goaf was 480 m^3/h, after which it continued to decline. Except for fluctuations in water inflow at 263 m and 2,800 m of advancement, the water inflow showed a relatively steady increase during other periods, followed by a gradual decreasing trend. No large water inrush from bed separation was observed.

Water quality analysis of samples from the goaf and roof drip water in the panel showed that the salinity of the water samples ranged from 1,990.68 to 2,814.8 mg/L, which differs from the salinity of the Cretaceous aquifer (252.84–761.48 mg/L). This indicates that the water inflow primarily originated from the Zhiluo Formation to the Yan'an Formation aquifers, with no infiltration from bed separation water. The grouting project effectively prevented and controlled bed separation water hazards, ensuring the safe mining of the panel.

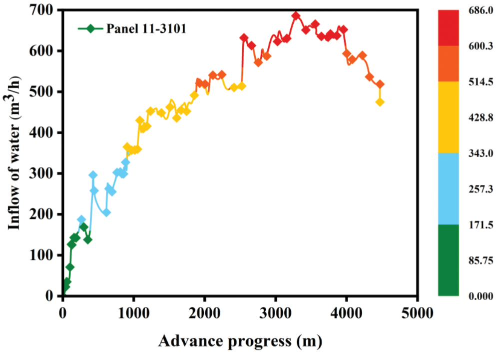

Figure 5 *Water inflow curve in the panel.*

Conclusions

(1) A three-dimensional numerical simulation model of overburden bed separation was constructed, simulating and revealing the distribution characteristics and development patterns of the bed separation space. As the panel advanced continuously, the separation space exhibited a phased development from low-order to high-order in the vertical direction and moved closely along the centre of the coal seam in the horizontal direction. Field verification demonstrated the accuracy of the model.

(2) The risk of water hazards from overburden bed separation in the panel was evaluated and zoned using a comprehensive weighting method. Based on the mechanism of water inrush from bed separation, the main controlling factors of water hazards were analysed, enabling precise identification and pre-grouting treatment of high-risk areas with high water pressure, thin aquicludes, and highly developed fracture zones.

(3) Through on-site monitoring of changes in water inflow, water quality analysis, it was confirmed that no sudden water hazards from bed separation occurred during the mining process, demonstrating effective prevention and control of bed separation water hazards.

Acknowledgements

The authors thank the financial support of the National Natural Science Foundation of China with a grant No. 42130706 and Deep Seek for the language translation help.

References

Bai J, Zhu Z, Liu R *et al.* (2021) Groundwater runoff pattern and keyhole grouting method in deep mines. Bull Eng Geol Environ 80(7):5743-5755. https://doi.org/10.1007/s10064-021-02102-y.

Cao Y, Yin Q, Zhang G. (2024) Study on the mechanism and prevention countermeasures of compound separation water inrush. China Min Mag 33(6):194-202. https://doi.org/10.12075/j.issn.1004-4051.20240108.

Gao Z, Xu G, Li H *et al.* (2023) Bed separation formation mechanism and water inrush evaluation in coal seam mining under a karst cave landform. Processes 11(12):3413. https://doi.org/10.3390/pr11123413

Jia J, Jia Q, Sang X *et al.* (2023) Review and prospect of coal mine geological guarantee system in China during 30 years of construction. Coal Geol Explor 51(1):86-106. https://doi.org/10.12363/issn.1001-1986.22.07.0564.

Qiao W, Wang Z, Li W *et al.* (2021) Formation mechanism, disaster-causing mechanism and prevention technology of roof bed separation water disaster in coal mine. J China Coal Soc 46(2):507-522. https://doi.org/10.13225/j.cnki.jccs.XR20.1972.

The Legacy of Hard Coal Mining Revealed by Isotopic Fingerprinting of Mine Waters, Ruhr Area, Germany

B.M.A. Teichert[1], H. Jasnowski-Peters[1], S.E. Nikutta[1], H. Strauss[2], S. Schlömer[3], S. Westermann[1]

[1]*Research Center of Post-Mining, Technische Hochschule Georg Agricola University, Herner Str. 45, Bochum, Germany, ORCID 0000-0003-1729-9064*

[2]*University Münster, Institute for Geology and Paleontology, Corrensstr. 24, Münster, Germany, ORCID 0000-0003-2639-1225*

[3]*Federal Institute for Geosciences and Natural Resources, Stilleweg 2, Hanover, Germany, ORCID 0000-0002-7706-4235*

Abstract

Hard coal mining ended in Germany in the Ruhr Area in December 2018. The cessation of mining activities and the associated changes in mine water management lead to a controlled mine water rebound. The geochemical composition of mine water is fundamentally influenced by sulfur cycling. Research results enable a deeper understanding of the sulfur and carbon cycles in mine water, and thus provide important information about ongoing biogeochemical processes in the now inaccessible underground mine workings. This in turn allows projecting expected biogeochemical changes into the future which is important for risk assessment.

Keywords: Ruhr Area, mine water, sulfate, methane, bacterial sulfate reduction, isotopic composition, iron sulfide oxidation

Introduction

The carbon and sulfur cycle in mine waters of shallow to deep mine workings in the Ruhr Area is mainly controlled by the presence of iron sulfide in hard coal deposits. Iron sulfide, mostly as pyrite, is oxidized under aerobic conditions in a complex hydrobiogeochemical process, often catalyzed by bacterial species such as *Acidithiobacillus ferrooxidans* and *Leptospirillum* sp.. Pyrite can be oxidized either by dissolved molecular oxygen (eq. [1]) or by ferric iron (eq. [2]; Singer & Stumm 1970). Oxygen in water ensures consistently high reaction rates (eq. [3]) as it accelerates the oxidation of ferrous iron (Fe^{2+}) to ferric iron (Fe^{3+}). This reaction may be catalyzed by microorganisms:

$$[1]\ FeS_2 + 3.5O_2 + H_2O \rightarrow Fe^{2+} + 2SO_4^{2-} + 2H^+$$

$$[2]\ FeS_2 + 14Fe^{3+} + 8H_2O \rightarrow 2SO_4^{2-} + 16H^+$$

$$[3]\ Fe^{2+} + 0.25O_2 + H^+ \rightarrow Fe^{3+} + 0.5H_2O$$

The sulfate formed during iron sulfide oxidation shows a diagnostic isotopic fingerprint because practically no fractionation occurs during oxidation. Therefore, the sulfur isotopic composition of the resulting dissolved sulfate reflects the signature of the original iron sulfide.

Bacterial sulfate reduction is an important process in which organic matter is mineralized under anaerobic conditions. Sulfate acts as an electron acceptor in this metabolic pathway. The following equation [4] illustrates organotrophic sulfate reduction, assuming a simple organic compound (CH_2O):

$$[4]\ SO_4^{2-} + 2\ CH_2O \rightarrow H_2S + 2\ HCO_3^-$$

Continued sulfate reduction leads to sulfate depletion if sulfate is not sufficiently replenished. The reaction product, hydrogen sulfide (H_2S), can precipitate as iron sulfide in the presence of reactive Fe^{2+}-species. Bacterial sulfate reduction is associated with a kinetic fractionation of the sulfur and oxygen isotopes of the dissolved sulfate. Bacteria preferentially use the lighter isotope. As a result, the reaction product (H_2S) is enriched in the lighter sulfur isotope ^{32}S, while the remaining dissolved sulfate becomes enriched in the heavier sulfur isotope ^{34}S. In natural environments, a sulfur isotope fractionation range of 20 ‰ to 40 ‰ is commonly observed between the sulfate and the resulting hydrogen sulfide during bacterial sulfate reduction (e.g., Canfield 2001). However, even larger fractionations have been observed (Sim *et al.* 2011).

In the presence of methane (CH_4), bacterial sulfate reduction can also be coupled to the anaerobic oxidation of methane (AOM, eq. [5]):

$$[5]\ CH_4 + SO_4^{2-} \rightarrow HCO_3^- + HS^- + H_2O$$

Terrestrial environments, especially in anaerobic groundwaters or mine waters, have been studied to a much lesser extent than marine environments (e.g. Banks & Boyce 2023, Dockins *et al.* 1980, Jakobsen & Postma 1994, Malik *et al.* 2023, Schulte *et al.* 1997). The goal of this project is to characterize the sulfur turnover using isotope analyses and to identify the influence of microbially controlled processes during the interaction between hard coal deposits and mine water.

Study area

The Carboniferous geology in the Ruhr Area is defined by hard coal-bearing strata that was formed in extensive swampy environments. These layers, rich in terrestrial plant material, were later buried (resulting in coal formation) and deformed by tectonic activity. Over time, they became unconformably overlain by Permian, Mesozoic and Cenozoic successions, reflecting a dynamic geological history of subsidence, sedimentation, and uplift. Today, Carboniferous rocks are only exposed in the southern part of the Ruhr Area. The strata are dipping to the northwest and mostly found beneath thick overburden.

Methods

Sampling

Since 2021, mine water was sampled every two months at nine different mine water pumping stations in the Ruhr Area (WA: Walsum, CO: Concordia, AM: Amalie, ZV: Zollverein, STI: Stinnes, CG: Carolinenglueck, RM: Robert Mueser, FN: Friedlicher Nachbar, HN: Heinrich). Due to the mine water rebound and the involved changes in mine water management, five mine water pumping locations were closed during 2022 and 2023. Therefore, only four locations (WA, HN, FN, RM) are being sampled since 2023.

Figure 1 *Mine water sampling locations since 2021 (yellow: until 2022/2023, red: ongoing).*

Isotope analysis

For sulfate sulfur and oxygen isotope analyses, dissolved sulfate was precipitated as barium sulfate at pH ≤ 2 and sub-boiling conditions using an 8.5% $BaCl_2$ solution following Dogramaci *et al.* (2001). Sulfur isotope measurements ($\delta^{34}S$) were performed in continuous-flow mode via EA-IRMS using a Flash EA Isolink elemental analyzer interfaced to a ThermoScientific Delta V Advantage isotope ratio mass spectrometer. Results are reported in the standard delta notation as per mil difference to the V-CDT standard. Reproducibility as determined through replicate measurements was generally better than 0.3 ‰. Analytical performance was monitored using international reference materials IAEA S1, S2, S3, NBS 127 and lab reference materials Ag_2S and CdS. Oxygen isotope measurements were carried out in continuous-flow mode using a high-temperature combustion unit (TC/EA) interfaced to a ThermoScientific Delta V Plus. Results are reported in the standard delta notation as per mil difference to V-SMOW. Reproducibility as determined through replicate measurements was generally better than 0.5 ‰. International reference materials IAEA SO-5, SO-6, NBS 127 and a lab $BaSO_4$ reference material were measured to monitor analytical performance.

Sulfide sulfur, stabilized during sampling with zinc acetate solution as zinc sulfide, was transferred to silver sulfide following Canfield *et al.* (1986). Sulfur isotope measurements were performed via EA-IRMS as described above. Results are reported in the standard delta notation ($\delta^{34}S$) as per mil difference to the Vienna Canyon Diablo Troilite (V-CDT) standard.

Carbon isotope signatures of methane were determined after injecting into a continuous flow GC-IRMS system (Agilent GC coupled to a Thermo Fisher Scientific MAT 253 via a GC-Combustion interface II/III). The different compounds were separated on a 25 m Porapak column and methane was combusted to CO_2 at a temperature of 960 °C. The reproducibility for $\delta^{13}C$ is ± 0.3‰. $^{13}C/^{12}C$ are presented in the standard δ-notation versus the reference standard V-PDB.

Compositional gas analysis

Sampling and analysis of dissolved hydrocarbon has followed the internal standard operation procedures. In short, 100 mL serum flasks were filled air-free, stabilized with 1 mL HCl (molarity 9 mol/L) and immediately crimped with Teflon-coated butyl-rubber seals. The dissolved gas concentrations were determined applying a headspace equilibration method as described in Schloemer *et al.* (2018). Hydrocarbon composition was determined by means of a Trace 1310 GC (Thermo Fischer Scientific, USA) equipped with a heated valve system and column switching. Pre-separation of hydrocarbons (C1 through C6) from a 500 µL sample was performed on a non-polar polysiloxane polymer column (Restek MX-1, 15 m, 0.28 mm ID, film thickness 3 µm). Molecular weight components >C7 were back-flushed. Full separation was performed on the main 50 m Al_2O_3 capillary column (0.32 mm ID, film thickness 5 µm). Both columns were operated non-isothermally. All components were detected on a Flame Ionization Detector (FID) with helium (He) as carrier gas. The quantification limit for dissolved methane is ~20 nL/L, with a duplicate error of ±10%. The ethane/propane quantification/detection limits are 10 nL/L and 3 nL/L, respectively.

Results and Discussion

The sampled locations show large differences in electrical conductivity (EC). The southern part of the Ruhr Area is characterised by a rather low EC with values between 2,000 µS/cm and 6,000 µS/cm (HN, FN, AM, RM) while medium EC values can be found at ZV and CG (19,500 µS/cm to 33,000 µS/cm). The highest conductivities have been measured at CO, WA and STI (63,800 µS/cm to 132,500 µS/cm).

The oxygen and sulfur isotopic composition of the dissolved sulfate (Figure 2) shows that each location has its characteristic isotopic signature. A positive correlation between $\delta^{18}O$ and $\delta^{34}S$ can be observed. This is indicative for the process of microbial sulfate reduction where microbes preferentially turn over the light sulfur and oxygen isotopes which results in an enrichment of the heavy

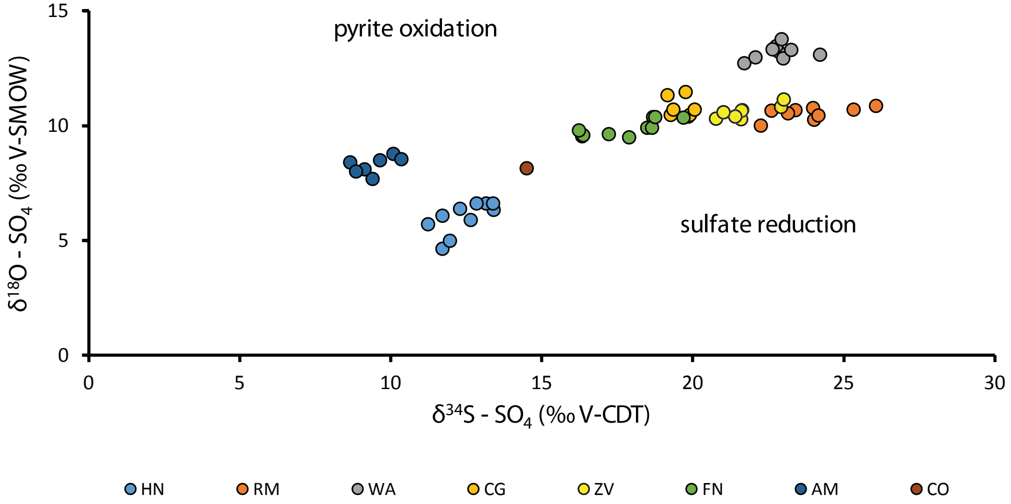

Figure 2 *δ¹⁸O and δ³⁴S values of dissolved sulfate in mine waters from the Ruhr Area.*

sulfur and oxygen isotopes in the dissolved sulfate.

The sampled sites show different geochemical characteristics based on the geological history of the Ruhr Area. In the southern Ruhr Area, the Cretaceous overburden is either low or completely missing and allows the infiltration of meteoric waters into the underground mine workings (HN, FN, AM, RM). These locations are characterised by varying δ³⁴S values and relatively constant EC values. This can be interpreted as mine workings with a rather constant water source (Figure 3).

In the northwestern part of the Ruhr Area, the sampled mine waters (ZV, CG, CO, WA) have medium to high salinities (Figure 3). Here, the influence of lateral fluid flow or a contribution from deep-seated groundwater dominates the mine water composition. An aquitard in the overlying Cretaceous strata (Emscher Formation) of negligible to low thickness might limit the infiltration of meteoric waters locally. The saline, deep

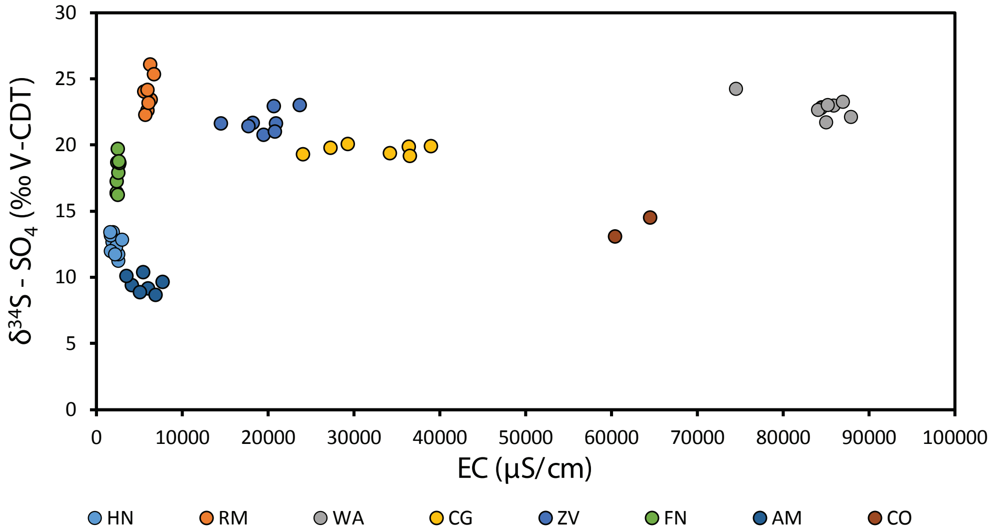

Figure 3 *Sulfur isotopic composition of sulfate versus electrical conductivity (EC) of mine waters.*

water mass is most probably derived from the dissolution of Permian evaporite deposits in the Lower Rhine region or from Cretaceous saline waters. Deep mine waters with high salt concentrations are found in many coal mining regions (e.g., England, Spain, Poland, China). Their origin is often unclear and remains a topic of discussion (Banks *et al.* 2020).

Geochemical characteristics of these saline mine waters is a variable EC, indicating changes in the composition of the supplied waters (Figure 3). The sulfur isotopic composition of the dissolved sulfate however shows no large variation. This indicates a rather homogenous sulfate source. Mainly high $\delta^{34}S$ values are typical for ongoing sulfate reduction.

The molecular as well as the isotopic composition of methane might provide some additional information on the main processes involving sulfate but also carbon in the mine waters of the Ruhr Area (Figure 4). Free methane, measured at combined heat and power plants (Teichert *et al.* in prep.), shows a mixture of microbial and thermogenic methane. Some of the sampled locations have an unambiguous microbial methane source. This observation has been previously made by Thielemann *et al.* (2004) and seems to be typical for the Ruhr Area. Some of the dissolved methane samples follow the same mixing trend as the free methane. However, most samples indicate a shift towards heavier $\delta^{13}C$ values with a consistent molecular composition (methane/ (ethane + propane)). This characteristic shift might be the result of anaerobe methane oxidation (AOM) where sulfate is bacterially reduced and methane anaerobically oxidized. While microbes preferentially oxidize the light carbon (^{12}C) isotope the remaining dissolved methane gets enriched in the heavier ^{13}C leading to increasingly heavier $\delta^{13}C$ values.

Conclusions

- If mine water contains oxygen through the infiltration of meteoric water (low EC), iron and sulfate are released through the process of iron sulfide oxidation. Iron will rapidly oxidize to FeOOH and may settle out. Sulfate has a typical light sulfur isotopic composition indicative of its origin from the oxidation of iron sulfide. This scenario can be observed at most sites in the southern Ruhr Area.

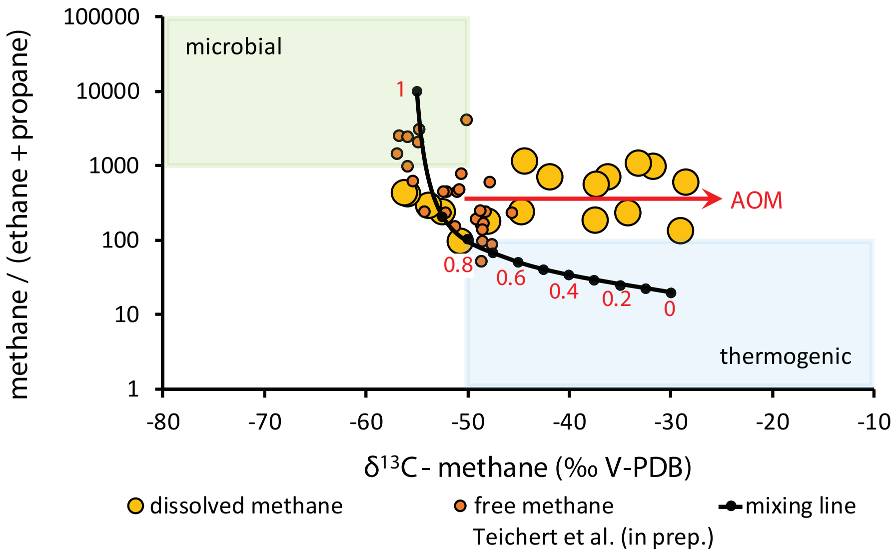

Figure 4 Carbon isotopic composition of methane versus methane/(ethane + propane) ratio. The mixing line shows mixing between an assumed microbial (-55; 10,000) and thermogenic (-30; 20) methane endmember. Small, black circles show 10% intervals; red numbers give 20% intervals. Red arrow indicates direction of isotopic shift due to anaerobe methane oxidation (AOM).

- Anoxic, highly saline mine waters derive their sulfate not only from the oxidation of iron sulfide but also from the dissolution of evaporites and/or fossil seawater. In deep, anoxic mine workings (with the exception of CO), the sulfate is bacterially reduced, resulting in the formation of hydrogen sulfide and isotopically enriched sulfur and oxygen isotope values of sulfate. This scenario can be observed at the sites in the northwestern Ruhr Area.
- At some locations (RM, FN) with a rather low EC and sulfate primarily derived from iron sulfide oxidation, there is indication for bacterial sulfate reduction.
- Abandoned mines which undergo mine water rebound and show bacterial sulfate reduction (with sulfate derived from iron sulfide oxidation), will experience a declining hydrogen sulfide production in the future due to declining sulfate concentrations over time.
- The molecular and isotopic composition of dissolved methane in the mine water supports ongoing microbial sulfate reduction combined with anaerobe methane oxidation.

Acknowledgments

The authors would like to thank L. Rose and T. Genth for help with water sampling. A. Fugmann is thanked for assistance in the laboratory (Univ. Münster) and T. Trieb (RAG AG) during mine water sampling. We greatly appreciate the support and discussion with the RAG AG as well as the financial support of this project. The authors thank two anonymous reviewers for providing critical comments which helped to strengthen this text.

References

Banks D, Boyce AJ (2023) Dissolved sulfate δ^{34}S and the origin of sulfate in coal mine waters; NE England. Quarterly Journal of Engineering Geology and Hydrogeology 56: 1–12.

Banks D, Boyce AJ, Burnside NM, Janson E, Roqueñi Gutierrez N (2020) On the common occurrence of sulphate with elevated δ^{34}S in European mine waters: Sulphides, evaporites or seawater? Int. Journal of Coal Geology, 103619: 1–18.

Canfield DE (2001) Biogeochemistry of Sulfur Isotopes. Reviews in Mineralogy and Geochemistry 43(1): 607–636.

Canfield DE, Raiswell R, Westrich JT, Reaves CM, Berner RA (1986) The use of chromium reduction in the analysis of reduced inorganic sulfur in sediments and shales. Chem. Geol. 54: 149–155.

Dockins WS, Olson GJ, McFeters GA, Turbak SC (1980) Dissimilatory bacterial sulfate reduction in Montana groundwaters. Geomicrobiology J. 2(1): 83–98.

Dogramaci SS, Herczeg AL, Schiff SL, Bone Y (2001) Controls on δ^{34}S and δ^{18}O of dissolved SO_4 in aquifers of the Murray Basin, Australia and their use as indicators of flow processes. Appl. Geochem. 16: 475–488.

Jakobsen R, Postma D (1994) In situ rates of sulfate reduction in an aquifer (Rømø, Denmark) and implications for the reactivity of organic matter. Geology 22: 1103–1106.

Malik C, Böttcher ME, Jenner A–K, Schmiedinger I, Löffler S (2023) Akkumulation von Sulfat und Karbonat in nordostdeutschen Grundwässern – Eine Multi-Isotopen-Analyse. Grundwasser 28: 331–344.

Schloemer S, Oest J, Illing CJ, Elbracht J, Blumenberg M (2018) Spatial distribution and temporal variation of methane, ethane and propane background levels in shallow aquifers – A case study from Lower Saxony (Germany). Journal of Hydrology: Regional Studies 19: 57–79.

Schulte U, Strauß H, Bergmann A, Obermann P (1997) Isotopenverhältnisse der Schwefel – und Kohlenstoffspezies aus Sedimenten und tiefen Grundwässern der Niederrheinischen Bucht. Grundwasser 3: 103–110.

Sim MS, Bosak T, Ono S (2011) Large sulfur isotope fractionation does not require disproportionation. Science 333(6038): 74–77.

Singer PC, Stumm W (1970) Acidic mine drainage: the rate-determing step. Science 167: 1121–1123.

Teichert *et al.* (in prep.) Abandoned mine methane – defining methane sources in the Ruhr area and Saarland, Germany. – to be submitted to International Journal of Coal Geology.

Thielemann Th, Cramer B, Schippers A (2004) Coalbed methane in the Ruhr Basin, Germany: a renewable energy resource? Organic chemistry 35: 1537–1549.

Utilizing pore pressure simulations with an unstructured mesh for closure design optimization of the Wanagon Stockpile at the Grasberg Mine

Mark J. Thomasson[1], Made Mahayasa[2], Larry Standridge[1], Drew Enns[1], Brad Ruddy[1], Steven C. Schmelter[1]

[1]*Call & Nicholas, Inc., United States of America*

[2]*Freeport-McMoRan Inc., United States of America*

Abstract

Estimating pore pressures distributions within stockpiles poses a significant challenge in industry as the distribution of hydraulic properties is linked to construction methodology, materials, and sequence. This paper presents a case study demonstrating how a FEFLOW 3D unstructured meshing approach can be used to simulate a complex hydrogeologic system. Advanced tools were developed and used to build numerical models supporting design and material optimization, locating monitoring targets, and developing Trigger Action Response Plans. Utilizing identical meshes for hydrogeologic and geotechnical models allows for direct transfer of pore pressure distributions and eliminates the need for interpolation between the models.

Keywords: Grasberg, heterogeneity, pore pressure modelling, design optimization, closure monitoring

Introduction

The Grasberg surface mine, operated by PT Freeport Indonesia and located in Papua Province, Indonesia, began ore production in 1990 until open pit mining operations ceased in 2020. The topography surrounding the Grasberg Mine is rugged with steep slopes, sharp peaks, and deeply incised valleys with elevations in the area between 3200 and 4600 m. The climate is considered alpine/sub-alpine with little variation of temperatures throughout the year, and rainfall occurring nearly every day. The extreme environment left few options for storing overburden removed to access metal containing ore and required operational and engineering controls to safely operate in this unforgiving and challenging environment. The Wanagon Basin, located to the west of the Grasberg open pit, was one of the locations selected for long term material storage. This basin included lakes and natural drainage channels that would be filled by OBS materials. Fig. 1 presents topographic contours of the Wanagon area prior to OBS filling and identifies important features. As open pit mining began, stockpile plans were developed and engineering work commenced to identify operational (Irwandy 2004), environmental (Miller 2003, Prawawa 2018, Widjijanto 2015), and long-term closure options (Mahayasa 2021).

OBS was placed in the Wanagon Basin with run of mine (ROM) material delivered by haul trucks and from a crushing and conveying (C&C) stacker system. Filling was completed using top-down construction forming continuous stockpile slopes with heights up to 400 m. Three primary placement elevations were used and include the upper area (4200 m), the middle area (3845 m) and the lower area (3685 m), with the toe of OBS material reaching the 3200 m elevation.

Using advanced tools developed by CNI, a 3D unstructured mesh was created for geotechnical and hydrogeological numerical analysis where material properties were uniquely defined based on the location, method, type, and sequence of material placement. A FEFLOW model was calibrated to match observed data then forward analyses and sensitivity studies were conducted to support Wanagon closure.

Wanagon Closure Goals

There have been numerous challenges because of site-specific conditions which include steep terrain, foundations containing lakes, vegetation, and alluvial deposits, and a high precipitation environment. These challenges during the operational and closure periods were mitigated through operational practices and engineering designs.

Closure design of the OBS had to include feature to prevent surface erosion and a basal drain zone to accommodate subsurface flows through the OBS. These surface and subsurface water conveyance systems must have the capacity to accommodate maximum precipitation events to manage safety risks during construction and for long-term facility stability.

Primary considerations for stability include:

1. Reclaiming the stockpile slopes to a geometry to accommodate erosional design elements to capture, direct, and discharge surface water flows in a controlled manner.
2. Resloping the overall stockpile to an appropriate slope angle considering stockpile geometry, foundation, and water pressures within the stockpile due to precipitation infiltration and flows through the basal drain system.
3. Engineering and constructing a stockpile underdrain exit structure at the toe of the stockpile to allow water discharge under maximum event flow conditions without erosion of the exit structure.

To achieve these goals, critical areas of the OBS were identified, TARPS and monitoring systems were developed for risk management, and locations for long-term monitoring systems were identified. Finally, the closure design, material requirements, and construction techniques were optimized to minimize construction time and costs.

Hydrogeological Setting

The final OBS facility has a volume of ≈465 Mm^3 equivalent to ≈837 M tonnes of fill, with an infiltration surface area of 3.1 Mm2. Ground water flow through the system is generally from the northern end at an elevation of 3960 m, to the south-southwestern end at 3,200 m. Using an approximate path length of 4,080 m, the overall topographic gradient is 0.18 %. Fig. 2 shows topography of the final Wanagon OBS Design along with adjacent excavations of the WWSS and the South Knob.

C-SUM Mesh Generation

Analyses in geotechnical engineering often involves complex three-dimensional geometries representing geologic structures and material properties coupled with a defined sequence of excavation or filling steps to assess stability during and after construction. Stability is assessed using numerical geomechanical stress models and plasticity criterion to determine yielding. When groundwater is present, pore pressures need to be incorporated in the stress analysis, as pore pressures can have a destabilizing effect. FEFLOW is a groundwater modelling software used to simulate pore pressure distributions needed for stress analysis.

Conditions that necessitate both stress-based geotechnical and hydrogeologic modelling can be expensive and time consuming, requiring the construction of multiple models for each analysis type. Unstructured meshing is available in FEFLOW, but it cannot generate a mixed element mesh. To simplify the modelling, CNI has developed proprietary tools and processes to create three-dimensional mixed element unstructured meshes for numerical analyses.

CNI Synchronized Unstructured Mesh (C-SUM) incorporates complex 3D model geometries and material property assignments which can vary both temporally and spatially. The mesh developed using C-SUM can be used in different numerical analysis packages allowing elemental and nodal values to be directly synchronized between analysis types, eliminating the need for interpolation between dissimilar model meshes. While not presented in this case study, a structured mesh was used for the same model volume. General observations between these two approaches indicates the C-SUM approach requires fewer elements and nodes, has more consistent element sizes, faster solve times, improved mass balance, and better numerical stability.

Model Definition

C-SUM was used to define a 3D FEFLOW model, for the end of year 2022 (EOY2022) and final (YRFinal) design surfaces, to simulate groundwater flows and pore pressure distributions throughout the OBS facility.

The OBS construction sequence and placement method were used to define three-dimensional material domains in twelve steps. Every element was assigned properties representative of the placement sequence, relative position, and material type. The YRFinal model contains ≈313 k nodes defining ≈317 k active elements.

Material types were categorized as: 1) ROM, 2) C&C, 3) screened coarse, or 4) rehandled. ROM and C&C materials were placed using a top-down method which resulted in gravity segregation with the coarsest particles at the base of the stockpile, and the finest particles retained near the crest. Particle sizes also vary with C&C being crushed to a maximum particle size of 8 inches. The screened coarse material was processed to provide a well sorted material for constructing the outflow exit structure. Lastly, rehandle material consists of material placed without segregation resulting in lower conductivity.

Boundary conditions representing the OBS system, as described above in hydrogeologic setting, were defined. Conventional groundwater flow boundary conditions were used to represent fluxes and forms the basis of the water balance of the system.

Model Methods and Results

The YR2022 model was used to generate a steady state solution to define initial conditions prior to transient flow analysis. Transient boundary conditions were defined along with modulation functions to represent fluctuating conditions that affect infiltration and groundwater flows. Simulations were conducted to adjust hydraulic conductivities to match the system response as observed by groundwater flows, and vibrating piezometer measurements collected during 2022. A calibrated model was achieved matching piezometer measurements in both magnitude and behaviour, as shown in Fig. 3, and to estimated flows into and out of the system.

The YRFinal model, which has two primary objectives, added additional material downstream of YR2022 geometry and incorporated the engineered toe exit structure. The first objective was to guide the material requirements and placement methodology to ensure the system has the capability of discharging high flows through an erosionally stable toe exit structure. The second objective was to verify flows can be transferred through the system without increased pore pressures that may impact stability.

Using the calibrated YR2022 model properties transferred into the YRFinal model, a steady state solution was generated for initial conditions for predictive transient simulations. Predictive simulations evaluated the capability of the system to transfer flows with and without a functioning WDD dewatering system.

Fig. 4 shows geometry, hydrogeologic units (HGU), head, and pressure contours along a section (Fig. 1), assuming the WDD is functional. Results indicate that the system including the engineered exit structure is sufficient to convey all flows through the system. No pressure increases were noted. With the WDD dewatering turned off, increased pressures were noted; however, the increases were insufficient to be detrimental for stability.

Using the model results, areas were identified 1) where pressure increases originate, and 2) where elevated pressures may result in stability concerns. TARPS were defined for critical areas and piezometers installed to trigger actions to manage operational risks. Once closure activities are completed and for long term facility management, additional piezometers are planned to monitor drain zone performance and to provide data needed for future calibrations and predictive analysis.

Conclusion

This case study demonstrates that an unstructured FEFLOW 3D mesh can be used to model a complex hydrogeologic system such as the Wanagon OBS. The model was successfully calibrated using as-placed materials, measured water flows, and pressures. TARPS were defined by using model results to identify critical areas.

With this new approach, the resolution of the pore pressure model was enhanced. Compared to a traditional structured (layered) mesh, improvements were observed. Numerical stability had a reduced error field, run times decreased, convergence improved due to element size consistency, and mass balance is easier to achieve.

For the toe exit structure, material and geometry requirements were determined. While results are not specifically presented in this paper, using an unstructured mesh approach allows results from the hydrogeologic model to be imported directly into geotechnical stability models without the need for interpolating values.

Acknowledgements

The authors would like to thank the staff at PT Freeport Indonesia for their contributions and support of the Wanagon OBS closure project and James Killian, P.G., of CNI and Numerical Solutions for contributions to the C-SUM technique.

References

Irwandy A, Sengara W, Adisoma G, Wawa JS, Stawski M, Nasution Y (2004) Post failure stability analysis and management of Wanagon Overburden Dump. In: Hardygora M, Paszkowska G, Sikora M (Eds), Proceedings of the Thirteenth Symposium on Mine Planning and Equipment Selection. p. 91–96.

Mahayasa M, Simanjuntak M, Johnson M (2021) Wanagon overburden stability; Grasberg surface mine closure. In: Fourie AB, Tibbett M, Sharkuu A (Eds), Mine Closure 2021: Proceedings of the 14th International Conference on Mine Closure, QMC Group, Ulaanbaatar, https://doi.org/10.36487/ACG_repo/2152_04.

Miller S, Andriana J, Richards D (2003) Overburden Geochemistry and Acid Rock Drainage Scale-Up Investigations at the Grasberg Mine, Papua Province, Indonesia. In: Proceedings Sixth International Conference on Acid Rock Drainage (ICARD), Cairns, QLD, July 12-18, 2003. p. 111–121.

Prabawa Y, Bugaleng L, Gautama R, Widiajanto E (2018) Blasting, fragmentation and wall quality result at West Wanagon slope stability project on Grasberg Mine. In: IOP Conf. Ser.: Earth Environ. Sci. 212 012066.

Widijanto E, Setiawan I, Prasetyo G (2015) Dedicated Underground Drainage Drift for Dewatering Wanagon Overburden Stockpile, Grasberg Mine – PT. Freeport Indonesia. *Prosiding TPT XXIV dan Kongres Perhapi.*

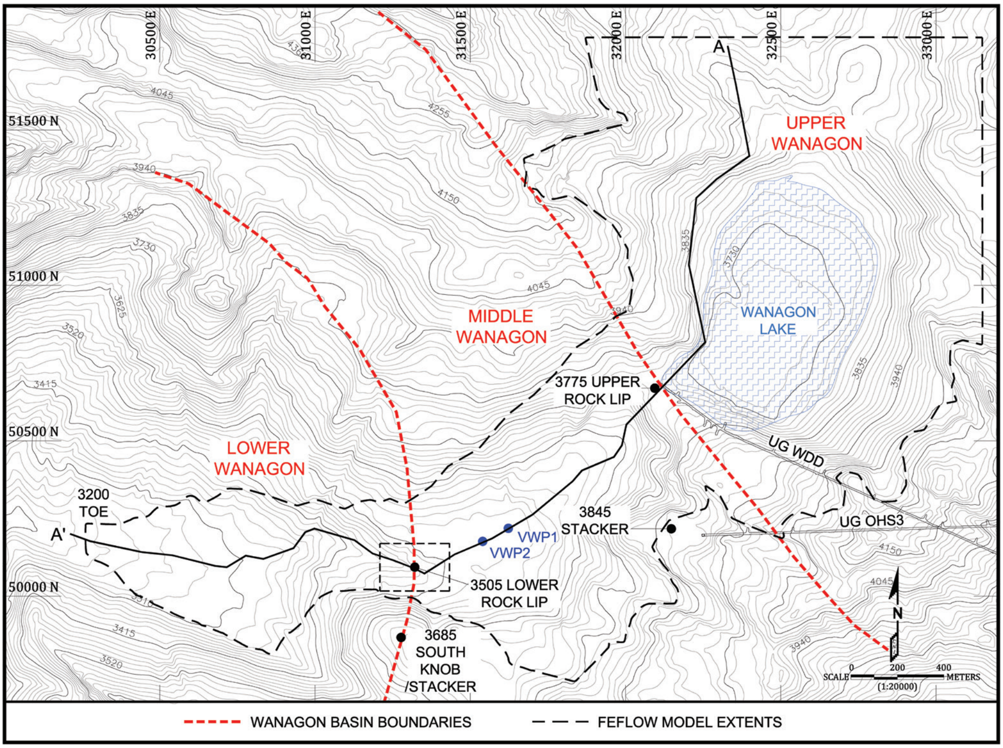

Figure 1 *Topography, features, and locations in the Wanagon Basin before stockpile placement.*

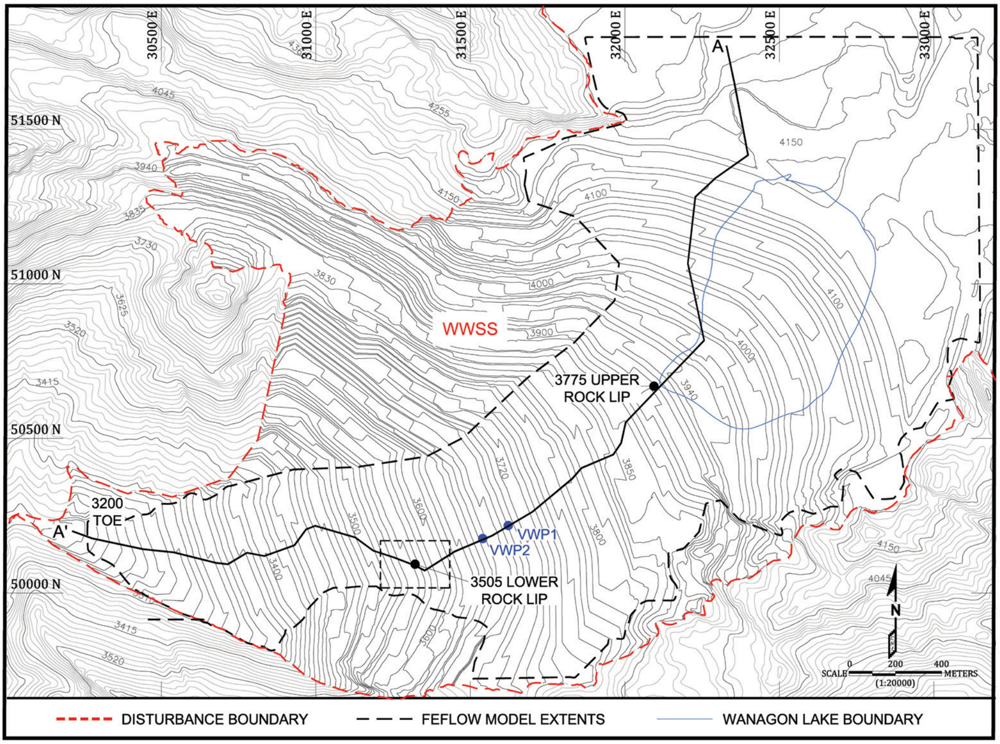

Figure 2 *Topography, features, and locations for the final Wanagon OBS Design.*

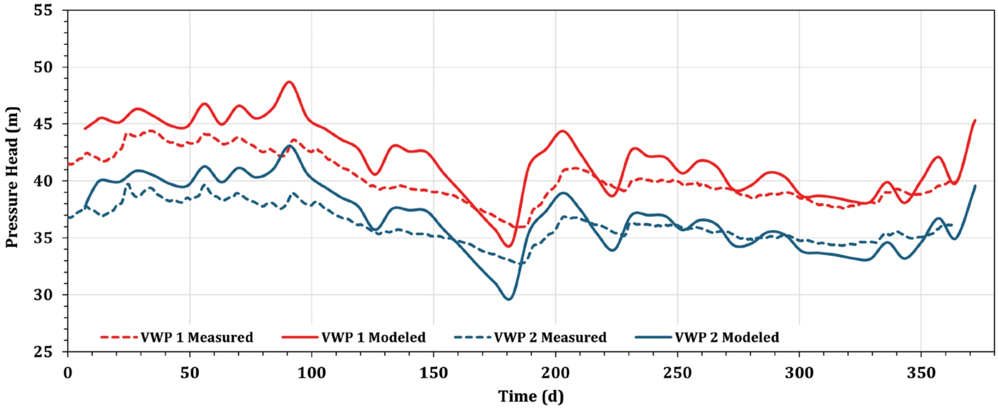

Figure 3 Calibration results for the YR2022 model.

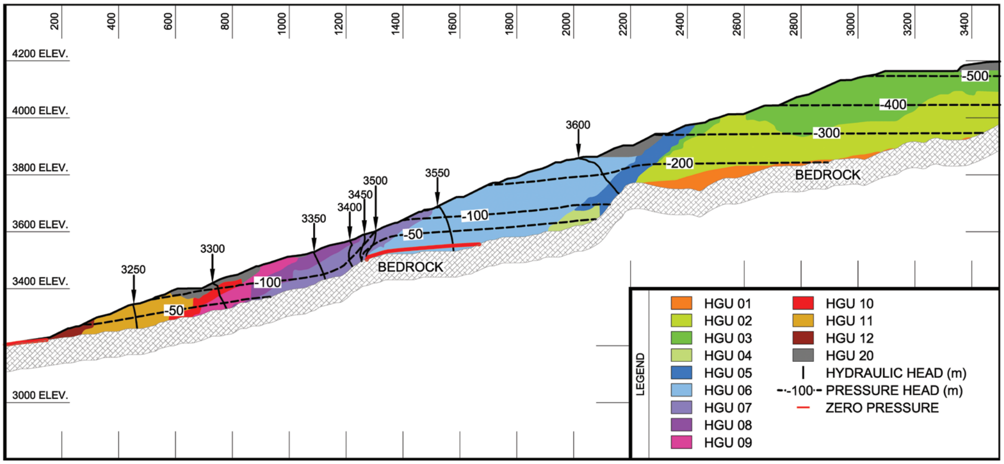

Figure 4 Results for the YRFinal model including the WDD dewatering along section A-A'.

Is the Water Balance of Your Waste Rock Pile Reliable? A framework for Improving Assessment of Water Inputs and Outputs for a Typical Storage Facility

Craig Thompson[1], Randi Thompson[2], and Willy Zawadzki[3]

[1]*BGC Engineering Inc., 234 St. Paul St., Kamloops, BC, Canada V2C 6G4, cthompson@bgcengineering.ca, ORCID 0000-0003-2315-1824*

[2]*BGC Engineering Inc., 234 St. Paul St., Kamloops, BC, Canada V2C 6G4, rthompson@bgcengineering.ca*

[3]*BGC Engineering Inc., 300–3 Fan Tan Alley, Victoria BC, Canada V8W 3G9, wzawadzki@bgcengineering.ca, ORCID 0009-0007-0046-4226*

Abstract

Piles of waste rock placed during mining operations commonly increase from initial heights of several metres to more than 100 m during the life of a mine. Depending on geochemical properties of the waste rock, seepage emanating from the base of piles may require collection and treatment which necessitates adequate planning through development of reliable estimations of the waste rock pile water balance. Using a suite of numerical simulations of a synthetic waste rock pile, consideration of the pile's temporal development is shown to be an important factor on the distribution of water within the waste rock and the timing and magnitude of basal drainage from the pile for a range of climate regimes.

Keywords: Waste rock, numerical model, groundwater, seepage, HydroGeoSphere

Introduction

Waste rock is a ubiquitous mining waste often produced in large quantities as rock mass surrounding the orebody is extracted from the subsurface. The waste rock is frequently stored at the land surface in piles that may be more than 100 m in height and cover several square kilometres. These piles may be temporary features during active mining operations with the waste rock backfilled into open pits and underground workings at the cessation of mining; however, more often they become permanent fixtures in the landscape.

Mine development and closure require estimation of water quantities emanating from these waste rock piles, which, together with geochemical assessment of water-rock interactions within the waste, allow effective short- and long-term planning for water management. Hawley and Cunning (2017) provide generalized guidelines for application of numerical models to estimation of waste rock seepage. Nevertheless, Smith (2021) notes that current state-of-the-science numerical models are not widely applied in practice due to the inherent uncertainty in quantification of waste rock material properties resulting from the wide range in waste particle size (i.e., clay to large boulders) distributions. Moreover, where applied, the numerical models are generally limited to simulation of a static configuration of the piles that does not consider their transient development.

Here results are presented from one-dimensional numerical simulations for a synthetic waste rock pile that gradually increases in height throughout the mine life. One-dimensional simulations were conducted under the assumption that flow through the unsaturated waste rock is primarily vertical. The simulations were used to illustrate the influence of considering the temporal development of the waste rock pile on the pile's water balance.

Methods

One-dimensional numerical simulations were conducted for a 100 m high waste rock pile using HydroGeoSphere (Aquanty 2024), a fully-integrated groundwater-surface water code. The simulations facilitated estimation of the partitioning of rain and snowmelt into infiltration, evapotranspiration, and overland flow at the land surface, changes in moisture storage within the subsurface, and drainage from the base of the waste rock using a physically-based approach. The numerical simulations were driven by daily atmospheric inputs of rain, snowmelt, and potential evapotranspiration derived from a range of climate regimes within Canada (Fig. 1) and marched forward in time using an adaptive time-stepping scheme that incorporated use of sub-daily timesteps as necessary.

The numerical simulations were conducted using 1 m^2 square column models extending vertically across the waste rock pile, and with a nominal ground surface slope of 1%. The vertical grid discretization ranged from 0.02 m at the top of the columns to 0.5 m at the base. Simulations were conducted for a period of 120 years (20 years active mining followed by 100 years closure) using either a static 100 m high column or a column that increased in height with 10 m of fresh (i.e., at low initial saturation) waste rock added every two years of active mining starting from an initial height of 10 m. At closure, a 1 m thick vegetated soil cover was placed at the surface.

Simulations were conducted that considered the waste rock as both "soil-like" materials limited to matrix flow (e.g., commonly encountered in coal operations) or "rock-like" materials with matrix flow and macropore (i.e., dual domain) flow (e.g., characteristic of hard rock settings; Smith, 2021). Specified material properties (Fig. 2) for the simulations were specified based on values reported in the literature (e.g., Smith 2021; Broda *et al.* 2014; Carsel and Parrish 1988) and assumed to remain constant in time. A set of simulations was also conducted using the Site A climate dataset that assumed seasonal freezing due to sub-zero temperatures which may inhibit percolation of water through the waste rock (Langman *et al.* 2017) due to clogging of pores with ice. For these simulations, the hydraulic conductivity of near-surface materials (i.e., upper 1 m) was decreased by a factor of 10^4 from the base case values to represent ice formation with freezing and thawing specified to occur over a three-week period each year. However, changes in waste rock hydraulic conductivity due to freezing may be variable and dependent on a number of factors (e.g., climate, pore size and geometry, water content).

Boundary conditions applied to the surface of the model consisted of daily atmospheric conditions that included inflow from precipitation and snowmelt (calculated externally from the numerical model) and

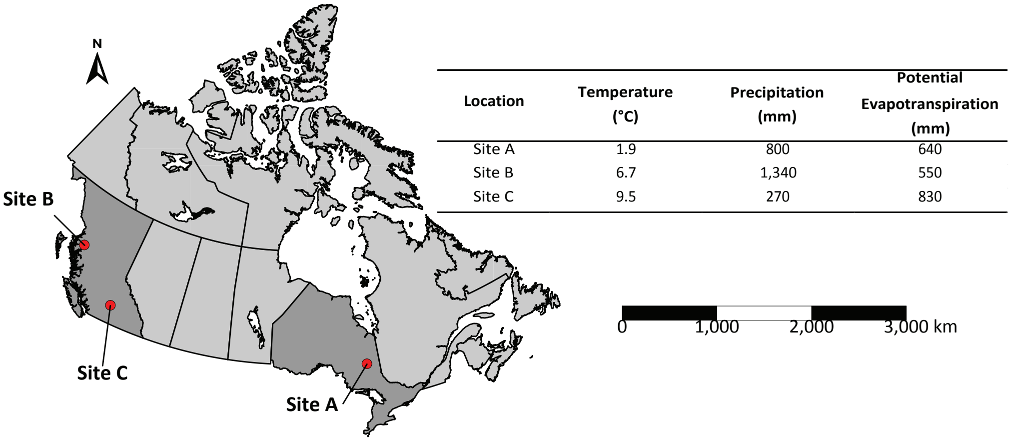

Location	Temperature (°C)	Precipitation (mm)	Potential Evapotranspiration (mm)
Site A	1.9	800	640
Site B	6.7	1,340	550
Site C	9.5	270	830

***Figure 1** Map of Canada showing simulated locations and annual average (1990 – 2020) climate variables. Daily temperature and precipitation were obtained from Environment and Climate Change Canada datasets; potential evapotranspiration was estimated using ClimateNA (Wang* et al. *2023).*

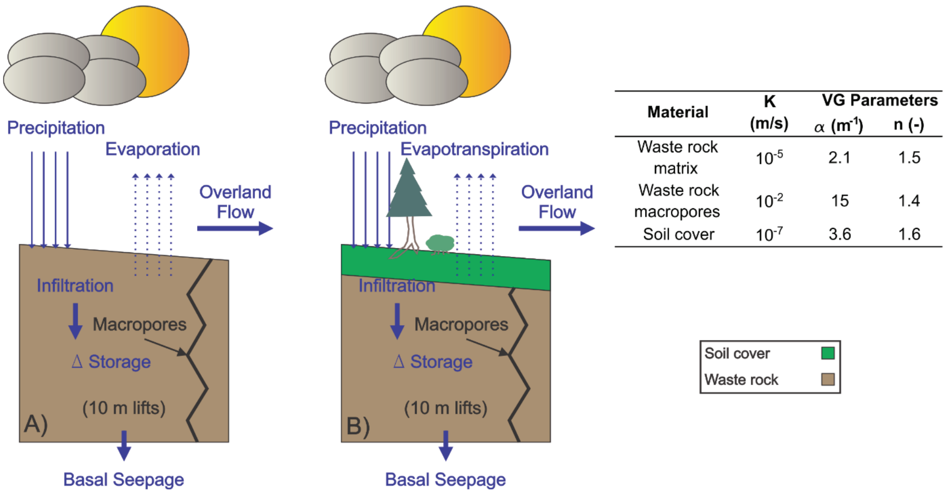

Material	K (m/s)	VG Parameters α (m^{-1})	VG Parameters n (-)
Waste rock matrix	10^{-5}	2.1	1.5
Waste rock macropores	10^{-2}	15	1.4
Soil cover	10^{-7}	3.6	1.6

***Figure 2** Diagram showing simulated waste rock configuration for A) mining operations and B) closure along with model parameters (K is hydraulic conductivity, α and n are VG or van-Genuchten parameters).*

outflow from potential evapotranspiration and overland flow (Fig. 2). At the base of the model, seepage emanating from the waste rock was simulated using a free drainage boundary condition under the assumption that the water table in the native materials underlying the pile remains below the pile's base.

Results and Discussion

Fig. 3 provides an example of the simulated saturation within the waste rock at the end of the 20-year mining period. Above a depth of approximately 20 m, predicted saturations are relatively similar (i.e., within 0.05) for all scenarios reflecting recent climate forcings. Below 20 m depth, predicted saturations generally cluster into two groups defined by the temporal representation of the waste rock pile within the simulations. In the first group (Group A) that includes scenarios that represented the waste rock as a static pile at its full height, the predicted saturations are higher and more uniform with depth. In the second group (Group B) that considered the temporal development of the pile, the saturations are lower due to drainage reporting to the base of the pile earlier in the mine life (Table 1) and more variable with depth due to saturation disequilibrium between waste rock lifts.

Predicted water fluxes and saturation at the base of the waste rock using the Site A climate dataset are provided in Fig. 4 for the 120-year simulations, considering "soil-like" and "rock-like" waste rock, static and increasing pile height, and near-surface freezing. Predicted evapotranspiration and overland flow rates, controlled by recent near-surface conditions, are similar between scenarios. A wider range in water flux is predicted for basal drainage rates during mining operations and the initial years of closure, as the basal drainage is influenced by the cumulative evolution of the pile (e.g., volume of waste rock and available storage). For the climate prevalent in Site A, where precipitation is somewhat higher than potential evapotranspiration, consideration of the early stages of pile development where the

***Table 1** Predicted waste rock pile wet-up times.*

Climate Location	Predicted Wet-up Time (yr) Assuming Static Facility	Predicted Wet-up Time (yr) Assuming Transient Facility
Site A	15 to 19	2
Site B	9 to 10	<1
Site C	80 to >120	7 to 31

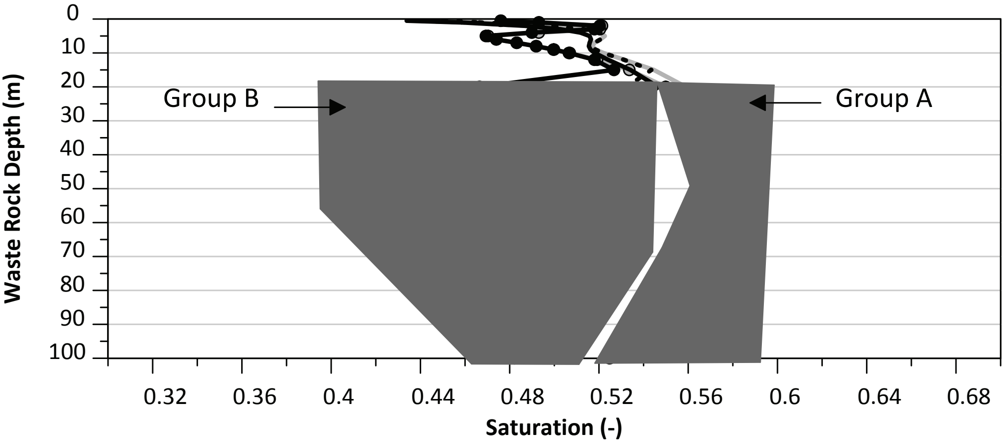

Figure 3 *Predicted saturation within the waste rock at the end of the 20-year mining period using the Site A climate data. Solid and dashed lines indicate respective "soil-like" and "rock-like" waste rock; grey and black lines indicate respective static height and increasing pile height, symbols indicate scenarios with seasonal near-surface freezing, and shaded areas are described in the text. Residual and initial saturation specified to be 0.08 and 0.18, respectively.*

waste rock is initially shorter with less available storage yields a wet-up time (i.e., time for drainage to start reporting at the base of the pile) of 2 years (Table 1). Representation of the waste rock pile with a static configuration (i.e., a more conventional analysis) results in longer predicted wet-up times of 15 to 19 years. For other climate regimes (Table 1), consideration of the pile's temporal development may alter predicted wet-up times on the order of years (e.g., wetter climate such as Site B) to decades (e.g., drier climates such as Site C).

Results of the simulations indicate that the temporal development of waste rock piles is an important factor that should be considered in waste rock seepage assessments where adequate information is available. The rate of pile development influences both the water distribution within the waste rock and the timing and magnitude of drainage rates at the base which may have important implications for mine developments due to costs associated with storage and treatment of waste rock effluent.

Mine planning and operations may require a large number of scenarios to be evaluated to address variants in mine development schedules and permitting requirements. Furthermore, extensive sensitivity analyses of predicted seepage quantities are commonly needed to adequately account for uncertainty in waste rock properties and climate variability. Nevertheless, the assessments are relatively efficient to conduct, particularly in a one-dimensional framework, with computational times on the order of two to five hours on a standard desktop computer.

Conclusions

The temporal development of waste rock piles is an important factor that should be considered in seepage assessments, as the rate of development influences the distribution of water within the waste rock and the timing and magnitude of drainage at the base. One-dimensional simulations conducted using HydroGeoSphere were used to derive predictions for a range of scenarios and climate conditions; however, the simulations could be extended to two- and three-dimensions based on project requirements and available data.

References

Aquanty (2024) HydroGeoSphere, Revision 2688, Build date May 3, 2024.

Broda, S, Aubertin, M, Blessent, D, Hirthe, E, and Graf, T (2014) Improving control of contamination from waste rock piles. Environmental Geotechnics, http://dx.doi.org/10.1680/envgeo.14.00023, Paper 14.00023

Carsel, RF, and Parrish, RS (1988) Developing joint probability distributions of soil water retention characteristics. Water Resources Research, 24 (5): 755–769. https://doi.org/10.1029/WR024i005p00755

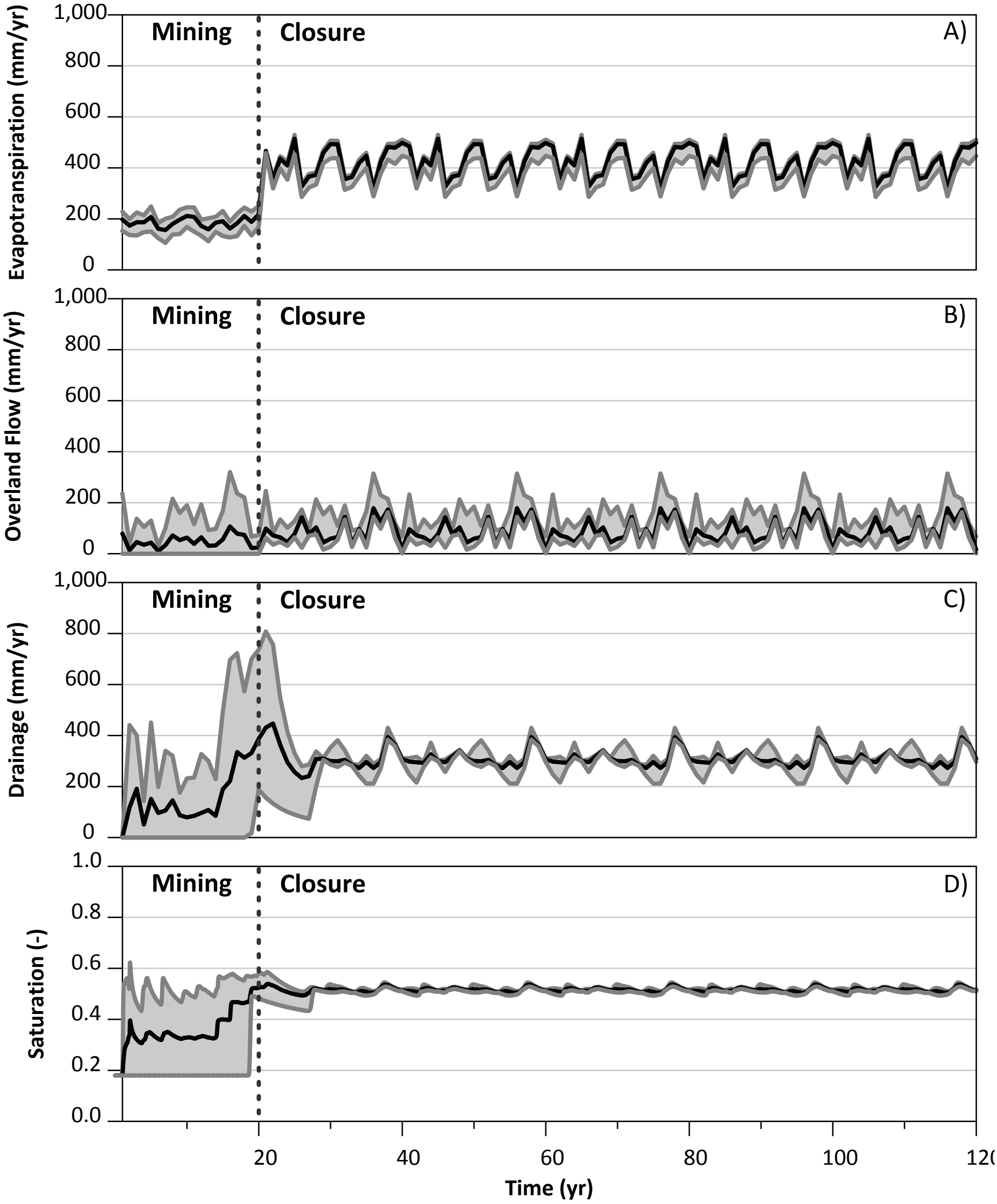

Figure 4 Simulated range in A) annual evapotranspiration, B) annual overland flow, C) annual basal drainage, and D) daily saturation at the base of the waste rock pile using Site A climate data. Shaded area bounds minimum and maximum predictions, black line indicates average of predictions, and dashed line indicates transition from active mining to closure.

Hawley, M, and Cunning, J (2017) Guidelines for Mine Waste Dump and Stockpile Design. CSIRO Publishing.

Langman, JB, Blowes, DW, Amos, RT, Atherton, C, Wilson, D, Smith, D, Sego, DC, and Sinclair, SA (2017) Influence of a tundra freeze-thaw cycle on sulfide oxidation and metal leaching in a low sulfur, granitic waste rock. Applied Geochemistry, 76: 9–21. https://doi.org/10.1016/j.apgeochem.2016.11.010

Smith, L (2021) Hydrogeology and Mineral Resource Development. The Groundwater Project, Guelph, Ontario, Canada.

Wang, T, Mahony, C, Spittlehouse, D, and Hamann, A (2023) ClimateNA (v7.42): A program to generate climate normal, annual, seasonal and monthly data for historical and future periods in North America.

Carbon Footprinting of Mine Water Treatment for Future CO_2 Emission Reduction

Oliver Totsche[1], Katja Kunze[2], Felix Bilek[3]

[1]*LMBV, Knappenstraße 1, 01968 Senftenberg, Germany, oliver.totsche@lmbv.de*
[2]*LMBV, Knappenstraße 1, 01968 Senftenberg, Germany, katja.kunze@lmbv.de*
[3]*GFI Grundwasser-Consulting-Institut, Meraner Straße 10-12, 01217 Dresden, Germany, fbilek@dgfz.de*

Abstract

This study provides an in-depth examination of the carbon footprint associated with neutralization measures implemented in post-mining landscapes, focusing on the activities of the Lausitzer und Mitteldeutsche Bergbau-Verwaltungsgesellschaft (LMBV). The research quantifies CO_2 emissions from the production, transport, and application of neutralization agents, as well as from different application methods. It also investigates and evaluates possible strategies for reduction of the carbon footprint of these essential remediation activities. The findings reveal relevant CO_2 emissions associated with neutralization measures and highlight opportunities for emission reduction through alternative technologies and management practices.

Keywords: Quick lime, chalk, hydrated lime, in-lake treatment, climate neutrality, outgassing

Introduction

Climate change poses one of the biggest global challenges of the century. To mitigate its effects, Germany and the European Union aim to achieve climate-neutrality by 2045 and 2050, respectively. This goal necessitates a drastic reduction in carbon emissions from mining rehabilitation activities, including mine water treatment.

Post-mining landscape rehabilitation is crucial for environmental restoration and sustainable land use. However, the neutralization measures employed to mitigate acidic mine waters contribute to greenhouse gas emissions, particularly CO_2.

Lime products, primarily limestone or chalk powder ($CaCO_3$), quicklime (CaO) and hydrated lime ($Ca(OH)_2$), are used for the majority of water treatment. CO_2 is released in various processes along the path of the lime products from their place of extraction to their place of use in the post-mining landscape. An overview of the CO_2 emitting processes is shown in Figure 1.

The aim of this study is to quantify and evaluate the carbon footprint of the neutralization measures carried out by the LMBV in the Lusatian and Central German mining districts. The objectives of this study are

- to calculate the carbon emissions associated with the production, transport and application of neutralization agents,
- to determine the CO_2 footprint of in-lake treatments compared to mine water treatment plants,
- to compare the CO_2-intensive application of lime products with the use of neutral buffered river water in in terms of carbon footprint,
- to investigate possible strategies to reduce the carbon footprint of neutralization measures.

Methods

Data on neutralization measures was collected from LMBV records for the period 2015-2022. This included qualities and quantities of various neutralization products used in in-lake treatments and water treatment plants.

CO_2 emissions were calculated stoichiometrically, for four main processes using complementary literature data:

1. Production: Carbon emissions from the manufacturing process of lime-based

products were estimated using industry-standard values (Franck & Knop 1979, Guminski *et al.* 2019, Kölling & Schnur 1977).

2. Transport: CO_2 emissions from transporting neutralization agents to application sites were calculated based on average transport distances and vehicle emission factors. (Süßmann & Lienkamp 2015)
3. Application: Emissions from the application process, including energy consumption for in-lake treatments and water treatment plants, were determined using operational data (LMBV 2021) and electricity emission factors.
4. Outgassing: When calcite-based neutralizing agents are added to a water body, the calcite dissolves. Due to a shift in the carbonate equilibrium, this leads to a proportional outgassing of CO_2. This was calculated stoichiometrically, taking into account the reactivity of the neutralizing agent.

Results and Discussion

From 2015 to 2022, LMBV utilized 280,000 t of lime-based neutralization agents, with 77% for in-lake neutralization and 23% for water treatment plants. This resulted in 188,000 t of carbon emission, 63% from in- lake treatment and 37% from conventional water treatment plants (Tab. 1).

In relation to the tonnages used in each case, however, less CO_2 was released by in-lake neutralization than during water treatment in stationary plants. This is due to various

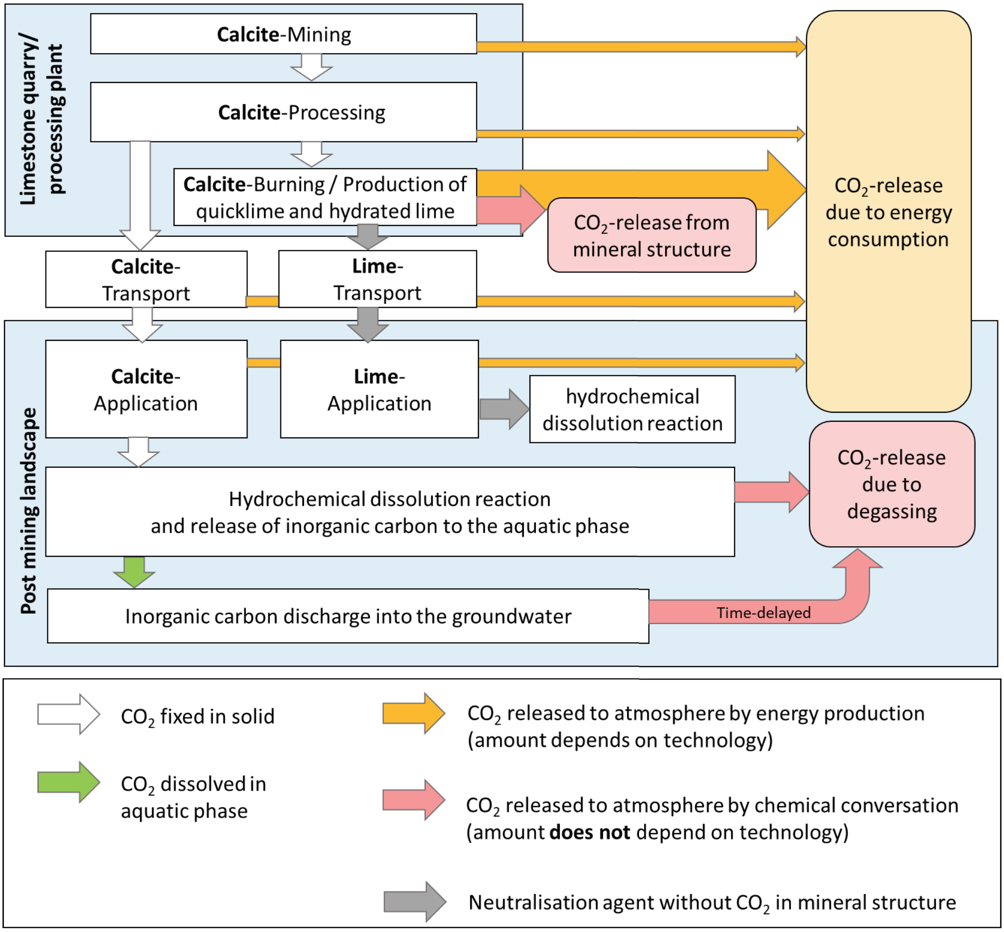

Figure 1 *Flow diagram for CO_2 emitting processes in mine water treatment.*

Table 1 Overall water treatment carbon footprint in the period of 2015 to 2022.

	Production	**Transport**	**Application**	**Outgassing**	**Total**
	t	**t**	**t**	**t**	**t**
in-lake treatment	82,212	2,085	1,280	33,518	119,095
water treatment plant	58,112	376	9,372	1,233	69,093
Total	140,324	2,461	10,652	34,751	**188,188**

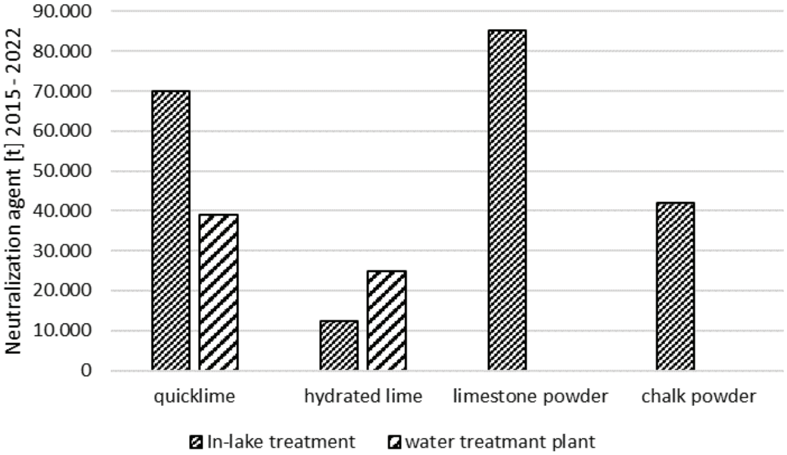

Figure 1 Quantities of neutralization agents utilized by LMBV for in-lake treatments and water treatment plants in the period of 2015 to 2022.

factors. The most important factor here are the differences in the main neutralizing agent used (Fig. 2). While all four neutralization agents are utilized in the in-lake treatment, with a focus on limestone and chalk powder, only quicklime and hydrated lime are used in the water treatment plants due to their better reactivity.

Neutralization Agent Production

The production of quicklime and hydrated lime is much more CO_2-intensive than limestone powder and chalk, with approximately 95% of the total carbon release being attributable to the burning process. The emissions from this sub-step result from the required heat energy (≈ 30%) and the amount of CO_2 separated from the calcite mineral phase (≈ 70%) (BVK 2017).

Transportation

Compared to the production and chemical solution of the neutralization agents in the treated water, the transportation and application of the neutralization agents only release small amounts of CO_2 and therefore offer little potential for savings (Tab. 1). However, the product-specific and absolute shares of transportation in the overall carbon footprint depend on the actual location of the quarries where from the raw materials originate.

Application

The amounts of energy required for discharge into the water (distribution, mixing) were calculated on the basis of ship operating times, fuel consumption and discharge quantities in the case of ship-based in-lake treatments and on the basis of electricity costs and electric power consumption in the case of stationary water treatment plants. Overall, the input of neutralization agents by means of in-lake technology is more favourable in terms of carbon emissions than the input via water treatment plants (Tab. 1).

Outgassing

When limestone and chalk powder are added to a water body, the calcitic part of the solid phase partially dissolves in the treated water, which initially produces carbonic acid under acidic respectively hydrogen carbonate under neutral conditions. Depending on the saturation state of the water in relation to the atmosphere, there is a partial outgassing of CO_2 (Cole & Caraco, 1998; Wetzel, 2001), which is in equilibrium with the aquatic species mentioned. Especially when the pH value decreases, typically in periods without in-lake treatment, there is an increased emission-relevant outgassing of CO_2 into the atmosphere. This process is more intense in fall, when the lakes transition from the stagnation phase into the circulation phase. This is because the increased inorganic carbon species concentrations of the hypolimnion, which have accumulated during summer, approach a steady state with the atmosphere. In spring, on the other hand, neutral lakes tend to incorporate carbonate species into biomass due to the increased biomass growth.

As a result of the calcite solution, a total of 34,750 tons of CO_2 have been released between 2015 and 2022 (Tab. 1), albeit with a time delay in some cases. Compared to limestone and chalk powder, quicklime and hydrated lime release substantially less carbon during application, as the CO_2 has already been released during the production process. Only the very low residual carbon content of the essentially carbon free solids is taken into account for the CO_2-balance.

Exemplary calculation

An examplary calculation for Lake Schlabendorf shows that over 50% more carbon is released when quicklime is used compared to limestone powder (Tab. 2, line 1 and 2). In general, it can be stated that the use of burnt lime products leads to significantly higher carbon emissions than the use of unburnt ones. This is due to the high-energy input for the firing process, but not due to the CO_2 released during firing, as this carbon is also largely released during the dissolution in case of application of unburnt limestone.

Another way of reducing the carbon footprint is to limit water treatment to the outlet of a post-mining lake instead of treating the entire lake. Treatment of the outlet is necessary to avoid harmful effects of the acidic water on the biocenosis in the downstream watercourse.

Comparative calculations were carried out for Lake Schlabendorf. This was based on an average discharge of lake water into the Lorenzgraben of 3.8 m^3/a with a maximum acidity of 10 mol/m^3, which the lake had before its first neutralization in 2013. If an outlet treatment had been installed instead of the initial neutralization, only about half of the acidity would have had to be treated

***Table 2** Comparison of CO_2 emissions with different treatment options of Lake Schlabendorf.*

	Neutralizing Agent	**Needed Alkalinity** Mmol/a	**Input Quantity** t/a	**Molar Equivalent** mol/t	**Efficiency Factor η** -	**Specific CO_2 release** kg(CO_2)/t	**Total CO_2 release** t(CO_2)/a
in-lake treatment	limestone powder	77.7	8,443	20,000	0,46	258	2,179
in-lake treatment	quick lime	77.7	3,108	35,714	0,70	1083	3,366
outflow treatment plant	quick lime	37.9	1,516	35,714	0,70	1,083	1,642

to date. Although the treatment would have to be carried out with quicklime, the carbon release would be substantially lower than the in-lake neutralization with limestone powder due to the lower quantity required (Tab. 2 line 1 and 3). However, it should not be forgotten that acidic lakes also have restrictions on subsequent use (tourism, fishing).

River water as a source of alkalinity

The discharge of river water into pit lakes is used not only to store water for times of low water supply but also to control the quality of the pit lake itself and its outflow. For this purpose in 2021, 19 million m^3 were withdrawn from the river Lausitzer Neiße, 95 million m^3 from the river Spree and 22 million m^3 from the river Schwarze Elster. As a result of the flushing of the pit lakes with an average alkalinity of the river water of 1.5 mol/m^3, 204 million mol alkalinity have been provided and the use of lime products was reduced accordingly.

Nevertheless using river water as an alkalinity source has its own CO_2 footprint. It results from the construction measures, which are required to build the technical flooding facilities (which are not assessed here), and the energy input for the transfer, in particular the pumping operation.

While the water from the river Schwarze Elster can be used without pumping, the water from the river Spree has to be pumped into some of the lakes. The water from the river Lausitzer Neiße has to be pumped even twice before it can be used.

Assuming an alkalinity of 1.5 mol/m^3, a specific CO_2 release of 45 to 51 g/mol alkalinity can be estimated for the use of Lausitzer Neiße water. This is of the same order of magnitude as the use of quicklime or hydrated lime and does therefore not improve the carbon footprint.

However, this only applies to the specific CO_2-emissions under the conditions of current electricity production. If specific CO_2 emissions of the electricity generation will decrease due to increasing renewable energy production, the CO_2-footprint of pumping will decrease and eventually will become climate-neutral.

Conclusions

The carbon footprint assessment can now serve as a basis for further measures to reduce CO_2 emissions in the LMBV's water treatment operations. There are some measures that can be implemented quickly and easily, while others still need to be developed, planned or installed.

Short-term measures such as the use of chalk and limestone powder for in-lake treatment or the prioritization of river water (without using pumping energy) with respect to the use of lime products have already been implemented.

In the medium term, alternative alkalinity carriers that do not have to be produced specifically but are generated as by-products in industrial processes (Uhlmann 2014) can improve the carbon footprint of the LMBV's water treatment measures. Research into by-products from industrial processes should therefore be intensified. However, extensive testing and approval procedures are to be expected until the by-products are ready for use, as well as initially elaborated monitoring. The LMBV is currently conducting a pilot project for the use of such a by-product (GFI 2022), which has the potential to replace more than 10% of the lime products used in in-lake treatment and the associated CO_2 emissions.

In the long term measures to minimize lake acidification by preventing the inflow of acidic groundwater should be implemented. This can be achieved, for example, by the construction of sealing walls. Another long-term option is the additional transfer of alkaline river water from other catchment areas. Although this can only be done by pumping, the power supply is expected to originate completely from renewable energy in the future. In this case, only the carbon emissions caused by the construction of the infrastructure need to be considered. If the price of electricity falls substantially as a result of renewable energies, electrochemical water treatment processes (Friedrich *et al.* 2007) could also become economically interesting. Such processes have already been tested by the LMBV in pilot projects, but were rejected due to high electricity costs.

The LMBV is a state-owned mining rehabilitation company financed by taxes. On the one hand, the state has the fundamental goal of becoming CO_2-neutral by 2045; on the other hand, strict attention must be paid to the economic use of taxpayers' money. There is a conflict of objectives between these two goals. While carbon neutrality is still a rather generally formulated goal, there are numerous regulations in public procurement law that make it difficult to finance CO_2 savings if they result in higher costs. This conflict of objectives will be defused by the expected increase in the price of CO_2 certificates. The switch to renewable energies will automatically eliminate a large proportion of carbon emissions in the long term.

As long as lime products are used, carbon emissions from quicklime production and the outgassing of CO_2 are unavoidable. However, if we consider not only water treatment, but the entire operations of the LMBV, things look different. While the LMBV's water treatment released an average of around 23.524 tons of CO_2 per year during the examined time period, conservative calculations of carbon storage show that around 86,000 tons of CO_2 are sequestered annually in the soils and forests recultivated by the LMBV since 1995 (with an upward trend). Even if other LMBV carbon emissions are taken into account, the LMBV already is a climate-positive institution.

By addressing the carbon footprint of neutralization measures, LMBV can contribute to broader climate change mitigation efforts while fulfilling its environmental restoration obligations. The implementation of the strategies identified in this study could lead to relevant reductions in CO_2 emissions associated with post-mining landscape rehabilitation.

References

BVK (2017) Bericht zu den 7 Leitlinien der deutschen Kalkindustrie. Kalk - die nachhaltige Lebensgrundlage, Bundesverband der Deutschen Kalkindustrie e.V., Köln Juni 2017

Cole JI, Carac, NF (1998) Atmospheric exchange of carbon dioxide in a low-wind oligotrophic lake measured by the addition of SF. Limnol Oceanogr, 43(4): 647-656

Franck HG, Knop A (1979): Kohleveredlung. Chemie und Technologie, Springer Verlag, Heidelberg

Friedrich HJ, Zaruba A, Meyer S, Kappnik R, Stolp W, Benthaus FC (2007) Verfahren und kleintechnische Anlage zur Aufbereitung schwefelsaurer Grubenwässer (RODOSAN®-Verfahren). Proceedings des Dresdner Grundwasserforschungszentrums e.V., Heft 31: 205-210.

Kölling G, Schnur F (1977) Chemierohstoffe aus Kohle, Thieme, Stuttgart

GFI (2022) Antrag auf ein Pilot- und Demonstrationsvorhaben bei der LMBV: Einsatz des alkalinen Produktes „RENACARB“ aus der Lebensmittelproduktion für die Wasserbehandlung in der Lausitz., Dresden 21. August 2022

Guminski A, Rouyrre E, Wiener M (2019) CO2-Verminderung in der Kalkherstellung. Präsentation vom 27.11.2019. Forschungsstelle für Energiewirtschaft e.V., http://ffe.de/wp-content/uploads/2021/08/CO2-Verminderung_in_der_Kalkherstellung.pdf

LMBV (2022) Nachhaltigkeitsbericht 2021 der LMBV. Lausitzer- und Mitteldeutsche Bergbau-Verwaltungsgesellschaft mbH, Senftenberg. April 2022

LMBV (2023) Nachhaltigkeitsbericht 2022 der LMBV. Lausitzer- und Mitteldeutsche Bergbau-Verwaltungsgesellschaft mbH, Senftenberg. April 2023

Süßmann A, Lienkamp M (2015) Technische Möglichkeiten für die Reduktion der CO2-Emissionen von LKW und Bussen. Fahrzeugtechnik 103, Carl Schünemann Verlag, Bergisch Gladbach

Uhlmann W (2014) Untersuchung des Einflusses der Einlagerung von Eisenhydroxidschlämmen in Tagebauseen auf deren Wasserbeschaffenheit. Dresden, 31. August 2014

Twenty-Five Years of Evolution of Integrated Water Management and Integrated Water Balance Modelling at Mine Sites

Lloyd R. Townley[1,2]

[1]GW-SW Pty Ltd, Dee Why NSW 2099, Australia, lloyd@gw-sw.com, ORCID 000-0003-2923-628X

[2]School of Environmental Science and Engineering, Nanjing Tech University, Nanjing, China

Abstract

Mine sites throughout the world are similar but different. They have different topography, climate, geology, target minerals, mining methods and processing methods, but mining and processing are always affected by water, and water in the environment is always affected by mining and processing on site. At every stage in the project pipeline, from Conceptual to Order of Magnitude Study (OoM) to Pre-Feasibility Study (PFS), from Feasibility Study (FS) to Engineering, Procurement and Construction Management (EPCM), from commissioning to operations, and then to expansion and closure studies, there are reasons to consider water management holistically, in an integrated way, to ensure success in operations and to mitigate risks. Simulation modelling can be used to support decisions during design and operations, and with 25 years of evolution of integrated water balance modelling, there are now clear patterns that show when integrated balance modelling is especially useful.

Keywords: Integrated water management, water balance modelling, mining

Introduction

To understand the concept and importance of integrated water balance modelling, it is first necessary to understand the concept of integrated water management. In essence this means consideration of all issues related to water management on a mine site in an integrated way, simultaneously or at least in sequence, to avoid the pitfalls of independent management of different issues in different silos within a site management team. This is harder than it sounds. The issues and the silos appear very early in the mining life cycle (cf. the project pipeline), and persist in similar and different forms during operations, unless specific efforts are made to ensure communication between these silos.

Focusing now on water balance modelling, there are several distinct times during the mining life cycle when integrated models are useful, and each requires a special kind of modelling. These times include: (1) during conceptual, OoM and PFS studies, when it is useful to understand water supply demands throughout the Life of Mine, in areas with intermittent rainfall and/or insufficient storage, and requirements for mine pit dewatering, e.g. in high rainfall environments where it may be difficult to store excess water that cannot be discharged; (2) after a mine has been commissioned, when an operational model predicting 12-24 months ahead can help mine managers to understand the risks associated with failing to build additional water management infrastructure; (3) when there is risk of poor quality water being released, and it is necessary to predict potential environmental impacts downstream, beyond mining lease boundaries, including the effects of dilution, adsorption and reactive transport in porous media, drains and streams; and (4) during expansion studies and closure planning, combining some aspects of each of these three types of models.

Which teams manage water?

It takes time to understand who has responsibility for water management on mine sites, and how and when problems may arise. How water is managed also depends on the owner of the project or mine:

- startup or junior mining companies (the "juniors", without any operations or perhaps with one) tend to run on shoestring budgets and rely on consultants for services, with specific services provided by different types of consultants, and sometimes with less, sometimes with more, communication between teams;
- mid-tier mining companies (the "mid-tiers", with a handful of operating mines (say 3-5) and a number of projects in the pipeline) usually use consultants, because they are not yet large enough to have technical specialists in-house, but some try to bridge the gap, operating more like a small major; and
- major mining companies (the "majors", with tens of operating mines and many projects in the pipeline) tend to have in-house technical expertise to oversee operations and to guide studies for projects, even if specialist consultants are also sometimes used.

During the **studies phase** (conceptual, OoM, PFS and FS studies, and sometimes during expansion studies), a mining company often contracts a large international consulting firm to manage the overall study. These firms often have specific in-house skills in one or more areas, for example in extractive metallurgy, process design and EPCM for all the civil, mechanical, electrical and other engineering required to build a process plant and all associated mine infrastructure; these firms sometimes have in-house expertise in geology and mine design, but they usually subcontract smaller companies to provide geotechnical advice (e.g. to recommend pit wall slope angles), to design tailings storage facilities (TSFs) and to provide hydrogeological advice (related to design of water supply borefields and/or active or passive mine dewatering) and hydraulic design (for diversion channels, dams, pipelines and pumps). The large consulting firms also usually contract a separate large consulting company to prepare an Environmental and Social Impact Assessment (ESIA, in modern parlance), and the latter subcontracts others to undertake baseline hydrological studies and to assess potential impacts of the proposed project on surface water, groundwater and the ecosystem. The use of so many specialised teams sometimes leads to a lack of integration.

Many teams make assumptions about the movement of water and make calculations, often relatively independently:

- process engineers nearly always assume steady flow, with water demand driven by the assumed percent solids in tailings, and they then estimate steady raw water makeup demand based on assumptions about tailings decant;
- tailings engineers collate climatic data and make many assumptions about water balance (including consolidation, beaching angles and return of decant to a process water pond), as well as leakage to underdrains, toe drains or the soil beneath the floor of a TSF (unlined or lined); they rarely assess environmental impacts;
- geochemists are engaged to recommend the placement of potentially acid forming (PAF) waste in Waste Rock Dumps (WRDs), and the management and possible treatment of acid rock drainage (ARD);
- geotechnical engineers often focus on the near field of pit walls and underground workings;
- civil/water engineers collate climatic data and design drainage systems and floodways and do not usually assess potential environmental impacts;
- hydrogeologists design water supply borefields and estimate mine pit inflows and potential environmental impacts; and
- environmental consultants also collate climatic data and assess environmental impacts.

It requires focus to complete all of these scopes of work in an efficient manner, with different teams making consistent assumptions. Integration is often difficult to achieve.

During **operations**, each mine has a mine manager, who is usually a mining engineer or a process engineer by training, depending on what is most critical on an individual mine site, and on rare occasions a geologist or environmental specialist. The mine manager is supported by a management team: a geology or geoscience manager, a mining manager, a processing manager, an infrastructure manager, an environmental (Environment, Health and Safety or EHS) manager, and perhaps another. Because an Environmental and Social Management Plan (ESMP) often includes an Environmental Management System (EMS) consistent with the ISO 14001 series of Standards, it is common for operations to commence with a Surface Water Management Plan (SWMP, or Surface Water Management and Monitoring Plan, SWMMP) in place, and perhaps a Groundwater Management Plan (GWMP or similar). These plans are written to help operations to comply with requirements (legislation, regulations and licence conditions) that are focused on environmental management, but they are not usually focused on operational water management issues and practices that are required within an operation to meet operational requirements. Water is always the "poor cousin" relative to the most important disciplines of mining and processing. There is almost never a "water manager" on site, although some majors understand the desirability of such a role, a "water czar", not a line management role, but a person (reporting to the mine manager) whose role is to oversee a less formal "water team" and to encourage if not ensure integrated water management. Often there is an assumption that water management should be the responsibility of the EHS manager, simply because WMPs include the word "water", and even though such plans may have been written by city-based consultants who have never been to site. Effective integration is always difficult.

Special challenges in mine water management

Why is integrated modeling at mine sites different or especially challenging? One could argue, correctly, that software for simulating the movement of surface water (hydrology, hydraulics and hydrodynamics) and groundwater in natural systems has evolved significantly in the past 20–30–40 years, and software for simulating movement of water in engineered systems (pipe networks, pumps, water treatment etc.) is also mature; there are many commercial and open-source software packages available in all these areas. However simulation of the movement of water on mine sites remains difficult largely because the geometry, features and properties of mine sites change every day, and at monthly and annual intervals they change noticeably. Some technical software allows for changes in geometry, but no software package can handle all aspects of water management on a mine site, including continuously changing geometry, or certainly not without unreasonable effort required to represent the dynamic changes of geometry. This is a major reason why different approaches have evolved and why software for mine site water management needs to be extensible.

So far we suggest the possible need for integrated water balance modelling. In fact we sometimes need integrated balances of water, mass and solutes. A mine schedule defines the sequence in which individual blocks in a 3D mine geological model are removed from the mine, whether open cut or underground. Each block includes volume and mass of mineralised ore that is sent to Run-of-Mine (ROM) pads or a processing plant and waste rock that is directed to WRDs; the rock in both cases contains some water that was not released in the drilling and blasting or other mining process. In many types of mining, ore that is crushed and milled ultimately reports to a TSF; in other types of mining, such as bauxite or nickel laterites, the ore is completely dissolved and precipitates as a residue, hence Residue Storage Facilities (RSFs) rather than TSFs. WRDs and TSFs/RSFs are constructed landforms that grow within expanding footprints throughout the Life of Mine. Management of water that falls on and within these landforms is important, to reduce the mobilisation and transport of solutes. Integrated mass balance modelling can help us to estimate or predict dynamic changes in catchment areas which are important for water balances.

Solutes of importance include tailings liquor, which can have concentrations as high as 50,000-100,000 mg/L. Such liquor is more dense than seawater and certainly more dense than groundwater below the land surface. Density becomes important when leakage reaches the water table, because dense groundwater often leads to dense plumes that can propagate in unexpected directions, following the topography of low hydraulic conductivity layers beneath the surface rather than surface topography. Acid rock drainage (ARD) can be produced within and discharged from mines or can be generated within WRDs and occasionally TSFs. Sometimes it is important and useful to compute solute balances in conjunction with water and mass balances, although estimation of source concentrations is challenging.

Evolution of balance modelling methods

Thirty years ago, in 1995, while simple balance modelling was possible using Lotus 1-2-3/W Release 5 (16-bit) and Microsoft Excel 95 (v7.0) (32-bit) for the Microsoft Windows 3.1x operating system, it was still quite common to write applications for specific purposes using languages such as Fortran. Barr and Townley (1991ab) developed a water and solute balance model for many coupled ponds, for application to solar salt production for the Shark Bay Salt Joint Venture in Western Australia, a special type of "mining" that is relevant because of the challenges of simulating many coupled storages. Perhaps this is the first important concept in integrated modelling on mine sites, the need to store water in many storages (dams, ponds and/or tanks), with water flowing from one to another under gravity or being pumped back according to agreed operating rules, sometimes with overtopping that cannot be prevented (but a destination must be assigned) and sometimes drying out. Drying, due to an excess of outflows over inflows, with ever-present evaporation, is the hardest phenomenon to represent in software, because the time at which dryness is reached is nearly always part way through a computational time step.

Twenty-five years ago, the author developed a sitewide water and solute balance model for the Mt Gordon copper mine in Queensland, Australia, using XPSWMM, which was first released under the Microsoft Windows operating system in 1997. Professionals working on urban stormwater drainage have been using the US EPA's Storm Water Management Model (SWMM) since 1971. The XP (expert) graphical user interface made it relatively easy to create a node-link model of flows between storages on site, with catchments generating runoff, but SWMM was not designed to handle the complexities of mining, especially with time-varying catchment areas. As mentioned above, this is a second important concept in integrated modelling: the geometry of catchments on mine sites is nearly always time-varying. XPSWMM is now supported by Innovyze (2024).

In the late 1990s, the author experimented with the use of other simulation software, notably STELLA and ExtendSim, both of which were first released in the mid-1980s. ExtendSim is used in the mining sector today, although perhaps not widely with application to water management. In fact the field of simulation modelling is very diverse, and there are many specific types of modelling; a review by Roberts and Pegden (2017) provides useful insights.

In 1990, a team inside Golder Associates in Seattle started to develop a general simulation package called GoldSim (see www.goldsim.com/Web/Company/History and a blog referred to therein; the “gold” in the product name comes from the name of the company, not the metal). GoldSim was first released in 1999, and the author first used GoldSim in 2006, at a time when Rio Tinto was encouraging the development of sitewide balance models for operating mines to assess short-term operational water-related risks. In the past nearly 20 years, the author has developed more than ten models of mine sites, at different stages of development, and reviewed many more. The current release of GoldSim (GoldSim Technology Group 2025) is popular in the mining sector, used at hundreds of mine sites, indeed mining and water balance make up 50-60% of the current user base. GoldSim is a general purpose simulation framework, that can be thought of as a high-level programming language that allows users to simulate many kinds of systems in a flexible way. GoldSim differs from spreadsheets, system dynamics software and discrete event simulators, (see www.goldsim.com/Web/Products/GoldSim/Comparison) but combines some of the best features of each. GoldSim has powerful Monte Carlo capabilities, making it ideal for quantitative risk assessment (QRA). GoldSim can use Excel for input and output (as well as databases) and is highly extensible using dynamic linked libraries (DLLs) for communication with other software. GoldSim has been linked to MODFLOW, FEFLOW, PHREEQC and many more packages used in the mining sector. The GoldSim Model Library (online) contains hundreds of examples of applications, as well as examples of how to use each of the individual "elements" that are used to construct a model. GoldSim 15 introduces a new Controller element that will find widespread application in mine water management modelling, for representing transfers between ponds.

In 2006, the author was also introduced to OPSIM (see OPSIM Pty Ltd 2025) and had the opportunity to develop a model for one mine in Australia. OPSIM was obviously a product written by water engineers for water engineers, using the terminology and naming conventions of water engineers, and focused specifically on the mining sector. OPSIM at that time could be configured relatively easily, but was far less extensible than GoldSim, which is a high-level development environment. While the learning curve for OPSIM was arguably shorter, it was not as powerful. Things have clearly changed, because OPSIM has continued to evolve and now boasts capabilities that include movement of water, mass and solutes, as well as special modules for geochemistry, real-time integration with online information systems and a Water Accounting Framework (WAF) aligned with the Global Reporting Initiative (GRI). OPSIM continues to be used in the mining sector, often by teams within mining operations (John Macintosh, pers.comm.).

What are the benefits of modelling? How can integrated modelling help?

Models should be designed to meet specific objectives, to answer specific questions:

- Typical objectives during the studies phase relate to design of dams and ponds, i.e. how big do they need to be, and what should be their operating rules, in order (i) to ensure sufficient water supply through months and years of drought, or (ii) to contain contaminated water when heavy rain falling into open cut pits, or onto WRDs and TSFs, leads to large volumes of mine-affected water, or when discharge of groundwater into mines is very large? Corollaries include the questions of how big pipes and pumps need to be for mine pit dewatering or to move water between storages according to operating rules.
- Typical objectives during operations are similar, but by this time most infrastructure is already in place, so questions relate to potential additional infrastructure or changes in operating rules. Looking ahead through the next dry season or two, what is the risk that available storage will not be sufficient to meet makeup water and process water demands, and if the risk is too high, what changes in infrastructure and/or operating rules would mediate that risk? Looking ahead through the next wet season or two, what is the risk that failing to lift a TSF could result in overtopping, or if storage on the surface of a TSF is used for emergency water storage (not generally recommended), what is the risk that there is insufficient storage on site to contain contaminated water, so that mining must cease?

In both sets of examples, the focus of modelling is on design, based on QRA.

Guidelines for integrated water balance modelling at mine sites

The author is not aware of any industry-wide guidelines for integrated (water, mass and solute) modelling at mine sites, nor is he suggesting that such guidelines are needed. It is useful however to read guidelines of other kinds, and to consider what can be learned and applied.

The Australian Groundwater Modelling Guidelines (AGMG) (Barnett *et al.* 2012) were written by many authors, following workshops with stakeholders from government and many industry sectors. The guidelines were not universally accepted, indeed the need for guidelines was debated and rejected by some, but nevertheless the guidelines have been useful for some stakeholders. One key feature is that the guidelines were not written for modellers, who learn their trade in universities and in the workplace, after gaining experience developing many models; the guidelines were written primarily for the people who read reports on the results of modelling, to help them to understand what a model is, how it is developed and how it can be useful. In some ways this paper is written with similar intent: it is not intended to teach modellers how to develop models, but rather to provide context and to tell some of the stories that are not so often told.

A key recommendation in the AGMG is that a model must have clear objectives. A model should never be developed simply because someone believes a model might be useful. A model should aim to analyse/explain behaviour of a system in the past or to predict specific behaviour in the future, usually related to flows of water or mass or solutes. It should be designed to answer specific questions, often related to design of mine and water management infrastructure and choice of operating rules. Specific objectives are essential to allow a modeller to design a model to achieve those objectives. Sometimes it is difficult to add more objectives later, because meeting those new objectives would require a different modelling approach or a different model structure. It is therefore important to invest time and effort into setting objectives at the start.

The AGMG also recommend a staged approach. This is especially difficult during the studies phase, where the lead consulting firm may prefer a single deliverable rather than multiple stages and workshops. Nevertheless, the AGMG recommend eight stages separated by three hold points where results are documented and reviewed: (1) planning, conceptualisation and model design (based on clear objectives), (2) model construction, calibration and sensitivity analysis, (3) prediction and uncertainty analysis, and (4) final reporting and archiving. This modelling process can easily be applied to sitewide integrated balance modelling, of course recognising that calibration is not always possible in early stage studies.

The importance of data

It is useful to distinguish between "monitoring" of levels, flows and water quality in natural surface water and groundwater, often managed by EHS personnel, and "metering" of levels, flows and water quality in engineered parts of a mine site, with data sometimes collected by Supervisory Control and Data Acquisition (SCADA) systems and stored in large database systems such as AVEVA PI System (previously known as OSIsoft PI Historian). It takes substantial effort to access both types of data, if indeed it is necessary. This depends on the question being addressed.

A bigger challenge in studies and even during operations is simply to obtain the mining schedule, the schedule for production of waste rock, the processing schedule and the tailings production schedule, to support a planned QRA. Sometimes the "poor cousin" needs to educate and encourage all the teams involved in a study, to allow integrated water, mass and solute modelling to succeed.

Conclusions

This paper is not intended to teach modellers how to develop models. Rather the author hopes to have provided some context and referred to many challenges, to help young modellers, experienced modellers and those who need to read and understand model predictions to gain perspectives on how the current state-of-the-art has evolved to where it is today.

Acknowledgements

The author is grateful for the friendship and support of: Anthony (Tony) D. Barr with whom he developed SALTPROD at CSIRO in 1989-90; Allan Goyen of Willing & Partners Pty Ltd and later XP Software Pty Ltd in Canberra, Australia, with whom he first collaborated in 1976 on urban flood modelling and who was developing XPSWMM on Apple Macintosh personal computers in the late 1980s, but the node-link interface was unable to support the author's AQUIFEM-N; Rick Kossik of GoldSim Technology Group in Seattle, USA, who provided personal training in his office in 2006; and John Macintosh of Water Solutions Pty Ltd and OPSIM Pty Ltd in Brisbane, Australia, who also provided personal training in OPSIM in his office in 2006. Thanks also to all clients who have understood the potential benefits of integrated balance modelling.

References

Barnett B, Townley LR, Post V, Evans RE, Hunt RJ, Peeters L, Richardson S, Werner AD, Knapton A, Boronkay A (2012) Australian Groundwater Modelling Guidelines, Waterlines Report Series No. 82, National Water Commission, Canberra, June, 203 pp.

Barr AD and Townley LR (1991a), SALTPROD: a program that simulates the flow of water and salt through a system of evaporation ponds, CSIRO Division of Water Resources, Consultancy Report 91/4, 58pp., plus software.

Barr AD and Townley LR (1991b) SALTPROD: a simulation model for systems of salt evaporation ponds, International Hydrology and Water Resources Symposium 1991, Perth, 2-4 October, Volume 3, 657–658.

GoldSim Technology Group (2025) GoldSim Version 15.0, www.goldsim.com.

OPSIM Pty Ltd (2025) OPSIM, www.opsim.com.au.

Roberts SD and Pegden D (2017) The history of simulation modeling, Proceedings of the 2017 Winter Simulation Conference, Chan WKV, D'Ambrogio A, Zacharewicz G, Mustafee N, Wainer G and Page E, Eds, 16pp.

Innovyze (2024) XPSWMM/XPStorm 2024.2, https://help.innovyze.com/space/xps.

006) Toxicological Profile for Cyanide. Table 8–1.

Forty Years of Evolution of Groundwater Flow and Solute Transport Modelling at And Near Mine Sites

Lloyd R. Townley[1,2]

[1]GW-SW Pty Ltd, Dee Why NSW 2099, Australia, lloyd@gw-sw.com, ORCID 000-0003-2923-628X

[2]School of Environmental Science and Engineering, Nanjing Tech University, Nanjing, China

Abstract

The nature of groundwater flow and solute transport modelling at and near mine sites has evolved because the objectives (the questions) have changed, simulation software has improved, model resolution has increased, graphical interfaces have become very powerful and stakeholders are asking more challenging questions, especially related to prediction uncertainty. Computing performance has increased by a factor of 10^6 or more (cf. Moore's Law and its corollaries), but stakeholder expectations have increased dramatically, so the time required to develop, test and apply a simulation model is not significantly less than it was 40 years ago. High-level modellers still need programming skills to extend available simulation software.

Keywords: Groundwater flow, solute transport, simulation, mining

Introduction

The application of groundwater flow and solute transport models at and near mine sites is not new. Simulation software has been used in the mining sector since it first became available, perhaps starting with PLASM (the Prickett and Lonnquist Aquifer Simulation Model, based on the finite difference method, Prickett and Lonnquist 1971), then with AQUIFEM-1 (Wilson *et al.* 1979, Townley and Wilson 1980), FEFLOW (Diersch 2014, but first released in 1979), MODFLOW (McDonald and Harbaugh 1988), AQUIFEM-N (Townley 1990) and many more.

Objectives of modelling: analysis and design

Working effectively within the mining industry requires an understanding of the types of questions that need to be answered, or problems that need to be solved, and how these questions and problems evolve during the many stages of mining projects, from Conceptual to Order of Magnitude (OoM) to Pre-Feasibility Study (PFS), from Feasibility Study (FS) to Engineering, Procurement and Construction Management (EPCM), from commissioning to operations, and then to expansion and closure studies, each of which involve multiple stages. Another important factor is the nature of the proponent or operator, because startup or "junior" miners are more willing to take risks than "mid-tier" mining companies, with multiple concurrent operations, and "majors", with many concurrent operations and many future projects at different stages of investigation; juniors employ consultants for most tasks while majors often have internal specialist teams. Forty years ago, the project pipeline was not as clear or as well understood, but now it is mature.

Developing a good model requires investment of resources (people, time and money), and every model therefore requires clear objectives. The objectives of a model should be to answer a question, or perhaps several questions. The Australian Groundwater Modelling Guidelines (Barnett *et al.* 2012) emphasise the difference between the objectives of a mining company (e.g. to design a borefield for water supply or mine dewatering, or to gain environmental approvals) and the objectives of a simulation model, which must start with its own conceptual model (conceptualisation of processes), leading to design, construction and execution of that model, with model calibration and often including sensitivity and uncertainty analysis.

An important distinction is between simulation of the past behaviour of a groundwater system and prediction of its future behaviour, without or with human and/or engineered interventions. Simulation of the past is necessary before it is possible to contemplate prediction, which can sometimes be a form of design. Modelling of groundwater near mine sites as part of baseline environmental and Environmental and Social Impact Assessment (ESIA) studies sometimes has the stated objective of developing understanding, but if the effects on environment are considered to be too great, regulators can force the redesign of a proposed mine. Simulation of groundwater flow and solute transport can also be considered in the context of sitewide or integrated water management at mine sites; water management issues can be categorised as being related to having "too little" water, "too much" water or water that is "too dirty".

All the types of studies described in Tab.1 are often described simply as "modelling", but it is useful to emphasise the distinction between analysis and design, partly to elevate our work as "groundwater modellers" to the level of "design engineers". This is not to say that groundwater modelling at or near mine sites is a form of engineering, although sometimes it is, but rather to remind stakeholders that the level of scepticism and criticism sometimes directed at groundwater "modelling" is sometimes much greater than the level of scepticism and criticism directed at all the other types of engineering "design" required to build and operate a mine (e.g. mining, geotechnical, process, civil, mechanical and electrical engineering). All engineering design requires clear design objectives, requires consideration of multiple scenarios and must deal with uncertainties. The use of groundwater simulation software in design is similar to the use of software in all other types of engineering, but with different levels of scrutiny by stakeholders.

Why is groundwater modelling especially challenging in the mining sector?

One of the special features of mining projects is that the geometry of the system is changing every day, through excavation (in either open cut or underground mines) and placement of waste rock in waste rock dumps (WRDs) at the land surface. In many kinds of mining, mineral processing requires crushing and grinding/milling rock, and this leads to construction of Tailings Storage

__Table 1__ Objectives of modelling: analysis versus design

Question/problem	At or near mine site?	Too little, too much, too dirty?	Analysis or design?
1. Groundwater resource assessment and borefield design	Near	Too little for processing	Both
2. Estimation of (passive) mine inflows	At and near	Too much	Analysis
3. Design of (active) dewatering bores	At and near	Too much	Design
4. ESIA of mine inflows and dewatering on regional groundwater (cone of depression, depressurisation)	Near	Too little for environment	Analysis
5. ESIA of mine inflows and dewatering on springs, groundwater dependent ecosystems (GDEs), stygofauna	Near	Too little for environment	Analysis
6. Assessment of pit slope stability and design of depressurisation (both saturated and unsaturated)	At	Too much	Both
7. Evaluation of leakage and migration of (often dense) plumes from water storage ponds, TSFs and WRDs; design of borefields to recover (dense) plumes	At and near	Too dirty	Both
8. Evaluation of the formation and control of acid rock drainage from within mines and WRDs and potential discharge to surface streams and lakes	At	Too dirty	Both
9. Prediction of evolution of mine pit lakes after closure	At and near	-	Analysis

Facilities (TSFs), another kind of constructed landform. When modelling software was first developed, it was based on the concept of a layered system, initially a sequence of sub-horizontal aquifers and aquitards. From the outset, using this available software to simulate mining and later the growth of constructed landforms was a bit like trying to fit the proverbial round peg in a square hole.

Another special feature of mining is the stress that it puts on a regional groundwater system. We use the terms "stress" and "forcing" partly because development of groundwater simulation software followed the development of software for structural engineering in the 1970s. Developing a water supply borefield, in either an unconfined or confined aquifer, leads to lowering of the water table or the piezometric surface over a large area; large borefields are rarely developed in aquifers without some previous history of pumping and without knowledge of aquifer properties. But in mining the opposite is true. Mining nearly always takes place in hydrogeological systems that have not previously been stressed and causes drawdown of the water table or piezometric heads or both by tens and often hundreds of metres. Conducting 72-hour or even 30-day pumping tests hardly stresses the hydrogeological system and rarely provides data to support calibration of a regional scale model. In the same way, three years of monitoring of a quasi-steady regional water table (as required in Australia, for example) is usually insufficient for model calibration.

Because mining leads to so much drawdown, this causes difficulties related to dewatering and draining of cells or elements in a model with a fixed mesh or grid. While this also occurs in borefields, the challenge is greater in mining. MODFLOW, MODFLOW-SURFACT and FEFLOW have similar but different approaches for handling large drawdown, with draining of many cells.

Representation of mines and other infrastructure in modelling software

Since the earliest attempts to estimate mine pit inflows, modellers have been faced with the challenge of how to represent mines in software. Most modellers use software that assumes that Darcy's Law (a linear gradient law, with flow proportional to the gradient in piezometric head) is sufficient to represent flow at a large scale, from tens or hundreds of metres to tens or hundreds of kilometres. Conservation of mass (or volume, if variations in density can be ignored) leads to a diffusion-type partial differential equation (PDE) for piezometric head which can be solved by finite difference, finite element, finite volume or other methods.

The PDE and resulting simulation software only allow three types of boundary conditions: 1st Type, prescribed head or Dirichlet boundary conditions, where piezometric head is known but flux through the boundary at that location is not; 2nd Type, prescribed flux or Neumann boundary conditions (Neumann when the prescribed flux is zero), where flux across the boundary is known but piezometric head at that location is not; and 3rd Type, mixed or Cauchy boundary conditions, where neither piezometric head nor flux across the boundary are known, but a relationship between head and flux is known.

Where do we get guidance on how to use groundwater flow simulation software in the mining sector? The author is not aware of any text or reference book focused on simulation of groundwater near mines. In the Large Open Pit (LOP) project led by CSIRO and supported by many large mining companies (Read and Stacey 2009), Chapter 6 (Hydrogeological Model, by Geoff Beale) introduces a modelling methodology, focused on estimating or predicting pore pressures in pit walls of large open pits, to support assessment of geotechnical stability. Chapter 6 led to a second book (Beale and Read 2013) which was longer than the first. However neither of these books provides detailed advice on how to set boundary conditions in models.

Hamilton and Wilson (1977) used an early version of AQUIFEM-1 to study the effects of strip mining of coal (see also Wilson and Hamilton 1978). Since AQUIFEM-1 was a 2D finite element model, modelling was undertaken in 2D plan and also in 2D vertical section, where it was possible to represent hydrostratigraphic layers with different properties. Typical finite element grids had more than 100 nodes and 200 triangular finite elements. A mine was represented using prescribed head boundary conditions, with head set equal to the elevation of the base of the mine. The AQUIFEM-1 user manual (Townley and Wilson 1980, Section 5.5) includes an example where a mine excavation is represented by only 4 nodes, using a so-called "rising water table" condition (Section 3.4.2), effectively a "seepage face" boundary condition where in this case the ground surface falls in time, and when water table elevation at such a node exceeds the ground elevation, water table elevation is fixed at that elevation until the next time step.

Users of MODFLOW and MODFLOW-SURFACT (HydroGeoLogic Inc. 1998, Panday and Huyakorn 2008) have long used a so-called "drain" boundary condition (DRN package) to represent the base of a mine. This is a mixed boundary condition, and if conductance is very large, this boundary condition is almost equivalent to a prescribed head condition. Some modellers use prescribed pumping first to design dewatering bores and then use drain nodes to check performance.

FEFLOW has an extensive range of special boundary conditions, such as a "seepage face" condition, which is like the rising water table condition in AQUIFEM-1 and AQUIFEM-N and it includes a constraint that the flux through the boundary must be out of the model domain. This, when combined with many other features in FEFLOW such as elements that can be deactivated and reactivated (mined and refilled), and control using the Interface Manager and special data files, makes FEFLOW by far the most powerful and flexible software for representing mines.

Evolution of groundwater modelling software

The last 40 years (or arguably a little more) have seen slow but steady evolution of groundwater modelling software, from PLASM to AQUIFEM-1 and FEFLOW, to MODFLOW, AQUIFEM-N and more (FEFLOW was first released in the former East Germany in 1979, the same year as AQUIFEM-1). These packages are described in two well-known reference books by Anderson and Woessner (1992) and Anderson *et al.* (2015). Other well-known packages are MODFLOW-SURFACT, HydroGeoSphere, HYDRUS and MINEDW (references for the last three are not provided here). MODFLOW-6 is now enormously different from earlier versions, indeed there are so many versions of MODFLOW that even experienced modellers struggle to understand the differences.

In parallel with simulation software itself, there has been evolution of graphical user interfaces (GUIs). In the 1990s the author collaborated with 3G Geotechnica s.r.o. in Prague to develop a GUI for AQUIFEM-N, and this was used for many mining applications by consultants in Australia during the 1990s. At the same time, AQUIFEM-N was embedded within Maptek's Vulcan 3D mining software, and MODFLOW was also embedded within Surpac mining software, but neither were released, largely because it became clear that geological data were collected very close to an orebody, and such data could rarely support the development of a regional scale groundwater flow model suitable for estimating mine inflows. Leapfrog Hydro (now from Seequent) and Geomodeller 4.0 (from Intrepid Geophysics in Melbourne, Australia) provide useful pathways from 3D geological models to 3D hydrogeological models to 3D simulation models, but FEFLOW is evolving rapidly with more and more 3D geological modelling capabilities built in.

MODFLOW and MODFLOW-SURFACT have been supported in many GUIs, such as ModelMuse, Visual MODFLOW, GMS and Groundwater Vistas. For some years the latter was the GUI of choice for users of MODFLOW in the Australian mining sector, but many advanced users are also using FloPy and PyEMU (https://help.pesthomepage.org/pest_and_pestplusplus.html) and Jupyter Notebooks. These methods provide flexibility and transparency, at least for the experts.

FEFLOW is extremely powerful because it is extensible via its Interface Manager (Ifm), with code that can be written in C, Python or other languages. Perhaps one reasonable conclusion is that modellers (users of modelling software) always need capabilities that are not yet available, so high-level modellers still need programming skills

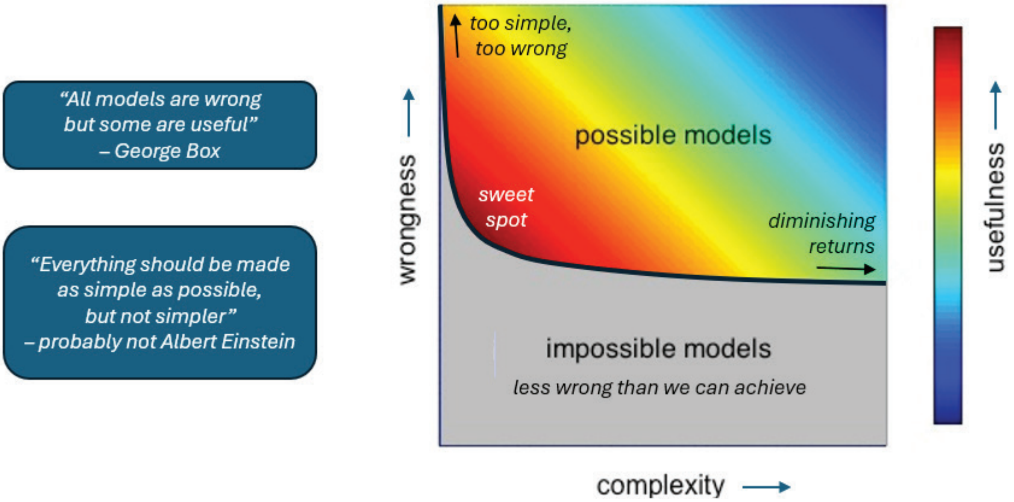

Figure 1 The Box-Einstein surface of mathematical models, after Noble (2016).

to fill the gap. It remains to be seen whether Large Language Models (LLMs), a form of Artificial Intelligence (AI), will reduce barriers to entry and allow non-programmers to achieve results that used to require years of experience.

Model complexity

While simple questions could be answered in the 1980s using 2D models with hundreds of nodes or cells, typical models today have 10^5–10^6 unknowns or more. The number of unknowns affects computation time but this is not the only measure of model complexity. The latter depends also on parameterisation (the way hydrogeological properties and boundary conditions are represented and the number of parameter values required to describe their spatial and temporal distributions). While some modellers subscribe to the philosophy of highly parameterised models, relying on parameter estimation software such as PEST (Doherty 2015) to estimate many parameter values, there may also be good reasons to keep models as simple as possible. Fig. 1 illustrates the possibility that it may be useful to resist the temptation to add complexity.

Expectations are rising

If computing performance is always increasing (see Tab.2), why can't we do much more? Perhaps there are many reasons. Expectations are now much higher than they were 10–20–30 years ago. Government and community stakeholders expect higher resolution in graphics and visualisation, and this implies finer resolution in grids, even though the graphics may then suggest a level of "rightness" that is not achievable.

Table 2 Corollaries to Moore's Law: Evolution in computing power since the 1970s

Performance Measure	Then	Now	Factor of Increase
Transistors (Moore's Law)	2300 in 1971	>20 billion in 2021	≈10^7
Processor speed	1 SPECint in 1978 (VAX 11/780)	11000 SPEC CPU 2006 in 2017 (Intel Xeon 8180)	≈10^5
RAM	16 KB in mainframe in 1976	128 TB in Dell T5820 workstation in 2021	≈10^7
Capacity of disks	360 KB on 5¼ inch floppy in 1978	8 TB in 2021	≈10^7
Network speed	110 baud on AUSTPAC in 1984	500 mbps in 2023	≈10^7
Time to develop and run a model	Weeks to months	Weeks to months	1

Stakeholders demand that more processes (e.g. unsaturated flow and reactive transport) should be included in models, even if there are not enough data to support such efforts. Development of models still takes time, even with sophisticated user interfaces, and because modellers need time to communicate with their teams and with other stakeholders. This part of the modelling process is not becoming easier or faster.

Conclusions

The objective of this paper was not to teach modellers how to develop models, but rather to provide context that partly explains why modelling remains difficult and time-consuming. High-level modellers still have needs that are not met by available software, so they often still need programming skills to extend the available capabilities.

Acknowledgements

The author is grateful to: the late Dr Jiří Bartůněk and his colleagues at 3G Geotechnica s.r.o. in Prague who from 1991 to 1996 used Borland Pascal and Turbo Vision to develop graphical user interfaces PreAQ and AQPost for the author's AQUIFEM-N simulation software, which was used in the mining sector in Australia throughout the 1990s; the late Dr Anthony (Tony) J. McNulty who led the integration of AQUIFEM-N within Maptek's Vulcan 3D mining software in the mid-1990s; and to his team at NTEC Environmental Technology and later CDM Smith (Australia) Pty Ltd in Perth, Western Australia, especially Dr Andrew M.H. Brooker, Dr Anthony (Tony) J. Smith, Rikito A. Gresswell and Isabelle Dionne, in the years 2010 to 2017, when together we worked on many models of many mines, pushing FEFLOW, MODFLOW- SURFACT and Groundwater Vistas to and beyond their limits.

References

Anderson MP, Woessner WW (1992) Applied Groundwater Modeling, Simulation of Flow and Advective Transport, Academic Press Inc., 381 pp.

Anderson MP, Woessner WW, Hunt RJ (2015) Applied Groundwater Modeling, Simulation of Flow and Advective Transport, Second Edition, Academic Press Inc., 564 pp.

Barnett B, Townley LR, Post V, Evans RE, Hunt RJ, Peeters L, Richardson S, Werner AD, Knapton A, Boronkay A (2012) Australian Groundwater Modelling Guidelines, Waterlines Report Series No. 82, National Water Commission, Canberra, June, 203 pp.

Beale G, Read JRL (Eds) (2013) Guidelines for Evaluating Water in Pit Slope Stability, CSIRO Publishing and CRC Press, 600 pp.

Diersch HJG (2014) FEFLOW: Finite Element Modeling of Flow, Mass and Heat Transport in Porous and Fractured Media, Springer, 996 pp.

Doherty J (2015) Calibration and Uncertainty Analysis for Complex Environmental Models. Watermark Numerical Computing, Brisbane, Australia. www.pesthomepage.org/pest-book.

Hamilton DA, Wilson JL (1977) A generic study of strip mining impacts on groundwater resources, MIT Energy Laboratory Report No. MIT-EL 77-017, September, 156 pp.

HydroGeoLogic Inc. (1998) MODFLOW-SURFACT v.3.0: A comprehensive MODFLOW-based flow and transport simulator, Code Documentation Report, Reston VA.

McDonald MG, Harbaugh AW (1988) A Modular Three-Dimensional Finite-Difference Ground-Water Flow Model, Techniques of Water-Resources Investigations 06-A1, USGS, 576 pp.

Noble R (2016) The Box-Einstein surface of mathematical models, www.thesefewlines.wordpress.com/2016/11/20/the-box-einstein-surface-of-mathematical-models.

Panday S, Huyakorn PS (2008) MODFLOW SURFACT: A State-of-the-Art Use of Vadose Zone Flow and Transport Equations and Numerical Techniques for Environmental Evaluations. Vadose Zone Journal, 7(2), 610. doi:10.2136/vzj2007.0052

Prickett TA, Lonnquist CG (1971) Selected Digital Computer Techniques for Groundwater Resource Evaluation, Illinois State Water Survey, Bulletin 55, 62 pp.

Read JRL, Stacey PF (Eds) (2009) Guidelines for Open Pit Slope Design, CSIRO Publishing and CRC Press, 496 pp.

Townley LR (1990) AQUIFEM-N: A Multi-layered Finite Element Aquifer Flow Model, User's Manual and Description, Townley and Associates.

Townley LR, Wilson JL (1980) Description of and User's Manual for a Finite Element Aquifer Flow Model AQUIFEM-1, Technical Report No. 252, Ralph M Parsons Laboratory for Water Resources and Hydrodynamics, MIT, 294 pp.

Wilson JL, Hamilton DA (1978) Influence of strip mines on regional groundwater flow, J.Hyd.Div. ASCE 104, 9, 1004–1011, September.

Wilson JL, Townley LR, Sa da Costa A (1979) Mathematical Development and Verification of a Finite Element Aquifer Flow Model AQUIFEM-1, Technical Report No. 248, Ralph M Parsons Laboratory for Water Resources and Hydrodynamics, MIT, 114 pp.

Water Geochemistry in the Former Hg-Mining Area of Abbadia San Salvatore: a Review

Orlando Vaselli[1,2], Federica Meloni[1,2], Barbara Nisi[2], Jacopo Cabassi[2], Francesco Bianchi[3], Giordano Montegrossi[2], Daniele Rappuoli[4,5]

[1] *Department of Earth Sciences, University of Florence, Via La Pira 4, 50121 Florence, Italy*

[2] *CNR-IGG Institute of Geosciences and Earth Resources, Via La Pira 4, 50121 Florence, Italy*

[3] *S.B.C., Geologi Associati, Via XX Settembre n. 78 – 50129 Firenze (Italy)*

[4] *Unione dei Comuni Amiata Val d'Orcia, Unità di Bonifica, Via Grossetana 209, Piancastagnaio, Siena 53025, Italy*

[5] *Parco Museo Minerario di Abbadia San Salvatore - Via Suor Gemma, Abbadia San Salvatore 1, Siena 53021 Italy*

Abstract

The mercury (Hg)district of Mt. Amiata (Tuscany, central Italy) has been one of the most famous mining areas to produce liquid mercury from cinnabar (HgS)-bearing ore deposits and the mining site of Abbadia San Salvatore was by far the largest exploiting and productive center of the whole district. In this work, we reviewed a large dataset of geochemical parameters, including As, Hg and Sb, using about 40 geochemical surveys of surface and ground waters from the mining areas and surroundings to provide evidence of the most important contaminants and to suggest remediation actions.

Keywords: Mercury mines, , Hg contamination, Abbadia San Salvatore, remediation

Introduction

Contamination of surface and ground waters represents one of the most important criticalities in decommissioned and active mines where poly-metallic sulfides have been or are exploited. This is due the fact that the interaction between meteoric waters and sulfides causes so-called acid mine drainage which is normally characterized by high concentration of potentially toxic elements (PTEs) and pH down to 2 (Nordstrom 2011a). However, mines showing circumneutral waters are also affected by anomalous concentrations of PTEs (Nordstrom, 2011b; Gandy *et al.* 2015; Vriens *et al.* 2019). The former mercury (Hg)-mining area of Abbadia San Salvatore (central Italy) is indeed showing pH values that very sporadically are clustering around 5, while most of them are between 6.3 and 7.3. Despite these pH values, arsenic (As) and antimony (Sb) concentrations are commonly found to be >10 μg L^{-1} while those of Hg largely exceed 1 μg L^{-1}, the latter being the targeted value for uncontaminated ground- and surface waters (Vaselli *et al.* 2015; 2021; Lazzaroni *et al.* 2022; Meloni *et al.* 2024).

This study reviews the ground- and surface water geochemistry of the Abbadia San Salvatore mine and its environs. The dataset includes dissolved major, minor and trace (As, Hg and Sb) concentrations of waters collected and analyzed since 2013 and new original data collected in 2024 as part of a collaboration between the local municipality and the Department of Earth Science at the University of Florence, Italy. This study's primary goal is to identify the geochemical facies, As, Sb, and Hg concentrations, as well as their seasonal variations, in order to reduce the remarkably high Hg concentrations and, to a lesser extent, As and Sb concentrations. These elements are considered rather dangerous since they have negative effects on the ecosystems and human health, therefore, minimizing their concentrations in aquatic environments is necessary (Fu *et al.* 2010). As reported by Vaselli *et al.* (2015), several approaches have been proposed to remove Hg from water, but no well-assessed methods are commercially available since most abatement systems are still at laboratory scale. Here, we report the main results related to two experimental methods, carried out at laboratory scale, where the initial concentration of dissolved Hg in groundwaters collected from the Abbadia San Salvatore mining was successfully and quantitatively reduced.

The study area

The Abbadia San Salvatore Hg-mine (Fig. 1) is part of the Mt. Amiata, a 300–200 ka old volcano, mining district that has been one of the most important sites worldwide for the exploitation of Hg from cinnabar (HgS) that lasted for more the 150 years (1846–1982). About 117,000 tons of liquid Hg were produced (Segreto 1991). It has been estimated that about 70% of the total production of Hg was from the Abbadia San Salvatore Hg-mine (Cipriani and Tanelli 1983; Rimondi *et al.* 2015). In contrast to As and Sb, which were found to be more dispersed and primarily related to tailings and calcines derived from roasting processes of ore deposits treated at Abbadia San Salvatore but exploited from other Mt. Amiata mines (e.g. Meloni *et al.* 2023), particularly high abundances of Hg were determined within the mining area and nearby (Vaselli *et al.* 2013; Rimondi *et al.* 2019). The initial phases related to the remediation of the Abbadia San Salvatore Hg-mine dates back to 2010, and due to the large variety of criticalities encountered (Vaselli *et al.* 2019), the operations have been extended up to the early 2020. Finally, at the end of 2025 the ground of the mining area is expected to be completed. The difficulties related to the removal of dissolved Hg from the surface and ground waters are still to be decided and are still a matter of debate. This is due to different problems, including: i) the Hg concentrations are extremely variable, and sometimes >100 µg L^{-1}, from piezometer to piezometer, although they are located a few tens of meters from each other (Vaselli *et al.* 2015), similar behavior is also shown by As and Sb, though to a minor extent; ii) there is not continuous shallow aquifer. According to Meloni *et al.* (2024), hydrological investigations did indicate that

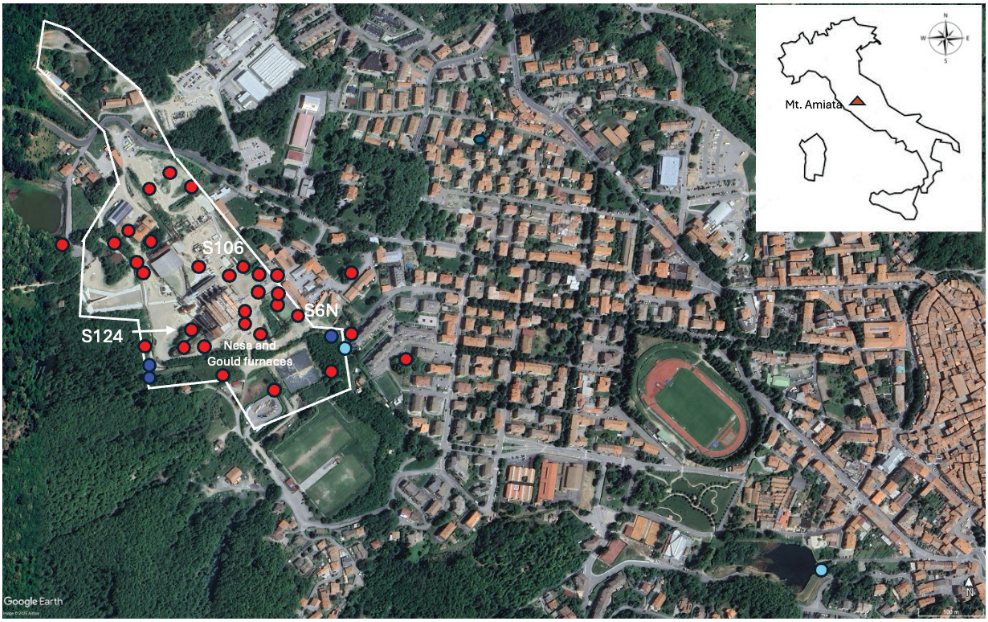

Figure 1 The Abbadia San Salvatore mining area. The white line surrounds the main mining structure (including the Gould and Nesa furnaces). Red circles: piezometers; Blue circles: spring; Light blue: surface waters. The sampling points refer to the geochemical survey activity carried out since 2013. Over time, some piezometers were covered due to the remediation operations while others were drilled. The water samples used for the laboratory tests related to the removal of Hg are reported (see text).

there are a few isolated subterranean water pockets with low transmittivity, meaning that the hydraulic connection is rather poor.; iii) the shallow aquifer in the mining area was formed when a small paleo-valley was filled with material derived from the mining activity, as observed during piezometer drillings that also showed the presence of drops of liquid Hg (Vaselli *et al.* 2015); iv) groundwaters located along the water flowlines and outside the mining area showed concentrations of Hg, As and Sb of <1, 10 and 5 µg L^{-1}, respectively (Meloni *et al.* 2024).

Methods

The sampling sites (collected in January/February, May/June and September/October) are shown in Fig. 1. The limits of the Hg-contaminated site are indicated with a white line that also defines the area where the main mining structures, such as edifices, Gould and Nesa furnaces, mineral conveyor belts, dryers and condensers, are hosted. It must be pointed out that since 2013 onward some piezometers were destroyed during the remediation activities and others were drilled to cover as much as possible the former mining area. All the chemical analyses were carried by titration (HCO_3), molecular spectrophotometer (NH_4, NO_2), ion chromatography (main cations and Cl, SO_4, Br, F and NO_3) and inductively coupled plasma-mass spectrometry (As, Hg and Sb) or by cold vapor with a Lumex device (Hg). Temperature, pH and electrical conductivity were measured in the field. All water samples were filtered at 0.45 µm prior analysis. Other trace elements were also determined but their concentrations did not show any specific peculiarity and thus, they will not be considered in this work. In order to provide suitable solutions to reduce the concentration of dissolved Hg in the Abbadia San Salvatore mine, laboratory tests were conducted by using two different approaches: i) Borraquero *et al.* (2018) proposed the use of highly Hg-selective microcapsules (MC-TOMAC) characterized by trioctyl-methyl-ammonium-chloride and applied to three waters with different Hg concentrations: from 1.4 to 257 µg L^{-1}; ii) Capterall® is an industrial patented product by Solvay industries. Capterall® is a synthetic bio-apatite used for wastewater treatments. It was tested in three different water samples with different amount of Hg: 21, 46.6 and 252 µg L^{-1}. In this three different waters, three different typologies (Mix 1, Mix 2, Mix 3) of Capterall® with 2 distinct dosages (D1: 0.4 and D2: 0.8 g/L, respectively) were given by the manufacturer. The pH of the water was stabilized at 7.5 with NaOH. The waters were left reacting with the three Mix products using the two distinct dosages overnight by means of a horizontal shaker. The samples were filtered afterwards with a Sartorius® filtering device.

Results and Discussion

Temperature was strictly dependent on the season, particularly for the surface waters (down to 4.8 °C and up to 17 °C). Groundwater temperatures ranged from 11 °C in the winter to up to 17 °C in the summer. The electrical conductivity ranged from 60 to 1800 µS/cm, and the pH was circumneutral, ranging from 5.5 (only four samples) to 7.9. The Ca(Mg)-SO_4 composition was mostly dominant and characterized most studied waters. This composition was linked to the water-rock interaction with gypsum, which is a gangue mineral that was probably employed during the roasting process of HgS. The Ca(Mg)-HCO_3 and (Na+K)-HCO_3 facies were identified as secondary. It should be noted, though, that seasonal differences were noted in water geochemistry. This was interpreted as being related to remediation actions carried out over time, such as construction of an artificial channel to convey the meteoric waters to minimize the interaction with the contaminated soils and the made-made material (such as concrete, bricks, tuff, tiles) of the mining area where concentrations of Hg as high as 73,000 and 46,000 mg kg^{-1} were measured, respectively (Vaselli *et al* 2017). High concentrations of Hg in soil were found in front of the Gould and Nesa furnaces where the mining materials were stored whereas those related to the construction material were related to the long-lasting contact with an Hg-rich atmosphere (up to >50,000 ng m^{-3}) (Vaselli *et al.* 2017; Lazzaroni *et al.* 2020). Table 1 summarizes the minimum, maximum, mean, and median concentrations of As, Hg, and Sb.

Table 1 *Minimum and maximum concentrations (μg L^{-1}) for As, Hg and Sb. These abundances refer to the seasonal surveys carried out from 2013 to 2024 in the waters from the former Hg-mining areas of Abbadia San Salvatore.*

Sampling period	Arsenic μg L^{-1}	Mercury μg L^{-1}	Antimony μg L^{-1}
Winter 2013–2024	<0.1–18.1	<0.1–853	<0.1–31.0
Spring 2013–2014	<0.1–18.4	<0.1–695	<0.1–31.4
Autumn 2013–2014	<0.1–30.4	<0.1–440	<0.1–199

To simplify, the three chalcophile elements' mean, minimum, and maximum values are listed by considering their contents on an annual seasonal basis.

Samples ranging from 22 to 42 were gathered throughout each survey. Only a few samples had very high levels of As and Sb, since most of them had values within the 10 and 5 μg L^{-1}, respectively, limits suggested by the European Community. Remarkably different is the situation concerning Hg. In fact, its abundance spanned over 4 orders of magnitudes and reached up to 853 μg L^{-1} (January 2014). The concentrations of Hg are not preferentially distributed in a specific area since they are mostly scattered throughout the mining site. The highest concentrations are indeed found in the eastern and western part although notable concentrations were also found close to the building hosting the Gould and Nesa furnaces (Fig. 1).When the current measured amounts need to be carefully reduced in the future, the randomly distributed Hg may cause some challenges. According to the new hydrogeological conceptual model and the geochemical data, the Hg-contamination seems to be presently limited to the mining area (Meloni *et al.* 2024) while the deeper aquifer appears to be not affected by Hg concentrations >1 μg L^{-1} (Vaselli *et al.* 2015).

The two different approaches test for Hg removal in waters have given excellent results. The MC-TOMAC approaches, at the current pH values, the laboratory results indicated that up to 99± 2.0% of the initial Hg was successfully removed.

The application of a commercial product, named Capterall®, to the water samples characterized by variable and increasing Hg contents provided satisfactory results. As previously mentioned, three different typologies of Capterall® with two distinct dosages were tested, containing bioapatite although the complete industrial receipt was not provided.

The results are reported in Table 2 for the S6N, S106 and S124 water samples (Fig. 1). Note that the initial concentrations of Hg are in μg L^{-1} whereas those after the application of Capterall® are in ng L^{-1}. The removal of Hg appears to be effective. In fact, in only two cases the concentration of Hg is about 1 μg L^{-1} whereas in most cases the remaining Hg in solution after the Capterall® is clustering around 1% of the original concentration.

Conclusions

A large variability of concentrations of As, Hg and Sb was observed in the former Hg-mining area of Abbadia San Salvatore. However, from an environmental perspective, As and Sb do not pose a serious problem since a very low number of samples showed concentrations higher than those expected for surface and ground waters. Dissolved Hg is thus the main issue in this site where remediation operations at the ground level in the mine are about to be completed at the end of 2025. The laboratory runs, conducted with two different approaches (MC-TOMAC and Capterall®), have produced satisfactorily results. The next step is to set up a pilot site that is planned by the end of 2025 to test the encouraging laboratory results although economic evaluations to select one of the two approaches are required.

Acknowledgements

The authors thank A. Esposito and F. Piccinelli for their help and patience during the many geochemical surveys carried out in the former mine of Abbadia San Salvatore and nearby. We acknowledge two reviewers for improving an early version of this extended abstract.

***Table 2** Laboratory tests carried out using different mixing products of Capterall® and dosages (D1 and D2). The second and third columns refers to the concentrations of the original content of Hg (μg L^{-1}) and those measured after the application of Capterall® (ng L^{-1}). The three samples (S6N, S106 and S124) were collected from the former Abbadia San Salvatore Hg mine (Fig. 1).*

Sample	Initial concentration (Hg) μg L^{-1}	Final concentration (Hg) ng L^{-1}
S6N Mix1 d1	252	595.2
S6N Mix2 d1	252	1516
S6N Mix3 d1	252	638.4
S106 Mix1 d1	21	811.6
S106 Mix2 d1	21	464.4
S106 Mix3 d1	21	676.4
S124 Mix1 d1	46.6	379.6
S124 Mix2 d1	46.6	267.6
S124 Mix3 d1	46.6	355.6
S6N Mix1 d2	252	402
S6N Mix2 d2	252	450
S6N Mix3 d2	252	282
S106 Mix1 d2	21	710
S106 Mix2 d2	21	1668
S106 Mix3 d2	21	443.2
S124 Mix1 d2	46.6	275.2
S124 Mix2 d2	46.6	193.6
S124 Mix3 d2	46.6	263.2

References

Cipriani C, Tanelli G (1983) Risorse minerarie ed industria estrattiva in Toscana. Note storiche ed economiche. Atti Mem. Accad. Sci. Lett. Colombaria 28:241–283. (In Italian)

Borreguero AM, Leura A, Rodríguez JF, Vaselli O, Nisi B, Higueras PL, Carmona M (2018). Modelling the mercury removal from polluted waters by using TOMAC microcapsules considering the metal speciation. Chem Engin J 341:308–316, doi.org/10.1016/j.cej.2018.01.113

Fu Z, Wu F, Amarasiriwardena D, Mo C, Liu B, Zhu J, Deng Q, Liao H (2010) Antimony, arsenic and mercury in the aquatic environment and fish in a large antimony mining area in Hunan, China. Sci Tot Environ 408:3403–3410, doi.org/10.1016/j.scitotenv.2010.04.031

Gandy CJ, Smith JWN, Jarvis AP (2007) Attenuation of mining-derived pollutants in the hyporheic zone: A review. Sci Tot *Environ* 373:435–446, https://doi.org/10.1016/j.scitotenv.2006.11.004

Lazzaroni M, Nisi B, Rappuoli D, Cabassi J, Vaselli O (2020) A New Low-Cost and Reliable Method to Evaluate the Release of Hg0 from Synthetic Materials. Processes, 8:1282, https://doi.org/10.3390/pr8101282

Lazzaroni M, Vetuschi Zuccolini M, Nisi B, Cabassi J, Caliro S, Rappuoli D, Vaselli O (2022) Mercury and Arsenic Discharge from Circumneutral Waters Associated with the Former Mining Area of Abbadia San Salvatore (Tuscany, Central Italy). *Intl J Environ Res Pub Health* 19(9):5131. https://doi.org/10.3390/ijerph19095131

Meloni F, Nisi B, Gozzi C, Rimondi V, Cabassi J, Montegrossi G, Rappuoli D, Vaselli O (2023) Background and geochemical baseline values of chalcophile and siderophile elements in soils around the former mining area of Abbadia San Salvatore (Mt. Amiata, southern Tuscany, Italy). J Geochem Expl 255, doi.org/10.1016/j.gexplo.2023.107324.

Meloni F, Montegrossi G, Cabassi J, Bianchi F, Nisi B, Rappuoli D, Vaselli O (2024) Geochemical Surveys of Ground and Surface Waters in the Abandoned Hg-Mine of Abbadia San Salvatore (Central Italy): A Preparatory Investigation before Remediation. Water 16(9):1210, https://doi.org/10.3390/w16091210

Nordstrom DK (2011a) Hydrogeochemical processes governing the origin, transport and fate of major and trace elements from mine wastes and mineralized rock to surface waters. Appl Geochem 26:1777–1791, doi.org/10.1016/j.apgeochem.2011.06.002

Nordstrom DK (2011b) Mine waters: acidic to circumneutral. Elements 7:393–398 doi: 10.2113/gselements.7.6.393

Rimondi V, Chiarantini L, Lattanzi P, Benvenuti M, Beutel M, Colica A, Costagliola P, Di Benedetto F, Gabbani G, Gray JE, Pandeli E, Pattelli G, Paolieri M, Ruggieri G (2015) Metallogeny, exploitatio and environmental impact of the Mt. Amiata mercury ore district (Southern Tuscany, Italy). It J Geosci 134:323–336, doi.org/10.3301/IJG.2015.02

Rimondi V, Costagliola P, Lattanzi P, Morelli G, Cara G, Cencetti C, Fagotti C, Fredduzzi A, Marchetti G, Sconocchia , Torricelli S. (2019) A 200 km-long mercury contamination of the Paglia and Tiber floodplain: Monitoring results and implications for environmental management. Environ Poll 255, doi.org/10.1016/j.envpol.2019.113191.

Segreto L (1991) Monte Amiata. Il mercurio italiano. Strategie internazionali e vincoli extraeconomici. Franco Angeli (Ed.)

Vaselli, O, Higueras P, Nisi B, Esbrì JM, Cabassi J, Martìnez-Coronado A, Tassi F, Rappuoli D (2013) Distribution of gaseous Hg in the Mercury mining district of Mt. Amiata (Central Italy): A geochemical survey prior the reclamation project. Environ Res 125:179–187. doi.org/10.1016/j.envres.2012.12.010

Vaselli O, Nisi B, Rappuoli D, Bianchi F, Cabassi J, Venturi S., Tassi F, Raco B (2015) Geochemical characterization of the ground waters from the former Hg-mining area of Abbadia San Salvatore (Mt. Amiata, central Italy): criticalities and perspectives for the reclamation process. It J Geosci 134:23–31.

Vaselli O, Lazzaroni M, Nisi B, Cabassi J, Tassi F, Rappuoli D, Meloni F (2021) Discontinuous Geochemical Monitoring of the Galleria Italia Circumneutral Waters (Former Hg-Mining Area of Abbadia San Salvatore, Tuscany, Central Italy) Feeding the Fosso Della Chiusa Creek. Environments 8(2), https://doi.org/10.3390/environments8020015

Vaselli O, Nisi B, Rappuoli D, Cabassi J, Tassi F (2017). Gaseous Elemental Mercury and Total and Leached Mercury in Building Materials from the Former Hg-Mining Area of Abbadia San Salvatore (Central Italy). Intl J Environ Res Public Health 14, doi:10.3390/ijerph14040425.

Vaselli, O., Rappuoli, D., Bianchi, F., Nisi, B., Niccolini, M., Esposito, A., Cabassi, J., Giannini, L., Tassi, F., 2019. One hundred years of mercury exploitation at the mining area of Abbadia San Salvatore (Mt. Amiata, Central Italy): a methodological approach for a complex reclamation activity before the establishment of a new mining park. El patrimonio geològico y minero. Identidad y motor de desarrollo. Publicaciones del Instituto Geològico y minero de España Serie: Cuadernos del Museo Geominero, n. 29. Proceed. XVII Congreso Internacional sobre Patrimonio Geológico y Minero, ISBN: 978-84-9138-081-8, 21–24 September 2017, Almaden (Spain):1109–1126.

Vriens B, Skierszkan EK, St-Arnalt M., Salzsauler K, Aranda C, Mayer KU, Beckie RD (2019) Mobilization of Metal(oid) Oxyanions through Circumneutral Mine Waste-Rock Drainage. ACS Omega 4:10205–10215, doi.org/10.1021/acsomega.9b01270

Surface Disposal of High-Sulfide Thickened Tailings at the Neves Corvo Mine, Portugal – Operational Observations

Rens Verburg[1], Mafalda Oliveira[2]

[1]WSP USA, Redmond, WA 98077, USA, rens.verburg@wsp.com

[2]SOMINCOR – Sociedade Mineira de Neves-Corvo, S.A., Castro Verde, Portugal, mafalda.oliveira@lundinmining.com

Abstract

The Neves Corvo mine in Portugal makes use of surficial disposal of high-sulfide thickened tailings. The environmental behavior of the tailings is assessed through an extensive monitoring program of interstitial, surface and seepage water quality as well as the solids. The ongoing monitoring of the tailings mass and operational experience at Neves Corvo indicate that surficial deposition of high-sulfide thickened tailings in an arid climate represents a feasible alternative that enhances operational flexibility, facilitates concurrent reclamation and permits co-disposal with waste rock.

Keywords: Paste, tailings, sulfide, surface, operations

Introduction

Neves Corvo is a world-class underground copper-zinc mine located in the south of Portugal, owned at the time of paper preparation by Lunding Mining Corporation but currently owned by Boliden. The mine has been operated since 1988 by SOMINCOR. The pyritic tailings produced by the operation contain up to 45 weight% sulfide sulfur. Additionally, they have negligible neutralization potential (NP), resulting in a very high acid generation potential. Following mine startup, the tailings were placed subaqueously in the Barragem Cerro do Lobo tailings storage facility (TSF), a large tailings pond created by a rockfill dam across a natural river valley. However, due to the finite capacity of the impoundment, alternatives for provision of sufficient storage capacity were studied by SOMINCOR in the early 2000s. Surface disposal of thickened tailings was identified as the preferred option, which was considered a novel approach at the time given the high reactivity of the tailings and the arid climate at Neves Corvo. More detail on the geochemical and geotechnical investigations that were conducted in support of this decision as well as results from infiltration and geochemical modeling can be found in Junqueira *et al.* (2009), Lopes *et al.* (2015) and Verburg *et al.* (2003, 2009).

The tailings facility was originally developed for sub-aqueous tailings deposition, with an area of 191.5 hectares or 1.9 km^2, allowing for a total of 17 Mm^3 to be deposited. In 2010, the TSF was converted from a sub-aqueous to a thickened tailings deposition facility, without requiring any future raises of the main and perimeter rockfill embankments. The design included disposal of tailings with run-of-mine waste rock, which is potentially acid generating, in a co-disposal system. The waste rock is used for construction of peripheral berms and covers while use of waste rock for internal dikes formed part of an older depositional scheme which is no longer in use. Waste rock dikes nowadays have become encapsulated in the tailings.

The storage capacity of the facility using this method was increased to 33.3 Mm^3, based on a vertical expansion of five tiers. In 2022, SOMINCOR received approval to expand the footprint of the TSF to the south area, to allow for sufficient additional storage capacity through 2033. Construction of a new south containment embankment started in 2022 and the deposition of thickened tailings in the new area started in April 2024. Additional lifts to the expanded facility will be constructed in accordance with the mine plan. The expanded facility occupies a total area of approximately 210 hectares. With this expansion, the TSF storage capacity has increased in capacity from 33.3 to 50 Mm3 of extractive waste (tailings and waste rock), maintaining the current system of co-disposing thickened tailings and waste rock. Fig. 1 shows a recent aerial photo of the TSF.

Monitoring data collected since late 2010 include records of tailings production and thickened tailings densities, yield stress, particle size distribution, and specific gravity. Settlement, deposition slopes and piezometric levels in the thickened tailings and underlying subaqueous deposit are also routinely monitored. The environmental component of the monitoring program includes, among others, the determination of ponded water quality. Due to the acidic nature of the near-surface tailings, surficial contact water in the TSF is acidic as well, with elevated sulfate and metals concentrations. This water is directed to Cell 15 where it is mixed with process water from the tailings thickener. It is then treated by Fenton reaction plus a high-density sludge (HDS) process and reused in the industrial process, reducing the requirement for fresh makeup water.

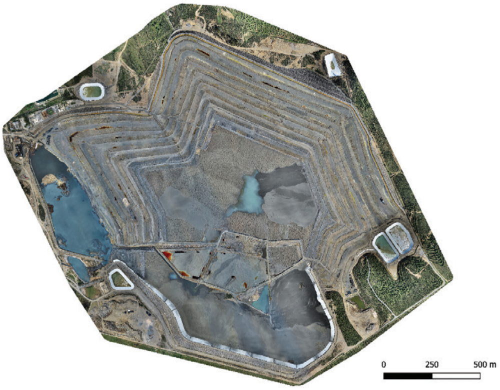

***Figure 1** Aerial photo of the Barragem Cerro do Lobo TSF (image: IRCLLevantamento GW20Fev2025_100cm).*

A second component of the environmental monitoring program consisted of periodic compositional profiling of the thickened tailings and underlying slurry tailings with depth, which is the focus of this paper. The aim of this effort was to develop a better understanding of the depth of oxidation as a function of location in the TSF, with special focus on locations near waste rock dikes vs. locations at some distance from the dikes as well as locations underneath waste rock covers vs. locations where thickened tailings were exposed.

Methods

The sampling program of the thickened tailings took place during two campaigns in 2021. A total of 70 thickened tailings samples were collected from different depths at 40 locations throughout the TSF.

The first campaign involved collection of 40 deeper samples at 10 locations up to depths of approximately 35 m using a piston sampler as part of a geotechnical program. A second campaign consisted of collection of 30 shallow core samples up to approximately 1 m deep at the same locations (each generating 10 subsamples corresponding to different depths within each sample core). The samples were collected along transects to support assessment of different aspects related to depositional age of the thickened tailings, exposure duration, and the presence or absence of a waste rock cover.

Samples obtained during the first campaign underwent comprehensive geochemical characterization and were analyzed for paste pH and electrical conductivity (EC), acid base accounting (ABA), net acid generation (NAG) testing, chemical composition, and short-term leach testing by the shake flask extraction (SFE) method. The second campaign focused on the determination of paste pH and EC for the assessment of oxidation of shallow thickened tailings either exposed or encapsulated by the waste rock cover.

Concentration profiles with depth (not shown) indicate that the composition of the tailings has been relatively consistent over time, with both the deeper, subaqueous tailings and the overlying, subaerial thickened tailings reporting similar overall compositions. Where compositional differences are observed, they occur in the shallower, near-surface samples. Differences between the shallower and deeper samples are most pronounced for the following parameters: sulfate sulfur (highest concentrations in shallow samples), total inorganic carbon (TIC) and NP (lowest concentrations in shallow samples), paste pH (lowest values of approximately pH 2 in shallow samples) and paste EC (highest values in shallow samples). Also, for some trace metals (e.g., cobalt, copper), the shallowest samples contain some of the lowest concentrations observed throughout the depth profile.

Discussion

The observed trends in the solids profiles are consistent with sulfide oxidation occurring. This process results in generation of sulfate and acidic conditions, an increase in paste EC, and depletion of TIC, NP and the trace metals mentioned due to their increased mobility under acidic conditions. The SFE results support the observed trace metal trends and are in good agreement with geochemical principles, with leaching of cationic trace metals (e.g., cadmium, cobalt, nickel, zinc) more pronounced under acidic conditions and leaching of anionic parameters (e.g., antimony, arsenic, molybdenum selenium) more pronounced under circumneutral to alkaline conditions.

Due to the high sulfide sulfur content of the tailings of up to 45 weight%, its depletion is not apparent in the shallow samples. Also, in the presence of elevated sulfide sulfur contents, the quantities of near-surface sulfur available for reaction with oxygen are such that an oxidation front typically does not extend to great depths. In the absence of a cover, the oxidation front typically extends to a depth of approximately 30 cm. Figure 2 shows a typical oxidation front of an uncovered tailings surface that has been exposed for four years. Oxidation is most pronounced along fractures and cracks.

The effects of the near-surface sulfide oxidation (e.g., depletion of TIC, NP and/or trace metals) reach a depth of up to approximately 1 to 1.5 m, with the greater depths typically associated with desiccation cracks or discontinuities related to, for instance, the presence of waste rock dikes. These effects are considered the result of downward percolation of acidic solutions resulting from the near-surface sulfide oxidation.

The effect of the presence of waste rock dikes is illustrated in Fig. 3. This figure shows that paste pH is typically lower in the vicinity of those dikes than some distance away. Paste EC (not shown) exhibits the opposite trend, with higher values found closer to the dikes.

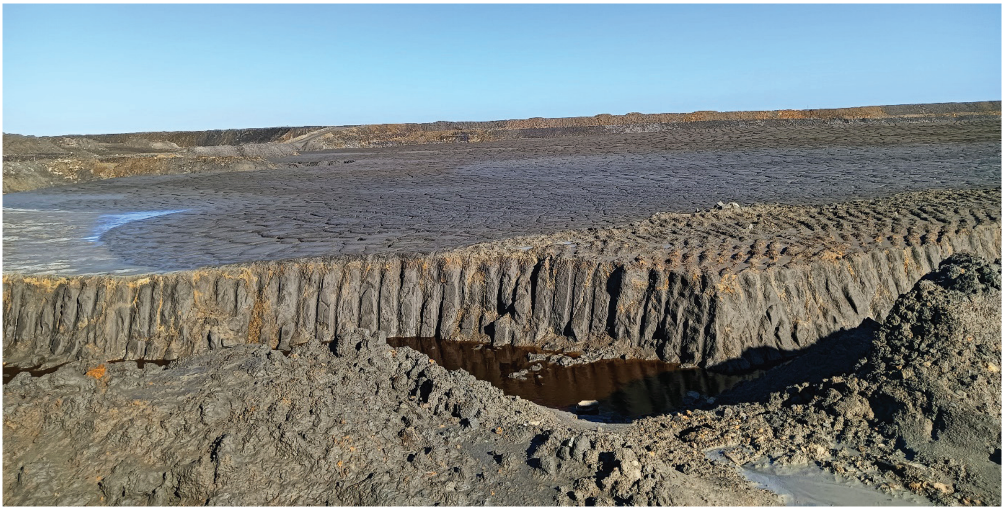

Figure 2 *Example photograph of oxidation profile.*

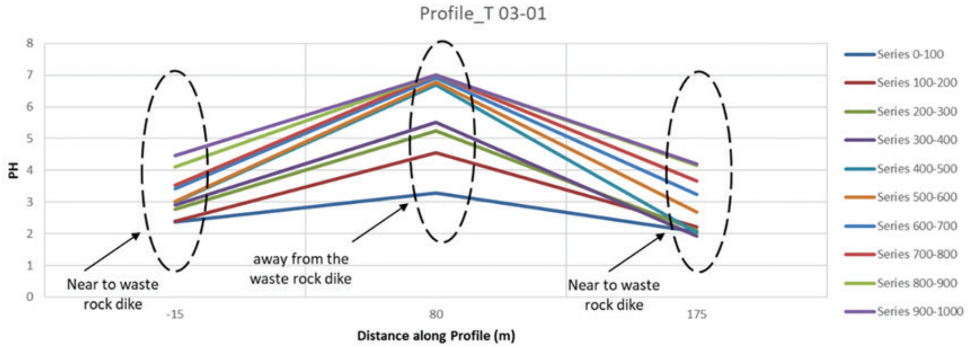

Figure 3 *Example cross section of paste pH near and away from waste rock dikes. Values in the legend refer to 100-mm depth increments of each sample below ground surface.*

This indicates that the dikes enhance sulfide oxidation relative to the regular thickened tailings surface, likely through promoting horizontal drainage and depression of the water table in the vicinity of the dikes, thereby reducing the moisture content of the thickened tailings and/or enhancing oxygen ingress by providing preferential pathways through cracking of the tailings. Sulfide oxidation is very sensitive to moisture content, with oxygen diffusion declining by approximately three to four orders of magnitude as the degree of saturation increases above 85% (INAP 2009). The effect of the dikes is typically more pronounced for the deeper samples, while shallower samples within the 1-m depth interval generally report lower paste pH than the deeper samples.

The effect of the presence of a waste rock cover is noticeable as well. Fig. 4 and 5 show paste pH trends for an uncovered and covered transect, respectively. Whereas paste pH in uncovered transects typically ranges from 2 to 6 (depending on depth), this range generally is 6 to 8 for covered thickened tailings, indicating that the waste rock cover has been effective at reducing sulfide oxidation. The average thickness of the waste rock cover is 1 m. The waste rock cover is applied as soon as the maximum tailings level defined for each lift has been reached.

Conclusions

In summary, the results obtained from the geochemical characterization program have demonstrated the following:

- Away from waste rock dikes and in the absence of a cover, the oxidation front reaches a depth of approximately 30 cm. The zone of oxidation is characterized by lower paste pH, higher paste EC, an increase in sulfate sulfur content, and depletion of TIC, NP and select trace metals. At greater depths (up to 1 to 1.5 m), infiltration of acidic solutions may result in depletion of TIC, NP and/or trace metals as well.
- The waste rock dikes promote sulfide oxidation relative to the regular thickened tailings surface, likely through increasing horizontal drainage and depression of the water table, thereby reducing the moisture content of the thickened tailings and/or enhancing oxygen ingress by providing preferential pathways.
- The waste rock cover has been effective at reducing sulfide oxidation relative to exposed conditions.

The ongoing monitoring of the tailings mass and operational experience at Neves Corvo indicate that surficial deposition of high-sulfide thickened tailings in an arid climate represents a feasible alternative that enhances operational flexibility, facilitates concurrent

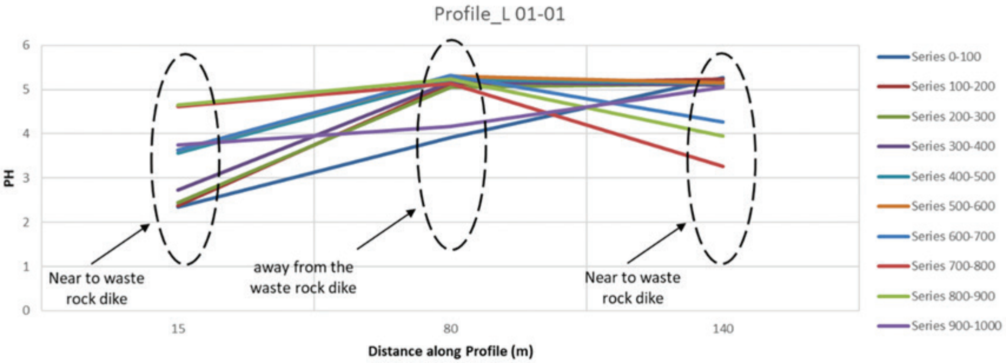

Figure 4 *Example cross section of paste pH in uncovered thickened tailings. Values in the legend refer to 100-mm depth increments of each sample below ground surface.*

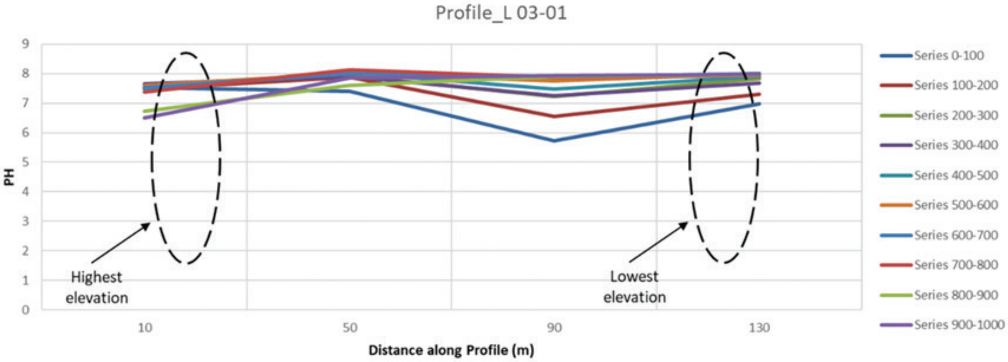

Figure 5 *Example cross section of paste pH in thickened tailings underneath waste rock cover. Values in the legend refer to 100-mm depth increments of each sample below ground surface.*

reclamation and permits co-disposal with waste rock.

Acknowledgments

The authors thank SOMINCOR for permission to present the results of the thickened tailings investigative program and Ricardo Bahia and Eduardo Afonso (WSP Portugal) for their support in paper preparation.

References

International Network for Acid Prevention (INAP) (2009) The Global Acid Rock Drainage (GARD) Guide. www.gardguide.com

Junqueira F, Wilson G, Oliveira M (2009) Surface Paste Disposal of High-Sulphide Tailings at the Neves Corvo Mine in Portugal. Part 1: Estimation of Tailings Desaturation and Implications for ARD Generation. Proc of the 8th Int Conf on Acid Rock Drainage, Skellefteå, Sweden, June 23–26, 2009

Lopes R, Bahia R, Jefferies M, Oliveira M. (2015) Upstream Stacking of Thickened Tailings at Neves Corvo. Proc of the 18th Int Seminar on Paste and Thickened Tailings, Cairns, QLD, May 5–7, 2015

Verburg R, Johnson B, Fordham M, Logsdon M (2003) A Rapid and Cost-Effective Method for Bench Screening of Geochemical Performance and Disposal Options for High-Sulfide Tailings. Proc of the 6th Int Conf on Acid Rock Drainage, Cairns, QLD, July 12-18, 2003

Verburg R, Ross C, Oliveira M (2009) Surface Paste Disposal of High-Sulphide Tailings at the Neves Corvo Mine in Portugal. Part 2: Field Trials, Cover Performance Monitoring, and Impact Assessment. Proc of the 8th Int Conf on Acid Rock Drainage, Skellefteå, Sweden, June 23–26, 2009

Catoca Diamond Mine – Implementation of an Advanced Monitoring Network for a Tailings Storage Facility (TSF)

Marçal Manuel Vicario[1], Manuel Fidel Sonhi Manassa[1], Enoque Makango Paiva[1],
Lukombo Eduardo Luzaiadio Carlos[1] & Kym L Morton[2]

[1]Catoca Mining Society, Luanda, Angola, Talatona Sector, geral@catoca.com, +226 624 7001

*[2]KLM Consulting Services Pty Ltd, 22 Central Road, Sunrella AH, South, P.O. Box, 119, Lanseria, 1748,
South Africa, kmorton@klmcs.co.za, ORCID 0000-0002-5865-1979*

Abstract

Catoca mine is an open-pit diamond mine belonging to Sociedade Mineira do Catoca in Angola that began in 1995. It has a large active tailings storage facility (TSF) and two smaller deactivated TSFs. Catoca aims to comply with Global Industry Standard on Tailings Management (GISTM) and has installed a comprehensive monitoring and fully automated control network infrastructure that is connected to a database and dashboard viewed by operators and managers. This interactive database can be accessed anywhere in the world. The enhanced monitoring network can be used in analysing the causes of TSF failures and providing early warnings for prevention of failures.

Keywords: Tailings Storage Facilities, Monitoring, Automation, Pore Pressures, Dam Failure, Diamond Mine

Introduction

Catoca mine is an open-pit diamond mine belonging to Sociedade Mineira do Catoca in Angola which started in 1995. The mine is in the Province of Lunda Sul, 1050 km east of Luanda(Capital of the Republic of Angola), very close to the border with the Democratic Republic of Congo (DRC). It has a large active tailings storage facility (TSF) and two smaller deactivated TSFs.

The pit is next to the Lova river, which drains to the North into the Tshikapa River which joins the Congo River then drains into the Atlantic Ocean through the DRC. The active TSF is on the Lupugo and Luite streams that join the Lova downstream of the main TSF wall. Fig. 1 shows the mine location, the main rivers, and the catchment area for the main TSF.

Catoca processes kimberlite ore to extract diamonds and has a large active tailings storage facility (TSF) and two smaller deactivated TSFs. The three TSFs are shown in figure 2.

Catoca is the largest of all kimberlite pipes in the Lucapa kimberlite structure in northeastern Angola, covering a surface area of about 64 hectares. It is the fourth largest known kimberlite. The pipe comprises volcanogenic-sedimentary rocks. The inner ring of the vertical pipe comprises porphyritic kimberlites, while the centre is primarily kimberlitic breccias. The type of kimberlite is relevant to the mineral processing method as the high clay content results in a high concentration of suspended sediments in the tailings pond, giving it its characteristic red colour.

The pipe is intruded into Archaean granite-gneisses and crystalline schists, overlain by Palaeogene to Neogene sands of the Kalahari Formation some tens of metres thick. A small kimberlite pipe to the southwest of the main pit has been mined out. The TSFs sit on Kalahari sand and weathered granites, gneiss and schists.

Groundwater levels are from 5 to 30 m deep, the aquifers are weathered rock, alluvium, and some fracture/fault structures.

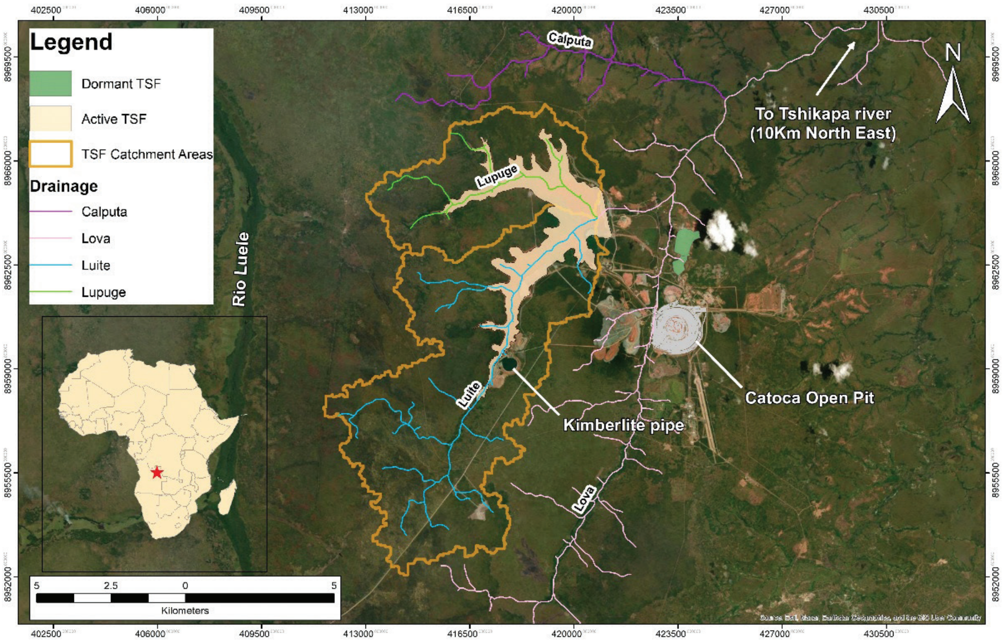

Figure 1 Catoca location and drainage.

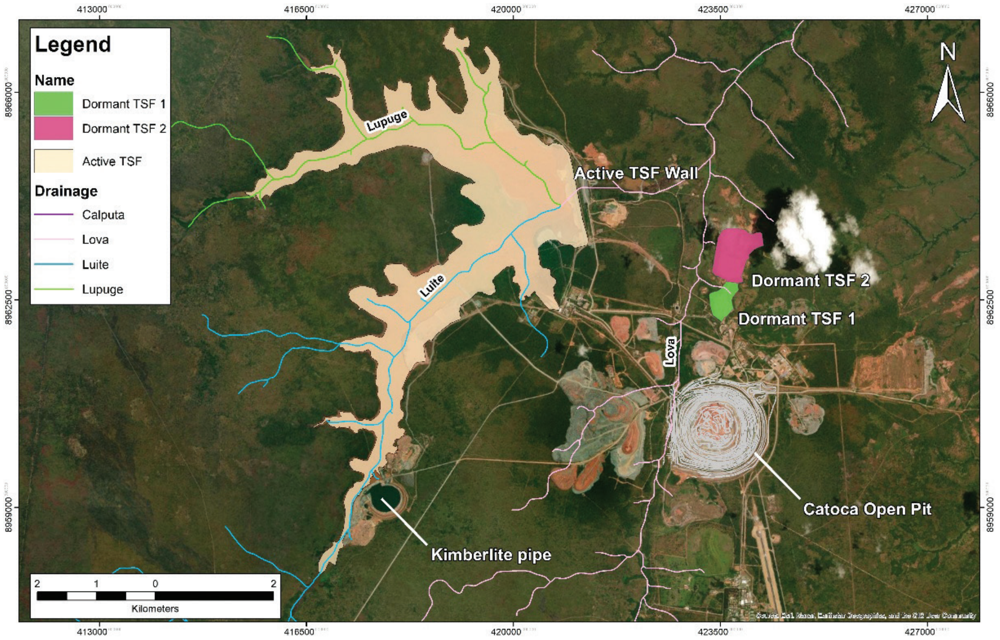

Figure 2 Three tailings storage facilities.

Monitoring objectives

Sociedade Mineira do Catoca, the owners of Catoca Diamond Mine, are working hard to become compliant with the Global Industry Standard for Tailings Management (GISTM 2020) (globaltailingsreview.org) and to meet recommendations listed in Morton *et al* (2020). Mine management are very aware of causes of failures of TSF installations worldwide. The failures are predominantly caused by excess and uncontrolled water (Shahid *et al* 2020) in the pond and in the dam walls. Over the last three years, Catoca has installed a comprehensive monitoring and control network infrastructure to monitor all aspects of the dam morphology. The Catoca system is fully automated and connected to a database-enabled dashboard which is viewed by operators and management at remote workstations. This bespoke interactive database can be accessed anywhere in the world and has also been designed to inform engineers, shareholders and stakeholders. With this interactive database, Angola now has an enhanced monitoring network capable of reducing risk by monitoring all aspects of the water and materials balance, analysing the causes of TSF failures and providing early warnings to enable risk reduction and prevent failures.

Historically, monitoring of TSFs around the world has tended to concentrate on the simple measurement of movement of the TSF dam wall. This is reactive monitoring; once unplanned movement of the dam starts it is too late to stop it. Catoca is proactive in its approach as it measures the inputs and outputs of the TSF (water and materials), interprets potential causes for movement of the TSF, sets targets for water control and then implements the required mitigation measures timeously.

Catoca TSF complex comprises three TSFs. Two dormant TSFs were commissioned in the 1980s and closed in the 1990s. These reach an elevation of 970 mamsl. The active TSF was started in 2000 and covers 1280 hectares and reaches an elevation of 950 mamsl. Fig. 3 shows the detail of the two dormant TSFs.

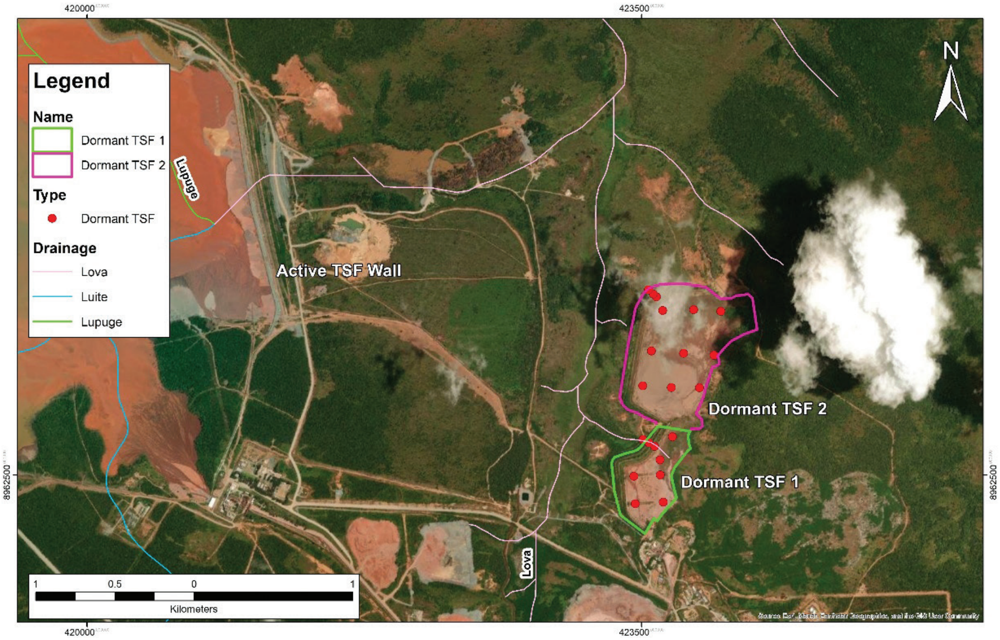

Figure 3 *Two dormant TSFs with vibrating wire piezometers.*

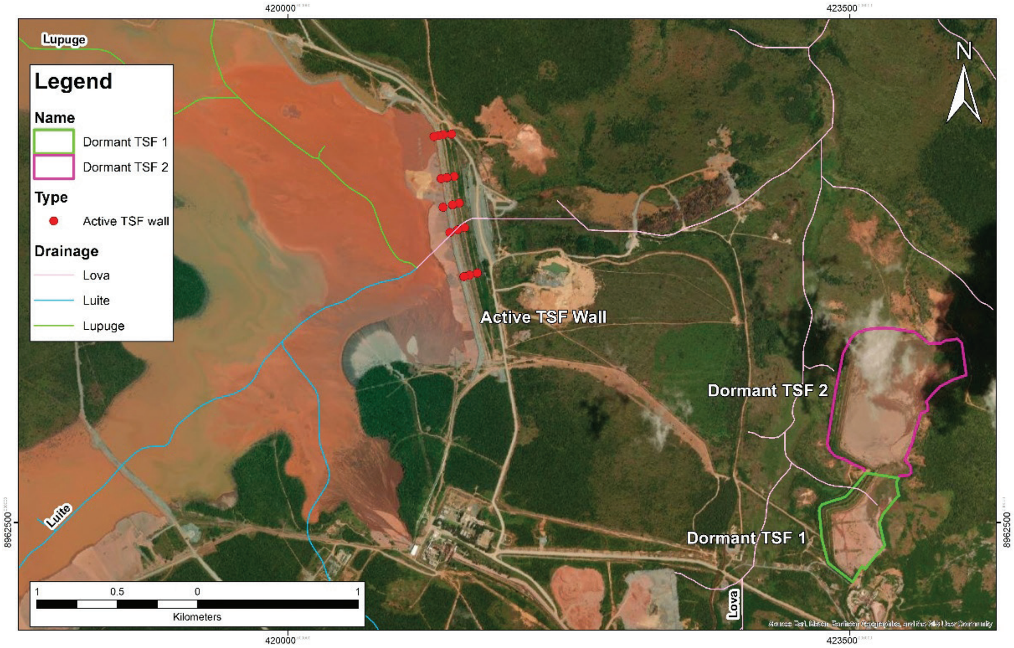

Figure 4 *Active TSF with vibrating wire piezometers.*

Description of monitoring network

Catoca collects data, collates it into useful information (graphs, cross-sections and tables), then interprets this information to generate knowledge, which is then used to manage the TSFs and reduce risk. Surface water levels and groundwater pressures are measured using Vibrating Wire Piezometers (VWP's), both sealed and suspended. Inclinometers are used to observe movement in the TSF wall.

Catoca's tailings team, working with TecWise Africa (https://www.tecwiseafrica.com) has installed:

- Three weather stations to measure rainfall.
- Twenty-two grouted and sealed vibrating wire piezometers in the active TSF to monitor the pore pressure and water levels in the wall of the TSF.
- Fifteen vibrating wire piezometers (suspended) in the dormant TSFs to monitor water levels in the dormant TSFs.
- Twenty-nine open groundwater level monitoring boreholes with suspended vibrating wire piezometers to monitor groundwater levels on the regional scale of the Catoca mine.
- Three inclinometers in the active TSF to measure lateral deformation or displacement of the TSF wall.
- Six water level flumes and sensors for measuring streamflow.

A dashboard system, created by Insight Terra https://www.insightterra.com, and described in Morton and Bovim 2023, is used to display data collected by the instruments. The dashboard displays live information obtained from the weather stations, vibrating wire piezometers and inclinometers. Regular measurements of beach lengths are collected using survey drones and hand surveys of vertical pegs located in the TSF wall, dikes, and beach area.

In cross-section, the active Catoca TSF is also supported by a new buttress, designed by Knight Piesold. Fig. 5 illustrates the profile from beneath the TSF to the main pond along the line of VWPs 8, 10 and 12. The cross-section shows the water levels in the pond, the beach length, the position of the VWP's and the topography.

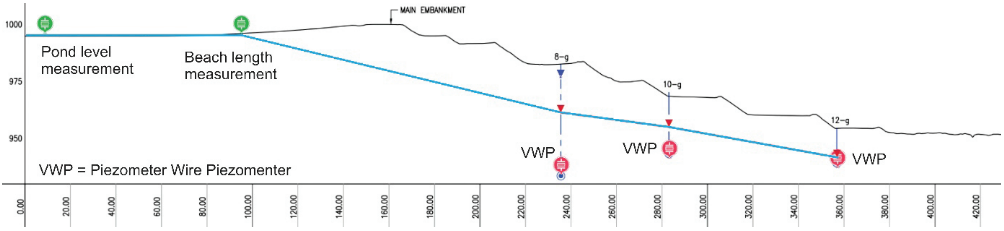

***Figure 5** Cross section of TSF profile*

All the TSF critical areas are now monitored. The management team can see in real-time dashboards, the health of the TSFs using graphics showing the water level in the pond, the beach length, the pore water pressures in the aquifer below the TSFs, the pore water pressures in the dam walls and dormant TSFs, inclinometer data and also the water balance budget including rainfall inputs and in/outflows from the streams feeding into the TSFs.

The data is collected automatically and then sent via a telemetry network to Insight Terra's platform, where data is automatically consolidated into graphs and cross-sections. This information is then presented as a live dashboard which has been configured to report in English and Portuguese in formats to suit the needs of the operators, managers, designers, and risk management practitioners. Fig. 6 shows the locations of the VWPs' in the Active TSF wall and Fig. 7 is a dashboard presentation of the VWPs' water level readings.

Trigger levels have been established for increases in water levels, the rate of increase and the maximum water levels. These trigger levels are linked to a warning system which ensures timely responses to mitigate risk. Fig. 8 shows the overall layout of the monitoring network, data transmission sites and linkage. The system has battery back-up, as well as solar panels to ensure there is no interruption of service during any power outages.

Conclusions

The implementation of an advanced monitoring network at the Catoca Diamond Mine has greatly enhanced the management and safety of both active and dormant tailings storage facilities (TSFs). By integrating

***Figure 6** Locations of the monitoring VWPs in the active TSF.*

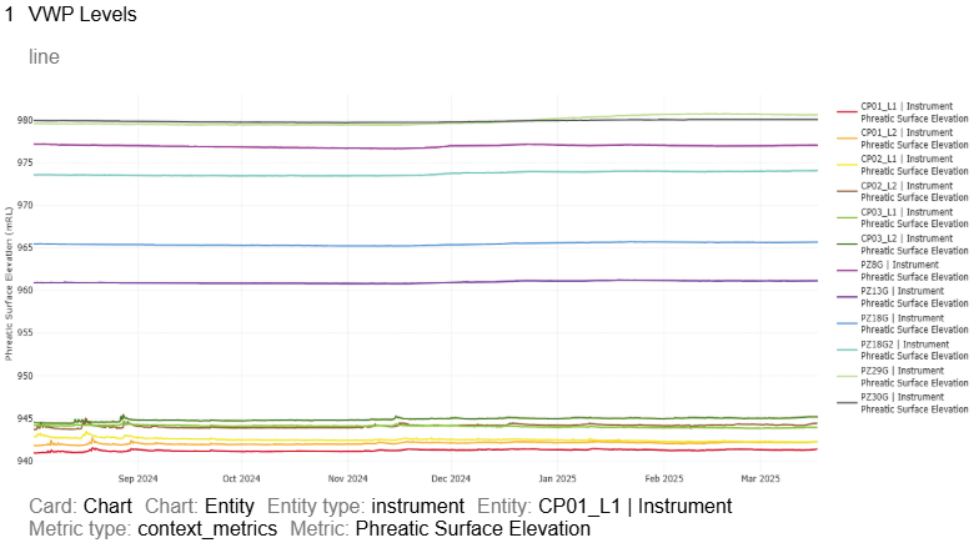

1 VWP Levels

line

Card: Chart Chart: Entity Entity type: instrument Entity: CP01_L1 | Instrument
Metric type: context_metrics Metric: Phreatic Surface Elevation

***Figure 7** Water level plots over time for VWPs in the active TSF.*

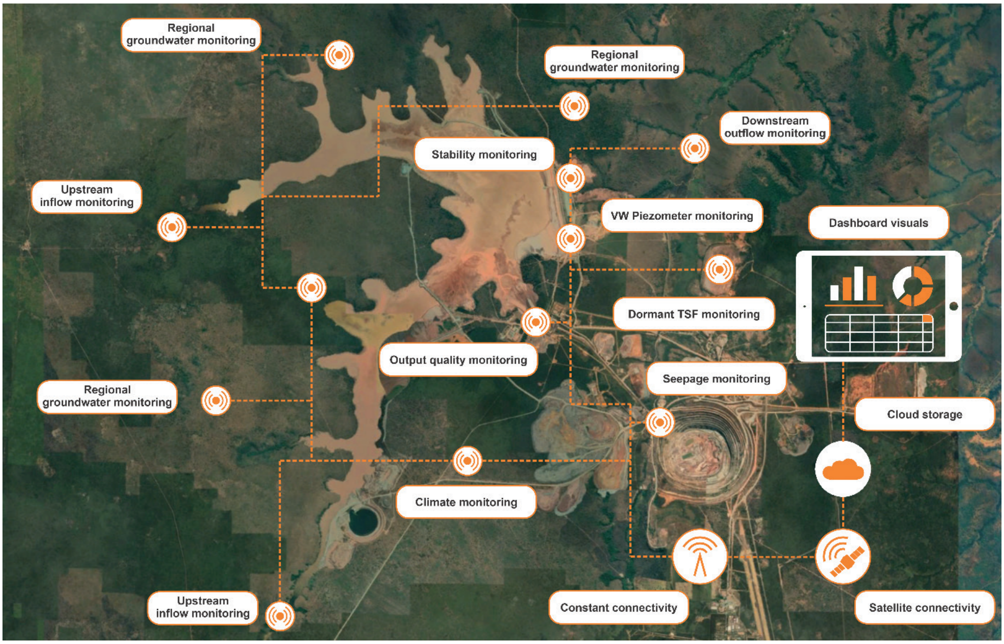

***Figure 8** Schematic of the monitoring infrastructure at Catoca.*

state-of-the-art instrumentation, including vibrating wire piezometers, inclinometers, weather stations, and instrumented groundwater monitoring boreholes, the system provides real-time data on key parameters such as pore pressure, beach lengths, water levels, and structural stability. This data is consolidated and visualised through a live dashboard, allowing operators and management to monitor TSF health remotely and respond proactively to potential risks. The adoption of the Global Industry Standard for Tailings Management (GISTM) principles ensures Catoca's TSF monitoring is aligned with international best practices. The comprehensive network not only reduces the risk of TSF failures, but also serves as a model for other mining operations seeking to enhance their tailings management strategies.

References

Global Industrial Standard for Tailings Management (GISTM) (2020) (globaltailingsreview.org)

Morton KL (2020) The use of accurate pore pressure monitoring for risk reduction in tailings dams. Mine Water and the Environment (2021) 40:42–49

Morton KL (2020) Tailings dam risk reduction using accurate pore pressure monitoring. Proc, South African Institute of Mining and Metallurgy Tailings Storage Conf. Online Available at: https://frstafricaguide.com/2020/02/06/tailings-dam-risk-reduction-using-accuratepore-pressure-monitoring/ [Accessed 6 Feb 2020]

Morton KL and Bovim AB (2023) Advanced monitoring of tailings storage facilities and dams to prevent failure. Illustrated with case studies from UK, Africa and South America. International Mine Water Association (IMWA) Conference 17 – 21 July 2023 ICC Wales in Newport

Shahid A and Q Li (2010) Tailings dam failures: a review of the last one hundred years. Geotechnical News Waste Geotechnics pp51

Methodology for Estimating Hydrogeological Risk for Open Pits

José Luis Villa[1], Fernanda Andrade[1], Ignacio Álvarez[1], Martin Brown[2], Cati Sesmero[3]

[1]Itasca Chile, Providencia, Santiago, Chile, joseluis.villa@oneitasca.com
[2]Itasca Australia, Scarborough, WA 6019, Australia, martin.brown@oneitasca.com
[3]Minera Escondida Ltda, Antofagasta, Chile, maria.sesmero@bhp.com

Abstract

Groundwater affects open pit slope stability by reducing effective stress and shear strength. To improve slope management, it is necessary to identify which areas of the pit may present stability issues triggered by groundwater.

This paper proposes a methodology for assessing hydrogeological risks to open-pit stability by integrating geotechnical and hydrogeological data through field measurements, numerical modeling (MINEDW and FLAC3D) and uncertainty analysis. This approach enables the generation of hydrogeological risk maps to support decision making on depressurization, monitoring, and mine design adjustments by quickly and efficiently identifying critical areas where groundwater affects stability, improving slope management, reducing failure risks and enhancing safety.

Keywords: Open Pit, Slope Stability, Numerical Modelling, Uncertainty, Reliability, Pore Pressure

Introduction

It is well documented that water presence can result in a loss of performance of the pit slopes (Read & Stacey 2009; Beale & Read 2013). Water pressure within discontinuities and pore spaces reduces the effective stress, leading to a decrease in shear strength of the rock mass (Sullivan 2007; Devy & Hutahayan 2021). As a result, slopes must be depressurized, designed with a lower factor of safety, or flattened to compensate for the reduced rock mass strength. When excess water pressures occur below the pit floor, groundwater pressure is the only geotechnical parameter in pit slope engineering that can readily be modified (Wyllie & Mah 2004). Therefore, it is crucial to have accurate hydrogeological characterization that enables the development of robust numerical models used to support decision making. An adequately calibrated groundwater model can provide reliable pore pressure predictions that combined with slope stability models can help understanding their impact in stability of open pit slopes.

This study outlines a new approach to quantify the risk linked to the hydrogeological component of slope stability in open-pit operations. It integrates geotechnical and hydrogeological data, focusing on the influence of pore pressure and water table variations on slope performance. Through the combination of field measurements, hydrogeological numerical modelling (developed using MINEDW software, Itasca Denver Inc 2019) and stability analysis (simulated by FLAC3D Software, Itasca Consulting Group Inc 2023), this methodology provides a comprehensive tool for evaluating potential risks and supporting the design of mitigation strategies.

As a result, a contour map is obtained that provides a quick and simple method to assess the implications of hydrogeology on slope stability. It identifies areas where depressurization is required, zones where improvements in hydrogeological characterization and monitoring are needed, and sectors where the mine planning design should be revised.

Background. Conceptual Hydrogeological Model of the Pit

The open pit used in this study has been excavated in a complex hydrogeological environment, characterized by a main aquifer hosted in alluvial materials and in the leached supergene unit which overlies an aquitard (low hydraulic conductivity medium with low storage) composed of andesitic rocks where porphyritic activity occurred forming the deposit. A 3D groundwater flow model has been developed for this open pit in MINEDW code, which is used to make seepage flows and pore pressure distribution predictions. A FLAC3D (Itasca Consulting Group Inc, 2023) model uses these pore pressure predictions to conduct slope stability analysis.

Methodology

The hydrogeological risk map aims to geographically identify sectors of the mine with higher geotechnical risk triggered by pore pressures, considering slope susceptibility to pore pressure variation, uncertainties in pore pressure modeling, hydrogeological data gaps, as well as regulatory safety requirements for maintaining operation.

Thus, a risk index (eq.1) was developed by combining information from field measurements, groundwater and slope stability numerical models, and safety standards for slope stability design. Specifically, it considers: (1) the density of hydrogeological data at the mine site, (2) the deviation of the pore pressures calculated by the groundwater model during calibration compared with field measurements, (3) the sensitivity of safety factors to pore pressure variations, and (4) compliance with pore pressure targets to maintain safety factors above required thresholds.

1. Hydraulic tests and groundwater monitoring databases were considered to calculate the information density, which reflects the existing knowledge of the hydrogeological regime affecting the site, the rock mass hydraulic properties and the groundwater level evolution during the mining operation (Eberhardt & Stead 2011). Furthermore, this knowledge is essential for effectively evaluating the performance of the slope design, including depressurization programs, and reducing uncertainties regarding pore pressure variations, which, in some cases could reach levels that compromise the slope stability (Dunnicliff *et al.* 2012; Brawner 1982). The data were georeferenced within the open pit. Subsequently, radial isocontours were generated from each data point, divided into 8 bands. These bands were categorized based on the greatest distance between a point and the excavation area not covered by hydrogeological information (800 m). As a result, 8 ranges of 100 m were created for each point. The information density map can be observed in the Fig. 1a.

Deviation between simulated (from model calibration) and observed (measured) pore pressures was also used to construct the index. An uncertainty analysis was conducted over predictive simulations of the groundwater model (Middlemis *et al.* 2019; Alvarez & Brown 2023; Gutierrez & Brown 2023). During the analysis, 100 realizations were executed with different hydraulic properties (conductivity, specific storage and specific yield) (Fig. 2a), covering the full conceptual range defined for each hydrogeological unit and adhering to the calibration standards established by groundwater modeling guides (SEA 2012; Barnett *et al.* 2012). In this analysis, the realizations are considered equiprobable, however, each model calibrates a particular monitoring well to greater or lesser degree. For the development of the map, the deviation marked by 80% of the models was associated with each monitoring point and isocontours were generated for the entire pit area, considering 8 bands, each representing a 10 meters deviation from 0 to 80. The deviation map is shown in the Fig. 1b.

2. Sensitivity analysis of the safety factors for different pore pressures distributions (higher or lower) is also considered. This variable was obtained using the geotechnical software FLAC3D to evaluate the safety factors of each sector of the pit with varying pore pressures as input. The evaluated pore pressures corresponded

to the base scenario obtained from the calibrated model, along with six additional scenarios with variations in the pore pressure field for the entire pit: ± 15, ± 30 and ± 45 m w.c. (i.e. ±147KPa, ±294 KPa and ±441 KPa). Fig. 3 shows a cross-section example of how pore pressures were modified in the base case ± 15 m w.c. As a result, the pit sectors where safety factor is most sensitive to pore pressure variations, were identified (Villa *et al.*, 2024). For example, some sectors show no variation in their safety factor, indicating they are not susceptible to changes in pore pressures. In contrast, other sectors become unstable when pore pressures increase by 15 m w.c. or become stable when pore pressure decrease by 15 m w.c. To standardize criteria, sensitivity was divided into 8 bands, each corresponding to the variation in m w.c. required for the slope to lower its safety factor below the thresholds established by the operation. The sensitivity of the safety factors map can be observed in the Fig. 1c.

3. The final component of the index is compliance with pore pressure targets required to maintain the safety factors above defined thresholds. Compliance is measured as the difference between the target level and the current measured level. The target level is set by the operation based on depressurization targets, which are derived from geotechnical and hydrogeological numerical models, accounting for associated uncertainties and reliability criteria (Dowling *et al.* 2020; Rougier *et al.* 2020; Villa *et al.* 2024) (Fig. 2b). Once again, a map associated with this component was created, with isocontours divided into 8 bands. The targets map is illustrated in the Fig. 1d

To calculate the hydrogeological risk index, each of the four factors was divided into 8 classes (bands), which were assigned a rank from 1 to 8. The ranking depends on the nature

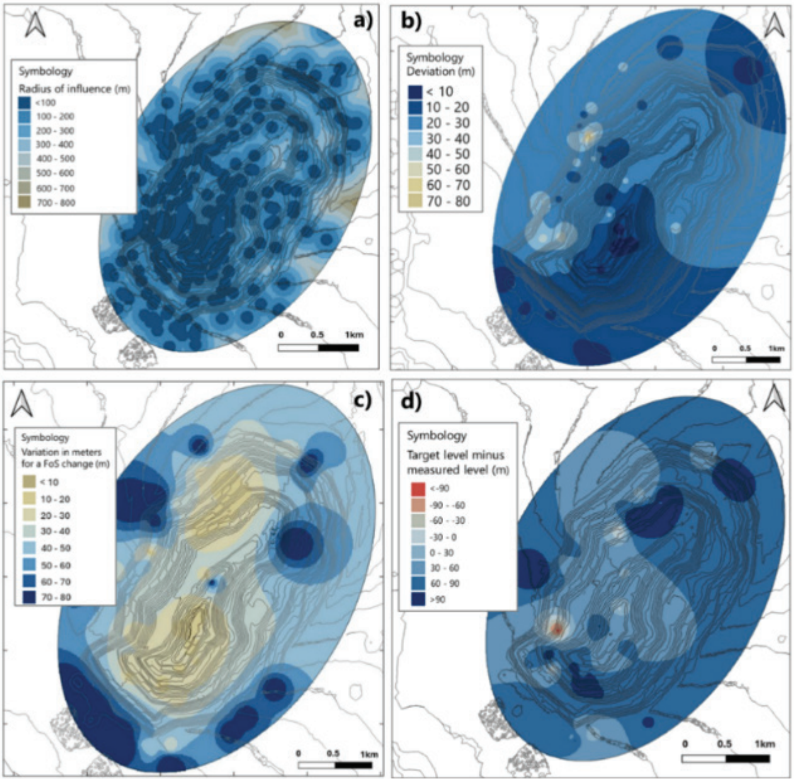

Figure 1 *Maps used to generate the Hydrogeological Risk Map associated with slope stability in the open pit. a) Information density map, b) Deviation level for 80% of the uncertainty models (P80), c) Slope stability sensitivity to the pore pressure and d) Difference between target level and measured level.*

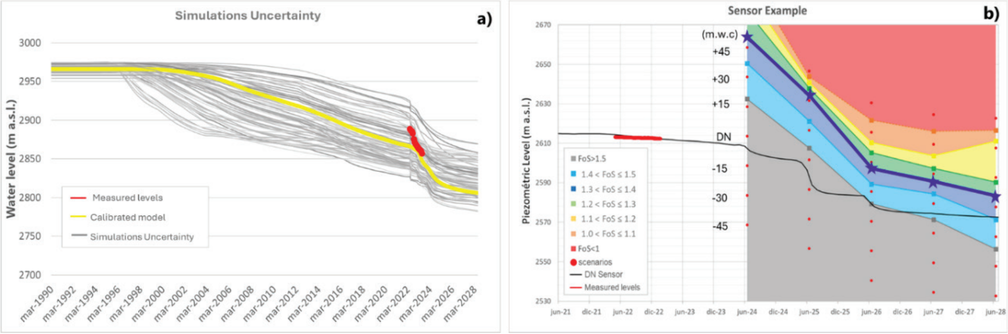

Figure 2 *Uncertainty analysis and impact of pore pressure on slope stability: a) Uncertainty simulations, measured level, and best-calibrated model. b) TARP chart linking the water table level to the Factor of Safety.*

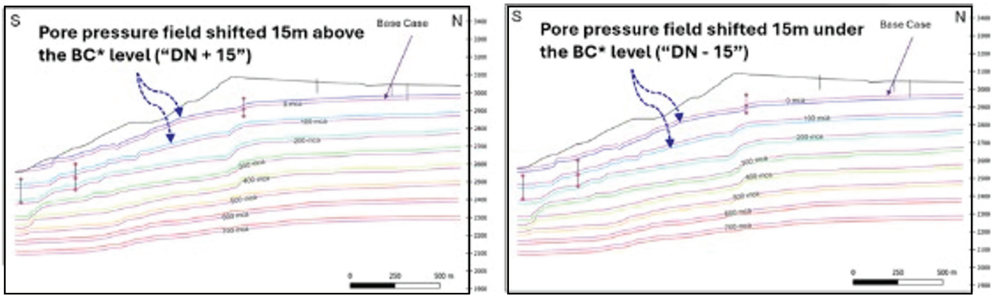

Figure 3 *Example of additional scenarios with a ±15% variation in the pore pressure field.*

of the variable: for favorable variables such as data information density and compliance with pressure targets, higher values (e.g., more data, better compliance) received higher ranks. In contrast, for variables representing higher uncertainty or risk – such as model deviation or safety factor sensitivity – the ranking was inverted, assigning lower ranks to higher-risk conditions (e.g., larger deviations = lower rank).

Finally, for each 10 × 10 m grid cell, the hydrogeological risk index was calculated by multiplying the four ranked values according to Equation 1, allowing spatial identification of sectors with higher or lower hydrogeological risk within the pit.

Hydrogeological Risk = Data Density × Model Deviation × Safety Factor Sensivity × Compliance (eq.1)

In Fig. 1, the four generated isocontours maps can be observed, which serve as the basis for creating the hydrogeological risk index of the open pit. The risk index was conceptualized as a simple combination of equally weighted factors.

Results

The calculated risk index for every 10x10 m is plotted to create the hydrogeological risk map Fig. 4. The map illustrates the risk arising from non-compliance with the operational targets and slope stability susceptibility to pore pressure variations, integrating the uncertainty due to hydrogeological data gaps and numerical modeling of pore pressures.

To ease interpretation, the risk map has been divided into three categories, although it could consider further discretization if more detailed information were needed. In this case study, the pit exhibits overall intermediate risk, with low-risk sectors mainly on high slopes, and high-risk sectors concentrated in the west and northwest.

The map supports decision making regarding sectors that require additional hydrogeological characterization such as pore pressure monitoring and new hydraulic tests, that inform the hydrogeological model and can serve as an input to interpret other numerical models used in the slope design

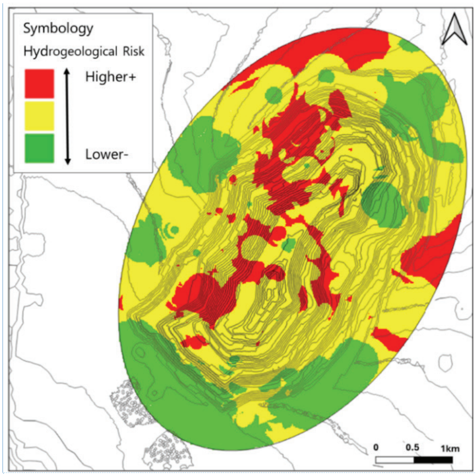

Figure 4 *Hydrogeological risk map associated with slope stability in the open pit.*

process, such as geological, geotechnical, structural and hydrogeological.

At the same time, the map provides relevant information to communicate hydrogeological needs (exploration and depressurization campaigns) to stakeholders in a simple and quick manner.

Discussion

This methodology successfully achieves its objective of quantifying the hydrogeological risk of an open pit mine, producing visual results that can assist stakeholders in their interpretations and analysis of the pore pressures effect on slope stability in the different sectors of the operation.

The proposed risk index was conceptualized as a simple combination of equal weighted factors, following risk definition for natural disasters outlined by UNDRO (1980) and Cordona (1993), which considers total risk as a product of hazard and vulnerability. Furthermore, considering the IPCC (2020) statement that adds the concept of incomplete knowledge or uncertainty as a key element in the definition of risk.

In these definitions, hazard refers to the possibility of an event, such as the natural phenomenon. On the other hand, vulnerability refers to the impact of the natural phenomenon, represented by physical factors like early warning systems. In this work, hazard is the probability of excessive pore pressure and its associated uncertainties, while vulnerability is reflected by the susceptibility of the slope stability and its potential reduction below the threshold due to variations in pore pressure.

Although, this index provides a simple way of conceptualizing risk, several factors can be considered (Ramli *et al.* 2020). One such factor is exposure, which refers to the infrastructure, ecosystem or population at risk. In this analysis, the entire pit is considered exposed; however, it is also possible to focus on specific areas, such as the slopes that will be excavated in the coming years.

Other factors could also be used, such as the uncertainty associated with the inputs of the numerical models, such as geological, geotechnical and structural information, which, in this case, are assumed to be implicitly incorporated in the results of the groundwater model's uncertainty analysis. Additionally, the uncertainty related to the FLAC3D model, which was not addressed in this study, as well as historical information on slope movements, could be important.

Moreover, if necessary, weights could be assigned to each factor based on their reliability or perceived importance. For instance, low confidence in numerical models, conceptualizations, target compliance measurements, or field data could reduce the weight of certain factors. Similarly, high compartmentalization or significant variation in geotechnical parameters might also affect the factor weighting.

On a different note, risk maps can be used dynamically to track the evolution of risk over time. This approach allows for the evaluation of past work by comparing 'before' and 'after' scenarios and helps assess future risks by analyzing the lack of information and the results of predictive simulations. This can guide data collection and slope depressurization campaigns aimed at reducing risk, as well as support the assessment of compliance with the operation's depressurization targets.

References

Alvarez I, Brown M (2023) Uncertainty Analysis in Groundwater Flow Models as A Tool to Support Decision Making: Assessing the Influence of Infiltrations From A TSF Over an Open Pit. – In:

Stanley, P.; Wolkersdorfer, C.; Wolkersdorfer, K., Mugova, E.: IMWA 2023 – Y Dyfodol | The Future. – p. 6–12; Newport, Wales, UK (International Mine Water Association).

Barnet B, Townley LR, Post V, Evans RE, Hunt RJ, Peeters L, Richardson S, Werner AD, Knapton A, Boronkay A (2012) Australian Groundwater Modelling Guidelines – June 2012. National Water Commission Australia, Waterlines Report Series No. 82, ISBN:978-1-921853-91-3.

Beale G, Read J (2013) Guidelines for evaluating water in pit slope stability. CSIRO Publishing, Collingwood.

Brawner, CO (1982) Control of groundwater in surface mining. International Journal of Mine Water, 1(1). pp. 1–16.

Cardona OD (1993) Evaluación de la amenaza, la vulnerabilidad y el riesgo En A. Maskrey Los Desastr. no son Nat. 51–74.

Devy SD, dan Hutahayan, PP (2021) Groundwater Effect on Slope Stability in Open Pit Mining: a Case of West Kutai Regency, East Kalimantan, Indonesia, Journal of Geoscience, Engineering, Environment, and Technology, 6(4), 192–205. https://doi.org/10.25299/jgeet.2021.6.4.6226

Dowling J, Beale G, Haas P, Kaya B, Mak S, Tejada LC, Kramer K, Johnson J, Zea RE, Palmer C (2020). Development of an integrated workflow for pit slope pore pressure reconciliation. Slope Stability 2020: Proceedings of the 2020 International Symposium on Slope Stability in Open Pit Mining and Civil Engineering, Australian Centre for Geomechanics, Perth, pp. 1267–1280.

Dunnicliff J, Marr WA, Standing J (2012) Principles of geotechnical monitoring. In J. Burland, T. Chapman, H. Skinner & M. Brown (Eds.), ICE Manual of Geotechnical Engineering, Volume II. pp. 1363–1377. ICE Publishing.

Eberhardt E, Stead D (2011) Geotechnical Instrumentation. In P. Darling (Ed.), SME Mining Engineering Handbook. pp. 551–571. USA: Society for Mining, Metallurgy, and Exploration, Inc

Gutierrez M, Brown M (2023). Use of Groundwater Numerical Model to Support Decision Making At large Open Pit. – In: Stanley, P.; Wolkersdorfer, C.; Wolkersdorfer, K., Mugova, E.: IMWA 2023 – Y Dyfodol | The Future. – p. 178–184; Newport, Wales, UK (International Mine Water Association).

Itasca Consulting Group, Inc. (2023) FLAC3D – Fast Lagrangian Analysis of Continua in Two-Dimensions, Ver. 9.0. Minneapolis: Itasca.

Itasca Denver Inc (2019) MINEDW – 3D Groundwater Flow Code, Version 3.06. Denver.

IPCC (2020) The concept of risk in the IPCC Sixth Assessment Report: a summary of cross-working group discussion. Guidance for intergovermental panel on climate change.

Middlemis H, Walker G, Peeters L, Richardson S, Hayes P, Moore C (2019) Groundwater Modelling Uncertainty – Implications for decision-making. Summary report of the national groundwater modelling uncertainty workshop, 10 July 2017, Sydney, Australia. Flinders University, National Centre for Groundwater Research and Training.

Morales M, Panthi K, Rostad R, Holmøy K, Botsialas K (2019) Assessment on the hydrogeological condition of an open pit mine based on piezometric measurements. J Mining Engineering and Research 1: 16–34. doi:10.35624/jminer2019.01.03

Ramli MWA, Alias NE, Yusop Z, Taib SM (2020) Disaster Risk Index: A Review of Local Scale Concept and Methodologies.

Read J, Stacey P (2009) Guidelines for Open Pit Slope Design. CSIRO Publishing, Collingwood.

Rougier M, de Graaf PJH, Desjardins M, O'Leary M, Yugo N, Kilbride B. (2020). Managing ice walls and another operational challenges while optimising Victor Mine late-stage opportunities. Slope Stability 2020: Proceedings of the 2020 International Symposium on Slope Stability in Open Pit Mining and Civil Engineering, Australian Centre for Geomechanics, Perth.

Servicio de Evaluación Ambiental (SEA) (2012) Guide for the use of groundwater models in the SEIA [in Spanish]. Santiago, Chile.

Sullivan T (2007) Hydromechanical Coupling and Pit Slope Movements, in Y Potvin (ed.), Slope Stability 2007: Proceedings of the 2007 International Symposium on Rock Slope Stability in Open Pit Mining and Civil Engineering, Australian Centre for Geomechanics, Perth, p 3–43.

Villa JL, Rivero V, Sesmero C, Sanchez A, Andrade F, Ramirez A (2024). Depressurization Targets Based on 3D Slope Stability Analysis at the Escondida open pit. Slope Stability 2024: Proceedings of the 2024 International Symposium on Slope Stability in Open Pit Mining and Civil Engineering; Belo Horizonte, Brasil.

UNDRO (1980) Natural disasters and vulnerability analysis: report of Experts Group Meeting of 9 12 July 1979.Day TJ (1977) Field Procedures and Evaluation of a Slug Dilution Gauging Method in Mountain Streams. J Hydrol New Zealand 16(2):113–133

Wyllie C, Mah W (2004) Rock Slope Engineering Civil and Mining. In: Hoek, E. and Bray, J.W., Eds., Rock slope Engineering, Taylor & Francis Group, London and New York, 431 p.

Sensible Communication Strategy in Mine Water Licensing Processes

Thomas Walter

Ministerium für Umwelt, Klimaschutz, Mobilität, Agrar und Verbraucherschutz,
Keplerstraße 18, D-66117 Saarbrücken,Germany, t.walter@umwelt.saarland.de

Abstract

Mine water licensing processes often face strong public scrutiny and legal challenges, due to water quality concerns and the lack of technical expertise among plaintiffs and judges in administrative courts. This paper highlights how translating technical concepts into clear legal language and in-dependently assessing applicant data can strengthen permits in legal review. The case of the Saar-land mine water rebound project serves as an example of best practices.

Keywords: Mine water permitting, environmental law, hydrochemistry, administrative court procedures, water re-source management, legal-scientific communication

Note: This paper does not aim to provide a comprehensive account of the entire permitting pro-cess under water and mining law, nor does it elaborate on related aspects such as the Environmen-tal Impact Assessment (EIA), which has been conducted. Instead, the focus lies on the perspective of the water authority and the specific legal considerations under water law that guide the assess-ment and supervision of the mine water rebound.

The Legal Challenge of Mine Water Rebound Processes

Mine water licensing processes often face strong public scrutiny and legal challenges, due to water quality concerns and the lack of technical expertise among plaintiffs and judges in administrative courts. Licensing authorities must therefore communicate transparently without compromising scientific or legal accuracy. This paper highlights how translating technical concepts into clear legal language and independently assessing applicant data can strengthen permits in legal review. The case of the Saarland mine water rebound project serves as an example of best practices. In recent decades, mine water-related projects have faced increasing public scrutiny, particularly in developed countries governed by the rule of law. Environmentally aware societies often see changes to the status quo as potential threats to health and well-being. Mining projects, in particu-lar, are frequently suspected of causing harm to groundwater and surface water systems, fueling concerns about environmental degradation and long-term health impacts. As a result, administra-tive courts often become the final decision-makers.

A key challenge in this process is that neither plaintiffs nor judges typically possess the necessary scientific or technical expertise to fully assess the potential environmental effects of a project. As a result, a fundamental objective in mine water permitting must be to lower the barriers to under-standing, ensuring that administrative judges can grasp both the technical foundations and regulatory rationale of a permit. This is particularly critical for licensing authorities, which not only issue permits based on legal provisions but must also defend them in court against legal challeng-es.

As the German saying goes, "Vor Gericht und auf hoher See sind wir in Gottes Hand" – "Before the court and on the high seas, we are in God's hands." This highlights the unpredictability of legal The Interplay Between Legal and Scientific Approaches in Mine Water permitting proceedings, especially when scientific complexity meets legal interpretation.

The Interplay Between Legal and Scientific Approaches in Mine Water Permitting

One of the fundamental differences between the legal and scientific approaches in mine water per-mitting is how each side perceives and processes information. The legal perspective is focused on properly describing a given situation to determine which legal norms apply. Judges and legal pro-fessionals must categorize facts within existing legal frameworks to establish compliance, liability, and regulatory obligations. Their challenge lies in ensuring that a project is accurately represented in a manner that allows for proper legal classification.

On the other hand, the scientific and technical perspective is primarily concerned with identifying, analyzing, and solving complex environmental and engineering challenges. Experts focus on water flow dynamics, chemical processes, and system interactions, aiming to predict outcomes and miti-gate potential risks. Their challenge is translating these complexities into a clear, structured form that non-experts can understand.

A viable permit requires mutual understanding between legal and technical experts. However, in practice, legal and technical professionals often communicate in a formal, text-based manner without actively ensuring that mutual comprehension is achieved. This can lead to misinterpretations, incomplete assessments, and legal vulnerabilities. The key to bridging this gap lies in an iterative process of information exchange, where both legal and technical professionals continuously refine descriptions, verify interpretations, and ensure alignment. Each step must include cross-checks to confirm that a shared understanding has been reached.

Crucially, the description of the underlying factual situation is entirely within the hands of the scientific and technical side. A well-structured and precise technical description will almost inevi-tably lead to the correct legal classification. In other words, the technical side plays a decisive role in shaping the legal outcome. By carefully framing the environmental and engineering realities of a project, scientific experts effectively guide the legal determination of whether a project meets reg-ulatory standards. Thus, an accurate and strategically framed technical description can predefine the legal solution, ensuring that the permit conditions align with both scientific realities and legal requirements.

Comprehensive Understanding as the Basis for a Defensible Permit

To achieve a robust and defensible permit, the licensing authority must possess a deep under-standing of the project and its environmental context. This requires comprehensive and accurate information, necessitating close collaboration between applicants, experts, and regulatory bodies. Engaging early with authorities helps align applications with regulatory and scientific expecta-tions, streamlining approval.

While the application documents themselves should maintain scientific and technical accuracy, the wording of the final license must adhere to legal language. However, directly translating complex technical descriptions into the legal text can create ambiguities and misinterpretations, particular-ly among the general public and legal professionals who may lack specialized background knowledge. To mitigate this risk, the permit should be structured using clear and accessible lan-guage wherever possible. This includes rewording technical concepts into legally precise yet comprehensible terms, ensuring that the reasoning behind the permit conditions is transparent.

A critical component of this strategy is the independent assessment and refinement of technical descriptions provided by the applicant. Instead of merely adopting the terminology and conclu-sions of the applicant's reports, the licensing authority should actively reframe key hydraulic and hydrochemical concepts, demonstrating a critical and independent review process. This approach not only strengthens the authority’s credibility in court but also reassures judges that the permit is based on a thorough and impartial evaluation rather than a passive endorsement of the appli-cant’s claims.

To further enhance the effectiveness of this strategy, the following principles should be applied:

1. **Clarity in Communication** – Technical terms should be translated into accessible language without losing scientific accuracy. Judges and the public must be able to under-stand the key aspects of the project, including water flow dynamics, contamination risks, and mitigation strategies.
2. **Legal and Scientific Consistency** – The permit should be legally sound while maintaining scientific integrity. Balancing legal precision with scientific clarity prevents misunderstandings and strengthens the permit's defensibility in court.
3. **Independent Review and Critical Assessment** – The licensing authority must demonstrate an independent assessment of the application. Reformulating key technical concepts and supplementing them with additional expert reviews ensures credibility.
4. **Precautionary Approach** – Where scientific uncertainties exist, the permit should explicitly acknowledge them and integrate precautionary measures such as contin-uous monitoring, adaptive management, and contingency planning.
5. **Early and Continuous Engagement** – Close coordination with experts, applicants, and stakeholders throughout the process ensures that the final permit reflects a well-informed and balanced assessment of risks and mitigation measures.

Mine Water Rebound Project in Saarland, Germany

The mine water rebound project in Saarland is one of the most significant water management initi-atives in the region. It involves the controlled rise of mine water in decommissioned coal mines while ensuring environmental protection and compliance with regulatory requirements.

After more than 250 years of coal mining and the extraction of about 1,400,000,000 metric tons of coal, in 2012 mining activity in Saarland come to an end. In the neighbouring and hydraulically connected coalfield of Lorraine in France, coal mining already had ended in 2004 and in Summer of 2006 the

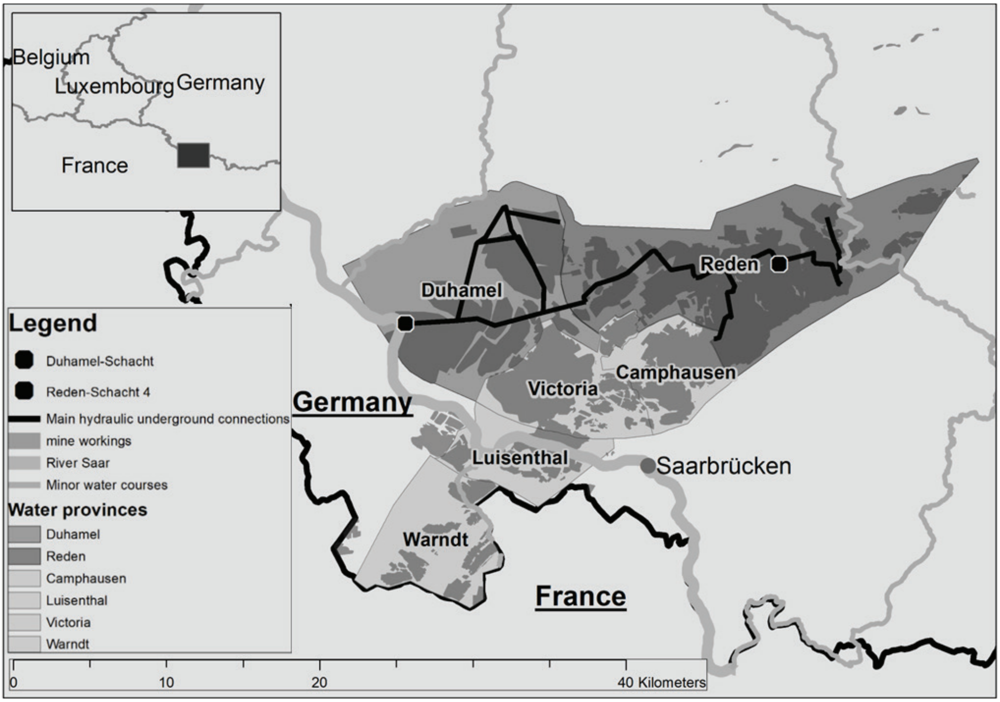

Figure 1 Saar Coalfield with its different water provinces. Dewatering in Reden will be stopped and mine water will rise to -320 m asl, so that Duhamel will dewater both provinces.

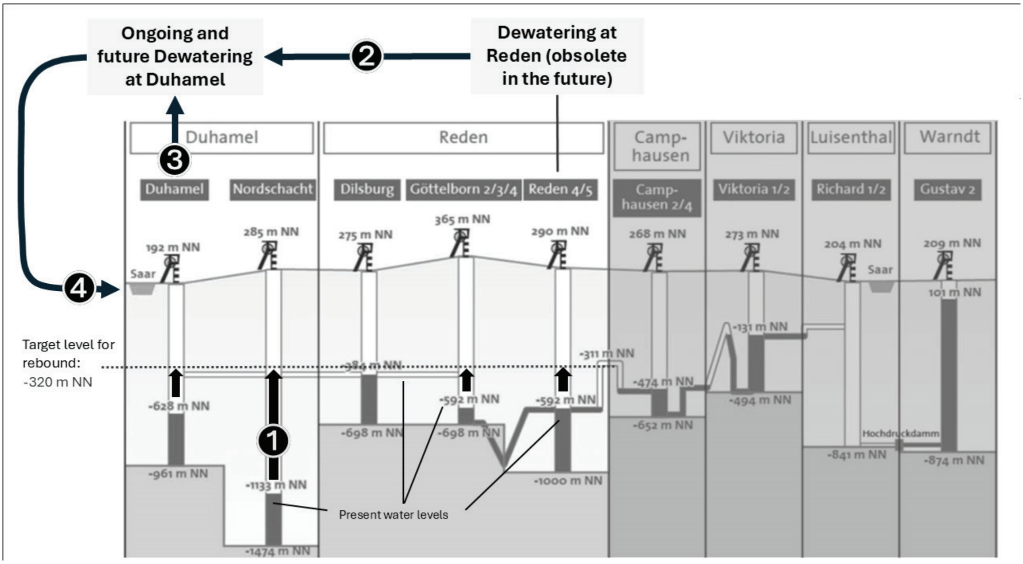

Figure 2 *Current Dewatering System and Planned Target Levels in the Saar Coalfield. Under Water Law the following aspects where considered as relevant: the potentially harmful effect of first flush due to the rebound (1), the transfer of mine water from one province to the next (2), the final abstraction of mine water at Duhamel shaft (3) and the injection of the water into the river Saar (4)*

controlled process of mine water rebound was started (Westermann *et al*., 2019). After a first outline of a complete rebound in 2014 (RAG AG, 2014), RAG AG presented the application for a partial rebound in the water provinces Reden and Duhamel in 2017, which resulted in the permit issued in 2021 after a long process of assessments and discussions with the applicant and external experts.

The project is primarily governed by the German Federal Mining Act (Bundesberggesetz, BBergG, 1980) and the German Water Resources Act (Wasserhaushaltsgesetz, WHG, 2008), the latter set-ting out strict conditions for groundwater management, water body transfers, and pollution con-trol. For the decision on the project, a mining law planning approval procedure was required, in which the mining authority, under German law, grants not only the mining-related but also the water law permits; however, this must be done in agreement with the competent water authority.

Key WHG provisions relevant to the Saarland project include:

Section 8 WHG (Water Use Permit) – Any use of ground- or surface water is subject to a permitting procedure.

Section 9 WHG (Types of Water Use) – The extraction as well as discharge of mine water into surface water bodies are considered as direct water uses and therefore subject to permits. This was also seen by the applicant and thus applied for, while a permit for the transfer of mine water between underground compartments had not been requested by the applicant. This also applies to the so-called indirect use of groundwater as the rise of mine water, due to its potentially detrimental impact on groundwater quality. These as-pects have been included in a permit for the first time in Germany.

Section 48 WHG (Obligations to Prevent Harmful Changes to Water Bodies) – The project must include monitoring and mitigation strategies to prevent detrimental changes to wa-ter quality and flow regimes.

One important aspect is the transfer of mine water between different water bodies, including un-derground reservoirs and its longevity. This was legally a new concept in the licensing process. The permit needed to establish clear conditions under which such transfers are allowed, address-ing both quantitative and qualitative impacts as in accordance with WHG regulations.

The concept of indirect water use plays a crucial role in the licensing process. The gradual rise of mine water influences regional groundwater levels and interconnected water bodies, which can have significant environmental and hydrological consequences. It also can cause substantial hy-dro-chemical changes of the mine water itself, but also of all connected water bodies due to the first flush effect, where rising mine water mobilizes contaminants (Younger *et al*, 2002, Wolkers-dorfer, 2008). This aspect so far has been considered for the first time in a permit related to mine water rebound. The permit therefore considers not only direct discharges but also secondary effects, ensuring that regulatory requirements for both direct and indirect water use are fully ad-dressed.

The licensing process for mine water rebound in Saarland regarding water law issues involves multiple administrative steps and coordination between regulatory bodies:

- **Pre-Application Consultation** – The mining company (applicant) engages with the envi-ronmental and mining authorities to clarify legal and technical requirements.
- **Submission of Application** – The applicant submits detailed documentation, including hydrogeological studies, environmental impact assessments, and risk evaluations.
- **Public Participation and Stakeholder Engagement** – In line with transparency princi-ples, the application undergoes public review, allowing objections and concerns to be ad-dressed.
- **Technical and Legal Evaluation** – The Water Authority (Ministry of Environment) inde-pendently assesses the documentation, revising key descriptions to ensure clarity and compliance with legal standards. In order to be able to being able to properly do so, Saar-land's government had several reports prepared by external independent experts includ-ing a ground- and a minewater model.
- **Coordination with the Mining Authority** – The mining authority ensures that mine safe-ty and subsurface stability are considered alongside environmental concerns. Under Ger-man law, the mining authority is the primary permitting body for mining-related activities, making final decisions in agreement with the water authority.
- **Permit Issuance and Conditions** – A final permit is granted with clear conditions, moni-toring obligations, and contingency plans (OBA SL, 2021).
- **Judicial Review** – In case of legal challenges, administrative courts review the decision, where the clarity and legal robustness of the permit text play a decisive role

Comparison of Key Permit Elements

Drinking Water Protection: Applicant's Argument vs. Permit Language

The applicant originally described the risk to drinking water resources in terms of generalized hydrogeological models, emphasizing that no substantial effects were expected due to the natural separation of mine water and the overlying aquifers by more than 300 m. While these statements were scientifically not wrong, they did not address the fact that it's primarily the hydraulic gradient and not – as described in the text – the distance of the mine water from the bottom of the aqui-fer that controls a potential flow of mine water into an aquifer.

In contrast, the permit text corrected the wording and redefined the risk assessment with a more detailed analysis of local groundwater flow, introducing additional monitoring requirements and contingency measures. This demonstrated that the authority had not simply accepted the applicant's assurances but had critically assessed and expanded the evaluation to include a more pre-cautionary approach.

Transfer Between Water Bodies: Expanding Beyond the Applicant's Scope

The applicant's documentation primarily focused on local water retention and discharge but pro-vided only limited discussion on the regulatory implications of transferring mine water between hydrologically distinct water bodies. This aspect was crucial from a legal perspective, as inter-basin transfers could have broader regulatory consequences under the Water Resources Act (WHG).

The permit addressed this gap by explicitly defining the conditions under which mine water trans-fers were permissible, including legal references and additional environmental impact assess-ments. By doing so, the licensing authority demonstrated independent expertise and regulatory foresight, reinforcing the robustness of the permit in legal proceedings.

Conclusion

By bridging the gap between scientific accuracy and legal clarity, the licensing authority enhances both public trust and judicial comprehensibility. This strategy ultimately reduces the risk of legal challenges succeeding due to misunderstandings or perceived regulatory weaknesses. The key to success in administrative court proceedings lies in presenting a well-documented, legally sound, and scientifically justified permit in a language that is accessible to both legal professionals and the wider public.

So, we are not necessarily "in God's hands" before the courts. The strategy of full transparency, clear communication, and independent assessment has proven its worth. In every legal challenge faced so far, the courts have upheld our decisions, often citing directly from the permit in their reasoning: Three of these lawsuits have already been heard and dismissed, three additional cases were recently tried, and decisions are expected in the coming days,14 further lawsuits have since been withdrawn. This demonstrates that a well-structured, scientifically sound, and legally pre-cise permit is the key to success—not only in public administration but also in the courtroom.

References

Bundesministerium der Justiz (2009) Wasserhaushaltsgesetz (WHG) – Gesetz zur Ordnung des Wasserhaushalts. Bundesgesetzblatt I: 2585–2616

Bundesberggesetz (BBergG, 1980): https://www.gesetze-im-internet.de/bbergg/BJNR013100980.html

Bundesverwaltungsgericht (BVerwG, 2022): Urteil vom 23.06.2022 -BVerwG 7 C 1.21, https://www.bverwg.de/de/230622U7C1.21.0

Gesetz zur Ordnung des Wasserhaushalts (Wasserhaushaltsgesetz, WHG, 2009): https://www.gesetze-im-internet.de/whg_2009/BJNR258510009.html

OBA SL (Oberbergamt des Saarlandes, 2021): Planfeststellungsbeschluss für den Rahmenbetriebsplan zum Heben und Einleiten von Grubenwasser am Standort Duhamel in die Saar als Folge des Ansteigenlassens des Grubenwasserspiegels auf minus 320 m NHN in den Wasserprovinzen Re-den und Ensdorf der RAG Aktiengesellschaft, Im Welterbe 10, 45141 Essen; https://www.saarland.de/mwide/DE/downloads/sonstiges/grubenwasseranstieg_planfeststellungsverfahren/planfeststellungsbeschluss

OVG SL (Oberverwaltungsgericht des Saarlandes, 2023a): Entscheidung vom 20.06.2023 – 2 C 220/21 – Bergrecht (Grubenwasser), PDF, 1MB https://www.saarland.de/ovg/DE/institution/aktuelle-meldungen/spruchpraxis

OVG SL (Oberverwaltungsgericht des Saarlandes, 2023b): Entscheidung vom 20.06.2023 - 2 C 250/21 - Bergrecht (Grubenwasser), PDF, 1MB, https://www.saarland.de/ovg/DE/institution/aktuelle-meldungen/spruchpraxis

OVG SL (Oberverwaltungsgericht des Saarlandes, 2023c): Entscheidung vom 20.06.2023 – 2 C 251/21 – Bergrecht (Grubenwasser), PDF, 933KB, https://www.saarland.de/ovg/DE/institution/aktuelle-meldungen/spruchpraxis

RAG AG (2014): Konzept zur langfristigen Optimierung der Grubenwasserhaltung der RAG Akti-engesellschaft für das Saarland gemäß $ 4 Erblastenvertrag zur Bewältigung der Ewigkeitslasten des Steinkohlenbergbaus der RAG AG im Rahmen der sozialverträglichen Beendigung des subven-tionierten Steinkohlenbergbaus in Deutschland vom 14.08.2007. – 17 p.; Herne. https://www.bergbau-unser-erbe.de/fileadmin/user_upload/Grubenwasserkonzept_Saar.pdf

Westermann S, Dogan T, Reker B, Goerke-Mallet P, Wolkersdorfer C and Melchers C (2019): Evaluation of Mine Water Rebound Processes in the German Coalfields of Ruhr, Saar, Ibbenbüren, and the Adjacent European Countries., Berichte zum Nachbergbau, Issue 1, Forschungszentrum Nachbergbau, Technische Hochschule Georg Agricola; Bochum, https://fzn.thga.de/wp-content/uploads/sites/4/2021/02/Berichte-zum-Nachbergbau_Heft1_Evaluation-Mine-Water-Rebound_encoded.pdf

Wolkersdorfer C (2008) Water management at abandoned flooded underground mines. Springer, Heidelberg

Younger PL, Banwart SA, Hedin RS (2002) Mine water: hydrology, pollution, remediation. Kluwer Academic Publishers, Dordrecht

Treatment Of Copper-Containing Acid Mine Drainage By Combined Use Of Multiple Technologies

Xingjie Wang, Ling Liu, Liyuan Ma, Rui Deng, Yuxuan Yang, Jianwei Zhou

China University of Geosciences, Wuhan, China, wangxingjie@cug.edu.cn

Abstract

This work provided a promising methodology for removing iron ions and recovering copper ions from copper-containing AMD by incorporating the copper ions sulfide precipitation, iron ions biomineralization, and lime neutralization. The experimental results indicated that nearly all copper ions were removed in the sulfide precipitation process and 82.2% of iron ions were removed after biomineralization treatment. Additionally, the consumption of lime slurry was reduced compared to the conventional direct neutralization method. By integrating various techniques, it is possible to improve the removal efficiency of iron ions, reduce the consumption of lime, and recover the copper and sulfur from the AMD.

Keywords: Acid mine drainage, copper ions, sulfidation, biomineralization

Introduction

The management of acidic mine drainage (AMD) is a global challenge faced by numerous countries due to its serious threat to the environment (Kefeni *et al.* 2017). A variety of active and passive methodologies have been developed and used for AMD treatment. Neutralization by adding alkaline materials, particularly lime slurry, is the most widely used AMD treatment technology, especially for the emergency management of AMD with high concentrations of metal ions and low pH (Chen *et al.* 2021; Johnson and Hallberg 2005). However, the neutralization process consumes a substantial amount of lime and generates large volumes of sludge containing hazardous metals. Theoretically, the consumption of alkaline materials is usually several times of the theoretical value for the neutralization of H^+ ions and the precipitation of the metal ions, especially for the AMD with high iron ions concentration (Cheong *et al.* 2022). Therefore, iron ions in AMD are critical to the consumption of the alkaline materials in the application of neutralization technology, as well as the cost of subsequent disposal of the residual sludge (Djedidi *et al.* 2009). Consequently, integrating multiple treatment technologies represents an essential strategy for effective AMD management (Mosai *et al.* 2024).

Biomineralization has been identified as a promising method for the removal of iron ions, to reduce the consumption of lime in the neutralization process, but still limited by the low removal efficiency (Jiang *et al.* 2024). It has been reported that the required doses of lime to neutralize AMD can be reduced by nearly 80% after biomineralization treatment (Song *et al.* 2022). To improve the biomineralization efficiency, many measures have been explored, including cyclic biomineralization and pH-controlled biomineralization (Jiang *et al.* 2024; Jin *et al.* 2020). A constant pH of 2.5 could lead to a greater fraction of iron precipitating during the biooxidation of Fe^{2+} (Liu *et al.* 2024). However, the pH-controlled biomineralization treatment still cannot completely remove iron ions from AMD. Consequently, subsequent neutralization with lime slurry is still required, generating neutralization residues containing hazardous metal ions.

The sulfide precipitation method has increased interest for a long time due to its ability to selectively separate dissolved metals from AMD, producing metal sulfide residues with a high concentration of the element recovered (Li *et al.* 2024b). These advantages have promoted the study of sulfide precipitation for removing and recovering several metals, such as copper, zinc and iron from AMD (Li *et al.* 2024a). Theoretically, Cu^{2+} and Fe^{2+} can react with sulfide to form precipitates, while Fe^{3+} can be reduced by sulfide to Fe^{2+}. According to the differences in reaction conditions, copper ions can be preferentially precipitated and removed from copper-containing AMD (Choi *et al.* 2006), but the influences of iron ions were unclear.

In this work, we propose a comprehensive treatment scheme that combines sulfide precipitation, biomineralization, and lime neutralization for the effective treatment of copper-containing AMD. Specifically, sodium sulfide is added to precipitate copper ions. Subsequently, *Acidithiobacillus ferrooxidans* is inoculated for biomineralization. During the biomineralization process, the pH is maintained at 2.5±0.1 by adding lime slurry. Following the completion of the biomineralization reaction, lime slurry is continuously added until the pH is elevated to 9.0. The combined use of these multiple technologies demonstrates significant advantages in improving the removal efficiency of iron ions, reducing the consumption of lime, and facilitating the recovery of copper and sulfur from the copper-containing AMD.

Materials and methods

Simulated copper-containing AMD

The initial iron concentration of the simulated AMD was 1000 mg/L with a Fe^{2+} to Fe^{3+} ratio of 7:3, and the Cu^{2+} concentration was 15 mg/L, in consistent with the AMD sample collected from a pyrite mine in Anhui Province, China. The stock solution of 3000 mg/L Fe^{3+} was prepared from the biogenic Fe^{3+}, which was derived from the cell-free supernatant of *Acidithiobacillus ferrooxidans* cultures after bacterial harvesting via centrifugation, and the stock solution of 150 mg/L Cu^{2+}, 7000 mg/L Fe^{2+} was prepared by analytical grade $CuSO_4·5H_2O$ and $FeSO_4·H_2O$ using deionized water. 0.01 mol/L H2SO4 solution and 1.0 g/L lime slurry were used for pH control.

Reaction between sulfide and metal ions

The sulfidation experiments were performed in 50 mL centrifuge tubes. In the stoichiometrically matched experiments, Na_2S at molar ratios of 0, 0.25, 0.5, 0.75, and 1 to the Cu^{2+} and Fe^{3+} were added. The stock solution of 7.8 g/L Na2S was prepared by analytical grade Na2S·9H2O. The metal ions solution at pH 2.5 and the Na_2S solution were well mixed with a total volume of 50 mL, and then placed in a rotator mixer at 170 rpm and 30°C.

Biomineralization

The biooxidation experiments were conducted in a 250 mL conical flask containing 100 mL of simulated AMD. *Acidithiobacillus ferrooxidans* ATCC23270 provided by the Key Lab of Biometallurgy of the Ministry of Education of China was used. The inoculated cell density was approximately 1.0×10^8 cells/mL. The pH was adjusted by lime slurry every 8 hours. The flask was placed in a rotating shaker at 170 rpm and 30 °C to initiate the biooxidation process. After biomineralization, the AMD was filtered to collect precipitates and filtrate.

Neutralization

The simulated AMD and the filtrate obtained after the biooxidation treatment was subsequently neutralized by lime. $Ca(OH)_2$ slurry (10.0 g/L) was quantitively added to the filtrate until the solution pH was maintained at about 9.0. The sludge was filtered by 0.45 μm MCE filter paper (Jinteng, China), washed, dried at 70°C, and then weighed.

Analytical methods

The pH was measured using a pH meter (Beier 620, China). The Fe^{2+} concentration was determined using the 1,10-phenanthroline method (Pham *et al.* 2009). The morphology and elemental composition of the precipitates were identified by scanning electron microscopy and energy dispersive X-ray spectroscopy (SEM-EDS, SU8010, Japan).

Results and discussion

Interaction between iron and copper ions with sulfide ions

To identify the interaction between Fe^{3+} and S^{2-}, Na_2S was added to synthetic AMD without copper ions. The Fe^{2+} concentration was monitored to give a measure of the Fe^{2+} ions as a function of the S^{2-} ions. Theoretically, a ratio of $n(S):n(Fe^{3+}) = 0.5$ serves as a threshold point (Wei and Osseo-Asare 1996).

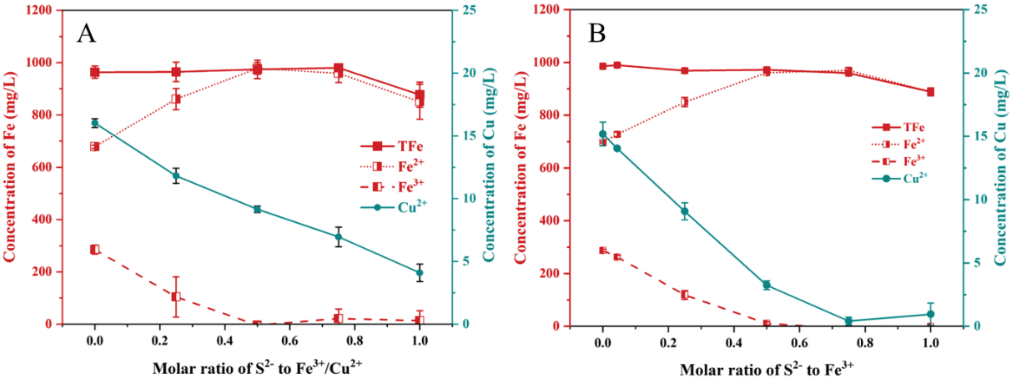

Figure 1 *Variation of copper and iron ions concentration under different sodium sulfide concentrations.*

The results suggested that each S^{2-} ion reduced two Fe^{3+} ions, which was inconsistent with the theoretical value (Fig. 1A). The sludge generated during the Fe^{3+} reduction process was sulfur. No FeS precipitates were formed during the reduction process due to the relatively high solubility of FeS under acidic conditions (Rickard 2006).

For the sulfide precipitation reaction of Cu^{2+}, Na_2S was added to the iron-free simulated AMD. It has been reported that the copper precipitate produced by reacting with sulfide ions is considered to be a form of CuS (Choi *et al.* 2006). In this work, Cu^{2+} was not completely removed when the ratio of n(S): n(Cu^{2+}) was 1:1, with a residual concentration of 4 mg/L (Fig. 1A). When the pH is within the range of 2 to 5, the precipitation rate of Cu^{2+} decreases as the pH drops (Choi *et al.* 2006). Specifically, at a pH of 2, the precipitation rate of Cu^{2+} only reached about 82%. Therefore, we speculated that some S^{2-} may have combined with H^+ to form H_2S or HS^-.

The experiment of the interaction between iron and copper ions with sulfide ions was conducted by introducing Na_2S into the copper-containing AMD. Compared to the Fe^{3+} reduction and the Cu^{2+} precipitation experiment, it can be found that the precipitation of Cu^{2+} from the AMD occurred synchronously with the reduction of Fe^{3+} (Fig. 1B). However, Cu^{2+} is not completely precipitated when Fe^{3+} is reduced. Instead, complete precipitation of Cu^{2+} occurs at the molar ratio of n(S): n(Fe^{3+}) higher than 0.5. The result at this point exhibited consistency with prior experiments, hypothesizing that partial S^{2-} ions may undergo protonation to form H_2S or HS^- species, thereby influencing the precipitation reactions.

Biomineralization of the AMD at pH 2.5

The metal ions removal efficiency by the direct biomineralization and sequential sulfidation treatment followed by biomineralization was investigated. It has been reported that a constant pH of 2.5 could lead to a greater fraction of iron precipitating during the

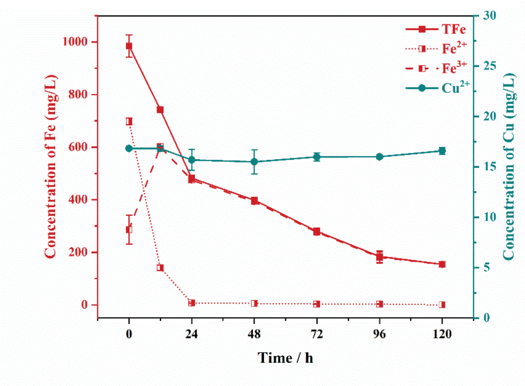

Figure 2 Variation of the metal ions concentration in AMD during the biomineralization process.

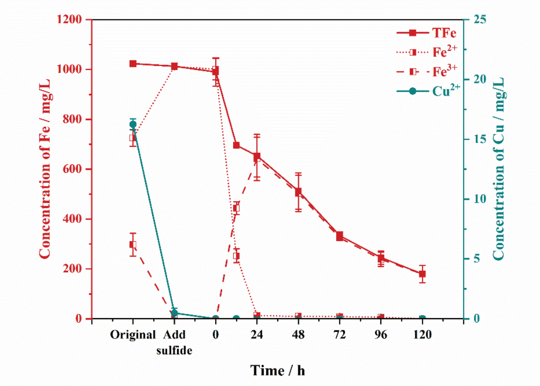

***Figure 3** Variation of the metal ions concentration in AMD during the sulfidation and biomineralization process.*

biooxidation of Fe2+ (Liu *et al.* 2024), therefore, the pH was maintained at 2.5 during the biomineralization process.

In the direct biomineralization group (Fig. 2), the Fe^{2+} was oxidized to Fe^{3+} within 24 hours. The total iron concentration decreased fastest in the first 24 hours, and then slowly decreased to the final concentration of about 150 mg/L, at which point the mineralization efficiency was 84.3%. Additionally, it could be found that the Cu^{2+} was not removed during the biomineralization process, indicating that the formed secondary minerals did not contain Cu and did not adsorb Cu^{2+} at the experimental condition.

The results of the sulfidation-biomineralization group indicated that the Fe^{3+} was reduced to Fe^{2+}, and Cu^{2+} no longer existed in the solution after sulfidation treatment (Fig. 3). After inoculation, the Fe^{2+} was oxidized to Fe^{3+} within 24 hours, and the final mineralization efficiency was 82.4%. Compared to the direct biomineralization experiment, the total iron removal rate is essentially the same. However, the rate of decrease in total iron was reduced, indicating that the biomineralization rate was decreased. This could be due to an increase in ferrous ion concentration after sulfide reduction, thereby delaying the mineralization reaction. The sulfidation treatment did not improve the efficiency of iron ions removal but could completely remove copper ions. After biomineralization treatment, the concentration of Fe^{3+} was about 150 mg/L, lower than the initial concentration of Fe^{3+} in the simulated AMD (300 mg/L). Combining the results of these two experiments, it can be inferred that for the simulated AMD used in this work, biomineralization for iron removal followed by sulfidation precipitation for copper removal can reduce the amount of sodium sulfide used.

Neutralization of the AMD and pretreated AMD by lime

The lime slurry was used to neutralize the simulated AMD and the pretreated AMD. The results showed that at a final pH of approximately 9, the remaining total Fe concentration was 9.29 mg/L and 0.86 mg/L for the simulated AMD group and the pretreated AMD group. Notably, Cu2+ was completely removed in all groups. The lime consumption was 12.4 mL and 4.5 mL, respectively. When taking the lime slurry used to maintain the pH into consideration, the total lime slurry consumption was 12.4 mL and 9.4 mL. Therefore, the sulfide precipitation and biomineralization treatment can reduce the amount of alkali required for neutralization (Song *et al.* 2022). In terms of the sludge, including the sulfide precipitation, the biomineralization and the neutralization sludge, the total weight of the sludge generated after pretreatment was higher than that without pretreatment. This is primarily due to the greater quantity of biomineralization slag, which consists mainly of schwertmannite containing sulfate ions

(Schoepfer and Burton 2021). In summary, the pretreated AMD drastically reduced the required lime slurry in the subsequent lime neutralization process and improved the removal efficiency of iron ions.

Identification of the sludges

The morphology and elemental composition of the sludges generated at each stage were analyzed by SEM-EDS, including the sulfidation sludge, the biomineralization sludge and the neutralization sludge.

The results revealed that the primary components of the sulfide precipitation residue were copper sulfide and elemental sulfur (Fig. 4A). The elemental sulfur existed in a granular form with particle sizes exceeding 10.0 µm, while the copper sulfide was found in a loose aggregated state. The biomineralization sludge exhibited a morphology highly consistent with schwertmannite, namely, they were comprised of spherical aggregates resembling pincushions with diameters of approximately 3.0 µm (Fig. 4B). The neutralization residue exhibited distinct calcium sulfate crystals, while the iron oxides formed during neutralization did not show visible crystalline structures. This is also the primary reason why the neutralization residue is difficult to settle and filter (Fig. 4C).

Conclusion

The sulfidation treatment facilitated the complete precipitation of copper ions from AMD, and resulted in the reduction of Fe^{3+} to Fe^{2+}, which can facilitate the recovery of copper as CuS. No FeS precipitates were generated during the sulfidation process. The stoichiometric ratio of Fe^{3+} to S^{2-} was approximately 0.5, whereas the ratio of Cu^{2+} to S^{2-} exceeded 1.0. After biomineralization treatment, 88.2% of iron ions were removed. The usage of lime slurry was also reduced compared to the conventional direct neutralization method, with the residual iron ions concentration decreased to 0.86 mg/L. SEM-EDS analysis confirmed that the main phase of the sulfidation sludge was CuS and elemental sulfur, the biomineralization sludge was schwertmannite and the neutralization sludge was calcium sulfate and iron oxide. This work provided a promising integrated approach for the efficient removal of iron ions and recovery of copper ions from AMD by incorporating the copper ions sulfide precipitation, iron ions biomineralization, and lime neutralization.

Acknowledgments

This work was supported by the National Key R&D Program of China (2022YFC3702203).

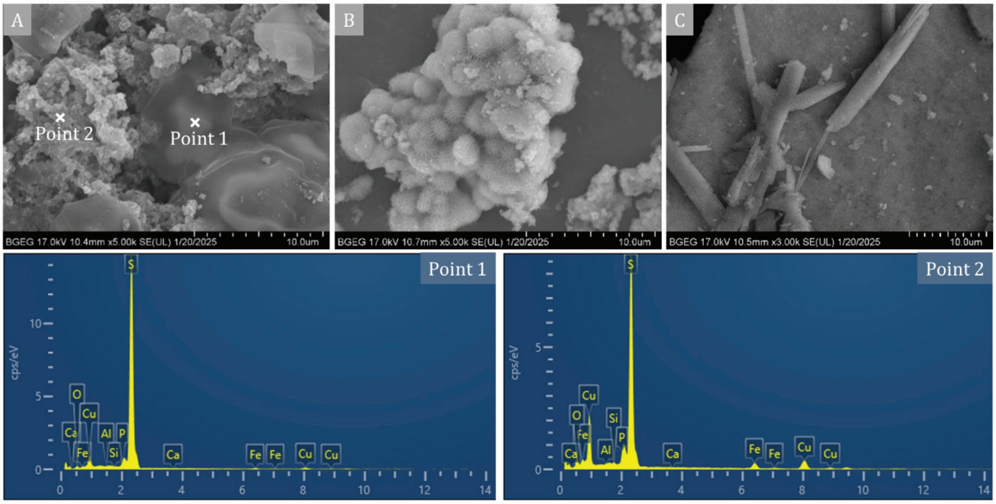

Figure 4 *SEM-EDS of the sludge generated at the sulfidation stage (A), the biomineralization stage (B) and the neutralization stage (C).*

References

Chen G, Ye Y, Yao N, Hu N, Zhang J, Huang Y (2021) A critical review of prevention, treatment, reuse, and resource recovery from acid mine drainage. Journal of Cleaner Production 329:129666. https://doi.org/https://doi.org/10.1016/j.jclepro.2021.129666

Cheong Y-W, Cho D-W, Lee J-S, Hur W (2022) Estimation of Alkali Overdosing in a Lime Neutralization Process for Acid Mine Drainage. 공업화학 33(1):109–112. https://doi.org/10.14478/ACE.2021.1096

Choi J-Y, Kim D-S, Lim J-Y (2006) Fundamental Features of Copper Ion Precipitation Using Sulfide as a Precipitant in a Wastewater System. Journal of Environmental Science and Health, Part A 41(6):1155–1172. https://doi.org/10.1080/10934520600623059

Djedidi Z, Médard B, Cheikh RB, Mercier G, Tyagi RD, Blais J-F (2009) Comparative study of dewatering characteristics of metal precipitates generated during treatment synthetic polymetallic and AMD solutions. Hydrometallurgy 98(3):247–256. https://doi.org/https://doi.org/10.1016/j.hydromet.2009.05.010

Jiang F, Lu X, Zeng L, Xue C, Yi X, Dang Z (2024) The purification of acid mine drainage through the formation of schwertmannite with Fe(0) reduction and alkali-regulated biomineralization prior to lime neutralization. Science of The Total Environment 908:168291. https://doi.org/https://doi.org/10.1016/j.scitotenv.2023.168291

Jin D, Wang X, Liu L, Liang J, Zhou L (2020) A novel approach for treating acid mine drainage through forming schwertmannite driven by a mixed culture of Acidiphilium multivorum and Acidithiobacillus ferrooxidans prior to lime neutralization. Journal of Hazardous Materials 400:123108. https://doi.org/https://doi.org/10.1016/j.jhazmat.2020.123108

Johnson DB, Hallberg KB (2005) Acid mine drainage remediation options: a review. Science of The Total Environment 338(1):3–14. https://doi.org/https://doi.org/10.1016/j.scitotenv.2004.09.002

Kefeni KK, Msagati TAM, Mamba BB (2017) Acid mine drainage: Prevention, treatment options, and resource recovery: A review. Journal of Cleaner Production 151:475–493. https://doi.org/https://doi.org/10.1016/j.jclepro.2017.03.082

Li Q, Xiao Z, Zhang WJME (2024a) Sulfide precipitation characteristics of Mn, Ni, Co, and Zn in the presence of contaminant metal ions. 215:108814

Li T, Cheng F, Du X, Liang J, Zhou L (2024b) Efficient removal of metals and resource recovery from acid mine drainage by modified chemical mineralization coupling sodium sulfide precipitation.

Liu L, Li J, Su L, Fang D, Zhou L (2024) An integrated process incorporating pH-controlled biomineralization and sulfate bioreduction to facilitate recovery of schwertmannite and sulfated polysaccharides from acid mine drainage. Chemical Engineering Journal 487:150614

Mosai AK, Ndlovu G, Tutu H (2024) Improving acid mine drainage treatment by combining treatment technologies: A review. Science of The Total Environment 919:170806

Pham AL-T, Lee C, Doyle FM, Sedlak DL (2009) A Silica-Supported Iron Oxide Catalyst Capable of Activating Hydrogen Peroxide at Neutral pH Values. Environmental Science & Technology 43(23):8930–8935. https://doi.org/10.1021/es902296k

Rickard D (2006) The solubility of FeS. Geochimica et Cosmochimica Acta 70(23):5779–5789. https://doi.org/https://doi.org/10.1016/j.gca.2006.02.029

Schoepfer VA, Burton ED (2021) Schwertmannite: A review of its occurrence, formation, structure, stability and interactions with oxyanions. Earth-Science Reviews 221:103811. https://doi.org/https://doi.org/10.1016/j.earscirev.2021.103811

Song Y, Guo Z, Wang R, Yang L, Cao Y, Wang H (2022) A novel approach for treating acid mine drainage by forming schwertmannite driven by a combination of biooxidation and electroreduction before lime neutralization. Water Research 221:118748. https://doi.org/https://doi.org/10.1016/j.watres.2022.118748

Wei D, Osseo-Asare K (1996) Particulate pyrite formation by the $Fe^{3+}HS^{-}$ reaction in aqueous solutions: effects of solution composition. Colloids and Surfaces A: Physicochemical and Engineering Aspects 118(1):51–61. https://doi.org/https://doi.org/10.1016/0927-7757(96)03568-6

Monitoring of Water Quality in Post-Mining Pit Lakes – Why, How and How Long?

Anne Weber[1], Katja Kunze[2], Susann Wilhelm[2], Felix Bilek[3], Elke Kreische-König[1]

[1]Lausitzer und Mitteldeutsche Bergbau-Verwaltungsgesellschaft mbH (LMBV), Walter-Köhn-Straße 2, 04356 Leipzig, Germany, Anne.Weber@lmbv.de, ORCID 0000-0003-2582-5327

[2]Lausitzer und Mitteldeutsche Bergbau-Verwaltungsgesellschaft mbH, Knappenstraße 1, 01968 Senftenberg, Germany, Katja.Kunze@lmbv.de, Susann.Wilhelm@lmbv.de

[3]GFI Grundwasser-Consulting-Institut GmbH Dresden (GFI), Meraner Straße 10, 01217 Dresden, Germany, fbilek@gfi-dresden.de

Abstract

Over a hundred lignite-mining pit lakes exist in East Germany, most of them flooded for more than a decade. A specially developed monitoring program tracks their hydrological and chemical conditions and, encouragingly, many lakes show progress towards stable conditions. In recognition, 16 pit lakes were included in a preliminary monitoring under the European Water Framework Directive, which provides a standardized framework for assessing lake water quality across Europe. The coexistence of these two monitoring systems has prompted consideration of potential synergies. However, a comparison reveals differences in frequency, parameters, and quality requirements. Ultimately, defining 'stable lake water quality' remains the key relinquishment criterion to conclude the mining-hydrological monitoring.

Keywords: European Union Water Framework Directive; Mine Closure; Lignite; Germany

Introduction

Monitoring is data collection for answering specific system questions. According to INAP (2018) it is 'routinely, systematically, and purposefully gathering information for use in management-decision making'. As such, when the system in consideration evolves over time or questions alter, the monitoring must be adapted. Regarding pit lakes – which are artificial, and as such juvenile, characteristic surface water bodies resulting from open cut mining (Lund & Blanchette, 2022) – monitoring must consider their typical evolution. Four typical stages of pit lake monitoring are described in Schultze *et al.* (2024) and encompass monitoring during a) mine planning and operation, b) pit lake filling, c) being full before closure, d) after closure.

During the 1970s and 1980s, the former East Germany was the world's largest producer of lignite. Surface mining devastated large areas and changed water resources in the two mining regions Lusatia and Central Germany. After German reunification in 1990, East German lignite mining largely ceased, and since 1994, the Central German Mining Administration Company (LMBV), a state-owned company, has been responsible for rehabilitation of these former lignite mines (LMBV, 2023).

Numerous lignite mining pit lakes have evolved in Lusatia and Central Germany. More than 200 are monitored and 75 of them will have a final area of more than 0,5 km^2. The majority of the larger pit lakes were flooded with river or mine drainage water, whereas others filled from groundwater rebound.

Mine-specific legal requirements from mining operation plans, water regulations, and planning approvals obligate LMBV to monitor the creation and restoration of water bodies.

Figure 1 *Cospuden: The lignite mine in 1993 a few months after mining ceased (left, source: LMBV); 30 years later as rehabilitated pit lake within a new landscape, lignite power plant Lippendorf in background (right, source: LMBV, Peter Radke).*

To ensure consistent monitoring practices across its operations, LMBV developed a Mining-Hydrological Monitoring (MHM) standard in the 2000s which, amongst others, targets pit lakes. Its overall purpose is to support the survey of geotechnical stability, to guide water management measures, and to verify the success of implemented water management measures during rehabilitation (LMBV, 2022). For this, the standard summarizes the generally applicable rules and establishes uniform company-wide practices for planning measurement points, sampling procedures, and analysis programs. This monitoring reveals that several pit lakes have been progressing towards stable (meaning steady) chemical composition since being flooded over a decade ago.

Parallel to LMBV's mining rehabilitation, the European Water Framework Directive (WFD) came into force in December 2000, with the primary purpose of establishing an integrated water protection policy across Europe. Its primary target is to achieve a 'good status' for all water bodies in Europe (EC, 2000). These overall regulations were implemented into national law, where the German Surface Water Ordinance ('Oberflächengewässerverordnung', OGewV) addresses the environmental quality standards for surface water bodies. The WFD recognizes lakes with a surface area > 0.5 km^2, and besides natural lakes it also includes artificial lakes such as mine pit lakes. For such artificial water bodies, the objective is to achieve a 'good ecological *potential*' and a 'good chemical status'.

In Germany, authorities at the *federal* level are responsible for conducting monitoring programs to assess the status of the surface water bodies according to the WFD. In perspective, this is relevant for about 75 of LMBV's pit lakes with a surface area larger 0,5 km^2. Given that these pit lakes are in their early stages of development, the LMBV and relevant authorities are still discussing how to monitor and manage these water bodies in accordance with the WFD. This, because it is not well-defined *when* lignite mining pit lakes can be considered 'ready' to fall under the WFD regulations. Further, the East German pit lakes are located on the territory of four federal states: Brandenburg, Saxony, Saxony-Anhalt, and Thuringia and practical application of the regulations differ slightly between them.

In preparation for the WFD reporting, 16 pit lakes in the Federal State of Saxony have been included in a preliminary sovereign monitoring under the OGewV mostly due to their stable hydrodynamic and hydrochemical conditions. For these 'candidate pit lakes', the temporally limited MHM has now been accompanied by a regulatory OGewV monitoring for several years. This raises the question of whether one or both monitoring systems could be optimized due to potential redundancies.

This work offers insight into the parallel implementation of LMBV's Mining-Hydrological Monitoring and the initial monitoring according to OGewV. To uncover potential synergies, both programs were compared in terms of monitoring frequency, location, parameter sets, and quality requirements (GFI, 2024). Two pit lakes are described in more detail. A dialogue, initiated by the Federal State of Saxony, revealed options for monitoring agreements between LMBV and the authorities. Finally, the work addresses the long-term challenges for LMBV, including establishing a definition of stable lake water quality as a criterion for discontinuing its mining-hydrological monitoring.

Comparison of Monitoring Systems for Mining Rehabilitation and EU Regulations

Characteristic of Two Example Pit Lakes

To exemplify the application of both monitoring systems, two pit lakes were selected which are included in both monitoring systems. Key characteristics of both pit lakes are provided in Table 1. Lake Cospuden was flooded with mine drainage from a nearby active lignite mine, whereas Lake Berzdorf received river water. Both are circumneutral (pH 7–8) and oligotrophic with Lake Cospuden having elevated concentrations of sulfate (800–1000 mg/L).

Monitoring Scope

For MHM as well as the preliminary regulatory OGewV monitoring, the main sampling location aligns to the coordinate of the lake's maximum depth. Additional sampling locations typically target sub-areas that are affected by acidic groundwater inflow. Both pit lakes differ in the number of current sampling points (see Fig. 2) with slight deviations in their locations.

Sampling and Analysis

Table 2 summarizes the main features of the MHM and the preliminary OGewV monitoring for both lakes. The list of analyzed biological parameters is comparable. However, only a part of the MHM's mining-specific chemical parameters is analyzed in the preliminary OGewV monitoring. On the other hand, the OGewV covers dozens of chemical parameters potentially relevant for this surface water monitoring, which are beyond the scope of MHM.

Comparability of Monitoring Results

The monitoring results were compared for several mining-specific parameters, among them pH, electric conductivity, alkalinity, acidity, concentrations of SO_4, Fe, Zn, Ni, NH_4, o-PO_4, P^{tot}, TOC, chlorophyll-a. These parameters were both collected in the MHM and used to assess the lakes according to the preliminary OGewV monitoring.

As an example, figure 3 shows alkalinity in Lake Cospuden from the two monitoring programs. The overall comparison shows that most analysis data are essentially congruent but allow for different evaluations due to widely differing sampling intervals. Besides differences in parameter lists, detection limits and norms (which are not discussed here) the obviously main difference is the sampling frequency of both monitoring systems, mentioned above.

Table 1 *Key characteristics of the two pit lakes where application and results of two monitoring programs are compared in this study (LMBV, 2025).*

Pit Lake		Lake Berzdorf (Lusatia)	Lake Cospuden (Central Germany)
Maximum depth	m	72.5	54.2
Final volume	Mio m^3	333	111
Start flooding		01.11.2002	05.08.1993
Flooding until		06.02.2013	02.08.2000
Flooding with		River water	Mine drainage
Lake area	km^2	9.56	4.39
Shoreline	km	16.5	12.5

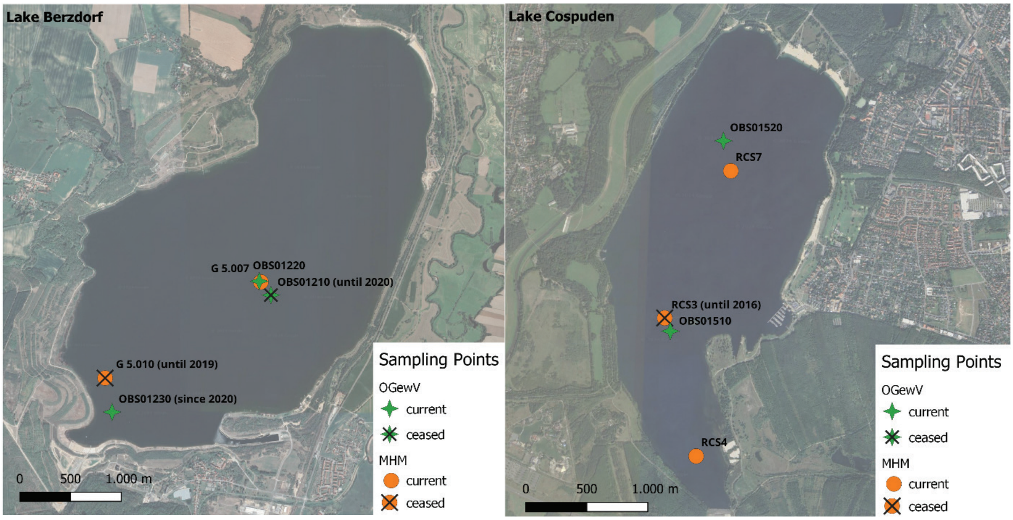

Figure 2 *Locations of sampling points for the two pit lakes Berzdorf (left) and Cospuden (right). Comparison of preliminary regulatory monitoring according to OGewV and monitoring for mining rehabilitation of LMBV.*

Table 2 *Comparison of the implementation of Mining Hydrological Monitoring and preliminary regulatory OGewV monitoring. S: Summer stratification, C: Circulation, *: Plus several lake specific parameters to define the chemical status or the ecological potential (GFI, 2024).*

Pit Lake	Lake Berzdorf		Lake Cospuden	
Monitoring	**MHM**	**OGewV**	**MHM**	**OGewV**
Sampling locations	2	1 (same location)	2	2 (1 slightly differing, 1 different location)
Frequency	annual	every 2–3 years	annual	every 2–3 years
Campaigns per monitoring year	3 × S, 1 × C	4-6 × S, 1 × C	2× S, 2 × C	4 × S, 2 × C
Sampling method	By boat, depth specific sample collectors, nets for plankton sampling (partly different mesh size); slightly differing practice in vertical sample location during stratification			
Chemical parameters	22	13 covered in MHM*	31	14 covered in MHM*
Biological parameters	Chlorophyll, Phaeophytin, phytoplankton cell numbers and volume, zooplankton cell numbers and volume			
Analytical norms	MHM refers to national and European norms, most of them compatible to international norms requested in OGewV			
Results due	Few weeks	6 weeks after a quarter of the year	Few weeks	6 weeks after a quarter of the year

Experiences for Monitoring Transition during Mine Closure and Relinquishment

For many of the 16 Saxon pit lakes with candidate status the preliminary bi- to triennial WFD assessment suggests that temporal changes are still too large to assume stable water quality and that continued measurements should be included in the assessment (GFI, 2024). On the other hand, with a frequency four times a year, LMBV's MHM can reveal stable conditions earlier.

Regarding the long-term perspective, all involved parties agree with a transition phase finally leading to cessation of MHM

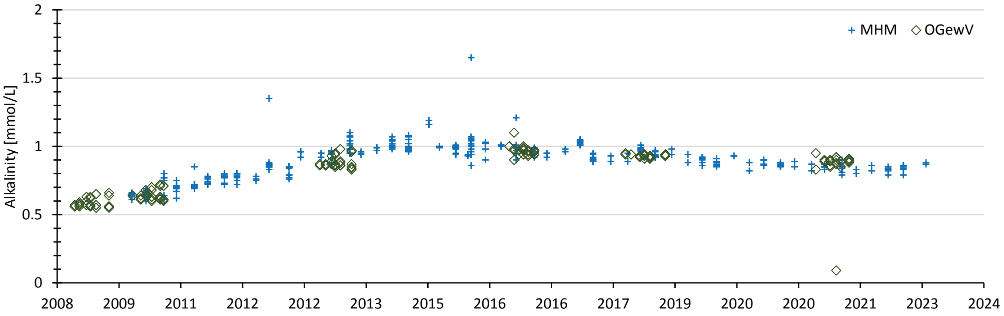

Figure 3 *Alkalinity ($K_{A4.3}$) in pit lake Cospuden. Comparison of preliminary regulatory monitoring according to OGewV and mining-hydrological monitoring of LMBV (basing on GFI, 2024).*

monitoring and sole continuation of the regulatory lake water monitoring. The difficulty now lies in shaping this transition phase. One consideration was to transfer the monitoring of the parameters which are measured in both programs to one monitoring program. However, in addition to the different sampling frequencies, the differences in the analytical requirements and reporting deadlines also proved to be an obstacle. As a result, the two monitoring programs still coexist.

On some points, however, optimization is possible. LMBV's monitoring and reporting could be streamlined or support the preliminary OGewV monitoring by the following: A) Besides monitoring itself, MHM includes reporting to authorities. Whereas monitoring should be continued annually, written reports and their discussion suffice every two years. This practice was already implemented for western Saxon pit lakes in 2021 and is now being discussed for East Saxon pit lakes. B) Since the benefit of plankton counting in MHM is considered disproportionate to the effort, it is currently discussed to conduct these determinations only through OGewV monitoring. C) There is a common understanding that parameters of OGewV monitoring should be included into MHM in case they are mining related (e.g. Ni, Zn, Se) and specific concerns exist. With annual results, authorities then have a broader basis for evaluation of these parameters which they would monitor every 2 or 3 years only.

Saxon authorities recommend and implement a preparatory OGewV monitoring already during the pit lake development. It is pointed out that finalization of pit lakes is generally not completed with the achievement of target water levels and the target quality values (e.g. pH) but sometimes requires further aftercare to achieve stable conditions. Further, the ecological potential of pit lakes can only be assessed once stable water quality conditions have been established and the species communities have been able to establish themselves as representative and stable colonization.

As mentioned above, implementation of regulatory OGewV monitoring differs between the involved federal countries. To date, discussions with the Federal State of Saxony have resulted in the biggest progress and most detailed agreements. As a crucial point to decide, when LMBV's MHM can be ceased the definition of '*stable lake water quality*' has emerged. A similar definitional question will also become relevant for terminating the monitoring of pit lakes in Saxony-Anhalt. There, the definition of a '*largely self-regulating water balance*' is crucial for the completion of post-mining lakes. The LMBV, in turn, is responsible for this verification.

Conclusion

The coexistence of the Mining-Hydrological Monitoring (MHM) and the preliminary regulatory monitoring under the European Water Framework Directive (WFD) for post-mining pit lakes in East Germany presents both challenges and opportunities. This study has revealed several key insights into the monitoring of these unique water bodies:

1. The MHM, developed by LMBV, is finite by definition and focuses on guiding

water management measures and verifying the success of rehabilitation efforts. In contrast, the preliminary WFD monitoring aims to assess the 'chemical status' and 'ecological potential' for these artificial water bodies, also for quantifying eventual future public costs of long-term rehabilitation.

2. While both systems target similar locations within the lakes, they differ substantially in sampling frequency, parameter sets, and quality requirements. Typically, MHM conducts more frequent sampling (4 times each year) compared to WFD monitoring (6 times every 2–3 years).
3. Despite some overlap, each monitoring system provides unique data. The MHM covers a broader range of mining-specific chemical parameters, while the WFD monitoring includes additional parameters relevant to surface water quality assessment.
4. The transition from MHM to sole WFD monitoring is complicated by differences in sampling frequencies, analytical requirements, and reporting deadlines. This requires the continuation of both monitoring programs to date.
5. Several potential improvements have been identified, including streamlining LMBV's reporting, adjusting plankton counting practices, and incorporating relevant WFD parameters into the MHM for mining-related concerns.
6. A crucial challenge lies in establishing a clear definition of 'stable lake water quality', which is one essential prerequisite for determining when LMBV's MHM can be discontinued.

These findings underscore the complexity of managing and monitoring post-mining pit lakes as they transition from rehabilitation to integration into natural water systems. The experience gained from the parallel implementation of these monitoring systems in East Germany provides insights for other regions facing similar challenges in mine closure and water body management.

A key challenge for future discussions with state authorities remains the definition of criteria for stable lake water quality. This is crucial for determining when these artificial lakes have reached a state of balance and are fully integrated into natural water management systems. Further investigation into the long-term ecological development of pit lakes could inform more effective management strategies and contribute to our understanding of ecosystem restoration in post-mining landscapes. As pit lakes evolve and stabilize, collaboration between mining companies, regulatory authorities, and researchers is crucial in ensuring the successful integration of these water bodies into the landscape.

References

EC (2000) Directive 2000/60/EC of the European Parliament and of the Council of 23 October 2000 establishing a framework for Community action in the field of water policy, OJ L 327, 22.12.2000, p. 1–73

Lund MA, Blanchette ML (2022) Closing pit lakes as aquatic ecosystems: Risk, reality, and future uses. WIREs Water e1648, doi:10.1002/wat2.1648

GFI (2024) Comparison between the LMBV's mining hydrological monitoring and the sovereign monitoring for the assessment according to the EC-WFD. GFI, Dresden, Germany, 14.06.2024. Report (in German)

INAP (2018) Global Acid Rock Drainage Guide. International Network for Acid Prevention https://www.gardguide.com

LMBV (2022) Mining-Related Hydrological Monitoring of LMBV mbH – Code of Practice for LMBV. LMBV Senftenberg, Germany, original version from 2007, last updated in June 2022 (in German)

LMBV (2023) Views – Redevelopment and recultivation of mining landscapes. Lausitzer und Mitteldeutsche Bergbau-Verwaltungsgesellschaft mbH, available: https://www.lmbv.de/medium/lmbv-broschuere-einblicke-views-deutsch-englisch/

LMBV (2025) LMBV-Mapviewer. https://www.lmbv.de/service/geoportal/

Schultze M, Vandenberg J, Castendyk D, Schleußner H-P, McCullough CD (2024) Monitoring for pit lake planning, filling and use: Why? When? What? In: Fourie AB, Tibbett M, Boggs G (eds.) Mine Closure 2024: Proceedings of the 17th International Conference on Mine Closure, Australian Centre for Geomechanics, Perth, p 1049—1062, doi:10.36487/ACG_repo/2415_75

If we had a Consistent System for Using Pyrite in Coal Mining in the State of Santa Catarina, Brazil, What Would the Scenario Be?

Jéssica Weiler[1], Ivo André Homrich Schneider[2]

[1]*Universidade Federal do Pampa, Campus Caçapava do Sul, Caçapava do Sul, Brazil, jessicaweiler@unipampa.edu.br, ORCID 0000-0002-2808-7502*

[2]*Universidade Federal do Rio Grande do Sul, Departamento de Engenharia de Minas, Porto Alegre, Brazil, ivo.andre@ufrgs.br, ORCID 0000-0001-9056-1925*

Abstract

In Santa Catarina State, Brazil, almost 400 million tons of coal waste rich in pyrite have already been deposited on the surface, causing severe environmental damage due to acid mine drainage (AMD) generation. In the 1980s, coal waste was reprocessed to concentrate pyrite for the production of sulfuric acid; however, the practice was discontinued. This study assessed the benefits that would have occurred if pyrite recovery had continued. The results showed that pyrite recovery would reduce waste mass by 14.1%, decrease the total sulfur content in the waste from 6.9% to 2.2% and lower acid generation and lime consumption in AMD treatment. This would help simplify the decommissioning and recovery of degraded areas, and improve sulfuric acid supply in Brazil.

Keywords: Acid mine drainage, pyrite recovery, coal waste, degraded areas

Introduction

Coal mining in Brazil only occurs in three states in the southern region (Fig. 1). The state of Santa Catarina is facing the greatest environmental challenges. Coal mining began in the late 19th century and, for decades, occurred without environmental care. The coal in the region has a high sulfur content, and the mechanised underground mining process promotes the transport of a large volume of rock waste to the surface. To meet the standards of the local thermoelectric plant, the coal needs to be processed to remove pyrite and associated rocks, generating 50–70% waste. It is estimated that almost 400 million tons of coal waste have already been deposited on the surface of the Santa Catarina Coalfield (Weiler and Schneider, 2019). The result is a legacy of immense waste deposits with a high pyrite concentration (10-12%), presenting a major environmental problem. Acid mine drainage (AMD) has contaminated the soil, groundwater, and surface water.

Currently, the recovery of environmental liability has been addressed through public civil action with local mining companies. These actions are gradually mitigating the effects of AMD on the soil, groundwater and rivers of the region. However, many areas remain 'orphan sites' and continue to impact the environment (Rocha-Nicoleite *et al.*, 2017). Although legislation and actions to mitigate environmental damage have advanced since the 1990s, some areas remain affected. Models indicate that AMD may continue to be generated for over 500 years, requiring effluent treatment and long-term monitoring of these areas. Fig. 2(a) represents an area of irregular waste disposal directly on the soil, and Fig. 2(b) shows a river contaminated by AMD in the coal mining region of Santa Catarina.

Geologically associated with carbonaceous matter, there are pyrite nodules. The production of elemental sulfur, sulfuric acid, and other products from pyrite can provide the country with essential raw materials for industry without the need for imports. In

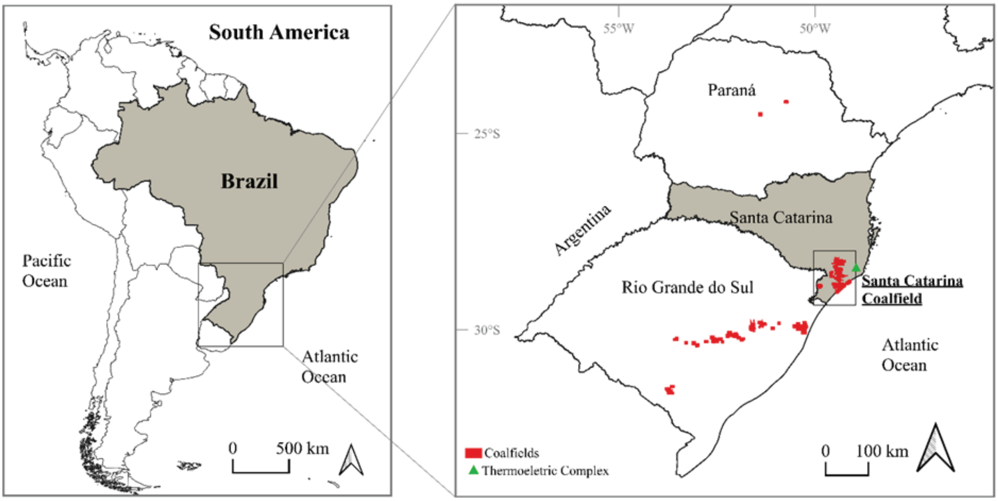

***Figure 1** Location of the study region, in Santa Catarina Coalfield, which supplies the Jorge Lacerda Thermoelectric Complex.*

1968, semi-industrial scale studies conducted by the fertiliser company, later transformed into ‘Indústria Carboquímica Catarinense’ (ICC), demonstrated that 70–80% of sulfur could be recovered from pyrite concentrates. The importance of sulfuric acid production for fertiliser manufacturing was highlighted. It is estimated that during its operational period, ICC consumed around 2.3 million tons of pyrite, supplying 15% of Brazil’s sulfuric acid demand between 1985 and 1988 (Souza, 2007; Goularti and Moraes, 2009).

However, ICC closed in 1992, declaring bankruptcy and abandoning the pyrite concentration plant near the coal production site and the sulfuric acid plant near the Imbituba port, SC (Souza, 2007). Some mining companies attempted to include pyrite concentration in their beneficiation plants, but the small volume produced and the lack of a consumer market restricted this initiative. Thus, the practice was discontinued and is considered one of the major setbacks in the sector because it shifted from a clear circular economy to a linear economy (coal to thermoelectric power).

Based on the problem presented, this study assessed the benefits that the use of pyrite could have brought to the southern region of Santa Catarina if pyrite concentration had continued. This would have prevented the disposal of a substantial amount of pyrite with the waste on the surface, reducing AMD and all related impacts while also providing a raw material source for sulfuric acid production.

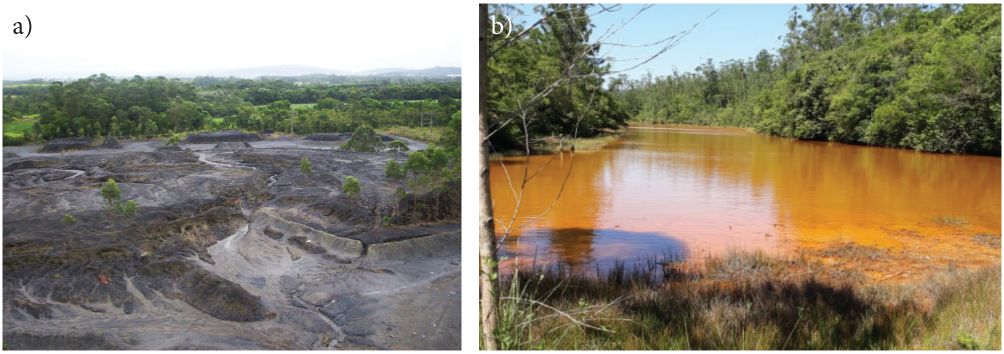

***Figure 2** Irregular coal waste disposal on the surface (a) and a river contaminated by acid mine drainage (AMD) in the coal mining region of Santa Catarina (b).*

Methods

Quantitative data on coal production and waste generation in Santa Catarina from 1925 to 2022 was provided by 'Sindicato Indústria de Extração Carvão Estado de Santa Catarina' (SIECESC) (2025). The quantity produced in the period from 2023 to 2025, not yet disclosed, was estimated based on the trend of recent years.

The mass balance of the pyrite fraction was obtained from the work of Weiler and Schneider (2019), who separately evaluated the two main coal layers explored: the 'Barro Branco Seam' and the 'Bonito Seam'. The values do not differ much in terms of sulfur content and mass recovery, and an average value was adopted. Only the gravimetric processing of the coarse fraction (50.8 + 2.0 mm) was considered, which was used by ICC in the concentration of pyrite.

Briefly, representative samples from both seams were gravimetrically processed in a dense medium of iron–silicon (Fe-Si) to obtain two density fractions: below 2.7 g cm^{-3} (waste rock with low pyrite content) and above 2.7 g cm^{-3} (pyrite concentrate). The processing products were characterised in terms of sulfur content (pyritic, organic, sulfate, and total) and acid generation potential. The total sulfur analysis was conducted using a Leco SC 457. Sulfur forms (pyritic and sulfate) were analysed using titration procedures according to ASTM D2492–02 (ASTM, 2012). Organic sulfur was calculated from the difference between total sulfur and pyritic and sulfatic sulfur. The account provided that approximately 82% of S is in the form of pyrite, 15% in the form of organic S, and 3% as sulfate. The acid generation potential was determined using the classical acid–base accounting method described by Sobek *et al.* (1978).

Results and Discussion

Fig. 3 presents historical data regarding waste production in the Santa Catarina coal region. An increase in waste production can be observed in the 1970s and 1980s, resulting from the Brazilian Government's encouragement of coal production due to the 1973 Oil Crisis. In the following decade, due to incentives for the sector, a coal waste processing plant was also implemented to concentrate pyrite, intended for the production of sulfuric acid for fertilisers. Since the 1990s, the production of coal waste in the region has averaged 4.1 million tons per year (SIECESC, 2025).

Table 1 presents the result of the densimetric separation of the waste, considering the pyrite fraction above 2.7 g cm^{-3}. The mass fraction density above 2.7 g cm^{-3} (pyritic concentrate d ≥ 2.7) accounted for 14.1% by mass, with a total sulfur content of 35.4% (54% pyrite). The remaining fraction (waste fraction d < 2.7) makes up 85.9% of

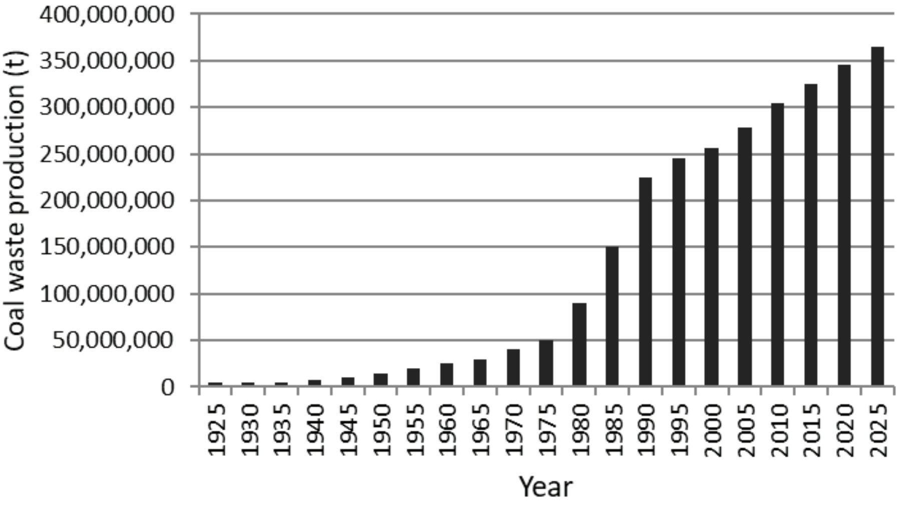

***Figure 3** Accumulated coal waste produced in the carbonific site of Santa Catarina, Brazil.*

Table 1 *Results in terms of mass and sulfur content of the raw waste and after its densimetric division at a density of 2.7 g cm⁻³.*

	Raw waste	Waste Fraction ($d < 2.7$ g cm^{-3})	Pyrite Concentrate ($d \geq 2.7$ g cm^{-3})
Mass (%)	100.0	85.9	14.1
Stotal (%)	6.9	2.2	35.4
Spyrite (%)	5.7	1.6	31.1
Ssulfate (%)	0.2	0.1	0.5
Sorganic (%)	1.0	0.5	3.8

the mass, with only 2.2% of total sulfur (3.3% pyrite). Basically, with a gravimetric process of coarse particles of coal waste, there is a potential to remove 77% of the pyrite present in the waste.

Fig. 4 compares the historical accumulation of the discarded mass of coal waste and the amount of coal waste if the waste was processed to concentrate pyrite. The historical reduction in the period from 1925 to 2025 would not exceed 6%.

Fig. 5 compares the historical accumulation of total sulfur in the discarded mass of coal waste and the amount of total sulfur if the waste was processed to concentrate pyrite. In this scenario, the historical reduction in total sulfur discharged in coal dumps in the period from 1925 to 2025 decreases to 27%.

The data presented here related to the concentration of pyrite do not solve the problem of the volume of waste deposited. However, they make it possible to restrain the amount of pyritic sulfur deposited in the environment. Previous geochemical tests by Amaral Filho *et al.* (2017) showed that the coal desulfurisation process in Santa Catarina does not prevent AMD generation; however, it substantially decreases the rate and net amount of metals, salts, and acidity. Additionally, it was estimated by Weiler *et al.* (2016) that a cut in the costs of reagents (basically lime) of approximately 85% is expected in acid mine treatment plants if coal desulfurisation procedures were adopted.

Currently, with the disruption of the pyrite production chain, actions are mainly focused on the safe land disposal of waste

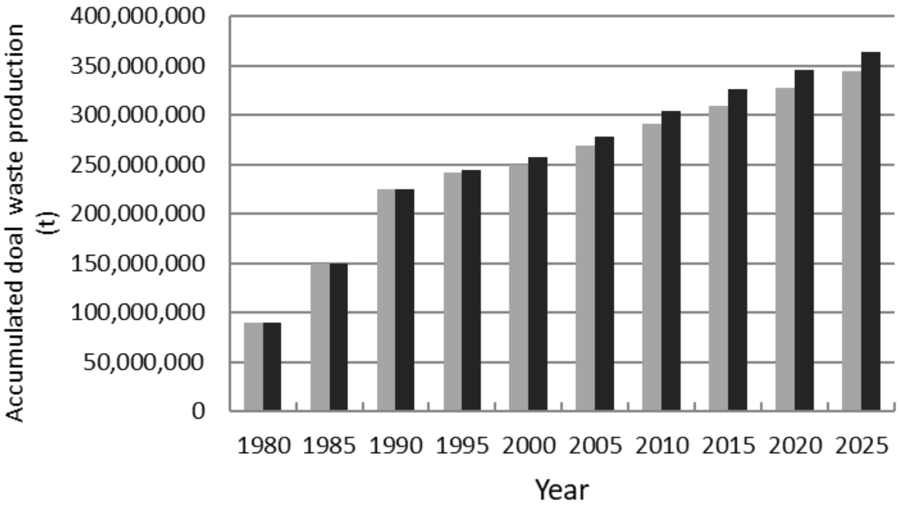

Figure 4 *Accumulated coal waste produced from 1980 to 2025 (right, black) and simulated coal waste production in the same period considering the use of the pyritic fraction (left, grey).*

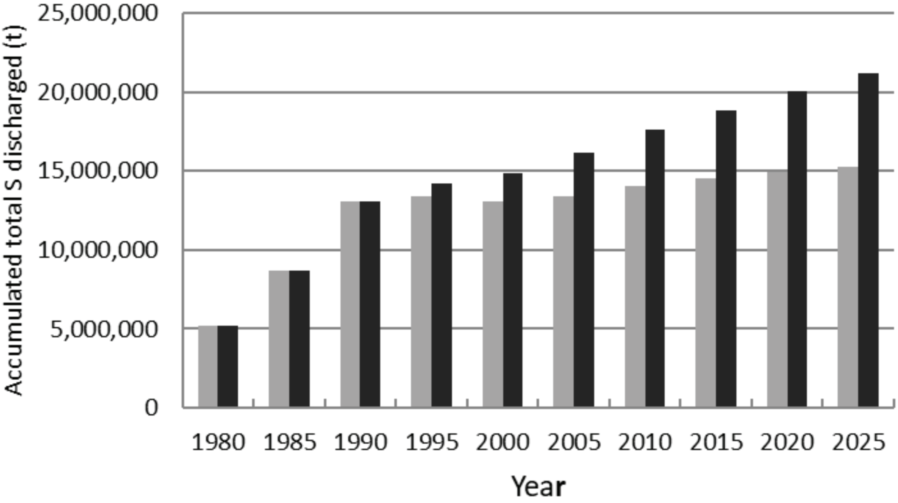

Figure 5 *Accumulated total sulfur discharged from 1980 to 2025 (right, black) and simulated total sulfur discharged in the same period considering the use of the pyritic fraction (left, grey).*

in modules, with a small fraction of pyrite concentrates being sold to sulfuric acid production units in central Brazil and some backfill initiatives (returning waste to open chambers in the mining process) (Amaral Filho *et al.*, 2013). However, the sector's active community agrees that utilising pyrite is part of the necessary set of actions for the environmental recovery of the coal mining region in Santa Catarina (de Oliveira *et al.*, 2019; Weiler *et al.*, 2019; Ferreira *et al.*, 2021).

In addition, the region has the potential to supply 400,000 to 800,000 metric tons of pyrite concentrate (50–60% pyrite) per year. If converted into sulfuric acid, this would represent an increase of at least 500,000 tons of the acid annually to Brazil's production (Weiler and Schneider, 2019). This amount could help meet this Brazilian deficit in this input. It is important to remember that Brazil plays a key role in global food supply and that 80% of the sulfuric acid required in the country is used for fertiliser production.

Conclusions

The decommissioning of the coal mining sector in Brazil is in progress. The pollution scenario might not have been resolved by pyrite concentration and utilisation, but the level of the damage would have been lower, and finding solutions would have been easier. If the region had been seen both as a coal and a sulfide deposit, environmental management would have been facilitated, and less of a pollution legacy would have been left for future generations. Therefore, it is suggested that new coal mining projects in the region consider waste processing for pyrite concentration and that existing operations be restructured accordingly. Additionally, another opportunity would be to reprocess surface-disposed wastes, treating this material as ore rather than waste. Naturally, this should be based on technical, economic, environmental and legal feasibility, highlighting the importance of future studies focused on these aspects.

Acknowledgements

The authors thank all co-organisers for hosting the IMWA 2025 Conference and Jo Burgess, Amy Kokoska, Hetta Pieterse, and Glenn MacLeod for providing critical comments on earlier versions of this text. We also acknowledge the financial support of CNPq (Process 314880/2020-8) for the development of this work and for enabling us to attend the IMWA 2025 conference.

References

Amaral Filho JR, Schneider IAH, Brum IAS, Sampaio CH, Schneider C (2013) Caracterização de um depósito de rejeitos para o gerenciamento integrado dos resíduos de mineração na região carbonífera de Santa Catarina, Brasil. REM. Revista Escola de Minas (Impresso) 66:347–353.

Amaral Filho JR, Weiler J, Broadhurts, JL, Schneider, IAH (2017) The use of static and humidity cell tests to assess the effectiveness of coal waste desulfurization on acid rock drainage risk. Mine Water and the Environment 36(3):429–435.

ASTM (American Society for Testing and Material) (2012). ASTM D2492 – 02: Standard Test Method for Forms of Sulfur in Coal.

De Oliveira CM, Muller TG, Ferreira LP, Cechinel MAP, Paterson M, Raupp-Pereira (2019) Valorization of iron pyrite from coal mining in southend Brazil. Journal of Environmental Chemical Engineering 7(1):102931.

Ferreira LP, Muller TG, Cargnin M, de Oliveira CM, Peterson M (2021) Valorization of waste from coal mining pyrite beneficiation. Journal of Environmental Chemical Engineering 9(4):105759.

Goularti Filho A, Farias de Moraes, F (2009) Formação, expansão e desmonte parcial do complexo carbonífero catarinense. Revista História & Perspectivas 40: 251–267.

Rocha-Nicoleite E, Overbeck GE, Müller SC (2017) Degradation by coal mining should be priority in restoration planning. Perspectives in Ecology and Conservation 15(3):197–200.

SIECESC – Sindicato das Indústrias Extratoras de Carvão do Estado de Santa Catarina (2025) Dados estatísticos. In: http://www.satc.edu.br/siecesc/estatistica.asp. Accessed 02 January 2025.

Sobek AA, Schuller WA, Freeman JR, Smith RM (1978) Field and laboratory methods applicable to overburden and minesoils, EPA 600/2-78-054.

Souza ML (2007) A indústria carboquímica catarinense em Imbituba: uma breve história encoberta pela fumaça vermelha. Santa Catarina em História 1(1):99–107.

Weiler J, Amaral Filho JR, Schneider IAH (2016) Processamento de rejeito de carvão visando a redução de custos no tratamento da drenagem ácida de minas - estudo de caso na Região Carbonífera de Santa Catarina. Engenharia Sanitária e Ambiental 21: 337–345.

Weiler J, Schneider IAH (2019) Pyrite utilization in the carboniferous region of Santa Catarina, Brazil - Potentials, challenges, and environmental advantages. REM: International Engineering Journal 72(3), 515–522.382.

Estimation of Drainage Composition Sourced from Lime-Iron Ore Tailings Mixture in Dry Stack Deposit: Laboratory Testing and Numerical Modeling

Mariana Werle[1], Eduardo dos Santos Costa[1], Carolina Bittencourt de Abreu[1], Rafael Cavalcanti de Albuquerque[1], Lara Lange[1], Maria Luiza Silva Ramos[2], Maria Isabel Pereira Teodoro[2], Ana Caroline Cambraia Trindade[2], Lorena Guimarães[3], Ruberlan Silva[3], Rogerio Kwitko[3], Thaís de Paula Marteleto[1]

[1] Water Services and Technologies (WST), 30220-140 Belo Horizonte, Minas Gerais, Brazil contato@waterservicestech.com

[2] Vale S/A, Belo Horizonte, Minas Gerais, Brazil

[3] Vale S/A (CDM), 34505-120 Belo Horizonte, Minas Gerais, Brazil

Abstract

The closure of traditional tailings dams has driven the adoption of dry stack disposal, presenting both geotechnical and environmental challenges. A critical concern is the chemical composition of effluents generated by these new structures, demanding robust predictive assessments to mitigate environmental risks. Global guidelines advocate for predictive chemical studies prior to constructing tailings containment structures, while the Global Industry Standard on Tailings Management (GISTM) underscores the critical role of such studies alongside multidisciplinary approaches in geochemistry, water quality, hydrology, and geotechnics for the effective design of tailings facilities, including dry stacks. In this context, this study evaluates the environmental and hydrogeochemical implications of mixing iron ore tailings with lime, a strategy to reduce moisture content of filtered tailings and enhance the geotechnical stability of dry stacks. The study was conducted during the project's conceptual phase, adhering to best environmental practices. The methodology integrated laboratory testing with hydrogeochemical numerical modeling to predict the long-term behavior of the tailings-lime mixture. Laboratory tests encompassed static and kinetic drainage predictions, along with chemical and mineralogical analyses of pure iron ore tailings and those mixed with lime in various proportions. Hydrogeochemical modeling, conducted using PHREEQC software, simulated the deposition of the material in a dry stack, accounting for scaling factors, rainwater percolation, site-specific hydrogeology, and partial gas pressure. Results indicate that lime addition induces alkaline pH conditions, promoting silicate dissolution and neo-mineral formation via pozzolanic reactions. Additionally, kinetic tests results showed that alkaline conditions favor the release of metals (e.g. Al, Cr, Cu, Ni), which would otherwise remain relatively inert under neutral pH. Numerical modeling predicts calcium carbonate precipitation under atmospheric exposure, potentially creating low-permeability zones and preferential flow paths within the dry stack. These findings underscore the need for integrated geochemical and geotechnical evaluations in tailings management to ensure compliance with environmental best practices and global standards.

Keywords: Dry stacking, Lime treatment, Hydrogeochemical modeling, Effluent quality, Calcium carbonate precipitation

Introduction

The increasing global demand for sustainable and environmentally responsible mining practices has guided the development of innovative solutions for tailings management. In this context, various organizations and research programs have provided valuable guidance and resources for understanding and addressing these challenges. Examples include the ARD Test Handbook (AMIRA 2002), the GARD Guide (INAP 2009), and the Prediction Manual for Drainage Chemistry from Sulfidic Geologic Materials (MEND/CANMET 2009). These comprehensive resources offer critical methodologies and frameworks to evaluate and manage the environmental risks associated with mining waste, underscoring the importance of integrating standardized approaches into innovative stabilization techniques.

In Brazil, the rupture of iron ore tailings dams in 2015 and 2019 has led to novel approaches in the tailings management methods. In this context, dry stack tailings emerge as a viable substitute for conventional tailings dam projects, aiming to reduce stored water volume and associated hydraulic failure risks. Among these, chemical stabilization using lime presents a promising approach to improve the geotechnical properties of tailings as a mean to control the humidity of the medium. However, the environmental implications of lime addition, including changes in pH and the mobility of potentially toxic metals, remain important concerns that require careful consideration.

This study focuses on the conceptual and practical aspects of chemical reactions involving lime in the context of dry stacking and dam closure, with particular attention to the stabilization of iron ore tailings. To address these challenges, this work integrates laboratory experiments and hydrogeochemical modeling to evaluate the interactions between lime and iron ore tailings. Laboratory tests, including static and kinetic drainage prediction and mineralogical characterization were conducted to assess the chemical and mineralogical transformations induced by lime addition. Numerical modeling using PHREEQC simulated the long-term geochemical behavior of lime-treated tailings under field-relevant conditions, providing insights into the precipitation of calcium carbonate, changes in permeability, and potential environmental impacts. By combining experimental and modeling approaches, this study contributes to the understanding of lime-induced stabilization mechanisms, offering practical guidance for the design and management of dry stacking systems and dam closures in mining operations.

Conceptual Model – Chemical Reactions Involving Lime

Calcium lime is produced from calcitic limestones or marbles via calcination at 900–1,200°C, converting calcite ($CaCO_3$) into lime (CaO) and CO_2. Lime reacts with water at low temperature, forming portlandite [$Ca(OH)_2$], raising solution pH to 12.45 and releasing calcium ions, which can trigger further chemical reactions. Lime is extensively applied to modify the physical properties of fine-grained soils, particularly those containing plastic clays. The addition of lime initiates cation exchange and flocculation/agglomeration, enhancing soil plasticity, workability, and strength.

The reactions between lime, water, soluble silica, and alumina in soil produce various cementitious materials, known as pozzolanic reactions. These include Calcium-Silicate-Hydrates (CSH) and Calcium-Aluminate-Hydrates (CAH), also formed during Portland cement hydration (Terrel *et al.* 1979). The process increases the soil mixture's pH to approximately 12.4, enhancing the solubility of silica and alumina and sustaining pozzolanic reactions as long as sufficient residual calcium and high pH persist (Little 1987). The possible primary sources of silica and alumina in typical fine soils include clay minerals, quartz, feldspars, micas, and other similar natural silicates and aluminosilicates, both crystalline and/or amorphous. The following reactions illustrate the transformation of lime into cementitious products through interaction with soluble silica and alumina: (1) $Ca(OH)_{2(s)} \rightarrow Ca^{2+}_{(aq)} + 2(OH)^-_{(aq)}$; (2) $Ca^{2+}_{(aq)} + OH^-_{(l)} + SiO_{2(aq)} \rightarrow$ CSH and (3) $Ca^{2+}_{(aq)} + OH^-_{(aq)} + Al_2O_{3(aq)} \rightarrow$ CAH. Another reaction, carbonation, occurs when lime reacts with atmospheric or organic-derived CO_2, forming stable calcium carbonates instead of the cementitious compounds CAH and CSH. This process can interfere with soil stabilization efforts, especially in exposed or operational waste piles.

Methods

Laboratory tests

Laboratory tests were conducted on pure iron ore tailings as well as on tailings mixed with lime in varying proportions. These tests included paste pH measurements, kinetic testing, and mineralogical analyses.

Paste pH analysis is a static test designed to determine whether a sample contains readily available acidity or alkalinity. This analysis involves mixing a specific amount of the solid sample with deionized water, typically in a 1:1 or 2:1 water-to-solid ratio, to create a paste. The pH of this paste is then measured using a pH meter, providing a rapid assessment of the chemical reactivity of the material. Kinetic tests were conducted in humidity cells following ASTM Standard D5744 (2012). The tests lasted 50 weeks and involved 7 tailings samples: one pure tailings sample (Sample 01) and six iron ore tailing mixed with lime in different proportions (Samples 04, 07, 10 13, 16, 19). The tests involved wet-dry cycles and flooding events. Leaching tests began (week 0) with cells flooded with 1000 mL of deionized water, followed by chemical analysis of the solution after 1 hour. Samples were then exposed to three days of dry air (1.5 ± 0.5 L/min), three days of humid air (95% humidity, 18.1°C–30.4°C), and one day of water percolation. This cycle was repeated throughout the 50-week test period. Weekly measurements included pH, redox potential (mV), electrical conductivity (µS/cm), and temperature (°C). Liquid effluent sampling occurred over 20 weeks (at weeks 0, 1, 2, 3, 4, 6, 8, 10, 12, 14, 16, 19, 22, 25, 28, 31, 35, 40, and 45) for chemical analysis.

Mineralogical analyses were conducted with the QEMSCAN system using a Scanning Electron Microscope (SEM), FEI Quanta 650F model, operating at 25 kV and 10 nA. Microanalyses were conducted pixel-by-pixel using two Bruker XFlash 6|30 EDS spectrometers. Images were generated by phase recognition combining Backscatter Electron Imaging (BSE) and EDS microanalysis. The modal distribution of minerals, expressed as weight percentage per sample or fraction, was calculated based on area percentages weighted by the density of each phase.

Hydrogeochemical numerical modeling

Hydrogeochemical modeling was performed using PHREEQC software (version 3; Parkhurst and Appelo 2013) to simulate the deposition of the material in a dry stack, considering scaling factors, rainwater percolation, hydrogeology, and partial gas pressure. For the simulation of chemical reactions with lime and the water percolation model, the kinetics of reactions (*KINETICS* data block), chemical equilibrium (*EQUILIBRIUM_PHASES* data block), and 1D (one-dimensional) transport (*TRANSPORT* data block) were simulated.

Results and Discussion

Mineralogical analysis indicates that the iron ore tailings are predominantly composed of quartz and Fe oxides, followed by phyllosilicates and Mn and Al oxides. Additionally, CaAl silicates (anorthite) and CaFe silicates (tremolite) were identified. In the iron ore tailings mixed with lime, the formation of calciosilicate phases was observed, which were absent in the iron ore tailings. These phases are likely formed through pozzolanic reactions between portlandite and soluble silica, resulting in the generation of CSH-type minerals. Fig. 1 illustrates details of the lime agglomerate, as well as neoformed calcium silicate, identified as the mineral tobermorite.

The pH paste results for the iron ore tailings samples show an average value of 7.35. For the tailings samples mixed with lime, the pH values range from 12.18 to 12.32. This high pH is related to the presence of lime in the tailings and does not vary with the proportion of lime added to the mixture. This aspect indicates that the pH range measured in the samples mixed with lime is due to the thermodynamic equilibrium of the reactions.

The results of the kinetic tests indicate that pH conditions are neutral to slightly basic for the iron ore tailings samples and basic for the iron ore tailings mixed with lime samples. The iron ore tailings sample (Sample 01) exhibited a pH of 6.95 during the first effluent discharge (Week 0) and maintained a pH range of 6.95 to 8.00 in the leachates from Week 1 to Week 50 (Fig. 2). The effluents from the iron ore tailings mixed with lime (Samples 04, 07, 10, 13, 16 and 19) display pH values close to 12 in Week 0, then decreased to a range of 7 to 10 between Weeks 1 and 4 and stabilized between 7 and 9 from Week 5 through Week 50 (Fig. 2). These results indicate the precipitation of mineral phases that reduce the pH to near-neutral values.

Kinetic tests showed that the alkaline conditions favor the release of metals into solution, which would otherwise remain relatively inert under neutral pH. Higher concentrations of aluminium (Al) were identified in Week 0 in the iron ore tailings mixed with lime samples compared to the pure tailing sample, followed by a more evident decline starting from Week 1 (Fig. 2). The iron ore tailings mixed with lime showed an average Al concentration of 0.27 mg/L, while the pure tailing sample exhibited <0.02 mg/L of Al.

Copper displayed higher values, particularly in Weeks 0 and 1, with fluctuations until Week 6. Chromium (Cr) concentrations exceeded 0.05 mg/L in the effluents during the initial weeks for most iron ore tailings mixed with lime samples, while the pure tailings sample showed no variation in Cr levels (Fig. 3). Tailings samples exhibited higher concentrations of Cr up to approximately Week 10, with peaks observed during Weeks 1, 6, and 8. These characteristics suggest that the initial shift to basic pH, followed by a transition to neutral pH, promotes the progressive leaching of mineral phases, enabling the chemical mobility of metals during the early weeks. It is worth noting that some of these values exceed the maximum limits permitted by Brazilian legislation for surface waters, thus raising an environmental concern.

The hydrogeochemical numerical modeling were performed using the software PHREEQC to investigate reactions between lime and iron ore tailings and their impacts on effluents and precipitates. In Simulation 1, a closed system without CO_2 were simulated. The results display that lime is completely

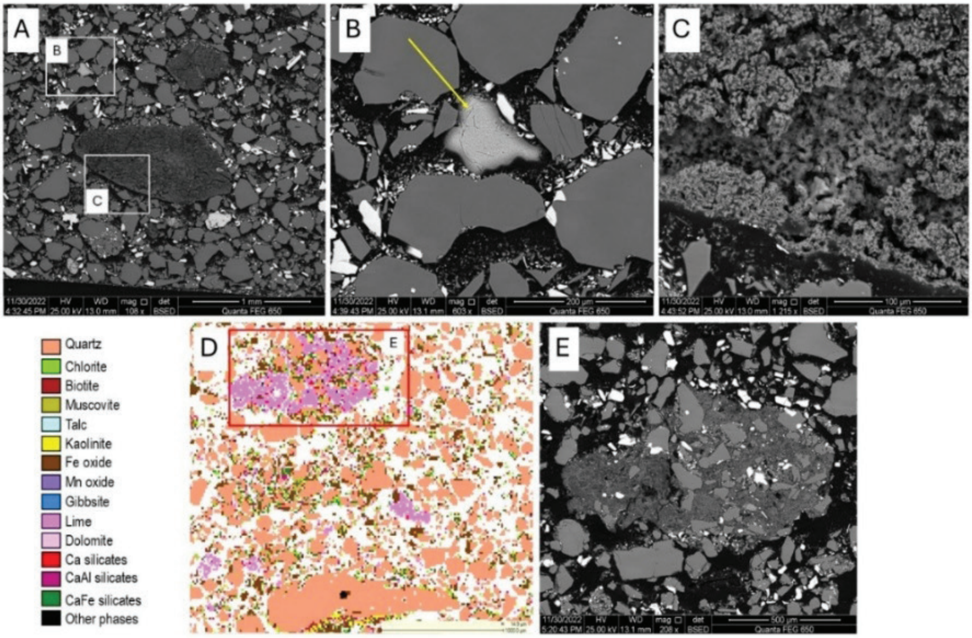

Figure 1 *A) Backscatter Electron Imaging (BSE) of iron ore tailings mixed with lime. B) Neoformed calcium silicate C) Detail of lime agglomerate. D and E) QEMSCAN and BSE images of iron ore tailings mixed with lime.*

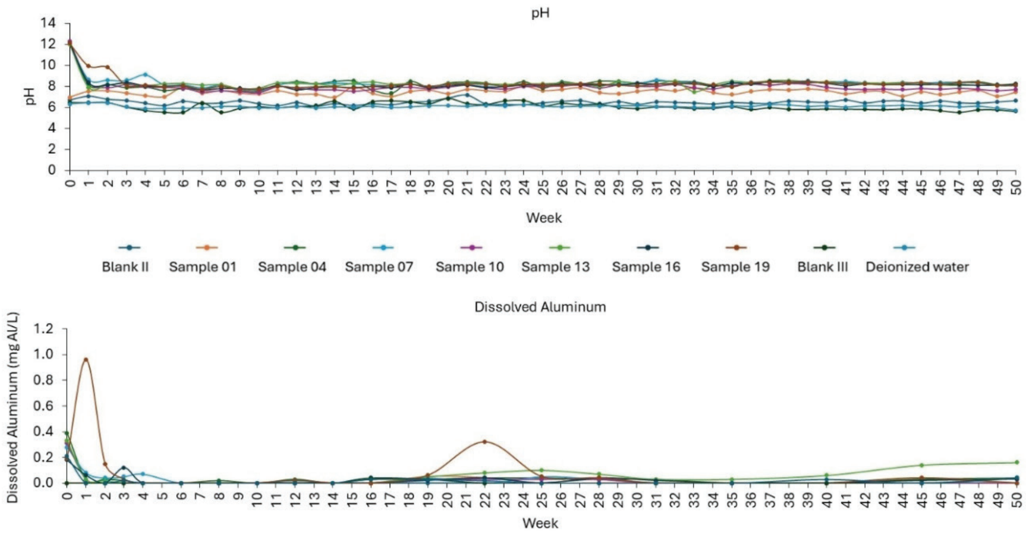

Figure 2 *Kinetic Test Results for pH and Aluminum Concentration Over Time.*

consumed, forming portlandite and raising the pH to an average of 12.26, similar to what was observed in pH paste tests. The pH remains high, and the amount of lime does not limit the reactions or pH increase. In Simulation 2, considering an open system with CO_2, the reaction with lime consumes CO_2, resulting in calcite supersaturation and a slightly lower pH of 11.56 compared to the closed system. The calcite saturation index is 6.15. Tests with varying PCO_2 values (-3.5, -2.5, and -1.5) showed no significant changes in pH or calcite saturation, regardless of the CO_2 concentration.

Simulation 3 aimed to simulate reactions with lime in the presence of silicates and iron oxide in an open CO_2 system. Hematite and kaolinite were considered at equilibrium,

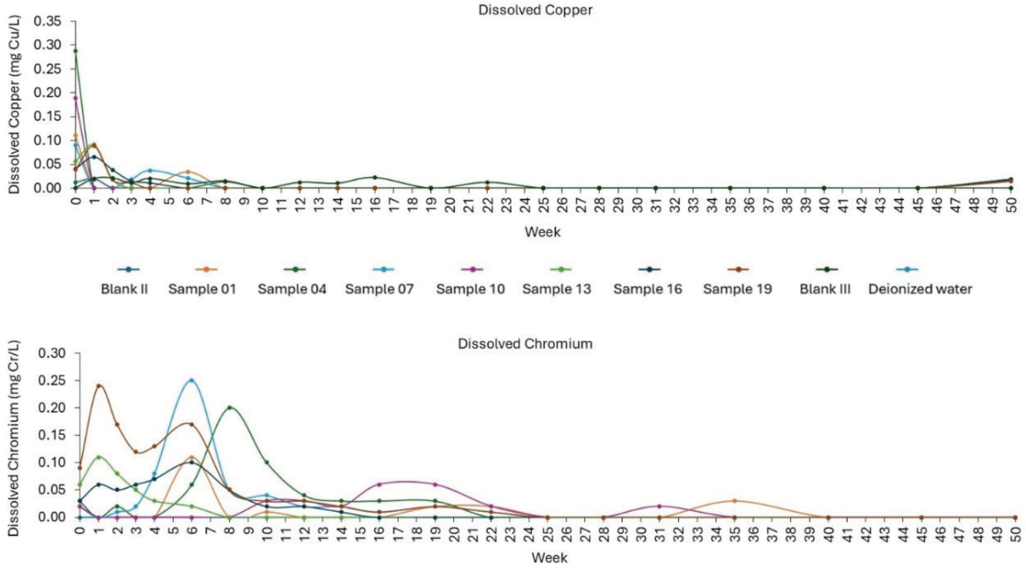

Figure 3 *Kinetic Test Results for Dissolved Copper and Dissolved Chromium Concentrations Over Time.*

while the reaction kinetics of anorthite were included. The high pH promotes silicate dissolution, releasing silica and alumina, which react with lime in pozzolanic reactions to form CSH and CAH minerals. Mineralogical analyses revealed increased amounts of calcium silicates, calcium-aluminum silicates, and calcium-iron silicates, interpreted as neoformed silicates. The simulation showed supersaturation of both calcite and neoformed silicates. Simulation 4 evaluated calcite and neoformed silicates at chemical equilibrium in an open CO_2 system. The presence of both calcite and neoformed silicates caused a further pH reduction due to mineral precipitation.

In addition, a simulation was conducted on a hypothetical dry stack accounting for scaling factors, rainwater percolation, site-specific hydrogeology, and partial gas pressure. The results showed that lime is instantly consumed in the first equilibrium (step 0 in the transport model), transforming into calcite. As calcite precipitates, it captures alkalinity and Ca^{2-} ions, reducing the pH to near-neutral values. However, this occurs only after all lime is depleted. With a constant addition of lime-treated tailings, reactions may continue, maintaining the pH near 12. A significant effect of these reactions is mineral precipitation, which can alter the material's physical properties, such as porosity and permeability.

The numerical modeling indicates that calcium carbonate precipitation may occur under atmospheric exposure, potentially creating low permeability zones and preferential flow paths within the dry stack structure. These factors should be carefully considered in geotechnical designs. This study highlights key factors related to effluent quality and environmental impacts that must be addressed in projects involving the mixing of iron ore tailings with lime.

Conclusions

The study demonstrates that mixing iron ore tailings with lime has both environmental and geotechnical implications. The elevated pH can dissolve mineral phases that are stable under neutral conditions, releasing chemical species previously confined to the solid phase. These released species may pose environmental risks and complicate wastewater treatment processes. Conversely, in the presence of CO_2, lime reacts to form carbonate, which lowers the solution's pH to near-neutral levels. This precipitation process tends to fill the material's interstitial spaces, reducing porosity and potentially causing chemical clogging within the structure. Such intense precipitation can lead to the formation of cemented zones with low permeability in the tailings, a critical factor to consider in geotechnical design. The study was conducted during the project's conceptual phase, in adherence to best environmental practices.

References

AMIRA (2002) ARD test handbook. AMIRA P387A project: prediction and kinetic control of acid mine drainage. Melbourne, VIC: AMIRA International.

ASTM – American Society for Testing Materials (2012) ASTM D5744-07e1 Standard Test Method for Laboratory Weathering of Solid Materials Using a Humidity Cell, 19p. DOI: 10.1520/D5744-07E01

GISTM (2020) Global Industry Standard on Tailings Management. Global Tailings Review, 40p.

INAP (2009) The International Network for Acid Prevention. Global Acid Rock Drainage Guide (GARD Guide). http://www.gardguide.com

Little DL (1987) Fundamentals of the Stabilization of Soil with Lime (Bulletin 332), NLA, Arlington, VA. http://www.lime.org/publications.html

MEND/CANMET (2009) Mining and Mineral Science Laboratory. Prediction Manual for Drainage Chemistry from Sulphidic Geologic Materials. MEND Report 1.20.1.

Parkhurst DL, Appelo CAJ (2013) Description of input and examples for PHREEQC version 3–A computer program for speciation, batch-reaction, one dimensional transport, and inverse geochemical calculations: U.S. Geological Survey Techniques and Methods, book 6, chap. A43, 497p. http://pubs.usgs.gov/tm/06/a43/

Terrel RL, Epps JA, Barenberg EJ, Mitchell JK, Thompson MR (1979) Soil Stabilization in Pavement Structures: A User's Manual, Volumes I and II, FHWA.

System and Process Understanding of Mine Gas Release of Closed Hard Coal Mines in the Context of EU Methane Regulation

Sebastian Westermann[1], Barbara M.A. Teichert[1], Stefan Möllerherm[1]

[1]Research Center of Post-Mining, Technische Hochschule Georg Agricola University, Herner Str. 45, 44787 Bochum, Germany, sebastian.westermann@thga.de

Abstract

Even after the closure of a mine, degassing of methane on the surface is observed. EU regulation 2024/1787 obliges companies to continuously measure and reduce these emissions, which is a major challenge given the thousands of degassing sites (shafts, adits, boreholes, faults) in the Ruhr region alone. Integrated monitoring, including hydraulic and geochemical analyses, can shed light on release mechanisms. The rise of mine water level can be an effective method to control degassing. This contributes to the regulation of methane emissions and supports compliance with the new EU emission reduction targets for the energy sector.

Keywords: Mine gas release, mine water rebound, methane, integrated monitoring

Introduction

Methane is released from fossil deposits, e.g. those of lignite and hard coal, as well as of oil fields, moors and swamps; it is also released during the exploitation and decomposition of organic materials (e.g. in agriculture or landfills). In the atmosphere, it acts as a greenhouse gas that is harmful to the climate and it harbours an equivalent of global warming potential (GWP) that is between 28 and 80 times higher (EC 2024) than that of carbon dioxide (CO_2). In 2020, almost 13 billion tons (EC 2021) of CO_2-equivalent methane was released into the atmosphere worldwide. The largest contributor was agriculture and livestock farming (47%), followed by the energy sector (oil, natural gas, coal; 28%), waste management (13%) and other industries (12%). The Global Methane Initiative (GMI, US EPA 2025) states that in 2020 it was China which made the largest contribution to global methane emissions with 18%, followed by Russia with approx. 11%, the US with 8% and India with 7% (GMI, US EPA 2025).

There are regular observations of degassing processes at the surface of (former) mining areas; during the active mining stage, the mine gas flows into the mine workings through loosened rock above and below the seams. For safety purposes, this mine gas is diluted using technical measures such as fresh air supply (ventilation), or it is extracted from bore holes (pre-degassing).

In the post-mining phase, methane continues to degas from open mine workings, the deposit itself, and adjoining rocks. A proportion of the mine gas remains in the mining areas as natural residual gas. Even where mine workings are flooded, methane may continue to degas. At low barometric pressure the mine gas escapes from the mine workings to the atmosphere through a network of fissures that has occurred either naturally or as part of the exploitation. This migration can be enhanced by the rise of the mine water level which often results from the adjusted mine water pumping during the post-mining stage. In some cases, this effect is often not fully recorded, analysed or clearly communicated to the public. This approach leads repeatedly to annoyance and fear among the population, and this in return has negative effects on the public acceptance or the natural environment.

On 15/11/2023, the EU Parliament and the EU Member States agreed on a submission to pass a regulation on reducing methane emissions; this regulation is based on the EU-wide strategy to reduce methane emissions of 14/12/2020 and on a draft regulation of the European Parliament and of the Council on the reduction of methane emissions in the energy sector of 15/12/2021. The EU Regulation 2024/1787 of the European Union aims at reducing methane emissions, improving the air quality, and strengthening the global leadership of the EU in the fight against climate change.

Degassing behaviour of an underground mine during mine water rebound

Methane gas from abandoned mines can reach the surface through the rock mass (which consists of hard coal seams, overburden, faults/remoulding) and via boreholes and degassing pipelines. The overburden often shows different types of consolidation, porosity, crevasse formation and permeability. Due to crevasses and fissures in the overburden mine gas can naturally escape into the atmosphere. Because of the low permeability, the flow resistance inside the coal seams and overburden strata is relatively high compared to that in the open mine workings. Mostly, there is a slow flow in a porous or fissured medium at low speed and Reynolds number.

If a seam comes in contact with the surface due to galleries, shafts, crevasses or fissures, the methane content in the hard coal is reduced until the gas pressure inside the seam is identical to the atmospheric (air) pressure. This process is stopped when mine water accumulates at the hard coal or a water column forms. In this case, the degassing of the methane can be reduced; the mine water acts as a barrier and prevents the exchange of the methane from the coal to the ambient air. Thus, the pressure gradient decreases and the potential release of methane is reduced. This process can result in less methane escaping to the surface.

According to an examination by Krause & Pokryszka (2013), the degassing velocity is reduced by a factor of 9 as soon as the seam is flooded with mine water and hydrostatic pressure is exerted on the hard coal. This result shows that the presence of mine water influences the degassing velocity and considerably reduces the release of methane. A seam with a gas pressure of 10 bar can no longer degas at a water column of 90 m (corresponding to 9 bar) and the additional atmospheric pressure of 1 bar. The pressure inside the water column and the atmospheric pressure exceed the pressure inside the seam and, as a result, no further methane is released. An equilibrium is created, and the degassing process is stopped. Although methane may dissolve in the mine water and move also towards the surface through diffusion in water, the diffusion velocity of methane in water is lower than that of methane in air, to be precise, by a factor of approx. 10,000 (Stephan *et al.* 2019). This means that the methane molecules move much slower in mine water than in air; consequently, the degassing of methane from mine water happens at a much slower pace and can be substantially delayed.

Isotope geochemistry of methane

The isotopic composition of methane can provide insights into its mode of formation. Methane can be generated either biogenically or thermogenically. In biogenic methane production, microorganisms known as methanogens or methane producers are involved. These organisms obtain energy either through the fermentation of acetate or the reduction of carbon dioxide using hydrogen (Whiticar *et al.* 1986). Since these microorganisms preferentially use the lighter carbon isotope ^{12}C for their metabolism, isotopic fractionation occurs, leaving a characteristic signature in the carbon of the methane. The isotopic composition is expressed in delta notation. This represents the relative difference between the isotopic ratio in a sample and a standard (PDB, Peedee Belemnite), where the ratio of the heavier to the lighter isotope ($^{13}C/^{12}C$) is measured. The $\delta^{13}C$ values for biogenic methane typically range between -110‰PDB and -50‰PDB (Whiticar *et al.* 1986).

$$\partial^{13}C = \frac{\left(\frac{^{13}C}{^{12}C}\right)_{Probe} - \left(\frac{^{13}C}{^{12}C}\right)_{Standard}}{\left(\frac{^{13}C}{^{12}C}\right)_{Standard}} \times 1000\ ‰$$

In thermogenic methane formation, organic material (plant matter, aquatic organisms) is thermally decomposed under high-pressure and high-temperature conditions (Tissot & Welte 1984). Thermogenic methane is isotopically heavier, with $\delta^{13}C$ values typically ranging between – 50‰PDB and -30‰PDB (Tissot & Welte 1984). During thermogenic methane formation, higher hydrocarbons such as ethane, propane, and butane are also produced (Tissot % Welte 1984). Thus, the ratio of methane to the sum of ethane and propane can serve as an additional indicator for distinguishing between thermogenic and biogenic methane. Thermogenic methane has a characteristic value of <100 (Whiticar *et al.* 1986), while biogenic methane shows values >1,000 (Bernard *et al.* 1977). In biogenic metabolic activities, higher hydrocarbons are formed only in trace amounts.

Microbial degradation of methane also influences the isotopic signature. Microorganisms that oxidize methane and convert it to carbon dioxide or bicarbonate preferentially use the lighter ^{12}C isotope (Barker & Fritz 1981). As a result, the remaining methane becomes increasingly heavier, which can lead to pseudo-thermogenic isotopic values (Humez *et al.* 2019).

Other processes affecting the isotopic signature of methane include its migration (diffusion) and the desorption and adsorption of methane onto coal (Gaschnitz 2001). Both processes lead to isotopic fractionation, i.e., the preferential mobilization of the lighter ^{12}C isotope.

EU methane regulation

In October 2020, the European Commission adopted an EU strategy to reduce methane emissions ('the Methane Strategy') setting out measures to cut methane emissions in the Union, including in the energy sector, and at global level (EC 2020). According to the Union's greenhouse gas inventories data, the energy sector is estimated to be responsible for 16% of methane emissions within the Union in 2022, the second highest methane emitting sector after agriculture (EEA 2024). In the energy sector, methane emissions are primarily linked to mining activities, both in active (coal mine methane, CMM) and abandoned mines (abandoned mine methane, AMM). They account for 38% of methane emissions within the energy sector in 2022, but the situation varies greatly among the EU countries (EEA 2024). For instance, methane emissions from mining activities account for 0% to 4% in France and Belgium since all coal mines were closed at least 20 years ago, while they account for 70% in Poland due to ongoing mining activity.

In this context, the European Parliament and the Council adopted a new regulation on the reduction of methane emissions in the energy sector (EU) 2024/1787, including those from abandoned underground coal and lignite mines (EC 2024). According to the Regulation (EU) 2024/1787 Member States shall:

- set up and make publicly available an inventory of all closed coal mines and abandoned underground coal mines in their territory;
- measure methane emissions in all closed and abandoned underground coal mines where operations have ceased since August 3rd, 1954, and
- designate one or more competent authorities responsible for monitoring and enforcing the application of this regulation in each state.

Finally, the regulation requests the coal mining companies and the authorities to create and implement an emission reduction plan to tackle methane emissions from abandoned underground coal mines that ceased operations after 3rd August 1954.

The new regulation raises two main challenges regarding its implementation without providing any standard or technical guidance. The first one concerns the methodology to carry out the inventory at such a large scale with the need to deal with archives and historical and incomplete data for ancient, abandoned mines. Indeed, the feedback from US inventories carried out by the U.S. Environmental Protection Agency (EPA) highlights the lack of data for mines closed before 1972 and the difficulties to develop methods to assess methane emissions from abandoned mines (US EPA 2004a, 2004b). The situation is probably worse in Europe due to the different regulations and mining situations in the respective countries. Hence this diversity raises questions about how to deal with different mining data reporting systems, which may not have the same reported data. Furthermore, the challenge is likely to increase as the number of abandoned mines is likely to increase, especially in countries with ongoing mining activity such as Poland, and therefore their share in the methane emissions will increase, too (Kholod *et al.* 2020).

The second challenge concerns the emission threshold of 0.5 t_{CH4}/a adopted and the obligation to continuously acquire and collect data at each mining emitting component for more than 90% of the period for which it is used to monitor the emissions. The low value of the threshold raises questions about the sensitivity of the current methane and flow sensors. For instance, according to the review of the Yale Carbon Containment Lab carried out in 2022, aerial methane measurement technologies (e.g. UAV, manned aircraft, satellites) currently are not likely to reach such levels of sensitivity although they allow to quickly investigate large areas (Yale Carbon Containment Lab 2022). State-of-the-art UAV technology currently allows to estimate CH_4 flux down to ca. 1 g/s (Shaw *et al.* 2021) while the EU threshold of 0.5 t_{CH4}/a corresponds to a flux of 0.02 g/s. However, Hollenbeck *et al.* (2021) mention the existence of a small unmanned aircraft system (sUAS) with a minimum detection limit of 0.06 g/s and the existence of a hyperspectral camera that was found to measure flux down to 0.006 ± 0.0006 g/s (23 ± 2.3 g/h) and that can potentially be mounted to an aerial platform. Moreover, large diversity of emissive component configuration, depending on the seal quality, function of its aging and its sealing procedure (Foreman 2016), and the type of component (e.g. shafts, galleries, tunnels), is expected to be encountered. Hence, different methods to measure CH_4 flux must be used or developed if they do not exist. Furthermore, CH_4 fugitive emissions are known to vary greatly depending on atmospheric pressure (Fleming *et al.* 2021; Hatch *et al.* 2018; Mønster *et al.* 2019; Nambiar *et al.* 2020); hence aggregation methods must also be developed to obtain a single value for the CH_4 flux for each component that is representative of the temporal variations.

Techniques for handling methane

In the past, technologies for extracting and reducing methane degassing in active coal mining primarily served the purpose of keeping the methane concentration in the mine air below the explosive range (4.5 vol. % to 16 vol. %). Depending on local safety regulations, this upper limit is 1 vol. % to 2 vol. %.

Provided suitable measures of explosion protection are applied, mine gas can be used as fuel in gas turbine plants or combined heat and power (CHP) plants to generate energy. To burn methane at concentrations of less than 3 vol. %, energy must be added to the chemical reaction which is usually done by adding more fuel gas, heat or electric energy. Fuel gas is often generated during gas extraction whereas heat can be generated by the incineration process in the reactor itself; electrically heated reactors can burn lean gas flows of approx. 0.18 vol. % and higher. Above this threshold, the combustion heat of the methane itself can be used to generate energy.

Usually, regenerative thermal oxidation (RTO) reactors are used to burn lean gases. These systems can be operated with up to 1.5 vol. % CH_4 because the explosion protection required for higher concentrations in the reactors would be technically too complex. RTOs control the lean gas flowing back and forth between two heat exchangers. The heat exchangers are heated by the combustion heat and preheat the incoming lean gas flow for combustion after the reversal. RTOs for industrial use are offered by various plant manufacturers and are in use worldwide with throughput capacities of over 1.2 million Nm^3/h.

The RTO reactors are relatively large because of their valve control system and double heat exchangers. An alternative is the thermal recuperative oxidation (TRO) process; here, the shaft gas flows through the combustion chamber and heat exchanger in a co-current flow. According to the manufacturer, TROs only require around ¼ of the space (and presumably the cost) of an RTO. However, TROs for lean methane gas combustion have only been available as laboratory and pilot plants so far.

Conclusion

The degassing of methane from abandoned hard coal mines provides a major challenge for climate change as methane is a highly effective greenhouse gas. Since the EU Methane Regulation (EU 2024/1787) came into force, the overarching goal is to control and minimise methane emissions. The controlled mine water rebound is one key factor that has the potential to dramatically influence the release of methane.

After mine closure, the mine water rebound may cause a continuous methane release as gas is pushed upwards to the surface; with continuously increasing mine water levels, however, the mine water floods successively the coal seams, i.e., the source of the methane. With each flooded seam the mine water seals the methane inside the coal seam as soon as the hydrostatic pressure exceeds the gas pressure. The process of flooding will diminish the degassing dramatically and finally methane emissions will stop completely.

An essential factor needed here is integrated monitoring which considers the hydrological and geochemical conditions and helps to understand and purposefully control the processes at work. The combination of mine water measurements, gas concentration and isotope analyses and geological data collection enable us to forecast dynamics of methane degassing and identify possible migration paths. It is in particular the signature of the gas that provide valuable information on the origin of the methane and possible extraction processes.

Furthermore, the active control of the mine water rebound provides the opportunity of targeted methane regulation. In conjunction with thermal or energy procedures, measures such as the use of gas extraction systems which are also suitable for low methane concentrations can ensure an effective reduction of methane.

Earlier technologies for methane reduction in coal mining were primarily used for safety reasons by keeping the methane concentration below the explosive range. Today, mine gas can be used to generate energy. Thermal oxidation processes such as RTO or TRO can be used to efficiently burn even lean methane gas.

To summarise: a mine water rebound does not only provide a natural barrier against methane emissions; it also offers technical methods of emission control. Optimising the mine water management and combining it with innovative monitoring and reduction technologies is a promising tool not only to meet the requirements of the EU Methane Regulation but to actively contribute to the fight against climate change.

References

Barker JF, Fritz P (1981) Carbon isotope fractionation during microbial methane oxidation. Nature 293: 289–291, doi: 10.1038/293289a0

Bernard B, Brooks JM, Sackett WM (1977) A geochemical model for characterization of hydrocarbon gas sources in marine sediments. Proc. Offshore Tech. Conf., 435–438

EEA (2024) EEA greenhouse gases – data viewer (European Environment Agency)

EC (2020) COM/2020/663 Communication from the Commission to the European Parliament, the Council, the European Economic and Social Committee and the Committee of the regions on an EU strategy to reduce methane emissions

EC (2021) Impact assessment report accompanying the proposal for a regulation of the European Parliament and of the Council on methane emissions reduction in the energy sector and amending Regulation (EU) 2019/942

EC (2024) Regulation (EU) 2024/1787 of the European Parliament and the Council of 13 June 2024 on the reduction of methane emissions in the energy sector and amending Regulation (EU) 2019/942

Fleming NA, Morais TA, Mayer KU, Ryan MC (2021) Spatiotemporal variability of fugitive gas migration emissions around a petroleum well. Atmospheric Pollut. Res., 12(6), doi: 10.1016/j.apr.2021.101094

Foreman J (2016) Engineered structures for sealing underground mines

Gaschnitz R (2001) Gasgenese und Gasspeicherung im flözführenden Oberkarbon des Ruhr-Beckens

Hatch MA, Kennedy MJ, Hamilton MW, Vincent RA (2018) Methane variability associated with natural and anthropogenic sources in an Australian context. Aust. J. Earth Sci., 65(5), 683–690, doi: 10.1080/08120099.2018.1471004

Hollenbeck D, Zulevic D, Chen Y (2021) Advanced leak detection and quantification of methane emissions using sUAS. Drones, 5(4), 117, doi: 10.3390/drones5040117

Humez P, Mayer B, Ing J, Nightingale M, Becker V, Kingston A, Akbilgic O, Taylor S (2016) Occurrence and origin of methane in groundwater in Alberta (Canada): Gas geochemical and isotopic approaches. – Sci. Total Environ. 541: 1253–1268

Kholod N, Evans M, Pilcher RC, Roshchanka V, Ruiz F, Coté M, Collings R (2020) Global methane emissions from coal mining to continue growing even with declining coal production. J. Clean. Prod. 256, doi: 10.1016/j.jclepro.2020.120489

Krause E, Pokryszka Z (2013) Investigations on methane emission from flooded workings of closed coal mines. J. Sustain. Min. 12(2): 40–45, doi: 10.7424/jsm130206

Mønster J, Kjeldsen P, Scheutz C (2019) Methodologies for measuring fugitive methane emissions from landfills – A review. Waste Management, 87, 835–859, doi: 10.1016/j.wasman.2018.12.047

Nambiar MK, Robe FR, Seguin AM, Endsin M, Aliabadi AA (2020) Diurnal and seasonal variation of area-fugitive methane advective flux from an open-pit mining facility in Northern Canada Using WRF. Atmosphere, 11(11), doi: 10.3390/atmos11111227

Shaw JT, Shah A, Yong H, Allen G (2021) Methods for quantifying methane emissions using unmanned aerial vehicles: A review. Philosophical Transactions of the Royal Society A: Mathematical, Physical and Engineering Sciences, 379(2210), doi: 10.1098/rsta.2020.0450

Stephan P, Kabelac S, Kind M, Mewes D, Schaber K, Wetzel T (2019) VDI-Wärmeatlas

Tissot BP & Welte DH (1984) Petroleum formation and occurrence

US EPA (2004a) Methane emissions from abandoned coal mines in the United States: Emission Inventory Methodology and 1990–2002 Emissions Estimates (US Environmental Protection Agency)

US EPA (2004b) Proposed methodology for estimating emission inventories from abandoned coal mines (US Environmental Protection Agency)

US EPA (2025) Non-CO_2 Greenhouse Gas Data Tool (US Environmental Protection Agency). Last accessed on 3/2/2025

Whiticar MJ, Faber E, Schoell M (1986) Biogenic methane formation in marine and freshwater environments: CO2 reduction vs. acetate fermentation-Isotope evidence. Geochim. Cosmochim. Acta 50: 693–709

Yale Carbon Containment Lab. (2022) Measuring Methane from Abandoned Wells and Mines. Carbon Containment Lab

Evaluating the Effectiveness of Various Aggregate Cleaning Methods

Neil Wolfe, Robert Hedin, Benjamin Hedin, Olivia Weaver

Hedin Environmental, 195 Castle Shannon Blvd, Pittsburgh, PA, 15228, USA, nwolfe@hedinenv.com

Abstract

Aggregate used in passive mine water treatment systems can become fouled over time with metal solids that decrease chemical reactivity and hydraulic retention. Replacement of fouled stone is expensive. We evaluated the effectiveness of various physical methods for cleaning aggregate in oxic limestone beds. All the methods involved tumbling the stone in mine water which removed Fe and Al solids. We measured the effects of cleaning on chemical and hydraulic characteristics of the beds. All the methods restored aggregate porosity, increased hydraulic retention time, and increased alkalinity generation. Thus, cleaning aggregate is an effective alternative to replacement of fouled stone.

Keywords: Passive treatment, limestone aggregate

Introduction

Aggregate is commonly used in passive mine water treatment systems. Calcareous aggregates, such as limestone (calcite) and dolomite, are used to neutralize acidity and generate alkalinity. Non-calcareous aggregates, such as granite and sandstone, are used to promote surface-dependent reactions (e.g. Mn removal). The fouling and plugging of aggregate is a problem in systems where metal removal occurs within the bed. One way to deal with this problem is to avoid creating or maintaining redox conditions that inhibit the formation of solids. Anoxic limestone drains and vertical flow ponds (also known as reducing and alkalinity producing systems (RAPS)) are such systems (Hedin *et al* 1994; Younger *et al* 2002). However, for mine waters that contain metals whose solubility is not redox dependant (e.g. Al), metal removal within the aggregate cannot be avoided. Design features such as flushing systems can remove a portion of the accumulated metal solids, but long-term treatment plans should consider management of the solids that cannot be flushed. One solution for the long-term maintenance of these systems to replace the aggregate. In these cases, valuable chemical or physical characteristic of the aggregate are masked by the solids and useful aggregate is disposed of. An alternative action is removal of the solids and renewal of the useful attributes of the aggregate.

This project studied methods being used to clean aggregate in passive mine water treatment systems in the eastern U.S. We cleaned aggregate in 10 oxic limestone beds contained in passive treatment systems. We evaluated how the various cleaning methods affected factors that influence impact treatment effectiveness such as porosity, hydraulic retention time, and chemical reactivity. We evaluated how the various methods handled solids cleaned from the aggregate. This paper provides a review of the general results of our project.

Methods

The effects of aggregate cleaning were evaluated by measuring chemical and physical parameters before and after a cleaning event. The treatment effectiveness of the beds was evaluated by collecting water samples from influent and effluent locations. Flow rates were measured by the timed-volume method. Conductivity, pH, and temperature were measured in the field with a calibrated combination pH/conductivity electrode and meter. Alkalinity was measured by titration to pH 4.5 with sulfuric acid. Raw and acidified (nitric acid) water samples were collected and submitted to a laboratory for analysis of acidity, Fe, Al, Mn, and sulfate by standard methods. The samples were not filtered, and results represent total concentrations.

The porosity of aggregate beds was determined by measuring the amount of water needed to fill a known volume of aggregate. A water level transducer was installed in an effluent water level control structure. The bed was drained and then allowed to refill by a known flow of mine water while the transducer measured the water level. Construction plans were used to calculate the volume of the aggregate at various elevations. Porosity was calculated:

Porosity, % = Volume (L) / flow (L/min) / time (min) x 100 (1)

where volume is the amount of aggregate filled, flow is the inflow rate of mine water in, time is the number of minutes needed to fill the aggregate, and 100 converts the result to a percentage. The transducer reported water levels on ten-minute intervals. Bed dimensions were determined for each water level, allowing calculation of porosity for sections of the beds.

Porosity measurements were not conducted on the full depth of aggregate at all sites. In order to standardize comparisons within and between sites, porosity measurements presented in this paper represent the top 45 cm of the aggregate beds (unless otherwise indicated).

The theoretical hydraulic retention of water flowing through a bed, THRT, was calculated from the bed volume, porosity, and flow rate.

THRT (h) = bed volume (L) × porosity (%) / flow (L/h) (2)

This value represents the retention time if water travels through the bed without any preferential or short-circuiting flow paths. The actual hydraulic retention time, HRT, was determined through a tracer addition. The flow rate of mine water through the bed was measured. A calibrated Na-fluorescein sensor (Cyclops-7 Logger) was placed in effluent of the bed and set to make measurements every ten minutes. Uranine, a Na-fluorescein dye, was added to the influent. The tracer addition was calculated from limestone volume and Na-fluorescein concentration in the injection dye with a target concentration of 10 ppb in the pore spaces of the limestone bed.

After at least twice the estimated THRT had elapsed, the detector was retrieved and data downloaded into a spreadsheet. Tracer masses were calculated for each interval from the concentration, flow rate, and elapsed time. The total recovery of tracer was determined by summing the individual masses. The amount of tracer recovered varied from the injection, presumably due to adsorption onto solids in the bed and/or overestimation due to scattering from turbidity (Naurath *et al.*, 2011). The individual mass measurements were divided by the total recovered tracer, converted to percentages, and summed. The hydraulic retention time was determined as the time for 50% of the tracer recovery.

The HRT for bed varies depending on the flow rate at the time of testing. While we had several cases where pre-clean and post-clean HRTs were measured under similar flows and direct comparison of HRTs was reasonable, most comparisons occurred under different flow rates. To standardize for this variation, we calculated an efficiency value by comparing the HRT to the THRT

HRT efficiency (%) = HRT / THRT (3)

Cleaning methods

Aggregate was cleaned by four methods as outlined below.

Dozer: A bulldozer pushes aggregate from the flooded bed onto a berm and then back into the bed. The aggregate's tumbling action removes solids which either settle to the bottom of the bed flow out into a settling pond by gravity or pumps. Support with an excavator may be necessary.

Mix and Rinse: And excavator mixes aggregate within the flooded bed. A sump is dug in the bed in which aggregate is mixed with the excavator and sprayed with a pump. Clean stone is placed aside and the process repeated until logistics require establishment of a new cleaning sump. Solids washed off the aggregate are carried out of the bed by gravity flow and pumps or settle in the sump and are periodically excavated and disposed of outside the bed or left in the bed.

Screening bucket: This method utilizes a specialized attachment that replaces the bucket on an excavator. There are two primary types of screening bucket: basket and drum. The basket type has a screen that rotates on an axis parallel to the boom of the excavator. It is similar in appearance and function to the basket in a vertical axis clothes washer. The drum type has a barrel-shaped screen like a trommel screen that rotates on an axis that is perpendicular to the boom of the machine.

Both types of screening buckets are loaded like a standard excavator bucket. The loaded bucket is held in a partially curled position and rotated to tumble the aggregate. Dipping the screen in water while it rotates washes solids from the aggregate. Basket screening buckets are unloaded like a standard bucket while drum screening buckets are unloaded by reversing the drum rotation.

Cleaning can take place within the aggregate, but a preferred method utilizes a dedicated container to serve as a wash basin such as a stone boat or roll of container. Clean water is pumped into the wash basin while solids laden water is simultaneously pumped out of the wash basin during the cleaning work. Coarse solids tend to accumulate in the wash basin and must be removed periodically by either excavation or by tipping the basin over. Solids are then disposed of outside the limestone bed in either a settling pond or by burial.

Trommel: A trommel is a cylindrical rotating screen that allows fines to fall through the screen while clean aggregate is discharged out the end of the cylinder. For this project a mobile trommel unit was modified so that aggregate would be sprayed with water as it tumbled through the screen. Solids washed off the aggregate were captured in a pan beneath the screen and pumped away. The trommel used in this project was powered by a farm tractor and fed by an excavator.

Results and Discussion

Table 1 shows the characteristics of 10 aggregate beds included in this project. The size of the beds and flow rates of mine water varied widely. Nine of the beds received low pH water containing Fe, Al and Mn. One of the beds received an alkaline influent containing Fe. All the beds were constructed with high-calcite limestone aggregate and operated as oxic systems where the formation of Fe, Al, and Mn solids was encouraged. Seven of the systems contained operational automated flushing devices that drained the beds empty once/week. The draining removes a portion of the metal solids which prolongs the effectiveness of the beds (Wolfe *et al.* 2010). However, after several years of operation the aggregate in the beds requires rehabilitation or replacement to maintain effectiveness.

We observed two types of solids that form within aggregate beds. Suspended solids accumulate within the aggregate pores that appear to be Fe and Al oxides and hydroxides. These solids can be partially removed by flushing and are readily removed by washing. Solids also form scales attached to aggregate particles. These Fe and Al solids are not removed by flushing but can be removed with washing. Fig. 1 shows stone fouled with Al and Fe solids before and after cleaning. Mn oxide solids also form as attached coatings, but they are not readily removed by washing (evidenced by black coatings remaining on stones after cleaning).

Table 2 shows changes in alkalinity generation and hydrologic characteristics of the beds before and after cleaning. Water chemistry assessments were made for all beds. A primary goal of the cleaning was to increase alkalinity generation. All the cleaned beds discharged more alkalinity than pre-cleaning. All the effluents from the cleaned beds had pH 6–8 and contained <1 mg/L Fe and Al (data not shown).

Measurements were made of porosity and hydraulic retention time at five sites. Fresh well-sorted aggregate typically has a porosity between 40% and 45%. The porosity of fouled aggregate was as low as 10–12%. Cleaning increased porosity, generally to values consistent with fresh aggregate. Fig. 2 shows porosity values measured at the Kentucky Hollow site where aggregate was cleaned by the screening bucket method and porosity was increased from 33% to 44%.

Hydraulic retention time was measured by tracer additions. Fig. 3 shows tracer test results for the Scootac Site-1 bed where cleaning by the mix/rinse method increased HRT from 10 hr to 17 hr. Cleaning increased

HRT at all sites. This change can be attributed to the increased void space (porosity) and the elimination of preferential flow paths. The increased retention time provides more times for limestone dissolution and increased alkalinity where its generation is limited by contact time. Cleaning did not eliminate hydraulic inefficiency (HRT/THRT). Many of the beds have design features that promote the creation of "dead spots" or preferential flow paths. Cleaning the aggregate will not correct these problems.

All the methods tested improved the treatment effectiveness of the systems. The methods vary in how they handle solids produced during cleaning. The dozer and mix/rinse methods clean the aggregate *in situ*. While a portion of the solids produced may be removed by piping/pumping turbid water to a settling pond, solids also settle and are retained in the bed. These solids decrease the bed volume and porosity, especially in the bottoms of the beds (Hedin Environmental, in review). Eventually the accumulation of these solids would be expected to impair the effectiveness of the system. The screening bucket and trommel methods collect solids in a box or pan and provide the opportunity to remove solids permanently from the bed. This practice likely allows more sustainable treatment by the system.

Conclusions

The treatment effectiveness of oxic limestone beds containing fouled aggregate was evaluated restored through cleaning of the aggregate. Four cleaning methods were tested and all were effective. Cleaning increased aggregate porosity, increased the hydraulic retention time of the mine water in the beds, and increased the generation of alkalinity from limestone dissolution. The main differences between the methods were that the dozer and mix/rinse methods uses standard construction equipment but the washed off solids were retained in the limestone bed compared to the screening bucket and trommel methods which required specialized equipment but removed the washed off solids from the limestone bed.

References

Hedin R, Watzlaf G, Nairn R (1994) Passive treatment of acid mine drainage with limestone. Journal of Environmental Quality 23:1338–1345

Hedin Environmental (in review) Oxic Limestone Bed Maintenance and Performance, Final report. Contract with the Western Pennsylvania Conservancy funded through the Pennsylvania Growing Greener Program

Naurath L, Weidner C, Rüde TR, Banning A (2011) A New Approach to Quantify Na-Fluorescein (Uranine) in Acid Mine Waters. Mine Water Environ 30:231–236, doi:10.1007/s10230-011-0138-4

Wolfe N, Hedin R, Weaver T (2010) Sustained treatment of AMD containing Al and Fe^{3+} with limestone aggregate. in, Wolkersdorker and Freund (Ed.) Proceedings of the 2010 Meeting of the International Mine Water Association, Nova Scotia, CA. pp 29–32

Younger PL, Banwart SA., Hedin R (2002) Mine Water: Hydrology, Pollution, Remediation, Kluwer Academic Publishers

Figure 1 *A) Aggregate fouled with AMD solids; B) aggregate after cleaning Both photos from the Kentucky Hollow oxic limestone bed.*

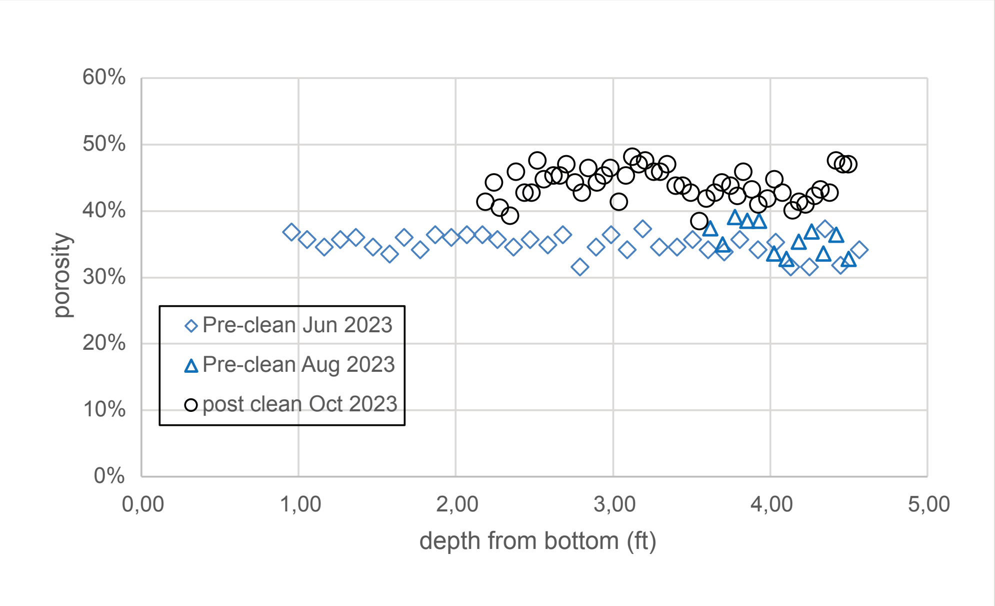

Figure 2 *Porosity measurements made at the Kentucky Hollow oxic limestone bed which was cleaned via the screening bucket method.*

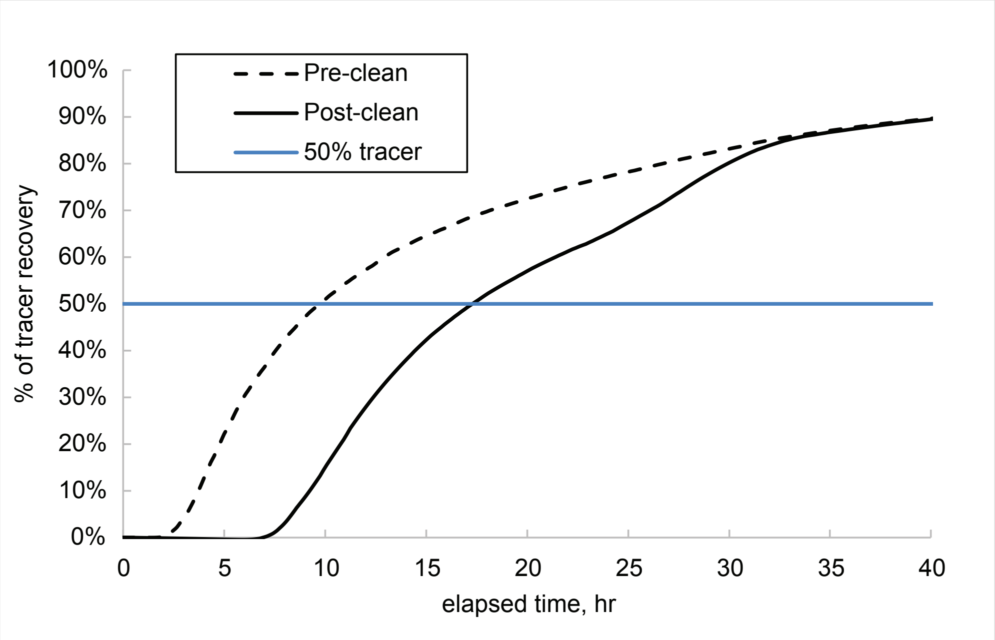

Figure 3 *Tracer recovery at the Scootac Site-1 site. HRT is determined at 50% tracer recovery. Both tests done at flow rate of 150 L/min.*

Table 1 Characteristics of sites included in the study. Flow and chemistry are average values.

	Bed size t	Installed a	flow L/min	pH s.u.	Acid mg/L	Fe mg/L	Al mg/L	Mn mg/L	SO4 mg/L	Cleaning method
KH-W	680	2019	128	3.5	85	0.9	7.8	0.9	397	SB[a]
Mud MR-4	635	2014	191	4.5	30	0.2	2.6	4.5	174	SB
Scootac	900	2010	219	4.0	85	0.2	10.2	23.1	880	mix/rinse
FB DLB1	3,000	2015	857	3.6	78	0.3	8.1	10.4	475	Dozer
Gib FLB-1	3,400	2018	184	3.5	39	1.2	3.2	2.7	139	trommel
Sterrett-S	1,600	2015	219	3.4	95	9.2	8.5	16.8	447	Dozer
Sterrett-N	1,600	2015	202	3.4	95	9.2	8.5	16.8	447	mix/rinse
Mor MR-8	360	2016	78	3.7	128	2.7	9.3	6.5	226	trommel
BT DLB-1	540	2005	23	2.6	520	196	6.3	4.6	597	SB
BTDLB-2	540	2005	28	7.6	-46	2.7	0.2	3.2	540	SB

[a]screening bucket

Table 2 Effects of aggregate cleaning on alkalinity generation and hydraulic characteristics.

	Effluent Alkalinity		Bed size	Porosity		Hydraulics – Pre				Hydraulics – post			
	Pre mg/L	Post mg/L	m³	Pre %	Post %	Flow L/min	HRT h	TRT h	HRT/THRT %	Flow L/min	HRT h	TRT h	HRT/THRT %
KH-W	110	162	375	33	44a	79	24	26	92	68	34	40	83
Mud MR-4	78	112	405	30	37	25	48	81	59	25	76	102	74
Scootac	122	190	601	10b	31b	151	10	7	146	151	15	21	75
Gib FLB-1	49	53	1,258	42	48a	93	95	94	101	178	68	57	119
FB DLB-1	0	79		32	22		10	8					
Sterrett-Sc	33	183	709		40					83	25	57	44
Sterrett-N	39	174											
Mor MR-8	28	70											
BT DLB-1	62	123											
BT DLB-2	82	105											

[a]5–45 cm depth; [b]0–30 cm depth; [c]Sterrett-S porosity and HRT measurements made 2 years after cleaning

Hydrodynamic Investigation of a Density-Stratified Underground Mine – Tracer Test Challenges and Results in the Georgi-Unterbau Mine, Tyrol, Austria

Christian Wolkersdorfer

South African Research Chair for Acid Mine Drainage Treatment, Tshwane University of Technology (TUT), Private Bag, X680, Pretoria, 0001, South Africa, christian@wolkersdorfer.info, ORCID 0000-0003-2035-1863

Abstract

Understanding hydrodynamics in stratified underground mines is critical for effective mine water management. In Tyrol's Georgi-Unterbau mine, density stratification in a subvertical shaft between levels 20 and 40 enabled the study of flow and tracer dispersion using four solid tracers and a fluorescent dye introduced at varying depths. An inclined rise connected to the shaft required adding table salt as a tracer, disrupting the delicate density layering with a 0.1–0.2 K difference. While flow paths and velocities were measured, the stratification breakdown caused by the injected brine highlighted the sensitivity of such systems. This study underscores the challenges of external interventions and provides insights for managing stratified mine water.

Keywords: Mine water tracer test, Tyrol/Austria, underground mine, density stratification, lessons learned

Introduction

Density-stratified underground mines typically discharge Mining Influenced Water (MIW) with better water quality than non-stratified mines. This is because cooler and fresher mine water is superimposed on warmer, mineralised mine water in the deeper parts of the mine. To understand the process causing this density stratification and the subsequent layering of mine water into cold fresh (CF) and warm mineralised (WM) water bodies, research in flooded underground mines is required (Mugova and Wolkersdorfer 2022). This research needs to investigate the hydrodynamics, chemistry, geochemical reactions and physico-chemical parameters in the MIW. Tracer tests in flooded mine pools are part of these investigations, as the velocity of the tracer or its flow path is an indication of the mine water hydrodynamics (Wolkersdorfer 2005). Understanding the processes that cause density stratification will allow mines or mine closure procedures to be designed to minimise the discharge of polluted MIW, as illustrated by the cases of the abandoned Metsämonttu, Finland and Urgeiriça, Portugal mines (Mugova and Wolkersdorfer 2022, 2024). In these mines, the highly mineralised mine water in the WM water body is overlaid by the better water quality of the CF layer, which ultimately discharges into the receiving water courses.

Initial measurements of temperature and electrical conductivity (EC) in the 100 m deep sub-vertical shaft ("Blindschacht") of the Austrian Georgi-Unterbau mine showed stable stratification at the three working levels connected to the shaft (Unger 2002; Wackwitz 2002). This was indicated by a temperature jump of 0.1 to 0.2 K of the 8.5–8.6 °C warm, circum neutral MIW and a more or less constant EC of 280 to 340 µS/cm (Wolkersdorfer et al. 2002). The persistence of this density stratification over a three-month period prompted an investigation of the stratification. This included measurements of temperature and EC, water chemistry and a multi-tracer test using microspheres, a fluorescent dye and a water-soluble salt. The injection locations of the various artificial tracers were determined during preliminary investigations of the 38,200 m³ mine pool, where six locations were identified for the injection of microspheres and uranine.

During the preparation of the multi-tracer test, a rise (possibly an ore chute) from level 20 to the level of the Georgi-Unterbau was discovered. This was overseen in the pre-investigation as it was not mapped in the digital map provided, but was later identified in supplement 30 of Krischker (1990). An additional tracer, sodium chloride (NaCl), was to be injected into this rise to determine its role in the density stratification. This additional tracer, which had not been considered during the planning phase of the survey, ultimately made part of the results difficult to interpret.

This paper describes the results of the August 2001 multi-tracer test in the Austrian Georgi-Unterbau mine and the implications of the incorrectly injected uranine and NaCl tracers. It will describe the characteristics of the used tracers and the local conditions encountered during the tracer tests.

Location and Investigation

The Georgi-Unterbau is an access adit to the Großkogl mine ("Bergbau Großkogl") in the Brixlegg mining district, which mined for fahlore (silver, copper) and barite within the Reither Kogel mountain range east of St. Gertraudi in the Austrian Inntal valley. It is 38 km ENE of Innsbruck and geologically dominated by the Devonian Schwazer Dolomit of the Oberalpin (Zentralostalpin) Grauwackenzone (Pirkl 1961; Schmidegg 1953; Schönlaub 1980). Mining in this Kogel complex dates back to the 19th century when the Georgi-Unterbau adit was started in 1887, and the sub-vertical shaft therein was sunk after 1900. After baryte mining until 1968 (Hanneberg and Schuster 1994; Mutschlechner 1984) the operations temporarily closed ("gefristet"). At the time of the author's investigations, the sub-vertical shaft had been flooded since at least 1990 (pers. comm. Peter Gstrein, 2001), meaning that the hydraulic system had been in equilibrium (stationary conditions) for at least a decade at the time of the tracer test. In 2021 the shaft was dewatered down to level 40 for research purposes (pers. comm. Armin Hanneberg, 2025). To reach the sub-vertical shaft ("Blindschacht"), a 320 m long adit had to be followed. The shaft itself is a 100 m deep two-compartment shaft connected to levels 20, 40, 70 and 100 of the mine (Fig. 1)

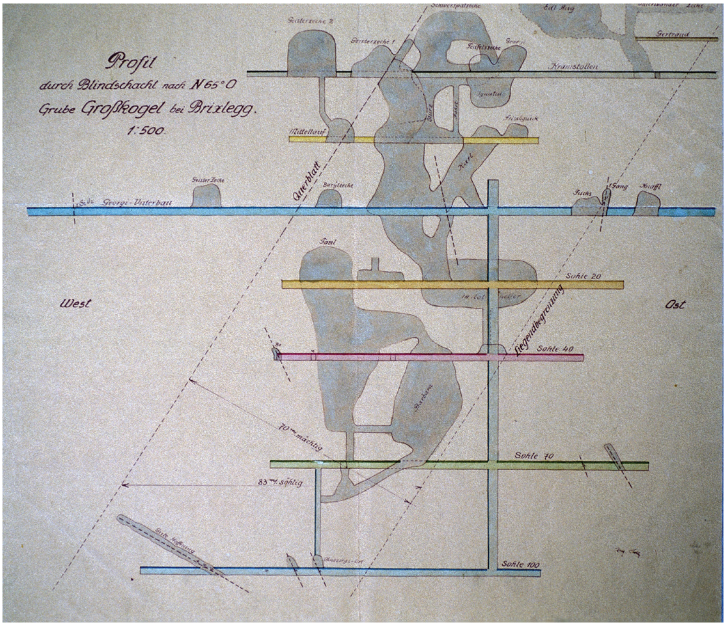

Figure 1 *Cross section of the Georgi-Unterbau and sub-vertical shaft (courtesy: Armin Hanneberg; from former Berghauptmannschaft Innsbruck, today Montanbehörde; IRIS register MB 30205).*

with a cross-sectional area of 6.23 m². Other hydraulic connections exist with the older workings of the "14 Nothelfer" and "Barbara" pits, an ore shoot and the "Large" and "Small" lakes (the latter resulting from the connection of the two aforementioned pits with the "Schwerspat" pit). Prior to the start of the tracer test, the temperature and EC within the shaft were measured using a 6-parameter borehole probe (DL1-512, Login Gommern GmbH, Gommern, Germany), and 12 mine water samples were taken within the shaft and its underground surroundings. These samples were analysed for major ions (unfiltered and unacidified samples) and trace elements (0.45 µm filtered and acidified samples). At all sites, temperature, pH, EC, redox and oxygen concentrations were measured in situ with an Ultrameter 6P (MyronL Company, Karlsbad, USA) and an OxiCal SL oxygen probe connected to a WTW Multiline P4 (WTW Weilheim, Germany).

Three different tracer classes were used to investigate the hydrodynamic and stratification conditions of the mine: a fluorescent dye (uranine, CAS 518-47-8), particle tracers (15 µm fluorescent microspheres, FluoSpheres, Triton Technology, San Diego, USA) and a water-soluble salt (sodium chloride, NaCl, CAS 7647-14-5; animal food grade: 98.3% NaCl, 1.2% SO_4, 0.47% Ca, 0.03% Mg). All of them are considered ecologically safe (Behrens et al. 2001). For the tracer test in August 2001, 900 g of uranine powder were filled into a LydiA injection probe (Wolkersdorfer et al. 1997), 4 times 20 mL of microspheres (yellow, orange, red, green, $1 \cdot 10^6$ per colour) into three LydiAs as well as the large lake and 200 kg of NaCl (dissolved in 600 L of mine water) directly into the rise. These tracers were injected on 5 August 2001 between 8:02 and 10:10 o'clock using the LydiAs (10, 30 and 85 m below surface for microspheres, 55 m below surface for uranine), green microspheres into the large lake and pouring the NaCl solution via Dirac injection (300 g/L, 68 minutes injection time to avoid immediate disturbance of the stratification) into their respective injection locations.

Microspheres were collected from the mine water using a specially designed filter set, uranine was measured photometrically (HACH DR/2500 Scanning Spectrophotometer, Loveland CO, USA) at a wavelength of 489 nm (experimentally determined), and NaCl was measured with an EC probe at a depth of 0.66 m below the shaft water surface (DL1-512, Login Gommern GmbH, Gommern, Germany). Additionally, measurements were taken down the shaft before and after the tracer test. Two Pleuger Worthington mini submersible pumps were used to extract the mine water from a depth of 10 cm in the sub-vertical shaft. The flow from the shaft to the dewatering gully was measured every ≈ 11 h with a calibrated V-notch weir, as were the pumping rates through the photometer and the microsphere filter sets (volumetric method, every ≈ 47 h).

Results

The flow rate of mine water leaving the shaft increased from 9.8 to 31.4 L/min (average 22.3 L/min, error range 7%) during the 16-day tracer test. The pump rate for the microsphere filters was 0.26 L/min and the photometer 0.04 L/min (error range 1–3%). This increased flow rate from the shaft was due to three intense rain events with a cumulative rainfall of 103.1 mm (meteorological station Rotholz, 5 km W of mine adit) during the tracer test (August 4, August 9 and August 16). The filtered water totalled 4.57 m³ and the water flowing through the photometer was 0.84 m³, compared to 511.41 m³ discharged from the shaft during the tracer test.

All three tracer classes were detected at the shaft outlet, but at substantially different concentrations and satisfaction. The LydiA filled with 900 g of uranine powder was only partially opened, resulting in average uranine concentrations between 50 and 100 µg/L at the shaft outlet (theoretically a concentration of 1.4 mg/L would have been expected). Measurement of the uranine concentration at 10 m intervals along the first 90 m of the shaft showed that the uranine is close to a Gaussian normal distribution around the injection point at 55 m, with a maximum concentration of 563 µg/L at the injection point (curve fitting showed that the distribution is closer to a Weibull distribution with $r^2 = 0.956$, but as the number of data points is small, the simpler Gaussian distribution with $r^2 = 0.946$ describes the data well enough; in both cases

$p < 0.0005$). This result corresponds to 109 to 114 g of uranine being released into the shaft (12% release rate). When the LydiA injection probe was lifted, the reason for the low uranine concentration at the photometer and in the shaft, and hence the very low recovery rate, became clear: the two halves of the probe were stuck together because the uranine had agglutinated as soon as the shaft water entered the partially opened LydiA probe. It took a chisel and hammer to remove the uranine block from the probe (≈ 870 g of uranine were recovered this way, but it was not possible to fully dry the block even after five months).

Despite this negative result, the uranine tracer distribution in the shaft allowed the calculation of a longitudinal dispersion coefficient D_L of 0.015 m^2/min and an effective velocity of 0.009 m/min (Tab. 1). These data give a Peclet number Pe ≈ 34, indicating advective flow of the tracer (diffusive flow was assumed in previous reports, but a recalculation updated this assumption). In the time between tracer injection and shaft measurement, approximately 220 m^3 of water flowed past the probe, which is about half of the outflow at the shaft. If this water would have come predominantly from below the level 40, the tracer would not have shown a Gauss distribution around the injection location, but an upward skewed distribution, indicating an upward flow. Yet, the tracer distribution is indicative of convective upward and downward flow of the MIW in the section of the tracer injection. This could be proven by a numerical model with ANSYS FLOWTRAN which showed low flow between levels 40 and 70 but upward advective flow above level 40 (Unger 2002).

Microspheres were injected at four locations: three in the shaft at 10, 30 and 85 m depth and into the large lake. Only microspheres from the large lake and 10 m depth could be identified during the tracer test. Considering the result of the uranine test, which calculated the time from 55 m depth to the discharge to be 100 h, it would have been expected that the microspheres from the 30 m injection point would also have been found. However, combined with the microspheres from 10 m depth, which arrived 10 days after injection, it may be that the sampling time was too short, and the tracers injected below 10 m depth were not detected. This also means that the tracers from the 85 level did not arrive during the sampling period. Similarly to the uranine tracer, the green microspheres from the large lake had a mean effective velocity of 0.017 m/min with a D_L of 0.016 m/min.

The results for the NaCl tracer were disappointing, as the increase in EC at the shaft outlet was not as high as expected. Assuming equal dilution of the salt in the 623 m^3 of shaft water, an increase in EC of 580 ± 30 µS/cm would have been expected. Yet, the EC increased by 71 ± 1 µS/cm, which relates to a flow based NaCl discharge of 3.9 ± 0.2 kg, representing a recovery rate of 1.9 ± 0.2%. Depth dependent measurements of EC, Na, Cl and Ca showed a statistically significant increase in these chemical parameters with depth. Electrical conductivity at 90 m increased from 410 to 449 µS/cm, Na from 0.7 to 15 mg/L, Cl from < 0.7 to 20 mg/L and Ca from 60 to 65 mg/L. This result indicates that the high density NaCl brine (ρ ≈ 1.18 g/L) sank to the deeper parts of the shaft and did not mix uniformly with the MIW therein.

Two measurements of on-site parameters in the shaft after tracer injection showed that the initial stratification which the project was designed to investigate had broken down. Instead of two layers before NaCl injection, there were three distinct water bodies with different average EC values of ≈ 360, 390 and 470 µS/cm. They were separated by levels 40 and 70, confirming the flow conditions previously identified and used in the numerical modelling.

During the tracer test in February 2002, the on-site and chemical parameters were analysed again. It was shown that the Cl concentration was still higher than before the NaCl injection, but substantially lower than immediately after the 2001 tracer test. Before the injection it averaged ± 1 mg/L, after the test 20 mg/L at a depth of 90 m and 5 mg/L at 55 m, all other sites had pre-injection concentrations. In 2002, five months after injection, all eight sampling points in the shaft and the three lakes were around 4 mg/L, showing (1) that the stratification had broken down and (2) that the accessible MIW appears to be well mixed and to be rising from deeper parts of the mine to the shaft surface.

Discussion and Conclusions

Based on preliminary measurements in the sub-vertical Georgi-Unterbau, a stable mine water stratification with a temperature difference of 0.1–0.2 K was observed. The aim of the 2001 tracer test was to investigate the reasons for this stratification and the hydrodynamics in this flooded Großkogl underground mine. The conceptual model before the tracer test assumed a stable stratification at level 40 with flow from the "Schwerspat" pit into the "14 Nothelfer" pit and from there via level 40 into the sub-vertical shaft. Below level 40, convective, possibly free flow driven by the geothermal gradient through the shaft and the Barbara pit was assumed (Fig. 1 has geometric details). To verify the conceptual model, a multi-tracer test was carried out in 2001 using uranine, microspheres and rock salt (NaCl).

It was shown that the conceptual model had to be adjusted and that the tracer test design had three weaknesses that rendered the tracer test partially unusable, which are described here:

1. The mass for the uranine tracer was not only too high, but the injection method was also inappropriate. Assuming a uniform dilution of uranine in the 623 m^3 of shaft water, the concentration would have been 1.4 mg/L, well above the visibility limit of 10 to 100 µg/L. A yellow to greenish plume would most likely have been visible for several kilometres in the receiving water courses of the Geyerbach and Inn rivers. Therefore, it was ultimately a favourable situation for tracer design weakness 2. to occur. Also the assumption that the tracer would spread into the whole mine pool and the uranine concentration being 23 µg/L was, under the given hydrodynamic circumstances, wrong.
2. The uranine was injected as a powder into the LydiA injection probe. Water was allowed to slowly seep into the probe at a depth of 55 m before the tracer was released. This probe was completely filled with the uranine and therefore the water seeping into the probe did not find enough pore volume to dissolve the tracer, causing the uranine to clump. This procedure contradicts most of the recommendations in tracer testing guidelines to dissolve the powder before injecting it into the water course (e.g. Benischke et al. 2007). Why this recommendation was not followed in the tracer test design could not be determined anymore at the time of the first evaluation and article in 2002 (Wolkersdorfer et al. 2002).
3. The application of an almost saturated NaCl solution with a density of 1.18 g/L directly into a slightly stratified system caused a rapid breakdown of the initial stratification. This resulted in a newly stratified system where the density of each new layer overprinted the initial conditions.

Although the 2001 tracer test failed in verifying the initial conceptual model, it was possible to use the results to interpret the hydraulics in the Georgi-Unterbau (Tab. 1). However, the conclusions – and they are not new *per se* – are that the tracer masses must be carefully selected based on the real situation, for example using the EHTD code (Field 2003). This code gave good results in all tracer tests subsequently carried out by the author. In addition, water-soluble tracers must always be dissolved before the tracer

***Table 1** Effective velocities of the MIW in the sub-vertical shaft of the Georgi-Unterbau based on various evaluation methods.*

Test Conditions	$\bar{v}$, m/min	v_{max}, m/min	D_L, m^2/min
Model set 1	0.008	0.017	–
Model set 3	0.029	0.058	–
Uranine 2001, 55 m	0.009	–	–
green Microspheres 2001, 20 m	0.017	0.024	0.016
Uranine 2002, 10 m	0.049	0.078	0.07
Average	0.022	0.044	–

test and mixed outside the test area to avoid contamination. Finally, when using saturated brine, it is essential that it does not sink into areas where it could become trapped or negatively affect the initial conditions of the mine. In the author's other tracer tests using saturated brine, the injection points were chosen so that the brine could flow into the mine workings without affecting the system or hydrodynamics too much.

Acknowledgements

The investigations described were carried out by Thomas Wackwitz and Kati Unger. Access to the underground mines was provided by Montanwerke Brixlegg (Robert Stibich) and accommodation as well as logistical support during the tracer tests by "Team 2000" (now: "Bergbau Aktiv Team"). Thanks to Armin Hanneberg for his continuous support and excellent historical information. Additional support was provided by Gerold Sturmmeier, Andrea Hasche, Andreas Hechenblaikner, Leopold Weber and Erwin Schinner. Part of the project was financed through the EU project PIRAMID (EVK1-CT-1999-00021).

References

Behrens H, Beims U, Dieter H, Dietze G, Eikmann T, Grummt T, Hanisch H, Henseling H, Käß W, Kerndorff H, Leibundgut C, Müller-Wegener U, Rönnefahrt I, Scharenberg B, Schleyer R, Schloz W, Tilkes F (2001) Toxicological and ecotoxicological assessment of water tracers. Hydrogeol J 9(3):321–325. https://doi.org/10.1007/s100400100126

Benischke R, Goldscheider N, Smart C (2007) Tracer techniques. In: Goldscheider N, Drew DP (eds) Methods in Karst Hydrogeology. Taylor & Francis, London, p 147–170. https://doi.org/10.1201/9781482266023

Field MS (2003) Tracer-Test Planning Using the Efficient Hydrologic Tracer-Test Design (EHTD) Program. vol EPA/600/R-03/034. U.S. Environmental Protection Agency – Office of Research and Development; National Center for Environmental Assessment, Washington

Hanneberg A, Schuster H (1994) Geschichte des Bergbaus in Schwaz und Brixlegg. Mineralien Magazin, Lapis 19(7-8):13–21

Krischker GA (1990) Die Baryt-Fahlerz-Lagerstätte St. Gertraudi/Brixlegg. Unveröff. Dipl.-Arb. Univ. Innsbruck, Innsbruck

Mugova E, Wolkersdorfer C (2022) Density Stratification and Double-Diffusive Convection in Mine Pools of Flooded Underground Mines – A Review. Water Res 214:118033. https://doi.org/10.1016/j.watres.2021.118033

Mugova E, Wolkersdorfer C (2024) Advancing sustainable mine water management through understanding stratification in flooded underground mines. Paper presented at the West Virginia Mine Drainage Task Force Symposium & 15th International Mine Water Association Congress, Morgantown, WV, USA:471–472.

Mutschlechner G (1984) Erzbergbau und Bergwesen im Berggericht Rattenberg. Eigenverlag Gemeinden Alpbach Brixlegg Rattenberg und Reith im Alpbachtal, Innsbruck

Pirkl H (1961) Geologie des Trias-Streifens und des Schwazer Dolomits südlich des Inn zwischen Schwaz und Wörgl (Tirol). Jb Geol B-A 104(1):1–150

Schmidegg O (1953) Die Erzlagerstätten am Reiter Kopf und am Reiter Kogel. Schlern-Schr 101:17–25

Schönlaub HP (1980) Die Grauwackenzone. In: Oberhauser R (ed) Der geologische Aufbau Österreichs. Springer, Wien, p 265–289. https://doi.org/10.1007/978-3-7091-3744-4_16

Uerpmann E-P (1980) Hydrogeologische Fragen bei der Endlagerung radioaktiver Abfälle. Unveröff. Diss. TU Clausthal, Clausthal-Zellerfeld

Unger K (2002) Hydrodynamische Verhältnisse im gefluteten Unterbau des Bergwerks Großkogel/Tirol – Numerische Modellierung mit ANSYS-FLOTRAN [Hydrodynamic conditions in the flooded substructure of the Großkogel mine/Tyrol – Numerical modelling with ANSYS-FLOTRAN]. Unveröff. Dipl.-Arb. TU Bergakademie Freiberg, Freiberg

Wackwitz T (2002) Multitracerversuch im gefluteten Blindschacht des Bergwerks Großkogel/Tirol: Vorbereitung, Durchführung und GIS unterstützte Auswertung [Multitracer test in the flooded subvertical shaft of the Großkogel mine/Tyrol: preparation, implementation and GIS-supported evaluation]. Unveröff. Dipl.-Arb. TU Bergakademie Freiberg, Freiberg

Wolkersdorfer C (2005) Tracer Tests as a Mean of Remediation Procedures in Mines. In: Merkel BJ, Hasche-Berger A (eds) Uranium in the Environment. Springer, Heidelberg, p 817–822. https://doi.org/10.1007/3-540-28367-6_84

Wolkersdorfer C (2006) Acid Mine Drainage Tracer Tests. ICARD 2006. vol 7. Proceedings 7th International Conference on Acid Rock Drainage (ICARD), St. Louis, p 2490–2501 [CD-ROM]. https://doi.org/10.21000/JASMR06022490

Wolkersdorfer C, Hasche A, Unger K, Wackwitz T (2002) Tracer Techniken im Bergbau – Georgi-Unterbau bei Brixlegg/Tirol. Wiss Mitt Inst Geol 19:37–43

Wolkersdorfer C, Trebušak I, Feldtner N (1997) Development of a Tracer Test in a flooded Uranium Mine using Lycopodium clavatum. In: Kranjc A (ed) Tracer Hydrology 97 – International Symposium of Underground Water Tracing. vol 7. Balkema, Rotterdam, p 377–385. https://doi.org/10.1201/9781003078142-62

Experimental Study on the Damage Mechanism of Coal Pillars in Abandoned Mines under Immersion Conditions

Xu, Zhimin[1,2]; Yuan, Huiqing[1]; Lu, Weining[1,3]; Han, Yuhang[1]; Xiong, Shijie[1]

[1]*China University of Mining and Technology, School of Resources and Geosciences, Xuzhou 221116, China.*

[2]*Fundamental Research Laboratory for Mine Water Hazards Prevention and Controlling Technology, Xuzhou 221116, China.*

[3]*China Railway Liuyuan Group Co., Ltd., Tianjin 300308, China.*

Abstract

Coal mining often leaves large abandoned spaces where acidic mine water accumulates, threatening the stability of boundary coal pillars. Rising water levels and corrosive mine water can severely weaken these pillars, risking water inrush disasters. Understanding the damage mechanisms is crucial for enhancing mine safety and preventing environmental hazards. This study assesses the long-term effects of immersion on coal pillar strength, with implications for mine safety and water management.

A new high-pressure mine water-rock coupling test device simulated immersion conditions under varying pressures and solutions. The study introduced the "damage coefficient" to quantify the reduction in compressive and tensile strength of coal pillars due to prolonged immersion. CT scanning provided insights into internal structural changes, such as crack expansion and mineral dissolution.

Results show that after 150 days of immersion in synthetic acidic solutions, the tensile strength of coal samples was most affected, with a damage coefficient of 0.775. CT scans revealed significant crack growth and dissolution of minerals like calcite and feldspar, further weakening the pillars. These findings highlight the substantial impact of prolonged immersion in corrosive solutions on coal pillar strength and stability.

The results are important for designing and evaluating water-proof coal pillars in abandoned mines, especially in reducing the risk of water inrush disasters. This work guides future efforts to protect both active and abandoned mines from water-related risks.

Keywords: Water-rock interaction, damage mechanism, damage coefficient, coal pillar stability, immersion test

Introduction

Abandoned mines can have a negative effect on regional groundwater systems and threaten adjacent operating mines with water inrush. Under high water flow pressure, the boundary coal pillars and waterproof walls between abandoned and operating mines suffer long-term damage from aggressive mine water(as shown in Fig. 1), severely affecting their mechanical stability and resistance to failure(Sun *et al.* 2020; Andrews *et al.* 2020). This leads to reduced water resistance of coal pillars and increased risk of water inrush accidents. Cases of water inrush from abandoned mines or old workings have shown that the water-coal (rock) interaction under high water flow pressure and the long-term influence of aggressive mine water can significantly weaken the mechanical properties of rocks. Under water-saturated conditions, the chemical dissolution and leaching of mineral components in coal (rock) intensify, intergranular bonding strength decreases, and stress corrosion accelerates the expansion of pores and growth of fractures. Although scholars have made achievements, research on the erosion and destruction of boundary coal rock pillars due to rising water levels in abandoned mine spaces, water flow conditions, and resulting water inrush disasters is relatively insufficient. The lack of quantitative studies has become the main reason for the frequent occurrence of such water-related accidents(Duan *et al.* 2012; Wu *et al.* 2022; Zhu *et al.* 2024). Existing research mostly focuses on theoretical analysis and numerical simulation, with insufficient study on the stability impact of actual coal rock bodies under long-term water immersion, especially in the damage evolution and deterioration mechanisms under aggressive water solutions(Chen *et al.* 2025).

This paper shows how we conducted simulated pressurized water immersion tests on coal and mine water samples from Mine A in the Xuzhou Mining District of the North China Carboniferous-Permian coalfield. Through laboratory analyses and theoretical analysis, we comprehensively analyzed the structural evolution and mechanical damage of coal samples under long-term water immersion and clarified the physicochemical mechanisms. This provides a theoretical basis and parameters for quantitatively evaluating water-induced "damage" to boundary waterproof coal pillars.

Sampling and Methods

Coal and mine water samples were collected from Mine A in the Xuzhou Mining District of the North China Carboniferous-Permian coalfield. A total of 350 kg of coal blocks were extracted from the main 9# coal seam. The samples were processed into standard cylindrical coal samples according to the ISRM standards(Ulusay 2015), with an end-face non-parallelism of less than 0.02 mm. Cylindrical coal samples with dimensions of Φ50×100 mm were used for uniaxial compression tests, and those with dimensions of Φ50 mm×25 mm were used for Brazilian splitting tests. A whole-rock analysis was conducted on the coal samples before soaking to determine their mineral composition. The main minerals in the initial coal samples were quartz (4.3%), albite (12.5%), muscovite (30.9%), kaolinite (24.5%), calcite (17%), gypsum (4.3%), and hematite (6.5%).

We sampled 350 L of water from the abandoned goaf area of Mine A, with the pH of the abandoned mine water measured at 5.8. To assess the erosive effects of acidic mine water, we prepared simulated mine water (pH = 3.0) and deionized water (pH = 7.0) as controls. Specimens were immersed for 150 days under two pressure conditions:

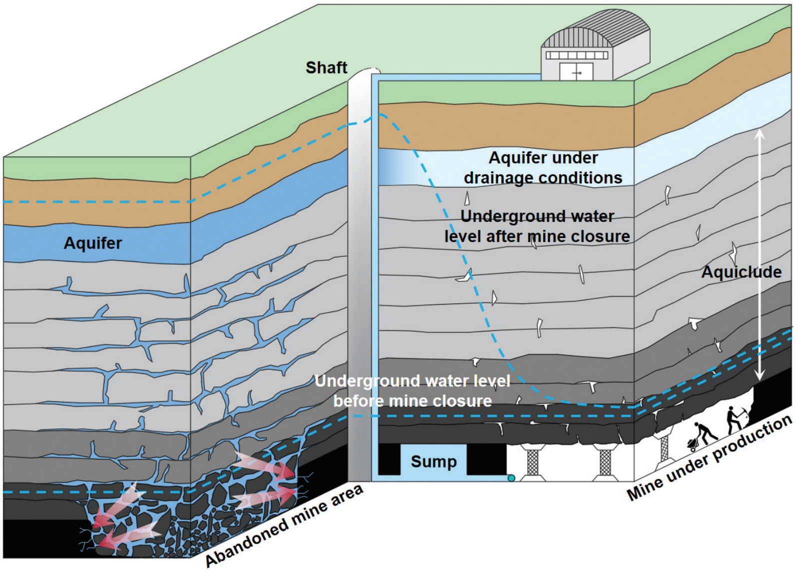

Figure 1 *Characteristics of groundwater level variation before and after mine closure.*

atmospheric pressure (0.1 MPa) and elevated pressure (0.8 MPa).

The experimental scheme, detailed in Table 1, included 74 groups. To assess the impact of water immersion on coal properties, we conducted uniaxial compression and Brazilian splitting tests on each group(Packulak *et al.* 2024). We analyzed the mineral composition of coal samples after different immersion durations and the changes in cations and anions in the soaking water.

Uniaxial compression and Brazilian splitting tests on coal samples were conducted using a high-pressure servo-compression system. In the uniaxial test, axial load was applied at 0.2 MPa/s until failure. In the Brazilian test, a linear load was applied at 0.05 MPa/s in the diameter direction until the sample fractured due to horizontal tension.

Before X-ray diffraction (XRD) analysis, coal samples were ashed and etched using a low-temperature plasma ashing instrument (LTA, Quorum K1050X) to oxidize organic matter. Mineral composition of the ashed samples was then analyzed using XRD (ThermoFisher ARL EQUINOX 3000). Jade 6.0 software was used for qualitative mineral identification, and the Rietveld method for quantitative analysis of mineral components. The pH of the soaking solution was measured using a pH30 meter.

Results and Discussion

CT scanning produced high-resolution 2D slice images of the coal samples in their original dry state and after 45 and 150 days of soaking in simulated mine water, as shown in Fig. 2. These slices were reconstructed into 3D models using VGSTUDIO MAX and AVIZO software, including detailed models of pores and fractures.

Fig. 3(a) shows that the number of pores and fractures in the coal samples increased over time, while the area, volume, and average size of individual pores and fractures initially increased and then decreased. In the acidic environment, the evolution of pore and fracture structure exhibited nonlinear characteristics, possibly due to substance dissolution and pore filling/reorganization. Compared with the initial samples, the porosity of the coal samples significantly increased from 0.25% to 1.2% after soaking in simulated mine water for 45 and 150 days. As the water-coal reaction continued, the pores inside the coal samples gradually transformed from fewer and larger to more and smaller. Although the porosity continued to increase, the rate of increase decreased with soaking time, indicating a slowdown in the water-coal reaction. The pores and fractures were categorized into 14 size ranges from less than 100 μm to greater than 5000 μm, with statistical parameters presented in Table 2. Overall, the coal samples were predominantly characterized by micro-pores with a diameter of less than 400 μm, accounting for over 95%, while the distribution of pores and fractures with a diameter greater than 3000 μm was minimal.

In the simulated mine water environment, as soaking time increased, porosity rose in initially low-porosity areas of the coal samples, while porosity in dense areas, especially the centers, changed little. Chemical reactions promoted new pore formation and expansion of existing small pores in loose areas, increasing porosity. This was seen as: (1) new pores and fractures

***Table 1** Table of preparation scheme of immersed coal sample.*

Immersion pressure MPa	Immersion solution pH	Immersion time of coal sample Day
	3 (Simulated mine water)	5
0		10
	5.8 (Abandoned mine water)	20
		45
0.8	7(Deionized water)	90
		150

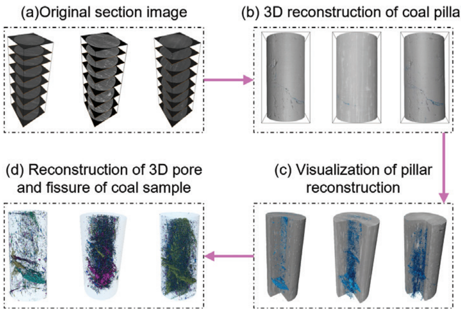

Figure 2 *Flowchart of 3D pore reconstruction using CT.*

forming, possibly due to mineral dissolution or organic matter decomposition; (2) irregular pore and fracture shapes, especially where acidic solution eroded unevenly; (3) more uneven pore distribution, with varying reaction involvement; (4) more complex pore and fracture structures, including more types; (5) increased specific surface area due to more pores and fractures, enhancing surface activity.

XRD results showed that the mineral composition of coal samples changed over time (Fig. 3b). From 0 to 150 days, the main minerals were quartz, albite, muscovite, kaolinite, calcite, gypsum, and hematite. In unsoaked samples, muscovite, kaolinite, and calcite were dominant, making up 72.4% of total content. As soaking time increased, their relative content dropped to 53.7%. After 150 days, albite, calcite, and hematite decreased from initial 12.5%, 17%, and 6.5% to 9.6%, 10.9%, and 4.9%, while quartz increased from 4.3% to 29.1%.

In the acidic solution, water-coal interaction was key to the initial increase in most mineral components. As soaking time increased, albite, calcite, and hematite content decreased, while quartz content rose. This was due to chemical reactions between these minerals and H+ ions in the solution, forming new substances and reducing their content. Quartz, being chemically stable, did not easily react with acid and generated additional SiO_2 during albite's reaction with H^+ ions, increasing its overall content.

Table 3 *Main mineral reaction equations during coal sample soaking.*

Mineral	Chemical equation
albite	$NaAlSi_3O_8 + 4H^+ = 3SiO_2 + 2H_2O + Al^{3+} + Na^+$
calcite	$CaCO_3 + 2H^+ = Ca^{2+} + H_2O + CO_2$
hematite	$Fe_2O_3 + 6H^+ = 2Fe^{3+} + 3H_2O$
kaolinite	$Al_4[Si_4O_{10}](OH)_4 + 4H_2O = Al_4[Si_4O_{10}](OH)_4 \cdot 4H_2O$

Clay minerals show more water absorption and swelling than other minerals when interacting with aqueous solutions(Ju *et al.* 2019). In this experiment, kaolinite exhibited significant water absorption and swelling, occurring more rapidly than new substance formation. This led to a notable impact of clay minerals in coal fractures early in soaking and increased their mineral content. The pH trends of the three soaking solutions from 0 to 150 days are shown in Fig. 3(c). pH values rose significantly initially as coal minerals reacted with H^+ ions, consuming them and causing the solution pH to increase rapidly. Over time, pH stabilized around 8.

Dry coal samples had a compressive strength of 27.21 MPa and tensile strength of 1.42 MPa. Mechanical properties decreased significantly with soaking time, especially in simulated mine water. After 150 days, compressive strength dropped by 69.9-72.9% and tensile strength by 70.4-77.5%. This shows that solution acidity, soaking time, and pressure all affect coal strength, with acidic water causing the most damage. Thus, we propose a "damage coefficient," defined as the ratio of the reduction in physical and mechanical parameters after soaking to dry state strength. As illustrated in Fig. 3(d) the growth rate of the damage

Table 2 *Distribution of pore fracture parameters in coal samples under different soaking duration.*

Diameter range µm	0d	45d Counts	150d
<400	106158	263718	500441
400–3000	5584	5380	20850
>3000	3	2	2

coefficient exhibits a progressive deceleration over time. The damage coefficient reaches its maximum in simulated mine water and minimum in deionized water, demonstrating significant environmental sensitivity. Pressurized soaking generally caused higher damage coefficients. As coal moisture neared saturation, the soaking effect transitioned to a water-coal coupling reaction stage. Aggressive solutions interacted physically and chemically with coal minerals, dissolving clay minerals and increasing porosity, leading to mechanical damage.

$$d = \frac{S_{dry} - S_i}{S_{dry}} \times 100\% \qquad (1)$$

Coal samples were soaked in three solutions for 5–150 days, with ion concentration trends shown in Fig. 3(e). Initially, most ions in abandoned mine water showed no significant change, likely due to coal adsorbing ions, indicating ion exchange capacity. In simulated mine water, high initial H^+ concentration caused frequent reactions between coal minerals and H+, rapidly increasing metal cation concentrations. Among the solutions, K^+, Na^+, Cl^-, and SO_4^{2-} concentrations initially decreased then increased, while Ca^{2+} and Mg^{2+} concentrations rose continuously. Coal samples, containing abundant albite and calcite, reacted with H^+, increasing Ca^{2+} and Na^+ concentrations. In deionized water, low initial H^+ concentration limited reactions, with Ca^{2+} and Na^+ increases mainly due to coal surface dissolution.

Water-induced damage to abandon mine coal pillars results from multiple factors. Aggressive water solutions with different pH values affect coal pores and fractures, directly influencing their development. Clay, feldspar, and carbonate minerals in coal react

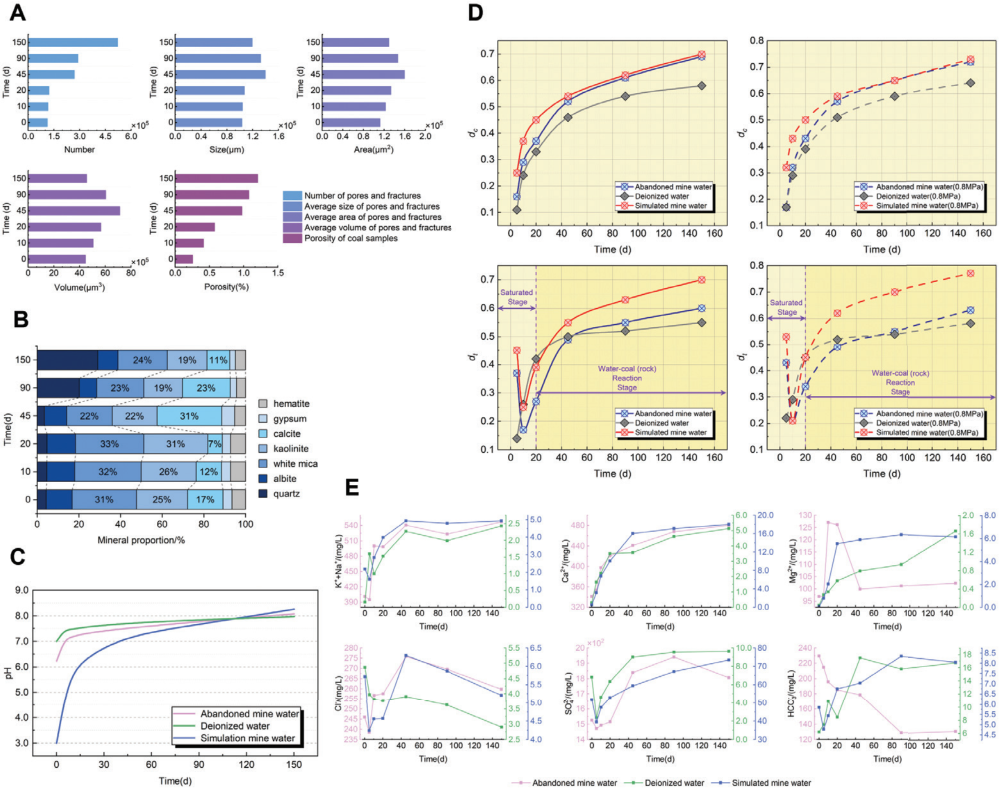

Figure 3 Soaking test results,(a) data of pore fracture parameters of coal sample un-der different soaking duration;(b) mineral composition ratios of coal samples at different soaking time;(c) pH value of soaking solution changed with different soaking time;(d) mechanical damage coefficient under different soaking conditions;(e) The ion concentrations in different soaking solutions change with different time, respectively.

differently in various pH solutions, causing coal edge dissolution, clay swelling, and particle migration, exacerbating fractures and weakening coal structure, leading to strength loss. In acidic environments, pronounced H^+ reactions with coal minerals generate CO_2, potentially causing coal dissolution and further damage.

Main Conclusions

Long-term soaking and XRD/CT scans showed that aggressive mine water caused significant internal pores and fractures in coal pillars from Mine A, increasing porosity from 0.25% to 1.2%. Pore development heterogeneity decreased over time. Coal samples' strength dropped significantly, with compressive strength falling 58−72.9% and tensile strength 54.9%–77.5% from 0 to 150 days. Soaking time, pressure, and solution pH affected the coal samples' strength, with soaking time being especially influential.

The study clarified the physicochemical mechanisms of structural evolution and damage in boundary coal pillars in abandoned goaf areas under high water flow pressure and long-term aggressive mine water influence. Pressurized water immersion has two key stages: initial water saturation, marked by physical water absorption and expansion, causing compressive strength to drop and tensile strength to initially decrease then increase; and water-coal coupling reaction, characterized by combined physical and chemical effects, where clay mineral dissolution and increased porosity lead to mechanical damage. As coal pillars transition from water saturation to water-coal reaction, water chemistry changes, with K^+, Na^+, Ca^{2+}, and SO_4^{2-} concentrations in the solution first decreasing then increasing, and pH becoming weakly alkaline.

The "damage coefficient" was defined as the ratio of the reduction in physical and mechanical parameters after soaking to the dry-state mechanical strength. Empirical values of the "damage coefficient" for water-soaked coal pillars were determined, providing a new quantitative indicator for the mechanical performance evaluation of coal rock pillars in abandoned mines or goaf areas.

Acknowledgments

The authors thank all co-organisers for hosting the IMWA 2025 Conference.

References

Andrews BJ, Cumberpatch ZA, Shipton ZK, Lord R (2020) Collapse processes in abandoned pillar and stall coal mines: Implications for shallow mine geothermal energy. Geothermics 88:101904. https://doi.org/10.1016/j.geothermics.2020.101904

Chen C, Wang W, Cao Y, *et al* (2025) Effect of hydro-chemical corrosion on mechanical properties of red sandstone under uniaxial and triaxial compression. Int J Rock Mech Min Sci 185:105967. https://doi.org/10.1016/j.ijrmms.2024.105967

Packulak TRM, Day JJ, McDonald MR, *et al* (2024) Measurement of true tensile strength from brazilian tensile strength laboratory tests. Can Geotech J cgj-2023–0204. https://doi.org/10.1139/cgj-2023−0204

Ulusay R (ed) (2015) The ISRM suggested methods for rock characterization, testing and monitoring: 2007–2014. Springer International Publishing, Cham

Wu K, Xiong Y, Tan X, *et al* (2022) Research Progress on Crystallization Kinetics of "Water-Rock" Reaction in Reservoir Pore System. Acta Sedimentologica Sinica 40(4): 996–1009. https://doi.org/10.14027/j.issn.1000–0550.2021.029

Sun Y, Chen G, Xu Z, *et al* (2020) Current Status and Research Progress of Water Environment and Mine Water Treatment and Utilization in Coal Mining Areas of China. Journal of China Coal Society, 45(1): 304–316. https://doi.org/10.13225/j.cnki.jccs.YG19.1654

Zhu C, Xie G, Wang L, *et al* (2024) Characteriza-tion of Coal Mass Fracture Evolution and Destruction State Based on CT Scanning. Journal of China University of Mining and Technology, 53(1): 93–105. https://doi.org/10.13247/j.cnki.jcumt.20230298

Duan H, Jiang Z, Zhu S, *et al* (2012) Mi-cro-mechanism of water stability and characteristics of strength softening of rock in deep mines Chinese. Journal of Ge-otechnical Engineering, 34(09):1636–1645.

Ju J, Li Q, Xu J, *et al* (2019) Water-CO_2 – rock interaction experiments to reveal the self-healing effect of fractured mining damaged rock. Journal of China Coal So-ciety, 44(12): 3700–3709. https://doi.org/10.13225/j.cnki.jccs.SH19.0447

Mine Water and Rock Engineering – A Winning Partnership in Cave Mining

Yungwirth, Grace[1], Nazaruk, Sofia[1], Redfern, Hannah[1], Booth, Thomas[1], Cammack, Jessica[1], Singh, Givarn[1], Buckwalter-Davis, Martha[1], Digges La Touche, Gareth[1], Sweetman, Ryan[1], Smith, James[2], Bewick, Robert[2]

[1]WSP UK Ltd, 70 Chancery Lane, WC2A 1AF, UK, Grace.Yyungwirth@wsp.com, Thomas.Booth@wsp.com, Redfern.Hannah@wsp.com, Sofia.Nazaruk@wsp.com, Jessica.Cammack@wsp.com, Givarn.Singh@wsp.com, Ryan.Sweetman@wsp.com, Martha.BuckwalterDavis@wsp.com, Gareth.DiggesLaTouche@wsp.com

[2]WSP Canada Inc. 6925 Century Avenue Mississauga, Ontario, L5N 7K2 Canada, James.Smith@wsp.com, Robert.Bewick@wsp.com

Abstract

Bulk mining methods such as cave mining allow the production rates necessary to provide the needed near term supply of critical minerals to support the energy transition. Mine planning studies benefit from integration of rock engineering and mine water considerations to optimise and increase project value and limit project risks. This paper outlines a procedure developed to integrate these aspects. Each step of the process is described along with a case study demonstrating the value of the approach. The developed workflow can be used as a checklist to guide future integrated mine water studies supporting the development of cave mines.

Keywords: Mine water, rock engineering, integrated studies, ESG, Cave Mining

Introduction

In the drive to secure the world's supply of critical minerals, mining projects are being developed in more complex locations and at greater depth. Bulk mining methods such as caving are becoming increasingly common to allow the production rates necessary to secure suitable project economics and to provide the urgently needed near term supply of critical minerals to support the energy transition. Should appropriate geotechnical conditions exist, cave mining methods can allow for high production rates following a period of large initial investment in the substantial infrastructure development required to support this mining method. Consideration of water is essential for the successful development of these types of mining operations, both to limit production risks, costs, and safety risk as well as to meet Environmental, Social, and Governance (ESG) requirements.

When undertaking water management studies and design at deep underground cave mines, it is fundamental to consider geotechnical conditions throughout every aspect of the mine water study. In this light, a workflow has been developed to support full integration of geotechnical considerations into mine water aspects of cave mining studies. The workflow supports all aspects of a typical mine water study from site investigation through to development of the Conceptual Site Model (CSM), integrated modelling, risk management, planning and thereafter engineering of the water management scheme.

Although the integration of geotechnical and hydrogeological field investigations is common practice in the mining industry to limit drilling costs, the key value of this study was the production of a tested workflow which allows geotechnical integration through every aspect of a cave mining focused mine water study, thereby limiting project risk.

The developed workflow in this paper is expected to be used as a checklist to guide future mine water studies supporting the development of cave mines. A case study is used as an example of the workflow, applied to advance the development of a cave mining study and demonstrating the effect and importance of geotechnical integration to the outcomes of the mine water study.

Approach

Rock mechanics and hydrogeology professionals worked together to produce a workflow procedure to integrate geotechnical and hydrogeological programmes, to optimise data collection efforts and to feedback outcomes into integrated engineering designs. The procedure was developed over the course of a Front End Loading (FEL) 3 (Batavia, 1999) cave mining study and included the following steps:

1. **Integrated Field Investigation Design:** Consideration of integrated geotechnical and hydrogeological field investigations with feedback to hydrology and geochemistry.
2. **Integrated Interpretation of Field Data:** Delineation of mine scale faults and fracture network considering both geotechnical and hydrogeology significant fracture sets.
3. **Geomechanical Model:** Appropriate geomechanical modelling should be undertaken to understand the development of caving conditions over time and their effect on surrounding strata. Potential development of a Discrete Fracture Network (DFN) model (with feedback to Step 1).
4. **Integrated development of the CSM and water management concept:** Consideration of geotechnical ground disturbance in the CSM and water management conceptual design (with feedback to Step 1).
5. **Mine Plan Optimisation:** Optimisation of the mine plan and engineering considering the above integrated CSM and conceptual design (with feedback to Step 4 and Step 1).
6. **Integrated Modelling:** Outcomes of the optimised mine planning should be considered in water balance and geochemical modelling. Consideration of development of the cave and stress/strain conditions in the surrounding strata within the hydrogeological model (with feedback to Step 4).
7. **Inrush Assessment:** Hydrogeological model and integrated water balance should be considered alongside the geomechanical model to predict the potential risk of catastrophic inrush to the mine workings.
8. **Water Management Plan:** Consideration of the above in the development of groundwater control options and detail of the site water management plan (with feedback to Steps 5 & 7).
9. **Detailed Engineering:** Progression to detailed engineering and monitoring plan.

This process is represented graphically as Fig. 1 with each step discussed further in the following sections.

1. Integrated Field Investigation Design

Integration of geotechnical and hydrogeological field investigations is common practice to limit drilling costs. However, it is critical that these investigations are planned together, with appropriate feedback from conceptual mine planning,

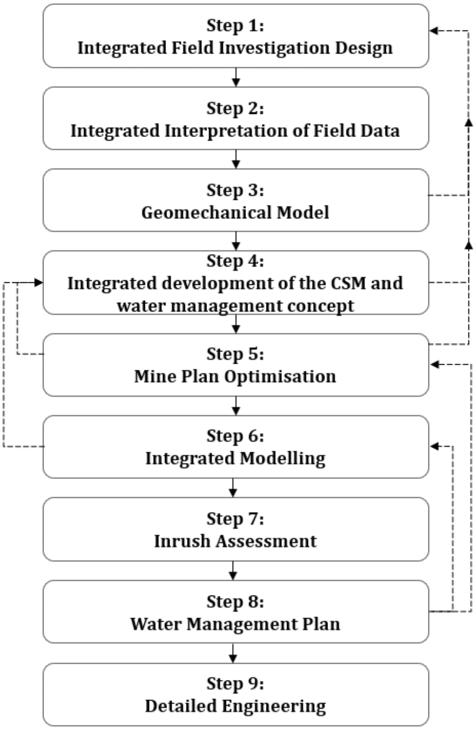

Figure 1 *Workflow Procedure with Feedback Loops.*

geomechanical modelling, and CSM development (Steps 3, 4 and 5 as above), and integration of hydrology and geochemistry studies. Not only can drillhole locations be optimised for combined data collection but they can be used for geological, geotechnical and hydrogeological logging, testing and instrumentation and water quality sample collection (for both geochemistry and hydrology considerations). Factors to be considered and planned for in design of these investigations include:

- Ground stability and suitability for various types of testing.
- Sampling and ability to investigate units and areas key to the mine plan and associated infrastructure.
- Positioning and suitability to install long term monitoring equipment (e.g. drill hole diameter and collar location).
- Need for high quality structural geology data collection aligned with hydrogeological parameter identification.
- Drilling and testing equipment limitations.
- Experience of local contractors in specialised testing and installations.

2. *Integrated Interpretation of Field Data*

Delineation of mine scale faults and fracture network considering both geotechnical and hydrogeology significant fracture sets (potentially DFN model).

High quality data collection of the mine scale faults and fracture networks is essential to cave mining studies. This information feeds into both geotechnical and hydrogeology analysis and understanding. The use of the information may be different since geotechnical analysis considers both open fractures and healed or infilled fractures as a critical part of the ground conditions predictions. Traditional hydrogeology analysis considers open or interconnected fractures as conduits to flow. However, as the cave propagates, disturbance of the blocks of rock is designed to cause a change in the stress/strain regime of the healed rock structures which may then become open or conduits to flow. The changes in the connectivity and openness of the caved area and surrounding rock affected by caving should be considered.

3. *Geomechanical Model*

Appropriate geomechanical modelling should be undertaken to understand the development of caving conditions over time and their effect on surrounding strata.

The extent and magnitude of ground disturbance expected from caving activities should be evaluated and fed into the development of the CSM and water management concept. One approach is to produce an integrated DFN model of the site considering these aspects however the suitability of this approach will be dependent on the site conditions and availability of suitable datasets.

Key outputs include:

- The footprint and magnitude of surface subsidence over time.
- The extent and magnitude of ground disturbance developed over time expected to cause a change in hydrogeological condition.

The calculation of these values can be site and materials specific.

4. *Integrated development of the CSM and water management concept*

Consideration of geotechnical ground disturbance in the CSM and water management conceptual design (with feedback to Step 1).

Consideration of geotechnical ground disturbance should generally focus on the following aspects relevant to groundwater and surface water management plans:

- At the surface via predictions of surface subsidence.
- Between hydrogeological units causing increased connection of the area to capture groundwater inflow.
- Causing increased infiltration rates from surface or other water bodies due to increased hydraulic connection.

The extent and magnitude of ground disturbance can affect:

- Positioning of surface infrastructure;
- Need for surface diversions around subsidence zones;
- Need for removal or decommissioning of potentially connected water storage facilities;

- Positioning of groundwater control infrastructure; and
- Potential effects on groundwater quality and discharge considerations.

Feed back to the ground investigation (Step 1) to allow the study to characterize:

- Areas relevant to surface infrastructure and surface water bodies;
- Targeted testing of structural features which may eventually be conduits to flow;
- Testing of units that may eventually be in hydraulic connection with other units which are currently disconnected; and
- Baseline water quality analysis and geochemical characterisation to approximate the predicted water quality and set discharge location and/or treatment requirements.

5. *Mine Plan Optimisation*

Optimisation of the mine plan and engineering considering the above integrated CSM and conceptual design.

The outcomes of the CSM and conceptual water management plan should be fed back and integrated with the mine planning works to:

- Optimise mine sequencing to achieve project goals such as minimising mine inflows during early time and staging water management infrastructure development to allow the mine to achieve ramp up production targets;
- Optimise mine infrastructure positioning to limit the potential need to relocate key mine infrastructure; and
- Appropriately consider water storage and discharge locations and treatment requirements.

6. *Integrated Modelling*

Outcomes of the optimised mine planning should be considered in water balance and geochemical modelling. Consideration of development of the cave and stress/strain conditions, which may be influenced by geochemical weathering, in the surrounding strata within the hydrogeological model (with feedback to Step 4).

Optimised mine planning should be integrated into the relevant water balance and geochemical water quality modelling so that all relevant aspects are considered.

If appropriate, the numerical hydrogeological model should aim to represent the relevant hydromechanical coupled effects induced by the cave mining when running predictive simulations. There are several methods to allow for this including consideration of a full integrated DFN model or by modifying the hydraulic parameters and recharge rates of equivalent porous media models according to the results provided by the geomechanical models. In particular, the model should represent the effects of the cave and strain zones, along with any surface subsidence over time if this information is available.

Predictive simulations should consider these changing conditions over time and their effect on potential inflows to the mine including the influence of hydraulic connections which may develop as the effect of cave related ground disturbance propagates. It is essential that modelling extends to cover the mine closure period as well as the extent of the propagation of geomechanical effects.

7. *Inrush Assessment*

Hydrogeological model and integrated water balance should be considered alongside the geomechanical model to predict the potential risk of catastrophic inrush to the mine workings.

The potential risks arising from the possibility of inrush or mud rush should be assessed as appropriate to be informed by the mine plan and predictive hydrogeology and water balance modelling. The assessment should include consideration of the potential magnitude and frequency of inrush events and associated safety and operational considerations.

The assessment shall consider:

- Any enhanced hydraulic connections between the mine workings and the ground surface associated with the cave and strain zone, and to the potential development of subsidence fractures or a subsidence zone at surface level; and
- The potential existence of additional preferential pathways for ingress of groundwater or surface water.

Outcomes of the assessment should feed into the project risk assessment and inform Water management and operational monitoring plans developed in Steps 8 & 9.

8. *Water Management Plan*

Consideration of the above steps in the development of groundwater control options, site water management plan and associated infrastructure.

Optioneering of water management solutions should consider the positioning of both groundwater and surface water management infrastructure in relation to the predicted ground disturbances. The hydrogeological model and water balance model ideally should be used to set performance specifications and assess options against other project requirements (e.g. the need for pre-dewatering of some mining areas) and will inform the inrush assessment (Step 7). The transient outputs of the model predictions are essential to develop this planning and mine plan optimization (feedback to Step 5) and should extend to consider mine closure.

9. *Detailed Engineering*

Progression to detailed engineering and monitoring plan.

Detailed engineering of water management infrastructure to consider the outcome of Step 8 including the progression of geomechanical ground disturbances from mining over time.

Detailed engineering should be advanced to consider the following integrated geomechanical and mine water considerations aligned with the requirements of the water management plan (developed in Step 8):

- Timing of decommissioning or lining of surface water bodies and storages;
- Design of surface water diversions and the mechanism for staged dewatering;
- Positioning and interaction of key infrastructure;
- Integrated design for closure and consideration of passive water management and passive treatment options;
- Consideration of the optimised mine plan, dewatering and mine safety infrastructure; and
- Controlling the quantity and quality of site discharges and the need for water treatment prior to discharge aligned with project requirements.

Monitoring plans should be developed and managed during operations and closure to consider timing and progression of the mine through the operations and closure period and associated ground disturbance. Typical monitoring considerations could include:

- Instrumentation and monitoring of surface water features and storages;
- Piezometric pressures in area of potential ground disturbances;
- Real time inflow monitoring within the mine at key locations and draw points noting that sudden changes in inflows can be an indication of inrush risk; and
- Changes in water quality and sediment loading which also can be an indication of changing geomechanical conditions; and
- Monitoring of changes in geomechanical conditions which also may provide early indications of changes to the groundwater or geochemistry regime.

Case Study

The above process was developed and tested while working on an integrated FEL 3 study of a deep cave mine by a collaborative team of geotechnical, rock mechanics, modellers, mine water professionals, and mine planners. The process was validated by this multidisciplinary team who were able to include the feedback opportunities indicated in the process to the benefit of the study. The following aspects were noted as being valuable to the project and study:

- A key aspect of development of the CSM was interaction of the cave with local water storages and the near surface weathered bedrock. Timing of this progression from the geomechanical model was essential to the assessment.
- This understanding directed field investigations and monitoring installation locations and positioning of key surface infrastructure.
- It also directed the requirement for pumping tests in the weathered bedrock zone to more accurately evaluate key parameters such as Storativity.
- This monitoring and the outputs formed a critical part of the hydrogeological mod-

elling input and allowed for an optimisation of the dewatering efforts by considering the option of pre-dewatering from the weathered bedrock zones which reduced pumping effort and also reduced the inrush risk.

- Mine planning options were also optimised to consider the advancement of development to allow staged implementation of the mine and associated dewatering infrastructure to achieve early time production targets limiting cost & schedule risks for the mine operator.

Study planning and timeline had to be updated to consider this integrated feedback and allow for associated updates to the field investigations, interpretation, mine planning and infrastructure design. This consideration should be built into the project schedule, which may be challenging given commercial pressure to meet cost-driven deadlines.

Conclusions

When undertaking water management studies and design at deep underground cave mines, it is fundamental to consider geotechnical conditions throughout every aspect of the mine water study, ideally with feedback to mine planning aspects. A tested workflow has been developed to support full integration of geotechnical considerations into mine water aspects of cave mining studies.

The procedure outlined in this paper has been shown to provide positive and integrated value in the development of the FEL3 cave mining study. The primary application is a proven approach to support the advancement of bulk mining methods underground with opportunity to optimise water management and mine planning aspects aligned with project focused business drivers, such as ESG aligned project metrics and limiting risks to production and schedule.

A case study has been presented as an example of the workflow, applied to advance the development of a cave mining study and demonstrating the effect and importance of geotechnical integration to the outcomes of the mine water and overarching FEL3 study.

Key success factors of the process were the close collaboration between project teams and the mine owner and the iterative feedback process through various phases of the study. Time allowance for this feedback should be built into the project schedule and/or considered as projects advance through study phasing. The developed workflow can be used as a checklist to guide future integrated mine water studies supporting the development of cave mines.

References

Batavia, R (1999). *Front-End Loading – A Path to a Successful Project.* – In: Proceedings of the 30th Annual Project Management Institute 1999 Seminars & Symposium. Philadelphia, Pennsylvania, USA: Available at: https://www.wcu.edu/pmi/1999/OG02.PDF (Accessed March 2025).

ESG & Mine Water Stewardship: A benchmarking approach to targeted investment and project decision making

Grace Yungwirth[1], Simone Bailey[2], Sean Capstick[2], Mattia Lanzani[1], Givarn Singh[1], Alex Russell[1], Pamela Phanouvong[1], Linda Mazzoni[2], Erin Jerome[2], Madeleine MacIsaac-Sun[2], Emily Cline[2]

[1] *WSP UK Ltd, Chancery Lane, NG12 5BL, UK, grace.yungwirth@wsp.com, mattia.lanzani@wsp.com, givarn.singh@wsp.com, alex.w.russell@wsp.com, pamela.phanouvong@wsp.com*

[2] *WSP Canada Ltd. 6925 Century Avenue Mississauga, Ontario, L5N 7K2 Canada, simone.bailey@wsp.com, sean.capstick@wsp.com, linda.mazzoni@wsp.com, erin.jerome@wsp.com, madeleine.macisaac.sun@wsp.com, emily.cline@wsp.com,*

Abstract

Mines and mining companies are challenged to translate corporate water stewardship goals to site-level investment plans that are defensible to stakeholders and realistic to what is practically achievable. A tested quantitative benchmarking methodology has been developed to allow mining companies to use benchmarking to support their planning and investment processes, reporting, and stakeholder engagement. It can be used to guide executives in setting company commitments and to provide the basis for project-level investment decisions. It can support building trust with project stakeholders when reporting on progress and setting future targets, satisfying ESG commitments, and focusing on practical solutions.

Keywords: Water stewardship, benchmarking, ESG, responsible mining, investment

Introduction

Mines and mining companies face two main challenges to translate broad corporate water stewardship goals to meaningful site-level investment plans to manage their water projects and, in turn, to link these site-level actions to wider water resource goals:

1. Firstly, the level of investment needed to bring mining projects to the desired level of maturity, depending on corporate commitments, is challenging given the cost pressures of changing commodity pricing, the requirements of the project and other priorities competing for investment.
2. Secondly, mining companies are challenged to present their position to their stakeholders in a transparent manner that justifies investment decisions and presents a realistic picture of where they are in terms of what is achievable.

Benchmarking can be considered to address these two challenges as a useful tool to both understand what is achievable versus level of investment and to build trust with stakeholders on the current state of maturity of the project portfolio. However, quantitative benchmarking of mine water use within the mining industry has been difficult to achieve given the varying ways this information is measured and reported as opposed to other industry where systems are highly monitored. Also, the number of factors affecting mine water benchmarking is substantial, and it is therefore not meaningful to compare all mines with one another as may happen when standard ESG frameworks are applied. An innovative methodology has been developed to undertake meaningful quantitative benchmarking making use of publicly available information and industry understanding which compares mines of technical similarity in terms of mine water metrics.

This paper focuses on the use of benchmarking data and the factors to consider in the interpretation of publicly available water data, along with the limitations of such a benchmarking exercise. The tested quantitative benchmarking methodology has been developed to allow mining companies to use benchmarking in a way that is meaningful to their planning and investment processes, reporting, and stakeholder engagement. Relevant examples are provided to demonstrate the value of and potential use of the benchmarking outcomes.

This tested approach can be used to guide project-level investment decisions to execute projects aligned with informed corporate commitments. Finally, the approach can be used to build trust with project stakeholders when reporting on progress, making future commitments, satisfying ESG requirements, and supporting understanding of what is practically achievable.

Approach

The project team worked together with several mining companies to produce a workflow that allows a mine site or a portfolio of sites to evaluate their current position on key water metrics against their peers with similar mines. Factors affecting water benchmarking can be categorized into two key areas: corporate water reporting metrics; and site- or portfolio-level water metrics.

This paper shall focus on the site-level water metrics and the associated quantitative benchmarking process and outcomes. A separate paper is in development on the corporate metrics related to water reporting and company maturity in this space noting that an integrated benchmarking effort incorporating both aspects can be of great value to many mining companies, particularly those committed to the Water Stewardship programmes as defined by the ICMM (2023a) water stewardship maturity framework.

The process developed to undertake the site- or portfolio-level quantitative benchmarking exercise is outlined as follows:

1. Identify appropriate quantitative water metrics for benchmarking;
2. Identify factors affecting water use metrics and site-level performance;
3. Develop benchmarking comparison metrics; and
4. Undertake the benchmarking study and outcomes:
   A. Data gathering and benchmarking library production;
   B. Data review and interpretation; and
   C. Development of site-level action plans.

Each of these steps is discussed further in the following sections.

Step 1: Identify Appropriate Quantitative Water Metrics for Benchmarking

Water metrics considered as part of this process include typical site water use metrics, primarily based on ICMM definitions (ICMM, 2023b). It is important that an understanding of the definition of these terms is used by the data collection teams so that quantitative outputs are comparable. Where possible these data were collected per site and can be compiled into portfolio-level metrics as needed.

Step 2: Identify Factors Affecting Water Use Metrics and Site Level Performance

Key performance factors when considering mine water metrics have been categorized as the following for consideration in a benchmarking study:

- Mine/site-type factors – related to the nature and design of the operation;
- Location-based factors – related to site environment and location; and
- Time-based factors.

These factors are often integrated and overlapping.

The water use metrics of mines vary based on the inherent nature of the mine (e.g. commodity, mine type, etc.) and whether the mine site is water positive or water negative. Factoring in the aspects of mine type and design that account for the greatest water use or loss is necessary to create a meaningful comparison.

Extensive experience of the project team's mine water practitioners in examining mine site water balances has led to the following general understanding of water use and losses on mine sites. The most common sources of water losses and operational water use on mine sites include:

- Losses to evaporation;
- Losses of water entrained in mine tailings and mine waste facilities; and
- Other water uses for processing activities and other machinery or domestic uses etc.

Comparison metrics that allow for evaluation of these factors must therefore be considered in the benchmarking exercise.

When considering location-based factors the site's environment can affect the integrated or catchment-based water balance affecting overall water metrics. Additionally, resource availability at the site location, often influenced by geopolitics, can also affect a mining operation's performance. Factors including the availability of and access to energy; capital; supporting resources such as chemicals or technology supply within the local supply chain; and access to skilled talent etc. are also aspects to factor in when considering the performance of mining operations. These aspects are considered location-based factors.

Time-based factors are also important to consider given the rate of change of climate predictions and also the ongoing development of new technologies.

A quantitative benchmarking assessment must aim to compare similar operations in relation to these key performance factors. Additionally, these factors will affect the type and number of opportunities for improvement and therefore the maximum performance metrics possible by an operation.

Step 3: Development of Benchmarking Comparison Metrics

To address the factors set out in Step 2, the benchmarking comparison metrics were developed and collected for individual operations. The development of benchmarking comparison metrics builds on experience from several projects and the work originally published in Yungwirth *et al.* (2023) as follows:

- Mining operation type – open-pit mine, underground mine, mineral processing facility, or a combination of these;
- Stage of operation and age – design, construction, operation or closure;
- Climate – arid, equatorial, warm, temperate, arctic;
- Climate projections;
- Project location – delineated by continent and country;
- Commodity and production – primary and secondary commodity produced and production method; and
- Type of tailings – conventional (slurry), thickened, filtered, mixed (if known).

Additionally, the following corporate factors were also considered related to the ownership of the sites as a mechanism to compare some of the factors identified in Step 2:

- Company size (by market capitalisation) and number of operations; and
- Maturity assessed through membership of ICMM or other relevant industry associations committed to responsible mining and water stewardship practices.

Changes in comparison metrics over time were noted where possible.

Step 4: Undertaking the Benchmarking Study and Outcomes

The benchmarking study was progressed through sub-steps A through C as described below.

A. Data Gathering and Benchmarking Library Development

Publicly available data from sustainability reporting was the primary source of information used to undertake the benchmarking exercise and form the basis of a benchmarking library. Data was also obtained from other published sources including government and other publicly available reporting frameworks such as South Africa's Department of Water and Sanitation (DWS) Water Conservation and Water Demand Management Guide (WCWDM) (2016), Minerals Council of Australia's Water Accounting Framework (WAF) (2022) and the Chilean Copper Commission's (COCHILCO) Best Practices and Efficient Use of Water in the Mining Industry Guide (2008). The aim was to collect a dataset that contained at least 10 years of data for each site (if possible) so that trends over time could be tracked.

The following factors were considered challenges and limitations of the benchmarking exercise:

- Water reporting methodologies differ in terminology and metric definition. Two of the primary reporting standards are ICMM and WAF, however others also exist. An understanding of water reporting metrics is required to interpret the reported results and to translate the metrics so that metrics of equal definition are being compared.
- Reporting formats vary and not all companies report based on ICMM or WAF requirements which may differ or may not require site-level detail.
- Some companies' data are self-reported and not externally verified which can cause some challenges when using it as a comparison point.
- In practice, data from public sources often do not contain an appropriate level of detail to allow site level comparisons. Technical understanding by the data gathering team interpreting this information and applying experience to estimate key parameters is essential to produce useful information for comparison.

B. Data Review and Interpretation

Information from the benchmarking library was presented in a graphical format allowing comparison of sites against other similar operations globally. The graphical format allows selection of comparison metrics relevant to the site or portfolio of sites to allow useful comparisons to be made. **The selection of appropriate comparison metrics and the context around this selection is a critical component of the interpretation.**

A temporal assessment of metric changes over time coupled with future predictions is also a useful aspect of the interpretation of the results.

The benchmarking assessment was then used to further prioritise the focus of the study within the selected portfolio. Comparison of priorities across the site or portfolio of sites aligned with material ESG and project considerations. Presentation of the results via a graphical output aided interaction with project stakeholders in setting priorities or criteria based on the benchmarking exercise. Some ways that water benchmarking can add value:

- To support informed setting of reasonable and actionable water savings targets aligned with corporate goals;
- To transparently understand and present the performance of a site or portfolio of sites against similar mines. This can be used to communicate both performance and technical realities to project stakeholders;
- To further investigate water savings options and understand maximum possible performance (based on current technologies); and
- To target investment in sites or projects that will add the largest value. Opportunities can be prioritised based on water savings versus cost or other relevant metrics (as described below).

C. Development of Site-Level Action Plans

Typical objectives of the benchmarking exercise are to plan future programmes, prioritise investment, and to understand target setting. It's therefore important to follow the benchmarking exercise with workshop-based opportunity development to produce a prioritised site level action plan. The action plan should set clear goals for each site or portfolio that are aligned with business and stakeholder needs. To promote transparency, it is important to document the evaluation and selection process to allow acceptance of the proposed solutions by the project stakeholders.

Building on the previous work (Yungwirth *et al.*, 2023) the following process was developed to support investment decisions and target setting:

1. Identification of priority sites/portfolio. Consideration of sites in water-stressed regions or those underperforming are typical criteria.
2. Interrogation of site water balance and water management plans alongside workshops with multi-disciplinary site stakeholders to identify opportunities.
3. Selection of a short list of potentially applicable opportunities for improvements using a ranking exercise. Appropriate

implementation of technology should be considered in the assessment. A list of water savings technologies typically applicable to mining and smelting sites can be found in Yungwirth *et al.* (2023).
4. Development of concept-level engineering (to support cost estimation) and estimates of timeline and potential water savings using predictive modelling.
5. Cost estimation (CAPEX, OPEX, and standardised Net Present Value (NPV)) and evaluation of results based on cost per water Megalitre (ML) saved, timeline, or other project requirements (see below).
6. Presentation of results through transparent engagement with relevant stakeholders.

Dependent on the site or portfolio, considering other material ESG concerns such as energy requirements (e.g. NetZero commitments) alongside potential water savings may be valuable.

Results of the study were presented in a graphical format which allowed evaluation of options individually or as a combination of portfolio metrics. The following were critical to the success of the evaluation and development of site-level action plans:

- Appropriate interpretation of the benchmarking exercise;
- Setting a common baseline year for comparison of water metrics;
- Understanding corporate level priorities;
- Understanding that solutions are inherently site-specific;
- Standardising cost estimation criteria and predictive modelling over a timeline of interest;
- Engagement with relevant stakeholders; and
- Transparent and graphical presentation of results.

It may be useful to consider the maximum possible metrics at some of the sites based on practical limitations of technology, mining method etc. so that the water use metrics are viewed in this context. However, this type of assessment requires significant site monitoring data and understanding to undertake successfully.

Case Studies

A selection of case studies is presented here to illustrate the value the benchmarking approach provided to several different mining companies.

Case Study 1: The benchmarking approach (and subsequent action plan) was used by the mining company to set realistic operational site-level actions which then were combined to set corporate targets. The benchmarking approach was also used to transparently present the company's position to stakeholders to justify investment decisions, mid-term operational targets and to feed into corporate reporting.

Case Study 2: Benchmarking was used to support the mining company's decision to focus on recycle-reuse efficiency at their sites as they were in the process of designing updated water treatment solutions which then could be optimised while achieving significant improvement in efficiency metrics aligning with their corporate goals.

This action plan was aided by implementation of the Mine Water Pinch process at site level (after Dama-Fakir *et al.*, 2024). The Mine Water Pinch process is a tool that can be applied to optimise water reuse/recycling by identifying water users where high quality water may not be needed and aligning these uses with existing lower quality water streams on the site, allowing direct reuse with limited or no treatment, limiting costs and energy use associated with water treatment and optimising water intakes.

Conclusions

Mines and mining companies face increasing challenges to translate broad corporate water stewardship goals to meaningful site level investment plans and practical targets. A quantitative benchmarking approach has been developed to assist companies in targeting investment to the most impactful projects amongst competing priorities for investment in their portfolio. Presentation of interpreted benchmarking results has also been shown to support transparent interaction with project stakeholders to justify both investment decisions and realistic targets.

This paper presents a methodology to undertake meaningful quantitative benchmarking making use of publicly available information and industry understanding which compares mines of technical similarity in terms of mine water metrics. Context and technical interpretation of the public data is essential to allow meaningful comparisons to be made between similar projects. The factors essential to these benchmarking comparisons have been presented.

The benchmarking approach outlined in this paper has been shown to transparently support the integration of corporate water stewardship targets with prioritised site-level action plans, proactively supporting investment decisions. The approach also supports the evaluation of opportunities to improve water metrics demonstrating that solutions are highly site-specific and must be evaluated on a per site basis.

Key success factors in the development of aligned site-level action plans were: appropriate interpretation of the quantitative benchmarking exercise; setting a common baseline; understanding corporate level priorities; understanding that solutions are inherently site-specific; standardising cost estimation criteria and predictive modelling over a timeline of interest; engagement with relevant stakeholders; and transparent and graphical presentation of the results.

This paper presents a tested and defensible methodology to produce and use water metric benchmarking to guide practical site-level action plans and investment decisions. The process has been demonstrated to be meaningful and defensible to the mine site- and portfolio-level planning and investment processes, reporting, and stakeholder engagement at mine sites aligning corporate ESG and water stewardship goals with practical site-level actions.

References

Chilean Copper Commission (COCHILCO) (2008). Best Practices and Efficient Use of Water in the Mining Industry. (English) I.S.B.N: 978-956-8242-10-7

Dama-Fakir, P.; Coleman, T.; Yungwirth, G.; Wille, P. (2024). Mine Water Pinch - increasing reuse/recycle efficiency while optimising water treatment on a mine sites. – In: Kleinmann, B., Skousen, J., Wolkersdorfer, Ch.: West Virginia Mine Drainage Task Force Symposium & 15th International Mine Water Association Congress. – p. 105 – 110; Morgantown, WV, USA (International Mine Water Association).

Department of Water and Sanitation (2016). Benchmarks For Water Conservation And Water Demand Management (WC/WDM) In The Mining Sector. Johannesburg, South Africa.

ICMM (2023a). *International Council on Mining and Metals, Mining with Principles – Water Stewardship Maturity Framework.* London United Kingdom: Self Published. Available at: https://www.icmm.com/en-gb/guidance/environmental-stewardship/2023/water-stewardship-maturity-framework (Accessed January 2025).

ICMM (2023b). *International Council on Mining and Metals, Water Reporting Good Practice Guide, 2nd Edition.* London United Kingdom: Self Published. Available at: https://www.icmm.com/website/publications/pdfs/environmental-stewardship/2021/guidance_water-reporting.pdf?cb=59625 (Accessed January 2025).

Minerals Council of Australia (2022). Minerals Industry Water Accounting Framework (WAF) User Guide Version 2.0. Sydney, Australia. Self Published. Available at: https://minerals.org.au/wp-content/uploads/2022/12/MCA-Water-Accounting-Framework-User-Guide-2.0-2022.pdf (Accessed January 2025).

Yungwirth, G., Coleman, T., Norwood, W. J., Dama-Fakir, P., Bruton, B., Ali, N., Singh, G. (2023). ESG & Mine Water: A Procedural Approach to Support Setting Water Savings Targets in the Mining Sector. – In: Stanley, P.; Wolkersdorfer, C.; Wolkersdorfer, K., Mugova, E.: IMWA 2023 – Y Dyfodol | The Future. – p. 564 – 569; Newport, Wales, UK (International Mine Water Association).

Post-Mining Water-Soil Interaction in Au-Mine Area: Piedmont Region (NW Italy) Case Studies

Linda Zaniboni[1], Giovanna Antonella Dino[1], Manuela Lasagna[1], Isabel Margarida Horta Ribeiro Antunes[2], Domenico Antonio De Luca[1]

[1]University of Turin, Department of Earth Sciences, 10125 Turin, Italy, linda.zanboni@unito.it, ORCID 0009-0009-0586-7563

[1]University of Turin, Department of Earth Sciences, 10125 Turin, Italy, giovanna.dino@unito.it, ORCID 0000-0002-1577-0337

[1]University of Turin, Department of Earth Sciences, 10125 Turin, Italy, manuela.lasagna@unito.it, ORCID 0000-0003-3464-2370

[1]University of Turin, Department of Earth Sciences, 10125 Turin, Italy, domenico.deluca@unito.it, ORCID 0000-0003-2718-4359

[2]University of Minho, Campus de Gualtar, Institute of Earth Sciences, 710-057 Braga, Portugal, imantunes@dct.uminho.pt, ORCID 0000-0003-3456-5926

Abstract

Mining activities can affect water quality long after the mines have closed. This study focuses on the current status of water in two abandoned gold mines - Crocette and Pestarena - in the Western Alps (Piedmont, Italy). Surface and groundwater samples were collected in three monitoring campaigns in 2024. The results showed arsenic contamination in 75% of the samples. Contamination by aluminium, iron, lead, manganese and nickel was also found in groundwater close to the tailings. These results highlight the long-term impact of abandoned mining activities and the need for continuous monitoring to assess environmental and human health risks.

Keywords: Abandoned Au-mines, PTE mobility, soil, water, Italy

Introduction

Mining activities can have a substantial effect on soil and water quality both surface (SW) and groundwater (GW). Environmental problems often persist long after operations have ceased, especially when processing plants are not properly managed and mining waste is not effectively disposed (Antunes *et al*. 2014; ISPRA 2023).

The most substantial effect of Au mines are related to acid mine drainage (AMD), which is generated by the erosion and leaching of mining waste and by water drainage from mining tunnels (Karaca *et al*. 2018). AMD in Au mines is caused by the oxidation of sulfide minerals (e.g. pyrite and arsenopyrite) and it promotes the mobility of potentially toxic elements (PTEs) in the environment. The most commonly occurring PTEs include arsenic (As), cadmium (Cd), copper (Cu), lead (Pb), nickel (Ni), manganese (Mn), iron (Fe) and zinc (Zn)(Hou *et al*. 2023). Added to this are the pollutants generated by Au mining process, such as mercury and cyanide (Ritcey 2005; Hou *et al*. 2023). These persistent pollutants pose a serious threat to ecosystems and human health due to their toxicity and their non-degradable nature (BRGM 2001).

These long-term environmental impacts need to be thoroughly assessed through effective monitoring. The aim of the study is to investigate the current status of soil, SW and GW affected by past Au mining activities in northern Italy, more than 60 years after closure. The obtained results will allow assessing the environmental and human health risk associated with the abandoned Au mines.

Study area

The Monte Rosa mining district (Piedmont, Western Italy) represents one of the most important Au mining districts in the Western Alps, with a history of exploitation since Roman times. This study focuses on two abandoned Au mines located in the municipalities of Crocette and Pestarena in the Anzasca Valley. The Valley is mainly drained by the Anza River; Pestarena is located on the left bank of the river, while Crocette is situated on the left bank of the Quarazza stream, a tributary of the Anza River (Fig. 1a).

Au mineralisation is hosted by the Monte Rosa Unit comprising a basement of paragneiss and micaschist intruded by orthogneiss (Dal Piaz 2001) (Fig. 1b). Veins mineralogy is dominated by quartz; carbonates are ubiquitous but always less abundant. Au is associated with sulfides, typically pyrite and arsenopyrite and subordinate galena, sphalerite, pyrrhotite, chalcopyrite (Stella 1943; Lattanzi *et al.* 1989). From a hydrogeological point of view, Pestarena and Crocette fall within the Crystalline Complex of the Alpine Chain; the metamorphic rocks of this complex are essentially impermeable or weakly permeable to fracturing (De Luca *et al.* 2020). The metamorphic rocks at the valley floor are covered by fluvial and debris flow deposits that host a phreatic aquifer connected to surface water bodies. GW circulation in the area occurs in fractured rocks, deposits and mining tunnels.

Mining in the Anzasca Valley began at the end of the 13th century with the exploitation of underground Au deposits. Over the centuries, Au production gradually increased, reaching a peak between 1938 and 1961, when about 5.4 tonnes of Au were mined. In the early years of this period the Au ore had a grade of 11 g/t, but there was a significant decline during the Second World War, culminating in the final closure of the mines in 1961 (Bruck 1985; Preite *et al.* 2007).

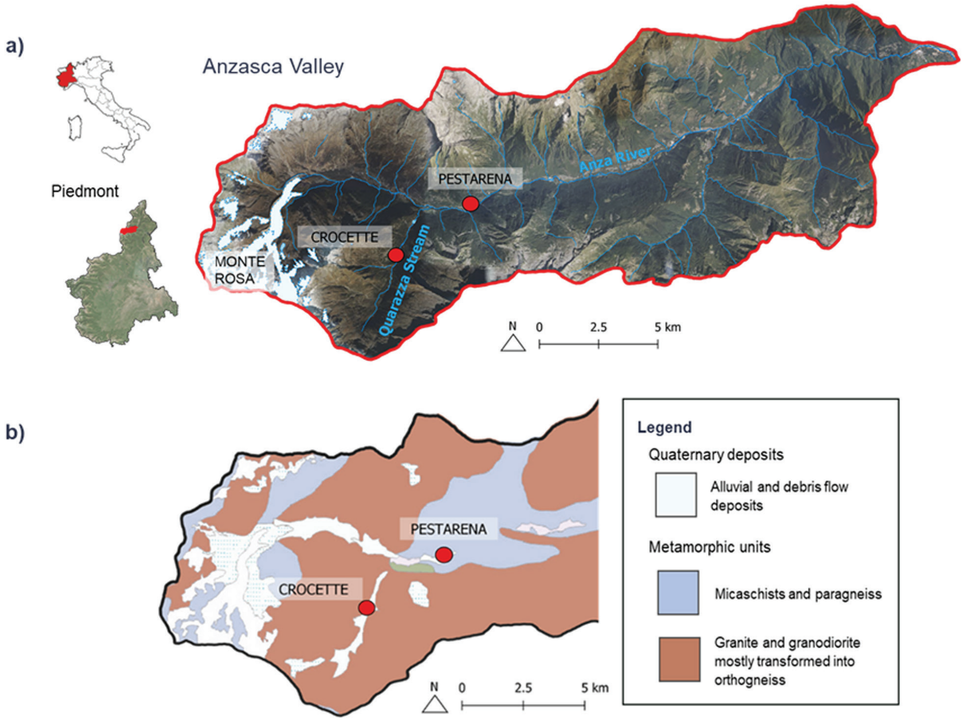

Figure 1 *Geographical, hydrographical (a) and geological (b) framework of the study area. Modified from Piana et al. 2017.*

Processing plants for the mined ore in the study area were located near the Pestarena and Crocette mines (Cerri and Fantoni 2017). Two main methods were used for Au extraction. Mercury amalgamation, a technique widely used since the Middle Ages, and cyanidation, which was introduced in the 1890s and became the dominant method until the mine's closure. The waste rock excavated and mined from the underground operations and the tailings from the processing of the ore were abandoned in the large area around the processing plants and deposited in waste dumps.

Previous studies

Previous studies (Bruno 2005; Nepote Valentin 2007; Rolando 2008) have shown that areas around mining processing plants have high levels of contamination due to the presence of abandoned processing waste (tailings), some of which is now covered by vegetation. The mine soil samples collected at Pestarena confirmed the presence of tailings with high concentrations of As, Hg, Pb and Sb, characterised by very acid pH values ranging between 4.0 and 6.85. Similarly, samples collected at Crocette showed high concentrations of arsenic and lead, with even more acidic pH values, ranging from 3.21 to 4.95 (Bruno 2005; Nepote Valentin 2007; Rolando 2008).

On a larger scale, soil samples collected in the Quarazza stream basin, where Crocette is located, and downstream along the Anza River near Pestarena, indicate arsenic concentrations higher than the threshold concentration set by Italian legislation (Legislative Decree 152/2006) for residential soils (20 mg/kg) (Caviglia *et al.* 2014; Allegretta *et al.* 2018). For these areas, the natural background value for soils was defined using the 95th percentile statistical method, resulting in a value of 414 mg/kg. This value is a fundamental reference point for distinguishing between natural geochemical enrichment and anthropogenic impacts. Many values founded in soils near the mining areas, were higher than the background of some order of magnitude. SW samples collected from the Quarazza Stream and the Anza River indicate that As concentrations in the most contaminated samples exceed the Italian threshold concentration for water (10 µg/L), reaching a maximum of 279 µg/L. The highest concentrations were found in areas close to mining activities. However, until now, no studies have evaluated the GW quality in these areas.

Materials and methods

In 2024, three monitoring campaigns were carried out in the areas of Pestarena (PE) and Crocette (CR) to analyse soil and water quality. The sampling, carried out in May (I), July (II) and September (III), was planned to study the temporal variability based on seasonal conditions and to ensure the accessibility of the sites, which is limited by the winter conditions of the alpine environment.

During the campaigns 19 SW samples and 13 GW samples were collected mainly at the same monitoring points during each campaign (Fig. 2). At Crocette, the GW sampling points were: the existing piezometer near the mining facilities and tailings dump (CR_1) and a spring (CR_2). The SW sampling points were: surface runoff (CR_4, CR_6); the Quarazza stream (CR_3 upstream of the mining facilities, CR_5 in correspondence, and CR_7 downstream); The lake that receives the waters of the Quarazza stream before the confluence with the Anza River (CR_8). At Pestarena, the GW sampling points were: three existing piezometers situated near the mining facilities, one upstream of the tailings dump (PE_1) and two downstream of the tailings dump (PE_2, PE_3); and a mine tunnel effluent (PE_4). The SW sampling points were: the Anza River (PE_5 upstream of the mining facilities, PE_6 in correspondence, and PE_7 downstream).

A total of 26 soil samples (Fig. 2) were collected during the second and third campaigns to assess the extent of potential contamination and its evolution over the years. Sampling points were selected in the area affected by mining activities, identified in previous studies and characterised by the presence of both dumps and scattered deposits of mining waste. Additional samples were taken up to 2.5 km upstream and downstream of the mining facilities.

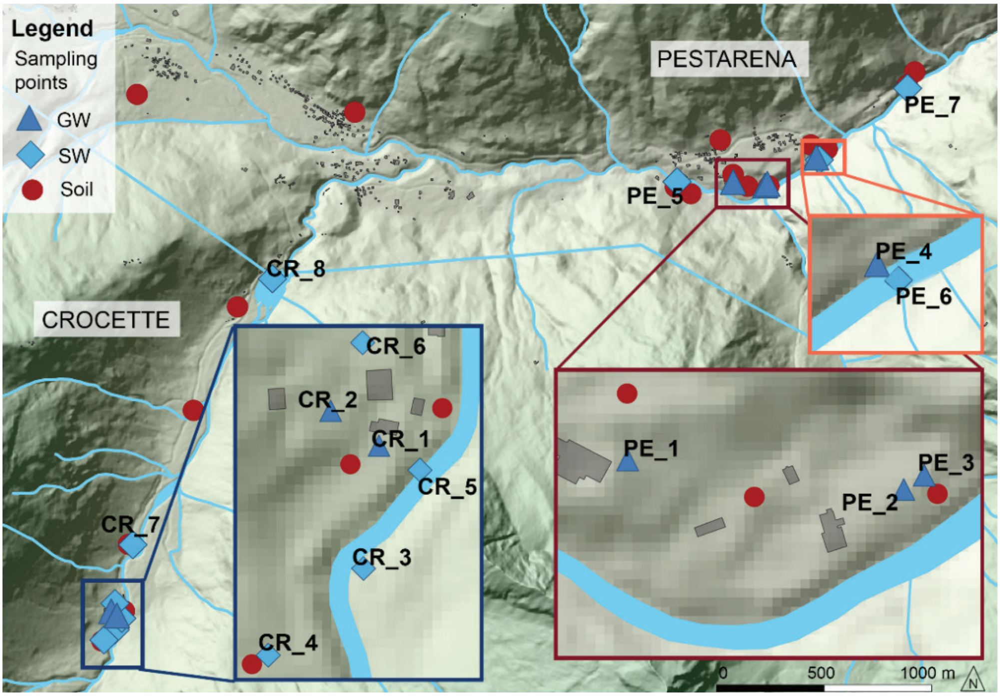

Figure 2 *Location of the sampling points of the three monitoring campaigns in 2024.*

The pH, total dissolved solids (TDS), electrical conductivity (EC) and temperature were measured in situ. Anions and cations were determined on non-acidified samples by ion chromatography. Metals and metalloids (Al, As, Cd, Co, Cr, Cu, Fe, Mn, Ni, Pb, Sb, Zn) were analysed by ICP-MS on filtered (membranes with 0.45 μm porosity) and acidified with HNO_3 samples. The analyses were performed at the Department of Earth Sciences, University of Turin. Analyses for mercury and cyanide concentrations in water, as well as concentrations of PTEs in soils, are currently underway.

Results and discussion

Most water samples show a low mineralisation (EC = 8–58 μS/cm), which is also supported by the TDS ranging from 5 to 45 mg/L; except for GW in Pestarena close to the tailings dump (PE_2, PE_3) with high values (EC = 484–1190 μS/cm and TDS = 245–596 mg/L). The pH is neutral or acidic in most of the samples ranging from 3.2 to 7.8, with more acidic values during May campaign in the GW samples (CR_1, PE_3, PE_4). The acidic waters were usually due to oxidation of sulfides from the mineralised veins and consequently from the tailings.

According to the Piper classification (Fig. 3), SW at Crocette is mainly of bicarbonate-calcium type while SW and GW at Pestarena is mainly of sulfate-calcium facies. The GW samples collected in piezometers downstream of the tailings (PE_2, PE_3) have a more pronounced tendency towards sulfates probably related to mining wastes. In fact, dissolved sulfate is remarkably persistent through mine water systems, and discharge waters commonly retain a strong dissolved sulfate signature (Craw *et al.* 2015).

The comparable composition of SW and GW suggests a relationship between these water bodies and also suggest that SW at Pestarena could be more influenced by the presence of highly mineralised and exploited areas than Crocette.

The analyses of metals and metalloids in the water samples are presented in Tab. 1. 75% of the water samples show arsenic contamination, with concentrations exceeding the limits set by Italian legislation (Legislative Decree 152/2006). Mining activities have increased the exposure of

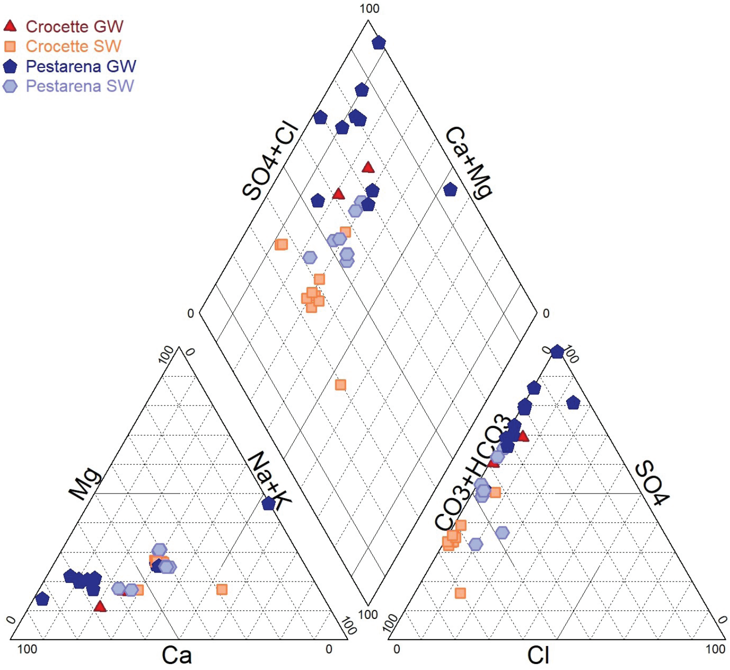

Figure 3 Piper diagram of the samples collected during the three campaigns in 2024.

arsenic-rich rocks, resulting in the presence of arsenic in the water. While the other metals remain at low concentrations in the SW, threshold values are exceeded in the Pestarena GW (PE_2, PE_3) downstream of the tailings, including aluminium (up to 7266 µg/L), iron (up to 1785 µg/L), lead (up to 25 µg/L), manganese (up to 276 µg/L) and nickel (up to 86 µg/L). These values highlight the impact on GW quality of abandoned mining activities and inadequate waste management.

Conclusions

This study highlights the long-term effects of two Au mines in the Alpine environment.

At Crocette and Pestarena, soil and water were found to be contaminated with arsenic more than 60 years after closure. The contamination of SW and GW with arsenic persists into the present day. Moreover, the presence of elevated arsenic and other metals concentrations in the Pestarena GW, along with acidic pH and high EC and TDS, underscores the persistent impact of mining waste.

This research provides insight into the environmental impacts of abandoned mining activities and highlights the need for continuous monitoring. Future studies will focus on assessing and mapping soil contamination and evaluating potential leaching into water bodies. By collecting this additional information, it will be possible to assess the ecological and human health risks associated with abandoned Au mining activities.

References

Allegretta I, Porfido C, Martin M, *et al* (2018) Characterization of As-polluted soils by laboratory X-ray-based techniques coupled with sequential extractions and electron microscopy: the case of Crocette gold mine in the Monte Rosa mining district (Italy). Environ Sci Pollut Res 25:25080–25090. https://doi.org/10.1007/s11356-018-2526-9

Antunes IMHR, Albuquerque MTD, Sanches FAN (2014) Spatial risk assessment related to abandoned mining activities: an environmental management tool. Environ Earth Sci 72:2631–2641. https://doi.org/10.1007/s12665-014-3170-4

BRGM (2001) Management of mining, quarrying and ore-processing waste in the European Union

Bruck R (1985) La miniera d'oro di Pestarena e gli altri giacimenti auriferi italiani. Comunità montana Valle Anzasca

Table 1 Concentration of metals and metalloids in water samples collected from sampling points during the three campaigns in 2004 (n: I-May; II-July; III-September).

Sampling point	n	Al µg/L	As µg/L	Cd µg/L	Co µg/L	Cr µg/L	Cu µg/L	Fe µg/L	Mn µg/L	Ni µg/L	Pb µg/L	Sb µg/L	Zn µg/L
Threshold		200	10	5	50	50	1000	200	50	20	10	5	3000
CR_1 GW	I	191.8	14.0	0.0	0.2	0.1	0.9	18.0	11.1	1.4	0.2	0.1	8.4
	III	215.9	10.6	0.0	0.1	0.2	15.3	49.4	6.3	1.2	2.0	0.1	27.5
CR_2 GW	I	54.4	51.6	0.0	0.1	0.1	0.5	9.1	7.7	0.2	0.0	0.6	2.5
CR_3 SW	I	32.9	5.6	0.0	0.0	0.0	0.5	4.6	0.5	0.1	0.0	0.0	0.8
	III	17.6	14.0	0.0	0.1	0.1	2.4	8.8	2.5	0.6	0.0	0.3	11.1
CR_4 SW	II	118.5	6.7	0.0	0.1	0.1	45.0	19.2	1.8	0.6	0.2	0.0	20.1
CR_5 SW	I	38.4	6.0	0.0	0.0	0.0	0.4	4.3	0.5	0.1	0.0	0.1	2.1
	II	24.1	13.8	0.0	0.1	0.1	2.9	42.6	4.0	1.1	0.1	0.4	23.7
	III	26.4	15.9	0.0	0.1	0.2	4.4	23.6	3.5	1.0	1.2	0.3	34.2
CR_6 SW	I	213.9	6.0	0.0	0.1	0.1	0.5	7.2	10.6	0.4	0.1	0.0	6.6
CR_7 SW	II	24.8	12.4	0.0	0.1	0.1	1.8	18.5	1.6	0.6	0.2	0.2	15.0
	III	25.6	12.9	0.0	0.3	0.1	3.4	13.7	2.5	1.1	0.7	0.2	38.5
CR_8 SW	II	31.7	16.3	0.0	0.2	0.3	3.5	23.6	15.3	1.4	0.1	0.3	25.8
	III	37.8	29.7	0.0	1.1	0.5	5.5	178.0	189.2	2.2	0.4	0.2	33.3
PE_1 GW	I	8.6	4.1	0.0	0.2	0.1	1.8	8.9	1.0	1.1	0.1	0.4	8.9
PE_2 GW	I	70.4	43.7	0.3	3.4	0.1	5.6	137.3	62.5	18.3	0.4	0.1	76.2
	II	2.8	45.6	0.0	1.2	0.0	2.0	270.5	15.1	15.7	0.0	0.1	14.3
	III	3.9	69.6	0.0	1.6	0.3	4.2	438.8	27.9	20.5	0.1	0.2	26.2
PE_3 GW	I	7265.4	11.9	1.5	13.5	1.8	78.7	1785.3	234.5	29.4	25.0	0.1	278.4
	II	94.5	20.3	0.4	11.3	1.2	8.8	310.8	151.1	61.3	0.5	0.5	235.9
	III	92.1	22.4	0.6	19.8	0.7	8.1	672.5	276.4	86.2	0.3	0.2	265.7
PE_4 GW	I	178.5	3.2	0.1	0.7	0.1	2.6	49.8	13.3	2.2	1.5	0.2	23.5
	II	98.0	44.1	0.0	0.6	0.1	2.0	163.2	19.6	2.9	0.6	0.2	12.1
	III	103.9	67.1	0.0	0.4	0.2	3.9	132.7	10.8	3.1	0.8	0.2	39.5
PE_5 SW	I	27.6	10.6	0.0	0.1	0.1	2.0	12.0	1.1	0.8	0.6	0.1	11.0
	II	14.7	4.4	0.0	0.4	0.1	2.2	24.4	12.5	3.6	0.1	0.1	9.5
	III	19.6	12.0	0.0	0.2	0.1	1.8	25.2	5.2	2.7	0.0	0.1	20.1
PE_6 SW	I	29.4	10.5	0.0	0.0	0.1	1.1	10.9	0.9	0.5	0.4	0.1	10.4
	II	37.7	21.2	0.0	0.4	0.1	1.9	57.6	12.3	3.9	0.8	0.1	13.6
	III	43.2	16.7	0.0	0.3	0.9	3.1	49.6	7.3	3.2	0.3	0.2	33.3
PE_7 SW	II	11.8	5.2	0.0	0.4	0.3	1.7	15.3	11.1	3.8	0.0	0.1	9.4
	III	25.0	18.5	0.0	0.3	0.2	2.5	34.4	6.6	3.0	0.1	0.2	14.0

Bruno C (2005) Comportamento geochimico e mineralogico dell'arsenico nell'area circostante le miniere aurifere della Valle Anzasca

Caviglia C, Destefanis E, Masciocco L, Re D (2014) Environmental Problems Related to the Presence of Arsenic in the Anza Valley (Piedmont, North-Western Italy)

Cerri R, Fantoni R (2017) L'oro del Monte Rosa. In: L'attività mineraria nelle Alpi. Il futuro di una storia millenaria. CAI Sezione di Varallo, Gorno (BG), pp 9–24

Craw D, Cavanagh J, Druzbicka J, *et al* (2015) A Geoenvironmental Model for Orogenic Gold Deposits to Predict Potential Environmental Effects. Mine Water Environ 34:388–403. https://doi.org/10.1007/s10230-015-0358-0

Dal Piaz G (2001) Geology of the Monte Rosa massif: Historical review and personal comments. Schweizerische Mineralogische und Petrographische Mitteilungen 81:275–303

De Luca DA, Lasagna M, Debernardi L (2020) Hydrogeology of the western Po plain (Piedmont, NW Italy). Journal of Maps 16:265–273. https://doi.org/10.1080/17445647.2020.1738280

Governo Italiano (2006) Decreto Legislativo 3 aprile 2006, n. 152 – Norme in materia ambientale. Gazzetta Ufficiale della Repubblica Italiana, n. 88, 14 aprile 2006

Hou Y, Zhao Y, Lu J, *et al* (2023) Environmental contamination and health risk assessment of potentially toxic trace metal elements in soils near gold mines – A global meta-analysis. Environmental Pollution 330:. https://doi.org/10.1016/j.envpol.2023.121803

ISPRA (2023) Siti di estrazione di minerali di prima categoria (miniere) | Indicatori ambientali. https://indicatoriambientali.isprambiente.it/it/georisorse/siti-di-estrazione-di-minerali-di-prima-categoria-miniere. Accessed 16 Oct 2024

Karaca O, Cameselle C, Reddy KR (2018) Mine tailing disposal sites: contamination problems, remedial options and phytocaps for sustainable remediation. Rev Environ Sci Biotechnol 17:205–228. https://doi.org/10.1007/s11157-017-9453-y

Lattanzi P, Curti E, Bastogi M (1989) Fluid inclusion studies on the gold deposits of the upper Anzasca Valley, northwestern Alps, Italy. Economic Geology 84:1382–1397. https://doi.org/10.2113/gsecongeo.84.5.1382

Nepote Valentin G (2007) Contaminazione da arsenico in un'area circostante una miniera d'oro (Pestarena, Valle Anzasca)

Piana F, Fioraso G, Irace A, *et al* (2017) Geology of Piemonte region (NW Italy, Alps–Apennines interference zone). Journal of Maps 13:395–405. https://doi.org/10.1080/17445647.2017.1316218

Preite D, Ciriotti M, Appiani R (2007) Pirrotite di Pestarena. Micro 2007:59–62

Ritcey GM (2005) Tailings management in gold plants. Hydrometallurgy 78:3–20. https://doi.org/10.1016/j.hydromet.2005.01.001

Rolando A (2008) Inquinanti inorganici intorno alla miniera d'oro di Pestarena (Valle Anzasca) e proposta di un intervento di bonifica

Stella A (1943) I giacimenti auriferi delle Alpi italiane. Memorie descrittive della carta geologica d'Italia, vol 27. Istituto Poligrafico dello Stato, Roma, 134 pp.

Key Drivers of Metal Removal in Constructed Wetlands Treating Acid Mine Drainage Revealed by Machine Learning

Jingkang Zhang[1,2], Xingjie Wang[2, 3], Liyuan Ma[1,2,3*], Jianwei Zhou[1,2]

[1]*School of Environmental Studies, China University of Geosciences, Wuhan 430074, China*
[2]*Institute of Geological Survey, China University of Geosciences, Wuhan 430074, Hubei, China*
[3]*School of Engineering, Cardiff University, Cardiff CF243AA, United Kingdom*

Abstract

Constructed wetlands (CWs) have been used for treating acid mine drainage (AMD), yet their metal removal mechanisms remain unclear. Herein, machine learning (ML) was employed to predict multi-metal removal efficiencies, with XGBoost achieving highest accuracy ($R^2 > 0.8$) for total Fe, Mn, Al, and Zn removal. Feature importance analysis identified operation days (1–185) and inflow chemical oxygen demand (COD, 6.5–1027.6 mg/L) as dominant predictors. Partial dependence plots revealed interactions between predictors. Inflow parameters contributed 57.6% to metal removal, surpassing time series and wetland properties. This study provides data-driven insights for optimizing CWs in AMD treatment.

Keywords: Acid mine drainage; Machine learning; Constructed wetland; Metal removal efficiency

Introduction

Acid mine drainage (AMD), generated from sulfide mineral oxidation, poses severe environmental risks due to high metal content and acidity (Younger *et al.*, 2002; Stumm and Morgan, 2013; Blowes *et al.*, 2005). Constructed wetlands (CWs) offer sustainable AMD treatment through metal precipitation and biological processes (Jouini *et al.*, 2020), yet their performance is affected by a variety of factors. Traditional statistical methods fail to capture these complex interactions inherent in such systems, while machine learning (ML) has shown promise in decoding multivariate systems (Palansooriya *et al.*, 2022). Various ML methods, such as Random Forest (RF), Extreme Gradient Boosting (XGBoost), k-Nearest Neighbors (kNN) and Neural Networks (NN), have been utilized to monitor and map contaminants in soil (Wu *et al.*, 2013) and groundwater (Lopez *et al.*, 2021). However, ML applications in CWs for AMD treatment remain limited. This study aims to bridge this gap by developing five ML models to predict multi-metal removal efficiencies (total Fe, Mn, Al, Zn). As the quality of the dataset brought into a model profoundly affects the validity of the model (Briscoe and Marin, 2020; Kim *et al.*, 2022), it was crucial to ensure the robustness of the initial datasets. Therefore, we devoted much effort to the construction of the dataset and feature engineering to obtain a practice-oriented dataset. This data-driven ML approach elucidated the complex interactions in constructed wetlands, providing a deeper understanding of how varying parameters affect the removal efficiency of metals in AMD treatment.

Materials and methods

Data from 31 published studies (from 2006 to 2023) were collected, focusing on CWs treating AMD. Key parameters included wetland properties (length, width, height, plant type), inflow/outflow parameters (pH, COD, metals concentration), and time series (operation days). Missing data were imputed using RF, Histogram Gradient Boosting Regression (HGBR) and Hot Deck imputation, with outliers removed via Kolmogorov-Smirnov tests.

The final dataset comprised 354 data points with 29 features and 7 target variables (total Fe, Mn, Al, Zn, Ni, Co, Cr removal efficiencies). To simplify the ML model and improve its performance, feature filtering was performed based on feature correlation and ML-based feature importance analysis (Palansooriya *et al.*, 2022). Hierarchical clustering grouped correlated features based on Pearson correlation coefficients (PCC). Further, feature importance analysis was conducted with ML-based model to determine the significance of each feature in predicting the target variable (Zhu *et al.*, 2019). By integrating results from feature importance and correlation analysis, the most important feature within a cluster was selected as input features.

RF (Zhao *et al.*, 2023), XGBoost, Support Vector Regression (SVR) (Palansooriya *et al.*, 2022), kNN (Yin *et al.*, 2024) and Artificial Neural Network (ANN), were selected for this study and built based on Python 3.9.7. StandardScaler in Scikit-Learn (version 1.4.1.post1) was used to standardize the input features. Following data standardization, 80% of data were randomly extracted from each input dataset and used for model training, while the remaining 20% were used for testing (Yin *et al.*, 2024; Zhang *et al.*, 2023). The method of grid search with cross-validation (5-fold) was employed during the initial training process to conduct hyperparameter tunning, aiming to enhance model performance and mitigate the risk of overfitting (Yan *et al.*, 2021; Bergstra and Bengio, 2012; Zhu *et al.*, 2023). The coefficient of determination (R^2) and root-mean-square error (RMSE) were utilized to compare the prediction accuracy and quantify the prediction performance (Hu *et al.*, 2022). Feature importance was assessed using SHapley Additive exPlanations (SHAP). Partial dependence plots (PDPs) were utilized to visualize the interaction effects between key predictors (e.g., inflow COD and operation days) on metal removal efficiency. Fig. 1 shows the framework and detailed steps for this study.

Results and discussion

Across the initial dataset, missing data were identified for 19 variables. Subsequent the complete dataset (Dataset A) is obtained by missing data filling based on RF, HGBR and Hot Deck imputation methods. Following the completion of dataset filling, an extensive feature analysis ensued, which included PCC, hierarchical clustering (Fig. 2a) and model-based feature importance analysis (Fig. 2b). **Inflow COD** was discovered to be the most important feature for predicting metal removal efficiencies. To refine the dataset and enhance model generalization while reducing computational complexity, a feature filtering process which involved integrating the outcomes of hierarchical clustering with feature importance assessments was conducted. Following this procedure, six representative features were selected from Dataset A to form Dataset B. Despite the apparent optimality of dataset B from an ML perspective, it is crucial to acknowledge that the selection of input features based solely on their correlation and importance may not consistently adhere to domain expertise and real-world necessities. Therefore, through the

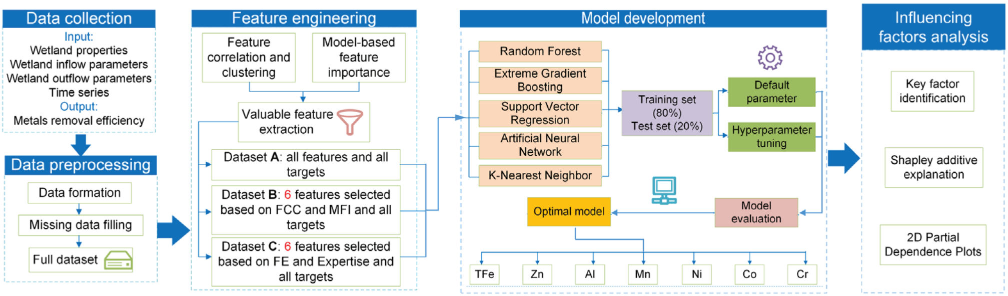

***Figure 1** The flowchart provides a detailed overview of the strategy employed for predicting the efficiencies of metals removal in AMD treated by constructed wetlands using a machine learning framework. Note: FCC: feature correlation and clustering; MFI: model-based feature importance; FE: feature engineering; TFe: total Fe.*

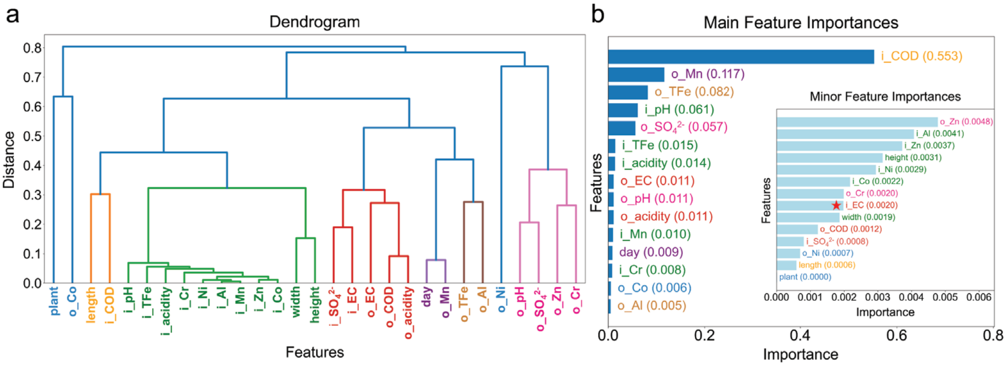

Figure 2 *Input feature analysis: (a) hierarchical clustering and (b) feature importance from the XGBoost model. Note: the prefix "i_" represents inflow parameters, while the prefix "o_" represents outflow parameters.*

integration of particle experiment conditions and feature analysis results, Dataset C was built. Three datasets were defined:

Dataset A: All features and targets (full dataset).

Dataset B: Six most important features (inflow COD, inflow pH, outflow EC, outflow Mn, outflow TFe, outflow SO_4^{2-}).

Dataset C: Six practical features (inflow COD, inflow pH, inflow acidity, inflow EC, wetland height, operation days), selected based on monitoring feasibility and domain expertise, alongside the assessment of feature importance and correlation.

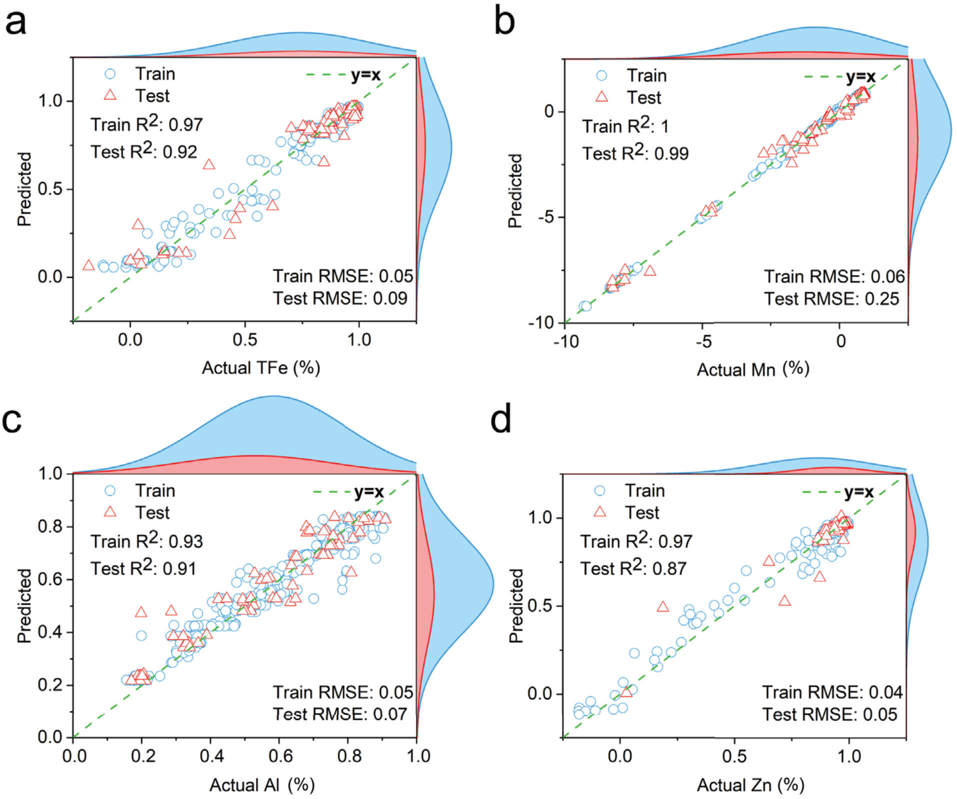

Figure 3 *The predictive performance demonstration of the optimal model XGBoost for (a) TFe removal efficiency, (b) Mn removal efficiency, (c) Al removal efficiency, and (d) Zn removal efficiency based on dataset C, evaluated using R2 and RMSE as assessment metrics. RMSE = root-mean-square error.*

In assessing the fundamental predictive performance of different models, Dataset A, encompassing all inputs from the full dataset was utilized. This strategy aimed to mitigate the potential reduction in predictive accuracy resulting from the exclusion of valuable features by Datasets B and C.

Five ML models (RF, XGBoost, SVR, kNN, ANN) were evaluated for predicting metal removal efficiencies (Fe, Mn, Al, Zn). XGBoost achieved the highest accuracy ($R^2 > 0.8$) across all datasets. Dataset A, with comprehensive features, yielded the best predictions, while datasets B and C showed slight declines due to feature selection. XGBoost demonstrated robust performance on the test set, particularly for TFe and Mn removal (Fig 3).

In accordance with previously published research, both Fe and Mn were identified as two key metals requiring particular attention in the treatment of AMD using constructed wetlands (Chen *et al.*, 2023; Singh and Chakraborty, 2020). During the process of Fe conversion to hydroxides, the transformation of aluminum often accompanies (Singh and Chakraborty, 2020). Additionally, research indicated that aluminum played a significant role in plant growth and can mitigate the toxicity of metals such as Fe, Mn and H^+ in acidic soils (Nguegang *et al.*, 2022). Furthermore, it was found that the concentration of Zn significantly exceeds the standard limits. Therefore, this study focuses on predicting the removal efficiency and analyzing the influential factors of TFe, Mn, Al and Zn. This aligns with the emphasis on key pollutant metals in relevant published studies (Singh and Chakraborty, 2020).

To quantitatively decipher the factors influencing the prediction of metal removal efficiencies, we employed the SHAP analysis on optimal model to reflect the importance of these factors (Fig. 4a, b). The comparison of feature importance rankings between the two analysis methods reveals discrepancies, but inflow COD and operation days were both considered to be the key factors. PDPs revealed nonlinear relationships between predictors and metal removal efficiency (Fig 5). For example, Fe removal efficiency peaked at low COD (<300 mg/L) and declined after 80 days of operation. Mn removal efficiency was highly sensitive to COD, with negative removal observed at high COD (>800 mg/L). These findings highlight the importance of optimizing COD levels and operational duration for effective metal removal.

Conclusions

In this study, we utilized ML to predict and analyze multi-metal removal efficiencies in constructed wetlands treating AMD. The main findings are summarized as follows:

- Five ML models were developed, with the **XGBoost** model emerging as the most effective, achieving high predictive accuracy ($R^2 > 0.8$) for the removal efficiency of total iron, manganese, aluminum and zinc.

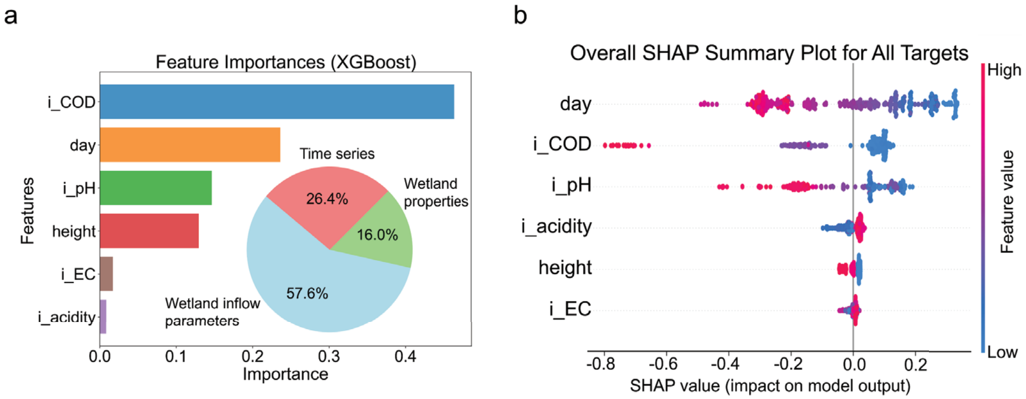

Figure 4 *Influential factors analysis based on dataset C and the optimal XGBoost model: (a) feature importance assessment based on XGBoost model and (b) Shapley additive explanation method.*

- Detailed feature analysis using the XGBoost model identified **operation days** (1–185) and **inflow COD** (6.523–1027.631 mg/L) as significant predictors of metal removal efficiency. These factors were found to have a substantial impact on the effectiveness of the wetland treatment process.
- The empirical categories for metal removal efficiency, ranked by importance, were wetland inflow parameters in first place, followed by time series, and wetland properties in last place. Inflow parameters were quantified to exert the highest influence on metal removal efficiency at 57.6%.
- Partial dependence plots elucidated the non-linear relationships between key predictors and metal removal efficiencies. This analysis revealed that specific ranges of operation days and COD levels are critical for optimizing the removal processes, providing actionable insights for the monitoring and management of constructed wetlands.

The findings offer a foundation for further research and practical applications aimed at enhancing the performance of constructed wetlands in treating acid mine drainage.

References

Bergstra J, Bengio Y (2012) Random Search for Hyper-Parameter Optimization. J Mach Learn Res 13:281–305

Blowes D, Ptacek C, Jambor J, Weisener CJEG (2005) The geochemistry of acid mine. 9:149

Briscoe J, Marin O (2020) Looking at neurodevelopment through a big data lens. Science 369 (6510). doi:10.1126/science.aaz8627

Chen D, Wang G, Chen C, Feng Z, Jiang Y, Yu H, Li M, Chao Y, Tang Y, Wang S, Qiu R (2023) The interplay between microalgae and toxic metal(loid)s: mechanisms and implications in AMD phycoremediation coupled with

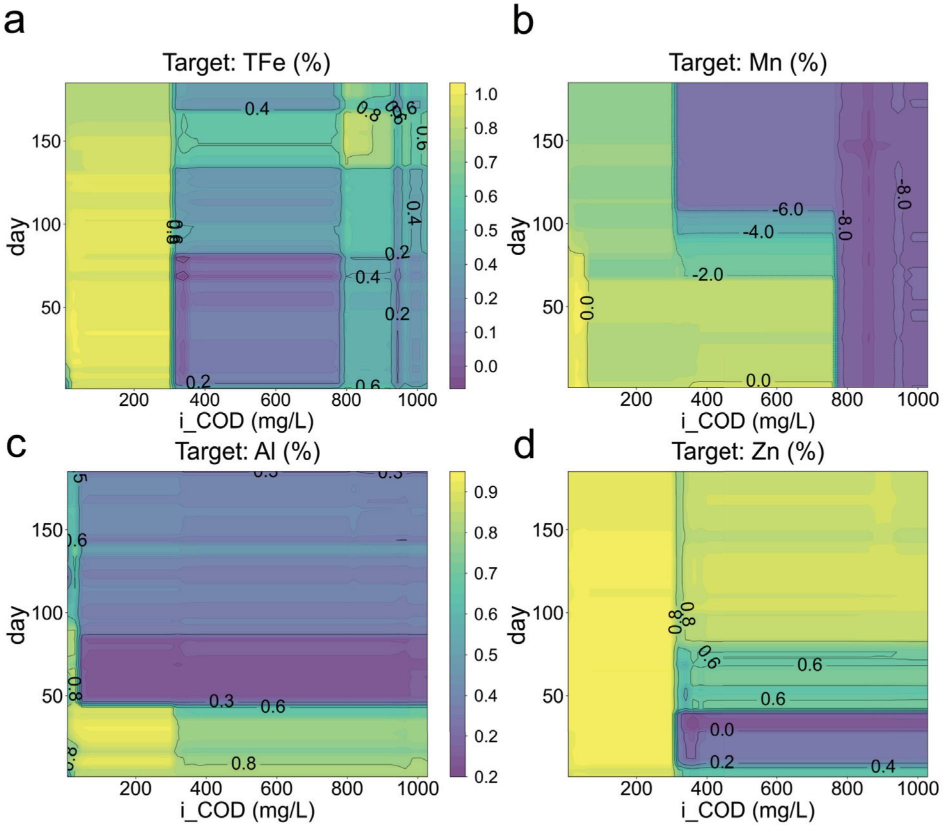

Figure 5 The interaction between inflow COD and operation days was analyzed to assess its impact on the (a) TFe removal efficiency, (b) Mn removal efficiency, (c) Al removal efficiency, and (d) Zn removal efficiency.

Fe/Mn mineralization. J Hazard Mater 454:131498. doi:10.1016/j.jhazmat.2023.131498

Hu S, Liu G, Zhang J, Yan J, Zhou H, Yan X (2022) Linking electron ionization mass spectra of organic chemicals to toxicity endpoints through machine learning and experimentation. J Hazard Mater 431:128558. doi:10.1016/j.jhazmat.2022.128558

Jouini M, Benzaazoua M, Neculita CM, Genty T (2020) Performances of stabilization/solidification process of acid mine drainage passive treatment residues: Assessment of the environmental and mechanical behaviors. J Environ Manage 269:110764. doi:10.1016/j.jenvman.2020.110764

Kim T, Shin J, Lee D, Kim Y, Na E, Park JH, Lim C, Cha Y (2022) Simultaneous feature engineering and interpretation: Forecasting harmful algal blooms using a deep learning approach. Water Res 215:118289. doi:10.1016/j.watres.2022.118289

Lopez AM, Wells A, Fendorf S (2021) Soil and Aquifer Properties Combine as Predictors of Groundwater Uranium Concentrations within the Central Valley, California. Environ Sci Technol 55 (1):352–361. doi:10.1021/acs.est.0c05591

Nguegang B, Masindi V, Msagati Makudali TA, Tekere M (2022) Effective treatment of acid mine drainage using a combination of MgO-nanoparticles and a series of constructed wetlands planted with Vetiveria zizanioides: A hybrid and stepwise approach. J Environ Manage 310:114751. doi:10.1016/j.jenvman.2022.114751

Palansooriya KN, Li J, Dissanayake PD, Suvarna M, Li L, Yuan X, Sarkar B, Tsang DCW, Rinklebe J, Wang X, Ok YS (2022) Prediction of Soil Heavy Metal Immobilization by Biochar Using Machine Learning. Environ Sci Technol 56 (7):4187–4198. doi:10.1021/acs.est.1c08302

Singh S, Chakraborty S (2020) Performance of organic substrate amended constructed wetland treating acid mine drainage (AMD) of North-Eastern India. J Hazard Mater 397:122719. doi:10.1016/j.jhazmat.2020.122719

Stumm W, Morgan JJ (2013) Aquatic chemistry: chemical equilibria and rates in natural waters. John Wiley & Sons,

Wu G, Kechavarzi C, Li X, Wu S, Pollard SJT, Sui H, Coulon F (2013) Machine learning models for predicting PAHs bioavailability in compost amended soils. Chem Eng J 223:747–754. doi:10.1016/j.cej.2013.02.122

Yan J, Yan X, Hu S, Zhu H, Yan B (2021) Comprehensive Interrogation on Acetylcholinesterase Inhibition by Ionic Liquids Using Machine Learning and Molecular Modeling. Environ Sci Technol 55 (21):14720–14731. doi:10.1021/acs.est.1c02960

Yin M, Zhang X, Li F, Yan X, Zhou X, Ran Q, Jiang K, Borch T, Fang L (2024) Multitask Deep Learning Enabling a Synergy for Cadmium and Methane Mitigation with Biochar Amendments in Paddy Soils. Environ Sci Technol 58 (3):1771–1782. doi:10.1021/acs.est.3c07568

Younger PL, Banwart SA, Hedin RS, Younger PL, Banwart SA, Hedin RS (2002) Mine water hydrology. Springer,

Zhang Y, Feng Y, Ren Z, Zuo R, Zhang T, Li Y, Wang Y, Liu Z, Sun Z, Han Y, Feng L, Aghbashlo M, Tabatabaei M, Pan J (2023) Tree-based machine learning model for visualizing complex relationships between biochar properties and anaerobic digestion. Bioresour Technol 374:128746. doi:10.1016/j.biortech.2023.128746

Zhao W, Ma J, Liu Q, Dou L, Qu Y, Shi H, Sun Y, Chen H, Tian Y, Wu F (2023) Accurate Prediction of Soil Heavy Metal Pollution Using an Improved Machine Learning Method: A Case Study in the Pearl River Delta, China. Environ Sci Technol 57 (46):17751–17761. doi:10.1021/acs.est.2c07561

Zhu JJ, Yang M, Ren ZJ (2023) Machine Learning in Environmental Research: Common Pitfalls and Best Practices. Environ Sci Technol 57 (46):17671–17689. doi:10.1021/acs.est.3c00026

Zhu X, Li Y, Wang X (2019) Machine learning prediction of biochar yield and carbon contents in biochar based on biomass characteristics and pyrolysis conditions. Bioresour Technol 288:121527. doi:10.1016/j.biortech.2019.121527

Abstracts and Extended Abstracts – Reviewed

Water Management in Iron Ore Mining: Regression Models for Optimizing Water Use in Mining Complexes

Renata Andries[1], Renato Silva Júnior[2], Guilherme Alves[3]

[1] *Vale Technological Institute, Botafogo Beach, 186, Rio de Janeiro, RJ, Brazil,*
renata.andries@vale.com, ORCID 0009-0005-2002-512X

[2] *Vale Technological Institute, Boaventura da Silva Street, 955, Belém, PA, Brazil,*
renato.silva.junior@itv.org, ORCID 0000-0001-8875-6299

[3] *Botafogo Beach, 186, Rio de Janeiro, RJ, Brazil,*
guilherme.alves@vale.com, ORCID 0009-0008-3638-4655

Abstract

Mining plays a crucial role in economic development by providing raw materials that drive social progress. In this context, water is a transversal and indispensable element at all stages. However, with the increasing demand for water and climate change, efficiency in the use of water resources has become a priority. Therefore, it is essential to develop tools that enable effective water resource management in mining, promoting cost reduction, mitigating water risks, and meeting environmental and social requirements, as well as creating competitive advantages for the sector through transparency and attracting investments.

The innovative approach of this work lies in the development of regression models to analyze the relationship between iron ore production, mineral beneficiation method, rainfall seasonality, and water demand. Using data from six Brazilian mining complexes over 89 months, the research seeks to establish correlations that can guide strategic decisions and increase water efficiency. Additionally, it is important to highlight that there are few studies in the literature that quantify water use in relation to production, differentiating Operational Water, Total Intake, and Reuse.

The main findings indicate that simple linear regression (SLR) is more effective for analyzing Operational Water and Reuse, while generalized Poisson linear regression (GPLR) presents lower errors for Total Intake. The research also reveals that both Total Intake and Reuse have lower correlation with the production variable. This is because total intake is more related to the volume of dewatering water than to the ore processing itself. In other words, most of the dewatering volume is returned to the environment without use and is not part of the operational water computation. Regarding the reuse portion, it is mainly related to units with dams, i.e., units with wet beneficiation. Furthermore, it occurs to a greater extent when there is robust water infrastructure capable of treating/reusing non-new water volumes.

The applications of this work are vast, including the planning and analysis of water use in mining enterprises. The developed models can be used as tools to increase transparency, attract investments, and create competitive advantages. The implications include promoting sustainable practices, reducing operational costs, and mitigating environmental impacts, contributing to water security and the sustainability of the mining sector.

Keywords: Water, water resources, sustainability, regression models, mining

Introduction

Mining is essential for economic and social development, with water being a critical input throughout all mining phases. In 2023, Brazil exported 378.5 million tons of iron ore, valued at US$30.5 billion, and consumed an average of 0.305 m^3 of new water per ton of ROM (IBRAM 2023, 2024). Consequently, it is estimated that the sector utilized approximately 115.4 million m^3 of new water in its production processes that year.

However, freshwater consumption limits are rapidly approaching (GERTEN *et al.*, 2013) or the available volume may have already been exceeded (Grafton *et al.* 2013; Rosa *et al.* 2019). The increasing water demand is driven by population and economic growth across various sectors, including industry, agriculture, livestock, energy, and mining. The World Resources Institute reports that a quarter of the global population lives in countries with extreme water stress, with over 1 billion people projected to face this situation by 2050.

Considering the reliance on water in iron ore mining, the rising water demand over the years, and the increasing frequency of global water scarcity events, it is crucial to thoroughly understand the operational water balance and actual water demand in mining projects. This understanding enables the prioritization of sustainable sources, the selection of water management strategies, the proper planning of necessary water infrastructure, and the enhancement of freshwater use efficiency, thereby preparing the sector for potential shortages or changes in supply conditions.

Water estimates for iron ore processing are limited in the literature, particularly when accounting for various components of the operational water balance, such as water capture for drawdown, freshwater, and reused water. Additionally, beneficiation methods (dry, wet or natural moisture processing) must be differentiated when calculating the project's overall water demand, as each method has distinct water requirements and infrastructure, influencing the feasibility of water reuse.

In the book "Perspectives and Advances in Water Resources Management in Mining" (ANA and IBRAM, 2024) the average specific water use per ton produced for different products was calculated by dividing the annual volume declared in grant applications by the annual ore production. However, this granted volume does not account for water capture needed for drawdown or the water used in the production process. Additionally, this indicator overlooks reused water, which constitutes most of the water consumption in an iron ore plant (approximately 80%) and treats all iron ore mining methods (natural moisture and dry processing) as similar.

NORTHEY *et al.*, (2019) analyzed 359 public mining reports for various minerals and found water withdrawals ranging from 0.13 m^3 to 17.29 m^3 per ton of processed ore. This research supports the assertion that it is not feasible to group or model a range of water use for different production processes. Furthermore, the indicator used in the research refers to total water withdrawal, not the new water used in operations. Therefore, in the case of iron ore, the water quantification presented by the author is more related to the water demand for drawdown than the operational use of new water.

The objective of this work is to develop a tool to quantify the water demand required for an iron ore mining project, from extraction to the final product. This tool will consider the total water collected, water used in the production process, and reused water. Linear regression models will be employed to compare water demand relative to the volume of raw ore processed (ROM) for different mineral processing methods. The following sections present the theoretical framework, methods, results, and conclusions necessary for understanding and executing the project.

Methods

The methodological steps of this study are as follows: 1) Data collection, including the definition of samples and variables; 2) Statistical treatment and analysis; 3) Correlation analysis; 4) Development of linear regression models (both simple and generalized); and 5) Model diagnostics. The following sections provide detailed descriptions of each step.

Database, variables and sample

The primary data utilized in this study encompass operational water monitoring and mining reports from six Brazilian iron ore mining complexes over a period of 89 months (January 2017 to May 2024). The analyzed complexes include Serra Sul (PA/BR), Serra Leste (PA/BR), Serra Norte (PA/BR), Itabira (MG/BR), Vargem Grande (MG/BR), and Paraopeba (MG/BR), resulting in a total of 2,670 observations. The variables incorporated into the linear regression model are Operational water, Total water withdrawn, Reused water, Plant feed, and Type of mineral processing.

Statistical treatment and analysis

During the analyzed period, operations experienced several events, including production shutdowns, changes in the production process, alterations in data consolidation personnel, and variations in water volume estimates. These factors increase the likelihood of data variability due to the absence of a verification or standardization process. Therefore, it is crucial to analyze and process the data, identifying and removing potential outliers to enhance data reliability before utilizing them in the proposed models.

Outliers were detected using the Interquartile Range (IQR) rule, which employs values estimated by regression methods (Jeong *et al.* 2017) to define acceptance or rejection limits for measured values. The normality of the data will be assessed using the Shapiro-Wilk test to determine whether parametric or non-parametric hypothesis tests should be applied. Visualizations such as boxplots, histograms, and scatter plots will be generated to examine the data set.

Correlation analysis

To understand the correlation between the variables in the model, Pearson's correlation coefficient will be employed. This coefficient is a bivariate measure of the association (strength) of the relationship between two variables (Paranhos *et al.* 2014). It ranges from -1 to 1, where the sign indicates the direction (positive or negative) of the relationship, and the value indicates the strength of the relationship. A perfect correlation (-1 or 1) signifies that the value of one variable can be precisely determined by knowing the value of the other (Elian 1988; Paranhos *et al.* 2014). Conversely, a correlation of zero indicates no linear relationship between the variables.

Simple linear regression model (SLR)

According to *(Elian 1988)*, linear regression is a global method and is based on the use of only one equation to explain the relationship between the variables studied (dependent and independent). The simple linear regression model (SLR) expected for the present study is given by the equation below.

$$y_i = \beta_0 + \beta_1 . X_1 + \varepsilon_i$$

Where y_i is the i-th value of the response variable, β_0 e β_1 are the parameters (regression coefficients), X_1 is the i-th value of the predictor variable and ε_i is the random error term.

Generalized linear model (GLM)

When aiming to associate a dependent variable with independent variables, linear modeling is commonly employed. However, a limitation of linear models is that the dependent variable must follow a normal distribution Akaike (1974). Therefore, it is necessary to seek an alternative method to satisfactorily associate the dependent and independent variables.

According to Dobson (2001), the generalized linear model (GLM) allows for the adjustment of regression models for univariate response data that follow a distribution from the exponential family. The exponential family includes distributions such as normal, binomial, Poisson, geometric, negative binomial, exponential, gamma, and inverse normal.

The generalized linear model with Poisson distribution is given by the equation below:

$$\ln(y_i) = \beta_0 + \beta_1 . X_1 + \beta_2 . X_2 + \dots + \beta_n . X_n + \varepsilon_i$$

Where y_i is the i-th value of the response variable, β_0, β_1 e β_n are the parameters (regression coefficients), X_1, X_2 e X_n are known constants and ε_i is the random error term.

Table 1 Descriptive statistics of the variables Operational water, Total water withdrawn and Reused water (m^3) and Production unit (t).

Complex	Variable	Mean	Median	σ	Minimum	Maximum
Itabira Complex	Operational water (m^3)	782,288	706,551	389,185	176,184	2,134,528
	Water Withdrawn (m^3)	1,239,970	1,177,568	418,597	607,152	2,610,282
	Reuse water (m^3)	5,248,472	5,121,209	742,584	3,942,365	6,855,672
	Production unit (t)	4,194,529	4,209,416	470,050	3,056,534	5,270,583
Paraopeba Complex	Operational water (m^3)	484,760	509,734	185,883	194,557	1,009,908
	Water Withdrawn (m^3)	1,243,860	1,202,686	263,204	356,785	1,859,243
	Reuse water (m^3)	1,154,011	790,026	921,491	162,860	2,916,920
	Production unit (t)	1,694,792	1,414,756	897,347	385,308	3,442,221
Vargem Complex Grande	Operational water (m^3)	860,612	877,598	359,375	82,480	1,602,300
	Water Withdrawn (m^3)	1,815,025	1,761,688	266,792	1,403,991	2,662,421
	Reuse water (m^3)	4,447,241	1,589,233	5,415,777	0	18,295,521
	Production unit (t)	3,306,432	3,261,708	1,454,959	125,848	6,023,899
Serra Leste Complex	Operational water (m^3)	18,834	18,054	8,159	4,494	38,574
	Water Withdrawn (m^3)	19,654	20,664	8,791	4,494	40,645
	Reuse water (m^3)	0	0	0	0	0
	Production unit (t)	429,488	410,497	95,215	73,559	573,849
Serra Norte Complex	Operational water (m^3)	645,536	606,621	271,821	168,415	1,221,619
	Water Withdrawn (m^3)	1,563,351	1,544,904	581,663	386,026	5,185,788
	Reuse water (m^3)	2,856,345	2,841,263	818,965	1,127,990	6,475,531
	Production unit (t)	9,687,420	9,646,836	2,458,428	4,669,465	13,838,155
Serra Sul Complex	Operational water (m^3)	86,213	82,216	27,926	34,392	151,884
	Water Withdrawn (m^3)	580,961	369,284	569,485	34,392	1,795,160
	Reuse water (m^3)	5,513	2,123	7,717	0	34,665
	Production unit (t)	6,038,252	6,447,528	2,098,740	934,899	9,643,820

Model diagnosis

The selection of the optimal regression model will be based on statistical criteria, including the coefficient of determination (R^2), standard error (σ), root mean-square deviation (RMSD), and Akaike information criterion (AIC). RMSD measures the difference between the values predicted by a model and the observed values, calculated as the square root of the mean of the squared errors. The AIC method, proposed by Akaike (1974), addresses model identification from the perspective of statistical decision theory, facilitating the selection of the most appropriate loss function for model adjustment.

Results

Statistical treatment and analysis

Statistical analysis of the data was conducted by calculating the means, medians, standard deviations, minimums, and maximums (Table 1). Comparing the standard deviation (σ) with the mean of the variables (Operational water, Total water withdrawn and Reused water) reveals significant variability within the complexes, as well as for plant feed. This variability can be attributed to the dynamic nature of operations, which experience fluctuations in production due to market demand, climatic seasonality, process maturity, changes in production routes, and other factors.

The Shapiro Wilk test was used to analyze the normality of the data. Most of the variables in the complexes do not follow a normal distribution. Although a non-normal distribution of most of the variables was observed, it is possible to perform a regression model with the data from the 6 complexes to analyze the relationship between the variables and the Production Unit. Linear regression assumes that the residuals (errors) of the model follow a normal distribution, not necessarily the independent or dependent variables. Furthermore, if the residuals do not follow a normal distribution, transformations in the variables (such as logarithm or square root) can be considered to improve the normality of the residuals.

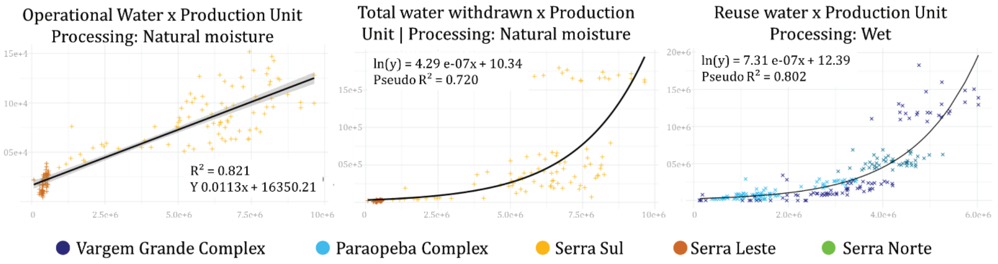

Figure 1 *Model behavior: 1) SLR Operational Water processing at natural moisture, 2) GLM Total water withdrawn at natural moisture and 3) GLM Reuse water at wet processing.*

Table 2 *Summary of analysis of SLR and Poisson GLM. Gray color indicates the best-fitting model.*

Operational Water (m^3) x Production Unit (t)

Proc.	Model	β0	σ (β0)	β1	σ (β1)	R²	σ (Res.)	p-value	AIC	RMSD
H	SLR	-1.01E+05	8.60E+04	7.70E-02	8.61E-03	0.485	1.96E+05	< 2e-16	1.87E+03	2.13E+04
	GLM	1.28E+01	2.03E-04	2.24E-07	5.59E-11	0.410	2.33E+07	< 2e-16	2.33E+07	2.61E+03
NM	SLR	1.64E+04	2.08E+03	1.13E-02	4.29E-04	0.821	1.69E+04	< 2e-16	2.49E+03	1.38E+03
	GLM	1.00E+01	7.37E-04	2.04E-07	1.16E-10	0.790	9.41E+05	< 2e-16	9.43E+05	1.65E+03
W	SLR	2.59E+05	3.99E+04	1.53E-01	1.24E-02	0.407	2.74E+05	< 2e-16	4.79E+03	1.84E+04
	GLM	1.22E+01	5.93E-04	1.21E-07	5.56E-11	0.490	4.98E+06	< 2e-16	4.98E+06	1.53E+03

Total capture (m^3) x Production Unit (t)

Proc.	Model	β0	σ (β0)	β1	σ (β1)	R²	σ (Res.)	p-value	AIC	RMSD
H	SLR	4.19E+05	2.22E+05	1.18E-01	2.22E-02	0.249	5.07E+05	8.64E-07	2.03E+03	5.50E+04
	GLM	1.40E+01	1.25E-04	5.64E-08	3.75E-11	0.090	2.39E+07	<2e-16	2.39E+07	2.33E+04
NM	SLR	-7.34E+04	4.45E+04	1.14E-01	9.17E-03	0.505	3.62E+05	< 2e-16	3.41E+03	2.95E+04
	GLM	1.03E+01	4.96E-04	4.29E-07	6.77E-11	0.720	2.48E+07	<2e-16	2.49E+07	7.26E+02
W	SLR	1.23E+06	5.76E+04	8.27E-02	1.79E-02	0.088	3.95E+05	6.70E-06	4.79E+03	1.84E+04
	GLM	1.35E+01	3.68E-04	7.58E-08	3.53E-11	0.280	1.17E+07	<2e-16	1.17E+07	4.41E+02

Reuse (m^3) x Production Unit (t)

Proc.	Model	β0	σ (β0)	β1	σ (β1)	R²	σ (Res.)	p-value	AIC	RMSD
H	SLR	3.59E+06	3.52E+05	-7.55E-02	3.52E-02	0.051	8.02E+05	3.48E-02	2.11E+03	8.70E+04
	GLM	1.24E+01	1.37E-04	7.31E-07	3.12E-11	0.802	1.67E+08	<2e-16	1.67E+08	2.33E+04
NM	SLR	-1.25E+03	6.35E+02	1.21E-03	1.31E-04	0.362	5.17E+03	<2e-16	2.13E+03	4.21E+02
	GLM	4.54E+00	6.88E-03	5.83E-07	8.92E-10	0.620	5.11E+05	<2e-16	5.11E+05	7.26E+02
W	SLR	-2.61E+06	3.49E+05	2.07E+00	1.09E-01	0.623	2.39E+06	<2e-16	5.74E+03	1.61E+05
	GLM	1.51E+01	2.56E-04	-2.65E-08	2.60E-11	0.050	1.87E+07	<2e-16	1.87E+07	2.33E+02

Correlation analysis

The linear correlation matrix was generated by calculating Pearson's correlation coefficients between the dependent and independent variables used in the study. A stronger correlation was observed among the variables associated with the natural moisture beneficiation type. This can be explained by the fact that, in this type of beneficiation, the primary use of water is for ore processing itself. Generally, in natural moisture processing, water is used more for particulate control than for ore processing. In other words, water use is more related to the mining area, roads, and piles that need to be sprayed.

Regarding operational water, an R^2 greater than 0.6 was obtained when comparing the production unit, suggesting that this variable can be used as a dependent variable in a model explaining the use of operational water in relation to the plant's feed. However, the same correlation is not observed for total water withdrawal or reuse. This is because total water withdrawal is more related to the volume of drawdown water than to ore processing itself. In other words, most of the water withdrawn is returned to the environment without being used and is not included in the calculation of operational water.

The potential for water reuse is mainly associated with units that have dams, i.e., units with wet processing. Additionally, reuse is more prevalent when there is a robust water infrastructure capable of treating and reusing non-new water volumes.

Simple Linear Regression Model (SLR) and Generalized Linear Regression Model (GLM)

Below is the graphical representation of the models with the highest R^2 values (Fig. 1), a comprehensive presentation of the results (Table 2), and a summary of the results analysis.

- Operating Water | Hybrid (H): The SLR model is considered the best due to its higher R^2 and lower AIC, despite the GLR model having a lower RMSD.
- Operating Water | Natural Moisture (NM): The SLR model is the best due to its higher R^2, lower AIC, and lower RMSD.
- Operating Water | Wet (W): The SLR model is preferred due to its lower AIC, despite the GLR model having a higher R^2 and lower RMSD.
- Total Water Withdrawal | Hybrid (H): The SLR model is the best due to its higher R^2 and lower AIC, despite the GLR model having a lower RMSD.
- Total Water Withdrawal | Natural Moisture (NM): The GLR model is the best due to its higher R^2 and lower RMSD, despite the SLR model having a lower AIC.
- Total Water Withdrawal | Wet (W): The GLR model is the best because it has the highest R^2 and lowest RMSD, despite the SLR model having a lower AIC.
- Reused Water | Hybrid (H): The GLR model is the best because it has the highest R^2 and lowest RMSD, despite the SLR model having a lower AIC.
- Reused Water | Natural Moisture (NM): The SLR model is the best because it has the lowest AIC and RMSD, despite the GLR model having a higher R^2.
- Reused Water | Wet (W): The SLR model is the best because it has the highest R^2 and lowest AIC, despite the GLR model having a lower RMSD.

Conclusion

Regarding the models studied, it was found that simple linear regression (SLR) presents the greatest gain when analyzing the Operational Water and Reuse coefficient. However, for Total Water Withdrawn, the generalized linear Poisson regression (GLPR) models generally presented smaller errors.

For both Total Water Withdrawn and Reuse, a lower correlation was observed with the Production Unit variable (Plant feed). This is because Total Water Withdrawn is more related to the volume of drawdown water than to the processing of the ore itself. In other words, most of the drawdown volume is returned to the environment unused and is not part of the calculation of operational water.

The potential for reuse, on the other hand, is mainly related to units with dams, i.e., units with wet processing. Additionally, it occurs to a greater degree when there is a robust water infrastructure capable of treating/reusing non-new water volumes.

Finally, the models proposed in this work, both the SLR model and the GLPR model, present an important technical-scientific contribution, as they can be used as useful tools for planning and analyzing water use in iron ore mining projects. Furthermore, there are no studies in the literature that estimate water use in relation to production by dividing the uses into Operational Water, Total Water Withdrawn, and Reuse.

References

Akaike H (1974) A New Look at the Statistical Model Identification, 6th edn. Boston

ANA (National Water and Sanitation Agency), IBRAM (Brazilian Mining Institute) (2024) Perspectives and Advances in Water Resources Management in Mining. Brasília (DF)

Dobson A (2001) An Introduction to Generalized Linear Models, Second Edition. Chapman and Hall/CRC

Elian SN (1988) Regression analysis. São Paulo

Grafton RQ, Pittock J, Davis R, *et al* (2013) Global insights into water resources, climate change and governance. Nat Clim Chang 3:315–321. https://doi.org/10.1038/nclimate1746

IBRAM (Brazilian Mining Institute) (2023) Mining in Numbers 2023. https://ibram.org.br/wp-content/uploads/2024/02/mineracao-em-numero-2023.pdf. Accessed 5 Aug 2024

IBRAM (Brazilian Mining Institute) (2024) ESG Results for Brazil Mining 2024. https://ibram.org.br/wp-content/uploads/2024/07/IBRAM-ESG_Resultados23_ColetivadeImprensa-1.pdf. Accessed 5 Aug 2024

Jeong J, Park E, Han WS, *et al* (2017) Identifying outliers of non-Gaussian groundwater state data based on ensemble estimation for long-term trends. J Hydrol (Amst) 548:135–144. https://doi.org/10.1016/j.jhydrol.2017.02.058

Northey SA, Mudd GM, Werner TT, *et al* (2019) Sustainable water management and improved corporate reporting in mining. Water Resour Ind 21:100104. https://doi.org/10.1016/j.wri.2018.100104

Paranhos R, Figueiredo Filho DB, Rocha EC da, *et al* (2014) Unraveling the Mysteries of the Pearson Correlation Coefficient. Leviathan (São Paulo) 66. https://doi.org/10.11606/issn.2237-4485.lev.2014.132346

Rosa L, Chiarelli DD, Tu C, *et al* (2019) Global unsustainable virtual water flows in agricultural trade. Environmental Research Letters 14:114001. https://doi.org/10.1088/1748-9326/ab4bfc

Arsenate and chromate attenuation in acid mine drainage systems

Juan Antelo[1], Sarah Fiol[1], Ivan Carabante[2], Isabela Filardi[3], Ana Barroso[4], Teresa Valente[4]

[1]Cross-disciplinary Research Center in Environmental Technologies (CRETUS), Universidade de Santiago de Compostela, Spain; [2] Department of Civil, Environmental and Natural Resources Engineering, Luleå University of Technology, Sweden; [3] Soils Department, Federal University of Viçosa, Brasil; 4 Institute of Earth Science, University of Minho, Portugal

Abstract

The oxidation of iron sulfide minerals in mining environments generates acid mine drainage (AMD), leading to acidic pH waters with relatively high concentrations of potentially toxic elements. The formation of secondary iron minerals, such as ferrihydrite (Fh) and schwertmannite (Sch), plays a critical role in controlling the mobility of these elements. In these environments, iron mineral surfaces are involved in adsorption reactions that mitigate the spread of metals and metalloids. Additionally, the coprecipitation of ions and their incorporation into iron oxides modify the surface properties, affecting their stability and reactivity. Knowledge of the binding behaviour of iron mineral surfaces in AMD is needed to establish the mechanisms of pollution sequestration at the solid-solution interface and to develop remediaton procecures to minimize AMD pollution.

This study investigates the reactivity of iron minerals surfaces in AMD. Batch adsorption experiments were carried out with ferrihydrite, schwertmannite, and goethite in the presence of arsenate or chromate and organic acids. Key factors influencing the reactivity of these AM-formed iron minerals, such as pH, redox conditions, and the presence of co-precipitated species like Al, were examined. By integrating the macroscopic information with microscopic data, surface complexation modeling was used to characterize the ion-binding behavior on these minerals.

Results showed that increasing pH, sulfate concentration or the presence of organic acids enhances the mobility of both arsenate and chromate. This is likely due to changes in surface charge, competition for the binding sites, and the decrease of the anion-exchange reactions with the sulfate groups. On the other hand, the incorporation of Al ions in the mineral structure also leads to an increase on the mobility of these oxyanions, which is caused by changes in the surface area and surface charge, and the alteration of the binding site concentration. These observations were modelled using a surface complexation model, specifically the CD-MUSIC model. The spectroscopic data was used to constrain the surface complexes, e.g. monodentate and bidentate inner-sphere complexes identified as the main complexes for chromate, and monodentate inner-sphere and bidentate outer-sphere complexes selected for sulfate.

A major challenge lies in predicting when these iron minerals will transition into more crystalline forms, as these changes may result in the re-mobilization of adsorbed pollutants, increasing environmental risks. This study enhances the understanding of the physicochemical conditions driving such transformations, contributing to the development of more effective remediation strategies for managing AMD-related pollution.

Secondary Minerals from Evolved Mine Waters: A Detailed Survey in Almadén Historic Mercury Mine Gallery

Ana Barroso[1], José Ignacio Barquero[2,3], Efrén García-Ordialesa[4], Judith L. Jaeger[2,3], Pablo Higueras[2,3], Teresa Maria Valente[1]

[1] *Universidade do Minho, Campus de Gualtar, Institute of Earth Sciences, 710-057 Braga, Portugal*

[2] *Instituto de Geología Aplicada, Universidad de Castilla-La Mancha, Pl. Manuel Meca 1, 13400 Almadén, Ciudad Real, Spain*

[3] *Escuela de Ingeniería Minera E Industrial de Almadén, 13400 Almadén, Ciudad Real, Spain*

[4] *ISYMAResearch Group, Mining, Energy and Materials Engineering School, University of Oviedo, C/ Independencia 13, 33011 Oviedo, Spain*

Abstract

Mercury (Hg) is a significant global pollutant, primarily associated with mining and industrial activities. The accumulation of waste containing elevated concentrations of Hg has resulted in the contamination of numerous sites, which presents a risk to human health and the integrity of ecosystems. In response to identifying Hg as one of the most harmful toxic metals, regulatory measures have been introduced that restrict the disposal of Hg without prior treatment. Despite a decline in mining activity due to economic and environmental concerns, it remains paramount to understand the environmental liabilities associated with historical mining districts. Investigating the formation of secondary minerals in these areas may assist in mitigating the risks associated with Hg pollution and its toxic legacy.

The primary objective of this study was to compile a comprehensive inventory of secondary minerals resulting from mine water precipitation within a Hg mine gallery in the Almadén mining region, Spain. This region has a mining history dating back to Roman times; however, it gained prominence during the 16th and 17th centuries. Open-pit and underground mining operations targeted cinnabar deposits, and the region's intensive exploitation established Almadén as a benchmark in Hg production until its gradual decline in recent decades.

Sampling was conducted in June 2024, with temperatures between 17 and 19 °C within the gallery at a depth of 50 m. To avoid mineralogical changes, samples were preserved in closed containers and analyzed promptly upon arrival at the laboratory. Temperature and relative humidity (RH) were recorded at each sampling point. The samples were initially examined using a binocular lens for morphological assessment, and subsequently separated for X-ray diffraction and energy-dispersive X-ray fluorescence analysis. The mine gallery exhibited a range of efflorescence, particularly in areas with elevated RH, highly faulty, and with water percolation. Secondary minerals of diverse colors and morphologies were documented, such as white minerals with saccharoidal or dendritic habits, yellow minerals exhibiting pulverous to globular habits, and globular pink minerals. The paragenesis included gypsum, jarosite, melanterite, bieberite, cinnabar, diadochite, and carbonates. Chemistry indicates Hg concentrations ranging from 17 to 470 mg/kg.

This study successfully establishes an inventory of secondary minerals on the gallery's walls, now classified as a mining park. It details the characteristics of the minerals, including habits and colors, with particular emphasis on those present in small stalactites. Furthermore, analyzing the mineralogy and chemistry of the efflorescent salts has provided valuable insights into the processes underlying their formation.

Keywords: Mercury, efflorescence, paragenesis, geochemical analysis

Advanced Monitoring of Abandoned Mining Sites with High-Resolution UAV Technology

Ana Barroso[1], Renato Henriques[1], Ângela Cerqueira[1], Patrícia Gomes[1], Teresa Maria Valente[1], Isabel Margarida Horta Ribeiro[1], Amélia Paula Marinho Reis[1,2]

[1] *Universidade do Minho, Campus de Gualtar, Institute of Earth Sciences, 710–057 Braga, Portugal*

[2] *GEOBIOTEC, Geosciences department, University of Aveiro, Campus Universitário de Santiago, 3810–193 Aveiro, Portugal*

Abstract

In the past decade, unmanned aerial vehicles (UAVs), or drones, have become invaluable tools in the mining industry, supporting applications ranging from mineral exploration to environmental remediation. When equipped with high-resolution image sensors, UAVs enable high spatial and temporal resolution surveying, making them particularly effective for monitoring abandoned mining sites. This paper presents a case study demonstrating the application of UAV technology for monitoring an abandoned mining site affected by acid mine drainage (the Trimpancho mining complex in the Iberian Pyrite Belt, southwestern Spain).

The study was conducted on two selected waste dumps: one at the upstream and the other at the downstream of the mining complex. The primary objective was to estimate the volume of waste material accumulated in these areas. To achieve this, a DJI Phantom 4 RTK UAV was employed to conduct comprehensive aerial surveys of the sites. The imagery collected enabled the generation of orthophotomaps and digital surface models (DSMs), which provided detailed spatial information for accurately delimiting waste accumulations and identifying dominant runoff zones contributing to the degradation of the Trimpancho stream.

The three-dimensional models and orthomosaics produced from the UAV data provided an in-depth visualization of the waste distribution. This enabled precise volume estimations that are essential for long-term monitoring and management of the mining system. By comparing these models with future surveys, it is possible to track changes in waste dump morphology over time. Additionally, the models offer a valuable tool for assessing the potential valorization of critical materials accumulated in the abandoned dumps.

The results confirm that UAV technology is highly effective in obtaining the detailed and accurate data needed for monitoring abandoned mining sites. This information is crucial for planning and implementing remediation strategies adapted to the site's specific topography, hydrology, and geology. UAVs present an innovative, efficient solution that optimizes safety, accuracy, and cost-effectiveness. By enhancing assessment precision and enabling targeted reclamation strategies, UAVs technology contributes to the restoration and sustainable management of degraded mining areas, while also advancing environmental monitoring efforts.

Keywords: Unmanned Aerial Vehicles, mining, environmental remediation, acid mine drainage, orthophotmaps

Acknowledgements

Ana Barroso acknowledges FCT - Foundation for Science and Technology, I.P., by the support of ICT through the research fellowship with reference UI/BD/151330/2021. FCT also co-funded this work in the framework of the UIDB/04683 and UIDP/04683 – Instituto de Ciências da Terra programs.

Influence of Reactive Media on Microbial Sulfate Reduction at Two Distinct Temperatures

Laura Nina Bettoni[1], Maria Hellman[2], Sara Hallin[2] & Roger B. Herbert[1]

[1] *Uppsala University, Uppsala, Sweden, lauranina.bettoni@geo.uu.se, roger.herbert@geo.uu.se*

[2] *Swedish University of Agricultural Sciences, Uppsala, Sweden, maria.hellman@slu.se, sara.hallin@slu.se*

Extended Abstract

Mining activities are a major source of sulfate (SO_4^{2-}) to surrounding freshwater systems, as it commonly results from the oxidation of sulfide minerals found in mine waste. High concentrations can be detrimental for aquatic life and surface water quality criteria on sulfate are starting to be imposed in Sweden (Soucek and Kennedy 2005; Swedish Agency for Marine and Water Management 2018). To meet the quality criteria, mining companies must implement removal strategies. Biotechnologies using sulfate-reducing bacteria (SRB) offer an effective method for removing sulfate by reducing it to hydrogen sulfide (H_2S), which can be precipitated as a solid phase metal sulfide (Runtti *et al.* 2018; Pudi *et al.* 2022). Microbial sulfate reduction is influenced by various key factors including pH, temperature, organic matter availability, microbial competition and other physical factors (Middleton and Lawrence 1977). This study aims to evaluate the effects of different solid reactive media as carbon sources and temperature on microbial sulfate reduction to optimize conditions for enhanced sulfate removal.

In this study, woodchips (WC), woodchips with biochar (BC) and woodchips with potato peels (PP) were selected for column experiments at 5 °C and 15 °C. Woodchips and woodchips-biochar were chosen based on previous experiments at 22 °C showing over 90% sulfate removal with lactate as a carbon source (Parvage and Herbert 2023). Biochar was included due to its high porosity, which supports microbial activity, including sulfate-reducing bacteria (Lehmann *et al.* 2011; Easton *et al.* 2015). To sustain sulfate reduction without external carbon sources, a material that releases substantial dissolved organic carbon (DOC) is needed. Potato peel were selected due to its high DOC release (Kiani *et al.* 2020). The columns (40 cm in length and 10 cm in inner diameter) were run in triplicate for each medium with an upward flow direction of 0.2 mL/min yielding a theoretical hydraulic residence time of 5 days. Prior to the start of the experiment, each medium was inoculated overnight with a mixture of activated sewage sludge (10 mL/100 g material) and inflow water to establish an initial microbial community. The inflow was composed of 10 mM sulfate and calcium, major components of waste rock leachate. After 39 days, lactate ($CH_3CH(OH)COO^-$, 16.5 mM), commonly used as an external carbon source to promote sulfate reduction (Widdel 1988), was added to the inflow solution. This addition would theoretically contribute to a maximum of 82.5% sulfate removal based on stoichiometry (reaction 1). The removal produces acetate (CH_3COO^-) and carbonate alkalinity as bicarbonate (HCO_3^-). The 5 °C experiment concluded after 117 days, while the 15 °C experiment extended to 213 days. In the latter, the effects of a higher lactate concentration (33 mM) added on day 150 and the supplementation of macronutrients (phosphate 5 mM and ammonium 18.7 mM) on day 176 on sulfate removal rates were evaluated.

$$SO_4^{2-} + 2CH_3CH(OH)COO^- = H_2S + 2CH_3COO^- + 2HCO_3^- \qquad (1)$$

At the start of the experiment, sulfate concentrations remained relatively unchanged, and no sulfide production was observed (Fig. 1). Following lactate addition, sulfate concentrations decreased in treatments, with BC columns showing the fastest and highest reduction in the first 30 days (approximately 40% sulfate removal at 5 °C and >90% at 15 °C) before gradually declining in efficiency (Fig. 1.B). This suggests that SRB are inhibited by hydrogen sulfide that is likely adsorbed by the biochar material (Janyasuthiwong *et al.* 2016; Kanjanarong *et al.* 2017). WC (Fig. 1.A) and PP (Fig. 1.C) columns displayed a slower increase in sulfate removal, stabilizing at 24% and 55% at 5 °C and 58% and 24% at 15 °C, respectively. Although higher temperature benefited the process in WC and BC columns, PP columns performed better at 5 °C. Other microbial processes can influence sulfate reduction, either by releasing additional carbon sources for SRB or competing for them (Zhang *et al.* 2022), which is currently under investigation. Additionally, excess lactate improved sulfate reduction and it could be further improved by nutrient addition, allowing a maximum of 58%, >90% and 47% sulfate removal for WC, BC and PP respectively.

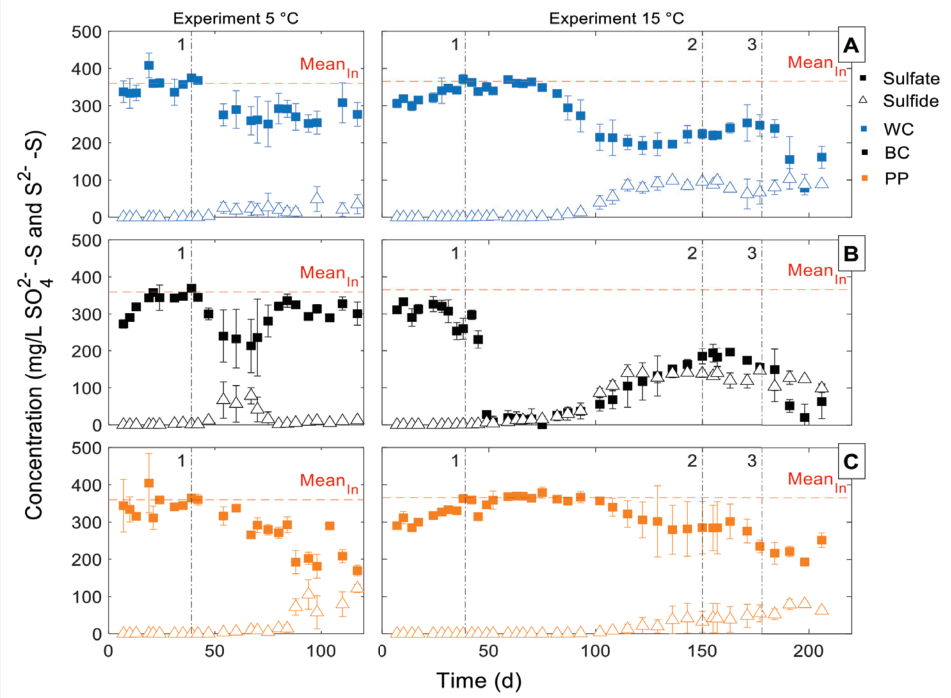

Figure 1 *Mean outflow concentrations of sulfate-sulfur (square) and sulfide-sulfur (triangle) from columns containing (A) woodchips, (B) woodchips with biochar and (C) woodchips with potato peels during the experiment at 5 °C (left) and 15 °C (right). The red dashed line denotes the average* SO_4^{2-}*-S concentration at the inlet. Error bars represent standard deviations on the mean values. The vertical dashed line indicates changes in the inlet composition with (1) lactate addition, (2) double lactate addition and (3) nutrients addition.*

This study highlights the significance of both temperature and carbon source selection in optimizing sulfate reduction for mine water treatment. The enhanced sulfate removal observed in BC columns followed by a decline in treatment performance, particularly at higher temperatures, underscores the role of biochar in influencing microbial activity and hydrogen sulfide dynamics. While WC and PP columns exhibited variable performance

across temperatures, the results suggest that microbial competition and carbon source availability play crucial roles in sustaining sulfate reduction. Additionally, the positive effect of lactate and nutrient supplementation reinforces the need for tailored dosing strategies to maximize efficiency. Future research should further explore microbial interactions and long-term stability to refine biotechnological approaches for sulfate removal in mining-affected waters.

Keywords: Biological sulfate reduction, bioreactor efficiency, carbon source, column experiments, temperature effect

Acknowledgements

This study is part of the SULFREM project, which is conducted within the program Swedish Mining Innovation and funded by the Swedish Innovation Agency (VINNOVA, project number 2021-04669), Boliden Mineral AB and LKAB.

References

Easton ZM, Rogers M, Davis M, Wade J, Eick M, Bock E (2015) Mitigation of sulfate reduction and nitrous oxide emission in denitrifying environments with amorphous iron oxide and biochar. Ecol Eng 82:605–613. https://doi.org/10.1016/j.ecoleng.2015.05.008

Janyasuthiwong S, Rene ER, Esposito G, Lens PNL (2016) Effect of pH on the Performance of Sulfate and Thiosulfate-Fed Sulfate Reducing Inverse Fluidized Bed Reactors. J Environ Eng 142:C4015012. https://doi.org/10.1061/(ASCE)EE.1943-7870.0001004

Kanjanarong J, Giri BS, Jaisi DP, Oliveira FR, Boonsawang P, Chaiprapat S, Singh RS, Balakrishna A, Khanal SK (2017) Removal of hydrogen sulfide generated during anaerobic treatment of sulfate-laden wastewater using biochar: Evaluation of efficiency and mechanisms. Bioresour Technol 234:115–121. https://doi.org/10.1016/j.biortech.2017.03.009

Kiani S, Kujala K, T. Pulkkinen J, Aalto SL, Suurnäkki S, Kiuru T, Tiirola M, Kløve B, Ronkanen AK (2020) Enhanced nitrogen removal of low carbon wastewater in denitrification bioreactors by utilizing industrial waste toward circular economy. J Clean Prod 254:119973. https://doi.org/10.1016/j.jclepro.2020.119973

Lehmann J, Rillig M, Thies J, Masiello C, Hockaday W, Crowley D (2011) Biochar effects on soil biota - A review. Soil Biol Biochem 43:1812–1836. https://doi.org/10.1016/j.soilbio.2011.04.022

Middleton AC, Lawrence AWm (1977) Kinetics of Microbial Sulfate Reduction. J Water Pollut Control Fed 49:1659–1670

Parvage MM, Herbert R (2023) Sequential removal of nitrate and sulfate in woodchip and hematite – coated biochar bioreactor. Environ Sci Water Res Technol. https://doi.org/10.1039/D2EW00499B

Pudi A, Rezaei M, Signorini V, Andersson MP, Baschetti MG, Mansouri SS (2022) Hydrogen sulfide capture and removal technologies: A comprehensive review of recent developments and emerging trends. Sep Purif Technol 298:121448. https://doi.org/10.1016/j.seppur.2022.121448

Runtti H, Tolonen E-T, Tuomikoski S, Luukkonen T, Lassi U (2018) How to tackle the stringent sulfate removal requirements in mine water treatment—A review of potential methods. Environ Res 167:207–222. https://doi.org/10.1016/j.envres.2018.07.018

Soucek DJ, Kennedy AJ (2005) Effects of hardness, chloride, and acclimation on the acute toxicity of sulfate to freshwater invertebrates. Environ Toxicol Chem 24:1204–1210. https://doi.org/10.1897/04-142.1

Swedish Agency for Marine and Water Management (2018) Remittance on the revision of regulations (HVMFS 2013:19) on the classification on environmental quality standards with regard to surface water

Widdel F (1988) Sulfate- and sulfur-reducing bacteria. Biol Anaerob Microorg

Zhang Z, Zhang C, Yang Y, Zhang Z, Tang Y, Su P, Lin Z (2022) A review of sulfate-reducing bacteria: Metabolism, influencing factors and application in wastewater treatment. J Clean Prod 376:134109. https://doi.org/10.1016/j.jclepro.2022.134109

Lake Affected by Acid Mine Drainage – A Case of Extreme Contamination

Patrícia Gomes[1], Teresa Valente[1]

[1]*Universidade do Minho, Campus de Gualtar, Institute of Earth Sciences, 710-057 Braga, Portugal*

Abstract

Sulfide mining, commonly associated with metal and coal deposits, produces reactive wastes typically stored in piles. These wastes pose a critical environmental problem, causing acid mine drainage (AMD) and contributing to the degradation of aquatic ecosystems.

The São Domingos mine in the Iberian Pyrite Belt was closed without environmental protection. Two streams that cross this mine have several acid lakes along their 20 km length and over a relative surface area of 6,000 ha, which flows into the Chança water reservoir used for public supply. One of the acid lakes, PAT7, is particularly notable for its massive presence of sulfate efflorescence. Therefore, the main objective is to understand the mineral-water interaction processes that influence the hydrochemical behavior of this lake. For this purpose, the mining waste surrounding this lake and twelve water sampling have been carried out over a complete hydrological year.

The results indicated a highly acidic environment, as evidenced by very low pH values (0.4) and high acidity concentrations (429.25 g/L $CaCO_3$). The driest months, July and August, coincided with the most extreme results, where salts completely covered the area. However, the electrical conductivity did not show the same trend. This parameter was highest in October (26,200 µS/cm) and May (27,300 µS/cm). PAT7 also has high concentrations of potentially toxic elements (PTE): Fe (134 g/L), Al (24.8 g/L), Cu (4.42 g/L), Ti (7.83 mg/L), Pb (27.3 mg/L), and Cd (18.7 mg/L), exceeding many severe cases of AMD contamination worldwide. The Spearman correlation between sulfate and acidity is high (0.991). This is also true for most PTE, sulfates, acidity, and among the elements themselves, which typically show values around 1. These results may be related to the location of the lake. PAT7, close to the metallurgical center of the mine, has surrounding dumps of fine sulfide-rich waste from ore treatment and extraction.

Understanding the evolutionary processes undergone by the wastes and the seasonal variations is crucial to assessing the drinking water reservoir's contamination risk. In this way, the present study supports future monitoring efforts and informs the relevant authorities of the critical need for urgent environmental remediation. This is particularly important as the mine is in the Mediterranean region, facing persistent droughts and critical water shortages.

Keywords: Iberian Pyrite Belt, mining waste, hydrochemistry characterization, extreme contamination, potentially toxic elements

Acknowledgments

This work is co-funded by the framework of the UIDB/04683 and UIDP/04683 – Institute of Earth Sciences programs.

Five Years Of Hydrogeological Consulting For A Mining Company: Lessons Learned For Successful Work

Manuel Gutierrez[1], Laura Tapias[2], José Luis Delgado[3]

[1]*Itasca Chile, Providencia, Santiago, Chile. manuel.gutierrez@oneitasca.com*

[2]*Itasca Chile, Providencia, Santiago, Chile. laura.tapias@oneitasca.com*

[3]*Itasca Chile, Providencia, Santiago, Chile. joseluis.delgado@oneitasca.com*

Abstract

Mining operations face different groundwater challenges, often addressed by various consultants with differing scopes. This leads to repetitive work and knowledge loss with consultant turnover. Five years of consulting experience at a large open pit mine highlighted some key lessons. Critical data review, even repeated data, is crucial due to potential inconsistencies. Permanent peer review improves work quality, identifies issues, and generates new ideas. Long-term engagement fosters deep understanding of hydrogeological conditions, enabling knowledge sharing and building internal expertise within the mining company to address future challenges.

Keywords: Consultancy, Data Review, Mining Operation.

Introduction

Chile's expansive copper mining sector relies heavily on open pit operations, most of which penetrate below the natural water table. This necessitates significant groundwater management, presenting a range of complex challenges, as seepage in pit slopes (Fig. 1) or the reduction of pit slope stability due to pore pressure (Hoek & Bray 1981; Sullivan 2007).

Figure 1 *Pit floor flooding due to seepage.*

These challenges span different aspects such as:

- Data acquisition: This includes piezometer installation and monitoring through time, water quality sampling, and geophysical surveys.
- Hydraulic testing: Pumping and slug tests.
- Seepage and pore pressure control: Design and implementation of depressurization and drainage systems (D&D) and cut-off walls.
- Groundwater modelling: to predict inflows, pore pressures, assess environmental impacts, and optimizing water management.

Mining operations frequently engage external consultants to address these multifaceted issues. However, this often leads to a fragmented approach, with consultants tackling specific scopes, such as regional groundwater modelling for environmental impact assessments or mine-scale models for slope stability. While sometimes unavoidable, this piecemeal strategy can create inconsistencies and redundancies, especially with consultant turnover. This paper leverages five years of continuous consulting experience at a large Chilean open pit mine to discuss key lessons learned regarding data management, the importance of peer review, the advantages of long-term engagement, and the critical integration of diverse data sources.

Consultant Turnover and Knowledge Loss

Hydrogeological studies at large mines are inherently long-term endeavours, often spanning decades. Certain tasks, such as groundwater monitoring data collection, numerical model calibration and updates, and reporting, are typically repeated annually, forming a continuous cycle of investigation and refinement. This cyclical nature, coupled with the complex and evolving hydrogeological systems characteristic of mining environments, necessitates a consistent and comprehensive understanding of the site. However, the mining industry frequently experiences consultant turnover, often driven by competitive bidding processes and economic factors. This frequent change in consulting personnel presents a significant challenge to maintaining continuity and preserving institutional knowledge, leading to several detrimental consequences.

When a new consultant team takes over a project, they face a significant learning curve. They must familiarize themselves with the site's specific hydrogeological characteristics, the existing data, the conceptual and numerical models, previous reports, and the rationale behind past decisions. This process often involves repeating previous work, such as re-evaluating existing data or re-running model simulations, to gain a sufficient understanding. This duplication of effort wastes valuable time and resources, affecting project timelines and budgets. Furthermore, the time spent getting up to speed delays progress on critical tasks and potentially postpones crucial management decisions.

It must be noted that in some cases keeping a consultant for many years without implementing new technologies, or without generating extra value to the company it is not the best case, consultants should be continuously adding value to their work, being able to implement new methodologies to improve efficiency and safety to the mine operation.

The Importance of Rigorous Data Review

A critical lesson learned emphasizes the vital importance of reviewing all data, regardless of apparent similarity to previous datasets. Even when data is received repeatedly for recurring tasks, inconsistencies can arise (Fig. 2). Values for previously recorded data points may differ, suggesting potential errors in measurement, recording, or data management. Therefore, a thorough review, including comparison with historical data, is essential.

This review process not only identifies errors but also offers valuable insights into the evolution of the hydrogeological system, highlighting potential areas of concern such as changes in water levels, water quality, or seepage patterns. For example, discrepancies in piezometric data might reveal previously unknown fault zones or shifts in recharge rates. Neglecting this crucial review step can lead to flawed models and incorrect interpretations, ultimately affecting decision-making related to mine dewatering, slope stability, and environmental compliance.

The example (Fig. 2) in particular shows incoherency in data after a period of time without records, at the end this difference in measured values was caused due to change in the calibration parameters of the instrument that recorded the water levels measures, leading to different values with the new set of parameters.

The Value of Consistent Peer Review

Consistent peer review has proven invaluable, as mentioned in various groundwater numerical guidelines (Barnett *et al.* 2012), providing a crucial external perspective that identifies potential improvements and uncovers overlooked issues. Peer reviewers offer fresh ideas for fieldwork, refine conceptual models, and enhance numerical models. A structured, regular peer review process ensures the quality and robustness of hydrogeological studies, helping identify potential biases or limitations in the existing approach.

Our experience demonstrates that consistent peer review, even for repeated tasks, significantly improves overall work quality and fosters innovation. Furthermore, it facilitates the sharing of best practices and the adoption of new technologies in hydrogeological investigations.

Benefits of Long-Term Engagement:

Long-term engagement with the mine has proven crucial for developing a deep understanding of its complex hydrogeological conditions. This extended involvement allows for the observation of seasonal variations, the identification of long-term trends, and the development of a comprehensive conceptual model. This deep understanding facilitates more effective problem-solving and enables the development of tailored solutions.

For instance, a long-term perspective allows for accurate assessment of the long-term effects of mine dewatering on regional groundwater resources. Furthermore, it fosters strong relationships with mine staff, facilitating open communication and collaboration, which is crucial for effectively addressing hydrogeological challenges and ensuring studies align with the mine's operational needs.

Integrating Diverse Data Sources and Advanced Modelling:

Effective hydrogeological management requires the integration of diverse data sources, including geological data, hydrochemical

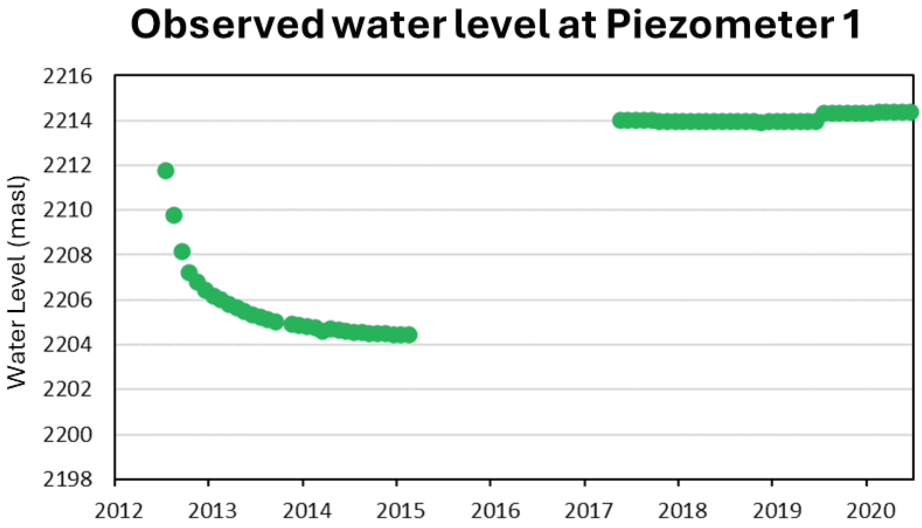

Figure 2 *Inconsistencies in measured water levels*

data, geophysical surveys, and remote sensing data. Our long-term engagement has allowed us to effectively integrate these data sources into comprehensive hydrogeological models. Furthermore, we have utilized advanced modelling techniques, such as stochastic modelling approaches, to better understand the complex interactions within the hydrogeological system. These advanced techniques allow for a more robust assessment of uncertainty and provide valuable insights for decision-making (Fig. 3).

Knowledge Transfer and Internal Expertise Development:

A significant benefit of long-term engagement is the ability to transfer knowledge to mine personnel and new consultants. We have been able to assist in training new staff, providing context for existing data, and explaining the rationale behind previous studies. This knowledge transfer helps build internal hydrogeological expertise within the mining company, enabling them to better manage groundwater-related challenges. This internal expertise is invaluable for addressing future issues, reducing reliance on external consultants for routine tasks, and ensuring continuity in hydrogeological management. This also empowers the mine to critically evaluate the work of future consultants and ensure that it aligns with their needs and objectives.

Conclusions

Our five years of consulting experience at a large Chilean open pit mine have highlighted the importance of rigorous data review, consistent peer review, long-term engagement, and the integration of diverse data sources. These practices are essential for overcoming the challenges associated with consultant turnover and ensuring the effective management of groundwater resources. By embracing these lessons, mining companies can build internal expertise, improve the quality of hydrogeological studies, and make more informed decisions regarding groundwater management. This ultimately contributes to the long-term sustainability and success of the mining operation. Further research could explore the development of standardized data management protocols and knowledge transfer mechanisms to further enhance the efficiency and effectiveness of hydrogeological consulting in the mining industry.

References

Barnett *et al.* (2012). Australian groundwater modelling guidelines, Waterlines report, National Water Commission, Canberra.

Hoek E., Bray J.W. (1981). Rock Slope Engineering, London: Institution of Mining and Metallurgy, 527.

Sullivan, T. (2007). Hydromechanical Coupling and Pit Slope Movements, in Y Potvin (ed.), Slope

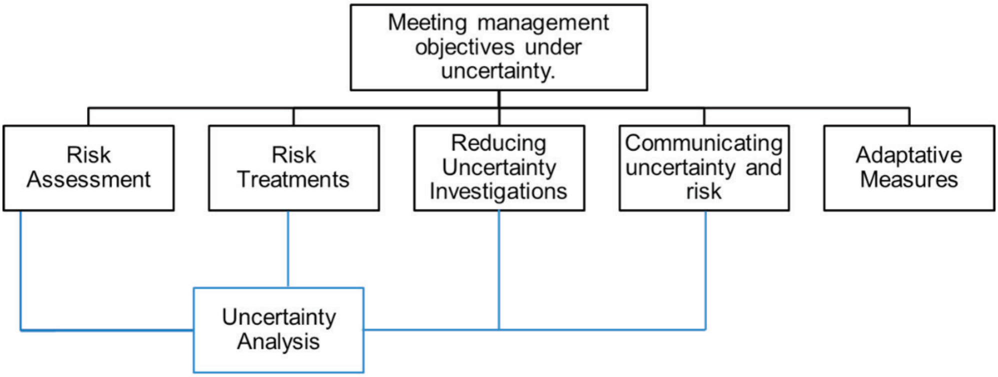

Figure 3 *Decision-making under uncertainty could be supported with long-term tasks. (Adapted from Walker 2017)*

Stability 2007: Proceedings of the 2007 International Symposium on Rock Slope Stability in Open Pit Mining and Civil Engineering, Australian Centre for Geomechanics, Perth, pp. 3-43.

Walker G. (2017). Predictive uncertainty in groundwater modelling: how is it best used? Discussion paper no.1 in Middlemis *et al.* 2019. Groundwater modelling uncertainty – implications for decision making. National Centre for Groundwater Research and Training, Australia.

Manganese(II) Removal Bioreactor System of Mine Drainage is Dominated by Chemolithotrophic Manganese Oxidizing Microorganisms

Taiki Katayama[1], Miho Watanabe[2], Naoyuki Miyata[2], Yuto Komura[1], Sereyroith Tum[1], Tetsuo Yasutaka[1]

[1] *Institute for Geo-Resources and Environment, National Institute of Advanced Industrial Science and Technology (AIST), 1-1-1 Central 7, 305-8567, Tsukuba, Ibaraki, Japan, katayama.t@aist.go.jp*

[2] *Department of Biological Environment, Akita Prefectural University, 241- 438, Shimoshinjo-Nakano, 010-0195, Akita, Japan*

Abstract

A key environmental issue at mining sites is the unregulated release of hazardous metals, particularly manganese ions (Mn(II)), from mine drainage. Conventional chemical methods for Mn removal are costly and require high pH. Mn-oxidizing bacteria (MnOB) offer a biological alternative, capable of oxidizing Mn(II) at circumneutral pH. This study investigated the use of bioreactors to treat mine drainage in Japan without the addition of organic substrates, achieving over 98% removal efficiency for Mn(II) and zinc. Metagenomic analysis revealed that chemolithotrophic MnOB, including Mn(II)-oxidizing and carbon monoxide-oxidizing bacteria, dominated the bioreactor community. Consistently, six MnOB strains isolated from the bioreactor oxidized Mn(II) under nutrient-limited conditions but not under nutrient-rich conditions, even though some strains did not exhibit cell growth under nutrient-limited conditions. These findings clearly indicate the presence of MnOB adapted to oligotrophic conditions and highlight the potential of an organic-free solution for mine drainage treatment.

Keywords: Manganese, manganese-oxidizing microorganisms, chemolithotrophs, oligotrophic

Introduction

Environmental issues related to mine drainage arise in both active and abandoned mining sites, encompassing tunnels, operational mines, open pits, waste rock heaps, and mine tailings. A key concern is the unregulated discharge of hazardous metals, with manganese ions [Mn(II)] being a major contaminant due to their high solubility and prevalence in the Earth's crust. Conventional treatment methods for Mn(II) removal from mine drainage involve chemical neutralization, where caustic agents are used to oxidize and hydrolyze Mn, requiring a high pH (>9). Subsequent reverse neutralization with acids is also employed to meet effluent standards, which contributes to the overall cost of Mn removal.

Mn-oxidizing bacteria (MnOB) offer a biological alternative, as they can oxidize Mn(II) at circumneutral pH. Microbial treatment strategies for Mn-containing mine wastewater often involve the addition of organic materials. This is because most known MnOB are heterotrophs and rely on organic substrates like carbohydrates and organic acids as sources of carbon and energy for growth. Given that many mine environments harbor poor organic substrates, the exploration of a biological Mn oxidation system that can operate effectively under oligotrophic conditions holds importance in the advancement of Mn-containing mine drainage treatment. However, little is known about microbial lifestyle involved in Mn(II) oxidation in such nutrient-limited settings. In this study, we deployed in-situ pilot-scale bioreactors to treat mine drainage containing 20 mg/L of Mn(II) and 6 mg/L of zinc (Zn(II)), without the supplementation of organic substrates, in Japan. Physiology and ecology of MnOB in the bioreactors were characterized by cultivation-dependent and -independent experiments.

Results and Discussion

Two biological contact oxidation systems were installed and operated in an underground tunnel of an abandoned mine site. Limestone was utilized as an inorganic carrier in the system for stabilization and promotion of microbial activity. The fiber filter materials were also utilized as the inorganic carriers to increase the effective volume of the bioreactors. Each system contained three water tanks with a working volume of 600 L. The reactor was filled with mine drainage without pH adjustment, and a suspension of Mn deposit collected from the drainage ditch was added as an inoculant source of MnOB.

After four months of operation, with a hydraulic retention time of 0.5 days, the system achieved more than 98% removal efficiency for both Mn(II) and Zn(II). A total of 6 MnOB strains were isolated from the bioreactor. All of these isolates can oxidize Mn(II) under nutrient-limited conditions, but not nutrient-rich conditions. Metagenomic analysis revealed that chemolithotrophic MnOB dominated the bioreactor community, likely oxidizing Mn(II) via extracellular electron transfer for energy production and CO_2 fixation. Additionally, other chemolithotrophs, such as hydrogen- and carbon monoxide-oxidizing bacteria, which possessed non-energy-yielding Mn oxidation ability, were also detected in a major proportion.

Conclusions

These findings highlight the critical role of microorganisms adapted to oligotrophic conditions in facilitating Mn(II) oxidation within bioreactors. This approach indicates potential for mine drainage remediation without the need for added organic materials, offering a cost-effective and environmentally friendly alternative. Future investigations include how costly aeration affects the Mn oxidizing activity of these MnOB.

Acknowledgements

This study was partly funded by Ministry of Economy, Trade, and Industry, Japan (METI) under the research project on Advanced Technology for Mine Drainage Treatment in Closed Mines for the year 2023 and 2024.

References

Watanabe M, Tum S, Katayama T, Gotore O, Okano K, Matsumoto S, Yasutaka T, Miyata N. (2024) Accelerated manganese(II) removal by in situ mine drainage treatment system without organic substrate amendment: metagenomic insights into chemolithoautotrophic manganese oxidation via extracellular electron transfer. J Environ Chem Eng, 12, 113314, doi:10.1016/j.bej.2023.109187

Active treatment experiments including coprecipitation-adsorption of arsenic for mine drainages in Peru

Duk-Min Kim[1], Joyce Carol Bottger-Gamarra[2], Carmen Rodriguez-Vasquez[2], Jong-Wook Jeon[3], Eun-A Choi[3], Yeon-Jun Im[3], Seyoung Kang[4]

[1]*Department of New Energy and Mining Engineering, Sangji University, Wonju, Gangwon state, Republic of Korea, kdukmin8@sangji.ac.kr, ORCID 0000-0002-1537-6866*

[2]*Ministry of Energy and Mines, Lima, Peru*

[2]*Byucksan Engineering, Seoul, Republic of Korea*

[4]*Korea Mine Rehabilitation and Mineral Resources Corporation, Wonju, Gangwon state, Republic of Korea*

Abstract

Two metalliferous mine drainages from El Triunfo 1 (ET) and Santa Teresita (ST) mines in the Ancash region of Peru were selected to assess the feasibility of (semi-) active treatment methods, including the efficiency of As coprecipitation with Fe in inflows. Elevated concentrations of Al, Fe, Mn, and Zn at both mine drainages were reduced to target levels at pH 10. Additionally, the As concentration of 1.69 mg/L at the ET mine was reduced by approximately 93%, reaching 0.124 mg/L at pH 10, suggesting that coprecipitation and adsorption by Fe in the mine drainage played a substantial role in As removal.

Keywords: Active treatment, coprecipitation of arsenic, manganese, Peru, mine drainage

Introduction

Peru is the second largest producer of Cu and Zn in the world. Mining of porphyry copper ores and hydrothermal multimetal ores leads to the enrichment of various metals, often resulting in water contamination by Al, As, Cd, Fe, Mn, and Zn. Therefore, it is essential to assess the feasibility of conventional (semi-)active treatment methods, including the efficiency of As coprecipitation with Fe in inflows.

Methods

Two metalliferous mine drainages of El Triunfo 1 (ET) and Santa Teresita (ST) in the Ancash region were selected. ET adit drainage exhibited Al, As, Cd, Fe, Mn, and Zn concentrations of 13.5, 1.69, 0.084, 31.3, 7.73, and 21.0 mg/L, respectively, while ST adit drainage exhibited Al, Cu, Fe, Mn, and Zn concentrations of 15.1, 0.49, 11.4, 43.1, and 6.79 mg/L, respectively.

Hydrated lime was injected into ET and ST mine drainages in stepwise. At each step, pH, Eh, electrical conductivity (EC), and dissolved oxygen (DO) concentration were analyzed using Hach HQ 2200 multimeters immediately after sampling. Alkalinity was determined using Hach AL-DT digital titrator. Collected samples were filtered using 0.45 μm syringe filter papers and samples for cation analysis were acidified to $pH < 2$ using concentrated nitric acid. Cations were analyzed using a inductively coupled plasma optical emission spectroscopy (ICP-OES) at the Certimin, Lima, Peru. Anions were analyzed using a ion chromatography (IC) at the Certimin, Lima, Peru. Relative standard deviations (RSD) were less than 5% for ICP-OES and IC analyses.

Results and discussion

Increasing pH to 9.0 resulted in reductions of Cd, Cu, Fe, and Zn concentrations to below 0.03, 0.02, 0.2, and 0.2 mg/L, respectively, at both ET and ST mine drainages, meeting effluent standards. However, decreasing Mn concentrations to <1.3 mg/L required an increase in pH to 10.0 at both mines. While Al concentration increased slightly due to redissolution at these pH levels, they remained below 0.7 mg/L. In the ET drainage, As concentrations were reduced by approximately 93%, reaching 0.124 mg/L at pH 10, suggesting that coprecipitation and adsorption by Fe in the mine drainage played a substantial role. Further reduction of As concentrations to below 0.08 mg/L by adsorption is still necessary to meet effluent standards.

Conclusion

The Fe present in the mine drainage facilitated a reduction in As concentration by up to 93% through coprecipitation and adsorption. Given the diversity of contaminants in these mine drainages, this treatment approach could be applied to a wide range of mine sites where contamination by Al, As, Cd, Cu, Fe, Mn, and Zn is a concern.

Acknowledgements

This work was supported by the Korea International Cooperation Agency (KOICA) through a project (Improving Peru's Mine Closure and Mining Environmental Liabilities Remediation Procedure in Support of SDG Achievement). The authors gratefully acknowledge the contributions of the people at Ministry of Energy and Mines, Peru, for conducting experiments.

Passive treatment experiments including slag reactor and As adsorption reactor for mine drainages in Peru

Duk-Min Kim[1], Carmen Rodriguez-Vasquez[2], Joyce Carol Bottger-Gamarra[2],
Jong-Wook Jeon[3], Eun-A Choi[3], Yeon-Jun Im[3], Seyoung Kang[4]

[1]*Department of New Energy and Mining Engineering, Sangji University, Wonju, Gangwon state, Republic of Korea, kdukmin8@sangji.ac.kr, ORCID 0000-0002-1537-6866*

[2]*Ministry of Energy and Mines, Lima, Peru*

[2]*Byucksan Engineering, Seoul, Republic of Korea*

[4]*Korea Mine Rehabilitation and Mineral Resources Corporation, Wonju, Gangwon state, Republic of Korea*

Abstract

Drainages from two mines in the Ancash region of Peru were enriched with Al, As, Fe, and Mn, and Zn. Both pilot-scale and laboratory-scale slag reactors were employed to remove Mn and Zn. The column system effectively reduced Mn and Zn concentrations to <0.1 mg/L for both mines, with a residence time of 14.4 hrs in the slag reactor. Additionally, As was removed to <0.09 mg/L, likely due to coprecipitation and adsorption by Fe, even in the absence of a dedicated As adsorption reactor. These results suggest efficacy of the complex passive treatment system to treat Al, As, Fe, Mn, and Zn as well as possible utilization of coprecipitation-adsorption by Fe to reduce As and Zn concentrations in passive treatment system. The adsorption efficiency can be further enhanced by design improvement in the future.

Keywords: Slag reactor, arsenic adsorption, manganese treatment, Peru, mine drainage

Introduction

Peru is the second largest producer of Cu and Zn in the world. Its porphyry copper ores and hydrothermal multimetal ores are rich in various metals, which can lead to water contamination by Al, As, Cd, Fe, Mn, and Zn. To address this, eco-friendly, low-carbon, and cost-efficient passive treatment technologies are crucial for metalliferous mines.

Methods

Among several candidate mines, two metalliferous mine drainages of El Triunfo 1 (ET) and Santa Teresita (ST) in the Ancash region, Peru, were selected. The ET adit drainage exhibited high concentrations of Al (13.5 mg/L), As (1.69 mg/L), Cd (0.084 mg/L), Fe (31.3 mg/L), Mn (7.73 mg/L), and Zn (21.0 mg/L). Meanwhile, the ST adit drainage had high concentrations of Al (15.1 mg/L), Cu (0.49 mg/L), Fe (11.4 mg/L), Mn (43.1 mg/L), and Zn (6.79 mg/L). Both pilot-scale and laboratory-scale slag reactors were employed to remove Mn and Zn, following the treatment of Al and Fe by SAPS and oxidation pond system, for both mines.

Columns to treat ET drainage consisted of SAPS, VFR (Vertical Flow Reactor), and slag reactor, while the columns for ST drainage consisted of SAPS and slag reactor. Diameter and height of each column was 50 mm and 300 mm, respectively, and the flow direction was downward. SAPS column had a upper organic matter layer of 45 mm and a lower limestone layer of 150 mm. Volume of water in the limestone pore space was 147 mL. VFR column had a limestone layer of 45 mm and a open water layer of 175 mm. Total volume of water in the open water and limestone pore was 417 mL. Slag reactor column had a layer of steel slag mixed with limestone of 150 mm. The volumetric mixing ratio between the steel slag and limestone was 4:6. Porosity and pore volume of the mixed substrate were 36% and 141 mL, respectively. The outflow tube of each column was hung to the column at a specific level to maintain the water level in the column. ET and ST drainages flowed into each column set using a peristaltic pump.

Additionally, As adsorption reactor was applied for ET drainage. The drainage was pretreated using limestone and steel slag to decrease Al, Fe, Mn, and Zn concentrations. The adsorbent used was CMDS-bead, which was a bead-shape adsorbent made from Fe-rich sludge from a coal mine drainage treatment facility in South Korea. Upward flow was applied with empty bed contact time (EBCT) of 20 min.

Pilot-scale treatment facilities for both mines consisted of SAPS 1 - Settling pond/VFR 1 – SAPS 2 – Settling pond/VFR 2 – Slag reactor – Aerobic wetland – As adsorption reactor. Two consecutive series of SAPS and settling pond/VFR were applied due to the excessive acidity at both mines. Settling ponds were designed to be able to be converted to VFR. After accumulation of Fe-rich sludge, the flow will be changed from horizontal to vertical direction to induce enhanced adsorption of As by the Fe sludge layer. Aerobic wetland was installed to decrease pH again after the slag reactor.

The inflow and outflow samples for the column sets and each pilot-scale treatment unit were collected and actual flow rates were measured using a bucket-and-stopwatch method. Electrical conductivity (EC), temperature, pH, and dissolved oxygen (DO) concentrations were analyzed using Hach HQ2200 multimeters immediately after sampling. Alkalinity was determined using Hach AL-DT digital titrator. Collected samples were filtered using 0.45 μm syringe filter papers and samples for cation analysis were acidified to pH < 2 using concentrated nitric acid. Cations were analyzed using a inductively coupled plasma optical emission spectroscopy (ICP-OES) at the Certimin, Lima, Peru. Anions were analyzed using a ion chromatography (IC) at the Certimin, Lima, Peru. Relative standard deviations (RSD) were less than 5% for ICP-OES and IC analyses.

Results and discussion

Column experiments

The column system could decrease Mn and Zn concentrations to <0.1 mg/L for both mines, with a residence time in the slag reactor of 14.4 hrs. Effluent standard in Peru for Zn concentration is 1.5 mg/L, and stream water quality standard in Peru for Mn concentration is 0.2 mg/L. The effluents met those standards with a much higher efficacy. Mn and Zn may have been precipitated as hydroxides and carbonates in the slag reactor which may have increased pH sufficiently. The pH values of final outflow samples were 7.7–8.8, which was decreased again by dissolution of atmospheric CO_2 after the slag reactor.

Concentrations of Al, Cd, Cu, and Fe decreased to <0.8, <0.001, <0.01, and <0.2 mg/L, respectively. These values were far less than the effluent standard concentrations in Peru for Cd, Cu, and Fe, which are 0.05, 0.5, and 2 mg/L. Moreover, As was removed to <0.09 mg/L, which was less than the effluent standard of 0.1 mg/L in Peru. This was likely due to coprecipitation and adsorption by Fe, even without an As adsorption reactor.

Additionally, in the adsorption column experiment for As removal, the reactor successfully decreased As concentrations from 1.69 mg/L to <0.008 mg/L.

Pilot-scale experiments

At ET mine, treatment efficiencies were assessed after five months of the pilot-scale system installation. At the SAPS 1, pH increased from 4.70 to 6.37, to decrease Al concentration from 7.93 to 0.07 mg/L. Zn concentration also decreased from 19.00 to 1.32 mg/L. As the pH was not high enough to precipitate Zn hydroxides, precipitation of Zn carbonates and sulfides and/or adsorption onto Fe (oxy)hydroxides and coprecipitation with Fe which decreased from 92.6 mg/L to 41.8 mg/L may have decreased Zn concentrations. At Settling pond 1, Fe was efficiently oxidized to be 0.12 mg/L. During this process, As concentration decreased from 2.04 mg/L to 0.35 mg/L by adsorption and/or coprecipitation by Fe. At the slag reactor, Mn concentration decreased from 4.3 to 2.5 mg/L at pH of 8.54. As the DO concentration and Eh of slag reactor inflow were only 2.25 mg/L and -5 mV, the reducing condition may have inhibited the oxidative treatment of Mn. Organic matter still flowed out from the organic matter layer of SAPS 2 to make reducing conditions in following treatment units.

Conclusion

Given the broad spectrum of contaminants addressed in these mine drainages, the passive treatment technology demonstrated here can potentially be expanded to treat diverse mine drainages contaminated with Al, As, Cd, Cu, Fe, Mn, and Zn. The results in this study suggest efficacy of the combined passive treatment system as well as the possible utilization of coprecipitation-adsorption by iron to reduce As and Zn concentrations in passive treatment system. The As adsorption efficiency by Fe in mine drainages can be further enhanced by design improvement in the future.

Acknowledgements

This work was supported by the Korea International Cooperation Agency (KOICA) through a project (Improving Peru's Mine Closure and Mining Environmental Liabilities Remediation Procedure in Support of SDG Achievement). The authors gratefully acknowledge the contributions of the people at Ministry of Energy and Mines, Peru, for conducting experiments.

Factors Controlling Manganese(II) Removal Efficiency in a Passive Treatment Bioreactor with Mn(II)-Oxidizing Microorganisms

Yuto Komura[1], Taiki Katayama[1], Tetsuo Yasutaka[1], Sereyroith Tum[1], Miho Watanabe[2], Naoyuki Miyata[2]

[1]Institute for Geo-Resources and Environment, Geological Survey of Japan (GSJ), National Institute of Advanced Industrial Science and Technology (AIST), 1-1-1, Higashi, Tsukuba, Ibaraki, 305-8567, Japan

[2]Department of Biological Environment, Akita Prefectural University, 241- 438, Shimoshinjo-Nakano, Akita, 010-0195, Japan

Abstract

A pilot-scale bioreactor with Mn(II)-oxidizing microorganisms achieved 98% Mn(II) removal without added organic substrates. To assess its stability and applicability, a lab-scale bioreactor was used to examine the effects of water temperature and pH. Mn(II) removal rate declined from 95% to 88% as temperature decreased from 15 °C to 6 °C. Even from acid mine drainage with a pH2.6, over 90% Mn(II) removal was achieved when pH exceeded 7 due to limestone neutralization. These findings highlight the importance of pH control and temperature stability for maintaining high Mn(II) removal efficiency in this bioreactor.

Keywords: Mine drainage, passive treatment, Mn(II)-oxidizing microorganisms, pH, temperature

Introduction

Removal of manganese (Mn) from mine drainage using active treatment requires the addition of large amounts of caustic chemical reagents to precipitate Mn ions [Mn(II)] (Neculita and Rosa 2019). To reduce the cost associated with chemical reagents, a pilot-scale passive treatment bioreactor system with Mn(II)-oxidizing microorganisms was installed at Legacy Mine X. This system removed 98% Mn(II) from mine drainage including 20 mg/L of Mn(II) without the need for additional organic substrates (Watanabe *et al*. 2024; Tum *et al*. 2024). Given that mine drainage is typically poor in organic matter, this bioreactor is effective for the passive treatment of mine drainage (Miyata *et al.* 2024). However, in the winter of 2023, when the water temperature decreased, the Mn(II) removal rate of the bioreactor declined by nearly 50%, indicating that maintaining stable operation remains a challenge. Moreover, the pilot-scale tests have only been conducted using mine drainage with a neutral pH where Mn(II)-oxidizing microorganisms naturally occur, so it remains unclear whether the bioreactor is applicable to acidic mine drainage from other mine sites. In this study, to ensure stable operation and assess its applicability to acidic mine drainage sources, a laboratory-scale bioreactor was set up to evaluate the effects of temperature and acid mine drainage.

Methods

The Lab-scale bioreactor used in this study was divided into 5 lanes, each lane is filled with limestone medium inoculated with Mn(II)-oxidizing microorganisms from the pilot-scale bioreactors at Legacy Mine X (Sunouchi *et al*. 2022) (Fig. 1).

To evaluate the effect of temperature, and establish stable operating conditions for the pilot-scale bioreactor, mine drainage from Legacy Mine X (pH7.4, Mn(II) concentration of 20 mg/L) was used, with water temperature set at 15 °C, 10 °C and 6 °C.

Under each temperature condition, the mine drainage was continuously supplied to 3 lanes of the lab-scale bioreactor. Hydraulic retention time (HRT) was set to 0.3 days, which corresponds to the HRT during the period when Mn(II) removal rate decreased in the pilot-scale bioreactor.

To investigate the applicability of this bioreactor to acidic mine drainage from other mines, 10 mg/L of Mn(II) containing acid mine drainage sourced from Mine Y (pH2.6) and Mine Z (pH2.8) was used. Each mine drainage was initially supplied at HRT = 4 days and then increasing the flow rate to HRT = 1 day at a temperature of 15 °C.

Mn(II) concentrations and pH were measured at both the inlet and outlet of the bioreactor. Sludge precipitated on the limestone medium was collected for 16S rRNA gene amplicon sequencing at the end of each experimental run.

Result and discussion

As a result of the temperature evaluation, the average Mn(II) removal rate in the lab-scale bioreactor decreased from 95% to 88% as the temperature decreased from 15 °C to 6 °C. On the other hand, in the pilot-scale passive treatment bioreactor system at Legacy Mine X, Mn(II) removal rate decreased by nearly 50% in winter (December 2022 to February 2023), when the water temperature in the bioreactor dropped from approximately 15 °C to 12 °C. Therefore, the nearly 50% decrease in Mn(II) removal rate in the pilot-scale bioreactor cannot be attributed solely to the effect of water temperature.

The investigation of pH effects revealed that a strong positive correlation ($r = 0.92$) was observed between pH and Mn(II) removal rate, indicating that pH significantly influences Mn(II) removal of the bioreactor. At a low flow rate of HRT = 4 days, the pH of both mine drainages increased to above 7 because of reaction with limestone in the lab-scale bioreactor, and more than 90% Mn(II) removal was achieved. However, when the flow rate was increased to HRT=1 day, the pH in the lab-scale bioreactor dropped to 4.5, and the Mn(II) removal rate also decreased to a minimum of nearly 1%.

Based on Bray-Curtis dissimilarity calculated from amplicon sequencing variants, the decrease in pH from 7 to 4.5 caused more than 2.5 times greater changes in β-Diversity of the microbial community compared to the temperature decrease from 15 °C to 6 °C.

Conclusions

The lab-scale bioreactor removed over 90% of Mn(II) even from pH2.6 mine drainage due to the neutralization effect of limestone. This suggests that the Mn(II)-oxidizing bioreactors operating without organic substrates, has wide applicability for treatment of mine drainage treatment, which is often acidic and poor in organic matter. On the other hand, water temperature is not considered a major factor contributing to the nearly 50% decrease observed in the pilot-scale passive treatment bioreactor system. Identifying other environmental factors that affect Mn removal rate of the bioreactor remains an important challenge.

Acknowledgements

The authors sincerely appreciate the efforts of all co-organizers in hosting the IMWA 2025 Conference. This study was funded by Ministry of Economy, Trade, and Industry, Japan (METI) under the research project on Advanced Technology for Mine Drainage Treatment in Closed Mines for the year 2023 and 2024. The funders had no role in the study design, data collection, data analysis, or decision to publish.

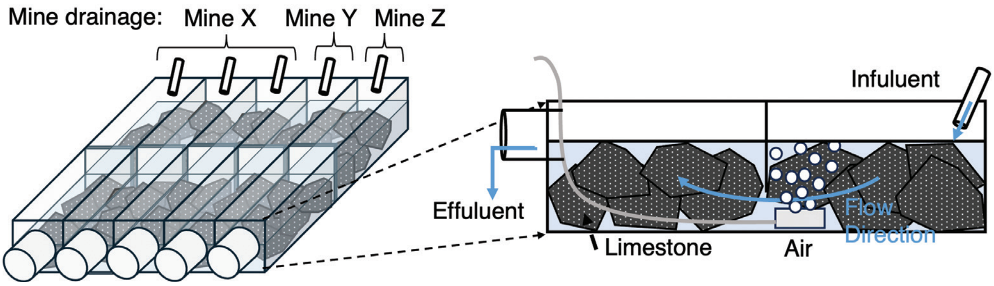

Figure 1 The schematic illustrates of Laboratory-scale bioreactor.

References

Neculita C M, Rosa E (2019) A review of the implications and challenges of manganese removal from mine drainage, Chemosphere 214: 491–510, doi: 10.1016/j.chemosphere.2018.09.106

Miyata N, Suganuma R, Sunouchi K, Okano K, Fuchida S, Watanabe M, Fujibayashi M, Sato Y, Tokoro C (2024) Biological Mn(II) oxidation under organic substrate-limited conditions and its application in mine drainage remediation. Biochem Eng J 203:109187, doi:10.1016/j.bej.2023.109187

Watanabe M, Tum S, Katayama T, Gotore O, Okano K, Matsumoto S, Yasutaka T, Miyata N (2024) Accelerated manganese(II) removal by in situ mine drainage treatment system without organic substrate amendment: Metagenomic insights into chemolithoautotrophic manganese oxidation via extracellular electron transfer. J Environ Chem Eng 12:113314, doi:10.1016/j.bej.2023.109187

Tum S, Katayama T, Miyata N, Watanabe M, Hashimoto Y, Nishikata M, Yasutaka T (2024) Geochemical insights and model optimisation for pilot-scale passive treatment of manganese and zinc in a legacy mine in Japan. Heliyon 10:e40363. doi:10.1016/j.heliyon.2024.e40363

Sunouchi K, Watanabe M, Okano K, Masaki Y, Sakoda M, Miyata N (2022) Removal of Mn(II) and Zn(II) Ions from Synthetic Mine Drainage Using a Laboratory-Scale Mn(II)-Oxidizing Bioreactor. Jpn J Water Treatment Biol 58:25-34, doi:10.2521/jswtb.58.25

Phytoremediation of Mine Influenced Waters: Comparing the Efficiency of Alyssum, Virginia Mallow and Giant Miscanthus in Removing Metals

Martyna Lalik[1]

[1]*University of Silesia, Faculty of Natural Sciences, Będzińska 60, 41–205 Sosnowiec, Poland, martyna.lalik@us.edu.pl, ORCID 0009-0007-2515-2800*

Abstract

Mine influenced waters, rich in metals, pose a significant environmental challenge due to their toxicity and potential effects on ecosystems and human health. The contamination of mine-influenced waters with metals such as chromium (Cr), cadmium (Cd), copper (Cu), mercury (Hg), nickel (Ni), lead (Pb), and zinc (Zn) represents one of the most pressing ecological challenges. Given the toxicity of these elements to living organisms and their persistence in the environment, developing effective and sustainable methods for their removal is a priority. Phytoremediation, which utilizes the natural ability of plants to accumulate metals, offers a promising alternative to costly physicochemical technologies.

The review of studies and experiments focused on phytoremediation using Giant Miscanthus (Miscanthus × giganteus), Virginia Mallow (Sida hermaphrodita), and Alyssum (Alyssum spp.). The comparison of the plants' effectiveness in environmental remediation was based on the bioconcentration factor (BCF), bioaccumulation factor (BF), and translocation factor (TF).

Research findings revealed that Virginia mallow exhibits higher accumulation capacities for metals such as zinc (Zn) and cadmium (Cd), attributed to its well-developed root system and biomass accumulation capabilities. Conversely, giant miscanthus, due to its rapid biomass growth and tolerance to harsh environmental conditions, effectively removes contaminants on a larger scale, making it more efficient overall. Studies on alyssum indicated that its capacity for cadmium (Cd) and nickel (Ni) accumulation is considerable in controlled conditions; however, its effectiveness in water remediation is limited compared to other studied species, and it cannot be classified as a suitable accumulator for pollutants. The results highlight that the efficiency of phytoremediation depends on environmental factors such as pH, metal availability, and the physicochemical characteristics of soil and water. Additionally, employing supportive technologies, such as the addition of chelators or microorganisms that enhance plant growth, can further improve the efficiency of this process.

The potential of phytoremediation as a tool for reducing metals is substantial. Environmental remediation using this method aligns with sustainable development principles and is economically advantageous compared to traditional remediation methods. Field studies, the integration of various approaches, and the development of supporting technologies can further enhance the effectiveness and applicability of this technology in the removal of pollutants from mine influenced waters.

Keywords: Phytoremediation, metals, mine influenced waters, contamination

References

Bang J, Kamala-Kannan S, Lee KJ, Cho M, Kim CH, Kim YJ, Bae JH, Kim KH, Myung H, Oh BT (2015) Phytoremediation of Heavy Metals in Contaminated Water and Soil Using Miscanthus sp. Goedae-Uksae 1. International Journal of Phytoremediation, 17(6), 515–520, doi: 10.1080/15226514.2013.862209

Kocoń A, Jurga B (2017) The evaluation of growth and phytoextraction potential of Miscanthus x giganteus and Sida hermaphrodita on soil contaminated simultaneously with Cd, Cu, Ni, Pb, and Zn. Environmental Science and Pollution Research, 24, 4990-5000, doi: 10.1007/s11356-016-8241-5

Nurzhanova A, Pidlisnyuk V, Abit K, Nurzhanov C, Kenessov B, Stefanovska T, Erickson L (2019) Comparative assessment of using Miscanthus× giganteus for remediation of soils contaminated by heavy metals: a case of military and mining sites. Environmental Science and Pollution Research, 26, 13320-13333 , doi: 10.1007/s11356-019-04707-z

Pusz A, Wiśniewska M, Rogalski D (2021) Assessment of the Accumulation Ability of Festuca rubra L. and Alyssum saxatile L. Tested on Soils Contaminated with Zn, Cd, Ni, Pb, Cr, and Cu. Resources, 10(5), 46, doi: 10.3390/resources10050046

Mine Water in the Global Industry Standard on Tailings Management

Kevin Leahy[1], Thomas Collin[2], Sia Tanhai[3], Simon Gibbons[4]

[1]*ERM UK Ltd., Suite 15 & 25, New Barclay House, 234 Botley Road, Oxford, OX2 0HP, United Kingdom, kevin.leahy@erm.com*

[2]*ERM UK Ltd., 4th Floor, One New York Street, Manchester, M1 4HD, United Kingdom, thomas.collin@erm.com, ORCID 0000-0002-8883-2594*

[3]*ERM UK Ltd., 5 Callaghan Square, Suite C, 2nd floor, CF10 5BT, Cardiff, United Kingdom, sia.tanhai@erm.com*

[4]*ERM UK Ltd., 1st floor, 40 Queen Square, Bristol, BS1 4QP, United Kingdom, simon.gibbons@erm.com*

Abstract

Brumadinho and Samarco Mariana tailings storage facilities (TSF) failures in Brazil caused deaths and environmental damage, prompting the Global Industry Standard on Tailings Management (GISTM) in 2020. The International Council on Mining and Metals (ICMM) required members to disclose information on extreme and very high consequence TSFs by 2023 and all TSFs by 2025. This study analyses the integrated knowledge base developed for 56 TSFs across various geographies and commodities, assessing data sufficiency across 25 water topics. Despite generally high compliance, systematic gaps exist globally. The findings are relevant to mining companies, environmental professionals, and the ICMM for GISTM compliance.

Keywords: Integrated knowledge base, Global Industry Standard on Tailings Management, Gap analysis

Introduction

The catastrophic failures of the Brumadinho and Samarco Mariana tailings dams in Brazil resulted in hundreds of fatalities and widespread environmental devastation, highlighting the urgent need for improved tailings storage facility (TSF) management. Tailings dams continue to fail at an alarming rate (Islam and Murakami 2021, Rana, *et al.* 2022). These events spurred the development of the Global Industry Standard on Tailings Management (GISTM), released in August 2020 by the International Council on Mining and Metals (ICMM), the United Nations Environment Programme, and the Principles for Responsible Investment (ICMM; UN Environment Programme; PRI 2020). GISTM aims to establish a comprehensive framework for TSF safety, with ICMM requiring its members – some of the largest mining corporations globally – to implement the standard for extreme and very high consequence TSFs by August 2023, and for all TSFs by August 2025.

GISTM comprises six topics and 15 principles encompassing up to 77 requirements for TSFs. Mine water management is explicitly addressed in four critical areas: (i) breach modelling, (ii) the knowledge base, (iii) tailings water management, and (iv) mine water balance. Breach modelling estimates the potential inundation area in the event of a dam failure. The knowledge base demands a comprehensive characterisation of the TSF site, integrating climate data, geomorphology, geology, hydrology, and water usage patterns, among other factors. Tailings water management requires ongoing monitoring of water levels, seepage, pore pressure, and surrounding water bodies, while the mine water balance emphasises the need for a holistic water accounting approach at the catchment and mine site scale.

This paper explores the integral role of mine water in achieving GISTM compliance by drawing from extensive data analysis conducted in developing integrated knowledge bases for TSFs ahead of the

GISTM disclosures. A total of 56 TSFs at 53 mines or former mine sites are used to investigate compliance against water-related topics, and reflect on the wider implications of knowledge gaps for TSF management. The 53 selected mines are from 13 nations across Africa, Australasia, the Americas and Europe, that produced copper, nickel, lead, zinc, aluminium, vanadium, chromium, gold, silver, platinum, molybdenum and cobalt, as well as examples of TSFs at non-metal mines with four from coal mines.

Methods

ERM developed a staged approach to build Integrated Knowledge Bases (IKB) supporting the GISTM Disclosures, including: (i) logging documents held by the mining companies, (ii) logging data against the specific topics, (iii) extracting the relevant information, (iv) conducting a data gap analysis for each topic, (iv) review by the mine team and update of the gap analysis.

In total, 3,502 documents were logged, and 11,646 data inputs were extracted, covering the 56 TSFs, against eight main topics: (1) Basemapping, (2) Environment, (3) Geology, (4) Historic environment, (5) Hydrology, (6) Infrastructure, (7) Site Infrastructure, and (8) Socio-Economic. The focus of this paper is on sub-topics broadly related to water management (Tab. S-1 in Supplementary Material). Following data extraction, knowledge gaps were assessed against each topic, and conversations with mine teams were undertaken to discuss these with the intention to fill these gaps.

Technical data on the 56 TSFs was extracted from the Global Tailings Portal (GRID-Arendal 2020) which has been developed based on responses from the "Investor Mining and Tailings Safety Initiative" launched by The Church of England Pensions Board and The Council on Ethics of the Swedish National Pension Funds (Church of England 2019). Specifically, this included data relating to the status (active, inactive and closed), and the construction year and design (Tab. 1).

The analysis then considered if there was or was not sufficient water-related data such that a given TSF could be considered as compliant with the requirements of the IKB within GISTM and if not then what gaps remained. A data gap is defined as a missing dataset, or one considered insufficient to be complaint with the GISTM requirement. For example, if a TSF lacked groundwater monitoring records, this was classified as a data gap under the "Groundwater Quality". In this analysis, compliance referred to whether a TSF was considered to have sufficient, relevant and up-to-date water-related data to meet requirements within GISTM.

Many aspects of the IKB can be obtained by accessing online databases, either freely or supplied by third parties, such as mapping of water courses, locations of licenced landfills or private well locations. This analysis excludes these generic, free or third-party water data that are generally available. Instead, the 56 TSFs were assessed if there was or was not sufficient data for 25 specific and comparable water topics within, or as a

Table 1 *Location, construction decade and status of the studied TSFs.*

	Construction decade								Status		
Region	Pre-1950	1950	1960	1970	1980	1990	2000	2010	Active	Inactive	Closed
Africa		1			1	3	6	2	12	2	0
Australasia		1		1		3			3	1	1
Eurasia	*2*	1	2	1					2	1	3
North America	1	1	4	3	1	2		1	6	3	7
South America				1	4	4	1	1	6	2	3
Total	3	4	6	6	6	12	7	4	29	9	14

Notes: 'Active' refers to facilities currently receiving tailings material from on-going mining operations, 'Inactive' are facilities not presently receiving tailings but not yet fully closed, 'Closed' refers to facilities for which the closure plan has been implemented and has been approved by the competent authorities.

sub-set of, the eight categories such that they could be considered as compliant with the requirements of the IKB within GISTM, or if not, what the number of gaps were. The 25 specific topics are listed and defined in Tab. S-1 in Supplementary Material.

Results

Compliance and Status

The average compliance rate across the 25 studied topics was evaluated at 65%, 74% and 70% for active, closed and inactive TSFs respectively (Fig. 1) with a statistically significant difference observed between active and closed TSFs (t-test, α = 0.1). This difference is likely to be explained by the additional data required to attain 'closed' status in most jurisdictions, which implies that active TSFs are more likely to have inadequate water data, not only to comply with GISTM but also to attain closure.

Compliance and Geographies

The median compliance values with water topics that are required for a complete IKB, as assessed across the 25 studied topics, were relatively consistent regardless of mine location, including Africa, Australasia, and North and South America (Fig. 2). However, Eurasian mine sites demonstrated a distinct compliance pattern with three sites out of six having a compliance of 36%. Notably, these three sites, located in the same country, achieved the lowest compliance across the sample, hinting at region-specific challenges.

The relatively uniform median compliance across regions suggests that broad challenges to achieving GISTM compliance are shared globally, such as limitations in data availability, monitoring infrastructure, or technical expertise.

Compliance and Construction decade

The most notable observation when assessing average compliance with the TSF construction decade and status (Tab. 2), are the lower levels of compliance for older active facilities. To illustrate, facilities built before the 1980s had an overall compliance of around 50% while active facilities built since the 1980s are around 70% compliant. This may relate to a focus on business-as-usual operations at older active TSFs that probably underwent little or no environmental impact assessment at the time of construction and during early

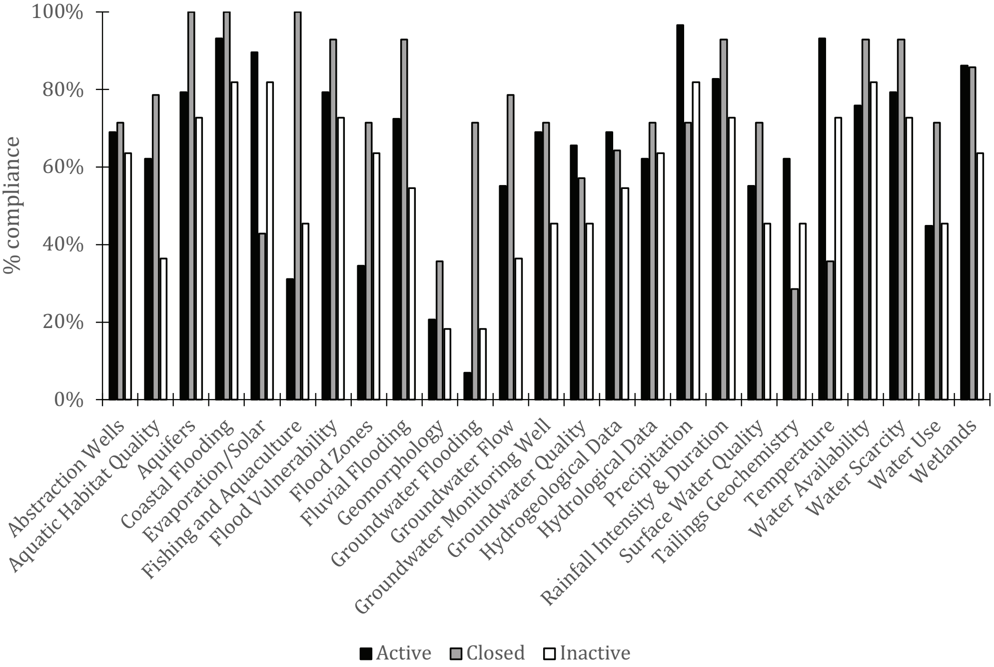

Figure 1 *Evaluated compliance across all water-related topics.*

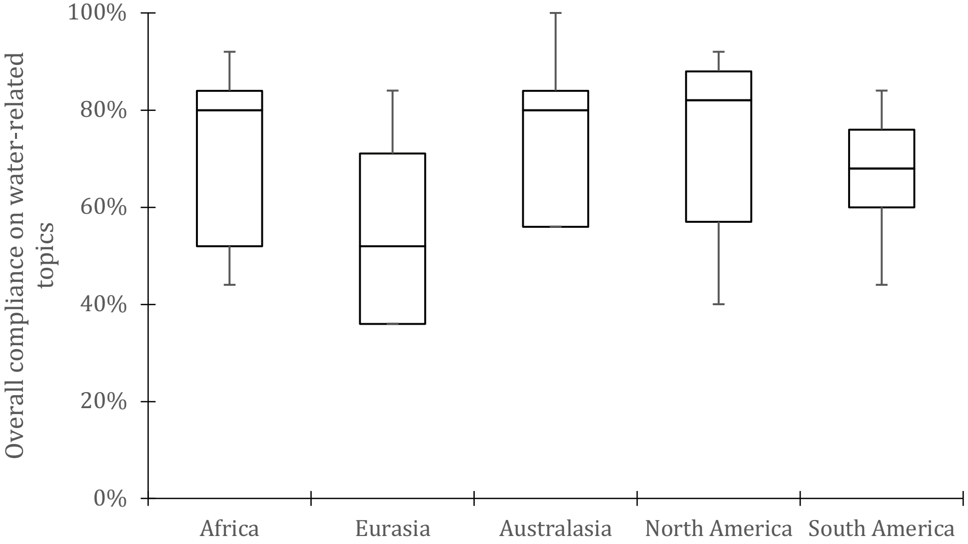

Notes: the lower end of the box represent the first quartile (Q1), the median is the line inside the box, and the third quartile (Q3) is the upper end of the box, representing the 25th, 50th and 75th respectively. The whiskers indicate both minimum and maximum values.

***Figure 2** Average TSF compliance reported against geographies.*

operations, with few drivers prior to GISTM to more fully understand the water context.

General Patterns of Compliance

Overall, of the 25 topics assessed, Geomorphology and Groundwater Flooding were the least understood and had the highest number of data gaps (Fig. 1). By contrast, topics relating to Climate Change (i.e. Flood Vulnerability, Rainfall Intensity & Duration, Water Scarcity) were generally covered for most TSFs. Often this data was found to have been obtained from Climate Change Risk Assessments or by utilising third-party data, such as the World Resources Institute's Aqueduct (World Resources Institute 2024). However, reliance on external datasets did not always guarantee that climate change effects were adequately accounted for at the TSF level, potentially leading to site-specific risks being overlooked.

Similar observations were made for the Aquifers and Water Availability topics, which were often addressed using third-party datasets. This highlights an important implication: while leveraging third-party data can bridge knowledge gaps, it should be supplemented by localised assessments tailored to the specific context of each TSF. Without such localised assessments, there is a risk of overlooking critical factors that could compromise TSF safety and water

***Table 2** Evaluated compliance based on status and construction decade.*

Construction decade	Active	Inactive	Closed
Pre-1950s	–	–	87%
1950s	50%	36%	65%
1960s	48%	–	86%
1970s	55%	76%	40%
1980s	73%	56%	72%
1990s	72%	81%	78%
2000s	73%	–	72%
2010s	69%	–	–

management strategies, particularly in areas with complex or poorly understood hydrogeological settings.

Notably, only one TSF out of the 56 studied achieved full compliance with the water-related topics for the IKB, pointing to a significant and systemic gap in meeting GISTM requirements at TSFs globally.

Compliance gaps

A lack of available data was identified as the most prevalent data gap by far, accounting for 79% of all deficiencies. The second most common gap, representing 15%, was categorised as "limited coverage," which referred to instances where data existed but did not encompass the inundation area, estimated by Breach Analysis to simulate the case of TSF failure.

Geomorphology, identified as the least compliant topic (Fig. 1), was predominantly associated with a lack of available data (Fig. 3). However, further discussions with subject matter experts suggested that this issue might not solely result from data unavailability but also from a fundamental lack of clarity regarding what data should be collected and analysed for this topic. This gap underscores the need for clearer guidance on geomorphological parameters. Specifically, it may prompt the need to incorporate a clear definition under Requirement 2.2 of GISTM explicitly outlining the parameters to be assessed ensuring consistency in interpretation across stakeholders.

Notably, "limited coverage" was particularly significant for groundwater-related topics, such as groundwater monitoring wells and groundwater quality (Fig. 1). This gap highlighted that groundwater monitoring was often confined to the immediate vicinity of the TSF, failing to comprehensively evaluate effects within the inundation area. Given the potential correlation between groundwater flow direction and the inundation area—likely influenced by local topography—this limitation raised concerns about inadequate groundwater monitoring downgradient of some TSFs, where seepage could have affected groundwater quality. However, further research is required to explore this causal relationship.

Conclusion

The analysis demonstrates that despite observing relatively high levels of sufficient water data that is required for IKBs within GISTM, there are systematic shortcomings

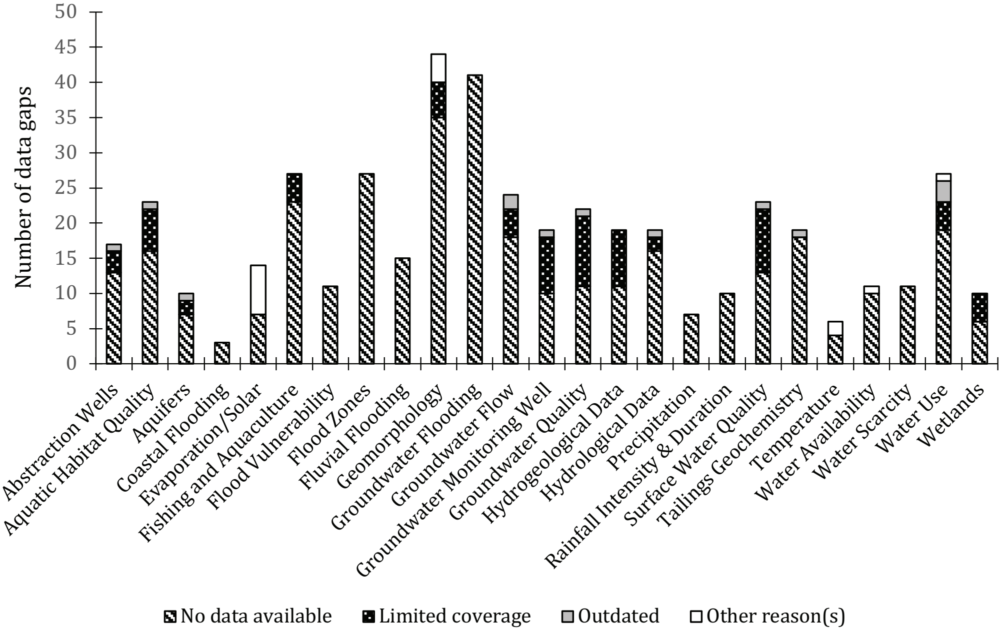

Figure 3 Reason for identified gaps.

in the collection of water data. The evidence is that these challenges in gathering sufficient water data for TSFs are a global phenomenon, across geographies and commodities. The study findings also indicate that older active TSFs are less likely to have sufficient data than closed TSFs, not only for compliance with GISTM but also to be able to obtain regulator-approved closure.

Some specific water topics, such as geomorphology, point to not just a lack of data gathering and understanding at the site-level, but also a lack of clear definition as to what is required and why within the GISTM framework. Another important implication is that monitoring well arrays and other water data are often focussed on the immediate surrounds of the TSF, with too little coverage of downstream and downgradient areas, failing to characterise the inundation zone in the event of rare catastrophic failure, and the much more common groundwater plume that is present at most TSFs.

Mining companies operating TSFs within the GISTM framework need to overcome these limitations in data availability by assessing their gaps in compliance and improving monitoring infrastructure and technical expertise, as required, to fill them. Reliance on third-party datasets does not always provide sufficient understanding of complex water issues and risks at the site-level, both to the environment, site operations and wider communities.

Fundamental to GISTM moving forward is the use of data within the knowledge base to support decision making around safe tailings management. The continued reference back to GISTM requirements may well elevate the need to collect more of the right kind of data to better understand risks and it is hoped that new facilities, as they come online, will inherently capture a greater variety of pertinent water data to ensure the safe operation and closure of these facilities in the future.

Acknowledgement

We thank the IMWA 2025 Conference organizers for the opportunity to present this work. We also acknowledge the staff involved in data extraction for their invaluable contributions.

References

Church of England. 2019. *Thousands of Tailings Dams revealed for the first time as over 200 companies disclose.* https://www.churchofengland.org/media/finance-news/thousands-tailings-dams-revealed-first-time-over-200-companies-disclose.

GRID-Arendal. 2020. *Global Tailings Portal*. https://tailing.grida.no/disclosures.

ICMM; UN Environment Programme; PRI. 2020. *Global Industry Standard on Tailings Management*. https://globaltailingsreview.org/wp-content/uploads/2020/08/global-industry-standard_EN.pdf.

Islam, K., and S. Murakami. 2021. "Global-scale impact analysis of mine tailings dam failures: 1915–2020." *Global Environmental Change* 70: 102361, DOI: https://doi.org/10.1016/j.gloenvcha.2021.102361.

Rana, N. M., N. Ghahramani, S. G. Evans, A. Small, N. Skermer, S. McDougall, and W. Andy Take. 2022. "Global magnitude-frequency statistics of the failures and impacts of large water-retention dams and mine tailings impoundments." *Earth-Science Reviews* 232: 104144, DOI: https://doi.org/10.1016/j.earscirev.2022.104144.

World Resources Institute. 2024. *Aqueduct – Water Risk Atlast*. https://www.wri.org/applications/aqueduct/water-risk-atlas/.

Occurring Challenges in the Development Process of Geothermal Mine Water Projects and Possible Solutions

Kevin Mannke[1], Florian Hahn[1], René Verhoeven[1], Stefan Klein[1], Jonas Enno Lehmann[1]

[1]*Fraunhofer IEG – Fraunhofer Research Institution for Energy Infrastructures and Geotechnologies IEG, 44801 Bochum, Germany, kevin.mannke@ieg.fraunhofer.de ORCID-ID: 0009-0000-1130-8551*

Abstract

In the context of the ongoing energy transition, characterized by a shift from fossil fuels towards renewable energy sources, it becomes imperative to present local energy suppliers with technically and ecologically viable solutions. In regions formerly dedicated to coal mining, the utilization of warm mine water and its geothermal application can play a significant role in the energy transition, functioning as a heat source and a heat reservoir. The implementation's feasibility has been thoroughly investigated by various studies, particularly within the Ruhr region of Germany, elucidating the pertinent challenges and the development of solutions for addressing them, which will be subsequently presented.

Keywords: Mine water, legal challenges, geothermal, post-mining exploitation

Introduction

In the context of the transformation of the heat supply in Germany, away from fossil fuels towards renewable energies, geogenic energy sources play a vital role, as they offer the advantage of providing energy locally and thus secure independence from external energy sources. In the former coal mining regions, mine water can represent a part of these locally available heat sources and can be compared with the other heat sources in terms of technical and economic feasibility. In the course of conducting various feasibility studies on the implementation of geothermal mine water systems, challenges that need to be overcome for numerous reasons and using diversified methods quickly come to light. Recognizing and compiling these important findings is essential in order to create a more profound basis for future projects, so that obstacles that arise again can be dealt with more effectively using the lessons learned. In the following, typical problems that emerged in recently completed or in-progress case studies are highlighted, and respective solutions and/or circumventions are discussed.

Technical challenges

As part of three feasibility studies on the conversion of heating networks for a local energy supplier serving three municipalities in the eastern part of the Ruhr area, mine water was investigated as a regenerative heat source in addition to other energy sources. In the three areas that were investigated, a comprehensive evaluation was conducted to ascertain the requirements and conditions for implementing geothermal mine water utilisation. It was observed that each of the three supply areas presented distinct possibilities for mine water utilisation, accompanied by a range of challenges.

The northernmost areas of the former "Königsborn" coal mine are located directly below the smallest of the three district heating grids that were the focus of the study. The location of the heat network and the former underground parts of the mine are shown in Fig. 1. The existing underground data was overlaid with a buffer zone representing a larger area around the original data points. This buffer serves to anonymise the specific location of the data by adding an extra spatial margin around it, according to legal restrictions.

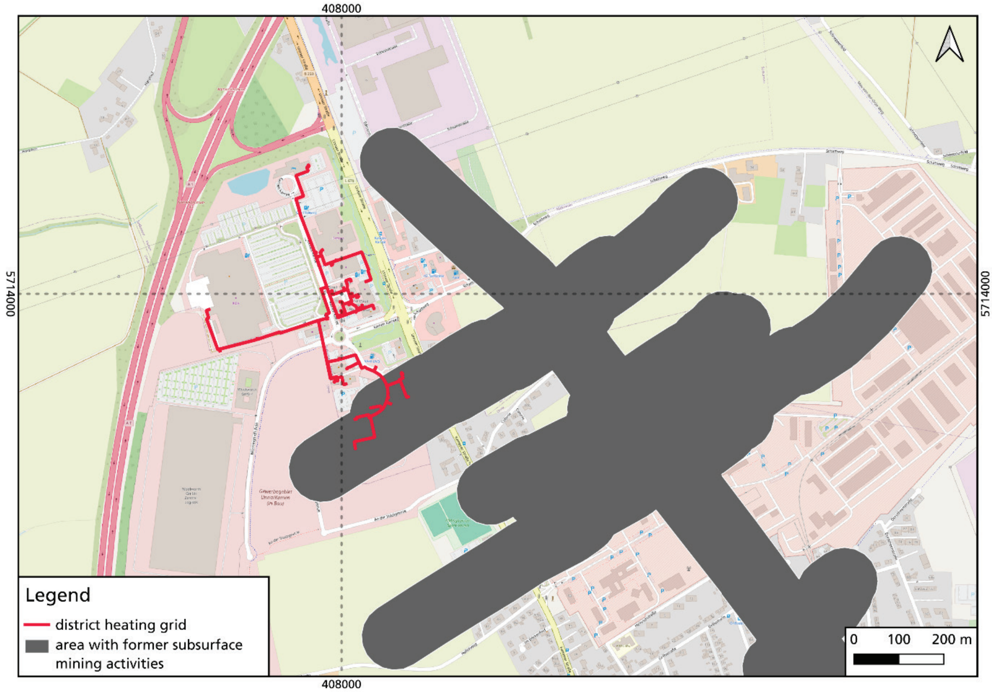

Figure 1 *District heating network (red) with a representation of the former underground structures of a coal mine (grey, due to restricted permission anonymised).*

The former drifts and crosscuts of the colliery lie at a depth of -200 to -300 meters below sea level, while the upper edge of the site is at a level of +70 meters above sea level. The mine workings are part of a mine that is isolated from the central mine water drainage system that often dominates the mine water levels in the Ruhr area and is therefore completely flooded. With a current measured mine water level of just over 45 meters above sea level (Bürgerinformationsdienst, 2025), this results in a pumping height of just under 25 meters at an expected temperature of 18 °C. Based on these facts alone, especially the low head and the perfect location of the mine below the current network, the use of mine water as a geothermal source seems obvious and logical. However, there are two major obstacles that make technical implementation problematic: the age of the mine and its location within the mine. The part of the mine below the heating network is one of the oldest parts of the mine and was created around 1890. At that time the mine was mainly built with wooden beams, and discussions with experts from the responsible mining company suggest that these beams have barely survived the last 130 years intact, leaving only a small residual mine void volume from the former workings. This means that only a small part of the former cavity is likely to be available for geothermal use. The second obstacle to the development of the mine is the location of the existing drifts in relation to the rest of the mine. The drifts are very isolated areas in terms of their location and are only connected to the rest of the mine by a single drift. This makes it difficult for the mine water to exchange with the rest of the mine, which means that the mine workings would cool down more and more over time. For these two reasons, the use of mine water for the existing local heating network was not the preferred option for the project.

As the underground conditions cannot be changed retrospectively, a different solution must be found for the utilisation of mine water for this project, which relates to the surface. One possible solution, which was discussed and developed with the energy supplier and grid operator, would be a possible extension of the grid to the south.

This would allow the network to move into areas of the mine that were created much later and therefore offer more residual mine void volume and at the same time open up areas of the mine that allow better exchange of the mine water to prevent the mine water from constantly cooling down. By creating a mine model and simulating the underground thermal-hydraulic situation, the influence of larger residual cavity volumes can be modeled and well estimated. The mine water can then once again become a valuable geothermal heat source for a future expansion of the heating network.

Legal Challenges

The second and largest heating network of the energy supplier is located in proximity to one of the six central mine water dewatering sites, with the future intention of permanently pumping mine water from this location to ensure a constant mine water table in the mine water province. These pumping sites offer a high potential for the geothermal utilisation of mine water, as the necessary infrastructure has already been established to bring the water to the surface. The existence of this infrastructure greatly enhances the economic viability of the project and facilitates expeditious and technically uncomplicated execution.

While technical implementation at this location can be very straightforward, the legal and contractual challenges here are more complex and need to be clarified in advance. First of all, the water law in Germany issues had to be clarified, as these can have an influence on the subsequent operator model. In principle, the energy from the mine water can be transferred to three locations. (1) at the surge chamber of the mine drainage system, (2) behind a heat exchanger and finally (3) behind a high-temperature heat pump. Each of these three options offers advantages and disadvantages for both the operator of the mine dewatering system and the operator of the heating network.

In the case (1) of a transfer downstream of the surge tank, the mine water management operator would lose control over its own water and would transfer responsibility for the extracted mine water to the network operator, and thus also the potential problems associated with this. The advantage of this variant would be that the supplier could plan everything from a single source and that no additional costs would be incurred by the mine water management company. In variant (2), the operator of the mine water drainage system would continue to have sovereignty over its own mine water, but would have to pay for the investment and operation of the heat exchanger. The network operator would avoid problems with the mine water and would have lower investment costs, but these would probably be offset by a slightly higher price for the heat provided. Option (3) would save the supplier the large investment for a large heat pump, but the potential margin from refining the heat would also be lost. The mine water operator could offer the heat at grid temperature in a complete package and thus increase its own margin, but this would come with high investment costs as well as the responsibility of becoming an energy supplier. After constructive discussions with both stakeholders, it became clear that variant (2) turned out as the most practicable option for the time being, as a clear separation of responsibilities is evident for both sides and, above all, the legal issues relating to the ownership of the mine water are clearly resolved.

Another legal obstacle that can be encountered in the implementation of mine water geothermal projects is the exploration fields for the use of geothermal energy. At the present time in North Rhine-Westphalia, these legally cover the areas of medium-depth and deep geothermal energy as well as the use of mine water for geothermal purposes from a level of less than 100 meters. As part of the “Act to speed up the approval procedures for geothermal systems, heat pumps and heat storage facilities”, the lowering of the limit to 400 m is currently being examined, which may offer more scope for implementation in the future (BMWK, 2024). This means that if such a field was to be used by the owner for the exploration of deep geothermal energy, the realization of projects that want to use thermal energy from mine water could be hindered. Here too, an agreement would have to be reached with the owner of the field in order to find a joint legal solution. Alternatively, such a problem could also be solved technically. If the mine workings and the conditions above ground are suitable for use as a mine heat storage facility, consideration could be given to adapting the concept into a storage concept. The storage of heat is not covered by the rights of the exploration fields for geothermal energy and therefore a possible legal obstacle could be circumvented here by adapting the technical layout.

Conclusions

The challenges that can arise during the planning, development and implementation of mine water projects are multiple and complex. For some, there are direct solutions that ideally only require intensive and constructive discussions among the stakeholder and can often be resolved with a contract. These are mainly issues that have either a legal, social or contractual dimension. Although these problems can be solved, the processes can be extremely delayed, as it is not always clear who is responsible, which areas are affected and which other stakeholders may need to be involved in finding a solution. As this can take a very long time, it is important to address these issues at an early stage of the project, to avoid further delays during the actual implementation.

Problems that are based on geological, chemical or technical reasons can be much more complex, due to the many different aspects, but can often be solved or circumvented with the right methods and approaches. However, if this is not the case, an alternative solution must be sought or the expansion must be postponed to a later stage, when the framework conditions for the successful implementation of a geothermal mine water utilization are more favorable.

Acknowledgements

The author thanks the project partners helping in the development of geothermal mine water projects. Florian Hahn and Tobias Rolf provided critical comments on earlier versions of this text.

References

Bürgerinformationsdienst (2025): RAG Aktiengesellschaft, https://geodaten.rag.de/mapapps/resources/apps/bid/index.html?lang=de, last accessed 09.02.2025.

BMWK (2024): Entwurf eines Gesetzes zur Beschleunigung der Genehmigungsverfahren von Geothermieanlagen, Wärmepumpen und Wärmespeichern sowie zur Änderung weiterer rechtlicher Rahmenbedingungen für den klimaneutralen Ausbau der Wärmeversorgung. https://www.bmwk.de/Redaktion/DE/Artikel/Service/Gesetzesvorhaben/20240628-entwurf-beschleunigung-genehmigungsverfahren-geowg.html

Competitive Adsorption of Toxic Metals Using Activated Carbon Derived from Sargassum for Polymetallic Acid Mine Drainage Treatment

Patricia I. Melendez-Torres[1],*, Máximo E. Reynoso-Ortega[1], Pamela R. Tejada-Tejada[1], Teresa Valente[2], Ulises J. Jauregui-Haza[1]

[1]Instituto Tecnológico de Santo Domingo, Distrito Nacional, Dominican Republic

[2]Instituto de Ciências da Terra, Polo da Universidade, Universidade do Minho, Braga, Portugal

**Corresponding and presenting author: ulises.jauregui@intec.edu.do*

Abstract

Acid mine drainage (AMD) represents a significant environmental threat due to high concentrations of potentially toxic elements. Adsorption with activated carbons is one of the processes used to treat these waters. In scientific literature, activated carbons are widely recognized as effective materials for the adsorption of contaminants, but activation methods and the choice of base material affect their performance. This work uses sargassum, an algae that has proliferated excessively in areas of the Caribbean, as an alternative and economic resource for producing activated carbon, thus contributing to managing this environmental waste.

This study investigated the competitive adsorption efficiency of three metals (Mn, Al, and Zn) in acid mine waters using activated carbon derived from sargassum. The relevance of this study lies in its innovative and sustainable approach to reduce metallic concentrations in AMD. The adsorption kinetics of the three study metals in an aqueous solution on activated carbon from sargassum were established. Activated carbon from sargassum was obtained by acid activation, achieving the prevalence of acid groups on its surface. The simple and competitive adsorption isotherms were determined for the three metals at different pH to evaluate this factor's influence on adsorption at room temperature.

The concentration of metals is higher in acidic water at pH 3 when compared to the model solution at pH 7. The isotherm models that best described the adsorption were the Langmuir and Jovanovic models, with a random distribution of settling times for the cases of simple and competitive adsorption. The breakthrough curves for simple and competitive adsorption on activated carbon for the three metals were determined experimentally. The results were validated in a real acidic water matrix from Barrick Gold's gold mine, demonstrating the effectiveness of acid-surfaced sargassum activated carbon under real-world conditions.

The next step will be to design a pilot adsorption column to evaluate the efficiency of the process under real-world working conditions at the mine. Using sargassum as a base material, the study offers a solution to metal contamination in AMD and takes advantage of a low-cost and abundant biomass. This presents an economically viable and sustainable alternative to conventional methods of remediating acidic mine water, which are often expensive and generate secondary by-products.

Keywords: Sargassum, gold mine, sustainable treatment, Dominican Republic

Characterization of Core Samples and Mechanisms of Zinc Leaching in a Waste Rock Dump of Abandoned Mines

Miu Nishikata[1], Yohey Hashimoto[2], Tomoko Oguri[1], Tetsuo Yasutaka[1]

[1]*Institute for Geo-Resources and Environment, Geological Survey of Japan (GSJ), National Institute of Advanced Industrial Science and Technology (AIST), 305-8567, Higashi 1-1-1, Tsukuba, Ibaraki, Japan*

[2]*Department of Bioapplications and Systems Engineering, Tokyo University of Agriculture and Technology, Koganei, Tokyo 184–8588, Japan*

Abstract

Mine drainage containing toxic elements discharged from abandoned mines and waste rock dumps is causing pollution of rivers, farmland and groundwater around the world. In Japan, there are many abandoned mines and there is a need to reduce the cost and improve the efficiency of mine drainage treatment. In order to reduce the cost and improve the efficiency of mine drainage treatment, it is necessary to understand not only the characteristics of mine drainage, but also the elution mechanism of toxic elements. In this study, we conducted a drilling survey of a waste rock dump at an abandoned mine where leachate containing zinc has been confirmed, and identified the minerals contained in the drilling core using XRD (X-ray Diffraction) analysis, determined the total potentially toxic metals content, and identified the chemical form of zinc using XAFS (X-ray Absorption Fine Structure) to understand the spatial distribution of environmental information within the dump. We also carried out leaching tests to investigate the leaching mechanism of zinc in terms of the influence of contact with groundwater in the waste rock and the form in which zinc is present, and considered countermeasure options to reduce the concentration of zinc in mine drainage from the waste rock dump. The borehole reached groundwater, and the groundwater quality showed that the contamination was not uniform (table1). The results of the analysis of the drilling core and the leaching test showed that the main cause of zinc leaching in the waste rock dump was the sulfate form, and that the sulfate form of zinc was more abundant in areas with high groundwater concentrations. XRD analysis and SEM (Scanning Electron Microscope) observation confirmed the presence of pyrite, galena, sphalerite, anglesite, and jarosite (containing lead, zinc, and copper). The waste rock contained high concentrations of zinc (1000mg/kg to 53,000mg/kg). The maximum concentration of zinc in the batch elution test was 151 mg/L. Furthermore, XAFS analysis confirmed that the chemical form of zinc in the samples with high elution amounts was sulfate and clay minerals, and SEM observation showed that jarosite was observed, suggesting that the source of elution was sulfate rather than sphalerite. The results of this study suggest that the amount of zinc leaching is affected by groundwater. If the pathway of groundwater inflow into the waste rock deposit site can be identified, and if the inflow of rainwater can be prevented by using a water-proof sheet to prevent the rise in groundwater levels, it is thought that the leaching of zinc that affects groundwater can be prevented, and the load on wastewater can be reduced.

Keywords: Waste rock dump, zinc, x-ray absorption fine structure, batch leaching tests

***Table 1** Groundwater quality of cores with high concentrations of potentially toxic metals and cores with low concentrations of potentially toxic metals in waste rock. (August/2021).*

	pH	EC (mS/m)	SO_4^{2-} (mg/L)	Zn (mg/L)	Cd (mg/L)	Pb (mg/L)
High concentration	3.6	308	140	7.9	0.068	1.9
Low concentration	5.7	231	110	1.5	0.013	0.001

Investigating the Effects of Storm Events on the Temporal Dynamics of Acid Mine Drainage Loads in Receiving Streams of the Lusatian Lignite Mining District (Germany)

Extended Abstract for Poster Presentation

Erik Nixdorf[1,2], Maik Boehmeke[1], Marcus Fahle[1]

[1]*Federal Institute for Geosciences and Natural Resources, Cottbus, Germany, 2Helmholtz-Centre for Environmental Research UFZ, Leipzig, Germany*

Keywords: Lignite mining, acid mine drainage, surface water quality, event-driven monitoring

For more than 100 years, opencast lignite mining in the Lusatian Mining District has transformed more than 800 km^2 of landscape in East Germany, forming a distinctive pattern of active mines, post-mining lakes, reclaimed agricultural land and forests (Krümmelbein *et al.* 2012). Dewatering, aeration, and rewetting of iron sulfide containing sediments during the mining cycle led to the formation of strong acid mine drainage (AMD) loads. The AMD pollution of the River Spree, which drains the central part of the mining district, mainly originates from an area in the southern part of the mining district, the Spreewitz glacial channel (Fig. 1, left). Extensive AMD management and remediation measures are required to reduce the negative influence on the water quality of the Spree River (Pflug 1998).

Water quality can be strongly impacted by storm events due to event-driven dilution or enrichment patterns in the catchment, which overlay seasonal and long-term trends (Musolff *et al.* 2021; Knapp and Musolff 2024). In former mining areas, it has been shown that storm events can increase pollutant loads, including potentially toxic metals, iron, and sulfide by orders of magnitude, highlighting the critical role of flood events in accurately estimating the annual dissolved pollutant load in surface waters (e.g. Blake *et al.* 2003; Cánovas *et al.* 2008; Mayes *et al.* 2021).

In this context, we investigate the temporal dynamics of AMD loads by deploying high-frequency LTC (Level-Temperature-Conductivity) data loggers of type Solinst Levelogger 5 LTC at the Spree River and its tributaries along a 15 km long river section, the Spreewitz glacial channel (Fig. 1, left). Loggers were placed on the streambed in proximity to gauges using concrete slabs (Fig. 1, right).

Data was monitored at a resolution of 10 minutes covering an observation period between April, 10th 2024 and January, 10th 2025 (Fig. 2). In addition, surface water samples at each deployment location have been taken bimonthly. Samples for cation analysis were filtered through 0.45 μm teflon filters, acidified with suprapure nitric acid to a pH <2 and refrigerated until analysis in the laboratory.

Due to the predominance of sulfate as the most relevant electro-active species in the AMD-impacted water of the Spree River and its conservative behaviour, electric conductance measured by each datalogger at high frequency serves as a very good proxy for sulfate concentration. According to the data of our samples, we found a linear correlation of R^2 = 0.97 (Fig. 3, left). Hence, we set up a mass balance model for the section of the Spree River between Sprey and Spreewitz by interpreting the

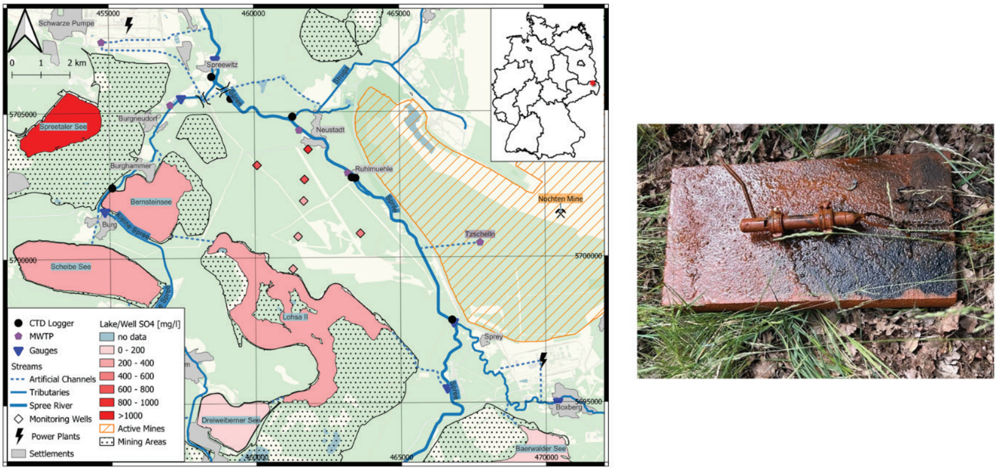

Figure 1 Left: Map of the study site with relevant installations. Water quality of groundwater wells and mining lakes is provided by (LMBV 2024; Uhlmann et al. 2024). Right: LTC logger anchored on a concrete slab taken out of the water at location Spreewitz. The reddish color is caused by iron hydroxide deposits.

product of measured flow rate provided by gauging stations and corresponding EC as the electroactive load. This parameter, representing the total load of electroactive species in the water, serves as a proxy for estimating AMD loads entering the stream.

The results indicate that exchange fluxes and their directions vary both spatially and temporally, resulting in a net loss of stream water to the groundwater but a net gain of AMD loads (Fig. 2, lower plot). Analysis of nine major storm events revealed an average increase of approximately 75% in AMD loads entering the stream compared to pre-event conditions, potentially driven by the mobilization of pre-event water stored in sediments. Peaks in AMD loads occurred, on average, 5.6 ± 7.4 hours before the peak discharge, while excess AMD loads ceased 5.2 ± 7.0 hours after the peak discharge. As the events progressed, AMD loads fell below pre-event conditions due to the dilution by stormwater inflow becoming the dominant factor (Fig. 3, right).

Our findings highlight the importance of high-frequency measurements to accurately

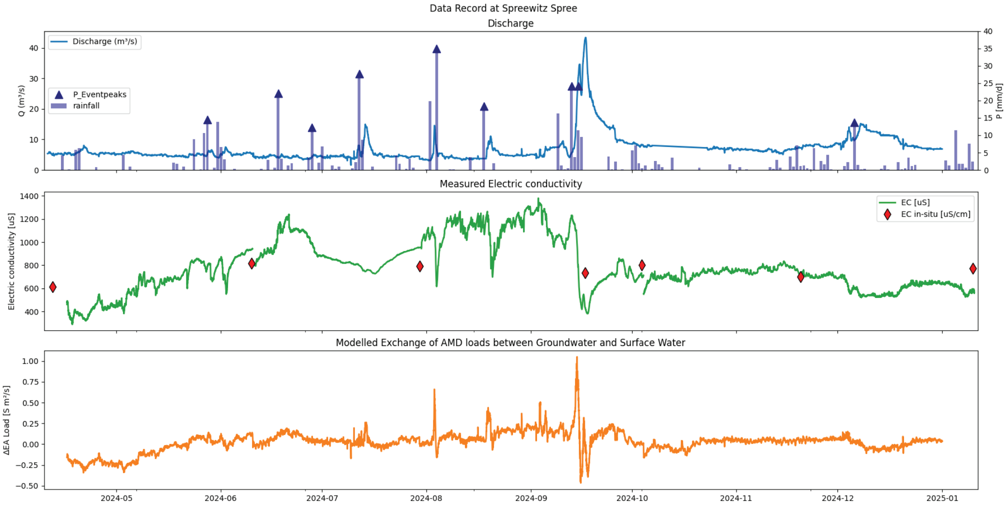

Figure 2 Time series of discharge and precipitation (top), monitored EC (middle) and derived exchange of AMD loads between surface and groundwater (bottom) in the Spree River at the community Spreewitz.

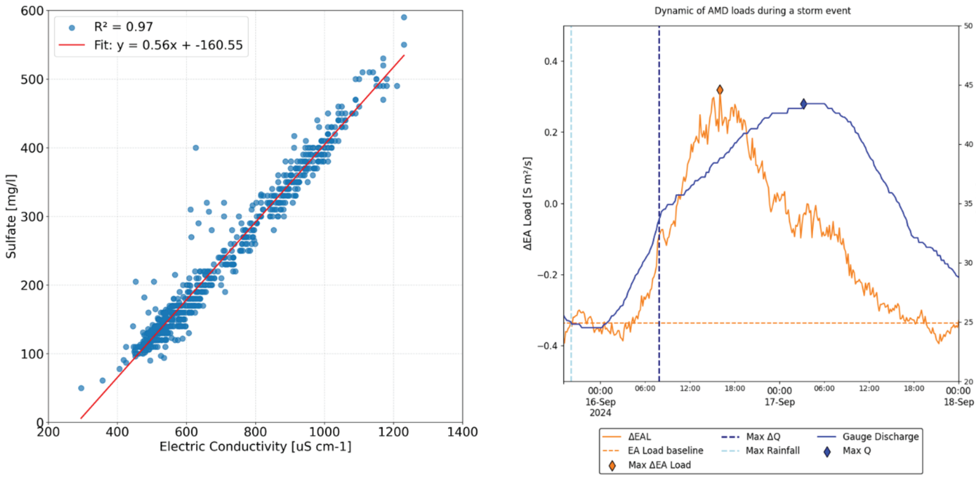

Figure 3 *Left: Correlation between sulfate and EC in the Spree River at the investigation site (586 samples over 30 years at three locations, provided by the local water authorities). Right: Dynamics of exchange of AMD loads between surface and groundwater in the investigated river section during a one in ten years flood event observed in September 2024.*

account AMD loads. They may contribute to enhance AMD load management in receiving waters by adopting measures to reduce peak loads during storm events. Possible measures like optimizing drainage designs and implementing sediment control practices may save costs and improve water quality in surface water bodies affected by acid mine drainage. In addition, accurately accounting outflows of event-induced AMD loads from tailings can improve estimates of remaining AMD stocks in the tailings, allowing for a more precise forecast of the remaining timeframe required for remediation efforts in the receiving waters until pollutant levels drop below environmental standards.

References

Blake WH, Walsh RPD, Barnsley MJ, *et al* (2003) Heavy metal concentrations during storm events in a rehabilitated industrialized catchment. Hydrological Processes 17:1923–1939. https://doi.org/10.1002/hyp.1218

Cánovas CR, Hubbard CG, Olías M, *et al* (2008) Hydrochemical variations and contaminant load in the Río Tinto (Spain) during flood events. Journal of Hydrology 350:25–40. https://doi.org/10.1016/j.jhydrol.2007.11.022

Knapp JLA, Musolff A (2024) Concentration-Discharge Relationships Revisited: Overused But Underutilised? Hydrological Processes 38:e15328. https://doi.org/10.1002/hyp.15328

Krümmelbein J, Bens O, Raab T, Anne Naeth M (2012) A history of lignite coal mining and reclamation practices in Lusatia, eastern Germany. Canadian Journal of Soil Science 92:53–66

LMBV (2024) Wasserwirtschaftlicher Jahresbericht der LMBV mbH 2023. Lausitzer und Mitteldeutsche Bergbau-Verwaltungsgesellschaft mbH, Senftenberg

Mayes WM, Perks MT, Large ARG, *et al* (2021) Effect of an extreme flood event on solute transport and resilience of a mine water treatment system in a mineralised catchment. Science of The Total Environment 750:141693. https://doi.org/10.1016/j.scitotenv.2020.141693

Musolff A, Zhan Q, Dupas R, *et al* (2021) Spatial and Temporal Variability in Concentration-Discharge Relationships at the Event Scale. Water Resources Research 57:e2020WR029442. https://doi.org/10.1029/2020WR029442

Pflug W (1998) Braunkohlentagebau und Rekultivierung: Landschaftsökologie–Folgenutzung–Naturschutz. Springer

Uhlmann W, Hiekel, Robert, Giering, Niklas (2024) Quellenmonitoring und Grundwassermonitoring im Südraum – Hydrologisches Jahr 2023. Institut für Wasser und Boden, Dresden

Hydrogeological and Hydrological Modelling of the Impact of Water Resources on Mineral Resource Production

Mariam Taki, Nicolas Flipo, Damien Goetz

Mines Paris PSL, Geosciences department, 77300 Fontainebleau, France, mariam.taki@minesparis.psl.eu

Abstract

The increasing global demand for mineral resources, particularly copper, nickel, lithium, and cobalt, driven by the energy transition, presents challenges to the mining industry, especially amidst increasing global water scarcity. Water plays a vital role in all stages of mineral extraction and, as water stress intensifies, its availability becomes a limiting factor for mining operations. Given that global water consumption is increasing at twice the rate of population growth, concerns over water availability are intensifying, particularly in regions experiencing severe scarcity.

This study introduces HYIR (HYdrological and Industrial Resilience), a global-scale integrated tool designed to assess water availability for mining operations by combining multiple data layers and models. HYIR utilizes climate data from the Coupled Model Intercomparison Project Phase 6 (CMIP6) (Eyring et al., 2016), driven by Shared Socioeconomic Pathways (SSP) scenarios, to simulate future climate scenarios. These projections provide critical insights into expected changes in precipitation patterns and other climate variables that will influence water resources in the world in general and in mining regions in particular.

To evaluate the effects of these climatic changes on water resources, HYIR incorporates hydrological models and global databases (Oki, 1998) to simulate river networks and large-scale hydrological processes. The tool also takes into account data on surface water bodies, including lakes, dams (Lehner, 2023), and groundwater reservoirs (aquifers).

HYIR's key capability will lie in its ability to generate spatiotemporal assessments of water availability, accounting for both climate and hydrological dynamics. By integrating climate projections, river routing data, and surface and groundwater storage data, HYIR will be able to evaluate water availability at specific locations and times. This allows for the identification of regions at risk of water scarcity, providing insights into the future viability of mineral extraction in those areas.

In particular, HYIR aims to assess whether certain mineral deposits are likely to remain exploitable in the future or if they are vulnerable to water stress. This tool shall serve as a decision-support framework, facilitating assessments of the risks associated with water scarcity for mining operations and informing long-term planning and resource management.

Keywords: Hydrology, water stress, climate change, mining, water availability, global water resource, mineral production

References

Eyring V, Bony S, Meehl GA, et al (2016) Overview of the Coupled Model Intercomparison Project Phase 6 (CMIP6) experimental design and organization. Geoscientific Model Development 9:1937–1958. doi:10.5194/gmd-9-1937-2016

Oki T, Sud YC (1998) Design of Total Runoff Integrating Pathways (TRIP)—A Global River Channel Network. Earth Interactions 2:1–37. doi:10.1175/1087-3562(1998)002<0001:DOTRIP>2.3.CO;2

Lehner B, Döll P (2004) Development and validation of a global database of lakes, reservoirs and wetlands. Journal of Hydrology 296:1–22. doi: 10.1016/j.jhydrol.2004.0

Evaluating the Sustainability of Passive Treatment for Acid Mine Drainage of a Legacy Mine via Life Cycle Assessment

Sereyroith Tum[1], Taiki Katayama[1], Naoyuki Miyata[2], Takaya Hamai[3], Yuki Semoto[3],
Tetsuo Yasutaka[1]

[1]Institute for Geo-Resources and Environment, Geological Survey of Japan (GSJ), National Institute of Advanced Industrial Science and Technology (AIST), 305-8567, Higashi 1-1-1, Tsukuba, Ibaraki, Japan

[2]Department of Biological Environment, Akita Prefectural University, 010-0195, Shimoshinjo-Nakano 241-438, Akita, Japan

[3]Metals Environment Management Department, Japan Oil, Gas and Metals National Corporation, 105-0001, Toranomon 2-10-1, Minato, Tokyo, Japan

Abstract

Legacy Mine X in Japan has employed an active treatment system since 1979, generating high CO_2 emissions and operational costs. In 2021, a pilot-scale passive bioreactor achieved 98% manganese (Mn) and zinc (Zn) removal, but the comprehensive environmental impact assessment has not been yet evaluated. Using life cycle assessment (LCA), the passive treatment system was found to emit approximately 130 g CO_2 equivalent/m^3, with a unit cost of 37.91 Japanese Yen/m3. Scaling up passive treatment presents a sustainable and cost-effective remediation strategy.

Introduction

The active treatment system at Legacy Mine X has effectively prevented mine drainage from contaminating surrounding water bodies and aquatic environments, although at a high cost (Hengen *et al.* 2014; Miyata *et al.* 2024). To reduce operational expenses and CO_2 emissions, passive treatment was introduced to the study area. The pilot-scale passive treatment successfully removed Mn and Zn from the mine drainage using limestone gravel to enhance the activity of Mn-oxidizing bacteria (Watanabe *et al.* 2024). However, the environmental impacts, particularly CO_2 emissions and operational and maintenance costs of scaling up the passive treatment system have not yet been fully investigated. Therefore, this study employs LCA of the full-scale passive treatment system scenarios to estimate the CO_2 emission and operational cost of the passive treatment.

Methods

Full-scale passive treatment scenario

The full-scale passive treatment plant scenario was designed to treat mine drainage at an average flow rate of 2.84 m^3/s (Iwasaki *et al.* 2022) (Fig. 1), based on the pilot-scale passive treatment described in Tum *et al.* (2024). The system is designed to operate on a daily basis for at least 30 years. Regular maintenance is planned every three years to remove the formation of birnessite and woodruffite coatings on the limestone surface, which could otherwise affect the efficiency of the system.

Life cycle assessment approach

The assessment uses a midpoint evaluation method to focus on CO_2 emissions, using kilograms of CO_2 equivalent per m3 (kg CO_2 eq/m^3) as the functional unit during the operational period. The system boundaries include all aspects of the treatment plants, such as energy consumption, water sampling, sample handling, transportation, sludge management, and labour. Operation and maintenance costs are included in the LCA to facilitate economic comparison. In addition, the study explores strategies to reduce CO_2 emissions in the passive treatment system using the alternative energy sources. The cost of the active treatment system was determined based on annual mine drainage treatment costs and the volume of mine drainage treated.

Result and discussion

The mine drainage at the study site contained Mn and Zn concentrations of 20 mg/L and 8 mg/L, respectively (Watanabe *et al.* 2024). The pilot-scale passive treatment system exhibited removal efficiencies of 98% for Mn and 82% for Zn, attained with a hydraulic retention time (HRT) of 0.5 days within the limestone tank (Tum *et al.* 2024). These removal rates signify the system's capacity to adhere to regulatory mandates for treated mine drainage.

The LCA study revealed that the passive treatment system emits approximately 97,000 kg CO_2 equivalent annually, with an operational cost of 28.2 million JPY. By comparison, the active treatment system is more resource-intensive, costing approximately 147 million JPY annually (METI 2010). Furthermore, the unit processing cost of the passive system (37.91 JPY/m^3) is 2.6 times lower than that of the active system (99.5 JPY/m^3), underscoring its economic viability.

The transition to nuclear or solar energy has the potential to enhance the environmental and economic sustainability of the passive system (Fig. 2). It is important to note, however, that while nuclear energy sources have been posited as a means to minimize CO2 emissions, this is an option that has been largely overlooked since the 2011 Fukushima nuclear incident (Yamagata 2024). Conversely, the utilization of solar energy has been shown to result in a 16,210 kg CO_2 eq annual reduction in CO_2 emissions, accompanied by a 10 million JPY annually decrease in energy expenditures. This finding underscores the importance of energy source selection in reducing the carbon footprint and operational expenses of passive treatment systems (Fig. 2).

Despite its apparent advantages, the passive system faces challenges related to maintenance. The necessity of limestone replacement every three years results in substantial expenditures and CO_2 emissions. Nevertheless, the negative environmental impacts of the passive system remain comparatively less substantial than those associated with the active system. This is primarily due to the reduced consumption of raw materials and the consequent decrease in greenhouse gas emissions.

Conclusion

The findings indicate that expanding the passive treatment system offers a sustainable and cost-effective solution for mine drainage remediation. The associated reductions in CO2 emissions and treatment costs are highly beneficial to mine wastewater operations

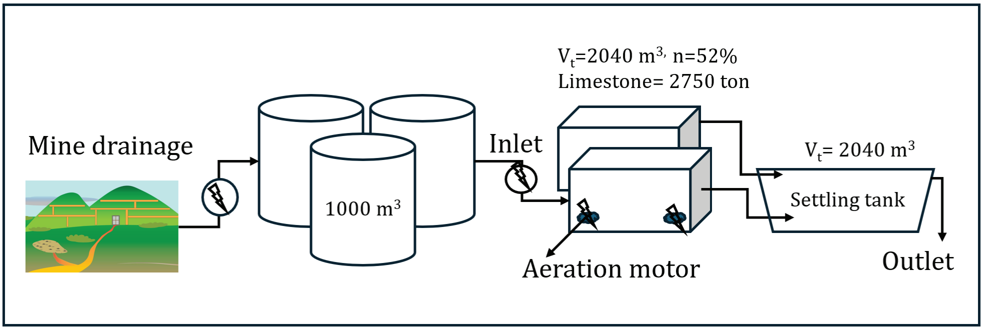

Figure 1 The schematic illustrates the passive treatment pants scenario.

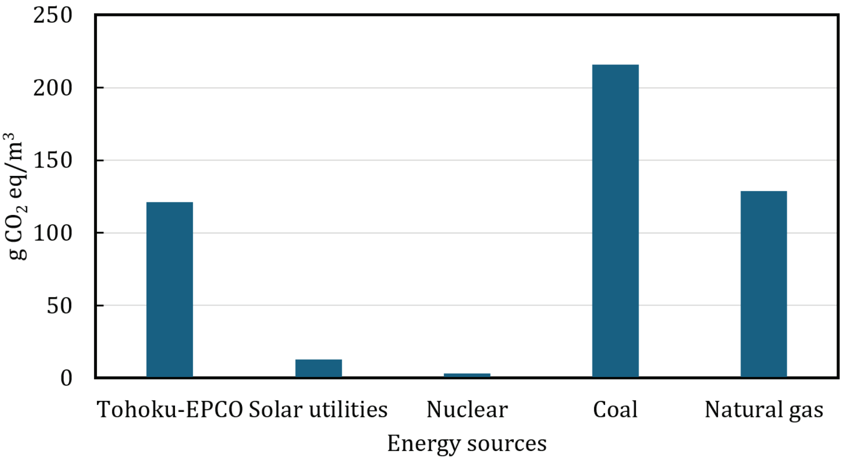

Figure 2 *CO_2 emissions from the passive treatment plant during the treatment of 1 m^3 of mine drainage according to various energy sources, Tohoku-EPCO: a local electric company in the Tohoku region, Japan.*

and align with the CO_2 zero-emission goals. Future research should prioritize optimizing maintenance practices and further reducing energy consumption to enhance the long-term viability of the system. Additionally, evaluating the applicability of this approach to other legacy mine sites will be essential to assess its broader scalability and impact.

Acknowledgement

The authors express their sincere gratitude to all the co-organizers for hosting the IMWA 2025 Conference. Additionally, the authors would like to extend their heartfelt thanks to all individuals, both directly and indirectly involved, who have made valuable contributions to this research project. This study was partly funded by METI (Ministry of Economy, Trade, and Industry).

References

Hengen TJ, Squillace MK, O'Sullivan AD, Stone JJ (2014) Life cycle assessment analysis of active and passive acid mine drainage treatment technologies. Resources, Conservation and Recycling 86:160–167. https://doi.org/10.1016/j.resconrec.2014.01.003

Iwasaki Y, Murata M, Kawaguchi T, *et al* (2022) 坑廃水原水を放流する場合に休廃止鉱山下流の水質測定地点の金属濃度は環境基準を達成できるか？. Journal of MMIJ 138:28–32. https://doi.org/10.2473/journalofmmij.138.28

METI (2010) Central Mine Safety Council (METI/Ministry of Economy, Trade and Industry). https://www.meti.go.jp/shingikai/hoankyogikai/015.html. Accessed 14 Jan 2025

Miyata N, Suganuma R, Sunouchi K, *et al* (2024) Biological Mn(II) oxidation under organic substrate-limited conditions and its application in mine drainage remediation. Biochemical Engineering Journal 203:109187. https://doi.org/10.1016/j.bej.2023.109187

Tum S, Katayama T, Miyata N, *et al* (2024) Geochemical insights and model optimisation for pilot-scale passive treatment of manganese and zinc in a legacy mine in Japan. Heliyon 10:e40363. https://doi.org/10.1016/j.heliyon.2024.e40363

Watanabe M, Tum S, Katayama T, *et al* (2024) Accelerated manganese(II) removal by in situ mine drainage treatment system without organic substrate amendment: Metagenomic insights into chemolithoautotrophic manganese oxidation via extracellular electron transfer. Journal of Environmental Chemical Engineering 12:113314. https://doi.org/10.1016/j.jece.2024.113314

Yamagata H (2024) Public opinion on nuclear power plants in Japan, the United Kingdom, and the United States of America: A prescription for peculiar Japan. Energy Policy 185:113939. https://doi.org/10.1016/j.enpol.2023.113939

From Deep Mineral Exploration to Mine Closure: Why Groundwater Matters?

Magdalena Worsa-Kozak

Politechnika Wrocławska, Faculty of Geoengineering, Mining and Geology, Wybrzeże Wyspiańskiego 27, 50–370 – Wrocław, Poland, magdalena.worsa-kozak@pwr.edu.pl, ORCID: 0000-0001-8119-3075

Extended Abstract

Groundwater plays a critical yet often overlooked role in the lifecycle of mineral resource development, from exploration to mine closure. As global demand for minerals intensifies, deeper and more complex deposits are being targeted, and the sustainable management of groundwater resources has become a pivotal factor in successful operations. This work highlights the importance of groundwater investigation at the earliest stage of the mining project life cycle and the need to integrate groundwater management into every mining stage, emphasizing its influence on environmental stewardship and operational success. Addressing deep mineral exploration challenges, we bring the idea of miniaturized robotic tools for deep exploration of inland mineral deposits closer, with a particular focus on groundwater challenges. Early hydrogeological exploration can minimize environmental risks, reduce costs, and ensure the long-term viability of mining projects. This is crucial as the industry faces increasing scrutiny from regulatory bodies and local communities.

Based on the MINOTAUR EU-funded project approach (MINOTAUR, 2024), we present a novel concept of a miniaturized robotic exploration tool for deep land deposits (Fig. 1) that will support developing an integrated hydrogeological framework combining advanced geophysical surveys, hydrogeochemical information, and long-term monitoring data to assess groundwater conditions at each stage of mining project life and to plan effective and sustainable mine water management.

The implementation of the Logging-While-Drilling (LWD) and Measure-While-Drilling (MWD) approach by integrating novel sensors and technologies into the MINOTAUR robotic tool (Fig. 2) is expected to allow for direct identification and measurement mainly of rock geochemical and geomechanical properties but also of groundwater basic parameters like pressure, temperature or electric conductivity. This information is often lacking at the stage of early mineral exploration. However, it is crucial for future mine operation planning, e.g., drainage design, mineral processing design, or mine closure design.

The key applications of our work include improving risk assessments and mine planning, enhancing regulatory compliance, and providing tools for effectively monitoring groundwater throughout the mining process. Our integrated framework supports decision-makers in designing more resilient and environmentally responsible mining operations. The implications of our findings are particularly relevant for developing sustainable mineral resource extraction practices in a world increasingly focused on climate change and water security, ensuring that groundwater is protected and utilized efficiently across the entire mining lifecycle.

Acknowledgements

The work is funded by the European Union under Project 101178775 — MINOTAUR.

References

MINOTAUR – Miniaturized Robotic Systems for Autonomous In-Situ Exploration of Critical Raw Materials In Deep Land Deposits – project proposal, 2024, DOI: https://doi.org/10.3030/101178775

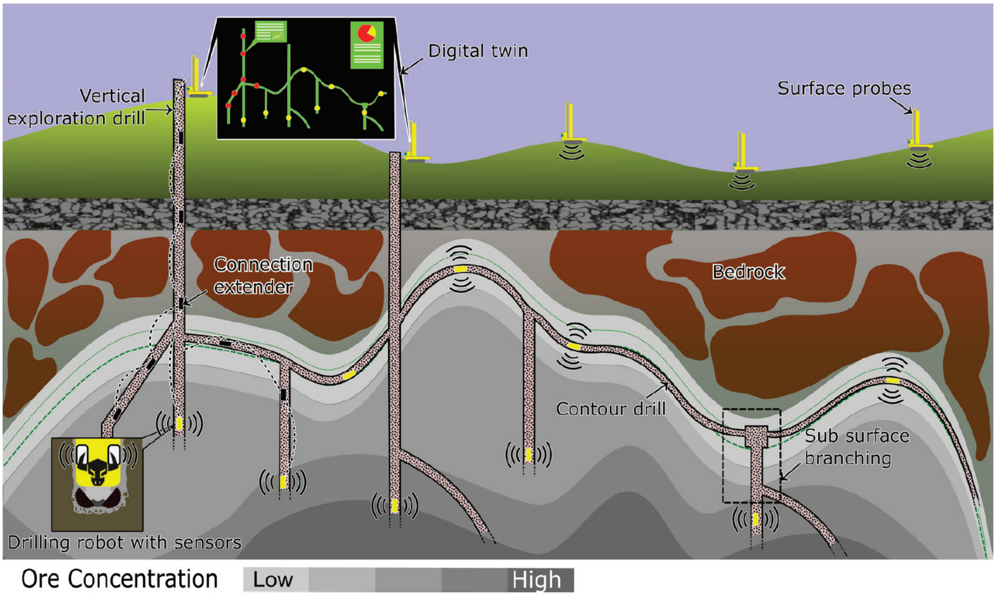

Figure 1 Minotaur concept for exploratory drilling, with novel technologies, such as robotized drilling machines, autonomous contour drilling and ore-tracking, in-situ sensing and AI based resource characterization and geo-modelling. (MINOTAUR, 2024).

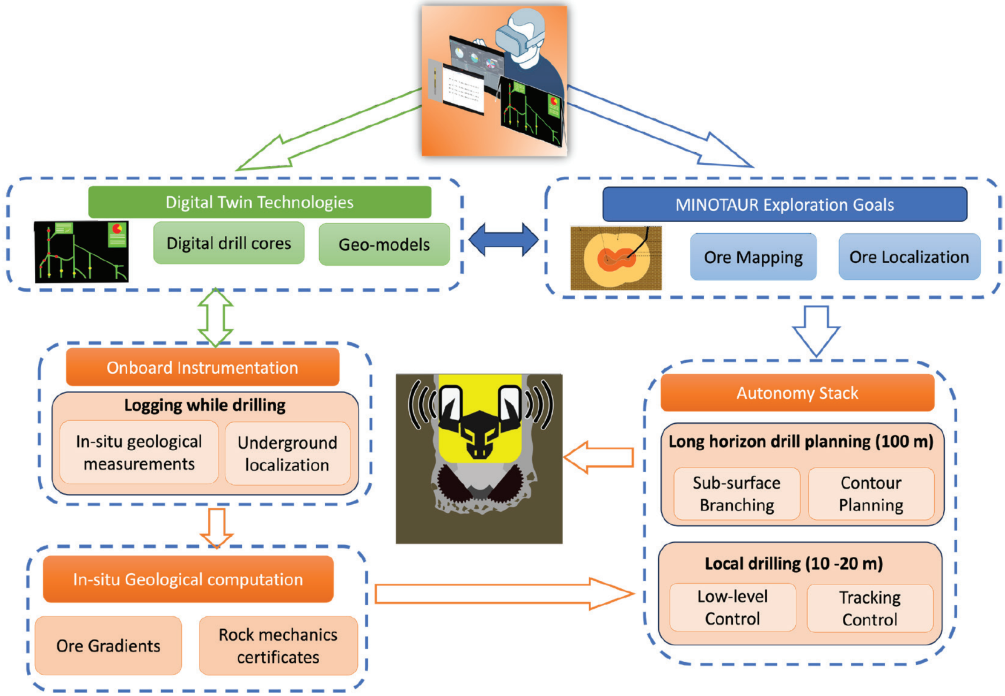

Figure 2 A workflow diagram of the conceptual MINOTAUR system. (MINOTAUR, 2024).

Author Index

Keyword Index

Dear IMWA 2025 participant, dear reader!

Experience the enchantment of Portugal and Spain!

The IMWA 2025 Organising Committee is delighted to present the proceedings of the International Mine Water Association Conference, which takes place at the University of Minho in Braga, northern Portugal, from 6–11 July 2025, and will be co-hosted by the University of Oviedo in Spain.

This year, we welcome the international community to a region with a rich mining heritage dating back to pre-Roman times. Both Portugal and Spain have long-standing traditions of mineral exploitation and innovation, and we are honoured to be hosting IMWA 2025 – "Time to Come" – within this legacy.

The proceedings feature 170 peer-reviewed full papers from oral presentations, as well as 20 extended abstracts from poster sessions. Contributions come from 592 researchers and professionals representing 40 countries across five continents, showcasing the event's global and multidisciplinary scope.

With over 300 delegates in attendance, IMWA 2025 presents a broad spectrum of innovative research, case studies, and technologies relating to mine water management, environmental effects, remediation, hydrogeology, geochemistry, policy, and sustainable mining practices.

We are also proud to acknowledge the substantial backing of numerous industry sponsors, including companies from the mining sector, environmental consultancy, and equipment manufacturing. This support strengthens the connection between science and practice.

All papers accepted for inclusion in this volume have undergone rigorous peer review, ensuring high-quality contributions to the field. These proceedings serve as a lasting, citable scientific record of the knowledge, ideas, and advancements shared at IMWA 2025.

We thank all the authors, reviewers, and sponsors who contributed to the success of the IMWA 2025 edition and joined us in Braga to strengthen the global mine water community.

Teresa Valente | Conference Chair
Almudena Ordoñez | Conference Co-Chair
Christian Wolkersdorfer | IMWA President

ISBN 978-3-9825293-3-2